LUND UNIVERSITY

NSB 2014 - 10th Nordic Symposium on Building Physics - Full Papers

Arfvidsson, Jesper; Harderup, Lars-Erik; Kumlin, Anders; Rosencrantz, Bitte

2014

Link to publication

Citation for published version (APA):
Arfvidsson, J., Harderup, L.-E., Kumlin, A., & Rosencrantz, B. (Eds.) (2014). *NSB 2014 - 10th Nordic Symposium on Building Physics - Full Papers*. Building Physics, LTH, Lund University.

Total number of authors:
4

General rights
Unless other specific re-use rights are stated the following general rights apply:
Copyright and moral rights for the publications made accessible in the public portal are retained by the authors and/or other copyright owners and it is a condition of accessing publications that users recognise and abide by the legal requirements associated with these rights.
• Users may download and print one copy of any publication from the public portal for the purpose of private study or research.
• You may not further distribute the material or use it for any profit-making activity or commercial gain
• You may freely distribute the URL identifying the publication in the public portal

Read more about Creative commons licenses: https://creativecommons.org/licenses/

Take down policy
If you believe that this document breaches copyright please contact us providing details, and we will remove access to the work immediately and investigate your claim.

LUND UNIVERSITY

PO Box 117
221 00 Lund
+46 46-222 00 00

BUILDING PHYSICS IN THE NORDIC COUNTRIES

NSB 2014

10th Nordic Symposium on Building Physics

15-19 June 2014 Lund, Sweden

FULL PAPERS

LUND UNIVERSITY

FUKT CENTRUM

NSB 2014

10th Nordic Symposium on Building Physics

15-19 June 2014 Lund, Sweden

FULL PAPERS

Editors:
Jesper Arfvidsson, Lars-Erik Harderup, Anders Kumlin, Bitte Rosencrantz

ISBN: 978-91-88722-53-9 (TVBH-3061)

Photographer:
Frontpage: Lasse Strandberg

Print: Grafisk gruppen AB
Layout: Malmö Kongressbyrå AB

CONTENT

Introduction	4
Scientific committee	5

FULL PAPERS

Air-tightness	7-117
Building Envelope Systems	119-320
Building Materials and Structures	322-515
Challenges of the Future	517-598
Historical Buildings	600-669
Low energy Buildings	671-945
Moisture Safety	947-1170
Retrofitting of Buildings	1172-1356
RAP-RETRO	1358-1406
Author Index	1407-1411
Sponsors	Back page

INTRODUCTION

The Nordic Symposium on Building Physics started in Lund in 1987 on an initiative by the Moisture Research Centre in Lund and has been arranged every third year. The venues of the previous symposia were Lund (1987), Trondheim (1990), Copenhagen (1993), Espoo (1996), Gothenburg (1999), Trondheim (2002), Reykjavik (2005), Copenhagen (2008), and Tampere (2011). Now it is organized for the 10th time and will again, 27 years later, be hold in Lund.

Over time, the symposium has become the biggest international conference focusing on Building Physics. A total of about 300 abstracts were submitted to the 2014 symposium and an international scientific committee of external referees reviewed nearly 180 papers. The symposium provides a broad presentation of Building Physics research, especially in Europe.

During the last decades Building Physics research has increased all over the world. Good indoor environment in combination with sustainability and low environmental impact, to reduce the global climate changes, is a challenge across the world. It is of great importance to have a holistic view and include all the different aspects, such as energy, moisture safety, ventilation, acoustics, fire safety, economy etc., sometimes interacting in a very complicated way.

This symposium presents two tracks, one practical and one more theoretical, divided in ten topics, and presented in three parallel sessions. Two new topics are introduced; “Historical Buildings” and “Challenges for the future”. The intention of adding Historical Buildings is to gather people with different backgrounds, for example Building Physicists, Building antiquarians, Building Biologists, Architects, City planners etc. in a common forum. The interest for questions related to “Challenges of the Future” is growing rapidly. This area requires competence from many different specialities for example environmental impact, climate change, meteorology, and risk assessment.

Three keynote lectures related to the above subjects will be given at the symposium. Professor Johnny Kronvall, who organized the first symposium in 1987, will speak about “Building Physics – an attempt to a 30 years´ evolution story”, M.Sc. Anders Kumlin will concentrate on the practical applications in ”Practical Moisture Problems”. The last keynote lecture is Professor Mark Bomberg who will present his thoughts in ”A personal view on Building Physics: An address in the Nordic BP Symposium 2014”.

We want to thank all the people that took part in the realisation of this symposium; especially members of the Scientific committee for their great work in reviewing abstracts and papers. A special thank to Amelie Rönngård at Anagram and Lotta Ahlbertz at Malmö Kongressbyrå for all help in planning and correspondence with the authors. We are also grateful to all the authors who wrote the papers making this 10th symposium an interesting one. Finally we express our gratitude to the sponsors who financially supported the implementation of this symposium.

Lund, May 2014

The Organizing Committee of NSB2014
Jesper Arfvidsson, Lars-Erik Harderup, Anders Kumlin and Bitte Rosencrantz

SCIENTIFIC COMMITTEE

Dr. **Karin Adalberth**, Sweden
Prof. **Miimu Airaksinen**, Finland
Jim Althinsson, Sweden
Prof. **Jesper Arfvidsson**, Sweden
Björn Becker, Sweden
Prof. **Thomas Bednar**, Austria
Prof. **Folke Björk**, Sweden
Assoc. Prof. **Bert Blocken**, Netherlands
Prof. **Mark Bomberg**, USA
Lic. Eng. **Peter Brander**, Sweden
Steven Burke, Sweden
Dr. **Helena Bülow Hube**, Sweden
Peter Carlsson, Sweden
Prof. **Robert Černý**, Czech Republic
Jan Christensson, Sweden
Dr. **Malcolm Cunningham**, New Zeeland
Civ. Eng. **Martin Engman**, Sweden
Prof. **Vasco Peixoto de Freitas**, Portugal
Dr. **Hua Ge**, Canada
Dr. **Stig Geving**, Norway
Prof. **John Grunewald**, Germany
Rickard Henriksson, Sweden
Prof. **Carl-Eric Hagentoft**, Sweden
Dr. **Lars-Erik Harderup**, Sweden
Prof. **Per Heiselberg**, Denmark
Prof. **Shuichi Hokoi**, Japan
Prof. **Andreas Holm**, Germany
Dr. **Linda Hägerhed Engman**, Sweden
Assoc. Prof. **Hans Janssen**, Denmark
Anders Joelsson, Sweden
Prof. **Guðni Jóhannesson**, Iceland
Dr. **Peter Johansson**, Sweden
Dr. **Targo Kalamees**, Estonia
Dr. **Kurt Kielsgaard Hansen**, Denmark
Dr. **Johnny Kronvall**, Sweden
Dr. **Hartwig Künzel**, Germany
Mr. **Teppo Lehtinen**, Finland
Prof. **Ralf Lindberg**, Finland
Mathias Lindskog, Sweden
Prof. **Ardeshir Mahdavi**, Austria
Dr. **Peter Matiašovský**, Slovakia
Civ. Eng. **Anders Melin**, Sweden
Prof. **Nathan Mendes**, Brazil
Prof. **Kristina Mjörnell**, Sweden
Dr. **Phalguni Mukhopadhyaya**, Canada
Prof. **Anker Nielsen**, Denmark
Dr. **Tuomo Ojanen**, Finland
Dr. **Rudy Plagge**, Germany
Dr. **Nunu Ramos**, Portugal
Prof. **Carsten Rode**, Denmark
Prof. **Staf Roels**, Belgium
Assoc. Prof. **Ingemar Samuelson**, Sweden
Dr. **Chris Sanders**, United Kingdom
Ass. Prof. **Angela Sasic Kalagasidis**, Sweden
Ass. Prof. **Jos van Schijndel**, Netherlands
Prof. Dr. **Klaus Sedlbauer**, Germany
Dr. **Anders Sjöberg**, Sweden
Prof. **Svend Svendsen**, Denmark
Dr. **Berit Time**, Norway
Prof. **Lars Wadsö**, Sweden
Prof. **Juha Vinha**, Finland
Niclas Wahl, Sweden
Dr. **Maria Wall**, Sweden
Prof. **Monika Woloszyn**, France
Dr. **Petter Wallentén**, Sweden

TOPIC
Air-tightness

Page.....7-117

A quantitative evaluation of airtightness measurement experiences

Thomas Olofsson, Ph.D and Ingrid Allard, M.Sc.
Applied Physics and Electronics, Umeå University, Sweden

KEYWORDS: *Air tightness, Buildings, Field Measurements, Survey, ZEF*

SUMMARY:
Evaluation of building air tightness based on field measurements is an important aspect in the process to provide good indoor environment and energy efficient buildings. The measurements are generally conducted by experts. To improve field methods for evaluation of building air tightness, experience of these experts can be useful.

The scope of this paper is to problematize usefulness of methods for airtightness measurements, how and when methods are used and potential for future development. Surveyed Swedish and Finnish experts have valued the performance and usefulness of methods in the perspective of being used for singe family, multifamily, new, inhabited, under construction, renovation, leaky and air-tight buildings. They also valued the future potential, as well as their own level of experience and expertise, of the methods.

Although the results of the survey were based on a small set of collected data, it indicated that the experts favored methods with their highest assessed experience and expertise, i.e. Blower door and Surface temperature measurements/Thermography. Potential of future development within quantitative and component methods was assessed to be positive in general and in particular for the favored methods.

1. Introduction

Uncontrolled ventilation from air leakage has an impact on the indoor environment and the building energy efficiency. In that context, the air tightness is generally an important issue calling for evaluation. However, that evaluation is not an easy task (Sherman 2004, Sikander 2008, Gränne 2001, Bankvall 2013). Evaluation of building airtightness**,** based on field measurements for new buildings, buildings under construction, as well as for inhabited buildings is often conducted by trained experts. For their use there are several available methods. Based on the conditions in question and the demands on the evaluation, each method demonstrates its strengths and drawbacks, described in the literature (Allard 2012, Nirvan 2010, Lee 2011, Sherman 1992, Hassan 2013). The reported evaluations were often based on experimental conditions. It can be assumed that the experts' experience from field measurements can differ from what is documented under controlled laboratory conditions. Field experiences can supplement the experimental findings in general but also be useful for future development of field measurements.

In this paper we have investigated how a number of Finnish and Swedish experts value their expertise, the performance and usefulness, and expected future use of a selected number of identified methods for measuring airtightness. The scope of the paper is to problematize usefulness of the methods, how and when they are used and their potential for future development. The intension was for the findings of this pre-study to be used for a future similar, but more qualitative, investigation.

2. Survey background

The survey was based on statements and answered using a parametric Likert scale, with the range 1 to 5, in accordance with an increasing level of agreement. The survey was conducted on a selected set of methods and specified conditions of building types and life stages, introduced in this section.

2.1 Surveyed methods

The surveyed methods are arranged in three different groups: quantitative methods, component methods and experimental methods, see table 1 below. The methods in the quantitative group are used for verification of air tightness. The methods in the component group are used to enhance air tightness of building components, e.g. a wall. The methods in the experimental group are not used commercially today, but may have advantages and future potential.

Table 1. The methods analyzed in the study, arranged in categories.

Quantitative	Component	Experimental
1. *Fan pressurization - blower door*: A common method that uses a mounted fan to maintain a defined pressure inside the building, in order to estimate the air permeability and is standardized in (ISO 9972/EN 13829).	4. *Ocular inspection/light measurements:* Ocular (visual) inspection of air tightness on the test object. It requires experience and knowledge by the user. Ocular inspection is not standardized (Allard 2012).	8. *Acoustic measurements:* Pressurization operates by inducing a sinusoidal volume change pulse of about 1 Hz. By measuring the pressure pulse, information about air leakages can be extracted and is described by (Sherman 2004)
2. *Fan pressurization - ventilation:* A method that uses the fan in the ventilation system to maintain a defined pressure inside the building, in order to estimate the air permeability and is standardized in (ISO 9972/EN 13829).	5. *Surface temperature measurements/thermography:* Surface temperature measurement determines the temperature distribution, performed with a surface thermometer or an IR camera. It demands a temperature difference > 5°C (Nordtest 1997), standardized in (SS EN 13187).	9. *Pulse pressurization, SECA:* Pulse pressurization or sudden expansion of compressed air (SECA) can be obtained from e.g. a compressed air tank. A power law equation predicts a finite recovery time for the decay and can be used with the measurements to calculate leakage and volume (Lee 2011).
3. *Tracer gas:* SF_6 or N_2O, is diffused in the building or a single zone. With time the tracer gas will become diluted by inflowing air. Based on the gas decay and knowing the building geometry, the air permeability can be calculated, described in (NT VVS 055).	6. *Air velocity measurements/hand method:* Carried out with suppressed pressure inside the building. The anemometer (or hand) is moved along the analyzed area and air velocity (leakage) can be detected and is described in (ISO 7726, ISO 7730).	
	7. *Smoke methods*: With an overpressure, inside air leakages can be detected using smoke released with a smoke pen, bottle, machine or pistol smoke and is described in (ASTME 1186).	

2.2 Surveyed building types for the quantitative methods

Five building types where investigated with the quantitative methods: Single-zone, Multi-zone, High rise, Leaky building and Air tight buildings. Single-zone buildings are defined as single family buildings. Multi-zone buildings are for example apartment buildings or other houses with single-zone living compartments that border both to the outside and another single-zone. High rise buildings are defined as buildings with four floors or more. This definition is based on building conditions in the northern parts of Europe. Leaky buildings are buildings with high air permeability and air tight

buildings have low air permeability. The latter are often some kind of energy efficient building, such as a passive house.

2.3 Surveyed life stages for the methods

The different life stages of buildings, considered for component and experimental methods, are listed in table 2 below, with comments. Component methods can be used for all building types without significant mutual disadvantages. Experimental methods are considered too untested to analyze with respect to building type, and thus with concern of the questionnaire length, the questions for experimental methods related to all building types. New buildings are buildings which are built, but the inhabitants have not moved in. Forecast and background questions were asked considering all life stages and building types simultaneously.

Table 2. The life stages considered and comments.

Life stage	Comment
1. Under construction or renovation	Not used for quantitative questions
2. New building	Climate envelope is finished but inhabitants have not moved in
3. Inhabited Building	Inhabitants are living in the building

3. Questioner

The questionnaire used for the survey is developed by a Finnish marketing company (ZEF 2013) and utilizes a graphical 2D-interface.The results are reported in Fig 1-3, below, where the smaller circle with a number (1..n) is referring to the evaluated questions. The position of the point is based on the average of all who have answered the question. Around each circle there is a darker area/ellipse, calculated with a standard deviation formula. It shows, in a graphical way, how much answers from the respondents (experts) vary from each other. The smaller the ellipse is, the more persons agree on that topic. The model of the ellipse also tells you in which direction/criteria (horizontal/vertical) agreement is smaller or bigger.

The questions were categorized into three levels; Background, Recommendations and Forecast, all further introduced in this section.

3.1 Background: Expert awareness questions

The background question is supposed to give information about expertise and practical experience of the methods among the participants. This shows which methods are most commonly used within the expert group. The background question was stated as: “I assess my expertise and practical experience to be good”. Therefore, both information on expertise (which may be only theoretical) and practical experience will be gathered. This information may be used for qualitative assessments of the answers in combination with the other questions.

3.2 Recommendations: Method recommendation questions

The recommendations are supposed to indicate which methods that is appropriate to use under certain circumstances. The circumstances, or scenarios, depend on building type and life stage. The recommendation question was stated as: “I would recommend this method by the terms of ease of use and performance for this building type and life stage”. The question was modified to apply to the different building types and life stages.

3.3 Forecast: Future method use questions

The questions were asked about the potential and future use of the investigated methods. The forecast question was stated as: “I believe there is likelihood of use and potential of performance for this method in the future”. The term ‘future’ is used since the exact date is not important.

4. Results

The survey was conducted on a number of identified Finnish and Swedish experts. In total 16 Finnish and 4 Swedish experts were asked to participate. Finally, 8 Finnish and 2 Swedish experts completed the survey.

In this section, the results are illustrated in graphs based on the method categories: quantitative, qualitative and experimental. The results are also presented as quantitative scoring based on the Root Means Square of the assessed value of x-axes (0-100) and of the y-axes (0-100), where the Likert scoring of 1 to 4 was transformed to a scale 0-100. The calculated scoring is referred to as "high" if it is larger than 67. The scoring is referred to as "low" if it is less than 33. "Medium" is used if the scoring it is between 45 and 55. A scoring of 55 to 67 is referred to as "above medium", and a scoring of 33 to 45 is referred to as "below medium".

4.1 Qualitative methods

For the three investigated quantitative methods, the experts assessed their expertise and practical experience of fan pressurization with a blower door as high, marked with circle (1) in Fig 1a. The expertise and practical experience of fan pressurization using ventilation (2) and the tracer gas method (3), in Fig 1a, was assessed below medium.

When the experts assessed recommendations for the three methods, blower door (which the experts were most familiar with) gained high and the best score, applied to all investigated types of new buildings; i.e. single-zone, multi-zone, high rise, leaky, and air tight, see the circle with (1,4,7,10,13) in Fig 1b, as well as for all investigated types of inhabited buildings, see (1,4,7,10,13) in Fig 1c. The performance and ease of use of fan pressurization using ventilation was assessed above medium and lower for all investigated types of new buildings, see circle with (2,5,8,11,14) in Fig 1b, as well as for all investigated types of inhabited buildings, see (2,5,8,11,14) in Fig 1c. The tracer gas method was rated below medium and lowest for all investigated types of new buildings, see circle with (3,6,9, 12,15) Fig 1c , as well as for all investigated types of inhabited buildings, see (3,6,9,12,15) Fig 1d.

The investigation of potential and future use indicated that the by experts favored blower door method gained a high score. Fan pressurization using ventilation was rated lower, but high, and the tracer gas methods was rated below medium, see Fig 1d.

An overall indication of the investigation of qualitative methods is that the assessment was rated according to the experience of the experts, i.e. blower door method, which the experts seamed accustomed to, were found superior in all investigated situations.

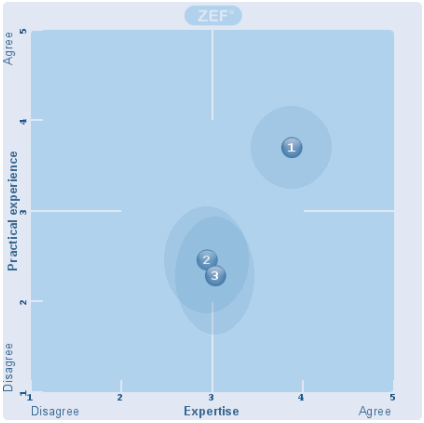

FIG 1a. Expertise and practical experience of fan pressurization with a blower door, fan pressurization using ventilation and the tracer gas methods

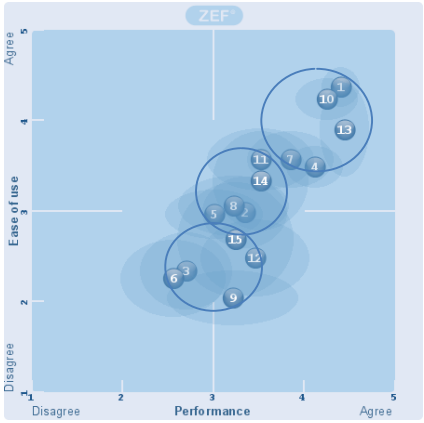

FIG 1b. Performance and ease of use for qualitative methods: Recommendations for single-zone, multi-zone, high rise, leaky as well as air tight and new buildings

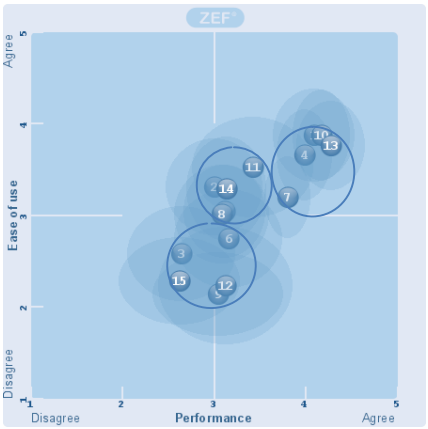

FIG 1c. Performance and ease of use for qualitative methods: Recommendations for single-zone, multi-zone, high rise, leaky as well as air tight and inhabited buildings

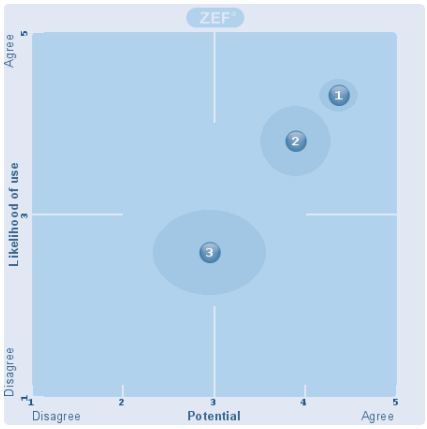

FIG 1d. A forecast of potential and future use of fan pressurization with a blower door, fan pressurization using ventilation and the tracer gas methods

4.2 Component methods

The experts assessed their expertise and practical experience of ocular inspection/light measurements and surface temperature measurements/thermography to be good and above medium, see circle with (1,2) in Fig 2a. The experts assessed their expertise and practical experience of air velocity measurements/hand method and smoke methods to be medium, see (3,4) in Fig 2a.

The experts assessed a high recommendation for surface temperature measurements/thermography for buildings under construction or renovation, new buildings and inhabited buildings, see circle with (2,5,6), as well as ocular inspection and light measurements for a building under construction or renovation, see (1), in Fig 2b. The recommendation of air velocity measurements/hand method and smoke methods, for a building under construction or renovation were assessed above medium, see (3,4) in Fig 2b.

The experts made a forecast of potential and future use of component methods. The scoring of potential and likelihood of use were ranked similar as the scoring of expertise and practical experience. The forecast of ocular inspection/light measurements and surface temperature measurements/thermography was scored high, see circle with (1,2) Fig 2c. Air velocity measurements/hand method and smoke methods was scored above medium, see (3,4) Fig 2c.

The results indicate that the experts in general assessed high rating for methods they are accustomed to, i.e. the favored ocular inspection/light measurements and surface temperature measurements/thermography.

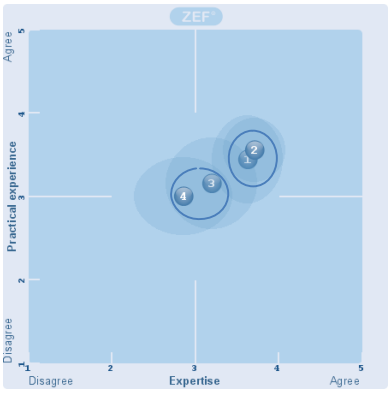

FIG 2a. Expertise and practical experience of ocular inspection and light measurements, surface temperature measurements and thermography, air velocity measurement/hand method, and smoke methods

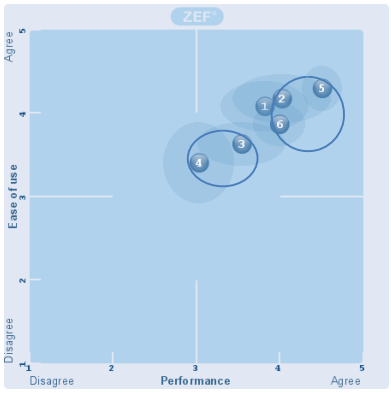

FIG 2b. Recommendations for buildings under construction/renovation, new buildings or inhabited buildings for component methods

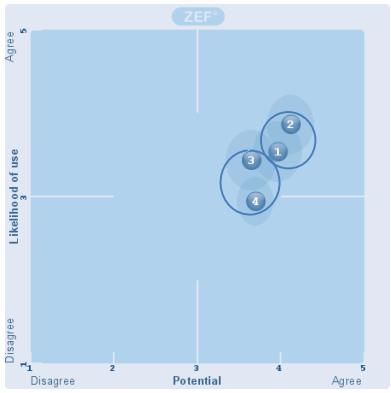

FIG 2c. A forecast of potential and likelihood for component methods

4.3 Experimental methods

The expertise and experience of the experts was assessed below medium for acoustic methods see (1) in Fig 3a. The expertise and experience of pulse pressurization or sudden expansion of compressed air (SECA) was assessed low, see (2) in Fig 3a.

The experts recommendations of acoustic measurements was rated above medium for new buildings, see (2) in Fig 3b and medium for new buildings and inhabited buildings, see circle with (1,4) in Fig 3b. Sudden expansion of compressed air (SECA) was assessed below medium, lowest for buildings under construction and new buildings, see circle with (3,5) in Fig 3b.

The experts assessed the likelihood of future use and potential of performance for acoustic measurements above medium, which can be interpreted as a small optimism for the future, see (1) in Fig 3c. The forecast for pulse pressurization or sudden expansion of compressed air (SECA) was assessed lower, medium, see (2) in Fig 3c.

It can be assumed that the experts have limited practical experience of these methods and consequently the interpretation of the results has less significance.

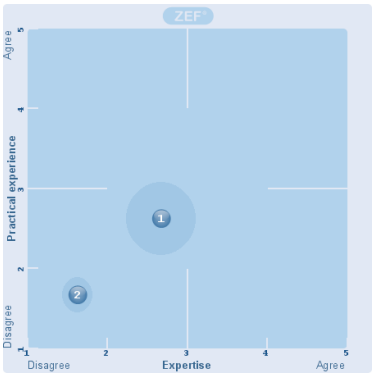

FIG 3a. Expertise and experience of experimental methods

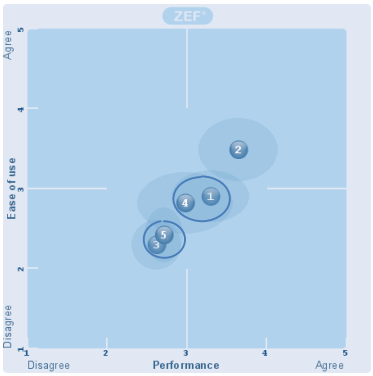

FIG 3b. Performance and ease of use for experimental methods

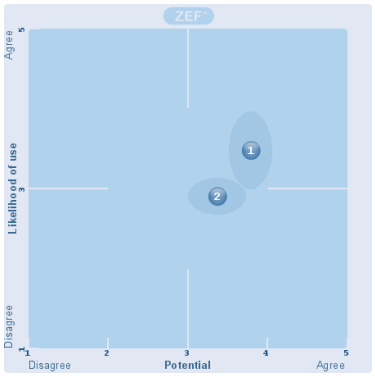

FIG 3c. Potential and likelihood of use for experimental methods

4.4 General results

The identification of experts for survey in this pre-study was based on mapping procedure supported by the national research institutes. It was found difficult to identify Swedish and Finnish experts of the investigated field measurement methods. For the study, 20 experts were identified and the

participation rate was 50%. From a statistical perspective that is small. For a larger study it would be beneficial with a more comprehensive mapping of experts.

Although the statistical material was limited, the standard deviation in the rating of the experts was relatively small, illustrated as the darker area around each circle in Figs 1-3. Additionally, the experts claimed their own expertise to be rather high. For the three categories of methods: quantitative, qualitative and experimental, the expert rating of recommendations were in accordance with their rated expertise and practical experience, which in general is rated medium to high. This indicates that the surveyed experts have sufficient expertise to answer the questionnaire. Thus it is assumed that the results can at least be used to give some guidance and some general trends can be discussed. An overall illustration of the results is presented in Tab 3.

Tabel 1.-Summary of the results for the investigated methods. The calculated root mean square can be found within the brackets.

Categories	***Methods***	***Expertise & Experience***	***Recommendations***	***Future forecast***
Quantitative	*Fan pressurization - blower door*	*High (70)*	*High for all applications (74)*	*High (83)*
	Fan pressurization – ventilation	*Below medium (43)*	*Above medium for all applications (56)*	*High (71)*
	Tracer gas	*Below medium (42)*	*Below medium for all applications (43)*	*Below med. (44)*
Component	*Ocular inspection/light measurements*	*Above medium (64)*	*High for buildings under construction (74)*	*High (69)*
	Surface temp measur./ Thermography	*Above medium (66)*	*Best component method, high for all stages (78)*	*High (75)*
	Air velocity measure-ments/hand method	*Medium (54)*	*Above medium for buildings under construction (65)*	*Above med. (64)*
	Smoke methods	*Medium (48)*	*Above medium for buildings under construction (56)*	*Above med. (59)*
Experimental	*Acoustic measurements*	*Below medium (41)*	*Above medium for new build., medium under construction and inhabited buildings (55)*	*Above medium (66)*
	Pulse pressurization, SECA	*Low(16)*	*Below medium for new and inhabited buildings(38)*	*Medium (54)*

The results showed an obvious correlation between high assessed recommendations and future expectations and high assessed experience and expertise of, e.g. Blower door and Surface temp measurements/Thermography. According to the experts, the potential for future development of quantitative and component methods reflects the recommendations of the favored methods. However, for experimental methods, the experts express a positive expectation of development, although the present recommendation was moderate. The rating of the future forecast in the study corresponds to the rated expertise and practical experience. The experts also indicated a general difficulty to measure air tightness in high rise and multi zone buildings, regardless of the method used.

Some overall suggestions of explanation can be proposed. The experts seems to prefer methods they are accustomed to before selecting method from actual condition, such as building type and the life stage of the building. Additionally, there is a general positive expectation from the experts in terms of a general large and growing future potential of field measurements in general for all three method categories.

5. Conclusions

The study was made on a rather small set of participating experts and should thus be interpreted as a pre-study. The investigated methodology was found applicable and useful and some trends and

findings were found that can be subject for future studies, e.g. of how and when the methods are used as well as future expectation.

For an interpretation in more detail, a future extended investigation is proposed, where more effort should be taken to get a larger set of experts, perhaps including more countries. Further, the study in this paper was conducted on a single survey. To collect more information and get more comprehensive results, it could be based on a methodology such as the Delphi method. In a future study experience based on findings in the literature could also be used to complement the findings from the surveyed experts.

6. Acknowledgement

This project has been funded by the Intereg IV project IEEB and the Kolartic project SBHN. The foundation of the survey presented in this paper was made by the Energy Engineering MSc-student Ragnar Björkén, at Umeå University, who is gratefully acknowledged. The authors would also express their gratitude to the experts who participated is the survey.

References

I. Allard, T. Olofsson, and O.B. Hassan, (2012) “Methods for air tightness analysis for residential buildings in Nordic countries" WIT Transaction on Ecology & the Environment, pp. 311–322

ASTME 1186-03 (2009), Standard Practices for Air Leakage Site Detection in Building Envelopes and Air Barrier Systems

C. Bankvall (013), "Luftboken : luftrörelser och täthet i byggnader", Studentlitteratur

F. Gränne (2001), “Air and Water Tightness in Building Envelopes - Evaluation of Methods for Quality Assurance,” KTH, Stockholm

O Hassan (2013), An alternative method for evaluating the air tightness of building components, Building and Environment, Vol. 67, pp. 82-86

ISO 7726 (2001), Ergonomics of the thermal environment, Instruments for measuring physical quantities (British Standard)

ISO 7730 (2005), Ergonomics of the thermal environment -- Analytical determination and interpretation of thermal comfort using calculation of the PMV and PPD indices and local thermal comfort criteria

ISO 9972:2006 (2006), Thermal performance of buildings -- Determination of air permeability of buildings -- Fan pressurization method

M. J. Lee, N. Il Kim, and H. S. Ryou (2011), “Air tightness measurement with transient methods using sudden expansion from a compressed chamber,” Building and Environment, vol. 46, no. 10, pp. 1937–1945

G. Nirvan, F. Haghighat, L. Wang, and H. Akbari (20012), “Contaminant transport through the garage – House interface leakage,” Building and Environment, vol. 56, pp. 176–183

Nordtest (1987), “Buildings: Total Outdoor Air Inflow (NT VVS 055),” pp. 1–11

M. Sherman (1992), “A Power-Law Formulation of Laminar Flow in Short Pipes,” Berkeley, Journal of Fluids Engineering, Vol.114, pp 601-605

M. H. Sherman and R. Chan (2004), “Building Airtightness: Research and Practice,” Lawrence Berkeley National Laboratory Report No. LBNL-53356, Berkeley

E. Sikander and P. Wahlgren (2008), “Alternativa metoder för utvärdering av byggnadsskalets lufttäthet,” SP-Borås

SS-EN 13187 (1999), Byggnaders termiska egenskaper - Kvalitativ metod för lokalisering av termiska ofullkomligheter i klimatskärmen - Infraröd metod

ZEF Solutions Ltd.,” 2013, Available: http://www.zef.fi/en/. [Accessed:10 Nov 2013]

Analysis and prediction of transient flow during night ventilation in a full scale test room

Sarah Leenknegt, PhD[1]

Dirk Saelens, Professor[1]

[1] Building Physics Section, Department of Civil Engineering, KU Leuven, Leuven, Belgium

KEYWORDS: *measurement, mechanical ventilation, unsteady ventilation, tracer gas, night ventilation, full scale test room*

SUMMARY

A full scale test room was constructed for the analysis of the energy performance of a room with night ventilation with air supply through a hopper window, supported by an extraction fan. Contrary to typical climate rooms, the room was exposed to realistic climatic conditions. This paper illustrates by means of measurements the air flow phenomena during night ventilation. The room includes a concrete floor and ceiling and detailed monitoring is done of local air and mass temperatures, air flow rate and local air velocities and surface heat flux. Based on a selection of summer nights, an assessment is made of the flow pattern occurring during night ventilation. Furthermore, to allow taking into account such flow changes in BES models, the timing of the flow changes are connected to the Richardson number. Three air flow typologies were identified: forced flow with short-circuit between supply opening and outlet (Coandă at ceiling), transition flow with limited Coandă effect, and buoyancy dominated flow with supply air falling down upon entry. The implications for assumptions used in BES models are discussed shortly, as the flow pattern will strongly influence the surface heat transfer.

1. Introduction

Night ventilation is a promising technique, able to reduce the cooling load through use of cold outdoor air at high air change rates to cool down the internal thermal mass of a building in moderate climates with sufficiently cold nights. A previous study focussed on the determination of the transient surface convection during night ventilation through numerical simulations using the commercial CFD package Fluent (Leenknegt et al. 2013). A simplified 2D geometry was simulated with unsteady RANS, using constant boundary conditions. Various supply air temperatures and velocities were studied, for a flow time of up to eight hours. Results from this numerical study showed the prevalence of unstable flow behaviour during constant high ventilation rates. Three flow regimes were observed, illustrated in FIG 1. Buoyant flow was defined as air falling down upon entry, with the main flow path over the floor surface. At a critical point, the air detaches from the wall under the inlet, moves upwards and attaches to the ceiling. The transition flow regime is then defined as a flow adhering to the ceiling with variable attachment length. During the simulations, this flow regime was only an intermediate regime, typically lasting only up to half an hour. Finally, the room air flow stabilizes into forced flow, with maximum ceiling attachment length and supply air short-circuiting via the ceiling towards the outlet. These flow regimes strongly influence the surface convection on the different surfaces during the intensive ventilation period. This influence was particularly noticeable at the ceiling where the evolution from buoyant to forced flow increased the surface averaged convective heat transfer coefficient (CHTC) by a factor 10. This illustrates the importance of taking into account this unsteady flow behaviour in rooms with night ventilation. However, this is currently not taken into account in Building Energy Simulation (BES) models.

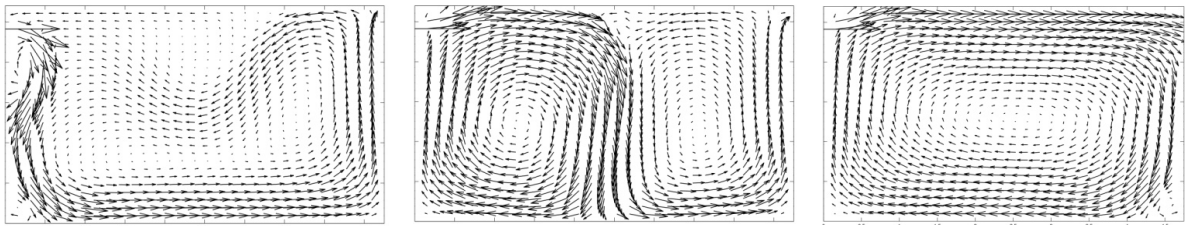

(a) Buoyant flow (b) Transition flow (c) Forced flow

FIG 1. Three flow regimes, observed in numerical simulations (Leenknegt et al. 2013)

Indeed, the most advanced but pragmatic convection model, used in BES models, is the adaptive convection algorithm, developed by Beausoleil-Morrison (2000), which defines five categories, assuming stable convection regimes during the (de)activation of HVAC. For instance, night ventilation would fall in the fifth category of mixed convection, as there is a system that supplies air to the room, combined with large temperature differences. Mixed convection correlations are then applied at the internal surfaces (Beausoleil-Morrison 2000). However, the numerical study showed that, during buoyant flow, the ceiling displayed very low heat transfer, corresponding to natural convection with stratified flow. To allow implementation of these insights in a refined convection model in BES, a criterion is required to predict the flow pattern. Therefore, the flow development was coupled to the dimensionless Richardson number. A critical value of Ri = 1 was suggested by the simulations, to indicate the transition from buoyant to forced flow.

This test room was constructed inside the Vliet test building of the Building Physics Section of KU Leuven, Leuven, Belgium. This is a 25.2 m long and 7.2 m wide test building, designed for the study of wall, window and roof components under real field conditions. The room differs from typical full scale test rooms in similar research (Artmann et al. 2010; Goethals et al. 2012), as it is exposed to real climatic conditions through a south-west oriented hopper window. High air change rates are provided through an extractor fan. As ventilation is done with outdoor air, the supply air temperature is not controlled and the thermal response of the room in case of realistic boundary conditions can be investigated. This limitation in ventilation control is compensated by more than 200 sensors, allowing a detailed monitoring of the air, surface and mass temperatures, as well as local air velocities, surface heat flux and pressure difference. This paper focusses on the determination of the air flow pattern during intensive night ventilation. It is investigated whether the same flow regimes are observed during the measurements as during the simulations. Furthermore, the prediction of the flow regime is studied.

2. Description of test cell

Although several researchers have performed detailed measurements regarding night ventilation (Artmann et al. 2010; Goethals et al. 2012), these measurements were limited to well controlled climate rooms under constant ventilation rate and supply air temperature. It was deemed interesting to investigate the thermal response of a full scale room during more realistic boundary conditions.

2.1 Location

The main orientations of the building are north-east and south-west, with the room located on the north-western side, façade facing south-west. The most prevalent wind direction in Belgium is south-west, so the building was oriented to have one long façade exposed to normal wind forces. However, as the room is located at the corner of the building, the wind climate at the window will be more unstable. The wind climate during the measurements was summarized in FIG 2b, showing the wind velocity as a function of the wind direction during the measurements. These were measured using an ultrasonic anemometer, placed on a mast (M) at a height of 10 m at approximately 20 m south-west of the building. Remaining outdoor climatic conditions were measured in the weather station (W),

located on the roof of the building. The outdoor air temperature varied between 12.8 °C and 20.4 °C during 80 % of the time.

FIG 3 shows a vertical section of the test room. The room internal dimensions are 1.80 m wide, 3.45 m long and 2.40 m high. A window with dimensions 1.25 m wide and 1.60 m high is placed centrally in the façade, starting at a height of 0.68 m above room floor level. The top part of the window is a hopper window, with a maximum opening angle of 30°. Opposite the window, an outlet opening is placed, with dimensions of 1.00 m wide and 0.10 m high and located at a height of 2.10 m and at 0.20 m distance from the ceiling. In front of the outlet, a grid is placed with horizontal lamellae with 2 cm spacing. The outlet opens into a metal plenum box, which is 40 cm deep. The plenum is connected with an extractor fan via a 1.50 m long flexible channel with 125 mm diameter, able to generate up to 18 h^{-1}. An exhaust opening is made in the NW-façade of the building and provided with a wind shield. A flexible duct leads 3.20 m upwards, connecting the fan to the exhaust opening.

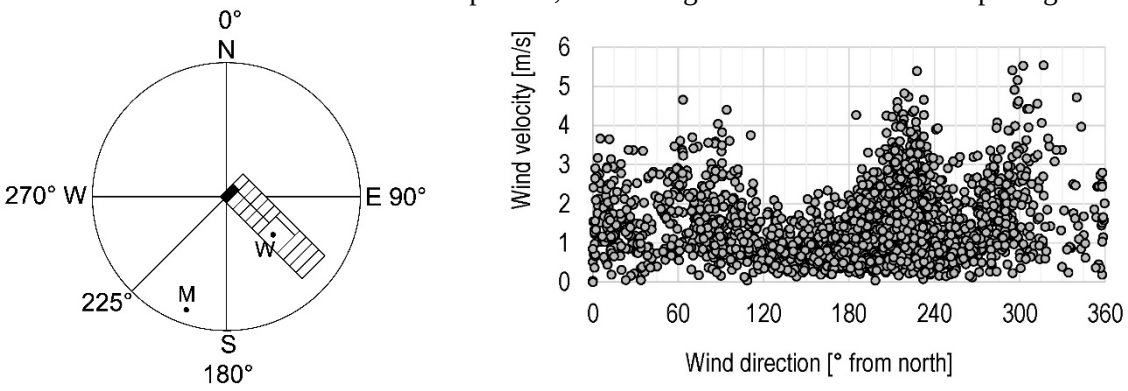

(a) Orientation of Vliet building and room (black) (M = wind mast, W = weather station)

(b) Wind velocity as a function of the wind direction

FIG 2. Overview of Vliet test building orientation and environmental parameters

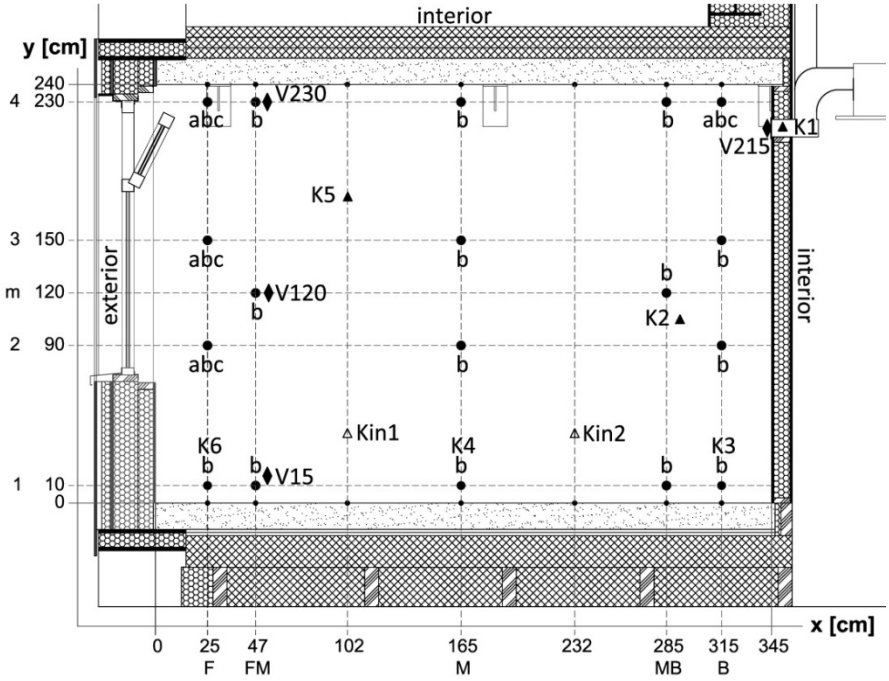

FIG 3. Vertical section over the length of the test room with sensor locations (round black: thermocouples, black triangle: tracer gas injection (Kin) and sampling (K), black diamonds: anemometers (V)

2.2 Measurement equipment

Thermal monitoring of the room air is provided by 26 thermocouples (TC), whose locations are shown in FIG 3 with black dots. One extra TC is placed in the extraction plenum to measure exhaust temperature. This figure further shows the measurement planes used to organise the TC locations. Five measurement planes are defined over the length of the room, from window to outlet: F, FM, M, MB and B, at a distance from the façade of respectively 25, 47, 165, 285 and 315 cm. Furthermore, five measurement planes have been defined over the height, from floor to ceiling: 1, 2, m, 3 and 4, at heights of respectively 10, 90, 120, 150 and 230 cm. Finally, three measurement planes have been defined over the width, from left to right (when facing the window): a, b, c, with distances from the right wall of respectively 120, 90 and 60 cm. For each TC in FIG 3, its location on the a/b/c planes is indicated. The temperatures are logged by two Fluke 2625a data loggers. All recorded values are instantaneous values, recorded every 30 s.

The air flow in the room is estimated from the measurement of the local air velocity in front of the inlet and outlet opening, as well as the pressure difference over window and extraction duct orifice. The sensor locations are indicated in FIG 3 with black diamonds (V). Three hot-wire anemometers from Sensor Electronics (AirDistSys 5000) are located in a vertical gradient, in the symmetry plane at 50 cm from the façade, just adjacent to the FM-plane (V). Two additional hot-wire anemometers (TSI, type 8475) are placed just in front of the outlet grid, in the middle of the opening height and 25 cm from the left and right edge. They are used to verify the calculated air flow rate. A 125 mm iris valve (Air Trade Center) was placed in the exhaust channel before the extractor fan. The pressure difference over this orifice is measured with a Halstrup differential pressure meter with range of 0 to 250 Pa. The orifice has seven manually adjustable opening positions. As the pressure-flow curves of the orifice are known, the flow rate can be calculated. This value was corrected based on tracer gas measurements, taking into account two-way flow at the window opening (Leenknegt & Saelens 2014).

2.3 Measurement campaign

A dataset of 60 nights is selected, consisting of six periods, spread from June to September 2012. The used data are taken from summer nights with night ventilation, but without mixing fans for tracer gas measurements. From June 29th on a 40 cm deep perforated box was placed in front of the window. The purpose of the box is to limit the influence of wind fluctuations and stabilize the flow rate. Five different ventilation settings were used during the selected nights, resulting in roughly four ranges of ACH: 10 h^{-1}, 14 h^{-1}, 16 h^{-1} and 17.5 h^{-1}. These values are based on the pressure difference in the exhaust channel, with the above mentioned correction based on the tracer gas measurements. These ventilation rates are high, compared to values expected in realistic implementations. The reasons are twofold: the uncertainty on the measured ACH is lower in case of higher ACH and the high flow rate made it possible to study more dynamic flow behaviour. The room is free-floating, so no pre-conditioning was made before each night ventilation cycle.

3. Results

3.1 Classification according to flow type

The same three flow typologies that were defined in the numerical study, namely buoyant flow (BF), transition flow (TF) and forced flow (FF), can be used as well to classify the flow pattern observed during the measurement campaign. However, the following differences with regard to timing and occurrence were noted. Firstly, the forced flow pattern was only observed at near isothermal cases or when the supply temperature is warmer than the room air temperature, placing the room in heating modus. Secondly, the transition flow, defined by a ceiling attachment length x_{cl} larger than zero but smaller than room depth D, will be shown to be a near stationary condition, rather than a short

intermezzo between buoyant and forced flow. Finally, the buoyant flow pattern was clearly observed, with supply air falling down immediately upon entry.

In order to classify the measurement data according to these three flow patterns, formal definitions are required. These are based on FIG 4, visually illustrating the different typologies. The forced flow pattern is active whenever the outdoor temperature is warmer than the indoor temperature at the window opening. For the locations and coding of the TCs, the reader is referred to FIG 3, with T_{AFb4} located in the F-plane just adjacent to the window opening, in the symmetry plane (plane b) and at a height of 230 cm (plane 4). In case of forced flow, the incoming warm air will initially attach to the ceiling and short-circuit to the outlet, also known as the Coandă effect. The ceiling is then actually in heating mode during this period. Depending on the outdoor temperature, this may continue throughout the night or cease due to a decrease of the outdoor temperature. In this dataset, the former does not occur, but the latter is seen during 18 nights.

The buoyant flow pattern, indicated by a higher temperature at the window opening edge (AF-b4) than outside, is defined for nights where the incoming air flows downwards on either side of the hopper window. In this case, the outdoor air temperature is often more than 1 K lower than the temperature in AF-b4. The transition flow is defined for nights during which the incoming air flows over the horizontal edge of the hopper window and penetrates at least shortly into the room, which causes a limited Coandă effect at the ceiling. In this case, the air temperature in AF-b4 closely follows the outdoor air temperature. Many of these cases display a variable penetration depth throughout the night. Of course, the flow pattern is not stable, so some nights display a shift from forced flow to transition or buoyant flow. On FIG 4a, three typical air temperature profiles are shown, comparing the temperature in AF-b4 with the outdoor air temperature (Text). In black, one night is shown which displays all three flow types. In dark and light grey, a full night with transition and buoyant flow are shown respectively. To sort the data into flow patterns, a number of criteria are defined, based on the characteristics of the supply air, and summarized in TABLE 1, with T_e the outdoor air temperature.

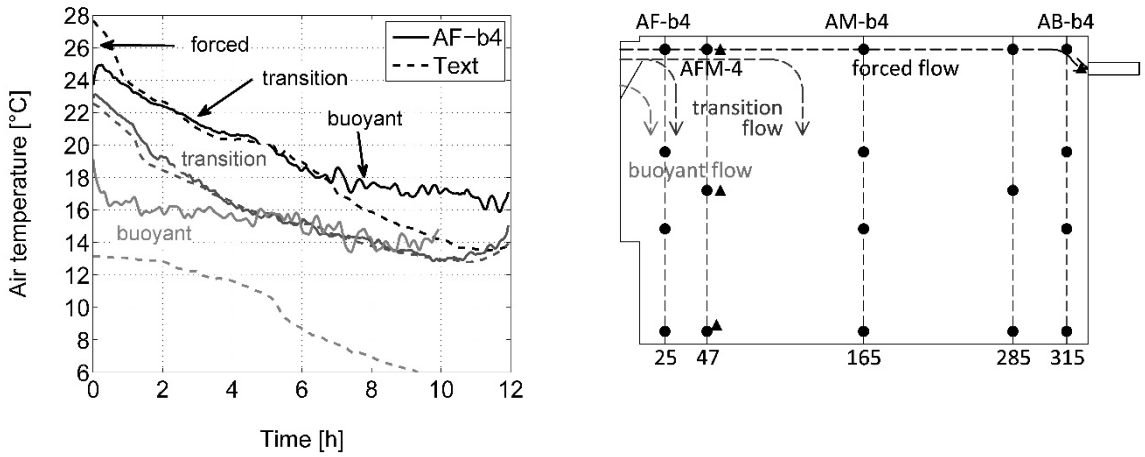

(a) Air temperatures for different flow types (b) Schematic visualisation of flow types

FIG 4. Illustration of different flow types

TABLE 1. Criteria to sort measurement data per night according to flow development

Flow type	Criteria	Number of nights
forced (FF)	$T_e > T_{AFb4}$	0
transition (TF)	$T_e < T_{AFb4}$ & $T_e \approx T_{AFb4}$	18
buoyant (BF)	$T_e < T_{AFb4}$ & $T_e << T_{AFb4}$	20
FF → TF	$T_e > T_{AFb4} \rightarrow T_e \approx T_{AFb4}$	5
FF (→ TF) → BF	$T_e > T_{AFb4} \rightarrow T_e << T_{AFb4}$	3
TF → BF	$T_e \approx T_{AFb4} \rightarrow T_e << T_{AFb4}$	14

The forced flow type only displays Coandă effect when the room is not in cooling mode, and night ventilation should be avoided. Note that a realistic case with night ventilation should have a control system to limit ventilation, in case the indoor-outdoor temperature difference is too low or even negative. In combination with the low supply air velocity, typical for this configuration, it is expected that the buoyant flow pattern will be prevalent most of the time, with transition flow occurring only rarely. Therefore, the transition and buoyant flow regimes are most relevant. However, the evolution of forced to transition or buoyant flow can provide useful information regarding the timing of the flow changes, which is required to improve the convection modelling in BES. Literature study showed that attempts have been made to use the Richardson or Archimedes number, both of which are defined as Gr/Re^2 (Leenknegt & Saelens 2013), with Gr the Grashof number and Re the Reynolds number. Therefore, the Richardson number will be used to predict flow pattern changes, as it was already used for the numerical study. The definition of Ri_H is given by equation (1).

$$Ri_H = \frac{g\beta H\left(T_{r,c} - T_e\right)}{\left(\dot{V}/bh\right)^2} \quad (1)$$

Where
- g gravitational acceleration (m/s²)
- β thermal expansion coefficient of air (K^{-1})
- H room height (m)
- $T_{r,c}$ central room air temperature (°C)
- T_e outdoor air temperature (°C)
- $\dot{V}$ volumetric air flow rate (m³/h)
- b, h opening width and height of supply window in façade (m)

3.2 Global evaluation of flow type as a function of Ri

A total of 39 nights were found with fluctuations. Out of this dataset, 12 nights showed a drastic change from forced to buoyant flow. They start with the outdoor air warmer than or nearly equal to the indoor air, which results in a forced flow pattern at the start of the night ventilation with Coandă effect over the full length of the ceiling. As the outdoor air cools down, the attachment length was seen to decrease rapidly. One such night is illustrated in FIG 5. On the left hand side, the local air temperatures are shown and the changes are indicated. The right hand side graph gives the corresponding Richardson number as a function of the supply air velocity. Two reference temperatures are compared: either the central air temperature ($T_{central}$) or the temperature at the window opening (AF-b4). It is clear that the central room air temperature is a more relevant reference value, even though Ri also indicates local flow variations. As soon as the Richardson number reaches zero, i.e. the outdoor temperature is no longer higher than the central room temperature, the air starts to detach from the ceiling at the outlet, indicated by a diverging air temperature in point AB-b4. About two hours later, the temperature profile at the centre of the ceiling (AM-b4) also shifts towards stratified flow, and one more hour later, the air detaches next to the window (AFM-4) as well. This full change in flow pattern takes about three hours.

A similar analysis is performed by hand for these 39 nights with flow pattern changes for which the Richardson number at the time of the change is logged. Five flow pattern changes are defined here, presented schematically in FIG 6. They are categorized by comparing the local air temperatures in following four locations: AF-b4, AFM-4, AM-b4 and AB-b4. Flow pattern changes A, B and C represent forced flow or transition flow, with air flowing over the horizontal edge of the window and at least partially continuing along the ceiling. A indicates that the Coandă effect at the ceiling decreases to at least the middle of the ceiling (AM-b4). B and C indicate a further decrease, respectively past AFM-4 and AF-b4. D and E represent buoyant flow, with air predominantly falling down on either side of the hopper window. D then indicates the change from transition flow to buoyant flow, but with turbulences at the window opening, resulting in very similar temperatures in AF-b4 and AFM-4. Finally, E marks that AFM-4 lies within the stratified zone at the ceiling. This

analysis results in a range of values for Ri corresponding to each of the flow pattern changes, which is shown in FIG 7. Note that the A/B/C ranges show some overlap, indicating for example that on some nights, the full transition from forced flow to transition flow with minimal ceiling attachment length occurs between Ri-values of 3-5 and on other nights between 0 and 2. More measurement data are needed to deduce a more definite critical value.

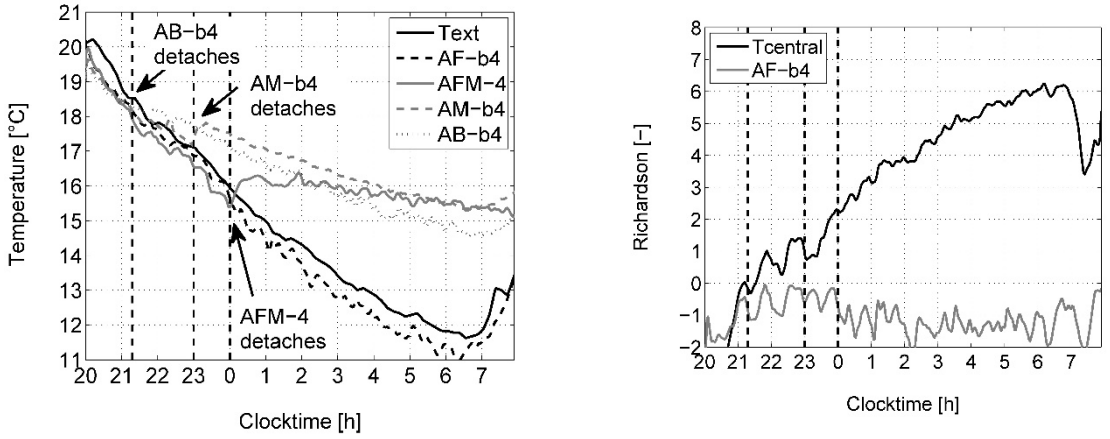

(a) Change in flow pattern (b) Richardson number

FIG 5. Indication of Richardson value during flow changes

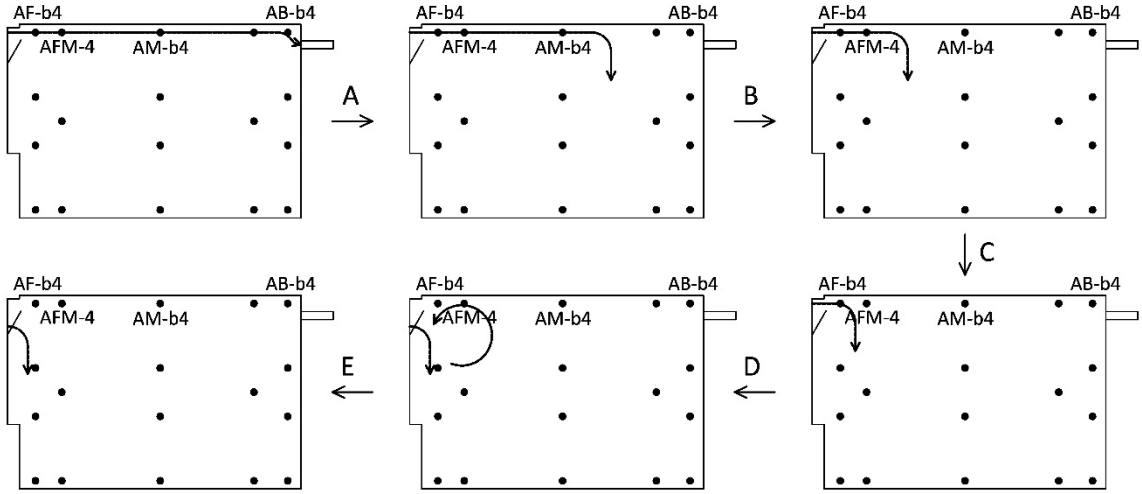

FIG 6. Schematic presentation of flow pattern changes

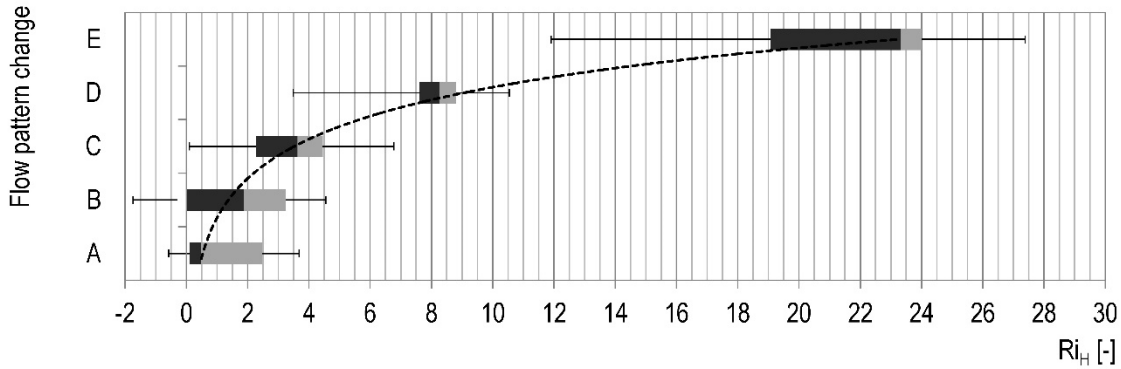

FIG 7. Range of Richardson values for which flow pattern changes occur (dataset: 39 nights)

4. Conclusions

A full scale test room was constructed for the study of night ventilation under realistic conditions. Air was supplied through a south-west oriented hopper window, supported by an extractor fan, ensuring high flow rates. Previous work on the transient surface convection during night ventilation through numerical simulations showed the importance of the unsteady flow development. Therefore, the main topic of this paper is to analyse the flow patterns in a dataset of 60 summer nights with ventilation rates ranging from 10 to 17.5 h^{-1}. Three flow regimes were identified, which were also observed during the numerical simulations, i.e. buoyant, transition and forced flow. Forced flow displayed a short-circuit flow between supply opening and outlet (Coandă at ceiling), transition flow was seen in case of limited Coandă effect, and buoyancy dominated flow was classified when the supply air falls down upon entry. The CFD simulations illustrated that the flow pattern strongly influences the surface convection. Therefore, the aim of this research is to develop criteria to predict the dynamic flow behaviour.

The level of buoyancy of the supply air was expressed with the dimensionless Richardson number. This number was defined using the room height, the supply air velocity and the indoor-outdoor temperature difference. Based on four local air temperatures, five flow pattern changes were defined. The first one, corresponding to the shift from forced to transition flow, was situated for a Richardson number between 0 and 2. Various stages of transition flow could be seen for Ri between 0 and 9. Buoyant flow can be assured for Ri higher than 19. Further measurements are required to refine the determination of the flow changes.

5. Acknowledgements

This research was funded by the Research Foundation Flanders (FWO Vlaanderen). Their financial contribution is greatly appreciated. Furthermore, Patricia Elsen was a great help in conducting the measurements.

References

Artmann, N. et al., 2010. Experimental investigation of heat transfer during night-time ventilation. *Energy and Buildings*, 42(3), pp.366–374.

Beausoleil-Morrison, I., 2000. *The adaptive coupling of heat and air flow modelling within dynamic whole-building simulation*. University of Strathclyde, Glasgow, UK.

Goethals, K. et al., 2012. Experimental investigation of the impact of room/system design on mixed convection heat transfer. *Energy and Buildings*, 49, pp.542–551.

Leenknegt, S. et al., 2013. Numerical study of convection during night cooling and the implications for convection modeling in Building Energy Simulation models. *Energy and Buildings*, 64, pp.41–52.

Leenknegt, S. & Saelens, D., 2014. Determination of ventilation rate in a full scale night ventilation experiment through tracer gas measurements. In *submitted to Nordic 2014*.

Leenknegt, S. & Saelens, D., 2013. Use of dimensionless numbers to classify room air flow and convection regimes: part 1 - literature review. *Building and Environment*, submitted,.

Determination of the ventilation rate in a full scale night ventilation experiment through tracer gas measurements

Sarah Leenknegt, PhD[1]

Dirk Saelens, Professor[1]

[1] Building Physics Section, Department of Civil Engineering, KU Leuven, Leuven, Belgium

KEYWORDS: *measurement, mechanical ventilation, unsteady ventilation, tracer gas, night ventilation, full scale test room*

SUMMARY

A full scale test room was constructed for the analysis of the energy performance of a room with night ventilation with air supply through a hopper window, supported by an extraction fan.. Contrary to typical climate rooms, the room was exposed to realistic climatic conditions. The determination of the air change rate is paramount in a night ventilation system. This paper compares two methods for the determination of the air change rate: (1) the pressure difference over the orifice in the exhaust channel and (2) tracer gas measurements using the averaging method on the tracer gas mass balance. The latter method allowed accounting for the back flow through the hopper window, which was not captured via the orifice method. A large underestimation was seen in case of the pressure based ACH, as this method does not take into account two-way flow via the large supply opening. Therefore, a correlation was developed to correct the pressure based flow rate, to be able to determine the flow rate in future measurement campaigns, which cannot be combined with tracer gas experiments.

1. Introduction

Night ventilation is a promising technique, able to reduce the cooling load through use of cold outdoor air at high air change rates to cool down the internal thermal mass of a building in moderate climates with sufficiently cold nights. To investigate the energy performance of night ventilation, a full scale test room was constructed inside the Vliet test building of the Building Physics Section of KU Leuven, Leuven, Belgium. The room differs from typical full scale test rooms in similar research (Artmann et al. 2010; Goethals et al. 2012), as it is exposed to real climatic conditions through a south-west oriented hopper window. High air change rates are established through an extractor fan. As ventilation is done with outdoor air, the supply air temperature is not controlled and the thermal response of the room in case of realistic boundary conditions can be investigated. This limitation in ventilation control is compensated by more than 200 sensors, allowing a detailed monitoring of the air, surface and mass temperatures, as well as local air velocities, surface heat flux and pressure difference. One of the key parameters in the analysis of the energy performance is the ventilation rate. Therefore, it is crucial to have a reasonable estimate of the air change rate during the night ventilation experiments. This is complicated by the influence of wind on the large supply opening. Therefore, the objective of this paper is to determine the air change rate in this mechanically ventilated case.

One of the commonly used methods to asses ventilation rate is the use of tracer gas, which is also the main method discussed here. Alternatives found in literature are hot wire anemometry or pressure difference measurements either by wind on the façade or over an orifice in a extraction/supply duct (Van Buggenhout et al. 2009; Shen et al. 2012). Furthermore, an orifice was placed in the exhaust channel to allow determination of the flow rate through the orifice using the measured pressure difference. This paper will discuss the determination of the ventilation rate through tracer gas

measurements, and compare these results with the calculated ACH based on the pressure difference over the orifice in the exhaust channel. As the window is exposed to the influence of wind, unsteady air change rates are observed, combined with two-directional flow, even at high fan power. This latter behaviour will not be captured by the orifice method. In the following, first the test room is described. This is followed by a discussion of the results, starting with a short theoretical introduction on tracer gas measurements and continuing with a comparison of both methods.

2. Description of test cell and measurement methodology

Although several researchers have performed detailed measurements regarding night ventilation (Artmann et al. 2010; Goethals et al. 2012), these measurements were limited to well controlled climate rooms under constant ventilation rate and supply air temperature. It was deemed interesting to investigate the thermal response of a full scale room during more realistic boundary conditions.

2.1 Location

The Vliet test building is a 25.2 m long and 7.2 m wide building, designed for the study of wall, window and roof components under real field conditions. The main orientations of the building are north-east and south-west, with the room located on the north-western side, façade facing south-west. The most prevalent wind direction in Belgium is south-west, so the building was oriented to have one long façade exposed to normal wind forces. However, as the room is located at the corner of the building, the wind climate at the window will be more unstable. The wind climate during the measurements was summarized in FIG 1b and c, showing a box plot of respectively the wind direction and wind velocity. These were measured using an ultrasonic anemometer, placed on a mast (M) at a height of 10 m at approximately 20 m south-west of the building. The box plot is based on the 10th and 90th percentile, with conditions occurring only 2 % of the time not considered in the calculation of the spread. Remaining outdoor climatic conditions were measured in the weather station (W), located on the roof of the building. FIG 2 shows a vertical section of the test room. The room internal dimensions are 1.80 m wide, 3.45 m long and 2.40 m high. A window with dimensions 1.25 m wide and 1.60 m high is placed centrally in the façade, starting at a height of 0.68 m above room floor level. The top part of the window is a motorized hopper window, with a maximum opening angle of 30°. Opposite the window, an outlet opening is placed, with dimensions of 1.00 m wide and 0.10 m high and located at a height of 2.10 m and at 0.20 m distance from the ceiling. In front of the outlet, a grid is placed with horizontal lamellae with 2 cm spacing. The outlet opens into a metal plenum box, which is 40 cm deep. The plenum is connected with an extractor fan via a 1.50 m long flexible channel with 125 mm diameter. A maximum air change rate of up to 18 h^{-1} could be realized. An exhaust opening is made in the NW-façade of the building, provided with wind shield. A flexible duct leads 3.20 m upwards, connecting fan to exhaust.

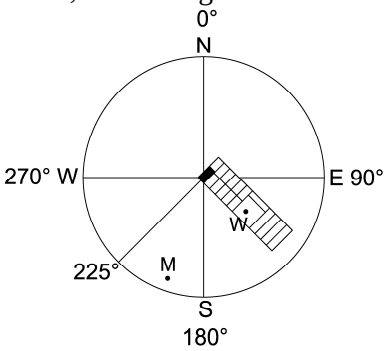

(a) Orientation of Vliet building and room (black) (M = wind mast, W = weather station)

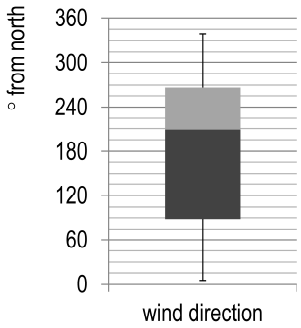

(b) Spread on wind direction during analysed nights

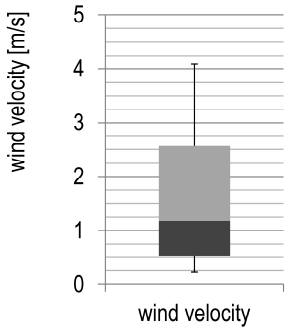

(c) Spread on wind velocity at 10 m high during analysed nights

FIG 1. Overview of Vliet test building orientation and environmental parameters

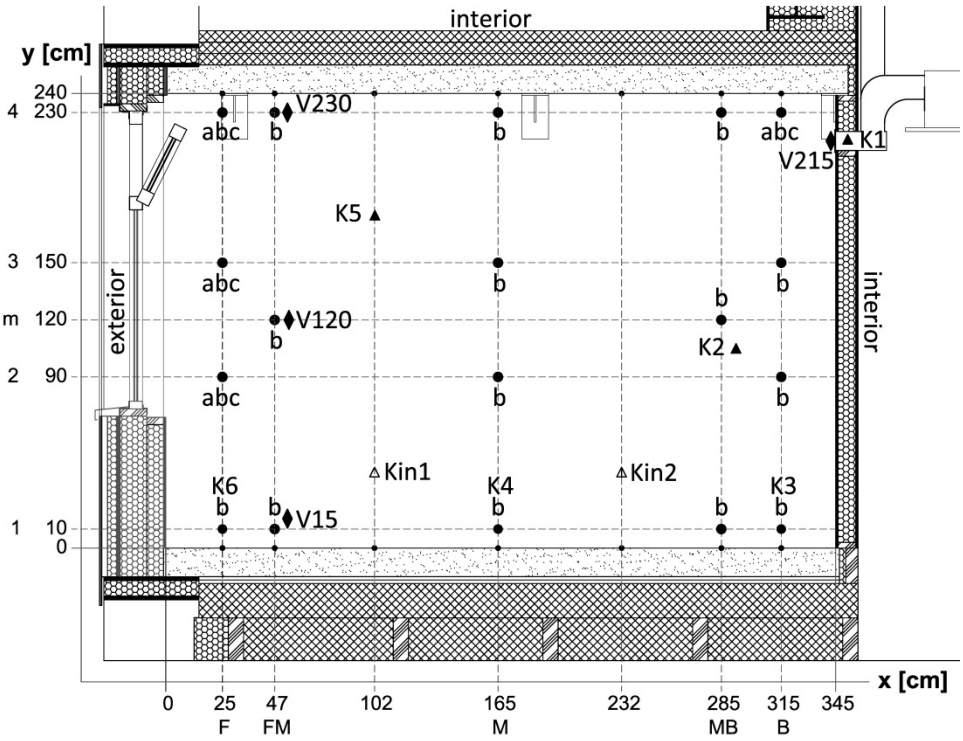

FIG 2. Vertical section over the length of the test room with sensor locations (black circles: thermocouples, black triangles: tracer gas dosing (Kin) and sampling (K) points, black diamonds: anemometers (V))

2.2 Measurement equipment

The air flow in the room is monitored through measurement of the local air velocity in front of the inlet and outlet opening. Furthermore, the air flow rate is monitored through the pressure difference over window and exhaust channel orifice. The sensor locations are indicated in FIG 2.Three hot-wire anemometers from Sensor Electronics (AirDistSys 5000) are located in a vertical gradient, in the symmetry plane at 50 cm from the façade, just adjacent to the FM-plane (V). Two additional hot-wire anemometers (TSI, type 8475) are placed just in front of the outlet grid, in the middle of the opening height and 25 cm from the left and right edge. They are used to verify the calculated air flow rate. The pressure difference over the window is monitored through a Halstrup differential pressure meter with range 0 to 25 Pa. Additionally, a 125 mm iris orifice (Air Trade Center) was placed in the exhaust channel before the extractor fan. The pressure difference over this orifice is measured with a Halstrup differential pressure meter with range of 0 to 250 Pa. The orifice has seven manually adjustable opening positions, going from maximum opening at setting 1 to minimum opening at 7. As the pressure-flow characteristics of the orifice are known, the flow rate can be calculated.

The tracer gas equipment consists of a dosing- and sampling unit (type 1303) from Bruel & Kjær Innova, containing six dosing and six sampling channels. The air samples are analysed in a multi-gas monitor (type 1302), which measures the gas concentration using photo-acoustic gas detection. The gas used for the tracer gas experiments is sulphur hexafluoride or SF_6. The health related threshold for SF_6 is 1000 ppm and it is an artificial gas. However, it has the downside that it is about five times heavier than air, with a density of 6.2 kg/m³. This results in a risk of stratification, where the gas sinks to the floor, especially for low air velocity situations. Furthermore, it is a strong greenhouse gas, whose use should be limited. The location of the six sampling points (K) and two injection points (Kin) is illustrated in FIG 2. Two small mixing fans are located on the floor adjacent to the injection points, directed away from window and outlet opening.

2.3 Tracer gas techniques

The standard tracer gas analysis techniques are well known and will not be further discussed here, instead the interested reader is referred to Sherman (1990). All methods are based on the tracer gas mass balance, also called the continuity equation, given in equation (1).

$$V\frac{dC}{dt} = Q_T - QC \quad (1)$$

Where V zone volume (m^3)
C tracer gas concentration in the zone (10^{-6} mol/mol)
t time (h)
Q_T injected tracer gas volumetric flow rate (m^3/h)
Q volumetric flow rate (m^3/h)

Sometimes however, the standard techniques are not usable, for example if the air change rate is unstable and the controller is too slow to follow the changes. When no assumptions are made regarding constant injections and concentrations apart from the continuity equation itself, Sherman describes three different approaches for determination of the ventilation directly from the concentration data: (1) regression, (2) integral and (3) averaging techniques, of which the latter technique is used here (Sherman 1990). The continuity equation cannot be used to determine instantaneous ventilation, but it can be averaged over a measurement period T to get the average ventilation, as given in equation (2).

$$\bar{Q} = \frac{\overline{Q_T}}{C} - \frac{V}{T}\ln\left(\frac{C_{final}}{C_{initial}}\right) \quad (2)$$

Where $\bar{}$ average value over period T
T averaging period (h)
final/initial: final and initial tracer gas concentration during averaging period

3. Results

The following results will start with a description of the ventilation rate based on the averaging method applied to the measured tracer gas concentrations. The influence of wind climate is shortly discussed, resulting in unstable flow rates. These results can then be compared to the air change rate based on the pressure difference over the orifice in the exhaust channel. The problems concerning this latter method are identified and addressed.

3.1 Tracer gas based determination of ACH

Over the course of three months, starting in May 2012, 45 tracer gas experiments have been conducted. Each measurement had a duration of minimum two and up to eight hours and was conducted during night. Two different tracer dosing control methods were used: constant concentration (target 20 or 50 ppm) and constant dosing (18 mg/s). FIG 3 shows the range of the unsteady air change rate n_{Tr30m} for each measurement, based on the averaging technique by equation (2), using an averaging period of 30 minutes. Each box plot represents one experiment. The results have been sorted according to increasing fan power and orifice opening.

At fan power 1, only small orifice openings were tested, as this setting would mainly be used to achieve low ACH. The minimum ACH achieved here however is still at least 5 h^{-1}, though most ranges are higher than 7 h^{-1}. Remarkable is the large range of calculated ACH for each measurement, despite the constant fan power and orifice opening. During most measurements, there is a significant fluctuation of the wind direction (not shown here). Even though the wind velocity is relatively low (most of the time < 3 m/s), this causes an unstable flow rate. Indeed, analysis of the air temperatures in the room when the mixing fans were not active, showed a highly unsymmetrical flow, illustrating the

strong influence of the wind. Therefore, a perforated box was installed in front of the window to equalize the wind pressure and reduce the effect of wind direction fluctuations. The box was placed halfway through the measurement period at the end of June 2012. It is 40 cm deep, constructed with 4 mm thin plywood, and about 13 % of the area is perforated with 8 cm diameter holes. In FIG 3, the measurements conducted with the box in front of the window are coloured grey-black, instead of grey.

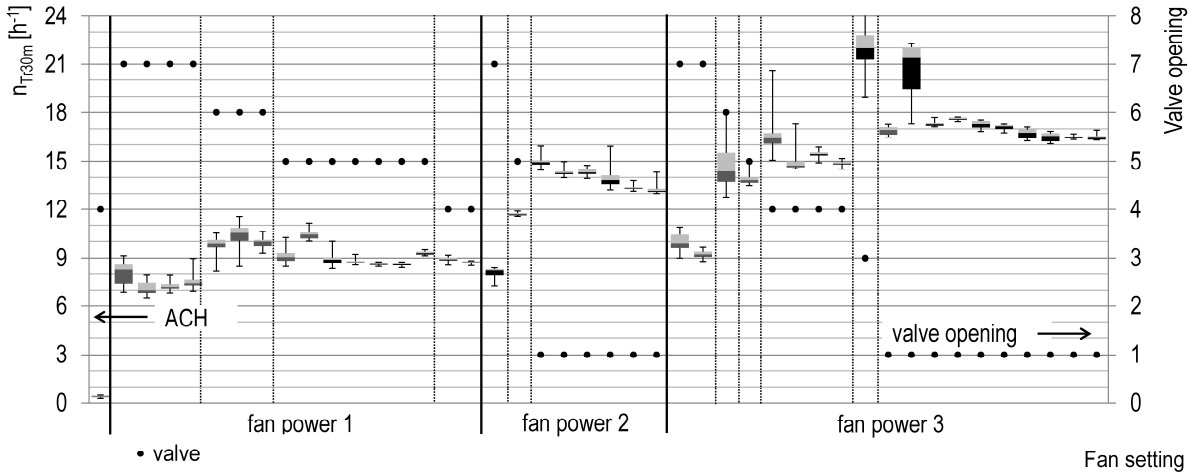

FIG 3. ACH based on averaging technique from equation (2) over 30 minute periods as a function of orifice opening and fan setting (wind box present: black bars, no wind box: grey bars)

For the measurements with fan power 1, the effect of the wind box is clearly visible, with much more stable flow rates. At fan power 2, all measurements are conducted with the wind box in place. Most of the calculated ACH display only a very limited range, indicated by the box plot. Nevertheless, the minima and maxima, indicated by the vertical lines, are still quite far apart. The measurements with the widest ACH-range correspond again to the moments with the most unstable wind direction.

At fan power 3, measurements were conducted with and without wind box. At this high fan power, the correlation between wind direction and ACH range is less strong. Some measurements show a very stable ACH, despite a large variation in wind direction. Nevertheless, the wind box again results in much more stable air flow rates. One case at fan power 3 and orifice opening 1 is an exception, with the air change rate ranging from 17 to nearly 23 h^{-1} in one night, illustrated in more detail in FIG 4a, displaying the ACH, along with current wind direction and velocity. The tracer gas based air change rate n_{Tr} is calculated for a 30 minute averaging period (nTr30m), which is indicated on the graphs by horizontal bars. The wind velocities (WindVel) are rather low, i.e. equal to or lower than 2 m/s. However, the wind direction (WindDir) is continuously nearly perpendicular to the window. This could explain why the moderate wind still has such a high influence on the air flow rate. However, the increase in ACH over the presented period seems not correlated with the wind climate and could not be explained.

Another interesting case is shown in FIG 3 at fan power 1, orifice opening 5 and with wind box, but nevertheless with a large spread. The main dataset is very stable at 8.5 to 9 h^{-1}, though a peak up to 10 h^{-1} is seen. This day is shown in more detail in FIG 4b. Cross-referencing with wind climate explains this variation. During the stable phase, the wind velocity is rather low, i.e. equal to or lower than 2 m/s. However, the local peak in ACH coincides with a sudden increase in wind velocity up to 5.5 m/s.

3.2 Pressure difference based determination of ACH

The ACH was also calculated based on the pressure difference over the orifice in the extraction duct. The pressure differential deducer in the exhaust channel has an accuracy of ± 0.2 % on the reading with a minimum of ± 0.15 Pa. The ventilation rate of the room is calculated based on the airflow rate

determined through the pressure-flow characteristics, supplied by the product information of the orifice. The product information stipulates an uncertainty on these curves of ± 7 % if the minimum straight pipe length after a bend and before the orifice is higher than the orifice diameter, which is the case in this experimental set-up.

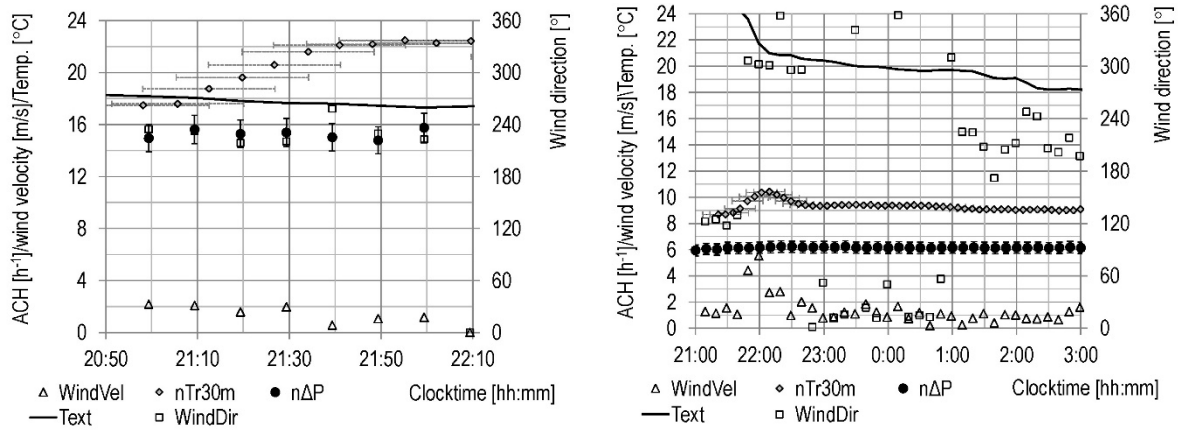

(a) Tracer gas based ACH on day 62 (F3V1) (b) Tracer gas based ACH on day 48 (F1V5)

FIG 4. Detail of tracer gas based ACH, correlation to climatic data

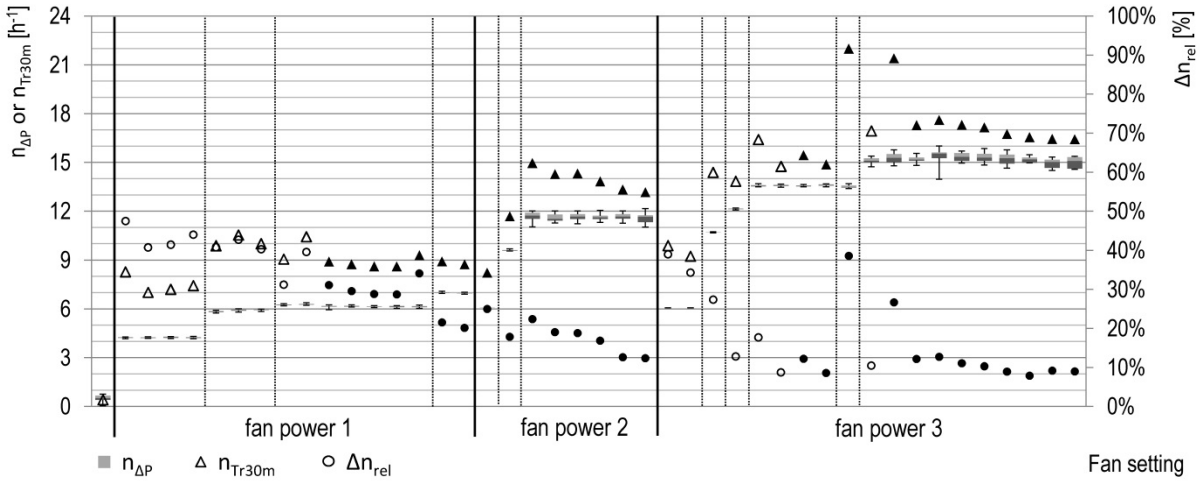

FIG 5. Comparison of pressure based ACH ($n_{\Delta P}$) and tracer gas based ACH (n_{Tr30m}), see equation (3) for Δn_{rel} (filled markers = with wind box, not filled markers = without wind box)

During the analysed periods of intensive ventilation, the pressure difference is always 10 Pa or higher, resulting in an uncertainty on the calculated ACH of approximately ± 7 %, as the uncertainty on the measured pressure difference is very small. FIG 4 shows for both days also the pressure based ACH, indicated by $n_{\Delta P}$. The uncertainty is indicated by the vertical error bars, based on the uncertainty on the pressure difference measurement, combined with the pressure-flow characteristics. Also the outdoor temperature is indicated by Text. Two conclusions can be drawn: firstly, the pressure based air change rates $n_{\Delta P}$ are significantly lower than the tracer gas based air change rates n_{Tr}, and secondly, they are independent of the wind climate. They may fluctuate somewhat by the indoor-outdoor temperature difference, although no clear correlation was found. Furthermore, the ventilation rate is driven by the extraction fan in all measurements. The pressure based ACH for the full measurement period are shown in box plots in FIG 5. The tracer gas based median values n_{Tr30m} of each measurement are shown as well. To illustrate the difference between both methods, the relative difference Δn_{rel} according to equation (3) has been plotted on the right axis, with n_{Tr30m} based on the 30 minutes

averaging value and $n_{\Delta P}$ based on the pressure difference over the orifice. Filled markers refer to measurements with wind box. The time-average of the full measurement was used. Often a large difference between both methods to determine the ACH is observed. Particularly at low fan power n_{Tr} is often 30 to 50 % higher than $n_{\Delta P}$.

$$\Delta n_{rel} = \frac{\overline{n_{Tr30m}} - \overline{n_{\Delta P}}}{\overline{n_{Tr30m}}} \quad (3)$$

3.3 Corrected ACH

The difference between the two calculated air change rates, based either on the pressure difference or on the tracer gas measurements, is illustrated in FIG 6a, showing the relative difference as a function of $n_{\Delta P}$. The overestimation of the tracer gas based results can be explained by air leaking back through the window to outside, which means that the incoming air could be contaminated by tracer gas, causing an underestimation of the ACH in the tracer gas analysis so far. To check this,19 further measurements were performed in winter showing that 1 to 9 % of the tracer gas concentration in the room is found outside the window, depending on the strength of the extractor fan. At air changes rates as high as 10 h^{-1}, a tracer gas concentration of 5 % of the inside value was measured outside, which went up to 9 % at lower ACH. Based on these measurements, an exponential function was found, correlating the calculated air flow rates with the tracer gas percentage outside. With this correlation, the previously calculated ventilation rates were corrected. The average difference with the initially calculated values was only 3.4 % with a total range of 1 to 6 % of underestimation.

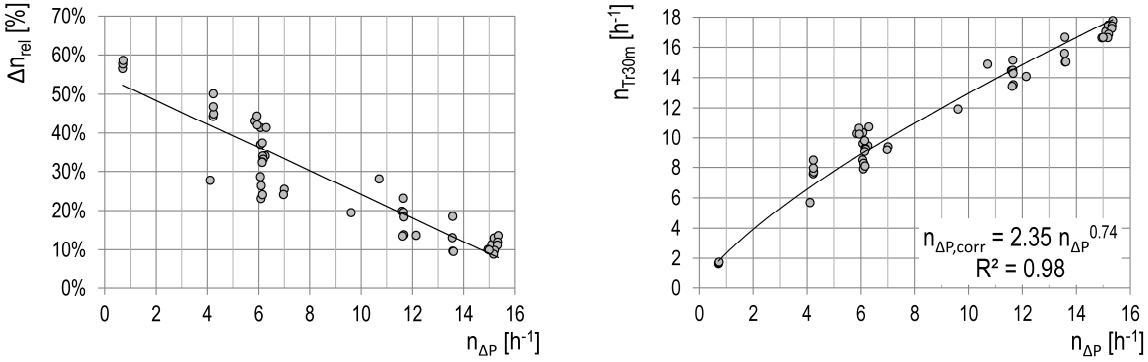

(a) Relative difference between tracer gas based and pressure based ACH

(b) Correlation between pressure-based on tracer gas based ACH

FIG 6. Correlation to predict actual ACH based on pressure-based ACH

Future research is aimed at predicting the air flow pattern in the room during intensive night ventilation, as this strongly influences the local surface convection. This was shown in previous research through numerical simulations (Leenknegt et al. 2013) . The presence of mixing fans would disrupt the flow pattern, which is a crucial part of the research. Therefore, it is impossible to perform tracer gas measurements during the night ventilation experiments and the ACH must be determined based on the pressure difference over the orifice. It was shown before that this value only takes into account the flow rate leaving through the extraction duct and ignores the additional air leaving through the window opening. As such, the pressure based ACH is an underestimation of the actual value and a correlation was sought and found between n_{Tr} and $n_{\Delta P}$ to obtain a corrected value $n_{\Delta P,corr}$. This correlations is illustrated in FIG 6b and given by equation (4). Despite the good correlation, there is still some scatter, and the corrected value will have an uncertainty which is estimated at ± 15 %, based on the typical difference between the measured values and the correlation.

$$n_{\Delta P,corr} = 2.35 n_{\Delta P}^{0.74} \quad (4)$$

4. Conclusions

A full scale test room was constructed for the study of night ventilation under realistic climatic conditions. Air was supplied through a south-west oriented hopper window, supported by an extractor fan, ensuring high flow rates. For the analysis of the night ventilation performance, knowledge of the ventilation rate is paramount. This paper analyses the results of two methods to determine the ventilation rate. As a first method, an orifice was placed in the exhaust channel, calibrated to allow calculation of the volumetric flow rate based on the opening size and pressure difference. However, this method does not provide an evaluation of the unsteady air flow rate. Indeed, due to the influence of wind on the large hopper window opening, unstable air ventilation rates were observed, even at high fan power. This could however be evaluated with tracer gas measurements, the second method. The averaging technique was applied to the continuity equation to determine a profile of the unsteady air flow rate. Furthermore, the results of these two methods could be compared. It was shown that the pressure based air change rate was consistently lower than that based on the tracer gas method. This was attributed to the back flow at the large supply opening of the hopper window, caused by the wind and resulting in two-way flow. The influence of the indoor-outdoor temperature difference was low, as the ventilation rate was driven by the extraction fan throughout all measurements. The results were corrected, taking into account the tracer gas contamination of the supply air. As the pressure based ACH only takes into account the air leaving the room via the exhaust channel, this value underestimates the actual air flow rate. However, future research is focussed on the energy performance of this night ventilated room. A crucial part of the research is dedicated to the prediction of the air flow pattern, as this is closely related to the local surface convection regimes. Therefore, the activation of mixing fans is not possible and tracer gas experiments cannot be used for the determination of the air change rate. To solve this, a correlation was developed, providing a correction on the pressure based ACH.

5. Acknowledgements

This research was funded by the Research Foundation Flanders (FWO Vlaanderen). Their financial contribution is greatly appreciated. Furthermore, Patricia Elsen was a great help in conducting the tracer gas measurements.

References

Artmann, N. et al., 2010. Experimental investigation of heat transfer during night-time ventilation. *Energy and Buildings*, 42(3), pp.366–374. Available at: http://linkinghub.elsevier.com/retrieve/pii/S0378778809002412.

Van Buggenhout, S. et al., 2009. Influence of sampling positions on accuracy of tracer gas measurements in ventilated spaces. *Biosystems Engineering*, 104(2), pp.216–223.

Goethals, K. et al., 2012. Experimental investigation of the impact of room/system design on mixed convection heat transfer. *Energy and Buildings*, 49, pp.542–551.

Leenknegt, S. et al., 2013. Numerical study of convection during night cooling and the implications for convection modeling in Building Energy Simulation models. *Energy and Buildings*.

Shen, X., Zhang, G. & Bjerg, B., 2012. Comparison of different methods for estimating ventilation rates through wind driven ventilated buildings. *Energy and Buildings*, 54, pp.297–306.

Sherman, M.H., 1990. Tracer-gas techniques for measuring ventilation in a single zone. *Building and Environment*, 25(4), pp.365–374.

The impact of leakage properties onto the flow-through of single leakages

Jens Schmidt, [1]
Oliver Kornadt, Professor [2]

[1, 2] Technical University of Kaiserslautern, Germany

KEYWORDS: *convection, leakage flow, discharge coefficient, air tightness, simulation*

SUMMARY
Leakages in the building envelope may lead to increase of primary energy demand and carbon footprint of buildings. Additionally, particle and bacteria infiltration or exfiltration are possible. Furthermore, the building shell may be damaged by hygric enveloping surface infiltration. For investigation of the impact of leakages in the building envelope, different measurements and simulations are used. The disadvantage of the both is that the knowledge on discharge coefficient of leakages in real buildings is limited. Therefore, the discharge coefficient is estimated or based on sharp edged, circular standard orifice. But real leakages are different, e.g. the shape is not comparable to a standard orifice. Due to these, the flow through different leakages in perforated air tightness layers of light-weight timber frame constructions was analysed. The applied pressure differences were real measured values of long term investigations on building shells. At these specific pressure differences, the flow profile through leakages is different to studies of standard orifice. The volumetric flow through leakages is significantly influenced by this difference. The results show the impact of the different leakage parameters onto the discharge coefficient. Thus, simulations should not be based on standard orifice investigations.

Introduction

In walls of new or refurnished buildings, it is common to integrate different insulation. Thus, a reduction of energy losses through the building envelope is possible. However this climate separation of interior and environment represents also a potential danger. If the water vapour diffusion resistance of the room side materials is too small, condensation may arise in the wall construction. For prevention, room-side diffusion inhibiting or blocking materials e.g. vapour barriers are arranged. According to (Schulze H. 2011), awareness regarding diffusive moisture transport processes has increased. Therefore, moisture problems caused by diffusion in constructions of new buildings are infrequent at present time. A far bigger problem is given by the deficient air tightness of the building envelope. According to (Biskop R. 2008), these leakages are caused by mistakes in planning and execution. Especially during the heating season, bacteria, particle and moisture may be transported by convection from the interior to the environment. This transport of matter may lead to deposits in the wall structure. This might result in growth of mould and mildew or the formation of heat bridges e.g. in case of condensation in non-capillary active components. Additionally, the convective heat exchange leads to increased energy losses. Light-weight timber constructions are particularly at risk concerning leakages. Damages in the air tight and protection layer are easily possible and the used insulation materials are frequently air permeable. In addition, the convective leakage flow is promoted by the non-obligatory air tightness of the weather protection layer. These findings led to the development of simulation software with the aim of analysing the disadvantages of leakage flows on buildings. The best-known algorithms are implemented in the software of Delphin and WUFI. These algorithms are based on leakage flows caused by density differences (Häupl P. et al. 1997, Künzel H.M. 2010). Only a few calculation models are developed for leakage flow analyses under real

pressure difference conditions of wind and buoyancy. They are frequently based on the existing calculation approaches of Delphin and WUFI (Langmans J. 2013, de With G. et al. 2009, Zirkelbach D. 2009, Kurnitski J. et al. 2000). In these new approaches, the contraction influence on the leakage flow is either estimated or refers to unpublished references. Currently, standards and knowledge about the discharge coefficient are exclusively based on standard orifice and materials which are used in technical building equipment (ASHRAE 2009, DIN EN ISO 5167-2). However, leakages in buildings may differ e.g. in shape, compared to standard orifice. Nevertheless, for investigation of the equivalent leakage area with the pressure difference method, also a generalized discharge coefficient is used (DIN EN 13829, ASTM E779-10, ASTM E1186-03). Furthermore, the friction coefficient of pipeline materials for air and water transport is different, compared to the short channels which arise by perforation of the room-side layers e.g. in materials of light-weight timber frame constructions. Therefore, this work aims to analyse the impact of the leakage shape and size in air barriers onto the flow-through. Also, the influence of deformation of the air barriers onto the discharge coefficient was measured. Finally, a comparison of the volumetric flow through a single leak and several leakages of the same total leakage area and texture was carried out.

Basics

The pressure difference between interior and the surrounding area is the potential of flows through leakages in the building envelope. In naturally ventilated buildings, these are influenced by wind and buoyancy. The change of pressure differences occurs in intervals of seconds (Schmidt J. et al. 2010b). According to the Bernoulli equation, the leakage flow is from the higher to the lower pressure level. In order to analyse and simulate the exfiltration flow through a room-side layer with a single leak and adjacent permeable insulation in a light-weight timber structure, knowledge on the pressure loss caused by the leak is required. Commonly, the cross-section of a leak in the building shell is much smaller than the cross-section area of the room, which forces a constriction of the exfiltration flow. This results in contraction and velocity losses. The contraction factor Ψ is affected by the ratio of stream and leakage cross-section. In addition, the shape of leakage edge is crucial (fig. 1, 2). Ψ of e.g. sharp edged standard orifice is 0.61 … 0.64 (Bohl W. et al. 2005). The velocity coefficient Φ of the leakage flow is influenced by the macroscopic and microscopic geometry of the opening, the viscosity and the surface tension (if not air) of the fluid. Φ is in case of sharp edged standard orifice 0.97 (Bohl W. et al. 2005). The product of Ψ and Φ gives the discharge coefficient ζ. “Caused by the difficulty to investigate Ψ and Φ experimentally separated from each other, values of these coefficients are only scarcely documented in the literature.” (Bohl W. et al. 2005) Theoretical considerations were already carried out by Torricelli and Borda in 17th and 18th century (Borda J. C. 1769).

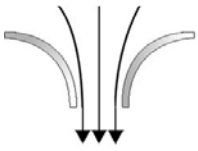

FIG 1. Circular opening

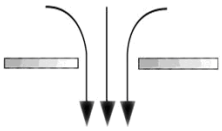

FIG 2. Sharpe edged opening

By comparison of pressure and impulse force, they determined a theoretical contraction coefficient of 0.5 (Bohl W. et al. 2005). Later, investigations of the discharge coefficient of standard orifice by E. Buckingham (1931) and J. Unger (1979) have resulted in the values given in (DIN EN ISO 5167-2). The discharge coefficient ζ of the air flow through a horizontal leak may be derived by the Bernoulli and continuity equation according eq. (1):

$$A_L \cdot \zeta \cdot \sqrt{\frac{2 \cdot \Delta p}{\rho \cdot \left(1 - N^2\right)}} = \dot{V}_{real} \qquad (1)$$

In eq. (1) A_L represents the leakage area, Δp the pressure difference and ρ the density of air. The ratio between room and leakage cross-section is given by N. Corresponding to eq. (2), it is possible to determine the discharge coefficient by experimental investigations. In this context represents $\dot{V}_{real}$ the measured and $\dot{V}_{theo}$ the undisturbed, theoretical volumetric flow.

$$\frac{\dot{V}_{real}}{\dot{V}_{theo}} \cdot \sqrt{\left(1 - N^2\right)} = \zeta \tag{2}$$

According to (DIN EN ISO 5167-2), the parameter N is powered by 4. An explanation of the exponent is missing in DIN EN ISO 5167. Due to the fact that N approaches to 0 the root expression is negligible. In contrary to the Darcy-Weisbach formulation in eq. (3), according to the (ASHRAE 2009) it is possible to investigate ζ without knowledge about channel friction, profile and velocity of the leakage flow through perforations of layers. Furthermore, the influences of inlet and outlet losses for integration in eq. (3) are scarcely documented (Langmans J. 2013). The impacts of these losses are integrated in ζ.

$$\left(\frac{f \cdot L}{d_h} + \Sigma C\right) \cdot \left(\frac{\rho \cdot \overline{u}^2}{2}\right) = \Delta p \tag{3}$$

In eq. (3) ΣC is representing the sum of local losses. f is the Darcy-Weisbach friction factor. In case of fully developed laminar flow it is equal 96/Re (Langmans J. 2013). The other parameters in eq. (3) are L the length, d_h the hydraulic diameter and the mean square velocity $\overline{u}^2$ in the channel. Re denotes the Reynolds number, which defines the stream profile *(*laminar, $Re \leq 2300$*)*. DIN EN ISO 5167 provides additional opportunities for estimation of ζ under conditions of $0.05 \leq N \leq 0.64$ and $5 \cdot 10^4 < Re < 10^7$. A tabulation of some ζ-values of standard orifice is implemented in this standard. Furthermore the Reader-Harris/Gallagher equation may be used for estimation under knowledge of Re at $N \geq 0.1$ (Böswirth L. 2007). It is only applicable to pipes with circular standard orifice. Caused by the approach of $N \rightarrow 0$ and the laminarity of flows through common leakages in buildings, (Langmans J. 2013) values that these models are unsuitable for forecasts of pressure losses. Hence, the discharge coefficient was analysed using eq. (2).

Measurements

The investigations were carried out on vapour barrier foils of about 1 x 1 m in the “Measurement Setup for research on convective moisture transfer (MCMT)” (Schmidt J. et al. 2010a). Every investigated leakage was sharp edged by use of special tools. The climate conditions between the over and under pressure chamber were equal at all measurements. The perforated vapour barrier was the separation of these two connected chambers. For the early investigations, the foil was stiffened without influencing the flow. The volumetric flows through the leaks were measured parallel by use of Tracer-gas-system “TGS” and calorimetric flow meter “MSD”. According to (Böhle M. et al. 2002, Leick Ph. 2008), the flow-through was under open outflow wherein the air flow after overcoming the obstacle could open conically. First, the pressure difference between the inflow and outflow-side were calculated by weather data of a German test reference year (Christoffer J. et al. 2004). Later, these values were arranged based on long term measurements at real building facades. According to the design of the MCMT (Schmidt J. et al. 2012), the maximum total leak size was 10 cm ², at a maximum pressure difference of 350 Pa. Under real measured pressure differences (Schmidt J. 2013) the leakage flow is usually laminar. Due to poor execution of real buildings, cavities between the insulation and airtightness layer may occur. In order to analyse their influence on the leakage flow of perforated vapour barrier foils, double chamber measurements were carried out under free arching of

foils like before. Additionally, the deformation of 4-sided clamped, perforated vapour barrier foils was investigated in single chamber tests with onesided over pressure. For this, a 2D- traversal with rangefinder was installed behind the leakage at the under-pressure side.

Results

The first part of the study related to the analysis of the flow of differently shaped leaks. Therefore, leakages of the same cross-section and shape of edge were investigated in stiffened PE-foil.

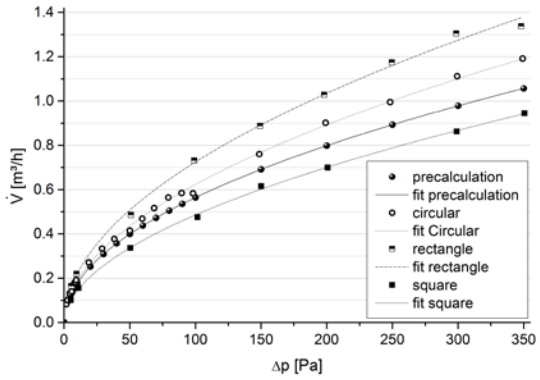

FIG 3. Volumetric flow through different shaped leaks, A_L = 0.2 cm²

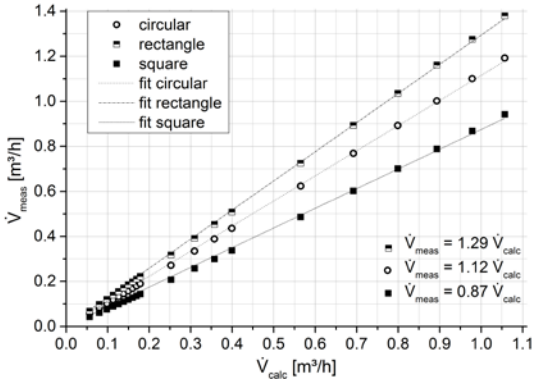

FIG 4. Comparison of volumetric flow through different shaped leaks to the calculated leakage flow, A_L = 0.2 cm²

Figure (3) shows the leakage flow through 0.2 cm² leakages of different shape at different pressure differences. In this context, the flow may be approximated by a leak according to (DIN EN 13829, ASTM E779-10, ASTM E1186-03) as a function of the applied pressure difference by an exponential function. As leakages in figure (3, 4) were used: an edged rectangular leak (0.1 x 2 cm), a squared leak (0.45 x 0.45 cm) and a circular leak (d = 0.5 cm). The measurement error between the carried out parallel measurements was about 3%. The association for air tightness in the building trade “Flib” (2008) suggests using a ζ-value of 0.61 to analyse the equivalent leakage area of a building. Calculated flows, using this ζ-value, were compared with the measurement results, see figure (3, 4). According to figure (4), the calculated flows had an average difference of about 20 % compared to the measured flows. When using the hydraulic diameter to calculate the flow rate, the error would increase further. For e.g.the rectangular leak, it would yield d_h = 0.19 cm. Thus, a much smaller calculation cross-section would be given.

The discharge coefficient is calculable by use of eq. (2) and neglecting *N*. According to figure (5), a linear relationship exists between theoretical and measured volumetric flow. The inclination of the linear fit defines the correlation between the two flow rates. Thus, the inclination resembles a resistance coefficient respectively the discharge coefficient. The properties of the ζ-value were investigated on sharp edged, circular leaks of different cross-section. As shown in figure (6), the discharge coefficient ζ is hyperbolic, approaching a limit value. This relationship can be approximated by an exponential function. The result for circular holes was similar (figure 7). Both, figure 6 and 7 show that the discharge coefficient approaches the theoretical, calculated contraction coefficient according to Torricelli and Borda (1769) with increasing leakage size. This suggests that the influence of the velocity on Φ decreases when the leakage area increases.

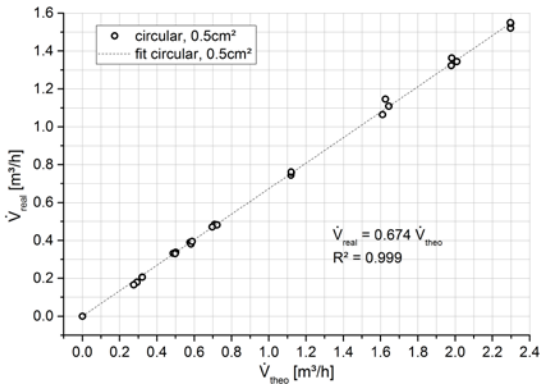

FIG 5. Linear relationship of theoretical and measured volumetric flow A_L = 0.5 cm², sharp edged, circular leak

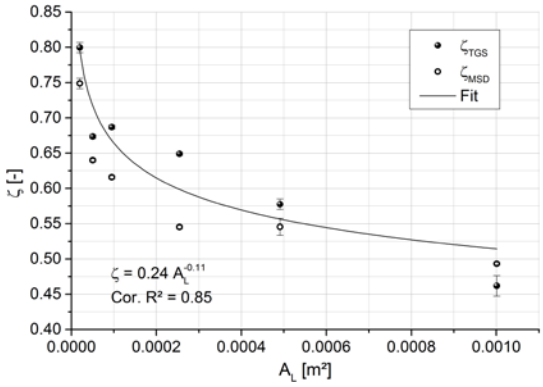

FIG 6. Change of the discharge coefficient in comparison of the change of the leakage area of circular, sharp edged leaks

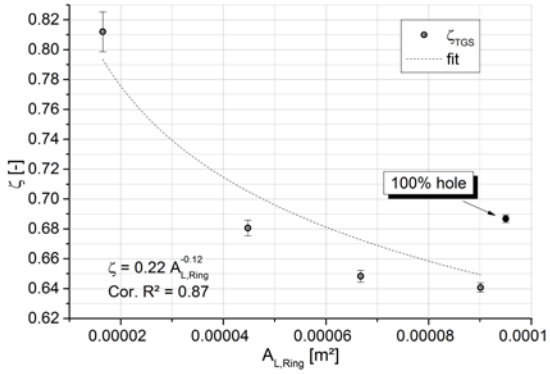

FIG 7. Change of the discharge coefficient in comparison of the change of the leakage area of annular, circular, sharp edged leaks

In the next step of this investigation, the deformation behaviour of a 1 m² large, 0.2 mm thick, perforated PE-foil was examined. In figure (8) is shown that the PE-foil is arching like a nozzle due to the one-sided pressure load. The maximum of arching was 7.4 ± 0.1 cm at a leak size of 0.2 cm² and 350 Pa of pressure difference (figure 9).

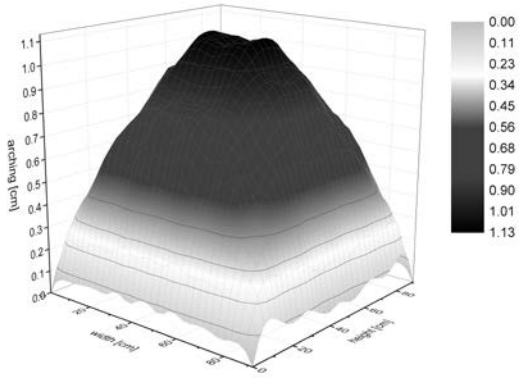

FIG 8. Arching of perforated PE-foil at Δp = 2Pa, A_L = 0.2 cm², circular, sharp edged leak

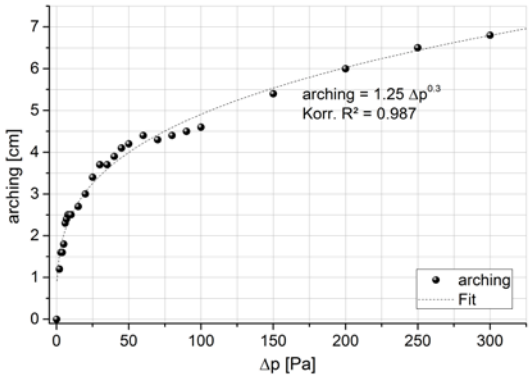

FIG 9. Maximum of arching of perforated PE-foil at different Δp, A_L = 0.2 cm², circular, sharp edged leak

The values for the volumetric flow through the holes in an arched and stiffened PE-foil were compared with the calculated flows for $\zeta = 0.61$ according to (Flib 2008). As can be seen in figure (10), the formation of a nozzle in the air tightness layer may lead to a change of the leakage flow at different pressure differences.

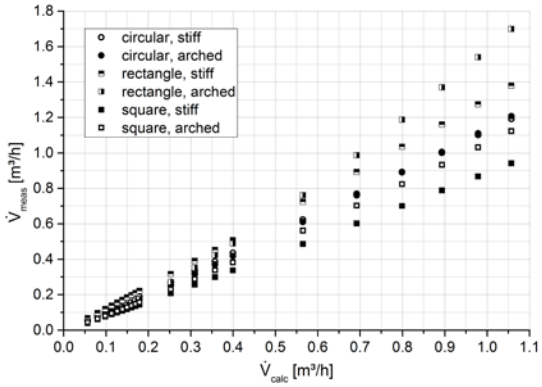

FIG 10. Impact of foil arching onto the leakage flow compared to calculated flow with $\zeta = 0.61$, $A_L = 0.2$ cm², circular, sharp edged hole

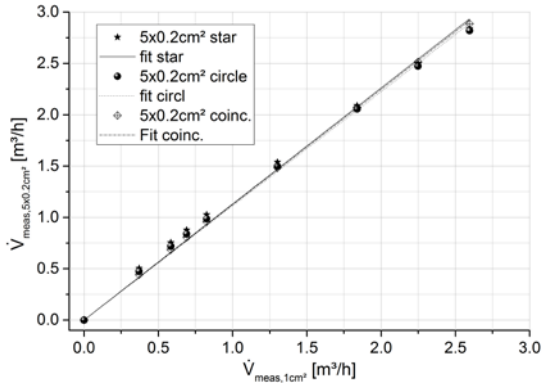

FIG 11. Comparison of leakage flows through a single leak with the total cross-section of 5 small leaks of the same properties in deformable PE-foil

In figure (10) is shown that the smallest variation between the flows through arched and stiffened PE-foil occurs for circular leaks. The difference of leakage flow between deformed and undeformed foil increases with increasing pressure difference (figure 10) for leakages of non-circular shape. The ratio between calculated and measured volumetric flows was never 1 for all measurements (figure 10). These results show that only one value for ζ is not generally valid for every single leakage.

Further investigations should clarify if the ζ-value of the volumetric flow of one leak is equal to the ζ-value of several leakages of the same total cross-section and properties. For the experiment, a leakage area of 1 cm² was chosen. The reference was the flow through a single, sharp edged, centred leakage in deformable PE-foil. The total flow at different pressure differences for the single leak was compared to 5 leakages of $A_L = 0.2$ cm² (total 1 cm²) with different positions.

In figure (11), circle means a uniform distribution of the small holes with a 30 cm radius around one central leak. The definition star describes a hole distribution with one centre leak and 4 leaks in a distance of 5cm on the ordinate and abscissa. Coincidence “coinc.” denotes a freely chosen, non-definable distribution of the small leakages. Figure (11) shows, that the total leakage flows are similar for all 5-leak-tests. The relationship of the flow through the single leak and the 5 holes of the same total cross-section is linear. However, the inclination of the flow fit between the 5 small to the one large leak shows a deviation of 11 to 13 %. In order to be able to define only one discharge coefficient for existing leakages in the building envelope, e.g. in Zone models or to determine the equivalent leakage rate, accurate knowledge about the existing leaks is essential. Even the size of the leakage can be critical.

Conclusions

The investigations of leakage flows through PE-foil show that the volumetric flow through a leak in lightweight timber structures and the adjacent layers is significantly influenced by the discharge coefficient ζ of the room-side leak (exfiltration). It is shown, that the assumption of a discharge coefficient of standard orifices to describe a leakage flow under real pressure differences (wind + buoyancy) may contain errors. The ζ-values of building leakages deviate to ζ-values of standard

orifice in pipes due to the ratio of usual leakage area and room cross-section that approaches zero. Furthermore, leakage flows through building structures under real pressure differences are mainly laminar, in deviation to studies of standard orifice. The investigations show that the discharge coefficient of building leaks is significantly influenced by size, shape and edge properties of a leak. Additionally, leakage edge deformations may influence the ζ-value for PE-foil. Furthermore, caused by poor workmanship, cavities between airtightness and insulation layer may affect the flow through the leakages. In case of PE-foil as air tightness layer, arching of the foil is possible. Depending on the shape of leakage and the applied pressure difference, this may affect the leakage flow in various ways. Only for circular holes were similar volumetric flows for stiffed and deformable foils detected. The theoretical value of $\zeta = 0.61$ for the discharge coefficient (based on shape-independent, stable standard orifices at $N \geq 0.1$) could not be measured for stiffened or deformable foils with single leaks. Furthermore, the discharge coefficient of a single leakage and several leakages with the same properties and the same total cross-section did not match. The obtained results demonstrate that the assumption of only one ζ-value for the whole variety of leakages in the building envelope, e.g. in zone models and for the determination of the equivalent leakage area in differential pressure tests, may be incorrect. The findings of this study can help to optimize simulation models of convective transports through leaks in the building envelope of lightweight timber constructions. However, the study refers only to the leakage flow through perforated air tightness foils. Therefore, the presented measurements should be continued for multi-layered, room boundary layers. It can be assumed that non-negligible factors will be the channel roughness, the material thickness and the propagation behaviour of the air stream in the leak channel.

References

ASTM E1186-03, 2009, Standard Practices for Air Leakage Site Detection in Building Envelopes and Air Barrier Systems.

ASTM E779-10, 2010, Standard Test Method for Determining Air Leakage Rate by Fan Pressurization.

ASHRAE Standards Committee, American National Standards Institute, 2009, ASHRAE Handbook - Fundamentals. Atlanta: ASHRAE Customer Service.

Biskop R., 2008, Bauphysikalische Probleme - Fallbeispiele aus der Praxis des mo-dernen Bauens, 1. Workshop InnoProfile / nuBau, CD, Bauhaus-Universität Weimar (editor), Germany.

Bohl W. & Elmendorf W., 2005, Technische Strömungslehre, Stoffeigenschaften von Flüssigkeiten und Gasen, Hydrostatik, Aerostatik, inkompressible Strömungen, kompressible Strömungen, Strömungsmesstechnik, 13.th ed., Vogel, Würzburg, Germany.

Böhle M., Etling D. et al., 2002, Prandtl - Führer durch die Strömungslehre, Grundlagen und Phänomene, 11th ed., Vieweg, Braunschweig, Germany.

Borda J. C., 1769, Mémoire sur l'Ecoulement des. Fluides par les Orifices des Vases, Mémoires de l'Académie, Royale des Sciences, Paris, France.

Böswirth L., 2007, Technische Strömungslehre: Lehr- und Übungsbuch, 7th ed., Vieweg, Braunschweig, Germany.

Buckingham E., 1931, Beitrag zur Berechnung der Kontraktionszahl, Mitteilung des Bureau of Standards, Washington, Rundschau, Forschungsband, vol. 2., 5th ed., Fritz W. (editor), Berlin, Germany, pp. 185–192.

Christoffer J., Deutschländer Th. et al., 2004, Testreferenzjahre von Deutschland für mittlere und extreme Witterungsverhältnisse TRY, Selbstverl. des Deutschen Wetter-dienstes, Offenbach a. Main, Germany.

de With G., Cherry N. et al., 2009, Journal of Building Physics, Thermal Benefits of tiled roofs with above-sheathing ventilation, vol. 33, 2nd ed., pp. 171–194.

DIN EN 13829, 02/2001, Bestimmung der Luftdurchlässigkeit von Gebäuden, Differenzdruck-verfahren.

DIN EN ISO 5167-2, 01/ 2004, Durchflussmessungen von Fluiden mit Drosselgeräten in voll durchströmten Leitungen mit Kreisquerschnitt-Teil 2: Blenden.

„FLIB“ Fachverband Luftdichtheit im Bauwesen e.V. (editor), 2008, Gebäude-Luftdichtheit, vol. 1, Kassel, Germany.

Häupl P., Grunewald J. et al., 1997, International Journal of Heat and Mass Transfer, Coupled heat air and moisture transfer in building structures, vol. 40, 7th ed., pp. 1633–1642.

Künzel H.M., 2010, Holzbau die neue quadriga, Trocknungsreserven schaffen, Ein-fluss des Feuchteeintrags aus Dampfkonvektion, 1st ed., pp. 28–32.

Kurnitski J. & Vuolle M., 2000, Simultaneous calculation of heat, moisture, and air transport in a modular simulation environment, Proceedings of the Estonia Academy of sciences / Eesti Teaduste Akadeemia Toimetised, Engineering / Tehnikateadused, vol. 1, Aben H. & Kurnitski V. (editors), The Academy, Tallinn, Estonia, pp. 25–47.

Langmans J., 2013, Feasibility of exterior air barriers in timber frame constructions, PhD Thesis, KU, Building Physics Section, Leuven, Belgium.

Leick Ph., 2008, Quantitative Untersuchungen zum Einfuss von Düsengeometrie und Gasdichte auf den Primärzerfallsbereich von Dieselsprays, Dissertation, Technischen Universität Darmstadt, Fachbereich Maschinenbau, Germany.

Schmidt J., 2013, Konvektiver Feuchtetransport, Schlussbericht zum InnoProfile Forschungsvorhaben: Methoden und Baustoffe zur nutzerorientierten Bausanierung, Vogel A., Völker C. et al. (editors), Universitätsverlag, Weimar, Germany, pp. 39–41.

Schmidt J. & Kornadt O., 2010a, Verfahren und Untersuchungsvorrichtung zur Untersuchung eines konvektiven Feuchtetransports in einem Bauwerkelement, Bauhaus-Universität Weimar (applicant), 09.07.2010, publication number: DE102010031141.3.

Schmidt J. & Kornadt O., 2010b, Konvektiver Feuchtetransport durch Bauteilleckagen in Bestandsgebäuden, Nutzerorientierte Bausanierung, vol. 1., 1st ed., Völker C. & Kornadt O. (editors), Universitätsverlag, Weimar, Germany, pp. 109–116.

Schmidt J. & Kornadt O., 2012, Der Bausachverständige, Konvektiver Feuchtetrans-port durch die Gebäudehülle – neuartiges Messsystem zur Klärung relevanter Fra-gen, 4th ed., pp. 29–33.

Schulze H., 2011, Feuchtebedingte Schäden an Wänden, Decken und Dächern in Holzbauart, Schadenfreies Bauen, vol. 5, 2nd ed., Fraunhofer IRB Verlag, Stuttgart, Germany.

Unger J., 1979, Forschung im Ingenieurwesen, Strömungen in zylindrischen Kanälen mit Versperrung bei hoher Reynolds-Zahl, vol. 45, 3rd ed., pp. 69–80.

Zirkelbach D., 2009, Dampfkonvektion wird berechenbar-Instationäres Modell zur Berücksichtigung von konvektivem Feuchteeintrag bei der Simulation von Leichtbaukonstruktionen, 4th International Symposium on Building and Ductwork Air tightness, Berlin, Germany, pp. 1–8. www.hoki.ibp.fhg.de, last call 19.01.2012.

Full paper no: 5

Effect of different façade systems on the cooling capacity of a cooled ceiling – Tracer gas measurement of the air flow

Katharina Eder [1]
Hannes Konder [1]
Thomas Bednar [1]

[1] Vienna University of Technology, Institute for Building Construction and Technology, Department for Building Physics and Building Acoustic, Austria

KEYWORDS: *Air flow, tracer gas measurement, comfort, façade systems, cooling ceiling, cooling capacity*

SUMMARY:
The aim of the work is to clarify how the façade system and the cooling ceiling impacts the air movement within a room. Therefore tracer gas measurements with different inject locations and different room set-ups were done.

One part of the results show the impact of different façade systems – a single skin façade and a single storey double skin façade – on the air movement. The measurements show an increase of concentration within the ceiling zone which is attributed to a higher air flow rate over the ceiling. Furthermore different set ups of the cooling ceilings were measured – one with natural ventilation over the suspended cooling ceiling and one without natural ventilation. The measurement results show that there is a decrease of concentration due to missing natural ventilation.

The measurement results show a clear difference in the rate of concentration on different room points due to solar radiation, the location of impact and the room set up.

1. Introduction

This paper presents the impact of different room boundary conditions (façade system and ventilation rate over cooling ceiling) on the air movement inside an office room. The motivation for this work is that the calculation of comfort in the common areas of buildings plays a key role for the acceptance of new concepts. In the completeness the calculation of complex flow processes in closed and open façades, the dynamic of building elements' performance in combination with the control system is at the moment, if possible, very time consuming. The aim is to develop a simplified room model for the evaluation of building concepts in terms of energy efficiency and comfort.

Measurements for the model validation are one part of the development. A series of measurements according to the operative temperature and the cooling capacity have been carried out and the results show that there is an impact on the cooling capacity with respect to different façade systems. There is an increase of the cooling capacity of about 20 W/m²cooling area in dependency of the temperature difference between the operative temperature in the middle of the room and the mean medium temperature due to a second internal glazing (Eder, 2012).

For verification of the assumption, that the capacity increase is due to a higher air flow rate over the ceiling and therefore to a higher convection load, a mathematical model is built. The validation of this model is done by a series of tracer gas measurements and the results of these measurements are presented in this paper. Chen (2010) describes an overview of ventilation assessment methods. The methods are divided into analytical, empirical, small-scale experimental, full-scale experimental,

multizone network, zonal and CFD models for ventilation in buildings. The advantage of full-scale measurements is, that the real situation is studied, although they are mostly limited by the numbers of measurement points in the tested area.

2. In-situ measurement –Building Information

The measurement was done in an existing office building. On the 34th floor a test room of about 10.8 m² has been built, this is typical for a single person office in Austria. As the room is situated on the 34th floor, there is no shading due to other buildings or geographical surroundings. The façade is a west-orientated totally glazed façade.

Figure 1 shows the floor plan (left side) and the section view (right side) of the measurement room. The floor is raised which is caused to its air leading properties (the supply air is realized over the raised floor) open throughout the whole storey. It is not possible to close the floor, because then the test room would be without fresh air. The suspended ceiling of the measurement rooms is separated by a foreclosure (mineral wool) around the room. The suspended ceiling in the corridor area is used as exhaust air duct.

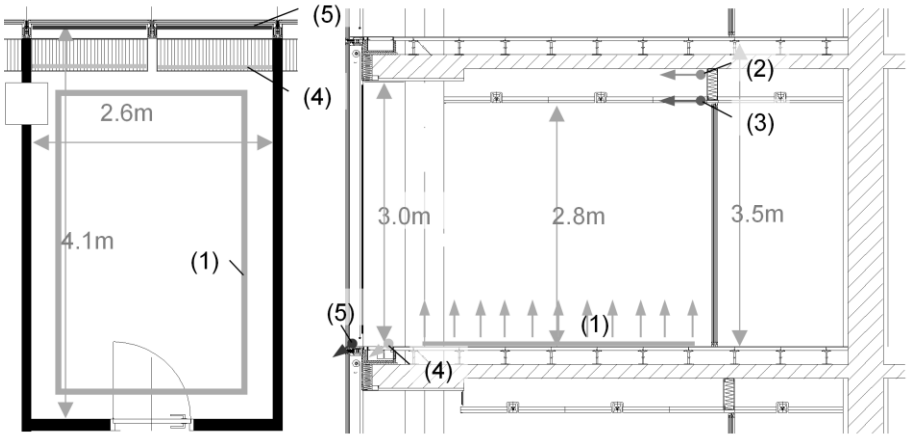

FIG 1. Floor plan (left side) / section (right side); location of tracer gas injection is highlighted; floor plan: direct injection to the room (1); concrete ceiling (2) cooling ceiling (3); supply air area (4); façade area (5)

The U-Values of the surrounding areas of the room are summarized in the following list:

- glazing: U = 1.10 W/m²K
- frame (percentage 8%): U = 2.95 W/m²K
- ceiling / floor: U = 1.47 W/m²K
- Interior wall (gypsum cardboard): U = 0.65 W/m²K
- Interior door: U = 1.80 W/m²K

There is the possibility to change the façade system from a single skin façade to a single storey double skin façade by adding a second internal glazing element. These two façade systems were tested, both with an internal shading element. The difference between these two façade variations are shown in figure 3, there the difference is highlighted between picture 1 and 3, and between 2 and 4 respectively.

2.1 Cooling

The cooling of the rooms is done by a suspended cooling ceiling with capillary pipe mats, which are placed in the ceiling panels. The cooling area is splitted into a façade area and a room area, these are overlapping so that there is a higher capacity in the façade area. For the room area of the measurement room the active area of the cooling ceiling is 5.56 m² and for the façade area it is 3.19 m². Overall

there is an active cooling area of 8.75 m², based on the room area (10.8 m²) there is a rate of cooling area of about 80 %.

Through the measurement the boundary conditions of the suspended cooling ceiling was changed, one time with and one time without natural ventilation over the cooling ceiling. The difference on room conditions is shown in figure 3, for the cooling ceiling picture 1 and 3 are without natural ventilation and the 2nd and the 4th one are with natural ventilation.

2.2 Ventilation

There is a mechanical ventilation system. The design of the ventilation system is as full air conditioning – heating, cooling / dehumidification and humidification.

The supply air for the room is realized via the raised floor, the whole floor is air leading. The air outlet is over "slot diffusors" next to the façade. There is a flow rate of about 50 m³/h for the room, which means an air change rate of about 2.0 1/h with a supply air temperature of about 21 °C.

The exhaust air is realized by exhaust air lights (light fixture combined with extract air terminals). There are flexible ducts between the lights and the suspended ceiling in the corridor. The idea of doing the return air in this way is to remove the heat were it is generated. The suspended ceiling in the corridor is air leading as well.

3. Measurement Set up

The goal of the measurement is to paint a picture of the air flow movement in the room and to see if it is changing with different façade situations. Therefore a series of tracer gas measurements was done. The ASHREA Handbook of fundamentals (2009) describes three different tracer gas methods to determine the air change rate:

- concentration decay or growth method
- constant concentration method
- constant injection method

The concentration decay method, measuring the decay of tracer gas is the simplest and most often used method. The following three conditions should strictly be satisfied using single point measurements. For single point measurements the tracer gas should be uniformly mixed in the enclosure, there should be no unknown tracer gas sources and the ventilation flow should be the dominant means of the tracer gas removal from space to get reliable results (according ASHREA Handbook of fundamentals (2009)).

According to Charlesworth (1988) it is very difficult to achieve a uniformly mixture of the tracer gas in the entire enclosure of in-situ measurements. To solve this problem tracer gas concentrations should be measured at several points of the considered areas and it is assumed that the mean value is the average concentration for the entire enclosure.

As tracer gas carbon dioxid (CO_2) was used, as described in Laussmann (2011) it fulfils a number of the specification of a good tracer gas.

1.1 Sensor Location

To measure the room a grid of 27 CO_2 sensors was set up. In figure 2 the position of the CO_2 sensors is shown, where the left side is the floor plan and the right side shows the section of the room. To measure the air flow in the room, a grid of CO_2 sensors was built.
The measurement itself was done by CO_2 injections and the concentration at the measurement points was logged. A defined amount of CO_2 was injected on five different positions of the room (Figure 1 shows the different impact locations of tracer gas):

- Inj 1: directly into the room, floor area (by a frame with small openings)
- Inj 2: ceiling – height of the concrete ceiling
- Inj 3: ceiling – height of the suspended cooling ceiling
- Inj 4: Supply air area
- Inj 5: Façade area

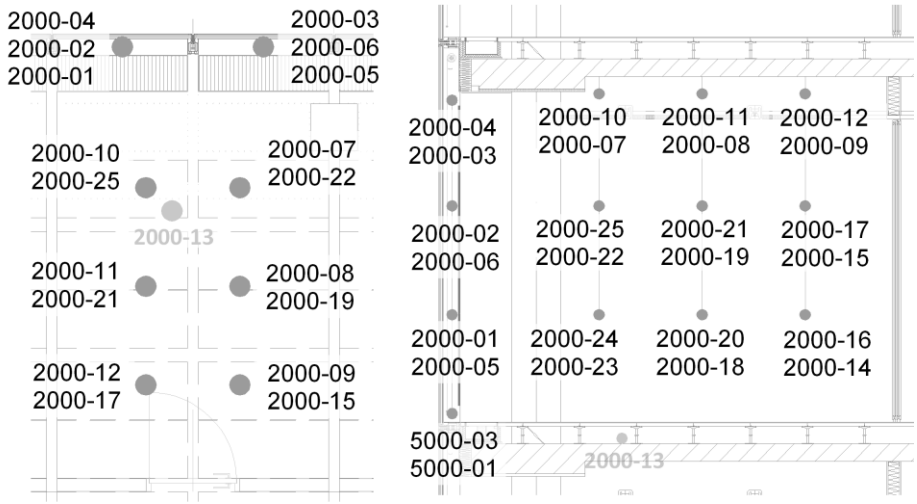

FIG 2. Measurement set up – floor plan (left side) and section (right side) including the sensor numbers, where the first 4 numbers are the maximum concentration rate and the last 2 are the numbers referring to the evaluation diagrams

1.2 Measurement Variations

The measurement was done with a single skin façade and a single storey double skin façade and with an open suspended ceiling and a closed suspended ceiling (figure 3).

The measurement was done with the following 4 different room types:

- Room type 1: **s**ingle **skin** façade, **closed** suspended cooling **c**eiling (sskin+closedc)
- Room type 2 **s**ingle **skin** façade, **open** suspended cooling **c**eiling (sskin+openc)
- Room type 3: single storey **d**ouble **skin** façade, **closed** suspended cooling **c**eiling (dskin+closedc)
- Room type 4: single storey **d**ouble **skin** façade, **open** suspended cooling **c**eiling (dskin+openc)

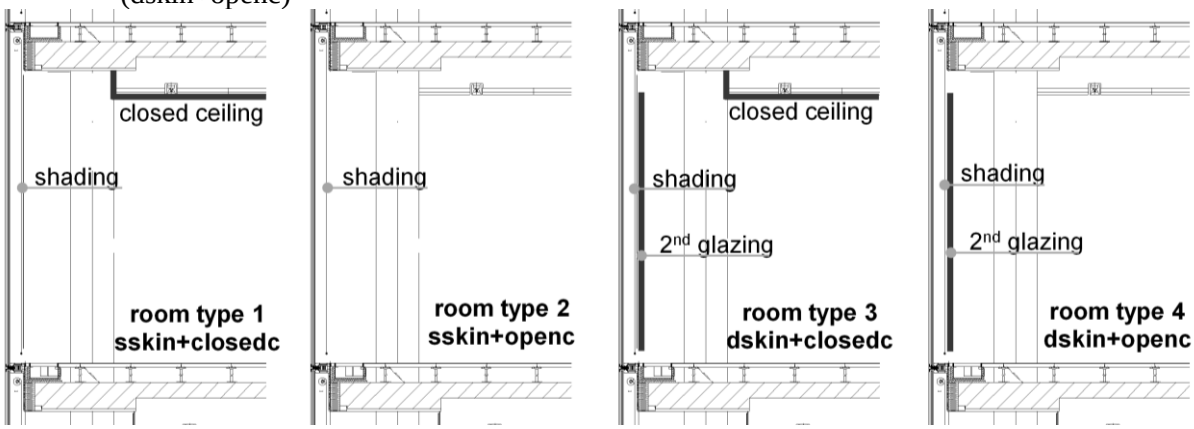

*FIG 3. Schematic overview of the four different room types; from left to right: **s**ingle **skin** façade+**closed** suspended cooling **c**eiling; **s**ingle **skin** façade+**open** suspended cooling **c**eiling, single*

*storey **d**ouble **skin** façade+**closed** suspended cooling **c**eiling; single storey **d**ouble **skin** façade+**open** suspended cooling **c**eiling*

In total there were measured 40 different variants with different boundary conditions. Each variant was measured twice, one time with a clear sunny sky and the other time with a cloudy sky. The measurement period for each variant is 1 hour due to the air change rate of the room. The measurement interval is 10 seconds.

2. Results

2.1 Decay curves – CO_2 concentration

As a result of the measurement there are curves of concentration for each variant and each sensor. The measurement period for one variant is 1 hour, but the main air movement is within the first 10 minutes, then the concentration is equal within the room (see figure 4 and 5).

Figure 4 represents the measurement results for room type 4 (single storey double skin façade+open ceiling) for the different locations in the room. The results are for a clear sunny day and the CO_2 impulse was injected directly into the room. In the diagram there are results for different room heights, where the black line represents the measurement points at 1m height, the black dotted line the measurement results at 2m room height and the grey line the measurement results for the ceiling. The location of the measurement is marked in the diagram at the right corner. The figure shows the change of concentration for different locations within the room and the measurement results indicate that there is no big difference of concentration with respect to the room location, the existing difference can be explained by the supply air location next to the façade.

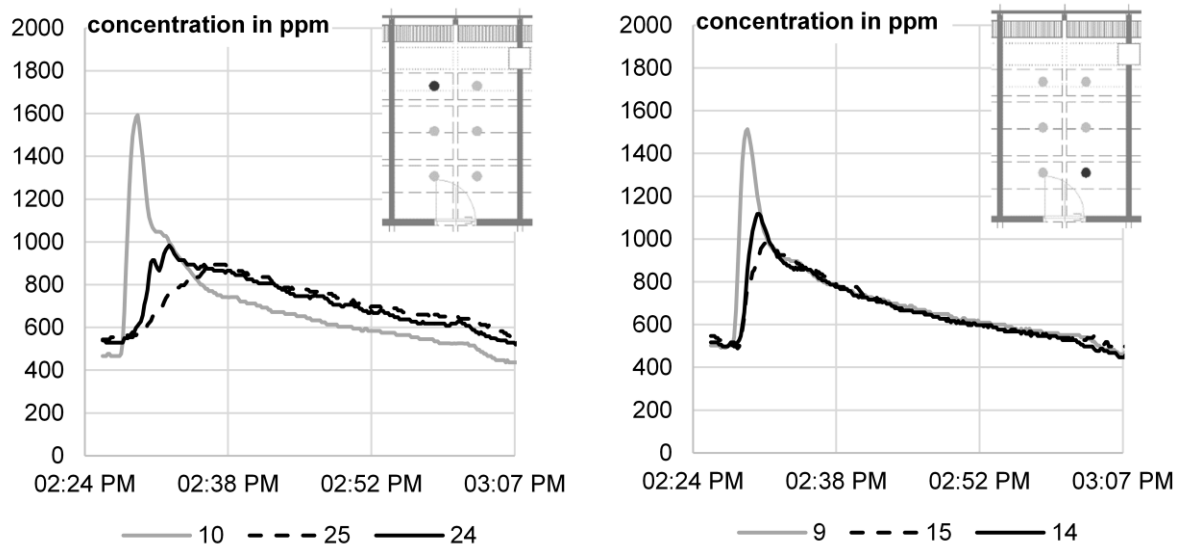

FIG 4. Measurement result of CO_2 concentration a different location in the room with the impact in the room for room type 4, the numbers shown in the legend are referring to the numbers of the sensor (last two numbers in fig 2). The measurement results of the air temperatures (t) for the different room zones are: t_{room}= 24.5 °C, t_{facade} = 31.2 °C, $t_{ceiling}$ = 23.5 °C and t_{floor}= 21.8 °C.

2.2 Impact Location of Injection

The summary of the results for the difference of the CO_2 concentration in the different room areas by different location of injection are shown in figure 5 for room type 04 (single storey double skin façade+open suspended ceiling).

The grey line represents the concentration in the raised floor and is constant within the whole measurement period. The marked black lines show the different room areas (the room itself, the façade area and the ceiling area). The diagram shows that there is an “air roll”, the highest concentration rate with the injection direct to the room is in the façade area, the second highest concentration rate is in the ceiling area and the room itself has the smallest concentration rate. With the injection of tracer on the cooled layer (third part of the diagram) the results show a rapid declension of a cold airstream, first the concentration raises within the room and then in the façade and the ceiling area.

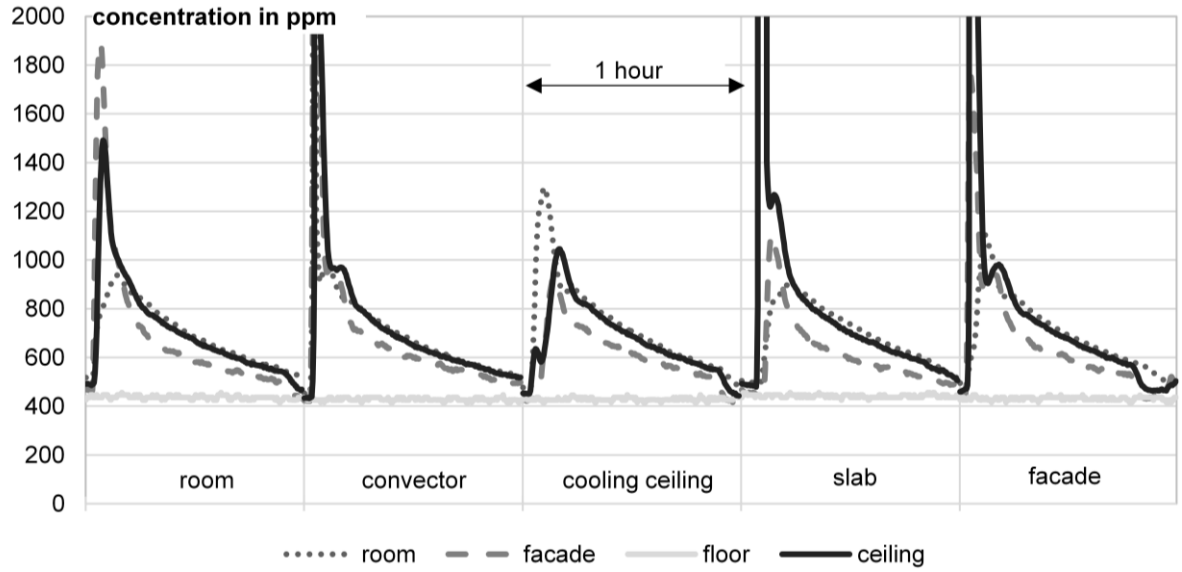

FIG 5. Measurement result of CO_2 concentration with respect to different impact location for room type 4 (dskin+openc); with solar radiation; measurement period 1 hour for each variant; different concentrations in the specified areas within the first 10 minutes, after the first 10 minutes the concentration is equal in each area independent of the impact location

2.3 Summary of results for a day with solar radiation

In figure 6 there is the summary of the measurement results for the four different room types for a day with solar radiation visualized.

Figure 6 shows the first 10 minutes after the CO_2 injection directly into the room. The values in the diagram are the mean values of concentration for the room area, the façade area, the suspended ceiling and the raised floor. The concentration of the raised floor is not changing during the whole measurement, so there is no mass flow from the room to the floor.

The different rate of concentration in the suspended cooling ceiling show the difference in the air flow over the cooling ceiling. The measurement results show an increase of air flow due to the single storey double skin façade (comparing room type sskin+openc and dskin+openc) and a decrease of air flow due to the closed ceiling (comparing room type sskin+openc and sskin+closedc to room types dskin+openc and dskin+closedc).

2.4 Summary of results for a day without solar radiation

In figure 7 the results for the four different room types for a day without solar radiation are visualized. There is almost no difference of concentration between the room types. Due to the lack of buoyancy there is no air roll and the air movement is very small.

In figure 7 the first 10 minutes after the CO_2 injection direct into the room are shown. The values in the diagram are the mean values of concentration for the room area, the façade area, the suspended ceiling and the raised floor.

The different rate of concentration in the suspended cooling ceiling show the difference in the air flow over the cooling ceiling due to the tested boundary conditions of the room. The measurement results for the case without solar radiation show almost no difference of concentration.

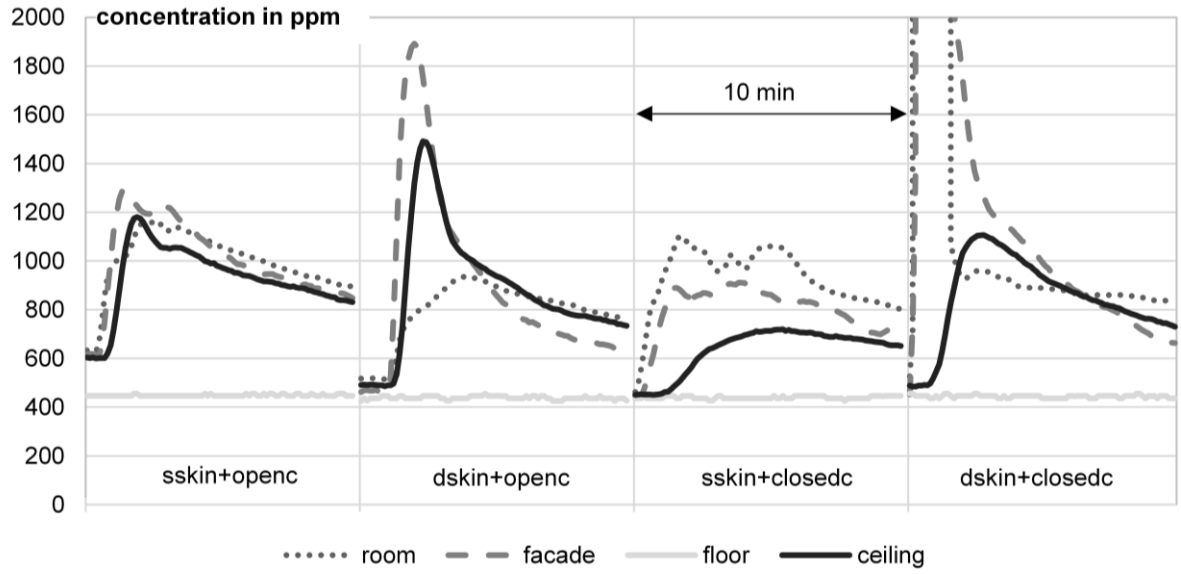

FIG 6. Measurement results of CO2 concentration for the different room types with solar radiation, the tracer gas injection directly into the room (floor area). The diagram shows an increase of concentration in the ceiling area due to the single stores double skin façade and a decrease due to the lack of natural ventilation for the cases with the closed suspended ceiling.

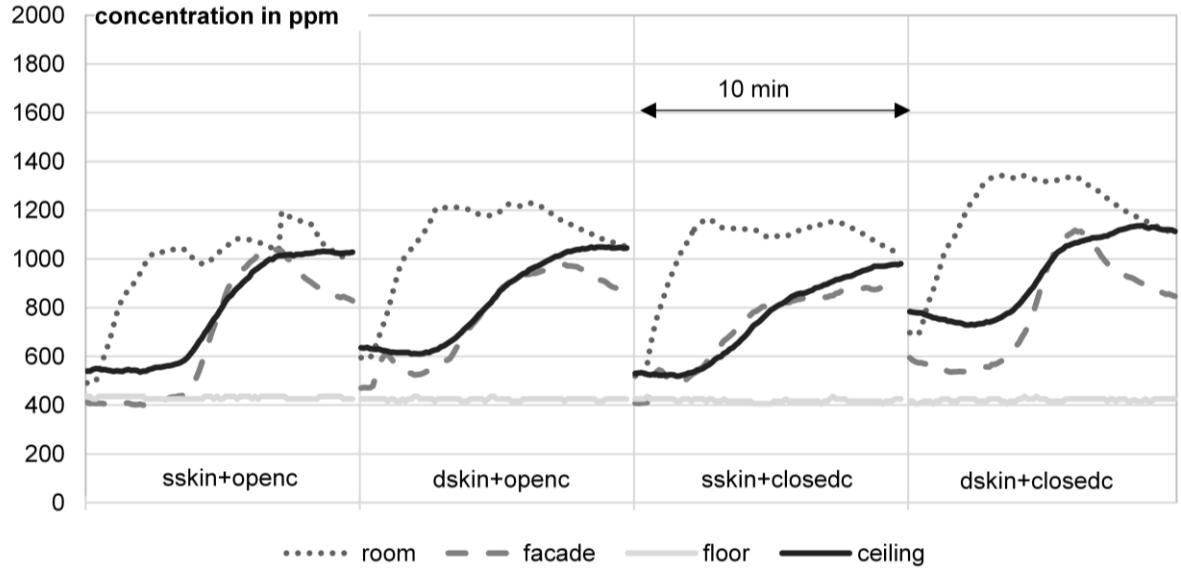

FIG 7. Measurement results of CO2 concentration for the different room types without solar radiation, the tracer gas injection directly into the room (floor area). The diagram shows that there is almost no difference of concentration between the room types

3. Conclusion

Through an intensive set of measurements the impact of air flow due to different room conditions (façade system, cooling system) were evaluated. The tracer gas measurement results show the impact by different concentration rates. The location of injections has no impact on the decay curves after the first 10 minutes.

The single storey double skin façade leads to a significant increase of tracer gas concentration within the ceiling zone. The maximum concentration within the suspended ceiling variate between 720 ppm (room type 1) and 1491 ppm (room type 4). Due to the second glazing there is an increase of 350 ppm. The difference between the open and the closed ceiling is about 420 ppm.

For further evaluation of the measurement results an ideal multi zone model was assumed and mass balances were calculated. Furthermore a mathematical model (CFD) is built and the measurements are used to validate the air flow model.

The measurement results show an impact on the air flow due to different boundary conditions. The next step for the model development is the detailed mathematical modeling of the air flow network within the room, which is done by CFD. To reach the aim of the research, which is the development of a computational model that can determine the impact on comfort with reasonable accuracy, the set of tracer gas measurement is one part of the model validation.

Based on the validated room model, recommendations for future building designs in net energy producing buildings can be formulated.

4. Acknowledgements

The doctoral program “Energy Systems 2030 (ENSYS 2030)” is an internal research project funded by the Vienna University of Technology, which has the main goal to provide doctoral students within the research area "Energy and Environment," a remarkably structured and interdisciplinary education. 10 PhD positions are advertised and supported as part of the College of the Vienna University of Technology.

Energy and Environment is part of the development plan of the Vienna University of Technology 2010+ as one of the five research priorities. The doctoral program ENSYS 2030 has the following key themes: solar energy, energy storage, electro mobility and energy active building.

References

ASHRAE. Handbook of fundamentals.2009. Atlanta, USA: American Society of Heating, Refrigerating and Air-Conditioning Engineers, Inc.

Charlesworth P.S.1988. Air exchange rate and airtightness measurement techniques - an applications guide. Coventry, UK: Air Infiltration and Ventilation Centre

Chen, Q., Lee, K., Mazumdar, S., Poussou, S., Wang, L., Wang, M., and Zhang, Z. 2010. “Ventilation performance prediction for buildings: Model Assessment,” Building and Environment, 45(2), 295-303.

Eder K., Steininger C., Bednar T. 2012 “Enhancing the performance of a cooling ceiling by an innovative façade system”; Proceedings of the 5th International Building Physics Conference, IBPC, 2012, Kyoto

Laussmann D., Helm D. 2011. Air Change Measurements Using Tracer Gases: Methods and Results. Significance of air change for indoor air quality. Chemistry, Emission Control, Radioactive Pollution and Indoor Air Quality, Dr. Nicolas Mazzeo (Ed.), ISBN: 978-953-307-316-3, pp. 365-399

Full paper no: 6

Effect of different façade systems on the cooling capacity of a cooled ceiling – CFD modeling

Katharina Eder [1]
Maximilian Neusser [1]
Thomas Bednar [1]

[1] Vienna University of Technology, Institute for Building Construction and Technology, Department for Building Physics and Building Acoustic, Austria

KEYWORDS: *façade systems, natural ventilated double skin façade, computational fluid dynamics, operative temperature, cooling capacity, comparison measurement and CFD calculation*

SUMMARY:
One of the key issues for the calculation of a room's condition and the resulting thermal comfort is the knowledge of the air flow distribution in the room. A simplified but still accurate enough CFD model should be developed to determine the effect of different façade types on the cooling capacity of a cooling ceiling. A parametric study using the program COMSOL Multiphysics 4.3a was done. The output of the calculations was compared with the results of a series of in-situ measurements and is presented in this paper.

The measurement and the calculation results show an impact on the cooling capacity by changing air flow conditions within the room. The design of the façade system can increase the capacity of a cooling ceiling and therefore decrease the operative temperature in the room. Neglecting the flow characteristics in the room can lead to incorrect results, especially for complex façade systems in combination with component activation (e.g. cooling ceiling).

Therefore an enhanced building model for the design of future buildings, taking into account the interaction of building envelope and building service systems should be developed using the results of the CFD calculation. Recommendations for energy active buildings related to room conditions, room comfort and the energy demand can be formulated by simulations over yearly periods.

1 Introduction

This study presents results of the cooling capacity of a cooling ceiling in dependence of two different façade systems – a single skin façade and a single storey double skin façade. The influence on the cooling capacity due to the façade systems was measured by an intensive set of measurement and the results are presented in Eder et al. (2012) and are used for the validation of the mathematical model.

Due to multiple coupled physical phenomena (air flow, convection, conduction and radiation) the behaviour of double skin façades is very complex. Both, experimental and numerical models for the optimization of the performance of double skin façades have been developed e.g. network models (Tanimoto et al., 1997), zonal models (Jiru et al., 2008), energy simulation with coupled air flow models (Stec et al. 2005) and detailed computational fluid dynamics studies (Manz, 2004).

Most of the developed models are for external double skin facades. This paper studies the effect of a (internal) single storey double skin façade on the HVAC system. The diving force is natural buoyancy, therefore the air flow is not easy to control and the dependence on weather conditions (mainly solar radiation) makes it discontinuous. The validated results of the air flow calculation should be

integrated in an enhanced room model which takes flow phenomena that influences the cooling capacity, the operative temperature - and therefore the comfort within the room - into account.

2 Theoretical background

The software program COMSOL Multiphysics version 4.3a was used, with the aim to calculate the impact of air movement with different façade systems. As physical model non isothermal flow was used to describe the problem. The main equations are the Navier Stokes (momentum balance and mass balance), heat balance and energy transport (convection and conduction).

One of the main topics is the modeling of the façade. Because the simulation program COMSOL Multiphysics version 4.3a consider all radiation as the same, it is not possible to make a distinction between large infrared radiation and the solar spectrum (UV, light & short IR). Within this study the interaction between the façade system and the cooling ceiling is the main topic, therefore the surface to surface radiation has to be considered. For this work the incident solar radiation was realized by heat impacts to the individual layers of the façade according to its absorption and solar transmission coefficient.

3 2-D Model

3.1 Geometry and mesh properties

The geometry of the simulation model is according to the architectural plans, a section through the room. A simplification of the model, from three dimensions to two was done. The symmetry is along the depth of the room (see figure 1).

The main geometric data of the room is summarized in table 1.

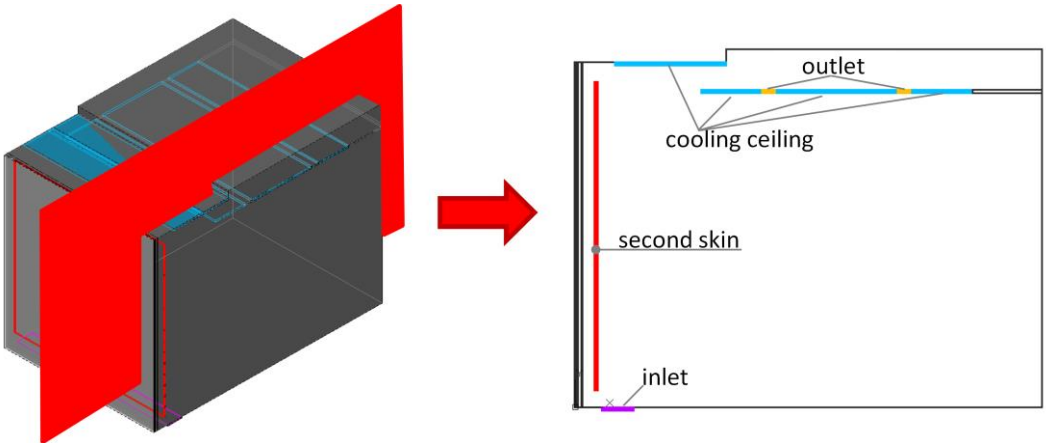

FIG 1. Simplification of the model geometry from three dimensions to two dimensions

TABLE 1. Room / model dimensions

Outside pane	height in m	width in m
Room height	3.40	-
Room depth	4.10	-
Façade – exterior glass	3.07	0.01
Argon	3.07	0.01
Façade – interior glass	3.07	0.01
Gap between glass and screen	3.07	0.03
Screen	3.07	0.01

Gap between screen and 2nd glazing	3.07	0.11
2nd glazing extern	2.74	0.01
2nd glazing argon	2.74	0.01
2nd glazing intern	2.74	0.01

3.2 Façade systems

With the CDF Model the impact of two façade systems – Façade system 1: single skin façade with internal shading element; Façade system 2: single storey double skin façade with a shading element between the 2 glazing elements should be tested. Figure 2 shows the schematic overview and table 2 summarize the technical data for the façade systems. The total solar energy transmittance g-value of the glazing is g = 0.36 according to the technical data sheet. The air permeability of the shading systems was not considered within this study.

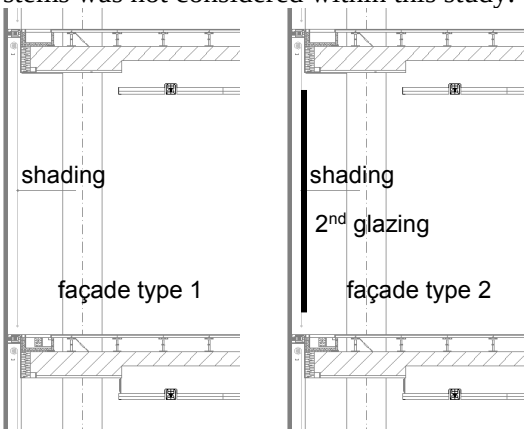

FIG 2. Façade type 1 (left side): single skin façade with internal shading element / façade type 2 (right side): single storey double skin façade with a shading element between the glazing elements.

TABLE 2. Technical data façade system

Parameter description	Outside pane	Shading system	2nd skin
Total solar energy transmittance:	g = 0.36	---	---
Solar transmittance:	τ = 0.33	τ = 0.11	τ = 0.55
Reflectance:	ρ = 0.41	ρ = 0.39	ρ = 0.24
Absorptance outside pane:	a_c = 0.25	a = 0.50	a_c = 0.25
Absorptance inside pane:	a_i = 0.01	---	a_i = 0.01
Light transmittance:	---	τ_L = 0.10	---

3.3 Boundary Conditions

The heat flux of the external wall is defined by an inward heat flux, the heat transfer coefficient for the external wall is 20 W/m²K and the external temperature is 32 °C. The surface temperature for the cooling ceiling panels was measured by thermography with a reference temperature measurement. The temperatures of the enclosing surfaces are summarized in table 3.

TABLE 3. Temperatures surrounding surfaces

Surface	Temperature in °C
Floor	23.0
Partition wall	25.0
Ceiling – room	23.0

Ceiling façade	32.0
Cooled ceiling (bottom)	18.5
Cooled ceiling (top)	18.5

3.4 Material Properties and Initial conditions

The material properties of the surrounding surfaces and used materials are shown in table 4 and the the surface emissivity is shown in table 5. The initial temperature condition t_0 is 294.15 K, the initial pressure p_{ref} is 1 atm. The dynamic viscosity, the heat capacity and the thermal conductivity of the layer ”air” are temperature dependent and the density is calculated in dependency of the air temperature and the air pressure.

TABLE 4. Material data

	dynamic viscosity	ration of specific heat	heat capacity at a constant pressure	density	thermal conductivity
	Pa s	-	J/kg K	kg/m³	W/mK
Air (room)	eta(T[1/K])	1.4	cp(T[1/K])	rho(pA[1/Pa],T[1/K])	k(T[1/K])
Façade external glazing			480	2200	1.1
Argon			520	1.7837	0.0177
Façade internal glazing			480	2200	1.1
Screen			1700	1150	0.26
2nd glazing – external			480	2200	1.1
2nd glazing – internal			480	2200	1.1
Aluminium			900	2700	160

TABLE 5. Surface emissivity

Surface	Surface emissivity
Floor	0.97
Aluminium – grey paint	0.95
Glass	0.80
Screen	0.88
Concrete – ceiling	0.96
Plaster – partition wall	0.94

3.5 Mesh and Solver setting

One output of the CFD calculation is the cooling capacity of the cooling ceiling, due to this issue, the calculation was done with the Low Reynolds number k-ε turbulence model. The mesh of the complete model consists of 100298 (façade type 1) and 120508 (façade type 2) elements.

The summary of the solver settings is shown in table 6

TABLE 6. Solver settings

description	type
Type of analysis: non isothermal flow	Non-isothermal flow
Linear system solver:	MUMPS

Relative tolerance	0.001
Pivot threshold	0.1
Memory allocation factor	1.2

4 Results

4.1 Operative Temperature

In figure 3 the results of the operative temperature in the middle of the room are shown for the two façade systems. The results for the single skin façade show an increase of the operative temperature from 24.7 to 28.5 °C with an increasing solar impact. The mean capacity of the cooling ceiling variate between 40 and 80 W/m²$_{\text{cooling area}}$. The effect of the single storey double skin façade is a smaller increase of the operative temperature in the middle of the room due to a higher efficiency of the cooling ceiling. The diagram shows, that the operative temperature stays around 26 °C and the cooling capacity increases with respect to the solar impact.

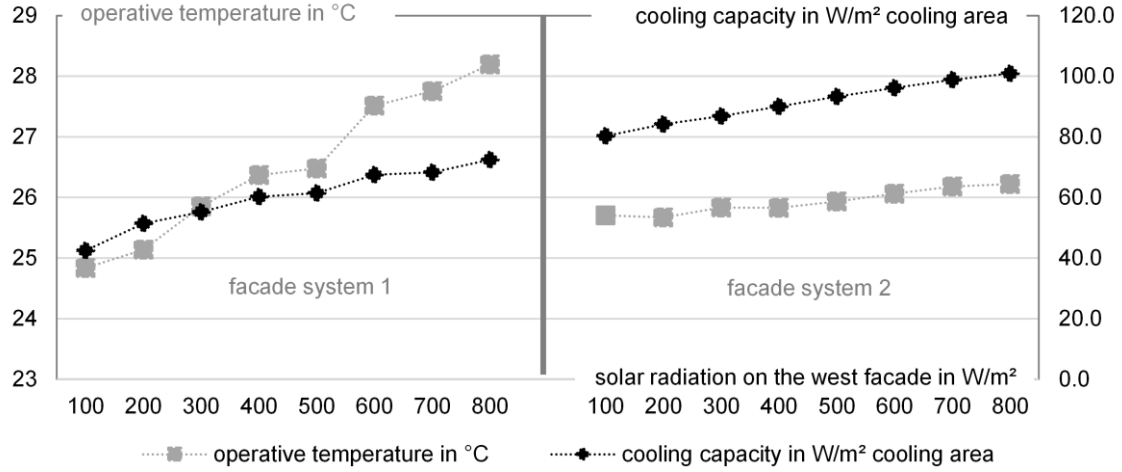

FIG 3. Comparison of operative temperature and the cooling capacity for façade type 1 (left side) and façade type 2 (right side); the temperature is below 27°C with façade type 2, the cooling capacity is increasing with increasing solar radiation; with façade type 1 the operative temperature is getting above 27°C and the cooling capacity is lower.

4.2 Cooling capacity

The definition for the test bed measurements for the cooling capacity of cooling ceilings is done in the standard EN 14240. According to the standard the cooling capacity is based on the average temperature difference between the operative temperature in the middle of the room and the mean medium (flow and return) temperature and is referring to the active cooling area.

The cooling capacity was calculated for both façade types with different incident radiation (from 100 W/m² to 800 W/m²): In figure 4 the results on cooling capacity in relation to the room depth for façade type 2 for a temperature difference between the mean medium temperature and the operative temperature in the middle of the room of 9 K are visualized.

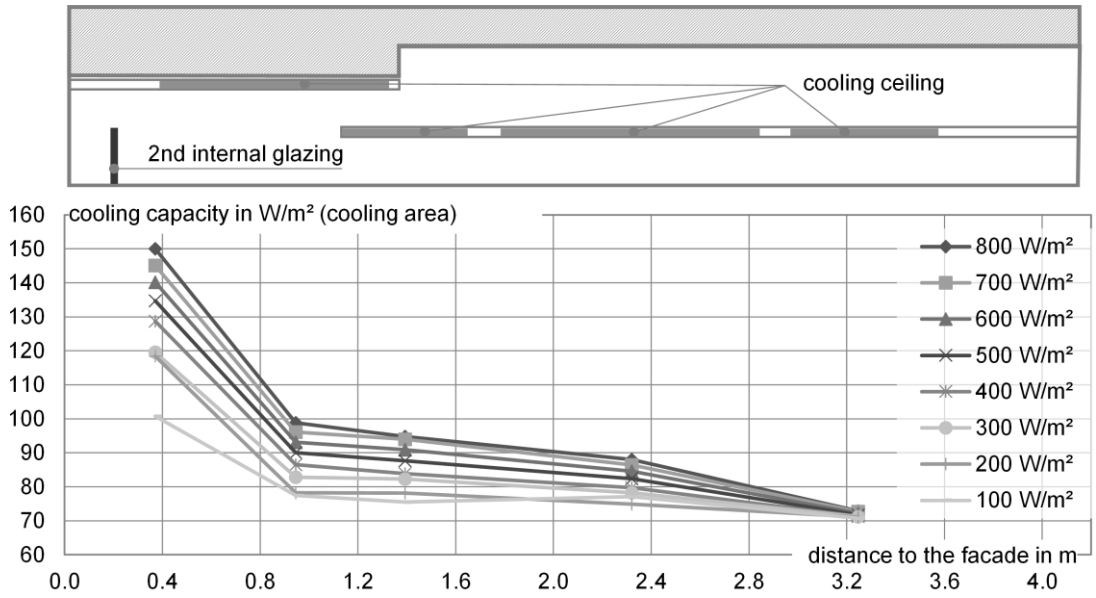

FIG 4. Cooling capacity in dependence of the room depth for façade system 2; temperature difference between mean medium temperature and operative temperature in the room is 9 K

The results for the cooling capacity of the cooling ceiling as a function of the depth of the room for the 2 façade systems is shown in figure 5. The calculation results show that there is an increase of the cooling capacity by comparing the single skin façade (grey line) and the single storey double skin façade (black line). Especially next to the façade but also throughout the room, the difference is minimal where the cooling ceiling is arranged overlappingly.

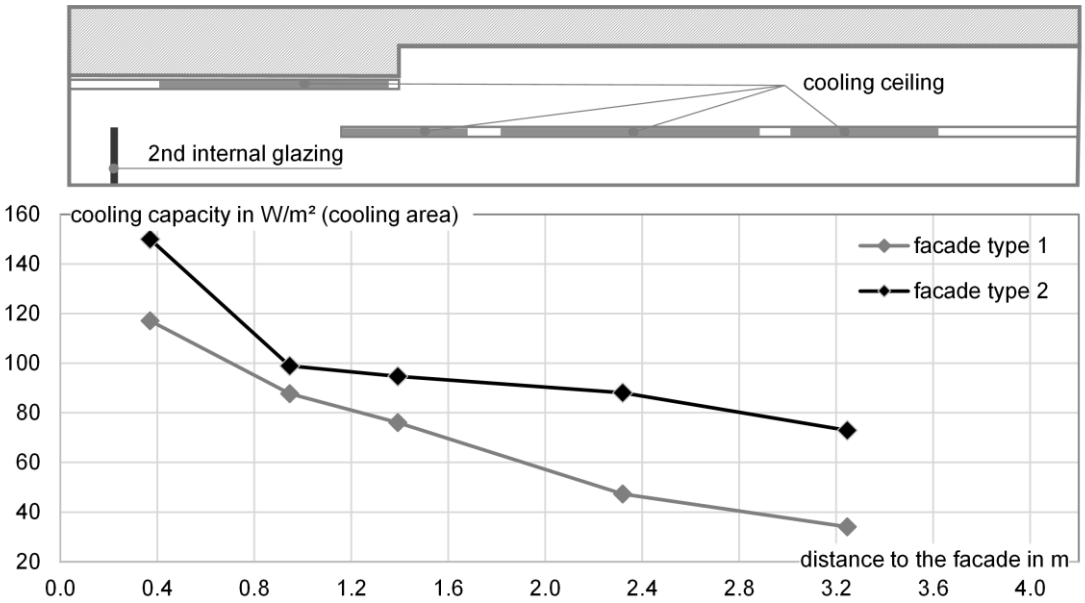

FIG 5. Cooling capacity in dependence of the depth of the room with an incident solar radiation of 800W/m² and a temperature difference of 9 K between the mean medium temperature and the operative temperature in the middle of the room.

Figure 6 shows the resulting mean cooling capacity with different impacts due to the incident solar radiation for the two façade systems. The temperature difference between the mean medium temperature and the operative temperature in the middle of the room is 9 K.

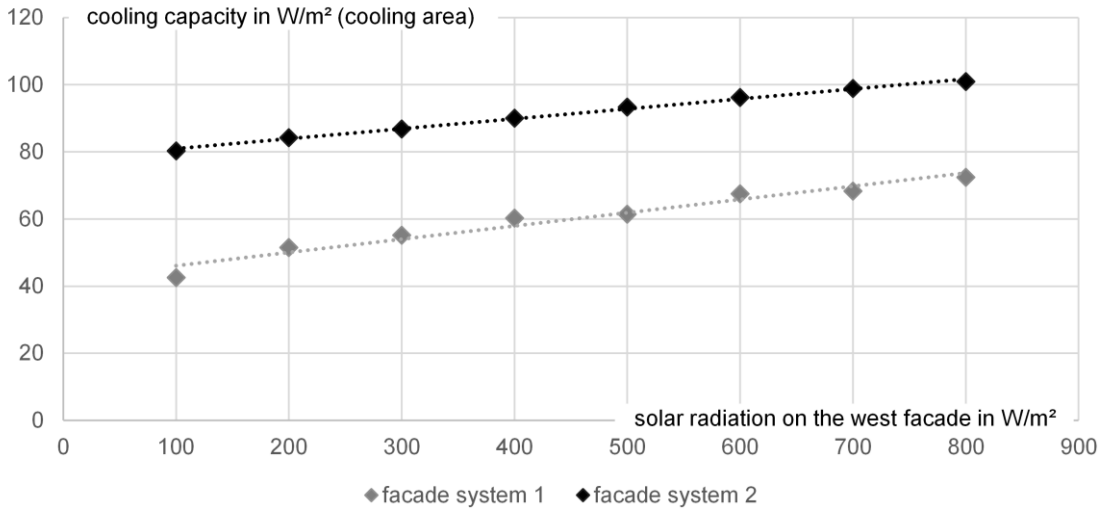

FIG 6. Resulting cooling capacity in dependence of the incident solar radiation; the temperature difference between the mean medium temperature and the operative temperature in the middle of the room is 9 K

The comparison of the measurement results and the results of the CFD calculation is shown in figure 7. There is a good agreement between both for the operative temperature and the cooling capacity. The measurement results are taken by a series of measurement in an existing building, the description is found in Eder et al. (2012).

In figure 7 on the left side the operative temperatures for both façade types are shown, the left part in this diagram represents the result of the CFD calculation and the right part the measurement results. The difference of the operative temperature in the middle of the room is about 0.2 K. The right side diagram in figure 7 show the results of the cooling capacity in dependence of the temperature difference between the mean medium temperature and the operative temperature in the centre of the room. The lines represent the measurement results. The points are the results out of the CFD calculation for the different tested boundary conditions. The diagram shows a good agreement between the measurement results and the results of the CFD calculation.

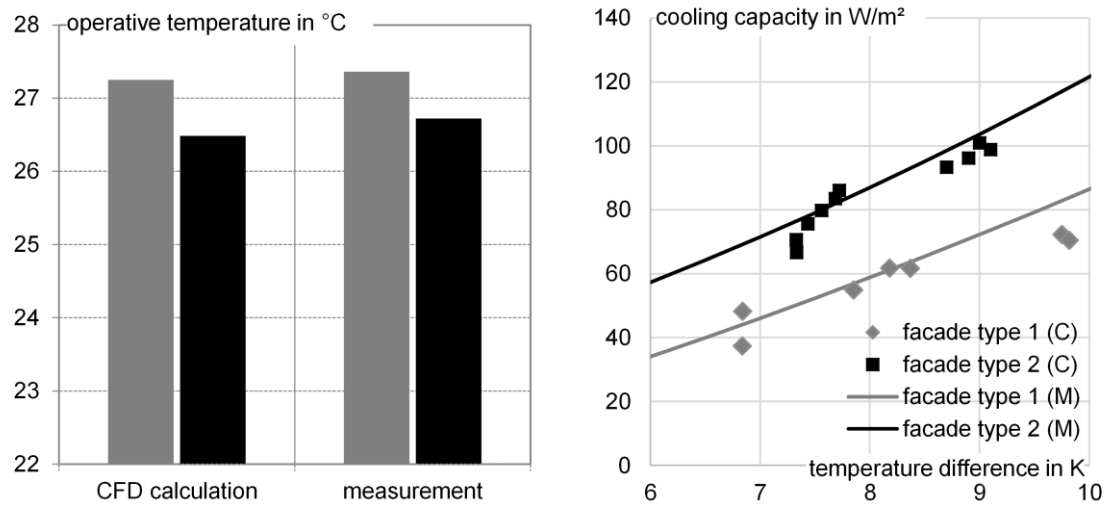

FIG 7. Measurement results on operative temperature (left side) and cooling capacity (right side; (M)..measurement; (C)..CFD calculation) – there is a good accordance between the measurement results and the CFD calculation; the difference of operative temperature is about 0.2 K;

5 Conclusion

The comparison of in-situ measurements of operative temperature and the cooling capacity of a cooling ceiling and the calculation results of the CFD calculation show good agreement. The CFD model can therefore be used to characterize different façade systems regarding their impact on operative temperature and the capacity of the cooling ceiling.

The comparison of the two façade systems – the single skin façade (type 1) and the single storey double skin façade (type 2) – shows that there is a decrease in operative temperature and an increase of the cooling capacity.

The CFD calculation results show the cooling capacity in dependence of the solar radiation the temperature difference between the mean medium temperature and the operative temperature in the middle of the room and the depth of the room. The results show, that there is an impact due to the solar radiation and the characteristics of the cooling capacity within the room geometry. The increase of the cooling capacity due to a higher air flow rate is limited on the first 3 m from the façade, there is no longer an impact due to solar radiation further in the back.

The results of the CFD calculation can be used for an enhanced building model for future building design. Recommendations for net energy producing building according to room comfort and energy demand can be formulated by simulations over yearly periods.

6 Acknowledgements

The doctoral program "Energy Systems 2030 (ENSYS 2030)" is an internal research project funded by the Vienna University of Technology, which has the main goal to provide doctoral students within the research area "Energy and Environment," a remarkably structured and interdisciplinary education. 10 PhD positions are advertised and supported as part of the College of the Vienna University of Technology

Energy and Environment is part of the development plan of the Vienna University of Technology 2010+ as one of the five research priorities. The doctoral program ENSYS2030 has the following key themes: solar energy, energy storage, electro mobility and energy active building.

References

Eder K., Steininger C., Bednar T. 2012 “Enhancing the performance of a cooling ceiling by an innovative façade system”; Proceedings of the 5th International Building Physics Conference, IBPC, 2012, Kyoto

EN 14240. 2004. Ventilation for buildings - Chilled ceilings - Testing and rating

Jiru T.E., Haghighat F., 2008 “Modeling ventilated double skin façades – a zonal approach”, Energy and Buildings 40, 1567–1576.

Manz H. 2004 “Total solar energy transmittance of glass double façades with free convection”, Energy and Buildings 36, 127–136.

Safer, N., Woloszyn, M., Roux, J.J., 2005 "Three-dimensional simulation with a CFD tool of the airflow phenomena in single floor double-skin façade equipped with a venetian blind", Solar Energy 79, 193–203.

Stec W.J., Van Paassen A.H.C. 2005, “Symbiosis of the double-skin façade with the HVAC system”, Energy and Buildings 37, 461–469.

Tanimoto J., Kimura K., 1997 “Simulation study on an airflow window system with an integrated roll screen”, Energy and Buildings 26, 317–325.

Air leakage and hygrothermal performance of an internally insulated log house

Üllar Alev, M.Sc [1]
Andres Uus, M.Sc [2,3]
Marko Teder, M.Sc [2]
Martti-Jaan Miljan, M.Sc [2]
Targo Kalamees, Professor [1]

[1] Tallinn University of Technology, Estonia
[2] Estonian University of Life Sciences, Estonia
[3] Hobbiton OÜ, Estonia

KEYWORDS: *air leakage, internal insulation, log house, test-house, corner notch*

SUMMARY:
In this study the air leakage of four different log corners and hygrothermal performance of three different interior insulation materials are studied in a log test house. Field measurements of the air leakages were analysed in a test house built with different types of log junctions: corner post, dovetail notch, Scandinavian saddle notch, and double notch with wind lock. One wall made of logs (average thickness of 270 mm) in a test house was internally insulated with three different materials: cellulose fibre, mineral wool and reed mat. The air leakage rate of the overall house was also measured using the standardized building pressurization technique. Hygrothermal performance of walls was measured with t&RH sensors and heat flow plates.

The mean air leakage rate of the overall house at the pressure difference of 50 Pa was q_{50}=2.8 $m^3/(h \cdot m^2)$ and mean air change rate was n_{50}=5.0 h^{-1}. The air leakage rate lowered slowly over time. The lowest air leakage was through the Scandinavian saddle notch - 6.7 $m^3/(h \cdot m)$.

Simulation models on the hygrothermal performance of the studied test walls were validated based on the measurement results. Temperature, relative humidity and heat flux showed good agreement between the measured and the calculated results.

1. Introduction

Log houses have a long history and they represent a variety of building techniques employed in Estonia and in other Nordic countries. Results of measurements of old log houses have shown that this building type is typical of the highest air leakage (Alev & Kalamees 2013). In a new log house, the quality of the envelope has to be higher than a century ago, because the requirements for comfort, function, and energy-efficiency of today's residents are different.

Uncontrolled air movement through a building envelope leads to problems related to the hygrothermal performance, health, energy consumption, performance of the ventilation systems, thermal comfort, noise and fire resistance. Air leakage through the building envelope depends on the results of the air-pressure differences across the envelope, the distribution of air leakage places and the airtightness of the building envelope.

Many studies have analyzed the possibilities to use the internal thermal insulation for improving the thermal resistance of external walls, including those focused on stone walls (Stopp et al. 2001; Häupl et al. 2004; Toman et al. 2009) and only few have studied the internal insulation of log walls (Ojanen 2007; Alev et al. 2012; Arumägi & Kalamees 2012; Arumägi et al. 2011). Ojanen (2007) studied the

internal insulation only numerically and assumed that the log wall was completely airtight, but vertical air channels between the log and the insulation layer were suggested to reduce the moisture level. Arumägi & Kalamees (2012) and Alev et al. (2012) studied old walls with high leakage rate and found that the log wall is not completely airtight and to validate the simulation model the air change through the log wall had to be added. Other differences between mentioned studies include the type and usage of the house, used insulation materials, moisture excess etc. Therefore the measurements of new log wall were needed.

This study had two main objectives:

- to study the air leakages of different corners and the whole building of a new log house;
- to validate the simulation model of three different internal insulation constructions (materials).

2. Methods

2.1 Tested house

The field measurements were carried out in a small test house (one room with a net area of 18 m^2) specially designed and built for current study (FIG 1). The house was made of square logs with an average thickness of 200 mm (except the back wall with half round logs and an average thickness of 270 mm, insulated from the internal side). Every corner had a different type of log junction (FIG 2).

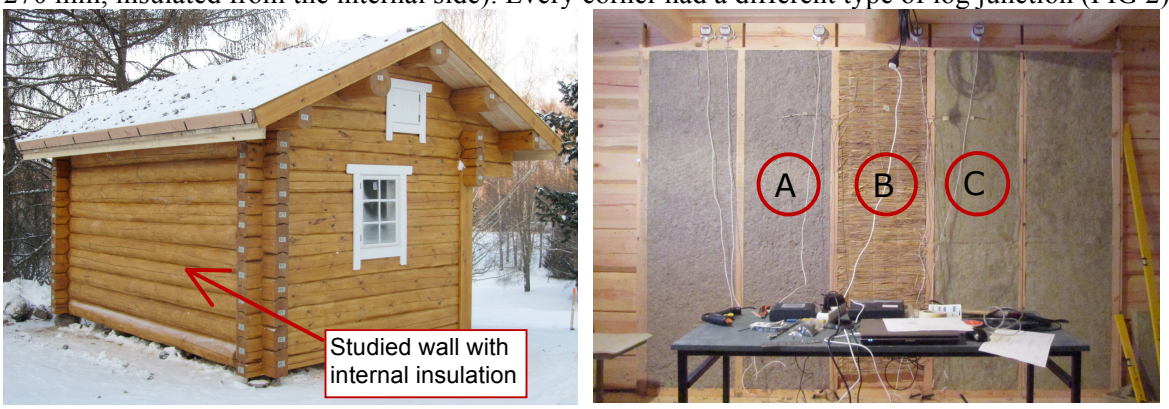

FIG 1. View of the test house from the back (left) and internally insulated wall (right).

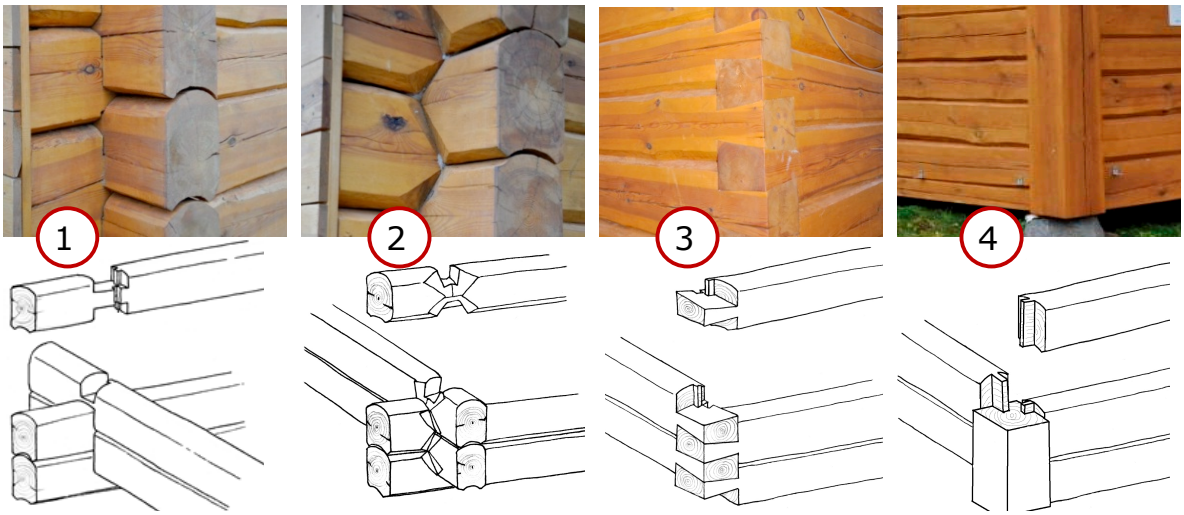

FIG 2. Different corner notches of the log wall: double notch with wind lock (1), Scandinavian saddle notch (also known as Norwegian notch) (2), dovetail notch (3) and corner post (4).

The types of corner notches were selected based on popularity among log house construction companies in Estonia. In the corner notches, a special self-expanding sealing tape for log houses (Classic Log Home Tape LHC 20-20-06) was used.

One wall was insulated internally with three different materials (FIG 1, left): mineral wool, cellulose fibre (both covered with vapour retarder and gypsum board) and reed mat with clay plaster. The internally insulated wall faced west and it was shaded with wooden boards (not present in FIG 1 (left), between the boards and the log wall there was a ventilated air gap of 250 mm) to protect the wall and sensors from direct sunlight. The indoor climate conditions created in the house were based on the results of a study in Estonian wooden apartment buildings (Kalamees, Arumägi, et al. 2011). The room was heated with an air-air heat pump with the heating setpoint of 21°C. The room was also humidified, the target of the automatic humidification system was to hold the moisture excess of 5.5g/m^3 in the winter period and 2.5g/m^3 in the summer period constant.

2.2 Measurement methods

The air tightness of the entire test building was measured with the standardized (EVS-EN13829 2001) fan pressurization method, using ‘‘Minneapolis Blower Door Model 4’’ equipment with an automated performance testing system.

A special timber framed structure with the width of 1414 mm made of 20x80 mm planks was set inside the pre-milled 50mm deep gaps in the log walls at each corner of the test house. The timber frame, ceiling and floor were sealed with a 0.15mm thick PVC-membrane with an opening of ø110mm to measure air leakage of every corner separately using an anemometer. A special self-expanding sealing tape was used to ensure the air tightness between the log wall and timber frame. In the calculations the air leakage of the plain wall was subtracted from the total air leakage rate of the corner based on the wall area and the air leakage rate of the plain wall.

To determine the air tightness of the building envelope, depressurizing and pressurizing tests were conducted. Measurements were made at 10 Pa pressure difference step from 0 to 60 Pa. An exponential trend line was calculated according to the measurement points and an exact 50 Pa reading was taken from the trend line. Measurements of every corner were repeated for 11 times during one year. The pressure difference was generated with “Minneapolis Blower Door Model 4” equipment, the air flow was measured with an anemometer (Ahlborn FVA 915 MA1; measurement range 0.2…20 m/s ±0.5%) and the pressure difference was measured with a pressure sensor (FD8612DPS; measurement range was 1 mbar (100 Pa) ±1%), both were continuously recorded with a data logger (Almemo® 2890-9) over a period of 30 s with a 1 s interval.

The values of the temperature, the RH both inside and outside the wall and the heat flux were measured over a one-year period at one-hour intervals. The following sensors were used: temperature sensors (TMC6-HD; measurement range: -40 °…+100 °C, accuracy: ±0.25 °) with HOBO U12-013 data loggers; temperature and RH sensors (Rotronic HygroClip SC05 ∅5mm×51mm, measurement range: -40 °…+100 °C and 0…100%, accuracy: ±0.3 °C and ±1.5%); and heat flux plates (Hukseflux HFP-01-05, measurement range ±2000 W/m^2, accuracy: ±5%). Measurement results were saved with a Grant Squirrel SQ2020 data logger. Together with airtightness measurements the moisture level in the logs at different heights was measured with Gann Hydromette HT 85 (with puncture probe M40, accuracy ±2%) to observe the drying out process of the logs.

2.3 Simulations

The measurement results were compared with a complex hygrothermal simulation model, WUFI 5.1 Pro. The comparison was made to validate the simulation model for future simulations with different initial and climatic conditions as well as with different dimensions of the building envelope layers.

3. Results

3.1 Air tightness of the corners and the envelope

The airtightness of the entire house was measured for seven times during a one-year period. The average air leakage rate of all measurements of the entire envelope at the pressure difference of 50 Pa was q_{50}=2.8 $m^3/(h \cdot m^2)$ (FIG 3 left) and the mean air change rate was n_{50}=5.0 h^{-1}. The air leakage rate lowered slowly over time until the two last measurements in spring; these measurements show more than 1 $m^3/(h \cdot m^2)$ higher value than before. The air-tightness of the log house is influenced by several factors: volume changes of the logs due to water vapour (de-)sorption processes, the efficiency of insulation and sealing in notches and grooves (joints of logs), accuracy of notches and grooves, tightening of walls caused by the weight of the roof, and the overall building quality. The change of airtightness in time can be explained in several ways. The reduction of air leakages was probably caused by the weight of the roof that tightened the joints between the logs (grooves and notches). By the time of the last two measurements, the weight of the roof was significantly decreased, because the thick layer of snow had melted. Another reason for increased air leakages during spring was the drying process of the logs caused by intensive solar radiation (FIG 3 left). The drying process is more intensive near the ends of the logs and therefore the shrinkage of the logs near the corners is higher and the cracks (grooves) will widen. The wider cracks near the corners increased the air leakage both of the whole house and also in every corner (FIG 3 right).

The air leakages of the corners were measured for 11 times during the study. The average air leakage rate of all measurements in every corner was 10 $m^3/(h \cdot m)$. The air leakage of the corners were (FIG 3 right):

- Scandinavian saddle notch 6.7 $m^3/(h \cdot m)$;
- dovetail notch 6.8 $m^3/(h \cdot m)$;
- corner post 10.4 $m^3/(h \cdot m)$;
- double notch with wind lock 17.3 $m^3/(h \cdot m)$.

When comparing the change of the air leakage rate in time, all the corners except the Scandinavian saddle notch started to improve after the second measurement. In the case of the Scandinavian saddle notch, it can be explained as the combination of drying of the logs (shrinkage of volume), effectiveness of sealing and tightening of the wall due to weight. During winter the snow layer added extra weight to the roof and to the wall, thus the tightening process of the corners was the greatest.

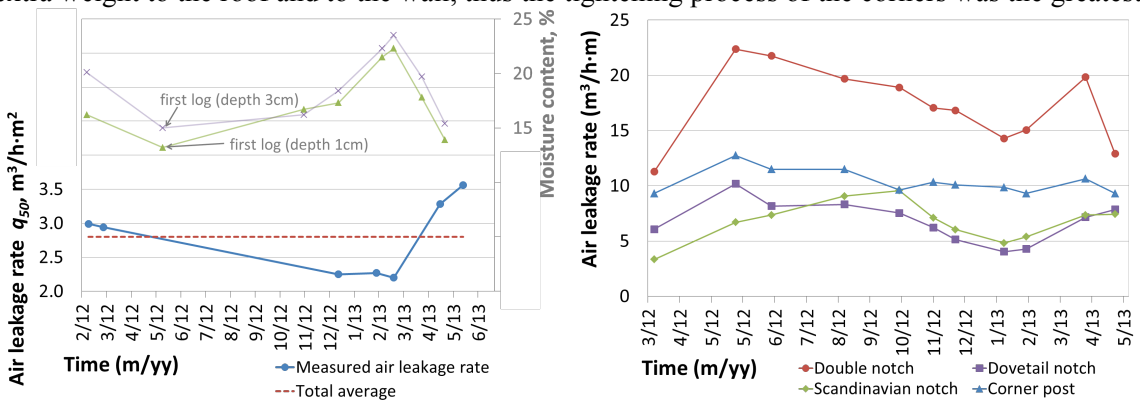

FIG 3. Air leakage rate of the total house (left) and the corners (right).

3.2 Hygrothermal performance and validation of the simulation model

The daily average outdoor microclimate near the test wall varied between -27 °C and +28 °C. The average outdoor temperature during summer (June…August) was +17.9 °C and during winter (December…February) was -4.5 °C and the RH was accordingly 72% and 89%.

Modified material properties were used from the WUFI database. Table 1 shows the properties of the materials used in comparison of the simulated measured and results when the best correlation was obtained. Although the wall was made as airtight as possible, the air change through the log wall was necessary to match the calculated results with the measured results. The air change rate of 0.3 h^{-1} was added during the cold period (November to the February). The RH level of kiln dried logs at the time of building was 21.6% at the depth of 3 cm.

Table 1. Main hygrothermal properties of the materials used in the simulation

	Wooden log	Mineral wool	Cellulose fiber	Reed mat	"Intello" membrane	Clay mortar	Gypsum board
Bulk density ρ, kg/m^3	390	60	60	136	425	1568	850
Porosity f, m^3/m^3	0.75	0.95	0.95	0.9	0.001	0.41	0.65
Specific heat capacity c, J/(kg·K)	1600	850	2000	2000	2300	488	850
Thermal conductivity λ, W/(m·K)	0.12	0.04	0.037	0.075	0.17	0.48	0.2
Vapour diffusion resistance factor μ, -	108	1.3	1.5	2.0	37500	20	8.3
Built-in moisture w, kg/m^3	65	4.5	4.5	6.0	0	100	2.0

Two methods may be used to compare the thermal performance of the test walls: to compare temperatures on the inner surface of the log, or to compare the measurement results of the heat flux plate. The simulation model and this experiment were validated in both ways. The figures below show the difference between the measured and the calculated temperatures (FIG 4), RH (FIG 5) and water vapour pressure (FIG 6) between the log wall and the insulation layer for three materials. Thin lines on both figures represent the measured values and thick lines the calculated values. There is a good correlation between the measured and the calculated results in addition to the temperature and the RH, also with the heat flux. Differences in the temperatures reflect the different thermal resistances of the insulation materials. Reed mat has higher thermal conductivity and therefore the temperatures between the insulation layer and the log wall were higher during the winter period.

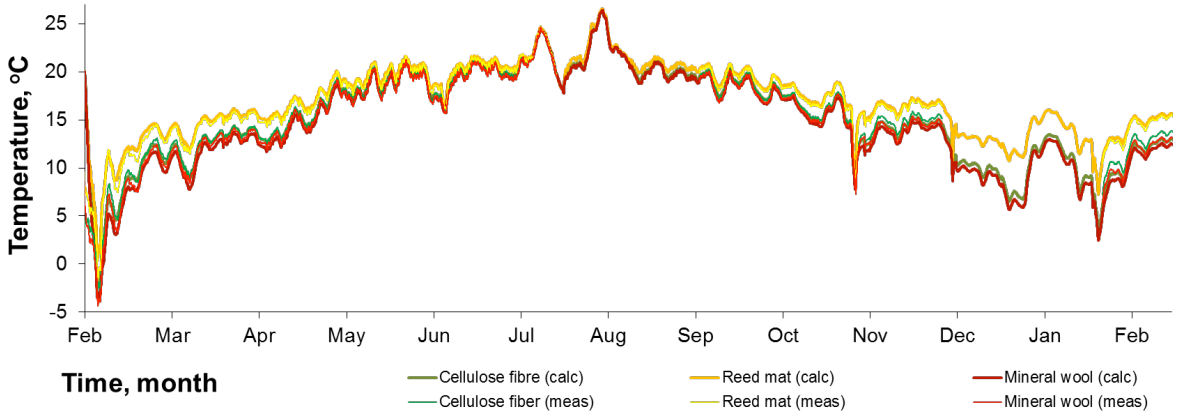

FIG 4. Measured and calculated temperatures on the inner surface of the log wall.

The log wall with an average thickness of 27 cm had a thermal transmittance of U=0.49 W/m^{2}K. After adding internal insulation, the thermal transmittance decreased to U=0.31 W/m^{2}K in the case of cellulose fibre, U=0.28 W/m^{2}K in the case of mineral wool, and U=0.36 W/m^{2}K in the case of reed mat.

The RH level of different materials was different due to different construction methods. Insulation with cellulose fibre was most critical, because it was installed by a wet spray method. While the

cellulose was covered with water vapour barrier, the drying out of moisture was also slow (about six months). The reed mat itself was dry, but the added plaster layer added a significant amount of water into the insulation layer, therefore the RH was high during the first month. The drying process was faster than in the cellulose fibre part, because the water vapour resistance of the clay layer is much lower than the resistance of the PE-membrane used for water vapour barrier on the cellulose fibre and on the mineral wool part. The mineral wool part had no additional moisture during installation and therefore the RH level was low at the beginning of the measurements. The RH level increased because of the moisture dried out from the logs. The RH in the reed mat in summer was about 10% lower than in the mineral wool and cellulose fibre because the moisture can dry out to the room side easily. In the mineral wool and cellulose fibre part the moisture mainly dried out to the external side due to air convection through the log wall, which is much more intensive during the cold period (beginning from November).

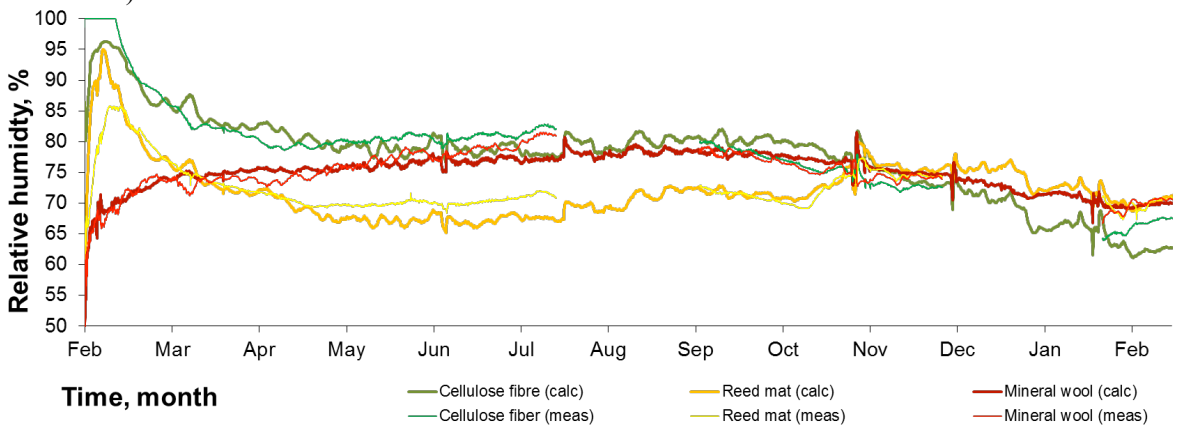

FIG 5. Measured and calculated RH on the inner surface of the log wall.

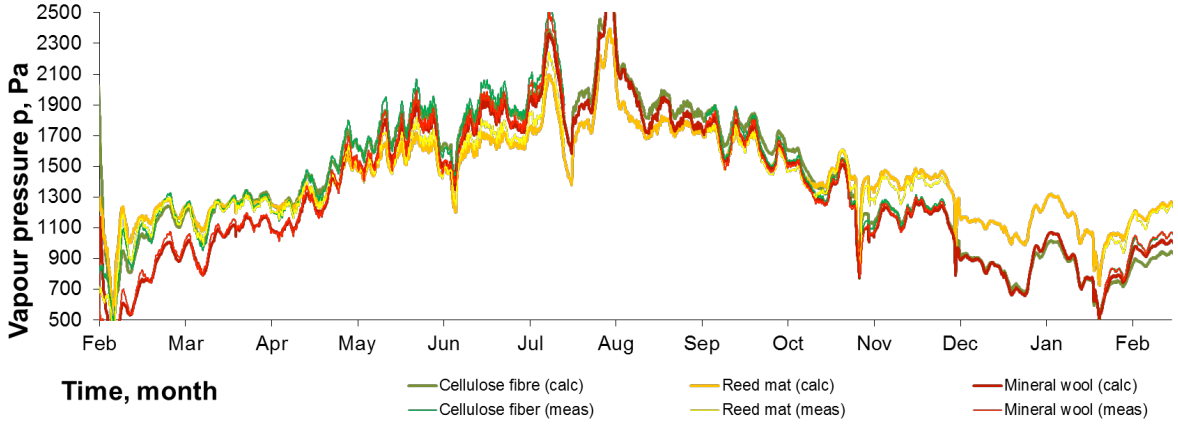

FIG 6. Water vapour pressure on the inner surface of the log wall.

The required moisture excess was guaranteed over the first half year without the use of air humidifier, caused by the drying out of the logs and the absence of ventilation. The vertical temperature gradient was small due to air movement in the room caused by the air-air heat pump.

4. Discussion

Comparison of airtightness measurements of this specially built house (2.8 $m^3/(h \cdot m^2)$) and previous measurements in the log houses in Estonia reveals substantial improvements using the new sealing method and the quality of work: the average airtightness of 12 log dwellings was 9.2 $m^3/(h \cdot m^2)$ (Kalamees 2008); the average of 35 measurements in wooden apartment buildings (made of logs) 10

$m^3/(h \cdot m^2)$ (Kalamees, Arumägi, et al. 2011) and the average airtightness of 24 old rural log houses was 15 $m^3/(h \cdot m^2)$ (Kalamees, Alev, et al. 2011).

When sealing different corners, especially the double notch with the wind lock, the placement and the choice of seal has an important role. A wide seal (15 cm) expanded less than a narrow one (2 cm). Also, the logs should be as dry as possible before erecting the house to prevent the cracks caused by the shrinking of the logs.

In this study the process and influence of the drying out of the logs on the internal insulation layer is visible (FIG 5). On the one hand, it is reasonable to let the logs dry out more easily as in reed mat part. On the other hand, the moisture level in reed mat raised to the same level as other insulation materials during the winter period when the humidifier produces extra moisture to the room to hold the moisture excess of 5.5g/m^3. In the cellulose fibre part the RH stayed above the critical level for mould growth (80%) more than half a year. The mould growth index (calculated according to Hukka & Viitanen (1999)) on the surface of the log behind the cellulose fibre insulation layer had the highest value of 1.3 during April, which means that there could be some growth detected by microscopy. After removal of insulation there was no mould growth detected visually and it was not viewed with a microscope.

5. Conclusions

The average air leakage rate of all measurements of the entire envelope at the pressure difference of 50 Pa was q_{50}=2.8 $m^3/(h \cdot m^2)$. The average air leakage rate of all measurements in every corner was 10 $m^3/(h \cdot m)$. The lowest air leakage was through the Scandinavian saddle notch - 6.7 $m^3/(h \cdot m)$, almost the same was through the dovetail notch - 6.8 $m^3/(h \cdot m)$), the corner post had much higher leakage rate of 10.4 $m^3/(h \cdot m)$ and the double notch with the wind lock was the leakiest - with 17.3 $m^3/(h \cdot m)$.

The internal insulation parts were constructed differently from the hygrothermal point of view. The mineral wool part was constructed as a dry wall, cellulose fibre was installed using a wet method and the reed mat was covered with clay plaster that added also moisture to the reed mat. Cellulose fibre and mineral wool were covered with water vapour barrier, which prevented these wall parts to dry to the room side. The reed mat with clay plaster dried out within less than a month. The RH in the cellulose fibre part was over 80% for over 6 months and the RH level in the mineral wool part had increased to the same level as in the cellulose fibre part after 6 months and both started to dry out to the external side during the winter period. During the warm period the RH was about 10% lower than in other parts, during the cold period the RH level increased at the same rate as in other parts.

The simulation models of three internally insulated log walls were validated using long-term field measurements. The WUFI was selected for the hygrothermal performance simulations. A good correlation between the calculated results and the measured values was achieved after the modification of the material properties and adding a factor as the air change rate in the material layers inside the wall. The thermal transmittance decreased by 27..43% in different internally insulated wall parts as compared to an uninsulated wall. Drying and wetting are determined more accurately if the convective air flow is included in the hygrothermal simulation model. The drying out moisture from fresh, but a kiln-dried log with an average RH level of 21.6% caused significant moisture excess to the room and increased the RH in the internal insulation layer. The validated model will be used in our further studies to focus on the performance of the internally insulated log wall in cold climates.

6. Acknowledgements

The research has been conducted as part of the projects IUT1-15 “Nearly-zero energy solutions and their implementation on deep renovation of buildings” financed by Estonian Research Council.

References

Alev, Ü. et al., 2012. Comparison of thermal performance of mineral wool and reflective insulation on internally insulated log wall. In *Proceedings of Healthy Buildings 2012*. Brisbane: Queensland University of Technology.

Alev, Ü. & Kalamees, T., 2013. Field Study of Airtightness of Traditional Rural Houses in Estonia. In M. L. Karel Kabele, Miroslav Urban, Karel Suchý, ed. *Proceedings of CLIMA 2013*. p. 6882.

Arumägi, E. et al., 2011. Field study of hygrothermal performance of log wall with internal thermal insulation. In *International Conference on Durability of Building Materials and Components. Proceedings*. pp. 811 – 819.

Arumägi, E. & Kalamees, T., 2012. Validation of a Simulation Model for Hygrothermal Performance of Log Wall with Internal Thermal Insulation in Cold Climate. In *Proceedings of 5th IBPC*. Kyoto, pp. 345–352.

EVS-EN13829, 2001. *Thermal performance of buildings—determination of air permeability of buildings—fan pressurization method.*, Estonian Centre for Standardisation.

Häupl, P., Fechner, H. & Petzold, H., 2004. Interior retrofit of masonry wall to reduce energy and eliminate moisture damage: Comparison of modelling and field performance. In *Thermal Performance of the Exterior Envelopes of Buildings IX*. Florida.

Hukka, A. & Viitanen, H.A., 1999. A mathematical model of mould growth on wooden material. *Wood Science and Technology*, 33, pp.475–485.

Kalamees, T., Arumägi, E., et al., 2011. *Eesti eluasemefondi puitkorterelamute ehitustehniline seisukord ja prognoositav eluiga*, Tallinn.

Kalamees, T., 2008. *Elamupiirete õhupidavus: Uurimistöö „Elamute õhulekkearvu baasväärtuse väljaselgitamine ja õhulekkearvu muul viisil tõendamise metoodika väljatöötamine“ raport.*,

Kalamees, T., Alev, Ü., et al., 2011. *Maaelamute sisekliima, ehitusfüüsika ja energiasääst I*, Tallinn: Tallinna Tehnikaülikool.

Ojanen, T., 2007. Low Energy Log Walls Under Cold Climate Conditions. In *Proc. Thermal Performance of the Exterior Envelopes of Whole Buildings X International Conference*. Clearwater Beach, Florida, p. 9.

Stopp, H. et al., 2001. The hygrothermal performance of external walls with inside insulation. In *Thermal Performance of the Exterior Envelopes of Buildings VIII*. Clearwater Beach, Florida.

Toman, J., Vimmrová, A. & Černý, R., 2009. Long-term on-site assessment of hygrothermal performance of interior thermal insulation system without water vapour barrier. *Energy and Buildings*, 41(1), pp.51–55.

Full paper no: 8

Apartment's air-tightness in an apartment block area from the 1960s

Dan Jönsson, PhD [1]
Dennis Johansson, PhD [2]
Hans Bagge, PhD [3]

[1] Building Services, Lund University, Sweden
[2] Building Services, Lund University, Sweden
[3] Building Physics, Lund University, Sweden

Keywords: *Air Leakage, Pressure Testing, Thermography.*

Summary

It is important that the building envelope is airtight, to prevent outside air to leak into the house and cause draught, excessive energy use and moisture convection which affects people's health and satisfaction. Increased energy use is caused by cold outside air that blows into the building which must be heated to the indoor temperature. Moisture convection can cause damage to the exterior walls and roof when warm moist air condenses inside the wall and ceiling of the exterior parts that are colder. The result for the ten apartments showed values between 0.59 to 2.29 l / (s · $m^2_{exterior}$). In today's Swedish building regulations, there is no particular requirements but a certain annual energy use is required. In other regulations there are requirements in the form of a specific value. This value should then be less than 0.3 l / (s · $m^2_{exterior}$) according the passive house regulation in Sweden and less than 0.8 l / (s · $m^2_{exterior}$) in the former building regulation. This study shows that the studied multi-family houses that were built of concrete with infill walls of lightweight concrete have a lower air leakage than a multi-family house that was built of concrete with infill walls with wood frame. Thermal imaging showed that a large leakage flow occurred at the junction between the outer wall and the concrete floor slab. This is probably due to poor sealing. In an ongoing project these apartments block will be investigated with destructive methods to help renovations and remodeling of the large existing housing stock with the construction techniques from that time.

1 Introduction

It is important that the building envelope is airtight, to prevent outside air to leak into the house and cause draught, excessive energy use and moisture convection which affects people's health and satisfaction. Increased energy use is caused by cold outside air that blows into the building which must be heated to the indoor temperature. Moisture convection can cause damage to the exterior walls and roof when warm moist air condenses inside the wall and ceiling of the exterior parts that are colder.

Air leakage as the result of poor air tightness can be measured by a pressurization test where a fan is controlled to keep a 50 Pa pressure difference between indoors and outdoors. The airflow through the fan is measured and presented with a functional unit that can be for example envelope area or floor area. The EN-13829 standard states that the resulting value should be weighted from one test with under pressure and one with over pressure. Simultaneously with the pressurization test, it is common practice to perform thermal imaging of the interior building envelope to find locations of thermal bridging and air leakage.

Swedish building regulations have subsequently introduced requirements on air leakage after the 60's. The instruction to the building regulations of 1960 does not mention any requirement for air leakage, but there is a text that a vapor barrier should be provided in the construction where required to avoid buildup of moisture in the materials contained in the building structure. In the building regulation BBR 10 2002:19 there was a requirement that the leakage flow through the building envelope must not exceed 0.8 l / (s·m^2) with the area referring to envelope area. This was replaced 2006 with a text in the current regulation BBR 19 that the building envelope shall be designed with sufficient air tightness regarding both energy use and moisture convection (The Swedish National Board of Housing, Building and Planning 1).

A lot of studies have been presented investigating the air tightness of buildings, both in Sweden and internationally. Internationally, usually, the functional area unit is the air exchange per hour at measurements pressure. An example of a Swedish survey is Stein (2008) who examined the uncertainty depending on leakage between apartments which is not described in the standard EN 13829, in a building built in 2001. In Stein's measurements of the air leakage at 50Pa pressure difference, the apartments ranged between 0.74 and 2.70 l / (s · m^2) with an average of 1.53 l / (s · m^2) referring to the exterior envelope area, and between 0.20 to 0.69 l / (s · m^2) with an average of 0.43 l / (s · m^2) referring to the interior apartment envelope area. The leakage flow per apartment volume was between 0.21 and 0.74 l / (s · m^3) which are equivalent to an air exchange of between 0.77 to 2.67 /h with an average of 1.66 ACH. Leakage flow per apartment floor area was between 0.59 and 1.97 l / (s · m^2) with an average of 1.23 l / (s · m^2).

An example of an international investigation is Kalamees (2006) who examined 32 new houses built in the years 2000-2001 in Estonia, of which only 41% passed the Estonian criterion of 3 m^3 / (h · m^2) with the function denominator area as envelope area. The leakage depended largely on leaks at holes of the air barrier and at junctions between ceilings and walls, and at junctions between exterior walls and interior walls. For the nine one floor houses the average resulting value was 1.9 m^3 / (h · m^2). The 23 houses that had professional supervision during the construction got a average value of 3.0 m^3 / (h · m^2) and the 15 houses with prefabricated wall or volume elements got an average value of 2.9 m^3 / (h · m^2). Kalamees had an average value of 4.2 m^3 / (h · m^2) for all his measurements.

The existing measurements of air tightness in buildings were generally performed in new buildings. To meet the future energy requirements of the society, there is a need for extensive energy measures and renovation in existing buildings. There is a lack of measurements of air tightness in old, existing buildings. In this study ten apartments were measured to add to the knowledge of deviations between apartments and the value and location of the leakage for houses built in the 1960's that are due to be renovated soon, and prior to such renovation, knowledge of shortcomings is important.

2 Method

For the pressurization tests, according to the standard EN 138 229, all air inlets and devices and other intentional openings through the building envelope must be sealed. Before the measurements were carried out, all supply and exhaust devices were taped and, sewage traps were filled with water and all doors and windows were closed. A Minneapolis Blowerdoor with fan model 4 was used. The fan was mounted in an outgoing balcony door. The fan was mounted in a Blowerdoor custom canvas that was stretched on adjustable aluminum rails with a rubber strip on the side facing the door frame to get it completely tight in the opening.

A pressure meter of model DG-700 measured the pressure difference between indoor and outdoor. A pc application, Tectite Express 3.1, controled the fan to obtain a set point pressure difference and another pressure meter gives the airflow through the fan. The standard specifies a number of set point pressure differences that will be tested up to 50 Pa.

The pressurization tests were carried out simultaneously with the thermal imaging with a Flir ThermoCAM 45 both before and during pressurization testing. By thermal imaging before pressurization and during under pressure indoors, the combination will make it possible to specify whether a cold spot is due to thermal bridging or cold air leaking in. Notes on the walls were used to compare cold spots before and after pressurization. When positive and negative pressure tests were carried out, the fan was set to 50 Pa for about 15 minutes so that cold outdoor air could cool down surfaces at locations with air leakage.

The apartments were located in Kiruna, northern Sweden, 500 meters above sea level and about 200 kilometers north of the Arctic Circle. Normal winter is seldom colder than -20 °C and the period of snow extends from late October to late May (Kiruna a, 2013). Predominant wind direction is between south and west, while the winds that give large amounts of snow and rain along with strong winds often come from the west or northwest (Kiruna b, 2013). Average annual temperature is -1.6 °C, average annual vapor content is 3.7 g/m^3 and the mean annual relative humidity is 76% (Elmarsson and Nevander , 2006). The residential area where the test was performed was built in the 1960s. It had natural ventilation hydronic heating with a boiler in a particular building. The residential area was built with four groups of houses surrounding a recreation area in form of a lawn with integrated playground. Each group of houses consists of three three-floor buildings and one two-floor house. The two-floor houses had lightweight concrete walls on bottom floor, gables and infills. At the second floor the end walls and the apartment separation walls were of lightweight concrete, while the remaining walls were built with wooden frame. All walls in the three-story buildings were of concrete, except for non-supporting infill walls were of lightweight concrete while the infill walls above and below the window section in the living room were built with a wooden frame. All concrete floor slab was built of concrete. On top of the attic floor a low-sloped roof was built.

3 Results

During the testing day the weather was sunny, the wind light and the temperature -6 ° C. The pressurization test showed that apartment number seven which is an apartment on the second floor of a two-floor house, has an airflow at 60 Pa of 499 l / s, compared to the nine other apartments that have a maximum airflow of between 82 and 159 l / s. The high value of apartment seven was due to a construction defect close to the shaft penetration to the attic space. Because of this large leakage in apartment seven, its result was excluded from further analysis. However, it is included in Table 2 to show the difference in airflow. Table 2 shows the leakage flows normalized to quantities depending on the different surfaces and volumes in the apartments. This is to compare the apartments with each other but also with the results of other studies. Table 1 gives the quantity description used in Table 2.

Table 1 Quantities of Table 2

Quantity	Unit	Description
V_{50}	l/s	Leakage airflow
Q_{50}	l/(s·m^2)	Leakage airflow per apartment envelope area
$Q_{50.ext}$	l/(s·m^2)	Leakage airflow per apartment exterior envelope area
$Q_{50.V}$	l/(s·m^3)	Leakage airflow per apartment volume
W_{50}	l/(s·m^2)	Leakage airflow per floor area
n_{50}	m^3/(h·m^3)	Leakage air Change rate
A_{ext}/A_O	m^2/m^2	Ratio between apartment exterior envelope and envelope area
B_{50}	l/(s·m)	Leakage airflow per concrete floor slab edge length

The study did not measure airflow to adjacent apartments which makes it impossible to compare the survey results with the requirement from the former building regulation, which specified airflow per envelope area for the entire building. Leakage airflow in apartments can also enter adjacent apartments. The flow at 50 Pa per exterior envelope area ($Q_{50, ext}$) varies between 0.59 (APT 8) to 2.29

(APT 3) l/s. APT 7 had a leakage of 1.43 l / (s · m^2) for Q_{50} while the other apartments in the test have values ranging from 0.28 to 0.45. This gives a ratio of 3 between APT 7 and APT 5 which have the highest value of the other. However, the difference is not as extensive for the leakages through the building envelope as APT 7 is located on the top floor of two-floor houses and has an exterior surface of 60 percent of the enclosing surface. It gives a ratio of 1.05 (2.4 / 2.29) between APT 7 and APT 3 which have the highest value of the other.

Table 2 Air leakage when tested with a differential pressure of 50 Pa. In the column to the right of each quantity its placement in the ranking is given. The largest value is ranked number 1.

APT	V_{50}/(l/s)		Q_{50}/(l/(s·m^2))		$Q_{50,ext}$/(l/(s·m^2))		$Q_{50,V}$/(l/(s·m^3))	
1	117,50	4	0,42	3	0,86	8	0,51	3
2	119,17	3	0,40	4	1,76	5	0,49	4
3	72,22	9	0,35	6	2,29	1	0,48	5
4	85,00	7	0,30	8	1,79	4	0,39	8
5	132,78	2	0,45	1	1,86	3	0,54	2
6	133,33	1	0,44	2	1,60	6	0,55	1
8	78,06	8	0,28	9	0,59	9	0,35	9
9	116,11	5	0,39	5	1,98	2	0,48	6
10	93,33	6	0,32	7	1,27	7	0,42	7
Max/Min	1,85		1,61		3,88		1,57	
7	438,89		1,43		2,40		1,77	

APT	W_{50}/(l/(s·m^2))		n_{50}/(m^3/m^3)		(A_{ext}/A_O)/(m^2/m^2)		B_{50}/(l/(s·m))	
1	1,28	3	1,85	3	48%	1	6,48	1
2	1,22	4	1,76	4	23%	6	4,40	7
3	1,21	5	1,75	5	15%	9	5,09	2
4	0,98	8	1,41	8	17%	8	4,48	6
5	1,35	2	1,95	2	24%	5	4,66	4
6	1,36	1	1,96	1	27%	3	4,01	8
8	0,88	9	1,27	9	46%	2	4,56	5
9	1,19	6	1,72	6	20%	7	4,95	3
10	1,06	7	1,52	7	26%	4	3,18	9
Max/Min	1,54		1,54		3,2		2,04	
7	4,42		6,37		60%		13,07	

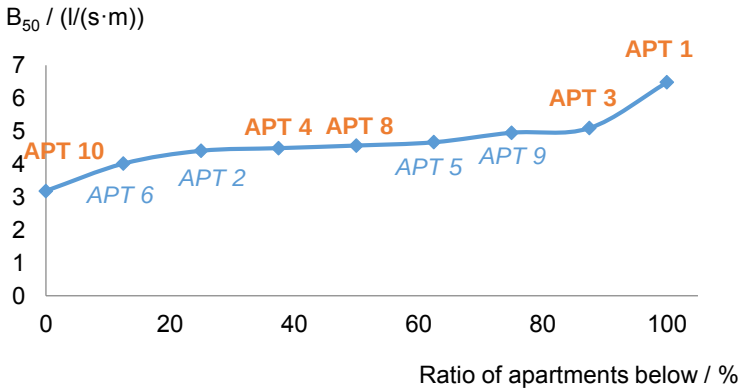

Figure 1. Leakage airflow B_{50} per concrete floor slab edge length.

Figure 1 shows apartments' leakage airflow per concrete floor slab edge length to the outdoor sorted in order. The apartments belonging to two-floor buildings is marked blue, italic, and the label is

positioned under the curve while the apartments from the three-floor houses are marked red, bold and the tag is located above the curve.

Figure 2 gives the leakage airflow parameters Q_{50}, $Q_{50,\ ext}$ and n_{50}. The values are sorted. APT 8 had the lowest leakage by 0.59 for $Q_{50,\ ext}$ and 0.28 for Q_{50} and minimum air change rate of 1.27 for n_{50} while it is different for the other apartments. APT 3 had the highest leakage of 2.29 l/ ($s \cdot m^2$) based on on exterior envelope area while APT 5 had the highest leakage based on the envelope area with an airflow of 0.45 l / ($s \cdot m^2$). Based on the envelope area, the apartments have a flow of 0.28 to 0.45 which means that there is a ratio of 1.6 between them, while based on the exterior envelope area, the airflow was 0.59 to 2.29 l / ($s \cdot m^2$) with a ratio of 3.9. APT 8 had the lowest air change rate of 1.27 /h and APT 6 had the highest of 1.96 /h, a ratio of 1.54 regarding n_{50}. APT 2, 5, 6 and 9 in the two-floor houses generally had higher leakage airflow than the apartments 1, 3, 4, 8 and 10 in the three-floor houses. This applies to both Q_{50} and $Q_{50,\ ext.}$. The ratio between the highest and lowest values was 3.9 for $Q_{50,\ ext}$, 1.5 for n_{50} and 1.6 for Q_{50}. The ratio of external wall area was lower for the apartments that had adjacent apartments on both sides and above and below compared to a gable apartment at the highest floor, which leads to a rather high difference in dynamics between $Q_{50,\ ext}$ and Q_{50}.

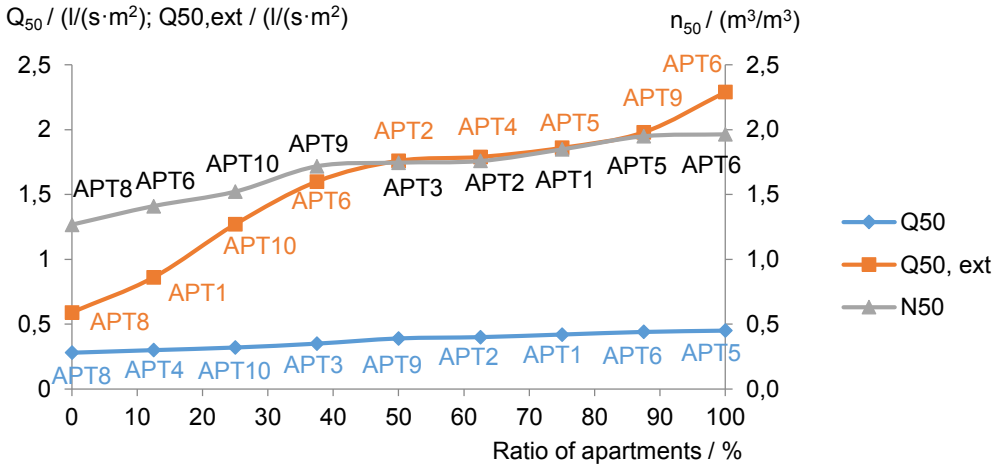

Figure 2. Leakage airflow parameters for the apartments.

APT 1 had the maximum leakage airflow of 6.48 l / (s·m) regarding concrete floor slab edge length. APT 10 had the lowest of 3.18 l / ($s \cdot m$). This gives a ratio of 2.04 regarding $B_{50,\ max}/B_{50,\ min}$. Much of the leak seemed to occur in the junctions between building elements in the apartments which Figure 3 indicates, since the leakage airflow increased with the concrete floor slab edge length in the apartments. APT 3 had 14 m concrete floor slab edge length and a leakage airflow of 72 l / s, which is the smallest in the range. APT 6 had the longest concrete floor slab edge length and the maximum leakage flow. Two points do not follow the indicated correlation line of the curve. APT 1 had a concrete floor slab edge length of 14 m and a leakage flow of 117 l / (s·m). APT 10 had a concrete floor slab edge of 29 m and a leakage flow of 93 l / (s·m), both apartments in three-floor houses. Figure 4 shows that the air change rate in the three-floor houses are overall larger than in the two-floor houses.

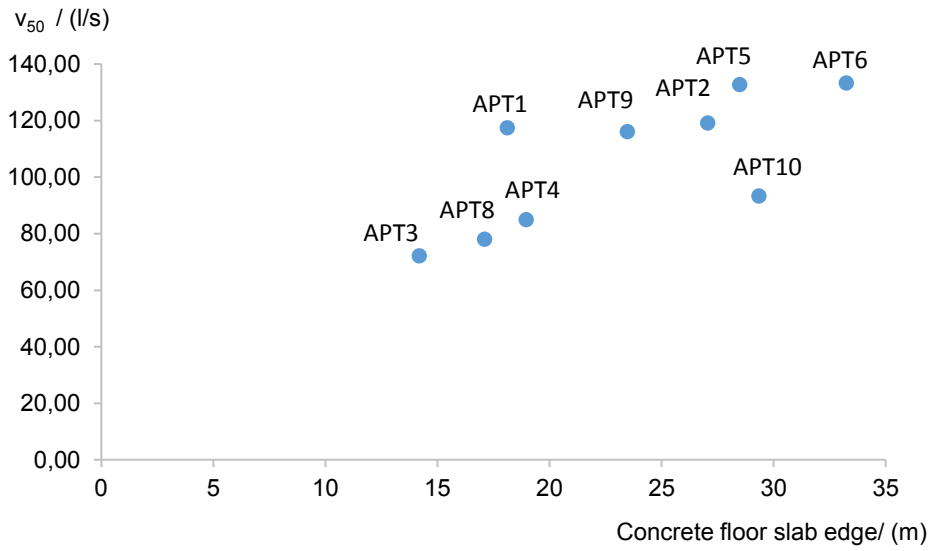

Figure 3. Leakage airflow as a function of concrete floor slab edge length.

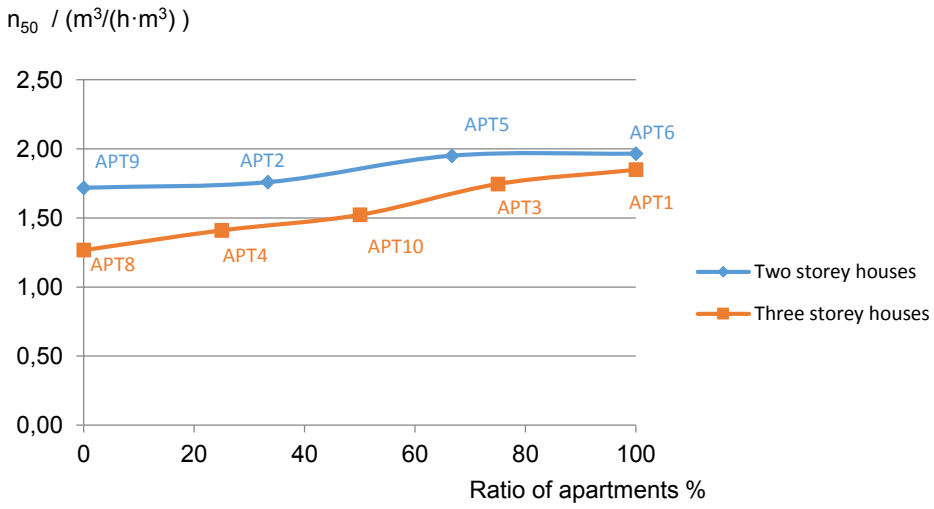

Figure 4. Air change rates.

The results of thermal imaging indicated leakage in the junctions between building elements. Figure 5 and 6 shows the outer wall of the bedroom in APT 1 where it is suspected that the seal between the wall elements and the concrete slab are not in order.

41.7°C

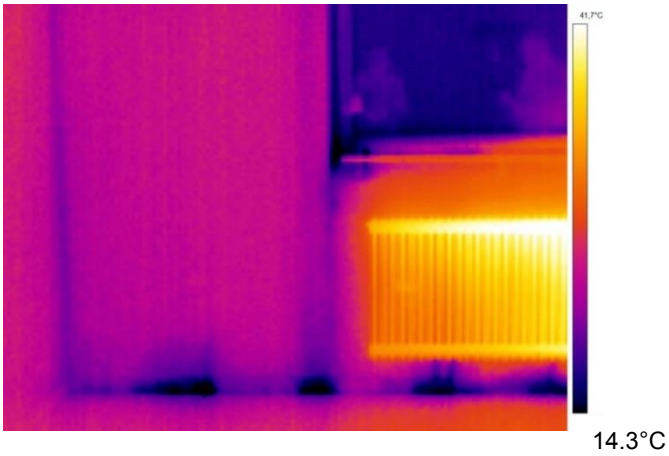

Figure 5. Left side of the bedroom in APT 1 towards outdoors.

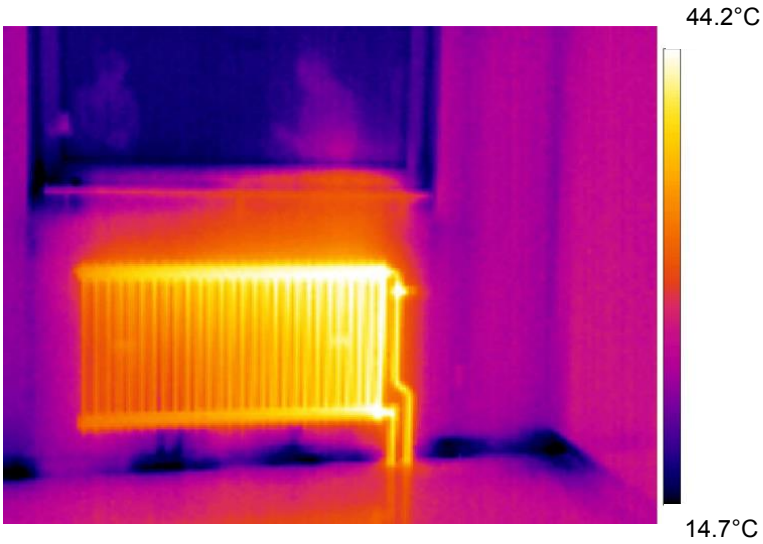

Figure 6. Right side of the bedroom in APT 1 towards outdoors.

4 Discussions and Conclusion

For the purpose of increasing the available reference material and showing variations in apartments in old, existing buildings and analyze where such leakages occur, this study measured leakage from ten apartments with the help of thermal imaging to distinguish between thermal bridging and leaks. The result from the measurements of leakage in ten apartments with one excluded due to extremely high leakage, are between 3.2 and 4.9 m^3 / (h· $m^2_{exterior}$) with an average of 4.2 m^3 / (h· $m^2_{exterior}$) to be compared with Kalamees (2007) who found an average of 4.2 for all their measurements. Kalamees however, had 41 percent below the 3 m^3 / (h · m^2 $_{exterior}$). The rather high variation between different apartments indicates a need to measure in many apartments when buildings are verified.

The comparison with Stein (2008) is interesting because the investigated building constructed in the south of Sweden in 2001 have approximately the same intensive leakage airflows as the buildings in the present study which were built about 40 years before. In comparison, Q_{50} and W_{50} were even slightly lower for the 40 years old apartments. For $Q_{50, ext}$ and W_{50}, the results are close.

According to the thermal imaging results, leakage occurred especially along the joints between the wall and floor and roof. Here, it appeared that thermal bridging and leakage points were the same in the apartments for the entire apartment stock in the studied residential area. This suggests that either the structure had been degenerated over time or that the mounting of the building elements were poorly done as it was not now sealed in a proper way. It was clear that the seal between the floor slabs and wall light weight concrete elements was not satisfactory and more or less leaked along the entire

element length. The present study as well as the study by Kalamees (2008) indicates that much of the leakage occurs along the concrete floor slab edges. The results from the studied apartments built in the 1960s when the air tightness was not regulated by building regulations give values close to the much newer building studied by Stein (2008). There was no special air sealing in the buildings. Gable walls of concrete and lightweight concrete are supposed to be airtight if there are no cracks, but infill walls built by wooden frame lack air barriers. The presently studied buildings were located in an area where cracks can be suspected due to mining below the buildings, which can have influenced the leakage but reasonably only towards higher values.

The measurements were performed in apartments without pressurization of adjacent apartments. There are several reasons for using this method that was also used in the referred literature. It is more economical to perform and there are reasons such as smell, fire, heat transfer and rebuilding to avoid leakage through the internal walls and therefore there are reasons for having requirements on apartment level. The different presented parameters show different results. N_{50} does not normalize for the size of the apartment, which Q_{50} and $_{Q50,\ ext}$ do. The shown difference between Q_{50} and $_{Q50,\ ext}$ indicates both that the ratio between them varies and that there is a leakage through internal walls that are in the same magnitude as the external walls. Even if the result from this study is a help for determining where to put efforts in a renovation, it would be interesting to extend the measurements and pressurize adjacent apartments to determine the flow patterns though different internal walls, which will be a matter of future research.

5 Acknowledgements

This study is funded by the Research Council Formas.

6 References

Stein J. (2008). Air tightness in multifamily - measurements and analysis. THID-08/5098 (In Swedish)

Kalamees T. (2007). Airtightness and air leakages of new lightweight single-family detached houses in Estonia. Building and Environment, 42 (6), pp2369 – 2377

Nevander, L.E. and Elmarsson, B. (2006). Moisture Manual - practice and theory. ISBN 9173331562 Stockholm: Swedish Building Centre Ltd

Kiruna a 2013, Climate. [www]. Retrieved from <http://www.kiruna.se/kommun/Kommun-politik/Kommunfakta/Geografi/Klimat/>

Kiruna b 2013, Event Handling new city hall. [www] . Retrieved from <http://www.kiruna.se/PageFiles/6614/134368%20t%C3%A4vlingsprogram_uppslag_low.pdf?epslanguage=sv>

The Swedish National Board of Housing, Building and Planning 1 2013, <http://www.boverket.se/Bygga--forvalta/Regler-om-byggande/Boverkets-byggregler-BBR/>

On the coupling of a zonal model with a multizone building energy simulation model

Lien De Backer, M.Sc [1]
Jelle Laverge, Ph.D [1]
Arnold Janssens, Professor [1]
Michel De Paepe, Professor [2]

[1] Ghent University, Department of Architecture and Urban Planning, Belgium
[2] Ghent University, Department of Flow, Heat and Combustion Mechanics, Belgium

KEYWORDS: *Building simulation, vertical temperature distribution, coupling, multizone model, verification*

SUMMARY:
The conditions in one zone are often treated as 'fully mixed' in Building Energy Simulation programs (BES) e.g. TRNSYS. By contrast, Computational Fluid Dynamics (CFD) are too complex and time-consuming to predict temperature and relative humidity in a building for a longer time period, such as one year. Nevertheless, several building applications require a prediction of the vertical distribution of the indoor relative humidity and temperature under transient boundary conditions. This paper presents the development and possibilities of a coupled TRNSYS-zonal model, which allows accounting the stratification in a room. The zonal model is based on the so-called block model proposed by Togari[1] and describes a one-dimensional heat and mass transfer between horizontal layers. The goal of this preliminary study was to examine the effect of parameters such as the number of layers, the value of the heat convection coefficient and the value for the time step. To validate the model, the case of natural convection in a test room (3m x 3m x 2.5m) described by Arai and Togari has been used .

1. Introduction

'Energy use' is a concept which we could not ignore nowadays: every day we are flooded with information and publicity about energy saving measures and cutting down on power consumption. However, when dealing with historical buildings, architectural and deontological criteria e.g., the rules of the Flemish monumental Guard complicate the idea of sustainability. Due to increased thermal comfort expectations from churchgoers, in recent decades heating systems have been installed in the historical church buildings. Even today the demand for new or additional heating is still large. So despite the idea of energy saving and despite the fact that a church building represents a large volume to be heated, one can ask whether heating a church is ecologically and financially wise.
There also is the additional problem that a lot of churches contain valuable and historic pieces of art. Hence, the heating systems, which often only operate during service, significantly alter the microclimate in the church and these fast-changing indoor conditions may result in a faster deterioration of the artworks. To avoid the damage of the artworks, guidelines can be found in literature for the acceptable indoor temperature and relative humidity variations (Anon 2011). To reconcile these preservation needs for the artworks with the heating demand, computer simulations provide an alternative for experiments and measurements. Because heating often leads to stratification in this type of buildings, the simulation study must correctly estimate the stratification. Therefore, the calculation of the airflow in the space is also necessary, next to the calculation of the energy exchange. To predict this temperature and humidity distribution in building, different modelling approaches have been used; namely the CFD-method and a zonal airflow model. The CFD-method is a widespread approach to simulate the airflow in a building. The models based on the CFD-method predict

accurately the temperature, velocity and other flow parameters by the Navier-Stokes equations. However, in order to assess the damage risk of art works such as wooden panel paintings, the fluctuations in temperature and humidity over a longer time period are of interest. To simulate this, the mentioned CFD models are less suitable for their need for powerful computers with a large amount of memory, even for a short-time simulation. In reality, these requirements are often not available. So to be able to predict the airflow in a building in a fast way and for a longer time period, the use of macroscopic airflow models offers a solution. In literature, several macroscopic airflow models can be found. An overview of the most common models is given by Megri and Haghighat (Megri and Haghighat 2007). The different macroscopic airflow models differentiate themselves by the simplifications they make in the conservation equations. A suitable zonal model to predict the temperature distributions in a large space is the so-called temperature zonal model proposed by Togari (Togari et al. 1993), which is based on temperature differences (Heiselberg et al. 1998).
The goal of this paper is to develop a suitable dynamic simulation tool to predict the temperature and humidity distribution in a church building. To this end, the authors expanded the Togari block-model with mass conservation equations for water vapour and integrated this zonal model into the BES-software TRNSYS v17.

2. Simplified Modelling of the vertical temperature and relative humidity distribution

The model selected for this work was first proposed by Togari et al.(Togari et al. 1993) and has been used by others (Wang et al. 2009, Arai et al. 1994, Takemasa et al. 1996). This model is a simplified model for calculating the vertical temperature distribution in a large space building. To calculate the temperature distribution in the room the model starts from a given inside wall temperature. The authors assumed the supply airstreams and the airflows along the vertical wall surfaces to be the main components of the air movement in the large space. Further, it was also assumed that the horizontal temperature was uniform, except for the regions affected by supply air jet ventilation. This zonal model would be more useful when it could be used in an energy simulation, starting from other boundary conditions than the wall temperature, e.g. given outside conditions. Therefore the zonal model was implemented in an existing BES-software. To do so, the software TRNSYS was used.

2.1 Governing equations of the zonal model

In the zonal model, the space is divided into a finite number of horizontal layers or blocks. Each layer consists of a core cell and wall cells, as displayed in

FIG 1. The core cell represents a horizontal layer and when the layer is bounded by a wall, a wall cell is defined which accounts for the mass flow along the wall. This wall cell is a fictive cell and has no dimensions. Flows are defined as positive in the upward direction and from the wall cells to the layers. There is an exchange of mass and energy between a “wall cell” and a “zone cell”, but, the conservation of momentum in the zone is not considered (Schlichting and Gersten 1979) because the velocity in the “zone cell “ is assumed to be very low.

2.1.1 Conservation of mass

The mass balance for a layer i is expressed as:

$$0 = m_s + m_e + m_{cur} + m_{lay} \qquad (1)$$

Where
- m_s net air mass flow from a source or to a sink, kg/s
- m_e net air mass flow from a jet, kg/s
- m_{cur} net air flow between the wall current and the zone, $=m_{in(i,K)} - m_{out(i,K)}$, kg/s
- m_{lay} net air flow to the layer underneath (m_{i-1}) and above(m_i), kg/s
- $m_{out(I,K)}$ mass of flow from layer i to wall current of wall K, kg/s

$m_{in(I,K)}$ mass of flow from wall current of wall K to layer i, kg/s

The mass transfer along the wall is modelled using a wall current model based on the boundary layer theory for natural convection for a vertical wall (Schlichting and Gersten 1979). The model assumes that heat convection drives mass flow $m_{out(I,K)}$ with an average temperature $T_{D(i,K)}$ from layer i to its related boundary layer (
FIG 1). To calculate $m_{out(I,K)}$ with temperature $T_{D(i,K)}$, the following assumptions were made:

$$T_{D(i,K)} = 0.75T_i + 0.25T_{w(i,K)} \quad (2)$$

$$m_{out(i,K)} = 4\,\frac{\alpha_{C(i,K)} \cdot A_{w(I,K)}}{C_i} \quad (3)$$

Where $T_{w(i,K)}$ the average temperature of the wall K adjacent to layer i, °C
T_i the average temperature of the layer i, °C
$T_{D(i,K)}$ the average temperature of the mass $m_{out(I,K)}$, °C
$\alpha_{C(i,K)}$ heat convection coefficient, W/m²K
$A_{w(I,K)}$ area of wall K adjacent to layer i, m²
C_i specific heat of the air in layer i, J/kgK

When the currents are descendent, as shown on
FIG 1, the currents flow from wall $cell_{K,i+1}$ to wall $cell_{K,i}$ and will combine with the current flow from layer i to form a total flow with mass $m_{m(i,K)}$ and an average temperature $T_{m(i,K)}$, yielding:

$$m_{m(i,K)} = m_{out(i,K)} + m_{md(i+1,K)} \quad (4)$$

$$T_{m(i,K)} = \frac{m_{out(i,K)} T_{D(i,K)} + m_{md(i+1,K)} T_{m(i+1,K)}}{m_{m(i,K)}} \quad (5)$$

Where $m_{m(i,K)}$ the mass of the wall current of wall K adjacent to layer i, kg/s
$m_{md(i+1,K)}$ the mass of the wall current of wall K adjacent to layer i+1 or i-1 to layer i, kg/s
$T_{m(i,K)}$ the temperature of the wall current of wall K adjacent to layer i, °C

Some of the air returns to the air layer i ($m_{in(i,K)}$) and some continues to the cell down/up($m_{md(i,K)}$). The splitting of the mass $m_{m(i,K)}$ into $m_{in(i,K)}$ and $m_{md(i,K)}$ is calculated by the ratio P(i,K).

2.1.2 Conservation of vapour

The moisture balance equation for a layer i can be expressed as:

$$\rho_a V_i \frac{(Y_i^{t+\Delta t,m} - Y_i^{t})}{\Delta t} = G_{lay} + G_{walls} + G_{currents} + G_s \quad (6)$$

Where G_{lay} the mass flow rate of water vapour from layer i-1 and layer i, kg/s
$= \max(m_{c,i-1}, 0)\, Y_{c,i-1} + \min(m_{c,i-1}, 0) Y_{c,i} - \max(m_{c,i}, 0) Y_{c,i} - \min(m_{c,i}, 0) Y_{c,i+1}$
G_{walls} the mass flow rate of water vapour at the wall surface K, kg/s
$G_{currents}$ the mass flow rate of water vapour of the wall current of wall K adjacent to layer i, kg/s, $= Y_{i,K} m_{in(i,K)} - Y_i m_{out(i,K)}$
G_s vapour flow produced by people, systems, activities such as washing, ...
m number of the iteration step

2.1.3 Conservation of energy

In the air the heat transfer equation can be written as:

$$V_i \frac{(\rho C)^{t+\Delta t,m} T_i^{t+\Delta t,m} - (\rho C)^{t} T_i^{t}}{\Delta t} = Q_s + Q_{lay} + Q_{cur} + Q_b \qquad (7)$$

Where
- V_i volume of layer i, m³
- Q_s heat sources or sinks, W
- Q_{lay} the heat flow due to mass transport from layer i with layer i-1 and layer i+1, W
- Q_{cur} the heat flow from or to the wall currents, W
- Q_b the heat flow from inversion between layers expressed as $q_{b=} C_b A_b (T_{(i-1)} - T_{(i)})$, W
- C_b the value obtained when a stable (2.3W/m²°C) or unstable (112W/m²°C) temperature stratification is formed
- A_b cross section area of the top or bottom layer, m²

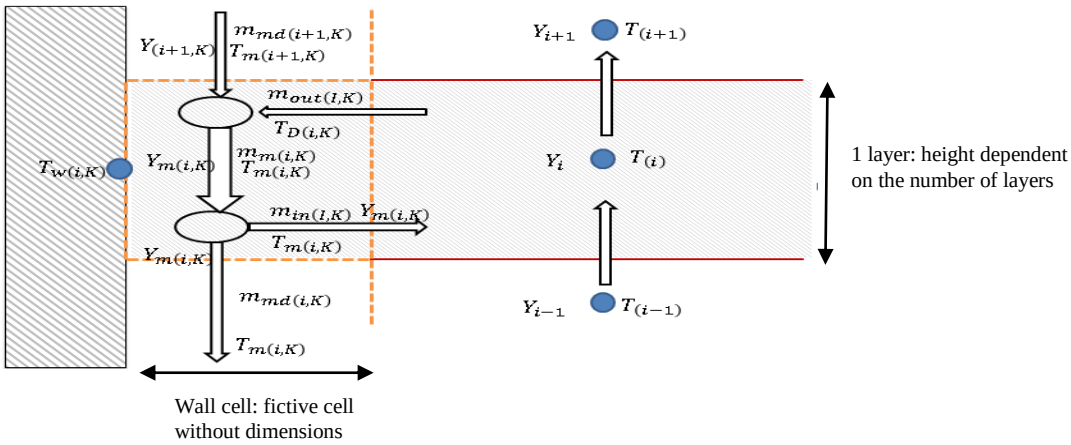

FIG 1. Schematic representation of the wall currents and air flows in one layer

2.2 Coupling of the zonal model with TRNSYS

TRNSYS (Solar Energy Laboratory 2010) is a TRaNsient SYStems Simulation program with a modular structure. Next to its own library of components, this software allows for implementing an own written component as a dynamic link library in the simulation environment, which is called 'the Simulation Studio' (SEL 2013). The multizone building model of TRNSYS is represented by 'Type 56' and calculates the heat and moisture balance of a building for given boundary conditions such as temperature, solar radiation, heat and moisture gains. The building can contain different zones. Each zone represents one or more rooms in which T and RH is typically assumed to be well-mixed.
The zonal model is written as a new component for TRNSYS v17. This version of TRNSYS has the possibility to divide one zone into several air nodes (Solar Energy Laboratory 2012). Each air node of the building model must be connected with a layer in the zonal model. FIG 2 shows a schematic overview of the procedure used to couple the thermal zonal model with the building energy simulation program TRNSYS. The interior surface temperature (T_{si}) and the heat transfer coefficient (h_{is}) act as boundary conditions for the zonal model. Initial values of the temperature and relative humidity from each air node are used as an input of the zonal model, together with the vapour mass flux of the walls. This can be done by the implementation of a HAM-model for TRNSYS(Steeman 2010) or by using a simplified model provided by TRNSYS.

Once the boundary conditions are given to the zonal model, the latter calculates the wall currents and the heat and mass conservation equations for all the layers until convergence is reached. As a convergence criterion, the maximum temperature difference in the layers between successive iterations is chosen. Afterwards, the net heat and moisture gain for every layer is passed on to the multizone building model (TRNBuild). So the coupling of the BES-software with the zonal model consists of a convective heat and water vapour gain for every air node in TRNSYS calculated by the zonal model. Looking closer to the heat conservation in TRNSYS, TRNSYS calculates in every air node a convective heat gain. To avoid to count in twice this heat gain (one by the wall currents in the zonal model and one by TRNSYS), the convective surface heat flows calculated by TRNSYS may not be taken into account. Therefore, this value also has to be passed to the zonal model, in which it will be taken into account. The radiative heat gain, which is decoupled of the convective heat gain, will be calculated by TRNSYS.

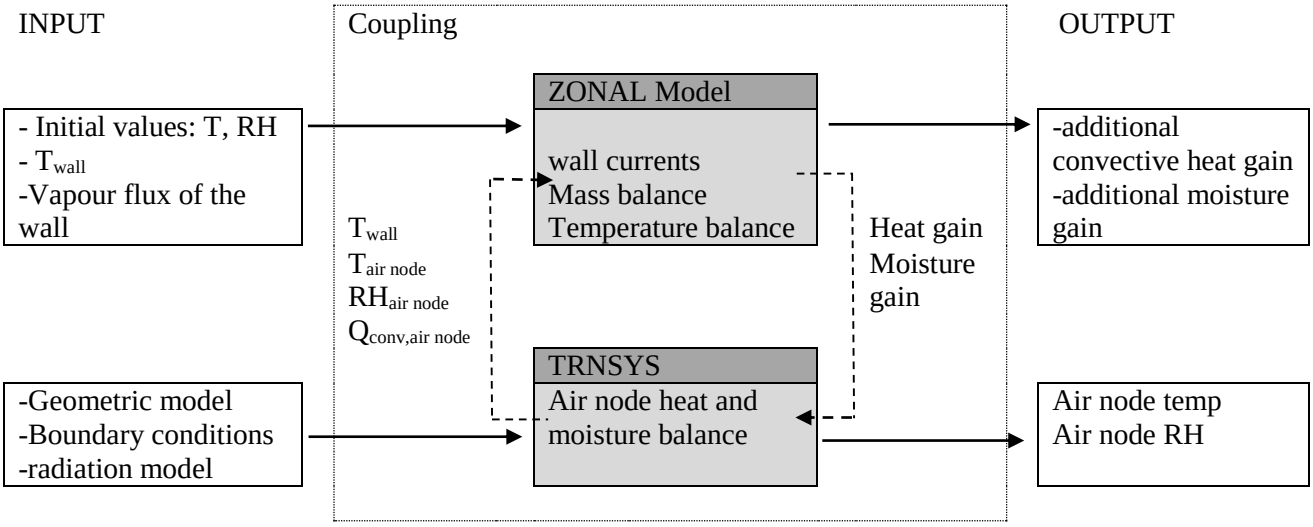

FIG 2. Schematic overview of the coupling between the multizone building model in TRNSYS and the developed thermal zonal model.

3. Initial results

3.1 Test case

The case studied in this paper was the case that can be found in the report of Togari et al. (Togari et al. 1993) and that of Arai et al.(Arai et al. 1994) which was used for evaluating the implemented model. The geometrically simple test room had a ground plane of 3m x 3m and measures 2,5m in height. The room consisted of insulation boards (three vertical walls, a ceiling and a floor) and one glass wall. In the wall opposite to the glass wall, two openings were foreseen in the symmetry plane: a supply inlet at 0,625 m above the floor and a return outlet at 0,250m above the floor. Several configurations were measured in this test room e.g. air heating or cooling and natural convection.
To validate the calculated results of the newly implemented model, the natural convection case (N10) has been used in this paper. In this case, the temperature outside the room was kept at about 12°C and was then raised to 42°C, while 24 hours later it was again lowered to 12°C. The response of the test room was monitored, while no air was supplied into the room. The moisture transfer between the air wall surface and the air was not considered in this case study.
The first calculation with the zonal model was a steady-state calculation of the layers temperature using the measured interior surface temperatures at two hours of testing as boundary conditions.

Measured surface temperatures according to TABLE 1 were used together with constant heat transfer coefficients. The coefficient was 3.5 W/m²K for the glass wall and the insulated wall. For the floor and the ceiling, the coefficient was 4.6W/m²°K when heat flow was upward, and 2.3W/m²K when the heat flow was downward. The calculated temperatures are given in TABLE 1. These results show that the average room temperature was slightly overpredicted. This could be due to the constant heat transfer coefficients and the use of a C_b coefficient for stable or unstable stratification.

TABLE 1.Measured temperature for the wall and glass surface and the zone temperature at different heights (0,25m – 0,75m – 1,25m 1,75m 2,25m) in the test case presented by Togari and the calculated temperature in the zonal model.

height (m)	$T_{zone0.25m}$ [°C]	$T_{zone0.75m}$ [°C]	$T_{zone1.25m}$ [°C]	$T_{zone1.75m}$ [°C]	$T_{zone2.25m}$ [°C]	T_{wall} [°C]	T_{glass} [°C]	$T_{calculated}$
0.25	16.7	16.9	17.1	17.4	17.6	16.3	28.4	17.4
0.75	17.4	17.5	17.6	18	18.5	17.2	27.7	18.8
1.25	18.2	18.1	18.4	18.9	19.1	17.9	27.6	19.5
1.75	19.9	19.2	19.2	19.4	19.7	18.1	26.2	20.1
2.25	19.5	19.5	19.9	20.1	20.1	17.9	27.2	20.8

The next step was to perform a dynamic calculation taking transient terms in eq.6 and eq.7 into account. For that, 48 hours were simulated with coupled TRNSYS - zonal model. The goal of this study was to examine the effect of physical and numerical parameters such as the thermal resistance of the walls, the value of the heat convection coefficient, the number of layers and the value for the time step. In this case, the full test room was modelled.
Because material parameters were unknown, several compositions for the walls were tested. Good agreement was found for the thermal resistance R=1.6 m²K/W for the insulated walls and with the glass wall as a massless layer. However, the surface temperature of glass was slightly under predicted. On FIG 3, results were depicted for the first seven hours in which outdoor temperature was raised from 12 to 42°C. The measured outdoor temperature served as boundary conditions, while the temperatures for the insulated walls and the glass surface were calculated by TRNSYS. This was opposite to the calculated results of Togari in which all interior surface temperatures at each time step (one hour) were given by the experiment (steady-state calculation for every hour). The calculated results were compared to the measurements and the calculations of Togari (FIG 3). The zone temperature was lower than was seen in the calculations of Togari, which was probably due to the lower surface temperatures of glass and the dynamic character of the calculation (Togari adapted the boundary conditions every hour based on his measured results).
On FIG 4, the effect of the number of layers on the zone temperature and relative humidity was visualised. The temperature and the relative humidity in the zone represented the values for whole the volume. The more layers, the more the stratification was detailed. Further, it could be noticed that the number of layers has an impact on the zone temperature and the surface temperature of the floor and the ceiling. The more layers, the higher the temperature and the lower the relative humidity became. In future, further research needs to be done on the allowed maximal number of layers. Next, the effect of the time step has also been investigated, which had no effect on the calculated results, and the value of the heat convection coefficients (FIG 5). In the first calculation, heat transfer coefficients were considered as simple constant values as described earlier. In the second calculation, heat transfer coefficients were adapted for every time step based on the temperature in the layer. In first instance

the algorithms for natural convection proposed by TRNSYS were used. Using these algorithms led to a slower heating up and a slower cooling down.

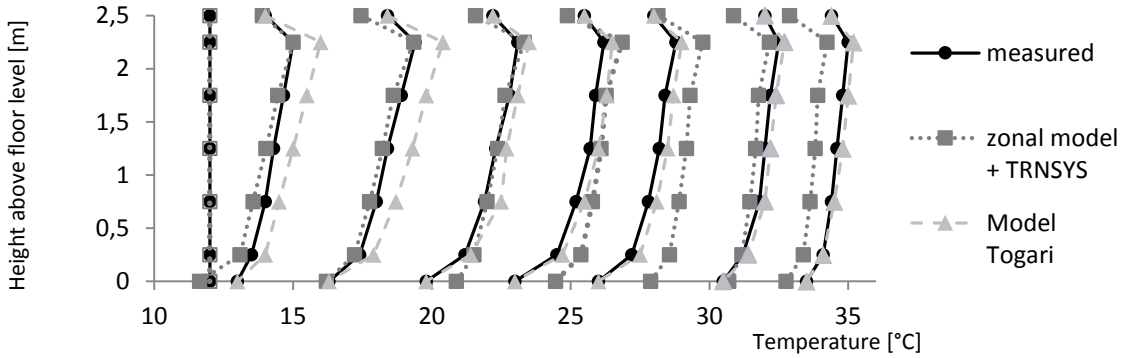

FIG 3:Comparisons between calculated values, measured values and the calculations of Togari in case where outside was heated for every hour, during seven hours(N10).

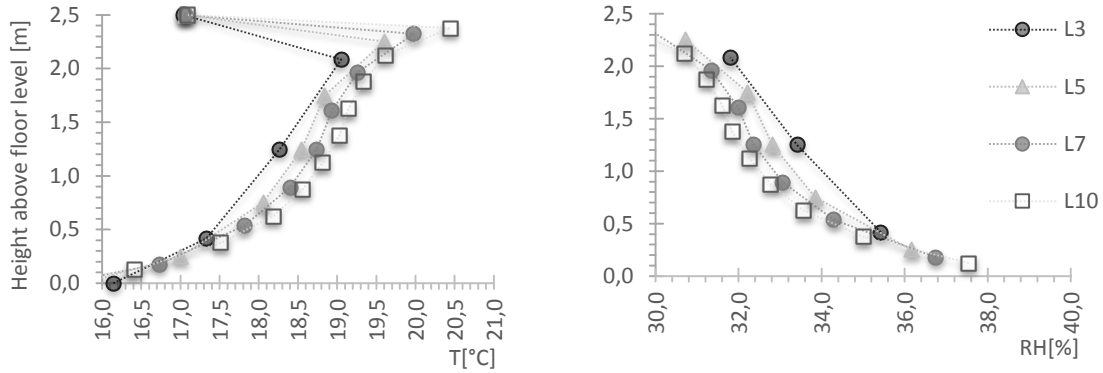

FIG 4: Comparison between the calculated temperature and relative humidity after two hours of heating for a different number of layers.

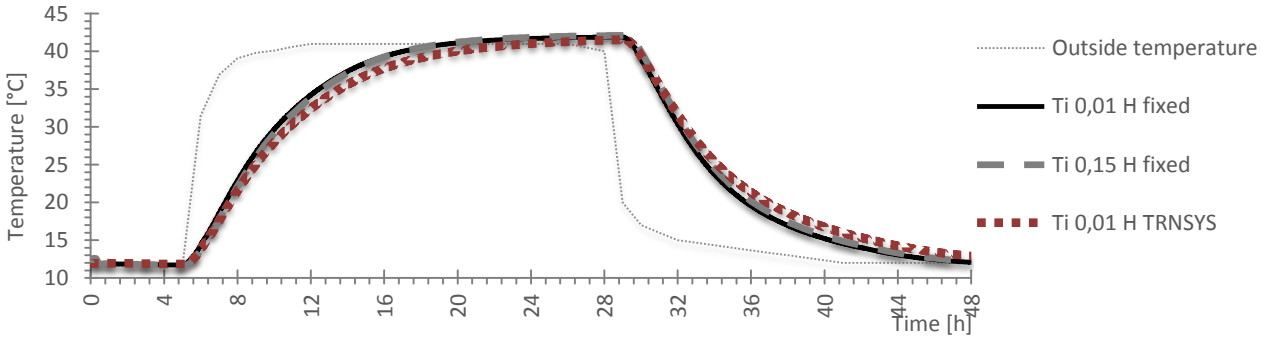

FIG 5. Comparison between the calculated values with a time step of 0,01h and 0,15h and between a constant heat transfer coefficients and the heat transfer coefficients calculated by the algorithms from TRNSYS

4. Conclusion and further work

Currently the thermal-zonal model is operational in the version of TRNSYS v17. This version of TRNSYS has the possibility to divide one zone into several air nodes. For each air node, the zonal

model defines a convective heat gain and a gain in vapour mass. To validate the zonal model, the case of natural convection described by Togari was used. The initial testing has been positive in order of the prediction of the temperature stratification. However, some fundamental work still must be done. As shown, the results are dependent of the choice of heat transfer coefficient and the number of layers. Also the choice for the Cb coefficients will have an impact. For these parameters, a more detailed sensitivity analysis will be done. Further must it be kept in mind that the model is a simplification, in which some assumptions were made such as the value of the C_b coefficient. Also, if the number of layers increase, one can question the physical background accepted in the simplifications. So the allowable number of layers and the choice of the C_b coefficient need further study.
In the next stage the model will also be further developed. The equations for the jet flows will be implemented and there will also be looked at the possibility to combine the model with TRNFLOW in order to make more complex models.

References

Anon (2011) 'ASHRAE handbook: Heating, ventilating, and air-conditioning applications, SI edition' in, American Society of Heating, Refrigerating and Air-Conditioning Engineers, 23.1-23.22.

Arai, Y., Togari, S. and Miura, K. (1994) 'Unsteady-state thermal analysis of a large space with vertical temperature distribution', *ASHRAE Transactions,* 100(part 2), 396-411.

Heiselberg, P., Murakami, S. and Rulet, C.-A. (1998) *Annex 26: Ventilation of large spaces in buildings. Part 3. Analysis and Prediction Techniques*, *Denmark, Aalborg, Aalborg University*

Megri, A. C. and Haghighat, F. (2007) 'Zonal Modeling for Simulating Indoor Environment of Buildings: Review, Recent Developments, and Applications', *HVAC&R Research,* 13(6), 887-905.

Schlichting, H. and Gersten, K. (1979) *Boundary-Layer Theory,* Seventh Edition ed., New York and London: MacGraw-Hill.

SEL, U. o. W.-M. (2013) 'A TRaNsient SYstems Simulation Program TRNSYS 17', [online], available: http://sel.me.wisc.edu/

Solar Energy Laboratory, U. o. W.-M. (2010) TRNSYS 17: A Transient System Simulation Program,

Solar Energy Laboratory, U. o. W.-M. (2012) *Mult izone Building modeling with Type56 and TRNBuild*, Volume 5, Solar Energy Laboratory, University of Wisconsin-Madison.

Steeman, M. (2010) *Hygrothermal modelling for building energy simulation applications*, unpublished thesis Ghent University.

Takemasa, Y., Togari, S. and Arai, Y. (1996) 'Application of an unsteady-state model for predicting vertical temperature distributions to an existing atrium', *ASHRAE Transaction,* 102(part 1), 239-247.

Togari, S., Arai, Y. and Milura, K. (1993) 'A Simplified Model for Predicting Vertical Temperature Distribution in a Large Space', *ASHRAE Transaction,* 99(part 1), 84-90.

Wang, X., Huang, C. and Cao, W. (2009) 'Mathematical modeling and experimental study on vertical temperature distribution of hybrid ventilation in an atrium building', *Energy and Buildings,* 41(9), 907-914.

Full paper no: 10

A heat-airflow model for simulating the effects of air leakage on the temperature field in porous insulation

Clément Belleudy, Ph.D. Candidate [1,2,3]
Ahmad Kayello, M.A.Sc. Candidate [2]
Monika Woloszyn, Professor [1]
Hua Ge, Assistant Professor [2]
Paul Fazio, Professor [2]
Marx Chhay, Ph.D. [1]
Daniel Quenard, Ph.D. [3]

[1] LOCIE, CNRS UMR 5271, Université de Savoie, Chambéry, France
[2] CZEBS, BCEE, Concordia University, Montréal, Canada
[3] CSTB, Saint-Martin-d'Hères, France

KEYWORDS: **air leakage**, **building envelope**, **numerical model**, permeability, heat loss, defect

SUMMARY:
Air leakage through the building envelope can result in an increase in energy consumption and in potential moisture damages. In this paper, the development of a simplified coupled heat-airflow model is presented. The model is applied to a ceiling section insulated with blown-in cellulose, separating an attic space from a heated indoor space. This ceiling section, part of a full scale test-hut built in an environmental chamber, is tested experimentally with and without air leakage, where temperature sensors in the cellulose provide a map of the temperature profile at various locations about the air leakage point. A comparison of the experimental data and the simulation results is performed.

1. Introduction

Ineffective design and poor workmanship can both lead to a dramatic decrease in building's air tightness. Occupants can also inadvertently create additional openings in the building envelope after the building is delivered. Excessive air leakage can result in significant heat losses, as well as condensation formation and mould growth in the building envelope. Statistical surveys carried out in France over the past decade identified the areas of the building envelope where air leakage is more often observed (Litvak, 2005). Excluding electrical conduits and thin gaps between window frames and the walls, airflow due to air leakage through building defects generally flows through the insulation material. The model developed here aims to assess the effect of the airflow on the temperature profile in porous insulation materials. Following a brief overview of the existing research work on heat-airflow coupling, the governing equations, geometry, and boundary conditions of the model are presented. A comparison between the experimental data and the simulation results demonstrates the ability of the model to predict the temperature conditions in the insulation.

2. Numerical model

2.1 Current state

The influence of air leakage on the performance of porous insulation has been investigated since the late eighties. An experiment conducted at the Fraunhofer Institute of Holzkirchen showed that a 1 mm crack in an air membrane placed on fibrous insulating material could reduce its effective R-value by a factor of 4.8 (Wagner, 1989). Langlais et al. (1990) presented a numerical model to assess natural

convection within horizontally placed mineral wool insulation caused by temperature gradients between the indoor and outdoor air.

Follow-up research has focused on different wall configurations with cracks on the interior and exterior sheathings to investigate different air paths through insulation materials (Buchanan & Sherman, 2000; Abadie et al., 2002). Svoboda (1999) developed a 2D model which accounts for heat and air transfers, introducing a convective linear thermal transmittance $\psi_{\Delta P}$ similar to the linear heat loss coefficient of a thermal bridge. Similar work has been done by Barhoun (2006), who developed a simplified model of a wall subjected to air leakage (inlet at the bottom, oulet at the top) and calculates an effective U-value accounting for this defect. More recently, several heat-air-moisture (HAM) models have been developed, some with a uniform flow rate on the whole wall section (van Schijndel, 2008; Li et al., 2009; Tariku et al., 2010), and some modeling air fluxes through cracks between different materials of wall assemblies (Saber et al., 2012). Moreover, Langmans (2013) developed a 2D HAM model, implemented in the software Delphin simulating airlfow entering and exiting cracks located in a wall's vapour/air barrier, flowing through fibrous insulation material in the wall, and assessing its impact on the wall drying capacity.

The objective of this research is to develop a HAM model versatile enough to deal with two-dimensional airflow through both porous media and through thin air gaps, while implementing suitable boundary conditions with respect to the defect configuration. This could aid in development of guidelines for modeling various permeability defect configurations and can lead to a catalog similar to those for thermal bridges. The flow through a thin crack will be dealt the same way as through a porous medium, using an equivalent permeability based on Poiseuille law. The first step of our work, presented in this paper, is a heat-air (HA) model applied to a permeability defect where air enters a porous medium via an opening in the air barrier and exits through an open interface.

2.2 Governing equations

To describe coupled air and heat transfer in porous insulation, classical conservation laws are used. All properties are averaged on representative elementary volumes (REV) within the continuous medium approximation (Bories et al., 2008). This allows the local mass, momentum and heat conservations equations to be written using partial differential equations (PDE). The continuity equation on a REV is

$$\frac{\partial \rho_{air}}{\partial t} = -\nabla \cdot (\rho_{air} \times v) \text{ which reduces to } \nabla \cdot v = 0 \text{ for incompressible flow} \quad (1)$$

where ρ_{air} density of dry air (kg/m^3), assumed incompressible
v intrinsic velocity of air (m/s)

In the case of a porous medium, the REV contains matter in both solid and fluid states. Therefore, an averaged velocity over this volume, called the Darcy velocity (u), is introduced. The Dupuis-Forchheimer relationship provides the link between v and u:

$$u = \varepsilon \times v \quad (2)$$

where ε porosity of the material

Therefore, (1) becomes:

$$\nabla \cdot u = 0 \quad (3)$$

The momentum conservation for laminar airflow is described by the Navier-Stokes equation, which is highly nonlinear and often solvable only with numerical methods.

$$\rho_{air} \frac{\partial v}{\partial t} + \rho_{air} (v \cdot \nabla)\, v = -\nabla P + \mu\, \Delta v - \rho_{air} g \quad (4)$$

where P air pressure (Pa)
μ dynamic viscosity of air (Pa·s)
g gravity acceleration (m/s^2)

For a flow through a porous medium, an additional drag due to the resistance of porous matrix against the flow appears. This drag is described by a volume force in the Navier-Stokes equation. For a pore Reynolds number of order unity or smaller and for incompressible steady-state flow, neglecting edge effects, the momentum equation is called Darcy law, which is widely used:

$$0 = -\nabla P - \frac{\mu}{k_{mat}} u \tag{5}$$

where k_{mat} permeability of the material (m^2)

To deal with interfaces between a porous material and air, taking into account the shear induced momentum transfer is required (Nield and Bejan, 2006; Vafai and Thiyagaraja, 1987). As in Navier-Stokes equation, a Laplacian term is added. The transient Darcy-Brinkman equation is written as follows:

$$\frac{\rho_{air}}{\varepsilon}\left(\frac{\partial u}{\partial t} + (u \cdot \nabla)\frac{u}{\varepsilon}\right) = -\nabla P - \frac{\mu}{k_{mat}} u + \mu\, \Delta u \tag{6}$$

The pore Reynolds number provides information on the flow regime in the porous medium and is expressed as

$$\mathrm{Re}_p = \frac{L_c \rho_{air} u}{\mu_{air}} \tag{7}$$

The characteristic length (L_c) for the flow can be approximated by the square root of the material permeability (Nield and Bejan, 2006).

$$L_c = \sqrt{k_{mat}} \tag{8}$$

In building physics, the infiltration/exfiltration air velocity driven by pressure differences typically do not exceed 0.5 m/s (Chan et al., 2003). For our experiment, given that the permeability of cellulose insulation is 7.67×10^{-10} m^2 (Trechsel, 2011) and the inlet airflow rate is 2 or 5 LPM (see section 3):

$$\mathrm{Re}_p = 4.8 \;\rightarrow\; 1 < \mathrm{Re}_p < 10 \tag{9}$$

For Re_p>10, the flow regime is still laminar but the friction drag becomes quadratic as described in the Forchheimer equation:

$$\frac{\rho_{air}}{\varepsilon}\left(\frac{\partial u}{\partial t} + (u \cdot \nabla)\frac{u}{\varepsilon}\right) = -\nabla P - \frac{\mu}{k_{mat}} u - c_F k_{mat}^{-1/2} \rho_{air} |u| u + \mu\, \Delta u \tag{10}$$

where c_F dimensionless constant

Because this transition is quite smooth, and our velocity is much smaller in the vicinity of the inlet because of widening of the air section, we will use (6) in our model (Nield and Bejan, 2006). The diffusion-convection equation is written in the general form:

$$\frac{\partial h}{\partial t} = -\nabla \cdot (q_{conduction} + q_{convection}) \tag{11}$$

Where h volume enthalpy (J/m^3)
$q_{conduction}$ heat conduction flux density (W/m^2)
$q_{convection}$ heat convection flux density (W/m^2)

The first step is to determine whether thermal equilibrium can be considered between fluid and solid phases of the insulation. If not, two coupled equations with a sink and source term must be considered to describe the heat transfer between the two phases. The temperature of the solid matrix, T_s, and the temperature of the fluid, T_f, would be the dependent variables. For an airflow velocity of 0.08 m/s at T_f= 0ºC passing through glass fiber insulation at 25°C, it has been proven (Buchanan and Sherman, 2000) that the air reaches the temperature of insulation at a distance of 1.5×10^{-5} m from the inlet. This assumption is made for this study. The heat balance equation is a follows:

$$\rho_{mat} c_{mat} \frac{\partial T}{\partial t} = -\nabla \cdot (-\lambda_{mat} \nabla T) - \nabla \cdot (\rho_{air} c_{p_{air}} T\, u) \qquad (12)$$

Where ρ_{mat} density of the material (kg/m^3)
c_{mat} specific heat of the material (J/kg·K)
λ_{mat} thermal conductivity of the material (W/m·K)

3. Experimental Setup

A test hut built inside an environmental chamber at Concordia University provides the experimental setup for this study. The test hut contains an unvented attic space insulated at the ceiling level with 380 mm of blown-in cellulose above 38 mm of rigid polyisocyanurate (PIR). The PIR also acts as the air and vapor barrier of the ceiling. To simulate air leakage, sampler pumps installed in the indoor space are used to continuously deliver indoor air into the attic space at a controlled rate. The air is supplied at the bottom of the cellulose insulation through an orifice in the PIR using a tube with a 6.4 mm inner diameter. In the case where there is no airflow into the attic, the orifice is sealed with tape at bottom of the PIR.

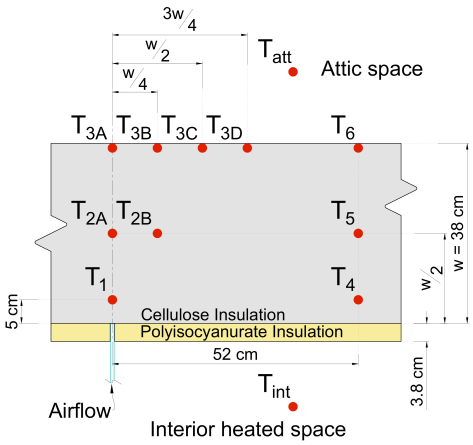

FIG 1. Location of temperature sensors across the ceiling

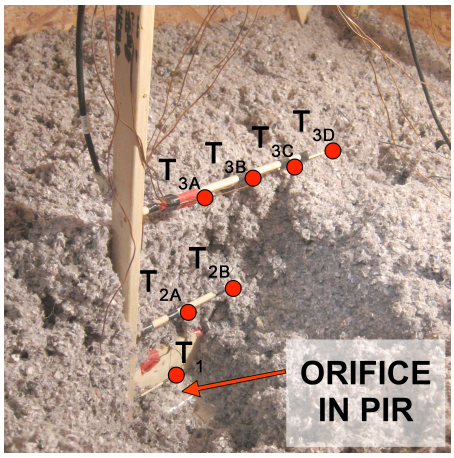

FIG 2. Temperature sensors held in place with a low-profile wooden support system

Figure 1 shows the location of the temperature sensors in the indoor, ceiling, and attic space. T_{att} and T_{int} are the attic and indoor space temperature sensors, respectively. A way to indirectly map air leakage through building components is to measure temperature in the vicinity of the hole (Desmarais et al., 2000), so the remaining sensors are located within the cellulose insulation at three different heights and at various horizontal distances away from the air leakage orifice in the PIR. T_{att}, T_{int}, T_{3A} and T_6 are resistive temperature detectors embedded in relative humidity sensors with an accuracy of ±0.3ºC. The other temperatures are measured by thermocouples (30AWG, NSB special limits of error

±0.5ºC). The temperature sensors in the cellulose insulation are supported by a thin wooden structure to ensure proper placement of the sensors without risk of displacement (Figure 2). Horizontal wood members less than 10 mm in diameter support the sensors at each of the three heights in the cellulose insulation; the horizontal members are themselves supported by vertical members at least 100 mm away from the sensors. The indoor and outdoor temperature conditions were maintained at 22ºC and 5ºC, respectively. The air leakage rates used are 0, 2 and 5 LPM. At each air leakage rate, thermal steady-state conditions are attained.

4. Numerical simulation

The model in this study uses COMSOL's built-in physics of "heat transfer in porous media" and "Brinkman equations" to implement the conservation equations in the different domains as described in section 2. To reduce computational time, the transfer phenomena are considered to be rotationally symmetric about the longitudinal axis that starts at the air orifice and points upward, neglecting therefore the thermal bridge induced by the truss and wooden structures supporting the sensors (Figure 2). The simulation is therefore performed on a 2D axisymmetric plane, creating the 3D rotational polar coordinate system.

TABLE 1. Input Parameters

Parameter	Symbol	Units	Value	Source/Note
Thermal conductivity of cellulose	λ_{cel}	W/(m·K)	0.038	Manufacturer
Thermal conductivity of PIR	λ_{poly}	W/(m·K)	0.022	ASHRAE
Thermal conductivity of air	λ_{air}	W/(m·K)	0.026	At 20°C
Dynamic viscosity air	μ_{air}	Pa·s	1.8×10^{-5}	At 20°C
Surface film coefficient int.	h_{int}	W/(m^2·K)	9.26	ASHRAE
Surface film coefficient attic	h_{attic}	W/(m^2·K)	4.32	ASHRAE
Permeability of cellulose	k_{cel}	m^2	7.67×10^{-10}	(Trechsel, 2011)
Porosity of cellulose	ε_{cel}	-	0.95	CSTB (Optimob)
Air density	ρ_{air}	kg/m^3	1.2	At 20°C
Thermal capacity air	cp_{air}	J/(kg·K)	1006	Assumed constant

Boundary conditions for air and heat must be chosen on each boundary. The measured temperatures T_{int} and T_{att} are used as boundary conditions for the model. To simplify the geometry, polyisocyanurate insulation has been integrated as thermal boundary condition with the interior surface film coefficient in an equivalent global heat transfer coefficient (Figure 3):

$$h_{eq} = \frac{1}{R_{polyiso} + \frac{1}{h_{\text{int}}}} \tag{13}$$

The interior temperature is imposed at the entrance of the hole, and both open boundary and natural convection are assigned to the top of the cellulose. The heat flux brought by air can both enter and leave the domain on interfaces with the thermal open boundary condition (COMSOL, 2011):

$$\begin{cases} T = T_{att} & \text{if} \quad n \cdot u < 0 \\ -\nabla T \cdot n = 0 & \text{if} \quad n \cdot u \geq 0 \end{cases} \tag{14}$$

where n unit vector normal to the surface

For the cut section 1 m away from the axis, adiabatic conditions are considered. The air inflow is imposed at the inlet. A no-slip condition is applied to the interface between PIR and cellulose. An open boundary with no viscous stress is imposed at the upper interface. COMSOL's built-in meshing

is used; the meshing is refined in narrow regions and in regions where high temperature/velocity gradients are expected. The mesh size is refined until the flux and temperature calculated become stable. The geometry has a total of 233,220 meshes and the fully-coupled model requires approximately 7 minutes to converge using an Intel® Core i7-2600 CPU at 3.4 GHz and 8 GB RAM.

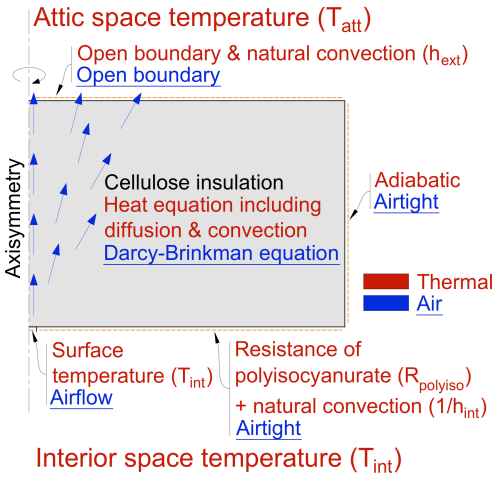

FIG 3. Domain physics and boundary conditions of simulation

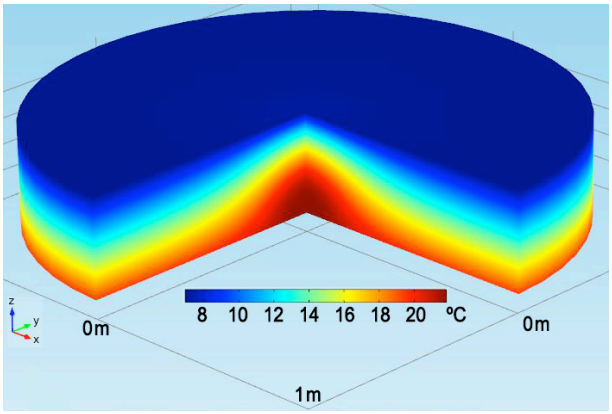

FIG 4. 3D plot of the temperature field for a flow rate of 5 LPM

5. Results and discussion

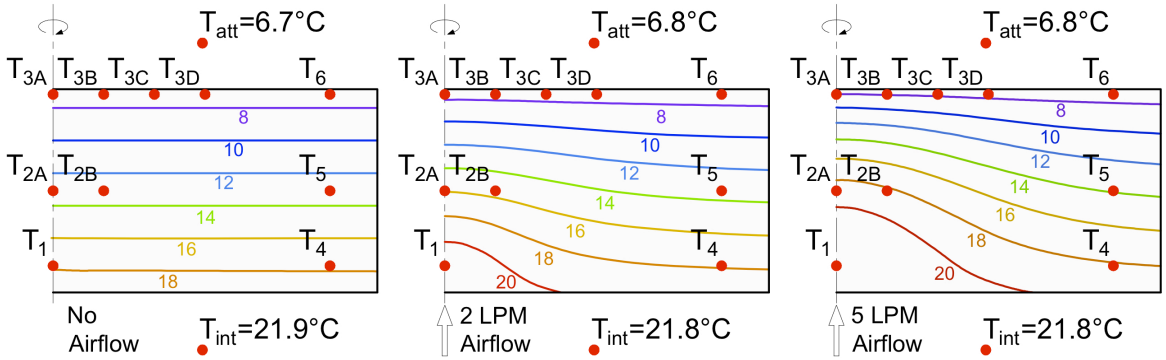

FIG 5. Isotherms obtained from simulation, values are in ºC

TABLE 2. Temperature data from the experiment and simulation, values are in ºC

	Experiment			Simulation		
Data Point	No airflow	2 LPM	5 LPM	No airflow	2 LPM	5 LPM
T_{int}	21.9	21.8	21.8	21.9	21.8	21.8
T_1	16.6	20.3	20.8	17.7	21.5	21.8
T_{2A}	12.1	16.1	19.4	13.1	15.9	18.9
T_{2B}	12.1	15.7	19.0	13.1	15.5	18.3
T_{3A}	6.4	6.8	7.9	7.2	7.5	8.0
T_{3B}	6.4	6.6	7.5	7.2	7.5	8.0
T_{3C}	6.4	6.6	7.2	7.2	7.4	7.8
T_{3D}	6.3	6.4	6.8	7.2	7.4	7.6
T_4	16.3	16.9	17.3	17.7	17.9	18.2
T_5	12.0	12.6	13.3	13.1	13.4	13.9
T_6	6.4	6.5	6.6	7.2	7.3	7.4
T_{att}	6.7	6.8	6.8	6.7	6.8	6.8

The results from the simulation are shown in isotherm graphs in figure 5; the temperature values from both the simulation and the experiment are tabulated in table 2. Figure 4 shows the temperature field of the 3D section with an air leakage rate of 5 LPM.

Compared to the case with no air leakage where the isotherms are horizontal and equidistant in the cellulose insulation, imposing air leakage shifts the isotherms upwards at the axis of the orifice, creating bell-shaped curves. The increase in temperature in the cellulose is more pronounced with higher flow rates, as expected. The simulation results compare well with the temperature readings from the experiment. With no air leakage, the simulated temperatures in the cellulose are roughly 1ºC higher than the measured ones. This discrepancy may be partly due to variations in the material properties, the simplified boundary conditions in the model, as well as a possible lack of homogeneity of the cellulose in the test setup. Also, the temperature of the top layer of the cellulose in the experiment is lower than the attic air temperature, which may be attributed to heat loss by radiation to colder surfaces in the attic such as the roof sheathing.

When simulating air leakage through the section, the flow rate is calculated on several horizontal planes at different heights to verify mass conservation. The simulation and the experimental results are in good agreement with regards to the altered temperature field in the cellulose caused by air leakage. The simulation tends to slightly overestimate the temperature increase by up to 1ºC, except at T_{2A} and T_{2B} where it is underestimated by up to 0.5ºC. Again, the non-homogeneity of the cellulose can partly be the cause. Accounting for moisture conditions and moisture transport can improve the accuracy of the model; for example, the moisture content of the insulation has an effect on its thermal conductivity.

6. Conclusion

Air leakage is a major contributor to moisture problems and energy losses in buildings. Airflow through the building envelope often occurs through porous insulation materials, and understanding its effect on the enclosure performance is of importance. This study presents a simplified, coupled heat-airflow model, applied to an experimental setup. The experiment focuses on the temperature profile of cellulose insulation in an attic of test hut, subjected to a 15ºC temperature difference and various air leakage rates. The results from the experiment and simulation show good agreement. Ongoing research aims to expand this model to couple moisture transport, which can further increase its applicability, especially for greater temperature differences and transient processes. Parametric and sensitivity analyses with multiple orifice areas, thicknesses of insulation, and flow rates could also be performed.

7. Acknowledgements

This work is financially supported by ADEME *(Agence De l'Environement et de la Maîtrise de l'Énergie),* CSTB (*Centre Scientifique et Technique du Bâtiment)*, and the *Région Rhône-Alpes*. The experimental data is taken from a project under the NSERC Smart Net-Zero Energy Buildings Strategic Research Network (SNEBRN), sponsored by the Natural Sciences and Engineering Research Council of Canada (NSERC) and 14 industrial partners including KOTT Group. The project is also supported through a NSERC discovery grant. The materials and installation of the test hut are supplied by KOTT Group.

8. References

Abadie, M.O., Finlayson, E.U., Gadgil, A.J., 2002. Infiltration heat recovery in building walls: Computational fluid dynamics investigations results. Lawrence Berkeley National Laboratory.

Barhoun, H., 2006. Influence des transferts aérauliques dans les parois sur leurs performances thermiques. Institut National des Sciences Appliquées de Lyon.

Bories, S., Mojtabi, A., Prat, M., Quintard, M., 2008. Transferts de chaleur dans les milieux poreux: Conduction, convection, rayonnement. Tech. Ing. Génie Énergétique.

Buchanan, C.R., Sherman, M.H., 2000. A mathematical model for infiltration heat recovery. Lawrence Berkeley National Laboratory.

Chan, W.R., Price, P.N., Sohn, M.D., Gadgil, A.J., 2003. Analysis of US residential air leakage database.

COMSOL, 2011. Comsol Multiphysics User´s Guide - Version 4.2.

Desmarais, G., Derome, D., Fazio, P., 2000. Mapping of Air Leakage in Exterior Wall Assemblies. J. Therm. Envel. Build. Sci. 24, 132–154. doi:10.1106/BWH8-9D3J-R939-957E

Langlais, C., Arquis, E., McCaa, D.J., 1990. A theoretical and experimental study of convective effect in loose-fill thermal insulation.

Langmans, J., 2013. Feasibility of Exterior Air Barriers in Timber Frame Construction. KU Leuven, Belgique.

Li, Q., Rao, J., Fazio, P., 2009. Development of HAM tool for building envelope analysis. Build. Environ. 44, 1065–1073. doi:10.1016/j.buildenv.2008.07.017

Litvak, A., 2005. Campagne de mesure de l'étanchéité à l'air de 123 logements RT2000 - Rapport final. CETE de Lyon.

Nield, D.A., Bejan, A., 2006. Convection in porous media. Springer, New York.

Saber, H., Maref, W., Elmahdy, H., Swinton, M., Glatzer, R., 2012. 3D heat and air transport model for predicting the thermal resistances of insulated wall assemblies. J. Perform. Simul. 75–91.

Svoboda, Z., 1999. The analysis of the convective-conductive heat transfert in the building constructions. Presented at the 6th Building Simulation Conference, Kyoto, pp. 329–335.

Tariku, F., Kumaran, K., Fazio, P., 2010. Transient model for coupled heat, air and moisture transfer through multilayered porous media. Int. J. Heat Mass Transf.

Trechsel, H.R., 2011. Moisture analysis and condensation control in building envelopes. ASTM International, West Conshohocken, Pa.

Vafai, K., Thiyagaraja, R., 1987. Analysis of flow and heat transfer at the interface region of a porous medium. Int. J. Heat Mass Transf. 30, 1391–1405.

Van Schijndel, A.W.M. van, 2008. Heat and Moisture Modeling Benchmarks using COMSOL. Presented at the COMSOL conference, Hannover.

Wagner, H., 1989. Luftdichtkeit und Feuchteschutz (beim Steildach mit Dämmung zwischen den Sparren). Dtsch. Bauz. Heft 1289 1639–1646.

Airtightness of office and school buildings in Sweden – measurements and analyses of the implication for the energy use

Åke Blomsterberg, Assistant Professor [1]
Stephen Burke, Ph.D. [2]

[1] WSP and Lund University, Sweden
[2] NCC Construction, Sweden

KEYWORDS: *Airtightness, blower door, energy, measurement, office building, pressurisation, school.*

SUMMARY:
The airtightness of office and school buildings influences energy use and thermal comfort. A leaky building is likely to have a high use of energy and thermal discomfort. The knowledge of real airtightness levels of entire buildings and their impact on the energy use is very low, except for a study carried out in the USA. Therefore two different methods of airtightness testing were applied to six entire Swedish office and school buildings built since 2000. The first method involves using the ventilation system of the building and the second one to use a number of blower doors. Information on 30 other airtightness tests of similar buildings was collected. During the airtightness testing the air leakage paths were detected using infrared scanning and smoke sticks. Most of the tested buildings showed a very good airtightness level. All previously tested office buildings in the USA, Canada and the UK are much leakier. The tested buildings had some leakage paths, which could easily have been taken care of during construction, but are rather difficult to stop now. The infiltration rate for these buildings was estimated by a simplified calculation procedure to be low, implying a low energy use caused by infiltration. For most of the buildings stringent airtightness requirements had been applied.

1. Introduction

It is well-known that the building sector plays an important role in the work towards sustainable development. The sector represents extensive economic, social and cultural values, at the same time as it causes extensive environmental impact due to its high use of energy and materials. An important part of the energy use within the building sector is related to office and school buildings. The total energy use of an average Swedish office building is 220 kWh/(m²year) (heated usable floor area) of which electricity stands for 108 kWh/(m²year). Of this 108 kWh/(m²year), 57 kWh/(m²year) is due to office equipment, of which 23 kWh/(m²year) is lighting. This was shown in a study of 123 office and administrative buildings of different ages (Persson 2007). Of the floor area in all office buildings, 69 % is heated by district heating and the average use of district heating energy is 110 kWh/(m²year) (SCB 2006). Both new and old office buildings have a substantial potential for energy savings and improvement of indoor climate. While many new office buildings may have a low energy use for heating compared with older office buildings, they may have a higher electricity use. This is due to a high use of electricity for ventilation, cooling, lighting and office equipment. The situation for school buildings is similar, with the exception of cooling which is rare in school buildings. An important parameter affecting the energy use for space heating and cooling, and thus the indoor climate, is the airtightness of the building envelope. In a leaky building the energy use increases due to uncontrolled infiltration/exfiltration. The air leaking in and out through the building envelope increases the energy use as it, for example, does not pass through a heat recovery unit. The uncontrolled air leakage can contribute to discomfort such as draught, which can result in the indoor temperature being raised to improve the comfort, causing a further increase in energy use from the user's behaviour.

Unfortunately, there is no simple and accurate method of relating the airtightness of a building to the air leakage for an office or school building in operation. This is due to difficulties in determining the location and characteristics of all leakage paths and determining the wind pressure coefficients (Blomsterberg 1990).

The aim of this project (Blomsterberg 2012) was:

- to use different measuring methods for determining the airtightness of school and office buildings,
- to determine the airtightness for modern school and office buildings,
- to estimate the influence of airtightness on the energy use for space heating.

2. Method

The hypothesis is that, in many cases, the airtightness can be measured using the ventilation system of the building instead of using a number of blower door units. Two different methods were used:

- Airtightness testing using the ventilation system of the building. Canadian standards were applied (CGSB 1986, CGSB 1996).
- Airtightness testing using a number of blower doors (portable fans), www.energyconservatory.com. European standard 13829, Method B was applied (CEN 2000).

The measurements involve pressurizing and depressurizing the entire building and measuring the corresponding air flow to maintain the different pressure differences between inside and outside. Ventilation openings and lead-throughs are sealed before the measurements. Thus the airtightness of the building envelope is determined. The location of leakage paths are determined using thermography and smoke.

When using the ventilation system of the building the following has to be investigated before proceeding:

- Assess the building automation system to ensure that the ventilation air flows can be controlled and that it has the capacity to provide the necessary air flows. It is usually easier if the building has a demand controlled ventilation system.
- Ensuring that the air flows can be measured and that it can be done with adequate accuracy.

Within this project three schools and three office buildings were tested. Additional tests had been carried out before by other Swedish organizations.

To determine the air infiltration/exfiltration rate from the results of pressurization tests there are different ventilation models. The ventilation models can be divided into: “air change” methods, reduction of pressurization test data, regression techniques, theoretical network methods, simplified theoretical methods (Liddament 1986). The first three models are empirical techniques, which tend to be loosely based on the physical principles of air flow. The other models are theoretical models, which are based on a much more fundamental approach involving the solution of the equations of flow for air movement through openings in the building envelope. Empirical methods are usually straightforward to use, but tend to be unreliable and have a limited field of application. On the other hand, theoretical models have a potentially unrestricted applicability but are often demanding in terms of data and computer execution time. Theoretical calculation techniques can be divided into: single zone network models, multi zone network models and simplified theoretical techniques. These models require a lot of information e.g. wind pressure coefficients, air leakage distribution for the building envelope, local wind speed, geometry of the building. Due to the limited amount of information on the tested

buildings the method using reduction of pressurization test data was chosen in order to determine an order of magnitude for the average infiltration/exfiltration rate.

The reduction of pressurization test data method does nevertheless provide valuable information concerning the average infiltration performance of the building. The artificial pressurisation/depressurisation of a building to determine air leakage performance is now fairly common practice. The test only provides data regarding the "leakiness" of the building. The result provides no information on the distribution of openings or on how infiltration will be affected by wind, temperature, terrain, or shielding. However, several experimental results have shown that the approximate air infiltration rate in practice will be in the order of one twentieth of the measured air change rate at 50 Pa (ASHRAE 2009), i.e.:

$$Qinf = Q50 / 20 \quad (1)$$

Where Qinf infiltration rate (h-1)
Q50 air change rate at 50 Pa.

Calculations have shown that the ratio can vary between 6 and 40 depending upon the house, the climate and the shielding (Blomsterberg 1990).

To determine the energy use caused by air infiltration/exfiltration the infiltration/exfiltration rate was first calculated from the pressurization tests and then the energy use was calculated using degree days for Stockholm. For most of the buildings the only available information was the floor area, the volume, type of ventilation system and type of building technology, the results of a pressurization test.

3. Tested building

The aim was to test school and office buildings built after the year 2000 with a floor area preferably larger than 1000 m². They should be a mix of buildings both with and without specific airtightness requirements.

3.1 Outside this project

Thirty buildings had previously been tested by different organisations e.g. SP - the Technical Research Institute of Sweden, Akademiska Hus, Skanska, WSP. All the buildings were built between 2007 and 2012. The buildings are mainly schools and offices, but also include homes for the elderly, shops, and sports centres. The smallest building had a floor area of 800 m² and the biggest 17 000 m². All buildings had balanced mechanical ventilation with heat recovery. The building envelopes varied, ranging from prefabricated concrete to stud walls.

3.2 Within this project

Six buildings were tested for the purpose of this project, three office and three school buildings. All the buildings were built between 2007 and 2011. The smallest building had a floor area of 1,030 m² and the biggest 20,000 m². All buildings had balanced mechanical ventilation with heat recovery. The building envelopes varied, ranging from prefabricated concrete, prefabricated glass facade to stud walls.

4. Results

All the buildings tested outside the project were very airtight (see table 1). The average airtightness was 0.3 l/sm² @ 50 Pa which is equivalent to the voluntary Swedish requirement for passive houses (Nollhus 2012). The best building had a value of 0.1. For most of the buildings airtightness requirements ranged from 0.2 to 0.8 l/sm² @ 50 Pa, which can be compared with the requirement of the previous Swedish building code (before year 2006), of 1.6 l/sm² @ 50 Pa. The current building code does not have any specific requirement. Only two buildings did not meet their requirement. All

previously tested office buildings in the USA, Canada and the UK are much leakier (Blomsterberg 2009). Common leakage paths were exterior doors and connections between façade elements and floors/roofs, most of which would be difficult to tighten afterwards. Most buildings were tested with blower doors. Some were tested with the ventilation system.

TABLE 1. Measured air leakage and leakage paths.

Type of building	Year of con-struction	Envelope area, m²	Airtight-ness require-ment, l/sm² @ 50 Pa	Measured airtight-ness, l/sm² @ 50 Pa	Main leakage paths
Shop	2011	18,721	-	0.18	Concrete element joints, exterior doors
Sport Centre	2011	6,616	0.4	0.44	Exterior doors etc.
Office	2008	2,580	-	0.34	Entrance parts/windows/exterior doors
Office	2010		0.4	0.27	
Office	2010	4,237	0.5	0.43	Connections between floor and wall
Office	2010	14,610	0.6	0.55	
Office	2007	-	0.8	0.7	Connection between facade elements, facade and roof elements
Office/industry	2009	4,560	0.25	0.26	Connection between ceiling and wall/workshop – exterior doors
Storage/workshop/office	2011	10,034	0.3	0.29	Exterior doors
Food store	2011	3,995	0.8	0.62	TRP/expanded clay, windows, Entrance parts
School	2009	4,912	0.5	0.36	
School	2011	2,607	0.2	0.13	
School	2008	3,335	0.45	0.41	
School	2008	5,180	0.4	0.21	
School	2009	2,832	0.6	0.27	Exterior doors
School	2008	2,414	0.3	0.26	
School	2010	2,460	0.6	0.23	Exterior doors and windows
School	2010	2,460	0.6	0.19	Exterior doors and windows
School	2010	2,182	0.6	0.57	
School	2010	2,054	0.5	0.38	Exterior doors
School	2010	5,513	0.2	0.09	No major leakage paths
School	2011	2,520	0.4	0.28	Exterior doors
School	2011	4,973	0.25	0.17	Exterior doors
School	2007	3,941	0.4	0.45	Exterior doors etc.
School	2011	2,261	0.6	0.48	Roof, windows and doors
School	2010	2,295	0.3	0.4	Connection wall-ceiling,

					exterior door
School	2011	4,822	0.2	0.16	
School	2010	5,641	0.8	0.88	
Home for the elderly	2012	4,081	0.3	0.20	Exterior doors
Home for the elderly	2011	3,900	0.2	0.14	
Average			0.44	0.30	

For twelve of the buildings information on the volume was available and the airtightness could be recalculated to ach @ 50 Pa (see table 2). A comparison of the buildings is now different due to different ratios between volume and envelope area. Using a simple method of calculating the infiltration (see Method) an average infiltration rate was estimated. The result was an average air infiltration rate during the heating season of 0.03 ach (air changes per hour), varying between 0.01 and 0.06. This is equivalent to an energy use for space heating of 4 kWh/m²year. If the buildings would have only met the requirements of the previous building code the energy use might have been five times higher i.e. 20 kWh/ m²year.

TABLE 2. Measured air leakage and calculated energy use for heating infiltrating air.

Type of building	Year	Measured airtightness l/sm² @ 50 Pa	Measured airtightness ach @ 50 Pa	Infiltration/exfiltration, ach	Energy use for heating infiltration, kWh/m²year
Shop	2011	0.18	0.20	0.01	2
Office	2008	0.34	0.60	0.03	3
Office	2010	0.43	0.43	0.02	3
Food store	2011	0.62	1.11	0.06	10
School	2010	0.09	0.13	0.01	1
School	2011	0.17	0.34	0.02	2
School	2011	0.48	1.18	0.06	7
School	2010	0.4	1.04	0.05	7
School	2011	0.16	0.24	0.01	2
School	2010	0.88	1.28	0.06	9
Home for the elderly	2012	0.20	0.20	0.01	1
Home for the elderly	2011	0.14	0.18	0.01	1
Average		0.34	0.58	0.03	4

Also the recently tested six buildings were fairly airtight, but not as airtight as the previously tested buildings (see table 3). One contributing factor might be that there were only two buildings which had a specified airtightness requirement.

TABLE 3. Measured air leakage and leakage paths.

Type of building	Year of construction	Test method	Envelope area, m²	Airtightness requirement, l/sm² @ 50 Pa	Measured air tightness, l/sm² @ 50 Pa	Main leakage paths
Exhibition /office	2011	Ventilation system, the whole building	40,400	0.4	0.39	Connection between façade elements and columns, between facade and roof, exterior doors.
Office	2009	Ventilation system, storey 3, back pressure storey 2, 4, atrium and staircase	5,600		0.85	Connection between infill walls and steel columns, windows
School	2007	Blower Door	3,923	-	0.87	Lead-throughs, windows
School	2011	Blower Door	2,775	-	0.45	Doors, windows
School	2009	Blower Door	4,307	-	0.62	Lead-throughs, windows, doors.
Average					0,64	

For the recently tested buildings, information on the volume was available and the airtightness could be recalculated to ach @ 50 Pa (see table 4). The comparison of the buildings is now different due to different ratios between volume and envelope area. Using a simple method of calculating the infiltration (see Method) an average infiltration rate was estimated. The result was an average air infiltration rate during the heating season of 0.06 ach (air changes per hour), varying between 0.01 and 0.14. This is equivalent to an energy use for space heating of 6 kWh/m²year. If the buildings would have only met the requirements of the previous building code, the energy use might have been three times higher at about 20 kWh/ m²year.

TABLE 4. Measured air leakage and calculated energy use for heating infiltrating air.

Type of building	Year	Measured airtightness l/sm² @ 50 Pa	Measured airtightness ach @ 50 Pa	Infiltration/exfiltration, ach	Energy use for heating infiltration, kWh/m²year
Exhibition/office	2011	0.39	0.28	0.01	5
Office	2009	0.85	0.36	0.02	2
Office	2009	0.68	2.77	0.14	4
Education	2007	0.87	1.44	0.07	8
Education	2011	0.45	1.51	0.08	7
Education	2009	0.62	1.34	0.07	8
		0.64	1.28	0.06	6

5. Conclusion

Two different methods of measuring the airtightness of entire buildings have been used, using the building's ventilation systems or using a number of blower doors. Both methods can be used separately or combined. Choice of method depends on the prerequisites of the individual building. For large buildings using the ventilation system can be preferable. This presupposes that the air flow can be controlled within the desired range and measured accurately enough. Usually this is the case for demand controlled ventilation. Tests during construction, which are recommended to ensure good airtightness, can often only be carried out using blower doors. The two methods can be applied to office buildings, apartment buildings, industrial buildings and other premises. For apartment buildings the blower door technique is often the only method as the ventilation system often has insufficient capacity, unless the building is very airtight. Complete testing includes determination of the location of leakage paths.

This study clearly shows that it is possible to build very airtight school and office buildings i.e. which fulfils the Swedish criterion for passive houses at 0.3 l/sm² @ 50 Pa. This seems to be possible with a building envelope which is prefabricated or framework construction or curtain wall. Most likely, the energy use for infiltration in these buildings is almost negligible i.e. in the order of magnitude of a couple of kWh/m²year. This number can be compared with the total energy use for space heating for a typical average Swedish office building of 110 kWh/m²year, where infiltration might account for 10-20 kWh/m²year if only the airtightness requirement of the previous building code is fulfilled, which is likely.

An important prerequisite for arriving at a very good airtightness is obviously that requirements regarding airtightness are set at an early stage. These requirements have to be specified as a maximum air leakage value, which should be tested during the building process.

6. Acknowledgements

The project was funded by SBUF (Development Fund of the Swedish Construction Industry), NCC and WSP.

7. References

ASHRAE 2009. ASHRAE Handbook Fundamentals. ASHRAE, Atlanta, USA.

Blomsterberg, Å., 1990. Ventilation and airtightness in low-rise residential buildings - Analyses and full-scale measurements. Swedish *Council for Building Research, D10:1990, ph.d. thesis.

Blomsterberg, Å. 2009. Airtightness and energy use of an Swedish office building – measurements and calculations. Presented at the 30th AIVC- and the 4th BUILDAIR-Conference in Berlin.

Blomsterberg, Å., Burke, S. 2012. Real airtightness of large buildings – Measurements and calculations (in Swedish). SBUF (Development Fund of the Swedish Construction Industry), NCC and WSP.

CEN 2000. Thermal performance of buildings - Determination of air permeability of buildings – Fan pressurization. European Committee for Standardization, EN 13829.

CGSB 1986. Determination of the Airtightness of Buildings envelopes by the Fan Depressurization Method Using the Buildings's Air Handling Systems, Canadian General Standards Board, Standard 149.10-M86, National Standard of Canada.

CGSB 1996. Determination of the Overall Envelope Airtightness of Buildings by the Fan Pressurization Method Using the Buildings's Air Handling Systems, Canadian General Standards Board, National Standard of Canada.

Liddament, M. 1986. Air Infiltration Calculation Techniques – An Application Guide. AIVC.

Nollhus, 2012, Kriterier för passivhus m.m. (Criteria for passive houses etc.), www.nollhus.se .

Persson, A. 2007. Improved energy statistics for premises – Report for year 1 – Inventory of offices and administrative buildings (in Swedish). The Swedish Energy Agency, rapport ER 2007:34.

SCB 2006. *Energy statistics for premises 2005*. Swedish Statistics, EN16SM0603, www.scb.se.

Manageable supervision of air tightness for large buildings

Mikael Kläth [1]
Peter Sunvisson [1]

[1] Dry-IT, Sweden

KEYWORDS: *Air tightness, air leakage, blower door, pressure test, building envelope*

SUMMARY:
It is important to approach issues concerning building air tightness systematically and implement this throughout the building process to ensure that air leakage requirements are met for large buildings. Air leakage testing needs to be applied early on during construction to better understand how to increase the quality of the building and efficiency of the construction process. This paper explains how to work with air tightness management in the different construction phases and gives a practical example of a large building that met high ambitions for air tightness.

1. Introduction

Several benefits can be derived from testing air tightness in the early stages of constructing large buildings. The key to making this possible is to use a systematic approach to managing issues concerning air leakage throughout the construction process.

Difficulties that occur concerning air leakage testing during the production phase of large buildings are foremost of the practical types. Examples include limitations of the equipment capacity, the scale of the provisional sealing methods and time consumption of the capsuling techniques and other operation steps. Different parties may participate in different ways to contribute towards an air-tight end result, through defining requirements, technical collaboration meetings or workshops, coordination for difficulties in practice, storage and use of sustainable materials and well thought-out modifications.

This paper aims to answer how to efficiently manage air tightness issues from experience of working in projects for the construction of large buildings. First we present the authors' general method of practice for implementing air-tightness management in the different stages of the building process. Furthermore a project with a high ambition level is presented where the actions taken concerning air tightness are mapped out and how the issued air leakage requirements were met.

2. Air tightness management in the building process

Regrettably, air tightness (or building physics in general) engineers and consultants are rarely involved early on in the construction process, during the time where many decisions of importance to air tightness issues are set. This chapter describes how air tightness consultants should be utilized in the different stages of the building process.

2.1 Air tightness management during the design and development phases

A project developer can set an ambition level for air tightness that can be regulated as a part of the company's standard for construction or it can be project specific. Air tightness in this phase is often related to energy efficiency, which has a strong connection to the attractiveness of the building as a product, i.e. if it can be promoted as a "green" building by itself or with an environmental classification system.

It is important that relevant information concerning air tightness issues is updated and spread through the project organisation during the course of the design phase. A dialogue between the air tightness consultant and the designers (as well as other consultants in other fields of expertise) needs to be managed and documented systematically. This can be achieved by creating an Air Tightness Description, which is a document that describes project specific air tightness aspects that needs attention so as to ensure that requirements and regulations from the developer and authorities can be met. The contents of this document are dynamic and may be revised if any conditions are changed. There are many disciplines that need coordinating in this phase so as to strive towards the same goal. An example of this is when the architect is weighing on how far to recede the windows in the wall construction, then the construction engineer needs coordination on how this affects the choice of sealing method between the walls' air barrier and window.

The consequence of choices made early on in the design phase may be beneficial in one aspect but negative in another, which for example is sometimes the case for detail designs in relation to insulation thickness. It is therefore advantageous if the coordinating role has experience in building physics (building physics coordinator) and has enough knowledge in different fields to be able to identify if a design may lead to problems for the indoor environment.

2.2 Air tightness management during the construction phase

Air leakage restrictions that are set by the developer or client (often a result of requirements set by environmental classification systems such as Miljöbyggnad, BREEAM or LEAD) need to be related to the contractors' process for construction. During the construction phase it is therefore important to involve air tightness engineers that can lift these issues within the project's organisation early on in the construction phase. An effective method to assist this process is to create a Plan for Air Tightness, which is a document that establishes how issues and secondary aspects related to air leakage are to be dealt with, so as to create efficient models to monitor and achieve the requirements governed by the Air Tightness Description. Within the documentation an organisational chart is set, that for instance points out specific personnel that carry responsibility for different aspects to make sure that regulations are met; eventual planning that affects procurement, scheduling, testing and monitoring, education and quality assurance.

Necessary for large buildings, provisional encapsulations are used for sectioning off building parts during the ongoing construction to enable pressurised testing. The air leakage index is measured with computer operated fan equipment, e.g. Blower-door, attached to customised tents or makeshift walls that enclose the area of interest. Improvement measures for air leakages sought out during the test are prescribed for the following building parts of the same type to be installed. Furthermore, problems that need to be solved concerning practice methods are informed to the involved carpenters and other craftsmen so that lessons can be learnt from previous mistakes. It is important that experiences from the ground level are documented and that the information is quickly distributed to the right people so that the organisation has a chance to adapt.

Suitable parts of the building for air leakage testing are identified together with the contractor during a start-up meeting, preferably before the procurement process of materials and subcontractors. The scale of the testing areas may vary due to the complexity of the building and the level of prefabrication. Sometimes it is more suitable to test samples of for example window connections, prefabricated wall sections, prefabricated bathroom modules, a fire cell, a whole floor, two floors to check the wall knee, material joints, wall corners, stairwells, before a commissioning test is relevant. For some buildings a full scale pressurised test isn't technically possible before the ventilation system is functional or that several buildings are internally connected and individual air leakage indexes are irrelevant. Common tools for localising discrepancies in the building envelope or air barrier include an anemometer, thermography imaging (during the colder period of the year) and smoke machines (note that the choice of gas mixture affects the natural smoke movement due to its density).

2.3 Air tightness management during the operational phase

During the operational phase it is important to spread knowledge to the involved parties concerning air tightness issues and to do so in a systematic approach toward the property manager and tenant of the building. This can be achieved by developing routines for sustainable air tightness management related to renovation maintenance, outer refurbishment, internal repairs and tenant modifications, aging of materials, technical lifespans and unexpected changes to the buildings air permeability conditions.

3. A practical example of air tightness management in the construction phase of a large building

3.1 Project description

A good example of how air tightness management can be implemented for the construction of a large building is Uarda 5, see figure 1, located in Solna, Stockholm. The building's floor area (A_{floor}) amounts to roughly 55,000 m^2 and area for the building envelope to nearly 28,500 m^2(A_{env}). The property received the highest Miljöbyggnad certification grade: Gold. The maximum air leakage allowed was set to 0.3 l/s,m^2(A_{env}) @ 50 Pa differential pressure over the building envelope. The authors' company was involved in the project during the design stage, mainly for consultation in the area of moisture safety, where there are concerns that are closely related to air leakage. Further regulations for air tightness management were expressed under a chapter in the Moisture Safety Description. The resulting air leakage index was measured to 0.27 l/s,m^2(A_{env}) @ 50 Pa.

FIG 1. Illustration of Uarda 5.

3.2 Work methodology

Management of the issues concerning air tightness to achieve the requirements was initially planned through a start-up meeting and executed through continuous discussions with the contractor. An Air Tightness Control Plan was established in accordance with the projects conditions and the critical parts of the construction were identified for further examination. Technical meetings were set when the subcontractors had been procured to discuss the steps that had to be taken to achieve an airtight result.

Some of the critical building parts that were identified included the roofing, skylights, exterior walls, windows, outer glazing, ventilation aggregates, garage doors, airlocks, basement walls and details around the foundation. It was concluded that pressurised air leakage testing (SS-EN 13829) was to be conducted to a skylight, a few sections of the exterior walls and a larger coherent section of the outer glazing. After testing the first of each building section to be installed, experiences were documented and improvement measures were taken for the following building sections that were in line to be installed. The ventilation aggregates had tougher requirements and were subdued to a more vigorous

testing procedure (VVS-AMA Täthetsklass B). The rest of the critical building parts were surveyed to find air leakage paths through thermography during the commissioning pressurised test.

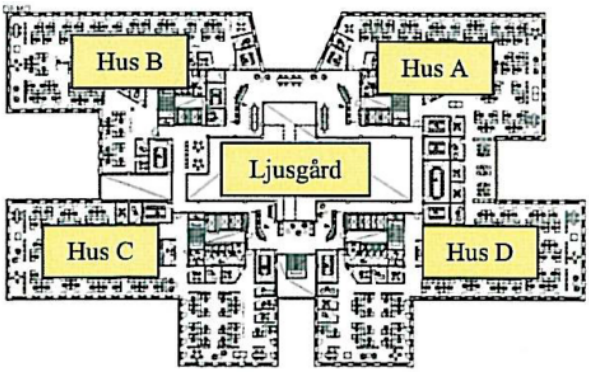

FIG 2. Sketch of the floor plan.

The areas of interest for testing were marked out on overview plans and the contractor was given instructions on the method for constructing the provisional encapsulations, which were also explained in detail beforehand on site together with the carpenters.

FIG 3. Blower-door equipment attached to a provisional wall with a smoke machine placed at the fan inlet.

3.3 Exterior walls

Initially the exterior walls were air leakage tested in smaller sections, for example some of the wall joints on a few floors. Later on whole flights in one of the four building corners was subdued to pressurise testing. The provisional capsuling consisted of a wooden framework c/c 400 - 600 mm, MDF or plywood sheeting and an exterior polyethylene foil with taped joints and clamped with screws to the framework with battens. An acrylic sealant is applied between the polyethylene foil and concrete to fill any voids that may occur due to imperfections in the batten, joist or the concrete. The provisional capsulations sectioned off the testing area between the stairwell and to the adjacent building corners, see “Hus D” in figure 2. The Blower-door equipment was attached to the capsulation and the smoke generator was placed at the fan inlet at the time that pressure was applied to the testing volume, see figure 3, or used inside the testing area by applying smoke directly to the building envelope, see figure 4. Personnel on the inside and outside of the testing volume monitored the envelope for smoke leakage during the test.

FIG 4. Air leakage testing of window details with smoke.

3.4 Ventilation aggregates

The building's four ventilation aggregates were each approximately the size of an apartment and had tough air tightness requirements to fulfil. The aggregates were depressurised with a pressure difference of 50 Pa. The result was extrapolated using the air leakage coefficient and exponent to estimate a value at 200 Pa, which was the specified output. Later the aggregates were pressurised at 200 Pa to compare the extrapolated air flow result to the actual measurement.

3.5 Skylights

The skylights are situated over the atrium in the core of the building with a vast open space underneath, see figure 5. The provisional encapsulation that was constructed around one of the skylights was made up of a customised polyethylene tent that was sealed to the floor of the scaffolding. The air tightness engineer and representatives from the contractor and subcontractors enclosed themselves inside the testing area during the testing. The fan was mounted to the polyethylene foil and the test area was pressurised and inspected for air leakage with the use of thermography, anemometer and a smoke machine. It turned out that the attachment of the capsulation to the scaffolding could not ensure an air tight test result during pressurisation but air leakages could still be found and repair work was prescribed.

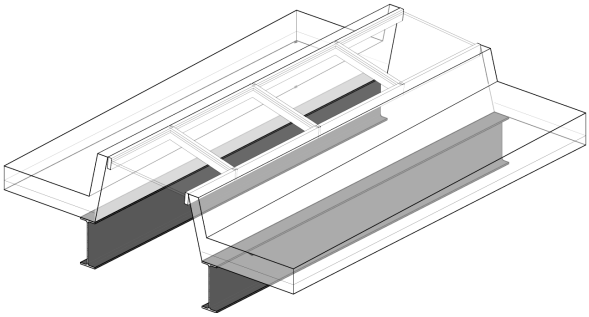

FIG 5. Rendered illustration of the skylight construction.

3.6 Commissioning air tightness test

The buildings own air-handling equipment was employed for the commissioning air tightness test (CAN/CGSB 149.15-96). Simultaneously air leakage paths were exposed, especially for details around the drains, doors, windows and installations through the façade using thermography (SS-EN 13187). The few parts of the building that had yet not been completed at the time of the commissioning test were applied with complementary provisional encapsulations. To ensure that the

measured air leakage index was reasonable, the test was redone by a two separate ventilation aggregates.

The set requirements for maximum air leakage index (0.3 l/s,m^2) was met and measured to 0.27 l/s,m^2 for the project Uarda 5. The property was awarded the title of SGBC Green Building Award 2012 and the highest classification Miljöbyggnad Guld. We are at this point unable to present a calculation of the benefits concerning reduced energy consumption for this building due to concerns of the buildings safety regulations set by its current occupants. The extra energy consumption for changing the design air leakage index from 0.3 to 0.5 l/s,m^2(A_{env}) has been calculated for a similar project of this scale, which amounts to a difference of 2 kWh/m^2(A_{floor}). If applied to Uarda 5, the consequence would be an extra energy demand of 110 MWh/y.

4. Conclusions

There are several benefits for air tightness management throughout the building phases and to scale down planning for manageable testing methods to be applied during the course of the construction. One of the foremost reasons for these benefits is that the air tightness engineer or consultant may implement systematic routines for spreading information to the different organisational parts of the building process, so that the end installer or carpenter is up to date with accurate knowledge on how to effectively work with these issues and why they are important. There are vast possibilities to engage these issues early on to affect the building process and have an impact on the end result.

Work that is needed to ensure a comprehensive grip on air tightness is implemented during the design phase, when construction designs are made that are critical to air tightness issues and need to be identified and analysed in an Air Tightness Description, for issues that concern both the construction and operational phase of the building. Before commencing the production, a Plan for Air Tightness needs to be established, which describes the execution of critical steps that are practically explained through technical meetings. The choice of suitable building sections to be tested is of great importance, especially for buildings where it is not applicable to pressurise the total area of the building envelope at once, for results from these sections will represent the whole building. It is important to work with air leakage surveillance and apply pressurised testing to strategically chosen parts of the building during the course of construction, to assure the quality of execution so that the end result amounts to less than the design value. Through a systematic approach to air tightness management throughout the construction process and documenting the path taken, lessons may be learnt and a more widespread knowledge of the importance of air tightness may infiltrate the building industry.

5. Acknowledgements

The authors wish to thank Fabege for involving us early in the project Uarda 5 and Peab Sverige AB for the partnership surrounding air tightness testing.

References

CAN/CGSB-149.15-96. Determination of the Overall Envelope Airtightness of Buildings by the Fan Pressurization Method Using the Building's Air Handling System, Canadian General Standards Board, Ottawa, Canada, 1996.

SS-EN 13187. Thermal performance of buildings - Qualitative detection of thermal irregularities in building envelopes - Infrared method. Swedish Standards Institute SIS, 1999.

SS-EN 13829. Thermal performance of buildings - Determination of air permeability of buildings - Fan pressurization method (ISO 9972:1996, modified). Swedish Standards Institute SIS, 2000.

AMA VVS & Kyl 09. Allmän material- och arbetsbeskrivning för vvs- och kyltekniska arbeten, Svensk Byggtjänst, 2010.

Method for measuring the air-tightness of facing formworks

Paul Wegerer [1]
Thomas Bednar, Professor [1]

[1] Vienna University of Technology, Austria

KEYWORDS: *air-tightness, durability, facing formwork, in-situ measurement, tracer-gas*

SUMMARY:
Air-tightness of constructions is essential when evaluating a building's energy efficiency and durability. Even in connection with refurbishment air-tightness is becoming increasingly important. Especially when using facing formworks with vapour barriers as interior insulation to thermally renovate an existing building, air-tightness is an essential parameter. It has a significant influence on the proper functioning of the construction because convective moisture entry can lead to considerable damage.

In this paper an in-situ measuring carried out on a real object is being presented, which allows to assess and to proof the air-tightness of facing formworks. This method was developed on a testing wall in the laboratory of the Research Centre for Building Physics and Sound Protection of Vienna University of Technology.

The measurement starts after the completion of the construction by using a tracer-gas (CO_2) and by adjusting excess pressure in the testing room. At the same time the increase of CO_2 in the facing formwork is recorded. Measurements are carried out with at least two different pressure ranges. From the results gained, the air flow volume coefficient C and the leakage exponent n are calculated in accordance to EN 12114.

1. Introduction

A construction's air-tightness substantially influences its functionality as convective moisture entries contain a high risk of causing damage. The quality of the airtight layer often does not meet the planned requirements. This has been pointed out in many publications. For example, Sandberg (2005) described typical problems caused by poor air-tightness of constructions and specified experience from site visits. Wahlgren (2010) presented a method detecting air leakages at an early construction stage by using negative pressure. However, the given examples of joints and connections solely refer to the entire building envelope as an airtight structure.

A building's air-tightness can be determined by negative- or excess-pressure-measurement using standardised measuring methods (Blower-Door-measurement according to EN 13829). Thereby, the total air-tightness at a difference in pressure of 50 Pa is given as a n_{50}-value in air exchange rate per hour or as a q_{50}-value in m³/(m²h) according to the formulas (1). There is, however, no differentiation whether the leakiness occurs in the area of the windows, doors or joints and connections. Because of this, size and form of leakages cannot be quantified with this method. Furthermore, a judgement concerning a construction's durability cannot be drawn from these measurement results.

$$n_{50} = \frac{\dot{V}_{50}}{V} \qquad q_{50} = \frac{\dot{V}_{50}}{A_E} \tag{1}$$

If, on the other hand, the air-tightness of a single building component or a single construction layer is to be determined, a different measurement concept must be used. In this case the focus is not on

determining the whole building's air-tightness but a single component layer, e.g. gypsum board planking, the vapour retarder or a foil in general is observed. This is especially relevant when using a facing formwork as interior insulation as with this method of construction leakiness of the vapour retarder may lead to damage. In this paper, a method to measure the air-tightness of a facing formwork as interior insulation will be introduced.

2. Air flow through facing formwork constructions

The calculation of air flows in building components has already been validated in several publications. In Bednar et al. (2010) the convective moisture entry into a flat roof is shown. In this case, two holes of the same size are assumed as entry- and exit-leakages. Wegerer et al. (2012) demonstrated the influence of leakiness of inside insulated walls using the example of a wooden beam bearing. He showed that untight facing formworks used as interior insulation bear a huge potential for damage.

Facing formwork constructions normally consist of a post-and-beam-construction which is covered with panels, commonly gypsum boards. To implement an airtight layer and to restrict moisture entering the construction a vapour barrier is fitted between the post-construction and the planking. The quality of this component layer is directly linked to the functionality of the whole component. Leakages resulting from improper bonding as well as penetrating the vapour retarder with screws lead to an air flow through the facing formwork. This may result in moisture entering the component from the air of the room.

In the following two depictions (FIG.1) possible paths of air flows are shown schematically. In the picture on the left, you can see a one-dimensional structure in the form of a typical facing formwork with a possible air-path. The picture on the right shows possible air-paths using the example of a ceiling-to-wall connection.

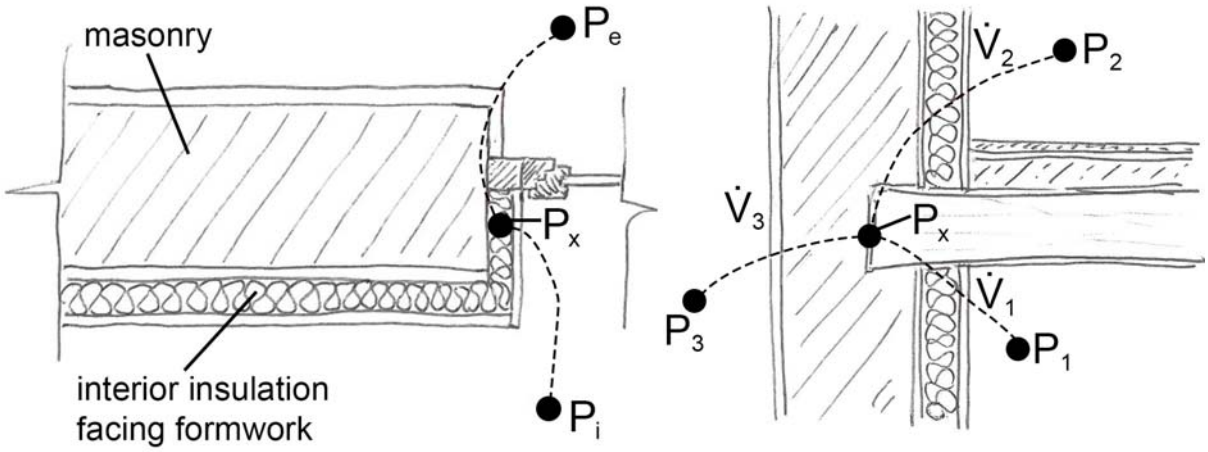

FIG. 1 left: reveal with facing formwork as interior insulation; right: ceiling-to-wall connection with facing formwork as interior insulation

It is noticeable that the air-tightness of the facing formwork depends on at least two layers. In the one-dimensional case these are the vapour barrier within the construction and the exterior load-bearing wall, e.g. the masonry. With multi-dimensional component connections flow-paths to neighbouring rooms or storeys may exist. As a prerequisite for a convective moisture entry into the facing formwork there has to be an air-path from the facing formwork to the outside or a neighbouring room additionally to the crack in the vapour retarder. Thus, to determine the airflow through the facing formwork, all leakages in the construction's interior and exterior cladding must be scrutinized. The volume flow rate into the construction in essence depends on the leakage size and the difference in

pressure between the room and the facing formwork and can be expressed according to the following equation:

$$\dot{V} = C \cdot \Delta p^n \qquad (2)$$

Where $\dot{V}$ airflow in $m^3/(m^2s)$
C airflow coefficient in $m^3/(sPa^n)$
Δp pressure difference between the two spaces in Pa
n leakage exponent

Hall (2003) has examined the connection between difference in pressure and volume flow rate through certain leakages in laboratory tests. Thereby, various practice-oriented situations such as slashes or distortions in the vapour barrier and holes and tears in various materials were measured. This study serves as the basis for the following laboratory tests concerning an in-situ method of measurement.

3. Measuring convective moisture entry in facing formworks

In the following a test set-up which serves to measure convective moisture entry in a facing formwork will be introduced. This in-situ method of measurement may be conducted on existing constructions, and thus provides information about the construction's actual air-tightness.

3.1 Laboratory measurements and analysis

The method of measurement was developed using a facing formwork in a laboratory test rig. Mass entry into the construction was determined using CO_2 as a tracer gas. The facing formwork (5 cm thick) consists of three fields separated by vertical wooden uprights. In addition, each field is divided into three horizontal segments. In total, there are nine fields, with fields 2, 5 and 8 being filled with mineral wool as shown in FIG. 2 on the right. The remaining six fields are without mineral wool and thus have a closed plenum filled with air. Furthermore, these six fields are fitted with tiny fans to ensure permanent and even airflow. All nine fields are fitted with CO_2 sensors. In the measuring room there are two sensors, one at the bottom and one in the upper region of the ventilated room.

FIG. 2 facing formwork in laboratory test rig; left without foil, right with foil and indication of fields

The facing formwork is lined with a foil which is stuck to the existing wall around the test construction in a manner as to provide an airtight space. Furthermore, the foil is attached to the facing formwork's vertical uprights with wooden strips to simulate planking with plasterboard. Deliberately, no full planking was provided and see-through foil was used in the laboratory test rig for us to be able

to closely observe the processes in the facing formwork. The CO_2 sensors‘ and fans‘ cables were led out via an airtight cable gland in field 7.

Additionally, an air hose is mounted to the vapour barrier in field 3 as shown in FIG. 3. It connects the air space in the facing formwork to the outside air. This air hose thus simulates the outer leakage of the whole construction.

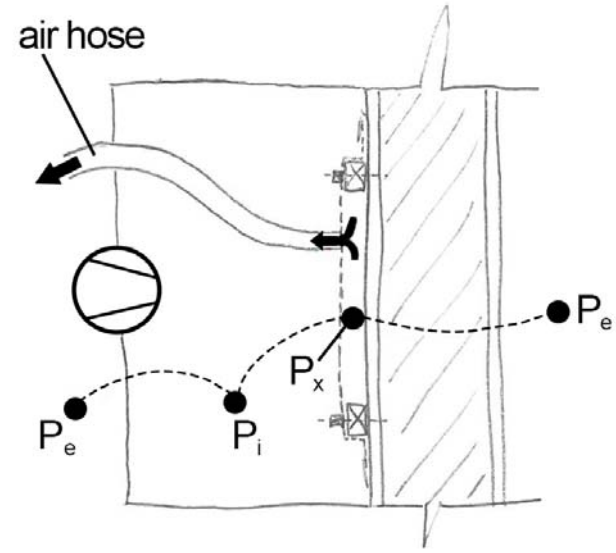

FIG. 3 left: hose leading from facing formwork to the outside; right: schematic depiction of the test set-up (layout)

During the test excess pressure is set up in the measuring room using a Blower-Door device. At the same time, CO_2 is released. The concentration of CO_2 in the room is set to approximately 2.000 ppm and kept on a constant level. Because of the difference in pressure between the test room and the facing formwork resp. the exterior the CO_2-air-mixture runs into the facing formwork through leaks in the foil, thus increasing CO_2-concentration in all nine measuring fields. In this test, the connection hose attached to the facing formwork simulates the leakage towards the exterior and thus favours the mass through cracks on the inside.

If one looks at a period of time with approximately constant CO_2-concentration in the test room, the mass entry ṁ into the facing formwork can be calculated in kg/d. This is effected by determining a linear regression from the CO_2-concentration measured in the facing formwork and by averaging over the period of time with approximately constant CO_2-concentration in the test room.

$$\dot{m} = \frac{\Delta c}{c_R - c_c} \cdot V \cdot \rho = \rho \cdot C \cdot \left(\Delta p\right)^b \qquad (3)$$

Where

ṁ	massflow rate of air into cavity in kg/s
Δc	rise of CO_2-concentration in test field in facing formwork in ppm/d
c_R	CO_2-concentration in test room in ppm
c_c	CO_2-concentration of test field in facing formwork construction in ppm
V	volume of the air space in test field in facing formwork in m³
ρ	air density in kg/m³
Δp	Pressure difference in Pa
C	air flow coefficient non-dimensional
b	air flow exponent non-dimensional

Should the measurements be conducted for at least two pressure stages, the volume flow rates can be plotted against the related difference in pressure and the air flow coefficient and the air flow exponent can be determined. This will be presented in chapter 3.2 on the example of an in-situ measurement.

Results of measurements in the laboratory

Various parameters were examined during the measurements on the test wall in the laboratory. At first, the influence of standing and mixed air was examined in a hollow test field. At that, small fans were mounted in fields 1, 4, 7, which are not filled with insulating material, and 3, 6 and 9. These fans ensure the air's thorough-mixing. Then a number of trials with and without fans were conducted. Furthermore, artificial leakages at various points were examined in both variants (mixed/not mixed). The following two diagrams show the influence of the air's thorough-mixing in the facing formwork's cavity using the example of an artificial leakage in field 7.

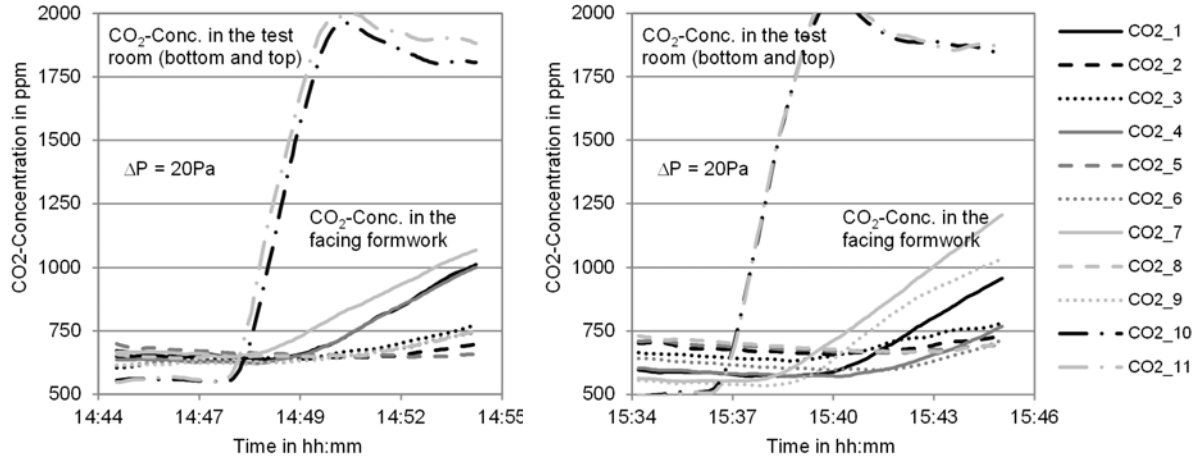

FIG. 4. CO_2-concentration in facing formwork at pressure difference of 20 Pa and leakage in field 7; left: with thorough-mixing; right: without air's thorough-mixing in facing formwork's cavity

It is clearly visible in the left diagram that the CO_2-concentration in fields 1, 4 and 7 rises markedly as CO_2 entering through the leakage in field 7 is mixed with the surrounding cavities. The right diagram also shows a steep rise of the CO_2-concentration in field 7 right behind the artificial leakage. Because of the low mixing of the air within the construction the remaining sensors react later to the air entering. The following two depictions FIG. 5 and FIG. 6 show measurement alternatives with insulation in the facing formwork (left) compared with alternatives without insulation in the facing formwork (right).

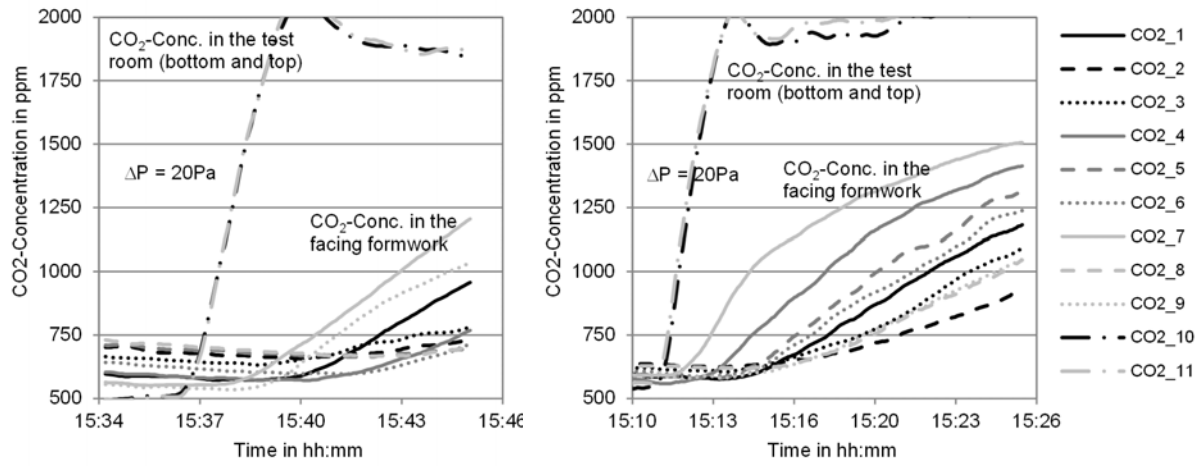

FIG. 5. Leakage in field 7; left with insulation in field 5; right without insulation in field 5

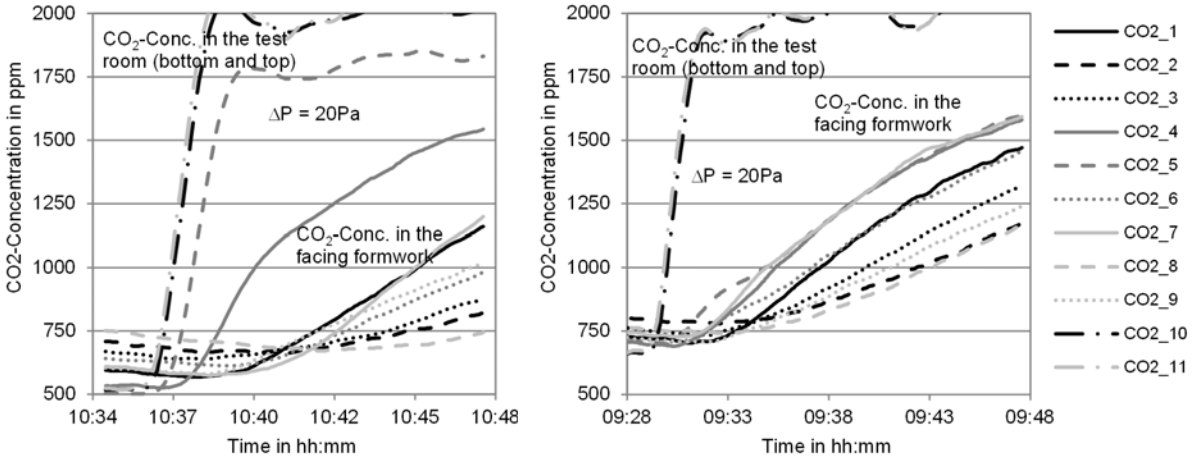

FIG. 6. Leakage in field 5; left with insulation in field 5; right without insulation in field 5

Based on the CO_2-progressions it becomes clear that the measurement of hollow facing formworks provides a solid mean regarding the actual airtightness of a wall-area. When measuring facing formworks with insulation, however, heavily varying results are gained. This is presumably due to flowpaths and cavities within a construction filled with insulation material causing an uneven spread of the tracer gas.

3.2 In-situ measurements of facing formworks on the building site

Based on the method described the air-tightness of an existing construction will now be determined. The measurement is prepared with the following steps:

1. The planking (most commonly gypsum board) is opened carefully between two vertical uprights without damaging the foil underneath. Possible damage to the foil caused by opening must be repaired carefully to restore the initial condition.
2. The vapour barrier is opened at two positions. One aperture is to be made just under the ceiling, the other near to the floor as a cross section. The filling material – usually the insulation material made of mineral wool – can be removed through these openings. It is crucial for the test that the facing formwork's entire test field is empty and has a defined air-volume. The dimensions of this air space must be measured as the air-volume is needed for the evaluation.

3. Two fans are mounted in the cavity to guarantee thorough-mixing of the air in the facing formwork's examined segment.
4. Two to three CO_2-sensors are inserted into the facing formwork through the upper aperture and hung at different heights in the cavity. The cable passage through the vapour retarded must be sealed airtight.
5. An air hose connecting the facing formwork to the outside air is mounted to the lower aperture in the vapour retarder. This hose represents the outer leakage. The connection to the vapour barrier also must be airtight.
6. After checking the cable passages for air-tightness, the gypsum board planking must be restored. This is done by sticking on an additional film to the existing planking in the area of the test field.

The measurement is conducted according to the laboratory test. At least two pressure stages are examined. Furthermore, the air-tightness of the entire inner layer (gypsum board and vapour barrier) as well as just the vapour barrier's air-tightness are measured. This is done by removing the foil attached according to the description in 6. Thus, the build quality of the vapour barrier is quantified.

Not the entire facing formwork of a room is examined, but particular fields between two vertical construction components. In FIG. 7 a wall is depicted schematically. For instance, three of the facing formwork's fields were chosen arbitrarily, the insulation material was taken out and the measuring equipment was built in. Thus, all existing leakages in the entire construction are statistically factored in. In FIG. 7 all possible alternatives of flowpaths are mapped. The black arrows show leakages and air-flowpaths recorded in the measurement. At that, the facing formwork's inner leakage is either located in the area of a test field or an air-flowpath crosses a test field creating a rise of tracer-gas-concentration in this area. The dotted arrows represent air-flowpaths not taken into account during the measurement as they do not run through a test field. As all test fields of a test room are measured at the same time, the mean airtightness per square metre of wall area can be stated.

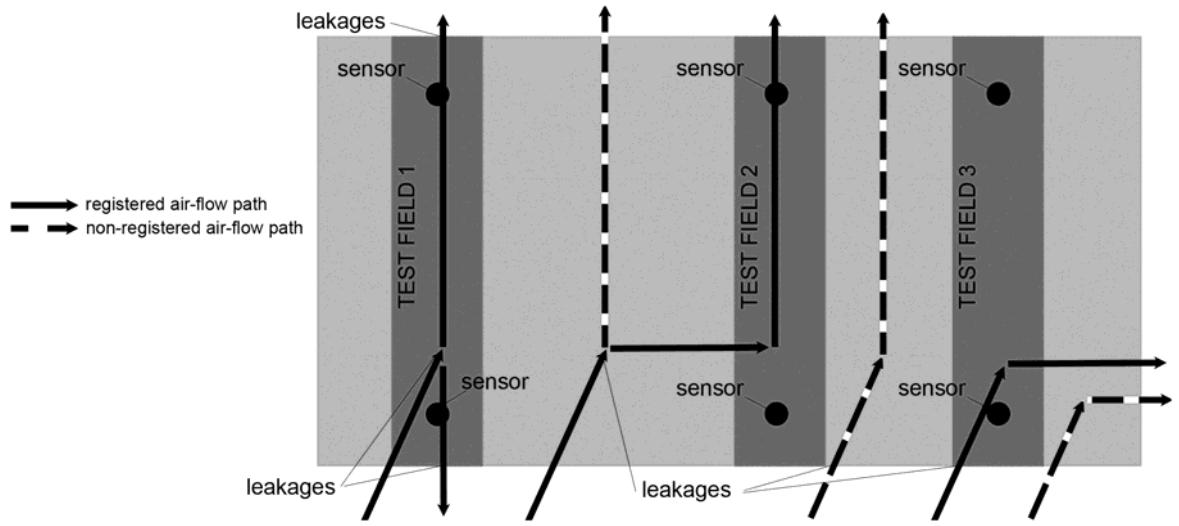

FIG. 7. Schematic view of wall area with three test fields and possible flowpaths both taken and not taken into account. Each test field contains multiple sensors to detect flowpaths.

In FIG. 8 some results of the in-situ measurements are presented. In this case three test fields – one in the reveal and two in the wall left and right to the window – were analysed. The results show that the increase of CO_2 in the window reveal (field 3) and in the neighbouring test field 1 are approximately the same. It stands to reason that a connected plenum exists between these two test fields, whereas test field 2 shows no connecting flowpath to the other test fields. The measurements were done at three stages of pressure differences. Thus, the coefficients C and n could be determined.

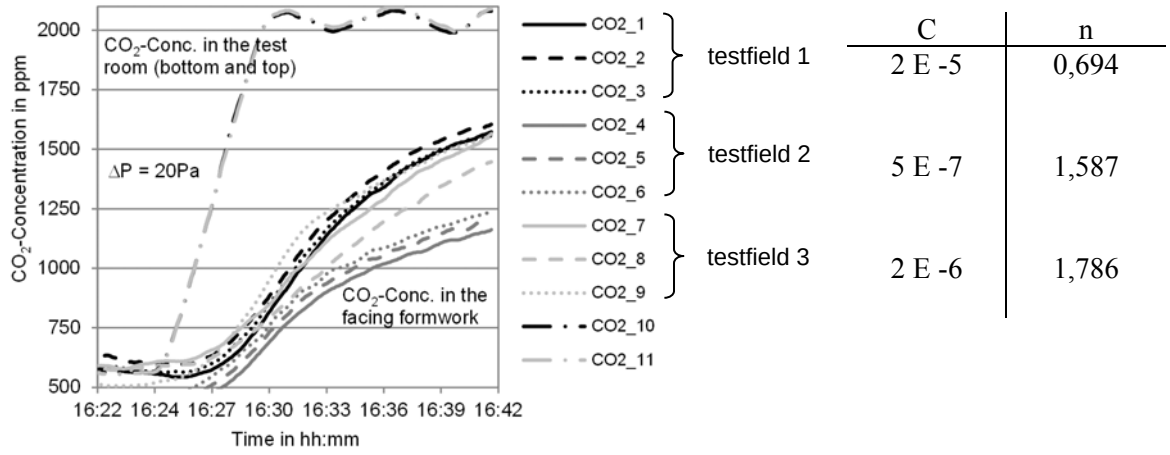

	C	n
testfield 1	2 E -5	0,694
testfield 2	5 E -7	1,587
testfield 3	2 E -6	1,786

FIG. 8. CO_2-concentration in three fields of facing formwork (left); Coefficients C and n (right)

4. Conclusions

Measurements in the laboratory test rig were conducted with and without insulation in the facing formwork. The results clearly show that the insulation material must be removed from the construction to obtain a defined volume of air which then serves as basis for evaluation. Furthermore, it was shown the air-volume in the test field examined in the facing formwork has to be thorough mixed with small fans to achieve an average airtightness. The measurements in the laboratory test rig have also shown that CO_2 entering the facing formwork does not only depend on leakage size and difference in pressure, but also on the dimension of the connection hose between facing formwork and outside air (i.e. the outer leakage). Because of this connection the mass-flow into the construction can be depicted in dependence of the relation between inner and outer leakage. This thesis will be the topic of future laboratory tests.

The in-situ measurement on a real object has shown that all test fields of a cohesive facing formwork provide similar results. It may thus be assumed that the tracer gas does spread immediately after entering the construction and forms flowpaths to neighbouring rooms. This means that more test fields must be arranged for more air-tight constructions to gather a statistic figure for the construction's air-tightness. The sizing of the artificial outer leakage in the form of a hose makes for further need for research.

References

Bednar T. & Deseyve C. & Jung M. & Nusser B. & Teibinger M. 2010. Impact of Airflow on the Risk Assessment of Flat Roofs. in: 7th International Conference on Indoor Air Quality, Ventilation & Energy Conservation in Buildings - IAQVEC 2010, Syracuse University, (2010)

Hall M. & Hauser G. 2003. In situ Quantifizierung von Leckagen bei Gebäuden in Holzbauart.

Sandberg P.I. & Sikander E. 2005. Airtightness issues in the building process. Proceedings of the 7th Nordic Symposium on Building Physics NSB 2005

Wahlgren P. & Sikander E. 2010. Methods and Materials for an Airtight Building. Buildings XI, 2010

Wegerer P. & Neusser M. & Bednar T. 2012. Auswirkungen der Luft(un)dichtheit auf die Feuchtebelastung von Konstruktionen mit Innendämmsystemen. 7th International Symposium on Building and Ductwork Air Tightness in Practice May 11 – 12, 2012, Stuttgart, Germany

EN 12114:2000 Thermal performance of buildings – Air permeability of building components and building elements – Laboratory test method

EN 13829:2001 Thermal performance of buildings – Determination of air permeability of buildings – Fan pressurization method

Airtightness variation over the year

Paula Wahlgren, Senior lecturer [1]

[1] Chalmers University of Technology, Sweden

KEYWORDS: *Airtightness, season, fan pressurization method, air leakage*

SUMMARY:
An airtight thermal envelope is important to achieve buildings with high energy efficiency and moisture safety. The airtightness is commonly measured using the fan pressurization method, and international studies have shown large variations in the measured airtightness at different seasons. In this paper the airtightness variation at different seasons is studied using measurements on two wooden frame, one-family residential buildings. Numerical simulations are presented that show the variation in airtightness due to varying air densities of the air.

The airtightness measurements in the two buildings have been performed during seven months, from summer to winter. The trend in the measurements is that the airtightness is lower (more leaky envelope) when the indoor air is drier (low relative humidity). Consequently, the air leakage is largest during the winter measurements. The decrease in airtightness during the measurement period (from summer to winter) is in the order of 8-10%.

1. Introduction

The airtightness of a building has an impact on the energy use and on the moisture safety of a building. It also affects the thermal comfort, the air quality in a building, sound insulation and the spread of fire gases (Sandberg et al. 2007a and 2007b). Measuring the airtightness of a building has become more common lately, much due to the increased energy use in leakier buildings. The airtightness of a building can be measured in order to attain a certification or on demand from a developer. The consequences if failing the target can sometimes be severe. Therefore, it is of great importance to obtain a correct and representative measure of the airtightness.

The airtightness in a building is created by a continuous and airtight thermal envelope. The airtight layer in a thermal envelope can be either a thin layer, such as a polyethylene foil, a board, such as plywood, a homogeneous construction (e.g. a concrete component) or an outer coating, such as rendering. In all examples it is of great importance that the joints are properly sealed.

Airtightness measurements are usually performed in accordance with EN 13829:2000 (Fan pressurization method). In this standard there are limitations with respect to the climatic conditions during measurements. There is for example a limit on the maximum allowed wind speed and the maximum allowed temperature difference over the thermal envelope. The purpose of the limitations is to assure a correct measured airtightness. Nevertheless, measurements have shown that there is a variation in the measured airtightness with respect to the time of year for the measurement. Yoshino (2012) described variations of ±20% over the year. Boorsboom et al. (2012) analyzed airtightness measurements, from the 80ies, made on 21 window frames mounted in masonry or concrete walls. The average difference in air tightness between summer and winter was about 30% (higher leakage during winter) and the maximum seasonal difference was 120%. To be noted, some window frames showed a lower leakage rate during winter. Boorsboom et al. suggest measurements during three subsequent seasons in order to obtain correct values. Also Kim and Shaw (1986) showed increased leakages during winter time. The highest leakages occurred in winter and early spring, and the lowest

in late summer and fall. Two wood frame constructions were studied and the effect was more pronounced in the leakier building. The measurements indicate that there is a correlation between indoor humidity and envelope leakage.

There are also measurements showing a higher leakage during the summer. An example is Dickinson et al. (1986) who, in one out of three residential, wooden frame houses, measured a lower air leakage in winter time. They do however speculate in the influence of snow and ice on the airtightness. Bracke et al. (2013) measured the airtightness in two new buildings during almost four months (December to April). In the masonry building, there was an increase in air leakage over time. A possible explanation is the different thermal expansion of the masonry/concrete structure and the plaster that assures most of the airtightness in these buildings. This difference in thermal expansion could create cracks in the plaster. Another possible explanation is a gradual deterioration of the ventilation ductwork due to repeated dismantling for the preparation of the pressurization tests.

In order to investigate the possible variations in airtightness at different seasons and the relation to climate, full scale measurements and numerical simulations have been be performed.

2. Methods

The air tightness' variation over season and climate will be studied by measuring the air tightness of three buildings, during one year, and by performing numerical simulations on the climate and the effect on airtightness. The first measurements, on two one-family wooden buildings, started in June 2013. Measurements on a multi-family concrete building will start March 2014. The measurements have been performed by SP, Technical Research Institute of Sweden. Initial numerical calculations have been made on the influence of wind, and on air properties.

The first airtightness measurements were performed on two residential one family houses, both located in the south west part of Sweden, one house in Landvetter and one in Sevred, located outside Borås. The houses are light weight wooden houses in two floors (plain wood in Landvetter and light weight wooden beams/joists in Sevred) and they both have slab on ground and cold attics. Both buildings have mineral wool insulation and polyethylene foil on the inside (between insulation and board) as air barrier and moisture barrier. The house in Landvetter is built in 2004 and the house in Sevred is built in 1993. Both houses have mechanical exhaust ventilation systems.

The airtightness quantity used is air permeability, q50 (l/sm²). It is the amount of air that passes through the thermal envelope at a pressure difference of 50 Pa, per area of thermal envelope (l/sm²). The air flow is measured both when the building is pressurized and depressurized and the mean value is used. The airtightness measurements are made according to EN 13829:2000, using a Minneapolis BlowerDoor. Temperature and relative humidity, indoor and outdoor, is measured at each measurement occasion, as well as the outdoor wind speed. Air leakage search was performed during the first airtightness measurements (June 2013) using air velocity meter and thermal camera, and will be performed again during winter conditions. The airtightness measurements are performed approximately every 1.5 month in order to study the different seasons and climate conditions.

3. Numerical simulations

Simulations have been performed in order to study how the measured air flow is affected by different densities of the air. The density of the air is different due to variations in temperature and relative

humidity over the year. Both high temperatures and high relative humidities result in low densities. Numerical investigations have also been performed on the effect of wind.

During a pressurization test, the air is drawn into the building through leakages in the air barrier of the thermal envelope. These leakages can have different geometry and surface roughness and the air flow can also pass through an air permeable material. The magnitude of the air flow depends on the pressure difference over the leakage path, of the characteristics of the leakage path, but also on the characteristics of the air. The density of the air changes due to temperature and relative humidity and is thus not the same for all measurement conditions. When measuring according to standard EN 13829:2000, the density change that affects the measurement equipment is corrected for. However, there is also the air flow through the leakages, which is slightly different at different air densities. This is investigated with numerical simulations.

The geometry of the building in the calculations is a box with an equal amount of leakages on all sides (including the roof). The effect of air temperature and relative humidity (RH) is determined by investigating two temperature conditions, -20°C and 30°C (RH=40%), and two relative humidity conditions, 0 and 100% (T_{mean}=10°C). A pressure of 50 Pa is used for the calculations and the resulting airtightness of the building is approximately 0.8 l/sm² (varying slightly in the different cases).

Assuming simple leakage geometry with a gap between two plates, the expression for the air flow, *Ra* (m³/s), as a function of pressure difference, *ΔP* (Pa) and leakage geometry is

$$R_a = \frac{\Delta P}{S_g} \tag{1}$$

$$S_g = \frac{12\mu \cdot L}{b^2 \cdot A} \tag{2}$$

Here S_g (Pa·s/m³) is the air flow resistance, *L* is the length of the air gap (m), μ (Ns/m²) is the dynamic viscosity, *b* (m) is the height (or width) of the gap and *A* (m²) is the entrance (or exit) area. In order to include the entrance and exit pressure losses, the air flow resistance at entrance and exit S_e needs to be known. The air flow resistance S_e depends on the air flow which requires the use of a parameter $S_e^{'}$ (Pa/(m³/s)²).

$$S_e^{'} = \frac{1.8 \cdot \delta_a}{2 \cdot A^2} \tag{3}$$

The density of the air δ_a (kg/m³) is included. Total air flow through a crack is determined by

$$R_a = \frac{1}{2 \cdot S_e^{'}}\left(\sqrt{S_g^2 + 4 \cdot \Delta P \cdot S_e^{'}} - S_g\right) \tag{4}$$

As previously mentioned, the leakages are evenly distributed over the building. By investigating extreme temperatures and relative humidities, the factors that possibly influence the airtightness measurements are determined.

The investigation shows that the temperature of the air can affect the measurements by affecting the air flow through the air gaps, see Table 1. Using -20°C, the measured airtightness is 0.76 l/m²s and at a temperature of 30°C the measured airtightness is 0.81 l/m²s. Consequently, the difference between the two extreme measurement situations is 5.7%.

Different relative humidities, however, have minor importance. At 0% relative humidity the airtightness is 0.789 l/m²s and at 100% it is 0.791 l/m²s. The difference is 0.14%, thus negligible. The effect of the air density on the measurement equipment (not leakages as above) is compensated for when measuring according to EN 13823:2000.

TABLE 1. Airtightness at different temperatures and relative humidities.

Air tightness at minimum temperature (l/sm²)	Air tightness at maximum temperature (l/sm²)	Air tightness at minimum relative humidity (l/sm²)	Air tightness at maximum relative humidity (l/sm²)
0.763	0.807	0.789	0.791
5.7%		0.14%	

The simulations on wind are made to investigate if different wind speeds give different airtightness results. Since the average wind speed can be different during different seasons of the year, this could be a part in explaining why different seasons have different airtightness.

In the standard, it is noted that if the meteorological wind speed exceeds 6 m/s or reaches 3 on the Beaufort scale, it is unlikely that a satisfactory zero flow pressure difference will be obtained. Three kinds of zero flow pressure is measured before and after the pressurization test and if either of these zero flow pressures is over 5 Pa, the test does not meet test conditions according to EN 13823:2000.

The shape of the simulated building is quadratic, with a flat roof. The shape factor C_p (-), that determines the pressure difference over a wall at a certain wind influence, is for the windward wall, 0.4, of the leeward wall, -0.2, and for the other walls, -0.3. The roof is -0.6 and the shape factor of the inside of the building, C_{pi}, is determined by a mass air flow balance. The pressure difference, ΔP (Pa), over a wall subjected to wind is

$$\Delta P = (C_p - C_{pi}) \cdot \frac{v^2}{2} \qquad (5)$$

The building is first simulated with equally distributed leakages, and then with a windward side that is twice as leaky as the other sides.

The results from the simulations show that there in many cases is a small difference in the measured airtightness values for pressurization and depressurization when wind is present. However, the average value is not affected until the wind speed increases. For example, at a wind speed of 9 m/s, the building is estimated 2% more airtight with wind than without wind. At a wind speed of 9 m/s, the zero flow pressure difference is most likely exceeding the value accepted in EN13823:2000. In the simulations, a higher wind speed resulted in lower calculated air permeability (more airtight building).

For the case of a non-uniform air leakage distribution, simulations were made for a wind speeds up to 9 m/s. The results are similar to those of the equal leakage distribution, i.e. unless the wind speeds are high there is little error due to wind.

4. Airtightness measurement results

Full scale airtightness measurements have been performed in the buildings described in Section 2. The families living in the buildings are not at home at the time of measurement. Consequently, there is only little moisture production in the buildings at the time of measurement. The moisture supply is in all cases but one below 2 g/m³. The lowest measured relative humidity outdoor is 54% (July, Landvetter) and it reaches 100% in November in Landvetter. Indoor, the relative humidity ranges from 23% (January, Landvetter) to 60% (September, Landvetter).

In the house in Sevred, there is a constant decrease in relative humidity indoor from July to November, while the house in Landvetter has the highest indoor relative humidity at the measurement in September. Both buildings have the lowest relative humidity indoor at the winter measurements. The wind speed is low, at most 3.5 m/s during the measurements.

Both buildings have the lowest airtightness at the winter measurement (January-February). This coincides with the lowest indoor air relative humidity. The measured airtightness (expressed as air permeability) as a function of time is shown in Figure 1, and as a function of relative humidity indoor in Figure 2.

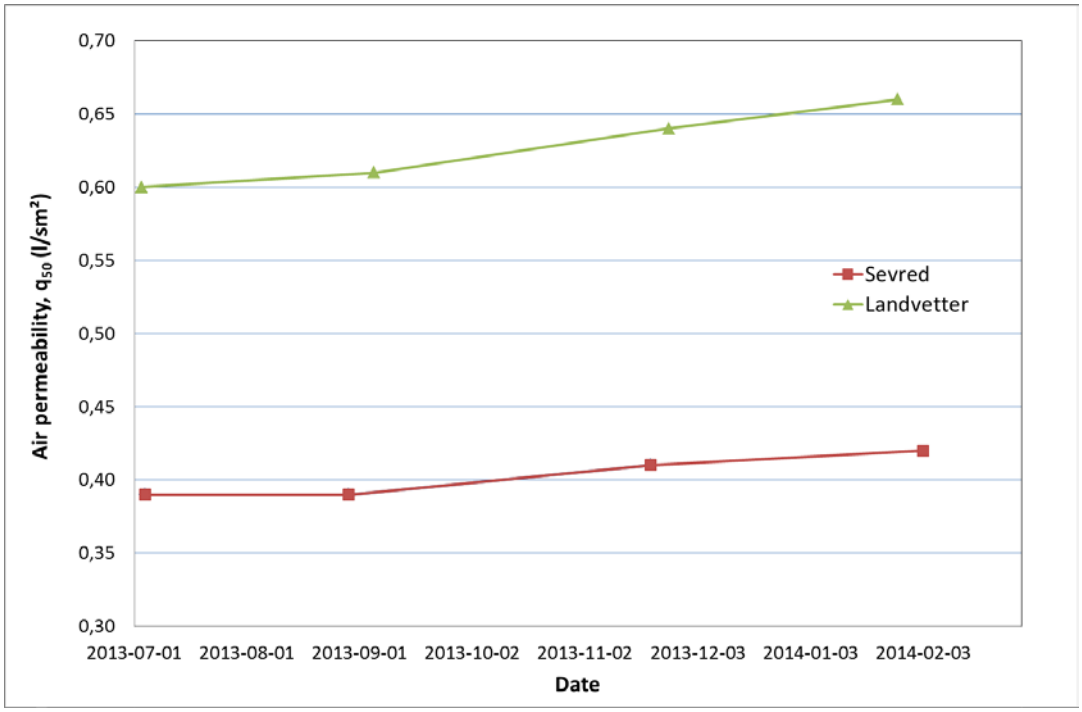

FIGURE 1. Measured airtightness as a function of time for the two buildings.

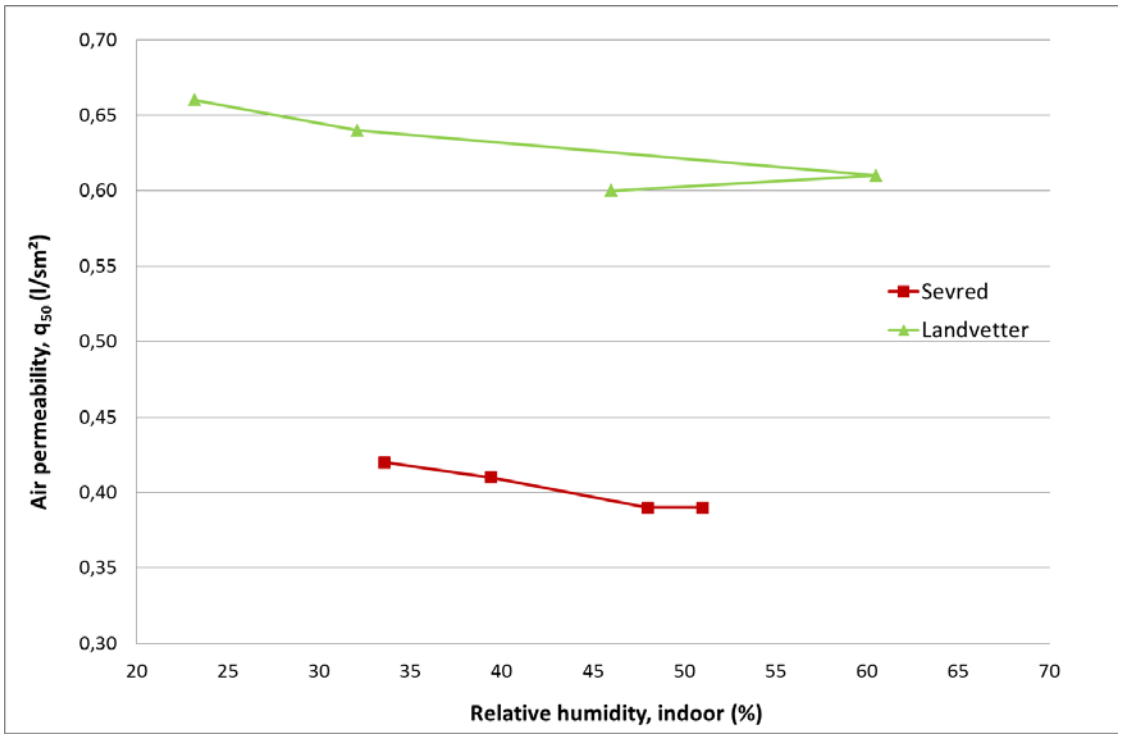

FIGURE 2. Measured airtightness as a function of relative humidity indoor.

There is an increase in air leakage over time. The increase from the first measurement is 10% for the building in Sevred and 7.7% for the building in Landvetter. For both buildings, the airtightness is less when the indoor relative humidity is the lowest. There is no clear correlation with indoor or outdoor temperature, or outdoor relative humidity. The variations in airtightness can be noticeable for stakeholders aiming for a certification.

The measurements will continue and will also include a concrete building (from March 2014). In the two measured wooden buildings shown above, the reason for the increase in permeability could be that the wooden construction dries when the relative humidity indoor decreases. The main leakages in the leakiest building (Landvetter) are found around the windows in the bottom floor, around the attic hatch (see Figure 3) and at the connection between the top and bottom floor (see Figure 4). The reason is probably a poor connection between window and polyethylene for the windows, a poor connection between hatch and polyethylene foil plus a leaky hatch (poor seal) for the attic hatch and a discontinuous polyethylene foil in the exterior wall.

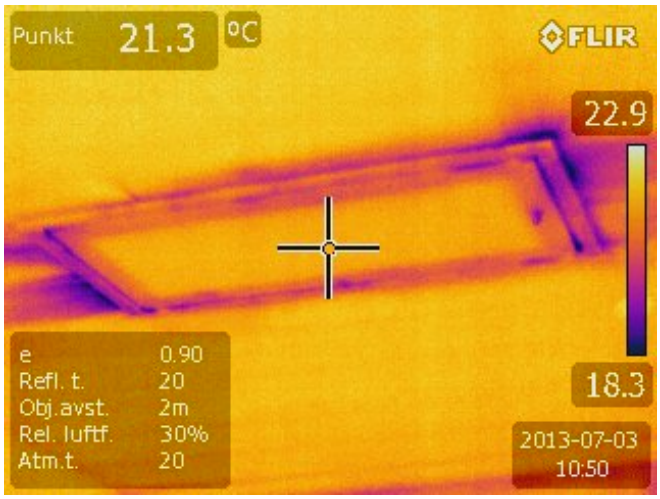

FIGURE 3. Thermographic image of a leaking attic hatch.

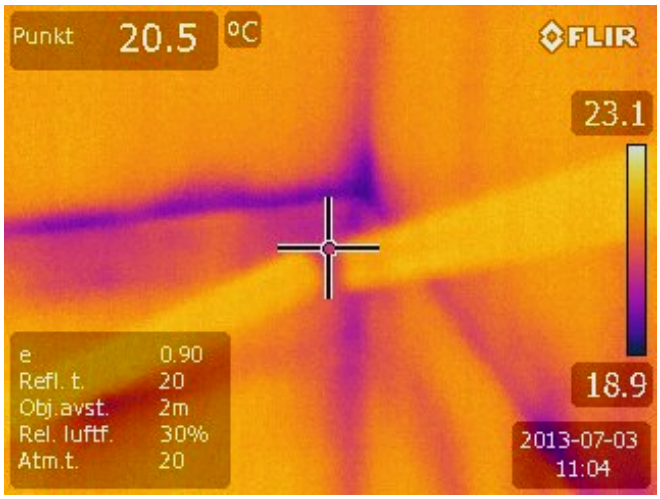

FIGURE 4. Thermographic image of the connection between the upper and lower floor, the brighter diagonal part in front is the hand rail in the stairs.

5. Conclusions

Airtightness has been measured in two residential wooden buildings. The trend in the airtightness measurements is that the airtightness is lower when indoor air is drier. The winter measurements (last reported measurements) have the lowest airtightness of all measurements during the seven months that the measurements have been ongoing. The decrease in airtightness during the measurement period is in the order of 8-10% (from July to February).

The simulations show a small change in air flow through the leakages due to high or low air temperatures (affecting the air density of the air that flow in the leakages), but no change in air flow due to different relative humidities. The effect of the air density on the measurement equipment (not leakages) is compensated for when measuring according to EN 13823:2000.

The measurements will continue to cover a whole year, and in March 2014 a concrete building will be included.

6. Acknowledgements

The research and the measurements have been financed by SBUF, the Development Fund of the Swedish Construction Industry, and supported by FoU-väst (regional comittee), which is greatly appreciated.

References

Borsboom W. and de Gids W. 2012. Seasonal variation of facade airtightness: field observations and potential impact in NZEB. *Proceedings of the AIVC-TightVent International Workshop*, Bryssel, Belgium, March 2012

Bracke W. Laverge J. Van Den Bossche N. Janssens A. 2013, Durability and measurement uncertainty of airtightness in extremely airtight dwellings. *Proceedings of the AIVC-TightVent International Conference*, Athens, Greece, September 2013

Dickinson J.B, Feustel H.E. 1986. Seasonal variations in effective leakage area, *Thermal performance of the exterior envelops of buildings III*, Atlanta, ASHRAE, 144-160.

Kim A.K. Shaw C.Y. 1986. Seasonal Variation in Airtightness of Two Detached Houses, *Measured Air Leakage of Buildings*, *ASTM STP 904*, 1986

Sandberg P-I. Sikander E. Wahlgren P. Larsson B. 2007a. Lufttäthetsfrågorna i byggprocessen- Etapp B. Tekniska konsekvenser och lönsamhetskalkyler, SP Report 2007:23 (in Swedish only)

Sandberg P-I. Bankvall C. Sikander E. Wahlgren P. Larsson B. 2007b. The effects and cost impact of poor airtightness- Information for developers and clients. *Proceedings of the Thermal Performance of the Exterior Envelopes of Whole Buildings X*, Florida, USA, December 2007

EN 13829:2000 (Thermal performance of buildings - Determination of air permeability of buildings - Fan pressurization method (ISO 9972:1996, modified))

Yoshino. H. 2012. System for ensuring reliable airtightness level in Japan. *Proceedings of the AIVC-TightVent International Workshop*, Bryssel, Belgium, March 2012

TOPIC
Building Envelope Systems

Page.....119-320

Performance of internal wall insulation systems - experimental test for the validation of a hygrothermal simulation tool

Valentina Marincioni, M.Sc. [1]

Hector Altamirano-Medina, Ph.D. [1]

Ian Ridley, Ph.D. [2]

[1]University College London, UK

[2]RMIT University, Australia

KEYWORDS: *internal wall insulation, hygrothermal simulation*

SUMMARY: *In the UK, transient models of heat, air and moisture transport (HAMT) are common tools used by building practitioners to better understand moisture movement within building elements and construction systems. Enforced by BS 5250:2011, hygrothermal simulations are also used for condensation risk analysis and to estimate the likelihood of mould growth and fabric decay. This paper describes the methodology applied in the validation of a hygrothermal-modelling tool used in the evaluation of internal wall insulation. Wall assemblies typically constructed for internal insulation were exposed to transient boundary conditions derived from vapour pressure profiles and their response to step changes and fluctuations were analysed. The wall assemblies were constructed using one wall substrate (aerated clay blocks and gypsum plaster) and eight commonly used internal insulation systems. Relative humidity and temperature levels measured at the interface between the wall substrate and each insulation system were used to assess the hygrothermal performance of each insulation system. As a result, the wall assemblies were clustered in three subgroups; dense capillary-active insulation, lightweight vapour-permeable insulation and synthetic vapour-closed insulation, and the hygrothermal performance of the proposed clusters compared with the results provided by the simulation tool. It was found that simulated assemblies have similar hygrothermal performance as those monitored.*

1 Introduction

In England, approximately 6.5 million homes are built of solid wall – 31% of the total housing stock, of which around 60% have been built before 1920. Solid wall dwellings are considered "hard-to-treat-homes", since they cannot be upgraded with easy or cost-effective fabric energy efficiency measures (BRE, 2008). Improving the energy efficiency of these dwellings becomes even harder in conservation areas, listed buildings, or building with decorative façades where the only feasible solution is internal wall insulation (IWI); planning permission for external wall insulation (EWI) is often denied. However, the installation of IWI may affect the interstitial temperature and vapour permeability of the building envelope leading to moisture accumulation and the reduction of the building durability; high interstitial relative humidity is ideal for mould growth and timber decay.

This paper describes the experimental test carried out for the validation of a numerical tool for heat, air and moisture transport. The experiment was designed to help understand the hygrothermal behaviour of internal wall insulation exposed to transient boundary conditions of relative humidity and temperature, and to validate a simulation tool commonly used to estimate moisture movement within building elements and the likelihood of mould growth and fabric decay in buildings. Two walk-in environmental chambers are utilised for the experiment; wall samples were exposed to climate conditions set independently in each chamber.

2 Methodology

2.1 Experimental method

Eight internal wall insulation systems were built and assessed under transient boundary conditions of temperature and relative humidity; these were controlled to define specific vapour pressure levels, to trigger vapour diffusion (varying direction and magnitude) and enhance moisture transfer within the construction assemblies. Similar methodologies have been used for the analysis of the hygrothermal behaviour of internal wall insulation systems exposed to a winter condition, combined with X-ray tomography on moisture distribution in samples (Vereecken and Roels 2011) and for the analysis of timber frame wall samples under external vapour pressure excess (Carmeliet and Derome 2012).

Temperature and relative humidity at the critical interface between the masonry substrate and the insulation system were measured and the data were used in the validation of a numerical tool for the evaluation of capillary active internal wall insulation.

2.1.1 Wall assembly

A partition wall between the two environmental chambers was constructed considering assemblies of one wall substrate and eight different internal insulation systems (Figure 1). The wall substrate consisted of 175mm-thick aerated clay block and 10mm-thick gypsum plaster (outside to inside). The eight wall samples are described in Figures 2-3 and considered capillary active and conventional insulation technologies. The assemblies were constructed as individual units to avoid moisture movement between them; each side of the assemblies was sealed using a polyethylene membrane, leaving only the surface of the aerated clay block and the surfaces of each insulation system in contact to the set exterior and interior climate conditions.

a) 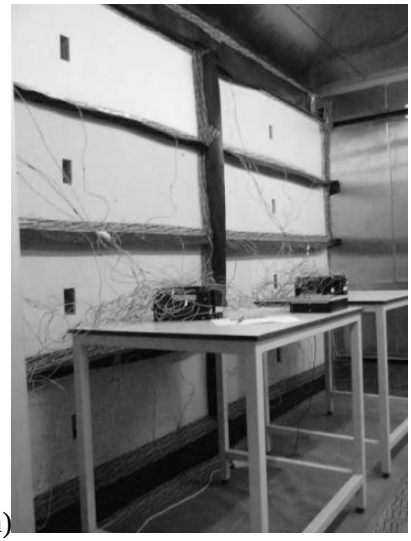 b)

FIG 1. Test wall built between the environmental chambers a) view of eight insulation systems exposed to internal boundary conditions b) view of clay block wall exposed to external boundary conditions

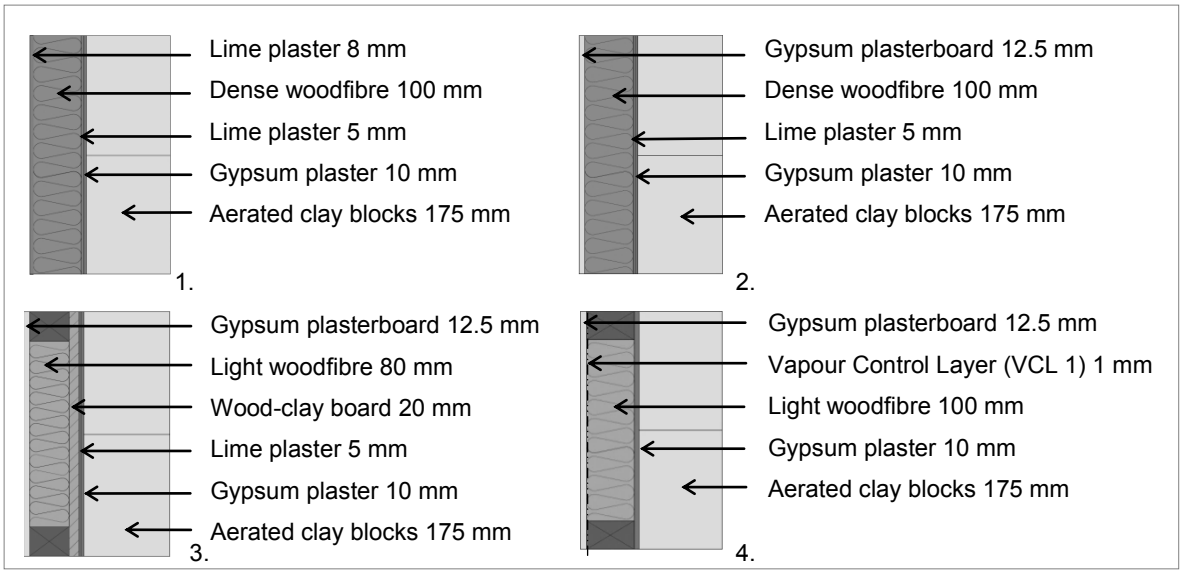

FIG 2. Construction assemblies of the capillary active insulation systems, samples 1 to 4

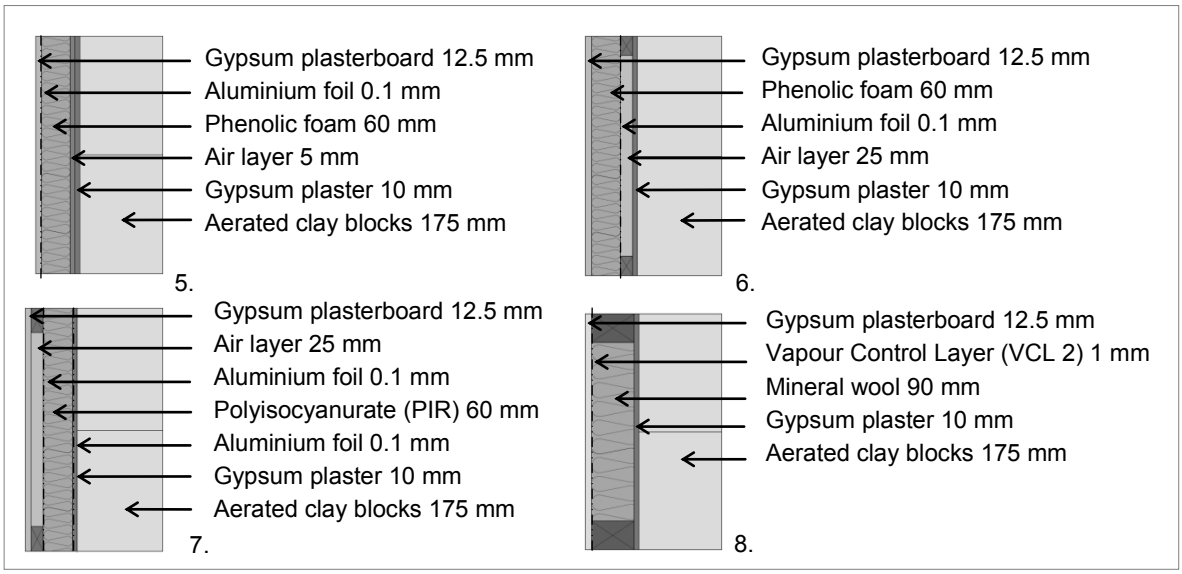

FIG 3. *Construction assemblies of the conventional insulation systems, samples 5 to 8*

2.1.2 Boundary conditions

Profiles of temperature and relative humidity (Table 1) were used to create two vapour pressure gradients between the environmental chambers and within the insulation samples. The first set of boundary conditions (Set 2) considered an internal vapour pressure excess of 400 Pa ($p_{v,int} - p_{v,ext}$ = 400 Pa), while the second set (Set 3) an external vapour pressure excess of 400 Pa,($p_{v,ext} - p_{v,int}$ = 400 Pa). Vapour pressure p_v (Pa), was calculated using equation 1, where T and ϕ represent temperature (ºC) and relative humidity (%) respectively.

$$p_v = \phi \cdot exp\left(22.565 - \frac{2377.1}{T} - \frac{33623}{T^{1.5}}\right) \quad (1)$$

Hygrothermal equilibrium within the wall was achieved by setting similar profiles of temperature and relative humidity (initial conditions) in both chambers. Samples were exposed to T=15 °C and ϕ=80 % for a period of 30 days and to Set 2 and Set 3 for 30 days and 13 days respectively.

TABLE 1.Boundary conditions for experimental test

	Internal T (°C)	ϕ (%)	$p_{v,\,int}$ (Pa)	External T (°C)	ϕ (%)	$p_{v,\,ext}$ (Pa)	Average $\Delta p_v = p_{v,int} - p_{v,ext}$ (Pa)
Set 1 (initial conditions)	15	80	1364	15	80	1364	0
Set 2	18.4 ± 1.5	58 ± 2	1228 ± 158	6.6 ±1.9	85	828±109	400
Set 3	18.4 ± 1.5	29 ± 5	614 ± 164	11.1 ± 3.7	75	991 ± 245	-377

2.1.3 Monitoring

The relative humidity at the interface between the insulation and the substrate wall was monitored using six temperature and relative humidity sensors applied to the gypsum plaster and subsequently covered by the insulation system (total of 96 sensors). Thermocouples and capacitive sensors were used for temperature and relative humidity respectively. Also, room temperature and relative humidity were monitored in each environmental chamber. Data were collected every 5 minutes, for 43 days, and averaged every hour. The collected data were then used as the boundary conditions input in the simulations for the tool validation.

2.2 Simulation method

The paper presents a validation of a heat, air and moisture transport (HAMT) tool; the tool used for the one-dimensional hygrothermal simulations is WUFI® Pro, developed at Fraunhofer IBP and compliant with EN 15026:2007. The material properties, boundary conditions and method of simulation are described below.

2.2.1 Wall assembly

The wall samples analysed in the experiment were reproduced in the simulation tool using material data provided by the respective manufacturers and properties taken from the simulation tool database (Table 2).

TABLE 2. Material properties for simulation

	ρ (kg/m^3)	ψ_o (m^3/m^3)	C_p (J/kg K)	λ (W/mK) at 0% RH	μ (-) at 0% RH
Aerated clay block	1400	0.74	850	0.58	10
Gypsum	850	0.65	850	0.2	8.3
Lime	1600	0.3	850	0.7	7
Dense woodfibre	155	0.981	2000	0.042	3 (1.5 at 60%RH)
Light woodfibre	53	0.96	2100	0.039	1.35 (1.58 at 72%RH)
VCL 1	130	0.001	2300	2.3	3500
VCL 2	130	0.001	2300	2.3	100000
Air	1.3	0.999	1000	0.155	0.51
Aluminium foil	130	0.001	2300	2.3	1500000
Phenolic Foam	43	0.95	1500	0.04	30

2.2.2 Boundary conditions

The boundary conditions considered in the simulation were those monitored in the experimental test and differed slightly from those set in the experiment. Boundary conditions used in the simulation are described in Table 3.

Initial conditions used in the simulation were those measured at the interface between the insulation systems and the wall substrate when the samples were in equilibrium and Set 2 was introduced (time t = 0) as shown in Table 4.

TABLE 3. Boundary conditions for simulation

	Internal			External			Average $\Delta p_v = p_{v,int} - p_{v,ext}$ (Pa)
	T (°C)	ϕ(%)	p_v (Pa)	T (°C)	ϕ (%)	p_v (Pa)	
Set 1 (initial conditions)	15	80	1364	15	80	1364	0
Set 2	17 ± 1.5	60 ± 2	1163 ± 150	6.9 ± 1.9	81 ± 5	806 ± 156	357
Set 3	17 ± 1.5	31 ± 4	601 ± 135	10.8 ± 3.4	76 ± 1	984 ± 237	-383

TABLE 4. Interstitial initial conditions for simulation

	T (°C)	ϕ (%)
Sample 1	15.5	83.8
Sample 4	15.5	74.36
Sample 5	15.7	84.11
Sample 6	15.5	86

2.2.3 Monitoring methodology

Similar to the experimental test, the simulation was set to last for around 42 days. Temperature and relative humidity levels were monitored using virtual monitoring sensors positioned between the wall substrate and the insulation, in the layer representing gypsum plaster.

3 Results and discussion

The experimental test was designed to generate data for the validation of the heat, air and moisture transport model as well as to understand the effect of environmental conditions on the moisture levels at the interface between wall substrate and insulation. The relative humidity at the substrate-insulation interface of 8 internal wall insulation systems was measured and analysed considering the level of humidity and the fluctuation amplitude of the humidity curves after the steps change between the two sets of boundary conditions.

An increase in the relative humidity of sample 5, sample 8 and capillary active insulation systems, ($\Delta\phi/\Delta t$ = 0.283 to 0.779 %/h) was observed in the first 12-hour period after the step change between Set 2 and Set 3. On the other hand, the variation of relative humidity in sample 6 and sample 7 was found to be minimal ($\Delta\phi/\Delta t$ = 0.049 and -0.108 %/h respectively). Similar results were observed after the step change between Set 2 and Set 3; the relative humidity of capillary active systems, sample 5 and sample 8 decreased with a rate of $\Delta\phi/\Delta t$ = -0.124 to -0.048 %/h, whereas sample 6 and sample 7 show negligible variations ($\Delta\phi/\Delta t$ = -0.007 and 0.015 %/h).

Samples 1, 2, 3, 6, 7 showed a daily fluctuation of negligible amplitude. Sample 5 on the other hand, showed a small fluctuation under Set 2, more visible during Set 3. Samples 4 and 8 presented visible fluctuations throughout the test.

TABLE 5. Results

	Set 2		Set 3	
	Δϕ/Δt (%/h)	Peak-to-peak amplitude (%)	Δϕ/Δt (%/h)	Peak-to-peak amplitude (%)
Sample 1	0.283	0.48	-0.105	0.39
Sample 2	0.309	0.32	-0.065	0.46
Sample 3	0.308	0.40	-0.048	0.42
Sample 4	0.613	1.18	-0.199	1.34
Sample 5	0.291	0.76	-0.078	1.06
Sample 6	0.049	0.32	-0.007	0.48
Sample 7	-0.108	0.55	0.015	0.42
Sample 8	0.779	1.78	-0.124	1.53

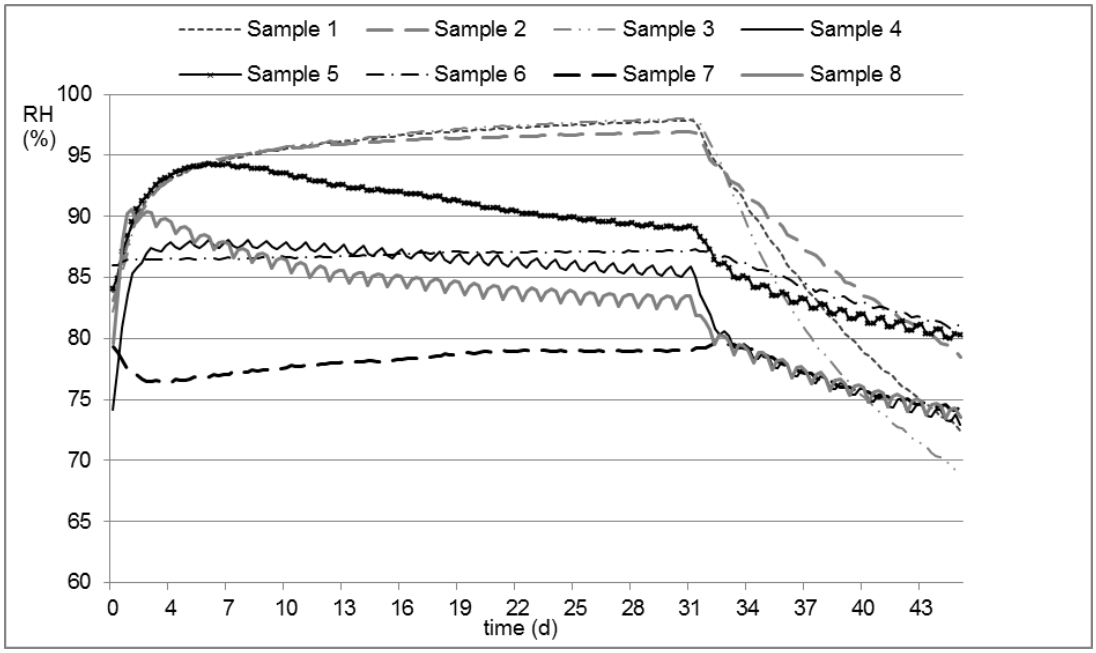

FIG 4. Hygrothermal response to a step change

The results showed that the hygrothermal performance of the insulation systems does not relate exclusively to their generic materials (e.g. wood). For instance, samples 1, 2, 3 – all based on woodfibre – show a comparable hygrothermal performance, while samples 4 and 8 have a similar performance but different materials (woodfibre and mineral wool respectively). For this reason, the samples were clustered in three groups according to their hygrothermal behaviour: Cluster A (samples 1, 2, 3) included samples largely affected by the step change between boundary conditions but showing a negligible amplitude of the daily fluctuations; these samples feature woodfibre-based dense boards with low vapour diffusion resistance coefficients. Cluster B (sample 4 and sample 8) included samples affected by the step changes and with significant daily variations; these samples are made of lightweight fibrous material (light woodfibre batt and mineral wool respectively) and feature a vapour control layer with low to medium vapour diffusion resistances (s_d=3.5 m and s_d=100 m are the respective equivalent air layer thicknesses). Cluster C (sample 6 and sample 7) included samples which presented minor correlations between boundary conditions and interstitial relative humidity; common characteristics of these samples are the presence of foam insulation (preventing moisture movement) and the use of a highly resistant vapour barrier, with μ=1500000. Sample 5, which has similar material properties to sample 6 (see Figure 3), presented a hygrothermal behaviour comparable to samples 4 and 8; this is due to undesired air convection occurring in the sample.

A comparison between the experimental test and the simulations was carried out taking into account the measured and calculated profiles of relative humidity. A sample of each cluster was selected and simulated. Results of the hygrothermal tool were considered acceptable if the profile of predicted relative humidity fell within the data intervals monitored, including a variation/error (ε_ϕ) in the measured relative humidity of ± 3.5 %. Sample 1, sample 4 and sample 6 were used as representative of Cluster A, Cluster B and Cluster C respectively. Sample 5 was also simulated and compared to the measured data.

Results of the simulations showed that the predicted profiles of relative humidity were most of the time in agreement with the measured data. Relative humidities of sample 6, fell the entire period within the range of measured data, whereas relative humidities of samples1 and 4 were at times slightly off from the range of the monitored data, yet following a similar trend. It might be possible that there was a higher actual error of the measured relative humidity; at low temperatures the error (ε_ϕ) of the relative humidity sensors could be as high as ± 30 % (Fossa and Petagna, 2004). In contrast, the trend and the levels of the relative humidity modelled for sample 5 were completely different to the monitored data. These results suggest a likely inaccuracy when constructing the sample; samples 5 and 6 have similar materials and construction assembly, yet dissimilar measured and modelled data.

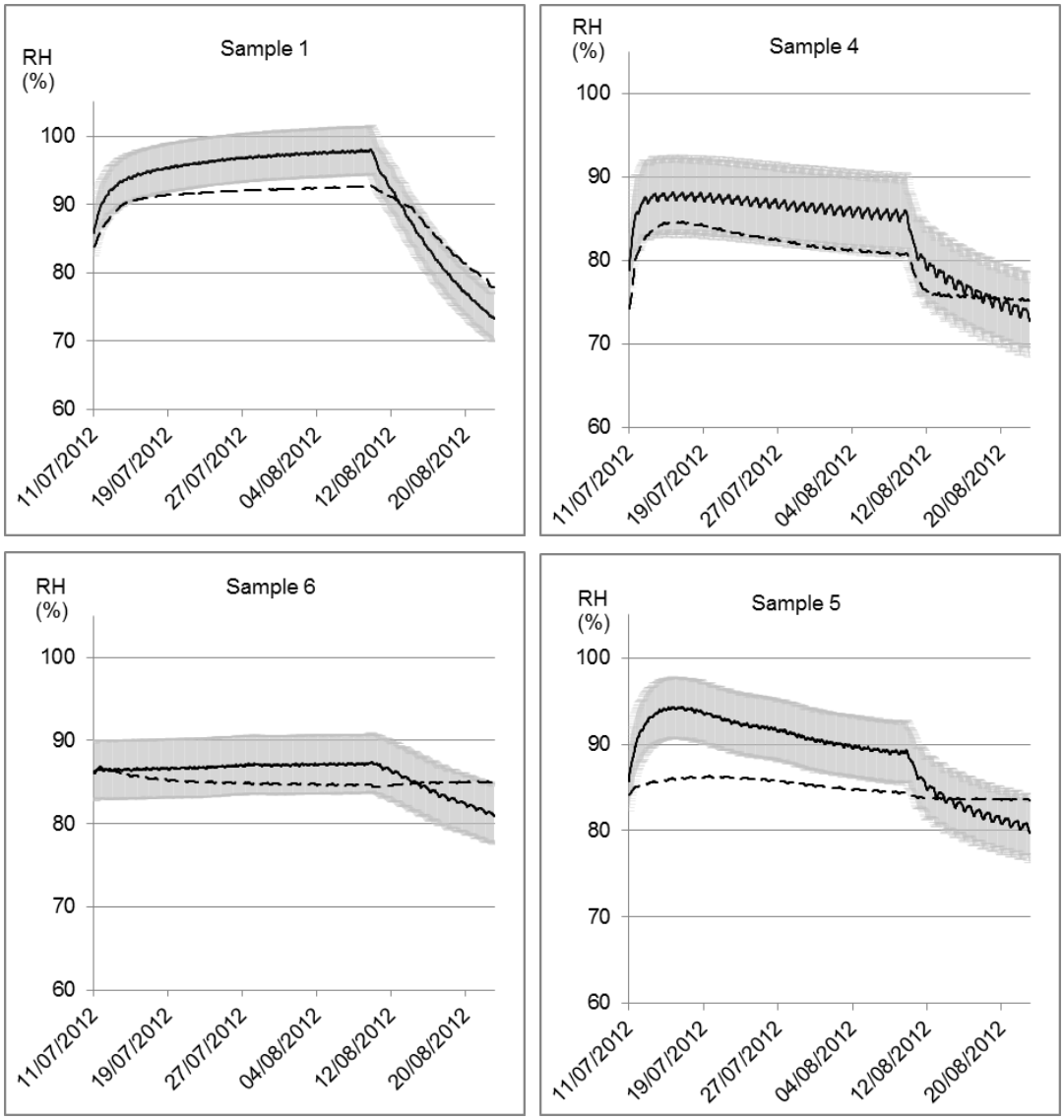

FIG 5. Comparison between experimental data (solid line) and simulation results (dashed line).

4 Conclusion

For certain building typologies, internal wall insulation is the most likely measure for increasing the walls thermal resistance. However, it may have other effects; internal wall insulation may as well help to reduce the temperatures and increase the vapour diffusion resistance of the retrofitted walls, raising the relative humidity at the existing wall-insulation interface, therefore increasing the risk of mould growth and timber decay.

This paper has presented the methodology and results of a test developed to help understand the hygrothermal behaviour of internal wall insulation and to provide data for the validation of numerical simulation tools. The hygrothermal behaviour of eight internal wall insulation assemblies exposed to transient boundary conditions of relative humidity and temperature were analysed by measuring the temperature and relative humidity at the interface between the masonry substrate and the insulation systems. Results of the experimental work showed that the insulation systems had a different response to same boundary conditions and the interstitial relative humidity varied considerably. The difference in hygrothermal behaviour was not only related to the generic materials used in the insulation assemblies, but to the specific properties of the insulation system. Similar differences were observed when the assemblies were modelled and the hygrothermal simulation tool validated.

Acknowledgments

The authors would like to thank Natural Building Technologies and Technology Strategy Board who funded the research project.

References

BRE. 2008. A Study of Hard-to-treat Homes Using the English House Condition Survey. Part 1 — Dwelling and Household Characteristics of Hard-to-treat Homes. Watford, UK, Building Research Establishment.

Carmeliet J. & Derome D. 2012. Temperature driven inward vapor diffusion under constant and cyclic loading in small-scale wall assemblies: Part 1" Building and Environment. 48-56.

Fossa M. & Petagna P. 2004. Humidity measurements inside Atlas and CMS: notes on sensor calibration. [http://proj-jcov.web.cern.ch/proj-JCOV/EBmeeting_22/040422_Rh_Sensor_calibration.pdf accessed on 13/12/2013]

Vereecken E. & Roels S. 2011. Hygric performance of different interior insulation systems: an experimental comparison. 12th International conference on Durability of Building Materials and Components, Porto, Portugal.

Watertightness of window-wall interfaces in wood-frame construction

Nathan Van Den Bossche, Assistant Professor[1]
Glenn De Meersman, M.Sc. [1]
Lynn Devos, M.Sc. [1]
Silke Maertens, M.Sc. [1]
Arnold Janssens, Full Professor[1]

[1] Ghent University, Belgium

KEYWORDS: *Watertightness, airtightness, window-wall interface, wood-frame construction.*

SUMMARY:
In recent years there has been an increased use of wood-frame construction in Belgium, which likewise requires an increased focus on both hygrothermal analysis as well as best practice guidelines to ensure the longevity of this construction type in a temperate maritime climate. This experimental research investigates both the airtightness and watertightness of window-wall interfaces, and the interrelation between both. Three different approaches to secure the watertightness on the exterior side were evaluated, more specifically the use of a watertight layer, spray-in-place polyurethane foam, and self-expanding tapes. The sensitivity of these installation methods was analyzed in respect to the airtightness of the window-wall interface. Based on 3 airtightness performance levels, it was found that the airtightness, and hence the pressure equalization, has a significant effect on the risk for water ingress. Furthermore, the amount of water ingress was also quantified under a range of pressure differences under both static and dynamic boundary conditions. This quantitative approach is also of importance to evaluate the moisture sensitivity and moisture tolerance of wood-frame constructions. Finally, the paper highlights typical installation errors, and provides practical guidelines for airtight window installation in wood-frame construction.

1. Introduction

The market share of wood-frame construction in Belgium is increasing. Studies show that the market share of wood-frame construction for newly built residential dwellings was 5.6% in 2004, it rose to 11% in 2009, and it is expected to increase up to a market share of 20% by 2020 (BBRI, 2020). In Belgium, residential buildings are typically constructed with brick cavity walls with about 8 to 20cm of insulation in the cavity. Consequently, the majority of technical guidelines and sector documents refer to that building practice, and little to no information is available on wood frame construction. Furthermore, Viitanen et al. (2010) report the modelled mass loss of pine sapwood for all of Europe, which shows that the climatic conditions in Belgium are among the worst in respect to wood decay.

In Belgium, the BBRI (2007) reported that 24% of all interventions for buildings relate to moisture, and water infiltration is the most important cause of building damage (condensation, absorption due to capillary action and initial moisture content are excluded). Brick cavity walls are the predominant construction type in Belgium, and this type of wall has the specific capacity of absorbing significant amounts of water without leading to premature deterioration or failure. Commonly, there is an exterior brick leaf with solid bricks, a ventilated air cavity, insulation, an extruded and perforated interior brick wall, and a stucco finish. A limited amount of inadvertent water ingress past the insulation layer may be stored by the interior brick wall, and due to the high vapour permeability of the construction

on both sides, the water may dry out without causing any damage. In general, water ingress will only cause damage when the storage and drying capacity of the construction are superseded, from which it may be evident that wood frame construction will be more prone to risk of failure when occasional water ingress occurs.

Wood frame construction is a relative new typology in Belgium, the Belgian climate shows to be rather severe in respect to wood conservation, moisture problems are the predominant type of building mitigation, and wood frame construction is probably less robust when considering occasional water ingress. Consequently, more research is required to evaluate to what extent the introduction of a new construction typology in a county with a history of moisture problems may lead to excessive damage.

Based on a review of 50 buildings in Alberta, 57 out of 105 rainwater penetrations were situated around windows and doors (Ruest, 2000). RDH (2000a, 2000b) found 15 failing window-wall interfaces in 127 field tests in British Columbia. For the same area, a different report on 37 buildings which experienced envelope failures showed that at least 25% of all problems were related to the windows or the window-wall interface (Rousseau, 1999). Similar conclusions were drawn in Florida (Lstiburek, 2005). Even though no scientific data were found for Europe, building practitioners often report that the window-wall interface is prone to water ingress problems, and hence, the window-wall interface was selected for this research paper. In this paper, the watertightness of several types of window installation methods are evaluated both qualitatively as quantitatively, under static and dynamic conditions, and taking into account a range of typical airtightness performance levels of window-wall interfaces. In the subsequent chapters, an overview of literature on the watertightness of window-wall interfaces is provided, followed by the description of the experimental setup, test results and conclusions.

2. Literature on the watertightness of window-wall interfaces.

A query in the database of the European Committee for Standardization yields over 2000 standards solely related to the performance of building components and materials (excluding products related to building services). When an architect draws a window-wall interface for a masonry brick wall, 148 standards may apply to the window, 73 to the glass, 85 to the masonry, 94 to the insulation, 70 to fire safety, 167 to concrete, 55 to acoustics… Additionally, ISO standards, national and regional codes can add to the complexity. Only nine standards relate to watertightness: concrete, windows, doors, curtain walls and roof coverings are addressed (query executed 04/12/2013). For the watertightness of window-wall interfaces, there are no specific test standards.

Nelson and Norris (2010) evaluated the watertightness of window-wall interfaces, for storefront windows installed in stucco walls (storefront windows: US terminology for windows without flanges, i.e. similar to European practice). Interestingly, although all perfect barrier systems failed, the authors do not question the concept of perfect barrier systems, and only insist making it more perfect. In New Zealand a new window installation method was advocated by the national window association (Knowles, 2002). Here a double-stage joint is applied at the window-wall interface, but drainage is poorly designed. The weather resistive barrier underneath the sill is not sloped, certain locations prone to wetting are not drained, and the design of the front seal is typical for perfect barrier systems. In 2003 it was even suggested in the New Zealand parliament to forbid the use of silicone sealant as primary means of weathersealing systems (2003).

Lacasse et al. (2008) compared the performance of a face-sealed window installation with a rain screen joint. It was concluded that the most airtight plane should not coincide with the rain screen. The exterior side of the joint should not be airtight, to reduce the driving force for water to enter. Consider that the location of the drainage plane is not clear at the top and sides. Consequently water ingress was reported due to insufficient drainage design (Lacasse et al. 2009). Salzano et al. (2010)

also found that drained systems perform better than perfect barrier installation methods in a rain screen wall. Conversely, for a concrete masonry wall, designed as perfect barrier system, the installation method with a single barrier performed better. Consider that for these test results the leakage paths were not described, the installation method in the concrete wall is not described in detail, and the sill flashing is level instead of sloped. Why the single-joint performs poorly in one situation and reasonably well in a different situation is not explained.

Note that the necessity to apply the rain screen principles to window-wall interfaces was already described explicitly and in great detail in 1957 by Birkeland (1957), who ends his paper with the sentence "Tightness is not increased by caulking the joint". Even though the use of drained joints is often advocated (Edgar, 1999; Finn, 1991), it seems that currently it still cannot be considered as common building practice in the US.

3. Experimental setup

A non-operable wooden window (1.55m high by 1.23m wide) was installed in a typical wood frame wall of 2.28m high and 1.94m wide. This wall comprised an interior airtight sheeting of taped oriented strand boards, an air-open exterior impregnated fibre board, but for reasons of visual inspection by means of an endoscope, no insulation was installed between the studs. On the exterior side, the cladding consists of slender horizontal planks, which was assumed the be rather permeable for wind driven rain. At the sill and top of the window, cross cavity flashing was installed by means of an aluminium profile, with end dams at the sill. The wood frame wall was installed perfectly airtight in a steel test box.

At the bottom side of the rough window opening a water collection tray and drainage system was installed, to measure the amount of water ingress into the window wall interface. Infiltration water from the drainage was directed to a hermetically sealed gravimetric trough and weighing system. The drainage system was designed in such a way that the water that was drained did not occlude the drainage tube, and in order to avoid artificial pressure gradients caused by the weighing system itself, the collection through was connected to the window wall interface with a pressure tube. That allowed for perfect pressure equalization, omitting any inadvertent pressure gradients due to perturbations in the collection system.

3.1 Test protocol

There is no specific test standard to evaluate the watertightness of joints or interfaces. For windows, a static test sequence is provided in EN 1027. The European standard EN 12865:2001 describes a test protocol to determine the resistance of external wall systems to driving rain under pulsating air pressure. According to this standard, water is sprayed at two locations: 72l/h-m at the top as run-off, and 90L/h-m² on the whole area to simulate direct Wind driven rain. The pressure difference is applied in a step-wise approach to determine at which level water entry occurs. Furthermore, the standard offers two procedures: one for qualitative testing (A - steps of 10 minutes after 20 minutes of initial wetting), and the other for quantitative testing (B - steps of 60 minutes). Although there is no standard for window-wall interfaces, the interface is perhaps expected to perform well according to both test sequences (windows and walls). Consider that the EN 12865 only provides a test sequence, without information on the required performance levels as a function of exposure to climate conditions. Consequently, the samples will be tested according to the static test protocol up to 750Pa (EN 1027) and the cyclic test protocol up to 600Pa (EN 12865).

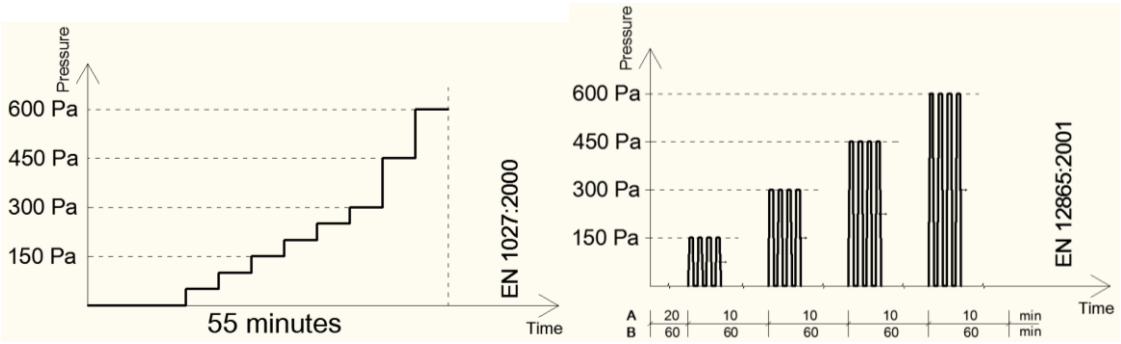

Figure 1. Dynamic test sequence according to EN 12865.

To assess the effect of the airtightness of the window-wall interface on the risk for water ingress, the airtightness of every setup was also determined based on EN 12114. Please refer to (Van Den Bossche et al., 2012) for more information on the airtightness measurements and error analysis.

3.2 Test parameters

Four different parameters were varied during the test sequence: mechanical installation of the window to the wall, installation method to ensure the watertightness, position of the window in respect to the wall, and the level of airtightness of the interface.

3.2.1 Mechanical installation

In Belgian brick construction practice, windows are typically fixed to the wall using steel brackets. Direct fixation with screws through the window frame itself – typical for German window installation in ETICS – is not advocated in Belgium, and flanged windows are not available. The brackets allow for a practical and flexible installation, but conversely hamper the easy installation of airtightness membranes at the window perimeter. The alternative is a plywood casing around the window frame, which in turn replaces the brackets. The plywood provides a solid ground for the finish of the window reveal, and allows to secure the airtightness easily.

3.2.2 Position of the window in respect to the wall

The position of the window frame might depend on the alignment with the thermal insulation, esthetical or mechanical boundary conditions, but by consequence will also affect the exposure to wind driven rain. Four positions are considered (see figure 2): behind the impregnated fibre board (a), onto the back of the fibre board (b), aligned with the fibre board (c), or projected outwards (d). Mind that the critical pathways for water ingress also shift from the bottom to the top as the position of the window shifts to the exterior. The highest risk for infiltration is located at the corners, where – depending on the position of the window – complex folding may be required to ensure the continuity of the foil. When the window is aligned with the fibre board, the foil can easily be installed with a low risk for installation errors.

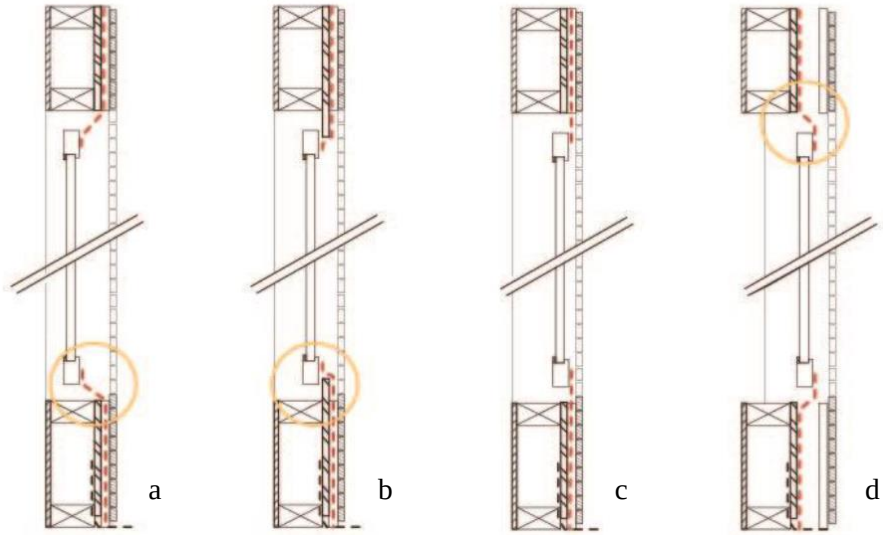

Figure 2. Position of the window in respect to the wall.

3.2.3 Installation method

The watertightness of the interface is primarily determined by the joint between the window frame and the impregnated fibre board. For this joint, three options were evaluated: foil, self-expanding sealant tape, and spray in place polyurethane foam. On one side the foil is adhered to the window frame with caulking, on the other side there is an adhesive with release liner to adhere it to the wall. The self-expanding sealant tape consists of an open cell impregnated foam, that is designed to act as a single stage joint for watertightness (type BG1). The spray in place polyurethane foam is a one-component flexible and low expansion foam. The main advantage of flexible foam is that it is capable of following the movements of the window frame induced by wind pressures, thermal gradients and forces due to opening and closing the sash.

Figure 3. Installation with self-expanding tape (left) and foil (middle and right)

3.2.4 Airtightness

The amount of water that enters into the cavity will depend upon the pressure gradient over the exterior, that in turn will be affected by the pressure equalisation and the airtightness of the interface. Based on stochastic analysis of the Belgian building stock, Van Den Bossche et al. (2012) derived three performance levels for the airtightness of window wall interfaces. Good installations entail an air leakage below 0.33m³/h.m; poor installations cause air flows above 3.3m³/h.m, and average performance is characterized by an air flow rates between the threshold levels reported above.

4. Results

4.1 Mechanical installation

The tests indicate that the type of mechanical installation did not affect the watertightness performance when self-expanding sealant tape or watertightness foil was applied. This was most evident for installations with a good airtightness, whereas installations with significant air leakages tend to show small discrepancies. Nevertheless, differences in water ingress could be attributed to executing performance. In general, installations using a plywood frame around the window frame proved to be less susceptible to errors in the airtightness: the use of metal brackets typically introduces more difficulties to ensure the airtightness, but for equal airtightness similar performances were found. When spray in place polyurethane foam was applied, a difference in failure behaviour was noticed. The foam itself did not show any leakage, but local deficiencies at obstacles may lead to water ingress. When installing metal brackets, it is important to make sure that the bracket itself does to protrude to the exterior, where it is exposed to runoff. Even though the foam was installed carefully, it does not provide a continuous barrier. For the installation with plywood frames, small wood blocks are used as spacer to position the window frame in respect to the rough window opening. At these blocks, the continuity of the foam is interrupted, which also gave rise to water ingress.

4.2 Position of the window in respect to the wall

Only for the case where the watertightness was ensured by a water resistive barrier as flashing, the effect of the position of the window was evaluated. As the window is located more inwards, the flashing at the bottom is more exposed, and inadequate drainage may lead to local accumulation, hydrostatic pressure and infiltration. Likewise, as the window is located more towards the exterior, the flashing at the top is similarly more exposed. However, the results show that more problems can be expected at the sill, as the window itself causes a high runoff rate at the sill, whereas at the top most of the water is diverted by the cross-cavity flashing.

4.3 Installation method and airtightness

The installation with sealant tape did not perform well. At the sill, the installation of the sealant tape apparently led to accumulation of water, which caused a hydrostatic pressure. Next to that, additional repetition tests showed that the specific sealant tape used in this study displayed shrinkage and swelling behaviour under wetting and drying cycles. With each cycle the sealant tape shifted slightly downwards due to gravity. Consequently, horizontal joints should be avoided with this type of tape, and otherwise these must be shielded from rain and runoff as much as possible. The compression of the tape should be adequate to prevent any sinkage of the tape. For a good airtightness the amount of water infiltrating to the interior was rather limited, whereas the water ingress increased as the airtightness decreased. The results reported in table 1 are those for window location b. The installation with a self-adhering flashing membrane to the window frame proved to be very susceptible to execution errors. The adhesion was found inadequate, and the joint between window and flashing was henceforth sealed by means of caulking (reported in the table below). Without caulking, water ingress rates of 14,7 up to 34,6 gram/min were measured under static conditions, and also under dynamic conditions the infiltration rates were higher. Table 1 again indicates that a good

airtightness has a beneficial effect on the occurrence and amount of water ingress. Even though the average airtightness seems to entail a better watertightness compared to the airtight situation, this can be attributed to the premature failure of the flashing adhesion: during the cyclic loading the membrane failed, leading to high air flow speeds and water ingress. Furthermore, it may be evident that the amount of water ingress is also affected by the exposure to direct rain impingement and runoff. By installing an additional shielding that diverts most of the water away from the flashing, the infiltration rate reduced by as much as 63%. Additionally, tests were done on a different damage pattern as well: during installation of the sill, local forces may induce excessive stress in the adhesion of the flashing. A representative installation error increased the infiltration rate from about zero to 23.2, 14.2 and 12.3 gram/min under static test conditions for a poor, average and good airtightness respectively, and likewise an increase for dynamic conditions to 27.8, 18.5 and 18.5 gram/min.

Table 1.Overview of a selection of test results

Rain barrier	***Airtightness***	***Water ingress (gram/min)***		***Pressure at infiltration (Pa)***	
		Static	**Dynamic**	**Static**	**Dynamic**
Sealant tape	Poor	X	X	0	0
	Average	13,33	9,9	0	0
	Good	0,48	0,15	300	450
Flashing	Poor	6,6	9,5	150	0
	Average	0	0	n.f.	n.f.
	Good	0	0,6	n.f.	450
PUR	Good	X	X	150	300

X: water ingress could not be measured; n.f.: no failure up to at least 600 Pa. The results reported in this table are the average infiltration rate monitored at 0, 150, 300, 450 and 600Pa for both static and dynamic pressure conditions.

When polyurethane was installed, the cavity between the window and the rough window opening was filled and thus blocked any infiltrating water to run down towards the collection through. Next to that, the airtightness of the setup could not be altered easily as the polyurethane itself secured the airtightness, and consequently only measurements were done for installations with good airtight sealing. Table 1 does not comprise measured infiltration rates, but water infiltrated at rather low pressure differences: 150 and 300 Pa for static and dynamic conditions respectively. Mind that the accompanying infiltration rates were very limited. The leakage pathways that did arise could be attributed to the presence of oversized spacers between window and rough opening. When no spacers are present, no infiltration was evident up to 600Pa.

5. Conclusions

The watertightness of window-wall interfaces in wood-frame constructions was evaluated in lab conditions, under static and cyclic wind pressure loadings. Two types of mechanical fixing to the interior wall were evaluated: steel brackets and plywood casing around the window. The steel brackets require more attention when installing the airtightness foil, but no significant effect was found on the level of watertightness. When polyurethane foam is used, one should ensure a continuous layer of foam, avoiding any crossing brackets or other obstructions. Tests on the position of the window were not reported in detail, but for all positions the sill was most prone to water ingress probably due to higher local runoff rates. The use of sealant tape led to high infiltration rates

at lower pressure differences. Even though reasonable results were found when the airtightness was good, this installation showed to be susceptible to errors in execution as well. The results for the water resistive barrier show a clear correlation between water infiltration rate and air leakage. Polyurethane foam only showed infiltrations when to foam was breached by means of steel brackets or spacers. Note that the static and cyclic watertightness tests do not lead to identical results in terms of infiltration rates and pressure difference at moment of failure. Next to that, it is unclear which of both is most severe: the failure initiation phenomena differ from installation to installation, leading to different interpretation under different test sequences. Note that all results are highly sensible to installation, materials used in the setup and craftsmanship.

References

BBRI, 2010. Research on new building concepts, and the impact on natural resources. (in dutch). Belgian Building Research Institute, VITO, KULeuven.

Viitanen H., Toratti T., Makkonen L., Peuhkuri R., Ojanen T., Ruokolainen L., Räjsänen J., 2010. Towards modelling of decay of wooden materials. European Journal of Wood and Wood Products 68, 3: 303-313.

BBRI, 2007. Annual report. www.wtcb.be

Ruest K., Wall moisture problems in Alberta dwellings. CMHC Research Highlights (2000) CMHC, Ottowa, Canada.

RDH, 2000a Water penetration resistance of windows – study of manufacturing, building design, installation and maintenance factors, RDH Building Engineering Limited, Vancouver, 2002.

RDH, 2000b Water penetration resistance of windows –study of codes, standards, testing and certification. RDH Building Engineering Limited, Vancouver, 2002.

Rousseau M., An Overview of the Survey of Building Envelope Failures in the Coastal Climate of British Columbia, performed by Morrisson-Hershfield Limited for CMHC (1996). Journal of Building Physics (1999) 22: 364-367.

Lstiburek J.W., Rainwater management performance of newly constructed residential building enclosures during august and September 2004. (2005) Building Science Corporation, MA.

Nelson C., Norris R.E., Mock-Up Water Test Results of Sample Flashing Systems for Storefront Windows in Stucco Walls. Interface (2010) RCI inc., Raleigh, NC.

Knowles S., WANZ Window Installation System. Window Association of New Zealand. Wellington, NZ, 2002.

House of Representatives, Weathertightness of Buildings in New Zealand. Forty-Seventh Parliamant, March 2003.

Lacasse M.A., Rousseau M.Z., Cornick S.M., Manning M.M., Nicholls M., Nunes S., Performance evaluation of Wall-Window Interface Details Phase 1 – Watertightness, Air Leakage and Rainwater Management of CMHC Specified Assemblies. Report B-1229.1. National Research Council, 2008.

Lacasse M.A., Rousseau M.Z., Cornick S.M., Manning M.M., Ganapathy G., Nicholls M., Williams M.F., Assessing the effectiveness of window-wall interface details to manage rainwater – selected results from US window installation practice. Journal of ASTM International (2009) 6, 8: 1-35.

Salzano C.T., Masters F.J., Katsaros J.D., Water penetration resistance of residential window installation options for hurricane-prone areas. Building and Environment (2010) 45: 1373-1388.

Birkeland Ø. The design of multi-layer walls. Report No 24, Norges Byggforskningsinstitutt. Oslo, 1957.

Edgar J., Performance of Source Drainage Exterior Insulation Finish System at the window/wall junction. Journal of Building Physics (1999) 23: 57-77.

Finn D., Rain penetration control of the window-wall joint. Institute for Research in Construction, NRC. NRCC-38747, 1991.

Van Den Bossche N., Huyghe W., Moens J., Janssens A., Depaepe M., 2012. Airtigthness of the window-wall interface in brick cavity walls. Energy and Buildings 45: 32-42.

An Outdoor Hut Testing Platform for Evaluating Advanced Building Enclosures

Bryan Urban, *S.M.*[1]
Nitin Shukla, *Ph.D.*[1]
Anthony Fontanini, *Ph.D. Candidate*[2]
Jan Kosny, *Ph.D.*[1]

[1] Fraunhofer Center for Sustainable Energy Systems, USA. Email: burban@fraunhofer.org
[2] Iowa State University, USA

KEYWORDS: *thermal testing, heat flux, insulation, R-value, measurement*

SUMMARY:

Evaluating the thermal performance of novel advanced building enclosures is challenging, and there is a need for better and more cost effective methods for doing so. Laboratory testing of components provides accurate results under special conditions, however, these may fail to represent complex dynamic interactions between system components. Field testing can offer more realistic performance evaluation, however, studies involving occupied buildings suffer from many confounding factors, such as occupant interactions and unknown building material properties that make it difficult to generalize results. Whole building energy modeling is the ultimate goal for evaluating and designing new building systems, however, without proper validation, the models cannot be trusted. In this paper we present a flexible approach for cost effective evaluation field testing of building advanced enclosures.

1. Introduction

New building components or systems must be evaluated and tested before going to market. From an energy and durability standpoint, it is desirable to measure performance on several dimensions, including thermal performance (heat gain or loss through components), occupant comfort (temperature and humidity in occupied zones), moisture performance (moisture accumulation and material durability), air tightness (and its impact on energy consumption), and energy performance (HVAC energy reduction, peak load shifting). Various testing approaches have been developed and tried in the last century. This paper is not meant to be a comprehensive review of such methods; however, it does illustrate some different philosophies and why the proposed approach may be appropriate for specific testing goals.

We present a flexible, nearly-calorimetric testing platform that combines the advantages of outdoor field testing with the controllability of a laboratory experiment. The platform is comprised of multiple small testing structures, or huts. One hut is built to standard construction practices (e.g., typical residential construction) and acts as a control or baseline case. The other hut(s) are constructed identically, with the exception of the novel building materials or components. All huts are conditioned with identical HVAC systems and control strategies, and HVAC energy consumption is metered during the experiment. Air tightness of each hut is measured prior to each experiment. Detailed temperature and heat flux measurements are made across assemblies of each hut. A weather station records outdoor conditions. Resulting data may be used to support the validation of energy models for advanced systems or to rapidly evaluate prototype building systems or components.

This paper presents the results of testing measurements made during the fall in three huts used to evaluate an advanced insulation material. Here we focus on description of the platform, construction and experimental technique, and the measurements obtained during testing. Through a six month

experiment, we have determined that this platform may be used to effectively test and compare thermal performance of insulation systems.

2. Description of Testing Platform

2.1 Testing Platform Architectures

In the testing platforms we consider, test structures are used to represent a specific type of building construction. Unlike experiments that completely isolate all components except for the one of interest, this platform seeks to obtain results that are more representative of a fully constructed system. Since real systems will have measurable air leakage and 3D conduction effects, it is important to test new products in situations where these effects may be non-negligible. The dynamic interaction of heat flow and thermal storage between various building components during the daily heating and cooling cycle is difficult to match in a laboratory experiment.

Two main approaches (single-structure and multi-structure) and two testing methods (serial and parallel) exist for performing direct-comparison in-situ building tests, each with distinct advantages depending on the situation and goals of the test.

2.1.1 Serial vs. Parallel Testing

In serial testing experiments, the performance measurements of components are made in sequence. This is akin to “before and after” testing or pre- and post- retrofit comparison. Serial testing is challenging since environmental conditions are often not identical or equivalent during both testing periods and it can be difficult (though not impossible) to control or adjust for variations by using simulation or engineering calculations.

In parallel testing, all systems are tested simultaneously. In this way, uncontrollable environmental factors are kept consistent during the test, eliminating an important source of error. When practical, parallel testing is preferred for its higher accuracy and more consistent results for making direct comparisons between systems.

When direct comparisons between systems are desired, parallel testing is often preferred. Parallel testing requires more infrastructure than serial testing, since it is necessary to have enough instrumentation for each product that will be tested. Serial testing, conversely, requires less equipment but more labor and time to remove and replace sensors before and after each reconstruction phase. The cost/benefit tradeoffs depend on the goals and resources of the experiment.

2.1.2 Single-Structure vs. Multi-Structure Testing

Single-structure testing, naturally, involves only one test structure. In the case of a serial single-structure test, this single structure is used to measure both baseline and retrofit conditions through a pre- and post- retrofit measurement study. This option suffers from uncertainty driven by environmental variability between measurement phases. In a parallel testing single-structure experiment, the single structure is made large enough to accommodate several different test elements within the same building so testing can be done simultaneously. For instance, one wall could be divided into several subsection sections, each one used to test a different type of insulation material. It may be easier to maintain consistent and uniform internal hut conditions in a single-structure test than in a multi-structure test, however this depends on what HVAC system types are used to control the space temperature. If multiple systems are tested simultaneously in a single-structure test, it is necessary to provide sufficient spacing between test elements so that lateral conduction does not influence the measurement results.

Multi-structure testing involves constructing multiple, independent, yet identical test structures. At least one structure represents a control or baseline condition, built to standard or typical construction

practices. The other structures are modified in some way, perhaps by with a new kind of insulation or roofing system.

2.1.3 Examples

Two example of a single-structure test is the test room of (Athienitis et al. 1997), which compared phase change material board temperature with that of ordinary wall board and developed mathematical models of material performance, and the test room of (Shilei et al. 2007), which tested phase change wallboard energy performance by measuring electric heating energy and temperature.

A more sophisticated, but slightly different type of single-structure test is a calorimetric testing chamber that exposes one side of a test element to the exterior environment and controls the interior side precisely. All remaining sides of the test chamber are heavily insulated and instrumented with heat flux sensors to obtain a careful heat balance of the space. This kind of apparatus has been used and tested extensively throughout research laboratories in Europe under various names DYNASTEE, PASLINK, and PASYS (e.g., Baker 2008). This approach is useful for obtaining assembly-specific parameters that can be used in simulation, but it may not capture the full system-level interactions between multi-zone spaces.

Examples of multi-structure testing include (Szymocha et al. 2005), which tested an advanced thermal solar system with heat storage and compared surface temperature, surface irradiance, and space heating with three test structures; (Medina et al 2007) tested a phase change material structural insulated panel using arrays of thermistors and heat flux sensors with two test structures; (Khudhair and Farid 2007) tested phase change material load shifting in two test structures

In some (intentionally unnamed) cases the researchers have mistakenly relied on insufficient data to produce conclusions about energy savings. For instance, measuring only interior temperature and cumulative heating or cooling energy consumption is normally not sufficient to convincingly show that (1) savings do exist, and (2) savings originate from the element in question. Accurate and sufficient measurement is the cornerstone of any evaluation. Since, in many cases, the effect of improving a building component can be small (say 5% improvement), it is essential to use sensitive equipment and sample frequently enough to measure these effects reliably.

2.2 Example Multi-Structure Test Huts

2.2.1 Experiment

In this experiment, we set out to measure the thermal and energy performance of two proprietary insulation systems against an uninsulated baseline structure. Each hut was conditioned to an identical setpoint temperature, and allowed to run for several months during the summer and fall of 2013 in the desert climate of Albuquerque, NM. We monitored temperature and heat flux through the assemblies, energy consumption of the cooling equipment, and climate conditions. We used the results to analyze energy reduction potential, peak load shifts and reductions, and zone temperature behavior.

The insulation systems were identical other than the presence of a reflective surface foil. Ordinarily, the baseline condition would include some standard insulation materials; however, in this case, the uninsulated case was more representative of the particular end-use application.

2.2.2 Hut Structures

We constructed three identical structures composed of uninsulated 8’x12’ wood framing with 2x4 studs spaced 16” on center. The exterior walls and roof deck are composed of oriented strand board (OSB). A hinged door on the north-facing side of each hut is the only means of access to the interior. The unvented gable roof consists of a layer OSB beneath a dark green colored metal roof. The huts were positioned on the test site to minimize solar shading.

The floors are made of tongue-in-groove plywood and rest above 2x4 floor joists with the floor cavities insulated with R-3.3 fiberglass insulation. The floors were insulated with a further R-1.8 foam board above the plywood layer. Initially, the huts were built without a ceiling to permit the installation of insulation on the interior side of the roof deck. In this state, the huts were tested for initial air tightness to ensure similar air leakage rates in the baseline condition.

Figure 1: Three identical test huts, pictured from the North-east corner of the lot.

Figure 2: Left to right: uninsulated hut interior without ceiling, non-reflective insulation installed on the roof interior of Huts 2 and 3, reflective insulation installed on the walls of Hut 3 with ceiling installed.

The test insulation was then nailed to the wall and roof deck studs of Huts 2 and 3, while Hut 1 remained uninsulated. Afterwards, ceilings were installed in each hut to separate the interior conditioned zone from the unconditioned attic space. Hut 2 received the insulation packaged in a non-reflective facing surface, while Hut 3 received insulation packaged with a reflective foil surface on both sides of the batts. The purpose of the reflective facing on the Hut 3 insulation was to reduce radiative heat transfer across the stud cavities created by the insulation. After the insulation was installed in Huts 2 and 3, OSB ceilings were installed on all three huts to create a separate, unconditioned attic space.

2.2.3 Space Conditioning

One of the most important and challenging aspects of running a multi-structure experiment is in maintaining similar interior conditions through controlled space conditioning. Several strategies exist, each with strengths and weaknesses.

For cooling, one can select from a number of air conditioners on the market, including portable or fixed room or window AC units, central AC units, ductless mini-split units, chillers with fan coil units, and others. For cost and simplicity reasons, we have experimented with fixed through-the-wall style and portable AC units. These are relatively inexpensive, and fairly straightforward to install and replace. Disadvantages include inability to use external thermostat control and the introduction of some additional air leakage as a consequence of the hot exhaust. In the case of a through-the-wall unit, there will be some air leakage through the unit itself. Some portable AC units have one or two venting ducts. Systems with two ducts (one for intake, one for exhaust) reduce pressure build-up within the huts and result in more controlled air exhaust. Systems with one exhaust duct force air out of the hut, creating a low pressure interior space. Exhausted air is replenished through uncontrolled infiltration. Depending on the importance of air tightness in the experiment, there may be advantages of one of these approaches. Ductless systems, meanwhile, do not need to exhaust air, as heat is carried away in

the refrigerant line; however these systems tend to be more expensive and it is more difficult to monitor refrigerant temperature and flow rate.

For heating, the easiest and most straightforward approach is to use a simple fan-assisted electric resistance space heater. Some portable air conditioners include a heating mode that works via a heat pump or through resistance heat.

Since individual space conditioning units may have slightly different performance characteristics, despite being of the same make and model, one should not rely on power consumption values alone when comparing systems. It is also essential to monitor the space temperatures of all huts (of a multi-structure test) during an initial testing period to ensure they are being cooled to a similar temperature. If a single-structure test is used, it is important to ensure the zone temperature distribution is uniform.

In this experiment, we were principally concerned with cooling loads, so we installed a portable air conditioning unit (4.1 kW cooling capacity) in each test hut. These units have two vents, an intake and exhaust vent that are used to cool the condenser and expel the heat from the huts. We sealed the perimeter of the vent penetration with caulk and expanding foam insulation to minimize air leakage from the gaps and cracks. Additionally, we wrapped the hot air exhaust duct with fiberglass insulation to prevent heat from conducting or leaking back into the huts. A moisture drain was installed on each air conditioner to expel any condensed moisture outside of the hut.

3. Instrumentation and Measurement

To monitor material performance, we installed a profile of temperature and heat flux sensors across all elements of key assembly components, including all six walls of the conditioned zones, the roof assembly, and the exterior surface of all walls. We sampled data at 20 second intervals, providing a high time-resolution of thermal performance.

3.1 Weather Station

As with most building experiments, we measure the usual climatic conditions, including solar radiation, outdoor air temperature and relative humidity, and wind speed and direction. Since this work was completed at our outdoor research facility, we made use of the existing permanent weather stations used for photovoltaic research. For many projects, a basic logging weather station is sufficient. If detailed calibrated simulation will be performed, more accurate measurements may be preferred.

3.2 Temperature

We measured temperature across all key wall assembly components, as well as the interior zone temperatures of all huts. By measuring temperature across lightweight construction materials of known properties, it becomes possible to estimate the heat flux through those materials. This provides a backup method for calculating heat flux through surfaces where sensors fail or where cost prohibits their use.

The temperature measurements were obtained using NIST Calibrated type T thermocouples with specified accuracy of ±0.5°C or 0.4%. Further laboratory tests were conducted to determine the accuracy by measuring thermocouples in conjunction with a calibrated thermistor in a metrology well from a range of 0°C to 60°C. To more accurately measure temperatures with our data logger, an external reference junction box was used. The isolated isothermal external reference junction box (zone box) is used instead of the data logger’s internal reference junction, minimizing fluctuations that could be caused by rapid changes in the outdoor temperature.

3.3 Heat Flux

As with the temperature sensors, we installed heat flux transducers on all six walls of the conditioned zone, and on one roof deck surface of each hut. This allowed us to construct a virtual energy balance on the huts by estimating the heat flow through each component surface. We calibrated the sensors in a heat flow meter, with the transducers sandwiched between layers of insulation sheets or smart boards siding (ASTM 2012).

To keep a flat contact surface between two gypsum boards without any air gap, shallow grooves were cut into the 6x6" board panels to make room for the heat flow transducer and its wires, and the sensor was then secured with thermal epoxy. This method allowed good thermal contact between the sensor and its surrounding components. When installing sensors on a reflective surface, we covered the sensors with matching reflective tape to ensure the sensors have the same radiative properties as the surrounding surface (ASTM 2007).

Figure 3: Installing temperature and heat flux sensors. Left to right: temperature sensor on exterior wall, heat flux sensor on interior side of OSB and thermocouple array through assembly, and installing heat flux sensor on reflective insulation with reflective tape.

3.4 Electricity

We monitored electricity consumption of each hut in one-minute resolution to approximate the cooling energy required by each hut. In this experiment, the instrumentation power was very low (<5W), and there were no additional internal building loads.

3.5 Air Tightness

Test hut structures are often too small and too air tight to use standard, full-sized blower door equipment to measure air tightness accurately. Instead, we used a duct-blaster system with a blower-door frame system that was capable of measuring air flow in the appropriate pressure range. In this experiment, there were no windows in the hut. In prior experiments, it was possible to perform air tightness measurements using the window as the test orifice to measure air leakage through the door.

In our experiments, air tightness was similar among all huts, and within typical ranges for U.S. residential construction (3-10 ACH), depending on the system. Because the huts have a high surface to volume ratio, the ACH value may be larger than normal without causing significant concern. If the air tightness of the huts is appreciably different, it may be necessary to perform additional air sealing, or, if that is not possible or effective, control holes may be drilled into the envelope of the tightest building until a similar tightness value are achieved.

4. Sample Results

The following results from a sample week illustrate the sample data results and relative differences in performance among the three test huts.

4.1 Temperature

Figure 4 illustrates the air temperature in the conditioned zone and in the unconditioned attic among the three huts, and Figure 5 indicates the interior wall temperatures.

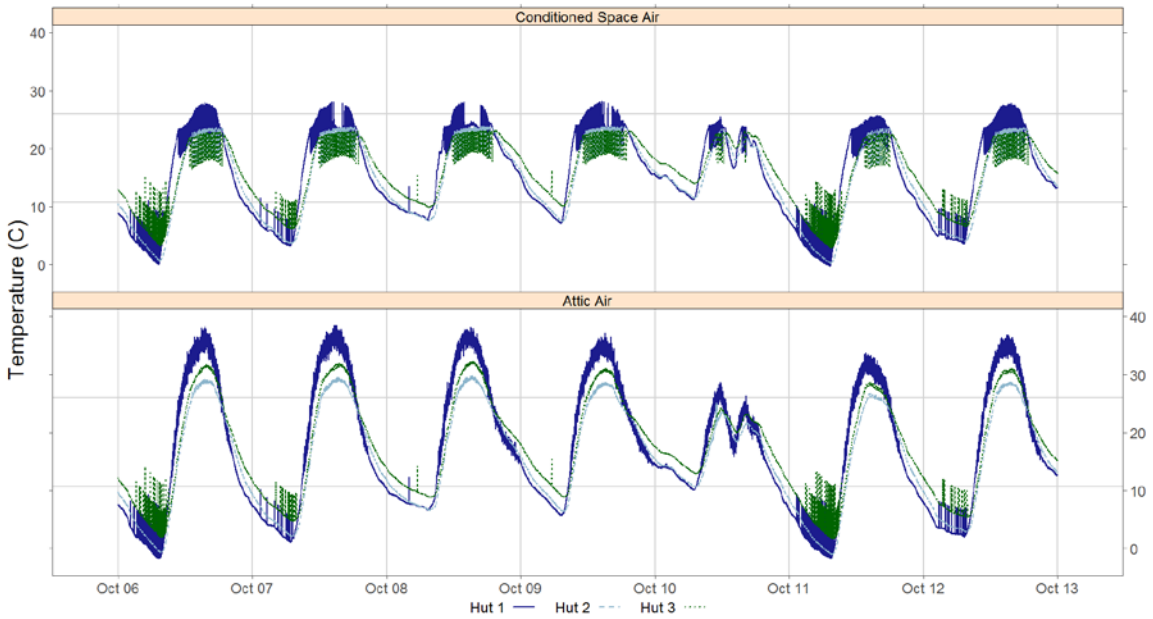

Figure 4: Interior zone temperatures.

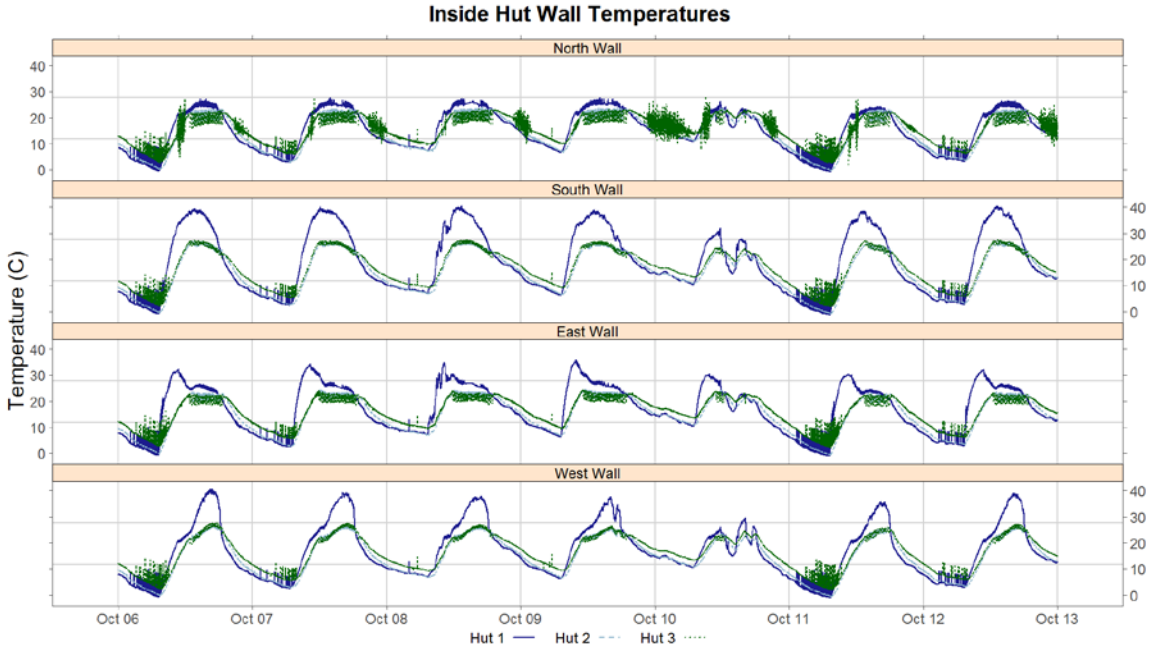

Figure 5: Interior wall temperatures.

During the daytime, the temperature oscillates due to air conditioner cycling. The air conditioner in the uninsulated Hut 1 struggles to supply enough cooling to maintain a matched temperature. Huts 2 and 3 maintain similar indoor temperatures during the experiment. Slight adjustments to the setpoint temperatures in all three huts were made during the initial testing phase of the experiment to bring interior space temperatures as near as possible. The occasional night-time temperature spikes were identified as a predictable source of electronic noise, which were later filtered out.

4.2 Heat Flux

Figure 6 shows the measured heat flux across each principal vertical wall. Here we can see that the magnitudes of the heat flux was similar for Huts 2 and 3, while Hut 1 displays daytime heat fluxes at least twice as high, and often exceeding 100 W/m^2.

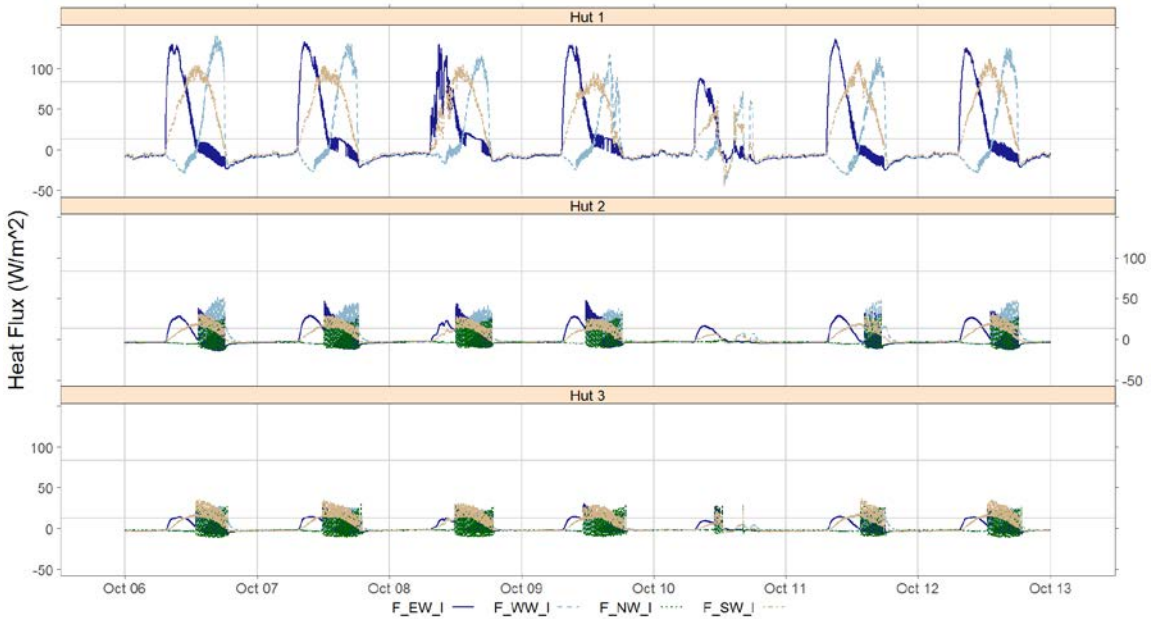

Figure 6: Wall heat flux from different surfaces: EW=east wall, WW=west wall, etc.

4.3 Energy Balance and Power Consumption

Using the heat flux from each hut surface and multiplying by the facing area of the corresponding wall, we are able to construct an estimation of the instantaneous zone load for each hut. We also show the air conditioning power, which follows the calculated load curves fairly closely. In the uninsulated hut, peak loads are highest, onset of cooling occurs hours earlier in the day, and nightly cooling occurs most quickly. The peak load shift was 44 min. between Huts 1 and 2, and 51 min. between Huts 1 and 3.

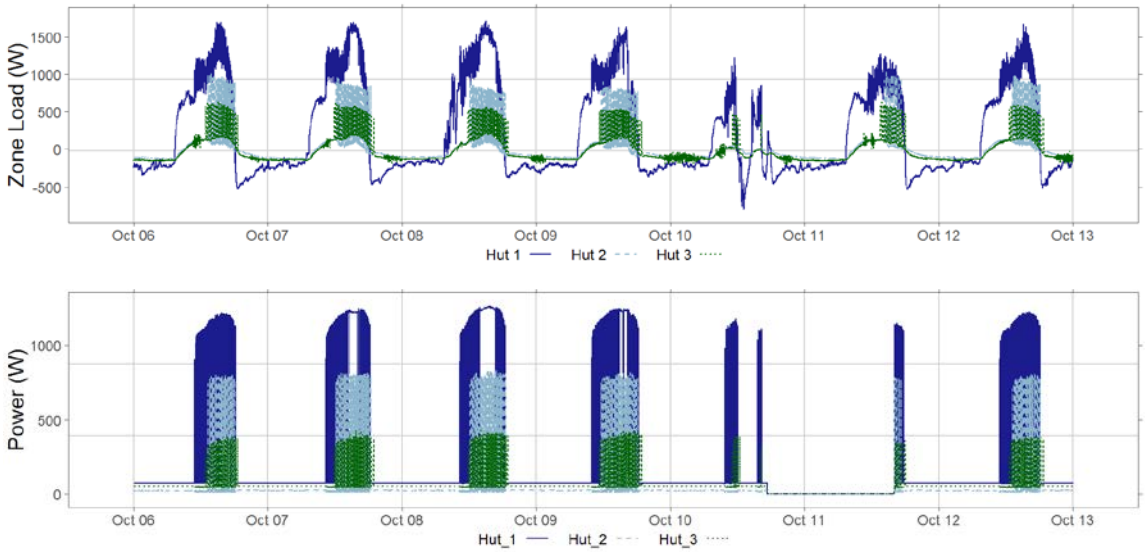

Figure 7: Zone Load (calculated from surface heat flux measurements) and AC Power draw.

By calculating the cumulative electricity usage from the power curves of Figure 7, we determined that that Hut 2 used only about 22% of the energy as Hut 1 for space conditioning, while Hut 3 used only 12%. On the surface, this makes it seem like Huts 3 performs considerably better than Hut 2, owing to the reflective insulation. On further investigation, however, the analysis of zone loads indicates that Huts 2 and 3 behave similarly, with 19-20% the cumulative heat gain of the uninsulated hut. This may be at least partially due to internal differences in the AC systems. For this reason, it is not advisable to base performance conclusions strictly on energy comparisons in multi-structure experiments.

5. Conclusion

We have described and demonstrated a flexible platform for accurately testing the thermal performance of advanced building systems through the use of small outdoor test structures. By carefully measuring key building parameters, we have found that is possible to study and characterize the performance of building systems in scaled-down versions of realistic building constructions.

In the materials we tested we found that insulated structures consumed about 20% of the energy needed by the uninsulated structure. Future work will use the detailed thermal measurements to develop calibrated energy models for the test huts, and energy savings will be simulated with buildings that have similar characteristics.

6. Acknowledgements

This material is based upon work supported by The Small Business Innovative Research (SBIR) program and the Engineer Research and Development Center – Construction Engineering Research Laboratory (ERDC-CERL) under Contract No. W9132T-12-C-0012. Special thanks to Bob Andrews and Alliston Watts for their many important contributions to this project.

References

ASTM. 2007. C1046-95(2007). “Standard Practice for In-Situ Measurement of Heat Flux and Temperature on Building Envelope Components.” American Society for Testing and Materials.

ASTM. 2012. C1130-07(2012). “Standard Practice for Calibrating Thin Heat Flux Transducers.” American Society for Testing and Materials.

Athienitis, A.K., C. Liu, D. Hawes, D. Banu and D. Feldman. 1997. “Investigation of the Thermal Performance of a Passive Solar Test-room with Wall Latent Heat Storage.” Building and Environment, Vol. 32, No.5, pp. 405-410.

Baker, P.H. and H.A.L. van Dijk. 2008. “PASLINK and dynamic outdoor testing of building components.” Building and Environment. 43(2008)143-51.

Khudhair, A.M. and M.M. Farid. 2007. “Use of Phase Change Materials for Thermal Comfort and Electrical Energy Peak Load Shifting: Experimental Investigations. In: GOSWAMI, D. Y. & ZHAO, Y., eds. Solar World Congress 2007, September 18-21. Beijing, China. Solar Energy and Human Settlement.

Medina, M.A., J.B. King, and M. Zhang. 2008. “On the Heat Transfer Rate Reduction of Structural Insulated Panels Outfitted with Phase-change Materials” Energy. Vol. 33, Issue 4:667-678.

Shilei Lv., F. Guohui, Z. Neng, and D. Li. 2007. “Experimental Study and Evaluation of Latent Heat Storage in Phase Change Materials Wallboards.” Energy and Buildings. Vol. 39 (2007), pp 1088-91.

Szymocha, K. 2005. “Advanced Thermal Solar System with Heat Storage for Residential House Space Heating.” Proceedings of SESCI 2005 Conference British Columbia Institute of Technology, Burnaby, British Columbia, Canada, August 20-24.

Stochastic Modelling of Hygrothermal Performance of Wood-frame Wall Assemblies: the Influence of Cladding Ventilation

[1]Lin Wang, M.A.Sc., Ph.D Student
[1]Hua Ge, Ph.D., P. Eng. Assistant Professor

[1]Department of Building, Civil and Environmental Engineering, Concordia University, Canada

KAYWORDS: *Wood-Framed Wall, Hygrothermal Performance, Cladding Ventilation, Stochastic Modelling*

Summary
The modeling of hygrothermal performance using computer programs has increasingly become a common task in building envelope design. Typically, the deterministic approach is used in hygrothermal modeling to assess the Heat, Air and Moisture responses and moisture risks of various designs. However, in reality factors influencing the hygrothermal responses are stochastic in nature such as the variability of material properties, boundary conditions, construction quality, and environmental loads, especially the wind-driven rain and runoff loads. To improve the reliability of hygrothermal modeling, stochastic modeling approach can be used to establish the correlation between input uncertainties with the output uncertainty and identify the most influential parameters. However, the importance of these parameters is not constant and varies with wall configurations, boundary conditions, and moisture loads. To investigate the importance of various design parameters, stochastic modeling approach is applied to a brick veneer wood-frame wall assembly. Four scenarios with different cavity ventilation rates and rain leakage deposition positions are tested. For each scenario, Monte Carlo simulation and multiple regression analysis are performed to rank the influential parameters. The results indicate that the importance of material properties is largely influenced by the cavity ventilation and the deposition location of rain leakage.

1. Introduction

Hygrothermal performance modeling has increasingly become a common tool used in building envelope design in recent years, especially for innovative and energy efficient buildings. Typically, the deterministic approach is used in hygrothermal modeling to assess the Heat, Air and Moisture responses and moisture risks of various designs. However, in reality factors influencing the hygrothermal responses are stochastic in nature such as the variability of material properties, boundary conditions, construction quality, and environmental loads, especially the wind-driven rain and runoff loads. The stochastic approach has been applied in several studies in hygrothermal performance simulations to investigate the influence of material properties (Salonvaara et al. 2001; Holm and Kuenzel, 2002; Defraeye et al. 2012). Zhao et. al. (2011) also looked into the influence of boundary conditions and ranked the importance of each parameter using multiple regression analysis. The influence of environmental conditions including rain loads and internal moisture gains on the hygrothermal performance of wall assemblies was also investigated by parametric studies and scenario analysis (Cornick, et al. 2009 and Pallin, 2013).

Previous studies mainly focused on the influence of the stochastic nature of material properties. As indicated in the study by Zhao et al. (2011), the importance of each influential parameter was not constant and varied with the weather conditions. To provide a reliable hygrothermal performance assessment of building envelopes, especially for those highly insulated or with innovative materials, a stochastic approach taking into account the combined influence of material properties, boundary conditions, and moisture loads is necessary. The objective of this paper is to develop a methodology to assess the moisture damage risks of wood-frame construction using a stochastic approach. A brick

veneer wood-frame wall, which was tested under the coastal climate of British Columbia (Simpson, 2010), is selected as an example. The influence of cavity ventilation, rain leakage, and material properties is investigated using the stochastic approach.

2. Background of the Field Test

To investigate the drying and wetting effect of cladding ventilation on rainscreen walls in the coastal climate of British Columbia, twelve test walls with two types of cladding, i.e. brick veneer and fiber cement panels, were installed on the southeast side of a Building Envelope Test Facility. All of the wood-frame back wall assemblies were identical and built using common building materials and construction method. The size of the back wall was 1.22m by 2.44m. The assembly is consisted of:

- 12mm unpainted gypsum board with a vapor barrier of 6 mil polyethylene
- 38mm x 140mm wood frame with R20 fiber glass batt insulation
- 12mm plywood (Douglas fir) sheathing
- Spun bonded polyolefin (SBP) sheathing membrane

The test period was from the beginning of January 2008 to the end of June 2008. The change of the moisture content (MC) in plywood was used as an indicator to evaluate the impact of cavity ventilation. Further information can be found in Simpson (2010).

3. Stochastic Hygrothermal Modeling

3.1 Material Properties

The stochastic hygrothermal model is constructed based on the typical wood framed wall with red clay matt brick as the rainscreen, as tested. The configuration of the wall assembly is presented as follows:

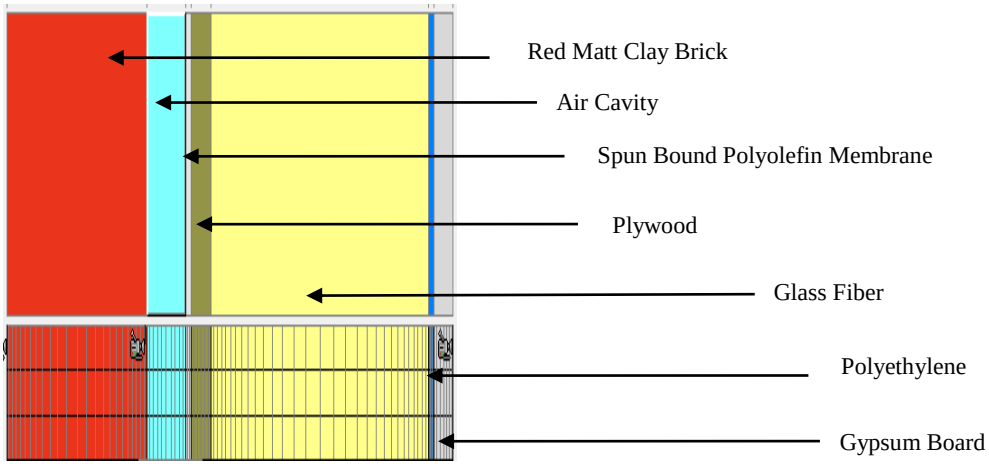

Figure1 Wall Configuration

According to Zhao et al. (2011), the thermal properties seem having insignificant influence when MC is taken as the performance indicator. Therefore, only the hygric properties are considered as stochastic variables. To examine the effect of cavity ventilation and rain leakage, the material properties of red brick, SBP sheathing membrane and plywood are selected for the stochastic analysis. Both the deterministic and stochastic parameters are listed in Table 1. The material properties are taken from the database in WUFI Pro 5.0. The properties of stochastic variables, mean value with a standard deviation in the bracket, are determined based on the measurement results reported by Kumaran (2002). All the stochastic variables are assumed to follow a normal distribution.

3.2 Environmental Conditions

The weather data collected at the test facility are used as inputs in the hygroghermal simulations, including outdoor temperature, relative humidity, solar radiation, rainfall, wind speed and wind direction. The indoor conditions are kept at 21°C and 40% RH. The wall faces southeast, the prevailing wind-driven rain direction at the test site. The initial moisture content of each layer is specified based on the measurements of RH and MC readings taken in the experiment. They are: Brick (2.9kg/m^3), Plywood (121.96kg/m^3), Glass Fiber (0.17kg/m^3), and Gypsum Board (4.6kg/m^3).

Table 1 Material Properties

	Unit	Red Matt Clay Brick	Air Layer	SBP Membrane	Plywood	Glass Fiber	Polyethylene	Gypsum Board
Thickness	mm	90	25	0.2	12.7	140	0.15	12.5
Density	kg/m^3	1935	1.3	448	432	88	130	625
Porosity	-	0.217	0.999	0.001	0.69	0.999	0.001	0.706
Heat Capacity	J/kg.K	800	1000	1500	1880	840	2300	870
Heat Conductivity	W/m.K	0.495	0.155	2.4	0.084	0.043	2.3	0.16
Water Vapor Diffusion Resistance Factor	-	137.8 (9.11)		328.4(22.5)	730.8 (115.8)	1.21	50000	7.03
Reference Water Content	Kg/m^3	1.25 (0.085)			64.4 (4.5)			
Free Water Saturation	Kg/m^3	56.11 (3.8)			550 (36.2)			
Water Absorption Coefficient	Kg/$m^2s^{0.5}$	0.0268 (0.0018)			0.0042 (0.00028)			

3.3 Scenario description

In order to examine the effect of cavity ventilation and rain leakage, four scenarios are investigated:
Scinario1: Cavity ventilation, no rain leakage, which is the same as the tested scenario.
Scinario2: Cavity ventilation with rain leakage deposited on the SBP membrane.
Scenario3: Cavity ventilation with rain leakage deposited on the plywood sheathing.
Scinario4: No cavity ventilation but with rain leakage deposited on the SBP membrane.

The range of air cavity ventilation is between 1 and 11ACH, which was predicted based on measured wind pressure differential and buoyance induced pressure differential between the ambient and inside of the air cavity (Simpson, 2010). Therefore, an air source with ACH 1~11 is added in the air space in WUFI simulations to account for cavity ventilation. The cavity ventilation rate is assumed to follow a normal distribution. According to ASHRAE160-2009 (ASHRAE, 2009), the default value for water penetration through exterior surface should be 1%, which deposits on the exterior surface of the water-resistive barrier. Therefore, a moisture source with 1% rain penetration is added on the surface of the SBP membrane to simulate the rain leakage. A 1% rain leakage deposited directly on the plywood sheathing is also investigated, i.e. scenario 3. Driving rain load is also considered as an

uncertainty source for the stochastic analysis. According to ASHRAE160, the driven rain load can be calculated as following:

$$r_{bv}=F_E \bullet F_D \bullet F_L \bullet U \bullet \cos\theta \bullet r_h \quad (1)$$

where

F_E rain exposure factor
F_D rain deposition factor
F_L empirical constant, 0.2kg.s/(m^3.mm)
U hourly average wind speed at 10m (m/s)
θ angle between wind direction and normal
r_h rainfall intensity, horizontal surface (mm/h)
r_{bv} rain deposition on vertical wall (kg/(mm^2.h))

The rain deposition factor is considered as a stochastic variable. As suggested by ASRHAE 160P, the range of the deposition rain factor is 0.35~1.0

4. Monte Carlo simulations

There are four steps in Monte Carlo simulations.

Step 1: Random number generation
A group of random numbers following a normal distribution is generated. In this paper, the hygric parameters, ventilation rates, and wind driven rain deposition factor are considered as stochastic variables. According to Lomas (1992), the improvement of accuracy becomes insignificant after 60-80 simulations. Therefore, 80 samples of each parameter have been generated.

Step 2: Sampling
Random sampling is commonly used in Monte Carlo analysis and in this paper the generated parameters are combined randomly. Each combination represents an individual hygrothermal simulation.

Step 3: Simulations
For each randomly generated sample, a group of parameters are input into the hygrothermal modeling program and a set of hygrothermal simulation results are obtained.

Step 4: Regression analysis
This step examines the relationship between the inputs and the outputs. In this paper, partial correlation coefficient (PCC), a measure of the linear dependence of a pair of random variables from a collection of random variables in the case where the influence of the remaining variables is eliminated, has been used as an indicator for the sensitivity of MC of plywood to each influencing parameter.

5. Result analysis and discussion

Figures 2-5 show the stochastic results of MC of the plywood for the four scenarios. The blue line is the mean value of the moisture contents and the grey lines are the stochastic results. The initial MC of the plywood is 28% and it stays at that level for over one month due to the wet weather. For Scenario 1, where no simulated rain leakage, the mean MC of plywood picks up a bit during the month of Feb. with a very slow drying rate until mid-April. Starting from mid-April quick drying occurs due to the warm up of the weather and less rain and the MC level decreases to below 10% in June. In some cases the plywood picks up moisture from the beginning up to mid-April and then slowly dries to below 10% in June. These cases typically have a higher rain deposition factor. In some cases, the plywood starts drying from mid-Feb. These cases typically have a lower rain deposition factor. For scenario 2, in which both cavity ventilation and rain leakage are simulated, the results are almost the same as that of Scenario 1, which indicates that the simulated rain leakage does not have much influence on the MC

level of the plywood. This may be because the rain leakage was specified at the surface of SBP membrane, which is supposed to shed any leakage water away. As expected, the MC of plywood is higher in Scenario 3, where the rain leakage is added on the layer of plywood. Without the protection of the SBP weather resistive barrier, the MC of plywood is more sensitive to the rain deposition factor. In scenario 4, the MC of plywood starts to pick up at the beginning of February, when a high rainfall occurred as shown in the weather data. This is followed by a gradual increase with the MC of plywood reaching the peak around mid-April. Without the cladding ventilation, the drying effect starts from mid-April, when there was less rain. The drying starts almost two months later than the scenarios with cavity ventilation and the peak of the MC of plywood is about 6% higher than that of scenario 1 and scenario 2

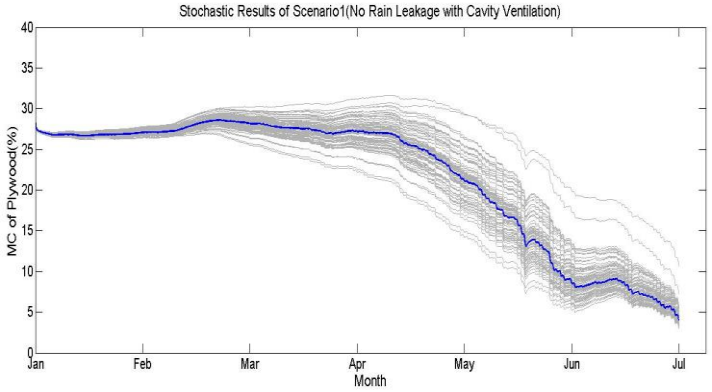

Figure 2 Stochastic Results of Scenario 1 (no rain leakage with cavity ventilation)

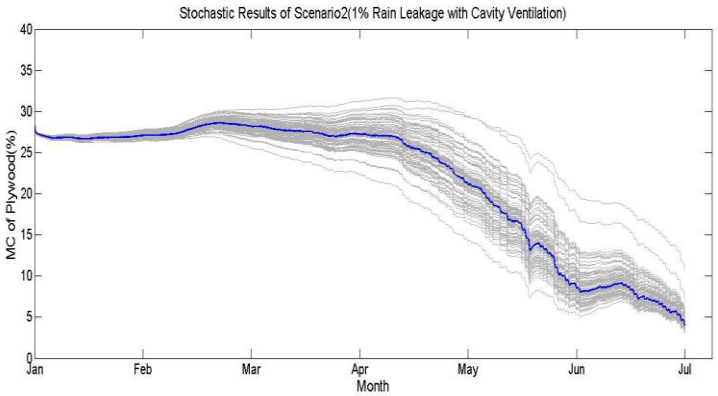

Figure 3 Stochastic Results of Scenario 2 (1% rain leakage on SBP membrane with cavity ventilation)

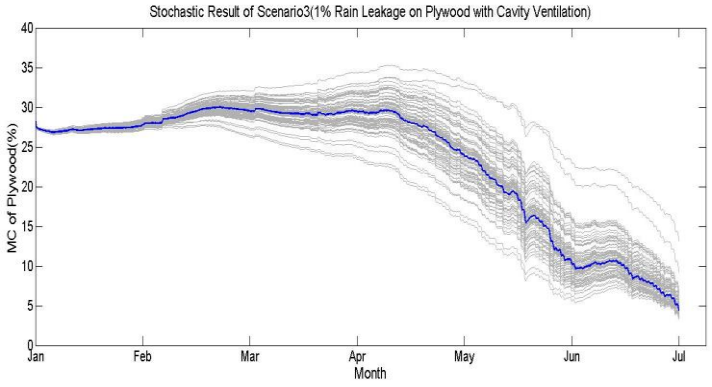

Figure 4 Stochastic Result of Scenario 3 (1% rain leakage on Plywood with cavity ventilation)

Figure 6 and Figure 7 show the PCC of each parameter under different scenarios at specific dates. The typical winter rainny day of Feb. 5th and a summer sunny day of June 30th are selected for the analysis. Figure 6 shows that the most influential factor in winter is the reference moisture content of plywood, which is used to generate the moisture storage curve in WUFI. It has a positive effect on the MC of plywood. The PCC of mr_plywood under scenario 1, scenario 2 and scenario 3 is slightly lower than that under scenario 4, which has no cavity vantilation. This reflects that cavity ventilation does promote drying, therefore, the MC of plywood is relatively less sensitive to the variation of moisture storage function. The free water saturation of plywood has the similar effect on the MC of plywood. When comparing scenario 3 with senario 2, the PCC for the most influential material parameters is lower, which indicates that with rain leakage deposited directly on the plywood, the influence of rain deposition factor increases while the influence of material properties slightly decreases. Figure 7 indicats that during summer conditions the reference moisture content of plywood is also the most influential factor, while the influence of free water saturation become less significant. This reflects that the moisture transport is mainly in the diffusion region. Because the rainfall in the summer is lower than that in the winter, the moisture accumulated in the plywood may mainly come from the moisture in the air. The cladding ventilation may bring more moisture from the ambient air into the cavity, therefore, wet the plywood. Therefore in the summer time the PCC of the influential parameter with ventilation is higher than that without ventilation.

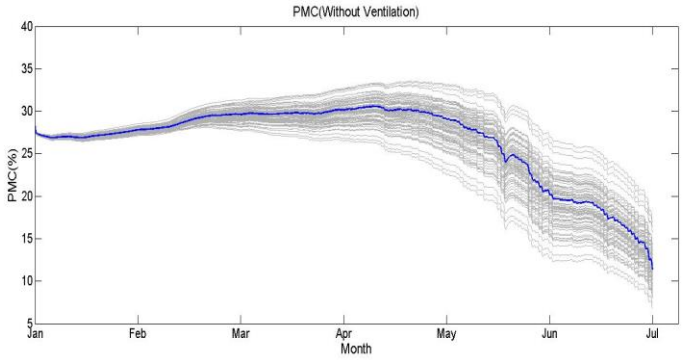

Figure 5 Stochastic Results of Scenario 4 (1% rain leakage on SBP membrane without cavity ventilation)

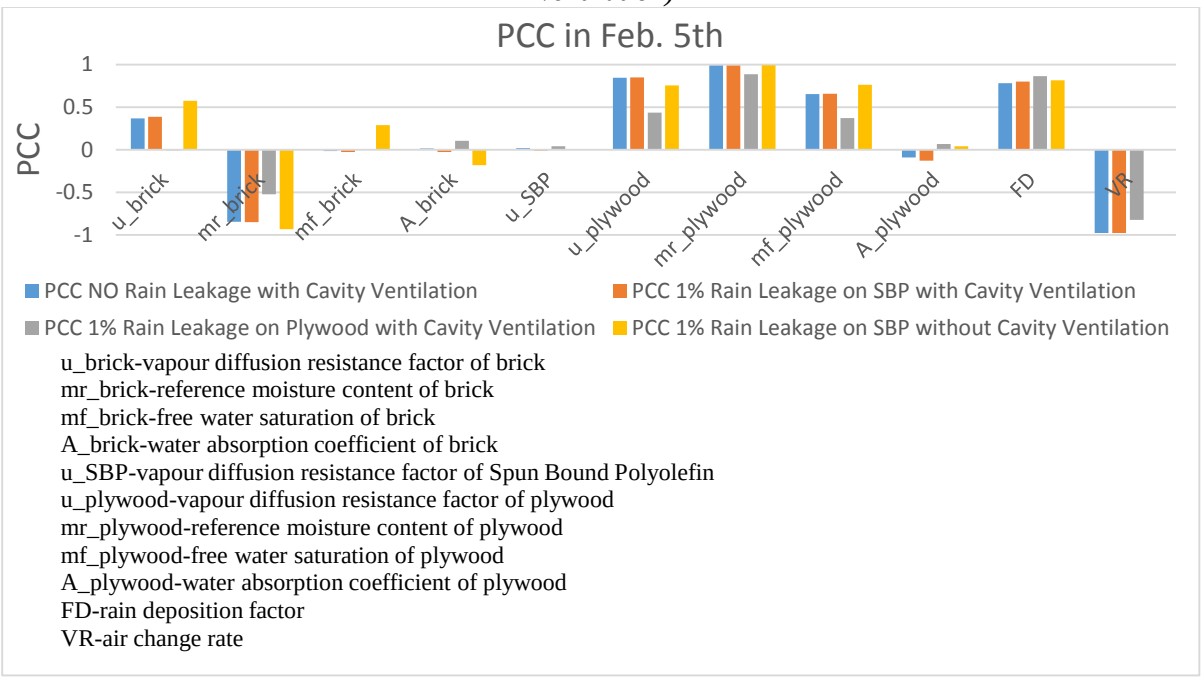

Figure 6 PCC of Each Parameter for February 5th

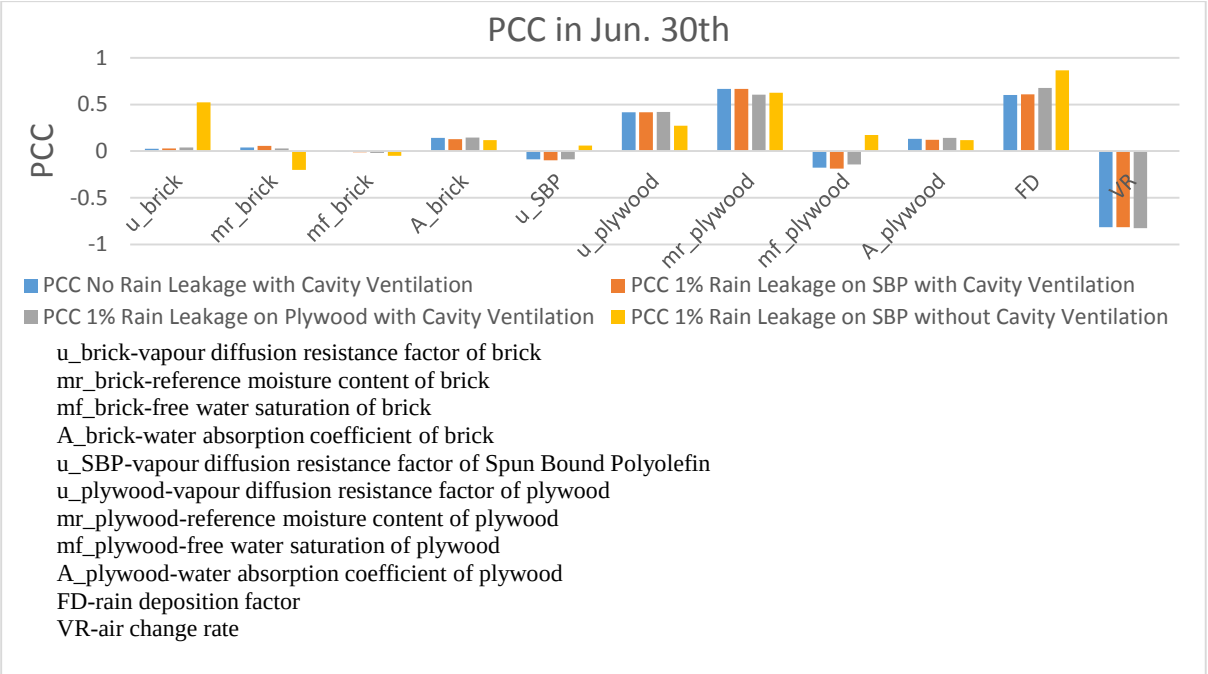

Figure 7 PCC of Each Parameter for June30th

What worth mentioning is the discrepancy between the stochastic results and the measured MC. As shown in Figure 8, the simulated MCs are much higher than that measured MC between February and June. This difference may be attributed to the approximation of material hygric properties. To consider the influence of moisture storage function, the reference moisture content and free water saturation has been considered as the stochastic variables. While the approximated moisture storage function cannot reflect the material property exactly, the difference between the approximated moisture storage function and the actual moisture storage function may have been amplified by the stochastic simulation process. As the results of sensitive analysis have shown, the reference moisture content and free water saturation are significant parameters that influence the MC of plywood. This means that the moisture storage function is an important material property that should be determined as accurate as possible for the hygrothermal simulations. The discrete isotherm data instead of approximation, which are included in WUFI material database, is used in the deterministic simulation. The simulated results are compared to measurements. As shown in Figure 9, the simulations have a better agreement with measurements.

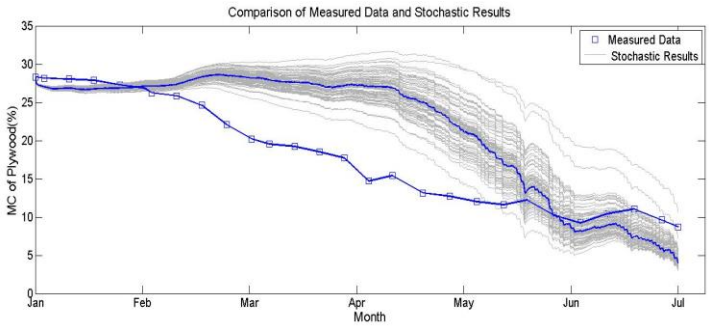

Figure 8 Comparison of Measured Data and Stochastic Modeling Results

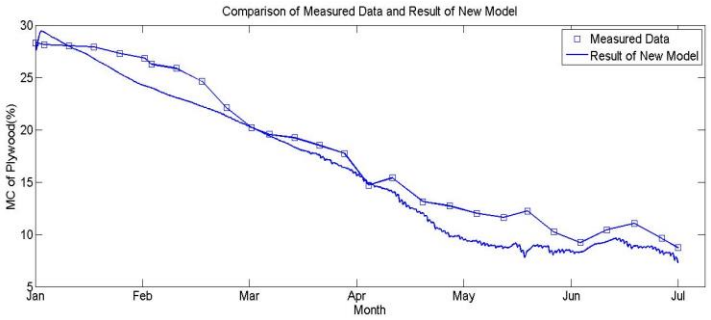

Figure 9 Comparison of Measured Data with simulation results with discrete Isotherm Data

6. Conclusion

Stochastic modeling can be used in the sensitivity analysis of hygrothermal performance of building envelopes. The sensitivity of the performance indicator in relation to input parameters often varies with wall configurations, environmental conditions, and moisture loads. To examine the combined effect of material properties and environmental conditions, both stochastic analysis and scenario analysis are performed using hygrothermal simulations. A typical wood framed building envelope with cladding ventilation is used for the stochastic modeling. The influence of ventilation rates and deposition rain factor is investigated by performing stochastic simulations under four different scenarios. The results indicate that the importance of the material properties is largely influenced by the cavity ventilation and the deposition location of rain leakage. Further research should be focused on developing wall configurations that are less sensitive to the variation of local environmental conditions and rain loads.

References:

ASHREAE. 2009. ASHRAE Standard 160-2009 Criteria for Moisture-Control Design Analysis in Building. American Society of Heating, Refrigerating and Air-Conditioning Engineers, Inc.

Cornick, S.M., Dalgliesh, W.A. & Maref, W. 2009. Sensitivity of Hygrothermal Analysis to Uncertainty in Rain Data. Journal of ASTM International, 6 (4): 1-17.

Defraeye, T., Blocken, B. & Carmeliet, J. 2013. Influence of uncertainty in heat-moisture transport properties on convective drying of porous materials by numerical modelling. Chemical Engineering Research and Design , 91(1): 36-42.

Holm, A. & Kunzel, H.M. 2002. Practical application of an uncertainty approach for hygrothermal building simulation-drying of an AAC flat roof. Building and Environment. 37(8-9): 883-889.

Kumaran, K., Lackey, J., Normandin, N., van Reenen, D. & Tariku, F. 2002. Summary Report from Task3 of MEWS Project. Institute for Research in Construction, National Research Council Canada. Ottawa, Canada, (NRCC-45369), pp.1-68.

Lomas. K.L., & Eppel, H. 1992. Sensitivity Analysis Techniques for Building Thermal Simulation Programs. Energy and Building, 19(1): 21-44.

Pallin, S. 2013. Risk Assessment of Hygrothermal Performance-Building Envelope Retrofit. Ph.D Thesis. Chalmers University of Technology. Goteborg, Sweden.

Salonvaara, M., Karagiozis, A., & Holm, A. 2002. Stochastic Building Envelope Modelling-The Influence of Material Properties. Proceedings for Performance of Exterior Envelopes of Whole Building Ⅷ: Integration of Building Envelope, Clearwater Beach, Florida.

Simpson, Y. 2010. Field evaluation of ventilation wetting and drying of rainscreen walls in coastal British Columbia. MASc. Thesis. Concordia University. Montreal, Canada.

Zhao, J., Plagge, R., Nicolai, A. Grunewald, J. & Zhang, J. 2011. Stochastic Study of Hygrothermal Performance of a Wall Assembly- The influence of Material Properties and Boundary Coefficients. HVAC&R Research, 17(4): 591-601.

LOW CARBON ECONOMY IN CITIES OF CHINA
POSSIBILITIES TO ESTIMATE THE POTENTIAL OF CO_2-EMISSIONS

Hans-Peter Leimer, Professor Dr.-Ing.[1,*]

University of Applied Sciences and Arts – HAWK Hildesheim, Germany
Hefei University, Anhui, China
Nanchang University, Jiangxi, China
BBS INSTITUT, Wolfenbuettel, Germany

KEYWORDS:
CDM, Cities, Thermal Energy Simulation, CO_2-Emissions, Energy Demand

SUMMARY:
Increasing urbanisation and climate change are one of the greatest challenges in the 21st Century. Many regions already face different negative impacts on cities such as growing local pollution, solid and liquid waste, traffic congestion and noise. A growing consumption of fossil fuels in cities leads to increasing CO2-emissions accelerating climate change. All over the world and also in China, cities are trying to reduce their carbon footprint. In that context, the concept of so called "low carbon cities" is promoted. Currently, 79 cities in China are considering low carbon concepts. To build a low carbon city is not an easy task as there are various barriers to be removed, such as financial, traditional and institutional barriers. Building belong to the most traditional and slow-changing innovative areas in industry. Further solutions are different for hot and warm climates than for cold climates. Due to a very fragmented and divided structure in smaller enterprises and in different areas, a holistic approach is hardly to get.

1. Introduction[1]

The Chinese government decided to reduce the domestic emission reduction goals in the 12th Five Year Plan (2011-2015) according to the goals of international emission reduction. The reduction of carbon intensity per unit of GDP (Gross Domestic Product) in China is supposed to be reduced by 40-45% in 2020 against the intensity of 2005 levels.

The implementation of CDM[2] in the United Nations is in the beginning; therefore China has the chance to implement these systems as the first and the most important Nation worldwide in the building sector for LOW Carbon Cities. Germany, as one of the leaders in Low Carbon projects, has the chance, in collaboration with China, to increase the leadership in this working field and to become the master in the implementation of CDM projects in buildings worldwide. An excellent possibility to reach this goal is therefore the implementation on financial incentives by pCDM (Programmatic

[1] Corresponding author email: h-p.leimer@BBS-INTERNATIONAL.com

[1] This report is part of the final report of the study for the German Federal Ministry for the Environment, Nature Conservation and Nuclear Safety, Chapter 1602 Title 896 05, 2009 as granted by the notification dated December 3rd, 2009

[2] The Clean Development Mechanism (CDM), defined in Article 12 of the Protocol, allows a country with an emission-reduction or emission-limitation commitment under the Kyoto Protocol (Annex B Party) to implement an emission-reduction project in developing countries. Such projects can earn saleable certified emission reduction (CER) credits, each equivalent to one tonne of CO2, which can be counted towards meeting Kyoto targets. [http://unfccc.int/2860.php]

CDM) or other advanced methods with this project. In consequence of the development of the city planning in china during the next years and the increasing building industry, the Chinese government needs a set of guideline and reliable prediction methods for the regional LOW Carbon potentials and their application. This project offers China the possibility to receive a forecast of the Low Carbon potentials for their NEW LOW CARBON CITIES. With these tools China can influence and lead the market under the aim of LOW CARBON reduction during the next years to full fill the domestic emission reduction goals. The project will provide the methodology for the implementation of pCDM for the different climate regions in China as well as the guideline during the planning and realisation phase of Low Carbon Cities. Only with both approaches it will be possible to find solutions for the practical implementation for different climate situations (heating, cooling, heating and cooling) and for suitable requirements.

2. Calculation of CO_2 - Emission-Reduction for the most important Building Types – Example for Xiamen - China

This chapter describes the basic approach to evaluate the energetic behaviour of buildings as well as to provide a calculation methodology for the CO_2-emission reductions in the PoADDs (Program of Activities Design Documents). In order to detect and to investigate the CO_2 saving potential in the different building types, the following steps of work are necessary:

- Numeric simulation of the range of the energy demand from the selected building types for heating, cooling and dehumidification
- Setting a baseline for each building type
- Calculation of the energy saving-/ CO_2 emissions saving potential of each building type
- Forecast of the CO_2 emissions saving potential for a whole pilot-region

In scope of this investigation, the available values from measurements of buildings/building categories will be compared to numeric calculations of energy requirement.

3. Identification of the baseline

The detection of the CO_2 saving potential is based on baselines, which are set by the energy standard of national requirements and/or regulations.

4. Thermal energetic simulations of buildings (TES)

In this project, three simulation computer models are used:

- TRNSYS
- LEC
- China GB-50189-2005 by the computer program BEED developed by MoHURD

TRNSYS delivers the calculation of the final energy demand of each building type, LEC will deliver an easy method to estimate the primary energy demand taking into account the primary energy and CO_2-emissions used to produce and transmit the final energy for the use in buildings.

4.1 TRNSYS

TRNSYS is a complete and extensible simulation environment for the transient simulation of thermal systems including multi-zone buildings.

It is used by engineers and researchers around the world to validate new energy concepts, from simple solar domestic hot water systems to the design and simulation of buildings and their equipment, including control strategies, occupant behaviour, alternative energy systems (wind, solar, photovoltaics, hydrogen systems), etc. Throughout its thirty year history, TRNSYS has been under continual enhancement by an international group. TRNSYS is based on a model developed by the Solar Energy Laboratory at University of Wisconsin-Madison, USA, 1992.

4.2 LEC

LEC (Low Energy Certificate) is the result of two years of research to develop a planning tool to evaluate the energy performance of buildings. Thanks to the evaluation programme it is possible to evaluate nearly all building types and parts of a building with regard to their energetic quality separately after the heating period and after the cooling period. The examination of the buildings with regard to the regional climate conditions is based on a pure physical basis. In this context it is important to mention that the calculations are exclusively based on results of analysis of the thermal equations.

The basis for the evaluation of the heating period is a comparison with similar buildings (Reference–building) which is in accordance with a building according the standard of the 80ies. As far as the cooling periods are concerned, the evaluation is based on comparisons with an “optimal” envelope of a building. The evaluation of the energy for cooling and heating are re-evaluated, classified and shown with regard to certain criteria. The result of the energetic verification is presented with a simple star system. An increase of stars clearly shows the energetic quality of the building, which means that the user can immediately recognize the energetic quality of the building thanks to a simple illustration.

4.3 BEED

Building Energy Efficiency Design, Calculation and Economy Analysis Software was developed by the Centre of Science & Technology of Construction Minister of Construction; P.R. China cooperates with Beijing E-house building science and technology development Co. Ltd. to finish the task of the World Bank "economy analysis about building energy efficiency measures and stimulation calculation module in BEED". The result has passed the MOC evaluation and the level is in the top in China. BEED was designed according as "Thermal design code for civil building" and "Energy conservation design standard for new heating residential building.

4.4 Calculation results

The simulation by TRNSYS delivers the Energy demand (kWh/m²) and the Maximum energy load (kW/m²) for heating, cooling and dehumidification.

LEC calculates the energy level considering the outer surface only. Other methods such as China GB-50189-2005 calculate a more general use of energy, based not only on the building surface, but also on system engineering and on political conversion factors. The evaluation tool offers the possibility to evaluate almost every building and construction part regarding to its energetic quality, separated by cooling period and heating period. The evaluation of the buildings under consideration of regional climatic circumstances is strictly based on fundamentals of physics. The calculations are based on results of thermo technical equations.

5. Calculation of the CO2-emissions of buildings

Basis of the classification are the 18 types of buildings according to the MoHURD-Ministry of Housing and Urban-Rural Development typology. For these types of buildings the energy demand and other relevant data are available in 23 cities of China. For the Xiamen project, however, the analysis of

18 building types is too detailed. Therefore, there was made a first selection of 7 main categories divided in

- Residential Buildings
- Non Residential Buildings

For residential buildings, a classification of the buildings was made on the basis of the building geometry. Here, the ratio of outer wall and roof to volume (A/V ratio) will be taken and the

residential buildings will be differentiated in

a) single family houses up to 3 stories;

b) multi-storage houses for multiple families.

Non-residential buildings will be differentiated in

c) office buildings; d) Shopping centres;

e) Hotels;

f) Buildings for trade and fair;

g) Schools and other buildings.

The simulation of energy demand is calculated by TRNSYS and based on a single-zone-model according to the standard room. Therefore, the standard room is calculated with different building components, different window to wall ratio and different utilization. Furthermore, the orientation and position of the room is varied.

The properties of the building parts fulfil the minimal requirement of the GB 50189-2005 and JGJ 75-2003. At this, the window to wall ratio fits the classification of the current Chinese requirements. Different user profiles have been provided for the utilization in accordance with the applicable standards in China.

Based on the determination of the final energy demand for cooling in Xiamen, CO_2-emissions of primary energy demand will be calculated by taking into account the primary energy structure, energy efficiency of energy transformation and the losses during transmission of electricity. For the PoA, to be conservative, additional reductions may be taken into account for user behaviour, planning and construction quality.

pCDM are based on the real energy consumption / real CO_2-emissions of a building or a side area. The problem is, that at the beginning of a Low Carbon building City planning phase (town planning phase) no detailed values of the CO_2-emissions are existent. In this phase, pCDM can be based on a calculation of the energy consumption / CO_2-emissions. Calculation methods offer the following advantages:

- considering the energetic behaviour of the building under repeatable boundary conditions
- provide the possibility to directly compare buildings (under the same boundary conditions)
- provide a forecast on the savings potential for CO_2 during the planning period

Summing up, they provide the possibility to compare the economical savings potentials from pCDM plus the saved amount of energy to the costs of the investment. Based on the variety investigation, an economical investigation is herewith possible.

6. Energy Demand of the 7 different building types

The aim was the calculation of the energy consumption and the CO_2 emissions of the 7 characteristic building types for new buildings in Xiamen, China under the climate conditions according to GB50189 for the region “hot summers and warm winters” by implementing a building energy efficiency simulation.

Table 1. *End Energy Demand of the building types (a-g)*

No.	Building type	**Simulated energy demand** (mean value) for cooling, heating, dehumidification current Energy Standard China	
		kWh/m²	kg CO_2/m²
a	Single family houses	43.10	36,59
b	Multi-storage/families houses	54.28	46,64
c	Office buildings	101.29	87,03
d	Shopping centres	114.02	97,97
e	Hotels	164.93	141,71
f.	Congress/Fair buildings	112.60	96,74
g	Schools	76.37	65,61

In this case, the possible variables, including building type, size, height, orientation according to azimuth of the buildings, the different ratios of the wall-/window areas of the facades, different uses and quality standards of the building services installations for energy distribution and energy production, are taken into account. Furthermore, the range of influence on planning- / arithmetic errors and execution mistakes had to be described.

7. Application of the models for the calculation of the CO_2-potential for Xiamen

The Chinese government decided the domestic emission reduction goals in the 12th Five Year Plan (2011-2015) according the international emission reduction goals the reduction of carbon intensity per unit of GDP in China by 40-45% in 2020 against 2005 levels. To fulfil these requirements the CO_2-potential for China has to be known. One of the parts in this research project is to know well the energy demand of buildings according to the CDM standard. With this information it will be possible, to get a forecast of the CO_2-potential for new buildings for whole China. To get this forecast based on the level of the baseline CDM the following information has to put into account in a bottom-up calculation process (see Figure 1):

The transfer of the results of the single buildings to complex new LOW Carbon Cities was reviewed by the city of Xiamen/Jimei.

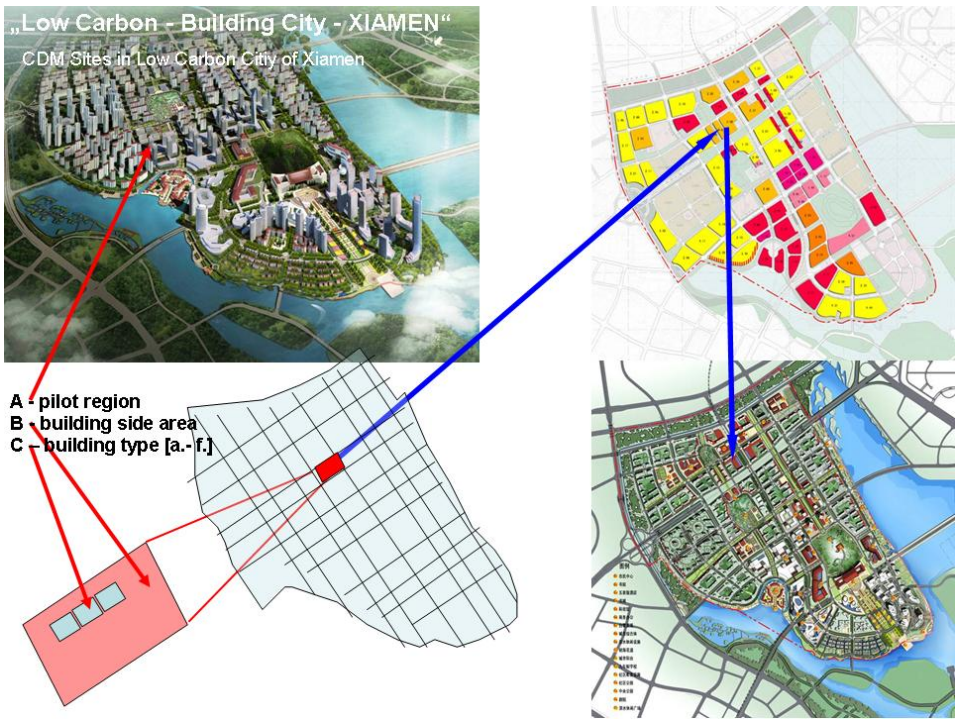

Figure 1. *Calculation of the CO_2 emissions' potential for the new LOW Carbon Building City Xiamen/Jimei*

Table 2. *– CO_2 emissions Jimei, different building standards according to the building standard LEC*

		(t CO_2/a)			
Building type	Floor area (m²)	Baseline	3 *	4 *	5 *
Single family houses	125969	4624	3081	2977	2664
Multi storage houses	1142439	47464	29545	27139	25180
Office buildings	946974	68184	61800	54332	46194
Multi storage houses / Office buildings (mix)	1247028	64288	43795	39312	36264
Shopping Centers	647986	52158	43418	40041	37955
Hotels	142016	16831	8503	7854	7083
Congress / Fair	11192	1078	834	772	733
Schools	68966	3493	1476	1249	1187
Other buildings	535384	40473	35351	31715	28292
TOTAL	**4867954**	**298594**	**227805**	**205390**	**191837**
Total (in % of baseline)		**100%**	**76%**	**68%**	**64%**
CO2-emissions for heating, cooling and dehumidification MIN values. Standards according to: Baseline = applicable Chinese standard 3* acc. Chinese Green Building Standard; 4* German ENEV 2001; 5* German ENEV 2009					

Even considering regional characteristics, it is shown that there is a possibility to determine the CO_2 potential for new „Low Carbon Cities" of China. The results will deliver the base to make decisions by implementing new CDM-Baselines to limit the energy demand in a special „Low Carbon Standard", a standard quite above the actual energy standard of China.

8. Outlook / Conclusions

The possible CO_2 savings potential of the new Low Carbon Cities currently being planned (see Figure 2) shows that an economic and ecological building process in China will be realisable once the requirements of the energetic quality of the buildings are reasonable increasing as well as the requirements for efficient energy distribution and energy production systems. This building process may lead the way to accomplish the global restriction of CO_2 emissions in the construction sector. To establish China as a pioneer for CDM in the building sector, actions have to be done in a short term.

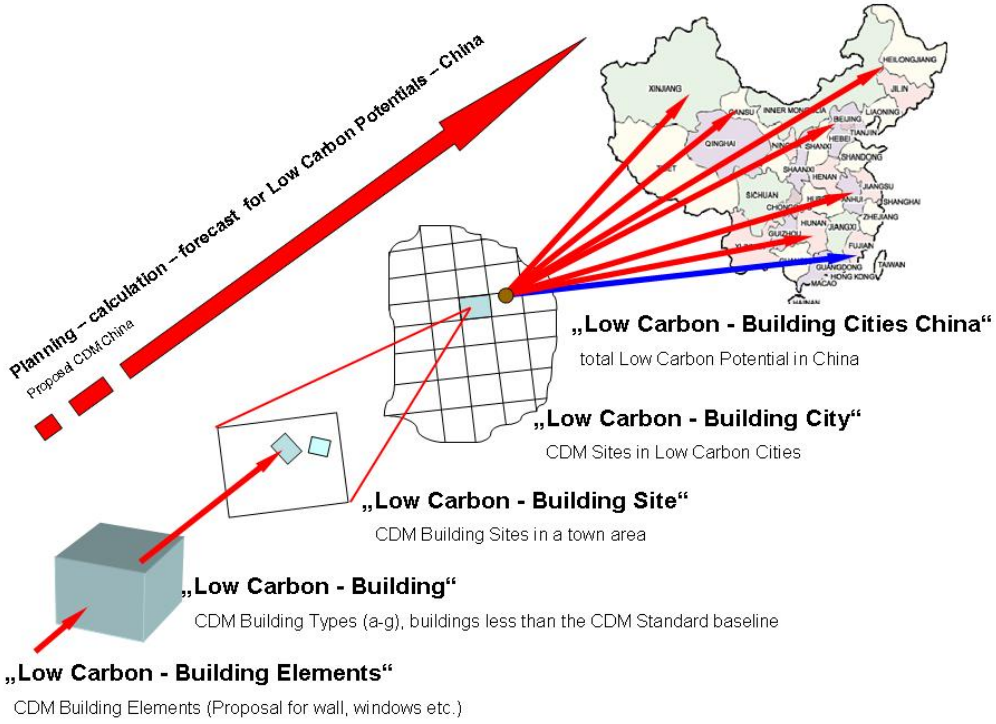

Figure 2. *Bottom-up-Calculation for the expected CO_2-Emissions in China*

References

PROPOSED NEW BASELINE AND MONITORING METHODOLOGIES - (CDM-NM)

CDM project activity categories – III.AE. Energy efficiency and renewable energy measures in new residential buildings

ASHRAE5 Guideline 14-2002, Measurement of Energy and Demand Savings, Whole Building Calibrated Simulation Performance Path6

GB 50189-2005 Chinese Guideline - public buildings

GB/T 50378-2006 Chinese Guideline - Green Building Standard

GB 50176-93 Chinese Guideline - residential buildings

Energieeinsparverordnung–EnEV2009 and DIN V 18599–Energetische Bewertung von Gebäuden (07/2005)

TRNSYS - Transient Energy System Simulation Tool; University of Wisconsin, Madison

LEC- Low Energy Certificate - http://www.lowenergycertificate.com

Innovative façade refurbishment with integrated air ducting for the existing building stock

Matthias Ziegler, M.Sc. [1]
Michael Krause, Dr.-Ing. [1]

[1] Fraunhofer Institute for Building Physics, Kassel, Germany

KEYWORDS: *Energetic retrofitting, façade integration, central ventilation system, air ducting*

SUMMARY:
For successful transition of the energy system being sustainable, the energetic retrofitting of the building stock is a crucial factor. About 40% of the current final energy consumption in Germany is caused by the building sector for heating purposes. Energetic retrofitting can reduce the heat demand of buildings considerably but extensive refurbishments often fail due to high costs, leading to only individual measures on the façade being carried out. New retrofitting concepts are required which are both energy efficient and cost-effective to increase the rate of retrofitting significantly.

A promising solution, developed by the Fraunhofer Institute for Building Physics, provides the implementation of the air duct system in the building envelope. Hereby, the air ducts for the installation of a central residential ventilation system are integrated directly in the mounted ETICS plate. Such a system has already been successfully tested in one and two family houses. However, the challenge of implementing the system in a multi-storey building is much larger due to structural dependencies on the façade, fire protection regulations and other limiting factors. These constraints have been identified to develop appropriate solutions for the planning of the air ducting on the façade.

1. Introduction

1.1 Importance of the building sector in our future energy system

In Germany, the building sector causes 40 % of the current final energy consumption. The main part of that energy is used in buildings for space heating and domestic hot water obtained from fossil energy sources. The energy concept of the German Federal Government (BMWi/BMU, 2010) assigns the energetic retrofitting of the existing building stock a significant role for the upcoming energy transition. Until the year 2050, the entire energy supply in Germany which is today mainly supplied by fossil and nuclear energy sources should be replaced by renewable energies. Furthermore these enormous efforts to rehabilitate the existing building stock are crucial to achieve the climate change objectives of the European Union.

Currently, the legislature in European countries has already reached a very high level of energy efficiency for new building, like the directive on the energy performance of buildings (EPBD) in 2003 or national ordinances like the Energy Conservation Act (EnEV) in Germany. New energy standards for buildings have been developed like the passive house concept, a building without a conventional heating system due to a high level of thermal insulation and optimized passive solar energy gains or the plus energy house, which produces throughout the year due to a large photovoltaic system more energy than it consumes. These concepts are proven, technically mature and well-established in building practice (Erhorn, 2012). Despite these technical processing, throughout all European countries the existing building stock contributes about 80 % of the overall energy consumption. The

possibilities for governmental requirements for energetic retrofitting are limited because of economic reasons like cost effectiveness and manageable payback periods. There are several ways to overcome these restraints for example with new innovative concepts for retrofitting like minimally invasive and multifunctional concepts to reduce the costs for renovations. These innovations are urgently needed to increase the rate of retrofitting significantly which is currently about 1% per year.

1.2 State-of-the art

Extensive renovations are costly, so that normally only single measures like the replacement of the old windows or the refurbishment of the building envelope with an external thermal insulation composite system (ETICS) are being carried out. Single measures are less energy efficient and one of the reasons why no more retrofitting is realized at towards a significant period on a certain building. Building retrofitting is traditionally planned and executed separately by trade with lack of coordination. This can often lead to problems because basic building physics principles, like thermal bridges or air tightness are not considered in an optimal way (Stiegel 2012). Structural enhancements like ETIC system or new windows can reduce the transmission loss of a building and the associated energy demand significantly but the increased sealing of the building envelope can lead to moisture related problems due to improper or insufficient ventilation. The installation of a user-independent central ventilation system with heat recovery can ensure the necessary hygienic air change and provides many advantages. So the indoor air quality can be improved and saving at the same time additional energy due to the recovery of the thermal energy contained in the exhaust air. Retrofitting barriers, such as the high cost of the internal ductwork and the impairments caused by dirt and noise for the tenants often prevent the installation of a central ventilation system. Other solutions with independent and decentralized ventilation units are cheaper but have a lower heat recovery and require more maintenance.

2. Innovative Retrofitting with façade integrated air ducting

The Fraunhofer Institute for Building Physics in Kassel developed in cooperation with an industry partner a promising solution for the subsequently installation of a central ventilation system in ETICS façades – “the FreshAirWall” system (FAW). The air ducts are integrated in the insulation panels, so that the functions thermal insulation and air ducting are combined in one construction. In figure 1 an ETICS plate with the integrated air duct is shown. The air duct is separated by a divider due to structural reasons and has a cross section of about 30 mm x 300 mm. For better processing on the building site and enhanced connection the plate features a groove and tongue system around the duct. Figure 2 shows an example how the panels are arranged on the façade. The panels are connected alternately to form the complete vertical duct.

FIG 1: ETICS panel with integrated air duct (FAW)

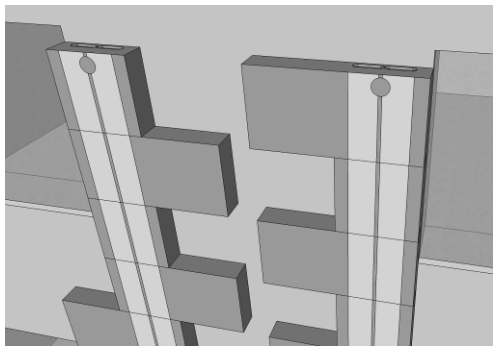

FIG 2: Air ducting on the façade

2.1 Current design and functionality

The current design of the insulation panels is specified for the ventilation of one or two rooms with fresh air. For this reason the cross section of the air duct corresponds hydraulically to a round duct with a nominal pipe size of DN90. The air ducting on the façade should be exclusively vertical, to avoid deflections and necessary fittings which would complicate the positioning on the building envelope. A wall bore hole connects the room with the air duct and all of the distribution pipes are located in the basement or the attic depending where the ventilation unit stands.

2.2 Previous investigations

The FAW system was examined by simulation, in-situ measurements and experimental investigation in the flow laboratory. These examinations are necessary to determine the basic functionality of the retrofitting system and to identify possible optimization for the system.

First, the System was implemented in the dynamic simulations program TRNSYS regarding the heat losses of the air ducting on the façade and the achievable heat recovery for a certain building. The air flows in all rooms provided by the ventilation system were calculated with a multi-zone air flow model and the results are already published (Ziegler, 2012). During a research project, the innovative retrofitting system was carried out in a two-storey residential house in Kassel (GER) and monitored for three years with long-term measurements to determine the heat recovery, the achievable air temperatures as well as an energy efficient operation with low pressure losses and minimal electrical energy demand for the fans. The hydraulic performance of the air ducts integrated in the insulation panels was mostly unknown, that is why experimental investigations in the flow laboratory to determine the pressure drop of the straight air ducts were carried out. The results of the examinations showed that the measured pressure drop of the air ducts corresponds to calculated pressure drop of a sheet metal duct with the same geometry (Ziegler, 2013). The pressure drop of the fittings like the 90° deflection and the wall connection to the room were comparatively higher.

3. Application in different types of residential buildings

The results of the investigations on the two-storey building described above demonstrate that an energy efficient and cost effective system is technically feasible and simple to plan. The application of this retrofitting system in larger buildings like multi-storey buildings has not been investigated yet.

Buildings from the post-war period constructed from the 1950s to 1970s in Germany are quite suitable for the renovation with the FAW system. These buildings are often in a poor condition because most of them are made of debris or substitute materials. Their high energy demand promises a high potential of energy saving. Especially, when the renovation of the building envelope is pending, a new ventilation concept must be evolved, e.g. the planning of a mechanical ventilation. The external appearance of the post-war buildings is mainly dominated by plaster façades without any ornaments or decorating elements. Due to this, constraints caused by preservation order are rarely found. Cubic structure and plain cubature simplify the arrangement of the air ducting on the façade.

Based on the example of several buildings the fundamental dependences for the planning of the air ducting on the façade should be identified to develop appropriate solutions. The selection of the buildings is aligned to the building classes of the German model building code (MBO, 2002) since it contains the relevant requirements concerning fire protection like building material classes or fire resistance classes compared to the pertinent building typologies. In table 1, the building classes for residential buildings according to German Model Building Code are listed and the image of a typical building is attached. High rise buildings and special structures are not considered. The height, mentioned in table 1, is measured from ground floor level to the finished level of the highest storey suitable for accommodation.

TABLE 1:Residential building classes according to Model Building Code (MBO) in Germany

Building class	Description	Example
Building class 1 (GK1)	detached buildings up to a height of 7 m and not more than two units with a max. area of 400m²	
Building class 2 (GK2)	buildings up to a height of 7 m and not more than two units with a max. area of 400m²	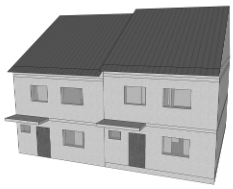
Building class 3 (GK3)	other buildings up to a height of 7 m	
Building class 4 (GK4)	Buildings up to a height of 13 m and each unit not more than 400 m²	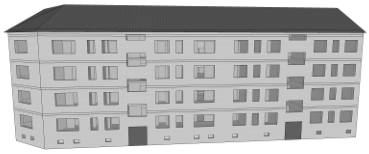

For every building class, a typical building was selected and examined regarding possible solution for air ducting on the façade with the FAW system. Class 1 building is a detached residential house with two dwellings and class 2 building is a terraced house with one dwelling. Furthermore, the example building for class 3 is a three-storey residential building which you can find mostly in larger cities. Also class 4 building is a typical multi-storey building in urban area with four floors.

3.1 Fire protection

For the planning of air duct systems on the façade the observance of the applicable fire protection regulations and their impacts are important. In general, in Germany there is a difference in requirements regarding building materials and building components.

Building materials are characterized according their fire behavior in different building material classes. There is a distinction between nonflammable materials A, flame resistant materials B1 and normal flammable materials B2. Air ducts integrated in the thermal insulation made of polystyrene can be produced as flame resistant by chemical additives. Flammable materials are allowed to use in building of class 1-3 but in class 4 buildings only flame resistant materials are permitted. For energetic retrofitting of building façades with ETIC systems, the thickness of thermal insulation must extend 100 mm due to regulations. These ETIC systems (thickness ≥ 100 mm) need further fire protection measures to obtain the flame resistance (FVWDVS, 2009). One possible solution is the installation of a fire barrier above every second floor with a minimum height of 200 mm. Another solution is a window lintel protection above every window to prevent the fire from spreading vertically to the next storey. Both additional fire protection measures are displayed in figure 3. As shown, these measures have a great influence on the planning of the air ducting because of less space on the facade. Either the air ducts must be arranged around the window linter protection or alternatives to match fire protection and air ducting on the façade need to be developed.

FIG 3: Additional fire protection for class 4 buildings with fire barrier above every second floor (left) and with window lintel protection (right)

When connecting two rooms of different units via one air duct, further fire protection measures are needed to prevent fire and smoke from spreading to another unit. The installation of maintenance free fire dampers for example can eliminate that danger.

3.2 Structual dependences on the façade

The arrangement of the air ducting on the façade is difficult in larger buildings like multi-storey buildings because of structural dependences on the façade and the layout of the floor plan. Below, these constraints and restriction are analyzed using the example buildings listed in table 1.

3.2.1 Floor plan design

The floor plan design can have a significant influence on the planning of air duct systems on the facade. Especially the position of the supply and exhaust air areas affects the air ducting. In most buildings the floor plans in the individual storeys do not differ, so similar rooms are always located above each other. This rather simplifies the design of air ducting. Many buildings of the 1950s and 1960s contain old chimneys which were used earlier for single fired ovens. Here, it would be possible to install subsequently several ducts in the chimneys for one room in each floor to minimize the number of ducts on the façade. The ducts could be made of flame resistant materials and the space between them in the chimney could be filled with an intumescent substance which foams and seals the duct in case of fire. An image of this concept can be seen in figure 4.

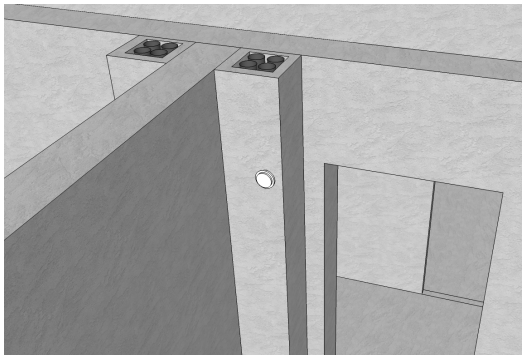

FIG 4: Subsequently installation of air ducts in existing chimneys

The ventilation unit can be positioned either in an unused or not extended attic or the basement of the building. For maintenance reasons, the ventilation device should be easily accessible. Usually, in the basement is not enough space for the installation of the central ventilation station because of rented cellars. Another limiting factor is the low ceiling height in the basement, so that the horizontal distribution air ducts are difficult to arrange. Possible solutions for the connection of the air duct to

the attic and the basement are illustrated in figure 5. The jamb wall and the cellar wall are suitable for linking the ducts together. In range of the basement window, the air ducting needs to be planned very carefully.

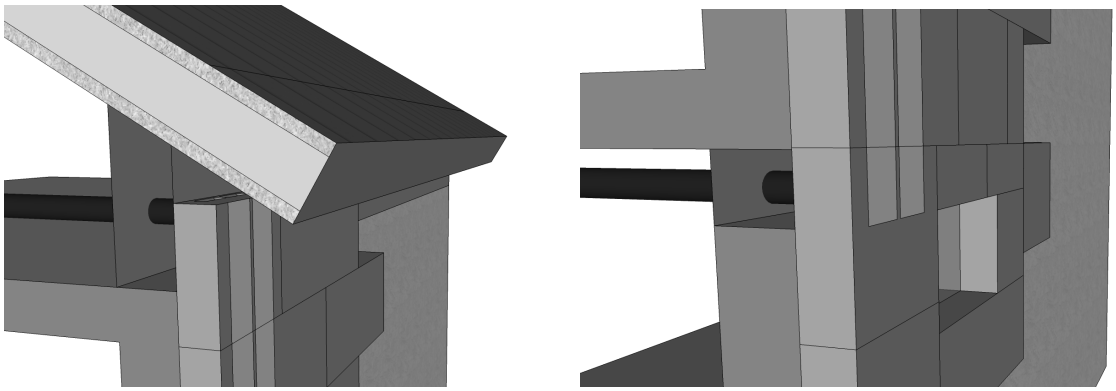

FIG 5: Connection between the inner distribution channels and the air ducting integrated in the thermal insulation in the attic through the jamb wall (left) and in the basement through the cellar wall (right)

3.2.2 Façade design

The available wall area between two windows in multi-storey buildings is limited assuming an exclusively vertical air ducting. This should be explained by the following example in the class 3 building. In figure 6 a front view of the class 3 building with the adjacent inner and outer walls is illustrated. The location of the lateral walls is important because the air ducts are connected to the room via a wall breakthrough. So, the usable wall surfaces in certain rooms are partially less than 50 cm wide, which is not sufficient to put multiple air ducts next to each other.

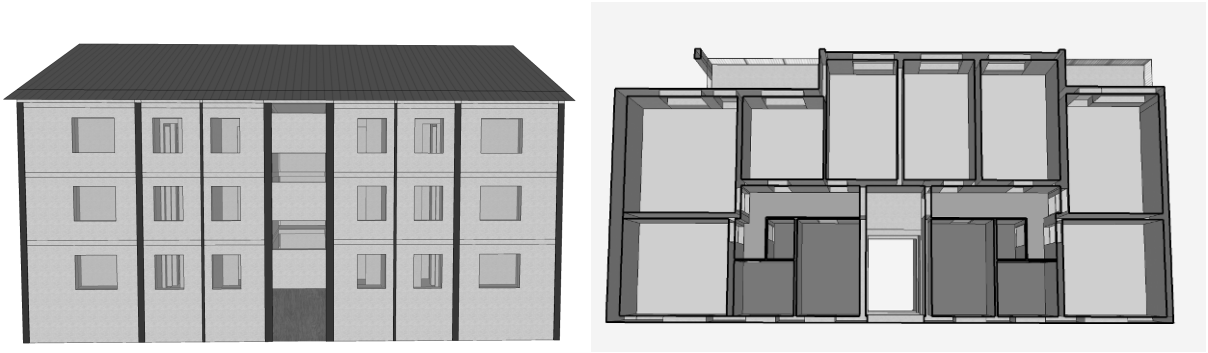

FIG 6: Front view of class 3 building with lateral inner and outer walls in dark lines (left) and the associated floor plan (right)

Buildings from the reconstruction years in Germany rarely have projections and recesses on the façade but on the rear side often recessed balconies or loggias can be found. The rooms located behind the balconies cannot be connected to a vertical air duct without using deflections on the façade. These constraints are shown in figure 6 (right side) to illustrate that challenge. Therefore, the air ducting in the area of the balcony can be realized for example by breaking through the ceiling selective. However, the sealing of the balcony should be maintained and the process of retrofitting should be preferably with little effort. Another possibility is to provide the lateral surfaces for air ducting, when they are not needed otherwise.

4. Possible solutions for multi-storey buildings

The constraints and structural dependencies in multi-storey buildings demonstrated above leads to significant challenges for the planning of the air duct system on the façade. Now, in this part appropriate solutions are being developed.

The arrangement of the air ducts is to a decisive extent dependent on the available wall surfaces between the windows. Usually, it is not possible to connect all the rooms on each floor with its own vertical duct. Using the example of the three-storey buildings of building class 3, two options are shown to integrate the air ducting on the façade. First option provides the connection of two rooms with one duct. In this case, the dispersion of fire and smoke from one dwelling to another must be prevented for a certain time period. The second option would be to separate the first two floors from the third floor. Two ventilation devices are required, one in the basement and one in the attic. Both possible solutions can be seen in figure 7.

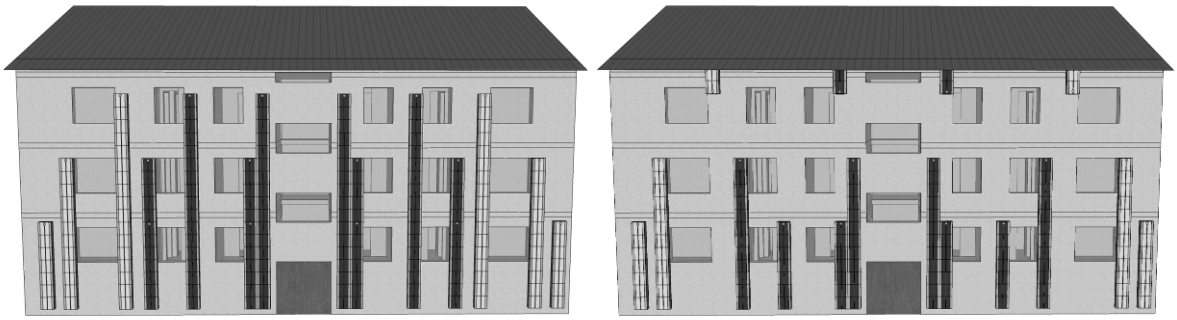

FIG 7: Solution for the air ducting on the façade with limited space between the windows: connection of two rooms with one duct (left) and with air ducting through the attic and the basement (right)

For large buildings (building class 4) additional fire protection measures are required e.g. fire barriers. The concept of separation of floors, described above, can be applied (figure 8). The fire barrier then splits two floors and the rooms are either supplied via air ducts from the attic or the basement. If only one ventilation device is desired, the fire barrier will be crossed by air ducts. This is technically possible with nonflammable ducts made of metal and laminated with an intumescent coating. For this purpose, further investigations are necessary to evaluate the performance in case of fire and smoke.

FIG 8: Fire barrier and separated supply air ducting through the attic and the basement, exhaust air ducts installed subsequently in existing chimneys

5. Conclusion and outlook

The retrofitting system with air ducts integrated in the thermal insulation (FAW system) is energy efficient and cost effective and has been tested both with theoretical and experimental investigations in one and two family houses. There are almost no limiting factors for the air ducting for class 1 and 2 buildings regarding structural dependencies or fire protection regulations. The planning of the air ducts on the façade for multi-storey buildings, however, is subject to much more constraints by obliged fire protection measures, flanking balconies and narrow available wall surfaces. For these limitations suitable solutions have been developed in order to realize the air ducting on the façade.

In further investigations an appropriate planning tool for the air ducting on the façade should be developed. In addition to that an enhanced design of the air duct in the insulation plates with same fluid dynamic properties and minimal heat losses can improve the system.

6. Acknowledgements

The author wants to thank the German Federal Environmental Foundation (DBU) for the PhD scholarship and the associated promoting of the research project. Furthermore, the authors are grateful to ABG Nova for the providing of the demonstration building that is to be renovated within the EU Project (EU RetroKit, 2012).

References

Erhorn H. 2012. Das Effizienzhaus Plus. Fachtagung „Die neue Plus-Energie-Welt“. Berlin http://www.forschungsinitiative.de/PDF/Plusenergie_IBP.pdf

European Union. 2002. Directive on the energy performance of buildings (EPBD). http://eur-lex.europa.eu/LexUriServ/LexUriServ.do?uri=OJ:L:2003:001:0065:0065:EN:PDF

European Union. 2012. RetroKit project. http://www.retrokitproject.eu/web/guest

Federal Government of Germany. Energiekonzept für eine umweltschonende, zuverlässige und bezahlbare Energieversorgung. Press information Office of the Federal Government. Berlin. Germany

Fraunhofer Institute for Building Physics. 2010. Innovativ saniert! – mit integrierten Lüftungskanälen in der Außendämmung, press release. Kassel. Germany

Hauser G. &Kaiser J. 2013. Dämmstoffintegrierte Kanäle für zentrale Lüftungsanlagen mit Wärmerückgewinnung. Article Bauphysik 6/2013. Ernst & Sohn. Berlin.

IS-Argebau. 2002. Musterbauordnung (MBO). Model Building Code. Berlin. Germany

Stiegel H. & Krause M. 2012. Minimalinvasives Sanierungssystem mit vorgefertigtem, multifunktionalem WDVS-Fassadenmodul. GI Gesundheits-Ingenieur. 133(2012) Heft 6.pp. 290-302

WDVSysteme. Fachverband Wärmedämmverbundsysteme e.V. 2009. Technische Systeminfo – „Brandschutz“. specialized information. Baden-Baden. Gemany

Ziegler M. 2012. Thermische und strömungstechnische Simulation einer Fassadendämmung mit integrierter Luftführung für die Bestandssanierung. conference BauSim 2012. Berlin. Germany

Ziegler M. & Krause M. 2013. Innovative façade refurbishment with integrated air ducting for the existing building stock. conference SB13. Munich. Germany

Achieving Sustainable Roof Systems through Innovative Design

Thomas W. Hutchinson, AIA, CSI, FRCI, RRC, RRP [1]

[1] Hutchinson Design Group, USA

KEYWORDS: *Long-Term Performance, Roof System Design, Durability, Sustainability*

SUMMARY:
The discussion on sustainability is now over a decade long. How this concept relates to roof systems is unique in that the variety of potential solutions is almost endless. If one accepts the conclusion of the CIB/RILEM Joint Committee on Sustainable Low Slope Roofing (2001), that established the 21 Tenets of Low Slope Roofing (which have become the international standard bearer for sustainable low slope roofing), that the essence of sustainability is 'Long Term Service Life', then designers must move beyond current fad and use empirical experience and innovative methods to achieve sustainable roof systems. This paper will present two roof system design case studies in which the author called upon his 25 years of roof system design experience, empirical in-field service performance, and architectural background to design roof systems whose long-term service life expectations are 50 years or more. Design concepts, details and photographs from these projects will be presented.

1. Introduction

Prior to any new concept implementation, such a Sustainable Roof Systems, the ultimate end goal should be clearly and definitively stated and understood through the definition of terms. Make no mistake about it: Sustainability is about long-term performance. Additionally, in combination with the concept that roofs are systems that are only as good as their weakest component, the idea of sustainability must be holistic in approach, involving the entire roof system. The inclusion of green parameters, which are only one part of sustainability, and without the other key parameters will not result in the realization of long-term performance. Thus, the keys to sustainability are not independent, but must act synergistically so that they result in a system that results in long-term performance, achieving the owner's and designer's desired sustainability goals.

Keys to sustainability that have been developed over years and have been proven by the test of time are as follows (Hutchinson 2007):

1. Achieving the owner's buy-in.
2. Be aware of budget appropriateness. Quality cannot be achieved with under-developed budgets.
3. A roofing system designed for long-term performance.
4. Use of quality materials that support long-term performance.
5. Inclusion of thermal insulation performance appropriate for the region in which the roof is installed.
6. Environmental considerations.
7. Use of qualified contractors.
8. Quality assurance.
9. Management of rooftop equipment.
10. Maintenance.

The following is a discussion of each of the above-mentioned 10 keys to sustainability.

1.1 Achieving owner buy-in

Designers and contractors work with a variety of clients who have differing performance goals, needs, and budgets. All clients must be educated in the development of their new roof system design and

enlightened not only as to the importance of long-term performance, but also to its benefits. Clients and building owners are becoming more sophisticated, requiring and demanding greater performance from their building systems: roofing systems are no less. Many clients assume warranties are justification for long-term performance; on the contrary, warranties are issued by manufacturers as a minimum standard, and are a promise to render a leak watertight, not a promise of a leak-free roof. Additionally, all too often this author has had to discuss owner concerns such as, “I only want to hold the building for 10 years”; “It’s not financially responsible to do so”; and “It’s just a roof”. All concerns suggested above have been dissuaded when resale value, altruistic values, return on investment, environmental benefit, etc. are reviewed and explained in a factual manner to those who doubt.

1.2 Roof systems designed for long-term performance

In the quest for long-term performance, roof system design requires specialized and concerned individuals. Long-term performance is defined as a 30-year minimum service life. However, as an industry we should be striving to achieve even greater performance duration. Achieving this goal encompasses much more than just roofing system design; it is giving consideration to how the, building’s architectural elements impinge upon the roofing system; such as masonry, EIFS, HVAC, and telecommunications equipment, as well as roof top access and traffic, and incorporating them into the roof system design. Qualified roofing system designers are mandated. They must be educated, knowledgeable, and in many instances licensed to perform design in the locality in which the construction project is to take place. The roof system must be appropriate not only for the building, building use, and anticipated roof top use, but also for the climatic and geographical conditions where it will be installed. Additionally, minimizing penetrations and foot traffic upon a roof go a long way to assist in the roof system’s performance.

This author is convinced that quality long-term roof system performance cannot be achieved without detailed building to roof specific details. The use of only specifications describing installations, and manufacturer’s details, is inappropriate and unacceptable for the attainment of long-term performance.

1.3 Materials

It continues to amaze this author that new materials (note: new material are not only those coming on the market, but also those whose formulation are revised, changed and modified in an attempt to correct in field performance issues). In the U.S.A. the primary example is TPO (thermoplastic polyolefin membrane), which are so readily and easily accepted by the building design community, when there is no proven history of performance for these materials in the roofing industry, nor in the region or locality in which the materials are being installed. Therefore, a key of all materials implemented on a new roof system looking to achieve sustainability is that each material has an established history of long-term in situ performance for the system in which it will be installed. The roof installation methodology should also be appropriate for the roof system involved.

Additionally, if possible, roof system materials should also be restorable, recyclable or reusable after their service life. What is the availability of roof system materials and their recycling programs in the locale in which the system it is being installed? Can the roof be restored? One fine example is the restoration of EPDM roofs after they are either out of warranty or their service life, resulting in an extended service life.

1.4 Thermal performance

The U.S. Department of Energy recently released data that suggests that it is the heating load that dominates, not cooling (U.S. Department of Energy 2011). Therefore, rendering an opinion that is diametrically opposed to that of the cool roofing proponents. Consequently, most buildings should be

designed for their heating loads rather than their cooling loads, as energy costs have historically risen over time; appropriate consideration of potential energy savings options is prudent.

There is a number of parameters that will affect thermal performance that should be given consideration. One such parameter affecting thermal performance to consider is the use of vapor and air retarders. Not only should consideration be given to these retarders during the installation process as a method for achieving a more homogeneous installation, but also to reduce construction induced moisture drive; they will thus protect the roof system through the new construction and/or re-roofing construction process. They will also reduce the amount of air transport into the roof system. Air transport is one of the greatest causes of heat-loss, and the movement of moisture into the roof system.

Through this author's experience, it is mandatory that multiple layers of insulation be installed to achieve the highest level of energy conservation. Recent inspections by this author on a multitude of roofs have shown that the allowable dimensional change of insulation (typical with polyisocyanurate or EPS) results in open gaps between insulation boards of up to ¾ inch (1.9 cm) in thick layers of insulation, resulting in numerous concerns including heat loss, unsupported roof covers, and the potential for moisture condensation at the roof cover. While this is not necessarily a performance concern of the material, but actually a characteristic of the material that is not properly described in product literature or communicated to the building designer. Thus, this author has required that all insulation voids at perimeters, penetrations, roof curbs, and drains be sealed with spray foam insulation to eliminate these thermal shorts.

Recent studies by Desjarlais et al. (2008) at the Oak Ridge National Laboratories (ORNL) have shown that the use of ASTM #4 ballast and/or concrete pavers can provide the same benefit as reflective roof surfaces, while additionally moving heat load away from peak periods.

1.5 Environmental considerations

Consideration of the environmental concerns is only one of the keys, not THE key, to sustainability. The goal of environmental consideration should include:

- Minimizing the burden on the environment;
- Using products with known long-term service lives; and
- Recognizing regional and climatic factors in the design of the roof system.

The practitioner must remember that it is often more appropriate to use a material that at first review appears less environmentally friendly than others, but who's long-term benefit is superior. For example, if a superior material is manufactured at a greater distance from the construction site, it may be worth the transport rather than using a local material that may not achieve long-term system performance.

Garden roofing has become a popular environmental treatment for a variety of roof surfaces. While the potential for extending a roof's service life is high when incorporating an overburden that protects a roof covering from thermal shock and UV degradation, thin overburdens and improper or reduced quality system design are resulting in systems of less than anticipated performance.

1.6 Contractor qualifications

This author cannot emphasize enough the necessity of pre-qualifying contractors. This is important not only for installation of the roof system and its related components, but also for value with regard to how business opportunities are viewed.

1.7 Quality assurance

Twenty-five years of roof system design and construction experience have led this author to realize that even with high quality drawings, specifications, budget appropriations, and quality contractors; nothing can supplant the continuous on-site observation of the roof system installation by qualified

roof consultants. On-site observation provides the opportunity to address questions, to verify compliance with the contract documents, and at times, to enforce quality related concerns. Even the best contractors occasionally have installation quality issues, such as joints in the insulation that are greater than ¼ inch (0.6 cm), or joints that are not offset as specified. Field observation will allow for the clarification of unknown or difficult conditions that may need resolution. Pre-construction meetings, weekly project coordination meetings, a view of the clear-cut definition and goal of the project should all be included under the auspices of "quality control".

1.8 Pro-active maintenance

All roof systems require maintenance. This bears repeating: all roof systems require maintenance! It is required by the warranty. Good roofing practices require it. It is key to achieving sustainability. All roof systems require maintenance. Keeping roof drains clean and free of debris; minimizing unnecessary maintenance crew's (HVAC and cable techs, etc.) access to the roof will go a long way to achieving a long-term service life and preventing unwanted damage to the roof.

2. Case Studies

In the past 5 years this authors has been involved with educational, healthcare and fortune 50 companies whose building stock is substantial, and for whom the concept of long-term service life is especially appealing. The decided upon long-term service life goal was to exceed 30 years. Design, detailing, material selection, contactor qualifications, and on site observation raised the authors prediction of long-term service life to 50 years.

A couple of the main parameters (concerns) of designing roof systems for 50 years are: 1.) How will the material perform under UV radiation, and its potential deleterious effects on the roofing material, and 2.) What type of in situ performance does the material have. In regard to the case study projects, the material selected was EPDM. This author's experience with the material is excellent, with numerous projects installed over 25 years ago still performing. In fact, studies by SKZ (Süddeutsche Kunststoff Zentrum) in Würzburg, Deutschland (Zahn 2003), declared that EPDM should have a service life of 50 years. Furthermore, this author and the EPDM Roofing Association (ERA) undertook a study looking at EPDM roofs over 30 years old, tested the material for the physical characteristics, and found that 90% held characteristics at levels above the minimum level for new materials. A second study heat aged the 30 year in situ material for an additional 30 year equivalency, and then performed physical characteristics tests. Not surprisingly the results were positive (a paper on the results and conclusion of these findings entitled *Characteristics of In-Service, 30-Year Old EPDM Roof Membrane* will be presented at the 2014 Durability of Building Materials and Components Conference in Sao Paulo, Brasil, in October 2014).

2.1 Case Study 1: Hawthorn School District 73: Middle School North

Client:	Hawthorn School District 73
Building:	Middle School North
Location:	Vernon Hills, IL (20 miles north of Chicago)
Building Use:	Middle School for grades 6-8
Size:	145,000 ft^2 (13,471 m^2)
Height:	1 and 2 Story: Max height: 28 feet (8.5 m)

Project Goals:

- 30 Year Service Life: Increased to 50 by author after design
- Increase thermal value by 200%
- Budget: $1,650,000 (approx. 1,218,200 € / 10,816,500 kr)
- Roofing to be completed during summer break: June to mid-August

Design Concept and Innovation: Use the existing roof membrane as a vapor retarder and install a new roof system over the top.

The existing Middle School had its original roof replaced in 1986 with a fully adhered 60-mil EPDM system installed over two layers of 1.5 inches (3.8 cm) polyisocyanurate insulation (Pier) with a ½ inch (1.27 cm) fiber cover board. The budget at the time was minimal; consequently, the roof design was basic, as was the installation. Subsequent roof top equipment installations and unabated foot traffic resulted in some minor physical damage, and the low level of insulation did little for a school that is heated 7 or more months a year. After several repeating roof leaks, as well as high energy costs, the board budgeted for a new roof system.

2.1.1 Investigation:

Initial investigation of the existing roof system found that while there were several deficiencies, they were not wholesale, and that the roof system as it was, was in good structural condition: It wasn't deteriorating below the membrane, and its attachment to the structure was intact. As a consequence of this investigational conclusion it was decided to use the existing roof system as the base for a new, highly thermally sustainable roof system. A review with the roof membrane manufacturer of the concept found them to be a willing partner.

2.1.2 Design:

Utilizing the existing roof system required special attention to the attachment of the new roof system. As the concept was to utilize the existing roof system as a vapor retarder, penetration of the existing membrane would not be prudent. Thus we looked to adhesives. Following a review of potential materials it was decided to use a low rise insulating, two component spray polyurethane adhesive with enhanced plasticity. Test mock-ups in the field prior to the finalization of design and consequential construction documents were undertaken with the finding that the proper preparation (cleaning) of the existing membrane and compression of new insulation board were required to achieved the required attachment and uplift resistance.

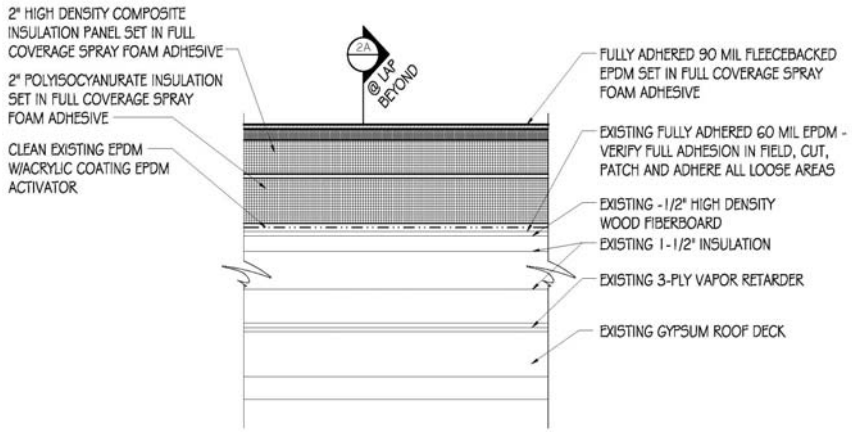

FIG 1. Typical Roof Section Detail

In order for the existing roof membrane to be used as a vapor retarder the new insulation above needed to be of an R value great enough to keep the membrane below the dew point. Dew point calculations determined that 2 layers of 2" (5.08 cm) polyisocyanurate insulation with R 24 were required. As this roof design called for long-term service life, a double coated fiberglass insulation facer, that does not support mold growth and provides a superior surface for adhesive attachment, was specified. To prevent foot traffic damage to the insulation, and insulation and membrane adhesive bond, the top layer of insulation was specified as a composite board with the top ½ inch (1.27 cm) being a high density polyisocyanurate of 100 psi.

A 90-mil fleece backed EPDM set in full coverage spray foam was specified for its superior wind uplift resistance, as well as its tenacity in deflecting foot traffic concerns. A section of the roof system design can be observed in Fig. 1 and Fig. 2. To enhance the roof system, 6" seam tape lap seams with self adhering cover strips were designed.

FIG 2A -B. Roofing crews set the 90-mil EPDM into the full coverage two component spray polyurethane adhesive, which will be rolled into place with a 90 # (41 kg) water roller. Note the two layers of insulation with offset joints and the roof edge sheet metal installation on the roof edges beyond. In the right photo the 45-mil vapor retarder has been installed, and the raising of the roof curbs and edges, replacing roof drains, and modifying mechanical equipment can take place.

Additional roof system design features included:

1. The roof edge had to be raised to accommodate the additional insulation. To reduce the number of horizontal layers of roof edge sheet metal, a vertical prefinished aluminum flush panel and coping were designed.
2. All roof drains were raised with extensions and new overflow roof drains added.
3. Abandoned equipment was removed, and the roof deck in-filled.
4. Smoke hatches were removed and replaced with new.
5. Roof hatches were removed and replaced with new.
6. Ladder and stair access to varying roof levels were added for maintenance.
7. Roof top mechanical equipment and piping was disconnected, curbs raised, and the integration with the new roof system coordinated.
8. Deteriorated masonry above the roof was restored.
9. Deteriorated areas of roof were removed and replaced with new to match.

2.1.3 Construction:

The project was bid in early spring 2012 with the main construction commencing in early June. The roof installation was observed by a Registered Roof Consultant (RRC) and took approximately 4 months. Roof edge sheet metal took another 2 months.

Contentedly, the owner reported an approximate drop in the total building energy usage in the first year.

2.2 Case Study 2: Moraine Valley Community College: Building L

Client:	Moraine Valley Community College
Building:	Building L
Location:	Palos Heights, IL (10 miles southwest of Chicago)
Building Use:	Educational
Size:	67,500 ft^2 (6,271 m^2)
Height:	2 Story: Max height: 26.0 ft (8.0 m)

Project Goals:

- 50 Year Service Life.
- Improve roof drainage.
- Recycle the existing ballast, PVC membrane, insulation, and sheet metal.
- Budget $1,056,000 US (approx. 777,500 € / 6,889,340 kr)

Design Concept and Innovation: Use 45-mil EPDM as vapor retarder, mold resistant insulation, 90-mil ballasted EPDM with filter fabric protection.

The existing ballasted PVC membrane served the college well for the first 10 years of its service life, after which the PVC migration into the ballast resulted in a rigid membrane prone to splits, especially under foot traffic. Numerous roof leaks into the interior disrupted the educational process and created unsafe slip conditions, as well as manifesting staff concerns with mold.

This project was second in a series of three required to complete this large multiple building complex. Prior to the projects HDG met with the college Building and Grounds Director, 'Green' Consultant, and Vice President to review the concepts of sustainability. The Green consultant immediately asked for a cool roof membrane, armed with incorrect precepts: It will save energy and reduces the urban heat island. After a review of the facts, that ballasted roof systems are a greater energy saver than cool roofing, the reflective roofs actually increase the ambient air temperature above the roof surface, and that with the exception of one commercially available in the US market, reflective roofing has an unproven track record in the field; with formula's being revised almost yearly they could even be considered "experimental"! A ballasted 90-mil EPDM system with enhancements was decided upon for the colleges preferred roof system.

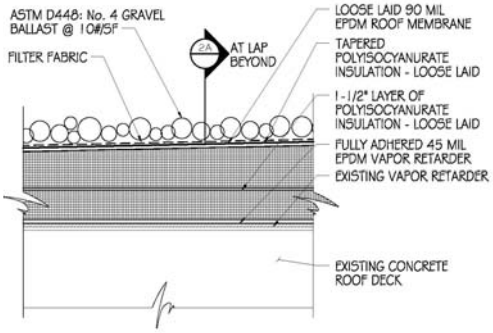

FIG 3. Typical Roof Section Profile

2.2.1 Investigation:

Roof cores revealed expanded polystyrene insulation below the 45-mil PVC membrane on a 2 ply built-up roofing vapor retarder on a concrete roof deck. The existing vapor retarder was found to be in good condition and very well adhered to the concrete. Removal of the vapor retarder would be costly and without merit, so it was decided to be allowed to remain.

2.2.2 Design:

While ballasted roof systems have been around for decades, and this author has observed numerous ones over 25 years of age and still performing, the goal for this roof system was 50 years of service life. As this project involved the removal of the existing roofing, roof edge raising, roof drain removal and replacement, as well as renovation, it was decided to enhance the existing vapor retarder with fully adhered 45-mil EPDM (see Fig. 2B) so that the entire existing roof could be removed, the ancillary details performed, and the new roof system installed in a more monolithic manner.

Additionally, high PSI polyisocyanurate, which is more stable, and with double coated fiberglass facers, which are mold resistive, was selected. A 90-mil EPDM membrane with 6" seam tape, and with all lap seams covered with self-adhering seam tape was designed. Looking forward 25 to 30 years

when the ballast might start to shatter and create shapes, a protective filter fabric was installed over the EPDM as a buffer between the EPDM and ballast (see Fig. 3). As the thickness of 90-mil EPDM, even with its flexibility, is difficult to install tight into the angle changes from horizontal to vertical, and heavy to extend up and over roof edges, this condition was designed and detailed with anchoring the field sheet to the wall, and using a 60-mil base flashing sheet with 6" seam tape and cover strip. To raise the roof edge a pre-fabricated metal roof curb in lieu of wood blocking was designed.

Additional roof system design features included:

1. Sealing of all voids between the insulation and roof edge perimeters, pipe and roof curb penetrations, and roof drains to eliminate thermal shorts and avenues for air transport.
2. Heavy gauge prefinished roof edge sheet metal copings.
3. Pipe penetration and roof curb flashing enhancements to resist anticipated abuse.
4. Protective 2'-0" x 2'-0" x 2" thick rubber walkway pads used to access roof top equipment.

2.2.3 Construction:

The construction commenced in mid-March 2013 and was completed in late June. The author observed the construction and several anomalies were observed. The existing roof edge wood blocking was found to be in good condition and was allowed to remain. Even with a high caliber contractor, their project organization and crew management was less than desirable and lengthened the construction time. Undulating concrete roof decks challenged the tapered insulation, and the required detailing on what many would consider the simplest of roof systems took considerable time to install.

3. Conclusion

In over twenty-five years of roof system design, this author has had the opportunity to design numerous long-term performance roof systems, even before the concept of sustainability was popular. To this author's knowledge, 90% of all the roof systems that he has designed are still in place and functioning properly. Through empirical observations and discussions with roofing contractors, building scientists, and others in the building industry such as manufacturers and owners, the keys to sustainability have actually been known intuitively by all of us for years. Now they are stated and need to be put into universal practice. Building owners, architects, the roofing industry, 'Green Activists' need to move forward with enthusiasm, to embrace the concept of long-term service life and thus sustainability (long-term performance), and to accept the challenges to achieving roof systems that will perform for half a century: for our clients, for ourselves, and for our children.

References

CIB W083 / RILEM 166-MRS Joint Committee on Roofing Materials and Systems. 2001. Towards sustainable roofing. CIB Publication No. 271. *http://cibworld.xs4all.nl/dl/publications/Publi271.pdf*

Desjarlais A.O. et al. 2008. Evaluating the energy performance of ballasted roof systems. ORNL Report Number UF-04-396

Hutchinson T. W. 2007. Keys to sustainable roofing. Roofing Canada, p. 16-30.

Hutchinson T.W. 2014. Characteristics of in-service, 30 year old EPDM roof membrane. Proceedings of 2014 Durability of Building Materials and Components Conference in Sao Paulo, Brasil.

U.S. Department of Energy. 2011. Building Energy Data Book.

Zahn A. et al. 2003. Final Results of Study to Estimate the Service Life of Hertlan EPDM roof sheeting. Life expectancy of EPDM roofing membrane over 50 years. SKZ (Süddeutsche Kunststoff Zentrum) Final report no. 37236/99-IV. SKZ - TeConA GmbH, Würzburg, Germany.

External insulation with cellular plastic materials – thermal properties, long term stability and fire properties

Lars Schiøtt Sørensen, Senior Researcher, Ph.D. [1]

Anker Nielsen, Professor [1]

[1] Danish Building Research Institute, Aalborg University, Denmark

KEYWORDS: *External insulation, Cellular plastic material, Fire properties, Thermal insulation, Moisture, Long term stability, ETICS*

SUMMARY:

External thermal insulation composite systems (ETICS) can be used as extra insulation of existing buildings. The system can be made of cellular plastic materials or mineral wool. There is a European Technical guideline, ETAG 004, that describe the tests that shall be conducted on such systems. This paper gives a comparison of systems with mineral wool and cellular plastic, based on experience from practice and literature. It is important to look at the details in the system and at long time stability of the properties such as thermal insulation, moisture and fire. Investigation of fire properties must be done before utilisation of the system, including the risk of fire spread from one storey to the next for practical solutions. An elaboration of fire spread risks require thermo physic knowledge about ignition temperatures, critical radiation, upward flame spread velocities etc. of the actual insulation.

1. Introduction

External insulation is a good solution for many buildings as it reduces the effect of cold bridges and in most cases does not need to disturb the inhabitants in the building. It can be used for both single family houses and blocks of flats. In most cases it will change the architecture of the building as we get a new outer layer. This can be a problem for old houses, where we will keep the exterior look. The external insulation can be mineral wool or cellular plastic material covered of an external layer of plate material or plaster. There is a European Technical guideline (ETAG 004 from 2011) for external insulation systems. The systems are called ETICS, an abbreviation for External Thermal Insulation Composite Systems. The guideline describes the tests for each component and the system that has to be done to get a CE-mark. The acceptance of the system is based on the whole system, so it is not allowed just to change for instance the insulation material without a new approval. The European Association for External thermal insulation (EAE) has made a report (EAE 2011) that describes a quality system for external extra insulation. In Denmark it has not been allowed to use plastic insulation as external insulation and an overview of the experience from other countries is interesting. We will specially focus on the use of cellular plastic material and the problems related to fire. But we will also discuss the use of mineral wool and compare systems with plastics and mineral wool, as they have different properties on some important parameters.

2. Components

The systems consist of:

- Adhesive (binds the insulation to the existing wall surface)

- Insulation material
- Anchors (to fix the insulation if the adhesive is not sufficient)
- Base coat of plaster
- Reinforcement (glass fibre mess)
- Top coat of plaster
- Accessories (strips, corner and bottom profiles, expansion profiles etc.)

For anchors a European approval (ETAG 014) defines the properties needed for plastic anchors. For each of the insulation materials are also found European standards that define the tests that have to be done.

2.1 Existing wall

An external insulation can be performed on existing walls. The outer surface material of the wall will influence the solution.

- Heavy constructions. This includes walls of lightweight concrete, concrete and masonry of different types. In these cases it will normally be easy to fix the insulation systems with anchors and/or glue.
- Light constructions. This can be wood, plywood and gypsum. The mechanical strength of the material can be limited and there is a higher risk for movements of the surface. So the fixing is more complicated. In this case it is important to keep water away from the light construction.

In ETAG 004 are described test methods that must be used to evaluate the system for different outer surfaces. In the EAE guide is a check list to avoid mistakes in design and execution.

2.2 Insulation material

The thermal insulation material must have a CE-mark and the most important factor is the thickness and the thermal conductivity. The thermal conductivity shall be declared by the producer. For external insulation we can normally use the declared value as the insulation should be kept dry. The declared values for mineral wool are 0.034 -0.040 W/mK. For cellular plastic materials there is more variation depending on the type – polystyrene, polyurethane, polyisocyanurate or phenol foam. For polystyrene the value will also depend on the production method – expanded polystyrene (EPS) 0.034 – 0.041 W/mK and extruded polystyrene (XPS) 0.025 – 0.038 W/mK. For phenol, polyurethane and polyisocyanurate foam, the values can go down to 0.022 W/mK. This is caused by gases used in the production process. The declared value takes into account the change in gas concentration during the lifetime.

2.3 Fixing system and surface

The insulation must be fixed to the wall without air gab between wall and insulation material, as this will reduce the heat resistance of the system. For EPS or mineral wool it is normal to glue all over the surface or along the borders of each plate and some points in the centre. It is very important to consider details as corners and connections, so thermal bridges are reduced. The insulation layer must be fixed with anchors if the glue is not sufficient. In the description of the ETICS it must be described which type of anchors (and how many) that are needed. Insulation of plastics does not tolerate ultraviolet-radiation as it can degrade the material, so is it important that the surface plaster is put on

as soon as possible. For the outermost plaster layer it is important to take into account all the details with windows, doors, overhang, roof connections and all pipes or cables going through the façade. Examples are fixings for outdoor light and ventilation pipes. These points are critical for the risk of driving rain penetrate into the insulation material and hits the surface of the old wall. The EAE guide includes examples of these details, but each producers of a system must show how these details are solved.

3. Thermal properties

The systems must keep the thermal insulation properties over time, so we still get the energy savings we calculated for the system, also after 10-20 years. We will normally expect that if we calculate the transmission heat loss after the European standards then this is a good estimate for the energy savings. It is possible to measure U-values before and after the installation, but it is very difficult in real buildings to be sure that the indoor (and outdoor) climate is the same and the inhabitants behave in the same way. So a theoretical calculation is sufficient, but we have to look at possible problems.

3.1 Change of U-value over time

For most materials there will be no change in thermal conductivity over time. Only cellular plastics with a foam gas that can diffuse out will increase the thermal conductivity over time, but this should be included in the declared conductivity.

3.2 Gaps in the insulation

With air gaps between the insulation material and the wall or between the insulation panels, then cold outer air can flow into the insulation layer, and we do not achieve the expected U-value. This is important to avoid in the construction phase. Furthermore we must ensure that the fixing of the panel not loosen during the lifetime of the system.

3.3 Moisture in the insulation

Moisture in the insulation will increase the U-value. The moisture can come from the outside in the form of driving rain or from the inside, if the moisture barrier is poor. Most critical is driving rain. If the extra moisture only comes in short periods it will probably dry out.

4. Fire properties

Cellular plastics are made of plastic which is foamed by injecting a gas. The final foam material consists of approximately 95-98% gas. Cellular plastic insulations are flammable, unlike mineral wools which are non-combustible. Fire characteristics for cellular plastics are, of this reason, important to investigate. The risk of fire spread, especially vertically from one storey up to the next, is important for practical solutions. An elaboration of fire spread risks requires thermo physic knowledge about ignition temperatures, critical radiation, flame spread velocities etc. Additives as fire retardants could be relevant to slow down the fire speed or reducing the flammability. This is discussed further below.

Cellular plastic insulation materials have very different fire characteristics, and there exist a number of opportunities to improve these through the addition of varying amounts of fire retardants. The

plastic-based insulation materials are found in a variety of configurations, which provide different fire properties.

We do not have one common European test method for facades. Some countries apply their own national tests, other utilize test methods, which in principle are developed for other purposes. This applies to the use of the EN 13823 single burning item (SBI) test for construction products` reaction to fire. Sweden and Norway use a Swedish full-scale test (SP Fire 105).

Cellular plastic has a large surface area relative to body mass, i.e. a large specific surface, and the material has great access to oxygen. These factors result in a fast and clean combustion of the material. The cell structure results in a low density of the material and consequently a relatively low energy production by combustion, measured by volume unit (Troitzsch 2004). (DBI 2012) provides an overview of the typical cellular plastic type density, thermoplastic properties and energy, and is summarized below in Table 1.

Material	**Thermo plastic or thermal curing** **(Rakic 2003)**	**Density** **(Davies 2001)**	**Energy content**		**Heat conductivity** **(EST, 2004)**
			Per Mass (Davies 2001)	Per Volume	
EPS	Thermo plastic	20 kg/m^3	40 MJ/kg	800 MJ/m^3	0.035-0.045 W/mK
XPS	Thermo plastic	35 kg/m^3	40 MJ/kg	1400 MJ/m^3	0.025-0.038 W/mK
PUR	Thermal curing	45 kg/m^3	26 MJ/kg	1170 MJ/m^3	0.022-0.035 W/mK
PIR	Thermal curing	45 kg/m^3	24 MJ/kg	1080 MJ/m^3	0.021-0.022 W/mK
PF	Thermal curing	45 kg/m^3	29 MJ/kg	1305 MJ/m^3	0.025 W/mK

Table 1. Overview of selected physical properties of typical plastic-based insulation materials (DBI, 2012).

4.1 Ignition temperatures

The ignition temperature is dependent on whether there is a pilot flame present or not. If the foam only is affected by heat radiation, the possibility of ignition depends on the exposure time, the radiation intensity and the size of the exposed area.

Table 2 from (DBI 2012) shows examples of ignition temperatures and critical thermal radiation of various cellular plastic insulation materials. The critical thermal radiation is the lowest thermal radiation which may cause ignition. Due to the materials very product specific properties, there may be a discrepancy between the table and some product values.

Material	Ignition temperatures			Critical radiation (auto ignition) (Babrauskas 2003)
	With pilot flame (Davies 2001)	Auto ignition (Davies 2001)	Auto ignition (Babrauskas 2003)	
EPS	245-345 °C	490 °C	440-448 °C	27 kW/m^2
XPS	245-345 °C	490 °C	-	-
PUR	285-310 °C	415-500 °C	457-494 °C	22-26 kW/m^2
PIR	415 °C	510 °C	-	23-24 kW/m^2
PF	490 °C	450 °C	-	-

Table 2. Examples of ignition temperatures and critical thermal radiation of the typical cellular plastic insulation materials (DBI 2012).

4.2 Fire retardant

By the addition of a fire retardant (additive) during production, the fire performance of the foam is changed. An additive can be used to alter cellular plastics ability to shrink or melt, char, slow down the fire speed or to reduce the flammability (DBI 2012). For example, the bromide flame retardants are widely used.

It may be noted that, for example ISOBYG`s EPS burn different than normal EPS, due to adding of flame retardant substances, which make the material does not burn in a self-sustaining reaction. That is, it turns off automatically when there is no direct flame exposure (ISOBYG 2012).

There are a large variety of additives. This coupled with a myriad of different combinations and proportions of different types of cellular plastics, makes it very difficult to accurately describe the additives effect on cellular plastics fire performance. Therefore, a fire-related classification of a foam material must be determined on the basis of a test of the exact composition of the foam and additive(s) (DBI 2012).

Fire and flame retardant additives have the greatest impact by initial heating, from small heat sources, i.e. corresponding to fire effects in the early course of the fire. In a fully developed fire, flame retardants have no effect on the fire performance (NFPA 2003).

4.3 Recommendations on the fire domain

The fire risk is not yet fully documented for cellular plastic insulation on facades. The risk of external flame spread seems to be the most critical parameter in this context. It is recommended that flame spread from one storey to the one above, should be further investigated in order to prove a fire safety level according to the Building Regulations. At the moment, there exists only the Nordic SP Fire 105 test, which in fact is developed for other types of facades. By the way the test is not suitable for handling molten material dripping from the burning facade.

5. Long term experience

The Fraunhofer institute of building physics has from 1975 to 2006 made a survey of ETICS systems in Germany, Austria and Switzerland (Künzel et al 2006). This is an investigation of outside plaster systems mounted on buildings from 18 to 35 years ago. The results show that there can be algae on part of the façade, but not very many mistakes in the form of peeling or cracks. The conclusions are that damage of the plaster is less than plaster direct on masonry. There are more algae on ETICS houses. The cost of repair and maintenance is similar to buildings with plaster on masonry. These systems are with 30 to 60 mm insulation on bricks. In Scandinavia it is important with a thicker insulation layer to improve the U-value.

The lifetime for plaster is important as it will give the lifetime for the ETICS systems. The information from literature is that the lifetime is similar to a masonry wall or a wooden panel. In all cases it is assumed that ordinary maintenance is carried out.

In Sweden it has been popular to build high insulated wooden wall with insulation and plaster on the outside as seen in Figure 1. An investigation of 800 buildings (Samuelson and Jansson 2009) shows that moisture will come into the construction. There is damage in 55 % of the buildings, mostly in houses with EPS as insulation. Using mineral wool as insulation reduces the damage to 32%. This is still a very high damage percentage. The problems are related to details as around windows, doors, shading roofs, balconies and cracks in the plaster at fixation of light or sunblinds. Testing the systems before it is used is important and also to reduce the number of special details, where there is a risk of damage. Later reports (Jansson 2011) confirm the results with EPS giving a high risk of moisture problems for light walls.

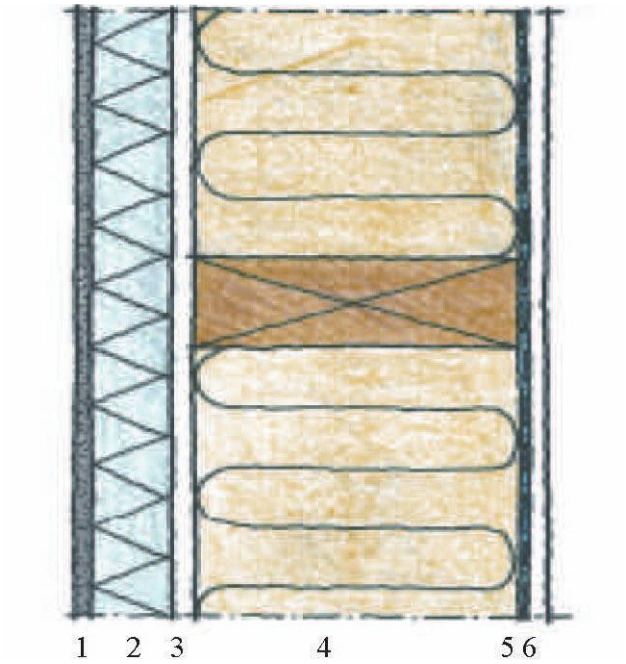

FIG 1. Sketch of system on a light wall from Samuelson 2009, 1- plaster layer 2- external insulation 3 gypsum plate 4 internal heat insulation 5 vapour barrier 6 gypsum plate

The Swedish problems are related to water in the insulation. Drying out of moisture in the external insulation layer is important. The most efficient way is to use a ventilated space behind the plaster or outer plate in the system. Swedish calculations from Falk and Sandin 2013 has shown large variations

in drying-out time. The relative drying out time for mineral wool with external plaster layer is 4 times longer than for a ventilated space. For plastic insulation with EPS and external plaster layer the factor is 20-30. So the plastic material increases the drying out time significantly.

6. Conclusion

External insulation of facades has, in Denmark, typically been done with systems of mineral wool as insulation material. This has worked very well, but it is interesting to look at the use of systems with cellular plastic material. Danish experience with plastic material in external insulation system is rather limited, primarily due to limiting building regulations, especially in relation to fire. Experience is taken from Sweden and Germany where it is widespread.

The fire risk is not yet fully documented for cellular plastic insulation on facades. The risk of external flame spread is found to be the most critical parameter in this context. It is recommended that flame spread from one storey to the one above, should be further investigated in order to prove a fire safety level that fulfils the building regulations.

There is no extensive documentation showing that houses with external placed insulation should have a higher general fire risk than buildings without external insulation.

References

Babrauskas, V. 2003. Ignition Handbook. Interscience Communications Ltd. 2003.

Davies, J.M. 2001. Lightweight Sandwich Construction. Blackwell Science Ltd. 2001.

DBI 2012. Dansk Brand- og sikringsteknisk Institut. Sandwichpaneler med celleplastisolering-Brandmæssige egenskaber. Rapport rekvireret af Beredskabsstyrelsen. Januar 2012.

EAE 2011; European guidelines for the application of ETICS (external thermal insulation composite system) - Quality with system, EAE – European association for External thermal insulation composite systems, March 2011.

EN 13823:2010 Reaction to fire tests for building products. Building products excluding floorings exposed to the thermal attack by a single burning item. 2010

ETAG 004 2011. Guideline for European technical approval of external thermal insulation composite systems with rendering, European Organisation for Technical Approvals, Brussels, 2011.

ETAG 014 2011. Guideline for European technical approval of plastic anchors for fixing of external thermal insulation composite systems with rendering. European Organisation for Technical Approvals, Brussels, 2011.

EST 2004; Information om brandteknisk dimensionering. Erhvervs- og byggestyrelsen. 2004

Falk, J. and Sandin, K.; 2013. Ventilated rain screen cladding: Measurements of cavity air velocities, estimation of air change rates and evaluation of driving forces, Building and Environment vol. 59 164-176. 2013

ISOBYG 2012. http://www.isobyg.dk fire information from 6. juli 2012.

Jansson, A. 2011. Putsade regelväggar - Erfarenheter från undersökningar som SP har utfört, Sveriges Tekniske Forskningsinstitut, SP rapport 2011:61.

Künzel, H., Künzel, H.M. and Sedlbauer, K. 2006; Long-term performance of external thermal insulation systems (ETICS), Architectura 5 (1) 2006, 11-24.

NFPA 2003. Fire Protection Handbook, 19. edition, Volume II. National Fire Protection Association. 2003.

Rakic, J. 2003. Fire rated insulated (sandwich) panels. Fire Australia. May 2003.

Samuelson, I. og Jansson, A. 2009; Pudsede regelväggar, Byggnadsfysik, SP Sveriges Tekniske forskningsinstitut, SP rapport 2009:16.

SP Fire 105. Swedish standard for large scale testing of facades system. SP Technical Research Institute of Sweden, Borås, Sweden.

Sørensen, L.S., Nielsen, A. and Wittchen, K.B. 2013. Udvendig efterisolering med plastbaserede materialer (external insulation with plastic based materials). Statens Byggeforskningsinstitut, Aalborg Universitet, København.

Troitzsch, J. 2004. Plastics Flammability Handbook. Published by Carl Hanser Publishers, Munich. 2004

U-value determination of masonry walls with complex shape units and thermal insulating mortars applied as rendering

Nuno M. M. Ramos, Assistant Professor [1]
Vasco P. de Freitas, Full Professor [1]
Pedro F. Pereira, M.Sc. [1]
Hipólito de Sousa, Associate Professor [1]
Rui Sousa, M.Sc. [1]
Ângela Nunes, M.Sc. [2]
Dina Frade, M.Sc. [3]

[1] University of Porto - Faculty of Engineering, Portugal
[2] Secil, SA
[3] Secil Argamassas, SA

KEYWORDS: *U-value, masonry, simulation, laboratory measurements*

SUMMARY:
Single leaf masonry walls with the application of thermal insulating mortar can be an interesting solution for façades, providing the performance of its components can lead to a competitive thermal resistance. The determination of the walls U-value will therefore be of most importance.

Laboratory tests were conducted in a wall composed of a thermal insulating mortar applied on a single leaf masonry of complex shape units. The objective was the evaluation of the U-value and the validation of calculation methodologies. The tests included material properties evaluation and U-value determination of the wall using a climate chamber and heat flow meters.

Numerical simulations were performed with the focus on the calculation of the thermal resistance of masonry using two approaches. One was a simplified 2D model based on EN ISO 6946 calculation methodology, and the other one a 3D model based on the finite element method (FEM).

The numerical results obtained from the simulations were compared with laboratory measurements leading to a difference of about 5%. The differences observed and the results obtained in the material characterization phase supported recommended strategies that can be used to improve the feasibility of U-value calculations for the studied wall, including manufacturer declared moisture dependence of key material properties.

1. Introduction

A growing interest in envelope solutions based on thermal insulating mortars applied on masonry walls of optimized geometry can be observed nowadays. The effective U-value of these solutions should however be carefully evaluated. Practitioners often use reference values available in literature or declared by manufacturers to determine U-values that will be computed in building thermal calculations. The case of masonry walls is typically sensitive in the sense that manufacturers frequently base the declared values on calculations using (EN-ISO-6946, 2007) methodology. For the case of masonry using complex shape units and thermal rendering the definition of the expected U-value raises additional problems that have to be tackled so that manufacturers declared values can be trusted.

This paper studies a façade system of the type described above. The study starts with the measurement of material properties that are used in the numerical model. The U-value was determined following the principles outlined in the standards (EN-1745, 2012) and (EN-ISO-6946, 2007). A wall specimen was tested in a climatic chamber according to (EN-1934, 1998) and (ISO-9869, 1994) for comparison with the calculated values.

2. Studied System

A specimen representing the wall system under analysis was installed in a climatic chamber. It includes a thermal insulation mortar applied as external rendering. The specimen is 3.61 m^2 (1.9 m x 1.9 m) and its constitution is described in TABLE 1 and FIG. 1

TABLE 1 - Materials applied in the test specimens.

Component	Description	Thickness [cm]
Masonry units	Commercially available lightweight concrete masonry units, vertically perforated	28.5
Laying mortar	Cork aggregates incorporating hydraulic binders, limestone and siliceous aggregates and additions.	1
Thermal insulating mortar (FIG. 2)	Dry mortar with EPS aggregates. Density 400 kg/m^3.	4
Final coat applied above the thermal insulating mortar (FIG. 2)	Dry mortar, pre-dosed, formulated from hydraulic binders, aggregates, adjuvants, fibers and resins. Density 1500 kg/m^3	0.15
Coat applied above the substrate (FIG. 2)	Dry mortar, pre-dosed, formulated from hydraulic binders, aggregates, adjuvants, fibers and resins. Density 1700 kg/m^3	1.5
Final coat applied above the substrate (FIG. 2)	Dry mortar, pre-dosed, formulated from mixed binders, fillers and limestone additions.	0.2

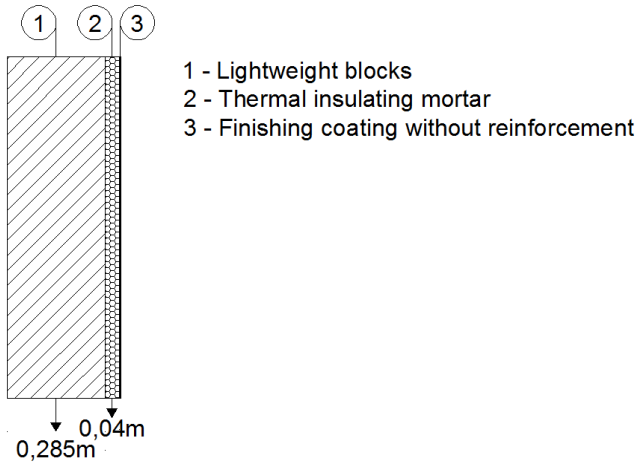

FIG. 1 – Wall system.

FIG. 2 – Application of renderings.

3. Material Properties

The thermal conductivity (λ) of the masonry units base materials and of the thermal rendering was determined. Conductivity can be affected by different factors. The λ is moisture dependent (Freitas, 1994), especially for these materials. Also, according to (Stahl et al., 2012) the pressurization used on the plastering machine can affect the actual performance of the insulating mortar. Hence, the actual insulating mortar applied on the wall was studied. Two 30 x 30 cm^2 panels were extracted from the specimen (FIG. 4). The λ of the masonry units material was determined from shell samples removed from the units. The determination of the thermal conductivity was been carried out using a thermal conductivimeter by Hot Wire "CT-mètre". The dry value was calibrated with measurements using the guarded hot plate according to (EN-12664, 2001).

The λ values of the samples of thermal insulating mortar (A) (bulk density ~400 kg/m^3) and masonry units (B) (bulk density ~440 kg/m^3) was obtained for different moisture content values, with results displayed in TABLE 2 and FIG. 3. In FIG. 3, the thermal conductivity as a function of moisture content of two types of lightweight concrete (Kumaran, 1996) is also included for comparison. The lightweight concrete and aerated concrete values from literature demonstrate an upgraded performance of the material applied in the masonry units of the studied system. The thermal insulating mortar performance is similar to the polystyrene concrete from literature, although its moisture dependence is higher.

TABLE 2 – Thermal conductivity values of the samples in various conditions.

Sample	Sample conditions	W [%-kg/kg]	λ [W/m.ºC]
A	Dried at 70ºC	0%	0.095
A	Laboratory conditions (RH ≈ 70%)	2%	0.107
A	Intermediate moisture content	28%	0.188
A	Saturated	47%	0.273
B	Dried at 70ºC	0%	0.178
B	Laboratory conditions (RH ≈ 70%)	1%	0.221
B	Intermediate moisture content	12%	0.320
B	Saturated	19%	0.360

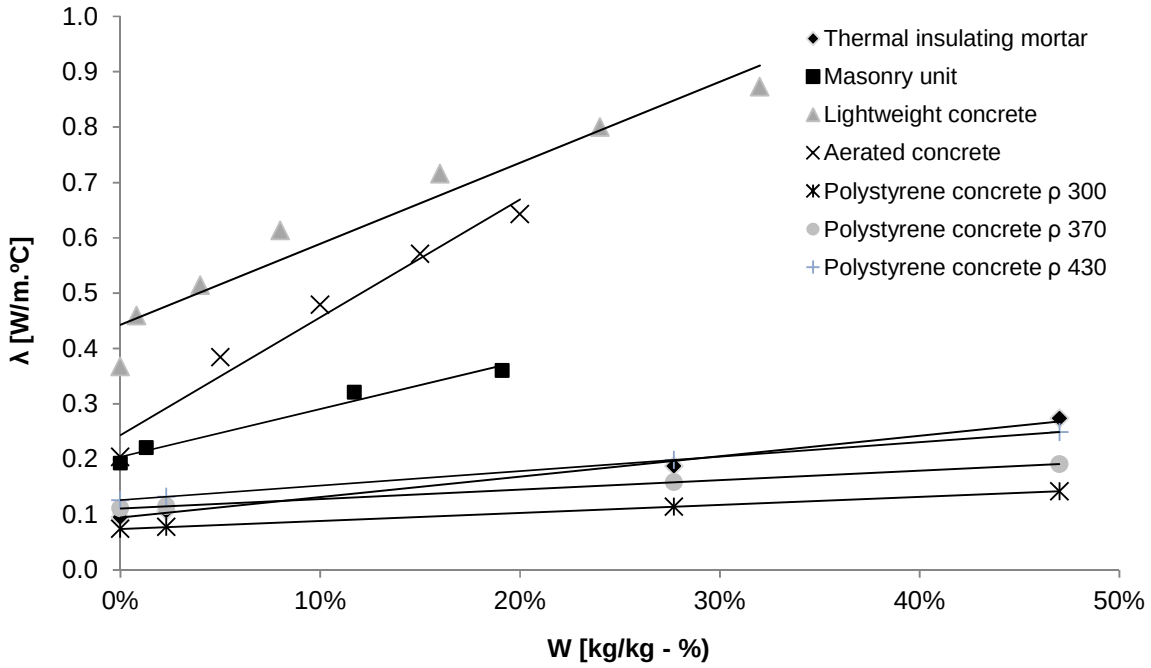

FIG. 3 –Thermal conductivity values obtained for the thermal insulating rendering sample.

FIG. 4 – Extraction of samples of insulating mortar from the specimen and shells from the masonry units

4. Numerical Simulations

Numerical simulations were performed to determine the thermal resistance of the masonry and the resulting U-value of the wall system, with two different procedures:

- 2D model based on a simplified geometry of the unit and vertical joints, and on the calculation methodology of (EN-ISO-6946, 2007) for the determination of the thermal resistance of the masonry unit with air spaces/voids and (EN-1745, 2012) used on the calculation of the overall resistance of the wall, i.e. with the influence of the mortar bed joints and rendering layers;
- 3D model based on the finite element method (Simulia), in which micro modelling of the masonry system was performed with an equivalent thermal conductivity for the air spaces (voids) calculated trough the method indicated in (EN-ISO-6946, 2007).

For practical reasons, in particular for the 3D model, the simulations were performed with a representative portion of the masonry system. The accuracy of both approaches was verified according to (EN-1745, 2012).

Two different conditions were considered in the simulations:

- Simulation 1: the constituent materials considered with a moisture content (W=2%) to reproduce the moisture equilibrium with the ambience of the laboratory (HR ≈ 70%);
- Simulation 2: the constituent materials considered in dry conditions (W=0%).

The thermal conductivity values, λ, of the constituent materials were adopted according to section 2 results. Except for the laying mortar (joints) and undercoat mortar (rendering), where conductivity values were obtained from the manufacturer, and were corrected according to (EN-1745, 2012) in order to consider a moisture content of 2%. Surface transfer coefficients were not a part of this specific problem as conventional Rsi=0.13 and Rse=0.04 were added to both numerical and experimental results.

The masonry was simulated with a temperature variation of 10ºC, and with a surface thermal resistance of 0.13 m^2.ºC/W and 0.04 m^2.ºC/W. The thermal conductivity values used for the materials, and results obtained for two situations are shown in TABLE 3.

The study by (Ghazi Wakili and Tanner, 2003) found a relevant effect of laying mortar penetration on the final U-value. In the present study, the masonry units in the zone of the laying mortar were probed and it was possible to see the penetration of the mortar into the unit voids. Because of the masonry unit geometry and the configuration of the laying mortar used in this study (FIG. 1), the penetration of laying mortar was only found on the two voids near each surface of the unit. On the bottom voids the penetration fills the voids up to a height of 1.3 cm. On the top voids of the unit the penetration was only visible in approximately half of the voids with a height of about 1.3cm. The simulations were repeated to include the mortar penetration effect.

TABLE 3 – Results obtained in the numerical simulations of the masonry system

Simulation	Materials	λ [W/m.ºC]	U without laying mortar penetration (2D/3D) [W/m^2.ºC]	U with laying mortar penetration (2D/3D) [W/m^2.ºC]
Simulation 1 (materials in equilibrium with 70% RH)	Thermal insulating mortar (rendering)	0.107	0.426 / 0.433	0.429 / 0.438
	Lightweight concrete (units)	0.221		
	Laying mortar (joints)	0.177		
	Undercoat mortar (rendering)	0.573		
Simulation 2 (materials dried at 70ºC and 10% RH)	Thermal insulating mortar (rendering)	0.095	0.384 / 0.390	0.387 / 0.393
	Lightweight concrete (units)	0.178		
	Laying mortar (joints)	0.167		
	Undercoat mortar (rendering)	0.540		

The U-value obtained from 2D and 3D approaches presented small differences. Although the masonry units are complex shaped, the voids are based on a simple rectangular shape. Moreover, one dimensional heat flux was considered (perpendicular to the thicknesses of the wall), since in stationary regimes other flux directions are usually too low, hence neglected for practical reasons. Therefore, the results obtained from simplified 2D models or 3D models are expected to be similar.

Nevertheless, the 3D models are expected to be more accurate than 2D models, since they can represent more realistically the geometry (e.g. irregular shaped voids/air spaces, thickness variation of the air spaces, amongst others aspects) and thermal behaviour of the walls.

5. Laboratory Tests

The specimen was conditioned by the climatic chamber Fitoclima EDTU 1000 (FIG. 5). The temperature provided by the device ranges from -50 to 180° C with an accuracy of ± 0.5°C while the relative humidity range is set from 10 to 98% with an accuracy of ± 2%. The test specimens were constructed in a detachable part of the climatic chamber (FIG. 5). The wall surface with thermal rendering is conditioned by the climatic chamber and the opposite surface is exposed to laboratory conditions. For the determination of the heat flow through the specimen, the equipment presented on the FIG. 6 was used. This equipment has an accuracy of 5%. The temperatures on the surfaces were determined using thermocouples of the type T as shown on FIG. 6. The temperature and the relative humidity near the specimen inside and outside of the climatic chamber was measured with Onset HOBO data loggers with a temperature range from -20 to 70 ºC with an accuracy of 0.35ºC while the relative humidity range is from 10 to 90% with an accuracy of 3% (FIG. 6).

FIG. 5 – Climatic chamber Fitoclima EDTU 1000.

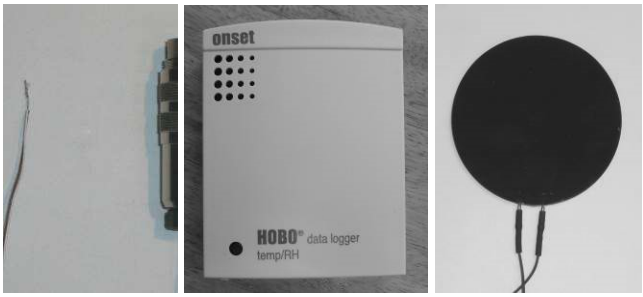

FIG. 6 – Thermocouple, HOBO and Heat flow meter.

In order to evaluate the influence of the mean temperature of the specimen and the moisture content value of the wall, the ambiance of the climatic chamber was changed and thus the conditioning of the test specimen. The climatic chamber was programed until nearly steady state conditions were achieved with set-points presented in TABLE 4, along with the test results. In the table, Ti is the climatic chamber temperature, RHi is the climatic chamber relative humidity, Tmean is the average temperature of the wall specimen and ΔT (Ti – Te) is the temperature difference between the climatic chamber and the laboratory. To ensure that the rendering moisture content was in equilibrium with the climatic chamber RH a sample was collected and weighed.

TABLE 4 – Specimen conditions and thermal transmittance values of the specimen.

Specimen conditioning	Ti (ºC)	RHi (%)	Tmean. (ºC)	ΔT (Ti – Te) (ºC)	U (W/ m^2.ºC)
Equilibrium with 70% RH	35.0	70.0	29.5	10.7	0.458
Dried at 70ºC and 10% RH	35.0	26.2	30.1	11.4	0.410

6. Conclusions

The main conclusions of this study are the following:

- The 2D and 3D numerical simulations demonstrated good accuracy with the experimental results, although 3D gave a better approach;
- A difference of about 5% was found between the numerical simulations (3D) and the experimental determination of the U value;
- Considering the penetration of laying mortar into the voids of the masonry units, reduces the difference between measured and calculated (3D) U-Value to 4%.
- A numerical procedure based on a 3D FEM model, in which the thermal conductivity values used in the model are obtained from laboratory tests made with samples removed from the masonry components, can be useful to determine the U values for several moisture conditions without using too many laboratory resources;
- The U-value of this wall system is very sensitive to moisture content even in the hygroscopic range and the manufacturers should clearly state it;
- This study is part of a work in progress and additional analysis will be performed on the hygrothermal behaviour of these systems.

7. Acknowledgements

The authors would like to thank Secil and Secil Argamassas for their technical support.

References

EN-1745 2012. Masonry and masonry products. Methods for determining thermal properties.

EN-1934 1998. Thermal performance of buildings. Determination of thermal resistance by hot box method using heat flow meter. Masonry. 1998-09-30: CEN/TC 89.

EN-12664 2001. Thermal performance of building materials and products - Determination of thermal resistance by means of guarded hot plate and heat flow meter methods - Dry and moist products of medium and low thermal resistance.

EN-ISO-6946 2007. Building components and building elements -- Thermal resistance and thermal transmittance - Calculation method.

FREITAS, V. P. 1994. A influência da humidade na resistência térmica de elementos de construção.

GHAZI WAKILI, K. & TANNER, C. 2003. U-value of a dried wall made of perforated porous clay bricks: Hot box measurement versus numerical analysis. *Energy and Buildings,* 35**,** 675-680.

ISO-9869 1994. Thermal insulation -- Building elements -- In-situ measurement of thermal resistance and thermal transmittance. ISO/TC 163/SC 1.

KUMARAN, M. K. 1996. *IEA ANNEX 24 - Heat, Air and Moisture Tranfer Through New and Retrofitted Insulated Envelope Parts (Hamtie) - Task 3: Material Properties,* Laboratorium Bouwfysica - Department Burgerlijke Bouwkunde - K.U. Leuven Belgium.

SIMULIA. *Abaqus/CAE User's Manual* [Online]. Available: https://www.sharcnet.ca/Software/Abaqus610/Documentation/docs/v6.10/books/usi/default.htm [Accessed 01/11/2013.

STAHL, T., BRUNNER, S., ZIMMERMANN, M. & GHAZI WAKILI, K. 2012. Thermo-hygric properties of a newly developed aerogel based insulation rendering for both exterior and interior applications. *Energy and Buildings,* 44**,** 114-117.

Experimental investigations of highly hygroscopic and vapour permeable walls exposed to real climate

Yannick-Ariel KEDOWIDE [1]
Amandine PIOT, PhD [2]
Monika WOLOSZYN, Professor [1]
Nolwenn LE PIERRES, Associate Professor [1]
Timea BEJAT, PhD [2]

[1] LOCIE, UMR 5271 Université de Savoie, France
[2] CEA, LITEN, Laboratoire d'Energétique du Bâtiment, at INES, Le Bourget Du Lac, France

KEYWORDS: *Heat and moisture transfer, outdoor experiment*

SUMMARY
An experimental facility consisting of a wall exposed to the external environment and installed on a cell with indoor controlled conditions is studied. The wall is timber framed with wood fibre panels for insulation. The first experimental results are presented. The results show the predominant effect in the short term of the temperature and insolation on the distribution of moisture in the walls, when for the long term it is rather the water content of inside and outside atmospheres that directs the walls' moisture distribution.

NOMENCLATURE

Symbol	Definition	Unit
λ	Thermal conductivity	mW/(m.K)
θ_m	Moisture content	kg/kg
HR	Relative Humidity	%
μ	Vapour diffusion equivalent air layer thickness	-
C_p	Specific heat capacity	J/(kg.K)
T	Temperature	°C
C	Water adsorption coefficient	$kg/(m^2.min^{0.5})$

1. Introduction

To study Heat, Air and Moisture (HAM) coupled transfers in building envelopes, many numerical studies have been done and many experimental facilities under controlled conditions or outdoor climate have been established [Kêdowidé et al., 2012]. Most of these studies concern realistic constructions, with high air and water tightness together with a vapour barrier, thereby limiting the impact of mass transfers on energy performance of the envelope. Yet moisture movements influence the temperature fields inside the walls [Labat et al., 2012] and indoor comfort [Teodosiu et al., 2003]. There is also a persisting need for precise assessment and understanding of the impact of mass transfer on the performance of highly hygroscopic wall assemblies, as well as for detailed validation of dedicated simulation tools. In order to better assess the effects of coupled transfers within wall assemblies, a new experimental work with highly vapour-permeable and very hygroscopic materials was used in the work presented below.

2. Experiment description

2.1 PASSYS cells

The PASSYS test cells were originally designed to test passive solar components under real weather conditions. Two of them were used in the present experiment in order to precisely control indoor conditions on one side of the tested façade. Both cells are located on the CEA-INES experiment platform in Le Bourget du Lac, south-eastern France. They are 8.44m long, 3.61m wide and 3.8m high. The cells are made of a metallic frame insulated by 48 cm of polystyrene and mineral wool to have 5 highly insulated (U=0.09W/m².K), water and vapour proof walls. The 6th face is reserved for a wall of maximum 3.6*3.3 m² to be tested. Each cell is placed on a dedicated rotating platform, for a free choice of orientation of the tested wall. Each cell has a HVAC system to control indoor temperature and relative humidity. Indoor temperature can be controlled from 15 to 35°C with +/-1°C tolerance; and indoor air moisture content from 6 to 14 g/kg of dry air with +/- 10% tolerance.

2.2 Walls layout

The tested walls are wooden framed. To have a highly-hygroscopic and vapour-permeable wall, the insulation was made using two layers of 80mm wood fibre panels. Those panels have 120-140 kg/m^3 density. Other characteristics of the panels are in the table below.

TABLE 1: Physical characteristics of the wood fibre panels

Property	Value
Thermal conductivity	$\lambda = 0.28 * \theta_m + (0.108*T+38)$
Sorption isotherm	$\theta_m = 5 * 10^{-5} * HR^3 - 0.0053 * HR^2 + 0.2925 * HR$
Vapour permeability	μ = 1.26 (dry cup) - 4.97 (wet cup)
Specific heat capacity	Cp = 1551

The walls are then coated with a 3mm roughcast to protect the insulation from liquid loads such as rain (C<0.20 kg/m².min$^{0.5}$) [EN 998-1] without being a barrier to vapour diffusion (μ<25).

During the first period of the experiment, reported in the present paper, the 2 walls are identical, and exposed to the same indoor climate.

2.3 Monitoring system

83 sensors were implemented per wall, together with 8 sensors in rooms' volumes, as detailed in table 2. Temperature and relative humidity sensors have been placed in different specific areas within the wall: current part, close to wooden frame and within thermal bridges due to PASSYS cells frame. The different locations are presented in Figure 1. There are also different locations within the thickness: between the layers of insulation, in the middle of each layer (a dedicated hole was made), and on the two sides of the roughcast. For the sensors close to the timber frame, they are placed on the surface and inside the wooden beam.

The rooms' volumes were instrumented with seven Pt100 temperature sensors, in order to check the uniformity of indoor conditions. A thermo hygrometer has been added in the middle of each room, next to the central Pt100 sensor, to monitor the relative humidity inside the cell.

For exterior conditions, a weather station, located 50m from the cells, recorded meteorological data such as temperature, relative humidity, wind speed and direction, pluviometry as well as solar (direct, global) and infrared radiation. Also, a pyranometer was placed vertically on each façade, in order to anticipate errors due to calculation of the global radiation on each wall taking into account surrounding buildings, by recording that radiation.

The data was recorded every 5 minutes.

TABLE 2: Overview of sensors used on each wall of the experimental facility

Sensor	Number	Specifications	Accuracy
Thermocouple	36	Type T	+/- 1°C
Thermohygrometer	42	Manufacturer : Sensirion Model : SHT 75	+/- 0.3°C; +/1.8% RH
Heat flux sensor	3	Manufacturer : Captec Dimensions : 100*100mm Sensibility : 40µV/(W/m²)	0.06 W/m² + 0.003% * Measured Value
Differential pressure sensor	1	Manufacturer : Furness Controls Model : 332	+/- 0.5% of Measured Value
Pyranometer	1	Manufacturer : Kipp & Zonen Model : CMP 11 Location : On the wall Tilt : 90°	7 W/m² (Zero Offset)

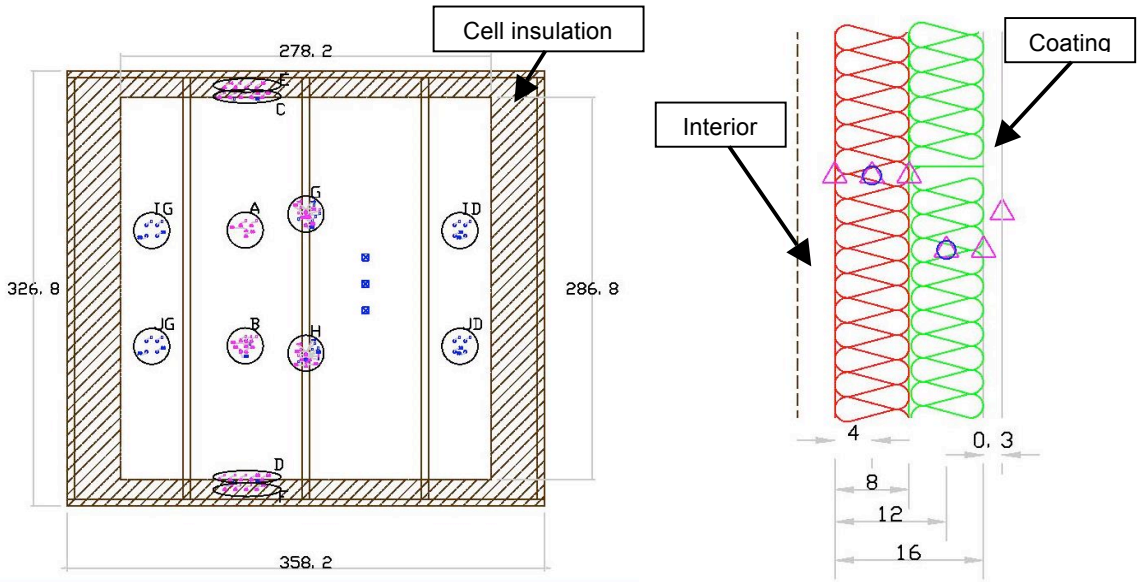

FIG 1: Position of the sensors: General view of the tested façade from the outside (left); Sensors in the thickness of the wall (right), dimensions in cm

3. Implemented tests

Tests on presented experimental facility began in March 2013, which corresponds to the end of winter - early spring. The figure 2 shows an overview of the experimental indoor (int) and outdoor (Ext) conditions over 5 months: temperature, relative humidity and vapour pressure. According to the weather data, recorded results can be divided into two main sessions.

3.1 Spring session

First, the two facades were oriented to the North. That objective was twofold: first to check whether both facades had identical behaviour while exposed to exactly the same conditions; and second, to study their responses to indoor hygric loads with a minimal solar radiation.

The results presented in the following focus on a two-weeks period (May, 18th to June, 1st) when the indoor temperature was set to 25°C, and a step-rise of relative humidity was made (from 40 to 70% RH); the duration of the step was one week.

3.2 Summer session

During summer (July, 1st to September, 15th), one of the walls (PASSYS cell n°2) has been turned to the south. Here the objective was to investigate the effect of sun on the behaviour of the wall. After 6 days, the indoor temperature has been decreased to 16°C (cooling mode) and as the vapour pressure was maintained constant; relative humidity increased from 40 to 70%. Those conditions were kept on 10 days and then RH was brought back to 40%, which dropped the inner vapour pressure.

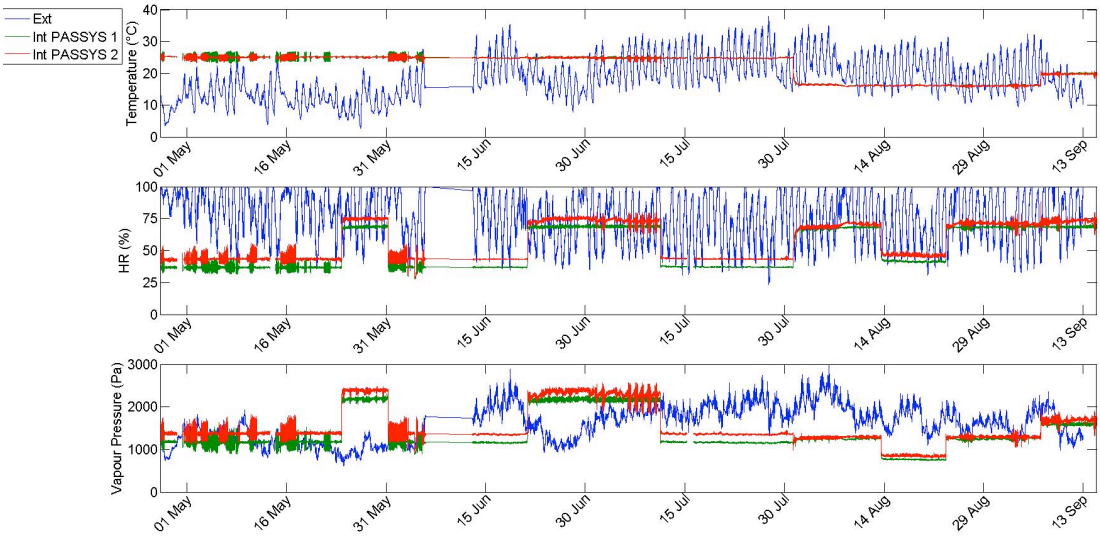

FIG 2: Overview of indoor/outdoor Temperature, Relative humidity and Vapour pressure

4. Results

4.1 Spring session

Here will be presented the first relevant test done with the experimental facility. Comparing pairs of sensors placed at the same position in the two tested wall showed that the responses were very similar; therefore, only one wall's results will be presented.

4.1.1 Before the step

The Figure 3 shows the measurements in the wall at the beginning of the session. A monotonous temperature gradient is observed within the insulation layer, except the temperature just under the coating (16 cm) because of the non-negligible solar radiation. The temperature difference between the inside and outside varies from 19°C to 9°C. A time lag for the highest temperatures during the day is also observed, from the outside towards the inside.

The vapour pressures within the wall intersect twice a day and the moisture flow is inverted from days to nights. The average values of vapour pressures inside the insulation are fairly close, but their amplitudes are bigger from the outside to the inside, and time lags similar to the ones recorded in temperature values are noticed. Daily variations of vapour pressure within the walls seem to be correlated with the variations of the temperatures.

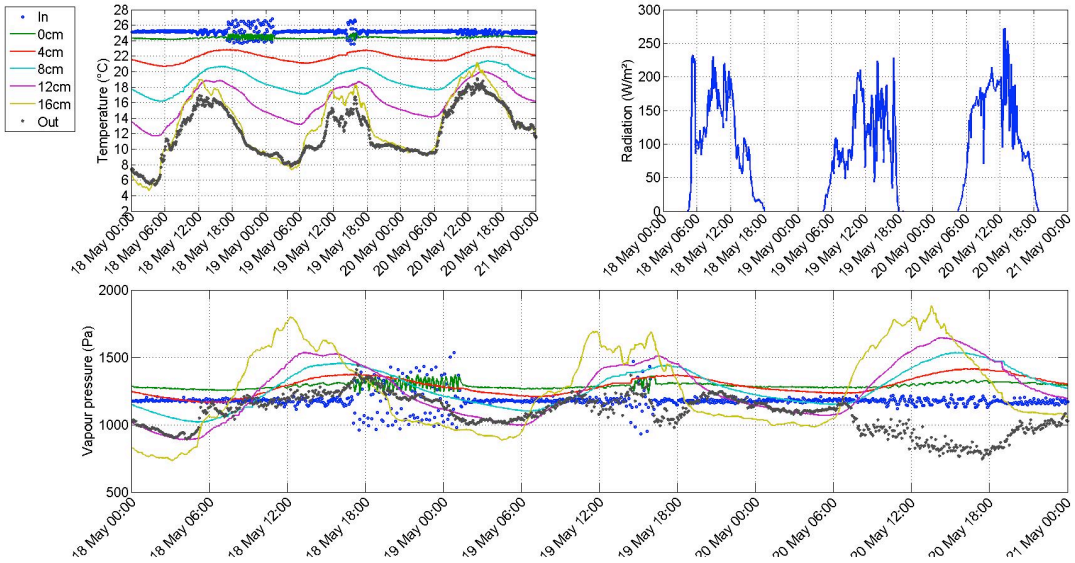

FIG 3: Temperatures, Vapour pressures and radiation in the wall

4.1.2 Step period

The 24th of May, the relative humidity inside the room was risen up to 70%. The Figure 4 shows the temperatures, vapour pressures in the wall and global solar radiation at the wall's surface during the entire step experiment. Just after the step from 40 to 70% of RH, a small increase in temperature values can be noticed on the inner surface (0 cm) and in the first four centimetres inside the wall. The difference between the surface temperature and the indoor air decreases simultaneously to the rise in the relative humidity. Those temperatures stayed higher than before the step (1 °C on the surface, 1.3 °C at 4cm) until the step back to 40% RH on the 31st of May. This effect is small, but could be seen at several places of the wall, and on the two test cells, although the indoor air temperature has not changed. The higher RH has also led to a redistribution of the vapour pressure, and there is a permanent gradient from inside to outside until the return to initial conditions. The disturbance on temperature and moisture distribution due to the steps made seems to be really short-term. A dynamic steady-state is reached after 5 days.

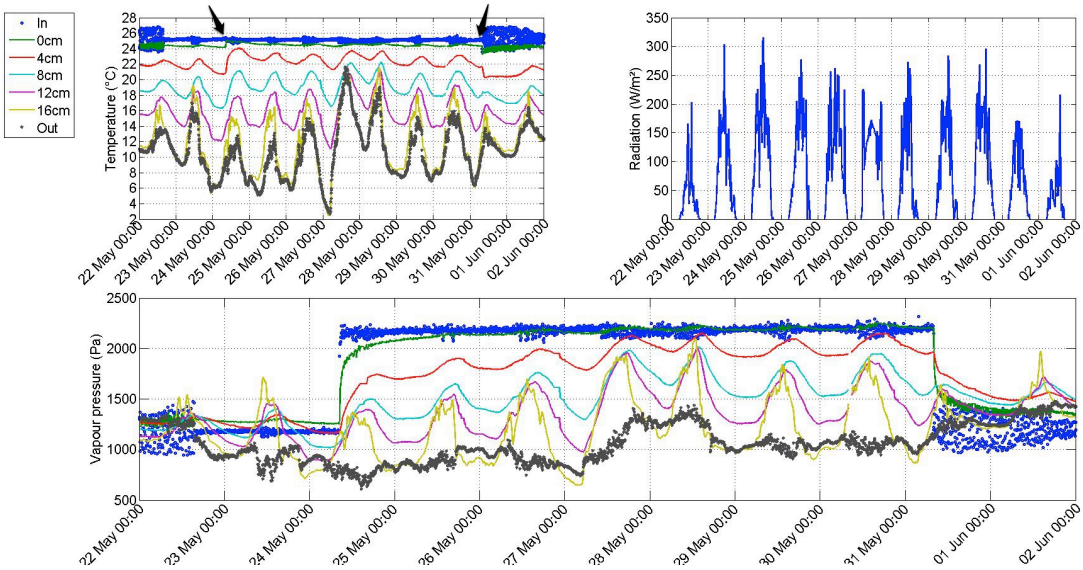

FIG 4: Temperatures, Vapour pressures and radiation on the walls during the steps experiment

4.2 Summer session

During that session, each condition (Temperature and Vapour pressure) was changed separately.

4.2.1 Cell turned to the south

The façade was turned to face South on the 25th of July. These results in temperatures in the wall higher than the outside air temperature during the day (see Figure 5). We can notice the same effect on the vapour pressure.

The internal temperature is maintained at 25°C, which is approximately the average temperature of the outside air; the heat flux therefore changes of direction between day and night. This is not true for the vapour pressure: the inner relative humidity being of 40% (see Figure 2), the associated vapour pressure is always lower than the outside vapour pressure.

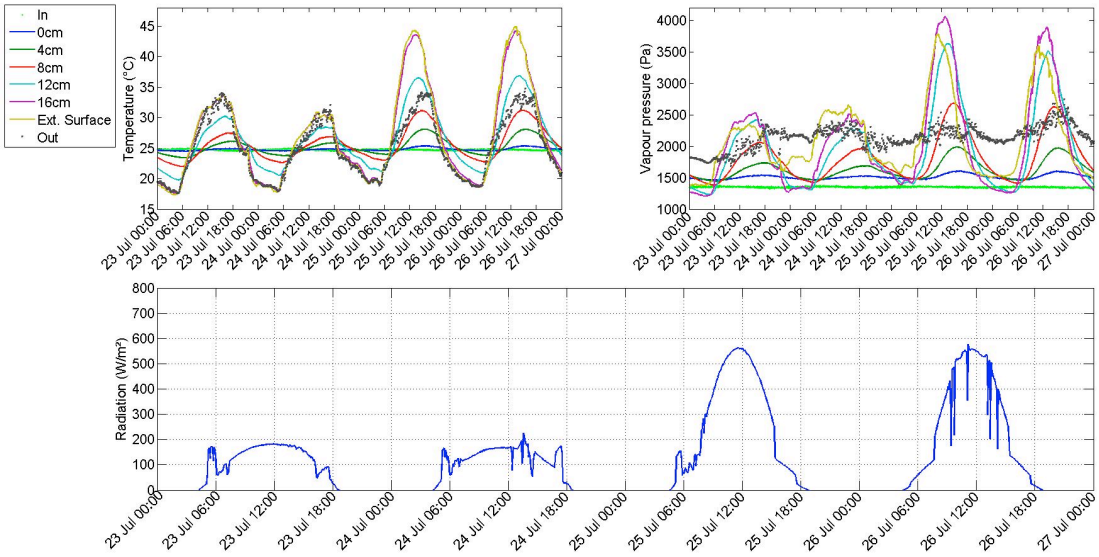

FIG 5: Temperatures, Vapour pressures in the wall and radiation on it when turned to the south

4.2.2 Change of inner temperature: Cooling mode

The temperature was changed on the 31st July (figure 6). The temperature was dropped to 16°C, while the relative humidity was raised from 40% to 70%, in order to keep constant the vapour pressure. This leads to a heat flux being always from outside to inside, as average temperature is no longer the same. However it does not disturb the distribution of vapour pressure in the wall; the only disturbances are due to regulation of the HVAC system.

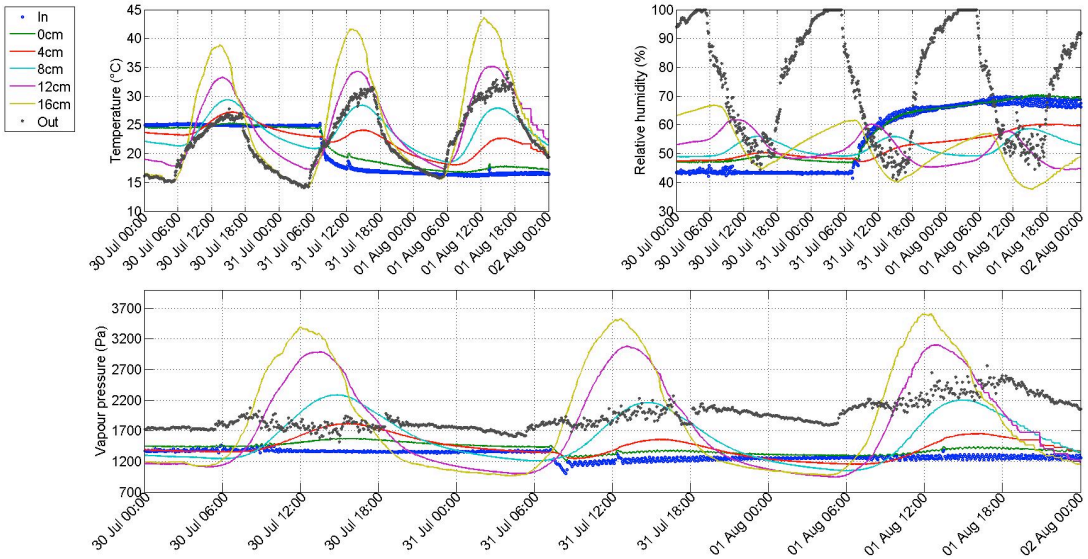

FIG 6: Temperatures, Vapour pressures and RH on the walls when temperature dropped

4.2.3 Change of inner vapour pressure

On the 13rd of August, the indoor relative humidity was decreased to 40% (see Figure 7). Vapour pressure drop causes a slight decrease of temperature at the inner surface (0.8°C) and inside the insulation of the wall, as could be seen in the step during the spring session. Yet the temperature decrease at the surface is close to the measurement accuracy of the sensor, and the decrease at 4cm inside the wall is under that accuracy, and could not be considered as relevant.

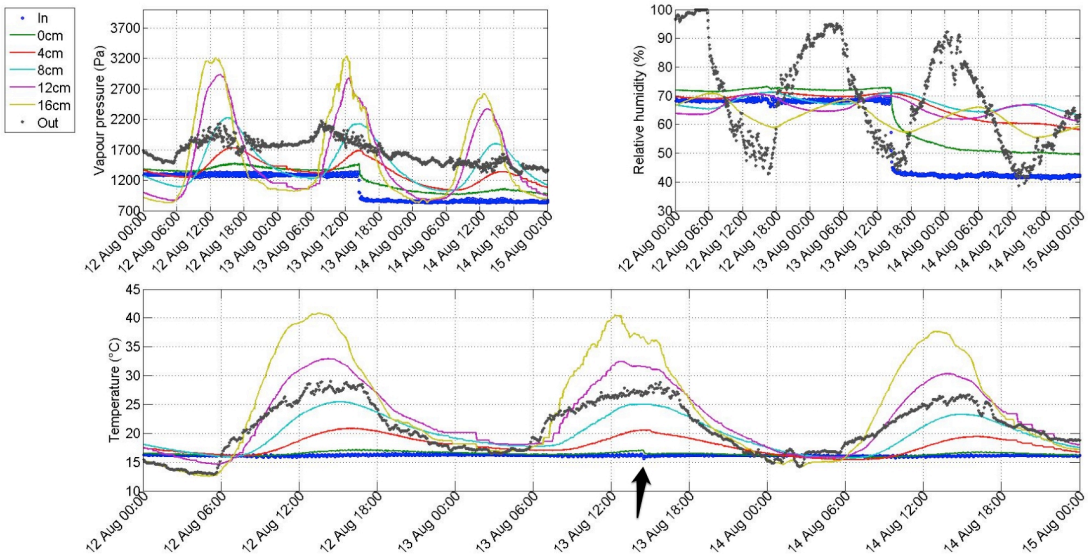

FIG 7: Temperatures, Vapour pressures and RH on the walls when vapour pressure dropped

4.3 Discussion of the results

Moisture content distributions represented here by vapour pressures variations from days to nights show us that the short time distribution of moisture inside the wall are mostly influenced by temperature. In fact, amplitude and time of variation are fairly correlated between vapour pressure and temperature. Thus, most short term moisture movements in the wall for that type of assembly are

thermal driven. Otherwise, the vapour pressure leads long term moisture distribution in walls, referring to the different distributions of vapour pressure during the test. An influence of vapour transfers on temperatures is also resorted. It could be explained by sorption (or desorption) for the short time moves, during the changing of internal conditions from 40 to 70% RH (or back from 70 to 40% RH). This shows up the hygroscopic characteristics of the wood fibre used for the walls. Long-time moves of temperatures could be explained by the change of heat fluxes due to latent heat or the change of internal convection coefficient and thermal conductivity in the thickness of the wall with adsorbed moisture due to the step; or it could be a mix of all those physical effects. Those hypotheses will be investigated through numerical simulations.

That experimental data may be used for the validation of HAM models, and presents the advantage of less problems for modelling external conditions due to air layer between claddings and the rest of the wall, such as encountered in (Desta et al. 2011).

5. Conclusions

A test made on a wall exposed to external environment was studied. The wall is a timber frame with wood fibre insulation, and a vapour permeable outer coating. The results show that for a very hygroscopic and vapour permeable wall, on the one hand the movement of vapour are directed by temperature fluctuations in the short term and the vapour pressure gradient between the exterior and interior in the long term, and secondly that the vapour pressure variation reciprocally influence the temperature of the hygroscopic material in the wall. Numerical studies should help better understand and assess these effects.

6. Acknowledgments

This study is done for the HYGROBAT (ANR-10-HABI-0005) project, financed by the National Agency of Research of France (ANR).

References

Desta, T. Z., Langmans, J., & Roels, S. , 2011. Experimental data set for validation of heat, air and moisture transport models of building envelopes. Building and Environment, 46(5), 1038-1046.

Kêdowidé Y., Woloszyn M., Le Pierrès N., 2012, Synthèse sur les dispositifs expérimentaux d'étude des transferts couplés de chaleur et d'humidité dans les parois des bâtiments ; Colloque International Francophone d'Energétique et Mécanique (CIFEM), Ouagadougou.

Labat M., Noel M., Woloszyn M., Piot A., Garnier G., Roux J.-J.. , 2012, Comparison of moisture and temperature measurements for six envelope types with different moisture transfer properties. 5th International Building Physics Conference. Kyoto, Japan, 28-31 May, 2012.

NF EN 998-1 (Décembre 2010) : Définitions et spécifications des mortiers pour maçonnerie – Partie 1

Teodosiu C., Hohota C., Rusaouën G., Woloszyn M., 2003, Numerical prediction of indoor air humidity and its effect on indoor environment, Building and Environment, Volume 38, Issue 5, Pages 655–664.

Co-heating test – state-of-the-art and application challenges

Geert Bauwens, Ir. Arch. [1]
Staf Roels, Prof. Dr. Ir. Arch. [1]

[1] KU Leuven, Building Physics Section, Department of Civil Engineering, Belgium

KEYWORDS: *Co-heating, reliability, state-of-the-art, heat loss coefficient, thermal performance*

SUMMARY:
Several studies show that the actual 'as-built' thermal performance of the building envelope can differ significantly from the theoretical, calculated value. Characterisation of building envelope performances based on in situ dynamic measurements can help to bridge this gap between 'designed' and 'as-built' performances. A common method to evaluate the thermal performance of a building in situ is the co-heating test, which is a quasi-stationary method based on linear regression analysis of dynamic measurement data.

After a short state-of-the-art on the co-heating test methodology, the limitations and opportunities associated with the use of the co-heating test method to characterise the thermal performance of buildings are investigated on the basis of a real full-scale experiment: a co-heating test performed on a terraced house in Herstal, Belgium. Renovation induced drops in the overall heat loss coefficient of the dwellings are characterised by the test method and compared with calculated values.

1. Introduction

In order to reduce the energy use of buildings, several countries have put forward more stringent demands on energy performance of new and renovated buildings. Without exception, these supervised buildings are characterised or awarded a label in the design phase. A theoretical energy use calculated on the basis of building plans and specifications determines the performance category. An important distinction needs to be made, however, between this theoretical energy performance and the actual as-built performance. Several studies have shown that these can differ rather significantly (Bell et al. 2010, Lowe et al. 2007).

The energy performance of a building is essentially determined by the (1) thermal characteristics of the building envelope, (2) installed services and (3) building usage. As the latter is not easily predicted nor controlled, the first two are decisive in achieving the envisaged building energy performance, both for new buildings and renovations. Hence, the thermal performance characterisation of a building envelope represents a crucial first step to bridge the gap between its designed and as-built energy performance. A common method to evaluate the thermal performance of a building envelope in situ is the co-heating test.

To the knowledge of the authors, (Sonderegger and Modera 1979) is first to mention the use of thermostatically controlled electric heating experiments to assess a building's energy performance. Real full-scale dwellings were alternately heated using the building's own services and electric heaters with known efficiency. Hence the name co-heating. Ever since it's conception, the co-heating test method has been used to (Sonderegger and Modera 1979):

- assess thermal efficiency of the installed services, e.g. distribution efficiency of duct systems (Sonderegger and Modera 1979);
- estimate thermal characteristics of the building envelope, e.g. overall heat loss coefficient and solar aperture (Bell et al. 2010, Lowe et al. 2007, Bauwens et al. 2012);
- load localisation (Sonderegger and Modera 1979)

The method was further explored during the 1980's and applied sporadically throughout the 1990's. Several transient and steady-state derived test procedures were proposed along the way. Recently, renewed interest in the characterisation of the thermal performance of buildings (Roels 2011) is apparent and has brought about a revival and further development of the co-heating test method (Bauwens 2012).

This paper tries to crystallise the current state-of-the-art on the co-heating test, as it is applied to assess the thermal characteristics of the building envelope. The co-heating test methodology is defined, with a clear focus on its data analysis part: basic heat balances are set up and applied simplifications are discussed. The analysis procedure is applied to measurement data collected during a co-heating test performed on a terraced house in Herstal, Belgium. During the test period multiple renovation steps were performed, allowing to, aside from a benchmark characterisation, characterise the renovation induced improvement of the fabrics' thermal performance.

2. Co-heating test methodology

During a co-heating test, the investigated dwelling is homogeneously heated to an elevated steady-state interior temperature (e.g. 25°C), using electric heaters. The electrical energy use necessary to retain this elevated temperature, the indoor and outdoor temperatures, wind speed and direction, and solar radiation are monitored throughout the test. Using regression analysis on averaged data, the monitored indoor and outdoor conditions are related to the electrical heating energy needed to sustain a constant indoor air temperature (Eq. 1(1).

$$Q_h + \sum(A_{sw,*}q_{sw,*}) = HLC(T_a - T_i) = HLC\Delta T \qquad (1)$$

where Q_h energy supplied by heaters and dissipated by ventilators (W)
$A_{sw,*}$ solar aperture coefficient of surface * (m^2)
$q_{sw,*}$ global solar radiation, normal to surface orientation * (W/m^2)
HLC overall heat loss coefficient (W/K)
$T_a - T_i = \Delta T$ indoor –outdoor temperature differential (K)

The coefficients describing the stationary heat balance in Equation 1 represent building thermal performance characteristics of interest: the overall Heat Loss Coefficient (*HLC*), in W/K, and one or more characteristics relating the heating energy to e.g. solar radiation. The overall HLC, on its turn, constitutes a combined transmission and ventilation heat loss. To decouple both, a co-heating test can be combined with a building air leakage test, i.e. blowerdoor or tracer gas test.

Notwithstanding a stationary heat balance is assumed, the measurement data are intrinsically dynamic, due to weather conditions. To diminish thermal dynamics resulting from charging and discharging of the buildings' thermal mass, the experiment period needs to be chosen sensibly and the collected measurement data averaged over a sufficient time span (mostly days, but possibly also several days or weeks). Hence, the co-heating test essentially represents a quasi-stationary test method based on linear regression analysis of building performance data.

3. Co-heating test data analysis

3.1 Revisiting the stationary heat balance: applied simplifications

3.1.1 Correlation between solar radiation projections

As a consequence of practical and statistical issues, Equation 1 is challenging to solve. When considering measurement data averaged over a larger time span, for instance 1 day, the global solar radiation normal to different orientations * naturally exhibit a strong mutual correlation. For example, on a sunny day, we are likely to monitor, on average, high global solar radiation values, regardless of how our pyranometer is orentied. Hence, $q_{sw,*}$ are linear dependent vectors and factors $A_{sw,*}$ in Eq. 1 cannot be estimated separately. The stationary heat balance equation is simplified accordingly:

$$Q_h + \sum(A_{sw,*}q_{sw,*}) = Q_h + A_{sw,*}q_{sw,*} = HLC\Delta T \qquad (2)$$

where $A_{sw,*}$ now represents the solar aperture coefficient corresponding to the sole global solar radiation component selected as input. For instance, in a next section, measurements of global solar radiation on a horizontal surface, $q_{sw,hor}$, is selected.

3.1.2 Disaggregation of transmission and ventilation heat loss

As mentioned earlier, the overall heat loss coefficient *HLC* actually comprises transmission heat losses, $\sum(AU)$, and ventilation heat losses, c_aG_a, as illustrated in Equation 3. On the basis of a separate estimate of the actual air change rate occurring over the course of the measurement period (Bell et al. 2010), both can be decoupled. The actual air change rate can be estimated on the basis of a blowerdoor tests or tracer gas tests. The latter comes with greater accuracy, but also with greater cost.

$$Q_h + A_{sw,*}q_{sw,*} = HLC\ \Delta T = (\sum(AU) + c_aG_a)\ \Delta T \qquad (3)$$

where $\sum(AU)$ transmission heat loss (W/K);
c_aG_a ventilation heat loss (W/K)

The blowerdoor test yields an estimate of the air change rate occurring at a pressure difference inside-outside of 50 Pa (n_{50}-value). Evidently, this pressure difference is not representative for real scenarios. Using a rule of thumb, following Kronvall and Persily (Sherman 1987), the n_{50}-value can be related to the average actual air change rate taking place under real pressure difference scenarios: $n_{actual} = n_{50}/20$. The corresponding average ventilation heat loss, c_aG_a, can then be calculated as:

$$c_aG_a = c_a(1/3600)\rho_a n_{actual}V \approx (1/3)n_{50}/20 \qquad (4)$$

where ρ_a density of air (kg/m³)
V air volume of dwelling (m³)

3.2 Estimating parameters using linear regression analysis

Assuming the heat balance in Equation 3 to hold, the parameters of interest, framed in Eq. 5, are generally determined by applying simple or multiple linear regression techniques on co-heating measurement data:

$$Q_h = \boxed{HLC}\Delta T - \boxed{A_{sw,*}}q_{sw,*} + \boxed{c} \qquad (5)$$

Where c describes the discrepancy between the regression model fit and the actual aggregated measurement data.

Essentially, three options can be discerned:

1. The energy supplied to the interior under the form of electrical energy can, on a daily average basis, be corrected for solar gains and plotted as a function of ΔT. This correction implies that an assumption is made for the solar aperture parameter $A_{sw,*}$. As illustrated in Fig. 1 (a), the slope of the regression line resulting from a simple linear regression on this corrected measurement data set yields an indication of the overall heat loss coefficient (Bell et al., 2010);
2. An alternative to the method described above is to, aside from ΔT, consider $q_{sw,*}$ as an additional independent variable explaining the variability of Q_h. Multiple regression techniques allow to determine both *HLC* and $A_{sw,*}$ in Eq. 5 (Lowe et al., 2007; Everett, 1985).
3. A third method is based on dividing all terms in Eq. 5 by ΔT. An equation is obtained on which a simple linear regression can be performed, assuming $Q_h/\Delta T$ as dependent variable and $q_{sw,*}/\Delta T$ as independent or explanatory variable, as in Eq. 6.

$$Q_h/\Delta T = \boxed{HLC} - \boxed{A_{sw,*}} q_{sw,*}/\Delta T \qquad (6)$$

As illustrated in Figure 1 (b), an estimate of *HLC* is then given by the intercept. Note that this mathematical transformation implicitly forces the above described multiple linear regression through zero. In both of the earlier mentioned methods, a non-zero intercept is possible due to discrepancies between the measurement data and the assumed stationary model to which it is fitted. In the third method, these errors are included in the *HLC*-estimate.

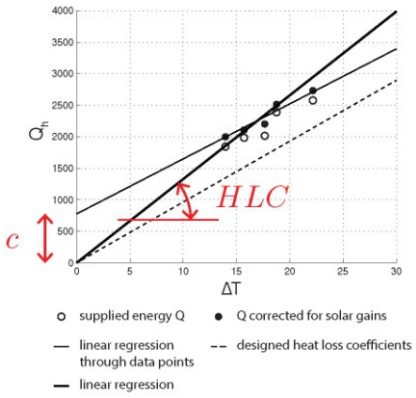

(a) Simple linear regression

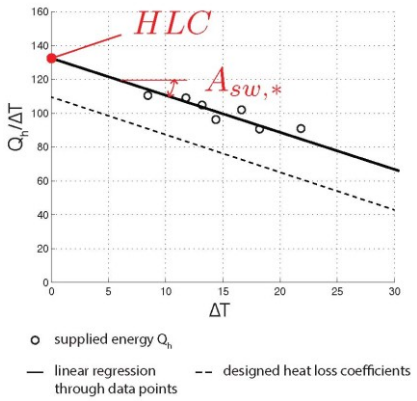

(b) Simple linear regression transformed equation

FIG 1. Estimation of HLC and $A_{sw,*}$ by applying simple linear regression

3.3 Thermal lag

From a harmonic analysis, it can be derived that the building fabric typically introduces a phase shift, between the internal heating power Q_h and the external temperature T_a and solar radiation $q_{sw,*}$. Due to this phase shift, ΔT at time t will not be representative for the needed energy supply Q_h at that time. To cope with this, Q_h at time t can be correlated with ΔT and/or $q_{sw,*}$ averaged over time step *t* and *t-1*:

$$Q_{h,t} = \boxed{HLC}\,(0.5\Delta T_t + 0.5\Delta T_{t-1}) - \boxed{A_{sw,*}}\,(0.5q_{sw,*,t} + 0.5q_{sw,*,t-1}) + \boxed{c} \qquad (7)$$

3.4 Reliability of co-heating test methodology

Regardless of the effort made to diminish the transient effects introduced by weather conditions and the investigated buildings' thermal mass, stationarity will never fully hold during a co-heating test. Averaging measurement data and taking into account thermal lags, as described in Section 3.3, only

partly addresses this issue. Hence, the estimates for HLC, $A_{sw,*}$ and possibly c, resulting from linear regression analysis are necessarily associated with a certain bias (e.g. if solar radiation is not taken into account) and error. In general, the reliability of co-heating test analysis results will depend on the investigated building, the imposed regression model and the period (start date and duration) in which the experiment is performed. To illustrate this, regression analysis can be performed on various subsets of the available co-heating measurement data, with each subset having a different starting date and a different duration. The reliability of the co-heating method can then be visualised by plotting the resulting collection of estimates. This is exemplified in Figure 2 (Bauwens et al. 2012). As the duration of the experiment increases, the regression result converges, hence the influence of the experiment starting date diminishes. For shorter measurement durations, however, the starting date is shown to be crucial. Fig. 2 (b) collects the results of applying multiple linear regression on measurement data, collected around winter. It can be seen that the results are generally reliable, and more so for high average Q_h monitored during the experiment.

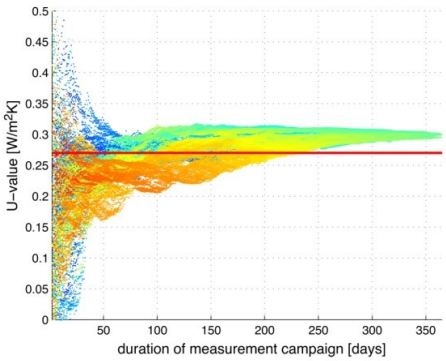

(a) Basic multiple linear regression: ΔT as descriptive variables, thermal lag not taken into account, intercept c.

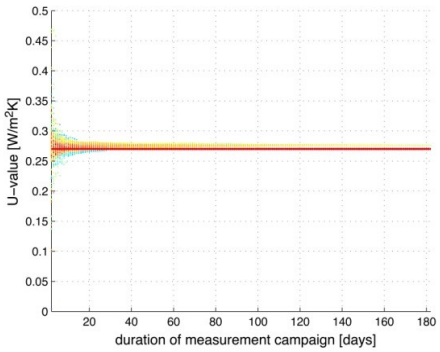

(b) Multiple linear regression when only considering winter months, ΔT and $q_{sw,*}$ as descriptive variables, taking into account thermal lags and forcing intercept through zero ($c = 0$).

FIG 2. U-value estimation through multiple linear regressions applied on data acquired during a simulated co-heating test on an insulated cavity wall component. Different subsets of the measurement data are considered: with different starting dates (vertically aligned points) and various durations (along the x-axis). The data points are coloured according to the average Q_h during the considered measurement data subset: red points indicate a high average Q_h, blue points indicate a low average Q_h.

FIG 3. Investigated terraced house in Herstal, Belgium. (a) Front façade; (b) Garden façade.

FIG 4. Co-heating test equipment: heat sources controlled by thermostats, ventilators, temperature sensors and pulse meters spread throughout the investigated dwelling. Sensor data (including weather station data) is transmitted to a central logger located on site.

4. Co-heating in practice: terraced house in Herstal, Belgium

From the 2nd of February to the beginning of May, an extensive co-heating measurement campaign was performed on a social row house in Herstal, north of Liège, Belgium. During the experiment, two renovation steps were executed:

- Renovation step 1: blowing in of insulation in the façade wall and party wall cavities and insulating the attic floor slab;
- Renovation step 2: insulating the floor above basement from underneath.

As depicted in Figure 4, the co-heating measurement equipment was fully deployed. A weather station was placed in the garden to monitor the outdoor air temperature, solar radiation, wind speed and wind direction. The indoor air temperatures in every room and the heat input necessary to elevate the indoor air temperature to 25°C were monitored throughout the test. Two blowerdoor tests were performed, before and after renovation step 1 (insulating wall cavities and attic floor slab).

4.1 Estimates of renovation induced performance improvement of fabric components

For verification purposes, the *U*-value reductions for the outside walls, cavity walls and ceilings are calculated on the basis of the applied insulation thicknesses and their respective λ-values (Table 1).

TABLE 1. Predicted thermal performance improvement induced by renovation step. d=thickness of applied insulation (cm); λ=heat conductivity (W/(mK)); R=thermal resistance (m^2K/W); hi = indoor surface heat transfer coefficient (W/m^2K), he=outdoor surface heat transfer coefficient (W/m^2K); U=heat transfer coefficient (W/m^2K), A=component surface (m^2).

	d (cm)	λ (W/mK)	h_i (W/m^2K)	h_e (W/m^2K)	ΔU (W/m^2K)	A (m^2)	$\Delta(UA)$ (W/K)
roof insulation	25	0.045	7.70	7.70	-2.00	40.32	-80.77
cavity wall insulation	5	0.034	7.70	23.00	-0.68	51.03	-34.94
party wall cavity insulation	5	0.034	7.70	7.70	-0.74	79.1	-58.40

Table 1 does not take into account certain aspects that could lead to an underestimation or overestimation of the corresponding reduction of the overall Heat Loss Coefficient *HLC*:

- Some areas of the cavity are not filled with insulation. The reason for this lies in the way the building was originally constructed. At the time of construction, it was common practice to close the cavity around the windows to facilitate installing and stabilising window frames. Where the cavity is closed no insulation will be added and thermal bridges are created. In other words, locally the thermal performance will not be improved. Other impurities in the cavity wall, e.g. interconnections of both masonry wall leafs, rubble in the cavity, …, further reduce the potential *HLC* reduction;
- The neighbours moved out shortly after the first renovation step, hence the party wall heat loss is expected to increase, leading to a possible overestimation.

4.2 Estimates of renovation induced HLC reduction

Figure 5 shows the *HLC*'s estimated on the basis of a multiple linear regression – Q_h as a function of ΔT and $q_{sw,hor}$, taking into account thermal lags and forcing the regression surface through the origin – applied on the co-heating measurement data before the renovation step, after renovation step 1 and after renovation step 2, respectively. Similar to Fig. 2, discussed in Section 3.4, different data subsets (different durations, different start dates) were considered in each case, effectively showing how the estimates for *HLC* converge towards the values reported in Table 2. As expected, renovation step 1, which included insulating the cavity walls and the attic floor slab, induces a far more significant

reduction of the *HLC (*110.92 W/K) than renovation step 2, during which the floor slab above basement was insulated (reduction of 27.79 W/K). It is seen that renovation step 1 only attains about 63.7% of the projected performance improvement. On the basis of the aspects listed in Section 4.1, however, this falls within the expected range.

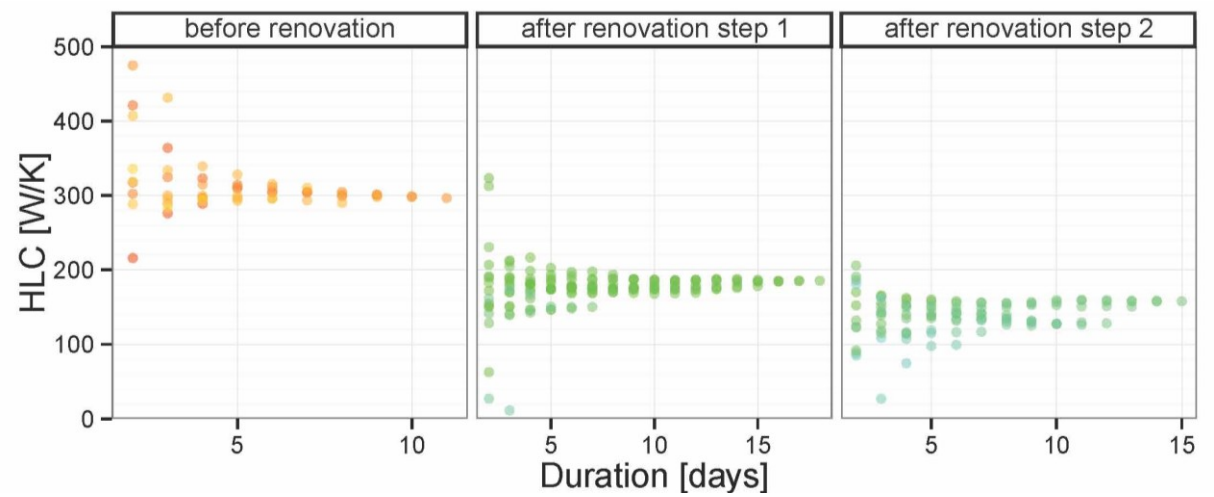

FIG 5. HLC estimates through multiple linear regressions with Q_h as a function of ΔT and $q_{sw,hor}$, taking into account thermal lags and forcing regression surface through the origin, applied on measurement data acquired during co-heating test on a terraced house in Herstal, Belgium. Different subsets of the measurement data are considered: with (1) different starting dates and (2) different durations. The data points are coloured according to the average Q_h over the course of the considered measurement data subset: red points indicate a high average Q_h, blue points indicate a low average Q_h.

TABLE 2. Results of applying simple and multiple linear regression on daily averaged co-heating test data, before and after renovation step 1 and 2: coefficient of determination R^2, estimates for HLC and $A_{sw,*}$, p-value Pr(>|t|). The p-value indicates the probability the variable is not significant.

	R^2	HLC	Std.Error	Pr(> |t|)	$A_{sw,*}$	Std.Error	Pr(> |t|)	
	-	(W/K)	(W/K)	-	(m2)	(m2)	-	ΔHLC
Before	0.9983	296.55	13.51	3.98e-09	3.15	3.85	0.433	
After step 1	0.9935	185.63	6.27	2.14e-15	4.76	0.69	3.70e-06	110.92
After step 2	0.9899	157.84	9.62	4.54e-10	2.48	0.68	3.06e-03	27.79

Both ΔT and $q_{sw,*}$ prove to be significant variables in all cases but one. Before renovation step 1, the average solar radiation was rather limited, which explains the fact that the solar radiation as a descriptive variable proves to be less significant in that case (p-value > 0.05).

4.3 Decoupling HLC into transmission and ventilation heat loss

Before renovation step 1, the measured n_{50}-value was 3.58 h^{-1}, corresponding to a ventilation heat loss of approximately (1/3) * (n_{50}/20) * V = (1/3) *(3.58/20) * 270.91 = 16.16 W/K. After the first renovation step, the n_{50}-value has risen slightly to 3.92 h^{-1}, corresponding to a ventilation heat loss of 17.70 W/K. During part of the measurement campaign following renovation step 1 (26th of March to 2nd of May), detailed air change rate measurements were performed, using a tracer gas test with constant tracer gas pressure. The average air change rate was found to be 0.48 h^{-1}, which is significantly higher than the air change rate estimated on the basis of the blowerdoor test result and the rule-of-thumb.

5. Conclusions

This paper investigated the applicability of a co-heating test to determine the overall Heat Loss Coefficient (HLC) of a dwelling. The co-heating test was introduced and the corresponding data analysis methodology developed.

A co-heating test was performed on a terraced house in Herstal, Belgium, over an extended period of time (three months). During the measurement period, two renovation steps were performed. The co-heating test proves to be a valuable tool here, not only to assess the *HLC* benchmark value, but also its reduction as a result of renovations. Multiple linear regression analysis was performed, with the heating power as a function of indoor-outdoor air temperature difference and global horizontal solar radiation, taking into account thermal lags introduced on both and forcing the intercept through zero. Confidence in the *HLC*-estimates is backed by the fast and rather steady convergence seen in scatter plots of *HLC*-estimates resulting from applying the regression analysis on measurement data subsets with different (increasing) duration and different start dates.

The blowerdoor test, generally used to decouple the *HLC* into its transmission and ventilation heat loss parts needs to be used with caution. Tracer gas tests showed that the average actual air change rate far outpassed the value estimated by reducing the measured n_{50}-value by a factor 20. The considerable cost associated with a tracer gas test, however, prevents its use on a frequent basis.

6. Acknowledgements

The authors wish to thank Knauf Insulation, for setting up an expert network concerned with investigating the gap between the ‘designed’ and ‘as-built’ thermal performances of building envelopes

References

Sonderegger, R. C., Modera, M.P. (1979). Electric Co-heating: A method for Evaluating Seasonal Heating Efficiencies and Heat Loss Rates in Dwellings. In *Second CIB Symposium on Energy Conservation in the Built Environment*. Lawrence Berkeley National Laboratory, March 1979.

Everett, R. (1985). Rapid thermal calibration of houses, ERG, Open University Energy Research Group, Milton Keynes UK.

Roels, S. (2011). Reliable Building Energy Performance Characterisation Based on Full Scale Dynamic Measurements. Annex text, November 2011. (http://www.kuleuven.be/bwf/projects/annex58/index.htm)

Bell, M., Wingfield, M. and Miles-Shenton D. (2010). Low carbon Housing. Lessons from Elm Treed Mews. Technical report, Joseph Rowntree Foundation.

Lowe, R.J., Wingfield, J., Bell, M. and Bell J.M. Evidence for significant heat losses through party wall cavities in load-bearing masonry construction. *Building Services Engineering Research and Technology*, 28 2:161-181, 2007.

Bauwens, G., Standaert, P., Delcuve, F., and Roels, S. (2012). Reliability of co-heating measurements. First Building Simulation and Optimization Conference. IBPSA, September 2012.

Max Sherman, Estimation of Infiltration for Leakage and Climate Indicators, in Energy and Buildings, 10, 1987, p.81.

The performance of unventilated wooden roofs with smart vapour barriers during winter conditions

Stig Geving, Professor [1]
Eirik Thorsrud, M.Sc [2]

[1] Norwegian University of Science and Technology, Norway

KEYWORDS: *smart vapour barrier, roof, moisture*

SUMMARY:
Unventilated wooden roofs typically need a vapor barrier at the warm side to avoid interstitial condensation due to vapor diffusion and air leakages from the interior. So-called smart vapour barriers (SVB) or retarders, could allow condensed moisture, built-in-moisture or moisture from minor leakages to dry to the interior. The concept of SVBs or retarders have been known for some time, consisting of a material that changes its vapour resistance according to the level of relative humidity in the surrounding air. SVB's should be relatively vapour open during summer conditions to allow drying to the interior. During winter conditions however, the vapour resistance should preferably be as high as possible to avoid condensation problems. Various commercial SVB's have different properties in regard to the level of their vapour resistance and variation with relative humidity.

In this laboratory study the level of moisture accumulation during winter conditions have been investigated for unventilated wooden roofs applying four various types of SVB's and compared with a standard roof with polyethylene foil as vapour barrier. Four levels of indoor air humidity were applied during the test period of three months. The measurement results were compared with hygrothermal simulations. The results showed that the various SVB's had very different robustness against condensation problems during winter conditions, and thus the type of SVB should be chosen in regard to the expected level of indoor air humidity.

1. Introduction

In Nordic climates a vapour barrier is typically used on the warm side of the building envelope to avoid interstitial condensation during the heating season due to vapour diffusion and air leakages from the interior. Often a polyethylene foil is used, which has a very high vapour resistance. Such a vapour tight product does however not allow moisture to dry to the interior. A more vapour open product could allow condensed moisture, built-in moisture or moisture from minor leakages to dry to the interior. This could be especially useful for constructions with reduced or no possibility to dry to the exterior, such as unventilated flat roofs. It might allow cheaper solutions, making it possible to use organic (wooden) materials in such constructions or skip the use of wooden preservatives.

The term "vapour retarder", as opposed to "vapour barrier", is often used on products that have a lower vapour resistance than recommended for vapour barriers. Such products may allow for some drying to the interior. While a vapour retarder has a given constant vapour resistance, some vapour barriers or retarders are sold (Note: "barrier" is used in the rest of this paper for simplification) on the European and North American market with adaptable vapour resistance in regard to what is actually needed. Popular terms for these products are "smart", "intelligent", "moisture adaptive" or "humidity dependent" vapour barriers. The physical behaviour of these products varies, but the main principle is that the vapour barrier should function as an ordinary vapour tight vapour barrier most of the time, preventing vapour diffusion into the construction from the indoor air – especially during winter conditions. If, on the other hand, the construction is wet, for example due to built-in moisture or

leakages, so that the relative humidity (RH) on the exterior side of the vapour retarder gets high, the vapour resistance will be reduced so that there may be possibilities for drying inwards - especially during summer conditions. Another possibility may be that the barrier layer has capillary properties with possibilities to transport condensed water to the interior surface.

Probably the first commercial product that can be put under the term “Smart Vapour Barrier” (SVB) was Hygrodiode that was developed in Denmark during the 80’s (Korsgaard, 1985). It consisted of synthetic fibres sandwiched between stripes of polyethylene, giving it a constant very high vapour resistance similar to the polyethylene film. If on the other hand moisture condensed on the exterior side of the vapour barrier, the water would be transported sideways through the fibres by the wicking action and be allowed to evaporate to the interior side.

In the mid 90’s another type of SVB was developed in Germany (Künzel, 1996). The product is named Difunorm Vario, but is also manufactured under other names, including MemBrain in the US, and Delta-Novaflexx in some parts of Europe. It consists of a polyamide film with no capillary prop-erties, but with a pronounced difference in vapour resistance for high and low ambient RH. The Sd-value is approximately 4-5 m when the RH is below about 40 % and Sd = 0,1-0,2 when the RH is above 80% (Künzel 1996). As for Hygrodiode, also this product was first introduced as beneficial for unvented wooden roofs. Most research from then and till today has been focused on use of this product.

Since then and up till today there have been developed various similar products with RH-dependent vapour resistance. Some of these new products may have a higher resulting vapour resistance for winter conditions, compared to Difunorm Vario, reducing the risk for interstitial conditions. And some may have a lower resulting vapour resistance for summer conditions, resulting in higher drying rate to the interior. Documented scientific studies of applications for these new products are however limited although they may have some advantages compared to Hygrodiode and Difunorm Vario.

This study is investigating and comparing the performance of two newer products (Intello and AirGuard Smart) with Delta-Novaflexx (i.e. Difunorm Vario) and Hygrodiode – applied in unventilated wooden roofs under winter conditions where condensation due to vapour diffusion from interior side may occur. In previous studies in this project the same products applied in the same construction has been investigated in regard to the drying potential for built-in moisture during summer conditions (Geving, Stellander and Uvsløkk 2013; Geving, Thorsrud and Uvsløkk 2013).

2. Laboratory tests

2.1 General

The purpose of these tests was to investigate the risk for undesirable vapour diffusion from interior air during winter conditions in unventilated wooden roofs with SVB’s, possibly leading to condensation, moisture accumulation or other moisture problems. SVB’s should be relatively vapour open during summer conditions to allow drying to the interior. During winter conditions however, the vapour resistance should preferably be as high as possible to avoid condensation problems.

In this laboratory study the level of moisture accumulation during winter conditions have been investigated for unventilated wooden roofs applying four various types of SVB’s and compared with a standard roof with polyethylene foil as vapour barrier. Four levels of indoor air humidity were applied during the test period of three months. The effect of having some part of the insulation at the interior of the SVB was also investigated.

The following type of compact unventilated wood frame roof was tested (from exterior side):

- Roofing membrane
- 200 mm glass wool
- SVB or PE-foil
- 13 mm gypsum board

Even though the construction considered is an unventilated compact roof, the results may also be applicable to assess the risk for moisture problems in walls and ventilated roofs with SVB's – although these constructions have drying possibilities to the exterior.

The measurements took place in the laboratories of Department of Civil and Transport Engineering, Norwegian University of Science and Technology, during spring 2013.

2.2 Experimental set-up

Five different configurations of the wood frame roof were tested, where the only difference was the type of vapour barrier used, i.e. four SVB's and PE-foil. Usually such constructions have a plywood sheathing or similar below the roofing membrane, but this was of practical reasons omitted in this test, and instead a thin cotton cloth was used to hold any condensed water below the membrane in place. This was considered acceptable since there was a constant vapour gradient directed outwards, and the roofing membrane was practically vapour impermeable. The five configurations were tested each with two specimens to get a better accuracy, i.e. a total of 10 specimens.

The roof specimens were built up in storage boxes of polypropylene; where the bottom of the boxes was used to imitate the roofing membrane and the rest of the materials were adjusted to fit the box, see Figure 1. The boxes had interior dimensions b = 0,28 m, l = 0,40 m and h = 0,22 m, and flanges onto which the SVBs and gypsum board were taped. The corners of the boxes were curved so the resulting "light-opening" of the boxes had an area of 0,105 m^2. The SVB was taped with double sided tape to the flanges of the box while the gypsum board afterwards was taped with vapour tight aluminium tape to the flanges.

FIG 1. Test box with RH/T-sensor before mounting of SVB (left) and after mounting of SVB and gypsum board.

To simulate a cold external climate on one side and a warm indoor climate on the other side the boxes were installed in a wall separating two different climate chambers with controlled temperature and relative humidity, as shown in Figure 2. A horizontal section through two of the boxes as installed in the wall is shown in Figure 3. This means the specimens were installed vertical instead of horisontal, that may potentially give some internal convection in the insulation layer. The insulation was however installed with no air gaps, so it is assumed that the effect of internal convection is insignificant. Since the main focus of this test was on the total moisture accumulation, any internal convection is anyhow considered of little importance. On the cold side a continuous wood fibre board layer was installed to

ensure airtightness of the test-wall. On all sides of the test boxes a glass wool and EPS layer was installed, see Figure 3.

FIG 2. The experimental set-up showing the 10 test boxes installed in the wall, seen from the warm side.

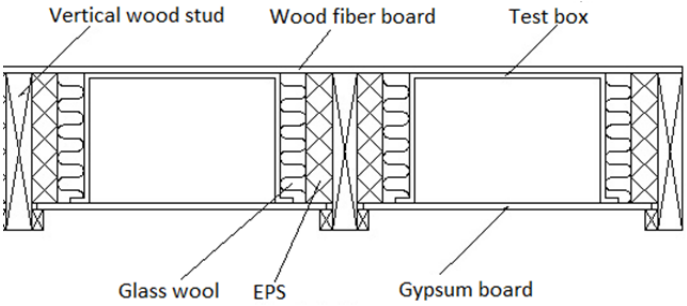

FIG 3. Horizontal section through two of the test boxes installed in the wall.

2.3 Materials

The four types of SVBs are;

- Delta-Novaflexx
- Intello
- AirGuard Smart
- Hygrodiode 200A

Delta-Novaflexx is a polyamide with an S_d-value ranging from 0,2–5 m. This product is manufactured under many different names, including MemBrain in the US, and Difunorm Vario in Germany. It was originally developed in Germany in the late 90's (Künzel, 1996), and was the first commercial available relative humidity dependent vapour barrier product for building applications. Most scientific studies on use of SVBs in building applications are limited to this product only. Intello is a polyethylene copolymer, where the copolymer is an acrylic with hygroscopic properties. The S_d-value ranges from 0,25-26 m (Pro Clima, 2006). AirGuard Smart is a polyvinyl alcohol film (with spun bond polypropylene as reinforcement and protecting layer) with an S_d-value ranging from 0,05 - 102 m (DuPont, 2012). Hygrodiode 200A is composed of a fabric of synthetic fibres with good capillary properties laminated with stripes of perforated PE-foil and polyamide-foil. It should be noted that this product is a further development of the original Hygrodiode mentioned earlier, i.e. the polyamide film giving the product drying possibilities also for conditions below 100% RH. The S_d-value ranges from

1-20 m (Icopal, 2005). The variation of S_d as a function of RH (data from manufacturer) is given for three of the SVBs in Figure 4 (detailed measurements have not been available for Hygrodiode). As a reference one configuration had 0,15 mm PE-foil with S_d = 70 m.The gypsum board has an S_d-value of approximately 0,10 m.

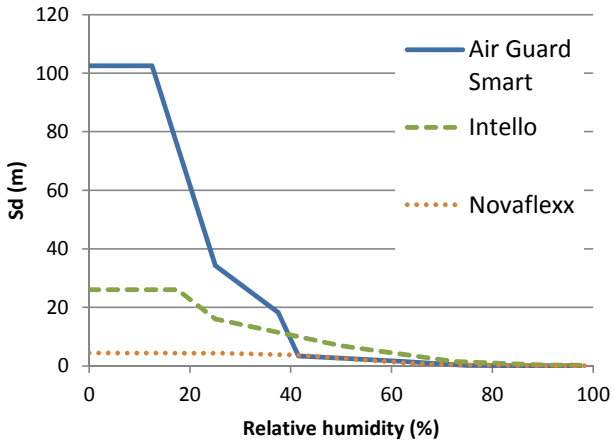

FIG 4. Sd-value as a function of RH

2.4 Boundary and initial conditions

The intention of the test was to study the risk for moisture accumulation during winter conditions, with varying indoor air humidity levels. It was chosen to do four cycles, each lasting three weeks, i.e. the test lasted a total of 12 weeks (84 days). The real measured average temperatures and RH, and the moisture supply Δv, for each cycle are given in Table 1. No built-in moisture was added, the initial moisture content of the materials used were according to a hygroscopic level of approximately 30% RH.

TAB 1. Measured average T and RH for each cycle

Cycle #	T_{cold} (Cº)	RH_{cold} (%)	T_{warm} (Cº)	RH_{warm} (%)	Δv (g/m^3)
1	-5,1	77,2	21,4	22,4	2
2	-5,1	77,5	23,0	32,8	4
3	-5,0	76,6	23,3	42,6	6
4	-5,0	77,0	23,2	51,7	8

2.5 Measurements

The rig and test boxes were constructed so that the boxes could be dismounted and weighed regularly to follow the total drying of the configurations. In addition the temperature and RH at the interface between the SVB and the 200 mm insulation were measured (logged each sixth minute) in all test boxes. The RH and temperature of the indoor climate were also continuously logged. The RH/T-sensors were controlled before and after the test, and the results were adjusted according to this calibration.

3. Hygrothermal simulations

The laboratory test setup were simulated for all the described configurations, except for the configuration with Hygrodiode where detailed material properties were missing, using WUFI 1D Pro 5.2 (WUFI 2013). WUFI 1D Pro 5.2 is a simulation program for coupled non-stationary, one-dimensional heat and moisture transport. The program includes the moisture transport by vapour diffusion and capillary transport, and takes into account the moisture capacity of the materials. The

boundary conditions and material properties given in chapter 2.3 and 2.4 were used. The sorption curve of the gypsum board is obviously important for these simulations with a focus on moisture accumulation. Swedish data for interior gypsum board ("Gipsskiva, innvendig") with density 625 kg/m^3, included in the material database of WUFI were used, with the following sorption curve up to 50% RH; 35%-3kg/m^3, 50%-4kg/m^3.

4. Results and discussion

The accumulation of water in the five roof configurations are shown in Figure 5, to the left is shown all specimens to give an impression of the variance. We see that the two specimens show a similar moisture uptake for all the five roof configurations, and very similar for the Intello and PE-foil configurations. This indicate that the repeatability of the experimental set-up is good. When it comes to the effect of type of vapour barrier on the moisture accumulation we see that the Novaflexx configuration accumulates the most, followed by Hygrodiode, Intello, AirGuard Smart and PE-foil. In general that is what could be expected when comparing the S_d-values for the various vapour barriers given in chapter 2.3. The average RH across the SVB's ranges from approximately 19 % for Cycle 1 till 36% for Cycle 4, i.e. according to Figure 4 Air Guard Smart has higher S_d-value than Intello during all cycles and Novaflexx has the lowest S_d-value. Regarding Hygrodiode we did miss a detailed description of S_d-variation as a function of RH, but it is interesting to observe that the moisture accumulation curve in Figure 5 lies between Intello and Novaflexx. The producer of Hygrodiode gives a dry S_d-value of 20 m, which seems reasonable when we know that the dry value of Intello and Novaflexx is 26 and 5 m respectively.

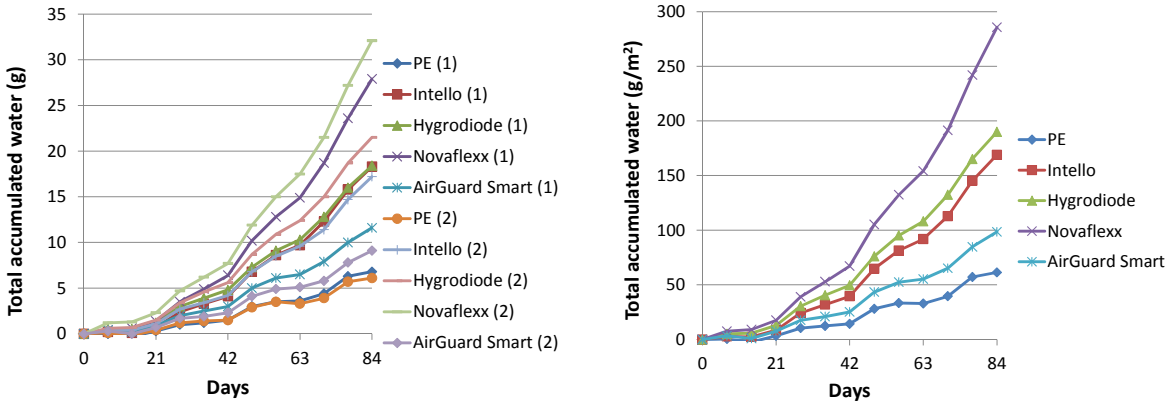

FIG 5. Total accumulated water in the five roof configurations, all 10 specimens to the left and the average of two specimens to the right.

In Figure 6 is shown the comparison of measured moisture accumulation with the hygrothermal simulations with WUFI. For the Novaflexx configuration the simulation compare very well with the measurements through all cycles. Also for the PE-foil and AirGuard Smart configurations the simulations and measurements compare very well, with the exception for some deviation for the last cycle. For AirGuard Smart the simulations give higher moisture accumulations than the measurements during the last cycle, while the opposite applies for the PE-foil. One explanation for the deviation in regard to AirGuard Smart could be that the S_d-value in reality is higher for the given RH levels than we see in Figure 4. New cup-measurements made for AirGuard Smart seem to confirm that explanation. For Intello the deviation between the simulation and measurements is however bigger, the simulation showing much lower moisture accumulation than the measurements. Due to the little deviation between the two test specimens of the Intello configurations we observe in Figure 5, the most obvious explanation may be that the real S_d-value for Intello is lower than given in Figure 4. It

should be noted that the S_d-value for Intello given in Figure 4 is linearly interpolated for measurement values between 25 and 50% RH, and thus the real S_d-value could be lower in this interval.

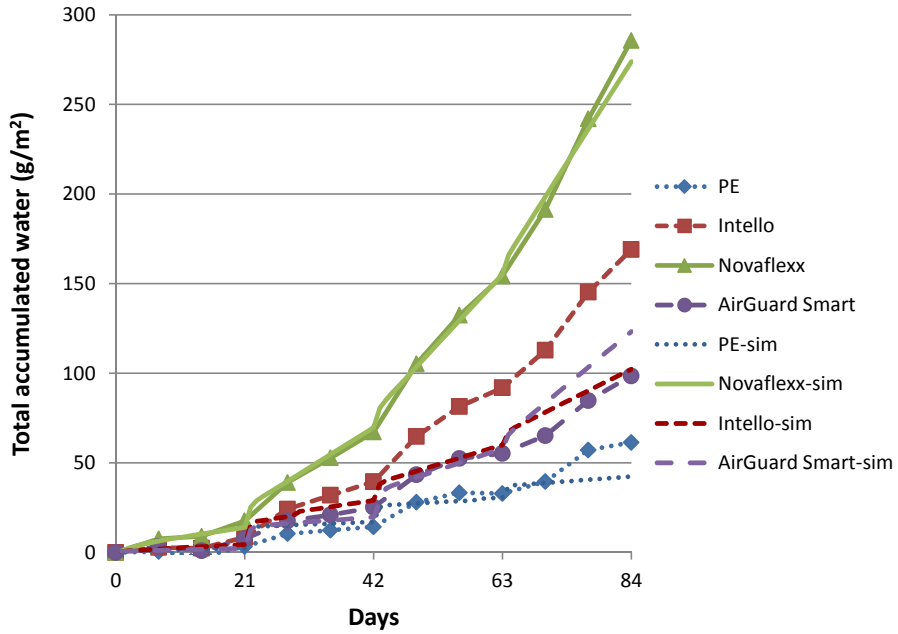

FIG 6. Comparison of measured and simulated ("sim") total accumulated water in four of the roof configurations.

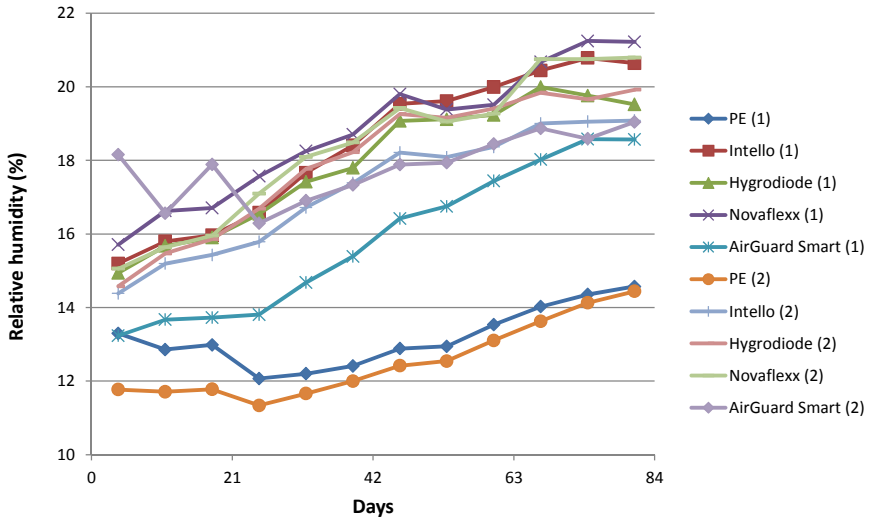

FIG 7. Measured RH at the interface between the glass wool and SVB/PE-foil for all test specimens.

The RH at the interface between the glass wool and SVB/PE-foils were measured and is shown in Figure 7. We observe that even if the various vapour barriers have very different vapour resistances, this do not influence the RH at the external side of the vapour barrier too much. For the PE-foil configuration the RH varies between approximately 12 – 14 %, while for the other SVB's the RH varies between approximately 14 – 21% - increasing somewhat as the indoor air humidity and water accumulation in the test specimens increases during the test. According to Figure 7 the average RH at the interface between glass wool and the SVS are approximately 16%, 17%, 19% and 20% for Cycle

1, 2, 3 and 4 respectively. This means that the average RH across the SVB's are approximately 19%, 25%, 31% and 36% for Cycle 1, 2, 3 and 4 respectively. To be able to make high quality hygrothermal simulations for winter conditions, we need good values/measurements of the S_d-value for the SVB in the regime 25-40%. Using linear interpolation of the S_d-value between for instance 25% and 50% as is the case for Intello (see Figure 4) is probably not satisfactory.

5. Conclusions

In this laboratory study the level of moisture accumulation during winter conditions have been investigated for unventilated wooden roofs applying four various types of SVB's and compared with a standard roof with polyethylene foil as vapour barrier. Four levels of indoor air humidity were applied during the test period of three months. The measurement results were compared with hygrothermal simulations.

The results showed that the various SVB's had very different robustness against condensation problems during winter conditions, and thus the type of SVB should be chosen in regard to the expected level of indoor air humidity. However, whether a certain level of moisture accumulation during winter conditions is a problem, also depends on the drying during summer conditions. It is for example interesting to observe that while built-in moisture drying experiments for summer conditions (Geving, Stellander and Uvsløkk 2013; Geving, Thorsrud and Uvsløkk 2013) show faster drying for Novaflexx and AirGuard Smart compared to Intello and Hygrodiode, Novaflexx show the highest moisture accumulation and AirGuard Smart the lowest for this experiment for winter conditions.

The simulations of the test conditions compared well with the measurements, except for a few cases – where one explanation for the deviations could be that the given S_d-values for those products may not be sufficiently correct or detailed.

6. References

DuPont. 2012. Tyvek ©. Product Brochure. http://construction.tyvek.co.uk.

Fraunhofer IBP. 2010. WUFI 1D (Version 5.1) [Computer Program]. Fraunhofer IBP, Holzkirchen, Germany.

Geving, S., Stellander, M. and Uvsløkk, S. 2013. Smart vapour barriers in compact wood frame roofs. Proceedings of Buildings XII Conference – Thermal Performance of Ecterior Envelopes of Whole Buildings, December 1-5, 2013, Clearwater Beach, Florida.

Geving, S., Thorsrud, E. & Uvsløkk, S. 2013. Smart vapour barriers in unventilated wooden roofs in a Nordic climate – laboratory study of drying effect under shaded conditions. Proceedings of 2nd Central European Symposium on Building Physics, September 9-11, 327-334.

Icopal, 2005. Hygrodiode ©. Product Brochure. www.icopal.dk.

Korsgaard, V. 1985. Hygro diode membrane: A new vapor barrier. ASHRAE/DOE/BTECC Conference: Thermal Performance of the Exterior Envelopes, Clearwater Beach, Florida, December 2-5.

Künzel, H.M. 1996. Humidity controlled vapour retarders reduce risk of moisture damages. Proceedings of the 4th Symposium on Building Physics in the Nordic Countries, Espoo, Finland, September 9-10.,447-454.

WUFI. 2013. http://www.wufi-pro.com

On the hygrothermal performance of applying exterior air barriers in Northern Climates.

Jelle Langmans, Ph.D.[1]
Staf Roels, Professor [1]

[1] Building Physics Section, KU Leuven, Belgium

KEYWORDS: *Exterior air barrier, HAM-simulation, DELPHIN 5, air flow, natural convection*

SUMMARY:
This paper studies the hygrothermal performance of timber frame wall configurations with exterior air barrier systems in various European climates. First, the impact of different insulation materials will be discussed for Belgium climate conditions. The simulation results demonstrate that the application of mineral wool insulated timber frame walls in combination with exterior air barriers result in increased moisture loads. Moreover, unavoidable (small) air channels between the mineral wool and the adjacent exterior air barrier significantly increase natural convection and add up to harmful moisture levels. Yet the use of cellulose insulation can avoid these issues. The second part of the paper studies the performance of these wall elements for 12 European climates, focussing on Nordic countries in specific. The simulation results indicate that the technique of exterior air barrier is more suitable for continental climates rather than for cold and moderate sea climates in Europe.

1. Introduction

The execution of exterior air barrier systems in timber frame construction has gained increasing interest in the aim to meet the severe airtightness requirements of Passive houses (n_{50}<0.6 ACH). In practice, fewer joints and perforations of exterior air barriers are an advantage compared to the traditional interior air barrier systems (Langmans, 2010). Also in Norway the practical advantages of exterior air barriers are mentioned (Myhre & Aurlien, 2005 and Holøs & Relander, 2010). Yet for cold and moderate climates, such as the Northern European countries, the hygrothermal impact of exterior air barriers remains unstudied. Consequently, the execution of wall systems with an exterior air barrier only is currently not recommended for these climate types.

The present paper performs numerical heat, air and moisture (HAM)-simulations on light weight walls with exterior air barrier systems to explore the risks involved. Yearly simulations under realistic climate conditions were conducted with an adjusted version of DELPHIN 5, capable to model forced and natural convection in interaction with detailed heat and moisture transport (Nicolai, 2007 and Langmans et al. 2012). The model applies a two-domain approach; (1) porous building materials with (2) adjacent air channels assuming fully-developed laminar flow. The applied model is extensively documented and evaluated with experimental results in previous work (Langmans, 2013).

The current article performs numerical simulations to investigate the hygric response of exterior air barrier systems in timber frame construction in a European climates. In a first step, interest lies in the impact of different insulation materials. Thereafter, simulation are conducted for various European climate conditions. Herein, focus is on the performance in Nordic countries. The transient simulations were conducted for yearly climate conditions and the mould index (M) (Hukka & Viitanen, 1999) and accumulated interstitial condensation (AC) were applied to assess the performance of these timber frame elements (M_{max} < 3 and AC_{max} < 0.1 kg/m²).
The following section will discuss the used wall configurations and climate conditions.

2. Wall configuration and climate conditions

2.1 Wall configuration

The simulations throughout this paper are restricted to wall elements only. Fig. 1 shows the general configuration which is in accordance with the current building practice of highly insulated timber frame construction in Belgium. Herein, the ventilated cavity of 25 mm contains top and bottom ventilation openings. The material properties of the cladding system are based on (Nore, 2009); the wooden cladding layer is modelled according to (Zillig, 2009) and its exterior paint layer has an sd-value of 0.1m. The wooden top and bottom plates have thickness of 40 mm and extend the full width of the insulation layer (30cm). A service cavity of 40 mm is applied at the inside of the wall element, which is covered with a gypsum board finishing layer. It is important to the note that both the interior vapour retarding layer (OSB) and the gypsum board layer are not continuously airtight, so, they will not act as an interior air barrier. Slots of 1cm are left at both 20 cm from the top and bottom of the wall. The air barrier, however, is positioned at the outer side of the insulation layer by sealing the joints in the exterior sheathing layer.

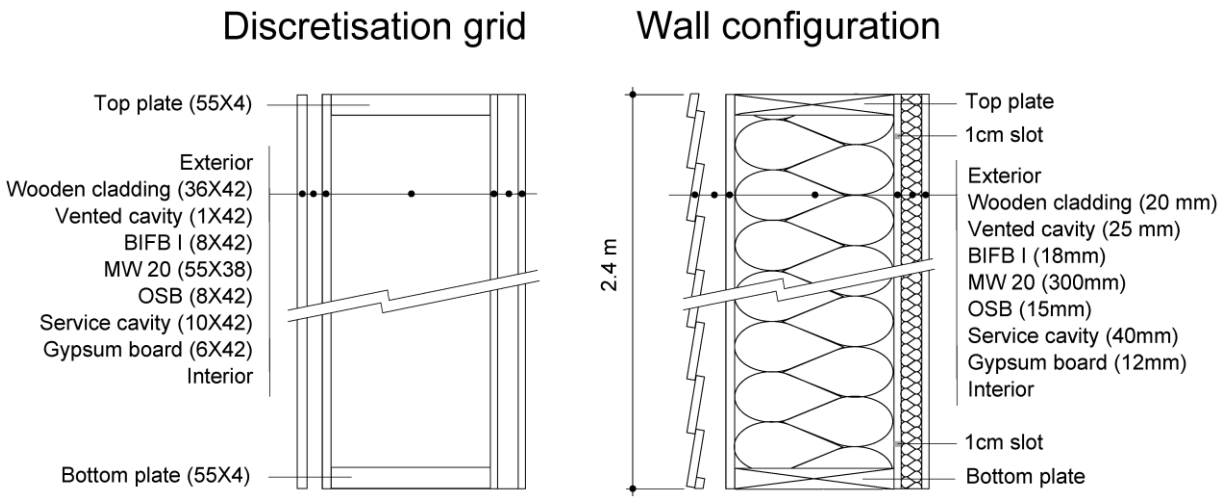

FIG 1.: Applied wall configuration and simulation grid.

The material properties of the applied materials are summarised in Table 1. Herein, a bituminous impregnated wood fibreboard (BIFB), a spunbonded foil (FOIL), oriented strand board (OSB), mineral wool of 20kg/m³ (MW20) and cellulose insulation of 60kg/m³ (CL60) are included. In addition, the simulations apply non-standard mineral wool with a density of 30 kg/m³ and cellulose insulation of 40 and 50 kg/m³. Yet these materials are excluded from Table 1 for brevity but can be found in (Langmans, 2013). Further, the properties of wood are adopted from (Zillig, 2009).

2.2 Climate conditions

The walls are oriented to the North and the applied climatic data is retrieved from the software package Meteonorm (TRY). The air pressure difference across the wall is a combination of (1) stack pressure, (2) wind pressure and (3) mechanical ventilation. For the simulations at hand, the stack pressure is calculated for a two-storey building, assuming that the main leakages are located near the foundation, wind pressures are calculated based on surface-averaged pressure in which the wind pressure coefficients are adopted from Swami & Chandra (1987) and a 5 Pa overpressure is assigned for mechanical ventilation. The inner temperature is assumed constant (20°C) throughout the year. Yet the inner humidity conditions are determined by a single zone model:

$$\left(\frac{V}{T_i R_V} + \frac{100\,HIR^{*}.V}{p_{v,sat}(T_i)}\frac{\partial p_{vi}}{\partial t} = (p_{ve} - p_{vi})\frac{nV}{3600 R_v T_i} + G_{vp}\right) \quad (1)$$

TABLE 1: limited overview of applied material properties (d (thickness), ρ (density), c_p (heat capacity), λ (thermal conductivity), K (air permeability) and sd (equivalent vapour diffusion).

	BIFBI	FOIL	OSB	MW20	CL60
d (mm)	18	0.2	15	300	300
ρ (kg/m³)	285	-	630	21.3	60
c_p (J/(kgK)	2068	-	1880	840	2544
λ (W/m/K)	0.045	-	0.1	0.031	0.034
$K^{\perp}$ (m²)	4E-14	airtight	8E-15	1.30E-09	8.8E-10
$K^{\parallel}$ (m²)	-	-	-	3.80E-09	8.8E-10
sd_{90} (m)	0.1	0.05	0.3	0.3	0.6
sd_{50} (m)	0.23	0.1	4.2	0.3	0.6

in which V (m³) corresponds to the volume of the room and HIR* (kg/m3%RV) to its hygric inertia, n (1/h) is the ventilation rate and G_{vp}(kg/s) is the vapour production in the room. The used parameters for the single zone model are chosen rather conservative: a small volume of 50 m^3 with a high moisture load of two active persons (120 gram/h) between 8h-22h. The nominal ventilation rate in living spaces is 3.6m^3/m^2/h according to the Belgium standard, corresponding to a ventilation rate of 1.51/h for this room. Several studies, however, indicated that the actual ventilation rate is often much lower in reality. Yet to include the effect of a realistic ventilation system in operation, the nominal ventilation rate was reduced to 0.5 1/h. Finally, a value of 1.5gram/m^3%RV was chosen for the hygric inertia.

3. Simulation results

3.1 Insulation material

First, the impact of the insulation material is investigated. Herein, two commonly applied groups of insulation materials are selected for the numerical investigation: (1) mineral wool and (2) cellulose insulation. Most often mineral wool insulation with a density of 20 kg/m^3 (MW20) is used in Belgium. Densities of 30 kg/m^3 (MW30) have only a limited market as they are more expensive. Nevertheless, both densities (MW20 and MW30) are included in the investigation here. For inflated loose-fill cellulose insulation, however, densities of around 60 kg/m^3, commonly applied in practice, are adopted here. In addition, cellulose insulations with lower densities (40 kg/m^3 and 50 kg/m^3) are examined as well. Table 2 presents the maximum mould index and accumulated condensate on the exterior air barrier (BIFB) for the reference configuration (Fig.1) with the discussed insulation materials. The predicted maximum mould index never exceeds the proposed limit of 3 and no condensation occurred for this type of insulation for the wall elements insulated with cellulose. For the mineral wool insulation, however, mould growth problems are predicted for the standard density of 20 kg/m^3. A mould index of 4.3 was found for this density, corresponding to a visual mould covering percentage between 10-50%. Mineral wool with increased density (30 kg/m^3), in contrast, meets the proposed moisture limit state. Finally, this table shows that no condensation on the BIFB exterior air barrier occurred for both the mineral wool and cellulose.

TABLE 2: Maximum mould index (M_{max}(-)) and accumulated condensate (AC_{max} (kg/m²).

	Cellulose			Mineral wool	
ρ (kg/m³)	40	50	60	20	30
M_{max} (-)/ AC_{max} (kg/m²)	2.3/-	1.8/-	1.6/-	4.3/-	2.3/-

The results of Table 2 correspond to an 'ideal' installation of the insulation layer, in that, perfect contact between the insulation and the adjacent layers is assumed. On the contrary, several experimental studies proved the importance of small discontinuities along the interface of mineral wool insulation layers (Brown et al., 1993). Such small air cavities are responsible for increased levels of natural convection and consequently higher moisture loads. As a result the presence of small air cavities around mineral wool insulation should be considered. Therefore, the simulations with mineral wool insulated elements were repeated, introducing imperfections along the interface for the insulation and the adjacent layers. Herein, five configurations are considered, varying the position of these air cavities: an air channel along the (a) cold side of the insulation, (b) on top of the insulation layer (c) both cold and warm sides, (d) both the cold and warm side and at the top of the insulation, and (e) at all four sides of the insulation. For these configurations the impact of channels of 1 mm, 3 mm and 5 mm have been studied. All combinations are simulated for both mineral wool with a density of 20 kg/m^3 and 30 kg/m^3 for which the corresponding simulation results are summarised in Table 3. This table confirms that the risk for moisture problems is highly influenced by the presence of small air channels along the mineral wool layer. Even a small air channel of 1mm at both sides of the insulation increases the mould index from 2.3 to 3.7 for MW30. As a consequence, the above-mentioned conclusion that higher mineral wool densities decrease the risk for moisture problems only holds for perfect contact conditions. From the moment imperfections around the mineral wool insulation layer (which are unavoidable in practice) are considered, the density of the mineral wool becomes of minor importance. In addition, Table 3 shows that most critical moisture limit state again corresponds to mould growth.

TABLE 3:Iimpact of air cavities (1mm, 3mm and 5mm) around insulation layer on the maximum mould index M (-) and maximum accumulated condensation MC (kg/m²) for mineral wool.

MC (kg/m²) / M (-)										
Density (kg/m³)	20	30	20	30	20	30	20	30	20	30
1 mm	4.5/-	2.8/-	4.5/-	2.9/-	4.6/-	3.7/-	4.8/-	4.1/-	4.8/-	4.1/-
3 mm	5.5/-	4.6/-	4.7/-	3.6/-	5.8/-	5.1/-	6/1.1	6/0.6	5.9/1.4	6/1.2
5 mm	5.9/-	4.9/-	4.7/-	3.7/-	6/0.1	5.6/-	6/>5	6/4.5	6/>5	6/>5

Fig. 2 depicts the hourly condensation along the height of the exterior air barrier for MW20 with air channels of 5mm at both sides. This graph demonstrates that condensation clearly occurs during winter periods and is concentrated at the upper height of this layer, indicating the importance of natural convection within the component.

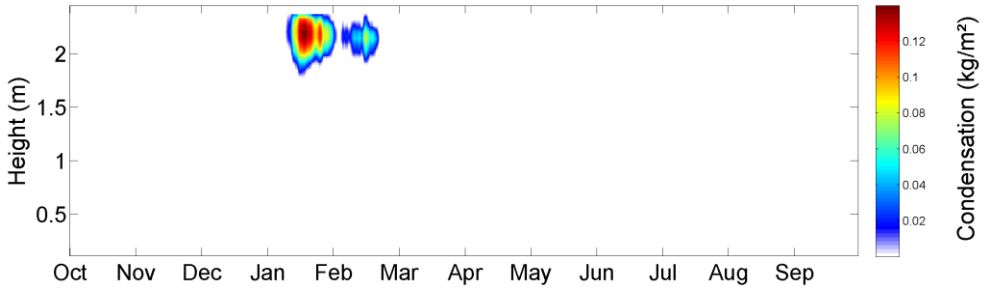

FIG. 2: Hourly condensation along the exterior air barrier for mineral wool of 20kg/m³ and air channels of 5mm on both vertical sides of the insulation layer.

3.2 Different climates

Finally, the hygrothermal response of wall elements with an exterior air barrier is studied for various European climate conditions. The selected locations cover a wide range of different climates from South to North Europe. Main focus is on the latter and particularly on Scandinavian regions. Recent building practice in Norway tends to focus on increasing the airtightness of the exterior layer, as stated by e.g. Myhre & Aurlien (2005), Holøs & Relander (2010). Therefore, special attention was given to this country by including Stavanger, Oslo, Bergen and Trondheim in the analysis. Figure 3 shows an overview of all locations studied. In addition, this figure compares the selected climates by means of averaged climate indicators.

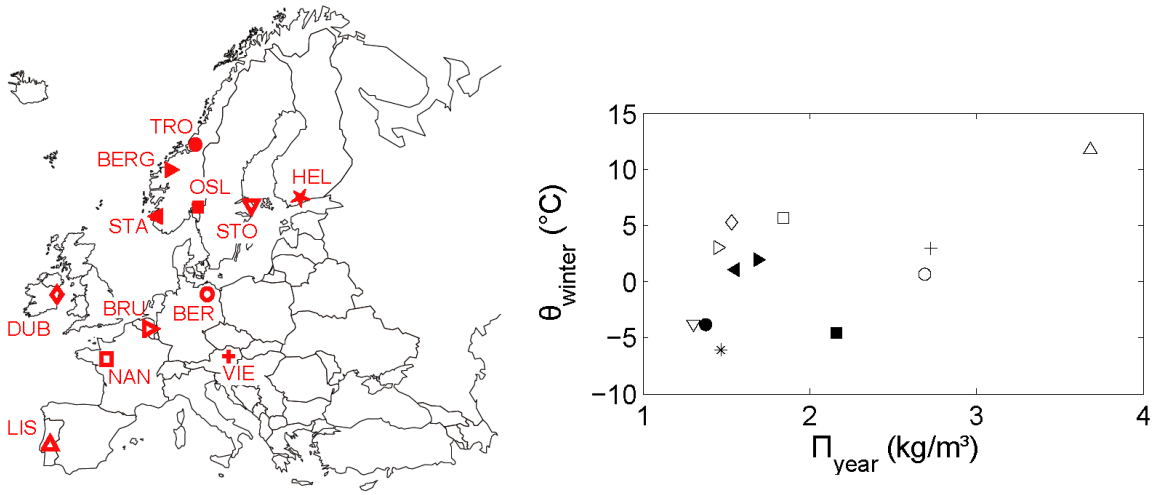

FIG. 3: Overview of the European locations for which simulations are performed.

First, the averaged outdoor winter temperatures (θ_{winter}), provides a direct indication of the potential for buoyancy driven air flow within the component, and thus, the increased moisture loads. Second, the Π_y -factor expresses the severity of the exterior climate. This factor (kg/m³), proposed by Hagentoft & Harderup (1993) for the selection of reference years, calculates the yearly averaged difference between the vapour concentration in the outdoor air and the maximum moisture concentration on the building envelope surface on hourly data:

$$\Pi_y = \overline{v_{out,sat}(\theta_s) - v_{out}}\,|_{\text{year}} \qquad (2)$$

in which $v_{out,sat}$ (θ_s) represents the saturation vapour concentration at the buildings surface for a North oriented wall and v_{out} corresponds to the moisture concentration of the outdoor air. As this value is calculated on a yearly basis, it represents the drying potential of the climate, and is thus, a relevant

indicator for the severity of the climate for the purpose of this study. Both the averaged outdoor winter temperatures (θ_{winter}) and the Π_y -factor of the climates investigated are depicted in Figure 3. This graph illustrates how the Southern European climate, Lisbon, combines a high averaged winter temperature with a high Π_y -factor. Furthermore, this figure clearly shows higher Π_y -factors for Eastern European climates (Berlin, Vienna) compared to the Western European locations (Brussels, Nantes, Dublin). In contrast the Western European climates tested correspond to milder winter temperatures. Most critical locations expected are Helsinki, Stockholm and Trondheim, in that they combine low winter temperatures with low Π_y -factors. Furthermore, this graph illustrates great differences between the four Norwegian climates included.

The simulations are performed for the wall configuration discussed in section 2.1 for which either MW30 with two vertical channels of 3mm on both sides or CL60 is applied. For the exterior air barrier material, on the other hand, two variants are included: (a) BIFB and (b) FOIL. Figure 4 depicts the simulation results for the wall elements insulated with mineral wool. Here, the maximum mould growth index on the walls using BIFB exterior air barriers is indicated in black and the maximum accumulated condensation amounts for the elements with a FOIL are given in red. These two graphs contain the same information, however, the left hand side is given as a function of θ_{winter} and the right hand side is presented as a function of Π_y . Out of the 12 climates tested only the Eastern European (Berlin, Vienna), the Southern European (Lisbon) and two of the Northern European locations (Oslo, Bergen) result in mould growth levels lower than 3. From this figure it follows that Π_y is the most dominating climate parameter in the prediction of mould growth. For these limited number of climates it appears that no problematic mould growth is observed for Π_y -factors higher than 2kg/m³. When it comes to condensation amounts on the non-hygroscopic foil, however, it appears that the temperature is the dominating climate parameter. Here only the coldest climates result in excessive condensation levels (Stockholm, Helsinki, Oslo and Trondheim).

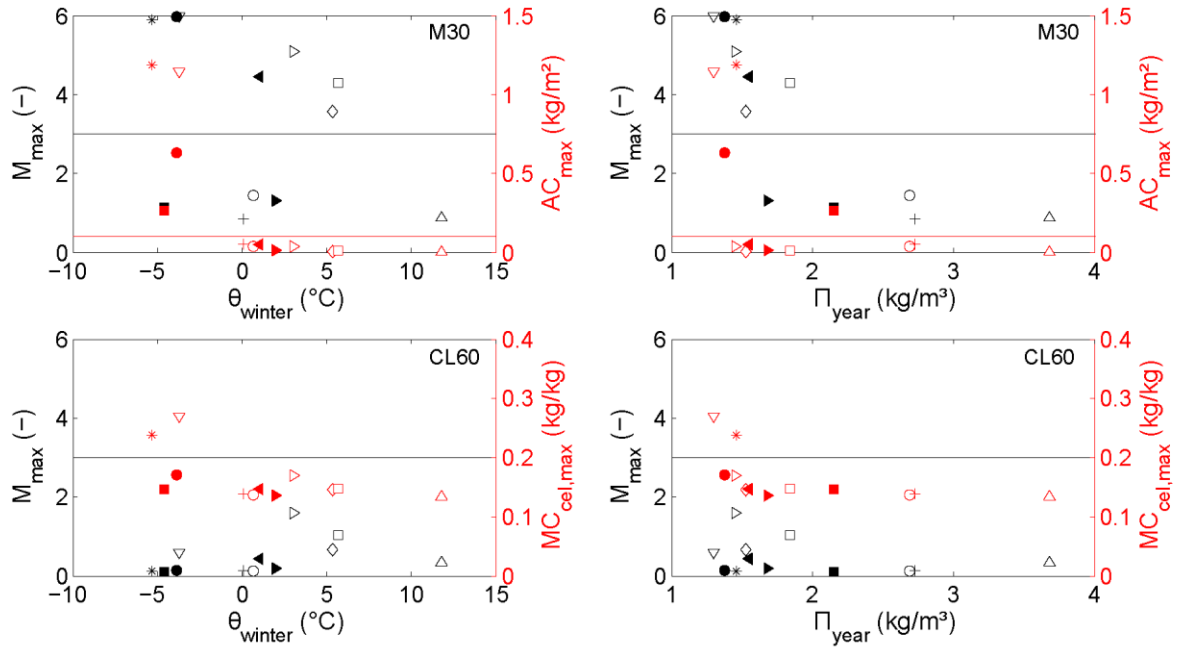

FIG. 4: Top: maximum mould index on BIFB and accumulated condensation on foil as a function of θ_{winter} (left) and Π_y (right) for MW30 insulated elements, bottom: maximum mould index on BIFB and maximum moisture content of cellulose insulation as a function of θ_{winter} (left) and Π_y (right) for CL60 insulated elements.

In contrast to the mineral wool insulated walls, no moisture problems were found for the wall elements simulated with loose-fill cellulose insulation. Because no condensation was found for these configurations, the highest moisture contents of the cellulose insulation are given here (in red). Highest moisture content of the cellulose insulation are found for Stockholm and Helsinki.

In summary, this section explored the hygrothermal response of highly insulated wall elements with an exterior air barrier in various European climates. In total 12 climates were verified, covering a range from North to South Europe. From this data it follows that Northern and Western Europe are most vulnerable to moisture problems when such wall systems are insulated with mineral wool. When these walls are insulated with loose-fill cellulose insulation, however, no moisture problems were obtained for the European climates tested.

4. Conclusions

This paper investigated the hygric response of a timber frame walls with an exterior air barrier in a Belgian climate. The simulation results identified a large impact of the applied insulation material on the hygrothermal performance of this component. No moisture problems were found for the walls insulated with loose-fill cellulose insulation. For mineral wool (glass wool) insulated walls, however, excessive mould growth levels were obtained on the upper parts of the exterior air barrier as a result of natural convection within the insulation layer. Furthermore, the simulations emphasised the importance of small air channels along the mineral wool and the adjacent layers. Such limited deficiencies increased the risk for mould growth and harmful condensation amounts against the exterior air barrier. The second part of the paper verified the performance of highly insulated walls with an exterior air barrier in 12 European climates. From the limited amount of locations tested, it followed that Northern and Western Europe regions were most vulnerable to mould problems. No mould problems were found for the (dryer) continental climates, such as Berlin and Vienna. For interstitial condensation on spunbonded foils, however, the decisive climate parameter appeared to be the winter temperatures. Excessive amounts of interstitial condensation were found for the coldest climates, such as Helsinki, Oslo, Trondheim and Stockholm.

5. Acknowledgements

Research funded by a Ph.D. grant (grant number 81153) of the Institute for the Promotion of Innovation through Science and Technology in Flanders (IWT-Vlaanderen).

References

Brown, W. C., Bomberg, M. T., Ullett, J. M., & Rasmussen, J. (1993). Measured thermal resistance of frame walls with defects in the installation of mineral fibre insulation. Journal of Building Physics, 16(4), 318–339.

Hukka, A & Viitanen, H (1999), ‘A mathematical model of mould growth on wooden material’, Wood Science and Technology 33(6),475–485.

Holøs, S. B., & Relander, T.-O. (2010). Airtightness Measurements of Wood Frame Low Energy Row Houses. In BEST conference (pp. 1–11). Portland.

Langmans, J., Klein, R., De Paepe, M. & Roels, S. (2010), ‘Potential of wind barriers to assure airtightness of wood-frame low energy constructions’, Energy and Buildings 42(12), 2376–2385.

Langmans, J., Andreas Nicolai, Ralf Klein, and Staf Roels. (2012). “A quasi-steady state implementation of air convection in a transient heat and moisture building component model.” Building and Environment 58 (12) 208-218.

Langmans, J. (2013), Feasibility of exterior air barriers in timber frame construction, PhD thesis, Department of Civil Engineering, Section Building Physics, KU Leuven. (http://bwk.kuleuven.be/bwf/PhDs/phdLangmans)

Myhre, L., & Aurlien, T. (2005). Measured airtightness in low-energy houses. In 7th Nordic Building Physics Symposium. Reykjavik, Iceland.

Nicolai, A., (2007). Modelling and numerical simulation of salt transport and phase transitions in unsaturated porous building materials, PhD thesis, Syracuse University, USA.

Nore, K. (2009), Hygrothermal performance of ventilated wooden cladding, PhD thesis, Norwegian University of science and technology, Norway.

Zillig, W. (2009), Moisture transport in wood using a multiscale approach, PhD thesis, Catholic Universtity of Leuven, Belgium.

Swami, M. & Chandra, S. (1987), Procedures for calculating natural ventilation airflowbrates in buildings, Technical report, FSEC-CR-163-86, Florida Solar Energy Center, Cape Canaveral, Florida, USA.

Computational simulation of hygrothermal performance of hollow brick-based building envelopes

Václav Kočí, Ph.D. [1]
Jiří Maděra, Ph.D. [1]
Miloš Jerman, Ph.D. [1]
Robert Černý, Professor [1]

[1] Department of Materials Engineering and Chemistry, Faculty of Civil Engineering, Czech Technical University in Prague, Czech Republic

KEYWORDS: *building envelope, hollow brick, computational simulation, heat and moisture transport, hygrothermal performance*

SUMMARY:
Computational analysis of hygrothermal performance of several types of hollow-brick based building envelopes is presented, aimed at the optimal hygric properties of hollow brick and exterior plaster. In the simulations, Künzel's mathematical model of coupled heat and moisture transport is used. Dynamic climatic data in a form of Test Reference Year for Prague are utilized as boundary conditions. The computational results show that for a suitable hygrothermal performance of the analyzed envelopes the key factor is the hygric properties of the exterior plaster, whose value of moisture diffusivity has to be reduced to at least $1 \cdot 10^{-10}$ m^2/s*, e.g. using hydrophobic agents. In that case, moisture content can be held under the hygroscopic threshold for almost the whole reference year, which ensures the elimination of the presence of liquid moisture inside the envelope.*

1. Introduction

Hollow brick blocks have found a widespread use in building industry during the last decades. The increasing requirements to the thermal insulation properties of building envelopes (Uygunoglu and Kecebas 2011) given by national standards in Europe led the brick producers to reduce drastically the production of common solid bricks. The brick blocks with complex systems of internal cavities (da Silva Almeida et al. 2013, Alhazmy 2010, Arendt et al. 2011) replaced the traditional bricks and became dominant on the building ceramics market. However, the development of the new types of bricks was very fast and their properties are often not known with a sufficient accuracy. Consequently, in the current durability assessment of hollow brick-based building envelope systems a complex view is often missing. Precise and serious analyses of hygrothermal performance based on sound scientific knowledge are not performed very frequently. However, hollow brick-based building envelopes should be designed as a system consisting of hollow bricks, internal and external finishes and possibly also thermal insulation layer, and in this design process, the details have to be solved using suitable methods. In this paper, influence of the effective hygric parameters of hollow brick and exterior plaster on the hygrothermal performance of building envelope is analyzed, in order to identify possible problems related to the coupled heat and moisture transport. Main objective of this paper is to find such combination of hygric parameters of exterior plaster and hollow brick, which will reduce the moisture content in the envelope as much as possible.

2. Computational simulation

2.1 Description of building envelope

As the load bearing material, hollow brick in a thickness of 500 mm, with the cavities filled by expanded polystyrene, was assumed. This brick was provided with 10 mm thick lime-metakaolin plaster in the interior and 30 mm thick thermal insulating plaster in the exterior. Scheme of analyzed building envelope is shown in Figure 1.

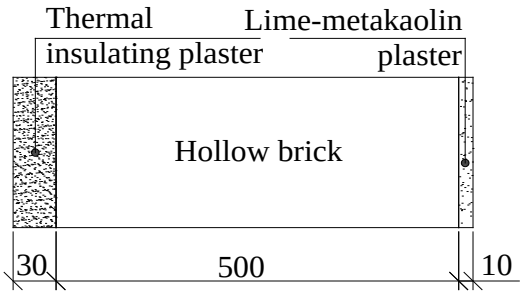

FIG 1. Description of analyzed building envelope

2.2 Material parameters

All material parameters were measured in the laboratories of transport processes of the Department of Materials Engineering and Chemistry, Faculty of Civil Engineering, Czech Technical University in Prague using the methods common in building physics (Černý, 2010). The properties of lime-metakaolin plaster were taken from Vejmelková et al. (2012). The properties of the thermal insulating plaster have not been published so far. The hollow brick was assumed in the form of a continuum comprising brick body and expanded polystyrene in the cavities and its properties were obtained using homogenization principles according to the procedure described in Pavlík et al. (2013), Korecký et al. (2013). The data are summarized in Table 1. The particular symbols denote: ρ – bulk density (kg/m^3), ψ – porosity (%), c – specific heat capacity (J/kg K), μ – water vapor diffusion resistance factor (-), λ_{dry} – thermal conductivity in dry state (W/mK), λ_{sat} – thermal conductivity in water saturated state (W/mK), κ_{app} – apparent value of moisture diffusivity (m^2/s), w_{hyg} - maximum hygroscopic moisture content by volume (m^3/m^3). Determination of optimal moisture diffusivity of both hollow brick and thermal insulating plaster was an objective of the computational analysis.

TAB 1. Material parameters

	Lime-metakaolin plaster	Hollow brick filled with expanded polystyrene	Thermal insulating plaster
ρ (kg/m^3)	1637	793	434
ψ (%)	33.9	w_{sat} = 27 %	40.7
c (J/kgK)	922-1404	1052 - 1995	646-1703
μ (-)	8.5-23.6	10.6-12.8	3.1-13.9
λ_{dry} (W/mK)	0.664	0.084	0.097
λ_{sat} (W/mK)	1.847	0.187	0.198
κ_{app} (m^2/s)	1.85e-7	*objective of analysis*	*objective of analysis ($1\cdot10^{-8}$; $1\cdot10^{-9}$; $1\cdot10^{-10}$)*
w_{hyg} (m^3/m^3)	0.0299	0.005	0.02

Moisture diffusivity of porous building materials is highly dependent on moisture content and the shape of the moisture diffusivity curve is often exponential (Carmeliet et al. 2004). It can be written that

$$\kappa(w) = a \cdot e^{bw}, \tag{1}$$

where $\kappa(w)$ moisture diffusivity as a function of moisture content (m^2/s)
a, b constants determining the shape of exponential curve
w moisture content by volume (m^3/m^3)

The constant b determines the range of functional values of $\kappa(w)$ function and was set to 2, 10 and 20 according to the characteristic shapes of $\kappa(w)$ function (Carmeliet et al. 2004). The apparent values of moisture diffusivity usually correspond to its values at about 2/3 of water saturation (Drchalová and Černý, 2003), therefore the constant a can be estimated using the equation

$$\kappa_{app} = a \cdot e^{b \cdot \frac{2}{3} w_{sat}}, \tag{2}$$

where κ_{app} apparent moisture diffusivity (m^2/s) (see Table 1)
w_{sat} saturated moisture content (m^3/m^3)

The apparent moisture diffusivity of hollow brick was estimated using homogenization principles in a similar way as in Pavlík et al. (2013), with the result $1 \cdot 10^{-10}$ m^2/s. The corresponding $\kappa(w)$ functions are summarized in Fig. 2.

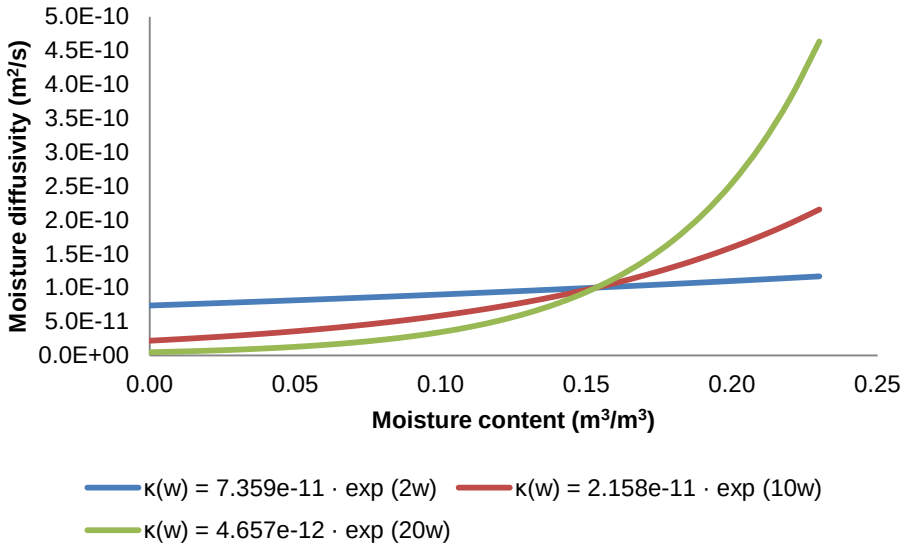

FIG 2. Moisture diffusivity vs. moisture content functions

2.3 Boundary condition

On the exterior side, dynamic climatic data in the form of Test Reference Year for Prague were applied, in order to describe the conditions as realistic as possible. Test Reference Year contains average hourly values of long-term climatic data, such as temperature, relative humidity, wind velocity, wind direction, different types of sun radiation, or rainfalls. On the interior side, constant values of temperature (21 °C) and relative humidity (55 %) according to the CSN 73 0540-2 (2011) were used.

2.4 Mathematical model and computer code

The computer simulation tool HEMOT (HEat and MOisture Transport) (Černý et al. 2010), which is based on the general finite element package SIFEL (SImple FInite Elements) (Kruis et al. 2010), was used for the assessment of hygrothermal performance of the analyzed building envelope. Mathematical model of coupled heat and moisture transport formulated by Künzel (1995) was implemented in HEMOT for the calculations throughout this paper. The balance equations of moisture (3) and heat (4) were formulated as follows:

$$\frac{d\rho_v}{d\varphi}\frac{\partial\varphi}{\partial t} = div\left[D_\varphi grad\varphi + \delta_p grad(\varphi p_s)\right] \tag{3}$$

$$\frac{dH}{dT}\frac{\partial T}{\partial t} = div(\lambda grad T) + L_v div\left[\delta_p grad(\varphi p_s)\right], \tag{4}$$

where
ρ_v partial density of moisture (kg/m^3)
φ relative humidity (-)
δ_p water vapor permeability (s)
p_s partial pressure of saturated water vapor (Pa)
H enthalpy per unit volume (J)
L_v heat of evaporation (J/kg)
λ thermal conductivity (W/(m K))
T temperature (K)

This model has been verified (Künzel and Kiessel 1996) and successfully applied in many hygrothermal simulations before, dealing with hygrothermal performance of building envelopes (Maděra et al. 2010), optimization of building envelope composition (Kočí et al. 2012), or service life estimates (Kočí et al. 2009). The simulations were performed as one dimensional. All the material parameters were determined using one dimensional experimental setup.

3. Results and discussion

The investigated variations of building envelopes were marked according to Table 2.

TAB 2. Investigated variations of building envelopes

		Moisture diffusivity of hollow brick (m^2/s)		
		7.359e-11 · e^{2w}	2.158e-11 · e^{10w}	4.657e-12 · e^{20w}
Moisture diffusivity of thermal insulating plaster (m^2/s)	$1 \cdot 10^{-8}$	A1	A2	A3
	$1 \cdot 10^{-9}$	B1	B2	B3
	$1 \cdot 10^{-10}$	C1	C2	C3

The results of hygric and thermal behaviour of studied building envelopes are presented in the form of temperature and relative humidity profiles for November 22 of the reference year. This day appeared statistically as one of the most critical from the point of view of hygric performance. According to the reference climatic data for Prague, a 3-day period with highly increased relative humidity of the air (> 97 %) due to the effect of rainfalls ends in this day. Such high value of the relative humidity corresponds to the overhygroscopic (liquid) moisture content, thus the presence of liquid moisture in the pore space of exposed building materials is to be expected. Although in the subsequent days the relative humidity of the air is still very high, it remains in the hygroscopic range and the liquid

moisture in the materials of surface layers can already begin to evaporate. Therefore, the moisture content in the external layer of the studied envelope at the end of the mentioned 3-day period can be considered to belong to the highest; this was confirmed in the test calculations. Taking into account the subsequent weather development, this moisture could get frozen within the next weeks.

According to the results, hygric parameters of hollow brick did not significantly affect hygric behaviour of the building envelope. Because of the presence of exterior plaster, moisture content of hollow brick remained very low and almost invariable, therefore it hardly reached high values, when the differences between moisture diffusivities of particular variations were considerable. Small differences are visible in the part of hollow brick which is closer to the exterior. Comparison of relative humidity profiles of variations A1 and A3 are captured in Figure 3.

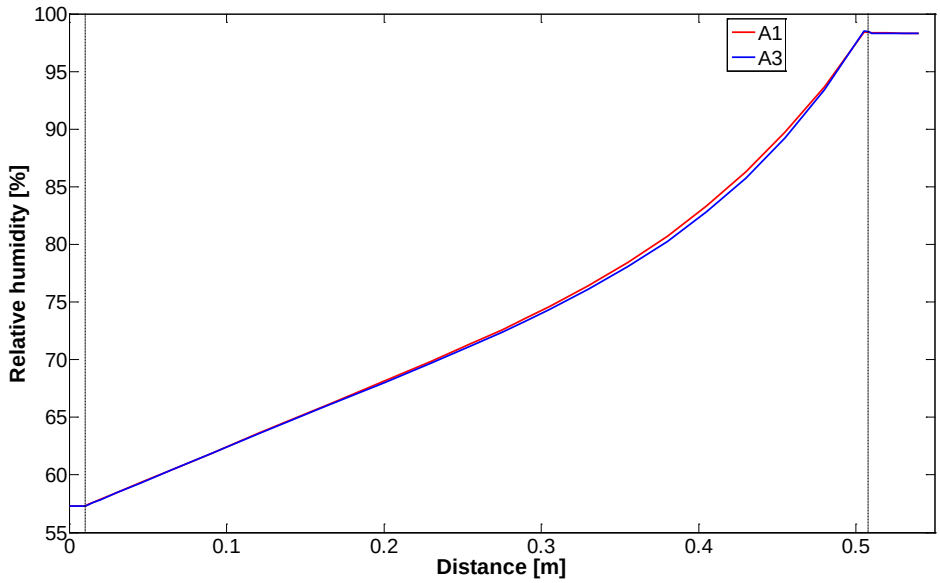

FIG. 3 Relative humidity profiles, A1 vs. A3

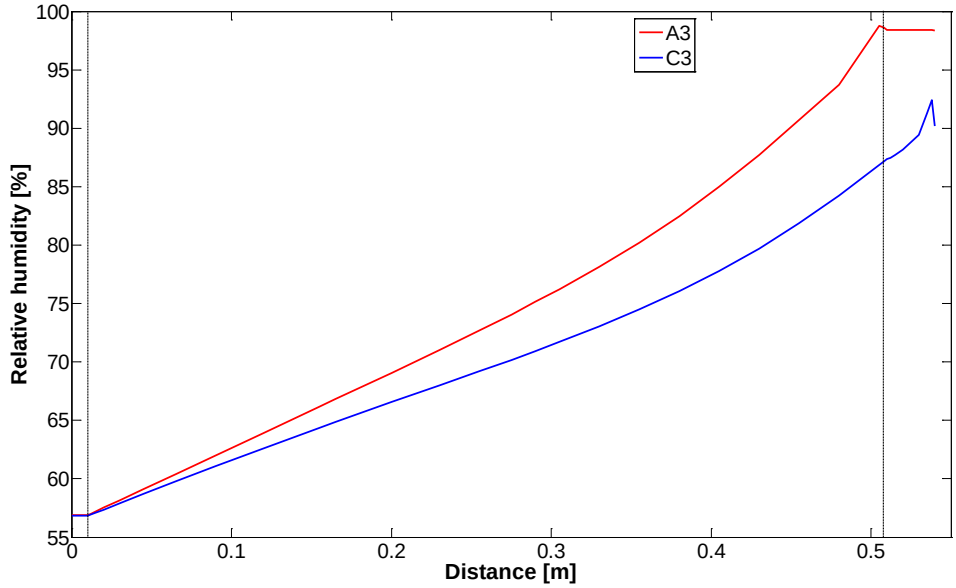

FIG. 4 Relative humidity profiles, A3 vs. C3

While the hygric properties of hollow brick had only small effect on the hygrothermal behaviour of the whole building envelope, the same could not be stated about the hygric properties of the exterior plaster. Because it is exposed directly to the effects of weather conditions its hygric properties are decisive, as for the amount of moisture transported inside the envelope. For this reason it is suitable to apply external plaster with low value of moisture diffusivity; otherwise the moisture content can reach very high values, as it is shown in Figure 4, where building envelope marked as A3 easily approaches overhygroscopic values of moisture content.

Comparing Figs. 5 and 6 which show long-term relative humidity distribution of variations A1 and C3 during three reference years, the differences are apparent.

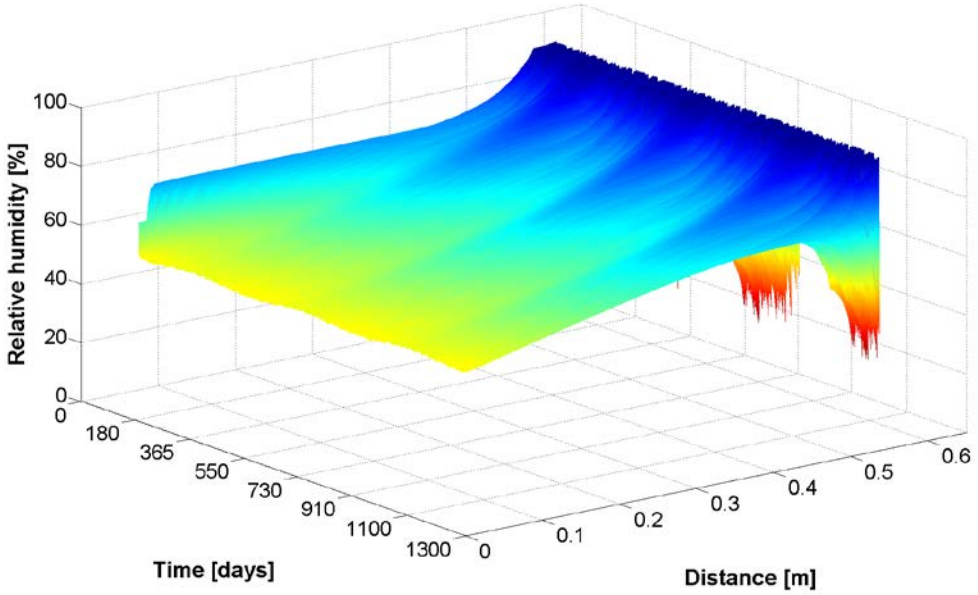

FIG 5. Long-term relative humidity distribution, variation A3

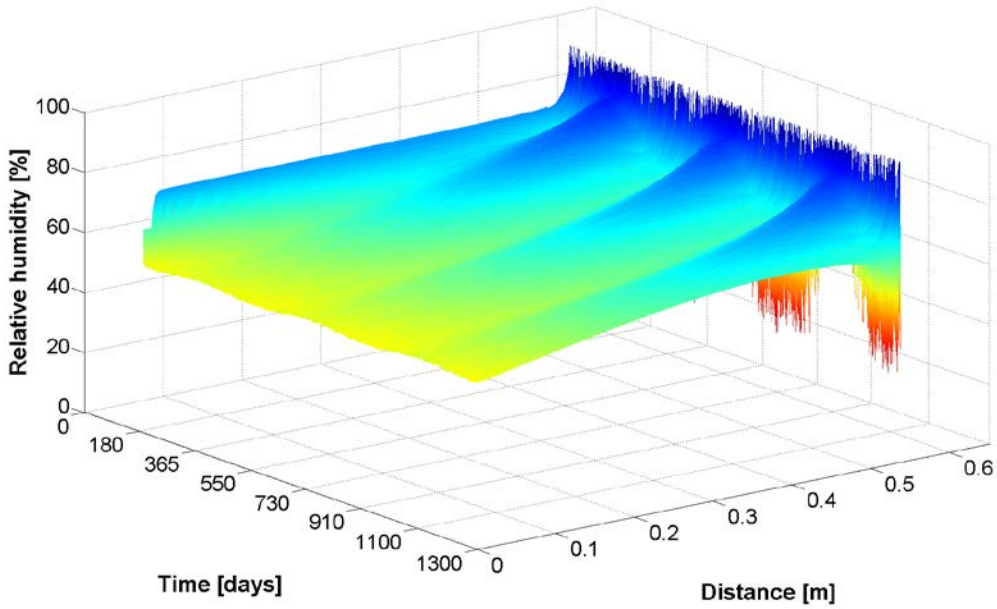

FIG 6. Long-term relative humidity distribution, variation C3

Unlike hygric conditions, temperature profiles of all the investigated variations were very similar. Therefore, only one example (variation C3) is presented (Fig. 7). Because of the exterior surface layer, the presence of liquid moisture was limited only to the external plasters and its subsequent worsening of thermal properties did not significantly influence the thermal behaviour of the building envelope.

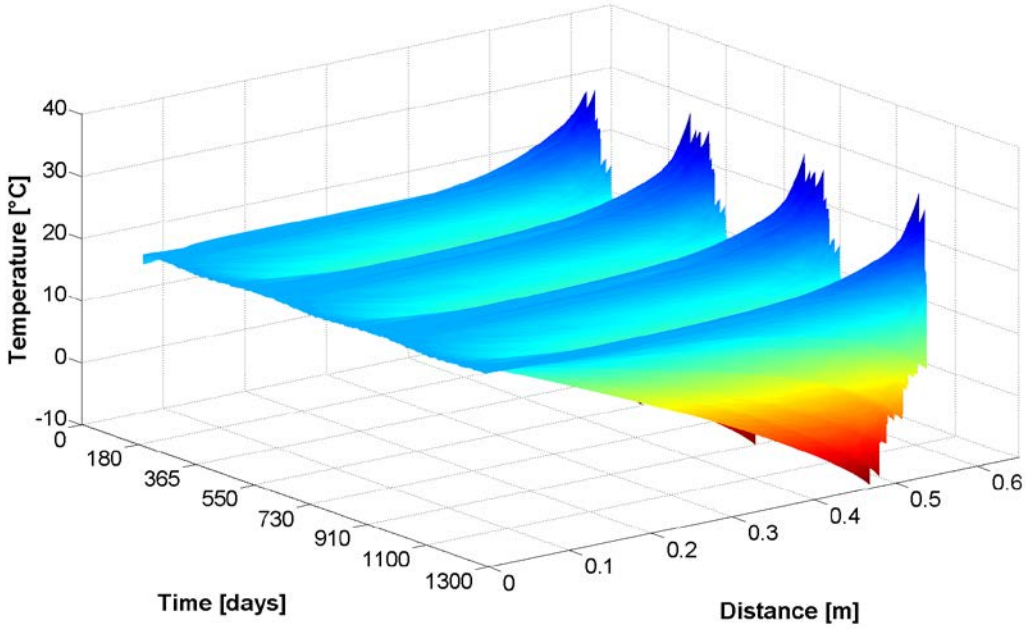

FIG 7. Long-term temperature distribution, variation C3

4. Conclusions

The effect of hygric properties of hollow brick and external plaster on the hygrothermal performance of hollow-brick based envelopes was analyzed in the paper. According to the results, hygric parameters of hollow brick did not play as significant role as the hygric parameters of the external plaster. This confirmed that the properties of surface layers of building envelopes are very important from the point of view of hygrothermal performance of whole building envelopes. In order to reduce moisture intake, it is necessary to decrease the value of moisture diffusivity of external plaster. Among all investigated variations, the apparent moisture diffusivity of external plaster equal to $1 \cdot 10^{-10}$ m^2/s provided the best results. This value can be easily reached using external plasters with hydrophobic admixtures.

5. Acknowledgements

This research has been supported by the Ministry of Industry and Trade of the Czech Republic, under project No FR-TI3/085.

References

Alhazmy M.M. 2010. Numerical investigation on using inclined partitions to reduce natural convection inside the cavities of hollow bricks, International Journal of Thermal Sciences 49 2201-2210.

Arendt K., Kraczek M. & Florczuk J. 2011. Numerical analysis by FEM and analytical study of the dynamic thermal behavior of hollow bricks with different cavity concentration, International Journal of Thermal Sciences 50 1543-1553.

Carmeliet J., Hens H., Roels S., Adan O., Brocken H., Černý R., Pavlík Z., Hall C., Kumaran K. & Pel L. 2004. Determination of the Liquid Water Diffusivity from Transient Moisture Transfer Experiments. Journal of Thermal Envelope and Building Science 27 277- 305.

Černý R. (ed.). 2010. Complex System of Methods for Directed Design and Assessment of Functional Properties of Building Materials: Assessment and Synthesis of Analytical Data and Construction of the System, CTU, Prague, Czech Republic.

ČSN 73 0540-2. 2011. Thermal protection of buildings – Part 2: Requirements. Prague: Czech Office for Standards, Metrology and Testing.

da Silva Almeida G., da Silva J.B., e Silva C.J., Swarnakar R., de Arújo Neves G. & de Lima A. G. B. 2013. Heat and mass transport in an industrial tunnel dryer: Modeling and simulation applied to hollow bricks, Applied Thermal Engineering 55 78-86.

Drchalová J. & Černý R. 2003. A Simple Gravimetric Method for Determining the Moisture Diffusivity of Building Materials, Construction and Building Materials 17 223-228.

Kočí V., Maděra J., Černý R. & Rovnaníková P. 2009. Application of a combined computational-experimental approach for service life estimate of exterior plasters of historical buildings, In: Structural Studies, Repairs and Maintenance of Heritage Architecture XI. WIT Press, Southampton, UK, 303-314.

Kočí V., Maděra J. & Černý R. 2012. Exterior thermal insulation systems for AAC building envelopes: Computational analysis aimed at increasing service life, Energy and Buildings 47 84-90.

Korecký T., Jerman M., Vejmelková E. & Černý R. 2013. Homogenization of physical parameters of filled hollow bricks, Stavební obzor 22 44-47 (in Czech).

Kruis J., Koudelka T. & Krejčí T. 2010. Efficient computer implementation of coupled hydro-thermo-mechanical analysis, Mathematics and Computers in Simulation 80 1578-1588.

Künzel H. M. 1995. Simultaneous Heat and Moisture Transport in Building Components, Ph. D. Thesis. IRB Verlag, Stuttgart, Germany.

Künzel H.M. &, Kiessl K. 1996. Calculation of heat and moisture transfer in exposed building components. International Journal of Heat and Mass Transfer 40 159-167.

Maděra J., Kočí J., Kočí V., Výborný J. & Černý R. 2010. Computational prediction of hygrothermal conditions in innovated AAC-based building envelopes. In: Advanced Computational Methods and Experiments in Heat Transfer XI. WIT Press, Southampton, UK, 291-301.

Pavlík Z., Fiala L., Vejmelková E., Černý R. 2013. Application of Effective Media Theory for Determination of Thermal Properties of Hollow Bricks as a Function of Moisture Content, International Journal of Thermophysics 34 894-908.

Uygunoglu T. & Kecebas A. 2011. LCC analysis for energy-saving in residential buildings with different types of construction masonry blocks, Energy and Buildings 43 2077-2085.

Vejmelková E., Keppert M., Keršner Z., Rovnaníková P., Černý R. 2012. Mechanical, fracture-mechanical, hydric, thermal, and durability properties of lime–metakaolin plasters for renovation of historical buildings, Constructions and Building Materials 31 22-28.

Comparison of Direct and Iterative Linear Equation System Solvers for Building Component Simulation

Anne Paepcke [1]
Andreas Nicolai [1]

[1] Institute for Building Climatology, Faculty of Architecture, Dresden University of Technology, Germany

KEYWORDS: *building envelope, numerical methods, modelling, 2D, hygrothermal transport, building simulation, linear equation solvers*

SUMMARY:
Transient hygrothermal simulations of two-dimensional detailed wall constructions set high demand on computational capacity. When using implicit time integration combined with spatial Finite-Volume discretization the resulting system of equations contains a large number of unknowns and the Jacobian matrices are sparse. This motivates the application of iterative solvers, particularly Krylov Subspace methods, to the resulting linear equation system. We compare two representative algorithms for direct and iterative linear equation system solvers: the Gaussian elimination with LU-decomposition versus the ILU-preconditioned GMRES. The numerical study covers three classes of problem types that may occur in the hygrothermal simulation: diffusion-dominated transport problems with highly nonlinear coupling of heat and moisture, diffusion-dominated transport inside constructions with extremely varying material properties, mixed convection-diffusion hygrothermal transport problems. The aim of the study is to evaluate the applicability of Krylov Subspace methods to different problem types and to provide advice for the choice of the linear equation system solver.

1. Introduction

Building component simulation considers the dynamic thermal and hygric transport inside wall constructions. We use the transport equations based on porous media theory by (Grunewald 1997) that include both liquid water convection and vapor diffusion. The transport equations are highly nonlinear and stiff. Therefore, only implicit time integration methods combined with established nonlinear solution methods may solve these equations sufficiently stable and efficient.

The numerical solution requires a time and spatial discretization. When using implicit time integration methods, many linear equation systems have to be solved. With increasing complexity of the construction the solution of the linear equation system dominates the simulation performance (Vogelsang 2013, Nicolai 2014). Therefore, the demand for an acceptable simulation time limits the problem dimension. Consequently, efficient numerical solution methods are of high interest.

The discretization of partial differential equations (PDE) results in matrices with characteristic pattern. This fact offers a high potential for optimizing the linear equation solver. The classical approach focuses on banded matrices. Alternatively the matrix can be considered as sparse with most elements of the matrix equal to zero. These matrix properties motivate the application of sparse matrix linear solvers.

2. Implementation of the Numerical Solution Method

In order to guarantee unconditional stability we apply an Implicit Euler method as time integration method to the dynamic equations. Additionally, we ensure accuracy of the numerical integration by an automatic time step adjustment scheme based on local truncation error control (Hindmarsh 2005), (Nicolai 2008, ch. 4.3).

For each of these integration steps a nonlinear problem is solved using a Newton-Raphson method. The method requires solving a sequence of linear equation systems consisting of Jacobian matrix and right hand side vector.

2.1 Direct linear equation solver

We use the Gaussian elimination which is a well-known representative of direct linear equation system solvers. The method is implemented via decomposition of the discretization matrix into the product of a lower triangular and an upper triangular matrix, the LU-decomposition (Meister 2008, ch. 3.1). To reduce the computational effort a special variant is used, taking into account the banded structure of the Jacobian matrix. The decomposition algorithm is the computational expensive part of the equation system solver.

Further, the LU-factorization strategy allows the re-use of already calculated decomposition matrices for the solution of several equation systems, i.e. several Newton iterations, a procedure described as modified Newton-Raphson method (Hindmarsh 2005). If the Jacobian matrices do not change significantly this may reduce simulation time substantially. In our implementation the Jacobian is generally only updated once at the beginning of a Newton iteration. It is then kept in factorized form until either a convergence failure occurs, or the time step size changes significantly.

2.2 Iterative linear equation solver

Iterative methods only approximately solve the linear equation system. Krylov Subspace methods are established algorithms for the solution of sparse linear equation systems (Saad 2003, ch. 6). As the discretized transport equations result in nonsymmetric matrices we choose the Generalized Minimal Residual (GMRES) method as a suitable candidate.

The GMRES solver is particularly efficient if it converges within a few iterations. For larger number of iterations error propagation from rounding errors and memory requirements may be problematic.

Fast convergence of the GMRES solver may only be reached by using preconditioning techniques. Preconditioners usually approximate the inverse of the original matrix. They modify the linear equation system with the aim to achieve better convergence of Krylov subspace methods. For the current study we choose a standard Incomplete LU (ILU) – preconditioner (Saad 2003, ch. 10.3) and an error bound from CVODE (Hindmarsh 2005) to check for convergence of the GMRES method.

3. Simulation examples

Typical for practical applications are two-dimensional simulation problems with a high geometrical complexity. Sufficiently refined spatial discretization is necessary and leads to critical demand on computational capacity. Further, for hygrothermal transport problems the intensity of nonlinear interactions varies highly for each simulation case. Consequently, we take into consideration different levels of physical model complexity for the current study.

We start with a thermal simulation, continue with a moderately nonlinear hygrothermal simulation, and finish with a discussion of a highly nonlinear hygrothermal simulation of a steel detail in the presence of real climate conditions.

3.1 Simulation of a thermal bridge

We choose a thermal bridge example with constant boundary conditions defined in the norm (EN ISO 10211:2007 2007) for the linear problem case. A cross section of a concrete wall with insulation and integrated aluminium/wood detail (see FIG. 1) is simulated. On the upper side of the geometry a constant outside temperature of 0°C is assumed, at the lower side a constant inside temperature of 20°C.

The norm provides reference results with a tolerance band. In order to achieve this requested accuracy we apply a non-equidistant discretization clustered near boundaries and material interfaces, resulting in 13674 elements and a Jacobian matrix dimension of 13674x13674. The requested steady-state temperature distribution is shown in FIG. 2.

Contrarily to the norm we are interested in the dynamic development of the temperature profile during the first 5 days, when starting with a constant initial temperature of 10°C.

TABLE 1. Thermal bridge: simulation performance

Numerical method	Number of integrator steps	Average time/ integrator step [s]	Overall simulation time
Modified Newton, Band Solver	746	0.08	59 s
Modified Newton, GMRES + ILU	748	0.5	6.168 min

This simulation case is a good candidate for the Modified Newton method. Because the problem is linear only a few matrix assemblies and few expensive LU-decompositions for the Band Solver are required. The actual time needed for the solution (backsolving-step) after the decomposition of the matrix is small, explaining the short overall simulation time (see TABLE 1).

The choice of the linear equation system solver should not affect the convergence of Newton-Raphson method and consequently lead to the same time step regime and the same number of integrator steps. Despite this fact, the GMRES variant takes a significantly longer overall simulation time.

Generally, Krylov Subspace methods demand higher computational effort for solving the linear equation system than needed for a backsolving-step of a Band-Solver with already decomposed matrix. Contrarily, the effort for the preparation of the equation solving is small compared to the Band-Solver that performs an LU-decomposition. Effectively, using GMRES shifts computational time from setup of the equation system to solving.

Note, for a few Newton iterations the embedded GMRES solver did not converge, resulting in additional Newton iterations. In two cases convergence failures occurred explaining the larger number of integration steps.

3.2 Hygrothermal simulation of a floor construction

The hygrothermal study of a floor construction in contact with ground is a typical application case. We choose real climate data of Potsdam (Germany) including rain and perform an annual simulation, see (Paepcke 2014).

The construction is shown in FIG. 3. It consists of a brick wall that is protected by a bitumen layer which is considered as watertight. Thus, the rain only infiltrates into the ground on the left side of the geometry. Rising damp, water vapour diffusion and capillary condensation cause moisture accumulation in the brick wall, see FIG. 4. The XPS layer inside the floor construction also is enclosed by a bitumen layer and therefore it is protected from water transport.

We rate this simulation case as a moderate nonlinear hygrothermal problem. The Finite Volume method discretizes the simulation domain into 7395 elements, a moderate problem size, with a total of 14790 unknowns.

Simulation runs for Band Solver and GMRES variants with modified Newton showed, that simulation times for GMRES are now lower (see first two lines in TABLE 2). In contrast to the first test case, the nonlinearity of the problem requires many more expensive LU factorizations for the Band Solver, which dominates the overall simulation time.

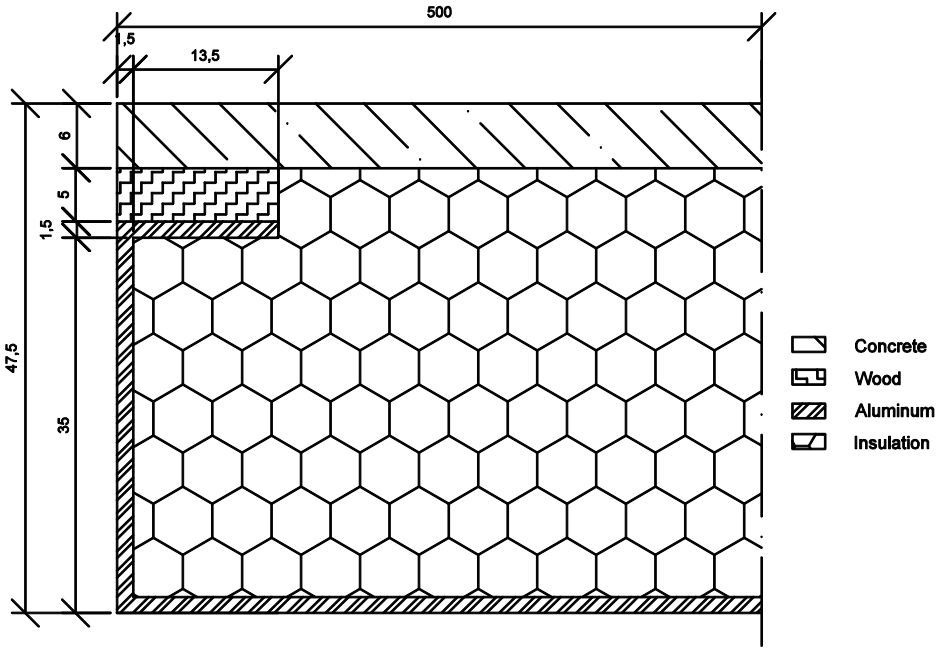

FIG 1. Thermal bridge: geometry.

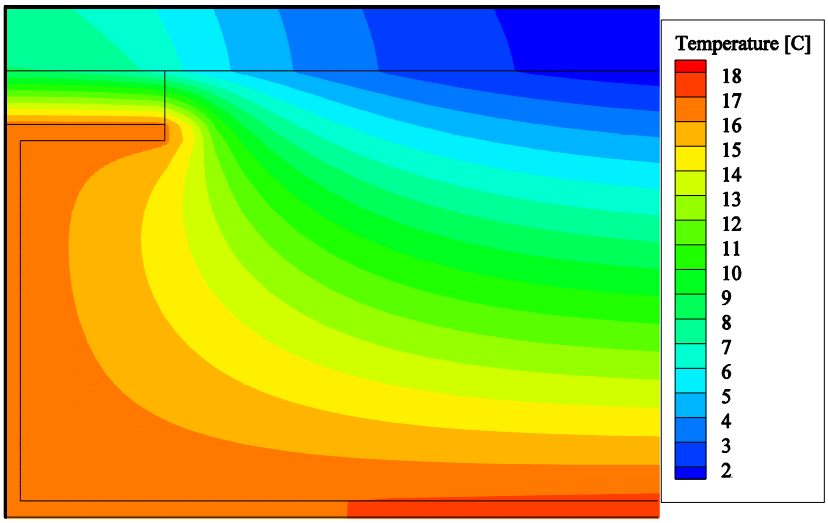

FIG 2. Thermal bridge: temperature distribution at steady-state.

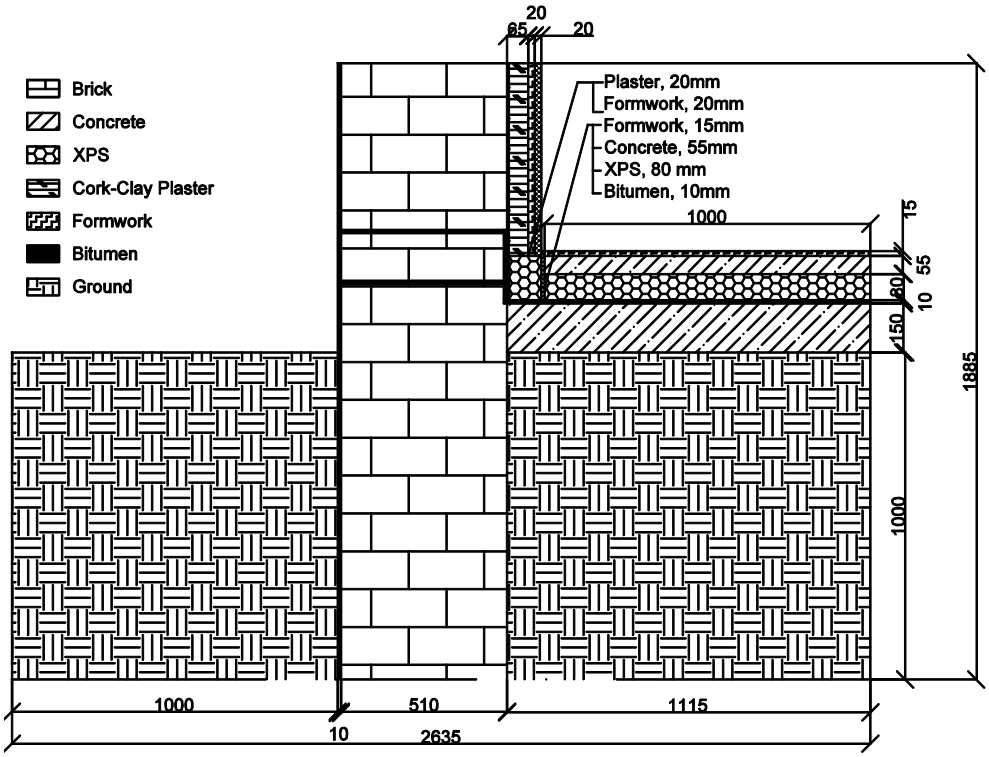

FIG 3. Floor construction: geometry.

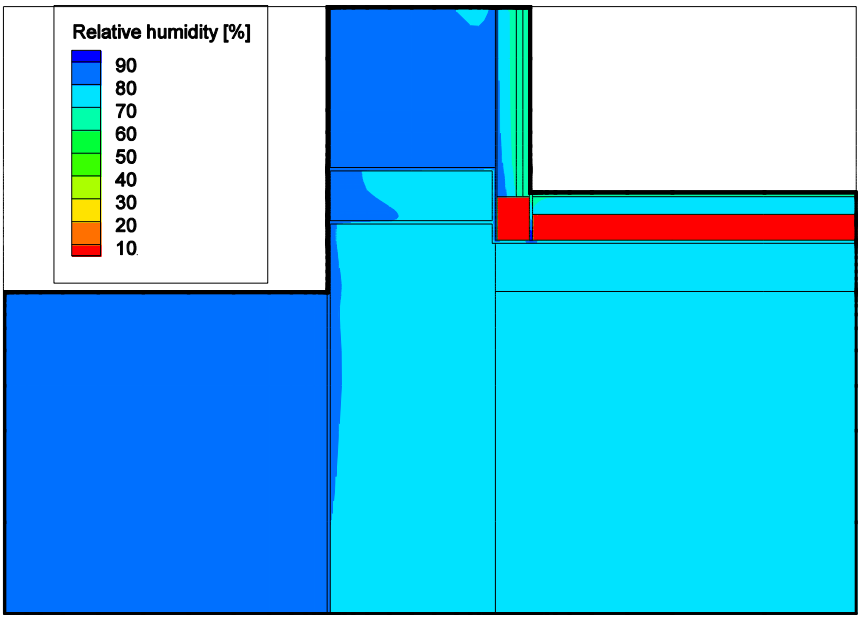

FIG 4. Floor construction: relative humidity at November 28 th.

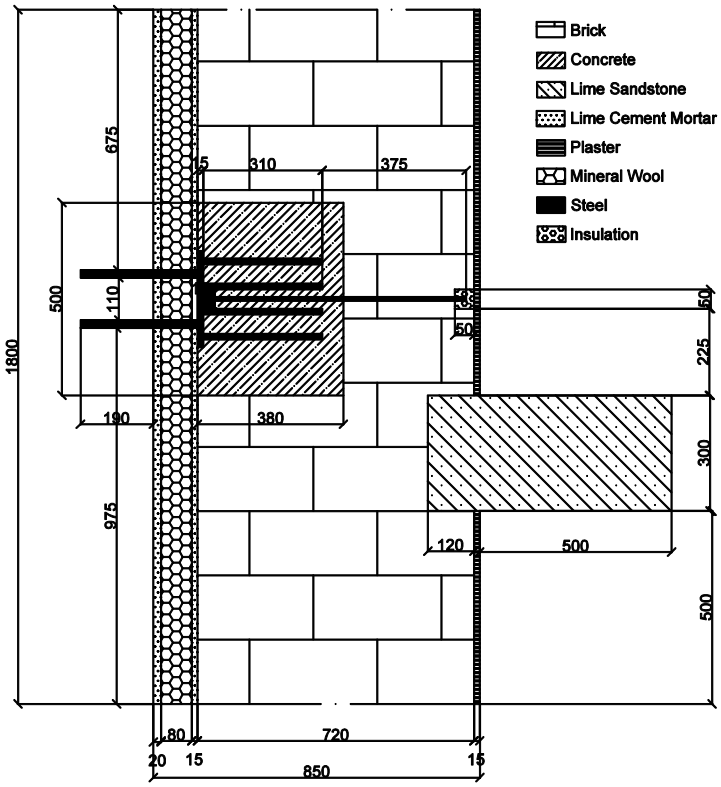

FIG 5.Balcony bearing: geometry.

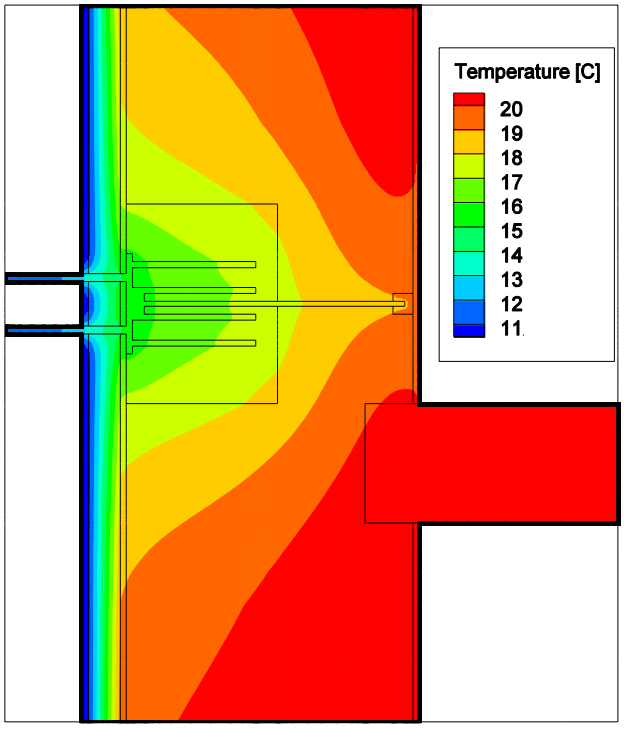

FIG 6. Balcony bearing: temperature distribution at June 11 th.

Another consequence of the now very nonlinear equations may be an increasing number of Newton iterations required, and also more Modified Newton convergence failures because of outdated Jacobians. This motivates analysis of both Modified and Standard Newton-Raphson methods. The Standard Newton algorithm updates the Jacobian matrix data for each nonlinear iteration and performs an LU-decomposition for the Band Solver. It improves convergence of the algorithm, hereby also reducing the number of Newton convergence errors. Consequently, the number of integrator steps is reduced (compare first and last two lines in TABLE 2).

TABLE 2. Floor construction: simulation performance

Numerical method	Number of integrator steps	Average time/ integrator step [s]	Overall simulation time
Modified Newton, Band Solver	20522	1.2	6.6 h
Modified Newton, GMRES + ILU	20632	0.3	1.7 h
Standard Newton, Band Solver	17554	3.0	14.4 h
Standard Newton, GMRES + ILU	17552	0.25	1.1 h

As expected, the Standard Newton further increases computational effort for the Band Solver. Clearly, for this case the Modified Newton approach is best when using a direct Band Solver.

For the GMRES solver the time needed per integration step is approximately the same for Modified and Standard Newton. Consequently, the overall simulation time decreases similarly as the number of integrator steps. Already in this case a Standard Newton method in combination to a Krylov Subspace linear solver can decrease simulation time by a factor of 6 if compared to the best direct variant.

3.3 Hygrothermal simulation of a balcony bearing

The last test case considers a balcony bearing consisting of a steel and concrete detail inside a brick wall (see FIG. 5). The wall is insulated from the outside by mineral wool and the steel beam leads to a thermal bridge. This fact motivates the application of simulation software in order to get information about hygrothermal conditions inside the wall. We apply climate data of Potsdam including solar radiation and rain. The simulation starts at May 15th and continues for one month, see (Paepcke 2014).

In order to guarantee a sufficient accuracy of the results a high-resolution discretization is necessary. We use 17204 elements and the number of unknowns is increased to 34408 for the hygrothermal simulation.

The problem is of highly nonlinear type. The steel beam conducts heat very well and therefore dynamic changes of the outside climate immediately affect a large part of the construction detail. Additionally, high temperature gradients occur at the contact between the steel and the external mortar layer (FIG. 6, left side of the construction) that are also rapidly changing in time. This effect results in very frequent variations in moisture content and temperature in the mortar close to the beam.

This simulation example reveals the limits of the classical Band Solver. The simulation time for this problem size and the Modified Newton variant is hardly in an acceptable range (see TABLE 3). For this highly nonlinear problem the Modified Newton method with our current update strategy is obviously an unsuitable choice.

As before, the GMRES method drastically improves the numerical efficiency.

Note, for this case the application of the Standard Newton method drastically improves convergence and the number of integrator steps is much lower compared to the Modified Newton variant. This even leads to a reduction of simulation time in the case of the direct Band Solver. Obviously, the current Modified Newton update strategy is unsuitable for this problem type.

TABLE 3. Balcony bearing: simulation performance

Numerical method	Number of integrator steps	Average time/ integrator step [s]	Overall simulation time
Modified Newton, Band Solver	151080	12.8	22.4 d
Modified Newton, GMRES + ILU	151083	1.3	2.2 d
Standard Newton, Band Solver	2840	74.6	2.5 d
Standard Newton, GMRES + ILU	2841	5.2	4.1 h

Since GMRES does not share the high performance penalty of direct solvers during Jacobian setup it benefits directly from the reduced integrator steps.

4. Conclusions

The study considers three simulation cases that appear in practical applications. Requirements on sufficient accuracy lead to high grid detail and critical simulation times. Choosing suitable numerical methods may drastically reduce the computational effort and therefore give access to simulation problems with an increased complexity.

In the case of a linear problem (case 1) the Band Solver combined with a Modified Newton method proves to be a high-performance method. However, hygrothermal simulations are of nonlinear type. We have shown that Krylov Subspace methods prove to be a very efficient alternative to direct banded linear equation system solvers when applied to nonlinear transport problems. As the equation system setup does not demand significant simulation time the Modified Newton strategy is no longer necessary. We suggest the combination of the GMRES method with a Standard Newton procedure for large nonlinear problems.

However, the GMRES method is only applicable when problem-specific preconditioned. In our tests the standard ILU preconditioner provided a base-level for convergence acceleration. The development of suitable preconditioning strategies will be subject of the future work.

References

Thermal bridges in building construction - Heat flows and surface temperatures - Detailed calculations (ISO 10211:2007). German version EN ISO 10211:2007

Grunewald J. 1997. Diffusiver und konvektiver Stoff- und Energietransport. Ph.D thesis. Dresden University of Technology.

Hindmarsh A. C. et al. 2005. SUNDIALS: Suite of Nonlinear and Differential/Algebraic Equation Solvers. ACM Transactions on Mathematical Software. Vol. 31(3). pp. 363-396.

Meister A. 2008. Numerik linearer Gleichungssysteme. Vieweg & Sohn Verlag, Wiesbaden.

Nicolai A. 2008. Modeling and Numerical Simulation of Salt Transport and Phase Transitions in Unsaturated Porous Building Materials, Ph.D thesis, Dresden University of Technology.

Nicolai A. 2014. Performance improvement of HAM simulations through an optimized grid numbering technique, 10th Nordic Symposium on Building Physics. Lund.

Paepcke A. 2014. Building constructions for the performance test of dynamic hygrothermal transport solvers arising from practical application. In prep.

Saad Y. 2003. Iterative Methods for Sparse Linear Systems, SIAM Society for Industrial and Applied Mathematics. Philadelphia.

Vogelsang S. 2013. Parallel Hardware Architectures. EnTool 2013 – Symposiuum Dresden.

The effect of weather data on glazing U-value in building performance simulation

Steffen Petersen, Assistant Professor [1]

[1] Aarhus University Department of Engineering

KEYWORDS: *Energy use, Glazing, U-value, Building Simulation, Performance gap*

SUMMARY:
The certification of building energy performance according to the European Building Performance Directive is in many EU countries based on monthly quasi-steady-state calculation of the expected energy use. But does this calculated energy use correspond to the actual energy use? The aim of this paper is to contribute to the minimisation of the performance gap between calculated and actual energy use by improving the precision of the calculated energy use. It is common practice to use the declared U-value of a glazing in calculations of the expected energy use despite the fact that this U-value is varying with outdoor temperature, wind speed and direction. Data presented in this paper suggests that the dynamic changes in U-value due to weather conditions should be taken into account to obtain a more accurate calculation of the expected energy use of a building in the Nordic countries. Consequently, three alternative approaches to minimise the performance gap is suggested: 1) abandon the monthly quasi-steady-state method for certification in favour of a dynamic method, 2) use the approach suggested in this paper to reduce the performance gap and then visualise the remaining performance gap as an uncertainty of the overall calculation result, or 3) visualise the full uncertainty of the overall calculation result due to the performance gap.

1. Introduction

The European Building Performance Directive (EPBD 2010) has since 2006 been the framework for certification of building energy performance in European Union (EU) member states. The certification process varies from country to country but is very often based on a calculation of the expected energy use (Lausten et al. 2010). Various stakeholders in the building industry use this calculated energy use for estimating operating budgets, investment security, policy making etc. Consequently, an increasing number of stakeholders are raising the question: does the calculated energy use correspond to the actual energy use?

EPBD prescribes the use of a standardised energy calculation method for calculating the expected energy use. ISO 13790 (2008) describes two basic types of methods for this purpose where the monthly quasi-steady-state method is the most widespread method in the EU member states. This method has its benefits but it is also in many aspects a simplified representation of reality. In relation to the above raised question, it is therefore relevant to investigate the significance of these simplified representations. This paper focuses on the simplified representation of heat loss through glazings.

The monthly quasi-steady-state energy calculation relies on the so-called declared U-values of glazings in its calculation of the annual heat loss. The purpose of the declared value is product comparison and it is obtained by calculating the U-value according to EN 673 (1997) using a set of fixed standardised boundary conditions. But EN 673 (1997) also makes it clear that the U-value of a glazing is not a static value as it varies with the environmental temperatures on each side of the window, outdoor wind speed and direction, and indoor air flows at the window. This paper therefore investigate the theoretical effect on building energy calculations when taking into account the

variations in U-value due to weather conditions compared to the use of the static declared U-value. This investigation is used to suggest how the effect can be represented when calculating the expected energy use according to the monthly quasi-steady-state method in ISO 13790 (2008). The investigation is limited to encompass the U-value of the central area of the glazing, i.e. ignoring any two-dimensional effects when getting near to the window frame.

2. Method

This section describes a procedure for calculating the dynamic U-value of a glazing due to changes in hourly weather conditions. The procedure is used in two types of energy calculations:

1. *Simplified dynamic calculation.*
   The procedure is integrated in a simplified hourly-based tool called iDbuild (Petersen & Svendsen 2010). The purpose is to investigate the theoretical effect of a dynamic *U*-value on energy performance calculations compared to the use of the static declared *U*-value.
2. *Monthly quasi-steady-state calculation.*
   The procedure is used to calculate the mean monthly U-values. These values are used for calculating the energy use of an office space in the program Be10 (SBi 2011). Be10 is the Danish implementation of the monthly quasi-steady-state energy calculations method described in ISO 13790 (2008). The purpose is to investigate whether the use of mean monthly U-values in monthly quasi-steady-state energy calculations is a reasonable approach to take into account any effect of weather data on glazing U-value identified in the simplified dynamic calculations.

The results from the calculations and comparisons can be found in section 3.

2.1 Procedure for calculating monthly mean U-values of a glazing

The procedure is based on the approach given in EN 673 (1997). Here the *U*-value is given as:

$$\frac{1}{U} = \frac{1}{h_e} + \frac{1}{h_t} + \frac{1}{h_i} \quad (1)$$

Where h_e external heat transfer coefficient (W/(m^2·K))
h_t total heat transfer coefficient of the glazing (W/(m^2·K))
h_i internal heat transfer coefficient (W/(m^2·K))

h_e is the sum of a convective conduction and a radiation conduction. The convection part is the dominating and can be 3 to 4 times larger than the radiation conduction (Cooper 1981, Palyvos 2008). The convection conduction dependent on many factors such as the geometry of the building and its surroundings, the position at the building envelope, the building surface roughness, wind speed, wind direction, local airflow patterns and surface to air temperature differences. The research made in this area is extensive and on-going and there are many different calculation methods available. It is difficult to choose a model as there is large uncertainty associated with the use of them as they vary in scope and detail (Mirsadeghi 2013). The model for representing h_e in this procedure is the NBS polynomial model (Rowley 1930). This model correlates h_e to surface roughness and local surface wind velocity. This correlation is chosen because it includes radiation to sky, ground, and air, and we thus avoid the rather detailed calculation of the radiation conduction. h_e as a function of air velocity for 'very smooth' materials like glass is:

$$h_e = 11.56 - 0.036 V_s^2 \quad (2)$$

Where V_s air velocity at the surface (m/s)

V_s can be calculated using the procedure described by Ito et al. (1972). h_i is also the sum of a convective conduction (h_c) and a radiation conduction (h_r). Both conductions are dynamic as they change with the temperature of the internal surface of the glazing, the room surfaces and the indoor air. A simplified expression is therefore preferred because the monthly quasi-steady-state method do not involve calculations of these temperatures. h_i can be expressed in a simplified way according to EN 673 (1997):

$$h_i = h_c + h_r = 3.6 + \frac{4.4\varepsilon}{0.837} \quad (3)$$

Where ε corrected emissivity of the internal surface of the inner glazing pane (-)

According to EN 673 (1997) h_t can be expressed as the sum of the gas space conduction (h_g) and the conduction of the individual glazing panes (h_p). In this procedure, it is assumed that h_p is independent of weather conditions. h_g is the sum of the radiation, conduction and convection conduction which all are dependent on the environmental temperatures on each side of the glazing:

- The radiation conduction depends on the temperature difference between the glass surfaces surrounding the gas space (ΔT).
- The gas property (density, dynamic viscosity and conductivity) depends on the mean absolute temperature of the gas space (T_m) which affects the conduction as well as convective conduction. The gas property as a function of temperature can be found ISO 15099 annex B (2003).
- The convection conduction expressed by the Nusselt number also depends on ΔT.

The calculation of the *U*-value of the glazing, it is assumed that a state of equibrilium is reached in each weather data time step. This requires an iterative process because ΔT and T_m are not known beforehand. The iteration in each weather data time step starts with a guess of the temperatures ΔT and T_m:

$$\Delta T_{guess} = 0.75\frac{|t_i - t_o|}{n} \quad (4)$$

Where n factor depending on number of panes, n=1 for two-layer glazings and n=2 for three-layer glazings

$$T_{m,guess} = 273 + k|t_i + t_o| \quad (5)$$

Where k factor depending on number of panes, k=0.5 for two-layer glazings, k=0.25 for the cavity closest to outside in a three-layer glazing and k=0.75 for the cavity closest to inside in a three-layer glazing

These guesses are used to calculate the initial *U*-value of the glazing. The initial *U*-value is used to calculate the temperatures of the glazing pane surfaces facing the gas space ($t_{s,x}$). $t_{s,x}$ of a certain surface x can be expressed as:

$$t_{s,x} = t_i - (t_i - t_o)\frac{\sum_{z=i}^{x} h_z^{-1}}{U^{-1}} \quad (6)$$

Where t_i indoor air temperature (°C)
t_o outdoor air temperature (°C)
z index referring to the heat transfer coefficients in equation 1 starting with h_i

A proportion of the total solar radiation is absorbed in the panes and thus increases the pane temperature. For example, an incident solar radiation of 500 W/m^2 increases the temperature of an

outer pane with an absorbance of 0.07 by approximately 1.5 ºC. Taking the relationship between incident solar radiation and pane temperature into account complicates the calculation of the total heat loss coefficient as it then becomes dependent on the orientation and tilt of the glazing. The relationship is ignored in the analysis presented in this paper but it could be added in future more detailed analysis.

The surface temperatures $t_{s,x}$ are used for recalculating ΔT and T_m which then is used for recalculating the *U*-value. This process is repeated in each time step until the *U*-value converges on the third decimal.

The above described procedure can be used for calculating the glazing *U*-value for every hour of the year. As an example of this, FIG 1 depicts the variation in glazing *U*-value of a two-layer and a three-layer glazing, respectively, for a west-facing glazing in Kiruna, Sweden. Results will always differ with orientation because the convective part of the exterior heat transfer coefficient depends on orientation. The deviations from the declared *U*-value are considerable for the two-layer glazing. This is mainly due to the radiation conduction which is the conduction most sensitive to the difference between indoor and outdoor temperature. The *U*-value of the three-layer glazing is more stable as the difference between indoor and outdoor temperature is less governing. The *U*-values are, however, in general somewhat lower than the declared value which is due to weather-induced fluctuations in the external heat transfer coefficient which often is lower than the standardised boundary conditions in EN 673 (1997).

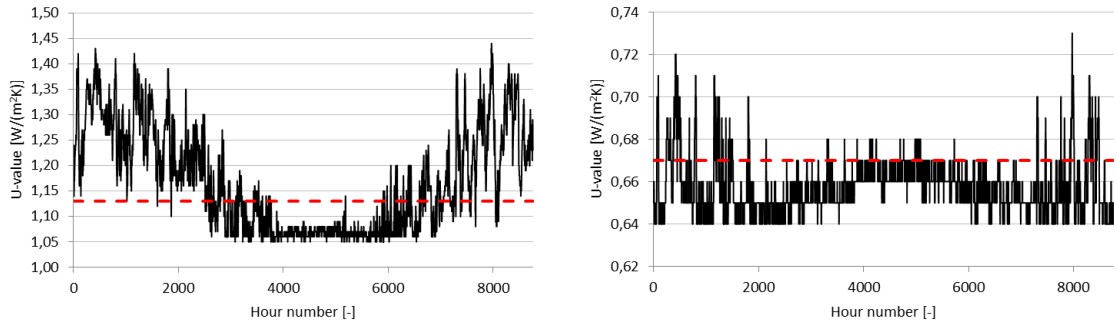

FIG 1. Hourly U-value of two-layer west-facing glazing in Kiruna, Sweden. The vertical dotted line is the declared U-value using the boundary conditions in EN 673 (1997).

2.2 Dynamic energy calculations

The procedure for dynamic calculations is in general as described in section 2.1. However, the radiant part of the internal heat transfer coefficient h_i can now be calculated as the mean radiant temperature is known:

$$h_i = \frac{\varepsilon\sigma\left(t_{s,x}{}^4 - t_{rm}{}^4\right)}{t_{s,x} - t_{rm}} \tag{4}$$

Where σ Stefan-Boltzmann's constant, $5.67 \cdot 10^{-8}$ (-)
t_{rm} mean radiant temperature of the room (K)

3. Results

The following case was used to investigate the impact of dynamic glazing *U*-value on energy need for heating and cooling using the formulas specified in section 2 compared to the use of the static declared *U*-value. Assume a single-sided, single-zone two-person office with a west-facing window.

The occupied period is from 8 a.m. to 5 p.m. every weekday. The lower limit for thermal comfort is set to 20ºC and the upper limit is set to 26ºC. Further data assumptions are shown in Table 1.

TABLE 1. Data assumptions for case.

	Parameter	Description
Room dimensions	Height × width × depth	2.8 m × 3 m × 6 m
Window	Height × width	1.8 m × 2 m
	Offset	Symmetrical, 0.8 m from floor
	Glazing (U/g/LT)	Two-layer (1.09/0.31/0.65) or Three-layer (0.73/0.34/0.58)
	Frame	Standard wooden frame, U=1.6 W/(m^2·K), width=0.08 m, ψ=0.05 W/(m·K)
Constructions	Façade	U=0.15 W/(m^2·K)
	Thermal capacity	120 Wh/(K·m^2)
Systems	Infiltration	0.10 l/s m^2, always active
	Mechanical ventilation in occupied hours	Min. ventilation rate 1.48 l/s m^2 corresponding to class II in EN 15251:2007. Max. ventilation rate is 2.96 l/s m^2. Average specific fan power of 1.0 kJ/m^3 air. No mechanical cooling available
	Mechanical ventilation in unoccupied hours	Min. ventilation rate is 0 l/s m^2, max. ventilation rate 2.96 l/s m^2
	Heat exchanger	Efficiency of 85 %
	General lighting	Dimming control, set point 200 lux, min. power 0.5 W/m^2, max. power 6 W/m^2, 3 W/m^2/100 lux. Only active in occupied hours
	Task lighting	Always on in occupied hours, set point 500 lux, 1 W/m^2.
	Internal load	300 W in occupied hours, 0 W in unoccupied hours
External conditions	Shadows from surroundings	None

Two glazing solutions are investigated: 1) a two-layer and 2) a three-layer glazing. Both solutions are simulated for four locations in the Nordic countries: Copenhagen (Denmark), Oslo (Norway) and Kiruna (Sweden), and Helsinki (Finland). IWEC data files normally used for EnergyPlus simulations (U.S. Department of Energy 2013) is used for representing hourly weather conditions.

3.1 Dynamic energy calculations

FIG 2 and FIG 3 depicts the annual sum of the hourly simulated energy need for heating and cooling using the static declared *U*-value and the dynamic *U*-value for the two-layer and three-layer glazing, respectively. For the two-layer glazing, simulations with dynamic *U*-value results in higher heating need and a slightly lower cooling need compared to simulations with declared *U*-value. For the three-layer glazing, simulations with dynamic *U*-value results in a somewhat lower heating need and practically the same cooling need compared to simulations with declared *U*-value.

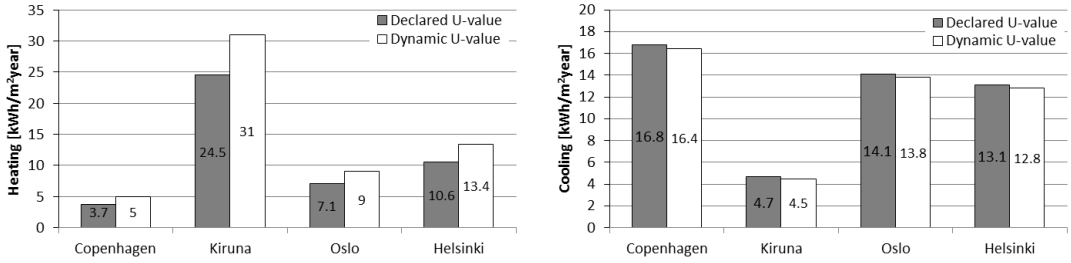

FIG 2. Energy use for heating and cooling, respectively, for the two-layer glazing at the four locations. Dynamic energy calculations.

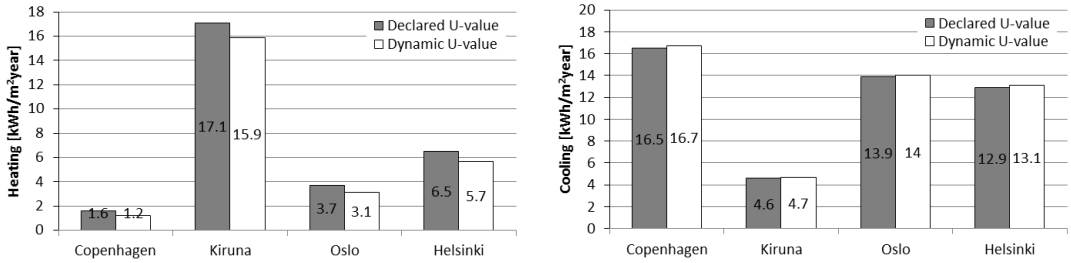

FIG 3. Primary energy use for heating and cooling, respectively, for the three-layer glazing at the four locations. Dynamic energy calculations.

3.2 Monthly mean quasi-steady-state calculations

It is investigated whether the use of monthly mean temperature-weighted *U*-values in monthly quasi-steady-state energy calculations is a reasonable approach to represent the dynamic effect of the *U*-value on energy need as documented in section 3.1. The monthly mean temperature-weighted *U*-value, $U_{month,}$ is calculated as:

$$U_{month} = \frac{\sum_{i=s}^{n} U_i T_i}{\sum_{i=s}^{n} T_{ref} - T_{out,i}} \quad (6)$$

Where s the annual hour number in the start of a certain month (-)
n the annual hour number in the end of a certain month (-)
ref a reference indoor temperature (°C), e.g. 20 °C

Results are depicted in FIG 4 and FIG 5. The heating demand for both glazing solutions shows the same tendency in deviations as the dynamic calculation in FIG 1 but not the same relative or absolute magnitude. The tendency for the cooling demand in the dynamic calculation is not repeated in the quasi-steady-state calculation.

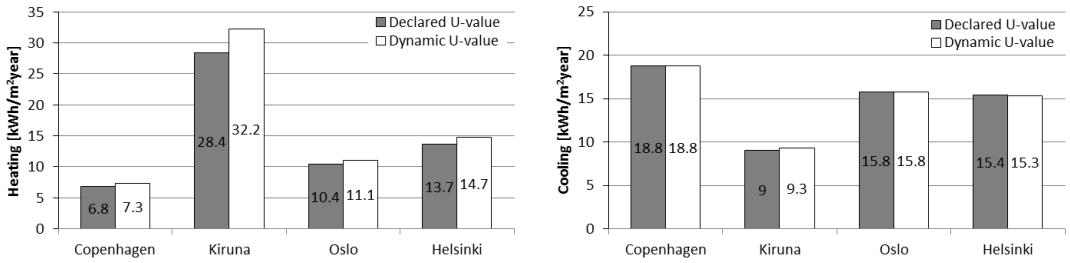

FIG 4. Primary energy use for heating and cooling, respectively, for the two-layer glazing at the four locations. Monthly mean quasi-steady-state calculations.

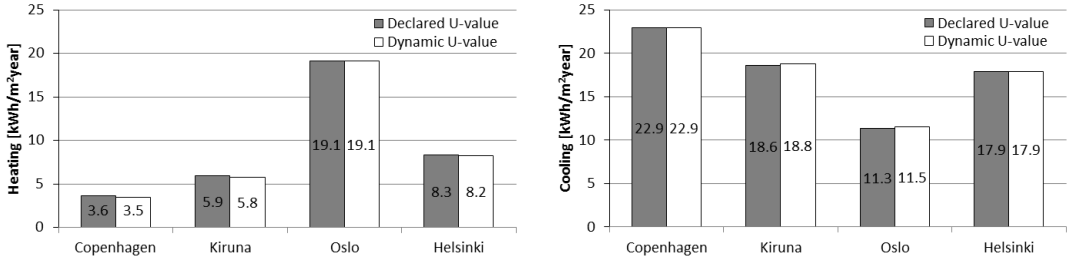

FIG 5. Primary energy use for heating and cooling, respectively, for the three-layer glazing at the four locations. Monthly mean quasi-steady-state calculations.

4. Conclusions

The aim of this paper is to minimise the performance gap between calculated and actual energy use by improving the precision of the calculated energy use. Focus is on the gap caused by the use of the declared U-value of a glazing as a static all-year input in energy calculations instead of the U-value as a function of hourly changes in weather conditions.

Data from dynamic hourly building simulations suggest that the dynamic changes in *U*-value due to weather conditions should be taken into account to obtain a more accurate calculation of the expected energy use of a building in the Nordic countries. The use of declared U-value in performance simulation of two-layer glazing solutions leads to an underestimation of the heating demand for all investigated locations and an overestimation of the cooling demand. For a three-layer glazing solution the use of dynamic *U*-value results in less heating demand whereas the cooling demand is practically the same. The use of declared *U*-values instead of dynamic *U*-values in energy performance calculations may therefore be a reason for performance gaps between calculated and actual energy use. Based on this data, the paper investigates whether the use of monthly mean temperature-weighted *U*-values is a reasonable approach to represent this effect when calculating the expected energy use according to the monthly quasi-steady-state method in ISO 13790. The conclusion is, assuming that the dynamic hourly calculation represents actual conditions, that the suggested approach is not sufficient to represent the identified effect even though the approach does compensate somewhat for the performance gap.

Three alternative approaches to minimise the performance gap is hereby suggested: 1) abandon the monthly quasi-steady-state method for certification in favour of a dynamic method, 2) use the approach suggested in this paper to reduce the performance gap and then visualise the remaining performance gap as an uncertainty of the overall calculation result, or 3) visualise the full uncertainty of the overall calculation result due to the performance gap.

5. Acknowledgements

The author gratefully acknowledges the support of this work through the project “Energy sinners in low energy buildings” financed by the Danish energy research and development program ELFORSK. The author would also like to thank Michael Dahl Knudsen at Aarhus University for discussions and generation of weather data files.

References

Cooper P.I. 1981. The effect of inclination on the heat loss from flat-plate solar collectors. Solar Energy 27 (5) 413-420.

EN 673. 1997. Glass in building – Determination of thermal transmittance (U value) – Calculation method. European Committee for Standarization. Brussels Belgium

EPBD. 2010. Directive 2010/31/EU of the European Parliament and of the Council of 19 December 2010 on the energy consumption of buildings (recast).

ISO 13790. 2008. Energy performance of buildings – calculation of energy use for space heating and cooling. International Organization for Standardization. Geneva Switzerland

ISO 15099. 2003. Thermal performance of windows, doors and shading devices – detailed calculations. International Organization for Standardization. Geneva Switzerland

Mirsadeghi M., Cóstola D., Blocken B. & Hensen J.L.M. 2013. Review of external convective heat transfer coefficient models in building energy simulation programs: Implementation and uncertainty. Applied Thermal Engineering 56 (1–2) 134-151.

Ito N., Kimura K., & Oka J. 1972. A field experimental study on the convective heat transfer coefficient on exterior surface of a building. ASHRAE Transactions 78 (1) 184-191

Lausten J., Brophy V. & Ryan L. 2010. Energy performance certification of buildings. IEA Energy Conservation in Buildings and Community Systems Annex 53 – Total energy use in buildings: analysis and evaluation methods. Paris France

Palyvos J.A. 2008. A survey of wind convection coefficient correlations for building envelope energy systems' modelling. Applied Thermal Engineering 28 (8-9) 801-808.

Petersen S. & Svendsen S. 2010. Method and simulation program informed decisions in the early stages of building design. Energy and Buildings 42 (7), 1113–1119.

Rowley F.B., Algren A.B. & Blackshaw J.L. 1930. Surface conductance as affected by air velocity, temperature and character of surface, ASHRAE Transactions 36 p. 429.

SBi 213. 2011. Bygningers energibehov. 5th ed. Copenhagen, Statens Byggeforskningsinstitut. 120 p.

U.S. Department of Energy. 2013. EnergyPlus Energy Simulations Software website, www.eere.energy.gov/buildings/energyplus/

Hygro-thermal and Energy Related Performance of Vertical Greening on Exterior Walls – A Field Measurement Study

Johnny Kronvall, Professor [1]
Hans Rosenlund, Ph.D. [2]

[1] Malmö University and Green Building Science, Sweden
[2] Malmö University and CEC Design AB, Sweden

KEYWORDS: *vertical greening, green walls, living walls, moisture conditions, evaporative cooling, energy balance, mould growth.*

SUMMARY:
Vertical greening on external walls has lately been the subject of increasing interest, where much hope is spent upon the benefits of enhanced energy performance of buildings. However, there is a lack of knowledge and experiences of the technical performance of such walls, especially their hygro-thermal and energy related behaviour under different climatic conditions.

This paper presents a long-term, full-scale field experiment study on a masonry wall in the southern part of Sweden. Different kinds of wall greening have been included in the experiment, mainly solutions based on commercially available cassettes, simple home-built pocket-like plant pots and different climbers.

Monitored parameters in the technical part of the program include outdoor and indoor climate, air gap and surface temperature and relative humidity, driving rain and thermal flux.

The wall greening systems studied quite strongly influence the hygro-thermal behaviour of the original walls; greening may even contribute to dryer conditions by protecting from driving rain. Caution must be paid to protect from water leakage, which may cause mould growth. The energy balance of poorly insulated walls is slightly improved in winter by raised air gap temperatures, and in summer by shading. No evaporative cooling effect has been found in this study.

1. Introduction

Vertical greening on external walls has during the last years been the subject of increased interest from city planners, architects and real estate developers (Köhler 2008). Much hope is spent upon the benefits of green walls, not only from an esthetical point of view, but also technically: e.g. enhanced energy performance with vertical greening, cooler street canyon climate during hot days and traffic noise reduction. Vertical greening concepts have been developed in a number of countries during the last decades, especially in Germany, Austria, the Netherlands and the US (Perini et al. 2013, Enzi 2011, Mir 2011, Tilley et al. 2012). In the northern parts of Europe and North America there exists however much less practice and thus experience of exterior wall greening and so little is known today about different greening systems and adequacy of different plants as well as the technical behaviour of wall greening in relation to the building under influence of e.g. more severe winter conditions.

In a collaborative research project with the Swedish University of Agricultural Sciences (SLU), Malmö University and the building developer and contractor PEAB as partners, research on the hygro-thermal and energy related performance forms one part which is performed by Malmö University and CEC Design AB. The results from this part of the project form the basis for this paper. The most extensive part of the project, however, is related to horticultural issues, such as planting systems, plant choice and adequacy, irrigation solutions etc. This research is mainly performed by SLU.

2. Hypotheses and methods

The following hypotheses were formulated for the behaviour and hygro-thermal and energy related performance of vertical greening on exterior walls:

- The vertical greening modifies the *microclimate for the exterior* wall behind the greening in the following respects:
    - Cooler summer conditions
    - Warmer winter conditions
    - Relative humidity is affected by the air temperature in the gap between the wall greening and the wall behind
    - Vapour content of air nearly equals that of ambient outdoor air
    - The wall behind the wall greening is effectively protected against driving rain
- The risk for mould growth behind the wall greening must be paid attention to when designing wall greening systems
- Vertical greening on exterior walls influence the energy balance of poorly insulated buildings:
    - in wintertime by creating an increased thermal insulation
    - in summertime by decreasing the cooling load of the building, while
    - for modern well-insulated buildings these effects are negligible

The hygro-thermal and energetic behaviour of outer walls with and without vertical greening was studied by means of field measurements described below.

3. Experimental setup

The study is using two experimental sites, both located in an industrial area in the city of Malmö in southern Sweden (N 55.6108, E 12.9896), see FIG 1.

FIG 1. Experimental sites overview. View from South (Source: Google).

3.1 Site 1 – Driving Rain

Site 1 is a south-west-facing corrugated steel façade of an industrial warehouse building. The wall was prepared for the propagation of climbers by mounting a standard reinforcement mesh #100 mm at a distance of 150 mm outside the wall surface, thus creating a trellis. A number of different climbers were planted and established in the ground and consequently climbing up in the trellis. The objective of the study at this site was to monitor the ability of wall vegetation to protect the wall behind against driving rain. In order to quantify this protection capacity, driving rain was monitored behind the vegetation layer and compared to the amount hitting the free, unprotected wall. A special meter device, the type of which has been used earlier and validated in a number of extensive studies of driving rain on buildings (e.g. Sandin 1984) was used, see FIG 2. The driving rain collected by the meter is further led to a standard tipping bucket rain gauge producing electrical pulses to the monitoring system depending on the intensity of the driving rain hitting the façade.

FIG 2. Site 1 with driving rain meters.
Left: Humulus lupulus (Hops)
Right: Fallopia baldschuanica (Bukhara fleeceflower)

FIG 3. The wall-greening systems (Site 2).
Left: Felt pocket module
Right: Modular panel

3.2 Site 2 – Temperature, Moisture and Thermal Flow

Site 2 is an old unoccupied, yet heated, office/workshop building with a south-facing ≈ 40 cm thick massive yellow masonry wall, rendered on the inside. Two different wall greening systems were mounted on the outside of the wall: 1) Modular panels (Vertigreen™) from *Zinco Gmbh*: a) placed with an air gap of 100 mm between the back of the panel and the wall and b) with mineral wool insulation bat (70 mm thick) close to the back of the panel leaving an air gap of 30 mm between the back of the bat and the wall and 2) On-site-made felt pocket modules placed with an air gap of 30 mm between the back of the panel and the wall, FIG 3. Also the microclimate close to the wall created by an already present and well-established plant of Virginia Creeper (Parthenocissus quinquefolia) growing on the wall was the subject of field measurements.

On locations on the inside of the exterior wall, where there was a greening system on the outside or where there was an undisturbed reference area without any greening, heat flow meters were glued to the wall. Further, indoor air temperature was monitored in the seasonally heated office room.

3.3 Monitoring System

Ambient weather conditions were monitored by means of a weather station built up with commercially available sensors for air temperature (radiation protected), relative humidity, total solar radiation hitting a horizontal plan, wind velocity and direction, precipitation and driving rain (site 1).

Weather data, as well as data regarding temperatures, relative humidity levels and heat fluxes were continuously collected for further analyses by means of two data loggers, see FIG 4.

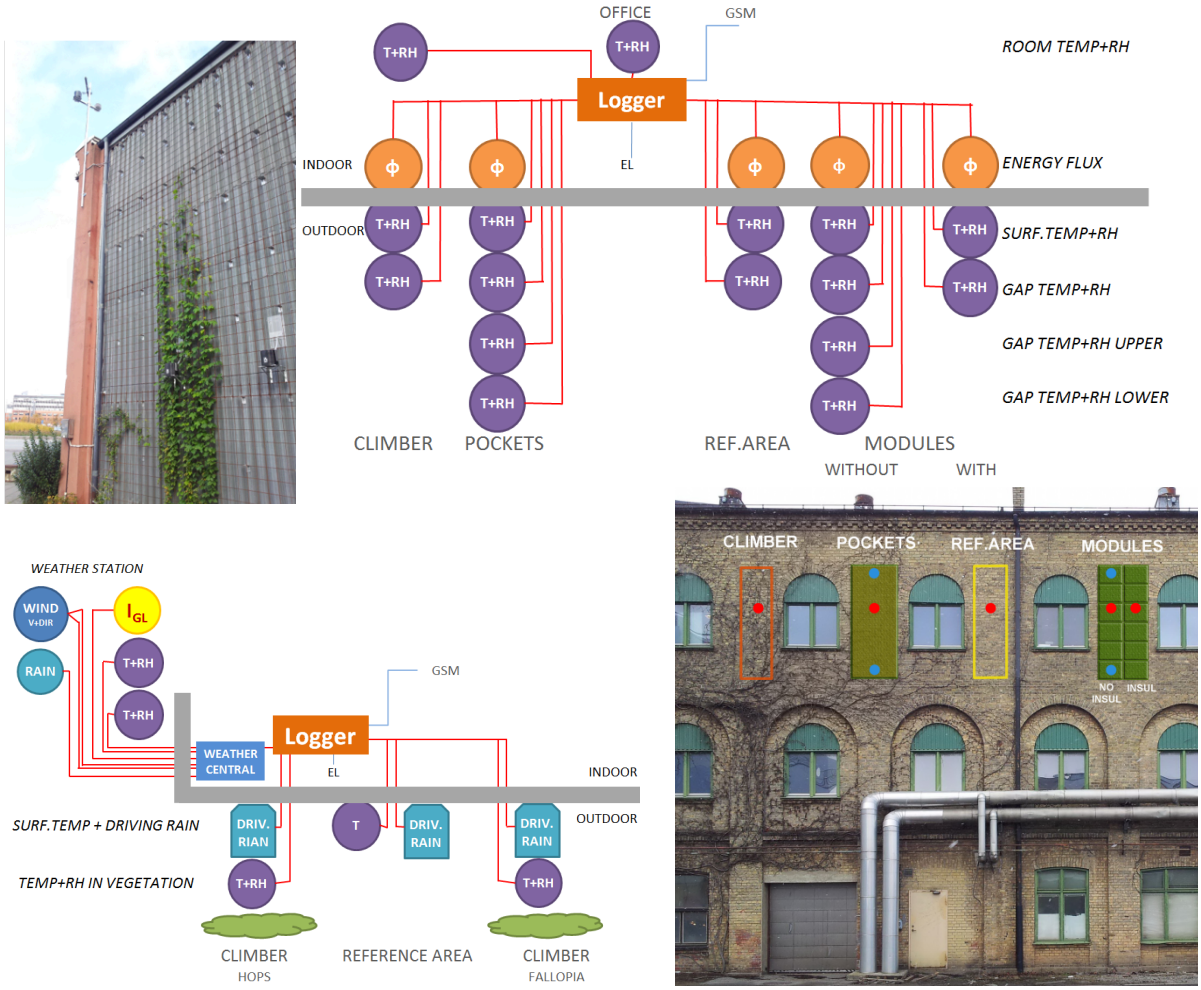

FIG 4. Monitoring setup. Left: Weather station and Site 1 with driving rain tests. Right: Site 2 with hygro-thermal and energy performance measurements.

4. Results and Discussion

This section presents measured data, either as monthly averages during a year or as details from two winter and two summer days. The days chosen; 17–18 January are cold with easterly wind, and 17–18 July are averagely warm and sunny with winds around west.

4.1 Thermal Performance

The thermal performance is evaluated through the temperature difference between the outdoor air and the air in the gaps or close to the wall surface (FIG 5).

The winter case shows considerable temperature rise, especially in the thinner gaps behind the insulated modules and pockets. The latter also has a steel sheet cover on top, decreasing the ventilation rate.

In the summer, the air space temperatures are closer to outdoor, except for the climber and the reference area, where the solar radiation makes temperatures increase during daytime. This effect is also seen in the January case, where the first day is sunny, but the second is not.

Also the wind affects the temperatures; higher wind speeds increase the ventilation rate and make the temperatures approach the outdoor ones.

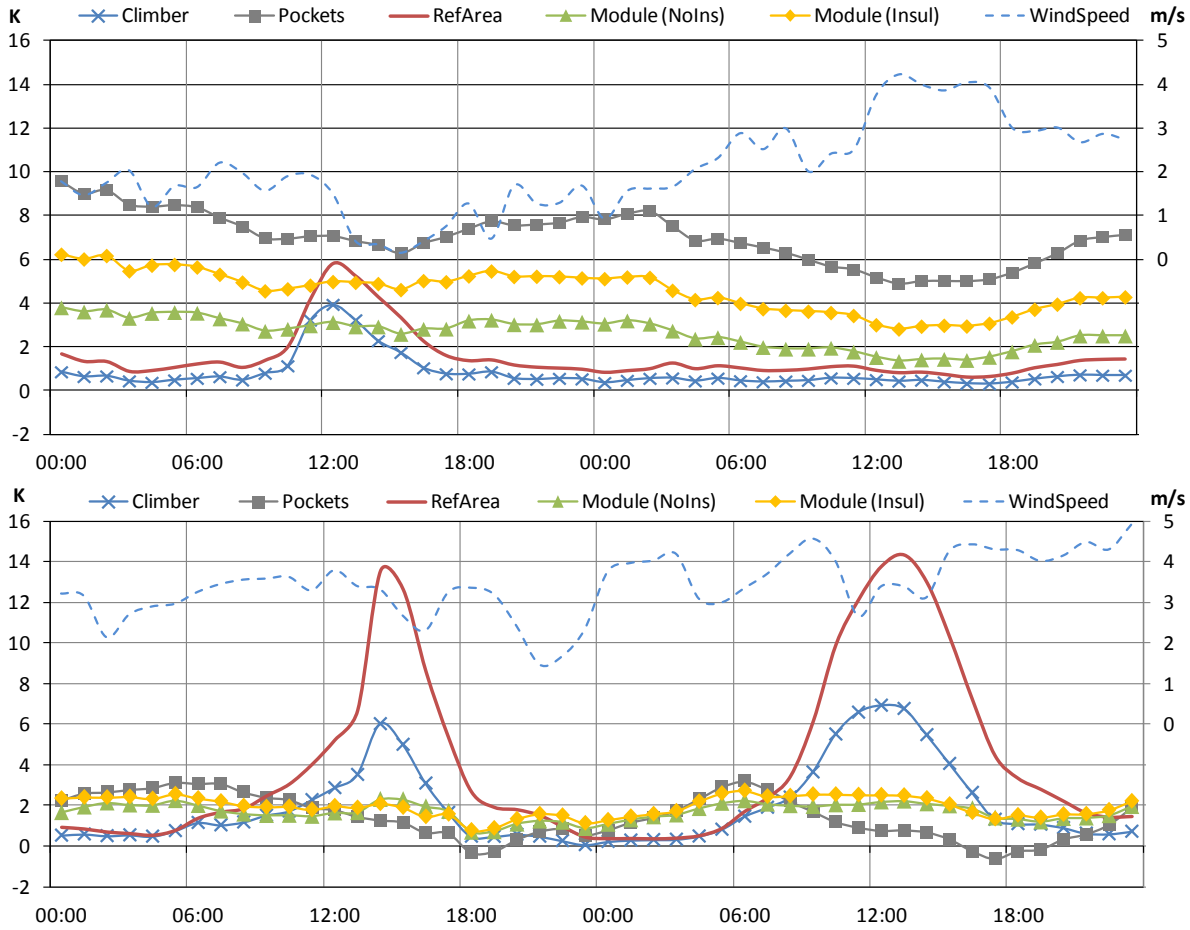

FIG 5. Air temperature differences in the air spaces or close to the wall compared to outdoor air during; 17–18 January (top); and 17–18 July (bottom).

It is often argued that vegetated walls and roofs generate a considerable evaporative cooling effect that reduces the need for active cooling of the building. The backside temperatures of the systems were not measured, but in FIG 6 we see the differences between *wall* surface and air gap temperatures of the test areas. A negative balance could thus indicate a radiative cooling effect from the green systems. However, this effect seems to be very marginal. Probably most of the evaporative heat exchange will take place between the plants and the surrounding air outside the plants, thus cooling the air in e.g. a street canyon. Later in the project this will be studied by means of simulations.

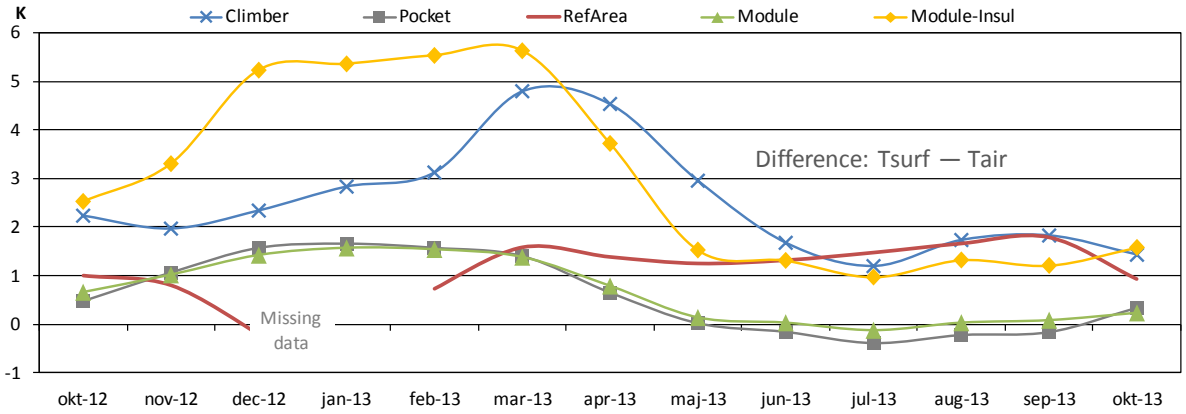

FIG 6. Monthly average temperature differences between wall surfaces and air gaps.

4.2 Hygric Performance

In both winter and summer, the vapour concentration levels are quite similar in all locations, except behind the pockets, where they are considerably higher (FIG 7). Winter conditions are stable, while in the summer moisture levels vary more due to evaporation processes from plants and surroundings.

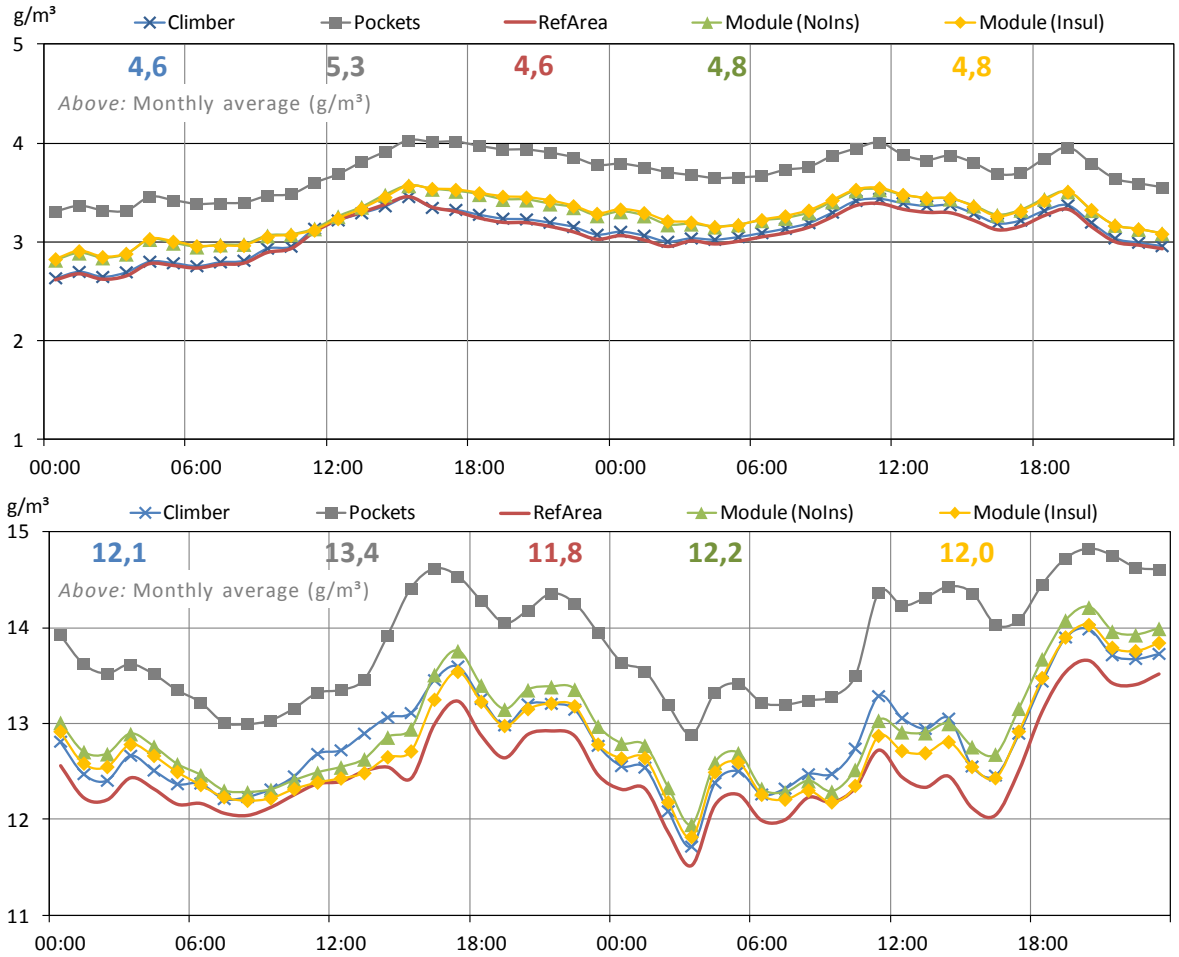

FIG 7. Vapour concentrations in the air spaces or close to the wall during; 17–18 January (top); and 17–18 July (bottom). Monthly averages also included.

There are two reasons for the higher moisture level behind the pockets; 1) the above mentioned steel sheet cover on top of the space reduces ventilation; 2) at the same time water transport through the felt structure into the space was discovered. Conditions suitable for mould growth occur from time to time and a preliminary investigation performed with an endoscope seems to confirm the existence of cob web and signs of mould growth. High moisture levels found in the wall surface could also indicate water leakage from the irrigation system. These issues will be further investigated.

4.3 Energy Performance

The thermal transmittance of the poorly insulated south-facing heavy brick wall varies considerably with outdoor weather conditions and seasons, see **Fel! Hittar inte referenskälla.Fel! Hittar inte referenskälla.**FIG 8. During the winter, when solar radiation is low, all test areas have similar transmittance values. However, increasing solar radiation accumulation in the summer counteracts energy losses from the building, clearly seen at the unprotected reference area. We also notice the effects of shading; by the modules, but also by the leaves of the climber from May to September.

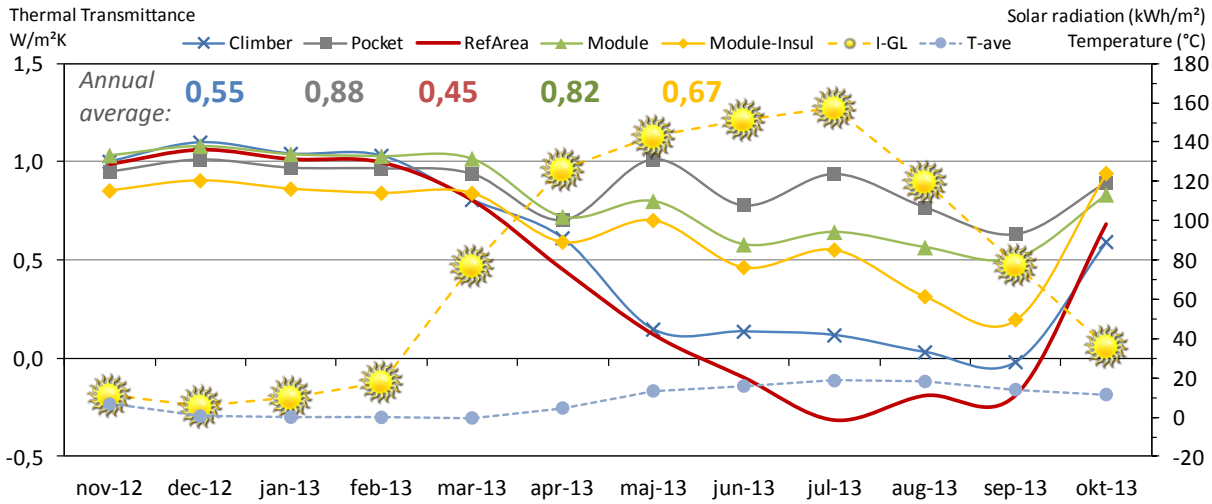

FIG 8. Annual and monthly average variations in thermal transmittance of the different test areas and the bare brick wall. Monthly global solar radiation and average outdoor temperature included.

The monthly values presented are based on diurnal averages, since such a representation of the thermal transmittance should fairly well reflect the thermal inertia effects of the approximately 40 cm massive masonry wall. The variations of the modules' performance in the warmer period, when the flux is not unidirectional, could thus be explained by the effects of time lag versus outdoor temperature stability. For instance, in May the range of average diurnal outdoor temperatures was 13 K, while in June only 6 K. Average monthly wind speeds during the summer were 2,5–2,9 m/s, which range should not affect the transmittance to a noticeable degree.

The average annual energy loss from this poorly insulated wall is lowest without any vegetation systems. However, the important winter transmissions are very similar, except for the insulated modules, which is slightly lower. Further, it should be kept in mind that in summer the heat gains through windows are usually dominating those through walls.

4.4 Driving rain

Even if the resolution of the driving rain gauges are rather coarse for detailed analyses, when summarized over the year we get remarkable differences between the reference area and the collectors behind the two climbers. The vegetation reduces the driving rain penetration of the wall by more than half, see FIG 9. Also during the winter, when only branches and some dead leafs remain, there is a clear protection effect of the vegetation.

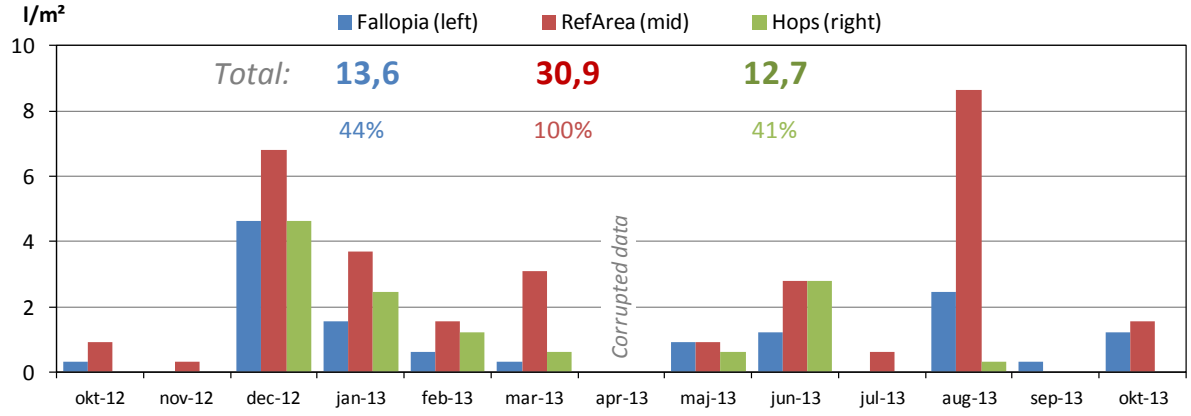

FIG 9. Driving rain. Two climbers compared to bare reference area on a wall facing prevailing wind.

5. Conclusions

The hygro-thermal and energy related performance of a number of vertical vegetation systems on outer walls in Malmö, southern Sweden, has been investigated in this year-round field measurement study. In summary, the result of the study can be concluded as follows:

The *thermal conditions* in air gaps behind the greening systems are slightly warmer in both winter and summer. However, solar radiation raises temperatures close to the bare wall and also in climbers.

Vapour concentrations are marginally elevated behind the greening, but since temperatures vary diurnally, relative humidity does not reach high and stable levels that indicate risk for mould growth. Nevertheless, mould growth was found in one case, where water leaked into the air gap, probably through the felt material and/or from the irrigation system. These risks require close attention at design and construction stages.

Wall greening effectively protects against *driving rain*. Climbers reduced the annual amount of driving rain on the facade by more than half.

The *energy balance* of poorly insulated buildings benefits from the slightly raised air gap temperatures. In summer the shading of the greening reduces solar heat load and thus risk for overheating. Climbers, dropping their leaves in the winter, combine this beneficial shading with allowing for solar access in the winter, thus reducing heat loss. These effects decrease with increasing thermal insulation, and is not estimated to play any significant role for modern standard buildings.

This study has not been able to identify any evaporative cooling effect of the green module systems – an effect that is often argued for in the debate.

6. Acknowledgements

The Swedish Research Council FORMAS and the building developer and contractor PEAB have financially supported the research study. The support is gratefully acknowledged.

References

Enzi V. et al. 2011. Leitfaden Fassadenbegrünung. (Guide book for vertical greening.) ÖkoKauf Wien, Arbeitsgruppe 25 Grün- und Freiräume. www.oekokauf.wien.at

Köhler M. 2008. Green facades – a view back and some visions. Urban Ecosystems, 2008, Vol. 11:423-436. Springer.

Mir M.A. 2011. Green facades and building structures. Master thesis CIE5060, TU Delft.

Nevander L.E. & Elmarsson B. 1994. Fukthandbok, Praktik och teori. (Moisture handbook, Practise and theory) 2nd ed. Stockholm, AB Svensk Byggtjänst and the authors. 538 p.

Perini K. et al. 2012. Vertical greening systems, a process tree for green facades. Urban Ecosystems, 2012, Vol. 16:265-277. Springer.

Sandin K. 1987. Fukttillstånd i autoklaverade lättbetongväggar. (The moisture condition in aerated lightweight concrete walls.) Report TVBM-3026. Div. of Building Materials. Lund Institute of Technology, Lund, Sweden

Tilley D. et al. 2012. Vegetated walls: Thermal and growth properties of structured green facades. Final report to Green Roofs for Healthy Cities – Green Walls Group. UM-09040836. Toronto. www.greenroofs.org

Characterising the actual thermal performance of buildings: round robin experiment within IEA EBC Annex 58

Staf Roels, Professor [1]
Geert Bauwens, M.Sc. [1]
Gilles Flamant, M.Sc. [2]
Peder Bacher, PhD [4]
Maria José Jiménéz, PhD [3]
Henrik Madsen, Professor [4]

[1] Building Physics Section KU Leuven, Belgium
[2] Belgium Building Research Institute, Belgium
[3] Energy Efficiency in Buildings R&D Unit, CIEMAT, Spain
[4] Technical University of Denmark, Denmark

KEYWORDS: *actual energy performance, in situ characterisation, dynamic data analysis, grey box models*

SUMMARY:
Several studies have shown that actual thermal performance of buildings after construction may deviate significantly from that anticipated at design stage. As a result, there is growing interest in full scale testing of components and whole buildings. The IEA EBC Annex 58-project 'Reliable Building Energy Performance Characterisation Based on Full Scale Dynamic Measurements' is developing the necessary knowledge, tools and networks to achieve reliable in-situ dynamic testing and data analysis methods that can be used to characterise the actual thermal performance and energy efficiency of building components and whole buildings. The research within this project is driven by case studies. As a first simple case, an experiment on testing and data analysis is performed on a round robin test box. This test box can be seen as a scale model of a building, built by one of the participants, with fabric properties unknown to all other participants. Full scale measurements have been performed on the test box in different countries under real climatic conditions. The obtained dynamic data are distributed to all participants who have to try to characterise the thermal performance of the test box's fabric based on the provided data.
This paper describes the rationale, aim and objectives of IEA EBC Annex 58 and presents more in depth the first results obtained on the round robin experiment. It is shown how different techniques can be used to characterise the thermal performance of the test box, ranging from a simple stationary analysis to advanced dynamic data analysis methods.

1. Introduction

The rise of living standards, the scarcity of natural resources and the awareness of climate change resulted in an international pressure to significantly reduce the energy consumption of buildings and communities. In several countries more stringent requirements are imposed by energy performance legislation and also an increased awareness for environmental issues in building codes can be noticed. Mostly, requirements and labelling of the energy performances of buildings is done in the design phase by calculating the theoretical energy use. Several studies showed however that the actual performance after realisation of the building may deviate significantly from this theoretically designed performance. Part of the deviations can be explained by user behaviour, but the other part has to be attributed to the physical features of the building and its systems. For the latter, building performance characterisation based on full scale testing – testing of building components or whole buildings under

realistic dynamic conditions – could help to bridge the gap between theoretically predicted and real life performance of buildings. Full scale dynamic measurements are e.g. helpful to investigate the performances of building components and whole buildings as built in reality, including the influence of workmanship. This is illustrated in Figure 1. The left image shows the impact of air looping due to poor workmanship on the U-value of a cavity wall (Hens et al. 2007). While the designed U-value corresponds to a high insulation level (U=0.2 W/m²K), the value based on full scale testing measures 0.8 W/m²K, which corresponds to an increase of more than 300%. The graph at the right in Figure 1 compares the designed and realised overall heat loss (W/K) of 18 dwellings in the UK. The overall heat losses are obtained with in situ co-heating tests (Wingfield et al. 2011). As can be seen none of the houses realises the intended performance and the measured heat losses of the houses may be up to 200% of the designed value.

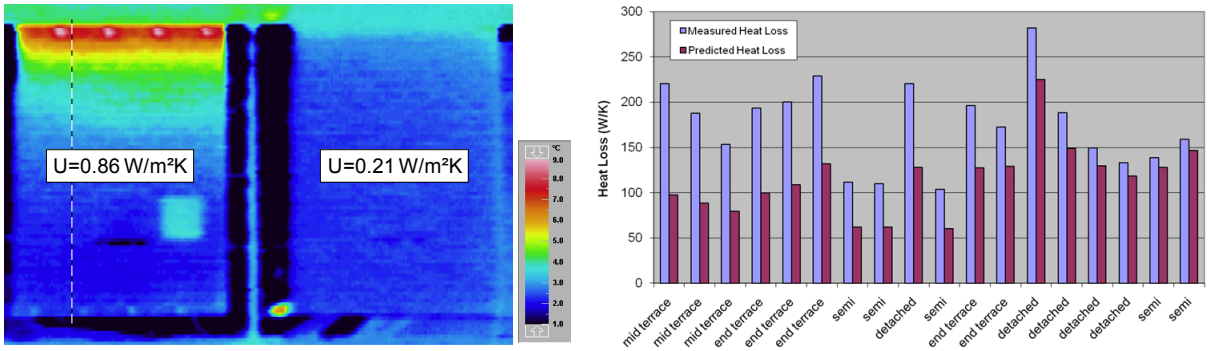

FIG 1. Left: infrared pictures of the outer leaf of two full scale highly insulated cavity walls in the VLIET-test building at KU Leuven. The impact of workmanship on the thermal performances of the walls is clearly visible. Right: Measured versus predicted whole house heat losses (W/K) for 18 new build dwellings in the UK. None of the houses is able to reach the designed values.

Examples as those mentioned above, explain why at present several in situ testing activities are going on. A recent international workshop showed the interest for full scale testing from all over the world (Janssens et al. 2011). A growing activity is observed in both full scale testing on building components (as e.g. in Paslink-cells or in situ on components of real buildings) and on whole buildings (to characterise thermal performance and energy efficiency of either test buildings or real buildings). So it is clear that, contrary to what was expected, the numerical building component and building energy simulation models did not make full scale testing of building (components) redundant. On the contrary, together with an increased application of numerical simulations, a renewed interest in full scale testing can be observed. This is not so strange, because dynamic full scale testing showed not only to be of interest to study building (component) performances under different real conditions – and as illustrated, quite often a huge difference is observed between predicted and realised performances –, it is also a valuable and necessary tool to integrate advanced components and systems into simulation models. Jiménez et al. (2008a) among others used full scale tests on BIPV-façade (BIPV: Building Integrated Photovoltaic Cells) to develop a so-called grey box-model. A grey box model is based on a combination of prior physical knowledge and statistics by identifying the unknown parameters of the system with dynamic data analysis. Once identified, the grey box model is able to predict the thermal dynamic response of ventilated photovoltaic double skin facades under different climatic conditions. This way it can be ensured that the behaviour of new advanced building components is integrated in a correct way in building energy simulation (BES) models. A similar approach of parameter identification based on dynamic measurements can be used to identify suitable models to describe the thermal dynamics of whole buildings including building systems (Bacher and Madsen 2011). Characterising the dynamic behaviour of buildings is an essential and very valuable input e.g. when optimising energy grids for building communities.

Despite the renewed interest in full scale testing, practice shows that the outcome of many on site activities can be questioned in terms of accuracy and reliability. The focus of nearly all full scale testing activities is on the assessment of the components and buildings, often neglecting the necessity of reliable assessment methods and quality assurance issues. Full scale testing however requires quality on all topics of the process chain (Strachan and Baker 2008), starting with a **good test environment**: test cells or real buildings, accuracy of sensors and correct installation, data acquisition software,… Only when this is present a **good experimental set-up** (test lay-out, imposed boundary conditions,…) can be designed producing reliable data that can be used for **dynamic data analysis** based on advanced statistical methods. This in order to come to a characterisation with reliable accuracy and **use of the results**. As soon as the required quality fails on one of the topics, the results become inconclusive or might even be wrong. To this extent an international collaboration in the framework of the 'Energy in Buildings and Communities'-programme (former ECBCS) of the International Energy Agency has been set up. Launched in September 2011, the IEA EBC Annex 58-project will work four years with international experts from all over the world on the topic of 'Reliable building energy performance characterisation based on full scale dynamic measurements'. The present paper shortly describes the Annex 58-project, but mainly focusses on a round robin experiment performed within the project. In this experiment a test box – a scale model of a building – has been built by one of the participants, with unknown fabric properties for all other participants. The test box is shipped to different institutes (different climatic conditions) with the aim to perform a full scale measurement of the box under real climatic conditions. The obtained dynamic data are distributed amongst all partners who have to try to characterise the thermal performance of the test box based on the provided dynamic data. A description of the round robin experiment is given in section 3, followed by a presentation and discussion of the first results of the experiment.

2. The IEA EBC Annex 58-project

The global objective of Annex 58 is to develop the necessary knowledge, tools and networks to achieve reliable in situ dynamic testing and data analysis methods that can be used to characterise the actual energy performance of building components and whole buildings. As the focus of the project is on the development of the testing and analysis methodology, no limitations are set to the type of components, nor to the type of buildings. The research project is organised around the full scale process chain as illustrated in Figure 2 and five subtasks are defined.

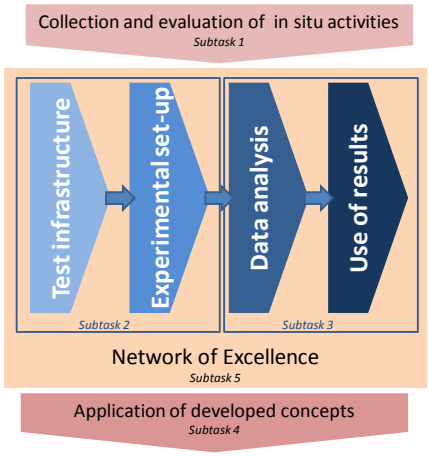

ST1. State of the art on full scale testing and dynamic data analysis

ST2. Optimising full scale dynamic testing

ST3. Dynamic data analysis and performance characterisation

ST4. Application of the developed framework

ST5. Setting up a network of excellence

FIG 2. Schematic overview of Annex 58 and organisation of different subtasks

Subtask 1 is a short introductory subtask. Based on a literature review an overview and evaluation is made of previous and ongoing in situ test activities. An inventory is made both on full scale test facilities available all over the world as well as on common methods to analyse dynamic data. **Subtask 2** establishes the procedure how to realise a good test environment and test set-up. A decision

tree will be developed to help research institutes and industry in setting up full scale dynamic testing, with emphasis on quality of test environment, measuring sensors and monitoring systems,.. in the light of the envisaged accuracy. **Subtask 3** focuses on the dynamic data analysis. The accuracy and reliability of different dynamic analysis methods will be compared by testing them on different data sets. This way quality procedures and guidelines for dynamic data analysis can be developed. **Subtask 4** will apply the developed concepts and show the applicability and importance of full scale dynamic testing for different issues with respect to energy conservation in buildings and communities. Finally in **Subtask 5** a network of excellence on 'in situ testing and dynamic data analysis' will be installed. To guarantee continuity when the Annex-project is finalised, a collaboration with DYNASTEE (http://www.just-pm.eu/dynastee) is established.

3. Round robin experiment

To determine the state of the art on full scale measurements and dynamic data analysis a round robin experiment has been set up in the framework of Subtask 3 of Annex 58. The global objective of the round robin experiment is to perform a well-controlled comparative experiment on testing and data analysis. To this extent, a test box (a scale model of a simplified building) has been built by KU Leuven. KU Leuven is the only partner within the Annex 58-project aware of the exact composition of the test box. After construction the box has been shipped to different partners (different climatic conditions and different acquisition equipment) with the aim to perform a full scale measurement of the test box under real climatic conditions. The obtained dynamic data is distributed to different institutes who have to try to characterize the test box based on the provided experimental data.

3.1 Description of the experiment

The investigated test box has a cubic form, with exterior dimensions of 120x120x120 cm³. Figure 3 gives an overall schematic view of the round robin test box. The floor, roof and wall components of the box are all identical and have a thickness of 12cm, resulting in an inner volume of 96x96x96cm³. One wall contains an operable wooden window with overall dimensions of 71x71 cm² and a glazed part of 52x52 cm². A structure is provided around the box, so that the box remains free from the thermal influence of the ground. Hence, the box can be considered as floating in free air.

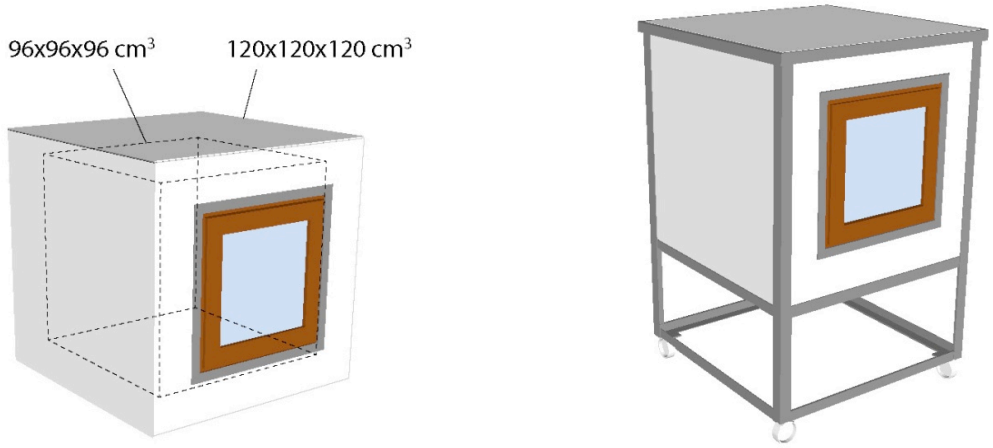

FIG 3. Overall schematic view of the round robin test box.

Winter 2012-2013 the test box has been tested at the premises of the Belgian Building Research Institute in Limelette, Belgium (50°41' N, 4°31' E). Afterwards the box has been shipped to Spain, where it was measured under summer conditions in Almeria (37.1° N, 2.4° W). In general, the weather conditions in Belgium are temperate, with a mild, but rainy, humid and cloudy winter. The weather at Almeria on the other hand is dry and extremely hot in summer, with large temperature amplitudes

between day and night. During day time, solar radiation is very high on horizontal surfaces and the sky is usually very clear. Figure 4 shows the test box at both sites.

FIG 4.Test box during winter at the measuring site at BBRI. Belgium (left) and during summer at the Plataforma Solar de Almeria, Spain (right).

At both sites, different experiments have been performed, ranging from co-heating tests with constant indoor temperature, over free floating temperature runs, to imposed dynamic heating sequences (ROLBS-signals). During the experiments, heat fluxes on all internal surfaces, together with internal and external surface temperatures, indoor temperature and delivered heating energy within the box have been measured. In addition, both test sites are equipped with an outdoor weather station, measuring all relevant boundary conditions (temperature, relative humidity, wind direction and speed, diffuse and direct solar radiation, long wave radiation,…). The measured data has been provided to all participants in the Annex 58-project. They are requested to characterise the thermal performance of the round robin test box as good as possible based on the provided dynamic data. Both stationary properties, e.g. the overall heat loss coefficient, and dynamic properties of the test box are aimed for.

3.2 Data analysis methods

Based on the provided dynamic data, different analysis methods have been used by the participants of Annex 58 to characterise the thermal performance of the test box. The techniques vary from simple stationary methods to advanced dynamic data analysis methods. In the next paragraphs a short description of the most important characterisation methods is given together with their main possibilities and limitations.

3.2.1 Averaging method

Averaging methods are typically used in winter conditions to estimate the thermal resistance of building elements from in situ surface temperature and heat flux measurements (ISO 9869, 1994). The method assumes that the (average) heat flow rate and temperatures over a sufficient long period of time give a good estimate of the values in stationary conditions. By averaging the (dynamic) measured data the steady state values are calculated. This way, making use of the measured heat input and indoor/outdoor temperature difference, the overall (stationary) heat loss coefficient of the box can be determined. The method is only valid if the thermal properties and heat transfer coefficients can be treated constant over the test period and if the effect of heat storage is negligible. As a result, it is clear that the method can be of use for the parts of the data measured during winter conditions in Belgium (when also the indoor temperature is kept constant and solar gains are negligible), but that the method

loses his applicability for the Almeria data. Furthermore, only the stationary thermal properties of the box can be determined.

3.2.2 Single and multiple linear regression

Apart from the averaging method, linear regression techniques are typically used to determine the stationary thermal properties. By fitting the linear correlation between the heat input and indoor/outdoor temperature difference, the overall heat loss coefficient can be determined. But where in the averaging method detailed (short interval data) can be used and the stationary values follow from the averaging technique, the linear regression typically makes use of daily averaged values, to cancel out short-term effects of thermal mass (Bauwens et al., 2012). Applying multiple linear regression, allows to determine not only the overall heat loss coefficient, but to gain also some information on the solar transmittance. Major drawback is again that only the stationary properties can be determined and no characterisation of the dynamic thermal behaviour of the box can be made.

3.2.3 ARX-models and ARMAX-models

Compared to the previous methods, ARX and ARMAX -models allow to include the dynamics of the system. In the abbreviation AR stands for AutoRegressive: the current output is related to the previous values of the output; MA (Moving Average) refers to the noise model used and X for the fact that eXternal inputs are used: the system relies not only on the current input value, but also on the history of the input. For identifying generic systems AR(MA)X-models are the standard methodology. The most used ARX model structure is the simple linear difference equation which relates the current output at time *t* to a finite number of past outputs and inputs. ARX and ARMAX models have among others been applied by Jimenez and Heras (2005) and Jimenez et al. (2008b) for modelling the heat dynamics of buildings and building components. Main problem when applying AR(MA)X-models on the data of the round robin box is first of all the selection and validation of the model, but then also how to interpret the model to get information on the thermal characteristics of the test box. Bacher and Delff (2013) show that by stepwise increasing the model order until most significant autocorrelation and crosscorrelation is removed, a reliable modelling of both stationary and dynamic properties of the box is feasible.

3.2.4 State space or so-called grey box models

A final methodology to characterise the round robin box is making use of state space models. State space models make use of simple resistance/capacitance schemes to simulate the dynamic behaviour of the box. Mostly a forward selection approach is used. In this approach the analysis starts with fitting a very simple model, which is then stepwise extended until the loglikelihood no longer increases significantly compared to the previous model and the model validation shows that the residuals (the difference between the measured and predicted output) correspond to white noise. As both the initial model as well as all possible extensions are expected to represent a simplified version of the round robin test box, this requires – in contrast to the ARMAX-model – some prior physical knowledge. That is why state space models are often also referred to as grey box models. Figure 5 shows as an example a two-state grey box model for the round robin test box, taking into account heat input by heater and solar radiation, capacity of the interior and walls of the box and (conductive) heat flow through the walls of the box. To identify all relevant dynamic characteristics of the box, preferably a predetermined heating power signal (e.g. ROLBS- or PRBS-signal) is imposed to excite the box around its expected time constants, whilst remaining uncorrelated with outdoor weather conditions.

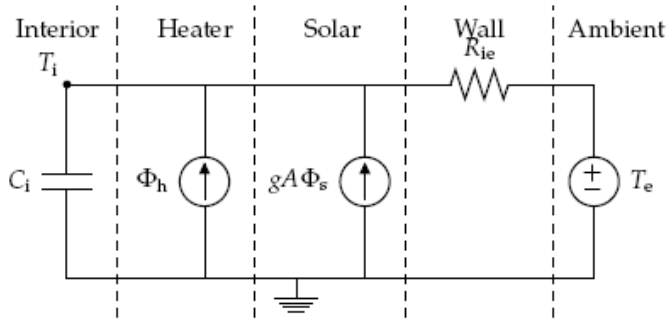

FIG 5. Example of a two-state grey box model applied by one of the participants (Bacher and Delff, 2013)

3.3 Characterisation of the test box – discussion of the results

As some of the methods are only able to determine the stationary properties of the box, Table 1 compares the obtained overall heat loss coefficient as determined by different participants. Comparing the results, it can be seen that most methods result in an overall heat loss coefficient around 4 W/K. Only when using the linear regression technique on short term data a significant lower value is found. At the moment a round robin task force has been initiated within Annex 58 to go in more depth on the pro's and cons of the different methodologies.

TABLE 1. Determined overall heat loss coefficient (W/K) of the round robin test box by different modelling teams and making use of different data analysis methods

Team		Winter data Belgium	Summer data Spain
1	Averaging method	3.77-3.92	
	State space model (RC using LORD)	3.07-3.42	
2	Averaging method	2.86-4.15	
	Linear regression (5'-data)	2.84-4.11	
	Linear regression (daily averaged data)	3.68-4.12	4.32-4.48
	AR(MA)X-models	4.06	4.07-4.32
	State space models (RC using LORD)	3.98-4.04	4.23
3	Multiple linear regression (hourly data)	4.77-5.24	
	Multiple linear regression (daily data)	3.73-4.39	
4	State space models	4.27-4.56	
5	Linear regression (daily averaged data)	3.99-4.08	
	State space models (RC using CTSM-R)	3.99	
6	State space models (RC using Matlab)	3.97	
7	ARX-models	3.95	4.05-4.10
	State space models (RC using CTSM-R)	3.84	3.96
8	Averaging method	3.72-3.99	
	Linear regression (5'-data)	2.98-3.94	
	AR(MA)X-models	4.01-4.08	
	State space models (RC using CTSM-R)	4.48	

4. Conclusions

The Annex 58-project of the IEA EBC-programme shows that there is currently a larger international interest in full scale testing and dynamic data analysis. This can be explained by the fact that full scale testing remains necessary for several reasons. It is for instance the only way to verify our numerical BES-models. Furthermore, full scale testing allows evaluation and characterisation of the thermal

performance of building components and whole buildings in reality. To illustrate this, as a first step a round robin test box experiment has been performed within the framework of Annex 58. The global objective of the round robin experiment was to perform a well-controlled comparative experiment on testing and data analysis. It is shown how different techniques can be applied to characterise the thermal performance of the test box ranging from (quasi)stationary techniques towards dynamic system identification. Where the first ones are only able to estimate the steady state properties of the box (e.g. overall heat loss coefficient), the latter can give additional information on the dynamic behaviour of the box and can be used to simulate the dynamic response of the box in a simplified way. In a next step the investigated methods will be applied to characterise real buildings.

5. Acknowledgements

The construction of the IEA EBC Annex 58 round robin test box was financially supported by Knauf Insulation. This as well as the input from the different Annex 58 members who participated in the common exercises is greatly acknowledged.

References

Bacher P and Madsen H, 2011. Identifying suitable models for the heat dynamics of buildings. Energy and Buildings, 2011, 43(7): 1511-1522.

Bacher P. and Delff P. 2013. IEA EBC Annex 58 Common Exercise 4: ARX, ARMAX and grey-box models for thermal performance characterisation of the test box. Internal report.

Bauwens G., Standaert P., Delcuve F. & Roels S. 2012. Reliability of co-heating measurements. Building Simulation and Optimization Conference 2012, Loughborough, UK. 348-355 p.

Hens H., Janssens A, Depraetere W, Carmeliet J. and Lecompte L. 2007. Brick cavity walls: a performance analysis based on measurements and simulations. Journal of Building Physics, 31(2): 95-124.

ISO 9869. 1994. Thermal insulation. Building elements. In-situ measurements of thermal resistance and thermal transmittance (ISO 9869:1994(E)). International Organization for Standardization ISO.

Janssens A., Roels S., Vandaele L. 2011. Full scale test facilities for evaluation of energy and hygrothermal performances. Proceedings of the International Workshop, Brussels, Belgium, 30-31 March 2011.

M.J. Jimenez and M.R. Heras. 2005. Application of multi-output ARX models for estimation of the u and g values of building components in outdoor testing. Solar Energy, 79(3):302–310.

M.J. Jiménez, H. Madsen, H. Bloem, B. Dammann. 2008a. Estimation of Non-linear Continuous Time Models for the Heat Exchange Dynamics of Building Integrated Photovoltaic modules. Energy and Buildings. 40, pp. 157-167.

M.J. Jimenez, H. Madsen, K. Andersen. 2008b. Identification of the main thermal characteristics of building components using matlab. Building and Environment, 43(2): 170–180.

Strachan P.A., Baker P.H. 2008. Editorial. Outdoor testing, analysis and modelling of building components. Building and Environment 43: 127-128.

Wingfield J., Miles-Shenton D., Bell M. 2011. Comparison of Measured versus Predicted Heat Loss for New Build UK Dwellings – Unpublished Data, Leeds Metropolitan University, Leeds, UK

The application of a modified co-heating test and grey-box modelling for predicting building thermal dynamics

Paul Steskens, Ph.D.[1]
Guillaume Lethé, M.Sc.[1]
Gilles Flamant, M.Sc.[1]

[1]Belgian Building Research Institute, Belgium.

KEYWORDS: *Grey-box modelling, co-heating, building thermal dynamics*

SUMMARY:
The applicability of the co-heating test for the estimation of a building's thermal dynamic characteristics, i.e. the heat loss coefficient, time constants, and effective thermal capacity, is investigated. Different grey-box models are identified based on a simulated co-heating test while the heating power supplied to the building is controlled using: (1) a constant indoor air temperature set-point, (2) multi-sinusoidal signals, and (3) a pseudo random binary sequence signals.

The study shows that measurement data obtained from a co-heating test with the indoor air temperature maintained constant is not suitable for estimation of the building's thermal dynamics, while multi-sine and PRBS based data provide a better basis for model identification. Multi-sine or PRBS signals covering a larger range of the frequency spectrum provided the best data set for identification heat dynamics, since the influence of the outdoor environmental conditions is reduced. While the advantage of the PRBS signal compared to a multi-sine signal is that its frequency spectrum is continuous, a PRBS is more stringent with respect to the selection of the sampling frequency for data collection. However, a multi-sine signal demands a well-designed frequency spectrum in order to excite the building properly.

1. Introduction

The consideration of the heat losses through the building envelope is crucial in order to develop energy efficient buildings and to reduce carbon emissions. During the last decades, the thermal insulation of building components has increased a lot, resulting in lower U values. However, experimental investigations and field studies (Hens et al. 2007) (Wingfield et al. 2009) indicated that the U values, and hence, the heat loss to the environment, in practice are often much higher compared to the theoretical U values resulting from calculations (EN ISO 6946). Moreover, the U value in practice depends strongly on the design and the installation of insulation layers.

A valuable test method to measure the heat loss of a building (both the building fabric and background ventilation) to the environment is a co-heating test. During the test, the building (often a dwelling) is heated electrically, using electric resistance point heaters, to an elevated mean internal temperature (typically 25°C) over a specific period of time, typically 3 winter weeks. The electrical energy consumption which is required for maintaining the building at the elevated temperature is measured, resulting in the heat loss coefficient (*HLC*) by plotting the daily heat input against the daily temperature difference between the inside and outside air. The development of the co-heating method started in the late 1970s and early 1980s and has been further developed, resulting in the current experimental guidelines available in the UK (Wingfield et *al*. 2011). Moreover, improvements to the co-heating test for characterization of the dynamic thermal properties of a building are currently studied in the European project IEA ECBCS Annex 58.

Nowadays, the co-heating method is mainly used for the estimation of the heat loss coefficient of a building assuming steady-state conditions and daily averaged measurement data, in an attempt to smooth the dynamic effects throughout the course of the day. However, dynamic effects and thermal inertia, represented by a building's time constants and effective thermal capacity, are important as well, for example when considering thermal comfort, overheating, and indoor climate control. In the standard EN ISO 13790 buildings are classified into inertia classes according to the value of the time constant, which is a function of the average active thermal capacitance C_m, defined as the heat accumulated inside the building, when the internal air temperature oscillates according to the sinusoid with the period t-24h and the amplitude 1K. However, the value of the internal thermal capacitance of the building depends on the amplitude of temperature oscillation in the premises. And, for indoor climate control the effective thermal capacity at other frequencies than the frequency corresponding to periods of 24h are important as well.

In this paper, the applicability of the co-heating test for the analysis of the dynamic thermal response of a building is investigated. A single zone building is selected for analysis. The building is modelled using the TRNSYS software for building energy performance simulation. A co-heating test is simulated while different input signals for the heating power supplied to the building are used: (1) a standard co-heating test, (2) multi-sinusoidal heating power, and (3) pseudo random binary sequence heating power. Based on the simulation results, grey-box models of the building's thermodynamics are developed. The grey-box models are used to estimate the dynamic thermal characteristics of the buildings, i.e. the heat loss coefficient, effective thermal capacity, and time constants. The influence of the different heating power signals on the accuracy of the estimated thermal properties is investigated.

2. Analysis

A case study building is selected and modelled using the TRNSYS software for building energy performance simulation. The software is used to simulate different co-heating experiments.

2.1 Case study

The geometry of a building which is defined along the lines of Common Exercise 1 of the IEA-ECBS Annex 41, is selected for analysis. The basic geometry of the test case building is presented in Figure 1. Table 1 shows the properties of the building, including the theoretically determined heat loss coefficients (UA values) for respectively the walls, floor, roof, and windows. Two building configurations have been used: a lightweight and a heavyweight building envelope, corresponding to a theoretical heat loss coefficient of 105.6 W/K. The walls of respectively the lightweight building and heavyweight building consist (from inside to outside) of a plasterboard (12mm), fibreglass quilt insulation (66mm), a wood siding (9mm), and of concrete blocks (100mm), foam insulation (62mm), wood siding (9mm). The floor of the lightweight building is an insulated timber floor, and an insulated concrete floor for the heavyweight building. The building is naturally ventilated with an air change rate of 0.5 h^{-1}, corresponding to a heat loss of 21.6 W/K.

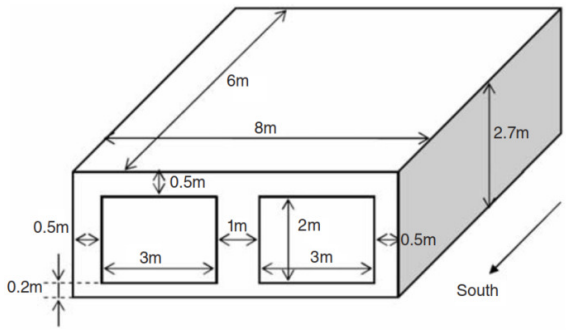

FIG 1: Geometry of the building

TABLE 1: Properties of the building

		UA [W/K]
Exterior walls [m^2]	63.6	32.4
Floor [m^2]	48	1.9
Roof [m^2]	48	15.2
Windows [m^2]	12	34.5
Constant air change rate [h^{-1}]	0.5	21.6

2.2 Heating power sequence

The co-heating tests have been simulated during two periods: a first period comprising a winter week from January 5 to January 19 and a second period consisting of a week in spring between April 1 and April 15. The building has been heated applying different sequences for the heating power supplied to the building. External boundary conditions were applied using the typical meteorological year for Belgian (Brussels) outdoor climatic conditions.

2.2.1 'Standard' co-heating: constant indoor air temperature

Figure 2 presents the outdoor and indoor air temperature, the solar radiation, and the predicted heating power during a co-heating test with a controlled indoor air temperature and a set-point of 25°C in January and April (only the results for the heavyweight building are presented in Figure 2).

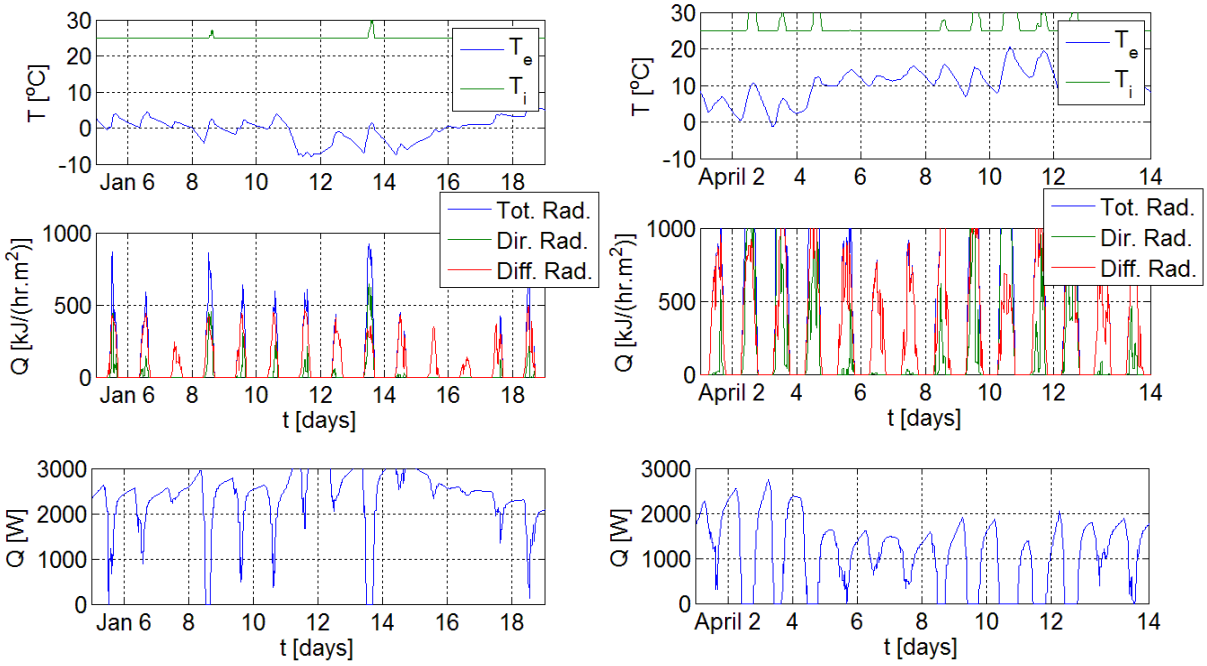

FIG 2. Indoor and outdoor air temperature (T_i and T_e [°C]), solar radiation (Q [kJ/(hr.m^2)]), and heating power (Q [W]) during the co-heating experiment with constant indoor air temperature in the heavyweight building during two weeks in January and April

2.2.2 Sinusoidal heating power sequence

Alternatively, the building is excited applying a signal consisting of multiple sines:

$$u(t) = \sum_{k=1}^{r} \alpha_k \sin(\omega_k t + \varphi_k) \quad (1)$$

with a user defined set of excitation frequencies $\{\omega_k\}_{k=1,\ldots,r}$ and associated amplitudes $\{\alpha\}_{k=1,\ldots,r}$. The phases $\{\varphi_k\}_{k=1,\ldots,r}$ are chosen in such a way that a minimal amplitude in the time domain, i.e. Schroeder-phased sines, is obtained. Obviously, when a system is excited with such a multi-sine, information is only obtained in a limited number of frequencies. The frequencies at which the system is excited are calculated based on the estimated system's lower and higher time constants, respectively τ_L and τ_H. The first identification attempts, which seem to be straightforward, are based on excitation of the system by generated sinusoidal signals with τ_L and τ_H corresponding to 60 and 240 minutes respectively, which may be sufficient in sense of building dynamics.

2.2.3 Pseudo random binary sequence PRBS heating power

As an alternative to a multi-sine signal, which only excites the system at a limited set of predefined frequencies, a pseudo random binary sequence is used for controlling the heater of the building. The heating power is a deterministic periodic signal fulfilling the requirement of continuous excitation of all modes in the system. The signal changes value (0 to 1) at a time point that is a multiple of the pulse period T, while the smallest and largest time constants are defined as $\tau_L = 2 \cdot T$ and $\tau_H = N \cdot T/5$. The shortest pulse is T time units and the longest $n \cdot T$ time units.

Table 2 presents the different signals and their properties which have been applied in the study.

TABLE 2. Properties of the different signals

Signal	Description	τ_L [h]	τ_H [h]
Const.	Controlled indoor air temperature, set point of 25°C	-	-
S1	Multi-sine function (10 sines)	1	24
S2	Multi-sine function (5 sines)	1	24
S3	Multi-sine function (5 sines)	5	120
S4	Multi-sine function (10 sines)	5	120
S5	Multi-sine function (20 sines)	5	120
P1	PRBS	5	120
P2	PRBS	1	24

3. System identification

The following iterative methodology has been applied for selecting, identification and validation of a suitable model of the heat dynamics of the building:

1. The first seven days of each data set, comprising respectively data from January 5 to January 12, and data from April 1 to April 8, are selected for model identification.
2. A sampling period containing sufficient information regarding the heat dynamics, is chosen. Average values of the signals are calculated for the sampling period.
3. The model's dependent variable(s) are selected, being the outdoor air temperature, total solar radiation on the horizontal plane and the heating power as input variables, while the indoor air temperature is selected as the output variable.
4. An ARMAX model is identified and validated with time series plots of the residuals and inputs, based on the auto-correlation function (ACF) of the residuals and cross-correlation functions (CCFs) from the residuals to the inputs. The data periods used for validation comprise January 12 to January 20 and April 8 to April 14.
5. If necessary, the mathematical order of the model is increased until the model's output does not contain any significant autocorrelation and cross-correlation.
6. The heat loss coefficient, time constants and effective thermal capacity of the building are determined.

3.1 ARMAX model

The heat dynamics of the building is modelled applying autoregressive integrated moving average models with exogenous input (ARMAX). While applying these models, it is assumed that the general properties of the building materials and the heat transfer equations are linear within the relatively narrow range of temperatures involved. And, causality exists between the different processes in the sense that the present value of the interior temperature is a unique function of the past values of the interior temperature, exterior temperature, auxiliary heat input, and solar heat gains.
The ARMAX model is written in the general form represented by:

$$A(q)Y = B(q)U + C(q)e \quad (2)$$

where $A(q)$, $B(q)$ and $C(q)$ are the p'th, s'th, and q'th order polynomials, respectively, in the backshift operator q, Y, U and e are respectively the model's output, input and the process noise. Considering the analysis of the thermal dynamics of the building, the most straightforward option is to choose the indoor air temperature T_i as dependent variable.

$$A(q)T_i = B_1(q)T_e + B_2(q)Q + B_3(q)G_v + C(q)e \quad (3)$$

where Q is the heating power [W], Ti and Te the indoor and outdoor air temperature [°C], and G_v the total horizontal radiation on the horizontal plane [W/m^2].

3.2 Interpretation of physical parameters

The physical parameters describing the heat dynamics of the building can be directly obtained from the ARMAX model's coefficients. The heat loss coefficient (HLC [W/K]) of the building is calculated based on the steady-state relationship:

$$Q = HLC(T_i - T_e) - gAG_v + e \quad (5)$$

where Q is the heating power [W], T_i and T_e the indoor and outdoor air temperature [°C], gA the solar aperture [-], and G_v the total horizontal radiation on the horizontal plane [W/m^2]. The equation is required to coincide with the steady-state equation representing the ARMAX model, where q=1, and the thermal characteristics are directly obtained from the ARMAX model's coefficients.

The transient behaviour can be characterized by the system's time constants, defined by the response to a sudden change of T_i, while all driving forces are held constant, i.e. the step response. As far as the change is concerned, the driving forces are set equal to zero. The system's time constants are derived from the ARMAX model's roots applying the methodology presented by (Jiminez et *al*. 2008) In order to calculate the building's effective thermal capacity, the methodology presented in (Rabl. 1988) is followed. Starting from a general differential equation describing the heat dynamics of a building, the effective thermal capacity is derived based on the system's time constants:

$$C_{eff} = HLC\left[(\tau_1 + \tau_2 + \cdots + \tau_N) - \frac{\alpha_{heat,1}}{\alpha_{heat,0}}\right] \quad (6)$$

where τ is a time constant and the term αheat,1/ αheat,0 could be interpreted as the sum of time constants for Q. With respect to the identified ARMAX models and the corresponding coefficients A, B1, B2, and B3 obtained. The coefficients α_i are replaced by the corresponding ARMAX parameters.

It should be noticed that the thermal capacity C_{eff} is only as exact as the coefficients of the model, which in practice are determined by means of the data set obtained. The normal diurnal cycling does not give enough time for a heat pulse to penetrate all parts of a massive building, which means that C_{eff} is an effective thermal capacity. It is a measure of the heat storable under normal cycling. For slower cycling C_{eff} would increase, and so would the time constants of the data fit. This illustrates to what extent the parameters of the model are dependent on the frequencies represented in the data.

4. Results

This section presents the simulation results and the physical parameters estimated by the different ARMAX models. Figure 3 presents a comparison of the measured indoor air temperature and the predicted indoor air temperature by a second order ARMAX model, while using a multi-sinusoidal heating power signal (S4). In addition, the figure presents plots of the ACF of the output's residuals and the CCFs between the residuals and the inputs, respectively the outdoor air temperature (T_e), the heating power (Q) and the solar radiation (G_v). No significant auto-correlation and cross-correlation is observed while the residuals lie near the confidence band of 95%. With respect to the indoor air temperature and the solar radiation, it could be argued that significant cross-correlation is observed. Additional investigations, which are not presented in this paper, showed that using a separate input for the direct solar radiation on each vertical facade instead of the total horizontal radiation on the

horizontal plane improves the model significantly. However, this increased the number of inputs with 4, i.e. one input for each facade. In order to reduce the complexity and the size of the models, it has been decided to use the total solar radiation as an input.

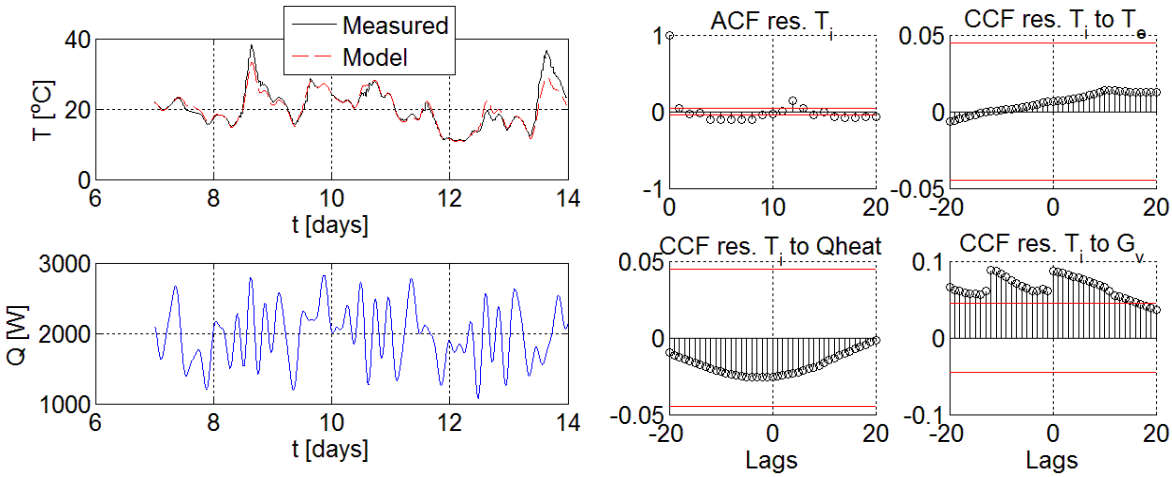

FIG 3. Comparison of the measured indoor air temperature and the indoor air temperature predicted by a second order ARMAX model using a multi-sinusoidal (S4) heating power signal and the corresponding autocorrelation and cross-correlation functions for the lightweight building

Figure 4 presents a comparison of the estimated *HLC* by the models based on the heating power signals (Table 2) both for the lightweight and the heavyweight building and for January and April. The ability of the models to predict the steady-state thermal properties of the building, i.e. *HLC* and the solar aperture are analysed. The models are compared using a relatively small sample time of 5 minutes (including both fast and slow system dynamics) and larger sample times of 15, 60, and 120 minutes focusing on the slow dynamics and the determination of the steady-state thermal parameters.

First of all, figure 4 shows that the models identified based on data obtained from the standard co-heating tests showed to be incapable of always giving a reliable prediction of the building's *HLC*. Since the indoor air temperature is constant during the measurement period, a reliable model describing the building's thermal dynamics is difficult to identify. Information regarding heat dynamics is only obtained from over-heating periods. If overheating does not occur or seldom occurs, which is the case in the heavyweight building, the capturing the building's thermal dynamics is impossible.

Second, the figure shows that the predicted *HLCs* for the lightweight building lie close to the theoretical value of 105.6 W/K, while the predicted standard deviation is relatively small, both for January and April based estimates. Moreover, model identification and prediction of the *HLC* was possible for every signal except for signal S3 in April. This signal contains too little information to excite the system sufficiently, comprising only 5 sines in a relatively large range of frequencies.

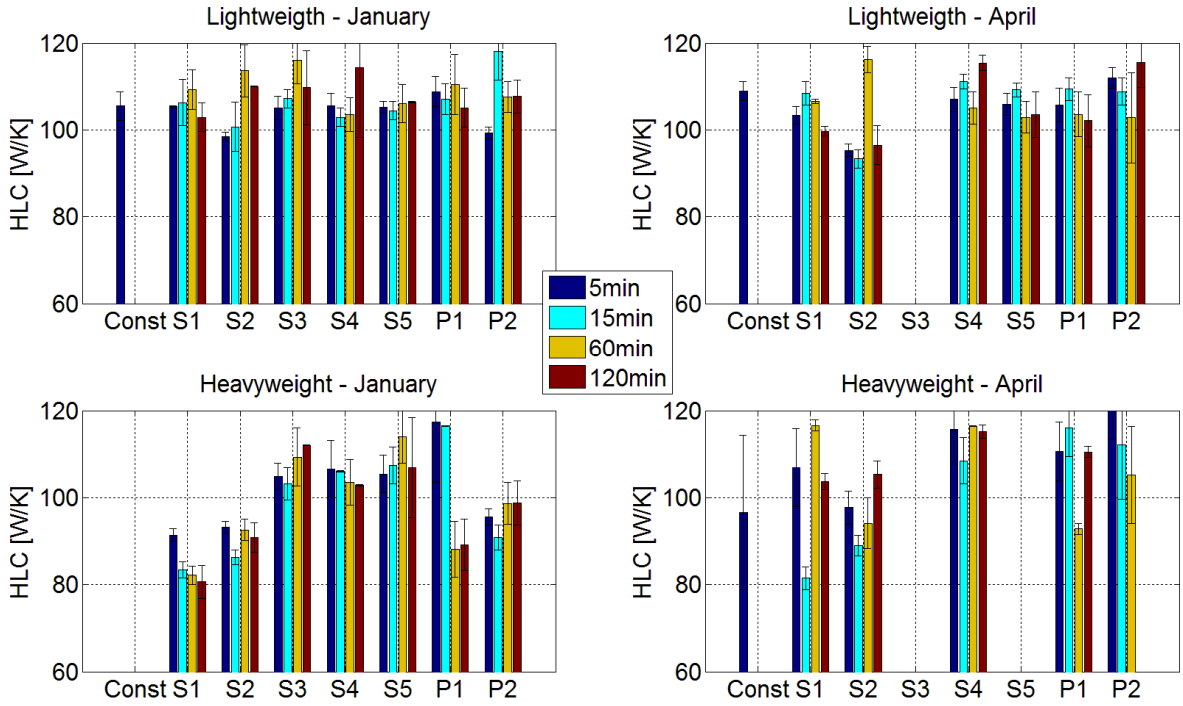

FIG 4. Estimated heat loss coefficient (HLC [W/K]) and solar aperture (gA [m^2]) for the lightweight building based on the data sets for January and April for sample times of 5, 15, 60 and 120 minutes.

Considering the predicted *HLCs* for the heavy weight building, a larger difference between the models is observed. The accuracy of the predicted *HLC* is largely influenced by the outdoor environmental conditions. The figure shows that the conditions in spring require a 'richer' signal in order to identify a reliable model. Model identification appeared only to be possible for those signals which cover a larger bandwidth of the frequency spectrum, i.e. a multi-sine signal consisting of 10 sines (S4) and PRBS signals. These signals showed to be capable of exciting the building dynamics in a wider range, clearly enhancing model identification.

Comparing multi-sine signal S4 and PRBS signals P1 and P2, the observations from this study showed that models based on PRBS heating power sequences are more susceptible to the sampling time of the data. Compared to the multi-sine signal based model, PRBS based models' predictions showed to be more influenced by redundance and reluctance of the data. If the sampling time T_s is too short the data become highly correlated (singular) and problems due to ill-conditioning arise, and redundance is observed. On the other hand, if the sampling time T_s is too long adjacent data points tend to become uncorrelated, i.e. reluctance.

TABLE 3. Estimated time constants for the lightweight building

	Lightweight		Heavyweight	
Const.	13.3	1.18	-	149.8; 0.018
S1	1.9	1.20; 0.010	7.7	10.0; 0.010
S2	2.1	1.15; 0.012	-	7.4; 0.010
S3	1.1	1.10; 0.012	7.3; 0.019	-
S4	1.1	1.20; 0.013	7.5; 0.018	7.3; 0.016
S5	1.2; 0.015	1.10; 0.012	8.1; 0.018	-
P1	1.4; 0.015	1.20; 0.013	11.8; 0.011	9.3; 0.011
P2	0.4; 0.04	1.15; 0.012	10.8; 0.012	12.0; 0.011

Table 3 presents the estimated time constants and effective thermal capacity for the lightweight and heavyweight building for the models based on different heating power sequences. For all identified

models, a sample time of 5 minutes has been applied. With respect to the lightweight building, two well-separated time constants of 0.012 and 1.1 hours and a corresponding effective thermal capacity of 0.12 kWh/K are predicted by the models based on multi-sine signals SINE3, SINE4, and SINE5. Similarly, the estimated time constants and effective thermal capacity of the heavyweight building are respectively 0.018 and 7.5 hours, and 0.8 kWh/K. With respect to the PRBS signal, slightly larger time constants are predicted.

In addition, the table shows that the models identified based on data obtained from the standard co-heating test showed not to be capable of giving a reliable prediction of the building's time constants. Since the indoor air temperature is constant during the measurement period, a reliable model describing the building's thermal dynamics and time constants could not be identified, resulting in a poor prediction of the building's thermal dynamics.

5. Conclusions and Recommendations

Based on the results presented in this study it is concluded the measurement data obtained from a co-heating test with the indoor air temperature maintained at a constant temperature is not applicable for the prediction of building thermal dynamics, i.e. the building's time constants and effective thermal capacity. Heating the building using a multi-sine or PRBS signal based heating power showed to provide a better data set for identification of the heat dynamics.

When applying multi-sine or PRBS signals covering a larger bandwidth of the frequency spectrum, the influence of the outdoor environmental conditions on model identification is reduced, and, hence, the thermal characteristics of the building can be predicted with a smaller uncertainty. The investigated PRBS signals showed always to be capable of identifying a reliable model, though these models appeared to be more influence by redundance and reluctance of the data compared to a multi-sine signal. The findings also showed that a multi-sine signal requires a well-thought signal design and selection of suitable frequencies to excite the system.

The observations and research results presented in this paper serve as a basis for additional study and analysis of the dynamic thermal characteristics of multi-zone buildings. In addition, they are applied for the design of the co-heating tests carried out at the Belgian Building Research Institute.

References

EN ISO 6946. 2007. Building components and building elements. Thermal resistance and thermal transmittance. Calculation method. (EN ISO 6946:2007). International Standards Organisation.

EN ISO 13790. 2008. Energy performance of building – Calculation of energy use for space heating and cooling. (ISO 13790:2008). International Standards Organisation

Hens H, Janssens A, Depraetere W, Carmeliet J, Lecompte J. 2007. Brick Cavity walls: performance analysis based on measurements and simulations. Journal of building physics 31(2), pp. 95-124.

Jiminez MJ, Madsen H, Andersen KK. 2008. Identification of the main thermal characteristics of building components using MATLAB. Building and Environment, vol. 43, pp. 170-180.

Madsen H. 2008. Time Series Analysis. Chapman and Hall.

Rabl. 1988. Parameter Estimation in Buildings: Methods for Dynamic Analysis of Measured Energy Use. Journal of Solar Energy Engineering, vol. 110, pp. 52-66.

Wingfield, J. Bell M, Miles-Shenton D, Seavers J. 2011. Elm Tree Mews Field Trial – Evaluation and Monitoring of Dwellings Performance Final Technical, Leeds Metropolitan University

Sensitivity analysis of the energy demand of existing buildings based on the Danish Building and Dwelling Register

Anker Nielsen, professor [1]
Kim B. Wittchen, senior researcher [1]
Niels H. Bertelsen, senior researcher[1]

[1] Danish Building Research Institute, Aalborg University, Denmark

KEYWORDS: *Energy demand; Danish Building Regulations; Calculation method; Uncertainty; Energy ratings*

SUMMARY:
The EU Directive on the Energy Performance of Buildings requires that energy certification of buildings should be implemented in Denmark so that houses that are sold or let should have an energy performance certificate. The result is that only a small part of existing houses has an energy performance certificate. The Danish Building Research Institute has described a method that can be applied for estimating the energy demand of dwellings. This is based on the information in the Danish Building and Dwelling Register and requirements in the Danish Building Regulations from the year of construction of the house. The result is an estimate of the energy demand of each building with a variation. This makes it possible to make an automatic classification of all buildings. The paper discusses the uncertainties and makes a sensitivity analysis to find the important parameters. The variations are compared with measured energy demand. The method can be applied in other countries with modifications for local building requirements, climate and building registers.

1. Introduction

In Denmark, energy performance certification has been in use since 1997 with energy performance rating and for new houses (since 2006), including sold or let buildings. The energy rating classifies the building on an efficiency scale ranging from A (high energy efficiency) to G (poor efficiency) (EPBD 2011). The rating is important when buying and selling houses. The problem is that many houses still do not have an energy rating, and that it will take many years to cover the entire building stock. Until ultimo 2013, only 22% of single-family houses had an energy rating. Energy ratings are given in connection with a visit by an energy expert and the result is a rating and a description of possible energy-saving measures. For houses that have not been energy rated, we do not know the energy demand and potential energy savings. An automatic calculation of the energy rating would thus be very useful. It is possible that some owners would make energy saving measures, if they were informed about the energy rating of their property. It would also make it possible for authorities to give an economic subsidy or tax deduction for the buildings with the poorest energy efficiency. The result should be more energy saved for the same money.

It is possible to apply a normal certification method based on monthly values and details on heating system and constructions to make energy demand calculations of existing houses. The problem is that we have to visit the houses and we will not always be able to obtain information about the constructions at the site or in drawings. Another important point is that this would be a very time-consuming and expensive method. The Danish Energy Performance Certification Scheme for existing buildings includes energy demand calculations based on a monthly calculation method (Aggerholm and Grau 2005). This can be used at the visit as you can find some information and have additional information from a guideline with typical constructions. The cost of this is paid by the owner before selling the building. As it will take many years before all buildings have been officially rated, the Danish Building Research Institute (SBi) has described a method (Bertelsen et al. 2011) that can be used without physically visiting the house but only based on available information.

2. BBR data

The Danish Building and Dwelling Register (BBR) has information that can form the basis for the calculation. This has to be supplemented with information from the Danish Building Regulations from the year of construction and some estimates from previous research and information collection (Wittchen 2009 and 2012) by SBi. The following data from BBR are used: building (building type), year of construction, useful floor area in m^2, number of storeys, building footprint in m^2,useful attic area in m^2, basement area in m^2 and external wall material.

The described method can be used for dwellings like single-family houses and blocks of flats. In the following, we only describe the use for single-family houses. The construction year is used to find the actual energy requirements in the Danish Building Regulations. In Denmark, we can expect that these requirements for thermal insulation are respected. We know that many buildings have better insulation or improved windows and we take that into account in the method.

The useful floor area is used for calculating the amount of heat from persons, light, equipment and solar radiation. The number of storeys, the building footprint, useful attic area, and basement area are used in the calculation of the geometry of the building. The external wall material defines the U-value level in the Danish Buildings Regulations.

3. Geometric model

BBR contains no information on building height, length or width. So we have to make an estimate of the geometry. The simplest form is a box-shaped building. We know the roof and floor area as it equals the building footprint. For buildings without attic and basement, we use a box-shaped building. We need the building width. Based on typical Danish buildings, we estimate the building width to be 9 m for single-family houses. The building length is the building footprint divided by the width. Calculations with other length/width proportions show that it does not influence the surface area very much. The storey height is assumed to be 2.8 m as a typical value. The volume and the external wall area can then be calculated.

If the building has a useful attic area, we get an extra wall area based on the attic which is also a box. The box is placed on top of the building box and does not change the floor or roof area. The length of the attic is estimated to be the length of the building. The width and volume of the attic and wall area can now be calculated.

For houses with a basement, this is calculated as a box placed under the building. As it is placed underneath the building, there is no change in floor or roof area. The walls of the box give the basement wall area. Note: We calculate as if the whole basement area is heated, as most people use it like that. The length of the basement is estimated to be equal to the length of the building. The width and volume of the basement and the basement wall area can now be calculated.

3.1 Areas used in the energy calculations

The roof area and the floor area are both equal to the building footprint. The external wall area is the sum of the wall areas of the building box and the attic box. The volume of the building is the sum of the volume of the three boxes. This is a simplification as some part of the volume might be unheated, e.g. staircases.

Another important information is the area of the windows of the building, as windows have a greater heat loss than the rest of the wall area. There is no information on window area or number of glass panes in BBR, so we need to estimate the values. The window area also includes door areas. It is estimated that before 1999 most buildings had a window area covering 15% of the façade area. After 1999, the windows covered 22% based on Wittchen 2009 and 2012. The basement wall has no windows. If we have an attic, then we estimate a window area covering 10% of the attic wall area.

Now we can calculate the window area for the building based on the construction year and possible presence of an attic. The wall area excluding windows is then easy to find.

4. U-value model

U-values for the different building parts are taken from the Danish Building Regulations in force when the building was constructed. Energy requirements were changed in 1961, 1967, 1972, 1977, 1982, 1985, 1995, 1998 and 2008. The five U-values used in the calculation are outer wall, basement wall, floor, roof and window. We do not take into account that we can have different outer wall constructions in the same house.

TABLE 1. Typical U-values and requirements in different periods

Heavy outer wall (> 100 kg/m^2)		Roofs		Windows	
Before 1930	1.2 W/m^{2}K	Before 1950	0.97 W/m^{2}K	Before 1930	3.7 W/m^{2}K
1931-1950	1.5 W/m^{2}K	1951-1960	0.6 W/m^{2}K	1931-1994	2.9 W/m^{2}K
1951-1960	1.5 W/m^{2}K	1961-1976	0.4 W/m^{2}K	1995-2007	1.8 W/m^{2}K
1961-1971	1.1 W/m^{2}K	1977-1994	0.2 W/m^{2}K	From 2008	1.5 W/m^{2}K
1972-1976	1.0 W/m^{2}K	From 1995	0.15 W/m^{2}K	Note: We assume that most old windows are upgraded.	
1977-1994	0.4 W/m^{2}K				
1995-2007	0.3 W/m^{2}K				
From 2008	0.2 W/m^{2}K				

BBR information on the exterior wall material is used to decide whether it is a light or heavy wall as the Danish Building Regulations define different U-values for these wall types. Data about older houses are supplemented by the experience of SBi. Table 1 is an example of the U-value variation over the years for heavy outer walls, roofs and windows. Data for other construction types and periods are given in a Danish report (Bertelsen et al. 2011).

5. Model for energy balance

The total transmission heat loss is found by multiplying the areas with the U-values from the construction year and making a summation of all constructions in the house. For floor and basement walls, we reduced the heat loss by 30% because of the ground.

The volume of the building is needed for calculation of the ventilation loss. As mentioned, the volume also includes internal construction and unheated areas such as staircases and basement. The ventilation is estimated based on SBi's experience gained from other projects. Here it was found that before 1961the air change rate (1/h) was 0.45, from 1961 to 1978 it was 0.4 and after 1978 it was 0.35.

Calculation of heat from sun, persons, and equipment can be complicated. It is theoretically possible to calculate the solar radiation through windows, but there are uncertainties in both the areas and orientation of the windows. The heat from persons, light, equipment etc. is also very uncertain. Another problem is that only part of this heat will reduce the heating energy demand of the building. The solution is to use a value for the useful part of the internal loads from SBi. The useful internal heat gain is estimated to be 55 kWh/m^{2}year, where the sun accounts for half the amount.

To calculate the energy loss, it is necessary to know the indoor and outdoor temperature. The indoor temperature is fixed at 20 °C. We use degree days. In Denmark the degree-day number for the energy calculation is 3600. The useful internal heat gain is calculated for the living area (given in BBR), and does not include for instance basement areas not accepted for living. The energy demand for heating the building in kWh/year (EX) can then be calculated as the sum of the heating and ventilation losses minus the useful internal heat gain.

6. Uncertainty of the parameters

The calculated energy demand is the best estimate based on the information in BBR and the estimates made by SBi based on the knowledge of the Danish building stock. Table 2 lists all the uncertainty parameters.

TABLE 2. List of uncertain parameters

Geometry	U-values	Energy calculation
Width	Walls	Ventilation rate
Length	Roof	Airtightness
Storey height	Floors	Useful heat (solar, persons, light and equipment)
Volume	Window type, number of glass panes translucent area, glass coating, orientation	Degree-hour number
Attic area and width		Renovation
Basement area and width		
Window area		

The method ignores complex geometric buildings like U or L shaped ones. The uncertainty of the U-values is large for buildings constructed before the first nationwide Danish Building Regulation in 1961 – after that time the uncertainty is lower as buildings are normally built in compliance with the Danish Building Regulations. There is no information in BBR as to whether extra insulation has been added after the construction year. In practice, we can expect that energy-saving measures have been implemented in many older buildings.

7. Variations of the result

Measurements of the energy demand of buildings show large variations for individual buildings in spite of their being uniform in construction (Petersen 1997). This is caused by the influence from the users and variations in workmanship etc. This calculation method is based on the variations in the building and only partly takes into account the variation caused by the users and their use of the building. If that variation was fully included, the variation would increase.

An estimation of the uncertainty of the calculations depends on the construction year. Old houses have a large variation and new houses a lower variation. The method provides an upper limit and a lower limit, as given in Table 3. The variation is not symmetric. These limits are in reality upper and lower quartiles as we estimate that 25% of houses have an energy demand higher than the upper limit and 25% of houses have an energy demand lower than the lower limit

TABLE 3. Variations in upper and lower limits during different periods

Upper limit	Lower limit
Before 1961: EX * 1.25	Before 1931: EX * 0.60
(it is 25% above the average)	(it is 40% below the average)
1961-1971: EX * 1.15	1931-1961: EX * 0.70
From 1972: EX * 1.10	1962-1977: EX * 0.80
	1978-1995: EX * 0.85
	After 1995: EX * 0.90

The lower limit has more variations than the upper limit which is explained by the fact that many old houses have been retrofitted with extra insulation and new windows. The result is an energy demand that is well below the average calculated value (EX). The values in kWh/year are calculated as energy demand per m^2 as this is the basis for the Danish Energy Performance Certification Scheme.

8. Automatic energy rating

The described method to perform automatic energy demand calculations can be used for automatic energy certification and rating of houses that do not have an official energy performance certificate. The auto-rating method can be described as follows:

Using the average energy demand per m^2 (EX) as a basis for automatic rating results in a number of houses would get a better rating than if they had been visited by an energy expert. This problem is solved by calculating the energy demand from the upper-limit energy demand (worst case). Use of this value makes nearly all houses obtain a better rating when an official certification is made later.

The method has been used in a case study of a street with 56 single-family houses. Figure 1 shows variations in energy demand, based on the construction year. It is seen that most houses are built from 1940 to 1960. Most houses with an automatic rating are rated either F or G, the two lowest ratings.

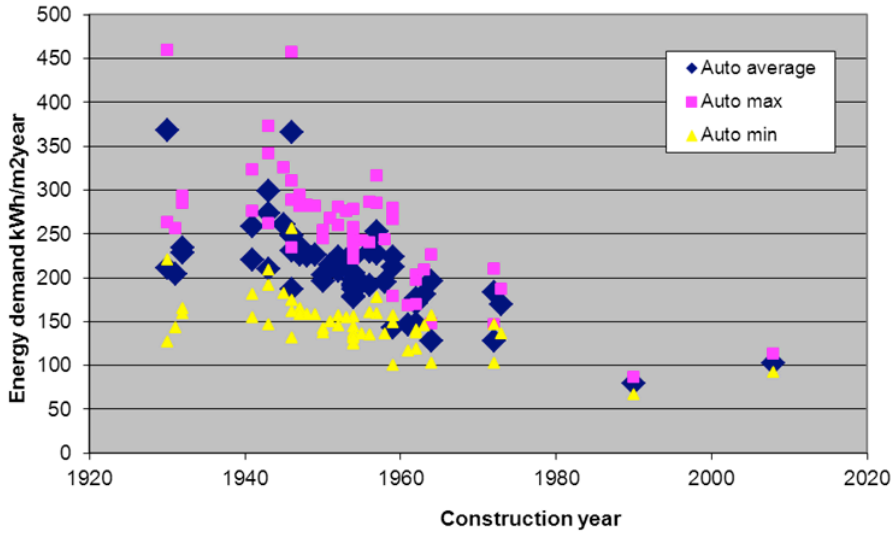

FIG 1. Calculated energy demand of 56 single-family houses versus construction year.

If we compare the official energy rating for the five houses that have an official energy certificate with the result of the automatic rating method based on BBR it is seen that the officially calculated energy demand by the energy expert lies between the upper and lower limits of the automatic method. As expected, the value is closer to the lower limit, as some energy-saving measures were made. These are typically additional insulation, tightening and retrofitting of windows and new heating system.

9. Sensitivity analysis for automatic calculation

A sensitivity analysis is done on a house from 1964 with a Monte Carlo simulation using random values to recreate the variation of the parameters. The calculation data is described in Table 4.

TABLE 4. Case of a single-family house with average values and variations

Geometry

- Building footprint 100 m^2 (variations from 95 to 105 m^2)
- Storey height 2.8 m (variations from 2.4 to 3.0 m)
- Length of house (area fixed – variation in length/width)
- Areas of windows 15% (variation from 10 to 25%)
- Insulations and constructions in W/m^2K. It is taken into account that there is a possible later insulation of the constructions.
- Walls 1964 1.1 W/m^2K (variation from 0.6 to 1.3 W/m^2K)
- Windows 1964 2.9 W/m2K (variation from 1.6 to 3.0 W/m^2K)
- Roof 1964 0.4 W/m^2K (variation from 0.25 to 0.5 W/m2K)
- Floor 1964 0.4 W/m^2K (variation from 0.3 to 0.5 W/m2K)

Other parameters

- Air change rate 0.4 1/h (variation from 0.2 to 0.6 1/h)
- Indoor climate – constant standard value
- Outdoor climate – constant standard value
- Heat from persons, equipment and solar radiation – constant standard value

The calculation of 10000 cases gives an average value and a variation for the building:

- Average energy demand 192 kWh/m^2
- In 10% of the cases, the demand is less than 157 kWh/m^2
- In 10% of the cases, the demand is higher than 226 kWh/m^2
- So 80% of all values ranged between 157 and 226 kWh/m^2

This variation is similar to the variation found in other research on buildings' from around 1965. The calculation makes it possible to evaluate the sensitivity of the parameters in the calculation. Table 5 show which parameters have the most influence on the final result.

TABLE 5. The calculated variance for the 9 parameters in the sensitivity analysis

Parameter	Variance	Sum of Variance
Wall U-value	36%	36%
Storey height	19%	55%
Air change rate	15%	70%
Window area	10%	80%
Roof U-value	7%	87%
Windows U-value	6%	93%
Building footprint	4%	97%
Floor U-value	2%	100%
Length/width proportion	0%	100%

The most important parameter is the U-value of the wall, and after that the storey height, air change rate and window area and hereafter the rest of the U-values and the built area. If we do a more correct calculation, we need more information. From this analysis, we see that if we can get better information on the U-values of the wall, the storey height and window area, we reduce the variance in the energy demand calculation as they account for 65% of the variation. The air change rate is very difficult to know without making measurement and it will change during the year – so it is not realistic to get better information on the air exchange rate. For the other three parameters, it is possible to ask the owner about the values and whether extra insulation has been added. It is interesting to note that an improvement of information for a number of the parameters does not have much effect on reducing the variance.

If we use the method to calculate the total energy demand for a group of houses, the estimate will be much better, if we assume that the houses have random variations. For instance we can estimate a single house with a variation of 56%, but for a group of 10 houses is it 18% and for more than 50 houses is it 8%.

10. Measured energy use

Is the assumption realistic if we compare with measured energy consumption in buildings? Figure 2 shows measured energy consumption for houses in relation to construction year (Jensen 2004). The red line is the level of the rules in the Danish Building Regulations from 1961 and onwards. It is seen that for most houses from 1960 to 1996, the energy consumption is below the requirement level. So our assumption that houses follow the rules is realistic and also that many has been improved. After 1996, more houses have a higher energy use than the Danish Building Regulations, probably because a slightly higher indoor temperature will only give a small increase in the energy bill. For older houses, this effect of the indoor temperature variation is blurred.

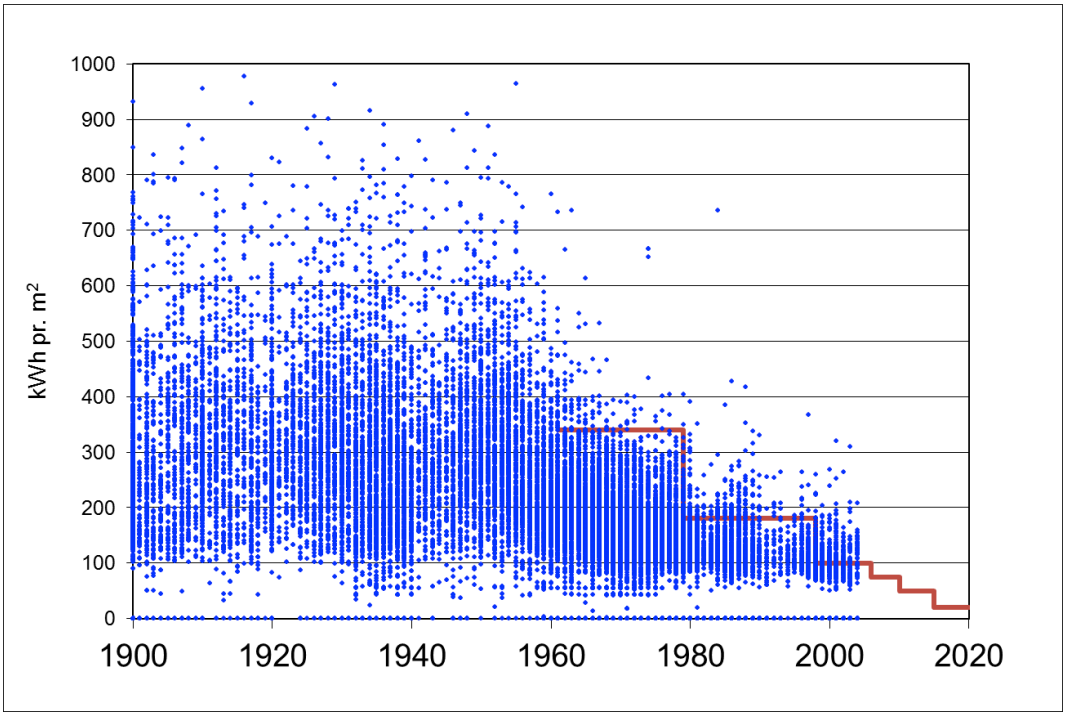

FIG 2. Measured energy consumption (dots) in Danish houses for different construction year. The red line is the requirement in the Danish Building Regulations.

Figure 3 shows that old houses have a high energy demand and large variation and new houses has lower energy demand and less absolute variation (Jensen 2004). The arrows indicate the average values. This shows that our assumptions for variations are realistic.

11.Conclusion and use in other countries

The comparison between the official Danish energy performance certification scheme and the automatic system shows that the automatic system can be used to identify buildings with potentially high energy consumption. This can be done based on information in BBR and the knowledge of typical Danish buildings. This provides a possibility of targeting incentives for better energy performance in the buildings, where you obtain the highest energy savings for the investment. The comparison with measurements shows that our assumptions are realistic.

This method can also be used in other countries using similar basic national building registers and building regulations over time, climate and information of the typical building and their use.

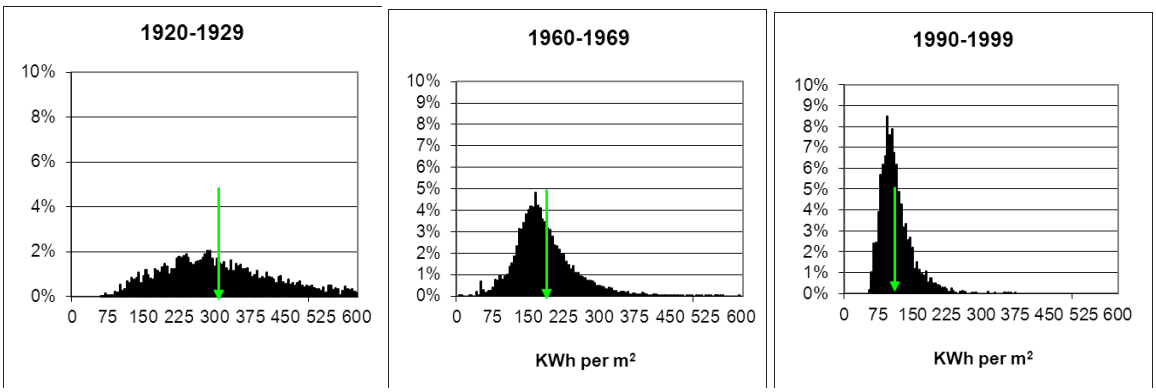

FIG 3. Variation in energy demand of houses with different construction year

References

Aggerholm, S. and Grau, K. (2005). Bygningers energibehov - PC-program og beregningsvejledning. (Building energy demand – PC program and user guide) SBi-Anvisning 213. Statens Byggeforskningsinstitut (SBi), Hørsholm, Denmark

Bertelsen, N. H., Nielsen, A., Sørensen, N.L. and Wittchen, K.B. (2011) Automatisk energirammeberegning for den eksisterende bygningsmasse (Automatic energy performace calculation for the existing buildings), SBi-rapport 2011-20, Statens Byggeforskningsinstitut (SBi), Hørsholm, Denmark

Danish Building Regulations (in Danish: BygningsReglementet. Erhvervs- og Byggestyrelsen, København. Use www.ebst.dk – to find older building regulations

EPBD (2011). Implementation of the Directive on the Energy Performance of Buildings - Country reports 2010. EPBD Buildings Platform, Brussels, European Commission ISBN: 978-92-9202-090-3.

Jensen, O. M. (2004). Barrierer for realisering af energibesparelser i bygninger. (Barriers for realisation of energy saving in buildings), Statens Byggeforskningsinstitut (SBi), Hørsholm.

Petersen, T.D. (1997). Uncertainty analysis of energy consumption in dwellings, NTNU, Dr.avh. 1997-122, Trondheim, Norway

Wittchen, K. B. (2009). Potentielle energibesparelser i det eksisterende byggeri. (Potential energy savings in existing buildings) Forskningsprojekt SBi 2009:05. Statens Byggeforskningsinstitut, Hørsholm, Danmark

Wittchen, K.B, and Kragh, J. (2012) Danish building typologies, Danish Building Research Institute, SBi 2012:01, Hørsholm, Denmark

Thermal performance of a window with in-between solar shading - Hot box measurements and simulated performance comparison

Steinar Grynning M.Sc, PhD-candidate [1,2*]
Berit Time, Senior Principle Research Scientist, PhD[2]
Egil Rognvik[2], Engineer
Arild Gustavsen, Professor, PhD [1,2]

[1] Department of Architectural Design, History and Technology, Norwegian University of Science and Technology (NTNU), NO-7491 Trondheim, Norway,
[2] SINTEF Building and Infrastructure, Building Materials and Constructions, Høgskoleringen 7b, Trondheim, Norway

* Corresponding author: steinar.grynning@sintef.no, tel. +47 97 56 61 03, fax +47 73 593380.

Keywords: *Windows, glazing, solar shading, thermal transmittance, U-value, Hot box, laboratory, simulation*

SUMMARY:
Shading systems are widely used in conjunction with glazed facades, especially in office buildings. Solar gains in combination with high internal gains will often lead to a cooling need during operational hours. Thus, shading devices are traditionally used in order to reduce cooling demands during the time of day when the sun is up.

The possible effects of a solar shading device on the thermal transmittance value (U-value) of the glazing unit has, however, not been given much attention.

In order to assess energy saving potentials by applying shading devices, detailed information about the component level characteristics is necessary. Thermal and optical properties of these components are important input data for simulation tools and the calculation of cooling and heating demands as well as daylight accessibility in buildings.

Shading systems can be categorized into three main types; external, internal and in-between panes shading devices. When an in-between pane shading device is deployed (i.e. closed shut), it can act as an additional layer in the insulating glazing unit (IGU) and thus reduce the U-value of the IGU. In a cold climate, such a system could be utilized in order to reduce heat losses during periods of time when a room is not occupied and when no view to the outdoors is necessary.

In this article, the thermal properties of such a system have been explored. Hot-box measurements have been carried out for a window with 4-panes. The glazing unit is built up as a 3-pane IGU with an external coupled fourth pane. A venetian blind shading device is placed between the outermost, coupled pane and the IGU. U-values have been measured for various slat-angles of the blinds. These results have been compared with calculated values using the THERM and WINDOW simulation software. This is software developed for calculations of thermal and optical properties of entire windows.

1 Introduction

Some of the previous work pertaining to louvered blinds has been done for a horizontal blind sealed between the panes of an Insulated Glazing Unit (IGU). Garnet et al. (1995) carried out an

experimental investigation using a guarded hot plate apparatus to determine the thermal performance of an IGU with a between-the-panes venetian blind. They found that the effect of the venetian blinds on the U-value of the glazing unit ranged from a 10 % increase for blinds in horizontal position to a 20 % decrease with the venetian blinds in a closed position. It is also concluded that, from a thermal performance perspective, it is better to close the blinds hot side up, i.e. the slats should point upwards on the warm side of the window. Similar blind configurations, within a sealed IGU, have also been studied using analytical and numerical models (Rheault and Bilgen 1989).

In spite of a large amount of theoretical work carried out in order to assess thermal and optical performance of solar shading systems, few measurement campaigns have been carried out. In 2001, Breitenbach et al. (2001) presented thermal resistance measurements for a two-pane IGU with integrated venetian blinds. The authors found that the thermal transmittance value (U-value) varied almost linearly with the slat angle from 2.92 ± 0.14 W/(m²K) with blinds retracted to 1.44 ± 0.21 W/(m²K) with the blinds shut and slats in vertical, closed position. This contradicts the values found by Tzempelikos (2005) during a measurement campaign performed on a double-pane window with in-between venetian blinds. Here it was found that a blind-tilt angle of 120° gave the lowest thermal resistance and that blinds closed with the slats in vertical (i.e. 180°) position gave the highest thermal resistance.

None of the two aforementioned publications present values for a situation with the blinds in a retracted position and only the centre-of-glass U-values are presented. Presenting only centre-of-glazing U-values does not take into account any effects caused by the mounting system and any motor of the venetians on the total U-value of the glazing unit. Such effects could be substantial as mounting systems and motors may contain large amounts of continuous metal spanning from the warm to the cold side.

In 2006 Huang et.al (2006) presented measurements performed using a Guarded Heater Plate apparatus (GHP). Here, centre-of-glass U-values (U_{cog}) for double-glazing units with and without shades, were measured using Heat Flow Meters (HFM). This was carried out by controlling the temperature on each side of the sample using the GHP. 12 sample configurations were measured. The measured values were used for benchmarking/validation of CFD simulations. Values are extrapolated to also include solar heat gain coefficients (SHGC) and visual transmittance (T_{vis}) values.

A study performed by Shahid H. and Naylor D. (2005) presents a numerical method for a window with internal shading. The method is validated by use of previous measurement results for tall vertical cavities. No validation using measurements on real windows was performed.

In 2009, Laouadi (2009) presented an overview of existing studies related to modelling of glazing units coupled with solar shading systems. A model for calculating properties of the centre-of-glazing area were proposed and found to correspond to measurements performed by Huang within a 7 % margin of error. The model is only verified for double pane glazing units with a limited (lower than 25 mm) cavity thickness. The U-value of IGU's with low-e coated glazings and higher cavity thicknesses (40 mm was modelled) were underestimated with the model. Furthermore, the authors point out that at that time, the models regarding the thermal performance of shading systems are based on simple algorithms and that further validation work needs to be carried out.

2 Methodology and experimental design

2.1 Window sample and test series overview

U-values are measured for a 4-pane window with integrated in-between-pane venetian blinds. The window consists of a 3-pane IGU with argon fillings. An external 4th coupled glass pane is mounted

on the exterior side. A manually operated (i.e.no motor) venetian type blind is mounted in the exterior cavity as shown in Figure 1.

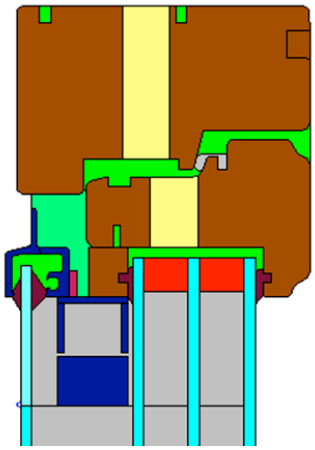

Figure 1. Graphical illustration of the 4-pane window. Shading device, in dark blue, shown in retracted position. The shading device is integrated in the cavity behind an exterior coupled glass pane. The frame is insulated with polyurethane foam (coloured yellow).

Table 1 shows an overview and description of the window configurations that have been measured. Generic data as described in ISO 15099 (ISO 2003) has been used as material data for the shading slats.

Table 1: Window sample description.

Window and material description	**Measurement description**

• Window size: 1200 x 1200 mm (w x h)
• Operable window
• 3-pane IGU + 1 exterior coupled pane
• Glazing construct: 4-24-4E-12Ar-4-12Ar-E4
• Venetian blind in external (coupled) cavity
• Wood frame insulated with 17 mm polyurethane foam
  ○ Sill width 101 mm
  ○ Jamb width 94 mm
  ○ Head width 105 mm
  ○ Frame depth (all parts) 105 mm
• Materials used in simulations
  ○ Wood thermal conductivity = 0.12 W/(mK)
  ○ Polyurethane thermal conductivity = 0.023 W/(mK)
  ○ Window spacer equivalent conductivity = 0.158 W/(mK)
• Slat material A from ISO 15099
  ○ Conductivity = 160 W/(mK)
  ○ Front- and back-side emissivity = 0.9
  ○ Front- and back-side reflectance = 0.7
	Blind position
	1. Retracted blind
	2. deployed blind horizontal slats
	3. deployed blind 45° slats
	4. deployed blinds vertical slats

Figure 2 shows the four blind positions as described in Table 1.

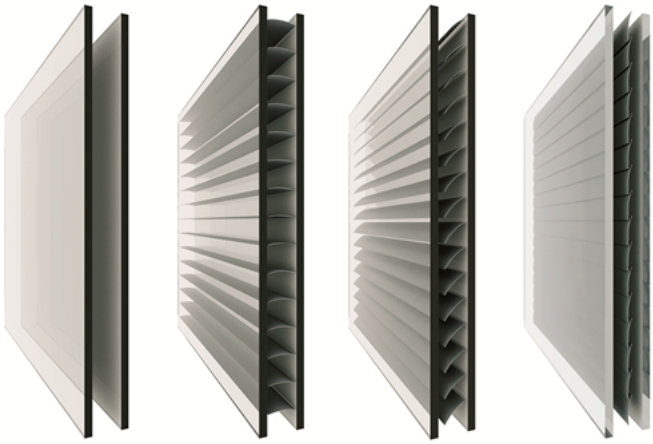

Figure 2. Blinds positions 1-4 as described in Table 1. Position 1 on the left and 4 on the right.

2.2 The hot box test facility – test procedure and instrumentation

Measurements have been carried out in a guarded hot box apparatus, as pictured in Figure 2, according to procedures described in ISO 8990:1994 *Determination of steady-state thermal transmission properties Calibrated and guarded hot box* (ISO 1994) and ISO 12567-1:2010 *Thermal performance of windows and doors - Determination of thermal transmittance by the hot-box method - Part 1: Complete windows and doors* (ISO 2010).

Figure 2. The guarded hot box test facility used for the measurements

The tests were performed at steady state conditions of +20 °C interior and 0 °C exterior temperatures. Window U-values are calculated based on the measured heat flows, surrounding temperatures and window area.

The window was mounted in a template constructed as a sandwich element consisting of a 100 mm thick Extruded Polystyrene (XPS) core, clad with 12 mm plywood on the faces exposed to the hot and cold sides of the hot box. The joints between the window and the surround panel are sealed with tape on both sides to ensure an air tight seal. Minor gaps between window frame and template were filled with Expanded polystyrene (EPS).

The metering area of the hot box is 2.45 m x 2.45 m. The window is placed in the middle of the metering area template wall at a distance of 1.0 m from the floor to the lower edge of the frame.

24 hourly, measured averaged values are used as basis for establishing the U-values. Each of the hourly measurement periods are again averages of values measured every 6-8 seconds.

Surface thermal resistances were adjusted close to the standardised ones prior to the tests by adjusting air flow velocities adjacent to the template surface on the cold side. Natural convection driven air-flow were maintained on the warm side. However, during the measurements the surface thermal resistances differ slightly from the standardized values. Corrections have thus been made for these deviations, so that all U-values are stated with normalised surface thermal resistance values as specified in ISO 8994:1994 (ISO 1994). The standardized conditions are; interior surface thermal resistance, R_{si} = 0.13 W/m²K and external surface thermal resistance R_{se} = 0.04 W/m²K.

Centre-of-glazing U-values (U_{cog}) were measured using two PU 43 T heat flow meters, from Hukseflux (Hukseflux), with a declared accuracy of ± 5 % at 20°C. These were mounted mid-height approximately 10 cm from the vertical symmetry axis of the IGUs on the warm side of the samples.

2.3 Uncertainty assessments

The uncertainties associated with the hot box measurements have been assessed in accordance with the procedure presented in ISO 12567-1:2010 (ISO 2010) The total uncertainty propagation of the measured U-value, $\Delta^P U_w/U_w$ has been derived using the root-mean-square method (RMS) as shown in Eq.1.

$$\frac{\Delta^P U_w}{U_w} = \sqrt{\left[\frac{\Delta^P \Phi_w}{\Phi_w}\right]^2 + \left[\frac{\Delta^P A_w}{A_w}\right]^2 + \left[\frac{\Delta^P \delta\theta_{ie}}{\theta_{ie}}\right]^2} \quad (1)$$

Where $\Delta^P\Phi_w/\Phi_w$ = Uncertainty in sample heat flow (W)
$\Delta^P A_w/A_w$ = Uncertainty of projected area of sample (m²)
$\Delta^P\delta\theta_{ie}/\delta\theta_{ie}$ = Uncertainty in temperature difference between warm and cold side (K)

The uncertainty in the sample heat flow is based on the heat balance equation for the metering chamber. The uncertainties in test sample specimen heat flow, $\Delta^P\Phi_w/\Phi_w$, is expressed using Eq. 2.

$$\frac{\Delta^P \Phi_w}{\Phi_w} = \sqrt{\left(\frac{\Delta^P \Phi_{IN}}{\Phi_w}\right)^2 + \left(\frac{\Delta^P \Phi_{sur}}{\Phi_w}\right)^2 + \left(\frac{\Delta^P \Phi_{EXTR}}{\Phi_w}\right)^2 + \left(\frac{\Delta^P \Phi_{FL,w}}{\Phi_w}\right)^2} \quad (2)$$

Where $\Delta^P\Phi_{IN}$ = Uncertainty in power input to metering chamber (W)
$\Delta^P\Phi_{sur}$ = Uncertainty in surrounding template heat flow (W)
$\Delta^P\Phi_{EXTR}$ = Uncertainty in metering chamber walls heat flows (W)
$\Delta^P\Phi_{FL,w}$ = Uncertainty in test sample flanking heat loss (W)

A calibration experiment for the thermocouples was carried out prior to the hot box measurements using a reference temperature bath. The relative scattering in measured temperatures between the thermocouples were found to be lower than 0.02 °C. Thus it can be concluded that the influence from the factor $\Delta^P\delta\theta_{ie}$ as described in Eq.1 is negligible.

The uncertainties stated in this work, are given with a coverage factor of two standard deviations and the corresponding 95 % confidence interval.

2.4 Numerical simulations

Simulations of the thermal properties of the window with the integrated shading device have been carried out using the THERM 7.1 and WINDOW 7.1 software developed at Lawrence Berkeley National Laboratories in Berkeley (LBNL 2013; LBNL 2013). THERM is a finite element method program suitable for calculating U-values of window frames, whereas the WINDOW software calculates thermal and optical properties of glazing units. Thus, THERM has been used for calculation of frame U-values and linear edge transmission losses caused by the spacer used. Cavities in the frames have been modelled according to the NFRC 100-2001 definitions in THERM. WINDOW has been used for calculating the centre-of-glazing U-values including the shading device. The results are compared to the values measured in the hot box.

3 Results

3.1 Measurement results

From Figure 3 and Table 2, one can see that the effect of operating the blinds has minor or no effect on the measured mean U-value. Deploying the blinds with horizontal slats, increases the U-value slightly, whereas closing the slats shut (vertical slats) will give a slight decrease in U-value. The alternations of the U-value as function of blind positions were found to be negligible in terms of statistical significance, which means that the individual measured mean U-values lies inside the measurement error boundaries.

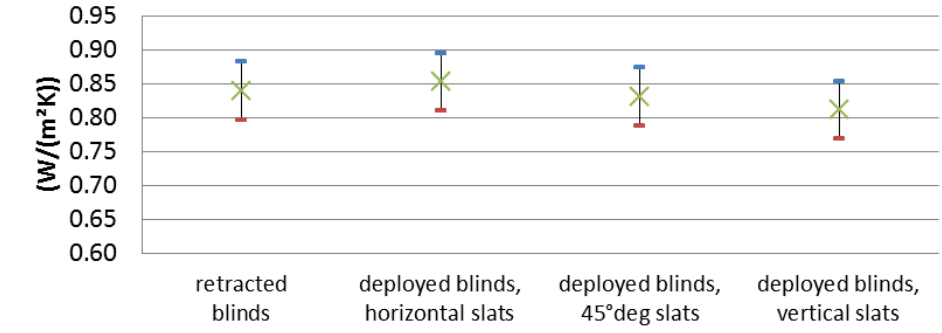

Figure 3. Measured U-values for the window. Upper and lower uncertainty values shown with lines.

The measured U-values for the whole window, U_{window}, and the center-of-glazing U-values, U_{cog}, are shown in Table 2.

Table 2. Measured mean U-values, U_{window}, and center of glazing U-values, U_{cog}, for the window.

Measured value	retracted blinds	deployed blinds, horizontal slats	deployed blinds, 45°deg slats	deployed blinds, vertical slats
U_{window} (W/m²K)	0.84 ± 0.04	0.85 ± 0.04	0.83 ± 0.04	0.81 ± 0.04
U_{cog} (W/m²K)	0.61 ± 0.03	0.60 ± 0.03	0.58 ± 0.03	0.57 ± 0.03

3.2 Calculation results

The outermost cavity in the glazing unit is an air filled cavity. Tests carried out using THERM to model this cavity treating the cavity as both a slightly ventilated and un-ventilated cavity according to the NFRC definition used in THERM (LBNL 2013), gave U-value-results comparable to the values calculated assuming an air-filled cavity using WINDOW. Assuming a slightly ventilated cavity gave center-of glazing U-values approximately 4 % higher than an un-ventilated cavity. However, based on the minor openings constricting air cross-flow in the cavity, it has been treated as an un-ventilated

cavity using the simulation results from WINDOW. Whole window, U_{window}, and center-of-glazing U-values, U_{cog}, calculated using THERM and WINDOW are shown in Table 3.

Table 3. Calculated mean U-values, U_{window}, and center of glazing U-values, U_{cog}, for the window.

Calculated value	retracted blinds	deployed blinds, horizontal slats	deployed blinds, 45°deg slats	deployed blinds, vertical slats
U_{window} (W/m²K)	0.65	0.66	0.65	0.64
U_{cog} (W/m²K)	0.52	0.53	0.51	0.50

4 Discussion and future work

The solar shading device positioned in the outermost cavity of the window does not have a statistically significant effect on improving the U-value of the window when in closed position compared to the open.

If one looks at the measured center-of-glazing U-values (U_{cog}), the same behavior as for the U_{window}-values can be seen. Thus the two independent measurments support each other in that the effects on the window U-value as function of shading device slat angle and position is negligible.

The U-values found from simulations using THERM and WINDOW were consistently lower than the measured values but also here, the effects of blind posistion and angle ion the U-value were found to be negligible. The deviation between the measured and calculated values can likely be explained by differences between declared (from the producer) and actual properties of the low-e coatings as well as the amount of argon in the gas-filled cavities of the IGU.

As opposed to finding any potential gains in U-value by the introduction of such a shading device, it was found to have a negative effect on the U-value of the window compared to one without the shading device. The protruding aluminum components of the shading device and venetian blinds, act as thermal bridges. Numerical simulations showed that the U-value of the window with the shading device will increase with approximately 5 % compared to a window without an integrated shading device. Thus, any beneficial effects expected to be achieved by using the venetians as an additional layer in the IGU, was found to be more than counteracted by the thermal bridging.

5 Conclusions

Measurements have been carried out in order to investigate the U-value of a window with a 4-pane glazing unit incorporating an in-between panes venetian blind shading device. The aim of the study has been to assess the effect of operating the blinds on the window U-value. Various slat angles and blind positions have been studied. It was found that no statistically significant effect could be found on the U-value as function of various slat angles.

Numerical simulations showed that the U-values were underestimated compared to the measured values. This can have several reasons, including deviations in gas-filling levels and quality of the low-emissivity coatings in the IGU. Identifying the reasons for these deviations is the aim of further studies that are currently being carried out within the Research Centre on Zero Emission Buildings (ZEB).

6 Future work

There are several possibilities which should be explored in order to achieve more effective shading devices, and the following should be explored

- Reduce slat thermal conductivity in order to reduce thermal bridging effects

- Improve surface properties of slats (i.e. reduce emissivity)
- Improve airtightness of shading layer by reducing openings between slats when in closed position

7 Acknowledgements

The authors gratefully acknowledge the support from the Research Council of Norway and several partners through the Research Centre on Zero Emission Buildings (ZEB).

8 References

Breitenbach, J., S. Lart, et al. (2001). "Optical and thermal performance of glazing with integral venetian blinds." Energy and Buildings **33**(5): 433-442.

Garnet, J. M., R. A. Fraser, et al. (1995). Effect of internal Venetian blinds on center-glass U-values. Window Innovations Toronto, Canada.

Huang, N. Y. T., Wright, J.L., Collins, M.R. (2006). "Thermal resistance of a window with an enclosed Venetian blind: Guarded Heated Plate measurements." ASHRAE Transactions **112**(2): 13-21.

Hukseflux. "PU Series." Retrieved 06.08.2013, from http://www.hukseflux.com/sites/default/files/product_brochure/PU%20series%20v0717.pdf.

ISO (1994). ISO 8990:1994 - Determination of steady-state thermal transmission properties Calibrated and guarded hot box.

ISO (2003). NS-ISO 15099 – Thermal performance of windows, doors and shading devices - Detailed calculations, International Organization for Standardization.

ISO, N.-E. (2010). NS-EN 12567:2010 Thermal performance of windows and doors - Determination of thermal transmittance by the hot-box method - Part 1: Complete windows and doors.

Laouadi, A. (2009). "Thermal modeling of shading devices of windows NRCC – 51121." NRCC-51121, ASHRAE Transactions **115**(2): 1-20.

LBNL. (2013). "THERM 7.1 beta." Retrieved 06.08, 2013, from http://windows.lbl.gov/software/therm/7/index.html.

LBNL. (2013). "WINDOW 7.1 beta." Retrieved 06.08, 2013, from http://windows.lbl.gov/software/window/window.html.

Rheault, S. and E. Bilgen (1989). "Heat transfer analysis in an automated Venetian blind window system." Solar Energy Engineering **111**(1): 89-95.

Shahid, H. and D. Naylor (2005). "Energy performance assessment of a window with a horizontal Venetian blind." Energy and Buildings **37**(8): 836-843.

Tzempelikos, A. (2005). A methodology for integrated daylighting and thermal analysis of buildings. Faculty of Engineering and Computer Science - Building, Civil and Environmental Engineering, Concordia University.

Modelling and Implementing efficient Three Dimensional Anisotropic Heat Air and Moisture Transport

Stefan Vogelsang[1]
Andreas Nicolai[1]

[1] Institute of Building Climate Control, Department of Architecture, Technische Universität Dresden, Germany

KEYWORDS: *simulation, framework, simulation and modelling techniques, transient transport simulation*

SUMMARY:
The development of complex physical models in building simulation creates a great demand for powerful and flexible transient simulation programs, and thus numerical solvers. Especially when turning to three dimensional models computational speed and memory use strongly limits the problem size of an application. The calculation complexity increases further more when taking anisotropic transport processes into account. This article describes a solution for a transient anisotropic three dimensional solver for combined heat, air, and moisture transport in porous materials of building envelop systems, utilizing the Delphin solver framework. After describing the physical model, boundary conditions, and certain aspects of internal solver optimisation regarding memory use and calculation speed, three initial academic verification examples will be presented. The influence of anisotropic material properties onto three dimensional simulation results is researched, targeting an evaluation of simulation performance and correctness while comparing to isotropic simulation results of the same experiments. The paper closes with an outlook onto parallelisation of the introduced solver solution.

1. Introduction

Prediction of damage in constructions (e.g. timber beam heads, interior insulations, etc.) is recently done by performing transient transport simulations. It is state of the art to utilise continuum physics for describing conserved quantities coupled through systems of partial differential equations. Our Delphin solver framework (Nicolai 2011) implements continuum physics models for porous media (construction materials) by defining a representative elementary volume (REV) following Whitaker (1969), Bear and Bachmat (1992) and Whitaker (1986). Grunewald (1997) and Nicolai (2007) defined essential conservation equations for hygrothermal, pollutant as well as salt transport. Moreover a lower bound (infimum) as a function of the pore radius spectrum was defined as a constraint for an accurately selected REV size.

The numerical solution of resulting partial differential equations is done using a spatial discretisation that introduces location-fixed control volumes and leads to a large set of ordinary differential equations to be integrated. Numerical integrators developed to solve such problems implement some form of time discretisation and solve the problem in a step-wise manner. Each integration step (time step) involved hereby a solution of a non-linear equation system, which in turn requires solving large sparse linear systems of equations. The actual implementation is done in several cascaded computational loops (see Listing 1).

Increasing dimension of simulation space (e.g. 1D, 2D to 3D) introduces new degrees of freedom, and thus complexity to all calculation procedures executed during a simulation. It basically increases

execution counts of the kernel loops. The cost of such a solution process is almost always governed by the solution of the linear systems especially for large scale problems (≥4.5 million elements).

LISTING 1. A general numerical integrator for systems of coupled ordinary differential equations

```
while (Time Integration) {
        while (Non Linear Iteration) {
                while (Linear Systems Solution) {
                        lots of computing work
                }
        }
}
```

Introducing anisotropic material properties into transient transport simulation creates a mapping problem for material characteristics defined in a materials reference system (anisotropic nature of the material) to a simulation reference system. Much research has been devoted to anisotropic material modelling (Zillig 2009; Segerholm 2007; Siau 1984; Krabbenhoft 2003, etc.) and anisotropic material properties as found in timber or sand stone.

We are interested in modelling three-dimensional transport in combination with anisotropy. Currently available hygrothermal simulation programs do not readily offer anisotropic and three-dimensional simulations. They are either limited to single materials, or single transformation orientations. A combination of wood-based construction elements with different longitudinal/radial orientations, or different anisotropic materials cannot be considered simultaneously. Hence, we decided to implement this functionality into the current Delphin 6 code. This paper presents the implemented anisotropic material model and related data handling.

Also discussed are optimisation approaches that make 3D simulations with anisotropy efficient. The new implementation presented here is labelled Delphin version 6.1 to distinguish it from the current Delphin 6 simulation code.

2. Three Dimensional Anisotropic Flux Calculation

Anisotropic transport models differ from standard isotropic hygrothermal transport models (Grunewald 1997; Nicolai 2008; Janssen 2007; Hagentoft et al. 2002) in the formulation of the flux quantities. Transport models within porous media define a linear relation between a flux and its driving potential, see Eq. (1).

$$\begin{aligned} \vec{j}^{k} &= \vec{\vec{L}}^{k}\vec{\nabla}X^{k} = R_T\overleftarrow{\overleftarrow{L}}^{k}\vec{\nabla}X^{k} \\ \overleftarrow{\overleftarrow{L}} &= \left(\overleftarrow{L}_u, \overleftarrow{L}_v, \overleftarrow{L}_w\right)^{\mathsf{T}} \end{aligned} \tag{1}$$

Where $\vec{j}^{k}$ is a flux density of a quantity *k*

X^{k} is the driving potential for quantity *k*

$\overleftarrow{\overleftarrow{L}}$ is the transport coefficient tensor formulated with respect to the MRS

$\vec{\vec{L}}$ is the transport coefficient tensor formulated with respect to the SRS

R_T is a transformation matrix

To emphasis additional effort of multidimensionality a vector arrow marks all divergence symbols, usually this vector arrow is implicitly defined in a divergence and therefore omitted. In isotropic models the transport coefficient is a scalar. In anisotropic models the transport coefficient tensor $\overleftarrow{\overleftarrow{L}}$ is

material dependent and such defined in an right-hand rectangular material reference system (MRS, with directions: u,v,w). The MRS may not necessarily be identical with the simulation space reference system (SRS). An anisotropic solver thus requires a transformation process from material to simulation reference system for each calculated flux in simulation space (see FIG. 1 for an example).

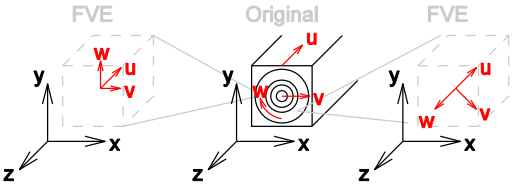

FIG 1. Example for a material and simulation reference system that are not aligned

The relation between material reference system and simulation reference system may change relative to the spatial location. In FIG. 1 the detail (right) shows the MRS for a specific location timber beam end. The direction W marks the tangential direction, V marks radial direction with respect to the material (MRS). Moving to a different location will change the orientation of the MRS within the global simulation coordinate system.

The mathematical transformation process responsible for mapping these two reference systems is thus location dependent. For completeness we briefly review the derivation of rotation matrices involved. Detailed information can be found in standard literature on the matter.

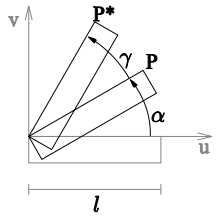

FIG 2. Rotation on Point P

Figure 2 shows an ordinary rotation of a point P by an angle γ. For a start respectively an end position of a rotation it is possible to deduce:

$$u_P = l\cos\alpha \qquad v_P = l\sin\alpha \tag{1}$$

$$u_{P^*} = l\cos(\alpha+\gamma) \qquad v_{p^*} = l\sin(\alpha+\gamma) \tag{2}$$

In this transformation the w-coordinate remains unchanged. A dependency between (u_P , v_P) and (u_{P^*} , v_{P^*}) becomes obvious, as soon as additional theorems of trigonometric functions are applied. Thus the equations for u_{P^*} and v_{P^*} can be reformulated as:

$$u_{P^*} = l\cos(\alpha+\gamma) = l(\cos\alpha\cos\gamma - \sin\alpha\sin\gamma) \tag{3}$$

$$v_{p^*} = l\sin(\alpha+\gamma) = l(\sin\alpha\cos\gamma + \cos\alpha\sin\gamma) \tag{4}$$

A starting position (u_P , v_P) may now be substituted, following equations (1 - 2) into the found equations (3 - 4) , which drops out all unknowns. The rotation equation, written in matrix notation, for a rotation by an angle β around the w-axis reads:

$$R_w = \begin{bmatrix} \cos\beta & -\sin\beta & 0 \\ \sin\beta & \cos\beta & 0 \\ 0 & 0 & 1 \end{bmatrix} \quad \text{with} \quad \begin{bmatrix} u_{P^*} \\ v_{P^*} \\ 0 \end{bmatrix} = R_w \begin{bmatrix} u_P \\ v_P \\ 0 \end{bmatrix}$$

The rotation axis u and v can be derived equivalently:

$$R_u = \begin{bmatrix} 1 & 0 & 0 \\ 0 & \cos\beta & -\sin\beta \\ 0 & \sin\beta & \cos\beta \end{bmatrix} \qquad (5) \qquad R_v = \begin{bmatrix} \cos\beta & 0 & -\sin\beta \\ 0 & 1 & 0 \\ \sin\beta & 0 & \cos\beta \end{bmatrix} \qquad (6)$$

A three dimensional point in a u,v,w coordinate system is transformed by stepwise execution of single direction rotations until it matches with the target x,y,z coordinate system.

$$\bar{p}_{xyz} = R_T \bar{p}_{uvw}$$

$$R_T = R_u R_v R_w$$

$$R_T = \begin{bmatrix} \cos\beta_v \cos\beta_w & \cos\beta_v - \sin\beta_w & -\sin\beta_v \\ -\sin\beta_u \sin\beta_v \cos\beta_w + \cos\beta_u \sin\beta_w & (-\sin\beta_u)\sin\beta_v(-\sin\beta_w) + \cos\beta_u \cos\beta_w & -\sin\beta_u \cos\beta_v \\ \cos\beta_u \sin\beta_v \cos\beta_w + \sin\beta_u \sin\beta_w & \cos\beta_u \sin\beta_v - \sin\beta_w + \sin\beta_u \cos\beta_w & \cos\beta_u \cos\beta_v \end{bmatrix}$$

In analogy a material parameter/transport coefficient tensor should be used in SRS, this coefficient tensor is first represented in MRS as $\overleftarrow{\overleftarrow{L}}^k$, and afterwards multiplied with the transformation matrix R_T . $\Rightarrow \overrightarrow{\overrightarrow{L}}^k = R_T \overleftarrow{\overleftarrow{L}}^k \square$

With respect to the numerical solution we have to keep in mind that the rotation matrix is location dependent.

3. Implementation and Numerical Solution

The Delphin 6 model framework is a modularized implementation of the governing equations for hygrothermal transport. Calculation of state variables from conserved quantities (Balance Equation modules), internal and boundary fluxes (Flux and BCFlux modules) and sources/sinks (FieldCondition modules) are customizable. For the purpose of anisotropic extension the modules for calculation of material transport properties and flux calculation modules were extended.

Since the Delphin 6 framework is built on top of a Finite Volume (FV) spatial discretisation method, the calculation of transport coefficients, both isotropic and anisotropic is done for each volume element and only one transformation matrix is computed for each element. Since transformation matrices may vary with spatial coordinates we work with volume-averaged transformation matrices. Hence, the size of the discretisation cells must thus be limited for accuracy reasons to avoid excessive changes in rotation matrices from one element to the next.

For the calculation of anisotropic fluxes the implementation requires local definition of materials and their respective orientations. The definition of material orientation within the construction definition (project file) is done in either simple or complex format. In the simple format each material assignments is a direct mapping of a material reference system to the simulation reference system. For example, if a timber stud (placed vertically) is modelled its u-direction shall be aligned to the y-direction. Then the mapping `VUW` (respective target coordinate system xyz) is specified alongside the

material placement within the calculation domain. The complex format allows arbitrary rotation matrices stored for each Finite Volume. Those rotation matrices are stored in simplified Euler-Matrix-Format. A line [1;0,0.5,-0.5;0,0.5,0.5] corresponds to the matrix: $\begin{bmatrix} 1 & 0 & 0 \\ 0 & 0.5 & -0.5 \\ 0 & 0.5 & 0.5 \end{bmatrix}$.

To assist in generation of rotation matrices we have developed a tool that generates matrices for materials with rotation symmetric material reference systems (i.e. wood/timber). Anisotropic measured material data and material functions including directional properties are stored and organised utilising the standardised IBK material format (Vogelsang et al. 2013).

For the purpose of integrating the set of ordinary differential equations resulting from the FV discretisation the Delphin 6 model is embedded into an advanced integration framework (Nicolai 2013). This framework implements several integrators including a BDF-type numerical integrator (backward-difference-formula) that is strictly mass and energy conserving and error controlled. The nonlinear equation systems arising from the BDF time discretisation are solved with a modified Newton-Raphson algorithm. In the standard configuration the integrator uses a direct solver for the solution of the linear equation systems within each Newton iteration.

The new implementation has been validated with isotropic validation cases from HAMSTAD benchmarks, DIN EN ISO 15026, and DIN EN ISO 10211 (Sontag et al. 2013) utilising an automated validation framework by Vogelsang et al. (2014). Since benchmarks or test cases for anisotropic simulations have not been published/defined yet, we are currently developing validation cases for the correct application of rotation and transformation matrices.

4. Improving Efficiency of Anisotropic Flux Evaluation

A transformation of material properties into the reference system of simulation space can be done automatically for each finite volume element when all rotation matrices are calculated in a preprocessing step of a simulation. Thus cost intensive evaluation of sinus and cosines functions during simulation time can be omitted. The additional effort of one transformation can such be minimised to six additions and nine multiplications per super positioned flux calculation (material parameter assignment). Moreover other de facto necessary projection methods, e.g. application of a two dimensional material in a three dimensional simulation space, can easily modelled through convenient R_m. For example: $R_m = \begin{bmatrix} 1 & 0 & 0 \\ 1 & 0 & 0 \\ 0 & 1 & 0 \end{bmatrix}$ maps a material parameter measured and rotated to simulation dimension X onto x, and y component and the Y dimension onto the z component of simulation space. When mapping matrix and rotation matrices are applied in a preprocessing step, the whole procedure can be realised by an single rotation matrix R_R: $\vec{\vec{L}}^k = R_m R_T \vec{\vec{L}}^k = R_R \vec{\vec{L}}^k$.

For large 2D and generally all 3D simulation setups efficient memory handling alongside a fast flux calculation is essential.

5. Efficient Solution of Three-Dimensional Problems

Solving sparse linear systems is one of the most challenging cost factors while executing transient transport simulations (see Figure 3). Two concurrent families of different solution methods exist:

Direct method solvers use a form of Gaussian elimination. Typically, an LU factorization of the linear equation system matrix is obtained, before one or more right-hand-sides (RHS) are solved (via backsolving). They are guaranteed to find a solution of a non-singular system in an exact count of arithmetic operations. They are therefore called robust and general. For instance LU decomposition with pivoting can be done for any non-singular matrix. In this sense the corresponding linear system is always solvable, a property required when the method is embedded inside a Newton iteration. In exceptional cases, the solution process of a linear system via LU is not backward stable, i.e. the backsolving process fails. However, this occurs rarely in practice. It depends on the so-called growth factor of the entries in the upper triangular matrix U, which may cause rounding errors to grow until they reach or exceed the magnitude of the desired solution. With respect to application in a Finite Volume solver, a pivoting version of a banded LU factorization routine will take into account the special structure of the Jacobian matrix involved.

An inevitable problem of direct methods is that calculated matrix factors are often denser than an original matrix. The resulting memory requirements dominate when large scale systems, as created by discretising three dimensional partial differential equations systems (large constructions), need to be solved. Also, banded LU factorisation routines have quadratic complexity with respect to bandwidth and linear complexity with respect to system size. This implies that factorisation time and memory use may grow beyond exceptional limits whenever system sizes become large. An application of direct methods is hence restricted by calculation effort and memory use.

Iterative methods approximate the solution rather than compute the solution exactly. The most relevant group of iterative methods are the Krylov subspace methods, projection methods where a subspace of search directions is enlarged with each iteration. The different Krylov subspace methods essentially differ in the choice of this construction of the subspace and the quality of the approximation to the solution obtained and improved in each step. An iterative solution of an equation system is finished once the solution is accurate enough, and consequently needs a suitable convergence criterion. Within a Newton iteration the accuracy of the Krylov subspace approximation must allow the Newton iteration to progress.

Unfortunately, Krylov subspace methods may converge very slowly or even stall without further improvement of the approximation. The latter problem may be caused by too large subspace dimensions and the involved rounding errors when increasing it further. Also breakdowns are possible. The details of the various methods are beyond the scope of this article and we refer to standard literature on the matter (Saad 2003).

With respect to hygrothermal transport problems the resulting Jacobian matrices may be very ill conditioned. This may lead to excessive iteration counts in the linear iterative solvers or bad approximations causing the Newton-Raphson method to fail. Therefore efficient preconditioning is mandatory. The preconditioning operation transforms the iteration matrix into another matrix that resembles the identity matrix more closely. Basically preconditioners (M) improve convergence properties of a linear system $\mathrm{Ax} = f$ by transforming it into a linear system $M^{-1}Ax = M^{-1}f$. The coefficient matrix $M^{-1}A$ then posses a (hopefully) better distribution of Eigenvalues (so called clustering) and approximates the identity matrix more closely than the original matrix A. Selecting M is done in a way that applying M^{-1} onto a vector is particular efficiently and preferably optimally scales on parallel computer hardware architectures. This procedures creates additional calculation costs at each iteration for creating M or M^{-1}, but may reduce iteration count substantially. Different classes of preconditioners exist that improve convergence speed (see Saad 2003 for a review).

One dimensional and small to medium two dimensional problems (less 10000 cells) are best solved by direct band solvers. For large scale two dimensional hygrothermal problems iterative solvers may be more efficient.

3D simulation models often have a grid cell count that exceeds practical limits for direct methods. Therefore, for large 2D grids (Paepcke 2014) and any 3D simulation, we always use Krylov subspace iterative solvers within our Newton iteration. Within the Delphin 6 framework, the ILU preconditioner is a standard accelerator for Krylov subspace methods and used in conjunction with single core GMRES implementation. This allows the computation of up to 4.5 million grid cells in reasonable time.

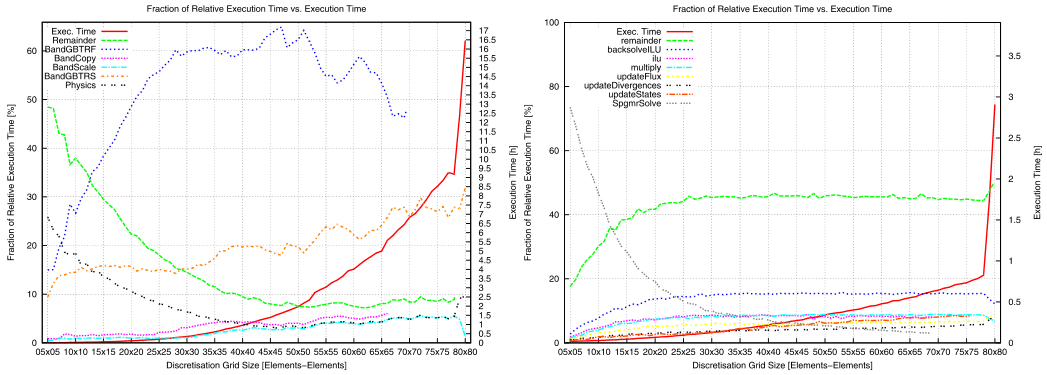

FIG 3. Simulation Time Comparison of the Direct (left) and the Iterative GMRES Solver (right) both utilizing the CVODE integrator.

6. Conclusions

An anisotropic three dimensional simulation model was developed and implemented in C++ within the Delphin 6 modelling framework. The framework was tested with scientific test cases to illustrate the functionality of the anisotropic property transformations with different mapping assignments (FIG 4).

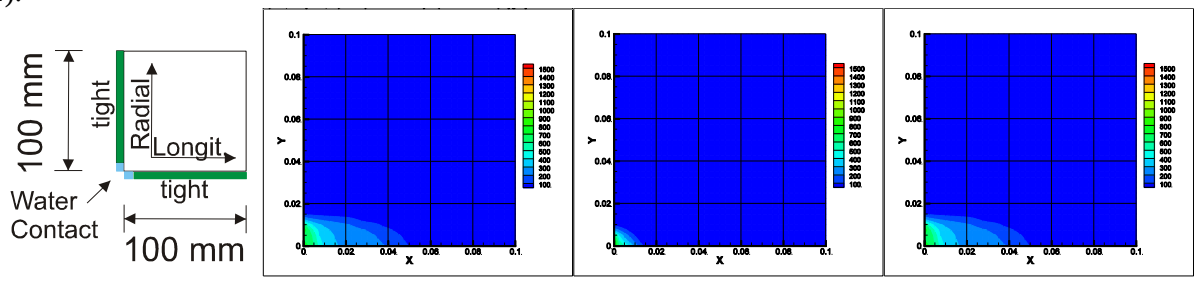

FIG 4. Anisotropic Transport for Spruce, Oak and Beech (24h) sorption in a corner experiment

The computational speed for the 3D tests was enhanced by selecting an iterative GMRES solver with ILU preconditioning. But large hygrothermal 3D cases take still too much time while running as serial iterative code, future work will be devoted to a parallel implementation of the Delphin 6.1 model. The preconditioner ILU must thus be replaced since its code is hard to parallelise. Another approach will be applying domain decomposition techniques to split large problems onto multiple processors.

For an accurate comparison of different solution algorithms a standardised set of three dimensional test benchmarks is required. Those test shall not only specify results, constructions, materials, and conditions but also truncation error control parameters to ensure a valid comparison of a simulations wall clock times or other convergence properties after valid simulation results are meet.

7. Acknowledgements

The authors gratefully acknowledge funding support by the German Federal Ministry of Economics and Technology under the Contract No. 0329663N.

References

Bear J., & Bachmat Y. 1992. Introduction to modeling of transport phenomena in pourous media, Kluwer Academic Publishers.

Grunewald, John. 1997 (September). Diffusiver und konvektiver Stoff- und Energietransport in kapillarporösen Baustoffen. Ph.D. thesis, Technische Universität Dresden, 01062 Dresden. pp. 104.

Janssen, J. & Blocken, B. & Carmeliet, J. 2007. Conservative modelling of the moisture and heat transfer in building components under atmospheric excitation, International Journal of Heat and Mass Transfer, http://dx.doi.org/10.1016/j.ijheatmasstransfer.2006.06.048

Kalagasidis, A.S. & Hagentoft, C. 2002. Simulink modelling tool for HAM system analyses in building physics, 6th Nordic Symposium on Building Physics

Krabbenhoft, K. 2003. Moisture Transport in Wood - A Study of Physical-Mathematical Models and their Numerical Implementation. Ph.D. thesis, Department of Civil Engineering, Technical University of Denmark, Denmark.

Nicolai, A. 2007 (December). Modeling and Numerical Simulation of Salt Transport and Phase Transitions in Unsaturated Porous Building Materials. Ph.D. thesis, Syracuse University, NY, USA. Printed at Institute of Building Climatology - Dresden University of Technology, Dresden, 2008.

Nicolai, A. 2011 (May). Towards a Semi-Generic Simulation Framework for Mass and Energy Transport in Porous Materials. Page 559ff. of: Vinha J. & Pirronen J. & Salminen K. (ed), 9th Nordic Symposium on Building Physics - NSB 2011, vol. 2. ISBN: 978-952-15-2573-5.

Paepcke, A. 2014. Comparison of Direct and Iterative Linear Equation System Solvers for Building Component Simulation. 10th Nordic Symposium on Building Physics. To be published.

Saad, Y. 2003. Iterative methods for sparse linear systems. SIAM, 2. ed., ISBN: 0898715342

Segerholm, I. 2007 (December). Moisture transport processes in Scots pine – Anomalous capillary suction. Nonisothermal diffusion. Ph.D. thesis, Chalmers University of Technology, Goteborg, Sweden.

Siau J. F. 1984. Transport processes in wood. Springer series in wood science. Berlin, New York: Springer-Verlag.

Sontag L. & Nicolai A. & Vogelsang, S. 2013. Validierung der Solverimplementierung des hygrothermischen Simulationsprogramms Delphin. Tech. rept. Technische Universität Dresden. http://nbn-resolving.de/urn:nbn:de:bsz:14-qucosa-128968.

Vogelsang S. & Fechner H. & Nicolai A. 2013. Delphin 6 Material File Specification. Tech. rept. Technische Universität Dresden. http://nbn-resolving.de/urn:nbn:de:bsz:14-qucosa-126274.

Vogelsang S. & Nicolai A. & Sontag L. 2014. Automated Validation of Building Performance and Building Envelope Simulation Tools. To be published.

Whitaker S. 1969 (December). Advances in Theory on Fluid Motion in Porous Media. Page 14ff. of: Flow Through Porous Media Symposium, vol. 12/61. Industrial and Engineering Chemistry.

Whitaker S. 1986. Flow in Porous Media I: A Theoretical Derivation of Darcy's Law. D. reidel Publishing Company.

Zillig W. 2009 (May). Moisture Transport in wood using a multiscale approach. Ph.D. thesis, Katholieke Universiteit Leuven, Kasteelpark Arenberg 40, B-3001 Leuven.

Evaluating the desired accuracy for mould index calculations and recommendations for crawlspace simulations

Anssi Laukkarinen, B.Sc. [1]
Petteri Huttunen, B.Sc. [1]
Juha Vinha, Professor [1]

[1] Tampere University of Technology, Finland

KEYWORDS: *Crawlspace, temperature field, simulations*

SUMMARY:
This text studies the required temperature accuracy criterion for mould growth index calculations in crawlspace. First outdoor air conditions data and the updated VTT-TUT mould growth model are used to evaluate the accuracy criterion for temperature field. Then heat conduction and air change simulations on crawlspace are made and the temperature accuracy criterion is used to give guidelines on modelling a crawlspace structure.

When the ground under the crawlspace is initially at outdoor air average temperature, it is recommended to have a minimum of three years pre-conditioning time. Based on the literature and simulations, it is recommended to have the cut-off planes in the ground at a distance of at least three times the periodic penetration depth or the width of the building. The temperature accuracy limit ±0.13 °C doesn't include many essential parameters, but gives direction on how sensitive the updated VTT-TUT mould growth model is for the change in temperature and humidity conditions.

1. Introduction

1.1 General

According to the European directive 2010/31/EU all new buildings must be near zero energy buildings by the end of year 2020. To design and build truly energy efficient and durable buildings it is essential to understand the hygrothermal behaviour of building structures. Numerical simulations provide a powerful way to contribute to this knowledge.

Calculation of temperature field is an essential part of evaluating the hygrothermal behaviour of building components. For example the relative humidity is a key factor in material moisture content and many degradation phenomena. Relative humidity depends essentially on temperature and because of that the temperature conditions should be evaluated as accurately as possible. Different authors however use different criterion for evaluating the applicability of a simulation model. This text aims to contribute to that by suggesting a method to determine limits for temperature accuracy.

Crawlspace is a building foundation type where there is an air space between the soil and living areas of the building. The structure allows making the building on several types of soils and for example on top of piles. Crawlspace structure is also suitable when making the building from volume elements and the crawlspace is also recommended in radon areas. However the major drawback of the structure is its inadequate hygrothermal behaviour in the summertime. The temperature accuracy criterion is used to give reference values when modelling crawlspace structure.

1.2 Literature review

International standard SFS-EN ISO 10211 (2008, chapter 5.2.4) gives guidelines on selecting the cut-off planes in the ground. For the calculation of both heat flows and surface temperatures the building

is divided from the symmetry plane. On the outside the ground is included for the length 2.5 x b in all directions, where the length b is the smaller length of the rectangular building foot (width). The cut-off planes on the symmetry plane and outside the building are adiabatic boundaries. For example, if the width of a building is 8 m, then 2.5 x 8 m = 20 m of soil is to be included in the calculation model outside the building.

International standard SFS-EN ISO 13370 (2008) states that the default values of $\lambda = 2$ W/(mK) and $\rho c = 2 \times 10^6$ J/(m^{3}K) as thermal conductivity and volumetric heat capacity of soil can be used as default values if no other information is available. These values for soil have been used in all calculations.

Cheng (2013) has used a selection of the IEA BESTEST cases and the calculation results from that project to evaluate the results of an approximate steady-state and dynamic 3D calculation model for uninsulated slab. The selected cases have a slab dimension of 12 m x 12 m, ground depth of 15 or 30 m (one case for shallow ground at 2 m depth) and the vertical cut-off plane 8, 15 or 20 m from the outside surface of the building wall. The deep ground boundary condition was the average outdoor air temperature and the vertical cut-off planes were adiabatic boundaries. It is also brought up that for a relatively shallow deep ground boundary the average temperature would be higher than the average outdoor air temperature. Because of that the use of average outdoor temperature would cause error in the calculations.

Pallin & Kehrer (2012) used a 1D model to evaluate the temperature conditions in 1 m depth in a free ground in absence of a building. Adiabatic boundary was set at 20 m depth from the ground surface and they used 10 years presimulation time. Moisture transfer was also included in the calculations.

Zoras et al. (2011) presented work on the numerical generation of response factors (NGRF). It was stated that in dynamic situation the time required to reach equilibrium can vary depending on the accuracy of the initial ground and structure temperature. It is also related to the meteorological conditions and the location. Three years simulation time for thermal equilibrium is given as an example.

Rees et al. (2007) compared 2D numerical simulations to full-scale measurements of a basement. Building foot was 6.5 m x 6.5 m and the building was divided from the symmetry line. The distance from outside wall surface to vertical cut-off plane was 9.7 m and the vertical distance to deep ground was 12.1 m. They used four annual cycles as pre-conditioning before the actual evaluation cycle. For the deep ground boundary condition a constant temperature was chosen, which was noticed to correspond well to preliminary simulation results.

Janssen et al. (2004) used numerical simulations to study the impact of soil moisture transfer on the building heat losses to the ground. When creating the 2D simulation model the building was first cut from the symmetry line. In the simulation model the basement was 5 m x 2.5 m and the amount of soil on the outside of the building was 15 m in the lateral direction and 12.5 m in the vertical direction. Adiabatic boundary condition was used in both vertical and horizontal cut-off planes. One-dimensional simulations were also done, which were started from average outdoor temperature and run for 15 years. The 2D simulations were initialised from the steady-state conditions where the deep ground conditions from 1D simulations were assigned to the outside surface. The 2D cases were simulated for 10-15 years until steady-periodical situation was attained with good accuracy.

Hagentoft (2001, ch. 3.2.5) has shown an analytical solution to the temperature response of a half-infinite slab to a sinusoidal temperature variation. The amplitude of the temperature variation drops exponentially when going deeper to the slab. At a depth of e.g. three times the periodic penetration depth the amplitude has dropped to 5 % of the amplitude at the surface. Periodic penetration depth δ_p [m] is defined as $\delta_p = \mathrm{sqrt}(a t_p/\pi)$, where a [m^2/s] is the thermal diffusivity of the material and t_p [s] is the period length. Example of $\delta_p > 2$ is given.

Adjali et al. (2000) discuss the selection of either constant temperature or adiabatic boundary condition to the deep ground. Temperature measurements from 10 m depth under a building showed 3 °C higher average temperature than the outdoor air average temperature. As stated also by Janssen (2004) the ground temperature depends also on the building itself and of the ground surface temperature, not the air temperature. Adjali et al. (2000) chose to use adiabatic deep ground boundary condition at 20 m depth. The vertical "far-field" cut-off planes were also adiabatic at 10 m distance from the external walls. Measured temperature values were used as initial conditions.

2. Methods

2.1 Temperature accuracy criterion

The temperature accuracy criterion was determined with the following steps:

1. Hourly T/RH data for 30 years was acquired from the Finnish Meteorological Station from four different localities (Sodankylä, Jyväskylä, Jokioinen and Vantaa).
2. For every hour of the year, new relative humidity was calculated by assuming a constant temperature change and a constant amount of water vapour in that time step. When temperature was decreased the relative humidity was limited to a maximum of 100 % RH.
3. The updated VTT-TUT mould growth model (Ojanen et al. 2010) was used to calculate the maximum value of mould index for every year and as a function of temperature change. Mould index calculation was done for the material class: "Very sensitive" (although no actual material surface was present).
4. Cumulative distribution function of the impact of temperature change was plotted for the set of 30 values (ΔM(ΔT)) at a time. Two maximum values (ΔM = 0.6 and ΔM = 1) were used and the temperature change where less than 90 % of the years stay under the limit was chosen.

2.2 Simulations

The crawlspace geometry and other simulation model information are shown in the next drawing.

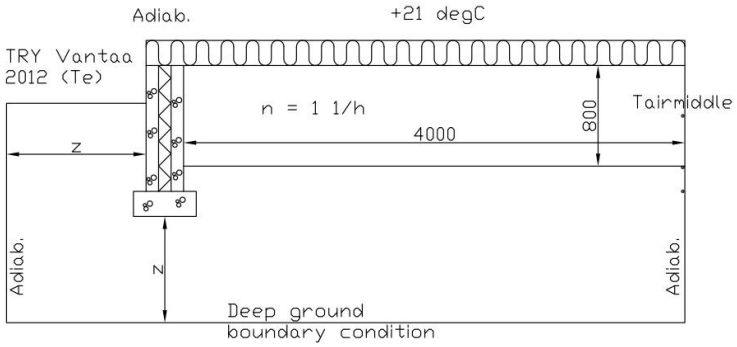

Figure 2.1 The geometry of studied crawlspace. Floor insulation is 200 mm and the thickness of foundation wall layers is 100 mm. The outside ground is 500 mm lower than the floor inside surface. For the 300 mm length of wall, adiabatic boundary condition is used. The amount of ground in the simulations (parameter z) is given values of 1, 2, 4, 8, 16 and 32 m. Monitoring point Tairmiddle is also shown.

As initial condition the yearly average of outdoor air temperature was used (5.63 °C). Long-wave radiation in the y-direction in crawlspace was taken into account where it was possible, but not between the wall and horizontal surfaces.

In Comsol Multiphysics the "Finer" Physics-controlled mesh was used for all calculations. For Wufi calculations the default discretization was used without modifications. In Delphin calculations first the

automatic discretization was done with minimum element width 1 mm and an expansion factor 1.6. Towards adiabatic surfaces the small elements were merged to reduce the amount of elements.

Material data and the boundary conditions that were used in the calculations are presented in the next table.

TABLE 1. Left: Material data. Right: Boundary heat transfer coefficients.

Material	λ W/(mK)	ρ kg/m^3	c_{pa} J/(kgK)	Boundary	Heat transfer coefficient, W/(m^{2}K)
Air (*, **)	100 or 2.353	1.25	1000	Indoor air (21 °C)	5.88
Concrete	2.3	2350	800	Outdoor air (TRY Jokioinen 2012)	25
EPS	0.039	35	800	Crawlspace top and	0.7 + Long-wave
Mineral wool	0.035	30	800	bottom (*)	radiation
Soil	2	2000	1000	Crawlspace wall (*)	7.7

(*) In Comsol and Delphin a large value for thermal conductivity of air was used and the surface heat transfer was taken into account with surface resistances or heat transfer coefficients. Long-wave radiation was included in the calculations. In Wufi the thermal conductivity of air was calculated from the surface heat resistances (2 x 0.17 m^{2}K/W) and height of the crawlspace (0.8 m).

(**) In Comsol Multiphysics the crawlspace air was handled in two ways: 1) Air was modelled as a material with high thermal conductivity and "Thin thermally resistive layers" were used at crawlspace surfaces or 2) Crawlspace air was analyzed as a lumped system, in which case the physics interface: "Global ODEs and DAEs -> Global equations" was used. In the latter case the lumped crawlspace temperature was named Tcs (`u` in Comsol documentation) and the equation to be solved (`f(u,ut,utt,t)=0`) was written as:

$$\dot{T}_{cs} - \frac{Q}{C \cdot V} \qquad (1)$$

Where $\dot{T}_{cs}$ first time derivative of lumped crawlspace temperature (`Tcst`), K/s
Q heating power from materials surfaces and ventilation, W/K
C volumetric heat capacity of air, constant value of 1250 J/(m^{3}K) was used
V volume of crawlspace air, (w x h x d) = 4 m x 0.8 m x 1 m = 3.2 m^3.

Initial temperature (`u_0`) was set to 5.63 °C (TRY average temperature) and the initial value of temperature time derivative (`u_t0`) 0 °C/s. The heating power was defined as a local variable and it was written as:

$$Q = (aveop1(T) - Tcs) \cdot h1 \cdot A1 + (aveop2(T) - Tcs) \cdot h2 \cdot A2 + nCV(Te - Tcs) \qquad (2)$$

Where aveop1 average operator (local definitions), which calculates the average temperature of crawlspace roof and ground surface, K
aveop2 average operator (local definitions), which calculates the average temperature of crawlspace wall, K
h, A convective heat transfer coefficients, W/(m^{2}K) and area, m^2
n air exchange rate between crawlspace and outdoor, 1 1/h
Te outdoor air temperature (global variable), which was interpolated from a text file, K.

For yearly variations the periodic penetration depth in soil is δ_{soil} = sqrt(1·10-6 m^2/s ·8760·3600 s/π) = 3.2 m

3. Results

3.1 Temperature accuracy criterion based on outdoor air conditions

The next figures show the impact of temperature change on the mould index calculated from the outdoor air conditions.

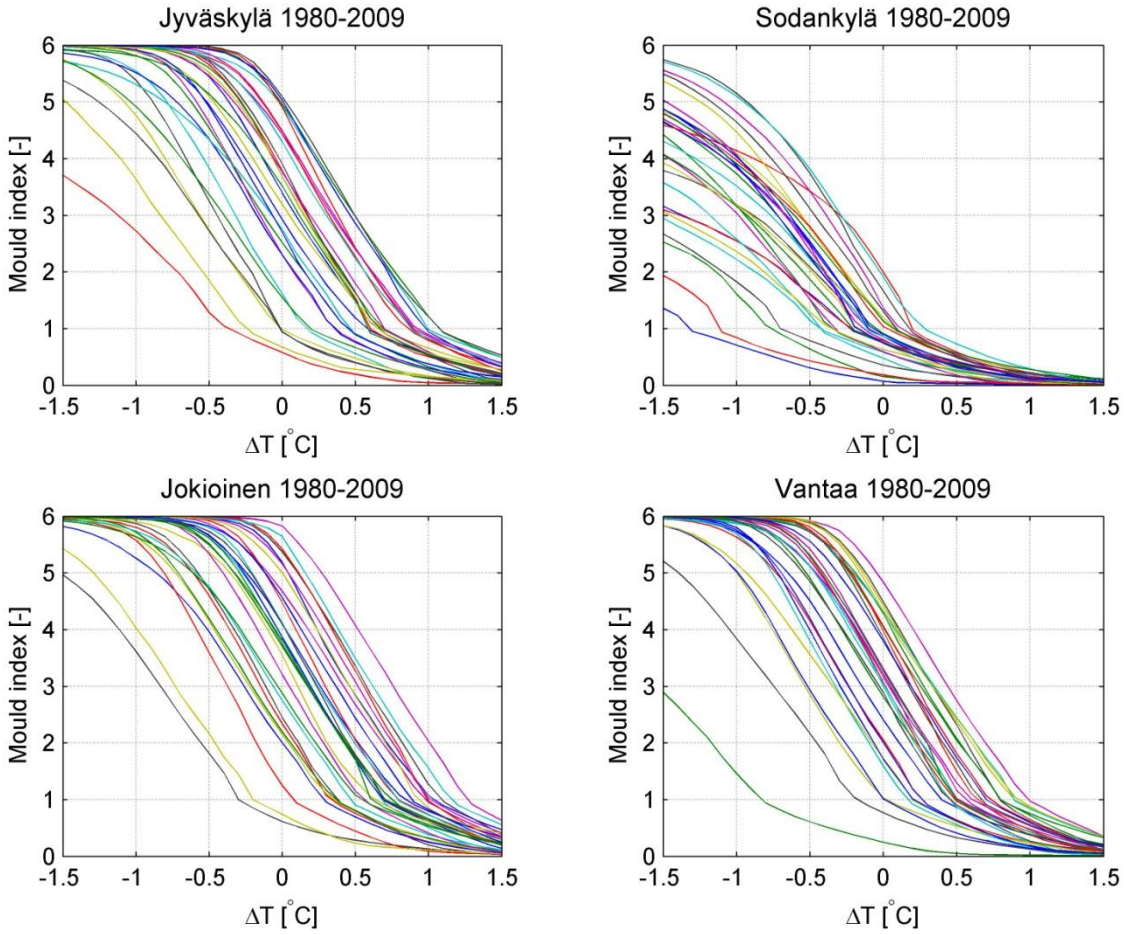

Figure 3.1. The impact of temperature change on the calculated mould index (sensitivity class: very sensitive). One line is associated with a one year of outdoor air T/RH conditions. The outdoor air moisture content is kept constant while the air temperature is decreased or increased. The maximum value of mould index is plotted against the temperature change.

Big differences exist between years. For example during 1980-2009 in Jokioinen the maximum value of the yearly outdoor air mould index has varied from 0.6 to 5.8 (ΔT = 0 °C). In Jyväskylä, Jokioinen and Vantaa the variability between years becomes smaller the better (warmer) or worse (colder) the conditions become. Sodankylä is located in Northern Finland and the average temperature there is lower than in the other three cities. It seems that the outdoor air conditions in Sodankylä are not as critical for mould growth as they are in other cities and even with some average temperature drop, the maximum mould index is not very high for all years.

The temperature has a big impact on the resulting mould index. A temperature change of 0.5 °C can change the mould index value over two units (scale 0...6). This leads to the conclusion that the determination of temperature field accurately is essential for accurate evaluation of mould growth and the hygrothermal behaviour of building envelope structures. A second conclusion is that it is possible

to either improve or impair the hygrothermal behaviour of building structures with solutions that affect the temperature field.

Desired accuracy can be chosen in different ways. One possibility is to allow error of 10 % (ΔM = 0,6) in 10 % of the years. Larger temperature difference than this means that less than 90 % of the years stay in the 10 % (ΔM=0.6) limit. This condition leads to the following values. Also limits for mould index error of ΔM = 1.0 are given.

TABLE 2. Minimum/maximum constant temperature error with different accuracy criterion.

City	$\Delta T_{allowed}$ ≥ 90 % of years ΔM ≤ 0.6	$\Delta T_{allowed}$ ≥ 90 % years ΔM ≤ 1
Jokioinen	-0.13...0.13	-0.22...0.21
Jyväskylä	-0.13...0.13	-0.22...0.21
Sodankylä	-0.15...0.28	-0.27...0.70
Vantaa	-0.13...0.12	-0.21...0.21

3.2 Simulation results

Crawlspace simulation results consist of hourly temperature data from certain monitoring points. From this data the yearly averages were calculated alongside with the hourly differences in each year compared to the last simulation year. The next figures show the development of yearly average temperatures in the crawlspace air and the maximum difference in each year compared to the hourly data of the last simulation year (15th year).

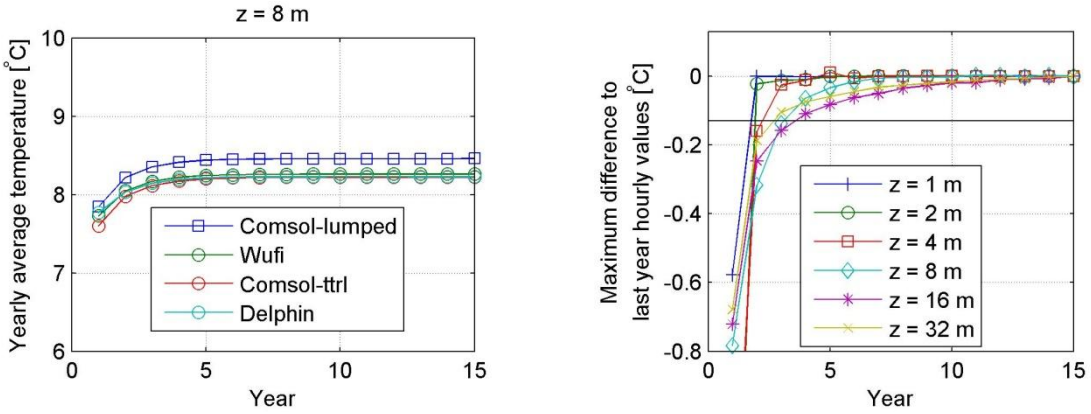

Figure 3.2 Results from crawlspace simulations. Left: Impact of simulation time and the choice of simulation software on the yearly average crawlspace temperature (z = 8 m, adiabatic). Right: Maximum difference in the hourly values compared to the last simulation year (Crawlspace air, Delphin, q = 0.03 W/m²).

Temperature changes faster in the beginning of the simulation than after a few years. The conditions approach asymptotically their periodical equilibrium. In the beginning of each year the conditions differ more from the last simulation year than the end of the year. In many cases two years pre-simulation time would have been enough but three years pre-simulation was enough in all calculated cases.

The next figures show the impact of increasing the amount of soil in the simulation model.

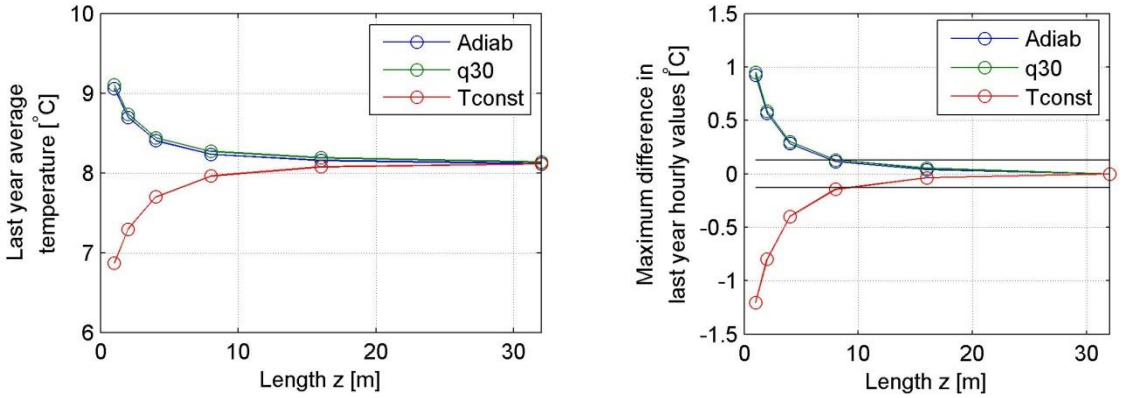

Figure 3.3 Crawlspace air average temperature for the last simulation year. Left: Impact of model size and deep ground boundary condition. Right: Difference to the largest (z = 32 m) simulation model.

When the amount of soil is small the periodic steady-state condition changes depending on the amount of soil in the simulation model and the deep ground boundary condition. The building itself behaves as a heat source and the amount of soil in the simulation model affects directly the amount of heat capacity and thermal resistance under the building. The yearly average temperature in crawlspace is few degrees higher than the average outdoor air temperature. If the average outdoor air temperature is used as a deep ground boundary condition it holds also the crawlspace temperature on a lower level. If adiabatic boundary condition is used the heat can't escape quickly enough from the ground below the building and the temperature of the thermal pillow rises. The constant heat flux 0.03 W/m^2 (= 2 W/(mK)) x (1.5 °C/100 m)) differs only little from adiabatic boundary condition.

Comparison with mould indices calculated from outdoor air vapour content and crawlspace air temperature doesn't give very much new information because in many cases the mould index for crawl space air (with very sensitive class) is very high. The mould index rises in the summertime and it is almost M = 6 as long as there is colder period in the summer than the outdoor air.

Modelling crawlspace air as lumped system produced similar results than in Fig. 3.3.

4. Discussion and conclusions

The required temperature accuracy is very high. If mould index accuracy of $\Delta M \leq 0.6$ is pursued the temperature accuracy should be in the range of ± 0.13 °C. With mould index accuracy $\Delta M \leq 1.0$ the temperature accuracy should be ± 0.21 °C. The accuracy of climate data, material parameters, mould growth modelling etc. is not explicitly evaluated at the moment. For example if more resistant mould growth class would be used the allowed temperature range would be wider. Conditions change also more slowly on materials surfaces, which likely also allow wider acceptable temperature range. Also the temperature change was now given constantly to the same direction. The simulation results can be however sometimes warmer and sometimes colder than the measured values, which is likely to even out differences. The values are seen as a starting point for evaluating results when simulations are compared to measurements.

The big influence of the temperature field on the calculated mould index also means that small favourable changes in structural solutions or boundary conditions can have a big positive impact on the hygrothermal behaviour of envelope assemblies.

When the initial ground temperature was set to the average outdoor air temperature, three years was enough for the crawlspace temperature changes to become smaller than the desired limit. Based on the literature and the simulations the amount of ground should be at least three times the periodic penetration depth or the width of the building, which one is larger.

Different deep ground boundary conditions produced the same results when the size of the simulation model was increased enough. However due to the wide use of adiabatic conditions as deep boundary condition in the literature, it is recommended with the use of large enough of amount of ground.

Setting up maximum time step was necessary if it wasn't already done in the calculation program. The impact of maximum time step wasn't varied but when hourly data was used, a maximum time step of half an hour was selected.

Crawlspace is known as a risky solution and the summertime temperature deficit appeared also in the current simulations. In summer the lower temperature compared to outdoor air causes relative humidity to rise and risk for mould and moisture problems to increase. Besides minimizing moisture loads, also the temperature behaviour of traditional crawlspace should be changed with structural solutions.

References

Adjali, M.H., Davies, M., Ni Riain, C. & Littler, J.G. (2000) In situ measurements and numerical simulation of heat transfer beneath a heated ground floor slab, Energy and Buildings 33 (2000) 75-83.

Cheng, Dong (2013) Dynamic three-dimensional heat transfer calculation for uninsulated slab-on-ground constructions. Energy and Buildings 60 (2013) 420-428.

Hagentoft, Carl-Eric (2001) Introduction to Building Physics. Studentlitteratur. Lund, Sweden. ISBN 91-44-01896-7

Janssen, Hans; Carmeliet, Jan & Hens, Hugo (2004) The influence of soil moisture transfer on building heat loss via the ground. Building and Environment 39 (2004) 825-836.

Ojanen, Tuomo; Lähdesmäki, Kimmo; Viitanen, Hannu; Vinha, Juha; Peuhkuri, Ruut & Salminen, Kati (2010) Mold growth modeling of building structures using sensitivity classes of materials. Presented at the Thermal Performance of the Exterior Envelopes of Whole Buildings XI International Conference.

Pallin, Simon & Kehrer, Manfred (2012) Hygrothermal simulations of foundations: Part I: Soil material properties. Journal of Building Physics 37(2) 130-152.

Rees, S. W., Zhou, Z. & Thomas, H.R. (2007) Ground heat transfer: A numerical simulation of a full-scale experiment. Building and Environment 42 (2007) 1478-1488.

SFS-EN ISO 10211. 2008. Thermal bridges in building construction – Heat flows and surface temperatures – Detailed calculations (ISO 10211:2007). Finnish Standards Association SFS.

SFS-EN ISO 13370. 2008. Thermal performance of buildings. Heat transfer via the ground. Calculation methods (ISO 13370:2007). Finnish Standards Association SFS.

Zoras, Stamatis; Georgakis, Chrissa; Kosmopoulos, Panagiotis & Dimoudi, Argiro (2011) Multi-year application of the three-dimensional numerical generation of response factors (NGRF) method in the prediction of conductive temperatures in soil and passive cooling earth-contact components. Solar Energy 85 (2011) 2275-2282.

Evaluation of the short-wave solar radiation transmission through complex fenestration systems in existing office buildings in Chilean warm climate

Sergio Vera, Assistant Professor, Ph.D. [1,3]
Waldo Bustamante, Professor, Ph.D. [2,3]
Alejandro Prieto, Research Associate, M.Sc. [2]
Claudio Vásquez, Associate Professor, Ph.D. [2,3]

[1] Department of Construction Engineering and Management, School of Engineering, Pontificia Universidad Católica de Chile, Chile
[2] School of Architecture, Pontificia Universidad Católica de Chile, Chile
[3] Center for Sustainable Urban Development (CEDEUS), Pontificia Universidad Católica de Chile, Chile

KEYWORDS: Complex Fenestration Systems, Short-wave solar radiation transmission, Office buildings, warm climate

SUMMARY:
Overheating, glare and high energy consumption for air conditioning and ventilation are recurrent problems in office buildings in Santiago of Chile over the whole year. Solar heat gains are the major cooling load. Large variety of complex fenestration systems (CFS) such as perforated screens, louvers and motorized rollers are being implemented on modern office buildings. However, it is unknown their effectiveness to control short-wave solar radiation before it is transmitted through the glazed building façades. This paper aims to study the performance of CFS currently used in existing office buildings in Santiago of Chile by measuring the transmission of short-wave solar radiation in four office buildings at different façade´s orientations. The main results show that perforated and undulated exterior screens and louvers and motorized rollers reduce peaks of solar heat transmission up to 2% of incident solar radiation, while solar transmissions can be as low as 8%. Also, this study reveals that CFS are more effective to reduce solar heat transmission than spectrally selective windows with low/medium SHGC. However, non-proper architectural arrangements of CFS can significantly diminish their performance.

1. Introduction

Overheating, glare and high energy consumption are recurrent problems in office buildings in Santiago of Chile over the whole year. This situation is consequence of the combination of a warm climate and modern architecture of office buildings. Figures 1a and 1c show the hourly temperature and beam solar radiation of an average day in January, March, July and October, while Figure 1b shows the global horizontal solar radiation during the whole-year (ASHRAE 2005). It is observed that Santiago's climate (S 33° 22'; W 70° 46') is characterized by high temperatures and solar irradiance for around 8 months of the year. This climatic condition exposes office buildings to large heat gains due to solar radiation and heat conduction.

This situation would not be a problem if office buildings would be properly designed for this weather condition. Otherwise, modern architecture imposes buildings with completely or large glazing façades as shown in Figure 2. Modern architecture, warm weather and internal gains (people, equipment and lighting) cause excess of solar heat gains and daylighting transmission to the indoor environment. For instances, it is observed in Figure 2b that internal rollers in Titanium Tower are down in the north

façade, which is either a sign of overheating or glare in perimeter offices despite of the low Solar Heat Gain Coefficient (SHGC) of the glazing system.

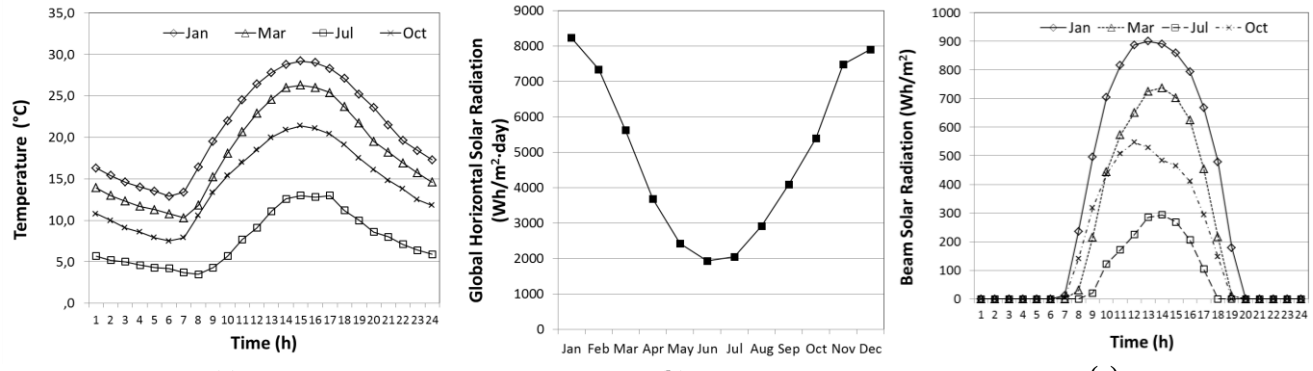

(a) (b) (c)

FIG 1: Weather data of Santiago of Chile. a) Hourly temperature. b) Global horizontal solar radiation. c) Hourly beam solar radiation.

Solar heat gains through windows are the major component of the building energy performance and occupant's comfort. Several authors have reported the large contribution to cooling loads of solar heat gains through fenestration in warm climates (Reilly and Hawthorne 1998; Li and Lam 2000; Winkelmann 2001; Kuhn 2006). Exterior shading devices are the most effective way to reduce solar heat gains through glazed façades because they intercept direct solar radiation before it reaches the glass. Fully shaded glazing façades can reduce solar heat gains up to 80% (ASHRAE, 2005).

CorpBanca Building

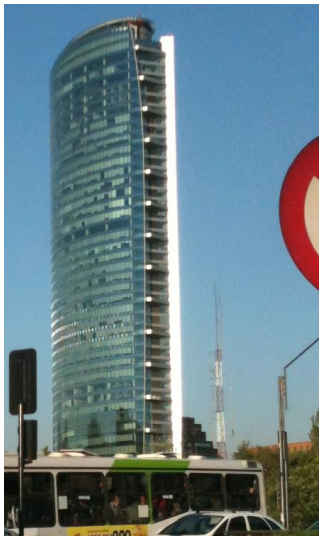

Titanium Tower

FIG 2: Buildings with large glazing façades in Santiago of Chile.

2. Case studies and monitoring methodology

2.1 Buildings studies

Short-wave (SW) solar radiation transmission was monitored in four office buildings in Santiago of Chile. Figure 3 shows pictures of the monitored buildings and their main characteristics are presented below:

- Building A: Itaú Bank Building is a 6th story office building. Its northwest façade consists of double glazing with unknown SHGC and visible transmittance (VT). This façade is implemented with external motorized rollers. The rollers are set to down at certain hour each day to control solar heat gains. According to the building manager these rollers only operate on weekdays, but it was found that they also operate on weekends sometimes. The rest of façades does not include the external rollers. Short-wave solar radiation transmission was monitored on the northwest façade only.

- Building B: DHL-Intersystems Building is an office building with large glazing façades. Northeast façade is composed of double glazing windows with SHGC of 0.39.

- Building C: San Agustín Building is a five-story university building with teaching labs, computer labs, classrooms and offices. The east façade is composed of single-pane clear glass, while the west façade consist of double glazed clear glass and exterior perforated and undulated screens on the 3rd and 4rd floors of the building.

- Building D: MideUC Building is a university building mainly composed of offices and meeting rooms. The envelope consists of double glazed clear glass with different CFS on each façade. The north façade includes perforated and undulated louvers, while undulated and perforated screens are placed on the east and west façades.

The CFS implemented in these buildings are motorized exterior rollers in Building A, perforated and and ondulated louvers in Building D, and ondulated and perforrated screens in Buildings C and D. Building B does not count with CFS but it has double glazing windows with medium SHGC. Finally, the east façade of Building C is composed of windows with a single clear glass.

FIG 3: Monitored buildings

The CFS, such as the undulated and perforated screen shown in Figure 4, are complex to be modelled in building energy simulation tools when their Bidirectional Scattering Distribution Functions (BSDF) are unknown, which is a common situation. Thus, this study aims to evaluate the effectivennes of CFS via monitoring how well they control solar heat gains in comparison with single glass windows and spectrally selective windows.

FIG 4: Undulated and perforated screen installed in Buildings C and D.

2.2 Methodology of monitoring

SW solar radiation transmission was measured using piranometers SP Lite2 of Kipp&Zonen at different locations of the fenestration system as shown in Figure 5a. The outer piranometer measures incident solar radiation on the CFS, while the inner piranometer measures how much solar heat is transferred through the fenestration system. When a CFS was part of the fenestration system, a piranometer was placed between the CFS and glass as shown in Figure 5a.

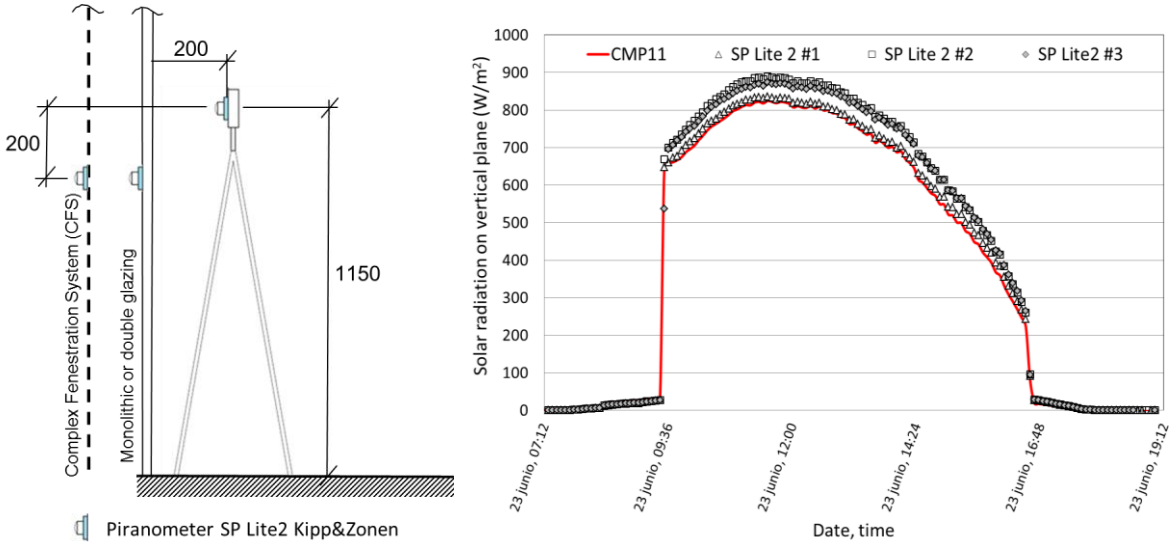

(a) (b)

FIG 5: a) Mounting diagram of piranometers (dimensions are in millimeters). b) Comparison of vertical solar radiation measurements of piranometers SP Lite 2 and CMP 11.

SP Lite2 sensor has a spectral range from 400 to 1100 nm. Since this range covers a fraction of the whole solar spectral range, thus they measure a range much smaller than more precise piranometers, it was necessary to evaluate if SPLite2 were suitable for this study. This was done by means of comparing the measurements of solar radiation of three sensors SP Lite2 against the measurements of sensor CMP11 of Kipp&Zonen, which has a spectral range from 285 to 2800 nm. Measurements were carried out for four days during winter in a vertical plane oriented to north. Figure 5b shows that

measurements of SP Lite 2 are in very good agreements with CMP11 measurements, which evidences that SP Lite2 sensors are suitable for measuring solar radiation on vertical planes. In consequence, piranometers SP lite 2 could be used to indirectly evaluate the performance of fenestration systems to reduce and control solar heat gains. The main limitation of this methodology is that long-wave solar radiation emitted to indoors by the window is not taken into account. However, the only method that allow to measure solar heat gains more precisely correspond to experimental calorimeters, which can not be implemented for measurements in existing buildings.

Monitoring was continuously carried for two or more days at different seasons in different building façades from July 2012 (winter in south hemisphere) to January 2013 (summer in south hemisphere). New measurements are being carried out to complete data for different façade orientations and types of fenestration systems. The objective of these measurements is to obtain experimental data for E, NE, N, NW and W façades for clear glass only (single or double glazed), double glazed with low SHGC, and glazing systems with CFS.

3. Results and analysis

Figure 6 summarizes the measurements (each circle) of the ratio between the daily integral of the measured SW solar radiation by the inner and outer piranometers. This ratio reflects the effectiveness of the fenestration system to control solar heat gains. This ratio varies between 0 to 1. Values close to 0 indicate very low SW solar radiation transmission, while values close to 1 evidence that large portion of SW solar radiation is transmitted indoors through the fenestration system. These results clearly show that CFS, such as screen rollers and undulated and perforated screens/louvers can effectively reduce the solar heat gains.

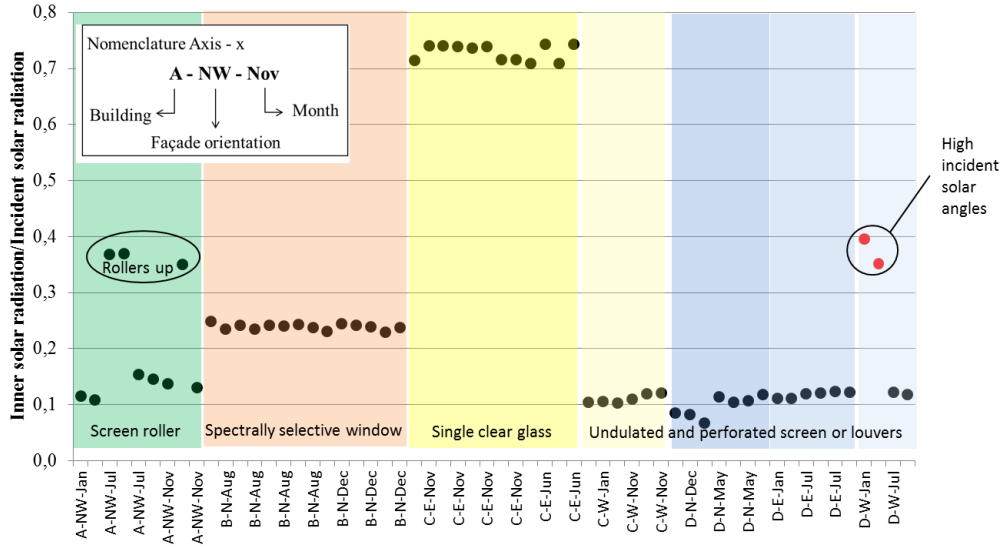

FIG 6: Measured SW solar radiation transmission through different fenestration systems, buildings, façade orientations, and season.

The following sections presents detailed results of incident solar radiation on building façades, solar radiation between the CFS and glass, and short-wave solar radiation transmitted through the fenestration system towards the indoor environment.

3.1 Building A

Figure 7 shows the measurements of solar radiation on the west façade in July 2012 (winter) and January 2013 (summer). In both figures is clear the effectiveness of exterior rollers to control the transmission of SW solar radiation. Despite of the high incident solar radiation on the northwest façade, the peak of transmitted SW solar radiation is below 20 W/m^2 in winter and summer. This

means this CFS blocks more than 85% of solar radiation when it is down and reduces the peak of transmitted SW solar radiation by more than 95%.

Figure 7a also shows a couple of days when rollers are not down during the weekend. During these days, the transmitted SW solar radiation is about 300 W/m^2, which is significantly higher than the transmitted SW solar radiation when the rollers are down. Figure 6 shows three days when this situation happened, thus the ratio between the inner and outer piranometer measurements is 0.37, which is significantly higher than the same ratio when the rollers are down.

Figure 7a also demonstrates that rollers should be down before midday in winter because the transmitted SW solar radiation increases significantly between 9 and 12 AM reaching a peak of 200 W/m^2. This could cause important cooling loads during the morning even though in winter.

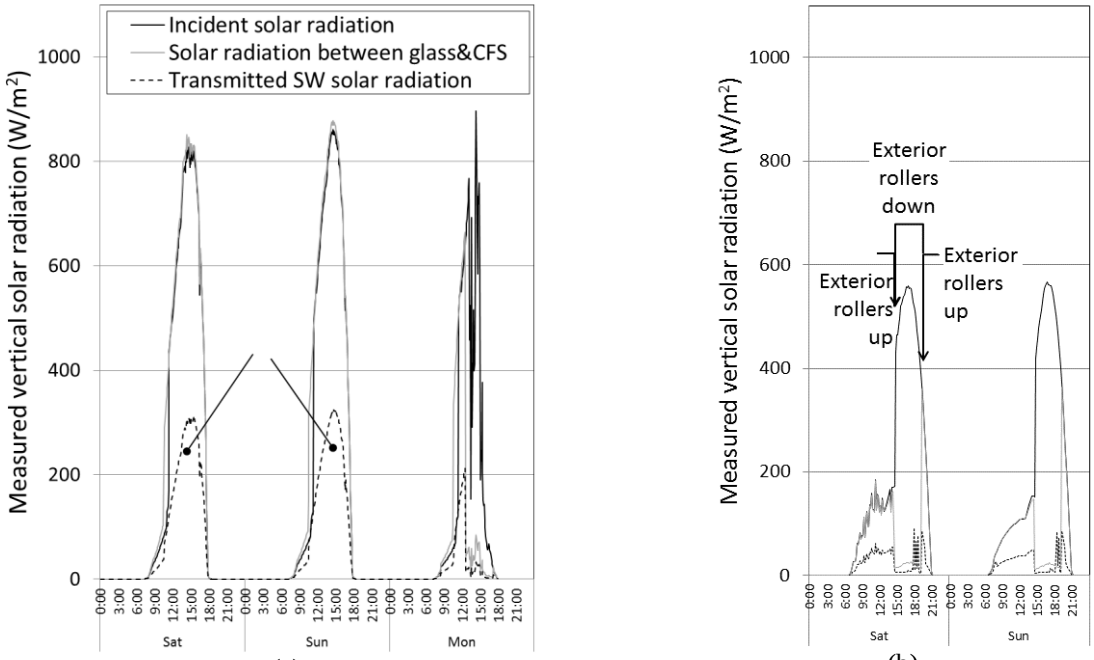

FIG 7: Incident and transmitted solar radiation through fenestration systems on northwest façade of Building A: a) July 2012. b) January 2013.

3.2 Building B

Figure 8 deploys the measurements of incident solar radiation on the northeast façade in August (winter) and October (spring). Figure 8a shows peaks of incident solar radiation around 800 W/m^2 and 600 W/m^2 in sunny days of winter and summer, respectively. In summer, incident solar radiation is lower than that in winter due to higher incident sun angles. Similarly to the measurements in Building A, it is shown that the transmitted SW solar radiation is higher in winter than that in spring and summer. This fact, in addition to that the people occupancy ratio of buildings is usually higher in Chile than that in North America and Europe, causes high energy consumption for cooling in office buildings even though in winter.

Figures 8a and 8b show that the double glazed window only transmits around 25% of the incident solar radiation. This indicates that spectrally selective windows with medium to low SHGC allow controlling solar heat gains effectively during the whole year. However, they still allow transmitting 20 to 25% of incident solar radiation, which is significant in climates with high solar radiation even in winter.

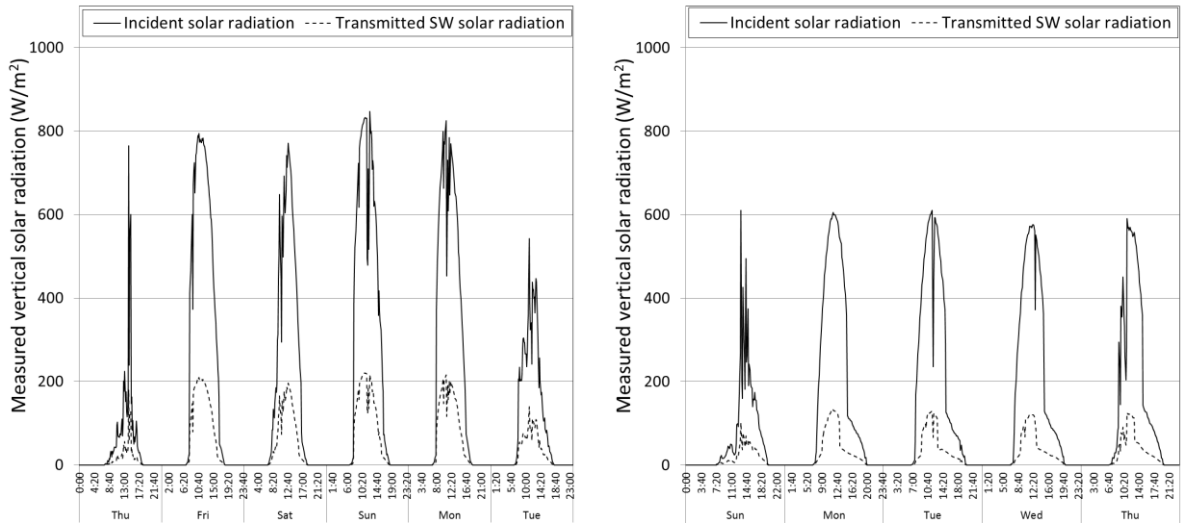

(a) (b)

FIG 8: Incident and transmitted solar radiation through northeast glazing façade in Building B: a) August 2012. b) October 2012.

3.3 Building C

Measurements were carried on the east and west façades in an unoccupied office and a small library, respectively, that are located on the third floor. Main results are presented below.

3.3.1 East façade: single clear glass

Figure 9a shows 8-day measurements on the east façades by the end of November 2012 (late spring). It can be seen that peaks of incident solar radiation on the east façade are around 900 W/m^2 in sunny days, which is a very high value. At the end of the measurement period is observed much lower values of incident solar radiation because these days were cloudy. Figure 9a also shows that transmitted SW solar radiation through the single clear glass is about 700 W/m^2 in sunny days. This means that around 75% of incident solar radiation is transmitted through the clear glass. As expected, these results show that this type of window do not allow controlling solar heat gains, especially at low incident angles that occur on the east façade early in the morning. This situation might cause high cooling loads, glare and uncomfortable indoor conditions in the work places close to the windows during the morning.

3.3.2 West façade: double glazed clear glass with CFS

Figure 9b shows the measurements on the west façades also in November 2012 (late spring). Peaks of incident solar radiation on the west façade have similar magnitude than the peaks observed on the east façade. On the contrary to what happened on the east façade, transmitted SW solar radiation through the fenestration system on the west façade is very small. This result is because the CFS blocks more than 85% of the transmitted SW solar radiation and reduces the magnitude of peaks by 90%. These results clearly show the effectiveness of the undulated/perforated screen on reducing solar heat gains. The CFS implemented on the west façade of this building is similar to the device shown in Figure 4, which blocks solar radiation very effectively but allows the transmission of natural light.

3.4 Building D

Figure 10 shows that the CFS on the east and north façades significantly blocks the incident solar radiation. On the east façade (Figure 10a), the peak of transmitted SW solar radiation is about 380 W/m^2 but it occurs for very short time (< 30 min). The rest of time when sun rays strike the east façade, the transmitted SW solar radiation is lower than 70 W/m^2, which is only 10% of the incident

solar radiation. On the north façade, the results are better due to the perforated and undulated fix louvers (Figure 10b), thus the peak of transmitted SW solar radiation is lower than 42 W/m^2. This represents less than 6% of the peak incident solar radiation. However, it should noticed that higher values of transmitted SW solar radiation might be found due to unshaded sections of the north façade due to architectural arrangement of the CFS as shown in Figure 11c.

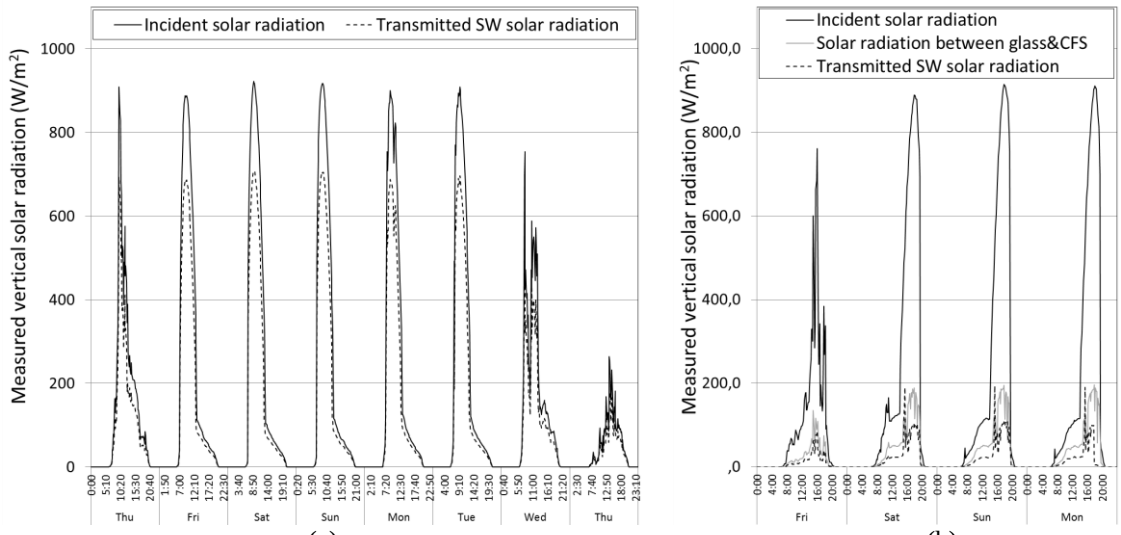

(a) (b)

FIG 9: Incident and transmitted SW solar radiation in San Agustín Building in November: a) East façade (single glazed clear glass). b) West façade (double glazed clear glass with perforated and undulated exterior screen).

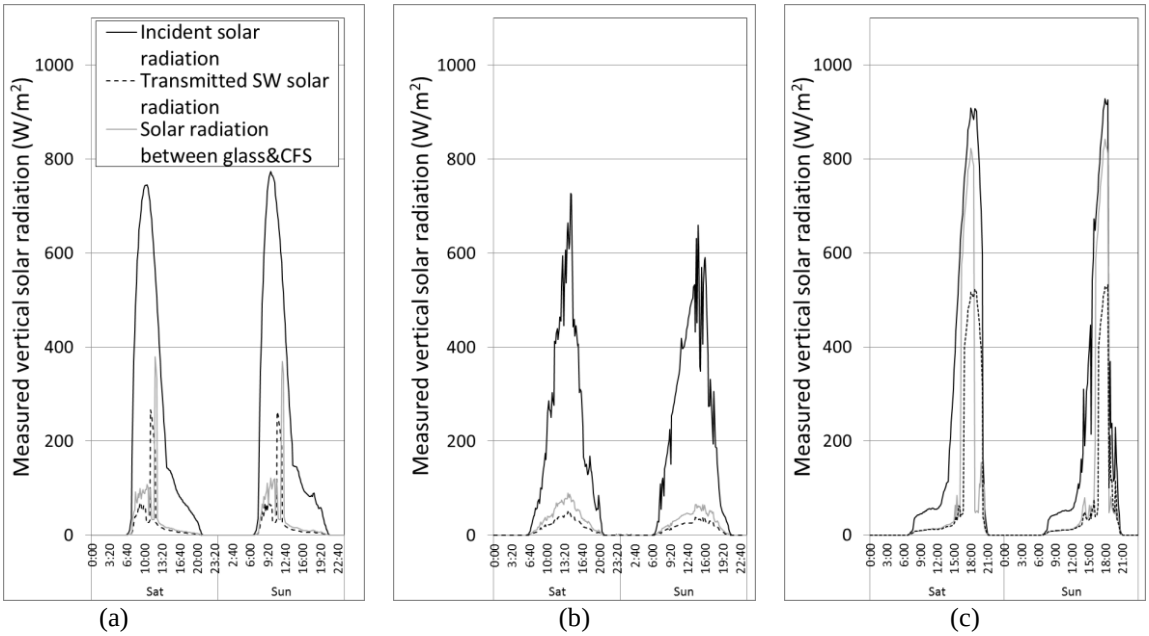

(a) (b) (c)

FIG 10: Incident and transmitted solar radiation through CFS in Building D: (a) East façade (January). (b) North façade (December). (c) West façade (January)

Despite that the east and west façades have the same CFS, Figure 10c shows that the transmitted SW solar radiation on the west façade is much higher than that in the east façade in summer. While the CFS on the east façade allows transmitted SW solar radiation around 12%, the same CFS on the west

façade permits the transmission of 35-40% of the SW solar radiation (see Figure 6). Moreover, the transmitted SW solar radiation through the west façade of this building is much higher than the value found for the west façade of building C (11%) that has a similar CFS. The high transmission of SW solar radiation on the west façade of building D is consequence of a non-proper architectural design of the CFS, which allows solar transmission at high solar altitudes through the large unshaded part of the window (see Figure 11a). This fact significantly deteriorates the performance of a good CFS.

Despite the architectural design problems of the CFS on the west façade of Building D, this CFS performs well in winter due to lower solar incident angles. Figure 6 shows that the transmitted SW solar radiation is about 12% of the incident solar radiation in July (winter).

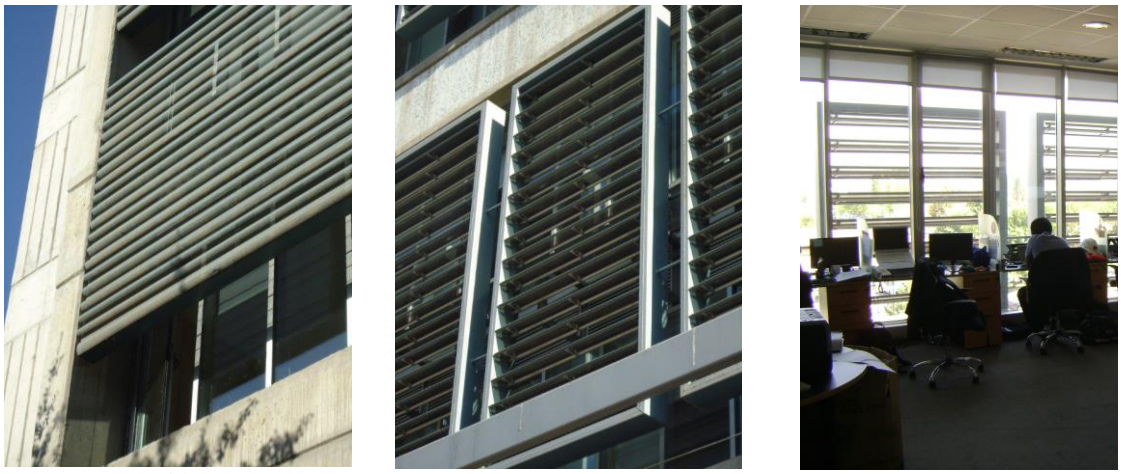

(a) (b) (c)

FIG 11: a) Perforated/undulated screen on west façade with uncovered sections. b) Perforated and undulated louvers on north façade. c) North façade with uncovered sections with louvers.

4. Conclusions

This paper presented a study of the effectiveness of typical glazing façades and CFS to control solar heat gains in existing buildings in Santiago of Chile. The main conclusions that could be drawn from this study are:

- CFS are more effective than double glazed windows with low/medium SHGC to reduce transmitted SW solar radiation. Perforated and undulated exterior screen/louvers and motorized rollers reduce peaks of SW solar radiation transmission up to 2% of incident solar radiation, while SW solar transmissions can be as low as 8%.
- Architectural design of CFS can extremely influence the effectiveness of CFS to control solar heat gains. When CFS are not arranged properly, their effectiveness to control solar heat gains can be significantly diminished. Therefore, it is important that designers take care how CFS are installed to maximize their effectiveness to control solar heat gains.
- Since high internal gains in Chilean offices buildings due to high occupancy ratios, significant SW solar radiation transmission during wintertime might cause the need for cooling even in winter. In consequence, designers should take into consideration the implementation of CFS to control solar heat gains over the whole-year.

5. Acknowledgements

This work was funded by the National Commission for Science and Technological Research (Conicyt) of Chile under the grant Fondecyt 1111001 and supported by the research grant CONICYT/FONDAP 15110020.

References

Appelfeld, D., A. McNeil & S. Svendsen. 2012. An hourly based performance comparison of integrated micro-structural perforated shading screen with standard shading systems. Energy and Buildings, 50: 166-176.

ASHRAE. 2005. Handbook Fundamentals. Atlanta: American Society of Heating, Refrigerating and Air-Conditioning Engineers, Inc.

Khun, T.E., S. Herkel, F. Frontini, P. Strachan & G. Kokogionnakis. 2011. Solar control. A general method for modeling solar gains through complex façades in building simulation programs. Energy and Buildings, 43 (1): 19-27.

Khun, T.E. 2006. Solar control: A general evaluation method for façades with venetian blinds or other solar controls systems. Energy and Buildings, 38 (6): 648-660.

Li, D.H.W. & J.C. Lam. 2000. Solar heat gain factors and the implications to building designs in subtropical regions. Energy and Buildings, 32 (1): 47-55.

Reilly, S. & W. Hawthorne. 1998. The impact of windows on residential energy use. ASHRAE Transactions, 104 (2): 791-798.

Winkelmann, F.C. 2001. Modeling windows in EnergyPlus. Proceedings of international IBPSA Conference, Building Simulation, Rio de Janeiro, august 13-15, pp. 457-464.

On the applicability of quantitative infrared thermography on window glazing

Kim Carbonez, M.Sc. [1]
Nathan Van Den Bossche, Assistant Professor[1]
Marijke Steeman, Assistant Professor [1]
Sven Van De Vijver, MEng. [1]
Arnold Janssens, Full Professor[1]

[1] Ghent University, Belgium

KEYWORDS: *infrared thermography, glazing, quantitative analysis, U-value,*

SUMMARY
Energy efficient buildings are an essential factor to reduce the energy consumption by 2020. New buildings have to meet severe requirements, whereas older buildings need renovation to reduce the heat losses through the building envelope. Infrared thermography (IRT) might be an improvement over existing methods to assess the thermal performance of an existing wall in a non-destructive way, or to check upon the as-built quality, specifically in the case of window glazing. The technique instantly visualises the surface temperature of a whole building part, and in turn might allow to deduce the thermal transmittance accordingly. However, many parameters can influence the surface temperature and lead to distorted conclusions. This paper reports on the impact of different indoor and outdoor boundary conditions for the assessment of the U-value of glazing, using the results from a numerical simulation model. After an analysis of 6 types of windows, it is concluded that for specific conditions, IRT might allow to estimate the U-value with an acceptable accuracy, based upon the instantaneous indoor surface temperature. In future research, experiments will be performed to validate this conclusion and the assessment methodology will be improved.

1. Introduction

Energy efficiency and sustainability are major concerns of our time. In 2011, the European Commission decided that the energy consumption in general should decrease with 20% by 2020 (compared to 1990) (EC, 2011). To reach this goal, the building industry has to comply with stringent regulations in respect to insulating performance, airtightness quality, renewable energy sources, etc. However, new buildings only constitute a minority of the building stock. In Belgium, 62 % of the buildings have been constructed before 1970 (WTCB, 2005), and typically do not comprise any insulation in the building envelope. Consequently, deep energy renovation and refurbishment has become essential to hit the target by 2020.
To verify whether the thermal performance of a building envelope meets the requirements, or to determine where renovation is necessary, the as-built state has to be evaluated. To this end, it is generally accepted to consider the thermal transmittance (U-value). This value can be calculated for steady-state conditions from technical standards (EN673, 1997, ISO6946, 2007) or be measured on site by means of heat flux sensors (ISO9869(E), 1994). The latter technique determines the U-value of a building element by measuring the heat flux on one side and the surface temperature on both sides. It is important to collect data during a considerable time span (preferably about 2 weeks) as in reality the boundary conditions are always fluctuating. With a substantial dataset it is typically possible to derive a precise U-value. This method is time consuming, and in principle different points on the wall should be analysed to exclude singularities, which renders this approach rather elaborate. Infrared

thermography (IRT) could potentially improve the efficiency of on-site U-value determination. The duration of the measurement procedure with a thermographic camera is short, and this technique allows to analyze the surface temperature of a whole building part at once. In this way a more complete overview of the heat flows of a building is attained, which is a clear advantage over the point wise data of the existing methods. Evidently, the instantaneous measurement only yields a single value in time, thereby limiting its applicability and accuracy.
Nowadays, IRT is a popular tool for qualitative building diagnostics (Lucchi, 2011, Kalamees, 2007, Straube and Burnett, 1999, Burn and Schuyler, 1980, Taylor et al., 2013, Balaras and Argiriou, 2002), either for supervision of the building quality during construction or to detect defects after completion. The temperature gradients on a building surface can indicate e.g. missing or damaged insulation, air leakages or sources of moisture. More recent studies focus on *quantitative* application of IR-images: Asdrubali et al. (2012) used IRT to classify thermal bridges, other researchers tried to derive the U-value of building components (Dall'O et al., 2013, Fokaides and Kalogirou, 2011, Lehmann and Ghazi Wakili, 2013). However, this is a complex procedure due to the fact that many variable parameters influence the instantaneous surface temperature of the object, such as solar radiation, atmospheric long wave radiation, wind velocity, outside temperature fluctuation, material characteristics, indoor heating. Lehman et al. (2013) performed a sensitivity analysis for a large number of parameters on 6 different *wall* types (brick cavity wall, concrete wall, timber framed wall and 3 types of plaster-brick walls). They concluded that the external surface temperature strongly depends on the wall assembly and its thermal performance. Solar- and IR-radiation turned out to impose the strongest restrictions for quantitative IRT, because these introduce a direct temperature increment on the surface of the object. It was concluded that sunshine had to be avoided somewhere between 1 hour and 2 days before the measurements, depending on the thermal capacity and assembly of the wall.
In general, the time that is needed to reach a uniform temperature over the section of a wall is called the time constant τ , which is proportional to the square root of the thermal conductivity (λ), the density (ρ) and volumetric heat capacity (c). The larger the time constant, the more stringent the boundary conditions for IRT become in order to reduce the impact of transient effects. Windows typically have a low time constant (30min for a 4mm glass pane vs. 12h for a cavity brick wall), hence the restrictions for quantitative thermography on *glazing* are perhaps less severe. The use of IRT on windows could be a powerful application in the case of renovation or energy audits, because flux measurements on glazing units are not evident. Even a visual inspection of the thermal performance of the glass is hardly possible on site, contrary to an insulated brick wall. Next to that, IRT could have the potential to reveal degradation in time due to gas leakage.
In this paper, the investigation to suitable boundary conditions for quantitative IRT on glazing is presented. As explained before, an IR-image is a record of one moment under specific circumstances, which typically does not correspond to the steady state. A robust assessment method of the U-value should thus include a confidence interval. Six glazing types are analysed, using numerical simulations. A sensitivity analysis to internal and external climatic variations is performed.

2. Method - numerical analysis

Every object emits radiant thermal energy from its surface as long wave radiation (heat). Hence the energy received by an infrared sensor of a thermal camera consists of the emitted energy of the target. But also the surroundings emit energy, which is partially reflected by the object and in this way captured by the camera as well. Furthermore, the infrared emission of the atmosphere between the camera and the object contributes, and in the case of transparent elements, long wave radiation from behind the element is partially transmitted through and should be taken into consideration as an additional term (FIG. 1). The standard equation for incident radiation of the camera becomes:

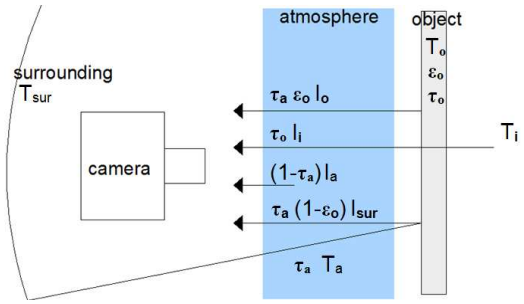

FIG. 1 Aspects of incident thermal radiation on the thermal sensor of an IR camera

$$I = \tau_a \cdot \varepsilon_o \cdot I_o^{\circ} + \tau_a \cdot (1-\varepsilon_o) \cdot I_{sur} + (1-\tau_a) \cdot I_a + \tau_o \cdot I_i \qquad (1)$$

Where τ transmittance
ε emissivity of the surface
I irradiance
$^{\circ}$ blackbody
$_{a,\ o,\ sur,i}$ atmosphere, object, surroundings, interior

The incoming energy is then converted to temperature values according to the Stefan-Boltzmann law. In other words, when the parameters for atmosphere and surroundings are correctly set to the camera software, thermography allows to determine the instantaneous surface temperature of a construction (either interior (θ_{si}) or exterior (θ_{se})).
Next to that, the internal and external air temperature (θ_i and θ_e) can easily be measured on site as well. With these data and an appropriate internal or external heat transfer coefficient (h_i or h_e), the heat flux (Q) through the wall can be calculated from the wall-air temperature difference.

$$Q = h_i \cdot (\theta_i - \theta_{si}) \quad \text{or} \quad Q = h_e \cdot (\theta_e - \theta_{se}) \qquad (2)$$

The heat flux can also be expressed in function of the indoor-outdoor air temperature difference,

$$Q = U \cdot (\theta_i - \theta_e) \qquad (3)$$

leading to the following expression of the U-value:

$$U = h_i \cdot \left(\frac{\theta_i - \theta_{si}}{\theta_i - \theta_e}\right) = h_e \cdot \left(\frac{\theta_{se} - \theta_e}{\theta_i - \theta_e}\right) \qquad [\text{W/(m}^2\text{.K)}] \qquad (4)$$

By definition, Eq. 4 is only valid under static boundary conditions, but it will be applied to transient conditions to assess to what extent it might provide useful information. Since the value for h_e is function of the strongly varying wind velocity (Emmel et al., 2007), this study emphasises on the determination of the U-value from the interior side. A sensitivity analysis of θ_{si} to variations in θ_i is performed by subjecting six types of windows to 3 different types of indoor temperature regimes. Additionally, the influence of the most critical outdoor parameters is analysed. Note that specific constraints in respect to thermography on glazing units are not addressed here. It is assumed that the surface temperature can be determined accurately with an IR camera. Evidently, uncertainties in emissivity and background temperature will propagate in the uncertainty interval of the estimated U-value, as well as the accuracy of the camera itself.

2.1 Cases

FIG. 2 illustrates the different glazing assemblies that are studied. These configurations are representative of those found in the Belgian building stock, and the broad variety of thermal performance levels ensures the wide applicability of the results. The properties of each layer are

derived from the European and international standards (EN673, 1997, ISO10456, 2007), and listed in TABLE 1.

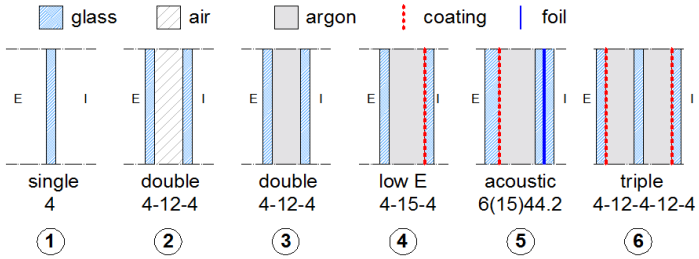

FIG. 2 Overview of the 6 investigated glazing types. Diversity in glass thickness, cavity fill and coating broadens the scope of the analysis.

TABLE 1 Properties of the 6 investigated glass types

Material Properties		t [m]	λ [W/m.K]	ρ [kg/m³]	c [J/kg.K]	ε [-]
A	Soda lime silica glass	0.004	1	2500	750	0.837
B	Air	0.012	0.025	1,232	1008	-
C	Argon	0.012	0.017	1.699	519	-
D	Low ε-coating	-	-	-	-	0.04
E	PVB-interlayer	0.0038	-	-	-	-

Glass type	Assembly (exterior - interior)	U-value[a] [W/(m².K)]
1. Single Glass (Si)	A	5.75
2. Double Glazing-air (Do+Ai)	A-B-A	2.85
3. Double Glazing-argon (Do+Ar)	A-C-A	2.67
4. Low E Glass (LE)	A-C (0.015m)-D-A	1.09
5. Acoustic Glass (Ac)	A (0.006m)-D-C (0.015m)-A-E-E-A	1.08
6. Triple Glazing (Tr)	A-D-C-A-C-D-A	0.7

[a] with standard internal and external heat transfer coefficient h_i = 7.7 W/(m².K) and h_e = 25 W/(m².K)

2.2 Simulation model

The numerical simulations are performed with the thermal analysis software VOLTRA . This program calculates transient heat transfer in 3D-objects, according to European and international standards. A solar processor takes into account of dynamic solar heat gains, based on the actual temperature and long wave radiation (Physibel, 2011).

The main purpose of the simulations is to calculate surface temperatures θ_{si} and θ_{se}, from which U-values will be deduced to evaluate the use of Equation 4 under dynamic boundary conditions. Heat transfer through conduction, convection and radiation is considered separately, according to EN 673 (1997): the radiative heat transfer is view factor based, whereas the convective heat transfer in the cavity is proportional to the Nusselt number of the gas and its thermal conductivity. The external convective heat transfer coefficient (h_{ec}) expressed in function of the wind speed (v) (Taki and Loveday, 1996), the internal convective heat transfer coefficient (h_{ic}) is calculated iteratively, using the temperature difference between the indoor air and surface (Thomas et al., 1990) :

$$h_{ec} = 5.85 \cdot v^{0.52} \qquad h_{ic} = 1.77 \cdot \sqrt[4]{\theta_i - \theta_{si}} \tag{5}$$

2.2.1 Outdoor boundary conditions

The simulations were carried out for a 10-days period during winter (December 17 - December 26). The meteorological data of a reference year of Uccle, Belgium was used as input. The chosen period

contains considerable variations in wind speed (v), sunny and overcast days (I_s) and variable outdoor air (θ_e) and sky (θ_{sky}) temperature, as can be seen from FIG.3.

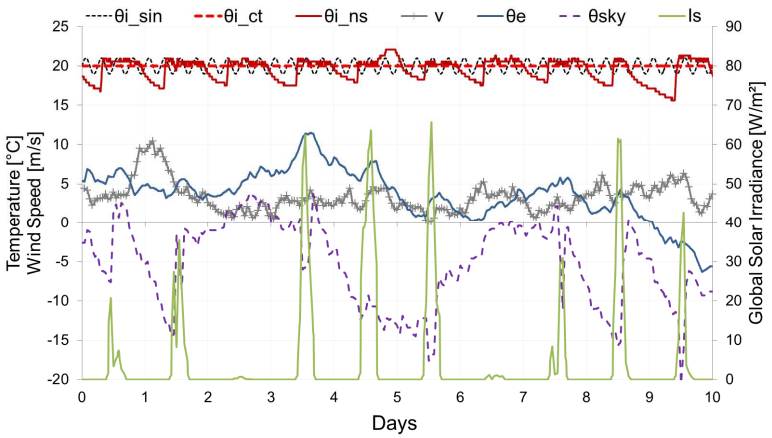

FIG. 3 Variable outdoor climate data for the period of December17-26, Uccle, Belgium, and 3 different temperature regimes for the indoor air (0= Dec 17 0h00, 10= Dec26 24h00)

2.2.2 Indoor boundary conditions

In this study, special attention was paid to the influence of variations in indoor air temperature. Because an IR-image shows the thermal state of a target for one specific moment, the thermal transmittance is derived by assuming these instantaneous circumstances as a steady-state condition. Nevertheless, in reality the indoor and outdoor temperatures are constantly fluctuating. To assess the effect of this assumption on the estimated U-value, simulations for each glazing assembly were carried out for 3 different indoor air temperature regimes (FIG. 3)

- θ_{i_ct}: constant temperature of 20°C
- θ_{i_sin}: fluctuating temperature 20±1°C, introduced as a sinus function with a period of 12h
- θ_{i_ns}: variable temperature with night setback (measurement data of a Belgian family house)

3. Results and discussion

3.1 Derivation of the thermal transmittance

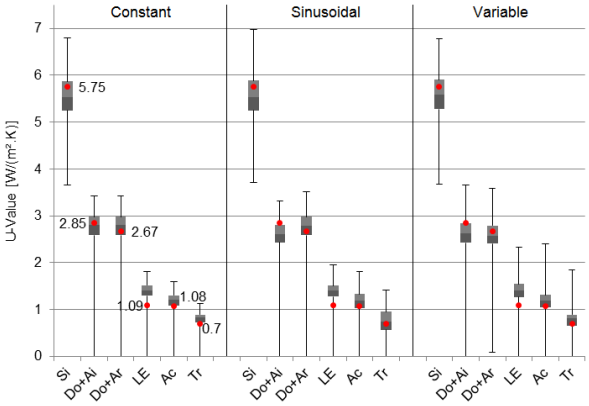

FIG. 4 U-value assessment based on θ_{si} for 3 θ_i- regimes and 6 glazing types. Note: in some cases the estimated U-value became negative, but these values are excluded from the graph.

For each indoor temperature regime, the U-value for the 6 types of glazing is estimated every 10 minutes, based on the internal surface temperature, using Equation 4 with h_i equal to 7.7 W/(m².K). In

FIG. 4 the distribution of the estimated U-value is reported. In general, it can be noticed that 50% of the assessed values (grey boxes) approximates the theoretical (red dots) thermal transmittance (an average deviation of 0.2W/(m².K), maximal 0.5W/(m².K)). Even though no restrictions to the boundary conditions are made yet, this already indicates the potential of quantitative IRT on glazing. However, strongly diverging outliers (up to 4W/(m².K) make it impossible to rely on the result of one specific moment, neither to determine the correct type of glazing based on a single measurement without any constraints.
It can be seen that the effect of a different indoor climates only has a minor influence for less insulating windows (type 1-3). As their time constant is small enough, the surface temperature can adapt at (almost) the same frequency as the ambient air temperature. For the better insulating windows (type 4-6), the error level becomes larger, due to the higher time constant. For type 1-3, the error interval increases with about 0.2W/(m².K), whereas for type 4-6, it augments up to 0.8 W/(m².K). This is especially true for glazing type 5, where the thickest glass pane is situated at the interior side.

3.2 Restrictions to the boundary conditions

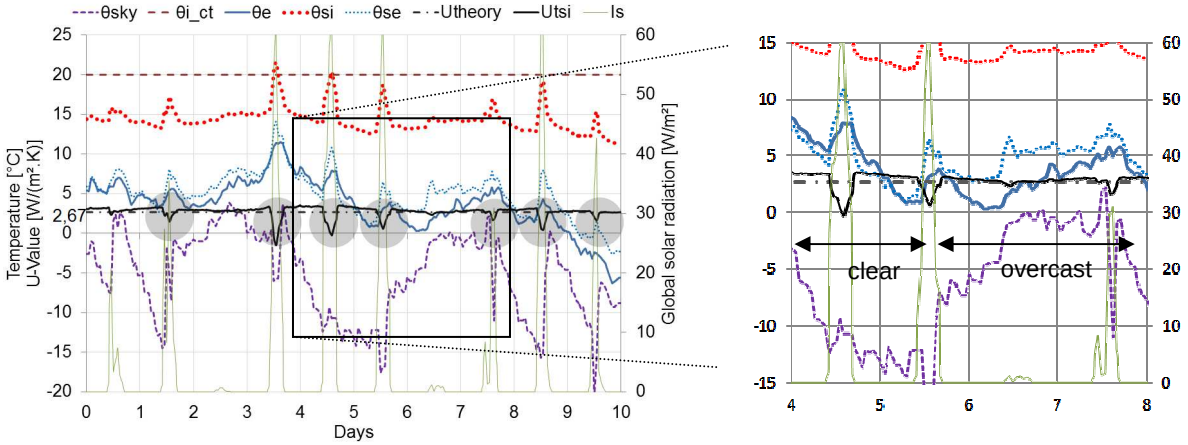

FIG. 5 Influence of the boundary conditions for the assessment of the U-value, illustrated for window type 3. During sunshine hours and clear skies, the deviation to the theoretical value increases.

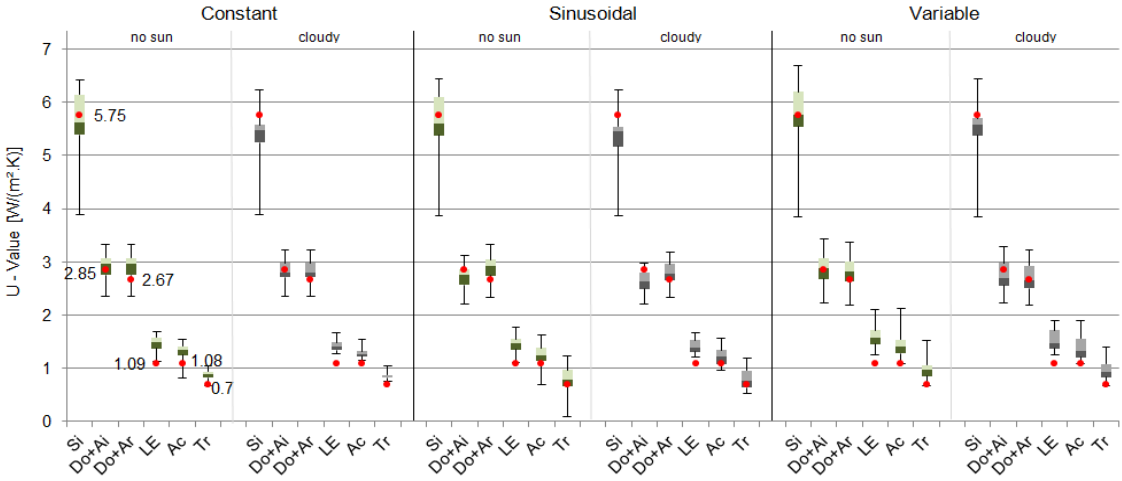

FIG. 6 Distribution of the assessed U-value(based on θ_{si}) for 3 θ_i - regimes and 6 glazing types. The results are either only excluding sunny periods (no sun) or also moments of clear sky(cloudy) .

To increase the reliability of the estimation, events that cause extreme aberrations should be excluded from the data. From FIG. 5 it is clear that the largest deviations of the estimated value (U_{tsi}) come to

front in the presence of sunshine (I_s) (grey circles). Due to the *solar radiation*, the internal surface temperature (θ_{si}) of the glazing augments. It gives the impression of a better insulating quality, leading to an underestimation of the U-value. As soon as the sun disappears, this effect fades quasi instantly. Next to that, the *long wave radiation from the sky* is one of the most influencing factors. This has also been pointed out by Lehmann et al. (2013) in the case of wall assemblies. Clouds reflect the earth's long wave radiation, leading to warmer surface temperatures of exposed objects. Consequently, a clear sky corresponds to a low sky temperature (θ_{sky}), which reduces the surface temperature of the glazing and therefore leads to a higher estimated U-value (FIG.5). To assess the influence of these two outdoor parameters, the data at moments of solar radiation ($I_s \neq 0$ W/m²) are excluded from the U-value assessment (*'no sun'*, FIG. 6). This roughly corresponds with the exclusion of data between 9AM and 5PM. Additionally, the data obtained during clear skies (θ_{sky}<-5 °C) are also excluded (*'cloudy'*, FIG.6).

3.3 Main findings

- The range on the results decreases substantially when direct solar radiation is avoided. Apart from single glazing, the maximal deviation from the theoretical U-value diminishes from 2.85 to 1.05 W/(m².K). It improves even more when clear sky moments are excluded, to only 0.81 W/(m².K). On average, the median deviation is only 0.24 W/(m².K), which is very accurate. Note that these values refer to the worst case scenario of internal heating pattern: night setback.
- In absence of solar radiation, this method allows to distinguish between poor insulation value (type 1), moderate insulation value (type 2, 3) and high insulation value (type 4, 5, 6).
- Assuming that the indoor temperature is kept constant, taking minor fluctuations of the heating system into account (sinusoidal regime – still realistic for on-site measurements), the U-value can be estimated with an uncertainty of at most 0.65W/(m².K) when the data is collected under the right circumstances (cloudy), except for single glazing.
- In general, the estimated U-value is systematically higher than the theoretical value. This can be attributed to a higher h_i that is used for the estimations (7.7W/(m².K)) compared to the variable value in the simulation model, which is typically depending on the type of glazing and boundary conditions and in the range of 7.0 - 7.5W/(m².K). This means that for 70 to 100% of the cases this approach yields a conservative estimation of the U-value.

4. Conclusions

This paper discusses the application of quantitative infrared thermography on window glazing. Based on numerical simulations for 6 window assemblies with different thermal performances, a sensitivity analysis has pointed out the most critical restrictions to the boundary conditions for a reliable assessment of the U-value from the interior surface temperature. Assuming that this temperature can be determined correctly, the limited simulation results show that the thermal transmittance can be estimated within a minor confidence interval of 0.65 W/(m².K) when direct sunlight and clear skies are avoided (except for single glazing). The regime of the indoor air temperature turned out to be of minor importance for the quality of the results. These findings are promising for the application of IR-thermography in assessing the insulation quality of glazing, but further research is needed to extend them to other types of windows and other periods of the year. Of course, the confidence interval will enlarge for on-site measurements because θ_{si} can only be determined within a certain range, e.g. due to the accuracy of the camera, the variability in emissivity, and the influence of the background. Future research will extend the error estimation by means of experiments, to verify the presented conclusions and include additional noise. Furthermore, the use of external surface temperatures for the assessment of the U-value will be investigated. Up to now, this data is ignored in the analysis, but including them might improve the methodology as information of both sides of the assembly is used. Also, consecutive measurements in a short time span may add to the accuracy of the U-value calculation.

5. Acknowledgements

This research is founded by the agency for Innovation by Science and Technology-Belgium (IWT), project 130210. The authors thank dr. P. Standaert for his help in the simulation modelling.

References

ASDRUBALI, F., BALDINELLI, G. & BIANCHI, F. 2012. A quantitative methodology to evaluate thermal bridges in buildings. *Applied Energy,* 97**,** 365-373.

BALARAS, C. A. & ARGIRIOU, A. A. 2002. Infrared thermography for building diagnostics. *Energy and Buildings,* 34**,** 171-183.

BURN, K. & SCHUYLER, G. 1980. Applications of infrared thermography in locating and identifying building faults. *journal of international institute for Conservation* 4**,** 3-14.

DALL'O, G., SARTO, L. & PANZA, A. 2013. Infrared Screening of Residential Buildings for Energy Audit Purposes: Results of a Field Test. *Energies,* 6**,** 3859-3878.

EC 2011. Europe 2020 targets. EU EUROPEAN COMMISSION.

EMMEL, M. G., ABADIE, M. O. & MENDES, N. 2007. New external convective heat transfer coefficient correlations for isolated low-rise buildings. *Energy and Buildings,* 39**,** 335-342.

EN673 1997. Glass in building. *Determination of thermal transmittance (U value). Calculation Method.* European Standard EN.

FOKAIDES, P. A. & KALOGIROU, S. A. 2011. Application of I thermography for the determination of the overall heat transfer coefficient in building envelopes. *Applied Energy,* 88**,** 4358-4365.

ISO6946 2007. Building components and building elements. *Thermal resistance and thermal transmittance - calculation method.* ISO International Organization for Standardization

ISO9869(E) 1994. Thermal insulation - Building elements. *In-situ measurement of thermal resistance and thermal transmittance.* International Organization for Standardization ISO.

ISO10456 2007. Building materials and products - Hygrothermal properties - Tabulated design values and procedures for determining declared and design thermal values. ISO International Organization for Standardization.

KALAMEES, T. 2007. Air tightness and air leakages of new lightweight single-family detached houses in Estonia. *Building and Environment,* 42**,** 2369-2377.

LEHMANN, B. & GHAZI WAKILI, K. 2013. Effects of individual climatic parameters on the infrared thermography of buildings. *Applied Energy,* 110**,** 29-43.

LUCCHI, E. 2011. Non-invasive method for investigating energy and environmental performances in existing buildings. *PLEA Conference on Passive and Low Energy Architecture.* Belgium.

PHYSIBEL 2011. Voltra 7.0 Manual. Physibel Software.

STRAUBE, J. & BURNETT, E. F. P. 1999. Rain Control and Design Strategies. *Journal of Building Physics,* 23**,** 41-56.

TAKI, A. H. & LOVEDAY, D. L. 1996. External convection coefficients for framed rectangular elements on building facades. *Energy and Buildings,* 24**,** 147-154.

TAYLOR, T., COUNSELL, J. & GILL, S. 2013. Energy efficiency is more than skin deep: Improving construction quality control in new-build housing using thermography. *Energy and Buildings,* 66**,** 222-231.

THOMAS, F., GLANZMANN, J., KELLER, B., QUEISSER, A. & RAGONESI, M. 1990. *Element 29: Wärmeschutz im Hochba,* Zürich, Faktor Verlag.

WTCB 2005. Visietekst 'Bouwen en Innoveren'- Bouwen aan de toekomst. Belgisch Bouwplatform.

TOPIC
Building Materials and Structures

Page.....322-515

State-of-the-Art and the Path to the Building Integrated Photovoltaics of Tomorrow

Bjørn Petter Jelle, Professor [1,2]

[1] SINTEF Building and Infrastructure, Department of Materials and Structures, NO-7465 Trondheim, Norway
[2] Norwegian University of Science and Technology, Department of Civil and Transport Engineering, NO-7491 Trondheim, Norway

KEYWORDS: *State-of-the-art, Review, Future, Building integrated photovoltaics, BIPV, Photovoltaics, Solar cell*

SUMMARY:
Building integrated photovoltaic (BIPV) systems may represent a powerful and versatile tool for achieving the ever increasing demand for zero energy and zero emission buildings of the near future. The BIPVs offer an aesthetical, economical and technical solution to integrate solar cells harvesting solar radiation to produce electricity within the climate envelopes of buildings. Building integration of photovoltaic (PV) cells are carried out on sloped roofs, flat roofs, facades and solar shading systems. PV cells may be mounted above or onto the existing or traditional roofing or wall systems. However, BIPV systems replace the outer building envelope skin, thus serving simultanously as both a climate screen and a power source generating electricity. Hence, BIPVs may provide savings in materials and labour, in addition to reducing the electricity costs. Nevertheless, in addition to specific requirements put on the solar cell technology, as the BIPVs act as the climate protection screen it is of major importance to have satisfactory or strict requirements of rain tightness and durability, where various building physical issues like e.g. heat and moisture transport in the building envelope also have to be considered and accounted for. This work summarizes briefly the current state-of-the-art of BIPVs, including both BIPV foil, tile, module and solar cell glazing products, and addresses possible research opportunities and pathways for the BIPVs of tomorrow.

1. Introduction

The world's demand and focus on renewable and non-polluting energy, together with energy efficiency, are increasing, thus zero energy and zero emission buildings are rapidly drawing attention. In order to become a zero energy or zero emission building, such a building need to harvest energy from its surroundings, where energy from the sun is one of the obvious choices. Building integrated photovoltaic (BIPV) systems, where solar cells are integrated within the climate envelopes of buildings and utilizing solar radiation to produce electricity, may represent a powerful and versatile tool for reaching these goals with respect to both aesthetical, economical and technical solutions. Building integrated photovoltaic (BIPV) systems replace parts of the conventional building materials and systems in the climate envelope of buildings, such as the roofs and facades. BIPV systems are considered as a functional part of the building structure, or they are architecturally integrated into the building's design (Peng et al. 2011). Hence, the BIPV system serves as a building envelope material and power generator simultaneously (Strong 2010). Accelerated climate ageing tests concerning the durability will also be important (Jelle 2012). This work summarizes first briefly the current state-of-the-art of BIPVs, including both BIPV foil, tile, module and solar cell glazing products, also mentioning building attached photovoltaic (BAPV) systems. Thereafter this work bridges today and

tomorrow by addressing and investigating several possible research opportunities and pathways for the BIPVs in the future. For further overview and elaborations within these aspects of BIPVs it is referred to the study by Jelle et al. (2012b).

2. Building integration and testing of photovoltaic cells

Building integration of photovoltaic (PV) cells are carried out on sloped roofs, flat roofs, facades and solar shading systems. PV cells may be mounted above or onto the existing or traditional roofing or wall systems. However, BIPV systems replace the outer building envelope skin, thus serving simultanously as both a climate screen and a power source generating electricity. Hence, BIPVs may provide savings in materials and labour, in addition to reducing the electricity costs. Nevertheless, as the BIPVs act as the climate protection screen it is of major importance to have satisfactory or strict requirements of rain tightness and durability. Several aspects have to be considered and evaluated related to the integration of the PV cells into the outer building envelope skin. One aspect is to ensure an air gap underneath the solar cells in order to provide an air flow reducing the temperature of the solar cells, as an elevated temperature decreases the efficiency of the solar cells, especially for mono- and polycrystalline Si cells. Another aspect to be considered are the inclination of the BIPVs, both with respect to existing and new buildings, as the solar cells necessarily need to follow the roof inclination (or the wall for that matter) to be integrated solutions. Geographical position and orientation towards the sun and area coverage are yet another aspects to be considered during integration of the BIPV systems. In fact, some BIPV manufacturers also offer dummy modules to provide a more aesthetical and consistent appearance of the roofs and facades. Hence, in short BIPVs have to fulfil all the requirements, with respect to several properties, of the building envelope skins they are substituting. Various building physical issues like e.g. heat and moisture transport in the building envelope also have to be considered and accounted for. The testing and evaluation of solar cells involve several properties, e.g. solar cell efficiency $\eta = P_{max}/(\Phi A)$ where Φ is the input solar radiation in W/m^2 and A is the solar cell surface area in m^2, maximum power point P_{max} in W or Watt-peak (Wp), open circuit potential or voltage U_{oc}, short circuit electrical current I_{sc}, fill factor $FF = P_{max}/(U_{oc}I_{sc}) = (UI)_{max}/(U_{oc}I_{sc})$, band gap E_g and quantum yield φ = number of photo-electrons divided by number of photons. The values reported by solar cell manufacturers are mainly obtained according to standard test conditions (STC) or nominal operating cell temperature (NOCT). Various standards exist for solar cells, where further information is given in the standards themselves as treated in the study by Jelle et al. (2012b).

3. State-of-the-art of BIPVs

3.1 BIPV categorization

The range of BIPV products is very wide, and they may be categorized in several different ways. Within this work the categorization is mainly performed based on the product descriptions from the manufacturers and what other material types the products are customized to be combined with. In this work the BIPV products or systems have been categorized into the following groups:

- BIPV foil products.
- BIPV tile products.
- BIPV module products.
- Solar cell glazing products.

In addition, related to the various BIPV products, the group building attached photovoltaic (BAPV) products should also be mentioned:

- BAPV products.

Building attached photovoltaic (BAPV) products are regarded as add-ons to the buildings, hence not directly related to the building structures' functional aspects (Peng et al. 2011). That is, BAPVs are not

BIPVs, i.e. the BAPVs are not integrated into the outer building envelope skin, thus not replacing the traditional building parts as the BIPVs are doing. Some BIPV products exhibit a variety of properties, thereby making it more difficult to categorize them. Yet in other cases it might even be rather difficult to determine whether a PV product should be considered as a BIPV product or not, e.g. due lack of of information and uncertainty about how the product is mounted. In the following there is given more details and some examples from each of the different BIPV product groups. For a comprehensive state-of-the-art review of these BIPV systems, including references and contact information, it is referred to the work by Jelle et al. (2012b).

3.2 BIPV foil products

BIPV foil products are lightweight and flexible, which is beneficial with respect to easy installation and prevailing weight constraints for roofs. The PV cells are often made from thin-film cells to maintain the flexibility in the foil and the efficiency regarding high temperatures for use on non-ventilated roof solutions. Unfortunately, currently there are few manufacturers on the market that provide weather tight solutions. Table 1 and Fig.1 present an example of one BIPV foil product. PV foil products have a low fill factor due to both the low efficiency and the large solar cell resistances of thin-film cells. However, it is possible to vary the degree of inclination of the product to a great extent providing flexible solutions.

TABLE 1. Literature data for one of the BIPV foil products (Jelle et al. 2012b).

Manufacturer	Product*	η (%)	U_{oc} (V)	I_{sc} (A)	P_{max} (W)	FF	Area (mm x mm)	P_{max}/area (W/m^2)
Alwitra GmbH & Co.	Evalon V Solar 408		138.6	5.1	408 /module	0.58	1550 x 6000	42.9
	Evalon V Solar 136		46.2	5.1	136 /module	0.58	1050 x 3360	38.5

*Several models are available from the producer in the Evalon V Solar series.

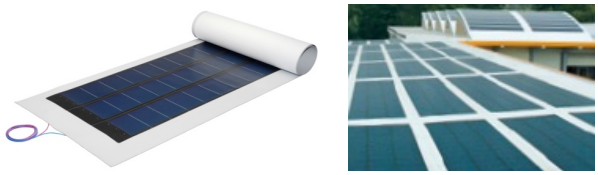

FIG 1. Example of a BIPV foil product from Alwitra GmbH & Co. using amorphous silicon cells from Uni-Solar (Alwitra 2011).

3.3 BIPV tile products

BIPV tile products may cover the entire roof or selected parts of the roof. They are normally arranged in modules with the appearance and properties of standard roof tiles and substitute a certain number of traditional roof tiles, thus also enabling easy retrofitting of roofs. The cell type and tile shape varies. Some tile products may resemble curved ceramic tiles and will not be as area effective due to the curved surface area, but may be more aesthetically pleasing. Some examples of BIPV tile products on the market today are given in Table 2, with two of them depicted in Fig.2. The BIPV products from Solardachstein, Lumeta and Solar Century (Table 2) provide the highest FFs indicating that the efficiencies are high. In fact, Solar Century reports an efficiency of 20 % per cell for their C21e Tile. The design concept of the STEPdesign and the Solé Powertile is one module appearing as standard roof tiles that displaces several standard roof tiles.

TABLE 2. Literature data for some of the BIPV tile products (Jelle et al. 2012b).

Manufacturer	Product*	η (%)	U_{oc} (V)	I_{sc} (A)	P_{max} (W)	FF	Area (mm x mm)	P_{max}/area (W/m^2)
Solardachstein	STEPdesign		23.15	2.40	1.36 /cell	0.76	8 units 100 x 100	136
SRS Energy	Solé Powertile		6.3	4.6	15.75 /module	0.54	868 x 457.2	39.7
Lumeta	Solar Flat Tile		7.4	5.2	28 /module	0.73	432 x 905	71.6
Solar Century	C21e Tile	20/cell	12.0	5.55	52 /module	0.78	1220 x 420	101.5

*Lumeta has also a Solar S Tile available.

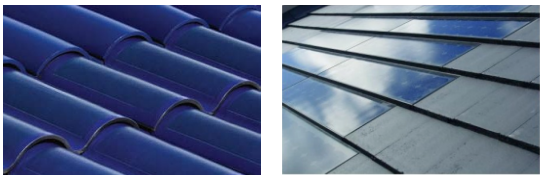

FIG 2. Example of BIPV tile products from SRS Energy (2010) (left) and Solar Century (2011) (right).

3.4 BIPV module products

The BIPV module products presented are somewhat similar to conventional PV modules. The difference, however, is that the BIPV modules are made with weather skin solutions. Some of the products may replace various types of roofing, or they fit with a specific roof solution produced by its manufacturer. These mounting systems increase the ease of installation. There is a large amount of products on the market and some of them are promoted as BIPV products without in fact functioning as weather skins, whereas other products are not very specific on how they are actually mounted which leads to uncertainty whether they are BIPVs or BAPVs. Some of the BIPV module products are premade modules with thermal insulation or other elements included in the body. Some examples of BIPV module products are given in Table 3, with two of them depicted in Fig.3.

TABLE 3. Literature data for some of the BIPV module products (Jelle et al. 2012b).

Manufacturer	Product*	η (%)	U_{oc} (V)	I_{sc} (A)	P_{max} (W)	FF	Area (mm x mm)	P_{max}/area (W/m^2)
Creaton AG	Creaton Solesia		13.86	8.46	90/module	0.77	1778 x 355	142.6
Rheinzink	PV Quickstep		17.10	5.12	68/module	0.78	2000 x 365	93.2
DuPont	Gevity	17.7 17.7	24.20 24.43	8.77 8.87	160 165	0.75 0.76	1332.5 x 929 1332.5 x 929	129.36 133.4
Solar Century	C21e Slate	20/cell	12.0	5.55	52	0.78	1174 x 318	139.3

*Several models are available from various producers.

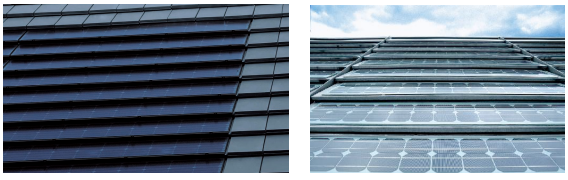

FIG 3. Example of BIPV module products from Creaton AG (2011) (left) and Rheinzink (2011) (right).

3.5 Solar cell glazing products

BIPVs as solar cell glazing products provide a great variety of options for windows, glassed or tiled facades and roofs, Different colours and transparencies can make many different aesthetically pleasing results possible. Some solar cell glazing product examples are given in Table 4 and Fig.4. The solar cell glazing modules transmit daylight and serve as water and sun protection. The distance between the solar cells depends on wanted transparency level and the criteria for electricity production, but normally the distance is between 3 and 50 mm. The space between the cells transmits diffuse daylight. Hence, both shading and natural lighting are provided while producing electricity. The solar cell glazing manufacturers usually offer customized products for specific projects, regarding shape, cell material, colour and transparency level, i.e. the distance between the cells, whereas Table 4 presents some predefined modules. For example, the transparency level varies from 16 % to 41 % for various Vidursolar models, while it is 25 % for the Abakus Solar AG Peak In P210-60 product. The different models from Sapa Building System depicted in Fig.4 are using either amorphous, polycrystalline or monocrystalline cells with different distances between the cells.

TABLE 4. Literature data for some solar cell glazing products (Jelle et al. 2012b).

Manufacturer	Product*	η (%)	U_{oc} (V)	I_{sc} (A)	P_{max} (W)	FF	Area (mm x mm)	P_{max}/area (W/m^2)
Abakus Solar AG	Peak In P210-60		36.50	7.70			2000 x 1066	
Vidursolar	FV VS16 C36 P120		21.6	7.63			1600 x 720	
Sapa Building System	Amorphous Si thin film	5/cell			32/cell		576 x 976 /cell	50
	Poly-crystalline	16/cell			1.46-3.85 /cell		156 x 156 /cell	120
	Mono-crystalline	22/cell			2.90-3.11 /cell		125 x 125 /cell	155

*Several models are available from various producers.

FIG 4. Example of various solar cell glazing products from Sapa Building System (2011).

3.6 BAPV products

As mentioned earlier, the BAPV products are added on rather than integrated in the roof or facade. For further details and examples of BAPV products it is referred to the study by Jelle et al. (2012b).

4. The path to the BIPVs of tomorrow

4.1 PV development and impact on BIPVs

Development within the PV materials and solutions and their technologies may have an even stronger impact on the development of BIPVs in the years to come if one is able from the PV based research to tailor-make solar cell materials and solutions for building integration. As for the advances in PV technology, in Fig.5 there is given a timeline for reported best research-cell efficiencies, depicting all verified records for various PV conversion technologies, including crystalline Si, thin-film, single-

junction GaAs, multijunction and emerging technologies, collected from solar companies, universities and national laboratories (NREL 2013). The advances in these PV technologies and their increasing efficiencies will naturally be exploited in the coming BIPV products to be made.

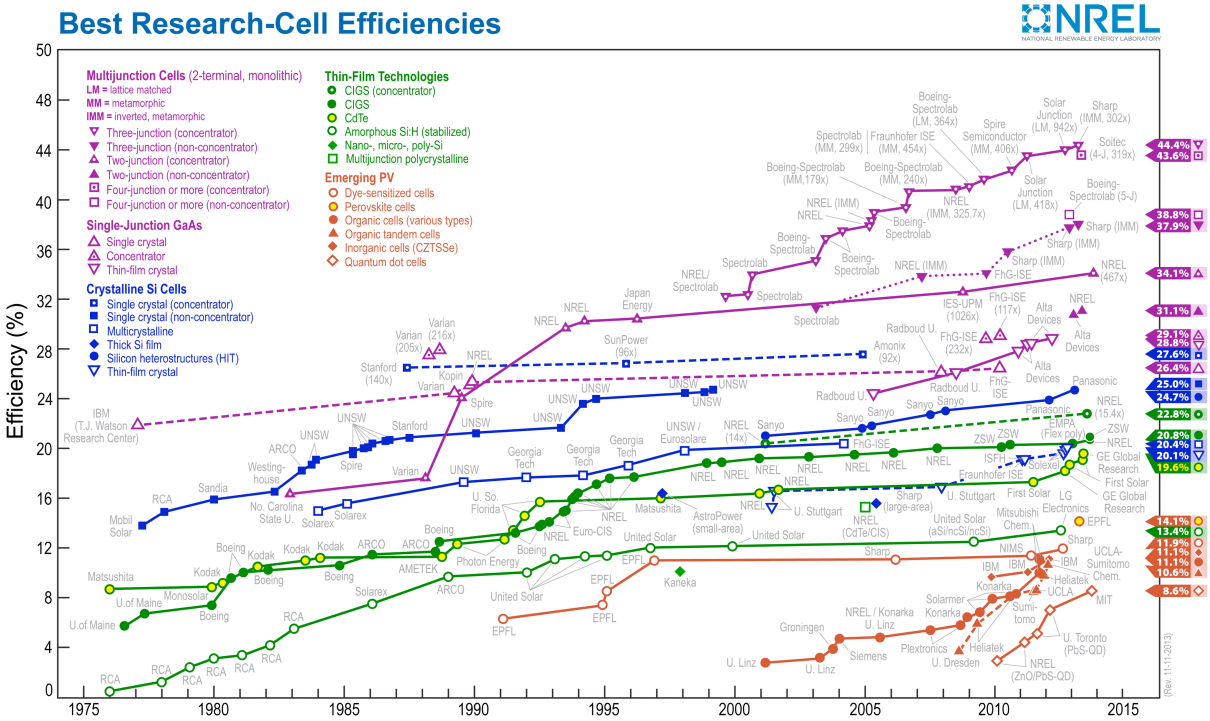

FIG 5. A timeline for reported best research-cell efficiencies, depicting all verified records for various PV conversion technologies (NREL 2013).

4.2 New materials and solutions for BIPVs

The research paths for possible new PV technologies that may initiate and advance into new innovations, and which may be developed into BIPVs, may be found in miscellaneous fields, e.g. ultra-low cost and low-medium efficiency organic based modules, ultra-high efficiency modules, solar concentrator and/or solar trapping systems embedded in the solar cell surface and material beneath, and flexible lightweight inorganic thin film solar cells, and several others some of them yet to be discovered. Carrying out the research and development of the PV and BIPV materials and solutions for the future one may bear in mind the following words: ”*think thoughts not yet thought of*” and ”*the more we know the more we know we don’t know*” (Jelle et al. 2010). In the following many new materials and solutions will briefly be mentioned, whereas further details may be found in the work by Jelle et al. (2012b) and referred studies therein.

As seen from Fig.5, research laboratories have for many years produced high-performance solar cells with efficiencies up to 25 %-44 %, the highest on currently being 44.4 %. One approach is to use materials with higher purity and to eliminate the impurities along in the process. Also the back surface can be passivated with silicon oxide and amorphous silicon to minimize recombination losses at the surfaces and contacts. Textured surfaces and buried contacts with minimal shading reduce optical losses. The total production is very expensive and is to date for use in laboratories only. Another way of increasing the efficiency may be concentrated photovoltaic (CPV) cells. Combining electrochromic materials with solar cell glazing solutions may also be possible (Jelle et al. 2012a), whereas another issue is to avoid snow and ice covering the solar cells (Jelle 2013). A strategy utilized to achieve high solar cell efficiencies is to make so-called sandwich or stack solar cells, which use several different material layers and cells with different spectral absorbances to harvest as much as possible of the solar

radiation in a wide wavelength range, see e.g. Fig.6 (DGS 2008). Hence, a much larger portion of the solar radiation is utilized.

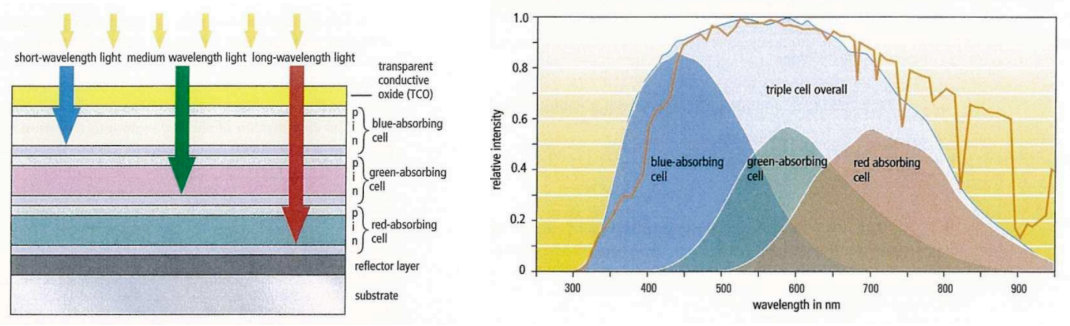

FIG 6. An amorphous triple solar cell with its configuration (left) and spectral responses (right) (DGS 2008).

Ultra-low cost and low-medium efficiency organic based modules are based on dye sensitized solar cells (DSSC), extremely thin absorbers, organic polymer cells and others. Organic semiconductors are less expensive than inorganic semiconductors like Si. Polymer solar cells are more sensitive to degradation, where ultraviolet solar radiaion and oxygen from the atmosphere may oxidize the organic layer. More stable devices have already been made and progress in this field is important for polymer solar cells to have a future as commercial devices and to be used in various BIPVs (Jørgensen et al. 2008). Dye sensitized solar cells (DSSC) usually have a titanium dioxide (TiO_2) substrate material like in the Grätzel solar cell. The technology is often compared with and stated to imitate the photosynthesis, and is by Grätzel (1991) called ”the artificial leaf”. Yet another innovative option for more effective harvesting of solar energy is so-called ”antennas”, which can harvest several wavelengths, i.e. a much broader spectrum of the solar radiation. This may be compared to the more ”traditional” sandwich solar cells. ”The use of antenna-sensitizer molecular devices may constitute a viable strategy to overcome problems of light harvesting efficiency in the spectral sensitization of wide-bandgap semiconductors.” (Amadelli et al. 1990).

Flexible CIGS (copper indium gallium selenide) and CdTe solar modules are shown in Fig.7. In an experiment performed by Buecheler et al. (2011), the flexible and lightweight CIGS and CdTe solar devices have yielded an active area efficiency of 14.7 % (CIGS) and 9.4 % (CdTe). ”The flexible solar modules can be laminated to building elements such as flat roof membranes, tiles or metallic covers without adding weight and thus, the installation costs can be reduced significantly” (Buecheler et al. 2011).

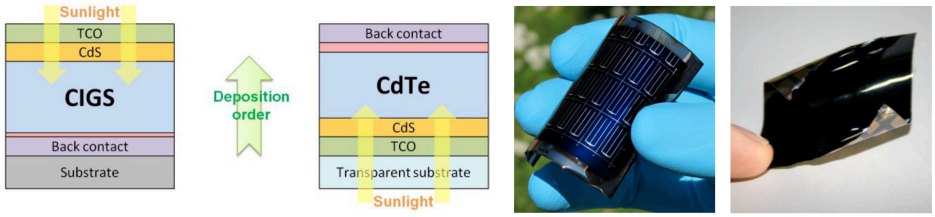

FIG 7. Schematic built-up and photos of CIGS and CdTe thin film solar cells on polyimide substrates (left and right, respectively) (Buecheler et al. 2011).

Other examples of innovative and on-going research on new solar cell materials may be quantum dot solar cells with photocurrent quantum efficiencies exceeding 100 % enabled by multiple exciton generation, solar radiation trapping mechanisms embedded in the surface (e.g. inverted pyramid texturing), integration with concrete plates (or other materials), thin laminate or paint layers enabling application by paint brush or spray, and several others (Jelle et al. 2012b).

5. Conclusions

Several state-of-the-art building integrated photovoltaic (BIPV) products exist on the market today, thus offering a wide range of integration of photovoltaic (PV) systems into buildings. Continued research and development within both PV and BIPV materials and technologies will continuously improve BIPV solutions in the years to come, e.g. with respect to increased solar cell efficiency, reduced production costs and improved building integration. New and innovative solutions may reduce costs and increase the market share, amongst other in the retrofitting market. The chosen solutions should be easily applicable, where one example of a future vision is paint applications of PV cells. It is crucial that all new technologies and solutions are thoroughly tested and approved in accordance with existing standards, and furthermore, there is also a need for development of new standards and methods, e.g. regarding long-term durability versus climate exposure.

6. Acknowledgements

This work has been supported by the Research Council of Norway and several partners through *The Research Centre on Zero Emission Buildings (ZEB)*.

References

Alwitra GmbH & Co. using amorphous silicon cells from Uni-Solar, <http://www.cythelia.fr/images/file/membranes/Brochure_evalon-solar_en.pdf>, 2011, (accessed December 6, 2011).

R. Amadelli, R. Argazzi, C.A. Bignozzi and F. Scandola, "Design of antenna- sensitizer polynuclear complexes", *Journal of the American Chemical Society*, **112**, 7099-7103, 1990.

S. Buecheler, A. Chirilă, J. Perrenoud, L. Kranz, C. Gretener, P. Blösch, F. Pianezzi, S. Seyrling and A.N. Tiwari, Flexible and lightweight solar modules for new concepts in building integrated photovoltaics, in: *Proceedings of the CISBAT*, Lausanne, Switzerland, September 14–16, 2011.

Creaton AG, <http://www.creaton.de/en/productrange/roof-accessories/photovoltaics/>, 2011, (accessed December 6, 2011).

DGS, The German Energy Society (DGS), Planning and Installing Photovoltaic Systems - A Guide for Installers, Architects and Engineers, Earthscan, 2008.

M. Grätzel, "The artificial leaf, molecular photovoltaics achieve efficient generation of electricity from sunlight", *Coordination Chemistry Reviews*, **111**, 167-174, 1991.

B.P. Jelle, "Accelerated climate ageing of building materials, components and structures in the laboratory", *Journal of Materials Science*, **47**, 6475-6496, 2012.

B.P. Jelle, A. Gustavsen and R. Baetens, "The path to the high performance thermal building insulation materials and solutions of tomorrow", *Journal of Building Physics*, **34**, 99-123, 2010.

B.P. Jelle, A. Hynd, A. Gustavsen, D. Arasteh, H. Goudey and R. Hart, "Fenestration of today and tomorrow: A state-of-the-art review and future research opportunities", *Solar Energy Materials and Solar Cells*, **96**, 1-28, 2012a.

B.P. Jelle, C. Breivik and H.D. Røkenes, "Building integrated photovoltaic products: A state-of-the-art review and future research opportunities", *Solar Energy Materials and Solar Cells*, **100**, 69-96, 2012b.

B.P. Jelle, "The challenge of removing snow downfall on photovoltaic solar cell roofs in order to maximize solar energy efficiency - Research opportunities for the future", *Energy and Buildings*, **67**, 334-351, 2013.

M. Jørgensen, K. Norrman and F.C. Krebs, "Stability/degradation of polymer solar cells", *Solar Energy Materials and Solar Cells*, **92**, 686-714, 2008.

NREL, National Renewable Energy Laboratory (NREL), Best Research-Cell Efficiencies, Rev. 11-11-2013, <http://www.nrel.gov/ncpv/images/efficiency_chart.jpg>, 2013 (accessed November 28, 2013).

C. Peng, Y. Huang, Z. Wu, "Building-integrated photovoltaics (BIPV) in architectural design in China", *Energy and Buildings*, **43**, 3592-3598, 2011.

Rheinzink, <http://www.rheinzink.com/en/products/roof-systems/roof-covering-systems/quick-stepr-the-rheinzink-stepped-roof/>, 2011, (accessed December 6, 2011).

Sapa Building System, <http://www.sapagroup.com/Companies/Sapa%20Building%20System%20AB/Pictures/brochures/Solar_BIPV_low.pdf>, 2011, (accessed December 6, 2011).

Solar Century, <http://www.solarcentury.co.uk/installers-and-roofers/products/solar-tiles/c21e-solar-roof-tiles/>, 2011, (accessed December 14, 2011).

SRS Energy, <http://www.srsenergy.com/maint/files/SPT16%20Technical%20Specifications%20090310.pdf>, 2010, (accessed October 5, 2010).

S. Strong, Building Integrated Photovoltaics (BIPV), Whole Building Design Guide, <http://www.wbdg.org/resources/bipv.php>, June 9, 2010, (accessed November 11, 2011).

Emissions from concrete – an indoor air quality issue?

Ingrid Johansson, M.Sc [1]
Peter Carlsson, B.Sc [1]
Mikael Sandberg [1]
Anders Kumlin, M.Sc [1]

[1] AK-konsult Indoor Air AB, Stockholm, Sweden

KEYWORDS: *Concrete, additives, emissions, ammonia, VOC, discoloration, indoor environment,*

SUMMARY:
Problems with indoor air quality, discolouration of oak flooring and odours are reported from newly constructed buildings. According to the industry emissions from concrete are more or less none existing. However on-site surveys in buildings with reported problems show that the concrete used in building constructions does emit volatile organic compounds, VOCs, and ammonia. Additives used in the concrete or unwanted impurities might be the source of the emissions.

Ammonia and VOC emissions levels have been measured on samples from buildings under constructions that were submitted to us for determination of RH. This study show that modern concrete, used in building construction today, does emit both ammonia and VOC even though it is presumably undamaged and does not have a surface layer coating. The majority of the samples have emission levels lower than 4 ppm for ammonia and 10 ppm for VOC. Diverging emission levels have mainly been found in samples from objects with a low water-cement ratio, which indicates that one or more of the ingredients in the concrete under certain circumstances can produce higher emission levels, however not all the samples from the same object with the same water-cement ratio have elevated emission levels hence more parameters than low water-cement ratio concrete seem to have an impact on the emission levels.

1. Introduction

Sweden historically has two well known emission damage types in concrete floor constructions. Both are initiated by elevated moisture levels due to insufficient drying during construction or later addition of moisture. One of the types is caused by degradation of casein (an amino acid) in self leveling compound that was common during a period (1974-84). The other well known floor damage type is the release of degradation products of plasticizers and other substances from glued flooring material with high moisture resistance. Indicator substances for the different damage types have been ammonia emissions from the concrete surface in the first case and 2-ethyl-1-hexanol and 1-butanol in the latter.

In recent years we have been asked to investigate the reason for discoloration of oak parquet floors, odour problems and/or health complaints in new dwellings on several occasions, in a few cases even during production. These objects neither had glued coating nor casein containing leveling compound. Nonetheless high levels of ammonia and volatile organic compounds (VOC) have sometimes been measured from the concrete, not only from the surface but also from samples taken deeper in the concrete slabs which indicate that the origin to the emissions this time is to be found within the concrete.

In recent years the use of additives has increased due to desired functionality, environmental considerations, time aspects in the building process and costs.

Our concern is that additives in concrete could be responsible for reported indoor environment problems possibly caused by unwanted synergetic reactions between different types of concrete

admixtures taking place in the reactive environment that concrete provides. Available information from the industry reports only low emissions from concrete.

The fact that the concrete formulas differ according to desired properties does not make the picture any clearer. There are references that modern concrete contains roughly 6-8 kg additives per m^3 (Naturvårdsverket, 1995, 2009), which means that the concrete in a normal sized room of 10 m^2, with a 200 mm thick concrete slag, contains 12-16 kg additives.

While the main ingredients in concrete (stone, gravel, sand, cement and water) are inorganic most concrete additives are organic and could therefore be a source of volatile organic compounds, in fact it has been shown that the emission from the concrete can occur when various additives are added to mixture (Johansson, 1994). The most commonly used additives are plasticizers that improve the workability of the concrete and thus also function as a water reducer. Additives often have unintended negative effect. According to Anderberg (2002) it was suggested by Byfors already in 1994 that preliminary investigations always should be made to ensure that unwanted effects do not occur. A Japanese study has shown that ammonia and VOC can be generated through alkaline hydrolysis within and emitted from hardened concrete (Tomoto, 2008). Urea-based antifreeze admixtures used in indoor concrete walls has been shown to be a source to indoor exposure to ammonia that may go on for a long period of time (Bai, 2006). Furthermore an unpleasant odor and mucous membrane symptoms have been linked to high levels of ammonia and benzene in a newly built office in Beijing (Lindgren, 2009)

Due to lack of information from the concrete producers regarding expected emission rates from the mixed concrete and the fact that samples submitted to us for analyses normally are from buildings with reported dampness and/or indoor air quality problems, our knowledge about what type of emissions and emission rates that can be expected from new undamaged concrete is insufficient. Therefore there is a need to establish normal emission levels (background levels) from concrete in newly constructed buildings without reported problems.

To get a better understanding of the type of emissions / emission levels expected from concrete in new buildings and also to compare some of the available, indicative methods normally used as a complement in on-site damage investigations, measurements have been performed on samples of concrete and floor leveling compound from new constructions.

2. Material and Methods

Measurements have mainly been performed on samples of concrete drill cores and in a few cases on floor leveling compound. All samples were taken from buildings during construction and, as earlier mentioned, were submitted to us for determination of moisture levels in terms of relative humidity (RH). None of the concrete samples have been subject to any kind of surface coating other than leveling compound and the leveling compound samples have not been coated at all.

In total we have performed measurements on 93 cores, 75 of concrete and 18 of floor leveling compound. RH and emission levels of ammonia, VOCs and water vapor have been measured on all the samples. The samples are from eleven different building projects with the number of samples included varying from one to 24.

2.1 Samples

As mentioned the samples were drilled out from buildings during production and submitted for RH-determination. The sampling have been carried out according to ‘RBK-metoden’, a standardized Swedish method for determination of RH in concrete structures, and the Swedish flooring industry's method for RH-determination in leveling compound respectively. The water-cement ratios for the different samples are known, with a few exceptions for the samples from hollow-core concrete

elements where w/c ratios of 0.4 or less have been assumed. No data regarding what additives that have been used have been available.

The concrete samples have, with a few exceptions, been taken from the equivalent measurement depth, which is defined based on the actual thickness and construction, while the leveling compound samples consist of the entire cross section. If, in the latter case, the sampled volume does not fit in a single test tube the material is mixed and divided into two test tubes. Hence in some cases there were two tubes with comparable content which allowed cross check evaluation of the used methods.

2.2 RH-determination

RH-determination has been carried out according to 'RBK-metoden' and the Swedish flooring industry's method for concrete and floor leveling compound samples respectively. The samples were collected prior to the application of the surface layer coating.

The uncertainty of these methods is approximately ± 2 % RH in the interval 75 – 95 % RH.

2.3 Ammonia, Organic compounds and Water Vapor in concrete, using modified OCIC method and B&K Multi Gas Monitor type 1302

The OCIC method is a modified head space technique where the sample is placed in a closed container which is kept at room temperature. The air in the pore system of the sample is allowed to reach equilibrium with the surrounding air which is then sampled and analyzed. The method was developed by Sjöberg (1998) to measure to what extent organic compounds, produced in the alkaline and moisture induced degradation process of plasticizers and other substances from carpet glue are deposited in concrete.

The sample is fractioned and placed in a gas tight 250 ml glass container fitted with stainless Swagelok tubing. The cover has an inner gasket of Teflon to prevent interference with the equilibrium process. This allows controlled extraction of air during sampling. The compounds in the sample and its pore system are allowed to reach equilibrium with the surrounding air in the glass container for 72-120 hours before air sampling.

Originally the sampling was carried out on a tube with Tenax TA sorbent which was analyzed for VOC with thermal desorption by gas chromatographic technique.

The method has been further modified and here the sampling was performed as follows: The sample was placed in the glass container after determination of RH, which in practice means minimum 4 days after it was drilled out, and left for 72-120 hours. The VOC and ammonia content in the equilibrated air were measured using the B&K Multi-gas monitor type 1302.

The B&K Multi-gas monitor type1302 is a gas analyzer. The principle of measurement is based on photo acoustic infra-red detection spectroscopy. The detection limit is gas-dependent but typically in the order of 10^{-3} ppm.

The VOC spectrum measured with B&K 1302 is broader than the normally used definition and includes VVOC, VOC and SVOC. Even though the filters used are calibrated for VOC (methane), ammonia and water vapor respectively cross sensitivity does occur. Measured levels are given with methane as reference. The sampling volume in each cycle is 140 cm^3.

The method in the applications used here should be viewed as an indicative method.

Before sampling an emptied glass tube is mounted directly on the Swagelok tubing outlet on the cover and connected to the instrument with a PTFE-tube. The inlet to the glass container is left open. The concentrations of ammonia, VOC and water vapor were measured. Before each measuring cycle, the background values were measured to ensure that one measuring cycle did not impact the next.

To evaluate the method the periods the samples were allowed to reach equilibrium before the first sampling have varied from a one up to 12 days. Where more than one cycle was measured new background levels were established before the next cycle.

FIG 1. Set up to measure VOC and ammonia with B&K 1302

Selected samples were left for an additional equilibration followed by measurement on Kitagawa detector tubes for ammonia.

2.4 Ammonia in concrete, using modified OCIC method and Kitagawa detection tubes

The preparations of the sample are the same as previously described. After the sample has been equilibrating air from the glass container is sampled on a Kitagawa detection tube for ammonia 0.2 – 20 ppm using the Kitagawa Gas aspirating pump AP-20.

As the detector tube does not have the right proportions to fit properly into the Swagelok coupling it has been fitted with thread tape and sealed with Parafilm to prevent leakage. When exposed to ammonia the color of the reagent changes from pink to whitish and the ammonia concentration in the sampled air is read on the scale of the tube.

The method in the applications used here should be viewed as an indicative method. The uncertainty in reading the detector tubes are reported to be ± 10-15%. Color change also occurs after exposure to other basic compounds such as organic amines, but with different scale.

FIG 2. Set-up to measure NH3 on detection tube

3. Results

A summary of the obtained results using the B&K 1302 modified methods for ammonia and OCIC and Kitagawa detection tubes on concrete samples can be found in table 1 and the distribution of values measured with B & K 1302 is shown in figure 3 below.

TABLE 1. Results from measurements using the B&K 1302 modified method for ammonia and OCIC and Kitagawa detection tubes on concrete samples.

	Sample age, days	NH_3, ppm B&K 1302	VOC, ppm B&K 1302	Water vapor, g/m³ B&K 1302	RH, %	NH_3, ppm Kitagawa
Minimum	11	0.476	3.77	11.9	61.2	2
Maximum	85	9.42	28.3	19.2	94.8	13
Mean	29.2	2.34	6.85	15.6	80.7	5.8
median	21	1.86	5.93	15.5	83.1	5
# samples		75	75	75	75	9

The majority of the measured concrete samples is comparable in both NH_3 and VOC respectively but diverges for some of the samples. 91 % of the sampled NH_3-values are below 4 ppm while 95 % of the sampled VOC-values are below 10 ppm.

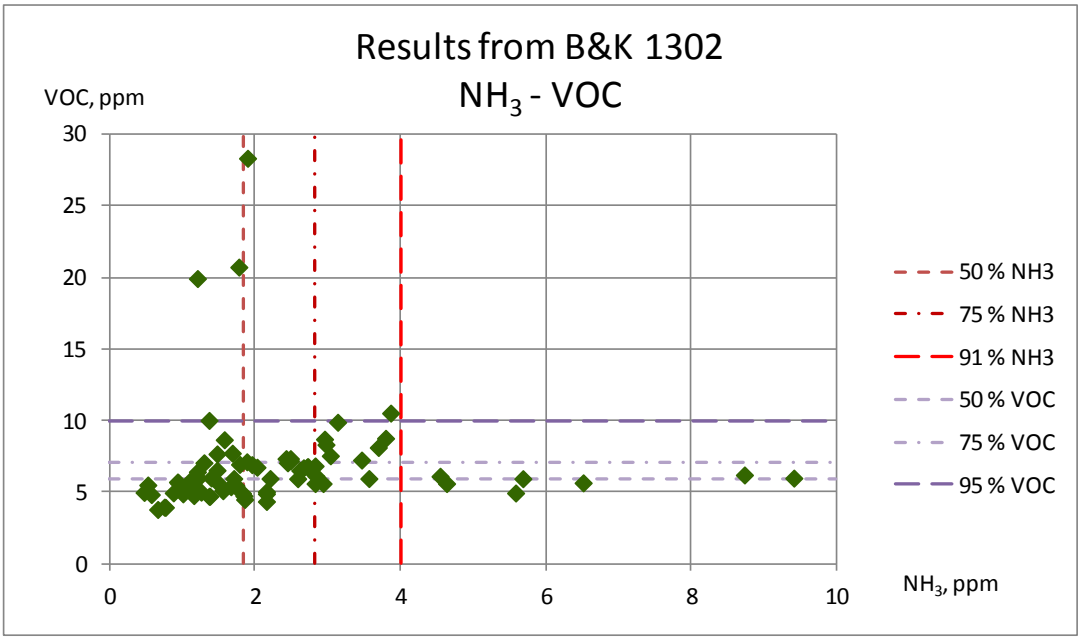

FIG 3. The distribution of values measured with B&K 1302 show that 50% are lower than 1.85 and 5.93 ppm, and 75% are lower than 2.83 and 7.1 ppm for NH_3 and VOC respectively.

The shares of measured values under 4 ppm for NH_3 and 10 ppm for VOC 95 and 97.5 % for samples with water-cement ratio higher than 0.4 and 85 and 95 % for samples with water-cement ratio 0.4 or lower respectively.

On nine of the samples ammonia emission levels were also measured on Kitagawa detection tubes. These measurements indicate that the correlation between the methods is relatively good, se figure 4.

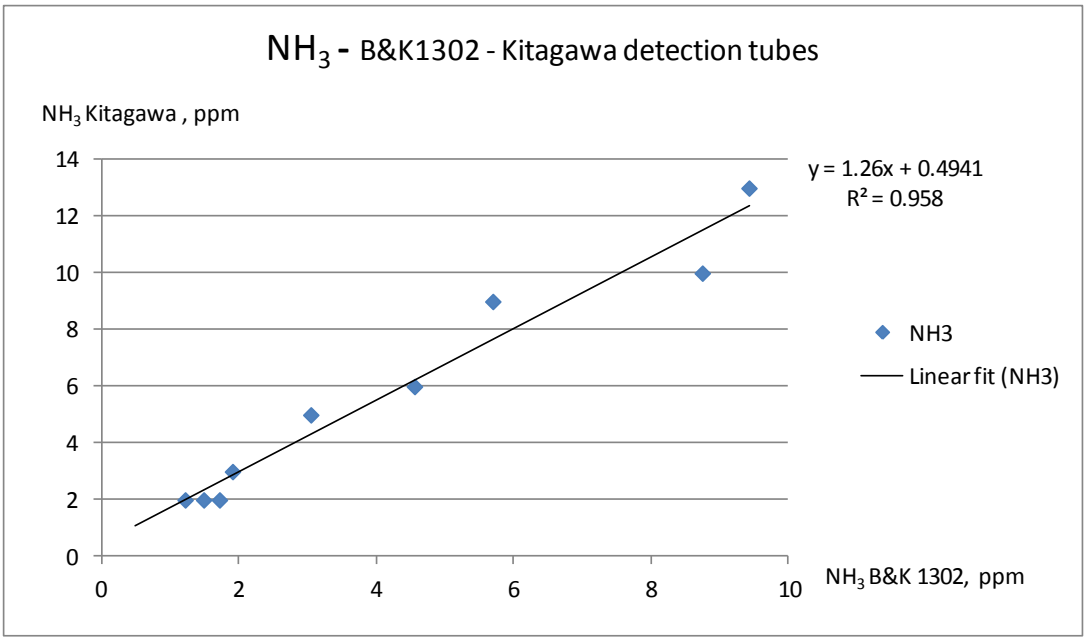

FIG 4. The correlation between NH_3values measured with B&K 1302 and Kitagawa tubes

The cross check evaluation of the double samples described in 2.1 shows that the modified method for OCIC with B&K 1302 is satisfyingly consistent for indicative measurements. Results are shown in table 2.

TABLE 2. Results from measurements using the B&K 1302 modified method for ammonia and OCIC and Kitagawa detection tubes on concrete samples.

Sample	NH_3, ppm A	NH_3, ppm B	Max/min ratio, NH_3	VOC, ppm A	VOC, ppm B	Max/min ratio, VOC	H_2O, g/m³ A	H_2O, g/m³ B	Max/min ratio, H_2O
1	1.94	2.43	1.25	9.65	10.70	1.11	19.80	19.10	1.04
2	2.41	1.98	1.22	11.40	9.61	1.19	19.10	17.40	1.10
3	2.23	2.40	1.08	7.21	6.07	1.19	17.60	16.70	1.05
4	2.21	2.00	1.11	9.94	7.36	1.35	17.00	17.00	1.00
5	3.22	3.02	1.07	18.40	17.00	1.08	19.00	19.40	1.02
6	3.11	3.45	1.11	11.70	11.60	1.01	19.50	20.30	1.04
7	1.09	1.23	1.13	5.81	5.33	1.09	12.40	12.70	1.02

The max/min ratio varies from 1.07-1.25, 1.01-1.35 and 1.00-1.10 for NH_3, VOC and water vapor respectively for the nine double samples with the corresponding mean values 1.14, 1.14 and 1.04.

4. Conclusions/discussion

In the present study, we have been referred to the submitted samples, one from each measuring point and each of them taken from an assigned depth in the structure. The recipe for the concrete regarding additives and all other parameters except water-cement ratios are unknown to us though we expect that they vary between, and in some cases maybe even within, the objects.

The results show that modern concrete, presumably undamaged, and with no surface layer coating, used in building construction today in fact does emit as well ammonia as VOC and that the emission levels in the majority of the so far investigated samples are less than 4 ppm ammonia and 10 ppm VOC. In this study this may be referred to as "normal concrete" in terms of emission levels. As the work proceeds and more samples are measured these reference values may have to be adjusted.

Considering that levels above 4-5 ppm NH_3 previously have been discussed as limits for discoloration of oak parquet flooring this is an interesting finding even though previous reference values were sampled with a different technique.

Among the results there are also a few samples with higher values for either ammonia or VOC which shows that high emission levels can arise from the concrete itself during the building process which indicates that one or more of the ingredients under certain circumstances can produce higher levels of emissions. An interesting fact is that while we have samples with higher emission levels of either ammonia or VOC, so far we have none with higher levels in both.

Some of the RH-values for the used samples are considerably lower than usually measured during the building process, 28 samples with RH lower than 80 %, however no disturbances were identified during the measuring process. As expected there is a correlation of water-cement ratio and RH but no connection could be seen between elevated emission levels and RH. Experiences from on-site surveys from buildings with reported discoloring of oak flooring and/or indoor problems as well as a small experiment with 150 mm concrete specimens indicate a correlation between high RH and high emission levels in samples from a specific cross section of the specimen. This study only includes 3 samples taken from the same cross section, these however indicates increasing values for both ammonia, VOC and RH which supports the earlier on-site survey findings and the theory that if other conditions are the same emission levels increases with moisture content.

Even though the number of samples with elevated emissions levels is small, especially for VOC emissions, a possible connection has been found regarding emission levels and water-cement ratio. In fact excluding the samples with water-cement ratio of 0.4 or lower also excludes most of the NH_3 values above 4 ppm and almost all the VOC values above 10 ppm. Yet another interesting fact is that while one of the objects, in all 24 samples with water-cement ratio 0.35 and obtained RH-values between 61.2 and 78.7 %, represents most of the samples with water-ratio of 0.4 or less and hence also most of the samples with elevated emission levels many of the other samples from this object had low emission levels of both ammonia and VOC.

While no specific information is available about the concrete formulas and additives used in these specific objects, a hypothesis is that low water-cement ratio concrete contains more additives, especially plasticizers, to increase the workability of the concrete and thus are more chemically complex. For instance plasticizers are based on organic compounds, concrete that contains more plasticizers potentially could emit more VOC. The fact that one object of 24 samples includes four samples with elevated levels of ammonia, three with VOC and the other 17 with low emissions of both indicates that while the chemical content, the additives or impurities in the concrete, appears to be a main contributor there are also other parameters that have a major impact on the outcome concerning emission levels.

Regarding VOC we still do not know enough to connect obtained values to potential indoor environment problems. The results from this study will give a better understanding of the expected emission levels of ammonia and VOC from new undamaged concrete and possibly what emission levels that are to be considered elevated and thus potentially could pose a negative impact on the indoor environment.

In addition to the results that are presented here, our intention is to carry out on-site FLEC measurements on concrete as well as OCIC on Tenax TA to link these to our modified methods of measurement and also to identify what compounds the emissions from new concrete contains.

The modified method for OCIC-measurements with B&K 1302 has been shown to work well for indicative measurements. The values from the floor leveling compound samples show good compliance for the double samples. Further analysis needs to be done to specify the method concerning the time period needed to optimize the equilibrating and to minimize leakage. The

comparison between measuring ammonia levels with B&K 1302 and Kitagawa detection tubes show good correlation for concrete samples, with a tendency for higher values for the detection tubes.

Questions of concern, among others, for the future are what emissions can be expected from concrete, in what way the use of fly ash in the concrete will affect the emissions and emission rates, what other chemicals will be added to the concrete? We believe there is a need that the concrete producers provide adequate information concerning expected emission levels for their concrete formulas including additives.

5. Acknowledgements

This work was carried out with support from our employer AK-konsult Indoor Air AB. The support, encouragement and understanding from our employer and our colleagues are gratefully acknowledged.

References

Anderberg A. 2002. Förändring av användbarheten hos betong. Rapport TVBM-3062. Lund. Lunds Tekniska Högskola. 48 p.

Bai Z., Dong Y., Wang Z. & Zhu T. 2005. Emission of ammonia from indoor concrete wall and assessment of human exposure. Environmental International 32, p. 303-311.

Johansson E. 1994. Emissioner från byggnadsmaterial. Rapport TVBM-3062. Lund. Lunds Tekniska Högskola. 50 p

Lindgren T. 2010. A case of indoor air pollution of ammonia emitted from concrete in a newly built office in Beijing. Building and environment 45, p. 596-600.

Naturvårdsverket. 1995 uppdaterad 2009. Branschfakta. Betongindustri - Anläggningar för framställning av betong och betongprodukter. 16 p

Nordtest Method NT Build 484. 1998. Building materials: Emission of volatile compounds - On-site measurements with Field and Laboratory Emission Cell (FLEC). Nordic Council of Ministers. 4 p

Sjöberg A. 1998. Transportprocesser och reaktioner i belagda betonggolv – olika faktorers inverkan på emission från golvkonstruktion. Göteborg. Chalmers Tekniska Högskola. 193 p.

Tomoto T., Moriyoshi A., Kiyoshi S., Eiji S. & Michihiro K. 2009. Identification of the sources of organic compounds that decalcify cement concrete and generate alcohols and ammonia gases. Building and Environment 44, p. 2000-2005.

Analytical model to calculate the temperature increase in a low conductive material covered by a highly conductive layer

Pär Johansson, Lic.Tech. [1]
Johan Claesson, Professor [1, 2]

[1] Chalmers University of Technology, Sweden
[2] Lund University, Sweden

KEYWORDS: *TPS method, quality assurance, vacuum insulation panel, thermal conductivity, analytical solution, numerical model*

SUMMARY:
There is a lack of measurement methods that can be used to determine the thermal conductivity of vacuum insulation panels (VIPs) on the construction site. With the transient plane heat source (TPS) method, the thermal properties of an isotropic material can be evaluated after a short measurement period. Heat is supplied in the TPS sensor which raises the temperature in the sensor. The thermal properties of the material are calculate based on the temperature increase. A novel analytical solution of the TPS method makes it possible to use the method on a low conductive material covered by a highly conductive layer. The aim of this study is to investigate the applicability of the analytical solution by comparing it to a numerical calculation model and TPS measurements. Five different setups were tested with good agreement between the analytical solution and the numerical calculation model. The TPS measurements deviated from the calculated temperature increase which could be explained by uncertainties regarding the influence of the contact surface between the sensor and material.

1. Introduction

The energy use in the European buildings should be decreased with 20% by 2020 and 50% by 2050 compared to the year 1990 (European Parliament 2010). To reach these goals, existing buildings need to be retrofitted to increase the thermal resistance of the building envelope (IVA 2012). One limitation when retrofitting existing buildings is the demand on a maintained rentable floor area which limits the possible additional thickness of the added thermal insulation layer. The façade of the building should also be protected for its architectural and historical features which limits the possible systems using conventional thermal insulation materials such as mineral wool and expanded polystyrene (EPS). A solution could be to use highly efficient thermal insulation components such as vacuum insulation panels (VIPs) in parts of the building envelope. The required thickness is reduced by a factor of 5-10 when using VIP instead of conventional insulation materials with the same thermal resistance.

Apart from the use of VIPs in buildings, they can also be used as thermal insulation in refrigerators and freezers, as pipe insulation, for insulating boilers, etc. The different purposes put high demand on the durability of the component which is composed of two parts; the open porous core material and the envelope separating the evacuated core from the ambient environment. The most common core material for VIPs in buildings is fumed silica and the envelope is composed of a metalized multi-layer polymer laminate. To reach the low thermal conductivity of the VIPs it is important to ensure a low internal gas pressure since the thermal conductivity increases with increasing gas pressure, decreasing the service life of the component.

At the production site different quality assurance measures can be taken to make sure that the internal pressure is low enough when shipping the panels to the construction site. The foil lift-off method can be used to determine the internal pressure by reducing the ambient pressure in a pressure chamber

until the laminate separates from the core material. Other available methods to measure the internal pressure are the spinning rotor gauge and remote sensing with active or passive chips using the RFID technique. Another approach is to measure the internal pressure by an indirect method, i.e. by measuring the thermal properties of the VIP. One of these methods is a patented technique where a metallic disk is inserted in the core material and a warm sensor is placed on the surface which is cooled down and the temperature decline registered for a short time period making it possible to determine the internal gas pressure (Caps *et al.* 2008). The transient plane heat source (TPS) method can be used in a similar way to determine the thermal conductivity by measuring the temperature increase in a sensor with a constant heat supply during a short time period.

The aim of this paper is to investigate the applicability and validity of a novel analytical solution of the TPS method on a low conductive material covered by a highly conductive layer. The analytical solution developed for this purpose is presented and elaborated in (Claesson 2012). In this paper it is compared to numerical simulations and TPS measurements exemplified in five setups: EPS, EPS covered by aluminum foil and VIP laminate respectively, and for functioning VIPs (evacuated) and damaged VIPs (punctured). The setup with EPS have been reported earlier in (Johansson *et al.* 2011) and (Johansson *et al.* 2012) where also the setup with EPS covered by aluminum foil was reported. The TPS measurements of the five setups were summarized in (Johansson 2012). The ultimate goal of this work is to develop the TPS method to be used at the construction site for measurements of VIPs after they have been installed in the building to ensure that the thermal performance becomes as good as possible.

2. Measurements with the transient plane heat source (TPS) method

The general and specific procedures of the transient plane heat source (TPS) method for measurements of thermal properties are described in ISO 22007-2. The method uses a sensor composed of a 10 μm thick double nickel spiral, sandwiched between two layers of 25 μm thick kapton (polyimide film). The spiral serves both as heat source and as electric resistance thermometer. A constant electric power is supplied through the spiral which develops heat by the electric resistance of the nickel, raising the temperature of the sample. The rate of the temperature increase depends on how quickly the heat developed in the spiral is conducted away through the surrounding materials. Heating is continued for a period of time, with the voltage across the spiral being registered. As the current is held constant, the voltage changes in proportion to changes in the resistance of the spiral. With knowledge of the temperature variation with time, i.e. variation of voltage, and the supplied heat flow, it is possible to calculate the thermal conductivity and volumetric heat capacity of the material. The sensor is clamped between two samples of the material as shown in FIG 1. It may be noted that the laminate surface becomes rugged due to the vacuum in the VIP that sucks the laminate inwards.

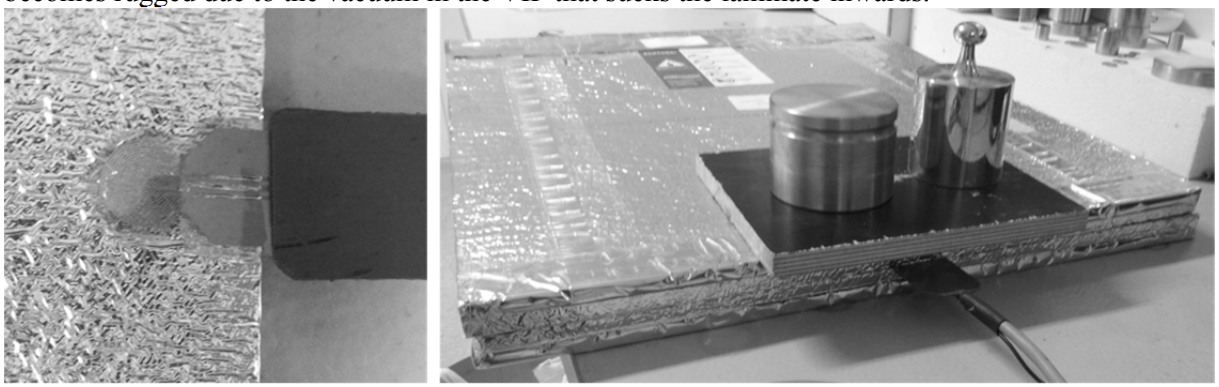

FIG 1. TPS sensor on a functioning VIP (left) and measurement setup with the sensor clamped between two VIPs (right). There is a pressure of 4.7 kPa applied on the upper sample to increase the contact with the sensor.

Measurements on the five setups with the TPS sensor was performed with a constant power of 20 mW applied during 160 s through the sensor with a radius of 6.4 mm. The average dimensions of the polystyrene were 70 mm x 70 mm x 20 mm (length x width x thickness) and the VIPs were 300 mm x 300 mm x 20 mm. The measured thickness of the aluminum foil and metalized multi-layer polymer laminate were 10 µm and 100 µm respectively. The samples were pressed together by applying a weight on top of the upper sample creating a pressure of 4.7 kPa. Each setup was tested at least 3 times with a break of 20 minutes between each measurement to make sure it was cooled down to the surrounding air temperature of 20.5°C.

2.1 Numerical model

The numerical model is based on the three-dimensional setup which is transformed into cylindrical coordinates. The heat source is clamped in the center of two identical material samples. During short calculation periods when only a small part of the heat has reached the boundary of the sample, the setup can be treated in the cylindrical coordinate system, see FIG 2. The thermal disturbance created by the heat source reaches the outer boundaries (two upper and four vertical ones) after a rather short time. These boundaries are treated as adiabatic, i.e. no heat passes through them. The solution presented here will not be correct when the thermal disturbance from the adiabatic boundaries reaches the heat source. The solution with these simplified boundary conditions is certainly correct during the first few minutes which are considered here.

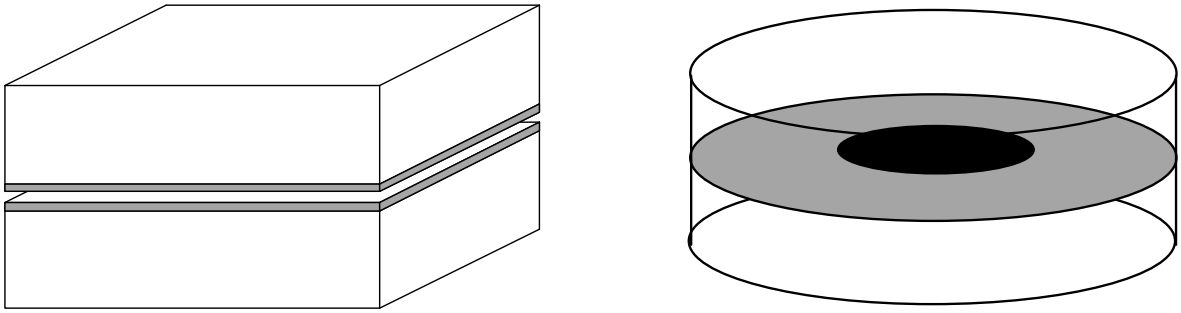

FIG 2. Test setup. Left: VIP with laminate in gray. Right: heat source in the center between two samples of the material. The three-dimensional setup is transformed into cylindrical coordinates.

The heat capacity and thickness of the sensor and the heat capacity of the laminate are disregarded in the model. The laminate is treated as an additional thermal conductance which is added to the thermal conductance of the first cell of the core material. The numerical calculations were performed in Matlab (R2009b) using a numerical finite difference calculation procedure (Hagentoft 2001). The numerical model was validated in (Johansson *et al.* 2012). The tabulated material properties that were used in the calculations are presented in TABLE 1. The weighted arithmetic mean of the thermal conductivities of the materials in the VIP laminate is 280-490 mW/(m·K). In this study a higher thermal conductivity was used which is based on the findings by Ghazi Wakili *et al.* (2011).

TABLE 1. Tabulated material properties for the materials used in the five setups. The properties of the EPS were measured with standardized measurement techniques.

Material	Thermal conductivity λ [mW/(m·K)]	Bulk density ρ [kg/m^3]	Specific heat capacity c [J/(kg·K)]	Thermal diffusivity $a = \lambda / (\rho \cdot c)$ [mm^2/s]
Aluminum	226 000	2 700	920	90.98
EPS	32	29	1 760	0.627
Silica (evacuated)	4	175	850	0.027
Silica (punctured)	20	175	850	0.134
VIP laminate	2 000	1 100	1 800	1.010

2.2 Analytical solution

The analytical solution for the heat supply over a part of a circular surface of an isotropic material can be derived from (Carslaw & Jaeger 1959). This solution is used for the setup with only EPS while for the four other setups there was no solution available in the literature. Claesson (2012) derived the analytical solution for the transient temperature in the point *r*, z (m) at time *t* (s) in an isotropic material covered by a thin highly conductive layer. The final solution is

$$T(r,z,t) = T_0 \cdot \int_0^\infty J_0(sr') \cdot J_1(s) \cdot f_c(s,z',t')ds \tag{1}$$

$$f_c(s,z',t') = \frac{2p}{s(a's+2p)} \cdot e^{-z's} - \frac{2}{\pi}\int_0^\infty e^{-s^2 \cdot t' - u^2 \cdot t'} \cdot I_f(u,s,z')du \tag{2}$$

$$I_f(u,s,z') = \frac{2pu}{s^2+u^2} \cdot \frac{2pu \cdot \cos(z'u) + \left[(a'-1)\cdot s^2 - u^2\right] \cdot \sin(z'u)}{\left[(a'-1)\cdot s^2 - u^2\right]^2 + 4p^2u^2} \tag{3}$$

$$T_0 = \frac{qR}{\lambda},\ r' = \frac{r}{R},\ z' = \frac{z}{R},\ t' = \frac{t}{t_1},\ t_1 = \frac{R^2}{a},\ p = \frac{R\rho c}{2D_0\rho_0 c_0},\ a' = \frac{a_0}{a},\ a_0 = \frac{\lambda_0}{\rho_0 c_0} \tag{4}$$

Here, T (°C) is the temperature increase due to the heat supply in the region $z = -D_0$ (m) with constant heat flux q (W/m^2) in the circular area with radius $r < R$ (m) and zero flux in $r > R$ (m). D_0 (m) is the thickness of the highly conductive layer with thermal conductivity λ_0 (W/(m·K)), density ρ_0 (kg/m^3) and specific heat capacity c_0 (J/(kg·K)). The properties of the isotropic material is given by λ, ρ and c, defined above. J_1 and J_0 are the Bessel functions of the first kind of the first and zeroth order.

The general solution for the *average* temperature increase in the sensor area is

$$T_{av}(t') = 2T_0 \cdot \int_0^\infty \frac{1}{s} J_1(s)^2 f(s,0,t')ds \tag{5}$$

with the parameters defined above.

3. Results

3.1 Measured temperature increase

Each setup was tested at least 3 times with a break of 20 minutes between each TPS measurement to make sure it was cooled down to the surrounding air temperature of 20.5°C. The results for the five setups are presented in FIG 3 where the average values for all the measurements of each setup have been calculated.

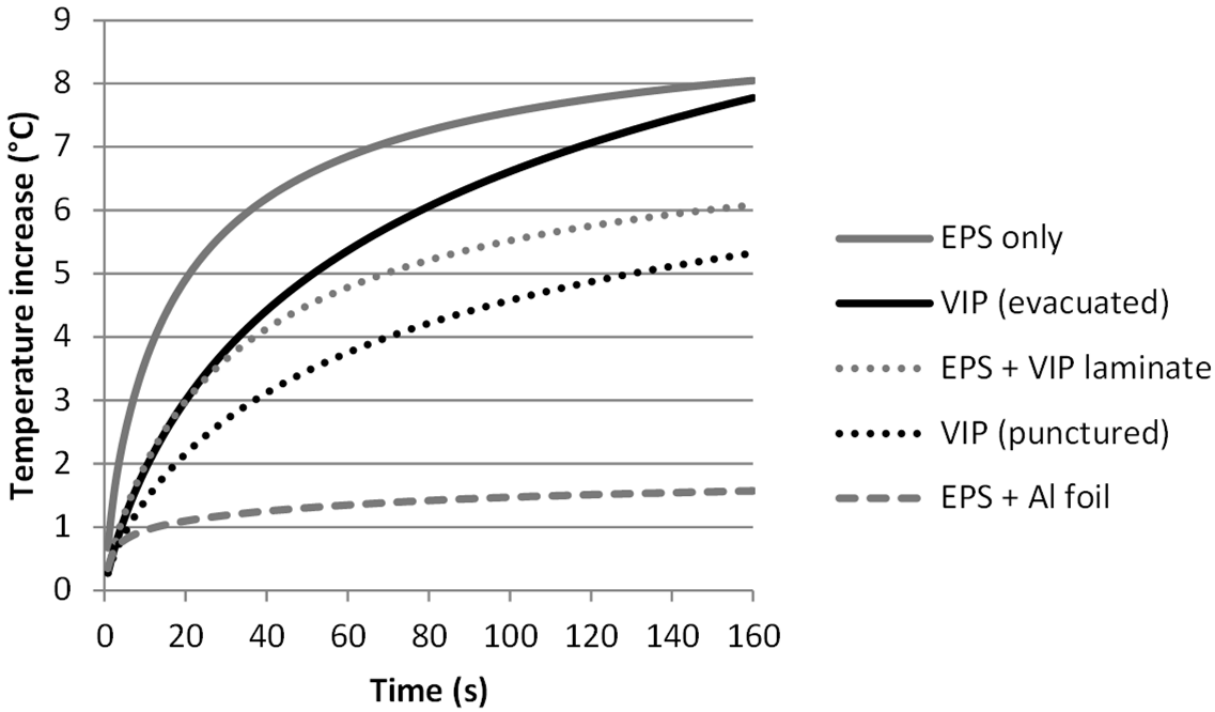

FIG 3. Average temperature increase in the five setups with a power of 20 mW supplied during 160 s in the 6.4 mm TPS sensor.

The temperature increased with 8.0°C in the EPS setup while it was lower for the two setups where the EPS was covered by the aluminum foil and VIP laminate. In these setups the heat was spread away from the sensor area through the highly conductive layer. The lowest temperature increase was found for the aluminum foil with 1.6°C while the VIP laminate gave a temperature increase of 6.1°C. Even though the VIP laminate is 10 times thicker than the aluminum foil, the heat was spread faster in the latter setup which shows the substantially higher thermal conductivity in the aluminum foil than in the VIP laminate.

To use the TPS method on the construction site to identify a damaged VIP, the difference in temperature increase has to be big enough between the evacuated and punctured VIP. For the evacuated VIP, the measured temperature increase was 7.8°C while it was 5.3°C for the punctured VIP. The thermal conductivity increases 5 times when the VIP is punctured while the temperature decreased with only 46%. Also, the temperature increase for the evacuated VIP and the EPS only differed by 0.2°C while the thermal conductivity of the evacuated VIP is one eighth of the EPS. This discrepancy shows the importance of the laminate and the possible influence by the contact heat transfer resistance between the sensor and laminate. The rugged laminate gets less rugged when the VIP is punctured compared to the evacuated VIP which increases the heat transfer through the laminate.

A reliable measurement procedure should have a low standard deviation for repeated measurements. One way to evaluate the reliability is by using the coefficient of variation (CV), i.e. the standard deviation divided by the average measurement result. The CV was 0.12% for the EPS setup while it was 0.79% and 0.21% for the EPS with VIP laminate and aluminum foil respectively. For the evacuated and punctured VIP setups, the CV was 0.56% and 0.18%. The low CV indicates a good reliability and repeatability of the TPS measurements on the five setups.

3.2 Comparison of the measured temperature increase to the calculations

The temperature increase from the numerical model, analytical solution and TPS measurements after 160 s are compared and presented in FIG 4. A constant power of 20 mW was applied during 160 s in the TPS sensor of 6.4 mm radius and the material data used in the calculations was presented in TABLE 1.

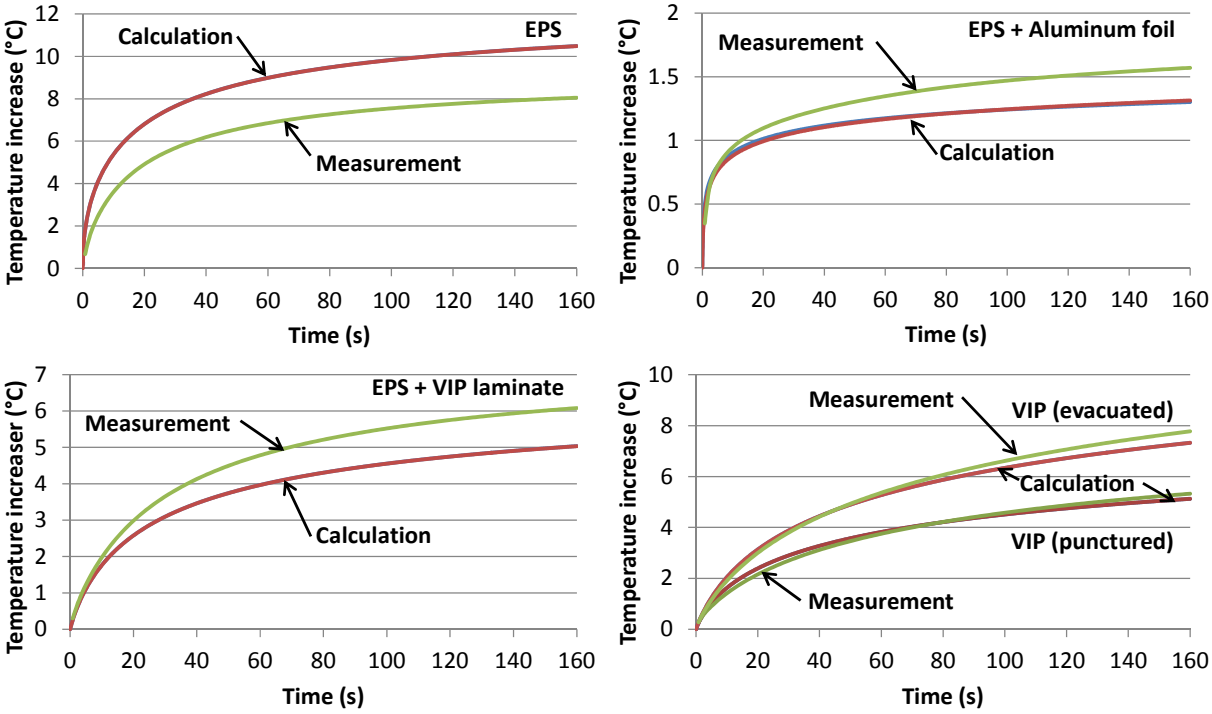

FIG 4. TPS measurements compared to the results from the numerical model and analytical solution for the five setups. EPS setup (top left), EPS covered by aluminum film (top right), EPS covered by VIP laminate (bottom left) and the punctured and evacuated VIP (bottom right).

The numerical simulations and analytical solution predicted a 30% higher temperature increase for the EPS setup than the TPS measurements showed. The difference between the numerical model and analytical solution after 160 s was 0.043%. The material properties used in the calculations of the EPS were measured with standardized measurement techniques which shows there is still more investigations needed for the effect of the contact heat transfer resistance between the material and the TPS sensor.

For the EPS covered by aluminum foil and VIP laminate, the measurement results were higher than the calculated temperature increase. The difference between the numerical calculation model and the analytical solution was 0.091% and 0.022% respectively after 160 s while the temperature increase was 17% lower than the measurements in both setups. The difference between the calculated and measured temperature increase could be caused by uncertainties regarding the thermal properties of the highly conductive layers and the properties of the contact surface.

The two VIP setups showed better agreement between the calculations and measurements. The difference between the numerical model and analytical solution was 0.037% and 0.029% for the evacuated and punctured VIP setups. After 160 s, the measured temperature increase was 5.8% and 3.8% lower than the calculated temperature increase for the two setups. Also here the different contact surfaces may be an important contributor to the difference between the calculated and measured temperature increase.

4. Conclusions

The analytical solution was compared to the numerical model with good agreement for all the five setups. The solution is therefore considered to be validated.

The CV was low for the five setups which indicate a good reliability and repeatability of the TPS method. The measurement conditions change when moving the equipment to the field which needs further investigations.

The measured temperature increase deviated from the calculated temperature increase in all the five setups. There are a number of factors which could influence the temperature increase in the area of the sensor. The thermal properties of the highly conductive layer on top of the low conductive material determine the spread of heat outside of the sensor area while the properties of the low conductive material determine how fast the heat is spread in the perpendicular direction. Only the thermal properties of the EPS were fully known by the use of standardized measurement techniques, while the other material properties were taken from the literature.

When the VIP is punctured and the pressure on the laminate around the core is reduced, the contact surface between the TPS sensor and sample is increasing. The changed gas pressure on the laminate changes the ruggedness of the laminate surface, which means that more heat can be transported away from the sensor area through the laminate. Therefore it is essential to know the thermal properties of the laminate and the required amount of pressure applied on the sample to increase the contact area with the sensor. The reduced ruggedness of the laminate gives a flatter surface, with less entrapped air which leads to a lower surface heat transfer resistance.

Research remains to make the TPS method applicable for measuring the thermal properties of VIPs in field. The contact heat transfer resistance needs further investigations and the influence by the loss of vacuum on the rugged contact surface should also be investigated. Also the material properties of the VIP laminate should be better determined by standardized measurement techniques.

5. Acknowledgements

The work is supported by the Swedish Research Council Formas. Thanks to Jimmy Forsberg and Remi Sørensen who made some of the TPS measurements in their Bachelor's thesis project at Chalmers University of Technology.

References

Caps, R., Beyrichen, H., Kraus, D., & Weismann, S. 2008. Quality control of vacuum insulation panels: Methods of measuring gas pressure. Vacuum, 82(7), 691-699.

Carslaw, H. S., & Jaeger, J. C. 1959. Conduction of heat in solids. 2nd ed. London, UK: Oxford University Press. (Eq. 4, p. 264).

Claesson, J. 2012. Mathematical report: heated disk in contact with insulation material covered by thin highly conductive layer (Report 2012:11). Gothenburg, Sweden: Chalmers University of Technology, Department of Civil and Environmental Engineering.

European European Parliament. 2010. Directive 2010/31/EU of the European Parliament and of the Council of 19 May 2010 on the Energy Performance of Buildings (recast). Retrieved from http://eur-lex.europa.eu/LexUriServ/LexUriServ.do?uri=CELEX:32010L0031:EN:NOT.

Ghazi Wakili, K., Stahl, T., & Brunner, S. 2011. Effective thermal conductivity of a staggered double layer of vacuum insulation panels. Energy and Buildings, 43(6), 1241-1246.

Hagentoft, C.-E. 2001. Introduction to building physics. Lund, Sweden: Studentlitteratur.

IVA. 2012. Energieffektivisering av Sveriges flerbostadshus: Hinder och möjligheter att nå en halverad energianvändning till 2050 (Energy efficiency in the Swedish multi-family building stock: obstacles and possibilities to reach a halved energy use by 2050). [In Swedish]. Stockholm, Sweden: Kungl. Ingenjörsvetenskapsakademien (IVA).

Johansson, P. 2012. Retrofitting of old Exterior Wall with Vacuum Insulation Panels: Meaurements of Thermal Properties, Moisture Performance and Practical Considerations (Lic. Thesis 2012:2). Gothenburg, Sweden: Chalmers University of Technology, Department of Civil and Environmental Engineering.

Johansson, P., Adl-Zarrabi, B., & Hagentoft, C.-E. 2011. Measurements of Thermal Properties of Vacuum Insulation Panels by using Transient Plane Source Sensor. Proceedings of the 10th International Vacuum Insulation Symposium, Ottawa, Canada, September 15-16, 2011.

Johansson, P., Adl-Zarrabi, B., & Hagentoft, C.-E. 2012. Using Transient Plane Source Sensor for Determination of Thermal Properties of Vacuum Insulation Panels. Frontiers of Architectural Research, 1(4), 334-340.

SS-EN ISO 22007-2:2008. Plastics - Determination of thermal conductivity and thermal diffusivity - Part 2: Transient plane heat source (hot disc) method. Geneva, Switzerland: International Organization for Standardization (ISO).

Moisture Transfer Study of Polyvinyl Chloride Roofing with Field Study and Computational Methods

Klaus Viljanen, M.Sc. [1]
Ari-Veikko Kettunen , M.Sc. [1]

[1] Vahanen Oy, Finland

KEYWORDS: *PVC, polyvinyl chloride, roof, moisture transfer*

SUMMARY:
Relative humidity and temperature was monitored from the thermal insulation layer of a building's PVC roof located in Southern Finland. The roof was a compact roof with 230 mm mineral wool insulation. The unventilated roof area and the area with underpressure vents but no ventilation grooves were not able to dry out the built in moisture during 18 months. The roof with ventilation grooves can remove moisture faster and is thereby more reliable option. However, the vapour barrier has to be airtight in ventilated roof structures to prevent moisture convection from the inside.

The calculations showed that the hygroscopic moisture dries out of the roof in 1 - 1.5 years. With built in moisture in the PVC roof this diffusive drying capability is usually not enough to achieve moisture safe roof structures. Computational methods were used to model hysteresis and temperature dependence of the sorption isotherm. Temperature dependent sorption isotherm improved the accuracy of the calculation however simple isotherm is usable in most common calculations.

The study showed that the extra moisture in the roof is usually in the miter (lowest point of the vapour barrier) and that large roof surfaces transfer moisture horizontally under the roofing (fluttering effect of the roofing in windy weather). In addition, temperature differences in the thermal insulation can cause moisture transfer to the shady roof areas which can result in interior water leaks.

1. Introduction

Polyvinyl chloride (PVC) roofs are relatively common for example in industry halls in Finland. The moisture transfer properties and especially the drying ability of a PVC roof was studied with a field experiment and with computational methods. The study was motivated by the uncertainties connected to the moisture transfer properties and drying ability of the PVC roof. The main goal of the study was to resolve if diffusion is a sufficient drying mechanism or should we use thermal insulation with ventilation grooves. This type of thermal insulation is used in roofs with bitumen roofings in Finland. An additional goal was to increase understanding of the movements of moisture in the PVC roof. The goals are based on an effort to enchance the moisture technical functionality of the PVC roof. The study was performed in co-operation with Kattoliitto ry. The results from the study are used in the upgrade process of publications Toimivat Katot 2013 (Kattoliitto ry 2013) and RIL 107-2012 Rakennusten veden- ja kosteudeneristysohjeet (Suomen Rakennusinsinöörien Liitto 2012).

2. The field experiment

2.1 The study program

The drying ability and moisture technical functionality of the PVC roof was studied in a field experiment in Southern Finland in Sipoo during 17.6.2011–9.1.2012. Relative humidity and

temperature was measured from the roof of a new storage hall between 17.6–28.12.2011. The roof areas were finished 15.4–24.4.2011 and had an area between 198 - 400 m^2 (fig. 1–2). The load-bearing structure of the roof areas was a hollow core slab or a load-bearing steel sheet and the thermal insulation was 230 mm of stone wool. The measurement period was extended in 26.7–31.10.2012, from which results are only shown in figure 4. The roofing was a dark grey PVC roofing with thickness 1.2 mm. There were 5 study areas in total, which were separated from each other with a strip of aluminium vapour barrier and PVC roofing one on the other, which were attached to the roofing and the vapour barrier. Areas 2,4 and 5 were unventilated, area 3 was ventilated with ventilation grooves and 160 mm underpressure vents and area 1 was ventilated with just 110 mm underpressure vents and no ventilation grooves. There were 4.5 grooves with a 20 x 30 mm^2 cross section per meter width of the thermal insulation in 50 mm depth in the insulation in area 3. The flow length between collector channels was 18 m and there was one underpressure vent in both 8 m long collector channel. The ventilation length of the roof without grooves, area 1, was 13.6 m.

The outdoor absolute humidity was 1 - 2 g/m^3 higher during the measurements than the annual average in Helsinki. The maximum hygroscopic moisture absorption in stone wool is approximately 0.56 kg/m^3. The built in moisture of the roofs was low but in areas 1 and 2 there was 2 cm thick and 80 cm wide layer of water in the miter. This equals to an amount of 0.35 kg/m^2 water for an area unit of the roof. The rainfall before the construction was 1.7 kg/m^2, from which 20 % remained as the built in moisture. The moisture management during construction utilized weather forecasts and weather shelters. In addition, water was moved from over the vapour barrier to the roof drain before the installation of thermal insulation. Study areas 1 - 3 are presented in figure 1.

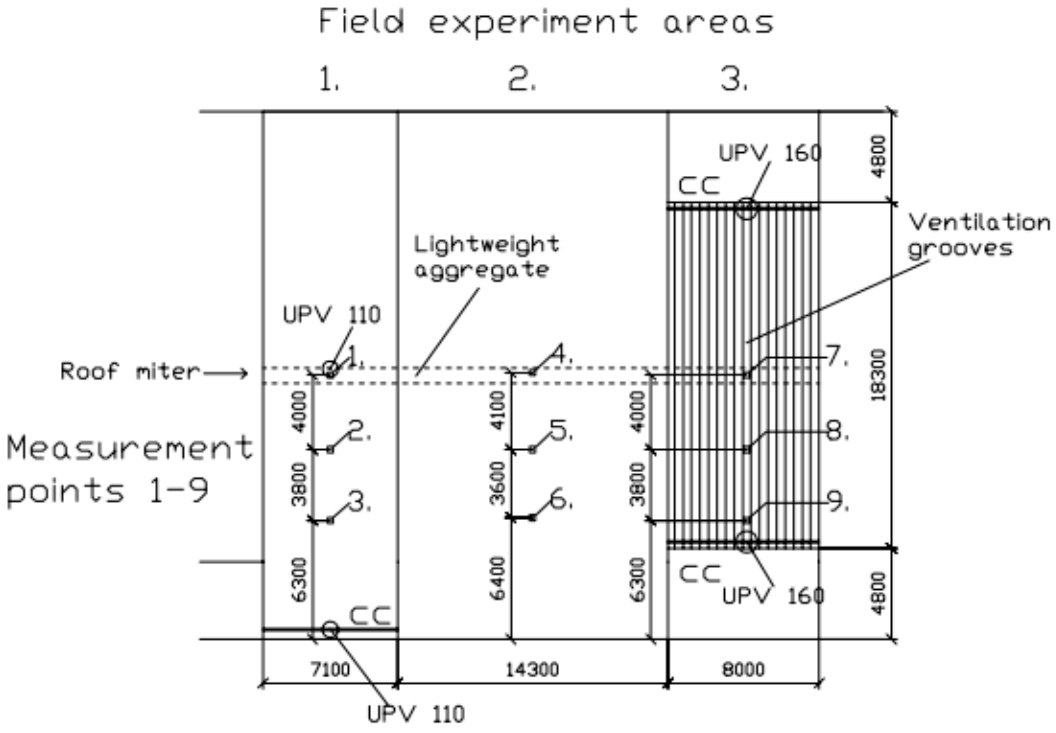

FIG 1. Measurement points 1 - 9 in field experiment areas 1 - 3. UPV = under pressure vent. cc=collector channel. The roof miter is presented in dashed line where the lightweight aggregate is placed under the mineral wool to ease the installation phase of the mineral wool.

Study areas 4 and 5 are presented in figure 2. Measurement points 10,11,13,14 and 16 were prepared but not measured due to the limited amount of sensors available.

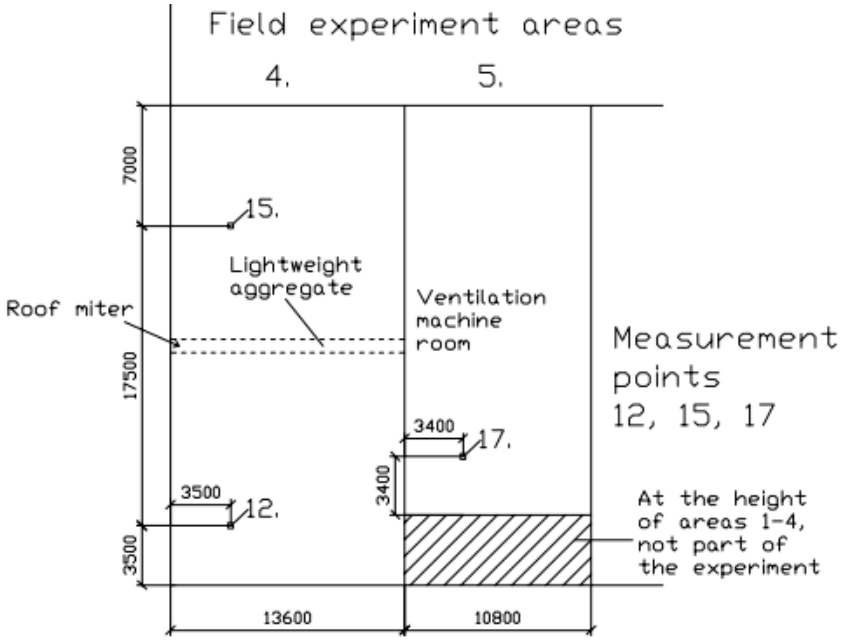

FIG 2. Measurement points 12, 15 and 17 in field experiment areas 4 and 5.

The roof structures and measuring heights A - C are presented in figure 3.

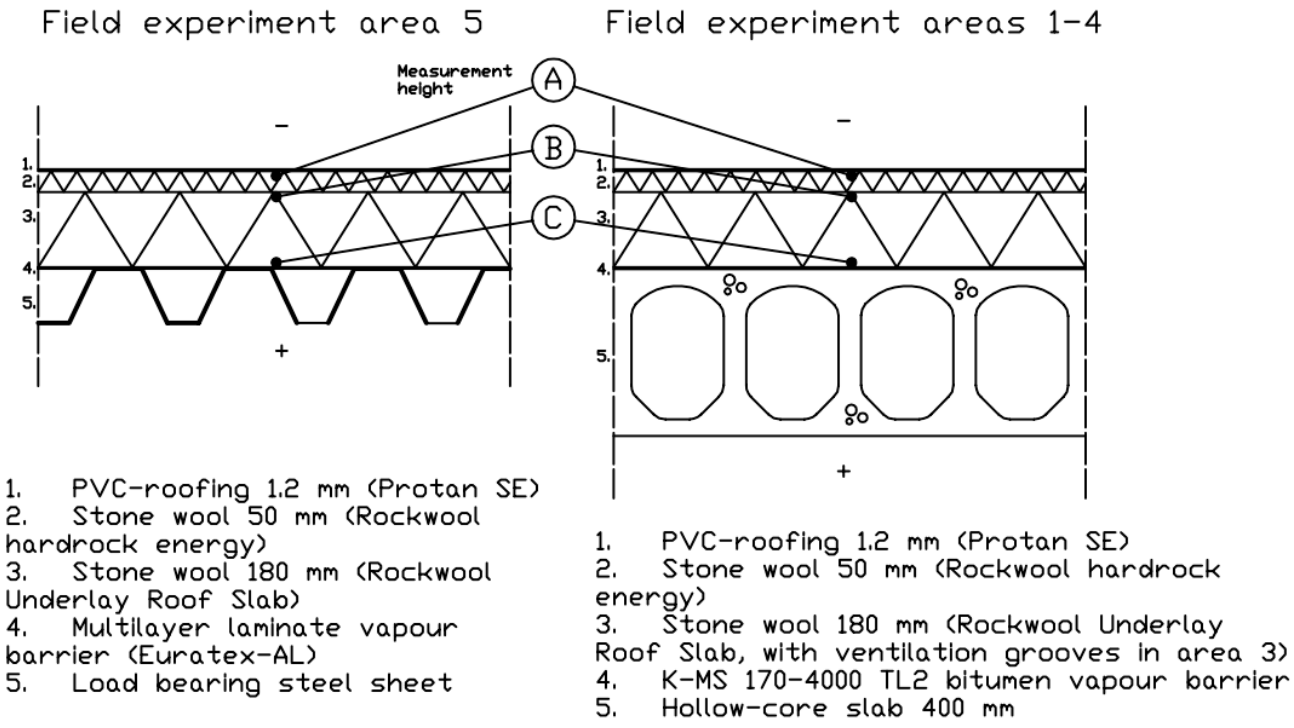

FIG 3. The roof structures in the field experiment. The experiment area five had a load-bearing steel sheet. In the other experiment areas the load-bearing structure was a hollow-core slab. The measuring heights A, B and C are also presented in the figure.

2.2 Results

The built in moisture 0.35 kg/m^2 did not dry out of the roof from areas 1 and 2 during study time which ended 18 months after the construction work. The underpressure ventilation without grooves in

the thermal insulation was not effective, because of the minor air flow in the pore structure of the thermal insulation. Calculation showed that the porous air flow rate is 100 times lower compared to the ventilation grooves. The calculation assumed groove velocity 0.01 m/s, groove cross section similar to area 3, pressure difference between underpressure vents 1 Pascal, porous flow distance 13.6 m and flow cross-area 50 mm height stone wool. Both areas 1 and 2 practically dried out with diffusion which was not fast enough to dry the areas during 18 months. The absolute humidity in the unventilated area 2 (which was the main interest in this study) was calculated from the measurement result and is presented in figure 4.

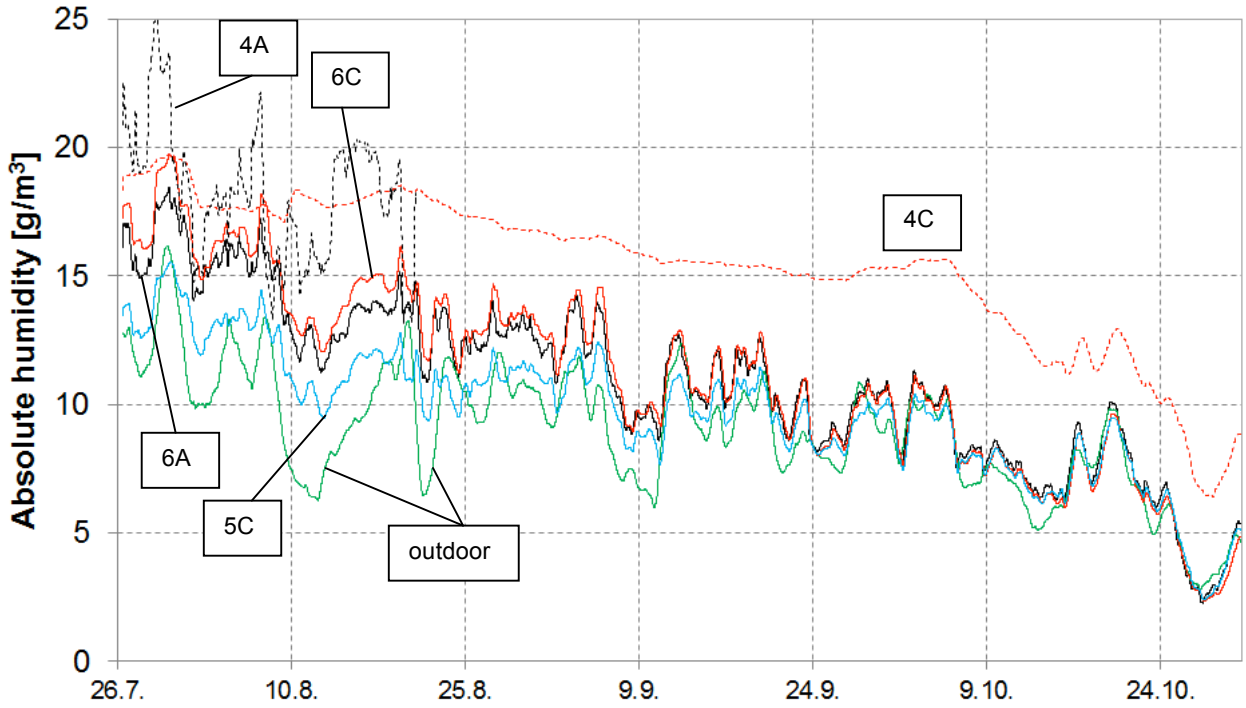

FIG 4. Daily mean values of absolute humidity in area two at points four (in the miter), five and six during 26.7–31.10.2012. In comparison to this figure, in area three the absolute humidity in the dry roof was at outdoor level even in summer.

The surface area of the unventilated experiment area 2 with built in moisture was 400 m^2. This area moved moisture from the miter to other areas of thermal insulation more effectively than the 198 m^2 large experiment area 1. This was noticed as clearly higher relative humidity far from the miter in area 2 compared to area 1. The smaller area had more joints in the roofing which lowered the fluttering (the roofing temporarily rises on the thermal insulation causing wavy motion) of the roofing by wind forces. The results suggest that it is beneficial to have large uniform roof areas in unventilated roofs. The fluttering effect was observed in the experiment areas. The wind velocity was 0.7 - 1.5 m/s during 17.6–23.9.2012 in the experiment areas. This was measured with Vaisala's weather station located in area two.

The built in moisture level was low in the experiment area 3 with ventilation grooves because there was no rain during the construction of this area. Therefore no drying was observed when the measurements started two months after the completion of the roof area. Nevertheless, the effective drying capability of the ventilation grooves has been tested in another study (Kettunen 2011). This study is not totally comparable to our case, since the conditions are always different in field studies. However, the results from Kettunen clearly showed the tendency that ventilation grooves increase the drying ability of a roof structure.

Our field study indicated that the experiment area with the ventilation grooves had the lowest absolute humidity of all of the areas and this absolute humidity was even clearly lower than outdoor absolute humidity due to the ventilation grooves. The unventilated area four with load-bearing steel sheet had similar built in moisture but had 1.5 g/m^3 higher absolute humidity compared to area 3. The ventilation grooves did not move moisture into the roof by convection and condensation although in January a small amount of snow was visually detected in the underpressure ventilator.

There was no built in moisture in the unventilated area 5. Therefore the drying ability of this area was high enough. The ventilation machine room below area 5 was eight meters high and there were holes and untighten seams in the vapour barrier. No moisture convection was detected from the indoor air to the roof in December although indoor air absolute humidity was 1 g/m^3 higher than in the stone wool of the roof.

A degree lower temperature was measured from the miter of area 4 compared to the dry miter in area 3 which implied that the moisture levels in the capillary region can reduce the insulation properties of the stone wool. This result is however uncertain due to the reduced accuracy of the temperature sensor in the humid conditions.

Moisture accumulation was detected in the shady north part of roof area 4. In December absolute humidity in the thermal insulation was 7 g/m^3 in the south part of this area, but in the north part 17.5 meters away the absolute humidity was 11 g/m^3. The moisture level in the north part of the roof was clearly elevated as in roof areas 1 and 2. There was horizontal moisture transfer in the roof due to the warm stone wool that released moisture from the pore surfaces in to the pore air. This moisture moved to the north part of the roof by the fluttering of the roofing, pump-effect and diffusion. The accumulated moisture did not even out in the year 2011. The uneven temperature change of the thermal insulation in area 4 is shown in figure 5.

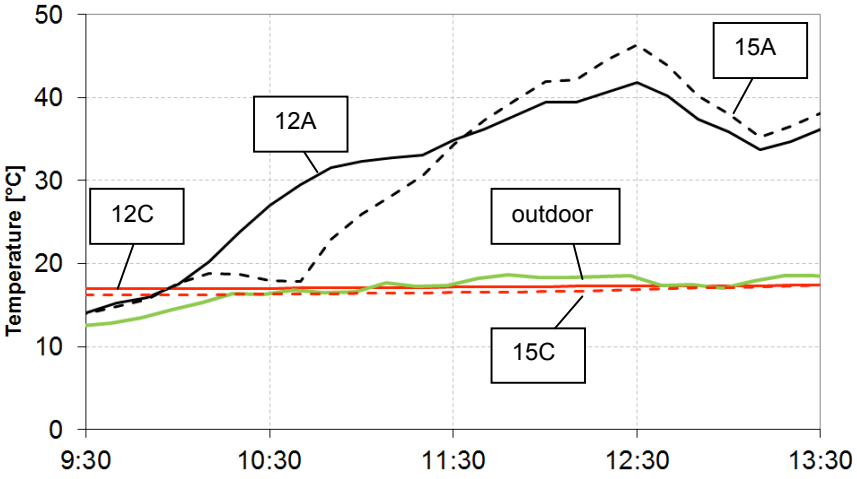

FIG 5. The warming up of PVC roofs occurs at different times in the shady areas. The measurement point 15 was shaded by a south-north wall in the right side of the point (figure 2).

The impact of sun radiation to moisture transfer should be considered in roofs that have shady areas and in roofs that warm up unevenly due to the shape of the roof. The condensation of moisture that is based on the sun radiation is more problematic in situations where the slope of the roof descends in the condensation area where there might be snow on the roof. In this situation the low sloped area is colder and easily condensates the moisture which moves in the thermal insulation. Unventilated thermal insulation might be a better option than insulation with ventilation grooves in pitched roofs and domes because thermal radiation induced moisture transfer is slower without grooves. Moisture transfer can be reduced with cellular plastic insulation because of the lower water vapour and air permeability. In addition, tight and dense fastening of the roofing reduces air flow beneath the roofing. Moreover, the temperatures of the roof can be lowered 10 °C with a light colour PVC roofing

compared to dark colour. This might be useful to reduce refrigeration energy costs. The effect of internal variable heat loads can be reduced for example with a load bearing structure with thermal mass such as concrete slab. However, it is justified to use watertight vapour barrier if the temperature difference induced moisture transfer cannot be prevented.

The relative humidity in the upper and lower part of the thermal insulation fluctuated strongly during sunny weather. The stone wool passes moisture when the temperature rises. This moisture moves downwards in the insulation by diffusion. The stabilization of the moisture content takes place when the thermal radiation ceases. Again, the absolute and relative humidity are almost equivalent between different heights of the stone wool on cloudy days. This suggests that the moisture is evenly distributed when it is in the hygroscopic moisture region. The variation of relative humidity in sunny weather should be taken into account in the moisture measurements of the roof. This variation can be even tens of percent in an hour. In summer the moisture measurements of the roofs should be made on cloudy weather or at night.

From October onwards the built in moisture condensated and frose in the upper parts of the thermal insulation. It is not recommended to perform moisture measurements in winter because most of the moisture is in the upper parts of the structure and on the underside of the roofing as water or ice making it difficult to interpret the results. Determining the water content from a material sample is a better option in that case.

The results of the field study apply exactly only to the type of roof that was investigated. The sizes of the experiment areas are smaller than what roof areas usually are which might lower the moisture transfer induced by the fluttering effect of the roofing. The experiment areas were bounded by a dark steel wall on one side that might have had a minor effect on the temperatures in the roof. Nevertheless, the temperatures where in accordance with the information from the roofing manufacturer (Protan 2005). The careful construction work of the experiment areas resulted in relatively low built in moisture levels in the roof.

3. Computational studies

The moisture loads against the PVC roof and the drying ability of the roof were evaluated in the calculations. The analysis was done in steady state with handmade calculations (by this we mean for example steady state diffusion equation and analytical expression for cavity flow) and time dependently with calculation programs. Based on the handmade calculation the moisture amounts from roofing leaks or moisture convection from indoor air are so large that an unventilated PVC roof is not able to remove this moisture in a short time. Moisture convection was largest through holes in the vapour barrier and gaps in the joints. In half an hour roofing leaks can cause equal moisture loads compared to moisture convection from indoor in a year. Moisture diffusion from indoor to the roof is minor, at most 0.17 kg/m^2 in a year. The drying of the roof by diffusion to outdoor air is 0.25 kg/m^2 in a year and 1 - 16 kg/m^2 with ventilation grooves (figure 6). The effect of the ventilation with grooves to the heat loss of the roof is low, approximately 1.5 % compared to the conduction heat loss. The results from the handmade calculations were analogous to the earlier studies. The handmade calculations utilized the measurement results from the field study, like temperature and relative humidity, which increases the validity of the results. However, there is always simplifications in the calculations that somewhat cause error to the results.

The moisture technical performance of the PVC roof was modelled with Comsol Multiphysics 4.2 and Wufi 4 -programs. The six years long Wufi model showed that the hygroscopic moisture (relative humidity below 97 %) dries out from the unventilated roof by diffusion in a year giving a drying speed of 0.05 - 0.08 kg/m^2/a. With a cellular plastic the drying time is under 1.5 years and drying speed 0.04 kg/m^2/a. Cellular plastics do not slow the drying significantly because the drying speed is determined mostly by the water vapour permeability of the PVC roofing. The type of the outdoor boundary conditions for temperature and humidity in Helsinki and Sodankylä were sinusoidal based on the

weather data. Boundary conditions in Helsinki were 4.5 °C (annual average), amplitude 12.1 °C and 79.9 %+10 % (two simulations with other simulation with 10 % higher value), amplitude 10 %. Boundary conditions for Sodankylä were -1 °C, amplitude 14.5 °C and 78.7 %+10 %, amplitude 12 %. The drying speed did not vary with locality, rise of indoor air humidity to 90 % or rise of outdoor relative humidity in Helsinki by 10 %. The vapour barrier was similar bitumen felt to the one in the field study. In practice, the drying time of the PVC roof is increased if there is built in moisture in the roof. A built in moisture of 0.23 kg/m^2 increases the diffusive drying time by a year. The sufficiency of the drying times by diffusion depends on the moisture durability of the thermal insulation and how much water leaks are allowed in the indoors. If necessary, a watertight vapour barrier can be used to prevent interior water leaks caused by extra water in the roof. Stone wool withstands moisture in the hygroscopic region and even some times in the capillary region but the long-term durability of wet stone wool should be investigated. It should be noted that the pressure difference across the roof affect the possibility of microbes that are harmful to humans moving into the indoor air. In addition, the moisture transfer inside the PVC roof increases the probability of interior water leaks in wet roofs.

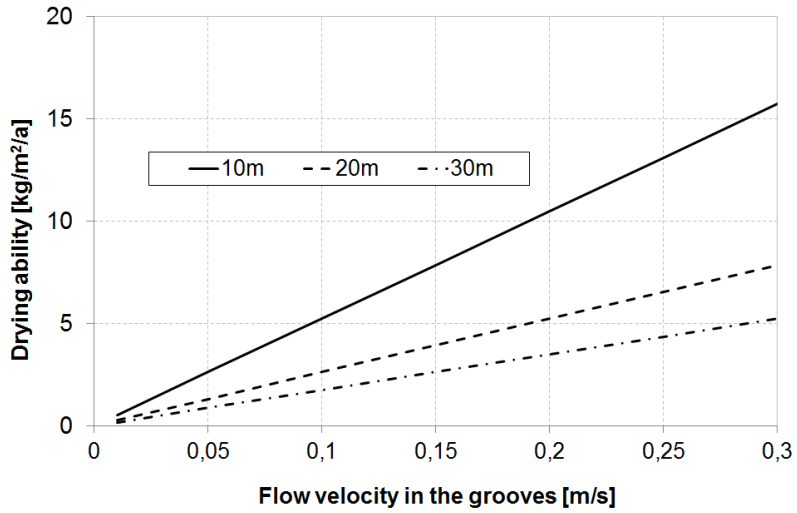

FIG 6. The drying ability of a PVC roof with ventilation grooves [kg/roof-m^2] in a year depends on the air velocity in the groove (horizontal axis), distance between collector channels (different curves), outdoor humidity and the amount of solar radiation. Outdoor humidity and solar radiation is not accounted for in the picture.

A calculation program (Comsol Multiphysics 4.2) was used to model the moisture transfer in a PVC roof (right structure in figure three) in a sunny day by using boundary conditions from the field study. Heat flux by solar radiation was calculated by temperature measurements and set for the boundary condition. By this method temperature simulation was almost identical to the measured values. Satisfactory results were obtained from the relative humidity in different height of the insulation. In sunny weather the calculation gave relative humidity 26 % (measured 17 %) for upper surface of thermal insulation, 37 % (measured 23 %) at groove depth and 68 % (measured 78 %) in the lower side of thermal insulation at night. One analysis accounted for temperature dependent sorption isotherm and the other hysteresis effect in the sorption isotherm. The temperature dependency was modelled with four temperature regions based on the moisture sorption measurements done in 5 °C and 23 °C temperatures. The sorption curves for temperatures 40 °C and 60 °C were determined so that the sorption moisture changed with similar amount per degree than in laboratory test. The adsorption and desorption curves in hysteresis were based on laboratory measurements that implied the difference between adsorption and desorption in 75 % humidity to be 0.01 kg/m^3. A larger hysteresis was also tested. The best results came from temperature dependent sorption curve, but the results did not improve substantially compared to the measured values. Therefore other models used a simple sorption isotherm depending only on relative humidity.

The moisture transfer was analysed likewise in a roof with EPS insulation. In EPS roofs the variation of relative humidity during sunny weather is 55 % in the upper part of the roof compared to 75 % with stone wool. In the lower part of the roof the variation is 6 - 8 % with EPS and 25 - 35 with stone wool. The vertical moisture transfer is less in roofs with cellular plastic insulation compared to stone wool insulation. The effect of ventilation grooves was added to the model similarly as was calculated with handmade calculation. The program gave a drying ability of 0.55 kg during 90 summer days which is less than in the earlier studies or the handmade calculation. Probably the model did not work properly and underestimated the effect of ventilation. The program showed that the moisture transfer into the roof with groove ventilation by night time condensation or spring condensation is minor. These models calculated the temperature under the roofing and at groove depth and the outdoor humidity was based on the field measurements. The outdoor humidity was compared to the saturation moisture values in the roof. The condensed amount was 0.006 kg/m^2 during 1.10–30.3. The spring condensation was investigated qualitatively and the probability was considered to be little. The condensation is little in winter due to the small amount of water vapour in the outdoor air.

4. Conclusions

It is important to keep the thermal insulation dry in a roof structures. It was found in the field study that unventilated PVC roof areas did not dry out the built in moisture during 18 months. The computational studies gave similar results. The drying ability of the roof by diffusion is 0.05 - 0.25 kg/m^2/a based on the calculation results. The theoretical drying speed varies for example due to its dependency on the outdoor conditions. The moisture loads directed to the roof are usually larger than the diffusive drying ability. In the field study there were no disadvantages in the moisture technical operation of the roof with ventilation grooves. In addition, this roof area was the driest one. To be sure of the sufficiently fast drying speed of built in moisture and moisture loads during operation it is recommended that PVC roofs in Finland are built as ventilated structures. An exception to this are certain roof types such as pitched roofs and domes where roof ventilation can induce unwanted moisture transfer inside the thermal insulation that might result in interior water leaks.

5. Acknowledgements

This master's thesis was ordered by Kattoliitto ry. The study was part of the PVC project 2011 organized by Kattoliitto ry. The project aimed to develop a classification for plastic and rubber roofings and a proper ventilation principle for PVC roofs. The research is funded by Kattoliitto ry via the Research Foundation of Helsinki University of Technology.

References

A-V. Kettunen. 2011. Technical analysis of moisture transfer qualities of mildly sloping roofs. 9th Nordic Symposium on Building Physics. Proceedings, Volume 1, s.255 - 261.

Kattoliitto ry. 2013. Toimivat Katot 2013. 117 s. Available: http://www.kattoliitto.fi/?s=146

Protan Oy. 2005. Lämpötilaolosuhteet vesikatteessa ja tasakatoissa. 2 s. Available: www.protan.fi

Suomen Rakennusinsinöörien Liitto. 2012. RIL 107-2012. Rakennusten veden- ja kosteudeneristysohjeet. 219 s.

Hygrothermal performance of hollow brick with foam polyurethane cavity filler

Zbyšek Pavlík, Associate Professor [1]
Jan Fořt, Eng. [2]
Robert Černý, Professor [3]

[1] Czech Technical University in Prague, Czech Republic
[2] Czech Technical University in Prague, Czech Republic
[3] Czech Technical University in Prague, Czech Republic

KEYWORDS: *Lightweight hollow bricks, foam PU cavity filler, hygrothermal performance, semi-scale testing*

SUMMARY:
Hygrothermal performance of newly developed type of hollow brick is studied in the difference climate conditions. The cavities of hollow brick are filled by foam polyurethane (PU). The experiment is done in semi-scale conditions. For that purpose, a system of two climatic chambers separated by the connecting tunnel for sample positioning is used. The studied brick block is provided with combined temperature/relative humidity sensors and thermally and vapour proof insulated in the tunnel between the climatic chambers. In the interior climatic chamber, constant temperature and relative humidity values typical for residential houses are set. On the exterior side, there are simulated hourly data of relative humidity and temperature corresponding to Prague climatic reference year. In this way, the 1-D heat and water vapour flux through the studied brick block is simulated. The obtained data provide a detailed information on the hygrothermal performance of the analyzed brick exposed to winter climatic conditions.

1. Introduction

Present age lays great emphasis on decrease of energy consumption for buildings conditioning, e.g. energy for heating in cold year period and energy for air conditioning in hot year seasons. Environmental protection and achieving sustainable development requires energy efficient solutions and energy conservation in buildings. The high demands on thermal insulation function of buildings led to the construction of passive and low energy buildings that are known to outperform conventional buildings in terms of living conditions and energy efficiency due to their heat recovery, good thermal insulation, and the overall optimization of the house (Mlakar & Štrancar 2013).

There are number of technical standards and recommendations on the proper indoor temperature and relative humidity of buildings. According to (Mlakar & Štrancar 2013), (Wolkoff & Kjaergaard 2007), the internal temperature is the best to be kept between 20 - 26 °C and the indoor relative humidity between 30% and 60%.

In order to meet the above given requirements on low energy consumption for buildings operation and to keep optimal conditions of interior climate, new sophisticated thermal insulation materials and systems are under development and testing.

Hollow bricks are used extensively in the construction of building envelopes because of their enhanced thermal insulation properties, attributed mostly to the presence of air holes. Concerning the mode of heat transport in hollow bricks, it is generally accepted that overall heat transfer trough the cavity is due to the convective, conductive and radiative transfers (Vasile et al. 1998), (Antar & Baig 2009), whereas this heat transport can be reduced by thermal insulation fillers of the cavities (Hazmy

2006), (Zzkowski & Haese 2010). On this account, a new type of hollow brick with original cavities arrangement and with foam PU cavity filler is studied in the paper.

2. Experimental details

2.1.1 Studied hollow brick

The hollow brick with internal cavities filled by recycled foam PU was designed for application in single layer thermal insulation masonry having a width of 500 mm. The view of the cross-section of researched hollow brick is given in Fig. 1. Similar brick body arrangement we studied in (Pavlík at al. 2013a), where we accessed the thermal conductivity of brick block having cavities filled by polystyrene balls.

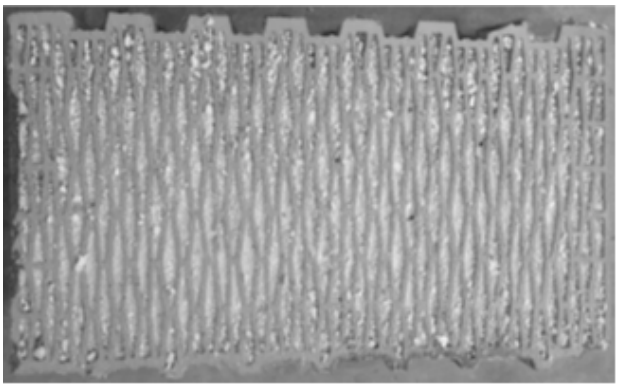

FIG 1. The view of the cross-section of the researched hollow brick block

Basic physical properties of the brick body we measured in (Pavlík et al. 2013b). Here, the bulk density was accessed from the measurement of sample size by digital length meter and its dry mass. The matrix density was determined on helium pycnometry principle. The total open porosity was then calculated from the bulk density and matrix density. In (Pavlík et al. 2013b) we determined also thermal conductivity of the brick ceramic body, whereas the measurements were performed in dependence on moisture content from the dry state to the water fully saturated state using impulse measurement technique. The basic properties of the brick body are given in Table 1. Thermal conductivity is presented in Table 2.

TABLE 1. Basic physical properties of the brick body

Bulk density (kg/m^3)	Matrix density (kg/m^3)	Total open porosity (-)
1 389	2 830	50.9

TABLE 2. Thermal conductivity of the brick body

Moisture content (m^3/m^3)	Thermal conductivity (W/m·K)
0.0	0.3
0.11	0.44
0.13	0.57
0.29	0.75
0.36	0.88
0.46	1.03
0.49	1.06

In above listed paper *(Pavlík et al. 2013b)* we tested also reference brick block without cavity filling, brick block with polystyrene balls filled cavities and brick block with mineral wool filled cavities. On

the basis of obtained data there was observed improvement of bricks thermal resistance by application of thermal insulation materials as cavity fillers. From the quantitative point of view, the best thermal insulation performance exhibited brick blocks with recycled foam PU and mineral-wool filled cavities. Their thermal conductivities were about 40% lower compared to brick block with air cavities. On this account, brick with PU filled cavities is studied, in order to approve its improved thermal insulation function.

2.1.2 Semi-scale experiment

Determination of hygrothermal performance of the studied hollow brick was done in the conditions of semi-scale experiment that enables testing of the whole brick block.

For the realization of the transient heat and water vapor transport experiment, the climatic chamber system originally designed in our laboratory was used (Pavlík & Černý 2008), (Pavlík & Černý 2009). This system consists of two climatic chambers for simulation of relative humidity and temperature, and connecting tunnel for placing the specimen (Fig. 2).

FIG 2. Climatic chamber system

Maximum volume of the tested specimen, which is possible to be placed into the connecting tunnel, is 0.35 m^3 with surface exposed to the simulated climatic conditions of dimension 0.7 x 0.9 m. The construction of the particular chambers is based on common commercial solutions for controlling temperature and relative humidity conditions but the solution of connections between the chambers and the tunnel and of the organization of additional admission holes for parallel measurements are designed in our laboratory. The dimension of the test space of the chambers is 0.72 x 0.72 x 0.60 m. In our case, the hollow brick of real dimension was studied.

FIG 3. Sensors positioning and sample insulation

Within the experiment, the investigated brick was placed into the tunnel, and then provided with the sensors and with the additional thermal insulation consisting of polystyrene boards and polyurethane

foam (Figs. 3, 4). Finally, the climatic chamber system was closed, and required temperature and relative humidity values were set. The whole experimental setup is schematically presented in Fig.5.

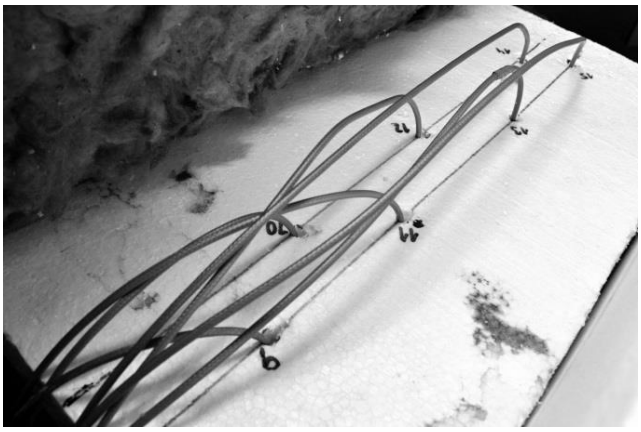

FIG 4. View of the sensors in thermal insulation board

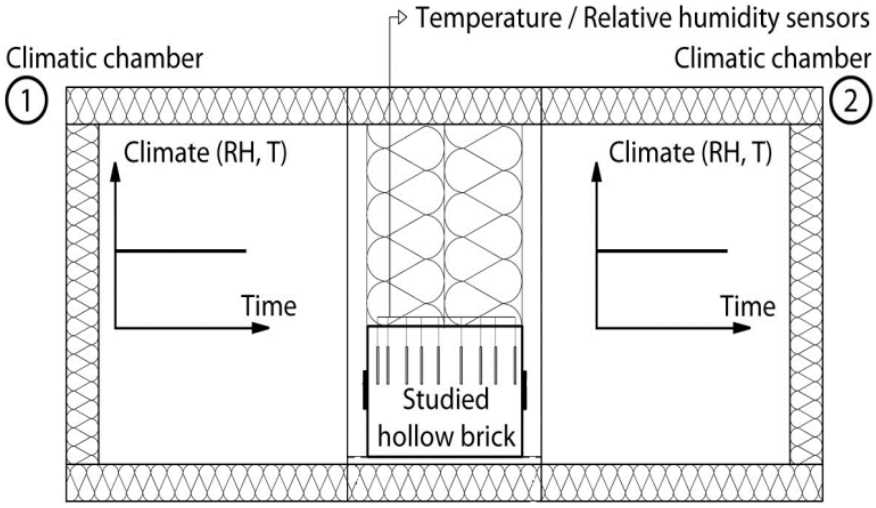

FIG 5. Scheme of the experimental setup

During the experiment, constant temperature 21 ± 0.5 °C and constant relative humidity 50 ± 2% were maintained in the interior climatic chamber. On the exterior side, there were simulated typical climatic conditions for Prague, whereas the climatic loading started with data corresponding to November 1 and the experiment was stopped with climatic data corresponding to March 31. Hence, the whole winter period, which is the most critical part of the year from the point of view of heat losses, was simulated. The airtightness of the climatic chamber system was monitored by anemometers for air flow velocity measurement. Continuous monitoring of temperature and relative humidity distribution along the hollow brick thickness was done using commercial combined sensors from Ahlborn, Germany. These sensors measure relative humidity on electrical capacity principle in the 5-98% relative humidity range with a ± 2% accuracy and temperature using NTC thermistor. The temperature measurement accuracy was for the temperature sensors applied in the measuring system ± 0.1°C.

3. Results and discussion

Climatic conditions typical for residential buildings measured in the interior climatic chamber are given in Fig. 7. We can see that both temperature and relative humidity were kept during the whole time of experiment almost constant.

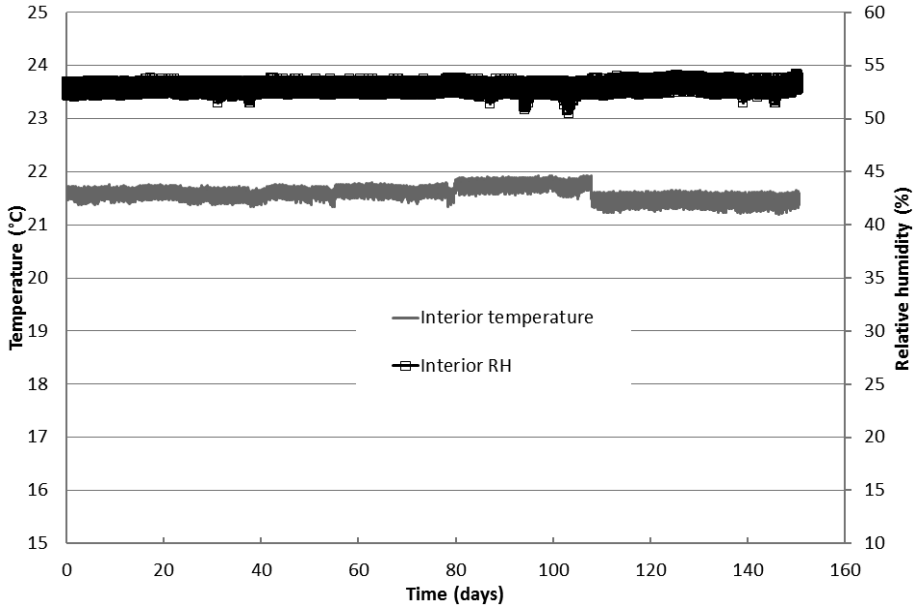

FIG 7. Interior climatic conditions

Simulated exterior climatic conditions corresponding to the time interval from November 1 to March 31 are graphed in Figs. 8, 9. Within the whole experiment, high values of relative humidity were simulated, what is typical for autumn and winter period of the year. Here, the temperature varied between -15°C and 15°C.

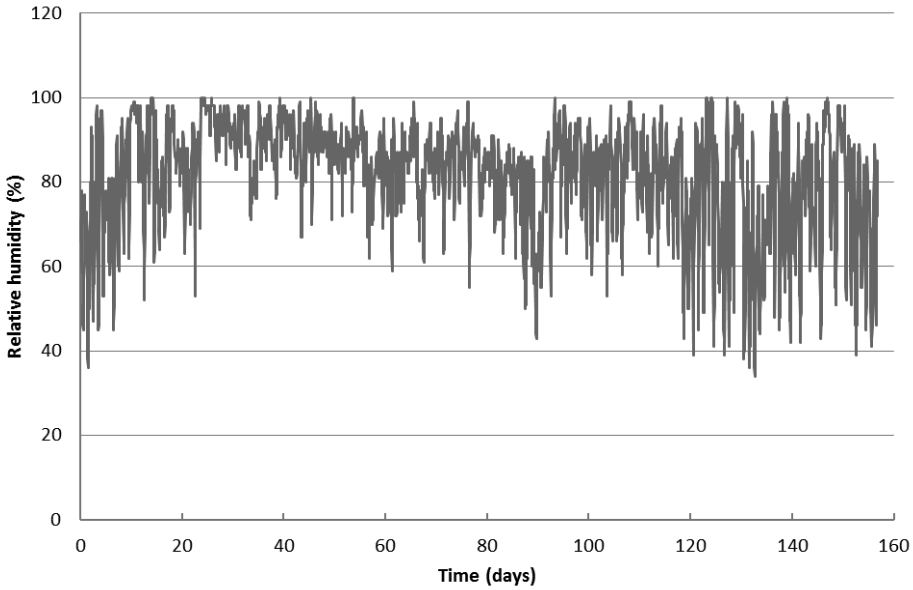

FIG 8. Exterior relative humidity

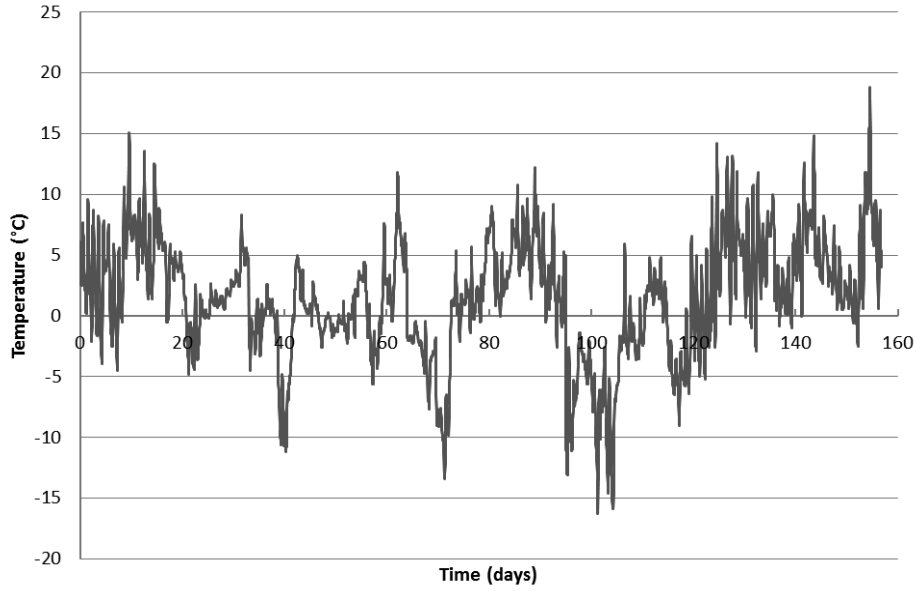

FIG 9. Exterior temperature

Temperature and relative humidity profiles measured along the brick thickness are presented in Figs. 10, 11. Looking at the temperature profiles one can observe high sensitivity of the researched brick block on the exterior temperature variations. The thermal insulation function of the brick can be considered good in general, what is promising for practical application of the developed material in building practice. At 150 mm distance from the interior surface, there were measured temperatures of the brick about 20°C, what is very good for the conditioning of the interior climate. Basically, there were only small differences between interior temperatures and the temperatures of the brick at the distance of 150 mm from the brick surface.

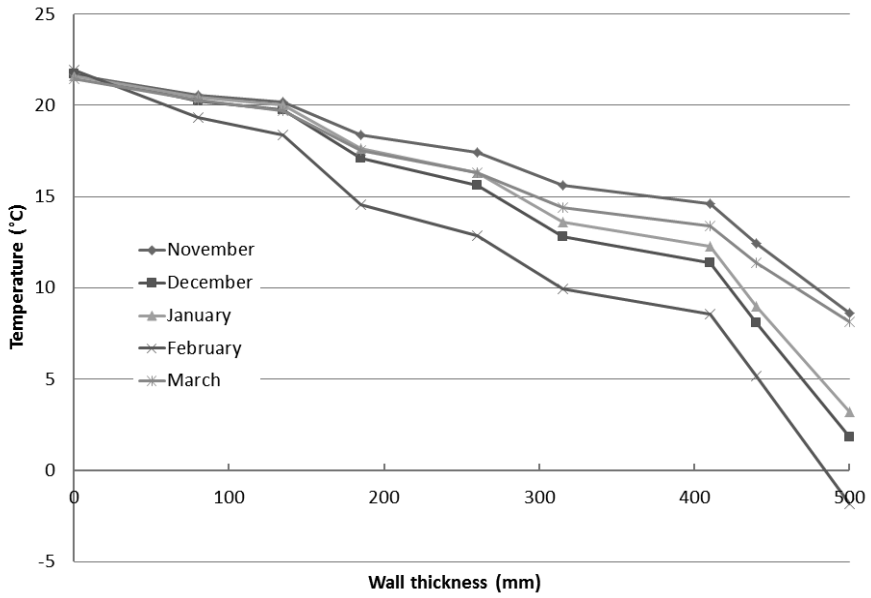

FIG 10. Temperature profiles measured along the sample thickness

Relative humidity profiles reflected the simulated relative humidity in the exterior chamber. Typically, the lowest values of relative humidity were measured for climatic loading corresponding to January and November. Here, the relative humidity values were < 60% up to 400 mm distance from the

interior surface of the brick block. Relative humidity in the exterior layers of the brick was then affected by high relative humidities simulated in the climatic chamber. In December, February and March, the measured relative humidity values slightly increased and varied typically from 55 to 65%. Also in this case, the exterior side of the brick was more affected by exterior climatic conditions changes.

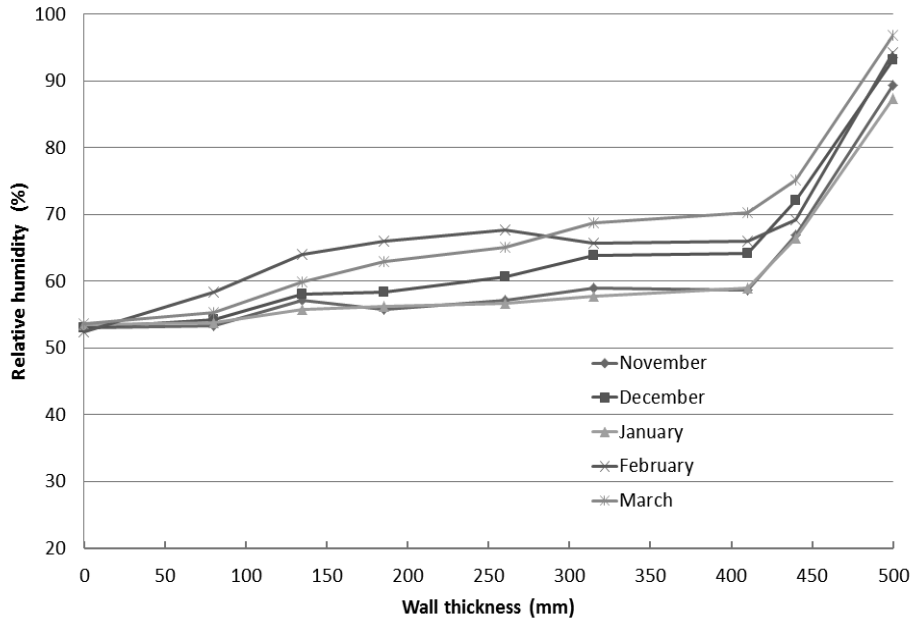

FIG 11. Relative humidity profiles measured along the brick thickness

4. Conclusions

The application of semi-scale arrangement for experimental assessment of hygrothermal performance of the newly developed hollow brick block was found to be effective way for such type of analysis. The relatively low cost of the experiment in a combination with the reasonable accuracy of measured temperature and relative humidity fields in long time interval makes good prerequisites for a widespread use of the technique.

The applied climatic loading allowed evaluation of the functionality of the tested wall segment in the winter period, which is the most critical part of the year from the point of view of the heat losses of the buildings. The obtained results revealed a very good hygrothermal performance of the brick block provided with foam PU cavity fillers.

5. Acknowledgement

This research has been supported by the Ministry of Industry and Trade of the Czech Republic, under project No FR-TI3/085.

References

Antar M.A. & Baig H. 2009. Conjugate conduction-natural convection heat transfer in a hollow brick block, Applied Thermal Engineering (29), pp. 3716-3720.

Hazmy M.M. 2006. Analysis of coupled natural convection-conduction effects on the heat transfer through hollow building blocks, Energy and Buildings (38), pp. 515-521.

Mlakar J. & Štrancar J. 2013. Temperature and humidity profiles in passive building blocks, Building and Environment (60), pp. 185-193.

Pavlík Z., Fiala L., Jerman M., Fořt J., Černý R. 2013a. Thermal properties of contemporary lightweight cavity bricks: A semi-scale experimental study, Proceedings of the 2nd Central European Symposium on Building Physics, 9-11 September 2013, Vienna, Austria, pp. 733-739.

Pavlík Z., Fiala L., Vejmelková, E., Černý, R. 2013b. Application of effective media theory for determination of thermal properties of hollow bricks as function of moisture content, International Journal of Thermophysics (34), pp. 894-908.

Pavlík Z., Černý R. 2008. Experimental assessment of hygrothermal performance of an interior thermal insulation system using a laboratory technique simulating on-site conditions, Energy and Buildings (40), pp. 653-678.

Pavlík Z., Černý R. 2009. Hygrothermal performance study of an innovative interior thermal insulation system, Applied Thermal Engineering (29), pp. 1941-1946.

Vasile C, Lorente S., Perin B. 1998. Study of convective phenomena inside cavities coupled with heat and mass transfers through porous media – application to vertical hollow bricks – a first approach, Energy and Buildings (28), pp. 1998.

Wolkoff, P. & Kjaergaard, S.K. 2007. The dichotomy of relative humidity on indoor air quality, Environmental Engineering (33), pp. 850-857.

Zukowski M. & Haese G. 2010. Experimental and numerical investigation of a hollow brick filled with perlite insulation, Energy and Buildings (42), pp. 1402-1408.

Wireless temperature sensors embedded in concrete

Magnus Åhs, Ph. D. [1]

[1] Div. of Building Materials, Lund university, Sweden

KEYWORDS: *Wireless communication, reinforced concrete, temperatures, signal strength*

SUMMARY:
Concrete is a very dense material with a high density which effectively shields radio signals. Therefore the transmitting power of a wireless sensor, e.g. RFID- tag, needs to be high in order to reach outside the concrete. The receiver also needs to have a high sensitivity to ensure that a weak signal is detected. Now there are small receivers that perceive signals with a signal strength of -100 dBm. Some benefits of a wireless sensor in contrast to a non-wireless sensor; the sensors are protected from an external impact; no wires to protect on the construction site; it is possible to monitor the temperature development, strength development and drying even after the building is in operation. This project is based on studying the potential of using wireless communication for continuous, wireless monitoring of concrete structures during curing, desiccation, at the construction site and in the operating stage. RFID-sensors were cast into concrete and the transmission signal strength was determined both at the transmitter and the receiver at different distances from the sensors. The distance between the sensor transmitter (embedded 40 mm into the concrete) and receiver was more than 70 meters. The sensors and the RFID tags works well in both fresh and hardened concrete and this implies that it is possible to manufacture a temperature monitoring system for concrete with wireless sensors.

1. Introduction

Sensors have been used for many years in the building industry worldwide to measure various physical quantities. In the case of the production of large concrete structures, such as bridges, tunnels and nuclear power plants, sensors are widely used to monitor the temperature development. These sensors are in most cases connected to a data logger by wires. A lot would be gained if these sensors could be read remotely by using wireless transmission of data. As reinforced concrete is a very dense material the radio signals' strength are substantially reduced, hence limiting the distance between the transmitter and the receiver.

A wireless sensor system was developed about ten years ago in order to log relative humidity, RH, in concrete (Åhs, 2005). The system was mainly wireless, but at the point of the measurement, there was a relatively large radio transmitter connected to the sensors inside the concrete structure. The radio transmitter was installed on the concrete surface and transmitted data to a data logger connected to the GSM-network. A connection to the data logging system could be attained by a software via the GSM network. The radio transmitter used in the system was too large to embed into the concrete.

Wireless sensors, such as RFID, have been used to determine temperature development in concrete. Such sensors have been embedded in concrete, but so far the distance between the transmitter and receiver has been short up to about 10 m, see TABLE 1. The reason for this short distance was most probably because of a weak transmitting power. Embedded wireless passive sensors have also been used in concrete structures to monitor the humidity (Norris et al., 2008, Ong et al., 2008, Stojanovic et al., 2010, Barroca et al., 2013). Unfortunately none of these authors stated the distance between RFID-tag and receiver. Passive sensors are not equipped with a transmitter which mean that they hence the short distance between sensor and receiver.

TABLE 1. Frequency and distance in air of the used wireless sensors embedded in concrete,

Author	Frequency	Distance in air [m]	Distance to concrete surface [m]
(Chang and Hung, 2012)	868 MHz	7.3-12.2	-
(Quinn and Kelly, 2012)	433 MHz	3.5-7.5	.5
(Saafi et al., 2010)	916.5 MHz	-	.1
(Sjöberg and Gerstig, 2009)	868 MHz	0.5-3	.2
(Sjöberg and Gerstig, 2009)	125 kHz	<0.7	.5
(Barroca et al., 2013)	2.4 GHz	35	.05
(Helbig et al., 2010)	-	-	-
(Jo et al., 2013)	2.4 GHz	120-300	

The objective of this work was to quantify the maximum distance of transmitting a signal sent from embedded RFID-tags with various configurations. Another objective was to explore to what degree the antenna design influences the signal strength.

2. Material

RFID tags were installed in a reinforced concrete column with a rectangular section, its foot print was 0.5*0.5 m^2 and 3.130 m tall. All sensors except one were installed 40 mm below the concrete surface; the last sensor was installed 265 mm below the concrete surface. Note that one sensor was installed at the bottom of the column 12A4. All sensors were installed before casting according to FIG 1.

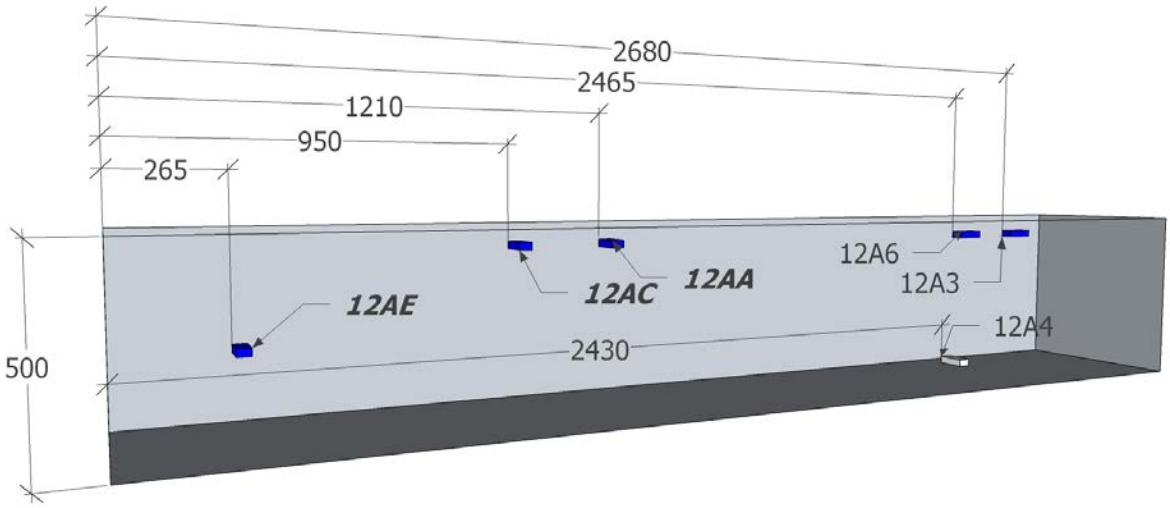

FIG 1. The sensors (small dark boxes except for one light grey) were installed in the horizontally oriented concrete column (big gray box) according to this drawing [mm].

This column was cast in a factory used for the production of prefabricated concrete structures. The water cement ratio of the self-compacting concrete was 0.4 and the composition is presented in TABLE 2.

TABLE 2. Concrete mixture proportion, quantities are in kg/m^3

Material	w/c 0.4
CEM 1 52.5 R	220
CEM II/A-LL 42,5 R	220
Sand 0-4 mm	395
Sand 0-4 mm (heated)	400
Gravel 4-16 mm	495
Gravel 4-16 mm (heated)	490
Sikament VS-1	3.96
Water (heated)	173.2

The RFID-tags had different configurations regarding antenna and booster. These configurations are shown in TABLE 3. The normal-mode dipole antenna, traded as a rubber ducky antenna, and the foil based dipole antenna, is an antenna which is integrated onto the electrical circuit board.

TABLE 3. RFID-tags with different configuration

RFID-tag	Antenna configuration
12A3	Foil based dipole antenna without booster
12A4	Foil based dipole antenna without booster
12A6	Normal-mode helical antenna without booster
12AA	Foil based dipole antenna with booster
12AC	Foil based dipole antenna with booster
12AE	Normal-mode helical antenna with booster
12A5 not embedded	Foil based dipole antenna without booster
12A7 not embedded	Normal-mode helical antenna without booster

RFID-tag configurations without booster transmitted with a signal strength of +10 dBm and the ones with a booster transmitted with a signal strength of +27dBm. The used signal frequency was 868.3 MHz in both directions, hence both the RFID-tags and the master unit operated with the same frequency. In addition to the RFID-tags embedded in concrete two RFID-tags was used as controls, to compare the achieved signal strength in air with the signal strength in both air and concrete. These tags were installed on steel plate fixture 150 mm above the concrete column, and were only active during the first 24 hours.

The master unit was equipped with a transmitter without booster. Its transmitting signal strength was +10dBm (10mW) and its receiver detected signal strengths down to -100dBm.

Another temperature monitoring system, Conreg maturity meter, was used as a control to compare with the temperature readings from the wireless sensor system.

3. Methods

In order to evaluate the maximum distance of successful communication, the master unit was installed at different positions inside a large factory, about 270 m long and 8 m high. The exterior walls of the factory were made of prefabricated concrete, and the roof was made of corrugated steel sheets. In this factory the master was left at each position for at least 20 minutes hence possibly receiving at least ten successful measurements of the signal strength, see FIG 2.

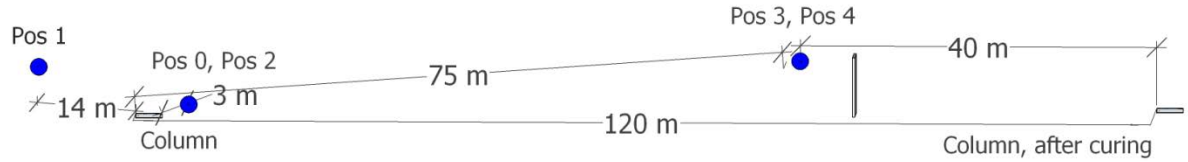

FIG 2. Various positions of the master unit, solid dots, versus the horizontally positioned concrete column at and after curing, small grey rectangle. Note that the concrete column was moved after curing. The standing rectangle to the right shows a concrete wall in between the master unit and concrete column.

The signal strength was registered and logged every second minute by the master unit and each RFID-tag. Pos 0 represents the position of the master unit before casting and Pos 2 after casting at approximately the same position within +/- 0.2 m. Those two positions made it possible to perform and evaluate the impact of the signal strength with and without concrete. Pos 1 is located 14 m from the concrete column about 3 m above the floor. Pos 3 is located around 75 m and about 5 meters above the floor. When curing was finalised the column was moved to a location for temporary storage about 40 m from the master unit, represented by Pos 4. Note that there was a concrete wall, 6 m tall and 4 m wide, between the master unit and the concrete column. This wall covered about one-sixth of the available cross sectional area of the factory building, which means that there was still plenty of open air left for transmitting radio signals, see FIG 3.

RFID-tags were installed inside a small plastic container which was sealed by using hot melt adhesive. The sealing was used to protect the electrical equipment from harmful liquid pore solution. The containers were fixed on to the reinforcement bars by using plastic stripes, see FIG 4.

FIG 3. The premises used in the experimental setup. Note the concrete wall partly shielding radio signals.

FIG 4. The RFID-tags were fixed by using plastic stripes looped around reinforcement bars.

4. Results and discussion

The mean signal strength from the master unit registered by each RFID-tag in each position is shown in TABLE 4. The mean was calculated by using each signal strength registration divided by the number of successful registrations. This means that if the signal strength was not registered it does not have an impact on the mean value. Such a calculation method was applied since there were moving objects in the factory that could intermittently obstruct the data transmission. Such factors may have interfered with the radio communication on a short or long time basis. Please note that RFID-tag 12AE

malfunctioned after concrete placement, most probably because of a leakage in the sealed plastic container, see TABLE 4 and TABLE 5.

TABLE 4. Mean value of the signal strength in, dBm, RxRSSI, from the master unit as registered by each RFID-tag.

RFID-tag	Pos 0	Pos 1	Pos 2	Pos 3	Pos 4	Pos 0-Pos 2
12A3	-63	-77	-70	-85	-81	-7
12A4	-54	-91	-89	-91	-94	-35
12A6	-50	-64	-73	-82	-74	-23
12AA	-42	-74	-65	-80	-85	-18
12AC	-46	-69	-70	-84	-81	-24
12AE	-49	—	—	—	—	—
12A5	-73	-79	-71	-86	—	2
12A7	-59	-69	-57	-65	—	2

The signal strengths from the RFID-tags without a booster, 12 A3 and 12 A6, are 3 dBm lower than the RFID-tags 12AA and 12AC, determined by each RFID-tag. Tag 12A4 was installed 40 mm above the bottom concrete surface and is therefore not comparable with the other RFID-tags.

Comparisons between transmitting radio signals through no concrete and concrete is displayed in the right hand column of TABLE 4. These show that the signal strength is reduced by at most 35 dBm, after the casting is performed. Fortunately, there is still about 10 dBm left to reach the operational limit of detection of -100 dBm. The reduction on the other RFID-tags is about 20 dBm and the surplus of signal strength is about 20 -40 dBm, which seems to be a reasonable margin.

Furthermore, the comparisons of the control RFID-tags show that there is a difference of signal strength between Pos 0 and Pos 2 of 2 dBm. This difference is small and is a validation that the positions, Pos 0 and Pos 2, of the master unit are reasonably equal before and after concrete placement. The result from the control RFID-tags also shows that the normal-mode helical antenna has higher signal strength in all positions, about 15dBm. Note that the control RFID-tags were both dismantled and were therefore not used at Pos 4. The signal strength of the RFID-tags equipped with a normal-mode helical antenna is on average 6 dBm higher than the foil based dipole antenna.

It was possible to transmit and receive radio signals from all positions of the master unit, which means that the maximum distance was about 70 m.

The mean signal strength that the master unit detects from each RFID-tag is presented in TABLE 5.

TABLE 5. Mean value of the signal strength, in dBm, TxRSSI from each RFID-tag respectively as registered by the master unit.

RFID-tag	Pos 0	Pos 1	Pos 2	Pos 3	Pos 4	Pos 0-Pos 2
12A3	-61	-74	-68	-82	-79	-7
12A4	-52	-88	-87	-91	-91	-35
12A6	-46	-63	-72	-79	-73	-26
12AA	-49	-78	-67	-80	-85	-23
12AC	-35	-57	-58	-71	-68	-23
12AE	-34	—	—	—	—	—
12A5	-70	-77	-67	-83	—	3
12A7	-58	-68	-55	-63	—	3

Comparing the signal strength from RFID-tags with a foil based dipole antenna, with and without a booster, shows that the strength is about 10 dBm higher for the boosted RFID-tags. This difference clearly decreases with an increasing distance, see RFID-tag 12AA in TABLE 5. The signal strength

registered by each RFID-tag with no booster is lower than the signal strength registered by the master unit. This difference is about 2 dBm. In contrast the master unit detects a signal strength on average 7 dBm higher from the RFID-tags equipped with a booster than in the opposite direction. Such a result is as expected as the signal strength is boosted from the RFID-tag but not from the master unit. The signal strength registered by the master unit from the RFID-tags equipped with a normal-mode helical antenna is on average 8 dBm higher than the foil based dipole antenna.

The signal strength from two individual RFID-tags, 12A6 and 12 AC are shown in FIG 5 and FIG 6.

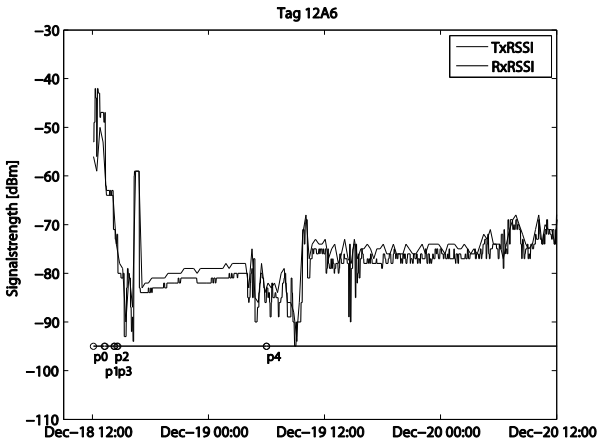

FIG 5. Signal strength of RFID tag 12A6, normal-mode helical antenna without booster.

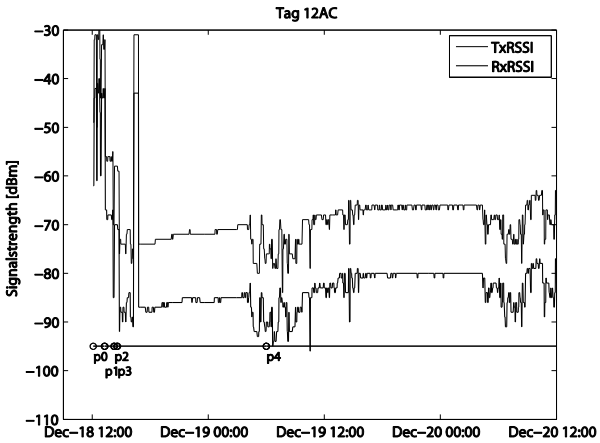

FIG 6 Signal strength of RFID tag 12AC, foil based dipole antenna with booster.

The x-axis represents the time and the y-axis represents the signal strength in dBm. Two solid lines are shown which represent the signal strength registered by the master unit, thin solid line, and registered by the RFID-Tag, thick solid line. The thin solid line with circles at -95 dBm shows when the master unit was located in Pos 0 to Pos 4, p0-p4.

There are a number of disturbances on the signal strength during working hours when there is personnel in the factory, from about 5am until 5 pm. The rest of the time the signal is quite constant and undisturbed. There is a small increase in signal strength during the first day after casting, about 3 dBm. This increase occurs from 4 pm at the 18:th of December until 5 a.m. at the 19:th of December, and this could be interpreted as an effect of the hardening of the concrete.

FIG. 7 shows the temperature development in the concrete column determined by two sensors, the wireless RFID-tag 12AC, and the Conregsystem sensor which is not wireless. The x-axis represents the temperature in °C and the y-axis represents time.

The two temperature curves show a similar behaviour, following an increasing and later a decreasing stage. The magnitude of the increase and following decrease are also similar. However, there is a notable difference in absolute temperature between the two sensors where the Conreg sensor registers a temperature about 5 °C higher than the RFID-tag sensor. This difference may have two different origins. Firstly the two different sensors are not located at the same spot; this is of course one major source of error. The conreg sensor was located deeper into the concrete, near the cross sectional centre of the column whereas the RFID-tag was located at a shallower depth. Secondly, despite efforts to make the clock time of both systems identical there may still be some time lag that unintentionally is interpreted as a difference in temperature. This effect is much smaller than the first effect. In addition there is also an uncertainty of the two sensor which means that the shown temperature differs from the true temperature.

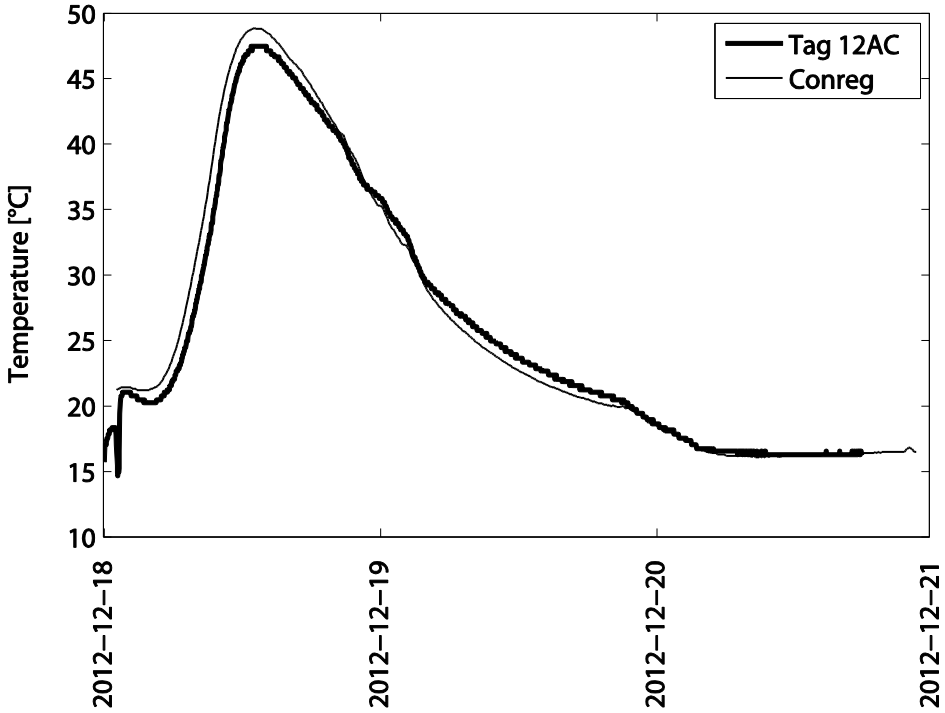

FIG 7. Temperature development after concrete placement inside the concrete column.

It should also be noted that the temperature sensor in the RFID-tag is not in direct contact with the concrete. The sensor is located inside the plastic container and is measuring the air temperature in the plastic container.

Finally, the results of the study clearly show that it is possible to embed RFID-tags of a suitable configuration and transmit data at a distance of >70 m. This finding confirms the results from the earlier studies in which the maximum distance was between 35 - 120 m (Jo et al., 2013, Barroca et al., 2013).

5. Conclusions

The results of the studied wireless system showed that the maximum distance between embedded sensors and the master unit is over 75 m, when RFID tags are installed 40 mm below the concrete surface. This result means that it is possible to monitor the temperature in large concrete structures without the need of sensors connected to a data logger by using long wires. If the RFID-tag is equipped with an external temperature sensor, the temperature could easily be determined deep into a concrete structure. It was also clearly shown that the RFID-tags normal-mode helical antenna is the configuration that demonstrates the highest signal strength.

The trueness of the temperature may be corrected for by calibration prevented that the sensor is put in direct contact with the concrete. This will make it possible to use such a system as a maturity meter system given a correct interpretation and recalculation of the temperature to a compressive strength.

6. Acknowledgements

This study was funded by SBUF, the Development Fund of the Swedish construction Industry. NCC Construction Sweden, Electrotech, Strängbetong, and Cementa are also acknowledged for their financial support. Juha Rajala, Urban Classon and Richard Hahto from Electrotech are hereby gratefully acknowledged for their valuable support and Örjan Petersson and Bengt Johansson for letting us testing the wireless system in the factory of Strängbetong in Långviksmon in Sweden.

References

Barroca, N., Borges, L. M., Velez, F. J., Monteiro, F., Górski, M. & Castro-Gomes, J. 2013. Wireless sensor networks for temperature and humidity monitoring within concrete structures. *Construction and Building Materials,* 40**,** 1156-1166.

Chang, C. Y. & Hung, S. S. 2012. Implementing RFIC and sensor technology to measure temperature and humidity inside concrete structures. *Construction and Building Materials,* 26.

Helbig, S., Steinke, A., Hummel, W., Janorschke, B. & Plagge, R. Entwicklung eines Sensorsystems zur Messung der Ausgleichsfeuchte in Estrichen. Proceedings of the First European Conference on Moisture Measurement - Aquametry, October 5-7 2010. 458-469.

Jo, B.-W., Park, J.-H. & Yoon, K.-W. 2013. The Experimental Study on Concrete Permeability of Wireless Communication Module Embedded in Reinforced Concrete Structures. *International Journal of Distributed Sensor Networks,* 2013**,** 10.

Norris, A., Saafi, M. & Romine, P. 2008. Temperature and moisture monitoring in concrete structures using embedded nanotechnology/microelectromechanical systems (MEMS) sensors. *Construction and Building Materials,* 22**,** 111-120.

Ong, J. B., You, Z., Mills-Beale, J., Tan, E. L., Pereles, B. D. & Ong, K. G. 2008. A Wireless, Passive Embedded Sensor for Real-Time Monitoring of Water Content in Civil Engineering Materials. *IEEE Sensors journal,* 8**,** 2053-2058.

Quinn, B. & Kelly, G. Feasibility of embedded wireless sensors for monitoring of concrete curing and structural health. 2012.

Saafi, M. A., Kaabi, L. B., Mccoy, M. C. & Romine, P. C. 2010. Wireless and embedded nanotechnology-based systems for structural integrity monitoring of civil structures: A feasibility study. *International Journal of Materials and Structural Integrity,* 4**,** 1-24.

Sjöberg, A. & Gerstig, M. 2009. Trådlös mätning av temperatur i nygjuten betong, Litteratur- och experimentell fältstudie.

Stojanovic, G., Radovanovic, M., Malesev, M. & Radonjanin, V. 2010. Monitoring of Water Content in Building Materials Using a Wireless Passive Sensor. *Sensors,* 10**,** 4270-4280.

Åhs, M. Remote monitoring and logging of relative humidity in concrete. Proceedings of the 7th symposium on building physics in the nordic countries, June 13-15 2005. The icelandic building research institute, 181-187.

Influence of input data uncertainty in school buildings energy simulation

Ricardo M.S.F. Almeida, Assistant Professor [1,2]
Nuno M.M. Ramos, Assistant Professor [2]

[1] Polytechnic Institute of Viseu, School of Technology & Management, Civil Engineering Department, Portugal
[2] University of Porto, Faculty of Engineering, Civil Engineering Department, Laboratory of Building Physics, Portugal

KEYWORDS: *Uncertainty analysis, sensitivity analysis, Monte Carlo simulation, building simulation, school building, heat demand*

SUMMARY:
In developed countries, the building sector is responsible for a very significant share of the total energy consumption. A more detailed and rigorous analysis of building energy performance became possible due to the building simulation software improvement. Traditionally, buildings energy simulation requires the definition of a set of input parameters, which are usually considered as deterministic, neglecting the fact that in reality they have a stochastic nature. Hence, if one intends to evaluate the uncertainty in simulation due to the uncertainty of the input parameters, stochastic methods, such as Monte Carlo simulations should be employed. This paper presents a methodology for the stochastic simulation of school buildings for tackling input data uncertainty. The Monte Carlo method application in the evaluation of the uncertainty of the heat demand of a school building provides an example case where the opportunities and difficulties of the method are explored. The methodology includes parameter characterization, sampling procedure, simulation automatization and sensitivity analysis. Its application results in increased knowledge of the building, allowing to define targets that include the stochastic effect.

1. Introduction

Dynamic energy simulation software is an essential tool for building designers and constitute an added value for both new construction and building retrofit projects. Traditionally, buildings energy simulation requires the definition of a set of input parameters, which are handled according to more or less complex mathematical models generating a final deterministic result. These input parameters can be obtained in national regulations, guidelines or standards, and is common to find different recommendations depending on the consulted document.

Thus, this methodology, although its simplicity, does not consider the stochastic nature of the input parameters, and, consequently, the obtained simulation results might be far from reproducing the real performance of buildings. Hence, if one intends to evaluate the uncertainty in simulation results due to the uncertainty in the definition of the input parameters, stochastic methods, such as Monte Carlo simulations should be employed. This uncertainty is particularly important in retrofit projects, where, sometimes, designers are limited by architectural reasons and, therefore, some flexibility in building regulations limits can be decisive.

Furthermore, over the past few years, there has been growing interest among researchers and consultants of building energy simulation in uncertainty analysis. This methodology is often applied to assess the risk of different energy conservation measures (Rodríguez 2013). Hopfe (2011) studied the

integration of uncertainty analysis into building simulation of energy consumption and thermal performance of an office building.

Monte Carlo simulations are based on a sequence of random numbers derived from the initial input variables, which probabilistic distributions are known or can be estimated. Thus, for each of the *i* input parameters analysed (X_1, X_2, ... X_i) a set of *N* random numbers is generated, in accordance with the initially assumed probability distributions. Simulations are performed and for output *Y*, *N* results will be obtained (Y_1, Y_2, ... Y_N).

The accuracy of the methodology depends on the number of simulations performed. However, no consensual rule exists to define the sample dimension. Sensitivity studies that address this issue can be found in Macdonald (2009) and Burhenne (2013).

This paper presents a methodology for the stochastic simulation of school buildings for tackling input data uncertainty. The Monte Carlo method application in the evaluation of the uncertainty of the heat demand of a school building provides an example case where the opportunities and difficulties of the method are explored. A school building model was simulated with EnergyPlus and five input parameters were considered as variables with an associated uncertainty: occupation, metabolic rate, lighting, ventilation and envelope thermal resistance. Parameters uncertainty was defined by a mean value and a standard deviation and a normal distribution was considered. Monte Carlo simulations were performed for 25, 50, 100, 200 and 500 cases, generated with Latin Hypercube Sampling, with the purpose of analysing the convergence of the results. The procedure for implementing a manageable simulation is explained and the sensitivity analysis of the results is performed.

2. Methodology

2.1 Parameters

Since the main goal of this research is to understand the influence of input data uncertainty in buildings energy simulation, the first step was choosing the input parameters. On the one hand, a large number of parameters would compromise the time-efficiency of the procedure and on the other, it is desirable that the most uncertain and potentially most influential parameters should be considered. Thus, 5 parameters were selected: occupation density, metabolic rate, lighting density, ventilation rate and external wall thermal resistance. For all it was assumed a normal distribution with the mean (μ) and standard deviation (σ) values presented in Table 1. Particular attention should be paid to the ventilation since several *in situ* measurements revealed that air change rates tend to be much lower than the ones predicted at design stage (Almeida, 2012). For that reason two mean values were considered for the air change rate.

TABLE 1. Normal distribution parameters

Parameter	Unit	μ	σ
Occupation density (*occ*)	person/m^2	0.1	25%
Metabolic rate (*met*)	W/person	94.3	10%
Lighting density (*lig*)	W/m^2	15.0	10%
Ventilation rate (*acr*)	h^{-1}	2.0 4.0	25%
External wall U-value (*wall*)	W/m^2 K	0.5	10%

2.2 Number of samples and output

Five sets of the parameters, with different dimension, were computed in order to evaluate the convergence of the results. These combinations of parameters were obtained by using Latin Hypercube Sampling method, which is a stratified sampling method and can produce more stable

analysis results than random sampling. The MatLab algorithm *lhsnorm* was employed. Therefore, Monte Carlo simulations were performed for 25, 50, 100, 200 and 500 cases. The software chosen for the simulation was Energy Plus. This software is particularly adequate for the implementation of this methodology since its input files are text-based and, consequently, it was possible to automate the procedure of writing EnergyPlus models by means of an Excel VBA code. 1750 models were created and simulated.

The building simulation output chosen was the heat energy demand (*Eannual*), both monthly and annual. Figure 1 illustrates the procedure.

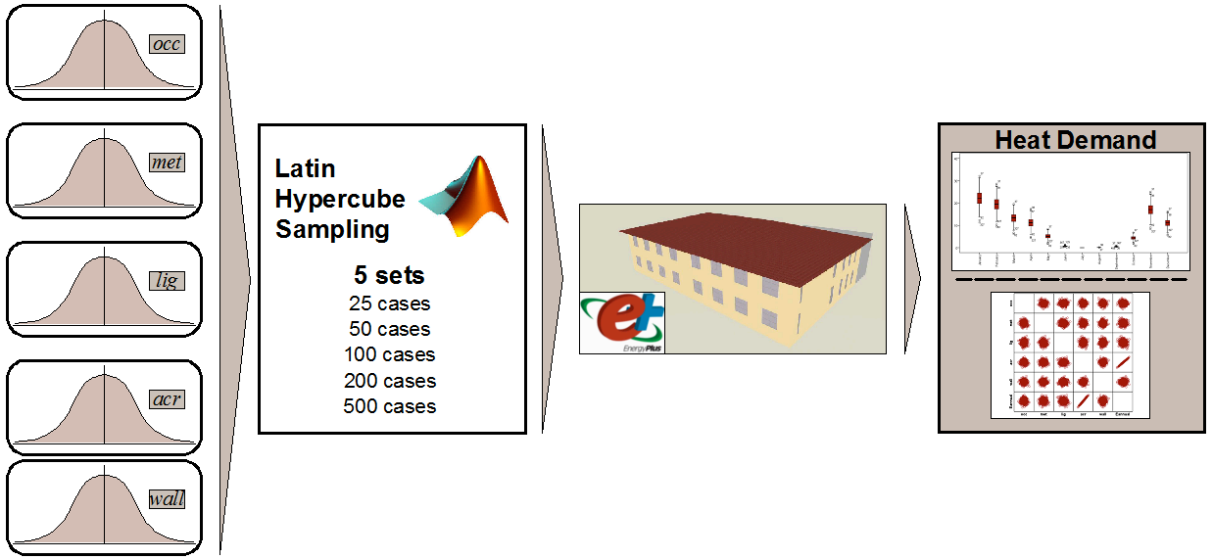

FIG 1. Methodology

2.3 Case study

The case study is a typical two storey Portuguese school building, dated from the 90's, and this project of simple rectangular schools was repeated throughout the country. The building model was created with DesignBuilder.

Four types of zones were considered, each with specific metabolic rates, occupation density and schedules: classroom (545 m^2), circulation (212 m^2), storage (130 m^2) and toilet (63 m^2). For the classroom zone was defined a metabolic rate of 94 W/person with an occupation density of 0.40 people/m^2.

An *in situ* complete survey was carried in order to characterize the most relevant construction elements properties. The school original walls and roof have no insulation and the windows are single glazed. Blinds with medium reflectivity slats were considered as shading devices, with operation by solar radiation control with a set point of 120 W/m^2.

Ventilation is natural and the heat systems are hot water radiators, with a temperature set-point of 20ºC, which is in conformity with the Portuguese regulation.

The simulations were performed on an annual base, with hourly outputs, and considering 10 time steps per hour.

3. Results

Two kinds of analysis were performed: a convergence analysis and a sensitivity analysis of the results. The sensitivity analysis produced a large amount of results since it was performed for monthly and annual heat demand. However, the scope of this paper is just to explore the opportunities and

difficulties of the methodology on the uncertainty evaluation of the input parameters. For that some demonstrative examples were chosen.

3.1 Convergence analysis

The study started with the base case simulation. This case corresponds to the scenario where the mean value is assumed for all the parameters (Table 1).

The five sets of simulations were then performed and the annual heat demand computed. The mean value was calculated, compared with the base case and the corresponding error was determined by the following equation:

$$error(\%) = \frac{\overline{E}_{annual} - E^0_{annual}}{E^0_{annual}} \times 100 \quad (1)$$

Where $\overline{E}_{annual}$ heat demand mean value obtained with Monte Carlo simulation (kWh/(m^2.year))

E^0_{annual} heat demand obtained with base case (kWh/(m^2.year))

Standard deviation convergence was also analysed. Figure 2 shows the plot of the results.

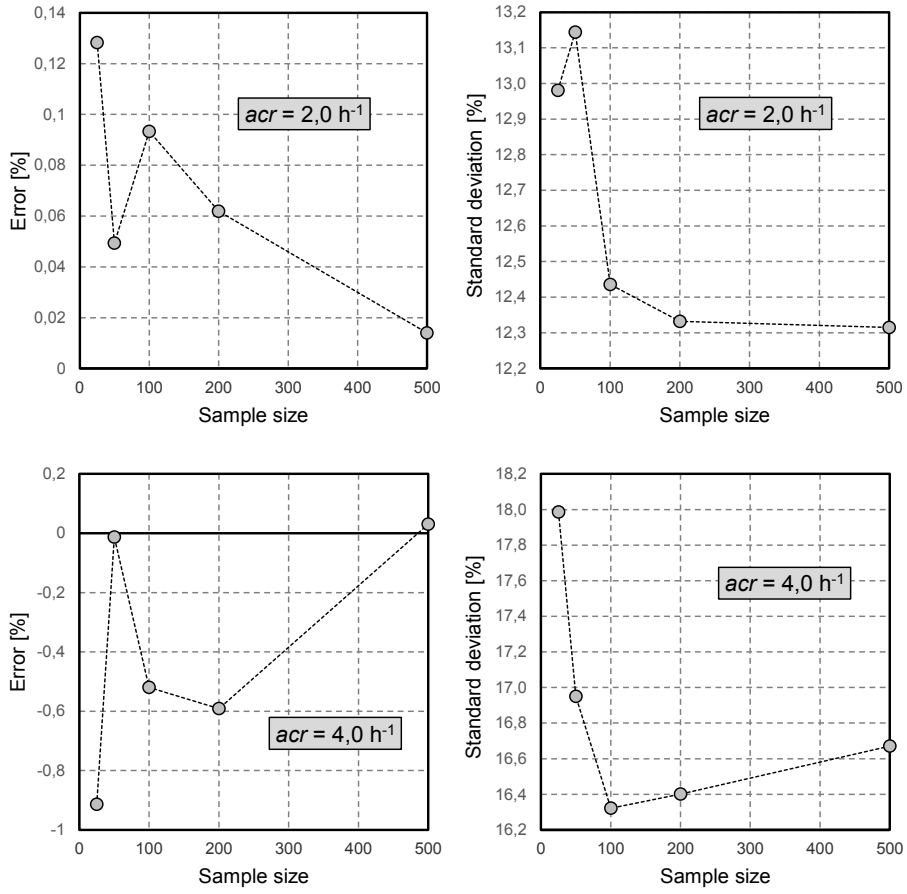

FIG 2. Convergence analysis of the annual heat demand

The most important finding of this analysis is that all the sets performed very well. Even for the set of 25 cases an error below 1% was observed. However, it is important to refer that this conclusion is only valid for this particular problem. As stated before, several studies revealed that the sample size is

important for the overall accuracy of the method and can be responsible for very significant errors, particularly when a large number of inputs and outputs are analysed.

For the scenario of $acr = 2.0\ h^{-1}$ the best performance was achieved with the largest set (500 cases); for $acr = 4.0\ h^{-1}$ the best performing set was the one with 50 cases, followed by the one with 500 cases.

Regarding the standard deviation, no convergence was found. However, differences between the sets are relatively small.

3.2 Sensitivity analysis

3.2.1 Monthly analysis

Figure 3 shows the mean, maximum and minimum monthly heat demand, obtained in the scenario of $acr = 2.0\ h^{-1}$ and a set of 500 cases.

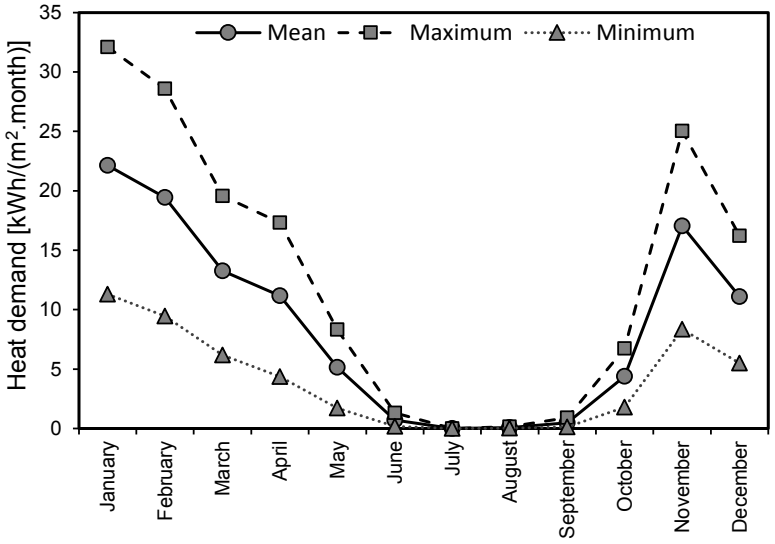

FIG 3. Monthly analysis

Another way to statistically analyse the distribution of these results is using the box-plot representation, where the outliers of the sample can be observed. Outliers should be investigated carefully. Often they contain valuable information about the process under investigation. This form of representation (Figure 4) allows to easily identify situations of abnormally high or low heat demand, and if one checks the input values of the parameters for those cases, the relative importance of each parameter can be assessed. As an example, Table 2 includes the parameters input values of case 37 and 82, the first corresponds to a situation of high energy demand and the second of low demand.

Results indicate that air change rate plays a vital role in the result. The situation is confirmed by the correlation analysis presented in section 3.2.2.

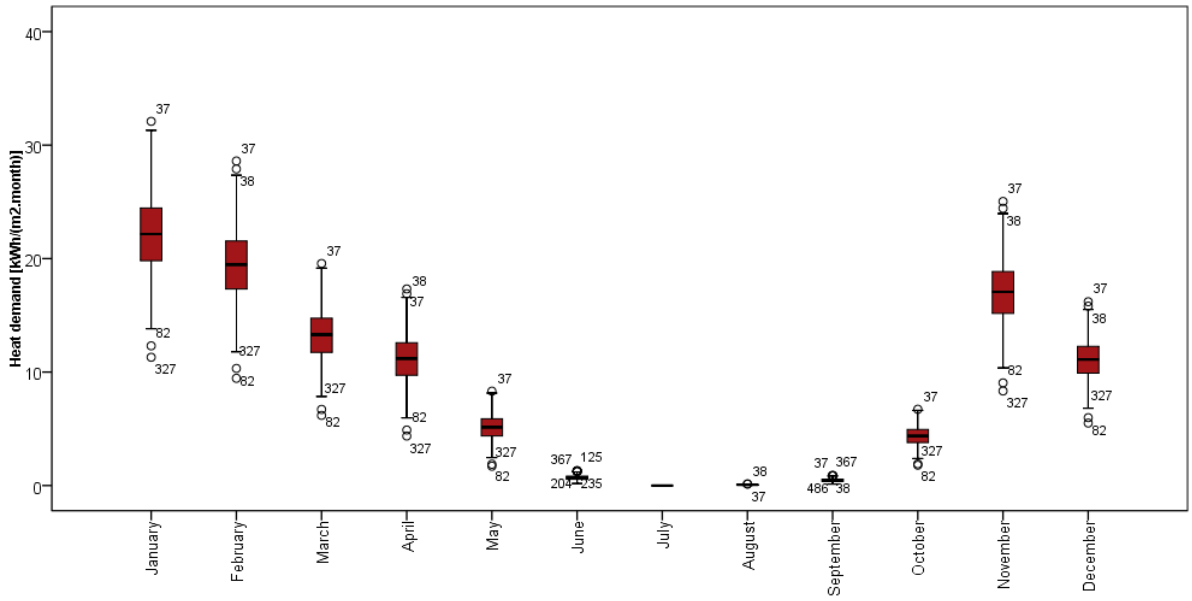

FIG 4. Monthly analysis: box-plot

TABLE 2. Outlier interpretation

Case	*occ*	*met*	*lig*	*acr*	*wall*
37	0.109	85.407	17.444	17.444	0.426
82	0.107	89.088	17.656	17.656	0.475
Mean	0.1	94.275	15.0	4.0	0.5

3.2.2 Annual analysis

Annual heat demand was also evaluated. The histogram of the normalized heat demand is illustrated in Figure 5 and Table 3 summarizes the results. As in the case of the monthly analysis, the example refers to the same data (*acr* = 2.0 h^{-1}; 500 cases).

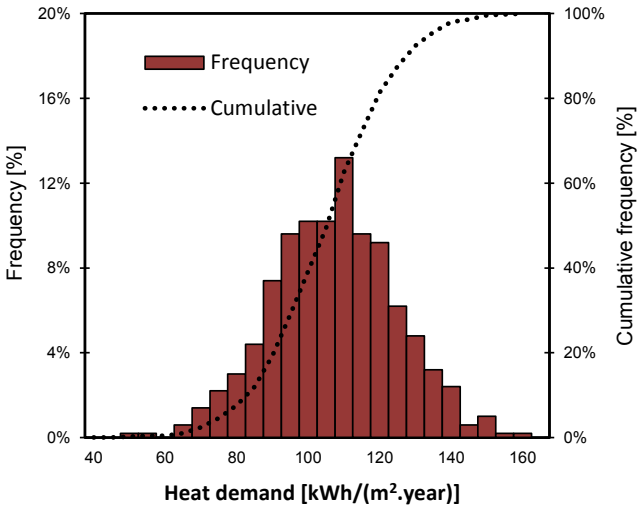

TABLE 3. Statistical indicators

μ	104.9
σ	17.5
Maximum	156.2
Minimum	49.0
Coef. of variation	0.17

FIG 5. Annual distribution

As it was expected a normal distribution of the results was obtained. The annual heat demand derived from the deterministic analysis (Table 1 input values for the five parameters) was also

104.9 kWh/(m^2.year). However, if one considers the stochastic nature of the input parameters the available information increases. For the example under study, the Monte Carlo simulation reveal that in 68% of the scenarios the heat demand is between 87.4 and 122.4 kWh/(m^2.year) ($\mu \pm \sigma$). Though, if one imposes a target of 90% probability an heat demand of 127.8 kWh/(m^2.year) should be considered. This kind of conclusions exposes the importance of stochastic analysis to technically support the decision-maker.

When one seeks to evaluate the influence of the uncertainty of the input data and in which manner they influence the result, giving the designer information about the relative sensitivity of the parameters, an interesting and simple method is a graphical sensitivity analysis (Burhenne 2010). Each parameter and its corresponding result (e.g. occ_1, $Eannual_1$; …; occ_n, $Eannual_n$) is plotted in a scatter plot. Figure 6 shows a matrix of scatter plots for the 5 input parameters and the correspondent heat demand (*acr* = 2.0 h^{-1}; 500 cases).

It can be seen that the annual heat demand of the building (*Eannual*) is very sensitive to air change rate (*acr*). Furthermore, an almost linear dependency between the parameter and the output can be observed. This result was confirmed by a correlation analysis between the input and output parameters whose results can be found in Table 4. A specific parameter can therefore arise as the only one relevant for the problem, alerting designers for the need of measures that increase robustness of, in this case, *acr* control during the school's operation.

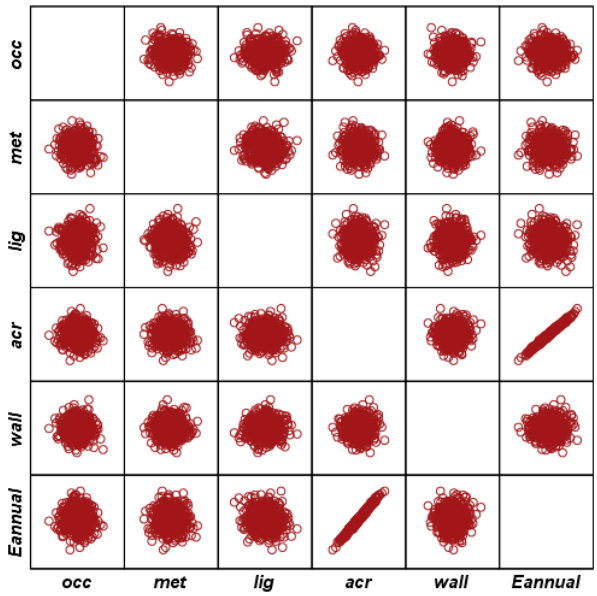

FIG 6. Scatter plot matrix for sensitivity analysis

TABLE 4. Correlation analysis

	occ	*met*	*lig*	*acr*	*wall*	*Eannual*
occ						
met	-0.06					
lig	0.03	-0.07				
acr	-0.07	-0.04	-0.02			
wall	-0.06	0.03	0.02	0.05		
Eannual	-0.08	-0.03	-0.12	**0.99**	0.06	

It is important to refer that all the considerations exposed here for the scenario of *acr* = 2.0 h^{-1} and 500 cases were similar to the ones obtained in the other setups.

4. Conclusions

Buildings energy performance is nowadays a motive of concern for all European governments. In developed countries, buildings are responsible for a significant share of the total energy consumption and increasing in recent decades mainly due to the users growing comfort demands. In this context all the measures to improve the energy efficiency of buildings are welcome. Building simulation is an essential tool in building energy optimization. However, its use should be prepared carefully since only realist input data would lead to valuable outputs. Therefore, the stochastic nature of input data should be taken into account and uncertainty analysis should be performed.

This paper proposes a probabilistic approach to the evaluation of the uncertainty of input data in a school building energy simulation. Monte Carlo simulation is performed considering uncertainty in five input parameters. Building heat demand is the output.

The study included a convergence analysis of the results and a sensitivity analysis. Convergence analysis exposed that, for this particular situation, a small number of cases (25) are enough to obtain an error below 1%. Sensitivity analysis revealed that air change rate was the most important input in school buildings energy simulation. In fact, a linear dependency between air change rate and the annual energy demand of the building was found. A stochastic database is the final piece missing, after which this methodology can actually be applicable in practice.

References

Almeida R. & Freitas V.P., 2010. Hygrothermal Performance of Portuguese Classrooms: measurement and computer simulation. In: *Proceedings of 1st Central European Symposium on Building Physics*. Cracow, Poland 13-15 September 2010.

Burhenne S., Tsvetkova O., Jacob D., Henze G.P. & Wagner A. 2013. Uncertainty quantification for combined building performance and cost-benefit analyses. *Building and Environment*, 62, pp.143-154.

Burhenne S., Jacob D. & Henze G.P. 2010. Uncertainty analysis in building simulation with Monte Carlo techniques. In: *Proceedings of Fourth National Conference of IBPSA-USA*. New York City, USA 11-13 August 2010.

Hopfe C.J. & Hensen J.L.M. 2011. Uncertainty analysis in building performance simulation for design support. *Energy and Buildings*, 43, pp.2798-2805.

Macdonald I.A. 2009. Comparison of sampling techniques on the performance of Monte-Carlo based Sensitivity Analysis. In: *Proceedings of Building Simulation 2009*. Glasgow, Scotland 27-30 July 2009.

Rodríguez G.C., Andrés A.C., Munoz F.D., López J.M.C. & Zhang Y. 2013. Uncertainties and sensitivity analysis in building energy simulation using macroparameters. *Energy and Buildings*, 67, pp.79-87.

Effect of Temperature on Moisture Buffering of Hemp Concrete

Florence COLLET, Assistant Professor [1]
Sylvie PRETOT, Assistant Professor [1]

[1] Université de Rennes 1- Laboratoire de Génie Civil et Génie Mécanique – EA 3913-Equipe Matériau-Thermo-Rhéologie- 35704 Rennes, France

KEYWORDS: *Hygrothermal behaviour, Moisture Buffer Value, Bio-based material*

SUMMARY:
Hemp concrete is a bio-based building material made of hemp shiv and lime. This material is not used as load-bearing due to low mechanical properties. Hemp concrete is thus mainly used as filling material associated to a wooden structure. The indoor side of the wall can be coated or not. On hygrothermal point of view, hemp concrete shows low thermal conductivity, about 0.1 W/m/K, and can be used without added insulation layer in buildings. The hydric characterization of hemp concrete shows high transfer and storage capacities.

Thus, this study deals with hydric characterization of hemp concrete under dynamic conditions. The experimental method is based on the NORDTEST protocol where specimens are exposed to daily cyclic variation of relative humidity. Generally, hygrothermal characterization is held at 23°C. This study deals with the impact of temperature on moisture buffer value of hemp concrete. Several temperatures are investigated from 11°C to 23°C. The results show that moisture buffer value increases with the temperature according an exponential law.

1. Introduction

In a context of sustainable development, buildings should be energy efficient, comfortable and made of environmentally friendly materials.

The environmental quality is studied from Life Cycle Analysis of materials and buildings.

In order to characterise the hygrothermal performance of building envelop, the hygrothermal characteristics of materials are needed. In a general way, these data are thermal conductivity, sorption curves and water vapour permeability. They are characteristics of steady state behaviour and are often given for one temperature and one humidity. It is shown that thermal conductivity varies with water content (del Coz Díaz and al. 2013)(Jerman and al. 2013). In the same way, hydric characteristics are impacted by temperature.

The prediction of energy needs and indoor conditions in building, under representative hygrothermal conditions, requires numerical studies. These one are developed to describe transient hygrothermal behaviour of building envelop. The input data should take into account the impact of water content on thermal conductivity and the impact of temperature on hydric characteristics. More, it was shown that the use of steady state data hamper reliable simulations of hygroscopic buffering (Roels and al 2010). Thus, investigations under dynamic conditions are developed, looking for more realistic characterisation of dynamic behaviour.

Hemp concrete is a bio-based building material made of hemp shiv and binder. It is used to build as well walls as floors or roofs. The main difference between practices is the hemp to binder ratio in the mix. Hemp concrete can be implemented by casting, spraying or precasting. More, the indoor side of the wall can be coated or not.

The apparent density of hemp concrete ranges from 200 for roofs to 500 kg/m3 for floors. The porosity of hemp concrete is high and mainly open. It includes wide range of pore size from macropore to micropore (Collet and al 2008). These pores are interconnected and are due to the arrangement of hemp shiv and hemp-binder adhesion, trapped air in binder and capillaries in hemp shiv.

This material shows poor mechanical properties with low mechanical strength and high deformability under stress (Murphy et al. 2010) (Amziane and Arnaud 2013). Thus it is mainly used as filling material associated to a load-bearing structure.

On hygrothermal point of view, hemp concrete shows low thermal conductivity linked to the density and the water content of the material. For wall, the thermal conductivity is about 0.1 W/m/K (Arnaud 2000)(Pretot and al. 2009), thus hemp concrete can be used without added insulation layer in buildings. The hydric characterization of hemp concrete shows high transfer and storage capacities (Collet and Pretot, 2012)(Collet and al. 2013). Its sorption curves are S-shaped with large hysteresis. Its moisture permeability increases with water content and is about 3.10-11 kg.m-1.s-1.Pa-1 for low and middle relative humidities. Lastly, the measurements of moisture buffer value performed at 23°C show that hemp concrete is an excellent hygric regulator.

Lastly, several studies on its environmental impacts were carried out at wall scale (Boutin and al. 2006) (Ip and Miller 2012) (Pretot and al. 2013). These studies considered several implementation methods (spraying or casting). They included the wood frame and the hemp concrete and some of them also included the coating of the wall. All of these studies show that hemp concrete is as an environmentally friendly material. Among the considered indicators, the balance of the climate change indicator is favourable as CO_2 uptake by photosynthesis and carbonation is higher than emissions.

This study investigates the effect of temperature on hygric behaviour of hemp concrete, used as exposed interior finishing material, under dynamic conditions. The temperatures range from 23°C to 11°C. The highest temperatures (from 23°C to 17°C) are commonly met in buildings, while the lowest temperatures (14 and 11°C) may be met during building vacancy. Firstly, the material is presented, and the experimental protocol and device are described. Then, the results are detailed.

2. Experimental method

2.1 Studied hemp concrete

The studied hemp concrete is manufactured by spraying. This spraying method is well adapted in order to construct buildings which maximum height reaches about 6 meters. It is used to build as well walls as floors or roofs. The main difference between practices is the hemp to binder ratio in the mix. This study concerns hemp concrete used to achieve walls.

FIG 1. Implementation by spraying

The spraying method requires a mixer and pumping equipment. Hemp and binder (mainly lime) are mixed together and constitute a dry mix that is blown along a pipe by means of an air-compressed flow. Water is added to the mix at the end of the pipe, it may be quantified by the operator with valves (FIG 1). Hemp shiv and binder are mixed in proportion of 22 kg of hemp shiv to 44 kg of lime binder (CBC Tradical 70).

For this study, hemp concrete was sprayed in moulds of 30×30×16 cm^3 (figure 1). The blocks are then stabilized at 23°C; 50% during three years and 10 months to ensure ageing. Tested materials are, thus, representatives of practical materials. The apparent density is in the range 410 to 450 $kg.m^{-3}$ with an average value of 420 $kg.m^{-3}$. This range is due to the variation of intergranular porosity and is linked to the spraying method.

Several specimens are cut from the blocks. Three of them are tested, they are chosen to be representative of the material from their density (FIG 2). Their size is chosen to meet the requirement of the NORDTEST protocol detailed in the paragraph 3. Their thickness (8 cm) is chosen to be higher than the penetration depth during the test. For each specimen, the exposed surface area is 15×15 cm^2 thus, the total exposed surface area is higher than 300 cm^2.

FIG 2. Specimen of hemp concrete

2.2 Protocol and device

In order to characterize the ability of a material, or of a system made of several material layers, to moderate variations of ambient relative humidity, the NORDTEST project defines the practical moisture buffer value (Rode 2005) (Rode and al. 2007) (Peuhkuri and Rode 2005). This value relates the amount of moisture uptake (and release), per open surface area, under daily cyclic variation of relative humidity according to equation (1).

$$MBV = \frac{\Delta m}{A.\left(RH_{high} - RH_{low}\right)} \quad (1)$$

Where MBV Moisture Buffer Value [g/(m².%RH)]
Δm Moisture uptake / release during the period [g]
A open surface area [m²]
$RH_{high/low}$ high/low relative humidity level [%]

The protocol to measure the moisture buffer value requires that specimens are sealed on all but one or two surfaces. After stabilization at (23°C; 50% RH), they are exposed to daily cyclic variations: 8 hours at high relative humidity (75 %RH) followed by 16 hours at low relative humidity (33% RH). Specimens are weighed continuously or at least five times during the eight hours absorption period during the last three days. The test goes on until the change in mass Δm is the same between the last three cycles with less than 5 % of discrepancies (Rode and al. 2007).

In this study, the effect of temperature on moisture buffer value is investigated. The measurements are held at 23°C, 20°C, 17°C, 14°C and 11°C. The aim is to identify if there is an effect of temperature on moisture uptake and release.

The device used for MBV test consists in a climatic chamber Vötsch VC4060. The switch in the chamber relative humidity (75 %RH; 33%RH) is done manually. Temperature and relative humidity are measured with sensors Sensirion SHT75 with a time step of 5 minutes. The accuracy of SHT 75 sensor is ± 0.3 °C in temperature and ± 1.8 % in relative humidity. The specimens are weighed out of the climatic chamber five times during absorption period and two times during desorption one. The readability of the balance is 0.01 g.
Within the NORDTEST project, a round robin test was held, at 23°C, on eight different building materials and systems. This leaded to a classification of moisture buffer value (FIG 3).

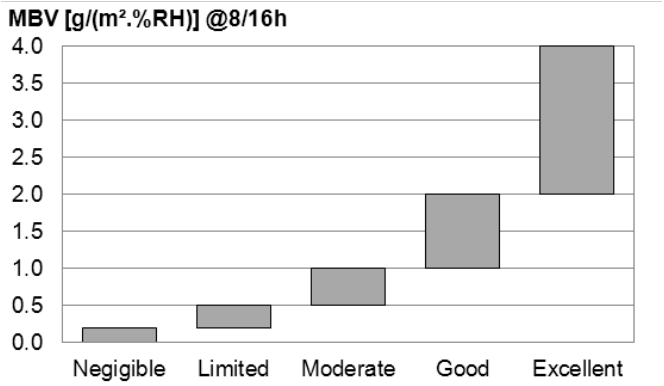

FIG 3. Classification of Moisture Buffer Values (Rode, 2005)

3. Results

3.1 Ambient temperature and relative humidity

Table 1 gives the average values of temperature and relative humidity for the five tests. Figure 5 shows the kinetic of ambient temperature and relative humidity during the test at 17°C.

Temperature and relative humidity are disturbed when the door of the climatic chamber is open to weigh specimens (peaks on the curves). The regulation of temperature is highly accurate as there is less than 0.1°C of discrepancy between the set value and the average value. During absorption, the relative humidity is slightly lower (resp. higher) than 75 % at 23°C and 20°C (resp. 17°C, 14°C, 11°C). During desorption, the relative humidity is slightly higher than 33%RH for the five tests. This leads to steps in relative humidity about 41.5 %RH for the tests performed at 17°, 14°C and 11°C and lower steps at 23° and 20 °C (resp. 33.0 and 30.7 %RH).

The step changes in relative humidity are achieved within 30 minutes from low to high RH and within one hour from high to low RH. This induces a nearly square wave of relative humidity. It was shown in (Roels and Janssen 2005) that the time need to achieve the step in relative humidity has a limited influence on the moisture buffer value (less than 5 %) even when it takes one hour and a half to achieve the required relative humidity.

TABLE 1. Ambient temperature and relative humidity for the five test

Temperature set (°C)	Average temperature (°C)	Average Relative Humidity Absorption (% RH)	Average Relative Humidity Desorption (% RH)
23	23.0	73.3	40.2
20	20.0	73.9	43.0
17	17.1	78.3	36.9
14	14.1	77.9	36.7
11	11.1	77.2	35.6

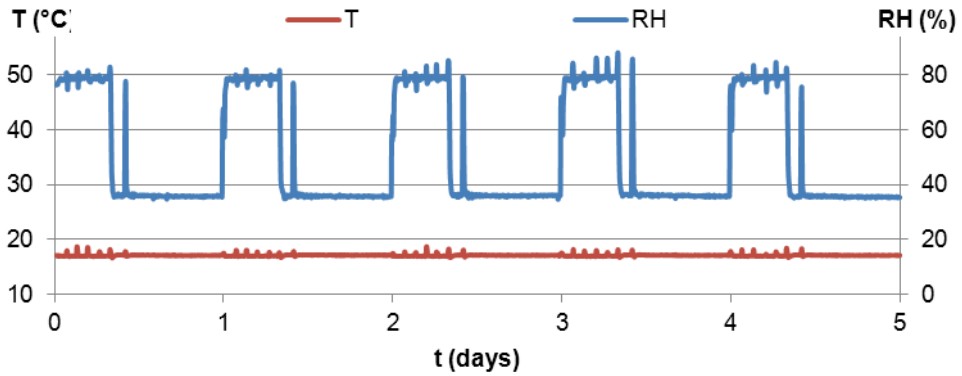

FIG 4. Ambient temperature and relative humidity during the test at 17°C.

3.2 Kinetics of mass

The measures performed on the three specimens of hemp concrete give similar results. Figure 5 gives the kinetic of mass of one specimen at 17°C, 14°C and 11°C. Previously to the test, specimens are stabilized at 50% and are then exposed to 75% RH. The decreasing tendency of the mass is due to the initial conditions that have been higher than the average of the steady state conditions. The cyclic amounts of moisture uptake and release are approaching each other, with less than 5 % within each cycle, from the third cycle. For similar steps in relative humidity, the moisture uptake and release is lower as the temperature decreases. This is due to the fact that the specific humidity of air (and thus its water vapour pressure) decreases with temperature for a given relative humidity (table 2).

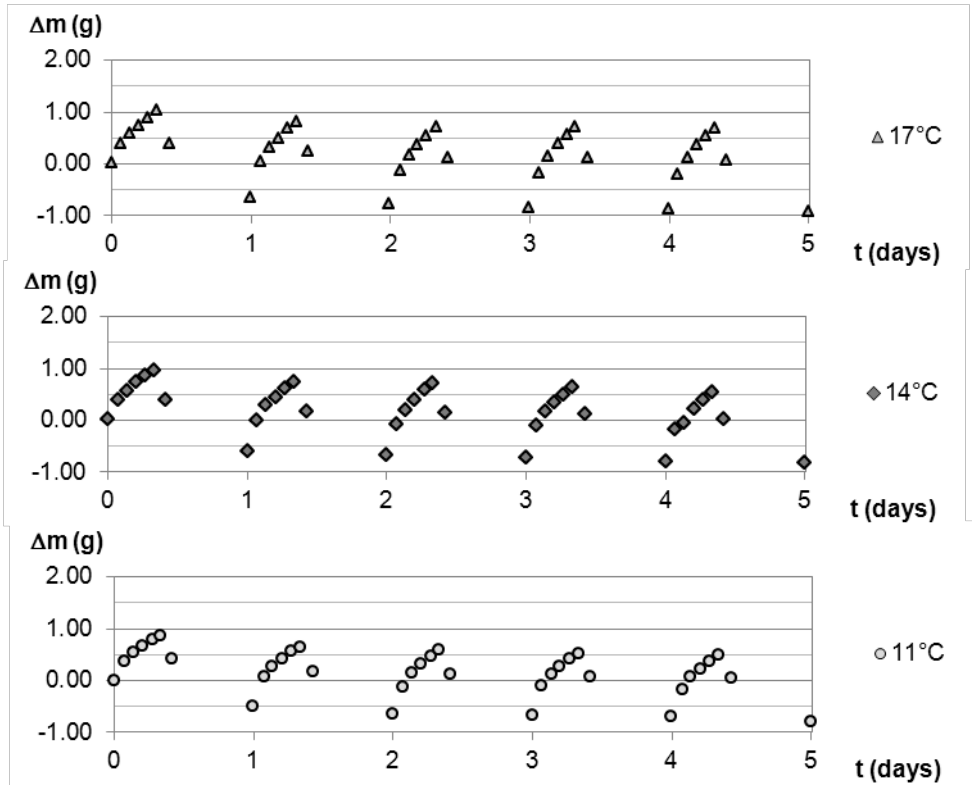

FIG 5. Kinetics of mass of one specimen at 17°C, 14°C and 11°C.

TABLE 2 Specific humidity of air ($g_{water\ vapour}/kg_{moist\ air}$) versus temperature and relative humidity

	23°C	20°C	17°C	14°C	11°C
33% RH	5.71	4.75	3.93	3.24	2.66
75% RH	13.03	10.83	8.96	7.39	6.06

3.3 Moisture Buffer Value

The results are similar for the three specimens of hemp concrete. Figure 6 gives the average MBV of the three specimens versus cycle. In link with the kinetic of mass, the values obtained for the first cycle are higher than the values of the following cycles; and the stabilisation is reached at the third cycle.

The average value of MBV, calculated from cycles 3 to 5 and from the three specimens, is plotted versus temperature on figure 7.

The MBV measured at 23°C classifies the hemp concrete as excellent hygric regulator, according to the NORDTEST classification (figure 3).

The MBV is highly impacted by the temperature as it decreases from 2.32 g/(m².%RH) at 23°C to 1.25 g/(m².%RH) at 11°C. The variation of MBV versus temperature is well fitted with an exponential curve given figure 7 (correlation coefficient >0.99). Like for the kinetic of mass, this variation is due to the fact that lower temperature induces lower vapour pressure. This variation may also be due to a thermo-dependant term in the hygric behaviour of hemp concrete. A study, taking into account the vapour pressure, could conclude on the thermo-dependency of hygric behaviour or not.

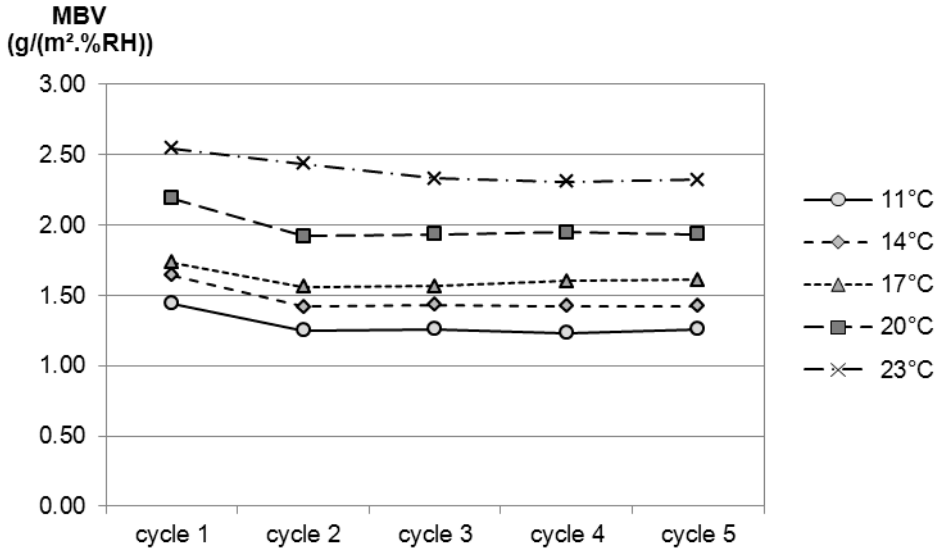

FIG 6. Variation of moisture buffer value versus cycle for the five investigated temperatures (average of the three specimens).

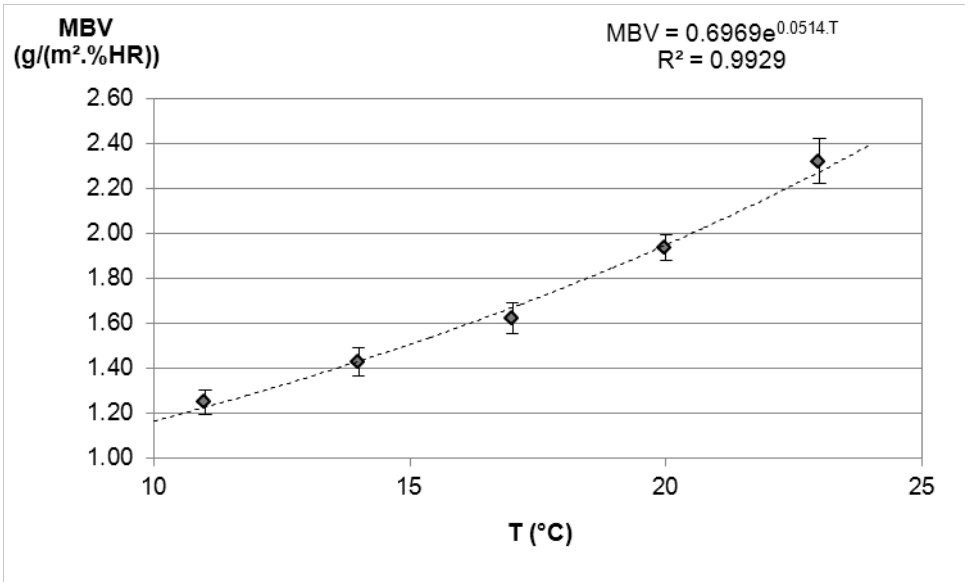

FIG 7. Variation of moisture buffer value versus temperature: experimental results (average value and standard deviation -three specimens / cycles 3 to 5) and fitting curve.

4. Conclusions

This study characterises the hygric behaviour of a bio-based building material under dynamic conditions. The investigations are performed at various temperatures. It is underlined that the temperature impacts the moisture uptake and release, and thus the moisture buffer value. The MBV increases with the temperature according an exponential law. This is due to the variation of vapour pressure with temperature, and may be to a thermo-dependant term in the hygric behaviour.

More, the results (kinetics of mass versus ambient conditions) can be used for benchmarking numerical moisture buffering models.

References

Amziane S. and Arnaud L. 2013. Bio-aggregate-based Building Materials, Applications to Hemp Concrete, ISTE Ltd and John Wiley & Sons, Inc.

Arnaud L. 2000. Mechanical and thermal properties of hemp mortars and wools: experimental and theoretical approaches, 3 Symp Int of bioresource hemp.

Boutin M.P., Flamin C., Quinton S., Gosse G. 2006. Paris, Ministère de l'agriculture et de la pêche, Lille I, Etude des caractéristiques environnementale du chanvre par l'analyse de son cycle de vie.

Collet F., Bart M., Serres L., Miriel J. 2008. Porous structure and water vapour sorption of hemp-based materials, Construction and Building Material 22,1271–1280.

Collet F., Pretot S.2012. Experimental investigation of moisture buffering capacity of sprayed hemp concrete., Construction and Building Materials, 36, pp 58-65.

Collet F., Chamoin J., Pretot S., Lanos C.2013. Comparison of the hygric behaviour of three hemp concretes, Energy and Buildings, 62, pp 294-303.

del Coz Díaz J.J., Álvarez Rabanal F.P., García Nieto P.J., Domínguez Hernández J., Rodríguez Soria B., Pérez-Bella J.M. 2013. Construction and Building Materials, 40, pp 543-555, Hygrothermal properties of lightweight concrete: Experiments and numerical fitting study.

Ip K, and Miller A. 2012, Resources,Conservation and recycling, 69, pp 1-9, Life cycle greenhouse gas emissions of hemp-lime wall constructions in the UK.

Jerman M., Keppert M., Vy´ borny´ J., Černy´ R. 2013. Construction and Building, 41, pp 352-359. Materials Hygric, thermal and durability properties of autoclaved aerated concrete.

Murphy F., Pavia S., Walker R. 2010. An assessment of the physical properties of lime-hemp concrete, Proc. of BRI/CRI. Ní Nualláin, Walsh, West, Cannon, Caprani, McCabe eds. Cork.

Peuhkuri R. and Rode C. 2005. Using dynamic moisture loading tests for the determination of moisture buffer value, Annex 41 Meeting, Montreal, 16-18 May.

Pretot S., Collet F., Glouannec P., Lang V. 2009. Variation des propriétés thermiques de bétons de chanvre en fonction de la formulation (in French), Congrès français de thermique-Efficacité énergétique, Vannes, Tome 2, pp 865-870, Editions Société Française de Thermique, ISBN: 2-905267-67-2

Pretot S., Collet F., Garnier C. 2013. Building and Environment, DOI information: 10.1016/j.buildenv.2013.11.010, Life Cycle Assessment of a hemp concrete wall : impact of thickness and coating .

Rode C., Moisture buffering of Building Materials.2005. Report BYG•DTU R-126, ISSN 1601 – 2917, ISBN 87-7877-195.

Rode C., Peuhkuri R., K. Hansen K., Time B., Svennberg K., Arfvidsson J., Ojanen T. 2007. Moisture buffer value of materials in buildings, Journal of ASTM international, vol. 4, issue 5.

Roels S., Janssen H. 2005. Is the moisture buffer value a reliable material property to characterize the hygric buffering capacities of building materials? Working paper A41-T2-B-05-7 for IEA Annex 41 project. Whole Building Heat. Air and Moisture Response, Trondheim.

Roels S, Talukdar P, James C, Simonson CJ. 2010. Reliability of material data measurements for hygroscopic buffering. Int J Heat Mass Trans ;53:5355–63.

Performance Results of a Prototype Ceiling Panel with Simultaneous Heat and Moisture Transfer

Melanie Fauchoux, Ph.D. [1]
Carey J Simonson, Professor, Ph.D., P.Eng. [1]
David Torvi, Professor, Ph.D., P.Eng. [1]

[1] University of Saskatchewan, Saskatoon, SK, Canada

KEYWORDS: *experimental testing, semi-permeable membrane, liquid desiccant, sensible effectiveness, latent effectiveness, heat flux, mass flux*

SUMMARY:
Maintaining adequate indoor air temperature and relative humidity (RH) is necessary to ensure good comfort for occupants, and maximize productivity. Radiant ceiling panels have been shown to provide good thermal comfort, while consuming less energy than typical all-air systems; however, they are unable to handle the latent load in a space. As such, a new ceiling panel has been designed which has the ability to transfer both heat and moisture, thus controlling the indoor temperature and relative humidity simultaneously. A prototype of this panel has been built and tested, to determine its performance under a variety of operating conditions. The results show that the sensible and latent effectivenesses and the total heat flux between the panel and the air are highest when operated under unstable air conditions, such as cooling and/or dehumidification. These values are lower for stable air conditions, such as heating and/or humidification. The total mass flux between the panel and the air is highest when the heat and moisture transfer are in the same direction, as the heat transfer enhances the moisture transfer. The mass flux is lowest when the heat and moisture transfer are in opposite directions, as the heat transfer diminishes the moisture transfer.

1. Introduction

The health and productivity of occupants in a building are linked to the indoor air quality and the conditions (temperature and RH) of the indoor air. The indoor temperature and RH must be kept within a certain range, in order to meet acceptable comfort standards (ASHRAE 2010). Conventional all-air systems supply air to a space at an appropriate temperature and RH in order to add/remove heat and moisture from the space. These systems however, typically consume large amounts of energy. An alternative method is to use radiant ceiling panels, which can control the indoor temperature of a space. Air is still supplied to the space to meet ventilation standards (ASHRAE 2013), but at much lower volumes than the all-air systems. Much research has been done on radiant ceiling panels, and the results show that they can provide good thermal comfort for occupants while consuming less energy than all-air systems (ASHRAE 2012, Vangtook and Chirarattananon 2006, Kim et al. 2005).

Although radiant ceiling panels are effective at maintaining the indoor temperature, they cannot remove the latent load from a space, as they are only capable of sensible heat transfer. This can result in unacceptable indoor relative humidity levels. High indoor relative humidity levels can cause occupants to feel uncomfortable (Toftum et al. 1998a,b, Fang et al. 1998), and can lead to mold growth, rot and deterioration of the building materials in a space (Chen et al. 2004, Moon and Yoon 2010). Low indoor relative humidity levels can lead to dry skin and eyes, and can cause irritation of the mucous membranes of the body, due to excess moisture transfer from the body (Wyon et al. 2006, Reinikainen et al. 1992).

This paper presents the results of research performed on a new type of ceiling panel, which has the ability to simultaneously transfer heat and moisture with the air in a space. The design of the new panel is similar to a radiant ceiling panel, with a few modifications to enable moisture transfer, in addition to heat transfer. As such, this panel has the ability to control both the indoor temperature and relative humidity of a space.

2. Prototype Heat and Moisture Transfer Panel

To test the concept of a ceiling panel that can simultaneously transfer heat and moisture with the air in a space, a prototype ceiling panel was built and tested in a small-scale facility (Fauchoux, 2012). Fig 1a shows a photograph of the prototype panel, which is built from an acrylic tray (22.8 cm x 22.8 cm x 2.5 cm). The surface of the panel is a semi-permeable membrane, which is permeable to water vapour, but impermeable to liquid water. This membrane allows for moisture to transfer between the panel and the air. A liquid desiccant solution is pumped through the panel, in cross-flow with the air flow, as indicated by the arrows in the photograph. The temperature of the solution is controlled, in order to heat or cool the air in the space as needed. With a liquid desiccant, the vapour pressure, or humidity ratio, at the surface of the panel can also be controlled, in order to humidify or dehumidify the space as needed. This prototype panel uses an aqueous lithium chloride solution, which has a surface relative humidity of 11% RH at saturation conditions (50% concentration at 20°C). By varying the concentration and temperature of the solution, the humidity ratio and temperature of the panel surface can be varied, to create different operating conditions.

The performance of the prototype panel is measured using a small wind tunnel facility, shown in Fig 1b, which provides hydrodynamically fully developed laminar airflow to the test section. The panel is placed in the top of the test section and air passes underneath at a low velocity (V = 0.005 m/s, Re = 65). The temperature and relative humidity of the air are measured at the air inlet and air outlet of the test section, as indicated in the photograph. The uncertainty in these measurements is ±0.3°C for the temperatures and ±1.0% RH for the relative humidities. The temperature and density of the solution are measured inside the panel. The temperature of the solution inside the panel does not vary during testing, so the panel is assumed to be at constant temperature and concentration. The uncertainty in these measurements are ±0.1°C for the temperature and ±11.7 kg/m^3 for the density. The density and temperature of the solution are used to calculate the equivalent surface relative humidity inside the panel, which has an uncertainty of ±0.5% RH.

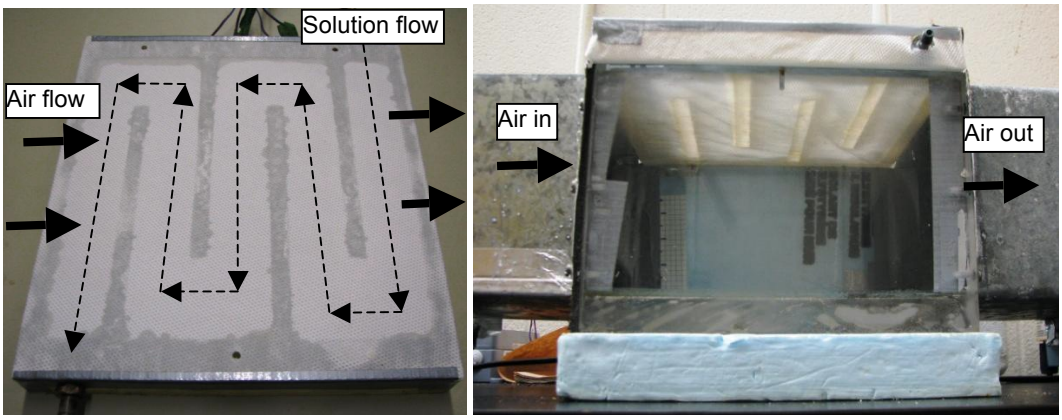

(a) *(b)*

FIG 1. Photographs of (a) the prototype panel and (b) the test section of the test facility.

3. Performance Parameters

The performance of a radiant ceiling panel is typically quantified by the total heat flux to/from the panel, either by convective transfer with the room air, or by radiative transfer with the other surfaces in the room. The magnitude of the heat flux is dependent on the temperatures of the panel, the air and the other surfaces in the space. The performance of the new heat and moisture transfer panel can also be quantified using the total heat flux, but also by the total mass flux between the panel and the air. The total mass flux is dependent on the humidity ratio difference between the panel and the air. The heat and moisture transfer panel can also be treated like a liquid-to-air energy exchanger. Energy exchangers are quantified by their sensible, latent and total effectivenesses. These performance parameters, which are defined in this section, will be used to evaluate the performance of the prototype heat and moisture transfer panel, under different operating conditions.

3.1 Total heat flux

The total heat flux between the panel and the air is defined by

$$q'' = U\Delta T_{lm} \tag{1}$$

Where U overall convection heat transfer coefficient (W/(m^2·K))
ΔT_{lm} log mean temperature difference between the airflow and the panel (°C)

The overall heat transfer coefficient is calculated from

$$U = \left[\frac{1}{h_{eff,air}} + \frac{\delta_{mem}}{k_{mem}} + \frac{1}{h_{sol}} \right]^{-1} \tag{2}$$

Where $h_{eff,air}$ effective heat transfer coefficient of the air (W/(m^2·K))
h_{sol} convection heat transfer coefficient of the solution (W/(m^2·K))
δ_{mem} thickness of the semi-permeable membrane, 2.2x10^{-4} m
k_{mem} thermal conductivity of the semi-permeable membrane, 0.334 W/(m·K)

The effective heat transfer coefficient of the air combines the radiation heat transfer coefficient and the convection heat transfer coefficient, as heat will be transferred through both of these modes. For typical radiant ceiling panels, the convection heat transfer coefficient makes up ~40% of the effective heat transfer coefficient. For the heat and moisture transfer panel, the value of the radiation heat transfer coefficient is approximately the same as it is for a radiant ceiling panel, but the convection heat transfer coefficient is smaller for the heat and moisture panel. The convection heat transfer coefficient makes up only ~20% of the effective heat transfer coefficient for the heat and moisture transfer panel. The convection coefficient is smaller for the heat and moisture panel prototype due to the low velocities of air used in the tests. The convection heat transfer coefficient of the solution is neglected, as the resistance to heat transfer inside the solution channel is very small compared to the air channel.

3.2 Total mass flux

The total mass flux between the panel and the air is defined by

$$\dot{m}'' = U_m \Delta W_{lm} \tag{3}$$

Where U_m overall convection mass transfer coefficient (kg_{air}/(m^2·s))
ΔW_{lm} log mean humidity ratio difference between the airflow and the panel (g_w/kg_{air})

The overall mass transfer coefficient is calculated from

$$U = \left[\frac{1}{h_{m,air}} + \frac{R_{mem}}{\rho_{air}} + \frac{1}{h_{m,sol}} \right]^{-1} \quad (4)$$

Where $h_{m,air}$ convection mass transfer coefficient of the air ($kg_{air}/(m^2 \cdot s)$)
$h_{m,sol}$ convection mass transfer coefficient of the solution ($kg_{air}/(m^2 \cdot s)$)
R_{mem} resistance to vapour diffusion of the semi-permeable membrane, 125 s/m
ρ_{air} density of air (kg_{air}/m^3)

As with the temperature, the different in the humidity ratio across the height of the solution channel is negligible, therefore the resistance to moisture transfer through the solution is negligible and the convection mass transfer coefficient of the solution can be neglected from equation (4).

3.3 Effectiveness

The effectiveness of an exchanger is defined as the ratio of the actual amount of transfer to the maximum potential transfer, and is calculated as

$$\varepsilon = \frac{X_{air,out} - X_{air,in}}{X_{sol} - X_{air,in}} \quad (5)$$

Where X temperature (°C) for sensible effectiveness, humidity ratio (g_w/kg_{air}) for latent effectiveness or enthalpy (kJ/kg) for total effectiveness

3.4 Dimensionless parameters

As heat and moisture are exchanged between the panel and the air, temperature and concentration gradients will form in the test section, which result in a density gradient between the air at the top of the test section and the air at the bottom of the test section. If the density of the air at the top of the test section is lower than the density of the bottom of the test section, the airflow remains stable and forced convection is dominant. If the density of the air at the top of the test section is higher than the density of the air at the bottom, the airflow will become unstable, and natural convection will become dominant in the test section. The Rayleigh number is used to determine when buoyancy forces are present in the duct (positive value) and when they are not (negative value). Also, the magnitude of the Rayleigh Number can be used to determine if the buoyancy forces are large enough that natural convection will dominate the flow.

3.4.1 Heat transfer Rayleigh number

The heat transfer Rayleigh number is used to determine when buoyancy forces are present in the test section, due to a temperature gradient and is calculated as

$$Ra_h = \frac{g\beta(T_{air} - T_{sol})L^3 Pr}{\upsilon_{air}^2} \quad (6)$$

Where g acceleration due to gravity, 9.81 m/s^2
β the volumetric thermal expansion coefficient (1/K)
T_{air} average temperature of the air (K)
T_{sol} temperature of the solution inside the panel (K)
L characteristic length (m)
ν kinematic viscosity of air (m^2/s)
Pr Prandtl number of air (-)

The heat transfer Rayleigh number will be positive when the panel is used for cooling and negative when used for heating. The opposite would be true if the panel was in the floor, instead of the ceiling.

3.4.2 Moisture transfer Rayleigh number

The moisture transfer Rayleigh number is used to determine when buoyancy forces are present in the test section, due to a concentration gradient and is calculated as

$$Ra_m = \frac{g\left(\frac{M_{air}}{M_w} - 1\right)\left(C_{air} - C_{sol}\right)L^3 Sc}{\upsilon_{air}^2} \quad (7)$$

Where M_{air} molecular weight of air (kg_{air}/mol)
M_w molecular weight of water vapour (kg_w/mol)
C_{air} average concentration (mass fraction) of water vapour in the air (kg_w/kg_{air})
C_{sol} concentration (mass fraction) of water vapour at the surface of the solution (kg_w/kg_{air})
Sc Schmidt number (-)

The moisture transfer Rayleigh number will be positive when the panel is used for dehumidification and negative when used for humidification.

3.4.3 Effective Rayleigh number

When both temperature and concentration gradients are present and both are positive, or both are negative, they will add together to create a larger positive, or negative, density gradient. If the two gradients are acting in opposite directions, the smaller gradient will be subtracted from the larger gradient, creating a smaller overall density gradient. The two Rayleigh numbers can be combined to form an effective Rayleigh number (Lin et al. 1992),

$$Ra^+ = Ra_h + Ra_m \quad (8)$$

4. Results

To determine the performance of the prototype heat and moisture transfer panel, the panel was tested under a large variety of operating conditions ($T_{air,in} \approx 24°C$, $RH_{air,in} \approx 3 – 87\%$ RH, $T_{sol} \approx 6$ - $35°C$, $RH_{sol} \approx 15$ - 61% RH). The results of six tests, which represent the different directions of heat and moisture transfer, will be presented here. Fig 2 presents the air inlet, air outlet and solution conditions, on psychrometric charts, for the six tests. These tests represent cases of: cooling and dehumidification; cooling and humidification; heating and dehumidification; heating and humidification; dehumidification only; and humidification only.

Each of the six tests presented create temperature and concentration gradients of different magnitudes and direction. The heat transfer, mass transfer and effective Rayleigh numbers are presented in Table 1 for the six tests. The information in this table illustrates how the temperature and concentration gradient can add together, or subtract from each other, depending on the magnitude and direction of each. For most cases, the concentration gradient is one order of magnitude smaller than the temperature gradient. However, in the last two cases, the temperature gradient was kept to a minimum to determine the performance of the panel when only moisture transfer is required in a space. For the dehumidification case, there is a small negative temperature gradient, while there is a slightly larger, positive concentration gradient. In this case, the concentration gradient was actually able to overcome the temperature gradient and reverse the direction of the overall density gradient. This was verified using flow visualization, where smoke was inserted upstream of the test section and the flow patterns through the test section were captured.

Table 1 also shows the sensible, latent and total effectivenesses of the prototype panel for each test. This information can also be inferred from Fig 2, by comparing the location of the air outlet to the air inlet and solution conditions for each test. The sensible and latent effectivenesses are highest when the panel is used for cooling and lower when the panel is used for heating. This corresponds to the

positive (unstable flow) or negative (stable flow) overall density gradients, represented by the effective Rayleigh number. The effectiveness is also higher in the case of dehumidification, compared to the case of humidification, due to the positive density gradient in the dehumidification case and the negative density gradient in the humidification case. In all cases, the latent effectiveness is higher than the sensible effectiveness. This is because the focus of this research is on achieving simultaneous heat and moisture transfer, and on maximizing the moisture transfer; the temperature gradients used in these tests were not very large, so the potential for heat transfer was much smaller than the potential for moisture transfer.

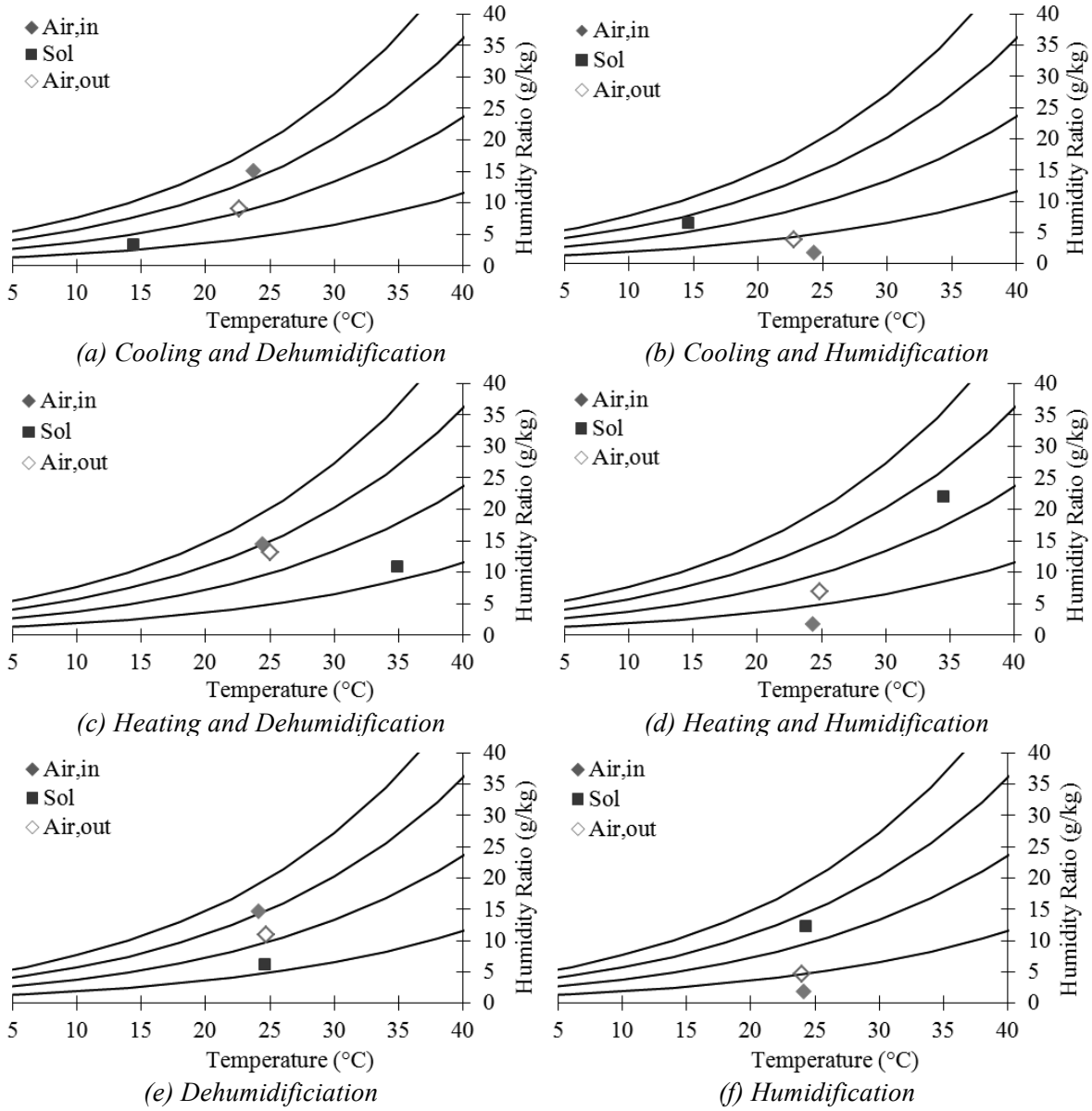

FIG 2. Psychrometric charts showing the inlet air, outlet air and solution conditions during six tests.

The total heat flux and total mass flux between the panel and the air are also presented in Table 1. The total heat and mass fluxes are calculated from equations (1) and (3) where U and U_m are calculated from the experimental results. These values are positive when the flux is from the air to the panel (cooling or dehumidification) and negative when the flux is from the panel to the air (heating or humidification). The total heat flux follows the same trend as the sensible effectiveness, where the values are highest for the unstable flow cases and lower for the stable flow cases. For the total mass

flux, the highest values occur when the heat and moisture transfer are in the same direction (cooling and dehumidification; heating and humidification) and the lowest values occur when the heat and moisture transfer are in the opposite direction (cooling and humidification; heating and dehumidification). Looking at the three humidification cases: the smallest mass flux occurs during the cooling case (positive temperature gradient, negative concentration gradient); the second highest mass flux occurs during the humidification only case (no temperature gradient); and the highest mass flux occurs during the heating case (negative temperature gradient, negative concentration gradient). This indicates that the total mass flux between the panel and the air is strongly dependent on the coupling between the heat and mass transfer.

Table 1. Dimensionless parameters and performance results of the prototype heat and moisture transfer panel, under different operating conditions.

	Ra_h	Ra_m	Ra^+	$\varepsilon_{sensible}$	ε_{latent}	ε_{total}	q''	$\dot{m}''$
	$[10^5]$	$[10^5]$	$[10^5]$	[%]	[%]	[%]	$[W/m^2]$	$[g_w/m^2 \cdot hr]$
Cooling, Dehumidification	32	5	37	11	51	41	5.4	104.4
Cooling, Humidification	32	-2	30	15	45	321	7.3	-36.0
Heating, Dehumidification	-32	1	-31	6	38	-200	-2.9	25.2
Heating, Humidification	-31	-9	-40	6	26	22	-2.9	-90.0
Dehumidification	-2	3	1	120	42	44	-0.5	61.2
Humidification	-	-5	-5	-50	28	30	-	-50.4

The total effectivenesses for the cases of cooling and humidification, and heating and dehumidification are outside the expected range of 0 - 100%. In these two cases, the enthalpies of the inlet air and the solution are approximately the same, resulting in very large total effectivenesses (> 100%). As well, the sensible effectivenesses for the dehumidification and humidification cases are outside of this range. In both of these cases, the solution temperature is slightly higher than the inlet air temperature. In the dehumidification test, the air leaves the test section at a higher temperature than the solution, resulting in a sensible effectiveness that is greater than 100%. In the humidification case, the outlet air temperature is actually lower than the inlet air temperature, resulting in a negative sensible effectiveness. This phenomenon is a result of the heat of phase change, which is added to the solution during dehumidification and removed from the solution during humidification (assuming that the phase change occurs on the solution side, as the membrane is impermeable to liquid water). The addition or removal of heat during phase change results in a slight change in the temperature of the solution between the inlet and the outlet. This effect is not noticed in most cases, as the temperature difference between the air inlet and the solution is large. However, in these two cases, the temperature difference is small and the effect of the heat of phase change is significant.

5. Conclusions

A prototype heat and moisture transfer panel has been constructed and tested under various operating conditions, to determine its performance. In terms of sensible and latent effectivenesses, the panel performs the best when operated under unstable conditions, such as cooling and/or dehumidification. The sensible and latent effectivenesses of the panel are lower when operated under stable airflow conditions, such as heating and/or humidification. The total heat flux from the panel also follows this trend, with higher results during cooling cases and lower results during heating cases. The mass flux however, follows a different trend. For the mass flux, the direction of the mass flux in relation to the direction of the heat flux is important. When the heat and mass fluxes are in the same direction, the mass transfer is enhanced and when the heat and mass fluxes are in opposite directions, the mass flux

is diminished, compared to the case with mass flux only. In addition, it was found that sensible effectiveness values can be negative or greater than 100% when the heat flux is small, due to the heat of phase change, which can add/remove heat from the solution, causing the outlet air temperature to be outside of the expected range.

6. Acknowledgements

The authors acknowledge financial support from the Natural Sciences and Engineering Research Council of Canada.

References

ASHRAE, 2012. HVAC Systems and Equipment Handbook, American Society of Heating, Refrigerating and Air-conditioning Engineers, Inc., Atlanta GA.

ASHRAE Standard 55 – 2010. Thermal environmental conditions for human occupancy, American Society of Heating, Refrigerating and Air-conditioning Engineers, Inc., Atlanta GA.

ASHRAE Standard 62.1 – 2013. Ventilation for acceptable indoor air quality, American Society of Heating, Refrigerating and Air-conditioning Engineers, Inc., Atlanta GA.

Chen, H., Deng, S., Bruner, H., and Garcia, J. 2004. Roots of mold problems and humidity control measures in institutional buildings with pre-existing mold condition, Proceedings of the 14th Symposium on Improving Building Systems in Hot and Humid Climates, Richardson, Texas.

Fang, L., Clausen, G., and Fanger, P.O. 1998. Impact of temperature and humidity on the perception of indoor air quality during immediate and longer whole-body exposures, Indoor Air, 8, 276-284.

Fauchoux, M. 2012. Design and performance testing of a novel ceiling panel for simultaneous heat and moisture transfer to moderate indoor temperature and relative humidity, Ph.D. Thesis, Mechanical Engineering, University of Saskatchewan, Saskatoon, SK.

Kim, T., Kato, S., Murakami, S., and Rho, J. 2005. Study on indoor thermal environment of office space controlled by cooling panel system using field measurement and the numerical simulation, Building and Environment, 40, 301-310.

Lin, J.N., Tzeng, P.Y., Chou, F.C. and Yan, W.M. 1992. Convective instability of heat and mass transfer for laminar forced convection in the thermal entrance region of horizontal rectangular channels, International Journal of Heat and Fluid Flow, 13(3), 250-258.

Moon, H.J., and Yoon, Y.R., 2010. Investigation of physical characteristics of houses and occupants' behavioural factors for mould infestation in residential buildings, Indoor and Built Env., 19, 57-64.

Reinikainen, L.M., Jaakkola, J.J.K. and Seppanen, O. 1992. The effect of air humidification on symptoms of perception of indoor air quality in office workers: a six-period cross-over trial, Archives of Environmental Health, 47, 8-15.

Toftum, J., Jorgensen, A.S. and Fanger, P.O. 1998a. Upper limits of air humidity for preventing warm respiratory discomfort, Energy and Buildings, 28, 15-23.

Toftum, J., Jorgensen, A.S. and Fanger, P.O. 1998b. Upper limits for indoor air humidity to avoid uncomfortably humid skin, Energy and Buildings, 28, 1-13.

Vangtook, P. and Chirarattananon, S. 2006. An experimental investigation of application of radiant cooling in hot humid climate, Energy and Buildings, 38, 273-285.

Wyon, D.P., Fang, L., Lagercrantz, L., and Fanger, P.O. 2006. Experimental determination of the limiting criteria for human exposure to low winter humidity indoors, HVAC&R Research, 12, 201-213.

Experimental analysis of the repeatability of vacuum saturation and capillary absorption tests

Chi Feng, Ph.D. candidate [1,2]
Hans Janssen, Associate Professor [2]
Ya Feng, Professorate Senior Engineer [3]
Qinglin Meng, Professor [1]

[1] Building Environment and Energy Laboratory (BEEL), State Key Laboratory of Subtropical Building Science, South China University of Technology, P.R. China
[2] Building Physics Section, Department of Civil Engineering, KU Leuven, Belgium
[3] China Southwest Architectural Design and Research Institute Corp. LTD, P.R. China

KEYWORDS: *repeatability, vacuum saturation, capillary absorption, porous building materials*

SUMMARY: *Vacuum saturation and capillary absorption tests provide information about bulk density, open porosity, vacuum moisture content, apparent matrix density, capillary absorption coefficient and capillary moisture content. These two tests are simple to perform but lack strict control, and the repeatability of them remains unknown. In this paper we perform vacuum saturation and capillary absorption tests on Chinese autoclaved aerated concrete, Belgian autoclaved aerated concrete, Belgian ceramic brick, and German calcium silicate at room temperature. To investigate the repeatability, both tests have been repeated three times on the same samples (five duplicates for each material). Results show that both vacuum saturation and capillary absorption tests have satisfactory repeatability, and the difference between replicate tests is negligible when compared with materials' heterogeneity. Moreover, the repeatability of vacuum saturation and capillary absorption tests is much better than their reproducibility in the EC HAMSTAD project, implying that there still are significant differences in the measurement and/or processing procedures in different labs.*

1. Introduction

Heat and mass transfer is important in soil science (Tuli, Hopmans et al. 2005), fire safety (Figueiredo and Costa 2004), environmental protection (Milt, Banús et al. 2010), energy engineering (LaManna and Kandlikar 2011), food processing (Yuan, Hanselmann et al. 2009), as well as in many other areas. In building physics, it is widely acknowledged that many crucial issues – energy efficiency, indoor air quality, service life… – are all closely related to heat and mass transfer processes (Abuku, Janssen et al. 2009; Geving and Holme 2010; Kwiatkowski, Woloszyn et al. 2011; Zhang, Yoshino et al. 2012).

To numerically assess heat and mass transfer processes in built constructions, many coupled heat, air and moisture transfer models (HAM models) are available. Although these models differ in many aspects, they all require an accurate input of material properties. Unfortunately, as is revealed by numerous tests, fairly large deviations exist in the determination of materials properties, especially for hygric properties (Galbraith 1993; Roels, Carmeliet et al. 2003; Time and Uvsløkk 2003; Rode, Peuhkuri et al. 2005; Roels 2008). It is hence crucial to examine the accuracy of these hygric material property tests and results. Furthermore, in most of the state-of-the-art HAM models, the influence of temperature on the hygrothermal properties is generally neglected. This is, however, without much theoretical or experimental support. In our current project we wish to analyze the influence of temperature on these material properties, whereto the accuracy of the tests becomes critical. If the temperature impact is smaller than or similar to the accuracy errors, then it is unlikely to be distinguished clearly. Also in this framework thus, it is of great significance to examine the accuracy of these hygric material property tests and results.

In general, the accuracy of experimental procedures and measurement outcomes can be described by trueness and precision (ISO 5725-1). Trueness refers to the closeness of agreement between the average result and the true or accepted reference value, while precision describes the closeness of agreement between multiple test results. Trueness and precision are often confused, and are therefore illustrated in FIG 1.

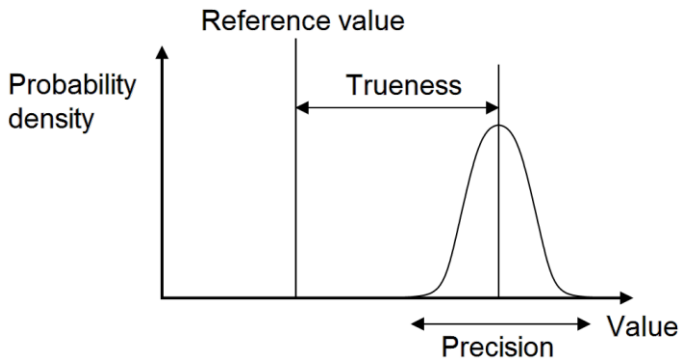

FIG 1. Illustration of trueness and precision

(Wikimedia: http://commons.wikimedia.org/wiki/File:Accuracy_(trueness_and_precision).svg)

Besides the extrinsic heterogeneity between the duplicate samples, precision is also affected by the intrinsic variations of the test itself, such as the operator, the equipment used, the calibration of the equipment, the environment, and the time elapsed between measurements. If all these factors are different in replicate tests, then the standard deviation of replicate test results is called reproducibility. If all these factors remain the same, then repeatability applies (ISO 5725-1). Obviously, reproducibility and repeatability are two extremes of precision.

Finally, we define variability as the standard deviation of different results from duplicate samples in the same test. Variability is not a well-defined concept in the standard, but it is still a kind of precision and facilitates our analysis a lot.

Within the field of hygric material properties, reproducibility has received most attention. As typical examples, we find the round-robin tests in the EC HAMSTAD project (Roels, Carmeliet et al. 2003) and in Subtask 2 of IEA Annex 41 (Roels 2008). In the former, 6 international labs determined various hygric properties of three different materials, each time on samples from the same batch of raw materials. In the latter, 14 international laboratories measured the water vapour transmission properties of (painted) gypsum board, again on samples from the same batch of raw materials. In both round-robin campaigns, the same test method was prescribed to all labs. Unfortunately, both campaigns demonstrated that the reproducibility of the basic hygric property tests is far below optimal. In order to shed some light on the observed deviations, this paper looks into the repeatability of these test methods, as these have received insufficient attention in the past.

The vacuum saturation and capillary sorption tests are very important, as they determine a lot of crucial material properties, such as bulk density, open porosity, vacuum moisture content, apparent matrix density, capillary absorption coefficient, and capillary moisture content. These two tests are simple but lack strict control, especially in the process of removing free water from the surfaces before weighing the samples. In this paper, we analyze the repeatability of vacuum saturation and capillary absorption tests experimentally.

2. Materials and methods

Two autoclaved aerated concretes (made in China and Belgium, from now on referred to as AAC-C and AAC-B respectively), a ceramic brick (made in Belgium, CB) and a calcium silicate insulation

(made in Germany, CS) are chosen as target materials. Both the vacuum saturation and capillary absorption tests have been repeated three times by the first author on the same 5 duplicate samples of each material going through the same procedure under the same condition with the same experimental setup (shown in FIG 2) at room temperature.

(a) (b)

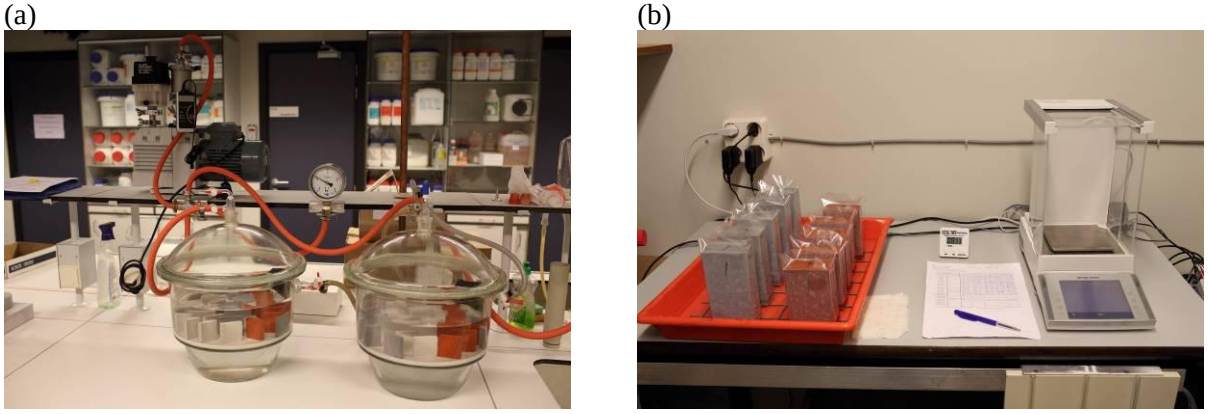

FIG 2. Experimental setup for: (a) Vacuum saturation tests (b) Capillary absorption tests

For the vacuum saturation tests, all samples have a size of 5cm×5cm×1cm. Oven dried samples are first put in empty desiccators connected to a vacuum pump and to a distilled water supply. The air in the desiccators is then pumped out gradually until the pressure inside is less than 20 mbar and the samples are kept under this condition for 4 hours. After that the water supply is turned on, and once the water rises to the bottom of samples, the water inflow rate is adjusted to keep the rise of water level in the desiccator at around 5 cm/h. When the water level is 5 cm above the top of samples, water supply and the vacuum pump are turned off. Samples are kept under water for 5 days, an interval longer than normal due to the arrangement of many other tests in the lab. Then samples are taken out of the desiccators for the underwater mass determination with a balance reading 0.001 g. Subsequently the water on the surfaces of the samples is removed with a moist cloth and the standard weighing is conducted with the same balance. The bulk density (ρ_{bulk}, kg/m^3), open porosity (Φ, %), apparent matrix density (ρ_{matrix}, kg/m^3) and vacuum moisture content (w_{vacuum}, kg/m^3) can be calculated with following equations:

$$\rho_{bulk}=(m_{dry}\cdot\rho_{water})/(m_{wet}-m_{under}) \quad (1)$$

$$\Phi=100\times(m_{wet}-m_{dry})/(m_{wet}-m_{under}) \quad (2)$$

$$\rho_{matrix}=100\times\rho_{bulk}/(100-\Phi) \quad (3)$$

$$w_{vacuum}=\Phi\cdot\rho_{water}/100 \quad (4)$$

Where
m_{dry} dry mass from the oven dried state (70 ℃), kg
m_{wet} wet mass weighed in the air, kg
m_{under} underwater mass, kg
ρ_{water} water density, 1000 kg/m^3

The apparent matrix density is rarely used in building physics. Moreover, the vacuum moisture content has the same repeatability as the open porosity. Consequently we only look into bulk density and open porosity in this analysis.

For the capillary absorption tests, all samples have a bottom surface size of 8cm×4cm. The heights for AAC-C, AAC-B, CB and CS samples are 6 cm, 6 cm, 12 cm and 15 cm, respectively. To minimize evaporation, samples are wrapped with plastic cling film on all surfaces except for the bottom. On the bottom 1 cm of the lateral sides, no film is present to avoid capillary uptake between the sample and the wrap. Two small holes are left at the top for air evacuation. Oven dried samples are place into a

water basin for the one-dimensional water absorption after cooling down in dry air. From time to time samples are taken out of water. The mass is determined to 0.001 g after removing the free water on the bottom with a moist cloth.

Ideally, the process for one-dimensional capillary absorption should be like FIG 3. In the first stage the sample is absorbing water quickly from the bottom. Capillary and viscous forces play dominant roles here. The capillary absorption coefficient (A_{cap}, kg/m^{2}s$^{0.5}$) is then defined as the slope of this stage. In the second stage, the waterfront has reached the top of the sample, and all entrapped air is now slowly diffusing out from the pores. The capillary moisture content (w_{cap}, kg/m^3) is determined from the intersection of the linear fits to the first and second stages.

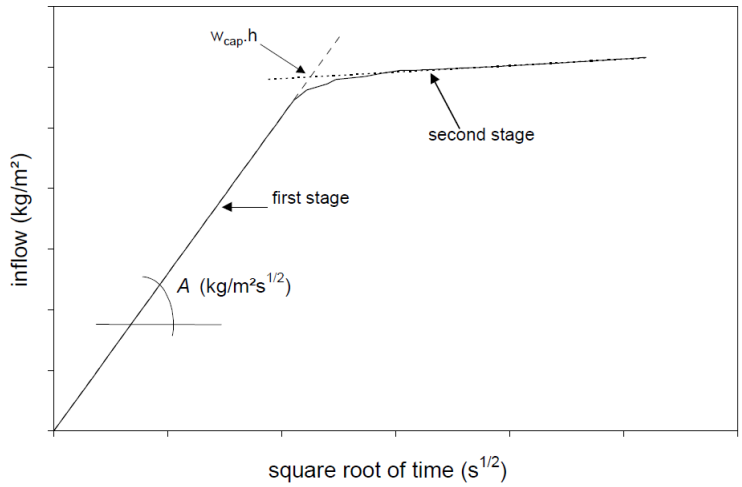

FIG 3. Ideal capillary absorption process (Roels, Carmeliet et al. 2003)

3. Results

The experimental results of vacuum saturation and capillary absorption tests are illustrated in FIG 4 and FIG 5 respectively. Five vertical bars represent five duplicate samples for each material, while error bars represent the standard deviations from three replicate measurements. Water temperature for three replicate vacuum saturation tests is 24.4 ℃, 24.3 ℃ and 24.4 ℃, which can be considered as the same. Due to evaporation the water temperature in the basin for capillary absorption tests is lower than ambient air temperature (25 ℃) and fluctuates. During our three replicate capillary absorption tests, the water temperature remains 22±1 ℃, which can be considered as sufficiently stable.

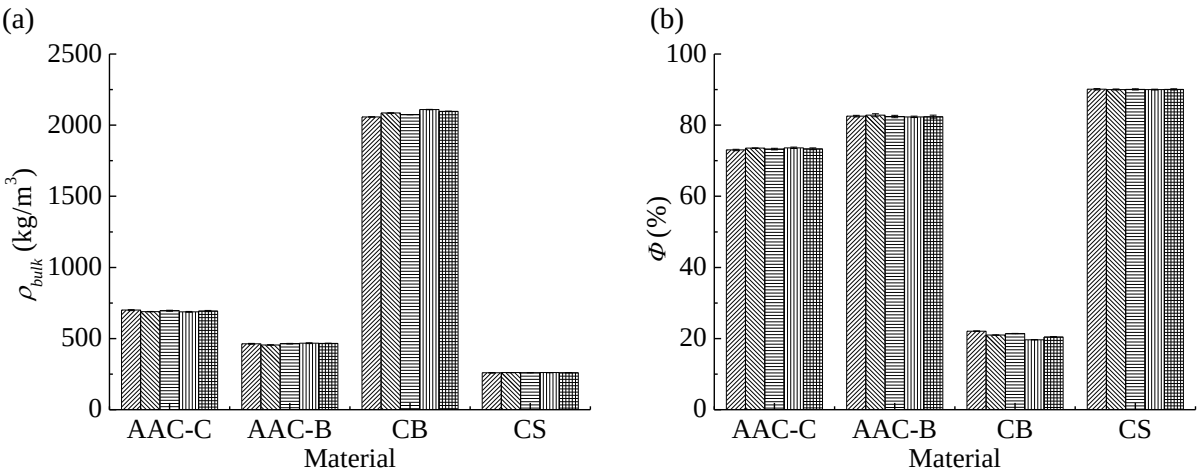

FIG 4. Repeatability of vacuum saturation tests: (a) bulk density (b) open porosity

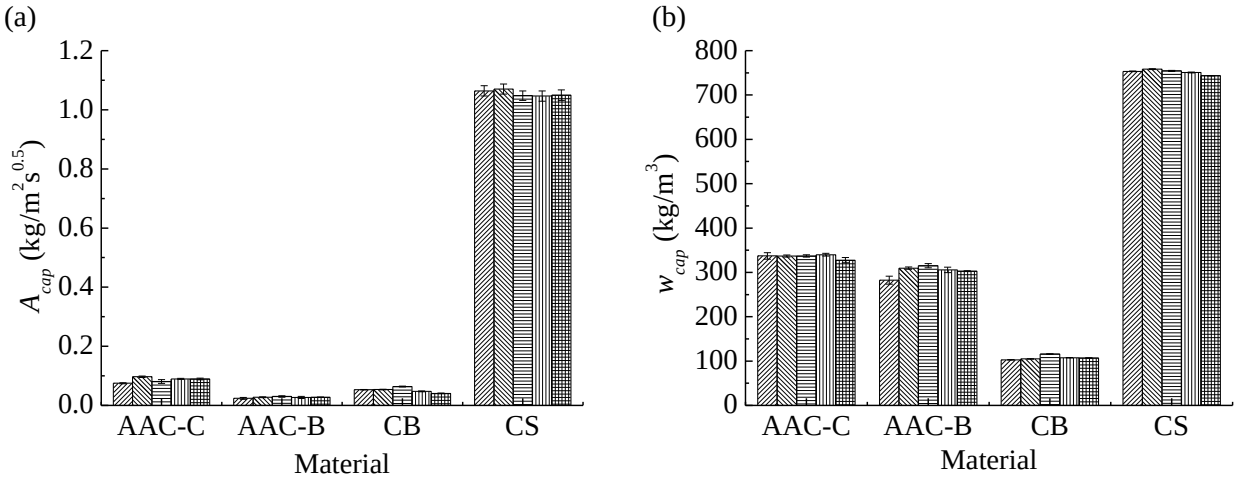

FIG 5. Repeatability of capillary absorption tests: (a) capillary absorption coefficient (b) capillary moisture content

As is clearly shown in FIG 4 and FIG 5, for both vacuum saturation and capillary absorption tests, the standard deviations of the results from three replicate measurements are extremely limited, indicating that the repeatability is quite satisfactory. Specifically, the relative standard deviations of bulk density and open porosity from three replicate measurements are within 0.44% and 0.38%, respectively. For most scientific research and engineering practice, this magnitude of deviation is negligible.

In addition, the relative standard deviations of capillary absorption coefficient and capillary moisture content from three replicate measurements are within 8.24% and 1.58%, respectively. These larger values show that the repeatability of capillary absorption tests is not as good as that of vacuum saturation tests. This can be partly attributed to the fact that more experimental procedures and more complicated data processing are involved in capillary absorption tests. However, the repeatability of capillary saturation tests is still satisfactory for most purposes.

To sum up, although the repeatability of capillary absorption tests is not as good as that of vacuum saturation tests, both tests have satisfactory repeatability.

4. Discussion

For a more in-depth understanding of the magnitude of repeatability, we compare the repeatability with the variability obtained in our tests, and with the variability and reproducibility from the reported results in the EC HAMSTAD project (Roels, Carmeliet et al. 2003) on similar materials (the same type but not exactly the same product). From our tests, with 5 duplicate samples in one test, we can obtain the relative standard deviation for variability by dividing the absolute standard deviation by the average value. Then the average results from three replicate tests can be calculated. Similarly, the average relative repeatability from duplicate samples can be obtained. From the EC HAMSTAD report, the minimum (from a single lab) and average relative standard deviation (from five labs involved) for variability can be obtained. The relative reproducibility can also be calculated by dividing the standard deviations among the results from different labs by the average values. All the results are summarized in TABLE 1 for comparison (in EC HAMSTAD only one kind of AAC was used). It should be note that the results from a specific lab in the EC HAMSTAD deviate from other labs' results extraordinarily in almost all the cases, and thus we exclude the results from that lab. Consequently, the reproducibility errors in TABLE 1 are conservative.

The results in TABLE 1 are quite informative. As a first step, we compare the variability from our tests and the reported results from the EC HAMSTAD project. As a kind of precision, variability is

determined by both the experimental method itself (we hereby define method precision errors) and the heterogeneity of materials (material heterogeneity errors). For all properties in TABLE 1, the variability errors for CS are the lowest among all materials. This is because CS is well known for its superb homogeneity. Moreover, the variability errors for CS in our tests are quite close to the minimum from the EC HAMSTAD project. This may be the best variability that we can achieve with current test method and experimental set-up. Now we assume that:

A. The (minimum) variability errors for CS are completely from the experimental method itself and have nothing to do with the material's heterogeneity. This means that no material heterogeneity error is assumed to exist for CS;
B. The method errors of a given test method for one property are the same for all materials (equal to that for CS). Thus the enlarged variability values for AAC and CB can thus be attributed to these materials' heterogeneity.

These two assumptions are, of course, ideal cases. But they should be reasonably close to the truth and facilitate our following analysis a lot. More importantly, it should be pointed out that it is meaningless to compare the homogeneity of different materials from their material heterogeneity errors. This is because all errors in TABLE 1 are relative (absolute standard deviations divided by the average value), and different bases give different percentages. As an example, for CB the material heterogeneity error of Φ is much larger than other materials. However, this is not because that CB is extremely heterogeneous, but results from the very small absolute Φ values. The same applies to the repeatability and reproducibility errors. Thus it is only reasonable to compare the variability, repeatability and reproducibility for the same material.

Based on the assumptions mentioned above, we can now start comparing variability, repeatability and reproducibility. Repeatability comes from replicate tests on the same samples. Consequently it should not be influenced by materials' heterogeneity. In our tests, the repeatability errors are either in the same order or much smaller than material heterogeneity errors, indicating that errors from replicate measurements are negligible when compared with materials' heterogeneity. This supports our previous conclusion that both vacuum saturation and capillary absorption tests have satisfactory repeatability.

TABLE 1 Comparison of variability, repeatability and reproducibility errors (%)

Test	Property	Material	Our tests		EC HAMSTAD (Roels, Carmeliet et al. 2003)		
			Variability	Repeatability	Variability (min)	Variability (aver)	Reproducibility
Vacuum saturation	ρ_{bulk}	AAC-C	0.74	0.44	1.59	2.31	2.53
		AAC-B	1.08	0.44			
		CB	0.98	0.06	0.34	0.58	0.80
		CS	0.30	0.26	0.29	0.50	0.98
	Φ	AAC-C	0.33	0.25	0.40	0.60	1.10
		AAC-B	0.24	0.38			
		CB	4.39	0.19	1.26	2.26	2.12
		CS	0.07	0.17	0.07	0.20	0.84
Capillary absorption	A_{cap}	AAC-C	10.16	3.74	7.80	10.51	19.95
		AAC-B	10.28	8.24			
		CB	16.51	2.13	5.38	8.78	14.51
		CS	1.02	1.61	2.05	3.59	5.22
	w_{cap}	AAC-C	1.65	1.27	5.04	8.48	13.40
		AAC-B	4.16	1.58			
		CB	4.61	0.32	2.06	4.11	7.20
		CS	0.73	0.11	0.25	0.67	2.60

Moreover, the errors in TABLE 1 for reproducibility include variability errors (both method precision errors and material heterogeneity errors), repeatability errors and the real errors caused by performing the same test in different labs (reproducibility errors). By excluding variability errors and repeatability errors, we still have very large reproducibility errors – which are often 1-2 orders greater than variability errors and repeatability errors. This implies that there must be significant differences in the experimental procedure or data processing in different labs. As a result, more specifics should still be defined to fully develop the potential of reaching converged results from different labs.

5. Conclusions

In this paper the repeatability of vacuum saturation and capillary absorption tests are analyzed experimentally. Three common porous building materials – namely autoclaved aerated concrete (made in China and Belgium), ceramic brick (made in Belgium), as well as calcium silicate (made in Germany) – are used as target materials. Experimental results reveal that:

A. Both vacuum saturation and capillary absorption tests have satisfactory repeatability. Vacuum saturation tests are better in terms of repeatability;

B. Errors from replicate measurements are negligible when compared with materials' heterogeneity;

C. The repeatability of vacuum saturation and capillary absorption tests is much better than their reproducibility in the EC HAMSTAD project, implying that there are significant differences in the experimental procedure or data processing in different labs. In order to come to a reliable material characterization, far more strict procedures for experimental actions and data processing are evidently required.

As a next step, we will study the repeatability of static gravimetric tests, cup tests and pressure plate tests – which determine sorption isotherms, vapor permeability and moisture retention curves – to complete our repeatability database. These results shall form an indispensable basis for our ongoing campaign to study the influence of temperature on the hygrothermal properties of porous building materials.

6. Acknowledgements

This project is supported by National Natural Science Foundation of China (No. 51278478). The first author (Chi Feng) is also financially supported by China Scholarship Council for his study at K.U. Leuven. The authors express sincere thanks to Patricia Elsen, Willem Bertels, Filip Vandenberghe and Paul Verbeek at Department of Civil Engineering, K.U. Leuven for their help in carrying out the experiments.

References

Abuku M., Janssen H., et al. 2009. Impact of wind-driven rain on historic brick wall buildings in a moderately cold and humid climate: Numerical analyses of mould growth risk, indoor climate and energy consumption. Energy and Buildings 41(1): 101-110.

Figueiredo A.R. & Costa J.J. 2004. Experimental analysis of the use of wet porous media for thermal protection against high intensity heat fluxes. International Journal of Heat and Mass Transfer 47(1): 11-19.

Galbraith G.H. 1993. Intercomparison on measurement of water vapour permeance, CEC BCR Report EUR 14394 EN.

Geving S. & Holme J. 2010. The Drying Potential and Risk for Mold Growth in Compact Wood Frame Roofs with Built-in Moisture. Journal of Building Physics 33(3): 249-269.

ISO 5725-1: 1994(E) Accuracy (trueness and precision) of measurement methods and results – Part 1:

General principles and definitions.

Kwiatkowski J., Woloszyn M., et al. 2011. Influence of sorption isotherm hysteresis effect on indoor climate and energy demand for heating. Applied Thermal Engineering 31(6-7): 1050-1057.

LaManna J.M. & Kandlikar S.G. 2011. Determination of effective water vapor diffusion coefficient in pemfc gas diffusion layers. International Journal of Hydrogen Energy 36(8): 5021-5029.

Milt V.G., Banús E.D., et al. 2010. Structured catalysts containing Co, Ba and K supported on modified natural sepiolite for the abatement of diesel exhaust pollutants. Chemical Engineering Journal 157(2-3): 530-538.

Rode C., Peuhkuri R.H., et al. 2005. Moisture buffering of building materials. Report BYG-DTU R-126.

Roels S. 2008. IEA Annex 41. Whole Building Heat, Air, Moisture Response. Subtask 2: Experimental Analysis of Moisture Buffering.

Roels S., Carmeliet J., et al. 2003. HAMSTAD Work Package 1: Final Report - Moisture Transfer Properties and Materials Characterisation, EU Contract GRD1-1999-20007.

Time B. and Uvsløkk S. 2003. Intercomparison on measurement of water vapour permeance. Nordtest – project agreement 1529-01.

Tuli A., Hopmans J.W., et al. 2005. Comparison of air and water permeability between disturbed and undisturbed soils. Soil Science Society of America Journal 69(5): 1361-1371.

Wikimedia: http://commons.wikimedia.org/wiki/File:Accuracy_(trueness_and_precision).svg

Yuan Q., Hanselmann W., et al. 2009. Characterization of vapor-induced and liquid-induced moisture migration through fractionated palm kernel (PKO) based multiphase systems. Journal of Food Engineering 95(3): 460-470.

Zhang H., Yoshino H., et al. 2012. Assessing the moisture buffering performance of hygroscopic material by using experimental method. Building and Environment 48(0): 27-34.

Moisture deformation of calcium silicate boards

Peter Matiasovsky, Dr.Ing.[1]
Peter Mihalka, Dr.Ing.[1]

[1] Institute of Construction and Architecture, Slovak Academy of Sciences, Slovakia

KEYWORDS: *Moisture induced deformation, poromechanical coupling, lightweight calcium silicate, elasticity modulus, damage*

SUMMARY:
Moisture induced deformations and elasticity moduli of calcium silicate boards were determined for the moisture contents within a whole water saturation interval. On the basis of micro-macro relations of poroelasticity the coefficients of coupling between moisture content and moisture deformation were identified. The moisture induced deformation of calcium silicates has a hysteretic character and it is given by different capillary pressures during the materials wetting and drying. With increase of capillary pressure the moisture induced strain is influenced by two opposing tendencies. For water saturation lower than critical moisture content the materials shrink due to water film thickness decrease. For the water saturation higher than critical moisture content the materials swell due to capillary menisci radius decrease. The elasticity moduli of the analysed materials are a function of capillary pressure. Their values are related with material damage parameter and they are proportional inversely to shrinkage.

1. Introduction

The calcium silicate is a porous material, originally manufactured as the refractory material, however owing to its high capillarity in the last decade it is applied also as thermal insulation at internal side of walls in construction industry.The calcium silicates deformation process due to changing moisture content is composed of two basic mechanisms and swelling is smaller than shrinkage: In the hygroscopic region the shrinkage is caused by the disjoining pressure or surface water film decrease (Maruyama 2010). In the over-hygroscopic region the disjoining pressure is accompanied with the contra-active capillary pressure (Gottfredsen et al 1997). The moisture content, at which the disjoining pressure without opposing influence of capillary pressure is maximal, corresponds to the critical moisture content (Kumaran 1996).

The fluid-skeleton interactions in nonsaturated porous materials can be expressed by constitutive equations of linear poroelasticity (Coussy 1995). The isotropic linear poroelastic behaviour is characterised by four independent poroelastic coefficients, which can be chosen in the following way: two undrained or drained coefficients from among the Lamé coefficients, the Young modulus, the Poisson ratio, the bulk modulus, altogether with the Biot coefficient and Biot modulus (Coussy 1995).

Carmeliet (2000) presented the approach enabling to determine the coefficients of coupling between moisture content and moisture induced strain in porous materials. For determination of the coupling coefficients of the porous material, the experimental procedure based on measurement of moisture deformations under isothermal sorption, and simultaneously on the measurement of the water sorption isotherms is necessary.

The equipment for measurements of moisture expansion, together with determination water sorption enabled the application of the complex methodology of poromechanical properties determination for capillary porous materials. In this paper an application of this approach was used to analyse the mechanism of calcium silicate moisture induced deformations.

2. Measurements of moisture induced strain and elasticity modulus

The analysis of poromechanical coupling issued from the measurements of moisture expansion and elasticity modulus of calcium silicate board, within the 0 – 90 % water saturation interval. The experiments consisted of the monitoring two subsequent processes: wetting and drying guided by changing the gravimetrically controlled moisture content. The length changes of the specimen with the dimensions of 0.04 x 0.04 x 0.5 m were measured by dilatometer in a climatic chamber at varied water saturation degrees.

TABLE 1. Basic parameters of calcium silicate

Parameter	Value
Bulk density	240 kg/m^3
Total porosity	0.91
Critical moisture content	0.24 m^3/m^3
Elasticity modulus under laboratory conditions	250 MPa
Poisson ratio	0.2

Simultaneously the measurements of elasticity modulus were carried out on the same specimen, supported as simply beam under a uniform load given by its own mass. At given moisture contents the change of top fibre length Δl of the beam was measured. The length change can be calculated by relationship:

$$\Delta l = \int_0^l -\frac{My}{EI}\,dx \tag{1}$$

The span of l is 0.45 m, E is the elasticity modulus, M is the bending moment as a function of the distance x from either support, I is the moment of inertia about the neutral axis, y is the perpendicular distance of the top fibre from the neutral axis to the cross section. Then the elasticity modulus could be calculated from the measured data on change of the top fibre length Δl and the mass of the beam m in the interval 0.186 – 0.921 kg.

Besides the moisture expansion and elasticity modulus measurements, the water vapour sorption isotherms in a climatic chamber and the pore size distribution by mercury intrusion porosimetry method were determined for the given material. The elasticity modulus of a dry material was also determined by a standard mechanical three point bending test under laboratory conditions. The basic material parameters of the analysed material are presented in Table 1. The results of the moisture expansion measurements for the analysed material are in Figure 1.

3. Analysis

The fluid-skeleton interactions in nonsaturated porous materials can be expressed by constitutive equations of linear poroelasticity in the form (Coussy 1995):

$$d\sigma = K \cdot d\varepsilon + b \cdot dp_c \tag{2}$$

$$\frac{dm_l}{\rho_l} = \frac{dp_c}{M} + b \cdot d\varepsilon \tag{3}$$

Where σ, ε respectively the stress and strain
p_c the capillary pressure
m_l, ρ_l respectively the fluid mass content and fluid density
K bulk modulus
b Biot coefficient.

In Figure 1 it can be seen that the zero deformation of the calcium silicate was at ca 0.24 m^3/m^3 moisture content and that all moisture induced deformations in the hygroscopic region are caused by the material shrinkage. The presented deformations course shows a significant hysteresis. The upper - wetting and lower - drying lines are significantly different. From the figure it is evident that for the calcium silicate two shrinkage minima are typical. Besides the first minimum, close to the critical moisture content, the second minimum occurs, close to the absolute water saturation state. During the moisture induced deformations courses two specific phases can be distinguished. The first phase is represented by the steep, almost linear change in the hygroscopic region corresponding to the moisture content interval 0 – 0.24. The second phase is characterised by weaker moisture induced strain changes in the over hygroscopic region.

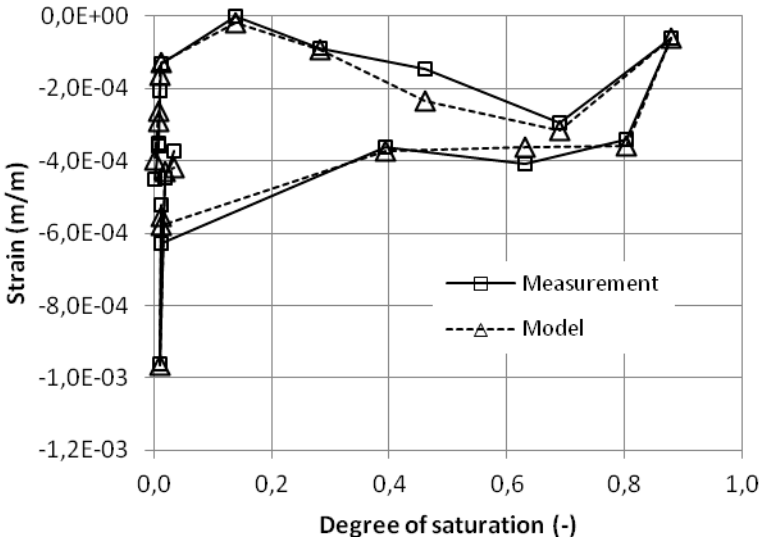

FIG 1. Moisture induced deformation of calcium silicate

Carmeliet (2000) expressed the free drying shrinkage from Equation (2), introducing $d\sigma = 0$ and the bulk modulus degradation factor (*1 - D*), in the form:

$$d\varepsilon = -\frac{b}{K(1-D)} dp_c \tag{4}$$

Where D damage variable.

The Biot coefficient which has in a case of the fibre reinforced material the form:

$$b = \left(1 - \frac{K}{K_m} - \frac{K}{K_f}\right) \cdot S \tag{5}$$

Where S degree of saturation
K_m bulk modulus of material solid matrix,
K_f bulk modulus of fibres.

In Equation (5) the parts K/K_m and K/K_f represent the solid matrix and fibres shrinkage restraint terms respectively. Using the parameter:

$$\kappa = 1 - \frac{K}{K_m} - \frac{K}{K_f} \tag{6}$$

the moisture induced linear strain of the calcium silicate can be expressed by the following relation (Coussy et al. 1999):

$$\varepsilon = -\frac{\kappa}{K(1-D)} \int_{p_{c\,\min}}^{p_{\max}} S(p_c)\, dp_c \tag{7}$$

The maximum elasticity modulus of the analysed cellulose fibre reinforced composite determined according to Equation (1) is equal to 600 MPa and the κ parameter is equal to 0.39 (Matiasovsky and Mihalka 2011).

The Equation (8) was applied at the analysis of the carried out moisture induced strain measurements described in Figure 1. The capillary pressures p_c, were determined from the retention curve (Fig. 2) using Equation (3), with neglected second term. The Biot modulus M is identified as an inverse value of the first derivation of the retention curve. The retention curve was determined from adsorption

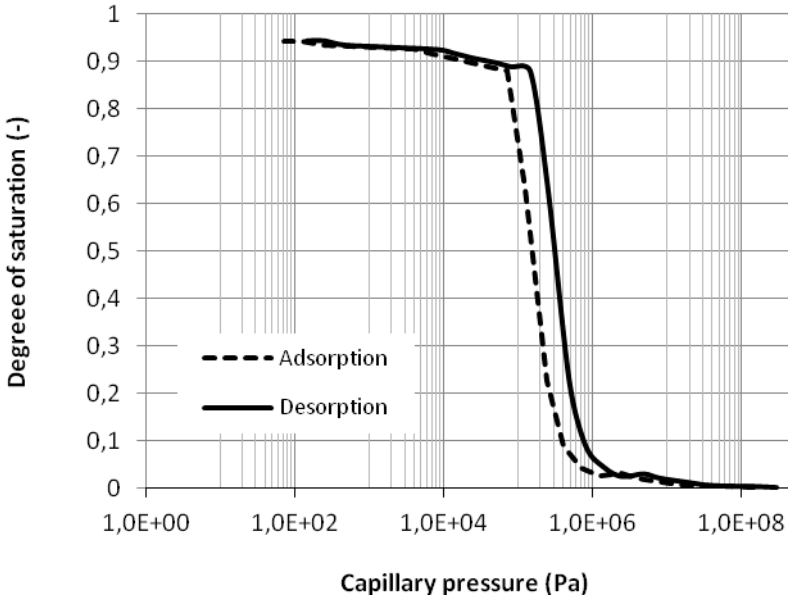

Figure 2. Retention curve of calcium silicate

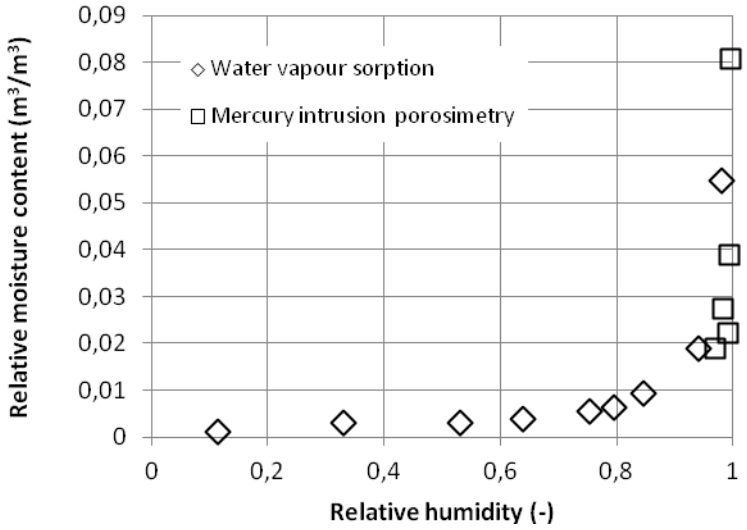

Figure 3. Water adsorption curve of calcium silicate

curve by transformation of the relative humidities to the capillary pressures, supposing the validity of capillary condensation sorption model (Gregg and Sing 1982), using Kelvin equation in the form:

$$p_c = -\ln\varphi \cdot k \cdot 135 \cdot 10^{\cdot 6} \tag{8}$$

Where $k = 1$ at adsorption and 2 at desorption.

The water vapour adsorption curve (Fig. 3) was constructed by joining the measured water vapour adsorption and pore size distribution curves (Hua et al. 1995), where the pore radius r (nm) was transformed into relative humidity φ for $k = 1$ by Kelvin equation in the form:

$$\ln(\varphi) = -\frac{k \cdot 0.535}{r} \tag{9}$$

As the moisture induced deformation of calcium silicate has a hysteretic character the calculation of water saturation integral in Equation (7) distinguishes a difference between the wetting and drying processes (Eq. 8). The strain evolution of the analysed material presented as the model solution in Figure 1 was calculated with the following considerations: The first water saturation phase represents the adsorption in hygroscopic region, guided by capillary pressure corresponding to cylindrical menisci of surface water film (k = 1). The second water saturation phase is the adsorption with capillary condensation and the macroscopic capillary pressure is guided by the mixed effect of cylindrical menisci proportional to the non saturated pore volume (with the capillary pressures p_{cads}) and spherical menisci (with the capillary pressures p_{cdes}) proportional to the saturated pore volume:

$$\int_{p_{c\,\min}}^{p_{\max}} S(p_c)\,dp_c = (1 - S(p_{cads}))\cdot \int_{p_{c\,\min}}^{p_{\max}} S(p_{cads})\,dp_{cads} + S(p_{cdes})\cdot \int_{p_{c\,\min}}^{p_{\max}} S(p_{cdes})\,dp_{cdes} \tag{10}$$

The drying is a desorption process guided by the capillary pressure corresponding to spherical menisci (k = 2).

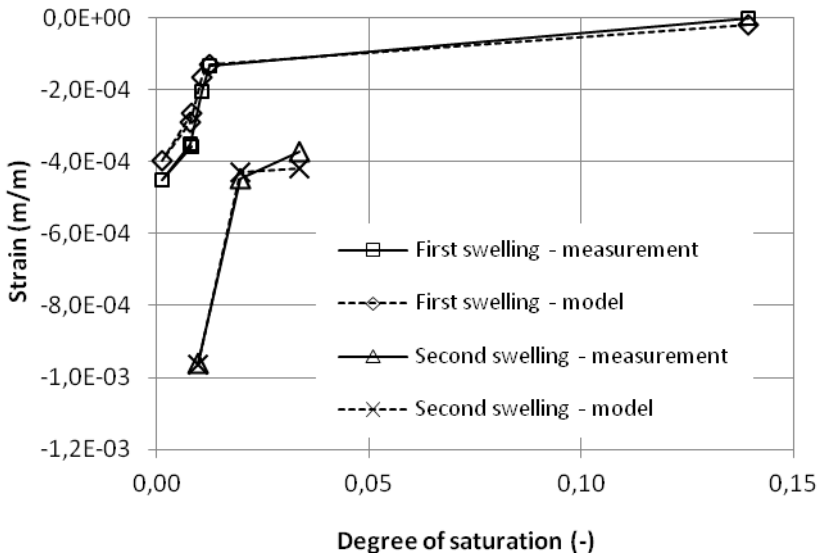

FIG 4. Moisture induced deformation of calcium silicate in hygroscopic region

Applying Equation (7), from the data on moisture induced strain ε and for the adequate water saturation integrals, considering the Biot coefficient b = 0.39 S and the composite bulk modulus $K = E/(1 - 2.\ \nu) = 1000$ MPa, the variable D was determined. The determined saturation dependent moisture induced strain in Figure 1. can be expressed as a continuous function of the saturation integral (Fig. 5).

4. Discussion

The damage variable determined from the moisture induced strain and compared with moisture content dependent elasticity modulus changes varies in the interval from 0 to 0.7 as it can be seen in Figure 6. The damage is proportional to the capillary pressure for saturation values lower than the critical moisture content and the minima are at the critical and maximum saturation moisture contents.

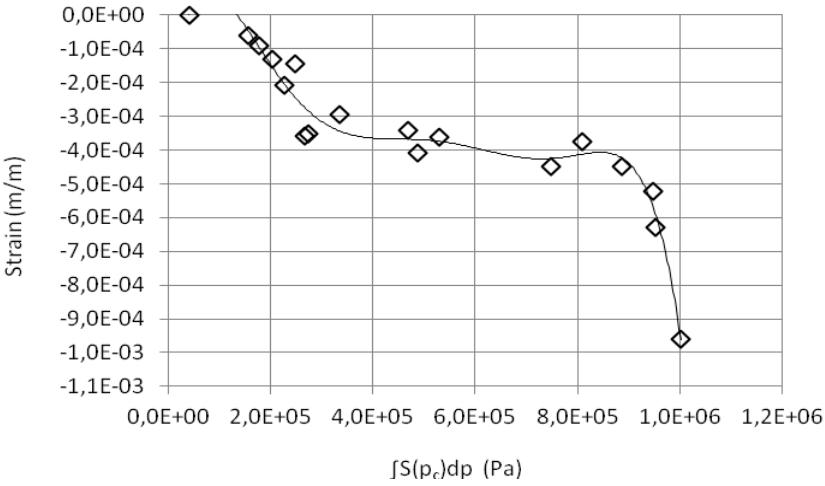

FIG 5. Moisture induced deformation of calcium silicate as water saturation integral function

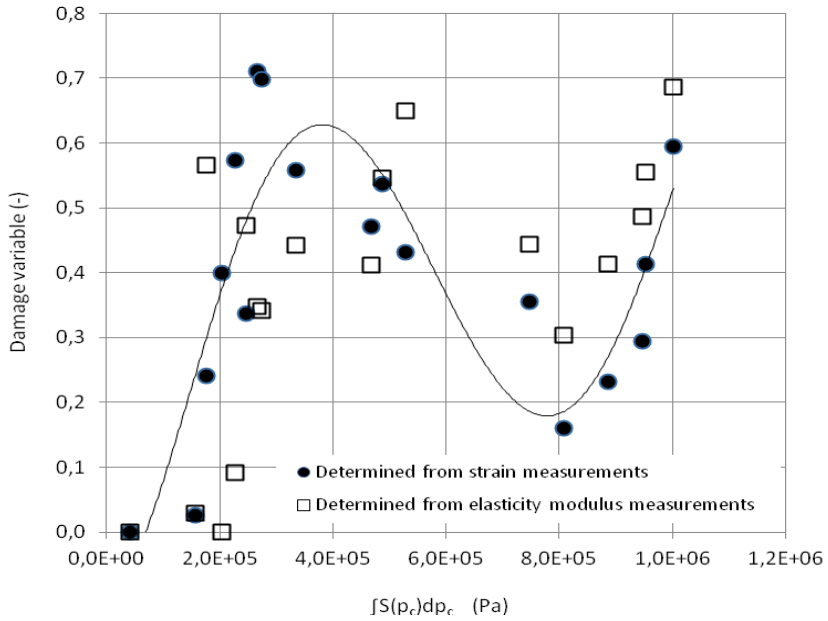

FIG 6. Comparison of damage variables of calcium silicate as water saturation integral functions determined from: 1- strain, 2 - elasticity modulus measurements

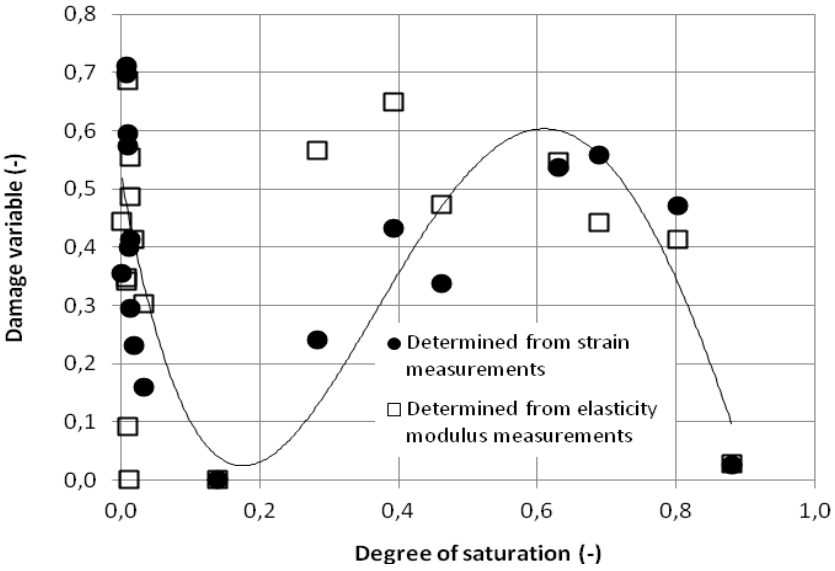

FIG 7. Comparison of damage variables of calcium silicate as water saturation functions determined from: 1- strain, 2 - elasticity modulus measurements

The maxima and minima correspond to the maximum and minimum shrinkage respectively.

Independently, the damage variable as the function of capillary pressure was calculated also from the measured elasticity modulus data. The obtained values are similar to the values determined from strain measurements. The maximum damage variable 0.7 determined from the strain measurements represents the degradation of maximum elasticity modulus from 600 to 180 MPa caused by the effect

of microcracking (Bažant et al. 1982). This interval is identical with the interval of measured moisture content dependent elasticity modulus values.

5. Conclusions

Moisture induced deformations and elasticity moduli of calcium silicate board were determined for the moisture contents within water saturation interval 0 - 90 %. On the basis of micro-macro relations of poroelasticity the coefficients of coupling between moisture content and moisture deformation were identified. The moisture induced deformation of calcium silicate has a hysteretic character and it is given by different capillary pressures during the material wetting and drying. With increase of capillary pressure the moisture induced strain is influenced by two opposing tendencies. For water saturation lower than critical moisture content the material shrinks due to water film thickness decrease. For the saturation higher than critical moisture content the material swells due capillary menisci radius increase. The elasticity modulus of the analysed material is a function of capillary pressure. Its value is related with damage and is proportional inversely to shrinkage.

6. Acknowledgements

The authors wish to thank the Slovak Research and Development Agency APVV, project No. 0032-10 for the financial support of this work.

This article has been produced with the financial assistance of the European Regional Development Fund (ERDF) under the Operational Programme Research and Development/Measure 4.1 Support of networks of excellence in research and development as the pillars of regional development and support to international cooperation in the Bratislava region/Project No. 26240120020 Building the centre of excellence for research and development of structural composite materials – 2nd stage.

References

Bažant Z. P. & Raftshol W. J. 1982. Effect of cracking in drying and shrinkage specimens. Cement and Concrete Research 12, 209 - 226.

Bentur A. & Diamond S. 1984. Fracture of glass fiber reinforced cement. Cement and Concrete Research 14, 31-42.

Carmeliet J. 2000. Influence of fluid-solid coupling on the damage behavior of quasi-brittle nonsaturated porous media. Emerging Technologies in NDT, Van Hemerlijck, Anastassopoulos & Philippidis (eds) Balkema, Rotterdam, 245 – 252.

Coussy O. 1995. Mechanics of Porous Continua, John Wiley, Chichester.

Coussy O., Ulm F. J. & Mainguy M. 1999. A Short Course on Environmental Mechanics of Concrete, Lecture Notes, Udine.

Ferraris C. F. & Wittmann F. H. 1987. Shrinkage mechanisms of hardened cement paste. Cement and Concrete Research 17, 453 - 464.

Gottfredssen F. R., Knutsson H. H. & Nielsen A. 1997. Determination of length changes due to moisture variations in autoclaved aerated concrete. Materials and Structures 30, 148 - 153.

Gregg S. J. & Sing K. S. W. 1982. Adsorption, Surface Area and Porosity. Academic Press, London. 1982.

Hua C., Acker P. & Ehrlacher A. 1995. Analyses and models of the autogenous shrinkage of hardening cement paste. I. Modelling at macroscopic scale. Cement and Concrete Research 25, 1457 - 1468.

Koronthályová O. & Matiašovský P. 2003. Thermal conductivity of fibre reinforced porous calcium silicate hydrate-based composites. Journal of Thermal Envelope and Building Science 4, 71 - 89.

Kumaran M. K. 1996. Heat, Air, and Moisture Transfer in Insulated Enveloped Parts. Final

Report. Task 3: Material Properties, IEA Annex 24, K. U. Leuven.

Lowell S., Shields J. E., Thomas M. A. & Thommes M. 2004. Characterization of porous solids and powders: surface area, pore size and density. Kluwer, Dordrecht.

Mangat P. S. & Azari M. M. 1988. Shrinkage of steel fibre reinforced cement composites. Materials and structures 21, 163 - 171.

Mangat P. S. & Azari M. M. 1990. Plastic shrinkage of steel fibre reinforced concrete. Materials and structures 23, 186 - 195.

Maruyama I. 2010. Origin of drying shrinkage of hardened cement paste: Hydration pressure. Journal of Advanced Concrete Technology 8, 187 - 200.

Matiasovsky P, & Mihalka P. 2011. Moisture induced deformations of calcium silicate boards. Building Research Journal 59, 217-227.

Morlier P. & Khenfer M. M. 1991. Effet de la longeur des fibres sur les proprietés mécaniques des ciments renforccés de fibres cellulosiques. Materials and Structures 24, 185 - 190.

Pihlajavaara S. E. 1974. A review of some of the main results of a research on the ageing phenomena of concrete; effect of moisture conditions on strength, shrinkage and creep of mature concrete. Cement and Concrete Research 4, 761 - 771.

Weimann M. B. & Li V. C. 2003. Hygral behavior of engineered cementitious composites (ECC). International Journal for Restoration of Buildings 9, 513 - 534.

Xi Y. & Jennings H. M. 1997. Shrinkage of cement paste and concrete modelled by a multiscale effective homogeneous theory. Materials and Structures 30, 329 – 339.

Zhang J. & Li V. C. 2001. Influences of fibers on drying shrinkage of fiber-reinforced cementitious composite. Journal of Engineering Mechanics 127, 37 – 44.

Influence of Frost-Induced Damage on the Microstructure and Physical Properties of Cement Mortars

Alicja Marciniak, M.Sc. [1]
Marcin Koniorczyk, D.Sc. [1]
Dariusz Gawin, Professor [1]

[1] Łódź University of Technology, Poland

KEYWORDS: *Cement mortar, Freeze-thaw cycles, Pore microstructure, Frost-induced damage, Multi-cycle Mercury Intrusion Porosimetry, Capillary suction, Strength properties*

SUMMARY: *The paper considers the change of cement mortar microstructures due to the water freezing. Frost resistance of a water-saturated cement based material is highly dependent on its pore structure. The pore sizes and their distribution determine, among other things, the freezing temperature of the water. The damage of pore microstructure for four types of cement mortars was investigated: two without air-entraining admixture (AEA) - series 01 and 02, and with 0.1% - series 05 and 0.2% - series 06 addition of AEA. Change of internal pore structure was determined by multi-cycle mercury intrusion test and capillary suction for the materials after 25, 50 and 100 freeze-thaw cycles. Additionally, strength properties were measured. The most extensive damage of micro-structure, was observed for samples without AEA with w/c ratio equal to 0.5. The smallest damage of microstructure was obtained by using AEA with addition 0.2% of cement mass and reducing w/c ratio to 0.4. This addition allowed to obtain mortar with not significantly changed coefficient of capillary suction and only slightly increased porosity from 27,5% up to 29,4% after 100 cycles of freezing. The specimens without AEA were damaged before reaching 100 freeze and thaw cycles.*

1. Introduction

The cement-based materials are widely used in civil engineering and exploited in various conditions, including severe climate and/or chemical action. The knowledge about their structure and its evolution due to the environmental loading is necessary for a more profound understanding of the physical and mechanical properties of the materials. The multi-cycle Mercury Intrusion Porosimetry (MIP) analysis allows to investigate the volume of capillary pores, their distribution and the existence of narrow channels connecting the ink-bottle type pores (Kaufmann et al. 2009). The capillary pores play the major role during the transport phenomena, hence an increase of their volume may accelerate the water and contamination migration into the pore system and cause accelerated deterioration of cement-based materials. The pore system microstructure is of primary interest when the durability of cementitious materials exposed to the frost damage is considered (Coussy & Monteiro 2008). Therefore the addition of air-entraining admixtures (AEA) is frequently applied to concrete, in order to help to redistribute the additional pressure induced by the growing ice volume.

Four kinds of cement mortar of different air-entraining admixture content were exposed to increasing number of freeze-thaw cycles in order to analyze the evolution of their pore microstructure and changes of strength properties caused by frost induced damage of the material. To this end, the changes of pore inner structure and pore shapes, as well as capillary suction coefficient were experimentally investigated after 25, 50 and 100 freeze-thaw cycles. Additionally, the bending and compressive strength tests were performed. The results of experimental investigation are analyzed and discussed in this contribution.

2. Materials

The variations of pore microstructure, as well as strength and transport properties for three cement mortars exposed to repeated freeze-thaw cycles are investigated in this contribution. The deterioration of microstructure was investigated for four mortars made of the CEM 1 32.5R cement with two different water/cement ratio w/c= 0.5 (series 01) and 0.4 (series 02, 05, 06), and with different amounts of plasticizer and air-entraining admixture (AEA): 0% (series 01, 02), 0.1% of the cement mass (series 05) and 0.2% (series 06), respectively. The Glenium admixture was used as a plasticizer, and the BASF Mischól LP75 as an AEA. For the cement mortars recipe cf. Table 1.

TABLE 1. Mixture composition, density and water absorption of the tested cement mortars.

Series	Cement [g]	Sand [g]	Water [g]	Plasticizer [g]	AEA [g]	Density [g/cm^3]	Water absorption [% weight]
01	900	2700	450	0	0	2.02	9.97
02	900	2700	360	18	0	2.13	7.82
05	900	2700	360	18	0.9	1.97	8.48
06	900	2700	360	8	1.8	1.70	8.84

After curing in water, the beams with dimensions of 4 x 4 x 16cm were weighed and measured. Next, the specimens were dried in the temperature of 60˚C and 105˚C until constant mass was reached. The measured values of density and water absorption (by weight) are given Table 1.

Then, the beams were placed in the freezing chamber. Three samples of each series were subjected to repeated freeze-thaw cycles. The mass loss due to frost damage and water absorptivity were measured after 25, 50 and 100 cycles. The results are presented in Table 2 (all three samples of series 01 and 02 were disintegrated before reaching 100 cycles). Each of the given values is an average from three samples tested. Analyzing the obtained results, one can observe an increasing mass (positive values in Table 2) and a decrease of water absorption (negative values in Table 2) for some specimens. This can be explained by water entrained into air voids and cracks, as well as by further hydration progress.

TABLE 2. The average loss of mass after 25, 50 and 100 freezing cycles

Series	The average loss of mass [%]			Increase of water absorption by weight after n frost cycles [%]		
	25	50	100	25	50	100
01	0.42	-1.30	-	14.89	27.31	-
02	0.36	-0.01	-	7.89	14.38	-
05	0.30	-0.05	-6.57	-1.9	11.5	33.0
06	0.45	0.19	0.30	-5.0	-5.2	-2.9

The microstructure of the analyzed materials was determined by means of the following techniques: mercury intrusion porosimetry (MIP) and capillary suction. The strength properties of the analyzed cement composites were also tested.

3. Methods

3.1 Mercury Intrusion Porosimetry

The multi-cycle MIP analysis gives information about dimensions of the channels connecting the capillary pores, which are essential for the water flow (Giesche 2006). The technique is very simple in principles. It is assumed that the material contains the set of cylindrical pores of different dimensions. The structure of the analyzed samples is unaffected by the pressure of intruded mercury. Since the mercury is a non-wetting fluid, the pressure must be applied in order to intrude it into the pore system.

The smaller are pores, the higher pressure must be applied. In order to assess the pore diameter, the Washburn equation was applied (Washburn 1921). According to this assessment cylindrical capillaries are inversely proportional to the applied pressure. The following properties of mercury were assumed in analysis: contact angle during intrusion ϑ_{in}=130º and extrusion ϑ_{ex}=104º and surface tension σ=0.48 N/m.

Microstructure damage of cement mortars caused by the freezing water were analyzed using mercury porosimeter AutoPore IV by means of multi-cycle MIP technique. This type of device is able to measure pores diameter from about 6μm to 3nm. Dried cylindrical specimens of each series were used in the experiment. The specimens were cut from the beams which had been subjected to repeated freeze and thaw cycles, respectively: 0, 25 and 50 cycles. The beams of series 05 and 06 were not damaged after 50 cycles and the investigation was carried out also after 100 cycles.

Applying two mercury intrusion - extrusion cycles, the change of the total porosity and the pore size distribution during the process of material frozen damage are investigated. It was observed that after the first cycle part of the mercury volume was entrapped in the pore system. The difference between the mercury volume intruded during the first and the second cycle might serve as a measure of the ink-bottle type pore content (Kaufmann et al. 2009).

The MIP technique does not give representative value of total porosity. One has to remember that this test gives information about some model of an internal structure, but not about the real microstructure of a cement-based material. The MIP method has some drawbacks (Diamond 2000). Most of them result from the fact, that the majority of pores in the cement based materials, called ink-bottle type pores, are connected with each other by thinner necks.

3.2 Capillary suction

Capillary suction is the ability of liquid to flow into narrow channels (material pores). It is caused by unbalanced force induced by the surface tension. The scale of the phenomenon depends on the amount, size and characteristics of air voids in the material. Additionally, the rising damp is inversely proportional to the pressure of capillary suction.

Testing the capillary suction in certain conditions is a method to investigate the ability of moisture absorption by a material (PN-EN ISO 15148:2004P). The specimens having dimensions of 40x40x80mm, were used in the experiments. Four sides of each sample were covered with silicon and then dried until constant mass was reached. During the test, which lasted for 48 h, samples were placed 1 cm below the water surface. The mass of the samples was measured every 60 s. As a result the charts of the mass increase as a function of square root of time for each series after different number of freeze-thaw cycles were performed.

4. Results and discussion

4.1 Mercury Intrusion Porosimetry

The results of MIP enabled to estimate the basic properties which characterize the porous structure of materials. The obtained data are presented in Table 3 where the signature stands for the number of series and the number of freeze-thaw cycles. The received values of parameters are the average of the three measurements.

After increasing number of freeze-thaw cycles the apparent density of the series 01 samples remained almost unchanged, while their porosity was increasing with the increasing number of cycles. The data in Table 3 show a visible increase of specific pore area after 25 cycles for the all tested materials. During next cycles the values of this parameter did not vary significantly. The damage of materials' micro-structure and the destruction of thin channels connecting the larger pores, were caused by the

increase of volume of freezing water. The process of ice formation, which generates tensile stress in the skeleton, can open the entrances to the smaller pores or to the pores which were initially inaccessible for mercury.

TABLE 3. Main material properties and inner structure characteristics of the investigated mortars.

Parameter	Unit	Series 01			Series 05			
		01_0	01_25	01_50	05_0	05_25	05_50	05_100
Total pore area	m^2/g	5.94	8.75	8.44	5.93	7.91	6.93	8.04
Bulk density	g/ml	2.03	2.04	1.88	2.10	2.04	2.05	1.87
Apparent density	g/ml	2.51	2.57	2.49	2.53	2.58	2.52	2.52
Porosity	%	19.04	20.70	24.51	16.93	21.02	18.90	25.95
Parameter	Unit	Series 02			Series 06			
		02_0	02_25	02_50	06_0	06_25	06_50	06_100
Total pore area	m^2/g	5.67	6.01	7.21	5.78	7.87	8.26	8.02
Bulk density	g/ml	2.10	2.20	2.04	1.81	1.79	1.84	1.80
Apparent density	g/ml	2.51	2.56	2.52	2.60	2.57	2.51	2.56
Porosity	%	16.44	14.11	18.93	27.49	30.38	26.68	29.36

4.1.1 Cement mortar without admixtures – series 01 (w/c= 0.5)

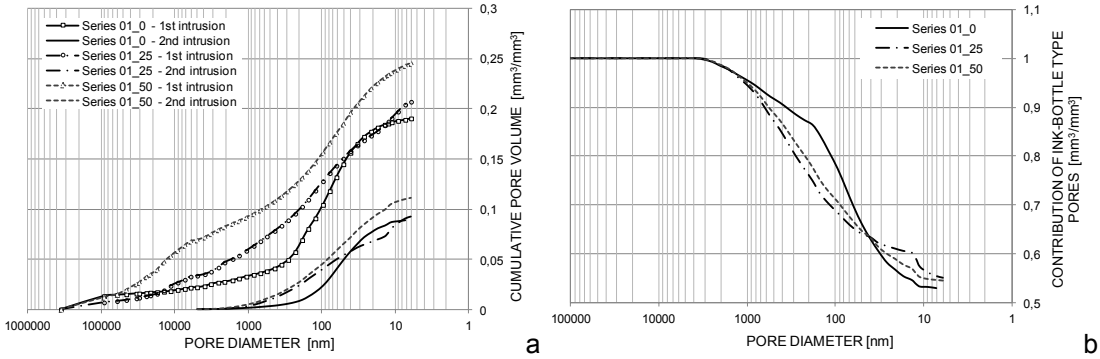

FIG 1. Comparison of the cumulative pore volume (a) and contribution of ink-bottle type pores (b) obtained by means of MIP for series 01after 0, 25 and 50 freeze-thaw cycles

Comparing the pore size distribution (Fig. 1a) and the contribution of ink-bottle type pores (Fig. 1b), one can observe some important differences between microstructure of the samples before and after the freeze and thaw cycles. The differences concern the pores of diameter from 10μm up to 50nm. For the pores of diameter 1μm – 40nm, the contributions of ink-bottle type pores for the specimens after freezing and thawing cycles were lower than in the reference samples. This was caused by the destruction of thin channels connecting the larger pores, induced by freezing water.

4.1.2 Cement mortar without admixtures – series 02 (w/c= 0.4)

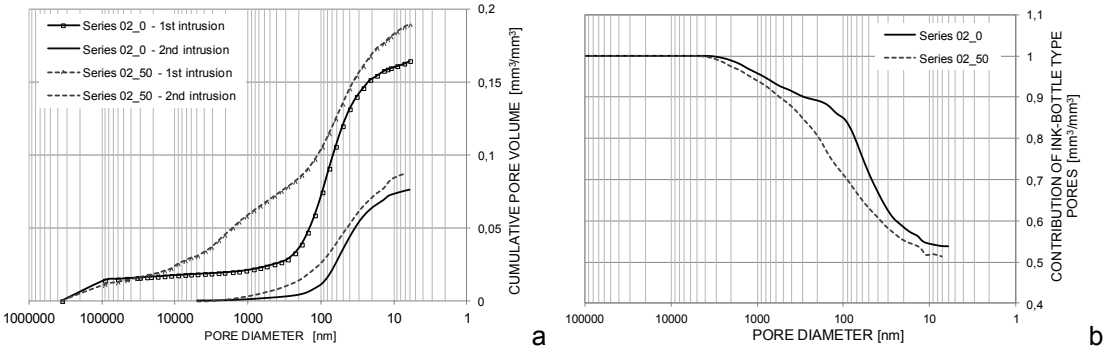

FIG 2.Comparison of the cumulative pore volume (a)and contribution of ink-bottle type pores (b) obtained by means of MIP for series 02 after 0 and 50 freeze-thaw cycles

The comparison of the cumulative pore volume and the contribution of ink-bottle type pores obtained for the samples of series 02, before and after freeze and thaw cycles, is shown in Figures 4a and 4b, respectively. The investigation of samples of series 02 after 100 freezing cycles was not possible because the specimens were destroyed before reaching this number of cycles.

The changes of the pore structures refer to the pores of diameter from 20μm to 100nm. The value of the average total porosity increased from 16,4% up to 18,9%. The investigation shows decrease of the quantity of ink-bottle type pores after successive freeze and thaw cycles.

4.1.3 Cement mortar with 0.1% AEA – series 05 (w/c= 0.4)

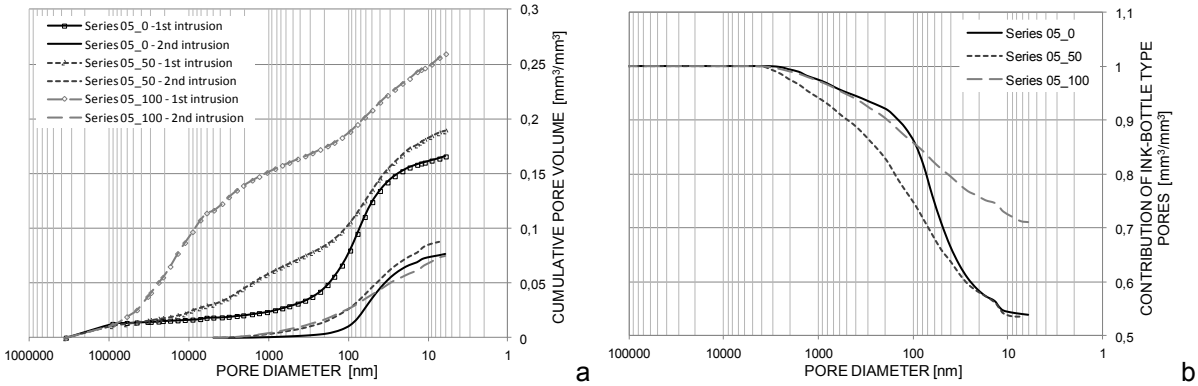

FIG 3. Comparison of the cumulative pore volume (a)and contribution of ink-bottle type pores (b) obtained by means of MIP for series 05 after 0, 50 and 100 freeze-thaw cycles

The results obtained for the specimens of series 05 are presented in Fig. 3. The differences between distribution of porosity for samples of this series after 50 cycles is small, when compared with the reference samples. However, there is a change in the range of pores with diameter of 20μm - 100nm. The average total porosity before the freeze and thaw test was equal to 16,9% and after the successive freezing and thawing cycles to 25,9%. With the increasing number of freeze-thaw cycles, the visible destruction of pores can be observed. Figure 3b indicates the increase of the contribution of ink-bottle type pores from 55% to 70%.

4.1.4 Cement mortar with 0.2% AEA – series 06 (w/c= 0.4)

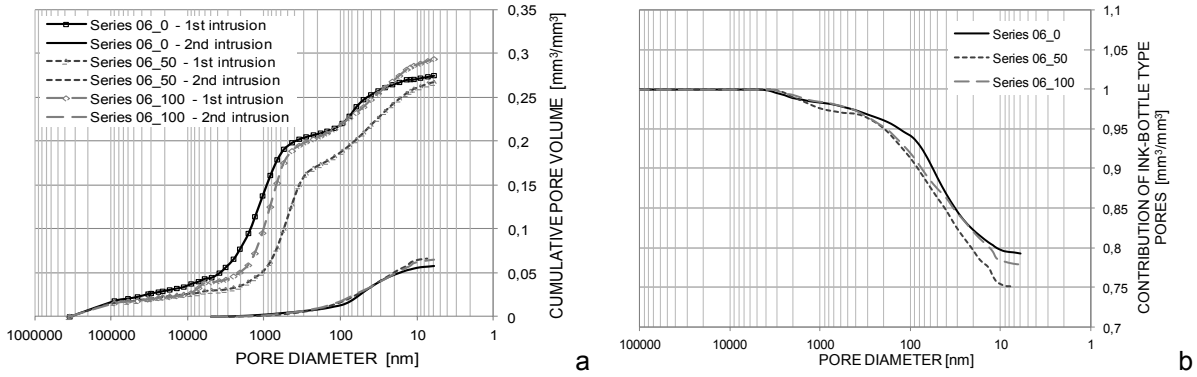

FIG 4. Comparison of the cumulative pore volume (a)and contribution of ink-bottle type pores (b) obtained by means of MIP for series 06 after 0, 50 and 100 freeze-thaw cycles

The results for the first and second mercury intrusion for series 06, before and after freeze - thaw cycles is presented in Figure 4a. The comparison of the contribution of ink-bottle type pores is shown in Figure 4b. With the increasing number of freezing and thawing cycles, no further destruction of the pore structure can be observed for this mortar. The volumetric contribution of ink bottle type pores is high and exceeds 80% for all the pore diameters. Another characteristic feature is also a small volume of mercury, which has been pressed during the further intrusions.

4.2 Capillary suction

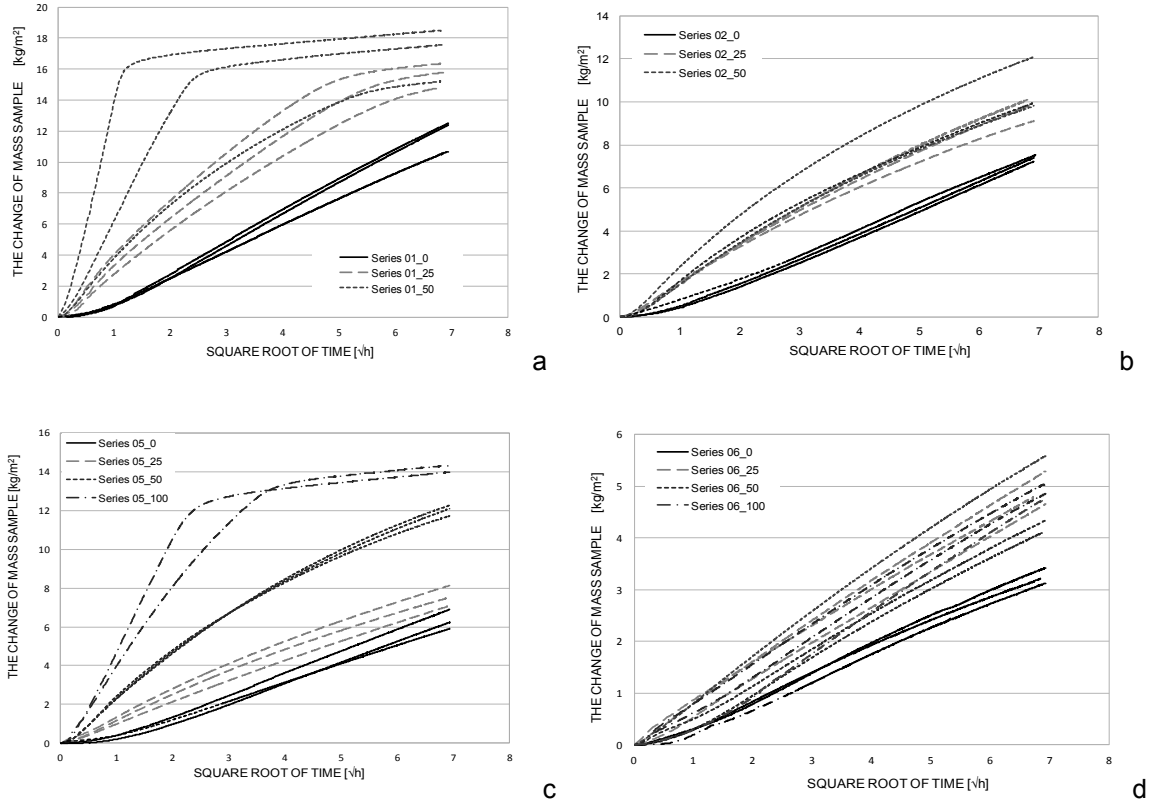

FIG 5. Mass increase as a function of square root of time for: a) series 01, b) series 02, c) series 05 and d) series 06, after different number of freeze-thaw cycles

The water mass increase due to capillary suction as a function of square root of time is presented in Fig. 5 for the all tested cement mortars after different number of freeze-thaw cycles. The highest value of the coefficient of capillary suction was measured for the mortars of series 01. One can also observe that samples which were subjected to freezing - thawing cycles, exhibit significantly higher rate of capillary suction, gradually increasing with the number of cycles. An exception was series 06 for which the increase of capillary suction coefficient was less pronounced, because of less visible pore microstructure changes (see Fig. 4 and Table 3). The observed increased water absorption rates can be explained by a gradual destruction of pore structure during freeze-thaw cycles (breaking narrow necks between the larger pores), as well as forming the micro-cracks or extension of pore diameter.

4.3 Strength properties

The investigation of strength properties changes due to the water freezing was performed for the reference samples and those exposed to 25, 50 and 100 freeze-thaw cycles. The values of compression and bending strengths for the four tested cement mortars after different number of cycles are presented in Table 4. Each of the presented data is an average value measured for three samples.

The increase of compressive strength observed after 50 and 100 freeze-thaw cycles for the mortar of series 06 can be explained by the progress of cement hydration. For all other series, after successive cycles of freezing and thawing one can observed a significant decrease of strength properties.

The value of bending strength decreased drastically after 25 freezing cycles. However, for samples from series 06 there was a less decrease then for the other ones.

TABLE 4. The average values of bending and compressive strengths after 0, 25, 50 and 100 freeze-thaw cycles

Series	The average bending strength [MPa]				The average compressive strength [MPa]			
	0	25	50	100	0	25	50	100
01	9.98	1.04	0.39	-	57.98	30.76	21.77	-
02	11.04	2.17	1.14	-	72.38	47.40	39.15	-
05	8.75	2.71	1.29	0.48	53.47	40.20	39.15	6.02
06	5.57	2.81	4.24	3.94	25.56	25.45	35.10	35.78

5. Conclusions

The damage caused by the water freezing - thawing cycles, repeated different number of times, was investigated for four types of cement mortars in the contribution. Changes of internal pore structure were analyzed by means of the multi-cycle mercury intrusion technique and capillary suction tests. The resultant changes of the compressive and bending strength were measured as well.

A significant damage of material microstructure was noticed for the cement mortars without any AEA, the most visible for series 01 (w/c= 0.5) and slightly less for series 02 (w/c= 0.4). The most pronounced micro-structure changes in the mortars of series 01, 02 and 05 were observed for the pores of diameter smaller than 20μm.

The smallest damage of microstructure was observed for the cement mortar of series 06. Despite of increasing number of freezing and thawing cycles, no further destruction of the internal structure and no significant change of the coefficient of capillary suction were observed. Moreover, only a slight change of the cumulative pore volume after subsequent cycles of freezing water was noticed. The porosity value increased from 27,5% up to 29,4%.

The obtained results allow to conclude that an addition of the suitably selected amount of AEA is an efficient protection measure against damage caused by repeated water freezing-thawing cycles to the inner structure of cement mortars.

6. Acknowledgements

This research was financially supported by the National Science Center - Poland, within the grant UMO-2011/03/B/ST8/05963 entitled "Degradation of building materials with microstructure induced by the development of expanding phases", realized at the Lodz University of Technology, Poland, in years 2012 - 2014.

References

Brandt A.M. & Kasperkiewicz J. (editors) 2003. Diagnosis of concretes and high performance concrete by structural analysis. Editions of the Institute of Fundamental Technological Research Polish Academy of Sciences. Warsaw, 218 p.

Coussy O. & Monteiro P.J.M. 2008. Poroelastic model for concrete exposed to freezing temperatures. Cement and Concrete Research 38: 40–48.

Diamond S. 2000. Mercury porosimetry: An inappropriate method for the measurement of pore size distributions in cement-based materials. Cement and Concrete Research 30, 1517-1525

Giesche H. 2006. Mercury porosimetry: A general (practical) overview. Particle & Particle Systems Characterization 23. 9- 19.

Kaufmann J. Loser R. & Leemann A. 2009. Analysis of cement-bonded materials by multi-cycle mercury intrusion and nitrogen sorption. Journal of Colloid and Interface Science 336, 730–737.

PN-EN ISO 15148. 2004P. Hygrothermal performance of building materials and products. Determination of water absorption coefficient by partial immersion (ISO 15148:2002).

Washburn E. 1921.Note on a method of determining the distribution of pore size in a porous material. Proceedings of the National Academy of Sciences of the United States of America 7,115-116.

Large scale measurements and calculations of wall elements with vacuum insulation panels (VIPs)

Silje Korsnes, M.Sc [1]
Berit Time, Ph.D [1]
Sivert Uvsløkk, M.Sc [1]
Arild Gustavsen, Professor [2]
Lars Gullbrekken, M.Sc [1/2]
Egil Rognvik, Eng [1]

[1] SINTEF Building and Infrastructure, Norway
[2] Norwegian University of Science and Technology, Norway

KEYWORDS: *Timber frame wall, Masonry block system wall, Hot-box measurements, Vacuum insulation panels, COMSOL Multiphysics, THERM*

SUMMARY:
Vacuum insulation panels (VIPs) are available on the market today. Although there might be some challenges, VIPs have the potential to bring down the wall thickness in wall constructions. However, calculating an accurate U-value for inhomogeneous wall constructions with a wide range of thermal conductivities might not be straight forward.

This study concerns calculation and measurements of two wall systems containing vacuum insulation panels (VIPs). Various computational models with varying complexity THERM 6, COMSOL Multiphysics 3D and a spreadsheet model have been used to calculate the U-value of the two walls. To verify the calculation models, large scale laboratory experiments has been performed in a guarded hot-box. The results show that the calculations and measurements of the timber frame wall have the best compliance. The deviations are in accordance with previous measurements and calculations of more traditional timber frame walls. The deviations between calculations and measurements for the masonry block system are slightly larger.

1. Introduction and background

Energy efficient buildings and passive houses has been in focus for many years. Plans are made for zero energy-, zero emissions and plus energy buildings in the near future. It is also desirable to decrease the material consumption in buildings by developing more efficient materials and building components.

Vacuum insulation panels (further referred to as VIPs) are available on the market today. They have a history of being quite expensive, but new technology and more efficient production reduces the prise. The panels consist of a porous core enclosed in a sealed vapor- and air-tight foil. The foil provides vacuum in the core material. The equivalent thermal conductivity of VIPs is dependent on the core material and the foil, but in general it's about 10 times lower than conventional insulation materials. Although there might be some challenges with VIPs, they have the potential to bring down the thickness in wall constructions considerably. The benefits of slimmer wall constructions are many. The size of the roof and floor construction gets reduced, leading to less material consumption. The costs of transportation gets reduced, and in areas with a high billing prize and/or small plots, slimmer walls implies increased floor space. A slim wall construction is also favourable in terms of more daylight.

But as more efficient materials and new building components are developed and the U-value (thermal transmittance) of building components is reduced, calculating accurate values are becoming even more important. This leaves no room for rough estimates. The U-values of walls in buildings used in calculations of energy and heating demand should represent the entire wall area from floor to ceiling, including sill beams and increased amount of loadbearing materials due to recesses etc.

It is our recommendation that the U-value of a new building system, especially those containing new and not well tested materials, should be measured in a guarded hot-box for the verification of the calculations. When calculations and measurements are consistent, the U-value of other sizes and thicknesses can be calculated with the corresponding calculation model.

Numerical calculations of complex building components might be challenging, especially for components containing materials with large variations in thermal conductivity. This study concerns calculation and measurements of two wall constructions containing vacuum insulation panels, a timber frame element and a masonry block system. Various computational models with varying complexity THERM 6, COMSOL Multiphysics and a spreadsheet model developed by SINTEF has been used to calculate the U-value of the two wall elements. To verify the calculation models, the U-value of the two walls have been measured in a large scale laboratory experiment performed in a guarded hot-box.

2. Test walls

2.1 Prefabricated timber frame wall element

The wall element consists of a timber frame wall with an ad on construction of horizontal laths on the inside. The element is 3036 mm wide and 2400 mm high. The timber frame is insulated with mineral wool and 12 mm VIPs from Va-Q-Tec is placed between the studs of the main construction, on the inside of the ad on construction. 2 of the 4 sill beams are 198 mm as the rest of the timber frame and 2 are only 148 mm to reduce the amount of wood in the construction.

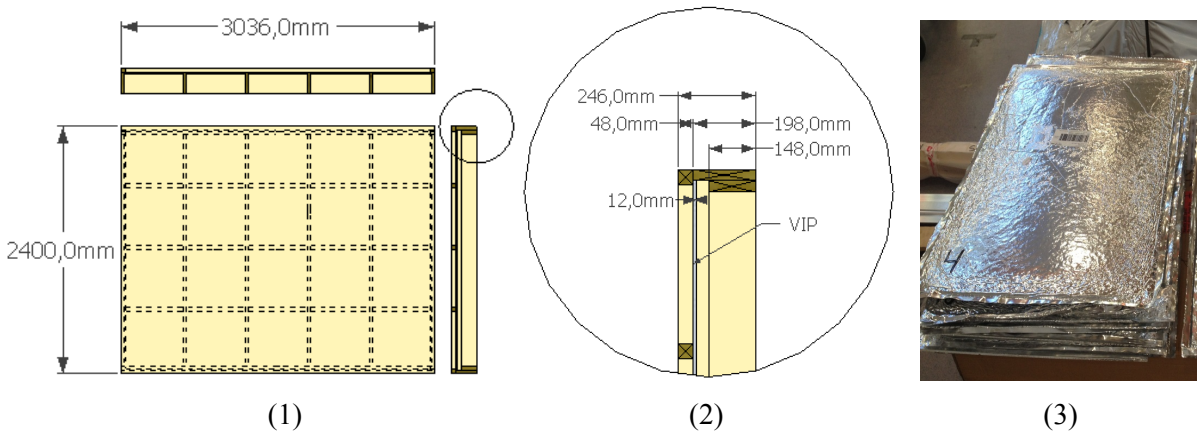

Figure 1: Timber frame wall element (1), details (2) and VIPs (3)

2.2 Masonry block system

The sandwich blocks consist of two light weight aggregate block leaves with a highly insulating core. The core consists of 50 mm thick VIPs enclosed in polyurethane (PUR). The horizontal joints consist of 12 mm of mortar between the masonry block leaves, and the space between the cores is filled with wrapped mineral wool, se figure 2 (7). The finished wall is plastered on both sides (10 mm).

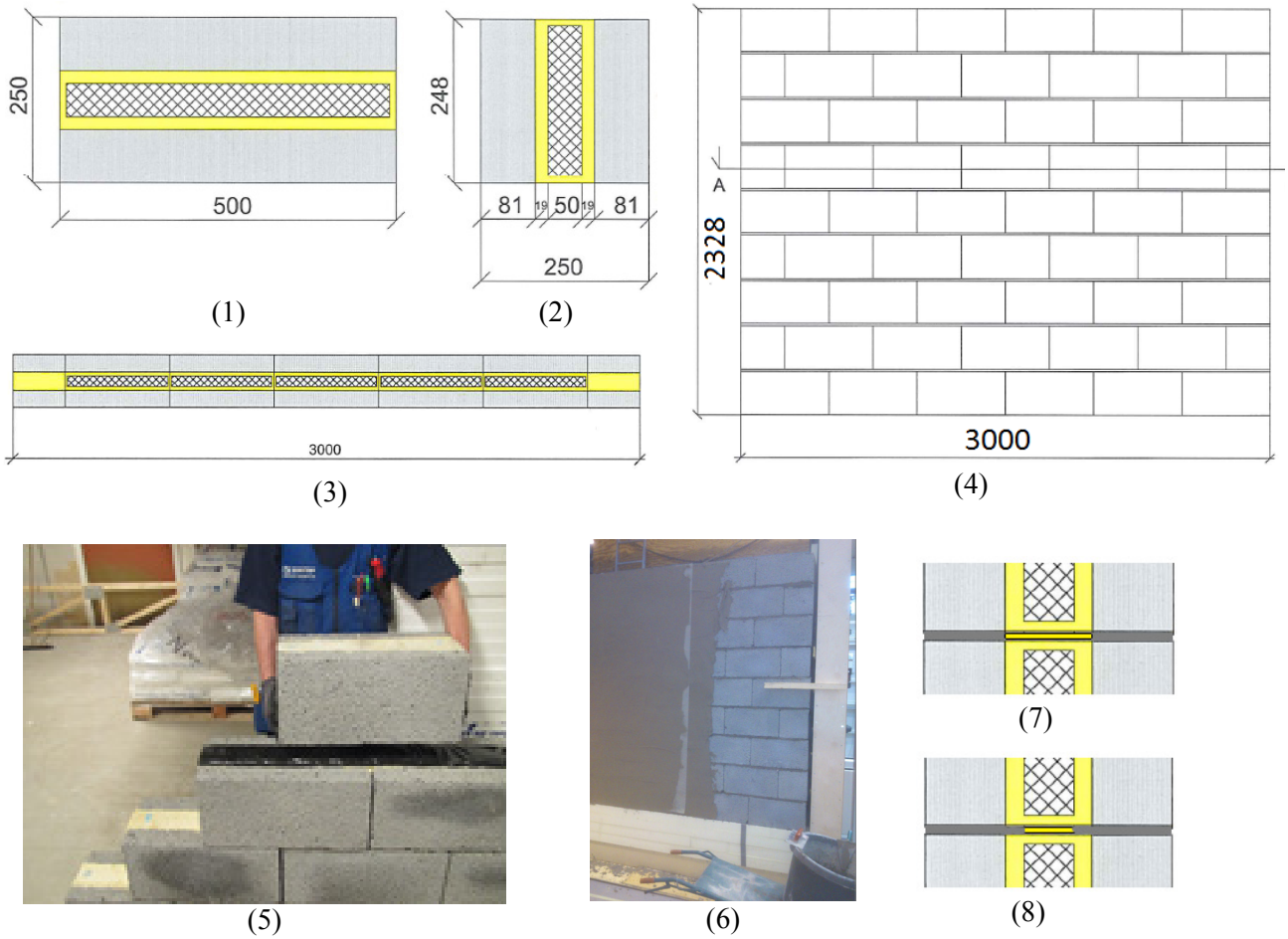

Figure 2: Masonry block system sections and front view (1, 2, 3 and 4), dry assembling of the wall (5), plastering of the wall (6), horizontal joints (7) and possible penetration of mortar in to the insulated space between the two cores (8)

3. Material properties and input values

When performing calculations on a real measured wall, one should aim at obtaining as accurate properties for the building materials as possible to secure a good correlation between calculations and measurements. This is because materials pproperties, even from well tested materials can vary between producers and even between samples from the same producer. Finding proper values for the properties of the building materials is very important for the quality of the calculations and the correlation between calculations and measurements.

The equivalent thermal conductivity of a VIP is dependent on the core material and the foil. The fresh equivalent thermal conductivity of the VIPs used in this project has been measured in the project. The 50 mm thick VIPs used in the masonry block system has achieved a value of 0.0039 W/mK and the 12 mm VIPs used in the timber frame wall achieved a value of 0.0032 W/mK.

Table 1: Input values timber frame wall

Material	**Thermal conductivity λ (W/mK)**	**Source**
Timber frame/laths	0.12	(Arnesen et al. 2009)
Mineral wool	0.033	From manufacturer
VIP core/foil	0.0032	Measurements performed in the project

Table 2: Input values masonry block system

Material	Thermal conductivity λ (W/mK)	Source
Mortar	1.2	From manufacturer
Leca	0.31	From manufacturer
PUR	0.024	Used in calculations
VIP core	0.004	Measurements performed in the project.
VIP foil	0.062	(Grynning et al. 2009)
Insulation strip	0.037	From manufacturer

4. Calculations

Various computational models with varying complexity THERM 6, COMSOL Multiphysics 3D and a spreadsheet model, all according to NS-EN ISO 6946 *Building components and building elements - Thermal resistance and thermal transmittance - Calculation method*, has been used to calculate the U-value of the two wall elements.

THERM is a Microsoft Windows™-based computer program, developed at Lawrence Berkeley National Laboratory (LBNL). THERM's two-dimensional conduction heat-transfer analysis is based on the finite-element method (THERM).

COMSOL Multiphysics® is a general-purpose software platform, based on advanced numerical methods, for modelling and simulating physics-based problems, both in two and three dimensions. The wall elements are modelled with the Heat Transfer Module. The module is used to study the mechanisms of heat transfer – conduction, convection, and radiation.

The spreadsheet model is developed at SINTEF Building and Infrastructure. The model is originally developed for standard timber frame walls and further developed for walls with I-beams. An ad on construction on the inside of the wall can be included.

4.1 Timber frame wall

The timber frame wall construction consists of vertical studs, two sill beams in the top, two in the bottom, and an ad on construction of horizontal lathes. Two of the sill beams are made smaller to reduce the amount of wood in the construction. The wall is insulated with mineral wool and VIPs. The VIPs are placed between the vertical studs. When modelling the construction in THERM some adjustments to the geometry have to be made.

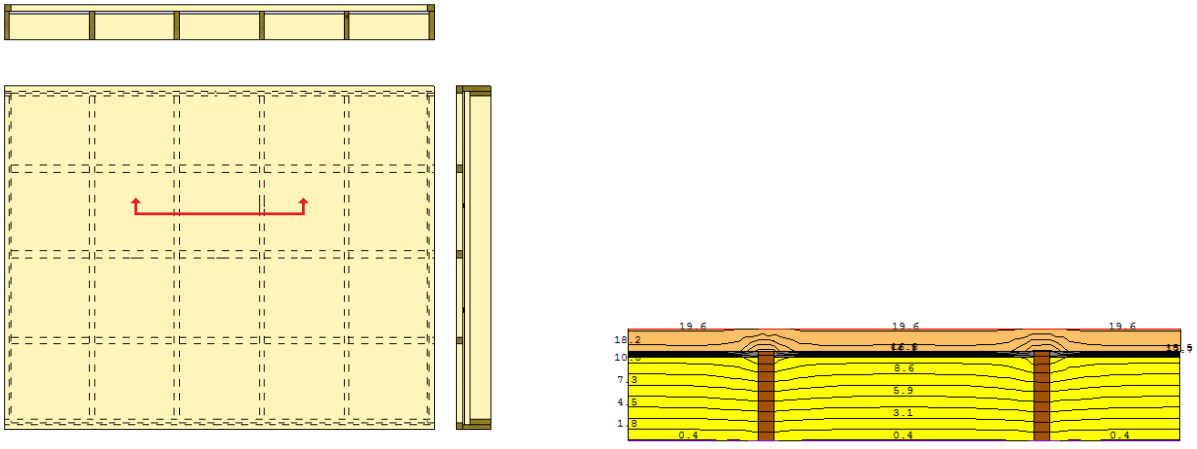

(1) (2)

Figure 3: Timber frame wall (1) and a horizontal section of the wall modelled in THERM (2)

A commonly used approach is to model a horizontal symmetry section of the wall showing the main studs, and then define the laths and insulation in the ad on constructions as a combined layer with alloyed thermal conductivity of the two materials, se fig 3. This simplification gives a U-value of the wall which is too low because it does not take into account the sill beams nor the increased heat flow which occurs in the laths due the thermal conductivity of the wood being higher than the mineral wood.

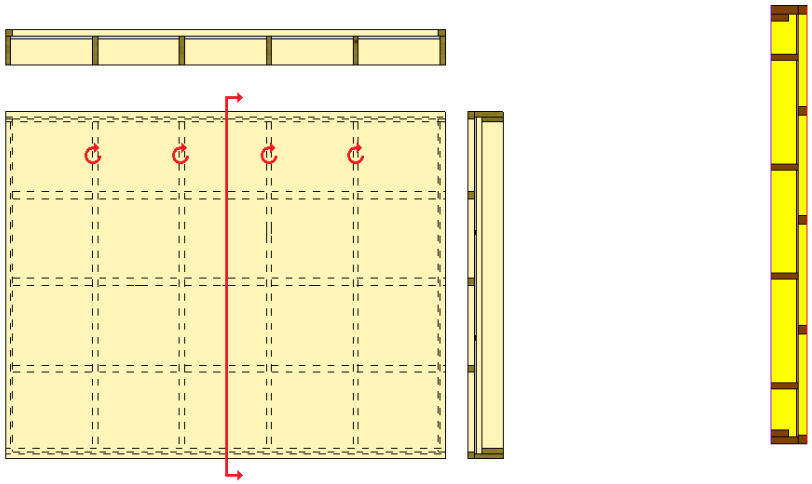

(1) (2)

Figure 4: Timber frame wall (1) and a vertical section where the mane studs are rotated (2)

An alternative model is made to take the sill beams and the laths into account. The model is a vertical section of the wall where the vertical studs are rotated sideways. The thicknesses of the studs are adjusted so that the amount of wood in the wall construction is the same as if the studs were vertical. This approach gives much more realistic results even though the small increase in heat flow in the intersection between the studs and the laths is not accounted for.

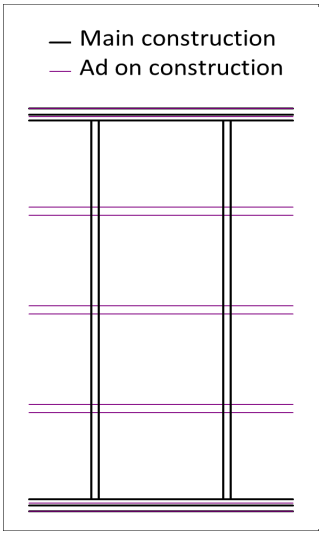

The spreadsheet model is developed at SINTEF Byggforsk and is basically based on calculations in Microsoft Excel. The model was originally developed for standard timber frame walls and has further been developed for walls with I-beams. The height of the wall, the centre distance and dimensions of studs and laths are defined. The areas of different combinations of materials are calculated and the U-value is a weighted average of the resistances of different combinations.

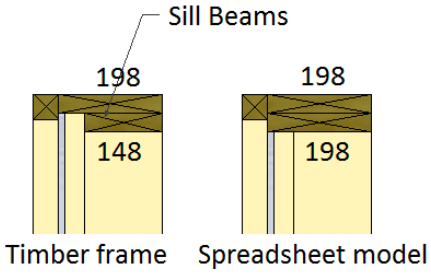

The only simplification in the geometry in this model is that the two sill beams which are supposed to be 148 mm are modelled as 198 mm.

(1) (2)

Figure 5: Geometry in the spread sheet model (1) and simplifications in the spreadsheet model (2)

Using COMSOL Multiphysics, complex geometry can be calculated without simplification or adjustments. One can easily model the entire wall construction, and then chose only to look at representative parts (symmetry section), se figure 6.

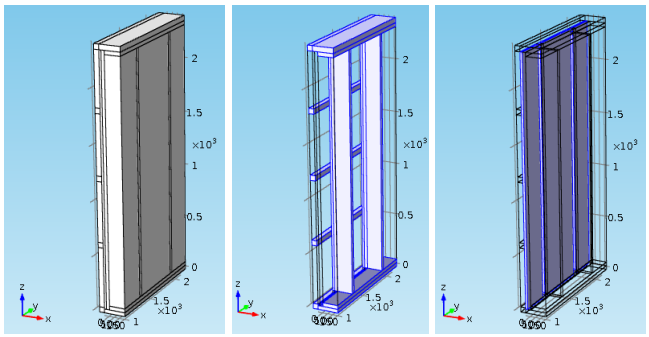

(1) (2) (3)

Figure 6: COMSOL Multiphysics can calculated complex geometry without simplification or adjustments. Representative section of the timber frame wall (1), timber frame (2) and VIPs (3)

4.2 Masonry block system

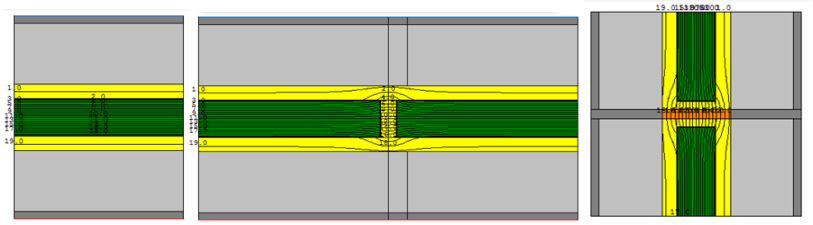

(1) (2) (3)

Figure 7: Geometry of the masonry block system modelled in THERM. Only the core (1), vertical joint (2) and horizontal joint (3)

When modelling the masonry block system with THERM, we encounter a similar challenge as for the timber frame wall. The geometry consists of different materials which are structured differently in the vertical and horizontal joints. A section of the core in a block without any joints is calculated first, se figure 7 (1). Then the vertical and horizontal joints are calculated separately, se figure 7 (2) and (3), and the additional heat transfer due to each joint is determined. The U-value of blocks with an addition for the joints constitutes the total U-value of the wall.

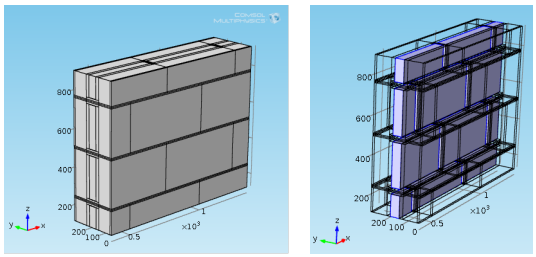

(1) (2)

Figure 8: Representative section of the masonry block wall modelled in COMSOL Multiphysics (1), and only the VIPs (2)

5. Measurements

The measurements are performed according to EN ISO 8990:1997 *Thermal insulation. Determination of steady-state thermal transmission properties. Calibrated and guarded hot box,* which is an international standard for measuring U-values for walls using a Hot Box, se figure 9 (1). The wall is placed in the middle of a template with an opening of 3.0 mx 3.0 m, EPS is used to fill out the rest of the gaps in the template. The metering area of the hot box is 2.45 m x 2.45 m. Corrections are done for the heat transferring through the EPS outside of the wall elements. The measurement is carried out

under stationary conditions with an ambient temperature of about 20 °C and 0 °C respectively on the hot and cold side of the wall panel.

In the measurements of the timber frame wall, the heat transfer coefficients may differ slightly from the standardized values during measurements, but this is corrected for so that the specified U-value includes the thermal resistance of a ventilated cladding. The U-value of the wall is calculated based on the measured heat flow, area -weighted surface temperatures and wall area.

(1) (2) (3)

Figure 9: Hot Box (1), masonry blocks system during construction (2) and timber frame wall ready for measurements (3)

6. Results

Results from calculations and measurements of masonry block system are shown in table 3 and the results from the timber frame wall is shown in table 4.

Table 3: U-values (W/m^{2}K) from calculation and measurements of the masonry block system

Calculation Tool		With VIP	
COMSOL 3D 4.3b		0.116	-20 %
THERM 1D 6		0.116	-21 %
Measurements Hot-Box, March 2013, vertical		0.146	
Input values	λ light weight aggregate (W/mK)	0.31	
	λ mortar (W/mK)	1.2	
	λ VIP foil (W/mK)	0.062	
	λ VIP core (W/mK)	0.004	
	λ PUR (W/mK)	0.024	
	λ wrapped insulation in joints (W/mK)	0.037	
The numbers in red are the difference between calculations and measurements			

Table 4: U-values (W/m^{2}K) from calculation and measurements of the timber frame wall

Calculation tool		With VIP		Without VIP	
COMSOL Version 4.3b, 3D		0.131	7 %	0,169	8 %
THERM Version 6, 2D		0.126	3 %	0,161	3 %
Spread sheet model (NS-EN ISO 6946:2007)		0.129	6 %	0,157	1 %
Measurements Hot-Box		0.122		0.156	
Input values	λ Mineral wool (W/mK)	0.033		0.033	
	λ Wood (W/mK)	0.12		0.12	
	λ VIP (W/mK)	0.0032		x	
	Thickness VIP (mm)	12		0	
The numbers in red are the difference between calculations and measurements					

7. Discussion and future work

The results show that the calculations and measurements of the timber frame wall have the best compliance. The deviations are in accordance with previous measurements and calculations of more traditional timber frame walls (Uvsløkk, 1990) and (Uvsløkk et al. 2010). The deviations between calculations and measurements of the masonry block system are slightly larger. The measured U-value is also higher than the calculated U-value which is normally not the case. A parameter study shows that a cause to the deviations might be penetration of mortar from the horizontal joints in to the space filled with wrapped mineral wool, se figure 2 (8).Convection in air gaps between the blocks might also contribute to a larger heat loss. Demolition of the wall showed mortar penetration of varying degrees in all the horizontal joints and gaps in some of the vertical joints (up to 5 mm). A combination of the two above-mentioned differences might explain the deviations between measured and calculated U-value. More detailed simulations in COMSOL Multiphysics will be performed to further investigate the impact of these differences and measurements of two old masonry block walls without VIPs will be used for comparisons with the results from this study. An uncertainty assessment of the measurements will be performed for both walls.

This study shows that some constructions are vulnerable to mistakes made during construction. It's debatable whether the U-values for these walls should be provided with a safety margin that takes the possible deviations into account.

8. Acknowledgements

This work has been performed within the Research Centre on Zero Emission Buildings (ZEB) and an R&D project between OverhallaHUS and SINTEF Building and Infrastructure. The authors gratefully acknowledge the support from the ZEB partners, the Research Council of Norway, OverhallaHUS and Innovation Norway.

9. References

Arnesen H., Holme J., Risholt B., Uvsløkk S., Grynning S., Jeller B. P. and Wærp S. 2009, Moderne trevinduer – funksjonalitet, levetid og design, Prosjektrapport 46. "*Modern wooden windows – functionality, lifetime and design. Project rapport 46* ". SINTEF Building and infrastructure.

COMSOL Multphysics, [http://www.comsol.no/] Downloaded 29.11.2013

Grynning S., Baetens R., Jelle B. P. Gustavsen A., Uvsløkk S. and Meløysund V. 2009. Vakuumisolasjonspaneler for bruk i bygninger – Egenskaper, krav og muligheter. Prosjektrapport 31. "Vacuum insulation panels used in buildings – Properties, demands and possibilities. Project rapport 31". SINTEF Building and infrastructure.

The measurements are performed according to EN ISO 8990:1997 (*Thermal insulation. Determination of steady-state thermal transmission properties. Calibrated and guarded hot box*)

NS-EN ISO 6946 (*Building components and building elements - Thermal resistance and thermal transmittance - Calculation method*),

THERM 6, [http://windows.lbl.gov/software/therm/therm.html] Downloaded 29.11.2013

Uvsløkk S. 1990. U-value determination of wall constructions. Proceedings of the 2th Symposium on Building Physics in the Nordic Countries. Trondheim, Norway.

Uvsløkk S., Skogstad H. B., and Aske I. J. 1996. Natural convection in timber frame walls with thick thermal insulation layer. Proceedings of the 4th Symposium on Building Physics in the Nordic Countries. Helsinki, Finland. Vol. 1, pp. 315-322

Moisture dependency of the resistance to moisture flow of thin-layer materials

Lars-Olof Nilsson, Professor

Building Materials Laboratory at Lund University, Sweden

KEYWORDS: *Resistance to moisture flow, thin-layer, barrier, paint system, floor covering*

SUMMARY:
The resistance to moisture flow of thin-layer materials is usually given as a fixed number, derived from a cup test. That number is relevant only for the RH interval where the material was actually tested, since the moisture transport properties of these materials are highly moisture dependent, as most other materials. Today, we have a number of examples where this simple fact is ignored. Additionally, most calculation tools do not include features where the resistance to moisture flow of a thin layer can be made moisture dependent.

The paper gives the theoretical background, describes the problems arising and gives examples when

a. measuring the moisture resistance of thin layers in different humidity intervals,
b. measuring the moisture resistance of a surface material on a substrate,
c. utilizing moisture resistances in intervals different from where it was tested.

The application examples involve floor coverings, paints on substrates and vapour and moisture barriers.

1. Introduction

The resistance to moisture flow of thin-layer materials is usually given as a fixed number, derived from a cup test. That number is relevant only for the RH interval where the material was actually tested, since the moisture transport properties of these materials are highly moisture dependent, as most other materials.

Today, we have a number of examples where this simple fact is ignored.

- The resistance to moisture flow of a surface material on a substrate may be measured without considering the moisture conditions in the substrate, with and without the surface material.
- The resistance to moisture flow of a thin-layer material is measured in an irrelevant moisture interval, giving results that are not applicable.
- The resistance to moisture flow of a thin-layer material is utilized in moisture intervals that are different from where it was tested.

Additionally, most calculation tools do not include features where the resistance to moisture flow of a thin layer can be made moisture dependent.

The theoretical background is summarized, the problems arising are described and some application examples are given.

2. Theoretical background

The moisture transport properties of a material may b described in many ways. As long as no temperature gradient is present, any description can be used since they are all possible to translate into each other.

A moisture transport coefficient that is commonly used in some countries is δ (m^2/s) that is defined by this flux equation

$$J = -\delta(RH)\frac{\partial v}{\partial x} \qquad (1)$$

where J is the flux of moisture (kg/m^2s)
v is the vapour content (kg/m^3)
δ is the moisture transport coefficient with v as transport potential (m2/s)
RH is the relative humidity in point x
$\partial v/\partial x$ is the vapour content gradient (kg/m^4)

Even though the vapour content is used as the moisture transport potential for the total flux of moisture the moisture transport coefficient is not a “vapour” conductivity, an expression that is commonly, but erroneously, used. The flux of moisture is almost never pure vapour diffusion in most building materials; flux of capillary condensed and adsorbed water is the major part of the flux of moisture.

The moisture transport coefficient is given as $\delta(RH)$, where RH is the relative humidity in a point of the material to show that it is strongly moisture dependent for most materials.

In figure 1 a moisture dependent moisture transport coefficient $\delta(RH)$ is shown, in principle.

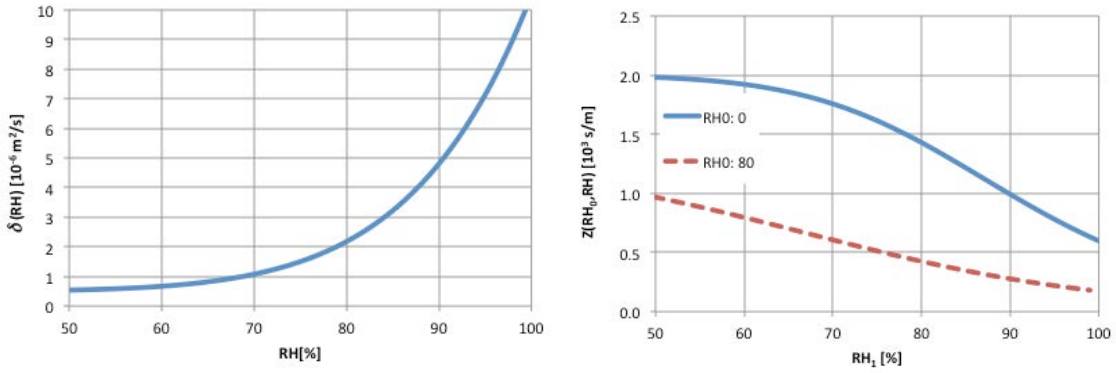

FIG 1. An example of a moisture dependent moisture transport coefficient δ(RH)(left), in principle, and the corresponding resistance to moisture flow $Z(RH_0,RH)$ for two levels of RH_0.

For a layer of a material with a defined thickness Δx (m) the moisture transport property is described as a resistance Z (s/m) to moisture flow that is defined by $Z = \Delta x/\delta$ (s/m). An alternative is to use the conductance for moisture flow $1/Z = \delta/\Delta x$ or δ/d (m/s).

The resistance to moisture flow Z(RH) is of course also strongly moisture dependent since δ(RH) is. That means that the resistance must be defined in the relevant humidity interval (RH_0, RH_1), that depends on the RH on the two sides of the layer

$$Z(RH_0, RH_1) = \frac{\Delta x}{\delta(RH_0, RH_1)} \qquad (2)$$

where $\bar{\delta}(RH_0,RH_1)$ is the average of the moisture transport coefficient in the humidity interval (RH_0, RH_1).

The resistance to moisture flow of a 1 mm thick layer of the material with a moisture transport coefficient as the left diagram in figure 1 is shown to the right in figure 1, as a function of RH on one side, for two RH-levels on the other side. The absolute value of the resistance to moisture flow of a layer of a material is obviously very different depending on the climatic conditions at the two sides. This must be considered determining or predicting the moisture flow through a combination of a surface material and a substrate.

2.1 Moisture distribution in a two-material combination

When a thin-layer material is combined with a substrate, the moisture conditions in the contact zone between the two materials will of course depend on the geometry, boundary conditions and the moisture transport properties of the two materials. In a steady-state, isothermal case the humidity interval (RH_0,RH_1) for the thin-layer material A is given by, cf. figure 2 (left)

$$RH_1 = RH_0 + \frac{Z_A\left(RH_0, RH_1\right)}{Z_A\left(RH_0, RH_1\right) + Z_{substrate}\left(RH_1, RH_3\right)}\left(RH_3 - RH_0\right) \quad (3)$$

where
- RH_0 is the relative humidity at the surface of the thin-layer material
- RH_3 is the relative humidity at the other side of the substrate
- $Z_A(RH_0,RH_1)$ is the resistance to moisture flow of the thin-layer material A
- $Z_{substrate}(RH_1,RH_3)$ is the resistance to moisture flow of the substrate

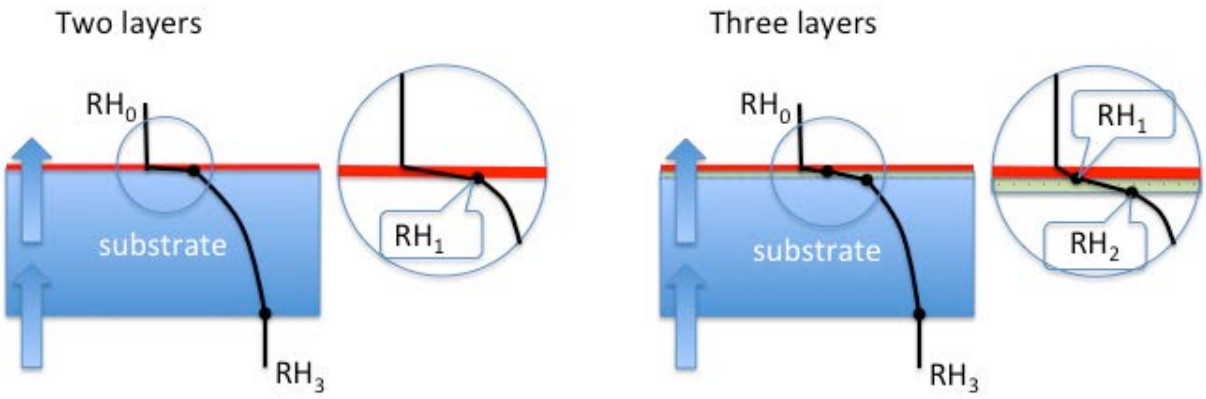

FIG 2. The steady-state, isothermal RH-distributions in a two- (left) and three-layer (right) material combination, in principle

2.2 Moisture distribution in a three-material combination

In the same way the steady-state, isothermal RH-distribution in a three-material combination, with two thin-layer materials A and B, can be calculated from, cf. figure 2 (right)

$$RH_1 = RH_0 + \frac{Z_A\left(RH_0, RH_1\right)}{Z_A\left(RH_0, RH_1\right) + Z_B\left(RH_1, RH_2\right) + Z_{substrate}\left(RH_2, RH_3\right)}\left(RH_3 - RH_0\right) \quad (4)$$

$$RH_2 = RH_0 + \frac{Z_A\left(RH_0, RH_1\right) + Z_B\left(RH_1, RH_2\right)}{Z_A\left(RH_0, RH_1\right) + Z_B\left(RH_1, RH_2\right) + Z_{substrate}\left(RH_2, RH_3\right)}\left(RH_3 - RH_0\right) \quad (5)$$

where RH_2 is the relative humidity at the interface between the two thin-layer materials A and B

$Z_B(RH_1,RH_2)$ is the resistance to moisture flow of the thin-layer material B

Note that the resistances to moisture flow of the two thin-layer materials A and B are moisture dependent. The ones in the two equations are in the humidity intervals (RH_0,RH_1) and (RH_1,RH_2), respectively.

Note as well that the humidity intervals to be calculated are required to calculate the humidity intervals! Here alternative calculation methods are required, preferably by using non-steady-state methods to eventually find the steady-state conditions.

3. Misuse of moisture dependent resistances to moisture flow. Examples

The main way of misusing the moisture dependent resistances to moisture flow of thin-layer materials is by utilizing a resistance from a humidity interval where it was measured and apply it into a situation where the humidity interval will be different. Some examples are shown here.

3.1 Surface cover/moisture barrier at a substrate

Floor coverings are exposed to room climate on top and the moisture from the substrate underneath. Recently, the resistance to moisture flow of a linoleum carpet was claimed to be some Z=788 ks/m (S_D=19.7 m), cf. Pointner (2009), roughly twice as high as previously understood. The test was performed according to EN 12086. First, this was believed to depend on the new carpet being different but later it was clear that the testing procedure was to blame. The test was done with 0 % RH on one side. Data from Haraldsson, cf. figure 3, shows a significant moisture dependency of the resistance to moisture flow of linoleum carpets. Such a material should be tested in a humidity interval where it is used.

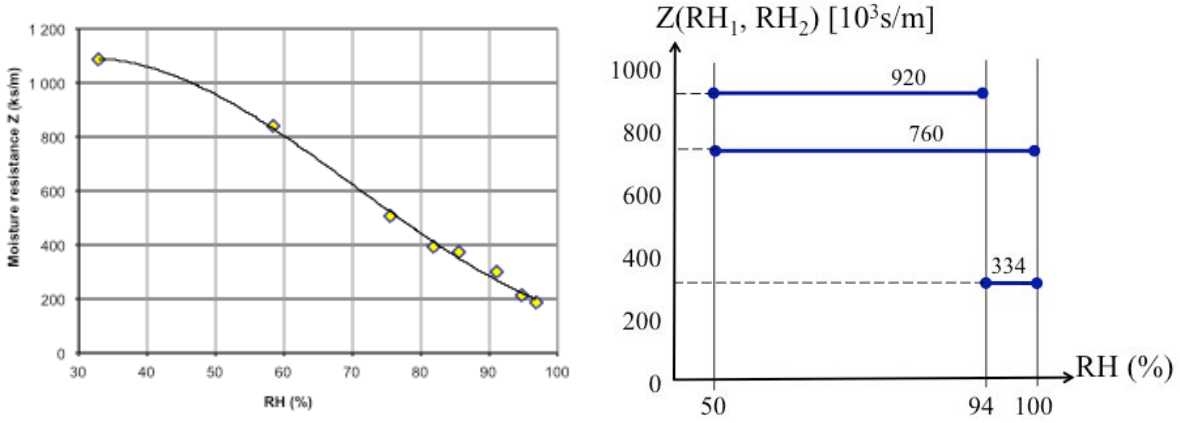

FIG 3. The moisture dependent resistances to moisture flow of two thin-layer materials, a 2.5 mm thick linoleum carpet (left), Haraldsson (2009), and a wet-room moisture barrier, Jansson (2006)

Wet-room moisture barriers were previously tested with a wet-cup method, with 94 % RH on the wet side. Jansson (2006) showed that such a material may very well be exposed to 100 % RH all the time. Jansson (2006) tested moisture barriers, cf. figure 3, with EN 12572 but used also more realistic humidity intervals. In figure 3 (right) the resistance to moisture flow is shown for two intervals (50,94) and (50,100). From those results the resistance in the interval (94,100) can be calculated according to the method by Anderberg & Wadsö (2004). The result is shown in figure 3.

Obviously, such a moisture barrier has very moisture dependent transport properties. This must be considered when testing the moisture transport properties. Today this is done in a much more relevant humidity interval (75,100).

3.2 Moisture barrier beneath a surface cover

An extreme example of misuse of the moisture dependent moisture transport properties is the testing of moisture barriers for use beneath PVC-flooring, cf. Nilsson (1977). Such a flooring material may have a resistance to moisture flow larger than Z=500 ks/m, corresponding to a moisture conductance of $1/Z=2\cdot10^{-6}$ m/s. To ensure an RH lower than 90 % beneath a PVC-flooring the moisture barrier need to have a resistance to moisture flow of more than Z=100 ks/m, cf. equation 5, equivalent to less than $1/Z=20\cdot10^{-6}$ m/s.

When using a wet cup method to measure the moisture transport properties, the humidity interval (40,90) was used. Nilsson (1977) showed that the transport properties of such a moisture barrier has a very large moisture dependency, see figure 4. A test in the interval (40,90) gives a conductance of $1/Z=12\cdot10^{-6}$ m/s but in the interval where it is to be exposed, (90,100), the conductance is much larger: $>50\cdot10^{-6}$ m/s.

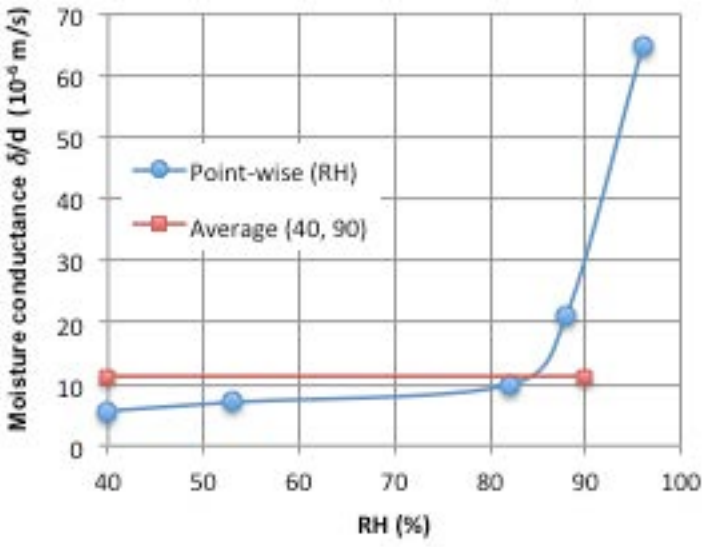

FIG 4. The moisture dependent conductance for moisture flow of an epoxy-based moisture barrier, Nilsson (1977)

4. Traditional methods to measure the resistance to moisture flow

Traditionally the resistance to moisture flow of a thin-layer material is determined by manufacturing a specimen as a layer of the material with a defined thickness or by covering the surface of a substrate with the thin-layer material and measure the steady-state flux out of or into a cup; i.e. the traditional cup method. In both cases the resistance to moisture flow is determined from the steady-state flux through the material. With a surface cover at a substrate the resistance of the substrate is determined in a separate measurement and subtracted from the resistance of the material combination. This is, however, not correct, see the next section.

To determine the moisture dependency of the resistance to moisture flow a series of cup method measurements must be done, usually with a constant humidity at one side. The steady-state flux as a function of RH at the other side can be used to evaluate the moisture resistance or conductance. The flux itself gives the moisture dependent “fundamental potential”, cf. Arfvidsson (1998). The derivative gives the moisture dependent moisture conductance, cf. Nilsson (1977). The transport properties in a small interval can be deduced from measurements in two larger intervals as described by Anderberg & Wadsö (2004).

5. A new method to measure the resistance of a surface cover on a substrate

The resistance to moisture flow of a combination of a surface cover and a substrate may be measured in a series of humidity intervals to quantify the moisture dependency. The resistance of the substrate only can then be determined in the same way. The difference between the two does not necessarily give the correct resistance of the surface cover, as is usually done. It would be erroneous to make an evaluation in that way. The result would only be close to correct if the resistance of the substrate is negligible but then, on the other hand, that resistance does not have to be quantified.

Instead, the results must be used in a new way by utilizing the two moisture dependent resistances. The principle is shown in figure 3.

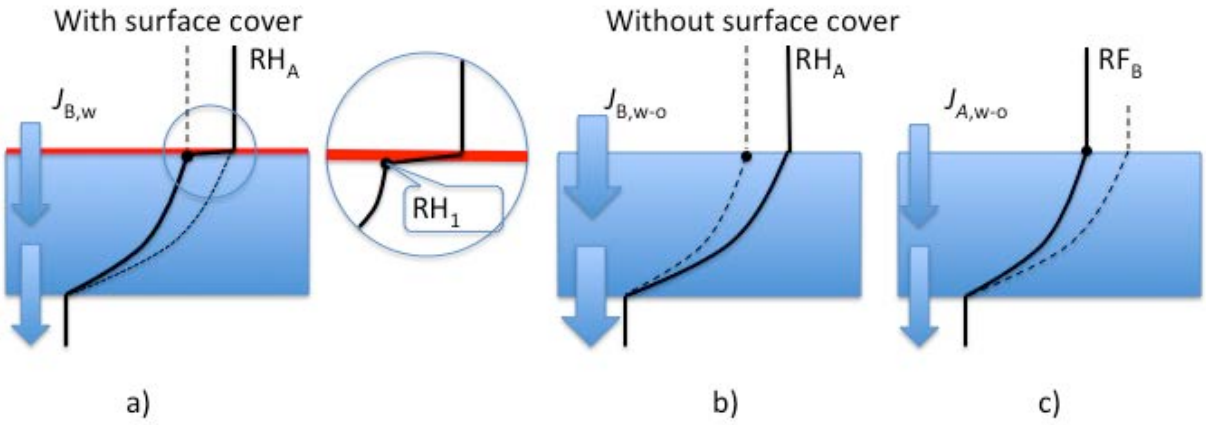

FIG 3. The steady-state RH-distributions in the substrate during the two measuring conditions

The measuring principle is to determine the resistance of the surface cover as the difference between

- the resistance of the surface cover plus the substrate (case a in figure 3) and
- the resistance of the substrate only, but at the same humidity distribution in the substrate in both cases (case c) in figure 3)!

By determining these two resistances to moisture flow in a series of humidity intervals the moisture dependency of the resistance to moisture flow of the surface cover can be evaluated.

5.1 Experimental

From a painted wooden beam a number of circular discs were cut out, with a thickness of 8 mm and a diameter of 63-64 mm, cf. Nilsson & Nilsson (2013). The discs were put as lids on glass cups containing a series of saturated salt solution giving an RH of 75, 85, 94, 97 and 100 % RH. Additionally one cup was turned upside down to give direct contact with water. The half of the discs that had the paint system at one surface was turned with the paint system inside the cups, against the more humid conditions. The cups were stored in a climate room with +20°C and 55 % RH until steady-state fluxes were achieved. The resistances to moisture flow are shown in figure 4.

5.2 Evaluation

A correct evaluation is based on finding the actual RH_1 at the interface between the paint system and the substrate, cf. figure 3. This is done step-wise by first estimating an RH_1, and use this to determine the $Z_{substrate}$ in the humidity interval (RH_3, RH_1) where RH_3 is the RH at the dry side of the discs, 55 %. From that RH_1 can be calculated. If it is not close to the first estimation, the estimate is updated, and so on. When the RH_1 is found, for each RH_0, the resistance of the paint system can be deduced. The results are shown in Table 1 and in figure 5.

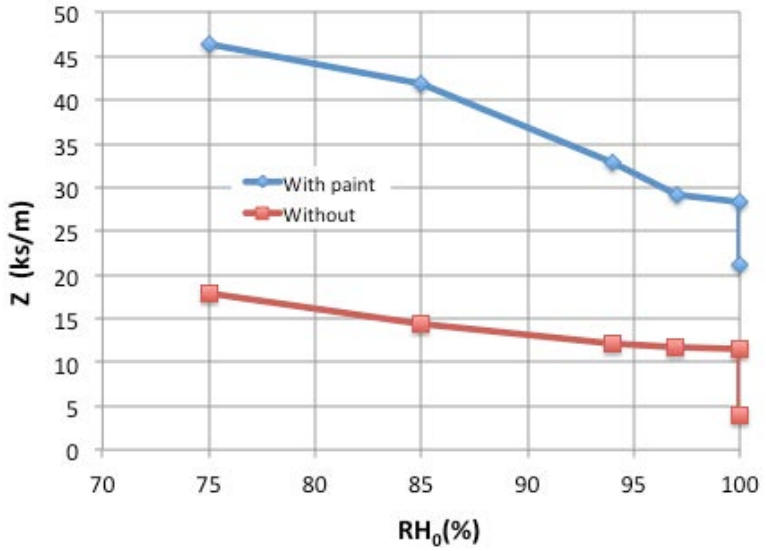

FIG 4. The resistance to moisture flow of the specimens in the two measuring conditions as a function of the RH at the surface of the exposed surface, with and without paint.

TABLE 1 Correct evaluation of resistance to moisture flow on a wooden substrate

RH_3(%)	RH_0(%)	$Z_{painted\ disc}$ (ks/m)	RH_1(%)	$Z_{substrate}$ (ks/m)	Z_{paint} (ks/m)
55	75.00	46.39	64.4	21.70	24.69
55	85.00	41.78	69.3	19.96	21.82
55	94.00	32.79	75.9	17.55	15.24
55	96.99	29.22	78.8	16.51	12.71
55	99.99	28.37	80.3	15.99	12.38
55	100.00	21.10	85.5	14.32	6.78

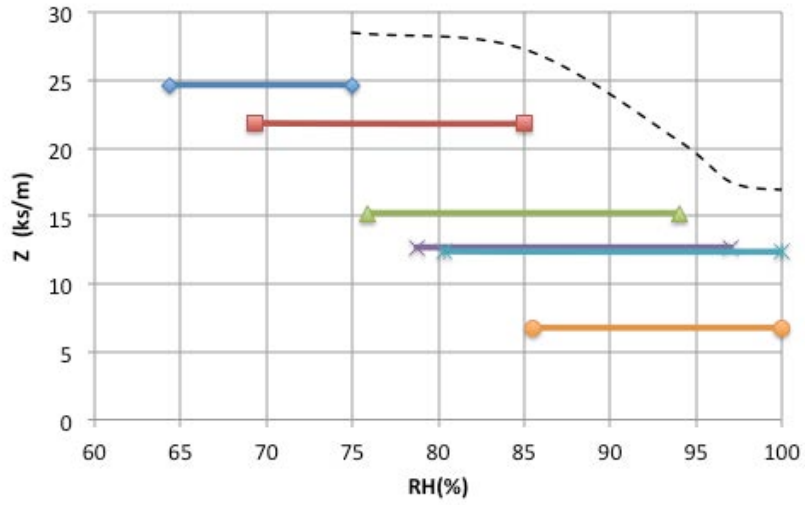

FIG 5. The resistance to moisture flow of the paint system as a function of humidity. The dashed line shows the erroneous results of a traditional evaluation

In figure 5 the incorrect results of a traditional evaluation is shown as well, where the difference between the two curves in figure 4 is used.

6. Conclusions

The moisture transport properties of thin-layer materials are in most cases strongly moisture dependent. Because of that these properties cannot be given by a single number, a resistance to moisture flow or a conductance. The moisture dependency must be described, and determined, in relevant humidity intervals. A number of cases were shown where this was not done.

From the experimental results it is obvious that the resistance to moisture flow of the paint system is strongly moisture dependent. There is a factor of 4 between the driest and wettest humidity intervals. When performing calculations of steady-state or non-steady state moisture distributions those differences must be considered. This is not easy to do with today's calculation tools where thin-layer materials usually are given a constant resistance to moisture flow.

The new evaluation method for moisture dependent resistances of thin-layer materials at a substrate works well. To cover a wider range of humidity intervals a larger RH-interval (lower RHs) could have been chosen for the discs without paint and thinner discs in the more humid intervals. This is recommended for future measurements of resistances to moisture flow of thin-layer materials at a substrate.

7. Acknowledgements

Part of the work is part of a project in WoodBuild, a research programme within the Sectoral R&D Programme 2006-2012 for the Swedish forest-based industry. This Programme is jointly funded by the government, industry and other stakeholders with interests related to the Swedish forest-based industry. Research engineer Bengt Nilsson performed all the measurements in the experimental part.

References

Anderberg. A & Wadsö, L. 2004. Moisture properties of self-levelling flooring compunds. Part I. Diffusion coefficients. Nordic concrete research Publication 32, 2/2004, pp. 3-15

Arfvidsson, J. 1998. Moisture transport in porous media. Modelling based on Kirchoff potentials. Report TVBH-1010. Div. Building Physics, University of Lund

EN 12086 - Thermal insulating products for building applications - Determination of water vapour transmission properties.

EN 12572 - Hygrothermal performance of building materials and products - Determination of water vapour transmission properties.

Haraldsson, N. 2009. Moisture properties of linoleum carpets. Unpublished results. Diploma work. Laboratory of Building Materials, University of Lund

Jansson, A. (2006) Sealing layer behind tiles in wet room exterior walls (in Swedish). SP-report 2006: 46. SP Swedish National Testing and Research Institute, Borås

Nevander, L. & Elmarsson, B. Fukthandbok, Praktik och teori. 2nd ed. Stockholm, AB Svensk Byggtjänst, Stockholm. 538 p.

Nilsson L.-O. 1977. Moisture problems at concrete floors (in Swedish). Report TVBM-3002, Laboratory of Building Materials, University of Lund

Nilsson L.-O. & Nilsson B. 2013. A method to determine resistance to moisture flow of paint systems on wood substrate. A project within WoodBuild C (in Swedish). Report TVBM-3174, Laboratory of Building Materials, University of Lund

Pointner, J. 2009. Report 59611. ÖTI – Institut für Ökologie, Technik und Innovation, Wien

Analysis of the weighing methods for oven-dried porous building materials

Chi Feng, Ph.D. candidate [1,2]
Hans Janssen, Associate Professor [2]
Qinglin Meng, Professor [1]
Ya Feng, Professorate Senior Engineer [3]

[1] Building Environment and Energy Laboratory (BEEL), State Key Laboratory of Subtropical Building Science, South China University of Technology, P.R. China
[2] Building Physics Section, Department of Civil Engineering, KU Leuven, Belgium
[3] China Southwest Architectural Design and Research Institute Corp. LTD, P.R. China

KEYWORDS: *dry mass, weighing methods, sample size, exposure time, moisture absorption, porous building materials*

SUMMARY: *The reliable determination of dry mass is the basis for characterizing the hygrothermal properties of porous building materials. Due to its efficiency, oven drying at elevated temperature is widely used. However, the weighing process for the oven dried samples can introduce an error due to the moisture absorption from ambient air. This paper experimentally studies the influence of this error on the dry mass determination for samples made of autoclaved aerated concrete, calcium silicate insulation and ceramic brick. Results show that for strongly hygroscopic materials, large samples are not sensitive to this error, and it is safe to take samples out of the oven and weigh them directly. Small samples, however, are more sensitive to this error. Consequently it is suggested to use sealing containers in the weighing process for them. For weakly hygroscopic materials, the moisture exchange flux is much less intensive, and thus the weighing protocol matters less. Last but not least, the linear correction method has been proven reasonable for both strongly and weakly hygroscopic materials. It is recommended in case of very critical requirements.*

1. Introduction

Heat and mass transfer is important in many areas, such as in soil science (Tuli, Hopmans et al. 2005), energy engineering (LaManna & Kandlikar 2011), food processing (Yuan, Hanselmann et al. 2009) and environmental protection (Milt, Banús et al. 2010). In building physics, energy efficiency, indoor air quality, service life and many other crucial issues are all closely related to heat and moisture transfer processes (Abuku, Janssen et al. 2009; Geving & Holme 2010; Kwiatkowski, Woloszyn et al. 2011). It is therefore of great significance to study them in built constructions.

In the analysis of heat and moisture transfer phenomena, hygrothermal properties are indispensable parameters. Almost all hygrothermal properties are related to the moisture content, for which the dry mass plays a crucial role (Hens 1991; Kumaran 2002; Roels, Carmeliet et al. 2003). It is therefore self-evident that the reliable determination of dry mass is of vital importance.

Oven drying at elevated temperature is the most popular method to determine dry mass in building physics, because of its drying efficiency and its equipment simplicity (Feng, Janssen et al. 2013). The ISO 12570 standard provides detailed descriptions of the experimental procedure (ISO 12570), which typically involves sample transportation between oven and balance. Unfortunately, in the process of taking samples out of the oven and weighing them on the balance, there is a momentary contact between samples and ambient air. During this period, moisture exchange between samples and air inevitably causes an error on the dry mass. This error may not always be negligible, but it has not received adequate attention.

There are several methods to tackle this error:

A. To perform the weighing process in a dry air environment;
B. To use air-tight containers to seal samples during the transportation and weighing process;
C. To measure the error experimentally and correct it mathematically;
D. To assume that the error has negligible magnitude.

Method A will provide reliable results. But since providing such a dry air environment is not straightforward, it is seldomly applied. Method B is suggested by both the ISO 12571 and the ASTM C1498 standards (ISO 12571; ASTM C1498), and can be proven to be effective (Feng, Janssen et al. 2013). However, not all samples can be sealed in containers for size reasons. As Method C, Richards suggested a linear correction method (Richards, Burch et al. 1992): by weighing the sample exposed to ambient air over a given time interval, a linear correction toward the initial mass can be performed. Although this method was originally used for the determination of equilibrium moisture content at different RHs, it should similarly apply to the determination of dry mass, too. However, for a large number of samples, this method may require much time and effort. More importantly, the validity of the linear correction has not been fully established yet. Method D is most widely adopted but without much theoretical or experimental support. To sum up, more in depth analysis of the drying and weighing procedure is desirable.

In this paper, we perform a comparative assessment of different methods for dry mass determination. To start with, oven dried samples are weighed with sealing containers, with linear correction, as well as in groups and one by one. The dry mass obtained from these methods is then compared. Next the validity and applicability of the linear correction method is analyzed. Finally the crucial influence factors in determining the dry mass of samples are discussed.

2. Materials and methods

Autoclaved aerated concrete (AAC, 440 kg/m^3), calcium silicate insulation (CS, 255 kg/m^3) and ceramic brick (CB, 2050 kg/m^3) are chosen as target materials. Raw materials are cut into samples of two sizes – 5cm×5cm×1cm and 12cm×8cm×4cm – to represent both large and small area to volume ratios. For each material and each size, 5 duplicate samples are used (numbered A to E). In this paper we call the 5 duplicates of the same material and the same size a group.

TABLE 1 Different weighing methods for oven dried porous building materials

Name	Corresponding method in *Introduction*	Description	Adopted by	
			Large samples	Small samples
Weighing with sealing containers	B	Seal all samples in glass containers (one group in each container) after opening the oven. Then take one container out of the oven each time. Finally take one sample out of the container each time and weigh.	No	Yes
Weighing with linear correction	C	Take one sample out of the oven each time and weigh it every 20 seconds for 2 minutes with linear correction toward the initial dry mass.	Yes	Yes
Weighing in groups	D	Take a group of samples out of the oven each time and weigh them one by one immediately.	Yes	Yes
Weighing one by one	D	Take one sample out of the oven each time and weigh it on the balance immediately.	Yes	Yes

All samples are dried at 70 ℃ in a ventilated oven supplied with dry air. After an initial drying period of approximately one week, samples are taken out of the oven every two or three days for the dry mass determination. Various weighing methods are summarized in TABLE 1. The method of weighing with linear correction has been performed only once on each sample, while all other methods have been performed four times on each sample. The temperature of room air is 23 ℃ and the RH is around 55%.

3. Results

3.1 Large samples

The dry mass of large samples obtained from different weighing methods is illustrated in FIG 1. The linearly corrected values are denoted as “Corrected linearly”, while “In groups” and “One by one” stand for the average values from the four weighings by weighing in groups and weighing one by one respectively. The error bars for “In groups” and “One by one” indicate the standard deviations for these four weighings.

It is clear that the dry mass obtained from different weighing methods is almost identical. The relative differences between different dry mass results are less than 0.05% for all materials, which is negligible in most cases for both scientific research and engineering practice. Moreover, the relative standard deviations for weighing in groups and weighing one by one are also very small, showing that their weighing precision is quite nice. Considering the low efficiency of linear correction for each sample, it is not recommended except for extremely accurate results. When it comes to weighing samples in groups and one by one, both methods provide satisfactory results. However, weighing samples in groups are more convenient because this method saves time, as well as avoids opening the oven too often and disturbing the conditions inside.

To sum up, for large samples, weighing in groups is the most convenient weighing method in terms of reliability and efficiency.

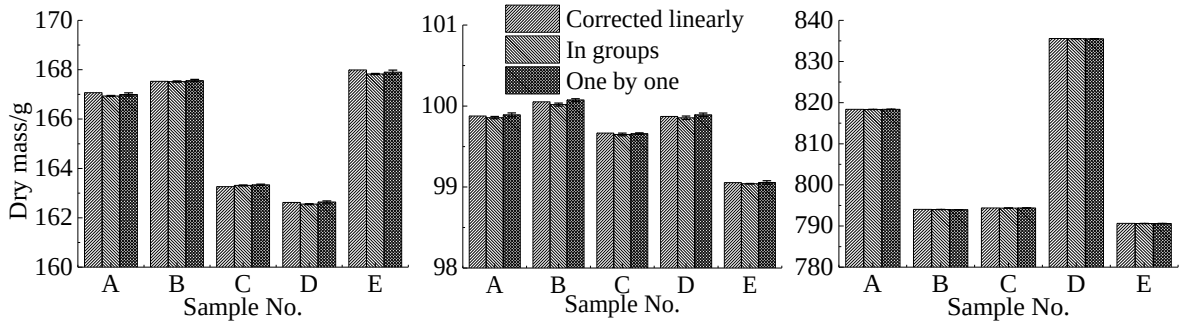

FIG 1. Dry mass of oven dried large samples determined from different weighing methods

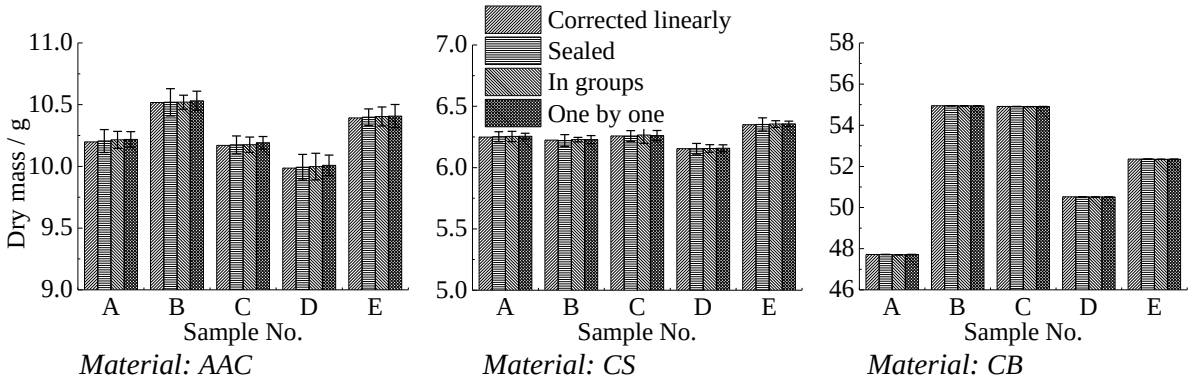

FIG 2. Dry mass of oven dried small samples determined from different weighing methods

3.2 Small samples

The dry mass of small samples obtained from different weighing methods is illustrated in FIG 2. Obviously, the situation is more complicated than that of large samples. To start with, we assume that the dry mass obtained with linear correction – which is the smallest in most cases – is the closest to the true dry mass of the oven dried state. Thus we take the corrected dry mass as the reference.

For the strongly hygroscopic AAC and CS samples, the dry mass increases proportionally with the exposure time, as revealed in the linear correction process (FIG 3). Due to the large area to volume ratio of small samples and the small density of these two materials, the influence of moisture absorption during the weighing process can be impressive. The relative difference between the correct dry mass and the dry mass determined without sealing is around 0.1% or even larger. According to the ISO 12570 standard, the dry mass determination should be within 0.1% fluctuation at 24h interval or longer (ISO 12570), meaning that a mass deviation larger than 0.1% is unacceptable. Consequently weighing in groups or one by one is not preferable for small AAC and CS samples, albeit that the four weighing results are close. On the contrary, if sealing containers are used, then the results are much closer to the corrected dry mass while the weighing scatters remains small. Although it requires extra effort to use these containers, experimental reliability should come first. In addition, it is still more convenient and straightforward to use sealing containers than adopting the linear correction method.

For CB samples, the impact of moisture absorption during the weighing process is very limited, due to the large density and limited hygroscopicity of the material. Thus the weighing procedure matters less.

To sum up, for small samples made of strongly hygroscopic materials, using sealing containers in the weighing process is preferable. For those made of weakly hygroscopic materials, the weighing protocol is not that crucial, but it is still reasonable to use sealing containers in the weighing process.

4. Discussion

So far we have recommended weighing in groups for large samples and using sealing containers for small samples for the dry mass determination process. As a further step, we analyze the validity and applicability of the linear correction method, and subsequently we aim at generalizing our findings.

4.1 The linear correction method

The basic assumption of the linear correction method is that within a short period of time, the mass increase due to moisture absorption from ambient moist air ($\Delta m_{moisture}$, kg) evolves linearly with time:

$$\Delta m_{moisture} = \beta \cdot A \cdot \Delta p_v \cdot t \qquad (1)$$

Where β the surface vapor transfer coefficient, kg/(m^{2}sPa)
A the surface area, m^2
Δp_v the vapor pressure difference between ambient air and sample surface, Pa
t time, s

TABLE 2 Linear fitting and β calculation (average values from 5 duplicate samples)

Material	Large samples			Small samples		
	Flux g/(m^{2}s)	β 10^{-8}kg/(m^{2}sPa)	R^2	Flux g/(m^{2}s)	β 10^{-8}kg/(m^{2}sPa)	R^2
AAC	1.76E-2	1.10	>0.99	1.78E-2	1.11	0.96
CS	1.35E-2	0.85	>0.99	1.72E-2	1.08	0.95
CB	1.30E-4	0.008	-	2.04E-3	0.13	0.60

Eq.(1) translates to the implicit assumption of a constant vapor pressure difference between samples and ambient air, or a constant vapor pressure at the samples' surface.

To evaluate the validity of such linear correction, we fit Eq.(1) to our measured results, with the moisture exchange flux $\beta \cdot \Delta p_v$ as the primary fitting result. Assuming a constant vapor pressure difference between sample surface and ambient air, this result can equally be expressed as the surface transfer coefficient β. For oven dried samples, the vapor pressure at the sample surface can be assumed close to 0 Pa. The vapor pressure in the ambient air is derived from the lab conditions – 23 ℃ and 55% RH – and comes to 1544 Pa. The average results are shown in TABLE 2.

If we look at the results for AAC and CS samples, the linear correction method works well. The R^2 is very close to 1.0. Moreover, the values of β are around 1×10^{-8} kg/(m^{2}sPa), which falls in the range of the measured and calculated values in the IEA Annex 41 Project (Kumaran & Sanders 2008). Last but not least, as confirmed in TABLE 2, the moisture exchange fluxes are almost the same for the AAC and CS samples, independent of their sizes.

Unfortunately, for CB samples the R^2 is either far from 1.0 or unavailable. Worse still, the calculated β values are 1-2 orders smaller than those for AAC and CS samples. This may result from the limited hygroscopicity of CB samples. According to our measurements, CB samples are only weakly hygroscopic, and hence have a very low moisture capacity. Thus a slight increase in the moisture content at the surface corresponds to a strongly increased vapor pressure there, which reduces the vapor pressure difference between the sample surface and the ambient air. As a result, the moisture absorption rate becomes limited and experimental errors play an important role in the determination of the mass increase.

For further interpretation, we turn to numerical simulations for the moisture absorption process of AAC and CB samples (to represent strong and weak hygroscopicity respectively). The software used is *Delphin (version 5.6)*, developed by the Institute of Building Climatology, Technical University of Dresden. Material properties in the software have been modified according to our material property measurements. Surface heat and moisture transfer coefficients are set as 8 W/(m^{2}K) and 1×10^{-8} kg/(m^{2}sPa), respectively. FIG 3 illustrates the simulated and measured mass increase of both large and small samples. It should be noted that we don't have measured weight values at the very beginning (time 0 s). Thus we calibrate the measured values at 20 s to be equal to the simulated values at that time, and modify the later measurement results accordingly.

Generally speaking, the agreement between simulated results and measured results is acceptable. Specifically, for both large and small AAC samples, the simulated mass increase is slightly lower than that from measurement. This may result from the conservative β value (smaller than that derived from our measurements) used in the simulations. More importantly, in our simulations, we implemented a linear adsorption curve between 0 and 11.3% RH. In reality, a more convex curve is expected in this region, which increases the actual moisture capacity valid for our circumstances. Such higher capacity would yield a higher simulated moisture absorption, improving the agreement between simulations and measurements. As we do not have more detailed sorption data in the 0 to 11.3% RH region, we can however not reliably quantify that. Notwithstanding, it is clear that the linear correction method is valid for AAC, as well as for other strongly hygroscopic materials. After applying the linear correction, a value close to the initial (and hence the "true") value can be obtained.

When it comes to CB samples, the situation is a bit different. First, for both simulations and measurements, the mass increase of CB samples is much less than their AAC counterparts. As explained before, this must originate from the limited hygroscopicity and moisture capacity of CB samples. Moreover, for small CB samples the simulated mass increase after 120 s is 0.004 g, while our measurement gives 0.002 g. This tiny mass change is close to the resolution limit of our balance, and

thus the readings from the balance are no longer reliable. For large AAC samples, the difference between simulated and measured values is somewhat larger. Unfortunately, we cannot explain this deviation very well. We have double-checked our simulation and measurement results very carefully, and all results are reasonable. Currently hence, this deviation remains as a question for the future. Nevertheless, it is again clear that the linear correction method is reasonable for CB (and other materials with limited hygroscopicity), even if it is not theoretically perfect due to the rise of surface vapor pressure.

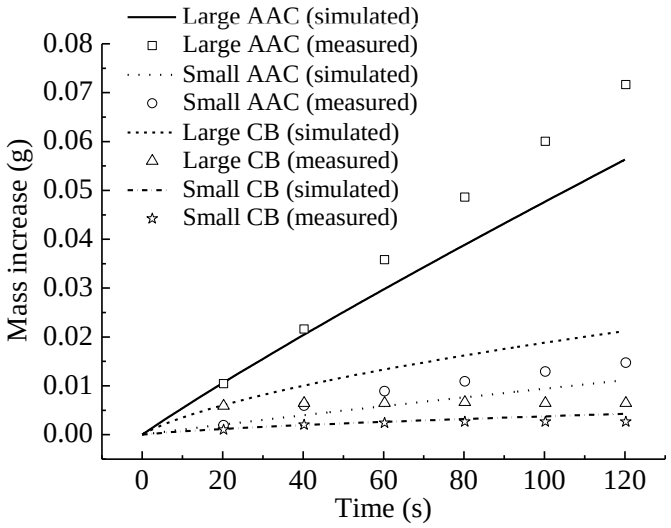

FIG 3. Comparison of the simulated and measured mass increase

4.2 Influence of absorbed moisture on dry mass determination

Now that we have confirmed the applicability of the linear correction method, the potential impact of moisture absorption during the weighing procedure is to be analyzed. As a general case, let's consider a material with bulk density ρ (kg/m^3). A sample with surface area A (m^2) and volume V (m^3) can absorb a certain amount of moisture $\Delta m_{moisture}$ (kg) from the ambient air within contact time t (s). The relative error of the absorbed moisture on dry mass (E, %) then becomes:

$$E(\%) = \frac{\Delta m_{moisture}}{m_{dry}} \times 100 = \frac{\beta \cdot A \cdot \Delta p_v \cdot t}{\rho \cdot V} \times 100 \qquad (2)$$

Where m_{dry} the dry mass of the sample, kg

For strongly hygroscopic materials, the vapor pressure on the surface remains close to 0 Pa after absorbing a small amount of moisture. Thus the vapor pressure difference Δp_v can be assumed equal to the vapor pressure of ambient air p_{ve} all the time. For weakly hygroscopic materials, the vapor pressure on sample surface climbs quickly and hence reduces the vapor difference. However, assuming that Δp_v remains equal to p_{ve} will in that case make E the upper limit for the error.

The ambient air can be assumed at 23 ℃ and 55% RH, giving a vapor pressure of 1544 Pa. Moreover, the value of β can be set as 1×10^{-8} kg/(m^{2}sPa). In addition, the weighing process for a single sample usually takes around 20 s, which can be assumed as the contact time. For common porous building materials, the bulk density is usually 300-2000 kg/m^3. For samples of different sizes, a 1m×1m×1m sample gives A/V=6 m^{-1}, while a 1cm×1cm×1cm sample gives A/V=600 m^{-1}. Thus we look into the situations of A/V=5-1000 m^{-1}. Taking all these values into Eq.(2), we obtain FIG 4. It is clear that both the surface to volume ratio and the material density have large impacts. For large and/or dense samples,

the error remains below 0.02 %, and is thus negligible. For small and light samples with strong hygroscopicity, on the other hand, the error becomes more significant. And as small samples are often preferred for their improved drying efficiency, protective measures may be required.

According to Eq.(2), the only changeable parameters are the vapor pressure difference and the contact time. By conducting the measurement in dry air the error can be reduced dramatically. However, providing such a dry air environment is not straightforward and is seldomly applied. To reduce the contact time, the adoption of sealing containers is effective. This method avoids the frequent opening of the oven, or the direct exposure of samples to ambient air. With sealing containers the average contact time can be reduced to around 10 s for each sample. If there is some desiccant in the sealing containers, the situation is even better. This method is practically feasible, and equally applies to the weighing process for the determination of the equilibrium moisture content at different RHs (Feng, Janssen et al. 2013).

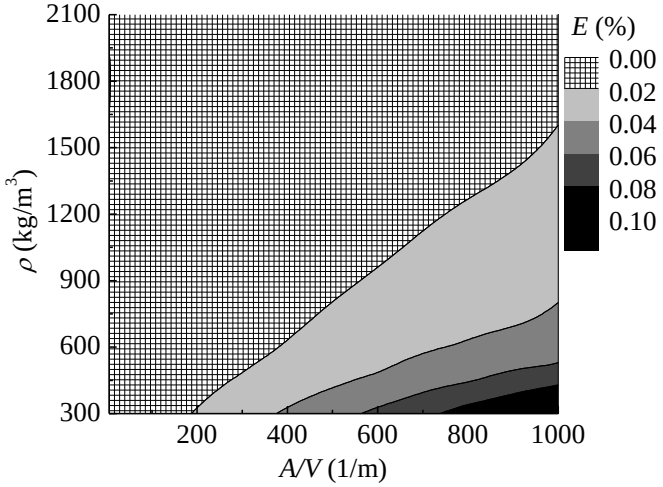

FIG 4. The relative error (E, %) of the absorbed moisture during weighing process (t=20 s, Δp_v=1544 Pa, $\beta = 1 \times 10^{-8}$ kg/(m^{2}sPa))

5. Conclusions

This paper studies different weighing methods for oven dried porous building materials. Samples are made of autoclaved aerated concrete, calcium silicate insulation and ceramic brick, and are cut into two sizes – 5cm×5cm×1cm and 12cm×8cm×4cm. Four weighing methods are compared: weighing with sealing containers, weighing with linear correction, weighing in groups and weighing one by one. Following conclusions are obtained:

A. For strongly hygroscopic materials, large samples are not sensitive to the error caused by the vapor absorption during the weighing process. It is recommended to take large samples out of the oven and weigh them in groups. Small samples are highly sensitive to this error. Consequently it is suggested to use sealing containers in the weighing process for small samples;

B. For weakly hygroscopic materials, the amount of vapor absorbed within a short period of time is limited. Thus the weighing protocol is not that crucial. For them it is still valid to adopt the recommendations for strongly hygroscopic materials;

C. The linear correction method is valid for strongly hygroscopic materials. For weakly hygroscopic materials, it is not theoretically flawless but still serves as an acceptable approximation. In case of very critical requirements, the linear correction method is recommended.

6. Acknowledgements

This project is supported the National Key Technology R&D Program of China (Project No. 2011BAJ01B01). The first author (Chi Feng) is also financially supported by China Scholarship Council for his study at K.U. Leuven. The authors express sincere thanks to Patricia Elsen, Willem Bertels, Filip Vandenberghe and Paul Verbeek at Department of Civil Engineering, K.U. Leuven for their help in carrying out the experiments.

References

Abuku M., Janssen H., et al. 2009. Impact of wind-driven rain on historic brick wall buildings in a moderately cold and humid climate: Numerical analyses of mould growth risk, indoor climate and energy consumption. Energy and Buildings 41(1): 101-110.

ASTM C1498 - 04a: Standard Test Method for Hygroscopic Sorption Isotherms of Building Materials.

Feng C., Janssen H., et al. 2013. Validating various measures to accelerate the static gravimetric sorption isotherm determination. Building and Environment 69(11): 64-71.

Geving S. & Holme J. 2010. The Drying Potential and Risk for Mold Growth in Compact Wood Frame Roofs with Built-in Moisture. Journal of Building Physics 33(3): 249-269.

Hens H. 1991. IEA Annex 14: Condensation and Energy, Volume 3: Catalogue of Material Properties.

ISO 12570: 2000(E) Hygrothermal performance of building materials and products - Determination of moisture content by drying at elevated temperature.

ISO 12571: 2000(E) Hygrothermal performance of building materials and products - Determination of hygroscopic sorption properties.

Kumaran M.K. & Sanders C. 2008. IEA Annex 41: Whole Building Heat, Air, Moisture Response. Subtask 3: Boundary conditions and whole building HAM analysis.

Kumaran M.K. 2002. A Thermal and Moisture Transport Property Database for Common Building and Insulating Materials. Final Report from ASHRAE Research Project 1018-RP.

Kwiatkowski J., Woloszyn M., et al. 2011. Influence of sorption isotherm hysteresis effect on indoor climate and energy demand for heating. Applied Thermal Engineering 31(6-7): 1050-1057.

LaManna J.M. & Kandlikar S.G. 2011. Determination of effective water vapor diffusion coefficient in pemfc gas diffusion layers. International Journal of Hydrogen Energy 36(8): 5021-5029.

Milt V.G., Banús E.D., et al. 2010. Structured catalysts containing Co, Ba and K supported on modified natural sepiolite for the abatement of diesel exhaust pollutants. Chemical Engineering Journal 157(2-3): 530-538.

Richards R., Burch D., et al. 1992. Water vapor sorption measurements of common building materials. Transactions-American society of heating refrigerating and air conditioning engineers 98: 475-485.

Roels S., Carmeliet J., et al. 2003. HAMSTAD Work Package 1: Final Report - Moisture Transfer Properties and Materials Characterisation, EU Contract GRD1-1999-20007.

Tuli A., Hopmans J.W., et al. 2005. Comparison of air and water permeability between disturbed and undisturbed soils. Soil Science Society of America Journal 69(5): 1361-1371.

Yuan Q., Hanselmann W., et al. 2009. Characterization of vapor-induced and liquid-induced moisture migration through fractionated palm kernel (PKO) based multiphase systems. Journal of Food Engineering 95(3): 460-470.

Effect of presence of salt on moisture accumulation and transport in burnt clay bricks

Olga Koronthalyova, PhD [1]
Lubomir Bagel, Dr [1]
Marta Kullifayova, Ing [1]
Tomas Ifka, PhD [1]

[1] Institute of Construction and Architecture, Slovak Academy of Sciences, Slovakia

KEYWORDS: *ceramic brick, water vapour adsorption, water vapour permeability, moisture dependence, hygroscopic salt*

SUMMARY:
In the work the effect of presence of a salt on parameters of moisture transport and accumulation, namely water vapour sorption and water vapour permeability moisture dependence is determined. The analysis is done for three types of commonly used burnt clay bricks with different hygroscopic ability. Experimental work consisted in determination of mineral composition, pore structure parameters, adsorption curves and water vapour permeability of the salt free and saline specimens. The presence of salt resulted in significant increase of the adsorbed water. For case of practically non-hygroscopic ceramic bricks, the sorption measurement has confirmed acceptable agreement with a simplified calculation, based on assumption of independence of the moisture adsorption by salt and by material. A deviation from the calculation was noticed in the range of high relative humidity, where obtained amount of moisture was lower than the calculated one. In case of the hygroscopic brick the interaction between the hygroscopic moisture of the material and the moisture of the salt was found out. Salt presence had practically no influence on water vapour permeability at higher moisture contents, where cumulated effect of the water vapour diffusion and the surface diffusion took place. On the other hand salt crust formation occurring during the dry cup measurements caused noticeable decrease of the resultant water vapour permeability.

1. Introduction

Numerical simulation is at present a common tool for determination of hygro-thermal state of building structures. However, reliable results of numerical simulation can be obtained only on condition of using correct moisture transport and accumulation parameters. Moisture transport and accumulation parameters are commonly measured in laboratory conditions where moisture in material pores is not contaminated. In reality, an interaction between the materials in building structures and chemicals from the surrounding air or water can take place and therefore pore water very often contains dissolved salt or different salts.

The issue of penetration and presence of salts in building materials is rather often discussed in literature but the existing works are focused mainly on an evaluation of the mechanical degradation of the saline materials or modelling the process of penetration of salt into porous building materials. The works dealing with moisture transport and accumulation parameters of saline building materials are not so frequent. A significant increase of the amount of adsorbed water in saline ceramic brick is presented for example in (Hansen 1986). Similarly Nielsen (1991) obtained substantially higher values of adsorbed water for ceramic brick and sandstone containing different salts. In the work also applicability of a simplified model for prediction of water vapour adsorption of saline building materials was analysed.

In this work the effect of the presence of sodium chloride on water vapour adsorption isotherm and the water vapour diffusion is quantified for three types of commonly used ceramic bricks with different hygroscopic ability. The analysis is limited to small salt concentrations having practically negligible effect on the material porosity. Based on the measured data the possibility of the prediction of the water vapour adsorption and water vapour permeability of saline bricks using the corresponding parameters of the salt free materials is discussed.

2. Materials and methods

The tested bricks are commonly used burnt clay bricks produced by three different Slovak manufacturers. Before the tests, a portion of the tested specimens was contaminated by sodium chloride solution. The samples were partly immersed in 4% NaCl solution (40 g NaCl in 1000 g of distilled water). The depth of the specimen immersion was kept at 3 mm in order capillary uptake of the salt solution take place. The samples were kept in contact with salt solution until the first phase of capillary uptake process was completed, i. e. until the water front reached the upper surface of the sample. It took from 1 to 3 hours, depending on the particular specimen and its height which varied between 15 and 28 mm. The saline samples were first dried by an air flow (the air flow velocity was about 1m/s) in air conditioned laboratory room (temperature of 23 ± 0.5°C and RH equal to 53 ± 1%) for 48 hours, then were oven dried to a constant mass and put to the tests. The salt content of the saline bricks was determined gravimetrically, from the weight of the original and saline dried out samples as well as from electrical conductivity of their extracts (Table of conductivity). The value determined from the conductivity of the extracts can be considered as a minimum level of the salt content. The extracts were prepared from 10g of dried powdered sample and 100 ml of distilled water. The whole extraction took about 24 hours. The pH and electrical conductivity of extracts was measured by pH meter LABIO pH 03 with combined glass electrode SEOJ 212 and conductivity meter WTW LF 96.

The tested materials were characterised by following basic parameters: bulk density, density, total porosity, open porosity and capillary moisture content. The bulk density was calculated from volume and mass of the dried out specimens (oven drying at 105°C). The density of ceramic body was determined by gas (N_2) pycnometer Pentapyc 5200e. The total porosity was calculated from density and bulk density. The open porosity was determined from water saturation test, the capillary moisture content from one dimensional time-controlled capillary water uptake experiment.

Mineral composition of the bricks was determined by X-ray diffractograf Philips. The device is equipped with goniometer PW 1050 and Ni filter, and use Cu-Kα radiation in the range of angles 4-62° 2Θ. X-ray tube works at 35kV and 20mA. Velocity of record is 2°/min 2Θ. The data were analysed using software BedeZDS Search/Match.

Nitrogen adsorption measurements were performed with the volumetric ASAP2400 instrument, enabling to obtain isotherms in the 0.01 – 0.98 relative pressure range. Prior to the measurement the samples were degassed overnight at 150 °C and 2 Pa. The specific surface area of pores was determined by the BET method.

Water vapour sorption isotherms were determined by the standard gravimetric desiccator method, which consists of conditioning the samples in desiccators under constant relative humidity (RH) and temperature until the static equilibrium is achieved (EN ISO 12571:2000). The desiccators were placed in an air conditioned test-room with the temperature controlled at 22.5 ± 0.5°C. The measurements were done for seven RH values: 11.3%, 33%, 53%, 75%, 85%, 94% and 98%. The samples were oven dried beforehand at 105 °C.

The water vapour permeability of the salt free brick specimens was measured by the standard cup method (EN ISO 12572:2001) using the RH differences: 0 – 53%, 11.3 – 53%, 33 – 53%, 53 – 75.4%, 53 – 84.7%, 53 – 94% and 53 – 100%. The water vapour permeability of the saline samples was measured under RH differences of 0 – 53% and 53 – 100%. Mass of the samples was checked before

and after each cup test. At the end of all cup measurements the samples were oven dried at temperature of 105°C in order to determine actual moisture contents of the samples. All water vapour permeability measurements were performed in an air-conditioned room at temperature of 23 ± 0.5°C and RH equal to 53 ± 1%. The required RH inside the cup was established by using silica-gel, water or saturated salt solutions.

3. Results and discussion

3.1 Basic material characteristics, mineral composition and pore structure parameters

The basic material parameters and the BET specific surface area of the tested bricks are presented in Table 1. Presence of sodium chloride (cf. also Tab. 3) has practically no effect on the density and porosity of bricks. The specific surface area values are slightly lower for all saline bricks but the noticed differences are insignificant and they can partly result from material non-homogeneity.
The crystal phases identified in the original brick specimens by X-ray diffractometry are summarized in Table 2. As follows from the data, the tested bricks have practically identical mineral composition, with an exception in case of the brick D, where also illite was identified. In case of the saline bricks the X-ray diffractometry detected also a small peak of halite (NaCl).

Determined values of salt content and pH are presented in Tab. 3. Despite the fact that the process of the immersion into the salt solution as well as the following treatment of all specimens was identical the resultant salt contents in particular types of bricks were different. The amount of the salt per volume seems to correlate with the open porosity of the bricks (Tab. 1, 3).

3.2 Water vapour adsorption isotherm

Figure 1 shows the measured water vapour and nitrogen adsorption isotherms for original bricks. It is obvious that the hygroscopicity of brick D is practically negligible up to the RH of 94%, the

TABLE 1. Basic material parameters and BET specific surface area (SSA) of tested bricks. Index sf indicates specimens in the original, salt free state, index s indicates the saline samples

Brick	Bulk density (kg/m^3)	Density (kg/m^3)	Total porosity (-)	Open porosity (-)	Capillary moisture content (m^3/ m^3)	SSA (m^2/ g)
D_{sf}	1780	2752	0.35	0.30	0.24	1.13
D_s	1789	2752	0.35	-	-	0.79
P_{sf}	1370	2788	0.51	0.42	0.36	14.2
P_s	1383	2757	0.50	-	-	11.9
S_{sf}	1460	2929	0.49	0.43	0.34	4.7
S_s	1475	2943	0.49	-	-	3.5

TABLE 2. Crystal phases identified in original bricks

Brick	identified phases
D	Quartz, illite, muscovite, feldspars, enstatite (Fe, Mg), hematite
P	Quartz, muscovite, feldspars, enstatite (Fe, Mg), hematite
S	Quartz, muscovite, feldspar, esseneite (Ca, Fe), enstatite, hematite

TABLE 3. Salt content in bricks determined gravimetrically and from electrical conductivity of extracts; pH of extracts

Brick	NaCl content (kg/m^3) determined gravimetrically	NaCl content (kg/m^3) determined from electrical conductivity	pH
D	8.8 ± 0.0	5.0	9.1
P	12.7 ± 0.2	10.7	8.8
S	14.6 ± 0.6	13.9	8.8

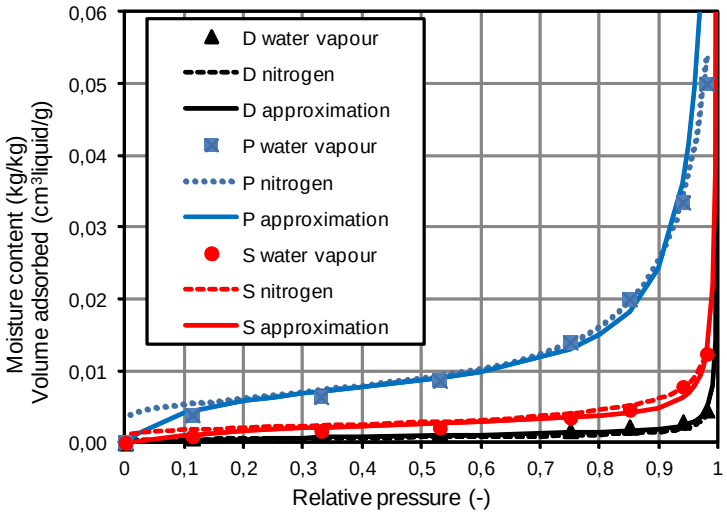

Fig. 1 Water vapour and nitrogen adsorption isotherms compared with Furmaniak's approximation. Bricks D, P, S in original salt free state.

TABLE 4. Parameters of Furmaniak's approximation

Brick	m_0	K	k	w
D	0.0029	0.88	0.99975	0.05
P	0.0083	2.5	0.9994	0.27
S	0.0045	9.1	0.994	0.062

hygroscopicity of brick S is more noticeable but still relatively low while the hygroscopicity of brick P is quite significant. In case of all three bricks very good correspondence between the nitrogen and water vapour isotherms was found. The good compatibility between water vapour and nitrogen adsorption of ceramic bricks had been noted already in previous works, as for example (Koronthalyova 2011). However in context of the analysed issue of the hygroscopicity of saline bricks it can serve as a proof that the tested bricks in original state did not contain hygroscopic salts.

The obtained water vapour adsorption curves were approximated by Furmaniak's relation (1), based on generalised D'Arcy and Watt model (Furmaniak 2012):

$$u_m = \frac{m_0 \cdot K \cdot \varphi}{1 + K \cdot \varphi} \cdot \frac{1 - k \cdot (1 - w) \cdot \varphi}{1 - k \cdot \varphi} \qquad (1)$$

Where u_m moisture content (kg/kg)
φ relative humidity
m_0 concentration of primary sites
K, k kinetic constants connected with sorption on primary and secondary centres
w parameter determining the ratio of molecules bonded to primary centres and converted into secondary ones

The applied parameters of equation (1) are presented in Tab. 4. The advantage of the used Furmaniak's approximation is that it covers the whole range of relative humidity, in contrary of other relations, analysed for example in (Pavlik et al. 2012).

In case of materials with negligible hygroscopicity it is supposed that there is no interaction between the hygroscopically bound water of the material and the hyroscopic water of the salt. Therefore the resultant adsorbed moisture content can be calculated by simple adding corresponding moisture content for salt free material and moisture bound by the salt (Nielsen 1991). The amount of the

hygroscopic water bound by salt is for RH higher than deliquescence relative humidity (DRH) given by the following relation (Nielsen 1991):

$$u_m = \frac{s}{c_s} \cdot \frac{1 - \varphi_s}{1 - \varphi} \qquad (2)$$

Where u_m amount of water bound hygroscopically by the salt (kg/kg)
s mass content of the salt (kg/kg)
c_s concentration of the saturated salt solution (kg/l)
φ relative humidity
φ_s relative humidity over saturated salt solution

In case of sodium chloride at temperature of 23°C the concentration of the saturated salt solution is 0.36 (kg/kg) and DRH is 0.75 (Tang and Munkelwitz 1993). In case of hygroscopic material an interaction between the hygroscopic moisture of the material and hygroscopic moisture of the salt takes place. It is possible especially in range of higher RH, where capillary condensed water is not so strong attached to the pore walls and therefore can dissolve the salt.

In Fig. 2 the measured water vapour and nitrogen adsorption isotherms of the saline bricks are compared with the moisture content calculated as sum of the moisture content of the salt free brick (Fig. 1) and the moisture bound by the salt (Eq. 2). In calculations the gravimetrically determined sodium chloride concentration (Tab. 3) was used. Compared to the salt free bricks, the nitrogen adsorption curves of the saline ones are slightly shifted to lower values. It is in accordance with the noticed lower values of specific surface area (Tab. 1) but it is practically impossible to decide if it is caused by presence of the salt or it results from material non-homogeneity.

In case of bricks D and S a sharp increase of adsorbed moisture can be noticed at DRH that indicate independence of the process of water adsorption by the salt and by the material. Correspondingly, the used simplified calculation gives sufficiently good estimation of the absorbed moisture content of brick D up to the RH of 90 %. In case of brick S, the calculated amount of adsorbed water is in acceptable agreement with the measured one up to the RH of 85 %. In case of hygroscopic brick P, the moisture content below DRH is higher and above DRH is lower than the value predicted by simplified calculation. It can be explained as a consequence of the interaction between the hygroscopic moisture of the material and the one of salt. However, starting from RH equal to DRH up to RH of 90 % the obtained moisture content corresponds approximately to the amount of hygroscopic water bound by salt (Eq. 2). At RH higher than 90 % the measured moisture content is lower than the value predicted by Eq. 2 for all three bricks.

3.3 Water vapour permeability

The obtained water vapour resistance factor/moisture content dependences and their approximations are presented in Fig. 3. Analysis of the measured water vapour resistance factor/moisture relations has shown that for original salt free brick samples they can be approximated by following hyperbolic function:

$$\mu = \mu_0 - a \cdot \frac{exp(\frac{u_m - u_{m1}}{u_{m2}}) - exp(\frac{u_{m1} - u_m}{u_{m2}})}{exp(\frac{u_m - u_{m1}}{u_{m2}}) + exp(\frac{u_{m1} - u_m}{u_{m2}})} \qquad (2)$$

Where u_m moisture content (kg/kg)
μ_0, a, u_{m1}, u_{m2} parameters

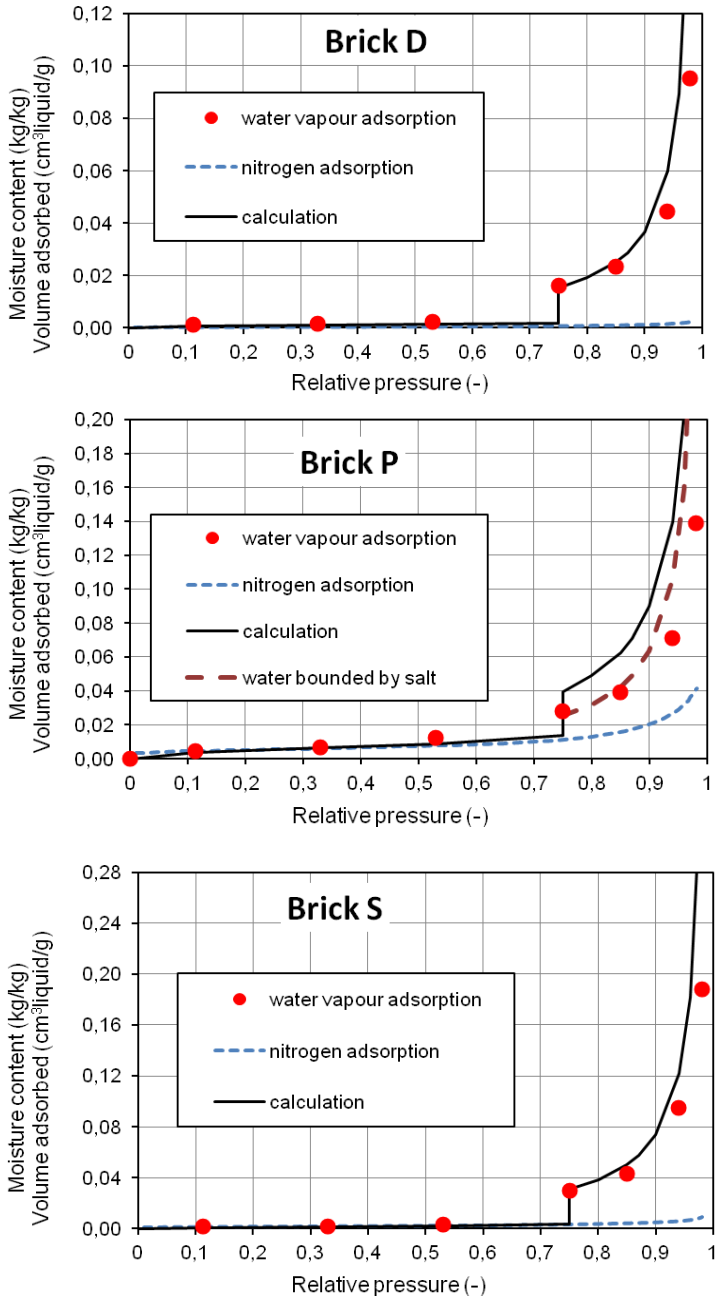

Fig. 2 Measured water vapour and nitrogen adsorption curves for saline bricks compared with water vapour adsorption estimated by simplified calculation

As can be seen from Fig. 3, the transition from the higher value of water vapour resistance factor, corresponding to the water vapour diffusion without the surface diffusion, to the lower value, following from cumulated effect of the water vapour diffusion and the surface diffusion takes place in a transition zone. The mean moisture content at which the transition occurs corresponds to parameter u_{m1}. The width of the transition zone is expressed by the parameter u_{m2} and corresponds to value of $2 \cdot u_{m2}$. The parameter μ_0 expresses the mean value of water vapour resistance factor and value of $2 \cdot a$ corresponds to difference between maximum and minimum μ value.

Compared to the salt free bricks the corresponding moisture contents of saline bricks are shifted towards the higher values (Fig. 3). The wet cup μ values of saline bricks are equal or slightly lower

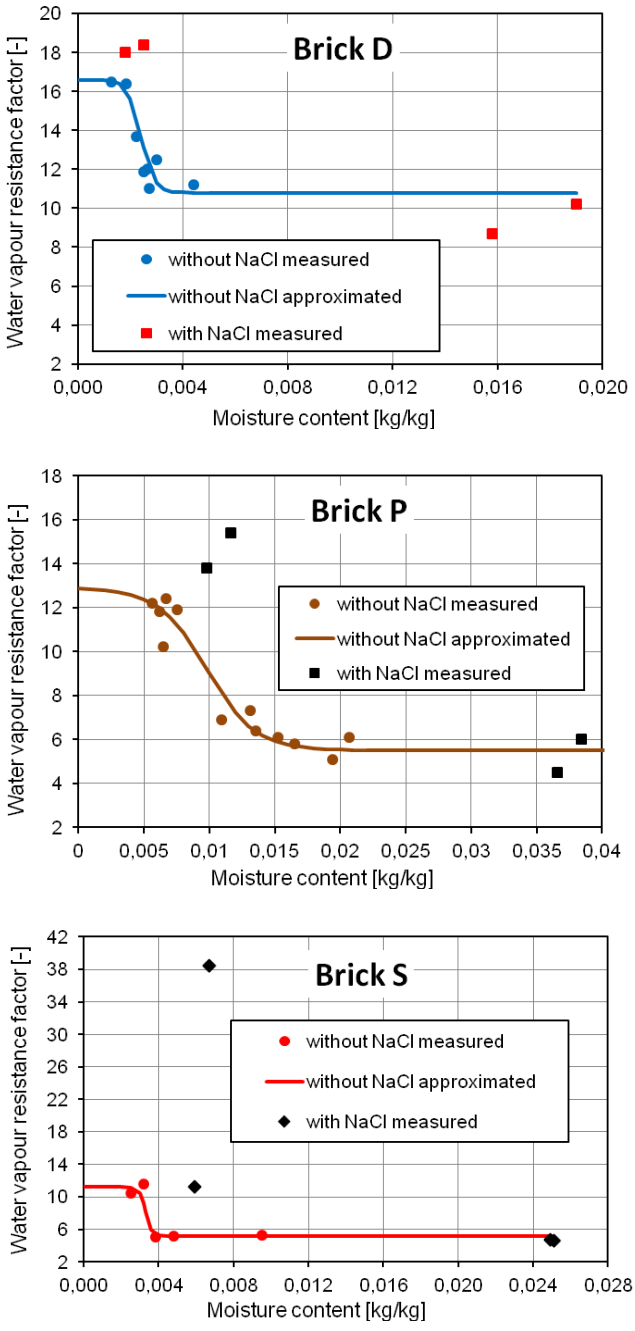

Fig. 3 Water vapour resistance factor vs.moisture content for brick D, P, S

than the ones obtained for salt free bricks. During the dry cup measurements efflorescence was noticed on the dry sides of all samples. The created salt crust causes higher dry cup μ values of the saline bricks. However, in spite of similar treatment of all specimens the salt crust thickness and continuity differs for particular samples, resulting in different increase of the dry cup μ values. The continuous crust was created only in one case (brick S), causing the increase from the original μ value of about 11.0 up to 38.5 (Fig. 3).

4. Conclusions

In the work the effect of presence of the salt on water vapour sorption and water vapour permeability moisture dependence was determined. The analysis was done for three types of commonly used burnt clay bricks with different hygroscopic ability and was limited to small salt concentrations having practically negligible effect on the material porosity.

The measurement has confirmed significant increase of adsorbed water caused by presence of salt. For practically non-hygroscopic ceramic bricks containing small amount of sodium chloride a prediction of the moisture adsorption by simplified calculation was possible, with an exception of the range of high values of relative humidity. However, in case of hygroscopic ceramic brick this prediction was not usable due to the present interaction between the hygroscopically bound water of the material and the hygroscopic water of the salt.

Presence of the tested salt amounts had practically no influence on the water vapour permeability of the bricks at higher moisture contents, where cumulated effect of the water vapour diffusion and the surface diffusion took place. On the other hand, salt crusts formatted during the dry cup measurements caused decrease of the resultant water vapour permeability. The significance of the decrease depended on the actual crust formation.

In order to get more general conclusions, the effect of different salt concentrations and another salts should be analysed.

5. Acknowledgements

This research was supported by the Scientific Grant Agency VEGA (Grant No. 2/0145/13).

References

EN ISO 12571:2000 Hygrothermal performance of building materials and products - Determination of hygroscopic sorption properties

EN ISO 12572:2001 Hygrothermal performance of building materials and products - Determination of water vapour transmission properties

Furmaniak, S. The Alternative Model of Water Vapour Sorption in Porous Building Materials, *Transport in Porous Media* 2012; 95: 21–23.

Hansen, K.K. Sorption Isotherms—A Catalogue. Technical report 162/86, TU Denmark, Lyngby (1986)

Koronthalyova, O. Moisture storage capacity and microstructure of ceramic brick and autoclaved aerated concrete, *Construction and Building Materials* 2011; 25: 879-885.

Nielsen, C. B. Salts in Porous Building Materials, Technical Report 243/91, Technical University of Denmark 1991

Pavlík, Z. – Žumár, J. – Medved, I. – Černý, R. Water Vapour Adsorption in Porous Building Materials: Experimental Measurement and Theoretical Analysis, *Transport in Porous Media* 2012; 91: 939–954.

Table of conductivity vs. concentration for common solutions: http://myweb.wit.edu/sandinic/Research/conductivity%20v%20concentration.pdf

Tang, I.N. – Munkelwitz, H.R. Composition and temperature dependence of the deliquescence properties of hygroscopic aerosols, *Atmospheric Environment* 1993;27A: 467–473.

Moisture diffusivities of calcium silicate board during absorption, wetting and drying

Peter Matiasovsky, Dr.Ing.[1]
Matus Holubek, PhD.[1]
Peter Mihalka, Dr.Ing. [1]

[1] Institute of Construction and Architecture, Slovak Academy of Sciences, Slovakia

KEYWORDS: *Moisture diffusivity, water absorption, drying, water vapour adsorption, TDR*

SUMMARY:
For the calcium silicate board successive water absorption, drying and wetting experiments were carried out. During the experiments the moisture content profiles were measured continuously by TDR method. The drying and wetting experiments were performed in a climatic chamber. Unlike the absorption the wetting was realised in a very high relative humidity environment maintaining the permanent surface condensation boundary conditions. From the determined moisture content profiles at particular moisture transport processes different moisture diffusivity curves were determined. The found differences were interpreted by different boundary conditions determining the different mechanisms of the occupation of pores during the water transport in the analysed material.

1. Introduction

At non-stationary transport regimes the water diffusivity can be calculated from the measured moisture content profiles. The methodology of liquid water diffusivity function during water absorption experiment is well described in detail in (Carmeliet et al. 2004). The study recommends not take into consideration diffusivity values at moisture contents within a hygroscopic region. Pel (1995), Pel et al. (1996) and Pel at al. (2002) focused on the diffusivity determination within hygroscopic region during drying tests. Adan (1995) determined diffusivity courses during drying and during water absorption and stated that satisfactory interpretation of the results and the moisture diffusivity modelling requires consider complex interaction of vapour and liquid water phases interaction in pore system.

In order to investigate the moisture diffusivity in a whole moisture content and its dependence on a type of moisture transport process within full moisture content range we realised the successive water absorption, drying and wetting experiments for calcium silicate board and consequently we determined moisture diffusivities from measured moisture content profiles. The obtained moisture diffusivities were analysed by modelling with use of capillary models.

As a testing material a calcium silicate was used. The calcium silicate has very high 90 % porosity and is originally manufactured as the refractory material, however owing to its high capillarity in the last decade it is applied in construction industry also as thermal insulation. Due to its high capillarity the experiments could be relatively fast.

For measurement of moisture content profiles the time domain reflectometry (TDR) method was used. A correct measurement by this method is conditioned by estimating the proper relative permittivity-moisture content dependence (the calibration function).

2. Absorption

Moisture diffusivity is usually calculated from the data obtained from absorption experiment, but its validity is limited to the moisture contents above the critical moisture. The absorption experiment was carried out during a standard 1-dimensional water uptake test.

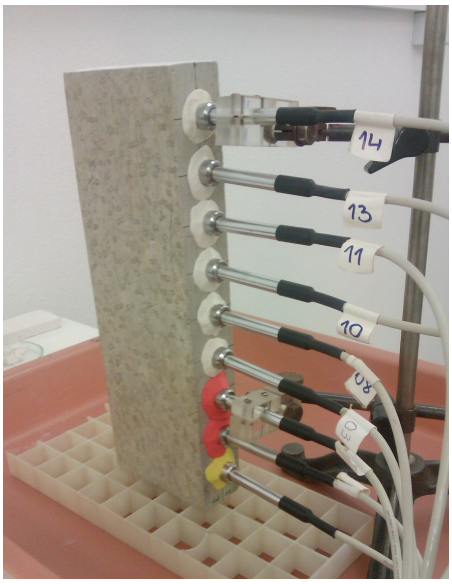

FIG 1. Water absorption experiment

2.1 Experiment

The diffusivity determination at absorption is determined from moisture content profiles measurement during liquid water absorption. The prismatic specimen of 0.3 m height and 0.10 x 0.04 m base was dried under 50°C temperature before the experiment. The lateral surfaces of the specimen were insulated by impermeable epoxy film. The top surface was covered by aluminium foil enabling the air outflow during the absorption process. The bottom surface represented the absorption area. The moisture content profiles were measured by 9 TDR probes with 0.03 m distances between them (Fig. 1), calibrated in ethanol and air before the measurement. Before the measurement starting the TDR probes were calibrated in water, ethanol and air. After the contact of specimen with water by its 0.003 m deep immersion the measurement started and the moisture content field development in the specimen was scanned in 2 minutes intervals. The 23°C temperature and 50 % relative humidity were maintained in the laboratory.

2.2 Determination of moisture diffusivity during water absorption

The TDR measurements provide the values of relative permittivity of moist material. With use of calibration curve we transform the measured permittivities to corresponding moisture contents. The measured data were represented in form of moisture content profiles (Fig. 2) and applying the Boltzmann transform the diffusivity was calculated from them. The moisture content profiles are plotted in Figure 2 at times displayed in the upper right corner.

To determine the diffusivity we used Boltzmann transformation (Crank 1975):

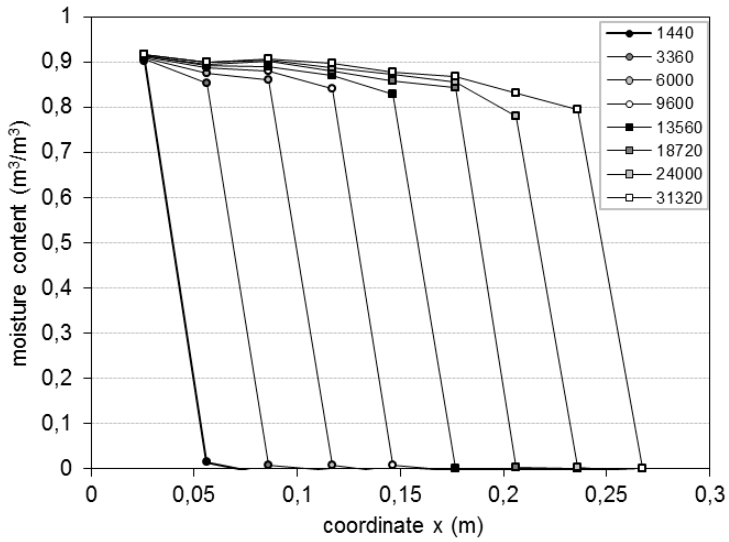

FIG 2. Moisture content profiles during absorption at selected times (s)

$$\lambda = \frac{x}{\sqrt{t}} \tag{1}$$

Where λ Boltzmann variable ($m^{-0.5}$)
x coordinate (m)
t and time (s)

The liquid water diffusivity can be determined from one-dimensional isothermal differential liquid water transfer equation:

$$\frac{\partial w}{\partial t} = \frac{\partial}{\partial x} \cdot \left(D(w) \cdot \frac{\partial w}{\partial x} \right) \tag{2}$$

Where w moisture content (m3/m3)
$D(w)$ moisture diffusivity (m^2/s)

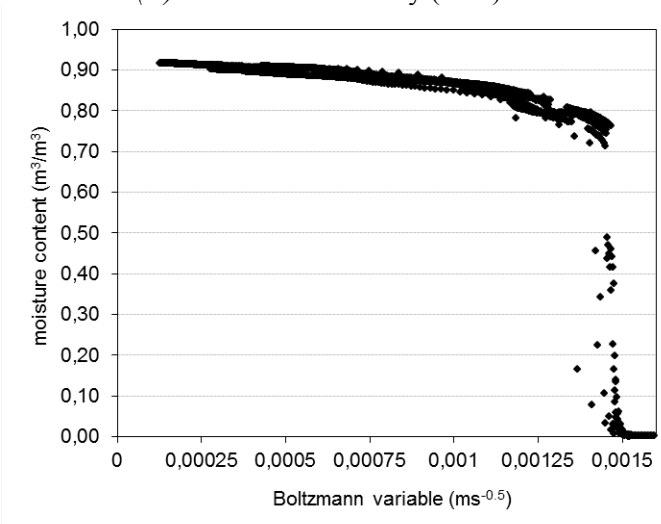

FIG 3. moisture profiles during absorption for 30cm sample of CaSi board, after aplycation of Boltzmann transformation

For initial conditions ($w = w_0$ at $x > 0$ at $t = 0$) and boundary conditions ($w = w_B$ at $x = 0$ and $t > 0$), the non-linear partial differential equation (2), after application of Boltzmann transformation (1), can be reduced to an ordinary differential equation.

$$-\frac{\lambda}{2}\frac{\partial w}{\partial \lambda} = \frac{\partial}{\partial \lambda}\cdot\left(D(w)\cdot\frac{\partial w}{\partial \lambda}\right) \tag{3}$$

If mentioned Boltzmann-conditions are fulfilled (a constant boundary condition applied to the semi-infinite homogeneous medium that is initially at a uniform moisture content) all the measured moisture profiles should fall on a single λ-w profile. Integration of equation (3) offers the liquid water diffusivity given by the expression (Crank 1975):

$$D(w) = -\frac{1}{2}\cdot\frac{\int_{w_0}^{w}\lambda dw}{\frac{\partial w}{\partial \lambda}} \tag{4}$$

The moisture diffusivity function resulting from the measurement is in Figure 7.

3. Drying

Moisture diffusivity determined from the absorption experiment covers a moisture region over the critical moisture content. Drying experiment is preferred by Pell especially to obtain moisture diffusivity for water contents contents lower then critical moisture content, within whole hygroscopic region.

The 1-dimensional drying experiment was carried out in steady state laboratory conditions under the surface water vapour transfer controlled by forced convection.

3.1 Experiment

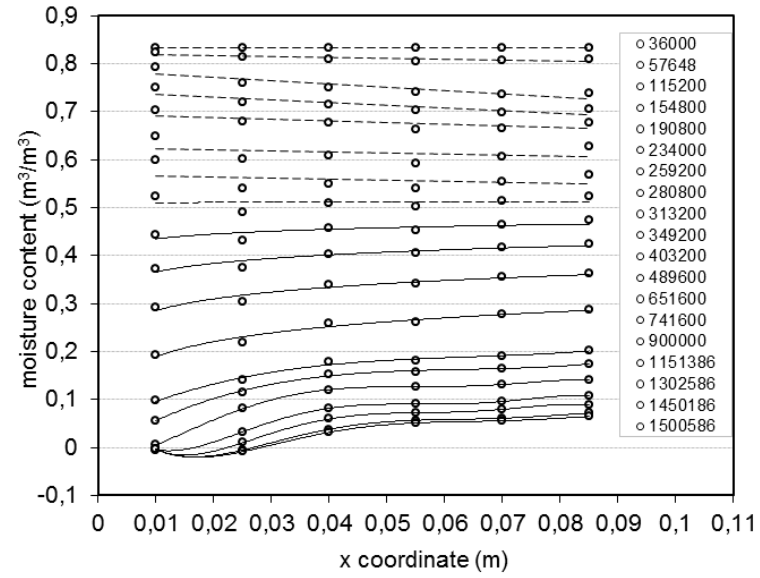

FIG 4. Drying profiles measured on 0.1 m thick specimen at specific times

The specimen had the prismatic shape of 0.1 m height and 0.1 x 0.04 m base. The first probe had the 0.01 m distance from drying surface and the other probes were placed in 0.015 m distance. The lateral surfaces were insulated by petroleum jelly. The drying surface had horizontal orientation and the evaporation was controlled by ventilator providing the air flow velocity ca 2 m/s. Temperature of 23°C and relative humidity 50 % were maintained in the laboratory. We started the experiment at capillary moisture content. A drying experiment has two stages. During the first stage the drying process is controlled by evaporation from the wet surface and the moisture content through the specimen is constant. After reaching the critical moisture content the second stage continues characterised by development of drying front. The moisture content profiles are plotted at selected times displayed in the upper right corner in Figure 4.

3.2 Determination of moisture diffusivity during drying

In order to derive $D(w)$ from the experimental moisture profiles (Fig. 4), Equation (2) is integrated with respect to x (Pel 1995), yielding:

$$D(w) = \frac{\int_{l}^{x'} \left(\frac{\partial w}{\partial t} \right) dx}{\left(\frac{\partial w}{\partial x} \right)_{x'}} \tag{5}$$

In this equation, use is made of the fact that the partial derivative of w with respect to x equals zero at the vapour-tight bottom of specimen ($x = l$). $D(w)$ is related to moisture content in coordinate $x`$. The resulting numerically calculated moisture diffusivity values are plotted against the corresponding moisture content in Figure 7.

4. Adsorption

The process of adsorption is an additional way to get diffusivity from the measured humidity profiles. This is a non-standard approach, which is time consuming and it is difficult to ensure the boundary conditions. Diffusivity which is calculated from the measured data falls within the range of low moisture contents. The water vapour adsorption experiment was carried out as 1-dimensional process in ca 100 % relative humidity environment controlled by the surface water vapour transfer under forced convection.

4.1 Experiment

The specimen and measuring set was identical wit the one used at drying experiment. Before the measurement it was dried under temperature 50°C. The experimental set is in Figure 5.

4.2 Determination of moisture diffusivity during adsorption

In order to derive $D(w)$ from the experimental moisture profiles (Fig. 6) Equation (5) was applied. The resulting diffusivity function is in Figure 7.

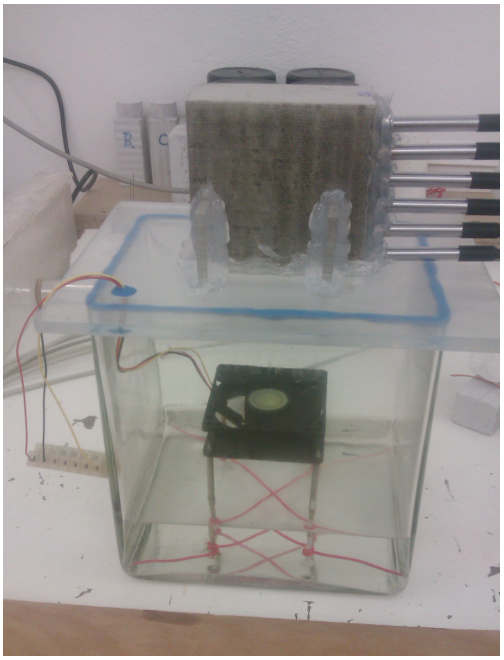

FIG 5. Adsorption experiment

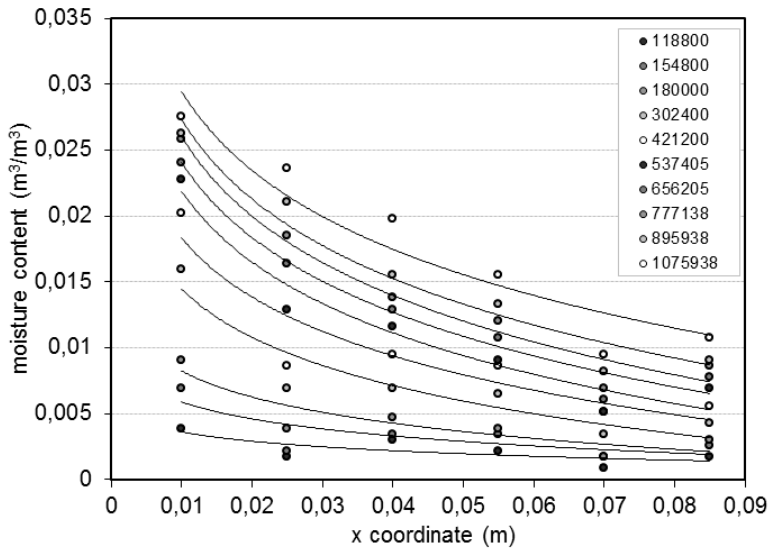

FIG 6. Adsorption profiles, measured on 0.1 m thick specimen at selected times (s)

5. Analysis

In Figure 7 we can see the lack of the data within the range of low moisture contents (below 0.05 m^3/m^3) in drying test. Due to the infrequent raster of measurement points (the locations of the TDR probes along the sample) we are unable to capture the shape of moisture content profiles in detail (Fig. 4). The mapping accuracy of the receding profile head significantly affects the calculated diffusivity in hygroscopic region.

To determine the diffusivity in this region we have designed the process of adsorption as a more suitable for the TDR method. The moisture flow into a dried sample is ensured by constant boundary conditions, with the relative humidity of the ambient air maintained at 100 %. The moisture content profiles are smooth in adsorption process (Fig. 6). The approximation of the profiles is well done from the sparse grid points (sparse spacing probes) available for the TDR method. The calculated values from these profiles excellently complement the course of diffusivity in hygroscopic region and smoothly follow its progress in overhygroscopic region (Fig. 7). Their slight overestimation in hygroscopic regions may be related to the uncertainty of the TDR probes, non-homogeneity of calcium silicate board and a choice of approximation function.

In order to interpret the obtained results the moisture diffusivity was modelled as the diffusivity of network of serial (for adsorption and drying) and parallel (for absorption) capillary pore fractions (Descamps 1997) and the diffusivity is then expressed as the ratio of moisture permeability and moisture capacity:

$$D(w) = \frac{K(w)}{\xi(w)} \tag{6}$$

The diffusivity model (6) has three forms according to the moisture content region or degree of saturation. In the hygroscopic region up to ca 60 % relative humidity the water vapour diffusion is a dominant moisture transport mechanism and the moisture permeability of pore volume fraction has the form (Carmeliet at al. 2004):

$$K(w) = \frac{D_a}{\mu}(1 - S)\frac{\varphi}{\rho_w R^2 T^2} \tag{7}$$

In Equation (7) the determining material parameter is the diffusion resistance factor μ dependent on degree of saturation S.

Under the relative humidity higher than 60 % up to critical moisture content the simultaneous water vapour diffusion and surface flow are active (Deryaguin et al. 1985) and the moisture permeability of a pore volume fraction has the form:

$$K(w) = \frac{D_a}{\mu}(1 - S)\frac{\varphi}{\rho_w R^2 T^2} + \frac{\Delta SSA \cdot t^3}{3 \cdot \eta} \tag{8}$$

The surface flow is determined by the specific surface area fraction ΔSSA and the water film thickness t at given moisture content.

The capillary flow is determined by the water filled fraction w and the pore radius corresponding to the pores saturation at given moisture content. If the moisture content is higher than critical the capillary flow is dominant and the moisture permeability of a pore volume fraction equals (Marshall, 1958):

$$K(w) = \frac{\Delta w^2 \cdot r^2}{8 \cdot \eta} \tag{9}$$

The permeability is determined by fraction pore radius r.

The modelled diffusivity courses in Figure 8 can be compared with the measured courses in Figure 7. An assumption that due to the water transport parameters dependence on the boundary conditions there is a difference between the water absorption moisture diffusivity during the water absorption, redistribution and drying and in a case of drying the diffusivity is smaller (Kuenzel 1995) was confirmed. In our case the absorption course gives higher values and this difference between adsorption/drying and absorption branches is smaller than one order of magnitude. This was confirmed also in the modelled diffusivity functions.

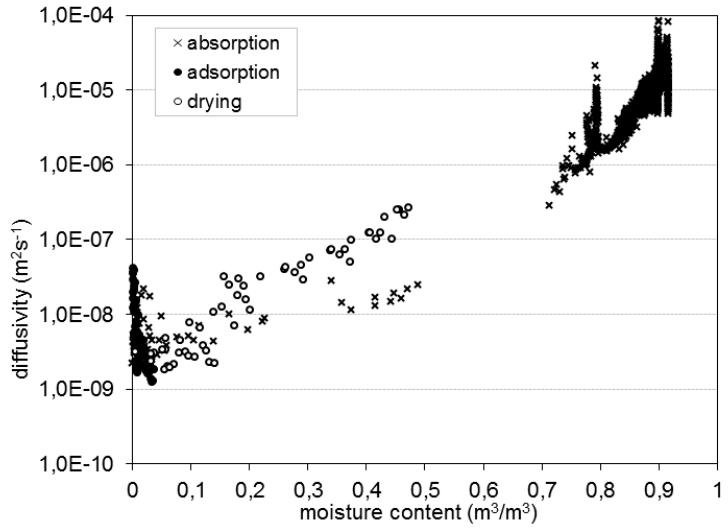

FIG 7. Comparison of diffusivities during absorption, drying and adsorption (measurements)

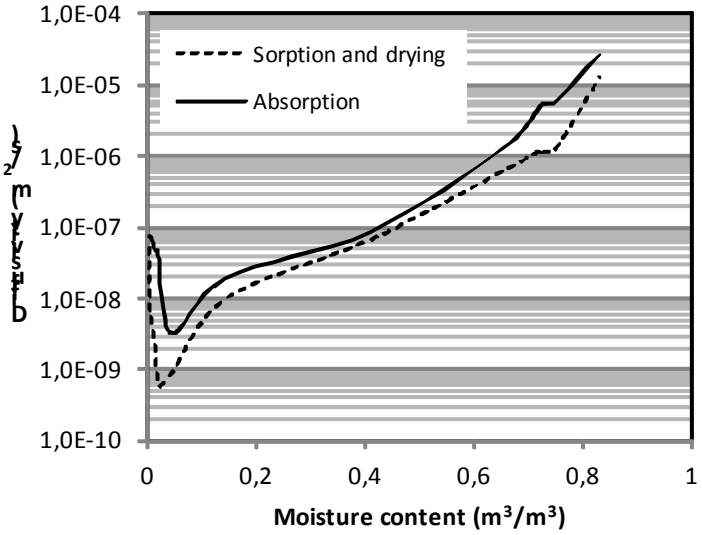

FIG 8. Comparison of diffusivities during absorption, drying and adsorption (modelling)

6. Conclusions

The moisture diffusivity functions for calcium silicate plate were determined from the various moisture transport experiments: absorption, drying and adsorption. Particular experiments give complex information on the moisture transport under different boundary conditions within the whole moisture content range. Obtained results were analysed by the serial and parallel capillary models of moisture diffusivity. The modelled diffusivities coincide with the diffusivities determined from measurements and confirm the applicability of the used TDR method as well as of capillary diffusivity models.

7. Acknowledgements

The authors wish to thank the Slovak Research and Development Agency APVV, project No. 0032-10 for the financial support of this work.

References

Adan O.C.G. 1995. Determination of moisture diffusivities in gypsum renders. HERON 40, 201-215.

Carmeliet J., Hens H., Roels S., Adan O., Brocken H., Cerny R., Pavlik Z., Hal, C., Kumaran K. & Pel L. 2004. Determination of the Liquid Water Diffusivity from Transient Moisture Transfer Experiments. Journal of Building Physics 27, 277-305.

Crank J. 1975. The Mathematics of Diffusion. Clarendon Press, Oxford.

Deryaguin B.V., Tshurayew N.V. & Muller V.M. 1985. Surface forces, Nauka, Moscow. (In Russian).

Descamps F. 1997. Continuum and discrete modelling of isothermal water and air transfer in porous media. PhD-dissertation. Leuven: K.U. Leuven.

Holubek M. & Matiasovsky P. 2012. Determination of liquid water diffusivity of building materials using TDR method. Building Research Journal 60, 89-108.

Kuenzel, H. M. 1995. Simultaneous Heat and Moisture Transport in Building Components, IRB Verlag, Stuttgart.

Marshall, T. J. 1958. A Relation Between Permeability and Size Distribution of Pores, Journal of Soil Science 9, 1-8.

Pel L. 1995. Moisture transport in porous building materials, PhD dissertation, T.U. Eindhoven.

Pel L., Brocken H. & Kopinga K. 1996. Determination of moisture diffusivity in porous media using moisture concentration profiles. International Journal of Heat and Mass Transfer 39, 1273-1280.

Pel L., Landman K.A. & Kaasschieter E.F. 2002. Analytic solution for the non-linear drying problem. International Journal of Heat and Mass Transfer 45, 3173–3180.

The effect of surface roughness on mould growth on wood

Annika Ekstrand-Tobin, Ph. D.[1]
Pernilla Johansson, Lic. Tech. [1]

[1] SP Technical Research Institute of Sweden, Sweden

KEYWORDS: *Wood, surface, mould resistance, natural spore exposure*

SUMMARY:
The purposes of the present study was to investigate if the surface geometry of wood has an effect on the rate of mould growth at the surface and also to evaluate if the spore suspension with high concentration of spores often used in laboratory testing is relevant to real conditions. New surfaces of pine wood with various roughnesses were compared with the original surface. One set of specimens were infested naturally with mould spores and another set by spraying a freshly made mixture of spores from six different moulds. The specimens were analysed after 60 days of incubation in 90% relative humidity and 22°C. The results showed no difference in mould growth for the different test specimens that had been sawn or planed and that the load of spores from artificial spore suspension and naturally infestation gives comparable results of mould growth on test specimens.

1. Introduction

The impact of surface roughness is regarded to be a parameter of significance considering mould growth. Earlier studies have shown that freshly planed pine lumber surfaces have significantly lower susceptibility to mould than its original surfaces (Terziev 1996, Johansson et al. 2013a, Johansson et al. 2013b).

Mould resistance tests are used to determine the susceptibility to mould of different building materials. These methods usually involves laboratory tests in which most often a mix of mould spores are applied to the material surface of specimens. This is followed by an incubation period at controlled relative humidity and temperature, during which the spores may germinate and are terminated with an assessment of mould growth.

The main purpose of the present study was to investigate if the surface geometry of wood has an effect on the rate of mould growth at the surface. In addition, it was evaluated if the use of a spore suspension with high concentration of spores often used in laboratory testing is relevant to in-situ exposures.

2. Materials and methods

2.1 Test material

In this study, spruce timber (*Picea abies*) from two sawmills in northern Sweden was used. The timber quality was ordered according to (SIS-EN Standard 1611-1). By selecting materials directly from sawmills more data of the material's history was obtained prior to testing than if the material had been purchased in a building supply store. In addition, the delivery corresponds to materials supplied to major construction projects. All data from the saw mills on the delivered timber is presented in TABLE 1.

TABLE 1. Timber description of the spruce wood sent from the sawmills

	Saw mill A	Saw mill B
Number of delivered wooden studs	4	3
Height x width	47x125 mm	50x125 mm
Moisture content	15,8 %	16,0 %
Drying method	Dry temperature 70°C Wet temperature 55°C No conditioning	Chamber dryer Dry temperature 70°C Wet temperature 60°C 6h conditioning 70/68°C
Drying time	4 days 4 h	-
Storage time before drying	2 days 18 h	-
Storage time after drying	16 days 23 h Sticked, under roof	10 days Sticked, under roof
Storage after adjustment	Open under roof at mill	22 days Open under roof at mill

2.2 Preparation of specimens

In total seven wooden studs of spruce timber were delivered from the two sawmills. Each of the seven wooden studs was cut into four parts, one for each of the three different surface treatments and one with remaining original surface.

The treatments were performed as two different sawn surfaces and one planed surface. This procedure was an attempt to create three different kinds of surfaces, one smooth (the planed surface), one more rough and one even rougher. The fourth parts used as references, were left with the original surface intact.

For the finest sawing, these fourth of the plank parts were prepared with a band saw INCA Type 342.186. With a saw blade with cutting width of 10/0.65 mm, length of 1874 mm, 6 teeth/inch, code 54.186.157. For the coarser sawing, these plank parts were prepared with a blade for coarse cutting in a wood working combination machine Luna Master W59, using a circular saw blade diameter 300 mm, bore diameter 30 mm, cutting width of 3.2/2.2 mm and 48 WZ number of teeth. The planed plank parts were also prepared in the combination machine. All treated plank parts were cut down to a depth of 2 – 5 mm from the sapwood surface. See FIG 1 below.

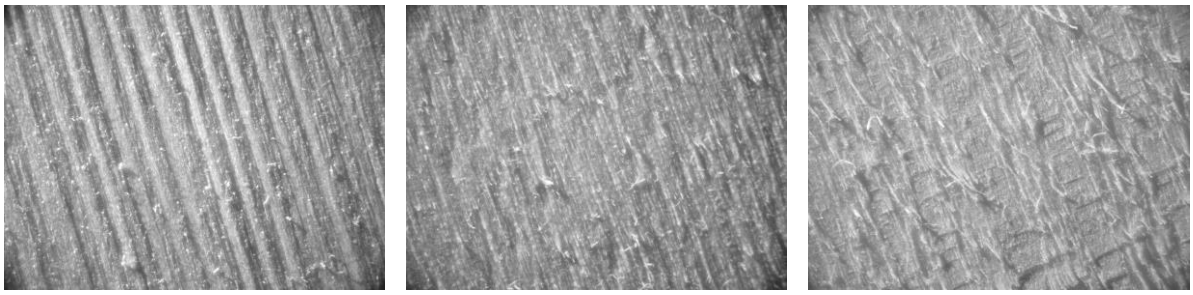

FIG 1. Surfaces with new treatments: Planed, sawed and coarser sawed surface. Magnification 40x.

All four plank parts, original surface and with different prepared surfaces, were cut into smaller test specimens, with an area of about 50 cm^2 each. Finally, all specimens were cleaned with compressed air in order to avoid leaving saw dust on the surfaces. Double sets of 7 specimens (1 from each plank) were prepared for each of the four categories.

2.3 Mould resistance test

2.3.1 Inoculation with mould spores

One set of specimens were exposed to natural spore contamination outdoors (in fall, abt. 15°C, weak wind) by placing specimens on a rack under a roofed shed outdoors for 8 hours before incubation in humidity chamber. The second set of specimens were sprayed with a freshly spore solution prepared from six species of mould (Johansson et al. 2012). The mould species used are presented in TABLE 2 below.

TABLE 2. Mould species included in the spore solution

Fungi species	CBS Nr
Cladosporium sphaerospermum	122.63
Stachybotrys chartarum	109292
Eurotium herbariorum.	516.65
Aspergillus versicolor	117286
Penicillium chrysogenum	401.92
Aureobasidium pullulans	101160

2.3.2 Incubation

Both the naturally infested and artificially inoculated specimens were incubated in a humid environment until all specimens had detectable growth of mould, in total for 60 days. The incubation was performed in 90% relative humidity, with a temperature of 22°C in test chambers (CTS C-20/350, CTS GmbH, Hechningen, Germany).

2.3.3 Microbial analysis

The detection of mould growth was performed with a stereo test microscope with x40 magnification and low angle light source according to a grading scale for mould growth in (Johansson et al., 2012). In this assessment 1 were considered as initial growth, with just one or some detected hyphae, 2 as clearly established but sparse growth scattered on the surface, occasionally with branched hyphae and few conidiophores, 3 as patchy heavy growth with mycelia and often well-developed conidiophores and 4 as heavy growth over more or less the entire surface of the specimen. No growth around the 0 – 5 mm zone along edges were considered.

2.4 Statistical evaluation

Two ways of considering the mould growth was used to statistically evaluate the data. One was to compare the different groups of variables (surface, spore exposure or sawmill) as the distribution of assessments at each time for analysis; that is the extent of mould growth at the surface was considered. This is described in boxplots and the extent of mould growth at each time of analysis was performed by using a Kruskal-Wallis test. Pairwise comparisons were performed with a Bonferroni correction for multiple comparisons.

The other way to evaluate the data was to consider the time before mould growth appeared on the surface of the test pieces. This approach is based on the assumption that what is important to study is not how much mould present on a material, but the event that mould growth occurs. Established growth was defined as rating equalling or exceeding 2 with the rating scale described in 2.3.3. The time to growth is described as survival functions in Kaplan-Meier plots. Survival in this case is then the event that mould growth has not been established, i.e. rating is 0 or 1. Pairwise comparison of the survival functions, shown as Kaplan-Meier curves in Fig 3, was performed with Wilcoxon tests (Singer and Willett, 2003).

3. Results

Within 60 days of incubation at 90% relative humidity and 22°C there was mould growth on all test specimens. The extent of mould growth and the time until fail varied.

FIG 2 displays the rating of mould growth for each of the four surface varieties at each analysis time. Pairwise comparisons between each of the treatments and the original surface showed a significant difference ($p<0.05$) in mould growth extension. The rating of mould growth on the specimens with original surface was higher than the treated surface specimens. No significant difference was found between different surface treatments.

The same pattern was found when considering survival functions; there is a statistical significant difference between each of the treated surfaces and the original surface but not between each of the surface treatments, see

FIG 3.

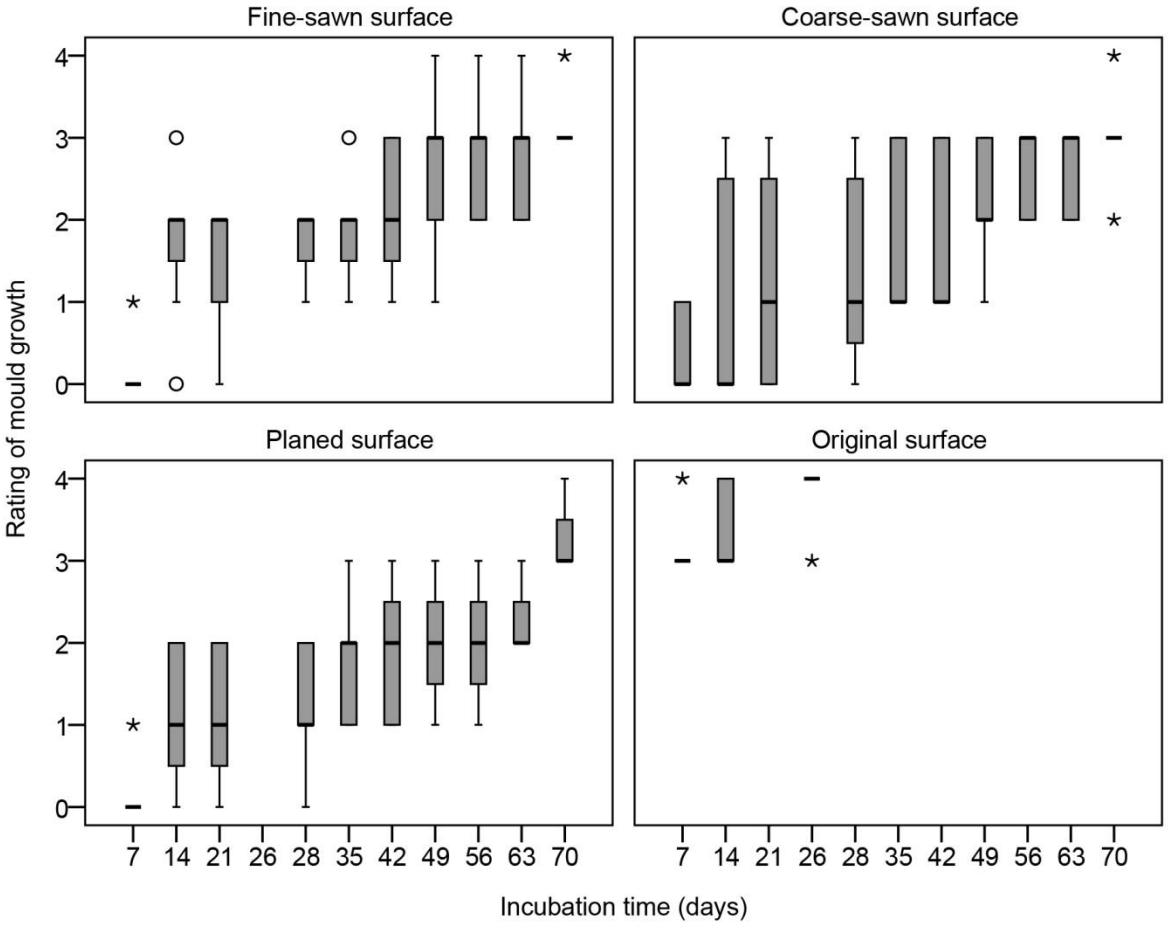

FIG 2. Rating of mould growth according to 2.3.3 from each analysis for all types of surfaces on the artificially inoculated test specimens.

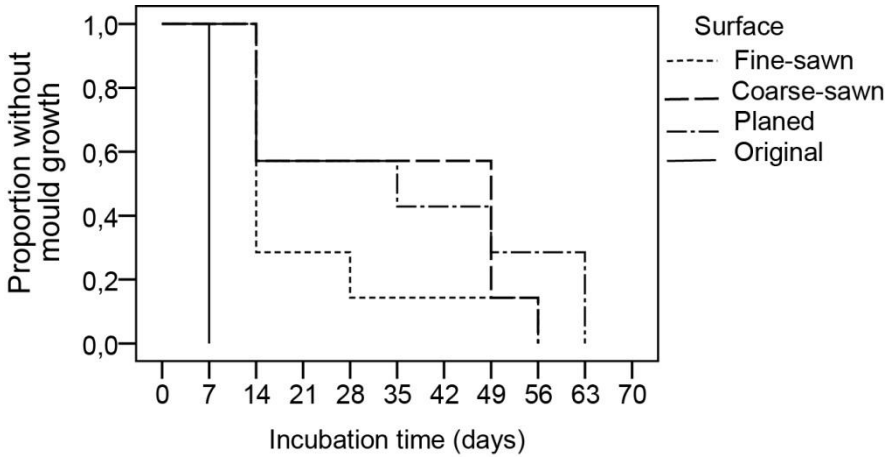

FIG 3. Kaplan-Meier plot of the survival functions for all four types of surfaces for all types of surfaces on the artificially inoculated test specimens. The horizontal axis shows the incubation time, the vertical axis the proportion of test specimens without established growth (rating < 2).

A statistical significant difference was found when comparing the survival functions of test specimens from the different sawmills, see FIG 4.

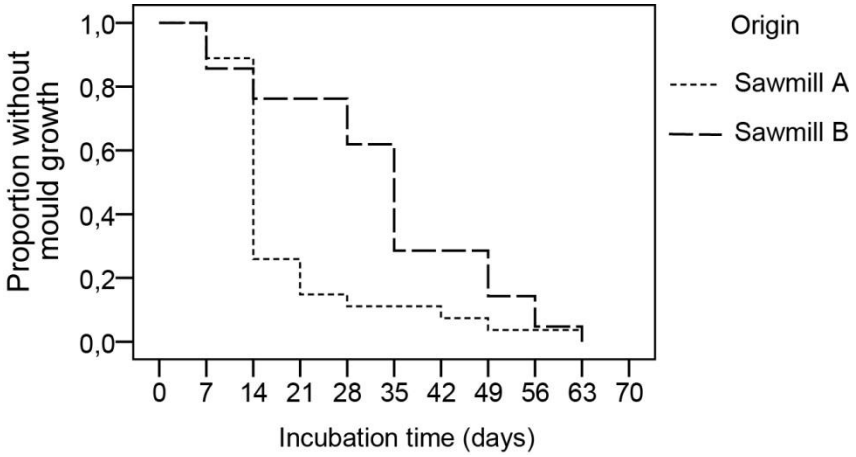

FIG 4. Proportion of test specimens, from the two sawmills, on which there was no established mould growth over incubation time (days).

When considering the spore exposure, the extent of mould growth on test pieces on each time was more or less the same for both natural contamination and spore-suspension at the majority of the analysis times.

4. Discussion

In this study we found no difference in mould resistance among wood that was planed or sawn, either coarse or fine. This indicates that surface roughness does not affect the mould growth on wood. However, a possible explanation to the lack of differences in the results is that the techniques here to

create the different surfaces were inadequate. When visually examined by the naked eye the impression was that the surfaces were quite similar in roughness. The roughness of wooden surfaces is although not an easy parameter to assess (Sandak and Negri 2005). An alternative explanation to the results might be that small differences in surface structure do not affect mould growth.

There was however, a significant difference between specimens that remained with the original surfaces in the test and each of the different treatments. This is consistent with earlier findings (Johansson et al. 2013b, Johansson 2003, Terziev 1996, Viitanen 1996) and indicates that it is not the effect of surface roughness that has been found affecting mould growth, but instead it is the treatment as such, i.e. a new surface has been created. This surface might be prone to mould growth in a lesser extent since the nutrients at the original surface has been removed (Terziev 1996, Theander et al. 1993). Some monoterpenes are known to be antifungal (Marei et al. 2012). Therefore, an alternative explanation is that when a new surface is created, the monoterpenes in the wood becomes volatile in the surface and inhibit the mould growth.

Laboratory tests are always simplified compared to real life conditions. When testing for mould resistance, a spore solution with a high amount of spores is often used in order to make the test reproducible. In this study we have shown that artificially inoculated specimens are comparable with naturally infested specimens. In other studies though (Johansson and Bok 2011) the time before mould growth occurred was shorter for the specimens with artificial inoculation than the naturally infested specimens directly delivered from single-house factories. The number of spores in outdoor air varies with time of year, time of day, weather conditions etc. (Mullins 2001). A possible explanation to the differences between the two studies is that this natural exposure varied.

5. Conclusions

The main conclusions in the study were:

- Small differences in surface roughness on newly treated fresh wood did not have any impact on mould growth.
- A significant difference in results was found between the group of specimens with original surface and the group with all the treated specimens.
- In future tests when the effect of surface roughness of mould growth is to be studied, the specimens should be exposed to clean indoor air for some time in order to allow any volatile compounds to evaporate from the surfaces.
- The spruce timber was selected according to standardized specifications. In spite of this, the results diverted significantly implying that there are difficulties in defining wood qualities of significance for mould resistance.

6. Acknowledgements

The present research is a part of the research program Woodbuild coordinated by SP Technical Research Institute of Sweden. The research is financed by Vinnova, the Swedish Federation of Forest Industries and a number of companies in the forest and building sector.

References

Johansson, P. 2003. Mögel på nytt och begagnat byggnadsvirke. SP Rapport 2003:17. Borås: SP Energiteknik.

Johansson, P. & Bok, G. 2011. Mould growth on building timber collected from three different single-house factories. SP Technical Research Institute of Sweden.

Johansson, P., Bok, G. & Ekstrand-Tobin, A. 2013a. The effect of cyclic moisture and temperature on mould growth on wood compared to steady state conditions. Building and Environment, 65, 178-184.

Johansson, P., Ekstrand-Tobin, A., Svensson, T. & Bok, G. 2012. Laboratory study to determine the critical moisture level for mould growth on building materials. International Biodeterioration and Biodegradation, 73, 23-32.

Johansson, P., Wamming, T., Bok, G. & Edlund, M.-L. 2013b. Mould growth on kiln-dried and air-dried timber. European Journal of Wood & Wood Products, 71, 473.

Marei, G. I. K., Abdel Rasoul, M. A. & Abdelgaleil, S. a. M. 2012. Comparative antifungal activities and biochemical effects of monoterpenes on plant pathogenic fungi. Pesticide Biochemistry and Physiology, 103, 56-61.

Mullins, J. 2001. Microorganisms in outdoor air. In: FLANNIGAN, B., SAMSON, R. A. & MILLER, J. D. (eds.) Microorganisms in home and indoor environments. Diversity, health impacts, investigation and control.: CRC press.

Sandak, J. & Negri, M. 2005. Wood surface roughness - what is it? [Online]. Available: http://www.boku.ac.at/physik/coste35/Rosenheim/article/art_Sandak_COST_E35_Rosenheim_2005.pdf.

Singer, J. D. & Willett, J. B. 2003. Describing Discrete-Time Event Occurrence Data. Chapter 10. Applied Longitudinal Data Analysis Modeling Change and Event Occurrence. Oxford; New York: Oxford University Press.

SIS-EN Standard 1611-1. 2000. Sawn timber - Appearance grading of softwoods - Part 1: European spruces, firs, pines and Douglas firs. Swedish Standards Institute.

Terziev, N. 1996. Low-Molegular Weight Sugars and Nitorgenous Compounds in Scots Pine. SLU.

Theander, O., Bjurman, J. & Boutelje, J. B. 1993. Increase in the content of low-molecular carbohydrates at lumber surfaces during drying and correlations with nitrogen content, yellowing and mould growth. Wood Science and Technology, 27, 381-389.

Viitanen, H. 1996. Factors affecting the development of mould and brown rot decay in wooden material and wooden structures. The Swedish University of Agricultural Sciences.

Strategy for visualisation of the activity of phase change materials by transient plane source technique

Angela Sasic Kalagasidis, Associate Professor [1]
Bijan Adl-Zarrabi, Assistant Professor [1]
Helén Jansson, Assistant Professor [1]
Billy Seng, BSc[2]

[1] Chalmers University of Technology, Gothenburg, Sweden
[2] Ecole des Mines d'Albi, Carmaux, France

KEYWORDS: *Phase change material (PCM), Passive control, Phase transition, Latent heat storage, Thermal energy storage*

SUMMARY:
Through a combination of theoretical and experimental research, this paper aims at evaluating the suitability of a transient plane heat source (TPS) method for the visualisation of the activity of phase change materials (PCMs). The TPS method provides measurements of thermal conductivity and thermal diffusivity of a material in a transient course. It has previously been tested on various building materials but not on PCMs. In this study TPS was tested in a laboratory environment on two inorganic PCMs (salt-hydrates), with melting temperatures 21 ^{o}C and 24 ^{o}C respectively. Based on the experimental trials, the technique has shown to be a valuable technique for the identification of the activity of phase change materials.

1. Introduction

From a sustainable point of view there is a need for the reduction of greenhouse gas emissions and the energy consumption in buildings. On the other hand, the constantly ongoing increase in living standard results in that both more greenhouse gases are emitted and more energy is consumed. Thus, to get this equation balanced, buildings must be more energy efficient and new types, or uses, of materials have to be taken into consideration.

Systems based on materials with thermal storage capacity could be used to reduce the use of fossil fuels used for heating and/or cooling of buildings. In principle it would be possible to use any material that undergoes phase transitions when it is heated or cooled, i.e. a more or less sudden change of the internal energy state of a material as a function of the temperature. Dependent on type of transition, e.g. solid-to-liquid or liquid-to-solid transitions, energy is either absorbed or released, respectively. If the transition involves large amounts of energy per unit mass and the transitions occur close to room temperature it is possible to use this type of materials for storing thermal energy. Such type of materials, which is commonly called phase change materials (PCMs), can be used for passive control of temperature and heat flow in in buildings

2. Thermal properties of salt hydrates

The most frequently used PCMs of today are based on organic (e.g. paraffins or fatty acids,) inorganic (e.g. salt hydrates) or eutectic (composition of two or more components) materials (Soares 2013). Salt solutions, or salt hydrates, generally have larger thermal effusivity than paraffin waxes mainly due to larger volumetric heat capacity. For that reason, salt hydrates show faster response to varying heat loads in

the environment and larger storage capacity per unit volume, which are preferable features for achieving efficient heat storage and release from building envelopes. Leakage from pouches, incongruent melting, large sub-cooling and corrosivity are still unresolved problems (Kosny et al. 2007, Hittle 2002), and the reasons why this type of PCM is used mainly in HVAC applications, (Hed 2009).

Even if this work is focused solely on salt hydrates, many thermal characteristics that are discussed hereafter are applicable also for other types of PCMs such as paraffin waxes.

Salt hydrates are available in a wide range of melting points of interest for building envelope applications, i.e. from +10 ^{o}C to 40 ^{o}C. Below the melting temperature, the PCM is in solid phase. Once the melting temperature is reached, typically after an increased heat load in the environment, the PCM absorb the excess heat at approximately constant temperature, i.e. the PCM starts to melt. When the whole amount of the PCM is melted, its temperature starts to increase. Similarly, when the heat load is reduced, the PCM cools down until the solidification starts. In the solidification period the stored energy is released to the environment. Examples of fully melted, partly melted and fully solidified salt hydrates in pouches are shown in Figure1.

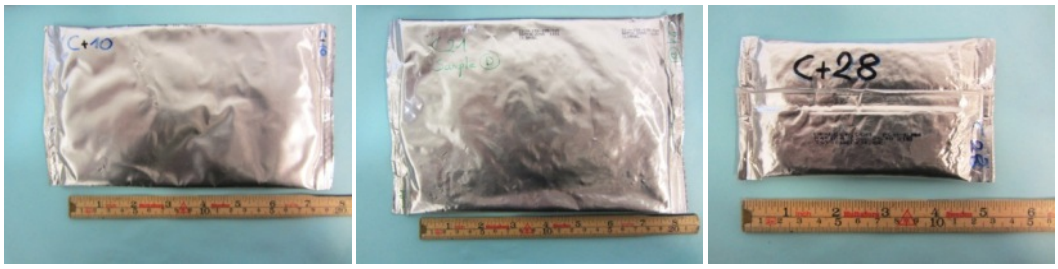

FIG 1. Pouches with ClimSel 10, ClimSel 21 and ClimSel 28 in laboratory environment at 21 ^{o}C. (photo B. Seng). Notations ClimSel 10, ClimSel 21 and ClimSel 28 stand for salt hydrates with melting temperatures at 10 ^{o}C, 21 ^{o}C and 28 ^{o}C respectively.

Depending on the mixture, the phase change process may happen at a constant temperature or within a temperature range. While eutectic salt solutions are characterized by a single melting temperature at a given pressure, non-eutectic solutions melt over a temperature range. For binary non-eutectic solutions, one can distinguish between start and end temperature, as shown in Figure 2. Besides, an apparent specific volumetric heat capacity can be found as the first derivative of energy, for example specific enthalpy h (J/kg of PCM), over temperature change T (^{o}C)

$$c_{apparent}(T) = \frac{dh}{dT}$$

This relation is usually highly non-linear and with a typical peak, as shown in Figure 2. For multi-component mixtures, several peaks can be detected each corresponding to the melting/solidification temperature of one of the components. The maximum apparent specific heat capacity can be several times larger than the heat capacity of a pure solid or pure liquid phase. As an example, Table 1 provides declared thermal properties of a sodium sulphate salt hydrates that were used in this investigation. Based on the data, the average apparent specific heat capacity of ClimSel 21, 10.4 kJ/kgK, can be found as a ratio between the enthalpy (156.5 kJ/kg) and the temperature range (15-30 ^{o}C) (see also Figure 2). This value is 2.5 times larger than the specific heat capacity of pure water (4.2 kJ/kgK) and 26 times larger than the specific heat capacity of dry sodium sulphate (0.4 kJ/kgK). In the same manner, the mean apparent specific heat capacity of ClimSel 24 is found to be 13.1 kJ/kg.

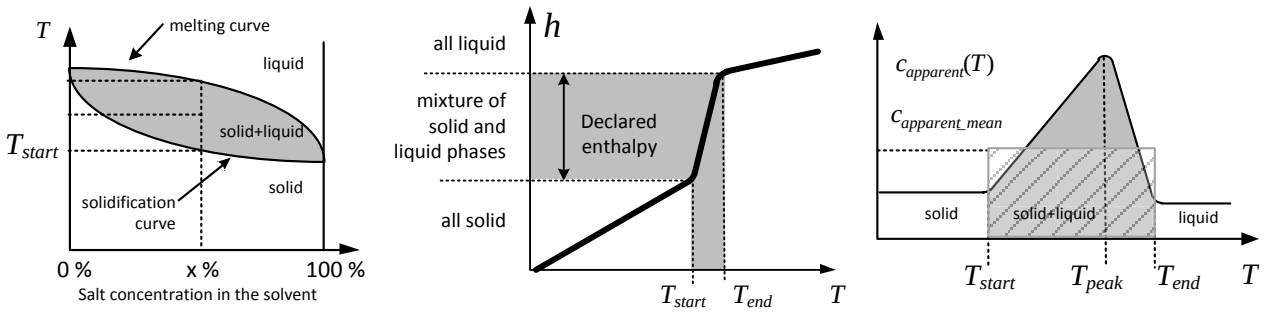

FIG 2. Left: Binary phase diagram. Middle: enthalpy change. Right: apparent specific heat capacity of PCM. All refer to a non-eutectic solution. Simplified representation.

Accurate thermal properties of PCM based materials and components are needed in numerical calculation related to energy performance of a building. The apparent specific heat capacity is a convenient thermal property for numerical modelling of PCMs (Sasic Kalagasidis 2013). Much more efforts are needed for the modelling of PCMs that melt at a constant temperature, as their apparent specific heat capacity is undefined. A multi-phase modelling is then an appropriate approach (Sasic Kalagasidis 2013).

TABLE 1. Thermal properties of ClimSel 21 from Climator Sweden AB

Name	Salt hydrate	Melting temperature [°C]	Latent heat [kJ/kg]	Density [kg/m^3]	Thermal conductivity [W/mK]	Storage capacity	
						Enthalpy [kJ/kg]	Temperature range [°C]
ClimSel 21	Sodium sulphate	21	112.1	1380	0.5-0.7	156.5	15-30
ClimSel 24	Sodium sulphate	24	151.3	1380	0.5-0.7	195.7	15-30

3. TPS method applied on PCM

Transient plane heat source (TPS) method is a transient technique for simultaneously determining thermal conductivity and thermal diffusivity of materials. A plane sensor is located between two halves of a specimen and acts as a heater as well as a detector of temperature increase. The sensor is insulated between two layers of kapton (polyamide) or mica (sheet silicate minerals). The thickness of this insulation is about 25 μm. By using the measured temperature increase at the surface of the sample and the constant power applied to the heater, it is possible to solve the partial differential equation that describes the heat transfer in the specimen, using curve fitting methods (Adl-Zarrabi, 2006). Results of the analysis are thermal conductivity and thermal diffusivity of the specimen.

The TPS method (ISO 22007-2:2008) is applicable for measurements on solids, liquids, anisotropic materials, powders and amorphous structures. The selection of power and measuring time can be based on literature or experience. The measuring time can be estimated from the ratio of the probe radius to the power of two and thermal diffusivity of the specimen.

Most often measurements on PCMs are performed by Differential scanning calorimetry (DSC), as shown in Figure 3, and the T-history method (Kuznik et al. 2011) but, to the best of our knowledge, TPS has not been applied on phase change materials before. Except for that TPS is a good complement to other techniques for heat and phase transition measurements, the choice of this technique is motivated by the small size of the probe, short measuring time and high precision proved on other materials.

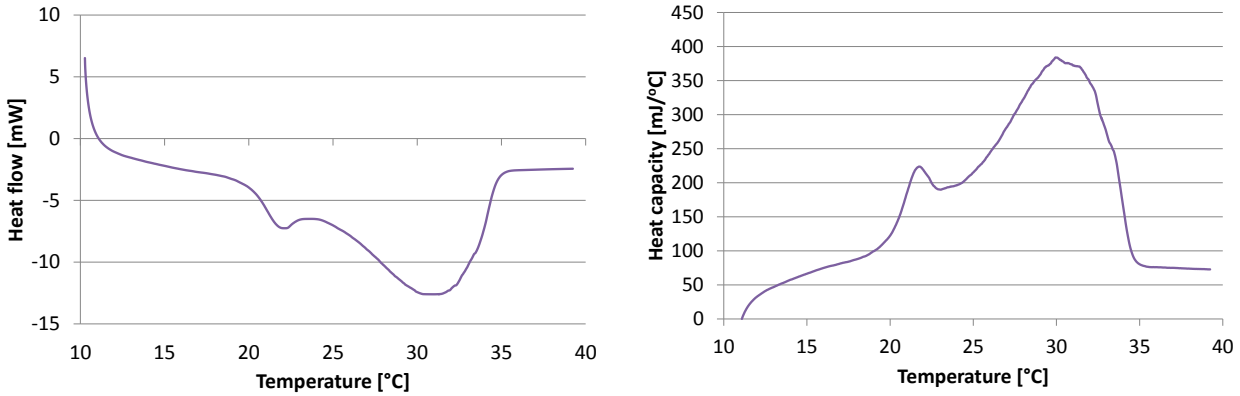

FIG 3. Curves showing the melting (left) and heat capacity (right) of ClimSel21 (Climator Sweden AB) obtained by Differential Scanning Calorimetry (DSC).

3.1 Direct measurements on PCM pouches

To evaluate the influence of the aluminium layer surrounding the PCM, the first attempt was to perform measurements with the probe placed directly on the pouches, both for the fully solidified and fully melted PCM. As the temperature response was almost identical in both situations, i.e. it was not possible to distinguish between the pouches with melted and solid PCM, it was concluded that the heat from the TPS-sensor was more dissipated in the aluminium layer than in the PCM. Similar issues were also described by Johansson et al. (2011) during measurements on vacuum insulation panels. Therefore, direct measurements on the PCM are suggested.

3.2 Direct measurements on PCM

In the second attempt, the sensor was thus placed in direct contact with a certain amount of PCM in a holder. The PCM was sampled from a newly opened pouch to prevent water loss since a control gravimetric analysis showed that the water loss from 2 gr of solid PCM, which was exposed to the ambient air in a Petri cup, was approximately 2 % / 4% / 6 % on a course of 1 h / 2 h / 3h. As any water loss from the PCM could lead to an alteration of the basic characteristics of the sample, the measurements were executed instantly after a sample was taken from the pouch.

A lack of standard holder for the measurements on granules of PCM was solved by using a sample holder made from a cup (120 ml) with a hole on the side through which the probe was inserted, as shown in Figure 4. The procedure was as follows: the cup was filled with the PCM up to the hole for the sensor; the sensor was inserted and an equal amount of PCM was filled over it; finally, the cup was sealed with a plastic paraffin film (Parafilm) to prevent any water loss from the specimen. The same setup was used for the measurements on melted PCM with an addition of a thermocouple, which was inserted in the cup to read the temperature of the specimen.

It was anticipated that the bulk density of the granules in the cup could vary due to irregular shape and size of the granules (see Figure 4), which would affect the results of measurements since the contact between the granules and the sensor would also vary. Therefore, the measurements were performed on differently compressed samples: without compression, i.e. with the bulk density obtained by normal filling of the cup, with small compression (slight patting), and with high compression (stronger patting).

All measurements were performed with a sensor, which is 12.8 mm in diameter and that gives the possibility to apply power of 0.1 W. The diameter of the cup was approximately four times larger than the diameter of the probe. The thickness of the PCM sample below and above the probe was about 1 cm.

FIG 4. Left: probe inserted in the cup. Middle: the cup sealed with Parafilm. Right: granules of PCM (photo B. Seng)

4. Results

4.1 Temperature response

Temperature response curves on 100 mW power supplied from the sensor are summarized in Figure 5, for melted (at 25 ^{o}C) and solid (at 20 ^{o}C) ClimSel 21. There is a clear separation between the curves obtained from the melted and solid samples. The curves obtained on the melted samples show a temperature increment of 1.2±0.1 ^{o}C after 20 s. The curves obtained on solid samples show larger temperature increment, from approximately 3.4 to 4.9 ^{o}C after the same time. The low temperature increment of melted samples can be explained by increased apparent volumetric capacity, which includes the impact of latent heat of melting. Among the solid samples, the lowest temperature increment (3.4 ^{o}C) is found on the high compressed samples, which is explained by a higher bulk density and, consequently, by a higher volumetric heat capacity of the bulk. High compressed samples are more likely to be found in the pouches from which air is evacuated, see Figure 1. Therefore, the temperature response of high compressed samples is more representative for the comparison with the results of melted samples. Note also that the response curves for all samples in the same group are closely gathered, which indicates a good repeatability and precision of the measurements.

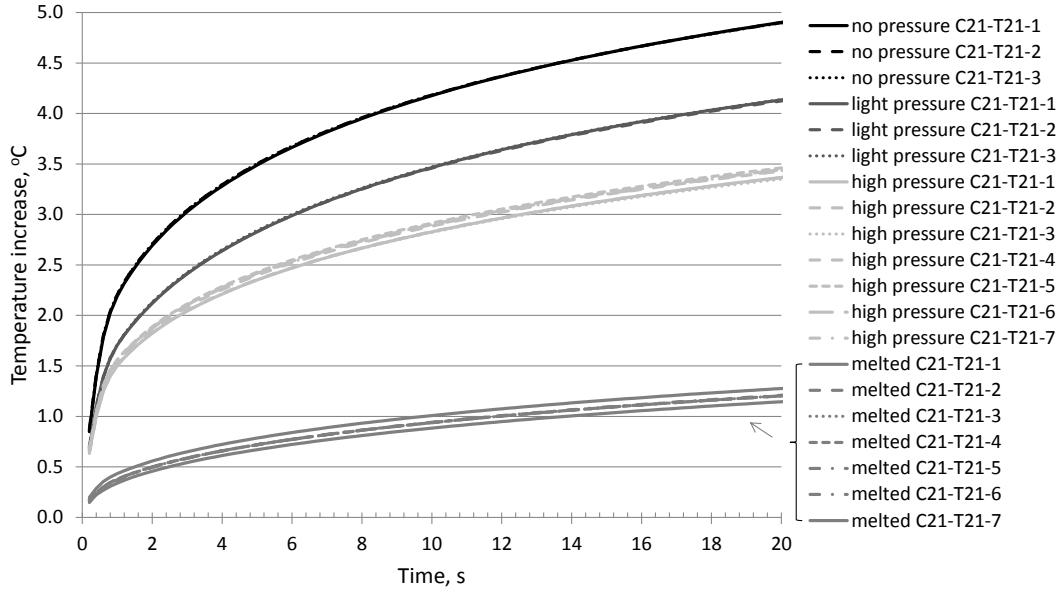

FIG 5. Temperature response curves for ClimSel 21obtained by TPS technique.

In order to verify the findings on ClimSel 21, the same measurements were done on ClimSel 24. This time, the measurements started from a melted sample (at 25 ^{o}C), after which they were repeated whenever the sample cooled down by one degree. The power supplied from the source was 200 mW. The idea was to

test the resolution of the measurements during transient phase change of the sample. The results of this attempt are summarized in Figure 6. As it can be seen, the cooling process is adequately presented with the measurements. The lowest temperature increment was found on the fully melted sample, and the highest response was recorded on the coolest samples. In this first trial of the method results for 23 ^{o}C and 24 ^{o}C were not recorded. Although the response curves are distinctly separated from each other, the difference between the fully melted and solidified[1] samples is not that large as in the previous example. One possible explanation is that the bulk density of the solidified samples was probably higher, which was achieved through a continuous process of solidification in which the air penetration in the sample was limited.

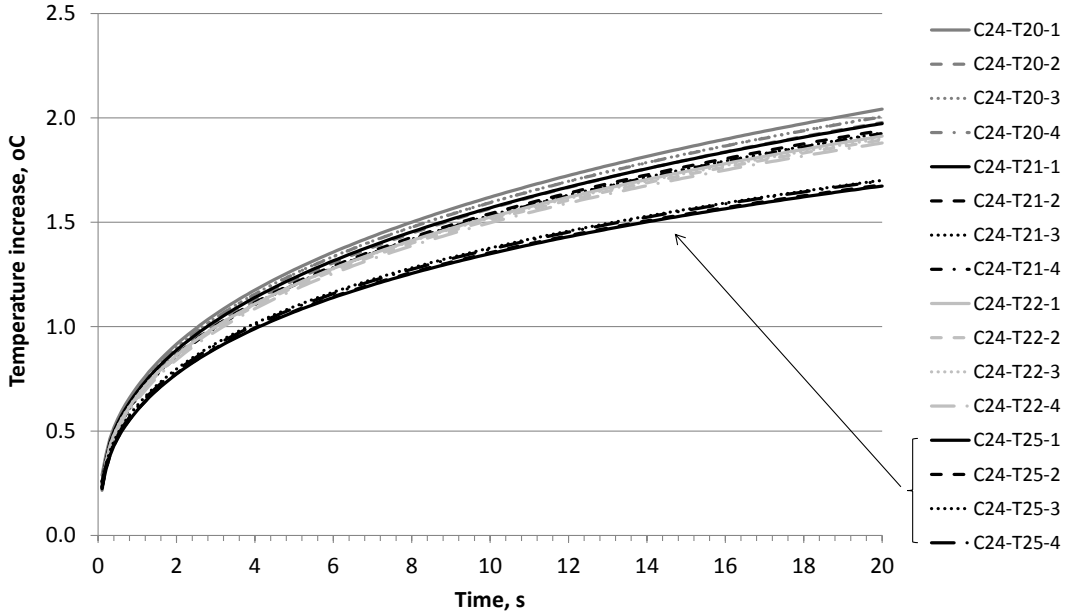

FIG 6. Temperature response curves for ClimSel 24 obtained by TPS in the continuous cooling mode.

4.2 Thermal properties

The TPS method was not designed for the evaluation of thermal properties of PCMs. Therefore, the results for thermal conductivity, thermal diffusivity and volumetric heat of ClimSel 21 and ClimSel 24, which were obtained by TPS and summarized in Tables 2 and 3 should be regarded as indicative. These results were determined from the temperature response curves in Figures 5 and 6 by built-in software provided together with the TPS by HotDisc (www.hotdiskinstruments.com).

The thermal conductivity of ClimSel 21 is close to the declared values in Table 1, with the lowest values found on the samples with the lowest bulk density (light compressed) samples and the highest on the melted samples. Likewise, the volumetric heat capacity increases with the bulk density of the samples while the thermal diffusivity decreases.

Similar but not exactly the same trend can be seen in the results for ClimSel 24 in Table 3. The values for thermal conductivity and volumetric heat capacity are much closer to each other and, in general, closer to the values obtained for the melted samples of ClimSel 21. As explained above, the density of these samples was less affected by air intrusion.

[1] It was not determined to what extent these samples were solidified

TABLE 2. Thermal properties of ClilmSel 21 determined by TPS technique. Bulk density n/a.

Sample (Number of samples)	Temperature °C	Thermal conductivity W/mK	Thermal diffusivity $\cdot 10^{-6}$ m^2/s	Volumetric heat capacity kJ/(m^3·K)
		Mean / Coefficient of variation (std. deviation/mean, %)		
Solid, light compression (3)	20	0.3370 / 0.26	1.0030 / 1.50	0.3360 / 0.25
Solid, high compression (7)	20	0.4003 / 0.68	0.4959 / 1.54	0.8077/ 1.45
Melted (7)	23-25	0.7657 / 4.32	0.3038 / 3.00	2.5295/ 11.77

TABLE 3. Thermal properties of ClilmSel 24 determined by TPS technique. Bulk density n/a.

Sample (Number of samples)	Temperature °C	Thermal conductivity W/mK	Thermal diffusivity $\cdot 10^{-6}$ m^2/s	Volumetric heat capacity kJ/(m^3·K)
		Mean / Coefficient of variation (std. deviation/mean, %)		
Solid[1] (4)	20	0.9588 / 2.01	0.3020 / 1.15	3.1768 / 5.64
Solid[1] (4)	21	1.0968 / 1.60	0.4359 / 1.12	2.5168 / 2.91
Solid[1] (4)	22	1.0812 / 1.76	0.3648 / 1.27	2.9649 / 5.64
Melted (4)	25	1.3217 / 0.53	0.4335 / 0.78	3.0497 / 5.39

For comparison, Figure 7 shows analytically obtained response curves for a material with the thermal diffusivity in the range of the values from Table 2 and 3. The analytical temperature solution is taken from Johansson et al.(2011); it represents a temperature response of a homogeneous material on heat (100 mW and 200 mW) injected from a circular plane source with radius 0.0064 m. The solution assumes maximum dispersion of heat in the material, a perfect contact between the source and the material and a perfect heat source. The theoretical temperature increment at the surface of the material, at around the circumference of the heat source is in the range 0.8-1.5 °C after 20 s, for thermal diffusivities $0.3 \cdot 10^{-6}$ m^2/s $-1 \cdot 10^{-6}$ m^2/s and for 100 mW power supplied from the source. The temperature increase is linearly proportional to the power supplied from the heat source and it's thus doubled for 200 mW (1.6-3 °C). These values can be compared to the ones in Figures 5 and 6, and Tables 2 and 3. The calculated temperature increment is in the range of the measured values by the TPS for the melted samples: 1.1-1.3 °C for ClimSel 21 and about 1.7 °C for ClimSel 24. For the solid samples with lot of air (i.e. loosely packing) between the granules, the analytical and measured response differ substantially. Nevertheless, the trend is still the same – the temperature increment is higher when the thermal diffusivity increases, as it is also shown by the measurements.

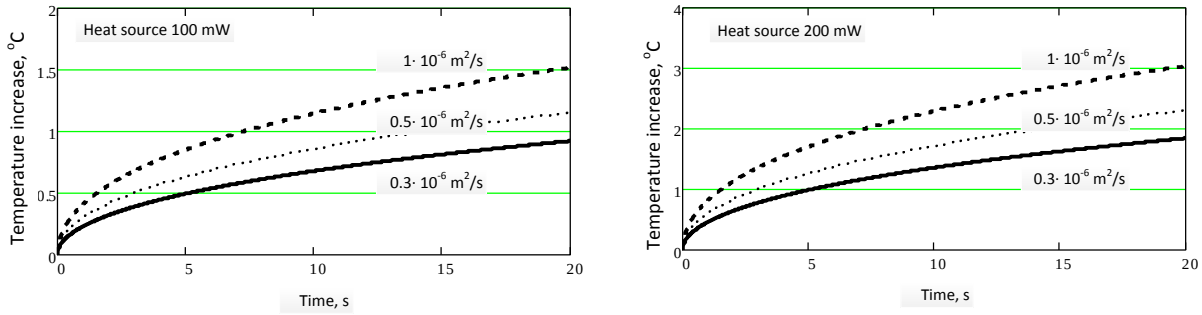

FIG 7. Theoretical temperature response curves for a material as a function of thermal diffusivity. The values for thermal diffusivity are based on the measurements, from Table 2 and Table 3.

5. Discussion

The results indicate that the TPS can detect the PCM activity with sufficient resolution. However, the results should be taken with caution due to some unresolved issues for the measuring procedure. While the

sensor was completely covered by the melted PCM, this was not the case during the measurements performed on the solid granules. The looser the packing of the grains, the less direct contact between the sensor and the grains is obtained. Ideally, a sample should be taken in a large block of compressed PCM or one should realize the measurement directly on the pouches after removing the aluminium layer. In that case, an environmental chamber at a specific atmosphere could be used to avoid any evaporation of the solvent. The original size of the grains is in millimetre range and a probe with larger radius than 6.4 mm, as used in this work, is probably more appropriate in order to account for the inhomogeneity of the sample. The issue with varying bulk densities of the solid sample could be overcome if the measurements should start from a melted sample.

6. Conclusions

The TPS technique was used in an innovative way, for the visualization of the activity of PCM (sodium sulphate hydrates) in the phase transition region. A sample holder for the TPS and the specimens was constructed and the measuring procedure was explained. The measurements with the TPS method provided temperature response curves for the fully solidified and fully melted samples with declared melting temperatures at 21 ^{o}C and 24 ^{o}C. It was found that TPS provided an exceptionally fine resolution for the temperature response curves, wherefrom it was possible to separate the samples in respect to their bulk density and the melting temperature. Based on the temperature response curves, the thermal properties of the samples were evaluated. Although these values varied in accordance with the bulk density and the melting temperatures of the samples, the absolute values were just indicative. This very first trial with using the TPS showed that the technique had potential to be used for the measurements of PCMs activation. The issues to be resolved in future are related to the bulk density of the specimen and to the size of the probe in relation to the granules of solidified PCM.

References

Adl-Zarrabi B. 2006. Using the TPS method for determining the thermal properties of concrete and wood at elevated temperature. Fire and Materials, 30:359-369.

Hed G. 2003. Use of phase change material for change of thermal inertia of buildings. In the proceeding of the 6th Expert Meeting and Workshop of Annex 17. Available on www.kth.se/abe/inst/byv/publ.

Hittle D. C. 2002. Phase Change Materials in Floor Tiles for Thermal Energy Storage. Topical Report. Award No. DE-FC26-00NT40999. Colorado State University. Fort Collins, CO 80523. Available on https://www.etde.org/etdeweb/servlets/purl/820428/820428.pdf

ISO 22007-2:2008. Plastics. Determination of thermal conductivity and thermal diffusivity. Part 2: Transient plane heat source (hot disc) method

Johansson P., Adl-Zarrabi B., Hagentoft C-E. 2011. Measurements of Thermal properties of Vacuum Insulation Panels by using Transient Plane Source Sensor. Proceedings of the 10th International Vacuum Insulation Symposium. Ottawa, Canada, pp. 18-21.

Kosny J., Yarbrough D., Miller W., Petrie T., Childs P., Syed A.M., Leuthold D. 2007. Thermal Performance of PCM-Enhanced Building Envelope Systems. *Proceedings of Thermal Performance of the Exterior Envelopes of Whole Buildings*, X International Conference.

Kuznik F., David D., Johannes K., Roux J-J. 2011. A review of phase change materials integrated in building walls. Renewable and Sustainable Energy Reviews (15) 379-391

Sasic Kalagasidis A. A multi-level modelling and evaluation of thermal performance of phase change materials in buildings. J of Build P Simulation, DOI:10.1080/19401493.2013.764547

Soares N., Costa J.,J., Caspar A.R., Santos P. 2013. Review of passive PCM latent heat thermal energy storage systems towards buildings' energy efficiency. Energy and Buildings (59), pp 82-103.

Modeling the moisture buffering behaviour of a bio-based building material

Dylan Lelièvre, Eng.[1]
Thibaut Colinart Associate Professor[1]
Patrick Glouannec, Professor [1]

[1] Univ. Bretagne-Sud, EA 4250, LIMATB, F-56100 Lorient, France

KEYWORDS: *Hemp concrete, Moisture Buffer Value, Hysteresis, Relative humidity measurement, Heat and moisture transfer, Numerical simulation*

SUMMARY:
In the present work, two extended cyclical adsorption/desorption tests are performed on a bio-based building sample (here hemp concrete), among which one is following the Nordtest protocol. Two improvements are done in the experiments: first, the mass variations are weighted continuously; secondly, the sample is instrumented at several positions with thermo-hygrometers and thermocouples to catch the local temperature and relative humidity variations within the material. Simultaneously, a heat and moisture transfer 1D-model accounting for hysteresis and phase change effect is developed with Comsol Multiphysics®. Input physical properties and their dependency with the temperature and the moisture content were defined by means of laboratory experiments. The comparison of numerical results with experimental data gives satisfactory results, in terms of mean mass variation, as well of temperature and relative humidity variations.

1. Introduction

During the last decades a large number of simulation works dealing with the energy efficiency of building have shown the positive effect of hygroscopic building materials on building energy demand (Osanyintola 2006), on HVAC system energy consumption (Woloszyn 2009) or on indoor air quality by reducing the amplitude of daily moisture variations (Simonson 2002). Among the numerous hygroscopic building materials, bio-based building materials, like hemp concrete, are currently interesting alternative products in the field of architecture and construction, since they have many environmental benefits, like a potentially very low carbon life cycle (Prétot 2013), and interesting thermo-hydric properties, like a low thermal conductivity (Pierre 2013) or a high hygric buffering capacity (Collet 2012). As expected, Tran Le (2010) showed also the positive effect of hemp concrete on the building energy consumption in comparison to cellular concrete.

Whatever the investigated material, the reliability of these numerical results depends however on the accurate quantification of heat and moisture transfer within the materials and at the interface with air. Therefore, numerous experiments aim to evaluate the hygroscopic building materials capacity to store and release moisture, and thus to validate their potential to moderate relative humidity changes inside a room/building (e.g. moisture buffering potential). This is mainly done by applying cyclical varying humidity conditions around the material. For instance, benchmark experiments on classical hygroscopic building materials like spruce plywood and cellulose insulation (Talukdar 2007a) or gypsum boards (James 2010) were performed in a wind tunnel in the framework of IEA Annex 41. This experimental facility allows particularly evaluating the temperature, the relative humidity and the moisture accumulation within materials subjected to convective boundary conditions. Alternatively, two more simple tests, the Nordtest protocol and the Japanese Industrial Standard, have been suggested to evaluate specifically the moisture buffering potential (Roels 2006). In such isothermal experiments, a preconditioned specimen sealed on all but one surface is successively exposed to high

and low ambient humidity for predefined time intervals in a climatic chamber. Mass evolution is recorded over time and a moisture buffer value (MBV) can be defined. These protocols were extensively applied to classical hygroscopic building materials, but also to hemp concrete (Collet 2012)(Maalouf 2013)(Dubois 2013). In particular, it was found that MBV are highly dependent on the sample thickness, the time scheme or the surface film resistance (e.g. the surface topology and the air velocity) (Roels 2006).

Simultaneously, numerous heat and moisture transfer models were developed to catch the benchmark experimental data (Talukdar 2007b)(Janssens 2008)(Steeman 2009)(Kwiatkowski 2009). Most of the model treat the moisture transfer only through an effective water vapour permeability and hysteresis or dynamic effects are often neglected although cyclical air relative humidity variations. Moreover, the interfacial transfer between the air and the material (boundary condition) is evaluated by calculating mean convective transfer coefficients. Adopting these assumptions, Dubois (2013) could predict the mass and surface temperature variations of a hemp concrete sample subjected to the Nordtest protocol. Even if no perfect match is found between numerical results and experimental data, the results are often considered as acceptable regarding the uncertainty in the properties. Maalouf (2013) and Aït Oumeziane (2013) proposed modelling improvements by considering liquid water transport and by accounting for hysteresis in the sorption curves. However, their results are validated only against the sample's mass variations in case of moisture buffering experiments.

The main purpose of this paper is to develop a heat and moisture transport model within bio-based building materials accounting for hysteresis and phase change effect. Contrary to the above-mentioned studies, this model is evaluated by comparing simulated results not only to global but also to local experimental data measured on hemp concrete during extended cyclical adsorption/desorption tests.

2. Experimental facility

The moisture buffering potential of hemp concrete is determined here by performing two cyclical adsorption/desorption tests in a climatic chamber (Memmert HPP 108, Schwabach, Germany) at a fixed temperature of 23 °C:

- A slow cycling test: 10 days at high relative humidity (75 %) followed by 10 days at low relative humidity (33 %),
- A fast cycling test (e.g. Nordtest protocol): 8 h at high relative humidity (75 %) followed by 16 h at low relative humidity (33 %) during 10 days.

The tested material is sprayed hemp concrete that was already investigated in previous studies (Pierre 2013)(Colinart 2013). The tested sample has a large open surface (148 x 148 mm) and a thickness of 100 mm, which is larger than the moisture penetration depth calculated for such a material (Collet 2012). For both experiments, the sample is conditioned as follow: first it is dried in a ventilated oven at 60 °C in order to get the dry mass/density (here, m_{dry} = 999,8g / ρ_s = 450 kg.m^{-3}), and then it is stored at 23 °C / 50% so that the initial state is well known. Before performing the experiment, the sample is sealed on all but one surface with aluminium tape and insulating material to ensure 1D heat and moisture transfer within the sample. During the experiment, the mass change is continuously measured by a weight-scale with a resolution of 0.01g (see Figure 1). Furthermore, temperature and relative humidity is monitored at different positions within the sample (at 15, 50, 80 and 100 mm ± 5 mm from the top surface) with K thermocouples and capacitive humidity sensors (Sensirion SHT 75, Staefa, Switzerland). Temperature and relative humidity uncertainties are evaluated to 0.5 °C and 5 % respectively. An additional humidity sensor is used to monitor temperature and relative humidity within the climatic chamber. Their variations are shown in Figure 1 in the case of the Nordtest protocol. Relative humidity set points are rapidly reached whereas temperature variations of about 0,2°C are observed at each relative humidity set point change. Furthermore, a fan is used to ensure good air homogeneity and measured air velocity does not exceed 0.3 m.s^{-1}. Last, temperature measured at 100 mm (i.e. bottom) presents similar variation as that of air temperature (see Figure 1).

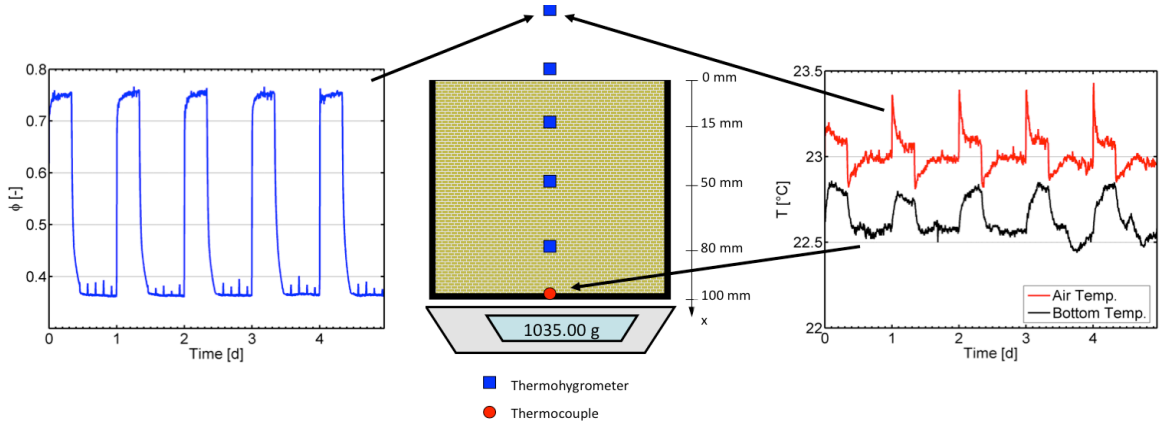

FIG 1. Experimental set-up and measured air relative humidity (left) and temperature in the ambient air and at the bottom of the sample (right).

3. Mathematical model

The modelling of heat and moisture transport processes in hygroscopic porous material has been an ongoing concern in building physics. Most of models involve the theory of Philip and De Vries (1957), which describes moisture transport as an addition of vapour and liquid flow and heat transfer according to Fourier's Law. The models differ in the assumptions and in the choice of state variable and driving potential (Delgado 2010). In the present work, temperature T and relative humidity φ are used in the view of stating the transfers through multi-layered component and we assume that:

- Porous material is regarded as continuous, homogeneous, stabilized (e.g. no chemical reactions) and non-deformable (e.g. no shrinkage),
- Local thermodynamic equilibrium is assumed at every point of the material,
- Gravity effects are neglected and total gas pressure p_g is constant, equal to the atmospheric one,
- Air transport is not taken into account.

3.1 Constitutive equations

Moisture conservation within the material is written as:

$$\rho_s \theta \frac{\partial \varphi}{\partial t} = -\nabla.\left(-\left(D_l^{\varphi} + D_v^{\varphi}\right)\nabla\varphi - \left(D_l^{T} + D_v^{T}\right)\nabla T\right) \quad (1)$$

Where ρ_s dry density (kg/m^3)

$\theta = dw/d\varphi$ sorption capacity (-)

w moisture content (kg/kg)

D^{φ}, D^{T} moisture transfer coefficients (kg/(m.s) and kg/(m.s.K))

Vapor and liquid diffusion coefficients are calculated as follow:

$$D_v^{\varphi} = \frac{\pi_a}{\mu_{dry}} p_v^{sat} \text{ and } D_v^{T} = \frac{\pi_a}{\mu_{dry}} \varphi \frac{dp_v^{sat}}{dT} \quad (2)$$

$$D_l^{\varphi} = \pi\, p_v^{sat} - D_v^{\varphi} \text{ and } D_l^{T} \approx 0 \quad (3)$$

Where π_a air vapour permeability, 2.10^{-10} kg/(m.s.Pa)

π material vapour permeability determined over the whole humidity range

μ_{dry} vapour resistance coefficient of the 'dry' material (-)

p_v^{sat} saturated vapour pressure (Pa).

Energy balance equation takes into account the thermal conduction and the phase change of water as:

$$\overline{\rho c_p}\frac{\partial T}{\partial t} = -\nabla.\left(-\lambda \nabla T\right) - K\left(L_v + \left(c_{p,v} - c_{p,l}\right)\left(T - T_{ref}\right)\right) \quad (4)$$

Where $\overline{\rho c_p}$ apparent thermal capacity (J/(m^{3}K))

λ apparent thermal conductivity (W/(m K))

$K = \nabla.\left(D_v^{\varphi}\nabla\varphi + D_v^T \nabla T\right)$

L_v heat of vaporization, 2500 kJ/kg

c_{pv}, c_{pl} vapour and liquid thermal capacity, 1860 (J/(kg K)) and 4180 (J/(kg K))

T_{ref} reference temperature, 273.15 K

3.2 Boundary conditions

Heat and moisture transfer equations are applied to one-dimension for sample in the case of cyclical adsorption/desorption simulations (see Figure 1): lateral sides are considered as impermeable and adiabatic. At x = 0 (bottom), impermeable condition is assumed for moisture whereas the temperature is set to the experimental one. At the top surface in contact with air (x = L), boundary conditions are:

$$-\lambda\nabla T - \left(\rho_s \nabla.\left(D_l^{\varphi}\nabla\varphi + D_l^T \nabla T\right)\right)\left(L_v + \left(c_{p,v} - c_{p,l}\right)T\right) = \left(h_c + h_r\right)\left(T_{air} - T_{surf}\right) \quad (5)$$

$$\rho_s\left[\left(D_v^{\varphi} + D_l^{\varphi}\right)\nabla\varphi + \left(D_v^T + D_l^T\right)\nabla T\right] = k_m \frac{M_v}{R}\left(\frac{p_{v,air}}{T_{air}} - \frac{p_{v,surf}}{T_{surf}}\right) \quad (6)$$

Where h_c convective heat transfer coefficient, 5 W/(m^{2}K)

$k_m = \frac{h_c a_{air}}{\lambda_{air}} = 7.3 \times 10^{-4} h_c$ convective mass transfer coefficient (kg/(m^2.s))

$h_r = 4\varepsilon_r \sigma\left(\frac{T_{air} + T_{surf}}{2}\right)^3$ radiative heat transfer coefficient (W/(m^{2}K))

ε_r material emissivity, 0.8

3.3 Material properties

To guarantee the accuracy of the input parameters in the modelling, material properties are measured in the lab. Sorption isotherms are determined gravimetrically at 23 °C using salt solutions to generate relative humidity according to ISO 12571. Figure 2 shows experimental results for the main adsorption and desorption isotherms.

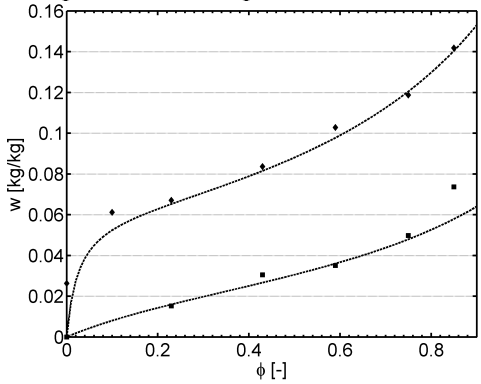

FIG 2. Main adsorption and desorption curves: measurements (points) and fitted curves (solid lines).

These data are fitted with a GAB model (Eq (7)), defined as:

$$w = \frac{w_m \times C \times K \times \varphi}{(1 - K \times \varphi)\left(1 + K(C-1)\varphi\right)} \quad (7)$$

Where w_m, C and K fitting coefficients (-). The fitting is done here not on the whole range of humidity but only in the range of interest (30 % – 80 %). Hence, we have w_m = 0.028, C = 5 and K = 0.68 for the main adsorption curve and w_m = 0.06, C = 60 and K = 0.68 for the main desorption curve.

To account for the hysteresis observed in the sorption's curves, adsorption and desorption capacities are described by the empirical approach proposed by Pedersen (1990):

$$\theta_{ad,hys} = \frac{B(w - w_{ad})^A \theta_{des} + (w - w_{des})^A \theta_{ad}}{(w_{des} - w_{ad})^A} \quad (8)$$

$$\theta_{des,hys} = \frac{(w - w_{ad})^A \theta_{des} + C(w - w_{des})^A \theta_{ad}}{(w_{des} - w_{ad})^A} \quad (9)$$

Where A, B, C empirical coefficients to be determined (-). Usually, A is set to 2 (Pedersen 1990).

The water vapour transmission properties are determined in accordance to ISO 12572. A value of $\mu_{dry} \approx 6.3$ is found for dry cup (0/50%) experiments performed at 23 °C and is in agreement with the one measured by Collet (2012) for the same material. The vapour permeability over the whole humidity range is taken from the literature (Collet, 2012):

$$\pi = 3.19 \times 10^{-10} + 5.18 \times 10^{-10} \varphi^{8.38} \quad (10)$$

Dry material's heat capacity c_{ps} is determined by a calorimetric measurement (Setaram µ-DSC III, Caluire, France): a value of 1000 $J.kg^{-1}.K^{-1}$ is found. Intrinsic thermal conductivity is measured using the transient hot-strip technique (to avoid evaporation effects) at temperatures ranging between -3 °C and 30 °C and relative humidities ranging between 0% and 95%. Its temperature and moisture dependence is evaluated as follow (Pierre 2013):

$$\lambda\left[W/(mK)\right] = 0.00818 + 2.76 .10^{-4} \times T\left[°C\right] + 0.24 \times w\left[\%\right] \quad (11)$$

3.4 Numerical resolution

The coupled and nonlinear partial differential equations are formulated in the ''PDE Modes" of COMSOL Multiphysics®, since it offers flexibility in the equation and boundary conditions writing and it may solve equations with variable time stepping (here the same as the experimental ones).

4. Comparison between experimental and numerical results

4.1 Slow cycling test

First, the slow cycling test is analysed: a comparison between experimental and numerical results are presented in Figure 3 for the mean moisture accumulation and in Figures 4 for temperatures and relative humidity's variations within the material. Before the experiment, the material is conditioned in sorption (φ increases from 0 to 50 %) and moisture content is measured to 0.032 kg/kg. This value is equal to the one predicted by the GAB model for the main adsorption curve and, thus, confirms the accuracy of the initial conditioning. During the adsorption stage (φ increases from 50 to 75 %), mean moisture content should theoretically follow the main adsorption curve: no hysteresis modelling is required in this case to predict the hygrothermal behaviour of hemp concrete and this stage can therefore be used to validate the material properties. As shown in Figure 3, a good agreement is found between numerical and experimental results for the mean moisture accumulation. Looking at the local

measurement (Figures 4), temperatures are accurately predicted over the entire thickness in terms of amplitude and phase delay whereas relative humidities are well caught at steady state close to the surface (at x = 15 mm and 50 mm) and less caught deeper within the material (at x = 80 mm). A sensibility analysis (not presented here) indicates that the main adsorption capacity is of great influence on the results, explaining why the fitting is performed only in the humidity region of interest. After 10 days, a primary desorption experiment starts (φ decreases from 75 to 33 %) in the view of determining the empirical coefficients B and C of the hysteresis model. Numerous simulation runs were performed: it is found that B is of no influence in this case whereas the coefficient C can be chosen between 0.7 and 0.9. Results obtained for B = C = 0.9 are plotted in Figures 3 and 4 (see between the 10th and 20th day): mean moisture accumulation is well caught at the beginning, and then a small difference appears from the 15th day. Temperatures variations are still accurately predicted within the whole material, contrary to the relative humidity variation.

Concerning the relative humidity prediction, two points should mentioned: first, sorption's curves are flat in the humidity region of interest, and, thus, a slight change in the moisture content may induce large humidity variations. Second, the small differences observed in the transient phase between experiments and simulation may be due to moisture dynamic effects (Janssen 2010). According to Scheffler (2011), this effect linked to sorption/desorption rate occurs not only in the capillary range but also in the hygroscopic range of low permeability material, like building materials.

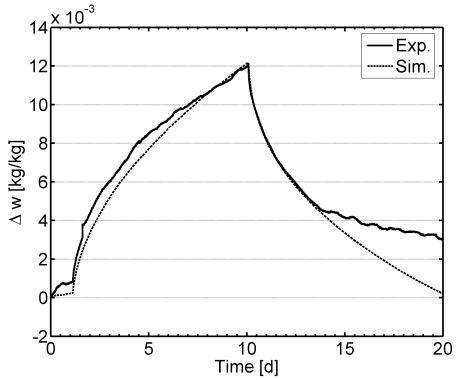

FIG 3. Measured and simulated mean moisture accumulation within the hemp concrete sample during the slow cycling test.

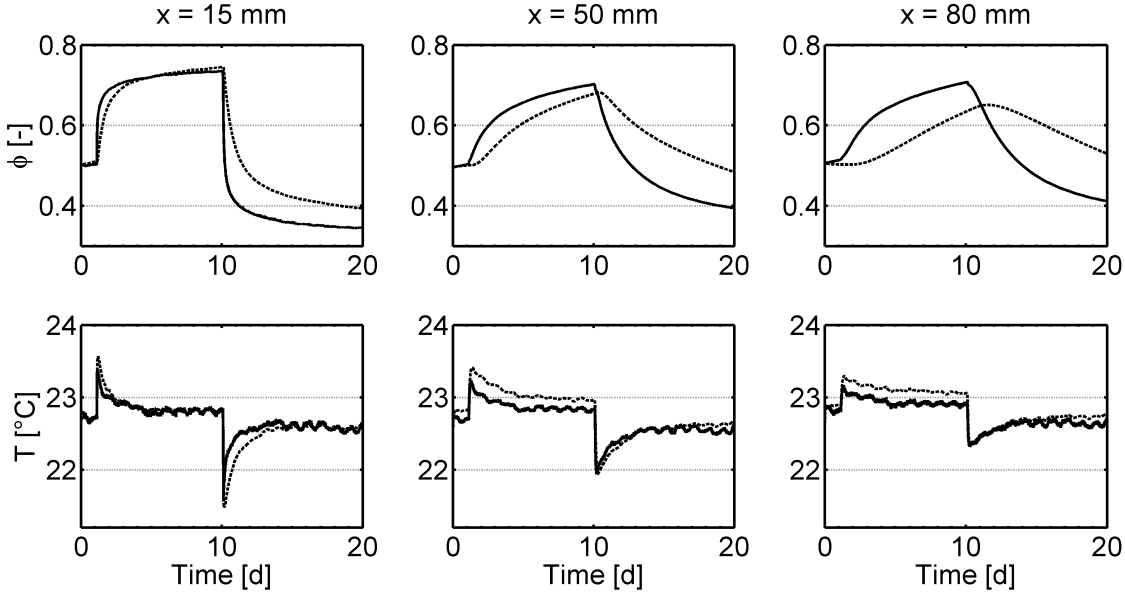

FIG 4. Measured and simulated (a) relative humidity and (b) temperature within the hemp concrete sample during the slow cycling test.

4.2 Fast cycling test

Based on the previous conclusions, a simulation of the fast cycling test was then performed and numerical results are presented in Figures 5. Mean moisture accumulations variations are well predicted during the first cycle, but numerical results differ slightly from the experimental ones as far the cycling proceeds. In this case, samples mean moisture content moves from the main adsorption curve toward the main desorption curve and the hysteresis model coefficients B and the main desorption capacity have progressively a greater influence on the results. Similarly to the slow cycling test, relative humidity's variations at x = 15 mm could not be well caught because of the uncertainty of the sensor position and accuracy, but also because the moisture dynamic effects.

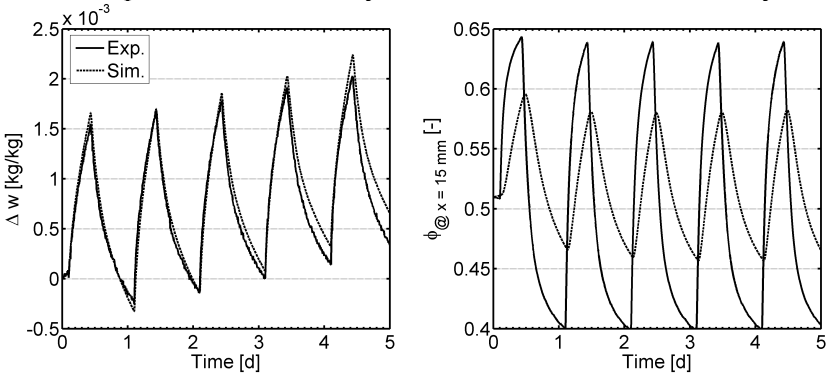

FIG 5. Measured and simulated (a) mean moisture accumulation and (b) relative humidity within the hemp concrete sample during the fast cycling test.

5. Conclusions

A model describing the hygrothermal behaviour of a bio-based building material was developed by considering hysteresis through the empirical model of Pedersen (1990). This model was solved for changing relative humidity conditions and the numerical results were compared to experimental data measured on instrumented samples during a slow and fast cycling test. First, the good agreement found in the analysis of adsorption stage indicates that the main adsorption curve is well fitted and that other materials properties are accurately defined. Secondly, while global variations of the sample mass as well the local variations of temperature have been successfully modelled during the desorption stage, differences still exist between the simulated and measured local variations of relative humidity, notably because of moisture dynamic effects. Accounting for this effect may concern a further development in the modelling. In addition, the empirical hysteresis model can be substitute by a physic-based hysteresis model. A last improvement consists in solving the model at the wall scale and in comparing the results with experimental ones (Colinart, 2013).

References

Aït Ouméziane Y. 2013. Evaluation des performances hygrothermiques d'une paroi par simulation numérique : application aux parois en béton de chanvre, Ph.D Thesis, INSA Rennes, France.

Colinart T., Glouannec P., Pierre T., Chauvelon P. & Magueresse A., 2013. Experimental Study on the Hygrothermal Behavior of a Coated Sprayed Hemp Concrete Wall, *Buildings*, **3**, 79-99.

Collet F. & Pretot S., 2012. Experimental investigation of moisture buffering capacity of sprayed hemp concrete, *Constr. Build. Mater.*, **36**, 58–65.

Delgado J.M.P.Q., Ramos N.M.M., Barreira E. & De Freitas V.P., 2010. A critical review of hygrothermal models used in porous building materials, *J. Porous Media*, **13**, 221-234.

Dubois S., Evrard A. & Lebeau F., 2013. Modeling the hygrothermal behavior of biobased construction materials, *J. Building Phys.*, in press.

James C., Simonson C.J., Talukdar P. & Roels, S., 2010. Numerical and experimental data set for benchmarking hygroscopic buffering models, *Int. J. Heat Mass Transfer*, **53**, 3638–3654.

Janssen H. & Scheffler G.A., 2010. Numerical Modeling of Dynamic Effects in Porous Media Flow, in Proceedings of "Thermal Performance of the Exterior Envelopes of Whole Buildings XI International Conference".

Janssens A., Woloszyn M., Rode C., Sasic-Kalagasidis A. & De Paepe M., 2008. From EMPD to CFD: overview of different approaches for Heat Air and Moisture modeling, in Proceedings of the IEA ECBCS Annex 41 Closing Seminar.

Kwiatkowski J., Woloszyn M. & Roux J.J., 2009. Modelling of hysteresis influence on mass transfer in building materials, *Build. Environ.*, **44**, 633-642.

Maalouf C., Lachi M., Mai T.H. & Wurtz E., 2013. Numerical and experimental study of the hygric inertia of a hemp-lime concrete, *Int. J. Math. Models Methods Appl. Sci.*, **7**, 149-156.

Osanyintola O.F. & Simonson C.J., 2006. Moisture buffering capacity of hygroscopic building materials: Experimental facilities and energy impact, *Energy Build.*, **38**, 1270–1282.

Pedersen C.R. 1990. Combined heat and moisture transfer in building constructions, PhD Thesis, Technical University of Denmark, Denmark.

Pierre T., Colinart T. & Glouannec P., 2013. Measurement of thermal properties of biosourced building materials, *Int. J. Thermophys.*, in press.

Philip J.R. & De Vries D.A., 1953. Moisture movement in porous material under temperature gradients, *Trans. Am. Geophys. Union*, **38**, 222–232.

Prétot S., Collet F. & Garnier C., 2013. Life cycle assessment of a hemp concrete wall: impact of thickness and coating, *Build. Environ.*, in press.

Roels S. & Janssen H., 2006. A Comparison of the Nordtest and Japanese Test Methods for the Moisture Buffering Performance of Building Materials, *J. Build. Phys.*, **30**, 137–161.

Scheffler, G.A. & Plagge R., 2011. Application of instantaneous profile measurement of moisture content and moisture potential in porous materials, *Mater. Struct.*, **44**, 1517–1536.

Simonson C.J., Salonvaara M. & Ojanen T., 2002. The effects of structures on indoor humidity—Possibility to improve comfort and perceived air quality, *Indoor Air*, **12**, 243–251.

Steeman M., Van Belleghem M., Janssens A. & De Paepe M., 2009. Coupled simulation of heat and moisture transport in air and porous materials for the assessment of moisture related damage, *Build. Environ.*, **44**, 2176-2184.

Talukdar P., Olutimayin S.O., Osanyintola O.F. & Simonson C.J., 2007a. An experimental data set for benchmarking 1-D, transient heat and moisture transfer models of hygroscopic building materials. Part I: Experimental facility and material property data, *Int. J. Heat Mass Transfer*, **50**, 4527–4539.

Talukdar P., Osanyintola O.F., Olutimayin S.O. & Simonson C.J., 2007b. An experimental data set for benchmarking 1-D, transient heat and moisture transfer models of hygroscopic building materials. Part II: Experimental, numerical and analytical data, *Int. J. Heat Mass Transfer*, **50**, 4915-4926.

Tran Le A.D., Maalouf C., Mai T.H., Wurtz E. & Collet F., 2010. Transient hygrothermal behavior of a hemp concrete building envelope, *Energy Build.*, **30**, 1797–1806.

Woloszyn M., Kalamees T., Abadie M.O., Steeman M. & Kalagsidis S.A., 2009. The effect of combining a relative-humidity-sensitive ventilation system with the moisture-buffering capacity of materials on indoor climate and energy efficiency of buildings, *Build. Environ.*, **44**, 515–524.

Impact of the moisture buffering effect of wooden materials on energy demand and comfort conditions

Matthias Winkler, M.Eng. [1]
Kristine Nore, PhD [2]
Florian Antretter, M.Eng. [1]
[1] Fraunhofer-Institute for Building Physics, Germany
[2] Norwegian Institute of Wood Technology, Norway

KEYWORDS: *Latent heat exchange, moisture buffering, wood, energy demand, comfort conditions, building simulation*

SUMMARY:
This paper assesses the effects of moisture buffering and related latent heat exchange in wooden surfaces on energy demand and comfort conditions in rooms. A parametric study on basis of an exemplary room varies surface material properties and areas, moisture production cycles, climatic conditions and air change rates for the zone. The study was conducted with the help of hygrothermal whole building simulation, which allows modelling all physical effects related to moisture buffering and latent heat exchange that occur in the surfaces that enclose spaces. Both long and short term simulations were performed, with time steps of one hour or one minute, to assess the associated influences on indoor climate and energy demand.
The study shows a distinct influence on indoor relative humidity. Moisture buffering effects of wooden materials reduce the fluctuation of relative humidity and lead to a more stable indoor climate. Because of that energy demand for humidification and dehumidification can be reduced clearly. Long term simulations show little or no impact for mean indoor and surface temperatures and herby connected energy demand for heating and cooling. Simulations with high temporal-resolution show temporary increase of room and surface temperatures coming with the application of wooden materials as long as moisture loads are available inside the room.

1. Introduction

The project Wood – Energy, Emission, Experience (WEEE) (NFR 216404, 2011) researches influences on energy demand, emissions and health effects coming with the application of wood surfaces. As contribution to the WEEE-project, this paper assesses the effects of moisture buffering and related latent heat exchange in wooden surfaces on energy demand and comfort conditions in rooms. Latent heat exchange happens when surrounding relative humidity changes and the wood needs to establish new moisture equilibrium. To do this, it takes up or releases water from the surrounding air to achieve equilibrium. When moisture is produced in a room, e.g. by cooking or showering, the indoor relative humidity rises slower if the interior surfaces are built of wood, as these surfaces interact with the room and store some of the additional moisture (Holm 2008). In terms of energy this storage process requires to transform the water vapor into liquid water. Due to the phase change, energy is released which heats up the surface and increases therefore the surface temperature. Preliminary studies showed a distinct increase of surface temperature (see Korsnes (2012) and Nore et al (2014)) and energy savings (see Korsnes&Nore (2011) and Antretter et al (2012)).

A parametric study on basis of an exemplary room is conducted to assess the influence of wood surfaces on energy demand and comfort conditions. For this purpose surface material properties and areas, moisture production cycles, climatic conditions and air change rates for the zone are varied. Hygrothermal building simulation software is used for this study.

1.1 Hygrothermal Whole Building Simulation

Hygrothermal whole building simulation is used to explore the possibilities which arise from the utilization of the effects related to the moisture buffering of wood. It allows modeling all physical effects related to moisture buffering and latent heat exchange that occur in the surfaces that enclose spaces. It also accounts for the impact of those effects on the energy demand of and comfort conditions within the space. For this study the hygrothermal building simulation software WUFI® Plus from Fraunhofer IBP is used. Its capabilities and verification is described in Lengsfeld (2007) and Antretter (2011).

1.2 Statistical Methods

Hygrothermal building simulations gives time-series of data with correlating simulation results. In this paper, the statistical distribution of relevant parameters is described by several values. These are minimum, maximum, mean, median and the 25% and 75% quantiles. They will be displayed as boxplots.

2. Simulation Study Set-Up

2.1 Geometrical Model

This parametric study is based on a rectangular room with a length of 5.0 m, a width of 4.0 m and a height of 2.5 m, see FIG 1. Both floor and ceiling as well as the eastern and northern wall are set against rooms with the same inner conditions. Exterior walls are located on the eastern and southern side. The latter one contains two windows, each measuring 1.5 x 1.2 m. The walls are modelled as wood frame constructions. Ceiling and floor consist of reinforced-concrete with $CaSO_4$-screed as top-layer. Painted gypsum plaster is applied to all inner surfaces, except the floor which is covered with tiles.

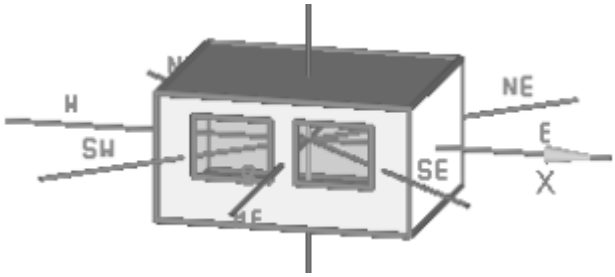

FIG 1. View of the exemplary room modelled in WUFI®plus

During this study the above described indoor surface material gypsum plaster is replaced with wooden materials with higher moisture buffer capabilities: Woodfibre and spruce, painted as well as unpainted. In this process each material is applied step-by step, starting with the ceiling until all surfaces, except the floor, consist of the same wooden material. Hygrothermal building simulations are performed for every application-step, so the resulting influence can be quantified. The materials used in this study were taken from the WUFI® Plus material database.

2.2 Climate Conditions

To assess different climatic conditions each variant of the exemplary room is simulated for four European locations: Oslo, Lund, Holzkirchen and Madrid. TABLE 1 shows an overview of their outdoor temperature and relative humidity. The climate data was taken from the WUFI® Plus climate database.

2.3 Boundary Conditions

Both temperature and relative humidity are controlled. The set-points for temperature are determined with 20 °C and 25 °C, the accuracy of the simulation is set to 0.1 K. These minimal and maximal temperatures are maintained by using ideal heating and cooling devices. Relative humidity is controlled within 30 and 65 %-RH, with an accuracy of 0.1 %-RH. Underrunning or exceeding these set-points results in humidification or dehumidification.

Ventilation is set to constant values, which vary between 0.3 – 1.0 h^{-1}. Infiltration is included in those values. Hygrothermal building simulations are performed for different ventilation cases.

2.4 Inner Loads

The usage of a room has a huge influence on its hygrothermal behaviour. To assess different impacts, four daily profiles with a time step of one hour were created which represent typical usage-types: Office, kitchen, living room and sleeping room. Bathrooms will be assessed in a separate study with another smaller exemplary room. These profiles incorporate heat-, moisture- and CO_2-production cycles as well as occupancy and human activity. Heat sources are based on EN ISO 13790 and moisture production is built from IEA ANNEX 41. CO_2-sources are derived from occupancy by using an internal WUFI® Plus calculator. These four usage-profiles are divided into a weekday- and a weekend-profile.

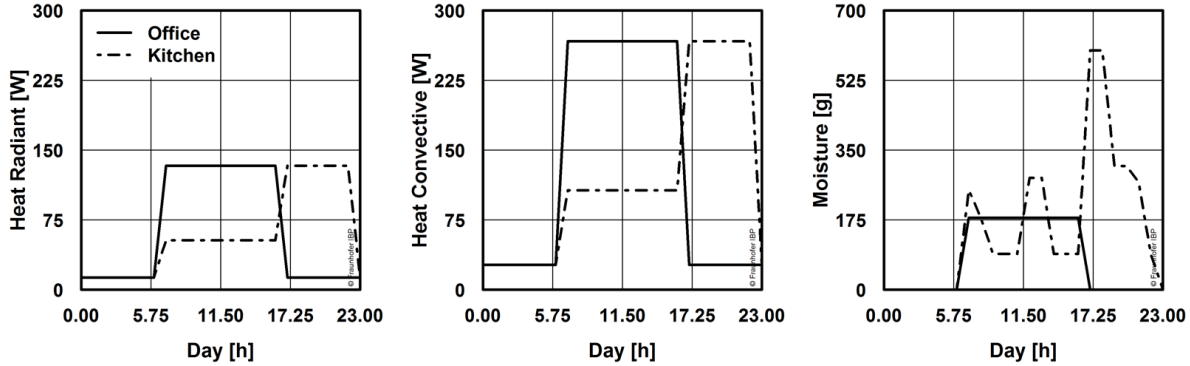

FIG 2. Inner loads for profiles "Office" and "Kitchen" during weekdays (Monday – Friday)

The hygrothermal-building simulations are performed over a year for all four profiles with a time step of one hour, to quantify the long-term effects of moisture buffering materials. In addition, more detailed simulations with a time step of one minute were performed to observe the short-time effects. These simulations cover a timespan of nine months from January to September and focus only on two profiles, which are shown graphically in FIG 2:

- Office: A profile which describes average usage with constant inner loads during weekdays. On weekends only small heat loads and no moisture- or CO_2-production occur.
- Kitchen: Cooking results in abrupt increase of inner moisture production, mainly during dinner time. This profile shows the highest moisture-loads, peak as well as daily sum. It is used both for weekdays and weekends.

2.5 Assessed Variables

Long term effects on the indoor climate are assessed with the statistical methods described in chapter 1.2 with focus on temperature and relative humidity inside the exemplary room as well as mean surface and mean ceiling temperature.

Comfort conditions for temperature are evaluated by using operative temperature, which describes the combined effects of convective and radiant heat transfer. For relative humidity, categories 1 and 2 defined in DIN EN 15251 are used. Category 1 represents a high standard for indoor climate, with an acceptable range for relative humidity between 30 and 50 %-RH. Values below or above these

thresholds are defined as “too dry” or “too wet”. Category 2 describes an average standard; its tolerable maximum and minimum are defined with 25 and 65 %-RH.

For energy demand, the yearly sums of heating and cooling energy are compared. Also humidification and dehumidification are taken into account.

TABLE 1. Outdoor climate conditions of the observed locations

Parameter	Min	Mean	Max
Holzkirchen – Temperature	- 20,1 °C	+ 6,6 °C	+ 32,1 °C
Madrid – Temperature	- 2,0 °C	+ 14,4 °C	+ 36.4 °C
Lund – Temperature	- 10,1 °C	+ 9,2 °C	+ 28,3 °C
Oslo – Temperature	- 14,8 °C	+ 6,8 °C	+ 29.3 °C
Holzkirchen – Relative Humdity	24,0 %	81,2 %	98,1 %
Madrid – Relative Humdity	16,0 %	63,0 %	99,0 %
Lund – Relative Humdity	25,0 %	81,0 %	97,0 %
Oslo – Relative Humidity	15,0 %	73,1 %	100,0 %

3. Results

3.1 Indoor Climate

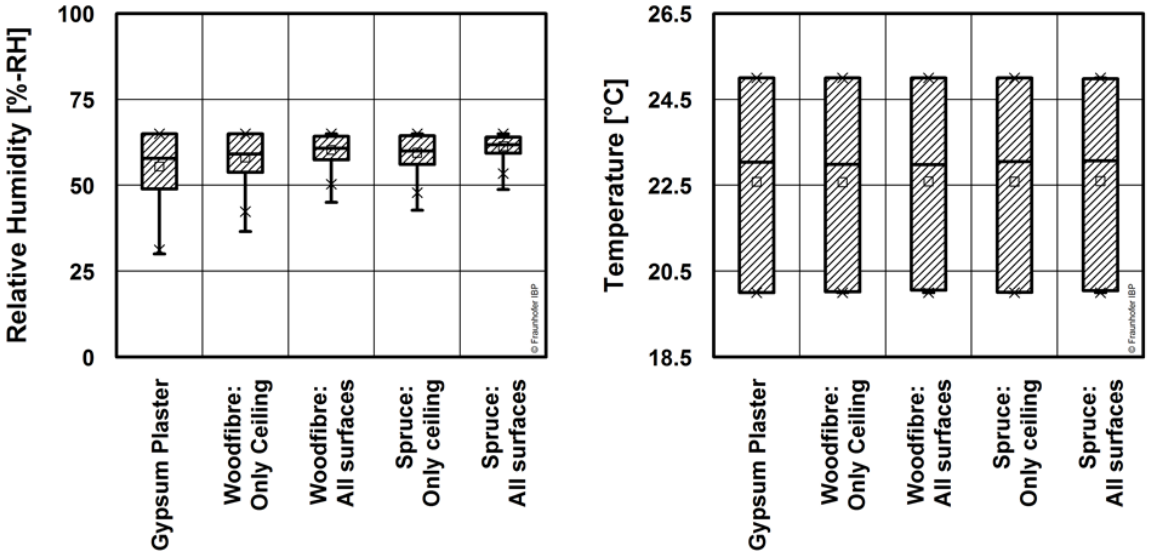

FIG 3. Lund, Kitchen, Ventilation 0.5 h^{-1}. Boxplots showing yearly relative humidity (left) and temperature in the middle of the exemplary room (right).

The application of wooden surface areas affects the indoor climate. Thereby, relative humidity experiences the highest impact: With increasing wooden surface areas the fluctuation of relative humidity declines and stabilises, see FIG 3 (left). Spruce shows a higher buffering-effect than woodfibre. For an air-change rate of 0.5 h^{-1} relative humidity stabilises around 50 %-RH for all inner-load profiles except kitchen. This profile implies the highest moisture production and stabilises around 60 %-RH. Increasing ventilation minimizes the influence of wooden surfaces and broadens the relative humidity spectrum. This buffering effect can be witnessed at all observed climatic locations.

For temperature inside the exemplary room, the statistical parameters of all simulated yearly variants vary on a small scale, see FIG 3 (right). Applying woodfibre areas increases the 1st quarter about 0.05 – 0.10 K in comparison with gypsum plaster faces. Also the temperature median drops around 0.10 K

for woodfibre. Spruce and gypsum plaster behave nearly identical. The statistical parameters of the long term simulations for mean surface temperatures also show very little effect.

Assessing the effects of moisture buffering materials on short term indoor temperature fluctuations needs more detailed building simulations with a time step of one minute. These short time simulations are only performed for two climatic locations, Holzkirchen and Lund, and two inner load profiles, kitchen and office. Ventilation is set to a constant value of 0.5 h^{-1}. Higher air-change would influence the moisture buffering effects too much, as described above. The simulations only use fully applied unpainted wooden surface areas. From the simulated data, three months were assessed in detail: January, representing cold winter climate with high heating demand, August, a typical summer month with high cooling demand, and March, with varying climate between summer and winter. This paper will focus on weekly results from Lund in March, where heating and cooling show low influence.

The detailed simulations show a short-term increase of indoor room, surface and ceiling temperatures comparing wooden materials with gypsum plaster surfaces. This applies to both inner load profiles. FIG 4 displays weekly temporal plots of room (left) and ceiling temperature (right) for the surface materials gypsum plaster (grey) and woodfibre (black). The peaks which are visible for both surface types appear simultaneous to peaks from inner moisture loads. So they can be linked directly to latent heat exchange effects. Surfaces applied with woodfibre show more distinct temperature peaks, with differences up to 1.5 K compared with gypsum plaster faces. The rises in surface temperatures are smaller for cold outdoor climate, where heating is necessary. This can be seen in the first three days of FIG 4. For a warmer climate and without any climate control, the impact grows. This can be seen in the last four days in FIG 4. Higher moisture loads lead to a higher increase of surface and indoor temperatures.

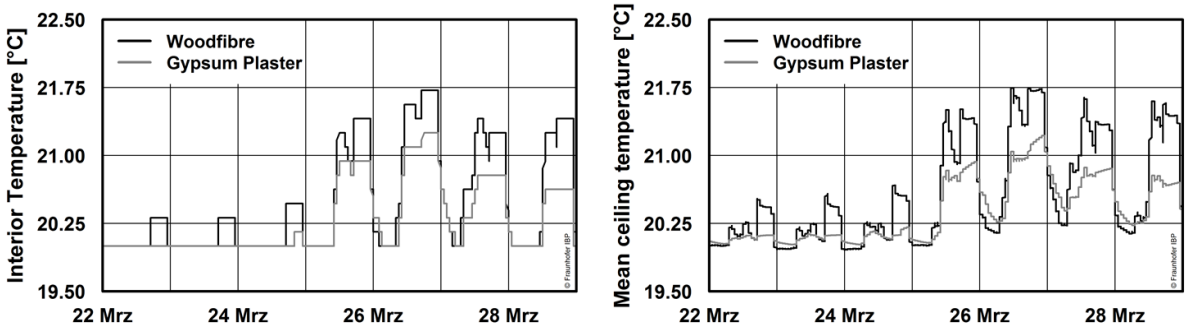

FIG 4. Lund, Kitchen, Ventilation 0.5 h^{-1}. Comparing full applications of woodfibre (black) and gypsum plaster (grey) on the exemplary rooms' inner surfaces. Temperature in the middle of the room (left) and mean ceiling temperature (right).

The simulations show higher temperature peaks for woodfibre surfaces than for spruce faces. The latter ones' surface temperatures are still about 0.1 – 0.2 K higher than for gypsum plaster surfaces. During summer the spruce variants show the lowest surface and indoor temperatures, being up to 0.1 – 0.3 K below gypsum plaster surfaces.

These observations also apply to the inner load profile office. Because of its smaller moisture loads the temperature peaks are lower than for the kitchen profile.

3.2 Comfort Conditions

Larger wooden surface areas buffer humidity inside the exemplary room in comparison with the original gypsum plaster surfaces, which effects the classification of the comfort conditions of EN 15251. For both categories the inner load profiles office, sleeping room and with reservations living room benefit thereof. Their relative humidity stabilises in all climatic locations around or below 50%-RH, with living room being slightly above. So, larger wooden surface areas result in higher

accordance for both categories one and two of EN 15251. Spruce performs better than woodfibre, see FIG 5.

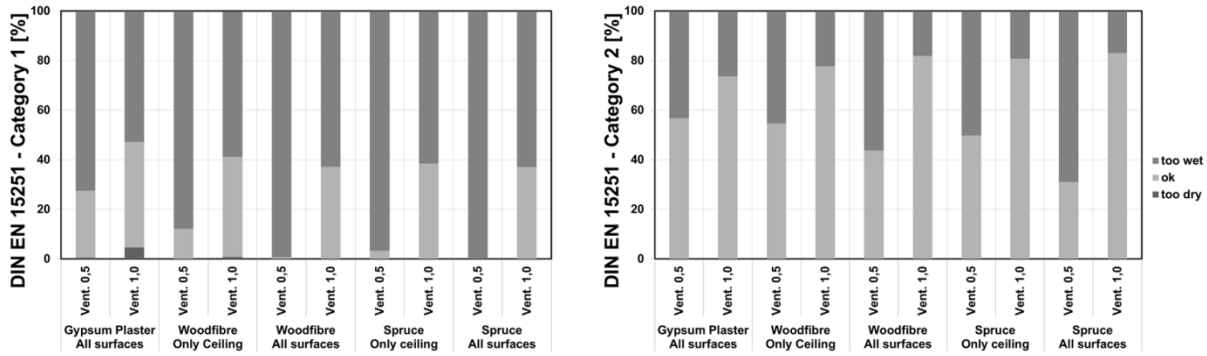

FIG 5. Lund, Kitchen, Ventilation 0.5 h^{-1} and 1.0 h^{-1}. Comfort Conditions of EN 15251 Category 1 (left) and 2 (right).

Because of the high moisture loads in the kitchen profile relative humidity stabilises between 55 and 65 %-RH. Larger wooden surface areas tend to higher values of relative humidity. In both categories of EN 15251 the upper thresholds are exceeded more often with increasing wooden surface areas, resulting in the classification “too wet”. Higher ventilation rates lead to lower relative humidity, as mentioned above. This results in higher accordance with the comfort categories of EN 15251, which can be seen in FIG 5.

As with indoor and surface temperatures, yearly simulations show hardly any impact on the statistical parameters of operative temperature. The additional simulations with a time step of one minute, as described in chapter 3.1, are necessary to quantify the short time effects on operative temperature. There, surface and room temperatures increase with the application of wooden surfaces. This also leads to higher peaks in operative temperature when compared with gypsum plaster. For woodfibre faces these peaks are about 0.3 – 0.7 K higher during winter and about 0.5 K lower during summer, which improves thermal comfort conditions.

3.3 Energy Demand for Air Conditioning

TABLE 2. Lund, Kitchen, Ventilation 0.5 h^{-1}. Yearly energy demand for heating and cooling, as well as necessary amount of dehumidification.

Surface condition	Heating [kWh/a]	Cooling [kWh/a]	Dehumidification [kg/a]
Gypsum Plaster	386.0 (± 0.0 %)	577.7 (± 0.0 %)	486.0 (± 0.0 %)
Woodfibre on ceiling	386.5 (+ 0.1 %)	604.2 (+ 4.6 %)	372.3 (- 23.4 %)
Woodifbre on all surfaces	388.0 (+ 0.5 %)	607.1 (+ 5.1 %)	287.4 (- 40.9 %)
Spruce on ceiling	388.5 (+ 0.6 %)	576.6 (- 0.2 %)	313.7 (- 35.5 %)
Spruce on all surfaces	398.5 (+ 3.2 %)	573.1 (- 0.8 %)	245.6 (- 49.5 %)

The hygrothermal building simulations over one year with an hourly time step show hardly any long term effects on heating energy demand by increasing the wooden surface areas for the exemplary profile kitchen in Lund, see TABLE 2. This can be stated for all observed climatic conditions. Larger

wooden surface areas generally tend to a slightly higher heating energy demand than gypsum plaster, with woodfibre being marginally lower than spruce.

Both wooden surface materials show different, but again small impact on cooling energy demand, see TABLE 2. The highest influences result from changing the ceiling material. Woodfibre tends to a slightly higher cooling demand than the gypsum plaster case, while the application of spruce areas decreases the necessity of cooling. These effects show their biggest impact in the climatic location Madrid.

The more detailed building simulations with a time step of one minute show an impact of moisture buffering effects on heating load. As with temperature, woodfibre surfaces show a higher influence than the other materials. FIG 6 (left) displays the heating power demand of an exemplary week during January for the surface materials woodfibre (black) and gypsum plaster (grey). The inner loads profile is kitchen. Rising moisture loads result directly in decreasing demand of heating power. Woodfibre surfaces lead to a higher drop than gypsum plaster. During high moisture loads, for example dinner time in the inner loads profile kitchen, the heating energy demand drops down to zero. These effects can be observed for all surface materials. With lower or no moisture loads, the necessary heating power increases for the exemplary room assembled with woodfibre and exceeds the demand of the gypsum plaster case. These short time effects can be witnessed at the two assessed inner loads profiles kitchen and office.

The simulations with high temporal resolution confirm the observations of the yearly simulations about cooling energy demand. Applying woodfibre surfaces results in more or less the same energy demand as gypsum plaster faces, while spruce reduces the peak loads of cooling demand a little, see FIG 6 (right).

Whereas the influence on annual energy demand for heating and cooling is low, the impact on humidification and dehumidification is distinct and shows the highest savings potential, see TABLE 2. Because of the high moisture buffering capabilities of wooden materials the relative humidity inside the exemplary room is more stabilised with increasing wooden area. This leads to less humidification or dehumidification demand. Simulations show up to 50 % lower necessity of humidification or dehumidification compared with gypsum plaster surfaces. For this purpose, spruce performs better than woodfibre.

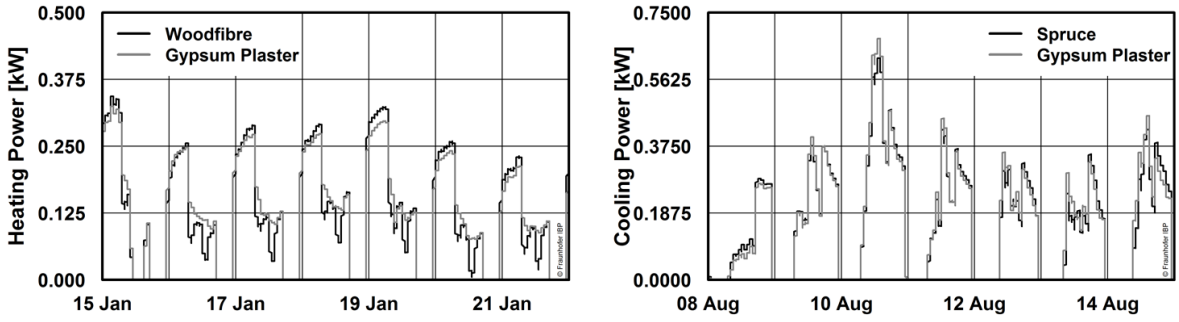

FIG 6. Lund, Kitchen, Ventilation 0.5 h^{-1}. Heating demand of the exemplary room (left) for woodfibre (black) and gypsum plaster (grey) surfaces during an exemplary January week. Cooling demand (right) during an exemplary August week for the materials spruce (black) and gypsum plaster (grey).

An overall comparison of the influence of the surface material on heating, cooling and dehumidification demand on all assessed climate locations is shown in FIG 7. A comparison of rooms completely equipped with either gypsum board, woodfibre or spruce on all surfaces shows the same trend as described above. Small impact is found for heating and cooling demand, the highest saving potential can be achieved for dehumidification.

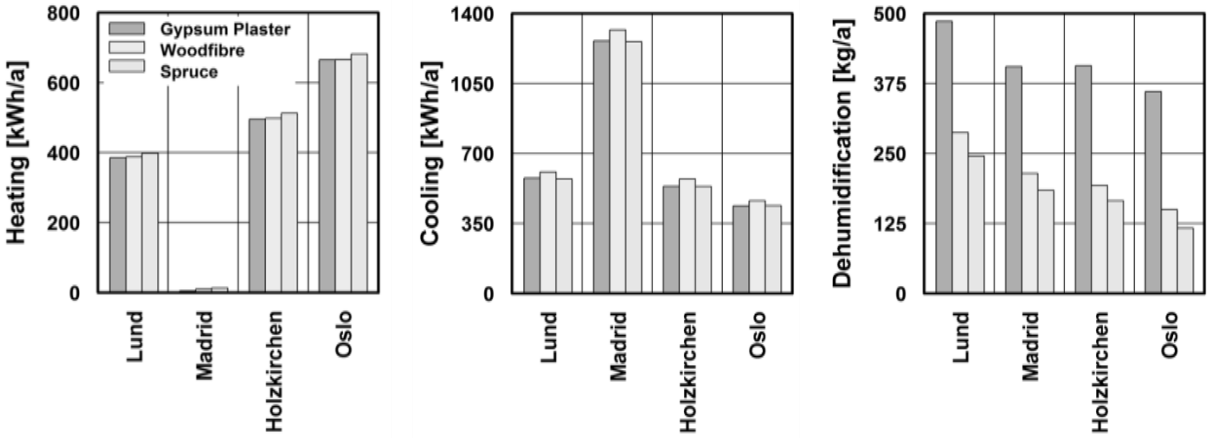

FIG 7. Kitchen, Ventilation 0.5 h^{-1}. Effect of moisture buffering on heating (left), cooling (middle) and dehumidification (right) demand for all climate locations. All inner surface areas covered with the related material.

4. Summary, Conclusions and Outlook

This paper gives a short overview on the effects of moisture buffering and related latent heat exchange in wooden surfaces. The highest influences on indoor climate can be observed for relative humidity, where fluctuations decline and stabilize with increasing wooden surface areas. This improves comfort conditions and clearly reduces energy demand for humidification and dehumidification. Room and surface temperatures show no long-term impacts. But short-term simulations indicate increasing peak temperatures which correlate with rising moisture loads and can therefore be connected to latent heat exchange effects. This also influences comfort conditions positively by increasing operative temperature.

Humidification and dehumidification show a high energy saving potential. The application of wooden surface materials had negligible long term effects on heating and cooling energy demand, but resulted in better comfort conditions. The higher the surface area where wooden materials are applied, the higher is the effect.

This paper shows potentials which arise from latent heat exchange effects. For a more detailed knowledge of these impacts further studies will be necessary. Simulations with high temporal resolution should be extended to other inner loads profiles and climatic conditions. The approach described in this paper will be applied to a smaller exemplary room, representing bathrooms, where high moisture loads should have a distinct impact on indoor climate. Furthermore ventilation should also be considered more detailed, for example the influence of non-uniform and rapid air exchanges.

It is shown that the application of moisture buffering materials on inner surfaces improves comfort conditions and energy demand for humidification and dehumidification. These effects can be assessed with a hygrothermal whole building simulation software, which models all buffering and latent heat exchange processes. It is to be researched, how an extrapolation to a verified real-scale building affects its performance.

5. Acknowledgements

The authors highly acknowledge the Research Council of Norway for funding the project WEEE together with the industry partners. Innovation Norway is acknowledged for funding part of the test house erection at Søråsjordet in Ås.

References

Antretter F., Sauer F., Schöpfer T., & Holm A. 2011. Validation of a hygrothermal whole building simulation software. Proceedings of Building Simulation 2011.

Antretter F., Mitterer C. & Young S.-M. 2012. Use of moisture-buffering tiles for indoor climate stability under different climatic requirements, HVAC&R Research, 18:1-2, 275-282

EN ISO 13790. 2008. Energy performance of buildings - Calculation of energy use for space heating and cooling. European Committee for Standardization.

EN 15251. 2007. Indoor environmental input parameters for design and assessment of energy performance of buildings addressing indoor air quality, thermal environment, lighting and acoustics. European Committee for Standardization.

Holm A. 2008. ANNEX 41 Whole building heat, air and moisture response (MOIST-EN), Volume 4: Applications: Indoor environment, energy, durability. Final Report International Energy Agency.

Korsnes S. K. 2012. Moisture and heat transfer of indoor surfaces. Master Thesis, in Norwegian. Norwegian University of Science and Technology, Trondheim, Norway.

Korsnes, S. K. & Nore, K. 2011. Potential energy savings due to latent heat exchange in indoor exposed wooden surfaces. CESBP 2013.

Lengsfeld K. & Holm A. 2007. Entwicklung und Validierung einer hygrothermischen Raumklima-Simulationssoftware WUFI®-Plus. Bauphysik 29 (3).

Nore K., Englund F., Aurlien T., Nyrud A. Q. 2014. Wood construction: Energy, Emissions and Experience. 10th Nordic Symposium on Building Physics 2014, Lund.

Vapour resistance of modern roof underlay products at real winter conditions

Sivert Uvsløkk, M.Sc.
Magnus Vågen, M.Sc.
Silje Korsnes, M.Sc.

SINTEF Byggforsk, Norway

KEYWORDS: *Roof underlay, vapour resistance, vapour flux, moisture uptake, winter conditions*

SUMMARY: (Style: Summary Heading)
Vapour resistance of ten vapour open underlay products has been measured at different temperatures in SINTEF 's laboratory. The purpose of the test was to check if the moisture transport properties of the underlay products changed at winter conditions, with condensation, rim or ice on the underside of the products compared with measurements performed by indoor temperature on both sides of the samples.

The measurements showed that all the examined products were "vapour open" even in cold weather. None of the examined underlay products became "vapour-tight" of frost or ice.

For most products, 7 of 10, the vapour resistance were about the same at freezing temperature as at room temperature. Only one product had a significant increase in vapor resistance at freezing temperature.

1. Introduction

After long cold winter periods in 2009 and 2010 several cases of "water leakages" were observed in new pitched roofs in Norway. The water came from melted ice or rim which had been accumulated on the roof underlay. This is well known phenomena in houses with leaky vapour barriers or when the vapour barrier is mounted too late in the building process. These winters however it also happened in properly constructed roofs. In the search for explanations, questions were raised about whether the new modern vapour-open roof underlays were equally vapour open even at freezing temperatures or if they became vapour-tight when it formed ice or rim on the underside. To investigate this question a laboratory project was carried out in co-operation between seven material manufacturers / suppliers and SINTEF Building and Infrastructure (Uvsløkk-2012).

2. Product description

Ten types of vapour-open roof underlay products were included in the test. They are identified by a letter and the main characteristics of the products are given in table 1.

3. Test method

The measurements were carried out according to the same principles as for regular "cup measurements" as described in NS-EN ISO 12572. 2001, but with some deviations to simulate moisture and temperature conditions in insulated, real roofs both summertime and wintertime. See the illustration in figure 1. As cups we used plastic containers of PE that were filled with approx. 170 mm mineral wool. Samples of the roof underlays were placed to the top and sealed to the boxes with ties of butyl. Between the insulation and underlay samples, there was about. 20 mm thick air gap to

prevent the insulation from freezing stuck to the underlay samples. About 0.55 litres of water were filled in the bottom of the boxes. The vapour pressure at the hot side of the insulation was therefore relatively high simulating a construction period with a lot of building moisture and high indoor temperature before the vapour barrier is mounted to protect the roof. The moisture uptake was measured on samples attached to removable plastic lids on separate boxes. It was corrected for moisture uptake on the plastic lid on the fringes around the samples. Moisture per area on the underside of the plastic part was calculated from measurements of the reference cap. Measurements were conducted at three different outdoor temperatures in the following order: +20 °C, -4 °C and + 4 °C. There was no acclimatisation or drying of the samples between these test periods.

TABLE 1. Overview of the roof underlay products included in the survey

ID	Type of product	Material	Thickness mm	Basis weight g/m²
A	Plate product	Wood fibre	32.0	2900
B	Roll product	Spun bounded PE-fibre, PP-felt	1.3	320
C	Roll product	Spun bounded PE-fibre	0.6	195
D	Roll product	PU and PP, PP-felt	1.2	300
E	Carton	Laminated paper	2.1	1400
F	Roll product	PP and PE	0.7	160
G	Roll product	PP	0.8	195
H	Roll product	PP and PE	0.8	140
I	Plate product	Wood fibre	20.5	4800
J	Roll product	PP	0.8	210

Legend:
PE = polyethylene, PP = Polypropylene, PU = polyurethane

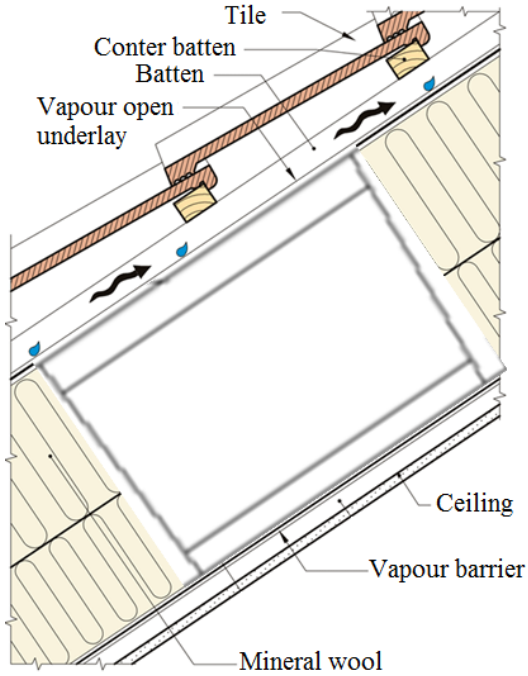

FIG 1. Sectional drawing of a roof with a plotted plastic box that illustrates what part of the roof that was simulated in the experiments

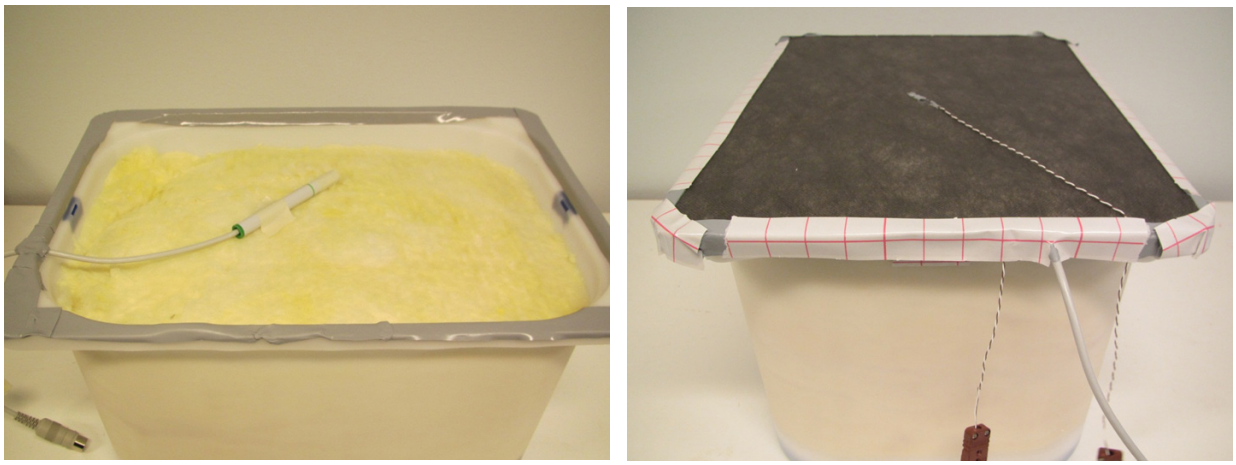

FIG 2. PE box with mineral wool insulation and a RH/temperature sensor before, left, and after, right, the underlay sample has been mounted. Thermocouples were fixed to both surfaces of the underlay samples for logging the surface temperatures during the experiments.

FIG 3. Picture of the test rig in the cold room, left. The boxes stood on a plate that was heated to normal indoor temperature of 20 °C. The boxes closest to the wall were used to measure water vapour permeance/resistance. On the other boxes, the row to the right, the underlay samples were attached to removable plastic lids for measuring moisture uptake. The weight changes of the boxes during the test period were measured by use of a balance as shown on the picture to the right.

4. Results

The results of the laboratory measurements are shown in the bar graphs in Figures 4 to 8. The results at the outdoor temperatures of +20 °C and -4 °C are also given in Table 2 along with the main test conditions. The results are average values for the stationary parts of the test periods.

4.1 Water vapour resistance

The results for all ten underlay products, at three different outdoor temperatures, is given by a staple diagram in figure 4. The measured water vapour diffusion resistance, which is usually referred to as water vapour resistance, is given as S_d-value [m]. S_d-value is a relative measure defined as the thickness of a motionless air layer which has the same water vapour resistance as the material layer. In table 2 the water vapour resistance is also given in SI units.

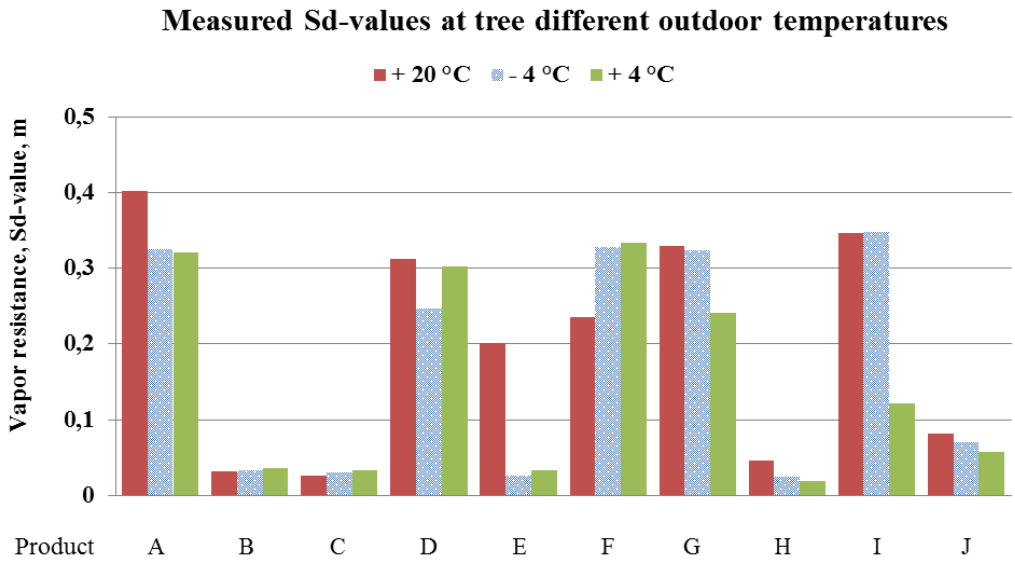

FIG 4. The graph shows the measured water vapour resistance, Sd-value [m], for all ten products at three different outdoor temperatures. See codes above the diagram

4.2 Water uptake

The moisture content of the ten underlay products at the end of each of the test periods at three different outdoor temperatures is given by a staple diagram in figure 5. For most of the products the moisture content was not in equilibrium at the end of the various test periods, but continued to increase in the following period. The specimens for measuring moisture uptake were not dried between the various test periods.

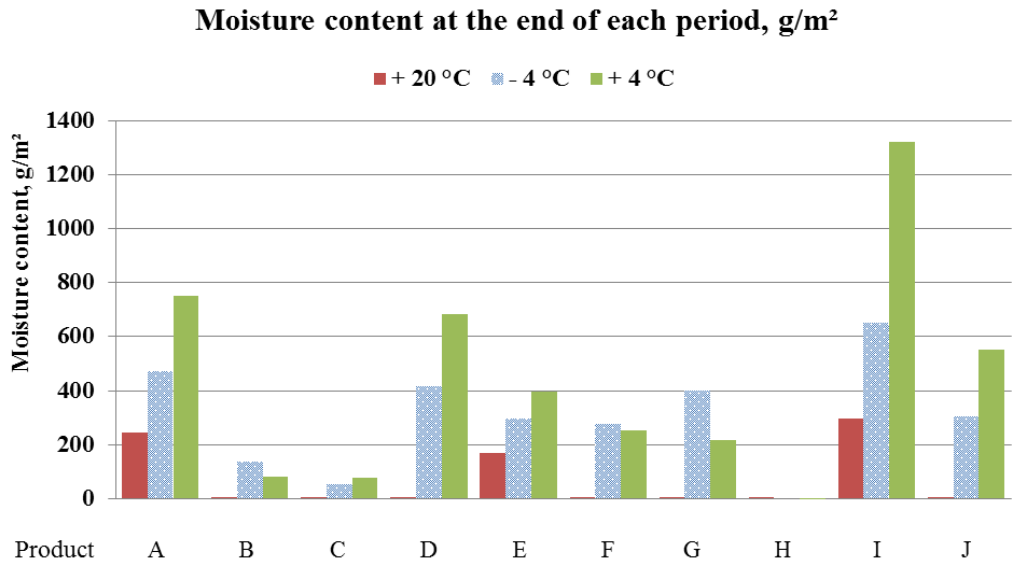

FIG 5. The graph shows measured water content, [g/m2], at the end of each of the tree measurement periods of different outdoor temperatures. See codes above the diagram.

4.3 Moisture flux and moisture uptake

The moisture flux and rate of moisture uptake during the hottest and coldest test periods is shown in staple diagrams in figure 6 and 7.

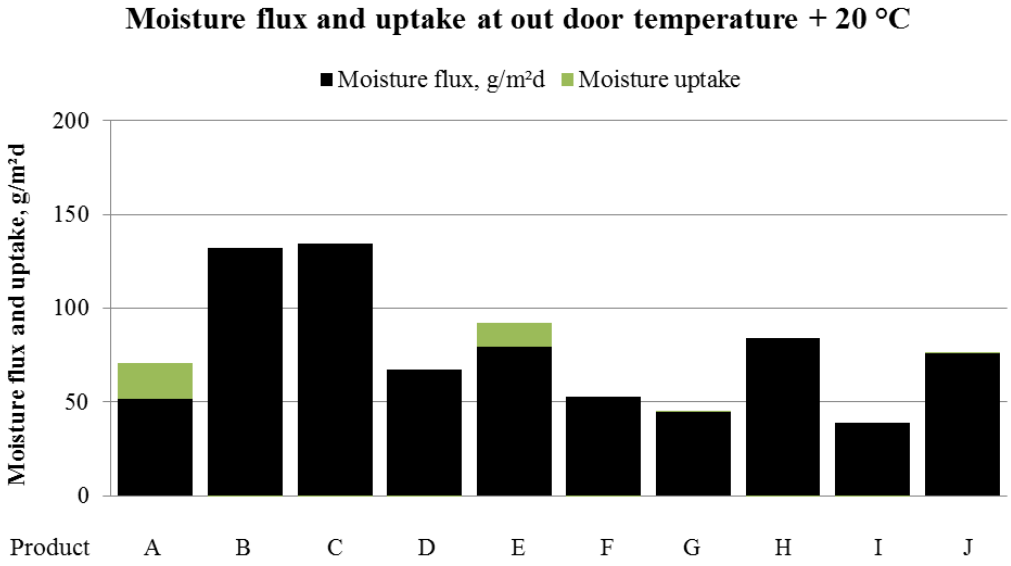

FIG 6. The graph shows the measured moisture transfer through the roofs, marked with black bars, at approximately the same temperature inside as out. The values are average values per area and time unit. The green bars on top of the black shows the average moisture uptake in the samples in the same period.

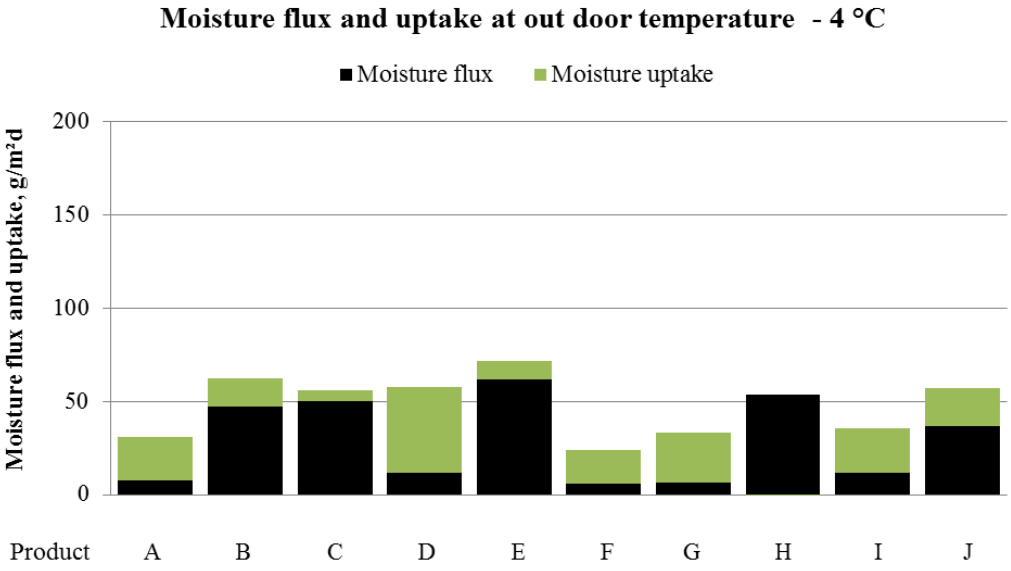

FIG 7. The graph shows the measured moisture transfer through the specimen, marked with black bars, at an outdoor temperature of – 4 °C. The values are average values per area and time unit. The green bars on top of the black shows the average moisture uptake in the samples in the same period.

TABLE 1. Results and test conditions from the tests at outdoor temperatures + 20 °C and – 4 °C

Results at outdoor temperature + 20 °C

Product		A	B	C	D	E	F	G	H	I	J
Air temp. cold side	°C	20.8	20.8	20.8	20.8	20.8	21.8	21.8	21.8	21.8	21.8
Sd-value	**m**	**0.40**	**0.03**	**0.03**	**0.31**	**0.20**	**0.23**	**0.33**	**0.05**	**0.35**	**0.08**
Vapour resistance	10^9 m²sPa/kg	2.06	0.16	0.13	1.60	1.04	1.20	1.69	0.24	1.77	0.42
Moisture content	kg/m²	0.24	0.00	0.00	0.01	0.17	0.01	0.01	0.01	0.30	0.00
Moisture flux	g/m²døgn	51	132	134	67	79	53	45	84	39	76
Moisture uptake rate	g/m²døgn	19	-6	-5	-2	13	0	0	0	-1	0

Test conditions at outdoor temperature + 20 °C, average values

Start date, year 2011		4.4.	4.4.	4.4.	4.4.	4.4.	14.6.	14.6.	14.6.	14.6.	14.6.
End date, year 2011		5.4.	5.4.	5.4.	5.4.	5.4.	23.6.	23.6.	23.6.	23.6.	23.6.
RH oudoor air	RH, %	36	36	36	36	36	42	42	42	42	42
RH specimen upper side, est.	RH, %	36	39	39	37	38	42	42	43	42	43
RH specimen lower side, est.	RH, %	84	48	47	86	75	68	75	51	71	57
RH insulation upper side, est.	RH, %	86	54	52	89	78	72	77	55	73	59
Air temp. cold side	°C	20.8	20.8	20.8	20.8	20.8	21.8	21.8	21.8	21.8	21.8
Temp. specimen upper side	°C	21.3	21.2	21.3	21.2	21.1	22.4	22.2	22.3	22.0	22.0
Temp. specimen lower side	°C	21.4	21.3	21.3	21.3	21.2	22.6	22.2	22.3	22.3	22.0
Temp. insulation upper side	°C	21.5	21.4	21.5	21.3	21.4	22.2	22.2	22.2	22.2	22.0
Temp water/insul. lower side	°C	24.5	24.5	24.5	24.5	24.5	22.3	22.3	22.3	22.3	22.3
Temp. diff. specimen, est.	°C	0.08	0.17	0.01	0.08	0.06	0.15	0.03	0.05	0.29	0.01
Press. diff. specimen, est.	Pa	1227	245	208	1248	951	733	876	233	798	371

(est. = estimated)

Results at outdoor temperature - 4 °C

Product		A	B	C	D	E	F	G	H	I	J
Air temp. cold side	°C	-4.2	-4.2	-4.2	-4.2	-4.2	-4.1	-4.1	-4.1	-4.1	-4.1
Sd-value	**m**	**0.32**	**0.03**	**0.03**	**0.25**	**0.03**	**0.33**	**0.32**	**0.02**	**0.35**	**0.07**
Vapour resistance	10^9 m²sPa/kg	1.79	0.18	0.16	1.36	0.14	1.81	1.79	0.14	1.92	0.39
Change rel. to + 20 °C	m	-0.08	0.00	0.00	-0.07	-0.18	0.09	-0.01	-0.02	0.00	-0.01
Change rel. to + 20 °C	%	-19 %	6 %	14 %	-21 %	-87 %	39 %	-2 %	-47 %	1 %	-15 %
Moisture content	kg/m²	0.47	0.14	0.05	0.41	0.30	0.28	0.40	0.00	0.65	0.30
Moisture flux	g/m²døgn	8	47	50	12	62	6	7	54	12	37
Moisture uptake rate	g/m²døgn	23	15	6	46	10	18	27	0	24	20

Test conditions at outdoor temperature - 4 °C, average values

Start date, year 2011		11.4.	11.4.	11.4.	11.4.	11.4.	23.6.	23.6.	23.6.	23.6.	23.6.
End date, year 2011		15.4.	15.4.	15.4.	15.4.	15.4.	8.7.	8.7.	8.7.	8.7.	8.7.
RH oudoor air	RH, %	76	76	76	76	76	75	75	75	75	75
RH specimen upper side, est.	RH, %	77	83	79	72	81	76	74	81	74	75
RH specimen lower side, est.	RH, %	100	98	96	100	97	100	100	96	100	100
RH insulation upper side, est.	RH, %	99	100	100	100	100	97	96	100	100	100
Air temp. cold side	°C	-4.2	-4.2	-4.2	-4.2	-4.2	-4.1	-4.1	-4.1	-4.1	-4.1
Temp. specimen upper side	°C	-3.8	-3.6	-3.1	-2.9	-3.0	-4.1	-3.8	-3.5	-3.6	-3.1
Temp. specimen lower side	°C	-3.5	-3.1	-2.9	-2.6	-2.7	-3.6	-3.5	-3.0	-0.9	-2.8
Temp. insulation upper side	°C	-2.3	-2.0	-2.0	-1.8	-1.3	-3.1	-2.5	-2.3	0.0	-1.3
Temp water/insul. lower side	°C	23.0	23.0	23.0	23.0	23.0	23.3	23.3	23.3	23.3	23.3
Temp. diff. specimen, est.	°C	0.32	0.56	0.12	0.33	0.32	0.55	0.27	0.50	2.75	0.29
Press. diff. specimen, est.	Pa	117	91	86	149	91	122	127	87	231	128

5. Discussion

Most of the tested products, seven out of ten, were about as vapour open with the same S_d-value at freezing temperature as at room temperature. See figure 4. Only one product (F) had a significant increase in vapour resistance at freezing temperature. The S_d-value of this product increased by 0.10 m (40%). One product (E) had a significant reduction in vapour resistance at freezing temperatures. The S_d-value decreased with -0.18 m (-85%). This probably reflects the fact that the moisture content also increased, see figure 5. It is a well-known phenomenon that wood and wood-based products become more vapour open when the moisture content increases.

Although the vapour resistance was about the same at summer and winter condition for most of the products, the vapour fluxes were much lower at winter temperatures compared to summer temperatures, + 20 °C, at the roof underlay. This is especially true for the least vapour open products A, D, F, G and I. The explanation for the decrease in water vapour transport at winter temperatures is the reduction in the water vapour pressure difference across the roof underlays, see table 2. The water vapour flux through the roof underlay and out of the roof is determined by both the S_d-value of the roof underlay and the vapour pressure difference across the roof underlay.

As shown in the diagram in figure 6 water vapour flux is relatively similar for all products at + 20 °C temperature both outside and inside even though the differences in S_d- value of the products are great.

The relative difference between the vapour transport through the most vapour open products and the other products are much larger at low winter temperatures than at summer temperatures. The difference between the water vapour pressure at the water layer at the bottom of the insulation and the vapour pressure in the air on the cold side of the roofs were approximately equal for all samples The vapour pressure difference across the underlay product however varies from sample to sample, especially in the "summer" period with the same temperature outside as inside.

As long as the RH is less than 100 % at the lower side of the sample the vapour pressure difference across the sample will be determined by the sample's share of the total water vapour resistance of insulation, air gap and roof underlay. The S_d-value of the insulation layer in the sample boxes are equal to the insulation thickness multiplied by 1.3 which is approx. 0.22 m. The vapour resistance of the most vapour open products therefore constitute only a small proportion of the total resistance.

When the temperature is high the vapour pressure at the lower side of the roof underlays also becomes high, especially for the products with the highest vapour resistance. The vapour pressure difference across the roof underlay is therefore much greater for these products compared with the most vapour open products. The higher Sd-values are somewhat "compensated" by higher vapour pressure differences giving relatively similar vapour transport through all products at "summer" conditions.

At winter conditions with low temperature the vapour pressure on the underside of the roof is rather low, even at high RH. When the RH on the lower side of the roof underlay is close to or equal to 100 %, the vapour pressure difference between the two sides of the roof underlay products is relatively similar for all products. Then the vapour transport is nearly proportional to the S_d-values of the products. Therefore it is primarily at winter temperatures the most open roof underlay products, B, C, E, H and J offer substantially faster drying than the other, A, D, F and G.

In a real timber frame roof with building moisture distributed in the rafters, parts of the moisture will have a shorter way out and the difference in drying rate will be somewhat larger in real roofs than shown in the diagrams in figure 6 and figure 7.

Provided that the accumulated moisture can be transported out through the roof underlay later, without dripping down through the insulation, a certain ability to absorb moisture may be an advantage. In the drying out period of the building moisture accumulation on the roof underlay to some extent may compensate for the higher S_d-value.

This requires, however, that the moisture dries out completely before the temperature becomes substantial higher than +5 °C to avoid mold growth conditions on the roof underlay.

6. Conclusions

The measurements showed that all the examined products were "vapour open" even at sub-zero temperatures. None of the examined roof underlay products became "vapour tight" of rim or ice.

Most products, seven out of ten, were about as vapour open with the same S_d-value at freezing temperatures as at room temperature. Only one product had a significant increase in vapour resistance at freezing temperatures.

One product had a significant reduction in vapour resistance at freezing temperatures. This probably reflects the fact that the moisture content also increased. It is a well-known phenomenon that wood and wood-based products become more vapour open when the moisture content increases.

Although the S_d-value for most of the product remained about the same at minus degrees as at + 20 °C the water vapour flux is substantial lower at minus degrees. This is especially true for the least vapour open products A, D, F, G and I. This decrease is due to the fact that the driving force for diffusion, vapour pressure difference across the roof underlay, is significantly lower when the temperature is lower

The relative difference between the vapour flux through the vapour open products and the other products are much larger at winter- than at summer temperatures.

It is primarily in winter temperatures that the most vapour open roof underlays, B, C, E, H and J offer substantially faster drying than the other, A, D, F and G.

Large vapour transport capacity, i.e. lowest possible S_d-value, is in our opinion the most important property of roof underlay products to counteract harmful wetting wintertime. Good moisture absorption ability will however also help to prevent dripping during a critical drying phase at low winter temperatures. It is however important that the accumulated moisture dries out during the late winter before the outside temperature becomes substantial higher than +5 °C to avoid mold growth conditions on the roof underlay.

The results and associated conclusions in this report apply only for the products involved in the project and cannot automatically be transferred to other underlay products.

7. Acknowledgements

We would like to thank the companies that have supported the project. The following seven material manufacturers and suppliers have contributed both financially and with technical input during both the planning and the implementation of the project: Hunton Fiber AS, Huntonit AS, Icopal AS, Isola AS, Monier Roofing AB, Nortett Bygg AS and Würth Norge AS.

References

NS-EN ISO 12572. 2001. Hygrothermal performance of building materials and products – Determination of water vapour transmission properties. Standard Norge.

Uvsløkk S. & Vågen M. 2012. Dampåpne undertak ved vinterforhold – Laboratorieforsøk. (Report in Norwegian). SINTEF Byggforsk Trondheim. 26 p.

Mould growth on building timber collected from three different single-house factories

Pernilla Johansson (First name and Last name), Title (see Summary)[1]
Gunilla Bok, Title[1] (Times New Roman 11 pt, Styles: Normal/ Superscript)

[1] Organisation 1 (name of the organisation only), Country

KEYWORDS: *mould, wood, small-house factories, moisture content*

SUMMARY: In this project, mould growth on the wood samples sourced from three different house manufacturers, using different wood suppliers, was studied. The results revealed differences in the wood quality supplied by different manufacturers, which could not be attributed solely to the differences in storage conditions. Instead, the susceptibility to mould growth seems to be a parameter that varies among different types of wood. In addition to the differences among the different manufactures, statistically significant differences between tongued and groove boards and wooden studs were found, the former being more susceptible to mould growth than the latter. The conclusion is that, when defining wood in the sense of mould growth susceptibility, several parameters must be taken into consideration.

1. Introduction

Mould growth on building materials is a consequence of a complex interaction among environmental factors (temperature and humidity), material properties, and the characteristics of the mould fungi present. In general, the availability of water in the material is regarded as the crucial element for growth to occur, whereby the amount of water required for growth is also dependent on the temperature.

Wood is a common building material in the Swedish building construction sector, and is typically used in manufacturing small family houses. During storage, if the wood is exposed to a suitable temperature and moisture sufficient for mould growth to occur, there is risk for mould growth. Due to differences in storage conditions at different warehouses, there may also be differences in mould growth on the stored wood. Although mould growth is not seen with the naked eye, the growth process may have started, which may affect subsequent mould resistance. In addition, the spore loads at different warehouses may vary and affect the mould resistance. Hallenberg and Gilert (1988) found differences in mould growth among timbers stored at different sawmills and concluded that this difference depends on the differences in spore exposure at these storage sites.

In this paper, we present the results of the mould growth tests performed on wood sourced from three different small house factories using different wood suppliers. The results are part of a bigger study, where mould growth on wood at different relative humidity and temperatures was studied (Johansson and Bok 2011).

2. Materials and Methods

2.1 Wood specimens

Tongue and groove board and wooden studs, commonly used in the construction of new single family houses, were used in the test. Wood sampling was performed in late October / November 2009, at the

factory warehouses of three single-family house manufacturers located in southern Sweden. In consultation with the staff of each factory, test boards were selected from timber that was intended for use in production. Clean timber with no visible damage was chosen and the intention was to take samples from different packages, thus ensuring that each test specimen would have different origins. The number of samples from each warehouse is presented in Table 1. The differences in the number of test specimens from the different factories are due to the limiting availability of wood packages from different sources at the time of sampling.

Once selected, the samples were stored in the laboratory, at conditions not favourable for mould growth. Before the trials commenced, the samples were cut into smaller test specimens sized approx. 50 × 100 mm.

Table 1 Number of samples from each factory warehouse.

Location	Wooden studs	Tongue and grooved board	Total
A	4	10	14
B	12	7	19
C	3	6	9
Total	19	23	42

2.2 Mould growth test

The specimens were incubated in climate chambers in (CTS C-20/350, CTS GmbH, Hechningen, Germany) set to RH 90 % and 22° C. Air with the desired relative humidity and temperature streamed over the test pieces at a velocity of 0.3–0.5 m/s. During the entire incubation time, the temperature and relative humidity in the climate chambers were measured and recorded. The data was adjusted according to values from calibration of the loggers used. A combined measurement uncertainty was calculated by using the calculated standard deviation and the measurement uncertainty from the calibration of loggers according to EA-4/02.

Prior to the incubation, the test specimens were either inoculated with spores from a spore solution, or were incubated with no prior inoculation. In the latter case, the test specimens were naturally contaminated with spores from the air. The aim was to investigate if possible differences in spore loads at the different test sites would affect the mould growth. By using a spore suspension with high amount of spores (1 000 000 spores/ml), the spore load from the different locations would be negligible. Thus, any differences in mould growth found in specimens from the different test sites would be due to other reasons. The two different tests, with and without spore suspension, were performed in two different moisture chambers.

The spore suspension containing *E. herbariorum, A. versicolor, P. chrysogenum, A. pullulans, C. sphaerospermum,* and *S. chartarum* spores was sprayed to the surface of the test specimens according to Johansson et al. (2012).

Twice a week, during the incubation time, the specimens were analysed for mould growth in a stereo microscope at 10-40 × magnification. Both mould growth visible to the naked eye and that visible only under the microscope were rated according to a five-point rating scale, where 0 = no growth; 1 = sparse, initial growth with only one or a few hyphae present; 2 = sparse but clearly established growth; 3 = patchy, heavy growth; and 4 = growth over most or all of the surface (Johansson et al. 2012).

2.3 Wood moisture content

When the samples arrived at the laboratory, up to maximum 4 hours after sampling, the moisture content at the surface was measured by momentary resistance with a hammer electrode (Protimeter BLD 5055 Hammerprobe) connected to a measuring instrument (Protimeter Timber Master). The procedure followed EN 13183-2 protocol.

2.4 Statistical analysis

During incubation, mould growth is a continuing process. In this study, we were interested in determining whether mould growth would establish on the test specimens and the time points at which this process occurred. Established growth was defined as mould growth assessed as rate 2, 3 or 4, according to the rating scale described above. The time that lapsed prior to this event was considered in a survival analysis. Survival functions for mould growth on specimens from different factories and from the two sawing patterns were described as Kaplan-Meier Curves and the equality of the survival functions was tested by using a log rank test. The data from different factories was assessed via pairwise comparisons. For this analysis, a Bonferroni correction was performed with a statistical significance accepted at the $p < .0167$ level. All tests were performed in SPSS.

3. Results

1.1 Moisture content at sampling

InFIG 1, the measured moisture content at sampling is shown. Significant difference was found among the different test sites for wooden studs.

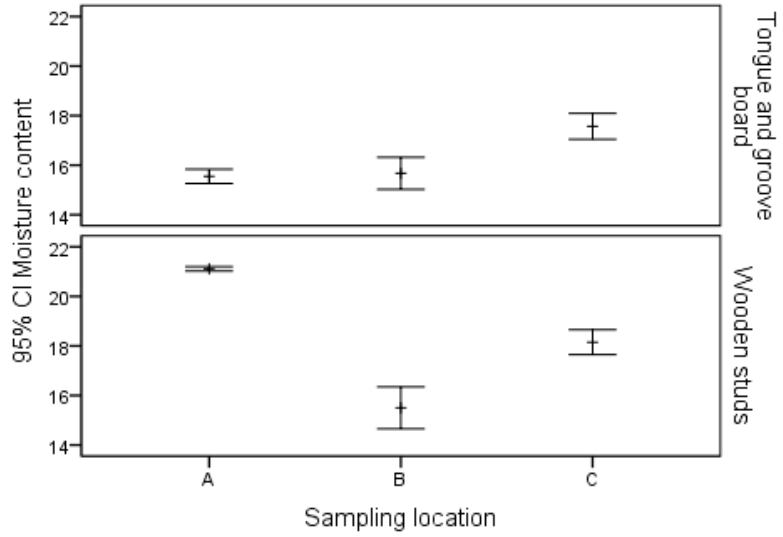

FIG 1. Moisture content at sampling, 95 % confidence interval of mean.

3.1 Incubation conditions

Mean temperature was the same in both tests, at 22 °C. With the exception of the 48-hour period, when the temperature was recorded at 15 °C, the temperature was very stable in the test chamber with naturally contaminated test specimens, and did not fluctuate by more than 0.5 °C.

The relative humidity during the incubation time for the two tests is shown in FIG 2.

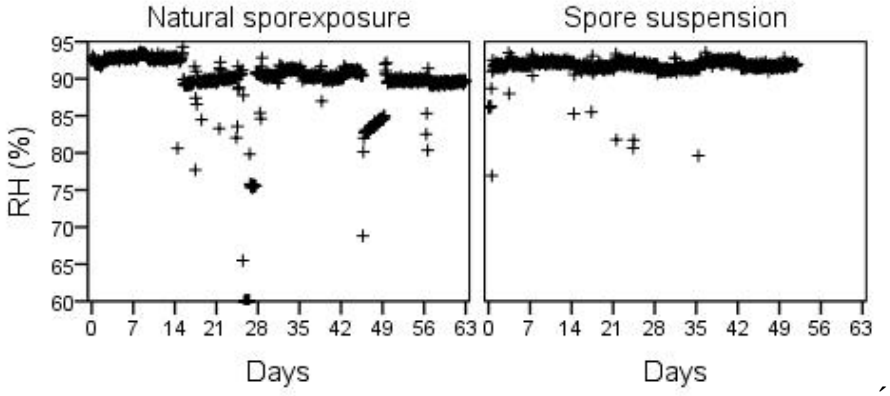

FIG 2. Relative humidity (RH) during the incubation period in the two tests.

3.2 Mould growth

The median incubation time before mould was established on the tongue and grooved board was 21 (95 % CI, 16.5 to 25.5) days, while it was 56 (95 % CI, 43.9 to 68.1) days for the wooden studs. The survival distributions for the two types of wood were statistically significantly different ($\chi^2(1) = 7.74$, $p < .0005$). Therefore, when analysing the effect of different sampling sites, these tongue and groove boards and wooden studs were considered separately.

InFIG. 3, the survival functions for tongue and grooved board from the different factories are shown as Kaplan Meier plots. In the case of natural contamination, the median time to mould growth was 21 (CI 95 %, 16.6 to 25.3) days for the specimens from Location A, and 49 (CI 95%, 36.5 to 61.5) days for specimens sourced at Location C. All cases from Location B werecensored, that is mould growth was not established on any of the test specimens during the incubation period. Statistically significant differences were found among the studied locations. However, since all cases were censored for Location B, no statists could be computed. The survival functions for Location A and Location C were significantly different at the $p < .005$ level ($\chi^2(1) = 12.3$).

When a spore suspension was used, the median time before mould established on the test specimens varied. For Location A and Location C, the median time of 7 days was measured, while it was 17 days for Location B (CI 95 %, 8.0 to 26.0 days). Pairwise log rank comparisons of the survival functions revealed a significant difference between Location A and Location B ($\chi^2 = 10.5(2)$, $p = .001$), as well as between Location B and Location C ($\chi^2(2) = 8.0$, $p = .005$). However, the survival distributions for Location A vs. Location C were not statistically significantly different ($\chi^2 = 0.1(2)$, $p = .736$).

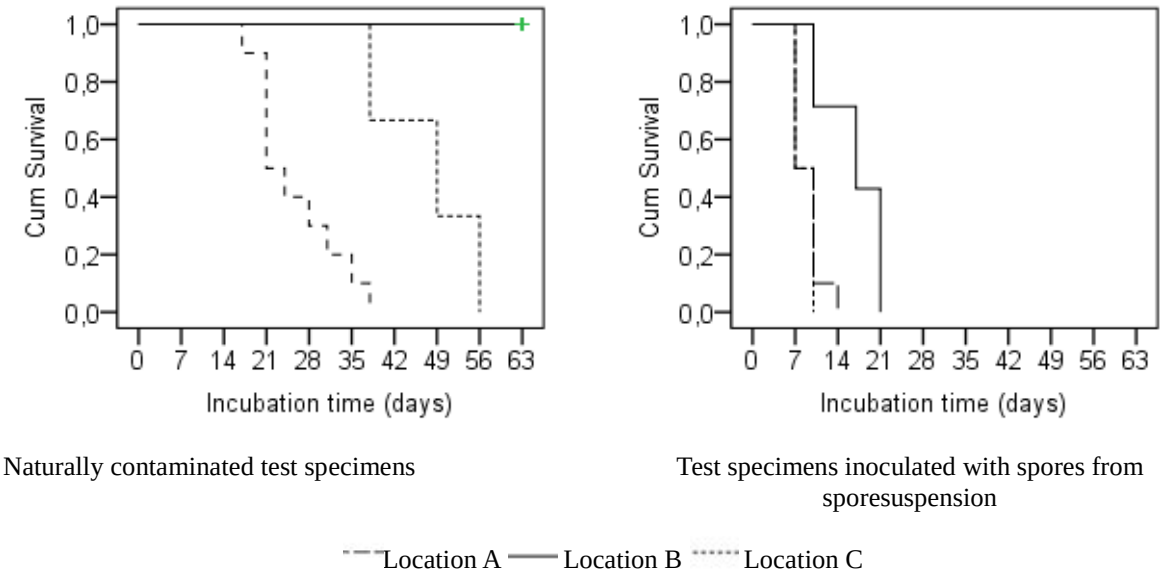

Naturally contaminated test specimens

Test specimens inoculated with spores from sporesuspension

Location A Location B Location C

FIG 3. Kaplan-Meier plot of the survival functions for tongue and groove boards from each sample location in the two tests. The x-axis is the incubation time to established growth and the y-axis is the cumulative survival. The greater the number of specimens on which mould growth had established, the lower the cumulative survival proportion and the lower the survival curve on the graph. Therefore, if the survival curve of one group is "above" the survival curve of another, the former is considered as less susceptible to mould growth than the latter.

In FIG 4, the survival functions for wooden studs are shown. The log rank test revealed no statistically significant differences in the survival functions corresponding to the test specimens from different locations, for either the naturally contaminated test specimens or the test specimens inoculated with a spore suspension.

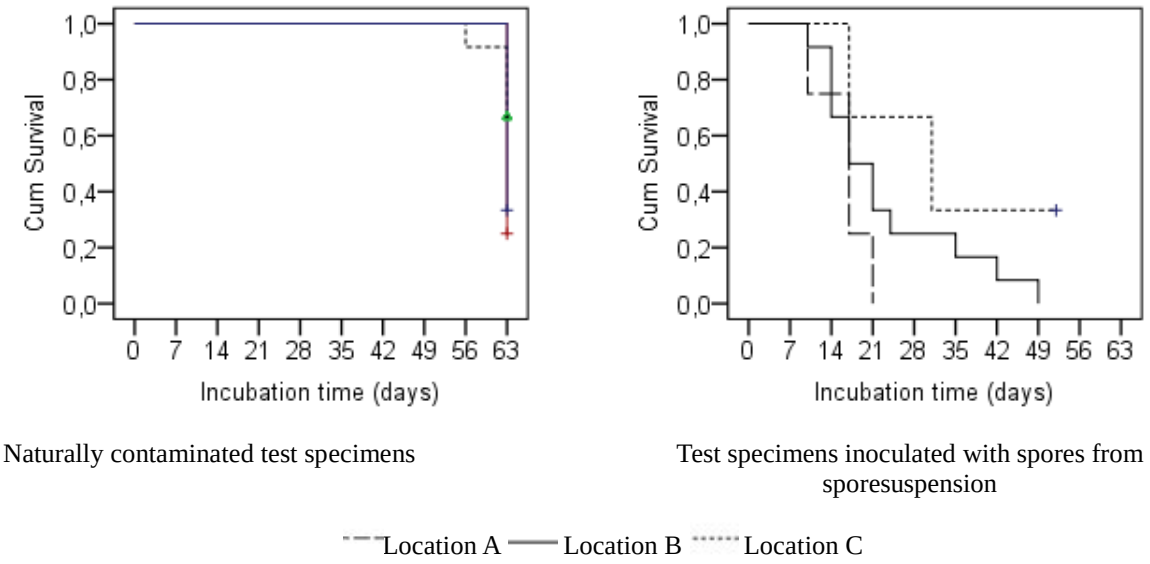

Naturally contaminated test specimens

Test specimens inoculated with spores from sporesuspension

FIG 4 Kaplan-Meier plot of the survival functions for wooden studs from each sample location in the two tests.

In general, the period before mould growth established was longer, with the median value 63(CI 95%, 57.5 to 68.5) days, for naturally contaminated test specimens, compared to the test specimens inoculated with a spore suspension, where the median survival was 14 (CI 95 %, 11.1 to 16.9) days. The survival functions were statistically significantly different (χ^2=65.1, $p < .001$).

In FIG. 5, the time that lapsed before mould growth established on each test specimens is shown in relation to the moisture content at sampling.

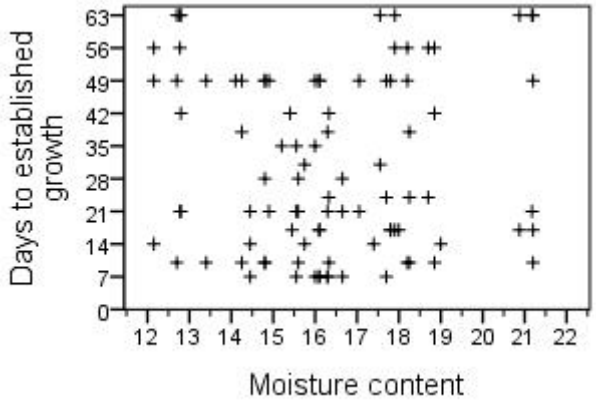

FIG 5. Days to established growth in relation to moisture content at sampling

4. Discussion

Differences among the survival functions for test specimens of tongue and groove board from different warehouses of small-house factories were found both when using a spore suspension before incubation and when test specimens were incubated with only the prior contamination of spores from the air. The wood from one of the factories (Location B) is noteworthy, as no growth on any of the tongue and grooved board specimens from this factory was found in the test where test specimens had not been sprayed with any spore suspension (i.e., the specimens were exposed to spores from the air only). Although the pattern of differences among different locations was not the same in both tests, the results indicate that the difference was not solely due to different spore loads at the warehouses.

No significant differences in mould growth on the wooden studs from the different factories were found, which may be explained by the low number of test specimens.

Although the moisture content at sampling is a momentary value, it can still be an indication of important differences in storage conditions among the different test sites, in particular with respect to exposure to humidity. The moisture content at sampling varied among the sampling locations; however, this had no effect on the differences on the mould growth on the samples from the different sites. For example, the mean moisture content was higher for the tongue and grooved board test specimens from Location C compared to those sourced at Location B. On the other hand, the survival function pertaining to Location C was above that associated with Location B. Neither was there any correlation between the moisture content at sampling and days until established growth. These results may indicate that different climate exposures at the different test sites had no effect on the mould growth.

For both types of wood tested, there time to mould growth was shorter for the test specimens treated with spore suspension compared to those that were naturally exposed to spores. In the climate chambers, the RH was set to 90% and the temperature to 22 °C. However, the actual RH varied and was slightly lower in the test with test specimens naturally exposed to spores. In addition, greater fluctuations in RH with time lapsed were also noted. Thus, the differences noted among different tests may be due to this difference in incubation conditions. However, based on our earlier findings (Johansson et al. 2012), this small difference cannot explain the difference in mould growth. Instead, we posit that different spore loads in the two tests are the main contributors to the mould growth rate.

The findings pertaining to the differences in wood from different warehouses, in addition to the differences between the tongue and groove board and wooden stud samples, indicated that there are parameters that differ among wood types used for construction that likely affect the mould growth. Further studies of those parameters and their effect on mould growth will be performed and published elsewhere.

5. Conclusions

In this study, the susceptibility of wood of different origin to mould growth varied. This finding can only partly be explained by different exposure conditions. Instead, we posit that the inherent difference in the wood quality is the main contributor to the observed mould growth rates.

Although, in this study, the time to mould growth was used to evaluate susceptibility to mould growth, the results cannot be used to predict how long a material can be exposed to environmental conditions without the risk of mould growth. The amount of spores present may affect the time until mould growth appears, since presence of a greater number of spores increases the probability that some of them would germinate and a hyphae grow.

References

EA-4/02. Expressions of the uncertainty of measurements in calibration. European Co-operation for Accreditation.

EN 13183-2 E. Moisture content of a piece of sawn timber - Part 2: Estimation by electrical resistance method. Swedish Standards Institute.

Hallenberg N, Gilert E (1988) Betingelser för mögelpåväxt på trä. Klimatkammarstudier. SP Statens Provningsanstalt, Borås.

Johansson P, Ekstrand-Tobin A, Svensson T, Bok G (2012) Laboratory study to determine the critical moisture level for mould growth on building materials. International Biodeterioration and Biodegradation 73:23-32.

Johansson P, Svensson T, Ekstrand-Tobin A (2013) Validation of critical moisture conditions for mould growth on building materials. Building and Environment 62:201-209.

Comparison of Different Methods for Evaluating the Thermal Conductivity of Granular Core Materials for VIPs

Peyman Karami, Ph. D. Candidate [1]
Kjartan Gudmundsson, Ph. D., Associate Professor [1]

[1] Department of Civil and Architectural Engineering, Royal Institute of technology (KTH), Sweden

KEYWORDS: *Vacuum insulation panels (VIPs), Core materials, Thermal conductivity tests, Hot plate apparatus, Transient Hot Bridge (THB) method, Transient Plane Source (TPS) method*

SUMMARY:
The superior thermal insulation properties of Vacuum Insulation Panels (VIPs) offer new possibilities to reduce the thermal losses of buildings. VIPs consist of an envelope enclosing a vacuumized core in which thermal conductivities as low as 0.004 W/(mK) can be reached. Despite the unique thermal advantages of VIPs, their relatively high costs limit the use in buildings. For economic reasons, new methods for developing low cost VIP core materials are therefore being pursued. It's obvious that fast and reliable methods for determination of thermal properties are needed. This study compares alternative methods for testing the thermal conductivity of three potential silica core materials for VIPs in terms of time, sample size and boundary conditions. In this study, a cylindrical device has been designed and used together with the Transient Plane Source (TPS) method that gives an opportunity to carry out thermal tests on silica powders at different gaseous pressure and mechanical loads. To verify the validity of this method, the thermal transmissivity is studied through stationary measurements with a hot plate apparatus and with the Transient Hot Bridge (THB) method. The thermal measurements in this study are conducted at atmospheric pressure and without using mechanical loads while the methods are compared experimentally and theoretically. The differences in some of the results indicate that the transient method is less suitable for testing very low-density silica materials with a comparatively large radiative heat contribution that can possibly affect the accuracy of the method.

1. Introduction

With a thermal conductivity between 4 - 8 mW/(mK) VIPs are an attractive solution for the thermal insulation of buildings. A vacuum panel consists of an impermeable envelope enclosing a porous core from which the air has been evacuated. There are many possibilities of combining alternative core materials and envelopes in different typologies. Granular materials such as aerogel, fumed silica and precipitated silica have excellent thermal properties due to a very low density, large surface area and small pores (Baetens et al. 2010a, Lu et al. 2004). Nanoporous silica materials are an example of a good core material due to their microstructure (Simmler et al. 2005). In case of aerogels, for instance, a low thermal conductivity in the range of 17- 21 mW/(mK) has been established at ambient pressure and a bulk density as low as 0.003 g/cm^3 has been reported, while aerogel for typical application has value of about 0.07-0.15 g/cm^3 (Baetens et al. 2010, Hüsing et al. 1998). Aerogels have a surface area that can be as large as 1600 m^2/g and pores in the range between 5 and 100 nm depending on the synthesis method and the silica source used. These pores occupy about 80 to 99.8% of their total bulk volume. As a result of these small pores and the high porosity, aerogels exhibit extraordinary physical, thermal, acoustical and optical properties. On the other hand in case of fumed silica materials, a thermal conductivity of about 20 mW/(mK) at atmospheric pressure has been proven while the material has porosity greater than 90% and a bulk density in the range of 0.06-0.22 g/cm^3 (Alam et al.

2011, Quenard et al. 2005). A range of 100-400 m^2/g is the specific surface area of fumed silica materials varies as function of particle size, while a maximum pore size value of about 300 nm has been reported by Gun'ko (2005). Despite the obvious technical advantages of fumed silica, their utilization as VIPs core material is limited due to their high market price. The current manufacturing processes of granular thermal insulations mentioned as laborious and uneconomical. (Hüsing et al. 1998, Quenard et al. 2005, Baetens et al. 2010a and Alam et al. 2011). Economical methods for producing new core material are therefore being pursued. This work calls for methods for testing thermal transfer properties of powder based materials.

1.1 Heat transfer through a porous media

Several studies put emphasis on assessing the heat and moisture distribution through building construction retrofitted with VIPs, while the investigation on contribution of different heat transfer mechanism at inside of the VIP core material is equally important. Gudmundsson and Karami (2013) did 2 and 3-dimentional dynamic simulations with Comsol Multiphysics® to illustrate the effect of retrofitting on heat and moisture distribution through a wall construction, while Baetens et al. (2010a) focused on VIPs envelope and gives a comprehensive account of foil encapsulated VIPs. Johansson et al. (2011) did measurement of the thermal conductivity of the VIPs using TPS method, while Bouquerel et al. (2012) and Coquard et al. (2013) did investigations on thermal transfer modelling through nanoporous silica applied for VIPs core materials. The total density of heat flow rate, q_{tot} (W/m^2), through a porous media used as VIP core material, can be approximated with calculating three different thermal transmission modes independently and summing them after all, with the optional coupling term, $q_{coupling}$. This procedure is widely applied in the literature (Fricke et al. 1989 and Heinemann 2008). The total rate becomes as

$$q_{tot} = q_{rad} + q_{sol} + q_g + q_{cv} + (q_{coupling}) \quad (1)$$

Where
- q_{rad} radiative heat transfer W/m^2
- q_{sol} heat transfer via conduction in the solid skeleton of the core W/m^2
- q_g heat transfer due to gas conduction W/m^2
- q_{cv} heat transfer due to gas convection W/m^2

Applying granular media with small pore sizes combined with low pressure prevents thermal transport through convection of gases in the core material and the heat transfer due to gas conduction can be reduced by using core material with pore size less than the mean free path of the gas molecules. In the case of nanoporous silica materials, for instance, the high porosity and small pore sizes enable them to retard the rate of heat transport effects of solid conduction, gas conduction and radiation (Gun'ko 2005). The report of Simmler et al. (2005) shows a relationship between bulk density and total thermal conductivity in porous materials comprising of solid conduction, gas conduction and radiation. It can be concluded that granular material with large amount of solid structure exhibits the largest heat flux due to solid conduction, while the radiation parameter will be decreased. Indeed, the lowest magnitude of the sum of the heat transfer due to radiation and solid conduction represents a good thermal performance for a granular core material. This in addition to the gas (air) conduction 26 mW/(mK) for conventional insulation gives a total thermal conduction down to a minimum around 30 mW/(mK). The gas conduction in aerogel or fumed silica granular powders may be reduced to a value of 15 mW/(mK) or below, even at atmospheric pressure due to their nanoscale pores see e.g. Coquard et al. (2013).

1.2 Measuring methods available for testing VIPs granular core material

The measurement of thermal transport properties of materials can be carried out with steady-state or transient methods. The effect of material properties on total heat transfer through a granular material can be included a long-term measurement with a Guarded Hot-Plate (GHP) or a Heat Flow-Meter

(HFM) apparatus, in which steady-state conditions are reached. GHP method is one of well-known stationary methods used for testing the thermal conductivity of commercial products such as thermal insulation for buildings, low density insulation for refrigerators as well as for the certification of reference materials of low conductivity. Xaman et al. (2009) did analysis of the temperature distribution in a GHP apparatus and point out that the GHP is more precise than HFM method. Recent work of Kim (2011) describes a GHP apparatus suited for controlling external compression as well as vacuum condition. Other stationary thermal methods are used by numerous authors as Zarr et al. (1990), Lu et al. (2012) and Coquard et al. (2013). Furthermore, transient methods such as the Transient Line Source (TLS) method, the Transient Hot Bridge (THB) method as well as the Transient Plane Source (TPS) method have been developed for measuring thermal conductivity W/(mK) as well as thermal diffusivity (m^2/s). The reports of Von Herzen R (1959), Jaeger et al. (1964) and Cull (1978) include theoretical proposals of transient temperature increase. The TPS method is a modified version of the Transient Hot Strip method (Gustafsson et al. 1967 and Gustafsson et al. 1979) later developed by Gustafsson (1991a) and Gustafsson (1991b). The TPS measurement technique has been described in detail by Log and Gustafsson (1995) and theoretical considerations have been summarized by He (2005). The method has been studied and used by numerous authors such as Bohac et al. (2000), Gustavsson et al. (2003), Gustavsson et al. (2006) as well as Jannot et al (2007) while they put emphasis on developing the accuracy of the technique. Recently, Jannot et al (2007) focused on the TPS methods and developed a complete model based on the thermal quadrupoles formalism to represent the TPS temperature variation. A report of Coquard et al. (2006) includes a comparison between transient and steady-state methods while a noticeable difference in results has been obtained. Coquard et al. (2013) tried to estimate the reliability of the transient technique for low-density thermal insulators addressing the probe. This study includes theoretical and experimental assessments of methods that may be used to evaluate the thermal transport properties of three potential core materials for VIPs in an accurate and reliable manner. The thermal experiments of this comparative study have been carried out with a TPS method connected to a self-designed device, with a THB method applied in an "outside" laboratory of the *Linsies Thermal Analysis Corporation* as well as with a stationary method with hot plate apparatus. The prerequisites of the different methods are compared and the applicability of the TPS method for testing transparent or semi-transparent low-density silica powders is investigated.

2. Theory

The conductive heat flux, q (W/m) in a point can be described with Fourier's law and a general equation for heat conduction in three dimensions can then be written as

$$\frac{\partial T}{\partial t} = \frac{\lambda}{\rho \cdot c}\left(\frac{\partial^2 T}{\partial x^2} + \frac{\partial^2 T}{\partial y^2} + \frac{\partial^2 T}{\partial z^2}\right) + \frac{\varphi}{\rho \cdot c} \qquad (2)$$

Where T temperature (K)
λ the thermal conductivity of material W/(mK)
ρ the density kg/m^3
c the specific heat capacity of material J/(mK)
φ the heat generation per unit volume W/m^3

2.1 Steady-state theory

When no heat is stored in or generated from a body the temperature in each point will remain constant with time and the conditions are defined as steady-state. The term on the left hand side of Eq. (2) will therefore vanish. Thus, with no heat being generated within the volume and zero net flow in the y- and z-direction Eq. (2) for evaluating the heat flux, q (W/m^2), in the x- direction through a material with thickness d, (m), between temperatures $T1$ and $T2$, (K), becomes

$$q = -\lambda \frac{T_1 - T_2}{d} \tag{3}$$

2.2 Transient theory

An equation for the increase of temperature with time in a semi-infinite medium subject to a source with a given heat flux density has been proposed by Carslaw and Jeager (1959). Further theoretical discussions of transient thermal measuring methods can be found in several reports (Blackwell 1954 and He 2005). It has been described by Gustafsson (1991a) and Gustafsson (1991b) that since the sensor is electrically heated, the time dependent resistance increase R(t) can be given as

$$R(t) = R_0 \{1 + \alpha \cdot [\Delta T_i + \Delta T_{ave}(\tau)]\} \tag{4}$$

where R_0 is the initial resistance of the disk at the time t = 0, the factor α is the Temperature Coefficient of the Resistivity (TCR), ΔT_i is the constant temperature difference, (K), that develops momentarily over the thin covering insulating layers located at both sides of the sensor, and $\Delta T_{ave}(\tau)$ represents the time dependent temperature increase, (s), at the surface of the testing sample on the other side of the insulating layer which is the same increase of temperature at facing the sensor.

With considering the Eq. 4, the temperature increase recorded by the sensor can then be written as

$$\Delta T_{ave}(\tau) + \Delta T_i = \frac{1}{\alpha} \cdot \left(\frac{R(t)}{R_0} - 1 \right) \tag{5}$$

Here ΔT_i is a quantity of the "thermal contact" between the sample surface and the sensor and becomes constant after a very short time Δt_i, (s), which can be estimated by

$$\Delta t_i = \frac{\delta^2}{k_i} \tag{6}$$

Where δ thickness of the insulating layer of the sensor (m)
k_i thermal diffusivity of a layer material m^2/s

The time-dependent temperature increase $\Delta T_{ave}(\tau)$ can then be written, based on the theory of He (2005), as a linear function of dimensionless time dependent function, $H(\tau)$

$$\Delta T_{ave}(\tau) = \frac{p_{av}}{4\alpha\lambda\sqrt{\pi}} H(\tau) \tag{7}$$

Where the dimensionless time τ, (-), defined by the corrected heating time ($t - t_c$) where t_c is the time correction factor for the sensor, (s), He (2005), and Θ is the characteristic time of the measurement, (s), which is unique to the test sample.

$$\tau = \sqrt{\frac{t - t_c}{\theta}}, \qquad \theta = \frac{a^2}{k} \tag{8}$$

Where a radius of the sensor (m),
k thermal diffusivity of the test sample m^2/s

The factor P_{av} in Eq. (7) is the average power released from the heat source during the thermal transport properties measurement, (V), (Gustafsson 1991a- 1991b and Rosenbaum 2007), and λ is the thermal conductivity, W/(mK) of the sample. Since P_{av} and a are constant factors for each sensor,

these are achievable by calibrating the sensor with a standard material. As Eq. (7) is linear, the slope factor can be used for calculating the thermal conductivity range of the test sample. As described by Gustafsson (1991a- 1991b) and Rosenbaum (2007), by making a computational plot of the recorded temperature increase $\Delta T_{ave}(\tau)$ versus $H(\tau)$, a straight line can be achieved, the intercept of which is ΔT_i and the slope factor is obtained by using experimental time steps much longer than Δt_i.

Since the factor of thermal diffusivity of the test sample and hence the characteristic times are not known before the experiment, the final straight line from which the thermal conductivity is calculated is obtained through a process of iteration. Thus it gives possibility to determine both the thermal conductivity and the thermal diffusivity from one single transient recording.

3. Thermal measuring procedure

3.1 Steady-state measurements with hot plate apparatus

A hot plate apparatus used in the experiment (Fig. 1) consisting of two independent flat tanks of stainless steel. The lower tank (warmer side) is connected to a temperature controlled liquid vessel (Lauda K4R) where the temperature is kept constant with an accuracy of ±0.2 °C, while the upper tank (colder side) is connected to a temperature control unit (Kebo-Grave) that kept the temperature constant with an accuracy of ±1°C. In order to minimize the surrounding effects on the heat flux between the tanks, the granular samples are placed in a cylindrical void in the center of a low conductive insulation material consisting of a hard polyurethane sheet with a size of 400×400×20 mm^3. Björk et al. (2009) gives further account of the use of a stationary hot plate apparatus. Two heat flow meters of the type PU43 are mounted in sheets of polymethylmetacrylate that are used to achieve a planar surface across the whole area of the sample. Two heat flow meters are used, one mounted above and the other below the test sample so that the heat flow in and out of the sample can be compared. The polymethylmetacrylate sheets are used to keep six copper-constantan thermocouples in place while the temperature is recorded every 15th seconds through the use of a data logger (Mitec AT 40g). Prior to the measurements, a standard reference material® (SRM 1450d) was used for calibrating the heat flow meters.

3.2 Transient measurements with THB and TPS methods

The commercially available THB method is an enhancement of the Transient Hot Strip method. A very thin strip comprising of a heat source and a temperature sensor is embedded between two “pieces” of the granular sample. A constant heat flow can be emitted during the experiment by supplying a constant current to the metal strip while it also serves as a resistance thermometer. The measuring procedure of the TPS is similar to that of the THB method but a difference can be observed between the measurement sensors. The TPS probe consists of a 10 µm thick double metal spiral which is fitted between two layers of 25 µm thick Kapton. Heat generates in the coil due to supplying a constant current to the prob. This causes the temperature to rise and an increase in the resistance of the spiral while the heat is being absorbed by the test sample. The voltage across the “meander spiral” is then registered. The rate of increase in temperature is due to the thermal transport properties of the samples surrounded the probe. The rate of change in the registered voltage corresponds to the resistance variation of the metal spiral when the electric power is held constant. The short time interval makes it possible to neglect the end effects of the finite size of metal strip and the temperature distribution around and in the coil is identical to that of an infinitely long plane heat source. The TPS sensor was connected to a self-designed cylindrical device (Fig. 1) for holding the powder in place and is capable of performing thermal tests from atmospheric pressure down to vacuum conditions combined with different external loads. This study includes the transient experiments performed at atmospheric pressure and without application of external loads. The device composes of two 15 mm thick Plexiglas cylindrical voids with 60 mm interior diameter, while two Plexiglas pistons with outer

diameter of 59.1 mm were placed into the vessels to keep the powder in place. The gap at between of the cylinders and pistons was sealed with 2 mm thick sealing rubber rings.

For the TPS method as described in the international standard ISO 22007-2, applied for carrying out a thermal test with measuring time *t*, (s), on a sample with a thermal diffusivity of *k*, (m^2/s), a "probing depth", Δp, has been defined as:

$$\Delta_p = 2 \cdot \sqrt{k \cdot t} \tag{9}$$

The constant 2 has been determined so that the influence of external sample boundaries on the temperature of the sensor cannot be detected when the probing depth Δp is limited to within the sample boundaries. In other words, the "thermal penetration depth" or "thermal wave" generated in a thermal experiment must not reach the outside boundaries of the test sample pieces during a thermal conductivity measurement based on transient temperature increase theories. In the TPS sensor case, it is essential to realize that the shortest distance from the spiral probe to the outside sample surface defines the available probing depth.

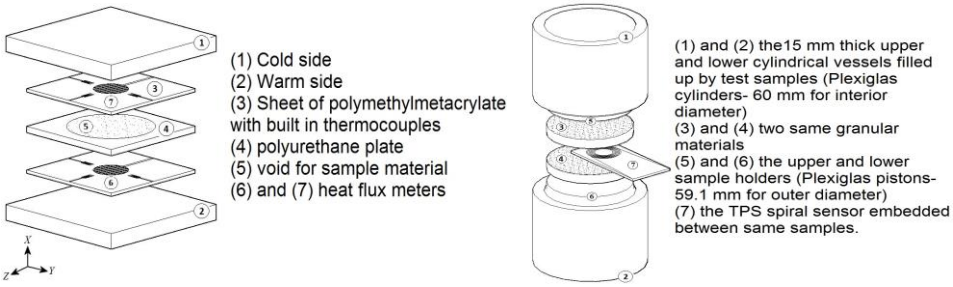

FIG 1. The Hot plate apparatus at the left hand side and self-designed cylindrical device at right

4. Results and discussion

Our previous work, concerning the development of low cost VIP core materials includes preparation of two new types "powders" of precipitated silica structure consist of white-colour particles (Twumasi et al. 2014). The same materials have been used in this study (samples B and C) for evaluation of thermal conductivity while the acquired values are compared with the results obtained for commercially available silica aerogel with known data from manufacture (Cabot Aerogel particles P100- sample A). This sample A consists of translucent aggregates. The particle size of sample A was 0.01 - 4.0 mm with pore diameter of about 20 nm, whereas samples B and C are precipitated silica powders with particle size of between 1.0 – 100 micron (0.001 – 0.1 mm) while having a pore diameter of 10 – 25 nm. Prior to the measurements, the samples were prepared through drying out at a temperature of 105°C during 24 hours. The temperatures of the granular sample were kept at 25°C during the transient experiments while the hot plate measurements had an average plate temperature of 25°C. In the case of steady-state measurements, all temperatures in the experimental setup are well above the dew point of the water vapour of the test room. The duration of the THB used in experiment was in the range of 45-60 seconds and the test duration of the TPS was set to 160 s. Whereas the measurement duration was as high as 24 hours when applying the hot plate apparatus. In fact, the calculation of the mean value must not include the initial transient for the temperature changes when the heat capacity in the samples has an influence on the recorded data. The duration of stationary experiments of samples was about 12 hours and measurements were done when a linear distribution of temperature has been reached through the powder. Table 1 includes the thermal conductivity values obtained for the three samples measured at ambient pressure and without external loads. This table also shows the thermal diffusivity acquired from the transient methods.

TABLE 1.The measured thermal conductivity measured at ambient pressure without external loads

Sample	Meas. Procedure	Temp. °C	Therm.Cond. mW/(mK)	Therm.Diff. Mm^2/s	Duration	Standard deviation
	Hot Plate App.	25	19.5	-	12 Hours	-
A(P100)	THB	25	23.5	0.1183	45-60 s	2 %
	TPS	25	29.1	0.216	160 s	< 5%
	Hot Plate App.	25	36	-	12 Hours	-
B	THB	25	36.4	0.2509	45-60 s	2 %
	TPS	25	38.7	0.328	160 s	< 5%
	Hot Plate App.	25	34.2	-	12 Hours	-
C	THB	25	38.5	0.2071	45-60 s	2 %
	TPS	25	38.8	0.249	160 s	< 5%

The methods show the greatest difference for material A with the hot plate method being much closer to the data from the manufacturer, showing a difference of only 1 % while the THB and TPS method differ by more than 16 % and 32%, respectively from the data of the manufacturer. The thermal conductivity measured for this material by Cohen (2011) is 19.7 mW/(mK), at ambient pressure. In the case of precipitated silica powders B and C, a much closer result values between the stationary and transient methods are shown. Since material A with a low actual density as 0.074 g/cm^3 consist of translucent spherical aggregates with comparatively bigger particles (0.01 - 4.0 mm) while materials B and C are more compact with a particle size of 0.001 – 0.1 mm having higher actual densities of 0.077 and 0.09 g/cm^3 respectively, this can possibly be explained by the relatively greater contribution of radiative heat transfer in sample A and its influence on the sensor of transient methods. Simmler et al. (2005) illustrates a graph that shows significantly greater radiative distribution thorough nanoporous silica materials in lower densities. Moreover, recent works of Coquard et al. (2006) and Coquard et al. (2013) have also pointed out to the effect of radiative heat exchange on accuracy of transient methods.

5. Conclusions

This study compares the viability of three methods for thermal conductivity determination of silica based powders that may candidate as VIP core materials. In general, the steady-state hot plate method might be considered somewhat simpler to conduct. Nevertheless, the method is restricted to large and standard dimensions of the testing samples as well as long measuring times. The transient methods offer other possibilities. Not only do they offer significantly less measurement time but the possibility to use a much smaller test sample, because the probe and measuring equipment of transient methods are physically small, simple and easy to use. The latter giving an advantage when producing new high cost materials in the laboratory. Furthermore, physically smaller sensor of transient method gives opportunity to be connected to other devices such as the self-designed equipment made in this study for measuring the thermal conductivity of nanoporous silica as a function of different gaseous pressure and mechanical loads. In addition, the transient methods also provide information about the thermal diffusion coefficient of the material. Nevertheless, at current the cost of acquiring the equipment for the transient measurements is also much greater while the method is less suitable for testing low-density silica materials with a comparatively large contribution of radiative heat transfer.

References

Alam M., Singh H., Limbachiya M.C. 2011. *Applied Energy*, 88, 3592– 3602.

Baetens R., Jelle B.P. et al. 2010(a). *Energy and Buildings*, 42, 147–172.

Björk F., Enochsson T. 2009. *Construction and Building Materials*. 23(6), 2189–95.

Blackwell J.H. 1954. *Journal of Applied Physics*, 25(2), 1954- 25.

Bohac V., Gustavsson M.K.et al. 2000. *Review of Scientific Instruments* , 71, 2452-55

Bouquerel M., Duforestel T., Baillis D., Rusaouen G. 2012. *Energy and Buildings*, 54, 320-336.

Carslaw H.S., Jeager J.C.1959. *Conduction of heat in solids*. Oxford, Clarendon.

Cohen E., Thermal Properties of Advanced Aerogel Insulation, *Master Thesis*, M IT 2011.

Coquard R., Baillis D., Quenard D. 2006. *J.of Heat and Mass Transfer*, 49, 4511–24.

Coquard R., Coment E., Flasquin G., Baillis D. 2013. *J. of Thermal Sciences*. 65, 242-53.

Coquard R., Baillis D., et al., Levitz P. 2013. *Non-Crystalline Solids*, 363(1), 103-115.

Cull J.P. 1978. *Journal of Physics E: Scientific Instruments*, 11(4), 323

Fricke J., Hümmer E., Morper H.J., Scheuerpflug P. 1989. *Revue de Physique Appliquée*, 24, 487–97.

Gudmundsson K., Karami P., 2013. *Journal of Civil Engineering and Architecture*, 77, 781-788

Gun'ko V.M. 2005. *Colloid and interface Science*, 289, 427-45.

Gustafsson S.E. 1991a. *U.S. Patent #*, 5044, 767

Gustafsson S.E. 1991b. *Rev. Sci. Instrum*, 62, 797–804

Gustafsson S.E., Karawacki E., Khan M.N.1979. *Journal of Physics D: Applied Physics*, 12, 1411-21

Gustafsson S.E., Naturforsch Z., Teil A., 1967, Chalmers University of Technology, Sweden, 1005.

Gustavsson M., Gustafsson S.E. 2003. *DEStech Pubs. Inc. Lancaster, Pennsylvania*, 338-46

Gustavsson M., Gustafsson S.E. 2006. *Thermochimica Acta*, 442, 1-5.

He Y. 2005. *Thermochim. Acta*. 436, 122–129

Heinemann U. 2008. *International Journal of Thermophysics*. 29, 735–49.

Hüsing N., Schubert U.1998. *Angew. Chem. Int. Ed.*, 37, 22-45

Jaeger J.C., Sass J.H. 1964. *British Journal of Applied Physics*, 15(10), 1-8.

Jannot Y., Acem Z. 2007. *Measurement Science and Technology*, 18, 1229-34.

Johansson P. et al. 2011, *Proceedings of the 10th Int.Vacuum Insulation Symp.* Canada.

Kim J., Song T.H. 2011, *Engineering and Technology*, (49), 765-768.

Log T., Gustafsson S.E.1995. *Fire and Materials*, 19, 43–9

Lu H., Lei Y., Jia Z.L., Jing K.Y. 2012. *Applied Mechanics and Materials*, 148-9, 1011-1015.

Lu G.Q., Zhao X.S. 2004. "Nanoporous Materials", Eds. Lu GQ and Zhao XS, 4, 1-12.

Quenard D., Sallee H. 13-16 Nov. 2005. *In 2th Int. Symp. on Nanotechnology in Construction*, Spain.

Rosenbaum E.J, English N.J., Johnson J.K., et al. 2007. *J. Phys. Chem*, 111, 13194–205.

Simmler H et al. 2005. *HiPTI- High Performance Thermal Insulation, IEA/ECBCS Annex 39*.

Twumasi Afriyie E., Karami P., Norberg P., Gudmundsson K. 2014. *Energy and Buildings*,75 (2014)210-215

Von Herzen R., Maxwell A.E. 1959. *Journal of geophysical research*, 64(10), 1557–63.

Xaman J., Lira L., Arce J. 2009. *Applied Thermal Engineering*. 29, 617-623.

Zarr R.R., Somers T.A. 1990. *Na. Inst. of Standard and Technology Gaithersburg*, 247-53.

TOPIC
Challenges of the future

Page.....517-598

An analytical method for calculating the thermal conductivity of a twin pipe in district heating system

Vahid Nik, Senior Lecturer [1, 2]
Bijan Adl-Zarrabi, Assistant Professor [3]

[1] Solar Energy and Building Physics Laboratory, Ecole Polytechnique Fédérale de Lausanne (EPFL), Switzerland
[2] Division of Building Physics, Lund University, Sweden
[3] Division of Building Technology, Chalmers University of Technology, Sweden

KEYWORDS: *Twin heating pipe, Heat Conductivity, Experimental Measurements, analytical Solution*

SUMMARY:
In this paper a simple analytical method is introduced for calculating the overall thermal conductivity of a twin pipe in district heating network. The method is developed based on calculating the conductive and convective heat transfer around the casing pipe in different perimetral sections. Temperature inside the supply and return pipes and also over the heating pipe is measured on different points. These data are imported to a computer program which was written to calculate the heat loss and the total conductivity of the heating pipe. The method has shown good agreement with measurements and it is simple and quick enough in calculating the thermal conductivity of asymmetric- geometries and their temperature distribution. The method is capable to make calculations for more complicated geometries, such as heating pipes with heterogeneous insulating materials.

1. Introduction

District heating systems are widely used in Sweden, mainly for residential and commercial space/water heating. The common medium for the distribution is water. Heat is distributed through underground networks of insulated pipes which consist of supply and return pipes. The higher the temperature difference between supply and return, the higher the efficiency of the delivered energy. .

By improvements in insulating buildings in Sweden there is less heating demand which results in lower temperature difference between the supply and the return pipes. As a consequence heat losses from the pre-insulated pipes to the surrounding environment apportion larger percentage of heat losses of the district heating network. Having the vision of energy plus buildings, smart grids and smart energy networks between buildings, motivates to make pipes better insulated and more efficient, i.e. more complex and more efficient designs such as twin pipes insulted with new materials such as vacuum insulated panels. Effectiveness of new designs and the efficiency of heating pipes are usually assessed by the combination of measurements and numerical simulations, which can be expensive and time consuming. More complex designs, geometries and materials, increase the complexity of the measurements and calculations. Therefore having easier methods for measuring/calculating the thermal performance of heating pipes is desired.

A simple analytical method for calculating the overall thermal conductivity of a twin pipe is presented in this paper. The experimental setup which was used to measure the temperature profile of the twin pipe and surrounding air is described briefly. The measured temperatures were used to calculate the thermal conductivity analytically.

2. The experiment

2.1 The experimental setup

Experiments were performed using a "guarded hot pipe" (more information available in (Berge 2013) and (ISO 8497:1994)) based on the standard for twin pipe assembly of steel service and return pipes, polyurethane thermal insulation and outer casing of polyethylene (15698-1:2009). A schematic figure of the twin pipe, casing and two steel pipes inside the casing, and the installed thermocouples is shown in FIG 1. One of the twin pipes is to supply heat (the pipe ion the bottom - red colour) and the other one contains the return flow (the pipe on top - blue colour). One heat rod was placed inside both of the supply and return pipes to simulate the warm fluid inside pipes. The electrical current in the heat rods were set to get a constant heat power depending on the desired temperature. Thermocouples were placed over the casing, 16 positions, and inside the steel pipes, 4 positions in each pipe – not visible in the figure – to measure temperature at different points. Temperature of the heat rods and the ambient air were also measured. The measured data were collected by two software programs. All the programs and thermocouples were calibrated before running the experiment to make sure about the accuracy of the collected data.

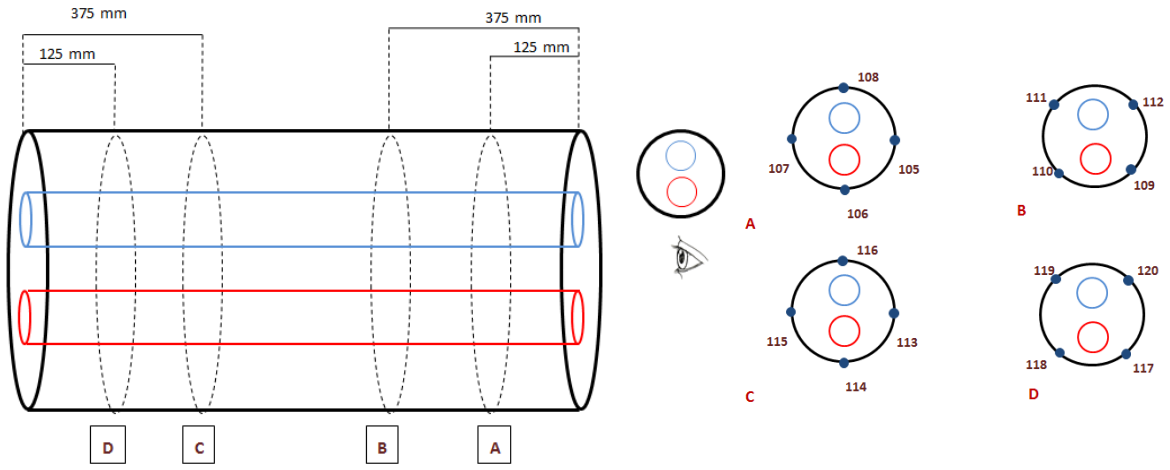

*FIG 1. Position of thermocouples on the casing pipe for the **vertical position** of the twin pipe. The red pipe (bottom) represents the supply pipe and the blue pipe (top) represents the return pipe.*

2.2 Measurements

Measurements were done in four different steps:

1. Horizontal: Supply flow of 78°C – Return flow of 78°C (supply and return pipes lay side by side)
2. Vertical: Supply flow of 78°C – Return flow of 78°C
3. Vertical: Supply flow of 70°C – Return flow of 50°C
4. Vertical: Supply flow of 80°C – Return flow of 40°C

Measurements were performed for two positions of the twin heat pipe; horizontal and vertical (as FIG 1). The aim was investigating the effects of rotating the twin pipe on the temperature distribution over the casing, since it affects the convective heat flow pattern around the casing. All the heat from the twin pipe transfers to the ambient air through natural convection, which the pattern of the air flow and its thermal properties can be influenced by the temperature profile on the casing and its variations. Comparing horizontal and vertical positioning (steps 1 and 2) helps to investigate the importance of positioning and the consequent difference in flow patterns on the temperature profile over the casing pipe. Main differences of the temperature profile are shown in FIG 2; the maximum difference caused by rotating the casing is for point **A** which its temperature increases for 2.6% when the casing turns to

the vertical position. Since the actual position of the twin pipe is vertical most of the measurements were performed for this position. Although for the real case the surrounding environment is soil and very different from air, but this sensitivity test enables to estimate the maximum divergence in results caused by positioning and the consequent difference in natural convection around the casing.

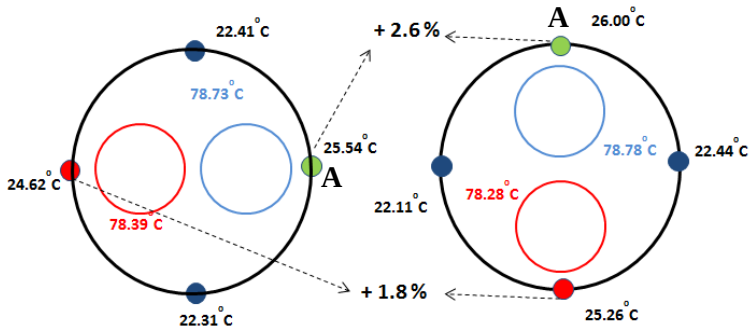

FIG 2. Differences in the temperature distribution on the casing caused by rotating the casing of the twin heat pipe.

3. The analytical method for calculating the thermal conductivity

An analytical method was developed to calculate the overall thermal conductivity of the twin pipe. The method is based on calculating the conductive and convective heat transfer around the heating pipe in different perimetral sections when steady state condition is achieved.

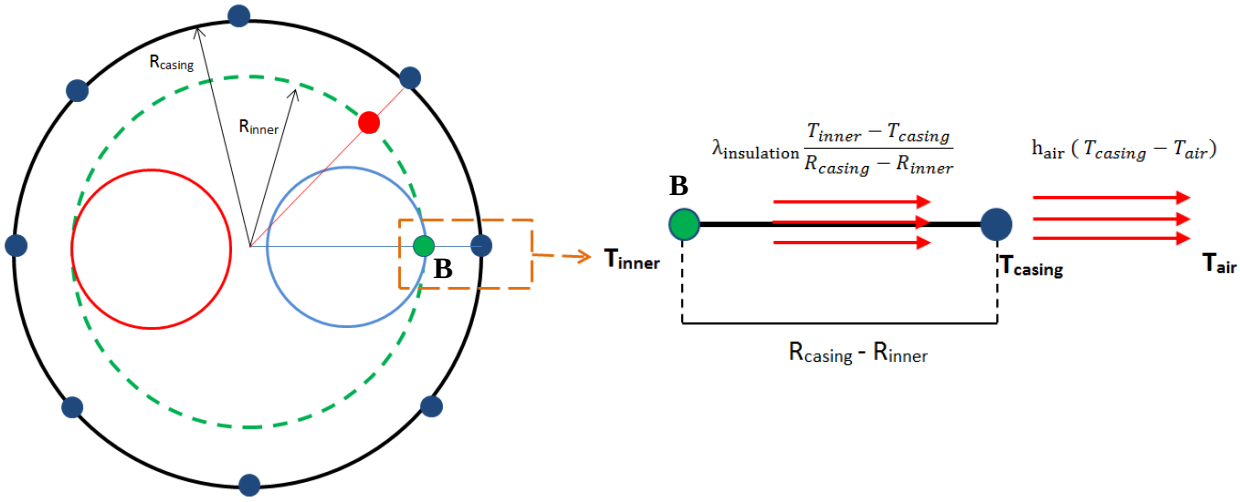

FIG 3. Left: Cross section of the twin heating pipe with an imaginary circle (green dashed circle) tangent to the steel pipe on the right side. Temperature of 8 points on the casing and one point on the steel pipe (**B**) *are known. Right: An infinite narrow section of the heating pipe; through conduction heat transfers from the imaginary circle to the casing where loses heat to the surrounding air through convection.*

Imagine a circle tangent to one of the steel pipes as shown in FIG 3. The amount of heat which passes through the imaginary dashed circle is equal to the heat which transfers to the surrounding air through the casing (the thermal capacity of the insulation and the casing is neglected, moreover measurements were done for steady-state condition). Assuming an infinite narrow section, the amount of conductive heat transfer from the imaginary circle, point **B** in FIG 3, is equal to the amount of convective heat transfer from the blue point on the casing to the air.

$$\lambda_{\text{insulation}} \frac{T_{inner} - T_{casing}}{R_{casing} - R_{inner}} = \text{h}_{\text{air}} \left(T_{casing} - T_{air} \right) \qquad (1)$$

Where $\lambda_{\text{insulation}}$ thermal conductivity of the insulation [W/m/K]

h_{air} convective heat transfer coefficient of air [W/m^2/K]

R_{casing} radius of the casing [m]

R_{inner} radius of the imaginary inner circle [m]

T_{air} temperature of the surrounding air [K]

T_{casing} temperature on the casing at the considered point [K]

T_{inner} temperature on the imaginary circle at the considered point [K]

T_{casing} is known for the 8 measured points on the casing and T_{inner} is known for the point on the steel pipe, point **B** on FIG 3. Since the geometry is not perfect the imaginary circle is not tangent to the other steel pipe and consequently temperature is assumed unknown for the imaginary circle located on the other steel pipe. The aim is finding the temperature profile of the imaginary circle based on equation (1). Three parameters are unknown in the equation; $\lambda_{\text{insulation}}$, T_{inner} and h_{air} .

The thermal conductivity of the insulation can be defined as a function of its temperature (Berge 2013):

$$\lambda_{\text{insulation}} = 26 + 0.1(T - 50) \quad (2)$$

Where the unit for conductivity in the equation is [mW/m/K].

Coefficient of the convective heat transfer for air, h_{air}, can be calculated in two ways:

1. By knowing T_{inner} for point **B** and using equation(2), h_{air} is calculated for that section of the casing. Afterwards the same h_{air} is used for all the other points around the casing.
2. The amount of heat which is generated inside the twin pipe is known. All the heat transfers to the surrounding air according to the following equation:

   $$Q = h_{air}\, A_{casing}\, (T_{casing} - T_{air}) \quad (3)$$

   Where T_{casing} is the average temperature of the measured points over the casing and A_{casing} is the surface area of the casing for a unit length. Using equation (3) it is possible to find an average h_{air} which can be used in the calculations.

Using the above mentioned equations and assumptions, T_{inner} is calculated for 8 points on the imaginary circle corresponding to the 8 measured points on the casing. The resulted temperature profile for the insulation inside the casing, located on the imaginary circle, helps to calculate the heat conductivity according to equation (2). Temperature values which are used in equation (2) are the average temperature of the casing and the imaginary circle:

$$T_{insulation,i} = (T_{inner,i} + T_{casing,i})/2 \quad (4)$$

i=1, 2,…,8

A Matlab program was written which reads the measured values out of experiments and calculates heat losses and the thermal conductivities based on the developed method.

4. Results and the calculated thermal conductivity

Measured and calculated temperature profiles for the four steps of the measurements are presented here. Thermal conductivity is calculated according to the previous section for 8 sections around the twin pipe. An average thermal conductivity is calculated as the mean value of the thermal conductivities at 8 points. The average thermal conductivity can be interpreted as the overall conductivity of the whole setup since it is based on the calculation of the amount of heat flow from the

twin heating pipe to the surrounding air. The following figures show the distribution of temperature and the thermal conductivity around the twin heating pipe. Tables compare the calculated thermal conductivities, calculated based on the two methods for calculating h_{air}.

4.1 Horizontal – Supply flow of 78°C – Return flow of 78°C

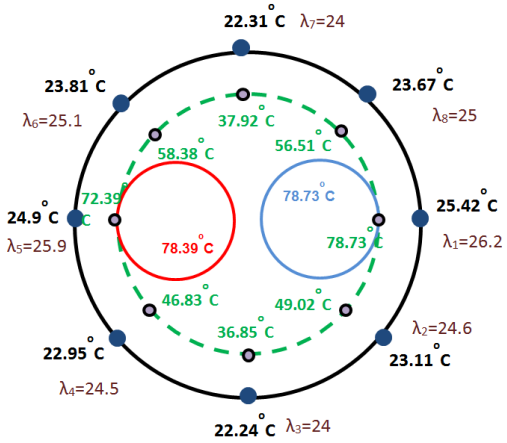

FIG 4. Temperature distribution over the casing and the imaginary circle (dashed green line). The calculated heat conductivity is shown at each section in mW/m/K.

TABLE 1. The calculated thermal conductivities for the twin district heating pipe at 8 points and the average value. Values are compared for the two methods of calculating the convective heat transfer coefficient of air.

	Temperature			$\lambda_{isulation}$ (or λ_{setup}) [mW/m/K]	
	T_{casing}	T_{inner}	T_{mean}	h_{air} was calculated for point **B**	h_{air} was calculated as a mean
1	25.42	78.73	52.075	26.2	25.8
2	23.11	49.02	36.065	24.6	24.4
3	22.24	36.85	29.545	24	23.8
4	22.95	46.83	34.89	24.5	24.3
5	24.9	72.39	48.645	25.9	25.5
6	23.81	58.38	41.095	25.1	24.8
7	22.31	37.92	30.115	24	23.9
8	23.67	56.51	40.09	25	24.8
Mean			39.07	24.9	24.7

4.2 Vertical – Supply flow of 78°C – Return flow of 78°C

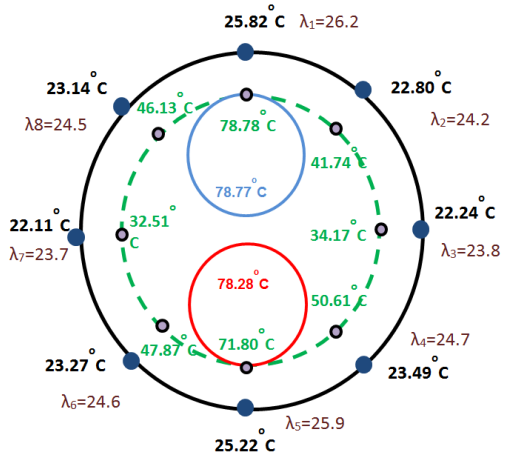

FIG 5. Temperature distribution over the casing and the imaginary circle (dashed green line). The calculated heat conductivity is shown at each section in mW/m/K.

TABLE 2. The calculated thermal conductivities for the twin district heating pipe at 8 points and the average value. Values are compared for the two methods of calculating the convective heat transfer coefficient of air.

	Temperature			$\lambda_{isulation}$ (or λ_{setup}) [mW/m/K]	
	T_{casing}	T_{inner}	T_{mean}	h_{air} was calculated for point **B**	h_{air} was calculated as a mean
1	25.82	78.78	52.3	26.2	26.1
2	22.8	41.74	32.27	24.2	24.2
3	22.24	34.17	28.205	23.8	23.8
4	23.49	50.61	37.05	24.7	24.7
5	25.22	71.8	48.51	25.9	25.8
6	23.27	47.87	35.57	24.6	24.5
7	22.11	32.51	27.31	23.7	23.7
8	23.14	46.13	34.635	24.5	24.4
Mean			36.98	24.7	24.7

4.3 Vertical – Supply flow of 70°C – Return flow of 50°C

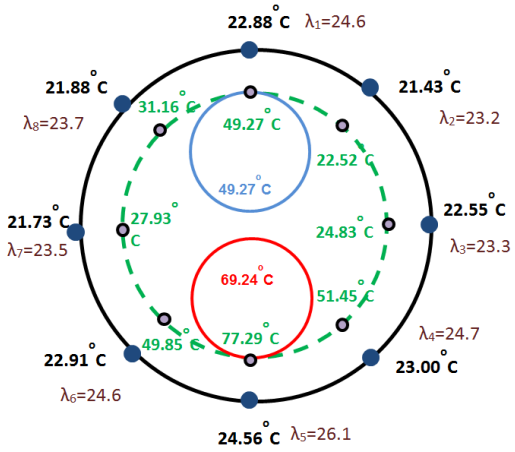

FIG 6. Temperature distribution over the casing and the imaginary circle (dashed green line). The calculated heat conductivity is shown at each section in mW/m/K.

In this case the calculated temperature for the imaginary inner circle is overestimated since it is higher than the temperature of the supply pipe (steel pipe on the bottom). Calculations were performed again by assuming temperature of the supply pipe as known, instead of the return pipe. There was almost no difference in the calculated conductivity; hence the overestimation of the calculation method could be neglected.

TABLE 3. The calculated thermal conductivities for the twin district heating pipe at 8 points and the average value. Values are compared for the two methods of calculating the convective heat transfer coefficient of air.

	Temperature			$\lambda_{isulation}$ (or λ_{setup}) [mW/m/K]	
	T_{casing}	T_{inner}	T_{mean}	h_{air} was calculated for point **B**	h_{air} was calculated as a mean
1	22.88	49.27	36.075	24.6	24.4
2	21.43	22.52	21.975	23.2	23.2
3	22.55	24.83	23.69	23.3	23.3
4	23	51.54	37.27	24.7	24.5
5	24.56	77.29	50.925	26.1	25.7
6	22.91	49.85	36.38	24.6	24.4
7	21.73	27.93	24.83	23.5	23.4
8	21.88	31.16	26.52	23.7	23.6
Mean			32.21	24.2	24.1

4.4 Vertical – Supply flow of 80°C – Return flow of 40°C

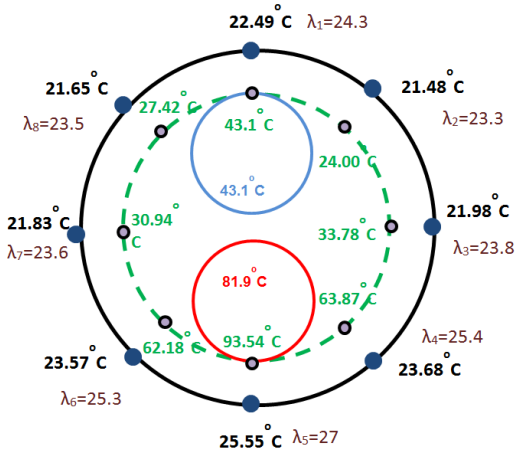

FIG 7. Temperature distribution over the casing and the imaginary circle (dashed green line). The calculated heat conductivity is shown at each section in mW/m/K.

TABLE 4. The calculated thermal conductivities for the twin district heating pipe at 8 points and the average value. Values are compared for the two methods of calculating the convective heat transfer coefficient of air.

	Temperature			$\lambda_{isulation}$ (or λ_{setup}) [mW/m/K]	
	T_{casing}	T_{inner}	T_{mean}	h_{air} was calculated for point **B**	h_{air} was calculated as a mean
1	22.49	43.1	32.795	24.3	24
2	21.48	24	22.74	23.3	23.2
3	21.98	33.78	27.88	23.8	23.6
4	23.68	63.87	43.775	25.4	24.8
5	25.55	93.54	59.545	27	26.1
6	23.57	62.18	42.875	25.3	24.8
7	21.83	30.94	26.385	23.6	23.5
8	21.65	27.42	24.535	23.5	23.4
Mean			35.07	24.5	24.2

5. Discussion and conclusion

According to the results, the two methods for calculating of the convective heat transfer coefficient of air do not affect the calculated thermal conductivity of the setup considerably. The maximum difference between the overall thermal conductivities is around 1.2% for the fourth case. For this case the maximum difference for $\lambda_{isulation}$ at a point happens at point 5 (see

TABLE 4) on the bottom of the heating pipe; 3.5% difference. Therefore it is possible to conclude that both methods for estimating h_{air} are valid. However using more accurate techniques to calculate h_{air} may give better results, although it will increase the complexity of the calculations and measurements.

The maximum difference between the calculated overall thermal conductivities is around 3.3% between the first case, 24.9 [mW/m/K] in TABLE 1 for the mean temperature of 39.07^{o}C, and the third case, 24.1 [mW/m/K] in TABLE 3 for the mean temperature of 32.21^{o}C. This maximum difference is induced by different positioning of the casing and also different temperatures. These two cases show the maximum differences in both positioning and temperature among the four cases, , which induces the maximum difference in the air flow around the casing and its thermal properties. This results in the maximum difference between the calculated $\lambda_{isulation}$.

Although there are differences between the calculated thermal conductivities, there are small enough to have a good estimate for the overall thermal conductivity of the twin heating pipe. The proposed method for calculating the thermal conductivity of the twin district heating pipe is simple and quick. Moreover it is not very dependent on the geometry inside the casing, for example it might be possible to use the same technique for estimating the conductivity of a twin pipe insulated partly by vacuum insulation panels. However more experiments and calculations will be performed in future.

References

15698-1:2009. 2009. “District Heating Pipes. Preinsulated Bonded Twin Pipe Systems for Directly Buried Hot Water Networks. Twin Pipe Assembly of Steel Service Pipe, Polyurethane Thermal Insulation and Outer Casing of Polyethylene.”

Berge, Axel. 2013. “Novel Thermal Insulation in Future Building and District Heating Applications - Hygrothermal Measurements and Analysis.” http://publications.lib.chalmers.se/publication/176926-novel-thermal-insulation-in-future-building-and-district-heating-applications-hygrothermal-measureme.

ISO 8497:1994. 1994. “Thermal Insulation -- Determination of Steady-State Thermal Transmission Properties of Thermal Insulation for Circular Pipes.”

Comparative assessment of in-situ thermal characterisation techniques.

An-Heleen Deconinck, M.Sc. [1]
Staf Roels, Professor [1]

[1] KU Leuven, Belgium

KEYWORDS: *In-situ thermal characterisation; Thermal performance; Building component testing; Full-scale testing; Dynamic data analysis*

SUMMARY:
A more precise knowledge of the as-built thermal performance of our buildings' fabric is of prime importance for the ongoing tendency to more stringent building performance demands. The methods that are commonly used for on-site thermal characterisation, such as the average method and linear regression technique, are based on stationary boundary conditions. As the latter are never encountered on site in practice, the methods' validity depends on outdoor weather conditions. This paper examines the practical applicability of different in-situ thermal characterisation methods based on simulated data for an insulated cavity wall. Common semi-stationary methods are compared with a more advanced dynamical data analysis method, giving special attention to the reliability of the methods' estimation results when confronted with data sets of limited measurement time spans and different measurement periods throughout the year. From this research, it can be stated that the use of semi-stationary methods for the characterisation of an insulated south-faced cavity wall can lead to accurate results in realistic measurement time spans when applied during winter months. The methods become less reliable when the temperature difference across the wall decreases. The dynamic method showed to be less sensible to the measurement period, provides more accurate results and needs shorter measurement time spans. The analysis itself however, showed to be more time consuming.

1. Introduction

A precise knowledge of the actual thermal performance of our buildings' fabric is of prime importance in the debate on energy efficient dwellings. Currently, the building envelope is assessed by a performance label in the design phase based on calculated thermal resistances of the consisting building components. Some studies, however, show that these theoretical values do not necessarily correspond with the as-built thermal performance of the building elements (Hens *et al.* 2007), (Lowe *et al.* 2007). The differences can among others be attributed to the applied materials that differ from the designated ones, poor detailing and/or workmanship issues and physical phenomena such as thermal bridging, wind washing, air looping, etc. The on-site thermal characterisation of building components is therefore an important step to bridge this gap between theory and reality.

The methods that are commonly used for in-situ characterisation, such as the average method and linear regression technique, are based on the linear steady state relationship between the thermal resistance of, the heat flux through and the temperature difference over the studied element. Yet, steady state boundary conditions are never encountered on site in practice and the methods require averaged data as an approximation for measurements under stationary conditions. For the methods to be valid, the averages should be taken over a sufficiently long period of time, which limits the practical applicability of the methods, as one wants as shortest measurement time spans as possible. Besides, the methods are dependent of the measurement period throughout the year: they are not valid when the heat flow through the element is negligible when compared to the heat storage in the wall. This means that small temperature differences between outside and inside boundary conditions,

typically occurring during the summer period, result in small fluctuating heat flows around zero and jeopardize the R-estimates of the semi-stationary analysis methods. In contrast with the quasi-stationary methods, more advanced dynamical data analysis techniques exist. The latter take advantage of the dynamic boundary conditions, as dynamics are an express condition for the functioning of the method. The use of dynamic parameter estimation in the field of thermal characterisation is rather new and the question can be raised whether they perform better than the quasi-steady state methods.

2. Methodology

This paper examines the practical applicability of different in-situ thermal characterisation methods. Common semi-stationary methods are compared with a more advanced dynamical data analysis method, giving special attention to the reliability of the methods' estimation results when confronted with data sets of limited measurement spans and different measurement periods. Ideally, however rarely the case, a good thermal estimation is independent of the measurement period throughout the year, i.e. in winter or summer, and results from short measurement terms. Most methods are accompanied by limiting conditions regarding the applicability and validity of the test method, however, these are not literally translated into a minimum test duration or delimited test period throughout the year. This paper aims to give an idea about those values in the case of a south-faced insulated cavity wall by applying the studied methods on various measurement data sets of this wall. The measurement data is generated by simulations in HAFMFEM, a finite element model based on the standard partial differential equations of heat, air and moisture transfer in porous building materials, developed at the KU Leuven. First the applied characterisation methods studied are presented, then the particularities about the wall's properties and simulation assumptions are described.

2.1 In-situ thermal characterisation methods

2.1.1 Average method

The International Standard ISO 9869 (1994) proposes an average method for the estimation of the thermal resistance of building elements from in-situ measurements. The method departs from the principle that the R-value can directly be obtained by measuring the heat flow rate through an element, together with the surface temperatures on both sides of the element in steady state conditions. However, since steady state conditions are never encountered on a site in practice, the method assumes that the mean values of the heat flow rate and temperatures over a sufficiently long period of time give a good estimate of these values in stationary conditions, leading to equation (1)

$$R = \frac{\sum_{j=1}^{n} \Delta T_{si/se,j}}{\sum_{j=1}^{n} q_j} \quad (1)$$

Where R total thermal resistance of the element ((m².K)/W)
$\Delta T_{si/se,j}$ difference between the internal and external surface temperature of reading j (K)
q_j heat flow rate of reading j (W/m²)

The assumption of averaging data equalling steady state data results in a valid method only if (1) the thermal properties of the materials and the heat transfer coefficients are constant over the range of temperature fluctuations occurring during the test and if (2) the change of amount of heat storage in the element is negligible when compared to the amount of heat going through the element. Besides these general conditions, the norm formulates additional criteria which determines, during the course of the measurements, when sufficient data has been recorded. These criteria include minimum test durations and minimum deviations between the subsequently obtained R-estimates computed after each measurement. According to the International Standard, the recording measuring interval is

typically 0,5h to 1h. In this paper, the average method is applied on (simulated) hourly measured data sets.

2.1.2 Average method with correction for thermal storage

The International Standard ISO 9869 provides criteria, indicating when sufficient data recordings for the average method have been obtained. If these criteria are not fulfilled, a correction procedure needs to be applied. The latter involves a rectification of the heat flow rates according to the thermal storage capacities of the element and is relevant for structures of high R-value and high thermal mass. The adjustment results from the assumption that all the heat flux measured at the interior surface passes through the test element. Strictly speaking, this will only be the case if the temperature profile throughout the element remains the same during the test. Equation (2) represents the adjustments to the measured heat flux at each data point, involving internal and external thermal mass factors for the structure concerned.

$$\sum q_j - \frac{F_i \delta T_i + F_e \delta T_e}{\Delta t} \qquad (2)$$

Where Δt the interval between readings (s)

$F_{i/e}$ internal/external thermal mass factor, relying on reasonable estimates of the thermal mass and resistance of the various layers of the structure

δT_i the difference between internal temperature averaged over the 24h prior to reading j and internal temperature averaged over the first 24h of the analysis period (K)

δT_e the difference between external temperature averaged over the 24h prior to reading j and external temperature averaged over the first 24h of the analysis period (K)

In this paper, hourly data is used as an input for the analysis procedure. According to the standard, the correction often permits a shorter measurement time.

2.1.3 Simple linear regression method

In essence, the simple linear regression technique fits a straight line through a set of points in such a way that the sum of the squared vertical distances between the points of the data set and the fitted line are as small as possible. To retrieve the R-value out of heat flux and surface temperature measurements, the stationary linear correlation between q and ΔT is assumed, as is the case for the average method. Equation (3) represents the equation of the resulting regression line approaching the relationship between the dependent variable q and the explanatory variable ΔT.

$$q = \frac{1}{\mathrm{R}} . \Delta T_{si/se} + c \qquad (3)$$

In contrary to the other methods, daily averages will be used for the application of the linear regression technique, for this permits to cancel out short-term effects of thermal mass (Bauwens *et al.* 2012). Theoretically, the regression line should go through the origin, which in practice will rarely be the case. Therefore, in this paper, this is forced by fixing the constant c at zero.

2.1.4 Dynamic parameter analysis

In contrast to the quasi-stationary analysis methods that are commonly used for in-situ thermal characterisation, this paper includes the application of a more advanced dynamic analysis technique. Essentially, dynamic parameter estimation is a way of inverse modelling: the method estimates the parameters of a physical model by tuning the behaviour of this model to the observed behaviour of the physical object, both subject to the same boundary conditions. The assumed physical models, or so called grey-box models consist of a set of continuous stochastic differential equations formulated in a state space form. The use of grey-box models is an approved method for identifying systems in a lot of

domains and is explored for modelling the heat dynamics of buildings and reported already in (Madsen & Holst 1995) and (Andersen *et al.* 2000).

The state space model structure used in this paper for modelling the insulated cavity wall is derived from the resistance capacitance model represented in FIG 1. The model's input variables are the in- and external surface temperatures $T_{si/e}$ of the wall, while the internal heat flux q serves as observation variable or output. This means that similar measurements as for the quasi-stationary methods are required. A third-order model is considered, meaning that the thermal mass of the wall is lumped to three capacitances. The state variables T_{wi} of the model represent the internal temperatures of those thermal capacitances. The estimation parameters of the model are the three capacities C_{wi} and the four linking thermal resistances R_{wi}. The total resistance R of the wall equals the sum of the individual model resistances. Note that the latter are not necessarily equally distributed over the wall: the identification procedure determines the values of the model resistances and controls the location of the capacities in the modelled wall. The model's parameters are estimated using the Continuous Time Stochastic Modelling (CTSM) toolbox implemented in the statistical software R (Rune *et al.* 2013). CTSM uses maximum likelihood estimation to identify the unknown parameters for the given model structure.

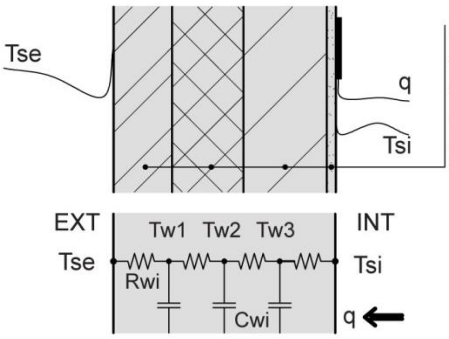

LAYER	thickness	thermal resistance	thermal capacity
- brick	0.090m	0.113 (m².K)/W	3.57e5 J/(m².K)
- thermal insulation	0.120m	3.429 (m².K)/W	7.06E3 J/(m².K)
- load-bearing brick	0.140m	0.187 (m².K)/W	2.36E5 J/(m².K)
- plaster	0.015m	0.088 (m².K)/W	1.80E4 J/(m².K)
TOTAL	0.365m	3.816 (m².K)/W	6.18E5 J/(m².K)

FIG 1. Representation of the studied insulated cavity wall and its thermal properties (top) and representation of the 3rd order resistance capacitance model used in the dynamic parameter analysis (bottom)

2.2 Case study

In this paper, an insulated south-facing brick cavity wall is observed, as depicted in FIG 1. The measurement data for the in- and external surface temperatures and for the internal heat flux through the wall are simulated in HAMFEM, a finite element model based on the standard partial differential equations of heat, air and moisture transfer in porous building materials, developed at the KU Leuven (Janssen *et al.* 2007). A refined mesh of 201 nodes is used. The thermal properties used for the one-dimensional simulations are represented in FIG 1. The goal value for the total thermal resistance of the cavity wall is calculated from the simulation's input properties and adds up to 3.82 (m².K)/W. A simulation with the length of one year and a calculation time step of one minute is performed for the typical moderate climate of Uccle (Belgium). Irradiance and outdoor air temperature data with a time resolution of 1 minute is obtained by Meteonorm v6.1 based on the period of 1981-2000. Other climate data is obtained with a time resolution of 1 hour and is interpolated to minutely data. For the inside boundary conditions, a constant indoor air temperature of 20°C is maintained during the whole year. This implies heating during the winter months and cooling during summer. The measurement output, e.g. surface temperatures and heat flux, are calculated at each minute of a whole year. This data is averaged to an hourly data set for the application of the average method, the average method with correction for thermal storage and for the dynamic parameter estimation method. For the simple linear regression method, daily averaged data is used.

3. Results

For comparison of the different analysis techniques, various data sets are considered: (1) data sets with different lengths ranging from 1 to 30 days and (2) data sets starting on the 1st, 2nd, …, till the 30th of January, April and July. The resulting estimates for the thermal resistance of the cavity wall are represented in FIG 2. The charts with heading *January* contain the results of the data sets with a starting day in January. The charts with heading *April* and *July* respectively contain the results of the data sets with a starting day in April and July. From here the data sets with a starting date in January will be denoted as the data sets in January, while they partly encompass data points in February. Analogous denotations will be used for April and July. The results are plotted in function of the length of the dataset. So, in January, there are 30 data points corresponding to a data set length of, for example, 20 days, notably the data set ranging from the 1st of January till the 20th of January, till the data set ranging from the 30th of January till the 18th of February. In fact, the different data sets are a moving window advancing with a step of one day, repeated for different window lengths. The results for the different analysis methods are ordered vertically, with a repetition of the results of the average method as a reference. Remark that the boundaries of the y-axis are adjusted for the results of the reference method in January and April and that some data points corresponding to the other methods or to July fall outside the boundaries of the graph.

Looking at the results of the **average method**, it can be seen from FIG 2 (first line) that in January all estimates of R lie within a 5%-accuracy band around the goal value for data sets with a length of 20 days or longer. All R-estimates resulting from data sets of minimum 7 days already satisfy the required accuracy of 10%. In April, the requisite length of the data sets for obtaining the defined accuracies of 5% or 10% increases to approximately 25 and 10 days respectively. In July, no meaningful estimates of R are acquired. This phenomenon of poorer estimates for warmer periods can be explained by the validity of the averaging method only in stationary conditions: the method assumes that the mean values of the heat flow rate and temperatures over a sufficiently long period of time give a good estimate of these values under steady state conditions. This assumption is no longer justified when the heat storage in the element is large compared to the amount of heat going through the element. Typically, the heat flow rate in summer is limited due to the small temperature differences between the in- and outside environment. For the studied case, cooling is allowed and larger negative temperature differences can be maintained during hot periods when compared to a situation without cooling. The latter situation would involve fluctuating small positive and negative heat flows through the element during the summer period. This situation is even less favourable than the studied one and implies worse results than those represented.

If the **correction for the storage effects**, as formulated in ISO 9869, is applied on the data (second line on FIG 2) an improvement of the estimation results in January and April are found compared to the average method. In January all results lie in the accuracy band of 10% and 5% for data sets of two and three days or longer respectively. In April, the required data set length reduces to 5 and 13 days for characterising a 10% and 5% accurately estimated R-value. The applied adjustments correct the measured data for the fact that not all the heat flux measured at the interior surface passes through the test element. For this cavity wall, an element with high R-value and high thermal mass, FIG 2 endorses the technique's potentials to shorten the required measurement time span for accurately characterising. Yet, it needs to be noticed that the thermal mass factors rely on estimates of the thermal mass and resistance of the various layers of the structure, which are exactly known for the studied wall. In reality, accurate thermal properties will often not be known and the improvement of the correction can be less effective. Besides that, by looking at the results for July, it is seen that the correction is not able to solve the problems when the measurements include small heat flow rates fluctuating around zero.

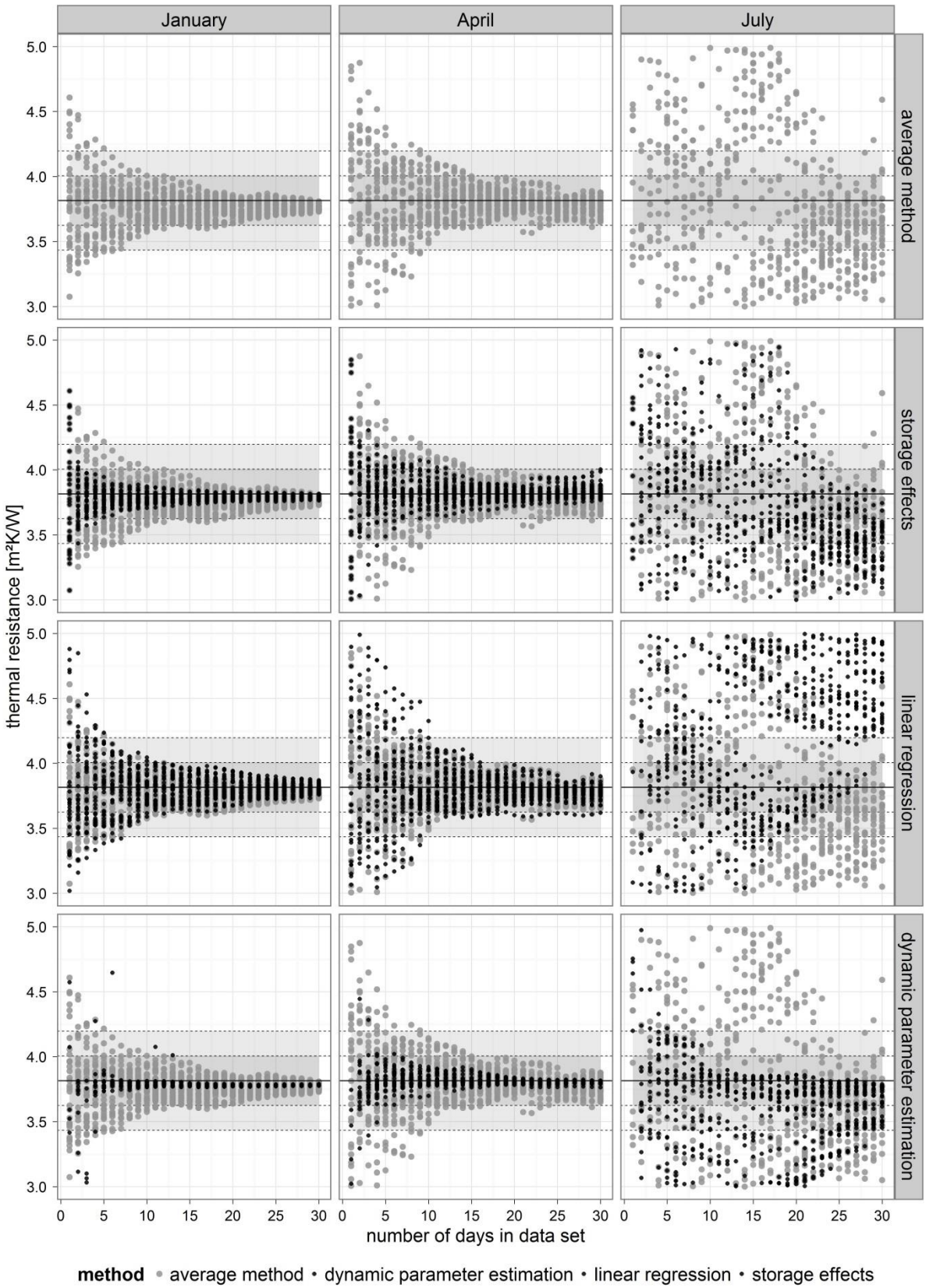

FIG 2. Comparison of the different analysis techniques regarding the data set length and period. The dotted lines and grey areas correspond to the 5% and 10% accuracy band.

The results for the **linear regression method** (third line on FIG 2) applied on daily averaged data points are similar to the results of the average method. As the same assumptions are made for both techniques, this may not surprise.

Finally, the results for the **dynamic parameter estimation method** are studied. At first sight, it is seen from FIG 2 (fourth line) that the estimation method achieves a fast and accurate convergence to the goal value in January and April. Nevertheless, some data points are missing because the estimation procedure did not converge to a parameter set that fits the adopted differential equations and observations. Next to that, a lot of solitary outliers are located outside the boundaries of FIG 2's graph. Yet, there is no stratification from the goal-value to these outliers, as it is for the other methods. This encourages the presumption that the outliers are due to unsatisfactory model assumptions. Contrary to the other methods, the application of the dynamic parameter estimation technique is not straightforward: initial values for the model parameters and model states have, among others, to be assumed and can affect the estimation results. The reliability of the assumed initial values and retrieved estimates can be examined by a set of post processed evaluation criteria. With this information reapplication of the estimation procedure with adapted initial values can still lead to correct R-estimates. However, this assessment procedure is not automatised and has not been applied for the series of dynamic estimations in this paper. Looking at the results for July, it is remarked that the presence of small heat flow rates does affect the dynamic estimation procedure too. Nevertheless, a denser cloud around the goal value is remarked. Further investigation should tell whether the application limitations due to limited heat flow rates are less tight than for the other methods.

4. Conclusions and discussion

To evaluate the reliability of the different methods in more detail, the standard deviation of the R-estimates is investigated for the different analysis methods as a function of the length of the measurement time span.

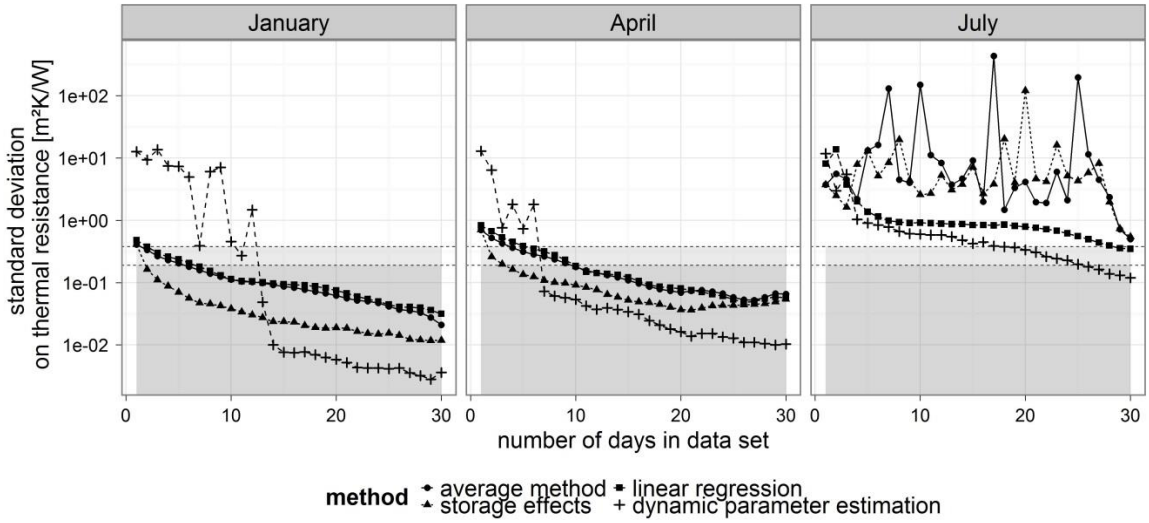

FIG 3. Standard deviation of R-estimates for a certain data set length and for each analysis method. The dotted lines and grey areas correspond to a deviation of 5% and 10% of the goal value.

The results are summarised in FIG 3. The graph represents the mean deviation from the goal value for the considered data points. Comparison of the semi-stationary results in January and April learns that the average method and the linear regression method with daily averages attain a similar accuracy for their results. The accuracy improves when the correction for the storage effects is applied, yet in contrast to real situations, in this study precise information about the thermal properties was present for the calculation of the in- and external thermal mass factors. The standard deviations for the dynamic estimation method show an irregular development for the shorter data set lengths. This is due

to the presence of large individual outliers. The presence of outliers disappears from a certain data set length, +/-15 days in January and +/-7 days in April. The question raises whether an individual assessment of the model assumptions could avoid outliers for shorter data set lengths. A look on the results of July learns that the average method, with or without a correction for thermal storage, is not valid in the presence of small heat flows. The linear regression methods appears to perform well, however, FIG 2 shows a convergence to a wrong value. The dynamic estimation method shows the smallest mean deviation from the goal value, however, the confidence intervals of the obtained results are larger in summer than in winter and do barely reach the defined accuracy band.

In general, it can be stated that the use of semi-stationary methods for the characterization of an insulated cavity wall can lead to accurate results in realistic measurement time spans, i.e. +/-5 till 7 days, when applied during the winter months. The dynamic estimation method is less sensible for low heat flow rates, provides more accurate results and, when individually assessed, in shorter measurement periods. One can question whether the additional time consumed on evaluation and reapplication of the method is worth the reduction in measurement time and the improved accuracy. However, the possibilities of a dynamic analysis procedure reach far beyond those of the stationary techniques. Where the latter are limited to the estimation of stationary parameters, the dynamic method is not. One can imagine the identification of a thermal resistance that includes it's temperature dependency or the identification of an R-value including dynamic effects as wind washing or air looping around the insulation layer, etc. As these dynamic phenomena do occur in practice, the potentials of the dynamic estimation method should be further investigated, for the possibility to characterise and quantify dynamic effects on the thermal performance of building components would be a significant improvement for in-situ characterisation.

5. Acknowledgements

This paper is realised thanks to a Ph.D. grant (grant number 121167) of the Institute for the Promotion of Innovation through Science and Technology in Flanders (IWT).

References

Andersen K.K., Madsen H. & Hansen L.H. 2000. Modelling the heat dynamics of a building using stochastic differential equations. Vol.31, Energy and Buildings. 13-24 p.

Bauwens G., Standaert P., Delcuve F. & Roels S. 2012. Reliability of co-heating measurements. Building Simulation and Optimization Conference 2012, Loughborough, UK. 348-355 p.

Hens H., Janssens A., Depraetere W., Carmeliet J. & Lecompte J. 2007. Brick Cavity Walls: A Performance Analysis Based on Measurements and Simulations. Vol.31, Journal of Building Physics, SAGE Publications, London, UK. 95-124 p.

ISO 9869. 1994. Thermal insulation. Building elements. *In-situ* measurements of thermal resistance and thermal transmittance (ISO 9869:1994(E)). International Organization for Standardization ISO.

Janssen H., Blocken B. & Carmeliet J. 2007. Conservative modelling of the moisture and heat transfer in building components under atmospheric excitation.Vol.50 (5-6), International Journal of Heat and Mass Transfer. 1128-1140 p.

Lowe R.J., Wingfield J., Bell M. & Bell J.M. 2007. Evidence for heat losses via party wall cavities in masonry construction. Vol. 28, Building Service Engineers Research and Technology. 161-181 p.

Madsen H. & Holst J. 1995. Estimation of continuous-time models for the heat dynamics of a building. Vol.22, Energy and Buildings. 67-79 p.

Rune J., Kristensen N.R., Bacher P., Kloppenborg J. & Madsen H. 2013. CTSM-R User Guide. 23 p.

The energy performance of urban rooftop greenhouses

Andrea Vickers, MBSc [1]
Mark Gorgolewski, PhD, Professor [1]

[1] Ryerson University, Canada

KEYWORDS: *Urban agriculture, greenhouse, rooftop food production, energy*

SUMMARY:
In many cities worldwide there is an interest in exploring food production within appropriate urban spaces. Rooftops have been identified as such an opportunity and increasingly rooftop growing spaces have been established in several major projects. To increase productivity and extend the growing season some projects have used greenhouses on top of buildings. These greenhouses are often operated year round and demand significant energy to maintain optimal growing conditions. This can significantly add to the carbon impact of the food that is produced within them. In general there has been little exploration of how the energy and water systems of such a food producing greenhouse can integrate with the systems of the building below to exploit synergies and reduce resource needs.

The paper reports on a study that explores the impact of adding a rooftop greenhouse to a typical six storey, detached office building design in Toronto. The research uses energy simulation software to explore the synergistic impacts on the total energy consumption of both office building and greenhouse, and how the specification of key parameters such as glazing, thermal mass, and location of roof insulation impact performance. The results provide a better understanding of how to design rooftop greenhouses to benefit from their unique location on top of a building.

1. Introduction

Urban agriculture is increasingly seen as an important step towards food security in cities. While there is considerable discussion about the proportion of food that can be supplied by urban food production (MacRae et al., 2010), urban agriculture is increasingly being considered as a potential sustainable food source in many cities. Furthermore, rooftop space is abundant in many cities, and is often an untapped resource that can accommodate various forms of urban agriculture. Specific examples of recently implemented projects include the rooftop farms such as Brooklyn Grange in New York City and Carrot Commons in Toronto, and commercial rooftop greenhouses such as Lufa Farms in Montreal and Gotham Greens in New York City (Gorgolewski, 2011). Such projects serve to intensify the use of urban land and diversify urban employment opportunities. Rooftop food production in the city provides opportunities for food education, reduces the distance that food has to travel, can improve nutrition, and, depending on agricultural intensity, can provide appealing leisure space for users of the host building. Their proximity to consumers also necessitates a level of accountability on the part of the growers and delivers unparalleled freshness.

Rooftop farming has significant technical implications on the buildings beneath, including: structurally, functionally and for maintaining appropriate internal environments. In particular, rooftop greenhouses can offer benefits from thermal integration both of envelope and HVAC systems. This paper presents an investigation using energy modelling of the potential impact of adding a rooftop greenhouse to a six storey, detached office building in Toronto on the total heating and cooling energy consumption of both structures operated year-round.

2. Background

According to Rodriguez (2009), a "very conservative" estimate of the productive potential of rooftops in London, UK, using greenhouse hydroponic production is 300 tons/ha/yr. This correlates well with the yields achieved by Lufa Farms in Montreal (Figure 1), a 2,880m^2 (0.288 ha) commercial operation that produces up to 100 tons of produce annually, which is the equivalent of nearly 350 tons/ha/yr, and feeds 2,500 people in Montreal (Rathmell, 2013).

Little research has been conducted on the energy performance of urban rooftop greenhouses, however, the idea has similarities to the concept of attached sunspaces and the impacts that these may have on the host building. Considerable research has been carried out on the passive benefits of attached sunspaces. Findings suggest that the parameters of the glazed space can be modified to decrease heating and/or cooling requirements in the host building although some studies suggest that without active heat transfer (by a ventilation system, or otherwise) this effect is not large (Hastings, 1981; Swann, 1996). Key parameters seem to include the form, glazing type, level of separation and insulation between host and sunspace, and the amount of thermal mass within the spaces.

Delor (2011) investigated building integrated agriculture focusing specifically on hydroponic rooftop greenhouses and found that a well-insulated office building, with the addition of a well-insulated rooftop greenhouse, could benefit from a 13% decrease in annual heating energy as compared with the identical separated building and greenhouse. In a poorly insulated building, the addition of a rooftop greenhouse saved 41% energy annually. This assumes an active transfer of waste heat from the greenhouse to the office building, and vice versa. Delor also indicates that while green roofs perform better than rooftop greenhouses to prevent heat loss, rooftop greenhouses can be used for both solar heat gains and evaporative cooling.

Also of relevance are studies of the effect of green roofs on the energy performance of buildings. Considerable research in recent years has found that green roofs provide reductions in cooling load and to some degree heating load of buildings through evapotranspiration of plants, and shading from foliage (Jaffal et al., 2012; Niachou et al., 2001).

FIG 1. Lufa Farms greenhouse in Montreal

3. Methodology

A typical six-storey, steel-framed office building in an urban location in Toronto, Canada was used as an example of a host building for this study which used IES-VE energy modelling software to investigate the impact of an agricultural greenhouse, operated year round on the rooftop. The thermal characteristics of the host office building remained the same through all iterations, except for the level of roof insulation between the building and greenhouse. The greenhouse was designed based on the office building roof conditions and geometry, and information from the Lufa Farms greenhouse.

Modelling was carried out using IES Virtual Environment (IES-VE 6.4.0.12) with Toronto climate data. The focus was to evaluate trends in the delivered energy required annually for heating and cooling in both the greenhouse and office building and to gather data on indoor environment. This paper will focus on the following variables:

1. Insulation levels between the top floor of the office building and the greenhouse.
2. Location of insulation below or above the roof slab which affects whether thermal mass of the roof slab is exposed to the greenhouse or to the top floor of the offices.
3. Glazing specifications.

The heating, ventilation and air conditioning (HVAC) systems were separate for each structure to allow for independent simulation of the greenhouse and the office building, and to distinguish to what extent each structure is impacted by their connection.

3.1 Office

A six-storey office building with 1,411 m^2 per floor for a total floor area of 8,467 m^2 was used as the host building. It was assumed to have sufficient structural capacity to support a rooftop greenhouse, have access to unobstructed sunlight, and the addition of a rooftop greenhouse is assumed to comply with zoning limitations. The specifications of the office building were to ASHRAE's Advanced Energy Design Guide (AEDG) for Small to Medium Office Buildings (ASHRAE, 2011).

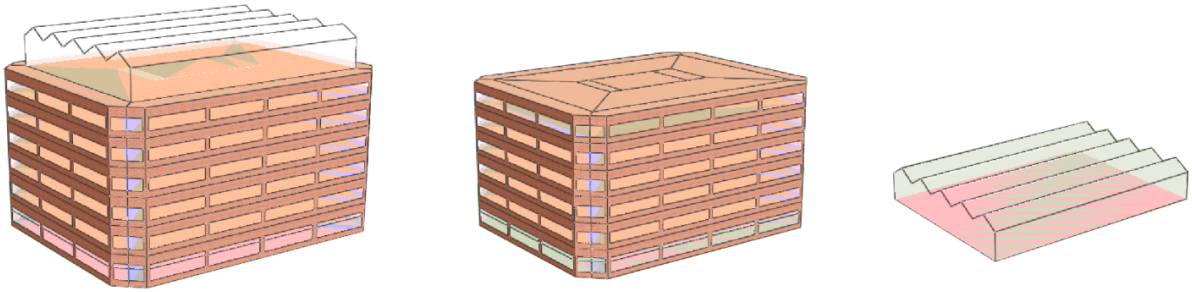

FIG 2. Office building with greenhouse (IES rendering)

The office building was divided into 7 thermal zones per floor, according to the recommendations for zoning set out in the EE4 Modelling Guide (Natural Resources Canada, 2008). Each zone was given internal loads corresponding to their use as laid out in the ASHRAE 90.1 standard, for equipment, lighting, and occupancy (ASHRAE, 2010). The heating system for the office is assumed to be a VAV-reheat with a condensing boiler (90% rated efficiency), and a EWC chiller.

3.2 Greenhouse

The 988m^2 greenhouse was designed to cover the largest possible area of the roof, approximately 70% of the office building roof, to deliver the maximum floor-to-wall-area ratio, in an east-west orientation for maximum solar radiation exposure. It is set back from the edge of the roof to allow for maintenance, some HVAC exits where necessary, and for compliance with fire code (i.e. glazing, in an urban fabric, requires a minimum separation from adjacent buildings).

The greenhouse is a typical Venlo design – multi-span construction with gable roofs – based on the operating rooftop greenhouse of Lufa Farms in Montreal; 4.2 m to the gutter, and an additional 1.5 m to the gable (Figure 3). The geometry was simplified in order to input the design into IES-VE simulation software; a pointed gable roof instead of curved vaults. It is assumed to be heated by a condensing gas boiler (90% efficient) with radiators.

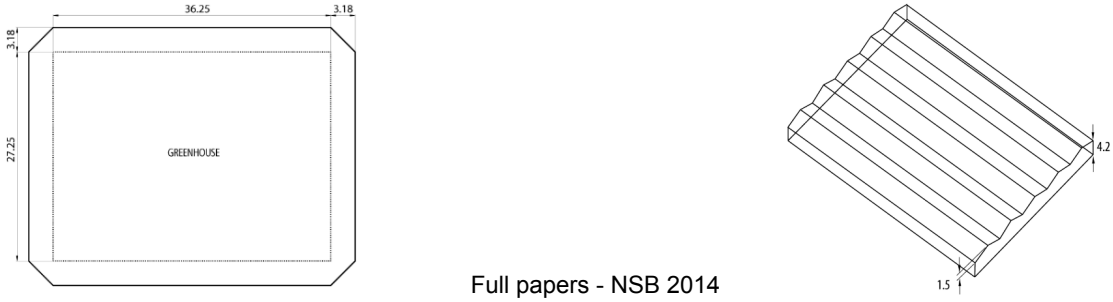

FIG 3. Office roof plan, greenhouse footprint, and axonometric

Shading in a greenhouse by the roof structure is typically between 5-6%, while the structure of the greenhouse accounts for additional 3% shading, therefore the overall vision area of the glass is 91%. Typically glazing for a greenhouse is 4mm tempered single pane glass, which has both high visible transmittance for good crop growth and high impact resistance for durability. This was the base case used in the simulations.

The minimum recommended temperature in a greenhouse is 10°C, however lettuce, tomato and cucumber night temperatures should be in the range of 13-18°C (55-65°F) (Aldrich & Bartok, 1994). Plant development is hinged on the daily average temperature, which is recommended to be around 21°C. Thus, the greenhouse heating set-point temperatures were 22°C during the day in the heating season, 18°C at night (based on those at the Lufa Farms greenhouse). In the cooling season ventilation only was used to try to keep temperatures within the limits acceptable for plants. Due to the poor thermal characteristics of the glass and the lack of active cooling, a certain lack of controllability in the greenhouse was accepted, and it was found that the temperature ranged from 10°C to 38°C. In the summer, temperatures approaching the maximum high are approached on almost a daily basis, while the minimum temperatures (when they fall far below the set-point temperature) are typically only reached a dozen or fewer times in the heating season and indicate that the heating system has trouble adjusting quickly to changing loads.

The basic internal loading was based on ASHRAE 90.1 space-by-space method for 'Active storage', with a moderate equipment and lighting load (ASHRAE, 2010). This moderate loading was recommended to best represent limited equipment use, and periodic task lighting (separate from supplementary crop lighting) (Truyens, 2013).

3.3 Variables

The following variables were investigated:

- Roof insulation- For this variable, the baseline for the thickness of insulation between the office and rooftop greenhouse was taken as RSI 5.28 m^2K/W as recommended by ASHRAE AEDG for Small to Medium Office Buildings. This parameter was varied from RSI 0, 0.88, 1.76, 3.52, 5.28, 7.04, 8.81 and 10.6 m^2K/W.
- Thermal mass - Baseline simulations used roof insulation located on top of the concrete roof slab, thus insulating the thermal mass from the greenhouse space but making it accessible to the office space below. In subsequent simulations this was modified so that thermal mass was incorporated into the greenhouse by modifying the roof assembly of the office building so that the concrete layer was exposed to the rooftop greenhouse with insulation below. This inverted assembly was tested with the same levels of insulation as in the previous roof insulation simulations, except placed below the concrete slab.
- Glazing – The purpose of a greenhouse envelope is to create an interior environment conducive to plant growth, which includes, in a northern climate, both thermal resistance, and high visible transmittance in the range of photo-synthetically active radiation of light (PAR), between 400-700nm. This corresponds closely to the visible spectrum, and therefore translates well to the visible transmittance property of glazing. The visible transmittance of the cover material can vary depending on the light needs of the crop grown in the greenhouse, though many agricultural crops typically grown in greenhouses (lettuce, cucumber, tomatoes) require mid to high light levels to thrive (Aldrich & Bartok, 1994). Ideally, an agricultural greenhouse will have a visible transmittance of 89-90%. In general, single pane horticultural glass is used due to its high light transmission qualities compared to double pane glass despite a large energy penalty. Double pane glass suffers from reduced light transmission both through the glass and resulting from a heavier support structure, resulting in overall reductions of plant

growth and yield. The baseline glazing in the greenhouse in this study was 4mm single-glazing. This was modified to test the effect of increasing the thermal resistance (but reducing light penetration) by using double-glazing, and glazing with low emissivity reflective coatings.

4. Results

The IES predictions of annual space heating and space cooling energy use (on site delivered energy) for the office building and greenhouse were compared, and internal temperatures in the greenhouse were also considered. Conversion to primary energy or resulting carbon emissions were not considered in this study. The predicted baseline simulation for the office heating and cooling energy use was 769 MWh and a total energy use (including appliances, pumps, fans, lighting, etc.) was 1667 MWh/yr or the equivalent of 200kWh/m^2/yr, which compares reasonably with a low energy office in the Toronto location. Commercial greenhouses typically use between 315.4-788.7 kWh/m^2 to maintain temperatures in the heating season, and 3.59-10.76kWh/m^2 over the cooling season (Aldrich & Bartok, 1994). The baseline simulated greenhouse uses 787.9 kWh/m^2 for heating, and 4.9 kWh/m^2 for ventilation.

4.1 Roof insulation

The results show the simulation with the lowest total annual heating and cooling energy for the office and greenhouse combined is achieved when there is no insulation in the office roof below the greenhouse (Table 1). Additionally, in this simulation, the maximum temperature in the greenhouse is shown to be lowest while the minimum temperature is highest of all the simulations. This suggests that there are benefits from thermal integration of the spaces. However, the variation is small and within the accuracy of the modelling. Nevertheless, this suggests that integration of the systems should be further investigated.

The trend in energy consumption in the greenhouse may also be explained by the effect of thermal mass: the simulation with no insulation separating the greenhouse from the office building leaves the 100mm concrete roof deck exposed to the interior of the greenhouse. When insulation is added above the deck, the thermal resistance isolates this mass from the space and so solar gains into the greenhouse become less useful. This highlights the importance of thermal mass in a highly glazed space. This also explains the trend of increasing heating consumption in the greenhouse (as the thermal mass is covered up), which levels out with resistances higher than RSI 1.76 m^2K/W in the separation. This phenomenon is discussed and tested further below.

The simulations for RSI 1.76 and 3.52 m^2K/W experienced instability and the only solution was to run the simulations using a much shorter time-step between calculations; 2 minutes and 6 minutes for RSI 1.76 and 3.52 m^2K/W respectively, instead of the typical 10 minutes. The annual results when run at a shorter time step tend to be higher therefore the results from these two simulations are less comparable to the other six points. It remains, however, that there is a trend towards higher heating and cooling energy consumption as insulation is added on top of the office roof.

TABLE 1. Effect of roof insulation (insulation above the slab), baseline simulation highlighted

	Office			Greenhouse						
Insulation level (m^2K/W)	**Annual space heating (kWh/y)**	**Annual space cooling (kWh/y)**	**Total (kWh/y)**	**Annual space heating (kWh/y)**	**Annual vent (kWh/y)**	**Total (kWh/y)**	**Total system (kWh/y)**	**max. temp (°C)**	**Min. temp (°C)**	**Hours above 30°C**
RSI 0	683,427	67,212	750,639	830,798	3,288	834,086	1,584,725	35.34	16.91	306
RSI 0.88	685,645	50,441	736,086	874,670	4,780	879,450	1,615,536	37.82	13.96	581
RSI 1.76	697,230	49,878	747,108	896,869	4,582	901,451	1,648,559	38.15	13.53	451
RSI 3.52	687,706	46,851	734,557	892,538	4,857	897,395	1,631,952	38.39	13.19	571
RSI 5.28	684,635	45,816	730,451	885,886	5,064	890,950	1,621,401	38.44	13.05	635
RSI 7.04	684,251	45,563	729,814	884,826	5,114	889,940	1,619,754	38.51	12.99	628
RSI 8.81	684,151	45,337	729,488	883,998	5,125	889,123	1,618,611	38.53	12.96	642
RSI 10.6	684,306	44,955	729,261	884,070	5,138	889,208	1,618,469	38.55	12.94	646

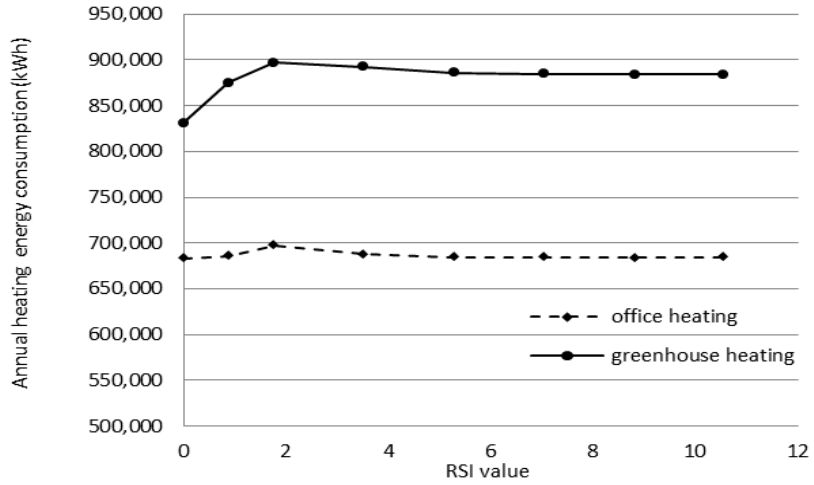

FIG 4: Effect of insulation in the roof between office space and greenhouse on the annual heating energy of office and greenhouse

Despite wide variations in roof insulation level, the office building does not differ in annual heating energy by more than 1%, (when the simulations with 1.76 and 3.52 m^2K/W insulation results are discounted because of instability in the simulation model). Even when those simulations are included, the variation is not more than 2% (Figure 4). This indicates that even when no insulation is present in the separation (and since the greenhouse envelope itself has little resistance), some property of the greenhouse must be providing a measure of thermal performance similar to additional insulation. This is likely due to the buffer effect as described by Swann (1996). As insulation in the roof increases the annual cooling energy in the office building decreases, while the greenhouse ventilation energy increases and the number of hours of extreme temperature also increase. This suggests that as the two structures decrease in thermal connection, the office building needs less cooling in order to compensate for the additional heat provided by the greenhouse, while the greenhouse begins to struggle to maintain acceptable temperatures particularly in the cooling season.

4.2 Thermal mass

As discussed previously, it appears that thermal mass in the greenhouse is a significant factor in the total annual heating/cooling load. The roof insulation simulations show lower total energy

consumption when the roof assembly incorporated no insulation on top of the roof slab allowing the thermal mass to be exposed to the greenhouse and the office space.

Further simulations (Table 2, Figure 5) included insulation in increasing thicknesses below the slab, thus providing increased isolation from the office but more effective use of mass for the greenhouse. These simulations show further benefit to the overall building energy use by added insulation below the slab. In contrast with the simulations reported above where insulation was above the roof slab, insulation placed below the slab marginally reduced the office annual energy use with increased RSI, and reduced greenhouse annual energy use. Thus overall energy use was reduced. However, the increased separation between the spaces led to an increase in the number of hours of extreme temperature in the greenhouse.

TABLE 2. Effect of thermal mass (insulation below the roof slab)

	Office			Greenhouse			Greenhouse			
Insulation level (m^2K/W)	Annual space heating (kWh/y)	Annual space cooling (kWh/y)	Total (kWh/y)	Annual space heating (kWh/y)	Annual ventilation (kWh/y)	Total (kWh/y)	Total system (kWh)	Max. temp (°C)	Min. temp (°C)	Hours above 30°C
RSI 0	683,427	67,212	750,639	879,572	4,051	883,623	1,584,725	35.34	16.91	306
RSI 0.88	687,399	50,813	738,212	820,036	5,002	825,038	1,526,811	36.02	16.56	440
RSI 1.76	703,741	51,412	755,153	799,020	5,154	804,174	1,547,850	36.1	16.64	335
RSI 3.52	687,212	46,473	733,685	782,515	5,235	787,750	1,509,255	36.21	16.53	470
RSI 5.28	686,809	45,904	732,713	776,482	5,311	781,793	1,506,666	36.25	16.47	470
RSI 7.04	687,270	45,711	732,981	772,555	5,379	777,934	1,506,015	36.27	16.51	471
RSI 8.81	687,540	45,450	732,990	769,931	5,362	775,293	1,505,191	36.28	16.49	470
RSI 10.6	687,565	45,164	732,729	768,555	5,384	773,939	1,504,457	36.29	16.49	474

N.B.: Again, there were problems with the simulation with RSI 1.76 m^2K/W insulation because of instability in the software

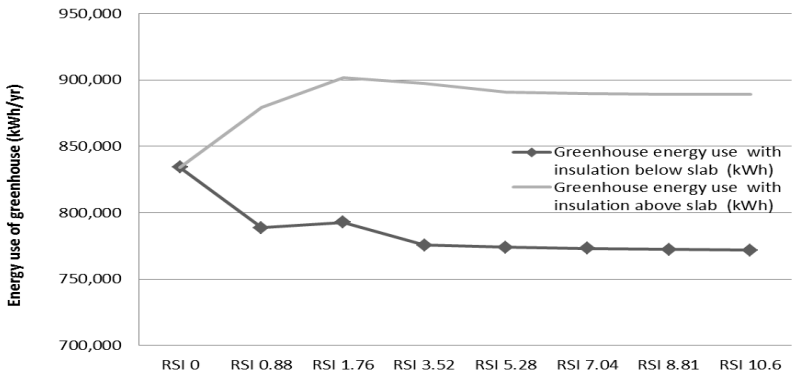

FIG 5: Annual energy required to heat and ventilate the greenhouse with insulation under the slab and over

4.3 Glazing

The results in Table 3 show, as expected, that as the U-value of the glazing decreases in the greenhouse, the annual heating energy also decreases significantly, while ventilation in summer increases marginally. This is consistent with the effect shown by Scott (2011) wherein an improved greenhouse envelope resulted in a lower heating requirement than single glazing. This confirms that glazing with better thermal resistance retains more of the heat, reducing the energy required for

heating. However, summer conditions lead to more overheating. The maximum greenhouse temperatures are highest with the best envelope (double glazed, low-e), consistent with the simulation of attached sunspaces done by Mihalakakou & Ferrante (2000). It is beyond the scope of this work to assess the reduced lighting impacts on the plants.

TABLE 3. Effect of greenhouse glazing envelope variations (office floor insulation RSI 5.28 m2/WK above the slab)

	Office			Greenhouse					
Greenhouse envelope glazing	Annual space heating (kWh/y)	Annual space cooling (kWh/y)	Total (kWh/y)	Annual space heating (kWh/y)	Annual ventilation (kWh/y)	Total (kWh/y)	Max. temp (°C)	Min. temp (°C)	Hours above 30°C (hrs)
single	685,623	46,045	731,668	883,634	5,094	888,728	38.44	13.05	635
single low-e	679,629	45,912	725,541	579,115	6,225	585,340	39.45	14.42	830
double	681,732	45,920	727,652	515,686	6,373	522,059	39.52	11.34	841
double low-e	681,577	45,849	727,426	433,861	6,821	440,682	39.74	8.56	898

Insulation in this scenario is above the roof deck; in retrospect, taking into account the implications of the thermal mass investigation, this insulation may be better placed below the roof deck, exposing the concrete layer's thermal mass to the greenhouse which may mitigate the additional cooling loads.

The issue of condensation is not addressed here and should be explored in future research as the simulation software gave preliminary indications of condensation on the greenhouse envelope, which can significantly reduce light transmission to plants in the greenhouse. Exploring other possible envelope systems including the numerous plastics available would be a logical next step, investigating combinations of high thermal resistance, and high transmittance. Plastic envelopes may have additional benefits because of their light-weight, although they are often less durable than glass.

5. Conclusions

This investigation of the performance of a rooftop greenhouse on an office building highlighted several key factors that affect energy and thermal performance. The first issue is the importance of thermal mass in the greenhouse. This is consistent with other studies on greenhouse or sunspace performance and suggests that integration of thermal mass can reduce heating and cooling loads and hours of extreme temperatures. Thus, insulation below the roof slab is preferable as this allows the slab to be thermally active within the greenhouse. Secondly, the glazing specification has the most significant effect on energy use. The energy use of a typical single glazed greenhouse can be reduced by 50% through the use of higher performance glazing. Although this will reduce visible light penetration, it may be possible that other benefits such as reduced condensation on the glass will to some degree compensate. These issues need to be investigated further.

Thus, it appears from the simulation results that the best performing rooftop greenhouses (i.e. with the lowest annual energy requirement for heating and cooling in the office building and greenhouse) will have a high thermal resistance greenhouse envelope and incorporate thermal mass in the greenhouse. With thermal mass present, the performance continues to improve as the level of insulation below the concrete roof slab is increased. Though it requires additional investigation, further improvement might be achieved by developing a separation with thermal mass facing both the office and the greenhouse, with insulation as an interior layer.

This study did not consider the potential of integrating HVAC systems of the greenhouse and office building, which may offer further benefits, particularly if the greenhouse can be used as a solar collector to warm air used for ventilation of the offices in the shoulder season, or if the expelled air

from the office HVAC can be used in the greenhouse. This may have additional benefit for plant growth as higher CO_2 concentrations can increase plant growth rates.

References

Aldrich, R. A., & Bartok, J. W. 1994. Greenhouse Engineering. Ithaca: Natural Resource, Agriculture and Engineering Service.

ASHRAE .2010. ASHRAE 90.1-2010 (I-P edition). Atlanta: American Society of Heating, Refrigerating and Air-Conditioning Engineers.

ASHRAE .2011.. Advanced Energy Design Guide for Small to Medium Office Buildings. Atlanta: American Society of Heating, Refrigerating and Air-Conditioning Engineers.

Astee, L. Y., & Kishnani, N. T. 2010.. Building integrated agriculture: Utilising rooftops for sustainable food crop cultivation in Singapore. Journal of Green Building, 5(2), 105-113.

Delor, M. 2011. Current state of Building-Integrated Agriculture, its energy benefits and comparison with green roofs - Summary. Sheffield: University of Sheffield.

Gorgolewski, M. Komisar, J. & Nasr, J. 2011. Carrot City: Creating places for urban agriculture, New York, Monacelli Press.

Hastings, S. R. 1981. Analysis of an attached greenhouse in a low isolation northern climate. Proceedings of the American Section of the International Solar Energy Society, Portland, Oregon , 6 251-255.

Jaffal, I., Ouldboukhitine, S., & Belarbi, R. 2012. A comprehensive study of the impact of green roofs on building energy performance. Renewable Energy, 43, 157.

MacRae, R., Gallant, E., Patel, S., Michalak, M., Bunch, M., & Schaffner, S. 2010. Could Toronto provide 10% of its fresh vegetable requirements from within its own boundaries? Matching consumption requirements with growing spaces. Journal of Agriculture, Food Systems, and Community Development, 1(2), 105-127.

Natural Resources Canada. 2008. EE4 Software, Version 1.7 - Modelling Guide. Retrieved from http://canmetenergy.nrcan.gc.ca/sites/canmetenergy.nrcan.gc.ca/files/files/pubs/EE4-English-2008-02-01.pdf

Niachou, A., Papakonstantinou, K., Santamouris, M., Tsangrassoulis, A., & Mihalakakou, G. 2001. Analysis of the green roof thermal properties and investigation of its energy performance. Energy and Buildings, 33(7), 719. doi:10.1016/S0378-7788(01)00062-7"

Rodriguez, O. 2009. London Rooftop Agriculture: a preliminary estimate of London's productive potential. (Unpublished MArch). Cardiff University, Cardiff.

Rathmell, L. 2013. personal communication, July 22,

Swann, B. 1996. Establishing design criteria for the incorporation of highly glazed spaces into the domestic building envelope. (PhD, Cranfield University).

Truyens, T. 2013. personal communication, May 28, 2013

EU Maps of Climate Related Building Performances using State-Space Modeling

A.W.M. (Jos) van Schijndel
Eindhoven University of Technology, Netherlands

KEYWORDS: *Climate, Map, State-Space, Building, Performance, Future*

SUMMARY:
Performances of building energy innovations are most of the time dependent on the external climate conditions. This means a high performance of a specific innovation in a certain part of Europe, does not imply the same performances in other regions. The mapping of simulated building performances at the EU scale could prevent the waste of potential good ideas by identifying the best region for a specific innovation. This paper presents a methodology for obtaining maps of performances of building innovations that are virtually spread over whole Europe. It is concluded that these maps are useful for finding regions at the EU where innovations have the highest expected performances.

1. Introduction

Due to energy efficiency, there exist a lot of studies on innovative buildings systems. The performances of these innovations are mostly very dependent on the external climate conditions. This also means that a high performance of a specific innovation in a certain part of Europe does not imply the same performances in other regions. Similar, innovations that did not perform very well due to local climate conditions, and therefore not commercialised, could still perform quite well in other climates. The latter can be seen as 'wasted' innovations. The mapping of simulated building systems performances at the EU scale could prevent this wasting of potential good ideas by identifying the best region for a specific innovation. This paper presents a methodology for obtaining maps of performances of building systems innovations that are virtually spread over whole Europe. This approach is based on previous research and literature: The model development, including State-Space models is presented in Kramer et al. (2012 & 2013). The use of Meteonorm (2013) climates files for generating maps is shown in van Schijndel& Schellen (2013). The computational tool HAMLab (2013) originating from van Schijndel (2007) was used to implement all models and climates. Finally the future climate files originates from the Regional Climate Model REMO by Jacob et al. (1997) and will become public available from July 2014 at the Max Planck Institute for Meteorology (2013).

The methodology consisted of (1) State-Space model development; (2) Validation with step-change experiments; (3) Simulation of one external climate; (4) Performance indicators; (5) Parameter study; (6) Mapping of using current external climates over the EU.

The above mentioned methodology covers a wide range of topics. Due to the length limitation of this paper, it is very difficult to provide all details for each topic. We try to focus on the most significant aspects taking the complete methodology into account. More details can be found in the references.

The next Section 2 demonstrates the method using a commercial case study. Section 3 presents a generalization of this approach by the development of a computational tool for simulation of performances using SS models and future climates. Section 4 provides the discussion and conclusions.

2. The simulated performance of a thermal active wall

A commercial case study is presented in this Section. Due to the patent protection of the industrial partner, some specific information is omitted without loss of generality. The innovation consists of a novel heat exchanger built inside a construction acting as a solar collector.

2.1 Modeling, validation and climate based performance

Figure 1 shows the principle construction of the solar collector (in reality this is much more complicated) and the involved mathematical model in the form of ordinary differential equations and State Space. The solar collector will be used for the heating of water that directly can be used or stored for later use.

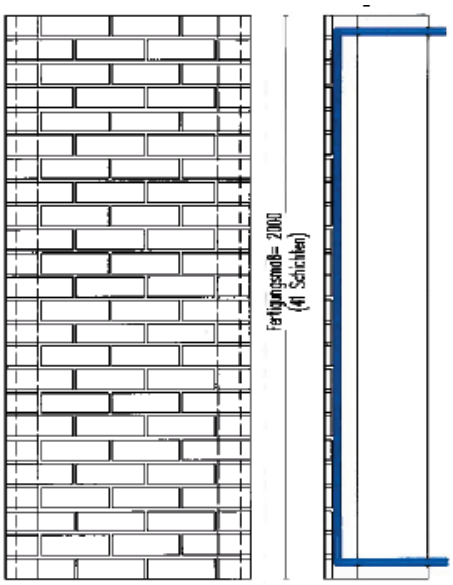

$$C_1 \frac{dT_1}{dt} = h\,A(\mathrm{Tamb(t)} - \mathrm{T_1}) - \frac{(\mathrm{T_1} - \mathrm{T_2})}{\mathrm{R_1}} + \mathrm{a_I\,A\,I(t)}$$

$$C_2 \frac{dT_2}{dt} = \dot{\mathrm{m}}\,\mathrm{c}\,(\mathrm{Tsup(t)} - \mathrm{T_2}) + \frac{(\mathrm{T_1} - \mathrm{T_2})}{\mathrm{R_1}} - \frac{(\mathrm{T_2} - \mathrm{T_3})}{\mathrm{R_2}}$$

$$C_3 \frac{dT_3}{dt} = \frac{(\mathrm{T_2} - \mathrm{T_3})}{\mathrm{R_2}}$$

Figure 1. Construction of the solar collector (Left), the model representation in ODEs (Right)

Where *Inputs* Tamb(t) = ambient (external) air temperature [^{o}C]; Tsup(t) = water supply temperature [^{o}C]; I(t)= external solar irradiance [W/m^2]; *States* T_1= external surface temperature [^{o}C]; T_2 = water return temperature [^{o}C]; T_3 = internal wall temperature [^{o}C]; *Parameters:* mdot = water mass flow [kg/s]; c = heat capacity of water [J/kgK] ; a_I = solar absorption factor [-];h = heat transfer surface coefficient [W/m^{2o}C]; A = surface [m^2]; d1 = distance pipe to surface [m]; d2 = distance pipe to insulation [m]; k = heat conductivity of concrete [W/mK]; R_1 = heat resistance [K/W] = d1/(kA); R_2 = heat resistance [K/W] = d2/(kA) ; C_i = heat capacity [J/ K];

The model was implemented using standard state-space modeling facilities of MatLab. State-space models (see for example Kramer et al. (2012 & 2013)) contain variables and matrices. Regarding the variables: We have 3 variables: the state vector x, the input vector u and the output vector y. For the ODEs of Figure 1 this means that, x=[T_1;T_2;T_3], u=[Tsup(t); Tamb(t); I(t)] and we chose y=x. Regarding the matrices: **A**,**B**,**C**,**D** can be calculated as shown in Figure 2 by using dx/dt = **A**x + **B**u and y = **C**x + Du. To simulate state-space models in MatLab, two commands are important: (I) creating a state-space system from the matrices: G=ss(A,B,C,D); (II) simulate the system (G) using input data u, time steps t and start values for x: lsim(G,InputData,t,Startvalues).

```
A=[ -(hA+1/R1)/C1   1/(R1*C1)                    0
    1/(R1*C2)    -(mdot*c+1/R1+1/R2)/C2     1/(R2*C2)
    0              1/(R2*C3)                -1/(R2*C3) ];

B=[ 0           hA/C1  aTA/C1
    mdot*c/C2   0      0
    0           0      0];

C=eye(3);

D=[0 0 0
   0 0 0
   0 0 0];

G=ss(A,B,C,D);

lsim(G,InputData,t,Startvalues);
```

Figure 2. The state space representation and simulation in MatLab

The next part shows the simulation and validations results. Laboratory experiments were used to validate the models. All experiments were simulated using the proper parameters and boundary conditions. The results were compared in order to evaluate the predictability of the model. In Figure 3 (Left) the results for a typical experiment, labeled A, is shown.

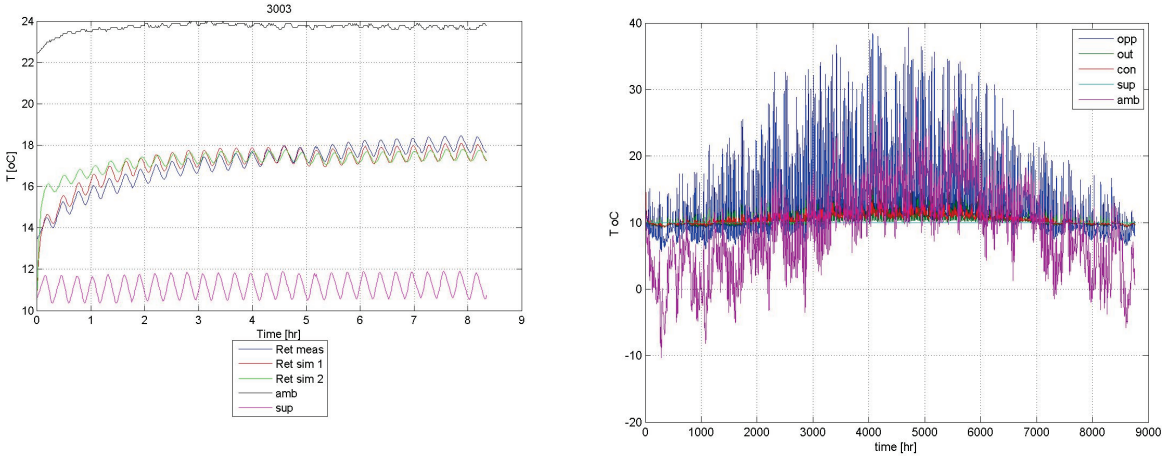

Figure 3. Temperatures vs time Left: Validation experiment A: The measured supply water(sup), the measured ambient air (amb), the simulated return water (Ret sim 1 & 2) and the measured return water (Ret). Right: Simulation of configuration A using a reference standard Dutch climate of deBilt. including the external wall surface (opp), the water return (out), the mid wall (con),

From Figure 3 left we observed that the predictability of model was satisfactory. All other tested configurations provided similar good results. Therefore we conclude that the model is quite usable for further use. The model configuration A was simulated using a reference standard Dutch climate of de Bilt. Figure 3 right presents the result. The water supply temperature was constant held at 10 ^{o}C. The other two input signals: Ambient air temperature and solar irradiation were taken from the climate file. The main output signal is the return temperature (out). With this signal the output power can be calculated. This is shown in the next Section. Figure 4 shows details of the model A configuration performance results

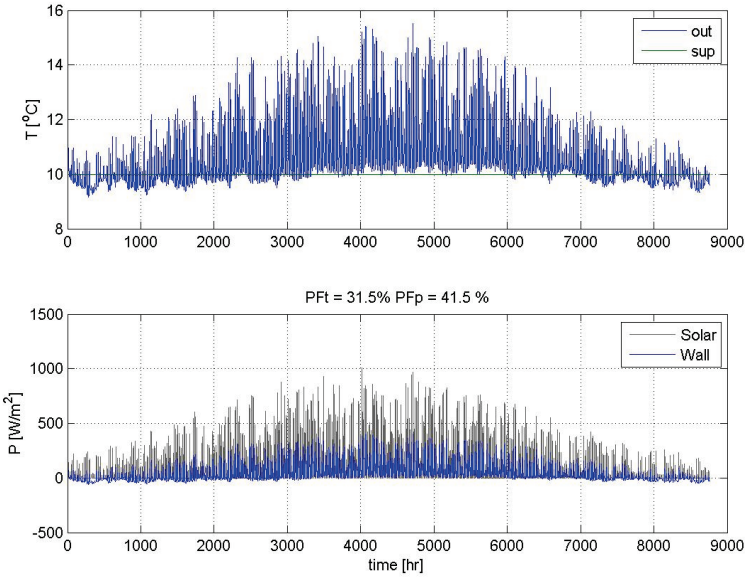

Figure 4. Performance evaluation. Top: The simulated supply and return water temperatures versus time. Bottom: The heat flux [W/m^2] of the incoming solar irradiation (Solar) and simulated output flux of the wall. 31.5 % of the year the wall system can be operated (PFt) The yearly mean efficiency is 41.5 % (PFp).

The output flux Pout is calculated by: Pout(t) =mdot*c*(Tret(t)-Tsup(t))/A [W/m^2]; The overall performance is evaluated as follows: Firstly, P50(t) is defined as Pout(t) with a threshold of 50 W/m^2. Below 50W/m^2, the water return temperature drops below 10.7 ^{o}C and the wall system is too inefficient. For these values P50(t) = 0. Secondly, two performance (PF) indicators are defined as follows: PFt = Percentage of time of Pout(t) above threshold of 50 W, i.e. percentage of time of possible operation [%]. PFp = 100* sum(P50(t)) / sum(I(t)) , i.e. the yearly mean efficiency [%]. From Figure 4 it follows for configuration A, PFt=31.5% and PFp=41.5%.

2.2 Parameter study

The following parameters were varied for the parameter study:

* The distance from the pipe to the surface (default 35 mm) was varied: 20, 35 and 50 mm.

* The mass flow (default 1 kg/min) was varied: 0.5, 1 and 2 kg/min.

The results are shown in Table I and II.

Table I. Efficiency Performance

Simulated yearly mean efficiency PFp [%]			
	d=20 mm	d=35 mm	d=50 mm
MF=0.5 kg/min	30.6	24.7	20.2
MF= 1 kg/min	39.0	30.9	25.2
MF= 2 kg/min	44.3	34.8	28.0

Table II. Operation Time Performance

Simulated Operation time PFt [%]			
	d=20 mm	d=35 mm	d=50 mm
MF=0.5 kg/min	29.8	26.5	23.7
MF= 1 kg/min	33.1	29.5	26.5
MF= 2 kg/min	34.5	30.9	27.7

The optimal efficiency performance for a Dutch climate is 44.3% with the accompanying mass flow of 2 kg/min and pipe depth of 20 mm.

2.3 EU Mapping of the standard configuration

By replacing the Dutch climate with the climates of weather stations presented in Figure 3, it is quite easy to simulate the response of the system to each external climate. From the responses the performance indicators can be calculated (See previous Section). The results of the standard wall performances are shown in Figure 5. These results are still based on the standard wall configuration A.

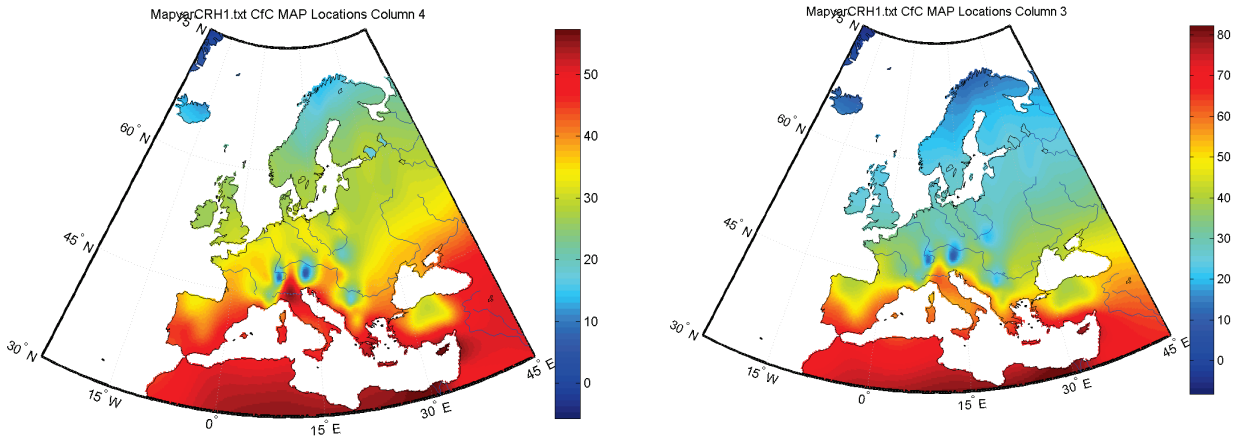

Figure 5. Left: Efficiency (PFp) of the standard wall configuration. Right: Percentage of time operation (PFt) of the standard wall configuration.

2.4 Simulation of optimized wall configurations

All nine configurations of the parameter study (see Table II and III) were also simulated on the EU scale. For each weather station the best configuration out of nine was selected. These optimized wall configuration performances are presented in Figure 6

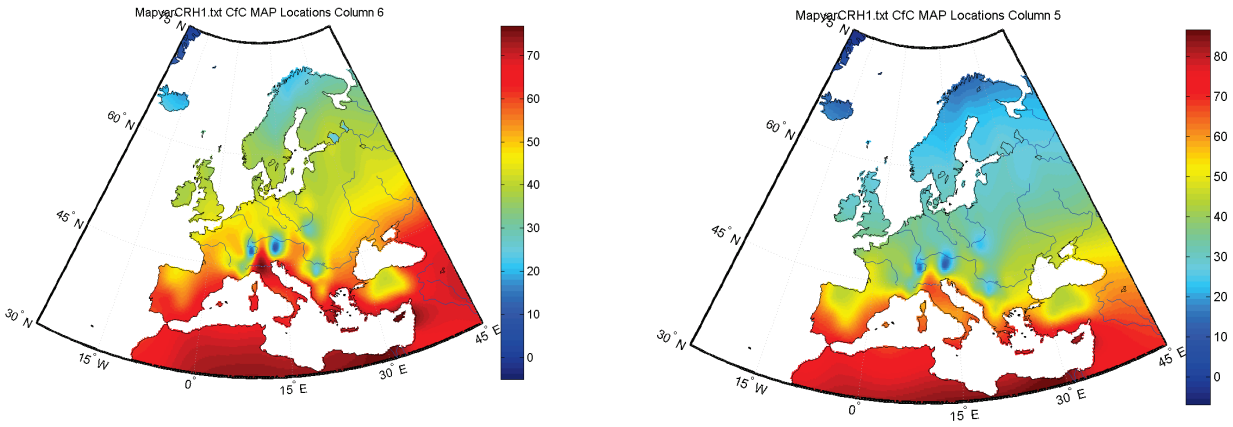

Figure 6. Left: Optimized wall configuration Efficiency (PFp). Right: Optimized wall configuration Percentage of time operation (PFt).

From Figure 6 left, it can be seen that large parts of Europe have efficiencies of at least 45%. From Figure 6 right, it can be seen that the areas near the Mediterranean have percentages of time of operation above 60%. The latter means that the wall collector is also operational during parts of the night.

3. Towards a tool for State-Space model simulations with Future Climate

One of the benefits of simulating State-Space (SS) models is its outstanding computational efficiency. To illustrate this: It takes longer to plot the maps of figures 5&6 than simulating them. Due to this excellent computational performance a practical tool for general purpose of simulating SS models using hourly based future climates is developed and will be public available together with the availability of the future climate files by the REMO model (2013).

3.1 How to use future hourly-based climate files for building simulation

The EU-FP7 project Climate for Culture (2013) is one of the first projects where high resolution EU future climate files where used for building simulation. Due to the stochastic behaviour and the time scale of about 250 years of the REMO climate model, it is recommend use three 30-year-periods for comparison purposes: „Recent Past“ (1960 – 1990), „Near Future“ (2020 – 2050) und „Far Future“ (2070 – 2100). An example from Winkler (2013) is shown in Figure 7. The left part shows the mean indoor temperature from the recent Past of a reference building. To compare this with the Near Future, the Near Future was simulated and the recent Past was subtracted. This generates the middle figure Past to Recent Future. Similar the figure on the right Past to Far Future was obtained. The reader should notice that from the experiences of the above mentioned project, it was concluded that the one-year-periods includes too much noise to be useful for analyzing and comparing purposes.

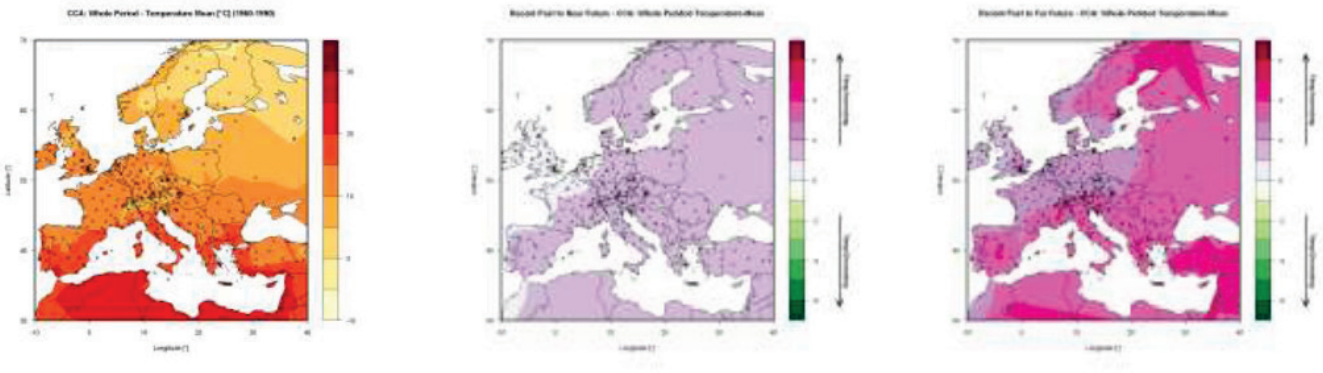

Figure 7. An example of the use of 30-year periods for comparison purposes of the indoor temperature of a reference room: Left: Recent Past, Middle: Past to Near fur, Right: Past to Far Future from Winkler (2013)

3.2 Current mapping visualisation tool

A MatLab mfile was developed for visualisation of EU maps. The input of this tool is in a single text file with performances related to longitudes and latitudes of the locations of the climate files. An example is shown in Figure 8. Here, over 130 external hourly based climate files were produced using commercially available software (Meteonorm 2013) using the so-called wac format. Figure 8 presents the distribution of the locations over Europe.

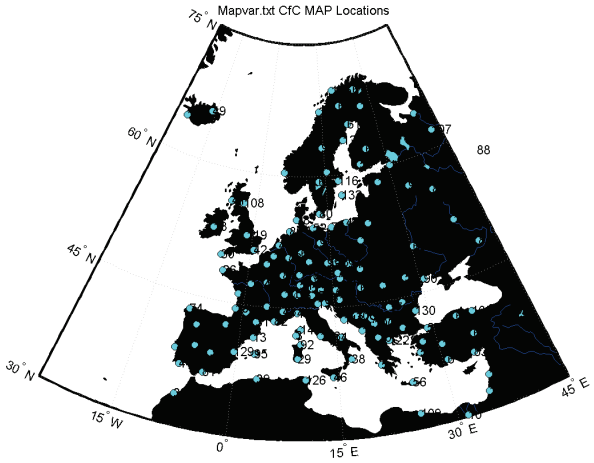

Figure 8. The distributions of the locations of the external climates in Europe.

Each climate file includes hourly based values for the common used external climate parameters: Horizontal global solar radiation [W/m^2] (ISGH), Diffuse solar radiation [W/m^2] (ISD), Cloud cover [0-1] (CI), Air temperature [^{o}C] (TA), Relative humidity [%] (HREL), Wind speed [m/s] (WS), Wind direction [0-360°] (WD), Rain intensity [mm/h] (RN), Long wave radiation [W/m^2] (ILAH). Each can be used as input file to simulate building energy performances for location. For the exact details of this mfile, we refer to the HAMLab website (HAMLab 2013).

3.3 State-space modeling and simulation tool

MatLab has been a very successful modeling tool for simulating state space systems over the last 20 years. For a recent built environment application, we refer to Kramer (2013).

4. Discussion and Conclusions

4.1 EU performance of the solar collector

Large parts of Europe have solar collector efficiencies of at least 45%, the exact details are provided in Figure 6. Furthermore, areas near the Mediterranean have percentages of time of operation above 60% (exact details are shown in Figure 6). The latter means that the solar collector is even operational during parts of the night. It is concluded that this study shows that the solar collector could be applicable in large parts of Europe. However, the reader should notice that the solar collector simulation results in this study are based on two assumptions: The supply water temperature is constant at 10 ^{o}C and all heat produced by the wall collector is usable at any time. Under most circumstances this is not very realistic. Therefore it is recommended to include buildings, systems and controllers details into the modeling for more realistic performance simulations and design of promising integrated configurations.

4.2 State-Space modeling tool using Future Climates

The main three work packages: (1) State-space modeling and simulation; (2) Getting reliable future hourly based climate data over the EU and appropriate use of them; (3) Visualisation of maps, are all implemented in MatLab. The complete tool, including climate files, will become public available after the official ending of the Climate for Culture project (2013). This is expected at July 2014.

References

Climate for Culture (2013), http://www.climateforculture.eu/ (accessed Nov 2013)

HAMLab (2013), http://archbps1.campus.tue.nl/bpswiki/index.php/Hamlab (accessed Nov 2013)

Jacob, D. and Podzun, R. (1997). Sensitivity studies with the Regional Climate Model REMO. *Meteorology and Atmospheric Physics*, 63, pp 119-129.

Kramer, R.P., Schijndel, A.W.M. van & Schellen, H.L. (2012). Simplified thermal and hygric building models : a literature review. *Frontiers of Architectural Research,* 1(4), 318-325.

Kramer, R.P., Schijndel, A.W.M. van & Schellen, H.L. (2013). Inverse modeling of simplified hygrothermal building models to predict and characterize indoor climates. *Building and Environment*, 68, 87-99.

Max Planck Institute for Meteorology (2013), www.mpimet.mpg.de (accessed Nov 2013)

Meteonorm (2013). http:/meteonorm.com (accessed Nov 2013)

Schijndel A.W.M. van (2007). Integrated Heat Air and Moisture Modeling and Simulation, PhD Dissertation, Eindhoven University of Technology

Schijndel, A.W.M. van & Schellen, H.L. (2013). The simulation and mapping of building performance indicators based on European weather stations. *Frontiers of Architectural Research*, 2, 121-133.

Winker, M. (2013), Development of an automated damage risk assessment method for the evaluation of the climate change impact on historic buildings and their interior in Europe MSc thesis TU Munich.

Monitoring-based dynamically updated occupancy models for predictive building systems control

Farhang Tahmasebi
Matthias Schuß
Ardeshir Mahdavi

Department of Building Physics and building Ecology,
Vienna University of Technology, Vienna, Austria

KEYWORDS: *Probabilistic occupancy models, predictive building systems control, evaluation statistics*

SUMMARY:
Knowledge of occupants' presence and behavior in buildings is of central importance to the implementation efforts concerning predictive building systems control. Specifically, prediction of occupants´ presence in office buildings represents a necessary condition for predicting their interactions with building systems. Implementation of occupancy prediction models in existing buildings can benefit from available occupancy monitoring data. In the present contribution, we focused on the evaluation of monitoring-based probabilistic occupancy models of a single-occupancy office, which are intended to be used for predictive room control. Thereby, we examined various scenarios to process the monitoring occupancy data obtained from this office toward developing stochastic occupancy models. These scenarios differ in terms of the duration and horizon (moving versus static) of the training intervals, as well as the grouping of the week days. To evaluate the stochastic occupancy models, we performed a Monte-Carlo study. Toward this end, a number of evaluation statistics were defined and the monitored and predicted daily profiles of occupancy were compared for individual days as units of observation to obtain the statistics. The results facilitate a discussion of the potential and limitations of occupancy models intended for incorporation in the control logic of buildings.

1. Introduction

Occupants influence thermal behavior of buildings due to their presence (e.g., via releasing sensible and latent heat), and via operation of control devices such as windows, shades, luminaries, radiators and fans (Mahdavi 2011). Specifically, knowledge of occupants´ presence represents a necessary condition for the development of predictive control action models. Performance simulation tool users typically deploy libraries of diversity factors and schedules to represent occupants' presence in buildings. These diversity profiles are derived from long term monitored data in different classes of buildings and are usually included in the simulation packages to facilitate the creation of building performance models. Obviously, in cases where the available information about the building in question differs from the default profiles, the modeler can modify these diversity factors and schedules. More recently, efforts are being made in the scientific and professional communities to develop probabilistic models that would capture the randomness of occupants' presence. As one of the first attempts, Newsham et al. (1995) considered the probabilistic nature of occupancy while developing a stochastic model to predict lighting profiles for a typical office. Their model deployed the probability of first arrival and last departure as well as the probability of intermediate leaving and returning. Reinhart (2001) further developed this model by using the inverse transform method (Zio 2013) to generate samples from the distribution functions of arrival and departure times. Moreover, days were divided into three phases (morning, lunch and afternoon) for which the probabilities of start

time and length of breaks were computed. Page et al. (2008) proposed a generalized stochastic model for the simulation of occupants' presence using the presence probability over a typical week and a parameter of mobility (defined as the ratio of state change probability to state persistence probability). They also included long absence periods (corresponding to business trips, leaves due to sickness, holidays, etc.) as another random component in their model.

In all these studies, monitored data has been used to derive a probabilistic model that generates random non-repeating daily profiles of occupancy for a long-term (e.g. annual) building performance simulation. Hence, models are suggested to perform well, if the entire set of generated random realizations of the daily occupancy profiles agrees in tendency with the monitored data over the whole simulation period. However, the synchronicity of these realizations with the monitored data (one-to-one agreement of the generated and monitored daily profiles) is not taken into consideration. Even in the case of considering long absences (Page et al. 2008), the unoccupied days are scattered randomly through the year and they do not necessarily match the dates of absences in the measured data. Thus, these practices cannot be said to "validate" the proposed models, if the actual day-to-day prediction of occupancy and control action probabilities are to be considered. Specifically, in a run-time use of a simulation model in building operation phase, where short-term predictions of occupancy and weather data are incorporated in the model to predict the future performance of the building, the agreement between the predicted and real future occupancy profiles in each day is of utmost importance.

Moreover, most of the work on validating the probabilistic occupancy models has focused on comparing the model outputs with the very set of data which has been used to derive the model. In contrast, Liao et al. (2010) used a fraction of data for calibration and the rest of the data for the validation of an agent-based occupancy model. In our view, a scientifically sound model evaluation approach must clearly separate the data segments used for model development and model validation. This is especially important while evaluating the predictive potential of an occupancy model, which is intended to be used for model-predictive control in buildings.

In the present study, we focus on evaluation of a stochastic model of occupants' presence to explore the potential of using past monitored data in predicting future presence of occupants. Toward this end, we selected a university campus office area, which is equipped with a monitoring infrastructure and includes a number of open and closed offices. For the purpose of this case study, we deploy long-term monitored occupancy data obtained from one office. Thereby, separate sets of monitored data are used to derive and validate the model. We examine various options to use monitored occupancy data toward developing occupancy models and we use a number of evaluation statistics to evaluate the model predictions. Thus, the results facilitate a discussion of the potential and limitations of occupants' presence models intended for incorporation in the control logic of existing buildings.

2. Approach

2.1 Overview

In this contribution, we derive and evaluate a probabilistic model of occupant's presence which is to provide predictions of daily occupancy profiles for predictive control of the building. We utilize monitored occupancy data obtained from a single-person office in Vienna University of Technology based on different scenarios to derive a stochastic occupancy model. To evaluate the model we use a number of statistics and a separate set of monitored occupancy data. Conducting a Monte Carlo simulation we evaluate the predicted daily occupancy profiles generated by the stochastic model and obtain the distribution of the statistics to discuss the reliability of predictions.

2.2 Data collection

To obtain occupancy data, wireless ceiling-mounted sensors (motion detectors) were used. The internal microprocessors of the sensors are activated within a time interval of 1.6 minutes to detect

movements. The resulting data log entails a sequence of time-stamped occupied to vacant (values of 0) or vacant to occupied (values of 1) events.
To facilitate data analysis, the event-based data streams were processed to generate 15-minute interval data, using stored procedures of the MySQL database (Zach et al. 2012). This procedure derives the duration of occupancy states (occupied / vacant) from the stored events and returns the dominant occupancy state of each interval. Occupancy periods before 8:00 and after 19:45 were not included in the study to exclude, amongst other things, the presence of janitorial staff at the offices. Occupancy data for a nine-month period (10th of November 2011 to 25th of July 2012) was used to derive and validate the occupancy model.

2.3 Data utilization scenarios for model extraction

We develop and validate a stochastic occupancy model, which is intended to be implemented in a continuous running mode in the building control system. In such an application, a number of questions arise with regard to occupancy data utilization: What length of past occupancy information shall be considered for model development? Would it be advantageous to differently treat days of the week? Shall the model training occur in static or shifting intervals?

To address these questions, we examined various scenarios in using empirical occupancy data to train the model. Concerning the number of days of monitored occupancy data as input to the model, we examined three alternatives, namely 5, 10 and 20 days. Days of the week were treated similarly in "All week's working days" mode and separately in "Specific week days" mode. Besides, fixed and moving training intervals were considered. In the fixed interval mode, the model is fed once with past data from a specific period (5, 10 or 20 days) and it predicts occupancy for future days (in this study, 90 working days). However, in the moving mode, the training interval advances as the model predicts the occupancy day by day. Table 1 summarizes different data utilization scenarios toward developing the occupancy model.

TABLE 1. Different data utilization scenarios for model extraction

Interval	Fixed						Moving					
Selected days	All week's working days			Specific week days in consecutive weeks			All week's working days			Specific week days in consecutive weeks		
Number of days	5	10	20	5	10	20	5	10	20	5	10	20
Scenario code	FW05	FW10	FW20	FS05	FS10	FS20	MW05	MW10	MW20	MS05	MS10	MS20

2.4 Stochastic model of occupants' presence

To derive a probabilistic occupancy model, which captures the random nature of occupants' presence, first, a specific period of the 15-min interval occupancy data (based on different data utilization scenarios) was deployed as the model input to extract following distributions:

1. The cumulative distribution function of first arrival times (CDF_a);
2. The cumulative distribution function of last departure times (CDF_d);
3. The probability distribution function of intermediate departure times (PDF_{id});
4. The distribution of the length of intermediate absences for different hours throughout the day.

Figure 1 shows an example of the above-mentioned distributions. A daily occupancy profile is then generated by identifying the first arrival time, last departure time, intermediate departure times and the associated length of intermediate absences as follows:

- Using a random number from the standard uniform distribution in the interval [0, 1] (u_1), the first arrival time (t_a) is derived from CDF_a such that CDF_a (t_a) = u_1.
- Using a random number from the standard uniform distribution in the interval [0, 1] (u_2), the last departure time (t_d) is derived from CDF_d such that CDF_d (t_d) = u_2.
- To decide if an intermediate departure event occurs at a certain time (t_m), a random number between 0 and 1 (u_m) is compared with the probability of intermediate departure at that time. Once an intermediate departure is identified (PDF_{id} (t_m) ≥ u_m), the length of the absence is obtained randomly from the associated set of the length of intermediate absences.

Compared with the previously developed stochastic models of occupancy, this model is most similar to the adapted stochastic occupancy model developed by Reinhart (2001). The main difference is that in our model, we used the hourly distributions of the length of intermediate absences, while in the other model, only three probability distributions, namely morning, lunch and afternoon, were used to randomly select the break lengths.

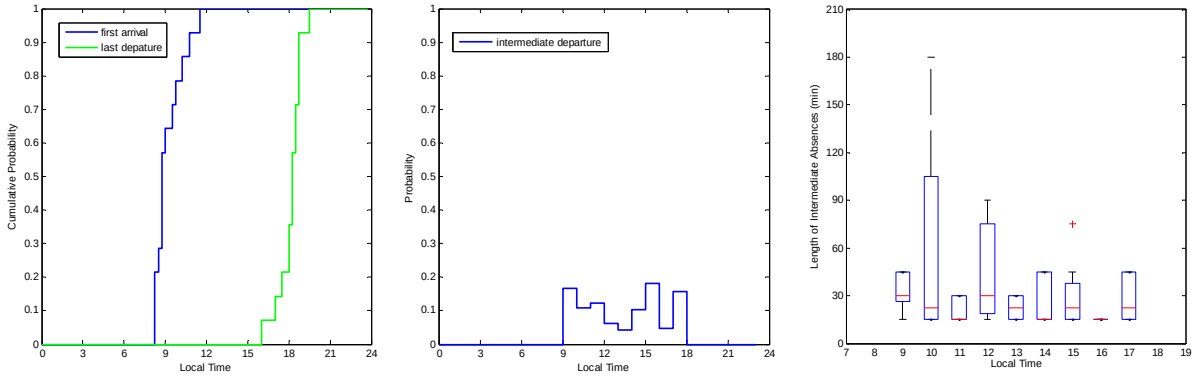

FIG 1. An example of distributions derived from monitored occupancy data. From left to right: The cumulative probability distributions of times of first arrival and last departure, the probability distribution of times of intermediate departures, the distribution of the length of intermediate absences.

2.5 Model evaluation

To evaluate the model, we compared predicted and monitored occupancy profiles of 90 working days between the 1st of April and the 25th of July 2012. This set of monitored data had not been used for deriving or calibrating the model. To evaluate the model predictions, we used five statistics:

1. Duration error [hour]: This metric represents the difference between the predicted and monitored daily presence duration. We calculated the presence duration by counting the number of occupied intervals.
2. First arrival time error [hour]: The predicted minus the monitored first arrival time.
3. Last departure time error [hour]: The predicted minus the monitored last departure time.
4. Asynchronicity index [-]: This novel indicator is calculated by averaging the differences between the number of predicted and monitored occupied intervals within each hour from 8:00 to 19:45. According to the definition, this statistics captures the asynchronicity of the predicted occupancy profiles (with reference to actual occupancy). A value of 1 for the Asynchronicity Index suggests zero temporal overlap between predicted and actual occupancy duration within a day. A value of zero would suggest full overlap between predicted and actual occupancy duration.
5. Number of transitions error [-]: The predicted number of daily occupied-to-vacant transitions minus the monitored number of daily occupied-to-vacant transitions.

Given the stochastic nature of this occupancy model, one cannot evaluate the accuracy of the model predictions by comparing the results of a single run with the measurements. Therefore we conducted a 100-run Monte Carlo simulation in order to analyze the distribution of the errors in predictions. The aforementioned statistics are calculated for each individual day during the validation period. Given the length of the validation period (90 working days) and the number of Monte Carlo simulations, we obtained 9000 values for each statistic.

Note that the current model is not intended to predict periods of long absences due to business trips, sickness, holidays, etc. Such whole-day absences can be presumably communicated to the building management system and reflected in the predictive building systems control. Therefore, in this contribution, we only included the actual working days in the validation process.

3. Results

Figures 2 to 6 illustrate the cumulative distribution functions of the obtained values for the introduced statistics.

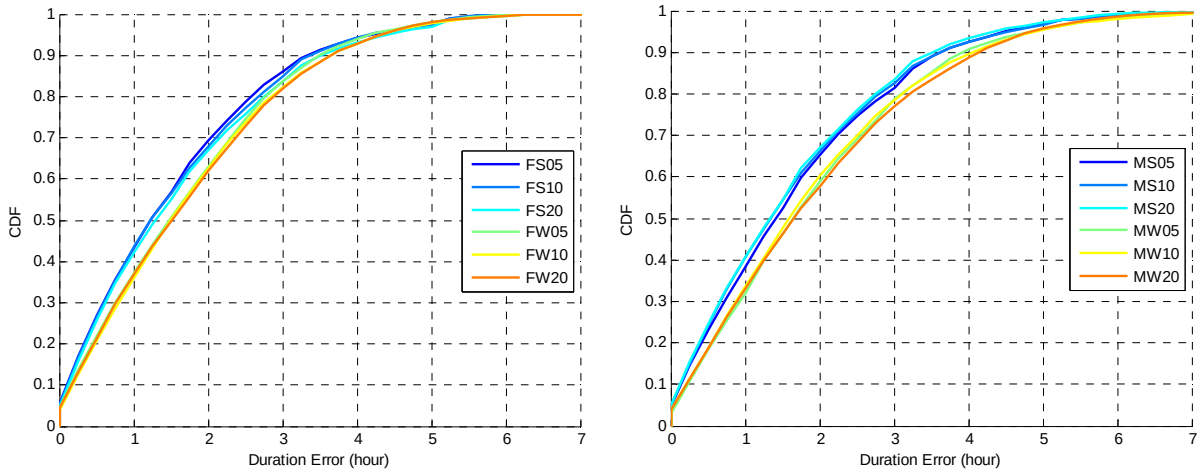

FIG 2. Cumulative distribution functions of duration error (left: fixed training interval; right: moving training interval)

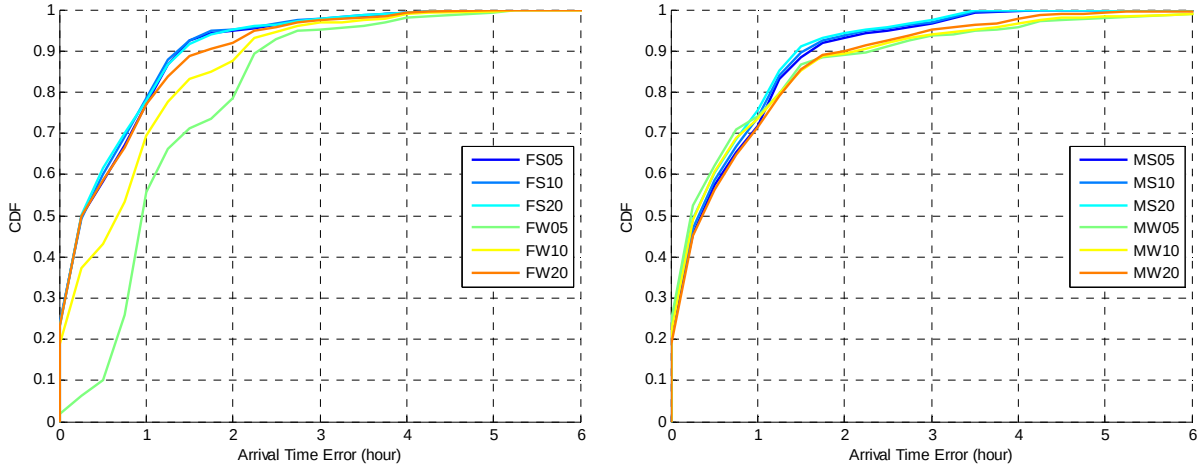

FIG 3. Cumulative distribution functions of first arrival time error (left: fixed training interval; right: moving training interval)

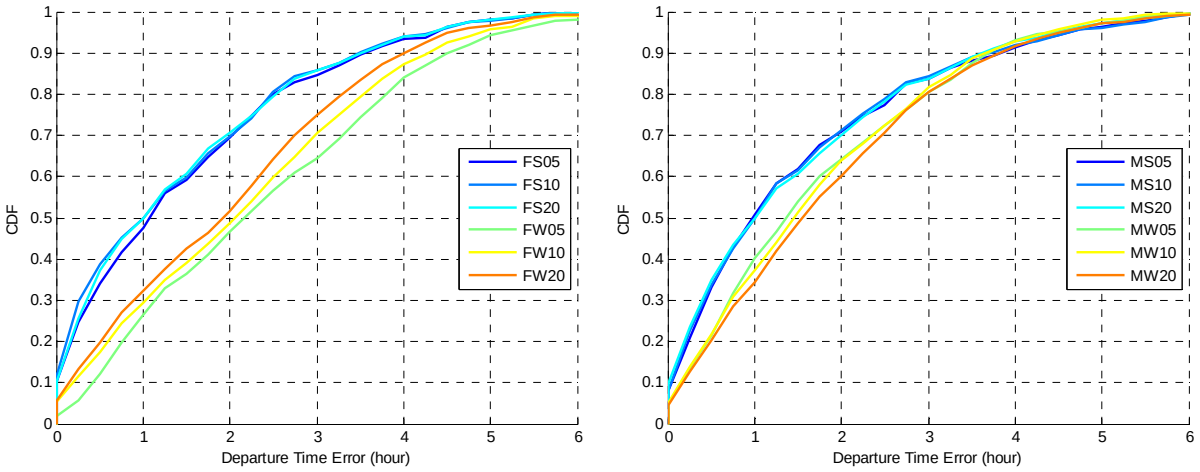

FIG 4. Cumulative distribution functions of last departure time error (left: fixed training interval; right: moving training interval)

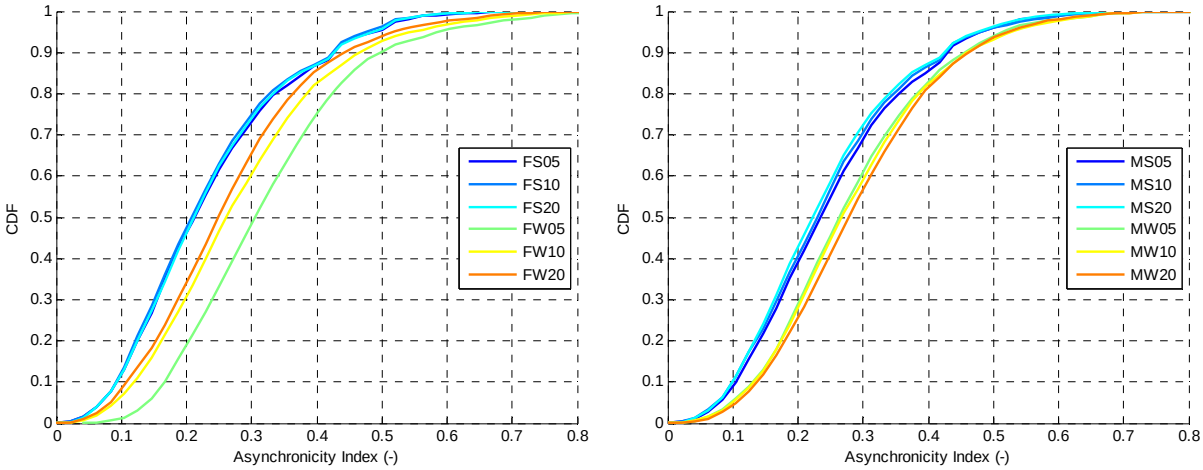

FIG 5. Cumulative distribution functions of asynchronicity index (left: fixed training interval; right: moving training interval)

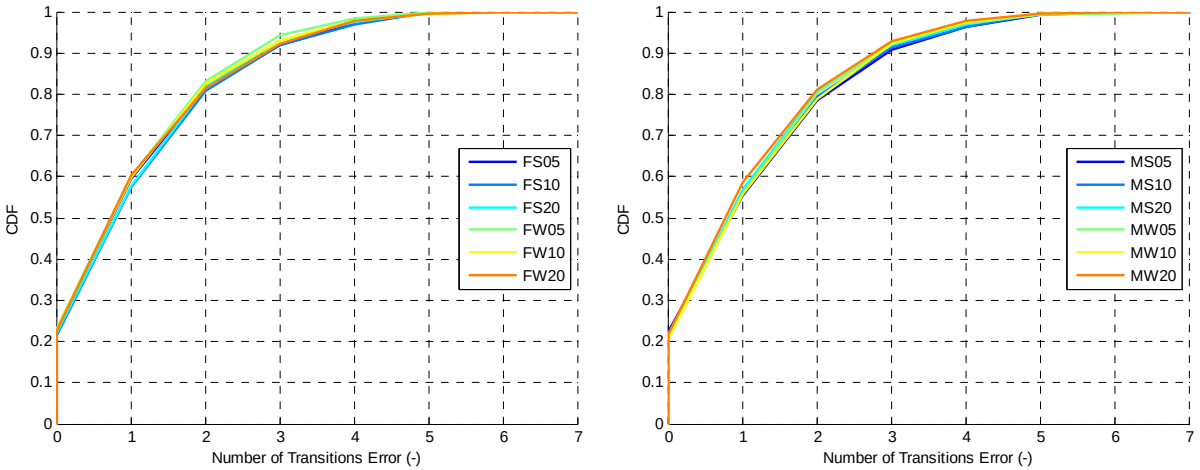

FIG 6. Cumulative distribution functions of number of transitions errors (left: fixed training interval; right: moving training interval)

4. Discussion and conclusion

Comparing different training data usage scenarios, models which distinguish between days of the week provide more accurate results in terms of almost all statistics. For these models, little difference in predictive performance could be found between the fixed and moving training modes. However, for models that do not distinguish between weekdays, the moving training mode offers more reliable predictions. Moreover, using longer intervals to train the models generally enhances predictive performance. However, this is much more evident in models with fixed training mode and no distinction between weekdays. In our study, no significant difference amongst the models could be found while predicting the number of transitions.

As noted at the outset of the paper, deployment of stochastic occupancy models in the context of building systems control requires a different standard concerning the evaluation of the models' predictive performance. Thereby, an important question concerns the extent to which short term occupancy prediction errors could be minimized. Table 2 summarizes, for the present study, the highest achieved accuracy in predicting daily occupancy profiles at 80 percent confidence level.

TABLE 2. The highest achieved accuracy in predicting daily occupancy profiles at 80 percent confidence level

Evaluation Statistic	Value at 80% confidence level
Duration error	2.5 hours
First arrival time error	1 hour
Last departure time error	2.5 hours
Asynchronicity index	0.32
Number of transitions error	2

The results reported here are derived from a single-occupancy office. Needless to say, using past occupancy data for prediction of future occupancy patterns may yield differing results. The error levels may be higher or lower based on factors such as the duration of the training period and the nature of the occupant's activity. However, the obtained results point out that there may be potentially a limit (lower uncertainty threshold) in predicting the occupants presence by using past data, as in this case, fairly detailed (high-quality) occupancy data was available and the nature of the occupant's task (mostly clerical) displayed a rather regular pattern.

Acknowledgements

The research presented in this paper is supported in part by funds from the project "Control & Automation Management of Buildings & Public Spaces in the 21st Century" (CAMPUS21, Project Number: 285729) as well as the project "Retrofitting Solutions and Services for the enhancement of Energy Efficiency in Public Edification" (RESSEEPE, Project number: 609377) under EU's Seventh Framework Programme.

References

Liao C, Lin Y, Barooah P. 2010. Agent-Based and Graphical Modeling of Building Occupancy. Journal of Building Performance Simulation 5(1), p. 5-25.

Mahdavi A. 2011. People in building performance simulation. In: Hensen J, Lamberts R, editors. Building Performance Simulation for Design and Operation. New York: Taylor & Francis; p. 56-83.

Newsham GR, Mahdavi A, Beausoleil-Morrison I. 1995. Lightswitch: a stochastic model for predicting office lighting energy consumption. In: Proceedings of Right Light Three, the 3rd European Conference on Energy Efficient Lighting. Newcastle-upon-Tyne; p. 60-66.

Page J, Robinson D, Morel N, Scartezzini JL. 2008. A generalized stochastic model for the simulation of occupant presence. Energy and Buildings, Volume 40, Issue 2, p. 83–98.

Reinhart CF. 2001. Daylight Availability and Manual Lighting Control in Office Buildings Simulation Studies and Analysis of Measurements. Ph.D. thesis, Technical University of Karlsruhe, Germany.

Zach R, Glawischnig S. Hönisch M, Appel R, Mahdavi A. 2012. MOST: An open-source, vendor and technology independent toolkit for building monitoring, data preprocessing, and visualization. In: Gudnason G, Scherer R, editors. eWork and eBusiness in Architecture, Engineering and Construction. Reykjavik: Taylor & Francis; p. 97-103.

Zio E. 2013. The Monte Carlo Simulation Method for System Reliability and Risk Analysis. 1st ed. London: Springer.

Combining Three Main Modeling Methodologies for Building Physics

A.W.M. (Jos) van Schijndel, Assistant Professor
R.P. (Rick) Kramer, M.Sc.
Eindhoven University of Technology, Netherlands

KEYWORDS: *State-Space, FEM, BES, Building, Energy, Modeling*

SUMMARY:
An overall objective of energy efficiency in the built environment is to improve building and systems performances in terms of durability, comfort and economics. In order to predict, improve and meet a certain set of performance requirements related to the indoor climate of buildings and the associated energy demand, numerical simulation tools are indispensable. In the paper we consider three types of numerical simulation tools: Finite Element Method (FEM), Building Energy Simulation (BES) and State-Space (SS) together. Commonly used within these tools are zonal approaches of the volumes, assuming uniform temperatures in each zone, and 1D modeling of the walls. Due to the rapid development of Finite Element Method (FEM) software and Multiphysics approaches, it should possible to build and simulate full 3D models of buildings regarding the energy demand. Another application consists of Building Energy Simulation using State space models identified from free floating data. It is concluded that the main benefits of FEM-SS-BES modeling exchange is the possibility to simulate building energy performances with high spatial resolution and low computational duration times.

1. Introduction

An overall objective of energy efficiency in the built environment is to improve building and systems performances in terms of durability, comfort and economics. In order to predict, improve and meet a certain set of performance requirements related to the indoor climate of buildings and the associated energy demand, numerical simulation tools are indispensable. In this paper we consider three types of numerical simulation tools: Finite Element Method (FEM), Building Energy Simulation (BES) and State-Space (SS). For each tool separately, there exist a vast number of references. Also on two tools combined, i.e. FEM-BES, BES-SS, FEM-SS, there is quite a lot of literature. However there is lack of research on an overall evaluation of the three tools FEM-SS-BES together. In this paper we present benefits of the FEM-SS-BES modeling exchange for building physics. The main reasons for converting models in each other are summarized in Table I.

TABLE 1. The main reasons for converting models in each other

<table>
<tr><th>To
From</th><th>FEM</th><th>BES</th><th>SS</th></tr>
<tr><td>FEM</td><td>*</td><td>Global effects
Lumped results</td><td rowspan="2">Computation Speed</td></tr>
<tr><td>BES</td><td rowspan="2">Local effects
High resolution results</td><td>*</td></tr>
<tr><td>SS</td><td>Inverse Modeling</td><td>*</td></tr>
</table>

In this work FEM is just a method of solving Partial Differential Equations (PDEs), like Finite Volume methods (FVM) or Finite Difference methods (FDM). We start with two combinations that are quite obvious and already commonly used. *BES to FEM* – BES is used to simulate the energy performance of buildings, using lumped parameter modeling. If local effects are important, FEM can be used to obtain high resolution results based on distributed parameter models and using BES simulation results as boundary values. *FEM to SS* – FEM based simulations can easily become computational time consuming. One of the methods to improve the computing time is to reduce the mathematical model to a lower order model by using for example a State-Space (SS) approximation. One of the main benefits of SS models is, that very efficient computation algorithms exist, that are able to almost completely reduce the computation time. If such a reduced order SS model is accurate enough, this method can be used for improving computation speed. This paper comprehends an investigation of the two other combinations. Each combination is presented in a separate Section, including background information and case studies. After these Sections a discussion of the results is provided. .

2. Application 1: Building Energy Simulation using 3D FEM with lumped parameter modeling for air.

BES using 1D FEM with lumped parameter modeling for air already exist. For example Wufi+ (2013) and HAMBase (de Wit 2006 & HAMLab 2013) are such tools. Commonly used within these tools are zonal approaches of the volumes, assuming uniform temperatures in each zone, and 1D modeling of the walls. Due to the rapid development of Finite Element Method (FEM) software and Multiphysics approaches, it should possible to build and simulate full 3D models of buildings regarding the energy demand. Moreover, the 3D models would also provide detailed (i.e. high resolution) results of the indoor climate and the constructions. The main problem regarding the use of FEM for BES is how to compare a distributed parameter model (FEM) with a lumped parameter model (BES)? Because BES and FEM have quite different approaches, we used the following method: Step 1, start with a simple reference case where both BES and FEM tools provide identical results. Step 2, add complexity and simulate the effects with both tools. Step 3, compare and evaluate the results. For step 1, a suitable reference case was found at the current International Energy Agency Annex 58. It concerns a test box with overall dimension 120x120x120 cm³. Comsol was used to build a 3D model of the test box. In order to compare the Comsol 3D FEM model with the BES lumped model (using HAMBase(de Wit 2006 & HAMLab 2013)), an equivalent heat conduction of the air is used in the FEM model. This provides identical FEM versus BES results.

For step 1, a suitable reference case was found at the current International Energy Agency Annex 58 (2013). It concerns a test box with overall dimension 120x120x120 cm³. Floor, roof and three of the four walls are opaque, one wall contains a window with opening frame. Details of the overall geometry with the exact dimensions can be found in figure 1.

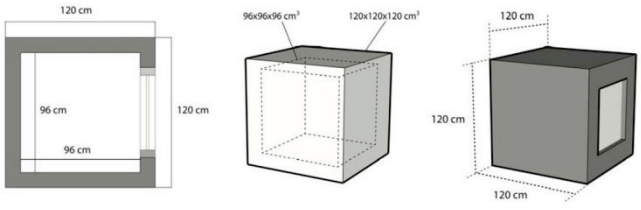

Figure 1. The reference case.

We started to build a 3D model of the opaque test box, heavy weight, air change rate: ACH=0 using Comsol (2013). In order to compare the Comsol 3D FEM model with the HAMBase (de Wit 2006 & HAMLab 2013) lumped model, an equivalent heat conduction of the air is used in Comsol instead of CFD. Equation (1) shows the PDE:

$$\rho c\, \partial T/\partial t = \nabla \cdot k \nabla T \qquad (1)$$

where T is temperature (K), t is time (s), ρ is density (kg/m^3); c is specific heat (J/kgK) and k is heat conduction coefficient (W/mK) . Equation (2) shows the boundary values:

$$q_{boundary} = h(T - T_e) + q_{irrad} \qquad (2)$$

where $q_{boundary}$ is the heat flux at a specific boundary (W/m^2) , h is the heat transfer coefficient (W/m^{2}K), T_e is the external air temperature (K) and q_{irrad} is the net radiation from the sun and sky to the surface (W/m^2). The temperature distribution in the test box is simulated using Dutch weather data. As mentioned above the model was implemented and solved using Comsol. The default second-order Lagrange element type was used. The mesh contained 4414 tetrahedral elements and with average element quality of 0.7512. The number of degrees of freedom solved for was 6679 using the PARADISO algorithm with absolute and relative tolerances of 0.001. The temporal convergence error was less than 10^{-5} for each time step. After the solution was obtained with these settings, the grid dependency was evaluated by a grid refinement study. The latter showed no significant changes in the solution. Figure 2 shows the 3D snapshots of the isosurfaces in simulated by the FEM software.

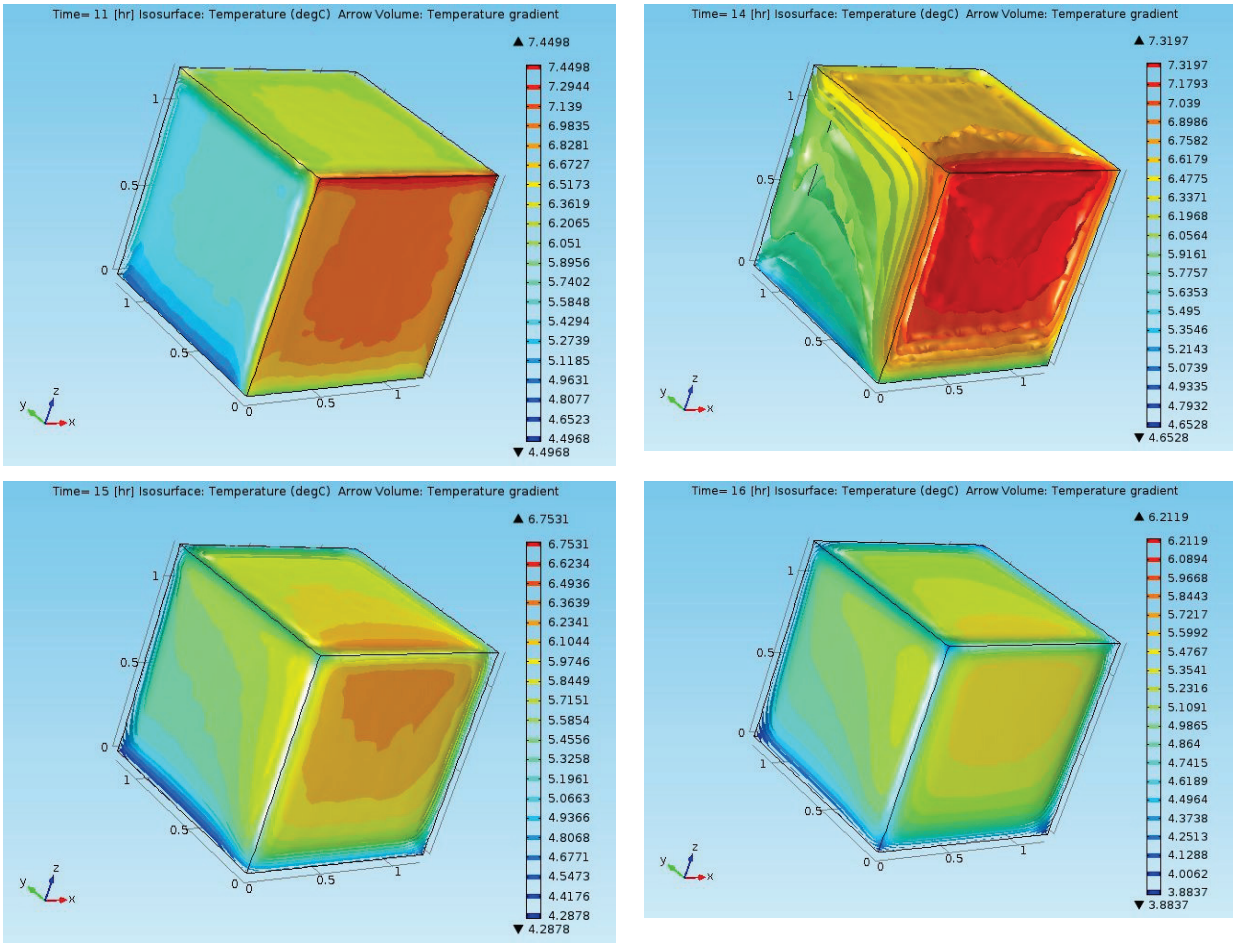

Figure 2. 3D snapshots of the temperature isosurfaces.

The main challenge now is how to match the high resolution distributed temperature results of Comsol with the lumped temperature results of the BES model. For this reference case (opaque test box, heavy weight, ACH=0) we were able to get a very good match by using a so-called equivalent heat conduction coefficient for the air inside the box in Comsol.

$$k_{eq} = d/R = 1 / 0.34 = 2.9 \quad (3)$$

Figure 3 shows the comparison of the simulated mean indoor air temperature using Comsol (thin line) and HAMBase (bold line) during the first month. The verification result is satisfactory.

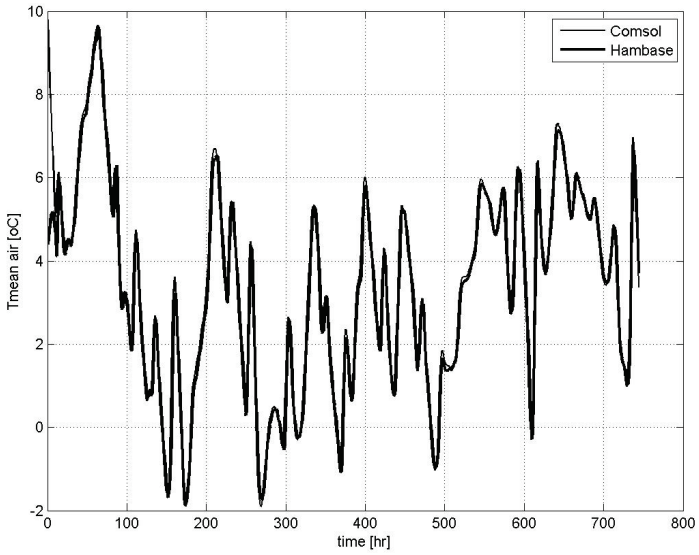

Figure 3. Comparison of the simulated mean indoor air temperature using Comsol (thin line) and HAMBase (bold line) during the first month for the opaque reference case.

From figure 3, two important facts can be concluded: Firstly, these results can be used as an additional verification benchmark for both Comsol as well as HAMBase. And secondly, it is seems to be possible to accurately reproduce a BES simulation using a relative simple heat conduction based FEM model with a equivalent heat conduction coefficient for the indoor air, but so far without CFD and internal radiation. The latter is left over for future research.

3. Application 2: State-Space models identified from measured data.

At the IEA Annex (2013) a test box was built to investigate it's thermal characteristics.

Figure 4. The test box from the IEA Annex 58 (2013), Left: design,Right: as built

The test box was tested at the premises of BBRI in Limelette, Belgium (Lat. 50°41' N, Long. 4°31' E). In general, the weather conditions here are temperate, consisting of mild winters and rather cool summers. The experiments extended over a period of one month. Testing was done under real outdoor weather conditions. The following outdoor climate sensors installed near the test box are included in the supplied data: air temperature (with a solar radiation shield and ventilated), vertical global solar radiation (parallel and next to the glazing) and horizontal long wave radiation from the sky. Additional meteorological sensors installed at the test site (200 m from the test box) are also included in the data sets : horizontal global solar radiation, horizontal diffuse solar radiation, vertical long wave radiation from the South direction, wind velocity, wind direction (North 0°, East 90°) and relative humidity. The following experiments have been carried out: Test A : free-floating temperature (with no heating power during 2 weeks) and Test B : co-heating test with constant indoor temperature of 25°C during 2 weeks,

3.1 Free floating experiment

Figure 5 shows the measured indoor and outdoor temperatures of the test box:

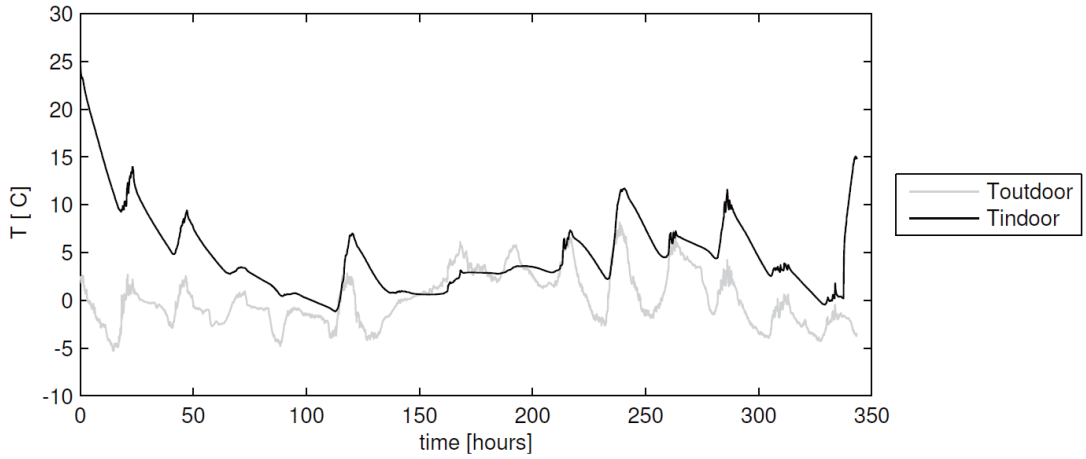

Figure 5: The measured indoor and outdoor temperature are shown. Both temperatures are averages of the two available measurement positions for respectively indoor and outdoor temperature

A model structure that is suitable for a thermal zone is provided by Kramer et al. (2013) and is shown in Figure 6.

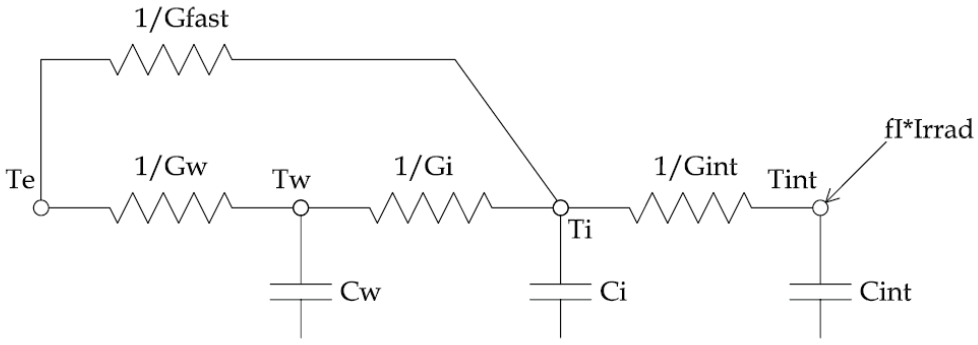

Figure 6: The used lumped thermal model with inputs outdoor temperature (Te) and solar irradiation (Irrad).

The thermal model is a 3rd order model with 7 parameters: Cw represents the capacitance of the envelope part, Ci represents the capacitance of the indoor air and Cint represents the capacitance of the interior parts which are not directly connected to the outdoor air. Gfast represents the heat loss due to ventilation and windows. The solar irradiation is placed on the interior node. This model structure proved to be the most suitable amongst several other assessed model structures. For more information see Kramer et al. (2013). The thermal model inputs are: Temperature outdoor and solar irradiation on vertical plane oriented on sooth. For this experiment, the solar input is limited to the global irradiation on the vertical south plane because this has the most influence. The objective is to identify the parameter values of the model by repeatedly trying different parameter values and comparing the simulated output with the measured output (Kramer et al., 2013). The result of the optimization procedure is shown in Figure 7. The measured indoor temperature is reproduced fairly accurately at first sight.

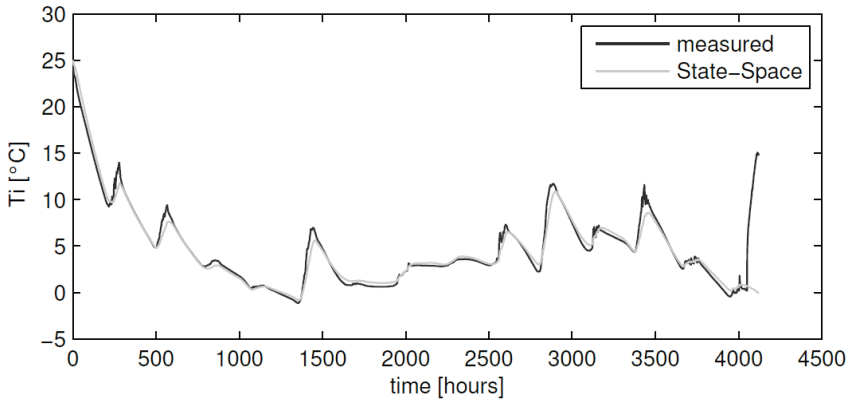

Figure 7: measured and simulated indoor temperature for the free floating situation using the thermal model from Figure 6 with inputs Te and global solar irradiation on vertical South plane (Gv).

3.2 Co-heating experiment

The state-space (SS) thermal model of the previous section was coupled with an PI controller (see Figure 8) in order to simulate the co-heating experiment.

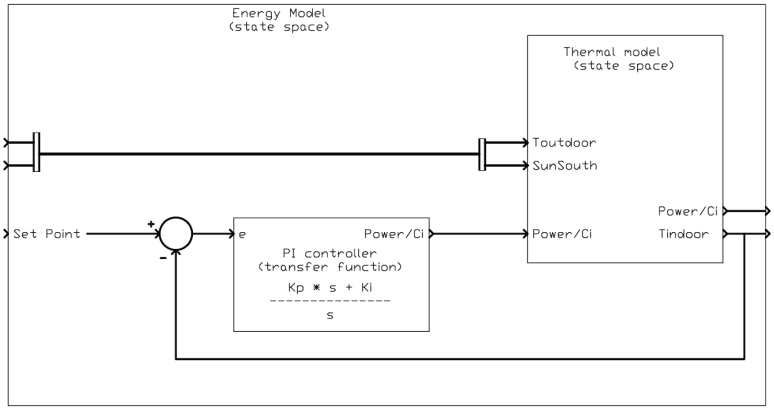

Figure 8: the identified thermal model is coupled to a PI-controller maintaining the indoor temperature at 25°C.

The simulation results compared with the experiments are shown in figures 9 and 10.

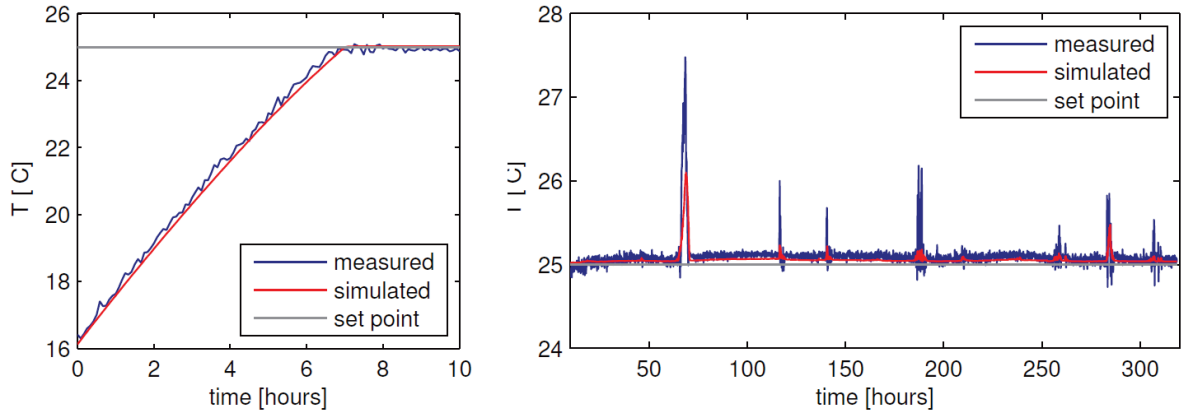

Figure 9: Simulated and measured indoor temperature for co-heating test. The first 10h (left) and 10 – 320h (right).

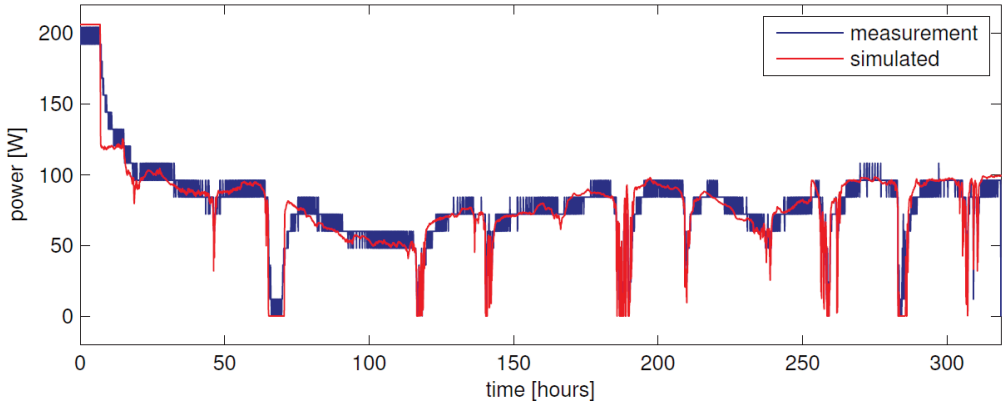

Figure 10: the simulated power is scaled by a factor 3.11e5 (Ci) and plotted with the measured power.

The results show a good agreement between simulation and measurement. Moreover, now that the indoor air capacitance Ci has been identified, the other parameters can be isolated. E.g., the individual parameters like Gi can be isolated, see Table 2:

TABLE 2. The identified parameters are split up by using the identified Ci.

#	Par.	identified	expected	unit
1	G_w	0.86	2.3	W/K
2	C_w	1.2e-1	41	J/K
3	G_i	3.11e4	43	W/K
4	C_i	3.11e5	1.1	J/K
5	G_{fast}	3.11	0.3	W/K
6	G_{int}	0.31	-	W/K
7	C_{int}	2.63e-4	-	J/K
8	fI-S	0.13	0.27	m^2

From Table 2 there it is noted that there is still a discrepancy between identified and expected values. The latter are estimated by hand calculations based on information provided by the IEA Annex 58. This is discussed in the next Section.

4. Discussion and Conclusions

The inverse modeling procedure presented at the previous Section provides a state-space model that is capable of accurately simulating the experiment. The indentified parameters should be interpreted as effective parameters. For example the air inside the box has a heat capacity of 1.1 J/K. However, in this experiment it is impossible to heat up the air alone because it immediately affects the construction also. Therefore it could be very difficult if not impossible to get the expected parameters from the inverse modeling method. Nevertheless, the model is a very accurate representation of the dynamics.

It is concluded that one of the main benefits of FEM-SS-BES modeling exchange is the possibility to simulate building energy performances with high spatial resolution and low computational duration times. Regarding FEM to BES – Firstly, these results can be used as an additional verification benchmark for both Comsol as well as HAMBase. Secondly, it is seems to be possible to accurately reproduce a BES simulation using a relative simple heat conduction based FEM model with a equivalent heat conduction coefficient for the indoor air, but so far without CFD and internal radiation. The latter is left over for future research. Regarding BES to SS - The paper presents case studies where SS models are successfully used for reducing computational times for BES models. Regarding SS to BES – Using this so-called inverse modeling approach, it is possible to obtain building energy performances from SS models. The FEM-SS-BES modeling exchange provides two alternative modeling approaches for each other. This may be beneficial if some specific limitations are encountered within one of the single FEM, BES, SS modeling methods.

References

Annex 58 (2013), http://www.ecbcs.org/annexes/annex58.htm

Comsol (2013), www.comcol.com

HAMLab(2013), http://archbps1.campus.tue.nl/bpswiki/index.php/Hamlab

Kramer, R.P., Schijndel, A.W.M. van & Schellen, H.L. (2013). Inverse modeling of simplified hygrothermal building models to predict and characterize indoor climates. Building and Environment, 68, 87-99.

Perez, R. et al., 1987. A new simplified version of the perez diffuse irradiance model for tilted surfaces. Solar Energy, 39(3), pp. p.221-231.

Schijndel, A.W.M. van & Wit, M.H. de, (1999). A building physics toolbox in MatLab, 7TH Symposium on Building Physics in the Nordic Countries Goteborg, pp81-88

Schijndel A.W.M. van (2007). Integrated Heat Air and Mois-ture Modeling and Simulation, PhD Dissertation, Eindho-ven University of Technology

Wufi+ (2013), http://www.wufi.de/

Wit, M.H. de ,H.H. Driessen (1988). ELAN A Computer Model for Building Energy Design. Building and Environment 23: pp285-289

Wit, M.H. de, (2006). HAMBase, Heat, Air and Moisture Model for Building and Systems Evaluation, Bouwstenen 100, Eindhoven University of Technology

Empirical and computational assessment of the urban heat island phenomenon and related mitigation measures

Ardeshir Mahdavi
Kristina Kiesel
Milena Vuckovic

Department of Building Physics and Building Ecology, Vienna University of Technology, Austria

KEYWORDS: *Urban climate Urban Heat Island, Mitigation Measure, Modeling, Evaluation*

SUMMARY:
A central strand of research work in the realm of urban physics aims at a better understanding of the variance in microclimatic conditions due to factors such as building agglomeration density, anthropogenic heat production, traffic intensity, presence and extent of green areas and bodies of water. This research has been motivated in part by phenomena associated with climate change and urban heat islands (UHI) and their implications for the urban microclimate. Note that the characteristics and evolution of the urban microclimate is not only relevant to people's experience of outdoor thermal conditions in the cities. It could be argued that the solid understanding of the temporal and spatial variance of urban microclimate represents a prerequisite for the reliable assessment of the thermal performance of buildings (energy requirements, indoor thermal conditions). In this context, the present paper entails a three-fold contribution. First, the existence and extent of the UHI phenomena are documented for a number of Central-European cities. Second, a number of variables of the urban environment are identified that are hypothesized to influence UHI and the urban microclimate variance. These variables, which pertain to both geometric (morphological) and semantic (material-related) urban features are captured within a formal and systematic framework. Third, to support the process of design and evaluation of UHI mitigation measures, the potential of both numerical (simulation-based) applications and empirically-based urban microclimate models are explored.

1. Introduction

An increasing number of people live in cities and are therefore influenced by the urban microclimate. The microclimate varies significantly within a city depending on factors such as urbanization, presence and density of industrial or commercial buildings, green areas, bodies of water, etc. (Grimmond 2007, Alexandri 2007). Furthermore, the geometry, spacing, and orientation of buildings and surrounding open areas greatly influence the climate in the city (Unger 2004, Kleerekoper et al. 2012, Shishegar 2013). Observations in many cities around the world point to significantly higher urban temperatures than the surrounding rural environment. This circumstance is referred to as the urban heat island (UHI) phenomenon (see, for example, Voogt 2002, Arnfeld 2003, Blazejczyk 2006, Oke 1981, Gaffin et al. 2008). Increase in average temperatures is believed to adversely affect the health of people living in cities (Harlan et al. 2011). Additionally, higher air temperatures have a direct effect on the energy use due to increased deployment of air conditioning (Akbari 2005). In this context, this paper presents the results of an ongoing research project. First the existence and extent of the UHI phenomena are documented for a number of Central-European cities. Thereby, certain features of the urban environment are hypothesized to influence UHI and the urban microclimate variance. The related variables, which pertain to both geometric (morphological) and semantic (material-related) urban features are captured within a systematic framework. Moreover, to support the

process of design and evaluation of UHI mitigation measures, the potential of both numerical (simulation-based) applications and empirically-based urban microclimate models are explored.

2. The Urban heat island in central Europe

2.1 Overview

The UHI is defined as the difference between urban and rural air temperature (Oke 1972). Generally, heat island intensities are quantified in the range of 1 to 3 K, but – under certain atmospheric and surface conditions – can be as high as 12 K (Voogt 2002). Material properties of urban surfaces (Akbari et al. 2001) as well as evapotranspiration, and anthropogenic heat emission (Taha 1997) can result in higher urban temperatures. The present contribution focuses on the frequency, magnitude, and time-dependent (diurnal and nocturnal) UHI intensity distribution (during a reference week) and the long-term development of urban and rural temperatures in eight Central-European cities, namely Budapest, Ljubljana, Modena, Padua, Prague, Stuttgart, Vienna, and Warsaw. The magnitude of the UHI effect can be expressed in terms of UHI intensity ($\Delta\theta$). This term denotes the temperature difference (in K) between simultaneously measured urban and rural temperatures.

As mentioned before, UHI intensity in observed urban areas was derived for a reference summer week selected by each participating city independently. Specifically the cities were asked to provide climate data recorded at two weather stations for a period of 7 consecutive days during the summer of 2011. The idea was to select a week with considerably high temperatures and relatively low wind velocities (preferably below 5 m/s). The collected information included hourly data on air temperature, wind speed, and precipitation from two representative weather stations (one urban and one rural). The participating cities were asked to select the weather stations according to the following guidelines: *i)* the urban station should be situated in a central area with a typical urban morphology/setting; *ii)* the rural station should be situated in a rural surrounding in the vicinity of the city (but not in the suburbs and not near an airport or similar structures). To obtain a long-term impression of the urban and rural temperature development, mean annual (urban and rural) temperatures and UHI values were derived for a period of up to 30 years, namely from 1980 to 2011 (Modena, Prague, Stuttgart, Warsaw), from 1994 to 2011 (Vienna, Padua), from 2000 to 2011 (Budapest).

2.1.1 Short-term (reference week) analyses of the UHI phenomenon

To facilitate the visualization and comprehension of the collected data for the reference week, we further processed it in terms of mean hourly urban temperature and UHI values for a reference day. These values provide thus an insight into the temporal characteristics of both air temperature and UHI.

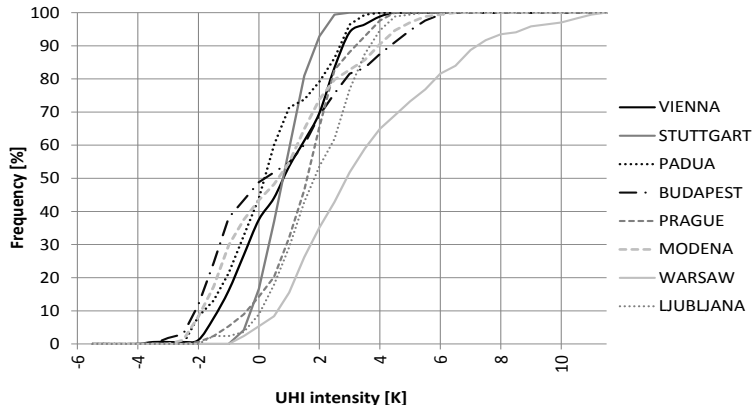

FIG 1. Cumulative frequency distribution of UHI intensity for a one week summer period

Figure 1 shows the cumulative frequency distribution of UHI values for the participating cities for the aforementioned summer reference week. Figure 2 shows the hourly UHI values for a reference summer day. The reference week data clearly demonstrate the existence and significant magnitude of the UHI effect in participating cities, especially during the night hours (Figure 2). However, the time-dependent UHI patterns vary considerably across the participating cities. The UHI pattern differences are also visible in the cumulative frequency distribution curves of Figure 1. In this Figure, a shift to the right denotes a larger UHI magnitude.

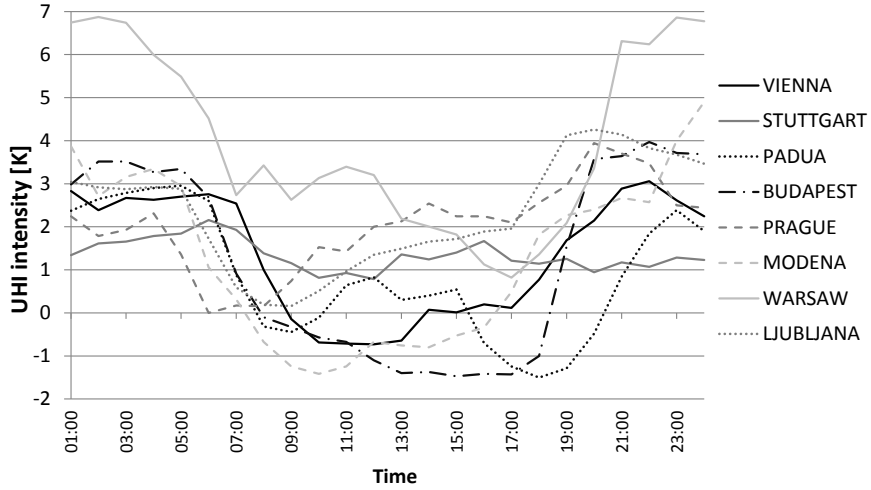

FIG 2. Mean hourly UHI intensity distribution for a reference summer day

2.1.2 Long-term analyses

Figures 3 and 4 show the (mean annual) urban and rural temperatures respectively over 30 years. Figure 5 shows the long-term UHI intensity trend over the same period. The historical temperature records suggest an upward trend concerning both urban and rural temperatures (see Figures 3 and 4). Consistent with regional and global temperature trends, a steady increase in rural temperatures of up to about 2.5 K can be observed in all selected cities (with the exception of Budapest). In the same 30-years period, the mean annual urban temperature rose somewhere between 1 K (Stuttgart) and 3 K (Warsaw). Note that, while both rural and urban temperatures have been increasing, the value of the UHI intensity has been rather steady. Our data suggest increasing UHI intensity trends in Warsaw and Ljubljana, whereas a slight decrease can be discerned from Stuttgart and Prague data (Figure 5).

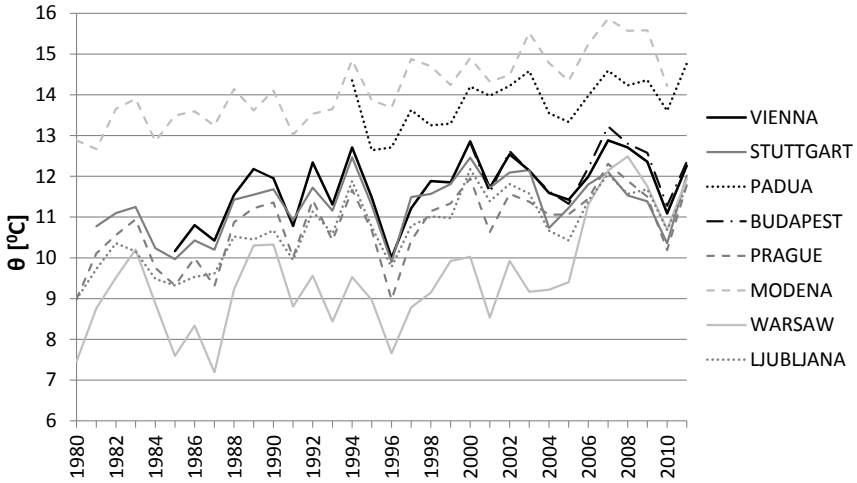

Year

FIG 3. Development of (mean annual) urban temperatures over a period of 30 years

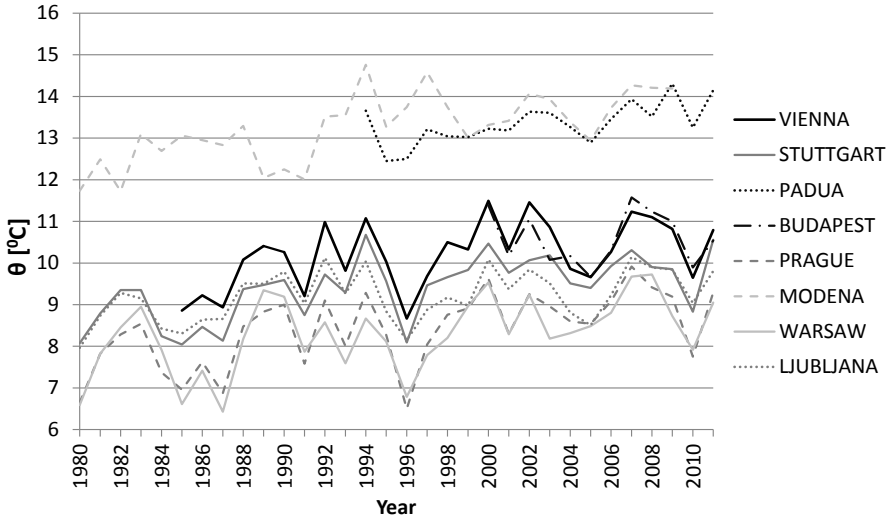

FIG 4 Development of (mean annual) rural temperatures

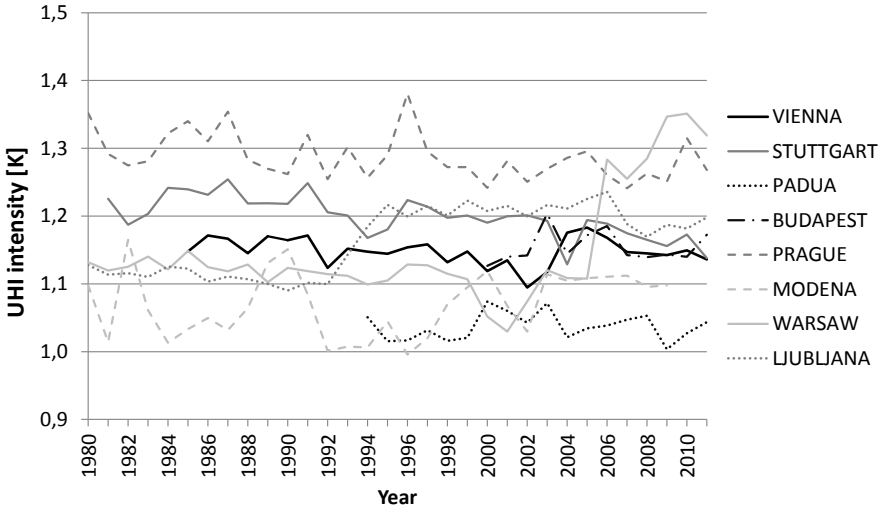

FIG 5. Long-term development of the UHI intensity

3. Systematic framework

Within the aforementioned project, a systematic framework was developed (Mahdavi et al. 2013) to assess – for a specific urban location, hereafter referred to as urban unit of observation (U2O) – the urban heat island phenomenon, to specify potential mitigation and adaptation measures, and to evaluate such measures via adequate modelling approaches. The framework involves the following steps: *i)* Definition of "Urban Units of Observation" (U2O): These are properly bounded areas within an urban setting selected as the target and beneficiary of candidate UHI mitigation measures*; ii)* Description of the status quo of U2O in terms of a structured set of geometric and physical properties; *iii)* Specification of the existing UHI intensity; *iv)* Specification of the candidate mitigation measures in terms of projected changes to the geometric and/or physical properties captured in step ii above; *v)* Prediction of the effect of mitigation measures using empirically-based and/or numeric models; *vi)* Expression of the mitigation measures' impact in term of predicted changes in UHI intensity; *vii)* Overall evaluation of the mitigation measures' effectiveness on the basis of modelling results together with their estimated financial and logistic ramifications.

In this framework, the notion of U2O is applied to systematically address the local variation of the urban climate throughout a city. A spatial dimension (diameter) of approximately 400 to 1000 m has been targeted for U2O, indicating common features in view of geometry, massing, or other aspects of the physical structure. As the urban microclimate is believed to be influenced by different urban morphologies, structures, and material properties, a set of related variables were identified and included in our framework.

3.1.1 The variables

In order to predict, estimate, and verify the effect of urban heat island mitigation actions on reduction of UHI intensity, we need to express such actions in terms of changes that they introduce in an U2O. Toward this end, a set of variables are suggested (Tables 1 and 2) based on past research (Mahdavi et al. 2013, Kiesel et al. 2013) and our own reasoning.

Table 1: Variables to capture the geometric properties of an U2O

Geometric properties	Definition
Sky View Factor	Fraction of sky hemisphere visible from ground level
Aspect ratio	Mean height-to-width ratio of street canyons
Built area fraction	The ratio of building plan area to total ground area
Unbuilt area fraction	The ratio of unbuilt plan area to total ground area
Impervious surface fraction	The ratio of unbuilt impervious plan area to total ground area
Pervious surface fraction	The ratio of unbuilt impervious surface area to total ground area
Mean building compactness	The ratio of built volume (above terrain) to total building plan area
Built surface fraction	The ratio of total built surface area to total built area
Wall surface fraction	The total area of vertical surfaces (walls)
Roof surface fraction	The total area of horizontal surfaces (roofs)
Mean sea level	Average height above sea level

Table 2: Variables to capture the surface and material properties of an U2O

Surface/material properties	Definition
Reflectance/albedo	Fraction of reflected direct and diffuse shortwave radiation
Emissivity	Ability of a surface to emit energy by radiation (longwave)
Thermal conductivity	Property of a material's ability to conduct heat, given separately for impervious and pervious materials
Specific heat capacity	Amount of heat required to change a body's temperature by a given amount, given separately for impervious and pervious materials
Density	Mass contained per unit volume, given separately for impervious and pervious materials
Anthropogenic heat output	Heat flux density from fuel combustion and human activity (traffic, industry, heating and cooling of buildings, etc.)

4. Evaluation of UHI mitigation measures

Once U2Os and their respective variables are defined, potential mitigation measures (see Table 3) may be expressed in terms of respective changes to the variable attributes. For example, introduction of green roofs or green facades in an U2O would modify the variables pertaining to surface albedo, emissivity, thermal conductivity, specific heat capacity, and density. Table 3 provides a concise summary of the most common mitigation measures. These measures can be divided into three main realms of interventions: buildings, pavements, and vegetation. Table 3 also includes a detailed description of expected benefits of such measures.

Table 3: A summary of principal mitigation measures

Category	Measure	Expected benefit
Buildings	Cool roofs	High solar reflectance and high thermal emissivity
	Green roofs	Shading and evapotranspiration
	Green facades	Reducing ambient air temperature, shading properties, natural cooling, control airborne pollutants, energy efficiency
	Façade construction and retrofit	Reducing cooling/heating load, reducing ambient air temperature, improving building envelope quality
	Geometry of urban canyon (new projects)	Fresh air advection , cool air transport into the city
Pavements	Cool pavements	Decreasing ambient air temperature
	Pervious pavements	Storm water management
Green areas	Planting trees within the urban canyon	shading and evapotranspiration, lower peak summer air temperatures, reducing air pollution
	Parks, green areas	

Finally the impact of those mitigation measures can be estimated based on appropriate calculation tools and modeling methods. For this purpose we considered two principal approaches: statistical analysis of empirical data and numeric (typically CFD-based) computational models. Correlations between measured urban heat island intensity in different locations within an urban environment and the physical features of these locations can be exploited to derive empirically based estimation methods. For numeric computation, different simulation tools can be applied, ranging from regional climate models to single-building models (Mirzaei 2010). To illustrate the application of the framework, a case study from the aforementioned EU project is presented below. The case study concerns a U2O in the center of Vienna, Austria with a total area of roughly half a square kilometer. Figure 6 shows the existing attributes of the variables for this U2O together with the changes in these variables as a consequence of three envisioned mitigation measures: *i)* Planting the maximum number of trees that could be reasonably accommodated within; *ii)* Implementing green roofs according to the "Gründachpotentialkataster", a document provided by the city of Vienna, which specifies roof areas with proper potential for conversion to green roofs (GREEN ROOF 2014); *iii)* A combination of measures *i* and *ii*. In this case, the estimation of the implications of the mitigation measures was conducted using a numeric simulation application (ENVI-met 2014).

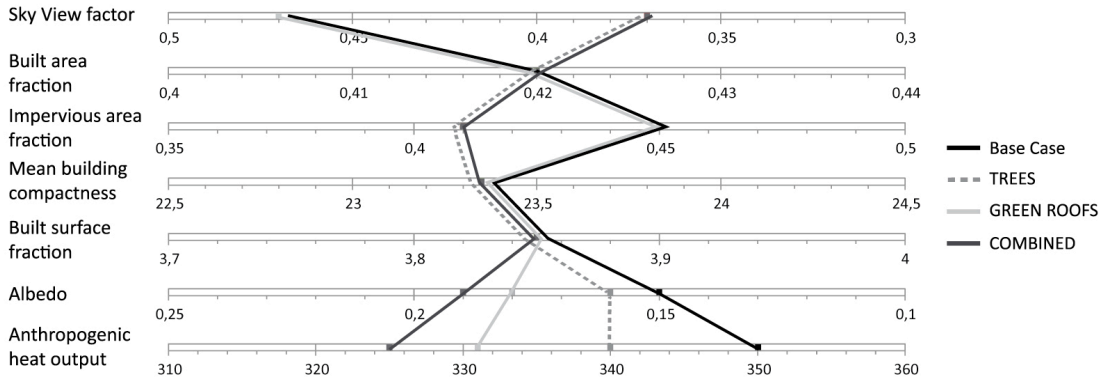

FIG 6. The existing values of the U2O variables for the Vienna case study together with modified values associated with proposed mitigation measures

Figure 7 shows the modeling results in terms of predicted reduction of UHI index in the course of a reference summer day. These results point to the considerable potential of tree planting toward the reduction of air temperature in the urban canyon. Green roofs, however, did not display a similar degree of effectiveness with regard to street level temperatures. Note that green roofs did not influence shading circumstances in the urban canyon. Nor did they have, in the present scenario, a noteworthy impact on the radiation exchange between (vertical) built surfaces and sky. Based on our current state

of information, we cannot conclude with certainty, if other positive implications of green roofs (e.g., evapotranspiration) are consistently and sufficiently considered in the computational tool deployed.

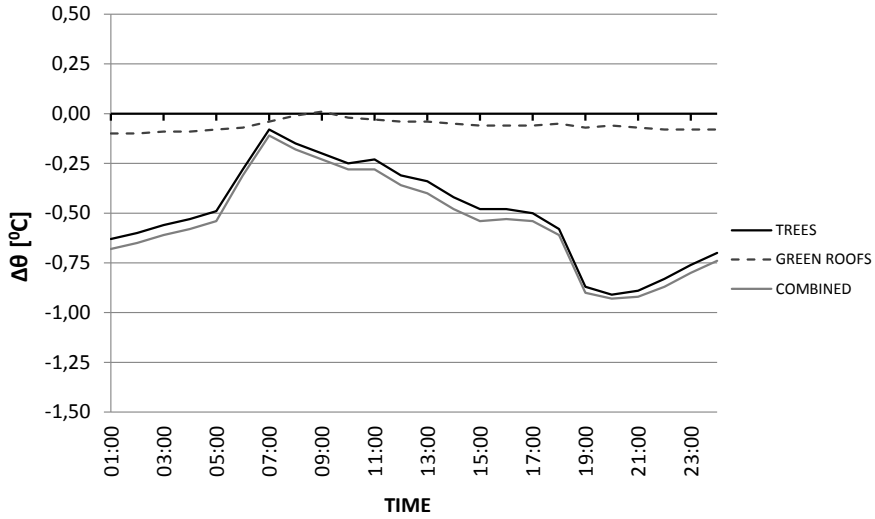

FIG 7. The modeled mean hourly temperature difference ("Innere Stadt", Vienna)

5. Conclusion

We presented the results of an ongoing EU-supported project concerned with the extent of the UHI phenomena in a number of Central European cities. The objectives of this project are to provide a common understanding of the UHI effects and to conceive and evaluate appropriate mitigation and adaptation measures. Short-term and long-term data with regard to urban and rural temperatures demonstrate the existence and significant magnitude of the UHI effect in a number of Central European cities. Furthermore observations based on hourly data display distinguished patterns implying larger UHI intensities during the night hours. To address the need for effective means of evaluating and mitigating UHI effects, a systematic framework was developed and tested within the collaborative context of an EU project. Thereby, a number of geometric (morphological) and semantic (material-related) variables of the urban environment were identified that are hypothesized to influence UHI and the urban microclimate variance. The deployment of this framework and a CFD-based urban climate modeling tool was exemplified using the case of an urban unit of observation in the city of Vienna. Ongoing work further explores and statistically analyses the link between UHI intensity and salient urban variables such as urban density and morphology, block layout, canyon geometry, surface properties, vegetation, bodies of water industrial sites, transportation systems and infrastructures. This work is expected to not only provide empirical data for the validation of numeric models, but also to support the formulation of simplified approaches toward estimation of mitigation measures effectiveness in view of UHI phenomena.

6. Acknowledgements

This project was funded in part within the framework of the EU-Project "Development and application of mitigation and adaptation strategies and measures for counteracting the global Urban Heat Island phenomenon" (Central Europe Program, No 3CE292P3).

References

Akbari, H., Pomerantz, M., Taha, H. 2001. Cool surfaces and shade trees to reduce energy use and improve air quality in urban areas. Solar Energy, Volume 70, Issue 3: 295–310.

Akbari, H. 2005. Energy Saving Potentials and Air Quality Benefits of Urban Heat Island Mitigation. Lawrence Berkeley National Laboratory, Berkeley, CA.

Alexandri, E. 2007. Green cities of tomorrow? Sustainable Construction, Materials and Practices, Portugal SB07: 710-717.

Blazejczyk, K., Bakowska, M., Wieclaw, M. 2006. Urban heat island in large and small cities. 6th International Conference on Urban Climate, Göteborg, Sweden, June12-16 2006: 794-797.

ENVI-met 2014. http://www.envi-met.com/ (last accessed Feb. 2014).

Gaffin, S. R., Rosenzweig, C., Khanbilvardi, R., Parshall, L., Mahani, S., Glickman, H., Goldberg, R., Blake, R., Slosberg, R. B., Hillel, D. 2008. Variations in New York City's urban heat island strength over time and space. Theoretical and applied climatology, Volume 94: 1-11.

GREEN ROOF 2014. http://www.wien.gv.at/umweltgut/public/ (last accessed Feb. 2014).

Grimmond, C.S.B., 2007. Urbanization and global environmental change: local effects of urban warming. Cities and global environmental change, Volume 173, Issue 1: 83-88.

Harlan, S L., Ruddell, D.M. 2011. Climate change and health in cities: impacts of heat and air pollution and potential co-benefits from mitigation and adaptation. Current Opinion in Environmental Sustainability, Volume 3, Issue 3: 126-134.

Kiesel, K., Vuckovic, M., Mahdavi, A. 2013. Representation Of Weather Conditions In Building Performance Simulation: A Case Study Of Microclimatic Variance In Central Europe, 13th IBPSA, August 25 - 28, France.

Mahdavi, A., Kiesel, K., Vuckovic, M. 2013. A framework for the evaluation of urban heat island mitigation measures. SB13 Munich Conference, April 23-26, Germany.

Mirzaei, P. A., Haghighat, F. 2010. Approaches to study Urban Heat Island – Abilities and limitations, Building and Environment, Volume 45, Issue 10, pp. 2192–2201.

Oke, T.R. 1972. City size and the urban heat island. Atmospheric Environment, Volume 7, Issue 8: 769-779.

Oke, T.R. 1981. Canyon geometry and the nocturnal urban heat island comparison of scale model and field observations. Journal of Climatology, Volume 1: 237–54.

Shishegar, N. 2013. Street Design and Urban Microclimate: Analysing the Effects of Street Geometry and Orientation on Airflow and Solar Access in Urban Canyons, Journal of Clean Energy Technologies, Volume 1, Issue 1, pp. 52-56.

Stewart, I.D., Oke, T. R. 2012. Local Climate Zones for Urban Temperature Studies. Bulletin of the American Meteorological Society, Volume 93: 1879–1900.

Taha, H. 1997. Urban climates and heat islands: albedo, evapotranspiration, and anthropogenic heat. Energy and buildings, Volume 25, Issue 2: 99-103.

Voogt, J.A. 2002. Urban Heat Island. Encyclopedia of Global Environmental Change, Volume 3: 660-666.

Unger, J. 2004. Intra-urban relationship between surface geometry and urban heat island: review and new approach, Climate research, Volume 27, pp. 253–264.

Wind Driven Rain and Climate Change: A Simple Approach for the Impact Assessment and Uncertainty Analysis

Vahid Nik, Senior Lecturer [1, 2]
Angela Sasic Kalagasidis, Associate Professor [3]

[1] Solar Energy and Building Physics Laboratory, Ecole Polytechnique Fédérale de Lausanne (EPFL), Switzerland
[2] Division of Building Physics, Lund University, Sweden
[3] Division of Building Technology, Chalmers University of Technology, Sweden

KEYWORDS: *Wind Driven Rain, Impact Analysis, Climate Change, Climate Scenarios, Uncertainty Analysis*

SUMMARY:
By increasing signs of climate change, growing knowledge about it and the availability of climate data, performing the impact assessment of climate change is becoming more feasible in different fields of science and engineering. However making practical conclusions out of the impact assessment is not easy since there are many climate scenarios for future. This introduces uncertainties in the impact analysis which should be considered. According to different climate scenarios Sweden faces warmer and moister climate. Rain shows strong signals of climate change; more rain in future and stronger and more often extreme raining events, which can increase the risks for buildings and the built environment.

This paper makes a preliminary impact assessment of climate change for wind-driven rain (WDR) on buildings. A simple method from ASHRAE is used to calculate the amount of rain deposition on wall, using the hourly values of rain and wind data from 6 climate scenarios during 1961-2100. Results show that the amount of rain deposition will increase in future, however there are considerable differences in results induced by climate uncertainties. Further research and numerical simulations of WDR is needed to evaluate the preliminary results.

1. Introduction

According to the fourth assessment report of the Intergovernmental Panel on Climate Change (IPCC, 2007), which is also confirmed by the Fifth Assessment Report (AR5), climate changes induces increase in climate variability and extreme events. Most of the future climate scenarios point to more frequent and extreme rain events in different parts of Europe which make buildings and the built environment more vulnerable. Signs of extreme climatic conditions and the corresponding high levels of precipitation have already appeared in Europe. For example during 2012 heavy rains in southern areas of Sweden caused flooding, many people were affected and buildings needed to be pumped dry (DN.se, 2012; Guibourg, 2012). Impacts of climate change on buildings in Sweden can often be associated with increased moisture stress. More intense precipitation events in future, changes in the timing of seasonal precipitation, rainfall, and the length of time surfaces are wet can result in increased and/or accelerated deterioration of the built environment (Moonen et al., 2012). Not preparing for these future changes increases risks, costs and the severity of damages, which can badly influence living conditions and economy of the country. Sustainability of the built environment depends on its adaptation to future climate. Adaption measures can reduce the risks of climate extremes and disasters, regardless of the degree of certainty around future changes (Field et al., 2012).

Wind-driven rain (WDR) is known as a damaging moisture source; out of all the exterior hygrothermal environmental loads which directly influence the moisture transport, WDR is the main reason for

critical damage to the building performance. WDR affects the hygrothermal performance and durability of building façades enormously. Rainwater is also an agent for most of the physicochemical deterioration processes (Moonen et al., 2012) (Blocken and Carmeliet, 2004). In future climate scenarios, precipitation shows the strongest signals of climate change along with temperature for future climate. Unlike precipitation wind has weak signals of climate change, therefore this study focuses on the rain precipitation in future. To estimate the importance of climate change on the hygrothermal performance of buildings in Sweden and to make the buildings resilient enough it is necessary to perform the impact analysis of climate change for WDR on buildings.

This paper presents a preliminary study about the impacts of climate change for WDR on buildings by using a simple method to calculate the amount of rain striking a vertical surface (ASHRAE, 2009). The main intention is to estimate how much situation for buildings can vary in future by estimating the amount of rain deposition on vertical wall surface. Moreover importance of three climate uncertainties - global climate models (GCMs), initial conditions and spatial resolution - in WDR calculations is considered. An earlier work of the authors looked into WDR and climate change by calculating the Stokes number for the driven rain (Nik et al., 2013). The approach in the present paper differs by using an empirical method which focuses more on characteristics of the wall surface than the driven rain. This study has been performed for the city of Gothenburg in Sweden during the period of 1961-2100.

2. Climate Data

Several climate models and scenarios exist. On a global scale, global climate models (GCMs) are used. GCMs consist of individual model components which describe the atmosphere and the ocean. They also describe the atmosphere-ocean interactions as well as interactions with the land surface, snow and sea ice and some aspects of the biosphere (Persson et al., 2007). Regional climate models (RCMs) are used to downscale results from GCMs dynamically, to achieve a higher spatial resolution over a specific region. The climate data used in this work are mainly results from the RCA3 regional climate model by the Rossby Centre which is the climate modelling unit of the Swedish Meteorological Hydrological Institute (SMHI).

Using the numerically simulated climate data in the building models introduces different uncertainties to the simulations. In this paper three climate uncertainties are considered. The first one concerns the changes in the large-scale circulation determined by the GCM. The second factor relates to the initial conditions which were assumed when running the climate models. The third uncertainty is the spatial resolutions of RCMs, since they can downscale data with different spatial resolutions.

2.1 Global Climate Models

RCA3 has been downscaling three different GCMs to 50km horizontal resolution. The GCMs are: 1) ECHAM5, 2) CNRM and 3) IPSL (for details see (Kjellström et al., 2011)). Different GCMs result in different climate conditions. Based on the previous research the uncertainties induced by GCMs are the most important ones in the hygrothermal simulation of buildings (Nik, 2012).

2.2 Initial Conditions

Climate simulations with global climate models for the 20th and 21st centuries generally start with preindustrial conditions. However the initial conditions are not fully known. Initial conditions are needed for the full three-dimensional fields in the atmosphere and oceans. Also starting conditions for the soil models and sea-ice models are needed. In addition to this there is a need to prescribe the physiography (orography, type of soils, vegetation cover, etc) (Nik, 2010). In this paper three simulations of a climate model (RCA3-EHCAM5-A1B) with three different initial conditions are compared. The evolution of time in these three simulations differs as the initial conditions are not the same. These differences are present throughout the simulations, i.e. both in the 20th and the 21st century.

2.3 Spatial Resolutions

RCMs downscale data from GCMs in different spatial resolutions, down to 5km. Data from two spatial resolutions of RCA3, 50km×50km and 25km×25km, are used in this work. RCA3 is set up so that a 50km grid is covered exactly by four grids in the finer-scale 25km integrations. Considering the availability of very fine spatial resolutions, it is important to investigate the uncertainty induced by different spatial resolutions.

3. Wind-Driven Rain

WDR is known as a potentially damaging moisture source. It especially affects the hygrothermal performance and durability of building façades. Out of all the exterior hygrothermal environmental loads which directly influence the moisture transport, WDR causes more than 90% of critical damage to the building performance (Karagiozis et al., 2003). Consequences of its destructive properties can take many forms. It enhances the dry and wet deposition of pollutants, façade surface soiling and façade erosion. The water layer on the façade can increase collection of pollutants. Rainwater is also an agent for most of the physicochemical deterioration processes, frost damage, moisture-induced salt migration, discolouration by efflorescence, and structural cracking due to thermal and moisture gradients (Blocken and Carmeliet, 2004; Moonen et al., 2012). More than that, WDR is one of the most important boundary conditions for HAM (heat-air-moisture) simulations of buildings (Blocken et al., 2007).

4. Methodology

For analysing WDR on buildings usually comprehensive models are used. In this work a simple model is used to estimate changes in WDR on buildings (ASHRAE, 2009). In this model the amount of rain striking a vertical surface is calculated using the following equation:

$$r_{bv} = F_E \cdot F_D \cdot F_L \cdot U \cdot \cos\theta \cdot r_h \quad (1)$$

Where F_E rain exposure factor [-]

F_D rain deposition factor [-]

F_L empirical constant, 0.2 [kg.s/m^3/mm]

U hourly average wind speed at 10 m [m/s]

θ angle between wind direction and normal to the wall [deg]

r_h rainfall intensity, horizontal surface [mm/h]

r_{bv} rain deposition on vertical wall [kg/m^2/h]

In this work the considered wall is facing west. F_E is influenced by the surrounding topography of the building and height of the building which is equal to 1.2 in this work, for a medium exposure and the building height between 10 m and 20 m. It is assumed that the wall is subject to rain runoff and therefore $F_D = 1$.

By programming in Matlab, the amount of rain deposition on the vertical wall was calculated for 6 climate scenarios in Gothenburg for the period of 1961-2100. Only the west-east component of the wind velocity, $\pm U_0$, is considered to simplify the calculations. The west-east component of wind is stronger than the south-north component in Gothenburg. Probable future conditions for WDR and differences induced by the climate scenarios are studied by looking into the distribution of the rain deposition, r_{bv}, during time. For simpler comparison of data sets, the square weighted moving average of the annual mean values is plotted. The dotted line in FIG 1 shows the annual average of precipitation while the black solid line shows the weighted average. The solid line shows the trend of changes with sufficient resolution. Divergence exists in the beginning of the period which occurs due

to the lack of data before 1960 in the calculation of lagging average. However since the focus of the paper is more on the future changes, this divergence can be neglected.

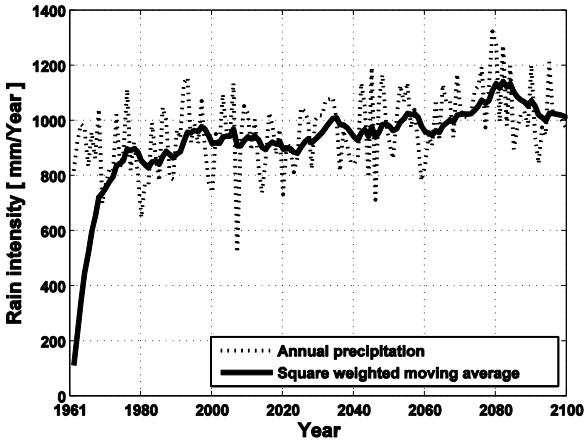

FIG 1. Annual mean precipitation and its square weighted moving average in Gothenburg during 1961-2100. Climate data are from RCA3, downscaling three GCMs with the same emissions scenarios and initial conditions (A1B-3) with the spatial resolution of 50km.

5. Results

As it was mentioned earlier strong signals of climate change are only visible in the rain data and not the wind.

FIG 2 shows the gradual increase in the amount of rain by time, while no considerable changes in the wind velocity are predicted. However climate uncertainties, different GCMs in this case, can affect both the rain and the wind data. Differences are more obvious for rain; although all scenarios point to more precipitation in future there can be differences up to 40% in the annual average of the rain intensity. Differences between scenarios for the WE wind velocity do not follow the same pattern as rain; RCA3-CNRM and RCA3-IPSL show less difference for wind velocity unlike the rain data.

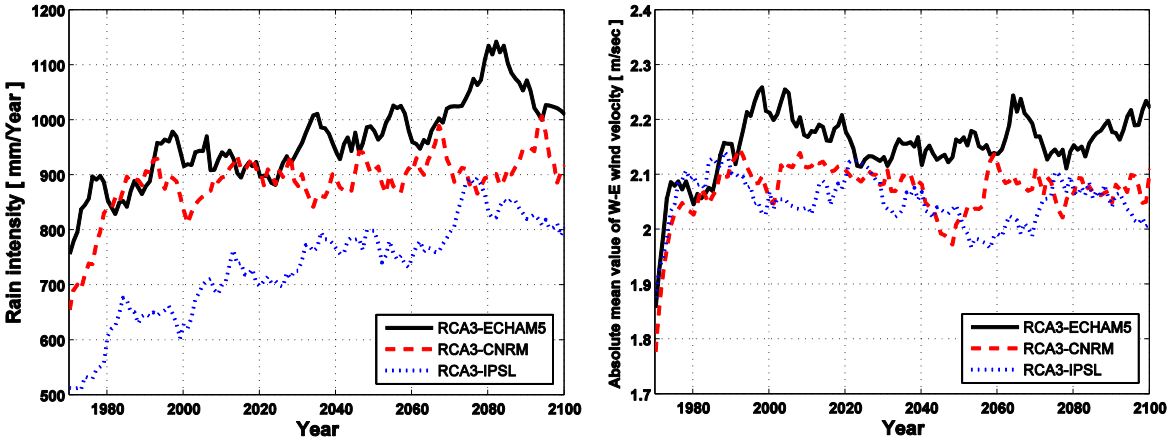

FIG 2. Square weighted moving average graphs for the annual mean value of (left) the rain intensity and (right) the absolute WE wind velocity in Gothenburg. Climate data are from RCA3, downscaling three GCMs with the same emissions scenarios and initial conditions (A1B-3) with the spatial resolution of 50km.

According to relation (1) the amount of rain deposition on vertical wall, r_{bv}, has linear correlation with both the rain intensity and wind velocity. As the distribution of r_{bv} shows in FIG 3, the amount of rain deposition can increase depending on the climate scenario, which RCA3-IPSL shows the maximum increase by time. There is no considerable change in the amount of deposition for RCA3-

CNRM, however sharp changes happen more often after 2050. A previous work showed that the trend of changes for the Stokes numbers in WDR are mostly affected by the wind data, but differences between scenarios are more influenced by the rain data (Nik et al., 2013). One conclusion was that it might be possible to use one wind scenario for WDR calculations and assess the differences induced by climate scenarios only by looking into the rain data. For the calculated r_{bv} in the present paper, differences between scenarios are still more affected by the rain data, however changes of r_{bv} by time can get equally influenced by wind and rain. Although still there are not considerable changes in the wind data by time, but to avoid underestimating the climate uncertainties in WDR calculations, it might better to use different wind scenarios with large differences. The true assessment of the climate uncertainties and the importance of wind/rain data is available when WDR calculations are performed by numerical simulations.

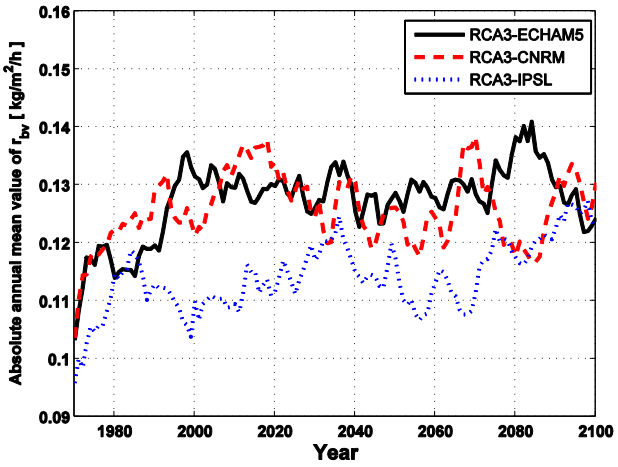

FIG 3. Square weighted moving average graphs for the annual mean value of the rain deposition on vertical wall [kg/m2/h] in Gothenburg. Climate data are from RCA3, downscaling three GCMs with the same emissions scenarios and initial conditions (A1B-3) with the spatial resolution of 50km.

Uncertainties in calculating the rain deposition induced by different initial conditions and spatial resolutions are visualized in figures 4 and 5. Increment of r_{bv} is obvious in FIG 4, specifically for A1B-1 & -2 scenarios. It is interesting to see that using scenarios with different initial conditions can result in considerable differences in calculating WDR. Differences between scenarios are both in the amplitude and the phase of distributions. The patterns of variations are very similar in FIG 5 which compares two scenarios with different spatial resolutions. There is almost no phase shift between the two scenarios since the climate models and the assumptions are unique and the only difference is in RCM downscaling with two different spatial resolutions.

We can get a better image about the influence of climate uncertainties in estimating the amount of rain deposition on a vertical wall by checking FIG 6. It shows the maximum difference due to the climate uncertainties in calculations, for 20-year mean values. For example the GCM graph is the absolute difference between RCA3-CNRM and RCA3-IPSL. Different GCMs can result in differences more than 20%, which cannot be negligible in WDR calculations. For initial conditions the uncertainty decreases to around 15%, which is still high. Difference between the two spatial resolutions of 25km and 50km are less than 7%. These results are in agreement with a previous research which looked into the climate uncertainties in hygrothermal simulation of buildings (Nik, 2012) and calculation of Stokes number (Nik et al., 2013).

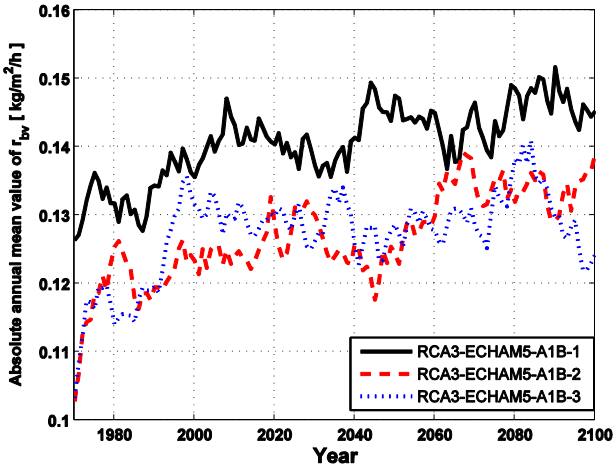

FIG 4. Square weighted moving average graphs for the annual mean value of the rain deposition on vertical wall [kg/m^2/h] in Gothenburg. Climate data are from RCA3-ECHAM5-A1B with three different initial conditions and the spatial resolution of 50km.

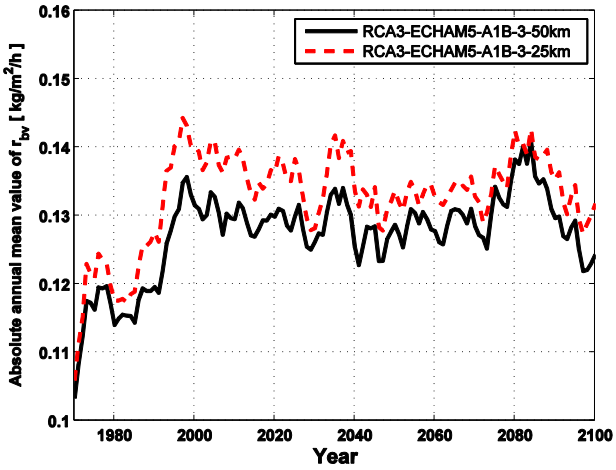

FIG 5. Square weighted moving average graphs for the annual mean value of the rain deposition on vertical wall [kg/m^2/h] in Gothenburg. Climate data are from RCA3-ECHAM5-A1B-3 with two spatial resolutions of 25km and 50km.

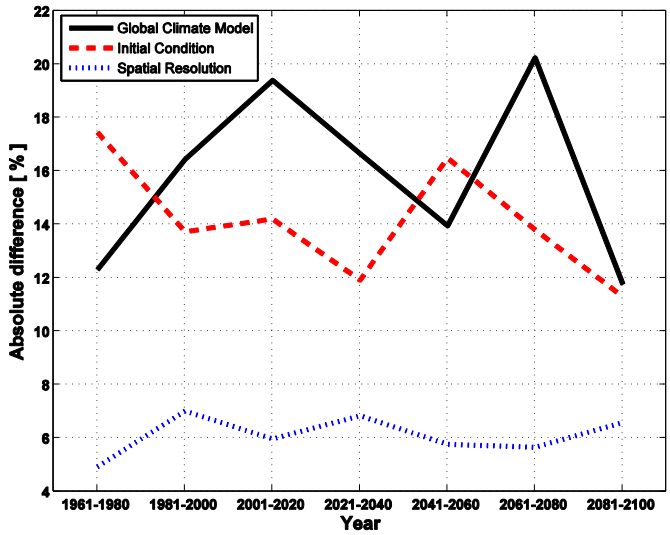

FIG 6. Comparing the importance of the uncertainty factors in WDR calculations; 20-year mean values for the absolute difference of r_{bv} are shown. Graphs represent the scenarios with the maximum difference in figures 3 to 5.

6. Conclusions

The probable effects of climate change on WDR were considered using a simple method to estimate the amount of rain deposition on a vertical wall. The simple method helps to investigate impacts of climate change on WDR and the importance of climate uncertainties before performing the WDR and CFD calculations. Results were in agreement with a previous research which was done by calculating the Stokes number. However this study is still in the preliminary phase and there is a need to perform numerical simulation of WDR.

Based on the results, the most important factor is the selected GCM. Spatial resolution had the least effect on calculations however further research with finer spatial resolutions should be performed. The importance of climate uncertainties in the wind data and its effects on WDR calculation should be investigated more thoroughly in future. It might be possible to use one reference wind data while different rain data sets are used to consider the climate uncertainties. This will help to decrease the calculation time considerably, especially when the CFD models are used to calculate the wind flow around buildings. However in this work the importance of the wind data and its uncertainties was larger than the case of calculating the Stokes number.

References

ASHRAE (2009) Standard 160-2009 -- Criteria for Moisture-Control Design Analysis in Buildings, ASHRAE.

Blocken, B. and Carmeliet, J. (2004) A review of wind-driven rain research in building science, *J. Wind Eng. Ind. Aerodyn.*, **92**, 1079–1130.

Blocken, B., Roels, S. and Carmeliet, J. (2007) A combined CFD–HAM approach for wind-driven rain on building facades, *J. Wind Eng. Ind. Aerodyn.*, **95**, 585–607.

DN.se (2012) Översvämningar i regnets spår på flera håll, *DN.SE*, 8th July, Available from: http://www.dn.se/nyheter/sverige/mariannelund-oversvammat-av-skyfall.

Field, C.B., Barros, V., Stocker, T.F., Dokken, D.J., Ebi, K.L., Mastrandrea, M., Mach, K.J., Plattner, G.-K., Allen, S.K., Tignor, M. and Midgley, P.M. (2012) *Summary for Policymakers. In: Managing the Risks of Extreme Events and Disasters to Advance Climate Change Adaptation*,

A Special Report of Working Groups I and II of the Intergovernmental Panel on Climate Change, Cambridge University Press, Cambridge, UK, and New York, NY, USA, 1–19.

Guibourg, C. (2012) Extreme rains flood southern Swedish town, *The Local*, 8th July, Available from: http://www.thelocal.se/41898/20120708/#.USNHtPLYE59 (accessed 20 February 2013).

IPCC (2007) Climate Change 2007: The Physical Science Basis, *Summ. Policymakers IPCC Genebra*.

Karagiozis, A., Salonvaara, M., Holm, A. and Kuenzel, H. (2003) Influence of wind-driven rain data on hygrothermal performance, Eindhoven, Netherlands.

Kjellström, E., Nikulin, G., Hansson, U., Strandberg, G. and Ullerstig, A. (2011) 21st century changes in the European climate: uncertainties derived from an ensemble of regional climate model simulations, *Tellus A*, 63, 24–40.

Moonen, P., Defraeye, T., Dorer, V., Blocken, B. and Carmeliet, J. (2012) Urban Physics: Effect of the micro-climate on comfort, health and energy demand, *Front. Archit. Res.*, 1, 197–228.

Nik, V., Sasic Kalagasidis, A. and de Wilde, P. (2013) Climate Change and Wind-Driven Rain – a Preliminary Study about Climate Uncertainties, University of Bath, United Kingdom.

Nik, V.M. (2010) *Climate Simulation of an Attic Using Future Weather Data Sets - Statistical Methods for Data Processing and Analysis*, Lic 2010:1, Sweden, Chalmers University of Technology, Available from: http://publications.lib.chalmers.se/records/fulltext/114053/114053.pdf.

Nik, V.M. (2012) Hygrothermal Simulations of Buildings Concerning Uncertainties of the Future Climate, PhD, Gothenburg, Sweden, Chalmers University of Technology, Available from: http://publications.lib.chalmers.se/records/fulltext/159222.pdf.

Persson, G., Bärring, L., Kjellström, E., Strandberg, G. and Rummukainen, M. (2007) *Climate indices for vulnerability assessments*, SMHI Reports Meteorology and Climatology, Norrköping, Sweden, Swedish Meteorological and Hydrological Institute, 64.

Towards efficient numerical modelling of hygrothermal transfers using Proper Generalised Decomposition

Julien Berger[1,2,*],
Sihem Tasca-Guernouti[1],
Monika Woloszyn[2]
Marx Chhay[2]
[1]CETE de l'Ouest, Nantes, France
[2]LOCIE, CNRS UMR 5271, Université de Savoie, Chambéry, France
[*]corresponding author. Tel.: +33240128461.
E-mail address : julien.berger@developpement-durable.gouv.fr

KEYWORDS: *Model Order Reduction, HAM transfers, Proper Generalised Decomposition*
ABSTRACT: *This paper proposes a reduced order model to simulate two-dimensional heat and moisture behaviour of material based on Proper General Decomposition (PGD). This innovative method is an* a priori *method. It proposes an alternative way for computing solutions of the problem by considering a separated representation (for instance time and space) of the solution. PGD allows considerables reduction of numerical cost. In this paper, the PGD solution is first compared with a finite-volume element solution in a 1D-case and then it is appliend on a 2 dimensional case.*

1 Introduction

Building can be affected by damage dues to action of moisture, such as mould growth, corrosion or reduction of thermal resistance of the insulation layers. The development of damage depends on hygrothermal fields in material. To address these issues of durability, detailed modelling exist for precise assessment of hygrothermal transfers in materials. Many 2- or 3- dimensional (2D-3D) heat and moisture (HAM) models are available in literature to assess material behaviour and durability issues (Woloszyn and Rode, 2008). They are used to determine the precise hygrothermal behaviour of complex multi-layered material assemblies. They enable us to take into account different moisture or heat sources. Their integration into whole building simulation tools is an interesting issue to assess durability of building, especially in case of retrofitting. Even if some examples can be found in literature (see for example (Steeman et al., 2009)), this integration is a complex task (Berger et al., 2013b). Such whole integrated building model has a high computational cost.

Thus, innovative and efficient ways of numerical simulation are worth investigation. Reduction techniques seems to be interesting alternatives. This paper proposes a reduced order model to simulate 2D heat and moisture behaviour of material based on *Proper Generalised Decomposition* (PGD). After a brief state-of-the-art of model reduction techniques, PGD strategy is detailed. Then results of the PGD reduced order model is compared to a finite volume resolution on a 1-dimensional case. In final part, possibility of use PGD on a 2-dimensional test case ins investigated.

2 State of the art

For modelling purpose, heat and moisture transfers in layers are generally solved with finite volume or finite elements techniques (in 1, 2 or 3 dimensions). A mesh of M nodes is considered and for transient problems, M values must be computed at each time step. Moreover for non-linear problems, it becomes computationally more expensive when M increases. Reduction techniques aim to approach this kind of highly-dimensional problem with a low-dimensional model. A short review of model reduction methods for non linear models was done in (Berger et al., 2013a). Other details on model reduction methods are given in (Palomo Del Barrio, 2011).

Two families of methods exist. One called *a posteriori*, needs an already-computed or experimental solution to build the reduced order model. Two beneficial approaches belong to this first technique. Firstly, the reduced order model is created with simulations of the large original model on a short time interval. Then the reduced order model is used for simulation on a longer time interval. The second approach is to create the reduced order model with the large original model on a large time interval. Then the reduced order model is used for problems on similar time intervals but with different boundary conditions or material properties.

Such an *a posteriori* method was tested on heat and mass problems in (Berger et al., 2013b). The method gave an interesting reduced order model with a good accuracy. Nevertheless, this kind of methods has important disadvantages. To build the reduced order model, preliminary results, i.e. *snapshots*, of large original model are needed. This requirement is time consuming. In addition, the reduced order model generally works in similar conditions to the ones used to produce the results of the large original models. This point is an important restriction.

The second family of reduction techniques is *a priori* methods. These techniques do not need preliminary informations on the studied problem. The basis of projection is not known *ab initio* and is built by an iterative process or by resolving Lyapunov's equation. Due to this substantial advantages, this type of method was chosen for the present study. Our works were based on *Proper Generalised Decomposition* (PGD). Many works on PGD done by CHINESTA et all. can be found in literature (Dumon et al., 2011), (Aghighi et al.), (Chinesta et al., 2011). This method offers an interesting numerical resolution of the problem and is detailed in next section.

3 Methodology

3.1 Heat and moisture transfers in materials

This part presents the hypothesis and equations of heat and mass transfers in building materials considered for PGD resolution in next section. It is assumed that materials are filled with a liquid phase composed of liquid water, and a gaseous phase, considered as a mixture of dry air and water vapour. The mass balance of water depends on moisture flow of the vapour phase v and of the liquid phase l. The conservation equation of moisture transfer can be expressed as :

$$\frac{\partial w}{\partial t} = -\nabla \cdot (\mathbf{g}_v + \mathbf{g}_l) \tag{1}$$

$\mathbf{g}_v$ is the mass flux of vapour and $\mathbf{g}_l$ is the mass flux of liquid water. Assuming, that air pressure is constant inside the material, the temporal variations of moisture content w can de expressed in function of vapour pressure :

$$\frac{\partial w}{\partial t} = \frac{\partial w}{\partial P}\frac{\partial P}{\partial t} + \frac{\partial w}{\partial T}\frac{\partial T}{\partial t} \tag{2}$$

Temperature variation of moisture content is neglected and $\xi = \frac{\partial w}{\partial P}$ describes the moisture storage. Therefore mass conservation in material (1) can be written as :

$$\xi \frac{\partial P}{\partial t} = \nabla(\delta_v + K_l \frac{\rho_l R_v T}{P}) \cdot \nabla P) \tag{3}$$

with $K_l(w)$ liquid permeability and $\delta_v(w)$ the vapour permeability of the material.

The energy balance equation is expressed in function of conductive and convective flux:

$$\frac{\partial E}{\partial t} = -\nabla \cdot (\mathbf{q}_{cond} + \mathbf{q}_{conv}) \tag{4}$$

where E is the internal energy. Air pressure is assumed as constant. $\{c_a, c_l, c_v\} \ll L_v$ so only latent flux is considered for the study and others flux are neglected. Therefore, energy balance equation is :

$$\rho_0 c \cdot \frac{\partial T}{\partial t} = \nabla \cdot (\lambda \nabla T + L_v \delta_v \nabla P) \tag{5}$$

with $c = c(w) = c(P) = c_0 + \frac{\rho_l}{\rho_0} * c_l$, where subscripts 0 and l indicates respectively properties of dry material and water and $\lambda(w)$ is the thermal conductivity, dependant with moisture. Eventually heat and moisture transport in Ω can be expressed as the following equation :

$$\begin{bmatrix} \rho_0 c & 0 \\ 0 & \xi \end{bmatrix} \cdot \begin{bmatrix} \frac{\partial T}{\partial t} \\ \frac{\partial P}{\partial t} \end{bmatrix} = \nabla \cdot (\begin{bmatrix} \lambda & L_v \delta_v \\ 0 & \delta_v + K_l \frac{\rho_l R_v T}{P} \end{bmatrix} \nabla \cdot \begin{bmatrix} T \\ P \end{bmatrix}) \tag{6}$$

The problem is a system of two non-linear partial coupled differential equations with temperature T and vapour pressure P as driving potentials.

3.2 Proper Generalised Decomposition

A problem is considered in a space of dimension d for the unknown field $u(x_1, x_2, \ldots, x_d)$. x_i can be a spatial coordinate, related to time or a problem parameter such as boundary or initial conditions, source term or material property. The solution is search for $(x_1, x_2, ..., x_d) \in \Omega_1 \times \Omega_2 \times \cdots \times \Omega_d$.

With the PGD method, the approximate solution is given by a separated representation:

$$u(x_1, x_2, \ldots, x_d) = \sum_{m=1}^{M} F_m^1(x_1) \otimes F_m^2(x_2) \otimes \cdots \otimes F_m^d(x_d) \tag{7}$$

The solution is a sum of M functional products involving d separated functions $F_i^j(x_i)$ that are unknown *a priori*. Functions are built by successive iterative enrichment. At a particular enrichment step n, the functions $F_i^j(x_i)$ are known for $i \leq n-1$ with the previous steps. Unknown functions $F_n^j(x_i)$ are computed using the equations of the considered problems.

the number of terms M required to approximate the solution depends on studied problem but might be between 10 to 100 in building physics application.

In present work, coupled heat and moisture transfers in porous materials, described by equation (6), are considered.. For $(\mathbf{x}, t) \in \Omega \times \Gamma$, $T(\mathbf{x}, t)$ and $P(\mathbf{x}, t)$ are search as solutions of the following equation:

$$\begin{bmatrix} c_{11}(T,P) & 0 \\ 0 & c_{22}(T,P) \end{bmatrix} \cdot \begin{bmatrix} \frac{\partial T}{\partial t} \\ \frac{\partial P}{\partial t} \end{bmatrix} = \nabla \cdot (\begin{bmatrix} d_{11}(T,P) & d_{12}(T,P) \\ d_{21}(T,P) & d_{22}(T,P) \end{bmatrix} \nabla \cdot \begin{bmatrix} T \\ P \end{bmatrix}) \tag{8}$$

TAB 1: Wood frame hygrothermal properties

Sorption curve $[kg/m^3]$	$m = 17.07$, $c = 8.076$, $k = 0.9699$	$w = m \cdot c \cdot \frac{\frac{P}{P_{sat}}}{(1-k\cdot\frac{P}{P_{sat}})(1-(k-c)\cdot\frac{P}{P_{sat}})}$
Liquid permeability $[s]$	$K_0 = 1.17 \cdot 10^{16}$, $a_1 = 0.2449$, $b_1 = 1.339$, $a_2 = -0.2441$ $b_2 = -93.79$	$K_l = K_0 \cdot (a_1 \cdot exp(b_1 \cdot \frac{w}{w_0})$ $+a_2 \cdot exp(b_2 \cdot \frac{w}{w_0}))$
Vapour permeability $[kg/m/s/Pa]$	$D_{v0} = 2.6 \cdot 10^5$	$\delta_v = \frac{D_{v0}}{462*T} \cdot (-18.14 \cdot 10^{-4} \cdot w + 1)$
Thermal conductivity $[W/m/K]$	$\lambda_0 = 0.107$, $b = 0.4747 \cdot 10^{-3}$	$\lambda = \lambda_0 + b \cdot w$
Heat storage $[J/m^3/K]$	$\rho_0 \cdot c_0 = 1551 \cdot 589$	

with coefficient for material properties corresponding to equation (6). Initial conditions are taken into account and Dirichlet or Neumann boundary conditions are associated to the problem. Noting $\Theta(\mathbf{x}, t)$ as $\Theta = \begin{bmatrix} T(\mathbf{x}, t) \\ P(\mathbf{x}, t) \end{bmatrix}$, such problems can be expressed with operator $\mathscr{A}$:

$$\mathscr{A}(\Theta) = 0 \tag{9}$$

N_x and N_t are assumed to be, respectively, spatial and time discretisation. Operator $\mathscr{A}$, is discretised by a tensorial product A_x^k and A_t^k, in space and time directions:

$$\mathscr{A} = \sum_{k=1}^{n_A} A_x^k \otimes A_t^k \tag{10}$$

Operator size A_x^k is $N_x \times N_x$ and A_t^k is $N_t \times N_t$. The PGD solution of this problem is sought in the form:

$$\Theta(\mathbf{x}, t) = \sum_{m=1}^{M} F^m(x) \otimes G^m(t) \tag{11}$$

with $(F^i, G^i)_{1 \le i \le m}$ the modes of PGD basis.

4 Proper Generalised Decomposition application on a 1D problem

4.1 Case study

To validate the resolution of heat and moisture transfers in material with PGD, a 1D case study, $x \in [0; d = 0.08m]$, is chosen. The material is wood fiberboard with hygrothermal properties given in table 1. The initial and Dirichlet boundary conditions for temperature T and relative humidity RH are:

$$\begin{aligned} &T(x, t = 0) = 23^\circ\text{C}\ ,\ T(x = 0, t \le 0) = 23^\circ\text{C}\ ,\ T(x = d = 0.08, t \le 0) = 15^\circ\text{C} \\ &RH(x, t = 0) = 0.4\ ,\ RH(x = 0, t \le 0) = 0.4\ ,\ RH(x = d = 0.08, t \le 0) = 0.9 \end{aligned} \tag{12}$$

The problem is solved by PGD and results are compared with a finite volume resolution. Details of the finite volume model are given in (Berger et al., 2013a). It was validated on Hamstad benchmarks. The problem is solved for a time period of 24 hours and a constant time step of 36 seconds. The layer is divided in 81 nodes with a constant spatial discretisation of 1 mm.

4.2 Results

The PGD solution is calculated with 60 modes. Different profiles of temperature and vapour pressure are compared at different moments in figure 2. In addition, the time evolution of temperature and vapour pressure for different nodes is given in figure 1. To compare both resolution of the problem, the maximum relative difference between both model is calculated and plotted in figure 3 according to the number of modes of PGD solution.

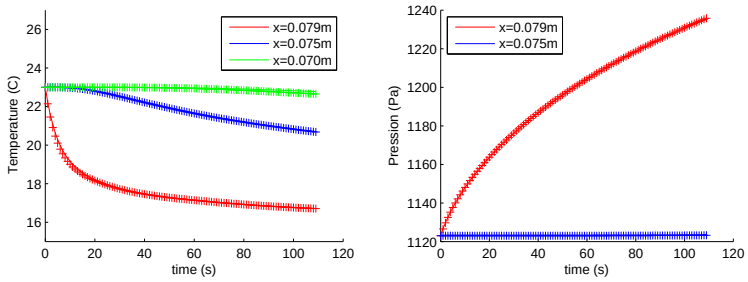

FIG 1: Time evolution of temperature and vapour pressure at different nodes for PGD solution (continuous line) and finite volume solution (+ points)

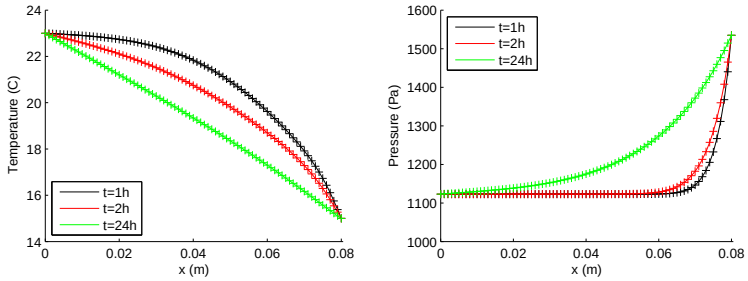

FIG 2: Profiles of temperature and vapour pressure at 1h, 2h and 24h for PGD solution (continuous line) and volume element solution (+ points)

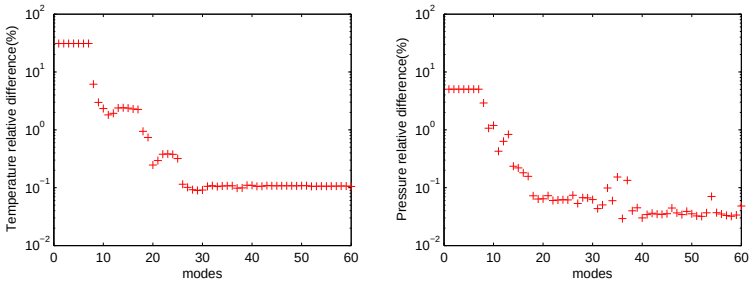

FIG 3: Maximum relative difference between both model for temperature and pressure in function of modes

4.3 Discussion

One can see that there is perfect accuracy of the PGD solution in figures 1 and 2. Absolute differences between the finite-volume model and PGD solution is less than 10^{-4} for temperature and pressure. PGD solution of the problem succeeds in representing temperature and vapour pressure inside material. The dynamic and amplitude of the hygrothermal field are well represented.

The choice of number of modes M for the separated representation is a relevant question. A number of 60 modes was chosen to compute the PGD solution in this test case. As shown in figure

3, the relative difference between the finite-volume solution and the PGD solution is less than 0.1% for a number of 40 modes. For the next simulations, a number of 40 modes was assumed sufficient to reach a good accuracy.

The separated representation of the PGD solution enables to have a low computational cost. With PGD techniques, two linear differential equations for x and t has to be solved. The cost of such PGD resolution is lower than solving equation 6 with finite-volume techniques. This point becomes more interesting when problem complexity increases. PGD solution offers interesting outlooks for modelling heat and mass transfers in 2- or 3-dimensional problems.

5 2D heat and mass problem

Results presented in previous section illustrate the possibilities with PGD techniques to solve heat and moisture problems with a good accuracy. The interest of the separated representation is illustrated for solving complex 2D problems. A *plate-type decomposition* is adopted to compute temperature and vapour pressure (Chinesta et al., 2011):

$$T(x,y,t) = \sum_{i=1}^{N} F_i^T(x,y) \cdot G_i^T(t) \text{ and } P(x,y,t) = \sum_{i=1}^{N} F_i^P(x,y) \cdot G_i^P(t) \tag{13}$$

5.1 Test case

The test case represents composition of an old building walls, associating timber pine filled with mortar. In the context of building retrofitting, this wall assembly should be insulated. Modelling tests with different types of insulations could be performed to assess durability of this type of improved wall assembly. One could be interested in studying the impact of a high or low hygroscopic insulation. In present work, such assembly was modelled with PGD techniques with two different types of insulate: PSE and wood fibre (figure 4. The issue is to study the impact of both insulate on moisture content in wall assembly.

Variations of properties as a function of water content and temperature are taken into account. Material hygrothermal properties were taken from (Kumaran, 1996). Sides ($\forall x, y = 0$) and ($\forall x, y =$ 0.9m) are considered as adiabatic. Conditions for the outside and inside faces are given in figure 4 with corresponding surface transfer coefficients given in table 2. Simulation was done for 20 days with a time step of 360 s and a spatial discretisation $dx = dy = 0.02$ m.

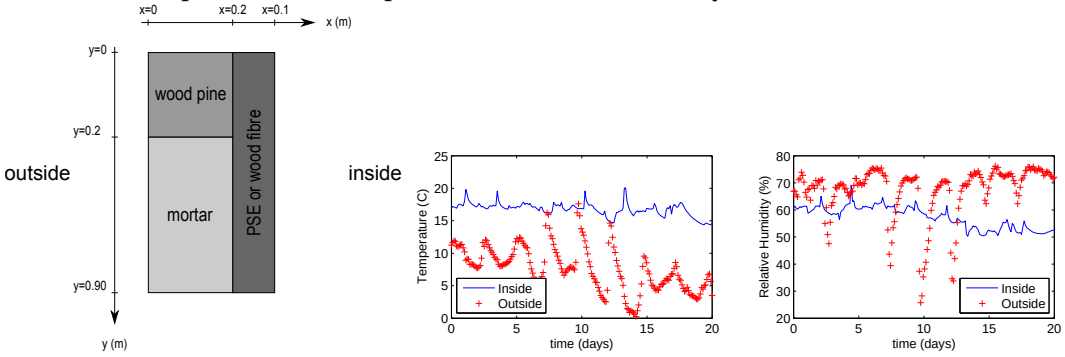

FIG 4: 2-dimensional multi-layered test case for PGD and boundary conditions

TAB 2: Surface exchange coefficients

	Inside	**Outside**
Heat surface transfer coefficient $[W/m^2K]$	8	25
Vapour surface transfer coefficient $[s/m]$	$1 \cdot 10^{-7}$	$3 \cdot 10^{-8}$

5.2 Results

The solution is calculated using $M = 40$ modes. In figure 5, hygrothermal fields are plotted for modelling considering wood fibre insulation. Figure 6 gives the total moisture content for mortar and wood for both wall assemblies. Figure 7 gives heat and vapour flux exiting insulation for both modelling.

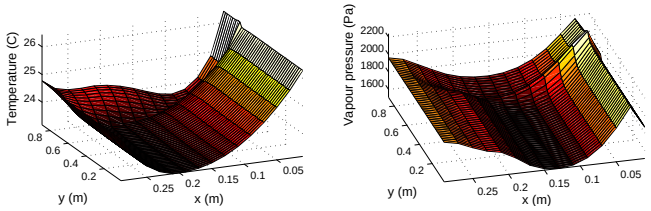

FIG 5: hygrothermal fields for the wood-fibre wall assembly at $t = 20 days$

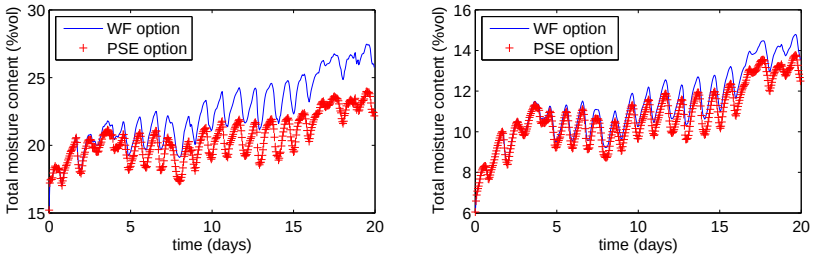

FIG 6: Total moisture content in mortar (left) and wood (right) for both modelling

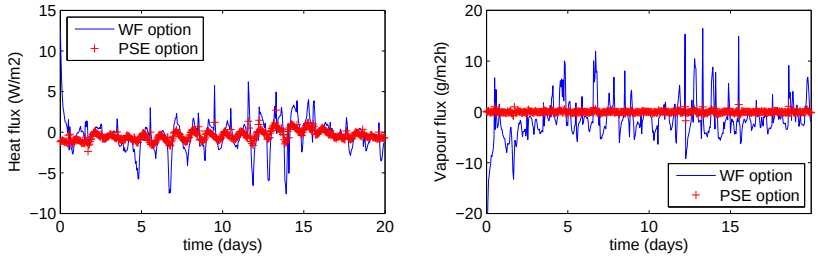

FIG 7: Heat and vapour flux exiting insulate for both modelling

5.3 Discussion

One can notice that PGD technique enables us to calculate precise hygrothermal fields in 2D wall assembly as mentioned for wood fibre as example on figure 5. Hygrothermal fields are correctly modelled in 2-dimensions. These hygrothermal results can be used for post-processing. The issue is to analyse which assembly is more efficient for insulating the old wall. As shown in figure 6, the total moisture content in wood and mortar is higher for the wall assembly with wood fibre, for these boundary conditions. Actually, wood fibre is more vapour-permeable than PSE. Dry vapour permeability considered is $8 \cdot 10^{-13}$kg/(m.s.Pa) for PSE and $9 \cdot 10^{-6}$kg/(m.s.Pa) for wood fibre. Therefore, for the wall assembly with wood fibre, moisture penetrates from both inside and outside borders. On the other hand, for the PSE wall assembly, moisture only penetrates from outside border. This results can also be seen in figure 7. Vapour flux is really smaller for wall assembly with PSE. In addition, figure 7 shows that heat flux is more important for the wall assembly considering wood fibre. This is due to the effect of vapour flux and to the higher dry thermal conductivity of wood fibre (0.042W/(m.K) opposed to 0.0251W/(m.K) for PSE).

With these considerations, one can see that the PSE wall assembly is more efficient for insula-

tion of the wall for these boundary conditions. To go further, the important point is that the PGD resolution enables us to model hygrothermal fields and to observe similar physical aspects as classic resolution (detailed finite-element or -volume resolution etc.). The interesting point is that PGD resolution has a lower computational cost due to the *plate-type decomposition*. The 2-dimensional problem is replaced by solving 2 differential equation for (x, y) and t. A brief comparison was done with a 2D finite volume resolution and computational gain was divided by 6 (with a AMD Phenom II, processor 2.99 GHz, 3.5 GO RAM). Gain might be increased by parallel computing.

6 Conclusion

This paper proposed a Proper Generalised Decomposition for solving heat and moisture transfers in materials. This technique is based on a space-time separated representation of solution. Comparing PGD solution with finite volume solution, the relative error is less than 0.1 %. This resolution strategy was illustrated on a 2-dimensional test case. PGD is efficient for addressing models defined in high-dimensional spaces with a low computational cost. Future works will concern integration of 2-dimensional PGD model into whole building simulation.

7 Acknowledgements

The authors acknowledge the french National Research Agency (ANR) for funding this work through its Sustainable Buildings and Cities programme (HUMIBATEX project n°ANR-11-BVD).

References

Aghighi, M., Ammar, A., Metivier, C., Normandin, M., and Chinesta, F. Non-incremental transient solution of the Rayleigh–Bénard convection model by using the PGD. *Journal of Non-Newtonian Fluid Mechanics*.

Berger, J., Tasca-Guernouti, S., Woloszyn, M., and Buhe, C. 2013a. Mould growth damages due to moisture: comparing 1D and 2D heat and moisture models. Chambéry.

Berger, J., Tasca-Guernouti, S., Woloszyn, M., and Buhe, C. 2013b. On the integration of hygrothermal bridges into whole building and HAM modeling. Chambéry.

Chinesta, F., Ammar, A., Leygue, A., and Keunings, R. 2011. *An overview of the proper generalized decomposition with applications in computational rheology. Journal of Non-Newtonian Fluid Mechanics*, 166(11):578–592.

Dumon, A., Allery, C., and Ammar, A. 2011. Proper general decomposition (PGD) for the resolution of Navier–Stokes equations. *Journal of Computational Physics*, 230(4):1387–1407.

Kumaran, M. K. 1996. *International Energy Agency energy conservation in buildings and community systems programme Heat, air and moisture transfer through new and retrofitted insulated envelope parts: [IEA] (Hamtie); Annex 24 Task 3/Final report: Material properties.* Laboratorium Bouwfysica, Dep. Burgerlijke Bouwkunde, K.U.-Leuven.

Palomo Del Barrio, E. 2011. *Solving high dimension thermal problems : reduction method (in French)*. Editions Universitaires Europeennes.

Steeman, H.-J., Van Belleghem, M., Janssens, A., and De Paepe, M. 2009. Coupled simulation of heat and moisture transport in air and porous materials for the assessment of moisture related damage. *Building and Environment*, 44(10):2176–2184.

Woloszyn, M. and Rode, C. 2008. Tools for performance simulation of heat, air and moisture conditions of whole buildings. *Building Simulation*, 1(1):5–24.

Road-map for future thermal insulation products and applications

Tuomo Ojanen, M.Sc. [1]
Isabel Pinto Seppä, D.Sc., [1]

[1] *VTT Technical Research Centre of Finland*

KEYWORDS: *Building envelope, thermal insulation, road map, future materials, energy efficiency*

SUMMARY:
The European energy efficiency policy sets challenging objectives both for new buildings and for retrofitting. The thermal performance of the building envelope is one significant part of the energy efficiency of the future buildings. There is on-going strong development of new insulation materials and also the properties and application systems of conventional insulation are improved.

This paper presents a road-map for research and technology development (RTD) priorities future thermal insulation materials, products and holistic solutions. The objective was to identify and verify the RTD topics and product development priorities and to identify current, emerging and promising technologies and materials that can support the development towards energy and resource efficient targets. The study was focused on Finnish market perspective, being applicable to Northern climate in general.

The study included state-of-the-art, analysis of key performance indicators of thermal insulation products, a patent search, interviews of building sector professionals and analysis forms a survey of the technology development in this field. The interviews revealed the expectations, barriers, trends and hypes that are related to the energy efficient building envelope applications. This paper presents the methodologies and part of the findings of the project.

1. Introduction

Challenges with climate change impacts and natural resources constrains has set multiple energy efficiency targets.
The EU aims to improve energy efficiency by 20% by 2020[1](from 1990 levels); however, the European Commission estimates that only half of the target can be achieved if new specific measures are not implemented. To attain the objectives of a maximum temperature rise of 2°C by 2050, a reduction of GHG emissions of 80-95% by 2050 will be necessary. Residential and commercial buildings are responsible for about 40% of the EU's total final energy consumption and 33% of CO2 emissions. Being the largest consumer of energy and the largest CO2 emitter, addressing the building sector is crucial for meeting the ambitious energy and climate objectives.

To achieve these targets requires an integrated approach including the deployment of energy-efficient technologies as well as the engagement of influential stakeholders on the market

[1]Communication from the Commission.(2006). Action Plan for Energy Efficiency: Realising the Potential.

supply and demand for those technologies. A well-insulated building envelope is recognized as key for high energy-efficient performance of buildings (IEA 2013).

Energy efficient and passive structures, in cold climates, typically use high volumes of thermal insulation leading to thick building envelopes. This causes architectural technical challenges, like the placement of windows, and also valuable building space is lost. New improved thermal insulation products and integrated envelope solutions are now emerging in the market. Developments in materials science, for different fields and industries, bring more suitable solutions for use in the construction in order to better manage the building envelope heat flows.

These new solutions are at different development stages from research to commercialization. Along this path their suitability for the building envelops needs to be analysed against key performance indicators and current legislation (WBCSD 2009). The presented roadmap was created to answer the needs on how building envelope insulation materials and products, at different development stages are positioned in this framework and how changes in the built environment affect existing products and create new emerging ones. This paper presents the highlights of the roadmap. The full report can be found in Ojanen et.al. (2014).

The study focused on thermal insulation materials and thermal performance solutions of the building envelope in cold climates. Out of the scope were the technical systems (HVAC), hygrothermal performance of structures and cost-efficiency issues.

Although many promising insulation materials and products solutions are emerging in the market there are many technical and socio-economic barriers to overcome before market upscale and mass production. The main drivers are the building directives and regulations, and the main barriers come often from non-technological issues. Together with the regulations, the market needs and expectations affect the demand for insulation products and envelope systems, performance and technical features. The combination of energy efficiency regulations and the challenge of the renovation of the old Finnish building stock raises demands for adaptable and integrated pre-fabricated products.

2. Roadmap methodology

2.1 State of the art

The state of the art of thermal insulation solutions for building envelops were analysed through their technical performance and current market environment. The study was done gathering qualitative information through literature surveys on innovation science publications as well as on patents database, product information and statistics and regulatory publications. In addition previous relevant roadmaps were reviewed as the E2BA multiannual roadmap (E2BA 2013); the SET plan materials roadmap (EU 2011) and national ones as the built environment (Airaksinen, M. et. al., 2011). These formed the baseline for the development of roadmap and future recommendations.

2.2 Interviews and workshop

The drivers, barriers and trends were studied through focused interviews and stakeholders feedback in an active workshop discussion. These were analysed and processedthrough the following steps:

1. Categorization of the main thermal insulation materials, products and systems
2. Identification of solutions that are in different stages of research or already commercialized
3. Evaluation criteria and performance indicators
4. Analysis of demand, potential usage scenarios
5. Description main innovation trends through analysis of main market players patents
6. Stakeholders interviews
7. Roadmaps for short, medium and long-terms
8. Recommendations

Altogether 23 building sector experts from construction industry, insulation material producers, architects, R&D, authorities and industrial associations were interviewed. A workshop for 30 participants was focussed on the most important gaps pointed by stakeholders during the interviews. Four discussion groups were set up based on the dimensions: People, business, processes and technology.

Figure 1 shows the method used in the workshop.

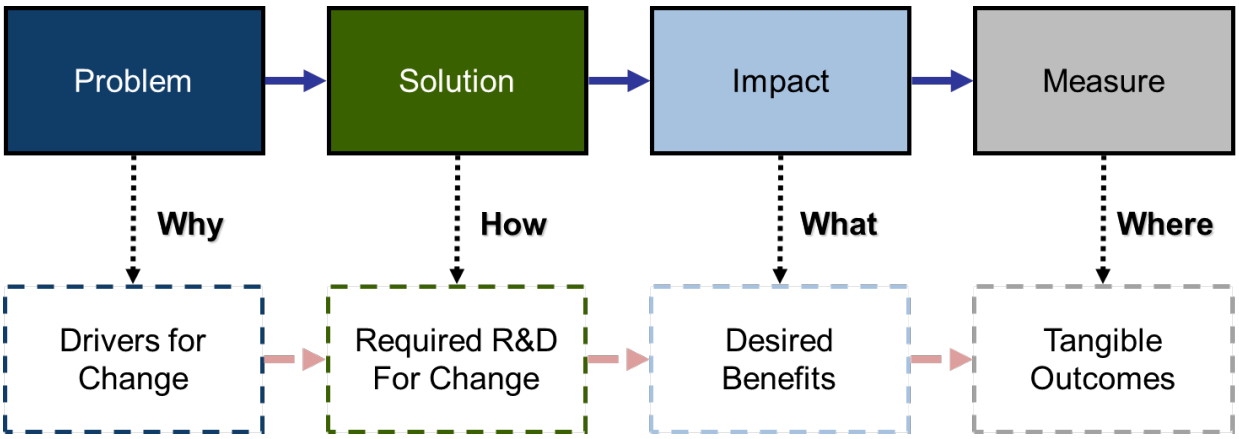

FIG 1. *A schematic presentation of the method used in the workshop.*

2.3 Materials and products analysis

The insulation materials and products were mapped into 3 key segment areas. The definition of these areas was based on market establishment of the main products as conventional versus emerging products. In addition a segment was created to analyse the trend for integrated special products and systems as not just only "thermal insulation solutions for building envelope" but also "energy efficient solutions for proactive envelopes". These areas are described in figure 2.

2.4 Key performance indicators

The CE-marking requires some basic performance indicators for the thermal insulation product. In addition, different performance indicators have to be known and for comparison of the products and their suitability for different building envelope applications. The main indicators are: Thermal conductivity, dimensions and dimensional stability, squareness, tencile strength, fire properties. In addition also properties like sound absorption, air permeability, health issues, sensitivity to moisture, technical lifetime expectancy, embodied energy, and those linked to buildability and recycling are important factors that have to be taken into account. The weight of each performance property depends on the application.

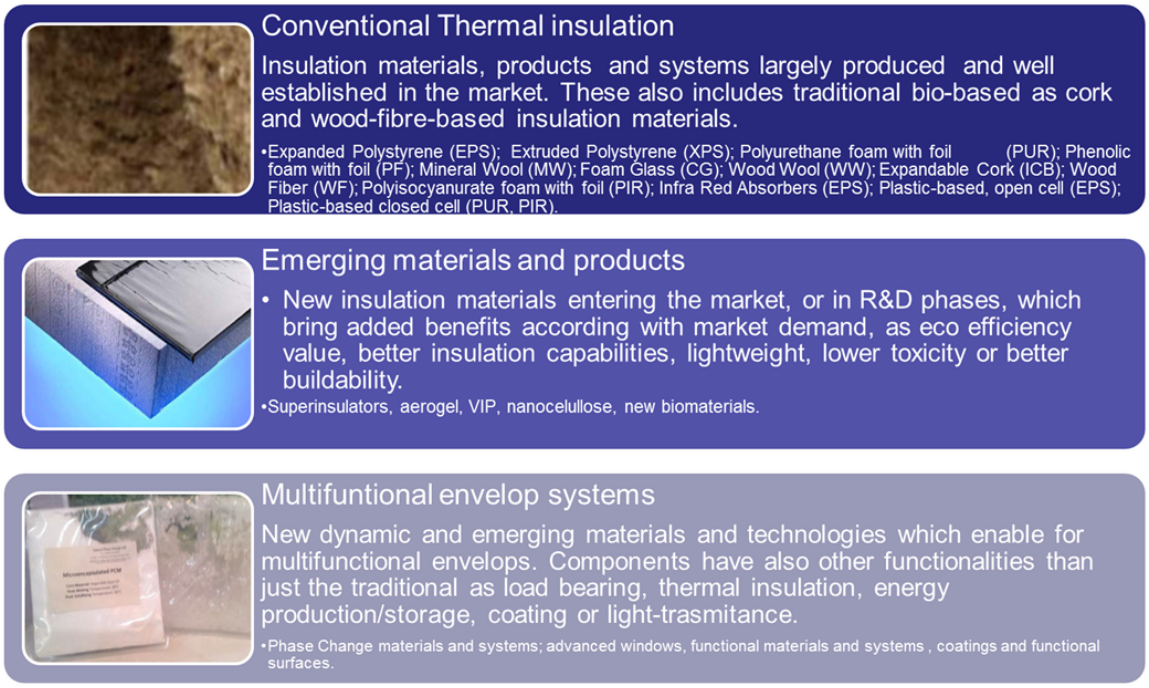

FIG 2.Thermal insulation product and application categories used in the study.

3. Roadmap for future thermal insulation products

Based on the gaps between the state-of-art and the visions, determine by experts and stakeholders the roadmaps were built separately for the industry processes, products and systems, regulations and for the research and development aspects. These form the overall roadmap for the energy efficiency development of the buildings.

The thermal performance of the building envelope couldn't be separated from the whole building performance and the building couldn't be separated from the building process. Therefore the result of the roadmapping process is not only an answer for the thermal insulation development or the development of the building as a whole, but it tended to open up the whole building sector. The segments developed in the roadmap were Markets and people, Regulations, Building services, Building products and Research. For this paper only some parts of the results are presented. Figure 3 shows the roadmap summary for the building envelope with target in nearly zero energy buildings and Figure 4 the roadmap for the building products segment.

When developing new thermal insulation materials, or any materials for the building envelope, the performance of the whole system must be taken into account as presented in Figure 5. A new material, even how good technical performance properties it has, is not yet a ready solution for the market. Suitable products have to be developed. If the products do not fit into the existing building systems, a new system has to be developed. Only after that the integration into the building can be done effectively.

This process requires both technical development and improved know-how in production process, design, installation, total performance analysis, etc. The existing products have relatively high level systems already. The new products have to adopted in the building system so that their technical benefits can be utilised in the best way.

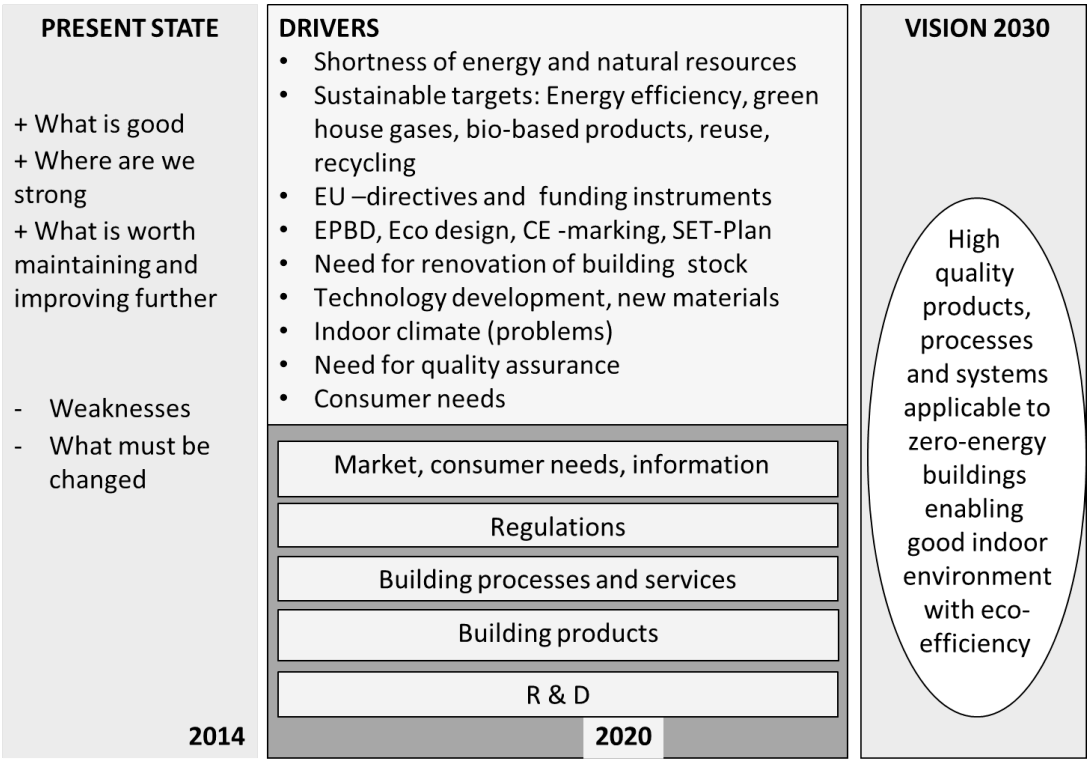

FIG 3. *Roadmap summary for the building envelope of nZeB*

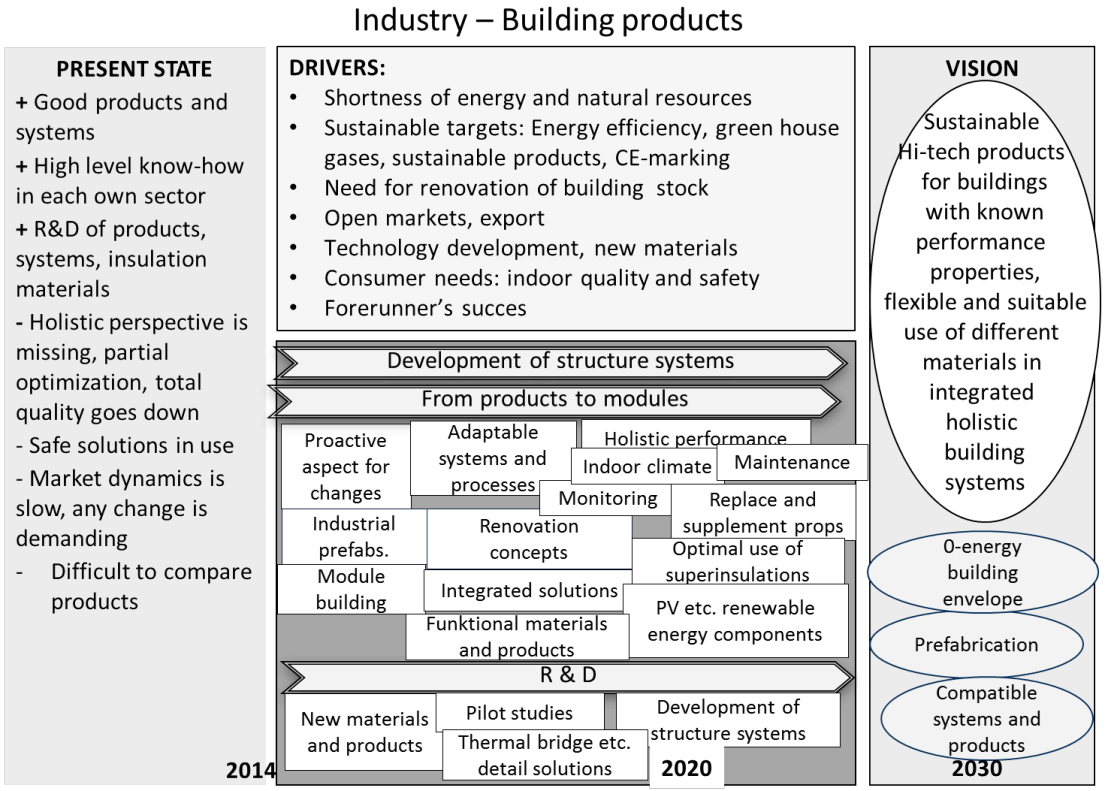

FIG 4. *Roadmap segment for the building products.*

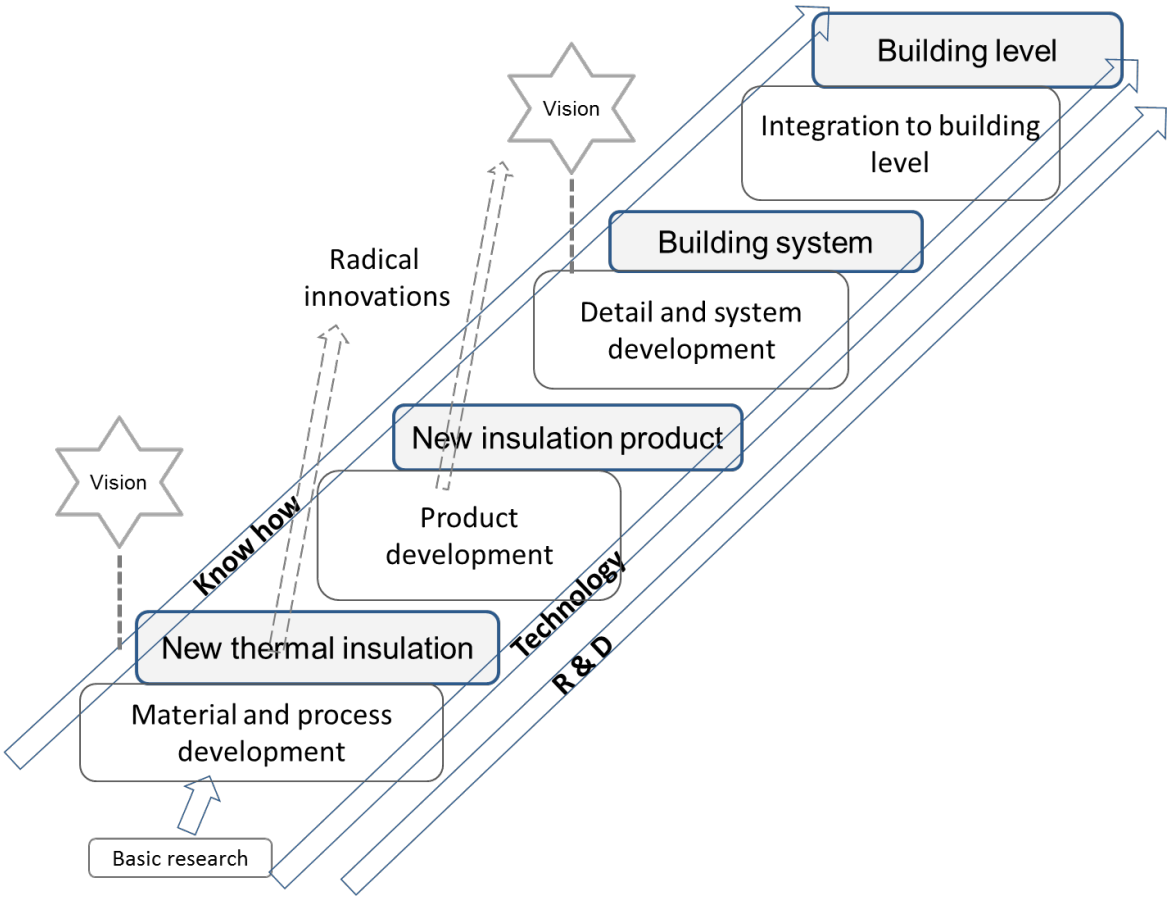

FIG 5. Product development steps from material to a product that can be integrated into highly energy efficient building.

Table 1 presents the summary of recommendation for different stakeholders. The recommendation are aimed to promote for the actions required for the target visions of the future building envelope development. The focus areas are is in the process and application of regulations in practice and also in the information of people in order to have trust and demand for quality of the building. High quality is essential in the nearly zero energy building applications.

4. Discussion and conclusions

The legislation and directives regarding sustainability, in general and energy efficiency in particular are becoming more tight. This is seen as a driver for the insulation products because it increases the market demand. However at the same time many stakeholders indicate it as a barrier because it slows down the business, creates challenges to the processes and creates barriers to the development and market up-take of new products.

The promising potential of new insulations solutions as aerogels, VIPs, bio-based materials and nano-based technologies, is seen as quite important for many of the R&D experts (Jelle 2011, Flynn & Sirén 2012). The industry does recognize these as promising solutions but does not see these as a threat in the near future. This is because the traditional products are well established and the construction industry is a slow adapter of new solutions. The building process is seen as one of the biggest barriers for the adaptation of new solutions.

TABLE 1. Summary of the recommendations for different stakeholder perspectives.

Effect on:	Who needs (to do) something					
	People	**Research**	**Regulations**	**Industry**		
				Building process	**Services**	**Products**
People, Markets	Quality requirements, demand for safe performance	True info on performance aspects	Supporting systems, possible to choose suitable materials, localized aspect, transparency of reasons for reg.	Show-cases	Adaptable solutions,	New products, comparable tech. info, educate sales people
Regulations		Impact analysis				Education, Benchmarking of new products, structures
Technology	demand	Tech.transport and development of new materials, products, applications	Guidelines prepared in good time, update fire regulations, district level	Integration of the building process, Hi-tech industry using pre-fabs	Integrated solutions and smart technologies	
Services	demand	Concept development, safe moisture performance processes	Requirement for quality certificate for buildings, building process and final performance responsibilities	Pre-fabrication concepts, coordination throughout the process, performance of the buildings	Form chain of companies Invest in skilful people, renovation solutions, support for pioneers	Modules, compatible products
Products	demand	Performance studies, material and product development	Information, guidelines, localized aspect, embodied energy in CE marking	Performance property matrix	Requirements for building components	Eco efficient , new materials
Research			Research result support system for decision making			

Promote positive thinking on the performance of buildings and Energy Efficiency, in combination with the correct choice of materials. Good concepts have been developed and significant research has been done. There is now a need to consolidate and invest on more public dissemination and awareness.

The impact of a good insulation cannot be separated from the total performance of the buildings energy performance or building physics. A holistic approach should be taken together with the use of materials. Material efficiency should be taken into account together with other measures as ventilation and automation and energy management systems. It is not only about reducing CO2 emissions or improving energy efficiency.

The forerunner companies and pilot studies should be promoted and supported in order to enhance the release of the good practices and the demand for them. The realization of the new approaches requires investing in education of professionals to design and apply the new systems in practice.

5. Acknowledgements

Project FUTBEMS (Future Building Envelope Material Solutions) was financed by The Ministry of Environment in Finland, The Confederation of Finnish Construction Industries RT and VTT (Technical Research Centre of Finland) and it was carried out by VTT during 2012 – 2013.

References

Airaksinen, M., Hietanen, O., Manninen, A.-P., Reijula, K. & Vainio, T. 2011. Roadmap for the built environment (in Finnish). Tekesin report 5/2011. Editor Suvi Nenonen, Helsinki 2011. 84 s.

E2BA. 2013. Towards the creation of a high-tech building industry. Turning energy efficiency into sustainable business. Research & Innovation Roadmap 2014-20. Energy-efficient buildings ppp.Draft version, March 2013. Avail-able http://www.ectp.org/cws/params/ectp/download_files/36D2534v2_E2B_Roadmap_draft.pdf

EU. 2011. Materials roadmap enabling low carbon energy technologies. Commis-sion staff working paper. SEC(2011) 1609 final. Brussels 13.12.2011. At http://ec.europa.eu/research/industrial_technologies/pdf/materials-roadmap-elcet-13122011_en.pdf

IEA International Energy Agency, Technology roadmap. Energy efficient buildings. IEA 2013. 64 p.

Jelle, B. P. 2011. Traditional, state-of-the-art and future thermal building insulation materials and solutions – Properties, requirements and possibilities. Energy and Buildings 43, pp. 2549–2563.

Flynn, C. & Sirén, K. 2012. Innovative thermal insulation materials and technolo-gies. RYM-SY Indoor Environment WP2 EECI. Allto University, Espoo 2012. 72 p.

Ojanen, T., Pinto Seppä I., Koukkari H. and Nykänen E. *Roadmap for the thermal insulation solutions of future building envelopes. VTT Technology -series report. VTT Technical Research Centre of Finland 2014 (In Finnish, in print). 114 p.*

WBCSD 2009. Energy efficiency in buildings. Transforming the market. World Business Council for sustainable development. 67 p. ISBN 978-3-940388-44-5. http://www.wbcsd.org/Pages/EDocument/EDocumentDetails.aspx?ID=11006&NoSearchContextKey=true

TOPIC
Historical Buildings

Page.....600-669

Quantifying the Influence of Hygroscopic Materials in the Fluctuation of Relative Humidity in Museums Housed in Old Buildings

Cláudia Ferreira, M.Sc. [1]
Vasco Peixoto de Freitas, Full Professor [2]
Nuno M. M. Ramos, Assistant Professor [3]

[1] Engineering Faculty, Porto University, Portugal
[2] Engineering Faculty, Porto University, Portugal
[3] Engineering Faculty, Porto University, Portugal

KEYWORDS: *Hygroscopic Materials, Relative Humidity, Museums*

SUMMARY:
The preservation of artifacts in museum collections is profoundly affected by fluctuations in temperature and, especially, relative humidity. Since the late 19th century, many studies have been carried out into the best way to control hygrothermal conditions. Today, however, the focus is less upon visitors' comfort than upon ensuring the stability of relative humidity.

In old buildings located in temperate climate zones with strong thermal inertia, and which have low ventilation rate (relative to the volume and number of visitors), daily and seasonal hygroscopic inertia may help to assure the maintenance of RH stabilization conditions. That is to say, active systems may be dispensed with if the buildings' passive behaviour is used to best advantage.

This paper presents the validation of an advanced hygrothermal model by comparing numerical and experimental results of RH fluctuation in the reserves of a museum housed in an old building, located in Porto. The quantification of the influence of hygroscopic materials with different characteristics in stabilizing the relative humidity when ventilation flows are reduced is also presented.

1. Hygrothermal conditions in museums

One of the main functions of museums all over the world is the conservation of artefact collections. For this, it is essential to control the climate conditions (i.e. temperature and particularly relative humidity) inside the museum buildings, as a number of studies have shown (MacIntyre, 1934; Rawlins, 1942; Thomson, 1986).

In the rehabilitation of museums in old buildings, active systems for interior climate control have generally been favoured over passive ones. However, in countries with a temperate climate, such as Portugal, hygroscopic inertia combined with adequate ventilation may help control relative humidity fluctuations in old buildings without need for complex active systems.

Hygroscopic inertia refers to the capacity of a room to store excess moisture from the air and restore it to the atmosphere when the relative air humidity is low. The finishings and the stored materials used in the rooms are the main factors responsible for the storage and restitution of humidity. Hygroscopic inertia may be assessed over short periods of time (short-cycle hygroscopic inertia of rooms) and for longer periods (long-cycle hygroscopic inertia of rooms).

In the Building Physics Laboratory at the Faculty of Engineering, University of Porto – FEUP, important research has been carried out in the domain of daily (i.e. short-cycle) hygroscopic inertia in order to quantify the performance of render materials (through parameters that indicate their water vapour adsorption and restitution capacity), find models with which to assess the influence of daily

hygroscopic inertia upon peaks of relative humidity, and develop experimental studies to measure the phenomenon and validate the models (Ramos, 2007; Freitas et al., 1988; Delgado et al., 2009; Ramos et al., 2009).

There have always been concerns about the climate conditions in museums. In the 1st century BC, Vitruvius mentioned the need to ensure wholesome conditions in the rooms where collections were kept (Casanovas, 2006). However, it was in the 20th century that the most significant advances were made in this area. In 1978, Garry Thomson published the book "The Museum Environmental", which gave priority to the museum's collections over its visitors and concluded that the control of relative humidity is much more important than the control of temperature (Thomson, 1986).

At the Ottawa conference of 1993 and 1994, Stefan Michalski contributed to an alteration of the dominant mindset by asserting that in museums there is no ideal relative humidity, but rather minimum and maximum values, and acceptable fluctuations that minimize the various types of deteriorations (Michalski, 1994). Till then, the reference values of temperature and relative humidity had been defined somewhat arbitrarily and were considered to be valid for any museum in any part of the world, whatever the exterior climate and the background of the collections and buildings.

In 1999, ASHRAE included in their manual for the first time a chapter devoted to museums, libraries and archives, in which they presented a methodology for the control of interior climate conditions based on reference values, maximum admissible fluctuations, and the risks and benefits for the collections, associated to each option (ASHRAE, 2007).

Between 1999 and 2001, a multidisciplinary European research project was under way which aimed to identify the main sources of risk to the cultural heritage due to the unconscious use of technology and mass tourism. The hygrothermal conditions were assessed in four museums exposed to different climate conditions and pollution levels, and it was concluded that museums located in historical buildings benefited from the heat and humidity storage action of their thick walls and the hygroscopic materials used in the renders inside the building. Air conditioning systems are generally designed for visitor comfort and often function only during the period in which the museum is open. However, this practice may be dangerous for the objects kept there, as it causes alterations in the temperature and humidity gradients over short spaces of time (Camuffo et al., 2001).

Another way of defining the hygrothermal conditions in museums is the confirmed fluctuation method, proposed by Stefan Michalski in a 2007 meeting organized by the Getty Conservation Institute in Tenerife. This method consists of defining the maximum temperature and relative humidity fluctuations to which the collection or object was subjected in the past, and respecting that interval (The Getty Conservation Institute, 2007).

In 2010, the CEN published a European norm (EN 15757), which established temperature and relative humidity specifications in order to limit the physical damage to organic hygroscopic materials (CEN, 2010). Then in 2012, the British Standards Institute published a specification that provided a series of requirements for the environmental conditions of storage, display and loan applicable to all types and sizes of collections (BSI Group, 2010).

It can be considered that, in addition to the developments summarized here, there is a need for an advanced hygrothermal approach to this problem that could enable the effect of hygroscopic inertia upon relative humidity peaks to be quantified.

2. Simulation vs Measurement: the hygrothermal behaviour of a museum

This study focuses upon the storage rooms used for paintings and sculptures in a Porto museum, located on the second floor of an old building. The storage rooms house works of art from the museum's painting and sculpture collection when they are not on display. They are visited sporadically by the technical staff. Ventilation is mechanical and consists of air extraction by a variable-speed ventilator in each room. The air extracted from the storage rooms comes from the exhibition gallery (A) through air inlet on the interconnecting doors.

The hygrothermal conditions in the storage rooms and exhibition gallery were monitored over the course of a year. This was done by distributing seven HOBO U12-011 dataloggers around the various rooms (FIG 1), located at a height of approximately 1.5 metres above the floor, which continuously recorded the temperature and relative humidity (FIG 2). The datalogger accuracy is, for temperature, ± 0.35 ºC in a range of 0 to 50 ºC, and for relative humidity, ± 2.5 % in a range of 10 to 90%.

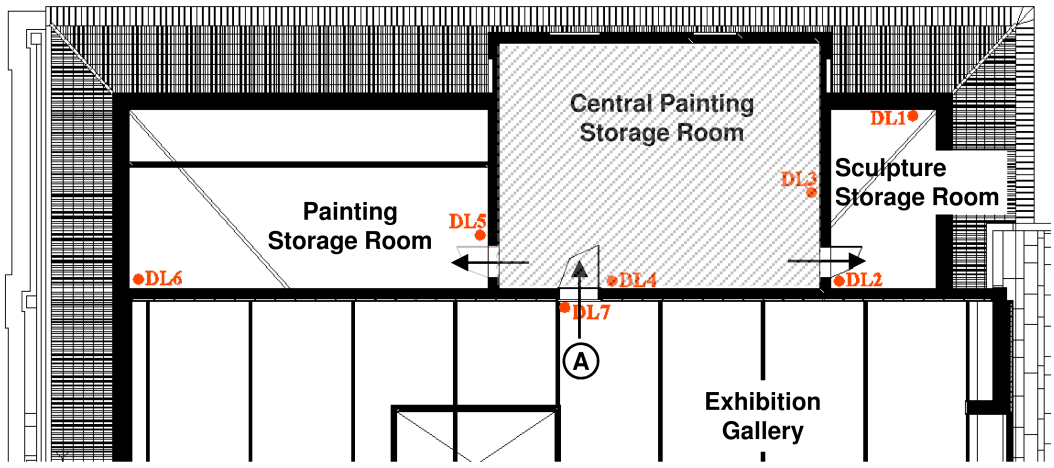

FIG 1. Location of the sensors in the museum storage rooms and exhibition gallery

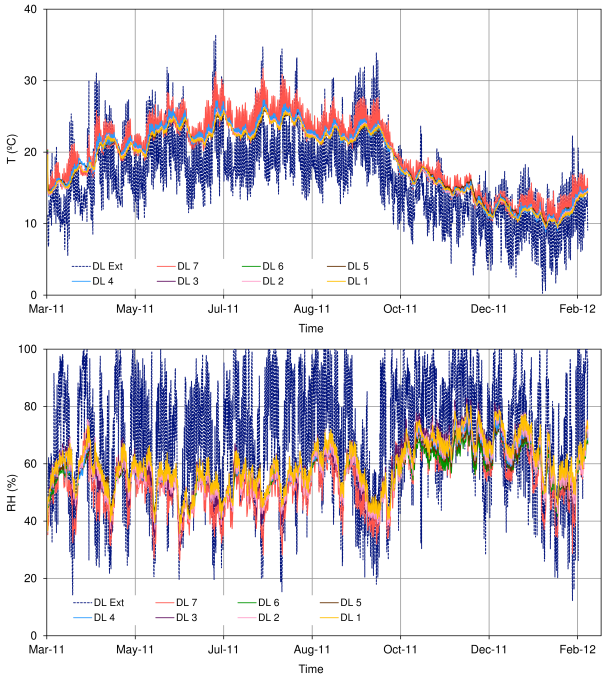

FIG 2. Temperature and relative humidity variations in the museum storage rooms and exhibition gallery over the course of a year

In order to assess the hygrothermal behaviour of museums and quantify the influence that the use of hygroscopic materials may have on the stabilization of relative humidity, an advanced hygrothermal numerical simulation model was selected. This was the *Wufi Plus*, a commercial programme developed by the *Fraunhofer Institut fur Bauphysik* to simulate the hygrothermal performance throughout the whole building. It was chosen because it had already been validated in various other studies (Woloszyn, M. and Rode, C. 2008).

In order to use any such advanced hygrothermal behaviour simulation programme, knowledge is required of the boundary conditions associated to the outside and inside climates, and the constitution

of the building's envelope. Thus, data concerning the orientation of the building, geometry (FIG 3) of each component of the envelope (materials and their properties), exterior climate and ventilation were introduced into the model. The exterior climate used was obtained at the Meteorological Station of FEUP. This station is located in the same city with the same urban climate and at a distance of 2 km from the museum.

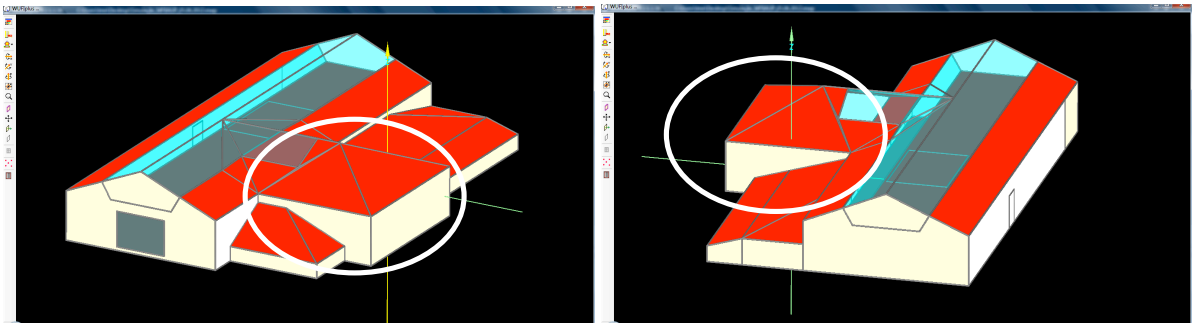

FIG 3. Model used for the exhibition gallery and storage rooms of the museum under study

The monitoring process provided the hourly temperature and relative humidity values, and the ventilation flows (extraction) in each storage room (TABLE 1). These flows were determined with the air speed in the air extraction opening, which was measured using an air speed and temperature measuring device associated to a *Micromec datalogger* for the acquisition and recording of data.

TABLE 1. Ventilation flows

Room	Type of ventilation	Source	Flow [m^3/s]	Flow [m^3/h]	ACH [h^{-1}]
Sculpture storage room	Mechanical	Central painting storage room	0.076	273.6	9.73
Central painting storage room	Mechanical	Exhibition gallery	0.056	201.6	0.98
Painting storage room	Mechanical	Central painting storage room	0.061	219.6	2.54

As regards the envelope, TABLE 2 gives a brief description of the constitution of each component and the material used in the final rendering. The properties of these materials were not determined experimentally. Instead, the database of the program *Wufi Pus* was used, which contained selected materials with similar properties to the finishing materials existing in the museum.

TABLE 2. Constitution of each component and respective finishing material

Component	Description	Finishing Material
Outer walls	Granite walls with ETICS	Lime Mortar with painting
Inside walls	Granite walls with lime-based rendering on both surfaces	Lime Mortar with painting
Roof of the sculpture and painting storage rooms	Pitched slab of reinforced concrete with thermal insulation and cellulose insulation on the interior surface	Cellulose Insulation with painting
Roof of the central painting storage room	Ceiling in gypsum board plus thermal insulation	Gypsum Board with painting
Floor	Reinforced concrete slab	Old Oak without varnish

TABLE 3 shows the properties of the finishing materials used for interior layer with higher relevance for the hygrothermal calculation.

TABLE 3. Main properties of the finishing materials

Properties	Lime Mortar	Cellulose Insulation	Gypsum Board	Old Oak
Bulk density	1785 kg/m^3	55 kg/m^3	850 kg/m^3	740 kg/m^3
Porosity	0.28	0.93	0.65	0.35
Specific heat capacity	850 J/kgK	2544 J/kgK	850 J/kgK	1600 J/kgK
Thermal conductivity	0.70 W/mK	0.036 W/mK	0.20 W/mK	0.1522 W/mK
Water vapour diffusion resistance factor	15	2	8.3	223
Hygroscopic sorption curves	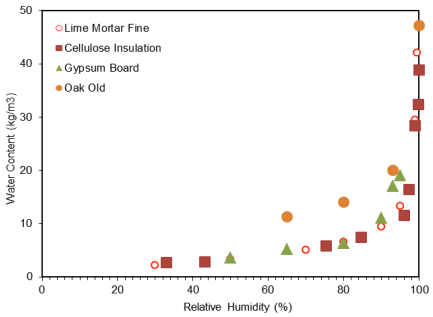			

Using the advanced hygrothermal behaviour simulation programme, a series of simulations were carried out enabling the temperature and relative humidity to be estimated inside the different rooms. These were then compared to the measurements taken. For example, the measured and simulated temperature and relative humidity values inside the central painting storeroom are shown in FIG 4.

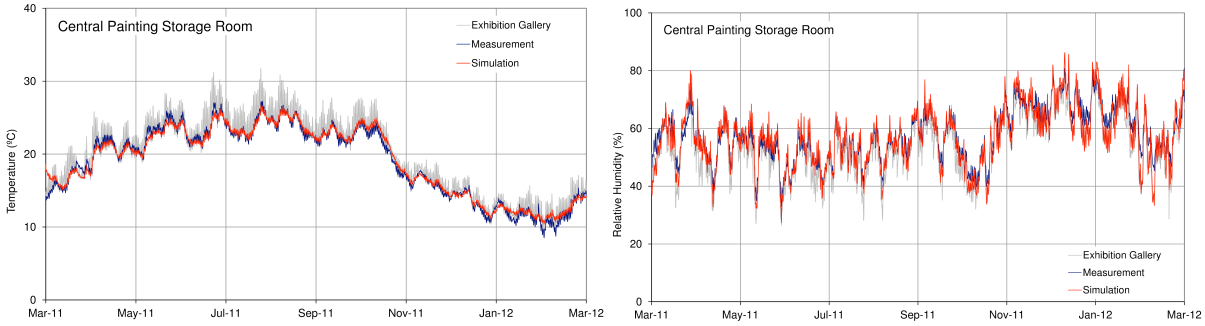

FIG 4. The measured and simulated temperature and relative humidity in the central painting store room

TABLE 4 shows the minimum, maximum and average temperature and relative humidity values obtained by measurement and simulation for the central painting storeroom.

TABLE 4. Minimum, maximum and average temperature and relative humidity

	Exhibition Gallery		Measurement		Simulation	
	T [ºC]	RH [%]	T [ºC]	RH [%]	T [ºC]	RH [%]
Minimum	9.15	26.35	8.51	32.92	10.39	27.198
Average	19.86	53.95	19.06	57.74	19.12	57.09
Standard Deviation	5.06	9.93	4.88	8.88	4.72	10.08
Maximum	31.75	80.64	27.25	80.82	26.69	86.25

From these figures and table, it is possible to observe that, on average, the simulated temperature differs from the measured temperature by about 0.5 ºC, while the simulated relative humidity differs from the measured by 2.5 % (calculus based in the hourly difference between measurement and simulation). Hence, the simulation and measured results are quite close, which validates the programme for the case study.

3. Assessment of the influence of hygroscopic materials

Having validated the numerical simulation model, the next step was to assess the influence of the use of hygroscopic materials upon the interior relative humidity stabilization. Thus, maintaining the ventilation flows and other conditions the same, the finishing materials of walls and ceilings of the rooms were changed for another material that was highly hygroscopic with high vapour permeability, namely spruce woodwool panels covered with mineral binders (M1). The properties of this material necessary for the hygrothermal calculation were inserted into the programme's database: bulk density (kg/m^3), porosity, specific heat (J/kgK), thermal conductivity (W/mK), water vapour diffusion resistance factor, and the respective hygroscopic sorption curve (TABLE 5).

TABLE 5. Properties of material M1

Spruce woodwool panels covered with mineral binders	Basic Material Data	Hygroscopic Sorption Curve
Bulk density	533 kg/m^3	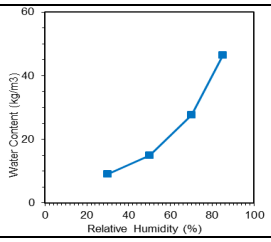
Porosity	0.50	
Specific heat capacity	1810 J/kgK	
Thermal conductivity	0.075 W/mK	
Water vapour diffusion resistance factor	1,1 (wc) e 3,2 (dc)	

The hygroscopic sorption curve and water vapour diffusion resistance factor enable the model to quantify the effect of the building materials upon the relative humidity stabilization. As shown in TABLE 5, the material used (M1) has good hygroscopic capacity in the 40 to 70% range of relative humidity (i.e. the recommended limits for relative humidity fluctuation inside museums).

FIG 5 shows the relative humidity variation of the central painting storage room, which resulted from the consideration of the original render materials and ACH – 0.98 h^{-1} (Simulation 1), the original render materials with a reduced ACH – 0.24 h^{-1} (Simulation 2), the adoption of buffering material M1 on the walls and ceiling and the original ACH – 0.98 h^{-1} (Simulation 3), and the adoption of buffering material M1 on the walls and ceiling with a reduced ACH – 0.24 h^{-1} (Simulation 4).

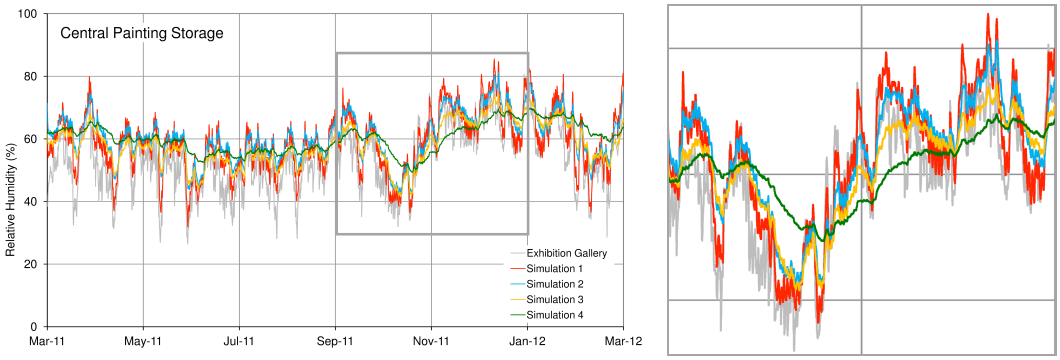

FIG 5. Comparison of relative humidity in the central painting storage room between: a) Simulation 1, which has a ACH of 0.98 h^{-1} and the original render materials; b) Simulation 2, with an ACH of 0.24 h-^{1} and the original render materials; b) Simulation 3, which has an ACH of 0.98 h^{-1} and buffering material M1 on the walls and ceiling; d) Simulation 4, which has an ACH of 0.24 h-^{1} and material M1 on the walls and ceiling

The use of buffering materials (FIG 5) which optimize hygroscopic inertia, improve the relative humidity stabilization. If the ventilation in the central painting storage room is reduced from 0.98 h^{-1} to 0.24 h^{-1}, the hygroscopic inertia effect is clearly visible.

TABLE 6 shows the minimum, maximum and average values of relative humidity in the central painting storage room obtained in the different simulations. It also shows a parameter called Relative Humidity Stabilization (RHS), which enables the performance of the various solutions on the relative humidity stabilization to be quantified, resulting from the sum of the different absolutes between average relative humidity and hourly relative humidity.

TABLE 6. Minimum, maximum, average relative humidity and RHS

Relative Humidity	Gallery	Simulation 1	Simulation 2	Simulation 3	Simulation 4
Minimum	26.35	27.19	42.50	41.56	49.38
Average	53.95	57.09	60.68	58.29	60.17
Standard Deviation	9.93	10.08	7.56	6.79	4.66
Maximum	80.64	86.25	81.25	74.38	69.84
$RHS = \sum_i \left\| \overline{RH} - RH_i \right\|$	70 738	70 073	52 795	48 469	33 794

From this one can conclude that:

- When the ACH value is around 1 h^{-1} and buffering material M1 is used on the walls and ceilings (Simulation 3), the value of parameter RHS reduces by 30 % compared to when the original materials are used (Simulation 1);
- When the ACH value is around 0.25 h^{-1} and buffering material M1 is used on the walls and ceilings (Simulation 4), the value of parameter RHS drops by 36 % compared to when the original materials are used (Simulation 2), and by 52 % compared to when the original materials are used and when a ACH value around 1 h^{-1} is considered (Simulation 1);
- When the ACH value is around 0.25 h^{-1} and buffering material M1 is used on the walls and ceilings (Simulation 4), the difference between the maximum and minimum relative humidity is 20 % compared to the 59 % of Simulation 1.

4. Conclusions

The main achievements and conclusions of this study are the following:

- The temperature and the relative humidity of a painting storeroom in a Porto museum were monitored. The ventilation air was admitted from the exhibition gallery with an ACH of 0.98 h^{-1}; the finishing materials used on the walls, ceiling and floor were lime mortar, gypsum board and old oak respectively;
- An advanced hygrothermal simulation model was used and validated with experimental results;
- The properties of buffering material M1 (spruce woodwool panels covered with mineral binders), were measured and were found to be the following: moisture content of 12 to 40 kg/m^3 for relative humidity values of 40 % to 80 %; water vapour diffusion resistance factor (μ) of 1.1 in the wet cup test and 3.2 in the dry cup test;
- When this particular buffering material was placed on the walls and ceiling of the storeroom, the difference between the maximum and minimum interior relative humidity changed from 59% to 33% for a ACH of 0.98 h^{-1};
- A parameter defined as Relative Humidity Stabilization (RHS), which reflects the performance of various solutions in stabilizing relative humidity, was quantified. This parameter is reduced by 59% compared to the reference situation (Simulation 1) when the finishing materials and ventilation are optimized.

5. Acknowledgements

Cláudia Ferreira would like to thank Fundação para a Ciência e Tecnologia (FCT), Ministério da Ciência, Tecnologia e Ensino Superior, Portugal, for financial support through the grant SFRH/BD/68275/2010.

References

MacIntyre, John. 1934. Some problems connected with atmospheric humidity. Some notes on atmospheric humidity in relation to works of art. *Courtauld Institute of Art, London*, p. 7-16.

Rawlins, F. Ian G. 1942. The control of temperature and humidity in relation to works of art. *Museums Journal,* Volume 41, p. 279-283.

Thomson, Garry. 1986. *The museum environment – Second edition,* Oxford: Elsevier Butterworth-Heinemann.

Ramos, Nuno.2007. *A importância da inércia higroscópica no comportamento higrotérmico dos edifícios,* Porto, Faculdade de Engenharia da Universidade do Porto.

Freitas, V. F. & Abrantes, V. 1988. Étude expérimentale de l'humidité de l'air dans l'intérieur dês bâtiments. Influence du comportement hygroscopique des matériaux. *Healthy Buildings'88, CIB*, Volume 2, p. 201-209.

Delgado, J.; Ramos, N. & Freitas, V. P. 2009. Can moisture buffer performance be estimated from sorption kinetics? *Journal of Building Physics*, Volume 29, n. º 4, p. 281-299.

Ramos, N. & Freitas, V. 2009. An experimental device for the measurement of hygroscopic inertia influence on RH variation. *Journal of Building Physics*, Volume 33, n. º 2, p. 157-170.

Casanovas, L. 2006. *Conservação preventiva e preservação das obras de arte. Condições-ambiente e espaços museológicos em Portugal,* Lisboa, Faculdade de Letras da Universidade de Lisboa.

Michalski, Stefan. 1994. Relative humidity and temperature guidelines: what's happening? [Online], Available: http://www.cci-icc.gc.ca/crc/cidb/document-eng.aspx?Document_ID=118 [Accessed 06 June 2011].

ASHRAE. 2007. Heating, Ventilating, and Air-Conditioning Applications. ASHRAE Handbook. Atlanta: American Society of Heating, Refrigerating and Air-Conditioning Engineers.

Camuffo, D. [et al.] 2001. Environmental monitoring in four European museums. *Atmospheric Environment*, Volume 35, Supplement n.º 1, p. S127-S140.

The Getty Conservation Institute. 2007. Experts' Roundtable on Sustainable Climate Management Strategies – Alternative Climate Controls for Historic Buildings. [Online], Available: http://www.getty.edu/conservation/our_projects/science/climate/climate_experts_roundtable.html#proceedings [Accessed 06 June 2011].

CEN – EN 15757: 2010. Conservation of cultural property – Specifications for temperature and relative humidity to limit climate-induced mechanical damage in organic hygroscopic materials.

BSI Group. 2010. New initiative on environmental conditions for cultural collections. [Online], Available: http://www.bsigroup.com [Press Release July 2010].

Woloszyn, M. and Rode, C. 2008. *Annex 41 Whole Building Heat, Air, moisture Response – Subtask 1 – Modelling Principles and Common Exercises*. International Energy Agency, Executive committee on Energy, Conservation in Buildings and Community Systems. ISBN 978-90-334-7057-8.

Hygrothermal performance of energy saving measures in a wooden building from the 1920s

Fredrik Ståhl, Ph.D. [1]
Thorbjörn Gustavsson, M.Sc. [1]
Tor Broström, Professor [2]
Petra Eriksson, Lecturer [2]
Linn Liu, Ph.D. student [3]
Patrik Rohdin, Ph.D. [3]
Bahram Moshfegh, Professor [3]

[1] SP Technical Research Institute of Sweden, Energy technology, Sweden
[2] Uppsala University, Conservation, Sweden
[3] Linköping University, Division of Energy Systems, Sweden

KEYWORDS: *Moisture safety, energy saving measures, heritage value, building*

SUMMARY:
About one third of Swedish buildings were built before 1945 and they constitute an important part of our built heritage. But these buildings also stand for a significant part of the Swedish energy use. This paper is part of the research project 'Potential and policies for energy efficiency in buildings built before 1945' that assess the capacity for energy saving in buildings built before 1945 with regard to historic values in the buildings.

The purpose of this paper is to assess energy saving measures that will reduce the energy use by 20, 50 and 70 % respectively in a typical single family wooden house from the 1920s. Primarily, this paper focuses on moisture safety. It also aims to highlight the difficulty of significantly reducing the building energy use without altering the building's character and historic value.

The work includes assessing the existing energy use in a fictitious 1920s building and identifies three packages of measures that reduce the building's energy use significantly at an optimal life cycle cost while considering conservation aspects. This is done using a methodology and a tool, OPERA–MILP, developed by the research project. The proposed energy saving measures, on both the building envelope and the building services, are then assessed from a hygrothermal performance perspective using the ByggaF methodology.

1. Introduction

The Energy Performance of Buildings Directive has set common targets for the EU; by 2020 there should be a 20% reduction in energy use and CO2 emissions. On a national level, the Swedish Government aims for a 50% reduction by 2050. In addition to this, new national building regulations require the same energy performance for an older building after major reconstruction as for a new building.

In this way, the pressure for improved energy performance in existing buildings is increasing, and carefully consideration has to be applied to balance energy conservation and building conservation. The Swedish research project “Potential and Policies for Energy Efficiency in Swedish Historic Buildings” aims to investigate the interdependency between political energy targets and effects on the built heritage.

Many energy saving measures will have a great impact on the hygrothermal conditions of a building. In the long run, this could jeopardise the indoor environment, damage the building and shorten its life span. Therefore, it is important to assess the hygrothermal conditions of the retrofitted building before planned energy savings are realised.

Today, there is no international or European standard for assessing and presenting moisture performance in buildings (Berggren 2013). However, the IEA research project Annex 55 RAP-RETRO is developing a tool to predict the energy use, cost and thermal performance of retrofitted buildings using probabilistic methodologies.

The purpose of this paper is to assess energy saving measures that will reduce the energy use in a typical single family wooden house from the 1920s, primarily, concerning the moisture safety.

2. Methodology

The research project 'Potential and Policys for Energy Efficiency in Swedish Historic Buildings' is proposing a methodology for decision making on energy interventions in historic buildings (Broström et. al. 2012). The developed procedure includes the following steps:

1. Categorisation of the building stock based on available data
2. Define targets for energy performance as well as for preservation of the building and its values.
3. A first assessment of risks and benefits based on a repository of measures for energy efficiency. The aim is to select the best measures and eliminate inappropriate ones.
4. A life cycle techno-economic optimisation to find the best combination of measures
5. Risk assessment with respect to cultural heritage values and hygrothermal risks
6. Analysis of the consequences in relation to the targets.
7. Iterative adjustments of measures and targets.

Through an iterative procedure, an interdisciplinary team of professionals can find a scenario that, in the best way, balances the benefit, in terms of energy saved, in relation to risks and costs. In the following, each step of the method will be described more in detail.

2.1 Categorisation of the Swedish building stock

An investigation of a large building stock cannot be made on a house by house basis. The building stock has to be reduced to a manageable number of categories that provide a satisfactory statistical representation of the whole stock. However, in this paper the ByggaF methodology for including moisture safety in the building process is tested on one possible building category specifically.

2.2 Targets for energy performance and preservation of buildings

Possible national targets for energy savings in buildings are: 20% by 2020 and 50% by 2050.

The Swedish building regulation indicate that the same property requirements shall be applied for both the construction of a new building as well as an altered building.

The built environment has a general protection in the Swedish planning law that states that historical, cultural historical, environmental and artistic values of the built environment should be protected. In addition to this, restrictions are given by local building plans. Thus preservation targets have to be defined in each context based on an interpretation of the legal requirements and the priorities of the owner.

2.3 Pre-selection of energy saving interventions

A gross list of the most common energy saving interventions is assessed with respect to the following risks and benefits: energy saving, economic return, cultural heritage values, durability, moisture

conditions and indoor environment. The risk and benefit is evaluated in five levels ranging from high benefit to high risk.

2.4 Techno-economic optimisation

In order to evaluate the economic efficiency of the suggested combinations of measures a optimization procedure has been applied. The used method, OPERA-MILP (Optimal Energy Retrofits Advisory-Mixed Integer Linear Program), is a mixed integer optimization method designed to minimize the life-cycle costs (LCC) of combinations of measures. The method, which is developed at Linköping University, is described more in detail in Gustafsson (2001) and Gustafsson (1998). Based on a mathematical model of the building and cost functions for all included measures, an iterative procedure determines the cost-optimal combination of measures.

The output from the optimization, which simultaneously includes building retrofits, ventilation retrofits and heating system retrofits, is a minimum of LCC for a package of these measures. The method also has the possibility to find combination of efficient solutions for a given rate of energy conservation, e.g. 20%, 50% etc.

2.5 Assessment of heritage values

In order to combine the assessment of cultural heritage values with a techno- economic assessment, a structured, transparent and reasonably simple method is needed. The generic elements of such a process are:

1. Assess the cultural significance of the building, group of buildings, building categories or the building stock.
2. Define the character (visual and material) of the buildings that contributes to and reinforces the significance.
3. Assess the vulnerability of change regarding the character with respect to each proposed measure.

2.6 Assessment of hygrothermal risks

The ByggaF method includes a number of routines, templates and checklists for clients to formulate requirements for moisture safety and to follow up and document the measures employed by different participants (Mjörnell et al. 2012). One of these templates is the tool ‘Moisture safety design and risk evaluation’ where each building part (e.g. Roof and attic) has its own template where possible moisture loads and what to consider are described for each load to guide the practitioner/user. Then the user has to describe the effect of the moisture load and assess the moisture conditions.

Overview of the stepwise procedure of the Moisture safety design and risk evaluation template:

1. Identification of moisture sensitive measures?
2. Identification of the moisture load
3. Estimate the effect/consequences of moisture load
4. Estimate moisture condition
5. Assess if the moisture level will be outside the allowable moisture conditions
6. Evaluation of the probability S (1-4) and consequence K (1-4). Risk Value (S * K = 1-16)
7. Estimate the need for risk reducing measures
8. Appropriate follow-up

The methodology supports the user by providing templates and tools but it is a qualitative analysis and dependant of the experience of practitioner. This methodology has been validated and revised when used in several projects (Mjörnell et al. 2012). The latest addition to the ByggaF method is step 6, Evaluation of probability and consequence, where the practitioner estimates the probability that the moisture conditions is outside the allowable range and, therefore, could cause damage or change the

properties of the building material. The consequence in terms of the moisture conditions is also estimated and both probability and consequences are rated in a scale of 1 to 4, where one is the lowest and four the highest. The risk value is the product of the value of the probability and consequence. Thus, the risk value is at least 1 and no more than 16. The risk value is rated accordingly: Low risk = 1-5 Medium risk = 6-8 High risk = 9-11 Extremely high risk = 12-16. If the risk value is high or extremely high, then some form of risk reducing measures should be performed. A risk reducing measure could be elimination or medication of measures or actions such as periodic controls.

3. Case study

The studied building is a single family one and a half storey wooden building from the 1920s. The outside comprises of a plank frame clad with vertical wood panelling, with cardboard dressed horizontal wood panelling on the inside. The coupled double-glazed windows are slightly larger on the 1st floor than on the 2nd floor. Many buildings from this time period were designed with a basement but in this case the building has a crawl space. The floor area is 164 m^2.

The building was original heated by stoves connected to a central chimney, presently it is connected to district heating that is distributed throughout the building using a hydronic heating system. The building is natural ventilated and, in general, the ventilation rate and the pressure conditions over the building envelope of natural ventilated buildings vary significantly depending on the weather conditions. However, in this case it is assumed that the requirement of minimum ventilation rate (0.35 l/s m^2) is fulfilled.

TABLE 1. The area and U-value of the case study building envelope parts.

Building envelope parts	U-value (W/m^2K)	Area (m^2)	U·A (W/K)
Roof	0.49	84	41
External wall (incl. thermal bridges)	0.94 (1,31)	156	147 (204)
Windows	2.70	18	49
Basement	0.30	84	25

The specific heat losses due to ventilation, a kitchen fan and air leakage are estimated to 70, 3 and 23 W/K, respectively. This gives a total specific heat loss of 415 W/K.

3.1 Preselecting energy saving measures for a 1920s wooden villa

The first step in selecting the “optimal” retrofit solution to the wooden building is to assess risks and benefits of a gross list of energy saving measures. This assessment is mainly designed to exclude inappropriate solution for this building category. In this case, the gross list consists of the energy saving measures that today are included in the OPERA-MILP optimisation tool. The gross list is: weather stripping (and other air-tightening measures), additional insulation on the attic floor, additional insulation on the outside or inside on the wall, additional insulation on the crawlspace or basement ceiling, replacement or upgrading of windows, heat pump, wood pellet burner.

TABLE 2. Example of pre-selection table where Interventions and their consequences are assessed.

	Assessment				
Intervention	**Energy use**	**Economic**	**Heritage values**	**Moisture perf.**	**Indoor environ.**
Insulation on the attic floor				Increased RH in attic space	Improved comfort
Exterior insulation on the wall		High investment	Visual and material changes		Improved comfort
Scale	High benefit	Low benefit	Neutral	Low risk	High risk

3.2 Techno – Economic optimisation using OPERA-MILP

In the next step the OPERA-MILP tool calculated three intervention packages to meet the energy reduction targets, 20, 50 and 70% respectively. These packages are presented in Table 3.

TABLE 3.Energy saving packages derived by OPERA-MILP.

Intervention	Package 1	Package 2	Package 3
Geothermal heat pump	x	-	-
Wood pellet burner	-	x	x
Weather-stripping	x	x	x
Attic insulation (mm)	600	160	360
External insulation of wall (mm)	-	60	160
Crawl space insulation (mm)	-	-	220
Window upgrade	Extra window pane	-	Triple-glazing, LE-coating

A more detailed description of the energy saving packages is presented in Broström et al. 2013.

3.3 Heritage values of a 1920s wooden villa

The building represents a common type of building from the 1920's, the cultural significance is mainly in the visual appearance including materiality and decorative details of the building. This category of building is not listed but is protected by the legal planning and building system where it is stated that the character of material and colours of the buildings in the area should be protected.

3.4 Hygrothermal risk assessment

The three energy saving packages in Table 3 were assessed according to the ByggaF method. As a comparison, Package 2 was also assessed using internal insulation (60 mm) of the exterior wall as an alternative to the exterior insulation. The prerequisite for the hygrothermal risk assessment is that the original construction works relatively well regarding moisture safety. The assessment focuses on identifying moisture risks associated with the proposed energy saving measures and, where necessary, suggest further technical investigation. In some cases, risk reducing measures was introduced to lower the estimated Risk value according to the 'Moisture safety design and risk evaluation' template. An extract from one of these templates is shown in Fig 1.

Design	Moisture load	To consider	The effect of moisture load	Estimation of moisture conditions	Probability	Consequence	Risk value	Risk reducing measures	Probability	Consequence	Risk value	Follow-up
Pitched roof, 45 ° Section A1	Snow and ice, melt water, drifting snow	• Dewatering warm roof, cold roof. • Risk of freezing in downspouts and gutters • Drfting snow in ventilated constructions • Are there pockets of snow on the roof? • Risk of re-freezing	The additional attic insulation will decrease the temperature of the roof and the probability for melting snow and forming of ice will decrease. Changing the heat source from district heating to heat pump is not expected to affect the temperature of the attic.	Cold roof, minor risk for ice forming	1	2	2		0	0	0	
	Moisture diffusion due to differences in moisture content	• Location of the vapor barrier • Check the moisture condition in winter and summer climate • Cut-in vapor barrier penetrations, attachments (especially important when difference in moisture content is great) must be sealed • Ventilate condensed water • Moisture buffring in roof materials • Critical moisture level of incliuded materials • Thermal bridges	Moisture diffusion from the interior to the attic will occur. However, the addition of moisture from the interior could vary considerably depending on the number of inhabitants and their habits. Due to the additional insulation, the temperature will be lower and, consequently, the relative humidity will be higher in the attic space during heating season. Changing the heat source from district heating to a heat pump is not expected to affect the temperature of the attic space or the indoor ventilation rate. In this assessment, it is assumed that the air sealing measures will not affect the moistrure diffusion significantly.	A Consequence rating of 2 shall apply provided that the natural ventilation works relatively well during the heating season and indoor moisture production is relatively low. At higher indoor moisture production will increased the consequence rating to 3.	4	2	8	Install a vapor barrier in the attic floor and stud walls. It is especially important to inspect the attic the first winter after the measures are implemented. Look for discoloration, changes, and measure the moisture content in wood constructions.	1	2	2	Placement of the diffusion barrier during the design phase.

FIG 1. Extract from one of the ByggaF templates.

A brief summary of the result of the hygrothermal risk assessment of the three energy saving packages is presented below.

3.4.1 Heating system

Changing from district heating to a heat pump will not affect the hygrothermal conditions of the building. On the other hand, the wood pellet burner (of Package 2 and 3) will probably ensure a negative pressure in the building during the heating season, thus decreasing the risk of moisture convection in the building envelope. The ventilation rate will also increase and a greater part of the additional moisture in the indoor air will be removed.

3.4.2 Weather-stripping

The air-tightening measures have a positive influence on the hygrothermal conditions in the building provided that the required minimum ventilation rate is maintained. Usually, air-tightening measures will decrease the risk of moisture convection in the building envelope but, depending on the measure, also moisture diffusion. However, the ByggaF methodology assesses moisture related problems due to convection and diffusion separately.

3.4.3 Additional attic floor insulation

In a building with a cold roof (cold attic space) it is easy to insulate the top floor ceiling from above. However, in the studied building, part of the attic is living space and both the stud walls and the ceiling have to be insulated. This measure will lower the temperature and consequently increase the relative humidity of the cold parts of the attic; hence increase the risk of moisture related damage of the attic space, the roof and the part of the exterior wall that is outside the stud wall. The hygrothermal risk assessment concludes that a vapour barrier and an air-tight layer have to be installed in addition to the insulation to prevent moisture diffusion and convection. The chosen heating system of Package 2 and 3 will provide some additional heat to the topmost attic space, thus counteracting the negative aspect of the attic floor insulation. However, ventilation of the attic can in some weather conditions cause problems. This moisture load is identified by the ByggaF assessment as the most difficult to counteract, especially for Package 1. A yearly inspection of the attic space is recommended.

3.4.4 Window upgrade

The ByggaF methodology does not include windows in the moisture safety assessment. Nevertheless, adding an extra window pane to an existing window will improve the hygrothermal conditions provided that indoor air is prevented from entering the space between the glass panes.

3.4.5 Additional external insulation of the outer walls

This measure will improve the indoor thermal comfort and the hygrothermal conditions of the wall, especially if the new façade is provided with an air space behind the outer panel that prevent driving rain to reach the interior of the wall. The heat losses will decrease significantly in the studied building. The greatest risk of moisture damage is during the construction phase when the wall is open and precipitation can reach the wall´s interior. Weather protection should be used. However, this measure has already during the pre-selection of measures been marked as an intervention that will have a great impact on the visual appearance of the building.

3.4.6 Additional internal insulation of the outer walls

Internal insulation will improve the thermal comfort in the building and decrease the heating need. On the other hand, the temperature of the wall structure outside of the insulation will be lower and the consequence of driving rain is adversely affected when the wall's drying ability is impaired. The risk of moisture diffusion is large and cannot be countered entirely by improved air circulation and removal of moisture via the wood pellet burner. This measure must be combined with a vapour barrier on the warm side of the wall.

3.4.7 Additional insulation of floor to crawl space

In general, adding insulation to the ceiling of the crawl space from below (as in Package 3) will improve the hygrothermal conditions of the floor structure above which usually is the most moisture sensitive part of a crawl space or basement. However, the crawl space itself will be colder and thus increasing the relative humidity and the risk of microbiologic growth.

4. Discussion and conclusion

One of the great benefits of the ByggaF methodology is that it considers every possible moisture load throughout the entire building process. On the other hand, ByggaF require detailed information about the building design in order to be fully exploited. In this case study of a wooden single family building, drawings of building details has been scarce but that is to be expected when more building categories are assess in the main research project.

The main goal of ByggaF is to support the production of a building, more or less, free of moisture related problems. However, this is very hard to achieve in an already existing building as the possibility to change the design is limited. Instead the objective of a moisture safety audit of energy saving measures in an existing building is to achieve a building/design less prone to moisture related problems than before.

One of the weaknesses of ByggaF is that it is dependant of the experience of the practitioner. There are a lot of parameters that with varying degree of uncertainty affect the hygrothermal conditions of the building and the practitioner has to account for all of them.

The above mentioned problems are accentuated in historic buildings where construction details and materials may not be well defined. For an individual building, further details are easily acquired if the building is inspected on site. Unfortunately, this amount of information is hard to attain for one category of the building stock.

It is worth noting that the methodology includes risk reduction measures which in some cases can affect other parameter being evaluated, e.g. conservation values.

It is possible to achieve great reduction in the energy use in a wooden single family building from the 1920s. Most of the presented interventions could be implemented in a moisture safe fashion, even though some might require some additional measures to decrease the risk of moisture damage. This is the case when insulation is added to the attic floor where moisture convection and diffusion can be prevented by air-tightening measures and vapour barriers but no risk reducing measure is proposed in the ByggaF assessment except to inspect the attic space regularly. The final Risk Value is assessed to be medium high and adaptive ventilation is one way to lower that Risk Value.

The major heat loss is through the exterior wall and heat losses can be decreased significantly by additional insulation on the façade. Unfortunately, this can hardly be done without tremendous impact on the visual appearance of the building. Sometimes insulation is added to the inside of the exterior wall to decrease the heat losses and improve thermal comfort. This solution requires an interior convection and diffusion barrier that is very hard to install in an existing building. The risk of moisture damage also increases dramatically if the installation of the vapour barrier is not perfect and the building's lifespan can be shortened considerably. But even with a perfectly installed vapour barrier, the lower temperature of the exterior wall, outside of the added insulation, will affect the wall´s drying ability and make it more sensitive to damage by driving rain.

5. Acknowledgements

This work is part of the Swedish national research program on energy efficiency in historic buildings: Spara och bevara which is financed by the Swedish Energy Agency.

References

Berggren B. 2013. Evaluating building envelopes for energy efficient buildings – Energy and moisture performance considering future climate change. Lund University. Report EBD-T--13/16.

Broström T., Eriksson P., Rohdin P. and Ståhl F. 2012. A method to assess the effect of energy saving interventions in the Swedish stock of historic buildings. Heritage 2012 Porto, juni.

ByggaF - Method for Including Moisture Safety in the Building Process http://www.fuktcentrum.lth.se/verktyg_och_hjaelpmedel/fuktsaekert_byggande/byggaf_metoden/

Eriksson P., Donarelli A. Arumägi E., Ståhl F. and Broström T. 2013. Energy efficient historic stone houses – a case study highlighting possibilities and risks. SB13 Munich -Sustainable Building Conference, Implementing Sustainability - Barriers and Chances, Munich April 24-26 2013.

Gustafsson S.I. 1998. Sensitivity analysis of building energy retrofits. Applied Energy, 61 (1998) pp. 31-38.

Gustafsson S.I. 2001. Optimal fenestration retrofits by use of MILP programming technique. Energy and Buildings, 33 (2001), 843-851.

Mjörnell K., Arfvidsson J. and Sikander E. 2012. A Method for Including Moisture Safety in the Building Process. Indoor and Built Environment 2012;21;4:583–594.

IEA ECBCS Annex 55: See http://www.ecbcs.org/annexes/annex55.htm.

Indoor climate and energy performance of traditional stone houses on Gotland, Sweden

Endrik Arumägi, M.Sc [1]
Targo Kalamees, Professor [1]
Tor Broström, Professor [2]

[1] . Tallinn University of Technology, Estonia
[2] . Uppsala University, Campus Gotland, Sweden

KEYWORDS: *historic building, indoor climate, air tightness, energy efficiency*

SUMMARY:
This study focuses on the rural stone houses built in the 18th and 19th century on the island of Gotland in Sweden. The study includes field measurements and simulations of renovation alternatives to improve energy performance of the studied houses.The annual average indoor temperature in the continuously used houses varied between +11.3°C...+27.2°C and RH between 20%...66%. During winter months the average temperature was +18.7°C and RH 36%. The RH levels were high in all unheated houses and in some periodically used houses causing possible mould growth problems.The average air leakage rate q_{50} *of the living houses was 14.5* $m^3/(h \cdot m^2)$*. The average air change rate measured with a passive tracer gas method during the winter time and in the normal use was 0.9* h^{-1}*. The air tightness measurements show that the studied houses are quite leaky.*

For historic houses, the renovation solutions concentrating on the building envelope are problematic due to the need to preserve cultural and architectural values. The largest energy saving potential of the historic stone houses lies in the heat source and in building service systems. Combining the new heat source with new windows, attic floor and base floor insulation, a maximum of 60% in primary energy and 86% in delivered energy can be achieved. For historic houses every renovation solutions has to be considered carefully.

1. Introduction

Through time, the use of historic and traditional rural houses has changed. Today people have different requirements for thermal comfort and energy performance of the houses. Therefore, old traditional houses have to meet the new indoor climate and energy requirements. All the studied houses can be classified as houses with very high energy consumption due to their size, construction and material. Around five times more energy is needed to keep up with the comfort standards of new buildings. It is questionable if the energy requirements are reachable in these houses without damaging heritage values and how large energy savings can be made.

The renovation solutions for historic buildings that concentrate on the building envelope are problematic due to the need for preserving cultural and architectural values. For historic, heritage, and traditional buildings the improvement of energy performance should be managed carefully aiming to find a balance between energy conservation and building conservation (Brostrom et al 2014, Fabbri *et al*. 2012).

This study focuses on the rural stone houses built in the 18th and 19th century on the island of Gotland in Sweden. The building type is considered important as part of the common heritage of the region and thereby well worth preserving. The study analyses renovation alternatives to improve energy performance of the studied houses. The study includes field measurements and simulations. In addition to the indoor climate measurements, the air tightness and air leakage measurements were conducted in some houses. For simulations one reference house was selected among the studied houses. Energy performance of renovation alternatives was calculated using the dynamic simulation software IDA ICE.

2. Methods

2.1 Studied buildings

Traditional Gotland's houses are built using dry wall technique (limestone or sandstone stones stacked on top of each other without mortar, stones are kept in place with smaller balance stones) (Fig. 1). The façades are plastered and painted with lime wash. The windows are either single or double glazed, allowing owners to remove inner window frames during the summer period. All the studied houses have different kinds of fireplaces (open fireplaces, tiled stoves, cast iron stoves). Also, different types of boilers with radiator heating or direct electric heating can be found to improve the original heating systems. Often direct electric heating is used if there is no water borne system. The studied dwellings had only natural ventilation.

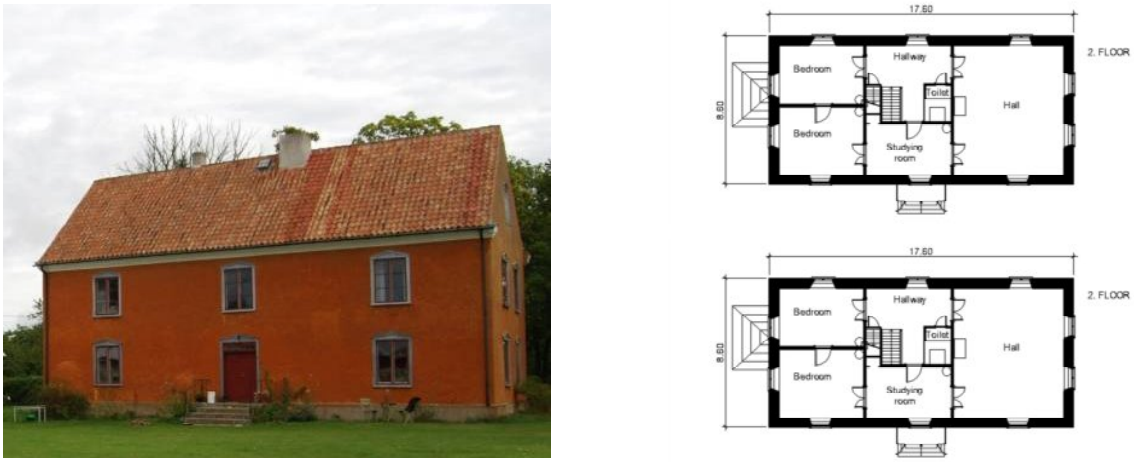

FIG 1. Front view and floor plans of a typical stone house on Gotland.

The average heated area of the studied houses was 180 m^2 (range 76…339 m^2). Average area of the building envelope was 412 m^2 (range 182…742 m^2) with an average of 10.6% (range 7.2%…17.8%) of windows from the total façade area. Thermal transmittance of the external walls varied between 1.5…2.0 W/(m^2K), attic floors 0.1…0.78 W/(m^2K), base floors 0.68…1.3 W/(m^2K) and windows 2.9…3.5 W/(m^2K). The characteristics of the reference house were as follows: heated floor area 244 m^2, area of building envelope 490 m^2 with 13% of windows from the total façade area, thermal transmittance of the external wall was 1.82 W/(m^2K), attic floor 0.33 W/(m^2K), base floor 0.68 W/(m^2K), and windows 2.9 W/(m^2K).

2.2 Field measurements

Field measurements included indoor climate studies, building surveys and measurements of the properties of the building's envelope. Indoor climate was studied in 23 houses. In each house indoor temperature and relative humidity (RH) were measured with data loggers (measurement range: –20 °C and +70 °C, 5 and 95 % RH with an accuracy of ±0.35 °C, ±2.5 % RH) at one hour intervals over a one-year period. Depending on the usage profile, 1 to 5 rooms (mainly master bedroom, living room, kitchen) were selected for the measurements.

The air tightness of each building was measured according to the EN 13829. 2001 standardized (EN 13829, 2001) fan pressurization method using "Minneapolis Blower Door Model 4" equipment with an automated performance testing system (flow range at 50 Pa 25 m^3/h – 7.8 m^3/h, accuracy ±3 %). Air tightness was measured under two different conditions, over-and under-pressurizing test was conducted. Measurements were made at 10 Pa pressure difference step from 10 Pa to 60 Pa.

In addition to the air tightness test, the air change rate in the buildings was measured with a passive tracer gas method (Sandberg 1989). The passive tracer gas method is based on passive sources and sampling tubes. Samplers were distributed per house depending on the volume and the number of rooms

to ensure the homogeneous emission in the whole house. The primary measured value called "local mean age of air" is equal to the inverted value of the local air change rate of the building. The inaccuracy of the PFT method is approximately ±10 % (based on laboratory measurement protocols).

2.3 Simulations

The multi-zone indoor climate and energy simulation program IDA Indoor Climate and Energy 4.5.1 (IDA ICE) (Sahlin 1996; Björsell etc 1999) was used for the simulations. The simulations were used to calculate the energy consumption of the buildings, to predict the energy savings and to propose the retrofit measures. Validated in different studies (Moinard 1999, Rode 2008), IDA ICE is a tool for building simulations of energy consumption, indoor air quality and thermal comfort.

A typical house used for the simulation was built in the 1850s. It is permanently inhabited, it has two floors, the attic is unfurnished and the house has no basement. The simulation model was calibrated based on the field measurements, user behavior, measured indoor climate and air tightness results.

The energy renovation measures were simulated with the standard use of the building (indoor temperature (≥ 21 °C); ventilation airflow 0.35 l/(s·m²) (an acceptable moderate level of expectation for indoor climate, category class III (EN 15251, 2007) per heated area; the usage rate of the building, lighting (8 W/m²) and equipment (2.4 W/m²); and the heat from the inhabitants (2W/m²) to reduce the influence of the user behavior. The use of domestic hot water is 45 l/(d·person). For outdoor climate, the measured temperature and RH from the year 2000 (HDD 3127 °C/d at t_i +17 °C) was used. In the calculations, delivered energy efficiencies of energy production and heat distribution systems were taken into account as follows:

Production (energy source)

- wood burning stove 0.6 (original), 0.8 (renovated, new)
- boiler 0.85 (pellet), 0.9 (oil/gas boiler)
- heat pump 2.4 (air to water), 2.8 (air to air), 2.9 (ground source)

Distribution (heating system)

- stoves 0.85
- hydronic radiators 0.85
- electric radiators 0.95

The energy performance of buildings is expressed as the use of the delivered energy (DE) and as the annual primary energy consumption (PE kWh/(m^2a) for space heating and heating of ventilation air. The delivered energy includes also energy for domestic hot water, fans and pumps. Additionally, the PE includes energy for lighting and household electricity. In the calculation of primary energy usage, the delivered energy is multiplied by the weighting factors for energy carriers (Svensk Fjärrvärme AB Rapport I 2009:18) as follows:

- wood 0.92
- pellet 0.97
- fossil fuels (gas, oil, coal) 1.0
- electricity 2.32

3. Results

3.1 Indoor climate conditions

Indoor climate was measured in all the studied buildings over a one-year period in a one-hour step. During the measurement period outdoor temperature varied between -20.0 °C…+27.6 °C and RH between 30%...100%. During winter the average temperature was -0.9 °C (min. -20.0 °C, max. +9.2 °C) and RH 87% (min. 55%, max. 100%). The annual average indoor temperature in the continuously used houses varied between +11.3°C…+27.2°C and RH between 20%...66%. During winter months the average temperature was +18.7°C (min. +11.3 °C, max. +21.5 °C) and RH 36% (min. 20%, max. 54%). The annual indoor temperature in the unheated houses varied between -8.2 °C…+24.8 °C and

RH between 47%...96%. During winter months the average temperature was +2.2 °C (min. -8.2 °C, max. +14.9 °C) and RH 76% (min. 47%, max. 96%).
Figure 2 shows the dependence of the indoor temperature and RH on the outdoor temperature. Each individual thin solid line represents the average value from the average daily indoor temperature and RH at the corresponding average daily outdoor temperature in one house. The dotted curve represents the average from all the houses with the same heating profile (continuous use, periodical use, unheated).

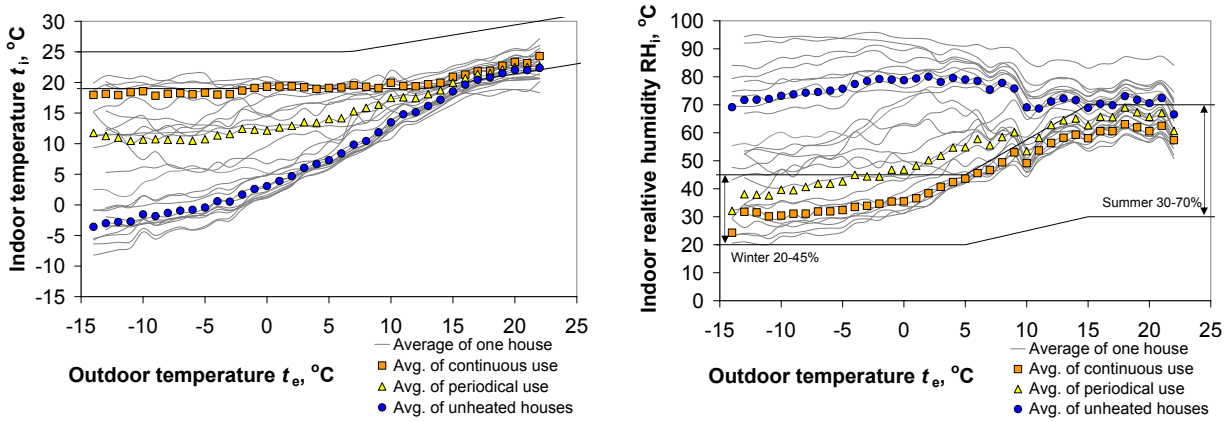

FIG 2. Dependence of the indoor temperature and RH on the outdoor temperature.

The RH levels were high in all unheated houses and in some periodically used houses. Figure 3 shows the mould growth index (Hukka and Viitanen 1999) representing the risk of the mould growth according to the measured indoor conditions in the studied houses and indoor climate conditions in one unheated example house. The mould growth depends on the RH and temperature. The mould growth can be detected with microscopy if the mould growth index is higher than 1 and visually if it is higher than 3.

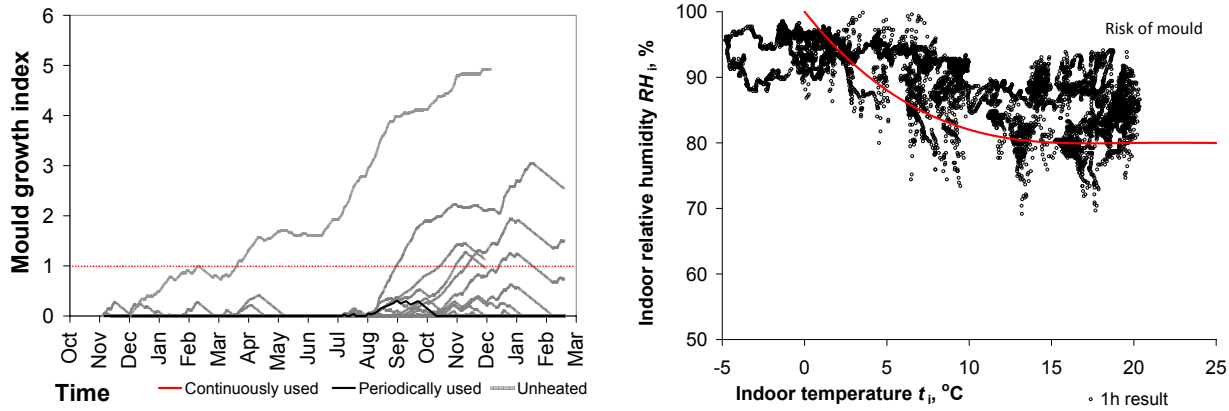

FIG 3.Mould growth index according to indoor conditions in the studied houses and indoor temperature and RH conditions in one example house.

3.2 Air tightness and infiltration of houses

To compare air leakage of different houses, the air flow rate at the pressure difference 50 Pa was divided by the envelope area of the house resulting in the air leakage rate q_{50} ($m^3/h)/m^2$) and by the internal volume of the house resulting in the air change rate n_{50} (h^{-1}). Based on 11 measurements, the average air leakage rate q_{50} of all the houses was 17.4 $m^3/(h \cdot m^2)$ (min. 11.5 $m^3/(h \cdot m^2)$, max. 33.1 $m^3/(h \cdot m^2)$) (FIG 4). The average air leakage rate q_{50} of the living houses was 14.5 $m^3/(h \cdot m^2)$ (min 11.5 $m^3/(h \cdot m^2)$, max. 21.1$m^3/(h \cdot m^2)$), leaving out two houses used as museums. The average air change rate n_{50} of the living houses was 12.4 h^{-1} (min. 9.6 h^{-1}, max. 18.4 h^{-1}).

The measurement result of the air change rate measured with a passive tracer gas method is an average value of the supply rate of outside air in the house during the measurement period. In the four-week period in winter, measurements were made in 7 houses. During the measurements the houses were used in the normal conditions. Average air change rate was 0.9 h^{-1} (min. 0.4 h^{-1}, max. 1.42 h^{-1}). Figure 4

shows the measured air leakage rate q_{50} and air change rate measured with a passive tracer gas during winter period.

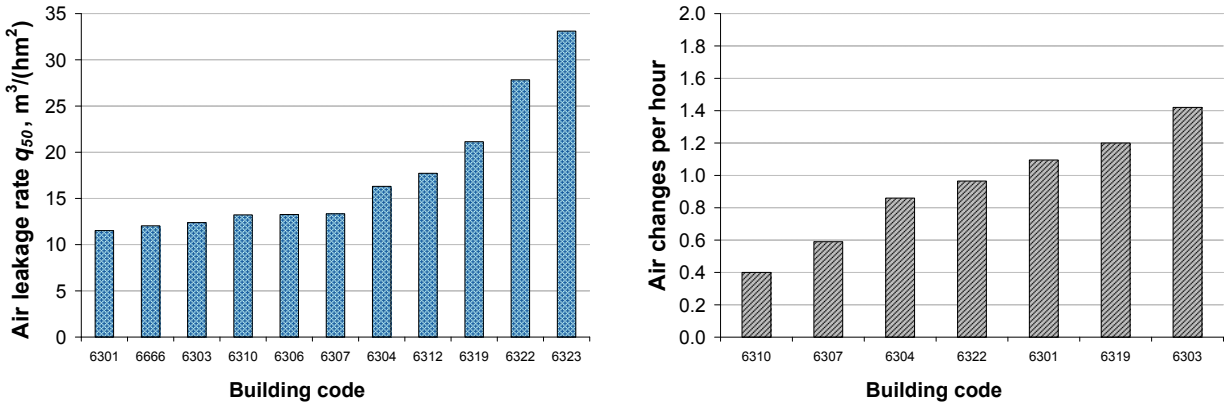

FIG 4. Air leakage rate q50 (left) and air change rate measured with a passive tracer gas (right).

3.3 Energy efficiency measures

To show the influence of single renovation measures, the delivered energy (DE) and primary energy consumption (PE) simulations were done using renovation measures one at a time and comparing the result to the reference case (see FIG 5.). The reference case is a building with its original structure, stove heating and natural passive stack ventilation. Energy renovation measures were applied to the building envelope (facade, attic floor, windows-doors, and basement floor) and the building's service systems (heating, ventilation, energy source). The thickness of additional insulation for the façade (λ=0.04 W/(m·K)) varied between 20…220 mm (*EW20...EW70*), for the attic floor 100…400 mm (*AF220...AF420*) and for the basement floor 200…300 mm *(BF200...BF300)*. Four renovation measures for windows were considered from the renovation of original windows (*U* 1.6 W/(m^2·K)) up to the installation of new windows (*U* 0.8 W/(m^2·K)) (*W1.6...W0.8*). A new wood burning boiler (*WBS*), a pellet boiler (*WPB*), an oil condensing boiler (*OB*), direct electric heating (*ER*), an air to water heat pump (*AWHP*), and a ground source heat pump (*GHP*) as new heat sources with hydronic radiators were compared with existing wood heating stoves. In addition to the heating system, solar collectors (*SC*) for the domestic hot water production and PV-panels (*PV*) for electricity were considered to improve the energy efficiency of the house.

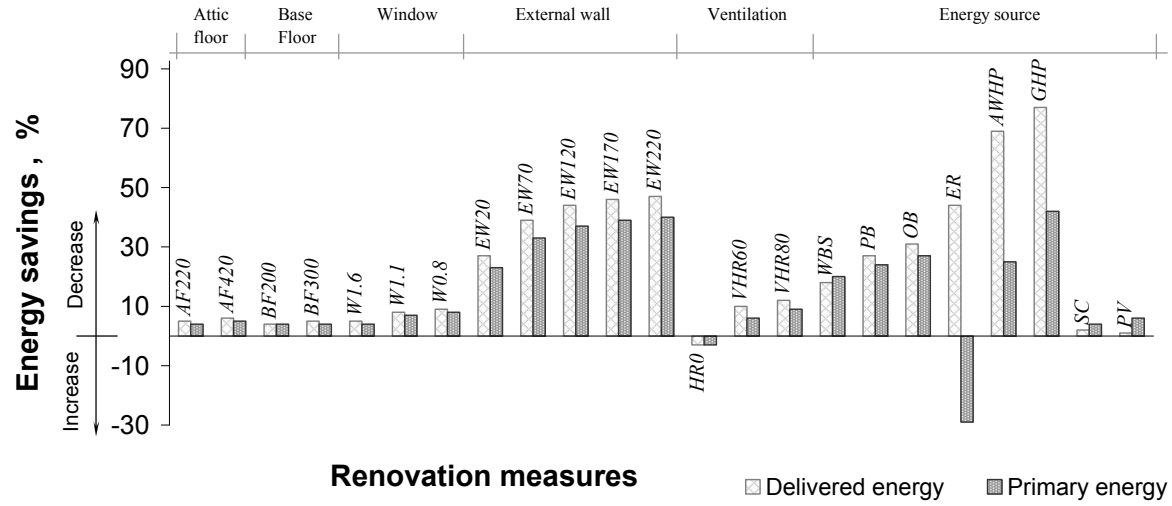

FIG 5. Influence of individual energy-renovation measure on the annual delivered energy (DE, kW/(m2·a)) and primary energy (PE, kW/(m2·a)) consumption.

3.4 Energy renovation packages

In the second step, the renovation packages were combined using single renovation measures. The packages are intended to attain different energy savings: -20% as minimum primary energy saving to -88% to reach the target in the regulation. The reduction of the annual delivered energy and the energy performance value from original levels were used as follows: >20% reduction from the original PE (EU overall level of the reduction of energy consumption); >50% reduction from the original PE (national level of the reduction of energy consumption); 80%/ 88% reduction from the original DE to reach the target values set in BFS 2011:26 BBR 19 for new and renovated buildings (80% when electricity is not used for heating, 88% with electric heating) (Table 2). In the renovation packages, the new mechanical exhaust-supply ventilation system with heat recovery was considered together with the improvement of air flows from 0.35 l/(s·m²) to 0.42 l/(s·m²).

The renovation packages were compiled considering three different aspects:

- 1st package: combining measures that alter the architectural appearance the least, starting from the less visible parts;
- 2nd package: concentrating on the improvement of thermal comfort starting from the building envelope (decreasing thermal transmittance of structures) and next service systems.
- 3rd package: improving energy performance starting from building service systems and next the structures.

Table 1 Energy-renovation packages for different energy saving levels.

Energy saving level	DE kWh/(m²×a) degrease from base case, %	PE kWh/(m²×a) degrease from base case, %	Energy-renovation measures: Attic AF220	Attic AF420	Base BF200	Base BF300	Windows W1.6	Windows W1.1	Windows W0.8	External walls EW20	External walls EW70	External walls EW170	External walls EW220	Ventil VHR60	Ventil VHR80	Energy source WS	WPB	AWHP	GHP	SC	PV
Ref.build.	553 / ±0%	603 / ±0%																			
-20% (EPV)	409 / -26%	474 / -21%	x		x		x								x						
	391 / -29%	457 / -24%	x		x					x											
	383 / -31%	463 /-23%												x		x					
-50% (EPV)	80 / -86%	244 / -60%		x	x				x						x				x		
	153 / -72%	240 / -60%	x		x		x				x				x	x					
	76 / -86%	233 / -61%		x	x				x						x				x	x	
-80%*	32 / -94%	129 / -79%		x		x			x				x		x				x	x	x
-88%**	110 / -80%	175 / -71%		x	x			x				x			x		x				
max	52 / 91%	179 / -70%		x	x		x				x				x				x		

* heating source other than electricity (wood, pellet, gas, oil);
** heating source is electricity (direct electricity, heat pumps)

4. Discussion

The indoor temperature is considered as the main factor in general thermal comfort. The acceptable temperature level in the existing buildings is considered to be in the range of +22±3 ºC (EN 15251 2007). During winter time the average indoor temperature is below the acceptable temperature level 37% of time in the continuously used houses. If the indoor RH level in the range of 25% to 45% during winter time is considered, then the average indoor RH is in an acceptable range in the continuously used houses.

In the houses that are used periodically or are unheated, the average RH level can be considered more critical than the temperature. In addition to the house as such, historic houses can contain numerous valuable objects that are to be preserved. Regarding preservation issues, the indoor RH can be

considered as the factor for mould growth. If the buildings stay unheated, there is no energy consumption but to avoid problems caused by moisture the need for the conservation heating or dehumidification prevails. If the buildings are considered in the condition they are, it may result in a failure to achieve the purpose of energy reduction.

The results of air tightness measurements show that the rural stone houses are quite leaky. Due to the low air tightness the air change rate measured with a passive tracer gas method showed a higher level of ventilation than that in standard use in energy performance calculations.

In terms of energy efficiency, as also indicated by other studies (Balaras 2005, Lechtenböhmer 2010), the main savings potential lies in the improvement of the building envelope. Heat losses can be reduced by adding insulation to the external walls, floors or roof, replacing the glazing or changing the windows. In addition, air tightness is an important factor of energy efficiency. Therefore, improving the building envelope may have a positive effect in the case of air leakages. If a renovation measure enables a reduction in air leakage, the air leakage rate was assumed to be reduced from the original value up to 50%: 5% from wall insulation, 10% from the renovation of windows and 15% from changing windows, 10% from insulating the base floor, and 20% from insulating the attic floor. From the insulation measures, insulation of the external wall has the highest potential. Adding 50 mm of thermal insulation to the external wall give the same amount of energy reduction as the less visible measures (adding insulation to the base floor, to the attic floor and changing windows) altogether.

As the studied buildings are an important part of the built heritage of the island, the architectural appearance should not be changed by external insulation and new windows. For the studied stone houses, the key to energy savings lies in more energy efficient energy sources and heating systems. Improvement of the building service systems (heating and ventilation) accounts for the largest energy saving potential because of the low efficiency of the existing systems. Improvement of the heating and ventilation systems has less significant influence on the architectural appearance of the house. Combining the building service systems with less visible insulation measures it is possible to achieve up to 60% reduction in PE consumption and 86% in DE consumption. To fulfill the target value set in the building regulation, the insulation of the external wall has to be included.

The indoor climate, the air change rate, energy consumption and preservation issues have to be considered when choosing suitable actions in historic buildings.

5. Conclusions

The indoor climate, air tightness and energy performance of the typical stone houses was studied. The indoor climate measurement results show that during the winter time the average indoor temperature is below the acceptable temperature level in the continuously used houses. The RH levels are problematic in the periodically used and in unheated houses causing suitable conditions for the mould growth.

The average air leakage rate q_{50} of the living houses was 14.5 $m^3/(h \cdot m^2)$. The average air change rate measured with a passive tracer gas method during the winter time and in the normal use was 0.9 h^{-1}. The air tightness measurements show that the studied houses are quite leaky.

The largest energy saving potential of the historic stone houses lies in the heat source and in building service systems. Combining the ground source heat pump with new windows, attic floor and base floor insulation, a maximum of 60% in PE and 86% in DE was achieved, having the least effect on the architectural appearance worth preserving.

The study is limited to the historic stone houses on Gotland, however there are some general conclusions to be made. The indoor climate is crucial to the use and preservation of the buildings and sometimes improving the indoor climate may require even more energy. Even though visible changes should be avoided, significant energy savings can be achieved by improving air tightness, control and by changing to more efficient heat source.

6. Acknowledgements

The research has been conducted as part of the IUT1-15 project “Nearly-zero energy solutions and their implementation on the full-scale renovation of buildings“ financed by Estonian Research Council, HELTH “Healthy and Energy-efficient Living in Traditional Rural Houses” financed by Central Baltic Interreg IV A program and the Swedish Energy Agency through the National Research Program on Energy Efficiency in Historic Buildings. The Publication of this article was supported by European Social Foundation financing task 1.2.4 Cooperation of Universities and Innovation Development, Doctoral School project "Civil Engineering and Environmental Engineering" code 1.2.0410.09-0080.

References

Balaras C, Droutsa K, Dascalaki E, Kontoyiannidis S. Heating energy consumption and resulting environmental impact of European apartment buildings. Energy and Buildings 2005;37:429–442.

BFS 2011:26 BBR 19. Boverket’s mandatory provisions on the amendment to the Board's building regulations (2011:6) –mandatory provisions and general recommendations.

Björsell N, Bring A, Eriksson L, Grozman P, Lindgren M, Sahlin P, et al. IDA indoor climate and energy. In: Proceedings of the IBPSA building simulation ’99 conference, Kyoto, Japan; 1999.

Brostrom T, et al. A method to assess the potential for and consequences of energy retrofits in Swedish historic buildings. The Historic Environment: Policy and Practice, (2014) 5(2)

EN 15251:2007. Indoor environmental input parameters for design and assessment of energy performance of buildings- addressing indoor air quality, thermal environment, lighting and acoustics.

Fabbri K, Zuppiroli M, Ambrogio K. Heritage buildings and energy performance: Mapping with GIS tools. Energy and Buildings 2012;48:137-145.

Fabbri K. Energy incidence of historic building: Leaving no stone unturned. Journal of Cultural Heritage 2013;14(3):e25-e27

Hukka A., Viitanen H.A. A mathematical model of mould growth on wooden material. Wood Science and Technology 33 (1999) 475 - 485

Lechtenböhmer S, Schüring A. The potential for large-scale savings from insulating residential buildings in the EU. Energy efficiency 2010;4(2):257-270.

Moinard S, Guyon G. Empirical validation of EDF ETNA and GENEC test-cell models. Subtask A.3, A Report of IEA Task 22, Building Energy Analysis Tools; 1999.

Sahlin P. Modelling and simulation methods for modular continuous system in buildings. PhD Thesis, KTH, Stockholm, Sweden; 1996.

Sandberg. M., Stymne. H. (1989), The constant tracer flow technique. Building and Environment. Volume 24, Issue 3, pp.209–219

Sustainable Cities’ Energy Demand and Supply for Heating and Cooling. Rapport I 2009:18 Svensk Fjärrvärme AB.

Woloszyn M, Rode C. Tools for performance simulation of heat, air and moisture conditions of whole buildings. Build Simulat 2008;1:5–24.

Energy conservation in museums via setpoint strategies: a case study for a state-of-the-art museum using building simulations.

Rick Kramer, MSc [1]
Jos van Schijndel, Assistant Professor [1]
Henk Schellen, Associate Professor [1]

[1] Eindhoven University of Technology, the Netherlands

KEYWORDS: *Energy conservation, museum, indoor climate, building simulation, preservation*

SUMMARY:

Museums are dedicated to protect their artwork collection and to display the collection as safely as possible. The indoor climate is of utmost importance to minimize collection degradation. Many museums employ tight climate guidelines, allowing only small fluctuations of indoor temperature and relative humidity, resulting in the following problems: huge energy consumption, the need for high-capacity HVAC systems, additional stress on monumental buildings. This research investigates the energy-saving potential of different setpoint strategies, while damage functions are used to assess the degradation risk of the collection, and an Adaptive Temperature Guideline is used to assess thermal comfort. A state-of-the-art museum in the Netherlands is modelled and the indoor climate is simulated. Energy demand includes simulated energy for heating, cooling, humidification and dehumidification. The main conclusion is that it is possible to significantly reduce the energy demand, significantly improve thermal comfort and even decrease chemical degradation.

1. Introduction

In the late 1980's, museums in the Netherlands paid little attention to collection preservation. Therefore, the Ministry of Health and Culture launched the Deltaplan in 1990 to initiate a paradigm shift by identifying areas for improvement, including indoor climate conditions. Consequently, museums installed Heating, Ventilation and Air Conditioning (HVAC) systems to control the indoor climate and provide a safer environment for the collection.

No indoor climate specifications were defined in the Deltaplan. So, new guidelines (Jütte 1994) were developed and international guidelines (ASHRAE 2007) were adopted that included several climate classes. However, over time the notion of a good indoor climate evolved: if fluctuations of ±5% RH are good, than ±3% RH must be better (Brown & Rose 1996). Consequently, museums chose the most strict climate classes.

During the 2000's, Ankersmit (2009) developed a risk-analysis procedure for museums, revealing that the employed guidelines are too strict in many cases: museums are often housed in historical buildings, requiring a huge amount of energy to meet the strict guidelines due to large heat losses. Moreover, strict indoor climates may cause stress on historical buildings (Schellen 2002), e.g. condensation problems.

Martens (2012) developed a method to assess the degradation risk of four museum objects based on T and RH data using damage functions. The method focuses on the influence of the indoor climate on the objects instead of focusing on the indoor climate directly. The study showed that the degradation risks of museum objects in old buildings with a simple installation often do not significantly differ from the risks in monuments equipped with modern HVAC systems.

This paper presents a holistic approach to investigate the energy saving potential of various setpoint strategies for T and RH: A state-of-the-art museum, which is housed in a renovated historical building located in the Netherlands, is modelled and simulated; damage functions (Martens 2012) were employed to assess the degradation risk of the collection; the Adaptive Temperature Guideline of van der Linden et. al (2006) was employed to assess thermal comfort of the simulated indoor climate. In the simulations, the HVAC systems are deliberately excluded, to reveal the effect of the different setpoint strategies on the building's energy demand.

Section 2 describes the methods, including a description of the case study building (2.1), data acquisition (2.2), the modelling (2.3), and how damage functions and Adaptive Temperature Guideline are used to assess collection preservation and thermal comfort, respectively (2.4). Section 3 presents the results, Section 4 provides a discussion with conclusions and Section 5 presents recommendations for future work.

2. Methodology

2.1 The museum

The case study comprises of a state-of-the-art museum that is located in Amsterdam, the Netherlands. The museum is housed in a late 17th century building. During the past centuries, many changes were made to the building, additional buildings were built and the layout was modified. Central heating was implemented in 1860. The building was substantially renovated in 1970 as it was transformed into a modern nursing home. The most recent renovation dates from the years 2007-2009 when the building was transformed into a state-of-the-art museum. FIG 1 shows the floor plan including two almost identical exhibition rooms with adjacent exhibition cabinets and their cross-section. The ceiling of the main exhibition hall contains a large glass area in the roof with interior sun blinds that are almost permanently closed. The exhibition rooms are conditioned by an all-air HVAC system.

The employed indoor climate specifications for T: setpoint 21°C, permissible fluctuation per hour is 2°C and per day is 3°C. The specifications for RH: paintings and furniture setpoint 55%, mixed collections 45-50% and metal collections 40-50%, all with tolerances ±5 %.

FIG 1. The floor plan of the first floor includes the two almost identical exhibition rooms between the red dots [left] and their cross-section [right], showing the main exhibition room in the center with the adjacent exhibition cabinets.

2.2 Data acquisition

2.2.1 Outdoor climate data

For calibration of the building model, outdoor climate data were used of the year 2011. The outdoor T and RH were measured at the museum in Amsterdam. Solar radiation data were retrieved from the Royal Netherlands Meteorological Institute's database (station Schiphol Airport). For simulation of the setpoint strategies, climate year 2003 was used: the year 2011 was a very mild year without very cold or hot periods, but the year 2003 had a cold winter and a hot summer. Therefore, the year 2003 is more suitable to discriminate between different setpoint strategies.

2.2.2 Indoor climate data

The exhibition room of interest is equipped with four combined T and RH sensors that are connected to the Building Management System (BMS). A data set for simulation and a data set for validation were constructed. Little preparation of the data was required by removing outliers and reconstructing missing values by interpolation.

2.2.3 Air Handling Unit data

The supply air for the entire building comes from four central outdoor air intake openings. The air handling system consists of ten Air Handling Units (AHUs). The exhibition area of interest is conditioned by one AHU that conditions the air by cooling, dehumidification and humidification by an electrical humidifier, heating, mixing-recirculation and filtering bacteria, spores, fungi, bacteria, harmful gases and particles. CO_2 measurements in the exhibition room are used to determine the required amount of fresh outdoor air. Data from measurement positions inside the AHU were extracted from the BMS. Supply air temperature and air flow data were used to calculate the supplied energy to the exhibition room used for calibrating the simulation model.

2.3 Modelling

A multi-zone model was developed using HAMBASE (Wit 2006), a Heat Air and Moisture modelling and simulation tool developed in the scientific programming environment MATLAB at the University of Technology Eindhoven. The model was used to simulate the indoor air temperature, the indoor air humidity and building's energy demand (excl. HVAC systems) for heating, cooling, humidifying and dehumidifying the multi-zone building.

The model of the museum consists of nine zones: one main exhibition room and all adjacent rooms. The HVAC systems were modelled for calibration but deliberately excluded in further simulations, so the simulated energy use only represents the building's energy demand.

The model was calibrated by comparing the simulated energy demand to the energy demand that was calculated based on measurements: air infiltration, internal heat gains (visitors and lighting) and internal moisture gains (visitors) were tuned to calibrate the model. The deviations of simulated energy use compared to calculated energy use, are +2% for heating, 0% for cooling, -9% for humidification and -8% for humidification.

2.4 Damage functions and thermal comfort

To assess whether the indoor climate is safe for the collection, the specific climate risk assessment method of Martens (Martens 2012) is used. The method focuses on the indoor climate as it is experienced by four typical objects: paper, panel painting, wooden furniture and wooden sculpture. To obtain the climate as it is experienced by the object, the response is approximated using a first-order filter including the response time of the object: minutes for paper (Michalski 1993), 4.3 days for

the panel painting's surface response and 26 days for the full response (ASHRAE 2007), 40 days for the furniture's full response (Bratasz et al. 2008), 10 hours for the sculpture's surface response (ASHRAE 2007) and 15 days for the sub-surface response causing maximum stresses (Dionisi Vici et al. 2006).

The specific climate risk assessment method assesses three degradation phenomena: Four degradation phenomena are assessed for four typical objects: biological degradation is based on Sedlbauer's theory (2001), chemical degradation is based on the Lifetime Multiplier (Michalski 2002) with E_a denoting the activation energy being 100 kJ/mol for paper and 70 kJ/mol for the other objects, mechanical degradation of the base layer is based on the theories of Mecklenburg et. al (1998), Bratasz et. al (2008) and Jakiela et. al (2007), and mechanical degradation of the pictorial layer is based on Bratasz & Rachwal's theory (2010).

Thermal comfort is evaluated using the Adaptive Thermal Guideline of van der Linden et. al (2006), taking the adaptive behavior of humans into account: the comfort limits depend on the running mean outdoor temperature of the current day and preceding three days. The museum is classified as building type 'beta': people can't control the indoor climate individually. Class 80% was used, i.e. 80% of the people are satisfied if the climate fits into the 80% class' comfort limits. Thermal discomfort is quantified by summing the hours that this comfort class is exceeded, only during opening hours (10am to 5pm). The used comfort guideline is specifically valid for offices, but is used in this study for a museum since comfort guidelines for museums are lacking. People spend more time in offices than museums, so the guideline's comfort limits may be more strict than necessary.

3. Results

One of the exhibition rooms of the museum was simulated. Different setpoint strategies for temperature (T) and relative humidity (RH) were studied to obtain energy savings while pursuing a safe indoor climate for the collection and a comfortable indoor climate for visitors and staff. The research is based on climate data for the year 2003 and simulated energy represents the building's energy demand. Energy savings were calculated by comparing different setpoint strategies to the reference situation. The strategies are numbered from 1 to 16.

3.1 Reference situation

The reference situation comprises of simulating the museum's exhibition room, with constant setpoints: 21°C for T and 48% for RH. TABLE 1 (strategy 1.) shows that maintaining a steady indoor climate all year round, 24h per day, provides a safe indoor environment for the collection, although chemical degradation is stimulated by the fairly high T and RH. Thermal comfort is unacceptable according to the ATG: the indoor climate is too cold during most of the opening hours, see FIG 2 (top left).

3.2 Setpoint strategies for T

This section deals with finding appropriate T setpoint strategies. Firstly, constant setpoints are assessed. Secondly, setpoints based on the dynamics of the outdoor climate are assessed. Thirdly, the chosen setpoint strategy is used during opening hours, and during closing hours night setback strategies are assessed.

3.2.1 Constant T setpoint

Three setpoint strategies are simulated, varying T and keeping RH at 48%: (2.) constantly 22°C, (3.) constantly 23°C, (4.) only a lower limit of 22°C (no cooling). TABLE 1 shows the results. Strategy 2 shows that increasing T to 22°C significantly improves thermal comfort (less undercooling hours).

However, this additional 1°C increases energy demand by 16%. Also, the LM drops to 0.8 indicating increased chemical degradation. Strategy 3 shows that an increase of 2°C makes things worse for collection and energy demand, but comfort is improved. Strategy 4 reveals that cooling is not needed for thermal comfort, only 7 discomfort hours, see also FIG 2 (top right). The main conclusion from this section is that cooling is not needed in the exhibition room with respect to temperature and that the fluctuation of T in the summer period does not have a negative impact on the collection. However, the LM is quite low due to the higher temperatures.

TABLE 1. Various setpoint strategies for T were simulated. Energy demand includes heating, cooling and (de)humidification. Collection preservation is assessed, visualized using the colors green (good), orange (moderate) and red (bad), for the degradation phenomena: biological (mold), chemical (LM) and mechanical. Thermal comfort is based on the ATG and expressed in hours discomfort.

	setpoint		energy		risk assessment				
	T [°C]	RH [%]	total [MWh]	vs. ref. [%]	mold	LM	base layer	pict. layer	discom-fort
1. ref.	21	48	146	-		0.92			812 h
2. const.	22	48	169	+16		0.80			63 h
3. const.	23	48	190	+30		0.69			28 h
4. no cool.	22 - ∞	48	168	+15		0.80			7 h
5. sine	20/22	48	142	-3		0.91			299 h
6. sine	19/23	48	139	-5		0.90			997 h
7. sine	20.5/22.5	48	153	+5		0.85			0 h
8. RMOT	~	48	133	-9		0.96			0 h
9. recirc.	RMOT	48	51	-65		0.96			0 h
10. setback	RMOT/FF	48	39	-74		1.10			0 h

3.2.2 T setpoint based on T outdoor

The constant setpoint strategies 2, 3 and 4 showed that thermal comfort can be improved significantly, but with increased energy demand. In this section, RH setpoints are kept constant at 48% and T setpoints vary with the outdoor T. Four strategies are simulated: (5.) a sine wave is used for T setpoints with an average of 21°C and amplitude of 1°C, (6.) a sine wave with average of 22°C and amplitude of 2°C, (7.) a sine wave with average 21.5°C and amplitude 1°C, and (8.) T setpoints based on the Running Mean Outdoor Temperature (RMOT). TABLE 1 shows the results. Strategy 5 shows that T-setpoints based on a sine wave improve thermal comfort and save energy compared to the reference situation. However, strategy 7 reveals that proper thermal comfort (0h discomfort) results in increased energy demand. Making T dependent on $T_{outdoor}$ using a sine wave is much more in accordance with the theory of adaptivity (ATG), see FIG 2 (bottom left). Strategy 8 gives the best results: Thermal comfort is maximized, see FIG 2 (bottom right), with a minimum of energy (-9%).

3.2.3 Tindoor based on RMOT and night setback

The best T setpoint strategy yet is based on the RMOT (strategy 8), since it provides both enhanced thermal comfort and energy conservation. Thermal comfort is only necessary during opening hours, therefore, two strategies were assessed for the closing hours: (9.) applying 100% recirculation, i.e. no air exchange with the outdoor environment and T is based on the RMOT; (10.) applying 100% recirculation and T free floating (FF), i.e. no heating and cooling. In the latter strategy, the recirculation ensures that the cooling down process is dampened by the building's thermal mass,

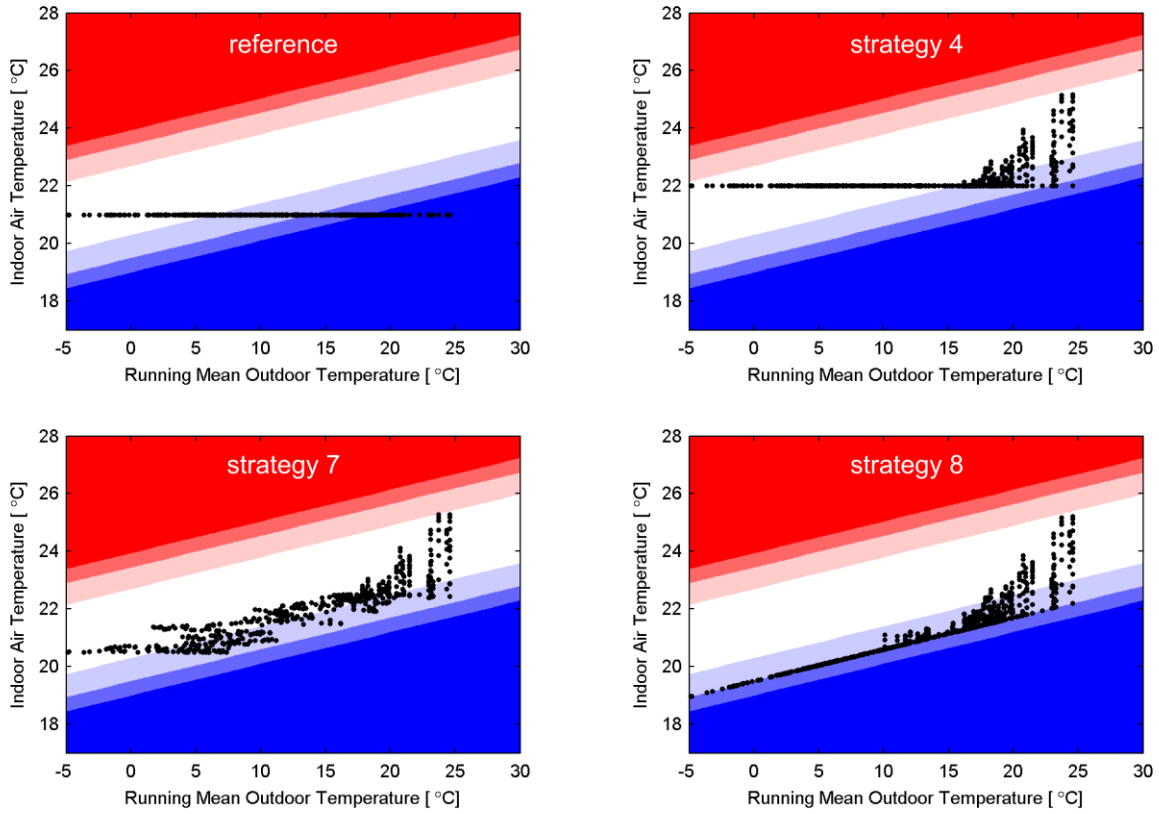

FIG 2. Comfort assessment. Top left: The reference situation, T is maintained at 21°C and RH at 48%. Top right: Strategy 4, the heating setpoint is 22°C and there's no cooling. Bottom left: Strategy 7, T-setpoints are based on a sine wave with average 21.5°C and amplitude 1°C. Bottom right: Strategy 8, T-setpoints are based on the RMOT.

limiting daily T fluctuations. The RH was maintained at 48% and strategy 8 is used during opening hours. TABLE 1 shows the results.

The application of 100% recirculation during closing hours significantly decreases energy demand. Strategy 10 combines the recirculation with free floating of T during closing hours. Due to the recirculation, the cooling down is limited during closing hours resulting in a safe indoor climate for the collection: allowing a lower T during closing hours even decreases chemical degradation as indicated by the increased LM. Thermal comfort is guaranteed by turning on the heating system one hour before the opening of the museum at 9 am.

3.3 Setpoint strategies for RH

Setpoint strategy 10 is used for T in this section. For RH, six setpoint strategies were simulated: (11.) RH free floating (FF), revealing the performance bound for energy savings; (12.) RH between 30% and 70%; (13.) RH between 40% and 60%; (14.) RH between 45 and 55%; (15.) RH between 40% and 50%; (16.) RH between two sine waves with average 40 and with average 50, both with amplitudes of 5%. Strategy 16 is used by several museums as it is considered to be superior compared to constant setpoints. TABLE 2 shows the results.

Strategy 11 shows, as expected, that free floating RH is harmful to the collection, all objects are affected by all mechanisms of deterioration, and the performance bound for energy savings is 84%. Strategy 12 shows that maintaining the indoor RH between 30% and 70% provides already a safe indoor environment regarding mold growth and mechanical degradation. Chemical degradation is still

too high, but chemically unstable artifacts may be moved to display cases. The energy saving is 82% which is very close to the performance bound. Moreover, the results show that adopting tighter requirements, ±20% (strategy 12), ±10% (strategy 13), ±5% (strategy 14), decreases chemical degradation, which is due to lowering the upper limit for RH (Michalski 2002), and more energy demand, see FIG 3 for a specification (notice that humidification is negligible). Chemical degradation is decreased by applying an upper limit of 50% (strategy 15), but this requires a lot of dehumidification which is very costly. Comparing strategy 15 to strategy 16 suggests to choose a strategy with fixed limits, instead of limits that depend on the outdoor RH, since this has no added value for collection preservation.

TABLE 2: Various setpoint strategies for RH were simulated. The energy demand includes heating, cooling and (de)humidification. Collection preservation is assessed, visualized using the colors green (good), orange (moderate) and red (bad), for these degradation phenomena: biological (mold), chemical (LM) and mechanical. Thermal comfort is according to strategy 10 (0h discomfort).

	setpoint		energy		risk assessment			
	T [°C]	RH [%]	Total [MWh]	vs. ref. [%]	mold	LM	base layer	pict. layer
11.	strat.10	FF	24	-84		0.70		
12.	strat.10	30-70	26	-82		0.78		
13.	strat.10	40-60	29	-80		0.88		
14.	strat.10	45-55	31	-79		0.95		
15.	strat.10	40-50	33	-77		1.06		
16.	strat.10	sine 40/50±5	33	-78		1.05		

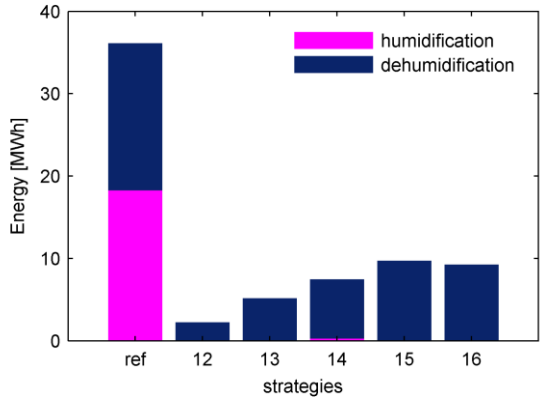

FIG 3. RH strategies' energy for (de)humidification.

4. Conclusions

The study involves a case study, therefore the results are applicable to well-insulated historical buildings. More research is needed that applies the method to other building types, especially to assess the suitability of free floating temperature during closing hours, which will be highly dependent on the building's thermal mass. Moreover, the applied *risk assessment* needs to be expanded to include more objects besides the included four reference objects.

HVAC systems were excluded to show the effect of the setpoint strategies on the *building's* energy demand and make the results more generally applicable to museums housed in well-insulated

historical buildings. Minimizing the building's energy demand is the first step in finding energy efficient operation strategies for museums.

The main conclusions are: (i) T is mostly determined by thermal comfort and RH by the collection; (ii) letting T free floating during closing hours with 100% recirculation saves the most energy and is not harmful for the collection for this case; (iii) T should depend on the outdoor climate, while RH should be maintained between fixed limits; (iv) it is possible to significantly save energy, significantly improve thermal comfort and improve collection preservation (strategy 15).

References

Ankersmit, B., 2009. *Klimaatwerk: Richtlijnen voor het museale binnenklimaat* B. Ankersmit, ed., Amsterdam: Amsterdam University Press.

ASHRAE, 2007. Museums, Archives and Libraries. In *ASHRAE handbook Heating, Ventilation and Air Conditioning applications*. American Society of Heating Refrigaration and Air-Conditioning Engineers, pp. 21.1–21.23.

Bratasz, L. et al., 2008. Conservation of the Mazarin Chest: structural response of Japanese lacquer to variations in relative humidity. *ICOM Committee of Conservation*, 2, pp.1086–1093.

Bratasz, L. & Rachwal, B., 2010. Computer modelling of dimensional response and stress fields in wooden artworks. In *Conference on allowable microclimate variations for polychrome wood*. Oslo: Institute of Catalysis and Surface Chemistry.

Brown, J.P. & Rose, W.B., 1996. Humidity and moisture in historic buildings: the origins of building and object conservation. *APT Bulletin*, 27(3), pp.12–24.

Dionisi Vici, P., Mazzanti, P. & Uzielli, L., 2006. Mechanical response of wooden boards subjected to humidity step variations: climatic chamber measurements and fitted mathematical models. *Journal of Cultural Heritage*, 7(1), pp.37–48.

Jakiela, S., Bratasz, L. & Kozlowski, R., 2007. Numerical modeling of moisture movement and related stress field in lime wood subjected to changing climate conditions. *Wood Sci Technol*, 42, pp.21–37.

Jütte, B.A.H.G., 1994. *Passieve conservering: klimaat en licht*, Amsterdam.

Van der Linden, a. C. et al., 2006. Adaptive temperature limits: A new guideline in The Netherlands. *Energy and Buildings*, 38(1), pp.8–17.

Martens, M.H.J., 2012. *Climate Risk Assessment In Museums: degradation risks determined from temperature and relative humidity data*. Eindhoven University of Technology.

Mecklenburg, M.F., Tumosa, C.S. & Erhardt, E., 1998. Structural response of painted wood surfaces to changes in ambient relative humidity. In *Painted wood: history and conservation*. Los Angeles: Getty Conservation Institute, pp. 464–483.

Michalski, S., 2002. Double the life for each five-degree drop , more than double the life for each halving of relative humidity. In R. Vontobel, ed. *13th triennial meeting Rio de Janeiro*. London: James & James, pp. 66–72.

Michalski, S., 1993. Relative humidity: a discussion of correct / incorrect values. *ICOM Committee of Conservation*, 2, pp.624–629.

Schellen, H.L., 2002. *Heating Monumental Churches, Indoor Climate and Preservation of Cultural Heritage*. University of Technology Eindhoven.

Sedlbauer, K., 2001. *Prediction of mould fungus formation on the surface of and inside building components*. Fraunhofer Institute for Building Physics.

Wit, M.H. de, 2006. *Heat Air and Moisture model for Building And Systems Evaluation* Bouwstenen., Eindhoven: Eindhoven University Press.

The importance of microclimate in at biodeterioration in historic wooden structures

Johan Mattsson, M.Sc. [1]
Anne Cathrine Flyen, M. Architecture [2]

[1] Mycoteam AS, Norway
[2] Norwegian Institute for Cultural Heritage Research (NIKU), Norway

KEYWORDS: *Biodeterioration, microclimate, growth rate, building survey.*

SUMMARY:
Due to long-term exposure to various climatic conditions, building materials in historic buildings are gradually deteriorated. Our studies have shown that a crucial factor in many cases of biodeterioration is the micro-climatic in the wooden cells. In an ideal situation could one hope for a good access to historic information about previous exposure and damages. Unfortunate does such information almost never exist. Since the established fungal attacks is a direct response to the long-term moisture exposure in the historic buildings, is it possible to read the information in the damages as a long-term logging of previous conditions. In order to understand the causes and prevent further deterioration it is by that reason important to identify the occurring species because their individual requirements for ecological conditions. By examine special details of the damages, e.g. the pattern of fungal decay and mixture of various species of organisms, can it be possible to identify the causative factors that has to be handled in order to avoid further damages. Our experience is that the methods for such survey are universal. By that reason damages caused by biodeterioration from the Polar Regions to the Tropics can be evaluated by the same procedures. This paper describes the effect of microclimate in some different cases at Svalbard.

1. Introduction

Fungal deterioration of wood occurs when the moisture content of the wood is sufficiently high, and the temperature is suitable. Moisture level is often the limiting factor for biodeterioration (Coggins 1980, Rayner and Boddy 1988). The extent of decay is dependent on the length of time these crucial conditions are present at the same time (Mattsson 1995). For that reason fungal decay of externally exposed wood is normally regarded to be correlated with climatic conditions, and maps of decay index have been made in order to describe the risk of deterioration of wood in an outdoor environment (Scheffer 1971, Grøntoft 2008). However, more recent research has shown that local climate has significantly larger impact than regional climate (Brischke et al. 2006). As a matter of fact, the critical conditions for fungal activity can be downsized to the actual piece of wood and the involved wooden cells where the fungus is situated (Gobakken et al. 2014).

It has been generally assumed that fungal decay is not possible in Polar Regions, due to the extremely cold and dry climate. At Svalbard (Spitsbergen) where wooden constructions are situated in a climate with an annual average temperature of -4,7 °C and a yearly precipitation of 271 millimetre (Wikipedia 2013a) it has by tradition been stated that deterioration caused by fungi due to the extreme climate was not a problem. However, despite this hard temperature and humidity conditions, extensive problems with fungal deterioration have been shown during several seasons of field work through 2001-2011 (Mattsson and Flyen 2011).

The decay of wood at Svalbard shows an important difference compared to decay damages in temperate areas. The dominating organism is *Leucogyrophana mollis*, which has been shown to cause almost all brown rot decay in wood exposed outdoors. Other species have been found only rarely (Mattsson et al, 2010). Other differences of decay pattern between wood exposed outdoors at Svalbard compared to the mainland of Norway is that the deterioration is almost never visible on the surface, fruiting bodies are never observed and the damages almost exclusively occur in wood in soil contact (Mattsson et al. 2010). Damages inside buildings, where the microclimate is governed by the climatic conditions inside the building or construction, the damage pattern differs from the damages in wood exposed outdoors. Indoors, the damages are more extensive, more visible, not necessarily in soil contact and caused by several fungal species (Mattsson and Flyen 2008).

This paper describes how the microclimate has a crucial importance for the risk of fungal deterioration, despite the extensive variations in temperature and humidity that can occur in constructions and materials. The resulting pattern of decay is described and explained, and comparisons are made with experiences from damages at Svalbard.

2. Materials and Methods

2.1 Field work

Field investigations were carried out at Svalbard at one occasion in 2010 and two occasions in 2012. During the survey in 2010, temperature and relative humidity in the soil at cable car bucks and wooden poles under several buildings in Hiorthhamn was examined. During the work in 2012, 82 cable car bucks around Longyearbyen and six buildings in Longyearbyen were controlled.

2.2 Visual investigations and measurements

The main method for the survey has been visual control of exposed wooden constructions. Investigation below the surface of the materials has been performed with knives or cutting steels. Temperature and relative air humidity has been measured in air in shadow and sunlight, soil from surface down to permafrost and wood (Rotronic Hygropalm with a 5 millimeter miniature probe). The accuracy of the sensor is ± 2 % RH under 90 % and ± 3 % RH over 90 %.

Logging of temperature and relative humidity at Svalbard was performed with a Rotronic Hygrolog-D, with a logging interval of 5 minutes. Wood moisture content has been measured using an electrical resistance moisture meter (AB-Wood Moisture meter) with a hammer electrode. The deviation of the device is +/-2%. A decay detecting drill has been used to evaluate the decay patterns of wooden constructions. The Resistograph E 300 functions by measuring the power needed to move a 2 mm drill probe forward at stable speed. The power measurement is plotted simultaneously on a paper roll, and is also committed to the memory of the apparatus for later digital analysis. Variations in density are shown directly in the power curve, and decay damages show as areas with lower drill power needed. The method leaves a 2 mm drill hole in the material, and is thus virtually non-destructive.

2.3 Sampling for microscopically analysis

In 2012, 126 samples were taken from cable car bucks and 53 from building fundaments. All 179 samples have been examined visually and by microscopic analysis. 126 of the samples have been examined for the thickness of sound wood in the surface (surface layer).

3. Results

3.1 Climatic conditions

Temperature measurements at in Hiorthhamn on the 31th July 2010 showed great differences in temperature between sun exposed surfaces and the air in a shaded location (table 1).

TABLE 1. Surface maximum temperatures 31. July 2010 at two facades at the blacksmith workshop at Hiorthhamn.

Place	Temperature (°C)	Relative humidity (%)
Air, in shadow	8,0 °C	70,1%
Eastern wall exposed to the sun, behind bitumen layer	50,1 °C	9,2%
Western wall, behind bitumen layer	8,6 °C	68,8%

Measurements of soil temperature have been investigated both by single measurements and by logging. The results from the single values are given in table 2. Table 2 shows that the soil temperature varied from close to zero near the permafrost and up to a temperature which approximates ambient air temperature closer to the surface. In direct sunlight on the dark surface temperature was much higher than the air temperature. The results show that there are high levels of relative humidity in the soil (90-100% RH), through the soil profile where the measurement is taken.

TABLE 2. Maximum temperatures and relative humidity in soil at Hiorthhamn 31th July 2010.

Place	**Depth in soil**	**Temp (ºC)**	**RF (%)**
Air, shadow		8,0	70,1
Air, sun		19,1	34,2
Cable car buck nr. 9, NE-pole	Surface	10,4	61,0
Cable car buck nr. 9, NE-pole	15 cm	7,1	96,3
Cable car buck nr. 8, shadow	Surface	9,6	62,7
Cable car buck nr. 8, sun	Surface	15,1	48,2
Cable car buck nr. 8, under a log	Surface	9,2	94,2
Cable car buck nr. 8, E pole	15 cm	5,8	93,9
Cable car buck, nr. 8, SW pole	25 cm	3,7	98,7
Cable car buck nr. 8, SW pole	50 cm	2,8	97,8
Cable car buck nr. 7, SW pole	5 cm	10,4	100,0
Cable car buck nr. 7, SW pole	30 cm	1,6	100,0
Cable car buck nr. 7, NE pole	5 cm	10,1	91,0
Cable car buck nr. 6, SW pole	5 cm	7,9	100,0
Cable car buck nr. 6, SW pole	15 cm	6,7	100,0
Cable car buck nr. 6, SW pole	40 cm	1,4	96,3
Manager's house, SE pole, in shadow	Air	6,8	87,2
Manager's house, pole under the building	5 cm	5,1	100,0
Manager's house, SE pole, (sun exposed)	5 cm	9,9	100,0
Manager's house, SE pole (sun exposed)	45 cm	5,6	100,0

The air temperature (in shadow) and relative humidity was logged in the air and 10 cm deep in the soil near two cable car bucks from July 31th to August 8th 2012. One buck was newly repaired and an

insulation mat was placed 20 cm under the soil surface, while the other buck was an old one without any insulation layer. Both bucks belonged to the transport line from coal mine 1B in Longyearbyen. The result of logging of temperature is shown in figure 1.

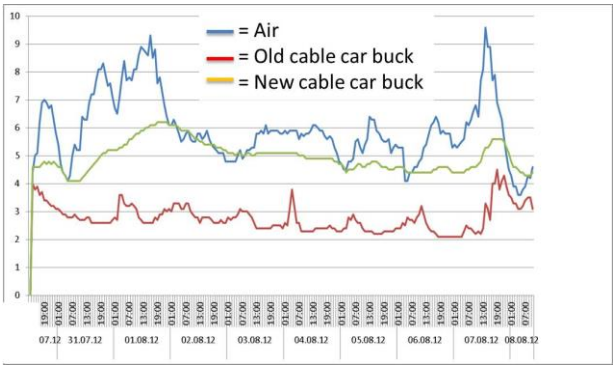

FIG 1. Temperature in air and 10 cm under the soil surface near an old cable car buck and near a repaired buck with a layer of mineral insulation placed 20 cm under the surface. The logging was done from 31. July – 8. August 2012.

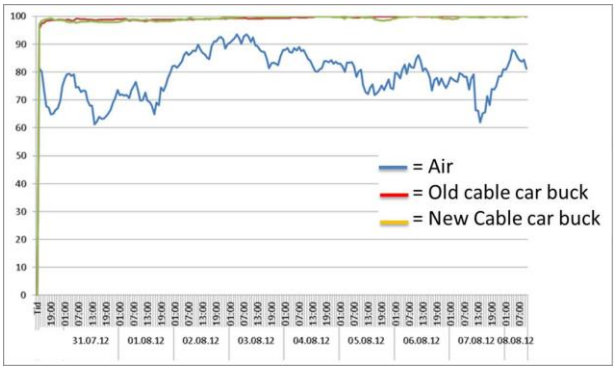

FIG 2. Relative humidity in air and 10 cm under the soil surface at an old cable car buck and at a repaired buck with an insulation mat placed 20 cm under the surface, from 31. July – 8. August 2012.

The results show that the insulation layer caused higher soil temperature above the layer than what the normal temperature would be. The difference is about two degrees Celsius. The relative humidity in the soil is the same, about 100% RH (figure 2), whether there is an insulation layer present or not.

3.2 Surface layer of unharmed wood

The thickness of the intact outer wooden layer outside the visibly decayed wood in 109 samples from the cable car bucks at Longyearbyen was 4.5 millimetre on average. The thickness of the unharmed wood in cracks in the surface was 2.8 millimetre on average (figure 3).

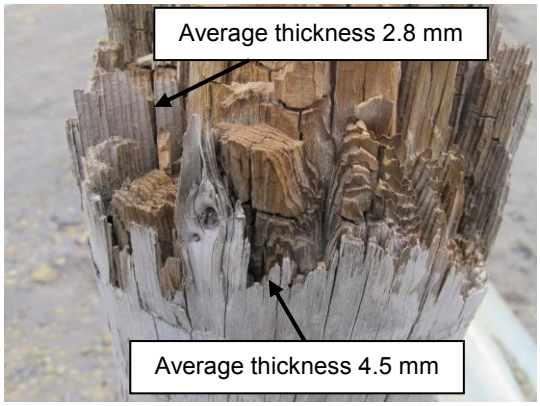

FIG 3. The surface of decayed wood at Svalbard is frequently without any visible damages due to the layer of unharmed wood.

3.3 Occurrence of decay fungi

In the present study, wooden materials in constructions from about 2 meters above the soil and down to about 15-20 cm under the soil surface were examined. The major part of decayed wood was found in areas close to soil contact. The samples of decayed wood were taken where there were visible

damages or where damages were expected (figure 4). In the cases where fungal damages were found above soil contact (figure 5), they occurred in connection with locations where precipitation easily could penetrate into the interior part of the wooden materials. Examinations of the wooden materials of buildings, building remains and cable car bucks have shown that the main area of deterioration is found to be from ca. 10 cm under soil surface to 20-30 cm above.

FIG 4. Decay damages were commonly found where the wood is in soil contact.

FIG 5. Decay in wood above soil contact is in areas where precipitation can penetrate into the wood, e.g. end grain and cracks.

Growth of visible mycelia does occasionally occur in brown-rot decayed wood in Norway, especially where there is high moisture content in the wood or high relative humidity in the surrounding air (Mattsson 2010). At Svalbard visible mycelia were only found in one case during the fieldwork in 2012.

4. Discussion

The climate at Svalbard is strongly affected by its northern location and polar climate. For a major part of the year all soil in Svalbard is frozen, and below a varying thawing zone the soil is frozen all year round (permafrost). Permafrost prevents biological activity both due to the low temperatures and by restricting the availability of water. At such low temperature it is in general not expected to be any fungal activity (Viitanen 1995).

Despite these tough conditions, our research has shown that fungal decay is commonly found in wood that has been in soil contact for 30-40 years or more. The extent of decay is clearly restricted to a limited area in the materials, from a few centimetres below the soil surface (i.e. the upper part of the thawing zone) to some decimetres above the surface. This indicates that these locations offer conditions that are suitable for biodeterioration (fig 6).

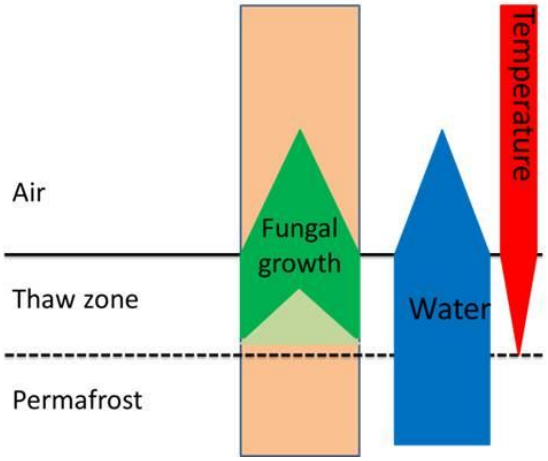

FIG 6. Fungal growth in wood with soil contact can be explained by the combination of stabile conditions of suitable access of water and favourable temperature.

In wintertime the soil is frozen due to permafrost and low air temperature. During the summer months, our measurements show that the temperature in the upper layer of the soil (the thaw zone) varies from 0 °C at the border against the permafrost to more than 10 °C in the soil surface. Measurements made in different locations near and on the surface of structures show large variations in climatic conditions over very small distances. One part of a building can offer hospitable conditions for microorganisms, while other parts offer neither necessary moisture levels nor sufficiently high temperatures for growth (Mattsson and Flyen, 2008). Measurements made in the soil in this study show that the relative humidity in the thaw zone is permanently close to 100 %. In the present study, measurements near cable car bucks with and without an insulation layer in the ground show that small changes can have a large impact on soil temperature. The intention behind the insulation layer was to reduce the heating of the soil by the sun, and thus keep the permafrost as close to the surface as possible. The effect of warmer soil and wood above the insulation was not anticipated. The temperature above the insulation layer was increased by approximately two degrees Celsius. Two degrees might seem as a small difference, but when the original temperature is so close to the lower limit for fungal activity, can even a few degrees increased temperature can have a significant impact on the risk of biodeterioration.

Several places in Svalbard have a dark soil surface, especially in the vicinity of coal mines. In the measuring location in Hiorthhamn, the surface of the cable car buck as well as the soil surface was covered with coal fragments, so the surface colour was almost black. This gives additional effect from solar radiation, warming the soil even more efficiently. The difference made by exposure to the sun can be seen in table 2, at the results from buck nr. 8 and the area under the Manager's house ("Direktørboligen"). In both cases, measurements made in locations exposed to the sun show higher temperatures than in shaded locations.

Optimal growth temperature for fungi is normally 20-25 °C, but fungal growth is possible down to a few degrees over freezing point, depending on species (Gravesen et al 1994). Fungi as a group are extremely versatile, and fungi are present in almost all locations and conditions on Earth (Stokland et al. 2012). It is well known that extreme conditions can make fungi that normally lose in competition with more efficient species dominant. In Svalbard, the pattern of species identified in decayed wood is clearly different from what has been reported from the mainland of Norway (Alfredsen et al 2006, Mattsson et al. 2010). Mattsson et al. (2010) reported that the dominating brown-rot fungus in Svalbard was *Leucogyrophana mollis*. This fungus was identified in 41,3% of the wooden samples that had been collected in that study, compared to a occurrence of 7,1% in samples in the Norwegian mainland (Mattsson et al. 2010). Mattsson et al. (2010) has shown that three commonly found

species of wood-decaying fungi in Norway (*Coniophora puteana*, *Antrodia* sp. and *Gloeophyllum sepiarum*) only has been found a few times each, and *Serpula lacrymans* has not been found at all. This is probably caused by the lack of suitable growth conditions for those fungi, especially *S. lacrymans*, while *L. mollis* obviously has many options for finding acceptable growth conditions. This show how great impact the microclimate has on the biodeterioration of wood at Svalbard, both with respect to occurrence of deterioration and the strong selection of few species with special tolerance for the extreme climate and growth conditions.

The impact of small variations in growth factors in the marginal conditions in Svalbard is illustrated by the sound outer layer found in wood exposed outdoors. The outer layer in the cable car bucks was 4.5 mm on average. This shows that growth is almost impossible in direct contact with the outdoor air. The combination of strong wind, ice crystals, UV-radiation and large variations in temperature and moisture level probably gives a difficult situation for both germination and growth for wood decay fungi. A similar surface layer was found in large cracks in the poles, but the layer was 60 % thinner in the cracks. This is probably due to more stable conditions regarding temperature and wood moisture content. This clearly shows the importance of the microclimate, as shown by Gobakken et al. (2014). The harsh conditions on the wooden surface in wood exposed outdoors are illustrated by the fact that limited growth of mildew fungi was found in these samples. This is very unlike the situation for outdoor exposed wood at the mainland of Norway where the wood surfaces fast get overgrown by various mould fungi (Mattsson 1995).

Measurements showed that the microclimate varied greatly within a few centimetres. Since the moisture conditions are essential if wood remains intact or whether it develops fungal decay, it is very important to clarify where the real dangers are in a construction and where it is unproblematic with regard to the risk of fungal decay. Managing this challenge, one can limit the need for action - which is beneficial for both economic and conservation reasons.

5. Conclusions

Growth of wood decaying fungi is shown to be limited by the harsh conditions offered in the polar climate in Svalbard. Nevertheless, decay has been shown to be commonly found in sheltered locations. The thaw zone offers feasible growth conditions during summer months, but the fungus *Leucogyrophana mollis* has been shown to dominate. Fungi that are more common on the mainland of Norway probably cannot survive the low winter temperatures.

Protected from the hostile surface, where there can be extreme variation in both temperature and moisture content of wood, the fungi have been shown to find quite good growth conditions inside wooden materials in soil contact. Only there a sufficient source of water can be found in combination with suitable temperatures for growth during a sufficiently long period of each year.

Both in an extreme climate and in constructions with potential high risk for critical moisture levels, even small differences in climatic conditions and distances can have an especially large impact. This has given a specific pattern in damage development, both regarding location, extent of damages and the organisms causing the damages. Due to the fact that almost all of the deteriorated constructions at Svalbard are protected cultural heritage, the extensive occurrence of fungal decay causes considerable concern. It is also important to not conduct improper or unnecessary measures in connection with listed buildings because of erroneous assumptions or lack of facts.

Further research concerning the impact of microclimate and possible solutions in order to reduce future decay problems is of large interest.

6. Acknowledgements

We would like to thank both Svalbard Environmental protection fund and Longyearbyen Community for financial support which made the surveys possible. We would also like to thank Store Norske and the department of Cultural heritage at the Svalbard Governor office for permission to examine the cable car bucks around Longyearbyen.

References

Alfredsen G, Solheim H, Jenssen KM, 2006. Råtesopp i norske bygninger. Agarica 2006, vol. 26, 78-86.

Brischke, C., Bayerbach, R., Rapp, A., 2006. Decay-influencing factors: A basis for service life prediction of wood and wood-based products. Wood Material Science and Engineering (1):91-107.

Coggins, C.R., 1980. Decay of timber in buildings. Dry rot, wet rot and other fungi. The Rentokil library, East Grinstead.

Gobakken LR, Mattsson J, Alfredsen G, 2014. The importance of critical in-situ conditions for in-service performance of wood. Agarica 2014, vol. 34, 29-36.

Gravesen, S., Frisvald, J. and Samson, R. A., 1994. Microfungi. Munksgaard, Copenhagen.

Grøntoft, T., 2008. Effekten av klima og klimaendringer på den bygde kulturarven. Online at http://www.klimakommune.no/kulturarv/Effekter_av_klima_og_klimaendringer_på_den_bygde_kulturarven_Nedbrytningsmekanismer_og_s_rbarhet.shtml .

Mattsson, J., 1995. Råte- og insektsskader. Tilstandsanalyse og utbedringstiltak. FOK-programmets skriftserie nr 23. Norges Forskningsråd

Mattsson, J., 2010. Råtesopp i bygninger. Mycoteam, Oslo

Mattsson, J. and Flyen, A.C., 2011. Preventive methods against biodeterioration of protected building materials in Svalbard. Polar Settlements – Location, Techniques and Conservation. ICOMOS. ISBN 978-82-996891-3-7. Pp. 44 – 50

Mattsson, J. and Flyen, A.C., 2008. Biodeterioration in buildings in Svalbard (Spitsbergen). Historical Polar Bases – Preservation and Management. ICOMOS. ISBN 978-82-996891-2-0. Pp 23 – 29.

Mattsson, J., Flyen, A.-C., Nunez, M., 2010. Wood- decaying fungi in listed buildings and structures at Svalbard. Agarica. Vol. 29, p. 5 – 14.

Nunez, M, Sivertsen, M.S, Mattsson, J, 2012. Indoor mould ecology: Substrate and construction preferences for Actinomycetes and 13 mould genera. Healthy Buildings 2012. Brisbane (In press).

Rayner, A.D.M, Boddy, L, 1988. Fungal decomposition of wood. Its biology and ecology. John Wiley & sons, Chichester.

Scheffer, T.C, 1971. A climate index for estimating potensial for decay in wood structures above ground. Forest products Journal, 21(10): 25-30.

Stokland, J.N., Siitonen, J., Jonsson, B.G., 2012. Biodiversity in dead wood. Cambridge University press.

Viitanen, H, 1995. Models of the critical time of humidity and temperature conditions for the development of mould fungi in pine and spruce sapwood. IRG/WP 95 – 20066. International Research Group of Wood Protection. Stockholm.

Wikipedia, 2013a. Online at http://en.wikipedia.org/wiki/Climate_of_Svalbard . Cited 28. November 2013.

Damp floor and humid interior in Hellerup Church, Denmark

Poul Klenz Larsen, Ph.D. [1]

[1] The National Museum of Denmark, Department of Conservation, Denmark

KEYWORDS: *Dehumidification, medieval church, humid interior, ground moisture, climate control*

SUMMARY:
The climatic influence of a damp floor in a typical Danish medieval church was monitored over four years. A dehumidifier was installed to control the RH all year. The energy consumption was approximately 2.5 MWh per year. Despite of this the water vapour content of the inside air was higher than outside most of the time, mainly due to evaporation from the floor. The water content in the ground below the tiled floor was monitored with a dielectric probe. The average water content of the soil 1,2 m below the floor was 9 -15 % by volume and it rose slightly during the four years . The source of moisture was a high water table which enforced a constant flux of water into the church. It is acceptable to control the RH by dehumidification all year, but a moisture membrane below the floor tiles would be a more sustainable solution.

1. Introduction

Medieval Danish churches often suffer from a humid interior climate (Larsen 2007). The source of the humidity is the building itself. A study in Kippinge Church showed that the evaporation from the walls can contribute significantly to the water vapour content of the inside air (Larsen 2011). In a similar study in Hellerup Church, the walls contributed less, but the floor was a possible source of humidity (Larsen 2011). The natural evaporation from the floor maintained a stable, high relative humidity all year. High RF is known to cause mould growth, which is considered to be a health risk for the church staff. In order to prevent mould growth it is essential to keep the relative humidity below 80%. This can be done by a combination of conservation heating and ventilation or by dehumidification (Larsen & Broström, 2012). Dehumidification is more energy efficient than heating for controlling the RH. But the question is if constant dehumidification will dry out the soil below the floor and thereby compromise the preservation of the archaeological remains associated with medieval churches. This aspect is addressed by a study over four years of the climatic influence of the ground below the floor in Hellerup Church, a typical church building in Denmark.

2. Structure and materials

Hellerup church is a 12th century brick building situated in a rural environment on the island Fyn (fig.1). The nave and chancel is 6 x 28 m, and the total volume of the spaces is 900 m^3. The solid 1.0 m thick walls are made of red brick and lime mortar, with plaster and lime wash on the inside and outside. The roof is tiled and there are no gutters to collect the rain. Instead there is a drain along the outer walls to reduce the water content of the ground. The nave has brick vaults without any thermal insulation. There are 8 windows with single glazing in cast iron frames. The floor is soft brick tiles that are permeable to evaporation of water vapour from the ground below. The church has electric heating elements mounted in the pews and on the walls.

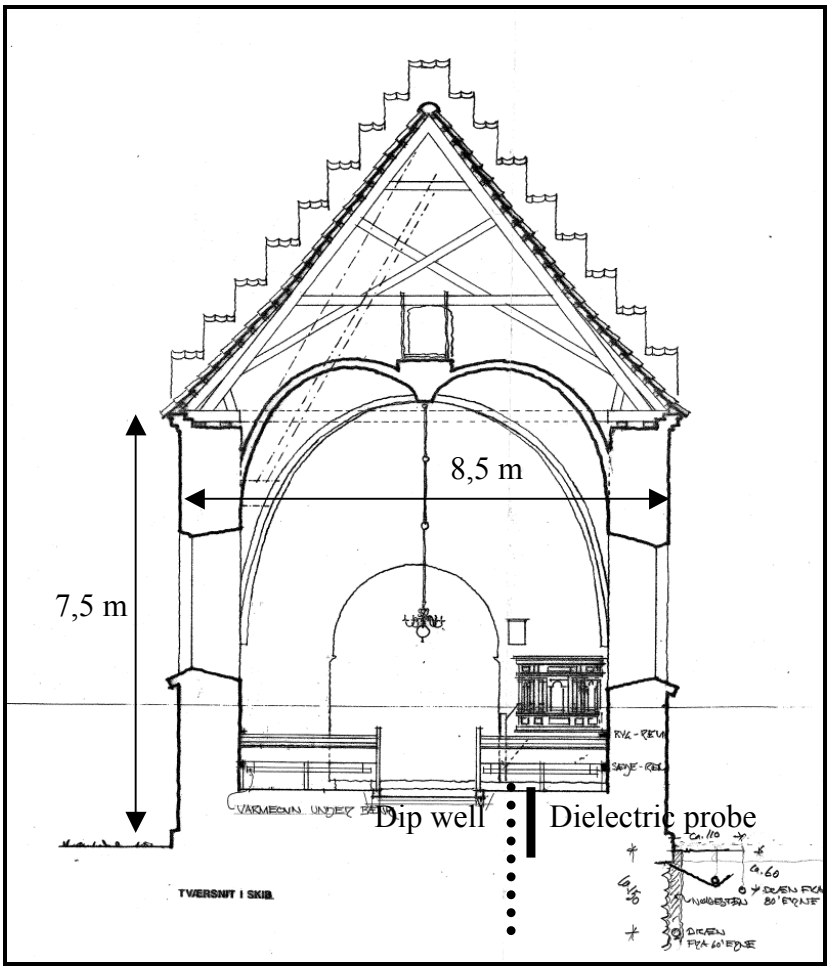

FIG.1. Cross section of Hellerup Church. Not to scale.

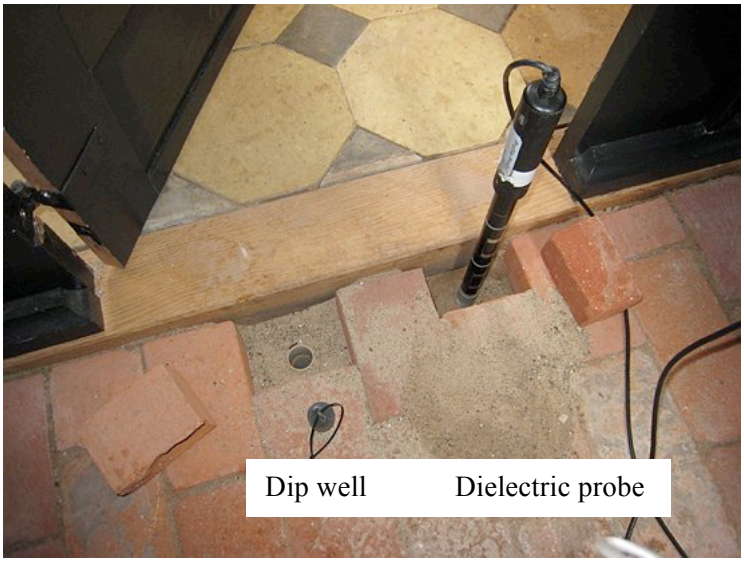

FIG.2. The dielectric probe used for monitoring the water content of the soil below the floor.

3. Measurements and results

3.1 Temperature and relative humidity

Temperature and relative humidity was monitored continuously inside and outside the church during four years, and in a cavity below the floor tiles in 2013. The inside climate records for two years are shown in fig. 3. The limit for mould growth is indicated by the dotted line. In the winter 2009/2010 the interior was heated to a basic temperature of 6-8 °C and to 18 °C for services. A condensing dehumidifier controlled the relative humidity in the autumn, spring and summer. In august 2010 the set point was raised from 70 %RH to 80 %RH, and dehumidification was used for humidity control all year, including the winter season. The dehumidifier had a defrosting cycle, since ice would form on the cooling element when the ambient temperature was below 8-10 °C. In the following winter the temperature was allowed to drop down to 2 °C, with on little basic heating. The RH rose to 90% on some occasions, but this was safe at low temperature, as indicated by the mould limit curve in the diagram. No incidents of mould infestation were observed after the change of climate control strategy.

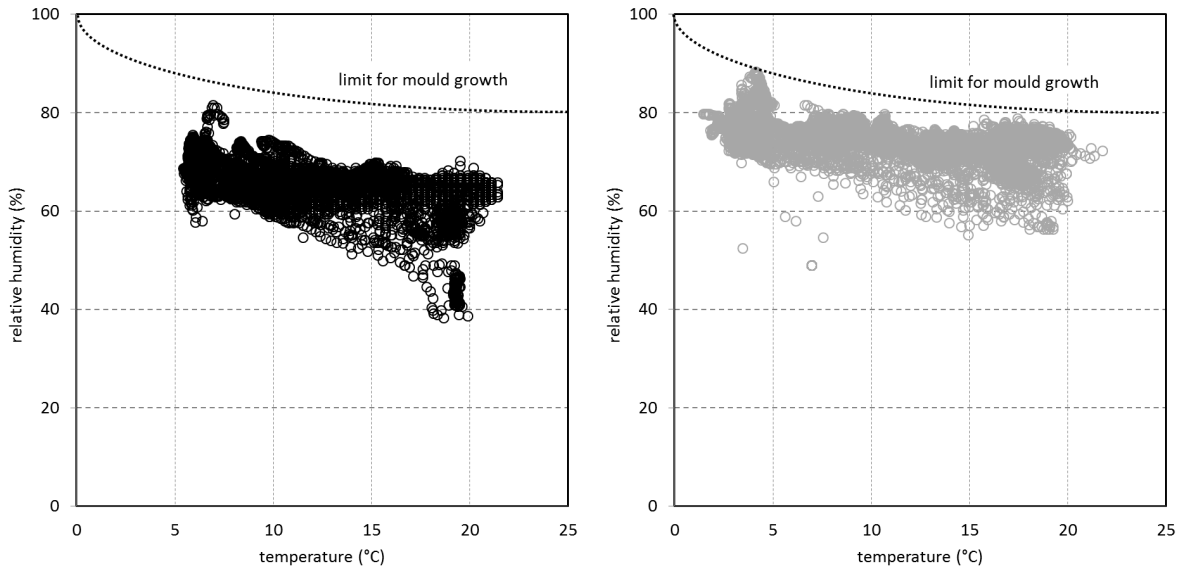

FIG 3. Climate record for Hellerup Church. Left diagram is the period 1 July 2009 – 30 June 2010 and right diagram is 1 September 2010 – 30 August 2011.

3.2 Energy consumption

The energy used for heating and dehumidification was recorded continuously during four years (fig. 4). Little energy was used during the summer, when only the dehumidifier was working. As the basic heat was turned on in December 2009, the energy consumption rose rapidly. The total annual energy consumption was 23.6 MWh for heating and 2.2 MWh for dehumidification the year 2009/2010. In the following year 2010/2011 the total heating energy was reduced to 13.9 MWh, because the basic heating was reduced. Next year 2011/2012 the basic heating was entirely abandoned, but service heating used 11.1 MWh, which was almost as much energy as before. The energy used for dehumidification rose slightly to 2.4 and 2.5 MWh. Detailed data for 2012/2013 is incomplete, but the total energy use was 18.6 MWh for heating and 2.2 for dehumidification. The rise in heating energy was due to the long and cold winter, which made the church ward to raise the basic temperature again.

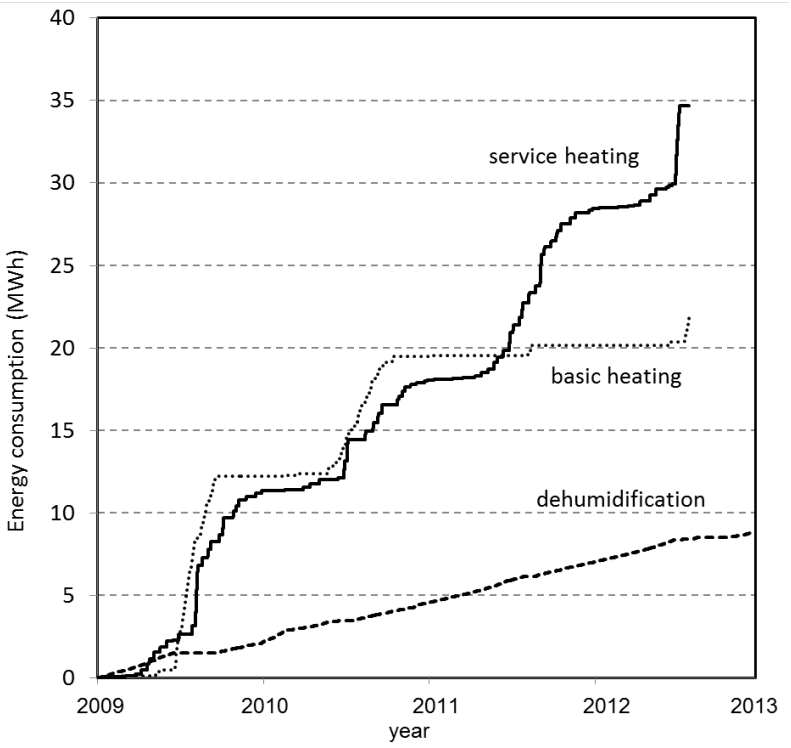

FIG 4. The measured energy consumption for heating and dehumidification summarized over four years.

3.3 Water content

The water content of the soil below the floor was measured with a dielectric probe type PR1/6 connected to a portable meter HH2. The instrument was developed for soil moisture measurements in agriculture. The probe was inserted into a vertical tube during operation (fig. 2). It was only allowed to install one tube in respect of the archaeological remains below the floor. Measurements were made at ten positions to a depth of 120 cm below the floor, with a distance of 10 cm between each position. The sensor is directional, so there were three readings separated by 120° turn of the probe at each position. The probe was calibrated for mineral soil, so the results were only indicative for the moisture content. The initial water profile is shown in fig. 5. The water content was in the range 9 -15 % by volume with considerable variation from one layer to the next. This reflects the inhomogeneity of the soil, which was mainly infill with different mixtures of clay and sand.

A dip well was installed 2.2 meters deep to monitor the ground water level below the church. The soil was homogenous clay from 0.7 m below the floor. Soil samples from the drilling were used for gravimetric determination of the water content. The gravimetric water content was recalculated to volumetric content assuming a soil density of 1500 kg/m^3. The water profile is displayed in fig. 5 together with the first reading of the dielectric probe.

The measurements with the probe were repeated twice every year, and the result is given in fig. 6. Each graph represents the average volumetric water content of the soil in five different depths, 30-70 cm and 70 – 120 cm below the floor. There was not much change in the water content during the four years. The position of the water table is shown in the same diagram. There is a slight indication that a high water table reflects in the water content higher up. Rainfall was not monitored, so it is not possible to detect any correlation with the natural precipitation.

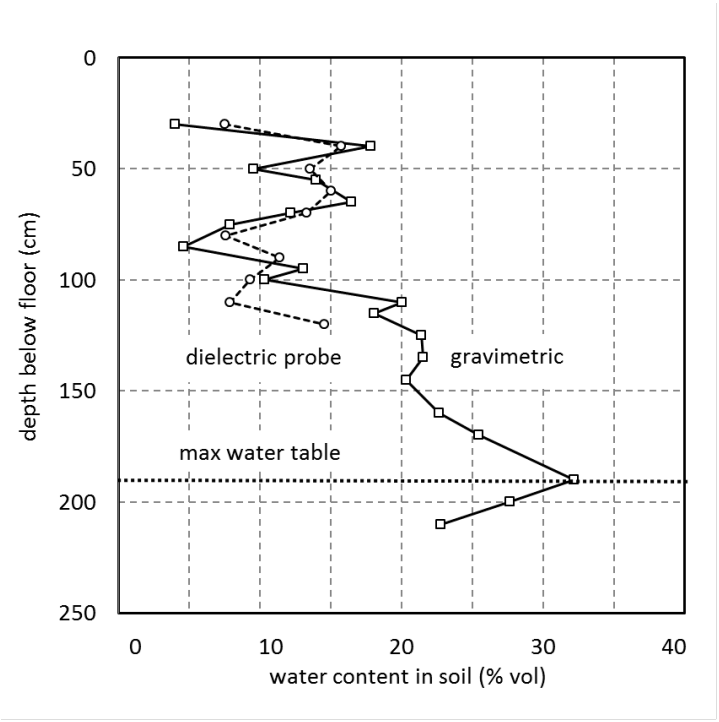

FIG 5. The initial water content of the soil in the ground below the floor. The gravimetric profile was determined by soil samples from the installation of the dip well.

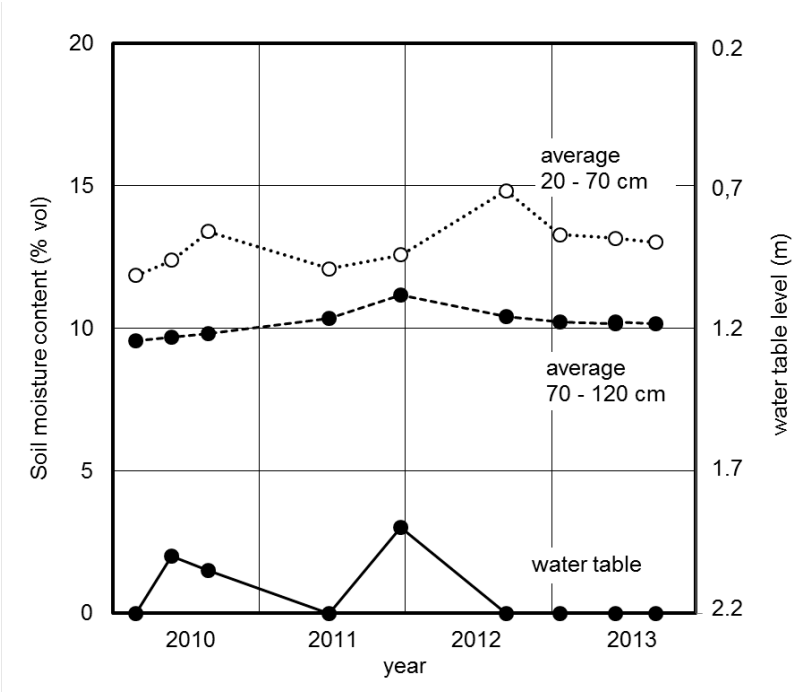

FIG 6. The result of soil moisture measurements with the dielectric probe. The ground water level is shown below in the diagram.

4. Discussion

The water vapour content of the inside and outside air was calculated from the climate records as a moving average over 7 days (fig. 7). The moisture is quoted in grams per kg of air, also known as the mixing ratio (MR). The difference for each week is shown as bars below the graphs. Most of the weeks the water vapour content of the inside air was higher than outside, on some occasions up to 3 g/kg. The surplus of moisture inside was maintained in spite of the constant dehumidification. The human activity in the church is very little with only 2 – 3 services each month. Evaporation from the damp floor is likely to be the source of the dampness. The water reservoir of the ground below the church is abundant as indicated by the soil moisture measurements.

The direction of moisture migration through the floor can be estimated from the microclimate measurements. Figure 8 gives the partial vapour pressure (VP) calculated for each hour during a six weeks period in the spring 2013. The inside VP is always higher than the outside VP. The saw-tooth shape of the inside VP reflects the intermittent heating practice, where each tooth indicates the increased evaporation caused by the rising temperature. At the end of week 13 the heating event is prolonged for several days. During this time the VP inside is up to 800 Pa above the outside VP. The evaporation from the floor is powerful enough to compensate the loss of water vapour by infiltration of outside air and dehumidification.

In between heating events the VP below the floor tiles is 250 Pa higher than inside the church. This constant difference will enforce a permanent flux of moisture into the church by a combination of capillary flow and diffusion through the porous floor tiles. The rate of diffusion is calculated by Ficks law, assuming a vapour permeability of the brick tiles of 30×10^{-12} kg/Pa m s. The diffusion is almost constant at 0.5 g/m^2 h. During the heating events the VP below the floor tiles is almost equal to the VP above the floor, so there is less potential for water vapour diffusion at this stage. The rapid release of water vapour originates from hygroscopic moisture stored by the floor tiles, and perhaps from the lime washed interior of the church.

Increased ventilation is the traditional advice for damp churches. This will remove the surplus of water vapour, but it will also lower the temperature in winter and increase the variations in RH all year. Any basic heating in between services must be abandoned, so the church becomes very cold in winter. Ventilation for humidity control is therefor mainly recommended for churches that are rarely or never used in winter. To keep the RH below 80% the ventilation must be controlled by the difference between inside and outside mixing ratio.

One way to prevent evaporation of water from the floor would be to install a moisture membrane below the floor tiles. Such interventions are usually not permitted in medieval churches in respect of the archaeological remains. Another argument is that a water impermeable floor will increase the rising damp in outer walls, since the water need to escape one way or another. However it is not likely that the water content on the walls of this church is much influenced by rising damp. Previous moisture measurements in the chancel walls showed that driving rain was the main source of water to the walls.

Drainage is often recommended as a precaution against dampness. In this case, three different drains were installed over the past 50 years in different positions, but none had any effect on the interior climate, which was always very humid. The position of the ground water level shown in fig. 5 gives an explanation for the failing drains. It was always below the level of the drain pipes, but high enough to supply water by capillary rise to the higher levels. The gravimetric moisture measurements shows a gradual decline in water content from 2 m to 1 m below floor level, which is typical for rising damp. Seasonal variations in the water table may also influence the water content of the soil higher up. Fig. 6 slightly indicates this dynamic. It is not safe to lower the ground water level by deeper drains or drain pumps. The risk of ground settlements and subsequent structural failure is too large.

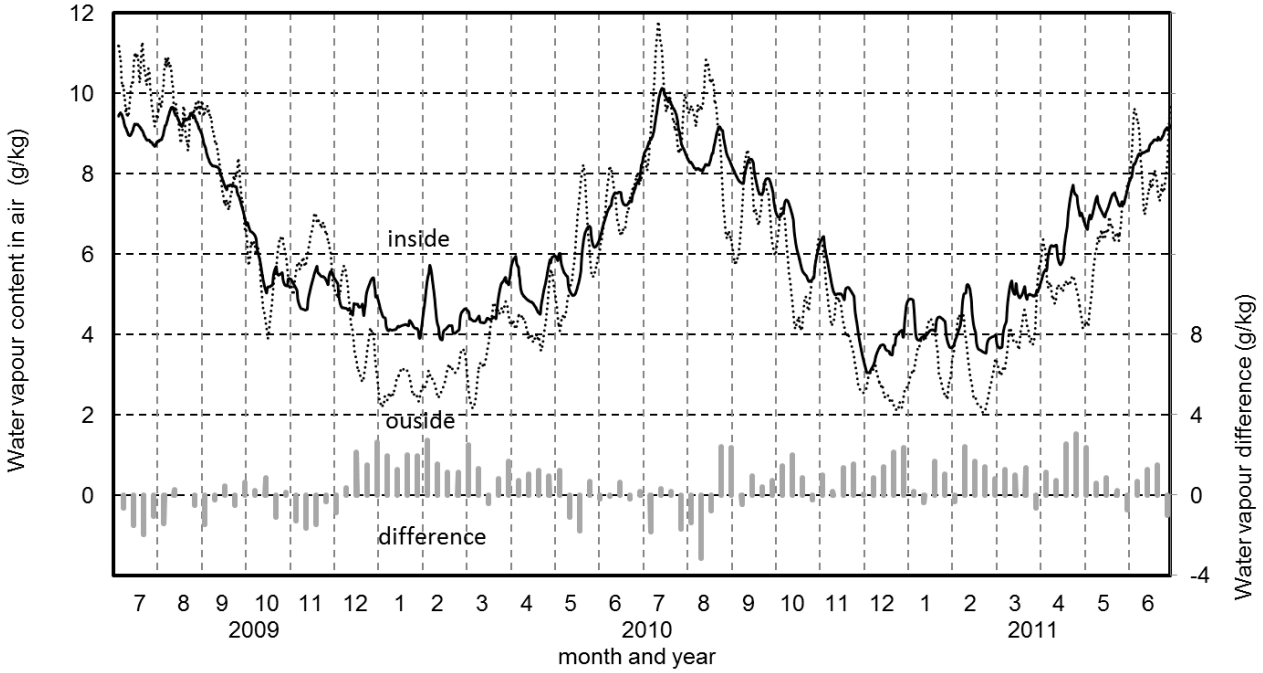

FIG. 7. The water vapour content in the air inside and outside the church calculated from the climate records as a moving average over 7 days. The difference for each week is shown with bars below the graphs.

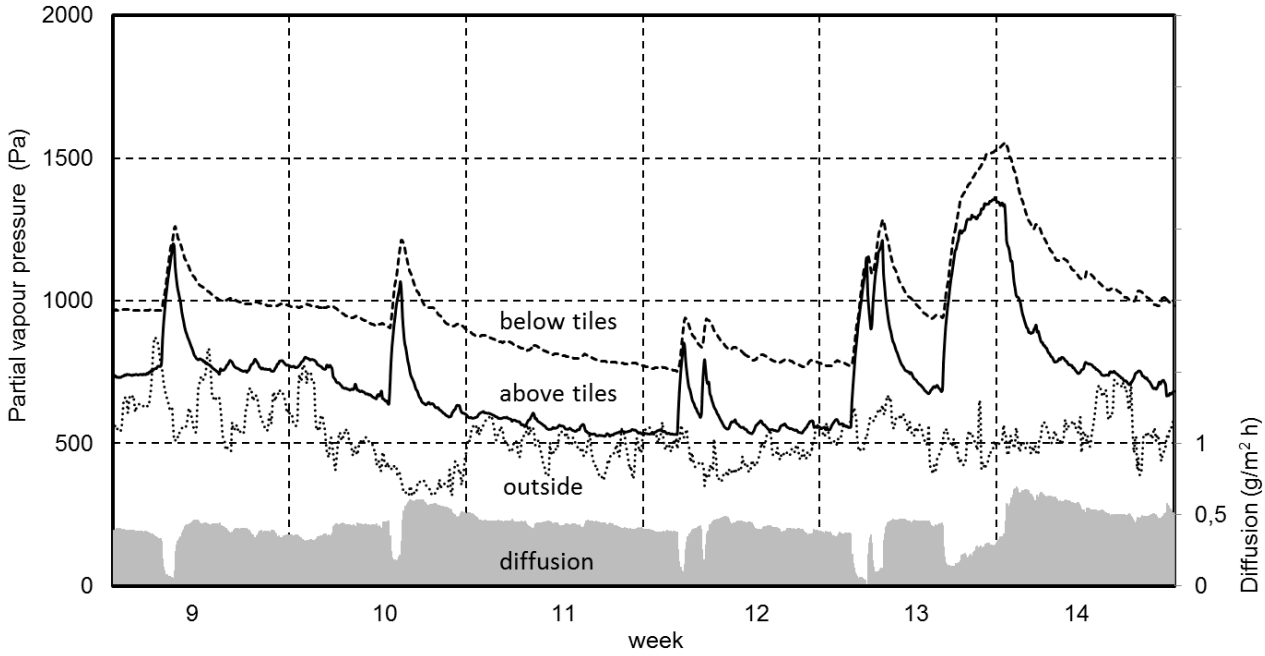

FIG. 8. The partial vapour pressure calculated from hourly data for temperature and relative humidity, measured at the positions indicated for each graph. The diffusion through the floor tiles is calculated by Fick´s law with a vapour permeability of 30 kg/Pa m s.

5. Conclusions

A new strategy for climate control in damp churches was evaluated over four years in Hellerup church. The aim was to keep the RH low enough to prevent mould growth on the one hand, and to avoid damage to the wooden furniture on the other hand. The combination of intermittent heating in winter and dehumidification all year was acceptable. The energy consumption was down to 11 MWh for heating, and 2.5 MWh for dehumidification in one year. This climate control strategy is relevant for churches and other historic buildings, which are rarely used, and therefore only needs heating on few occasions.

The need for dehumidification arises due to the constant flux of water vapour from the ground below into the church. Water is supplied from a high water table by capillary rise through the soil. The water evaporates from the floor into the church at a steady rate all year. Outside draining is not effective, because the drain pipes is located above the water level all times. It is not safe to install drain pumps due to the risk of ground settlement and subsequent structural failure of the solid masonry walls.

Even after four years of constant dehumidification there is no sign of drying in the soil just below the floor tiles. There is an abundance of water supply to the church from below, and that dehumidification does not affect preservation of the archaeological remains in the ground. A moisture membrane below the floor tiles would reduce the migration of water, but such intervention is usually not permitted in a medieval church. The demand for sustainable climate control in churches may be favourable for this solution in the future.

6. Acknowledgements

The project was supported by a grant from the Danish Ministry of Research (UMTS-project).

7. Instruments

Dielectric probe type PR1/6 connected to a portable meter HH2.

Delta-T Devices Ltd, 130 Low Road, Burwell, Cambridge, CB25 0EJ, UK, Phone : +44 1638 742922, Fax : +44 1638 743155, http://www.delta-t.co.uk/

References

Larsen, P.K., 2007. Climate control in Danish churches. Museum Microclimates, proceedings of the conference in Copenhagen 19-23 November 2007, pp.167-174

Larsen, P.K., 2011. The moisture equilibrium in Kippinge Church, Denmark. In: Proceeding of the 16th Triennial ICOM-CC conference, Lisbon, 19-23 September 2011 CD-ROM, 7 pages.

Larsen, P.K., 2011. The hygrothermal performance in Hellerup church, Denmark. Proceeding of the 9th Nordic Symposium on Building Physics, Tampere, June 2011 pp. 807-814.

Larsen, P.K., Broström, T. 2012. Climate control strategies for occasionally used churches. Heat, dehumidify, ventilate – or do nothing. In: Proceedings of the 2nd European Workshop on Cultural Heritage Preservation, Kjeller, Norway, 24th – 26th September 2012, pp 124 – 130

Solar energy augmented adaptive ventilation in historic buildings

Magnus Wessberg, M.Sc. [1]
Poul Klenz Larsen, Ph.D. [2]
Tor Broström, Professor. [3]

[1,3] Uppsala University, Sweden.
[2] Nationalmuseet, Denmark.

KEYWORDS: *Adaptive ventilation, climate control, mould growth, historic buildings*

SUMMARY:
Many historic buildings suffer from problems related to moisture and high relative humidity. Adaptive ventilation can be a low-energy and low impact solution to mitigate these problems. Previous studies have shown that adaptive ventilation can have a significant drying effect. However due to the covariance of temperature and absolute humidity in the outside air, the effect on relative humidity inside a buildings is limited in the short term. The present paper presents results from a medieval stone church where a novel integration of solar heating and adaptive ventilation has been implemented. Solar energy is collected in the day and stored. In the night, when the outside air generally is drier (in absolute terms), outside air is preheated using the energy stored in the daytime and added to the building.

The results show that adaptive ventilation can be a low-cost and low-energy option as compared to conventional humidity control.The average relative humidity and mould risk has decreased significantly. Auxiliary measures, such as dehumidification, would be needed, mainly in the summer. The energy from the photovoltaic elements has mitigated the cooling effect of the outside air.

1. Introduction

Many historic buildings with no heating or intermittent heating face problems related to high relative humidity (RH), mainly fungi and insects. Appropriate climate control is essential to preserve the building and its interiors. The conventional way to reduce relative humidity (RH) is through conservation heating or dehumidification (Larsen et al., 2012). However, these solutions are quite costly both in terms of investments and energy costs. In recent years adaptive, or controlled, ventilation has emerged as a potentially low-energy and low impact option.

The present paper presents results from a medieval stone church where a novel integration of solar heating and adaptive ventilation has been implemented. Solar energy is collected in the day and stored. In the night, when the outside air generally is drier (in absolute terms), the inlet air is preheated using the energy stored in the daytime.

1.1 Adaptive ventilation

Air exchange in a historic building, through infiltration or ventilation, has an important effect on the indoor climate. Depending on outdoor and indoor climate conditions, air exchange can either increase or decrease the RH in a building. The controlling principle of adaptive ventilation is to to ventilate only when the mixing ratio (MR), i.e. grams of water vapor per kg of dry air (g/kg), inside the building is higher than outside. Equally important is not to ventilate when MR outside is higher. Thus, both air tightness and ventilation must be controlled and adapted through the use of mechanical fans and dampers controlled by indoor and outdoor climate sensors.

1.2 Previous experiences of adaptive ventilation

The concept of adaptive ventilation was implemented in the Torhalle in Lorsch, Germany to avoid condensation on the wall paintings. Electric fans were controlled by indoor and outdoor climate sensors to keep the dew point of the inside air below the wall surface temperature (Reiss J et al., 1993). However the system was only in operation for a short time. In the church in Zillis, Schwitzerland, adaptive ventilation was used to stabilize RH in favour of the painted wooden ceiling (Bläuer-Böhm et al., 2001). The effort was not very successful due to a large infiltration rate and the fact that the ventilation was turned off in winter to reduce heat loss. A seasonal use was implemented in the Antikentempel in Potsdam-Sanssouci Park to prevent mould growth on the walls and ceiling. From May to September 2005 there was adaptive ventilation by a fan mounted in the skylight. The result was positive. The absolute humidity was 1-2 g/m^3 lower indoors than outdoors during the test period. In May to September 2007 measurements were carried out without adaptive ventilation and the absolute humidity was instead was 1-2 g/m^3 higher indoors than outdoors (Brockmann T et al., 2010).

In the above mentioned cases the control systems were custom designed for each building. There are commercial solutions available which are originally intended for attics and crawl spaces under houses (Hagentoft et al., 2008). Such equipment was used in a historic building on Gotland (Broström et al., 2011) and churches in Denmark and on Gotland (Larsen et al., 2013). The study on Gotland confirmed that adaptive ventilation is particularly useful when there are internal moisture sources in the building resulting in absolute humidity levels higher than outside. However due to the covariance of temperature and absolute humidity in the outside air, the effect on relative humidity inside a buildings is limited in the short term. In a typical diurnal cycle the temperature will be lower outside when the MR is higher inside and the fan is running. This means that the ventilation has a cooling effect that would tend to increase RH, even though moisture at the same time is removed from the building.

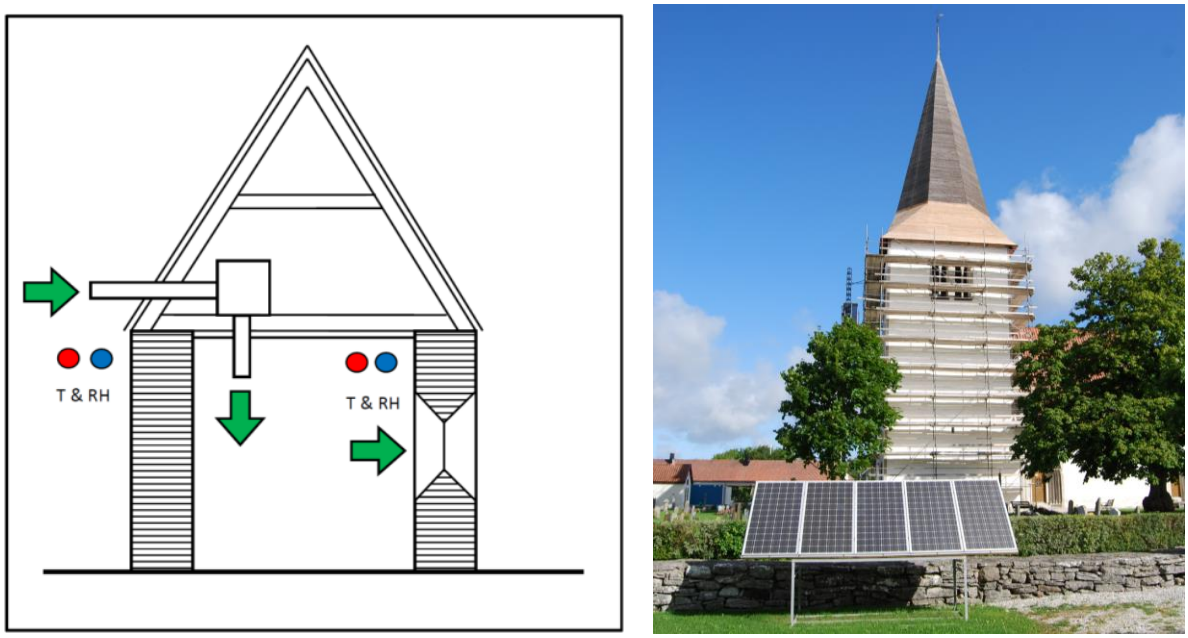

FIG 1 a, b. a) Adaptive ventilation: The operation of the fan is controlled by a control unit connected to the inside and outside sensors for temperature and relative humidity.
b) Hangvar church with the photo voltaic elements place outside the church fence.

1.3 Solar energy augmented adaptive ventilation

The previous studies have indicated that the cooling effect due to the covariance of temperature and MR is a limitation to the effectiveness of adaptive ventilation in historic buildings. The proposed solution is preheating of the inlet air through an integration of solar energy and adaptive ventilation. The concept operates as follows:

1. In the day time, solar energy is collected and stored.
2. At night, when the outside air generally is drier, the inlet air is preheated using the stored energy.

The system can either be electric (photovoltaic) or thermal (air based) depending on costs and practical aspects. In this study, an electric system was used. Solar energy was seen as a sustainable solution both in terms of resource use and economy, of course preheating can also be achieved by conventional means.

2. Case study

2.1 Hangvar church

Hangvar church is a 13th century stone church situated on the north west part on the island of Gotland, Sweden. The construction is typical for Gotland churches with outer walls and vaults made of lime stone in lime mortar and a roof construction of wood with tiles. The volume of the nave and chancel in total is 1000 m^3. The church is used only some 10 times per year, mostly for funerals and weddings. The church is intermittently heated for services and unheated in between. During winter the indoor temperature can go down below zero. The church has been very humid, during springtime there has been condensation on walls and floors. The members of the parish have complained about bad smell and there had been visual growth of algae and mould in corners and on the northern wall. Many tourists visit the church during summer and the church door has been left open in the day time.

2.2 Technical solutions

2.2.1 Adaptive ventilation system

The adaptive ventilation system was installed in July 2012. The system used is a commercial system (Hagentoft et al., 2008) mainly intended for attics. It consists of a control unit, an indoor sensor, an outdoor sensor and a fan. The fan runs if the outdoor partial pressure of water vapour is 10% lower than indoor value. The control unit has logging facilities for indoor and outdoor temperature and RH, fan speed and the relation between indoor and outdoor water vapour partial pressure.

The fan speed is adjustable and from July 2012 to December 2012 the ventilator speed was set to run proportional to the difference between indoor and outdoor water vapour pressure starting at 50% of max speed. From January 2013 the fan speed was set to run at 100% any time the water vapour pressure is 10% lower outdoors than indoors.

In the inlet air duct there are two electric heaters with a total power of 1800 W.

2.2.2 Photovoltaic elements

The case study was designed for 25 m^2 of photovoltaic elements. Due to costs and the fact that this set up is experimental, only 5 m^2 were installed. Therefore the amount of produced energy is multiplied by 5 in the control system. The photovoltaic elements where placed outside the church yard in order to avoid a discussion on the visual impact of roof placement. In this case the electric grid is used to store the energy, rather than a local storage. A DC to AC converter is connected between the photovoltaic panels and the grid via an energy meter which in turn is connected to the intake air heater control system.

2.2.3 Control in LabView

The heaters are controlled by control system developed In LabView. The system compares the amount of stored energy available from the photovoltaic elements and the consumed energy by the heater. The heater is turned on as long as the stored energy lasts.

3. Results

3.1 Indoor climate

From July 2010 to June 2012 there was no climate control in the church except for the heating periods for services. Adaptive ventilation was installed in June 2012. There was no climate monitoring between December 2011 and March 2012.

Figure 2 shows indoor climate over three years. It can be seen that the average relative humidity has decreased after the introduction of adaptive ventilation but the short term variations have increased.

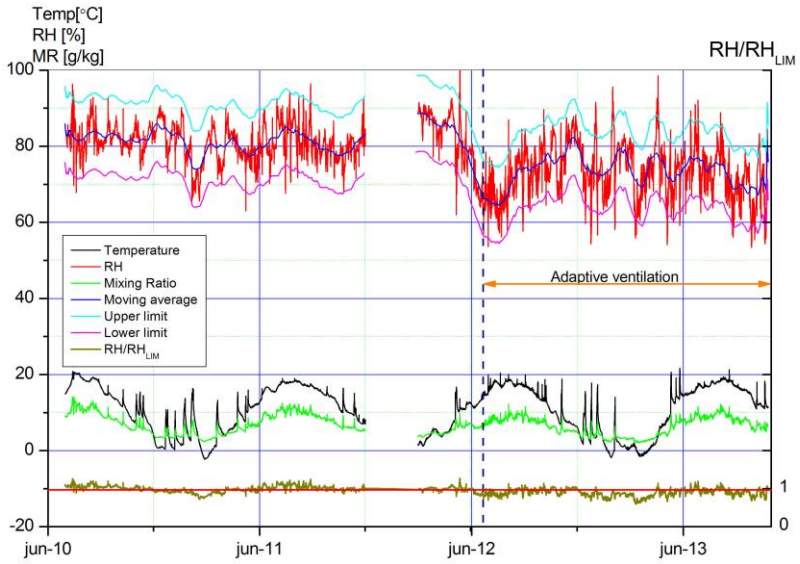

FIG 2. Indoor climate in Hangvar church. The graph shows that during the period with adaptive ventilation the relative humidity in average has decreased but the variations have increased

Table 1 shows a statistical comparison between the time period without any climate control, September 2010 to August 2011 and the time period with adaptive ventilation September 2012 to August 2013. The comparison shows that average relative humidity has decreased from 81 to 76 %. The average temperature is approximately the same the two periods, just 0,2 degrees of difference.

The short term variations in RH are important from a conservation point of view. A European standard, (EN15757) provides a method to determine a target range for short term variations in RH in relation to a moving seasonal average. Deviations of less than ±10% RH are considered safe. Figure 3 shows that when using adaptive ventilation there are more short term excursions outside the target range. The standard deviation, in relation to the moving average increase from 3,5 percentage points to 5,2.

TABLE 1. Statistics for the two periods

Period	Average Temperature	Average RH	Average MR	Standard deviation of short term fluctuations
Without climate control	9,6	81	6,5	3,5
Adaptive ventilation	9,3	75	5,9	5,2

3.2 Air tightness

Measurements of the church´s air tightness were carried out in August 2013. Two different methods were used. The blower door test (EN 13829, 2000) showed a result of Q_{50} = 0,89 L/s/m^2 and the pressure pulse method (Cooper Et Al., 2007) showed on a resulting equivalent leakage area at 4 Pa of 0,051 m^2. Both methods showed a result of Q_4 = 138 L/s which is on the same order of magnitude as adaptive ventilation at full speed.

3.3 Mould prevention

Mould risk is assessed in relation to the isopleth curve LIM I, biologically recyclable building materials (Sedlbauer 2001). Figure 3a shows the period without climate control and figure 3b the period with adaptive ventilation. It is clear that the risk for mould has decreased during the year with adaptive ventilation (Sedlbauer 2001). The year without climate control, 44% of the time the indoor climate was above the LIM. When the adaptive ventilation system was running only 16,7% of the time the indoor climate was above the LIM.

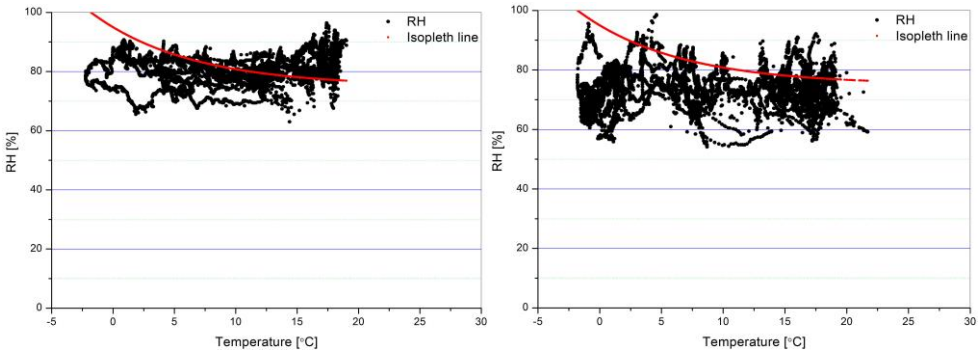

FIG 3 a, b. Damage functions for mould. a) time period without climate control. b) time period with adaptive ventilation.

Figure 4 shows RH/RH$_{LIM}$ where RH$_{LIM}$ is the lowest isopleth for mould that can be seen in Figure 3. If the value is above 1, the climate is beneficial for mould growth. The duration in the area above LIM is critical for mould growth. According to (Sedlbauer 2001) RH/RH$_{LIM}$ has to be above 1 for longer periods (days) for mould to grow. In the year without climate control the average duration length above LIM was 72 hours and the longest period was 826 hours. In the year with adaptive ventilation, the average was 32 hours and longest period 134 hours. In the latter case the extended periods were in the summer.

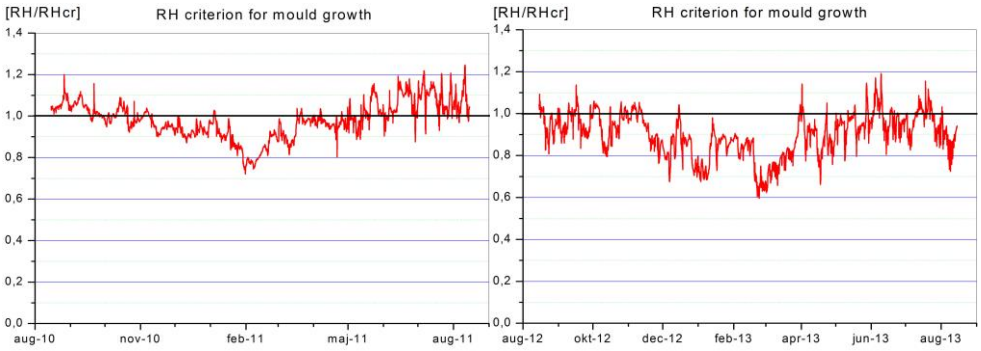

FIG 4 a, b. RH/RH$_{LIM}$. a) Time period without climate control. b) Time period with adaptive ventilation

The duration graph, fig 5, shows that even small changes in the RH levels have a significant impact on climate control requirements. Figure 5 shows the duration graph for RH/RH$_{LIM}$. If the control

requirement is $RH/RH_{LIM} < 1$ the time of operation for a dehumidifier was 1450 hours in combination with adaptive ventilation while it was 3750 hours without climate control.

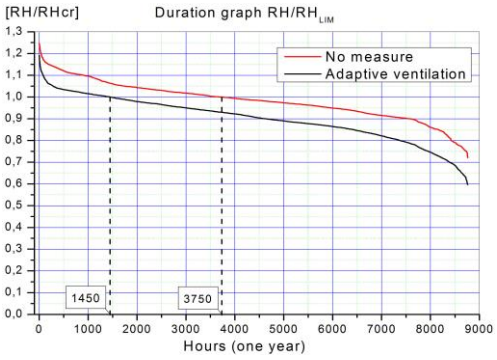

FIG 5. Duration graph of RH/RH_{LIM}.

3.4 Efficiency

Based on the difference between mixing ratio indoors and outdoors every hour and the air flow, the total moisture transport during the test period is calculated. From September 2012 to August 2013, 1100 kg of water was transported out of the church. The ventilator has consumed 250 kWh of electrical energy during the same period. This gives a drying efficiency of 4.4 kg water per kWh.

3.5 Energy from photovoltaic panels

The inlet air heaters are used only when there is stored solar energy available and the ventilator is running. In October, November, December and half of January the solar panels did not produce enough energy for preheating the whole time when the ventilation was in operation. In the rest of the year the produced energy was larger than the amount of consumed energy.

From September 2012 to August 2013 the $5m^2$ photo voltaic panels have produced 645 kWh, thus the imaginary panels of $25m^2$ produced $5 \cdot 645kWh = 3\ 225$ kWh. The amount of energy used for the inlet air heaters was 2 066 kWh.

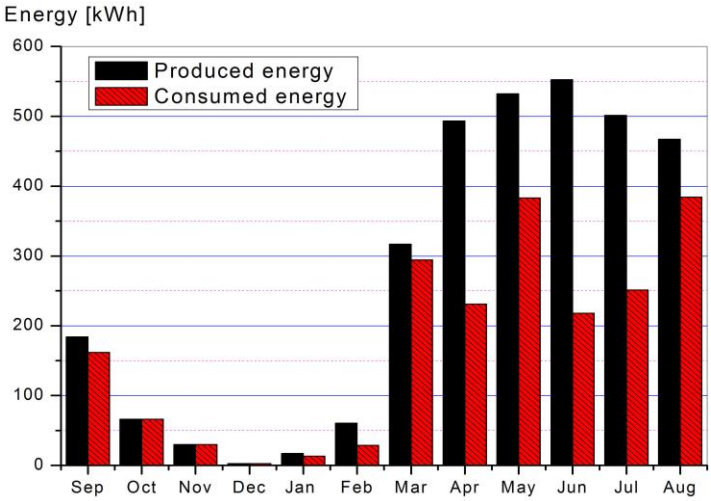

FIG 6. Monthly produced and consumed solar energy.

When the fan is running at full speed the heaters gave a temperature difference of 11°C. When solar energy has been available, this has generally been sufficient to counteract or mitigate the cooling effect without causing any harmful temperature variations.

In January 2013 there was no solar energy available. During one week, the adaptive ventilation ran without preheating and the indoor temperature decreased by 6 °C. At the same time the MR decreased and RH still was around 65%.

3.6 User aspects

The users of the church have perceived an improvement in indoor air quality, the bad smell is no longer a problem. The fan is too noisy to operate during services, it has been turned off manually. Overall the parish is positive towards this solution and wants to make it permanent.

4. Conclusion

This case study shows that adaptive ventilation has improved the indoor climate in the church. During one year, some 1100 kg of water has been removed from the building resulting in significantly lower RH level and reduced mould risk. The members of the parish have felt that the indoor air quality has improved, mainly in the elimination of bad smell. Short term variations have increased slightly, but they are still mainly within acceptable limits.

Adaptive ventilation is a low-cost and low-energy option as compared to conventional humidity control. The annual energy consumption for the operation of the fan was 250 kWh. Overall this gives an efficiency of 0,22 kWh/kg which is an order of magnitude smaller than for conventional dehumidifiers.

The preheating of the inlet air has counteracted the cooling effect that was reported in previous studies. During one year, the contribution from the solar panels was 2000 kWh. This is economically viable only if the solar panels are subsidised.

Generally, adaptive ventilation is best suited for unheated buildings. For buildings with comfort or conservation heating, more elaborate control strategies are needed.

In this case, adaptive ventilation is not sufficient to eliminate mould risk throughout the year; however it does significantly reduce the operational time and energy demand for auxiliary measures such as dehumidification. The results presented in this paper are from the first year of operation, over a longer time period the massive structure are expected to slowly become dryer thus reducing indoor RH levels.

A general problem with adaptive ventilation in historic buildings is achieving sufficient air tightness. The air tightness measurements indicate that the air leakage maybe of the same order of magnitude as the ventilator air flow.

Given the complex interaction between the thermal inertia and the RH and T of the incoming air, control by MR, rather than RH, has proven to be a robust method. In future investigations different strategies for the control of ventilation and preheating will be investigated through building simulations and further field trials, both over longer time periods. This would include an assessment of thermal solar air systems with local heat storage.

5. Acknowledgements

We gratefully acknowledge the support from the Swedish Energy Agency through the national research program for energy efficiency in historic buildings and the European Union Central Baltic INTERREG IVA program 2007-2013, for their support of the research program “Sustainable Management of Historic Rural Churches in the Baltic Sea Region (SMC)”.

References

Brockmann T. 2010. Langzeiterfahrungen mit dezentralen Kleinanlagen zur Feuchtegesteuerten Zwangslüftung. Klima und Klimastabilität in historichen Bauwerken, Wissenschaftlich-Techniche Arbeitsgemeinschaft für Bauwerkserhaltung e.V. Arbeitsgruppe 6.11., 2010, pp 59 – 76

Broström T., Hagentoft C.,Wessberg M. 2011. Humidity Control in Historic Buildings through Adaptive Ventilation: a Case Study. Proceedings of the 9th Nordic Symposium on Building Physics. Tampere, June 2011 pp. 783-790

Bläuer-Böhm, C., Zehnder, K., Domeisen, H. and Arnold, A. 2001. Climate control for passive conservation of The romanesque painted wooden ceiling in the church of Zillis (Switzerland). Studiea in Conservation 46 pp. 251-268

Cooper, E.W., Etheridge, D.W. and Smith, S., 2007. Determining the adventitious leakage of buildings at low pressure: part 2: pulse technique Building Services Engineering Research and Technology. 28(1), pp 81-96

EN 13829, 2000. Thermal performance of buildings - Determination of air permeability of buildings - Fan pressurization method

EN 15757, 2010. Conservation of Cultural Property - Specifications for temperature and relative humidity to limit climate-induced mechanical damage in organic hygroscopic materials.

Hagentoft C.E., Sasic Kalagasidis A., Nilsson S. et al. 2008. Mould growth control in cold attics through adaptive ventilation. Proceedings of the 8th Symposium on Building Physics in the Nordic Countries, Copenhagen, Denmark. pp. 1237

Larsen P.K., Broström T. 2012. Climate control strategies for occasionally used churches. Heat, dehumidify, ventilate – or do nothing. In: Elin Dahlin (ed.) Proceedings on the 2nd European Workshop on Cultural Heritage Preservation, Kjeller, Norway 24th–26th September 2012 pp124 – 130

Larsen P.K., Wessberg M., Broström T. 2013. Adaptive ventilation for occasionally used churches. Proceedings of the 3rd Erupean Workshop on Cultural Heritage Preservation, Bolzano, September 2013 pp. 55-62.

Mattsson M. 2013, Resultat av luftläckagemätningar i Hangvar & Fide kyrkor, Report

Reiss J., Kiessl K. 1993. Feuchtetechnicshe Untersuchung an Aussenwände der Torhalle Lorsch. Kunst in Hessen und am Mittelrhein, Heft 32+33, pp 91-98

Sedlbauer, K. 2002 Prediction of Mould Growth by Hygrothermal Calculation, Journal of Building Physics 2002 25, pp321-335.

Issues in calculation of infiltration in whole-building simulation: A wind-tunnel experiment studying wind pressure distribution on the facade in the case of Skokloster Castle

Torun Widström, Lic. Tech.[1]
Leif Claesson, Research Engineer[2]
Mats Sandberg, Professor[2]

[1] KTH, Royal Institute of Technology, Sweden
[2] University of Gävle, Sweden

KEYWORDS: *Wind tunnel, historic building, wind pressure coefficient, complex geometry, simplified models*

Summary
In this paper the impact of the wind pressure coefficient C_p on the air exchange in a historic building is investigated. Many historic buildings display complex geometry which gives rise to turbulence patterns unlike those of simpler forms, changing the wind pressure distribution and thus affecting the C_p coefficient. Natural ventilation and leaky building envelopes make the knowledge of the impact of the C_p coefficient important when performing whole-building heat, air and moisture simulations of such buildings, since a wrongly estimated air exchange rate can lead to erroneous simulation results and faulty predictions of the indoor climate. Assuming C_p coefficients of simpler forms to be valid when they are actually not may lead to such errors. In this paper an investigation of the wind pressure distribution around the façades of Skokloster Castle in a wind tunnel experiment is presented and the differences between different methods of estimating the C_p coefficients are displayed and discussed. In this case large differences in wind pressure distribution can be found between the actual and a simplified shape, due to the protruding corner towers of the castle.

1. Introduction

Ventilation in historic buildings is often natural and influenced by considerable leak flows. In such cases the wind pressure on the façades will impact the ACH and heat loss due to ventilation, but when the building is simulated using whole-building simulation tools variations in the pressure caused by turbulence are often neglected or taken into account based on simplified geometry as well as simplified calculation methods. This may lead to under- or overestimation of the leak flows, especially in cases where complex geometry causes deviating turbulence patterns.

A first step to evaluate the leak flows and the pressure drop over the building envelope is to examine the pressure distribution over the exterior building surfaces caused by the wind. The aim of the study presented has been to examine the differences between estimation of wind pressure coefficient based on actual geometry, based on simplified geometry and based on an even more simplified calculation method potentially used by a whole-building simulation program, all tested in the case Skokloster Castle. The actual air exchange rate of the castle displays signs of being significantly influenced by the exterior wind pressure, and the hypothesis is that the corner towers of the castle causes a build-up of overpressure where they block the path of the wind. The question is then to what extent this influences

the reliability of a simulation of the building and its resulting prediction of indoor climate, should estimates of the wind pressure be neglecting this effect.

This is part of a larger study included in the national research program Energy Efficiency and Preventive Conservation Through Climate Control, funded by the Swedish Energy Agency.

2. Method

2.1 The modelled building

The building has a square plan, about 46 m across, with octagonal towers placed at each corner. The plan, seen in fig. 1, is exteriorly symmetric in two directions. The height of the façades of the main building body is about 19.2 m and the roof-top of the building is about 33 m from ground level. The stagnation point is assumed to be at the level of the third floor, about 1.5 m from the floor level.

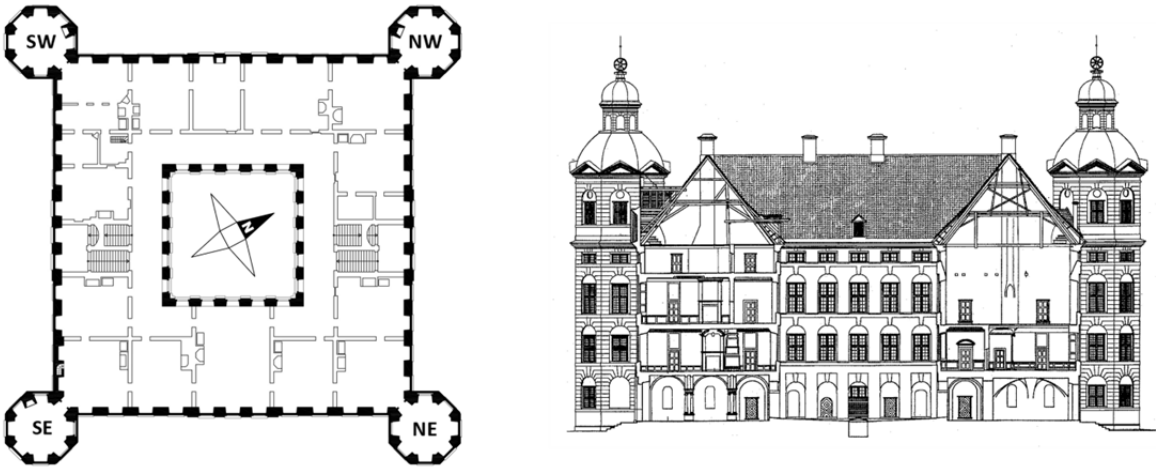

FIG 1: Plan for Skokloster Castle, showing its exterior symmetry, and section

A wooden model in scale 1:100 of the castle was produced and placed in a wind tunnel, figure 2. The building is surrounded by trees at three sides, but with different height and density on each side. This was taken into account in the first experiment, A, carried out in order to determine the adjustments to make to be able to calibrate the computer simulation model. In the following experiments, B and C, presented in this article, these surrounding elements were removed.

2.2 The wind tunnel

The wind tunnel is of closed circuit type with a width of 3 m and height of 1.5 m at the test section. The length of the test section is 11 m, making the wind tunnel of the short test-section type according to (ASCE 1999). The tunnel has a turntable, to mount the model on, with a diameter of 2.8 m and with its centre located 8.5 m downstream from the entrance to the test section.

To simulate the turbulence caused by the surrounding landscape roughness elements size 70 mm were placed throughout the first 7 m of the test section, upstream from the model location, thus reaching to the edge of the turntable, see fig. 2. The average wind speed during testing was measured to 12.9 m/s at roof-top level. Roof-top level was assumed to be the height of the roof of the main building, not the top of the steeples. The mean wind profile, normalized to maximum height of the measuring (800 mm) and maximum wind speed (18 m/s), and the turbulence intensity (standard deviation of velocity fluctuations/mean velocity), normalized to the same height, can be seen in figure 3. Temperature during the testing varied between 14 – 24 °C. The wind profile and turbulence intensity profile are recorded by use of hot-film anemometer at the centre of the turntable after removal of the model.

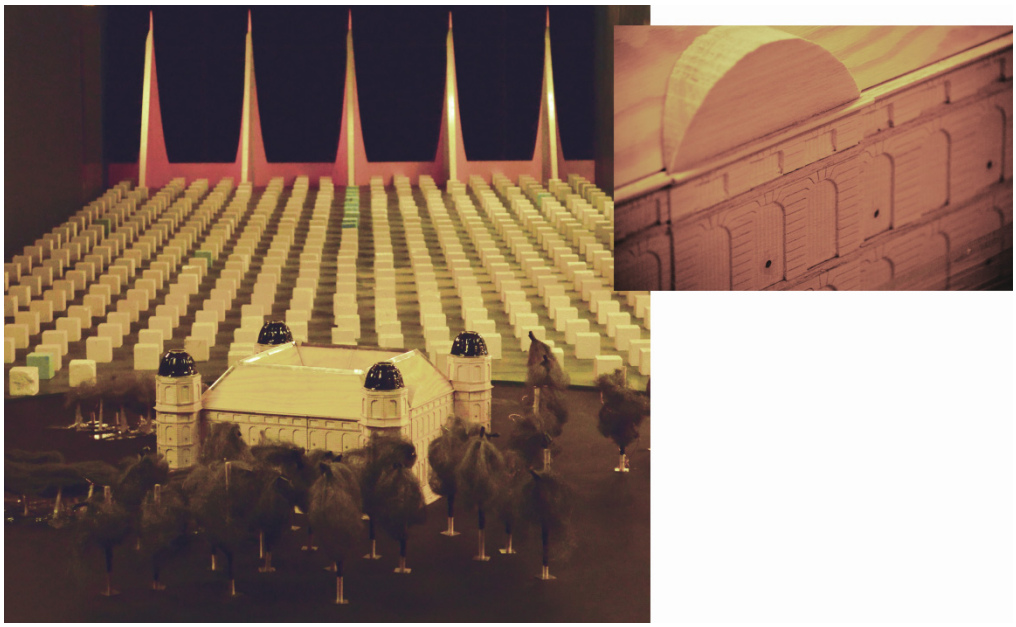

FIG 2: The model in the wind tunnel surrounded by existing trees and the roughness elements in the background, and inset a detail of the wooden façade of the model, featuring the measure points

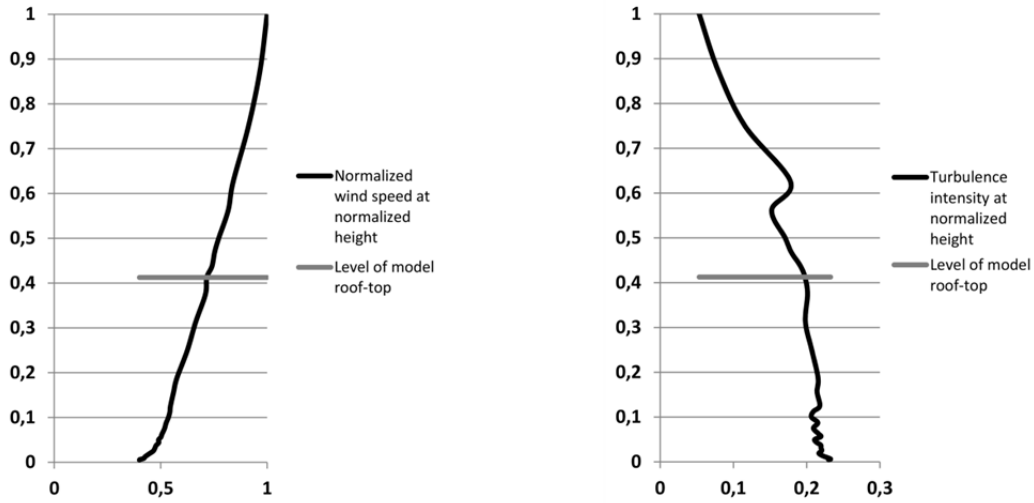

FIG 3: Wind profile (mean velocity) at the centre the turntable (left) and turbulence intensity at the same location (right)

2.3 Measuring

Measure points at the windows at the 2nd and 3rd floor of the castle were connected to the measuring device by means of plastic tubes with an inner diameter of 2.0 mm. Different sampling times were tested and 30 s found to deliver acceptable accuracy, though the values measured within that range were showing quite large fluctuations due to the turbulence. The atmospheric pressure was measured, as well as the static pressure at the wind tunnel ceiling above the model and at roof-top level, 330 mm above the wind tunnel floor, and also the total pressure at the roof-top level. The measurements at roof-top level were made upstream from the model, adjacent to the roughness elements, and near to the wind tunnel wall, as to not interfere with the testing of the model. However, the close proximity to the roughness elements turned out to cause large fluctuations in the measured values due to turbulence,

and the acquired values were deemed unfit for use. Instead a measuring was done after the model was removed, at the actual model location with more stable values. Thus these values were chosen instead of the ones measured parallel with the testing of the model. All measurements were normalized to temperature, 20 ºC, and atmospheric pressure, 1013.25 mbar.

2.4 Measured scenarios

Three experiments were carried out:

A. The building with surrounding trees and neighboring building
B. The building without the surrounding obstacles
C. The building with the corner towers removed

Measuring was performed at wind directions 360 degrees around the building in 15 degree intervals in experiment A, and with the same intervals but for a total of merely 90 degrees for experiments B and C, as the building's symmetrical geometry made more than 90 degree examination superfluous.

2.5 Calculations

The wind pressure coefficient C_p was calculated according to (Etheridge 2012):

$$C_p = \frac{P_{nor} - P_{sta}}{0.5\rho u_0^2} \quad (1)$$

Where P_{nor} the normalized total measured pressure at the measure points in the model (Pa)
P_{sta} the static pressure over the model center, at the wind tunnel ceiling (Pa)
u_0 the wind speed at the height of the model roof-top, measured after the model was removed (m/s)

3. Results

The results that will be shown in the following are from two wind angles and one level at the building only, as representative samples rather than a comprehensive account for the entire testing. The results are also not referring to the first scenario, A, with the surrounding trees and buildings, as that belongs to a more detailed study of the conditions of the object rather than the topic of this paper.

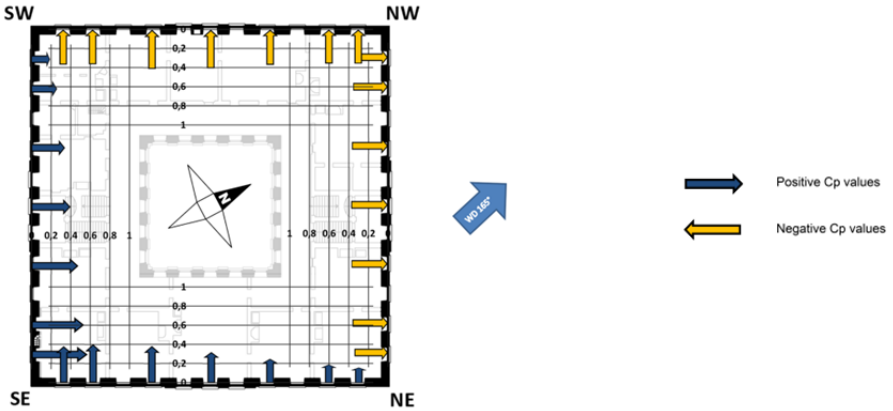

FIG 4: The C_p values for the wind angle 165 degrees in the no-tower scenario of experiment C, at level 2nd floor. Blue/dark arrows = positive C_d-values, yellow/light arrows = negative C_d-values.

3.1 Results of the testing of the model without towers, test C, angle 165 degrees

The largest deviations between the model with and without towers can be seen at wind angles close to 45 degrees on the main building body, straight at the towers. In a body without obstructions at the corners the wind pressure would generally be lower at corners that the air slips around, while a

building with obstacles trapping the air at such corners instead builds up a higher pressure at these points. For that reason the results for the angle 165 degrees from north are displayed here, as that wind angle gives an incidence angle on the main façades of 47 (east façade) and 43 degrees (south façade) from the respective normal to the façade surfaces, which gives the north-east and south-west towers maximum side-wind. In fig. 4 the calculated C_p-values from the second floor are displayed.

The wind exposed south-eastern corner displays the highest wind pressure, rather unsurprisingly, and then the pressure gradually decreases towards the following south-west and north-east corners as the air slips around them. The leeward sides show rather evenly dispersed negative pressure. A room in one of the affected corners between two façades, one leeward and one windward, would be exposed to a negative net exterior pressure, as opposed to the following scenario, the case B, with towers.

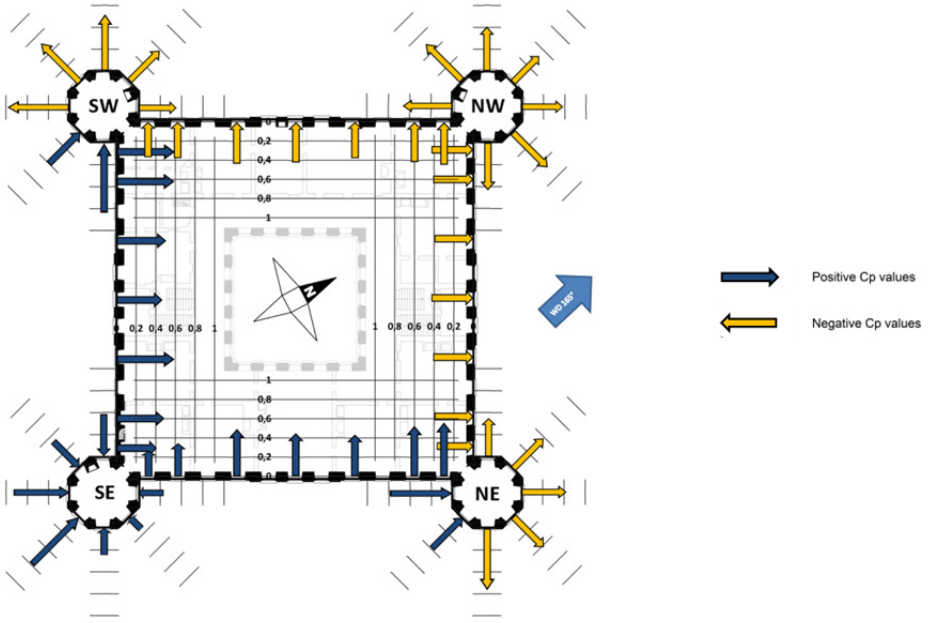

FIG 5: The C_p for the wind angle 165 degrees in the with-towers scenario of experiment B.

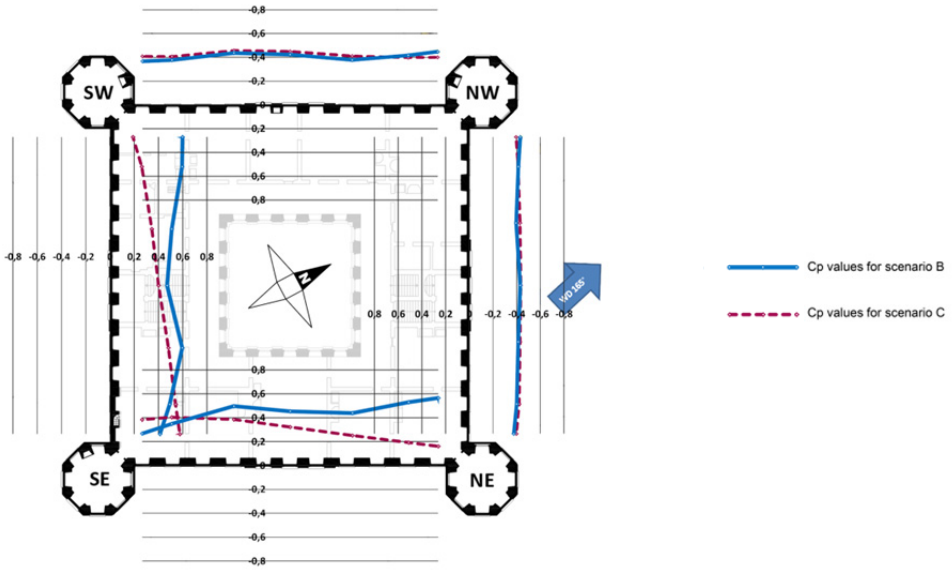

FIG 6: Comparison between B and C scenarios for the wind angle 165 degrees, at 2nd floor.

3.2 Results of the testing of the model with towers, test B, angle 165 degrees

The C_p-values at the measure points in test B are shown in fig. 5. As can be seen the leeward façades are almost identical to the no-tower case, case C, but the large difference, at largest a deviation of 254 %, is to be seen at the south-western and north-eastern corners. The towers obstructing the path of the wind flow there create an increasing instead of decreasing exterior overpressure towards these corners.

The comparison can also be seen in fig. 6. In this figure the values for the towers have been removed from the scenario B in order to be able to compare with the no-tower scenario C.

3.3 Results of the testing of the model with and without towers, angle 105 degrees

Another angle of interest is one where the wind hits one of the main façades more or less straight on, for example 105 degrees from north. In this case the angle of incidence on the eastern façade is 13 degrees from the normal.

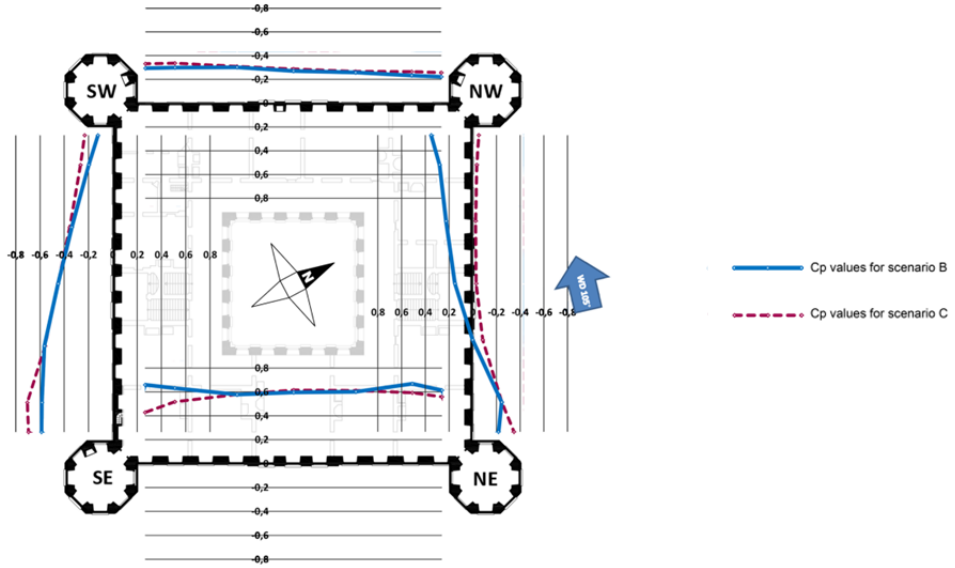

FIG 7: Comparison between B and C scenarios for the wind angle 105 degrees, at 2nd floor.

Figure 7 shows the comparison between the tests B and C. Again the leeward west façade show almost no difference. The values for the windward eastern façade are also rather similar but the effect of the obstruction of the towers is seen, more clearly in the southernmost part due to the wind direction.

The large difference in this case can be seen by the north-west tower, where the wind in the C- version travels along the façade causing a very low negative pressure while the tower blocking the path for the air movement in the B-version creates quite a large overpressure. Compared to the low reference value of scenario C the deviation in percent becomes very large, 800%.

3.4 Comparison of different methods of calculating the pressure coefficient

Two ways of dealing with the C_p-value to take into account have now been accounted for: One, C, ignoring the towers and assuming an unobstructed geometrical form, and the other, B, taking the effect of the towers into account. However, many whole-building simulation tools assume only one node for an entire façade, and may be calculating the wind pressure coefficient for that one node in different ways – if at all. One method could be to take an average from the simplified geometry, ignoring possible obstacles, and use that average for the entire façade. This even more simplified method may be included in a comparison with the two previous ones, as method S. To compare the influence of choice of method the predictable air exchange between indoor and the ambient air can be examined for the most deviating rooms in the two wind angles accounted for previously, based on the different C_p-

values. The potentially resulting air exchange, in m^3/s, disregarding interior air pressure, other interior air movements or buoyancy effects, can in a simplified manner be calculated according to (True 2003):

$$Q = C_d A u_{ref} \sqrt{\Delta C_p} \quad (m^3/s) \qquad (2)$$

Where C_d the discharge factor of the openings (-)
A the leak area (m^2)
u_{ref} the reference wind speed at the height of the leaks (m/s)
ΔC_p the difference between the wind pressure coefficient on the windward façade and the leeward façade (m/s)

Assuming that the C_d, A and u_{ref} are the same for both façades an estimate of a leak flow can be made for the two rooms, using the 3 methods of dealing with the wind pressure factor C_p: the methods of scenarios **C** (without towers), **S** (one average pressure coefficient for all points at one façade, average taken from the simplified geometrical shape = averages from scenario C) and **B** (with towers). For the sake of the example values are assigned to C_d, A and u_{ref}: $A = 0.038$ m^2 (a total of 2 mm cracks around all windows), $u_{ref} = 3$ m/s and $C_d = 0.3$ based on the previous values and (Baker et al 1987). The chosen corner rooms are the one in the north-west corner in the angle 165 degrees case and the north-east corner for the angle 105 degrees. Both rooms have a volume of 116.25 m^3, have equally long façades towards windward and leeward sides and have two windows each in each direction. The C_p for each façade wall of the rooms can be calculated as an average for the two windows/measure points of the façade in question.

The resulting potential leak flows and ACH (due to wind pressure only) of the rooms can be seen in table 1, along with deviation from scenario C for each result. The effect of the most extreme deviations in C_p value is obviously levelled out a bit by being combined with less extreme values.

TABLE 1: Potential resulting air flows due only to wind pressure for the corner rooms

Wind direction **165** degrees, NE corner room

Meth.	ΔC_p	Q	ACH	dev.
C	**0,558**	0,026	**0,79**	-
S	**0,717**	0,029	**0,90**	13%
B	**0,942**	0,033	**1,03**	30%

Wind direction **105** degrees, NW corner room

Meth.	ΔC_p	Q	ACH	dev.
C	**0,220**	0,016	**0,50**	-
S	**0,177**	0,014	**0,45**	-10%
B	**0,543**	0,025	**0,78**	57%

4. Discussion and conclusions

It is no surprise that the geometric complexity added by the towers causes additional turbulence compared to simpler geometry, as this investigation displays. Neither is it unexpected that that turbulence will affect the pressure coefficients influencing leak-flows nor that that effect will vary along the façades. What is interesting here is the size of the deviations and the consequences of simplifications not taking the additional turbulence into account.

The results show that the existence of the obstructions consisting of the towers potentially changes the air flow patterns not only around the building but also the air flow inside it if it is leaky. Skokloster's thick brick walls may, while still being made by something considered a porous building material, not let a lot of air through, and what is still getting through will take its time to reach from one side to the other. Thus the flow through the wall construction as such is not likely to be the large problem in this case. However, the large, single pane windows are old, most of them from the 1900th century, with noticeable cracks between the sashes and the window frames and large ones, several mm wide, between the window frames and the walls. The air flow through these cracks is not negligible and has a noticeable impact on the results achieved in a trace gas test performed at 4 occasions in the period July 2008 – May 2009 (Boman & Stymne, 2009).

It is possible to draw the conclusion that when calculating the wind impact on interior air movements these effects should be taken into account in any building with natural ventilation and/or where ventilation is significantly affected by leak flows, not just in the case of historic buildings such as Skokloster Castle. It is also worth keeping these effects in mind while calibrating a whole-building simulation model according to measured indoor temperature values, as these might well be influenced by the leak flows. Without taking the variations of the C_p coefficient into account the air flow calculations of this kind of objects may be flawed to such an extent that they are misleading, according to this study. This means a significant increase in uncertainty in the simulation model. It is thus important to be aware of the fact that this is the case and also of a plausible size of that additional uncertainty. And to determine that plausible size for other building shapes more studies are necessary.

It is hardly practical to make models of every building with leaky building envelope that deviate in shape from a simple block geometry and run them all in wind tunnel experiments, measuring every possible angle of wind. Thus more systematic wind tunnel tests of different generic geometrical layouts typical for historic buildings should be carried out, to establish approximate size of the deviations compared to simpler geometries so that estimates and manual adjustments can be done in the calculations where needed. However, to be able to make practical use of the results of such investigations the whole-building simulation software must also allow the user to adjust the model accordingly, and it must also be possible to perform these adjustments for the façade parts for each zone, not just for one node per façade as is often the case.

Hence, though the immediate practical use of this study is limited to Skokloster Castle, on a more general level the results point at an issue to be resolved in whole-building simulation of naturally ventilated geometrically complex buildings. Resolving it would require two steps. The first step would, as suggested, be to perform further wind tunnel tests on generic models to acquire a knowledge base enabling estimates of C_p -values, based on geometry. The second would be on the side of the software developers; it should be possible to deal with wall parts with deviating exterior pressure, preferably connected to C_p -curves for the different wind directions, even if they belong to the same façade. This would allow integration of the influence of geometry-induced pressure gradients over the façade.

5. Acknowledgements

We thank Professor Tor Broström, Gotland University, of the research program Energy Efficiency and Preventive Conservation Through Climate Control which this study is a part of, and its financer the Swedish Energy Agency. We also thank Professor Folke Björk for supervision and encouragement and Carl-Johan Wägner for generous assistance in the model-building.

6. References

ASCE. 1999. Manuals and Reports on Engineering Practice no. 67, Wind Tunnel Studies of Buildings and Structure. Ed. Isyumov N. Reston, USA: American Society of Civil Engineers. 214 p.

Baker P H, Sharples S & Ward I C. 1987. Air Flow Through Cracks. Building and Environment, Vol. 22, No. 4. Britain: Pergamon Journals ltd. pp 293-304.

Boman C. A. & Stymne H. 2009. Skokloster slott, Kungssalen och rum Bryssel. Infiltrationsmätning med passiv spårgasteknik. Report. Gävle, Sweden: Pentiaq AB. 20 p.

Etheridge E. 2012. Natural Ventilation of Buildings: Theory, Measurement and Design (3rd edition). John Wiley & Sons Ltd. 428 p.

True J et al. 2003. Wind Driven Cross-flow Analysed as a Catchment Problem and as a Pressure Driven Flow. International Journal of Ventilation, Vol.1 Hybrid Ventilation Special Edition. VEETECH Ltd. pp 89-101.

Accuracy Assessment of Hygrothermal Building Simulations of Historic Buildings

Ralf Kilian [1]
Martin Krus [1]
Klaus Sedlbauer [1]

[1] Fraunhofer Institute for Building Physics, Holzkirchen, Germany

KEYWORDS: *Hygrothermal Building Simulation, Measurements, Historic Buildings, Preventive Conservation, Damage Functions, Accuracy, Comparison*

SUMMARY:
The objective of this paper is the definition and development of new concepts to assess the hygrothermal simulation models of historic buildings in the context of preventive conservation. Preventive conservation is aimed at the permanent conservation of works of art and objects of cultural value by improving ambient conditions and by reducing or minimizing relevant risks. The quality of simulations is of significant importance especially in assessing the risks in historic buildings with precious interieur and works of art, since misjudgements of planned measures can result in irreversible damages. Moreover, hygrothermal simulations offer new opportunities in calculating the effect of different measures to improve indoor climate. Therefore, it is important to develop criteria to assess the results of simulation with regard to preventive conservation, and to verify them by means of case studies. A new method is presented to implement and calibrate simulation models of historic buildings.

1. Introduction

This work is a contribution to the further development of a preventive preservation strategy based on numerical simulation. Investigations to determine and assess the potential of this relatively modern method of hygrothermal building simulation in the field of historic buildings show that simulations are principally applicable in the field of preserving cultural assets and can advance preventive preservation decisively. Due to the global challenges like climate change, shortage of resources, population growth and destabilization of the financial system the requirements are growing to implement the criteria of sustainability also for the preservation of our cultural heritage. We must derive options for action, how to preserve the cultural heritage, more and more from simulations, since they allow breaking new ground with regard to risk assessment. Introducing the numerical simulation in the field of preventive conservation also means the initiation of a paradigm shift that has already been established in the fields of climate research or health care.
The chosen way to investigate these problems is the analysis of measured climate data in combination with the simulations of real historic buildings. A new method is presented to verify the necessary reliability of the simulation models for risk assessment and for the development of a concept of innovative measures for systematic quality assessment.

2. Development of a method for accuracy assessment of hygrothermal building simulations in the context of preventive conservation

2.1 Hygrothermal simulation of historic buildings

Simulations of historic buildings are in general concrete case studies. The causes of damage shall be clarified for an individual building or constructional changes shall be assessed, which have an influence on the indoor climate. This kind of simulation makes high demands on the precision of input data and the definition of boundary conditions.

Within the framework of this paper the following approach to hygrothermal simulation of a historic building is presented:

1. Definition of the objectives of simulation (Analysis of the causes of damages, prospects of constructional changes and changes of use, influence of technical building equipment, possible effects of climate change, etc.)
2. Determination of the relevant processes of damage and risks / definition of assessment criteria with regard to damage functions
3. Definition and determination of relevant input parameters for simulation (thermal and hygric material characteristics, building construction, utilization profiles, HVAC, etc.), measurement of indoor and outdoor climate
4. Realization, assessment and iterative calibration of the model by means of sensitivity analyses and modification of the relevant parameters and follow-up validation
5. Simulative work on the problem by means of calibrated / validated model / variable consideration
6. Documentation of the model and all variables

Solving this complex task requires great interdisciplinary cooperation. The question to be investigated is generally asked by the user, who is planning changes of a building or its utilization and therefore involves conservators and building physicists to make decisions. The objectives of simulation, the relevant damage processes to be considered, and the assessment criteria must be defined by all partners involved in the beginning. Principally, this can or must be done a long time before the simulation, since necessary data for calibration and validation of the model must be determined already then.

For later calibration of the model the indoor and outdoor climate but also other relevant boundary conditions of the usage of the building should be measured and documented in detail such as window and door ventilation, shading systems, operation of heating or air-conditioning systems, numbers of visitors etc. for a period of one year at least. Specific micro-climates, e.g. close to works of art or on the surfaces of building components to be considered by simulation, must be determined.

Relevant input parameters for simulation are derived from the objectives and damage functions defined in the beginning, which must be determined by building documentation, especially the thermal and hygric parameters as well as the surface shares of interior materials. These parameters must be taken into consideration with the calibration of the simulation later, and be within a realistic range. Sensitivity analyses help to assess the importance of unknown or insecure parameters for the calibration of the model.

Since the buildings are frequently not airtight and do not have any air-conditioning system, the indoor climate is predominantly determined by the outdoor climate within the course of a year in general. Temperature and absolute humidity adjust to the outdoor conditions in moderated form. If internal sources and sinks of temperature and humidity such as visitor, construction material moisture or HVAC systems remain unconsidered, the two factors that have the greatest impact on moderation and thus on climate stability will be the air change rate and the thermal and hygric inertia of the building.

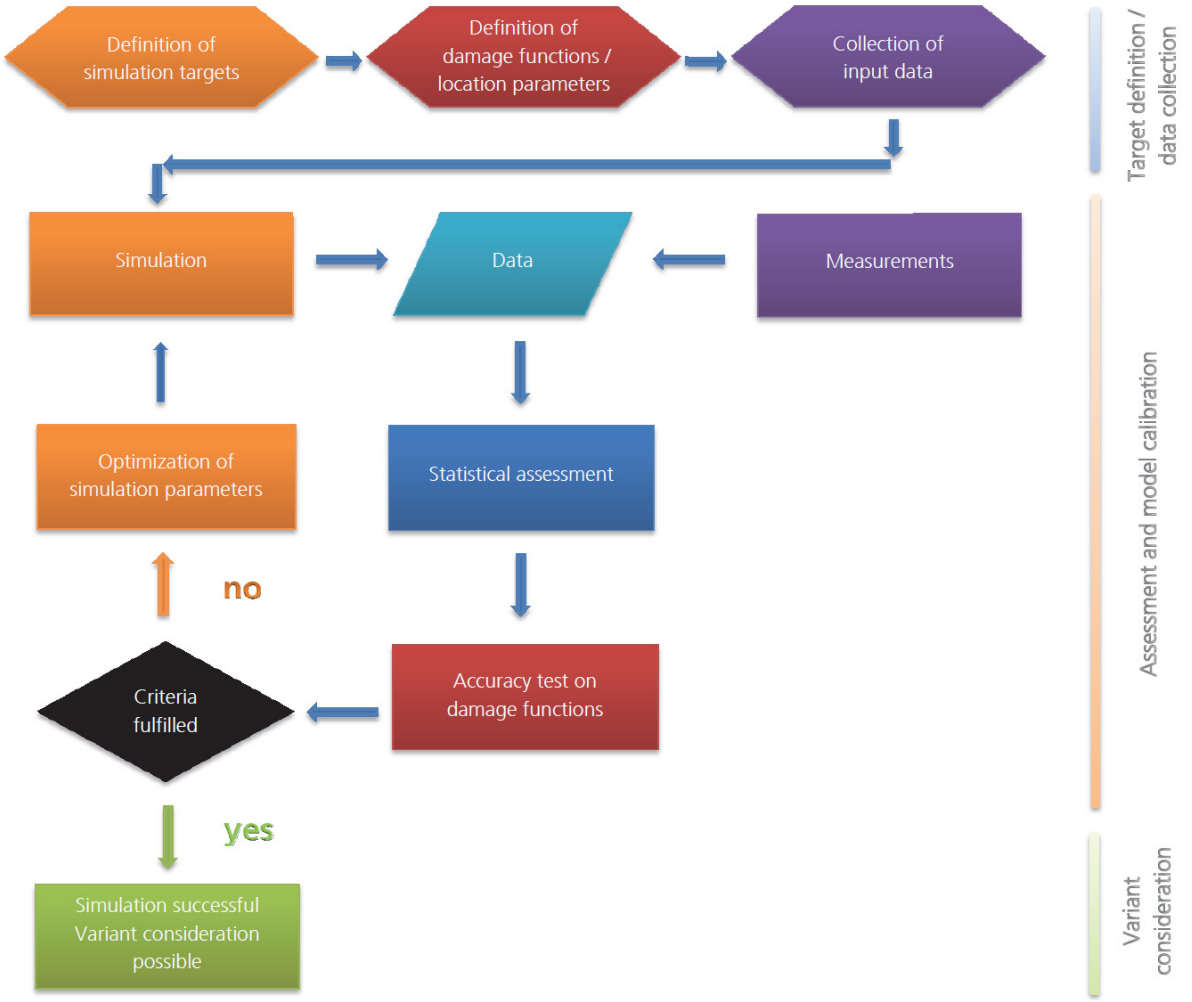

FIG 1. Course of a hygrothermal building simulation in the context of preventive conservation, definition of objectives, investigation of input data, iterative calibration of the model and assessment of the accuracy of the simulation by statistical comparison of the data sets of measurement and simulation as well as testing on the relevant damage functions.

This means the requirement for a high standard on the measurement of the outdoor climate for simulation. Weather data should be directly determined in-situ by measuring technique as precisely as possible and under standardized conditions. To use weather data from distant locations results in considerable insecurities in the model. Indoor climate data as well as data of the building construction and the interior materials should be measured with a high standard of precision for correct calibration concerning the quantity of surface shares and the hygric and thermal parameters. This latter kind of material characteristics is hardly available in the field of historic buildings, since hardly any measurements of the building material physical properties and their variation were carried out so far. Moreover, detailed data recording requires exact knowledge of the materials of the works of art and the historical techniques. All in all, the building simulation model is a system of different parameters with varying impact on the result of the simulation. In dependence of conditions and of the most important influencing factors on the indoor climate these relevant parameters must be identified and adapted in the most realistic way.

For the calibration of the calculated model usually the air change rate and the parameters of the moisture buffering function as well as of the vapour diffusion resistance are varied be-sides the thermal mass, since they have the greatest impact on the development of relative humidity in a room. The impact of visitors as source of humidity and air change rate for example in case of Linderhof Palace (Bichlmair et al. 2012) is predominant in comparison to the humidity buffering of internal surfaces, whereas it has a considerably higher impact on the indoor climate and thus on the results of the simulation in case of the King's House on the Schachen (Kilian et al. 2010). It is necessary to consider the relevant influences on the respective building. It must be avoided to generate artificial effects for example by unrealistic exaggeration of the number of visitors when calibrating the model.

The validation of the model must be carried out by means of a second independent data set, which is recorded separately. Only the validation will show whether the calibration was successful and realistic. Finally there is the opportunity to carry out variable calculations by means of the calibrated and ideally validated model to find answers to the questions asked in the beginning.

2.2 Assessment of the quality of hygrothermal simulations within the context of preventive conservation

Due to necessary restrictions of the model all simulations always represent only an approximate reproduction of reality. Thus, hygrothermal building simulation will never completely reproduce reality, but delivers a result showing the tendencies of possible measures. The comparison of simulation and measurement shows that it is impossible to reproduce every day correctly in detail. But it is important to understand, simulate and compare the characteristics of a specific indoor environment. To achieve reliable results from indoor climate simulation it is necessary to define criteria of precision. In this context, case-related relevant comparative parameters for the data sets of measurement and simulation with regard to the statistic parameters and damage functions must be defined as well as the respective quantitative criteria for these comparative parameters.From the point of view of preventive conservation the quality and thus the benefit of hygrothermal simulations is highly dependent on the precision in the reproduction of the real building. Since especially extreme weather events may cause damages – high humidity over a long period of time, extremely low values, frost and high material moisture or strong fluctuations of relative humidity – the correct reproduction is necessary. A second aspect are short- and medium-term climate fluctuations and their location in the data field, since they are a precondition for the advance of damages due to thermal cycling such as freeze-thaw cycling, moisture expansion and shrinkage or crystallization.

The process of assessment is principally conducted in two stages:

1. Statistical quality assessment of the reproduction of reality by simulation / check of conformity between measured and simulated data
    a. Assessment of statistical location parameters
    b. Assessment of the dynamics of indoor climate
2. Assessment of the correct reproduction of the relevant damage functions or of other problems by the model

The assessment of location parameters and of the dynamics of the indoor climate is conducted on the basis of criteria orientating on the present opportunities of hygrothermal building simulation and subject to individual adaptation, if necessary in the respective case. The assessment refers to the general statistical location parameters such as median, range of data as well as maxima and minima showing if the simulation represents the reality well enough. Furthermore a case-related individual consideration is necessary orientating on the actual damage and damage processes. Damage functions must be reproduced in dependence of the effects of damage and frequency of occurrence. As a clear and simple assessment of the quality of the forecasts of results, a forecast-quota can be used, describing the frequency of events in simulation and measurement in percentage.

2.3 Definition of assessment criteria of the reproduction of damage functions

Damage functions are aimed at reproducing a damage process / degradation process in a mathematical or logic function. In the last few years, damage functions were established in the different fields of conservation research to achieve a better understanding of the damage processes and to allow the assessment and prediction of aging and damage. Knowledge in the field of the quantitative courses of damage processes is still very limited. The correct reproduction of damage functions, however, is an essential assessment criterion to describe the quality of hygrothermal simulation in the context of preventive conservation. The respective criteria necessary for the accuracy of the simulations in the field of historic buildings must be defined for each individual case in a discussion of all relevant experts and decision-makers. Higher requirements for accuracy can be necessary for already pre-damaged buildings or collections.

TABLE 1. Examples of typical damage processes and functions and selection of adequate assessment criteria. To compare the frequency, a rate is developed from the result of the prediction by simulation and measurement.

Damage process	**Comparative parameter**	**Assessment criterion**
Level and frequency		
Crystallization and hydration of salts	Transition of deliquescence humidity	Comparison of frequency
Freeze /thaw cycling	Transition 0 °C / material moisture / duration	Comparison of frequency
Mechanical damage by cycling of high and low humidity	Short-term fluctuations / total range / exceeding of the Yield Point	Comparison of frequency / location parameter / comparison of frequency
Damage due to low temperature at organically bounded layers of paint	Temperature below glass transition temperature / exceeding of the Yield Points	Comparison of frequency
Level and duration		
Microorganisms	Duration of humidity and temperatures related to the quality of the substrate	Biohygrothermal and isopleth model [Sedlbauer 2001]
frequency of fluctuations		
Dynamics of cycling, mechanical damage	Daily fluctuation, or moving fluctuation range	Comparison of frequency

The following parameters with regard to the interactions of conservation and indoor climate must be considered separately for each case:

- High temperatures
  → Faster progression of the chemical degradation processes, more favourable for biological growth
- Low temperatures
  → Brittleness of organic binders below the glass transition temperature, formation of ice in the pore volume at a high level of moisture in the material and temperatures of < 0 °C over a longer period of time
- High humidity
  → Expansion, loss of stability, irreversible deformation, mould growth, salts dissolve
- Low humidity
  → Shrinking, crystallization of salts
- Fluctuations of temperature and humidity
  → Risk of advancing mechanical damage to materials by expansion and shrinking, freeze / thaw cycling or crystallization or hydration cycling of salts

Table 1 describes a selection of known and quantitative damage functions and indicates the assessment criteria to evaluate the quality of the prediction of certain damage processes.

3. Conclusions

A new method and its requirements for the calibration and assessment of accuracy of hygrothermal building simulation models in the context of preventive conservation were presented. The process of assessment is principally conducted in two stages. The first step consists of the statistical quality assessment of the reproduction of reality by the simulation. The check of conformity between measured and simulated data is done by an assessment of statistical location parameters as well as an assessment of the dynamics of indoor climate. As an additional step in the process of accuracy assessment in the context of preventive conservation for historic buildings, an assessment of the correct reproduction of the relevant damage functions or of other problems by the model is done. For each specific simulation case the relevant parameters and damage functions that should be reproduced by the model have to be defined by an interdisciplinary team doing the assessment. For this purpose building conservators and building physicists have to work together in an interdisciplinary team.

4. Acknowledgements

This research has been made possible by the European Commission funded project “Climate for Culture”, Grant Agreement N° 226973, FP7-ENV-2008-1 Theme 6 Environment (including Climate Change). We especially thank the Bayerische Verwaltung der staatlichen Schlösser, Gärten und Seen for the good and long-term cooperation in the field of heritage research.

References

Bichlmair S., Kilian R., Krus M. & Sedlbauer K. 2012. Building simulation modelling of the historic building Linderhof Palace taking account visitors. Proceedings of eSim 2012: The Canadian Conference on Building Simulation. Halifax, Nova Scotia, May 1-4, 2012. Halifax 2012.

Kilian R., Wehle B., Holl K., Radon J. & Holm A. H. 2010. “Climate Analysis of a Cultural Heritage Building determined by measurements and hygrothermal building simulation – The King’s House on the Schachen. In: Proceedings of the 1st Central European Symposium on Building Physics, 13-15. September 2010, Cracow – Lodz, Poland 2010.

Sedlbauer K. 2001. Vorhersage von Schimmelpilzbildung auf und in Bauteilen. Dissertation. Stuttgart.

TOPIC
Low Energy Buildings

Page.....671-945

Case study – Performances of a masonry house – Energy consumption and air-tightness

Anders Lidholm, M Sc Civil Engineering, Project leader Concrete and LECA®

Saint-Gobain Byggprodukter AB, Ollebovägen 14, 218 45 Vintrie, Sweden
anders.lidholm@weber.se

KEYWORDS
Masonry house, air-tightness, energy consumption, case study, measured values

SUMMARY
Air-tightness and energy consumption was measured in a one-family house built in 2009 and 2010. The air-tightness fulfilled the goals, which was set to 0,3 l/s, m^2. The energy consumption was measured from the start in May 2010. The figures in this report refer to measurements between May 2010 and October 2013 and are well below the authority demand of 55 kWh/m^2,year.

1 Introduction

In the last decade or so the energy performance for buildings have kept increasing. Focus has shifted from U-values to energy consumption. Houses with thick insulation, taped foils and many layers were in media focus. In the light of this a new sandwich block made of lightweight aggregate concrete has been developed and tested, with focus on how to build air-tight with few layers.
The air-tightness goal was <0,3 l/s, m^2 which is comparable with the demands for a passive house. Together with a consultant and close discussions with the building company, the air-tightness was measured three times during construction. Minor changes in the construction such as the thickness layer of the rendering and the direction of the plastic foil were made. When the house was finalized the final measurement showed 0,16 l/s, m^2. The energy consumption is approximately half of the authority demands.

2 Back ground

In the beginning of 2009 we had developed a new model of a well-tested masonry block. The next step was to put it on the market and build a house with as good performances as possible.

The back ground discussions were that we knew we had a very good masonry block, with a low U-value. Increasing the thickness would not necessarily give better energy performance compared to the cost increase for the product. We needed to work with other parts of the building process and the air-tightness was the obvious next big part, more or less directly connected to our products in order to decrease the energy demand for houses.

A family who was in the process of building a house for themselves was contacted. We agreed that we could follow the building process and do some follow ups. Their aim suited our aims. They wanted to build a low energy house with performances close to the demands for passive houses.
The main criteria were air-tightness and we agreed to have an air-tightness consultant involved in the project from the start.

3 Aim of the project

The goal for the company in this project, was to verify that with good communication between involved parties and only minor changes in erecting the building, it is possible to build a low energy and air-tight house with existing technology and modern architecture.

4 Technical aspects for the chosen materials

The building is a one-family house and is situated just outside Malmö in the south part of Sweden. It is a two story building with 192 m^2 living space (Atemp).

FIG. 1 3D-rendering of the house.

The outer walls of the lower floor consists of a masonry sandwich block with 150 mm of polyurethane foam and with 100 mm of lightweight aggregate concrete on both sides. On both sides of the wall there is a layer of 10-15 mm of rendering.
The outer wall of the upper part is a wooden frame with mineral wool.
To reduce the cold bridge in the roof beams they look like I-beams made of two wooden load bearing part connected with a wooden fiber board, with a thickness of 500 mm.
The foundation is a massive low density light weight aggregate concrete connected to a concrete slab.

TABLE 1. Thicknesses and U-values of different building parts.

Building part	**Thickness (mm)**	**U-value (W/m^{2}K)**
Outer wall, 1st story, LECA® Isoblock	370	0,15
Outer wall 2nd story, wooden frame	340	0,14
Roof	500	0,08
Windows		0,9

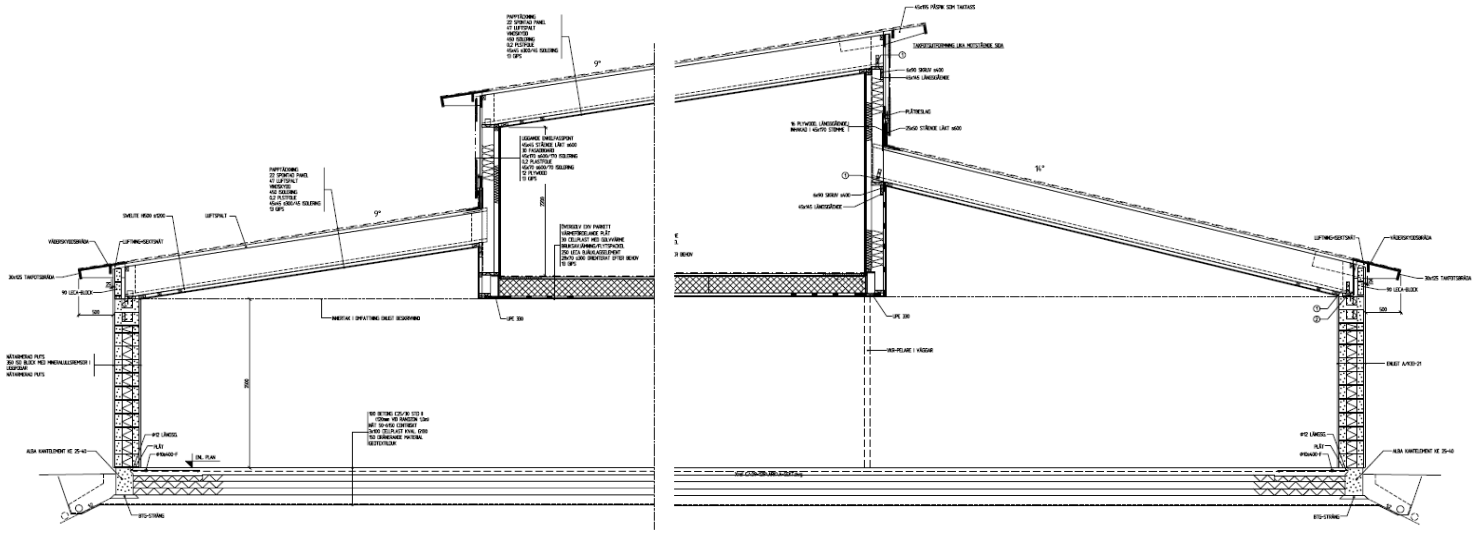

FIG 2. Cut through of the house with the different construction details.

The installations consist of a heat pump, solar panels and a storage pump (in a separate building).

5 The building process

Together with the construction company and the consultant we held a few meetings regarding important and critical points in the building process in order to achieve as good air-tightness as possible. Therefore everybody was “on their toes” already from the start.
The first layer of rendering is critical. Not only the façade part of the masonry needs to be rendered. But it is also very important to render the top of the masonry and door- and window-openings before doors and windows are installed. This is to ensure the air-tightness of the masonry structure.
Of equal importance was the way to connect the plastic foil from the roof to the masonry, which was pinched with expanding rubber tape between the top of the masonry and the roof construction.
The joints of the plastic foil were as far as possible taped and connected lengthwise to the roof beams in order to minimize air leakage.

FIG 3. Pinching of the plastic foil between top of the masonry wall and wooden beam.

Before closing the building with the finalizing layers we did an air-tightness measurement. This was to be able to do some enhancements if there might be some obvious errors. But after connecting the blower door we could not even achieve the proper pressure difference to get a value. It was however very easy to locate where the air leakages were and in this part of the process very easy to fix them. It was a few misses in the taped plastic foil joints and misses with the rendering in window openings. These were easily corrected in this phase of the building process.

We did a second blower door test with a fairly good result and some minor adjustments where done and then the building was finalized.

The air-tightness of the house was measured according to EN 13829 “Thermal performance of buildings - Determination of air permeability of buildings - Fan pressurization method (ISO 9972:1996, modified)”, commonly referred to as the “Blower Door Test”. And a Blower Door Modell 4 was used to receive an overpressure of 50-100 Pa.

FIG 4. The finalized house.

6 Results

The third and final blower door test was carried out in 2010 and gave us at the time a very good result. The few leakages were typically between frames and walls in both the masonry part and the upper wooden frame part.

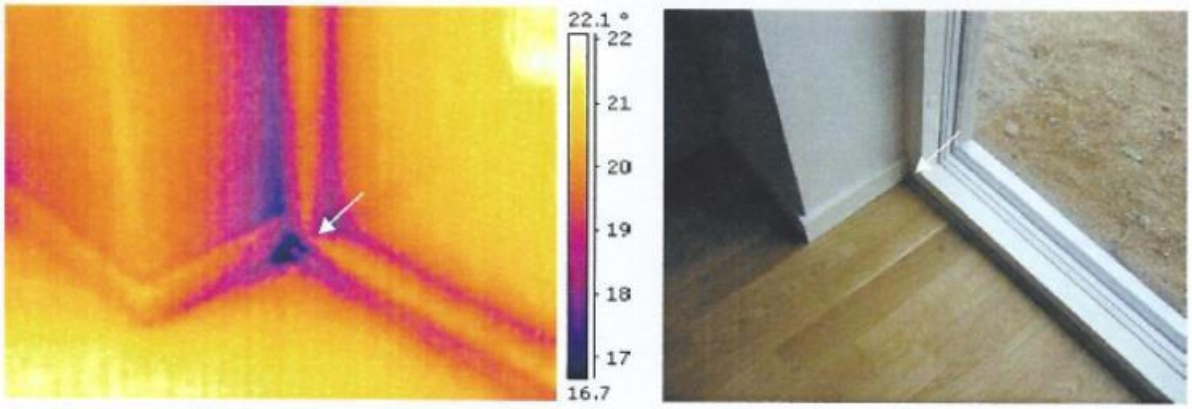

FIG 5.Small leakage between window and corner floor/wall, bottom floor.

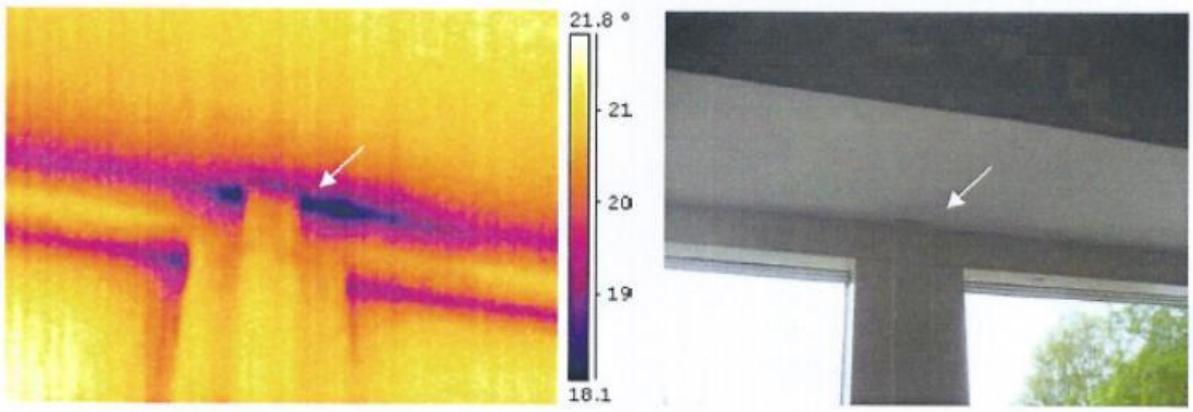

FIG 6.Small leakage between window frame and wall, upper floor.

The air leakage measured to 0,16 l/m^{2}s, compared to the goal of <0,30 l/m^{2}s. This goal was taken from the Swedish passive house regulations, FEBY.

The energy consumptions figures up to today are also very encouraging.

The separate storage pump building (heated) of 32 m^2 is not taken into account, which would have been beneficial for the calculations.
In this house it is possible to separate the energy consumption for hot water. And looking at the total monthly consumption for the summer months one can make a good estimate for the energy for lightning, TV, appliances etc.
Included in the figures for bought energy there is a huge computer server that uses 3000 kWh per year. I have pulled that out from the calculations. Below the table show a summary for the two complete years of 2011 and 2012, regarding energy and hot water.

TABLE 2. Summary of energy, taken from the appendix.

Year	Bought energy	Solar gain	Hot water
2011	12072	3204	2963
2012	11957	1344	2412
Mean	**12014**		**2687**

To make an estimate of the energy for lightening, washing machines etc I looked at the summer months for 2012 and 2013, where there are measured values.

TABLE 3. Summary of summer months, taken from the appendix.

Year	June	July	August
2012	710	703	710
2013	757	773	812
Mean	**744**		

The mean bought energy for 2011 and 2012 was approximately 12 000 kWh per year. This is for heating, hot water, light and appliances and the server. Looking at the summer months for 2012 and 2013 the bought energy is 744 kWh per month, that is 8 928 kWh per year. This is then energy for the kitchen appliances, TV, light, hot water etc and the server. Hot water is a little more than 200 kWh per month, which gives 2 687 kWh per year.

The total energy demand for heating and hot water is then 12 000 – 8 928 + 2 687 = 5 759 kWh per year. The heated area is 192 m^2. The energy demand per square meter and year is 30 kWh. This is a little more than the level for electrical heated passive houses according to FEBY. But on the other hand, this was not meant to be a passive house, since the installed heat exchanger had too high effect according to the FEBY-regulations at the time.

7 Conclusions and discussion

The goals that were set up where fulfilled. The level of the air-tightness was reached by far (0,16 l/m^2s). The energy consumption for heating and hot water is well below the regulations for normal houses (30 kWh/m^2, year). And it is a modern architecture.

There are some obvious energy loss points:

- First you have the storage tank that is situated in a separate building, which means that it is impossible to utilize the heat loss inside the house.
- Then there are losses from the pipes leading from that building into the house.
- The house has fairly normal windows with a U-value of 0,9 W/m^2K.
- And from an energy point of view, the architecture is not optimal.
- Another big source for the energy demand is that the indoor temperature in the house varies between 22 and 23 ^oC, according to the inhabitants. This is more than the 21 ^oC that is normally calculated.

8 Acknowledgements

The author gratefully acknowledges the owners of the house, for sharing their energy data, for letting me interview them and for fruitful discussions.

9 References

LTH rapport EBD-R-12/36; IVL rapport nr B 2027; ATON rapport 1201 (2012). FEBY12
"Kravspecifikation för nollenergihus, passivhus och minienergihus – Bostäder
Boverkets regelsamling, BBR
AK-konsult, Tätning och termografering, ordernummer 18556

Appendix

Monthly energy figures.

Month	Bought energy (kWh)	Solar gain (kWh)	Hot Water (kWh)
2010-05	**1053**		
2010-06	**1053**	492	230
2010-07	**1053**	548	240
2010-08	**1053**	474	194
2010-09	**1053**	456	206
2010-10	**1053**	325	219
2010-11	**1053**	0	181
2010-12	**1053**	59	264
Sum 8 months:	8424	2354	1534
2011-01	**1006**	21	321
2011-02	**1006**	178	247
2011-03	**1006**	417	258
2011-04	**1006**	618	330
2011-05	**1006**	592	310
2011-06	**1006**	706	291
2011-07	**1006**	**112**	**201**
2011-08	**1006**	**112**	**201**
2011-09	**1006**	**112**	**201**
2011-10	**1006**	**112**	**201**
2011-11	**1006**	**112**	**201**
2011-12	**1006**	**112**	**201**
Sum 12 months:	12072	3204	2963
2012-01	1460	**112**	**201**
2012-02	1236	**112**	**201**
2012-03	1016	**112**	**201**
2012-04	912	**112**	**201**
2012-05	726	**112**	**201**
2012-06	710	**112**	**201**
2012-07	703	**112**	**201**
2012-08	710	**112**	**201**

2012-09	798	**112**	**201**
2012-10	910	**112**	**201**
2012-11	1134	**112**	**201**
2012-12	1642	**112**	**201**
Sum 12 months:	11957	1344	2412
2013-01	1599	**112**	**201**
2013-02	1452	51	185
2013-03	1374	517	229
2013-04	993	615	243
2013-05	791		
2013-06	757		
2013-07	773		
2013-08	812		
2013-09	819		
2013-10	1044		
Sum 10 months:	10414		

Bold figures are calculated mean.

Statistical study on the link between real energy use, official energy performance and inhabitants of low energy houses

Marc Delghust, M.Sc. [1,2]
Arnold Janssens, Full Professor [1]
Wina Roelens, M.Sc. [3]
Tine Tanghe, M.Sc. [3]

[1] Ghent University (UGent), Belgium
[2] Ph.D.-fellowship of the Research Foundation Flanders (FWO) & the Flemish Institute for Technological Research (VITO), Belgium
[3] Flemish Energy Agency (VEA), Belgium

KEYWORDS: *low-energy houses, EPBD, survey, user behaviour*

SUMMARY:
Energy performance regulations are becoming increasingly strict and governments supply simplified calculation tools to assess whether new buildings fulfil the requirements. However, one can wonder what the accuracy of those tools is for assessing the next generation of houses, that will have to fulfil the upcoming energy requirements. In order to investigate the discrepancy between predicted and real energy use in low energy houses, 537 dwellings were analysed. Data on building characteristics and theoretical energy use from the Flemish EPBD-database was complemented with data from the energy utilities and a survey of the inhabiting households, providing information about the households, their user behaviour and real energy use. While an undeniable correlation was found between theoretical and real energy use, the EPBD-method overestimated the heating energy use for most of the cases. Two building related parameters and two user related parameters proved to have a significant impact on that gap: the use of default values for the air tightness of the envelop and for the efficiency of the gas boiler, the heating profiles of the master bedrooms and the amount of baths and showers taken by the inhabitants. However, two comments must be made. First, the dataset consists of early adopters who could afford such energy performance years before it would be imposed and are therefore not representative of the average household. In addition, the analysis showed significant correlations between household characteristics on the one hand and building characteristics and performance on the other. These last two points question the possibility to extrapolate findings from samples of existing forerunners towards prognoses on future, entire building stock level.

1. Introduction

It is often questioned whether theoretical improvements in the energy performance of buildings, imposed by European and national regulations, will be fully obtained in practice. This question is important not only to estimate the real reductions in CO2-emissions, but also to calculate the financial returns on investments and cost-optimal performance targets, as asked by the European Union to each member state. However, when defining the future energy standards that will be imposed, the question on prediction accuracy becomes even more difficult to answer as there are few houses already fulfilling those performance targets, resulting in less relevant data being available. Building simulation software allow researchers to calculate the energy performance of building more in detail and to compare those results with results from the simplified assessment tools. However, this approach might overlook unpredicted user behaviour as well as the varying thoroughness of the energy assessors when performing the calculations. One solution is to use large datasets, analysing

together both the officially reported building characteristics and performance on the one hand and real energy use and data on user behaviour on the other hand, as was done by Guerra Santin (2010). For this study, the approach was similar, though it focused solely on recent houses with good energy performances and therefore it is based on a much smaller dataset.

2. Material & methods

2.1 Data collection

Every new house in Flanders, built from 2006 onwards, must meet the energy performance requirements from the Energy Performance of Buildings Directive (EPBD). Technical building data and administrative data (e.g. address) of all these houses is kept in one centralized database by the Flemish Energy Agency (VEA). For this study, VEA selected 1850 projects, based on the four following criteria. (1) The energy performance had to meet at least the current energy standards. (2) The housing units had to have their own, individual heating system. (3) They had to be inhabited for at least two years. (4) Their EPBD-file had to be free of any major error or shortcoming with regards to data (e.g. missing data) or with respect to the energy performance requirements.

Three complementary data-sources provided the needed information for this study. (1) The EPBD-database itself provided technical data on the buildings and on their theoretical energy performance. The database does not contain the full inputs for the EPBD-calculation (e.g. data on each individual wall). However, it does contain some of the most important variables (e.g. the size and type of the building, the type of services, the average insulation levels etc.) as well as the intermediate and final results of the energy calculation. Those are expressed in monthly primary-energy use for sanitary hot water, heating, cooling and auxiliary energy for services, calculated with a primary energy conversion factor for electricity of 2,5. The database also contains the estimated monthly electricity production of the photovoltaic-panels (PV-panels). (2) Surveys of the households supplied additional data on the buildings as well as on the households, their behaviour and their real energy use. (3) Meter readings from the energy utilities further completed this dataset. The surveys obtained a response rate of 29%, resulting in a total dataset of 537 housing units. However, the response rate was not homogeneous over all energy performance levels: significantly higher response rates were obtained for the better performing houses, as will be further discussed in paragraph 3.2.

2.2 Data filtering & subsampling

A thorough analysis of the dataset revealed hidden shortcomings as well as contradictions, e.g. between the survey and the EPBD-database. As it was often impossible to elucidate the contradictions, several cases had to be removed from the dataset for further analysis. In order to keep the dataset as large as possible, those cases were only excluded from subsets for analyses depending on their specific erroneous or dubious data points. Thus, for example, faulty data on the PV-panels were not taken into account for the analysis on heating energy use based on gas combustion.

Three subsamples were identified within the full dataset, in order to analyse the total energy (subsample S1), the heating energy use for space heating and sanitary hot water (subsample S2) and the domestic electricity use (subsample S3) separately. Due to the relevant shortcomings in the dataset, these subsamples were reduced respectively from their original size of 350, 135 and 260 to 100, 75 and 150 cases. However, the analyses that didn't require real energy use, could be performed on much larger subsamples, with small variations depending on the specific analysis.

2.3 Normalization method

The statistical study of the data and further analysis were performed in SPSS, using multivariate regression analysis. However, prior to comparative, statistical analysis of the predicted, calculated

energy use and the real energy use, both have to be normalized to comparable boundary conditions such as similar climatic data. The most common way to do this, is to normalize the real energy use of all houses to one single, average climatic year, coinciding with the one used in the theoretical calculation method. However, this was impossible for this dataset due to several reasons. Normalization of the energy use requires to perform some regression, based on the real energy figures. However, data on real energy was provided for only one time period per dwelling and different types of energy demands were often aggregated into one single figure (e.g. sanitary hot water and heating on one single, yearly gas consumption bill). Therefore, individual normalisation regression could not be performed for the separate energy use types of the individual houses. Applying one common (e.g. degree-day based) formula on all the houses would neglect both the technical differences between the houses (e.g. thermal time constants) as well as the behavioural differences between households (e.g. heating profiles). Applying, on the real energy use data, a normalisation based on the theoretical EPBD-calculation of each separate house, would also ignore the impact of user behaviour of the individual household and it would assume an approximately correct, relative weight of the different energy demands of the house. However, these are two of the investigation topics of the study.

To tackle these issues, the procedure of normalisation was turned around: the theoretical calculation of each individual energy demand, according to the EPBD-method, was '(a)normalised' to coincide with the period of the real energy figures available. Redoing the full EPBD-calculation for the real climatic conditions was impossible, due to missing calculation input data in the EPBD-database. However, based on the formulas of the EPBD-method and on the main characteristics of the buildings and their services, accurate normalisation of the energy use was possible, using the monthly calculated values available for space heating, sanitary hot water, cooling, auxiliary energy and electricity-production for the PV-panels for each house separately. The limited variations in climatic conditions and time periods between the separate cases, were taken into account in the statistical, multivariate analysis, in order to ensure that these variations would not bias further analysis. However, their impact proved to be negligible, due to the relative homogeneity of the duration and average climatic conditions of the real periods.

3. Buildings & inhabitants

3.1 The buildings

The sample mainly consists of detached houses, with only a very low percentage of terraced houses, as shown in TABLE 1. Due to the very low number of apartments within the dataset, these were left out of the further analysis. With an average gross floor area of 257m² (median: 248m²), these relatively large houses are also not representative of the average size of new built houses in Flanders, though these numbers lie close to those of all detached houses within the EPBD-database (Defruyt et al. 2013).

TABLE 1. Distribution of housing typologies, showing the overrepresentation of detached houses

		Detached	Semi-detached	Terraced	Apartments
EPB-database:	total	26%	20%	8%	45%
EPB-database:	Single family houses	48%	37%	15%	-
Data sample		68%	28%	4%	-

In Flanders, each new building gets an 'E-level' as a label to indicate the primary-energy performance of the house with regard to space heating, sanitary hot water, cooling and auxiliary energy use for services, after deducting the electricity production of PV-panels if present. This level indicates the relative primary-energy use of a building, in comparison to a reference building of the same type dating from 2006. Reaching the same level as the reference building would deliver a level 'E100' (100%), but in the meantime, the requirements have been tightened towards E70. All of the selected

houses fulfil this current requirement, even though their building permits date from between 2006 and 2010. In addition to the total primary-energy use requirements, the insulation level of the houses is also subject to legal requirements. While all selected houses fulfilled the insulation requirements valid at the time of their building permit, only approximately 60% of the houses would fulfil the current, updated insulation requirement. This discrepancy within the sample is explained by the high performance of the building services and the very high presence of PV-panels, compensating the lower insulation levels within the calculation of the primary-energy demand. 83% of the houses have a mechanical, balanced ventilation system with heat recovery, 33% use heat pumps and 46% have PV-panels. While these numbers are not representative at all of current standard built houses, let alone standard practice three years ago, these numbers are representative for houses with similar E-levels, as illustrated by De Baets and Jonckheere 2013.

3.2 The inhabitants and their houses

Almost all of the households (co)owned their respective houses (99%) and were the original builders (99%). They are mainly young households (FIG.1), from the upper middle class (with high level of education, a good job and a good income). While this is to be expected for the average builder of a new house, this is not representative of the total population. These households having built their own houses, we can also assume they had their saying during the building process and were thus at the basis of the choice for an energy-performant house (considering the requirements and standard practice of that time). This assumption of looking at a sample of deliberate low-energy builders is strengthened by the response-rates to the survey: the response rate proved to be significantly larger for the higher performing houses within the sample, as shown in TABLE 2. The income of the households also proved to be significantly, positively correlated with the primary-energy performance of their houses. This could be directly linked to the correlation that was found between the income of the households on the one hand and, on the other hand, the possession of PV-panels or, even stronger, the area of PV-panels installed on the roofs. Looking further at the link between the households and their houses, one could expect to find a correlation between the size of the house and the size of the household. However, this was not found and the lack of correlation can be explained by the young age of the households, building for the future and, possibly, considering future family extension.

These tight links between household characteristics and building characteristics oblige us to be cautious with the further analysis as well as with possible extrapolation of further findings. These cross-correlations complicate the task of disentangling the relationships between the building characteristics, household characteristics and resulting energy use, let alone the goal to assess causality. Furthermore, due to the specificity of this sample, the applicability of findings on this dataset, onto the larger Flemish, Belgian or other population has to be questioned.

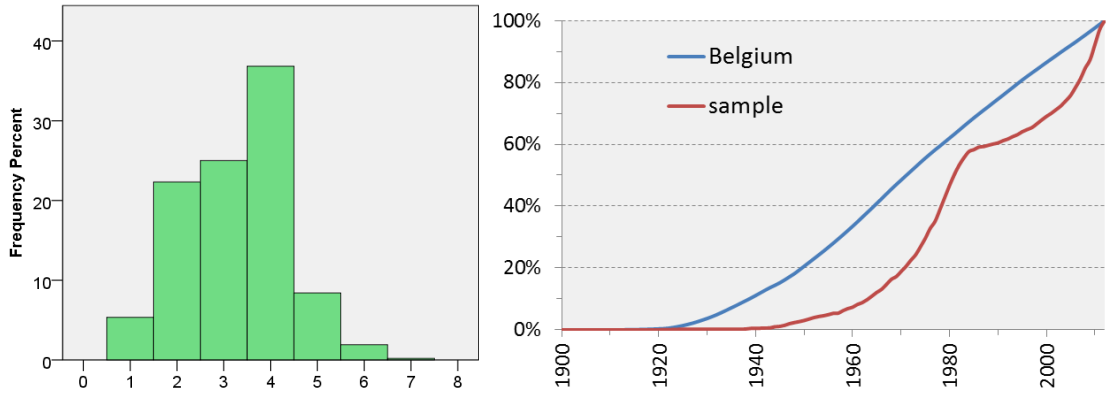

FIG 1. (a) Amount of inhabitants and (b) age distribution (date of birth): mainly young families

TABLE 2. Response rate to the survey, suggesting a sample of motivated low-energy builders

	≤ E40	E40-E50	E50-E60	E60-E70	TOTAL
Contacted	167	241	611	833	1850
Participated	70	86	183	199	537
Response-rate	42%	36%	30%	24%	29%

4. Real energy performance

4.1 Total energy use

Within the EPBD-calculation method, not all of the types of domestic energy demands are included. Foremost missing, are the energy demands for cooking, for lighting and for domestic electrical appliances (from refrigerators onto televisions). Further analysis in this paper will focus on the heating demand for space heating and for domestic hot water. As a reference, FIG. 2(a) compares the total primary energy demand of the households with the heating demand and the electricity demands (not for heating) according to data from the surveys and energy suppliers. The auxiliary electricity demand for building services, included in the EPBD-method, can be considered low in comparison to the other electricity demands. Furthermore, houses with active cooling were removed from the sample. Therefore, the total energy demand from subsample S1 in FIG. 2(a), can be (approximately) considered as the sum of the heating demand from subsample S2 and the electricity demand from subsample S3. Comparing real energy use with predicted energy use, FIG. 2(b) shows that the underestimation of the total, primary energy use is caused mainly by the higher domestic electricity use, as the heating-energy use is overestimated in most of the cases.

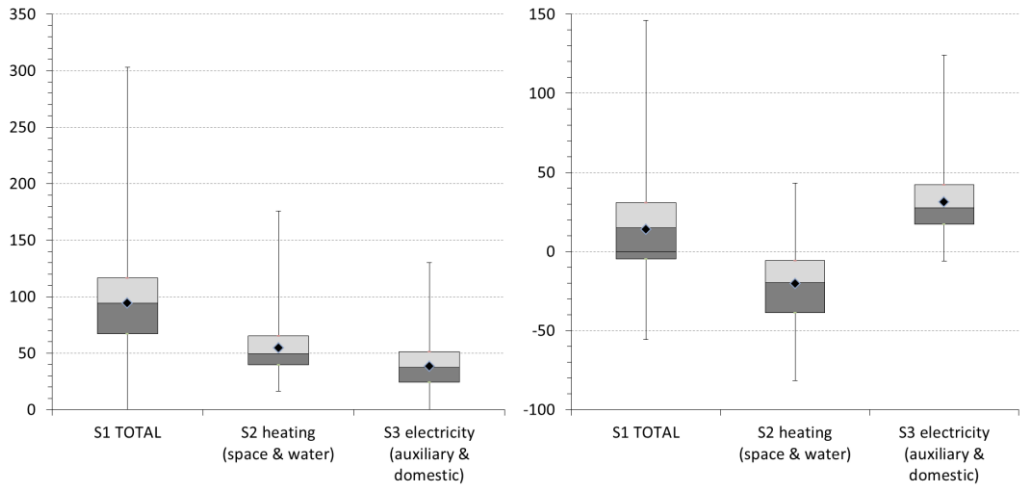

FIG 2. Yearly primary energy use per floor area [kWh/(m².y)]: (a) real values and (b) discrepancy with predictions

4.2 Heating & sanitary hot water

While an undeniable, positive correlation was found between the real and the predicted heating-energy use, there was no close fit between both. On average, heating energy use appeared overestimated by the EPBD-method. Furthermore, this gap between predicted and real values showed large variations, depending on the specific house and household. Four parameters were identified as a significant cause for these variations. Two of them are building related and two are user related.

4.2.1 Air tightness

The air tightness of the houses, or rather the way the air tightness is implemented within the calculation, proved to greatly influence the gap between real and predicted energy use. Within the EPBD-calculation, one can chose to perform the energy calculation with a default value for the air tightness, or with a measured value, based on an air tightness test performed after completion of the building. The overestimation of the heating energy use proved to be the largest for calculations using the default value. This seems to indicate that the real air tightness levels of the houses that were not measured, are better than that default value. This would also be in agreement with the most recent studies on air tightness of Belgian houses (Laverge et al.). However, statistical regression analysis on this or similar datasets cannot prove this, nor can they prove that the heat losses due to air infiltration are correctly modelled in the EPBD-method. The statistical analysis only proves the strong relative influence of choosing to use the default rather than a measured value.

The magnitude of this influence can be explained by the size and typology of the house and the unit used for the default air tightness. The default air tightness is expressed in v50-value, in cubic meter air infiltration rate at 50Pa pressure difference per square meter of envelope area [m³/(h.m²)]. Therefore, any difference with the real air tightness value is magnified within the EPBD-calculation by the large envelope area of the large, detached houses in this sample. The influence of the assumed air tightness rate was such that the calculations had to be corrected towards a more realistic default value, before performing further analyses.

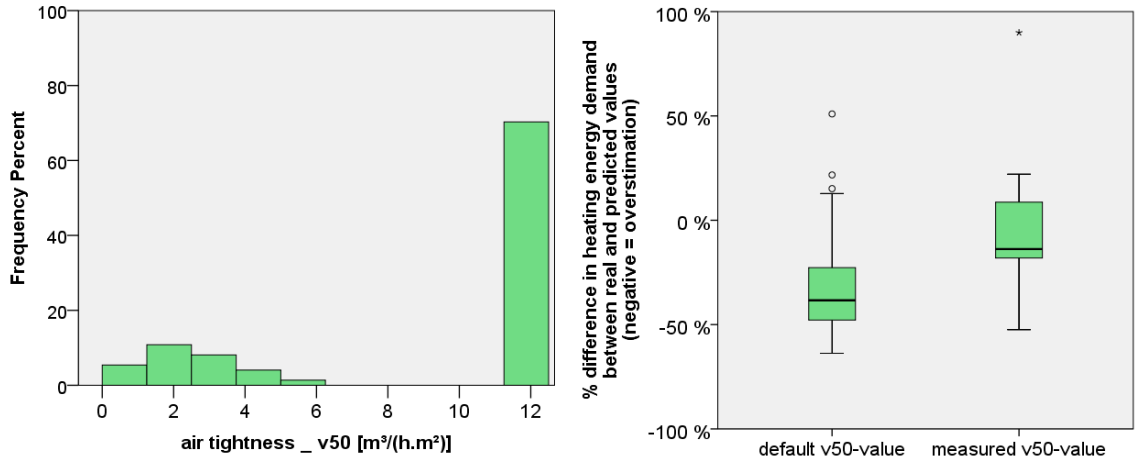

FIG 3. (a) Air tightness rates taken into account in the calculation (v50 in [m³/(h.m²)]) and (b) its effect on the gap between real and predicted heating-energy use

4.2.2 Gas boiler efficiency

The efficiency of the gas boilers, according to the EPBD-files, proved to be significantly, negatively correlated with both the absolute and the relative overestimation of the heating energy demand. The negative correlation with the absolute overestimation can be explained by the fact that a lower heat production efficiency would amplify any overestimation of the net heating demand. However, this would not explain the correlation with the relative overestimation. Three possible explanations were formulated, though none can be proven by statistical analysis on this type of data. (1) The formula used in the EPBD-method to correct the partial load efficiency from the manufacturer's data, based on the real return temperature of the system, might be flawed. (2) When a high performing boiler is chosen, one might be more inclined to use a lower return temperature to take full benefit of the investment and, consequently, to use that lower temperature in the EPBD-calculation, instead of keeping the fixed default value of 70°C. (3) Many houses had a combi-boiler, used both for space heating and for sanitary hot water. Due to the relatively low space heating demand of these houses,

the boilers would have to be sized based on the hot water demand. This could result in a lower, effective efficiency when the boilers are used for space heating only and have a larger, relative effect on the boilers with the highest theoretical efficiency. Further analysis on this problem is needed to identify whether its cause is related to the physical EPBD-model, to the varying scrupulousness of the EPB-assessor, to incorrect or imprecise installation on site or to any combination of these or other possible factors.

4.2.3 Heating profiles

The importance of user behaviour on energy use is generally acknowledged, as discussed e.g. by Guerra Santin (2010). However, the influence of the different heating profiles on the real energy use could not be proved directly from the answers to the surveys. Many different combination of heating profiles occurred within the sample, due to variations in daily heating times and heating set points over the different rooms of each different house, having also its own thermal time constants. Considering the size of the dataset, the amount of parameters for the regression analysis had to be reduced. This was achieved by clustering the daily heating times, set points and time constants of the buildings, using the simplified corrections formulas from EN 7120, resulting in one instead of three parameters per room. This allowed to identify the heating profiles of the master bedrooms as having the most significant effect on the real energy use. The statistical importance of the master bedroom can be explained by the fact this room is present in all houses (e.g. in comparison to a study or play room) and that its heating profiles showed larger variations than e.g. the living rooms, which almost all households heated to a similar set point.

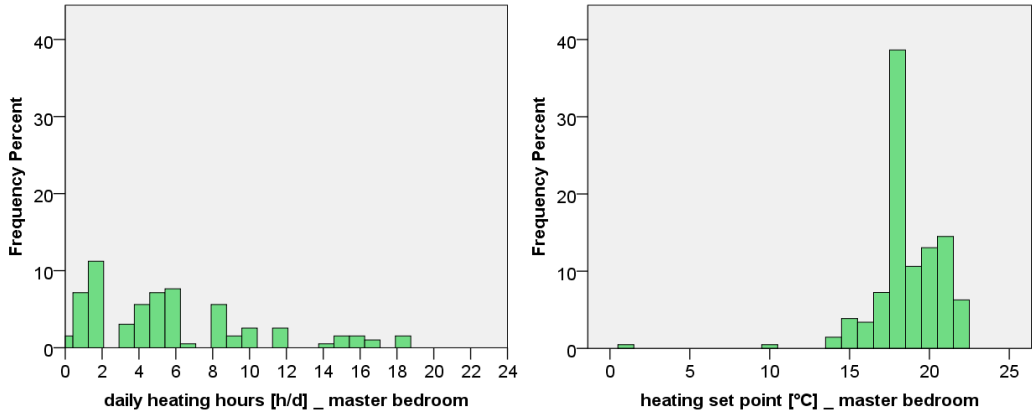

FIG 4. Heating profiles in the master bedrooms: (a) large spread in daily heating times [h] and (b) set points [°C]

4.2.4 Showers & baths

Neither the weekly amount of baths, nor the weekly amount of showers were proven to have a significant effect on the gap between real and predicted heating-energy use. This contra-intuitive finding was explained by the strong, negative correlation that was found between both ways of having a wash. Therefore, similar to the problem of multiple parameters for heating profiles, the parameters for baths and showers were merged. As the average heating-energy use for showers is not equal to that for baths, the weighted sum of weekly baths and showers, per household, was calculated. Based on EN 13203-2, the average energy use was estimated to be 3,6kWh for a bath and 1,4kWh for a shower. Using this aggregated parameter, the weekly amount of baths and showers taken by each household revealed itself as the second most influencing user behavioural factor explaining the divergent gaps between real and predicted heating-energy use.

5. Conclusions & discussion

This study aimed both at investigating the gap between real and predicted energy use in low-energy houses as well as at identifying the most significant parameters influencing this gap. This study proves the influence of both technical as well as user behavioural parameters on the gap between real and predicted energy use. The implementation (default values and formulas) of air tightness and combustion efficiency within the calculation method proved to be significantly correlated with the size of the gap. These issues could partly be tackled by choosing more realistic default values, improving the predictions' accuracy. However, this would oppose itself to the role of conservative default values, namely to admonish building teams to perform better and to prove it, by rewarding these efforts through better energy labels based on measured values. The realistic estimation of user behaviour is an even more complex task within energy performance regulations. The contradiction there lies between choosing a default user behaviour to enable comparison of energy labels on the one hand and delivering accurate predictions on energy use to the future, specific inhabitants and investors on the other hand. Therefore, one might question if it is realistic or even recommendable to aim both at labelling and at an accurate, case-specific prediction based on one single, simplified calculation.

The presented study pointed out some significant parameters. However, the limited representativeness of the sample, as well as the strong, direct correlations between building parameters and household parameters hinder further extrapolation towards building stock levels. These findings question the possibility of accurately predicting the effect of future, tightened building requirements, using data collected from past forerunners. Larger datasets would be needed for further thorough statistical analysis, due to the complexity of the problem, the large amount of influencing variables and the important possible amount of unknowns and contradictions within different datasets. However, collecting such size of datasets appears be in contradiction to the target of such study: the few forerunners.

6. Acknowledgements

The authors want to thank all inhabitants who participated to the data-collection.

References

De Baets K. & Jonckheere T. 2013. Cijferrapport energieprestatieregelgeving, Procedures, resultaten en energetische karakteristieken van het Vlaamse gebouwenbestand – periode 2006-2012. (in Dutch) 51p.

Defruyt T., Delghust M., Laverge J., Janssens A. & Roelens W. 2013. 'Evolution of Energy Performance of Houses and the Interaction with Energy Performance Regulation: An Analysis of the Flemish EPBD-Database'. In Proceedings of CLIMA 2013. Prague, Czech Republic.

Guerra Santin O., 2010. Actual energy consumption in dwellings. The effect of energy performance regulations and occupant behavior.(Ph.D. thesis), IOS Press BV, Amsterdam (The Netherlands)

ISO 13790. 2007. Energy performance of buildings – Calculation of energy use for space heating and cooling.

Laverge J. et al. 2010. Airtightness assessment of newly built single family houses in Belgium, Building and Ductwork Air-tightness, 5th International symposium, Proceedings (Buildair 2010).

NBN EN 13203-2, Gas-fired domestic appliances producing hot water - Appliances not exceeding 70 kW heat input and 300 l water storage capacity - Part 2: Assessment of energy consumption

NEN 7120+C Energieprestatie van Gebouwen - Bepalingsmethode (in Dutch). Delft, The Netherlands: NEN, October 2012.

Optimized energy concept for an office building with waste heat from IT cooling using building energy simulation

Dirk Weiß[1] and Hans Petzold[1]

[1] Dresden University of Technology, Institute for Building Climatology, Germany

KEYWORDS: *building energy simulation, EnergyPlus, waste heat, radiation heating*

SUMMARY: (Style: Summary Heading)
For the prognosis of the energy demand and the summer comfort as well as for the energy optimisation of a new office building in Potsdam, Germany, a building energy simulation was carried out with EnergyPlus. Summer conditions must be considered carefully in regard of on the occupancy and the inner thermal loads. The paper describes the tool chain used to model the complex geometry and the HVAC components as well as some inherent problems of the simulation software.

1. Introduction

The Potsdam Institute for Climate Impact Research (PIK) was founded in 1992 and currently has a staff of about 300 people. The historic buildings of the institute and its high-performance computer are located on Potsdam's Telegraphenberg campus, along with a number of other major research institutions. The most famous building at this location is the Einstein Tower (Einsteinturm).

Until 2015 a new building for ca. 200 employees will be erected, containing mostly office space and a computation centre in the basement. The design of the new building has the intention of being unobtrusive in respect of the historical buildings on the campus and being mindful of the green surroundings.

The waste heat from the cooling of the computation centre significantly exceeds the heat demand. The German Federal Ministry of Economics and Technology is funding a research project for exploring the options of using this waste energy for heating this building as well as other ones nearby, at the same time reducing the energy necessary for cooling. New technologies like vacuum glazing in parts of the facade, hot water cooling in the data centre and LED lighting will be applied. A main part of this project is the energy optimization of the new building with the help of simulations.

For the building energy simulations the software EnergyPlus is used. The aim is mainly to predict the energy demand, the room temperatures for a later comparison to measurements, and the optimization of the comfort in the offices and meeting rooms. The paper also describes some problems and weaknesses encountered during the simulations.

2. Building Description

The building is designed similar to a cloverleaf The outer areas contain the offices and meeting rooms. Inside are the sanitary, copy, and tea rooms and the staircases (Fig. 1). The public areas which also contain small areas for informal meetings are in between. In the centre an atrium stretches from the ground floor to the roof. The basement contains the computation centre, a conference room for 200 people and storage areas.

The heat source will be the waste heat from the computation centre. If necessary, the temperature level will be raised by a heat pump. The rooms are then heated by a panel heating system in the ceiling which can work with relatively low temperatures. It is planned to use "hot water cooling" for a part of

the racks - water cooling directly at the processors with a temperature of approx. 50°C which increases efficiency and provides waste heat with a higher exergy.

A ventilation system with heat recovery provides supply air. Heating and ventilation are operated via a building automation system, including individual room thermostats, presence detectors and window contacts for turning off ventilation and heating when the user opens a window.

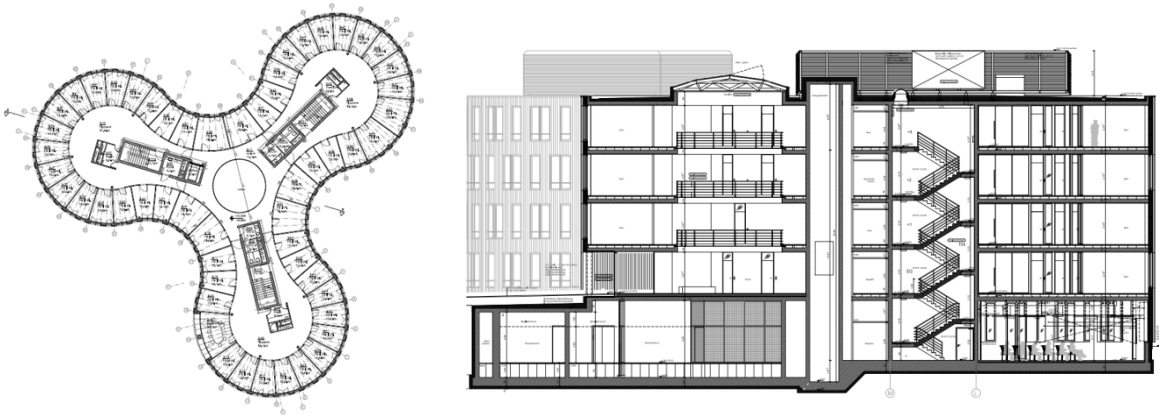

Fig 1.Groundplan shape and vertical cut of the building (2nd floor). Offices and meeting rooms are located at the facade, the atrium lies in the centre. The three cylinders contain staircases, sanitary, copy and tea rooms.

Supply air is provided from the cavity floor near the outside wall. The inner walls between office space and corridor contain an integrated overflow opening. Exhaust air openings are in the corridor and sanitary rooms central in the building. The office rooms (i.e. ground and upper floors) contain no active cooling systems. The lighting is daylight dependent.

3. Simulation Model and Input Parameters

Since the cardinal direction of each room in a floor is different, a simulation should provide individual room temperatures to ensure summer comfort. Additionally many of the rooms will be monitored. Therefore the simulation model was set up with more than 280 zones, which is a challenge for the simulation tool. For the same reason the individual control of room temperature, ventilation, lighting and shading are taken into account. To create the model and reproduce the complex building geometry as close to reality as possible, the software DesignBuilder was used.

DesignBuilder is a graphical user interface for the simulation program EnergyPlus, which enables the user to enter three-dimensional data for geometry, materials and constructions and schedules for all kinds of time dependent values. The user profiles (room use, lighting, shading, inner heat sources etc.) were created in agreement with the building owner to represent a realistic simulation environment.

Fig 2.Three-dimensional representation of the building model at building, floor, and room level. The screenshots are taken from the Designbuilder GUI.

It then creates an input file (IDF) for the simulation kernel EnergyPlus which can be edited if necessary. The HVAC system was implemented directly in the EnergyPlus IDF description including code written using the included programming language EMS. The postprocessing of the simulation results is mainly done with the help of self developed code in C++ generating key figures from the numerous outputs.

3.1 Schedules and user profiles

The simulation requires schedules for the energetically relevant values in each zone. The input can be very detailed, which on one hand enables an exact representation of the building in use. On the other hand, most of the values are unknown in the planning stage, and even in the practical case it will be impossible to measure them.

This concerns mainly the objects

- people - for inner thermal loads due to user presence,
- lights - for lighting,
- electric equipment,
- infiltration,
- and shading.

Since these schedules are interconnected in practice, emphasis was put on a logical set of values (this topic is connected to the EU research project ISES, http://ises.eu-project.info/). The flexible work time, with people coming in the morning and leaving in the evening, as well as lunch break can be taken into account. The default for the daily sums of the values was taken from the German code DIN V 18599 and adjusted with information from the building user. A sample representation of the user presence is given in Fig. 3 for some zone types.

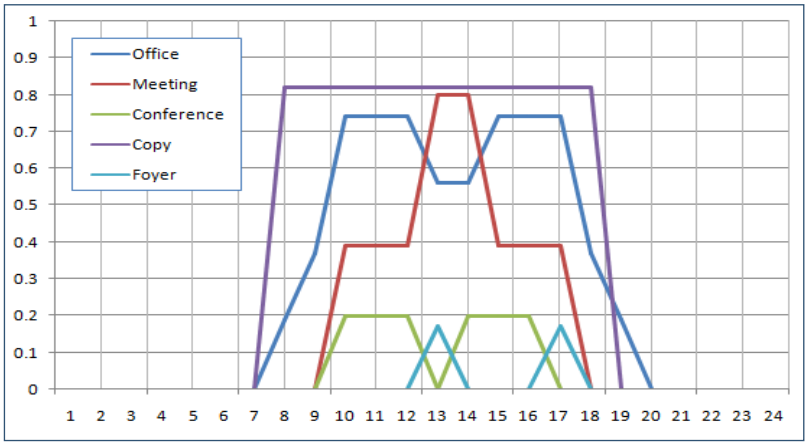

Fig 3. Occupancy schedules of several room categories. The daily sums for the zones correspond to the German code DIN V? 18599.

The artificial light calculation represents the daylight dependance of the building automation system.

3.2 Modeling of the HVAC systems

3.2.1 Heating

The following modules in EnergyPlus were tested to model heating:

- Ideal Loads Air System (ILAS)

- Baseboard heater
- Low Temperature Radiant System (LTRS) with variable flow

As the name implies, the ILAS is an idealized system where all heating/cooling is provided by the supply air and no other HVAC components are regarded. This is useful for approximations or for the case of an unknown HVAC configuration. This model has been thoroughly tested and validated.

The baseboard heater model contains parameters for a radiative part of the supplied heat. However, the simulation with radiation shows errors of partly neglecting the radiation part in the energy balance. Hence only a simulation with completely convective heat transfer delivers useful results.

The low temperature radiant system is provided as a module by EnergyPlus. In the current case the system works with a water loop. The water is heated to the required temperature by a heat source representing the waste energy.

Internally the simulation kernel calculates the thermal energy necessary for each zone for each timestep. For the low temperature panel heating this calculations are not working satisfyingly.

The reason for this can be seen in the EnergyPlus iteration strategy. First, the solver performs the wall calculations. These are carried out primarily without the heat source of the panel heating, independent of the zone balance. After finishing this calculation the zone balance is started, resulting in heat fluxes. Since the wall calculation is at this time already finished, the solver for the wall temperatures is not started again (Fig. 4).

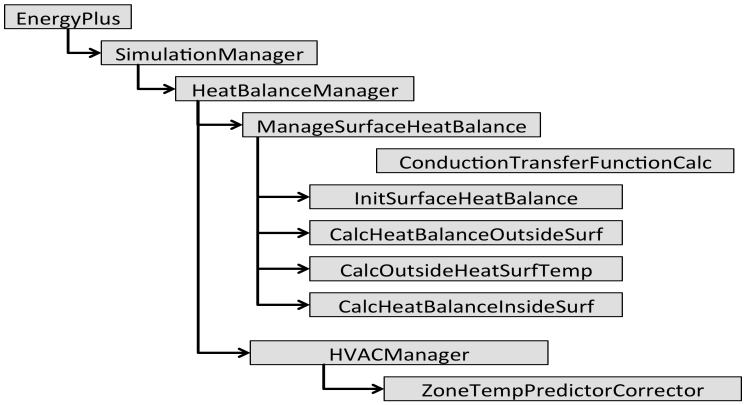

Fig 4. Iteration order in the EnergyPlus solver.

This leads to errors described below in more detail. It seems that the LTRS module was implemented without sufficient testing of its results.

3.2.2 Ventilation and air mixing

All zones with boundary to the outside air receive an infiltration corresponding to wind speed and temperature difference taken from the climate file. A ventilation rate per area and per person is provided by the ventilation system. The HVAC system contains a heat recovery system with an efficiency of approximately 60%.

The ventilation and the heat recovery unit is modeled with the "SingleDuct:Uncontrolled" module, regulated by code written in the internal EMS language. This enables a better control of the system for the individual zones including the detailed schedules.

The integrated overflow openings are modeled with an air mixing module of EnergyPlus. This module only considers the energy fluxes, which is sufficient for the current case of a pure energetic simulation. Moisture or contaminant fluxes are not regarded.

4. Problems during HVAC modeling with EnergyPlus

Several problems have been encountered in the application of heating and ventilation models of EnergyPlus. Though most modules of EnergyPlus work as expected when used alone, combinations can lead to unexpected and undocumented behavior. Therefore the following systems were tested to find a way to integrate the actual HVAC into a working EnergyPlus simulation model:

1. *Panel heating with ventilation system - regulation of the ventilation with "Controller:MechanicalVentilation" element*: Though the controller was implemented in the controller list, the connection with the system was not functional.

2. *Panel heating with ventilation - regulation of the ventilation with EMS code and "SingleDuct:Uncontrolled" element*: The ventilation system could be modeled in line with the demand. The air volume fluxes are then calculated from air change related to area and persons. A cooling by extended ventilation (if the inside temperature exceeds the comfort limits and outside temperature is lower, and extended night ventilation) could be realized.

The panel heating was not working physically correct. An example is given in Fig.5.

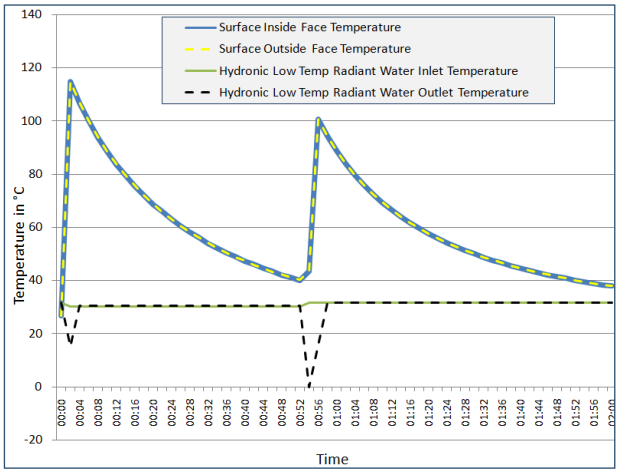

Fig 5. Physically incorrect results for a low temperature radiant element. When energy transfer from the surface to the room is required, the temperature in the water outlet decreases far below room temperature, and the temperature of the room surfaces take values of 100°C and more

It seems that these kinds of radiation heating are inherently not truly functional due to the reasons described above. Therefore the heating representation had to be changed to a simpler system with convection heat transfer only.

3. *Ideal system with ventilation - regulation of ventilation with EMS code and "SingleDuct:Uncontrolled" element*: The panel heating was simplified by an "IdealLoadsAirSystem". Both system parts are working correctly if applied individually. In combination, however, the volume fluxes show errors.

4. *Baseboard heating with ventilation system - ventilation energy balance is modeled by EMS code via "OtherEquipment" elements*: Because of the shortcomings described above the heating was described by a relatively simple water heating with baseboards as heat transfer elements. The ventilation was completely programmed in EMS code, including the heat recovery unit. With this approach it was possible to reproduce both the heating and the air volume flow combined in a consistent way.

Additionally, the following other errors were encountered:

The control of some desired values is not always described correctly. Thus, target values for feed and return flow can only be used with reservations. In this case the documentation states: "... the

component models and system solvers may or may not be able to use them." Therefore it is highly recommended to test implemented components before relying on the results.

Some serious problems occurred within the EMS programming language when comparing negative numbers. In if-statements or allocations the expressions "if (a == -1)" or "Set var1 = -var2" are not evaluated correctly. This leads to errors which are hard to find, especially since debugging is somewhat tedious within EMS.

5. Tool chain

As mentioned above, the software DesignBuilder was used for the input of the geometry. Despite the complex geometry, the graphical input in a 3D-CAD-like environment could be done relatively quickly.

For energy simulations, the software then writes an input file for EnergyPlus (a text file, so called input data file or IDF), calls the EnergyPlus solver internally and displays a limited set of results. Due to inefficient automatic writing of the IDF with lots of redundancies, the solver could not handle the input file for this large simulation model. Due to this fact and to provide for the detailed input of HVAC components the IDF had to be handled manually. Unfortunately the many redundancies and automatically generated quasi-random names make the file very impractical to use.

For this purpose a software tool was written which removes redundancies in construction definitions and schedules, creates zone lists, renames constructions and zones to human readable names while keeping all logical connections between all objects. In the case of the simulated buildings for instance the number of objects for the internal heat production related to people was reduced from over 250 to 10, more than 1000 schedules for time dependant input values were reduced to less than 40, and the output variable definitions from nearly 10000 to 50 output variables and variable groups, respectively.

The HVAC system as described above was partly added with usual IDF descriptions and in case of the ventilation system programmed in the EMS language.

6. Parametric study

To estimate energy demand and comfort for different scenarios, a number of variations have been analyzed with the simulation. The varied parameters are occupancy density, heat loads by electric devices, setpoint and setback temperature, and the ventilation control.

According to the code DIN V 18599, 12 m² are assigned to one office worker. The value of 10 m² is somewhat more realistic for the current building due to the size of the single offices. Since the number of employees might increase in the future, a case for increased occupancy was included with 6 m² per person, which represents roughly two employees in one office.

The values for electric devices, mainly be produced by computers and monitors, originates from own measurements. The used numbers represent cases of normal and high energy use of the devices. These two variations represent the inner thermal loads which in combinations result in a factor four between the lowest and highest inner loads.

The setpoint/setback temperatures of 21°C/17°C are taken from the DIN V 18599-10. A possible saving option is assessed by using 20°C/16°C.

The ventilation control is mainly planned for supplying fresh air for the offices. An additional amount of outside air for night cooling could increase the comfort level during warm periods, but will at the same time need energy for ventilation.

The energy gains and losses are shown in Fig. 6. Since the thermal standard of the building is high, the losses over the facade are comparatively small. The inner loads due to the internal sources are in the same order of magnitude as the heating energy provided by the HVAC system. The total energy

consumption should therefore consider both. In the current case, the pure heating energy consumption lies between 6 and 10 kWh/m²a, and the total consumption between approximately 20 and 40 kWh/m²a.

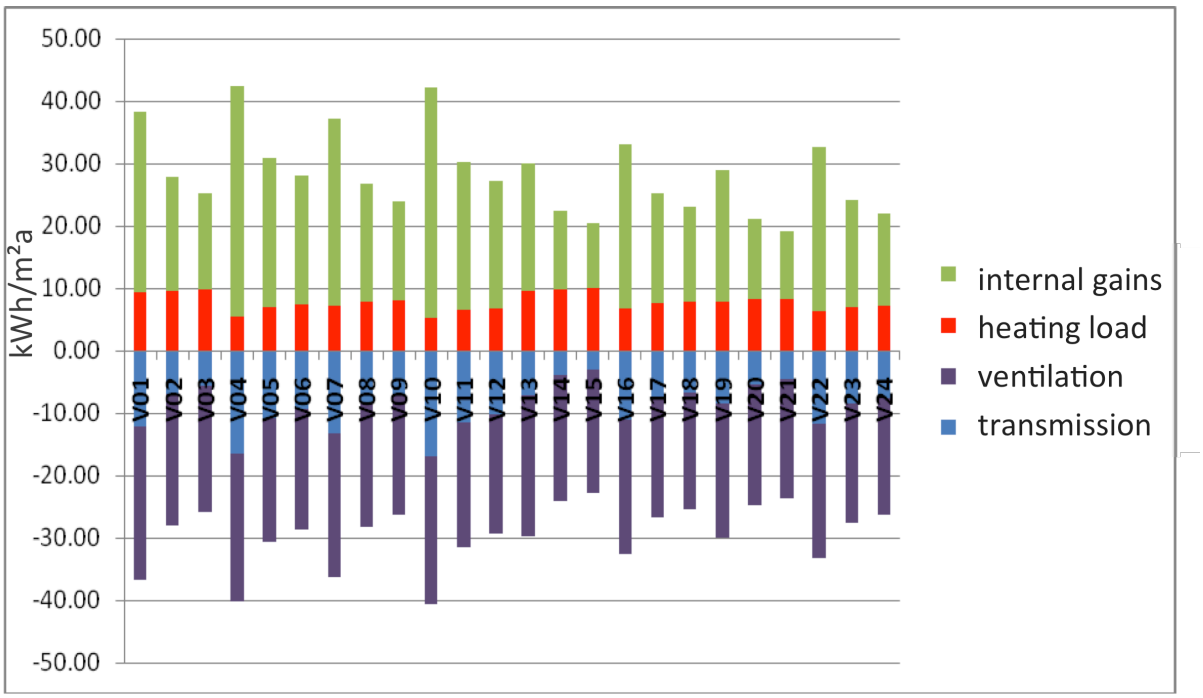

Fig 6. Energy consumption for the parametric cases.

In well insulated buildings the winter comfort is usually not a problem, since all room surfaces temperatures are close to the room air temperature. The summer case can be much more critical, especially for office buildings with a higher occupancy density. Therefore the summer comfort was evaluated for all the above variations in terms of Kelvin-hours ((Θroom - 26°C) · n with n: number of hours) over the limit of the EN 15251 category II under realistic conditions.

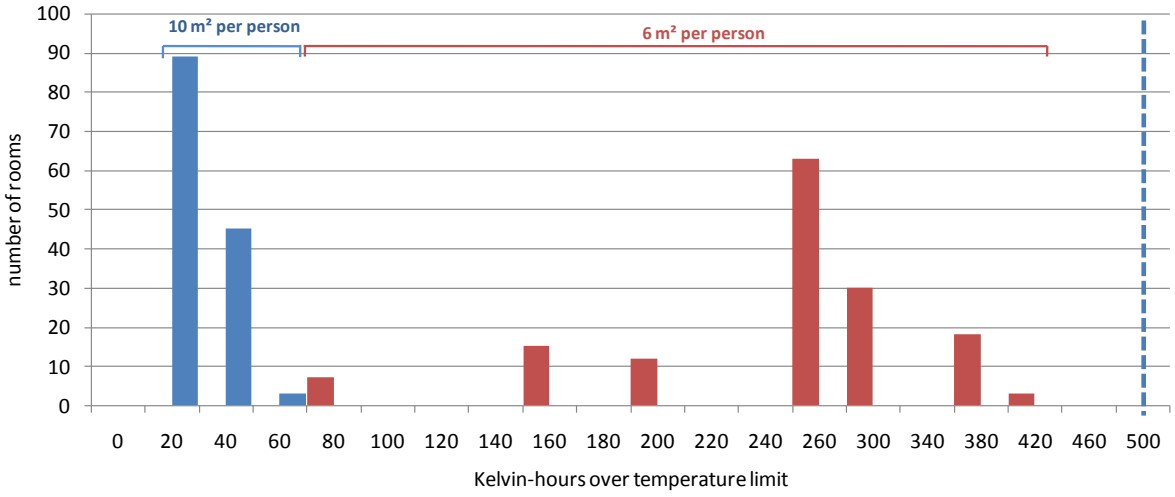

Fig. 7. Frequency distribution of the Kelvin-hours over the temperature limit of EN 15251 for all 137 office rooms with normal occupancy (10 m² per person, in blue) and high occupancy (6 m² per person, in red) and appropriate inner thermal and electric loads.

The German code DIN 4108 accepts a limit of 500 Kh over 26°C (under slightly different conditions). In the case of high occupancy density this limit is not reached but a number of rooms come near that value.

These parameter variations are only a limited approach. Naturally, there are many other values that will deviate in the practical case and should therefore be considered as variation parameters. This applies particularly for the user related values and will be part of further research.

7. Conclusions

For the satisfying modelling of the relatively complex building geometry a tool chain of different tools was used in the preprocessing to create the input for the EnergyPlus simulation kernel. The low temperature radiant elements of the heating system could not be modelled with the internal structure of the simulation solver. However, these elements become more and more important if energy from renewable sources is used in the building sector with a low temperature range. Despite these limitations, EnergyPlus remains a powerful and flexible simulation tool. A simulation software which will be able to describe such systems in detail and include them in thermal building simulation is currently in development under the EnTool research initiative (Tools and Data for Energy-optimized Buildings, Neighborhoods and Cities), see Nicolai (2012).

Two variations in input parameters reflect an influence in user behaviour (occupancy and inner loads mostly due to computational devices), while two others reflect some range of the HVAC control. As can be expected, the user influence in a building with good thermal quality is significant and exceeds most other input parameters. Summer comfort without active cooling can be achieved for most cases but will not be completely satisfying in all rooms if high inner loads are present.

8. Acknowledgements

The research project is funded by the German Ministry of Economics and Technology.

References

EnTool Symposium 2013. Conference proceedings, ISBN 978-3-86780-350-2

EnergyPlus Input Output Reference. EnergyPlus version 8.1.0, 2013

Nicolai, A. & Paepcke, A., 2012. Die Gebäudesimulationsplattform NANDRAD – physikalisches Modell, Umsetzungskonzept und Technologien im Überblick (The building simulation platform NANDRAD - physical model, realisation concept ant technologies). Conference proceedings BauSIM 2012 Berlin

DIN 4108-2:2013 Thermal protection and energy economy in buildings (Part 2), 8.4.

Zhen Tian & James A. Love, August 2006, Radiant slab cooling: a case study of building energy performance

The performance of subsoil frost protection system of mechanical heat recovery ventilation unit in a cold climate in the context of net zero energy building

Jaanus Hallik, M.Sc. [1]
Kristo Kalbe, M.Sc. [1]
Tõnu Mauring, Ph.D. [1]

[1] Energy Efficient Building Core Laboratory, University of Tartu, Estonia

KEYWORDS: *net zero energy building, frost-protection, ground-source brine heat exchanger.*

SUMMARY:
Mechanical heat recovery ventilation (MHRV) units with very high heat recovery efficiency are mandatory for achieving good indoor climate without excessive heat loss in cold climates. Higher heat recovery efficiencies, however, mean that more preheating energy is needed to avoid the frost formation in the heat exchanger. Typical methods for frost protection (electrical preheating coil or disbalancing the airflows) are not favourable solutions in cold climates with excessive period of low outside air temperatures. Several alternative systems with subsoil heat exchangers are possible for lowering the energy need for frost protection of net zero energy buildings (nZEB).

A subsoil-brine frost protection system in first certified passive house in Estonia and its performance during the first heating period has been further analysed in this paper. The measured performance data was compared to the modelled values in order to enable the subsequent retrospective analysis, but existing specific calculation routines could not be fully validated within this study. The variability of net energy demand for preheating was simulated using retrospective real climate dataset for time period between 1970 and 2000. The calculations show that the energy demand for the frost protection of MHRV can play significant role in overall energy use of the nZEB and the subsoil-brine heat exchanger is a viable solution for frost protection with additional cooling effect during the summer period.

1. Introduction

In the context of European directive on the Energy Performance of Buildings (EBPD) [2002/91/EC, 2002; 2010/31/EU, 2010] the energy demand of the buildings in the next decade is drastically reduced compared to previous practices. The transmission losses are significantly reduced by thick insulation layers, thermally optimized glazing and more compact architecture, which enable the reduction of cooling surfaces and thermal bridging. The infiltration and ventilation losses are minimized by careful realization of different air-tightness techniques and utilization of balanced mechanical heat recovery ventilation (MHRV) units with very high heat recovery efficiencies.

As the overall energy demand of the building decrease the auxiliary energy demand for powering the technical systems (ventilators, pumps, electronic controllers etc.) increases. In the case of ventilation units, higher heat recovery efficiencies, however, mean that additionally to ventilators and electronic controllers more preheating energy is needed to avoid the frost formation in the heat exchanger. This phenomenon is furthermore magnified in colder climates [Kragh *et al.* 2007] where excessive periods of colder temperatures endure. Although simple electric frost protection coils are widely used all over Europe, alternative systems exist such as ground-source air heat exchanger (GSHE), ground-source brine heat exchanger (GSBHE), hygroscopic heat exchanger (rotor systems, and improved plate heat exchanger systems), disbalancing the airflows, etc.

Although the disbalancing of the airflows or stopping the ventilation unit for defrosting is not useable for extended cold periods [Kragh *et al.* 2007] the use of other described alternative systems have to be considered as direct electricity use for frost protection in typical ventilation units can play a significant role in primary energy demand of the net zero and nearly zero energy buildings (nZEBs).

This paper concentrates on GSBHE systems comparing the simulation results with measured data from first Estonian net zero energy building, described in [Mauring *et al.* 2013]. Additionally theoretical net energy demand for frost protection in cold Estonian climate is calculated based on historical weather data for range of effecting parameters (ventilation air flow, frost-protection set point temperature) and is analysed in the context of overall energy demand of nZEBs.

2. Material and methods

2.1 Description of studied climate dataset

As a typical country bordering the Baltic Sea, Estonia is divided to two climatic zones – e.g. coastal area and inland area where conditions differ due to influence of nearby sea. The more detailed spatial division and climatic differences are given in [Kalamees and Vinha 2004]. The studied building is located in the town of Põlva at the South-East part of Estonia where more continental climatic conditions occur along with lower temperatures, deeper and longer lasting snow cover compared to coastal areas [Raik 1967 *cited in* Kalamees and Vinha 2004]. Based on national Test Reference Year for energy calculations the long- term average dry bulb temperature for inland part of Estonia in December is -2,5°C, in January -3,0°C and in February -5,2°C [Kalamees and Kurnitski 2006], however long-term average daily minimum values for each month from November to March are below -10,0 °C reaching -14,3 °C for January [Kalamees 2006].

In more extreme years the air temperature falls below -30 °C occasionally, staying frequently below -15 °C for several days [Estonian Meteorological and Hydrological Institute 2002] based on measurements in Tõravere station. For detailed analysis of variability of frost protection energy demand this measured sub-daily weather dataset for time period from 1970 to 2000 was used. The hourly data from measured data with sub-daily (3 hour) time steps was generated using linear interpolation between measured time steps.

Outdoor dry bulb temperature was used from the weather dataset to calculate the net energy demand of the frost protection system.

2.2 Description of studied building and ventilation system

The studied building has three stories, total net floor area of 305 m^2, external envelope surface area of 864 m^2 and enclosed volume of 1586 m^3. The building was planned and realized according to international passive house concept to achieve the average yearly net heating demand of 15 kWh/(m^2*year) [Passivhaus Institute 2012]. To further lower the energy demand, the studied building was equipped with split solar thermal system combined with ground source heat pump with vertical boreholes. Additionally an 90 m^2 photovoltaic solar (PV) system was built to cover the total final energy demand of the building making it net zero energy building. The more detailed description is given in [Mauring *et al.* 2013]. In table 1, estimated final energy demand (electricity) of the building is given.

The building has balanced mechanical ventilation system with PHI certified passive house ventilation unit (Paul Novus 300 with exhaust side heat recovery efficiency 93% according to PHI certification system) [Passivhaus Institute 2009]. Fresh air with no additional heating is supplied to living room and bedrooms and then exhausted from kitchen, bathrooms, etc. The airflows have been reduced to limit the risk of overly dry air during the winter season. The average airflow rate measured during the startup of the ventilation system is 280 m^3/h, which corresponds to average air change rate of 0,4 h^{-1}. On-site measurements showed that CO_2 levels are low enough to further lower the airflows if needed.

Table 1. Estimated final energy (electricity) consumption and production of the studied building.

Category	Electricity use / production, kWh/a
Estimated electricity production by solar PV (photovoltaic) system	10120
Total electricity demand of the building	10356
..including electricity demand of GSHP (vertical ground source heat pump	2149
..including estimated electricity demand of technical installations (ventilators, pumps etc.)	2000
..including estimated electricity demand of domestic appliances, lighting, sauna equipment etc.	6207

The frost protection of the ventilation unit is solely by sub-soil brine heat exchanger. The system features 226 m (with 40 mm diameter) of plastic pipe buried horizontally in the depth of approx. 1,0 to 1,2 m and connected to Paul Sole Defroster unit SD-550, which controls the fluid flow speed of the system according to air-temperature before the ventilation unit.

2.3 Measurements

After completion in December 2012 the studied building has been equipped with extensive monitoring system to gather information about indoor climate and performance of building system as well as exterior wall as a part of on-going joint research project between two universities in Estonia. In the context of this study the ventilation system is equipped with temperature and relative humidity sensors (∅5mm×51mm, measurement range: -40°…+100°C and 0…100%, accuracy: ±0.3°C and ±2%) to measure supply, extract, exhaust air parameters and additionally air parameters before and after frost protection system prior the ventilation unit.

2.4 Simulation procedure of GSBHE system

The net energy demand for regular frost protection and its variability over long term time period was calculated using statistical programming package R. A simplified hourly power estimations were calculated based air heat capacity using equation 1. Hourly power estimations were integrated for annual net heat demand values.

$$P = \dot{V} * c * \rho * (T_e - T_{sp}), \quad [1]$$

Where P – average hourly net power demand for preheating external air (W);

$\dot{V}$ – volumetric air flow (m^3/h)

c – heat capacity of air (1,006 kJ/kgK);

ρ – air density (1,225 kg/m^3);

T_e – dry bulb temperature of external air (K);

T_{sp} – setpoint temperature for frost protection (K).

The simulation of GSBHE system was carried out with calculation software *PHErde* (provided by Passivhaus Institute). The system configuration along with soil characteristics were input according to on-site conditions and details. For comparison of measured and simulated values a synthetic weather dataset was created from on-site measured average hourly values (for study period) and national Test Reference Year (hours outside study period). The dynamic simulation was carried out to acquire the temperature values after the GSBHE system. The length of the study period was determined according to external air temperatures when preheating would be required.

3. Results

3.1 Calculated net energy demand variability for frost protection

Average calculated long-term net energy demand for frost protection corresponding to airflow and frost protection set point described in the studied building is approx. 900 kWh annually. The net energy demand shows the energy physically needed for preheating the external air if no GSBHE is used or if direct electric preheating is used. In the case of properly dimensioned GSBHE this energy demand is omitted. The variability of net energy demand for frost protection is given in the Figure 1. It can be seen that depending on yearly differences the net heat demand varies in the range between 240 kWh and 1946 kWh annually.

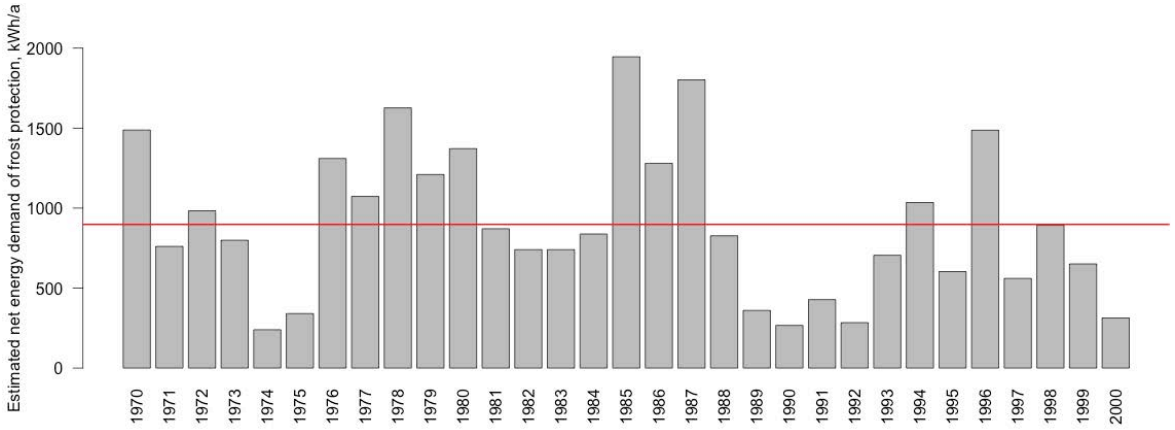

FIG 1. Calculated annual net energy demand for frost protection for historical period of 1970 – 2000 (volumetric air flow 280 m3/h, pre-heating set point temperature -3 °C). Long term average 897,9 kWh annually (marked with red line).

As estimated long-term average total energy demand of the building (heating, DHW, domestic and auxiliary electricity) is 10356 kWh, a direct electric preheating of external air can play considerable role in total energy and primary energy demand. For studied building the direct electric frost protection could account for 8,7% of total electricity use for average year. For colder years this percentage will be even higher because the room heating energy is produced with high efficient heat pump system. When omitting the consumption related electricity use (domestic appliances, lighting etc) the potential energy use of electric frost protection will be approx. 21,7% of the energy demand for heating, DHW and auxiliary electricity.

This signifies the use of alternative frost protection systems in low-energy and nearly zero energy buildings. Although the used GSBHE system in studied building avoids this surplus energy consumption it has to be acknowledged that this system has limited power output and in the case of higher frost protection demand (through higher volume flow rates or higher set point temperatures) the selection and dimensioning of the frost protection system has to be done carefully.

The effect of higher volume flow rate and set point temperature are given in figures 2 and 3. The estimated net frost protection energy demand for higher volume flow rates (0,6 h-1 and 0,8 h-1 accordingly) are given in figure 2. Compared to baseline situation the energy demand increases significantly.

The estimated net frost protection energy demand for lower and higher set point temperatures (-3 as baseline scenario and -6 °C, 0 °C and +3 °C accordingly) are given in figure 3.

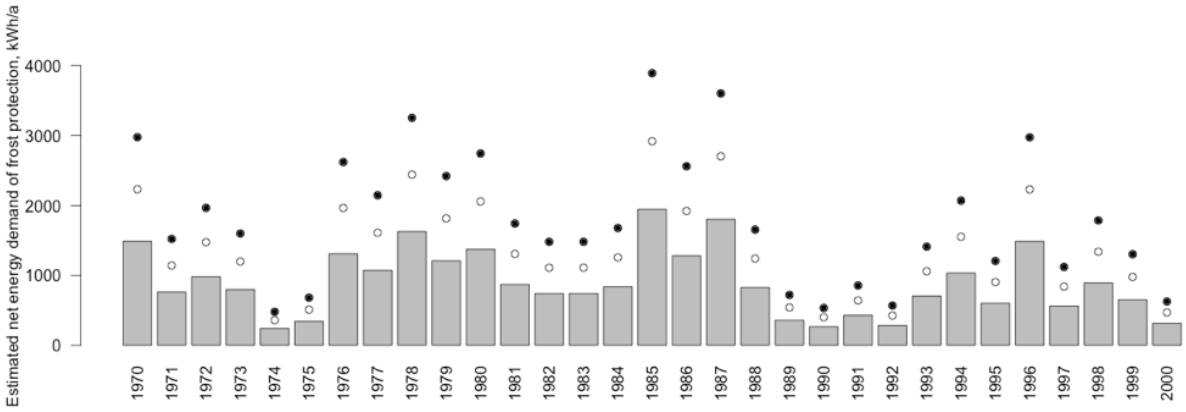

FIG 2. Calculated annual net energy demand for frost protection for historical period of 1970 – 2000 in the case of different volume flow rates (280 m3/h as baseline scenario with grey bars and 420 m3/h with empty and 560 m3/h with filled circles, pre-heating set point temperature -3 °C for all flow rates).

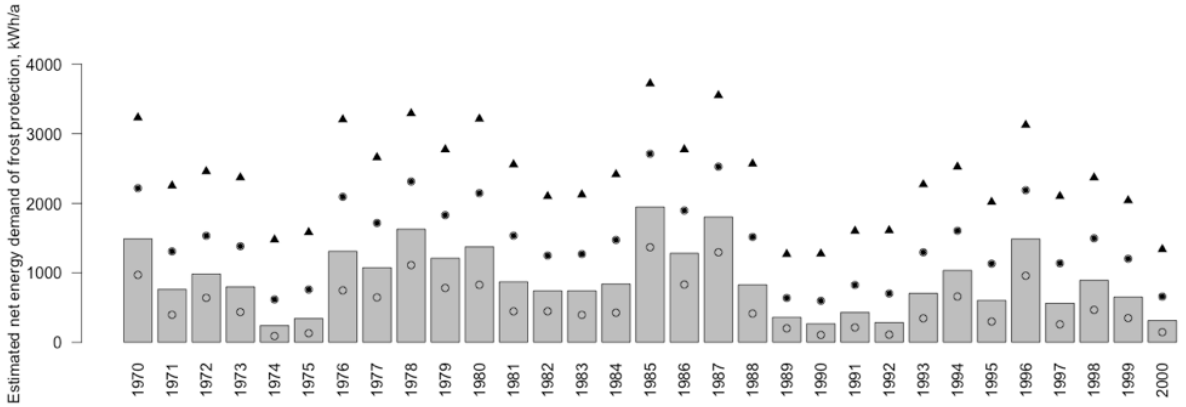

FIG 3. Calculated annual net energy demand for frost protection for historical period of 1970 – 2000 in the case of different set point temperatures for frost protection (- 3 C as baseline scenario with grey bars and -6 °C with empty circles, 0 °C with filled circles and +3 °C with filled triangles, volumetric flow rate 280 m3/h for scenarios).

Compared to the baseline situation the set point temperature of the frost protection greatly affects the energy consumption of the system. The use of lower set point temperatures, which is possible with hygroscopic heat exchangers, has great potential in context of minimizing the frost protection energy demand when direct electricity has to be used for preheating the outdoor air.

3.2 Measured and simulated performance of GSBHE system

The monitoring of dry bulb air temperature before and after GSBHE system started after setup and initial start-up of the GSBHE system as well as monitoring system. Initial stability issues with monitoring system were discovered and therefore results for full heating period of 2013/2014 are described in this paper excluding the measurements from the previous heating period. Monitoring results for time period between 01.12.2013 and 24.03.2014 are given in Figure 4 for each 5-minute time step.

It can be seen that although external dry bulb air temperature falls and stays frequently below -10°C the air temperature after the GSBHE system stays approximately between -1°C and +1°C during the coldest periods. At the beginning and at the end of the heating period the air temperatures after the GSBHE system are higher fluctuating between +2°C and +4°C. There are 3 irregular peak

measurements for single time steps, however these are related to manual shutdown of ventilation system during which the standing air warmed up in the ventilation ductwork.

Theoretical energy demand avoided by GSBHE system according to equation 1 based on measured air temperatures was 658 kWh for analysed heating period. Additionally approx. 43 kWh of electricity was used for the circulation pump – so overall energy avoided by GSBHE system was 615 kWh.

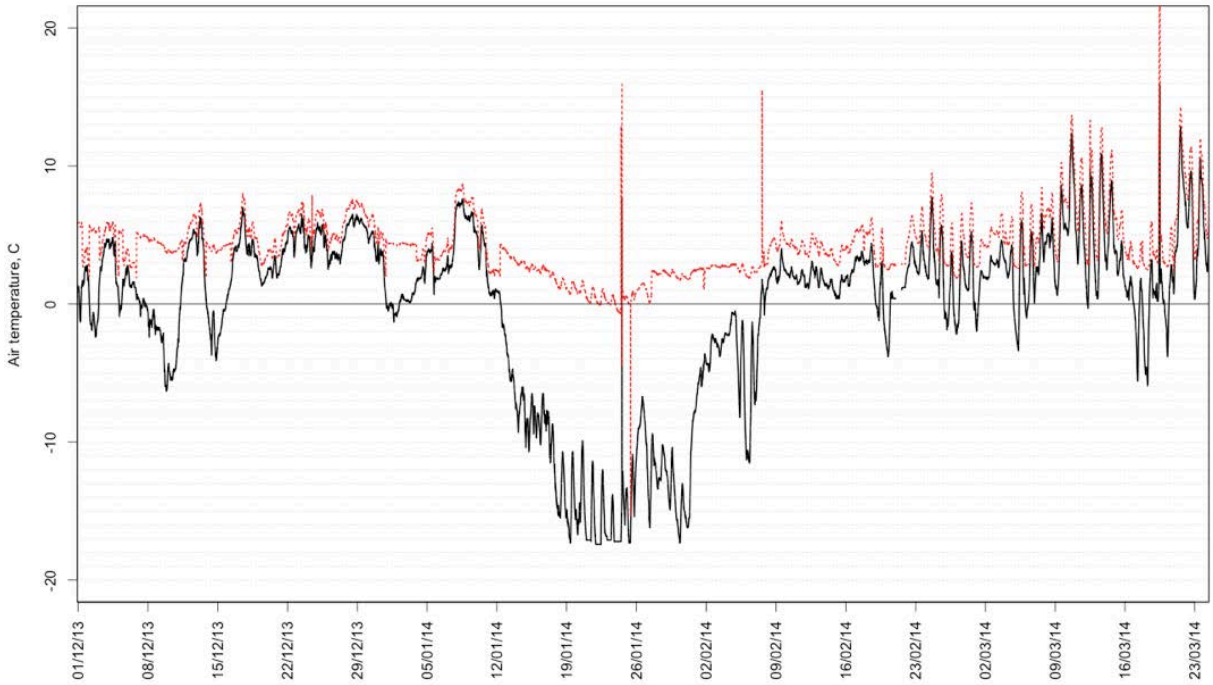

FIG 4. Measured air temperatures before (black solid line) and after (red dotted line) subsoil brine heat exchanger at 5 min intervals for whole heating period of 2013/2014

The measured temperatures before and after GSBHE system were averaged to hourly values in order to compare them to preliminary simulated values. These hourly temperatures along with simulated temperatures after the GSBHE system are given in figure 5.

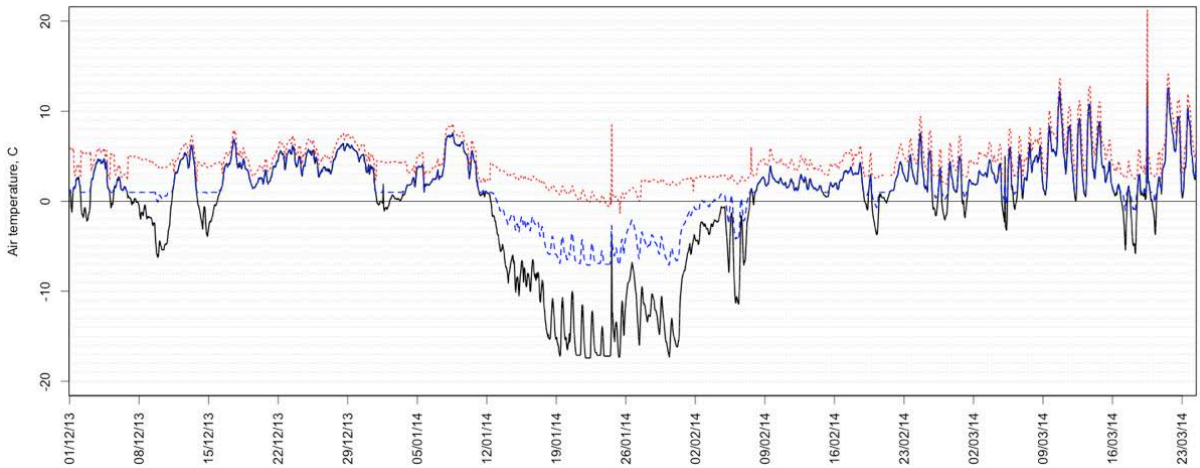

FIG 5. Measured average hourly air temperatures (black solid line – measured air temperature before GSBHE system, red dotted line – measured air temperature after GSBHE system) compared to simulated hourly temperatures (blue dashed line).

Although the pattern of hourly fluctuation of simulated values follow the measured values, the measurements do not correspond well to the simulated fluctuation amplitudes. Further calibration and fine-tuning of *PHErde* calculation model was performed after preliminary calculations (according to actually measured brine flow speeds, etc.), but calculation model could not be fully validated as can be seen from figure 5. This can be related to ground temperature modelling simplifications in *PHErde* tool and lack of possibility to include detailed solar radiation effect on ground surface and subsoil temperatures. Therefore, a multiyear retrospective simulation of GSBHE system is not currently possible to assess the long-term performance of such systems in Estonian climate.

4. Discussion

The theoretical calculation results given in figures 1, 2 and 3 show that net energy demand for the frost protection of the ventilation unit can account for significant part of total energy demand of the building even if the volumetric air flow rate and set point temperature for frost protection is lower than in historical practices. The higher airflow rates and higher set point temperatures will increase the net energy demand significantly. This means that in the context of nearly zero energy buildings where the overall energy demand is limited the frost protection of MHRV unit cannot be realized with direct electric heating coil. Alternative systems, such as ground-source air heat exchanger, ground-source brine heat exchanger, hygroscopic heat exchanger (rotor systems, and improved plate heat exchanger systems) and special systems utilizing double heat exchanger configuration etc are technically possible as stated in [Kragh *et al.* 2007].

The studied building features GSBHE system, which enables energetically effective frost protection without direct electric heating. This system was dimensioned and realized according to calculations with specific software models (*PHErde*), however the measurements from first full heating period show that calculations underestimate the real performance of the GSBHE considerably. The measurement results show that for entire heating period of 2013/2014 the system provided enough preheating energy for the ventilation unit even for excessive periods with air temperatures between -10°C and -17 °C.

Due to simplifications in specific software tools, the validation of calculation model and further performance analysis in even more extreme temperatures were not possible. As a future work we are trying to propose and implement enhancements to calculation procedures involved in GSBHE performance calculation software PHErde or develop a separate calculation method for such systems.

5. Conclusions

The performance of the ground source brine heat exchanger system of the first certified passive house in Estonia was monitored and assessed during the first full heating period after construction. The system performed well providing frost protection for the mechanical ventilation system without anyproblems. The measured values showed that mathematical simulation model used for dimensioning the system underestimated the system performance, which means that the calculation routines have to be further developed to achieve better match with the measured values. Thereafter a long-term retrospective analysis with historical climate data of cold Estonian climate can be performed.

Theoretical calculations of net energy demand for frost protection with different ventilation air flows and preheating set point temperatures showed that when utilizing typical electric preheating coil for frost protection a considerable energy demand can be expected which can contribute significantly to total energy demand of nearly zero energy building. Therefore, in cold climate, an alternative frost protection has to be used. Utilization of hygroscopic heat exchanger in MHRV unit enables lower set point temperatures for external air preheating independently from the volumetric airflow rates. However, when using GSHE or GSBHE systems, the power output is limited and therefore the dimensioning of these systems has to be carried out very carefully to match planned airflow rates ventilation unit requirements.

6. Acknowledgements

This research was supported by the European Union through the European Regional Development Fund.

References

2002/91/EC, E.-D., 2002. EU-Directive 2002/91/EC on the energy performance of buildings [WWW Document]. EU-Directive 2002/91/EC of the European Parliament and of the council of 16 December 2002 on the energy performance of buildings. European Commission. URL http://eur-lex.europa.eu/LexUriServ/LexUriServ.do?uri=OJ:L:2003:001:0065:0065:EN:PDF

2010/31/EU, E.-D., 2010. EPBD recast: EU-Directive 2010/31/EU [WWW Document]. EPBD recast: EU-Directive 2010/31/EU of the European Parliament and of the Council of 19 May 2010 on the energy performance of buildings. URL http://eur-lex.europa.eu/LexUriServ/LexUriServ.do?uri=OJ:L:2010:153:0013:0035:EN:PDF

Estonian Meteorological and Hydrological Institute. 2002. Raw measurement data at three-hour steps over the period from 1970 to 2001 in Tõravere weather station.

Kalamees, T. 2006. Hygrothermal criteria for design and simulation of buildings. Thesis, Tallinn University of Technology.

Kalamees, T. and Kurnitski, J. 2006. Estonian test reference year for energy calculations. Proceedings of the Estonian Academy of Sciences. Engineering 12 (1): 40-58.

Kalamees, T., Vinha, J. 2004. Estonian Climate Analysis for Selecting Moisture Reference Years for Hygrothermal Calculations. Journal of Thermal Envelope and Building Science 2004 27: 199 (2004)

Kragh, J., Rose, J., Nielsen, T.R., Svendsen, S. New counter flow heat exchanger designed for ventilation systems in cold climates, Energ Buildings. 39 (2007) 1151–1158.

Mauring, T., Reinberg, G.W., Hallik, J., Valge, M., Kalbe, K. 2013. A prototype architecture for passive and plus energy building in Estonia. Proceedings of Passivhus Norden 2013 conference 15-17 October 2013, Göteborg (Sweden).

Passivhaus Institute. 2009. [WWW document] Requirements and testing procedures for energetic and acoustical assessment of Passive House ventilation systems for Certification as “Passive House suitable component”, Passivhaus Institut (2009). URL http://passiv.de/downloads/03_Reqs_and_testing_procedures_ventilation_en.pdf

Passivhaus Institute. 2012. [WWW document] Certification criteria for residential Passive House buildings, Passivhaus Institut (2012). URL http://www.passiv.de/downloads/03_certfication_criteria_residential_en.pdf

Raik, A. 1967. Eesti klimaatilisest rajoneerimisest. Eesti Loodus, 2: 65–70.

Classification of building envelopes for solar energy applications

Elisabeth Kjellsson, Assistant professor

Lund University, Building Physics, Sweden

KEYWORDS: *Solar energy, Building envelopes, Solar radiation, Solar heat, PV, Solar map*

SUMMARY
Buildings are suitable as support structure for solar energy applications. The solar radiation on the envelope is depending on the orientation and tilt, as well as the geographical location and the time of the day and year. In order to utilize solar energy as solar heat and/or electricity, the envelope of the buildings can be categorized in different levels.

Category 1is the south facing roofs that receives the highest radiation, which includes tilts between 10-65° and the orientation from south-east to south-west. Category 2 includes the horizontal roofs and for the lower tilts (<30°) also east and west orientations. For very low tilts (<5°) also north facing roofs can be included. Category 3 includes south facing facades and low tilts for north facing roofs.

The potential of solar heat and solar electricity from the envelope of the buildings can be calculated and compared with the demand in the building depending on numbers of floors and category of irradiation. The ratio between suitable roof area and building floor area gives information about the potential of supplying energy within the building and the possibility to distribute the excess energy to a heating network or the electrical grid. Defining of categories can be a tool for potential calculations as well as structuring building types, blocks or areas according to utilization of solar energy. A Solar Map can also be used and one example is the solar map in Lund.

1. Introduction

The building envelopes can be used for heat- or micro power production and the energy may be used within the building and decrease the demand of the supplied energy to the building, as well as fed in the district heating network or the electricity grid. There is a large opportunity and challenge to transform buildings from just using energy to minimize the demand and also deliver more energy than needed over a year.

The solar radiation on the building envelopes can be converted to heat with solar collectors or to electricity by using photovoltaics (PV). In existing buildings the best surfaces should be used for installations and new buildings should be designed in order to optimize the output from the solar energy applications. There is not one solution for what is optimised, it differs depending on investment cost of the installations, the value of the solar energy, the possibility to use the energy directly within the building as well as the possibility for selling, taxes, incentives and supporting systems etc.

For each single building the decision support can be different regarding the economics, which controls the optimization of the size and design of the solar energy installation.

2. Solar radiation on building envelopes

The seasonal variation of the solar radiation increases with the distance to the equator and the more important is the tilt of the surface facing the sun. The tilt is here describing the angle between the

solar energy installation and the horizontal plane. The optimal tilt for the total irradiation is varying during the year. The optimal tilt per month for Lund, Sweden, for a south facing surface, is shown in figure 1.

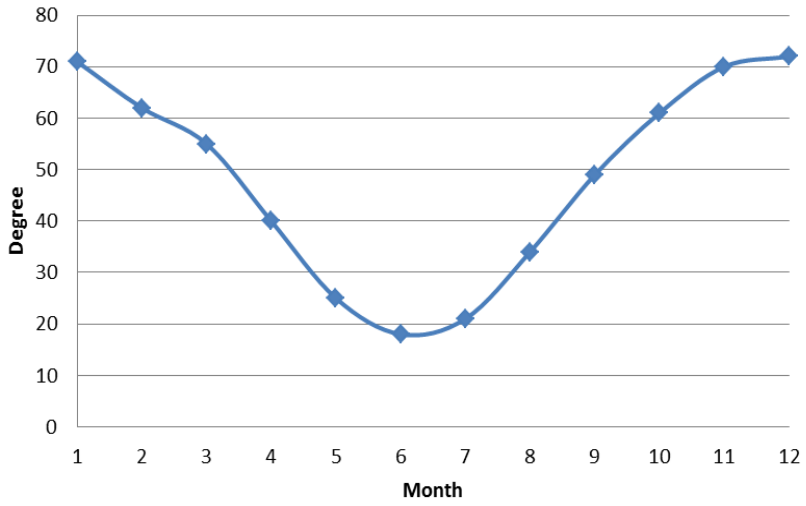

FIG 1. The optimal monthly tilt (inclination angle from horizontal) for solar radiation on a south facing surface in Lund, Sweden. (PVGIS 2013) (PVGIS © European Union, 1995-2013)

As the radiation is varying during the year, the main importance of the tilt is during summer and figure 2 shows the variation of the monthly total radiation for the south facing optimal angle (40°) as well as a horizontal plane and a vertical surface facing south in Lund.

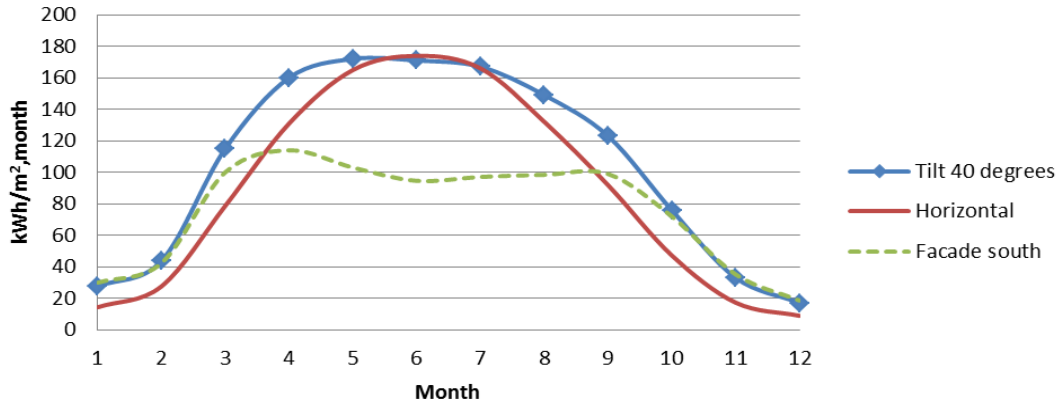

FIG 2. The monthly solar radiation in Lund for the optimal tilt 40 degrees, horizontal plane and 90 degrees tilt towards south (south facing facade) (PVGIS 2013) (PVGIS © European Union, 1995-2013)

The variation over the year is large as seen in figure 2. For the yearly optimal tilt 40° (towards south in Lund, Sweden), only about 10% of the yearly irradiation occurs during the 4 winter months: November to February. On the other hand about 65% of the annual solar radiation is obtained during the 5 spring- and summer- months; April to August and 75% of the yearly radiation during half the year from April to September.

The variation of the radiation for all tilts and angles for real weather data from Jönköping during 1961-1990 is shown in figure 3, as percentage of the maximum yearly radiation. By comparing solar radiation direct towards the south, the decrease is only about 5% for radiation towards southeast and

southwest. With increased angles from south, the optimal radiation is obtained on decreased tilts from horizontal, and for radiation towards east and west directions; the horizontal radiation is the maximal.

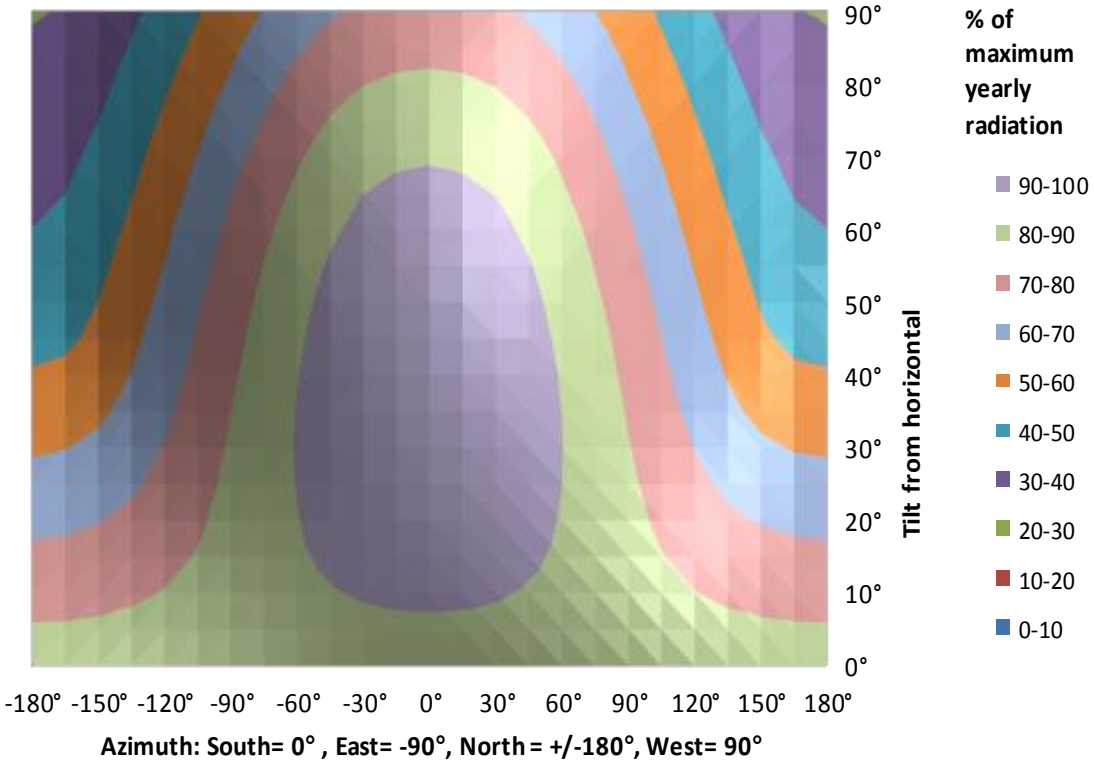

FIG 3. Total radiation depending on different azimuths and tilts in percentage of maximum annual radiation. Average for southern part of Sweden (Kjellsson 2000).

Figure 3 can be used in order to classify different surfaces according to level of radiation. The figure shows the relative radiation in percentage of the maximum radiation and the levels are divided in 10% ranges. A higher radiation means more output from the solar energy installation and also increased yield in economic terms.

The best 10% can be classified to Category 1 or "Very good radiation" and should be used first according to yield. In the figure 3 it is the central area including most of the used roof slopes and the orientation from south-east to south-west.

Category 2 may be called "Good radiation" and includes also the horizontal roofs and for the lower tilts (<30°) also east and west orientation. For very low tilts (<5°) also north facing roofs can be included.

Category 3 – "Less good" also includes south facing facades and low tilts for north facing roofs.

Finally, the rest may be categorized as not suitable for solar applications, at least not when optimizing the yield.

The corresponding maximum values depend on the actual location and varies in Sweden. The values for the different categories are calculated for the maximum radiation between about 1000 – 1200 kWh/(m^2,year), see table 1.

TABLE 1. Limits and mean of radiation for three categories based on 10-percentage levels of maximum yearly radiation.

Total maximum yearly radiation (kWh/(m^2,year))	**Yearly radiation (and mean) in Category 1 (kWh/(m^2,year))**	**Yearly radiation (and mean) in Category 2 (kWh/(m^2,year))**	**Yearly radiation (and mean) in Category 3 (kWh/(m^2,year))**
Max.	90-100% of max.	80-90% of max.	70-80% of max.
1000	900 - 1000 (950)	800-900 (850)	700-800 (750)
1100	990 -1100 (1045)	880-990 (935)	770-880 (825)
1200	1080-1200 (1140)	960-1080 (1020)	840-960 (900)

The economics and the yield from a solar energy application on a specific place are depending on the maximum radiation level, so the limit differs. Other limits may be used, as the actual economic circumstances vary in time. Anyhow it is of importance to investigate the most suitable areas.

The global irradiation for the optimal tilt for Sweden varies between 1200 kWh/(m^2, year) for the south of Sweden and some parts in the east of Sweden (north of Stockholm and Gotland), to the lowest figure of about 900 kWh/(m^2, year) in the very north parts.

The maximum annual radiation is received with a 2-axis tracking system, which is possible to use especially for PV. The increase of radiation is in the order of 500 kWh/(m^2, year) compared to optimal tilt, but the cost for for the movable support structure is much higher compared to fixed mounting supports and it is not an option for integrating in the envelope in buildings. One possible application may be to use tracking systems horizontal roofs.

3. Utilization of solar energy in buildings - combination of surface area, tilt and orientation

The envelopes of buildings have good opportunities to be used for solar energy installations. The roofs on many buildings have suitable tilts, which is between 20-55° and large areas. The orientation is to all directions, but in order to get the best radiation the most suitable is from southeast to southwest.

The roofs on single-family dwellings are suitable due to the large area compared to the floor area. For multiple-story buildings the ratio between the area of the roof and the area of the building's total floor area decreases with increased numbers of floors. This ratio can be calculated and indicates the possibility of utilization of solar energy within the building.

A typical single family building in the south of Sweden has gabled roof with a tilt of around 30°, which means that half of the roof can be classified to Category 1, if the roof is oriented between south-east and south-west. An ordinary size can be 130 m^2 floor space which means that the suitable tilted roof size can be 75 m^2.

If the whole roof is used, the ratio between the roof and floor area can be defined to 58%. This ratio can be used in order to compare the potential of producing heat or electricity, with the demand in the building.

The majority of the multifamily buildings constructed within the "Million building program" in Sweden have horizontal roofs, which means category 2, as described above. Comparing 4 and 8 floors respectively and calculating with the whole roof area, the ratio between roof and floor area is 25% and 12% respectively. In reality, one solution is to put a gabled roof upon the flat roof, which means

that halve of the roof can be in the category 1, if the orientation is OK. The ratio between suitable roof and floor area will be 14% and 7% for the 4 story and the 8 story buildings respectively. If the façade is oriented to the south, this can also be used but in category 3, which means less output/m^2. In high rise buildings this can be very large suitable areas.

Another possibility is to keep the horizontal roof and put supporting structures and tilt the solar devices. In order to maximize the output and minimize the shading, there must be distances between the rows. One rule of thumb is a distance between the fronts in each row of 3 times the module width, which means that only about 30% of the roof area can be used, although in category 1.

Finally here are many more considerations that must be taken into account in a building. Different kind of obstacles may be placed on roofs, which reduce the area and gives shadows.

If the building has fixed solar shading devices to the south, this may also be used for solar applications. The area is not so large but the radiation is in the best category for south facing shadings. In office buildings without solar shading there can be overheating problems, but after installing solar shading they can both save energy and produce electricity in the same time.

Shed roofs oriented to the south are the most efficient design for solar applications, see figure 4. Many new buildings are constructed with shed roof, but the importance of south orientation is not often considered.

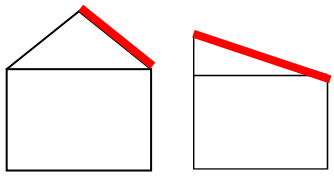

FIG 4. The suitable area for solar applications on gabled roofs is about half compared to shed roofs.

Comparing to the gabled roof, the whole area can be used (if no shading devices are placed on the roof), which means that the ratio between the roof and the floor area for a single store building and the tilt about 30° is 115%, see table 2. Normally the ventilation pipes are mounted on the roofs and for gabled roofs, they can be designed so the outlet is situated on the north side of the roof, but on shed roofs they may cause shading on the solar applications.

TABLE 2. The ratio between suitable roof area and building floor area, for different roof design facing south and number of floors.

Examples of buildings	**Ratio between suitable roof and building floor area (%)**	**Category of irradiation for the south facing roofs**
Gabled roofs (30° tilt), 1 floor	58	1
Gabled roofs (30° tilt), 4 floors	14	1
Gabled roofs (30° tilt), 8 floors	7	1
Flat roof, 4 floors	25	2
Flat roof, 8 floors	12	2
Shed roof (30° tilt), 1 floor	115	1

One way of using the category definition is to compensate the lower radiation with an increased area. Roughly 10% extra area is needed for category 2.

4. Comparing possible production solar heat and solar electricity with energy demand

4.1 Solar heat

Solar heat is mainly used in buildings for domestic hot water and for heating the building. In Sweden the normal system produce up to 50-60% of the yearly demand for domestic hot water. For optimal orientations the systems may produce between 400 and 650 kWh/m^2 solar collector (m^2 roof area), depending on system design. In combined systems, solar heat can also be used for heating the building in spring and autumn. Depending on the heat demand in the building the solar heat contribution varies. Normally there is almost no contribution with solar heat during the coldest days.

The heat demand for domestic hot water varies a lot depending on the users, and in new energy efficient buildings it may be 20 kWh/m^2 (heated area) for single family dwellings and 25 kWh/m^2 for multifamily dwellings (Feby 2012). For existing buildings this figure may be higher and a common average figure is 30 kWh/m^2 (heated area). When calculation for the existing buildings it may be possible to save 15 kWh/m^2 (heated area) with solar heat and the solar collectors will need an area on the roof of about 5-7 m^2 on a single family dwelling and about 3-5 m^2/flat on a multifamily dwelling.

On single family dwellings there is normally no problem to find the requested area but for multi-floor buildings the area may be limited. For an 8-floor building with gabled roofs that has a ratio between suitable roof and the floor area of 7% as indicated in table 2, an average area of a flat with 60-70 m^2 correspond to a roof area of 4-5 m^2, which is enough for a solar collector system for domestic hot water. It means that it covers the south facing roof more or less completely. For higher buildings the area is not enough and for lower – it is more than needed. For shed roofs, the area is almost the double, so this may cover up to 16 floor building.

For combisystems, that also heat the building, the requested area/dwelling are about the doubled compared to only heating domestic hot water systems. The combisystems (as well as domestic hot water systems) include heat storage for a few days but are not delivering substantial heat during the winter months, due to the low radiation as seen in figure 2.

Another design possibility is to use a local or central district heating network, which links the buildings together with a central unit for heat supply. In this case the best oriented roofs can be used for solar collectors and for new constructions the normal roof material can be replaced with solar collectors. For local district heating network a storage tank must be used, but in a large district heating network for a city, the solar heat can be delivered in the system without any storage tanks.

4.2 Solar electricity

The efficiency of photovoltaics (PV) is varying depending on the type. The common way of defining the size of PV modules are the photovoltaic power capacity. It is defined as the maximum power output under standardized test conditions (STC) in “Wp” (Watts peak). A rough figure for Swedish conditions is that the annual output is 1 kWh/Wp. The area conversion from power to m^2 is shown in figure 4.

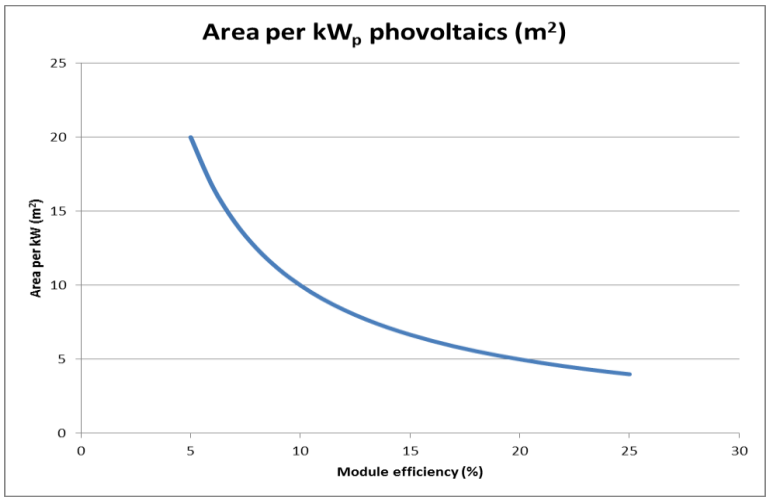

FIG 4. Conversion between 1 kWp PV module and the area for PV with different module efficiencys.

The most used PV modules are made of crystalline silicon cells but thin film cells are increasing. The module efficiency for single crystalline silicon is between 13-19% and for multi crystalline silicon 11-15% (EPIA 2011). Thin film PV modules vary between 7-13% (IEA 2013).

In a PV system there is also losses in the inverter, that is used for changing from direct current (DC) to alternate current (AC), as well as cables and due to high temperatures. For the further calculations the average figure of 15% efficiency has been used.

In Sweden the reference value for calculations of the demand of house-hold electricity in energy efficient buildings is 30 kWh/(m^2 (heated area), year) (FEBY 2012). The actual variation is very high and in dwellings there is also a demand for electricity for common purposes which may very significantly from single family dwellings with only a circulation pump to multi-family dweellings including e.g. elevators, lightning, heat recovary systems and laundry rooms.

PV on gabled roofs on single-family dwellings, which have a ratio between the roof and the floor of 58%, may cover the yearly demand of house-hold electricity. When calculating with 15% efficiency of the PV, the annual output from the PV-plant will be 150 kWh/m^2 roof area and compared to floor area this correspond to about 87 kWh/(m^2 (heated) floor area, year), almost 3 times the calculated demand of 30 kWh/m^2 (heated area). This means that 5 000-10 000 kWh electricity can be produced every year from the roof on an ordinary single family building. As PV-cells are very sensible to shading it might not be possible to use the entire roof area and the suitable area might decrease.

If the suitable roof area is large compared to the demand for household electricity, the PV can also be used for heating domestic hot water and heating the building, preferable with a heat pump. The price for PV has decreased rapidly during the last years and this solutions have became economical interesting.

For multifamily dwellings the suitable roof area is lower as discussed for solar heating , and the facades may be used.

PV-modules can also be used as a building component in other places like balcony railings, solar shadings and as architectural elements, when the energy production is not the decisive design factor.

Depending on the economical context all produced solar electricity can be deliverad to the grid, but in Sweden it is normally more economical to use the electricity within the building and decrease the amount of bought electricity. Depending on the number of floors and the actual demand, there is also a large potential of to produce electricity to the grid from the roofs of buildings.

The potential of using existing buildings for production of solar electricity in a city scale can be analyzed by using solar maps. A “Solar Map” for the whole municipality of Lund was launched in 2013, giving information of about 50 000 roofs with the potential of production of solar electricity by using the roofs, divided in four categories regarding irradiation levels. The solar map is available on internet and can be used as information to the house owners but also act as a benchmark for politicians, decision makers, investors etc. to define possibilities, strategies and goals (Solkartan Lund, www.solkartan.se).

The Solar Map can be used for analyzing the potential of producing solar electricity for single buildings, but also for comparing different blocks including similar buildings, comparing different blocks and types of buildings.

5. Conclusions

The potential of using buildings for production of heat and electricity is very large. There are although a lot of specific parameters that must be considered and the radiation on suitable surfaces is one important factor. By developing categories for levels of solar radiation on the surfaces, the potential of energy from the envelope of the building can be calculated and be developed to include building blocks, areas with types of buildings and whole cities.

The buildings can be transformed from only using delivered energy to be producer of heat and electricity, saving delivered energy or distribute heat and/or electricity to the network and grid. Old buildings can be refurbished and the most suitable surfaces can be defined, while new buildings can be constructed in an optimal design.

It is important to decrease the supplied energy to buildings and this can be done with a combination of improved energy efficiency and using the envelope for production of solar heat and solar electricity.

6. Acknowledgements

The author would like to thank the Swedish Research Council FORMAS, the Swedish Energy Agency, and the Swedish Environmental Protection Agency for their financial support.

References

EPIA 2011. European Photovoltaic Industry Association, Solar Generation 6, Solar Photovoltaic Electricity Empowering the World, Belgium

FEBY 2012. Kravspecifikation för nollenergihus, passivhus och minienergihus, Bostäder. FEBY 12, Justerad sept. 2012. LTH report EBD-R-12/36

Kjellsson E. 2000. Potentialstudie för byggnadsintegrerade solceller i Sverige. Rapport 2. Analys av instrålningsnivåer på byggnadsytor. Report TVBH-7216 Lund 2000, Dep. of Building Physics, Lund University

IEA 2013.Trends 2013 in Photovoltaic applications. IEA International Energy Agency PVPS Photovoltaic power systems programme. Report IEA-PVPS T1-23:2013

PVGIS 2013. Photovoltaic Geographical Information System – Interactive Maps. JRC European Commission. Webpage: http://re.jrc.ec.europa.eu/pvgis/apps4/pvest.php?lang=en&map=europe PVGIS © European Union, 1995-2013 (visited 2013-12-12)

Solkartan Lund. 2013. Kraftringen (f.d. Lunds Energikoncernen AB) Hemsida: www.solkartan.se

Indoor environment in four newly build low energy houses in Fairbanks, Alaska

Martin Kotol [1]
Colin Craven [2]
Carsten Rode, Ph.D. [3]

[1] Technical University of Denmark, Denmark
[2] Cold Climate Housing Research Center, AK, USA
[3] Technical University of Denmark, Denmark

KEYWORDS: *HVAC, Indoor air quality, Cold climates, Residential buildings, CO_2 concentration, Ventilation rates*

SUMMARY:
In cold climates living inside the heated space requires considerable amounts of heat. With the intention to decrease the heating demand, people are insulating their homes and make them more air tight. With the natural infiltration being brought close to zero there has been an increase of a new problem which is poor indoor air quality (IAQ). During summer 2012 four student homes were built in Fairbanks, Alaska as a part of Sustainable Village project. The aim of this project is to promote sustainable ways of living in the Arctic and to study new technologies and their applicability in the cold north. This paper presents the results of an IAQ survey performed in the homes during two weeks in December 2012. During this survey the air temperature, relative humidity (RH) and CO_2 concentration were measured in all occupied bedrooms along with monitoring of the ventilation units. The results have shown noticeable differences in IAQ between the four houses caused by different technical solutions. The ventilation rates were reduced by occupants or by frost protecting strategy of the ventilation units and the RH inside the living space was often very low. It is assumed that by introducing more advanced controls of the HVAC systems, better defrosting strategy and moisture recovery from the exhaust air the IAQ can be improved with minimum extra energy demand.

1. Introduction

Climate in the Arctic regions is cold so living inside the heated space requires quite some energy particularly during the long winters. With the intention to decrease the energy use for heating, people started insulating their homes more and making them more air tight (Kalamees 2007, Pan 2010). Consequently the natural infiltration was limited which led to reduced air change. Insufficient air change causes that the concentrations of various pollutants (including CO_2) generated indoors are increasing which may have a negative effect on human performance or even health (Wargocki, Wyon et al. 2000, Seppanen, Fisk et al. 1999). CO_2 it is often used as an indicator of IAQ. According to EN 15251 (Dansk Standard 2007) new buildings should have the indoor CO_2 concentration lower than 500 ppm above outdoors. ASTM Standard D6245 suggests CO_2 concentrations lower than 650 ppm above outdoors. ASHRAE 62.1 (American Society of Heating, Refrigerating and Air-Conditioning Engineers 2004) recommends 700 ppm above outdoors as an upper limit.

Another indoor environmental challenge in cold climates is humidity. In poorly ventilated buildings the moisture generated indoors may be too high for a poor air change which leads to high indoor humidity and may cause mold growth and house dust mite infestation (Pirhonen, Nevalainen et al. 1996, Emenius, Korsgaard et al. 2000). On the other hand proper air change in such dry climate often leads to extremely low indoor humidity which affects the comfort of the occupants as well (Reinikainen, Jaakkola et al. 1992).

To cope with risk of poor IAQ, ventilation systems were introduced to buildings. These systems can provide the buildings with required air change in more energy efficient way as they allow use of heat exchangers (HEs). Some HEs also allow the moisture recovery which may help to solve the low humidity issue, but the reliability and hygienic safety is considerable. In the cold and dry outdoor climate in HEs condensation and subsequent frost formation may arise and eventually put the entire system out of order. Preheating of supply air may be applied to cope with this issue; however, such solution is in cold climate with long winters very energy demanding. Alternatively, smarter heat recovery units may be used like the one used in Low Energy House in Sisimiut, Greenland (Vladykova, Rode et al. 2012).

1.1 Sustainable Village

In summer 2012 four student homes were built in Fairbanks, Alaska as a part of Sustainable Village (SV) project. The project was funded by University of Alaska Fairbanks (UAF) and contracted with Cold Climate Housing Research Center (CCHRC). The aim of this project is to promote sustainable ways of living in the Arctic and to study new technologies and their applicability in the cold north (Cold Climate Housing Research Center). Different energy efficient technologies were combined to create unique but still affordable homes. The homes have similar layouts and each of the homes accommodates 4 students; however they differ in used technologies. There are two types of heating systems used in SV: I) hydronic floor heating and II) unique forced air heating which combines delivery of heat and fresh air Br**HEAT**he in combination with a standalone heater (Cold Climate Housing Research Center). Three types of ventilation units were installed: I) Zehnder ComfoAir 350. This unit uses counter flow flat plate HE with an 800 W electric pre-heater to protect the HE from freezing. If the preheating is not sufficient (the outside air is too cold) the unit reduces the supply flow rate which puts the house into slight underpressure. II) Venmar EKO 1.5 HRV. The HE in this unit is a flat plate cross flow type. Unlike the Zehnder, Venmar units use recirculation cycle as a frost protection strategy. During recirculation cycle, the unit blocks the fresh air supply and exhaust and recirculates the air inside the house. III) Venmar EKO 1.5 ERV. The only difference from the HRV version is the type of HE. This unit uses cross flow flat plate energy exchanger which apart from heat also allows moisture recovery. Configuration of the homes is shown in Table 1.

Table 1. Description of the homes and systems

House:	**Birch House**	**Tamarack House**	**Spruce House**	**Willow House**
	North - West	**North - East**	**South - West**	**South - East**
Heating:	Br**HEAT**he + pellet stove	Hydronic floor heating	Br**HEAT**he + Steffes heater	Hydronic floor heating
Ventilation:	Zehnder ComfoAir 350	Venmar EKO 1.5 ERV	Venmar EKO 1.5 HRV	Venmar EKO 1.5 HRV
Defrosting strategy:	Electric preheating + Supply air flow reduction	Recirculation	Recirculation	Recirculation

The overall energy performance of each house is being continuously monitored by the CCHRC and UAF. Additional to the CCHRC and UAF monitoring there was a survey of (IAQ) performed in the homes during two weeks in December 2012. During this survey the air temperature, relative humidity (RH) and CO_2 concentration were measured in all occupied bedrooms. Additionally the temperature in all four connections to the ventilation units was measured. This paper presents the results of this survey which goal was to identify any possible issues with IAQ especially in relation to different ventilation units installed in the houses and to evaluate the performance of these units.

2. Methods

The survey was performed over the course of three weeks in December 2012. Due to the malfunction of the ventilation unit in the Tamarack house during the last week of measurements only the data obtained during the first two weeks were used for IAQ analysis. During this period the Tamarack, Birch and Willow houses had been fully occupied by 4 people whereas the Spruce house was only occupied by 3 persons. Therefore only 3 bedrooms were monitored in the Spruce house. The variables monitored and the equipment used are described below.

2.1 Air flows

The fresh air intake into the houses was measured by means of The Energy Conservatory Exhaust Fan Flow Meter (TECEFM) at the beginning of the survey. Before the measurements the ventilation units were balanced it can therefore be assumed that supply and exhaust air flows are equal. The measured values were compared with the requirements given by ASHRAE (American Society of Heating, Refrigerating and Air-Conditioning Engineers 2004) and BEES (Alaska Housing Finance Corporation. Research Information Center 2002).

2.2 IAQ

Onset HOBO loggers U12 were used to measure air temperature and RH inside the houses. The logging frequency was set to 2.5 min. The HOBO loggers were combined with CO_2 sensors Vaisala with a range of 0 – 5000 ppm. The sensors were placed far from the bed so the measurements were not affected by being too close to the breathing zone of a sleeping person and far from the air inlets.

With the outdoor CO_2 concentration in Fairbanks 400 ppm, the recommended indoor concentration according to ASTM Standard D6245 is 1050 ppm, according to ASHRAE 62.1 (American Society of Heating, Refrigerating and Air-Conditioning Engineers 2004) 1100 ppm and according to EN 15251 (Dansk Standard 2007) 900 ppm. Because the occupied period is of main concern, night only (10 p.m. – 8 a.m.) concentrations were taken into account when evaluating the CO_2.

The indoor humidity and temperature were evaluated for the entire measurement period as they do not only affect the comfort of the occupants, but also have effects on the eventual mould growth and overall heat loss (higher indoor temperature = higher transmission heat loss).

2.3 Ventilation units

The temperatures of all four air streams connected to the ventilation units were measured by temperature sensors TMC6-HD from Onset connected to HOBO loggers U12. In houses with Br**HEAT**he system, the temperature of the air right after the heater was also measured to identify the periods when the heater was on. The sensible heat efficiency of the heat exchangers for the periods with fresh air supply (no recirculation) was calculated according to (Eq.1.)

$$\varepsilon = \frac{T_{sa} - T_{fa}}{T_{ra} - T_{fa}} \cdot 100\ [\%] \quad (1)$$

Where T_{sa} is temperature of the supply air to the house (K)
T_{fa} is temperature of the cold fresh air (K)
T_{ra} is temperature of the return air from the house (K)

3. Results

3.1 Air flows

The measurements showed that three homes would fulfill the local ventilation requirements under normal operation of their ventilation system; however their actual air change was reduced by either occupants or frost protecting strategy. FIG 1 shows the correlation between the actual ventilation rate and amount of night time when the CO_2 concentration in bedrooms was above 1100 ppm.

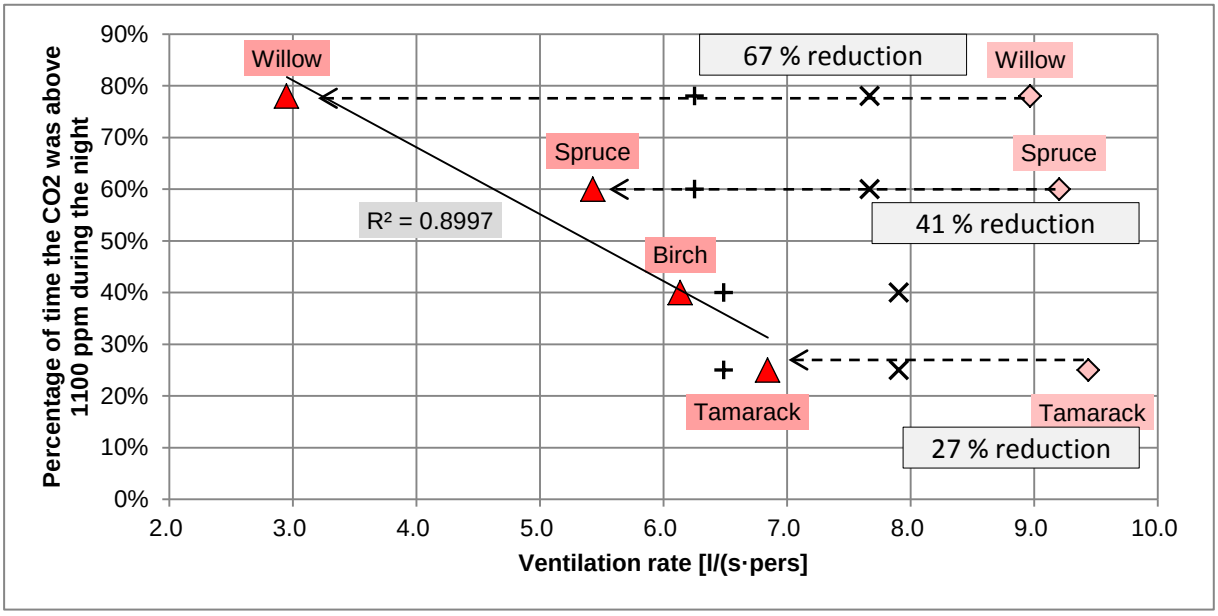

FIG 1. Night CO_2 concentrations above 1100 ppm and ventilation rates (the diamonds show the measured air flow and the triangles show the actual fresh air flow reduced by recirculation; the plus marks are ASHRAE 62.2 recommended values and X marks are BEES 2012 recommended values)

3.2 IAQ

The night CO_2 concentrations in each home along with the limits recommended by European and American standards are shown in FIG 2.

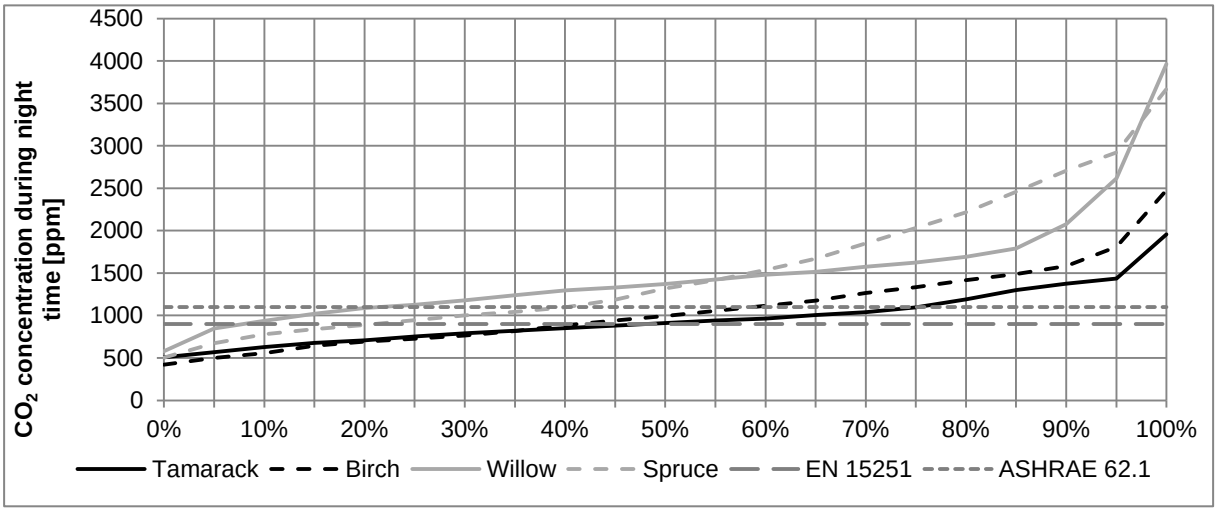

FIG 2. Cumulative percentage distribution of CO_2 concentrations in occupied bedrooms during night time (22:00 - 8:00)

Relative humidity measured in the bedrooms is shown in FIG 3. From there it is seen that the house with lowest air exchange (Willow) has the highest relative humidity. However the house with the highest air exchange (Tamarack) does not have the lowest relative humidity possibly as a result of the moisture recovery potential of the heat exchanger.

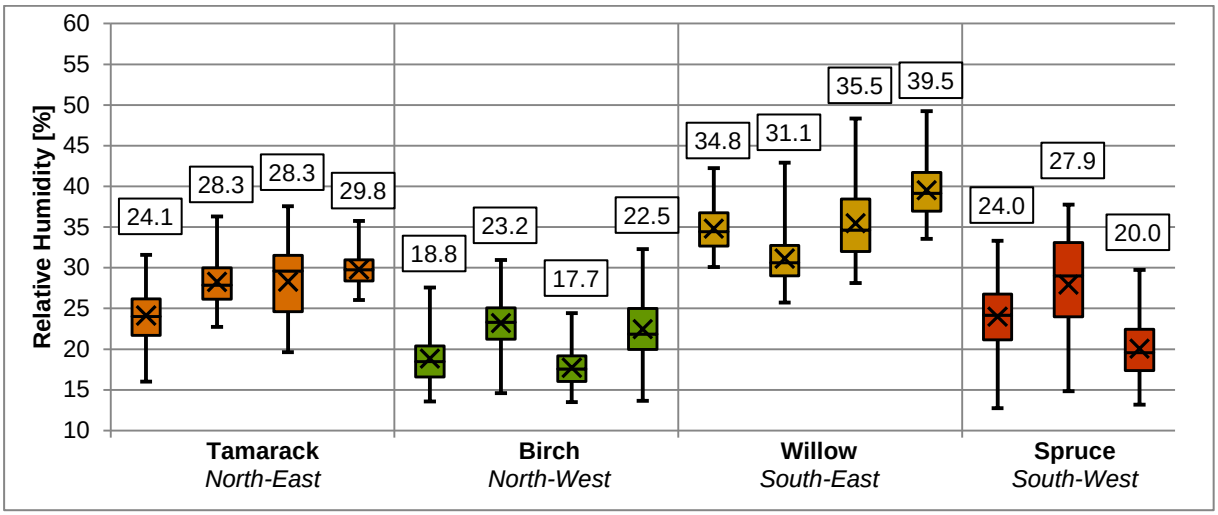

FIG 3. Relative humidity in all occupied bedrooms within the Sustainable Village (the X and values in the boxes are arithmetic averages)

The average temperature in most bed rooms was within the range 21.5 – 31.0 °C suggested by the Harbin study (Wang, Wang et al. 2003) to satisfy 80% of occupants. However according to the interviews with the occupants the large temperature swings leading to occasional overheating in Spruce and Birch house have caused some discomfort.

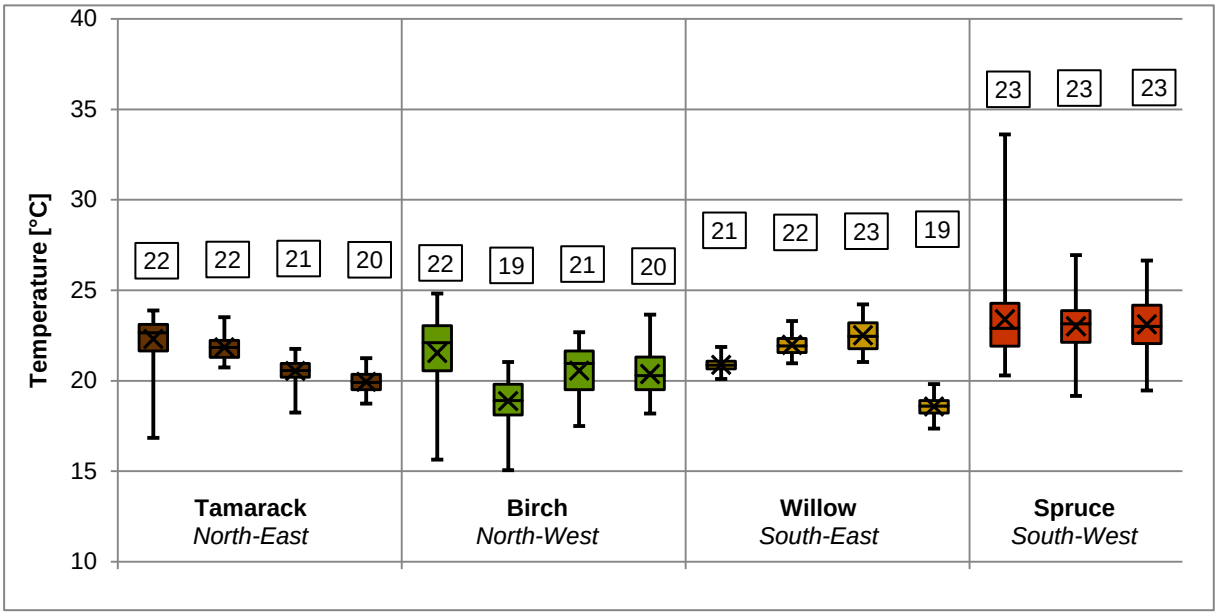

FIG 4. Temperature distribution in bedrooms. The boxes describe the lower and upper quartiles, the bands inside the boxes are medians, X and values in the boxes are mean values and the ends of the whiskers represent 1st and 99th percentiles.

3.3 Ventilation units

3.3.1 Venmar HRV

The average sensible heat efficiencies of the heat exchangers were 70.7 % and 76.6 %.

The hot air heater used for heating of Spruce house does not have a modulating heat output meaning that there is either 0 or 5 kW of heat being introduced to the air stream which causes large fluctuations in temperature of the air delivered to the rooms and consequently fluctuations in room temperatures. In average the heater turned on and off 14 times a day and was on for 58% of the time.

3.3.2 Venmar ERV

The average sensible heat efficiency of the heat exchanger when the unit was in air exchange mode was 76.5 %. The moisture recovery rate was not measured.

3.3.3 Zehnder

The average sensible heat efficiency of the heat exchanger was 71.7 % when measured after the electric preheater. The combination of 100% air exchange with no recirculation, hot air heating and no moisture recovery or humidification made the Spruce house the house with lowest indoor humidity, but also considerably low CO_2 concentration.

The hot air heater was on for 60% of the time and in average turned on and off 19 times every day.

4. Discussion

4.1 Air flows

In case of Birch house the low ventilation rate was due to low fan speed selected on the control panel by the users which can be fixed by reprogramming the controller of the unit in a way that it runs on higher speed. The ventilation rates in the other three houses were reduced significantly either by a) defrosting of the heat exchangers or b) by users selecting the recirculation mode manually on the control panel (one of the unit's operation modes is "20 min/h" in which the unit supplies fresh air for 20 minutes and then recirculates for 40 minutes). Reduced air change led to increased concentrations of indoor pollutants (such as CO_2). Possible solution for the homes where the Venmar units are installed could be an increase of the ventilation rate during periods when defrosting is active so that the reduced air change would be high enough to meet the requirement. To avoid unnecessary increase of the heat consumption, the increase of ventilation rates in all homes should only take place during occupied hours.

4.2 IAQ

The lowest CO_2 concentrations were measured in the Tamarack house which has the highest ventilation rate. Even that is however lower than recommended (due to defrosting) which can be the reason that in average 25 % of a night time the CO_2 concentration was above 1100 ppm recommended by ASHRAE. We believe that adjusting the ventilation systems to provide the required ventilation rates will help to eliminate the problems with elevated CO_2 concentrations. However the occupant's interaction with the systems can significantly affect the final results. Increasing the ventilation rates will increase the heating demand of the houses considerably. Variable air flow systems should be considered for the future projects to achieve good indoor air quality and lower energy use.

The occupants of the Birch house have been complaining about low humidity which according to the measurements is the lowest from all four houses (86% of the time below 25% RH). This house has the second largest air exchange and does not have moisture recovery which in combination with the hot

air heating gives a cause to such a low humidity. It can be expected that increasing the air flows up to a required levels will decrease the humidity even more. Moisture recovery, as demonstrated in the Tamarack house seems to have a potential for maintaining higher RH and thanks to the mass transfer potentially having higher energy recovery efficiency (this however needs to be further investigated). Air humidification or indoor plants may also help to solve the problem with too low humidity, but on the other hand may be very energy demanding and introduce new challenges such as mold growth.

Bedroom temperatures varied more in homes with hot air heating than in homes with floor heating which led to discomfort in occupants. The reason for such variation is that the hot air heaters do not have modulating power output and are controlled by a thermostat placed in a reference room (corridor). Therefore there are periods when the heat is delivered to bedrooms even though they do not need it and vice versa.

4.3 Ventilation units

The efficiency of the heat exchangers was in a range from 70.7 % to 76.6 % which is comparable to 68 % found in experimental heat exchanger in LEH Sisimiut (Vladykova, Rode et al. 2012). Increasing the air flows to meet the required air change might however cause that the efficiency will change.

The effect of frequent switching of the hot air heaters in BrHEAThe systems on a lifetime of the device is considerable. Modulating the power output of the air heaters would have a positive effect on the temperature fluctuations inside the houses as well as on the switching frequency.

Better control (possibly demand based) of the air flows would mean that the rooms would be ventilated sufficiently during all the time. Such control may bring energy savings and improve the air quality at the same time as the air flow will be reduced during unoccupied periods.

5. Conclusions

The houses in sustainable village are a great presentation of various ventilation systems and demonstrate quite well how important is the proper ventilation for healthy and sustainable homes.

The measurements showed that there are significant differences in IAQ in the four houses. These are partially attributable to variations in HVAC systems and occupant interactions with these systems.

The ventilation rate, even though it fulfills the ASHRAE standard requirements under standard operation, gets reduced either by the occupants or by the frost protecting strategy (recirculation). With the ventilation rate too low, the concentration of CO_2 along with other pollutants increases which may have an effect on comfort and performance of the occupants. In order to meet the requirements also during the Arctic winters system refinements and occupant education is recommendable.

Higher ventilation rate brings another issue which is too low humidity. To deal with this phenomenon moisture recovery proved to be efficient and despite being considered as incapable of working in our climate showed some good promise.

Zoning which would allow occupants to set their own room temperature would increase the comfort and could also decrease the heat demand thanks to set backs during unoccupied and night hours. Unfortunately zoning in hot air heating requires great deal of research and development before it is introduced to highly energy efficient residential buildings.

6. Acknowledgements

This study was generously supported by the Otto Mønsted and Idella foundation. Undertaking this study was only possible thanks to great collaboration with CCHRC and UAF. We would like to thank the occupants of the homes for their patient collaboration.

References

ALASKA HOUSING FINANCE CORPORATION. RESEARCH INFORMATION CENTER, 2002. *Alaska building energy efficiency standard.* Anchorage, Alaska: Alaska Housing Finance Corporation, Research & Rural Development Division, Research Information Center.

AMERICAN SOCIETY OF HEATING, REFRIGERATING AND AIR-CONDITIONING ENGINEERS, 2004. *Ventilation and acceptable indoor air quality in low-rise residential buildings.* Atlanta, Ga.: American Society of Heating, Refrigerating and Air-Conditioning Engineers.

AMERICAN SOCIETY OF HEATING, REFRIGERATING AND AIR-CONDITIONING ENGINEERS, 2004. *Ventilation for acceptable indoor air quality.* Atlanta, Ga.: American Society of Heating, Refrigerating and Air-Conditioning Engineers.

COLD CLIMATE HOUSING RESEARCH CENTER, , Integrated Heating and Ventilation. Available: http://www.cchrc.org/integrated-heating-and-ventilation2013].

COLD CLIMATE HOUSING RESEARCH CENTER, , Sustainable Village. Available: http://www.cchrc.org/uaf-sustainable-village2013].

DANSK STANDARD, 2007. *DS/EN 15251 - Indoor environmental input parameters for design and assessment of energy performance of buildings addressing indoor air quality, thermal environment, lighting and accoustics.* Charlottenlund: Dansk Standard.

EMENIUS, G., KORSGAARD, J. and WICKMAN, M., 2000. Window pane condensation and high indoor vapour contribution - markers of an unhealthy indoor climate? *Clinical and Experimental Allergy,* **30**(3), pp. 418-425.

KALAMEES, T., 2007. Air tightness and air leakages of new lightweight single-family detached houses in Estonia. *Building and Environment,* **42**(6),.

PAN, W., 2010. Relationships between air-tightness and its influencing factors of post-2006 new-build dwellings in the UK. *Building and Environment,* **45**(11), pp. 2387-2399.

PIRHONEN, I., NEVALAINEN, A., HUSMAN, T. and PEKKANEN, J., 1996. Home dampness, moulds and their influence on respiratory infections and symptoms in adults in Finland. *European Respiratory Journal,* **9**(12), pp. 2618-2622.

REINIKAINEN, L., JAAKKOLA, J. and SEPPANEN, O., 1992. The Effect of Air Humidification on Symptoms and Perception of Indoor Air-Quality in Office Workers - a 6-Period Cross-Over Trial. *Archives of Environmental Health,* **47**(1), pp. 8-15.

SEPPANEN, O.A., FISK, W.J. and MENDELL, M.J., 1999. Association of ventilation rates and CO2 concentrations with health and other responses in commercial and institutional buildings. *Indoor Air-International Journal of Indoor Air Quality and Climate,* **9**(4), pp. 226-252.

VLADYKOVA, P., RODE, C., KRAGH, J. and KOTOL, M., 2012. Low-Energy House in Arctic Climate: Five Years of Experience. *Journal of Cold Regions Engineering,* **26**(3), pp. 79-100.

WANG, Z.-., WANG, G. and LIAN, L.-., 2003. A field study of the thermal environment in residential buildings in Harbin, *ASHRAE TRANSACTIONS TECHNICAL AND SYMPOSIUM PAPERS* 2003, pp. 350-355.

WARGOCKI, P., WYON, D.P., SUNDELL, J., CLAUSEN, G. and FANGER, P.O., 2000. The effects of outdoor air supply rate in an office on perceived air quality, Sick Building Syndrome (SBS) symptoms and productivity. *Indoor Air-International Journal of Indoor Air Quality and Climate,* **10**(4), pp. 222-236.

Low-energy mechanical ventilation: a case study of two new office buildings

Claus Wessel Andersen, M.Sc. [1]
Christian Anker Hviid, Assistant Professor [1 2]

[1] ALECTIA A/S, Denmark
[2] Department of Civil Engineering, Technical University of Denmark, Denmark

KEYWORDS: *Mechanical ventilation, low-energy, ventilation, indoor climate, specific fan power*

SUMMARY:
In 2010 an internationally renowned company initiated an architectural competition for two new office buildings to be constructed in Denmark. The design objectives were to construct a sustainable office building according to Danish low energy class 2015, with a good indoor climate and with as little energy consumption as 41.1 kWh/m^2/year including heating and all building services with no use of renewable energy such as PV-cells or solar heating. One of the key means of reaching the objectives was to implement mechanical ventilation with low pressure loss and therefore low energy consumption. The project consists of two buildings, building one is 6 stories high, and building two is 4 stories high. The buildings have a gross area of 50,500 m^2 including underground parking. The ventilation and indoor climate concept was to use mechanical ventilation together with mechanical cooling and fan-assisted natural ventilation for free night cooling, hence minimizing the energy consumption for cooling. The paper describes the initial ventilation requirements and the implemented ventilation system. The specific fan power, SFP, with maximum air flow rate was measured to be 0.9 kJ/m^3 to 1.2 kJ/m^3, with an average of 1.1 kJ/m^3. The yearly mean SFP based on estimated runtime is approx. 0.8 kJ/m^3. The case shows the un-locked potential that lies within mechanical ventilation for near-zero energy consuming buildings.

1. Introduction

Mechanical ventilation has been the most widely used principle of ventilation over the past 50 years, but building services, including ventilation, represents a growing share of the total energy consumption. In the EU, HVAC systems accounts for 48% of the building sector energy consumption (Perez-Lombard et al. 2008) and, of this, fans accounts for 15-50 % depending on the type and design of the system (Wouters et al. 2001, Perez-Lombard et al. 2011).

To bridge the widening gap between the demand for fossil fuel reductions and the demand for improved indoor climate, other principles of natural and hybrid ventilation systems have emerged (Delsante 2002), intended to reduce the energy consumption for ventilation, specifically the power consumption of fans in mechanical systems. However, these alternative systems have many other flaws, e.g. ventilation heat losses, uncontrollable ventilation air supply and high risk of draught (Hviid 2010).

Meanwhile, little has been done to improve the performance of mechanical ventilation systems. The specific fan power (SFP), which expresses the ratio of power consumption to air flow rate of the ventilation system, is far from optimal. Terkildsen (2013) quotes four guidelines from the past 15 years that recommend 1.0 kJ/m^3, yet data from Hvenegaard (2007), Jagemar (2003), and Nilsson (1995) shows SFP-values of 2.5-3.5 kJ/m^3 with newer systems around 2.0-2.5 kJ/m^3. Only a few custom-designed systems comply with the guidelines. Berry (2000) reported a custom-made air handling plant with the specific fan power of 0.5 kJ/m^3. Hviid & Svendsen (2012) came as low as 0.6 kJ/m^3 with a prototype low pressure ventilation system, using custom build liquid-coupled indirect heat exchangers, diffuse ceiling inlets and low pressure dampers. In simulations, Terkildsen &

Svendsen (2013) came as low as 0.33 kJ/m^3 with an conventional mechanical ventilation system using different pressure reducing technologies like bypass of heat recovery unit, diffuse ceiling inlets, active electrostatic filtration and optimized pressure/flow control.

The discrepancy between guidelines and practice is mainly due to the industry focus on minimising space for building services, but it is also due to the low innovation focus in the ventilation industry to develop low-pressure solutions. This paper describes the ventilation system and the design process and the energy measurements on the completed system, thereby documenting the feasibility of conventional mechanical ventilation systems for realised low-energy buildings.

2. Design process

The core design team consisting of architects and engineers started from scratch with an integrated design approach where all stakeholders were included before the first lines were drawn. This approach, depicted on FIG 1, formalises the process by setting up initial design goals that are specific and measurable which enables concrete and continuous evaluations throughout the entire construction period. The expectations among the different stakeholders were aligned to match design goals that were sound, economically viable and socially responsible. These design goals formed the sustainability profile which the finalised building had to comply with. The profile was highly transparent and boosted the awareness of the different focus areas which the design team had to contribute to and comply with when the solutions were implemented.

By doing this, the design team was able to adjust the design pro-actively in order to combine the demands of the client with low energy consumption and a highly sustainable profile. The design outcome was a state of art building with indoor climate class I and II according to EN 15251.

The means of achieving low-energy consumption encompassed a few elements: optimised building form, a façade optimised for daylight and sufficiently high insulation level, low energy electrical lighting and low pressure VAV ventilation system. Especially the ventilation was under close review because badly designed ventilation would make it impossible to apply the highest indoor climate class with low overall energy consumption.

It was of particular interest to the client that there was no use of renewable energy sources such as PV-cells or solar heating, and that all solutions were proven and commercially available on the market.

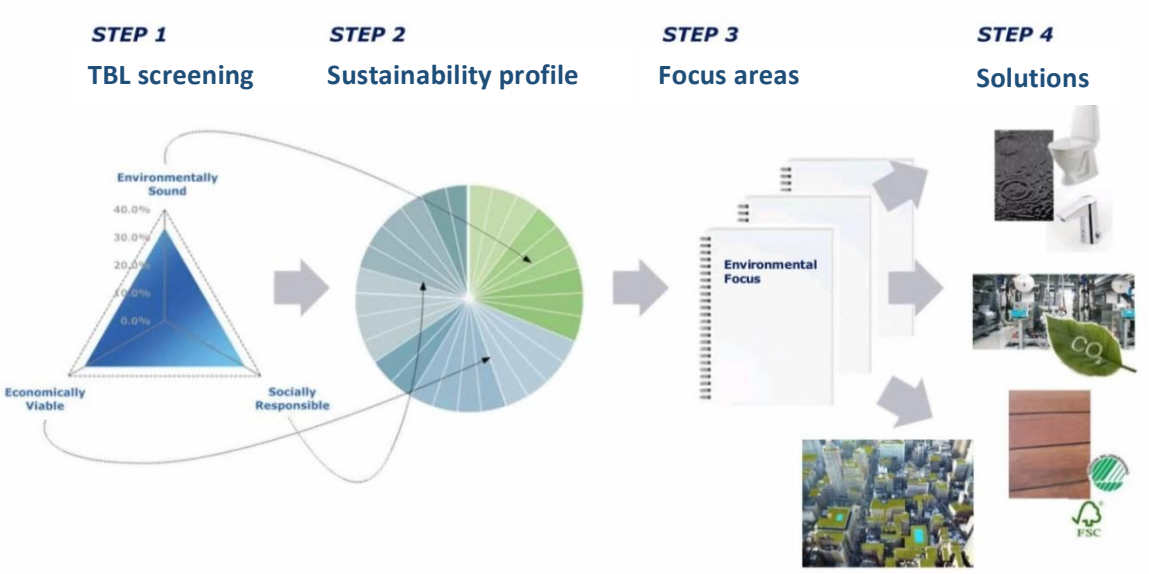

FIG 1. Integrated design process

3. Building

The project consists of two buildings, building one is 6 stories high, and building two is 4 stories high. The buildings have a gross area of 50,500 m^2 including underground parking. The ventilation and indoor climate concept was to use i) mechanical mixing ventilation together with mechanical cooling and ii) fan-assisted natural ventilation for free night cooling. In this manner, the energy consumption for cooling was minimised.

The core of each building is an atrium. At the ground floor and first floor the common facilities are located. The rest of the building floors are office spaces mainly along the outer façade. Rooms with none or less daylight requirements, e.g. service rooms, shafts, cafés and meeting rooms, are located between the perimeter spaces and the atrium,

The façade is optimised for optimal daylight access to the office space with large windows, but with insulated parapet below table height, preventing excessive solar heat gains and increasing the overall thermal insulation. The façades are equipped with external solar screens, and internal glare protection screens. The artificial lighting systems is low-energy and with dimmable daylight control.

3.1 Ventilation system

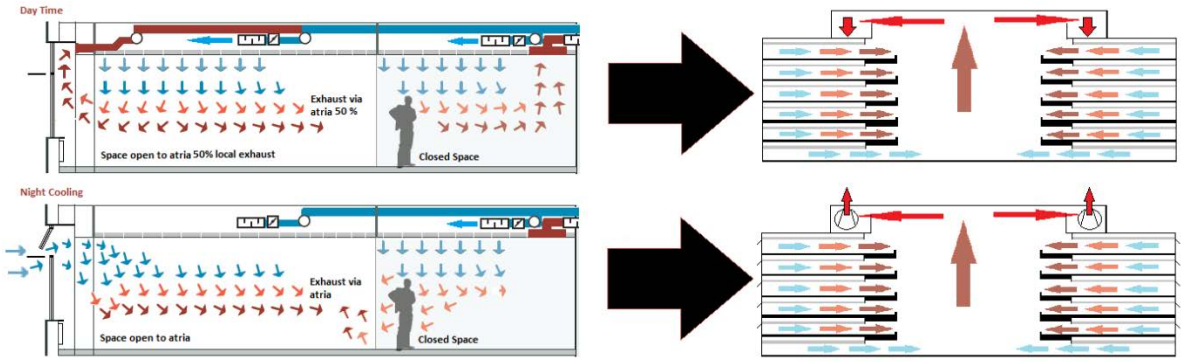

FIG 2. Principle of main building ventilation system; balanced mechanical day time ventilation and night cooling by operable façade windows and exhaust ventilation

The energy consumption of the ventilation system is related to the ventilation rate, resistance to the airflow, efficiency of the fan and motor, and operation time.

In mechanical systems, the fan power is approx. proportional to the ventilation rate cubed. Consequently, the first step was to minimise the ventilation rate demands, i.e. use low-emission building materials and exploit the fact that passive cooling means were implemented from the very first design phase.

The second step was to minimise flow resistance. This was achieved by planning the optimal duct routing, thus reducing the duct lengths. The central atrium was planned to function as non-ducted extract route. Plant rooms were located centrally. FIG 3 and FIG 4 depict parts of the ventilation routing while FIG 5 is more schematic.

The initial design pressure drop of the duct system was chosen to be maximum 150 Pa as a compromise between keeping the size of the air handling units down while still having an SFP value of 1.1 kJ/m^3 at maximum flow.

The design duct pressure loss was achieved with the following design criteria: Design pressure gradient of <0.4 Pa/m in general with, as additional constraint, maximum airspeed of 5 m/s in the main ducts.

For comparison the rule of thumb recommended by Nilsson (1995) and ASHRAE (2007) is 1.0 Pa/m; it is 0.8 Pa/m by Schild et al. (2009) while Hvenegaard (2007) accepts 1.5-2.0 Pa/m for systems with moderate operation time (offices).

The latter condition of 5 m/s was imposed because losses in bends and fittings are proportional to the air velocity squared. The break-even point of pressure gradient versus air speed was in this case Ø630 mm.

The air terminals were replaced by diffuse ceiling ventilation (Fan et al. 2013). Air is supplied in the plenum above the acoustic ceiling and distributed through cracks to the room below. The inlet velocity is very low and with no fixed jet direction, hence the term diffuse. The diffuse ceiling, which measured 5 Pa at 100 % airflow and 1-2 Pa at 30 % airflow, is employed in the office spaces to reduce the pressure losses of conventional mixing terminals (approx. 30 Pa) and to increase draught-free comfort.

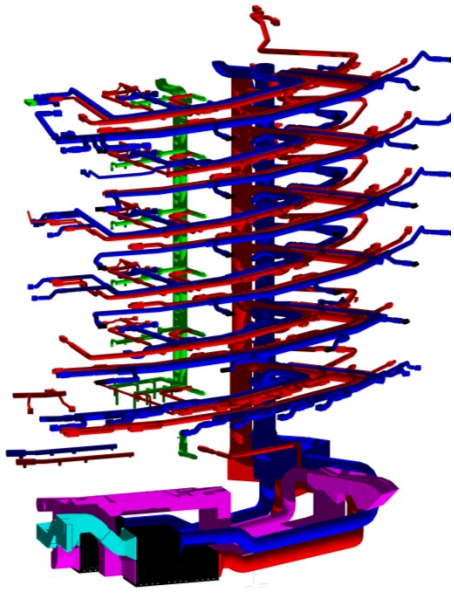

FIG 3. 3D view of ventilation system in Navisworks

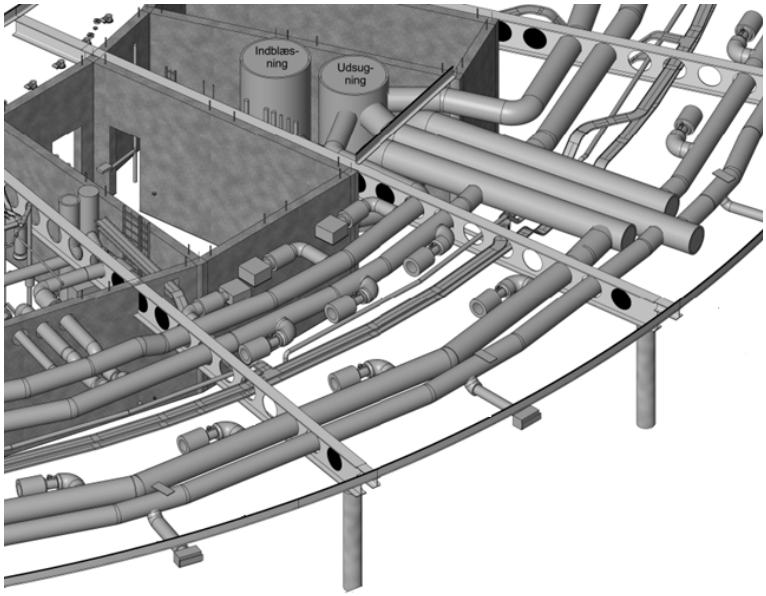

FIG 4. 3D view of floor section in Navisworks

With low-pressure ventilation systems, it is prudent to consider the motor, fan and drive efficiency because it can decrease significantly if the combination of airflow and pressure rise is not near the combinations giving peak efficiency. To avoid oversizing, smaller air handling units were installed in parallel two and two. At low load one unit shuts down, thus increasing flexible operation while maintaining fan efficiency. To recover heat, the air handling units were equipped with rotary heat exchangers with an efficiency of 80% or better.

3.2 Passive cooling strategy

The passive cooling strategy is four-legged with leg 1-3 depicted on FIG 2:

1. Automatic façade openings
2. Mechanical supply ventilation from the main air handling units to rooms with no façade and rooms on ground floor (safety reasons)
3. Mechanical exhaust from the atria

4. Cooling of IT-racks by room air

The first three legs of the passive cooling strategy reduced the energy consumption for night cooling considerably, from the initial all mechanical ventilation solution with 1-2 ACH (SFP = 0.5 kJ/m^3) to the final hybrid strategy with SFP = 0.11-0.125 kJ/m^3.

The fourth leg cools the IT-racks on each floor by simple mechanical exhaust with air supply from adjacent rooms. FIG 5 depicts this as red markings.

This makes it possible to turn off the main ventilation system outside office hours, while still cooling the racks with room temperature air supply. Depending on current building heat demand, the generated heat is either exhausted or distributed to the atrium depending on the current building heat demand which utilises the excess heat in a sensible manner and increases the overall building energy efficiency.

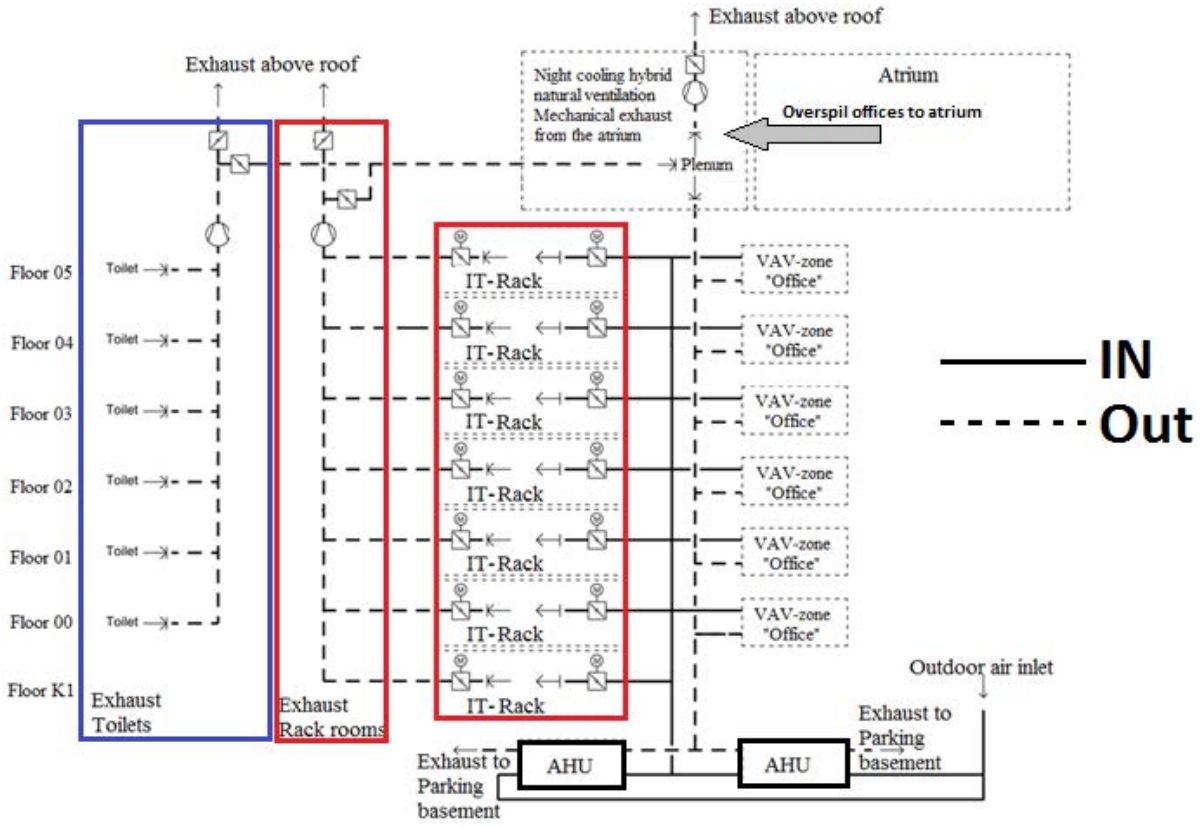

FIG 5. The ventilation system layout.

4. Results

The design pressure drops of the 19 air handling units with ductwork are 450 Pa to 550 Pa. This is the pressure drop from outdoor air intake to inlet to the office with full design air volume. In comparison, Hvenegaard (2007) reported the mean pressure drop from 100 mechanical ventilation systems in operation to be approx. 1400 Pa.

The energy efficiency, i.e. the specific fan power, is depicted on FIG 6. The figure shows measured values on the finalised installation at maximum flow rate. Systems for night cooling and exhaust systems have very low SFP values because of very short duct routing.

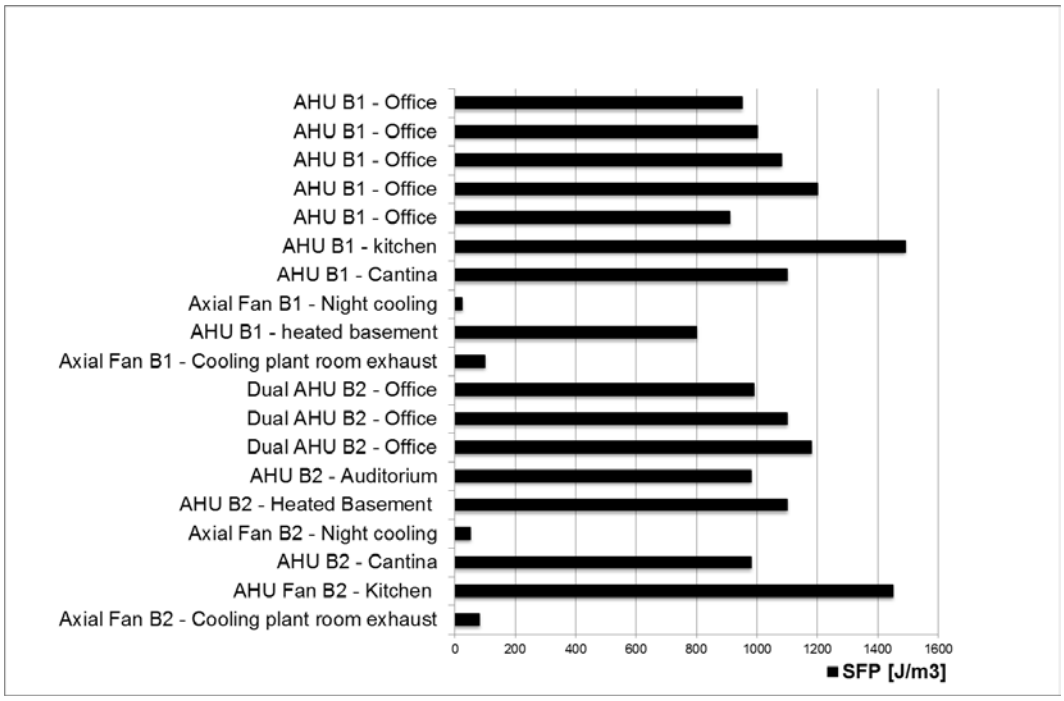

FIG 6. The specific fan power of the different air handling unit at maximum flow rate.

From FIG 6, the yearly mean specific fan power can be derived. SFP_{year} is a key performance indicator which is comparable across buildings and expresses the practical ventilation system efficiency. The results are shown in TABLE 1, however, the runtime can only be estimated at this current stage.

*TABLE 1. Yearly mean specific fan power [SFP_{year}]**

	Building one	Building two
Daytime ventilation**	0.80 kJ/m^3	0.79 kJ/m^3
Night cooling hybrid systems	0.125 kJ/m^3	0.11 kJ/m^3

* Time and flow weighted average SFP_{year} calculation: $q_{v1} \times SFP_1 \times t_1 + q_{v2} \times SFP_2 \times t_2 \ldots / q_{v1} \times t_1 + q_{v2} \times t_1 \ldots$ where q_v = air handling unit air flow, t= runtime and indices 1,2,…,n equals mode1,2,…,n; as an example mode 1 = 50 %, mode 2 = 75% etc.

** Ventilation during office hours, axial fans not included as they operate at night

In TABLE 2 the SFP is weighted by maximum flow rate. These results are not biased by the estimation of runtime, thus they are useful for evaluating the performance of the ventilation system before the final completion of the building.

*TABLE 2. Flow weighted specific fan power of max flow rates [SFP_{max}]**

	Building one	Building two
Daytime ventilation**	1.08 kJ/m^3	1.03 kJ/m^3
Night cooling hybrid systems	0.15 kJ/m^3	0.14 kJ/m^3

* Flow weighted SFP_{max} calculation: $(q_{v1} \times SFP_1 + q_{v2} \times SFP_1 + \ldots) / (q_{v2} + q_{v1} + \ldots)$ where q_v = air handling unit air flow and indices 1,2,..,n equals mode1,2…,n; as an example mode 1 = 50 %, mode 2 = 75% .

** Ventilation during office hours, axial fans not included as they operate at night

4.1 Energy consumption

The total calculated primary energy demand is 40.5 kWh/m^2/year for the two office buildings. Allowed primary energy demand is 41.1 kWh/m^2/year according to the Danish building code low-energy class 2015. The main thermal properties of the building envelope are listed in TABLE 3.

The distribution of the energy demand is depicted on FIG 7. It shows that the fans consume 23 % of the total energy consumption.

TABLE 3. Building insulation properties

Component	U-value	g-value	Visual transmittance
Curtain wall facade -glazing to floor ratio 30 % -glazing to façade ratio 60 %	Total 0.65 W/m^{2}K Opaque = 0.15 W/m^{2}K Transparent = 0.8 W/m^{2}K	g = 0.51 and ext. solar shading	71 %
Atria skylight: triple layer glazing	1.0 W/m^{2}K	g = 0.27	60 %
Roof	0.10 W/m^{2}K		
Basement walls	0.15 W/m^{2}K		
Basement floor slap	0.10 W/m^{2}K		

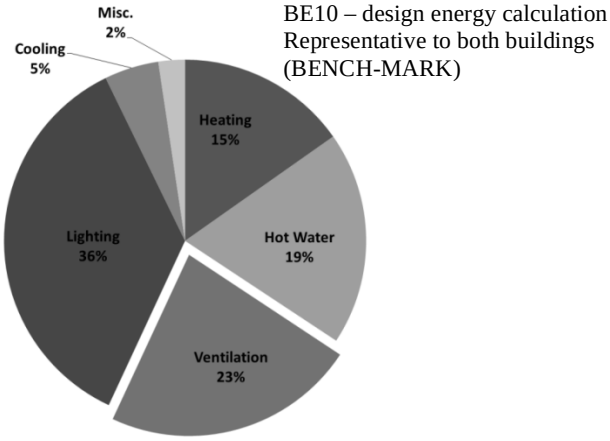

FIG 7. Primary energy demand in % - Total energy demand 41 kWh/m^2/year with no renewables.

5. Conclusion

The market for energy-efficient ventilation focuses on natural and hybrid solutions, leaving mechanical ventilation side-lined with a reputation of being energy-consuming and noisy. This paper shows a case where the design of conventional mechanical ventilation systems:

- was managed by a team of engineers, architects and contractors that understood their common goals, and agreed and adhered to a shared design process
- followed existing guidelines with some additional pressure-reducing technologies like diffuse ceilings and parallel air handling units
- was measured to be very energy efficient with an all units average SFP value of 1.0-1.1 kJ/m^3 (0.8 kJ/m^3 at yearly average airflow) compared to the Danish building code maximum allowed

SFP of 2.1 kJ/m^3. The energy use in this case is higher than custom best practice research systems with SFP as low as 0.6 and 0.33 kJ/m^3, but if these research systems were scaled to the same size as these buildings (one building has max. airflow approx. 180,000 m^3/h), they would take up significantly more building space

- the low pressure ventilation system is likely to be as low noise and it is low energy, resulting in less problems with noise
- low energy ventilation systems can help reduce energy demand in low energy buildings and subsequently reduce or remove the need for renewables. In other instances the reduced energy for ventilation can be “invested” in a less energy efficient layout or more freedom in the architectural expressions

6. Acknowledgements

The authors wish to express their gratitude to ALECTIA A/S for providing the case building.

References

ASHRAE. 2007. Handbook Applications. American Society of Heating, Refrigerating and Air-Conditioning Engineers

Berry J. 2000. Super-efficient mechanical ventilation. Indoor Built Environment 9. 87-96. 10p.

Fan J., Hviid C.A., Yang H. 2013. Performance analysis of a new design of office diffuse ceiling ventilation system. Energy and Buildings 59. 9 p.

Hviid, C.A. 2010. Building integrated passive ventilation systems. Ph.D. thesis, Dept. of Civil Engineering, Tech. Univ. of Denmark, Lyngby, Denmark.197 p.

Hviid, C.A., Svendsen, S. 2012. Wind and stack-assisted mechanical ventilation with heat recovery and night cooling, PSO project 339-24, Report R-282, Dept. of Civil Engineering, Tech. Univ. of Denmark, Lyngby, Denmark. 121 p.

Hvenegaard, C.M. (2007). Den lille blå om ventilation. 2nd edition. Dansk Energi. 120 p.

Jagemar, L. 2003. Målinger på ventilationsanlæg med lavt elforbrug i nyere kontorbygninger. By og Byg Dokumentation 039. Danish Building and Urban Research. Hørsholm. Denmark. 51 p

Nilsson L.J. 1995. Air-handling energy efficiency and design practices. Energy and Buildings 22. 1-13. 14 p.

Pérez-Lombard L., Ortiz J., Coronel J.F., Maestre I.R. 2011.A review of HVAC systems requirements in building energy regulations. Energy and Buildings 43. 255-268. 14 p.

Pérez-Lombard L., Ortiz J., Pout C. 2008. A review on buildings energy consumption information. Energy and Buildings 40. 394-398. 5 p.

Schild P.G., Mysen M. 2009. Recommendations on Specific Fan Power and Fan System Efficiency. Technical Note AIVC 65

Terkildsen S. 2013. Development of mechanical ventilation system with low energy consumption for renovation of buildings. Ph.D. thesis. Dept. of Civil Engineering. Tech. Univ. of Denmark. Lyngby, Denmark. 137 p.

Terkildsen S., Svendsen S. 2013. Performance potential of mechanical ventilation systems with minimized pressure loss. Internationl Journal of Ventilation 11. 13 p.

Wouters P., Delmotte C., Faÿsse J. C., Barles P., Bulsing P., Filleux C., Hardegger P., Blomsterberg A., Pennycook K., Jackman P., Maldonado E., Vitor L. and de Gids W. 2001. Towards improved performance of mechanical ventilation systems. EC JOULE- TIP-Vent project. 58 p.

Energy Balance Calculation and Nearly-Zero-Energy Standard of Industrial Buildings

Pascal Brinks [1,2]
Oliver Kornadt [1]
René Oly [2]

[1] TU Kaiserslautern, Department Building Physics / Low-Energy Buildings, Germany
[2] Lindab S.A., Astron Research & Development, Luxemburg

KEYWORDS *Industrial buildings, energy balance calculation, building simulation, nearly-zero-energy buildings, air tightness, infiltration, energy transport via ground*

SUMMARY
After 2020 all buildings in Europe have to be conceived and executed as "nearly-zero-energy buildings". For industrial buildings this poses an enormous challenge as their current energy standards are far behind and little research exists in this field. Due to few experiences the energy performance of industrial buildings is mainly still assessed with the same methods as residential buildings. This research project reviews the applicability of such methods for the industrial building sector using transient building simulation linked with a finite-difference ground model and air-flow network modelling. Required leakage data of typical light steel building components is measured in an air tightness test stand. The focus lies on air infiltration and thermal losses through large concrete slabs.

The main findings were that the current infiltration rating methods do not represent the variety of industrial buildings as inside temperature, building height and leakage distribution are not recognized. For zero-energy buildings it will further be required to introduce a monthly based method for infiltration rating to respect the irregular availability of renewable energy during the year. Further it is shown that vertical slab insulations are more reasonable for large slabs as energy gains by summer overheating can better be stored under the building when no horizontal insulation exists. For large slabs under low heated buildings this storing effect is an important saving potential. It is identified that current ISO standards are often not applicable for assessing industrial buildings.

1. Introduction

The adopted European directive on the energy performance of buildings sets a "nearly-zero-energy standard" for all buildings erected in Europe after 2020 (European Union, 2010). For the residential building sector this seems to be an ambitious but feasible goal as many new dwellings already reach a high energy standard and many lighthouse projects with this standard exist. Office buildings also caught up as many companies appreciate representing them as "green companies". But for industrial buildings no such high standards were built yet except some special single cases. In matters of energy saving these buildings still lag behind even if they have to meet the nearly-zero-energy requirements as soon as others. Reasons are not only the high pricing pressures in this sector but also a lack of technical solutions and holistic low-energy building concepts.

In the past many European countries did not even distinguish between the energy performance rating of industrial and residential buildings at all. First steps were made in the last years by implementing different requirements, assessment data or usage profiles in the energy rating methods as e.g. in the Méthode de calcul (2012) in France or the DIN V 18599 (2011) in Germany.

In spite of these first steps many parts of energy balance calculation methods are still based on the findings for residential buildings. For office buildings, schools or other similar buildings these methods may partially be applicable. But industrial buildings not only contain of different building components as for example light steel envelopes and dome -or skylights in the roof. They also have a very different building shape (large and flat). And further their usage is completely different as inside temperatures can range between 12 °C and 20 °C (partially with long night and weekend setbacks) and large open sectional doors can have a significant impact on the energy performance as well.

All these aspect have to be respected for future concepts. Especially when buildings shall be supplied by renewable energy it is crucial to know more exactly when which energy demand exists for a building. Thus current international energy balance methods were checked for their application for industrial buildings. Therefore the building simulation package TRNSYS and the air-flow network simulation TRNFLOW were mainly used. The focus of this project was on the air tightness of light steel building envelopes and the thermal losses via large concrete slabs on grade.

2. Air Tightness of Industrial Buildings

The air tightness of a building is important to reduce energy losses caused by infiltration during the heating period. In many European countries the infiltration during the year is calculated according to the static approach in EN ISO 13789 (2008). This method calculates the infiltration by reducing the n_{50}-value with a factor e. It shall reduce the infiltration as the difference pressure during the year is far lower than the 50 Pa generated during a fan pressurization test. This factor e is based on simulations carried out for residential buildings and can be chosen from a table dependent only on the wind shielding and the number of exposed facades.

Actually the difference pressures and therefore the infiltration depends significantly on other parameters such as building height, shape of the building, leakage distribution and very important the inside temperature (Younes *et al.*, 2011), (University of Wisconsin Madison, 2009). This is neglected completely in EN ISO 13789 (2008), so it can be assumed that the factors obtained in simulations for dwellings do not fit for large industrial buildings.

Further it is clear that the infiltration is not constant during the whole year. Due to buoyancy it considerably depends on the difference temperature between in -and outside which obviously varies between summer and winter. Future zero-energy buildings will surely be supplied by renewable energy, often based on solar energy. As solar energy is not constantly available during the year it is important to know when the energy losses by infiltration and therefore the energy demand occurs.

To check the applicability of the current method for future industrial buildings in simulations, input data describing the leakages of typical industrial buildings is required. This leakage data was measured in a new built tightness test stand.

2.1 Measurements in an Air Tightness Test Stand

In an air tightness test stand joints of standard connections used in typical light steel industrial buildings were measured. In detail the connections at the eaves, the verge, wall and slab and connections to accessories as well as between vapour barriers were analyzed. Figure 1 shows two different test set-ups. On the left side the connection between stapled vapour barriers was measured, on the right the joint between a concrete slab and a trapezoidal light steel wall was analyzed. The specimen had a length of 3 m.

A detailed description of the test stand cannot be given here but figure 2 shows the general set-up principle. The measurement in the test stand basically works like a blower door test of a whole building. A fan blows air into a tight box where the test items with the isolated joint are installed.

By the fan action a difference pressure between inside and outside the box is induced and measured by a manometer. At the same time the air flow into the box is measured by an anemometer. This air flow complies with the flow through the isolated joint between the building components. For every detail at least seven different pressure stages were measured.

FIG 1. Measurement of the joint between two vapour barriers (left) and between slab and wall (right)

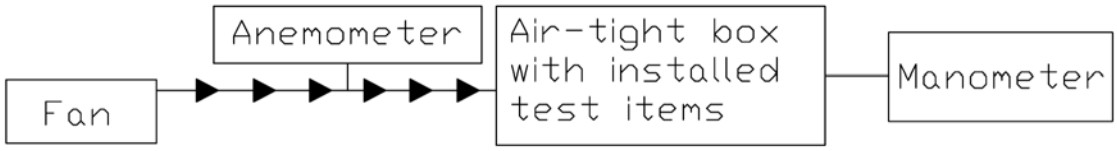

FIG 2. Principal test set-up of the air tightness test stand

The measurement results showed a relatively consistent leakage distribution all over the building envelope. Leakages in the roof usually comply with those in the wall which influences the following simulations of air infiltratin.

2.2 Simulation of Infiltration in an Air-Flow Network

The leakage data gained in the measurements could now be used for the simulations of air infiltration through the envelope of typical industrial buildings. For this the air-flow network model TRNFLOW was used which allows modelling every single crack of a building based on the measured leakage coefficients and flow exponents from the test stand.

The software TRNFLOW is coupled with the transient building simulation TRNSYS to create an interaction with the building. The simulations were carried out using time steps of 15 minutes. For detailed information about the network model it is referred to (University of Wisconsin Madison, 2009) and (Weber *et al.*, 2003).

Figure 3 and 4 show simulation results for different buildings all having the same n_{50}-value of 1.0 h^{-1}. For a better interpretation the infiltration is averaged for every month. All results show a clear dependency on the season. Due to stack effects caused by high temperature differences the infiltration is significantly higher in winter than in summer. For the chosen climate (German reference climate: city of Potsdam) the influence of strong winds in March is also visible.

For the simulations C_p-values generated by the C_p-generator by TNO (Knoll and Phaff) were used. These values required for estimating the pressure difference at the building envelope were chosen for a moderate shielding.

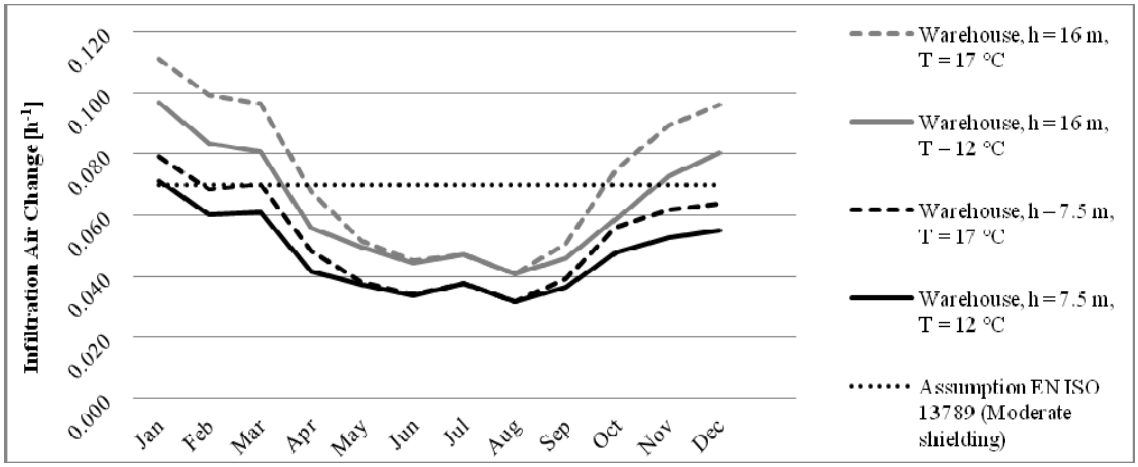

FIG 3. Simulated air infiltration during the year for buildings with different heights and temperatures

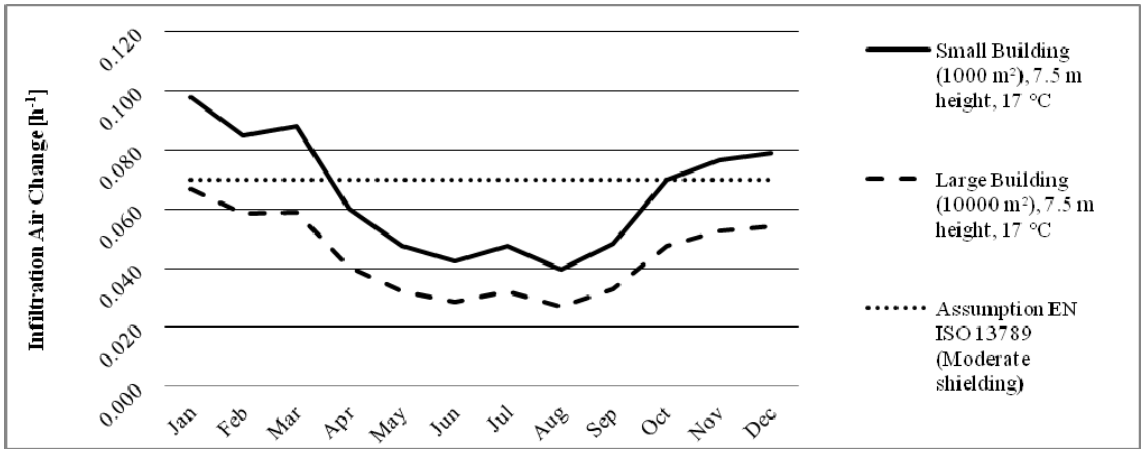

FIG 4. Simulated air infiltration during the year for buildings with different ground areas

In figure 3 industrial buildings with different building heights and different minimum inside temperatures are compared. A maximum temperature limit during summer was not set as industrial buildings usually do not have cooling devices. The impact of both parameters height and inside temperature on the infiltration is considerable. With an increasing height the wind velocity rises, which causes a higher pressure difference and therefore a higher infiltration. Further the stack effect increases with the building height and causes the same effect.

A buoyancy driven infiltration rise is also caused by a higher inside temperature. The importance of this effect can be seen when summer and winter months are compared. In winter the inside temperature has a clear impact on the infiltration. When the temperature difference disappears in summer, both curves merge again.

Figure 4 shows the influence of the building size. Here a rather small industrial building (1000 m² ground area) is compared to a building with the same length/width ratio and the same height but a larger ground area (10000 m²). The infiltration of the larger building is clearly lower than for the small one. The reason is the different roof/wall ratio and respectively a different leakage distribution. The simulations show that the variations between different industrial buildings are huge and general assumptions for an infiltration are not possible.

Thus the current method according to EN ISO 13789 (2008) does not seems to be appropriate for the assessment of infiltration losses of these diverse industrial buildings.

2.3 Losses via Open Doors in Industrial Buildings

In residential buildings and many office buildings the losses via open doors are negligible as doors are small and opening times are short. But for logistic or production buildings the energy losses through open sectional doors can amount for a considerable part of the total energy demand. The higher the insulation standard of a building is, the more important such ventilation losses get. But in current energy balance calculations losses via open doors are not considered. It is of course hard to estimate already during the design stage how long the opening times will be and the user behaviour can surely vary a lot in practice. But for zero-energy building design it will not be possible to neglect it anymore. To show the influence of this deciding parameter, transient simulations of the air flow through large sectional doors were carried out. For this purpose TRNFLOW was used again considering the air flow with a discharge coefficient according to Dascalaki (1995),(University of Wisconsin Madison, 2009).

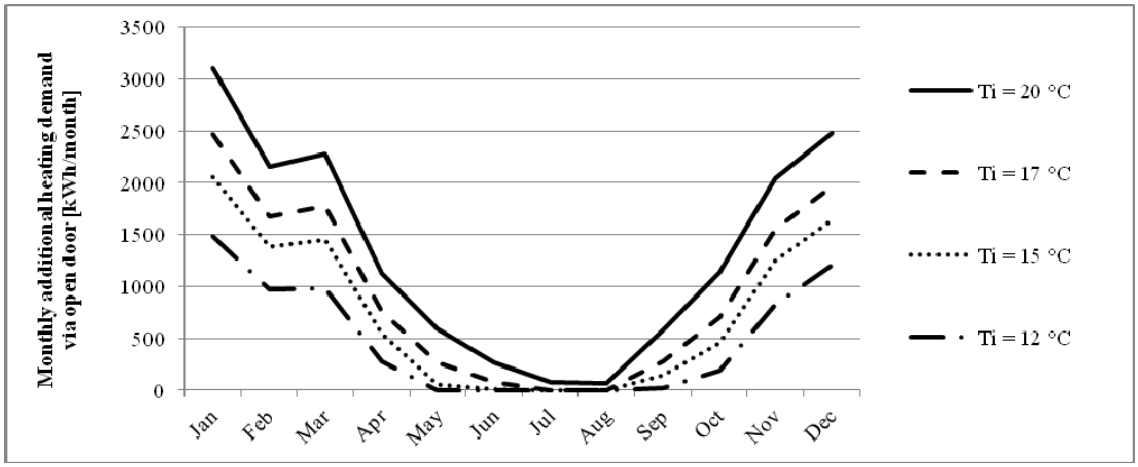

FIG 5. Additional energy demand by infiltration via open doors for 1 h opening time per working day

Results for the simulation of a 2000 m² large warehouse, located in Potsdam (Germany) are displayed in figure 5. It shows the additional heating demand during a year (monthly mean values) caused by an open sectional door of 4.80 m x 3.50 m with north orientation. The calculations assume that the door is opened for 1 h per working day distributed into short periods over the whole working shift. The inside temperature of a building is obviously a deciding parameter for the infiltration through an open door. Simulations only represent single sided ventilation. Opening two opposite doors can of course increase the infiltration by draft.

3. Energy losses via ground

Industrial buildings are usually built with a large slab on grade. These slabs can go up to some thousands of square meters, thus it is obvious that the thermal transport under industrial buildings differs significantly from the conditions under small dwellings. For appraising thermal losses via soil in Europe the EN ISO 13370 (2008) is often used for all kinds of buildings. To evaluate its applicability for large slabs on grade, simulations using the type 49 (Solar Energy Laboratory, 2012), a finite-difference model for ground modelling implemented in TRNSYS, were carried out. This transient 3D ground model was also utilized in IEA-Task 34/43 and testing results in comparison with other models were overall good (MCDowell *et al.*, 2009). Figure 6 shows the mean heat flow density through the slab of a small residential building with 20 °C inside temperature averaged per month. The heat flow was once simulated using the finite-difference model interacting with the building simulation model and once calculated according to EN ISO 13370 (2008). For the simulations the fourth year is shown which has an almost steady state.

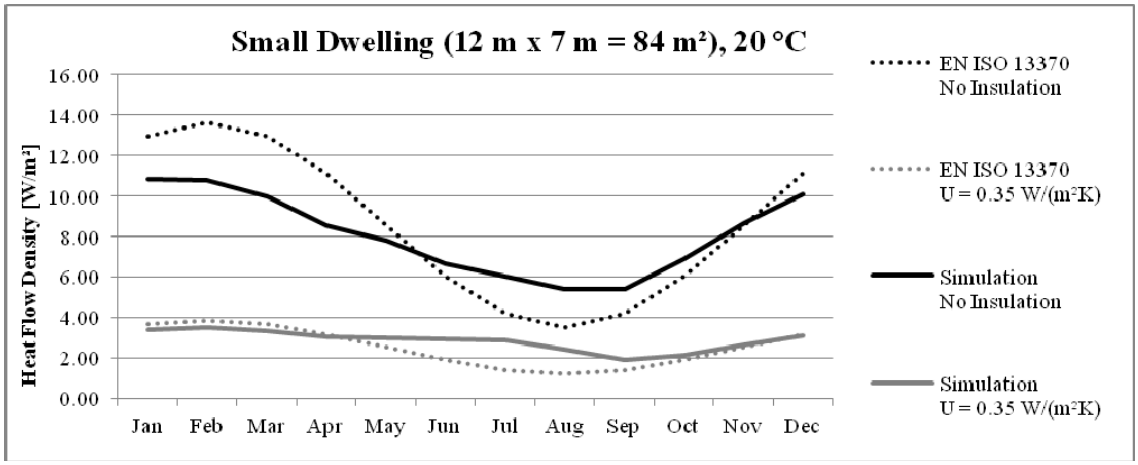

FIG 6. Heat flow density acc. to EN ISO 13370 versus transient simulations for a small building

The insulated slab shows a very good compliance between both models during the heating period. For an uninsulated slab the deviations are bigger, while the simplified EN method is up to 20 % on the safe side. In summer the heat flow is underestimated for both slabs as the EN ISO 13370 does not recognize the overheating of a building during summer in an appropriate way. Storage effects are only recognized by a periodic shift of about 1-2 months. In general the static method seems to be appropriate for such small buildings especially for insulated slabs where storage effects matter less.

Figure 7 shows the mean heat flow density through a large slab under an industrial building having a lower inside temperature of 15 °C. The storage effect in summer is directly visible. For uninsulated slabs or slabs with a vertical footer insulation it is even clearly bigger; in the middle of the slab temperatures of 20 °C and more arrise directly under the slab in summer. Until december the mean ground temperature under the slab still exceeds the low room temperature of 15 °C. Due to this energy gains can still be used until the turn of the year. Only in January first losses through the slab occur but they are still less than with a horizontal insulation. Only in March and April the losses through a slab without a horizontal insulation are bigger than with a short footer insulation. Using a horizontal insulation (holohedral or even a horizontal edge insulation) prevents the energy storing in summer. Besides the missing summer overheating protection this causes higher energy losses during the heating period and thus corrupts the total energy performance of a building.

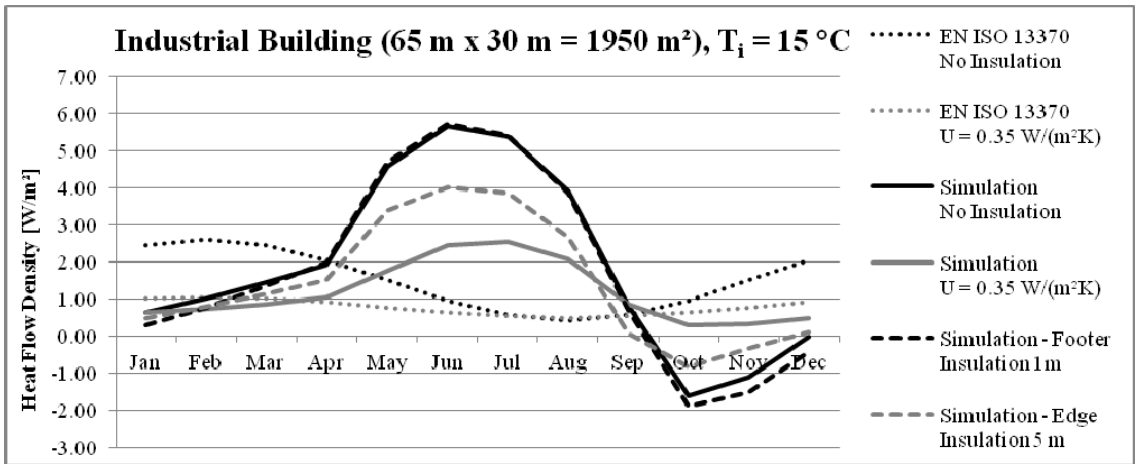

FIG 7. Heat flow density acc. to EN ISO 13370 versus transient simulations for an industrial building

In particular for zero-energy buildings supplied by renewable energy it is important to use the stored energy in months with few solar radiation (November – February). In March and April the higher losses by an only vertically insulated slab can easily be balanced by solar energy gains, which are already available in spring. Further a solution without a horizontal insulation saves costs and avoids design problems due to high loads on industrial buildings slabs.

4. Conclusions

The comparison of building simulations for industrial buildings with current appraisal methods showed that there are still lacks in their applicability to future low-energy industrial buildings. For a reasonable infiltration analysis the current static method is not sufficient. The infiltration should at least be determined dependent on the building height and the inside temperature. Further it should be based on monthly values and not averaged for the whole year. Moreover the infiltration losses via large open doors should be recognized in production and logistic buildings as it will not be possible to neglect these losses in future zero-energy building concepts.

In addition it was shown that horizontal insulations under large slabs can prevent storing energy from summer in the ground. Therefore vertical insulations seem to be the best solution for large industrial buildings. Unfortunately the thereby caused high U-values are partially not allowed by national energy balance regulations. For energy saving reasons this should be changed in the future. Further the possibility to use transient building simulation software for official energy performance certificates instead of static methods would be desirable. This would allow respecting the various parameters of industrial buildings better even if no universally valid methods yet exist.

5. Acknowledgements

This work was supported by the Fonds National de la Recherche Luxembourg (FNR). We thank the FNR for its kind support of the project “Concepts for nearly-zero-energy industrial buildings”.

References

Méthode de calcul Th-BCE 2012, Centre Scientifique et Technique du Bâtiment.

Dascalaki, E. and et al. (1995), “Predicting single sided natural ventilation rates in buildings”, Solar Energy, Vol. 55 No. 5, pp. 327–341.

EN ISO 13789 (2008), Thermal performance of buildings. Transmission and ventilation heat transfer coefficients. Calculation method

DIN V 18599 (2011), Energetische Bewertung von Gebäuden - Berechnung des Nutz-, End- und Primärenergiebedarfs für Heizung, Kühlung, Lüftung, Trinkwarmwasser und Beleuchtung.

EN ISO 13370 (2008), Thermal performance of buildings. Heat transfer via the ground. Calculation methods.

European Union (Ed.) (2010), DIRECTIVE 2010/31/EU OF THE EUROPEAN PARLIAMENT AND OF THE COUNCIL of 19 May 2010 on the energy performance of buildings (recast), L 153/13.

Knoll, B. and Phaff, H., “Manual for TNO Cp-generator”, available at: http://cpgen.bouw.tno.nl/cp/manual.asp (accessed June 2013).

MCDowell, T., Thornton, J. and Duffy, M. (Eds.) (2009), Comparison of a Ground-Coupling Reference Standard Model to Simplified Approaches.

Solar Energy Laboratory, U.o.W.-M. (2012), TRNSYS 17: Volume 4 - Mathematical Reference.

University of Wisconsin Madison (2009), TRNFLOW Manual: A module of an air flow network for coupled simulationwith TYPE 56 (multi-zone building of TRNSYS) Version 1.4, 19.11.2009, 19.11.2009.

Weber, A., Koschenz, M., Dorer, V. and Hiller, M. (Eds.) (2003), TRNFLOW, A new tool for the modelling of heat, air and pollutant transport in buildings with TRNSYS.

Younes, C., Abi Shdid, C. and Bitsuamlak, G. (2011), “Air infiltration through building envelopes: A review”, Journal of Building Physics, 35(3), pp. 267–302.

Experimental investigations of heat transfer in Thermo Active Building Systems in combination with suspended ceilings

Maria Alonso Alvarez, MSc [1]
Christian Anker Hviid, Professor, PhD [2]
Peter Weitzmann, Consulting engineer, PhD [3]

[1] Department of Civil Engineering, Technical University of Denmark, Denmark
[2] Department of Civil Engineering, Technical University of Denmark, Denmark
[3] COWI A/S, Denmark

KEYWORDS: *Thermo active building systems, suspended ceilings, heat capacity*

SUMMARY:
Thermo Active Building Systems (TABS), described as radiant heating or cooling systems with pipes embedded in the building structure, represent a sustainable alternative to replace conventional systems by using source temperatures close to room temperatures. The use of suspended ceiling in office buildings to cover acoustic requirements hinders the use of TABS. To measure the reduction of the heat capacity, several experiments are performed in a room equipped with TABS in the upper deck and mixing ventilation. The heat transfer is measured for different suspended ceiling covering percentages, occupancy scenarios and ventilation rates. The gained results indicate that the heat capacity coefficient of the ceiling surface is reduced by around 30% when the suspended ceiling covering is 70% of the total ceiling area, and 45% when the covering area is up to 87%. The results also demonstrate that the ventilation rate has a high influence on the convective heat capacity. When the ventilation rate is increased from 1.7 h^{-1} to 2.9 h^{-1}, the heat transfer coefficient increases up to 16% for the same occupancy and suspended ceiling layout.

1. Introduction

Global energy-related CO_2 emissions from human activities have continuously increased over the past years. Buildings account for around 32% of the total energy consumption of the countries members of the IEA, and it is in the provision of heating, cooling and ventilation where most of the energy is consumed (International Energy Agency 2013). Therefore the building sector must address the reduction of economic and environmental costs of energy used by means of technology developments, market strategies and government policies.

In this context, Thermo Active Building Systems (TABS), commonly described as radiant systems with pipes embedded in the building structure, recently appeared as a new alternative to cool or heat a space. The main difference with other radiant systems is that they benefit from the thermal storage capacity of the building structure. Due to the heat absorption of the thermal mass, the energy is stored and released over an extended period of time reducing the peak loads and temperature fluctuations.

These systems have been successfully implemented in mainly multi-storey office buildings where the benefits of the energy storage can be distributed from storey to storey (Schmidt 2004). Frequently office buildings require the installation of suspended ceilings to cover the acoustics requirements. However, the fulfilment of these requirements compromises the thermal performance of TABS by impeding the convective and radiant heat to be transferred to the space.

Previous researches have investigated the cooling capacity of TABS when the suspended ceiling is either totally or partially covered with acoustic ceilings. Contrary to what was expected, the results of the study performed by E. Pitarello (2008) shows that it is feasible to combine both techniques and still fulfil thermal and acoustic requirements. As a matter of fact, it was discovered that when covering up to 80 % of the ceiling, the cooling capacity was only lowered by around 25-30%.

Another study performed by H. Peperkamp and M. Vercammen (2009) investigates the cooling capacity reduction in relation with the covering percentage and the sound absorption of suspended ceilings. The study concludes that there is no noticeable reduction in the average sound absorption of the 500Hz to 4Hz band when the covering area is reduced from 100% to 80%.

The same embedded pipes can be used for both heating and cooling scenarios but until now, only cooling scenarios have been investigated in detail. Therefore this work investigates the heat transfer from heated ceilings for different suspended ceiling covering percentages and different occupancy scenarios.

2. Experimental Methods

2.1 Test facility

The experiments took place in a thermo active test facility with an internal area 21.6 m^2. The test facility includes a room surrounded by a thermal guard to control the outside conditions of the room. FIG 1 shows the exact geometry of the room and its surrounded guard.

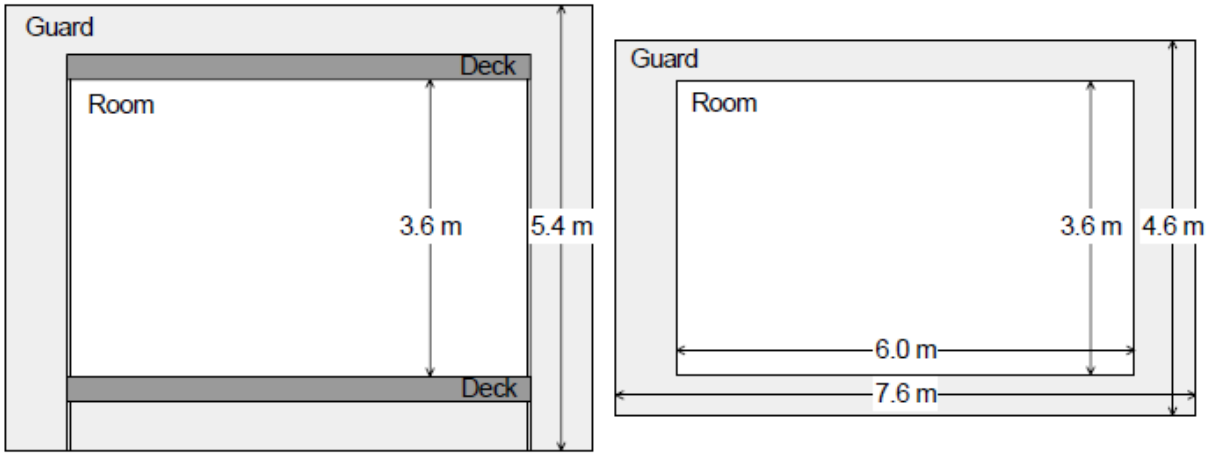

FIG 1. Front and plan view of the test facility with its corresponding dimensions

The upper deck consists of prefabricate hollow concrete slabs with integrated PEX pipes, that contains water at the desired flow rate. The height of the deck is 270 mm and the diameter of the pipes is 20 mm, positioned at 50 mm from the bottom of the deck as displayed in FIG 2.

FIG 2. Concrete hollow deck with integrated PEX pipes

During the investigations the temperature of the guard was set to be the same as the room temperature so that adiabatic conditions could be applied to room, walls and floor. .

2.2 Suspended ceiling

A suspended ceiling was installed in the test facility at a height of 2.7 m from the floor. It consisted of 600x600x15 mm mineral wool tiles mounted on wooden beams.

Three main suspended ceiling layouts were implemented varying in covering percentage (87%, 70% and 53%) as shown in FIG 3.

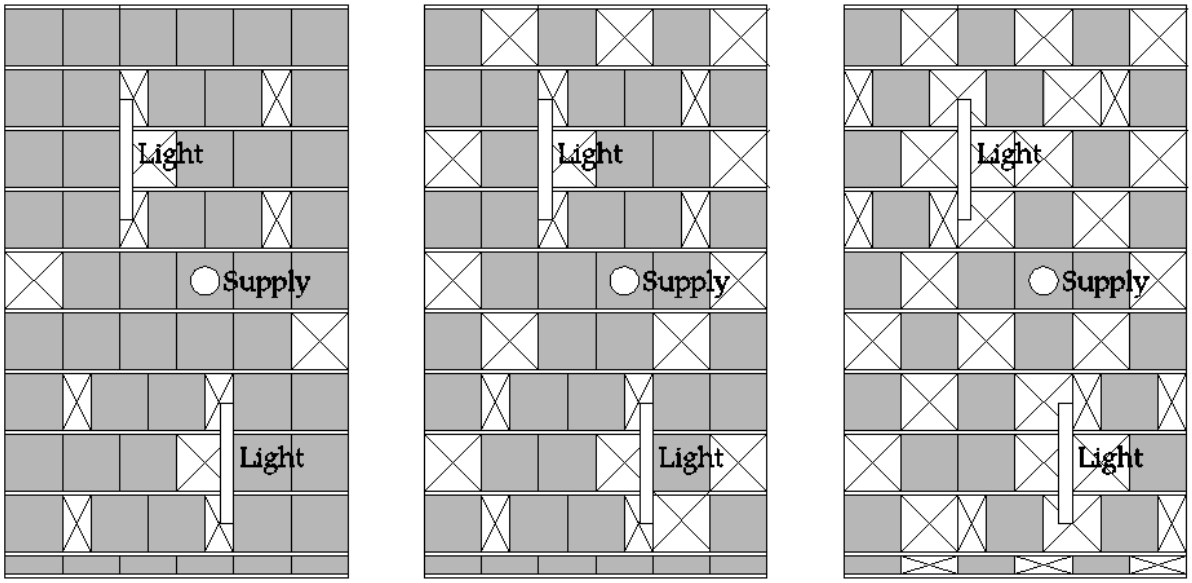

FIG 3. 87%, 70% and 53% suspended ceiling covering layouts

2.3 Equipment

A flow unit was used to provide the required supply water temperature at a constant flow (0.1 kg/s) to the upper deck pipes. A flow meter “Danfoss Mass 1100, DN10” measured the mass flow in the upper deck as an analog signal in the range of 0-20mA corresponding to 0-720kg/h.

In order to ensure the circulation of air at the desired temperature, two fans were positioned inside the guard. The temperature of the guard is controlled by a power controller with a 0-10V signal in order to obtain the desired conditions outside the room; in this case, adiabatic conditions were simulated.

A cooling coil was used to provide ventilation to the room. The temperature was controlled with a PID control system. The air was supplied to the room by a LCA ceiling diffuser.

Concerning internal loads, a double person office was simulated. by using two black barrels as dummies (100 W each), two desktop computers in stand-by mode (68 W each) and two lamps (36 W each) hanging 0.9 m from the upper deck. The total heat load during occupied hours was 18.84 W/m^2.

A LabVIEW application was used to measure and control the data collected by an Agilent 34970A data acquisition unit (data logger). Type TT (Copper/constantan) thermocouples measured absolute temperatures through a build-in function in the data logger, while thermopiles made of either three or five serially connected thermocouples measured temperature differences.

A micromanometer from Furness Controls model FCO510 measured the pressure drop across an orifice from Fläkt model EHBA-012-1 in the supply and exhaust ducts.

2.4 Measurements

The same temperature sensors were used during all the measurement series. Some of the sensors were placed during the construction process so that it was possible to measure the temperature of the concrete deck and the guard, as well as the fluid temperature. Surface- and air temperatures were measured in several locations in the occupied area and the plenum.

Steady state conditions were used during all the experiments. The heating investigations consisted of two series (series "a" and series "b") of 8 experiments each. Both series were identical except from the fan speed, and therefore the air flow supplied to the room. Experiments number 1a to 8a corresponded to a low ventilation rate (1.7 ± 0.1 h^{-1}) while experiments number 1b to 8b corresponded to a high ventilation rate (2.9 ± 0.1 h^{-1}).

The defined ceiling covering percentages (87%, 70% and 53%) and a non covered layout were tested as well as occupancy/ non-occupancy scenarios.

Each experiment lasted a minimum of 4 days in order to ensure steady state conditions. The data was measured within intervals of 30 seconds and the average of the data collected the last 12 hours of experiment was used for the heat capacity calculations.

2.5 Heat transfer

Energy balance of the deck is assumed. The flows composing the energy balance of the upper deck are defined in Eq. (1)

$$q_{fluid} = q_{down} + q_{up} + q_{guard} \quad (1)$$

Where q_{fluid} heat flow between the pipes and the deck (W/m^2)
q_{down} heat flow through the ceiling surface (W/m^2)
q_{up} heat flow through the floor (W/m^2)
q_{guard} heat losses through the sides of the deck (W/m^2)

The sides of the decks are insulated to minimized heat loss to the thermal guard, q_{guard} . This heat loss has been measured in previous studies demonstrating that it only accounts for around 2-3% of the total heat flows (Weitzmann 2004). In the current investigation, q_{guard} is thus neglected.

To obtain the heat flow through the ceiling surface of the upper deck, it is necessary to analyze first the heat flow through the floor and the heat flow between the pipes and the deck.

Temperature sensors located across the plywood layer used as floor covering make possible to calculate q_{up} through Eq. (2).

$$q_{up} = \frac{1}{R_{floorcovering}} \cdot \Delta T_{floorcovering} \quad (2)$$

Where $R_{floorcovering}$ thermal resistance of the floor covering (m^2K/W)

$\Delta T_{floorcovering}$ temperature difference across the floor covering (K)

The heat flow from the fluid to the deck can be calculated by multiplying the properties of the fluid and the temperature difference between supply and return as shown in Eq. (3).

$$q_{fluid} = \frac{m \cdot C_p \cdot (T_{return} - T_{supply})}{A_{deck}} \quad (3)$$

Where m fluid mass flow rate (kg/s)

C_p fluid heat capacity (J/kgK)

T_{return} fluid return temperature (K)

T_{supply} fluid supply temperature (K)

A_{deck} area of the deck (m^2)

The heat flow through the ceiling surface can be found through Eq. (1), (2) and (3), as simplified in Eq. (4).

$$q_{down} = q_{fluid} - q_{up} \quad (4)$$

Eq. (5) is used to calculate the heat capacity coefficient trough the upper deck.

$$U_{hc} = \frac{q_{down}}{(T_{fluid} - T_{room})} \quad (5)$$

Where U_{hc} heat capacity coefficient through the ceiling (W/m^2K)

T_{fluid} average temperature of the fluid (K)

T_{room} room temperature (K)

The thermal capacity of a heated ceiling can also by expressed as the ratio of heat flow through the ceiling to the temperature difference between the ceiling surface and the room as specified in Eq. (6). $h_{ceiling}$ is the total heat transfer or heat exchange coefficient of the ceiling surface including radiation and convection.

$$h_{ceiling} = \frac{q_{down}}{(T_{ceilingsurface} - T_{room})} \quad (6)$$

Where $h_{ceiling}$ heat transfer coefficient of the ceiling (W/m^2K)

$T_{ceilingsurface}$ surface temperature of the deck (K)

For the calculations, the room temperature is considered as the average between air temperature and mean radiant temperature. The temperature of the fluid is the average water temperature between supply and return.

3. Results

The heat flow through the ceiling surface as a function of the temperature difference between the fluid and the room is illustrated in FIG 4. The graph classifies the data according to the setup of the experiment but there is no distinction on whether internal loads are included or not. Two trend-lines are created to distinguish the results; each of the trend-lines corresponds to one series of experiments. For an equal temperature difference between the fluid and the room, the resultant heat flow is in average 2 W/m^2 larger in the high air flow series than in the low flow ones. The tendency also indicates that the experiments performed without suspended ceilings result in a larger heat flow as function of the temperature difference. And, as expected, the opposite occurs for the layout where 87% of the ceiling area is covered; in this case the results are clearly below their respective trend.

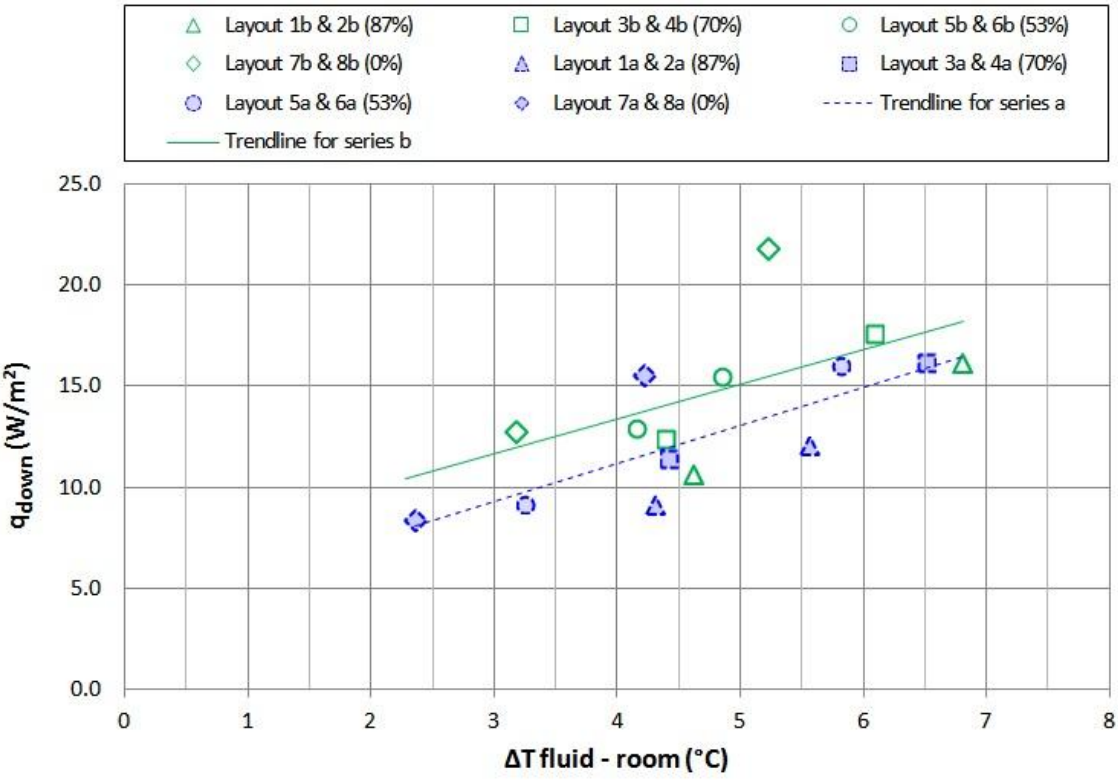

FIG 4. Heat flow through the ceiling surface, q_{down}, as function of the temperature difference between the operative temperature in the room, and the mean fluid temperature in the deck

FIG 5 combines the results of the heat capacity coefficient calculated based on Eq. 5 as function of the covering percentage and the results of the heat transfer coefficient defined in Eq. 6. In this figure, the experiments conducted with and without occupancy are not sorted since the differences between occupancy- non-occupancy layouts are not in any case larger than 5%. The heat capacity coefficient of the ceiling is reduced by 30% when the suspended ceiling covering rate is 70% of the total ceiling area. The reduction is increased to 55% when the covering rate is up to 87% of the ceiling area. It is also observed that series “a” results into a heat capacity coefficient up to 14% lower than series “b”. At the same time, the results of the heat transfer coefficient shows a variation between series “a” and series “b” which is up 16% when the ceiling is not covered. The heat transfer coefficient of series “b” for non covered layouts is up to 6.3 W/m^{2}K, whereas the same value for series “a” is 5.3 W/m^{2}K. At the same time, the results for a covering rate of 87% show a heat transfer coefficient of 3.1 W/m^{2}K and 2.7 W/m^{2}K for series “b” and series “a” respectively.

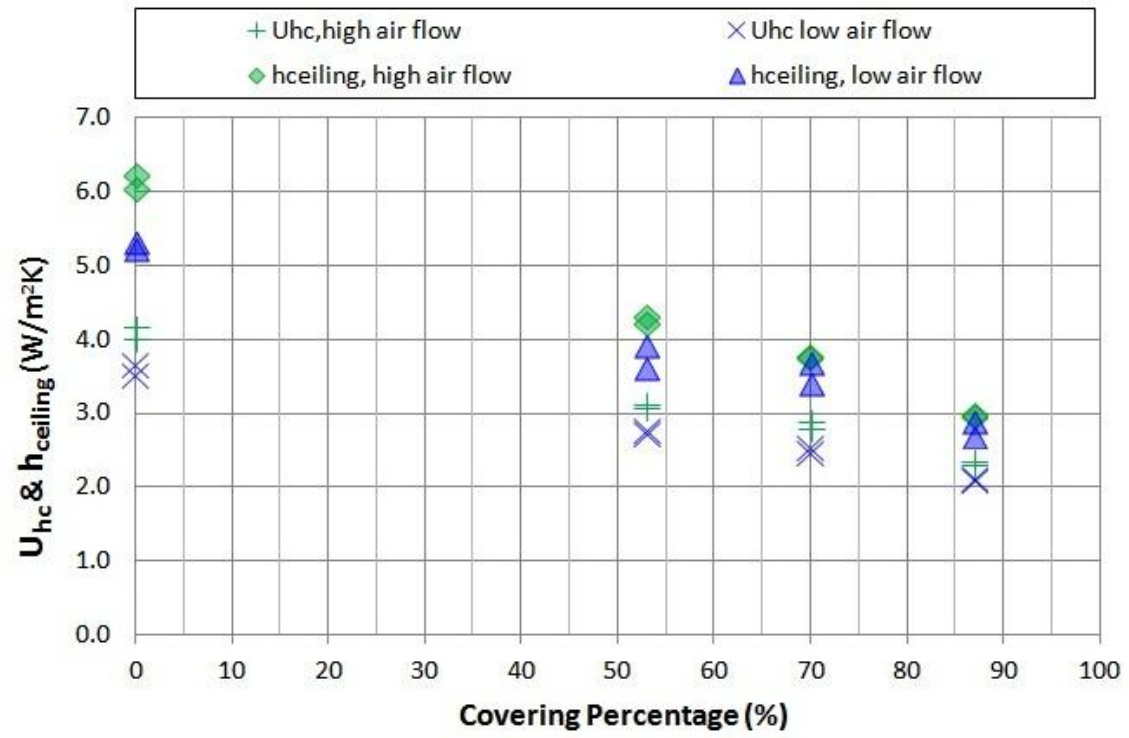

FIG 5. Heat capacity coefficient, U_{hc} and heat transfer coefficient, $h_{ceiling}$, as function of the covered percentage of the suspended ceiling

4. Conclusion

This project investigates the heat transfer of thermo active building systems in combination with suspended ceilings. The gained results show that the combination of suspended ceilings and TABS is a real alternative to conventional heating or cooling systems, especially for low energy or passive buildings where the heating and cooling demands are reduced.

The different layouts investigated show that both the covering rate and the ventilation rate have a great influence on the results. Those experiments conducted with a high ventilation rate result in up to a 16% higher heat transfer coefficient between the ceiling surface and the room than the same experiments performed with a low ventilation rate. The ventilation enhances the convective heat transfer between the ceiling surface and the room and therefore it is assumed that the variation between series correspond to an increase on the convective heat transfer coefficient.

Regarding differences between the results obtained in this project and previous investigations, it can be concluded that, as expected, the cooling capacity of the ceiling is higher than the heating capacity. The cooling capacity coefficient is reduced by 30% when using a suspended ceiling covering rate of 80%, whereas the heating capacity coefficient is reduced by the same range when using a covering rate of only 70%. This proves that the decline on the thermal performance is larger in the heating case.

It can be conclude that the thermal performance of TABS in combination with suspended ceilings is still acceptable for covering rates up to 70%. Coverings larger than that will considerably compromise the performance of the systems.

5. Acknowledgements

This research work would not have been possible without the help and support from the Civil Engineering Department in DTU as well as COWIfonden for financing the project.

References

International Energy Agency, I. 2013. Redrawing the energy-climate map, World Energy Outlook Special Report.

Peperkamp, H. and M. Vercammen. 2009. Thermally activated concrete slabs and suspended ceilings'.

Pittarello, E., P. Weitzmann, and B. W. Olesen. 2008. The cooling capacity of the Thermo Active Building System combined with acoustic ceiling.

Schmidt, D. 2004. Methodology for the modelling of thermally activated building components in low exergy design. Ph.D. thesis, Institutionen for byggvetenskap, Stockholm.

Weitzmann, P. 2004. Modelling building integrated heating and cooling systems. Ph.D. thesis, Danmarks Tekniske Universitet, Lyngby.

Estimating the input parameters of lumped building thermal models on the basis of standard design values

Pavel Kopecký, Ph.D.[1]
Kamil Staněk, Ph.D.[1]

[1] Czech Technical University in Prague, Faculty of Civil Engineering, Czech Republic

KEYWORDS: *building simulation, lumped parameters, estimation of input parameters*

SUMMARY:
This paper focuses on testing whether the input parameters of lumped parameter building thermal models could be estimated in advance on the basis of the known geometry and envelope composition of the building. The study was performed using a virtual test family house insulated in a low-energy standard. Two variants of the house were defined: a light one, made of timber structure, and the a heavier one, made of perforated brick blocks with external insulation. The reference results were calculated using a complex building energy simulation model. Then, simulations using four logical structures of lumped parameter models were conducted. The values of the lumped parameters in these models were estimated on the basis of available information on the test building, i.e. on the basis of basic drawings and known composition of building components. The results achieved on the lumped models were then compared with the reference solution. The results of this study show that input parameters of lumped parameter building thermal models can be estimated in advance only on the basis of standard information on the building.

1. Introduction

This paper deals with lumped parameter thermal models of a building. The lumped parameter thermal models divide building components into a small number of temperature-uniform parts on which heat balance is set. Thus, the lumped parameter models extensively reduce the number of unknown values which in turn considerably increases the speed of calculation. The general goal of such models is to exclude the variables with negligible influence, but at the same time maintain the physical nature of the problem and ensure reasonable accuracy. Since the input parameters to lumped models aggregate several aspects together, their interpretation can be ambiguous.

Lumped parameter thermal building models can be used for various purposes. (Nielsen, 2005) used a simple lumped model to develop a building design tool. (Kämpf, et al., 2007) developed a model which was used for calculations at the district level. (Huijbregts, Z., et al., 2012) used a lumped hygro-thermal building model to study the impact of global warming scenarios on museum buildings. (Prívara et al., 2011) used a simple lumped parameter room model to implement an advanced predictive controller of a heating system in a real building.

Model predictive control seems to be one of the most promising real applications of building lumped models. The identified lumped parameter building thermal model could be used to determine optimal set-point trajectories and optimize control of heating and cooling systems. Therefore, tons of literature about lumped building thermal models deal with the issue of applying system identification techniques using measured data. However, installation of sensors is labor-intensive, collection of a sufficient dataset needs some time and measurements cannot be performed in advance. This paper therefore tests whether the input parameters of lumped parameter models could be estimated on the basis of the known geometry and envelope composition of a building.

2. Lumped parameter thermal building models

Buildings are usually composed of:

- external components (walls, roof), all together marked with a lower index “ext”;
- transparent components (windows), marked with a lower index “w”;
- internal components (internal load bearing wall, partitions, ceiling, ground floor), all together marked with a lower index “int”.

As a starting point for the derivation of lumped parameter models, the following “parent” building thermal model is used, see Figure 1. (Hudson and Underwood, 1999) or (Gouda et. al, 2000) introduced similar model structures.

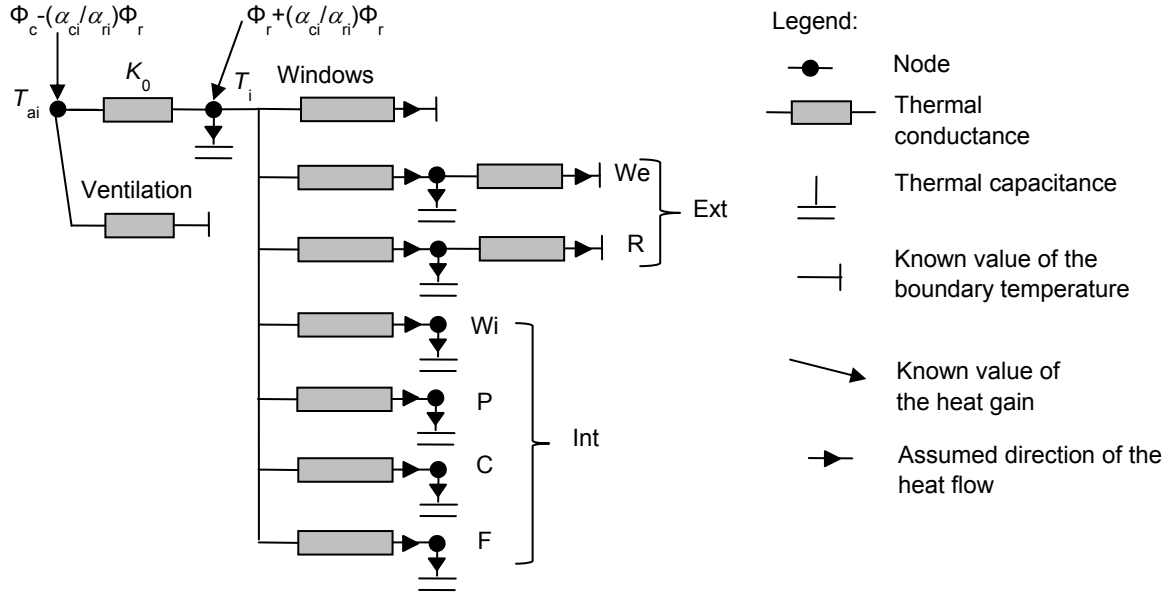

FIG. 1: Model composed of several one-node branches

This model has already been simplified because of the first order description of building components. Parallel paths in this model establish: one state for internal environment, two states for external components (external walls, roof), four states for internal components (partitions, internal load bearing wall, ceiling, floor on the ground) and two fast heat transfer paths representing the windows and ventilation. The model structure reflects the typical building components which have already been introduced. There is one missing, yet important aspect in the parent model. The model does not contain the heat transfer path through the floor on the ground to the external environment.

Lumped parameter models can be understood as even more simplified versions of the parent model depicted in Figure 1. Four lumped models are presented below (see Figure 2 and Figure 3). None of the lumped models decouples radiative and convective parts of heat gains. It corresponds to the very high value of the coupling conductance K_0 of the parent model. The internal temperature in the lumped models should be understood as a temperature composed of the internal air temperature and the mean radiant temperature of internal surfaces. Some error can therefore occur in the ventilation heat flow path.

The lumped model which is hereinafter designated as models 4 preserves the topology of external and internal components. The model 2 and the model 3 are reduced version of the model 4. In the model 3, it is assumed that the thermal capacity built in internal building components is negligible or easily accessible from the internal node. The model 2 replaces six parallel branches by just two branches and only one of these contains a capacity node. This model could well represent an office room with a glazed façade, i.e. a room where only negligible thermal capacity is built in external building

components. The model 1 could be seen as a special case of the model 2 with the infinite value of thermal conductance between the internal node and the capacity node.

Heat storage in model 1 is modeled using only one capacitance which is immediately accessible for the purpose of storing the heat gains, i.e. the temperature of internal mass is in equilibrium with the internal temperature. A similar one-node approach can be found in (Burmeister and Keller, 1998) and (Antonopoulos and Koronaki, 1998). The structure of model 2 was used by (Nielsen, 2005) to develop a simple building design tool.

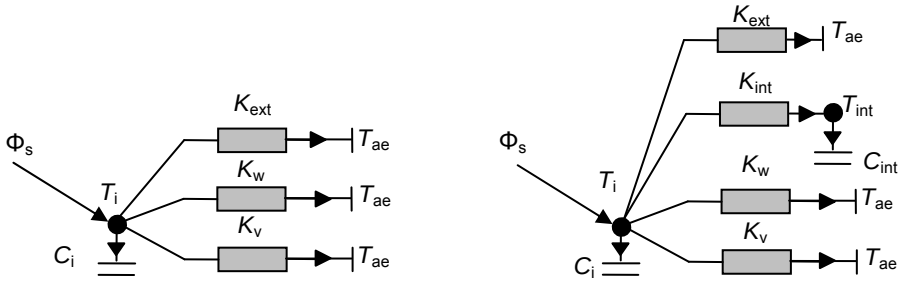

FIG. 2: Thermal circuit for the model 1 and model 2

The structure of model 3 was introduced by (Laret, 1981). (EN ISO 13790, 2008) and (EN ISO 13792, 2012) contain the first order analogy of the model 3 (capacity C_i is neglected). Model 4 logically combines the model 2 and model 3. (Kramer, 2012) used almost identical model structure and found it adequate even for the purpose of simulating heavy weight historical uninsulated buildings. The identical model structure was also presented in (Masy, 2007).

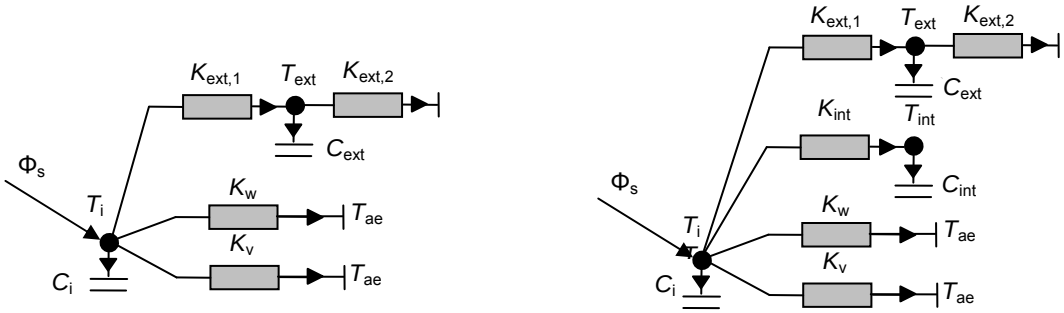

FIG. 3: Thermal circuit for the model 3 and model 4

3. Case study

3.1 Virtual test house

The virtual test house simulates a new family house corresponding to the low-energy standard. Two distinct variants of the house were defined: a heavier one, made of perforated brick blocks with an external insulation (V1) and a light one, consisting of a timber structure (V2). The detailed description of the house is not given here due to the lack of space. The reference simulation results were calculated using a complex thermal model of the virtual test house (Staněk, 2013). In order to reduce the complexity of the problem, following assumptions were used:

- One zone model was considered.
- Free-floating situation was simulated, i.e. thermal response of the building was driven by climatic conditions only. The simulation used the 2010 real measured data from the weather station in Prague Karlov.
- Air change rate was assumed to be constant during the whole year (0,3 h^{-1}).

- The floor on the ground was assumed to be adiabatic.
- Solar heat gains were calculated in advance using a separate solar model.

3.2 Estimation of input parameters

3.2.1 Standard design values

The transmission thermal conductance of a building component is defined as thermal transmittance multiplied by the corresponding area ($K = UA$). By way of analogy, thermal capacitance can be calculated as the areal heat capacity multiplied by the corresponding area ($C = \kappa A$). Table 1 contains the values of basic input parameters for the case of virtual test house.

Table 1: Standard design values

	K_{ext} (W/K)	K_w (W/K)	K_v (W/K)	C_{ext} (J/K)	C_{int} (J/K)
V1	67,7	66,2	39,6	$8{,}0\times10^7$	$7{,}2\times10^7$
V2				$2{,}5\times10^7$	$2{,}9\times10^7$

3.2.2 Position of temperature nodes in the parent model

There are some methods for the calculation of connecting conductance between the internal environment and the capacity node in one-node wall models, for details see (Mathews, 1994) and (Gouda, 2002). This case study uses a simpler approach. The proposed method situates the capacity node in the center of capacitance (analogy with the center of gravity). See the example of a two-layer wall depicted in Figure 4, where κ_1 (J/(m^{2}K)) denotes the areal thermal capacity of the layer 1, and κ_2 (J/(m^{2}K)) denotes the areal thermal capacity of the layer 2. In this case, the center of capacitance is located in the distance x_{cap} (m) from the internal surface of the wall.

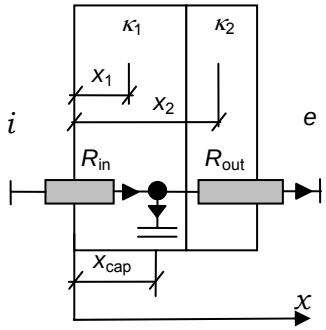

$$x_{cap} = \frac{\kappa_1 x_1 + \kappa_2 x_2}{\kappa_1 + \kappa_2}$$

FIG. 4: Center of capacitance for a two-layer wall with a corresponding thermal network.

3.2.3 Input parameters in lumped models

In simplified models, the input parameters have to be further lumped. In this study, thermal conductances and thermal capacitances acting in parallel are simply summed up. Thermal capacitances are considered as total values without any reductions. Estimated values of input parameters for the first three models are summarized in Table 2. In the model 1, the thermal capacity C_i (J/K) is assumed to be a sum of contributions from air, furniture, windows, internal building components and external building components. In the model 2, the thermal capacitance C_i (J/K) is assumed to be a sum of contributions from air, furniture and windows. Thermal capacitance C_{int} (J/K) is assumed to be a sum of contributions from internal and external building components. Conductance K_{int} (W/K) is assumed to be a sum of conductances which constitute the thermal link between internal temperature node and center of capacitance in a relevant building component of the parent model. In model 3, the thermal

capacitance C_{ext} (J/K) is assumed to be equal to thermal capacitance C_{int} from the model 2 and conductance $K_{ext,1}$ is assumed to be equal to K_{int} from the model 2.

Table 2: Estimated values of input parameters of the models 1,2,3

	Model 1	Model 2		Model 3	
	C_i (J/K)	K_{int} (W/K)	C_{int} (J/K)	$K_{ext,1}$ (W/K)	C_{ext} (J/K)
V1	$1{,}53\times10^8$	2470	$1{,}52\times10^8$	2470	$1{,}52\times10^8$
V2	$5{,}37\times10^7$	1319	$5{,}27\times10^7$	1319	$5{,}27\times10^7$

Estimated values of input parameters for the model 4 are summarized in Table 3. The thermal capacity C_{ext} (J/K) is assumed to be the contribution from external building components. The thermal capacity C_{int} (J/K) is assumed to be the contribution from internal building components. Conductances $K_{ext,1}$ and K_{int} (W/K) are calculated as the sum of conductances between the internal temperature node and the capacity node in a relevant building component of the parent model.

Table 3: Estimated values of input parameters of the model 4

	$K_{ext,1}$ (W/K)	K_{int} (W/K)	C_i (J/K)	C_{int} (J/K)	C_{ext} (J/K)
V1	715	1758	$9{,}57\times10^5$	See Table 1.	
V2	125	1193			

3.3 Simulation results

The free-floating internal temperature calculated using lumped parameter models was compared with the free-floating internal temperature calculated using the reference numerical model. The reference internal temperature was calculated as the weighted mean from the mean radiant temperature of all surfaces and the internal air temperature. The standard values of convective and radiative heat transfer coefficients were used as weights (3 W/(m^{2}K) and 5 W/(m^{2}K)).

For the sake of clarity, only the time-period between the 180th and 195th day is expressed in figures. Three variants are depicted: the reference course calculated using the reference numerical model (designated as “ref”), the course calculated using the estimated values of input parameters (designated as “estim”), and finally the course calculated using the optimized values of input parameters (designated as “optim”). Optimization process starts from the already estimated values of input parameters and attempts to find the values which are more appropriate. In this study, only thermal conductances have been assumed to be variable. Thermal capacities have been fixed to their total values. Goodness of fit was the objective function to be maximized.

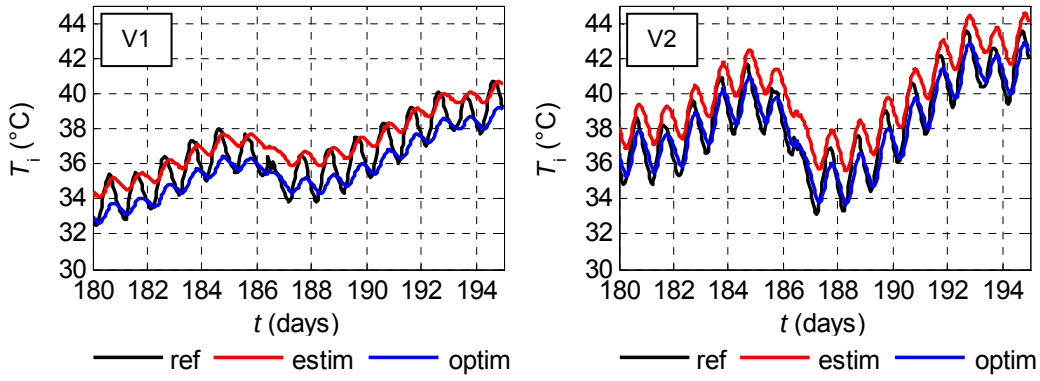

FIG. 5: Model 1 – Free-floating temperature.

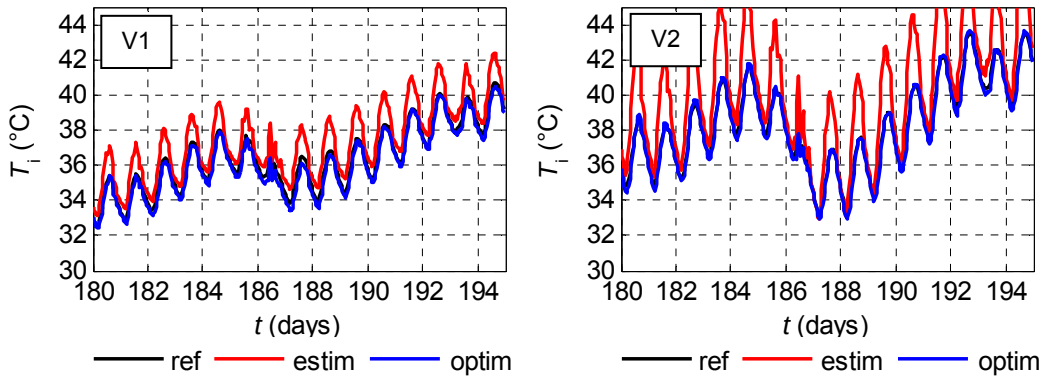

FIG. 6: Model 4 – Free-floating temperature.

As seen in Figure 5, the model 1 did not reproduce the daily dynamics correctly. The case calculated using the estimated inputs reached slightly higher values of daily means than in the reference case. Optimization determined the necessary correction of about 22 W/K (see Table 4) and it was similar for all other lumped models. As seen in Figure 6, the model 4 using the estimated values of input parameters resulted in reasonably good estimates of the free-floating temperature in case of the brick house (V1). In case of the wooden house (V2), the daily amplitude was overestimated. The capacity C_{int} was not sufficiently accessible to dampen the internal temperature fluctuation, i.e the thermal conductance between the internal environment and the capacity node was underestimated. After its optimization, the model 4 showed very good compliance with the reference case. It should be noted that the objective function was found to be very flat (see Figure 7). Rather different parameter sets thus can lead to very similar prediction of the internal temperature. Estimated and optimized values of time constants are summarized in Table 5.

Table 4: Estimated vs. optimized values of parameters of the model 1 and model 4

	Model 1		Model 4					
	$K_{ext}+K_v+K_w$ (W/K)		$K_{ext,1}$ (W/K)		K_{int} (W/K)		K_w+K_v (W/K)	
	estimated	optimized	estim	optim	estim	optim	estim	optim
V1	173,5	196,2	715	404	1758	3963	105,8	127,3
V2		194,5	125	517	1194	4252		126,8

Table 5: Estimated vs. optimized values of time constants in hours for all models

		M1	M2		M3		M4		
V1	Estimated	244	0,10	261,4	0,10	247,8	0,10	240,8	19,8
	Optimized	216	0,06	226,8	0,07	219,8	0,06	207,4	25,8
V2	Estimated	89	0,18	100,1	0,18	90,8	0,18	67,2	22,0
	Optimized	79	0,07	83,1	0,07	80,4	0,05	76,3	7,6

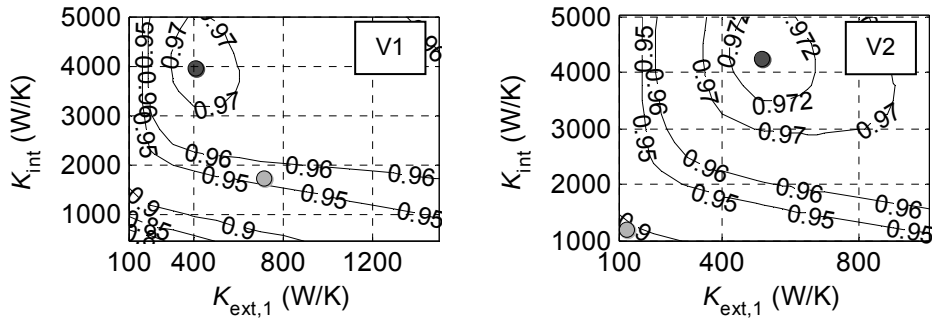

FIG. 7: Model 4 – the shape of objective function (conductance K_w+K_v was fixed to optimized value).

4. Discussion

Resulting differences between the reference solution and simplified models could be classified as differences in daily dynamics, differences in long-term dynamics, and systematic differences in annual mean values. The last type of error was common to all simplified models and hopefully was the result of the user uncertainty in modeling.

The values of connecting conductances between the internal environment and capacity nodes are important for good representation of daily dynamics. If the thermal conductance is too low (i.e. accesibility of the thermal capacitance behind conductance is poor), the internal temperature fluctuates too much. Unfortunately, the internal temperature amplitude is extremely sensitive to correct setting of the connecting conductance. The center of capacitance method led to fairly good estimates of accessibility in case of the brick house. This was not the case of the light wooden house, where the accessibility was set too low. Therefore, the evident question is: how could the estimation of thermal conductances between the internal environment and capacity nodes be improved. Another open question is, whether the lumped thermal capacitances should be to some extent reduced. This study was performed on the basis of total values of thermal capacitances. However, at least in case of the wooden insulated house, it is evident that the total value of the thermal capacity is not used to dampen the oscillation of the daily temperature swing.

Model 1 was not able to capture the internal temperature dynamics neither on the basis of estimated values nor after optimization of parameters. The total value of the building thermal capacity made it possible to reproduce longer dynamics, but the values of daily dynamics were reproduced very poorly. However, the daily means in the optimized model 1 were rather accurate. This is an important conclusion, as it means that the energy needs of insulated buildings could be estimated quite accurately and quickly even with this very simple dynamic model. The substantial advantage of the model 1 consists in the fact that the input parameters are standard design values.

5. Conclusions

The structure of all lumped parameter models investigated in this paper was derived from a typical topology of building components. Firstly, a parent thermal model was derived from this topology. Then, four lumped thermal models were derived by further reducing the parent model. The values of parameters in lumped models were estimated as the sum of thermal conductances or capacitances acting in parallel in the parent model. Thermal conductances in lumped models were derived from the position of capacity nodes placed in the parent model. A simple method to estimate the node position was used. Thermal capacitances in lumped models were assumed to be total values without any reductions.

The case study was performed using a virtual test family house insulated in a low-energy standard in free-floating conditions. It was observed that accurate representation of daily swings in the internal temperature is difficult. The daily amplitude of the internal temperature was very sensitive to the correct setting of thermal conductances connecting the internal node and other capacity nodes. It seems that these thermal conductances can only be roughly estimated in advance from drawings. With the exception of the first order model, all other lumped models using the estimated values of input parameters showed good compliance with the reference model (goodness of fit close to 90 %). It is therefore concluded from that the estimation of input parameter values based on the known geometry and envelope composition led to satisfactory results.

There are some open questions relating to future work:

- Under which conditions can the parent model be replaced by a lower-order model without significantly reducing accuracy? Why do simplified lumped models perform well; and under which conditions do they not work so well?
- What is an accurate lumped model of heat transfer through the slab on the ground?

- Which additional parts should be added to a lumped parameter building thermal model in order to accurately describe the HVAC system dynamics?

References

Antonopoulos, K.A. and Koronaki, E., Apparent and effective thermal capacitance of buildings, Energy 23(3): 183-192, 1998.

Burmeister, H., Keller, B., Climate surfaces: a quantitative building-specific representation of climates, Energy and Buildings 28, 1998.

EN ISO 13790, Energy performance of buildings – Calculation of energy use for space heating and cooling, 2008.

EN ISO 13792, Thermal performance of buildings – Calculation of internal temperatures of a room in summer without mechanical cooling – Simplified methods, 2012.

Gouda, M., M., Danaher, S., Underwood, C., P., Low order model for simulation of a building and its heating system, Build. Serv. Eng. Res. Technol. 21, 2000.

Gouda, M., M., Danaher, S., Underwood, C., P., Building thermal model reduction using nonlinear constrained optimization, Building and Environment 37, 2002.

Hudson, G., Underwood, C., P., A simple building modeling procedure for Matlab/Simulink, Proc. Of Building Simulation, Kyoto, Japan, 1999.

Huijbregts, Z., Kramer, R.P., Martens, M., H., J., van Schijndel, A., W., M., Schellen, H., L., A proposed method to assess the damage risk of future climate change to museum objects in historic buildings, Building and Environment 55, 2012.

Kämpf, J., H., Robinson, D., A simplified thermal model to support analysis of urban resource flows, Energy and Buildings 39, 2007.

Kramer, R., P., From castle to binary code. The application of inverse modeling for the prediction and characterization of indoor climates and energy performances. MSc. Thesis, Eindhoven University of Technology, 2012.

Laret, L., Contribution au développement de modèles mathématiques du comportement thermique transitoire de structures d'habitation, PhD thesis, Université de Liège, 1981.

Macy, G., Definition and Validation of a Simplified Multizone Dynamic Building Model Connected to Heating System and HVAC Unit, 2007.

Mathews, E. H., Richards, P. G., Lombard, C. 1994. A first-order thermal model for building design, Energy and Buildings 21(2): 133-145.

Nielsen, T. R., Simple tool to evaluate energy demand and indoor environment in the early stages of building design. Solar Energy 78, 2005.

Prívara, S., Široký, J., Ferkl, L., Cigler, J., Model predictive control of a building heating system: The first experience, Energy and Buildings 43(2011) 564-572

Richards, P., G., Mathews, E., H., A Thermal Design Tool for Buildings in Ground Contact, Building and Environment 29, 1994.

Staněk, K., A transient multi-zone model for heat transfer in buildings – unpublished work, 2013.

Reliability of meta-modelling in robust low-energy dwelling design

Liesje Van Gelder, M.Sc.
Hans Janssen, Professor
Staf Roels, Professor

Building Physics Section, KU Leuven, Belgium

KEYWORDS: *meta-modelling, probabilistic design, reliability*

SUMMARY:
In building design, energy demand and life-cycle costs are commonly calculated based on deterministic stationary or dynamic simulations. However, many contributing parameters are inherently uncertain, resulting in potentially unreliable performance predictions. To overcome this, a probabilistic design method is recommended to take uncertainties into account. Such an uncertainty-based optimisation often requires many simulations, making it extremely time-consuming. Here, meta-modelling can be of high interest. A meta-model aims to mimic the original numerical model with a simplified fast model. However, the simplicity of the meta-model - some aspects of the original model are inherently neglected - might affect the reliability of the results. This topic is investigated in this paper by means of a case study of robust cost optimisation of a low-energy dwelling. To maximise calculation efficiency, the meta-model has to be trained on as few samples as possible, taking into account meta-model reliability. Hence, a meta-modelling procedure is proposed and result reliability is investigated for meta-models based on different sample sizes. It is concluded that meta-models can be reliably used in probabilistic design and built with a reasonable sample size.

1. Introduction

Building performance optimisation typically uses deterministic simulations to select the best performing design according to one or more performance indicators, such as energy demand, life-cycle cost, … As many contributing parameters are inherently uncertain, such deterministic optimisation not necessarily leads to the best performing design. Therefore, probabilistic performance optimisation is recommended to take these uncertainties into account. The global framework of probabilistic design is described in section 1.1. Unfortunately, such a probabilistic design often requires significant simulation effort. To reduce calculation time, meta-modelling is of high interest as the original model is replaced by a fast simplified equation-based model, as described in section 1.2.

Because meta-model reliability is essential in probabilistic design, this paper investigates this aspect with a simplified robust cost optimisation of a low-energy dwelling. For that purpose, optimisation is performed on both the original model and several meta-models, differing in sample size.

The case study is described in section 2, the results are shown in section 3. The main observations and recommendations with respect to meta-model reliability are summarised in section 4.

1.1 Probabilistic design

In design problems, contributing input parameters can be divided into three categories. Design parameters, such as the thermal resistance of a wall, the type of ventilation system , … are fully controllable and their values are to be selected. Inherently uncertain parameters, such as the impact of workmanship, the actual ventilation rate value, … are uncontrollable by the designer. Finally, scenario parameters deal with future, for example economic or climate, scenarios. By ascribing these parameter

categories to a different layer in a multi-layered sampling scheme as shown in FIG 1, all design options are subjected to the same uncertainties and a direct comparison for several future scenarios is enabled.

This multi-layered scheme, combined with sampling efficiency and convergence control (Janssen 2013), is proposed in Van Gelder et al. (2014) as a global probabilistic design method. In this method, first all potential design options are chosen with for example a full factorial scheme of the design parameters. Then a small multi-layered scheme is created by independent sampling of both uncertainty and scenario parameters, preferably uniformly filling the probability space. To start the Monte Carlo loop, the first design option and first scenario are selected. The small uncertainty sample is run in the model and enlarged until the desired outputs are converged. After that, the next scenarios are analogously run and more scenarios can be added until convergence of the design options or until all potential scenario values are calculated. Then, one can continue with the next design option. If all design options are converged, the outputs can be evaluated. This methodology requires execution of numerous Monte Carlo simulations, which may easily become computationally (too) expensive. The latter barrier can be overcome by use of meta-models, which mimic the original time-intensive model with a simpler and faster surrogate model.

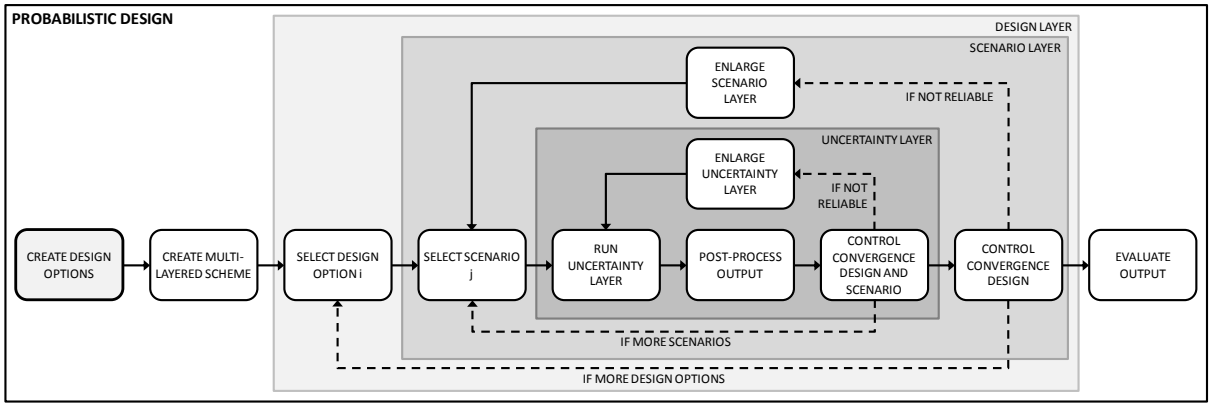

FIG 1. Probabilistic design method.

1.2 Meta-modelling

1.2.1 General aspects

Meta-models, also known as surrogate models, have the intention to mimic the original model but at a highly reduced calculation time. While for extreme cases, the original model might take days for one simulation, the meta-model only needs a fraction of this calculation time.

FIG 2 shows how to build such a meta-model based on several sample sets in order to enable cross-validation and to control calculation efficiency (Van Gelder et al. 2013b). First, all input parameters need to be sampled in a small scheme and run in the original model. Initially at least two sets are needed: one as training set to build the model, the other as validation set. Then a k-fold cross-validation is performed to control the reliability with validation indicators, which indicate how well the original model is approximated. This means that each sample set is once used as validation set, while the other sets act as training sets, resulting in as many validation indicator values as available sample sets (i.e. k). The coefficient of determination r^2, indicating the overall fit, and the maximal absolute error MAE can be used as indicators, among others. Sample sets are added until convergence of the minimal, maximal and average values of the selected validation indicators is satisfactory.

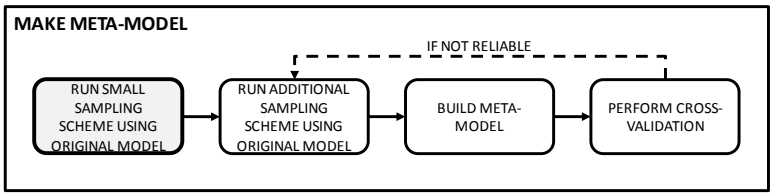

FIG 2. Meta-model construction.

1.2.2 MARS method

In this paper, cubic multivariate adaptive regression splines (MARS) (Friedman 1991, Jekabsons 2011) are used as meta-modelling method because of their good approximation ability and their fast calculation (Van Gelder et al. 2013b). Due to the use of hinge functions, model complexities can be taken into account. MARS models are of the form

$$\underline{y} = \sum_{i=1}^{m} c_i B_i(x) \tag{3}$$

Where $\underline{y}$ estimated output parameter
x input parameter vector
m amount of basis functions B_i, which can be a constant, a hinge function or a product of two hinge functions
c_i weight factors

2. Case study

To exemplify the probabilistic design method and to investigate the meta-model's reliability, a simplified case study of a semi-detached dwelling is used as shown in FIG 3. The dwelling has a floor area of 140 m², an uninsulated basement and overhangs for sun shading. Several low-energy design options are compared to select the most cost effective and robust option, with a comfortable indoor climate as auxiliary constraint. Therefore, both energy demand and maximal temperature are simulated, and net present costs are calculated afterwards.

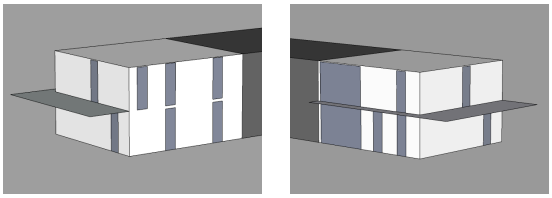

FIG 3. Dwelling model.

2.1 Output parameters

Following the European standard EN ISO 15459, the net present cost of all energy-related dwelling components is calculated over 30 years with a cost-calculation tool developed in research project IWT TETRA BEP 2020 (Verbeeck et al. 2013). The net energy demand is therefore simulated with a building energy simulation (BES) model (see section 2.3), which can be replaced by a meta-model (see section 2.4). Furthermore, the maximal temperatures in the dwelling are simulated with the BES model as well to be able to penalise those design options with a potential overheating risk.

Dwelling owners need confidence in selected design options as they require guaranteed net present costs for their investments in energy efficiency and indoor climate. Ideas from robust design are therefore incorporated by optimising mean performance and minimising spread (Zang et al. 2005).

That way, designs that best resist the uncertain and scenario parameters can be selected. Therefore, effectiveness ε and robustness R_p indicators were defined and illustrated in previous research (Van Gelder et al. 2013a). For a positive output parameter *y* to be minimised, the indicators are:

$$\varepsilon(x_n) = 1 - \frac{y_{50}(x_n) - y_{\min}}{y_{50} - y_{\min}} \quad (1)$$

$$R_P(x_n) = 1 - \frac{y_{50+P/2}(x_n) - y_{50-P/2}(x_n)}{y_{50+P/2} - y_{50-P/2}} \quad (2)$$

Where P user specified percentage of included sample points
y_q q^{th} percentile of distribution of *y* under full uncertainty
$y_q(x_n)$ q^{th} percentile of distribution of *y* after selecting design options x_n
y_{min} simulated minimal *y* value which is not an outlier, whereby an outlier is defined as a sample point smaller than y_{25}-1.5(y_{75}-y_{25})

Effectiveness ε thus describes how the deviation between median performance and optimal performance (y_{min}) improves compared to the design under full uncertainty. Robustness R_p is analogously determined as the improvement the performance spread of a design option makes in proportion to the spread under full uncertainty. According to these definitions, a solution with an effectiveness and robustness of one is the best possible, while negative values are to be avoided.

2.2 Input parameters

The design parameters considered in this paper are listed in TABLE 1. For each parameter, several

TABLE 1. Stochastic input parameters

	Parameter	Distribution*
DESIGN	Infiltration rate at 50 Pa	Dis(0.6, 1, 1.4) /h
	Ventilation system (and heat recovery)	Dis(exhaust, balanced 70% rec., balanced 80% rec.)
	U-value wall	Dis(0.1, 0.15, 0.2, 0.25) W/m²K
	Window type	Dis(1.29 W/m²K & g = 0.631, 1.31 W/m²K & g = 0.551, 0.7 W/m²K & g = 0.407)
	Sunscreen type	Dis(none, 30% transmission)
SCENARIO	Nominal energy price evolution	Dis(-1.5 %, 2.3 %, 10 %)
UNCERTAINTY	Set temperature occupancy day zone	Nor(21,1.35) °C
	Set temperature absence day zone	Dis(15°C, no reduction)
	Set temperature occupancy night zone	Nor(19,2) °C
	Internal heat gains	Uni(100,500) W
	Air change rate day zone	Wei(0.6576,4.67) /h
	night zone	Wei(1.7847,4.67) /h
	Workmanship error infiltration rate	Nor(1,0.1)
	Workmanship error U-value wall	Nor(1,0.1)
	Workmanship error heat recovery	Nor(1,0.1)

* Explanation of the symbols used:
Dis(a,b,c): discrete distribution with equal probability for a, b and c
Uni(a,b): uniform distribution between a and b
Nor(μ,σ): normal distribution wit mean value μ and standard deviation σ
Wei(λ,k): Weibull distribution with scale factor λ and shape factor k

low-energy design values are studied. To make probabilistic design with the original model feasible for this paper, calculation time is reduced by selecting only a limited set of design parameters and values. All combinations of these design values result in 216 design options.

As we are interested in the net present costs, the energy price evolution is of major interest. By considering this parameter as a scenario parameter, we are able to study the optimal results for each potential evolution. Three discrete values are considered, as shown in TABLE 1.

The inherently uncertain parameters, also listed in TABLE 1, deal with user behaviour and workmanship. The user behaviour variability is inspired by a measurement campaign of 70 new dwellings in Flanders (Belgium) (Staepels et al. 2013). 100 uncertainty layer values are sampled in sets of 20 with a *maximin* Latin Hypercube scheme (Husslage et al. 2008). In this case, this is sufficient for convergence as the maximal variation of the studied output percentiles is less than 6%. For simplicity in this paper, every design option and scenario combination is thus subjected to the same 100 samples, resulting in 64.800 simulation combinations.

Note that for clarity, in this case study, many other parameters are considered deterministic, such as occupancy profiles, climate and investment and maintenance costs.

2.3 Dynamic building energy model

The dwelling is modelled with two thermal zones and simulated in a transient BES tool developed in Modelica (Baetens et al. 2012) for the reference climate year of Uccle, Belgium (Van Gelder et al. 2013a). The adjacent dwelling is considered at a constant temperature of 19 °C. To simulate the heat demand, an ideal heating system is assumed, which is controlled using simplified occupancy and temperature profiles. A ventilation system is incorporated in the model with or without heat recovery. In summer, the heating system and heat recovery are switched off. To optimise the summer comfort, temperature of the day zone exceeds the user dependent comfort temperature, the air change rate is doubled for the next six hours or until the occupants leave the dwelling. This algorithm simulates the user behaviour to achieve a comfortable indoor climate.

2.4 Meta-models

Meta-models are built for both heat demand and maximal indoor temperature as described in section 1.2. The discrete distributions of the design parameters are transformed into uniform distributions to make other design options possible as well. All parameters are sampled together and both a sample size of 100 and 20 with up to ten sets of these sample sizes are used to build the models, as shown in FIG 4 and FIG 5. One can see that the model reliability increases with the total number of samples. Out of all presented models, four are selected to study the resulting reliability:

- reference meta-model: this is considered as the reference model as it is based on10 sets of 100 runs and is the most reliable out of the available models.
- meta-model 1: this model is built and validated on 2 sets of 100 runs and is considered as sufficiently reliable.
- meta-model 2: this model is built and validated on 10 sets of 20 runs, thus containing as many samples as meta-model 1, and the indicators are clearly converged.
- meta-model 3: this model is built and validated on 5 sets of 20 runs and is the model containing the minimal number of samples to create a reliable meta-model according to FIG 4 and FIG 5.

3. Results

As described in section 2, an optimisation is performed of the net present cost effectiveness and robustness. For that purpose, Pareto fronts are calculated. Those design options where the indoor temperature may rise above 28° C are penalised to avoid the risk on overheating. The cumulative

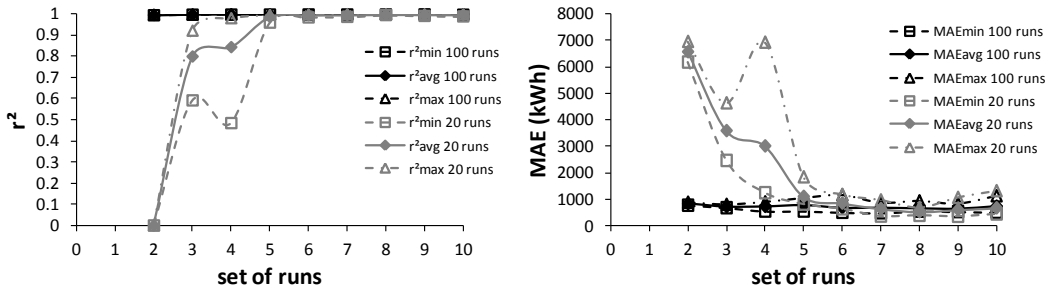

FIG 4. Minimal, average and maximal r² and MAE cross-validation indicators of the heat demand meta-model for different number of sets and samples.

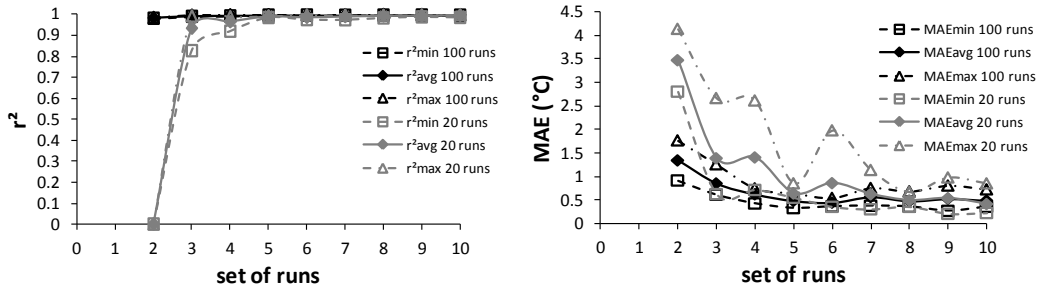

FIG 5. Minimal, average and maximal r² and MAE cross-validation indicators of the maximal indoor temperature meta-model for different number of sets and samples.

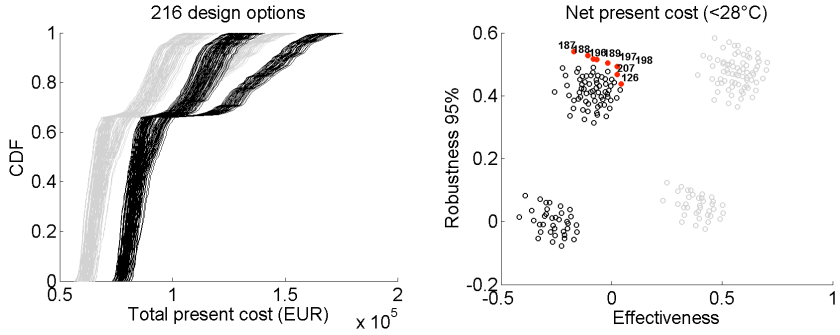

FIG 6. Cumulative distribution functions for net present cost for all 216 design options (left). Robustness R_{95} and effectiveness ε of net present cost (right). The design options with an overheating risk are indicated in grey. The Pareto front options are indicated with their design option numbers.

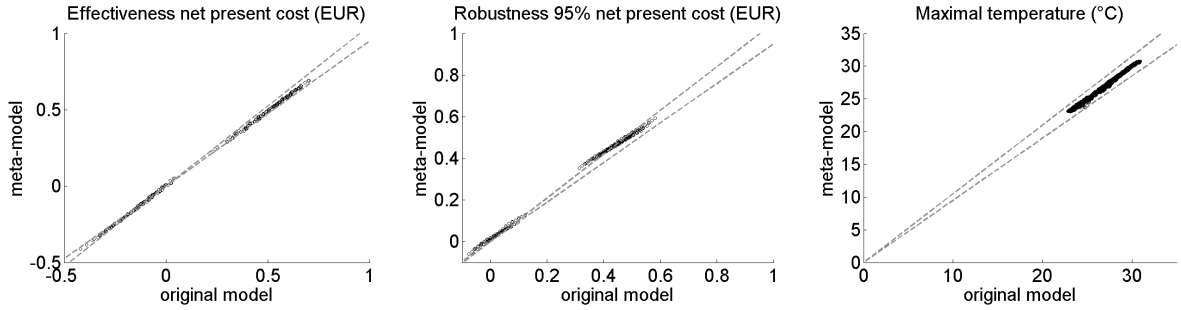

FIG 7. Comparison of outputs reference meta-model and BES model: effectiveness ε net present cost (left), robustness R_{95} net present cost (middle) and maximal indoor temperature (right). 5% deviation intervals are indicated with grey lines.

TABLE 2. Pareto front design options of dynamic BES model.

Design option n°	Infiltration rate at 50 Pa	Ventilation system (and heat recovery)	U-value wall	Window type	Sunscreen type
126	1.4 /h	balanced 80 % rec.	0.15 W/m²K	1.29 W/m²K	30 % transm.
187	0.6 /h	balanced 80 % rec.	0.10 W/m²K	0.7 W/m²K	30 % transm.
188	1 /h	balanced 80 % rec.	0.10 W/m²K	0.7 W/m²K	30 % transm.
189	1.4 /h	balanced 80 % rec.	0.10 W/m²K	0.7 W/m²K	30 % transm.
196	0.6 /h	balanced 80 % rec.	0.15 W/m²K	0.7 W/m²K	30 % transm.
197	1 /h	balanced 80 % rec.	0.15 W/m²K	0.7 W/m²K	30 % transm.
198	1.4 /h	balanced 80 % rec.	0.15 W/m²K	0.7 W/m²K	30 % transm.
207	1.4 /h	balanced 80 % rec.	0.20 W/m²K	0.7 W/m²K	30 % transm.

TABLE 3. Comparison effectiveness and robustness indicators of Pareto front design options. Grey italics indicate values which are not in the considered Pareto front.

Design option	BES model		Reference meta-model		Meta-model 1		Meta-model 2		Meta-model 3	
n°	ε	R_{95}	ε	R_{95}	ε	R_{95}	ε	R_{95}	ε	R_{95}
126	0.043	0.438	0.051	0.463	0.056	0.457	0.058	0.475	0.060	0.486
135	*0.038*	*0.418*	*0.049*	*0.445*	0.057	0.436	*0.056*	*0.451*	*0.059*	*0.464*
187	-0.171	0.540	-0.179	0.545	-0.176	0.535	-0.175	0.553	-0.177	0.556
188	-0.108	0.528	-0.113	0.536	-0.110	0.525	-0.112	0.540	-0.108	0.550
189	-0.067	0.515	-0.070	0.525	-0.067	0.515	-0.064	0.534	-0.065	0.540
196	-0.084	0.517	*-0.089*	*0.521*	*-0.087*	*0.513*	*-0.084*	*0.532*	*-0.091*	*0.533*
197	-0.018	0.505	-0.022	0.511	-0.021	0.503	-0.022	0.518	-0.022	0.526
198	0.025	0.493	0.020	0.501	0.022	0.492	0.027	0.512	0.021	0.517
207	0.025	0.467	*0.018*	*0.483*	0.023	0.471	*0.025*	*0.489*	*0.021*	*0.494*

distribution functions (CDF) of all design options, needed to calculate ε and R_{95}, and the Pareto front options of the BES-model optimisation are shown in FIG 6 and listed in TABLE 2.

When comparing net present cost effectiveness ε and robustness R_{95} and maximal indoor temperatures between BES model and reference meta-model, slightly deviating values are found, as shown in FIG 7. Although these deviations become slightly larger when fewer samples are used to build the meta-model, very similar Pareto fronts are obtained, as presented in TABLE 3. Only one option (i.e. 135) appears that was not in the original Pareto front. But this design option is very similar to option 126, as only the U-value changes (0.2 W/m²K). On the other hand, options 196 and 207 do not appear in the meta-model Pareto front, but they are almost equal to the other options and are still close to the Pareto front. Note that the optimal ε values are very small due to the fact that most effective solutions result in overheating risks.

Similar observations remain when comparing Pareto fronts per scenario. Those results are not explicitly presented here. When comparing Pareto fronts from meta-models built on fewer samples than meta-model 3, larger deviations are found. Moreover, design options with an overheating potential might be selected as this risk is unreliably detected. FIG 4 and FIG 5 show that these meta-models are indeed less reliable as they have low r^2 values and large maximal errors.

4. Conclusions

As illustrated in section 3, meta-models can be reliably used in probabilistic design of low-energy dwellings as output distributions and effectiveness and robustness are sufficiently mimicked and very similar Pareto optimal design options are found. This allows performing a generally time-consuming probabilistic design as presented in section 1.1, but now in only a fraction of the original time. The

presented method uses multi-layered schemes to classify parameters by their physical meaning as this enables the comparison of numerous design options and scenarios.

In order to reliably and time efficiently build a meta-model, a model procedure based on replicated sample schemes was proposed in section 1.2. Small schemes are preferred as it is seen that meta-model build on those schemes perform as well as the others, but less samples are needed.

5. Acknowledgements

The authors are very thankful for the funding of the Flemish government and companies for the IWT TETRA BEP2020 project (Verbeeck et al. 2013) and participating inhabitants for the related measurement campaign. Many thanks to Liesbeth Staepels to develop the cost-calculation tool according to the European standard EN ISO 15429. They would like to thank Bart Husslage and Gijs Rennen from the Tilburg University as well for sharing their MATLAB code for calculation of maximin sampling schemes (Husslage et al. 2008).

References

Baetens, R., De Coninck, R., Van Roy, J., Verbruggen, B., Driesen, J., Helsen, L. & Saelens, D. 2012. Assessing electrical bottlenecks at feeder level for residential net zero-energy buildings by integrated system simulation. Applied Energy, 96:74–83.

EN ISO 15459. Energy performance of buildings – Economic evaluation procedure for energy systems in buildings.

Friedman, J.H., 1991. Multivariate adaptive regression splines. The Annals of Statistics, 19(1), pp.1–141.

Husslage, B. et al., 2008. Space-filling Latin hypercube designs for computer experiments.

Janssen, H., 2013. Monte-Carlo based uncertainty analysis: Sampling efficiency and sampling convergence. Reliability Engineering & System Safety, 109:123–132.

Jekabsons G., 2011. ARESLab: Adaptive Regression Splines toolbox for Matlab/Octave, available at http://www.cs.rtu.lv/jekabsons/

Staepels, L., Verbeeck, G., Roels, S., Van Gelder, L. & Bauwens, G., 2013. Evaluation of Indoor Climate in Low Energy Houses. In Symposium on Simulation for Architecture and Urban Design, April 7-10. San Diego, USA.

Van Gelder, L., Janssen, H., Roels, S., Verbeeck, G. & Staepels, L., 2013a. Effective and robust measures for energy efficient dwellings : probabilistic determination. In Building Simulation 2013. Chambéry, France, pp. 3465–3472.

Van Gelder, L., Janssen, H. & Roels, S., 2013b. Metamodelling in robust low-energy dwelling design. In A. Mahdavi & B. Martens, eds. 2nd Central European Symposium on Building Physics, September 9-11. Vienna, Austria, pp. 93–99.

Van Gelder, L., Janssen, H. & Roels, S., 2014. Probabilistic design and analysis of building performances: methodology and application example. Energy and Buildings. Under review.

Verbeeck, G., Staepels, L., Roels, S., Van Gelder, L., Bauwens, G. & Deconinck, A.-H., 2013, IWT TETRA BEP2020: betrouwbare energieprestaties van woningen – Naar een robuuste en gebruikersonafhankelijke performantie (in Dutch), URL http://bep2020.pxl.be.

Zang, C., Friswell, M.I. & Mottershead, J.E., 2005. A review of robust optimal design and its application in dynamics. Computers & Structures, 83(4-5), pp.315–326.

The first year's results from the first passive house in Estonia

Targo Kalamees, Professor [1]
Leena Paap, M.Sc. [1]
Kalle Kuusk, M.Sc. [1]
Tõnu Mauring, Ph.D. [2]
Jaanus Hallik, M.Sc. [2]
Margus Valge, M.Sc. [2]
Kristo Kalbe, M.Sc. [2]
Alan Henry Tkaczyk, Ph.D[3]

[1] Chair of Building Physics and Energy Efficiency, Tallinn University of Technology, Estonia
[2] Energy Efficient Building Core Laboratory, University of Tartu, Estonia
[3] Institute of Physics, University of Tartu, Estonia

KEYWORDS: *nZEB, passive house, hygrothermal performance, indoor climate, overheating.*

SUMMARY:
A single-family detached passive house has been designed in cooperation with Austrian architects and built in Estonia. This paper presents and analyzes the thermal comfort and hygrothermal performance of the building envelope of this house during the first year after construction.

Results showed high temperature readings in most of the rooms, achieved mainly due to large windows with southern exposure and the small heat loss of the building envelope. Due to the high indoor temperatures, the relative humidity decreased to quite low levels. Humidity in the externally insulated cross-laminated timber panels was observed to be high, causing condensation and risk for mould development. This was caused by drying out of the constructional moisture and the high diffusion resistance of the wood fiber sheathing board. The indoor humidity loads were high indicating that the design of passive houses indoor humidity loads cannot be decrease. In summary, while planning buildings with high energy efficiency, more focused attention should be paid to the performance of the building service systems and moisture safety already in the preliminary stages of design.

1. Introduction

In the European Union (EU), buildings account for 40% of total energy consumption (2002/91/EC, 2002; 2010/31/EU, 2010). The 2010 EU directive on energy performance of buildings encourages the transition from fossil fuels to renewable energy sources in the building sector and underlines the importance of reducing energy dependency and greenhouse gas emissions in the EU. Europe has adopted an ambitious vision for the energy efficiency of its buildings. By the end of 2018 all new public buildings must meet nearly zero-energy building (*nZEB*) requirements.

The aforementioned directive describes *nZEB*-s as buildings with very high energy performance in terms of net energy consumption. The nearly zero or very low amount of energy required should be covered to a very significant extent from renewable sources, preferably produced on-site or nearby. In line with the EU directive, Estonian new energy performance regulations entered into force on 9.1.2013, establishing primary energy requirements for new and renovated buildings (RT I, 05.09.2012, 2010). The requirements and corresponding energy certificate classes are shown for three building types out of nine in Table 1.

TABLE 1 Energy performance certificate classifications (A-D) and corresponding maximum values of energy performance values (kWh/(m^2·a)) for three different types of buildings.

	Maximum energy performance values (Estonian legislation), kWh/(m^2·a)			
	A *nZEB*	B Low energy buidling	C Minimum requirements for new building	D Minimum requirements for major renovation
Detached house	50	120	160	210
Apartment building	100	120	150	180
Office building	100	130	160	210

In addition to national requirements, there are several internationally recognized energy-performance levels. The Passive House (PH) standard (PassivhausInstitut, n.d.) is one widely known energy performance standard. The PH standard requires thick insulation, minimized thermal bridges, airtightness, insulated glazing and heat recovery ventilation. For PH standard, the quantitative requirements are: annual specific net energy demand for heating at less than or equal to 15 kWh/(m^2·a) and total primary energy for space heating, domestic hot water and household appliances at less than or equal to 120 kWh/(m^2·a).

In Estonia, the renovation of a kindergarten with PH components marked the country's first experience with PH concepts ("Kindergarten 'Kaseke'," 2009). The first complete and certified PH in Estonia is a detached house located at Metsa 5a in the town Põlva, designed by Austrian architects and constructed by Estonian designers (Reinberg et al., 2013). Based on calculations, it achieves the annual basis "plus-energy" building classification in the Estonian legislation.

This paper presents and analyzes the thermal comfort and hygrothermal performance of the building envelope of the aforementioned PH during the first year after construction.

2. Methods

2.1 Studied house and structures

The PH concept has been fully implemented, in addition to utilizing extensive passive and active solar techniques. The design and construction of the house has taken into account the characteristics of Estonia's cold northern climate. For example, large transparent areas are concentrated toward the south, since the south façade windows have a favorable contribution from the sun and have potential to yield a positive heat balance over the heating season.

The house includes two stories (FIG 1, FIG 2) and a basement with total net floor area of 305 m^2. The building envelope surface area is 864 m^2 and has an enclosed volume of 1586 m^3, corresponding to a compactness factor (A/V) of 0.55 m^{-1} for the building.

The exterior walls feature an original design (FIG 3 left) with 94 mm thick cross-laminated timber (Kreuzlagenholz, KLH) block elements as the static layer and 400 mm cellulose insulation with external thermal insulation composite systems (ETICS). This house is the first building in Estonia based on KLH block elements, in addition to its other unique attributes.

Customization of the building design was necessary to accommodate the cold climate. Whereas a well-insulated undrained, rendered wooden exterior wall (see FIG 3 *left*) could be a good solution for a PH built in Austria, this option could result in serious moisture damage (Samuelson et al., 2008) and biological growth (Johansson, 2011) in a cold climate. Therefore, a new solution was proposed (FIG 3 *right*): the exterior wall was constructed with ventilated cavities covered mainly by rendering boards and partly by vertical solar collectors. Also the roof solution was changed: it was insulated with wedge shaped EPS insulation (380 mm – 550 mm).

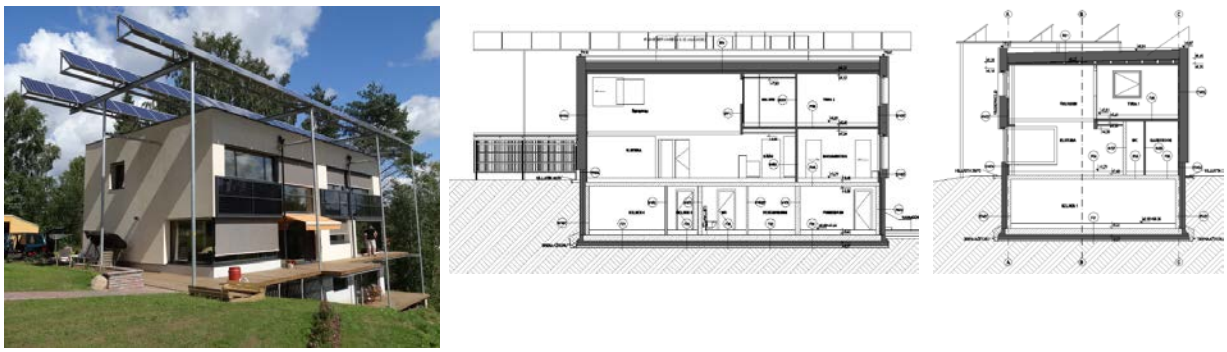

FIG 1 View from SW direction (left) and the sections (middle, right) from the house.

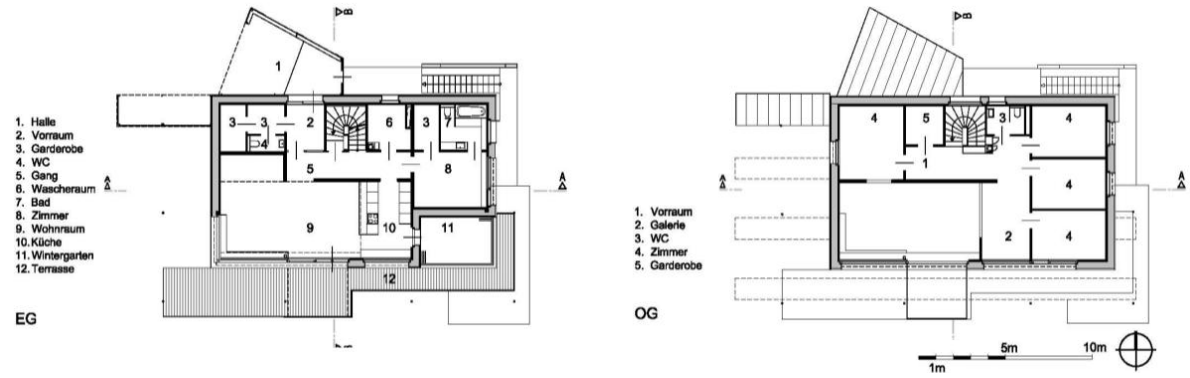

FIG 2 The plans of the first (left) and the second (right) floors.

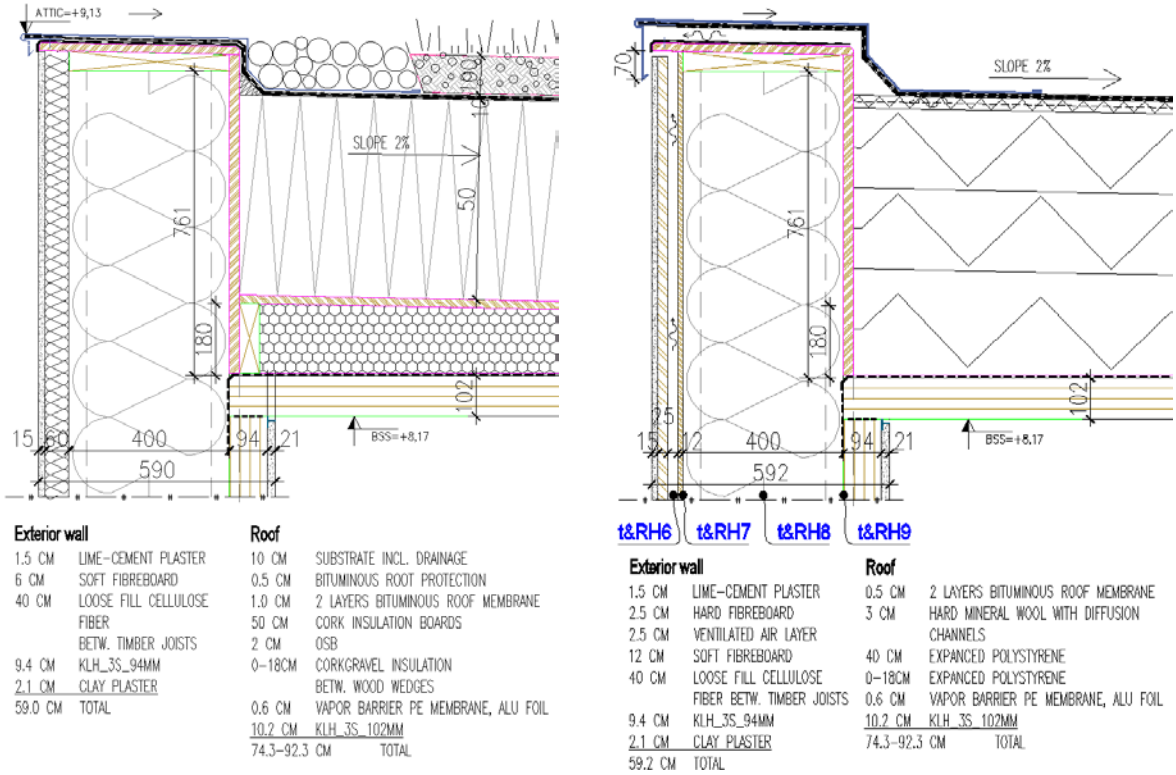

Exterior wall

1.5 CM	LIME-CEMENT PLASTER
6 CM	SOFT FIBREBOARD
40 CM	LOOSE FILL CELLULOSE FIBER BETW. TIMBER JOISTS
9.4 CM	KLH_3S_94MM
2.1 CM	CLAY PLASTER
59.0 CM	TOTAL

Roof

10 CM	SUBSTRATE INCL. DRAINAGE
0.5 CM	BITUMINOUS ROOT PROTECTION
1.0 CM	2 LAYERS BITUMINOUS ROOF MEMBRANE
50 CM	CORK INSULATION BOARDS
2 CM	OSB
0–18CM	CORKGRAVEL INSULATION BETW. WOOD WEDGES
0.6 CM	VAPOR BARRIER PE MEMBRANE, ALU FOIL
10.2 CM	KLH_3S_102MM
74.3–92.3 CM	TOTAL

Exterior wall

1.5 CM	LIME-CEMENT PLASTER
2.5 CM	HARD FIBREBOARD
2.5 CM	VENTILATED AIR LAYER
12 CM	SOFT FIBREBOARD
40 CM	LOOSE FILL CELLULOSE FIBER BETW. TIMBER JOISTS
9.4 CM	KLH_3S_94MM
2.1 CM	CLAY PLASTER
59.2 CM	TOTAL

Roof

0.5 CM	2 LAYERS BITUMINOUS ROOF MEMBRANE
3 CM	HARD MINERAL WOOL WITH DIFFUSION CHANNELS
40 CM	EXPANCED POLYSTYRENE
0–18CM	EXPANCED POLYSTYRENE
0.6 CM	VAPOR BARRIER PE MEMBRANE, ALU FOIL
10.2 CM	KLH_3S_102MM
74.3–92.3 CM	TOTAL

FIG 3 Exterior wall and roof structures, as originally designed (left), and as constructed (right, with measurement point for hygrothermal performance of exterior wall with temperature and relative humidity (t&RH6, t&RH7, t&RH8, t&RH9) sensors).

2.2 Measurements

Upon completion of house construction in December 2012, an extensive monitoring system was installed to continuously assess the indoor climate and performance of building systems and the exterior wall. The hygrothermal performance of exterior wall was measured on the northern façade with temperature and relative humidity sensors (∅ 5 mm × 51 mm, measurement range: -40°…+100°C and 0…100%, accuracy: ±0.3°C and ±2%) and heat flux plates (Hukseflux HFP-01-05, measurement range ±2000 W/m^2, accuracy: ±5%). Measurement results were recorded with a computer (Modbus RTU protocol). The indoor climate was measured with portable sensors (measurement range: -20°…+70°C and 10…95%, accuracy: ±0.35°C and ±3%).

3. Results

3.1 Indoor climate

To provide an overall view of the indoor climate, we analyzed the correlation of the indoor temperature and relative humidity (RH) with the outdoor temperature. Using green dots, the correlation of the hourly indoor temperature with the outdoor temperature outside the northern bedroom with east-facing window is displayed (FIG 4 left). Using black dots, the correlation of the average daily indoor temperature with the average daily outdoor temperatures outside the aforementioned room is displayed (FIG 4 left). This represents average thermal conditions in one room, and is depicted in FIG 4 right with a curve.

The correlation of indoor RH on the outdoor temperature was also analyzed, using a similar method as employed for the room temperature. In FIG 5 left, the average indoor RH values from one room are divided by the average outdoor air temperature. Based on each indoor RH sensor and the corresponding outdoor temperature, the daily average value was calculated to form the black dotted line. Each individual curve in FIG 5 right represents, for each room, the average value of the daily indoor RH and the corresponding average daily outdoor temperature.

The internal moisture excess was selected to characterize indoor humidity loads. FIG 6 left presents the daily moisture excess in one room during whole measurement period, and the black dotted line represents the weekly average moisture in excess in on 90% criticality level (design level). FIG 6 right presents the moisture excess during the winter period: the average value was 3.1 g/m^3, and the design value corresponding to 90% critical moisture level was 5.2 g/m^3.

Carbon dioxide (CO_2) concentrations were used to assess the indoor air quality. CO_2 concentrations at 500 ppm and 800 ppm above the outdoor concentration (400 ppm) correspond to the indoor climate category (ICC) target classifications of average (II) and third (III), as shown in FIG 7.

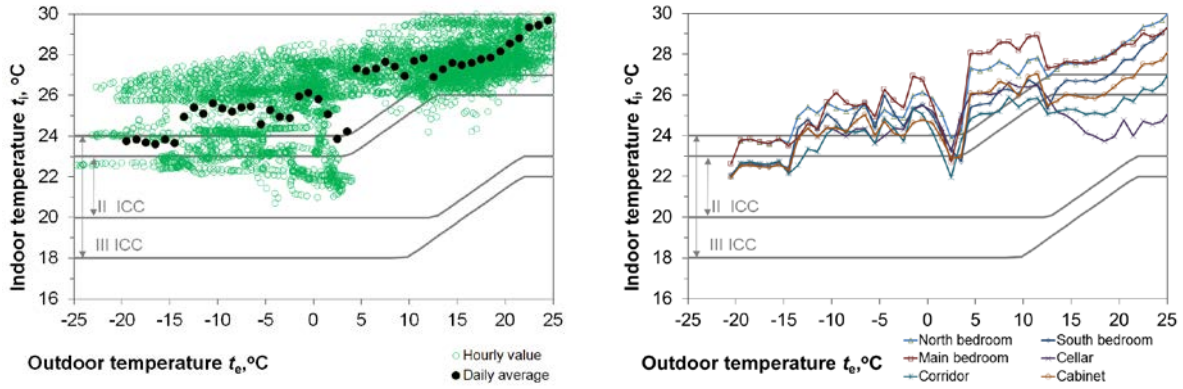

FIG 4 The dependence of the indoor temperature on the outdoor temperature in the north bedroom on the second floor with east-directed window (left) and the comparison of all rooms (right).

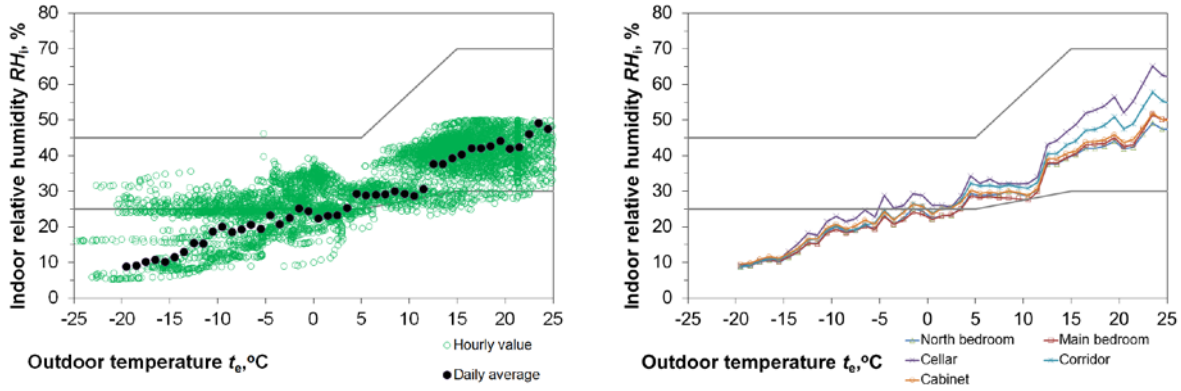

FIG 5 The dependence of the daily average indoor RH on the outdoor temperature in the north bedroom on the second floor (left) and the comparison of all rooms (right).

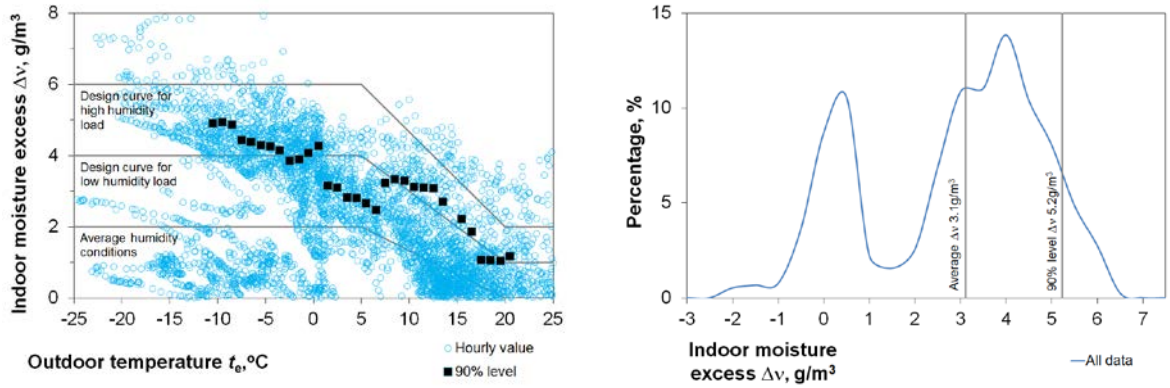

FIG 6 The distribution of moisture excess.

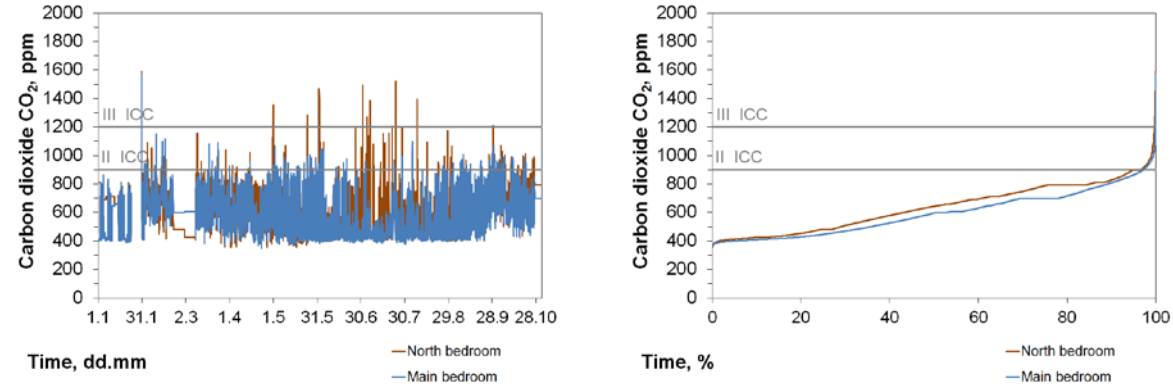

FIG 7 Carbon dioxide concentration in bedrooms.

3.2 Hygrothermal performance of exterior wall

The hygrothermal performance of the exterior wall was measured at different positions inside the 400 mm thick cellulose insulation (see FIG 3 right):

- on the internal edge of the insulation: between the insulation and the KLH;
- in the middle of the insulation;
- on the external edge of the insulation: between the insulation and the 12 mm thick wood fiber sheathing board (Kronopol DP50).

FIG 8 shows the temperature (left) and RH (right) inside the 400 mm thick insulation of the exterior wall. The RH was over 80% until the beginning of the summer (until 1.06.2013). As the exterior walls were insulated in September 2012, high moisture content in the walls lasted for approximately ten months. In the summer, when very high moisture conditions in the exterior wall were determined, two addional temperature and RH sensors (RH 7-2 and RH 7-3) were placed inside the wall. The measurement accuracy of the original sensor was open to discussion. However, similar humidity readings in the new sensors RH 7-2 and RH 7-3 assured the authors of the accuracy of the original sensor: the drying out of constructional moisture (KLH and cellulose insulation) had caused condensation and favourable conditions for mould growth (FIG 9) inside the exterior wall. Based on a mathematical model of mould growth in wooden material (Hukka and Viitanen, 1999), the mould index was near 3, meaning that some growth could also be detected visually and new spores could form.

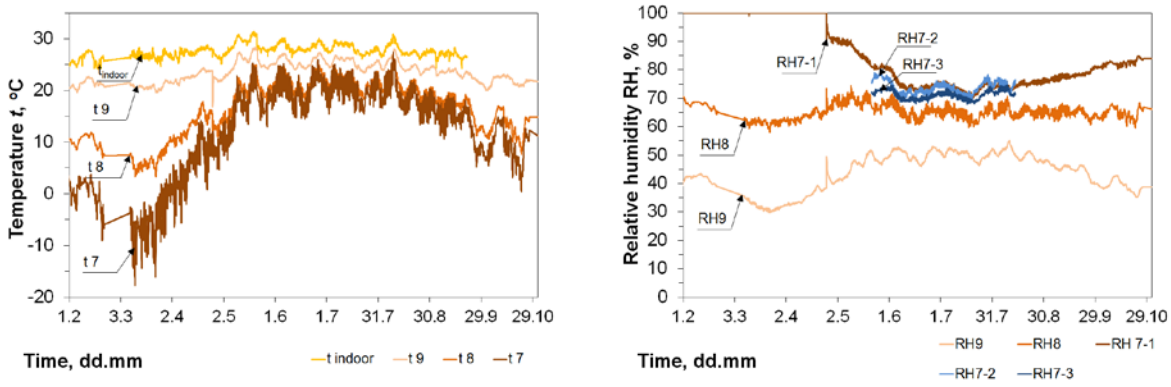

FIG 8 Temperature (left) and RH (right) inside the 400 mm thick insulation of the exterior wall.

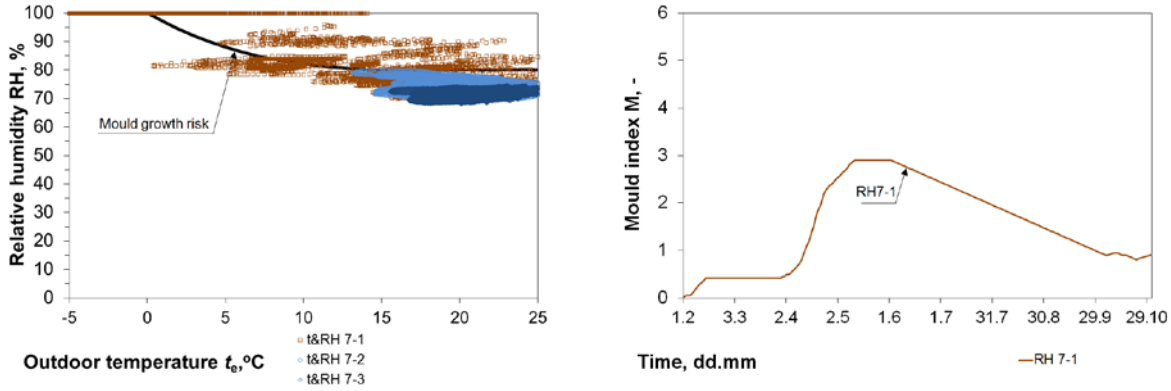

FIG 9 Temperature and RH between the cellulose insulation and the 12 mm thick wood fiber sheathing board (left) were suitable for mould growth, according to the mould growth index (right).

4. Discussion

The first certified passive house in Estonia was designed by Austrian architects in cooperation with Estonian designers, including the involvement of the co-authors of this paper. The indoor climate and hygrothermal performance measures of the exterior wall of this building were monitored and analyzed.

The passive utilization of heat gains is an important factor in the design of a passive house. In the cold Estonian climate, literature review suggests that only windows with southern orientation could yield energy-positive results (NorthPass, 2010). At the same time, large south-facing windows need flexible

solar protection to avoid over-heating indoor climate. South-directed windows could not be the only reason of overheating in the house under consideration, since the north bedroom with east-directed window reached high temperatures as well (FIG 4 left). During the summer months, only the basement maintained the average indoor temperature within the targets of indoor climate category II (normal level of expectation, for new buildings: Predicted Percentage Dissatisfied, PPD ≈ <10%).

Due to high temperatures, the indoor RH decreased to quite low levels. During the cold period ($t_e \leq +5$ºC), the indoor RH was below 20% (FIG 5). The indoor RH was similar in all rooms.

The indoor humidity loads were similar to typical dwellings with high humidity loads: the average value of moisture excess during the winter period was 3.1 g/m^3, and the design value of moisture excess was 5.2 g/m^3 (FIG 6). This indicates that in design of passive houses indoor humidity loads cannot be decreased despite the ventilation keeps the indoor air quality within the limits of indoor climate category II recommendations (FIG 7).

Humidity conditions in externally insulated cross laminated timber panels (KLH) were high (FIG *9* left), due to the drying out of constructional moisture (KLH and cellulose insulation) and the high diffusion resistance of the wood fiber sheathing board. Careful hygrothermal design and moisture safety considerations should be paramount in the construction of highly insulated building envelopes (Mundt-Petersen, 2013; Vinha et al., 2013). Otherwise, water vapour condensation or favourable conditions for mould growth could develop (FIG *9* right).

5. Conclusions

The performance of the first certified passive house in Estonia was monitored and assessed during the first year after construction, including detailed analysis of the indoor climate and hygrothermal performance of the exterior walls.

High temperatures in most of the rooms were achieved mainly due to the southern exposure of the large windows and the fact that the adjustable solar protection devices were installed only in the middle of the current monitoring period (May 2013). As the heat loss through the building envelope was small compared to the thermal transmittance of the interior walls and floors, a high average indoor temperature was maintained throughout the house, including the bedroom on the northern side of the building. Due to the high temperatures reached, the indoor RH decreased to quite low levels. The high indoor temperatures indicate that the large windows with southern orientation need adjustable solar protection or heat accumulation devices to avoid over-heating.

Humidity conditions in the externally insulated cross-laminated timber panels (KLH) were elevated for long periods, raising concern for condensation and the risk of mould development. Although the original hygrothermally risky design of the exterior walls, which would have used external thermal insulation composite systems (ETICS) with a wooden structure, was upgraded to a less moisture-prone design based on advice of the co-authors and other Estonian experts, excess moisture still became a problem. This was mainly caused by the shortcomings in the constructional technology, such as no rain protection for KLH, no moisture safety protocol during the construction period, and the high diffusion resistance of the wood fiber sheathing board. In parallel with energy performance, also the hygrothermal properties of the building envelope and its impact on the indoor climate should be top priority in the design of passive houses.

A key to successful completion of construction projects is clear communication and follow-up between designers and building crew, to ensure that the revised construction guidelines would be fully incorporated in the blueprints. This could reduce problems such as the overheating and moisture build-up encountered in this project. In design of buildings with high energy performance, focused attention should be paid on the performance of building service systems and moisture safety should be taken into account already in preliminary stage of design.

6. Acknowledgements

This research was supported by the European Union through the European Regional Development Fund. The research has been conducted as a result of the “Reducing the environmental impact of buildings through improvements of energy performance, AR12059” (financed by SA Archimedes) and IUT1−15 project “Nearly-zero energy solutions and their implementation on deep renovation of buildings“ (financed by the Estonian Research Council).

References

2002/91/EC, E.-D., 2002. EU-Directive 2002/91/EC on the energy performance of buildings. EU-Directive 2002/91/EC of the European Parliament and of the council of 16 December 2002 on the energy performance of buildings. European Commission.

2010/31/EU, E.-D., 2010. EPBD recast: EU-Directive 2010/31/EU. EPBD recast: EU-Directive 2010/31/EU of the European Parliament and of the Council of 19 May 2010 on the energy performance of buildings.

Hukka, A., Viitanen, H. a., 1999. A mathematical model of mould growth on wooden material. Wood Science and Technology 33, 475–485.

Johansson, S., 2011. Biological growth on rendered façades. 8th, NSB 2008; Symposium on building physics in the Nordic countries. Lund University, Division of Building Materials.

Kindergarten “Kaseke”, 2009. Promotion of the use of sustainable and low energy buildings and constructions in Latvia and Estonia (Active through Passive!). URL http://www.activethroughpassive.eu/en/passive-house-project-in-ee/example-house

Mundt-Petersen, O., 2013. Moisture Safety in Wood Frame Walls. Lund University.

NorthPass, I., 2010. Principles of low-energy houses applicable in North European countries and their applicability throughout the EU.

PassivhausInstitut, n.d. Passive House requirements [WWW Document]. URL http://passiv.de/en/02_informations/02_passive-house-requirements/02_passive-house-requirements.htm

Reinberg, G.W., Mauring, T., Kalbe, K., Hallik, J., 2013. First Certified Passive House in Estonia. In: Feist, W. (Ed.), Proceedings of 17th International Passive House Conference: 17th International Passive House Conference. Prototype architecture in Estonia demonstrates tha.

RT I, 05.09.2012, 4, 2010. Energiatõhususe miinimumnõuded (Minimum requirements for buildings energy performance) [WWW Document]. iigi Teataja - State Gazette of the Republic of Estonia. URL https://www.riigiteataja.ee/akt/105092012004

Samuelson, I., Mjornell, K., Jansson, A., 2008. Moisture damage in rendered, undrained, well insulated stud walls. In: Rode, C. (Ed.), 8th, NSB 2008; Symposium on Building Physics in the Nordic Countries. Lyngby, Denmark, pp. 1253–1260.

Vinha, J., Laukkarinen, A., Mäkitalo, M., et al. 2013. Ilmastonmuutoksen ja lämmöneristyksen lisäyksen vaikutukset vaipparakenteiden kosteusteknisessä toiminnassa ja rakennusten energiankulutuksessa. Tampere University of Technology. Department of Civil Engineering. Structural Engineering. Research Report 159.

LowEx Communities – Optimized Performance of Community Energy Supply System with Exergy Principles

Schmidt, Dietrich[1] , Ph.D.
Kallert, Anna[1] , M.Sc.

[1] Fraunhofer Institute for Building Physics, Department of Energy Systems, Kassel, Germany

KEYWORDS: Low Exergy Communities; Exergy Analysis; Low Temperature Supply Structures; Low Energy Buildings; Renewable Energy Supply

SUMMARY
Communities are characterised by a wide range of heating and cooling energy demands. This energy is mainly provided by the combustion of fossil fuels, which is responsible for greenhouse gas (GHG) emissions. While a lot has already been achieved there are still large potentials in providing heating and cooling energy more efficiently. At the community level, different renewable energy sources are available. These energies are characterised by high fluctuations and different qualities: e.g. photovoltaics as electricity (high-exergy) or low temperature (low-exergy) heat from e.g. thermal solar collectors or waste heat from industry facilities. Low energy qualities are of particular interest, because the low exergy (LowEx) supply of thermal energy is very efficient. The application of exergy principles is especially important, allowing the detection of different available energy-quality levels and the identification of optimal contribution to an efficient supply. From this, appropriate strategies and technologies with great potential for promoting the usage of low-valued energy sources (LowEx) and a high share of renewable energies for heating and cooling of entire cities can be derived. The paper presents the key ideas of the just started international co-operative work in the general framework of the International Energy Agency (IEA), the EBC Annex 64: "LowEx Communities – Optimized Performance of Community Energy Supply System with Exergy Principles"

1. Introduction

The energy demand of communities for heating and cooling is responsible for more than one third of the final energy consumption in industrialised countries. Commonly this energy is provided by different fossil fuel based systems. These combustion processes cause greenhouse gas (GHG) emissions and are regarded one core challenge in fighting climate change. National and international agreements (e.g. the European 20-20-20-targets or the Kyoto protocol) limit the GHG emissions of the industrialized countries respectively for climate protection. Country specific targets are meant to facilitate the practical implementation of measures. While a lot has already been achieved, especially regarding the share of renewables in the electricity system, there are still large improvement potentials in the heating and cooling sector and on the community scale. Exploiting these potentials and synergies, demands for an overall analysis and holistic understanding of conversion processes within communities. Communities are characterized by a wide range of energy demands in different sectors, for instance heating and cooling demands, lighting and ventilation in the building stock. Different energy qualities (exergy) levels are required as heat or cold flows or as electricity and fuels.

2. Description of technical sector

2.1 The LowEx Approach

To optimise the exergy efficiency of community supply systems the so-called LowEx approach (LowExergy) can be utilised. Simplified the physical property "exergy" can be described as a product of energy and "energy quality" q (carnot factor for thermal energy).

$$Ex_Q = Q \cdot \underbrace{\left(1 - \frac{T_0}{T}\right)}_{CarnotFactor=q} \quad (1)$$

As a part of the considerations of this project, the following simplifications will be used: The higher the temperature of a heat flow is above the temperature of the surroundings (reference temperature), the higher the energy quality. The LowEx approach entails matching the quality levels of energy supply and demand in order to optimise the utilisation of high-value energy resources, such as combustible fuels, and minimising energy losses and irreversible dissipation (internal losses).

To heat indoor spaces up to 20°C, heat has to be supplied at a temperature slightly higher than 20°C. An exergetic analysis shows that the required energy quality, the exergy fraction or quality factor q for this application is very low (q ≈ 7% only). If the production of domestic hot water is considered as heating water up to temperatures of about 55°C, the needed energy quality is slightly higher (q ≈ 15%). For operation of different household appliances and lighting, the highest possible quality (q ≈ 100%) is necessary. An adaptation of the quality levels of supply and demand could be managed by covering, for example, the heating demand with suitable energy sources, as there is available district heating with a quality level of about 30% (see FIG. 1)

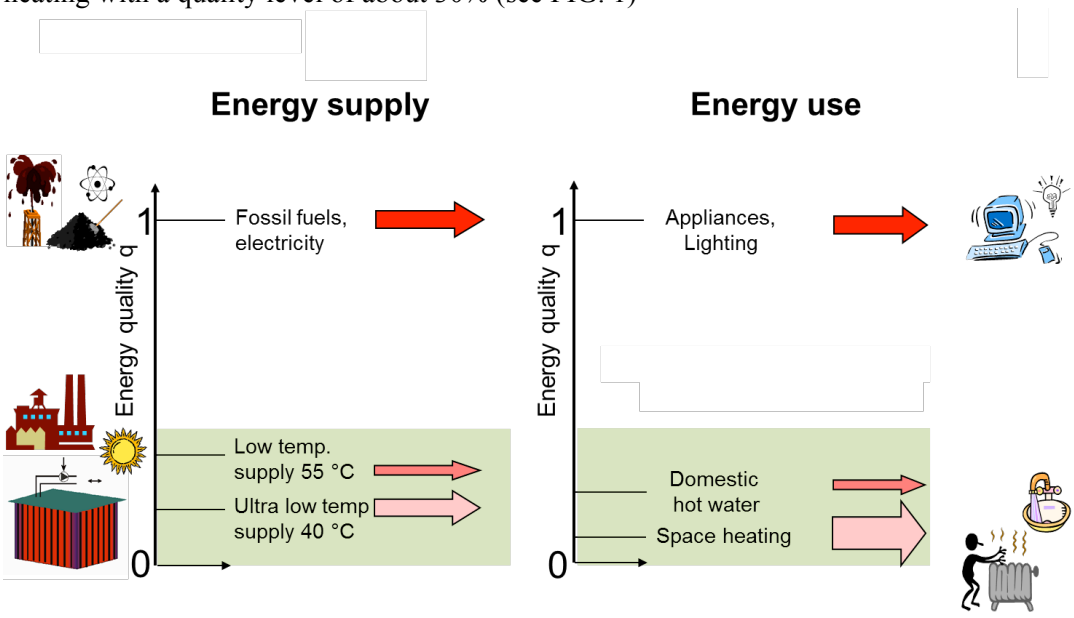

FIG 1: Application of LowEx approach for optimization of community demand adapted supply. The very efficient so called low exergy supply and use are of particular interest (see green boxes).

2.2 Scope

The scope of the annex covers the improvement of energy conversion chains on a community level, using an exergy basis as the primary indicator. The fundamental idea follows the hypothesis that by optimising the exergy chains, the overall system performance can be improved and CO_2 emissions can

be reduced. In particular, the method of exergy analyses has been found to provide the most accurate and insightful assessment of the thermodynamic features for any process as well as offering a clear, quantitative indication of both the irreversibilities and the degree of correspondence between the resources used and the end-use energy flows. In comparison to plain energy analysis, exergy based system optimisation facilitates the integration of renewable heat and cold sources that are most often available at fairly low temperatures. The optimal integration of decentralised supply modules of heat and cold enables the realisation of smart bi-directional supply chains in the heat and cold supply systems similar to 'smart-grid' approaches for the electricity sector. For conducting investigations on community level system boundaries have to be de-fined. The exact definition of the boundaries of the area to be examined (building, group of buildings, block, quarter or community) depends on the objectives of the involved research project (see: Focus of involved research projects).

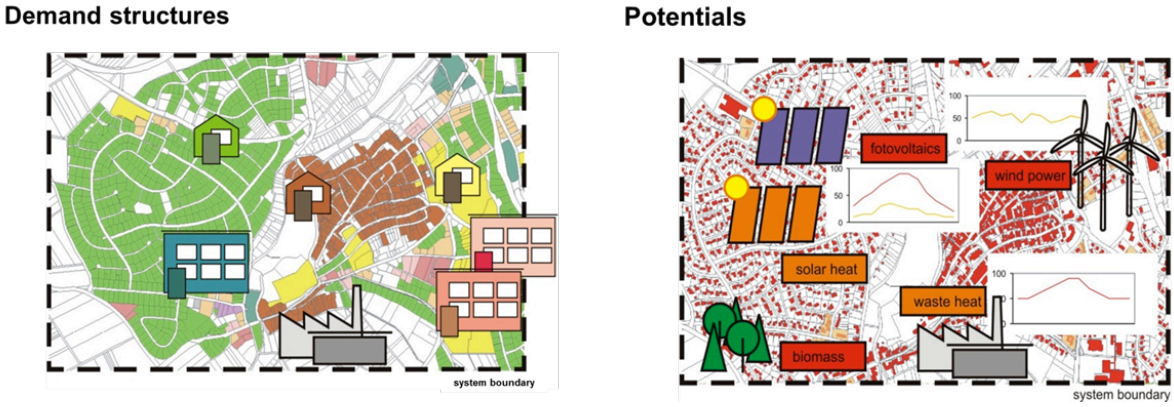

FIG 2: The boundary of the systems which are studied. Demand structures of different buildings and buildings groups (left). Sources and supply structures (right) adapted for supply of demand side.

2.3 Challenges and objectives

The main objective of the annex is to demonstrate the potential of low exergy thinking on a community level as energy and cost efficient solution in achieving 100% renewable and GHG emission-free energy systems. The intention is to reach these goals by providing and collecting suitable assessment methods (e.g. holistic balancing methods). Furthermore it is planned to provide guidelines, recommendations, best-practice examples and background material for designers and decision makers in the fields of building, energy production/supply and politics. During the course of this activity, the aim is to develop and improve means for increasing the overall energy and exergy efficiency of communities through demand adapted supply and inclusion of renewable energy sources. Therefore the central focus of all considerations is thermal energy at different exergy levels. Electrical energy will be taken into account as auxiliary energy. Electricity from a renewable fluctuating supply should be discussed as a contribution to the heat and cold supply of a community if it is thermally stored (e.g. storage tanks or usage of the building mass) and used for heating or cooling purposes (e.g. heat pumps). Further objective within the international co-operative work is discussion on appropriate additional indicators, supplementing the exergy assessment. The discussions should be initialised to come to a common understanding of how to weigh high-exergy electricity for heating and cooling purposes under the preconditions of local availability. Another objective is the application of exergy analysis as a basis for providing suitable material for designers and decision makers in the fields of low exergy generation, low exergy distribution and low exergy consumption. Central challenges in achieving the objectives are the identification of the most promising and efficient technical solutions for practical implementation and aspects of future network management and business models for distribution and operation. Aspects of transition management and policy will ensure the feasibility. A close cooperation with related IEA Annexes and activities is planned.

2.4 Benefits

The advantages of the application of the LowEx approach in the holistic assessment of a community are diverse:

- Customers benefit in various ways. First of all, the use of low exergy sources ensures a good comfort level and a sustainable supply. Customers do not have to worry about maintenance, fuel supply and optimal operation of heating systems.
- The environment benefits from the exergy concept. The total GHG emissions in communities can be substantially reduced as a result of the use of more efficient energy conversion processes. This new concept supports the setup of sustainable structures and secure energy systems for future developments on the community scale.
- From an economical point of view, high price stability can be expected due to the use of locally available, renewable, or surplus heat energy sources. An additional advantage of this is a lower dependency on foreign fuel supplies. The high overall sys-tem performance that can be achieved by using low temperature sources would lead to reduced resource consumption and therefore lower costs for fuels. This would also increase price stability and could potentially provide heat at very competitive prices.

The following three main target groups of the proposed annex benefit in different ways from the annex:

- The energy supply and technology industry will get development ideas for future products, business models and services in the field of dynamic energy supply systems. With the breaking down of traditional centralized top-down solutions in energy supply, new fields of business can be created in combination with overall system improvement.
- Communities will profit from the improved and more differentiated understanding of their local potentials and supply options. Greater local energy autonomy and impulses for local economy can support communities in regaining strategic competence in long-term development issues in the energy sector.
- Academic, research and education fields profit from the project by gaining a more holistic system understanding and a more differentiated view of community energy systems. A better understanding is created on the interaction and potential synergies of the different system modules.

3. Focus of involved research projects

Following chapters contain the key ideas of the new international co-operative work in the general framework of the International Energy Agency (IEA), the EBC Annex 64.

3.1 Optimisation of demand profiles

Energy demands currently are commonly supplied by centralised or decentralised systems designed and optimised for single demand profile. Therefore, energy demands of several yet different building types should be combined to pave the way for utilisation of unused synergies within existing communal building and supply structures. The research activities in field of “Optimisation of demand profiles” are strongly focused on the demand of buildings as part of multifarious community supply systems. As part of the work, the previously developed the exergetic assessment methods from IEA ECBCS Annex 49 (Torío, Schmidt 2011) will be applied and further developed. The focus here is particularly on so-called LowEx system distribution and supply concepts of different building classes. For this reason the optimisation potentials of heating and cooling tasks of buildings as well as building groups as one part of multifarious community supply systems. The following (FIG 3) figure illustrates the application of demand-optimized supply. An example, the waste heat of a cooling system for the heating of low-energy building could be used. For a sports centre, the waste heat from an ice rink could be used for heating a swimming pool.

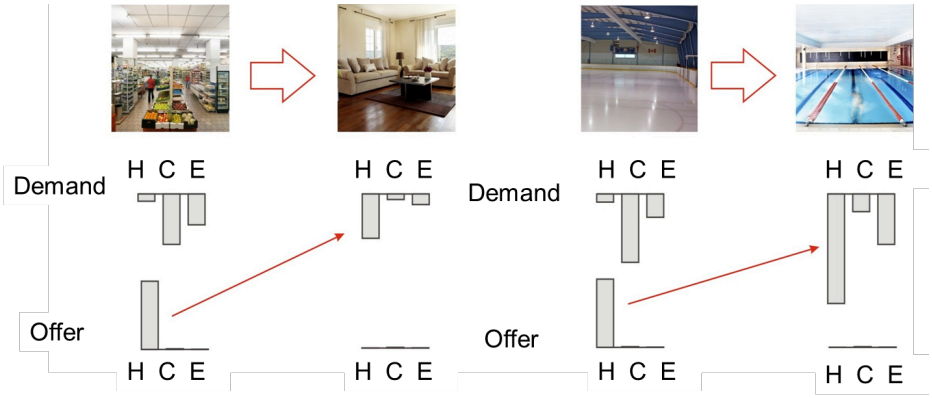

FIG 3: Presenting of demand adapted supply depending on different demand profiles.

3.2 Optimization of supply profiles

Development and identification of concepts allowing a flexible supply of different demands with maximum share of local and renewable energy sources. Thereby chances for an efficient use of decentralized renewable-energy based systems such as CHP units, heat pumps and solar thermal collector fields as well as surplus heat (secondary energy) are enhanced. In this context, an all electrical supply and the use of heat pumps for the heating and cooling of the building stock is a promising option, too. Electrical energy from fluctuating energy sources will only be considered if they are thermally stored (e.g. storage tanks or usage of the building mass) and used for heating or cooling purposes (e.g. heat pumps). In this case only, an exergetic assessment is required and the signified contribution to greenhouse gas reduction is available.

FIG 4 shows that available local sources have to be established to allow cascading of exergy flows. For this the location of both sources and sinks are crucial.

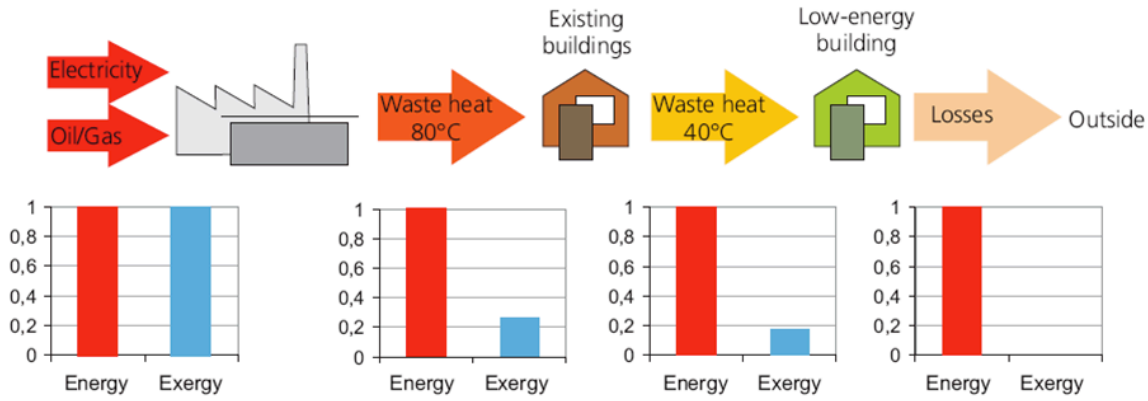

FIG 4: Presentation of demand adapted supply, e.g. cascading possibilities of the exergy flows at different exergy demand of different building energy classes.

3.3 Realisation and development of “model cities”

Development and identification of concepts allowing a flexible supply of different demands with maximum share of local and renewable energy sources. Thereby chances for an efficient use of decentralized renewable-energy based systems such as CHP units, heat pumps and solar thermal collector fields as well as surplus heat (secondary energy) are enhanced. In this context, an all

electrical supply and the use of heat pumps for the heating and cooling of the building stock is a promising option, too. Electrical energy from fluctuating energy sources will only be considered if they are thermally stored (e.g. storage tanks or usage of the building mass) and used for heating or cooling purposes (e.g. heat pumps). In this case only, an exergetic assessment is required and the signified contribution to greenhouse gas reduction is available.

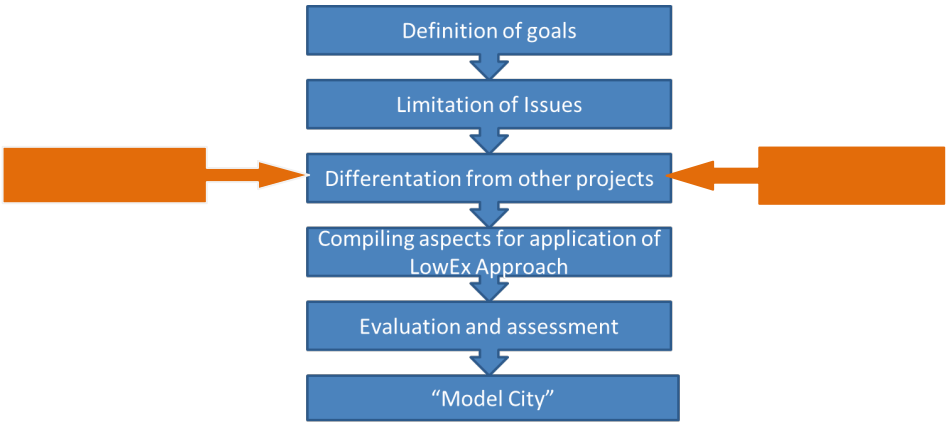

FIG 5: Opportunities for approach for the required steps to identify of a model city.

3.4 Assessment methodology

The main objective is to collect and further development of existing (exergy) assessment methods. This step is used to identify the most appropriate method (e.g. Excel Tools or Simulations Tools) for each user group. Based on the respective method it should be possible to display various stages of planning or design of buildings, groups of buildings and community supply systems. In particular, the further development of approaches from previous ECBCS Annex 37(Ala-Juusela, 2003) and Annex 49 (Torío, Schmidt 2011) is pursued here. In addition to these objectives, it is possible to develop a simplified approach or to identify new approaches. All method should contribute to a more flexible, efficient and renewable energy supply in community systems.

FIG 5 contains a description of the various planning stages. It should be clarified that the higher the resolution the less can be represented in detail. This shows the need for simplification in the modeling of complex community supply systems.

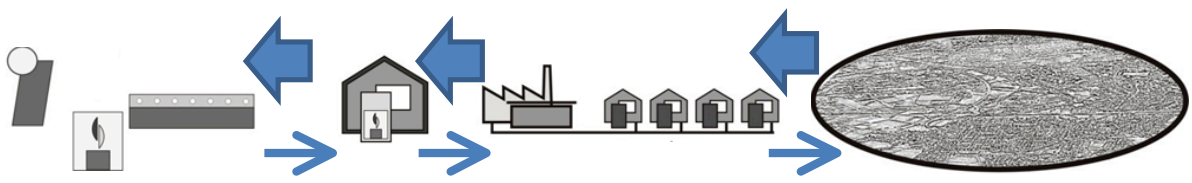

FIG 5: Schematic representation of application of evaluation methods for various stages of planning or design of buildings, groups of buildings and community supply systems.

4. Expected outcome and results from the project

The following results expected from the activities within the research activities within the framework of the International Energy Agency (IEA), the EBC Annex 64:

- Analysis concept and design guidelines with regard to the overall exergy performance of community supply and demand. This could include a possible classification of technologies in terms of performance, improvement potential and innovation prospects.
- Overview of the feasibility, efficiency potentials and impacts of integral energy system solutions for existing community settings, criteria for decision making in the project development phase.
- Analysis framework and open-platform software and tools for community energy system design and performance assessment.
- Summary of intelligent management and control strategies and system solutions for an efficient energy supply system at community level based on exergy principles.
- Set of existing and close to market systems and technological solutions and best integration into overall energy system design.
- Description and collection of good practices and examples of system concepts, technologies, management and control strategies for maximum share of renewable energy sources and maximum efficiency of the energy and exergy potentials available on a community scale.

The primary deliverable is an easy to understand and practical, applicable design guidebook for key people in communities. It is to contain an executive summary for decision makers and will cover issues on how to implement advanced supply technologies at a community level. Further it is focussed on how to optimise supply structures to ensure reduced costs for the system solution, while providing a high standard of comfort to the occupants of the buildings.

The dissemination of documents and other information is to be focussed on providing practitioners with research results. Methods of information dissemination are to include conventional means such as presentations at workshops and practice articles. The project homepage will be used extensively to spread information. Publications may be written in English and in the languages of the participants' countries. However, the translation of the key findings into English will allow for a broader distribution of knowledge. A communication platform will be developed using local networks and energy related associations. Regular workshops will be organised in all participating countries to show the latest project results and to provide an exchange platform for the target audience. Some of the workshops might be organised within the framework of national or international conferences or symposia.

5. Conclusions

Communities are characterized by a wide range of heating and cooling energy demands. This energy is mainly provided by the combustion of fossil fuels, which is responsible for greenhouse gas (GHG) emissions. National and international agreements limit the GHG emissions of industrialized countries, respectively, for climate protection. While a lot has already been achieved there are still large potentials in providing heating and cooling energy. At the community level, different renewable sources are available. These energies are characterised by high fluctuations and different qualities: e.g.

photovoltaic as electricity (high-exergy) or low temperature (low-exergy) heat from renewable energy sources. Low energy qualities are of particular interest, because the low exergy (LowEx) supply is very efficient. These described properties represent a major challenge. For solving these challenges, the identification of potential savings and synergies by performing holistic analysis of energy flows is necessary. The application of exergy principles is especially important, allowing the detection of different available energy-quality levels and the identification of optimal contribution to an efficient supply. From this, appropriate strategies and technologies with great potential for promoting the usage of low-valued energy sources (LowEx) and a high share of renewable energies for heating and cooling of entire cities can be derived.

In the framework of the new EBC project 'Annex 64 on LowEx Communities – Optimized Performance of Community Energy Supply System with Exergy Principles' advanced technologies have to be adapted and further developed to realize the identified potentials. For this reason, it is important to demonstrate the potential of low exergy thinking on a community level as energy and a cost efficient solution in achieving 100% renewable and GHG emission-free energy systems.

References

H.Torío, D.Schmidt, "IEA ECBCS Annex 49 Final Report-Low Exergy Systems for High-Performance Buildings and Communities-Detailed Exergy Assessment Guidebook for the Built Environment", 2011.

M. Ala-Juusela (Ed.); D. Schmidt; et. al. „Heating and Cooling with Focus on Increased Energy Efficiency and Improved Comfort". Guidebook to IEA ECBCS Annex 37, 2003.

D. Schmidt; "Low Temperature District Heating for Future Energy Systems", Annex Text to IEA DHC Annex TS1, http://www.iea-dhc.org, 2013

J. Kimman; A. Dütz; R. Jank; et. al."Case Studies and Guidelines for Energy Efficient Communities - A Guidebook on Successful Urban Energy Planning". IEA ECBCS Annex 51, 2013.

Frosting limit in Air-to-Air Membrane Energy Exchangers

Mohammad Rafati Nasr, M.Sc.[1]
Melanie Fauchoux, Ph.D.[1]
David Kadylak, M.A.Sc.[2]
Ryan Huizing, M.A.Sc.[2]
Carey Simonson, Professor [1]

[1] University of Saskatchewan, Canada
[2] dPoint Technologies Inc., Canada

KEYWORDS: heat exchanger, hydrophilic, hydrophobic, pressure drop, sensible effectiveness, latent effectiveness, frosting visualization

SUMMARY:
In this paper, three air-to-air membrane exchangers with (a) hydrophobic, (b) hydrophilic and (c) impermeable membranes are tested under a range of supply inlet air temperatures. The exhaust inlet conditions are ~22°C and ~45% RH, and the supply and exhaust airflow rates are 18.8 L/s. The frosting limit is defined as the supply air (i.e., outdoor) temperature below which frosting is observed in the exchanger after a specified time. The presence of frosting is determined by monitoring changes in effectiveness, pressure drop and visual inspection. The frosting limit is found to be approximately -1°C for the impermeable membrane exchanger and -6°C for the hydrophobic and hydrophilic membrane energy exchangers.

1. Introduction

Energy consumption in residential and commercial buildings makes up around 40% of the total energy use in Canada and 60% of the energy consumption in buildings is used for heating and cooling (Natural Research of Canada, 2009). Energy Recovery Ventilators (ERVs) are an essential part of heating, ventilating and air conditioning (HVAC) systems when designing energy efficient buildings, because they allow adequate outdoor ventilation air without excessive energy consumption. Membrane based energy exchangers are a new type of ERV that reduce energy use, while regulating relative humidity levels in buildings. In cold regions such as Canada or northern Europe, frost formation in the exchangers during the cold season decreases the performance of the equipment, and blockage of the air streams by frost may reduce the ventilation rate and decrease the indoor air quality (IAQ). Many researchers have studied frosting in air-to-air heat/energy exchangers, but frosting in air-to-air membrane exchangers has not been previously studied (Rafati Nasr et al., 2014). In this paper three different membrane energy exchangers are tested under frosting conditions to determine when frosting occurs for each exchanger. Additionally, different techniques to detect frost formation in the exchangers are compared. Frosting limit is defined as the temperature of the supply air inlet (at a specific exhaust inlet relative humidity) at which frosting is detected in the exchanger. In this paper heat exchanger or HRV refers to the exchanger with an impermeable membrane and energy exchanger or ERV refers to the exchangers with permeable membranes.

2. Test Facility

The three cross flow air-to-air exchangers were manufactured with identical geometries such that they all have the same surface area (FIG 1). The cores are made out of layers where the membrane is separated by corrugated aluminium foil spacers. For two of the exchangers, the polymer membrane

has a coating on one side, making that side more hydrophilic than the uncoated side. In one of these ERV exchangers the hydrophilic coating interfaces with the exhaust stream, while in the other exchanger the more hydrophobic surface is in contact with the exhaust stream. The third core is made with an impermeable polymer film with the same thickness as the polymer membrane used in the other two cores. This film blocks any water vapor, making it a heat recovery ventilator (HRV) with the same sensible performance, to compare it to the other ERV cores.

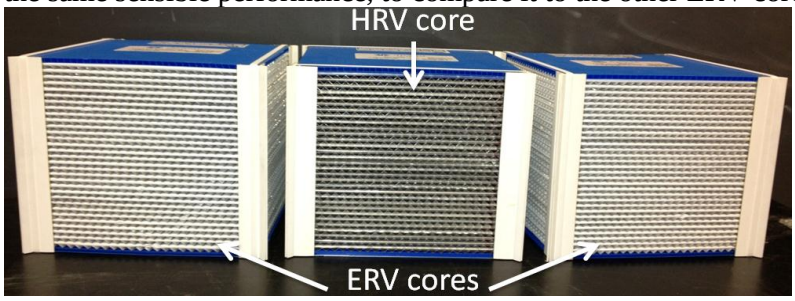

FIG 1. Three different cores used in the frosting tests.

FIG 2 shows the arrangement of the exchanger cores and the supply and exhaust air streams. Air is drawn from two environmental chambers at desired conditions (for the supply and the exhaust air inlets), and after passing through the exchanger, the air is discharged in to the laboratory. Fans are used both upstream and downstream to ensure balanced flow through the exchanger core. In order to determine when frosting occurs in the exchangers, several air properties are measured at different locations in the test facility.

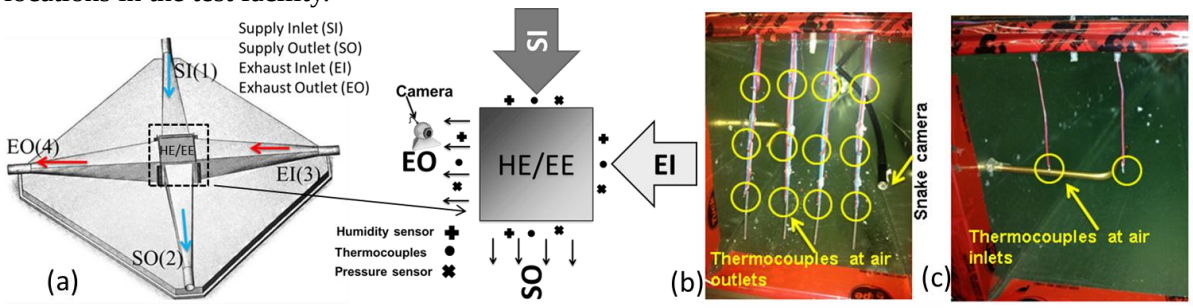

FIG 2. Arrangement of (a) exchanger core and headers and sensors location, (b) Configuration of the thermocouples at the outlets and (c) the inlets of the exchanger.

Temperature: The temperature of the air is measured using T-type thermocouples, which are calibrated over a temperature range of -30°C to 30°C. FIG 2 shows the configurations of the thermocouples at (b) the outlets and (c) the inlets of each stream.

Flow rate: Orifice plates are installed in the supply and exhaust ducts, both upstream and downstream of the exchanger, to determine the mass flow rate of dry air in each stream (ISO 5167-1, 2003).

Visualization: To observe frosting, a snake camera (endoscope) is installed at the exhaust outlet as shown in FIG 2 (a).

Relative humidity (RH): The relative humidity of each air stream is measured at the inlets and outlets of the exchanger, exactly where the temperature is measured. To achieve higher accuracy in measuring the humidity at very low temperatures, a chilled mirror dew-point sensor is used in the supply inlet side.

Pressure drop: Static pressure probes are placed before and after the core in each stream to measure the pressure drop across the exchanger (FIG 2 (a)).

3. Test Procedure

The experiments are designed based on the standard for testing air-to-air heat/energy exchangers (ASHRAE Standard 84, 2013). The performance of exchangers is evaluated using sensible effectiveness for HRVs and sensible and latent effectivenesses for ERVs.

3.1 Performance Evaluation

In this paper the performance of the exchangers is determined by their effectivenesses, and pressure drop, as described in (ASHRAE Standard 84, 2013). The nomenclatures in FIG 2 (d) are used in the remainder of the paper to designate locations.

Effectiveness: The effectiveness of an exchanger is calculated for the supply and exhaust streams from the following equations:

$$\varepsilon = \frac{q_{\text{actual}}}{q_{\text{maximum}}} \tag{1}$$

$$q_{\text{actual}} = C_{SO}(X_{SI} - X_{SO}) \qquad q_{\text{maximum}} = C_{\min}(X_{SI} - X_{EI}) \tag{2}$$

Where:
- ε effectiveness
- q sensible, latent, or total heat or energy (kW)
- X dry-bulb temperature (K or °C) for sensible effectiveness, humidity ratio (g/kg) for latent effectiveness or enthalpy (kJ/kg) for total effectiveness
- C $\dot{m}C_p$ for sensible, $\dot{m}h_{fg}$ for latent or $\dot{m}$ for total
- $\dot{m}$ the mass flow rate of dry air (kg/s)
- C_p the specific heat of dry air (kJ/(kg·K))
- h_{fg} the heat of vaporization of water (kJ/(kg·K))

The effectiveness in the supply side is more important and will be presented in this paper.

3.2 Mass and Energy Balance

Although tests with frosting or condensation may not meet the criteria for mass and energy balances, because of the continuous growth of the frost, in this paper, conservation of the mass flow rate of dry air and water vapour, as well as conservation of sensible and total energy for the HRV/ERVs according to (ASHRAE Standard 84, 2013) are satisfied in most tests.

3.3 Uncertainty

When conducting experiments it is important to determine the uncertainty in each measurement. The sensors are calibrated and the uncertainty of each sensor is determined according to (ASME, 2005). The uncertainty in the temperature measurements is ±0.2°C, in the relative humidity measurements is ±3% RH and in the pressure measurements is ±3-6 Pa. The uncertainty in the mass flow rates is ±2%, in the calculated sensible effectiveness is ±2% and in the latent effectiveness is ±5-8%. The higher uncertainty in latent effectiveness compared to sensible effectiveness is due to higher uncertainty in the humidity sensors compared to the thermocouples.

4. Results and Discussion

The three cores are initially tested under conditions with no risk of frosting, and then tests are conducted at low supply temperatures, with the possibility of frosting. In all of the experiments, the exhaust inlet conditions are maintained at 22°C and ~35-45% RH. The supply inlet temperature (T_{SI})

varies between 0°C and 11°C for the tests without frosting and between -10°C and 0°C for the frosting tests. The mass flow rate of dry air is ~23 g/s for both air streams.

4.1 Tests with no condensation or frosting

To make sure no condensation occurs in the test for HRV, the supply inlet temperature is 11°C. The mass flow rate of dry air in each stream is approximately the same, within uncertainty limits, which indicates negligible leakage in the test facility, and balanced flow through the HRV core. The effectiveness, as well as the pressure drop across the core, in each stream remain constant and the values for the two streams are approximately the same, again indicating equal flow rates.

Similar tests for the ERV with coating on the supply side (hydrophobic) and the ERV with coating on the exhaust side (hydrophilic) are performed. The sensible and latent effectivenesses in both these exchangers are constant as well. TABLE 1 presents a summary of results including the operating conditions and the performance parameters for the three exchangers. It can be seen that the sensible effectiveness of the hydrophilic ERV is 5% lower than the other two exchangers, but its latent effectiveness is slightly higher (within the uncertainty range), while the total effectiveness of both ERVs is the same.

TABLE 1. Summary of the performance tests of three exchangers without frosting.

	T_{EI}	RH_{EI}	T_{SI}	RH_{SI}	$\dot{m}_{dry}$	ΔP	ε_s	ε_l	ε_t
Type of exchanger	°C	%RH	°C	%RH	g/s	Pa	%	%	%
HRV	22.9	40	11.0	37	23	23	61	-	-
Hydrophobic ERV	23.1	55	4.5	39	23	24	61	30	45
Hydrophilic ERV	21.2	46	1.0	35	23	24	56	31	45

4.2 Frosting Limits

Many parameters may affect frosting, including air inlet conditions, flow rates, exchanger effectiveness and design. In this research, the exchanger designs are similar, and air flow rates are kept constant. The two main air properties are T_{SI} and RH_{EI}.T_{EI} is kept constant in all experiments, and RH_{SI} does not play a significant role in the frosting.

The methods used to detect frosting are:

- measuring the change in pressure drop across the core;
- calculating the change in effectiveness of the exchanger and
- visual observation using a camera at the outlet of the core.

4.2.1 HRV

Several tests are performed under frosting conditions to determine the frosting limit for each exchanger.. The supply side sensible effectiveness and pressure drop across the HRV over time are shown in FIG 3 for one test. The effectiveness stays approximately the same until 140 min, and then decreases by 2% over the last 30 min. The pressure drop on the exhaust air side increases gradually during the test, while the pressure drop on the supply side remains constant. This increase in pressure drop in the exhaust side is related to frosting, due to the high humidity and cold exchanger surface, which is consistent with the literature (Nielsen et al. 2009; Fisk et al. 1984). Photographs at the exhaust outlet show the formation of frost starting at an early stage of the experiment (FIG 4). After 10 min the amount of frost observed at the HRV outlet does not change with time, according to the photographs. It can be concluded that most of the frost is forming inside the core rather than at the outlet.

The exhaust side pressure drop is presented for all HRV tests, in FIG 5. The only case with no pressure change is the test with T_{SI} = -0.5˚C. From the results presented in TABLE 2, the frosting

limit of the HRV is determined to be $T_{SI} \approx -1^{\circ}C$ when $RH_{EI} \approx 45\%$ RH. The effectiveness results in TABLE 2 show a reduction in the average effectiveness with supply temperature, except for the test with $T_{SI} = -0.5^{\circ}C$. The higher average effectiveness in test 3 may be due to the condensation heat release in the exhaust air stream or an enhancement in heat transfer by the early stage of frosting (Fisk et al., 1984). However, this increase would be temporary and it is expected the effectiveness would decrease if left to frost for a longer period.

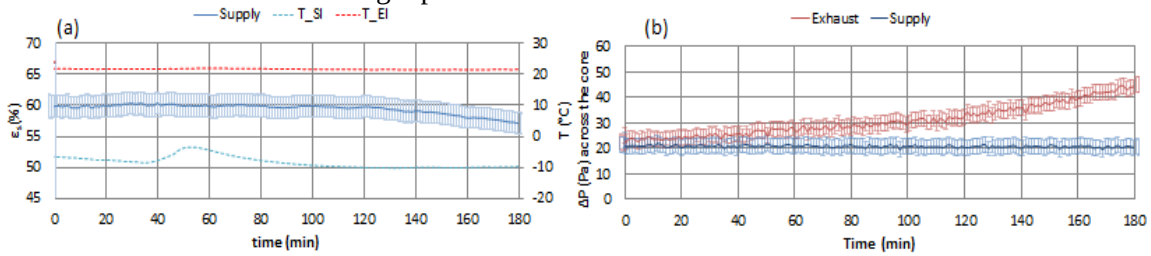

FIG 3. (a) Sensible effectiveness and (b) Pressure drop across the HRV with frosting.

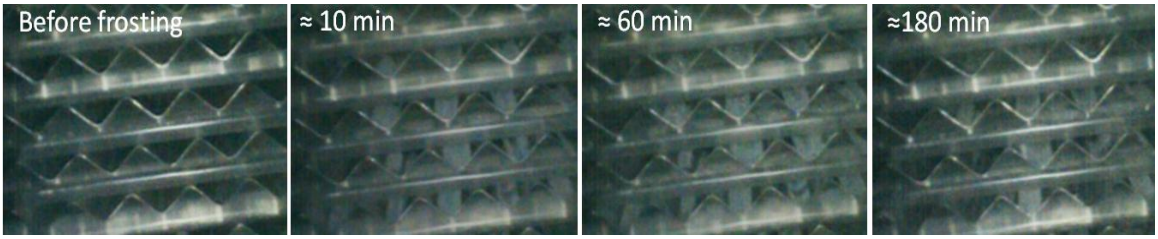

FIG 4. Photographs of frost formation in the HRV.

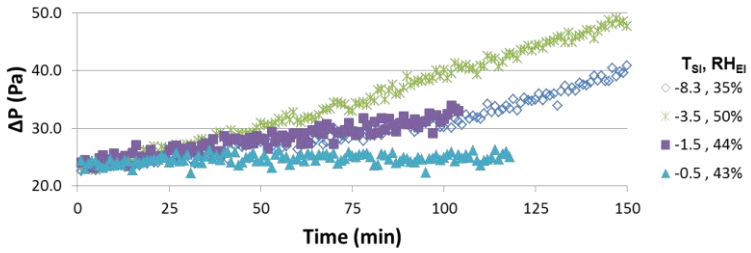

FIG 5. Exhaust side pressure drop for HRV tests.

TABLE 2. Summary of the frosting tests for the HRV.

Test No.	T_{SI} (°C)	RH_{SI}(% RH)	T_{EI} (°C)	RH_{EI}(% RH)	ε_s(%)	Frosting
1	-8.3	46	21.7	35	59	Yes
2	-3.5	29	21.7	32	60	Yes
3	-1.5	36	21.8	50	63	Yes
4	-0.5	36	21.9	43	59	No

The following can be concluded from the experiments on the HRV:

- visual observation shows the presence of frost earlier than the change in pressure drop,
- pressure drop shows an increase in the amount of frost over time, while the photographs do not,
- supply side pressure drop does not change under frosting conditions and
- change in sensible effectiveness is minimal; it is not a good indication of frosting in this test.

4.2.2 Hydrophobic ERV

Based on the results from the HRV, the frosting limit in the ERVs is expected to be lower than -1°C for the same RH_{EI}. FIG *6* shows the pressure drop across the core for a test with $T_{SI} \approx -4.5$°C and

RH_{EI} ≈ 49% RH. Again, frosting occurs only in the exhaust side of the ERV. This finding is important as it confirms that no frosting has occurred in the supply side, even with the use of a membrane in the exchanger.

The photographs in FIG 7 show a very small amount of frost at the outlet of the ERV. This amount does not change with time, although the pressure drop is still increasing. Again, it can be concluded that frost forms mostly in the middle of the core.

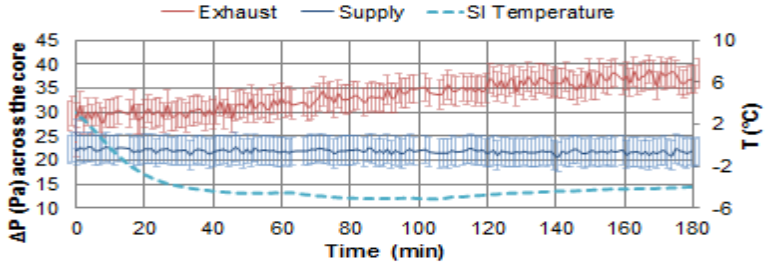

FIG 6. Pressure drop for the test with T_{SI} = -4.5˚C and RH_{EI} = 49% RH with the hydrophobic ERV.

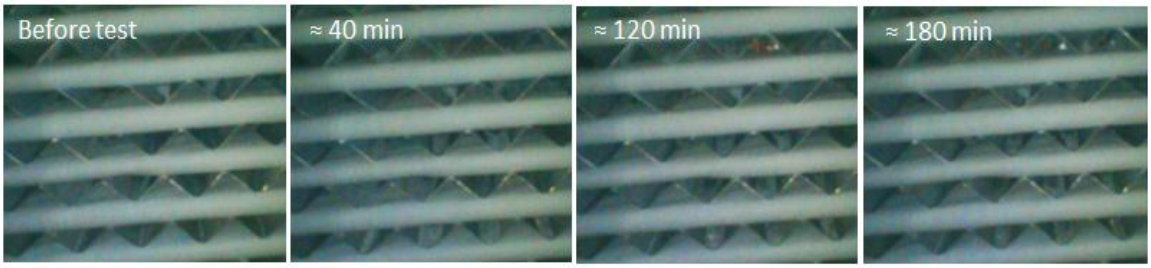

FIG 7. Photographs of frost formation in the hydrophobic ERV.

Sensible and latent effectivenesses are shown in FIG 8. The sensible effectiveness reduces by 2% at the end of the test, while latent and total effectivenesses stay fairly constant during the tests.

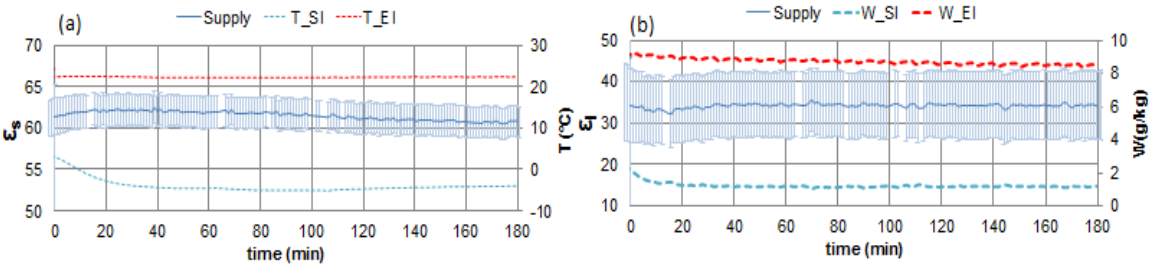

FIG 8. (a) Sensible and (b) latent effectiveness for the test with T_{SI} = -4.5˚C and RH_{EI} = 49% RH with the hydrophobic ERV.

Similar conclusions to those presented for the HRV can be extracted for the hydrophobic ERV, except for the frosting limit. A summary of the frosting tests for the hydrophobic ERV is presented in TABLE 3. There is a small variation in RH_{EI}, due to changes in the lab air conditions. This variation is the reason that frosting occurs during the test with T_{SI} = -4.5˚C, while no frosting occurs during the test with T_{SI} = -5.8˚C. Thus, it is predicted to observe frosting in the hydrophobic ERV at T_{SI} ≈ -6˚C when RH_{EI} ≈45% RH. In addition, comparing the effectivenesses for the frosting tests with the results in TABLE 1, the sensible effectiveness is 1-2% higher and the latent effectiveness is 2-4% higher when frosting occurs, compared to the frosting test. These increases in effectiveness are likely due to condensation heat release and the presence of condensed water on the membrane surface which may increase moisture transfer.

TABLE 3. Summary of the frosting tests for the hydrophobic ERV.

Test No.	T_{SI} (°C)	RH_{SI} (% RH)	T_{EI} (°C)	RH_{EI} (% RH)	ε_s (%)	ε_l (%)	ε_t (%)	Frosting
1	-6.2	43	22.3	49	62	35	51	Yes
2	-5.8	46	22.1	44	62	33	51	No
3	-4.5	44	22.2	49	62	34	50	Yes

4.2.3 Hydrophilic ERV

Based on the performance results from the previous section, the frosting limit in the hydrophilic ERV is expected to be close to the hydrophobic ERV. A summary of the results for the hydrophilic ERV is provided in TABLE 4. The pressure drop and effectiveness is shown in FIG 9 in FIG 10 respectively. The increase in pressure drop confirms the formation of frost in the exchanger. The pressure drop however, stays fairly constant after 140 min in FIG 9. This may be an indication of a reduction in the frost growth due to changes in the sensible effectiveness, which would reduce the heat transfer between the two air streams. On the other side, the sensible effectiveness decreases by 2% during first 140 min and stays fairly constant thereafter, with no change in latent effectiveness. The photographs of the outlet are similar to the observations in the hydrophobic ERV and so are not shown.

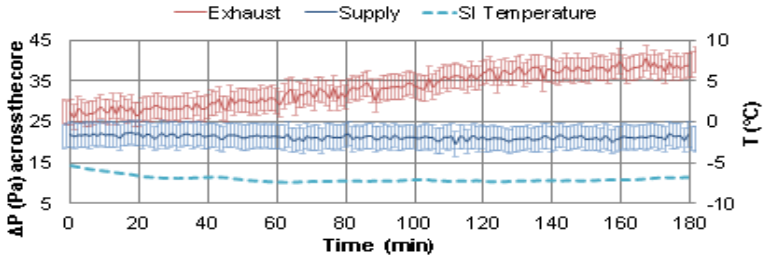

FIG 9. Pressure drop for (a) the test with T_{SI} = -7˚C and RH_{EI} = 47% RH, and (b) for the exhaust side for- all tests with the hydrophilic ERV.

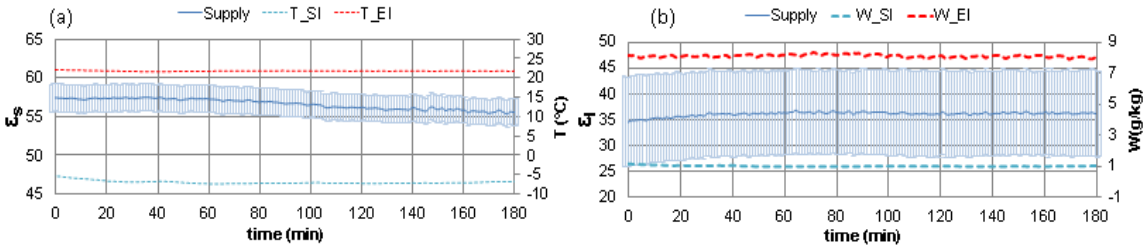

FIG 10. (a) Sensible and (b) latent effectiveness for the test with T_{SI} = -7˚C and RH_{EI} = 47% RH with the hydrophilic ERV.

TABLE 4. Summary of the frosting tests for the hydrophilic ERV.

Test No.	T_{SI} (°C)	RH_{SI} (% RH)	T_{EI} (°C)	RH_{EI} (% RH)	ε_s (%)	ε_l (%)	ε_t (%)	Frosting
1	-7	45	21.8	47	56	36	48	Yes
2	-6.8	41	21.9	43	56	35	48	Yes
3	-5.8	40	21.9	46	56	36	48	Yes
4	-4	41	22.8	46	56	34	47	No

By comparing the results in TABLE 4, the frosting limit for the hydrophilic ERV is between -4 to -5.8˚C when $RH_{EI} \approx$ 45% RH, which is a little higher than for the hydrophobic ERV. With further

analyse from the pressure drop graphs, the frosting limit is estimated at -5.5 ˚C. Although there is a little reduction in sensible effectiveness during the tests, the average sensible effectiveness of each test is the same as the test with no frosting, presented in TABLE 1. The average latent effectiveness is 3% to 5% higher with frosting than without frosting. This higher latent effectiveness might be the results of condensation in the exhaust air stream at low temperatures, which increases the moisture transfer through the membrane.

5. Conclusions

In this paper, three air-to-air membrane exchangers were tested under low supply inlet temperatures when the exhaust inlet conditions were ~22°C and ~45% RH, and the supply and exhaust airflow rates were 18.8 L/s. The frosting limit for the HRV is -1˚C, and for both the hydrophobic and hydrophilic ERVs is around -6 ˚C. In addition, the following points were concluded during this project.

- visual observation showed the occurrence of frosting sooner than pressure drop monitoring,
- the amount of frost throughout the test can be detected by an increase in the pressure drop, while the photographs from the outlet did not show this increase in the amount of frost,
- the pressure drop in the supply side did not change with frosting in any of the exchangers meaning that no frost formed in the supply side of the exchangers, and
- changes in effectiveness were not significant during the frosting tests, indicating that the effectiveness values did not show the initiation of frosting.

6. Acknowledgment

The authors acknowledge the financial support of Natural Sciences and Engineering Research Council of Canada (NSERC) Engage Grant, Smart Net-Zero Energy Building Strategic Research Network (SNEBRN), and dPoint Technologies Inc.

References

ASHRAE Standard 84, 2013. Method of Testing Air-to-Air Heat/Energy Exchangers, ANSI/ASHRAE Standard 84. American Society of Heating, Refrigerating and Air Conditioning Engineers Inc., Atlanta.

ASME, 2005. ASME PTC 19.1 test uncertainty. American Society of Mechanical Engineers, New York.

Fisk, W.J., Chant, R., Archer, K., Hekmat, D., 1984. Onset of freezing in residential air-to-air heat exchangers. ASHRAE Trans. 91, 145–158.

ISO 5167-1, 2003. Measurement of fluid flow by means of pressure differential devices - Part 1: Orifice plates, nozzles and Venturi tubes inserted in circular cross-section conduits running full. International Standards Organization, Geneva, Switzerland.

Natural Research of Canada, 2009. Energy Efficiency Trends in Canada 1990 to 2009. http://oee.nrcan.gc.ca/publications/statistics/trends11/pdf/trends.pdf

Nielsen, T.R., Rose, J., Kragh, J., 2009. Dynamic model of counter flow air to air heat exchanger for comfort ventilation with condensation and frost formation. Appl. Therm. Eng. 29, 462–468.

Rafati Nasr, M., Fauchoux, M., Besant, R.W., Simonson, C.J., 2014. A review of frosting in air-to-air energy exchangers. Renew. Sustain. Energy Rev. 30, 538–554.

Thermal comfort in summer in low energy buildings

Ansis Ozolins[1],
Andris Jakovics[1]

[1] University of Latvia, Latvia

KEYWORDS: *summer overheating, thermal comfort, low energy buildings*

SUMMARY:
The aim of this work is to analyse thermal comfort and overheating risks under Latvian climate conditions. Two cases were inspected: no cooling and heating applied indoors (temperature fluctuates due to free floating conditions) and cooling applied indoors. Results for 3 test houses significantly differ, despite the similar projected U-value for each external wall. Differences are analysed in detail. It is shown that the initial moisture on the external wall can significantly influence the thermal comfort in the room. Despite the temperate climate in Riga, Latvia, both the experiments and the calculations show that overheating risks are high in summer.

1. Introduction

By December 31, 2020, all the newly constructed buildings are to become the "nearly zero energy consumption buildings" according to (Directive of the European parliament and of the council 2010/31/EU). However, overheating risks can be observed for passive houses, especially in summer. A high indoor temperature combined with a higher relative humidity can influence the living conditions negatively, affecting human health. Therefore a comprehensive study of thermal comfort in passive houses is strongly recommended. Living conditions in summer have been widely researched. 207 across the England were chosen and summertime temperatures were analysed (Beizaee & Lomas 2013). A single Slovenian passive house was analysed and overheating risks in summer have been investigated in (Mlakar & Strancar 2011). In (Bravo & Gonzalez, 2013) thermal comfort in hot-humid climate has been analysed. (Brun & Wurtz & Hollmuller, 2013) applied a new free-cooling system in experimental houses with the aim to analyse summer comfort.

FIG 1. On the left: The test stands of houses. On the right: A cross-section of one test stand

Despite the countless researches dedicated to the thermal comfort in houses at the summertime, the research of houses having the same parameters (net volume, roof, floor, orientation, projected U-value of external walls), the only difference among the houses being materials used in external walls, has not yet been published.. Such experiments have been done in Riga, Latvia, where five test houses have been built (see Fig. 1). Thermal comfort conditions in the three test houses were analysed in

(Ozolins & Jakovics & Ratnieks & Gendelis 2013). However, that publication focussed on the heat and moisture transfer on the walls as well as on the temperature distribution in the room. Moreover, at the time the experiments were not started yet in the houses placed in Riga (see Fig. 1). The experimental results obtained from the test stands were discussed in (Ozolins & Jakovics & Ratnieks 2013). However, this paper focussed on moisture risks on the walls. Small test houses were created in (Mlakar & Strancar 2013). However, in this case the net volume was significantly lower, projected U-values of external walls were not equal and the aim of the given paper was completely different. INCAS platform with several test houses was described in (Spitz & Mora & Wurtz & Jay, 2012).

The aim of this work is to analyse thermal comfort and overheating risks under Latvian climate conditions.

2. Short description of test houses and measurements

This section provides a brief description of external walls of five test stands built in Riga, Latvia (see Fig. 1). Project homepage (EEM, 2011) provides a comprehensive image gallery of test stands as well as a detailed material description.

TABLE 1. Description of building construction's walls

AER house, 165 kg/m^2 $U_{projected}$=0.153 W/(m^{2}K) from outside to inside		CER house, 363 kg/m^2 $U_{projected}$=0.151 W/(m^{2}K) from outside to inside		PLY house, 79 kg/m^2 $U_{projected}$=0.154 W/(m^{2}K) from outside to inside	
Material	Thermal conductivity [W/mK], μ [-], $c_p \times \rho$ [J/(m^{3}K)]	Material	Thermal conductivity [W/mK], μ [-], $c_p \times \rho$ [J/(m^{3}K)]	Material	thermal conductivity [W/mK], μ [-], $c_p \times \rho$ [J/(m^{3}K)]
Wind protection slab, 0.03 m	0.034, 1, 59500	Wind protection slab, 0.03 m	0.034, 1, 59500	Plywood, 0.02 m	0.17, 700, 750000
Stone wool, 0.02 m	0.036, 1, 33200	Stone wool, 0.125 m	0.043, 1, 33200	Stone wool, 0.2 m	0.041, 1, 33200
Lime plaster, 0.015 m	0.7, 7, 1344000	Lime plaster, 0.015 m	0.7, 7, 1344000	Plywood, 0.02 m	0.17, 700, 750000
Aerated concrete, 0.375 m	0.072, 4, 255000	Aerated clay bricks, 0.44 m	0.175, 7, 595000	Fibrolite, 0.075 m	0.068, 2, 756000
Lime plaster, 0.015 m	0.7, 7, 1344000	Lime plaster, 0.015 m	0.7, 7, 1344000	Lime plaster, 0.015 m	0.7, 7, 1344000

In Table 1, the multi-layered external walls of each test house are characterized. For layers consisting of the stone wool effective λ is chosen taking into account the wood frame. Wood siding in front of walls for each test house was used to protect the walls from rain and solar radiation. Ventilated air layer with a thickness of 2 cm is located between the wood siding and the wall. The roof, floor, windows and doors of all test stands are similar. Triple-glazed window with solar heat gain coefficient 0.5 is built into the south-facing wall of each test stand. U-value is 0.72 W/m^{2}K for the

window and width, height and height above floor are 1.2 m, 1.5 m and 1 m, respectively. It can be noted that the inner loads due to the measuring equipment were approximately 3 W/m^2 for each of the test stands. More information about test stands and materials used for each of the test houses is available in (EEM, 2011).

3. Results and discussions

The current section consists of 2 parts:

- thermal comfort analysis based on the measurements in the test houses;
- analysis of the long term overheating risks based on the numerical calculations.

Numerical simulation has been implemented by using software WUFI PLUS: room climate model for calculation of the inner climate conditions.

3.1 Thermal comfort under different exploitation conditions

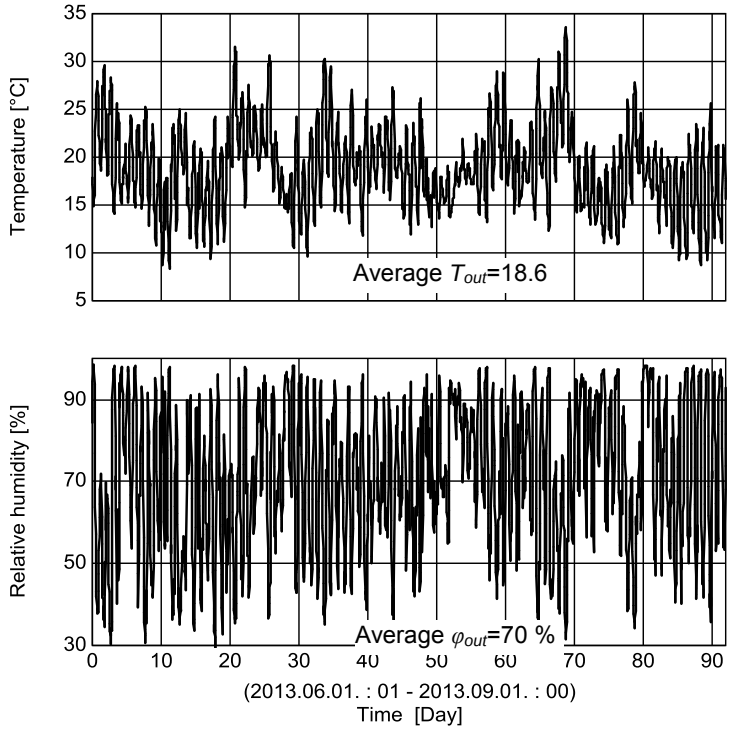

FIG 2. Outdoor temperature and relative humidity from June 1 to August 31

Measurements were implemented in test houses with the aim to estimate the room comfort under different conditions: no heating and cooling applied indoors in June, i.e. T_{in} and T_{out} fluctuated by free floating conditions. In July maximal T_{in} was set as +24 °C, i.e. cooling was ensured if indoor temperature rose beyond 24 °C. In August neither heating nor cooling were applied. However, the difference between the interior conditions in August and June was created by covering the windows from outside in August with the aim to observe the role of the solar radiation through the window. Air exchange coefficient was approximately 0.5 1/h and the indoor relative humidity fluctuated by free floating conditions for all time period. The outdoor climate conditions are shown in Fig. 2. The data has been obtained from the meteorological station created in the test polygon. The maximal outdoor temperature was observed on August 8, when maximum of T_{out} rose up to 33.6 °C. The average T_{out}

was 19.2 °C, 19.1 °C and 18.2 °C in June, July and August respectively. The average φ_{out} was 67 %, 71 % and 74 % in June, July and August respectively.

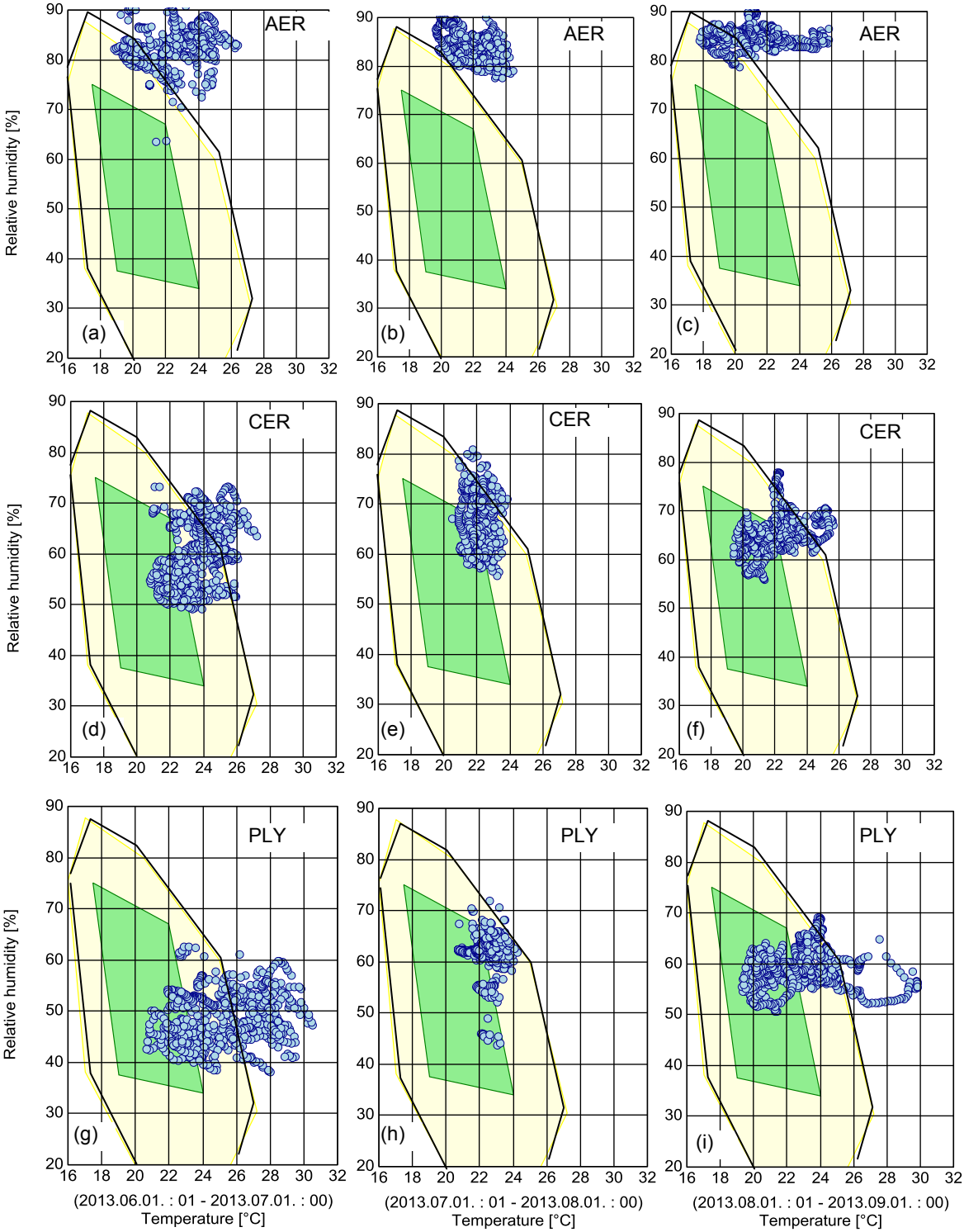

FIG 3. The measured indoor relative humidity compared to indoor temperature for 3 different test houses. Bounded regions are thermal comfort charts according to (ASHRAE Standard 55). Smaller region: comfortable. Larger region: still comfortable. On the left: room conditions in June when no heating and cooling was applied indoors. In the middle: room conditions in July when maximal T_{in}

was set at +24 °C. On the right: windows were covered in August, no cooling or heating applied indoors.

As it is shown in Fig. 3a, b, c, a high indoor relative humidity has been observed in case of the test stand of AER that can negatively influence human health. An explanation of high humidity is the high initial moisture for the aerated concrete that significantly influences the room conditions. The situation was not improved when the cooling was applied indoors. In the test stand of CER the room climate was significantly better (see Fig. 3d, e, f). For some time periods, the optimal thermal comfort was not ensured and circles slightly go out of optimal thermal comfort region due to the higher relative humidity (see Fig. 3e). When the windows were covered from the outside, the optimal comfort was also ensured almost throughout all days in August (see Fig. 3f). In case of the test house of PLY, a significantly lower relative humidity in the room (see Fig. 3g,h,i) was observed. However, a higher overheating was also observed, especially in June (Fig. 3g), when T_{in} fluctuates by free floating conditions and solar influence through the windows was observed. The problem is solved when cooling is applied indoors (see Fig. 3h). When windows were covered, the optimal comfort climate was also observed (see Fig. 3i), except during some warmer days that can be seen in Fig. 2. It can also be concluded that a significant impact of different building components used on the external walls to the thermal comfort has been demonstrated. The amplitude of T_{in} fluctuations was the lowest in case of the test stand of CER (Fig. 3d compared to Fig. 3g, Fig. 3f compared to Fig. 3i). It can be explained by higher volumetric heat capacity of aerated clay bricks incorporated in the external wall of CER that does not allow the heat to quickly transfer through the wall.

TABLE 1. Average outdoor and indoor temperatures for 3 test houses

	T_{out}	AER; T_{in}	CER; T_{in}	PLY; T_{in}
June	19.5	22.5	23.4	25.4
August	18.2	20.9	21.8	22.4

If we compare Fig. 3a to Fig. 3c, Fig. 3d to 3f, Fig. 3g to 3i, it can be seen that the average T_{in} between the months of June and August does not differ as much as it can be expected. More precisely, in June the average T_{in} was 3 °C, 3.9 °C and 5.9 °C higher than the average T_{out} for the test stands of AER, CER and PLY respectively (Table 2). The difference between T_{out} and T_{in} is explained with the inner sources and solar radiation through the window. In August average T_{in} was 2.7 °C, 3.6 °C and 4.2 °C higher than the average T_{out} for the test stands of AER, CER and PLY respectively (Table 2). It can thereby be concluded that a covered window only partially decreases the overheating risks.

3.2 Overheating risks in a long term

Measurements for estimating overheating risks in different building constructions were described in a previous subsection. However, only one summer was inspected, and the outdoor climate conditions can differ during other years. Therefore it is required to analyse the overheating risks in low energy houses during a long term. At first, WUFI PLUS model will be verified and the results compared with the experimental data obtained.

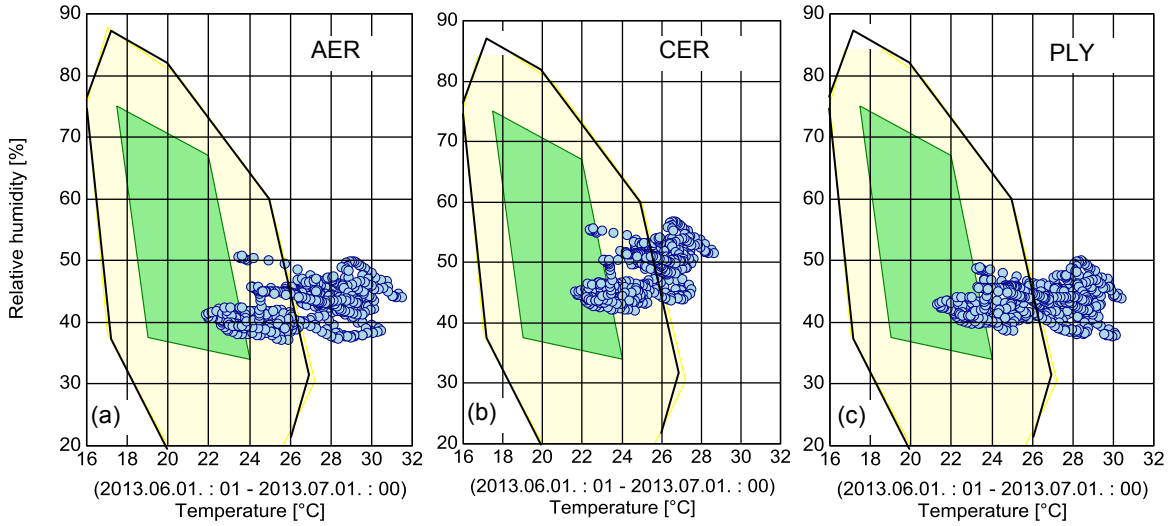

FIG 4. Calculated indoor relative humidity against indoor temperature for 3 different test houses.

It is shown that the numerical results (Fig. 4) significantly differ from the measurements (Fig. 3a, d, g). The differences in case of the test house of AER (Fig. 3a compared to Fig. 4a) are explained with a high initial moisture in aerated concrete that was not taken into account in numerical simulations. This moisture on the external wall promotes a higher indoor relative humidity, higher U-value and therefore lower indoor temperature. For the test stand of CER, the differences from measurements are lower (Fig. 3d compared to Fig. 4b). because the initial moisture for aerated clay bricks is not as high as for aerated concrete. For the test stand of PLY the range of T_{in} is similar both for measurements and numerical model (Fig. 3g compared to Fig. 4c). However, the measured range of φ_{in} is from 40-60 % despite the range of 40-50 % for numerical model.

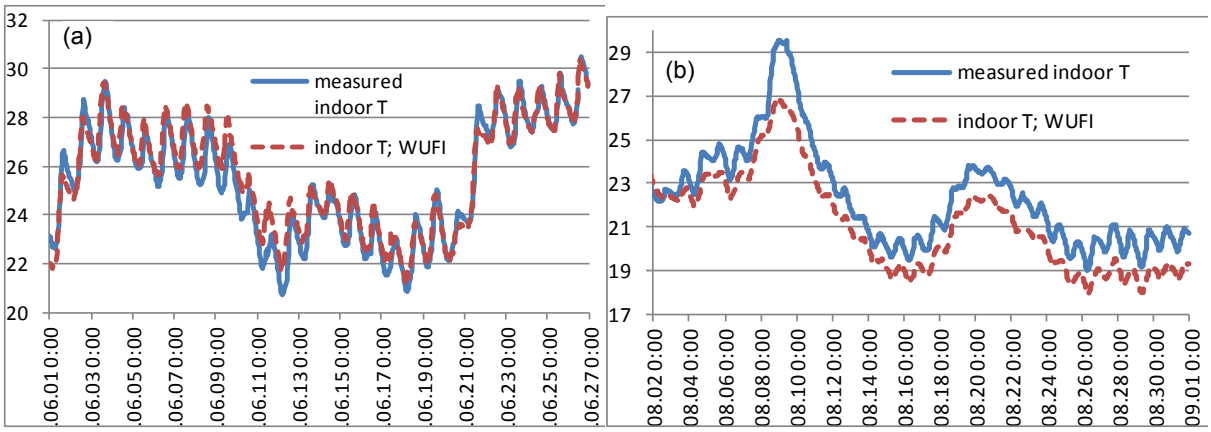

FIG 5. Experimental results (solid line) against numerical results (dashed line). Windows were: (a) uncovered; (b) covered

In Fig. 5 the dynamics of measured T_{in} are shown to verify the numerical model used in software WUFI PLUS. In June the numerical model is well fitted with measurements (Fig. 5a). However, measured T_{in} is for approximately 1-1.5 °C higher than the one obtained by numerical model in August (Fig. 5b). One explanation of this displacement is the overheating on the loft that can influence the room temperature more significantly, when the solar influence through the window is negligible

Since the numerical model shows reliable results for estimating room temperature for the test stand of PLY, a detailed analysis of overheating risks will be made in a long term, using the climate data from

2006 to2012 in Riga. It will be assumed that no heating and cooling is applied indoors in summer and solar influence through the window will be negligible.

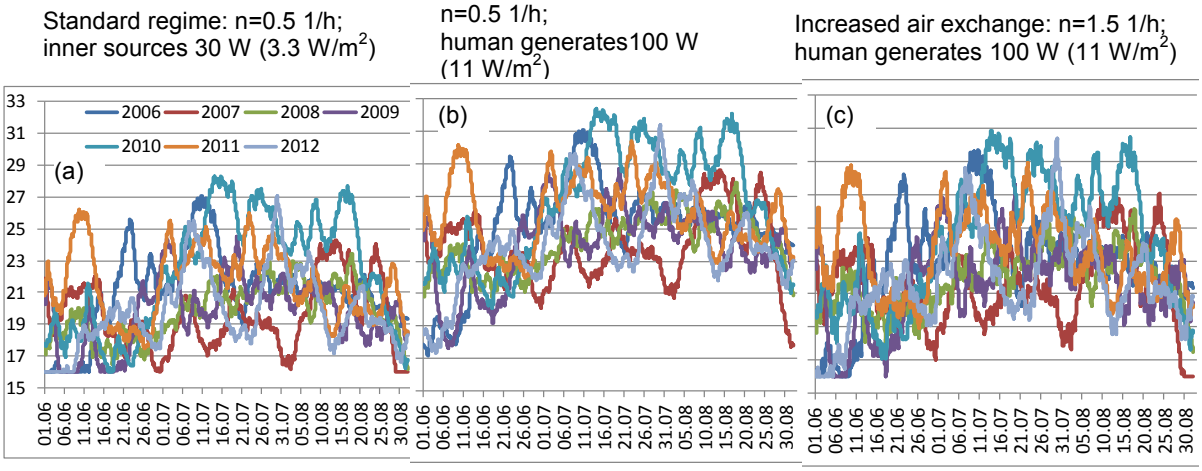

FIG 6. Calculated indoor temperatures for the test stand of PLY in a long term (2006-2012), solar influence through the window is negligible. (a) Standard room conditions that were applied on the real test house. (b) Inner loads 100 W due to the human activity. (c) Inner loads 100 W and increased air exchange from 0.5 to 1.5 1/h

Numerical calculations show that room temperature could increase above +25 °C in August only in 2010 (see Fig. 6a). It means that the situation, when T_{in} increases up to +29 °C (see measurement in Fig. 5b), is a rare phenomena at the given room conditions. However, T_{in} can increase above +25 °C several times during the 7 year period that can cause uncomfortable room living conditions. In a real situation, humans can produce additional heat or inner source. For the sake of simplicity it has been assumed that the inner loads are constant 100 W. The results obtained based on this assumption show a completely different situation (see Fig. 6b). Rooms can overheat for a longer time periods in several summers. Even T_{in}>30 °C can be reached. An assumption about an increased air exchange up to 1.5 1/h improves the thermal comfort (see Fig. 6c). However, the overheating risks remain and uncomfortable room conditions are often a case during the time period of 2006-2012. A better solution could be the night ventilation.

4. Conclusions

In the current paper three test stands of houses were compared and the experimental measurements of room living conditions for different cases (no heating and cooling applied indoors, covered windows, cooling) were obtained. The experiments show that the thermal comfort was not ensured for the house with external wall mainly consisting of the aerated concrete blocks and insulation materials. The living conditions were absolutely uncomfortable due to the high indoor humidity. The reason was a high initial moisture in the aerated concrete and very slow drying process. Thermal comfort also was not achieved in the test stands with the external walls mainly consisting of wooden materials and insulation layer. However, cooling or covering of the window significantly improves the situation. The best interior living conditions were observed in the test stand mainly consisting of aerated clay bricks and insulation materials.

Long term simulations based on the “light” test stand mainly consisting of plywood and stone wool shows that overheating risks could be observed for several time periods and for several summers despite the assumption about the window covered from the outside.

Since the initial moisture significantly influences the thermal comfort in case of one test house, it presents an interesting challenge to observe, how much the interior living conditions will improve for several subsequent summers. Such measurements will continue.

5. Acknowledgements

The current work was supported by the European Regional Development Fund in Latvia within the project No. 2011/0003/2DP/2.1.1.1.0/10/APIA/VIAA/041.

References

Ozolins, A. & Jakovics, A. & Ratnieks, J. & Gendelis, S. 2012. "Numerical modelling of thermal comfort conditions in buildings with different boundary structures", *Proceedings of the 11th REHVA World Congress & 8th International Conference on IAQVEC – CLIMA 2013,* Prague.

Ozolins, A. & Jakovics, A. & Ratnieks, J. 2013. "Moisture risks in multi-layered walls – comparison of COMSOL and WUFI@PLUS models with experimental results", *Proceedings of the COMSOL Users Conference 2013,* Rotterdam.

EEM, 2011. *Test stand of energy efficiency monitoring project*. [Online] Available from: http:/www.eem.lv.

Directive of the European Parliament and of the Council 2010/31/EU of 19 May 2010 on the energy performance of buildings.

Beizaee, A. & Lomas, K. & Firth, S. 2013. "National survey of summertime temperatures and overheating risk in English homes", *Building and Environment*. 65. p. 1-17.

Mlakar, J. & Strancar, J. 2011. "Overheating in residential passive house: Solution strategies revealed and confirmed through data analysis and simulations", *Energy and Buildings,* 43. p. 1443-1451.

Mlakar, J. & Strancar, J. 2013. "Temperature and humidity profiles in passive house building blocks", *Building and Environment,* 60. p. 185-193.

Spitz, C. & Mora, L. & Wurtz, E. & Jay, A. 2012. "Practical application of uncertainty analysis and sensitivity analysis on an experimental house", *Energy and Building,* 55 (2). p. 459-470.

Brun, A. & Wurtz, E. & Hollmuller, P. 2013. "Summer comfort in a low-inertia building with a new free-cooling system", *Applied Energy,* 112. p. 338-349.

Bravo, G. & Gonzalez, E. 2013. "Thermal comfort in naturally ventilated spaces and under indirect evaporative passive cooling conditions in hot-humid climate", *Energy and Buildings,* 63. p. 79-86.

ASHRAE Standard 55. *Thermal environmental conditions for human occupancy.*

Investigation of the Indoor Environment in a Passive House Apartment Building Heated by Ventilation Air

Mathias Young Bok Lysholt Hansen, M. Sc. [1]
Chrysanthi Sofia Koulani, M. Sc. [1]
Ruut Peuhkuri, Associate professor [1]
Jørn Toftum, Associate professor [1]

[1] Technical University of Denmark (DTU), Department of Civil Engineering, Denmark

KEYWORDS: *Low energy building, Passive House, warm air heating, thermal comfort, solar shading, field measurements, dynamic building simulation*

SUMMARY:
Experience has shown that appropriate design of very low energy dwellings can be a large challenge and that the final design may result in insufficient heating in winter and overheating in summer. The 126 certified Passive House apartments (Ravnsborghusene) in Køge, Denmark are a low energy building project finished medio 2012. The design challenge was met with a concept of air heating that is individually controlled in every room. It also applies external solar shading. This study used indoor climate measurements and dynamic simulations in one of these apartment buildings to evaluate thermal comfort and the performance of the air heating system and solar shading. Thermal comfort category B according to ISO 7730 was obtained in the building during field measurements, indicating that the air heating system was able to maintain comfort conditions in winter, when the outdoor temperature had been unusual low for a longer period. The dynamic simulations also indicated that air heating during winter can provide a comfortable thermal environment. Dynamic simulations also demonstrated that during summer, apartments with automatic external solar screens had no serious overheating, whereas in apartments with south oriented windows, static shadings by the balcony overhangs and low ventilation rates, resulted in excessive hours of overheating.

1. Introduction

From the Kyoto agreement in 1997 to the 2009 EU energy and climate package, the aim has been to reduce energy consumption of new and existing buildings. In the design of low energy buildings focus is to reduce the energy consumption. This may lead to design loads that are sensitive to variations in climatic conditions, user behaviour and changes during the building process.
The Passive House concept focuses on very low energy consumption for heating by efficient thermal insulation and utilization of the passive heat in the building. Here passive use of the solar load, occupants, electrical appliances etc. contributes considerably to heat up the space. Once the heating requirement is sufficiently low, the conventional water based heat distribution systems can be omitted and the dwelling heated by ventilation air alone. This may reduce the costs without compromising the indoor environment (Ellehauge et. al. 2008). However, recently published results found that poor design of air heating systems without individual control in each room and inadequate solar shading created problems with insufficient heating in winter and overheating in summer (Larsen 2011). These experiences from the first passive houses in Denmark have resulted in more detailed criteria on the space heating systems and on the performance of the indoor environment and namely thermal comfort. The current proposal for the future Building Regulations in Denmark, the current low energy class 2020, forbids the use of air heating alone and sets up concrete requirements for maximum acceptable indoor temperatures (Energistyrelsen 2013). But what if an air heating system is correctly dimensioned and gives occupants the possibility to control the room temperature individually and if the building has

an effective, external solar shading? Would the thermal indoor environment then meet the best indoor climate category A? This study focuses on evaluating the air heating system and solar shading systems of a newly constructed low energy apartment building, based on field measurements and dynamic simulations. The studied apartments are part of 126 certified Passive House apartments (Ravnsborghusene) in Køge, Denmark which were finished medio 2012.

2. Building description

The investigated apartment building is one out of nine certified Passive House apartment buildings. Each apartment building consists of 14 apartments spread over an eastern and a western section (see FIG 1). The eastern section consists of four floors with four 4-room apartments and four 2-room apartments. The western section comprises six 3-room apartments divided into three floors. The gross area of the east and west section is 689 m^2 and 490 m^2, respectively.

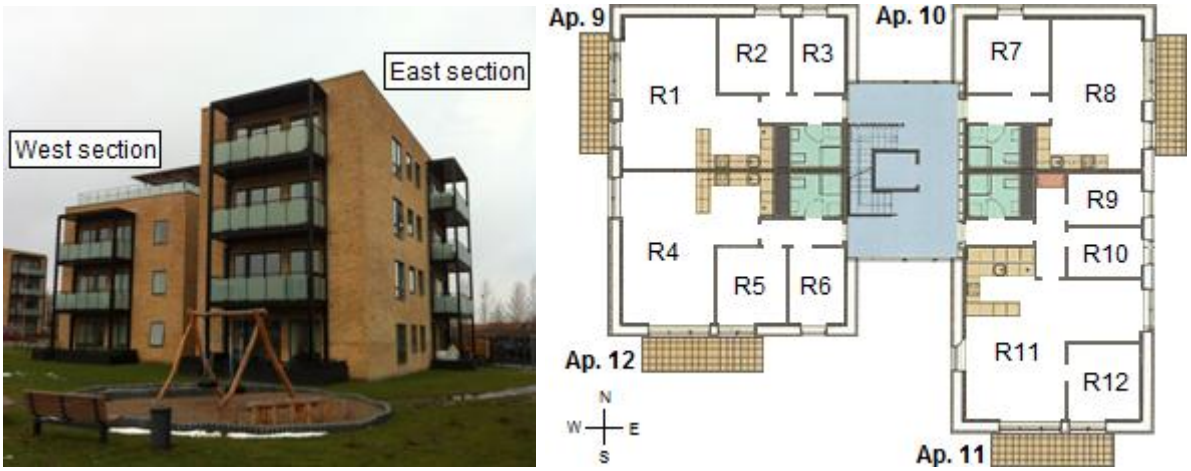

FIG 1. South east view of the investigated apartment building (left) and floor plan (right)

The apartment building is ventilated and heated by air from two centralized and balanced ventilation systems with heat recovery and pre heating coil. The supply air is heated by individual water based heating coils installed before each room inlet. The coil in each room can be individually controlled by thermostats. The heating system is based on three air to water heat pumps (AWHP) that supply heat to two domestic hot water tanks and a buffer tank. Automatic external solar screens are installed only at the east and west oriented windows. All 14 apartments have balconies towards east, west and south. These balcony overhangs operate as static shading.

3. Field measurements

3.1 Methods

Short and long term measurements were conducted to evaluate the thermal comfort and ventilation rates in the apartments.

3.1.1 Thermal comfort

Thermal comfort as well as local thermal discomfort was categorized according to ISO 7730 (2006), based on short term measurements. The purpose of the short term measurements was to evaluate if the air heating provided at specific locations in the living room was sufficient, during an unusual cold period where the outdoor temperature was approximately -8 °C. The average long term outdoor temperature in Denmark in January is -0.3 °C, the outdoor design temperature -12 °C and the design indoor air temperature is 20 °C. The short term measurements were conducted on January 25th 2013 in

each apartment on the 2nd floor, at three locations in the living rooms R1, R4, R8 and R11 (see FIG 1). The selected locations represented the approximate positions where occupants would stay for long time periods. At each location air temperature, air velocity, plane radiant asymmetry and relative humidity were measured at the heights 0.1 m, 0.6 m and 1.1 m during a minimum period of three minutes. A clothing insulation value of 1.0 clo and a metabolic rate of 1.2 met were assumed to best represent the average occupants clothing and activity level. The ASHRAE comfort tool software was used to calculate PMV and PPD (ASHRAE55 2013).

3.1.2 Ventilation rate

Occupant generated CO_2 was used to estimate the ventilation rates by applying a single-zone mass balance (Bekö et. al. 2010). The CO_2 concentration was measured during a period of one week (January 25th 2013 to February 1st 2013) by a Vaisala CO_2 transmitter connected to a HOBO data logger with a built in air temperature and relative humidity sensor. The placements of the HOBO data loggers were in representative locations in rooms R1-R11 (see FIG 1). The data acquisition interval was set to five minutes. In order to smooth the data and reduce extreme values, a 20-minute running average was used. Individual activity protocols for each room were completed by occupants for each day, in order to obtain behaviour related input to the calculation of the ventilation rates.

3.2 Results

3.2.1 Thermal comfort

Air temperature, mean radiant temperature, relative humidity and air velocity were found for all measuring locations. The average values over three locations in each apartment living room are illustrated in FIG 2 together with their standard deviations. The measured air temperature was close to the mean radiant temperature which also coincides with the high surface temperatures measured at the floor and ceilings. This indicates uniform thermal conditions in the measured rooms caused by well insulated building envelope and inner walls creating individual thermal zones.

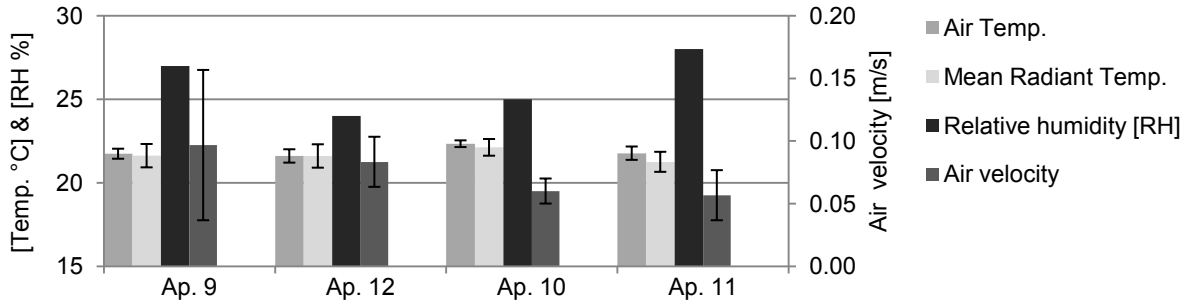

FIG 2. Parameters obtained in the 2nd floor apartments (Ap.9-12)

Based on the four obtained parameters and the assumed clothing insulation and metabolic rate, the PMV and PPD indices were calculated for the living room in each apartment shown in TABLE 1.

TABLE 1. PMV and PPD indices calculated for Ap. 9, 12, 10 and 11

Thermal comfort indices*	Ap. 9	Ap. 12	Ap. 10	Ap. 11
PMV [-]	-0.13	-0.13	0.04	-0.10
PPD [%]	5	5	5	6

*Calculation based on measurement at 0.6m height at three locations in each apartment living room.

According to ISO 7730 (2006), the PMV and PPD values for all apartments were within category A. In FIG 3, no noteworthy air temperature gradient occurred at any of the measurement locations. Also, the air velocity was generally below 0.15 m/s.

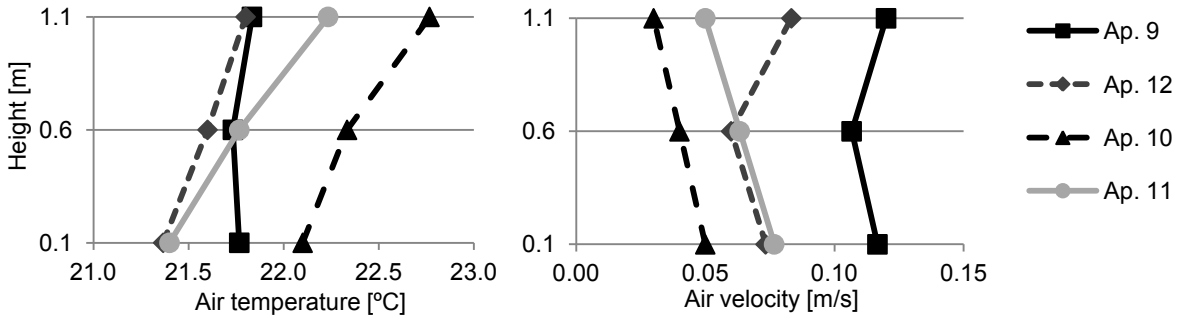

FIG 3. Vertical air temperature and air velocity profiles for the 2nd floor apartments

The local thermal discomfort measurements; draught rate (DR %), radiant asymmetry, vertical air temperature difference and floor temperature corresponded to category A for Ap. 12, 10 and 11, whereas Ap. 9 was in category B. The lower category was due to a slightly higher air velocity and lower air temperature, which resulted in 16 % draught rate.

3.2.2 Ventilation rate

In TABLE 2 the measured ventilation rates and the design values are shown. It can be seen that the measured ventilation rate, for most rooms, is comparable with the design ventilation rate. However, the ventilation rates for all rooms in Ap. 11 were much lower than the design values. The low ventilation rate in Ap. 11 may be due to the size and geometry of the apartment which created problems with sufficient ventilation or simply the fact that the ventilation system did not work properly for these rooms.

TABLE 2. Measured and design ventilation rates in the different rooms

Ventilation rates	Room [-]	Room Volume [m^3]	Measured* [l/sm^2]	Design [l/sm^2]
Ap. 9	R1/ R2/ R3	88.5/ 27.8/ 19.1	0.62/ 0.47/ -	0.6/ 0.7/ 0.7
Ap. 12	R4/ R5/ R6	88.5/ 29.8/ 19.1	0.72/ 0.63/ -	0.6/ 0.6/ 1.0
Ap. 10	R7/ R8	31.9/ 73.0	0.85/ 0.32	1.0/ 0.8
Ap. 11	R9/ R10/ R11	18.6/ 18.6/ 98.1	0.47/ 0.30/ 0.14	0.8/ 0.8/ 0.6

*The values are based on averages of the decay- and build-up periods throughout the measurement period.

4. Dynamic building simulation

4.1 Methods

The intended design of the heating and solar shading systems of the apartment building were evaluated by dynamic simulations performed with the simulation program IES- Virtual Environment, IESVE (IESVE 2013). The performance of the air heating and shading design was investigated throughout a one year period based on parameter variations. The parameter variations were compared with reference to the thermal environment categories I-IV given in EN 15251 (2007). The prerequisite for conducting parameter variations was to compare the simulated air temperature with measured data obtained from the HOBO data loggers during 25th of January 2014 to 1st of February 2014. The assumption was that if the simulated air temperatures approximated the measured ones, then the model setup would be sufficient in order to perform the parametric study.

4.1.1 Model setup

An IESVE model of the 2nd floor of the apartment building (see FIG 4) was set up, based on observations made during the field measurements and drawings of the building geometry. The rooms marked with black were included in the simulation while the grey ones were assumed adjacent rooms.

For the western apartment Ap. 9 and Ap. 12 additional heat loss is present compared to the eastern apartment.

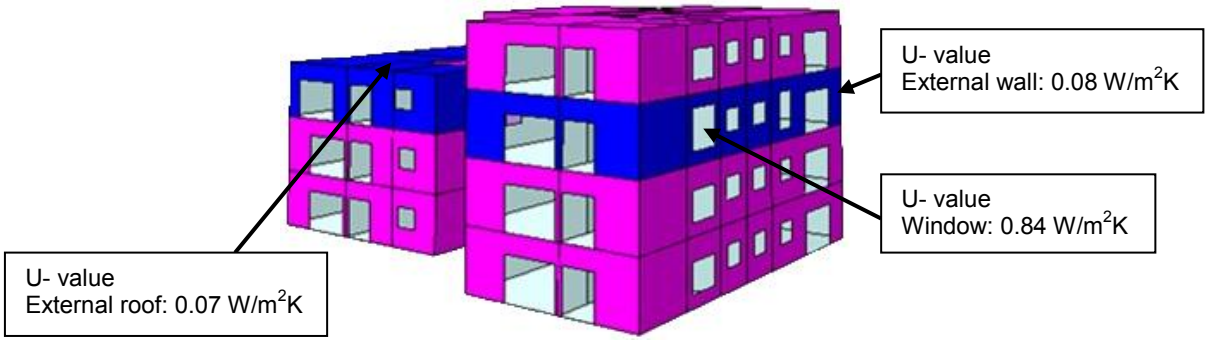

FIG 4. South east view of the IESVE model geometry of the apartment building and U- values

The location was set to Copenhagen/ Kastrup and the weather data file to 'CopenhagenDRY.ftw'. The automatic external solar screen system was set to roll down when the incident solar radiation was above 30 klx and to roll up again when it was below 25 klx. The static shading design from balcony overhangs had a shading angle of approximately 50°. According to fieldwork observations, internal curtains and vertical lamellas were included in Ap. 12 and Ap. 10.
Occupant and equipment profiles were created based on information provided from the activity protocols. The heat load emitted by the occupant was 90 W while the heat load from electrical appliances including illumination was approximated to 5 W/m^2 and 3 W/m^2 for the living rooms and bedrooms, respectively. The heat generated was assumed as 100 % sensible and 0 % latent. Venting was activated when the room temperature exceeded 26 °C during the occupied periods providing a venting rate of 0.9 l/sm² appropriate for manually operated windows (Aggerholm & Grau 2011). An overall infiltration rate of 0.07 l/sm^2 was estimated based on a Blower door test as a part of the Passive House certification ($n_{50} \leq 0.6$ h^{-1}).
The apartment building was ventilated and heated by a centralized Constant Air Volume (CAV) system with 85 % heat recovery based on two aggregates supplying the east and west sections. During the heating season, the heat exchanger was set to be active when the outdoor air temperature was below 15 °C and operated with a set point supply temperature of 18 °C. The heat exchanger was by-passed during the summer months when the outside temperature was above 22 °C. The individual heating coils installed before each room were set to regulate the air temperature as a function of the room air temperature. The coil adjusted the air temperature between 23 °C and 18 °C as the room air temperature varied.

4.2 Results

The results used for the evaluation of the model setup can be seen in FIG 5.

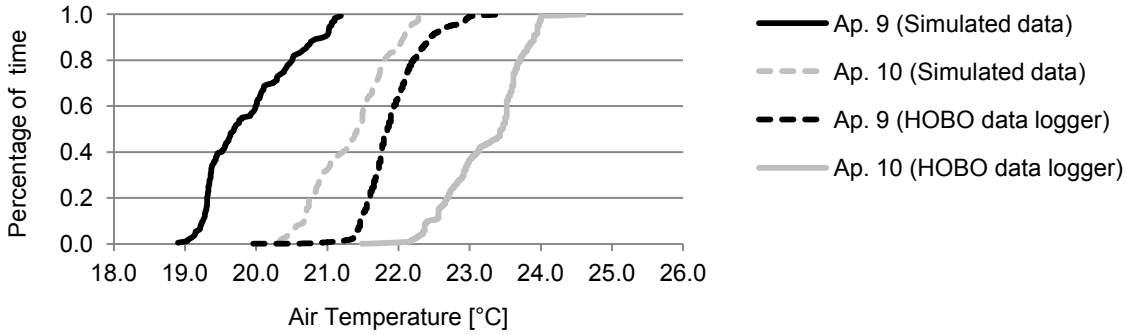

FIG 5. Simulated and measured air temperature distribution in Ap. 9 & Ap. 10 between 25th of January 2014 and 1st of February 2014.

The simulated and measured air temperature distributions ranged between 19-24.5 °C for the examined period (see FIG 5). In Ap. 9 the air temperature difference was approximately 2.5 °C where simulated temperatures were below 21 °C and measured ones mainly above 21 °C. In Ap. 10 simulated and measured data differed by 3 °C. In this apartment the simulated temperatures were below 22 °C and measured above 22 °C. The expected extra heat loss in the west apartment Ap. 9 and the air temperature difference between the apartments fit with both the simulated and measured air temperature distributions. The model setup was therefore considered sufficient to perform parameter variations where the intension was to compare the relative effect between different heating and shading designs.

4.2.1 Parameter variation

A parametric sensitivity analysis was conducted in order to evaluate the performance of the heating and shading system based on EN 15251 (2007). The parameter variations (P) are listed below:

- P1 was the reference model based on the intended model setup.
- P2 was similar to P1 but with a reduced supply set point temperature of 21°C, instead of 23 °C.
- P3 was similar to P1 but only with the balcony overhang as shading.
- P4 was similar to P1 but with added automatic external solar screens also on the south windows (controlled as the east and west windows).

To evaluate the air heating system the parameter variations P1-P2 were simulated. The results can be seen in FIG 6, where the annual thermal environment was compared.

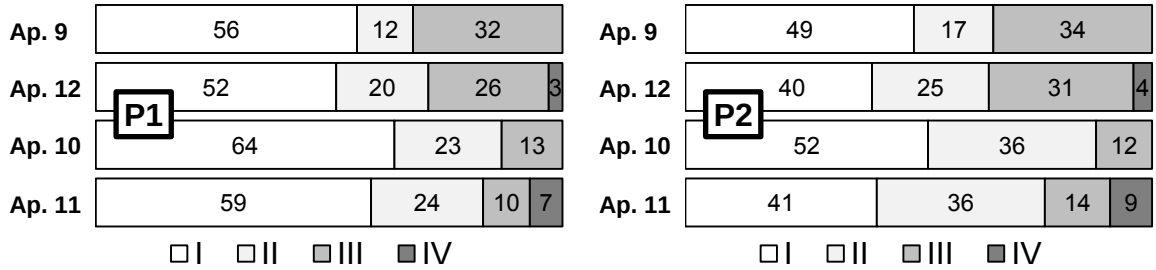

FIG 6. Annual thermal environment in % time in four categories for parameter variation P1 & P2

The reference model (P1) indicated a thermal environment within category III in Ap. 9, Ap. 10 and Ap. 12 whereas in the big south apartment (Ap. 11) 7 % of the occupied period was within category IV (see P1 in FIG 6). The reason for this was hours of overheating. When the supply temperature set point was reduced to 21 °C the occupied period within category IV increased 2 % (see P2 in Figure 6) and this was found to be caused by recorded hours below 20 °C as well.

To evaluate the influence of solar shading the parameter variations P3 and P4 were simulated and compared with the reference model (P1). According to FIG 6 the effect of the solar shading systems indicated that for P1 significant duration with overheating occurred in the South facing apartments (7 %). By removing the automatic external solar screens the duration of temperatures in category IV increased as illustrated in FIG 7.

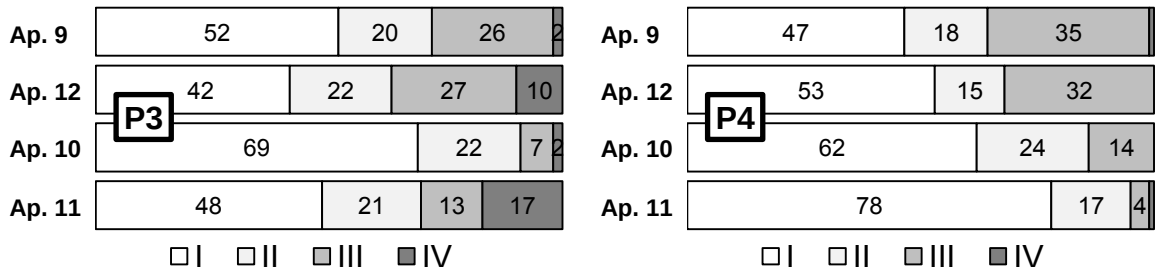

FIG 7. Annual thermal environment in % time in four categories for parameter variation P3 & P4

The design with no automatic external solar screens deteriorated the thermal environment in the living rooms with windows facing east and west, which in the actual case were the ones equipped with automatic external solar screens. This indicated that the design of the automatic external solar screens was effective in reducing the number of overheating hours. The apartment mostly affected was the large South oriented apartment (Ap. 11), where 17 % of the occupied period was within category IV. This was expected since it has a large glazing area facing south as well as windows oriented towards east and west. For apartments Ap. 9 and Ap. 10 with balconies facing east and west, the balcony overhang did not provide sufficient shading since the shading angle was designed for a high position of sun corresponding to summer midday (see P3 in FIG 7). Adding automatic external solar screens at the south windows of apartment Ap.12 and Ap.11, the number of hours with overheating was reduced significantly (see P4 in FIG 7).

5. Discussion

The results indicated PMV values within comfort ranges (-0.2 < PMV < 0.2) corresponding to the best indoor climate category A according to ISO 7730 (2006). Local thermal discomfort in Ap. 9 was within category B due to slightly increased draught rate. This showed that air heating alone with individual room control could maintain minimum thermal comfort category B in the apartments. The short term measurements also indicated uniform air temperature distribution as well as no air temperature asymmetry in the apartments where local discomfort could have been expected by the combined effect of heating by ventilation air and high measured ventilation rate.
Parameter variations illustrated that air heating was less sensible to change in supply temperature in the north apartments than in the south apartments, where a 2 °C lower supply temperature resulted in a 2 % increase of room air temperatures within category IV. Moreover parameter variations documented that automatic external solar screens were indispensable in order to achieve comfortable temperature ranges. The results also illustrated that the existing design can reduce overheating hours by 7-10 % in the south apartments. The simulations indicated that the design was likely to operate ineffectively during summer months as excessive hours of overheating were obtained in the south apartments even when venting was introduced. The simulation results should be validated in future work by performing field measurements during summer months while occupant observations is recommended to be taken into account by allocating questionnaires. By implementing automatic external solar screens to the south, thermal environment would improve further. However for dwellings this may constitute a problem since the user behaviour interacts with the shading control.

The ventilation rates in the apartment rooms were calculated based on the method of using occupant generated CO_2 to predict ventilation rate. The use of the single zone mass balance for estimating the air change rates does not take into account the distribution of CO_2 between rooms (interzonal air flow) and infiltration (Bekö et. al. 2010). The calculated air change rates could therefore be overestimated. In the current study the ventilation rates were calculated based on average values of decays throughout the measuring period. The consistency in well developed and continuing decays over the period increased the reliability of the estimated ventilation rate and provided a conservative measure for a total ventilation rate. In future work it is recommended to include airflow measurements at the air inlets or tracer gas measurements.

When performing dynamic building simulations uncertainties were involved as the indoor environment performance was estimated according to several assumptions regarding the schedule, occupant behaviour and heat loads. Fine tuning of the simulation model would be necessary in future work in order to comply with measured data. The intention of the dynamic simulation was to compare, based on a parametric study, the relative difference between temperature distributions. The results should therefore not be considered as absolute values since this would require a further validation of the simulation model and the use of specific located weather data.

6. Conclusions

Short term measurements documented that the provided heated air in the apartments could keep a minimum thermal comfort within category B according to ISO 7730 even in an unusual cold winter period. Using air heating with individual room control alone as well as higher ventilation rate can keep uniform operative temperatures without creating draught problems and is a sufficient mean of heating low energy apartment buildings.

Still an important factor to be considered for the design of low energy buildings is the correct implementation of external solar shading systems. This is possible by incorporating dynamic solar loads early in the design phase as static shading alone, caused by the balcony overhangs, cannot shade adequately the large south oriented windows. Building orientation, window distribution and dynamic shading need to be taken into account in order to utilize passive heating and still provide sufficient shading during summer.

References

Aggerholm S. & Grau K. 2011. Bygningers energibehov, SBi-anvisning 237. 2nd ed. Statens Byggeforsknings-institut. Hørsholm.

ASHRAE55. 2013. ASHRAE comfort tool program. Available from: http://www.cbe.berkeley.edu/comforttool/ [accessed 05-01-2013]

Bekö G., Lund T., Nors F., Toftum J. & Clausen G. 2010. Ventilation rates in the bedrooms of 500 Danish children. International Journal of Building and Environment, 45(10), 2289-2295. DOI: 10.1016/j.buildenv.2010.04.014. International Centre for Indoor Environment and Energy ICIEE. Department of Civil Engineering, Technical University of Denmark.

EN 15251. 2007. Indoor environmental input parameters for design and assessment of energy performance of buildings addressing indoor air quality, thermal environment, lighting and acoustics. 1st ed. Dansk Standard. Copenhagen.

ISO 7730. 2006. Ergonomics of the thermal environment, Analytical determination and interpretation of thermal comfort using calculation of the PMV and PPD indices and local thermal comfort criteria. 1st ed. Dansk Standard. Copenhagen.

Ellehauge K., Thomsen K.E. & Pedersen S. 2008. Passivhuse i dansk kontekst - vejledning, hjælpeværktøj og eksempler. Programområde EFP07-II – Energieffektivisering, Journal nr. 33033-0182.

Energistyrelsen. 2013. Bygningsreglementet, regler 2010. Available from: http://www.bygningsreglementet.dk/ [accessed 01-02-2013]

IESVE. 2013. Integrated environmental solutions (IES) software. Available from: http://www.iesve.com [accessed 20-02-2013]

Larsen T.S. 2011. Vurdering af indeklimaet i hidtidigt lavenergibyggeri - med henblik på forbedringer i fremtidens lavenergibyggeri. DCE Contract Report No. 100. Udarbejdet for Erhvervs- og byggestyrelsen, Institut for Byggeri og Anlæg, Aalborg universitet.

Integration of energy and indoor environment simulation tools into building design processes

Reinier Kok, B.Sc.[1]

[1] Technical University of Denmark (DTU), Denmark

KEYWORDS: *Design, process, method, energy, simulation, building, tool*

SUMMARY:
Building simulation tools can help make informed design decisions and improve the final building performance. A gap between building design processes and the implementation of building simulation tools exists because of a lack of knowledge on integrated design on the level of tool implementation. Yet, the gap can be bridged by fitting design processes and simulation methods to each other. This essay suggests a division of four building design processes in order to link these simplified processes to simulation methods. The four design processes range from being based on an architectural concept to being design based on computational input. The essay discusses that conceptual design process should sufficiently rely on (i) diverging and converging, (ii) cross-disciplinary input, and (iii) performance and intuition. The four building design processes relate to building simulation methods that implement certain types of tools for energy and indoor climate simulation. It is discussed how specific building design processes are more suitable for certain specific simulation methods. Energy and indoor climate simulation methods involve the use of simulation tools which may provide design input, optimise and/or evaluate a design prototype. The essay concludes with a table of building design processes related to simulation tool types aiming to stimulate knowledge-based design to achieve designs with better indoor environment quality and energy performance.

1. Introduction

It is buildings where we spend most of our time. They account for about 40% of the total primary energy consumption in Europe (International Energy Agency, 2011). Therefore it is essential to create buildings of high indoor environment performance with low energy consumption. This essay focusses on the conceptual design of a building. During the conceptual design the building geometry is largely defined, the building geometry alone can reduce the final energy consumption of a building up to 40% with no extra cost (Cofaigh et al., 1999). Therefore buildings have a high potential to save energy already in the conceptual design stage.

Building simulation tools can help make informed decisions and help improve the final building performance. Building simulation tools are currently mainly being used for building performance verification rather than design support. This lack of design support can partially be attributed to a lack of knowledge of the integration of energy simulation tools and methods into conceptual design processes. In the Integrated Design Process (IDP), designers are supported by tools that generate simulation-based design support in order to integrate energy performance and indoor environment requirements in their earliest design decisions (Löhnert et al., 2003). Even though the development of tools has mainly focused on building performance verification Petersen (2011) states:

> *"With minor adjustments to the workflow, building simulation tools could also become an active driver in the development of the building design."*

Typical research on integrated design focusses on a high level of abstraction of design and tends to omit specific design methods and tools when talking about integrated design. As integrated design is mainly understood on an abstract level, little is known on how to apply integrated design on a practical level where building simulation knowledge has design implications. Because of this lack of knowledge designers still struggle to effectively use building simulation tools to support their design decisions. This research attempts

to aid in bridging the universal gap between building design processes and the implementation of simulation tools. The term ‘simulation tools’ refers to both energy and indoor climate simulation tools. The research hypothesises that:

> **The gap between building design processes and the implementation of simulation tools can be bridged by fitting design processes to simulation methods and vice versa.**

The essay consists of an analysis of design focussing on conceptual design and building performance simulation. The research analyses four building design processes into which the integration of energy simulation methods are shown. Energy and indoor climate simulation methods are linked to simulation tools, bridging the gap from design process to implementing simulation tools.

2. Theory on conceptual design processes

Researchers have long been interested in the phenomenon of designing, since it is a complex process suitable for improvement. Moreover, design has an aura of mystery around it from which novel designs may seem to appear as sudden illuminations. This “creative leap” is considered to be essential to the design process (Cross, 1997).

The act of designing involves a workflow – the way you work. Such a workflow (indicated in FIG 1) is defined as a sequence of processes, for example creating a design team, visiting the site or designing the cooling system. Such processes involve methods. Methods involve a systematic way of performing a specific task. The use of tools can be a part of such a method. FIG 1 indicates the hierarchical order of acts of designing where workflow is placed at the top and tools at the lower end.

FIG 1. From workflow to method

It should be mentioned that every designer has adopted his or her own workflow, each involving a unique set of processes and methods. Designers tend to be rather protective of their workflows including their methods, described by Zimmerman (2011) in the following quote:

> *“Design methods are like toothbrushes. Everyone uses them, but no one likes to use someone else’s.”*

The upcoming paragraphs argue a conceptual design process should sufficiently rely on (1) diverging and converging, (2) cross-disciplinary input, and (3) performance and intuition.

2.1 Diverging and Converging

Östman (2005) defines conceptual design as the initial problem-setting and creative phase. The process of conceptual design is seen as a sequence of diverging and converging steps at different levels of abstraction (Turrin et al., 2011). In the divergent phase, the solution space is explored and a number of concepts are generated. In the traditional design process there is a lack of diverging steps; only a narrow solution space with a limited number of alternatives is explored (Turrin et al., 2011). Diverging allows the designers to increase the odds of finding good solutions in the infinite pool of possibilities.

In the convergent and exploiting phase, concepts are evaluated and selected. The concepts retrieved from the exploring phase must be developed and evaluated in order to select design – or ‘the best genomes from the generation’. Design alternatives can be compared to the design criteria to assess to what degree they meet the set requirements in order to select the best design.

2.2 Cross-disciplinary input

Design problems are wicked, ill-defined problems (Cross, 1997). Since the design problem cannot be completely defined, no ultimate, optimal solutions exists (Rittel & Webber, 1984) (Petersen, 2011). As no optimal solution exists, it is important to develop design processes and methods that test the solution space as

effectively as resources allow. Therefore, in order to develop a design that effectively tackles the full spectrum of the design problem, cross-disciplinary input is essential. Cross-disciplinary input also refers to generating solutions (diverging) from different disciplines and evaluating and selecting cross-disciplinarily (converging).

2.3 Performance and Intuition

Efficient and effective design can only be found by narrowing down the solution space, meaning the solution space is limited. For example, the freedom in architectural expression is limited in order to find an efficient and effective structural design. Consequently, the developed design is no longer evident to be a good design – in a holistic sense. Benjamin (2012) therefore warns us not to rely too heavily on performance and optimisation as the driver of design, since they might prevent finding a good, holistic design. Vice versa: dismissing performance and relying mainly on judgement and intuition may, similarly, prevent us from reaching good, holistic design.

3. Simulation Methods and Design Processes

3.1 Design Process

Architectural and building design processes have long been discussed in history as they lead to the creation of our environment. Below a division of four design processes are suggested based on B. Chandrasekaran (1990), Turrin (2011), and Benjamin (2012). The four building design processes are defined as (1) The Primary Generator, (2) Performance Based Design, (3) Synthesising the Parts, and (4) Optimising Creatively. It should be noted that the four listed design processes do not cover all possible design processes but are merely an attempt of listing the most prevalent ones.

3.1.1 The Primary Generator

The Primary Generator design process involves an abstraction of the problem. Based on the simplified problem an initial concept, or primary generator, is created and a crude design is developed which is evolved, through alterations, into the final conceptual design. The complex problem is addressed by some designers by seeking a ‘primary generator’ (Darke, 1979) which suggests the designer to define an important aspect of the problem in order to ‘develop a crude design’. Consequently the designer is to test the solution to see what else can be discovered concerning the problem. In general, the primary generator tends to be an architectural concept in the form of an analogy or configuration (Rittel & Webber, 1984). An example would be Fallingwater by Frank Lloyd Wright, where the analogy of a water fall lead to a design.

Turrin (2011) states “In earlier phases of traditional design, assessing the fulfilment of design requirements relies on the insight of the designer and focuses on a specific range of performances such as functionality and aesthetics.” The primary generator fulfils this definition of traditional design since the primary generator makes the designer focus on a narrow range of performances (such as functionality and aesthetics).

3.1.2 Performance Based Design

In the design process of Performance Based Design, designers use building simulation software to drive the design process. A concept for optimised evacuation, indoor environment or fire safety is promoted to be dominant and lead to the final design. Petersen and Svendsen propose a room-based simulation and design method; this method can be used in the defined process. In contrast to the primary generator, the evaluation takes place in the process of re-prototyping, this may be considered to be an optimisation process. The Energinet Building designed by Henning Larsen Architects is such a design, its façade has been optimised for energy and daylight levels (Henning Larsen Architects, 2014). An extreme example of performance based-design is ‘form follows performance’, where optimisation algorithms generate design form based on an initial set of parameters and requirements.

3.1.3 Synthesising the Parts

In the process of “Synthesising the Parts” the problem is divided into a set of sub-problems. Each sub-problem leads to a set of sub-solutions. In this exploring process all parties propose a number of sub-solutions. For example, the architect proposes a number of architectural sub-solutions and the energy engineer proposes a set of energy strategies. The architect then synthesises the wide range of both qualitative and quantitative sub-solutions into a prototype. The architect or designer coordinates the design team and ensures the timely consulting of experts.

Peter Zumthor appears to have synthesised sub-solutions in his design Werkhaus raum in Austria. The design consists of a roof supported by columns and an interior design containing various volumes creating a composition and routing within the building. The parts seem to tackle different sub-solutions: the roof encloses and is load-carrying, and the interior design of boxes facilitates functional requirements such as storage and reception. The sub-solutions are synthesised afterwards. The synthesis can be a complex task and requires simplification and insight by the architect. The synthesising is a subjective and value-dependant process. In the process of ‘synthesising the parts’ there is a danger of a lack of cohesion and of conflicting interests. In the example of ‘Werkhaus raum’ columns may for example collide with the inner volumes.

3.1.4 Optimising creatively

In the design process of ‘Optimising Creatively’ all design disciplines are stimulated to provide design prototypes based on the set of initial requirements: the sub-problems. A number of prototypes is selected by the design team and developed to the same level of detail for comparative evaluation. The evaluation is an act of multi-criteria decision-making. New alternatives are developed based on the comparison and the problem statement is sharpened. This process is repeated until resources are depleted and/or a satisfactory design is reached.

Masdar Institute Adu Dabi by Foster + Partners implements a variety of strategies ranging from shading, natural ventilation and electricity production to vernacular architectural expression. Such a large diversity in integrated concepts indicates a creative optimisation process as the design would have to accommodate multiple, possibly conflicting, strategies.

3.2 Energy and Indoor Climate Simulation Methods

This chapter describes how the four conceptual building design processes relate to methods of implementing energy and indoor environment simulation tools. Building simulation tools can (1) perform an evaluating role, (2) optimise given designs, or (3) provide design input. Each discussed building simulation process relates to a set of building simulation activities, these activities are executed by building simulation methods.

There are four types of building simulation methods (Citherlet, 2001):

- Stand-alone: the energy engineer acts as an external actor using stand-alone tools to perform evaluations with. Models have to be recreated and building information such as insulation values is not shared among disciplines through the building information model (BIM).
- Interoperable: the energy engineer uses simulation tools that can perform simulations on an exported BIM but not directly on the BIM. Interoperable tools are able to exchange or share models and information through different formats.
- Integrated: the energy engineer uses simulation tools that are an integrated part of the BIM software and performs simulations directly on the BIM as it contains a building energy model (BEM). Models and information are not exchanged across disciplines through exporting.
- Run-time coupling: simulation tools are coupled to the BIM software by the energy engineer who can run instant simulations on the BIM as the model is altered. Optionally, parametric design tools can be used to generate design solutions through optimisation algorithms available in for example Grasshopper.

3.2.1 The Primary Generator

The flow diagram FIG 2 depicts the design process known as ‘Primary Generator’. The dashed box involves the building simulation method where the related specialist, i.e. energy engineer, is involved. The energy engineer typically assesses the energy and indoor environment performance, optimises design and/or provides design input.

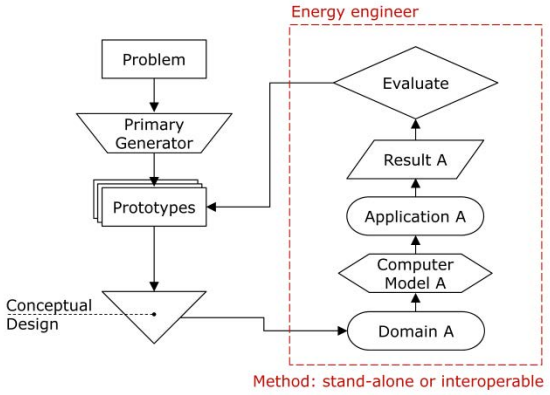

FIG 2. Methods in the flow diagram of The Primary Generator

In the ‘Primary Generator’ energy engineers are typically only involved in the evaluating of a design proposal. Energy engineers are typically provided with a design that has to be remodelled from scratch in a separate domain (Domain A in FIG 2). This is known as the stand-alone method. A digital building model is developed which is run in an application, providing results ready for evaluation. Depending on the outcome of the evaluation the engineer will suggest improvements and new prototypes may be developed. Alternatively, the conceptual design may include a BIM that can be used in an interoperable manner by the energy engineer meaning some useful information can be exported allowing for faster design evaluation. In the example of the Fallingwater the energy engineer would take no part in the designing of the house, but would merely evaluate its performance leaving little room for improved performance.

3.2.2 Performance Based Design

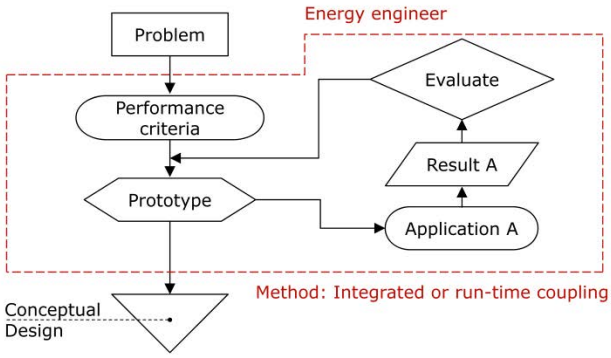

FIG 3. Methods in the flow diagram of Performance Based Design

In ‘Performance Based Design’ (FIG 3) the energy engineer is involved in the establishing of the performance criteria, as well as developing, evaluating and optimising the prototypes. The prototypes are typically modelled as a BEM, allowing for the implementation of the integrated or run-time coupling methods. The design performance can be assessed without the need of exchanging information or models between software tools. In the case of the office building Energinet by Henning Larsen Architects, the energy engineer suggests improvements to the design, in this case external vertical shading. He dimensions the shading system together with the design team in order to improve the daylight performance of the design.

This is an iterative optimisation process searching the solution space. The simulations were performed in Ecotect in which the shading geometry can be modelled acting as an integrated design tool for daylighting.

3.2.3 Synthesising the Parts

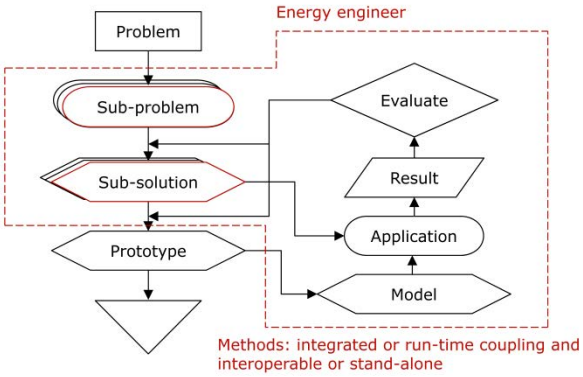

FIG 4. Methods in the flow diagram of Synthesising the Parts

In the process of 'Synthesising the Parts' (FIG 4) the energy engineer is involved in developing his own sub-problems and sub-solutions regarding for example indoor climate or energy conservation. When the energy engineer develops the sub-solutions, it is most likely he will do this through a stand-alone or run-time coupling method. In the act of evaluating sub-solutions from other disciplines or prototypes he will typically use a stand-alone or interoperable method. The integration of the sub-solutions is typically done by the architect but may be done by a design team consisting of more specialists than the architect alone. As the sub-solutions are synthesised, a BEM may be created allowing for design evaluation through an integrated or run-time coupling method.

In the example of 'Werkhaus raum' the energy engineer may perform analysis on his sub-solutions, such as the building services in order to optimise this sub-solution. This would typically be done in a stand-alone method where the engineer works in a tool that is not interoperable with those of the other disciplines. As the design is synthesised and a design or prototype is created the energy engineer may be involved to perform evaluation on the design. In the design of 'Werkhaus raum', sub-solutions appear to be integrated by the architects and no energy engineer was involved in this process.

3.2.4 Optimising Creatively

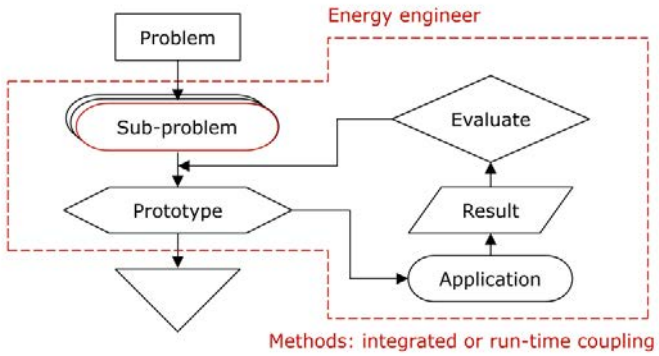

FIG 5. Methods in the flow diagram of Designing Creatively

In the design process of 'Optimising Creatively' (FIG 5), the energy engineer is involved in defining the sub-problem(s) from his discipline. He is involved in developing, evaluating and optimising the prototypes. In the developing of the prototype, the design is modelled as an integrated building information and energy model where designs can be evaluated consecutively through integrated method or real-time through run-time coupling method.

In the example of the Masdar institute this would entail that the design team suggested a number of prototypes each tackling the sub-problems through different strategies. Prototypes may have different configurations, building systems, building element properties, shading strategies etc. The prototypes are assessed and evaluated leading to the final design through a number of iterations.

3.3 Energy and Indoor Climate Simulation tools

Energy and indoor climate simulation methods involve the use of simulation tools which may provide design input, optimise and/or evaluate a design prototype. Energy and indoor climate simulation tools may affect the decision making process of the building's geometry, systems and components, envelope and material properties, and functional layout. The discussed design methods can be connected to simulation tools as shown in TABLE 1.

TABLE 1. Tool types and examples of energy and indoor climate simulation tools

Method	Simulation tool
Stand-alone	A+E3D, Bsim, BuildingAdvice, Design Advisor, eQuest, Parasol, IDbuild, Crawley, Energy+
Interoperable	Vasari, DesignBuilder, EcoDesigner, Ecotect, gModeller, IDA ICE, IESve, Velux
Run-time coupling	DIVA, Geco
Integrated	Building Design Advisor, OpenStudio, Sefaira, Revit

TABLE 2 shows the four design processes and connects them to the role of simulation methods and simulation tool types. Effective use of a design process involves the use of the right simulation method and tool and vice-versa; the effective use of a simulation tool involves the right implementation of a design method and process. Design processes, methods and simulation tools go hand in hand.

TABLE 2.The four design processes linked to simulation methods and tool types.

Design process	Role of energy simulation method	Methods
The Primary Generator	Evaluating	Stand-alone
		Interoperable (exchange only)
Performance Based Design	Creating, evaluating and optimising	Integrated
		Run-time coupling
Synthesising the Parts	Creating, evaluating and optimising	Stand-alone
		Run-time coupling
		Interoperable
Optimising Creatively	Creating, evaluating and optimising	Integrated
		Run-time coupling

This essay does not attempt to dictate a specific design process or simulation tool to designers. It merely attempts to help understand the relation between processes and simulation tools in order to help others design more effectively. It should be noted that every design team has a different specific skillset and is therefore more or less likely to be successful with a specific design process. This essay, in particular *TABLE 2*, should help designers define what design process and accordingly what tool types work best for them.

4. Conclusion and Discussion

This essay attempts to aid in bridging the gap between building design processes and the implementation of energy simulation tools by fitting design processes and simulation methods to each other. Design processes should sufficiently allow for diverging and converging in order to explore the solution space and exploit the design possibilities. Additionally, design processes should facilitate cross-disciplinary input and enable both performance and intuition based input to the decision making process.

By educating designers on the relation between designing and using simulation tools, this essay aims to help designers understand which design process they desire. The team of designers and engineers may adopt one of the four mentioned methods and integrate it into their workflow. Energy engineers can use the description of simulation methods to define their role in the design process. Desired design processes differ from firm to firm as they are dependent on the available knowledge, skills and resources. As simulation methods are successfully integrated into the design process, the performance of designs can be assessed and optimised at an early stage in the design process.

More research on the implementation of simulation tools and their integration into design processes is required and case studies should be performed. Performing case studies on the implementation of simulation methods would contribute to refining the fitting of design processes to simulation methods and vice versa. Moreover, case studies would show the potential as well as possible bottlenecks for the implementation of simulation methods.

5. Acknowledgements

First of all I would like to thank Toke Rammer Nielsen, associate professor at DTU, for being my mentor throughout this project. I would also like to express special thanks to Jakob Strømann-Andersen and Erik Holm Hansen at Henning Larsen for providing guidance and constructive feedback during my research.

6. Works Cited

Benjamin, D. (2012). *Digital workflows in architecture.* New York: Birkhauser.

Chandrasekaran, B. (1990). *Design Problem Solving: A Task Analysis.* Ohio: American Association for Artificial Intelligence.

Citherlet, S. (2001). *Towards the holistic assessment of building performance based on an integrated simulation approach.* Lausanne: Swiss Federal Institute of Technology Lausanne.

Cofaigh et al. (1999). *A green Vitruvius-principles and practice of sustainable architecture design.* London: James & James (Science Publishers).

Cross, N. (1997). *Descriptive models of ceative design: application to an example.* Elsevier: London.

Darke, J. (1979). *The Primary Generator and the Design Process.* Sheffield: University of Sheffield, The Arts Tower.

Henning Larsen Architects. (12. March 2014). *Energinet, lavenergikontorhuset*. http://da.henninglarsen.com/

International Energy Agency. (2011). *Europe's Buildings Under the Microscope.* Buildings Performance Institute Europe .

Löhnert et al. (2003). *Integrated Design Process; a guideline for sustainable and solar-optimised building design.* International Energy Agency.

Östman, L. (2005). *A Pragmatist Theory of Design.* Stockholm: Royal Institute of Technology.

Petersen, S. (2011). *Simulation-based support for integrated design of new low-energy office buildings.* Lyngby: DTU Civil Engineering.

Petersen, S., & Svendsen, S. (2010). *Method and simulation program informed decisions in the early stages of building design.* Lyngby: Department of Civil Engineering, Technical University of Denmark.

Rittel, H., & Webber, M. (1984). *Planning problems are wicked problems.* New York, USA.

Turrin et al. (2011). *Design explorations of performance driven geometry in architectural design using parametric modeling and genetic algoritms.* Delft: Elsevier.

Zimmerman, J. (2011). *Methods in Interactions, ACML.* (S. Harrison, & D. Tater, artists) Galli Design Process & Methods.

External shading control principles for low energy office buildings

Martin Thalfeldt, M.Sc. [1]
Jarek Kurnitski, D.Sc. [1]

[1] Tallinn University of Technology, Estonia

KEYWORDS: *External shading, low energy buildings, shading control principles, facades, windows*

SUMMARY: *An optimal control principle for external dynamic venetian blinds facades in a cold climate was determined based on generic office floor simulation. The cases were chosen so that the proportion of cooling in total energy use varied. The numbers of window panes, window-to-wall ratios and external wall U-values ranged from 3 to 5, 25% to 60% and 0.09 to 0.16 W/(m^2 K) respectively. The results show that controlling shade position according to internal temperature and desktop illuminance is most effective whereas suntracking can be used for slat angle adjustment. The room temperature setpoint for pulling down venetian blinds should be chosen slightly lower than cooling temperature (e.g. +24 °C) and the bandwidth for desktop illuminance should be chosen large enough to assure as good daylighting as possible (e.g. 1000 lx) while preventing unnecessary frequent changes in the position of blinds. Control methods according to external parameters such as vertical irradiance and outdoor temperature did not prove to be effective. The largest savings were obtained for cases with larger windows that had higher initial cooling energy use and the whole floor primary energy was decreased by up to 3.2 kWh/m^2 by using external venetian blinds. The savings in the primary energy of different orientations ranged from 2.5 to 6.6 kWh/m^2 in case of large quintuple windows.*

1. Introduction

External shading is considered an effective measure to improve a buildings indoor climate and energy performance. Cooling needs and summertime indoor temperatures are decreased by blocking direct sunlight and another benefit is that glare is also avoided. Severel studies have pointed out that the position of motorized shading is changed more frequently than of manual blinds, whereas when not controlled automatically a significant proportion of people formulate their decisions about blind position over a period of weeks or months, and not days or hours (Van Den Wymelenberg 2012). In a cold climate it is essential to utilize as much of sun radiation during heating period, however in case of low or nearly zero energy office buildings the heating need remarkably depends on the office use and internal gains (Thalfeldt 2013). Therefore simple control principles of automated blinds depending only on external conditions may not be optimal and might even increase energy consumption (Thalfeldt 2013). The possible energy penalty caused by external shading in the climate of Scotland was also pointed in a study by Littlefair (2010) and the importance of control strategy especially in case of balanced heating and cooling has been also stressed by da Silva (2012). One of the crucial aspects of automated dynamic solar shading is choosing the control parameters. In a study by Daum and Morel (2010) it was pointed out that at least two parameters should be used and the importance of internal temperature stood out. Controlling shades based on solar radiation is often used, however illuminance threshold might be a more appropriate solution (Tzempelikos and Shen 2013).

The purpose of this study was to determine an optimal control principle for external shading on different facades in a cold climate. An effective control principle of external venetian blinds was analyzed and the effect of algorith simplifications on the energy use was studied. A generic office

floor was analyzed and the cases were chosen so that the proportion of cooling in total energy use varied. The numbers of window panes, window-to-wall ratios and external wall U-values ranged from 3 to 5, 25% to 60% and 0.09 to 0.16 W/(m^2 K) respectively.

2. Methods

The study was conducted by simulating 3 different generic office floors with varying façade properties. External or internal automatically controlled dynamic venetian blinds were used. Initially an effective control method was used and then it was simplified to see the effect on energy use.

2.1 Office floor simulation model

Energy simulations were conducted on the basis of a generic open-plan office single floor model that was divided into 5 zones - 4 orientated to south, west, east and north respectively and in addition one in the middle of the building (figure 1). The longer zones consisted of 12 room modules of 2.4 m and shorter ones of 5 room modules, resulting in inner dimensions of the floor 33.6 x 16.8 m. In all cases the heating was district heating with radiators (ideal heaters in the model), and air conditioning with room conditioning units (ideal coolers in the model) and mechanical supply and exhaust ventilation with heat recovery was used. The working hours were from 7:00 to 18:00 on weekdays and the usage factor of heat gains during working hours was 55%. Ventilation worked from 6:00 to 19:00 on weekdays. The lighting was with dimmable lamps and daylight control with setpoint of 500 lx in workplaces. The position of workplaces used for the control is shown in figure 2. The initial data of simulation model is shown in table 1.

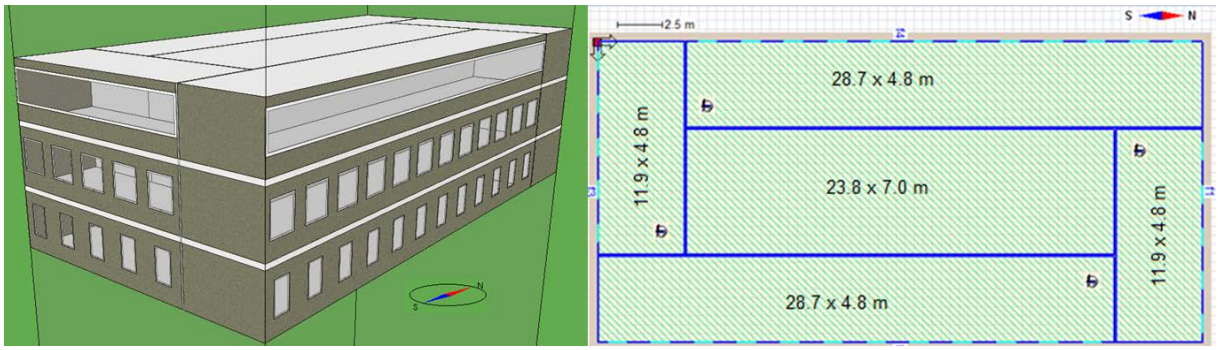

FIG 1. Description of simulation models' geometry. Office floor models with triple, quadruple and quintuple windows (from bottom to top in the 3D figure left) were simulated in separate models.

TABLE 1 Input data of office rooms and HVAC systems for energy calculations.

Occupants, W/m^2	5
Equipment, W/m^2	12
Lighting, W/m^2	5
Temperature set point for heating and cooling	+21 and+25 °C
Air flow rate	1.5 l/(s·m^2)
Illumination setpoint at locations (x,y,z)=(2.2, 4.0, 0.9), lux	500
Frame ratio of windows, %	15
Heating system (radiators) efficiency, -	0.97
Heat source (district heating) efficiency, -	1.0
Cooling system losses, % of cooling energy need	10
Mechanical cooling SEER, -	3.5
Temperature ratio of heat recovery, %	80

2.2 Simulation cases

The office floor façade solutions were chosen so that the balance of heating and cooling energy need would vary, which is achieved with differing thermal properties of windows and external walls and also window-to-wall ratios (see table 2 and figure 1). The case names are derived from the number of window panes used in the specific case. Detailed window models were used, which means that the thermal resistance depended on the temperature difference between internal and external conditions.

TABLE 2 Description of simulation cases.

	Glazing							
Case	No of panes*,	U-value**, W/(m^2 K)	g-value, -	Visible trans-mittance τ_{vis}, -	Gas filling	Gap width between panes, mm	Window-to-wall ratio, %	U-value of external walls, W/(m^2 K)
3	3	0.55	0.45	0.71	Argon	18	23.9	0.16
4	4	0.32	0.34	0.63	Krypton	12	37.5	0.13
5	5	0.21	0.25	0.56	Krypton	12	60.0	0.09

* - One is a simple highly transparent pane, the other panes have low emissivity coating (ε=0.03)
** - Given according to calculations of ISO 15099:2003/E at internal and external temperature difference of 20 °C

2.3 Control principles

The initial control principle for extrenal venetian blinds chosen as the base for optimization is described in figure 2 and has the following principles:

- The external shade position and slat angle was controlled according to room temperature (always) and illuminance on desktop (only during occupany)
- The shade position had on/off control with room temperature setpoint slightly below cooling setpoint and the bandwidth was 1.0 °, desktop illuminance setpoint was chosen so that the blinds would be drawn at 1900 lx and the bandwidth varied between 600 and 1400 lx
- The slat angle was adjusted with PI-controllers to keep the room temperature at setpoint and the desktop illuminance at 2000 lx.

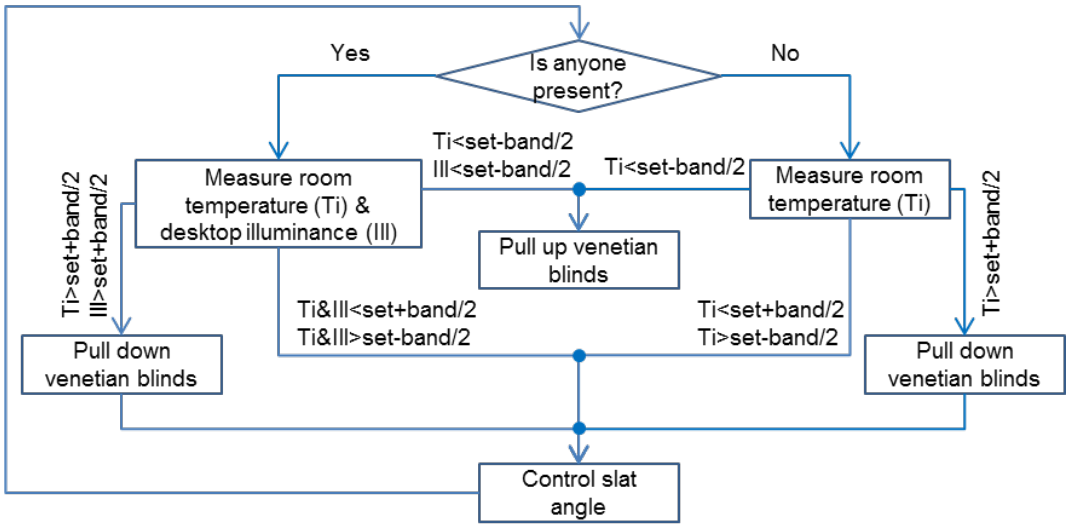

FIG 2. Description of the effective external shading control principle. The abbreviations set and band have been used for setpoint and bandwidth respectively.

The simpification/optimization of the control principle was done in the following order (see table 3):

- Cases with internal venetian blinds was simulated for reference (Internal)
- The room control setpoints of initial principle were optimized (Ideal)
- Slat angle was controlled according to sun altitude instead of PI-controllers (Suntracking)
- Vertical irradiance on the façade was used for shade position control (Ver. Irr.)
- External temperature was used for shade position control (Ext. temp.)

A control macro was created in the simulation program IDA ICE 4.5 for each control principle.

TABLE 3. Shading position and slat angle control principles of studied cases

Control principle	Shade position		Slat angle	
	Room temperature	Illuminance	Room temperature	Illuminance
Internal	Internal blinds, internal vertical irradiance 200 W/m^2			
Ideal	24.5 ± 0.5 °C	1400 ± 500 lx	24.5 ± 0.5 °C	2000 lx
	24.0 ± 0.5 °C	1400 ± 500 lx	24.0 ± 0.5 °C	2000 lx
	23.5 ± 0.5 °C	1400 ± 500 lx	23.5 ± 0.5 °C	2000 lx
	23.0 ± 0.5 °C	1400 ± 500 lx	23.0 ± 0.5 °C	2000 lx
	24.0 ± 0.5 °C	1600 ± 300 lx	24.0 ± 0.5 °C	2000 lx
	24.0 ± 0.5 °C	1200 ± 700 lx	24.0 ± 0.5 °C	2000 lx
Suntracking	24.0 ± 0.5 °C	1600 ± 300 lx	Sun altitude	
Ver. Irr.	Irradiance on facade 200 W/m^2		Sun altitude	
	Irradiance on facade 300 W/m^2		Sun altitude	
	Irradiance on facade 400 W/m^2		Sun altitude	
Ext. temp.	External temperature 10 ± 1.0 °C		Sun altitude	
	External temperature 15 ± 1.0 °C		Sun altitude	
	External temperature 20 ± 1.0 °C		Sun altitude	

3. Results

3.1 Optimizing setpoints

The results of the simulations of the effective control principle with different room temperature and desktop illuminance setpoints show that the most reasonable setpoint values are 24 ± 0.5 °C and 1400 ± 500 lx (table 4). However other setpoint values in the vicinity of the most optimal ones did not alter the energy performance significantly. Generally internal temperature setpoint value should be chosen slightly lower than the temperature for cooling and the bandwidth for desktop illuminance should be large enough to assure as good daylighting as possible while preventing unnecessary changes frequent changes in the position of venetian blinds. It has to be also stated that the setpoints for vertical irradiance and external temperature resulting in best energy efficiency were 400 W/m^2 and +20 °C respectively.

3.2 Simplifying control principles

The comparison of control principles showed that dynamic external venetian blinds offer energy savings in all cases compared to internal blinds however choosing the most effective control method is essential for reaching the decrease in energy use. The initial effective control method proved to be most effective for all cases but one, however the primary energy use did not increase significantly if

suntracking i.e. slat angle control according to sun altitude was used. The energy needs and primary energy uses for triple window cases are shown in figures 3 and 4, for quadruple window cases in figures 5 and 6 and for quintuple window cases in figures 7 and 8 respectively. When external shading was controlled according to vertical irradiance or external temperature then the energy use increased for almost all cases compared to effective principles. In most cases the cooling needs of offices with standardized use were fulfilled by supplying cooled air into the rooms, however less effective methods of blind control caused unnecessary additional heating and lighting energy use. The only façade where control according to external temperature seemed to work energy wise was the south, however glare was probably not avoided due to low sun angles in the winter time.

TABLE 4. The effect of of shading control setpoints of room temperature and desktop illuminance on the energy use of studied cases, the whole office floor results have been given and it has been marked if the optimal setpoint value of a façade zone differed from 24.0 ± 0.5 °C or 1400 ± 500 lx

		Room temperature setpoint, °C				Desktop illuminance setpoint, lx		
Energy use, kWh/m^2	Case	24.5 ± 0.5	**24.0 ± 0.5**	23.5 ± 0.5	23.0 ± 0.5	1600 ± 300	1400 ± 500	1200 ± 700
Heating	3	18.1	18.1	18.2	18.3	18.1	18.1	18.3
	4	17.2	17.2	17.3	17.5	17.2	17.2	17.4
	5	18.1	18.1	18.2	18.4	18.1	18.1	18.3
Cooling	3	2.2	2.2	2.2	2.2	2.2	2.2	2.2
	4	2.3	2.2	2.2	2.2	2.2	2.2	2.2
	5	2.4	2.2	2.2	2.2	2.2	2.2	2.2
Lighting	3	5.1	5.1	5.1	5.1	5.1	5.1	5.1
	4	4.8	4.8	4.9	4.9	4.9	4.8	4.9
	5	4.5	4.6	4.6	4.7	4.7	4.6	4.6
Primary energy	3	30.9^S	**30.8**	30.9^W	31.1	30.8	**30.8**	31.1
	4	29.7	**29.5**	29.7	29.9	29.6	**29.5**	29.8
	5	30.0^E	**29.9**	30.0^W	30.3	30.0	**30.0**	30.2

^{S} – lowest primary energy for south façade
^{E} – lowest primary energy for east façade
^{W} – lowest primary energy for west façade

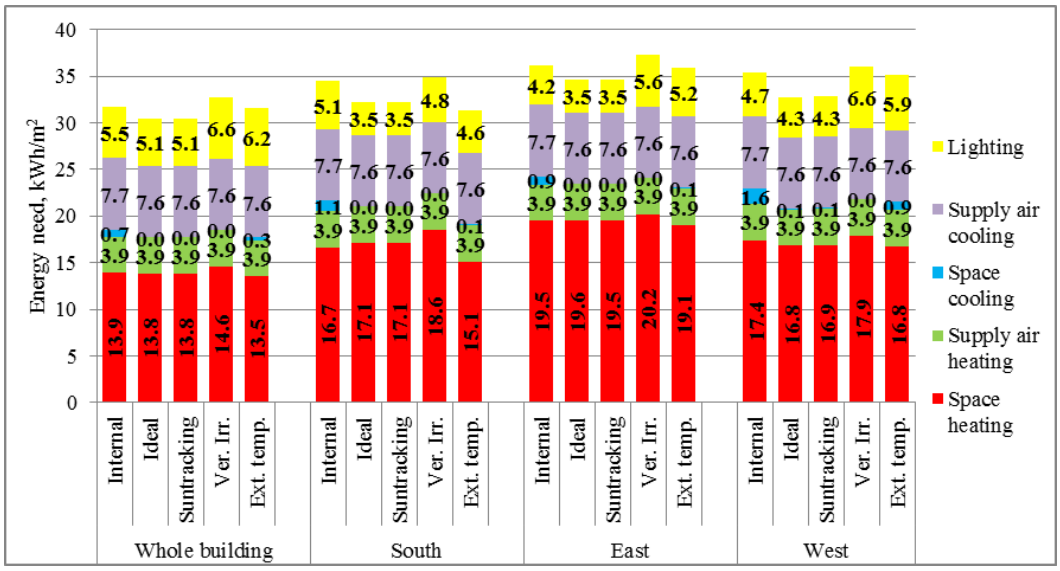

FIG 3. Energy need of cases with triple windows

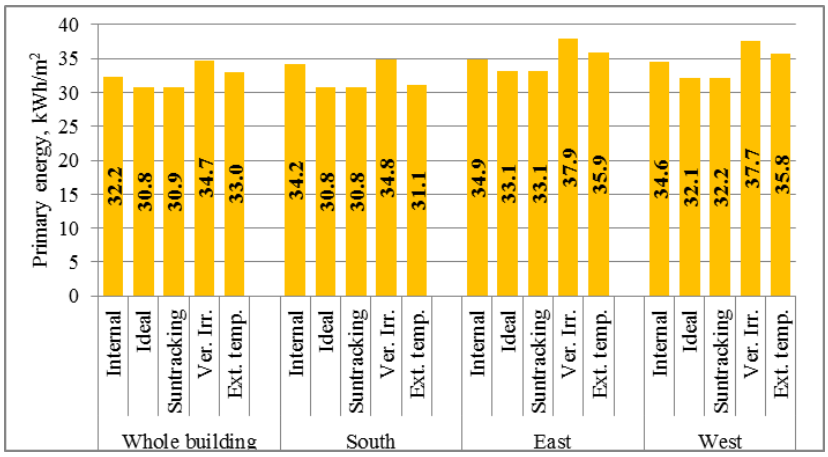

FIG 4. Primary energy of cases with triple windows

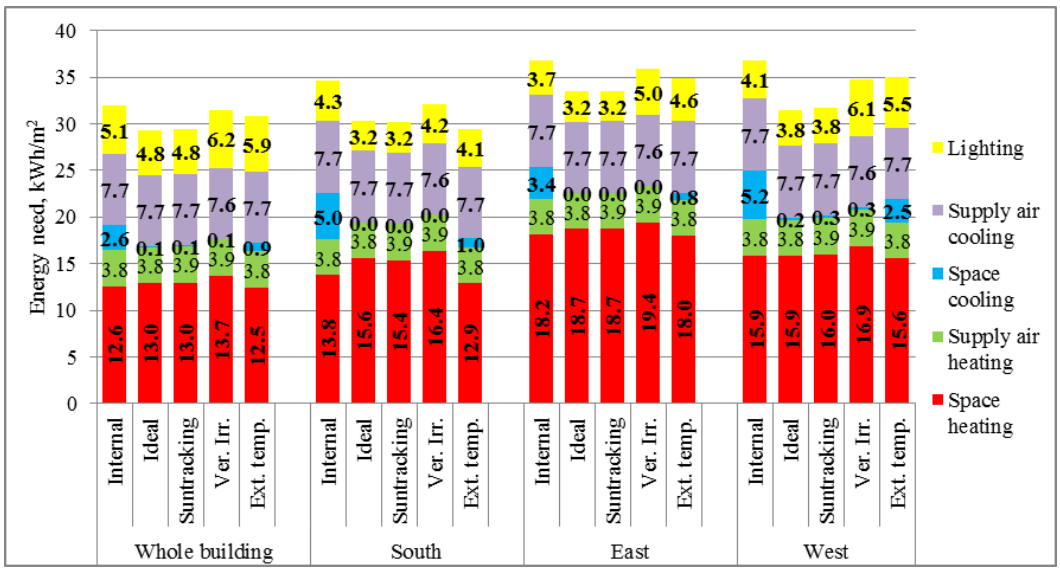

FIG 5. Energy need of cases with quadruple windows

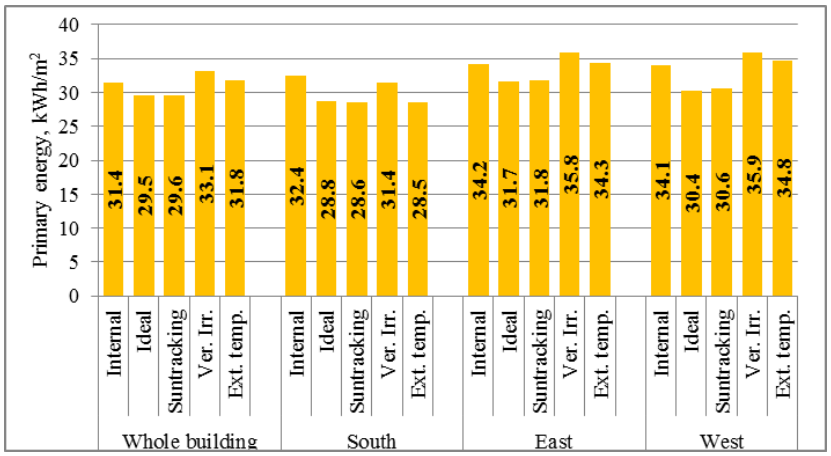

FIG 5. Primary energy of cases with quadruple window

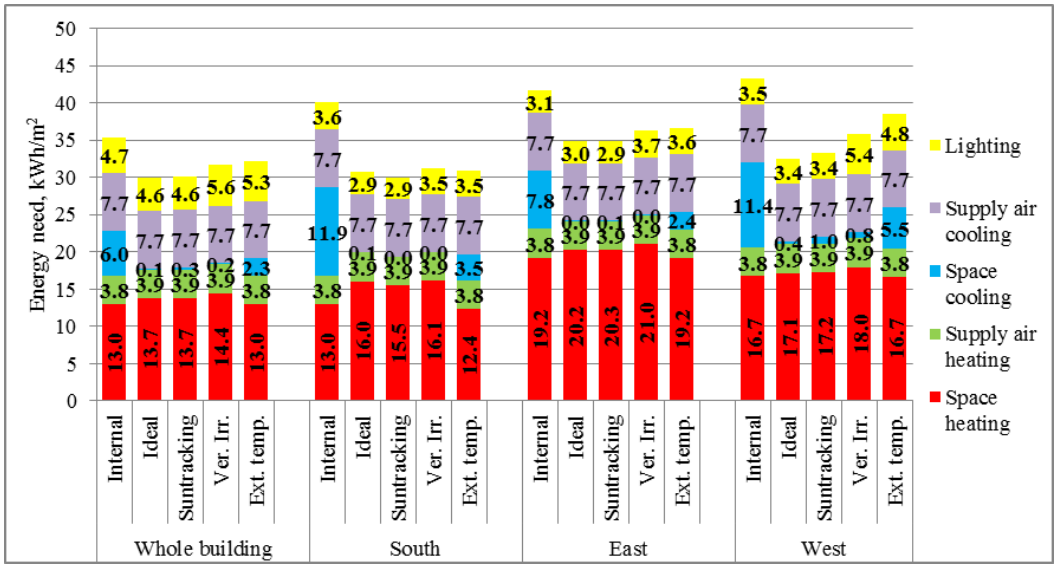

FIG 6. Energy need of cases with quintuple windows

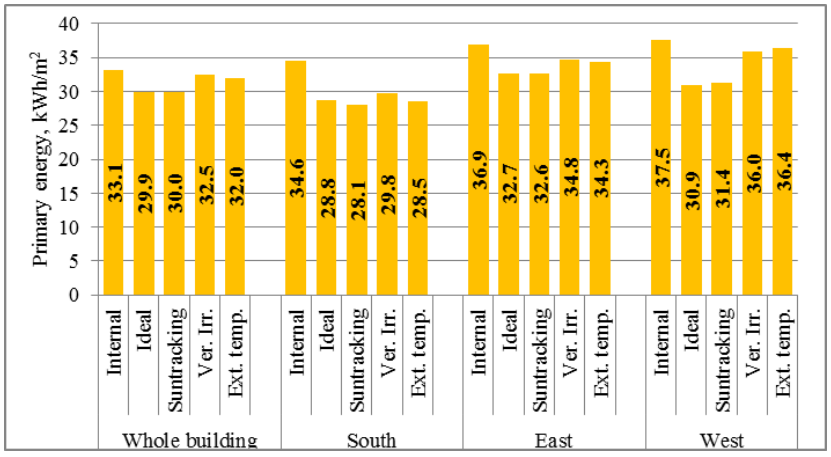

FIG 7. Primary energy of cases with quintuple windows

4. Conclusions

An optimal control principle for external dynamic venetian blinds facades in a cold climate was determined based on generic office floor simulations. Energy calculations of zones with different orientations were conducted and the results show that controlling shade position according to internal temperature and desktop illuminance is most effective whereas suntracking can be used for slat angle adjustment. The room temperature setpoint for pulling down venetian blinds should be chosen slightly lower than cooling temperature (e.g. +24 °C) and the bandwidth for desktop illuminance should be chosen large enough to assure as good daylighting as possible (e.g. 1000 lx) while preventing unnecessary frequent changes in the position of blinds. Control methods according to external parameters such as vertical irradiance and outdoor temperature did not prove to be effective. The largest savings were obtained for cases with larger windows that had higher initial cooling energy use and the whole floor primary energy was decreased by up to 3.2 kWh/m^2 by using external venetian blinds. The savings in the primary energy of different orientations ranged from 2.5 to 6.6 kWh/m^2 in case of large quintuple windows.

5. Acknowledgements

The research was supported by the Estonian Research Council, with Institutional research funding grant IUT1−15, and with a grant of the European Union, the European Social Fund, Mobilitas grant No MTT74 and Estonian Ministry of Education and Research European with Social Foundation financing task 1.2.4 Cooperation of Universities and Innovation Development, Doctoral School project “Civil Engineering and Environmental Engineering” code 1.2.0401.09-0080.

References

Da Silva P.C., Leal V. & Andersen M. 2012. Influence of shading control patterns on the energy assessment of office spaces, Energy and Buildings, vol. 50, pp. 35-48.

Daum D. & Morel N. 2010. Identifying important state variables for a blind controller. Building and Environment, vol. 45, pp. 887-900.

Estonian Government Ordinance No. 68 Energiatõhususe miinimumnõuded. (Minimum requirements for energy performance of buildings) (30.08.2012); RT I, 05.09.2012, 4, 2012.

IDA-ICE, IDA Indoor Climate and Energy 4.5. http://www.equa-solutions.co.uk/.

Kalamees T. & Kurnitski J. 2006. Estonian test reference year for energy calculations. In: Proceedings of the Estonian Academy of Sciences Engineering, vol. 12, pp. 40-58.

ISO 15009. 2003. Thermal performance of windows, doors and shading devices – Detailed calculations. International Organization for Standardization.

Littlefair P., Ortiz J. & Das Bhaumik C. 2010. A simulation of solar shading control on UK office energy use. Building Research & Information, vol. 38:6, pp. 638-646.

Thalfeldt M, Kurnitski J. & Mikola A. 2013. Nearly zero energy building without heating. Estonian Journal of Engineering, vol. 19 (4), pp. 309-328.

Thalfeldt M., Pikas E., Kurnitski J. & Voll H. 2013. Façade design principles for nearly zero energy buildings in a cold climate. Energy and Buildings, vol. 67, pp. 309-321.

Tzempelikos A. & Shen H. 2013. Comparative control strategies for roller shades with respect to daylighting and energy performance. Building and Environment, vol. 67, pp. 179-192.

Wymelenberg K.V.D. 2012. Patterns of occupant interaction with window blinds: A literature review. Energy and Buildings, vol 51, pp. 165-176.

Vertical temperature increase in multi-storey buildings

Mats Dahlblom, Lic.Tech.[1]
Lars Jensen, Professor [1]

[1] Lund University, Faculty of Engineering, Division of Building Services, Sweden

KEYWORDS: *Thermal indoor climate, indoor temperature, vertical temperature increase, case study, mathematical model, disturbance model*

SUMMARY:
Indoor temperature is by measurements stated to rise 0.1 – 0.2°C per storey upwards in multi-storey buildings, despite occupants' possibility to control the temperature. Due to upward air temperature gradient in rooms there will be a heat transfer through slabs upwards. The size of this depends on insulation degree of building envelope and slabs and air flow through the building.

With a linear mathematical model, considering 1 m² floor area, it is shown how some parameters affect the heat transfer. Starting position for the model is a building in the thermal balance from which deviations are calculated. The model gives, for a basic case, results that agree well with the measured values.

The vertical temperature increase, results in lower temperature in lower storeys and higher temperature in upper storeys. Total temperature rise for 4 – 28 storeys are in the range 0.5 – 0.7°C, which give vertical heat transfer of 0.6 – 1.1 W/m². A better insulated building envelope will increase the vertical temperature deviations. Better insulated slabs between the storeys will decrease the deviations. A building with well insulated envelope should also have well insulated slabs between storeys to limit the vertical heat transfer and temperature differences between storeys.

1. Introduction

For different reasons inhabitants desire different indoor temperature. In a building with individual measuring and billing (IMB) of space heating costs, it is desirable for each tenant to be able to control the temperature in their apartments, e.g. to keep a low indoor temperature to lower the heating cost.

However, this can be difficult to reach, as an apartment, through the slabs, is vertically thermally coupled with the apartment above and the apartment below and horizontally connected with adjacent apartments through the walls (Jensen 1999) and (Danilevskii 2011). The latter connection is normally weaker due to a smaller connection area. An apartment is also coupled to the surroundings via the external walls, bottom and top slabs and via the total air flow through the apartment.

The inner coupling, i.e. between adjacent storeys, depends on the slab construction. With in situ casted concrete slabs, without insulation, we will a U-value of about 2.7 W/m²K.

The thermal coupling for storeys in the middle of the building to surroundings depends on the U-values for facade walls and windows and the ventilation flow. For buildings erected in southern Sweden during 1960's typical facade U-value, U_f, are 0.6 – 1.3 W/m²K and for windows, U_w, 3.0 W/m²K (BABS 1960). Typical facade/floor area ratio is 0.4 – 0.5 m²/m² and window/floor area ratio 0.1 – 0.15 m²/m². With these measures the building, calculated per m² floor area, will have a thermal coupling through the facade in the range of 0.6 – 0.9 W/K.

The minimum fresh air flow is 0.35 l/s per m² floor area, which give a thermal coupling of 0.42 W/K per m² floor area.

Temperature measurements in one nine storey apartment building situated in Lund, in southern Sweden, has been done in a system for individual measuring and billing of space heating costs. Measurements from a period of 21 months have been analyzed and temperature differences between vertically adjacent apartments are noticed. Despite the occupants possibility to control their temperature a vertical increase in temperature was registered.

2. Aims and objectives

The overall aim of this study is to, with a theoretical model, show why and how vertically adjacent apartments thermally influence each other.

3. Methods and approach

Based on a case study of an apartment block, the temperature measurements are analyzed, mainly with help of Matlab. A mathematical model to simulate the heat transport upwards in the building is programmed and analyzed in Matlab.

3.1 Case study

3.1.1 Description of the building and its building services

The building with nine storeys and a basement was erected in Lund, in southern Sweden, 1965. It comprises 75 apartments, with 198 rooms, on totally 5150 m² heated area. See Figure 1.

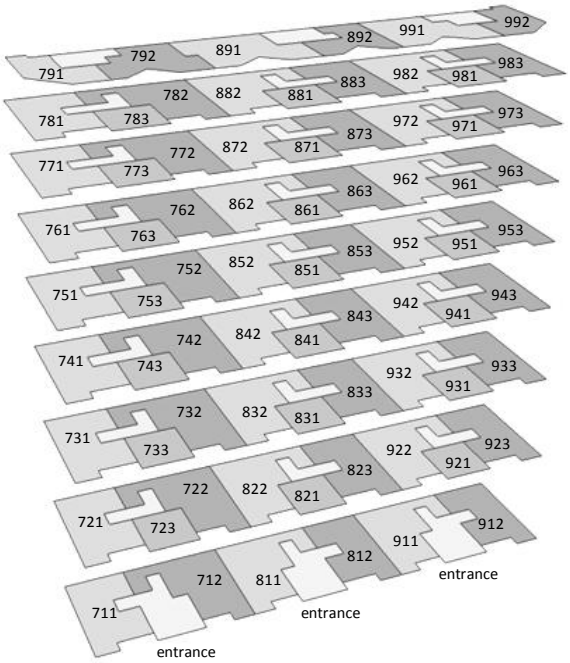

FIG 1. Location of the 75 apartments. Apartments directly above each other, e.g. 711, 721, …,791 are addressed as a column; numbered 1 – 9 from left to right. The entrances face close to south.

The construction is typical for the period, reinforced concrete frame with lightweight curtain walls and triple glazed windows, the slabs between storeys are of concrete with a plastic mat. The U-values are assumed to comply with Swedish building codes for the building year, see Table 1. The building is one of ten objects in a study with totally 1177 residential apartments (Dahlblom & Jensen 2011). The building is equipped with a two-pipe hydronic heating systems with radiators connected via a heat exchanger to the district heating system. The building is ventilated by a mechanical exhaust

ventilation system with constant air volume at a rate of 0.615 ac/h, which in this case means 0.41 l/(s·m²) floor area. The used principle for individual metering and billing (IMB) of space heating costs are based on achieved indoor temperature. The rent includes a "comfort temperature" of 21°C, for temperatures down to 18°C, tenants will be refunded and, vice versa, for temperatures up to 24°C tenants will be extra charged (Lunds Kommuns Fastighets AB 2011).

TABLE 1. Assumed properties for the basic case.

Building element	U-value W/Km²	Area m²
Facade walls	0.6	320
Windows and balcony doors	2.5	90
Ceiling above top floor	0.6	690
Slab above ground floor	0.6	690

3.1.2 Data collection and processing

A housing company has a system for individual measuring and billing of space heating costs (IMB) in about 3000 apartments, in size varying from one to six rooms. The method used for IMB is based on measurements of indoor temperature.

For the IMB-system the building is equipped with one temperature sensor in each room. For this purpose the temperature is measured every 15 minutes in all bedrooms and living rooms and it should, during the 21 months this study covers, at maximum been $12 \cdot 10^6$ readings, but due to shorter and longer interruptions there are $7.5 \cdot 10^6$ readings, i.e. a mean coverage of 62%. Though this data loss, it provides a unique opportunity to investigate indoor temperatures, absolute levels as well as temperature differences between apartments, in this study concentrated to differences between apartments above each other.

3.2 Vertical temperature differences between storeys for 21 months

Monthly mean temperature for each apartment was calculated for the covered period January 2010 until September 2011. Differences between seven vertical neighbours in the nine columns (Figure 1) were calculated and are presented in Figure 2.

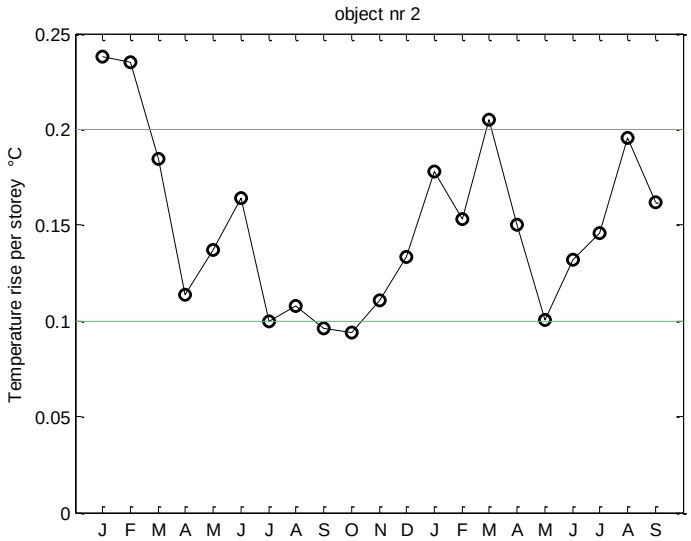

FIG 2. Monthly vertical mean temperature difference per storey for January 2010 to September 2011.

Only seven storeys are included due to floor plan nr 1 and nr 9 differ too much. This means 54 values on temperature differences per month. The temperature rise per storey is between 0.09°C and 0.24°C, in average over all 21 months 0.15°C, average during heating periods is 0.16°C and during non heating periods 0.13°C.

4. Temperature model

The model, illustrated in Figure 3, is normalized to calculate on one square meter floor area. The thermal coupling to the surroundings on each storey is related to one square meter floor area. The coupling depends on U-values for the façade and windows and on the ventilation air flow. The model comprises four temperatures on each storey, the air temperatures at floor level, $T_{air\ floor}$, and ceiling level, $T_{air\ ceiling}$, the floor surface temperature, T_{floor}, and the ceiling surface temperature, $T_{ceiling}$.

A temperature difference, ΔT, between air temperatures at ceiling and floor is set to a fixed value, 2°C. This temperature difference is actually created by up going air plumes from radiators, appliances and occupants and down going plumes at cold façades and window surfaces. Figures can be found in (Rietschel 1960). The model is, storey by storey, set up for the whole building.

The convective heat transfer, P_c, upwards in the room, is partly balanced by the radiant heat transfer, P_r, downwards, from ceiling to floor, described by the parameter h_r. The difference between the convective heat transfer, P_c, and radiant heat transfer, P_r, is equal to the slab heat transfer, P_s, if there are no heat losses, in the model $h_n = 0$. This means also that $T_{ceiling}$ is higher than the floor surface temperature on the next storey, $T_{floor\ above}$. The heat transfer through the slab is described with the parameter h_s.

The outdoor temperature set to zero as the model describes disturbances from steady state conditions. The model is described as a linear equation system, which means all temperatures are proportional to the assumed temperature difference, ΔT.

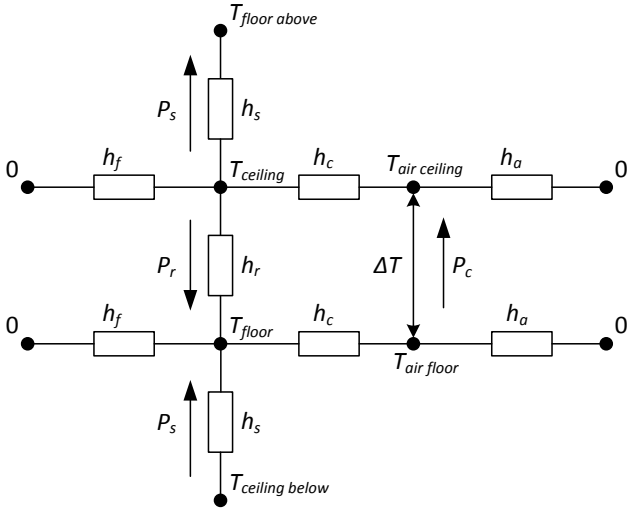

FIG 3. Model for heat transport for one storey

Total thermal coupling, except the vertical, to the surroundings through external walls and windows and air flow through the storey, per square meter floor, area is calculated by equation (1). The air flow is sum of ventilation air flow and infiltration, independent ventilation system type, i.e. it is valid both for exhaust ventilation and balanced ventilation.

$$h_n = U_w \cdot a_w + U_e \cdot a_e + \rho \cdot c_p \cdot q_e \qquad (1)$$

Where h_n total thermal coupling except the vertical versus floor area (W/(K·m²))
U_w U-value windows (W/(m²·K))
a_w window area versus floor area (m²/m²)
U_e U-value external walls (W/(m²·K))
a_e external wall area versus floor area (m²/m²)
ρ air density, 1.2 kg/m³
c_p specific heat capacity air, 1000 J/(kg·K)
q_e exhaust air flow versus floor area (m³/(s·m²))

This thermal coupling for one storey is in the model divided on four nodes, two connected via heat transport due to differences in surface floor and ceiling temperatures and two due to difference in air temperature, in the model described with h_f and h_a, see Figure 3.

$$h_n = 2 \cdot h_f + 2 \cdot h_a \quad (2)$$

How these couplings are distributed between those 4 nodes are not further investigated and therefore simplified set to be equal, i.e.

$$h_a = h_f = h_n / 4 \quad (3)$$

Losses through the top ceiling slab and the bottom floor slab are included in the model, named h_{se}.

4.1 Parametric study

To see the influence from different parameters a study, where some parameters are varied, has been carried out. The parameters for the basic case are, as close as possible, chosen to agree with the building in the case study above. Though, as only seven of the nine storeys have the same floor plan, this building height was chosen for the basic case. Note that the building has mechanical exhaust ventilation without heat recovery.

Following cases are studied, for details on parameters, see Table 2.

1. building with 4 storeys
2. building with 14 storeys
3. building with 28 storeys
4. better insulated slab between storeys (lower h_s)
5. better insulated bottom slab and top slab (lower h_{se})
6. better insulated facades, windows, bottom slab and top slab
7. better insulated facades, windows, bottom slab, top slab and slab between storeys

5. Results

Results from the parametric study are presented in Table 2 and Figure 4 and Figure 5. ΔT_{storey} in Table 2 was calculated as the total temperature difference between bottom and top storey divided by number of storeys. ΔT_{storey} for the basic case is 0.110°C, to be compared to the temperature rise per storey in the case study above, which was in the range 0.1 – 0.2°C. Corresponding heat transport upwards in the building according to the model is in average per storey 0.811 W/m².

For a building with only 4 storeys the temperature rise per storey seems to be linear; when studying buildings with 14 and 28 storeys respectively it is obvious that it is not, the disturbance in the middle storeys is close to zero. The mean temperature difference between bottom and top is approximately 0.7°C for 7, 14 and 28 storeys compared to 0.5°C for 4 storeys.

An insulated slab between the storeys, case 4, will decrease the mean temperature difference from 0.110°C to 0.079°C per storey, i.e. to 72% compared to the basic case, but the vertical heat transport $P_s=h_s \cdot \Delta T_s$ so this will decrease to 28% compared to basic case.

Better insulated bottom and top slabs, case 5, will increase temperature disturbances to 0.137°C per storey, compared to 0.110°C per storey for the basic case.

Case 6 have better insulated building envelope, close to what is required to meet present building codes. We can see a weaker coupling to surroundings and stronger coupling within the building; more heat is transported upwards in the building, the mean per storey, P_{sm} , is 0.583 W/m², compared to originally 0.811 W/m² for the basic case.

The last case, nr 7, is like nr 6 but with insulated slabs between the storeys. As can be expected, the temperature difference and hence the heat transport will decrease. The vertical heat transport is halved compared to the basic case, Table 2 and Figure 5.

TABLE 2. Input parameters for parametric study and results.

Case	Storeys	U_f	U_w	h_n	h_s	h_{se}	ΔT_{build}	ΔT_{storey}	P_{sm}
-	-	W/Km²	W/Km²	W/Km²	W/Km²	W/Km²	°C	°C	W/m²
basic	7	0.6	2.5	4.40	10	0.6	0.660	0.110	0.811
1	**4**	0.6	2.5	4.40	10	0.6	0.522	0.174	0.563
2	**14**	0.6	2.5	4.40	10	0.6	0.702	0.054	1.031
3	**28**	0.6	2.5	4.40	10	0.6	0.702	0.026	1.139
4	7	0.6	2.5	4.40	**4**	0.6	0.474	0.079	0.594
5	7	0.6	2.5	4.40	10	**0.1**	0.822	0.137	0.709
6	7	**0.1**	**1.0**	2.67	10	**0.1**	1.038	0.173	0.583
7	7	**0.1**	**1.0**	2.67	**4**	**0.1**	0.822	0.137	0.458

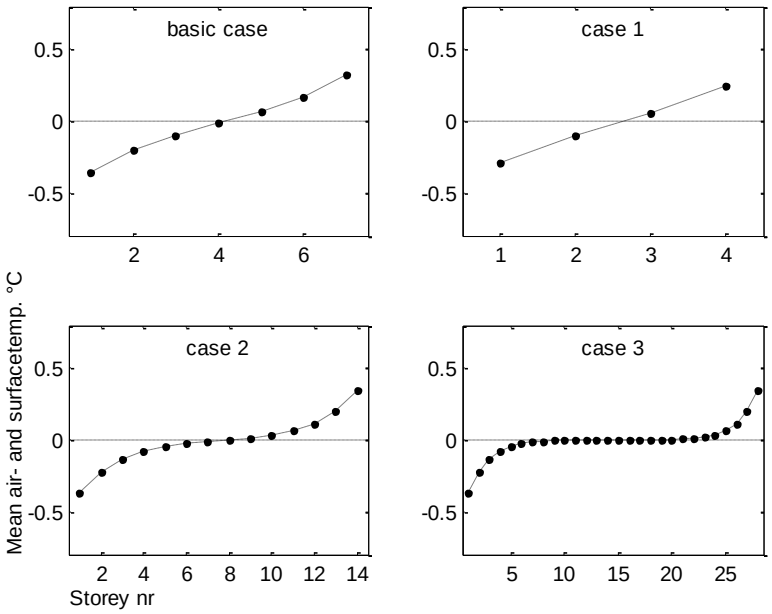

FIG 4. Mean temperature for the 4 nodes in each storey, i.e. deviation relative to a building in thermal balance, basic case and case 1 - 3.

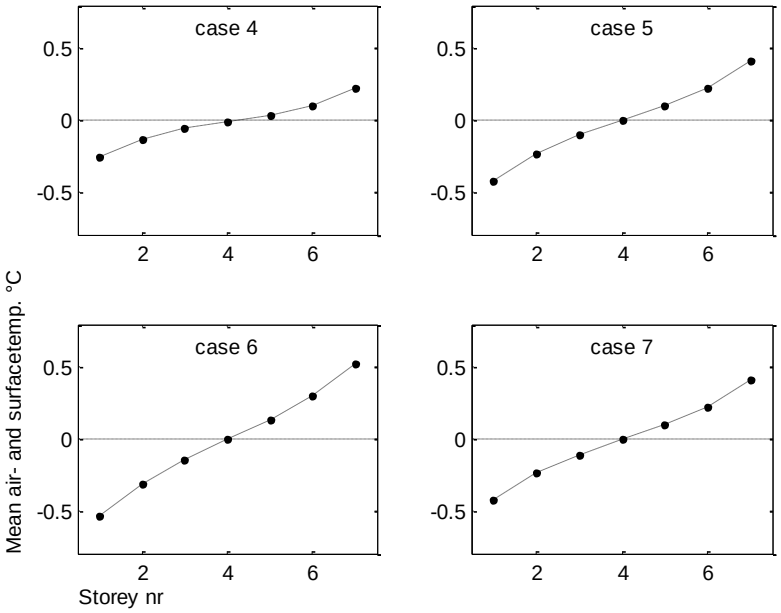

FIG 5. Mean temperature for the 4 nodes in each storey, i.e. deviation relative to a building in thermal balance, case 4 - 7.

5.1 Stationary model

Case 3, floor 10-20, show constant temperature conditions. Constant conditions mean that the temperature difference between floor and ceiling surfaces and across a slab is equal, i.e. there is no temperature increase for any level with constant conditions.

Therefore, if external losses are neglected, i.e. $h_n = 0$, the heat power through a slab can be written as $P_s = h_s \cdot \Delta T_s$, where ΔT_s is the temperature difference across a slab, or as $P_s = P_c - P_r$, i.e. the difference between the convective heat power upward and radiation heat power downward, which can be written as

$$P_c = h_c \cdot (\Delta T - \Delta T_s)/2 \tag{4}$$

$$P_r = h_r \cdot \Delta T_s \tag{5}$$

ΔT is assumed to be 2°C, while ΔT_s is unknown.

Inserting P_c and P_r make it possible to decide ΔT_s

$$\Delta T_s = \frac{h_c \cdot \Delta T/2}{h_s + h_r + h_c/2} = \frac{1}{2 \cdot h_s/h_c + 2 \cdot h_r/h_c + 1} \cdot \Delta T \tag{6}$$

Equation (6) shows that ΔT_s always is less than ΔT, as h_s, h_c and h_r always are positive.

The heat, P_s, upwards in the building can be expressed as

$$P_s = h_s \cdot \Delta T_s = \frac{h_s \cdot h_c \cdot \Delta T}{2 \cdot h_s + 2 \cdot h_r + h_c} \tag{7}$$

With values from the basic case, i.e. $h_s = 10$, $h_c = 2$ and $h_r = 5$, we get $P_s = 1.25$ W/m², compared to P_{sm} = 1.139 W/m² for case 3.

6. Conclusions

The results in the model are close to the measured temperature differences for the building in the case study, which indicates that the model gives reasonable values.

It can be concluded that there is an internal vertical heat transport upwards in multi-storey buildings.

The temperature difference between floor and ceiling causes a temperature difference over the slabs between storeys which drive the heat upwards. This results in lower temperature in lower storeys and higher temperature in upper storeys and hardly noticeable deviations in between, shown for buildings with a large number of storeys.

Better insulated slabs between storeys will decrease the temperature deviations.

Better insulated top ceiling and bottom floor will increase the temperature deviations.

Better insulated building envelope will increase the temperature deviations.

A building with these three cases of insulation can result in either decreased, increased or no temperature deviations at all versus the basic case.

A building with a well insulated building envelope should also be well insulated between storeys to limit the vertical heat transport upwards the building and the temperature differences between storeys.

7. Acknowledgements

This study was possible to complete thanks to the large data set provided by LKF.

References

Anvisningar till byggnadsstadgan: [BABS 1960]. (1960). [Instructions for the Swedish building statute]. Stockholm:

Dahlblom, M. & Jensen, L. (2011). *Reglering av värmesystem i flerbostadshus med individuell värmemätning. Slutrapport för forskning med stöd från CERBOF* [Control of heating systems in apartment buildings with individual heat metering. Final report of research supported by CERBOF]. (Rapport TVIT—11/3006). Lund: Building Services, Lund University.

Danilevskii, L. N. (2011). Temperature conditions and heat supply of apartments in an apartment house with individual regulators. *Journal of Engineering Physics and Thermophysics.* 84 (2) pp. 359-367.

Jensen, L. (1999). *Utvärdering av Hälsingborgshems system för komfortdebitering* [Evaluation of Helsingborgshems system for individual billing of space heating based on thermal comfort]. Lund: Building Services, Lund University.

Lunds Kommuns Fastighets AB (2011). Komfortvärme [Comfort heat]. [Electronic] Available: http://www.lkf.se/ImageVault/Images/id_5605/scope_0/ImageVaultHandler.aspx [2012-06-20].

Rietschel, H. (1960). *H. Rietschels Lehrbuch der Heiz- und Lüftungstechnik. 14. verb. Aufl. 2. Neudruck*. Berlin: Springer.

Optimized damper control of pressure and airflow in ventilation systems

Chrysanthi Sofia Koulani, M.Sc. [1]
Christian Anker Hviid, Assistant Professor [1]
Søren Terkildsen, Ph.D. [1]

[1] Technical University of Denmark (DTU), Department of Civil Engineering, Denmark

KEYWORDS: *ventilation system, HVAC control strategy, variable air volume, static pressure reset, modelling, Simulink, energy savings.*

SUMMARY:
Conventional control strategies in variable air volume (VAV) ventilation systems do not take fully into advantage the potential energy savings since the system operation is based on maintaining a constant static pressure (CSP) set point in the main duct irrespective of the actual pressure demand. The static pressure reset (SPR) control strategy can optimize the operation of the supply air fans by adjusting the pressure set point to be just enough to deliver the required airflow to the most critical zone.

This study investigated the operation and energy savings potential of an SPR control algorithm by using the Simulink programming tool which is add-on software to MATLAB mathematical programming language. A model of a VAV ventilation system was created in Simulink based on the International Building Physics Toolbox (IBPT); the IBPT thermal zone was remodelled in order to calculate dynamically the airflow demand according to the zone air temperature. The performance of the Simulink model was evaluated based on the experimental setup of the ventilation system. The SPR control method established stable system operation and was proven efficient to maintain comfortable space conditions while reducing by 14 % the fan energy used in a typical working day.

1. Introduction

In traditional control of variable air volume (VAV) systems the terminal boxes and the air handling unit (AHU) are operated independently without integration. The common practice is to control the AHU to a constant static pressure (CSP) set point corresponding to the pressure rise required under the design full load condition (Wei et al 2004).However in this way the AHU is regulated irrespective of the actual pressure demand. This is because under part load condition the fan is providing excessive static pressure (Wei et al 2004; Federspiel et al 2005; Liu et al 1997) which is dissipated by increasing the airflow resistance of the air distribution network via throttling at the terminal boxes. As a result significant fan power is wasted in mechanical energy losses. By integrating the control of terminal boxes into the building management system (BMS) it is possible to implement the static pressure reset (SPR) control strategy. This method regulates the AHU in real time according to feedback from several individual zones. In this case the fan generates the pressure required in order to satisfy the space conditions in the most critical zone while maintaining the airflow resistance of the distribution network at a minimum (Wang et al 1998). Consequently the fan pressure rise and thus the fan power is reduced. The control method of trim and respond based on zone pressure request alarms is the most efficient SPR strategy since it is more stable, flexible and it minimizes the impact of rogue zones (Taylor 2007). The objective of this paper is to investigate the operation and the potential energy savings of the trim and respond SPR control strategy. A mathematical model of a conventional VAV ventilation system is developed in Simulink (Simulink 2013) and the model is expanded by implementing the optimized SPR control algorithm. The Simulink model operation is validated by experiments performed on the full-scale test system.

2. The Simulink model

The model of the VAV ventilation system was created in the graphical environment of Simulink in Matlab (Matlab 2013) and it was built based on the blocks of the international building physics toolbox (IBPT). The IBPT toolbox (IBPT 2012) is a library of blocks added on Simulink, specially constructed for the thermal analysis in building physics. The construction blocks (external and internal surfaces, windows) provide detailed calculations of the thermal state of every subcomponent in the structure according to the surrounding conditions to which it is exposed. The thermal condition of the zone is calculated according to the heat gained through the building envelope, the systems used for heating, ventilation and air conditioning, the internal gains occurring in the zone and the weather data corresponding to a certain location. The default IBPT blocks for the internal gains and the ventilation system were rebuilt in order to fit the operation needs of the VAV ventilation system. FIG 1 illustrates the Simulink model which consists of three IBPT thermal zones.

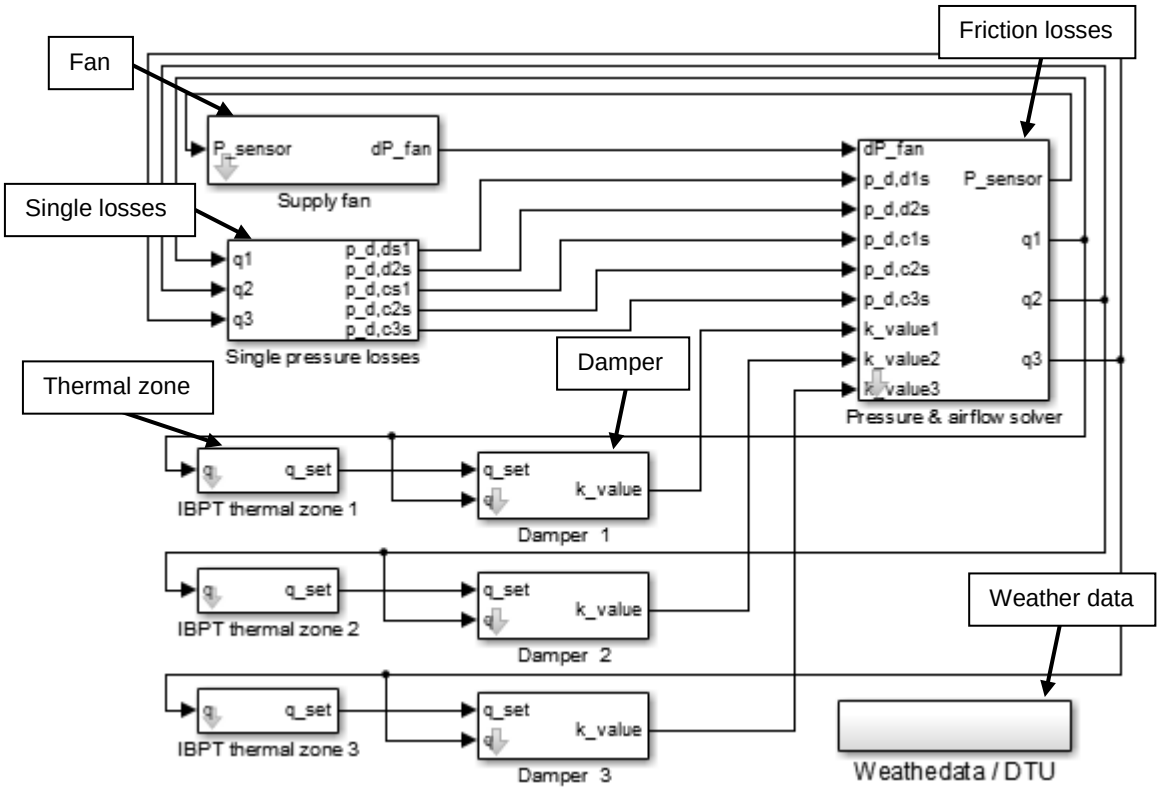

FIG 1. The Simulink model of the VAV ventilation system.

2.1 The internal gains

The IBPT internal gains block was configured to include an hourly load schedule of the ventilated zone. The modified block calculates the heat gains based on user defined profiles considering occupants, equipment and lighting use in the zone.

2.2 The ventilation system

The IBPT ventilation system block was remodelled to calculate dynamically the airflow demand (q_{dem}) according to the zone air temperature (T_a); the strategy is implemented with the ramp functions shown in FIG 2. The user defined data are the minimum ($q_{set,min}$) and maximum ($q_{set,max}$) airflow set point required in order to maintain a comfortable temperature range ($T_{set,min}$, $T_{set,max}$) in the zone.

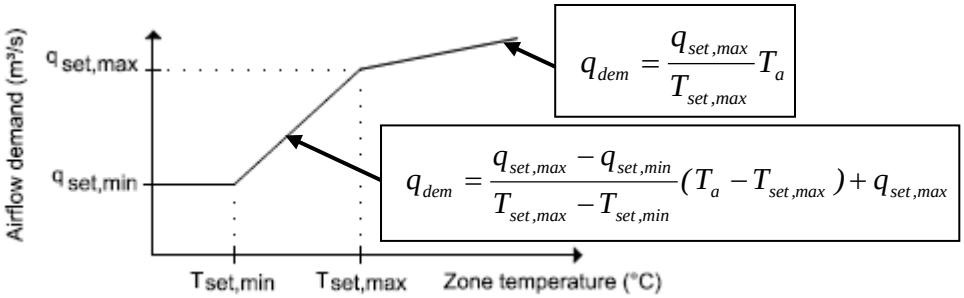

FIG 2. The dynamic calculation of the airflow demand according to the zone air temperature.

2.3 The fan

The fan operation is regulated according to the tracking error determined as difference between the CSP set point and the duct pressure at the sensor position; the block diagram is shown in FIG 3.

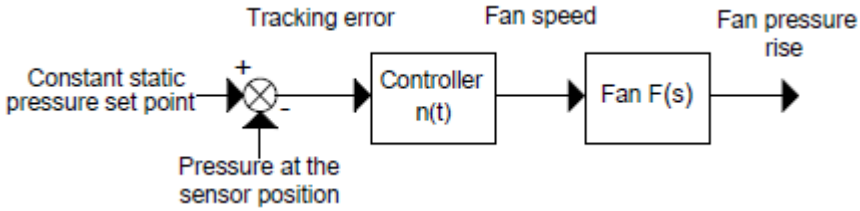

FIG 3. The fan operation principle.

The fan block receives the signal generated by the controller which corresponds to the fan speed. This control signal is used to calculate the new plant output, the fan pressure rise. The fan characteristics (F) are represented by using the first-order linear time-invariant (LTI) system (Franklin et al 1993) given in equation 1.

$$F(s) = \frac{k_f}{Ts + 1} \tag{1}$$

Where s representation of Laplace transformation (-)
k_f the process gain correlating the plant input with the plant output (Pa/rpm)
T the time constant is the time required to reach the system a steady state condition (sec)

The controller operation complies with equation 2; the tuning of the proportional integral (PI) controller is performed by using the simple analytic rules proposed by S. Skogestad (2002).

$$n(t) = K_{p,f} e_f(t) + K_{i,f} \int e_f(t) dt \tag{2}$$

Where e_f the tracking error between the CSP set point and the pressure sensor reading (Pa)
$K_{p,f}$ the proportional controller gain, 7.14
$K_{i,f}$ the integral controller gain, 17.85

2.4 The damper

The damper operates as shown in FIG 4; the damper position is adjusted based on the tracking error determined as difference between the zone airflow demand (see FIG 2) and the airflow provided to the zone. In the control process in FIG 4 the plant block is representing the damper system that receives the controller signal which corresponds to the damper position. The plant output, the resistance coefficient, is calculated accordingly. The second-order LTI system (Franklin et al 1993) presented in equation 3 approximates the operation of a typical damper (D).

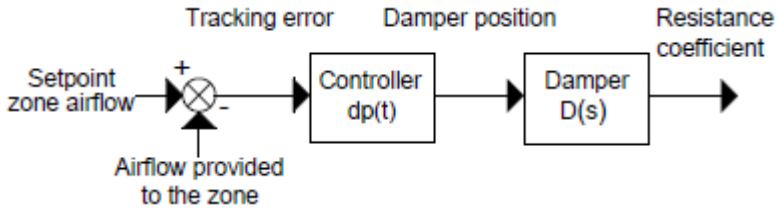

FIG 4. The damper operation principle.

$$D(s) = \frac{k_d \omega_n}{s^2 + 2\zeta\omega_n s + \omega_n} \quad (3)$$

Where k_d the process gain correlating the plant input with the plant output (m^3/s/Pa%)
ω_n the natural frequency relevant to the speed response of the system, assumed 10 rad/s
ζ the damping ratio relevant to the oscillation mode of the system, assumed 1

The controller operation is applied according to equation 4; the tuning gains of the PI controller are set based on typical product values.

$$dp(t) = K_{p,d} e_d(t) + K_{i,d} \int e_d(t) dt \quad (4)$$

Where e_d the tracking error between the demanded and the delivered airflow in the zone (m^3/s)
$K_{p,f}$ the proportional controller gain, 1
$K_{i,,f}$ the integral controller gain, 10

2.5 The pressure and airflow solver

The friction and single pressure losses blocks illustrated in FIG 1 implement the hydraulic calculation of the VAV ventilation system according to the duct design shown in FIG 5. The unknown pressure and airflow conditions are determined by setting up a system of equations expressing the pressure losses occurring in every component of the system. The hydraulic calculation determines the pressure demand (P) at the beginning and end of every component as well as the airflows (q) delivered to the different zones (see FIG 5). The system of equations cannot be solved analytically; therefore the Newton-Raphson numerical method is used instead.

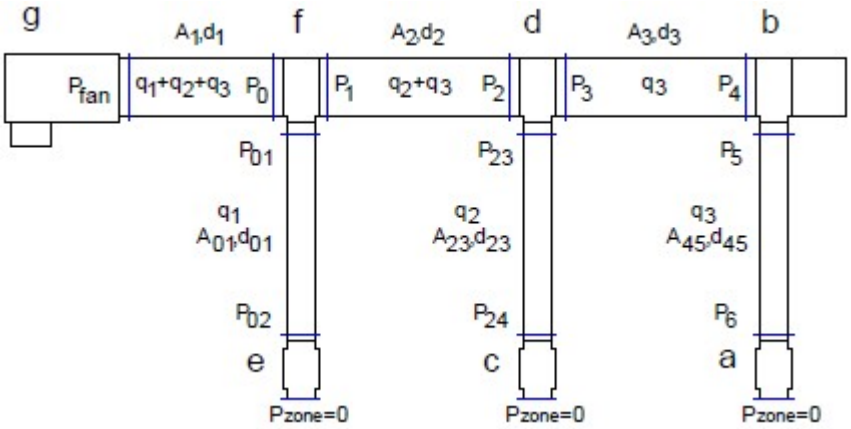

FIG 5. The duct design in the pressure and airflow solver block.

In a piece of duct the pressure losses due to friction are calculated according to the Darcy-Weisbach equation (White 1998) given in equation 5. The Darcy friction factor is obtained by the Swamme-Jain equation (Swamme et al 1976), which is an approximation of the implicit Colebrook-White equation (see equation 6).

$$\Delta P_{fr} = f_D \frac{L\rho}{d2} u_{air}^{\ 2} \quad (5)$$

Where f_D the Darcy factor (-)
L the length of the duct (m)
d the diameter of the duct (m)

$$f_D = \frac{0.25}{\left(log_{10}\left(\frac{5.74}{Re^{0.9}} + \frac{\varepsilon}{3.7d} \right) \right)^2} \quad (6)$$

Where Re the Reynolds number (-)
ε the roughness height, for thin plate ducts is equal to 0.15×10^{-3} m

The pressure losses due to connections and fittings are calculated according to equation 7.

$$\Delta P_{\text{sing}} = \frac{\zeta_r u_{air} \rho}{2} \quad (7)$$

Where ζ_r the resistance coefficient (-)
u_{air} the mean velocity of airflow (m/s)
ρ the density of air, 1.204 kg/m^3

The pressure losses introduced by the damper component are approximated based on equation 8.

$$\Delta P_{\text{sing}} = \left(\frac{q_{del}}{k_{value}} \right)^2 \quad (8)$$

Where q_{del} the airflow delivered to the zone (m^3/s)
k_{value} the damper resistance coefficient (m^3/sPa)

2.6 The static pressure reset algorithm

In order to implement the SPR control method of trim and respond based on zone pressure request alarms, one more block was added to the Simulink model presented in FIG 1. The operation principle of the applied control logic can be seen in FIG 6.

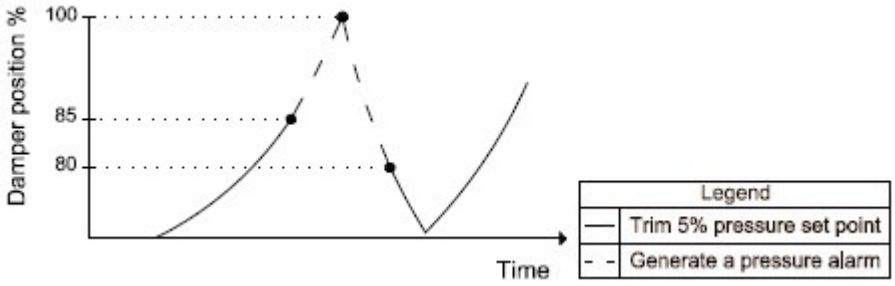

FIG 6. The control logic of the trim and respond static pressure reset method.

Every damper of the VAV system transmits an alarm signal when its position exceeds 85 % opening; the zone keeps generating a pressure request until the damper closes to a position of 80 % opening. The pressure requests from all zones are summed and when at least two zones give an alarm the fan pressure set point is reset 10 % upwards of the pressure demand at the sensor position. In the opposite case it is reset 5 % downward. The SPR is performed within a specific pressure range; the upper limit is set equal to the CSP set point while the lower SPR limit is determined according to the pressure demand ensuring precise damper operation. The SPR loop resets the pressure set point every 90 sec

and the fan adjusts to the new pressure set point.

3. The experimental setup

The performance of the Simulink model was validated on a full scale experimental setup; the experimental setup arrangement was identical to the duct design given in FIG 5 where the distribution duct had a diameter of 315 mm and the connection ducts a diameter of 160 mm. The setup consisted of three LeanVent DropDamper LERX and a box fan (Exhausto BESF1804-1EC). The VAV system was evaluated both with the CSP and the SPR control strategy; the two methods were modelled in LabVIEW (LabVIEW 2013). The validation was performed by providing the Simulink model and the experimental setup with the same airflow demand data; two different airflow demand profiles were used for testing the model performance with each control strategy (see FIG 7). Ventilation zone 3 behaved like a rogue zone with the SPR method because the lower limit of the pressure range, within which the fan operation set point reset, was insufficient for delivering the required pressure.

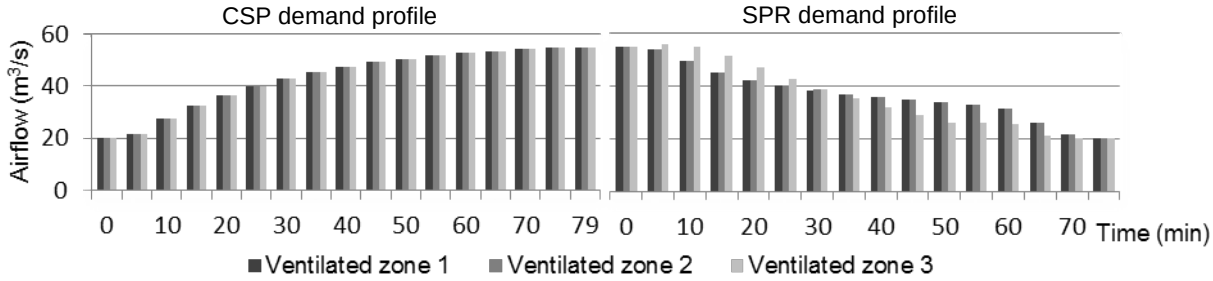

FIG 7. Airflow demand profiles with the CSP and the SPR control method, respectively.

4. Results

4.1 Simulink model validation

The graphs in FIG 8 compare the performance of the Simulink model and the experimental setup of the VAV ventilation system when the fan was controlled with the CSP and the SPR control method, respectively.

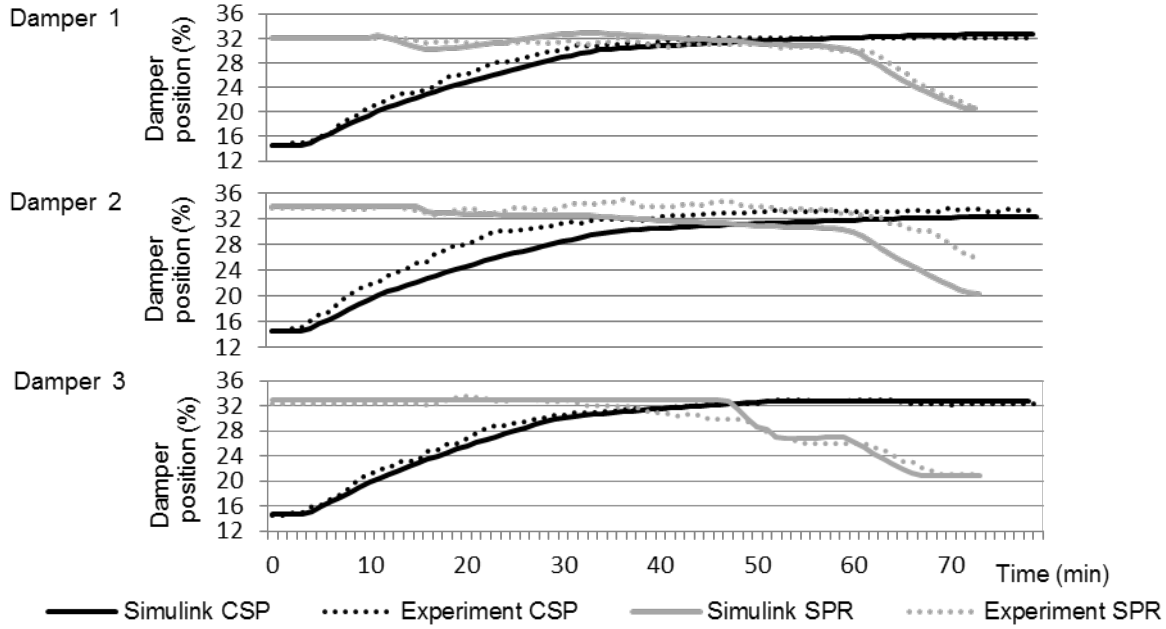

FIG 8. Response curves of the dampers with the CSP and the SPR control method, respectively.

According to the obtained results the Simulink model with both control strategies approximated satisfactory the actual operation conditions since the dampers followed a similar response trend. The largest deviation between the Simulink model and the experimental setup was obtained from damper 2 when the VAV system was regulated with the SPR control method. As presented in the second graph in FIG 8 the deviation was below 10 %, however in the last minutes it increased to 22 %. This occurred because the damper modelling represented insufficiently the actual speed response of the Dropdamper. The mathematical model of the damper should be tuned to coincide with the experimental data. The speed of the damper model is relative to the natural frequency parameter involved in the mathematical expression describing its response (see equation 3). In this case the speed of the damper was assumed; in order to accelerate the response, trial and error simulations have to be performed increasing the natural frequency.

4.2 Energy savings from optimized damper control

The energy savings potential of the SPR control strategy is determined based on the fan power used when controlling the ventilation system with the CSP and the SPR method, respectively. Considering that the fan efficiency varies according to the different pressure and airflow conditions that the fan is operating with, the fan efficiency was approximated from producer table values by using average hourly values of airflow and pressure rise delivered by the fan. The average hourly values were derived based on 24 hour simulation data obtained from the Simulink model of the VAV ventilation system when operated with both control strategies. The fan power was calculated according to equation 9.

$$Power = \frac{\Delta P_{fan} q_{tot}}{n_e} \tag{9}$$

Where ΔP_{fan} the fan pressure rise (Pa)
q_{tot} the fan airflow (m^3/s)
n_e the fan efficiency (-)

The fan energy used in a typical working day in winter when the occupancy period was set from 8 am to 17 pm with the CSP and the SPR was determined to 151 Wh and 130 Wh, respectively; the energy consumption was reduced approximately by 14 %. The highest energy savings potential of the SPR control method occurred under part airflow conditions as the fan operated with decreased static pressure. Due to the fact that the fan was correctly sized the combination of lower pressure set point and airflow improved fan efficiency and thus the energy savings were further increased. With the CSP control method the same airflow conditions combined with increased static pressure lowered the fan efficiency and as a result the fan operated inefficiently.

5. Conclusions

The results presented in this paper draw the following conclusions:

- The first and the second-order LTI systems were proven representative for the response of the fan and the damper, respectively. For the current study we assumed the parameters of the mathematical model of the damper (ζ, ω_n). The value of the natural frequency parameter turned to be inaccurate for representing the speed response of the Dropdamper as it introduced high deviation to the Simulink model when it was controlled with the SPR control. The damper mathematical model should be tuned to fit the experimental data.
- The SPR control method documented higher energy savings under part airflow conditions where the fan operated with decreased pressure set point.

In practical applications of the SPR control strategy caution should be given when determining the lower limit of the pressure range within which the variable fan operation set point is established. This

parameter is critical because in case that the minimum fan pressure rise is insufficient to satisfy the system pressure demand, the far located zones will act as rogue zones. Therefore it is advisable to perform airflow measurements in order to ensure that the set point selected is appropriate for the precise operation of the dampers. In order to maximize the energy savings potential of the SPR control method, the fan should be correctly sized; in this case the fan efficiency improves when the fan operates with decreased static pressure.

6. Acknowledgements

The authors acknowledge the financial support from the Energy Technology Development and Demonstration Programme (EUDP), Danish Energy Agency. Moreover the authors wish to express their gratitude to Remus Mihail Prunescu, Christos Papoutsellis and Vasilis Bellos.

References

Federspiel CC, Haves P. & Cohen T. 2005. Detecting critical supply duct pressure. ASHRAE Transactions, 111 PART 1, pp957-63.

Franklin G.F.; Powell J.D. & Naeini A.E. 1993. Feedback control of Dynamic Systems. 2nd ed. Addison-Wesley Longman Publishing Co., Inc. Boston, MA, USA.

IBPT. 2012. International Building Physics in Simulink. Available from: http://www.ibpt.org/ [accessed 01-02-2013]

LabVIEW. 2013. National instruments, version 2010. Available from: http://sine.ni.com/np/app/main/p/docid/nav-104/lang/da/ [accessed 05-08-2013]

Liu M.; Zhu Y.; Claridge D.E. & White E. 1997. Impacts of Static Pressure Set Level on HVAC Energy Consumption and Indoor Conditions. ASHRAE Transactions, 103, (2).

Matlab. 2013. Mathworks, version 2012b. Available from: http://www.mathworks.com/products/matlab/ [accessed 14-10-2013]

Simulink. 2013. Mathworks, version 2012b. Available from: http://www.mathworks.com/products/simulink/ [accessed 14-10-2013]

Skogestad S. 2002. Simple analytic rules for model reduction and PID controller tuning. Journal of Process Control, 14, (4), pp 465.

Swamee P.K. & Jain A.K. 1976. Explicit equations for pipe-flow problems. Journal of the Hydraulics Division (ASCE), 102, (5), 657-664.

Taylor S.T. 2007. Increasing Efficiency with VAV System Static Pressure Set point Reset. ASHRAE Journal 49, (6), pp24-32.

Wang S. & Burnett J. 1998. Variable-Air Volume Air-Conditioning Systems: Optimal reset of static pressure set point. Building Services Engineering Research & Technology, 19, (4), pp219-231.

Wei G.; Liu M. & Claridge D.E. 2004. Integrated damper and pressure reset for VAV supply air fan control. ASHRAE Transactions, 110, (2).

White F.M. 1998. Fluid Mechanics. 4th ed. McGraw-Hill Editions, 792 pp.

Variations in indoor temperature in residential apartments of different size and building category

Mats Dahlblom, Lic.Tech. [1]
Birgitta Nordquist, Assistant professor [1]
Lars Jensen, Professor [1]

[1] Lund University, Faculty of Engineering, Division of Building Services, Sweden

KEYWORDS: *Indoor temperature variations, residential apartments, thermal indoor climate, case study, individual metering and billing.*

SUMMARY:
In a case study, comprising 1177 residential apartments with 3248 rooms, temperature registrations every 15th minute in all living-rooms and bedrooms, during one year, in the system for individual metering and billing of space heating costs, were analyzed. The apartments were divided into two categories, apartment blocks from 1960th and row houses from about 1990. Apartments mean temperatures and standard deviations as a function of apartment size and category was compared. Corresponding was done on room level divided on apartment size for the two building categories. Finally, temperatures in bedrooms were compared to those in living-rooms for two objects from each category; presented in duration charts based on all single 15th minute values. The same pattern between different apartment sizes is kept for all month, though with a seasonal variation. The living-rooms are in mean warmer than bedrooms. The larger the apartments are the larger are the differences. The results provide a more nuanced picture of the temperature conditions in homes beneficial for better input data for building energy simulations.

1. Introduction

Knowledge of real indoor temperatures is important both in terms of thermal comfort and as the temperature affects the building's energy need for space heating. When performing simulations of the energy need in the design stage assumptions of what indoor temperatures the building will have must be done. To get reliable results it is necessary to use realistic indoor temperatures, an underestimation of 1°C give at least 5% error in the space heating need in Nordic climate. Both the absolute level and statistical measures of the variation of the indoor temperature are important to know.

Indoor temperatures in residential buildings have recently been studied by Pavlovas (2006), Bøkenes et al (2009), Yohanis et al (2010), Bagge et al (2011) and Kavgic et al (2012). Today's detailed knowledge of indoor temperature and its variations in different aspects, as dependency of apartment size, building age, time of the day, etc., in residential buildings is however limited. Bøkenes (2009) and Yohanis et al (2010) present detailed data for temperature variations between different rooms within apartments on Ireland. However, the habits in Northern Ireland do not agree with Scandinavian; the temperatures there are clear below what we can see in studies from Scandinavia. When looking at the residential building stock, it is of interest to know whether there are differences for example between rooms. People sometimes express a preference to have lower temperature in the bedroom. The type of homes and accordingly type of building technique may also be significant. Will the indoor temperature be different in older apartment blocks compared to newer row houses? Differences in plan, exterior surfaces and insulation level of the building envelope may imply different temperature and distribution. These are some objectives which this study strives to examine and gain increased detailed knowledge about.

In southern Sweden a housing company has implemented a system for individual measuring and billing of space heating costs (IMB) in about 3000 apartments, in size varying from one to six rooms. The method used for IMB is based on measurements of indoor temperature. The temperature is measured every 15th minute in all bedrooms and living-rooms. This provides a unique opportunity to investigate indoor temperatures, absolute levels as well as temperature distribution between rooms in different apartments.

2. Aims and objectives

The overall aim of this study is to investigate and present how indoor temperature varies between rooms in apartments of different size in multi-family buildings of mainly two types, apartment blocks and row houses, to give a more differentiated picture of the thermal climate in these types of buildings. A second aim is to contribute to more refined temperature data for energy simulations in apartment buildings.

3. Method and approach

In a case study of ten residential properties (here known as objects) with totally 1177 apartments and 85715 m² heated area, the temperature measurements, primarily used for individual metering and billing (IMB) of space heating costs, are analyzed from different aspects, mainly with help of Matlab.

3.1 Description of objects

Basic data for the ten objects this study covers are presented in Table 1. Nine of them are situated in the city of Lund in southern Sweden (55°42′N, 13°12′E) and one just outside. The climate in Lund (55°42′N, 13°12′E) is oceanic with relatively mild winters despite the northern location. Temperatures during winter are mainly around 0°C and summer 14-22°C; yearly precipitation approximately 600 mm, sparely as snow; prevailing wind direction W-SW.

The objects can, based on house type, be divided into two categories; apartment blocks (object 1-6) vs. row and semidetached houses (object 7-10). These two categories also represent two groups of age, the block houses are built 1963-1973, i.e. before the oil crisis, and houses in the other group are built during 1986-1995. Hence they are built according different building codes; the energy efficiency requirements got stricter step by step from 1973. Detailed information of building envelope construction was however not available. The apartment sizes in the first group are 1-4 rooms and kitchen with a total mean area of 69.3 m² and average room size of 26.2 m². The apartment sizes in the second group are 2-5 rooms and kitchen with a total mean area of 78.0 m² and average room size 26.6 m². More data about the studied building stock can be found in Dahlblom et al (2011).

The buildings are equipped with two-pipe hydronic heating systems with radiators. Nine objects are connected to district heating and the tenth has a natural gas fired boiler. Object 1-3 close to each other, share one substation, the other have one each and underground distribution pipes connecting the buildings in the object. The major part has exhaust ventilation systems with fans placed on the roof, two have balanced ventilation with heat recovery, see Table 1. The heating system was balanced and new thermostatic radiator valves were installed in all buildings before this study was performed. All buildings are subject to IMB of space heating. The set point indoor temperature is 21°C and the tenants can vary their indoor temperatures between 18 and 24°C with help of a thermostatic valve on each radiator.

TABLE 1. Basic data for the 10 objects.

Object number	1	2	3	4	5	6	7	8	9	10	Sum
Year built	1965	1965	1965	1973	1965	1963	1995	1989	1992	1986	
No of buildings	2	1	1	6	4	10	11	14	14	53	116
No of floors	2	9	9	2	3	3 – 4	1 – 2	2	1 – 2	1 – 2	1 – 9
No of apts	24	75	130	118	72	276	85	133	92	172	1177
- 1 RoK	0	21	31	34	0	28	0	0	0	0	114
- 2 RoK	2	7	29	41	18	48	22	56	37	74	334
- 3 RoK	9	25	68	31	36	144	34	46	35	53	481
- 4 RoK	13	22	2	12	18	56	26	22	10	36	217
- 5 RoK	0	0	0	0	0	0	3	9	10	9	31
No of rooms	83	198	301	257	216	780	265	383	269	496	3248
Heated area, m²	2096	5150	8017	7796	5908	19162	6705	10391	7786	12704	85715
Apt mean area, m²	87.3	68.7	61.7	66.1	82.1	69.4	78.9	78.1	84.6	73.9	72.8
Heating sup syst	DH/H	DH/H	DH/H	NG/S	DH	DH	DH	DH	DH	DH	
Vent type	EAH	EAH	EAH	EVS	EVS	EVS	EVS	EVS	BHR	EVS/ BHR	

DH = district heating, H = heat pump, NG = natural gas, S = solar collector, EAH = exhaust air heat pump, EVS = exhaust ventilation system, BHR = balanced ventilation with heat recovery.

3.2 Individual metering and billing of heating costs in the studied objects

The used principle for individual metering and billing (IMB) of space heating costs are based on achieved indoor temperature. The rent includes a "comfort temperature" of 21°C, for temperatures down to 18°C, tenants will be refunded and, vice versa, for temperatures up to 24°C tenants will be extra charged (LKF 2011). For the apartments in this study it will mean maximum of ±1200 SEK a year (135 € a year), to be compared with the mean rent 77000 SEK a year (8700 € a year) for the average apartment size.

3.3 Data collection and processing

The system for individual metering and billing of space heating registers indoor temperatures in all living-rooms and all bedrooms in the buildings. Thus, the number of sensors in each object is equal to the number of rooms in the object, see Table 1. The temperature sensor was calibrated during production to show a temperature reading with accuracy better than ± 0.15 °C (Sygel 2008). The temperature sensors are placed on internal walls, 3 – 4 m from the façade wall. They mainly measure the air temperature, but due to their position the difference between air temperature and operative temperature can be assumed to be small. Data from January until December 2010 was processed.

The system is supposed to register temperatures every 15th minute, which could have meant nearly 114 million readings for the studied period of 12 months. Unfortunately there have been data losses, partly due to interruptions in communication with the data server, partly due to scheduled interruptions during the summer. When communication is broken, the system inserts 21.0 °C, which leads to an overrepresentation of the temperature 21.0 °C. The retrieved data is processed by Matlab, excessive numbers of 21.0 °C readings are filtered and for shorter interruptions interpolated temperatures are inserted, longer are ignored. After this the available amount of data is 82 million temperature readings, i.e. 72 % average coverage over the year, and covering 79% of heating periods during 2010.

The living-rooms are generally about twice as large as the mean bedroom area, thus, when calculating apartment mean temperatures, living-rooms maybe should have been given double weight, which is not done here.

4. Results

4.1 Temperatures due to apartment size and building category

Figure 1 presents monthly mean indoor temperature and standard deviations for January-April and October-December 2010, i.e. months during heating periods, for varying apartment size divided on the two categories apartment blocks and row houses. Small variations in monthly mean temperature between apartments of different size can be observed, the same pattern is obtained for all months, e.g. apartment size 2 R&K in apartment blocks are always little colder than the others. The standard deviations do not differ much, but is somewhat larger for 5 R&K in the category row houses. There is also a seasonal variation, i.e. the indoor temperatures are not independent of outdoor temperature, and there are no cooling possibilities except free cooling by window airing.

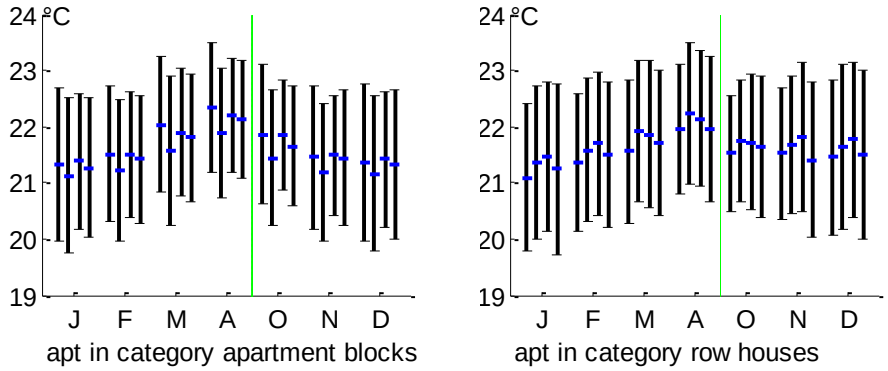

FIG 1. Monthly mean values and standard deviations for heating months on apartment level. Apartment size for category block houses are 1 R&K, 2 R&K, 3 R&K and 4 R&K respectively and for category row houses are 2 R&K, 3 R&K, 4 R&K and 5 R&K respectively.

4.2 Temperatures due to room type and building category

In Figure 2 and 3 the temperatures are further divided and, for the two categories, mean temperatures for living-rooms and bedrooms are separated. Broken down to room level, generally the living-rooms are warmer than bedrooms, the larger the apartment, the larger is maximal difference between living-rooms and bedrooms. About the same pattern can be observed in both categories and the pattern is kept for all month.

More detailed, on object level for apartment blocks, the mean values for the heating periods are between 21.3°C and 21.7°C with standard deviations in the range 1.11-1.34°C. Corresponding values on object level for row houses are mean temperatures between 21.5°C and 21.8°C with standard deviations in the range 1.22-1.40°C, i.e. objects in category row houses are warmer with larger standard deviations.

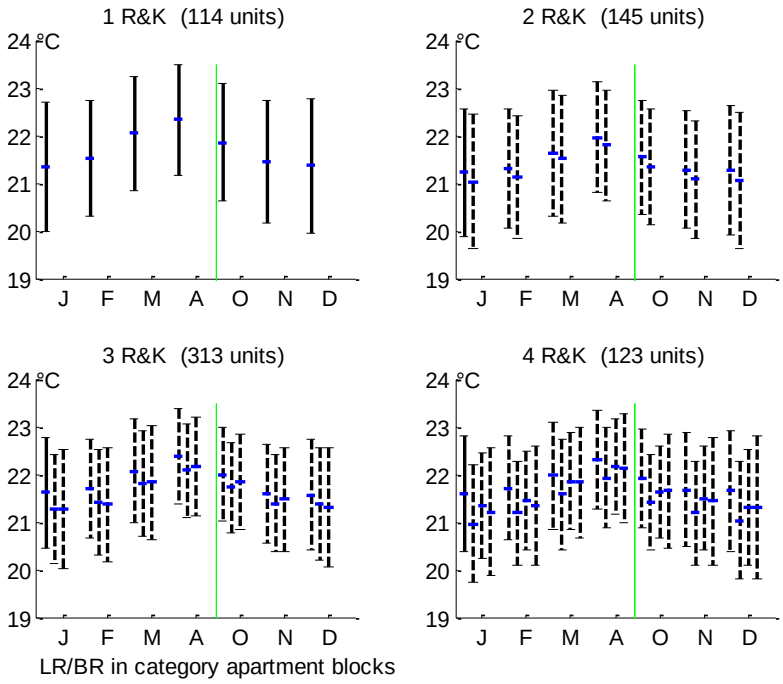

FIG 2. Monthly mean values and standard deviations for heating months on room level, divided on apartment size, for the category block houses. Solid lines are living-rooms, dashed lines bedrooms.

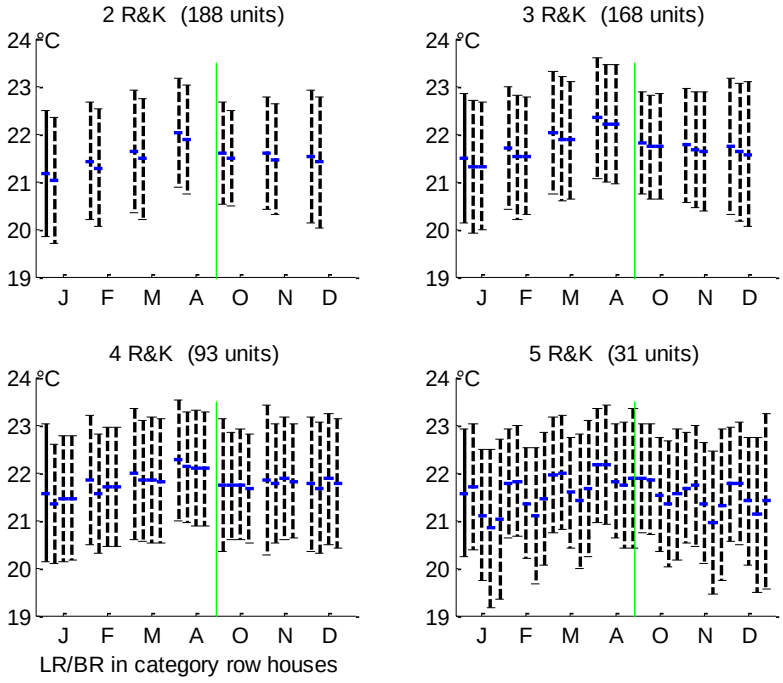

FIG 3. Monthly mean values and standard deviations for heating months on room level, divided on apartment size, for the category row houses. Solid lines are living-rooms, dashed lines bedrooms.

4.3 Temperature due to room type on object level

An even better overview of the differences between different rooms in apartments can be obtained from duration charts. Figure 4 – Figure 5 show, for two objects from each category, temperature differences between bedrooms and living-rooms, divided on apartment size. The scale on the x-axis is relative duration, i.e. compared to the total length of heating periods. The zero-line represents the mean temperature in the living-rooms in the object, the thick line represent the difference between mean temperature in living-rooms and bedrooms nr 1, the thin line d:o for the bedrooms nr 2, etc for broken and chain lines. The vertical lines show the breaking point when bedrooms mean temperature shift from colder to warmer than the living-rooms.

It can generally be noted that the temperature are lower in bedrooms, different bedrooms follow each other fairly well, with some exceptions, especially for larger apartments. Object 2 and object 8 are the two objects where the differences are largest, object 4 and 10 represent well the pattern in the other objects. Generally the differences are larger the larger the apartments are. From Figure 4 and Table 2 can for example be seen for object nr 2, apartment size 2 R&K that bedrooms nr 1 are colder than the living-rooms during approximately 35% of the heating periods (thick line). Accordingly, for apartment size 4 R&K, bedrooms nr 1 are colder during 94% of the heating periods, bedrooms nr 2 during 55% and bedrooms nr 3 during 27% of the heating periods (see Table 2). Remaining time the opposite situation is prevailing, i.e. bedrooms are warmer than living-rooms.

It is also possible to read out the largest differences in mean temperature, e.g. for bedrooms nr 1 in 4 R&K it is maximum 3°C colder, but only for a few hours. Temperature differences at 10th and 90th percentiles for the different bedrooms divided on apartment size and object are presented in Table 2, where also the relative duration for breakeven of bedroom and living-rooms temperature is reported. The temperature range between 10th and 90th percentile varies from 1.2°C to 3.1°C.

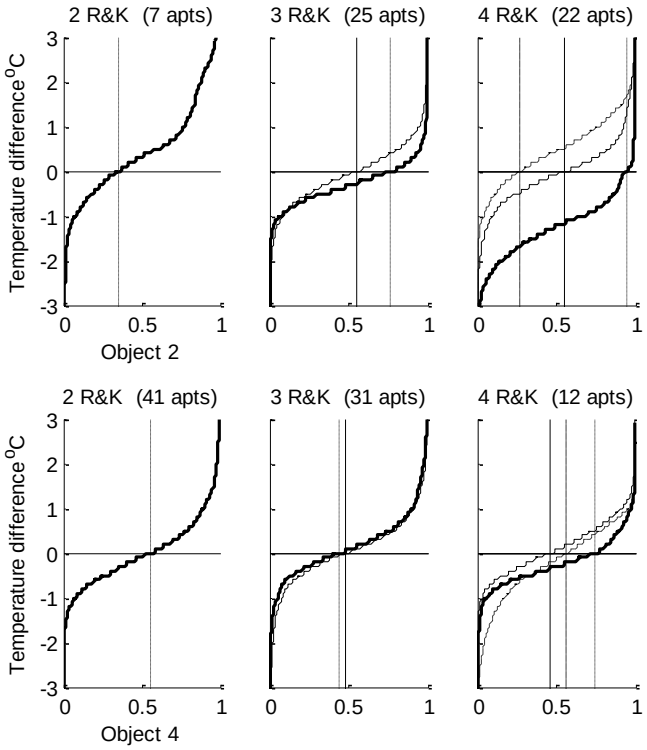

FIG 4. Duration for temperature difference between living-room and bedrooms; thick = bedroom 1, thin = bedroom 2 and broken = bedroom 3. Object 2 and 4, category apartment blocks.

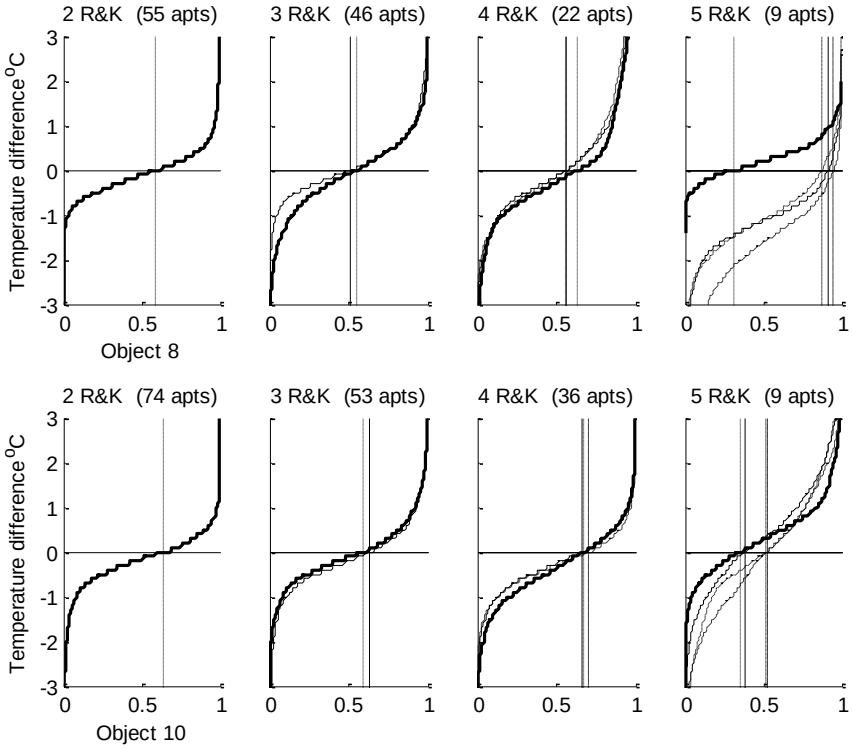

FIG 5. Duration for temperature difference between living-room and bedrooms; thick = bedroom 1, thin = bedroom 2, broken = bedroom 3 and chain = bedroom 4. Object 8 and 10, category row houses.

TABLE 2. Relative duration of equal temperature (dur_{dif0}) *and temperature differences at 10th and 90th percentiles* (ΔT_{p10} and ΔT_{p10}) *for bedrooms and living-room for different apartment size and object.*

size		2 R&K			3 R&K			4 R&K			5 R&K		
		dur_{dif0}	ΔT_{p10}	ΔT_{p90}	dur_{dif0}	ΔT_{p10}	ΔT_{p90}	dur_{dif0}	ΔT_{p10}	ΔT_{p90}	dur_{dif0}	ΔT_{p10}	ΔT_{p90}
obj	BR	-	°C	°C	-	°C	°C	-	°C	°C	-	°C	°C
2	1	0.35	-0.90	2.20	0.77	-0.90	0.30	0.94	-2.20	-0.30			
	2				0.55	-0.90	0.80	0.55	-1.00	0.80			
	3							0.27	-0.60	1.40			
4	1	0.55	-0.90	1.00	0.44	-0.60	1.00	0.74	-0.85	0.50			
	2				0.48	-0.85	0.90	0.46	-0.70	1.00			
	3							0.56	-1.40	0.80			
8	1	0.59	-0.70	0.50	0.55	-1.30	0.90	0.63	-1.30	1.80	0.31	-0.30	0.90
	2				0.51	-0.70	1.00	0.56	-1.20	1.90	0.92	-2.10	-0.10
	3							0.56	-1.30	2.30	0.95	-3.40	-0.40
	4										0.87	-2.20	0.20
10	1	0.64	-0.90	0.50	0.59	-0.90	0.90	0.67	-1.40	0.70	0.35	-0.70	1.30
	2				0.63	-1.00	0.80	0.66	-1.10	0.70	0.38	-1.20	2.20
	3							0.71	-1.10	0.50	0.52	-2.00	1.90
	4										0.52	-1.80	2.10

5. Conclusions and discussion

Based on the large data set it can be concluded that the indoor temperature for the category row houses are slightly higher than for category apartment blocks, though they have the same set point temperature, 21°C. The standard deviations are also slightly higher. In both categories apartment size 2 R&K has the lowest mean temperatures, all over the heating periods (Fig 2). Differences in mean temperatures between living-rooms and bedrooms, within apartments for all apartments in each category, are in the range 0.1°C – 0.5°C, larger for larger apartments (Fig 3).

The temperatures in bedrooms are generally below the temperature in living-rooms, but with large individual variations. The 10th percentile temperature difference is in the range -2.0°C to -0.6°C, with extremes on -3.4°C. Though the bedrooms are not always colder, the 90th percentile temperature difference is in the range 0.0°C to +1.9°C, with extremes on +2.3°C.

Only measuring one temperature in each apartment, as is done in some systems for IMB, may not give representative values. This study shows that deviations for single apartments in the dignity of 0.5°C, up to 0.75°C, can occur, if living-room temperature is used instead of apartment mean temperature.

The results can be beneficial as more refined temperature data for energy and moisture simulations in apartment buildings.

The floor plans and household size and composition are unknown and how these parameters affect the indoor temperatures have not been investigated. The fact that apartments of size 2 R&K have the lowest temperature may be explained by the number of person living in the apartment. Generally apartment of 1 R&K and 2 R&K are occupied only by one person, which means lower occupation density for 2 R&K, followed by lower heat gains from lighting, appliances etc.

6. Acknowledgements

This study was possible to complete thanks to the large data set provided by LKF.

References

Bøkenes, L., Mercer, J. B., MacEvilly, S., Andrews, J. F. & Bolle, R. (2009). Annual variations in indoor climate in the homes of elderly persons living in Dublin, Ireland and Tromsø, Norway. *European Journal of Public Health.* 21 (4) pp. 526-531.

Dahlblom, M. & Jensen, L. (2011). *Reglering av värmesystem i flerbostadshus med individuell värmemätning. Slutrapport för forskning med stöd från CERBOF* [Control of heating systems in apartment buildings with individual heat metering. Final report of research supported by CERBOF]. (Rapport TVIT—11/3006). Lund: Building Services, Lund University.

Kavgic, M., Summerfield, A., Mumovic, D., Stevanovic, Z.M., Turanjanin, V. & Stevanovic, Z.Z. (2012). Characteristics of indoor temperatures over winter for Belgrade urban dwellings: Indications of thermal comfort and space heating energy demand. *Energy and Buildings.* 47 (April 2012) pp. 506-514.

Lunds Kommuns Fastighets AB (2011). *Komfortvärme* [Comfort heat]. [Electronic] Available: http://www.lkf.se/ImageVault/Images/id_5605/scope_0/ImageVaultHandler.aspx [2012-06-20].

Sygel, K. (2008). *Interaktiva Tjänster. Systembeskrivning* [Interactive Services. System Description]. [Electronic] Available: http://www.compwell.biz/presentation/systemKS080505.pdf [2012-06-20]

Yohanis, Y.G. & Mondol, J.D. (2010). Annual variations of temperature in a sample of UK dwellings. *Applied Energy.* 87 (2) pp. 681-690.

SIMULATION STUDY OF SOLAR CHIMNEY ASSISTED SOLARIUM

[1]Afrooz Ravanfar, M.A.Sc.
[1]Zaiyi Liao, *Professor*, M.SC., Ph.D. (Oxford), Ph.D. (HKPU), PENG.
[2]Hua Ge, Assistant Professor,Ph.D., P.Eng.

[1]Ryerson University, Canada
[2]Concordia University, Canada

KEYWORDS: *Natural ventilation; Solarium; Solar chimney; Simulations*

SUMMARY:
The objective of this study is to develop a modelling method for optimizing the design of a Solar Chimney Assisted Solarium (SCAS) to maximize the ventilation rate in the solarium.
A thermal model is developed and implemented in SIMULINK to simulate the thermal response of the solarium combined with a solar chimney based on the first principle of thermal engineering. Thermal simulations are performed for critical summer days. The greenhouse air temperature and its ventilation rate with various geometrical configurations are calculated on the basis of solar irradiance intensity and ambient temperature. The preliminary numerical simulation results show that a solar chimney, combined with an appropriately inclined roof of a solarium, would be a better option for ventilation improvement in the solarium. The cross sectional air movement produced by a SCAS in an adjacent building maintains the interior condition within the adaptive and predictive comfort standard limits in about 85% of the month of July resulting in a potential cooling energy saving.

1. Introduction

The potential of a solarium system to reduce the temperature swing and heating demand of the house and achieve big savings in the operating costs of the building has been explored in several studies and was found to be satisfactory (Bastien and Athienitis, 2010; Mihalakakou 2000). Most of these studies, however, ignored the ventilation requirements of the solarium, despite the fact that Bryn and Schiefloe (1996) found that an improper design may cause overheating, resulting in an increase in the energy consumption of the building. Moreover, the solar chimneys can contribute to the production of the natural ventilation when they are applied to buildings (Marti-Herrero and Heras-Celemin, 2006). A solar chimney consists of one or more walls of a vertical chimney that are made transparent by providing glazed walls. The solar chimney contributes to building conditioning by using solar radiation to produce convective air flow. A study by Ekechukwu and Norton (1997) showed that the buoyancy force is proportional to the air density variation between the inside chimney air and outside air. Several studies on the ventilation of crop dryers and atriums have also been carried out. These studies demonstrate that using a solar chimney in conjunction with a highly glazed space can ensure stable natural ventilation performance even without encouragement of wind force (Afriyie et al., 2009 and Reuss et al. 1997). However, most of these studies were based on steady state conditions (Ong and Chow, 2003; Bassiouny and Koura, 2008). Studies subjected to dynamic climate conditions were mostly performed for typical buildings for hot and arid climates.

Research to date does not appear to consider the application of a solar chimney as the means of solar-driven natural ventilation in a solarium. To provide a more realistic assessment of the feasibility, benefits and potential improvement of this application, thermal and airflow simulations under dynamic conditions should be performed for solarium ventilated with solar chimney.

This paper develops a numerical model to investigate the dynamic performance of an inclined solarium combined with a solar chimney under transient conditions.

2. Physical model

In this study, a simple two-story residential building has been simulated with various solariums and solar chimney configurations. The simulated solarium is assumed to be located on the south side of a building in the region of Toronto, Canada with the glass wall facing south. A vertical solar chimney has been used in conjunction with inclined roof of the solarium to enhance the ventilation through the solarium. The schematic side section of the SCAS is presented in FIG. 1. As shown in this figure, air from the adjacent room in the house enters the solarium through a bottom inlet. This air is then heated up in the solarium and flows upwards and heated up further in the solar chimney. The air finally exits into the ambient, producing flow from living space to the outdoor. Uniform cross sections are assumed throughout the solar chimney in this application.

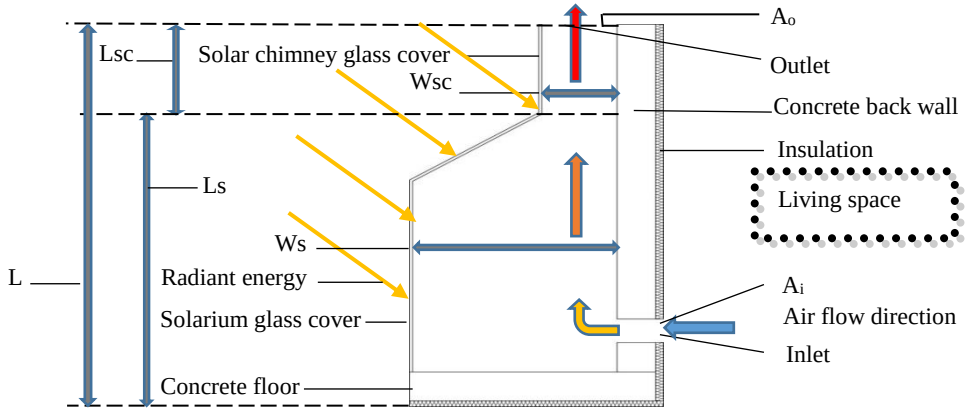

FIG. 1. Schematic side section of the SCAS: Ws and Ls are the width and height of the solarium (m); Wsc and Lsc are width and height of the chimney (m) and A_i and A_o are inlet and outlet areas of the openings (m^2)

The back walls in both chimney and solarium and the solarium floor are made of concrete, acting as thermal mass. Thermal inertia of these components converts them to a heat source for the air inside the SCAS when solar radiation is not available. These concrete elements are well insulated.

3. Mathematical model

3.1 Heating model

The energy balance method is employed to determine different temperatures inside the solarium and the solar chimney. FIG. 2 illustrates the physical heat exchange process in this model. Since the heat transfer in highly glazed spaces such as a solarium is a very complicated process, the following assumptions have been made to simplify the model.

- The air temperatures inside the solarium and the solar chimney are assumed to be well mixed and have values of T_{fs} and T_{fsc} at every time *n* respectively.
- The glass surfaces in the solarium and the chimney, concrete walls and floor in the chimney are also assumed to have constant temperature values of T_{gs}, T_{gsc}, T_{ws}, T_{wsc} and T_b respectively.
- Thermal inertia of the glass and the air inside the SCAS are negligible.
- Heat flow in the model is steady and one dimensional.
- The glass walls and roof are opaque to the long-wave radiation from thermal masses.

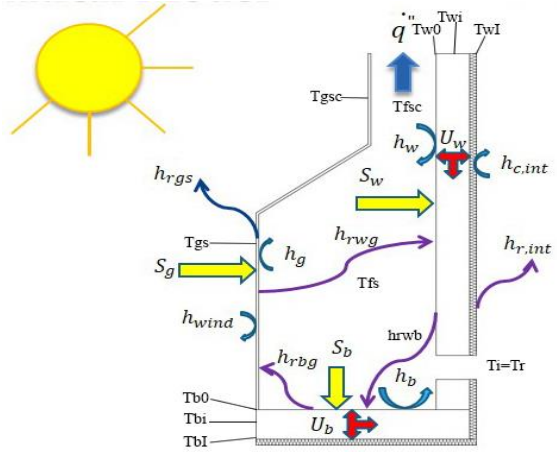

FIG. 2. Heat transfer process in the dynamic model of SCAC

In FIG. 2, S_g, S_w and S_b are solar radiation incident on the glass wall, concrete back wall and floor of the solarium respectively, h_{rwb}, h_{rwg} , h_{rbg} and h_{rgs} are radiative heat transfer coefficient between wall and floor, wall and glass cover, concrete floor and glass cover and glazing and the sky, h_w, h_b and h_g, is the convective heat transfer coefficients of wall, concrete floor and glass cover and air inside the solarium, $h_{c,int}$ and $h_{r,int}$ are convective and radiative heat transfer coefficients between wall and adjacent room, h_{wind} and h_{rgs} are convective and radiative heat transfer coefficients between glass cover and ambient due to the wind and sky respectively, U_w and U_b are the U values of the back wall and concrete floor, T_{wi} and T_{bi} are the temperatures of concrete wall and floor in each inside node, T_{W0}, T_{WI}, Tb_0 and T_{bI} are the surface temperatures of concrete wall and floor and T_i and T_r which have the same values are the temperature of adjacent living space which enters the SCAS.

3.1.1 Solarium and solar chimney concrete walls and solarium concrete floor heating models

The energy balance on the concrete wall of the solarium can be expressed as:

$$S_w + h_{rwb}(T_w^n - T_b^n) = h_{rwg}(T_w^n - T_g^n) + h_w(T_w^n - T_f^n) + U_w(T_w^n - T_r^n) + \rho C_p \frac{dT}{dt} \quad (1)$$

The energy balance on the concrete wall of the solar chimney is as follows:

$$S_w + h_{rwb}(T_w^n - T_b^n) = h_{rwg}(T_w^n - T_g^n) + h_w(T_w^n - T_f^n) + h_{rws}(T_w^n - T_{sky}^n) + h_{wind}(T_w^n - T_a^n) + \rho C_p \frac{dT}{dt} \quad (2)$$

Where T_{sky} sky temperature which is given by (Swinbank, 1963):

$$T_{sky} = 0.0552 T^{1.5} \quad (3)$$

Where T represents ambient temperature

The energy balance on the solarium concrete floor as follows:

$$S_b + h_{rbg}(T_b^n - T_g^n) = h_{rbw}(T_b^n - T_w^n) + h_b(T_b^n - T_f^n) + U_b(T_b^n - T_E) + \rho C_p \frac{dT}{dt} \quad (4)$$

The temperatures of each heat absorbing walls and the floor are characterized by 14 interior temperatures of T_{wi}, T_{bi} and 2 surface Temperatures of T_{w0}, T_{wI}, T_{b0} and T_{bI}. These are calculated employing conductive heat transfer equation in a solid.

3.1.2 Solarium and solar chimney fluid (inside air) heating models

The energy balance of the air inside the solarium and the solar chimney, considering the air being well mixed and having one unique temperature (T_f), has the following time dependant expressions:

Solarium:

$$h_g(T_f^n - T_g^n) + M(T_f^n - T_r^n) = h_w(T_{0w}^n - T_f^n) + h_b(T_{0b}^n - T_f^n) \quad (5)$$

Solar chimney:

$$h_w(T_{0w}^n - T_f^n) = h_g(T_f^n - T_g^n) + M(T_f^n - T_{fs}^n) \quad (6)$$

Where M is heat that leaves the solarium, can be expressed as:

$$M = \frac{\dot{m} c_f}{\gamma W L} \quad (7)$$

ṁ is the air volume that cross the solarium (kg/s) and has the following form ((Bansal et al., 1993 and Andersen, 1995)):

$$\dot{m} = C_d \frac{\rho_{fo} A_o}{\sqrt{1 + \left(\frac{A_o}{A_i}\right)^2}} \sqrt{\frac{2gL(T_{fsc} - T_r)}{T_r}} \quad (8)$$

c_f the heat capacity of the air

ρ density of the air (kg/ m^3)

v_o air velocity when leaving the chimney (m/s)

C_d coefficient of discharge of air channel, 0.57 (Flourentzou et al. 1997)

T_f mean fluid temperature ($\circ K$)

γ Coefficient of heat transfer to the air stream which flows out, Afriyie et al. (2011) found the value of 0.756 for the γ_{sc} and explored that for various configurations of the solarium γ_s is dependent on the tilt angle (ϴRad) and has the following form:

$$\gamma_s = -0.3856\theta^2 + 1.084\theta - 0.0844 \quad (9)$$

The heat transferred to the air stream inside the solarium can be rewritten as follows:

3.1.3 Solarium and solar chimney glass cover heating models

With assumptions stated in 3.1, the energy balances on the glass walls of the solarium and the solar chimney can be expressed as:

$$S_b + h_g(T_f^n - T_g^n) + h_{rwg}(T_{0w}^n - T_g^n) + h_{rbg}(T_{0b}^n - T_g^n) = h_{bwind}(T_g^n - T_a^n) + h_{rgs}(T_g^n - T_{sky}^n) \quad (10)$$

$$S_b + h_g(T_f^n - T_g^n) + h_{rwg}(T_{0w}^n - T_g^n) + h_{rbg}(T_{0b}^n - T_g^n) = h_{bwind}(T_g^n - T_a^n) + h_{rgs}(T_g^n - T_{sky}^n) \quad (11)$$

3.1.4 Heat transfer coefficients

Convective heat transfer coefficient due to the wind can be calculated using the following correlation (Palyvos, 2008):

$$h_{wind} = 7.4 + 0.4V \quad (12)$$

Where V the wind velocity (m/s)

According to Duffie and Beckman (1980) and Incropera et al. (2007), the convective heat transfer coefficients between air and wall, glass and solarium floor can be calculated using the following equations:

$$h_i = \frac{Nu \cdot k_f}{L_i} \tag{13}$$

Where i represents glass, wall and floor

k_f thermal conductivity of air (W/ m k)

Nu Nusselt number, has the following mathematical forms (Incropera and DeWitt, 1996):

Laminar flow, $Ra<10^9$

$$Nu = 0.68 + \frac{0.67Ra^{1/4}}{\left[1+(0.492/\mathrm{Pr})^{9/16}\right]^{4/9}} \tag{14}$$

In case of turbulent flow when $Ra>10^9$

$$Nu = \left[0.825 + \frac{0.387Ra^{1/6}}{\left[1+(0.492/\mathrm{Pr})^{9/16}\right]^{8/27}}\right]^2 \tag{15}$$

Ra Rayleigh number

Pr Prandtl number

α thermal diffusivity of air

β coefficient of expansion of air (1/K)

μ_f dynamic viscosity (kg/ m s)

g gravitational constant (m/s)

Physical properties of the air that were introduced by Ong and Chow (2003) have been used in the study. The convective heat transfer coefficient between collecting wall and the living space, $h_{c,int,}$ can be calculated as:

$$h_{c,\mathrm{int}} = 1.31\left|T_w - T_r\right|^{1/3} \tag{16}$$

The radiative heat transfer coefficient between back wall and the glazing and the linving space in both the solar chimney and the solarium can be calculated (Marti- Herrero and Heras-Celemin (2006):

$$h_{rwg} = \frac{\sigma(T_w + T_g)(T_w^2 + T_g^2)}{\frac{1}{\varepsilon_w} + \frac{1}{\varepsilon_g} - 1} \tag{17}$$

$$h_{r\,\mathrm{int}} = \frac{\sigma(T_w + T_r)(T_w^2 + T_r^2)}{\frac{1}{\varepsilon_w} + \frac{1}{\varepsilon_r} - 1} \tag{18}$$

Where σ is the Stefan–Boltzmann constant, $\sigma = 5.67\times10^{-8}$

The radiative heat transfer coefficients between solarium concrete floor with the glass cover and concrete, based on Afriyie et al. (2011) are expressed as follows:

$$h_{rbi} = \frac{\sigma}{A_b}\frac{(T_b + T_i)(T_b^2 + T_i^2)}{\frac{1-\varepsilon_b}{\varepsilon_b A_b} + \frac{1-\varepsilon_i}{\varepsilon_i A_i} + \frac{1}{A_b}} \tag{19}$$

The following equation represents the coefficient of radiative heat transfer between glass cover in the solarium and the solar chimney and also chimney back wall and the sky (Marti- Herrero and Heras-Celemin, 2006):

$$h_{ris} = \sigma(T_i + T_{sky})(T_i^2 + T_{sky}^2) \tag{20}$$

4. Results and discussion

A thermal simulation using MATLAB/SIMULINK was performed for the critical summer days (15-18 July) to predict the thermal performance of the greenhouse and the solar chimney using the actual weather data for Toronto (FIGs. 3-4). The results are shown in FIGs 5-8.

As shown in FIG. 5 the fluid (inside air) temperature of the chimney is notably higher than that of the solarium and fluctuates more than the solarium air temperature. The solarium fluid temperature stays at around the maximum ambient temperature over the period.

FIGs. 6-8 show that the inertial temperature shift is around 2-5 hours for the internal and external surfaces respectively. This number rises up to 8 hours delay for the exterior wall surface to reach its maximum temperature compared to the highest ambient temperature. The solarium floor has the highest interior temperature difference with the ambient temperature. This temperature variation follows almost the same pattern as the chimney air temperature.

FIG. 9 shows that the flow rate was higher than 0.07 kg/s during the whole simulation period. The flow rate was the lowest around the sunrise (5 am). The air flow rate reaches its maximum around 1 pm. As the FIGs 6-8 clearly show the temperature difference between the inner surfaces of chimney concrete wall and the solarium concrete wall and floor compared to ambient temperature reaches around 5, 5 and 15k at the midnight of July 15 producing a mass flow rate of around 0.1 kg/s or 1.2 ACH for the 300 m^3 adjacent residential building. Ventilation standards require a minimum of 3 ACH for residential buildings (ASHRAE, 2003). Therefore, it can be concluded that the investigated SCAS shall be able to provide more than one third of the desired ventilation in the attached building even with the lowest ventilation it produces.

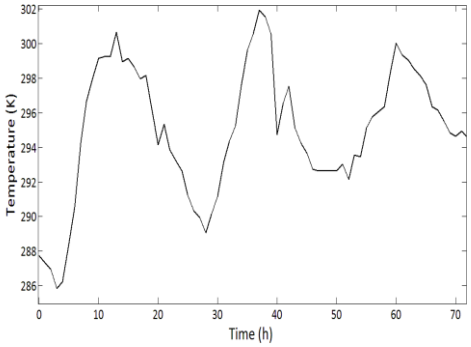

FIG. 3. Toronto weather data (ambient temperature) for July 15-18.

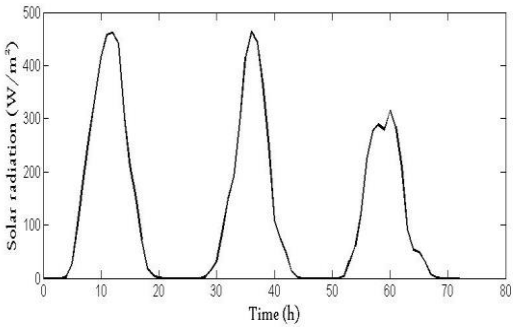

FIG. 4. Toronto weather data (solar radiation on south faced vertical surface) for July 15-18.

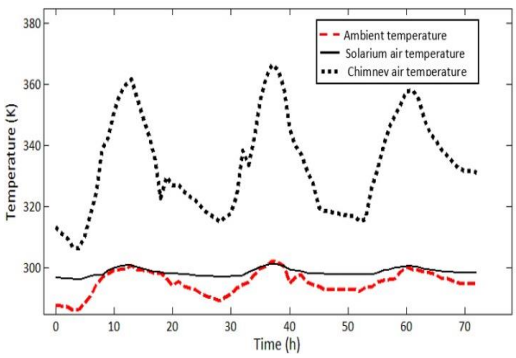

FIG. 5. The SCAS inside air temperature profile

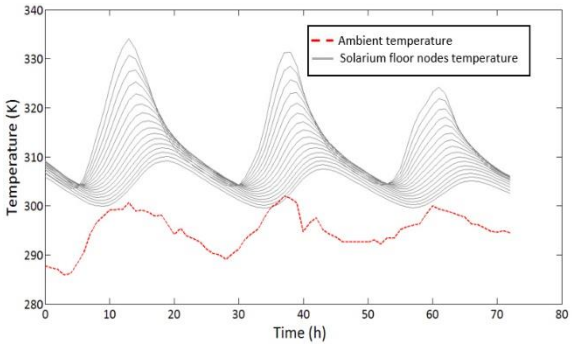

FIG. 6. The Solarium concrete floor nodes temperature profiles

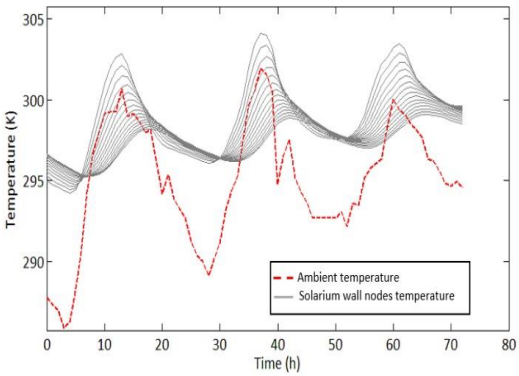

FIG. 7. The Solarium concrete wall nodes temperature revolution

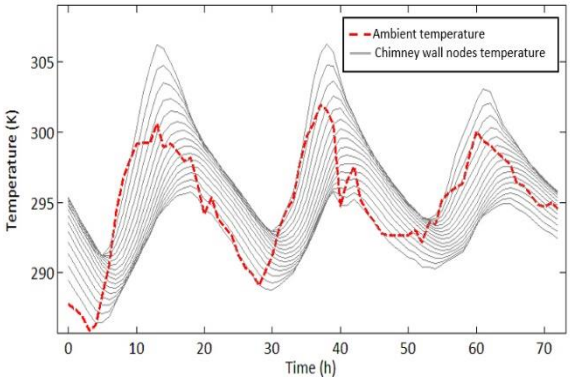

FIG. 8. The Solar chimney concrete wall nodes temperature revolution

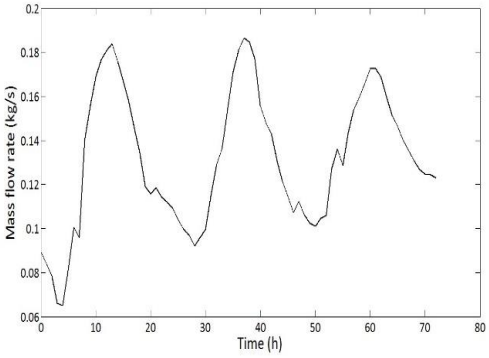

FIG. 9. The mass flow rate that crosses the SCAS for July 15-18

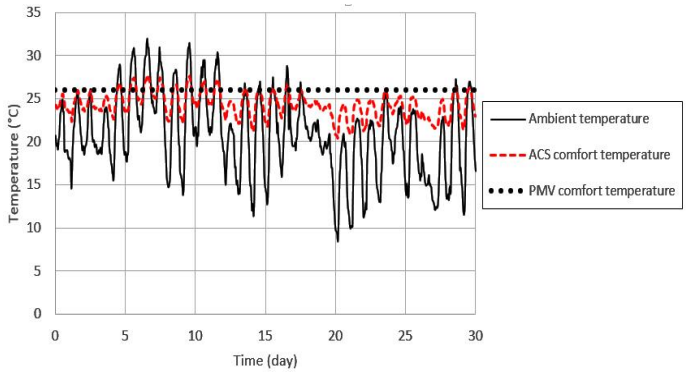

FIG. 10. Ambient temperature, adaptive and predictive mean comfort temperatures in the month of July

Moreover, Brager and de Dear (2002) compared naturally ventilated buildings with HVAC buildings. The study showed that occupants of naturally ventilated buildings become adapted to a vast range of air conditions close to outdoor air conditions. The researchers proposed the adaptive comfort standard (ACS) as an alternative to the predicted mean vote (PMV) method in ASHRAE standard 55 (2010). The study showed that higher air speed in occupied zone can lead to enhancing air quality by offsetting the enthalpy effect.

As can be seen in FIG. 10 the outdoor temperature for the month of July in Toronto is within the range of both adaptive (ACS) and predictive (PMV) mean comfort temperatures 85.7% of the time. Hence the proposed residential building interior condition is able to be maintained within ACS limits around 85% of the time during the warmest month of the year by natural means.

5. Conclusions

This study investigated the performance of a solar assisted ventilation system in a solarium attached to a residential building in Toronto at the initial design stage. Unlike the existing simulation process in the previous studies on ventilation of crop dryers and atriums, the actual weather data of Toronto was used in the simulation model. Simulation results showed that the 24cm concrete walls and floor provide up to 5-hour delay to reach up its peak temperature resulting in a temperature variation up to 15K and producing natural ventilation when solar radiation no longer exists. With the cross sectional air movement produced by a SCAS in an adjacent building, interior condition is able to be maintained within the ACS limits for about 85% of the time in month of July resulting in a potential cooling energy saving of 85% that would otherwise be used by an air-conditioner. The dynamic model proposed for the SCAS establishes a reliable and effective methodology for evaluating the performance of the SCAS, which can be a reliable reference for future experimental investigations and designing process.

References

Afriyie, J.K., Rajakaruna, H., Nazha, M.A.A., Forson, F.K., 2009. Experimental investigations of a chimney-dependent solar crop dryer, Renewable Energy 34(1): 217-222

Afriyie, J.K., Rajakaruna, H., Nazha, M.A.A., Forson, F.K., 2011. Simulation and optimisation of the ventilation in a chimney-dependent solar crop dryer, Solar Energy 85: 1560–1573.

Andersen, K.T., 1995. Theory for natural ventilation by thermal buoyancy in one zone with uniform temperature, Building and Environment 38: 1281–1289

ASHRAE, 2003. ASHRAE Standard 62.2: Ventilation and Acceptable Indoor Air Quality in Low-Rise Residential Buildings, American Society of Heating, Refrigeration and Air Conditioning Engineers Inc., Atlanta.

ASHRAE, 2010. ASHRAE Standard 55: Thermal Environmental Conditions for Human Occupancy, American Society of Heating, Refrigeration and Air Conditioning Engineers Inc., Atlanta.

Bansal, N.K., Mathur, R., Bhandari, M.S., 1993. Solar chimney for enhanced stack ventilation, Building and environment 28: 373–377.

Bassiouny, R. and Koura, N.S.A. 2008. An analytical and numerical study of solar chimney use for room natural ventilation, Energy and Buildings 40:865-873.

Bastien, D., Athienitis, A.K., 2010. Analysis of the Solar Radiation Distribution and Passive Thermal Response of an Attached Solarium/Greenhouse, International High Performance Buildings Conference.

Brager, G. S., de Dear, R. J., 2002. Thermal comfort in naturally ventilated buildings: revisions to ASHRAE Standard 55, Energy and Buildings, 34 (6): 549-561

Bryn, I., Schiefloe, P. A., 1996. Atrium models for the analysis of thermal comfort and energy use: a report of task 12, SINTEF Energy, Indoor Environment Technology, Trondheim.

Duffie, J.A., Beckman, W.A., 1980. Solar engineering of thermal processes, Wiley, New York.

Ekechukwu, O. V., Norton, B., 1997. Design and measured performance of a solar chimney for natural circulation solar energy dryers, Renewable Energy, 10 (4): 81–90

Flourentzou, F., Van der Maas, J., Roulet, C., A., 1997. Natural ventilation for passive cooling: measurement of discharge coefficients, Energy and Building 27: 283-292.

Incropera, F.P., DeWitt, D.P., 1996. Fundamentals of Heat and Mass Transfer, fourth ed. John Wiley, New York.

Incropera, F.P., De Witt, D.P., Bergman, T.L., Lavine, A.S., 2007. Introduction to Heat Transfer, fifth ed. John Wiley & Sons Inc., Hoboken, New Jersey.

Marti-Herrero, J., Heras-Celemin, M.R., 2006. Dynamic physical model for a solar chimney, Solar Energy 81: 614-622.

Ong, K.S., Chow, C.C., 2003. Performance of a solar chimney, Solar Energy 74: 1-17.

Palyvos, J.A., 2008. A survey of wind convection coefficient correlations for building envelope energy systems' modeling, Applied Thermal Engineering 28: 801-808.

Reuss, M., Benkert, S.T., Aeberhard, A., Martina, P., Raush, G., Rentzell, B.V., 1997. Modelling and experimental investigation of a pilot plant for solar wood drying, Solar Energy, 59 (4–6): 259–270

Swinbank, W.C., 1963. Long wave radiation from clear skies, Q.J.R. Meterol, Soc. 89: 339.

Tiwari, G. N., Din, Yadav, Y. P., Lawrence, S. A., 1988. Performance of a solarium: an analytical study. Building and Envinroment, 26: 203–215.

Perceived and measured indoor climate in new-family buildings including identifying technical deficiencies

Birgitta Nordquist, Assistant Professor [1]
Victor Fransson, M.Sc. [1]
Ola Lindberg, M.Sc. [1]

[1] Building Services, dept. of Building end Environmental Technology, Faculty of Engineering, Lund University, Sweden

KEYWORDS: *indoor climate, apartments, questionnaire, measurements, occupants, window opening, technical deficiencies*

SUMMARY:
When new buildings are constructed the indoor climate for the first period may differ from the one after some years due to various factors, for example may the emissions from the building materials be higher, possibly affecting the air quality, and the balancing of the technical systems; the mechanical supply and exhaust system and heating may not be completely finished. The perceived indoor climate in new-multi family buildings, with the aim of low-energy use and good indoor climate, has been examined by questionnaires when the buildings were new. In this follow-up study the same questionnaire has been performed after some years. Measurements of the indoor climate and the performance of the technical systems have also been made in some apartments. The objectives are to compare the resident's experience of indoor climate after some years of occupancy with when the buildings were new and to examine indoor climate and aspects influencing this after some years of occupancy. One objective being studied is the window opening in the apartments and factors related to this. No large difference in experience is seen after some years. A majority of the respondents open their windows during the heating season for rather long time periods and daily or almost every day. It was found that the resulting indoor climate is a complex interaction between the technical systems, the design of the building envelope and the behavior of the occupant. Several deficiencies in all this three areas have been identified and suggestions on possible improvements are included.

1. Introduction

When new buildings are constructed the indoor climate for the first period may differ from the one after some years due to various factors, for example may the emissions from the building materials be higher, possibly affecting the air quality, and the balancing of the mechanical supply and exhaust system respectively heating system may not be completely finished. The perceived indoor climate in new-multi family buildings in Malmoe, built with the aim of low-energy use and good indoor climate, has been examined by questionnaires in a study some years ago (Hansson, Nordquist, 2010).

The main findings were that the measured energy demand was higher than the calculated one and that the indoor climate overall was experienced as satisfying. Some questions were however identified to be worth looking into and ware also shown representative for new-built apartment buildings in general according to the nationwide study BETSI (Boverket, 2009). A follow-up study was therefore decided due to the possibility of gaining more knowledge on new-built apartment buildings both in respect of the outcome of energy use and experience of indoor climate.

One of the questions that were identified was the astonishing large amount of window opening reported by the residents. 59% reported that they aired all day/night or for some hours. The amount was in the same order of magnitude as in BETSI; 69%. 57% reported that they air daily or almost

every day during heating season, the corresponding amount in BETSI was 61%. Frequent airing has also been reported in other studies (Sandberg & Engvall, 2009). In the follow-up study the window opening was therefore one factor that was focused on as this influence both the indoor climate and the energy use. The frequent airing is made in these new-built buildings in which a vast majority is ventilated with modern mechanical supply and exhaust ventilation. In the first study it was also seen that several experienced a hot indoor climate especially in summer-time which also is experienced in general according to the BETSI study.

By both asking for the experience of the residents and also performing measurements of the real indoor climate and performance of the ventilation system it is possible to connect the experience of the residents to the real indoor climate in the apartments and aspects influencing this including the behaviour of the occupants. Other studies concerning window opening and occupant behavior have been made by for example Berge et al (2013).

The objectives of the present study are to compare the occupants experience of indoor climate after some years of occupancy with when the buildings were new and to examine indoor climate after some years of occupancy.

The results of the questionnaire concerning the window opening behaviour are more thoroughly presented in another paper (Fransson et al, 2014). This includes reasons for opening the windows respectively closing them. It could be mentioned that the reasons for opening the windows includes both reasons for a need of improving the thermal climate respectively the air quality. This paper focuses on the interaction and studying the conditions in individual apartments.

2. Method

The experience of the occupants has been studied by standardized and validated questionnaires, called the “Stockholms-questionnaire” and used by the city of Malmoe (Miljöbyggprogram Syd, 2009). To be able to compare the overall experience with the nationwide study BETSI (Boverket, 2009) two additional questions have also been added. In this follow-up study the same questionnaire has been performed after some years. Questions focusing on the specific issues have been added. The questionnaires were distributed to individual postboxes to each apartment in the staircases in the beginning of March 2012. Twelve different building owners and 32 staircases are included in the study. The residents should put their answered questionnaires in a paper box next to the postboxes in the staircases at the latest on the end of March 2012. All paper boxes were then gathered.

Based on the answers from the questionnaires a selection of nine apartments were chosen in which window opening for long time; window open for some hours to all day/night was reported. The residents were contacted and almost everyone who was asked on the phone agreed to participate. The selection included both rental apartment and condominiums and all existing combinations of mechanical ventilation systems; fans located central respectively fans and ventilation units located inside the apartments. A majority was ventilated with mechanical supply system but also one system which supplied the outdoor air directly to the rooms was included.

Measurements of the indoor climate for winter conditions and the performance of the technical systems have then been made in these apartments in 2013. The indoor climate and the factors influencing it have been studied both quantitative respectively qualitative. Measurements includes for example air flows, operative temperature (no airing, 0,1, 0,6, 1,1, 1,7m), throw, air velocity and focuses in the thermal, the hygienically climate and the ventilation system. Measurement equipment included SWEMA300 with SwemaFlow 125, SWEMAs ISO7730 for operative temperature and for long-term Onset HOBO loggers.

3. Results

3.1 Answers to questionnaire

The overall experience of the indoor climate during heating season is shown in Figure 1. The answers from the 256 people respondents are divided in two groups; one (2012) with the same buildings as in 2010 and one (new 2012) for the two buildings that were not included in the first study.

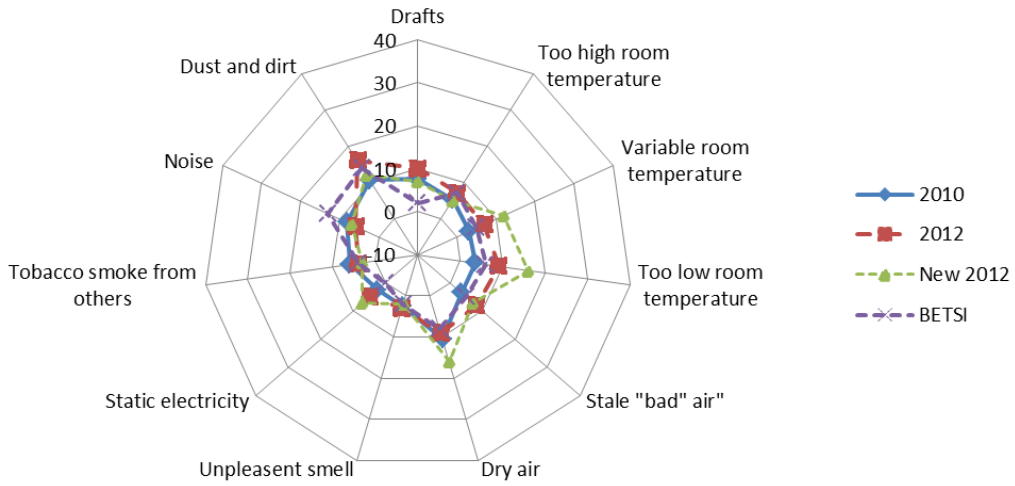

FIG 1. Proportion of the people; in percentage, who has answered "Yes, often (every week)" on the question "Have you during the latest 3 months felt bothered by one or some of the following factors in your home?"

Six of the factors are experienced of a somewhat higher percentage after some years; draft 10% (8% before), too high room temperature 7% (5%), variable room temperature 7% (3%), too low temperature 9% (4%), stale bad air 8% (4%) and static electricity 5% (3%), the difference is however rather small. One factor dust and dirt has increased somewhat more; 16% compared to 11% before. Three factors are reduced, dry air is reduced to 9% from 11%, tobacco smoke from others to 4% from 6%; and noise to 6% from 8%; also a small difference. The amount is in the same order of magnitude as the percentage in the nationwide study BETSI. Another measure that can be valid to compare with is the portion of people which are dissatisfied. If maximum 10% are dissatisfied then the indoor climate can be seen as very good (EMTF, 2013). For all factors but dust and dirt this is fulfilled.

The indoor climate is experienced somewhat less satisfying in the two new buildings. Four of the factors exceed the 10% guideline; variable room temperature (12%), too low room temperature (16%), dry air (16%) and dust and dirt (12%).

TABLE 1. Answers for two questions regarding window opening behaviour

Reported percentage	How often do You usually air during the heating season? *Daily +almost every day*	When You air do You usually air by? *Having open all day/night + Having open some hours*
2010	57%	59%
2012	53%	55%
BETSI	61%	69%

The amount of the respondents including also the newcomers which report that they apply window opening are shown in Table 1. The opening of windows have decreased somewhat.

3.2 Apartments

The results presented in this paper focuses, due to limited space, on some of the findings in the individual apartments and factors that stands out and deviates from the expected values as deficiencies and combines quantitative and qualitative data. In all apartments presented, window opening are reported to take place for long time periods except in building 4 in which airing are made for fully one hour each day. More extensive and complete results are presented in (Fransson, Lindberg, 2013) and (Karlsson, Nordquist, 2014).

Building 1, Mechanical supply and exhaust ventilation, central fan

Apartment 1
The resident reported that it will become too hot in the bedroom when going to sleep if the window in the bedroom isn´t opens all day. The residents assess a need of having relatively cool in the bedroom. The bedroom has *large windows facing west, no solar shading*, the whole apartment *only facing one west façade*. The radiator is working in the bedroom and is set on medium heat emittance by the thermostatic valve on the radiator in the hydronic system. Operative temp: 24,3-25,1°C in living room and 23,4-24,1 in bedroom. The Public Health Agency of Sweden recommends 20-23°C in homes. Measured air flow 18,0 l/s (Building code requirement: 21,3 l/s).
Comment: Both the plan of the apartment, the lack of solar shading and the behaviour of the resident; not reducing the heat from the radiator, contributes to the relatively high temperature during winter.

Building 2 Mechanical supply and exhaust ventilation, apartment unit, plate-heat exchanger (one of the added buildings)

Apartment 2
The residents report that it will become too hot in the living room and in the bedroom if the windows aren´t open. The apartment has an open plan with kitchen and living room as one large room. The living room has *very large windows facing south, no exterior solar shading*, the whole *apartment only facing south*. The solar shading consists of blinds positioned inside the room which means that the heat enters the room. Measured supply air flow 19,3 l/s. Supply air flow requirement according to building regulation 19,6 l/s. The ventilation unit is situated above the stove in the kitchen. The air flow can be varied by a control handle outside the unit. The handle is put on the mode intended for when no people are present (reduced air flow to save energy). When asking the resident why this mode is chosen the explanation is noise. The ventilation unit located inside the apartment creates *too high noise level* when the mode for being at home is used, so this mode is not possible to have when at home. The residents are bothered both in the living room but mostly in the bedroom in which the experienced noise level is far too high when going to sleep. The mode being at home fulfilled the building code in terms of air flows, however not being in operation. Operative temp: 23,7-24,8°C in living room.
Comment: The design of the building envelope, the location to the south and only one façade may contribute to create high temperatures. The air flow via the ventilation system is not really fulfilling the building code. This is explained by that the setting is wrong. The combination of the several identified deficiencies can contribute to an insufficient indoor climate both in terms of thermal and hygienically conditions.

Apartment 3

The resident reports insufficient air flows and a need of window opening in the bedroom. The measured supply air flow in the bedroom is 7,5 l/s. The air flow should be 4 l/s person according to the Public Health Agency of Sweden who are responsible for regulations for homes. Almost all nights

the bedroom is occupied by two adults and one 6-year old child. The requirement is accordingly 12 l/s in this room when three people are present. If two adults are present, which is the probable intended number of people, the requirement is 8 l/s.
Comment: The *air flow* in the bedroom via the ventilation system is *not fulfilling* the *regulation* for the number of people present. The air flow requirement for day time in an office or in a school would for the same number of occupants be 26,6 l/s in this size of room; almost 4 times more than the measured one.

Apartment 4

The residents report a need of having the window open in the bedroom during the whole night. They assess a need of having cool in the bedroom. They have closed the thermostatic valve at the radiator in the bedroom, which is situated to the west and keeps the door closed all the time. The whole apartment is situated to the south and west and they experience a too hot indoor climate especially in summer time. No exterior solar shading is installed. Operative temp: 24,7-24,8°C in living room. The ventilation unit is located above the stove. The control for the supply air heater after the heat exchanger is controlled by a very small circle located inside the equipment. This control cannot be found in the instructions which the residents have looked into several times. For all the three apartments the plate-heat exchanger should be replaced by a component for summer conditions, a sort of by-pass. All these components are reported by another resident to be in the cellar and not in use during summer time.

Comment: It is not clear how the heater and the plate-exchanger works and there could be a possibility of having the heat exchanger and the heater working all the year including the summer if this control is not adjusted.

Building 3 Mechanical supply and exhaust ventilation, apartment unit, rotary heat exchanger

Apartment 5

The residents report that they feel a need to have the windows open in the bedroom. The resident assess a need of having cool in the bedroom. Operative temp: 23,5-25,0°C in living room. The ventilation unit is located inside the apartment in the bathroom between the bedrooms. The air flow can be varied by a control panel outside the unit. The operating mode is the one intended for when no people are present – away-mode. The residents report that the reason for having this mode in operation is *noise*. The ventilation unit located inside the apartment creates *too high noise level* when the mode for being at home is used, that this mode is not possible to have when at home. The measured supply air flow was 23,8 l/s (Building code: 37,5 l/s). The throw in the bedroom (0,2 m/s) is 0,9 m, covering about 0,5 of the distance of the room intended to be covered.
Comment: *The air flow via the ventilation system is not fulfilling the building code*. This is explained by that the setting is wrong. The measured *throw is too short*, a general guideline value is that is should cover 0,75-1 of the room distance if assuring sufficient mixing conditions in the room. The fact that the throw is too short can contribute to an insufficient air movement and there by worse air quality in the room.

Apartment 6

The residents report that they feel a need to have the balcony door open. In the 110 m^2 apartment the air flow according to building regulation should be 38,5 l/s. Measured supply air flow were 25,2 l/s. The air flow of the ventilation unit located inside the apartment in the washing room/bathroom is controlled by a control panel located outside the unit. The mode in operation is the "away-mode", by which the air flow should be reduced when people are not at home. The resident answers when asking why this mode is in operation that "oh I don´t know anything about the ventilation system, I never change the setting."

Comment: The air flow via the ventilation system is not fulfilling the building code due to the wrong setting. The air flows has been significantly below the building code in this apartment who residents includes two adult and two small children.

Building 4 Mechanical supply and exhaust ventilation, apartment unit, rotary heat exchanger

Apartment 7
The residents report that they experience that it is too hot in the apartment. All thermostatic valves are closed on the radiators but it will become too still too hot. The bedroom directed to the north is aired before going to sleep and closed during night and the bedroom door is kept closed all time. They report a desire to open windows in the other rooms which are directed to the south but don´t, due to dirt which enters the apartment because of building activity in the area. No exterior solar shading to the south is applied. Operative temp: 23,4-24,1°C in living room. The apartment is 99 m^2; air flow according to building regulation: 34,7 l/s. Measured supply air flow is 14,4 l/s. The supply air flow requirement to the bedroom is 8 l/s and the measured one is 3,7 l/s. The ventilation unit is situated above the stove in the kitchen. The air flow can be varied by a control handle outside the unit. The display has no clear explanation for the different modes. The handle is put on the lowest mode which is found to be intended for when no people are present (reduced air flow to save energy). The resident have chosen this mode due to noise, they have no knowledge that this mode is intended for non-present situation. The moisture supply was measured to be in average 3,4 g/m^3 in the living room and 3,2 g/m^3 in the bedroom during two weeks which exceeds the recommended maximum value 3 g/m^3 by the Public Health Agency of Sweden.
Comment: The air flow via the ventilation system is not fulfilling the building code for the apartment and not fulfilling the requirement in the bedroom. This is explained by that the setting is wrong. The moisture supply is too high in the apartment which has a local rotary heat exchanger.

Building 5 Mechanical exhaust ventilation, apartment unit

Apartment 8
The resident report a need for having open the windows in both bedroom and living room and that it will become too hot in living room and bedroom if the windows aren´t open. The resident assesses a need of having cool in the bedroom. The apartment has an open plan with kitchen and living room as one large room. The living room has very large windows facing south, *no exterior solar shading*, the whole *apartment only facing south*. The solar shading consists of blinds positioned inside the room which means that the heat enters the room as in other apartments without exterior shading. The radiators are always closed also during winter. The operative temp: 21,7-23,5°C in living room how-ever the windows have been opened for a long time before the measurement.
Comment: Both the plan of the apartment and the lack of exterior solar shading con contribute to a thermal climate perceived by the resident to be too hot.

Apartment 9

The resident report a need for having open the windows in both bedroom and living room and a need of fresh air. The operative temperature is measured to 23,4-24,8°C in living room. The radiators are fully open in the living room and reduced in the bedroom. The resident smokes at home.

Comment: Both the relatively high operative temperature and the smoke may lead to a need of opening the windows.

4. Conclusions

The overall experience of the indoor climate during heating season reported by the respondents can be concluded to be satisfying. The amount which experience inconvenience have been somewhat increased for most of the indoor climate factors after some years of operation, however no large difference

can be concluded and the levels are satisfying for all factors but dust and dirt. The residents in the two new buildings report however a somewhat less satisfying indoor climate. There is still ongoing building project in the area which can contribute to the reported experience of dust and dirt. The suspected decrease in people experiencing inconvenience after some years is not met for most factors for the present buildings. One relevant parameter to this *dry air* is however reduced, but in a small amount. The conclusion is drawn that there is no significant difference in experience after some years.

The amount of airing has been somewhat reduced but no large difference can be seen. It is concluded that a majority of the respondents still open their windows frequently during heating season after some years of operation.

The measured operative temperature is rather high during winter conditions and the air flows are not fulfilling the codes in six of nine apartments, several of them significantly.

5. Discussion

There are several interesting results that can be discussed. It is interesting and a challenging matter that a majority of the people feel a need to apply window opening in the apartments which are ventilated with modern mechanical supply and exhaust systems.

Several deficiencies, some technical, have been identified in the limited number of studied apartments for example; too low air flows, no or not sufficient solar shading and perceived noise level. Some of the deficiencies emerge in the interaction of the users; reducing the air flows due to experienced noise, design of interface which leads to not understanding how to control the system. All of these can contribute to create an unsatisfying indoor climate in different ways and contribute to a need for increasing the air flow to the apartment; both for thermal and/or air quality reasons, which is done by window opening. The factors cover several areas; the building envelope, the building services systems and the interaction with the residents. The resulting indoor climate is a complex interaction between all these three areas. As several parameters can contribute to the total resulting indoor climate; all these factors must be observed and functioning. This implies that the area should be studied in a larger context in which several areas also are included; behaviour, design of inter-face and instructions to residents. The findings in the measured apartments in other words supports that research must be performed in a general inter-disciplinary way including both the performance of the building service systems, the interaction of the residents and the behavioural aspect of the people if an satisfying indoor climate is to be achieved.

The number of apartments studied is relatively few and no extensive conclusions can be made. The apartments are however situated in a nice area; nothing speaks for that these apartments should differ from other new-built apartments thus indicating that the apartments and the reported experience could be viewed upon as representative for newly-built well insulated apartment's buildings. This could be interpreted as that the identified short comings could be worth observing by other building owners and engineers both when building new apartments and also when upgrading and renovating existing one to modern technical equipment and components. Factors which could be worth observing and addressing in the planning process with the aim of creating an good indoor climate includes for example; solar shading, plan of the apartment, the design of building services systems and its interface; ventilation and heating in terms of noise, design of the control of the ventilation system, careful instruction to the occupants of the building services systems, especially if systems are to be controlled solely by the residents as the ventilation units placed inside the apartments.

The results also indicate several research questions to be addressed in the future; one of them is whether a ventilation system solely should be controlled by non-professionals as residents and if this will guarantee a good indoor climate.

In the hunt for saving energy; the ventilation air flows may be reduced. If the ventilation system supplies too low air flows; both in comparison with the Building code and possibly also perceived as too low by the occupants, this may lead to that the windows are opened. The air flow through an open window during heating season could be several times larger than via the ventilation system in a home, and this heat which leaves through the window is not recovered. An alternative could be to design for somewhat higher air flows via the ventilation system; which can both recover heat and also filter the outdoor air. This could be beneficial as the outdoor air pollution is recently classified by the WHO as a leading environmental cause of cancer deaths (WHO, 2013). This way could then be more efficient both in terms of energy use and air quality.

6. Acknowledgements

BEBO is acknowledged for financing the study. The energy part, not presented here, has been done by WSP. All the residents who answered the questionnaire are acknowledged for contributing to the knowledge on how the indoor climate is experienced in new-built apartment buildings. A special thank is directed to the residents who agreed to participate in the measurement study and so generously opened their homes and also gave valuable input on their experience of the indoor climate and the interaction with the building services systems.

References

Berge M. & Mathisen H. M. 2013. Post-occupancy Evaluation of Low-Energy and Passive House Apartments in the Lovåshagen Cooperative - Occupant behavior and Satisfaction. *Passivhuskonferens Norden, 15-17 okt 2013*, Gothenburg. 12 p.

Boverket. 2009. *Enkätundersökning om boendes upplevda inomhusmiljö och ohälsa – resultat från projektet BETSI*. ISBN pdf:978-91-86342-45-6, Boverket, Karlskrona

EMTF. 2013. *R1 – Riktlinjer för specifikation av inneklimatkrav.* EMTF Förlag AB, ISBN 978-91-976271-8-4

Fransson V. Nordquist B. Lindberg O. 2014. Window-opening and indoor climate in new multi-family-dwellings – A questionnaire survey. *NSB 2014, 10th Nordic Symposium on Building Physics*, 15-19 June, 2014, Lund, Sweden 8 p.

Fransson V. Lindberg O. 2013. *Undersökning av inneklimat och vädring i nybyggda lägenheter*. Building Services, Faculty of Engineering, Lund University, Lund. 205 p.

Hansson A. & Nordquist B. 2010. *Uppföljning Flagghusen Energi och inneklimat Slutrapport*, WSP, Avd. för installationsteknik, Lunds tekniska högskola. 110 p.

Karlsson E. & Nordquist B. 2014. *Energiuppföljning av området Flagghusen*. to be published in April 2014. WSP Malmö, Building Services, Faculty of Engineering, Lund University, Lund

Malmö Stad. 2009. *MiljöbyggprogramSyd*. Malmö and Lund city, http://www.malmo.se/Medborgare/Bo--bygga/Bygga-nytt---bygga-till/Bygglov-marklov--rivningslov/Miljobyggprogram-Syd.html

Sandberg. E. & Engvall K. 2002. *MEBY rapport Delrapport 3, Beprövad enkät – hjälpmedel för energiuppföljning*, Aton, Stockholm, http://www.aton.se/img/userfiles/file/Delrpport-3.PDF

WHO. 2013. *IARC: Outdoor air pollution a leading environmental cause of cancer deaths*. http://www.iarc.fr/en/media-centre/iarcnews/pdf/pr221_E.pdf . WHO; International Center for Research on Cancer. 17th of Oct. 2013.

HVAC Models coupled with hygrothermal building simulation software

Matthias Pazold; M.Eng. [1]
Florian Antretter, M.Eng. [1]
Jan Radon, Professor [2]

[1] Fraunhofer Institute for Building Physics, Holzkirchen, Germany
[2] Agr. University of Cracow, Poland

KEYWORDS: *Hygrothermal building simulation; detailed plant equipment simulation; HVAC; coupling simulation models; FMI for co-simulation*

SUMMARY:
This paper describes the integration of HVAC simulation models, developed with the multi-domain modeling language Modelica, into the hygrothermal building simulation software WUFI® Plus. With the existing software a hygrothermal building simulation, considering heating, cooling and air conditioning as ideal systems, can be performed in a user friendly way. Without detailed HVAC models, the software calculates the heating, cooling, humidification, dehumidification and ventilation demand which is necessary to keep the indoor climate in user defined design conditions. This output can be used for further investigation and sizing the plant equipment. However, a direct interaction between the detailed building model and the building equipment was not possible. This is improved with the newly developed Modelica HVAC models. They were exported via the common Functional Mock-up Interface (FMI), which was analyzed to assess the most effective coupling strategy. The FMI is the definition of an open interface between different software systems. The realization of a non-iterative coupling algorithm is illustrated by means of a simulation example. Furthermore, the implementation of the HVAC models into the hygrothermal building simulation program is validated using the results from a Modelica simulation environment as reference.

1. Introduction

1.1 Building model

Traditionally, many building simulation programs were written in high level languages like FORTRAN, or C/C++ with specialized solvers and algorithms for established and approved simulations. There is and always will be the aim to improve such simulation software. One of those traditionally software is the existing hygrothermal building simulation software, called WUFI® Plus (Holm, et.al. 2004; Lengsfeld & Holm, 2007). The holistic model is based on the hygrothermal envelope calculation model developed by Künzel (1994). This detailed model calculates the coupled heat and moisture transfer in building components and is written in FORTRAN and C++. The conductive heat and enthalpy flow by vapor diffusion with phase changes in the energy equation dependent on the moisture fields. The vapor flow is simultaneously governed by the temperature and moisture field due to the exponential changes of the saturation vapor pressure with temperature. The resulting differential equations are discretized by means of an implicit finite volume method. A stable and efficient numerical solver had been designed for the solution of the coupled and highly nonlinear equations..

The building envelope can consist of many and different components, such as exterior- and interior-walls, ceilings, and floors. A multi-zone model, written in C++, links them to the whole building model. Moisture sources or sinks inside the rooms or inside the components, exchange with the envelope due to capillary action, diffusion and vapor ab- and desorption as a response to the exterior and interior climate conditions as well as the thermal parameters are taken into account. The hygrothermal behaviour of the components affects the overall performance of the building and vice versa. The multi-zone model manages the simulation and interaction, even with further models, for windows, the solar radiation in different sun incidence angles, or the building air flow. The graphical user interface and the data management of the existing software WUFI® Plus is developed in C#. The model was validated by comparing simulation results with measured data of extensive field experiments or verification with standards (Antretter et al., 2011).

To simulate the indoor climate, the multi-zone model calculates heat and moisture balances for each zone, regarding all the sources, sinks and exchanges. As long as those balances are not satisfied during a time step, the interior temperature and humidity is adapted iteratively. For example, if the heat loss through the building envelope and ventilation is more than the solar and internal heat gain, the interior temperature is decreased as long as the loss and the gain are not equal.

The user can define design conditions for the indoor climate by setting minimal and maximal values, e.g. for the indoor temperature. Without the detailed HVAC models, ideal systems are regarded, calculating the heating, cooling, de- and humidification demand with the described heat and moisture balances. The systems are defined only per maximal capabilities. If the indoor climate would exceed the design conditions, the solution algorithm tries to get the necessary deficit to equal the balances from the defined systems capabilities. Back to the example before, if a user has set a space heating capacity, the interior temperature is kept by the minimal design condition as long as the space heating capacity is enough to fulfil the heat balance. The resulting actual heating demand is the difference in the heat balance.
However, in reality, the HVAC system may not deliver the demand instantly. It may have to load the water storage and heat up the radiator before energy is provided to the space. After that, the radiator may still heat up the room even the temperature has reached the set point temperature. This inertia of a heating system, regarding the warm-up time or the overheating of a room was not simulated with the ideal system. By coupling the detailed hygrothermal building simulation with the detailed HVAC systems, described later in this paper, the indoor climate may fluctuate more and is not kept exactly at the design conditions. Furthermore, many results regarding the dimensioning and planning of the HVAC system, in direct interaction with the building envelope, can be obtained. The multi-zone model also has to manage this simulation and interaction by setting boundary conditions, such as the radiator surrounding temperature and getting output, such as the heating power of the radiator calculated with the detailed HVAC system.

1.2 Modelica HVAC models

The aim was to create simple but realistic HVAC models, which can be used by practitioners. Following this, only necessary and obtainable plant information is required for the simulation. Also the computation time to simulate a building should not increase to times which are no longer acceptable for practitioners. The different HVAC devices to be simulated, plant equipment for heat generation, distribution, storage and controlling include, so far:

- Condensing gas boiler – simulating the heating power output in different operation modes

- Solar thermal collector – simulating the heating power output regarding the collector orientation, inclination and shading, depending on the position of the sun and surrounding temperature
- Combined heat and power plant – simulating heating and energy power
- Heat pump
- Bore hole heat exchanger
- Thermally activated building systems (TABS) – can be added as inner source directly in the building components
- Radiators – simulate the heat flow to a room regarding mass and nominal heat power
- Storage tanks – simulation of the temperature distribution within the tank
- Control equipment – controlling e.g. the mass flow rates, depending on set point temperatures and actual room temperatures
- PV system – simulate the power output, depending on orientation, inclination and sun irradiation

During the last years, the building simulation community discovered the advantages of using Cross-industry multi-domain modeling languages (CMML) such as Modelica (Elmqvist, 1997) for the development and verification of complex simulation models. Following this the model development of the detailed HVAC systems was done with the software Dymola 2012 (Dassault Systèmes AB, 2011). It was desirable to extend the existing program with the newly developed models to be able to use both, the existing tool as well as the CMML models.
To deliver realistic and validated plant equipment models, the above mentioned sub-models are merged to complete HVAC systems, an example is shown in FIG 1. This was done to increase the usability and avoid the risk of non-feasible system configurations. Finally, the user chooses one HVAC system configuration and has to set only a few necessary parameters or import them from a database.

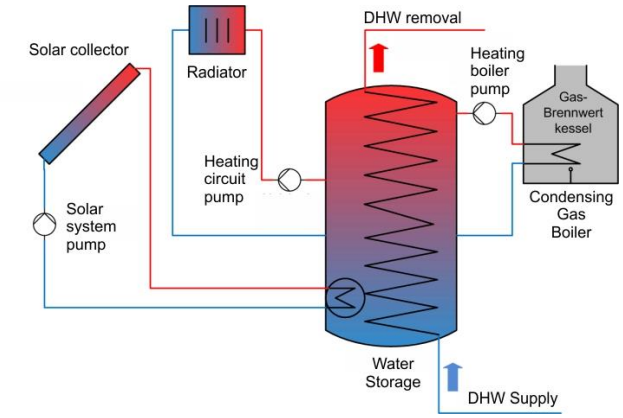

FIG 1: Exemplary HVAC configuration designed in Modelica and coupled with WUFI®Plus

2. Coupling

2.1 Preparing the HVAC models

As described above, all the different HVAC components, such as boiler, storage and solar collector are merged to whole plant equipment systems in order to increase the usability and to get feasible, proven and validated systems coupled with the building model. Each configuration can include different components, for example some include the condensing gas boiler, some others include heat pumps and some others include combined heat and power plants. The multi-zone model has to handle each of those configurations, just by changing the configuration type.

One necessary step to develop such models is to define the input, output and the parameters. Parameters are set at the beginning, respectively at the initialisation of a model. They can be computed with some other parameters, but regarded constant for the whole simulation. For example, the maximal gas-boiler output, or the maximal storage tank volume are such parameters. During the simulation the plant equipment has to interact with the building envelope, respectively the multi-zone building model. The multi-zone model has to send input, for each calculated time step. For example the actual interior building temperature and the set-point temperature is needed for the plant equipment, especially for the radiator sub-model to compute the heat flow to the room. Such time varying and simulation depending values must be sent to the plant model as input and delivered for the multi-zone model as output. Especially the model input has to be defined clearly as *input* in the model variable declaration; otherwise it is often not possible to set those values during the simulation in the exported model. Also the parameters have to be declared as *parameters* within the model. If not they might get the variability of a constant with the model export and constants cannot be changed.

One overall HVAC model exchange frame with all possible inputs, outputs and parameters for all the different kinds of included HVAC systems was defined. Each system is build up in this frame and using the inputs, outputs and parameters defined in the framework. If one configuration doesn't inherit the condensing boiler, for example, the parameters are just left empty.

A first coupling approach was to use Dymola specific export possibilities, the so called *Source Code Generation* or the *Binary File Export*. More details on this can be found in (Burhenne et.al. 2011). Finally the coupling with the *Functional Mock-up Interface* (FMI) for Co-Simulation was chosen because of its unified convention and possibilities to perform the co-simulation. Following this, all HVAC systems are exported using FMI for Co-Simulation. Those models include beside the simulation equations also a solver executing the co-simulation. The exported model is called *Functional Mock-up Unit* (FMU). It is a packed file (zip-file) containing the model binary file, a *dynamic link library* (.dll), with all the callable functions specified with the FMI application interface. Beside this model, the *modeldescription.xml* is included, containing all the necessary model information, especially the variables and parameter information.

Each input, parameter, or intern variable gets a model-unique identification number, a so called value reference number, during the export process. This number is documented in the model description file. The whole information exchange is handled via those value reference numbers. For example, the maximal boiler power with the model-variable name *qMaxBoiler*, gets the value reference number 16777216. With this number, and the transfer function `fmiSetReal(..)`, defined in the FMI specification, it is possible to set the value of the parameter, respectively the maximal boiler power. Even with the stiff configuration frame, the value reference numbers for the parameters and inputs change for different configurations or after a configuration is updated. It was decided not to hard-code the value reference numbers, but to develop a tool to setup the HVAC systems for the coupled simulation and merge the inputs, outputs and parameters.

2.2 Coupling the HVAC models

After a system is designed, validated and exported it can be loaded in the developed system configuration tool, shown in FIG 2 in the left bottom corner. The tool lists all the variables declared in the FMU, respectively the HVAC system. Besides the FMU variables, it also lists all the parameters, inputs and outputs provided within the graphical user interface of WUFI® Plus for the detailed HVAC Systems. They are partitioned per HVAC device, so each device type gets an identification number and the specified variables. For example, the gas condensing boiler has the ID 2 and the maximal heating power has the parameter index 1. Now the only thing to do, during the coupling process, is to find the variable name of maximal boiler power in the FMU (ordinary defined within the HVAC exchange framework before) and copy it behind the listed WUFI® Plus parameter. The tool merges the

Value Reference Number and checks the variability (input, output or parameter) and unit. It is visualised, if a connection is valid or not. The tool stores those links, and also some additional model information's, like model GUID (a unique number each exported model gets for exact identification) and the model binary file name in a HVAC configuration file.

The user of the software has not to do this. Only the model binary files, the HVAC configuration file and a FMU adapter is delivered with the software. The user only has to choose the desired HVAC system and set the values of the parameters within the graphical user interface.

The FMU adapter manages the simulation, also shown in FIG 2, without any user interaction. It gets all the parameter and input values from the building envelope model, connects them with the corresponding value reference number and sends this information to the HVAC model via the FMI-specification. It also manages the instantiation, initialisation and time step execution. Certainly it gets the outputs via the value reference numbers and sends it back to WUFI®Plus.

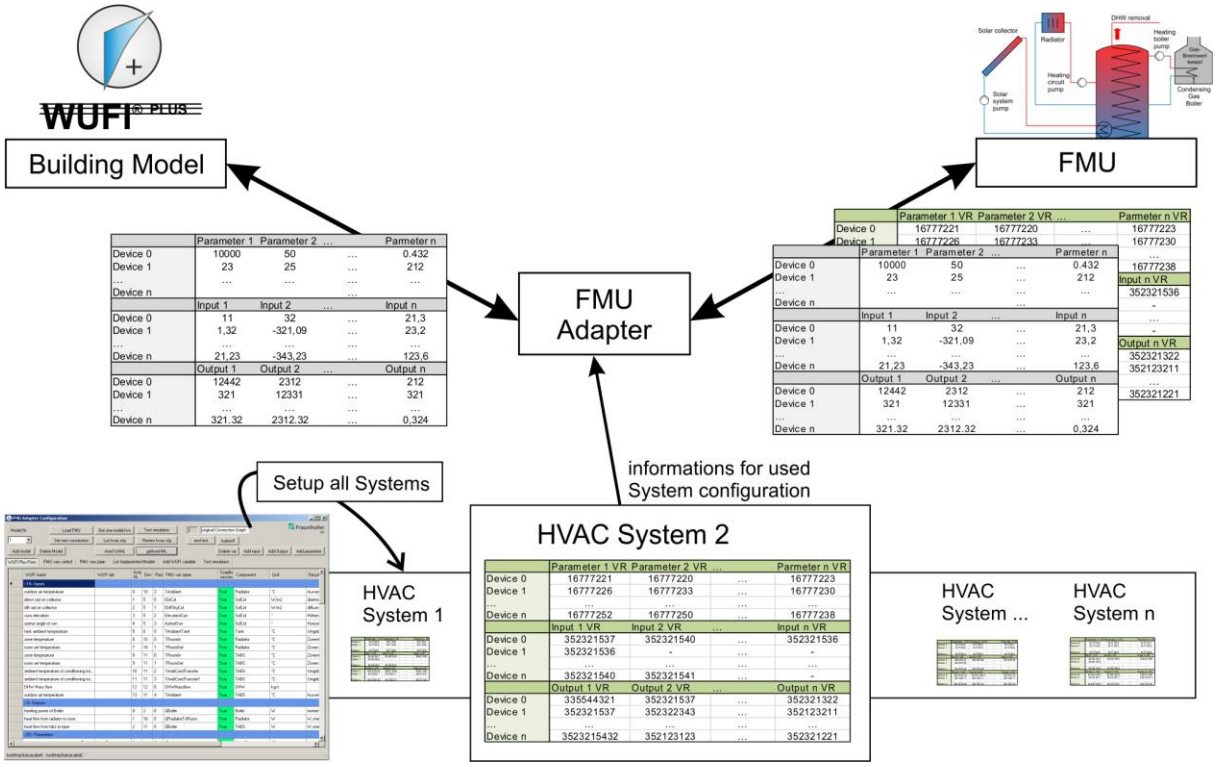

FIG 2: Coupling different HVAC Systems as FMU's with WUFI®Plus via the Coupling Tool

2.3 Simulation with the detailed HVAC models

As described before, the detailed HVAC models replace the ideal systems. Therefore, the implicit solution algorithm of the multi-zone model is replaced by an explicit method (Pazold et.al. 2012). This is required due to the unsupported rejection and repeating of time steps by co-simulation and particularly, because of the fast response to the indoor climate of the HVAC controlling devices and systems. The implicit method iterates each time step as long as the heat- and moisture in a zone is not balanced. With the explicit method, the indoor climate is adjusted for the next time step, regarding the heat- and moisture balances of an actual time step. The building model interacts with the HVAC system via a kind of *ping-pong* method. With an usual simulation time step size of one hour, to simulate one or more years, this alternative co-simulation would lead to unrealistic simulation results. Therefore, the explicit solution technique requires a decreased time step size, e.g. about five seconds. The computation of the indoor climate, and the heat and moisture field in the components has to be

done 720times each time step. The implicit method requires only 15 to 40 iterations, respectively computations. This and of course the detailed HVAC models increase the computation time. However, the results of the small sub time steps must not be stored, the time steps don't iterate, and the hygrothermal component simulation module computes a bit faster for such small time steps, which saves some computation time. First simulations, without any further computation improvements, increase the simulation duration about 3 to 5 times. Benefits from the coupled simulation

Some improvements, regarding the hygrothermal building simulation coupled with detailed HVAC systems are mentioned in the text before. Remember the indoor climate; it will be simulated quite more realistic because of HVAC reaction times or over powering. It may not stay exact at the defined design conditions if the plant equipment is active. This will also affect the exchanges across the building components. Furthermore, the interaction between building envelope and HVAC system can be investigated in more detail. For example, the operation mode of a condensing gas boiler or a pellet boiler is simulated. In combination with the dynamic interaction between the thermal storage mass of the building, the mass of the heating distribution system and the water storage tank, the estimated efficiency of the boiler can be investigated. Additionally the power output of a solar thermal collector is simulated regarding the collector orientation, inclination and of course shading - depending on the position of the sun and surrounding components.

Besides the efficiency and heating demand investigations, the comfort assessment within different rooms or zones benefits from the detailed HVAC systems simulation. For example, the operative temperature can be assessed. By choosing a system including the thermally activated building system the dynamically simulated heating power is regarded as inner source within a building component affecting directly the heat and moisture distribution within it, the surface temperature and the heat flow into the room. This simulation can check if the area of the TABS is enough to heat up the room, with a still comfortable surface temperature.

3. Application example

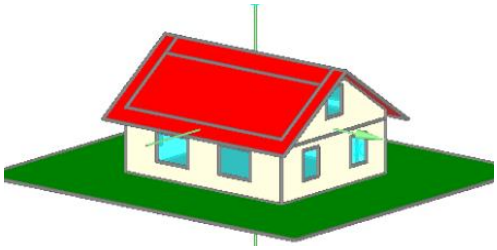

FIG 3: Application example test building

The effect of a coupled simulation is shown in this chapter. One exemplary case is chosen to show some of the results of a HVAC model and the interaction with the building envelope and the indoor climate. Therefore one small house, with one full storey and a developed attic is investigated as shown in FIG 3. The treated floor area of the building is 118 m² and the net volume 281 m³. It should be located in Lund, Sweden, with the respective climate. The heat transfer coefficient (U-value) of the timber constructed and insulated exterior wall is 0,15 W/m²K, of the roof 0,17 W/m²K and of the windows 1,76 W/m²K. The overall window area is 18,6 m², including window frames. Furthermore, standard internal loads for two residents are regarded. The air change rate is set constant to 0,4 per hour. The reference case is simulated with an ideal heating system with over dimensioned heating power. In a next step, the ideal system is exchanged with the detailed exemplary HVAC system shown in FIG 1. It includes a condensing gas boiler and a solar collector for heat generation, a storage tank and a radiator for heat distribution. The main parameters for the system are listed in TABLE 1.

TABLE 1. Parameter list for application example HVAC devices

condensing gas boiler	Maximal boiler power	5	[kW]
	Boiler and circuit mass	50	[kg]
	Temperature of tank which requires loading by boiler	60	[°C]
	Maximal mass flow of boiler supply	0,1	[kg/s]
	Top border temperature of tank	70	[°C]
Solar collector	Intercept (maximum) of the collector efficiency	0,8	[-]
	First-order coefficient in collector efficiency equation	3,5	[W/m²K]
	Second-order coefficient in collector efficiency equation	0,015	[W/m²K]
	Area of solar thermal array	6	[m²]
	Length of collector	3	[m]
	Orientation of array (positive east from north)	180	[°]
	Inclination angle of array	35	[°]
	Required temperature diff. between collector and tank	10	[°C]
	Maximal temperature of tank	90	[°C]
	Maximal mass flow of collector circuit	0,05	[kg/s]
Water storage tank	Thermal storage capacity	400	[Liter]
	Diameter tank	0,5	[m]
	Heat transfer coefficient tank fluid to ambient	0,25	[W/m²K]
	(relative heights of inlets, outlets and sensors)	0..1	[-]
	Thermal conductance of heat exchanger 1	500	[W/K]
	Thermal conductance of heat exchanger 2	500	[W/K]
Radiator	Nominal heat power of the used radiators	2	[kW]
	Mass of radiator including water	100	[kg]
	Radiator exponent	1,281	[-]
	Maximal radiator mass flow	0,1	[kg/s]
DHW	Domestic hot water profile (time scheduled)	variable	[kg/s]

As described before, the building is simulated twice. Once with the ideal heating system and in the next step with a coupled detailed heating system, described in this paper. The results of both simulations are compared and some additional results, only obtainable with the detailed system are shown.

The graphs in FIG 4 show the indoor air temperature and FIG 5 show the heating power, which was required to keep the indoor air temperature within the design conditions. The reference simulation with the ideal system calculates a quite constant minimum indoor temperature, because of the design condition at 20°C. The simulation with the coupled heating system gives a more fluctuating indoor temperature, because of the detailed simulation of the heating system. The system includes a thermostat, with a hysteresis, setting the heating circuit mass flow rate following the indoor temperature and set point temperature. The behaviour of the whole system, including supply and return temperature of the radiator is simulated. Exemplary, in FIG 6 the water temperature within the water storage at the bottom, the middle and the top of the storage volume is shown. Such new results, only available with the detailed system, may be used to adjust the storage capacity and properties to the whole building..

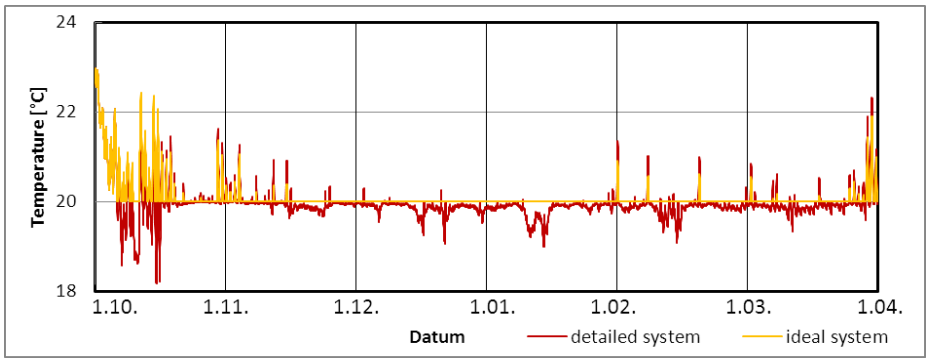

FIG 4: Comparison of the simulated indoor temperature of the application example building calculated with the ideal and the new detailed system. Because of the radiator hysteresis and the detailed heating system, the indoor air temperature fluctuating more and is not kept constant at the design condition at 20°C

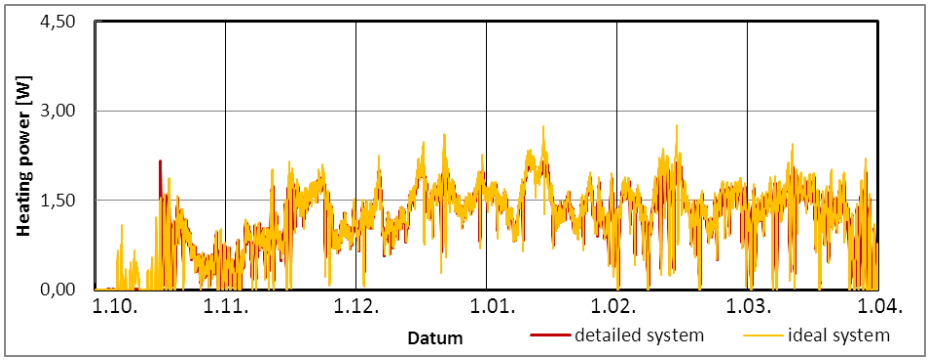

FIG 5: Simulated heating power, respectively heat flow from the radiator to the room, calculated with the ideal system compared to the simulation with the detailed system.

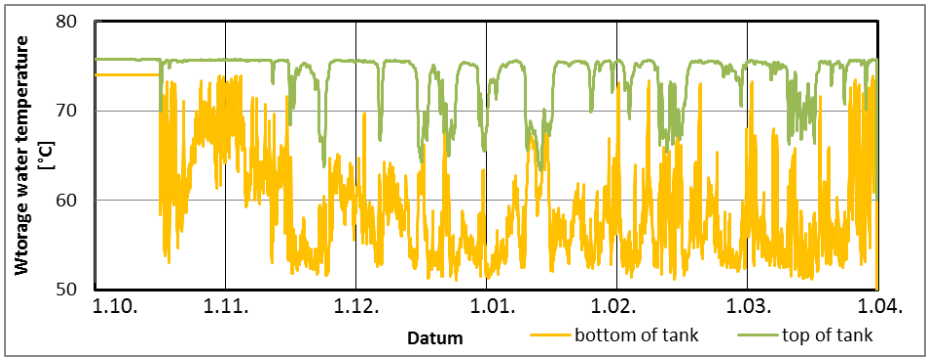

FIG 6: Further detailed system results, exemplary the simulated water temperature inside the water storage at different heights.

4. Conclusion

Cross-industry multi-domain modeling languages (CMML) provide a fast way to design and simulate different HVAC devices which are merged to pre-defined whole system configurations. Exporting those models with the standardized Functional Mock-up Interface (FMI) can be used to couple them with existing software, written in high level languages. However, some rearrangements of the existing software are necessary to adopt the models, respectively to implement the FMI functionality. The hygrothermal building model with a specialized solver and the HVAC systems are complex proven models, validated and stable for many kinds of simulations. The described coupling using the co-

simulation approach seems to be a reasonable technique to merge those models. The input and output of the different exported FMUs, acting as sub-models, can be defined using the developed tool. With the tool, it is possible to couple new or updated models without recurrent modifying of the source code of the existing software. A still acceptable computation time and realistic simulation results, e.g. a quite equal heating power to keep the indoor climate at the design conditions, leads to the conclusion, that the described coupling is a suitable and confiding method to improve the hygrothermal building simulation.

5. Acknowledgements

This study was funded by the German Federal Ministry of Economics and Technology (BMWi 0329663L).

References

Antretter F., Sauer F., Schöpfer T., Holm A. 2011. Validation of a hygrothermal whole building simulation software. Proceedings of Building Simulation 2011: 12th Conference of International Building Performance Simulation Association, Sydney, Australia.

Elmqvist H. 1997. Modelica – A unified object- oriented language for physical systems modeling. Simulation Practice and Theory 5, no. 6., 1997.

Künzel H. M. 1994. Simultaneous Heat and Moisture Transport in Building Components. Dissertation. University of Stuttgart, Download: www.building-physics.com

Holm A., Radon J., Künzel H. M., Sedlbauer K. 2004. Berechnung des hygrothermischen Verhaltens von Räumen. WTA-Schriftenreihe (2004), Heft 24, Seite 81–94. WTA-Publications, München.

Lengsfeld K., Holm A. 2007. Entwicklung und Validierung einer hygrothermischen Raumklima-Simulationssoftware WUFI-Plus. Bauphysik 29 (2007), Heft 3, Seite 178-186. Ernst & Sohn Verlag Berlin.

Dassault Systèmes AB 2011. Dymola. Dynamic Modeling Laboratory. Dymola Release notes, Lund, Sweden.

Burhenne S., Radon J., Pazold M., Herkel S., Antretter, F. 2011. Integration of HVAC Models into a Hygrothermal Whole Building Simulation Tool, Proceedings of Building Simulation 2011: 12th Conference of International Building Performance Simulation Association, Sydney, Australia.

Pazold M., Burhenne S., Radon J., Herkel S., Antretter F. 2012. Integration of Modelica models into an existing simulation software using FMI for Co-Simulation, Proceedings of the 9th International MODELICA Conference, September 3-5, 2012, Munich, Germany.

A comparison between a commercial energy calculation tool for buildings with calculations using a response model

Victoria Bonath, M.Sc. [1]
Eva-Lotta Kurkinen, Ph.D. [2]
Ulf Ohlsson, Ph.D., Assistant Professor [1]

[1] Luleå University of Technology, Sweden
[2] SP Technical Research Institute of Sweden, Sweden

KEYWORDS: *Energy calculation tool, thermal mass, building, VIP-Energy, Dynamic Thermal Networks (DTN)*

SUMMARY: (Style: Summary Heading)
The modeling of energy balances for buildings is a main task in building physics and a key issue in analyzing and developing new low energy buildings. On the market there exist many different calculation tools. They all have both benefits and draw backs in different cases. As a user it could be difficult to choose the most suitably tool.

In this paper a commercial energy calculation tool (VIP-Energy) is compared with the relative new methodology called DTN (Dynamic Thermal Networks). DTN is developed by Johan Claesson at Chalmers. The methodology is based on response functions which gives a very illustrative picture of a buildings thermal behavior. VIP-Energy is a commonly used simulation tool by consultants and designers in Sweden. VIP-Energy handle full dynamic energy balances with HVAC-systems (heat-ventilation- cooling systems).

The comparison is made in the following areas:

- *Accounting of thermal mass text*
- *Handling long and short time scales*
- *Influence from HVAC-systems*

The aim of this work is to find the most suitably tool to evaluate benefits of heavy thermal mass buildings and be able to make optimization in the construction in order to reach even more benefits of the mass. The considered benefits are; indoor temperature, low energy consumption and low installed power.

An early study shows that a combination of the two calculation tools is a good choice. The DTN methodology is to prefer to make detailed analyses and optimizations and the VIP-Energy is to prefer when analyze the complete energy balance including HVAC.

1. Introduction

Lowering the energy use has not only been an issue of the consumer for a long time. Nowadays utilization of the building structure in combination with adapted HVAC systems can increase the energy efficiency a lot. Buildings with high thermal inertia decrease the power peaks and moves the power demand in time. This is an important part to imply into smart energy systems. This combination can in the future be optimised by right operation of systems for heating, cooling and energy consumption.

Good energy calculation tools are necessary to individually optimise buildings for sustainable and best possible energy utilization. In order to generate an energy balance for buildings, different simulation models exist which are based on either steady state or dynamic conditions. When using these models it is important that the chosen method is reliable. Kalema et al. (2008) have done a comparison of in total 7 different tools to calculate energy balances in buildings. The focus was on analysing effects of thermal mass on cooling and heating energy. They found that the different results between the methods are mainly caused by different input data instead of differences between various calculation methods.

Within the Cerbof 2 project (Wadsö et al., 2012) different studies were done amongst others on optimising energy efficiency by utilizing heavy thermal mass buildings in combination with different operation conditions of HVAC systems. Two different calculation tools were used during these studies. VIP-Energy and is a dynamic method which is developed as a user-friendly, commercial tool for building industry. The relatively new method, called 'Dynamic thermic networks' has been developed by Claesson (2003).

The aim of this study is to evaluate both methods for their ability to optimise buildings by accounting for heavy thermal mass as effective as possible. The influence from HVAC-Systems and modified process energy on heavy thermal mass buildings is studied. The handling of long and short time effects of thermal inertia is compared.

2. Method

The two calculations methods are compared by calculating the indoor and wall temperature and the energy demand for a student apartment in north of Sweden. The student apartment is a heavy thermal mass construction. For evaluating the calculation methods, the influence of heat capacity for inner structures, ventilation systems, zone calculations and accuracy regarding input values were taken into account. A buildings response function was calculated in both VIP-Energy and DTN to illustrate how the buildings thermal inertia is accounted for. For the latter task, a simplified building structure is used. A constructions response function is the heat flow caused by one temperature step as a function of time.

3. Energy calculation programs

3.1 VIP-Energy

VIP energy is a thermal simulation program which covers the complete buildings energy balance. The calculations are based on dynamic equations where all parameters are updated with one hour time interval. Heat transfer coefficients are dynamic values which adapt hourly to the environmental circumstances. Input values are known or measurable values such as weather conditions and demands on indoor temperature or ventilation (VIP -Energy, 2002).

3.2 DTN

Dynamic Thermal Network, the theory means that the relations between boundary heat fluxes and boundary temperatures for any time-dependent heat conduction process in a solid material are represented in the same way as for an ordinary thermal network (for steady-state heat conduction). The calculations are based on step-response functions which mean that the heat fluxes through the surfaces are calculated for a unit step change at one surface while keeping zero temperature at the other surfaces. The relations between surface temperatures and heat flows for any time-dependent process are obtained by superposition of the basic step responses.

4. Indata

4.1 Student apartment

A student apartment consisting of two floors and four apartments at each floor is used as study object. The energy balance in VIP-Energy was calculated for the whole building as one zone. The apartments may have different indoor temperatures. Additional calculations were therefore done with the building divided into ten zones (one zone for each apartment and one zone for the stairwell at each floor). The energy balance is calculated for each zone while the heat flow between zones is taken into consideration. DTN calculates the whole upper floor as one zone. The structure is a heavy concrete structure with a thermal conductivity of 2.3 W/(m,K), the density is 4000 kg/m^3 and the heat capacity is 830 Ws/(kg,K). More material parameters are given in table 1. As DTN is only calculating for the upper part of the building, boundary conditions had to be applied which result in zero heat exchange towards the intermediate ceiling.

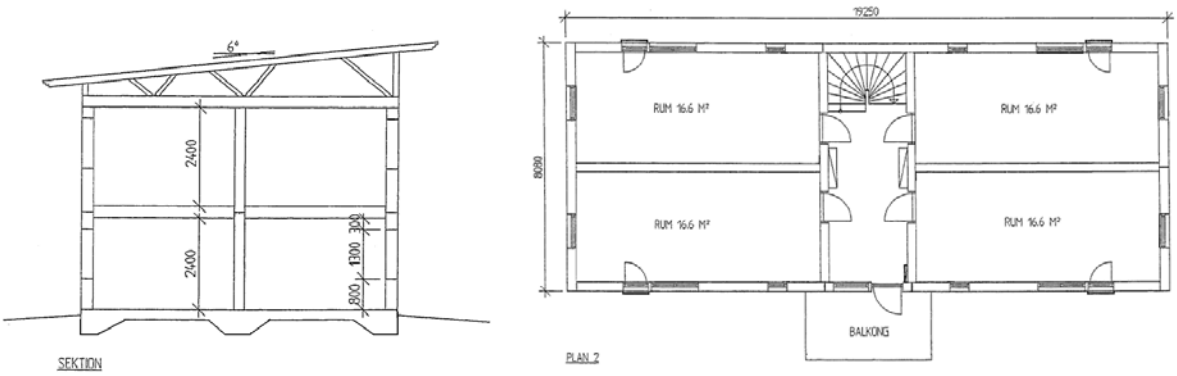

FIG 1. Studied building with four student apartment per floor.

TABLE 1. Input values for the construction used in chapter 4 and 5. U-values of some of the construction elements differ slightly for VIP-Energy and DTN.

Building part	Area (m^2)	U- Value (VIP)	U-Value (DTN)
Roof	155.5	0.097	0.087
Exterior wall	234.1	0.202	0.171
Interior wall	287	3.476	2.648
Intermediate ceiling	311	0.755	0.679
Window	50	1	1
Ground plate	155.5	0.142	-

Input values for process energy and ventilation are given in table 2.

TABLE 2. Input values for ventilation and process energy, same in both programs.

Ventilation:		
Volume of the upper floor:	373.295 m^3	
Air changes per hour:	0.525 if T_i < 24°C	1 if T_i > 24°C and |Ti-Ta| ≥5°C
Process energy:	5 W/m^2	

The weather data used is a synthesis of the years 1993 to 2003 for Luleå. Hourly values for air temperatures and solar radiation are used in both VIP-Energy and DTN. In addition to that are wind speed and relative air humidity included in the VIP-Energy calculations.

4.2 Input values for response functions

For calculating the response function in chapter 7 a simple construction as given in table 3 is used. The inside dimension is 12.5 m x 8 m x 2.5 m and no doors, windows, ventilation or infiltration are used.

TABLE 3. Input values for the construction used in chapter 7, where R are the inside and outside heat transfer coefficients, λ is the heat conduction, ρ is the density and c the specific heat capacity.

Heavy weight construction	R ($(m^2,K)/W$)	λ (W/(m,K))	ρ (kg/m^3)	c (Ws/(kg,K))
Inside	0,13			
150 mm Concrete		1,7	2300	800
200 mm EPS		0,036	25	1400
70 mm Concrete		1,7	2300	800
Outside	0,04			
	U-Value = 0,171 W/(m^2,K)			
Light weight construction	R ($(m^2,K)/W$)	λ (W/(m,K))	ρ (kg/m^3)	c (Ws/(kg,K))
Inside	0,13			
13 mm Plasterboard		0.21	700	1000
200 mm EPS		0.036	25	1400
13 mm Plasterboard		0.21	700	1000
Outside	0,04			
	U-Value = 0,171 W/(m^2,K)			

5. Accounting of thermal mass

Both the interior walls and intermediate ceiling have a high thermal mass. When removing the heat capacity of the interior construction elements, the total energy demand for heating is 1.26 % higher for DTN calculations. In VIP-Energy the energy demands increases only with 0.45 %.

TABLE 4. Energy demand for heating and average indoor temperatures calculated with and without heat capacity for interior walls and intermediate ceiling.

	With heat capacity		Without heat capacity	
Method	Energy demand (MWh/a)	T_{indoor}	Energy demand (MWh/a)	T_{indoor}
VIP -Energy (without zones)	8.85	22.18	8.81	22.20
DTN	4.53	22.90	4.47	22.90

Heat capacity for interior walls has more influence instead on the indoor climate, as shown in figure 2. Without considering thermal mass of interior construction elements, the indoor temperature increases faster during spring and decreases faster during autumn, this is also reflected in the demand of heating energy. In case of less thermal mass, higher daily variations of indoor temperatures are observed. Further the maximum effect needed for heating is slightly higher. The indoor temperatures calculated in VIP-Energy are constantly much lower than those resulting from DTN. Also daily

temperature oscillations are less extensive for VIP-Energy. Figure 3 shows the average wall temperature distribution with VIP-Energy. Both highest and lowest values for wall temperatures can be found for lower thermal mass. In VIP-Energy the wall temperature illustrates an average temperature value for those building materials that mainly are in contact with compartment air (VIP - Energy, 2002). It is not clearly formulated whether VIP-Energy takes a value in the middle of the wall or at the surface; anyhow it is a mean value for the whole building.

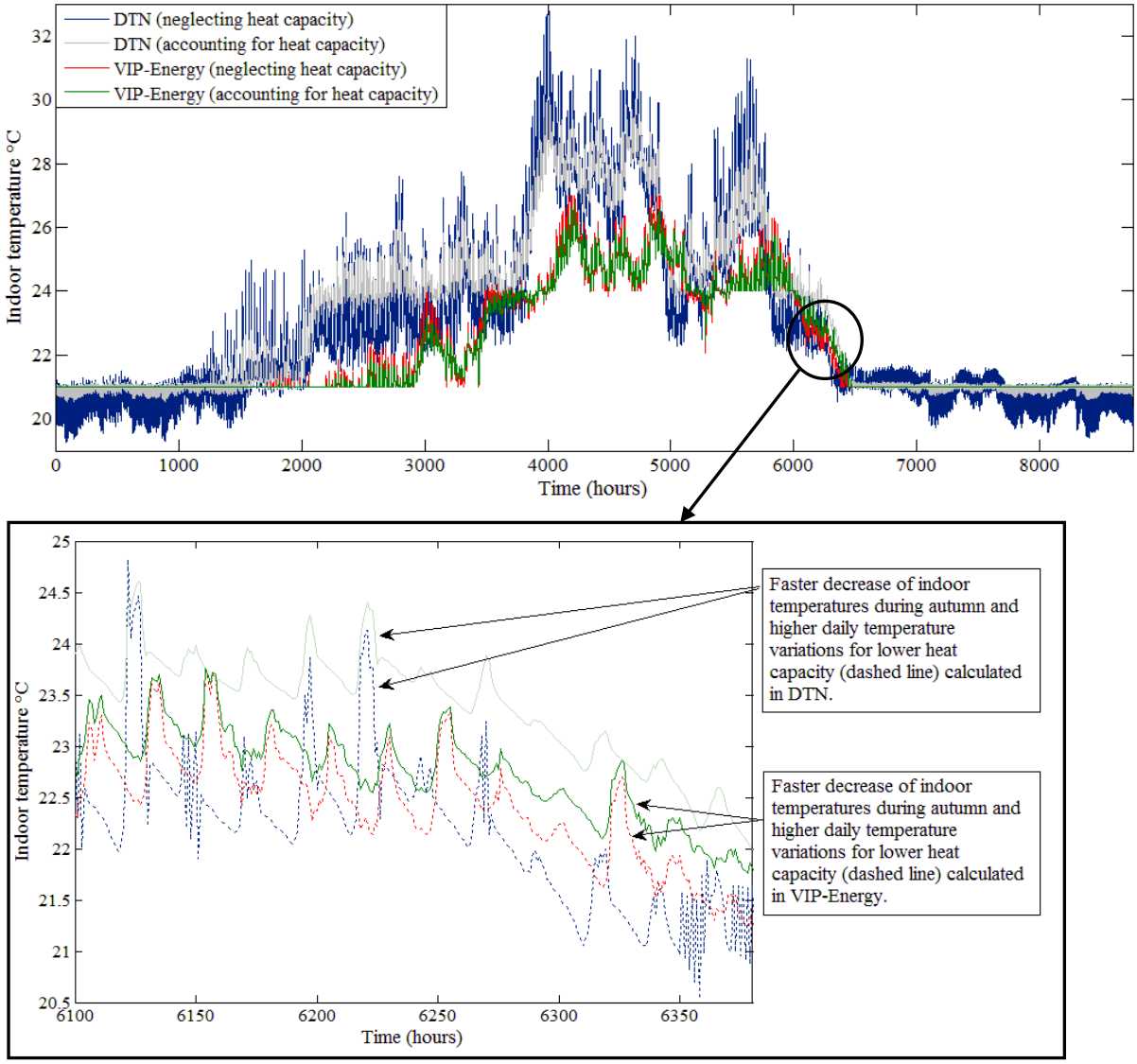

FIG 2. Indoor temperature during one year accounting for thermal mass of interior walls and neglecting thermal mass of interior walls calculated with VIP-Energy and DTN. Differences between the cases are scaled up for a period in late September.

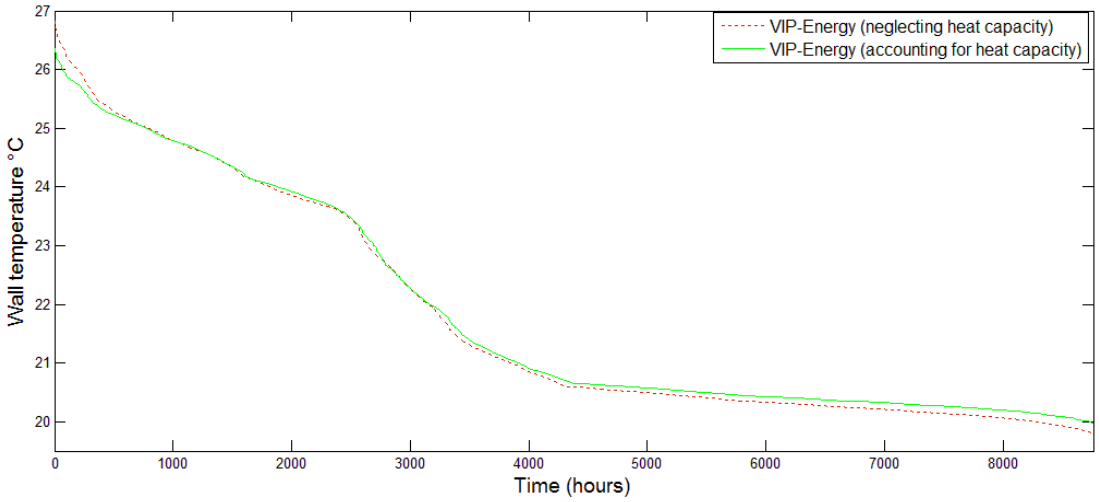

FIG 3. Wall temperatures during one year calculated in VIP-Energy accounting for thermal mass of interior construction elements and neglecting thermal mass of interior construction elements.

6. Constructive and functional impact on energy balance

Functional impact on the energy balance is studied with respect to varying operation of ventilation system and by taking into account different process energy distributions. Table 5 summarizes the mean room temperatures and demand of heating energy for 0% and 80 % ventilation heat recovery.

TABLE 5. Energy demand for heating and average indoor temperatures calculated with and without ventilation heat recovery.

	With 80% heat recovery		Without heat recovery	
Method	Energy demand (MWh/a)	T_{indoor}	Energy demand (MWh/a)	T_{indoor}
VIP -Energy (without zones)	8,82	22,03	17,55	22,18
VIP -Energy (with zones)	7,23	22,45	14,56	22,29
DTN	4,47	22,90	10,96	22,90

DTN calculates the lowest energy demand in both cases. Several factors can influence the lower values. In DTN the building is calculated for optimised conditions, where no air leakage or unwanted ventilation is assumed. VIP-Energy calculates with air leakage of 0.8 l/(m^2s), which equates to 3 MWh/a in zone calculations and 4.5 MWh/a when calculating without zones. Wind is taken care off in VIP-Energy so that the outer transient resistance is reduced and thus the U-values increases. In DTN no heat flow from ground is assumed whereas VIP-Energy calculates with heat exchange from the ground. When the whole building is regarded as on zone, then the energy for the upper floor is assumed to be 50 % of that for the whole building. This leads to an even higher heating demand for the upper floor. Heat losses through the ground have an even higher impact on the result.

With heat recovery DTN calculates 38.2 % lower heating demand, whereas without heat recovery DTN has only 24.7 % less heating demand. In DTN the ventilation is simply reduced to 20% whereas in VIP the efficiency for heat recovery in the ventilation system is set to 80%. From the energy balance we get that only in total 69 % of the energy losses due to ventilation are recovered. This is due to a function in the program that will reduce the heat recovery during warm periods in order to reduce high inner temperatures.

Further calculations in VIP – Energy were done considering different cases for ventilation, adapted process energy and sun protection. It turned out that through adapted ventilation system, the energy

demand can be decreased rapidly. From constant ventilation to different ventilation for day and night time already significant lower demands on both heating and cooling energy could be found. Even more effective use of ventilation could be achieved by temperature regulated ventilation. Different distributions of adapted process energy over the day may also make a significant influence of the inner temperature and the need for cooling. The possibility to divide the building in different zones and to be able to study the temperature variations and energy consumption in the coldest or warmest room is also a useful tool in VIP-Energy.

7. Long and short time effects

Thermal inertia of constructions is indicated by its response function. A constructions response function equates to the temporal gradient of heat flow caused by a single temperature step. For homogeneous material layers the response function can be calculated analytically in DTN and can therefore be considered as accurate. Thus the response function can be used as measure about how VIP-Energy takes into account thermal inertia. The in data used for heavy and light weight constructions are summarised in table 4.

Figure 4 shows the response functions for the heavy and light weight construction. Considering the heavy weight construction, the response function for VIP-Energy reacts directly whereas the analytical solution calculated by DTN shows a time lag of approximately three hours. After 15 hours the response functions overlap and fade to a reverse offset between the functions. Stationary values, where no difference between heat losses should occur anymore, are reached after 48 hours. The inner and outer surface thermal resistances in DTN are fixed. VIP-Energy does not use steady state values for the surface resistance they are a function of radiation and convection in the actual case and will vary during the calculation. It is not possible to know which values are used. Therefore the stationary value which should correlate to the thermal transmittance, U, of the construction will differ between VIP-Energy and DTN.

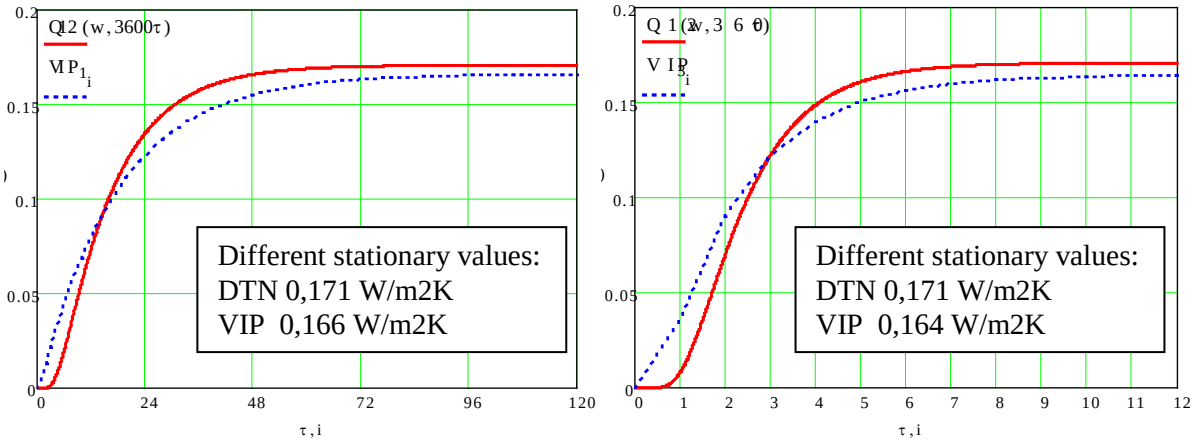

FIG 4. Response functions for the heavyweight construction (right) and for the lightweight construction (left).

The response functions show the same behaviour for the light weight construction, but the time lag is only approximately 0.5 hours. The functions overlap after 3 hours and no differences between heat losses are expected after 9 to 10 hours. Anyhow the stationary value for VIP-Energy is again lower than the constructions U-value.

8. Conclusions

The two energy calculation programs VIP-Energy and DTN have been compared. Focus has been on the ability to model the influence of thermal inertia in buildings. The studied parameters are energy consumption, variation of indoor temperature and variation and phase shift of transmission heat losses.

A student apartment in Luleå, Sweden, was used as study object. The calculations with the program VIP-Energy showed higher energy consumption then the DTN calculations. The differences can however be explained by different assumptions of air leakage and boundary conditions for the calculations and the two programs seem to predict similar energy consumptions.

Thermal inertia of constructions is indicated by its response to a single temperature step. The response function was tested on a simplified building model. The response function in VIP-Energy reacts much faster than the analytical calculated solution in DTN. The influence of thermal inertia may therefore be a little underestimated in VIP-Energy. After some time the response functions will overlap and change to a reverse offset between the functions so that the total heat loss will be the same for the two models. The response of a daily varying outdoor temperature and thermal load was also tested. The amplitude of the transmission heat losses is larger in the VIP-Energy model and the indoor temperature will therefore show a larger variation in that model. The total heat losses after 24 hours will however be the same for the two models.

A combination of the two calculation tools will be a good choice. The DTN methodology is to prefer to make detailed analyses and optimizations, especially for temperature cycles with a shorter period. VIP-Energy is to prefer when to analyse the complete energy balance including different HVAC systems with many options. The model can also be divided in different temperature zones to be able to reflect the real behaviour of a building.

9. Acknowledgements

We acknowledge the support from CERBOF – the Swedish Centre for Energy and Resource Efficiency in the Built Environment.

References

Claesson J. 2003. Dynamic thermal networks: a methodology to account for time-dependent heat conduction. Proceedings of the 2nd International Conference on Research in Building Physics. Leuven. Belgium. p. 407-415. ISBN 90 5809 565 7

Kalema T., Johanesson G., Hagengran P. & Elmarsson B. 2008. Accuracy of energy analysis of buildings: A comparison of a monthly energy balance method and simulation methods in calculating the energy consumption and the effect of thermal mass. Journal of Building Physics, 32 (2), pp. 101-130.

VIP-Energy.2010. VIP-Energy. Manual Version 1.5.0. Svensk. Structural Design Software 2010.

Wadsö L. et al. 2012. Energy saving through the utilization of the thermal behavior of heavy buildings, based on new materials, building frameworks and heat storage systems. http://www.byggnadsmaterial.lth.se/fileadmin/byggnadsmaterial/Research/CERBOF/Final_report_cerbof_project_heavy_buildings_number21.pdf [2013-02-15].

Wentzel E.-L. 2005. Thermal Modelling of Walls, Foundations and Whole Buildings Using Dynamic Thermal Networks. Doctoral thesis. Department of Building Technology. Chalmers University of Technology. ISSN 0346-718X.

Mathematical modeling of airflow velocity and temperature fields for experimental test houses

Jānis Ratnieks, B.Sc.[1]
Andris Jakovičs, Associate professor[1]
Staņislavs Gendelis Ph.D.[1]

[1] University of Latvia, Laboratory for Mathematical Modelling of Technological and Environmental Processes, Latvia

KEYWORDS: *CFD, energy efficiency*

SUMMARY:
Five equal size test houses of different constructional solutions have been built in Riga for building energy performance monitoring. Monitoring is done both during the heating and cooling seasons and necessary temperature is provided by an air-air type heat pump. An important issue regarding the heat pump is the coefficient of performance that changes for different outside temperatures. Therefore, even knowing the total power used by the heat pump, it is impossible to find out how much heat is taken into the room exactly. In this paper previously tested mathematical model is used to calculate coefficient of performance of the heat pump by exploiting the physical measurements of the inflow speed, temperature and air exchange in the room. A transient simulation is done results are compared to those of a stationary simulation and experiment. The integral model is also used to calculate coefficient of performance and compare it with numerical simulation.

1. Introduction

Energy efficiency of buildings and building materials is highly topical subject nowadays. To compare different building materials and constructions energy performance, five test houses with different constructional solutions have been built in Riga. The heating and cooling is done by air – air type heat pump (HP) that has velocity of 2 $m \cdot s^{-1}$. To try out different constructional options, a mathematical model is necessary as it is impossible to experimentally build a test house for every possible option. This experiment gives excellent verification options for the mathematical model.

The problem itself is transient both because the HP's cycle is time-dependent and because of fluctuating outside temperature. Period of time has been found form experimental data where temperature is constant and thermal radiation is negligibly small. These problems are studied in chapter 2 – experimental setup. Both - transient and stationary simulations have been made. The assumptions made, turbulence model used, meshing and other considerations regarding experimental implication in mathematical model are discussed in chapter 3 –modelling approach. The results acquired with mathematical model are compared with experimental data in chapter 4 – numerical results and discussion. Precision of numerical results are also discussed there.

2. Experimental setup

2.1 Test houses

As the detailed experimental setup is given in previous publication, the reader is referred to see the work of (Dimdina 2013) as only basic ideas are given here. The test houses (fig.1) are built of equal inner dimensions and cover the main locally produced building materials such as wood logs, ceramic bricks, aerated concrete and rock wool. The inner dimensions are 3x3x3 m that gives the total volume of 27 m^3. The calculated U-value is 0.16 $W \cdot m^{-2} \cdot K^{-1}$ for each construction therefore the expected heat

consumption is equal for every building type. The façade of all the houses are made ventilated to ensure equal conditions for every house. The data are gathered every minute for both the meteo station and sensors inside the building (fig.1).

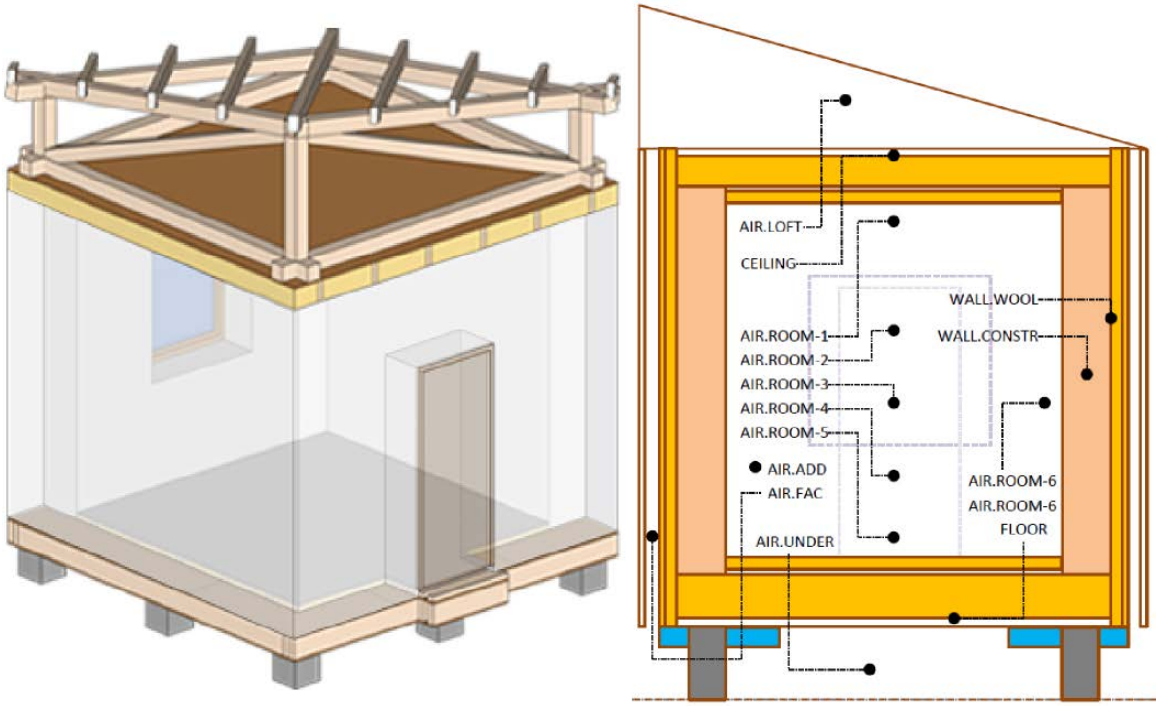

FIG 1. A) Test house geometry and B) monitoring sensor positions.

2.2 Heating cycles

Heating and cooling in test hoses are done with air – air type HPs that are located above doors (fig. 1) and ventilation opening is above the window. The air exchange (Gendelis 2013) in the test buildings have been measured to be n = 0.45 h^{-1}. This means that part of the air that is taken into the room by HP is forwarded to ventilation and some are taken back by the HP. The air – air type heat pump make a rectangular cycle every 51 second by changing the inflow angles form -45° to 45° on the horizontal plane and from -30° to -70°on vertical plane with respect to line that is made by cross section of both planes according to (Daikin Ltd. 2012). This makes the problem time dependent, as the transient simulations are computer resource demanding, it was decided to see if the stationary solution is a good approximation. For the latter the inflow angle was set constant for horizontal plane – 50° and for vertical plane 0°.

As the mathematical model is developed also for stationary case it is necessary to find a period of time when temperature is constant or at least changes a little around some fixed value. Such situation does not often appear in nature however, a period of time was selected from monitored data for outside temperature 5.1 °C that lasted for 2 h 52 min. The corresponding inside temperature should go asymptotically to a stationary temperature if the heating is done continuously with equal power. In experiment however temperature experiences a cyclic behaviour (fig. 2). This means that the HP is making some heating cycles with higher power then the rest. From temperature values it can be seen that last two cycles are approximately the same. Unfortunately no minute by minute power data are present during this particular cycle, only the heat consumption that cannot resolve the time when power was increased.

For the simplicity of the model and the lack of specific experimental data regarding inflow temperature and velocity the average data from experiment were taken into account for model verification. As it is not possible to find out how much mass is taken into the room, additional airflow velocity and temperature measurements were carried out.

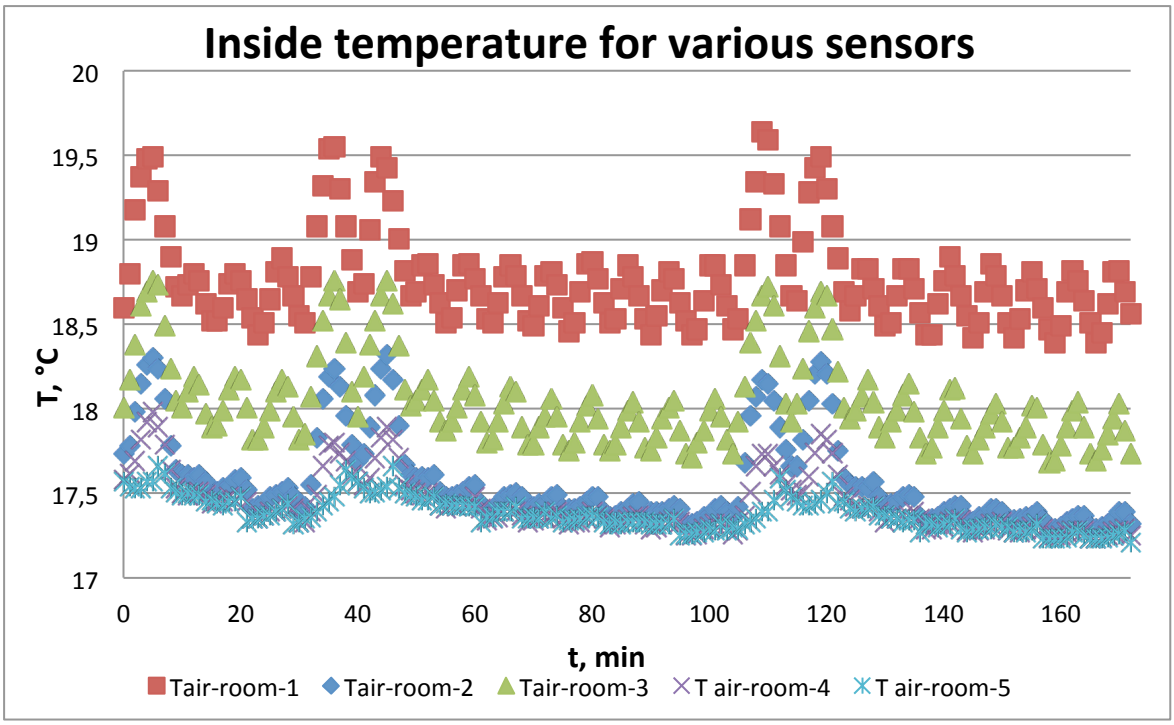

FIG 2. Inside temperature at monitoring points during the period of stationary temperature outside.

3. Modelling approach

3.1 Mathematical model

3.1.1 Governing equations and boundary conditions

For numerical realization the ANSYS/CFX program packet were used. The fluid flow is governed by Navier – Stokes (NS) equations that cannot be solved for this problem so the Reynolds averaged NS equations were used. These equations are derived multiple times in various standard texts on fluid dynamics like (Batchelor 1967) and (Versteeg 1995). The equation implementation in Ansys/CFX environment is described in user guide (Ansys Inc. 2011). Wall functions were used on solid – fluid interfaces that correspond to no slip conditions. Air inlet was defined as a constant mass flux and temperature with time-dependent or stationary direction depending on case. For air feedback to HP a constant mass flux boundary conditions were used because the free total flux would produce a negative outflow at some part of the boundary. For ventilation boundary there was an “opening” type boundary conditions where the relative pressure and outside temperature are defined. This was done to ensure that mass is conserved.

3.1.2 Model assumptions and numerical realisation

The thermal radiation was not taken into account because the radiation from wall to wall is negligibly small and there were negligibly small amount of thermal radiation in the night from the windows. As the air velocities are high – 2 $m \cdot s^{-1}$ the flow is turbulent and therefore a turbulence model was needed. The k-omega shear stress transport model was chosen, because it is robust and performs well both in the volume and near wall region. For buoyancy the *Boussinesq* approximation was used.

The initial conditions were taken as average temperature in test house that was T=17.84°C and the final result from stationary simulation were given as an initial condition for transient simulation. The transient simulation was run for 6 full cycles with time step of 0.05 s. With the given mesh the time required for simulation was 8 days on 3.2 GHz processor with 7 cores.

3.1.3 Geometry and meshing

As the test houses are built with from many layers that are slim or inhomogeneous, the model was simplified and the effective values of heat transfer coefficient, density and heat capacity were used. The meshes were made different for stationary and transient simulations to reduce computational time (Ozolinsh et.al. 2013). For stationary simulations results for coarser and finer mesh were compared.

3.2 Balance calculation and HP efficiency

The numerical simulation is only an approximation and convergence usually doesn't ensure that results are physically consistent. Heat balance for the model must show that heat gains are the same as heat loses. The heat gains by inflow and loses by both – the ventilation and feedback are calculated (1) as integral over surface (Ozolinsh et.al. 2013).

$$P_j = c_p \cdot \rho \oiint T \cdot \vec{v} \cdot d\vec{S} \qquad (1)$$

Where P_j – power by mass flux through boundary (W)
c_p – heat capacity at constant pressure (J/(kg·K))
ρ – density (kg/m^3)
T – temperature (K)
$\vec{v}$ – airflow velocity (m/s)

Heat loses through walls are calculated (2) as heat flux through outer surfaces.

$$P_\Phi = \oiint \Phi \cdot d\vec{S} \qquad (2)$$

Where P_Φ – power due to heat flux through solid material surface (W)
$\vec{\Phi}$ – heat flux (W/m^2)

For the various inflow temperatures the average temperature from the experimental points can be determined and compared to the experimental average. By doing two stationary calculations with the different temperatures interpolation can be done to find the inflow temperature that makes model average equal to experiment average. From these calculations the HP coefficient of performance can be determined by mathematical modelling. This result can be compared to integral model by taking into account experimental values.

4. Numerical results and discussion

To compare numerical experiments mutually a line perpendicular to the floor in the middle of room is considered. This is done because there are experimentally measured temperatures (fig. 1b) along it. The temperatures for stationary case are taken directly from final solution, but for transient case averaged over last HP cycle. For the verification that after six HP cycles the flow is stationary, the results were compared between the last two cycles and the difference was negligibly small.

The approximation that in the given time, when outside temperature is almost constant, heat flux through wall is quasi stationary will be better for constructions with lower heat capacity. Therefore for calculation the lightweight construction (made of plywood and rock wool) were taken and experimental data from this particular house was used for verification.

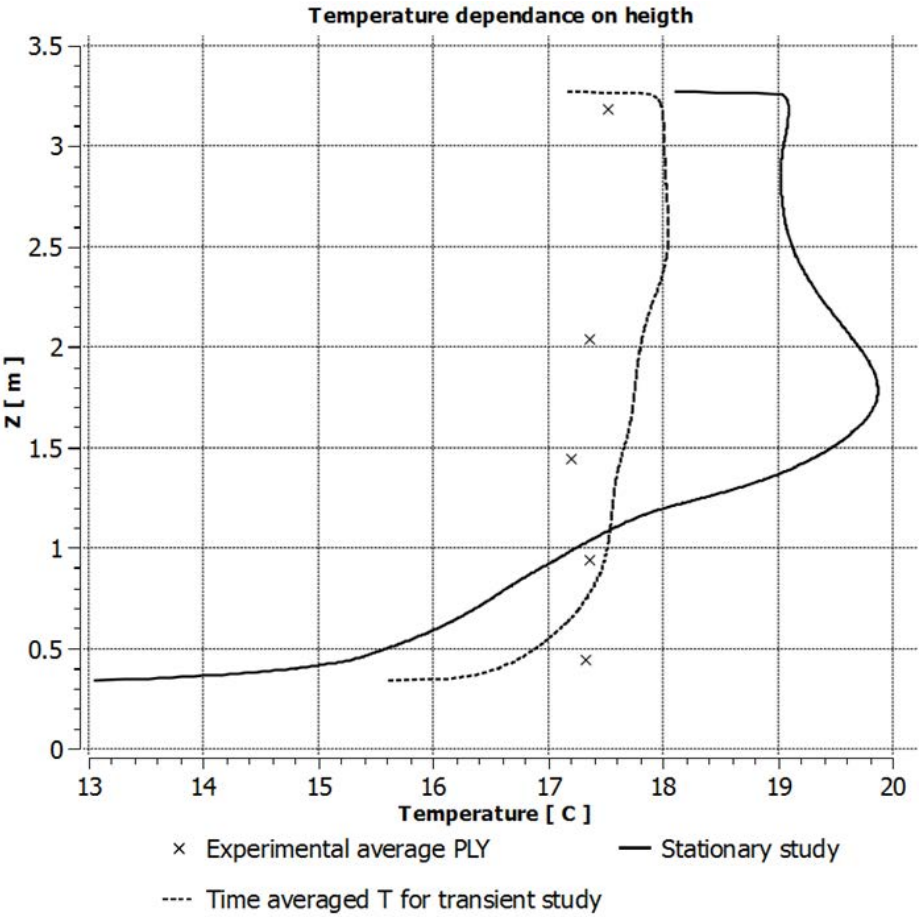

FIG 3. Temperatures at the middle line for mathematical models and experimental data.

The heat balance were computed (eqs. 1, 2) and the results (table 1) show that the heat balance is off by approximately 3%. This means that although the convergence was set to be 10^{-4} for maximum residual, the total error is considerably higher. This is due to third type boundary conditions. The temperature is not fixed at any point and therefore an error can occur.

TABLE 1. Heat balance for numerical simulation.

Heat gain	
Inflow	697.0
Heat loses due to ventilation	
Ventilation	-55.6
Feedback	-537.0
Heat loses due conduction	
Window	-15.0
Wall	-71.1
Floor	-15.8
Ceiling	-25.0
Doors	-13.1
Total loses	**-732.5**
Error, %	5

Temperature and velocity field plots (figs 4 and 5) for stationary simulation show that results are physically consistent. The overall velocity profiles are as expected and at the near wall region the flow are downward as expected for cold wall.

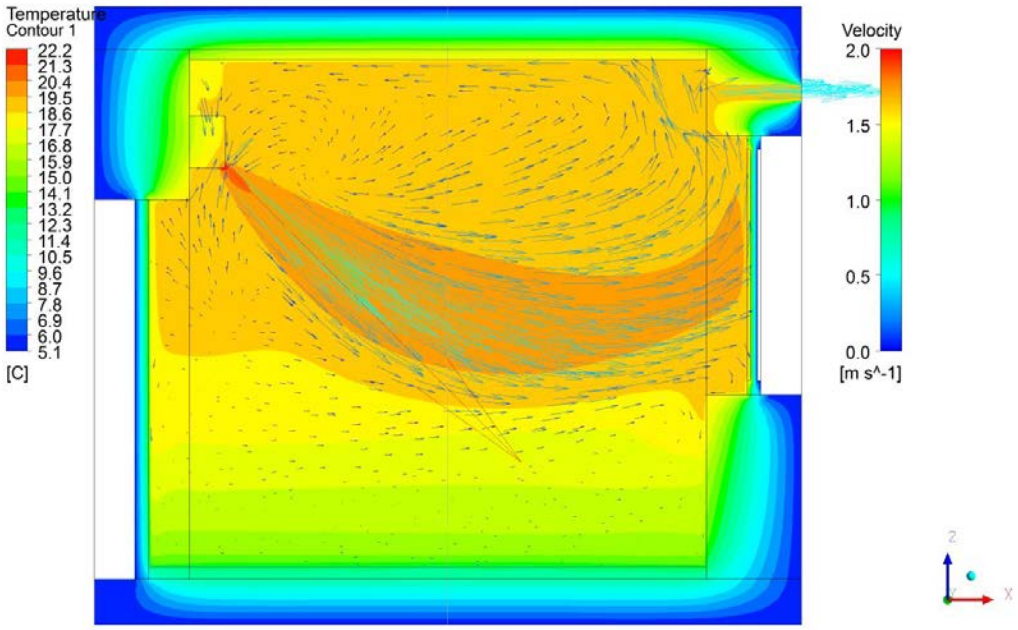

FIG 4. Temperature and velocity field for stationary study.

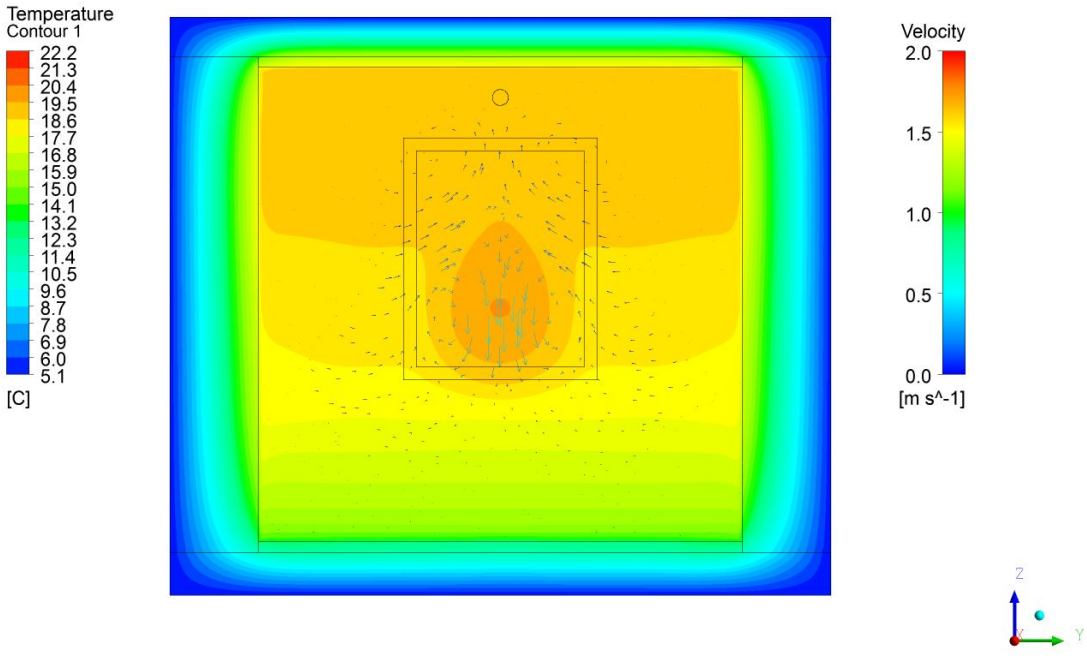

FIG 5. Temperature and velocity field for stationary study.

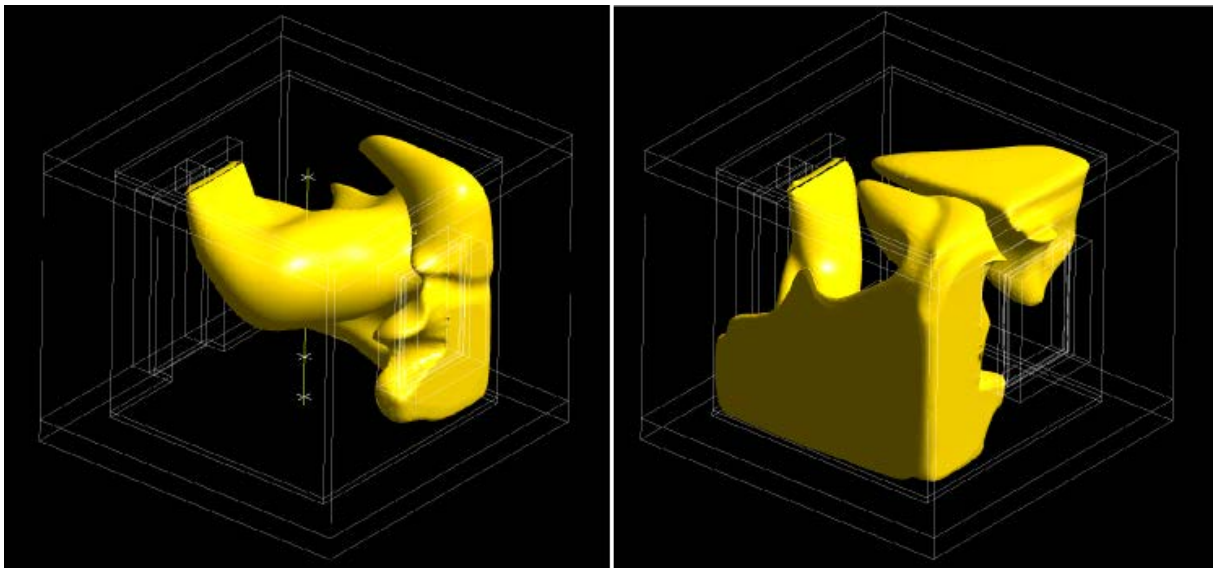

FIG 6. 18 °C isosurfaces at various time for transient study.

5. Conclusions

Mathematical model for airflow in the test houses have been set up and two types of calculations done. The numerical results seem to be qualitatively correct as the airflow directions at near wall regions tend to be physically consistent. Also the temperature gradients in the solid are as expected.

As it can be seen, stationary and transient model give similar volume average temperatures for the room, but the experimental point average is higher than model predictions. This is due to inflow angle that is directed toward the experimental point location. The values for each individual experimental point vary significantly in stationary model for points closer to ceiling and floor. This is due to bad mixing that stationary model offer. The transient model however gives much better results as the changing inflow ensures better mixing. Therefore we can conclude that for precise temperature fields in the room the stationary model is insufficient and transient model should be used. If, for example, only the average temperature of the room is necessary, the stationary model could be sufficient, but more tests for different temperatures must be made to verify this claim.

An important drawback for this model is that the power data weren't available at the time these measurements were carried out. The data is available now and therefore time averaging will be avoided in future studies and the full heating cycle will be included.

The first experimental results show that there are houses that perform in similar manner and therefore it has been decided to test the COP value for heat pump by letting the heating be done by inefficient heater that have COP value of unity.

6. Acknowledgements

This research was done at the University of Latvia with the financial support of European Regional Development fund support. Project nr. 2011/0003/2DP/2.1.1.1.0/10/APIA/VIAA/041

References

Ansys Inc. Ansys CFX user guide

Batchelor G.K. 1967 An introduction to fluid dynamics, Cambridge university press, ISBN 0 521 66396 2

Daikin Industries Ltd. 2012 Daikin room air conditioner user manual

Dimdina I. Jakovics A., Gendelis S., Klavins J. 2013. A Testing Ground for Measuring Influence of Building Envelope Materials on Energy Efficiency and Indoor Environment, Proceedings of the 11th REHVA World Congress & 8th International Conference on IAQVEC – CLIMA 2013

Gendelis S., Jakovics A., Nitijevskis A., Ratnieks J. 2013 Comparison of Different Air Tightness and Air Exchange Rate Measurements in Very Small Test Buildings, 34th AIVC conference: "Energy conservation technologies for mitigation and adaptation in the built environment: the role of ventilation strategies and smart materials". Athens, Greece, 2013

Ozolinsh A., Jakovics A., Ratnieks J., Gendelis S. 2013 Numerical Modelling of Humidity and Temperature Conditions in Buildings with Different Boundary Structures, Proceedings of the 11th REHVA World Congress & 8th International Conference on IAQVEC – CLIMA 2013

Ratnieks J. Jakovics A., Gendelis S. 2013. Stationary Heat Transfer and Airflow Simulation for Test Polygon Houses, CYSENI 2013, 10th international conference of young scientists on energy issues, Kaunas, Lithuania May 29-31, 2013 p. VI – 382-389

Versteeg H.K. Malalasekera W. 1995 An Introduction to Computational Fluid Dynamics. The Finite Volume Method, Longman group Ltd., ISBN 0 582 21884 5

A new Passive House Design Tool and its Application in Cold Climates

Florian Antretter, M.Eng. [1]
Marcus Fink, Dipl.-Ing. (FH) [1]

[1] Fraunhofer-Institut für Bauphysik, Germany

KEYWORDS: *hygrothermal building simulation; energy assessment; low energy buildings; passive houses*

SUMMARY:
Due to an increasing demand for sustainable low energy buildings, the application of the passive house design methodology spreads worldwide. The methodology applied to balance monthly heat gains and losses is developed for fast energy demand investigations in moderate climates; issues can occur in other climate zones. Furthermore, the hygrothermal effects within the building and the building components are neglected. The monthly method is not suitable for moisture relevant risk management, nor is it for transient effects that influence the building energy performance. This leads to the requirement of a dynamic simulation.

A new user friendly software tool is available that couples the established passive house design methodology, for quite instant energy demand simulation results, with an sophisticated hygrothermal dynamic simulation. The dynamic whole building simulation is based on a detailed building component model simulating the coupled heat and moisture transfer and a multi-zone building model, calculating hourly indoor climate and energy demand.

An advantage of the new tool is the opportunity to work with only one building model while conducting a monthly balance based energy assessment or a dynamic hygrothermal whole building simulation. The graphical user interface exchanges a small amount of parameters which are required by the respective setting. Additionally some results of the monthly method may be used automatically as approach for the dynamic simulation.

This paper includes the description of the coupling of both methodologies and an application example, explaining the usage of the tool for a building in cold climates. Furthermore the possible additional and in-depth analysis options and results by the application of the new tool are shown as well as some recommendations for the design process in cold climates.

1. Introduction

While designing energy-efficient buildings, a designer often uses different approaches to tweak the building in terms of energy efficiency, comfort and hygrothermal performance of the components. Common approaches for the assessment - and also for the certification - of the energy demand rely on steady state methods, using monthly balances, to compute the values used for the estimation of energy demand and for comparing different building designs under predefined boundary conditions. Those methods exclude all transient effects in buildings like the effects of thermal inertia. A comprehensive analysis of comfort conditions indoors is also not possible.

This causes the designer to switch to a dynamic whole-building model using hourly data to evaluate the dynamic behavior of the building. Often, very new and innovative building component

configurations are employed to meet the stringent energy criteria. Therefore, a third step is critical to performance and quality assurance: assessing the hygrothermal performance of envelope components. This third step evaluates the most critical components by employing a hygrothermal component simulation model.

This paper shows the development of a single tool that integrates all three steps. A steady-state approach for assessing the energy performance is combined with the dynamic modeling features of a whole-building simulation model including a full-scale hygrothermal component analysis.

2. Simulation Methodology

This section describes in short the basic equations for the calculation of the steady-state and dynamic model. Furthermore, it describes how integration into one tool for energy, comfort and hygrothermal component performance was implemented in the new WUFI Passive software.

2.1 Methodology for passive house assessment

The monthly balance based method depends strongly on overall heat transfer coefficients, temperature difference and considered time period. It is in accordance with the DIN EN ISO 13790, in particular the simplified approach. The heat transfer coefficient, the reciprocal of the thermal resistance, is an important input value for opaque components. It is calculated from the thermal conductivity and layer thickness of the building envelope materials. For transparent components, the heat transfer coefficient is input data. The monthly heat losses across the building envelope are calculated by determining the heat transfer coefficients, areas of the components and the appropriate temperature differences according to component location. The external boundary condition of exterior walls can be the ambient air temperature, it can also be the ground temperature in case of a basement wall or an increased or decreased derivative of the ambient air temperature in cases of attached spaces exterior of the thermal envelope, such as garages. With the temperature difference and a considered time period, the heating degree hours are calculated following [Feist 1992, Feist et.al. 2007]. Monthly heating degree hours consider the hour count of a month. The period under consideration for the annual demand depends on the monthly difference between the heat losses and the heat gains. If this difference is greater than 0.1 kWh the month will be considered in the calculation of the total annual heating demand. This means that the period under observation could be varying between the different cases. Ventilation heat losses are calculated considering the effective air change rate, building volume, effective heat recovery efficiency and annual heating degree hours as well.

Climate data contains information on the solar radiation for north, east, south, west and horizontal. Each component is associated with a cardinal or horizontal direction. For transparent components, the solar heat gain is calculated considering heat transmittance, shading reduction factors due to obstructions, overhangs and reveals. The solar heat gain of opaque components is computed considering the exterior absorptivity and emissivity. The required heating demand, over a specified time period, is calculated following [Feist et.al. 2007] and in accordance with [EN ISO 13790].

The monthly utilization factors indicate how much of the available heat gains can be used to counteract the heating demand during the heating period. It is calculated from the heat gain and loss ratio and a so-called time constant, depending on the internal heat capacity and the total heat loss coefficient of the building. For the time constant equation a continuously heated building (more than

12 hours per day) is considered.

The monthly losses are calculated using monthly heating degree hours and the annual losses using annual heating degree hours. The total heating demand, including the transmission heat losses for all components and thermal bridges and the ventilation heat loss is decreased by the total heat gain comprised of the solar and internal heat gain, multiplied by a utilization factor. Monthly heating degree hours are determined multiplying the hour count of the month with a temperature difference.

One of the passive house certification criteria is the total annual primary energy demand. To calculate the primary energy demand of a building the electrical and non-electrical demand of the mechanical system, including auxiliary energy, plug loads, appliances and lighting are summed up. The heating demand of the domestic hot water production and distribution is taken into account and if solar hot water generation is used, it is reduced by an estimated solar fraction. It is assumed that the energy use by any device or service is not necessarily continuous. The uses are either reduced by different usage or utilization factors stemming from predetermined utilization patterns or a certain frequency is assumed for each usage. If such energy use takes place within the thermal envelope it is added to the internal heat gains. Heat gains from people are already included in the heat gains. Then an annual specific internal heat gain is estimated. The total is then multiplied by the treated floor area and hours of the month resulting in the total monthly internal heat gains.

In addition to the heating demand the cooling demand is calculated using a very similar algorithm. One difference is that the heat gains are not weighted by the utilization factor as the heat losses are.

2.2 Hygrothermal whole building simulation

The dynamic hygrothermal simulation combines single building components such as walls, floors, and roofs to be modeled as a whole building. Coupled heat and moisture transport is simulated for each opaque component composed of different layers of materials such as wood, insulation, membranes or even air layers. This model was developed by Künzel [Künzel, 1994]. It considers capillary action, diffusion and vapor ab- and desorption. The conductive heat and enthalpy flow by vapor diffusion with phase changes strongly depends on the moisture field. The vapor flow is simultaneously governed by the temperature and moisture field due to the exponential changes of the saturation vapor pressure with temperature. Resulting differential equations are discretized by means of an implicit finite volume method. The component model was validated by comparing its simulation results with measured data of extensive field experiments [Künzel, 1994]. The temperature and moisture field within the component is simulated as a result of the model.

Coupling all the envelope components leads to the multi-zone building model. A zone constitutes one or more rooms with the same indoor climate. The zone boundaries are the components. There is also an outdoor zone. The outdoor climate is specified by location in the climate files assuming that the building itself does not influence the climate. However, the indoor climate is influenced by the simulation results of the component and vice versa - the component simulation is influenced by the indoor climate. Considering this interaction the indoor climate can be simulated. With every time step the zone temperature and humidity values are generated by solving heat- and moisture balance equations [Lengsfeld, Holm, 2007]. Besides the heat and moisture flow across the building the envelope internal heat and moisture sources and sinks are taken into account. They are caused by

people, lighting, mechanical equipment, infiltration and solar radiation. Such sources or sinks cannot only occur in the zones of the building itself but can also occur in the building envelope component with a direct influence on the heat- and moisture field of the component. Additionally transparent components, like windows, can be modeled more accurately. The solar transmission that passes through a transparent component is calculated taking into account the sun elevation and azimuth angle and the orientation and inclination of the component. Solar heat gain contributions that pass through the transparent components are apportioned out directly to the indoor air and to the inner-surfaces of opaque components according to a defined percentage (user defined, or estimated according to surface area). Besides the short wave solar irradiation also the long wave balance is considered for the opaque building components. Therefore not only the solar heat gains but also the long wave irradiation losses can be calculated.

The zone model was validated via cross-validation with other tools, experiments and standards like [ASHRAE 140, 2007]. The validation of both - the energetic and the hygric part of the zone model - is described in [Antretter et.al. 2011]. Currently the ideal mechanical system has the capacity to supply all minimized heating, cooling, humidification, dehumidification and mechanical ventilation loads. As long as the system's capacity is sufficient the indoor temperature and moisture can be maintained between defined design conditions and thus the hourly demand can be calculated. If the capacity is not sufficient then the temperature or moisture will rise above or fall below the specified design conditions. If there is no ideal mechanical equipment defined, a "free floating" indoor climate is simulated.

Every time step depends strongly on the previous steps because of the water content and thermal energy storage within the envelope and the air in the zones. A time step is characterized by these dynamic previous variables. New boundary conditions are created with each time step and varying input data like the outdoor climate. Using these initialization values the coupled heat and moisture transport is calculated and consequently the zone heat and moisture balance equations are created. Should these balances not be within an expected defined accuracy of the simulation then the indoor temperature and relative humidity is iteratively adapted.

2.3 Coupling of both methods

Both models, the monthly passive house calculation and the dynamic whole building simulation, rely on user inputs and assumptions. Some inputs are pre-defined, such as specific building materials, their dimensions, location and orientation. Some have to be estimated by measurements or experience.

The pre-defined input is fundamentally the same for both models, though quite more detailed for the dynamic simulation - not only because of the additional consideration of moisture. However, the building geometry, room and component dimensions, widths and heights, roof inclination are the same. Fenestration parameters like solar heat gain coefficients, frame geometries, shading reduction factors and many other boundary conditions such as the design indoor temperature, the overheating limit temperature and the natural air change rate are the same as well.

More different is the climate data. For the monthly method only monthly mean values for temperatures and solar radiation are necessary. For the dynamic hourly simulation, hourly input data for the outdoor climate must be provided. For the more detailed radiation calculation hourly diffuse and direct global solar radiation data is required. The static calculation method estimates ground

temperatures according to the given location and boundary conditions; those values can be used for the climate of the ground for the simulation by converting the data into a useable ground climate format. Additionally needed is information on wind velocity and the quantity of rainfall to calculate the driving rain on the external surfaces as well as the relative humidity of the outdoor climate to calculate the moisture balance. Aside from pre-defined input data some results of the steady-state method can be used for the dynamic simulation, as for example the mechanical ventilation volume flow rates for summer and winter ventilation, the simplified effective heat recovery efficiency, the space heating and cooling capacities of the mechanical equipment. Internal heat sources due to people, lighting, household and mechanical equipment are the same, but also have to be supplemented with moisture characteristics. For the monthly method it is possible to calculate these sources using a utilization factor depending on the average usage. For the dynamic hourly simulation this is a good first assumption, but it might be more realistic to create specific time schedules.

Basically, the main difference of both models is the level of detail. A much more detailed simulation needs more time to compute. The monthly method is fast. An ordinary PC can compute all results in real-time. The dynamic results may need some minutes up to some hours, depending on the complexity of the building model. Within the dynamic simulation not only the indoor air temperature is simulated. In addition the surface temperature of the surroundings of a room, e.g. to calculate the operative temperature, is computed and, once more, also the humidity. Assessments of comfort conditions become possible once those values have been generated. The predicted mean vote (PMV) or the predicted percentage of dissatisfied (PPD) is calculated hourly. Even if generally accepted boundary conditions are exceeded one can assess how long they will be exceeded.

The combination of both models using many of the same initial inputs, results in numerous positive synergy effects. On one hand it is possible to obtain very fast results using only the monthly method, including heating, cooling, electricity and primary energy demand and on the other, with some more calculation time, it is possible to get detailed information on risk of mould growth, rotting of components and of course detailed information on interior comfort conditions.

2.4 Basic application process

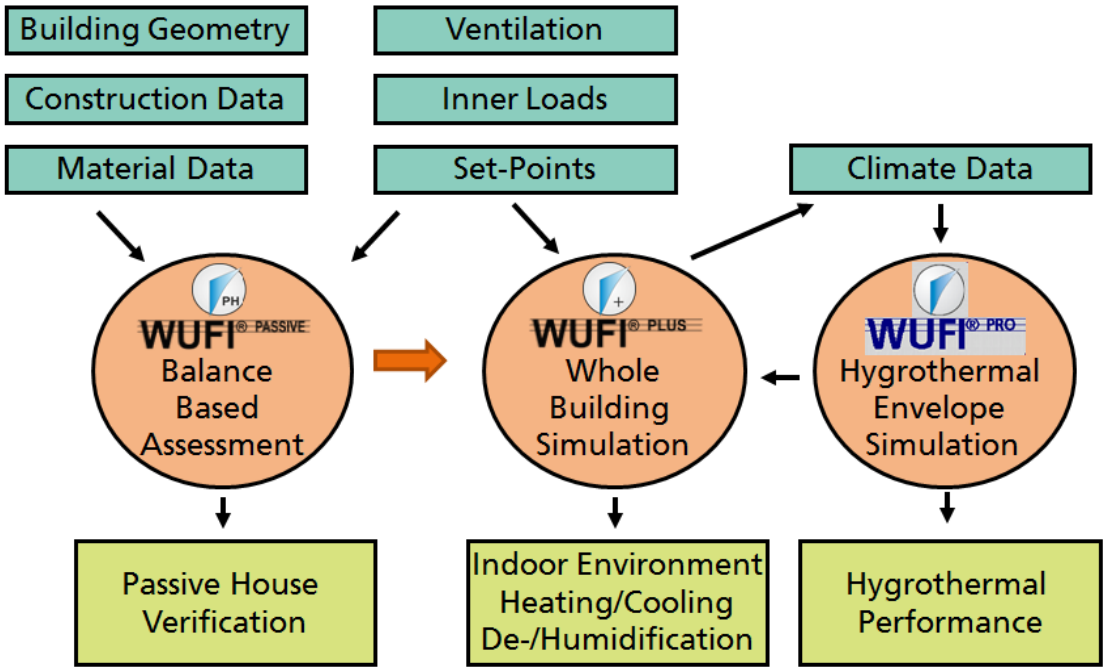

Figure 1: Inputs, interaction and outputs of the different parts of the simulation engine

To simulate a building different inputs for the desired results are necessary, as shown Figure 1. Typically a user starts with the passive house calculation. The first thing to do is to input the building geometry including structure, material, location and all essential passive house verification data. Once the geometry is set, thermal bridges and windows can be defined. The next step is to define the usage of the building (residential or non-residential) as the next input for inner loads is different for each type. Last but not least the user has to define the mechanical equipment. Therefore different systems for e.g. heating, domestic hot water production and ventilation can be defined as well as information about the distribution system. The software gives feedback at all times during the entry process to inform the user about still missing inputs and provides reasonable input values as well as explanations regarding the current input parameter. Once all inputs are complete, the heating demand and all other passive house verification results are calculated instantly.

For the dynamic hygrothermal simulation a user can switch to the “WUFI Plus” mode once the main passive house criteria are met to a degree. Some input screens change to the dynamic relevant input data. Certain boundary conditions are not applied automatically because more detailed information may be required (like the indoor set point temperature, which can be defined via time schedule), but there is an option to choose them with one click. If a user has used building materials or assemblies provided within the database, no additional information is needed but some additional parameters such as indoor moisture loads should be defined. The software will check all inputs for completeness and prompt the user for missing information before the simulation can start. During the simulation a user can monitor movies for the heat and moisture profiles of each component or the hourly heating demand. If the simulation is finished, detailed reports and graphs illustrate the

simulation results.

3. Application Example

In this example, a residential building in Göteborg, Sweden, is analyzed using WUFI® Plus simulation and the static passive house calculation approach. Results for heating demand are compared and further investigations of possible moisture risks are conducted.

3.1 Simulation Model and Boundary Conditions

3.1.1 Climate

Hourly values of the outdoor climate are required for the dynamic simulation which are available in the WUFI® Plus database (Figure 2, Figure 3). In contrast, the passive-house calculation method is based on monthly mean values. The climate of Göteborg has an amplitude of 48°C with 29.4°C as maximum and -18.6°C as minimum. There is also a significant amount of driving rain from the south.

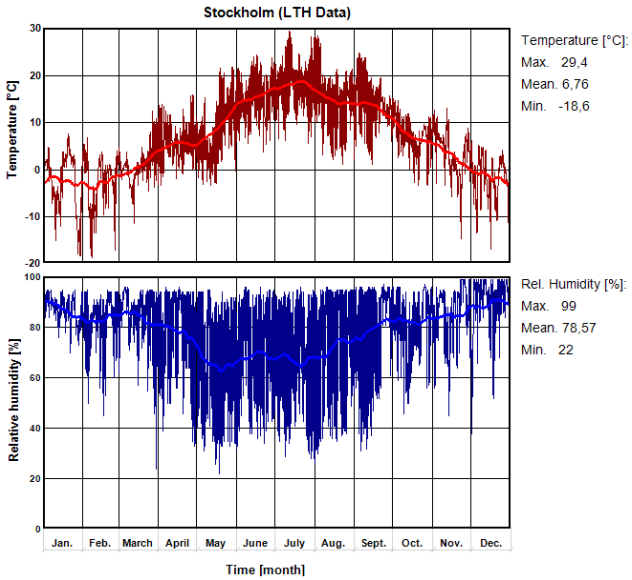

Figure 2: Outdoor climate - temperature and rel. humidity

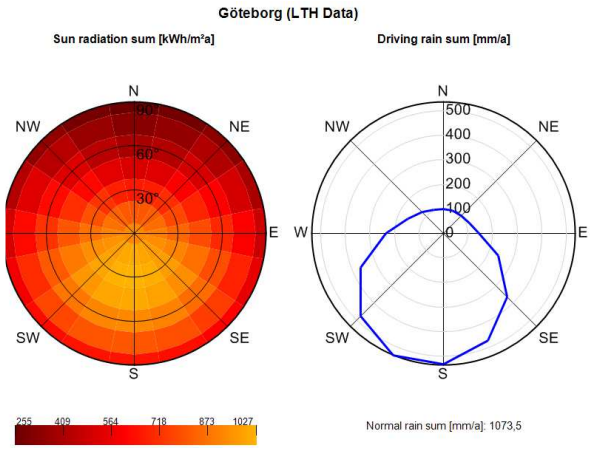

Figure 3: Outdoor climate - sun radiation and driving rain

3.1.2 Building and HVAC System

Within the framework of this paper a typical residential building model (Figure 4) has been used for both – the dynamic simulation as well as the static passive-house calculation method. The type of the residential building is a free-standing, two-story house with average wind exposure. In general, the assemblies of the building represent a typical Swedish construction type and are taken from (http://www.scanhome.ie/passive.php, also see 3.1.3). For detailed analysis, the building is subdivided into ten zones with individual internal loads and boundary conditions.

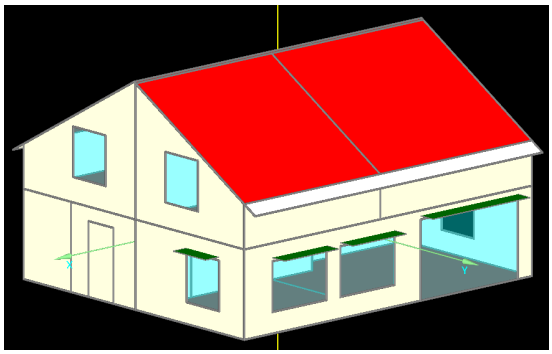

Figure 4: Reference Building 3D view

A heat pump with a capacity to ensure the indoor design conditions are met at any time for most of the zones (e.g. not for storage room) is used. Furthermore, a ventilation system with heat recovery efficiency of 85% is

installed. The use of photovoltaic or solar modules is not included in this case.

3.1.3 Components

The building envelope is specified that it fulfills the passive-house standard requirements of <= 15 kWh/m²a. For simplification, the construction is assumed to be without thermal bridges. For more information regarding the U-Values of the components see Table 1. As an example the exterior wall assembly is displayed in Figure 5.

Table 1: U-Values of components

Component	U-Value in [W/m²K]
Exterior Wall	0.14 [W/m²K]
Interior Wall *	1.93 [W/m²K]
Roof	0.13 [W/m²K]
Ceiling *	1.10 [W/m²K]
Floor Slab	0.14 [W/m²K]
Exterior Door	0.23 [W/m²K]
Interior Door *	1.76 [W/m²K]
Windows	0.80 [W/m²K], SHGC = 0.55

* (only relevant for heat storage)

Inhomogenous layers
Thermal resistance: 6,749 / 8,091 m²K/W (EN ISO 6946 / homogenous layers)
Heat transfer coefficient(U-Value): 0,14 W/m²K

Thickness: 0,337 m

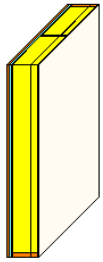

Nr.	Material/Layer (from outside to inside)	ρ [kg/m³]	c [J/kgK]	λ [W/mK]	Thickness [m]	Color
1	Hardwood	650	1500	0,13	0,022	
2	Air Layer 20 mm	1,3	1000	0,13	0,022	
3	Fibreboard with Paper Sheathing (one Surface)	284,4	1880	0,048	0,009	
4	Cellulose Fibre Insulation New (yellow)	30	1880	0,036	0,2	
5	vapour retarder (sd=100m)	130	2300	2,3	0,001	
6	Cellulose Fibre Insulation New (yellow)	30	1880	0,036	0,07	
7	Interior Plaster (Gypsum Plaster)	850	850	0,2	0,013	

Figure 5: Exterior wall assembly

3.1.4 Inner Loads and Design Conditions

The internal loads are set to the passive-house defaults for residential buildings (=2.1 W/m² treated floor area, in this case a total of 166.2 m²). For better comparison of the results between simulation and static calculation method, the internal loads are kept constant the whole day. The heat distribution to the room is 2/3 convective and 1/3 radiant.

The design minimum indoor temperature is set to 20°C for each zone apart from the stairway and storage room and the maximum temperature for overheating is defined to 25°C. If the set-point of 20°C is not reached, ideal heating is provided to the space up to the maximum heating power. Cooling devices are not available.

3.1.5 Ventilation

The building is constructed in such way, that a blower door test would result to n50 = 0.5 1/h which is below the passive-house requirements of 0.6 1/h. Empirical values suggest that a blower door test of 0.5 1/h corresponds to an infiltration rate of 0.03 1/h for this building. For sufficient fresh air supply a mechanical system is installed which runs at an air change rate of 0.35 1/h. The heat recovery efficiency is set to 85%. Manual window opening is not considered in this study.

3.1.6 Shading

For the simulation, a general shading factor (which is active at all-time) due to trees or neighboring buildings is specified to 0.9 (meaning reduction of incoming solar radiation of 10%). Furthermore, for the windows of the living room, there are overhangs of 50cm attached. To reduce overheating in the summer, a temporary sun protection (of 75% solar reduction) gets triggered whenever the design

temperature of 25°C is about to be exceeded. The shading for the static calculation method is estimated by the general factor, overhangs, reveal depth and shading objects.

3.2 Passive House Results

3.2.1 Passive House criteria

Apart from the heating load, all passive house criteria are met. Figure 5 shows a summary of all relevant values.

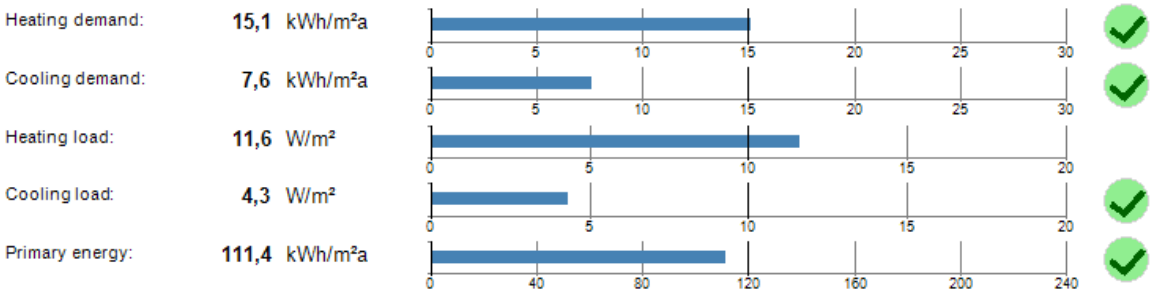

Figure 6: Passive-House criteria

3.2.2 Energy balance

The energy balances for the heating and cooling period are summarized in two graphs (Figure 7). In this case, the heat losses via windows are substantial to the overall heat losses during the winter months. For each section there are more detailed information provided for further analysis.

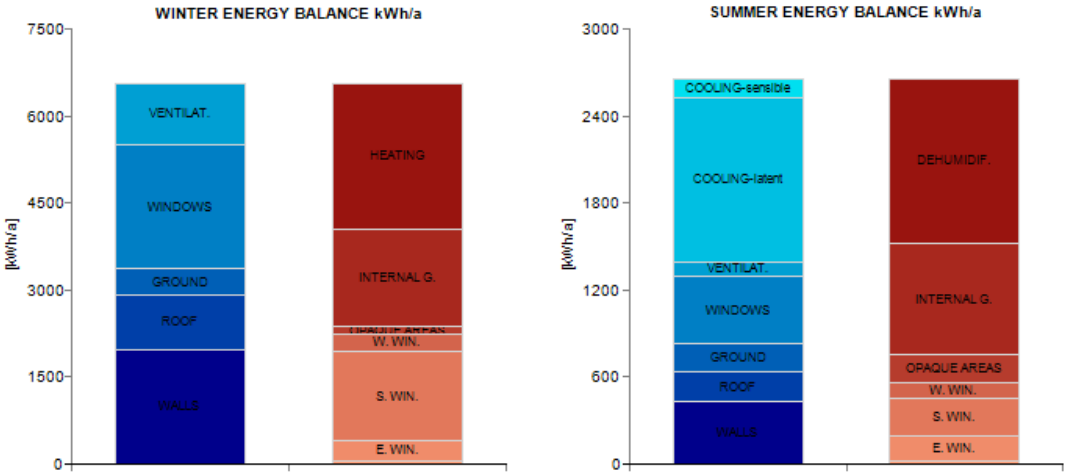

Figure 7: Passive-House result - energy balance

In case of windows for example there is an overview available (Figure 8), which can be used to quickly see the weak spots as well as detailed calculation for each window.

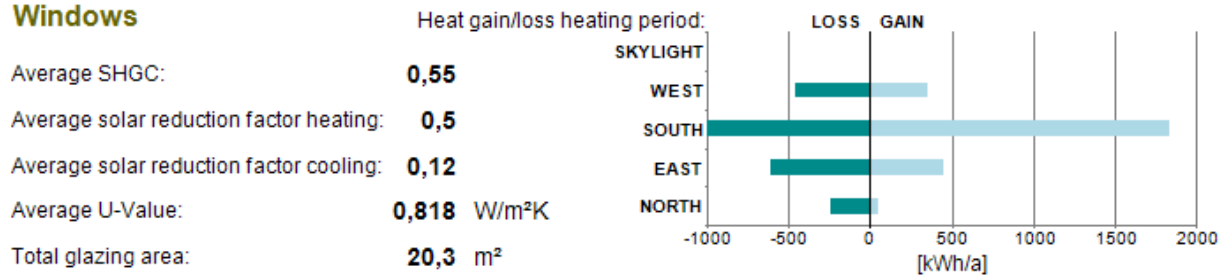

Figure 8: Passive-House result - window overview

A comprehensive output report is created, that shows all energy fluxes on building envelope, zone and systems level. All information required for certification is also included.

3.3 Dynamic Building Simulation Results

3.3.1 Main results

After completing the simulation, the main simulation results are listed in WUFI® Plus/Passive in a table displaying heating and cooling demand as well as computed indoor conditions. The total heating demand sums up to 2742,42 kWh which equals 15.5 kWh/m² (166m² treated floor area).

3.3.2 Energy balance

The energy balance for the heating period illustrates that the main fraction of the heat loss can be assigned to windows (for zone 1 = living room and south oriented, see Figure 9). It has to be pointed out, that the direct solar radiation on surfaces of surrounding components and radiant internal heating loads, are not considered in the energy balance graph, as is it only regards the zone balance (indoor air). Hence, the bars for heat gains and losses are slightly out of balance. Figure 10 shows the hourly heat fluxes for zone 1.

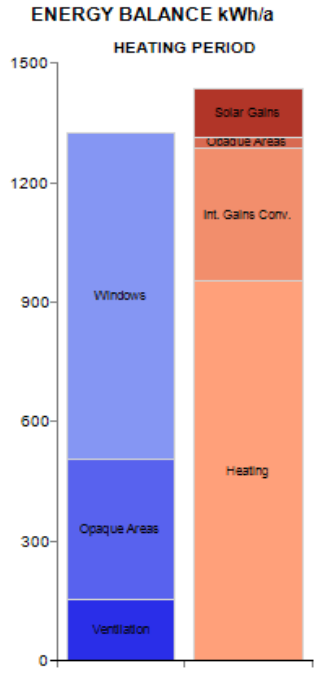

Figure 9: Simulation result - energy balance zone 1.

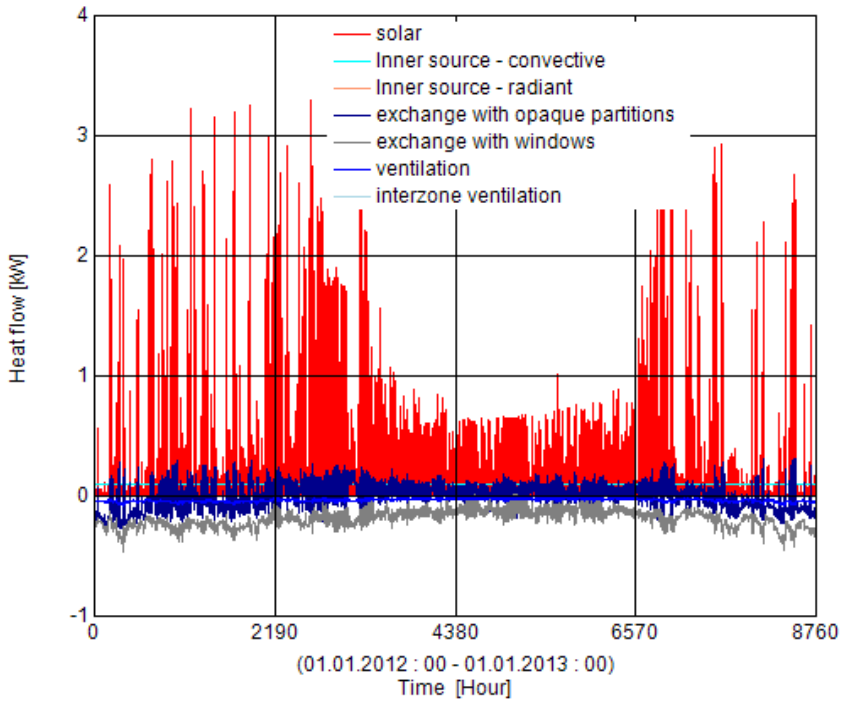

Figure 10: Simulation result - heat flow

3.3.3 Comfort, Moisture risks

The hourly output values allow assessment of comfort and potential moisture damages. Figure 11 shows a simple comfort diagram, plotting relative humidity over temperature in zone 1 in comparison to comfortable areas. Due to the high building standard and sufficient air supply, there are no moisture damages estimated by the simulation. The analysis of the comfort shows, that in most cases the optimum or at least good conditions are met. However, there is a noticeable risk of overheating in zone 1.

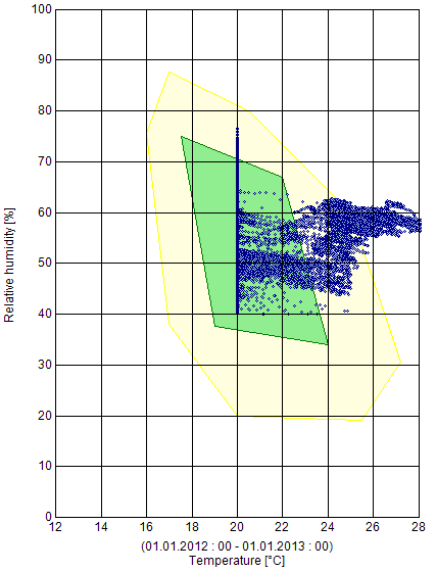

Figure 11: Simulation Comfort Assessment

The hygrothermal behavior of the components cannot be assessed by the static calculation approach, but is essential to evaluate potential moisture risks. In this example the water content of the fibreboard of the exterior wall is assessed depending on its orientation and the percentage of driving rain hitting this layer. A safety assessment according to ASHRAE 160 [ASHRAE 160, 2009] shows that with the application of 1% driving rain critical conditions might occur in the south oriented components (Figure 12). If the detail conditions are worse and 2% driving rain arrive at the fibreboard a net accumulation of the total water content is found and the building assembly will fail (Figure 13).

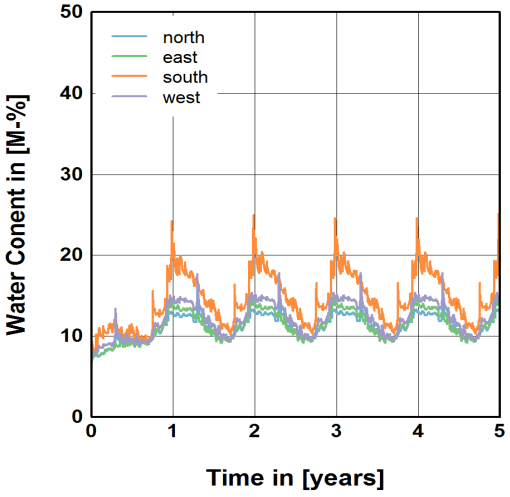

Figure 12: Water Content Fibreboard - Orientations

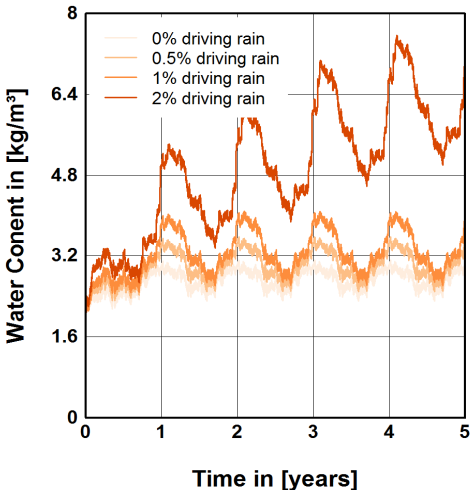

Figure 13: Total Water Content of the Ext. Wall – Percentage of Driving Rain behind cladding

3.4 Comparison and Summary

The static calculations method and the simulation show similar results in several aspects, while the simulation estimates rather higher overheating (see Table 2).

Table 2: Result comparison

	static calculation	simulation
Heating Demand	15.1 kWh/m²	16.5 kWh/m²
Heating Period	212 days	180.5 days *
Heating Load	11.6 W/m²	10.9 W/m²
Overheating Frequency (>25°C)	10.6%	18.6 % (critical zone 1)

* Sum of heating hours

Figure 14 shows the mean daily heating demand for the whole building and each zone over the whole simulation period computed with the selected climate file. A high heating demand can be found for only a very short period of time. Zone 1, the living room, is the main contributor to the overall building heating demand.

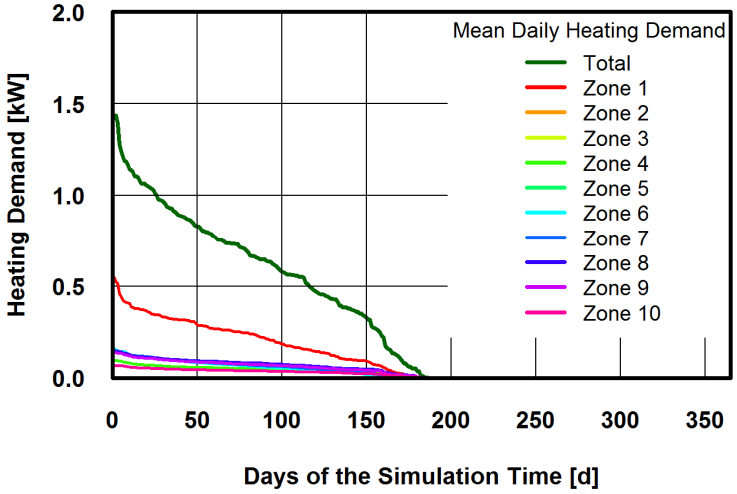

Figure 14: Annual load duration curve for mean daily heating demand of the whole building and single zones

Overall both approaches are viable as they complement each other. The static calculation method provides fast results and additional information regarding e.g. primary energy, electricity demand. WUFI® Plus on the other hand gives further information regarding hygrothermal behavior of the indoor climate and components including comfort assessment and potential moisture risks.

4. Summary, Conclusions and Outlook

The combination of both models – a monthly balanced and a dynamic simulation - into one tool has real potential to transform the passive building design process by making very complex processes accessible to more design professionals. Improvements start from a simple work flow perspective; it organizes the input process along a clearly guided path of the familiar tree structure of the WUFI software family while providing constant feedback on missing data entries. In addition, it supports the user by providing recommended and reasonable input values and explanation of the current parameter. Management help to optimize the design process in passive verification mode by allowing the modeler to store side by side an essentially infinite number of different cases is offered. The static calculation is fast and efficient and outputs include both numerical and illustrative graphical representations of the results, which are very helpful in discussions with clients.

Even more significant are the improvements in regards to the design process. Many designers have been forced to master and use separate hygrothermal tools and secondary dynamic energy models to assess wall component appropriateness by climate and thermal comfort by zone. All additional tools required some form of double entry of material properties, dimensions and mechanical specifications. In the design process many of those pieces of information are still in flux and lead to the need of updating three instead of one model when a design change is made. This is not only labor intensive but also increases the likelihood or error.

In conclusion, the most significant improvements aside from the more efficient and organized workflow is the all-in-one risk management capability. The next generation passive modeling needs to

include dynamic simulation and the ability to predict comfort issues such as overheating and high relative indoor humidity. And to conclude with a gaze into the future: as larger buildings with multiple zones also are being modeled to meet the passive building energy metrics it will become imperative to model and verify comfort in multiple zones in more complex buildings. WUFI Passive will meet those challenges on the horizon.

References

Antretter, F., Sauer, F., Schöpfer, T., Holm, A. 2011. Validation of a hygrothermal whole building simulation software. Proceedings of Building Simulation 2011: 12th Conference of International Building Performance Simulation Association, Sydney, Australia.

ASHRAE Standard 140 - 2007: Building Thermal Envelope and Fabric Load Tests.

ASHRAE Standard 160 – 2009: Criteria for Moisture-Control Design Analysis in Buildings.

DIN EN ISO 13790, 2008. Energy performance of buildings - Calculation of energy use for space heating and cooling; German version EN ISO 13790:2008Energieeffizienz von Gebäuden - Berechnung des Energiebedarfs für Heizung und Kühlung (ISO 13790:2008); Deutsche Fassung EN ISO 13790:2008

Feist, W. 1992. Passivhäuser in Mitteleuropa. Dissertation. University of Kassel.

Feist, W. et.al.. PHPP Handbook. 2007. PHI Darmstadt

http://www.eia.gov/emeu/recs/recs2005/c&e/spaceheating/pdf/tablesh8.pdf

Künzel, H.M., 1994. Simultaneous Heat and Moisture Transport in Building Components. Dissertation. University of Stuttgart, Download: www.building-physics.com

Lengsfeld, K., Holm, A. 2007. Entwicklung und Validierung einer hygrothermischen Raumklima-Simulationssoftware WUFI®-Plus, Bauphysik 29 (2007), Magazin 3, Ernst & Sohn Verlag für Architektur und technische Wissenschaften GmbH & Co. KG, Berlin

Development of a Solid Wood Panel for Heating and Cooling of Floor, Wall and Ceiling Constructions

Nadja Bishara, Dipl.-Ing.[1]
Rudolf Plagge, Dr.-Ing. [1]

[1] Institute of Building Climatology, Dresden University of Technology, Germany

KEYWORDS:

Multilayer solid wood panel, radiant heating, heating and cooling systems, tempering function, hygrothermal simulation, hygrothermal properties, performance- and damage analysis

ABSTRACT:
In the last years the usage of multilayer solid wood panels in the construction sector, has become increasingly popular. The ecological and sustainable production of wood is leading to this demand. In the frame of an industry driven project the development of a three layer solid wood panel with a functional pipe element in the middle layer is investigated. This functional element is used for heating and cooling of the wooden panel. Of course heat conduction of wood is adverse. Hence the challenge is to ensure the transfer of heat and cold to the wood and to handle the formation of condensation and moisture. Other aspects are to evaluate the pipe intervals and to reduce the thickness of the element. Therefore various hygrothermal simulations are carried out. Subsequently selected prototypes were produced and investigated in the laboratory at defined climatic conditions, using particular developed test benches with numerous sensors and infrared thermographic camera. Moisture, temperature and also strain are measured. The aim of these investigations is to create an energy efficient and optimal thermal behavior of the wooden panel heating/cooling system. In this context the results of the numeric simulations and the experimental investigations will be presented.

1. Introduction

Radiant heating systems increase the level of thermal comfort through the heating of surrounding surfaces. Those systems could be easily integrated in a buildings structure, especially into components surfaces, while merely low temperature is required. This enables the utilization of modern condensing technology, thermal heat pump systems and solar heat.

The most widely used radiant heating system is the floor heating. Operations are realized as hot water heating or electric heating. In case of water heating the system contents of water-flown pipes, made of plastic or multilayer composite. Also cooling of building components is possible. Here the heat of a component is dissipated through the tempering medium. Supply and removal of heat is enabled by the fluid which is flowing through the pipes.

The Department of Building Climatology of TU Dresden and the Institute of Wood Technology Dresden together with six industrial partners plan to create a new type of radiant heating/cooling system, using water-flown pipes for tempering of wooden panels. The base material is wood in form of a multilayer solid wood panel, which is frequently used for interior fittings with static functions in the construction sector. Thereby the diverse amenities of wood (ecological, sustainable, renewable, low weight, high load-bearing strength, natural moisture regulation etc.) are extended with a tempering function. This radiant system should be able to apply to the floor, wall and ceiling.

The structure of the proposed tempering system is shown in figure 1. The element is made of solid wood and consists of two top layers and a middle layer, twisted to around 90°. The layers are bonded together. The panel has a so called exterior top layer, which is faced to the building construction, and an interior top layer, which is faced to the room. In the middle layer a pipe system is embedded.

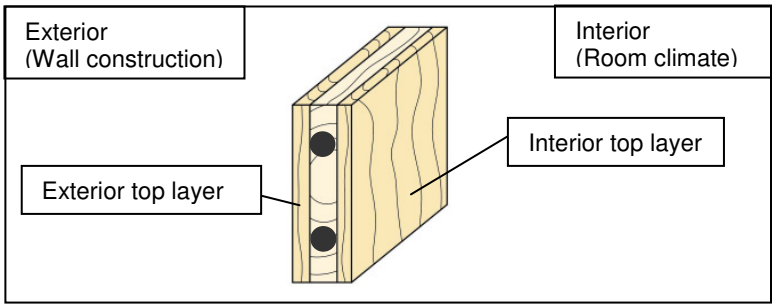

FIG 1. Structure of the proposed tempering system

2. Method

In a first step conceivable materials are examined for usability. These are solid wood lamellas for the face and middle layer, alternative materials for the middle layer (e.g. wood-based materials), adhesives, adhesive additives and pipe materials. The hygroscopic parameters of the selected layer materials are measured in laboratory and appropriate material functions are generated. These material functions form the basis for the numerical simulation with Delphin. In the second step the thermal and hygric behaviors of the different types of solid wood panels are simulated in Delphin, including the functional pipe element in the middle layer. Defined climatic conditions for the ambient climate and the pipe element are given. Upon completion of the first phase of optimization, a number of solid wood panels is manufactured and examined at pilot plant scale. Subsequently these panels are investigated laboratory in a climate chamber, during operation of the functional pipe element. Additionally the preferably variants are proved in climatic test chambers, to testify the performance of the solid wood panel with respect to a defined space. The data acquired from the laboratory tests enable statements about viability and capability of the prototypes. Based on these results a further optimization by means of the numerical software Delphin takes place. This step includes a performance- and damage analysis of the selected solid wood panels. Subsequently further optimized solid wood panels are manufactured in pilot plant scale and tested laboratory. In a further step the options for the connection of the pipe elements of two adjacent panels are investigated. The final aim of the project is the production of solid wood panels with functional pipe element in the middle layer on an industrial scale, as well as the laboratory examination of these panels in the laboratory.

2.1 Selection and testing of the material

In this initial step, potential materials for the element layers, adhesives and its additives and also the pipe elements are searched for. The solid wood lamellas should enable heat conduction in direction of the interior surface. In order to achieve a higher heat flux in the vertical axis of the middle layer, alternative materials are considered and investigated. For the basis variant spruce wood is selected for all layers, it is readily available and favourable. Two alternative types of wood used for the top layer are beech and oak, which have higher heat conductivity than spruce. The middle layer should also be produced with PB (particle board) and MDF (medium density fireboard), assuming that the tight fit between pipe element and middle layer will be better using wood-based materials than solid wood.

In the manufacture of multilayer solid wood panels the usual practice is to employ melamine-urea-formaldehyde (MUF) resin. This adhesive is selected to bond the layers to each other. The resin has to be moisture permeable to prevent moisture accumulation inside and of the surface of the wood panel. Also it has to enable heat flux to ensure the panels performance. To fulfil the heating and cooling task a multilayer composite pipe is chosen.

In this work package the selected wood materials are tested in laboratory to determine the respected hygrothermal properties. The following properties are measured: matrix density, bulk density, porosity, thermal conductivity and capacity, moisture storage, water vapour diffusion resistance, water conductivity and permeability and water absorption coefficient. Continuous measurement of water uptake and measurement of continuous drying are done. Subsequently material functions are generated and implemented in the software Delphin.

2.2 Calculations with numerical simulation software Delphin

The aim of this work package is to obtain an optimal panel construction relating to the progression of heat and moisture and also condensation that might occur.

The computer-aided examination of the solid wood panel is based on the numerical simulation tool Delphin. This heat-, moisture- and air transport software is based on a theory which is deducted from thermodynamic processes. The transport processes and transitions between the solid, the fluid and the gaseous phase are described in these thermodynamic processes. Delphin enables the simulation of a whole building component with diverse material layers und boundary conditions.

Especially the existing buildings are supposed to represent a potential market for the solid wood panel with functional pipe element in the middle layer. Thus the basis for simulating the solid wood panel is build through a wall construction with a U-value of 0.35 W/m²K. This value refers to the Energy Conservation Regulations (EnEV 2009) for existing buildings with interior insulation. The boundary conditions for heating function distinguish between interior (10°C/65% RH) and exterior climate (-5°C/80% RH). The temperature in the pipe element is set to 35°C. In case of cooling function boundary conditions are defined as follows: 28°C/75% RH interior climate and 32°C/60% RH exterior climate. The tempering fluid is supposed to have an average temperature of 16°C (Glück 1999). The temperatures for heating and cooling of the pipe element are chosen to use the environmental energy for tempering. Table 1 gives an overview of the implemented boundary conditions.

TABLE 1. Boundary conditions for the calculation with Delphin

Tempering function	Exterior Climate		Interior climate		Temperature Pipe Element
	Temperature	Relative humidity	Temperature	Relative humidity	
Heating	-5°C	80%	10°C	65%	35°C
Cooling	32°C	60%	28°C	75%	16°C

Additional to the material parameters, the geometry of the solid wood layers is very important such as thickness of the solid wood layers, pipe diameter and distance, piping route and also wood species. The required minimum thicknesses of the wood layers are essentially bounded by the limiting values of the manufacturing process. Standard thicknesses also vary from manufacturer to manufacturer. The included project partners provide top layers in diameters between 6.9 and 9.3 mm and middle layers between 9 and 20 mm.

The dimension of the middle layer is depending on the pipe diameter. The selection of pipe diameter and distance relate to performance criteria. A large pipe diameter in combination with a small distance would be the most powerful solution. Thus a diameter of 16 mm and a (standard) pipe distance of 10 cm is chosen. For the middle layer this leads to a thickness of 20 mm whereby the pipe element is located off-centre in the layer, directly on the adhesive plane.

A small radiation asymmetry represents a fundamental comfort condition (Glück 1999). Therefore the piping route should be symmetric. Two different balanced systems are usual: meander-shaped and spiral curse, as shown in figure 2. The spiral curse will create a more homogenous heat distribution. Here the warmer pipe of the flow is always next to the colder pipe of the return. For that reason the spiral curse is set as the basis variant for the following laboratory investigations.

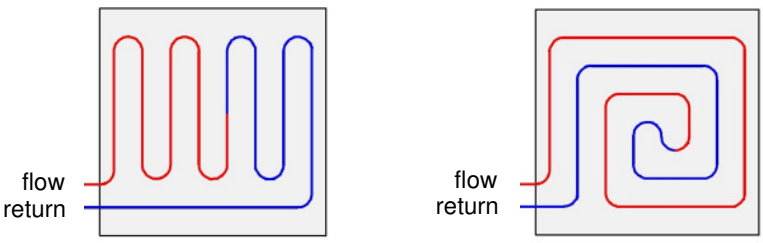

FIG 2. Piping routes: meander shaped (left) and spiral curse (right)

With these determinations a first design variant of the tempering panel is set, which forms the basis for the following simulations. In this variant the thicknesses of the top layers are set to 9.3 mm and the distances between the pipes is set to 10 cm. Furthermore the whole solid wood panel consists of spruce. A first simulation is performed for the heating mode. Figure 3 shows the basis variant and the corresponding simulation result for the panel in case of heating.

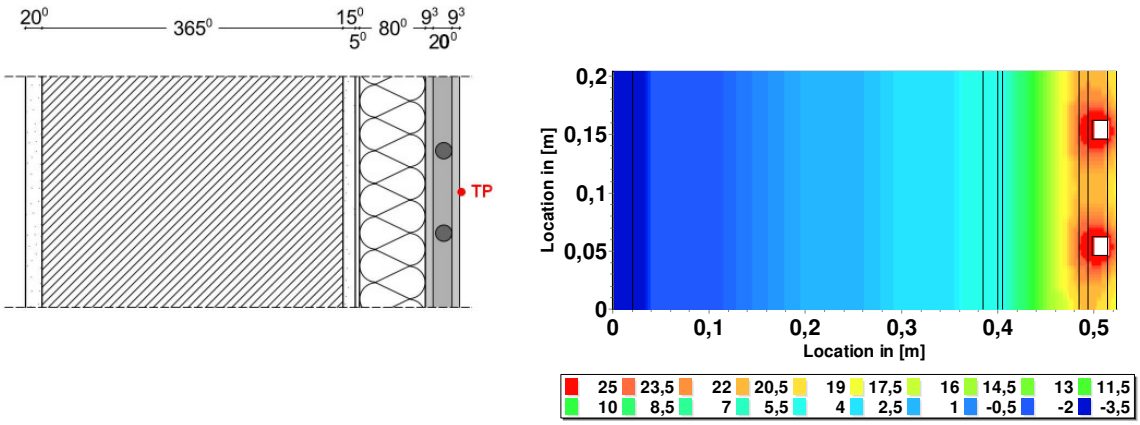

FIG 3. Simulation results in case of heating (left: wall construction, right: temperature field in [°C])

In order to improve the heat flux in vertical and horizontal direction diverse modifications regarding to the structural setup of the panel are done:

- Variation of the thickness of the top layers
- Variation of the pipe distance
- Variation of the wooden materials
- Implementation of a heat-conducting layer

2.2.1 Variation of the top layer thicknesses

It is assumed that the heat flux in interior direction increases with reducing the thickness of the interior top layer to 6.9 mm. This assumption is confirmed by the simulation results, which are shown in figure 4. The calculated output value refers to the surface point between the pipes (see the point “TP” in figure 3). The average temperature difference between the both variants is 0.7 Kelvin. Consequently the reduction of the thickness of the interior top layer achieves higher surface temperatures.

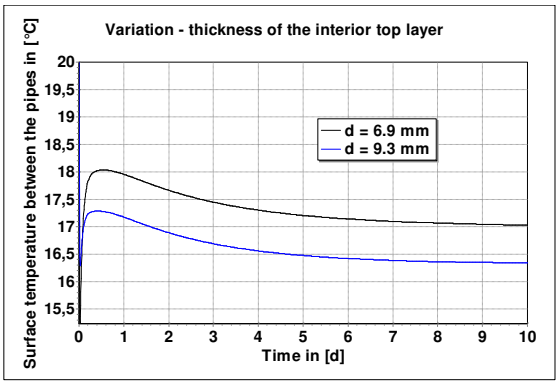

FIG 4. Variation of the top layer thickness – surface temperatures

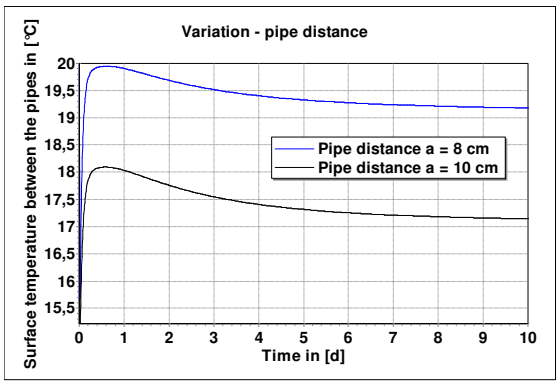

FIG 5. Variation of the pipe distance – surface temperatures

2.2.2 Variation of the pipe distance

A pipe distance of 10 cm is common and provides the basis variant. However, it is believed that the pipe distance should be as low as possible to increase the surface temperature and thus the amount of radiant heat. Determined by the minimum bending radius the minimal pipe distance is set to 8 cm. The result of this simulation is shown in figure 5. The temperature difference at the surface point “TP” is 2.1 Kelvin. Hence the reduction of the pipe distance leads to higher surface temperatures.

2.2.3 Variation of the wooden materials

A further step to increase the heat flux in the interior direction is to select another wood species. Therefore oak is chosen to substitute spruce, because of its high value of thermal conductivity ($\lambda = 0.16$ W/mK). At first only the interior top layer is refunded and then also the middle layer. The results of the simulations are shown in figure 6. In comparison to the base variant the variant with interior top layer made of oak reaches a higher surface temperature on point “TP” (0.3 Kelvin). If also the middle layer is replaced by oak, the surface temperature difference on point “TP” is 0.6 Kelvin in comparison to the base variant. Thus the aim is reached, to increase the heat flow in direction of the interior.

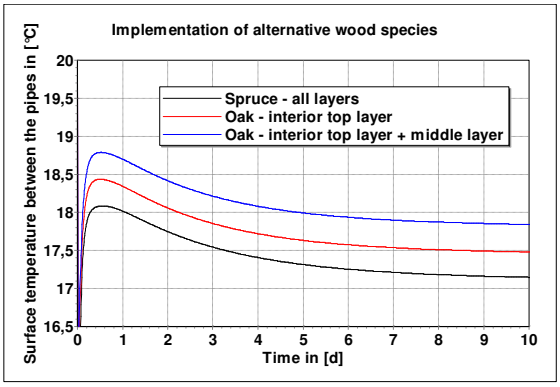

FIG 6. Implementation of alternative wood species – surface temperatures

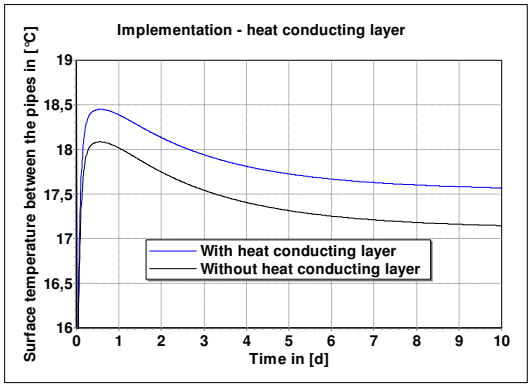

FIG 7. Implementation of a heat conduction layer – surface temperatures

2.2.4 Implementation of a heat conducting layer

The simulations reveal the significance of heat flux at a high level in the plane of adhesive between middle layer and interior top layer and also from this plane in the interior direction. To enhance the level of the heat flux, two capabilities are elaborated. The first one is a fine metal grid which is installed directly between middle layer and interior top layer and the second one is a thermoplastic material which is inserted in the same plane. In the subsequent simulation the plane between middle layer and interior top layer is added with a heat conducting layer ($\lambda = 0.8$ W/mK), such as for example a thermoplastic material. As figure 7 shows, the surface temperature difference between both variants at the point “TP” is 0.4 Kelvin. Hence the installation of a heat conducting layer conduces the increasing of the heat flux in vertical and horizontal direction.

Finally nine prototypes of solid wood panels with functional middle layer are selected to be produced in pilot plant scale. Table 2 below shows the components of the nine prototypes (i.=faced to interior, e.=faced to exterior, S=spruce, B=beech).

TABLE 2. Prototypes produced in pilot plant scale

Variant	Piping route		Pipe distance		Wood species			Exception
	meander-shaped	spiral curse	8 cm	10 cm	top layer (e.)	middle layer	top layer (i.)	
1	+			+	S	S	S	
2		+		+	S	S	S	
3		+	+		S	S	S	
4		+		+	S	MDF	S	
5		+		+	S	PB	S	
6		+		+	S	S	S	Metal Grid
7		+		+	S	S	B	
8		+		+	S	B	B	
9		+		+	S	S	S	Top layer (i.) 4mm

2.3 Measuring of the prototypes

The measuring setup consists of the solid wood element itself and a 10 cm thick insulation in its reverse field (DIN EN 1264-1). The tempering element is connected to a thermostat which is located outside the climatic chamber. The pipes chaining thermostat and solid wood panel are insulated to keep the temperature difference between flow and return as low as possible. Inside the climatic chamber a thermographic camera is placed (see figure 9). Also the data logger for gathering the measuring data is positioned in the chamber. Wires lead outside from the camera and the logger to a computer on which the external storage and analysis of the data takes place. Figure 8 provides an overview of the measuring setup.

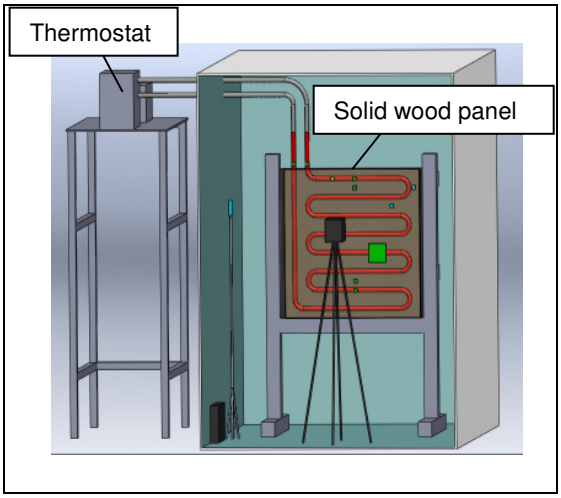

FIG 8. Measuring setup

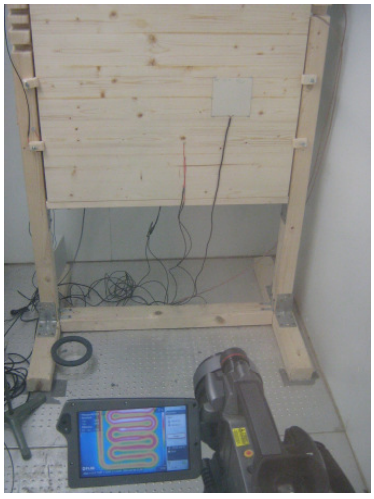

FIG 9. Measurement with the thermographic Camera

The measurement cycle should be determined from a periodic alternation of heating and cooling function, in order to define the impact of temperature change to the material behavior. The evaluation of the measurement course is done by using the software Delphin. The climatic boundary conditions for the heating function are: 15°C for exterior air temperature and 65% for exterior relative humidity. The temperature of the pipe element is 35°C. The aim of the simulation is to obtain statements about the transient state of the system. Figure 10 shows the result of the simulation. The pink curve shows the interior surface temperature between the pipes. The green curve displays the surface temperature at the point between the exterior top layer and the insulation, also between the pipes. After one day a

transient state is reached, which varies only very slightly in the further course. In case of cooling function a similar simulation is implemented. The boundary conditions are shown in table 3. The Figure 11 exhibits the results of this investigation. The transient state of the system is even after five days not yet reached.
The main focus of the laboratory investigation is on the element's hygrothermal behavior during heating. Since the transient state in case of cooling function is reached only after several days and time for the examination of the prototypes is limited the respective phase for heating and cooling is set to one day. The measuring cycle is now for each plate type as follows: preconditioning (2 days), heating (1 day), cooling (1 day), heating (1 day), cooling (1 day). The climatic boundary conditions are shown in table 3.

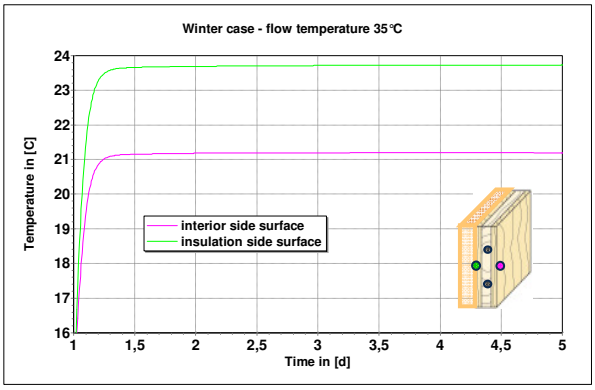

FIG 10. Transient state – heating mode

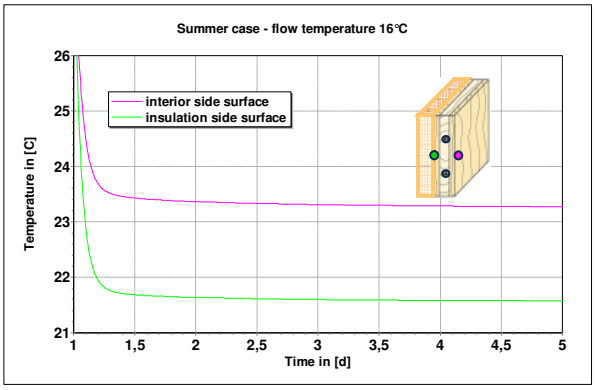

FIG 11. Transient state – cooling mode

TABLE 3. Measurement in climatic chamber – climatic boundary conditions

Tempering function	Exterior climate		Temperature pipe element
	Temperature	Relative humidity	
Preconditioning	15°C	65%	15°C
Heating	15°C	65%	35°C
Cooling	28°C	65%	16°C

In order to achieve a qualitative assessment for the hygrothermal behavior of the system measurements are performed during the operation. Here a distinction is made between the measurement plane on the panel's surface and the measurement plane between face and middle layer. The temperature and the relative humidity are measured at two different distances to the pipe element. On the elements surface the temperature is also measured perpendicular above and also between the pipes. Equally the temperature of flow and return is measured. A strain gauge, also positioned on the surface, provides information about the stretching properties of the wood. A heat flux plate measures the heat flux. By means of an infrared camera the homogeneity of the heat radiated form the solid wood surface is recorded. To verify the climatic boundary conditions (temperature and relative humidity) another sensor is applied in the climatic chamber. In figure 12 the measuring points are shown.

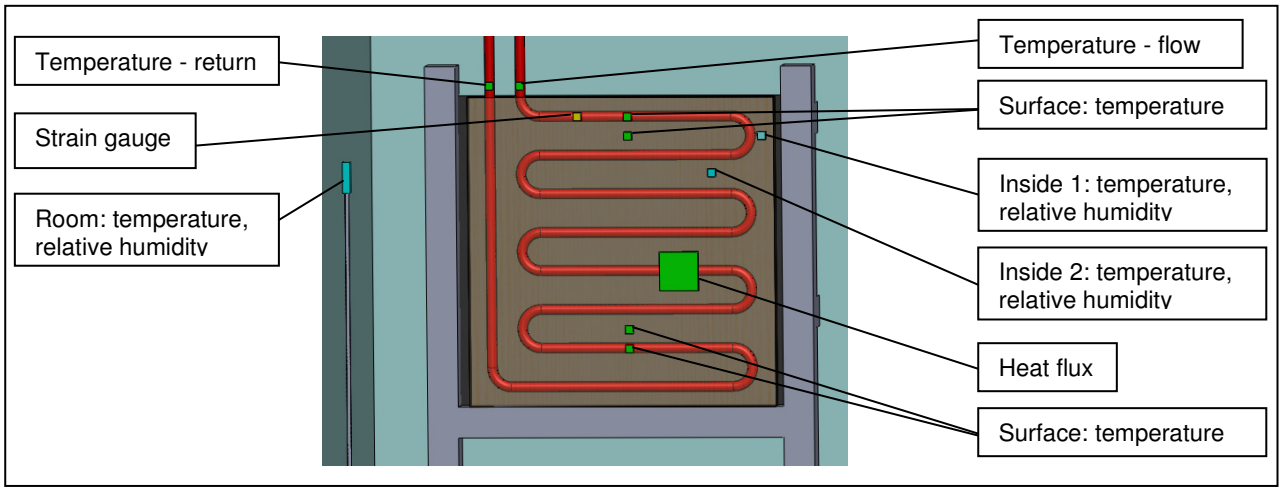

FIG 12. Measuring points

3. Conclusions and outlook

In the frame of an industry driven project the development of a three layer solid wood panel with a functional pipe element in the middle layer is investigated.

In the first step suitable materials were procured for the systems structure such as different kinds of wood, wood-based materials, pipe materials and adhesives. Types of wood and wood-based materials were examined in the laboratory for their hygrothermal properties. Based on these measured properties, material functions were generated and implemented in the numerical simulation software Delphin.

With the aim to obtain an optimized panel a simulation study was done regarding to the hygrothermal behavior of the element. Here parameters such as material selection, geometry of the layers and the pipe elements and pipe distance were varied. As a result, the following optimizations were obtained: The reduction of the thickness of the interior top layer achieves higher surface temperatures. The reduction of the pipe distance also leads to higher surface temperatures. Wood species with a higher thermal conductivity, implemented as interior top layer, increase the heat flow in direction of the interior. The installation of a heat conducting layer in the plane between interior top layer and middle layer conduces the increasing of the heat flux in vertical and horizontal direction.

With these concretions of the panel's structure, nine different prototypes of multilayer solid wood panels were manufactured with a functional pipe element in the middle layer to be tested in laboratory on their performance. The measurement setup and the measurement cycle were explained.

Currently the nine prototype panels are examined in the laboratory. First measurement results will be shown at the 10th Nordic Symposium on Building Physics in June 2014.

References

DIN EN 1264-1. 2011. Water based surface embedded heating and cooling systems – Part 1: Definitions and symbols. European Committee for Standardization

EnEV 2009. Energieeinsparverordnung - Verordnung über energiesparenden Wärmeschutz und energiesparende Anlagentechnik bei Gebäuden. BGBI

Glück B. 1999. Thermische Bauteilaktivierung. 1st ed. Heidelberg, C.F. Müller Verlag. 213 p.

Wood construction: Energy, Emissions and Experience

Kristine Nore, PhD [1]
Finn Englund, PhD [2]
Tormod Aurlien, Professor [3]
Anders Q. Nyrud, D.Sc. [1]

[1] Norwegian Institute of Wood Technology, Norway
[2] SP Wood Technology, Sweden
[3] Norwegian University of Life Sciences, Norway

KEYWORDS: *Wood, latent heat, thermography, indoor climate, wood, spruce, untreated panel emissions, health.*

SUMMARY:
Increased environmental awareness includes more consideration to indoor surface materials. The project Wood – Energy, Emission, Experience (WEEE) focuses on three aspects of interest when using wooden surfaces indoors: (I) The energy interaction of the air and the wooden surface – does the hygrothermal buffer capacity of wood contribute to improved indoor climate and possible reduce the energy need? (II) The emissions from wood panels – how does wood emissions differ and reach critical levels in residential buildings? (III) The experience of wood in our close surroundings – does exposure to wood environment and emissions influence our comfort and health, positively or negatively? This paper provides preliminary results from an ongoing project on untreated, solid wood.

1. Introduction

In the Western Hemisphere, people spend most of our time inside buildings. A substantial share of global energy consumption is used to accommodate desired indoor climate. There is an increased focus on actions to encounter energy-efficient buildings. This has resulted in concerns about possible human health effects from these actions.

The project Wood – Energy, Emission, Experience project (WEEE) (NFR 216404, 2011) examines the possibility to reduce primary energy input due to indoor wood surfaces, the expected emissions and following health effect. This paper sums up current results and presents future work. Each part is presented individually and commented on in the concluding remarks.

2. Do untreated wood surfaces contribute to the energy balance?

Based on the natural behavior of growing trees to provide the best growth environment at any climate, wood counteracts changes in the ambient environment in order to keep the vital moisture supply. Due to its water transport system, water on surface is absorbed in the capillaries (tracheides) and bound physically to the cell walls. Therefore wood can be seen as a natural phase change material (PCM). With varying relative humidity water molecules are bound and released, and this will respectively disengage and require energy. The authors investigate to which extent latent energy may be retracted from damp air with high enthalpy and this effect can be used to reduce the energy peaks.

Wood can be a conditioning component in the indoor environment because its open pore structure interacts with ambient air. This is defined as an active surface. Untreated wood has a surface of 200 m^2 per gram (Wimmer, 2012). Typical interior wall products in dwellings (often gypsum boards with wall paper or paint) have a much smaller capacity to interact with the indoor air and buffer moisture.

When including the pronounced hygroscopic capacity of wood, the energy gain from latent heat exchange may exceed the total energy gain of other materials with merely high thermal capacity (e.g. stone, concrete or glass). Energy gain from latent heat is studied on small samples in laboratory and with WUFI®plus simulations (Antretter and Winkler, 2014).

With the increasing need for energy efficiency in all buildings more efficient heating and advanced ventilation controls are receiving substantial attention. Research does, however, indicate that in spite of more efficient heating like from heat pumps, energy demand does not decrease like anticipated (Halvorsen and Larsen, 2013).

2.1 Initial simulations and laboratory test

Korsnes (2012) conducted hygrothermal simulations defining a potential energy outlet as a part of the phase change present from damp air to bond to the wood surface. A bathroom was heated, solely with damp air, by two degrees. This gives sufficient heat for comfortable dressing after a shower. The equal amount of energy is needed to dry the panels afterwards, but at this time no extra heat is needed; no one is getting dressed.

A laboratory test in a well controlled climate chamber has been conducted to verify the simulation results. Two wood surface samples (planed softwood, measuring105 x 205 mm^2) are subjected to change of ambient relative humidity from 20% to 90%. The temperature was kept constant and the relative humidity was rapidly changed within minutes. Both samples were from untreated wood, one exposed wood surface and one reference sample covered with low-emitting PE-foil to exclude moisture uptake, cf. FIG 1. The responding moisture uptake and heat release are measured by weight cells and thermography.

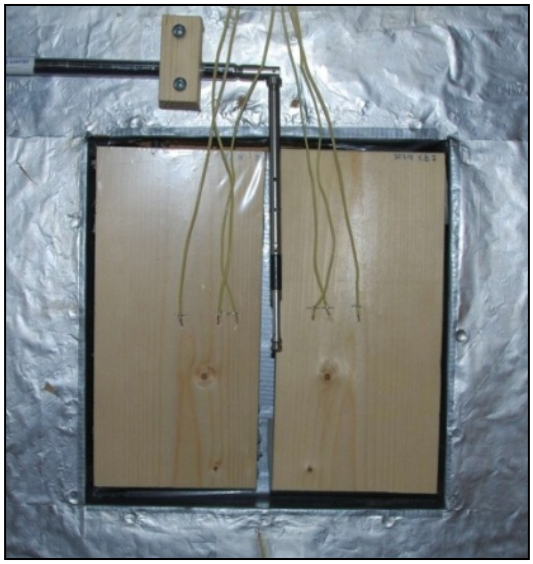

FIG 1. Samples mounted in housing. View Samples (covered left, uncovered right) and thermocouples mounted in the ceiling of a well controlled climate chamber. In center the air speed meter is placed.

Thermography is used to measure temperature differences on the two samples. Thermography detects the emitted magnetic waves from objects in the infrared spectrum and displays this as thermal images. Planed softwood reflects radiation with an emissivity of 0.86 while aluminium is an appropriative ambient material with a low emissivity of 0.02 at 25°C. Thermography has high sensitivity for temperature differences within areas and enables comparison of several spots at a time. Temperature is also measured with thermocouples in order to control the temperature measured by thermography. Ambient air velocity interacts with moisture uptake and is measured close to the surface. Weighting cells are used to measure the weight change (i.e. uptake of humidity) of the test samples

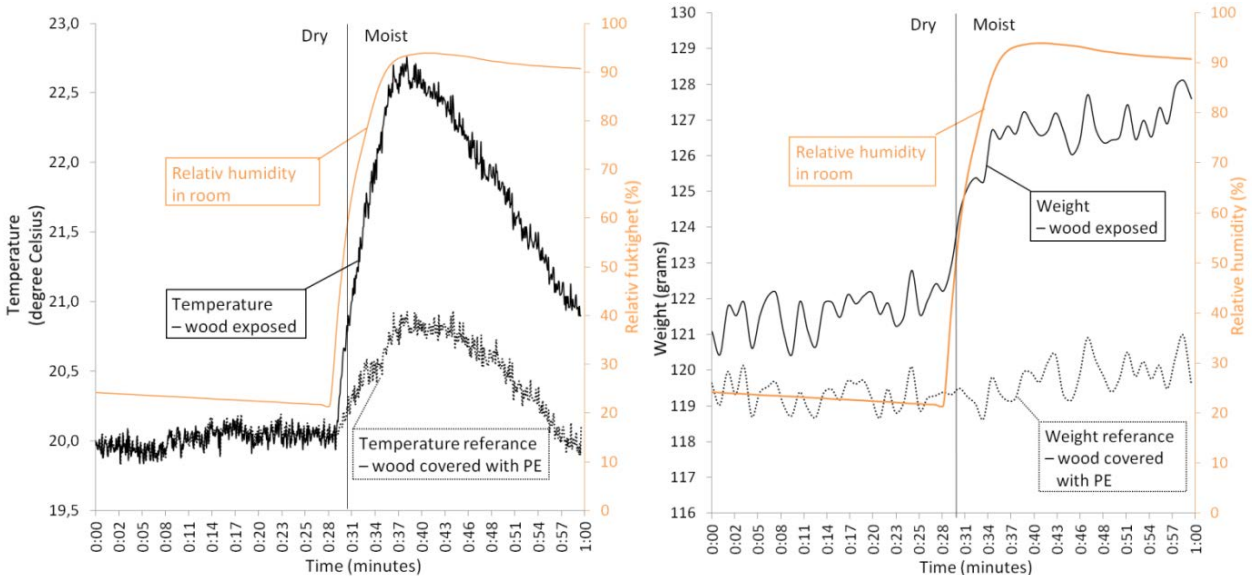

a *b*

FIG 2. a) Temperature change of exposed and covered reference wood samples. The graph clearly shows the increased surface heating on the exposed wood due to climate adaption. b). Moisture uptake of exposed and covered reference wood samples. The graph clearly shows the increased weight only of the exposed wood.

The results show a substantial difference between the two wood samples, both in temperature rise and moisture uptake when increasing the relative humidity of the room, cf. FIG 2a and 2b. The covered reference sample is also heated mainly due to moisture condensation, but no moisture is absorbed as shown in no weight gain in FIG 2b. The difference of the reference sample and the exposed wood reach nearly 2˚C. About six grams of water is absorbed in around five minutes.

2.2 Potential energy savings

The material buffer effect has been discussed the last decades. Large investigations have been made on the effect of furniture and room surfaces. However, the potential in latent heat is sparsely treated (Hameury, 2006).

The wooden surface act like a heat battery. The sun dries out the surface during the day and the heat is delivered back to the room as the humid night air is distributed. The wood moisture equilibrium may change up to 10 weight percent in one daily cycle if the surface air relative humidity reach around 30 % at daytime and 75 % at night. A living room with a floor space of 20 m^2 may have 50 m^2 active surface, including the ceiling and major part of the walls. The outer millimetre of the wood surface is considered active (Hameury, 2006). This millimetre then accounts for almost 50 litres of wood if the wood has a density of around 470 kg/m3 (Norwegian Spruce). With the change in moisture content, this gives around 2.5 litres of water fluctuating between being bound to the wood surface or part of the humid air. When considering the enthalpy of their compared to the water bound in wood this gives a difference around 4 J/g. The energy ready for cooling at daytime and heating at night-time then reach 10 kJ, which equals 2.8 kWh. This is a quite substantial amount of energy in such a small room. Do you still wonder why it feels good to live in a wooden house?

The next step is full scale testing. There is a need to unveil effects which may interrupt the heating from the hygroscopic capacity of the wood surfaces.

2.3 Field test

Two cross-laminated timber (CLT) test houses were erected and instrumented at the Norwegian University of Life Sciences (NMBU), cf. FIG. 3.

The natural wood surface in walls and ceilings of these modules provide perfect conditions for studying wood surface and indoor air interaction. Documenting these processes in a near to real scale by accurate measurements, will also serve as reference to parallel hygrothermal computer simulations.

The test houses have previously been used for testing impact of sound (Aarstad 2009). The test houses were moved during the autumn of 2012 out to a test field of the university, which also includes a national meteorological station for Ås County. They have high prior moisture content due to the storage and transportation. The modules are heated and monitored for an initial period, until a stable and representative indoor environment is established.

Ventilation flow, heat demand, resulting temperatures and relative humidity of air into and out from the modules are controlled and registered. Extract ventilation is installed and controlled at 0.5 h^{-1}|, according to ordinary levels in Norwegian regulations (TEK10). Electric resistant heaters (2 x 2 kW) are easy to control and register power consumption in to keep indoor temperatures at intended level.

In the following phase, moisture will be introduced into the indoor environment, simulating natural use of buildings. The moisture buffering response to this will be studied. Surface materials will be changed during the experiment. Different ventilation strategies may also be studied. One potential will be to document the experience that one “seldom see dew on the mirror a bathroom panelled with untreated wood”. A consequence may be that air exchange levels are reduced, in cases where the reason for these ventilation levels have been to control moisture level in indoor air to below acceptable threshold levels. Reducing air exchange levels is one of the possible steps to achieve ambitious levels of energy use in Scandinavian dwellings.

FIG 3. Field test at Ås. Two identical test-houses (7.0 m x 3.6 m x 2.2 m internal measurements).

3. Emissions from wood

Generally, standard emission testing and certification schemes require measurements of emissions from building products after 28 days. The international standard ISO 16000-9:2006 also requires measurements after three days, and optionally additional measurements depending on the purpose of the study.

In Norway, a national adaption of the international BREEAM environmental classification of buildings have developed into BREEAM-NOR. This classification scheme has adopted somewhat

stricter criteria, e.g. emission testing after both three and 28 days. Another criterion that differs greatly from the international BREEAM standard is the requirement of low polluting building materials in BREEAM-NOR, this is mandatory for classification levels of *very good* and higher. The criteria for low polluting are based on the Finnish Emission Classification of Building Materials and its class M1, also included in NS-EN 15251:2007 Appendix C. The emissions that are limited include total volatile organic compounds (TVOC), formaldehyde, ammonia, carcinogenic compounds and odour. For solid spruce and pine wood the TVOC criteria must be taken into consideration, cf. Table 1.

TABLE 1. M1 criteria and area specific emission rates of softwood after 28 days (Englund 1999, Englund 2010)

Examined qualities	M1 criteria	Spruce	Pine
		[$\mu g/m^2h$]	
The emission of total organic compounds (TVOC)	< 200	30-550	125-7000
The emission of formaldehyde	< 50	4-5	3-6
The emission of ammonia	< 30	0	
The emission of carcinogenic compounds	< 5	0	
Dissatisfaction with odour	< 15%		

For wood products, emission levels often show relatively high values after 28 days, but they are greatly reduced after further exposure to air. Perhaps the most striking observation is the considerable natural variation in emission source strength when testing a larger number of softwood samples with different origins. In the two publications by Englund, cited in Table 1, terpene emissions (and thereby TVOC) span over much more than one order of magnitude for a very limited number of samples. The same observation was made in a Nordic collaborative research effort in the late 1990's (Nordic Wood, 1998). Englund (1999) concluded that "The task of reaching a full and generalized picture of the emission characteristics of wood is a tremendous task, which hardly is possible to accomplish with realistic, limited resources… …To try to establish average values that could be used e.g. for all Nordic pine is, however, neither desirable nor meaningful. The only reasonable strategy is to acknowledge the large natural variations and to show their span, when necessary." The emission source strength is furthermore strongly dependent on kiln drying schemes (Steckel et al. 2011) or thermal modification processes (Hyttinen et al. 2010).

Current understanding is fairly incomplete regarding the contribution of individual compounds on the indoor air quality (IAQ), but also on how emissions vary with the moisture content of the material and the ambient air. Theoretical predictions can be made from distribution coefficients, but this project will attempt to shed further light on this through experiments. Emissions at different relative humidities will be investigated. Bearing in mind the limitations given by the natural variations of solid wood, the data will also serve to expand the bulk of base data to make the overall assessments of expected emission behaviour stand on firmer ground. Predictions of indoor air quality may also be estimated in WUFI®plus.

4. Health effect from wood emissions

4.1 State of the art

Research on health effects related to the built environment has mainly concentrated on the health impact of and various physical factors; ventilation, dust particles (Gyntelberg et al. 1994; Hauschildt et al. 1999), electrical fields (Skulberg et al. 2001) and emissions (Bornehag et al. 2010) as well as temperature, humidity and chemical substances (Wolkoff et al. 2003). Many indoor environment studies have measured the total volatile organic compounds (TVOC). No correlation between TVOC and health has been found (Andersson et al. 1997). However, several studies have found correlation between health outcomes and individual chemical substances such as formaldehyde, phthalates

(Fromme et al. 2004) and PGE (Bornehag et al. 2010), and mixtures of ozone and oxidizable compounds like terpenes can cause airway irritants (Wolkoff et al. 2000).

Cross-sectional design has been used most often in indoor environment studies. Questionnaires have been used in several Nordic studies, e.g. the Örebro questionnaire (Andersson et al. 1993), which aims at detecting three different groups of health outcomes: general symptoms (fatigue, headache, dizziness and failure to concentrate), irritation symptoms from mucous membranes (eyes, nose and throat) and skin symptoms (face and hands).

A few studies have specifically addressed health effects of indoor wood use, mainly focusing on subjective experience of wood materials, such as tactile and acoustic properties, thermal effects, odor or visual appearance and psychological effects and well-being. A few studies have also studied health effects as measured by objective physiological parameters (Gminski et al 2011), and all available results indicate that no adverse effects can be found. Nyrud and Bringslimark (2010) provide a review of relevant literature. Issues related to material use, building design and health have also been studied, e.g. Bringslimark, Bysheim and Nyrud (2010).

4.2 Laboratory experiment

A laboratory experiment evaluating occupant health in a controlled indoor environment was conducted in the indoor laboratory at the Oslo and Akershus University College of Applied Sciences (HiOA). The study addresses responses among human participants under two different conditions in a controlled environment, with different concentrations of emissions from wood. The aim was to evaluate the effect of emissions from Scots pine (*Pinus Silvestris*) on test persons in a simulated indoor environment.

Sixteen groups of two participants were scheduled for exposure to each of the two different conditions for two hours per condition. The control condition was without pine in the chamber, and the intervention condition was with fresh sawn pine wood in the chamber. The test subjects could not see whether there was pine in the chamber. Continuous measurement of Volatile Organic Compounds was conducted using a Proton-transfer-reaction mass spectrometer. The temperature and humidity were kept stable and monitored along with the CO_2-concentration. The experimental sessions for each group took place over a seven day period. The groups were exposed for one condition (no emissions/emissions) and subsequently for the other condition seven days later. The experiment consisted of 60 minutes of acclimatization, 30 minutes of introductory health tests, 120 minutes of exposure in the chamber and 30 minutes of post exposure health tests.

The order in which participants were exposed to the different conditions was balanced across groups. Participants were not informed about specific conditions in each session.

Before, during and after each exposure condition, participants completed a computer-based test of subjective health outcomes (c.f. Örebro questionnaire, Andersson et al. 1993) where they reported subjective evaluation of health symptoms related to indoor air quality.

The study was approved by the Regional Committee for Medical and Health Research Ethics (REK). Test subjects were mainly recruited among students at the HiOA. All test subjects were at least 20 years old, non-allergic non-smokers.

4.3 Results

Results are not fully analyzed. The concentration of monoterpenes in the control condition was less than 50 ppb, whereas the concentration in the intervention condition with pine wood in the exposure chamber reached levels of 1 000 – 3 000 ppb.

1000 ppb is equivalent to a concentration of 6000 $\mu g/m^3$ which equals an area-specific emission rate 3000 $\mu g/m^2h$. This is 15 times higher than the limit to M1 (200 $\mu g/m^2h$). There were no statistically significant health effects on test subjects from the exposure to emissions from wood. For several

outcomes (eye blinking ratio, neuropsychological test and self subjective health symptoms) there was, however, a statistically significant effect of participating in the experiment. This may be due to a learning or observer effect where test subjects may improve or modify behaviour in response to the fact that they know they are being studied.

5. Concluding remarks

Thermography provides an adequate method for measuring temperature differences due to moistening of wood. The comparison of reference samples and samples provided sorption and heat characteristics in correlation with the climate. This is with suitable accuracy for closer examination.

The latent heat exchange provides energy in indoor areas for hours after moistening. Thus untreated wood has energy saving potential in every kind of interior application.

The use of energy input and indoor climate levelling from untreated wood surfaces may increase the energy efficiency in our modern houses.

The monoterpene levels of the trial experiment showed a emission concentration which will be compared to as 15 times higher than the M1 criteria which must be fulfilled to deliver a BREAM certified building in Norway. There were no statistically significant health effects of the exposure to emissions from wood.

This research project will bring forward documentation of physical and experienced real wood behaviour.

6. Acknowledgements

The authors highly acknowledge the Research Council of Norway for funding the project WEEE together with the industry partners. Innovation Norway is acknowledges for funding part of the test house erection at Søråsjordet in Ås.

References

Aarstad J. 2010. Junction connections in multi-storey timber buildings. Report 81 Norwegian Institute of Wood Technology, Oslo, Norway

Andersson K, Bakke JV, Bjørseth O, Bornehag C-G, Clausen G, Hongslo JK, Kjellman M, Kjaergaard S, Levy F, Mölhave L, Skerfing S, Sundell J (1997). “TVOC and health in non-industrial indoor environments”, Indoor Air, **7**, 78-91.

Andersson K, Fagerlund I, Stridh G, Larsson B (1993). The MM-questionnaires. A tool when solving indoor climate problems, Örebro, Örebro Medical Center Hospital.

Antretter F. and Winkler M. (2014). Impact of the moisture buffering effect of wooden materials on energy demand and comfort conditions. Nordic Building Physics Symposium, Lund, Sweden.

Bringslimark T, Bysheim K, Nyrud AQ (2010). Design and health: Evidence-based biophilic design. Science without Borders. Transactions of the International Academy of Science H&E. Special Edition 35-42.

Choi H, Schmidbauer N, Spengler J, Bornehag CG. (2010) Sources of Propylene Glycol and Glycol Ethers in Air at Home. Int J Environ Res Public Health. 2010 December; 7(12): 4213–4237.

Englund F. (1999). Emissions of volatile organic compounds (VOC) from wood. Report I 9901001, Trätek, Sweden.

Englund F. (2010). Inredningsmaterialens korrosivitet, in Bevarande inomhusmiljö – Neutrala material i inomhusmiljö (ed. Monika Fjaestad), Report, Swedish National Heritage Board. (In Swedish).

Fromme H, Lahrz T, Piloty M, Gebhart H, Oddoy A, Rüden H (2004). Occurrence of phthalates and musk fragrances in indoor air and dust from apartments and kindergartens in Berlin, Indoor air, **14**, 188-195.

Gminski R., Marutzky R., Kevekordes S., Fuhrmann F., Bürger W., Hauschke D., Ebner W & Mersch-Sundermann V. (2011). Sensory irritations and pulmonary effects in human volunteers following short-term exposure to pinewood emissions. J Wood Sci, **57**, 436-445.

Gyntelberg F, Suadicani P, Nielsen JW, Skov P, Valbjørn O, Nielsen PA, Schneider T, Jørgensen O, Wolkoff P, Wilkins K, Gravesen S, Norn S (1994). Dust and the sick building syndrome, Indoor Air, 4, 223-238.

Halvorsen B and Larsen B.M., 2013. Who owns heat pump and what does it do to the power consumption. Economic Report 2/2013, Statistics Norway, Oslo. (In Norwegian)

Hameury S., 2006. The hygrothermal Inertia of Massive Timber Constructions. Doctoral Thesis. Royal Institute of Technology, Architecture and the Built Enviroment. Stockholm, Sweden.

Hauschildt P, Molhave L, Kjaergaard SK (1999). Reactions of healthy persons and persons suffering from allergic rhinitis when exposed to office dust, Scandinavian Journal of Work Environment & Health, **25**, 442-449.

Hyttinen M., Masalin-Weijo M., Kalliokoski P. & Pasanen P. (2010). Comparison of VOC emissions between air-dried and heat-treated Norway spruce (Picea abies), Scots pine (Pinus sylvestris) and European aspen (Populus tremula) wood. Atm. Env., **44**, 5028-5033.

Korsnes S. K. (2012) Moisture and heat transfer of indoor surfaces. Master Thesis, in Norwegian. Norwegian University of Science and Technology, Trondheim, Norway.

Korsnes, S. K. & Nore, K. (2011). Potential energy savings due to latent heat exchange in indoor exposed wooden surfaces. CESBP 2013.

NFR 216404, 2011. Wood - Energy, Emissions and Experience (WEEE) Research project Norwegian Research Council. Oslo, Norway.

Nordic Wood (1998). Emission from Wood-Based Products. Declaration Model – Main Report. Copenhagen: Danish Technological Institute

Nyrud AQ, Bringslimark T (2010). Is interior wood use psychologically beneficial? A review of psychological responses toward wood. Wood and fiber science **42**, 202-218

Skulberg KR, Høiskar BAK, Kolstad L, Rønning KA, Gjersø L, Torp KE. (2009), Kartlegging av ansattes vurdering av inneklima i skoler og barnehager. Allergi i praksis 3, 34-38

Steckel V., Welling J. & Ohlmeyer M. (2011). Product emissions of volatile organic compounds from convection dried Norway spruce (Picea abies (L) H. Karst.) timber. Int. Wood Prod. J., **2**, 75-80.

TEK 10, 2010. Plan and building act. Norwegian building regulations. Ministry of Local Government and Regional Development, Oslo, Norway.

Wimmer R. (2012). Holzkurier 41. University of Natural Resources and Life Sciences, Vienna, Austria.

Wolkoff P, Clausen PA, Wilkins CK, Nielsen GD (2000). Formation of strong airway irritants in terpene/ozone mixture, Indoor Air, 10, 82-91.

Wolkoff P, Skov P, Franck C, Petersen LN (2003). Eye irritation and environmental factors in the office environment – hypothesis, causes and a physiological model, Scand J Work Environ Health, 29, 411-430.

WUFI®Plus (2014). Software hygrothermal calculation for whole buildings. www.wufi.de.

Window-opening and indoor climate in new multifamily-dwellings –A questionnaire survey

Fransson Victor, M.Sc [1]
Nordquist Birgitta, Assistant professor [1]
Lindberg Ola, M.Sc[1]

[1] Building Services, Faculty of Engineering, Lund University, Sweden.

KEYWORDS: Window-opening, airing, comfort, questionnaire survey, indoor climate

SUMMARY: *The apartment-block of Flagghusen in Malmö in the south of Sweden was built and designed with the intention to achieve a lower energy use compare to the regulations and a good indoor environment. The outcome of this ambition was evaluated in a first report in 2010 that showed that the overall notion of the perceived indoor climate in the apartments were good but that the measured energy use exceeded the estimated values. It was revealed that the residents air their apartments frequently and for extended periods of time, which was in congruence with the previously made nationwide questionnaire survey BETSI. This observation in combination with the exceeded energy use resulted in the wish for a more comprehensive questionnaire study with in-depth questions concerning the window-opening behavior. A second questionnaire study took place in the heating season of 2012. This study aims at showing the magnitude and frequency of the window opening and to delve in the reasons why residents air their apartments with this second study as basis.*

1. Introduction

1.1 Background

The apartment-block of Flagghusen in Malmö in the south of Sweden was built and designed with the intention to achieve a lower energy use compared to the regulations and a good indoor environment. This was made by the initiative of Malmö Stad who at that time were a part of Bygga-Bo dialogen, a government financed program to promote sustainable city development. In 2010 a study was presented showing the outcome of the project both by comparing measured energy use with estimates from the design face and an evaluation of questionnaires concerning the indoor climate (Hansson and Nordquist 2010). The report showed that the overall notion of the perceived indoor climate in the apartments were good but that the measured energy use exceeded the estimated values. The evaluation of the questionnaire also revealed that the residents air their apartments frequently and for extended periods of time. More than 50 % indicated that they air daily or almost daily which is in congruence with the nationwide questionnaire survey BETSI (Boverket, 2009). Only the amount of airing could be concluded from this study. The reasons why the residents wanted to air their apartments were however not possible to attain. These reasons are one important part to examine if the behavior and the factors affecting it are to be understood. This observation in combination with the exceeded energy use resulted in the wish for a more comprehensive questionnaire study with in-depth questions concerning the window-opening behavior. This second questionnaire study took place in the heating season of 2012. The answers were then analyzed. Based on the answers from the questionnaire additional measurements were performed in selected apartments where extensive airing took place, the measurements was performed during the heating season of 2013. In connection with the measurements the residents were interviewed regarding their interaction with the heating system and airing. The conclusions from these short interviews and measurements in individual apartments is presented in (Nordquist et al 2014). The complete report for both questionnaire survey and measurements can be

found in Fransson and Lindberg (2013). The results presented in this paper is a compilation of results from the questionnaire survey regarding airing more extensively presented in the above mentioned report. An analysis concerning energy use and window-opening in this apartment block will be published this spring, Karlsson and Nordquist (2014). Other recent studies concerning window opening and occupant behavior in dwellings have been made by for example Berge et al (2013), Frontzak et al (2012) and Vinther Andersen et al (2008).

1.2 Paper Outline

This study aims at showing the magnitude and frequency of the window opening and to delve in the reasons why residents air their apartments. The window opening behavior will also be investigate by evaluating answers from questions mostly regarding thermal sensation. For determination of the impact of this comfort parameter on airing behavior.

2. Questionnaire survey

In the beginning of 2012 a questionnaire-survey was performed in the apartment-block of Flagghusen in Malmö in the south of Sweden. This study was a follow-up of a similar questionnaire-survey made a few years earlier in 2010 but now extended with comprehensive questions including airing behavior.

2.1 Method

The experience of the occupants has been studied by standardized and validated questionnaires, called the "Stockholm's-questionnaire" (Engvall, 2002) and used by the city of Malmoe (Miljöbyggprogram Syd, 2009). As mentioned above additional questions focusing on airing have been added from the previous study, the questionnaire consisted of a total of 62 questions. This paper will discuss the questions and answers regarding the issue of airing behavior and not the complete survey of 62 questions.

Questionnaires were distributed to 523 apartments in 12 different properties in between 5-7 of March 2012 and gathered during the end of the same month. The questionnaire were distributed to each member of the residence by the age of 18 or older and they were asked to be answered individually. 257 questionnaire were returned and the answers from these are the base for the conclusions in this paper. The response rate can be compared with the Swedish nationwide survey BETSI (Boverket, 2009). There is a slight difference between the Flagghusen study and the BETSI study as the former consisted of two questionnaires, one to be answered for each household concerning the residence and a personal questionnaire that was distributed to all persons in the household. The Flagghusen questionnaire were distributed to each adult of the residence but consisted of questions regarding both residence and the persons themselves so it can be viewed upon as a combination or merger of the BETSI study's two separate questionnaires. The response rate from the Flagghusen survey viewed upon as per person was 32 % compared to 46 % in the BETSI study, viewed upon as per household the response rate for Flagghusen was 45 % compared to 49 % for the BETSI study.

3. Results

3.1 General answers

This first part of the result chapter aims to give a general overview of how the residents that answered perceive their indoor environment together with the frequency and the cause for airing their apartments.

TABLE 1. How do you perceive the air quality in your apartment?

Very good	Good	Acceptable	Bad	Very bad
30 %	43 %	21 %	4 %	0 %

The results from Table 2 show that only 4 % of the inhabitants are dissatisfied with the air quality in their apartments.

TABLE 2. Do you think it is too cold or too hot in any of the rooms in your apartment during the heating season?

	Much too cold	Too cold	Equilibrium	Too hot	Much too hot
Kitchen	5 %	8 %	82 %	2 %	0 %
Livingroom	7 %	13 %	75 %	4 %	0 %
Bathroom	5 %	12 %	79 %	2 %	0 %
Bedroom	7 %	11 %	74 %	4 %	2 %

From Table 2 the answers show that the main reason for thermal discomfort is too low temperature but there are 6 % who experience the opposite in the bedrooms even during the heating season. The main part of the participants however are at an equilibrium state regarding the temperature in the apartment.

TABLE 3. How often do you usually air during the heating season?

	Daily/almost every day	Approximately once a week	A few times every month	Rarely or never air
Flagghusen	53 %	26 %	12 %	8 %
BETSI (1996-2005)	61 %	17 %	12 %	9 %

The answers about how often and for how long the residents air their apartments in Flagghusen has been compared with the answers from the BETSI-study for buildings completed during the period 1996-2005. The result concerning frequency is compiled in Table 3 and it is shown that the airing is slightly less frequent for Flagghusen.

TABLE 4. When you air, do you usually have...? (Sep-Apr)

	A window opened the whole day or night	A window opened for a few hours	Cross-ventilation for a few minutes	Never air
Flagghusen	12 %	43 %	44 %	4 %
BETSI (1996-2005)	19 %	50 %	27 %	4 %

Table 4 shows that the duration the occupants air their apartments is slightly longer for the BETSI-study compared to Flagghusen.

TABLE 5. When you air, do you usually have...?

Flagghusen	Window opened the whole day or night	Window opened for a few hours	Cross-ventilation for a few minutes	Never air
Airing daily	19 %	48 %	38 %	0 %
Airing once a week or less	3 %	38 %	52 %	8 %

In Table 5 the answer for Flagghusen in Table 3 and 4 have been cross-examined. Two groups were formed depending on how the residents responded in Table 3, “Airing daily” and “Airing once a week or less”. It is seen in Table 5 that the respondents who air more frequently also air for a longer period of time at the occasion of airing.

TABLE 6. For how long do you air your apartment each day?

	Winter (Nov-Mar)	Spring, autumn (April, Sep-Oct)	Summer (May-Aug)
No airing	9 %	5 %	1 %
0-15 min	41 %	21 %	2 %
15-30 min	12 %	14 %	3 %
30-60 min	7 %	16 %	13 %
1-2 h	7 %	13 %	14 %
2-6 h	3 %	5 %	21 %
6-12 h	5 %	7 %	14 %
12-18 h	1 %	2 %	7 %
18-24 h	0 %	2 %	11 %

Table 6 show the answers from one of the questions added in the second survey that gives a more detailed view of the amount of time the residents leave their windows open each day, also seasonal variations can be distinguished. During the coldest period of the year (Nov-Mar) 16 % have their windows opened one hour or longer each day. This number increases to 29 % in the spring and autumn (April, Sep-Oct) and further still to 67 % in the summer (May-Aug).

TABLE 7. What is usually the main reason for you to air your apartment during the heating season?

Habit, routine	Bad air quality	Too hot	Existing ventilation is not sufficient	Another reason
30%	29%	21%	10%	14%

Table 7 shows the main reasons for airing during the heating season and that there is no cause that stands out in particular, the main reason is habit closely followed by bad air quality. The thermal climate is another cause that the residents report. For this question multiple answers were accepted meaning that multiple reasons can occur in the same apartment. Under “Different reason” the residents had the opportunity to answer in free text and the most frequently occurring statement was the wish or notion of getting fresh air.

TABLE 8. What causes you to stop airing?

Habit, routine	Received sufficient amount of new air	Satisfactory indoor temperature reached	Too cold ambient air temperature	Too windy	Draught	Noise from the outside	Rain	Different reason
14%	44%	16%	25%	20%	5%	8%	10%	7%

Table 8 shows what causes the inhabitants to stop airing, for this question multiple answers were accepted meaning that multiple reasons occurred in the same apartment. The most significant cause for closing the windows, which occurred in 44 % of the apartments, was that sufficient amount of new air had been received. That ambient conditions influence residents to stop airing is also seen.

3.2 Cross examination of answers

By dividing the answers into different groups depending on the answer to a particular question enables the possibility to investigate the impact on one question upon another.

3.2.1 Groups divided depending on time they air their apartments each day

Here the answers from the questionnaire has been grouped according to the answers seen in Table 3 (winter, Nov-Mar) creating two groups, airing less or more than one hour each day. In this analysis the time chosen as the breaking point between frequent and lesser airing is one hour.

TABLE 9. With how large opening do you air your apartment during the heating season?

	Width less than 0,5 m	Width exceeding 0,5 m	Height less than 0,5 m	Height exceeding 0,5 m	Ajar (up to 10 cm)	Half open (between 20-50 cm)	Fully open (more than 50 cm)
< 1 hour/day	14 %	76 %	6 %	80 %	49 %	39 %	10 %
> 1 hour/day	24 %	73 %	9 %	80 %	71 %	24 %	2 %

In Table 9 it is shown by which mean these two groups air their apartments and there are two notable distinctions. The first is that the people who air a shorter period each day open the windows more fully (10 %) and those who air longer is more likely to put the window ajar (71 %). The second thing is that those who air longer tend to use a narrow window more often (24 %) than the other group (14 %).

TABLE 10. What is usually the main reason for you to air your apartment during the heating season?

	Habit, routine	Air quality issues	Too hot	Existing ventilation is not sufficient	Different reason
< 1 hour/day	31 %	31 %	19 %	10 %	17 %
> 1 hour/day	38 %	33 %	38 %	13 %	9 %

As mention earlier multiple answers were accepted for the question seen in Table 10. It can be observed that causes for airing occur more often in the group that air more than one hour each day. The most significant difference in comparison between the groups is regarding over-temperature, this cause occur twice as often in the group with above one hour airing. Habit is the main reason for airing in both groups together with air quality and temperature.

3.2.2 Groups divided into groups depending on their thermal sensation

Now three groups have been created from the answers of the last row in Table 2 regarding thermal sensation in the bedroom. The bedroom was chosen because there was the largest percentage dissatisfied as well as the biggest spread. Something that was noticed during the grouping was that those who thought it was hot or cold in the bedroom in most cases also had this experience for the other rooms so it is assumed that the answers for the bedrooms gives a good picture of the dwelling as a whole (there was no option in the questionnaire solely regarding the whole apartment for this question). The group “Cold” in Table 11, 12 and 13 consists of residents that answered both “much too cold “and “too cold” in Table 2. The same procedure has been made for the answers regarding too high temperature.

TABLE 11. For how long do you air your apartment each day?

	No airing	0-15 min	15-30 min	30-60 min	1-2 h	2-6 h	6-12 h	12-18 h	18-24 h
Cold	9 %	47 %	20 %	4 %	4 %	2 %	0 %	0 %	0 %
Equilibrium	10 %	41 %	11 %	8 %	7 %	3 %	6 %	1 %	1 %
Hot	0 %	31 %	13 %	6 %	13 %	13 %	13 %	6 %	0 %

In Table 11 the answers for the three groups concerning the time they air their apartment each day is shown. 6 % in the group that think it is too cold air longer than one hour each day, for the group experiencing equilibrium this number is 18 % and for the last group 45 %. Noticeable is that almost 20 % of those who experience equilibrium air longer than one hour each day, also this group consists of three quarters of the residents participating in this survey according to Table 2.

TABLE 12. What is usually the main reason for you to air your apartment during the heating season?

	Habit, routine	Air quality issues	Too hot	Existing ventilation is not sufficient	Different reason
Cold	31 %	38 %	11 %	22 %	9 %
Equilibrium	31 %	27 %	21 %	7 %	16 %
Hot	19 %	38 %	44 %	13 %	6 %

Table 12 shows the reasons for airing among the three groups. One observations is that the groups who feel it is too cold or too hot both experience a more significant reason to air due to air quality issues or insufficient ventilation compared to the group experiencing equilibrium. Airing out of habit is here the main reason only for the group who experience equilibrium.

TABLE 13. How can you control the temperature in your apartment?

	Airing	Knobs on the radiators	Display where the indoor temperature is chosen	No ability to influence	Different way
Cold	36%	40%	16%	11%	13%
Equilibrium	51%	70%	17%	2%	6%
Hot	69%	56%	0%	6%	13%

How the three groups believe they can control the temperature in their apartments is shown in Table 13. Airing as a way to control the temperature is most significant for those who experience too high temperature followed by the equilibrium group and least significant for the group who feel their apartments are too cold. Regarding the interaction with the heating system as a way of controlling the indoor temperature over 90 % of the equilibrium group consider it useful. This number is about 20 % lower for the other two groups. The ability to control the heating system is assumed to consist of answers from three categories “Knobs on the radiators”, “Display where…” and “Different way”. Under the category different way the residents mostly describe ways of controlling floor heating that does not fit under the other categories.

4. Conclusions and Discussion

The air quality is perceived good or acceptable by the vast majority of the residents, only 4 % think it is bad. Considering thermal comfort the experience of equilibrium conditions vary from 74 % to 82 % for the rooms in the apartment. Too low temperature is the main issue for those dissatisfied however 6 % deem the temperature too high in the bedroom. Both bad air quality and thermal climate are main causes which according to the answers can be reasons for airing. This leads to the conclusion that residents who experience good indoor air quality as well as good temperature conditions air their apartments for periods extending from one hour per day up to 18- 24 hours a day. The explanation for this cannot be certain but one theory is that the rather extensive airing is experienced as a necessary measure for achieving a desired indoor climate. This gives room for questions both regarding energy

use of the buildings and functionality of the ventilation system. The residents who experience good indoor air quality and good temperature conditions represent the majority of the answers from the survey. This fact can be interpreted in a way that possible deficiencies with the regulation of the heating system and the supply air-flow might be covered by the behavior of the occupant leading to acceptable indoor conditions first after airing is applied at the cost of higher energy use. This brings forth the subject of user related questions, how do residents interact with the heating system, what do they know about the management of the ventilation system etc. What demands can and should be laid upon the user and what will the consequences be. As mentioned in the introduction a separate paper (Nordquist et al 2013) will discuss several of these issues. Apart from bad air quality and temperature the main reason for airing is out of habit or routine according to the answers. What a habit is and from where it originate can be discussed. Perhaps it is a remnant from another living situation or maybe it is sprung from a repetitive need for airing due to a particular reason. This recurring action of airing due to a problem with for example too high temperature might in time turn into a habit and no longer be thought of as a way of solving an otherwise existing problem. This however is just a theory but definitely worth mentioning as this reason is such a big factor when considering window-opening behavior at least according to the answers in this study.

The last conclusion regards the way the resident's air depending on the duration. There is a very clear pattern showing that when airing longer than an hour the windows are less likely to be open wide but much more likely left ajar. And for short airing occasions a fully or half open window is more frequently used. One can assume that the short airing with fully open windows is to rapidly get rid of pollutants such as cooking fumes or other smells while airing with a smaller opening for a longer period of time is to lower the temperature. The answer in Table 10 gives a small indication that this might be a plausible explanation.

5. Acknowledgements

First of all BEBO; a cooperation between the Swedish Energy Agency and some large building owners in Sweden working for energy-efficient apartment buildings is acknowledged for financing the study. Secondly we wish to acknowledge those at the department of Building Services at Lund University who supported us throughout the study. Finally we wish to acknowledge the residents who participated in the questionnaire survey, without your share of experience this would not have been possible.

References

Berge M. & Mathisen H. M. 2013. Post-occupancy Evaluation of Low-Energy and Passive House Apartments in the Lovåshagen Cooperative - Occupant behavior and Satisfaction. 2013 *Passivhuskonferens Norden 15-17 okt 2013.* Gothenburg. 12 p.

Boverket. 2009. Enkätundersökning om boendes upplevda inomhusmiljö och ohälsa – resultat från projektet BETSI. ISBN pdf:978-91-86342-45-6, Boverket, Karlskrona, in Swedish

Engvall K. Sandstedt E. Norrby C. 2002. "The Stockholm Indoor Environment Questionnaire (SIEQ): A sociologically based tool for assessment of indoor environment and health in dwellings" *Indoor Air Feb 2004.* p. 24-33

Fransson V. Lindberg O. 2013. *Undersökning av inneklimat och vädring i nybyggda lägenheter*. Building Services, Lund. 252 p. in Swedish

Frontzak Monica, Vinther Andersen Rune, Wargocki Pawel, 2012, Questionnaire survey on factors influencing comfort with indoor environmental quality in Danish housing, *Building and Environment 50 (2012).* p.56-64

Hansson A. & Nordquist B. 2010. *Uppföljning Flagghusen Energi och inneklimat Slutrapport*, WSP, Department of Building Services, Faculty of Engineering, Lund University. in Swedish. 110 p.

Karlsson E. & Nordquist B. 2014. *Energiuppföljning av området Flagghusen*. to be published in April 2014. WSP Malmö, Building Services, Faculty of Engineering, Lund University, Lund, in Swedish

Malmö Stad. 2009. *MiljöbyggprogramSyd*. Malmö and Lund city

Nordquist B. Fransson V. Lindberg O. 2014. Perceived and measured indoor climate in new-family building including identifying technical deficiencies, *Nordic symposium on Building Physics 2014 Lund,* Building and Environmental Technology, Lund University. 8p

Vinther Andersen Rune, Toftum Jørn, Kaee Andersen Klaus, W. Olesen Bjarne, 2008, Survey of occupant behaviour and control of indoor environment in Danish dwellings, *Energy and Buildings 41 (2009).* p.11-16

Numerical investigation of diffuse ceiling ventilation in an office under different operating conditions

Christian Anker Hviid, Assistant Professor [1 3]
Steffen Petersen, Assistant Professor [2 3]

[1] Department of Civil Engineering, Technical University of Denmark, Denmark
[2] Department of Engineering, Aarhus University, Denmark
[3] ALECTIA A/S, Denmark

KEYWORDS: *Diffuse ceiling ventilation, ventilation efficiency, ventilation, draught, CFD*

SUMMARY:
Diffuse ceiling ventilation is a novel air distribution device that combines the suspended acoustic ceiling with ventilation supply. A diffuse ceiling distributes the supply air above the acoustic tiles and has proven performance in both laboratory and class room experiments. This paper is a numerical study of the performance of a six person office equipped with diffuse ventilation ceiling. In total six extreme, yet realistic, operation scenarios were simulated to study the performance including different occupancy, ventilation rates and supply air temperatures. The performance was studied with regard to air change efficiency, air movements, temperatures and stratification. In all scenarios the ceiling performed satisfactorily.

1. Introduction

The main purpose of the ventilation system in a building is to supply fresh air to the occupants and secondary to remove excessive heat. The ventilation system should do so energy-efficiently and with minimal risk of discomfort in the occupied comfort zone. A promising concept for this is diffuse ceiling ventilation which is a novel air distribution device that combines the suspended acoustic ceiling with ventilation supply. The principle of diffuse ceiling ventilation for comfort ventilation is to inject the supply air into the plenum above a standard suspended acoustic ceiling. The plenum thereby works as a pressure chamber and air is distributed to the room below through cracks and perforations. The flow velocity into the room is very small and irregular, hence the term diffuse.

The reported research in this area mostly relies on laboratory experiments where results have been promising. Nielsen & Jakubowska (2008) published results where diffuse ceiling ventilation outperformed five conventional air distribution systems in a laboratory office environment. The findings were supported by Hviid & Svendsen (2013) who carried out experiments in a test facility resembling a small classroom as well as in a real classroom (Hviid & Terkildsen 2012). Fan et al. (2013) has documented good performance of the concept both experimentally and numerically. Numerical investigations by CFD (Computational Fluid Dynamics) were shortly performed on an office by Nielsen et al. (2010) to investigate the level of stratification in heating mode. Hviid & Petersen (2011) demonstrated that diffuse ceiling ventilation may improve the night cooling potential of a classroom.

The objective of the research reported in this paper is to assess the indoor climate performance of diffuse ceiling ventilation in an office environment under six different operating conditions that stresses the concept. The performance is assessed numerically by CFD in terms of thermal conditions, air movements, stratification, and air change efficiency.

2. Test case

The investigations have been performed on an office located in a large newly erected building in the harbour of Aarhus, Denmark. The numerical solution domain has been established from the geometric model of the irregular office room depicted in FIG 1. This room was selected because the large façade/floor ratio has high solar gain and high thermal losses, thus imposing maximum stress on the HVAC strategy. The floor area of the office is 41.4 m^2 with a room height of 3.0 m. The room has two facades with the compass orientations 177° / 303°. The windows are arranged as transparent bands with a height of 1.8 m. The parapet is 0.875 m high.

FIG 1. Plan view of office. Furniture layout reflects potential meeting room

2.1 Diffuse ceiling

The suspended acoustic ceiling used as diffuse inlet consists of horizontal aluminium lamellas attached to a carrier as depicted on FIG 2 with 20 mm of black acoustic mineral wool batts overlying the lamellas. The finalized ceiling is depicted on FIG 3. The main air paths are the small holes in the universal carrier as well as cracks between batts and suspension profiles originating from the installation. This means that some air enters the room as linear microjets along the carriers, and some air enters diffusively.

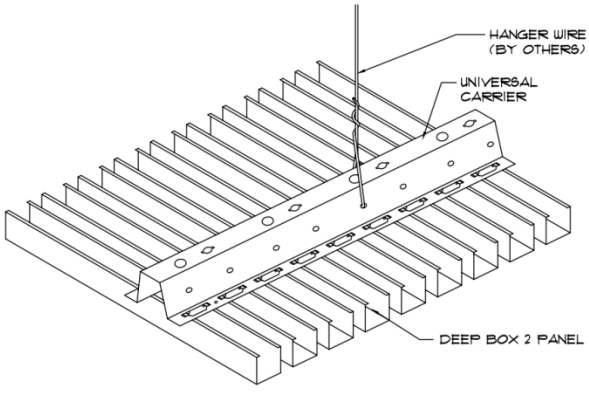

FIG 2. Aluminium lamellas with suspension system

FIG 3. Finalized ceiling

3. Method

3.1 CFD model

For the simulations the commercial CFD code Ansys CFX version 14.5 was used. FIG 4 depicts the CFD model with six workstations, occupants and computers. The lighting fixtures are not represented as they are off in all scenarios due to daylight control. All internal components of the model are simplified with box-shaped geometric models.

Heat transmission through the façade is modelled by the following U-values and the scenario-dependent external temperature:

- Opaque façade U-value: 0.14 W/(m^2·K)
- Window U-value: 0.8 W/(m^2·K), g-value perpendicularly: 0.3, incident angle dependent

Solar radiation is modelled by applying convective heat sources on the windows, i.e. it is not directional. The amount of incoming direct, diffuse and reflected solar and sky radiation depends on the simulation scenario as well as time of year and day, and the g-value of the glazing. Radiation exchange between surfaces in the model is not included in the calculations. The radiator is modelled as a surface under the window with a given heat flux depending on the simulation scenario. Each occupant provides a heat gain of 90 W and each computer a heat gain of 60 W.

The heat gains of the domain is balanced by making the internal walls absorb excess heat which occurs when, for instance, the room is heated with warm supply air.

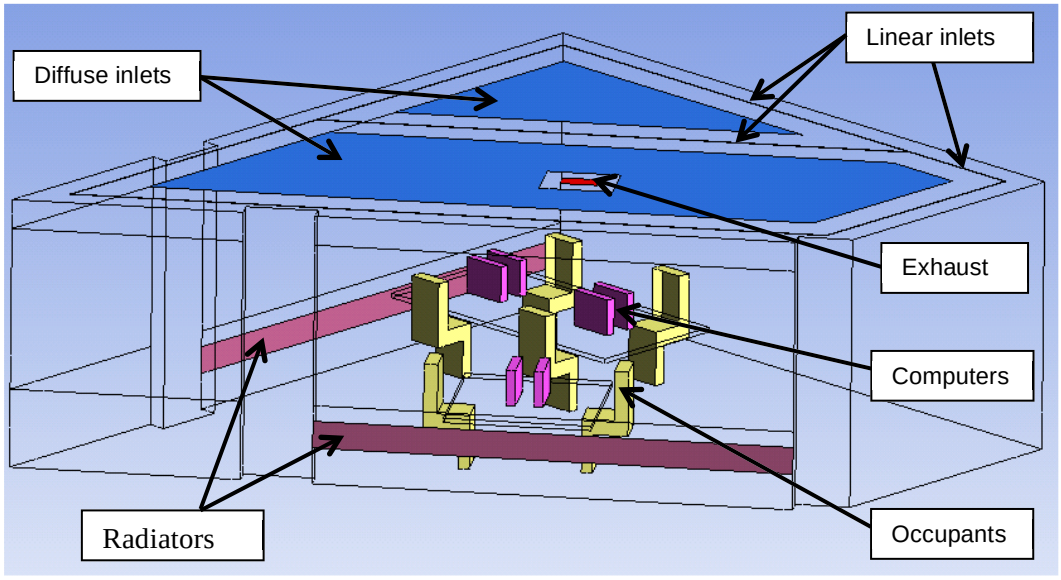

FIG 4. Solution domain with six workstations

The ventilation is supplied partly diffusively through the ceiling surfaces depicted on FIG 4, partly by microjets along the ceiling carriers (linear inlets). The latter are placed where the ceiling lamella finishes to the wall and every 3 m. The airflow distribution is assumed to be 70/30 with most air through the linear inlets. The width of the slot is adjusted to an inlet velocity of 0.23 m/s. The rest of the air is distributed over the diffuse surfaces.

The mesh comprises approx. 3.5 million cells and plane-parallel cell layers are implemented along the walls and heat sources to better capture the fluid flow. The Boussinesq approximation was chosen to model buoyancy driven forces as it provides faster convergence for many natural-convection flows. The applied turbulence model is the k-epsilon model, which is stable and with sufficiently accurate

results for most indoor applications. The turbulence model is combined with the CFX feature 'scalable wall laws', thus heat transfer between surfaces and air is made independent of grid size.

The convergence residual criteria were default values (0.0001) and no mass/heat flux imbalances were larger than 1 %. The reported results are transient since the temperature differences create weak unstable air currents which are unresolvable by steady-state calculations.

3.2 Investigated scenarios

The driving forces with diffuse ceiling ventilation are the thermal convective plumes that arise above any heat source. Thus, for air change efficiency we expect that the most critical scenarios are those with small temperature differences throughout the domain and small convective heat sources. Regarding thermal environment and elevated air movements, we expect that large airflow rate with low supply temperature to be the most problematic scenario. Six scenarios are therefore investigated:

1. **Normal operation.** Overcast winter day with occupants and computers. There are no expected critical aspects.
2. **Pre-conditioning.** Winter morning without occupants and computers. The critical aspect is possibly worsened air change efficiency with no occupants.
3. **Air-heating.** Winter morning without occupants and computers. The critical aspect is stratification.
4. **Cooling by low inlet temperature.** Summer day with occupants and computers. The critical aspect is the risk of draught due to low supply temperature.
5. **Cooling by high flow rate.** Summer day with occupants and computers on. The critical aspect is the risk of draught due to high airflow rate.
6. **Night ventilation.** Summer night without occupants and computers. The critical aspect is air change efficiency, subsequently night cooling efficiency, without heat sources present.

The design indoor air temperature is 21 °C in winter and 26 °C in summer. The specific data for each scenario is summarised in TABLE 1.

TABLE 1. Input to investigated scenarios. The emboldened values indicate the critical aspects.

	Season	Out. temp.	Flow rate	Supply air temp.	ΔT air	Work-stations	Radiator power	Solar radiation
1	Winter day	-5 °C	2 h^{-1}	16 °C	-5 °C	900 W	0 W	87 W
2	Winter morning	-12 °C	2 h^{-1}	21 °C	**0 °C**	0 W	**249 W**	0 W
3	Winter morning	-12 °C	3 h^{-1}	27 °C	**+6 °C**	0 W	0 W	0 W
4	Summer day	28 °C	4 h^{-1}	14 °C	**-12 °C**	900 W	0 W	1330 W
5	Summer day	28 °C	**6 h^{-1}**	18 °C	-6 °C	900 W	0 W	1330 W
6	Summer night	18 °C	2 h^{-1}	19 °C	-2 °C	**0 W**	**0 W**	**0 W**

3.3 Age of air

The age of air is a measure of the air quality. The air age (Sandberg & Sjöberg 1983) in a given point is a measure of how long a massless particle of air spent on transport from the inlet opening to that point. In the case of perfect mixing the air has the same age throughout the room. In locations with short circuiting or poor mixing, i.e. poor ventilation efficiency, the age differs significantly from the mean age. This age of air index is not dependent on the presence of specific pollutants or source location and eliminates the need for definitions of the occupied zone and breathing zone.

4. Results

4.1 Temperature performance

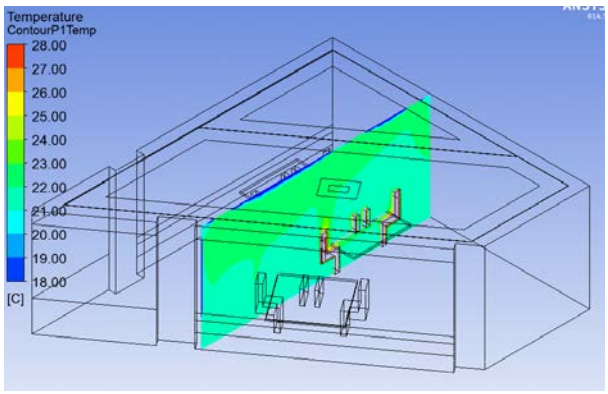

FIG 5. Thermal, scenario 1

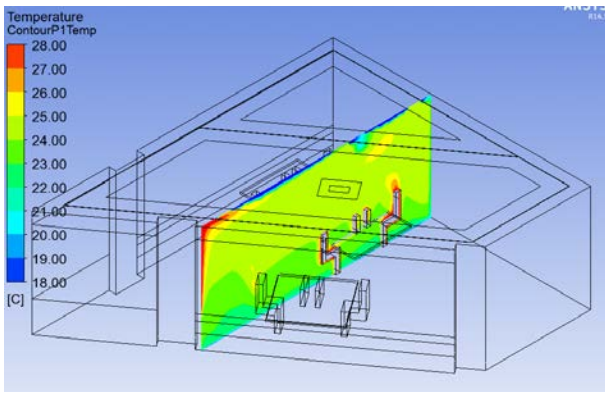

FIG 6. Thermal, scenario 4

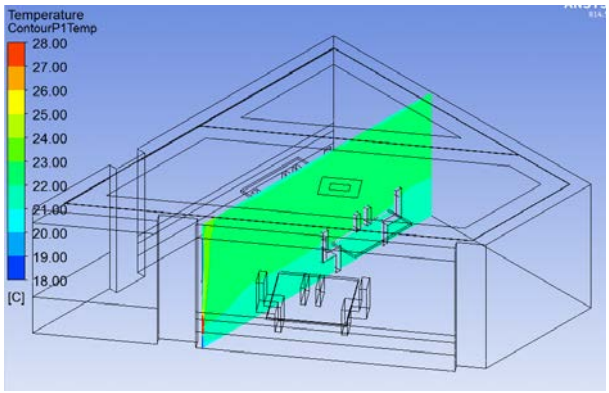

FIG 7. Thermal, scenario 2

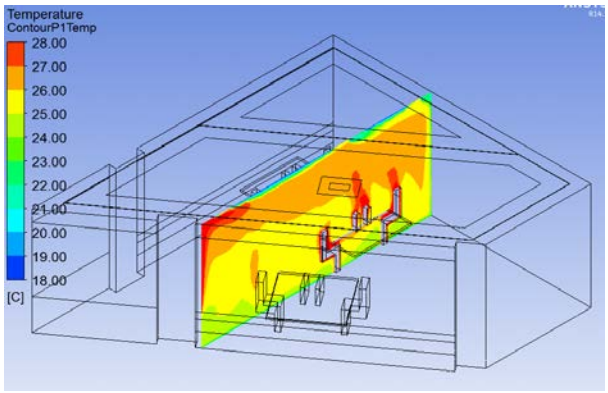

FIG 8. Thermal, scenario 5

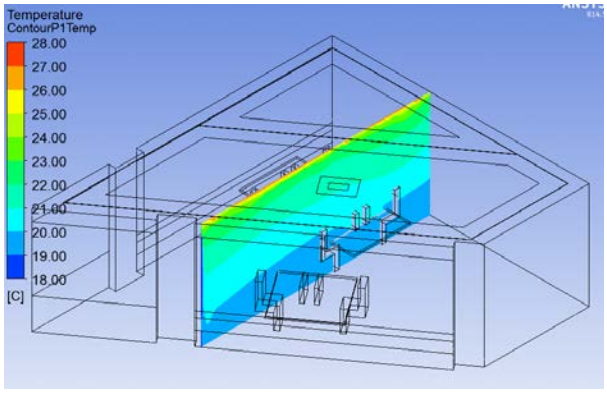

FIG 9. Thermal, scenario 3

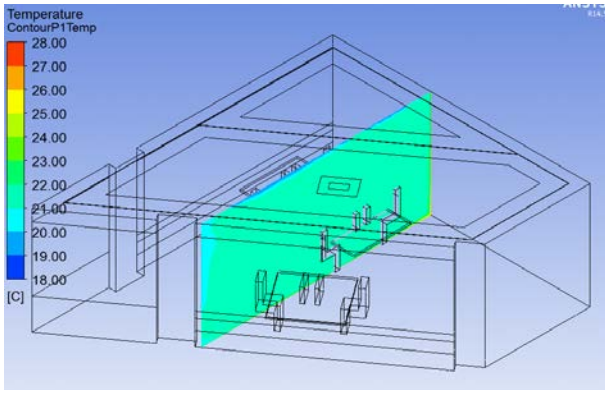

FIG 10. Thermal, scenario 6

The thermal performance of the scenarios, FIG 5-FIG 10, is in general satisfactory with very small stratification which is in good agreement with experiments (Hviid & Svendsen, 2012; Fan et al., 2013). Scenario 3 shows critical temperatures in the comfort zone partly due to cold downdraught from the window. Some stratification is present in scenario 5 but it is quite small, 1 K/m, and thus well within the limits of DS/EN ISO 7730.

4.2 Air movements

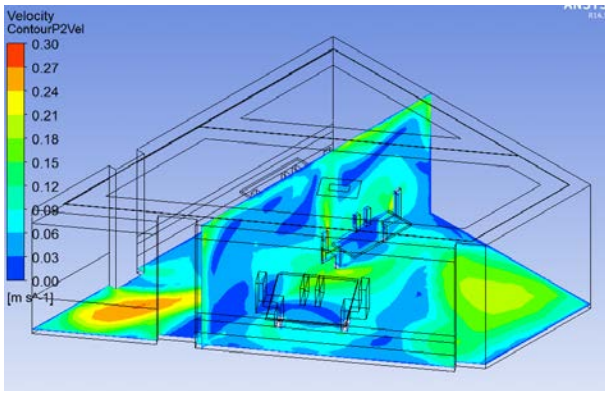

FIG 11. Air velocity, scenario 1

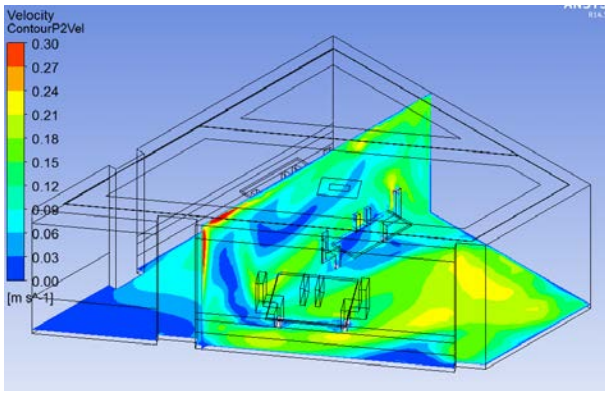

FIG 12. Air velocity, scenario 4

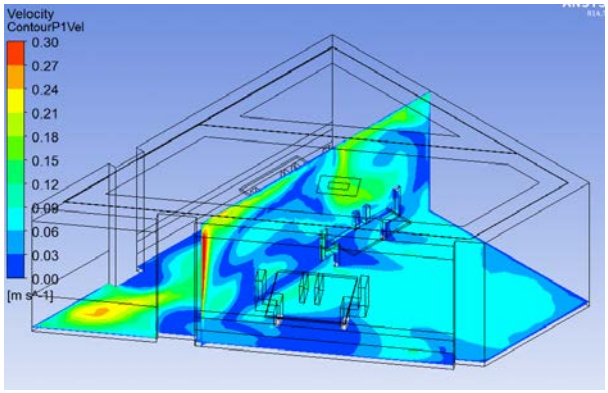

FIG 13. Air velocity, scenario 2

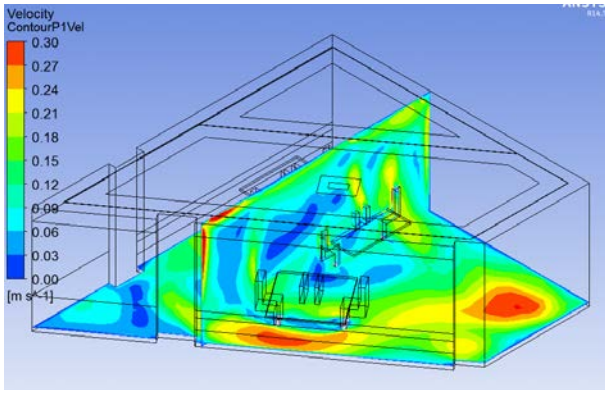

FIG 14. Air velocity, scenario 5

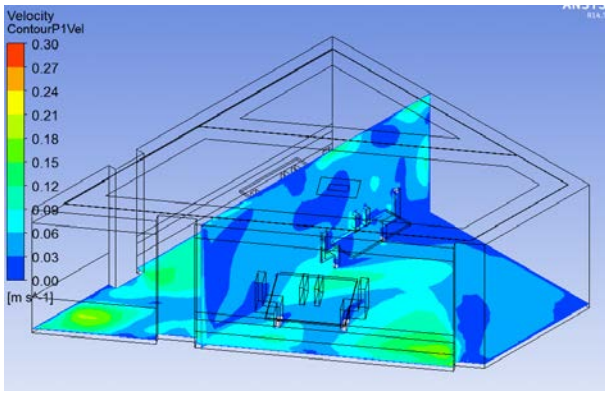

FIG 15. Air velocity, scenario 3

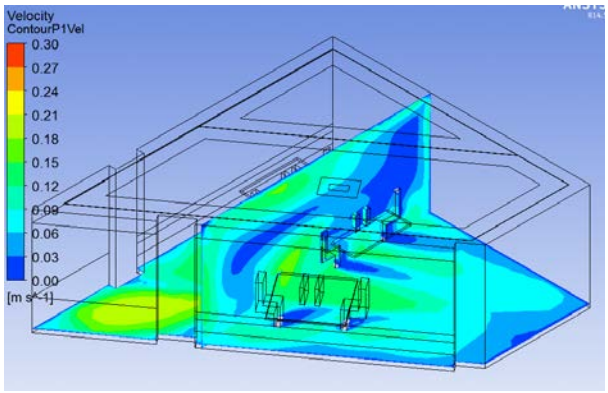

FIG 16. Air velocity, scenario 6

The air velocities in the winter scenarios, FIG 11 - FIG 16, are satisfactory, i.e. the air velocities in the comfort zone are below 0.15 m/s. In the summer scenarios, the two daytime scenarios (4 and 5) show elevated velocities (approx. 0.3 m/s) at ankle height in some areas. Analyses of these two scenarios show that cool, fluctuating ventilation air drops from the ceiling. This and the convective thermal plumes from occupants, computers, and the warm window create room size vortices along the floor. This behaviour has not been reported, neither by Nielsen et al (2010), nor by Hviid & Svendsen (2013) or Fan et al. (2013). However, a certain displacement effect is expected and this indicates the need for more investigations into the natural convection forces and transient behaviour of diffuse ventilation ceilings.

4.3 Air quality by age-of-air

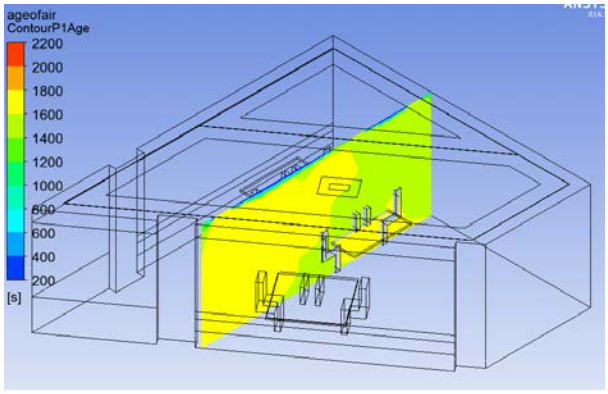

FIG 17. Age of air, scenario 1

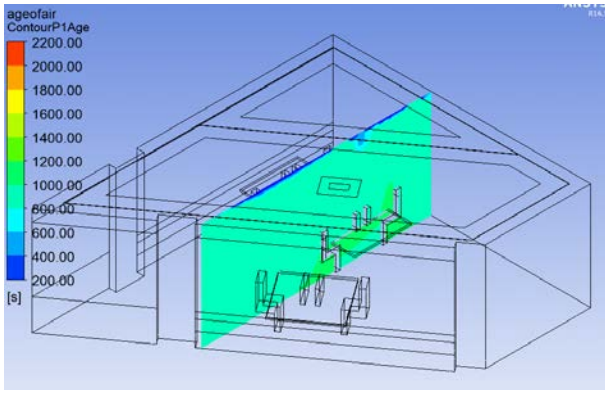

FIG 18. Age of air, scenario 4

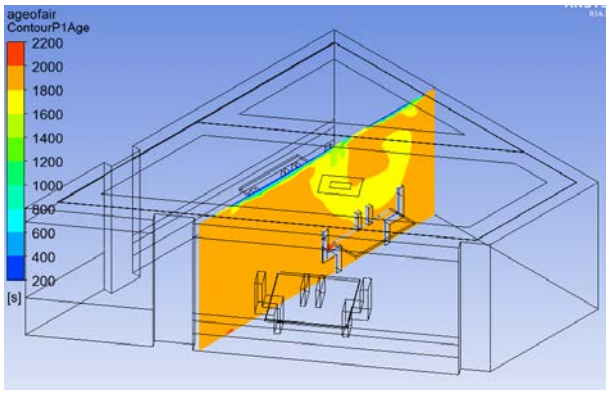

FIG 19. Age of air, scenario 2

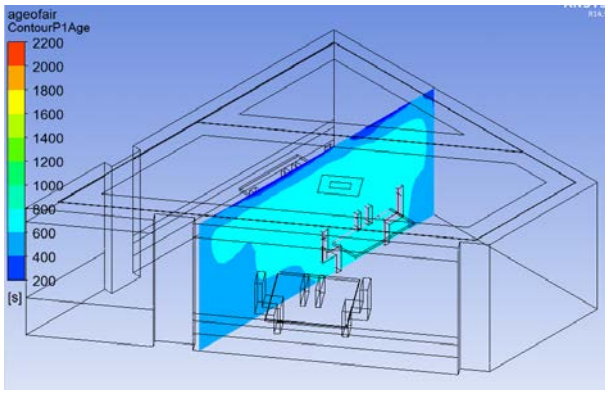

FIG 20. Age of air, scenario 5

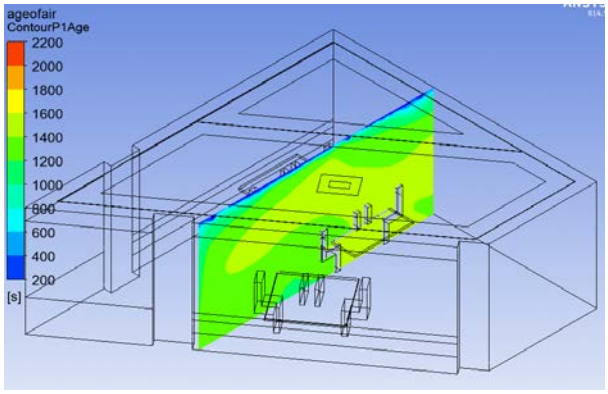

FIG 21. Age of air, scenario 3

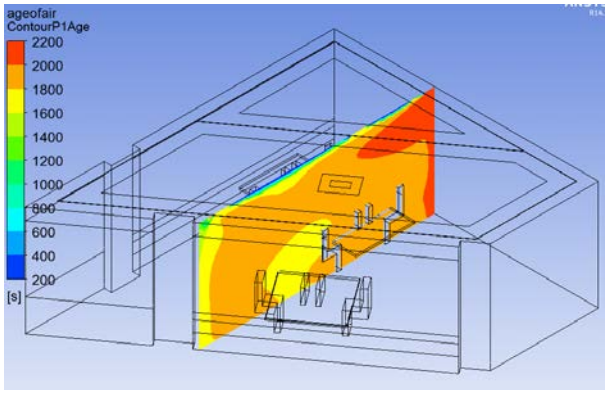

FIG 22. Age of air, scenario 6

The age of air shows the air change efficiency in different parts of the room in FIG 17-FIG 22. None of the scenarios show any sign of short-circuiting and stagnant zones.conventional mixing ventilation, which is also validated by experimental data from Hviid & Svendsen (2012), and Fan et al. (2013).

TABLE 2 compares the mean air change efficiency of the room with the analytically derived value of perfect mixing ventilation. The largest deviation is 9 %, hence the diffuse ceiling ventilation performs on par with conventional mixing ventilation, which is also validated by experimental data from Hviid & Svendsen (2012), and Fan et al. (2013).

TABLE 2. *Comparison of simulated air change efficiency with perfect mixing*

Scen.	Description	Perfect mixing	CFD-results @ outlet	Deviation
1	Winter day, normal operation	1800 s	1640	-9 %
2	Winter morning, pre-conditioning	1800 s	1793	0 %
3	Winter morning, air-heating	1200 s	1220	2 %
4	Summer day, cooling by low supply air temp.	900 s	901	0 %
5	Summer day, cooling by high flow rate	600 s	576	-4 %
6	Summer night ventilation	1800 s	1755	-3 %

4.4 Energy efficiency

In terms of energy efficiency, the pressure drop of diffuse ceilings was measured and reported by Hviid & Svendsen (2012) and Fan et al. (2013) to be approx. 0.5-3.5 Pa. Thus, in comparison with conventional mixing diffusers, the diffuse ceiling performs on par at 1/20 pressure drop. For current best-practice ventilation systems with a specific fan power of 1.1 kJ/m^3, the pressure savings by the diffuse ceiling constitutes approx. 10% of the supply pressure drop.

5. Conclusion

In general, the diffuse ceiling ventilation concept has performed on par with conventional mixing ventilation where the momentum forces of the supply jet entrains and mixes with the room air. The air change efficiency (age of air) documented that no stagnant zones or short-circuiting were present.

The thermal performance does not show stratification in the investigated scenarios, except when used with air-heating. Possibly, a radiator below the window will create sufficient thermal plume to avoid stratification.

The air velocities were satisfactory but the investigations in this paper have disclosed cold down draughts with this type of diffuse ceiling in an office setting during summer. However, these issues have not been reported in the literature, indeed, laboratory experiments performed on similar types of ceilings have not identified any problematic behaviour. Consequently, it is relevant to investigate further the behaviour and consequences of the transient convective forces.

References

Fan J., Hviid C.A., Yang H. 2013. Performance analysis of a new design of office diffuse ceiling ventilation system. Energy and Buildings 59. 9 p.

Hviid C.A. & Petersen S. 2011. Integrated ventilation and night cooling in classrooms with diffuse ceiling ventilation. 4th international conference on high-quality thermal retrofit of large-volume buildings (Ökosan). Graz, Austria. 7 p.

Hviid C.A. & Svendsen S. 2013. Experimental study of perforated suspended ceilings as diffuse ventilation air inlets. Energy and Buildings 56. 9 p.

Hviid C.A. & Terkildsen S. 2012. Experimental study of diffuse ceiling ventilation in a classroom. 33rd AIVC Conference, Copenhagen, Denmark. 10 p.

Nielsen P.V. & Jakubowska E. 2008. The performance of diffuse ceiling inlet and other room air distribution systems. Proceedings of Cold Climate HVAC. Sisimiut, Greenland. 7 p.

Nielsen P.V., Jensen R.L., Rong L. 2010. Diffuse ceiling inlet systems and the room air distribution. Proceedings of CLIMA 10th REHVA World Congress. May 9-12, Antalya, Turkey. 7 p.

Sandberg M. & Sjöberg M. 1983. Use of moments for assessing air quality in ventilated rooms, Building and Environment 18, 4, 181-197.

Application of the energy signature method for evaluation the effect of an exchange from electric coil heating system to a hydronic ground source heat pump system in a church building

Folke Björk, Prof
Navid Gohardani, PhD

Dept of Civil and Architectural engineering; KTH – Royal Institute of Technology, Stockholm, Sweden

KEYWORDS: *Energy use, Energy signature, Ground source heat pump,*

SUMMARY:
In this article, the energy performance of a church building built in 1978, where existing electric coil heating system is replaced by a hydronic ground source heat pump system, is assessed and discussed. The energy signature method is used in this analysis where it was found that this installation reduced energy consumption with approximately 66%. The use of billing data and the weather data from a public weather station was successful because they both were of good quality. Thus the problem with missing data was avoided. By only considering data for some of the periods of the day, disturbing effects by the activities of the building was minimized. Finally the energy signature method was found to be useful for evaluation of performance of a heating system in this case.

1. Introduction

The ground heat exchanger in ground source heat pumps (GSHP) is composed of a closed loop pipe system. In the winter, the fluid in the pipes extracts heat from the earth and transfers into the building, while in the summer, it is possible to reverse the system and transfer heat from the building and deposit it to the cooler ground (US Dept of Energy 2013). This method of reloading the system is an available option, but not the most common solution for ground heat exchanger systems utilized in Sweden. GSHPs operate based on a vapor – compression cycle as described by Björk et al (2012) and also in a review article by Mustafa (2006).

GSHPs are often dimensioned with the purpose of meeting the demand for heating and hot water. Generally this is carried out in order to meet 60–80% of the maximum thermal power demand of the building in question (Björk et al. 2012), leading to approximately 90% of the annual energy demand of the building is covered by the heat pump (Swedish energy Agency 2013). The rest will be covered by electricity.

1.1 Coefficient of performance

The coefficient of performance (COP) or heat output per unit of electricity for a heat pump is, is defined as the ratio between acquired useful energy and applied energy (Björk et al. 2012).

$$COP = \frac{E_u}{E_a} \tag{1}$$

Where E_u aquaired useful energy supplied to the system)
E_a *applied (bought) energy to the system*

An inventory of the system COP for a number of GSHP installations in apartment buildings has previously been carried out by Levin (2008). In that study, the system outputs were evaluated by metering of the electricity input and the thermal output. In that study COP over the year was in the range of 2,14 to 3,5 with a mean value of 3,0.

1.2 Geothermal energy usage in Swedish buildings

The best potential for geothermal energy in Sweden is believed to exist in regions where there are large bodies of groundwater at significant depths (2–3 km), i.e. areas with thick layers of sedimentary bedrock or fault zones (Geological survey of Sweden, 2013). In general, the rock or soil is reckoned to deliver two times the energy supplied by electricity to the system. Although the geothermal solution may be adequate for a large body of buildings, it is not applicable to all buildings. In particular, buildings where implementation of such a solution is difficult are those built on deep layer of soil. Additionally, buildings with only electric coil heaters require substantial renovation by the need for installation of a hydronic heating system. This however provides the option to choose a heating system with low emission temperatures, which is beneficial for the COP of the system. The most significant drawback of geothermal systems is their initial high cost.

2. Evaluation of energy consumption in buildings

When considering measures for improved energy performance, it is essential to have a reliable method in order to evaluate and compare the status prior to and after these were undertaken. Weather normalization of energy consumption in buildings is needed for comparison between various years, or parts of various years (Layberry 2009) [7]. One method for weather normalization is energy signature modeling which was utilized in this study, as it was considered to provide an adequate representation of the available data for the daily outside temperature and energy consumption (Schulz 2003). Estimation of energy performance indexes, such as the energy signature, call for data of energy use and the present outdoor temperature. The energy use of a building is plotted versus the outdoor temperature. The actual annual energy consumption for a building during a billing period is evident from the utility bills and the temperature can be taken from a weather station.

FIG 1. Åbyberg church (October, 2013)

2.1 Case study – The Åbyberg church

The Åbyberg church is located approximately 30 km north of Stockholm, Sweden. Built in 1978, the church consists of an octagonal brick church hall and a ground floor in stucco wall covering. The roof of the church hall is pyramid shaped whereas the acceding rectangular shaped building sections have a gable roof (Swedish National Heritage board 2013). The encircling area of the building is approximately 1400 m^2 with a total heated floor area of 740 m^2 and a total window area of 60 m^2. The overall heat transfer coefficient (U-value) for the windows, walls and the ceiling is given by 1.8 W/m^2K, 0.3 W/m^2K and 0.2 W/m^2K, respectively. The rectangular building consists of one floor and a basement with entrances recessed into niches.

With the aim of energy consumption reduction and improvement of the energy performance of the church building, an energy refurbishment measure was undertaken by exchanging the existing electric coil heating system to a hydronic ground source heat pump system. The system has three boreholes at a depth of 210 m. The hydronic heating system has a design output temperature (DOT) of 45ºC, which makes it a low temperature system. In this case no other measures for reducing energy consumption were done in the building.

2.2 Data acquisition

The data for energy consumption in this study was retrieved from the available electricity bills of the building. The data used consisted of readings per hourly basis, for the consumption of the entire building. Hourly reading is in Sweden offered all customers with main fuse larger than 63 amperes. The temperature data was acquired from the SLB weather monitoring station at Märsta (SLB 2013. which is a monitoring station with similar weather conditions as the location of the Åbyberg church.

2.3 Data processing

The calculated time periods both prior and subsequent to the GSHP system installation, have been divided into “non-heating” and “heating” seasons. The latter applies to the period from October, 15 until May, 15 while the rest of the year is considered as the “non-heating” season when the church building does not need additional heating.

The electricity consumption given by the billing data from the electricity provider includes both the consumption related to space heating and the consumption related to the activities in the building. Figure 2 depicts the energy consumption and outdoor temperature plotted against time for the first week of the year 2012. Special occasions, inclusive of social activities occurring on the Sunday morning service, are of particular interest and hence may contribute to higher consumption in daily energy. These peaks are for example explained by the chandeliers in the church room, having a rated power of 9.5 kW and the big dishwasher in the facility. These peaks in power load need to be removed when doing the analysis of the energy savings. In this energy signature analysis merely data for the hours between from 00.00 AM to 06.00 AM were considered, when customarily no other energy consuming activities take place and the electricity is only used for the GSHP system and for the base load of the church building.

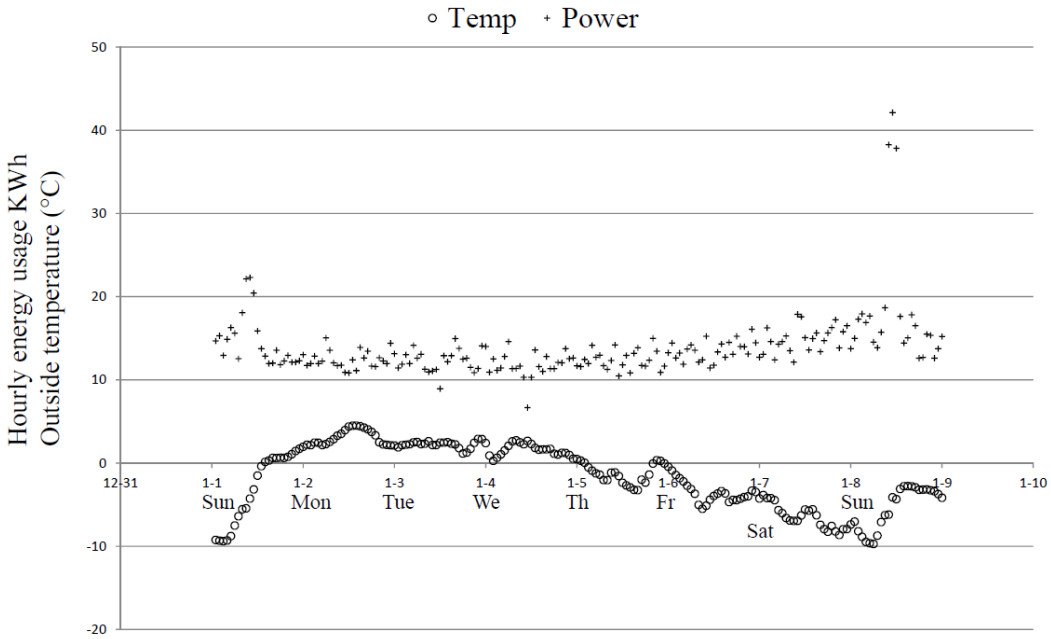

FIG 2. The hourly energy consumption and outdoor temperature during the first week of 2012.Note peaks on Sundays!

The average temperatures are calculated as

$$\bar{T} = \frac{1}{N}\sum_{m=1}^{N} T_m \qquad (2)$$

Where T_m temperature at each hour m
N Number of temperature readings

The linear regression of the data for non-heating and heating seasons respectively, a first order equations were produced, using the least square method.

TABLE 1. Coefficients of the regression lines given n Figures 3, 4 and 5.

	Heating season		Non-heating season	
	Base load factor	**Temperature dependent load factor**	**Base load factor**	**Temperature dependent load factor**
Prior to GSHP installment†	11.951	−0.4766	1.9348	−0.0093
Prior to GSHP installment‡ **(corrected base load)**	9.9903	−0.4766	−0.0259	−0.0093
Post to GSHP installment†	5.2670	−0.2358	1.9867	−0.0187
Post to GSHP installment‡ **(corrected base load)**	3.3063	−0.2358	0.0260	−0.0187

TABLE 2. Power consumption and utilised power, COP and energy savings at diffentoutdoor temperatures.

T [ºC]	Qprior [kW/h]	Qpost [kW/h]	COP	χ [%]
−20	19.55	8.00	2,44	59.1
−15	17.17	6.82	2,52	60.3
−10	14.78	5.64	2,62	61.9
−5	12.40	4.46	2,78	64.0
−2.3	11.11	3.82	2,91	65.6
0	10.02	3.28	3,05	67.3
5	7.63	2.10	0.275	72.5

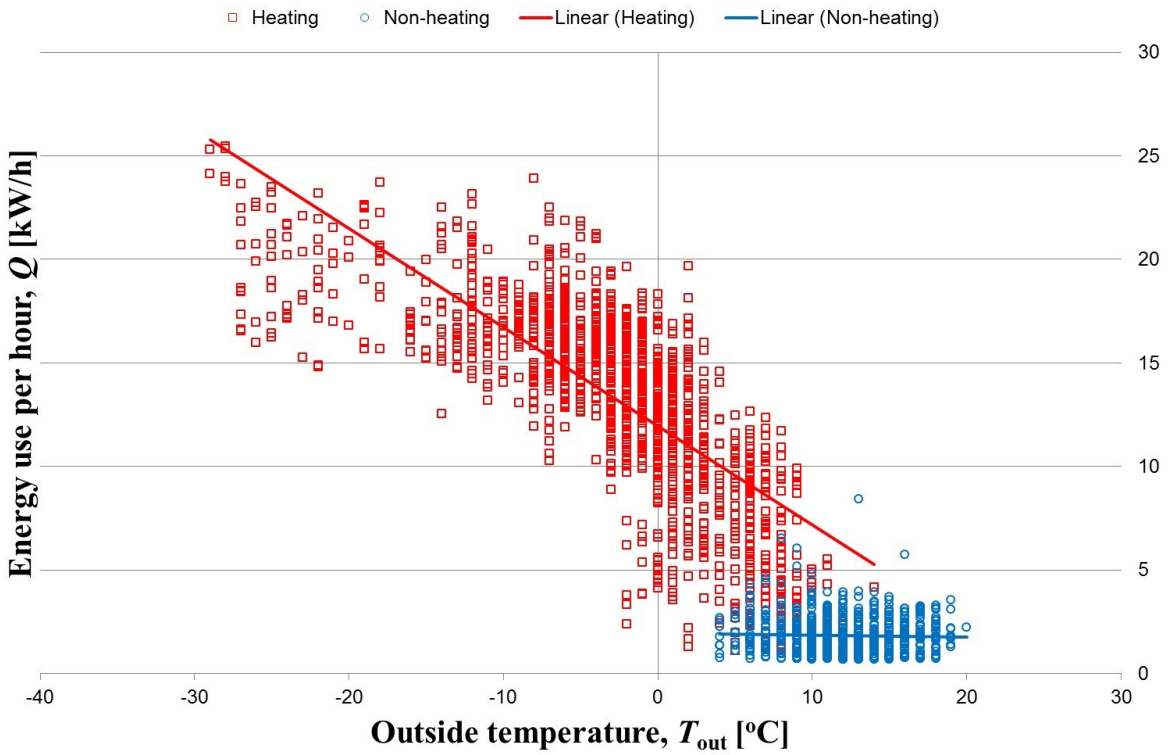

FIG 3. Åbyberg church (October, 2013) The energy use per hour versus outdoor temperature (in nighttime) versus oudoor temperature for the Åbyberg church for the time period October 15, 2010 to October 14, 2011. Before installment of GSHP.

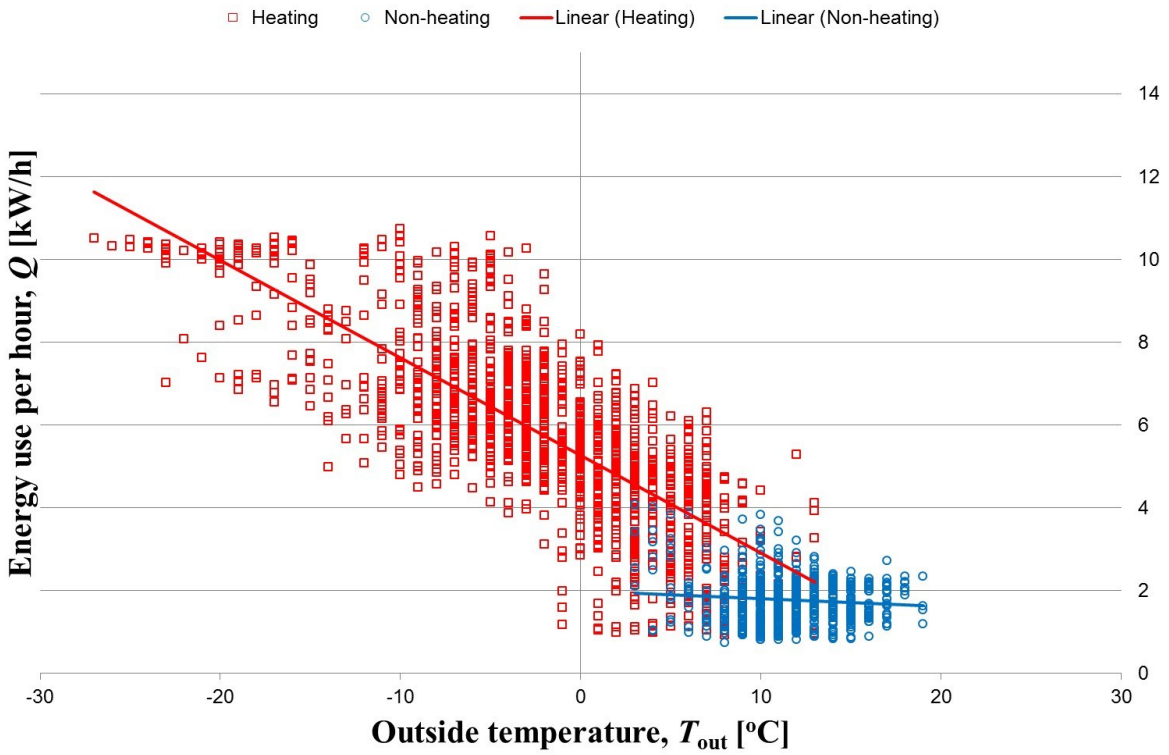

FIG 4. The energy use per hour versus outdoor temperature (in nighttime) for the Åbyberg church for the time period October 15, 2012 to August 25, 2013. After installment of GSHP.

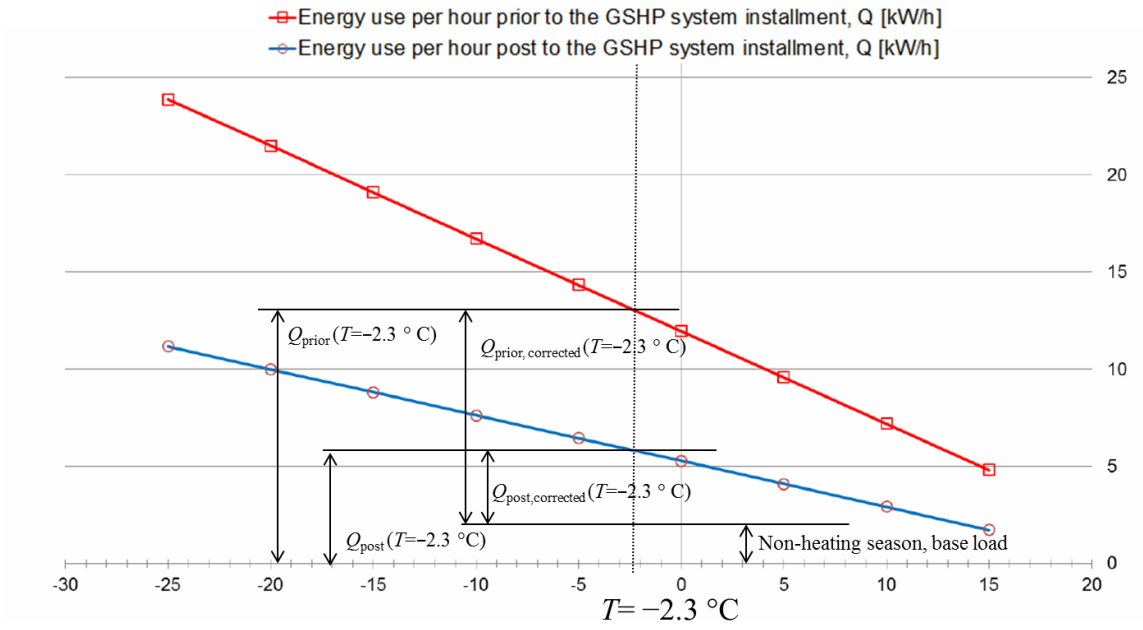

FIG 5. The daily energy usage(in nighttime) versus outside temperature for the Åbyberg church represented by two different linear functions. The base loads of the non-heating seasons and the corresponding corrected factors for the heating seasons are also shown in the figure.

3. Results

The behavior of the church, prior to installment of the GSHP system is calculated from the data shown in Figure 3 for the period October 2010 until October 2011. The new system started to operate in September 2012. Data for post installment is given in Figure 4 for the period October 2012 until August 2013. The coefficients of the regression lines for the energy signatures are presented in Table 1. They are provided with an accuracy of four digits, which obviously is higher than motivated by the input data.

A comparison between Figures 2 and 3 conveys that the installment of the GSHP system has contributed to a substantial decrease of the daily energy consumption. The regression lines from the data are compiled in Figure 5 which also shows how the base load factor of the non-heating season. This is approximately 1.96 kW and refers to the normal use of the building, also in nighttime. It should be adjusted for when calculating energy savings. This is done by subtracting the base load values for the non-heating season's pre and post to the GSHP installment from the power need, as illustrated in figure 5.

A comparison between the base load factors for the non-heating season prior to and after installment of the GSHP system exhibits an increase of the daily energy usage by 2.68%, which is virtually no difference. Nonetheless, the slope of the temperature dependent portion of the signature graph is considerably lower in the aftermath of GSHP system installment. The coefficients for the adjusted power need are given in Table 1 and results from these calculations at a few different temperatures are shown in Table 2. It is evident that the energy use was reduced because of the GSHP installation. An estimate of the saving can be performed by determining the ratio between the power need at a certain temperature prior and post to GSHP installment. This ratio is clearly temperature dependent and a comparison of the energy consumption is given in Figure 5. One choice that can be motivated is the mean temperature of the heating season post to the GSHP installment was −2.3 °C. Results for calculations at a few different temperatures are given in Table 2.

The reduction in need for electrical power at −2.3 °C becomes 65.6%, and practical COP 2,9, which is actually in the realm of results obtained in the study of Levin [6].

The process in these calculations is a bit different from what Levin did. In the calculation of the COP data for aquared energy E_a, is the energy consumption at a certain outdoor temperature prior to the installment and E_u is the energy consumption post the installment. The reduction in electric energy is in this case a measure of the coefficient of performance of the entire installation. This can be motivated because no other changes were made to the building. This is a way to use data available data in a quite simple but still efficient way.

4. Conclusions

The conducted study has exhibited the usage of a GSHP system as an energy refurbishment measure in an existing church building. The replacement of the original electric coil heating system with a GSHP system has resulted in an improvement of energy consumption of approximately 66% or a COP of 2,9. This is quite close to the results of Levin (2008).

The energy signature method is exemplified to be useful for evaluation of performance of a heating system. By only considering data for some of the periods, disturbing effects by the activities of the building users can be minimized. Otherwise a number of peaks would have partly hidden the effect of the heat pump. The billing data and the weather data from a public weather station are both of good quality. Thus the problem with missing data can be avoided.

Conclusively, it has been exemplified how the GSHP indeed is a useful and energy saving heating source for the considered church building. It has been shown that the energy signature method can be applied in order to assess the results of energy saving measures in buildings and that available data in terms of the daily outside temperature and hourly energy consumption, can be utilized for evaluation of the energy efficiency.

5. Acknowledgements

We express our gratitude to the Swedish research council Formas for financial support and to the Åbybergskyrkan congregation for provision of data.

6. References

Björk E, Acuña J, Granryd E, Mogensen P, Nowacki JE, Palm B, and Weber K. ”Bergvärme för den intresserade”, KTH and Geo and Power, 2012, ISBN: 978-91-7501-754-9.

Layberry RL. “Analysis of errors in degree days for building energy analysis using Meteorological Office weather station data”, Building Services Engineering Research and Technology, Vol. 30, Issue 1, 2009, pp. 79-86.

Levin P. ”Ekonomisk och driftserfarenhetsmässig utvärdering av bergvärmepumpar”. 2008.

Mustafa OA. “Ground-source heat pumps systems and applications” Renewable and Sustainable Energy Reviews 12, pp. 344–371, 2006.

Schulz L, ”Normalårskorrigering av energianvändningen i byggnader – en jämförelse av två metoder”, Report No. 2003:01. ISSN 1650-1489, 2003.

SLB: Stockholm - Uppsala County Air Quality Management Association, Electronic Source: www.slb.nu, Last accessed: 2013-10-14

Swedish EnergyAgency. The homepage of the Swedish Energy Agency, Electronic source: www.energimyndigheten.se, Last accessed: 2013-05-14

Swedish National Heritage Board. The homepage of the Swedish National Heritage Board, electronic source, www.bebyggelseregistret.raa.se, Last accessed: 2013-05-14

U.S Department of Energy. The homepage of U.S Department of Energy, Electronic Source: http://energy.gov/energysaver/articles/geothermal-heat-pumps, last accessed: 2013-05-14

Transfer of energy efficient building concepts to subtropical climate– The first MINERGIE P® based building in Japan

Yutaka Goto, D.Sc. [1]
York Ostermeyer, Assistant Professor [1]
Holger Wallbaum, Professor [1]

[1] Chalmers University of Technology, Sweden

KEYWORDS: *Subtropical climate, vapor-open building envelope, MINERGIE, Japan, design optimization, in-situ measurement*

SUMMARY:
While there are solid experience values for energy efficient buildings in moderate climate in Europe, the transfer of these concepts to differing climate and socio cultural conditions is a field of experimentation in building physics. Started as a cooperation project between Switzerland and Japan and now continued by including Sweden as a partner, the first Japanese residential building based on the MINERGIE P® standard has recently be realized in central Japan.

This presentation will offer a summary of the applied concept for the building envelope and housing services. The focus will be on measures to deal with the high humidity loads in subtropical industrialized country with related demand for comfort conditions and regular earthquakes straining the construction and the measures to achieve the MINERGIE P® targets in Japanese climate.

1. Introduction

With regard to the resource depletion and the global climate change, it is widely recognized that the construction industry is playing a key role for the rational use of resources and the realization of a more sustainable society (CIB 1999). On a global scale, the construction industry is contributing to about 50% of the manmade greenhouse gas emissions and to about 40% of the resource consumption (UNEP 2003). Energy consumption in buildings is of key importance in this regards and in order to improve the energy efficiency of buildings, several design protocols for building envelope and equipment have been proposed and implemented, though mainly in cold/mild climate regions. As a successful example the MINERGIE® Building Association of Switzerland has established an energy certification method labelling buildings to MINERGIE® and MINERGIE-P® standard. Due to the promotion driven by subsidies from local governments in Switzerland and the general perception that such labeled buildings are worth more in economic terms, more than 10,000 housings have been certified by this energy label in Switzerland so far. The Passivhaus Institute from Germany established similar energy labeling methods for buildings in Germany and other countries, mainly in Europe. A recent study has shown that the actual energy performance of certified Passivhaus buildings match the calculated energy demand (Passivhaus Institute) with the best exactness achieved again in cold and mild climates. These two examples show that the implementation of energy efficient building technologies accompanied by a labeling system can contribute to the further enhancement of the sustainability of the construction industry.

In order to address the energy performance of buildings on the global level, the implementation of such design protocols has been promoted recently. The key for a working concept as well as local acceptance is considering the local frame conditions when a certain technology is deployed in a certain place. Especially the climatic, craftsman skills and user behavioral difference may result in a serious damage in building components and/or inhabitants' health if not properly taken into account.

Within a series of research projects that started as a cooperation project between Switzerland and Japan and are now continued by including Sweden as a partner, the authors have developed an innovative vapor-open wooden building envelope system for subtropical regions. In June 2013, a test house, whose concept was based on MINERGIE®, was realized in central Japan. This paper introduces the concept of the construction system, introduces the framework of the adoption of MINERGIE® certification, reports the designing and construction processes of this test house and presents the preliminary results of the measurement of the indoor climate and the temperature and humidity inside the envelope.

2. Energy efficient building concepts for subtropical regions

2.1 Subtropical climate

Energy consumption by buildings is of growing concern in subtropical regions because of the high growth rate in urbanizing areas in these regions (CIB & UNEP-IETC 2002). FIG 1 shows the subtropical regions defined by Köppen-Geiger climate classification. The major difference between cold/mild regions and subtropical regions is the long and hot-humid summer. This causes significant energy consumption for cooling and dehumidifying in addition to the heating load in winter. From the view point of building physics, such a climatic condition is very challenging because it results in both heating and cooling demands in buildings. Consequently the direction of the moisture flux - due to the gradient of vapor pressure between exterior and interior - reverses throughout the year. In summer the moisture transfer happens from outside to inside and in winter vice versa. Inappropriate design of the building envelope, which fails to deal with the moisture flux in the exterior wall, may result in the interstitial condensation in the exterior walls.

One way to deal with this would be sealing both sides of the wall with water vapor tight layers. In order to create a robust solution the desirable way however is making the envelope vapor-open, especially in earthquake-prone regions where rifts in barriers can never be completely prevented. Directly implementing the conventional designing method for cold regions introduced above does not solve the fundamental problems in subtropical regions, but rather introducing a novel envelope system for subtropical regions has been required.

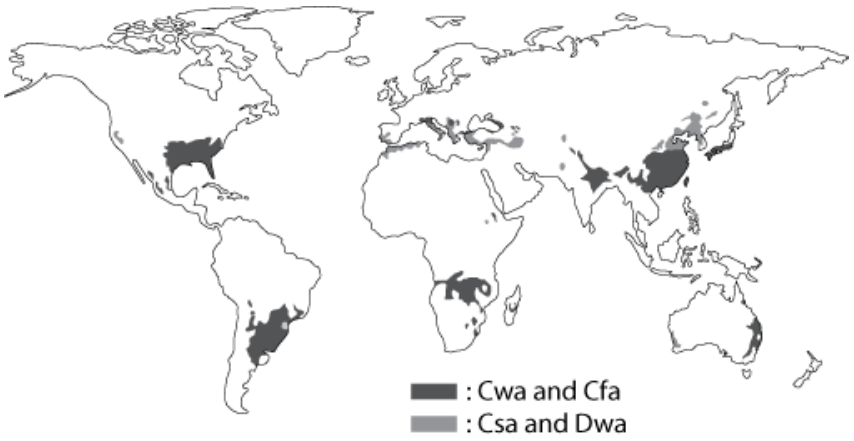

FIG 1. Subtropical regions according to Köppen-Geiger climate classification

2.2 Vapor-open envelope system for subtropical regions

A new building envelope system was developed within the research team led by the authors. This envelope system mainly consists of layers based on renewable, hygroscopic and vapor permeable materials, namely the external insulation layer made of wood fiber board, the structural layer made of

cross laminated wooden panel and the interior finishing layer made of a pre-dried composite of wood and clay. The illustration of the envelope system and the materials for each layer is shown in FIG 2. This system allows the moisture flux to move through the wall in both directions. By defining the appropriate thickness to each layer, it is possible to avoid moisture related problems inside the wall. Besides the building physical considerations, the design philosophy of the envelope also comprises ecological, economic and social aspects. The components are based on renewable materials, and so it may be produced using local resources, which contributes to the less transportation for each component. Local production also promotes the local economy creating local value chain. The local design conditions, namely local climatic conditions and socio cultural aspect such as user behaviors (preferred room temperature/humidity, heating/cooling strategies and so on) can be taken into account. Flexibility and adaptability to specific local conditions is assured by the layered structure of the envelope. This system enables the material of each layer and its thickness to be selected independently for its primary function alone. Therefore the thickness of the insulation layer, which gives not only the thermal resistance but also the moisture sorption capacity, can be determined according to the local climatic condition without interrupting the other components such as the structural element. By this flexibility, an actual wall make-up can be determined considering the local conditions of both sides of the wall easily.
By one dimensional transient heat and moisture transfer simulation program, hygrothermal property test and full scale testing with a climate chamber, the performance of the wall was verified (Goto et al. 2011). Then, the whole building heat and moisture balance simulation method for buildings with this system was also developed in order to predict the indoor climate and heating and cooling demand (Goto et al. 2012a). Combining these methods and Life Cycle Assessment (LCA) and Life Cycle Cost Assessment (LCCA), the authors proposed the optimization method for the thickness of the insulation layer within the Japanese economic and climatic conditions (Goto et al. 2012b).

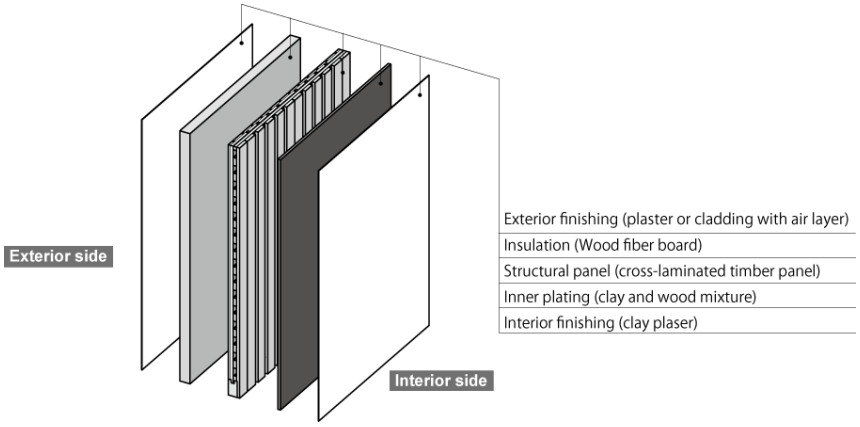

FIG 2. Layered make-up of the vapor-open envelope system

3. Adaptation of MINERGIE® to subtropical conditions

MINERGIE® is an energy label for new and refurbished buildings. It is mutually supported by the Swiss Confederation, the Swiss Cantons along with trade and industry. Assuring comfortable living environment is the origin of MINERGIE®. A wholesome level of comfort is argued to be made possible by high-grade building envelopes and the controlled ventilation. In Switzerland the MINERGIE® Standard is widely accepted and recent studies have found that on the free market labeled houses achieve a 6% higher sales price than non-labeled ones of similar performance (Salvi et al 2008). This shows the potential of such labels to be also perceived as a quality proof. By now, the building sector has developed a wide range of products and services for MINERGIE® buildings. Suppliers include architects and engineers as well as manufacturers of materials, components and systems. The diversity and competition of this market furthers quality and lowers costs.

Specific energy consumption is used as the main indicator to quantify the required building quality. Only the final energy consumption is relevant. The measures applied to achieve the goal are in many aspects not pre-described and the label follows the idea of naming the goal but not the way. This makes the label very flexible in regards to transferring it to different climate conditions as long as the target numbers are achievable. The experience with about 10.000 labeled buildings in Switzerland allows the association to identify the most cost competitive ways to achieve the standard (Mosteiro et al. 2014). These are listed in the figure below, being compared with the ones chosen for the building in Japan. In addition to the general criteria, it was decided to restrict the relative humidity in the exterior walls not to exceed 80%RH throughout the year in order to assure the longevity of the house in the case of prototype house.

TABLE 1. Comparison of MINERGIE P® *in Switzerland and Japan*

	MINERGIE P® (Switzerland)	Prototype house in Japan
Energy demand	Weighted energy index accounting for heating, ventilation, hot water, and air conditioning of 30 kWh/m^2 taking losses for extraction, transportation and distribution into account	Target as in Switzerland, based on a monthly calculation as well as dynamic modelling (29,2 kWh/m^2a)
Renewable energy	Prerequisite	PV (4.18 kWp) and solar thermal
Heating and cooling demand	<60% of legally allowed annual heat demand for new homes (SIA 380/1:2009 limit) or <15 kWh/m2, max. 10 W/m2 for air heating	Not applicable
Controlled outdoor air ventilation and indoor air quality	Controlled outdoor air ventilation prerequisite. Heat recovery required. Proof of thermal comfort during summer necessary	Enthalpy exchanger,
Air intrusion	<0.6 h−1 air exchange rate at 50 Pa pressure difference	Measured according to Swiss standards to be
Opaque walls Glazing	20–35 cm (U-value: <0.15 W/(m2 K)) Triple panes (U-value for glazing: <0.6 W/(m2 K))	18 cm, lambda 0,04 0,7 to 1,0 W/(m2 K)
Costs	Should not exceed construction costs of a conventional building by more than 15%	In range of upper class Japanese houses

Based on LCA, LCCA and hygrothermal analysis considering the specific design conditions as well as the MINERGIE P® criteria, the insulation thickness was decided to be 18 cm. For the openings air-tight and triple grazing windows (0.7 W/m^2K) were installed. PV panels cover the south roof (4.18 kWp) combined with solar water heater panels for domestic hot water. The building orientation and the shading of the openings were carefully decided considering the balance of solar gain in summer and winter. As for HVAC system, radiators for heating and cooling-dehumidification and mechanical ventilation with heat exchanger were employed. The façade consists of cladding with venting layer.

Three main differences can be identified when transferring the standard:

1. Any kind of solar technology (PV, solar thermic) is cost competitive to passive measures (insulation) at a much earlier stage. From a cost viewpoint there will be a focus on active technologies when limiting the assessment to an annual balance.
2. The envelope is affected by both energetic as hygro-thermal conditions in its design to a much higher extend than in Europe. In this case the minimal insulation thickness was 14cm out of hygrosorptive reasons and 18cm was chosen because the customer wanted some safety and at the same time felt to set an example for better insulated houses. 18cm of insulation results in the better environmental LCA result while in terms of an economic LCC a lower insulation combined with more PV would have performed better.
3. Controlled ventilation is mandatory simply to achieve comfort in summer within the set conditions. To avoid excessive de-humidification an enthalpy exchanger is an attractive option.

4. Construction of a test house

4.1 Planning

It was decided that a building with the envelope system would be realized in Ohmihachiman (central Japan) which has a typical subtropical climate with hot-humid summer and cold-dry winter. The general design of the building was done by local architects and the technical supervision was done by the research team. The building is a detached residential building where two to four persons (two adults and up to two children) are supposed to reside. The surface of the insulation was designed to be covered with vapor-open water-tight membrane. Air-tight membrane is employed between the insulation and the structural panel. The concrete foundation was designed to have a flat surface and to be covered with asphalt sheet so that the control of heat and moisture transfer through it becomes the least intricate. The roof was based on the conventional design with air venting layer. FIG 3 shows the plan and elevation of the test house.

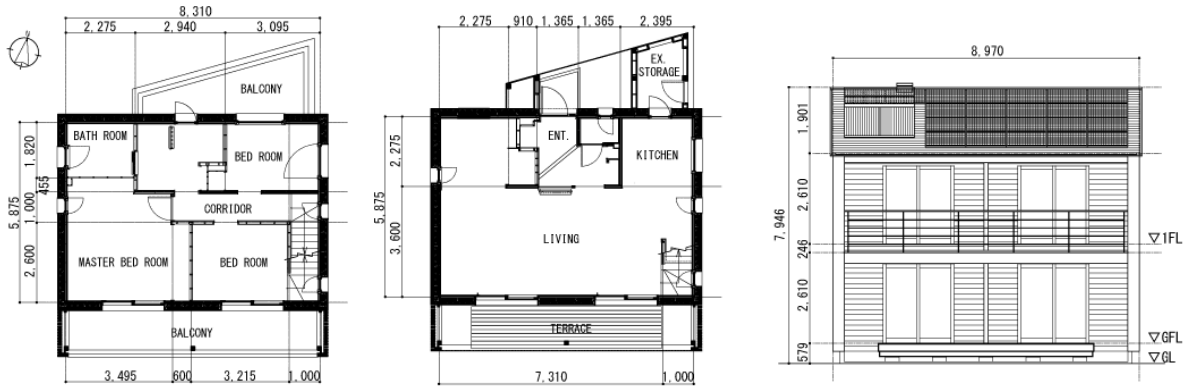

(a) Ground floor plan *(b) 1st floor plan* *(c) South façade elevation*

FIG 3. Plan and elevation of the test house

4.2 Construction

The structural panels were pre-cut and pre-assembled so that the work at the building site could be minimized. The assembled panels were carried in the building site on the 5th March 2013, and the building frame (floors, walls and roof) was constructed in three days. Subsequently, windows, plumbing, electric cables, insulation, housing services, façade, roofing and others were installed. FIG 4 shows the construction processes. The construction processes were carefully supervised by the research team so that no faulty works were to be done until the insulation and the water-tight membrane was completed. Because of the lack of experience with this construction system, several

significant faults were observed and modified (e.g. insufficient air-tightness at the bottom of the exterior walls between the structural panel and the insulation which would result in the direct flux of ambient air into the inside of the wall and eventually in moisture condensation).

FIG 4. The processes of the construction ((a): the erection of the load bearing element (b): the installing of wood fiber insulation)

4.3 Completion and measurement set-up

The construction was completed on the 26th June 2013. FIG 5 shows the finished house.
In order to measure the indoor climate and the conditions inside the external walls, 21 temperature and humidity sensors were installed. FIG 6 shows the sensor and sensor node. The measuring points are; northern side wall on the ground floor (5 points across the wall from the living room to the exterior), living room, kitchen, northern side wall on the 1st floor (5 points from the bathroom to the exterior), west side wall on the 1st floor (5 points from the master bedroom to the exterior), northern side roof (4 points from the attic to the exterior). Figure 1(b) shows a sensor installed inside the insulation layer. The measured results are available online simultaneously. The measurement started in September 2013.

FIG 5. The completed house ((a): east side façade, (b): living room on the ground floor)

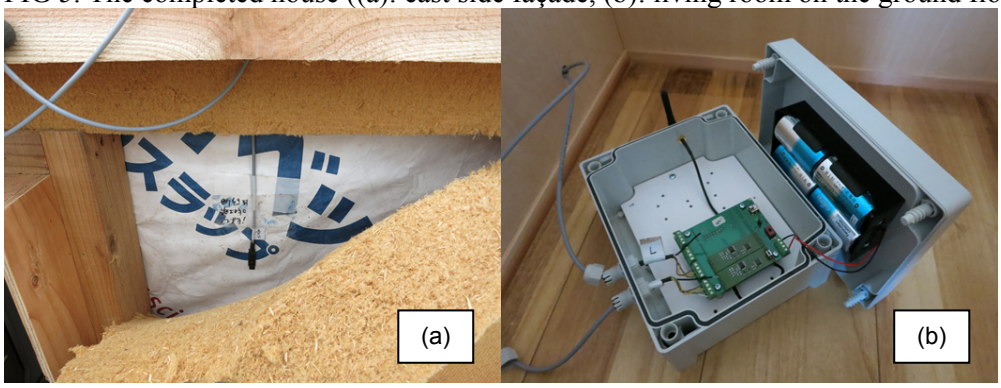

FIG 6. The installation of sensors. ((a) sensor inserted between air-tight membrane and insulation, (b) a sensor node box))

5. Result and discussion

The planning and the construction of the test house were successfully completed. Currently the monitoring is running. FIG 7 shows the temperature and humidity of the five points across the west side wall of the master bedroom (in ambient air in venting layer of the façade, inside insulation layer (80mm deep from the exterior side surface), between insulation and air-tight membrane, between structural panel and clay board and in master bed room).

Performance of the system is currently in line with the expectations but no final statement can be given yet as no full annual cycle has been recorded.

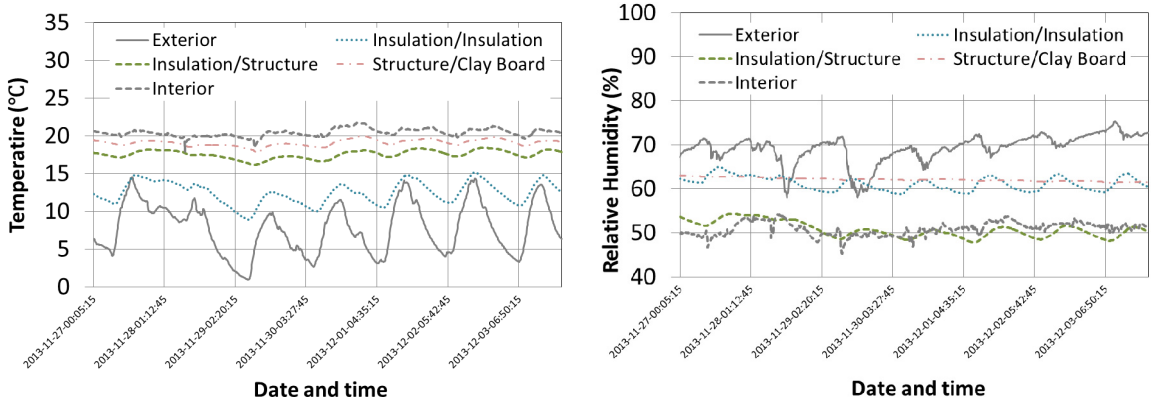

(a) Temperature *(b) Relative humidity*

FIG 7. Sensor data for temperature (a) and relative humidity (b) for the complete wall make-up

6. Conclusions

This paper reports the designing and the construction processes of a test house in central Japan with a novel vapor-open wooden building envelope system and based on the Swiss energy label MINERGIE P®. Throughout the designing and the construction process, it was found that close communications among the designers, the constructors and the client is essential in order to realize a building with new features as it is designed. Unless the construction work is carefully supervised, the measurement of the house in the use phase might not meet what is supposed to be measured.

The MINERGIE P® label in general was found to be of sufficient flexibility to allow for feasible solutions in the Japanese climate. In order to assess whether the frame conditions of the label finally lead to cost efficient solutions that are in line with the solutions that are optimal from an environmental viewpoint the market for such concepts first has to grow in Japan.

The energetic and hygrothermal performance of the building must be validated with the measured data once sufficient data becomes available.

7. Acknowledgements

The authors would like to express their special gratitude to the customers of the house in Japan, Iida family, for their perseverance, trust, willingness to try something new and kind allowance to monitor the performance of the building.

Acknowledgement also goes to the commission technical innovation (CTI) for whose funding enabled the initial project, Hans Ruedi Kriesi from the MINERGIE association for his support in the initial calculations and Stefan Wiesendanger from Zehnder group for his support on solutions concerning the heat exchanger.

References

CIB. 1999. Agenda 21 on sustainable construction. Available at online http://www.cibworld.nl/site/home/index.html (accessed on 12/12/2013)

CIB & UNEP-IETC. 2002. Agenda 21 for sustainable construction in developing countries. Available at online http://www.cibworld.nl/site/home/index.html (accessed on 12/12/2013)

Goto Y. & Ghazi Wakili K. & Ostermeyer Y. & Frank T. & Ando N. & Wallbaum H.. 2011. Preliminary investigation of a vapor-open envelope tailored for subtropical climate. Building and Environment, 46(3). pp719-728.

Goto Y. & Ghazi Wakili K. & Frank T. & Stahl T. & Ostermeyer Y. & Ando N. & Wallbaum H.. 2012a. Heat and moisture balance simulations of a building with vapor-open envelope system for subtropical regions. Building simulation 5(4). pp301-314.

Goto Y. & Ostermeyer Y. & Ghazi Wakili K. & Wallbaum H.. 2012b. Economic, ecological and thermo-hygric optimization of a vapor-open envelope for subtropical climate. Energy and Buildings 55. pp799-809.

Mosteiro-Romero, M. & Krogmann, U. & Wallbaum, H. & Ostermeyer, Y. & Senick, J. S. & Andrews, C.J. 2014. Relative importance of electricity sources and construction practices in residential buildings: A Swiss-US comparison of energy related life-cycle impacts. Energy and Buildings. 68. pp620–631.

Passivhaus Institute. http://www.passiv.de/ (accessed on 12/12/2013)

Salvi, M., Horejájová, A. and Müri, R. (2008) Minergie macht sich bezahlt, Centre for Corporate Responsibility and Sustainability (CCRS) and Zürcher Kantonalbank, Zürich, Switzerland.

UNEP. 2003. Sustainable building construction. Industry and Environment, Vol.26 No.2-3.

The potential of thermal energy storage in food cooling processes in retail markets for grid balancing

Tommie Månsson, M.Sc. [1]
York Ostermeyer, Assistant Professor [2]

[1] Chalmers University of Technology, Sweden
[2] Chalmers University of Technology, Sweden

KEYWORDS: *Energy efficient supermarkets, smart energy grid, adaptive energy consumption, energy efficiency, thermal buffering, electrical buffering*

SUMMARY:
An upcoming demand for higher energy efficiency in the society requires multiple actions to reduce the amount of unutilised energy. Supermarkets are part of the sixth largest energy consumers in Germany, the food industries, and hold a great potential for increase of its energy efficiency and at the same time contribute to buffering capacity needed in grids that have a large share of renewables.

A state of the art supermarket designed according to the demands of Passive House Institute has been built by REWE in Hannover Germany. Measurements are proving it to have energy consumption substantially lower than an average supermarket of the same size. Monitoring also proves a substantial amount of buffering capacity in the cooling processes.

Extrapolation shows a substantial potential for buffering grid fluctuations due to delaying cooling processes in Germany especially when complementing the system with ice storage.

1. Background – Storage demand in renewable grids

Any electrical grid with a large share of renewables faces problems with fluctuations in energy supply and therefore needs buffering or storage capacities (Farhangi 2010). In this context the NPO Agency for Renewable Energy (Agentur für Erneuerbare Energien e. V.) reviewed several governmental and non-governmental studies on future storage demands for the German grid (Renews, 2012). According to this the additional demand for electrical storage and buffering will likely reach 18 TWh by 2030 with renewables reaching 50% of power generation in Germany. By 2050 the demand of storage and buffering capacity will reach 30 TWh with renewables reaching 80% of power generation in Germany.

Besides direct storage the concept of delaying electricity consumption and therefore tailoring consumption to demand is another option to manage the grid. Large energy consumers should therefore be assessed on their potential to react flexible in their consumption. One such area of consumption is food cooling.

2. Energy consumption of food retail markets

Food production and distribution processes are two of the main consumers of energy in many societies. Together, they currently rank as the sixth largest within the processing industry in Germany, with an annual electricity consumption of 54 865 TJ and a heat consumption of 7 742 TJ in 2011(Destatis, 2013) . One dominating reason for this high level of energy consumption is the need for cooling food in warehouses, during transport, and finally in the supermarkets.

From monitoring of supermarkets in UK it's clear that the energy consumption for supermarkets is exceptionally high in comparison to residential buildings and even offices. FIG 1. shows the annual energy consumption of Saintsbury markets in the UK sorted by net sales area ranging from 500 to almost 3000 kWh/m^{2}a, offering similarly a high potential for shifting loads.

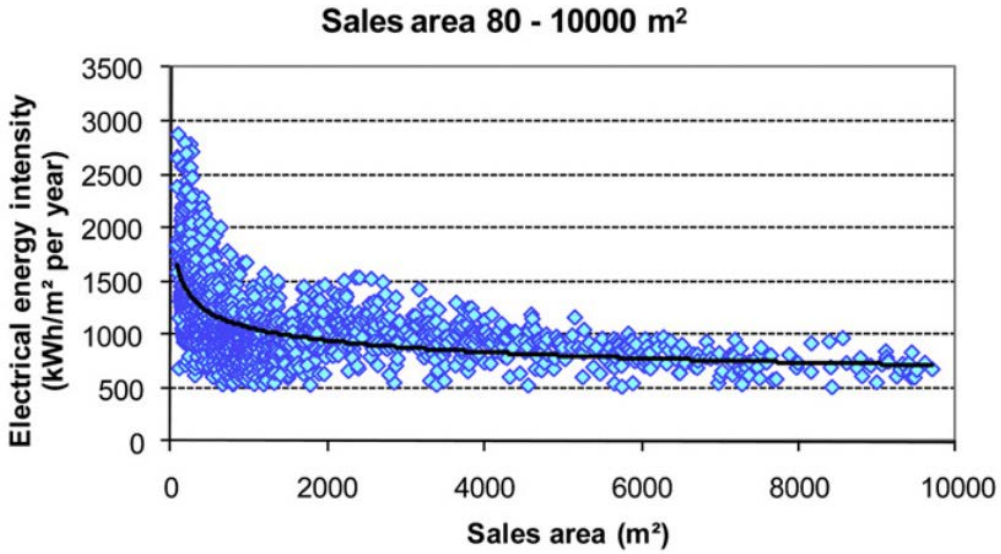

FIG 1. Variation of electrical energy intensity of 2,570 UK retail food stores with sales area from 80 m^2 to 10,000 m^2 (Tassou et al, 2011)

The implemented refrigeration system is found to be responsible for 39-47% of the annual energy demand in food retail markets in Sweden and the US in recent surveys (Arias, 2005).

These cooling processes offer the potential to buffer electrical energy in a thermal process with a higher efficiency than any kind of conventional electrical storage and are therefore in focus of the current discussion.

In general, supermarkets are not particularly energy efficient, as energy costs pale when compared with turnaround and profit (Arias et al. 2006). Rising energy prices and the need for companies to present themselves as environmentally friendly have, however, caused a re-think among supermarkets in recent years, resulting in a number of promising projects and technological developments (Arteconi et al. 2009 and Ostermeyer et al 2008). The potential for improving energy efficiency, reducing energy consumption, and the resulting emissions is very high in this sector (Ardito et al. 2013).

Obviously efficiency measures should be applied first in supermarkets from an environmental and in the end also from an economic viewpoint instead of designing inefficient cooling processes to create artificial consumption just to create load shifting potential. After applying economically feasible efficiency measures it has to be assessed how much energy is still consumed by the cooling processes. As the different components of cooling cabinets, cabinet, doors and heat pump are provided by different companies and the cabinets often run in complex networks the only sure way to assess the energy consumption is to monitor it in existing markets. This paper therefore takes measured data from a state of the art market and extrapolates from there.

3. State of the art food retail markets

Throughout the year, supermarkets need energy for heating to create a comfortable indoor environment and for cooling food storage at different temperature levels. Innovative concepts therefore utilize cascade heat pump systems to achieve high efficiency for the different temperature levels, and recover the process heat to help cover the heat energy demand by two-pipe or three-pipe based Cooling-Heating-Networks. With the heat recovery system alone, the heat energy consumption can be reduced substantially, about 30 to 40%, however peak demand related problems remain (Ostermeyer et al. 2008). The Passivhouse Institute Darmstadt in cooperation with Chalmers TU and REWE built on such concepts and designed the passive house standard for supermarkets to push even further.

3.1 The first Passive House Supermarket in Hannover/ Germany

In Hannover, the first Passive House Supermarket in Germany(Zero:e Park,2012), run by the REWE Group, was built in November 2012, based on a heating and cooling system as the one described above, and on specific tailoring of the envelope in order to reduce the additional heating demand after recovery to 15kWh/m^2, year.

All equipment within the supermarket was selected using a top-runner approach, which meant that only the most energy efficient products were installed. This includes high performance glazing in front of all cooling cabinets which, besides changing the energetic behaviour of the cabinet also resulted in complex hygro-thermal issues as humidity is not anymore condensing in the cabinets but remains in the sales room potentially causing the growth of fungi and mould.

Installing doors in front of the cooling cabinets and running them in a cooling network via a centralized heat pump in a cascade with the freezing cycle results in a consumption pattern that is extremely complex. The main challenge is that the performance of a single cabinet influences the complete system. The market therefore serves to assess the overall concept in general but the performance of the cooling and freezing processes in particular. FIG 2. shows some pictures of the market.

FIG 2. The first supermarket in Passive house Standard in Hannover

The market is monitored by nearly 200 sensors allowing for solid assessment of its performance. In addition it is equipped with a weather forecasting system. This will allow predicting future energy consumption based on similar conditions in the past which will be critical when starting to shift loads in the market at a later stage.

3.2 Monitoring results

The project results so far show that the energy consumption has been significantly reduced beyond the expectations in the design phase. FIG. 3 shows the overall consumption of the market which has now nearly completed an annual cycle. The consumption relatively stable at 8000 to 12000 kWh/week with a predicted annual consumption of around 250 kWh/m2 net floor area.

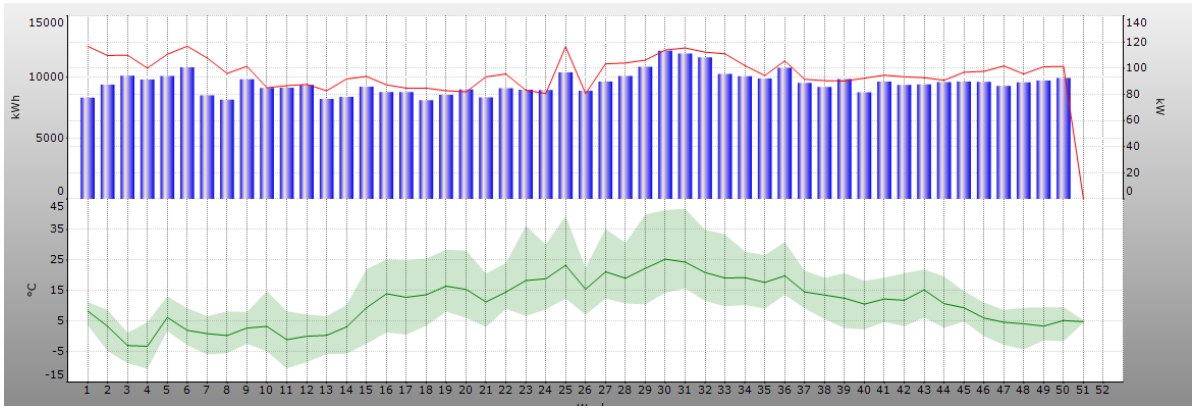

FIG 3: overall energy consumption (system border, market, all kWh in electricity), source FrigoData monitoring

FIG 4. Shows the cooling processes are in a range between 3000 kWh/week in winter and peaking at around 5000 kWh/week in summer.

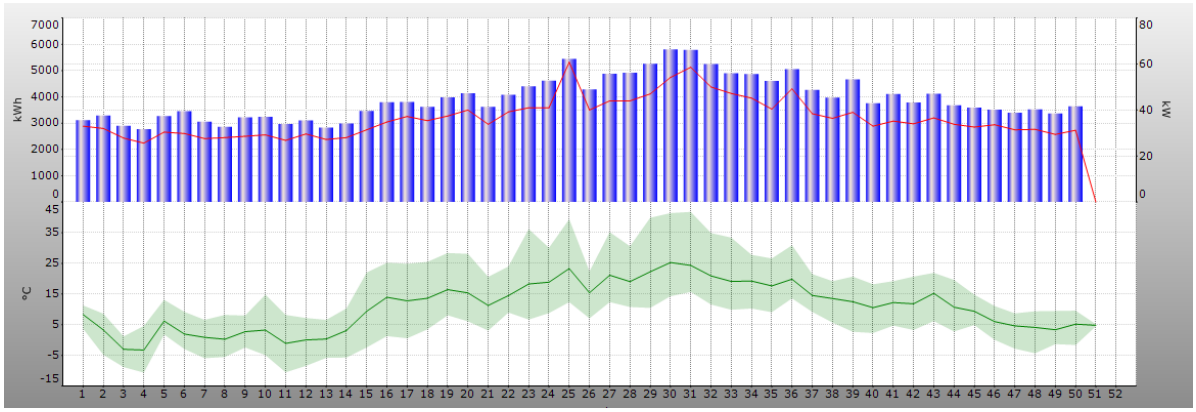

FIG 4: energy consumption for food cooling (system border, market, all kWh in electricity), source FrigoData monitoring

Peak loads in general are in line with the consumption with the exception of the starting phase of the market that included the heating of the formerly cold thermal building mass and some drying of still humid concrete parts.

Electricity consumption for food cooling (as opposed to freezing) is the most attractive consumption to be delayed in the market for two reasons:

1. The temperature level needed for the process allows for ice storage which would result in rather small modules making use of the phase change of water
2. The process heat from freezing processes is needed for regulating the sales room air temperature. Delaying both cooling and freezing would let the sales room cool down.

Delaying only freezing and not the cooling consumption is not possible because of the design of the cascade system.

Based on the current monitoring in the market in Hannover there is a potential to delay a consumption of 400 to 600 kWh/d. The necessary delay of 24 hours or more is currently not possible by thermal means alone which is limited to a delay of around 6 hours. 24 hours and more could be achieved though by ice storage modules which is the next step to be taken.
This also would create synergies with a remaining problem in the system which is the fluctuating energy demands of individual refrigerators and, to a lesser extent, the freezer units. As in order to be able to recover the process heat, all cooling devices have to be run in a combined cooling liquid grid (152a or 134a for cooling, CO_2 in the freezing area of the cascade system), erratic demand in a single device can affect all other devices and the overall system efficiency, as the refrigerators no longer have individual heat pumps. Ice storage could flatten the individual load of the cabinets and therefore improve the overall COP of the system.

4. Conclusions and outlook

Already with a single store buffering 100 kW over the time of six hours, impressive numbers would be achieved by the REWE Group alone. As their supermarkets are refurbished every 15-20 years, nearly all 3,000 stores could be fitted with these systems by 2030. Taking this idea even further, supermarkets in Germany could together contribute substantially to grid buffering. If they could be outfitted with ice storage the numbers would be even more impressive while at the same time further improving the performance of the cascade network.

In a long term scenario, about 5% of the needed storage and buffering capacity in Germany could be covered by food retail markets and cooling processes – without the need for new infrastructure and the resulting environmental effects.

The use of supermarkets as buffering and storage units for the electrical grid is a unique and world-first move. An increase in the proportion of renewable energy sources will result directly in the need for an improved storage and buffering capacity. The creation of such capacities therefore directly benefits society by allowing it to reduce its dependency on nuclear and non-renewable energy production and the problems associated with these.

What remains to be seen is whether the identified storage opportunity will result in supermarket consortia selling this capacity to power generators, like wind parks, or aiming to become self-sufficient via own energy generation for example by photovoltaic .

5. Acknowledgements

Special thank goes to the REWE Group for proving access to monitoring results and feedback on models and calculations. The ProKlima funds in Hannover is acknowledged for supporting the project and the necessary quality assurance financially. The Passivehouse Institute and especially Dr. Jürgen Schnieders is acknowledged for the discussions on feasible frame conditions for the market concept. Climate KIC is acknowledged for funding this research under the framework of the platform Transforming the Built Environment.

References

Ardito, Luca; Procaccianti, Giuseppe; Menga, Giuseppe; et al.(2013) Smart Grid Technologies in Europe: An Overview. ENERGIES (6) 251-281

Arias, J; Lundqvist, P (2006) Heat recovery and floating condensing in supermarkets ENERGY AND BUILDINGS (38) 73-81

Arias, J. (2005). Energy Usage in Supermarkets - Modelling and Field Measurements. Department of Energy Technology. Royal Institute of Technology, KTH Royal Institute of Technology.

Arteconi, A.; Brandoni, C.; Polonara, F.(2009) Distributed generation and trigeneration: Energy saving opportunities in Italian supermarket sector. APPLIED THERMAL ENGINEERING (29) 1735-1743

Destatis (2011) Energieverwendung der Betriebe im Verarbeitenden Gewerbe 2011, https://www.destatis.de/DE/ZahlenFakten/Wirtschaftsbereiche/Energie/Verwendung/Tabellen/Industriebranchen11.html;jsessionid=A81652FF29F3A3042C8FEF824F000294.cae1, (2013-05-10)

Duun, A. S.; Rustad, T. (2007) Quality changes during superchilled storage of cod (Gadus morhua) fillets. FOOD CHEMISTRY (105) 1067-1075

Egolf, P. W.; Kitanovski, A.; Ata-Caesar, D.; Vuranoz, D.; Meili, F. (2007) Cold storage with ice slurries. International Journal of Energy Research. 2008; 32:187-203

Farhangi, Hassan (2010) The Path of the Smart Grid. IEEE POWER & ENERGY MAGAZINE (8) 18-28

Lund, H.; Mathiesen, B.V. (2007). Energy System Analysis of 100 Per cent Renewable Energy Systems. 4th Dubrovnik Conference on Sustainable Development of Energy, Water and Environmental Systems.

Ostermeyer, Y.; Wallbaum, H.; Brand, C.(2008) Energy-saving concepts for supermarkets", peer reviewed conference paper and oral presentation. Nordic Symposium on Building Physics

Renews (2012) Spezial Ausgabe 57 / Februar 2012, www.unendlich-viel-energie.de . (2013-11-28)

Tassou, S. A., Ge, Y., Hadawey, A. & Marriott, D. (2011) Energy consumption and conservation in food retailing. Applied Thermal Engineering, 31 (2-3), 147-156.

Zero:e Park (2011). Klimaneutral einkaufen im zero:e park. http://www.zero-e-park.de/de/baugebiet/supermarkt . (2013-05-08)

TOPIC
Moisture Safety

Page.....947-1170

Accounting for unintended moisture sources in hygrothermal building analysis

Hartwig M. Künzel, Ph.D. [1]

[1] Fraunhofer-Institute for Building Physics, Germany

KEYWORDS: *Moisture control, hygrothermal simulation, standards and guidelines, unintended moisture sources, workmanship, moisture tolerant design.*

SUMMARY:
Moisture control analysis of building envelope components by hygrothermal simulation is state-of-the-art today and widely applied by architects and engineers. Compared to simple dew-point calculations, transient simulations according to existing standards (e.g. EN 15026-2009) have greatly improved the possibilities of moisture control analysis. However, the underlying assumption of building components without imperfections have remained a weak point, because unintended moisture sources due to e.g. rain-water penetration or air convection may have significant effects in real life. The new draft of the WTA guideline 6-2, whose original version served as blue-print for EN 15026, takes hygrothermal simulations a step further by introducing auxiliary models that account for unintended moisture sources likely to occur in building components, assembled and installed in best practice manner. Because bad workmanship is ruled out, applying these models offers the opportunity to differentiate between design errors and installation failures. Other guideline improvements include new boundary condition aspects such as safety margins for indoor climate conditions and consideration of envelope shading. Since capillary active insulation materials have become more popular in recent years a more accurate determination of liquid transport characteristics is also proposed. The new items in WTA 6-2 are summarized and their impacts on hygrothermal simulation results are discussed.

1. Introduction

Moisture in the building structure impairs thermal performance and accelerates ageing and degradation. Therefore moisture control has always been an issue for architects and engineers. Despite an improvement in construction quality, moisture problems have not diminished accordingly. This may partly be due to increasing energy savings requirements. More insulation and better air-tightness have resulted in lower temperatures at the exterior layers of the building envelope and higher indoor humidity. This increases the risk of interstitial condensation and reduces the drying potential. However, adequate moisture control design can help to prevent problems even in the most energy efficient structures. The necessary design tools are there but they have to be applied the right way. While it is fair to assume that a building has been erected according to best practice, a perfect seal against water, vapour or air entry is difficult to achieve. Therefore, the consideration of imperfections should be part of moisture control assessments based on hygrothermal simulation.

Another safety issue represents the choice of the exterior and interior boundary conditions. While at first sight it seems to make sense to select severe climate conditions and an unfavourable behaviour of the occupants, experience shows that even well-proven constructions may fail under these circumstances. Therefore a more sensible approach is desirable. Last but not least it is important that the material properties employed for the calculations represent the characteristics of the materials according to their intended use. This paper describes how the new draft of the WTA guideline 6-2

(WTA 2013) deals with all these issues. It also summarizes the background and rational for the new or modified items in the guideline.

2. Moisture control design by hygrothermal simulation

In the past, moisture control meant for most practitioners steady state vapour control calculations – often called dew-point or “Glaser” calculations – that were performed to determine whether there is a risk of harmful interstitial condensation in the building assembly during the heating season. However, due to numerous simplifications the results of these calculations may be misleading especially when short-term loads such as solar vapour drive or bulk water entry cannot be excluded. Therefore, modern hygrothermal simulation tools that calculate the transient temperature and moisture conditions in building envelope components under realistic boundary conditions have been increasingly applied by architects and engineers. To arrive at comparable results pertinent application standards for hygrothermal simulations have been developed which are under continuous revision in order to accommodate new approaches and feed-back from users.

The first guideline on moisture control analysis by hygrothermal simulation was issued in 2002 by the WTA, an association dealing with preservation and renovation of heritage constructions and rehabilitation of the building stock (WTA 2002). Five years later the European Standard EN 15026 (2007) which is largely based on the WTA guideline was published. However, both documents do not contain any information on how to deal with small defects in the building envelope. Parallel to the standard work in Europe a slightly more comprehensive standard on moisture control design has been developed in North-America (ANSI/ASHRAE 2009). As a result of numerous damage cases linked to rainwater penetration into constructions with rendered facades (Cheple & Huelman 2000), this standard has been the first that proposed the consideration of the effects of small leaks in the exterior finishes of exposed walls.

3. New items in hygrothermal simulation guideline WTA 6-2

Compared to the version from 2002 the new draft of WTA 6-2 (2013) allows the consideration of imperfections in the building envelope by simplified models. It also shows a way of dealing with ventilated cavities and contains some new information concerning boundary conditions. The new draft recognizes the problem of determining the material properties as accurately as possible for the intended use by a chart that recommends the test method as function of moisture range. This issue has come up in the context of capillary active insulation materials. These vapour permeable materials are supposed to prevent condensation at the cold side by compensating the diffusion flux with an opposed liquid flux. This means, liquid transport in capillary active insulation materials has to achieve a considerable magnitude well below 100% RH. Most of the currently employed methods have been designed to determine liquid transport properties in the high moisture range, i.e. when the majority of capillaries are filled with water. These methods turned out to be inappropriate to accurately determine liquid transport in the hygroscopic range. Therefore a new determination method has been developed by Binder et al. (2013) that tests the properties of interior insulation materials under the boundary conditions close to the real situation in practice application.

Since validation of the employed models is essential, the guideline now refers to some benchmark examples. One of the most important issues of a hygrothermal analysis is the interpretation of the results. Therefore a new chapter on result evaluation has been added which summarizes current assessment procedures. Concerning limit criteria it refers to existing WTA guidelines (e.g. WTA 6-3 (2007) and WTA 6-4 (2009)) as well as to a guideline on wood decay that is still in the making.

3.1 Rainwater penetration through imperfection in the exterior finish

As already mentioned the American moisture control standard ANSI/ASHRAE 160 (2009) requires the consideration of small rainwater leaks through the exterior finish which may result from gaps or cracks at joints and connections. It states: “In the absence of specific fullscale test methods and data for the as-built exterior wall system being considered, the default value for water penetration through the exterior surface shall be 1% of the water reaching that exterior surface. The deposit site for the water shall be the exterior surface of the water-resistive barrier. If a water-resistive barrier is not provided, then the deposit site shall be described and a technical rationale for its selection shall be provided.” In the case of ETICS on external walls the rainwater deposit site is likely to be the surface of the load bearing masonry beneath the insulation (see FIG 1).

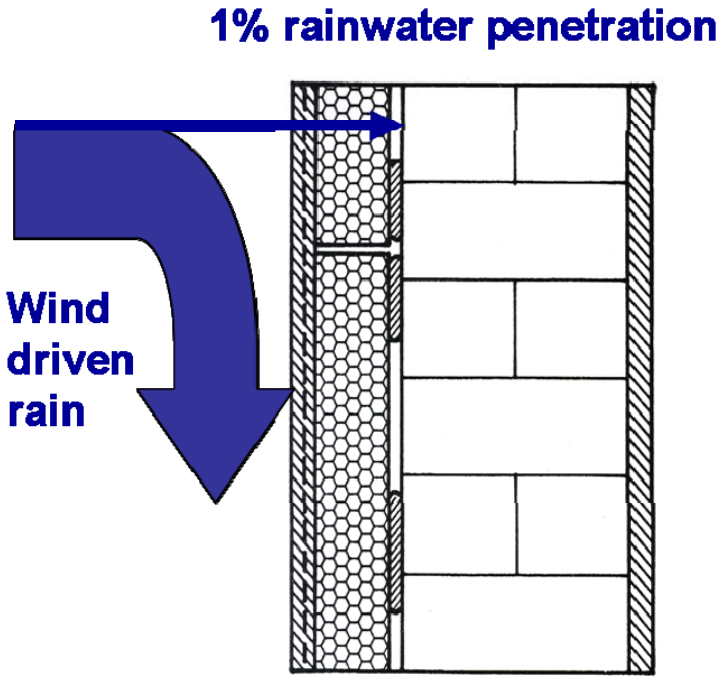

FIG 1. Example that shows the most likely deposit location for rainwater penetrating through leaks at joints and connections of a masonry wall with ETICS

It is obvious that neither the leaks nor the wind driven rain exposure are evenly distributed over the building envelope. But the standard committee chose this simple one-dimensional approach as a method to consider the effects of complex bulk water penetration phenomena observed in practice. The rainwater leakage rate proposed in the standard is not meant to be a worst case scenario. It is not based on field test results but on hygrothermal simulations (Desjarlais et al. 2001) that showed that more than 1% of rainwater penetration may be detrimental for a large portion of existing wooden wall structures. A recent literature review (Van Den Bossche et al. 2011), analysing data of leakage rates measured on different wall structures, confirmed the appropriateness of the “1% leakage” in ANSI/ASHRAE Standard 160. Therefore the rationale of this standard was also adopted for the new WTA guideline 6-2.

3.2 Moisture sources due to air flow through the building envelope

The convective moisture entry due to defects in the vapour respectively air control layer is a multidimensional effect, which cannot be captured directly by a one-dimensional calculation. However, also the application of multidimensional simulation tools hardly solves the problem, because the exact configuration of leakages is generally unknown and the complexity of relevant flow paths is exceeding the capacity of most models. Therefore it has been decided to choose an approach that

doesn't simulate the flow itself, but concentrates on the effects of vapour convection and subsequent condensation by introducing a moisture source inside the construction.

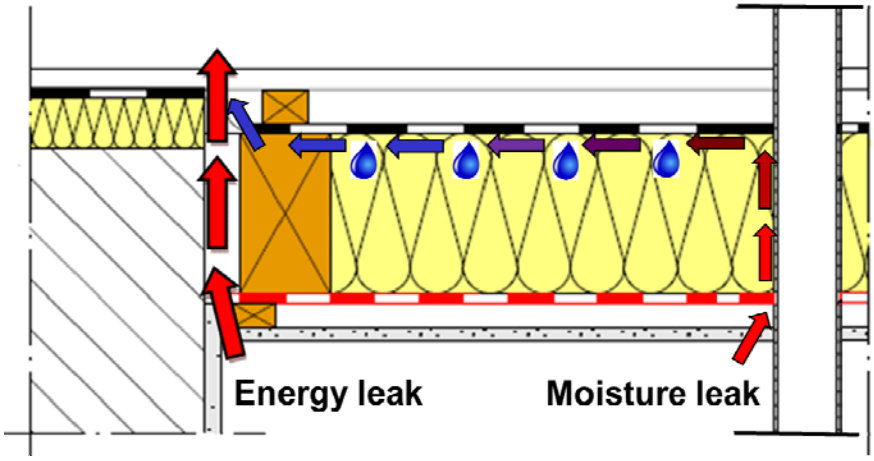

FIG 2. Indoor air leaking through a roof at joints and connections. If the flow path is short, it will be heated up by the air flow and only energy is lost. If the air flow creeps along the cold side of the structure before it finds its way out, its temperature may drop below the dew-point of the indoor air and cause condensation.

Based on experimental results from TenWolde et al. (1989), a simplified model to quantify the moisture sources due to vapour flow through the building envelope has been developed and checked for plausibility (e.g. Künzel et al. 2011). The model assumes that vapour contained in the indoor air, penetrating the envelope via so-called moisture leaks, condenses at the cold side of the insulation (see FIG 2). In contrast to energy leaks where the air remains warm because it flows in a short way from the room towards the outside, moisture leaks are small and tortuous channels where the air flow is slow and cools down in flow path. They represent only about 10% of all leaks in the building component. The position of the condensation plane has to be selected by the user. Its temperature, governed by the transient boundary conditions, is simulated without taking the latent heat of condensation into account. The right choice of this position depends on the construction. It must be cold enough for condensation to occur and it must be easily accessible for the indoor air that has penetrated the interior lining or air barrier. Examples are the exterior sheathing of wood frame walls or roofs and the interface between the interior insulation and the original wall after thermal retrofits of plastered masonry structures. The convective moisture source is equal to the amount of condensate that forms when the indoor air temperature is cooled down to the temperature of the selected condensation plane in the building assembly. Any increase in sorption water content that could occur in reality by the temperature drop is neglected. In order to remain on the safe side convective drying is excluded, i.e. the moisture accumulated by air convection can only dry out by vapour diffusion or liquid transport.

Thus the amount of condensation (moisture source S_{CL}), which results from vapour convection at the selected condensation plane p, is determined for each time step according to the following equation:

$$S_{CL} = k_{CL} \cdot \left(c_i - c_{sat,p}\right) \cdot (P_i - P_e) \qquad (1)$$

where

S_{CL}	moisture source due to vapour convection through the component	(kg/(m²h))
k_{CL}	air permeance of the "moisture leaks" of the component	(m³/(m²·h·Pa))
c_i	water vapour concentration of the indoor air	(kg/m³)
$c_{sat,p}$	water vapour saturation concentration at predefined plane p	(kg/m³)
$P_i - P_e$	air pressure difference over the considered envelope component	(Pa)

The air pressure difference is assumed to be due to buoyancy effects and pressure differentials generated by ventilation systems. Wind pressure effects are disregarded because they are difficult to determine and do not act on the building envelope in a continuous manner. Based on investigations in Künzel et al. (2011) the air permeance of the moisture leaks is set to 1,9·10-6 $m^3/(m^2s \cdot Pa)$ [0,007 $m^3/(m^2h \cdot Pa)$] for envelope components installed according to best practice. Buildings with higher k_{CL} would represent malpractice. Building components that can handle the moisture loads due to air convection are well-designed. Those that fail under these circumstances should either be redesigned or special care must be taken during installation which may include continuous moisture monitoring.

3.3 Boundary conditions

For the exterior boundary conditions EN 15026 (2007) recommends either hourly meteorological data of ten consecutive years or moisture design reference years that represent the worst year out of ten years. Alternatively an average year may be taken and 2 K may be added or subtracted every hour in order to arrive at a severe warm or cold year. WTA 6-2 (2013) discourages the use of severe meteorological data for assessing the long-term performance of building components because in reality sequences of such years are extremely rare and their repeated application may predict component failure of well-proven systems. Therefore the use of severe data files should be confined to the simulation of one year, preferably after a sequence of average years.

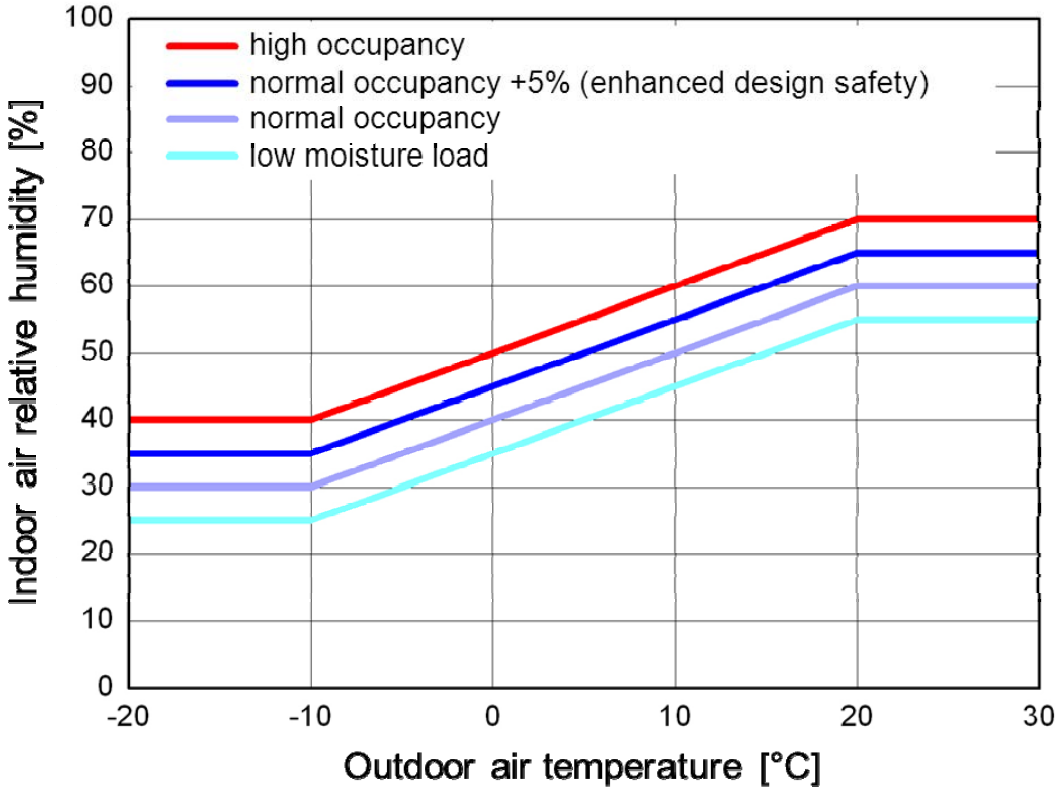

FIG 3. Chart to determine indoor RH from outdoor temperature according to WTA 6-2 (2013)

The recommended choices of indoor climate conditions are very similar in both documents. The widely used simplified method to determine indoor temperature and RH as function of outdoor temperature (Annex C in EN 15026) has been slightly refined (see FIG 3). The functions to determine the indoor temperature and humidity for normal and high occupancy are identical. Because the indoor boundary conditions for normal occupancy in WTA 6-2 guideline from 2002 resulted in somewhat

higher indoor humidity levels than the current function in EN 15026, the new draft of this guideline also proposes an increment of 5% RH to enhance the design safety of buildings with normal occupancy. However, for standard design purposes, indoor RH calculations based on the graph for normal occupancy in EN 15026 are still considered appropriate.

Since the guideline is also applicable to retrofit design, the assumption of having indoor conditions as derived for normal occupancy may limit the choice of retrofit measures. Therefore, it may make sense to choose the correlation for a low moisture load with indoor RH being 5% lower than that for normal occupancy, if a low moisture load can be guaranteed by adapted ventilation or dehumidification. Also non-residential buildings may be well represented by this category. However, it must be realized that moisture control design based on low indoor humidity levels set strict limits to other building operation modes.

4. Conclusions

The consideration of imperfections of the building envelope and its moisture related consequences represents an important step to improve the prediction performance of hygrothermal simulation tools. Unintended moisture sources due to rainwater penetration or vapour convection have often been a cause of severe structural damage. Therefore it is essential to increase the safety of moisture control design especially for light-weight structures. The approaches laid down in the WTA guideline 6-2 help to assess the moisture tolerance of building components with respect to different construction details and climatic parameters. Moisture damage risks caused by inadequate drying potentials, e.g. due to vapour tight layers on both sides of the construction, will be discovered and measures to improve the assembly can be evaluated. Finally, the balance between wetting and drying can be determined more realistically when the effects of potential defects are included in the hygrothermal simulation model.

So far, the results of simulations that included the consideration of imperfections according to the new WTA guideline have been very encouraging, i.e. they confirmed practical experience. However, there is a great need to improve the moisture source models and to elaborate their input parameters. This necessitates the investigation of typical imperfections of different constructions by especially designed laboratory and field tests. One of the most important issues is to differentiate between unavoidable moisture sources and bad workmanship. If consensus can be achieved about the definition of best practice for different construction types, hygrothermal simulation will not only lead to safer design, it will also be possible to use simulation tools for building forensics. That means, if a construction has failed, the simulations may show whether the architect or the installer is to blame.

5. Acknowledgements

The author wishes to express his gratitude to Daniel Kehl from TUD for having supervised as well as considerably enhanced the revision of the WTA guideline on moisture control by hygrothermal simulation. Equally valuable have been the contributions of all other WTA 6-1 working group members which merit special thanks.

References

ANSI/ASHRAE Standard 160 (2009). Criteria for Moisture-Control Design Analysis in Buildings.

Binder, A., Künzel, H.M. & Zirkelbach, D. (2013). A new approach to measure liquid transport in capillary active interior insulation. Proceedings 2nd Central European Symposium on Building Physics, TU Vienna, pp. 393-400.

Cheple, M. & Huelman, P. (2000). Literature Review of Exterior Insulation Finish Systems and Stucco Finishes, Report MNDC/RP B80-0130, University of Minnesota.

Desjarlais, A.O., Karagiozis, A.N. & Aoki-Kramer, M. (2001): Wall Moisture Problems in Seattle. Buildings VIII proceedings, ASHRAE, 8p.

EN 15026 (2007). Hygrothermal performance of building components and building elements - Assessment of moisture transfer by numerical simulation.

Künzel, H.M., Zirkelbach, D., Schafaczek, B. (2011): Vapour control design of wooden structures including moisture sources due to air exfiltration. Proceedings 9th Nordic Symposium on Building Physics (NSB), Tampere, pp. 189-196.

TenWolde A., Carll C.G., Malinauskas V. (1998). Air Pressures in Wood Frame Walls. Thermal Performance of the Exterior Envelopes of Buildings VII. Clearwater, Florida, USA.

Van Den Bossche , N., Lacasse, M., Janssens, A. (2011): Watertightness of Masonry Walls: An Overview. Proccedings 12dbmc Porto, 8 pp.

WTA-Guideline 6-2 (2002): Simulation wärme- und feuchtetechnischer Prozesse – Simulation of Heat and Moisture Transfer (English translation issued in 2004).

WTA-Guideline 6-2 (2013): Simulation wärme- und feuchtetechnischer Prozesse. Draft Oct. 2013.

WTA-Guideline 6-3 (2007): Rechnerische Prognose des Schimmelpilzwachstumsrisikos (Calculative prognosis of mould growth risk). Feb. 2007.

WTA-Guideline 6-4 (2009): Innendämmung nach WTA I (inside insulation according to WTA I). May 2009.

Results from laboratory tests of wind driven rain tightness in more than 100 facades and weather barriers

Lars Olsson, M.Sc.

SP Technical Research Institute of Sweden

KEYWORDS: *façade, wall, weather barrier, rain tightness, moisture, ETICS, EN 12865*

SUMMARY:
Over the past five years SP Technical Research Institute of Sweden have, for our clients, made more than one hundred wind driven rain tests in the laboratory of mock-ups of rendered stud walls or ETICS (External thermal insulation composite system) of existing and new designs and other types of facades and weather barriers.

More than 90 % of all tested objects failed and nearly 50 % of all details failed. Connections to windows got the worst results overall, despite windows being the most common details in facades. It is difficult to achieve good results in ETICS or undrained facades and even ventilated facades despite venting create pressure equalization across the façade. The weather barrier would be particularly important for the facades of multi-storey buildings, as leakages are added together downwards. If there are also flaws in the weather barrier there is an increased risk of leakage within the structure. Results from the tests of the weather barriers exposed to rain are similar to conclusions derived for facades. The consequence of leakage through the façade and to the structure has not been included in this study.

One can rarely visually determine whether façade detail solutions are rain tight before the test. It is hardly possible to determine the rain tightness of details only by theoretical assessment of drawings.

1. Introduction

During the last few decades rendered ETICS stud walls have been very popular in Sweden. Unfortunately, the combination of these systems with a wood frame structure has shown itself to be sensitive to moisture, which was revealed in Sweden in 2007 (Samuelson et al. 2007). Experiences from surveys of more than 1000 buildings show that the problem is moisture entering the structure - for example, at joints, poor connections to windows, doors, balconies etc. - wetting the materials inside the stud wall and causing rot and mould growth (Jansson 2011).

In Sweden it is no longer accepted to use ETICS in lightweight structures without improved and proven functionality, which partly led to facade providers need to develop new moisture-proof solutions. Additionally, other facades and weather barriers have got increasing demands for functional accounting.

Over the past five years SP have, for our customers, made more than one hundred wind driven rain tests in the laboratory of mock-ups of rendered stud walls or ETICS of existing and new designs and other types of facades and weather barriers as concrete element, wood panel, metal sandwich panel, weather barriers of fabric, board or slab. The test objects are usually constructed with the desired or common façade details, see FIG 1. The aim of this study is to show the driving rain tightness of facades, weather barriers and connections to joints, windows and balconies etc.

FIG 1. Example of test object, rendered stud wall with façade details.

2. Test objects and method

Various types of facades systems and weather barriers systems have been tested. Objects are divided with regard to function as undrained, drained or ventilated facades, sandwich elements of metal or concrete and second rain barriers (weather barriers) of fabric, board, or slab, see examples of designs in FIG 2 and FIG 3.

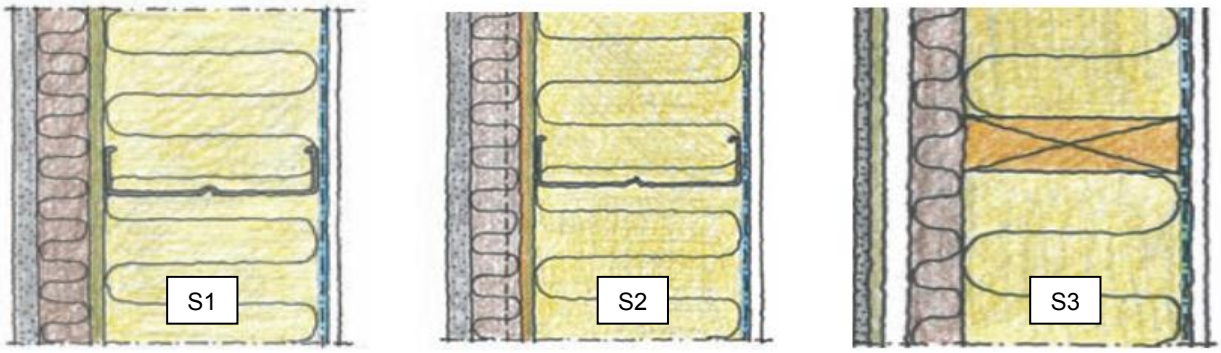

FIG 2. S1=Undrained (ETICS), S2=Drained, S3=Ventilated and drained

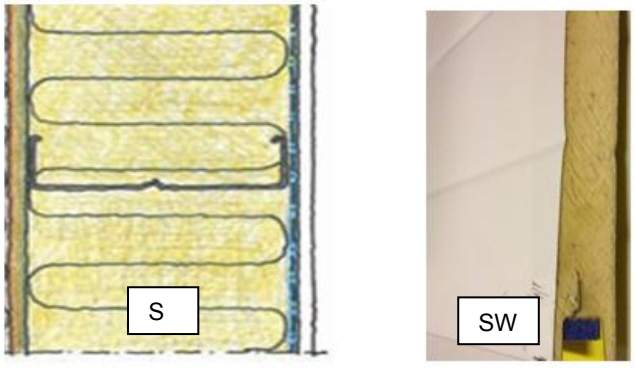

FIG 3. S=Second rain barrier, SW=Sandwich elements of metal or concrete.

The test objects were mainly mounted by the client in a steel test frame with the size of 3x3 meters in SP's laboratory. An airtight barrier of plastic film was attached to the inside of the frame walls. This film was perforated to create an air leakage of 1,6 l/s m2 at 50 Pa pressure difference, which represents the maximum allowable air leakage through the climate envelope according to Swedish building regulations 2002 (Boverket 2002). Before the testing started, each façade detail (except the movement joint) was subjected to between 5 - 10 blows (represented by a flat piece of wood hit with a hammer) to simulate the mechanical loading, which they would be subjected to in reality during nailing/construction.

Tests were carried out in accordance to SS-EN 12865 "Determination of the resistance of external wall systems to driving rain under pulsating air pressure" procedure B, with 300 minutes of total test time. The test starts with the object being exposed to 60 minutes simulated rainfall of 1.5 l / (m^2, min). After that pulsating pressure also starts for 60 minutes for each step 0-150 Pa, 0-300, 0-450 and 0-600 Pa. For objects that are not moisture absorbent method A is used, with a total test time of 60 minutes and the same pulsating pressure steps. When testing weather barrier the pressure difference used is usually up to 300 Pa and sometimes 600 Pa. Leakage of weather barriers of above 300 Pa is not reported in the results below.

Verification was carried out both visually and with moisture indicators which were attached underneath these details, see FIG 4. The moisture indicators were checked after each pressure level. Indicators consisted of absorption paper with thin electrodes for resistance measurement. At the end of the test, the wall was opened in order to investigate any further leakage and to estimate the leakage rate of each leak.

FIG 4. Indicators were placed just below all details behind the façade or exposed surface. The photo was taken after the rain test.

3. Summary of results

Failed = If water leaks through the rain exposed surface into the air gap, drainage gap, thermal insulation or structure. However, many walls may work even if the façade is not rain tight, in those cases the drainage rate, ventilation rate, dry out rate, rain tightness of the weather barrier or second rain barrier must be satisfied and may play an essential roll. The consequence of leakage behind exposed surface and to the structure has not been included in this study.

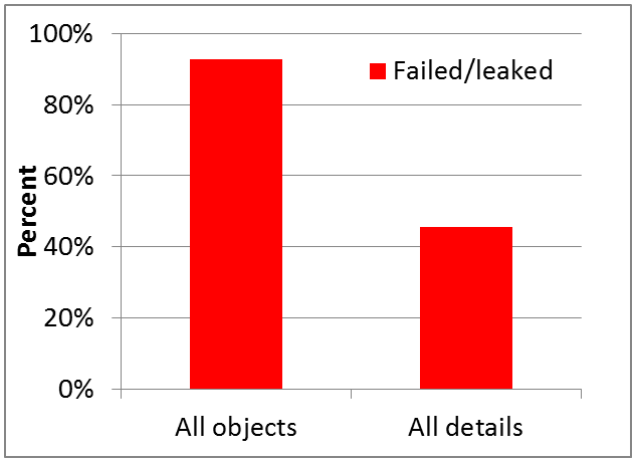

FIG 5. Percentage of objects and details that leaked or failed. 110 objects and 471 details were tested.

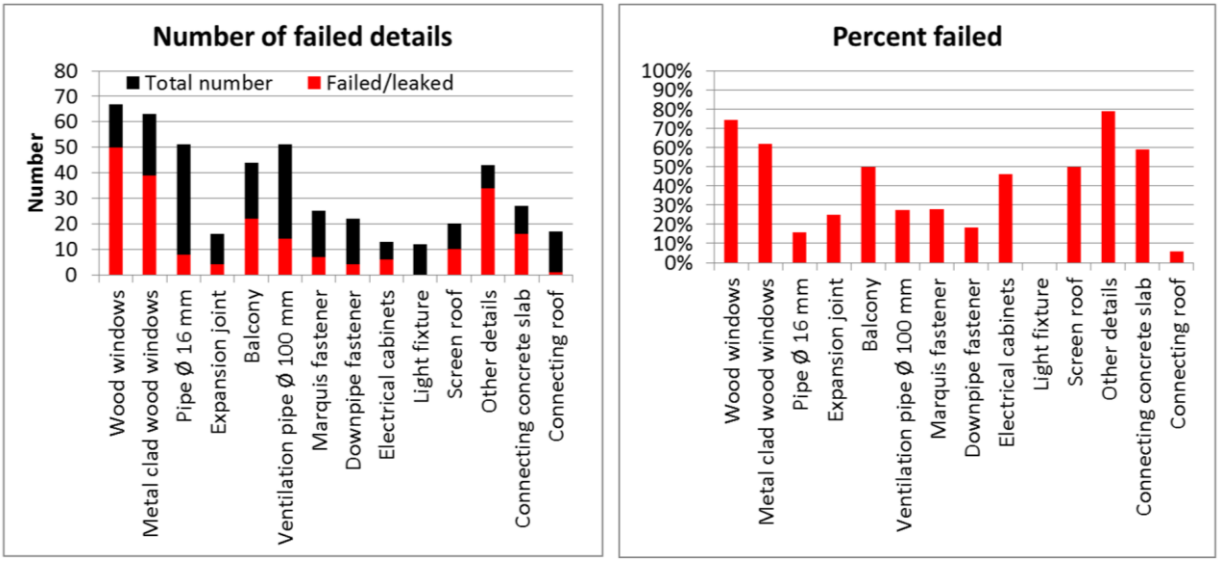

FIG 6.Number of failed details and total number tested (left). Percent of details that failed (right)

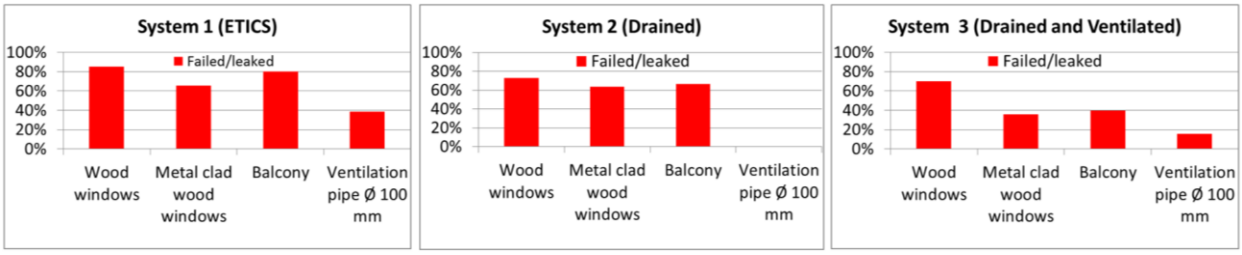

FIG 7. Comparison between system 1, 2 and 3 of failed details of common details.

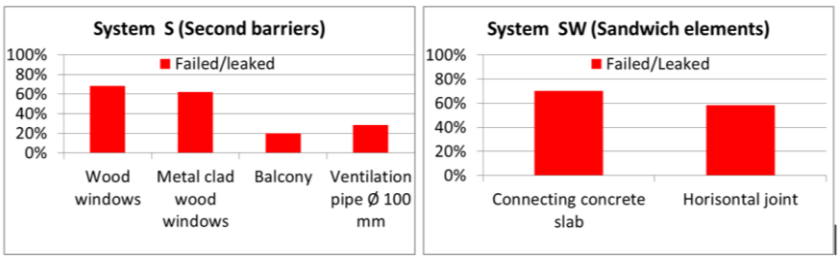

FIG 8. Comparison between system S, SW (and system 1-3, see FIG 7) of failed details of common details.

TABLE 1. Results of estimated leakage rate of failed objects. This result includes only the details that leaked most of each test object.

Description of the leakage rate	Leakage rate of failed objects [%]
1 - One or few drops	20
2 - Continuously dripping	53
3 - Low flow	26
4 - Modest flow	2
5 - Heavy flow	0

4. Conclusions

More than 90 % of all tested objects failed and nearly 50 % of all details failed. Connections to windows got the worst results overall, despite windows being the most common details in facades. It is difficult to achieve good results in ETICS or undrained facades. It is not quite as difficult to achieve good results with ventilated façades that provide almost no pressure difference over the façade cladding, compared to unventilated solutions where there is a pressure difference across the façade. The weather barrier would be particularly important for the facades of multi-storey buildings, as leakages are added together downwards. If there are also flaws in the weather barrier there is an increased risk of leakage within the structure. Results from the tests of the weather barriers exposed to rain are similar to conclusions derived for facades.

One can rarely visually determine whether detail solutions are rain tight before the test. It is hardly possible to determine the rain tightness of details only by theoretical assessment of drawings.

New designs and solutions need to be tested and evaluated. Ideally, there should be robust designs:

- that have at least two barriers against rain (even around details)
- that have good drainage
- without moisture retaining material where water optionally flows

- which can dry fast enough
- with sealing products tested for durability and compatibility (sustain at least 25 years).

5. Acknowledgements

Many thanks to our customers and staff at SPs wind driven rain laboratory that carried out the tests. The author made around 15 percent of all tests.

References

Boverket. 2002. Building Regulations, BBR. The Swedish National Board of Housing, Building and Planning, Karlskrona, Sweden.

Jansson A. 2011. Putsade regelväggar 2011, Erfarenheter från undersökningar som SP har utfört. SP Technical Research Institute of Sweden, SP report 2011:61.

Samuelson A. Mjörnell K. Jansson A. 2008. Moisture damage in rendered undrained well insulated stud wall. Proceedings of the 8th Symposium on Building Physics in the Nordic Countries, vol. 3, Copenhagen, Denmark

SS-EN 12865. 2001. Hygrothermal performance of building components and building elements, Determination of the resistance of external wall systems to driving rain under pulsating air pressure. SIS, Swedish Standards Institute.

Action against moisture damage in ETIC walls

Anders Jansson [1]

[1] SP Technical Research Institute of Sweden, Sweden

KEYWORDS: *moisture damage, one-stage barrier stud wall, remedial measures, follow-up measuring, in-situ sensors*

SUMMARY:

In Sweden today, it is widely recognised that there is a considerable risk of moisture damage in buildings with externally-rendered stud walls with a one-stage moisture barrier, particularly in locations exposed to the weather. In total, SP has investigated about 1000 buildings, and over 55 % of the buildings investigated have been so severely damaged that at least one entire façade has had to be rebuilt. The reason for damage is primarily inward leakage around poorly finished details and penetrations such as windows, window sills, balconies, sunshade fastenings, downpipe fastenings etc.

The extent of applied remedial measures has varied from completely rebuilt façade with a completely new design to partial repair of an existing façade. A common feature of all types of actions is that very few follow-up investigations with integral moisture sensors have been performed. This is unfortunate because such follow-ups indicate if measures are sufficient and are carried out in a proper manner. New inward leakages of varying amounts have been found in those buildings that have been monitored and this is not acceptable.

When damage has occurred, remedial work should be quality-assured, and the result be subsequently monitored through the use of integral moisture sensors. This applies regardless of the type of remedial work carried out.

1. Introduction

It is today widely recognised in Sweden (Jansson 2011) that there is a considerable risk of moisture damage in buildings having externally-rendered stud walls with one-stage moisture barriers, particularly in situations exposed to the weather. Damage has occurred in well-insulated stud walls having external insulation in the form of expanded polystyrene sheets or rigid mineral wool to which the rendered layer is applied, secured to a sheet of material that is often of organic origin. The outermost layer consists of plaster rendering, forming the façade. An air and vapour barrier in the form of a 0.2 mm PE sheet is normally applied to the inside, i.e. to the warm surface.

This system of plaster render on insulation was developed in Germany during the 1950s and 1960s for use as additional insulation of existing brick-built buildings. The energy crisis at the beginning of the 1970s provided the impetus for additional insulation of many Swedish buildings of lightweight concrete or brick in this way, without encountering any more serious problems.

A similar system, under the name of EIFS, Exterior Insulation Finishing System, started to be used in North America in the 1970s for insulation of stud walls using plaster-rendered foamed plastic insulation sheets. Questions started to be raised about this system at the end of the 1980s, as moisture damage started to be found in the walls (Hickman 2004). Based on the results of extensive investigations, buildings are now protected by a continuous layer of water-shedding but vapour-permeable material, known as house wrap. This external membrane is intended to ensure that any inward-leaking water drains out. It is applied outside the frame of the building, but inside the external

insulation. This means that the pressure drop occurs across the membrane, and that the weather seals in the façade are exposed to a lower water load than traditional one-stage barrier designs.

Sweden, and other European countries, started using plaster-rendered stud wall systems for new builds in the 1980s. This delivered a well-insulated, compact, externally-plastered wall design. This system is known in Europe as ETICS, External Thermal Insulating Composite System.

In Sweden, SP performed its first investigation of buildings having one-stage moisture barrier stud walls at the beginning of 2006. It found extensive inward leakage through façades around poorly sealed details, particularly on those exposed to the weather. Damage had previously been found in Hammarby Sjöstad in Stockholm, but this had been due to residual constructional moisture (Samuelson 2002). Many measurement programmes and investigations have been performed after SP published its results, warning that this design was sensitive to moisture, in specialist literature at the beginning of 2007.

1.1 The situation today

Just how many buildings have been built in Sweden using this particular design is not at present known. In 2009, in conjunction with the industry, SP estimated the façade area (m²) that had been erected using the method (Jansson, Samuelson 2009). Up to and including 2007, about 10,5 million m² of one-stage barrier stud walls had been produced, but we know that many more buildings have been put up using this method since 2007. It is therefore reasonable to assume that the actual area of such walls is today considerably more than 10,5 million m². We also know that there are construction companies that are still using the method, although with some modification in the form of thick plaster rendering on mineral wool and with improved detailing and penetrations.

As far as the extent of damage and inward leakage is concerned, SP has a very clear picture based on many measurements and opening up of walls. I, the author of this paper, have investigated 772 buildings having this method of façade construction. Many of them have been investigated in several stages, as follows:

Stage 1: Visual inspection and external moisture measurements

Stage 2: Local opening up from the inside and outside of the façade

Stage 3: Total opening up of the façade right through to the stud frame.

As the investigations have been carried out at different stages, and generally been very extensive, we have accumulated a substantial fund of knowledge and experience of one-stage barrier stud walls. In total, SP has investigated about 1000 buildings. We have also been in contact with other moisture consultants, who perform a considerable amount of damage investigations and surveys of buildings incorporating this form of construction. They share our understanding of the extent and occurrence of this type of damage.

According to SP, the extent and occurrence of damage in this particular type of structure is very considerable.

SP has found that the extent of moisture damage in this type of construction is very considerable. Over 55 % of the buildings that SP has investigated have been so severely damaged that at least one entire façade has had to be rebuilt. Naturally, not all buildings are damaged, but it can be safely said that there is an extensive risk of inward leakage through façades exposed to the weather and having poor-quality detailing. There is little risk of damage in areas protected from the weather and with good quality of detailing workmanship. Generally, it is weather and wind that directly determine whether damage occurs or does not.

The reason for damage that has been found is primarily inward leakage around poorly finished details and penetrations such as windows, window sills, balconies, sunshade fastenings, downpipe fastenings etc. Photographs 1 and 2 show examples of such leaking details.

FIG 1. Sunshade fastenings

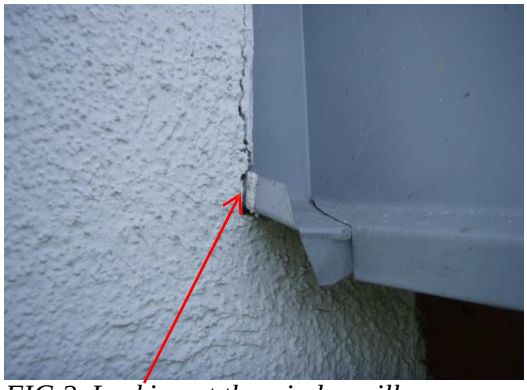

FIG 2. Leaking at the window sill

The above photographs show very clear leaks. However, in many places, extensive damage has occurred without any visible leaks. Even very small leaks or quality failures can result in relatively severe damage, particularly in areas exposed to the weather. Figures 3 and 4 show examples of such damage.

FIG 3. Extensive rot and mildew damage

FIG 4. Extensive mildew damage

SP has also performed many laboratory tests on this type of structure. Most of the laboratory tests of one-stage barrier façades have shown varying extents of inward leakage. However, they have also shown that it is possible, under laboratory conditions, to build a one-stage barrier wall that does not suffer from leakage if the correct materials are used, with careful detailing of fastening and penetration designs, and with absolutely correct construction of façades and details.

Many investigations have thus shown that there is a large number of buildings that are in need today of remedial measures. The question is, how should such measures be applied without creating a risk of new moisture damage?

1.1.1 What remedial measures are needed?

It is difficult to generalise as to what measures are needed, as each case is unique. However, remedial measures must be such as to remove moisture-damaged materials and prevent new leakage.

1.1.2 Which remedial measures have been chosen for application?

The extent of applied remedial measures has varied widely. Before it was realised that rot and mildew damage inside the structures were common, there were many 'repairs' made by applying an external mastic joint around leaking details. However, such repairs were insufficient, and inward leakage continued. We can also wonder how well these external mastic joints would work over time. Photos 5 and 6 show examples of poor joints that have failed.

FIG 5. Poor joint at window sill

FIG 6. Poor joint at electrical service

Three different remedial measures have tended to dominate over the last five years in Sweden:

- Completely rebuilt façade, with an air gap / drainage gap
- Completely rebuilt façade, with the same construction but better detailing
- Partial repair of an existing façade.

In most cases where there has been extensive moisture damage, the response has been to strip back the entire façade to the stud framework and remove all damaged materials. The façade has then been rebuilt with a two-stage barrier ventilated stud wall, as the risk of inward leakage through this construction is less, due to the fact that there is a different pressure distribution across the façade (Gustavsson 2009), and because drying-out proceeds more rapidly (Falk 2010) than in a one-stage barrier stud wall. In some cases, the façade has been restored with a two-stage barrier drained stud wall. From a technical point of view, there are no drawbacks in using a two-stage barrier ventilated stud wall to deal with the risk of moisture damage, but there are drawbacks in other respects as such a structure, having the same thickness of insulation as before, will be thicker than a one-stage barrier construction and therefore more expensive.

In many cases, the decision was taken to strip the façades back to the stud framework and remove all damaged materials. The façade was then rebuilt, using the same design, but with better detailing and less use of moisture-sensitive materials. The drawback of this method is that it still leaves a construction that is vulnerable to poor workmanship / detailing, with a resulting relatively high risk of damage if inward leakage recurs.

An example of better detailing at the joints between windows and external windowsills can be, for instance, extra window side metal sheeting that extends all the way down to the window sill.

1.1.3 Monitoring of remediated façades

Monitoring of the subsequent performance of remediated façades is an important element of dealing with the problem, as it shows whether the remedial actions were sufficient and were correctly applied. Unfortunately, monitoring has been carried out to only a limited extent, but new inward leakages of varying amounts have been found in those buildings that have been monitored. The following are brief descriptions of four such cases.

The work performed on three buildings in southern Sweden has been monitored over a two-year period, using sensors installed in the structure (Olsson 2011). Two of the buildings were remediated using the same type of one-stage barrier façade as before, but with improved detailing and other materials. The third building was remediated using a two-stage barrier ventilated construction. Both types of repair showed elevated measured values, indicating slight inward leakage, although the cause of the elevated values has not been found.

Partial repairs, varying in extent, were carried out in an area of about 20 buildings. The façades were rebuilt, using the same construction but incorporating a sheet of inorganic wind barrier material and better detailing. Instrumentation probes, known as passive moisture sensors, and requiring active reading, were inserted in the stud framework. However, no-one checked their readings after the repairs had been made. SP later performed an investigation of these buildings, finding extensive leakage and damage, both where the partial repairs had been carried out, and where no work had been done. Today, all the façades have been completely rebuilt, using a two-stage barrier ventilated construction.

Partial repairs were carried out in another area of about 45 buildings, varying in extent between buildings. In some cases, the façade was stripped back to the stud framework, and then rebuilt using the same construction, but with the addition of a sheet of inorganic windbreak material and improved detailing. Other buildings received partial repairs, with the same construction, but better detailing. SP then carried out an investigation of most of the buildings, and found extensive inward leakage and damage, both in areas where work had been performed and where nothing had been done. Today, all the façades have been completely rebuilt.

In another area of apartment buildings, remediation consisted of partial repairs of some buildings and total strip-back of façades in other buildings. The façades were rebuilt using different materials, better detailing and the incorporation of draining layers outside the wind barrier. The results were monitored in several of the buildings using moisture ratio sensors that had been built into the structure. Some of these test points have subsequently shown high moisture levels and the presence of free water.

Partial repairs have been carried out to various extents on several smaller apartment buildings, with the façades being rebuilt with improved detailing and different materials. Further moisture measurements, and localised exposure of the internal structure, have been carried out where elevated moisture levels have again been found.

Summarising, too few follow-up investigations have been performed to be able to say whether partial rebuilds can reliably deliver acceptable results. However, the few follow-ups that have been performed show clear indications that the repairs are not sufficient.

1.1.4 How can remediated façades be monitored?

In our opinion, it is relatively easy to follow up the performance of remediated façades as far as inward leakage is concerned. One way is to incorporate sensors in the wooden studs framework. Both passive and active systems are available: passive systems in which electrodes are inserted into the studs and provided with brought-out insulated cable tails to which a manual meter can be connected for a reading, and active systems in which electrodes are screwed into the wood and the moisture ratio read by wireless communication.

It is important that inserted sensors should be placed where the risk of inward leakage is highest. Reference sensors can be inserted in positions protected from the effects of weather, but the rest of the sensors should be in positions where the greatest risk of inward leakage is suspected. The reason for this is simple: the sensors are there to assess whether the façade is watertight or not. If passive sensors are used, they must be read after heavy rain, with the wind driving on to the façade.

The cost of inspection using in-situ sensors is small in relation to the cost of remediation work. It is therefore unclear as to why so few follow-ups of the performance of remedial work have been carried out.

2. Conclusions

A rendered one-stage barrier façade on a stud wall structure can be very difficult to make sufficiently watertight. Even very small leaks or defects can result in substantial inward leakage, particularly through walls exposed to the full force of the weather. There is therefore little allowance for carelessness or poor workmanship with this type of construction. It is our opinion that, if work and process installation instructions are not followed correctly, and if weather seals are not installed in the correct positions, the construction has no chance of providing its intended satisfactory performance.

The investigations that SP has performed of buildings with this type of structure have often found extensive inward leakage. The building's exposure to weather and wind, and the quality of workmanship of detailing and fitting of penetrations, are directly decisive in respect of the risk of damage.

Remedial works that have been applied vary from local partial repairs to total renovation with a new façade structure design. However, a common feature of all approaches is that very few have been quality-assured, or have had their performance monitored by integral moisture sensors. The follow-ups and investigations that have been performed indicate that the remedial works have not been entirely successful. Against this background, our advice to the construction industry is as follows:

- Avoid one-stage barrier façades on stud walls for new construction.
- When damage has occurred, remedial work should be quality-assured, and the result be subsequently monitored through the use of integral moisture sensors. This applies regardless of the type of remedial work carried out, but is more important in respect of one-stage barrier stud wall façades.

3. Acknowledgements

I would like to tender my thanks to my colleagues Ingemar Samuelson and Ingemar Nilsson at SP, for their valuable views.

References

Gustavsson Börje Fönstermontage. Byggnadsfysik, SP Sveriges Tekniska Forskningsinstitut. SP RAPPORT 2009:35.

Falk Jörgen. 2010. Ventilerad luftspalt i yttervägg – Luftomsättningar och konvektiv fukttransport. Lund, Lunds Tekniska Högskola. Rapport TVBM-3155.

Jansson Anders. 2011. Putsade regelväggar 2011, erfarenheter från undersökningar som SP har utfört. Borås, SP Sveriges Tekniska Forskningsinstitut. SP Rapport 2011:61.

Jansson Anders & Samuelson Ingemar. 2009. Putsade regelväggar. Borås, SP Sveriges Tekniska Forskningsinstitut. SP Rapport 2009:16.

Jansson Anders et al. 2005-2013. Enstegstätade regelväggar. Technical reports. Borås, SP Sveriges Tekniska Forskningsinstitut.

Hickman Ann Rudd. 2004. Insurers Slapping EIFS Exclusions on Insurance Policies. International Risk Management Institute, Inc. Construction Bulletin, 3/5/2004.

Olsson Lars. 2011. Fuktmätning under två år efter byte av putsfasad. Borås, SP Sveriges Tekniska Forskningsinstitut. SP Rapport 2011:67.

Samuelson Ingemar. 2002. Fukt och mögelskador Hammarby Sjöstad. Borås, SP Sveriges Tekniska Forskningsinstitut. SP Rapport 2002:15.

Hygrothermal simulation of green roofs – new models and practical application

Beate Stöckl, Dipl.-Ing. [1]
Daniel Zirkelbach, Dipl.-Ing. [1]
Hartwig M. Künzel, Dr.-Ing. [1]

[1] Fraunhofer Institute for Building Physics IBP, Germany

KEYWORDS: *green roof, simulation, moisture safety, growth medium*

SUMMARY:
Design and installation of green roofs on wooden constructions requires special care because of the low inward drying potential in the summer months. Within a research project new models to calculate green roofs reliably by the help of hygrothermal simulations were established. Based on experimental investigations of green roofs in Holzkirchen, Leipzig, Vienna, Kassel and Milan different models were developed which provide a reliable basis for moisture control design of extensive green roofs. After validation the model has been used to arrive at general practice recommendations for wooden light-weight green roofs. The critical condition in light-weight flat roofs is normally the water content in the exterior sheathing. For design purposes it shouldn't exceed a limit value of 18 % by mass – this is to prevent wood decay but includes a safety factor. To fulfil this requirement an additional insulation layer above the exterior sheathing is often necessary.

1. Introduction

Due to the fact that most city centres are soil sealed, green roofs become more and more popular as climatic compensation areas. The green roofs partly substitute the function of topsoil, because they can absorb and store rain water which subsequently can evaporate through growth medium and plants. The latent heat storage and the weight of the greening dampen diurnal and also seasonal temperature variation. The reduced temperature stress and strain increases the life expectancy of the roofing membrane and the substructure. Additionally undesirable heat gains in summer and heat losses in winter are generally lower than with other flat roof constructions. These benefits of green roofs are somewhat offset by potential moisture problems or construction damage. Such problems have been observed again and again in unventilated light-weight green roofs. One reason is the fact that flat roofs are vapour tight at the exterior surface and thus on the wrong side from the building-physics point of view. So drying is only possible towards the inside. In comparison to normal flat roofs, green roofs remain significantly cooler during summer time, which reduces the drying potential to the inside. The combination of greening and moisture sensitive wooden substructure may lead to a roof assembly, which is hardly fault-tolerant and requires special care for design and workmanship.

Until recently our knowledge about the hygrothermal conditions in the growth medium have been insufficient to accurately assess the moisture performance. This is the reason, why also advanced planners arrive at their limits and often recommend another roof assembly or require expensive preventive safety measures, for example a ventilated air layer, which can be unfavourable concerning energy performance. The missing basics for planning are opposed to the increased use of green roofs, which are ecologically worthwhile and energetically advantageous.

Within the research project (Zirkelbach & Schafaczek 2013) new models were developed in order to allow a green roof design by the help of hygrothermal simulations. The aim was to provide a reliable

basis for safe moisture control design of extensive green roofs to designers and manufacturers of building materials and constructions.

2. Green roof models

2.1 Generic simulation model

The generic green roof model shall serve as a common approach, which can be used without additional information of the type of the specific growth medium and with climate files which don't contain information about the atmospheric counter radiation. It was developed on the basis of field studies in Holzkirchen, Leipzig (Winter, Fülle & Werther 2007-2010), Vienna (Teibinger & Nusser 2010) and Kassel (Minke, Otto & Gross 2009). Based on the measurements of Holzkirchen for inverted green roofs in the period from 1985 to 2004 the material data, surface transfer conditions and rain water absorption behaviour were adapted by the help of hygrothermal simulations to achieve good agreement between simulation results and measured data. Therefore a growth medium layer is simulated together with the roof assembly considering its moisture balance during the year. The plant cover influence is represented by adapted values for surface heat transfer and radiation exchange, and an additional moisture source inserts a part of the rain water directly into the substrate, to accelerate the rain water uptake in comparison to only capillary transport. Details about the iterative adaption extend the scope of this paper but can be found in the detailed report (Zirkelbach D. & Schafaczek B. 2013) as well as on IBP homepage. The simulations are performed with WUFI® (Künzel 1994), a model to calculate the simultaneous heat and moisture transport in building components under real climate conditions, developed by the Fraunhofer IBP and validated by numerous field. It fulfils amongst others the requirements of (EN 15026) and (ASHRAE Standard 160).

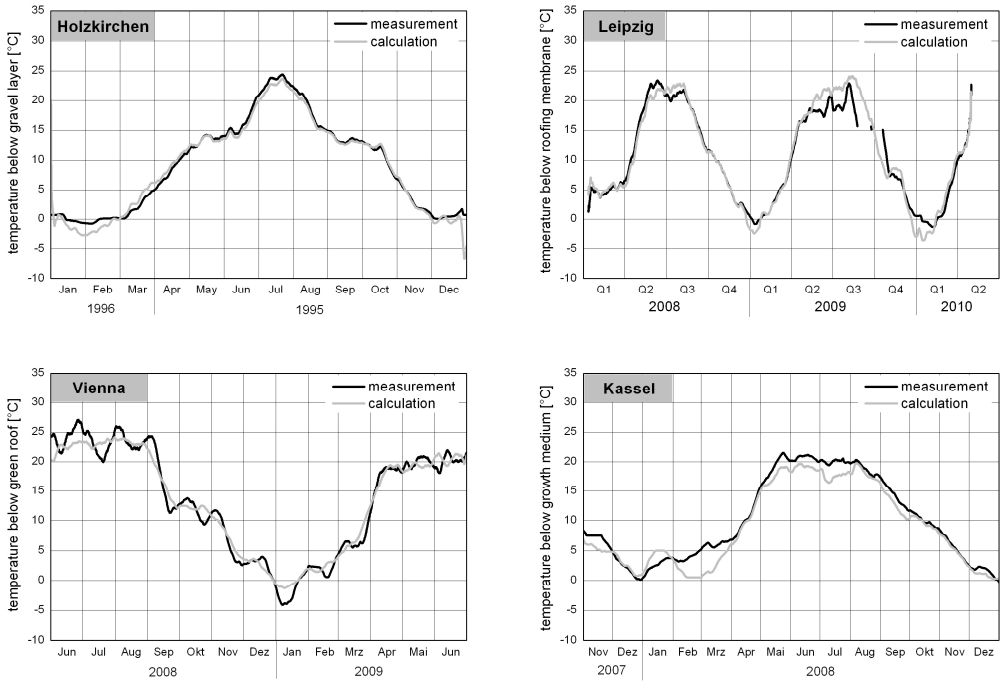

FIG 1. Calculated temperature (monthly average) below the green roof layers in Holzkirchen, Leipzig, Vienna and Kassel in comparison to the measured values.

The generic model for the simulation of green roofs generally shows a good agreement with the measured data at different locations and below different types of greening. Figure 1 shows the comparison between measurement and calculation of the temperatures below the green roof layers – i.e. on top of the insulated structure – as a monthly average for the investigated locations. In Leipzig

additionally also the water content in the OSB-sheathing was measured. A comparison with the calculated water content (Figure 2) shows also a very good agreement. In the winter months there are remaining differences between simulation and measurements because of the intermittent snow cover which is not considered in the calculation. It has been attempted to adjust the generic green roof model in such a way that generally the simulation leads to more unfavourable results than the measurement. This is necessary to allow the evaluation of a green roof assembly on the safe side.

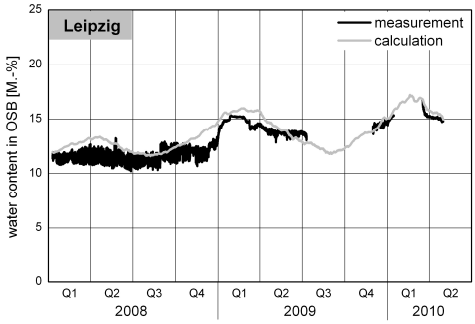

FIG 2. Calculated water content in the sheathing of a green roof in Leipzig in comparison to the measured data for the period January 2008 to April 2010.

The climate data available for the development of the generic model didn't contain any data for the atmospheric counter radiation, so it was necessary to consider this influence in a simplified way by the other climate data and appropriate surface transfer coefficients. This green roof model can be used if the radiation conditions are comparable to the ones at the examined Central-European locations. Other radiation conditions, especially those with clearly different cloud cover, should be considered by a detailed calculation of the long-wave radiation losses with one of the specific models.

2.2 Specific simulation models

To consider the long-wave radiation explicitly, new test roof sections with different growth media and thicknesses were established at the field test site in Holzkirchen (Figure 3). To provide product specific models different types of growth media were investigated:

- Single layer assembly with 8 cm growth medium
- Double layer assembly with 3 cm growth medium
- Multi-layer assembly with 10 cm new growth medium
- Multi-layer assembly with 10 cm ingrown growth medium

In each assembly the temperatures were recorded at two positions and in two resp. three levels. Additionally, in all test sections the moisture on the roofing membrane was determined indirectly by resistance measurements in thin wood specimens, because a measurement of the relative humidity in the mostly water saturated growth medium is not always accurate and the sensors often fail. On the other hand, even if the resistance measurement can only provide qualitative information it can show, if the growth medium dries out in summer time or if it remains humid all year round. Almost during the whole year the relative humidity in the growth medium layer didn't fall below 99 % - which is also the requirement for plant growth. An accurate measurement of the moisture in the growth medium layer is only possible by weighing. Therefore small baskets for manual weighing were installed in each test section.

The weather station on the field test side in Holzkirchen records all climate data required for a simulation. Additionally the interior surface temperature of the test roof was measured. To calculate the conditions in the different test sections detailed material data are required. Therefore, in addition to the manufacturer specifications, the following data were determined in the laboratory: density, diffusion resistance, water absorption factor, sorption moisture at different relative humidity levels

and free water saturation. Based on these field and laboratory tests the generic simulation model was extended to specific models, which consider the specific material properties and the detailed radiation exchange at the surface.

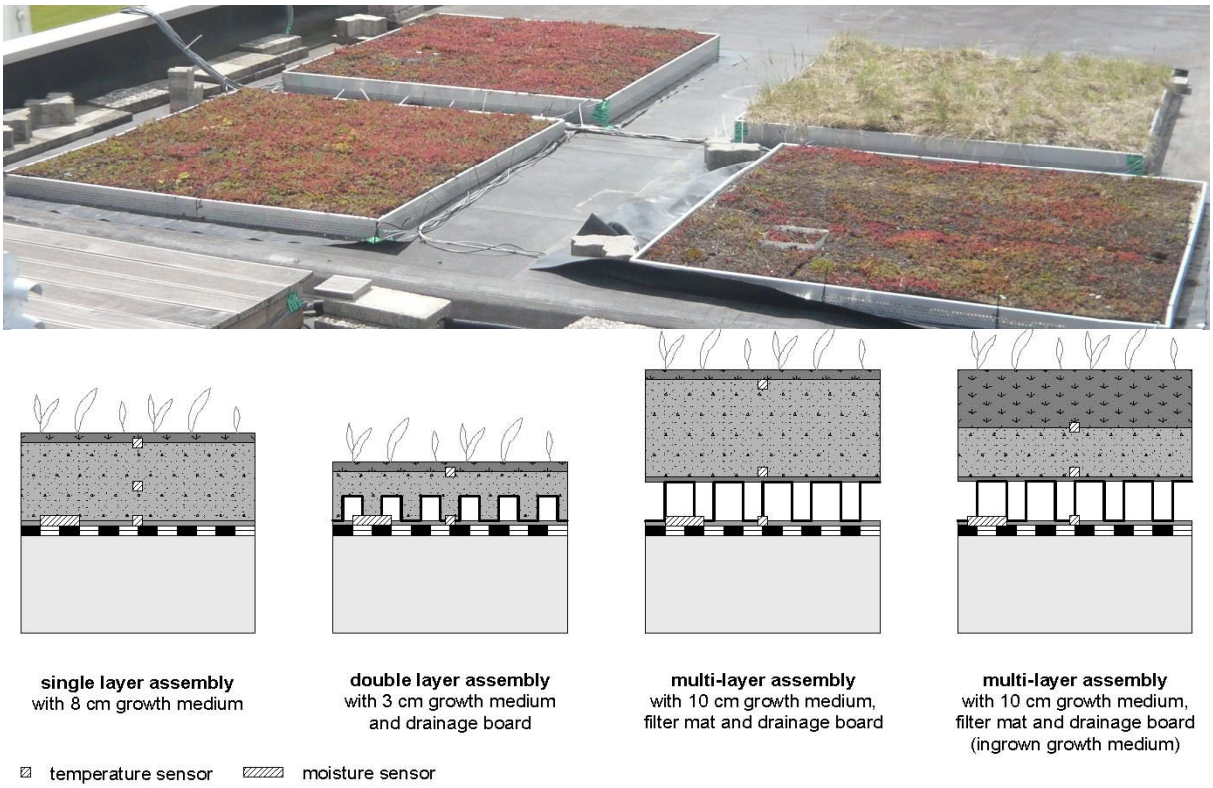

FIG 3. New field tests in Holzkirchen with different growth media and thicknesses. The drawing also shows the position of the temperature and moisture sensors.

During the iterative simulation of the hygrothermal behaviour of the different green roof assemblies the parameters which are unknown or difficult to determine experimentally due to their complexity are adapted to reach a good agreement with the measured values. The adaption was performed iteratively for each test section and each parameter to get an appropriate correlation between the variation of the input parameters and their influence on the results.

The following parameters had to be adjusted by this parametric study:

- the radiation exchange of the roof surface with the sky which is influenced by shading, changing colours and variability of the plant cover
- the moisture depending thermal conductivity of the substrate and the reduction of the effective heat transfer coefficient by the plant cover (the plants reduce the convective heat exchange and may even have an additional insulating effect)
- the influence of the drainage layers on moisture retention

The iteration steps and the results of the recalculation of the test fields are described in detail in the research report (Zirkelbach & Schafaczek 2013). Within this paper only the important results and the differences to the generic model will be explained.

On the exterior surface the detailed radiation exchange was considered by both the short-wave radiation absorption and the long-wave radiation emission. By introducing an additional plant cover layer at the surface also the insulation effect of the plants can be considered in the simulation. Furthermore the two dimensional and temporally variable properties of the drainage elements were

represented with average material data. The results have shown that there is a need to differentiate between a drainage element filled with substrate and an unfilled element.

The aim of the adaption has been to reach a good agreement between calculation and measurement. In Figure 4 (top) the comparison between the measured (solid lines) and the calculated (dotted line) temperatures on the roofing membrane of the single layer assembly are displayed. In average the agreement is quite good – but looking at the hourly values (Figure 4, middle) there are still short term peak differences of up to 8 K. But also the difference curve between the two measurement positions (Figure 4, bottom) shows, that the measured temperatures in the same roof and on the same level also differs up to 6 K. This is the result of the inhomogeneity of the substrate and plant layer as well as local differences in moisture contents. These uncertainties cause the described discrepancy between calculation and experiment and show that no “correct” solution but only a good approach to the measurements is possible. Compared to the measurements, the simulation results should show lower temperatures on average in order to remain on the safe side.

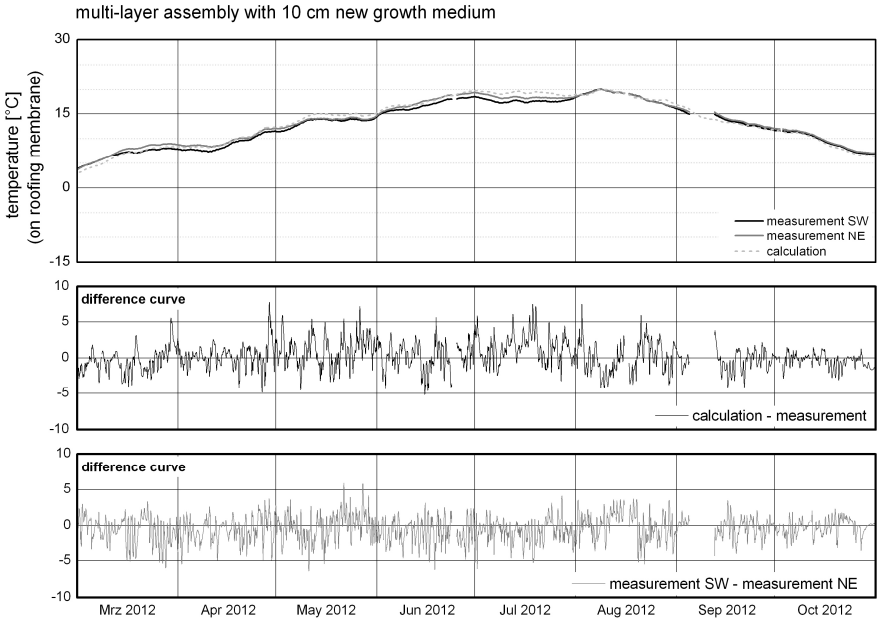

FIG 4. Monthly average of the calculated temperatures at the roofing membrane in comparison to the two measurement positions (top). In the middle and bottom diagram the difference curves are displayed.

Due to the fact that the specific models also consider the atmospheric counter radiation, there is the possibility to evaluate green roofs also in other climate regions with different radiation conditions. For additional validation some experimental data of a green roof research project in Milan were provided by Fiori & Paolini (2013). The first comparision over a short period have shown that the conditions below the green roof can be reproduced very well with the specific model. However, more validations are desirable and will be performed in future.

2.3 Verification of the green roof models by means of the impacts on a light-weight construction

Focus of the research project was a reliable design and evaluation of light-weight constructions. Therefore it is most important that the temperatures below the green roof on the roofing membrane can be well calculated. However, the simulations show temperature discrepancies up to 8 K to the measurement. Therefore, in the following it will be evaluated, if these short-time temperature differences have a significant influence on the hygrothermal evaluation of a roof.

Thus a light-weight construction with a very sensitive behaviour concerning the outdoor climate is analysed. To evaluate the remaining differences between measurement and calculation, as boundary conditions both, the directly measured values and the modelled conditions according to the new approach are used and compared.

The conditions below the green roof are considered as follows:

- measured temperatures on the roofing membrane in combination with a relative humidity of constant 100 %
- calculation of the green roof with the specific model using the measured outdoor climate data of Holzkirchen

For the evaluation, the water content in the OSB-sheathing of the two alternatives is compared. Experience shows that the OSB-sheathing presents the most likely location in the construction where damage due to high humidity conditions occurs. In Figure 5 the simulated water contents in the OSB-sheathing are displayed for two different boundary condition cases: For the first case the temperature of the roofing membrane is determined by the green roof model and in the second case the measured membrane temperatures from the green roof experiment are employed. For all considered assemblies the two curves run more or less parallel, whereby the water content of the approach with the green roof model is in case of difference maximum 1 M.-% higher than the one of the simulation with the measured values. That means that the hygrothermal results obtained by the new models are almost identical to those obtained by using real measured data as boundary conditions.

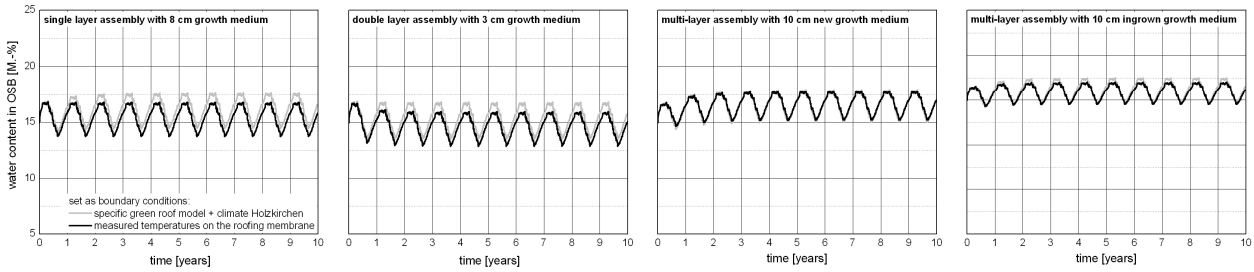

FIG 5. Calculated water content in the OSB-sheathing of a light-weight construction for the four roof assemblies using both the measured (black) and modelled green roof conditions (grey curve).

Altogether, it can be stated that the new green roof models can reproduce the conditions below the green roof very well. Thereby the temperatures of the simulation are slightly lower and consequently the calculated moisture conditions of the construction are on the safe side.

3. Application and practice recommendations

In wooden green roofs with vapour retarder only small moisture fluxes occur during the year. Therefore dynamic equilibrium is reached slowly – often only after a period of many years. Due to this fact the results of „short time“ field tests (less than five years) often provide only partially meaningful results to evaluate such constructions. The new green roof models allow a reliable simulation of the moisture conditions in light-weight assemblies as well as an evaluation of their long term behaviour.

Within the research project the hygrothermal behaviour of a typical light-weight roof was analysed depending on the green roof assembly, the insulation material, the thickness of the insulation layer and the vapor diffusion resistance of the interior surface materials. In this paper only one of these variation can be shown. In Figure 6 the calculated water content in the exterior OSB-sheathing in a roof with 20 cm insulation layer as function of the type of the vapor retarder is plotted: the left diagram shows the results for a membrane with a constant s_d-value of 2 m and the rigth one those with a variable vapour retarder (s_d-value < 0.5 m for humid and > 25 m for dry conditions). With previous

design (without additional insulation) and a s_d-value of 2 m for the vapor retarder the water content in the OSB-sheathing shows a strong increase both with the thin light-weight growth medium layer (grey solid line) and with normal growth medium thickness (black solid line) and reaches values of 25 to 45 M.-% after 15 years. Also with an additional insulation layer of 5 cm above the exterior sheathing both alternatives (grey / black dotted line) slightly exceed the value of 18 % by mass (a well-accepted limit to prevent wood decay that includes a certain safety factor). In comparison to these results the construction with a variable vapour retarder (diagram on the right) shows more favourable conditions. With the light-weight growth medium the water content remains below the limit value even without an additional insulation layer. But with the normal growth medium thickness and previous design the limit value is also exceeded and can only be kept with an additional insulation.

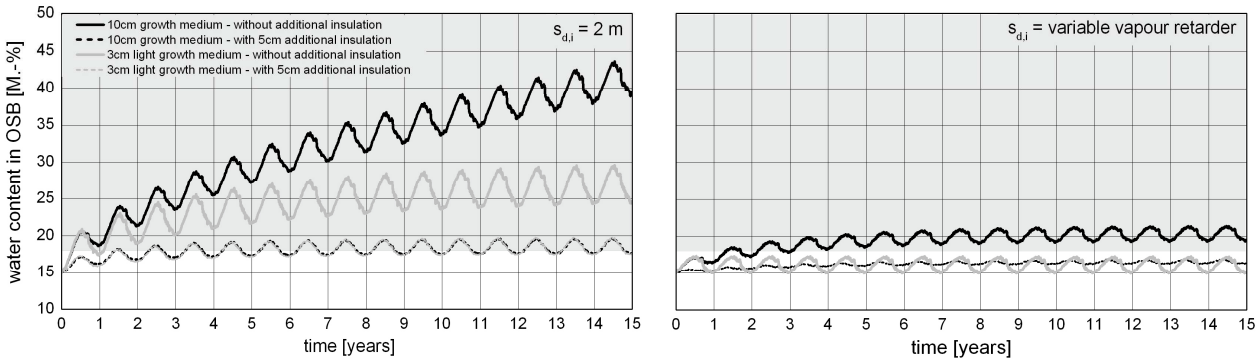

FIG 6. Calculated water content in the OSB-sheathing of a light-weight roof with 20 cm insulation depending on the thickness of the growth medium and the presence of an additional insulation layer. Vapour retarder with constant s_d-value of 2 m (left) and variable vapour retarder (right)

Due to the fact that the temperature on the roofing membrane rarely exceeds the outdoor air temperature and if so, only for a few degrees, drying towards the interior is only possible during a few weeks in summer time. A variable vapour retarder significantly improves the moisture balance and reduces the water content in the sheathing compared to a retarder with a constant s_d-value. Furthermore in almost all constructions an additional insulation of the exterior sheathing is necessary to keep the limit value. However, in practice wood decay can only occur if fibre saturation is reached at water contents above approximately 27 - 30 % by mass. Without the additional insulation the moisture level exceeds the safety limits within a couple of years in most cases, but usually remains within the range between 18 % and the beginning of fibre saturation.

As a result of all evaluated variations, the following practice recommendations can be given:

- variable vapour retarders provide a more favourable performance than retarders with constant sd-values
- for insulation layers thicker than 20 cm an additional insulation of the exterior sheathing is necessary to keep the limit values (for Central European climate conditions)
- the roofing membrane should be rather vapour tight, because drying to the outside doesn’t occur
- additional shading should be avoided
- high air-tightness level of the roof assemblies is recommended

4. Summary

The new green roof simulation models allow for a reliable calculation and design of green roofs by the help of hygrothermal simulations. This is of special importance for moisture sensitive wooden flat roofs.

The generic green roof model considers the effect of the atmospheric counter radiation in a simplified way by reduced short wave absorptivity and is suitable for locations in Central Europe or locations

with similar climate conditions, especially concerning the radiation loads. It can be used if no measured data for the atmospheric counter radiation or no detailed information about the applied growth medium are available. The specific green roof models include the atmospheric counter radiation and thus all relevant climate elements in detail and should be also suitable for other climate regions. Prerequisite is the availability of data for the atmospheric counter radiation. The validations showed good results for green roofs in Holzkirchen and Milan.

Based on the evaluation results general practice recommendations for unventilated light-weight green roofs were worked out. Especially two points are of importance: 1.Variable vapours retarder should be preferred to a retarder with a constant s_d-value to improve moisture balance and drying to the interior. 2. Thicker insulations layers in-between the rafters require an additional insulation on the top of the wooden sheathing to limit the moisture increase during winter. Rather uncritical remain structures with whole insulation on top of the load bearing wooden structure as well as ventilated roofs as far as a sufficient ventilation rate can be ensured (Zirkelbach, D., Künzel, H.M. & Bludau, Ch. 2008).

For further information please refer to the detailed research report (Zirkelbach & Schafaczek, 2013) or the IBP homepage.

5. Acknowledgements

The research project was funded by the “Forschungsinitiative Zukunft Bau” of the Federal Institute for Research on Building, Urban Affairs and Spatial Development (BBSR). Responsibility for the content of this publication remains with the author's.

References

Zirkelbach D. & Schafaczek B. 2013. Ermittlung von Materialeigenschaften und effektiven Übergangsparametern von Dachbegrünungen zur zuverlässigen Simulation der hygrothermischen Verhältnisse in und unter Gründächern bei beliebigen Nutzungen und unterschiedlichen Standorten. IBP-Bericht HTB-13/2013 (www.ibp.fraunhofer.de).

Winter S., Fülle, C. & Werther, N. 2007-2010. Forschungsprojekt MFPA Leipzig und TU München (Z 6 – 10.08.18.7-07.18). “Flachdächer in Holzbauweise”.

Teibinger M. & Nusser B. 2010. Ergebnisse experimenteller Untersuchungen an flach geneigten hölzernen Dachkonsturktionen. Holzforschung Austria, Wien (Forschungsbericht, HFA-Nr.: P412).

Minke G., Otto F. & Gross R. 2009. Ermittlung des Wärmedämmverhaltens von Gründächern. Abschlussbericht, AZ 24242-25. ZUB Kassel.

Künzel H.M. 1994. Simultaneous Heat and Moisture Transport in Building Components – One- and two-dimensional calculation using simple parameters. Dissertation Universität Stuttgart.

EN 15026. 2007. Hygrothermal performance of building components and building elements – Assessment of moisture transfer by numerical simulation.

ASHRAE Standard 160. 2009. Criteria for Moisture-Control Design Analysis in Buildings.

Fiori M. & Paolini R. 2013. Personal communication of project results. “Smart Building Envelope for Sustainable Urban Environment”. Politecnico de Milano, Dipartimento di Architettura, Ingegneria delle costruzioni e Ambiente costruito.

DIN 68800. 2012. Wood preservation. Beuth Verlag. Berlin.

Zirkelbach, D., Künzel, H.M. & Bludau, Ch. 2008: Begrünte Holzdächer ohne Dampfbremse. Festschrift „Umweltbewusstes Bauen“ zum 60. Geburtstag von G. Hauser, Fraunhofer IRB Verlag, Stuttgart 2008, S. 611-620

Moisture conditions in a cold attic – Case study of design

Kimmo Kurkinen, M. Sc. [1]

[1] University of Borås, Sweden & Chalmers University of Technology, Sweden

KEYWORDS: *cold attic, moisture, risk, performance*

SUMMARY:
To be able to design and construct robust, sustainable and well-functioning cold attics it is important to take into account the moisture loads involved. In this paper results from an ongoing field test on an innovative attic space of a building completed in 2009 are presented. The attic is constructed with light building technique. The floor area of the attic space is 370 m^2 and it is insulated with 400 mm loose wool insulation. The studied attic is divided into two parts, an eastern and a western part. The attic was designed with respect to moisture safety regulations according to the Swedish building code.

1. Introduction

In 2006 the National Board of Housing, Building and Planning in Sweden (Boverket) revised the Swedish building regulations for the building envelope suggesting a moisture level criteria of 75 % relative humidity (RH) for a material that is not well-researched and documented. A maximum permitted moisture level was introduced as well as recommendations for moisture safety design. This was done to ensure that the moisture level in any given material would not exceed critical moisture levels in an unpredictable way. In the regulations it is stated that these circumstances should be applied both on a finished building as well as during the execution phase. Due to this, the building industry in Sweden is concerned about whether existing technical solutions used for cold attics meet the new moisture demands and criteria set by Boverket.

In this paper, field measurements of the long time performance of a cold attic with an innovative design is presented. In Sweden there is a warranty period of 5 years on building constructions, therefore it is of interest for the contractor to analyse the performance of the attic. Measurements are also used to quantify the potential of mould growth in the wooden parts of the attic.

2. The object

The measurements presented in this paper come from an apartment building built in Borås, Sweden some 60 km east of Gothenburg. The building was finished in 2009, and contains 26 condominium apartments ranging in size from two to four-room apartments, in six floors. The frame construction of the building is made of concrete except for the top floor which partly consists of a wooden frame construction. Basically the building is made of concrete with a wood framed building on top as presented in Figure 1.

FIG 1. The considered apartment buildings in Borås. (Photo Wäst-Bygg)

In the spring of 2009 the structural engineer, who was in charge of the construction design of the building, was concerned about how to manage fire safety and moisture related design issues regarding the wooden construction parts on the top of the building, in other words the attic. He suggested a bachelor thesis work that would look into the fire safety and moisture aspects of the cold attic design. Cold attics are very common in Sweden, mainly among small houses. The cold attic design has gained more focus in Sweden since the new moisture criteria were implemented in the building regulations. This due to the fact that cold attics can induce high moisture levels which can lead to mould growth and other moisture related problems, which several studies have shown (Samuelson, 1995; Ahrnens & Borglund, 200); Arfvidsson & Harderup, 2008; Persson Lidgren, 2010).

To ascertain the best methods for reducing moisture/humidity levels in cold spaces/attics a bachelor thesis work was carried out in the spring of 2009. The results from the thesis work suggested that the top of the roofing should be insulted with a board and that the ventilation of the attic space should be as low as possible (Strand & Hansén, 2009). This would give the attic space the most favourable conditions with the lowest effort concerning material and installations.

The findings from this work was also presented at the last Nordic Symposium on Building Physics that was held in Tampere, Finland in 2011 (Kurkinen & Hagentoft, 2011).

2.1 The attic

The roof is built with what we in Sweden call “light construction technique”. This is often the case when wooden constructions are used in the building. Both of the attics are designed with wood trusses. The design of the roof structure from outside to the inside is as follows: waterproofing (class T), 20 mm insulation board (stone wool), roofing board, 22 mm tongue-in-groove board, trusses, 400 mm loose wool, vapour barrier, ceiling furring and gypsum board, Figure 2. The roof has a slope between 5.7 and 6.8 degrees.

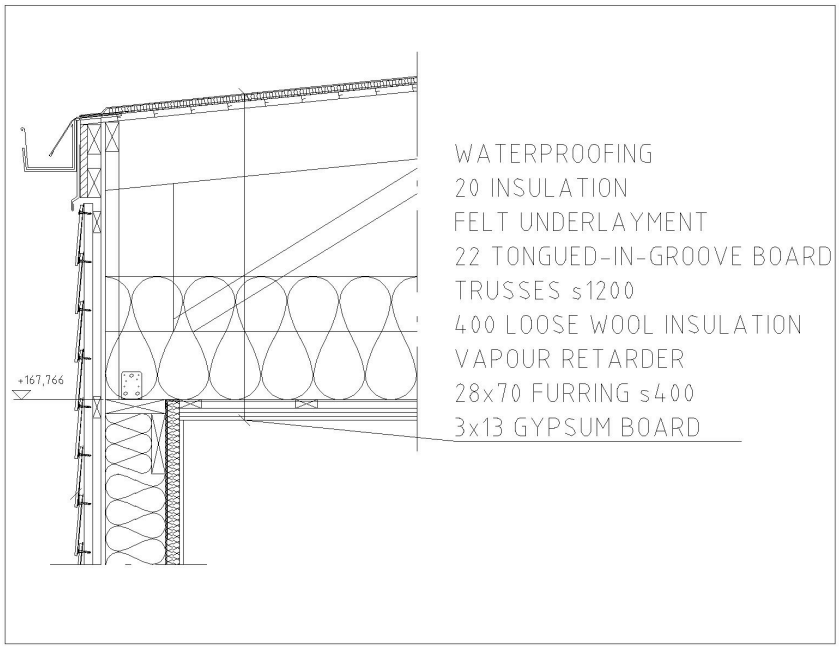

FIG 2. Detail of the considered attic. (Blueprint STIBA)

The attic space was designed to function without ventilation. Ventilation in spaces like these usually is constructed with vents in the gable of the building or through gaps in the soffit. The purpose of the

ventilation is to certify that the moist indoor air do not give moisture damages to the wooden parts of the cold attic. This happens when warm air condensates when the air hits cold surfaces in the attic.

The innovative with this solution of design is to minimize ventilation to prevent moist air to enter the attic space and condensate on cold surfaces such as the tongue-in-grooved board. Climate changes will lead to more moist weather in Scandinavia, which has implications for the design of ventilated constructions. For this building it was suggested that the ventilation of the attic space should be minimal to ensure that moist air would not enter the attic space. In this project it was stated that the moist air from the inside can be neglected or at least reduced due to the vapour barrier placed under the trusses. Therefore there is no need of ventilation to carry out warm moist indoor air. The ventilation of the attic space should be made minimal and only function as a pressure equalizer. Therefore it was decided that the ventilation system for the whole attic would be ventilation pipes, so-called “Kinahattar” Chinese hats), Figure 3. The building has three of these ventilation pipes.

FIG 3. Ventilation of the attic spaces.

3. Field measurements

After the building was completed and occupied, loggers were placed in the attic spaces to monitor the climate of the attic. Every 60 minutes the temperature and relative humidity is logged. In this paper measurements made from the 6th of May 2011 till the 22nd of February 2013, are presented. The data loggers that were used are called Tinytag Plus. The accuracy of these loggers is for the temperature ± 0,7 at 0 °C and for the humidity ± 3 % at 25 °C. The placement of the loggers was under the tongue-in-grooved board, Figure 4.

The attic space is divided into two parts, an eastern part and a western part. The measurements will be presented separately for these parts.

At the start of the summer in 2013 and at the very beginning of the autumn the same year, a visual inspection along with moisture content measurements on the wooden parts of the attic space was carried out. The visual investigation can tell us if mould growth can be spotted on the wooden parts of the attic like on the tongue-in-grooved board or on the trusses. During the inspections no visual mould growth could be observed. The moisture content in the wooden parts were analysed with a moisture content measuring instrument with a measuring range from 8.8 – 54.8 % by weight material moisture. The highest moisture content measured in the tongue-in-grooved board was 13.1 % in the beginning of autumn 2013. Before the summer the moisture content in to tongue-in-grooved board was 9.3 %.

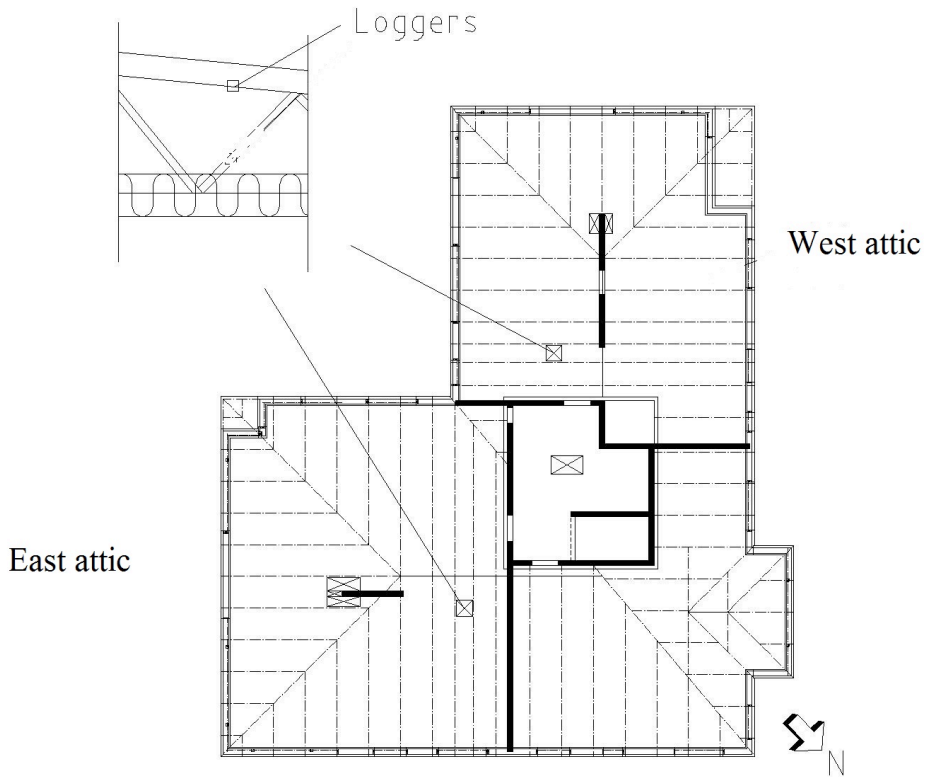

FIG 4. Floor plan of the attic space and the positions of the data loggers.

3.1 Results from field measurements

Figure 6 and Figure 7 shows the results from the field measurements. The average attic space temperature for the considered time period from the 6th of May 2011 till the 22nd of February 2013 was 12.5 °C for the attic part leaning west, and 13.3 °C for the attic part that is leaning to the east. At the same time the mean outdoor temperature was 8.1 °C. The corresponding values for the relative humidity in the attic spaces were as follows; 66.9 % for the western part, 63.2 for the eastern part and 86.7 % in the outdoor air. Figure 5 shows the corresponding values for the attics relative humidity. The main difference is that the western attic space differs from the east one with a higher percent of occurrences with a relative humidity between 70-80 %.

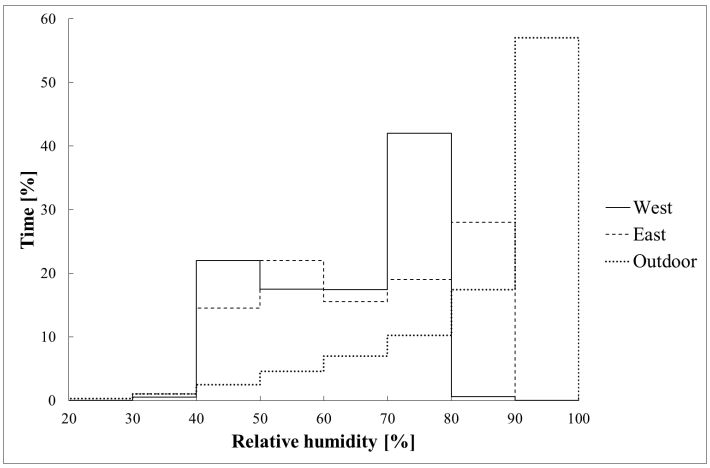

FIG 5. Results from the measurements in the attic presented as histograms.

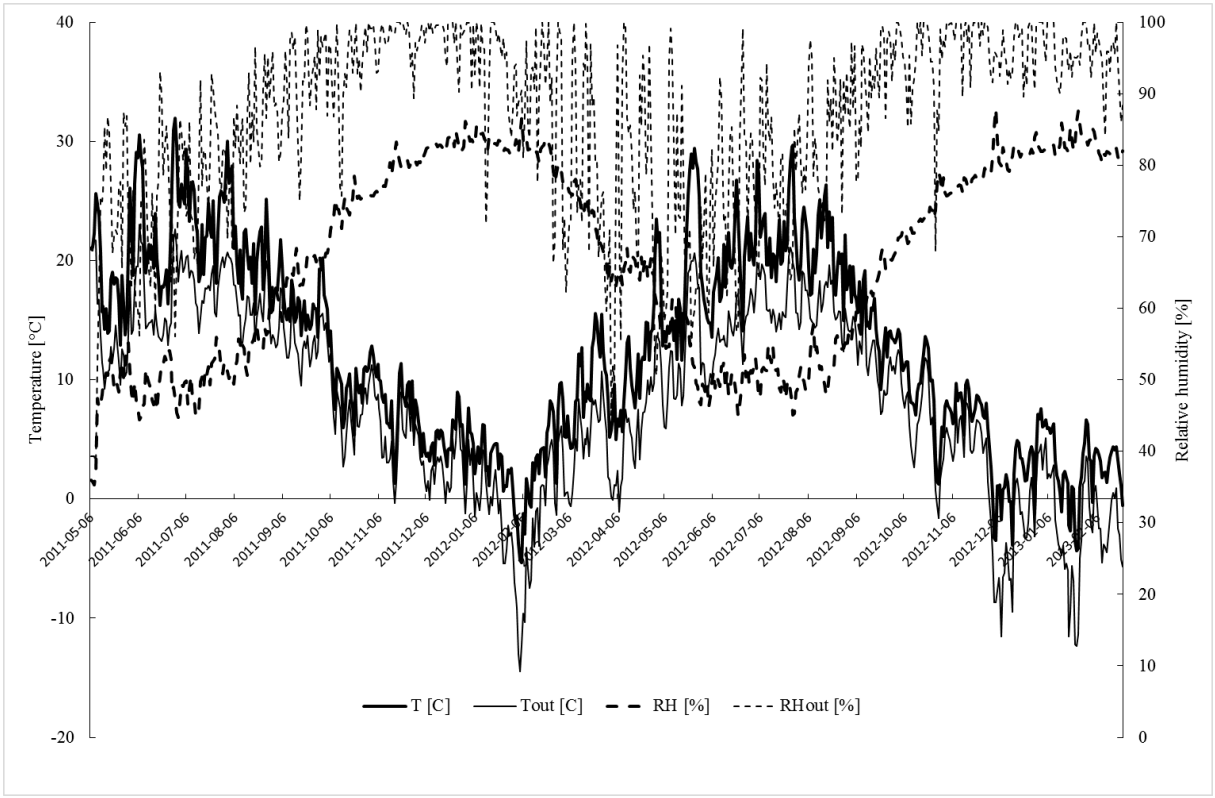

FIG 6. Results from the measurements in the western part of the attic

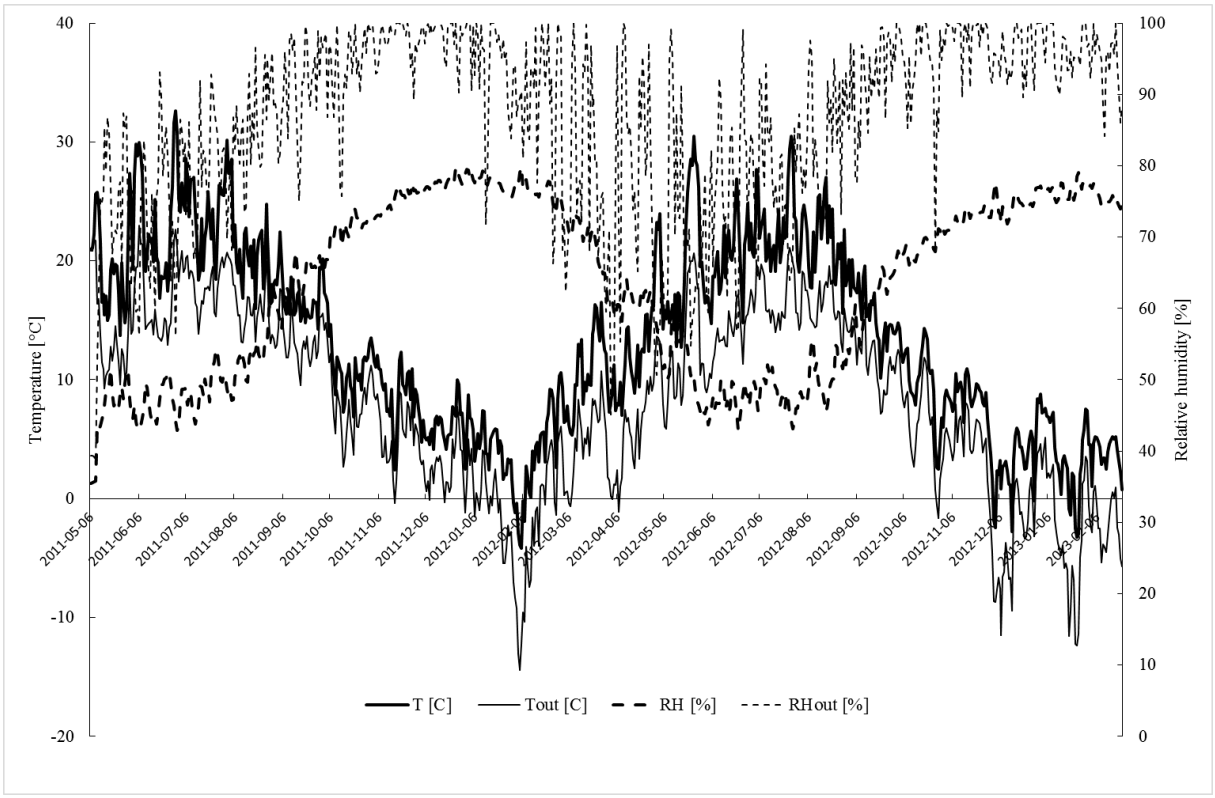

FIG 7. Results from the measurements in the eastern part of the attic.

4. Mould growth potential

As a method to assess the risk of mould growth in the attic space of the building, the mould growth potential *m* is used, (Hagentoft et al. 2008). The mould growth potential is the daily relative humidity divided by the critical relative humidity for mould growth to start, according to Hukka and Viitanen (1999). This potential is given by equation 1 and 2.

$$m = \frac{RH}{RH_{crit}} \qquad (1)$$

$$RH_{crit} = \begin{cases} -0.00267T^3 + 0.160T^2 - 3.13T + 100, T \le 20^{\circ}C \\ 80\%, T > 20^{\circ}C \end{cases} \qquad (2)$$

Using the mould growth potential a number exceeding 1 ($m > 1$) suggests a start of mould growth, i.e. an indicator of risk.

Figure 8 shows the results for the calculated mould growth potential of the attic spaces, according to equations 1 and 2 based on measured values of temperature T (°C) and relative humidity RH (%). The dotted line symbolizes conditions for a wood sample in corresponding outdoor air. For the considered time period from 2011-05-06 till 2013-02-22, the number of times when *m* exceeds one (m > 1) is as follows; western attic space 1 time, eastern attic space 0 time and for the outside 358 times.

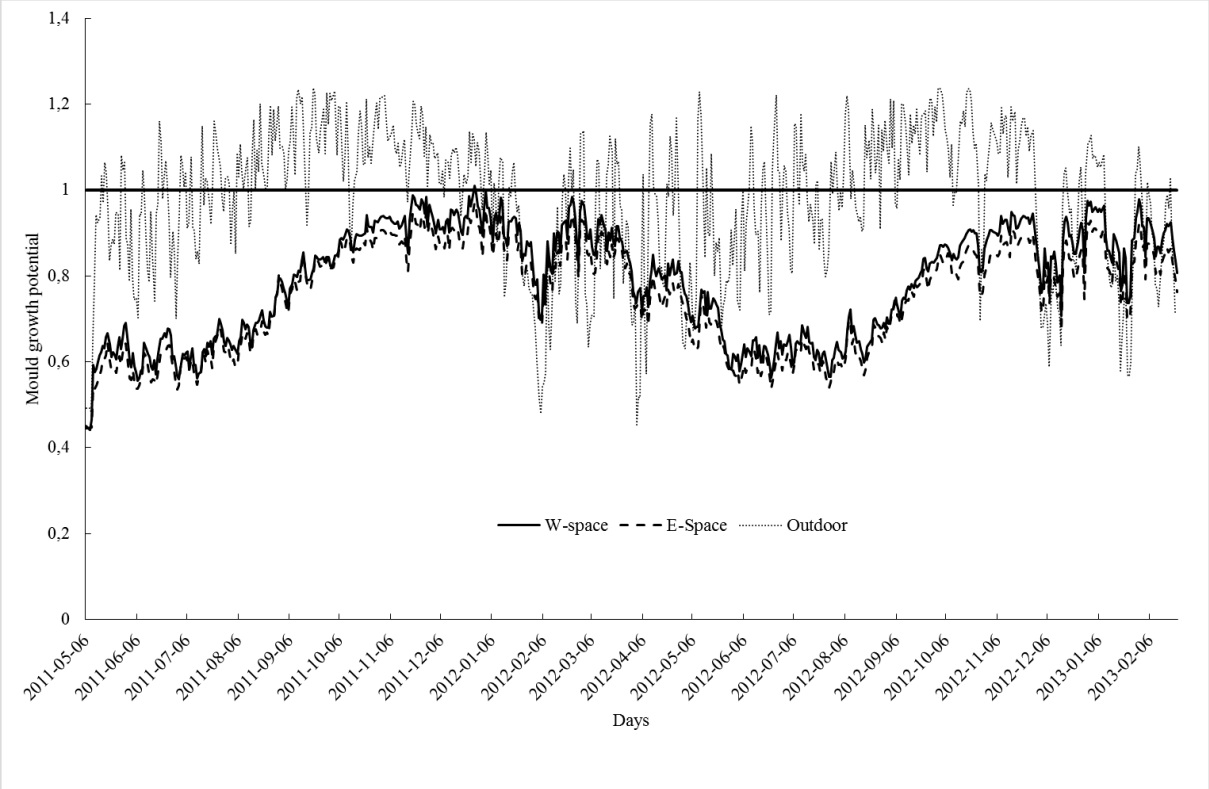

FIG 8. Mould growth potential plotted for the studied time period. Potential on Y-axis and time in days on the X-axis.

5. Conclusions

As the field measurements show an attic space constructed with an insulation board right beneath the waterproofing but over the tongue-in-grooved board and with minimal ventilation of the attic space, a mould growth potential under 1 can be obtained during the measured time period. This is good news for the construction companies using this method. During the visual observations of the attic space no mould growth can be noticed on the wooden parts.

From the earlier measurements presented in 2011, the attic of the building is now performing even better. Counting the times how often the mould growth potential was equal to or exceeded the value of one, $m =< 1$, we can conclude that for the earlier studies, the western attic space had a number of 75 times and the eastern attic space had a value of 45 times. The outside air had a potential of 95 times. The earlier study had a time frame of 234 days.

The new values show that during the measured time frame from the 6th of May 2011 till the 22nd of February 201, a time frame of 659 days, the circumstance in were a mould growth potential was reached happened once. Whereas for the outdoor climate the potential for growth happened 358 times.

The higher numbers from the earlier measurements can be derived to the dehydration of the building materials involved in the process of building the house.

The higher values of the relative humidity discovered in the attic space leaning to the west have to be studied more closely. This may be explained by the location of the building and/or shadowing from neighbouring buildings and trees etc.

Further research will be carried out on the importance of the ventilation openings, the so-called "Chinese hats". Their influence on the attic's climate needs to be investigated further.

6. Acknowledgements

The author of this study would like to thank Mr Joakim Österlund, structural engineer at Stiba AB and Jan Isberg lecturer at the University of Borås for their valuable contributions for this ongoing study.

References

Ahrnens C. & Borglund E. 2007. Fukt på kallvindar – En kartläggning av småhus i Västra Götalands län, Examensarbete 2007:11. Institutionen för bygg- och miljöteknik, Chalmers tekniska högskola.

Arfvidsson J. & Harderup L-E. 2008. Fuktsäkerhet i kalla vindsutrymmen – slutrapport. Avdelningen för Byggfyssik, LTH, Lund. Rapport TVBH-3050. ISBN 978-91-88722-38-6.

Hukka A. & Viitanen H. A. 1999. A mathematical model of mould growth on wooden material. Wood Science and Technology 33.

Hagentoft C-E., Sasic Kalagasidis A., Nilsson S. F. & Thorin M. 2008. Mould growth control in cold attics through adaptive ventilation. Nordic Symposium on Building Physics 2008, Copenhagen, Denmark.

Hägerhed Engman L. & Samuelson I. 2006. Redovisning av fältundersökning och forskningsprojekt: Kalla Vindar – problem och förbättringar. Bygg & Teknik 4/2006.

Kurkinen K. & Hagentoft C-E. 2011. Application of risk assessment technique to attics. 9th Nordic Symposium on Building Physics - NSB 2011, Tampere Finland

Nevander L.E. & Elmarsson B. 1994. Fukthandbok, Praktik och teori. 2nd ed. Stockholm, AB Svensk Byggtjänst och författarna. 538 p. (Times new Roman 11 pt, Style: Reference List)

Samuelson I. 1995. Fuktbalans I kalla vindsutrymmen. SP Sveriges Tekniska Forskningsinstitut, Borås. SP Rapport 1995:68. ISBN 91-7848-596-7.

Strand P. & Hansén M. 2009. Kallvindskonstruktioner – Hänsyn tagen till fukt- och brandkrav för kvarteret Tuppen i Brorås. Examensarbete. Institutionen Ingenjörshögskolan, Högskolan i Borås.

SFS-EN 13829. 2000. Thermal performance of buildings. Determination of air permeability of buildings. Fan pressurization method (ISO 9972:1996, modified). Finnish Standards Association SFS.

Data loggers used:

Tiny Tag Plus2, http://www.intab.se/System/FileArchive/295/File_32392.pdf [2013-11-27]

Moisture content measuring instrument:

Testo 606-2, http://www.testolimited.com/Content/downloads/testo606-2-manual-0560_6062.pdf [2013-11-28]

IAQ simulator for evaluating the effects of moisture and microbial problems on indoor air quality

Vuokko Lappalainen, M.Sc. [1,2]
Elina Sohlberg, M.Sc. [1]
Helena Järnström, Ph.D. [3]
Jarmo Laamanen, Eng. [1]
Hannu Viitanen, Ph.D. [1]
Pertti Pasanen, Professor [2]

[1] VTT Technical Research Centre of Finland, Finland
[2] University of Eastern Finland, Finland
[3] VTT Expert Services Ltd., Finland

KEYWORDS: *Indoor air quality, moisture damage, indoor air simulator, material relative humidity*

SUMMARY:
Clean indoor air is one of the most important factors for welfare of the building occupants. The Indoor Air Quality simulator (IAQ simulator) offers a research tool for building physics and building material research to evaluate the effect of materials in multilayer structures under different ventilation rates, pressure conditions and the air tightness of the structure. To understand and study the complex causality between severe microbial contaminations or moisture damage in building structures and indoor air quality, the IAQ simulator have been used in Microdiverbuild project at VTT and UEF. In this project, the IAQ simulator was used to assess the drift of various indoor air impurities from the moisture damaged wall structure into the indoor environment during changes in the relative humidity of the damaged material. Particle and TVOC concentrations did not show a clear difference between control and damage cases, but the single microbial VOCs indicated microbial growth inside the wall structure.

1. Introduction

Today people spend more and more of their time indoors and at the same time cases of unacceptable indoor air quality (IAQ) are increasing. Poor indoor air quality in schools and offices has been shown cause tiredness, unpleasant odour, discomfort, irritation, respiratory symptoms and other short- and long-term health problems (Smedje et al 1997, Apte et al 2000, Mendell et al 2008). Indoor air quality problems are usually complex and a sum of several factors or failures in the building or structures. The reparation of moisture, mould and decay damages fails often and there is a considerable need to develop further tools for monitoring and assessing the success of the renovation of a mould damaged building (Haverinen-Shaughnessy et al 2008).

The function of building structures and ventilation have an important role on maintaining acceptable indoor air quality. In a case of mechanical exhaust ventilation type, controlled intake air inlets are needed. In reality, when a building is in under-pressure and there is a lack of controlled inlets, intake air flows through window frames and cracks in the structures as a leakage. Especially in cold climates, under-pressure can be very high during winter time when the temperature difference can be more than 40 °C between indoor and outdoor air.

In the previous study (Airaksinen et al. 2004b), particle transport measurements for the wooden floor like structure were made under both high (20 Pa) and low (6 Pa) pressure differences. The penetration of particles in size range of <4 µm were in the same order of magnitude, but > 4 µm particles did not

penetrate through the envelope. However, in the case of the direct flow-path, these larger particles were transported into indoor air. This previous study showed that fungal spore transportation through the building envelope by sealing was difficult, and the only effective way to prevent the transportation of microbial contaminants into indoor environment was pressurising and balancing the building (Airaksinen et al. 2004b). In the other study (Airaksinen et al. 2004a), the fan controlled ventilation affected directly on the pressure difference between indoor air and crawl space but also on the airflow from outdoor into the crawl space. However, almost all of extract air of the crawl space flew into the apartment through the base floor leakages. The pressure difference between the apartment and the crawl space was about 6 Pa (under-pressure in the apartment). Three times a day the exhaust ventilation operated at higher speed and then the pressure difference increased up to 16 Pa (Airaksinen et al. 2004a).

In the Microdiverbuild project, the main aim is to develop a risk assessment model for indoor air failures. One part of the study was Indoor Air Quality simulator test runs. In these tests, the complex relationship between mould growth inside the structure and indoor air quality was simulated and the source strength of a mould growth inside the wall structure was assessed. In this investigation, the impact of relative humidity changes of the material with mould growth on IAQ were evaluated under normal pressure difference.

2. MATERIALS AND METHODS

2.1 The IAQ simulator and the setup of the experiment

The IAQ simulator gives a new point of view for indoor air quality assessment. In the Microdiverbuild project, the simulator was used to assess the drift of impurities from the mould damaged wall structure under various material relative humidity and pressure difference over the structure. The simulator was developed mainly at VTT (Paavilainen 2005), and it is based on the standard ISO 16000-9 (ISO 2006). The simulator consists of a supply air purification unit and a pressurisation unit and two test chambers (volume 0.5 m^3 per chamber). Between the chambers there was a frame where the tested structure was placed (see FIG 1).

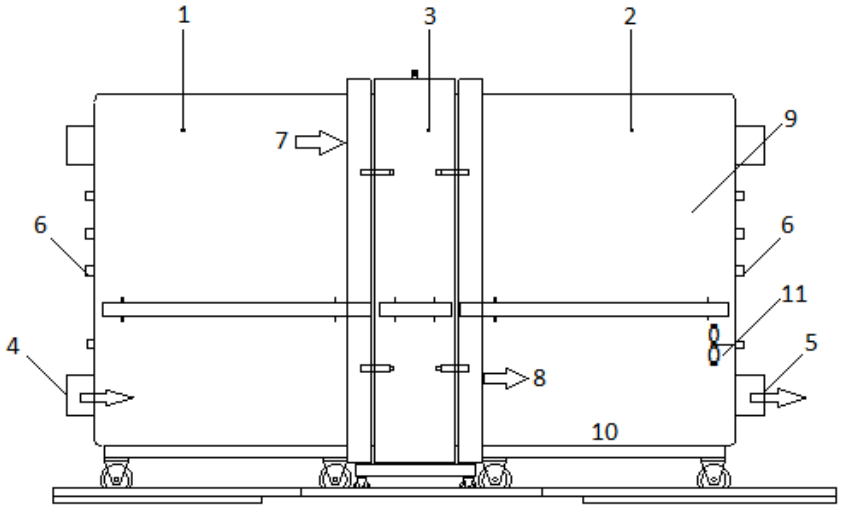

1: chamber 1 (outdoor air)
2: chamber 2 (indoor air)
3: test wall structure
4: incoming air for chamber 1
5: outgoing air from chamber 2
6: tubes for pressure measurements
7: airflow into the wall structure
8: leakage points
9: particle measurements
10: surface samples
11: air mixer fan

FIG 1. Principle of the IAQ simulator

The case presented in this paper, consists of a wall structure of two gypsum boards and five upstanding pine sapwood laths There were seven 6 mm in diameter drilled holes as leakage routes on

both of the gypsum boards. Other possible leakage routes from the borders of gypsum boards were sealed carefully with the aluminium tape. The computational leakage rate at 50 Pa pressure difference (n_{50}) of this wall structure was 2.87 h^{-1} what is a typical compactness for this kind of structure. The air change rate in the IAQ simulator was 1.0 1 h^{-1}, and incoming air flow was 8 l/min. The incoming air was purified from particles and VOCs, and humidified for clean and constant air quality. Also, all surfaces of the chamber and structures inside the simulator was cleaned with steam and 70 % ethanol dilution before and after every test runs.

In this test, the pressure difference was at normal, low under pressure level (-2…-5 Pa). Even low under-pressure has been found to cause infiltration of impurities in the indoor environment. Infiltration of microbial and gaseous contaminants from mould growth inside the structure decreases indoor air quality. In this case, infiltration or air leakage refers to the uncontrolled air flow through the wall structure.

The effects of moisture stress in the bottom of the wall were tested both with a mould damaged and an undamaged wall structure. In the moisture damaged wall, a mould suspension was inoculated on two sides of the wood laths and incubated for 4-6 weeks in high relative humidity. Inoculated species were *Aspergillus versicolor*, *Penicillium brevicompactum* (ATCC 58606), *Chaetomium globosum* (D-81079), *Cladosporium sphaerospermum*, *Paecilomyces variotii* (D-83214) and *Trichoderma viride.* An undamaged wall structure was used as a control case (no mould inoculated).

2.2 Measurements and analyses

The particle (0.5-5 µm) concentrations in the indoor air chamber were measured continuously with a BioVigilant® IMD-A™ (Azbil BioVigilant, Inc., Tucson, AZ, US) particle counter what fractionates biological particles (i.e. microorganisms) from non-biological particles by fluorescence detection. In the previous study, the most of the indoor air fungal spores from air leakages were in size range of 0.5-4 µm (Airaksinen et al 2004a). The relative humidity of the material was measured with a surface sensor (Tinytag TV-4506, Gemini Data Loggers Ltd., Chichester, UK) format a height of 10 cm from the bottom of the wood lath. The pressure difference between indoor and outdoor chambers was measured continuously (SwemaFlow 300, SWA10, Swema AB, Farsta, Sweden). VOC samples were taken on Tenax TA adsorbent tubes. The size of VOC samples varied between 2 and 6 litres. Tubes were analysed with ATD-GC/MSD (Agilent Technologies, Santa Clara, CA, US) SCAN technique, and calculated as toluene equivalents (ISO 2004).

Two parallel material samples (A and B) were taken from the surface (5.3 cm^2) of pine sapwood laths in both control and damage case with a sterile knife, and weighed. One part of the sample was used for cultivation and another part for DNA extraction and qPCR. The material samples for cultivation were extracted, diluted, and cultivated on two cultivation plates: tryptone yeast extract agar (THG) for bacteria and 2 % malt extract agar (M2) for fungi. Mould species were identified from cultivation plates after one week for fungi and two weeks for bacteria. DNA was extracted from the samples with PowerSoil DNA extraction kit (Mobio Laboratories, Inc., CA, US).

The quantitative PCR (qPCR) method was used to estimate the number of fungi and bacteria by quantifying the number of bacterial 16S rDNA or fungal ITS gene copies in pine sapwood lath samples. For the qPCR analyses the KAPA SYBR FAST Roche LightCycler 480 2x qPCR Master Mix (Kapa Biosystems, Woburn, MA, USA) and LightCycler 480 (Roche, Basel, Switzerland) was used using manufacturers protocol. 16S rDNA gene was amplified with the primer pair P1 and P2 (Muyzer et al, 1993) and ITS region with primer pair ITS1F (Gardes and Bruns, 1993) and ITS4 (White et al., 1990). The qPCR reactions were conducted in triplicate. No-template controls were included in every run. A standard curve for each run was included in each run reaching from $1.5x10^6$ to $1.5x10^0$ copies of 16S rDNA gene from *Escherichia coli* and $6.3x10^7$ to $6.3x10^1$ spores/ ng from *Aspergillus versicolor*.

3. Results

3.1 Pressure difference and material humidity

The average pressure difference over the wall structure was -2.2 Pa (range +0.4… -3.5 Pa) in the control case and -3.5 Pa (range -2.4… -4.6 Pa) in the damage case (FIG 2). The little distinction in pressure differences between control and damage cases probably came from a minor failure in the sealing of wall borders. The relative humidity (RH) of the material changed during the test because of drying. At the beginning of the test, water was added in a tub of the bottom of laths. The humidity changed during dehydration of water first from the tube and the slowly from wood material. The RH was 100% during first 6 days and dried slowly during next few days. The variation of the material relative humidity is presented in FIG 3. At the beginning, the relative humidity in the damage case was little higher than in control case. Also, the drying period of the material was started later in the damage case. This was probably caused by the heavy growth of mould on wood laths.

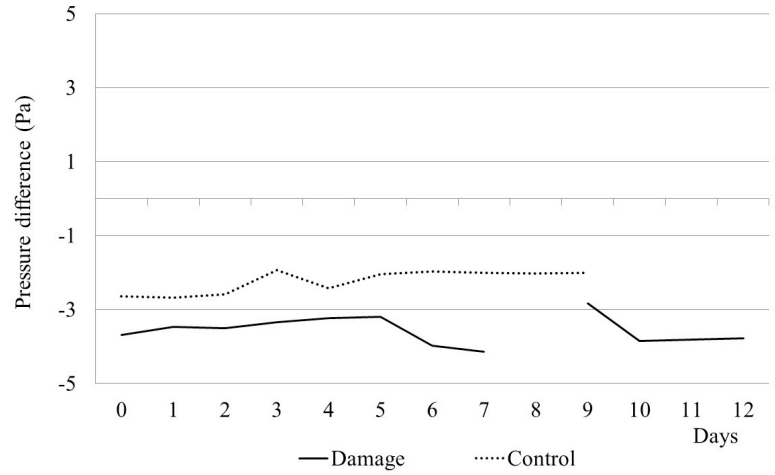

FIG 2. The pressure difference over the wall structure

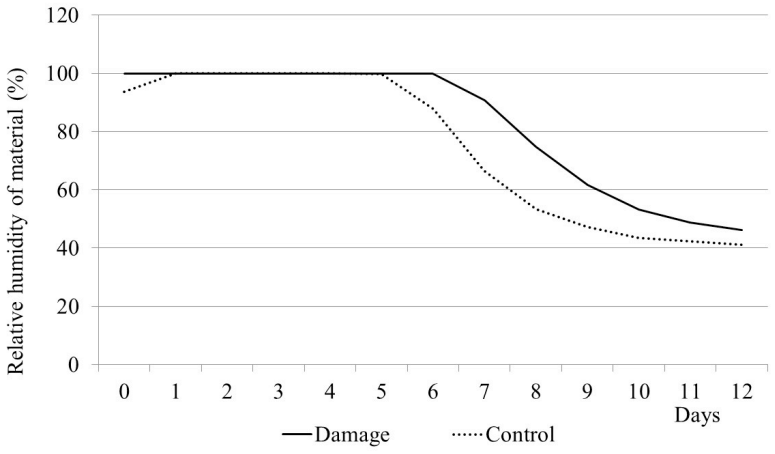

FIG 3. Relative humidity of the material

3.2 Microbial growth on the material

Material samples were taken from two (A and B) of five wood laths before and after the tests. In the control case, mould was not inoculated on the material. However, a little fungal growth was observed in samples after simulation test (FIG 4). This was probably caused by the moisture load during the test. Visible mould growth was not detected in the control case. Bacterial concentrations were in the same order of magnitude before and after the test.

In the damage case, the microbial concentrations in the material samples were high before and after the simulation test and mould growth was detected also visually (mould index 4 – 5 on the scale of 0-5; Viitanen et al, 2010). The short drying period after the high moisture load did not reduce the viability of microbes on the wood material. In cultivated samples, fungal growth was strong also in bacterial plates (THG agar). In the damage case, only three of six inoculated species were observed after the simulator test: *Aspergillus, Penicillium* and *Paecilomyces.* Also in the control case, *Penicillium* and *Paecilomyces* fungal genera were observed after the test.

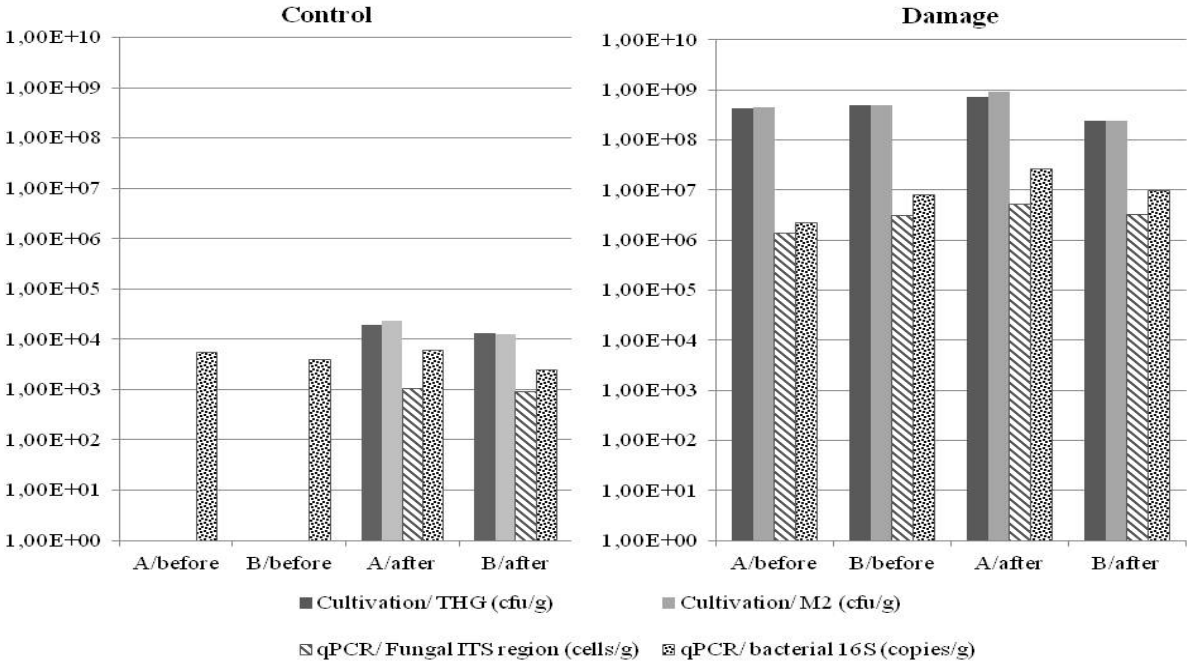

FIG 4. Microbial growth in two parallel wood laths (A and B) before and after the test

3.3 Particle concentrations in indoor air chamber

The particle concentrations were measured continuously in three size fractions: 0.5-1 µm, 1-3 µm and 3-5 µm. The particle concentrations did not vary much during high moisture load (days 1-6), drying (days 7-9) or dry period (days 10-12) in this test (FIG 5). On day 1, both biological and non-biological particle concentrations in two of the size fractions were significantly higher in the damage case. On day 6, non-biological particle concentrations were high in both control and damage cases. In the latter case, concentrations were significantly higher in all three size fractions. However, on days 9 and 10 non-biological particle concentrations were higher in the control case.

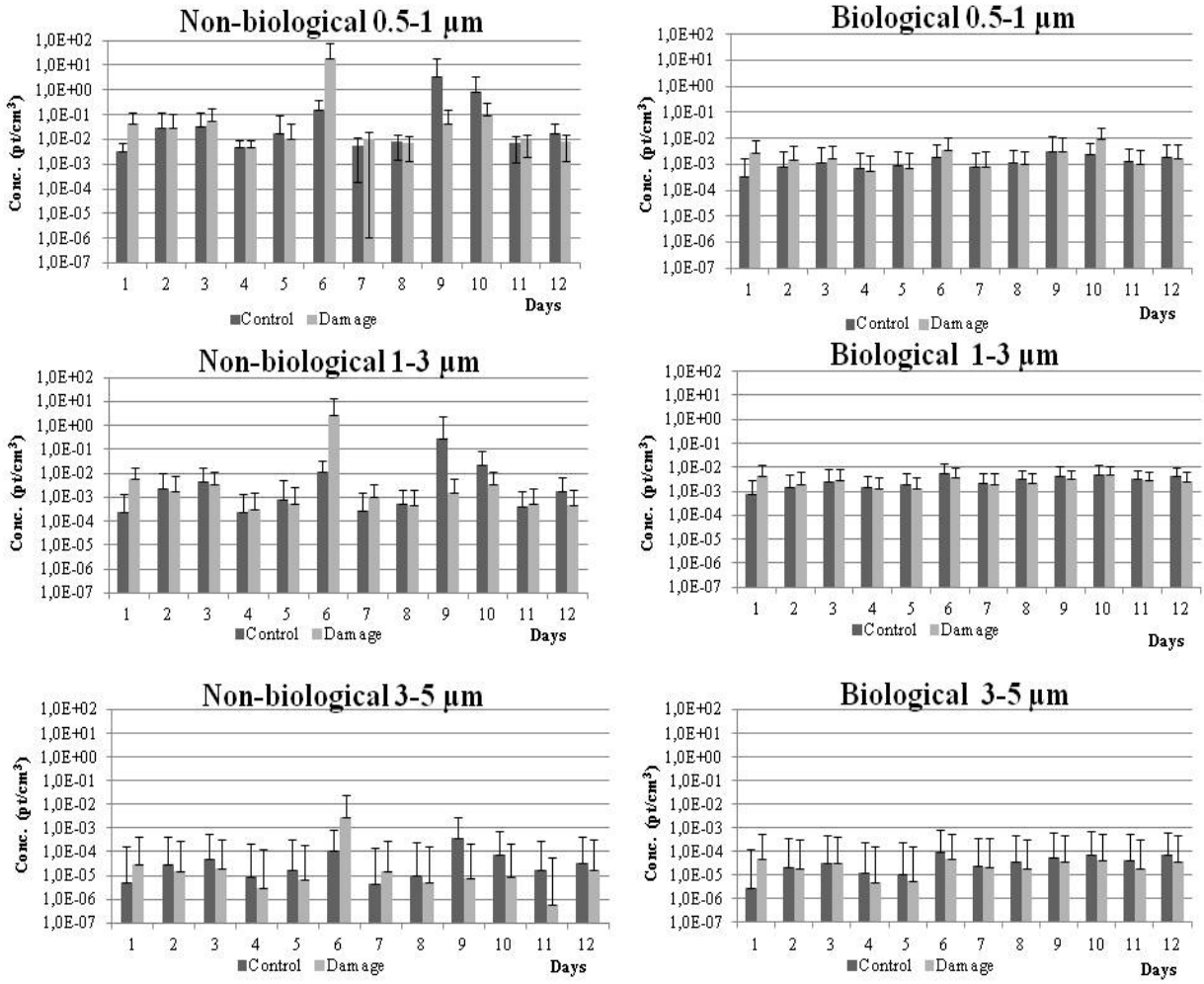

FIG 5. Biological and non-biological particles in three size fractions

3.4 Volatile organic compound concentrations in indoor air chamber

TVOC concentrations were clearly higher during the high moisture load period (days 0 to 6) than during the dry period (days 10 and 13) in both control and damage cases (table 1). However, the concentrations during the first six days were even higher in the control case but during the dry period, concentrations were higher in the damage cases.

Three VOCs were found as clear microbial metabolites (MVOCs). 2-pentanone, 2-heptanone and 2-hexanone were detected in damage case in high concentrations but were not found in control cases. These three compounds have been found as metabolites of *Paecilomyces, Penicillium* and *Thrichoderma* previously (Sunesson 1995).

TABLE 1. VOC concentrations in damaged and control case

Compound	Case	DAY 0	DAY 1	DAY 3	DAY 6	DAY 10	DAY 13
TVOC	Control (µg/m^3)	524	NA	702	942	140	159
	Damage (µg/m^3)	NA	916	561	744	246	204
2-Pentanone	Control (µg/m^3)	-	NA	-	-	-	-
	Damage (µg/m^3)	NA	197	138	125	11	7
2-Heptanone	Control (µg/m^3)	1	NA	5	3	-	-
	Damage (µg/m^3)	NA	78	53	60	6	3
2-Hexanone	Control (µg/m^3)	-	NA	-	-	-	-
	Damage (µg/m^3)	NA	35	22	24	2	1

(NA=not analysed)

4. Conclusions

The results presented in this paper are from the first stage of Microdiverbuild study. In this project, IAQ simulator tests have been done also in three other setups. The results from other simulator tests will be available soon. However, already this data showed that the emission of microbial VOCs from a mould damaged wall structure can be simulated by using the IAQ simulator. However, the microbial sampling methods still need adjustment to assess microbial growth.

The damaged wood laths were visually mouldy, and represented a severe mould damaged wall structure (mould index 4-5). These laths were inside the wall and the damage was hidden but there were air leakage routes on the envelope. The leakage rate n_{50} of the wall structure was 2.87 h^{-1} and pressure difference was in normal level (-2…-5 Pa). The simulation test showed clearly single MVOCs indicating microbial growth better than airborne particles or TVOC in the chamber test. However, it is known that MVOCs can be released from other sources in real buildings. The impact of relative humidity of the material found remarkable.

The IAQ simulator is a tool to evaluate the impact of mould growth on IAQ in a simulated case of the damaged structure taking into account the pressure difference over the structure. The simulator is designed for VOC measurements and it is optimal for example to investigate emissions from a multilayer structure at various ventilation rates. Particle measurements are available, but the air mixing system may need to rescale for larger particles. Microbial air samples for the cultivation or qPCR analysis were difficult because of the limited air flows in the simulator. Therefore, material samples were taken an analysed.

5. Acknowledgements

This study was funded by Academy of Finland (Microdiverbuild 253259), VTT Technical Research Center of Finland, Tekes (Bitefa project 40371/11) and University of Eastern Finland.

References

Airaksinen, M; Pasanen, P; Kurnitski, J; Seppänen, O. 2004a. Microbial contamination of indoor air due to leakages from crawl space: a field study. Indoor Air, 14, 55-64.

Airaksinen, M; Kurnitski, J; Pasanen, P; Seppänen, O. 2004b. Fungal spore transport through a building structure. Indoor Air, 14, 93-104.

Apte, M G; Fisk, W J; Daisey J M. 2000. Associations between indoor (CO2) concentrations and sick building syndrome symptoms in US Office Buildings: an analysis of the 1994-1996 BASE Study Data, Indoor Air, 10, 246-257.

Gardes, M., Bruns, T.D., 1993. ITS primers with enhanced specificity for basidiomycetes — application to the identification of mycorrhizae and rusts. Mol. Ecol. 2, 113–118.

Haverinen-Shaughnessy, U; Hyvärinen, A; Putus, T; Nevalainen, A. 2008. Monitoring success of remediation: Seven case studies of moisture and mold damaged buildings. Science of the Total Environment, 399, 19-27.

ISO 16000-6. 2004. Indoor Air Part 6: Determination of volatile organic compounds in indoor and chamber air by active sampling on Tenax TA, thermal desorption and gas-chromatography MSD/FID.

ISO 16000-9. 2006. Indoor air Part 9: Determination of the emission of volatile organic compounds from building products and furnishing. Emission test chamber method.

Mendell, M J; Lei-Gomez, Q; Mirer, A G; Seppänen, O; Brunner, G. 2008. Risk factors in heating, ventilating, and air-conditioning systems for occupant symptoms in US office buildings: the US EPA BASE study. Indoor Air, 18, 301-316.

Muyzer, G., De Waal, E. & Uitterlinden A. 1993. Profiling of Complex Microbial Populations by Denaturing Gradient Gel Electrophoresis Analysis of Polymerase Chain Reaction-Amplified Genes Coding for 16S rRNA. Applied and Environmental Microbiology (3) 59, pp. 695-700.

Paavilainen, J. 2005. Sisäilmasimulaattorin kehittäminen haihtuvien orgaanisten yhdisteiden emissioiden määritykseen. Master thesis. Helsinki University of Technology, Department of Chemistry.

Smedje, G; Norback, D; Edling, C. 1997. Subjective indoor air quality in schools in relation to exposure, Indoor Air, 7, 143-150.

Sunesson, A-L. 1995. Volatile Metabolites from Microorganisms in Indoor Environments – Sampling, Analysis and Identification. Department of Analytical Chemistry and National Institute for Working Life Analytical Chemistry Division, Umeå University, Sweden.

Viitanen, H; Vinha, J; Salminen,K; Ojanen, T; Peuhkuri, R; Paajanen, L; Lähdesmäki, K. 2010. Moisture and Biodeterioration Risk of Building Materials and Structures. Journal of Building Physics, 33, 201-224.

White, T.J., Bruns, T.D., Lee, S.B., Taylor, J.W., 1990. Amplification and direct sequencing of fungal ribosomal RNA genes for phylogenetics. In: Innis, M.A., Gelfand, D.H., Sninsky, J.J., White, T.J. (Eds.), PCR Protocols — a Guide to Methods and Applications. Academic Press, San Diego, CA, pp. 315–322.

Moisture status in municipal buildings

Anders Kumlin, M.Sc. [1]
Ingrid Johansson, M.Sc. [1]
Dan Norbäck, Associate professor [2]
Gui-Hong Cai, Ph.D. [2]

[1] AK-Konsult Indoor Air AB, Stockholm, Sweden
[2] Dept. of Medical Science, Occupational and Environmental Medicine, Uppsala University, Uppsala, Sweden

KEYWORDS: *damp buildings, moisture, mould, schools, day care centres, risk construction, fungal DNA*

SUMMARY:
An ocular inventory, e.g. identifying risk constructions and damages, by trained moisture consultants is a good method to get information on dampness status of all municipal buildings within one area. A significant association between levels of total Fungal DNA on indoor surfaces and risk construction grading of the buildings confirms that risk construction may lead to increased indoor mould contamination.

1. Introduction

Moisture in buildings, also called damp buildings or building dampness, is a common problem in many countries (WHO 2009). If the moisture level is increased in buildings, it may lead to growth of mould and bacteria (microbial growth) as well as chemical degradation of certain building materials. One well known problem in Sweden is alkaline degradation of water based adhesive in floor-constructions, or plasticizers in PVC materials, causing emissions of butanols and 2-ethyl-1-hexanol (Wieslander et al., 1999; Norbäck et al., 2000). A number of epidemiological studies have demonstrated that buildings with increased levels of moisture and microbial growth can lead to impaired health, with increased occurrence of asthma, asthma symptoms, respiratory infections and symptoms included in the sick building syndrome (e.g. eye and nose symptoms, headache and tiredness) (WHO, 2009). Some studies from Sweden have indicated that increased levels of moisture in the floor construction, causing degradation of water based adhesive or plasticizers in the floor, is associated with increased nasal inflammation (Wieslander et al., 1999) and asthma (Norbäck et al., 1999; Norbäck et al., 2000).

Moisture in buildings can occur for different reasons. Buildings can have water leakages. Moreover, buildings with high humidity production indoors combined with poor ventilation and temperature differences on indoor surfaces can lead to surface water condensation. This condensation may lead to microbial growth on indoor surfaces that can be observed. Visible mould growth on indoor surfaces is a relatively common problem in a warmer climate zones in Europe (Norbäck et al., 2013). However in a colder climate, such as in Scandinavia, increased moisture levels in buildings can occur inside wall, floor or roof-constructions without any visible signs of dampness or microbial growth (hidden moisture).

The concept of risk construction, e.g. risk construction due to moisture, has been used in Sweden to describe a building where the building construction leads to an increased number of buildings with moisture related problems. In Sweden, the focus has been on risk constructions related to type of floor construction. The home is the indoor environment where we spend most of our time, and most studies on health effects of building dampness and indoor mould growth have been performed in dwellings (WHO, 2009). However, indoor problems are often reported in public buildings such as schools (Simoni et al., 2011) and day care centres (Bröms et al., 2006). In such cases, when indoor problems

occur in a particular building, moisture consultants are often contacted to perform an investigation and suggest measures to solve the moisture related problem. However, there are few surveys investigating the prevalence of risk construction and moisture in all types of public buildings within a defined geographical area (e.g. one municipality).

The aim of this study was to survey municipal buildings in four municipalities in the Stockholm area for moisture status and risk for moisture problems. Moreover, this knowledge informs the property owners about moisture and risk status to be able to plan maintenance, corrective preventive actions and refurbish actions. The report sent to the property owners was kept short and was typically one page. Finally, the aim was to study the association between moisture status and risk for moisture problems and levels of indoor mould, measured as fungal DNA contamination on indoor surfaces.

2. Methods and results

2.1 Methods

Ocular inventory regarding moisture status was performed in municipal buildings in four different municipalities in the Stockholm area, mostly schools and day care centres. The inventory was an ocular inspection. Consultants performing the inventory were trained moisture consultants with long experience in investigating buildings with moisture problems. Total fungal DNA in dust from swab samples was analysed in day care centres in one of the four municipalities. Total fungal DNA is an indicator of mould contamination.

The buildings were graded according to a three level scale; low risk (level 1), risk (level 2) and damage (level 3). The levels were defined as follows: Low risk (1) means that no risk was associated with the building construction (a non-risk construction) and moreover no visible indoor mould, mould odour or visible moisture damage was observed. Risk (leve1 2) means that a risk was associated with the building construction (a risk construction) but no visible indoor mould, mould odour or visible moisture damage was observed. Damage (leve1 3) means that a risk was associated with the building construction (a risk construction) and moreover visible indoor mould, mould odour or visible moisture damage was observed.

A ground-construction that normally works well from a moisture point of view (a non-risk construction) in Swedish climate is described in fig 1. Three ground-constructions associated with a risk for moisture damage (a risk construction) in Swedish climate is described in fig 2-4. Calculations for concrete slabs have been done with assumed temperatures in the ground, annual mean 7°C, and known material moisture and heat resistant's. The crawl-space is simulated with the computer program CrawlRF.

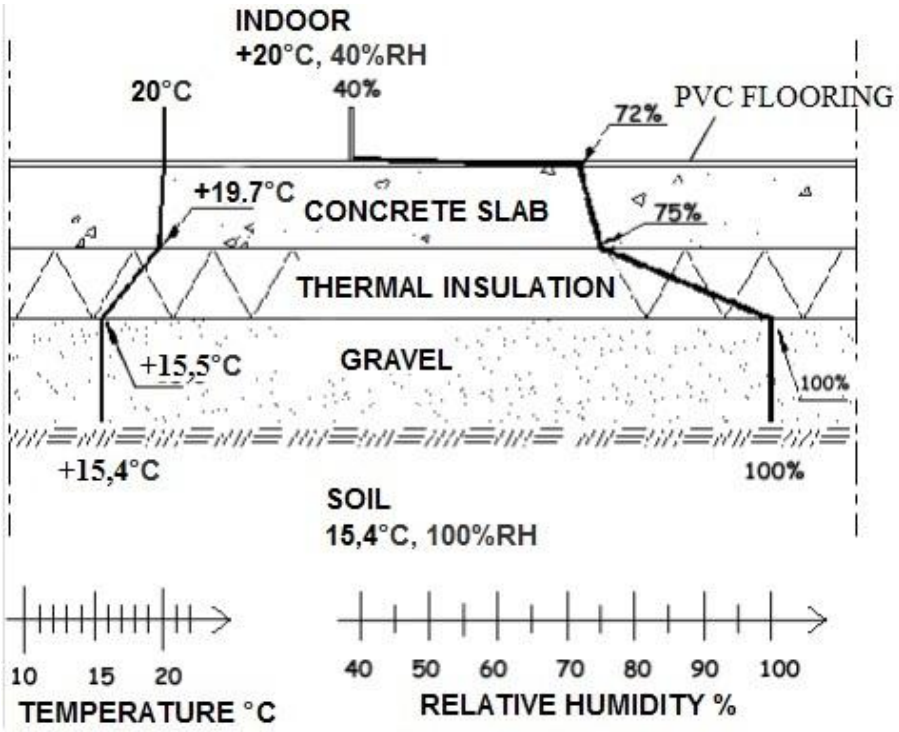

FIG 1. Expected humidity levels in a concrete slab with underlying thermal insulation

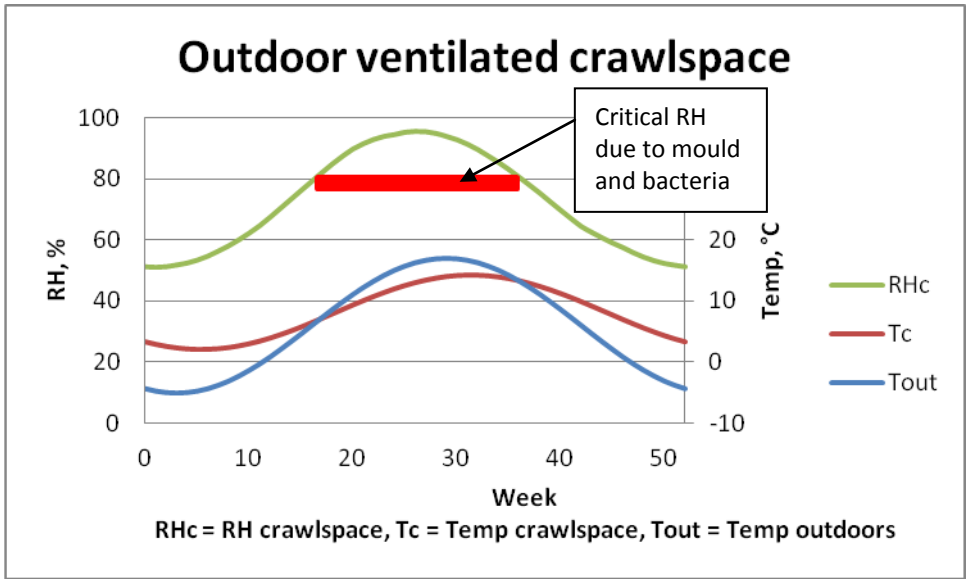

FIG 2. Expected humidity levels in an outdoor ventilated crawl space

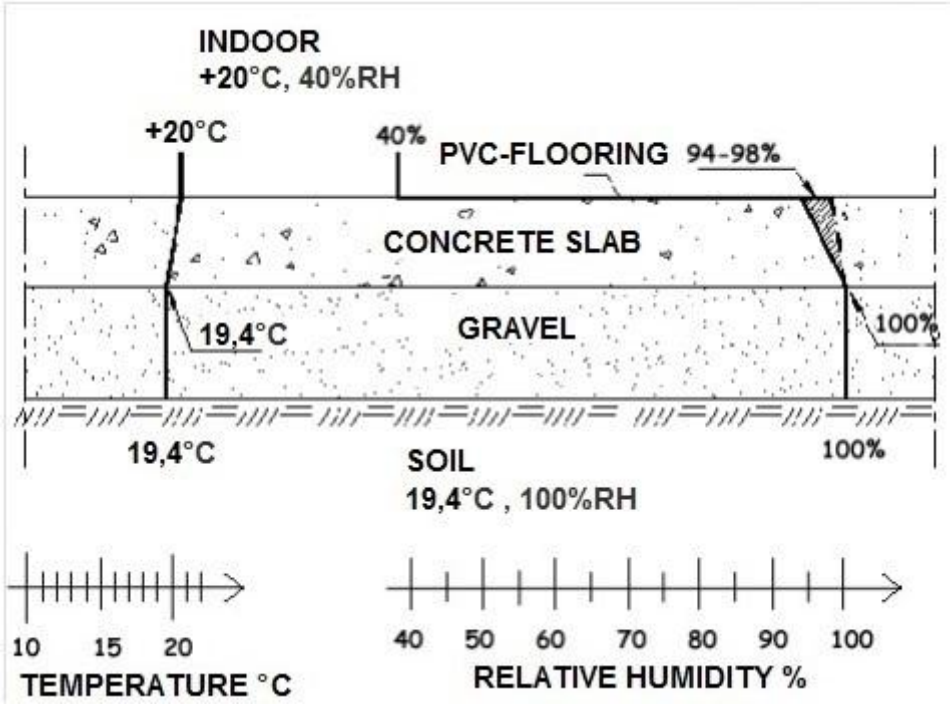

FIG 3. Expected humidity levels in a concrete slab with PVC flooring and no moisture barrier or thermal insulation under the slab

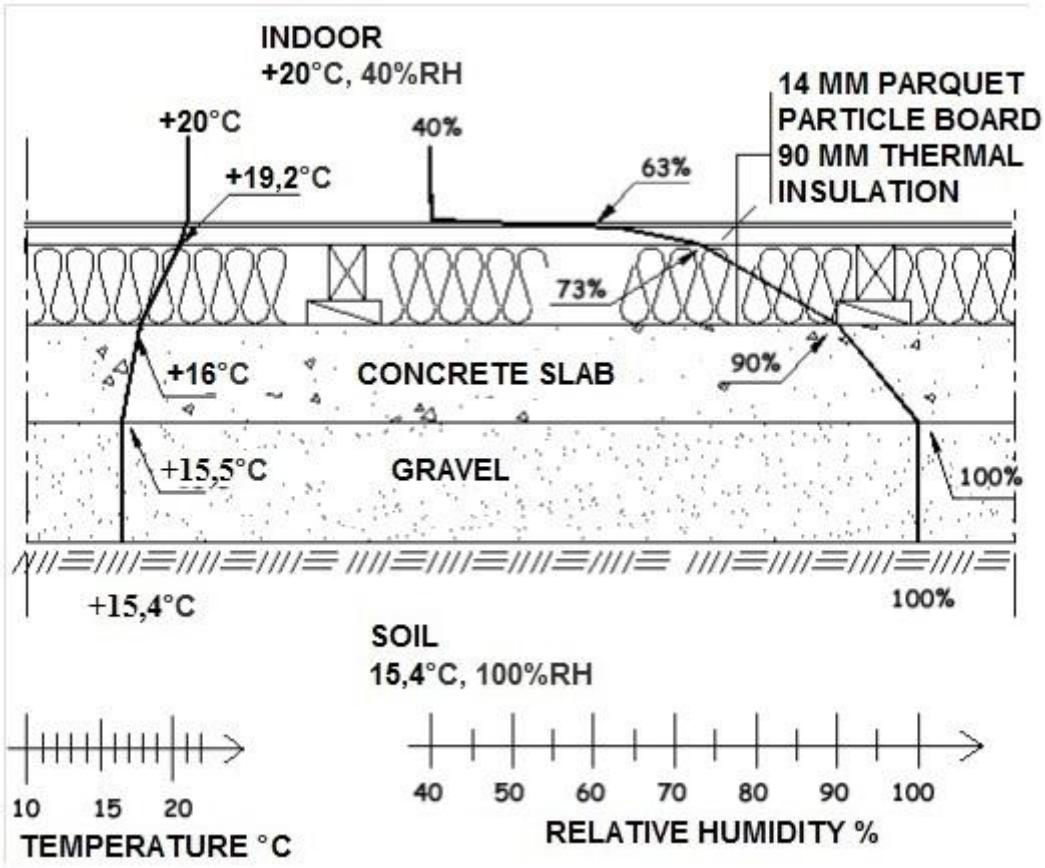

FIG 4. Expected humidity levels in a concrete slab with overlying thermal insulation

Dust sampling for fungal DNA analysis was performed in one municipality in the north east part of Stockholm. In total 24 day care centres were identified. Three of the day care centres were excluded in

this study since they were located in school buildings, and could be influenced by the school environment. Dust collection was performed in the remaining 21 day care centres (26 separate buildings). Surface dust was collected in 3-5 randomly selected rooms in each building. The number of rooms depended on the size of the buildings. Dust was collected by swabbing a 60 cm^2 surface (1×60 cm) of half of the upper part of the doorframe on the main entrance door to each room with a sterile cotton swab. If the main entrance door had a supply or exhaust ventilation duct above the doorframe, another doorframe without any ventilation duct was selected. Two samples were collected by dividing the doorframe into a left and a right side, and the left-side swab was used in this study. Fungal DNA was analysed by quantitative PCR (QPCR) by a previously described method (Cai et al., 2009; Cai et al., 2011). A fungal DNA sequence common for a large number of moulds (Universal Fungal assay 1) was analyzed, here described as total fungal DNA. The mould species detected by this total DNA method is available online at http://www.freepatentsonline.com/6387652.html. The mould level was expressed as cell equivalents (CE) assuming one copy per cell. The final results were presented as CE/m^2 of swabbed surface area. Data on total fungal DNA was log-transformed to get an approximately normally distributed variable. Associations between building factors and total fungal DNA were analysed by linear mixed models, to adjust for the hierarchic structure of the data (room and building level). A p-value below 0.05 was considered significant.

2.2 Results

Totally 316 buildings were investigated. In total, 53 buildings (17%) were rated with grade 1, 135 buildings (43%) with grade 2 and 128 buildings (41%) with grade 3. Among the 26 day care centre buildings where dust was collected for fungal DNA analysis, 4 buildings (15%) were rated with grade 1, 8 (31%) with grade 2 and 14 (54%) with grade 3. Among the rooms (N=103) in the 26 day care centre buildings, 13 rooms (15%) were in buildings rated with grade 1, 31 rooms (31%) in buildings with grade 2 and 59 rooms (54%) in buildings with grade 3.

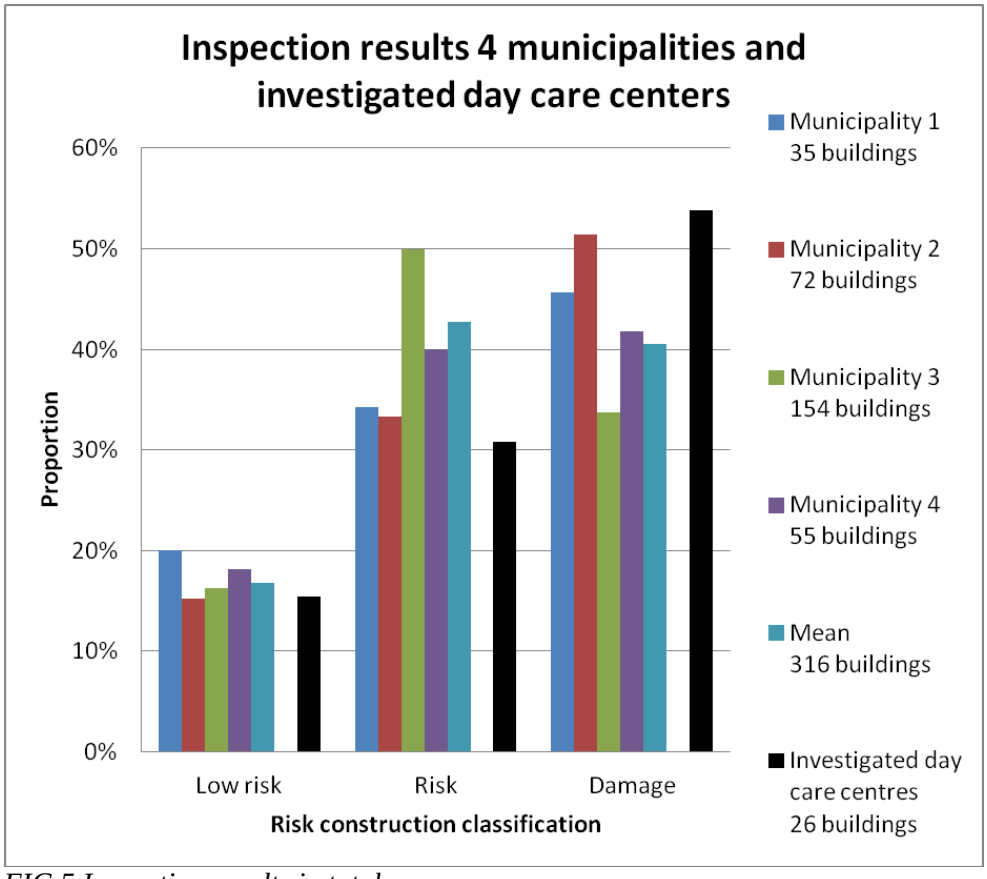

FIG 5.Inspection results in total

There were associations between total fungal DNA in swab samples and risk construction classification, rotating heat exchanger and linoleum floor material. The geometric mean (GM) of total fungal DNA was $3.0*10^6$ among rooms in buildings with risk level 1, $3.7*10^6$ among rooms with risk level 2 and $4.9*10^6$ among rooms with risk level 3 ($p<0.05$ for trend). Moreover, the GM of total fungal DNA was 2.1 times higher in rooms in buildings with linoleum floors as compared to PVC floors ($p<0.05$) and 1.5 times higher in buildings with a rotating heat exchanger ($p<0.05$). The associations between fungal DNA levels and risk construction classification remained significant even after adjusting for type of floor and rotating heat exchanger.

3. Conclusions

An ocular inventory by trained moisture consultants is a good method to get information on dampness status of all municipal buildings within one area. A dampness survey of all buildings within one area, e.g. one municipality, is important in terms of dampness prevention since it identifies building that are in most need for refurbish action. This is particularly important since many of the municipal buildings are schools and day care centres, important indoor environments for children. Adequate prevention measures may also lead to health improvements in the population. Finally the significant association between levels of total Fungal DNA on indoor surfaces and risk construction grading of the buildings confirms that risk construction may lead to increased indoor mould contamination.

4. Acknowledgments

The study was supported by grants from the Swedish Research Council for Environment, Agricultural Sciences and Spatial Planning (FORMAS) and the Swedish Asthma and allergy Association's Research Foundation.

References

Broms K., Svärdsudd K., Sundelin K. & Norbäck D. 2006. A nationwide study of indoor and outdoor environments in allergen avoidance and conventional daycare centers in Sweden. Indoor Air. 16, p. 227-235

Cai G.H., Bröms K., Mälarstig B., Zhao Z.H., Kim J.L., Svärdsudd K., Janson C. & Norbäck D. 2009. Quantitative PCR analysis of fungal DNA in Swedish day care centers and comparison with building characteristics and allergen levels. Indoor Air. 19, p. 392-400.

Cai G.H., Mälarstig B., Kumlin A., Johansson I. & Norbäck D. 2011. Fungal DNA and pet allergen levels in Swedish day care centres and associations with building characteristics. Journal of Environmental Monitoring. 13, p. 2018-2024

Norbäck D., Björnsson E., Janson C., Boman G. 1999. Current asthma and biochemical signs of inflammation in relation to building dampness in dwellings. Int J Tuberc Lung Dis. 3, p. 368-376.

Norbäck D., Wieslander G., Nordström K. & Wålinder R. 2000. Asthmatic symptoms in relation to measured building dampness in upper concrete floor constructions, and 2-etyl-1-hexanol in air. Int J Tubercl Lung Dis. 4, p. 1016-1025.

Norbäck D., Zock J.P., Plana E., Heinrich J., Svanes C., Sunyer J., Künzli N., Villani S., Olivieri M., Soon A. & Jarvis D. 2013. Mould and dampness in dwelling places, and onset of asthma: the population-based cohort ECRHS. Occup Environ. 70, p. 325-331.

Simoni M., Cai G.H., Norback D., Annesi-Maesano I., Lavaud F., Sigsgaard T., Wieslander G., Nystad W., Canciani M., Viegi G. & Sestini P. 2011. Total viable moulds and fungal DNA in classrooms and associations with respiratory health and pulmonary function of European schoolchildren. Pediatr Allergy Immunol. 22, p. 843-852.

Wieslander G., Norbäck D., Nordström K., Wålinder R. & Venge P. 1999. Nasal and ocular symptoms, tear film stability, and biomarkers in nasal lavage, in relation to building dampness and building design in hospitals. Int Arch Occup Environ Health. 72, p. 451-461.

WHO Guidelines for Indoor Air Quality: Dampness and Moulds. 2009. WHO Europe, Geneva.

Moisture in bathrooms and kitchens: the impact of ventilation systems

Jelle Laverge, PhD[1]
Marc Delghust, M.Sc.[1,2]
Arnold Janssens, Professor[1]

[1] Building physics, construction and services research group, Ghent University, Belgium
[2] Flemish Institute of Technology Development (VITO), Belgium

KEYWORDS: *moisture, bathroom, kitchen, ventilation*

SUMMARY:
Apart from the emission of bio-effluents, linked to the presence of the occupants themselves, moisture production related to household activities is one of the most important sources of indoor air pollution in dwellings. These activities are usually concentrated in bathrooms and kitchens. Since high humidity levels are a known stimulus for the development of mould and are associated with higher prevalence of asthma, most ventilation standards position exhaust vents in kitchens and bathrooms, so the moist air is directly extracted from the dwelling. Most occupants, however, operate their ventilation system at very low flow rates. Demand controlled ventilation often includes the humidity in the exhaust spaces as a trigger for higher flow rates. In this paper, we present monitoring results from 3 case study neighborhoods, with over 70 dwellings in total, with different ventilation systems (natural, exhaust, mechanical). The type of moisture profiles generated by the activities in kitchens and bathrooms is investigated and the effect of the different system types and measured exhaust flow rates on the measured humidity levels is analyzed and reported. It thereby provides a good overview of what kind of humidity levels are achieved in practice, and how these relate to the design intentions.

1. Introduction

When indoor air quality is discussed, a multitude of pollutants need to be considered, with the classification ranging from the chemical composition (eg. formaldehyde, ozone, carbon dioxide…), over physical appearance and properties (gaseous, particulates, VOC's, SVOC's) to the sources of the pollutants (Laverge, 2013). Although debatable, for the assessment of indoor air quality as a need for residential ventilation, the latter should be preferred. This creates 4 distinct categories of pollutants, each with their specifics: outdoor pollutants penetrating inside (Stephens and Siegel, 2012), emissions from building materials (Knudsen et al., 2007), bio-effluents from the occupants (Cen, 1998) and pollutants related to occupant activities (Abdullahi et al., 2013, Tung et al., 2010). For outdoor pollutants, mainly particulates, only filtration and tight construction are efficient measures. Ventilation, in this situation, is always a source of pollution rather than a solution for good indoor air quality. In the case of material emissions, source control is the most appropriate form of action. Therefore, ventilation is really only the appropriate course of action for the reduction of exposure to bio-effluents and pollutants generated by activities for which source control is not easily feasible.

In a residential context, both of these source types are mainly located in different rooms of the dwelling: bio-effluents are generated by the occupants and the exposure to them is therefore concentrated in the main living spaces such as the living room and the bedrooms. Due to its specific occupancy schedule, the bedroom heavily dominates this exposure (Laverge et al., 2013). Although a strong correlation between bio-effluents and perceived air quality exists (Fanger, 1988), the evidence for health effects related to exposure to them is much less convincing (Wargocki, 2009, Sundell et al., 2011).

For pollutants generated by various typical domestic occupant activities such as cooking, bathing and washing, there is, on the other hand, extensive evidence that they have a substantial impact on health: WHO (Who, 2010) lists both exposure to fumes from cook stoves and dampness as two of the main contributors to adverse health effects in indoor environments. Most of these activities take place in specific rooms, namely the kitchen, bathroom and, if available, service rooms.

While for exposure to fumes, the effects are mainly acute (with potential chronic consequences from repeated exposure), dampness exclusively affects us on the long term, both through its promotion of pulmonary affliction (Bornehag et al., 2001, Claeson et al., 2009) and mould growth (Viitanen et al., 2010, Isaksson et al.), which in its self is again associated with adverse long term health effects. Additionally mould growth has a negative impact on both the aesthetic value and the durability of the construction.

These are essential domestic activities, but, compared to the time spent in other rooms, are concentrated in relatively short intervals of time each day. Both of these properties of the exposure to pollutants from occupant activities make it a classic case for the application of local exhaust ventilation: evacuate the pollutants as close to the source as possible, before they have the chance to spread through the rest of the dwelling.

This strategy is adopted in most of the applicable residential ventilation standards (Nbn, 1991, Nni, 2006, Dimitroulopoulou, 2012), which specify that exhaust vents should be located in the ‘wet’ spaces of the dwelling (kitchen, bathrooms, service rooms) and fresh air is to be supplied to the main living spaces, creating an airflow network such as depicted in figure 1.

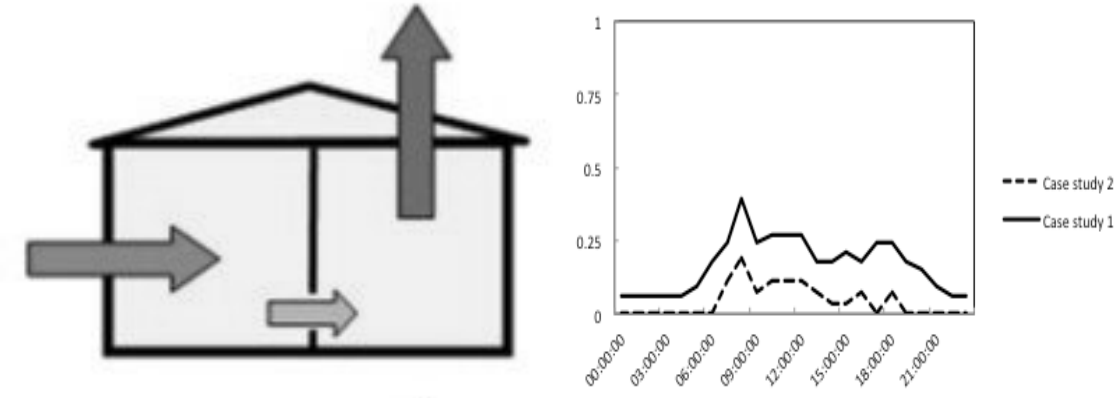

FIG 1. Classic residential ventilation scheme (left) and probability of opening of bathroom windows in case study 1 and 2 (right)

Although this general scheme is broadly applied for all types of ventilation systems, the flow rates generated by different approaches to ventilation, as well as their stability, can be very different. Most papers reporting on monitoring campaigns in residences focus on the living room (e.g. Stranger et al., 2012, Zhang and Yoshino, 2010), some include the bedrooms (Beko et al., 2010). In this paper, we focus on moisture in ‘wet’ spaces. If ventilation rates are reported, they are usually reported as whole building air exchange rates (Langer and Bekö, 2013) and not differentiated between the different wet spaces. Moreover, they usually focus on large cross-sectional cohorts of dwellings. We present the results from winter monitoring campaigns in 3 neighbourhoods in Belgium, with similar dwellings equipped with different types of ventilation systems and discuss the typically observed humidity profiles in kitchens and bathrooms for each of the options.

The following sections first present the case study neighbourhoods and the applied monitoring methods, followed by a discussion of the observed humidity levels and ventilation rates. At the end of the paper, the latter are summarized in general conclusions

2. Case studies and methods

As was explained in the introduction, three case study neighbourhoods in Belgium with different age, HVAC system and energy performance were selected for extensive winter monitoring. Thirty six, twenty and sixteen dwellings in case studies 1, 2 and 3 respectively were monitored. These monitoring campaigns are part of a larger project that focuses on the impact of user behaviour on the annual energy demand for space heating, the results of which were presented in earlier papers (Delghust et al., 2013, Delghust et al., 2012b, Delghust et al., 2012a). The monitoring and analysis of the indoor environment is a spin-off project. The results for the exposure to bio-effluents have also been reported earlier (Laverge et al., 2013).

The same monitoring scheme was adopted for all three case studies. A pressurization test (Cen, 2001b) was executed on each dwelling. If a mechanical ventilation system was available, the flow rates at each vent hole were measured, if applicable in different operation regimes of the system. An 'as built' file was compiled that contained all relevant building data and energy bills relevant for the current occupants were obtained from the utility companies. Temperature and relative humidity in each of the indoor spaces and of the outdoor environment were logged on a 5-minute interval for one to two weeks. Additionally, carbon dioxide concentration was monitored in the living room and master bedroom. After the monitoring campaign, the occupants completed an extensive questionnaire on their occupancy schedule and behaviour.

The typology of the dwellings in all three neighbourhoods is very similar. All are 2 floor semi-detached or terraced dwellings with a brick building envelope, concrete floors and unoccupied attics. The ground floor is always composed of a large living/dining room, a hallway, toilet and kitchen. The bathroom and three bedrooms are located on the second floor. All are built for the volume market and have a net floor area of about 100 m^2.

Where they are similar in size and typology, the energy performance of the dwellings is thoroughly different: the dwellings in case study 1 were constructed in the 1960's with no insulation what so ever. Although some local refurbishments have updated the performance of a few single components of the building envelope, e.g. the installation of a double pane window in a single room, the dwellings are still largely in the original state. This type of dwelling is not representative for recent construction, but is relevant for this analysis since this is the condition of the majority of the Belgian building stock. No dedicated ventilation is available, but it will be no surprise to the reader that pressurization tests show that these houses are very leaky, with an average of 10.8ACH_{50}. Occupants also reported much more frequent window openings in the 'wet spaces' than in the other case studies', as can be seen in figure 1. A boxplot of the measured leakage rates is shown in figure 2.

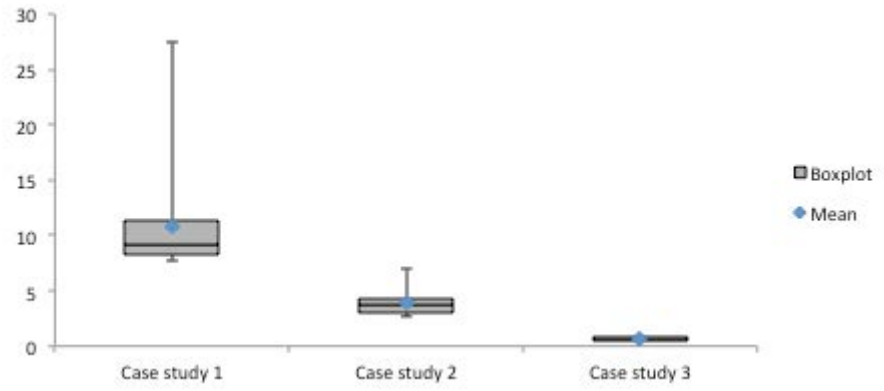

FIG 2. Boxplots of measured leakage levels (ACH_{50}) in each of the case studies

The second neighbourhood was built in 2007 and represents recent construction very well. It complies with the energy performance requirements of that time, without being very ambitious. It has moderate insulation levels (5-10 cm of insulation) and is relatively airtight with an average of 4.0 ACH_{50}. An exhaust ventilation systems, with trickle ventilators above the windows in the main living spaces and exhaust vents in the kitchen, service room, toilet and bathroom is installed in each dwelling. The measured airflow rates in the kitchen and bathrooms are reported in figure 3 (Delghust et al., 2013). The required design flow rate from the standard is never reached in the kitchens, while on average it is reached when the highest ventilation level is selected in the bathrooms. Almost all occupants report that they usually operate their systems at flow rates far below the design flow rate.

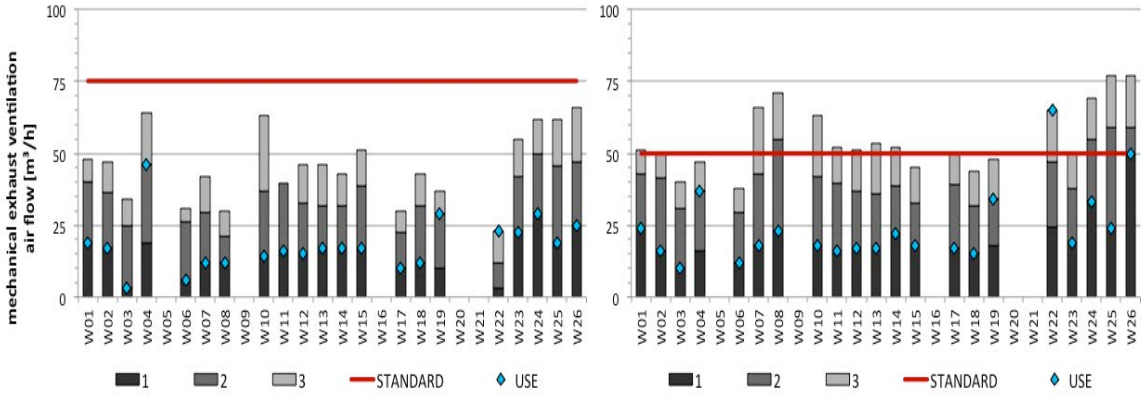

FIG 3. Measured air flow rates in kitchens and bathrooms in case study 2, at levels 1, 2 and 3 of the available 3 position switch of the system, the diamond indicating the flow rate usually selected by the occupants

The third case study consists of a number of recently completed passive houses. In agreement with the passive house standard (Feist et al., 2005), they have extensive insulation (up to 30 cm), are extremely air tight (average of 0.7 ACH_{50}) and are equipped with heat recovery ventilation. Again, supply vents are located in the main living spaces and exhaust vents are situated in the 'wet' rooms. Again, the results of the airflow measurements for kitchens and bathrooms are shown in figure 4 (Den Haese and Derudder, 2013). Note that is this case study, the flow rate of the ventilation system was logged. On average, we can say that the capacity of the ventilation systems comply with the design flow rates (although there is a large spread), but that they are operated at far lower flow rates.

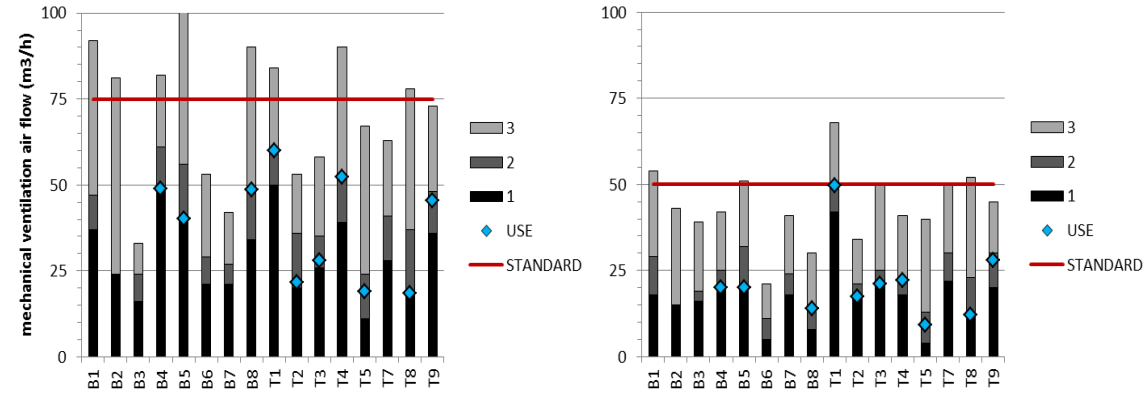

FIG 4. Measured air flow rates in kitchens and bathrooms in case study 2, at levels 1, 2 and 3 of the available 3 position switch of the system, the diamond indicating the average flow rate measured during the monitoring period

3. Results

This section reports and discusses the results of the monitoring with respect to humidity. First the observed moisture supply and relative humidity in the kitchens and bathrooms is discussed, followed by a discussion of the different humidity profiles observed in these spaces.

3.1 Moisture supply and relative humidity

Moisture supply, as it is defined in EN 13788 (CEN, 2001a) , is the average difference in moisture vapour pressure between the indoor and outdoor environment over a relevant measuring period that is long enough to cancel out short term buffering effects (Steeman et al., 2009, Janssen and Roels, 2009, Janssens, 2006). Plotted in function of the average outdoor temperature, it is a good measure to characterise the humidity levels in a space as a result of the actual production and ventilation.

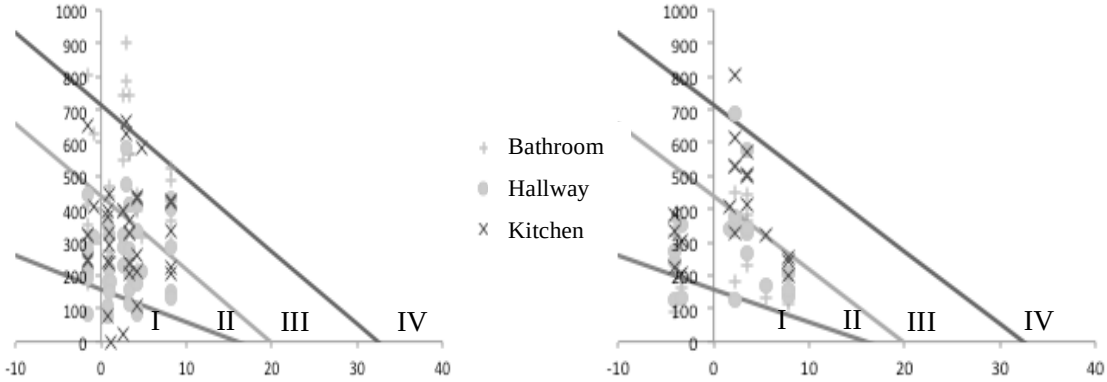

FIG 5. Moisture supply (Pa) as a function of outdoor temperature (°C) in kitchens and bathrooms in case study 1 (left) and 2 (right). The moisture supply in the hallway of the dwellings, where no moisture sources are found, is also shown as a reference.

Since no dedicated ventilation system is available in case study 1, ventilation of the 'wet' spaces exclusively depends on infiltration and window airing. Especially in the bathrooms, this leads to high moisture supply levels. In the kitchens, the moisture supply is similar to that of the main living spaces, which is on average somewhere in the middle between that of the hallway, where no significant moisture sources are found, and the bathroom. This is readily explained by the presence of a fume hood, which is operated during cooking and prevents most of the moisture produced to enter the space, and by the fact that in almost all dwellings, the kitchen is open to the main living room.

In case study 2, the difference between moisture supply in the bathroom and kitchen is much less obvious due to the continuous exhaust flow generated by the ventilation system. Nevertheless, the fact that this system is operated at low flow rates keeps the moisture supply in both spaces relatively high, mainly within class III, while in case study 1, this was only the case for the bathrooms and the kitchens were mainly within class II. Note that here too, kitchen fume hoods are available and the kitchen is open to the main living room.

The risk classes defined within the moisture supply framework are based on a constant indoor temperature of about 18 °C. Therefore it is a good indicator of the average production rate in the space. The risk of mould growth is a function of a high average relative humidity, which in turn depends on the vapour pressure and temperature. Bathrooms are often intermittently heated . With a lower indoor temperature, the same moisture supply will therefore lead to higher relative humidities. With relatively well designed thermal bridges in the building envelope, an average relative humidity of 70% is generally accepted as a threshold for the mould growth risk (Viitanen et al., 2010, Isaksson et al.).

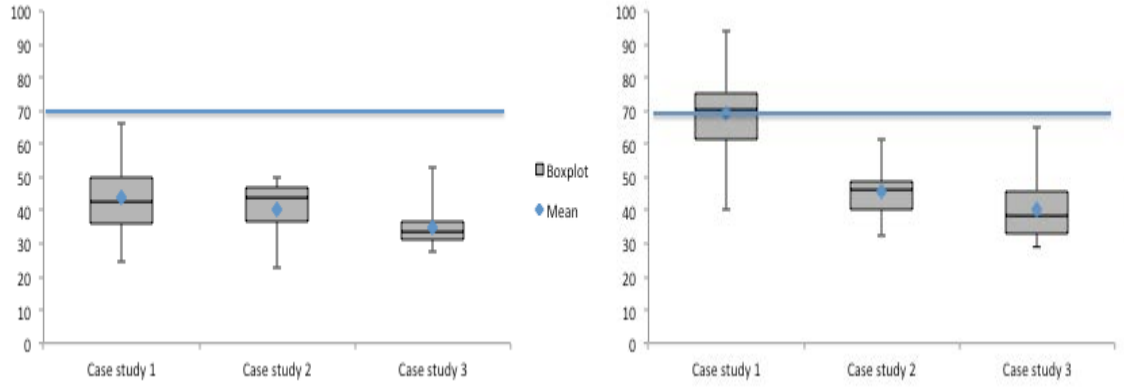

FIG 6. Boxplots of the average relative humidity (%) measured in kitchens (left) and bathrooms (right) in case study 1 and 2.

In case study 1, the bathrooms were scarcely heated, only during actual use of the space, leading to low average temperatures and high mould growth risks in the majority of bathrooms (Figure 6). This was confirmed by the frequent complaints from the tenants on this subject. In case studies 2 and 3, the better insulation, lower infiltration, warm airflows from the living spaces and longer heating due to control by a central thermostat (Delghust et al., 2013) inferred much lower average relative humidity.

3.2 Humidity profiles

Although, as stated before, moisture supply needs long averaging periods due to buffering effects etc., analysing the day profiles of the difference between indoor and outdoor vapour pressure is useful to understand the nature of sources that occur in different types of spaces. It needs to be stressed that, because instantaneous values are used to create average day profiles, buffering is completely ignored and this data can therefore not be used to calculate source strengths.

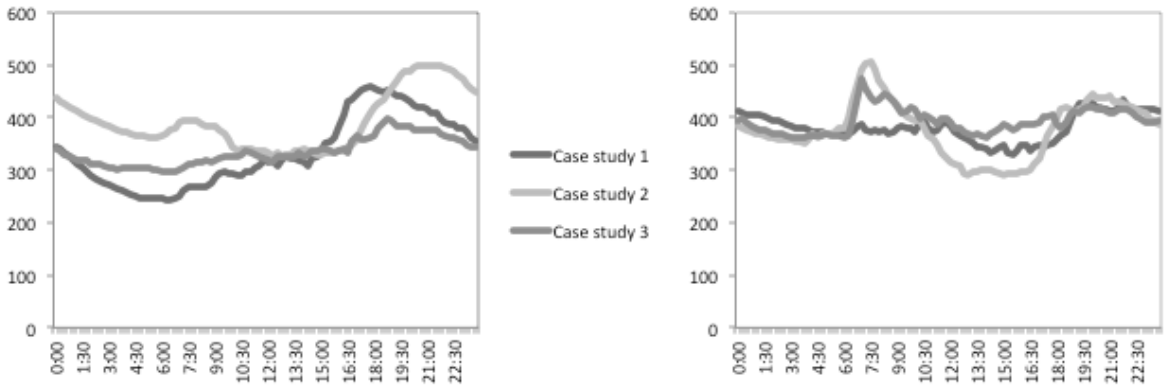

FIG 7. average day profiles of the difference between indoor and outdoor vapour pressure (Pa) for in kitchens (left) and bathrooms (right) in case study 1 and 2.

For the bathrooms, 2 distinct peaks in humidity levels occur over the course of the day: one in the morning and one at night. These are caused by large moisture loads generated by showers. This confirms that humidity based demand controlled ventilation has a good potential in bathrooms. In case study 1, this pattern is not seen since the occupants take very few showers and systematically open the bathroom window if they do. The sharp peaks seen in the bathrooms do not occur in the kitchens. Much flatter bumps occur during cooking activities, but the maxima observed in the evening are caused by occupancy of the living rooms adjacent to the open plan kitchens. The potential for humidity control is therefore much less obvious for kitchen ventilation.

4. Conclusions

This paper presented the results with respect to indoor humidity levels and ventilation in bathrooms and kitchens from extensive winter monitoring campaigns in three case study neighbourhoods in Belgium. The case studies includes old, recent and new construction with low, average and high energy performance respectively. The results demonstrate that, although they were continuously operated at low flow rates, mechanical ventilation systems effectively control the humidity levels within ‘wet’ spaces in a dwelling. Intermittent heating of bathrooms substantially increases the mould growth risk and bathrooms are particularly suited for humidity based demand controlled ventilation.

5. Acknowledgements

These case studies have been supported by the Flemisch Institute for Technoloy Research (VITO) and the Research Foundation – Flanders (FWO). We would like to thank all occupants of the three case study neighbourhoods for their cooperation and the graduate students of the department of civil engineering and department of architecture and urban planning at Ghent University that helped collect all the data.

References

Abdullahi K.L. et al. 2013. Emissions and indoor concentrations of particulate matter and its specific chemical components from cooking: A review, *Atmospheric Environment*, 71, 260-294.

Beko G. et al. 2010. Ventilation rates in the bedrooms of 500 Danish children, *Building and Environment*, 45, 2289-2295.

Bornehag C.G. et al. 2001. Dampness in buildings and health - Nordic interdisciplinary review of the scientific evidence on associations between exposure to "dampness" in buildings and health effects (NORDDAMP), *Indoor Air*, 11, 72-86.

Cen. 1998. Ventilation for buildings - Design criteria for the indoor environment, Vol. CR 1752, Brussels.

Cen. 2001a. Hygrothermal performance of building components and building elements - internal surface temperature to avoid critical surface humidity and interstitial condensation - calculation methods.

Cen. 2001b. Thermal performance of buildings - Determination of air permeability of buildings - Fan pressurization method (ISO 9972:1996, modified), CEN.

Claeson A.S. et al. 2009. Effects on perceived air quality and symptoms of exposure to microbially produced metabolites and compounds emitted from damp building materials, *Indoor Air*, 19, 102-112.

Delghust M. et al. 2013. The real influence of energy performance levels on the heating demand in dwellings: case study analyses on neighbourhoods. In: Proceedings of ASHRAE Buildings XII (submitted).

Delghust M. et al. 2012a. Analysing energy use in residential neighbourhoods: a comprehensive approach on complementary case-studies, *Energy Efficiency & Behaviour Conference, Proceedings*, Helsinki, Finland, Motiva Oy, 115-118.

Delghust M. et al. 2012b. The influence of user behaviour on energy use in old dwellings: case-study analysis of a social housing neighbourhood, *5th International Building Physics Conference, Proceedings*, Kyoto, Japan, 5th IBPC Organizing Committee, 809-816.

Den Haese M. and Derudder B. 2013 In-situ analyse van passiefhuiswijken: gebruikersgedrag, binnenklimaat en energiegebruik (in dutch). M.Sc., Ghent University, Architecture and Urban Planning.

Dimitroulopoulou C. 2012. Ventilation in European dwellings: A review, *Building and Environment*, 47, 109-125.

Fanger P.O. 1988. Introduction of the olf and decipol unit to quantify air-pollution perceived by humans indoors and outdoors, *Energy and Buildings*, 12, 1-6.

Feist W. et al. 2005. Re-inventing air heating: Convenient and comfortable within the frame of the Passive House concept, *Energy and Buildings*, 37, 1186-1203.

Isaksson T. et al. Critical conditions for onset of mould growth under varying climate conditions, *Building and Environment*, 45, 1712-1721.

Janssen H. and Roels S. 2009. Qualitative and quantitative assessment of interior moisture buffering by enclosures, *Energy and Buildings*, 41, 382-394.

Janssens A. 2006. Analysis of indoor climate measurements in recently built Belgian dwellings, *Annex 41 Moist-Eng working meeting lyon*, Lyon.

Knudsen H.N. et al. 2007. Sensory and chemical evaluation of odorous emissions from building products with and without linseed oil, *Building and Environment*, 42, 4059-4067.

Langer S. and Bekö G. 2013. Indoor air quality in the Swedish housing stock and its dependence on building characteristics, *Building and Environment*, 69, 44-54.

Laverge J. 2013. Ventilation: Thermal Efficiency and Health Aspects, In: Pacheco-Torgal, F. (ed) *Nearly Zero Energy Building Refurbishements*, Springer-Verlach.

Laverge J. et al. 2013. Bedroom IAQ: Where do we stand? In: Proceedings of ASHRAE IAQ 2013, pp. 8.

Nbn. 1991. Ventilatievoorzieningen in woongebouwen, Vol. NBN D 50-001, Brussels.

Nni. 2006. Ventilatie van gebouwen - Bepalingsmethoden voor nieuwbouw, Vol. NEN 1087, Delft.

Steeman M. et al. 2009. On including moisture buffering in the performance evaluation of humidity controlled ventilation systems.

Stephens B. and Siegel J.A. 2012. Penetration of ambient submicron particles into single-family residences and associations with building characteristics, *Indoor Air*, 22, 501-513.

Stranger M. et al. 2012. Clean Air, Low Energy - Schone Lucht, Lage Energie, Exploratory research on the quality of the indoor environment in energy-efficient buildins: the influence of outdoor environment and ventilation, Brussels, VITO, 117.

Sundell J. et al. 2011. Ventilation rates and health: multidisciplinary review of the scientific literature, *Indoor Air*, 21, 191-204.

Tung Y.-C. et al. 2010. Experimental performance investigation of ventilation schemes in a private bathroom, *Building and Environment*, 45, 243-251.

Viitanen H. et al. 2010. Moisture and Bio-deterioration Risk of Building Materials and Structures, *Journal of Building Physics*, 33, 201-224.

Wargocki P. 2009. Health-based Ventilation Guidelines for Europe.

Who. 2010. WHO guidelines for indoor air quality: selected pollutants, In: Who (ed), WHO.

Zhang H. and Yoshino H. 2010. Analysis of indoor humidity environment in Chinese residential buildings, *Building and Environment*, 45, 2132-2140.

Moisture problems in a narrow gap under the suspended floor: A case study

Kamil Stanek, Ph.D.

Czech Technical University in Prague (CTU), Czech Republic

KEYWORDS: *Sub-floor, moisture, ground cover, ventilation, measurement, numerical simulation*

SUMMARY:
This paper presents and explains moisture problems observed in the sub-floor space of a timber-framed kindergarten in the Central European climate. The floor structure (36 by 52 m) is suspended 0.27 m above the uncovered ground surface. The sub-floor is mechanically ventilated in one direction. Here, relative humidity constantly exceeds 95 % irrespective of the season. Furthermore, visual inspections revealed condensation and mould growth in the inlet area. A two-dimensional dynamic HAM model was written in Matlab in order to describe the sub-floor's behaviour and evaluate possible actions. The model was validated using measured data. The results show two principal moisture sources: (1) evaporation from the ground and (2) ventilation by the outdoor air. The ground source is active throughout the year and causes gradual increase in relative humidity in the direction of the flow. The outdoor air brings in excessive moisture from spring to autumn and causes condensation on the floor structure. Two measures can be adopted to cut off the sources, keep the relative humidity below 80 % and exclude the condensation: (1) ground cover and (2) adaptive mechanical ventilation. Unfortunately, practical realization of the former in the existing narrow gap is possible only at high costs, if at all, while the latter alone cannot solve the problem.

1. Introduction

Foundations with suspended floors (crawl spaces) have become more and more popular in the Czech Republic during the last two decades, especially for timber-framed houses. However, a lack of both experience and technical standardization sometimes leads to inconvenient design. This paper presents and explains moisture problems observed in the sub-floor space of a timber-framed kindergarten in the Central European climate. They are documented by both measured data and a numerical analysis. The numerical model is then used to simulate and evaluate possible actions, particularly with respect to various ground covers and ventilation regimes.

The 36 × 52 m single-storey kindergarten (Figure 1, left) is made of prefabricated timber-based elements supported by foundation footings at the distance of 0.27 m from the uncovered ground surface (Figure 2, top). There is no peripheral drainage and the perimeter of the sub-floor is not thermally insulated. In the initial design, the horizontal sub-floor gap was connected to the vertical gap of the northern façade to ensure ventilation by means of buoyancy and wind pressure differences.

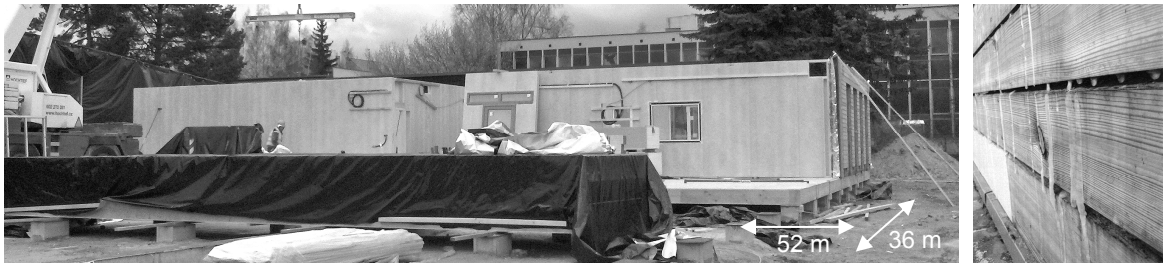

FIG 1. Prefabricated timber structure (left); northern facade with the freezing condensate (right)

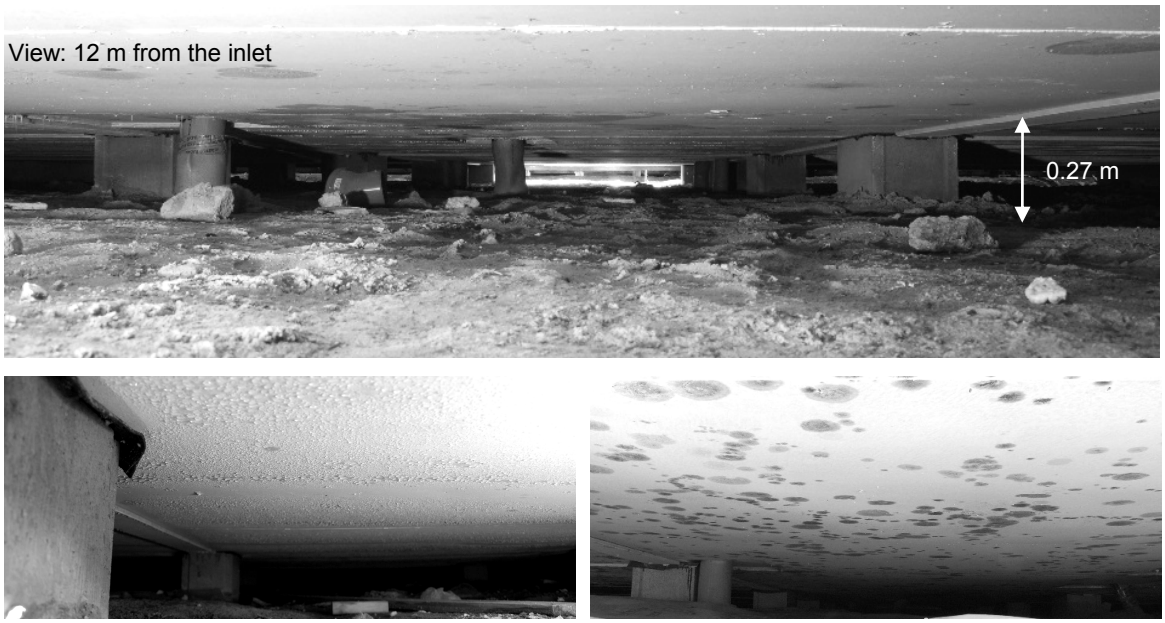

FIG 2. The sub-floor (top); condensation and mould growth in the inlet region (bottom)

During the first cold period after the opening in 2011, severe condensation appeared on the wooden cladding of the northern façade, as the moist and relatively warm air from the sub-floor was entering the façade (Figure 1, right). The system was redesigned in 2012 to avoid further damage to the cladding. A duct system with central suction fan was installed to ventilate the sub-floor in south–north direction with a constant air change rate of 1.5 h^{-1}. In 2013, visual inspections revealed condensation and mould growth (mainly Acremonium and Penicillium species) in the inlet area (Figure 2, bottom). It became clear that a further investigation was needed to describe the physical nature of the problem and propose adequate measures to ensure moisture safety of the sub-floor.

The literature survey showed that two design rules for crawl spaces are generally accepted: (1) site drainage and terrain grading to prevent ingress of rain water and (2) a ground cover to prevent moisture evaporation from the underlying soil (e.g. Rose and Wolde, 1994). There is, however, no explicit rule for the ventilation regime. In summer, venting by the outdoor air can significantly increase the relative humidity in the sub-floor. Samuelson (1994) reports values exceeding 85 % or even reaching 100 % for several weeks. Kurnitski and Matilainen (2000) and Airaksinen et al. (2003) suggest the crawl space may be left unventilated if the moisture evaporation is entirely prevented, but in other cases the ventilation is required. They also found out that the optimum air change rate varies seasonally and depends on the performance of the ground cover and on the heat input from the building. A current practice in North America often advises to seal and insulate the crawl space (e.g. InspectaPedia, 2013), while Carpenter (2000) warns against migration of bacteria, mould spores and radon from unventilated sub-floors into the living space. He also suggests a smart ventilation system controlled on the basis of water vapour concentrations (adaptive ventilation).

2. Methods

2.1 Experimental work

The aim of the experimental work was to document the hygrothermal behaviour of the sub-floor and gather enough information to design an appropriate numerical model for further evaluations. A number of temperature and humidity sensors was installed in the sub-floor space at positions denoted 1, 2 and 3, see Figure 3. In addition, the efficiency of the ventilation system was checked and soil samples were taken and analysed. The measurements and surveys were carried out during the spring season 2013.

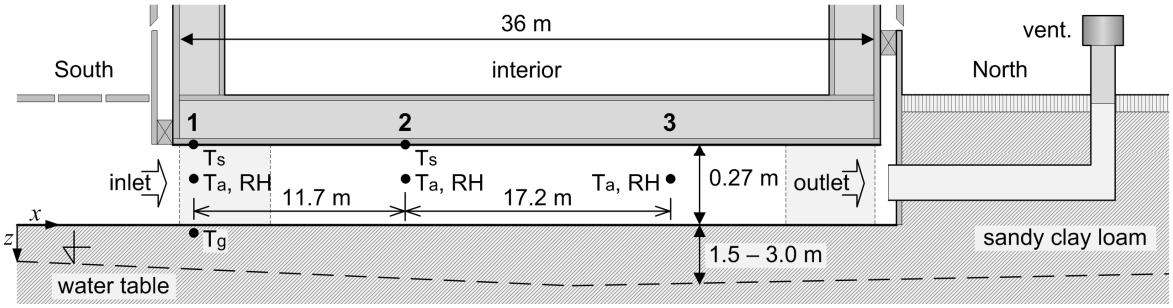

FIG 3. Vertical section of the sub-floor with measuring points (1, 2, 3)

The soil was classified as sandy clay loam with porosity of 45 % and dry bulk density of 1460 kg/m^3. The water table was found at the depth ranging between 1.5 and 3.0 m. The retention curve shows that the volumetric water content of the soil in the surface layer should range between 0.30 and 0.25 m^3/m^3 (Císlerová and Vogel, 2008). It was verified using soil samples taken from underneath the building. The measured values ranged from 0.19 to 0.32 m^3/m^3, with the average of 0.25 m^3/m^3. Thermal conductivity and volumetric heat capacity of the soil were then estimated at 1.3 W/(m·K) and 2.06 MJ/(m^3·K), respectively (Pallin and Kehrer, 2013). The moisture storage function of the soil indicates that the air in its pore system is close to full saturation (RH ≈ 100 %).

2.2 Numerical model

Although the measured data gives a valuable information on the sub-floor's hygrothermal behaviour, more complex picture can be derived from a numerical analysis. Therefore a 2-D dynamic HAM model was written in Matlab (Mathworks, 2013). The model includes three domains: (1) a large ground region around and under the building, (2) the ventilated sub-floor gap and (3) the floor structure. Local weather data were imported from the Meteonorm database (Meteotest, 2013). The principle of the numerical model is depicted in Figure 4.

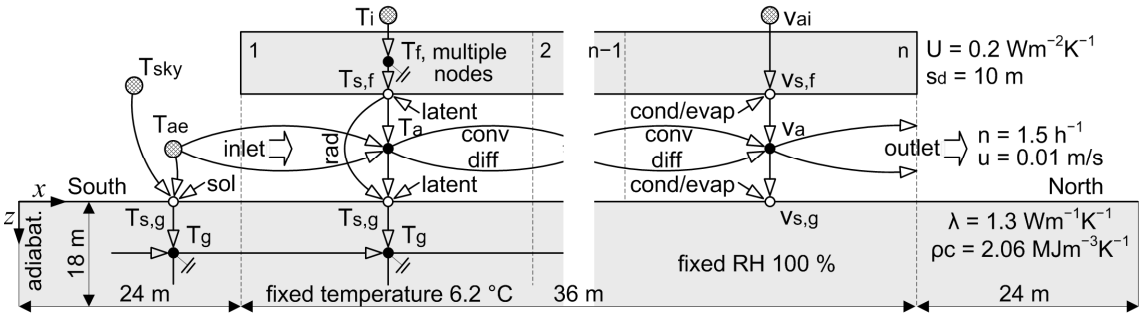

FIG 4. Principle of the numerical model – heat (left) and moisture (right) transport

3. Results and analysis

3.1 Measured data and model validation

The model was validated using a set of measured boundary conditions inserted into the Meteonorm climatic year. Measured and calculated courses of temperature and relative humidity at the individual measuring points are shown in Figure 5. The courses indicate strong temperature damping in the direction of the flow and steadily high humidity in the sub-floor (RH = 100 %). Figure 6 shows the derived moisture flux (*x*-averaged by principle) on the sub-floor's surfaces between the measuring points (1–2, 2–3). It is evident that most of the moisture exchange between the sub-floor air and the surfaces takes place in between the points 1–2, i.e. within the first 12 metres of the sub-floor. The negative values indicate frequent condensation in the inlet region (the inflowing air loses moisture).

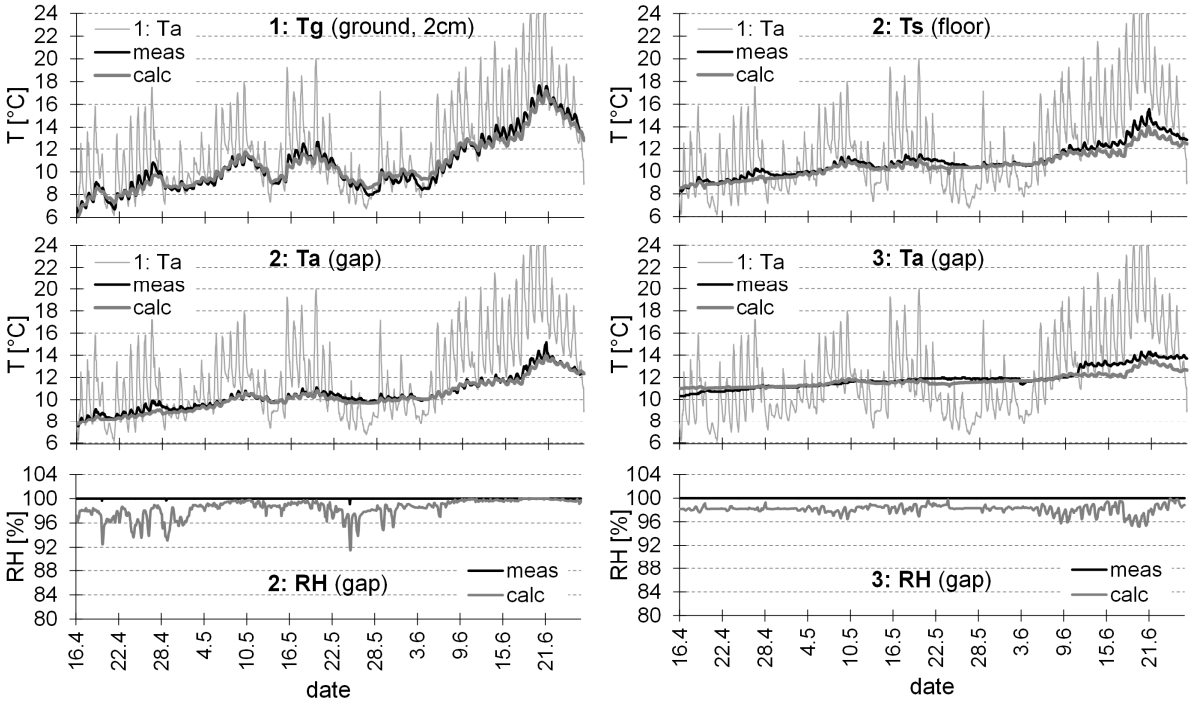

FIG 5. Temperature and relative humidity – measured and calculated values (16. 4. – 25. 6. 2013)

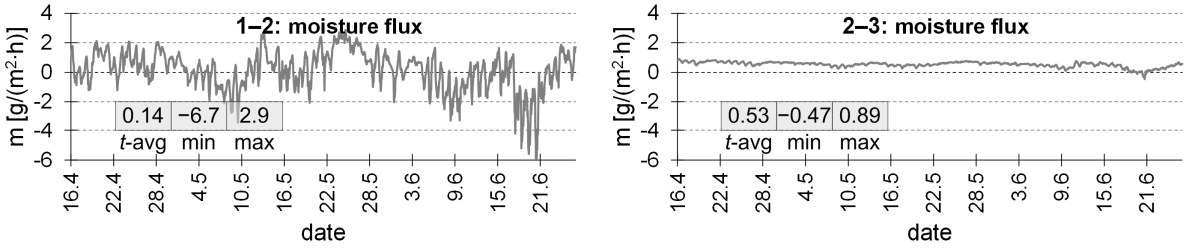

FIG 6. Moisture flux between the respective measuring points (16. 4. – 25. 6. 2013)

3.2 Simulations

3.2.1 Current state

The following figures show the results of the numerical simulation of the sub-floor's hygrothermal behaviour in the current configuration (constant mechanical ventilation, n = 1.5 h^{-1}; uncovered ground surface, s_d = 0 m). Figure 7 shows the temperature distribution in the ground in January and July.

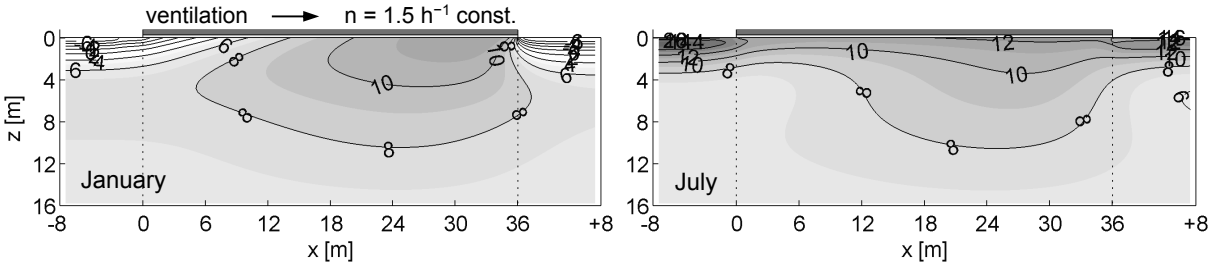

FIG 7. Temperature in the ground under the sub-floor: T(x,z,t), a cut-out from the ground domain

Figure 8 shows the course of the temperature (left) and relative humidity (right) on the floor surface (top) and in the air gap (bottom) in the direction of the flow (x axis) during the year (t axis). The figure also shows monthly averaged values (January, July) for the first and the last 1 meter of the sub-floor

(inlet, outlet), together with the average values for the whole length of the sub-floor (*x*-avg). The plots of the relative humidity start at 70 % and the states of full saturation/condensation are highlighted in black colour.

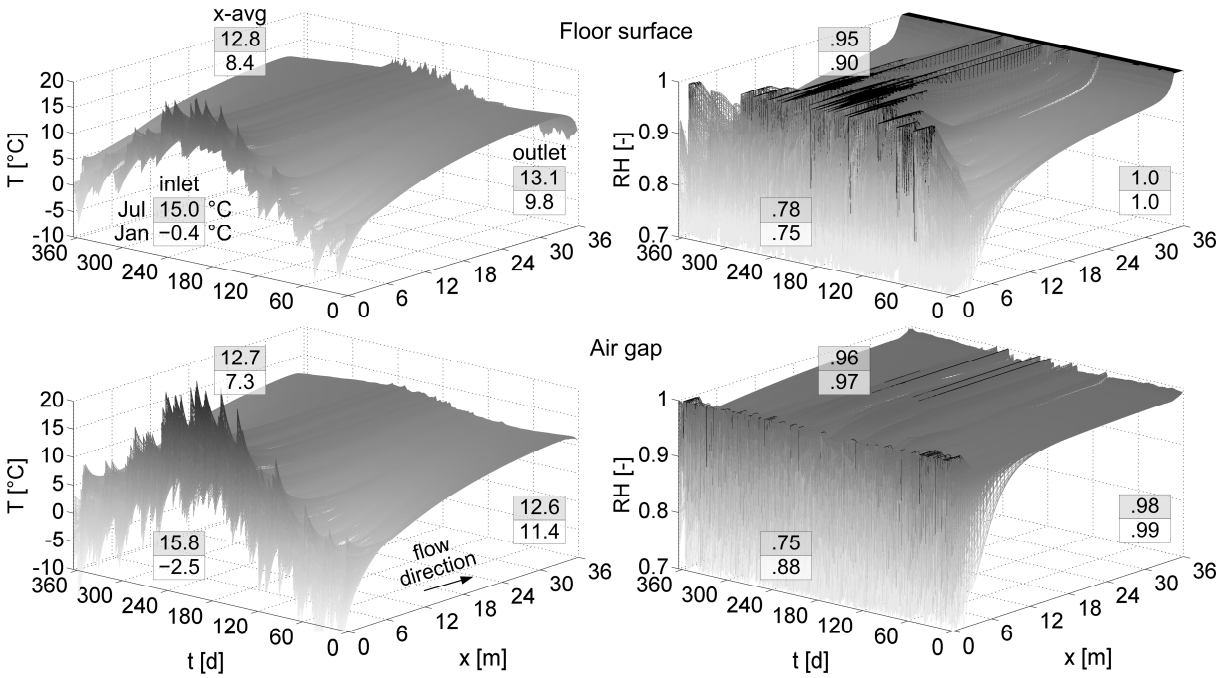

FIG 8. Temperature (left) and relative humidity (right) in the sub-floor: T(x,t), RH(x,t)

The thermal regime of the sub-floor is determined by several effects. The building constantly heats up the sub-floor and the underlying ground, but it blocks the direct influence of the outdoor climate. High thermal inertia of the ground causes strong damping and supresses short-term fluctuations (daily, weekly). Moisture evaporation from the uncovered ground surface lowers the sub-floor's temperature by approx. 2 °C. The radiation heat exchange draws near the temperatures of the floor and ground surfaces. Steady and unidirectional mechanical ventilation brings in long-term fluctuations (monthly, seasonal), which decline in the direction of the flow. The temperature of the inflowing air stabilizes and aligns with both of the surface temperatures within the first 12 metres. Further on, the system is thermally stable throughout the year, with temperatures ranging between 9 and 14 °C. The situation changes again in the outlet region, especially during the cold period – the surface temperatures here drop due to the proximity of the outdoor environment, while the temperature of the outflowing air remains unchanged. This "cold end" effect sets up conditions for moisture condensation at the outlet.

The moisture regime of the sub-floor is determined by two principal moisture sources: (1) evaporation from the uncovered ground surface and (2) ventilation by the outdoor air. Water vapour diffusion from the interior is not significant in the current state. The two sources are complementary and cause critical conditions in the sub-floor throughout the year.

- The ground moisture evaporation steadily saturates the sub-floor air in the direction of the flow. It is active throughout the year, but especially during the cold period and night times, when the moisture content in the outdoor air is lower than in the sub-floor. In winter, the relative humidity exceeds 90 % within the first 12 metres of the sub-floor. The average ground moisture flux here reaches 2.1 g/(m^2·h). Further from this point (12 – 36 m), the relative humidity slowly rises towards 100 % and the moisture flux drops to 1.3 g/(m^2·h). However, the ground moisture evaporation is not the cause of condensation in the sub-floor – except the outlet region.
- Ventilation moistens the sub-floor when the moisture content in the outdoor air is higher than in the sub-floor. It often happens in daytimes throughout the year, but the warm period is the most

critical. Moreover, when the dew point temperature of the outdoor air is higher than the temperature in the sub-floor, condensation occurs on the sub-floor's surfaces. It occurs from March to September, mostly within the first 12 metres, where the inflowing outdoor air cools down. After the air loses the excessive moisture, it retains high relative humidity (≈ 100 %) up to the outlet. The amount of the accumulated condensate on the floor surface reaches its maximum of 0.27 kg/m^2 in the early July at the distance of 5 to 6 m from the inlet. The longest period of uninterrupted presence of the condensate here is 25 days, starting at the late June.

Specific situation is observed in the outlet region, where high condensation rates are recorded for most of the year due to the "cold end" effect, while the drying potential here is basically zero.

3.2.2 Parametric study and possible improvements

The numerical model was used to evaluate possible actions with respect to various ground covers and ventilation regimes. The total of 28 combinations were studied based on two design variables:

- Air change rate, n in h^{-1}, provided by means of constant or adaptive mechanical ventilation: n = 0 (no ventilation); 0.5; 1.5 and 4.5 h^{-1}.
- Ground cover efficiency expressed in terms of an equivalent diffusion thickness, s_d in m: s_d = 0 (uncovered ground); 0.5; 2.0 and 10 m.

The concept of adaptive ventilation is based on the evaluation of actual moisture conditions. The fan is switched on when the moisture content in the outdoor air is lower than in the sub-floor. The reference point in the sub-floor is placed 11.7 m from the inlet (measuring point 2, see Figure 3).

The results of parametric study are presented in Figure 9 using two quantities. The graph shows x-averaged values of the relative humidity on the floor surface in terms of annual average (vertical axis) and averages in January and July (in brackets). The table shows annual amount of moisture condensed on the floor surface, M_c kg per unit width, summed over two regions: the whole sub-floor's length except the outlet region (0–32 m, "in") and the outlet region (32–36 m, "out").

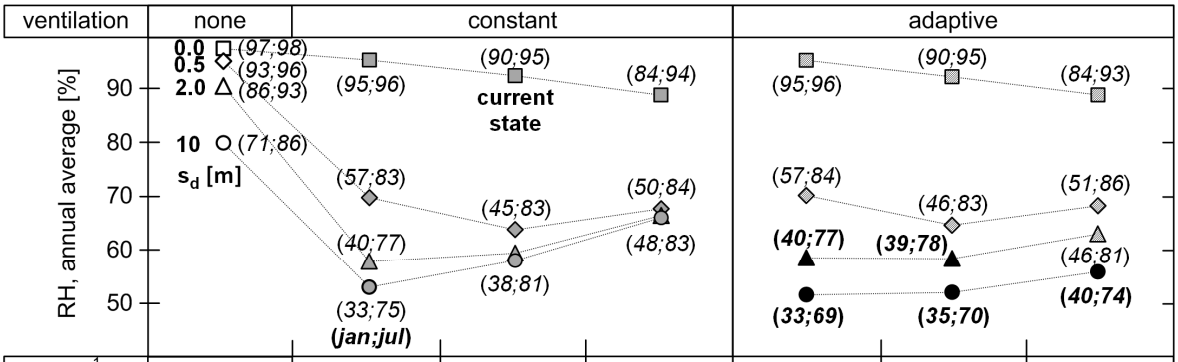

n [h^{-1}]			0		0.5		1.5		4.5		0.5		1.5		4.5	
			in	out	in	out	in	out	in	out	in	out	in	out	in	out
s_d [m]	0.0	M_c [kg]	0.1	2.8	1.8	35.8	6.3	16.9	20.5	2.4	0.3	35.4	0.2	16.6	0.2	1.8
	0.5		0	2.1	1.2	7.3	4.2	0	16.0	0.5	0.2	7.6	0.2	0	0.2	0
	2.0		0	2.8	1.2	0	4.2	0	16.0	0.5	**0.1**	**0.1**	**0.2**	**0**	0.2	0
	10		0	2.0	1.2	0	4.2	0	16.0	0.5	**0.1**	**0**	**0.1**	**0**	**0.1**	**0**

FIG 9. Results of the parametric study

Trends resulting from the study can be summarized in the following way:

- If the ground surface is left uncovered (s_d = 0 m), no ventilation regime can ensure moisture safety of the sub-floor. Adaptive ventilation prevents the condensation in the inlet region, but has little effect on the relative humidity in the sub-floor and the condensation in the outlet region.

- If the sub-floor is left unventilated (n = 0 h^{-1}), no ground cover, within the considered range of s_d-values, can ensure moisture safety, although the relative humidity drops with higher diffusion resistance of the cover and the condensation in the inlet region is excluded.
- Constant ventilation always leads to the condensation in the inlet region during a warm period. However, using a low air change rate (n = 0.5 h^{-1}) and efficient ground cover (s_d = 10 m) can significantly lower the relative humidity and prevent the condensation in the outlet region. In contrast, a high air change rate (n = 4.5 h^{-1}) results in lower temperatures in the sub-floor followed by a massive condensation during the warm period.
- Only adaptive ventilation in combination with an efficient ground cover ($s_d \geq 2.0$ m) provides a significant improvement in moisture conditions: (1) the relative humidity lower than 80 % throughout the year, and, (2) a negligible condensation in both the inlet and outlet regions. The differences among the respective n-values are small, only the number of fan operating hours drops with higher air change rates (0.5 h^{-1} ~ 4870 h/a; 4.5 h^{-1} ~ 2300 h/a; for s_d = 10 m).

Figures 10 and 11 show the sub-floor's hygrothermal behaviour in configuration with the highest level of moisture safety, i.e. with an efficient ground cover (s_d = 10 m) in combination with adaptive ventilation providing a low air change rate (n = 0.5 h^{-1}). Comparing with the current state (see Figure 8), there is a notable increase in temperature and a drop in relative humidity throughout the year. However, a short inlet region is still in risk of condensation and the conditions excluding mould growth might not be satisfied here. The operating scheme of the ventilation is shown in Figure 12. The times when the outdoor air would moisten the sub-floor, and thus the fan would be switched off, account for 45 % of the year.

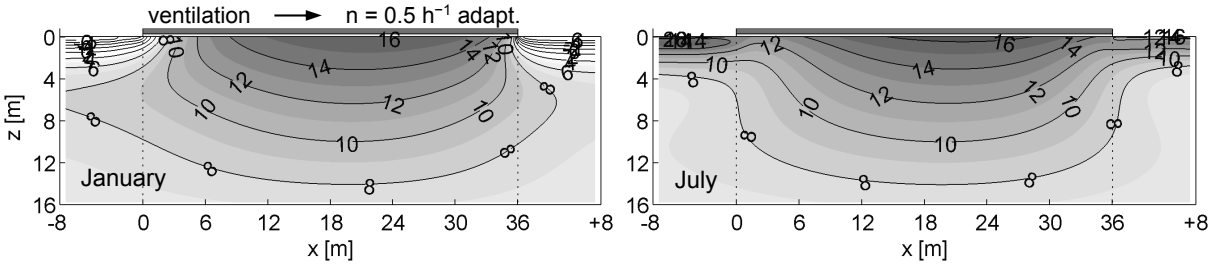

FIG 10. Temperature in the ground under the sub-floor: T(x,z,t), a cut-out from the ground domain

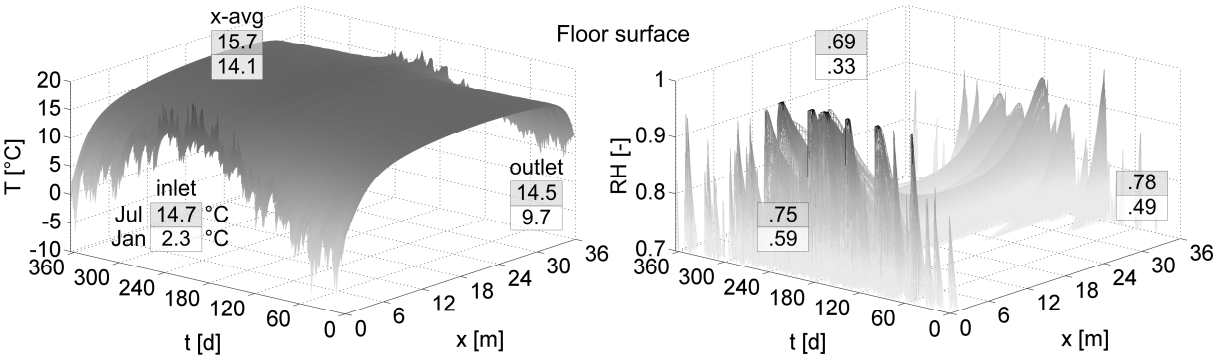

FIG 11. Temperature (left) and relative humidity (right) on the floor surface: T(x,t), RH(x,t)

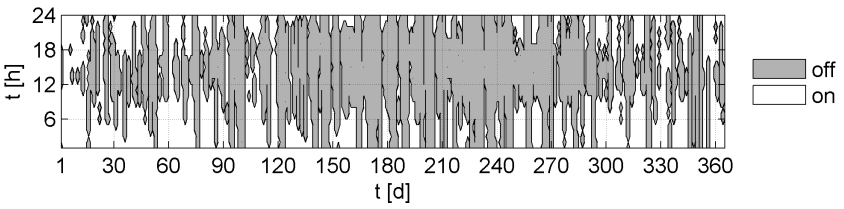

FIG 12. Operating scheme of the adaptive ventilation (fan on/off)

4. Conclusions

There are several decisive factors causing critical moisture conditions in the studied sub-floor:

- The sub-floor height (0.27 m) is disproportional to the floor area (36 × 52 m). Although it is possible to ventilate the sub-floor, even a weak ground moisture source inevitably leads to an excessive relative humidity. The sub-floor is also inaccessible for inspections and maintenance.
- The ground surface is not equipped with any cover that would act as a capillary break and provide a sufficient barrier against diffusion of the ground moisture into the sub-floor. A groundwater level at the depth ranging from 1.5 to 3.0 m in combination with the sandy clay loam guarantee steady moisture transport from the saturated zone to the surface.
- Constant mechanical ventilation moistens the sub-floor in daytimes and leads to moisture condensation on the sub-floor surfaces during the warm period.
- There is no peripheral drainage and the perimeter of the sub-floor is not thermally insulated.

A sheltered environment, high relative humidity, presence of liquid water (condensate) and stable temperatures also create favourable conditions for mould growth.

The two principal moisture sources: (1) evaporation from the uncovered ground surface and (2) ventilation by the outdoor air during unfavourable conditions can be cut off by using: (1) an efficient ground cover, together with (2) adaptive mechanical ventilation controlled on the basis of water vapour concentrations. Unfortunately, practical realization of the former in the existing narrow gap is possible only at high costs, if at all, while the latter alone cannot solve the problem.

5. Acknowledgements

This paper was supported by the EU grant CZ.1.05/2.1.00/03.0091 (OP VaVpI) – University Center for Energy Efficient Buildings (UCEEB).

References

Airaksinen M. & Kurnitski J. & Seppänen O. 2003. On the crawl space moisture control in buildings. In Proceedings of the Estonian Academy of Sciences Engineering, Vol. 9, Issue 1, pp. 34-58.

Carpenter P. 2000. Crawl Space Moisture Control – A Fundamental Misunderstanding. Available online: <http://www.smartvent.net/docs/crawlspacestudy.pdf>.

Císlerová M. & Vogel T. 2008. Transport Processes in the Vadose Zone (in Czech only). Czech Technical University in Prague, Faculty of Civil Engineering, Dept. of Irrigation, Drainage and Landscape Engineering. Available online <http://storm.fsv.cvut.cz/on_line/trpr/skriptum.pdf>

InspectaPedia, 2013 [online]. <http://inspectapedia.com/interiors/Crawl_Spaces.php>.

Kurnitski J. & Matilainen M. 2000. Moisture conditions of outdoor air-ventilated crawl spaces in apartment buildings in a cold climate. In Energy and Buildings, Vol. 33, Issue 1, pp. 15-29.

Mathworks, Matlab, 2013.

Meteotest, Meteonorm, 2013.

Pallin S. & Kehrer M. 2013. Hygrothermal simulations of foundations: Part I: Soil material properties. In Journal of Building Physics, Vol. 37, Issue 2, pp. 130-152.

Rose W. & Wolde T. 1994. Moisture Control in Crawl Spaces. In Wood Design Focus, Vol. 5, No. 4, pp. 11–14. Forest Products Society.

Samuelson I. 1994. Moisture control in crawl space. In ASHRAE Technical Data Bulletin, Vol. 10, Issue 3, pp. 58-64.

Convective drying of a calcium silicate sample: measurements and simulations

Marnix Van Belleghem, Ph.D [1]
Marijke Steeman, Assistant Professor [2]
Arnold Janssens, Professor [3]
Michel De Paepe, Professor [1]

[1] Ghent University, Department of Flow, Heat and Combustion Mechanics, Belgium
[2] Ghent University, Department of Industrial Technology and Construction, Belgium
[3] Ghent University, Department of Architecture and Urban Planning , Belgium

KEYWORDS: *calcium silicate, convective drying, coupled heat and mass transfer, hygroscopic, capillary active*

SUMMARY
This paper describes a drying experiment of a calcium silicate sample. Calcium silicate is an inorganic, hygroscopic and capillary active insulation material, that is often used as high-temperature or fire resistant insulation. During the drying experiment a small test sample (10cm x 10cm x 5cm), of which the sides and bottom were sealed for moisture, was saturated with water. The sample was placed in a climatic chamber, conditioned air was blown over the top surface of the sample. The temperature inside the sample at various depths as well as the mass change of the sample was monitored during the drying experiment.

The measurement results revealed an atypical drying behaviour of calcium silicate: during the second drying phase an intermediate temperature equilibrium seemed to occur. A recently developed heat and mass transport model that was implemented in a finite element solver, was used to study the observed phenomena in more detail. Based on the numerical simulations it was clear that as the material dries out, the dry top layer of the sample acts as an insulation layer on top of the wet material, causing the jump in temperature.

1. Introduction

Due to poor construction quality or deficiencies, building materials can be wetted due to surface condensation or interstitial condensation, rain penetration, water leakages, rising damp etc. If the building materials cannot dry out this may lead to severe moisture-related damage such as loss of thermal insulation quality, corrosion, wood rot, etc.

In the past a lot of research focused on the drying and wetting kinetics of porous (building) materials. Based on the knowledge of heat and moisture transfer in porous materials, several numerical models have been developed that help scientists and engineers to understand and predict the drying and wetting behaviour of porous (building) materials. Although the drying behaviour of most common building materials has already been studied, insulation materials were seldom addressed because, in contrast to building materials such as brick, wood or gypsum board, most insulation materials are non-hygroscopic and non-capillary. However, a building material such as calcium silicate (Ca_2SiO_4) combines a hygroscopic and capillary active behaviour with a relatively low thermal conductivity. The high moisture buffering capacity of calcium silicate enables it to dampen humidity variations and occasional interstitial condensation can be redistributed and transported out of the material due to the high capillary activity.

Due to its resistance to high temperatures this kind of material is often used as high-temperature or fire resistant insulation. Also, it is often used as thermal insulation material in interior insulation systems without a vapour barrier (Pavlík 2012).

In this paper the drying behaviour of calcium silicate when initially saturated with water is studied. Due to the combination of a high capillary activity and low thermal conductivity when dry, the material reveals an atypical drying behaviour.

2. Drying experiment

2.1 Set-up

In the drying experiment a calcium silicate test sample measuring 10cm x 10cm x 5cm was used. Both the sides and the bottom of the sample were sealed for moisture using silicone rubber. To insulate the sides of the sample, polyurethane foam (5 cm thick) was used, having a thermal conductivity of 0,023 W/mK. Various thermocouples were installed in the sample at a depth of 7mm and 17mm to monitor the temperature over time during the drying of the sample. Two thermocouples were installed respectively at the bottom of the sample and at the bottom of the PUR insulation. After calibration, temperature is measured with an accuracy of 0,1°C. The position of the thermocouples is shown in FIG 1.

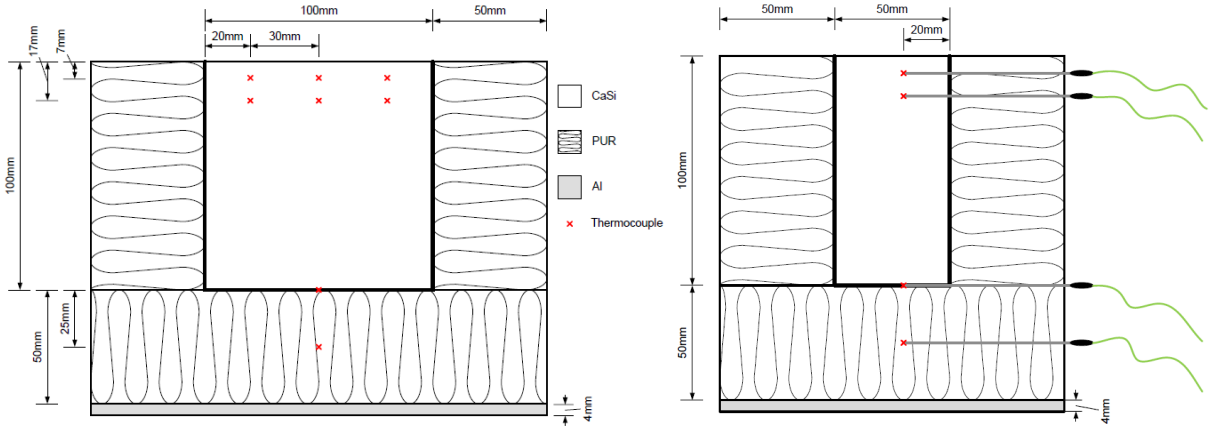

FIG 1. Longitudinal (above) and cross section (below) of the calcium silicate test sample: CaSi=calcium silicate; PUR = polyurethane insulation; Al = aluminium

The sample was placed in a climatic chamber, and conditioned air was blown over the top surface of the sample. Airflow flowing from one side over the sample could result in a leading edge effect: the leading edge may dry faster than the trailing edge. In order to evaluate this effect, three thermocouples were installed at 7mm and 17mm, centrally, upstream and downstream of the airflow. However, the measured temperatures at these locations did not indicate such leading edge effect.

Before the experiment, the sample was saturated with water by immersing it. Next, the sample was placed on a balance in a climatic chamber. The climatic chamber consists of an inner chamber (1,8m width x 1.89m depth x 1.8m height) and an outer chamber (3,0m width x 2,7m depth x 2,4m height) and was used to ensure well-controlled boundary conditions. Both chambers are well-insulated and vapour tight (Steeman 2010, Van Belleghem 2011). The climatic chamber contains an air handling unit that allows to control the supply air velocity, temperature and relative humidity. During the experiments, the inlet air temperature was controlled at 30 ± 0.1°C, the relative humidity of the inlet air was 20 ± 1.4%. The test room was ventilated with an air change rate of 10ACH.

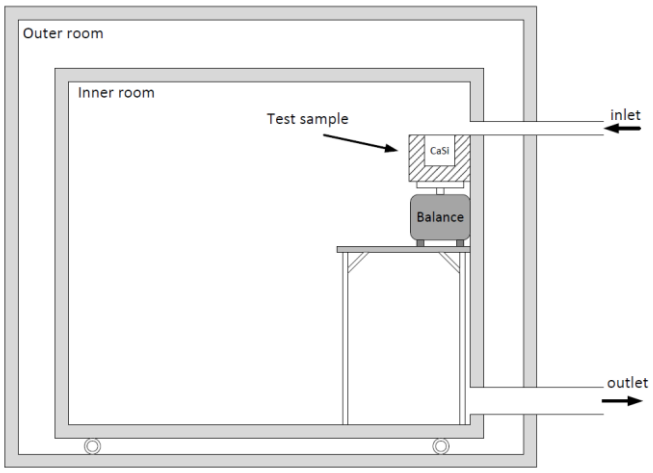

FIG 2. Vertical schematic section of the climatic chamber with the calcium silicate sample placed just beneath the air inlet on top of the balance.

The sample was installed in such a way that the air jet flows over the top surface of the sample (FIG 2). During the drying experiment, the mass change of the sample was measured over time. A precision balance (PE1200 Mettler-Toledo) was used, after calibration the precision was ± 2g.

2.2 Results of the drying experiment

2.2.1 Average mass loss

Because it was difficult to perfectly control the boundary conditions during the experiment (due to some imperfect insulation of the climatic chamber), the drying experiment was repeated several times. An average mass loss curve was derived from these measurements.

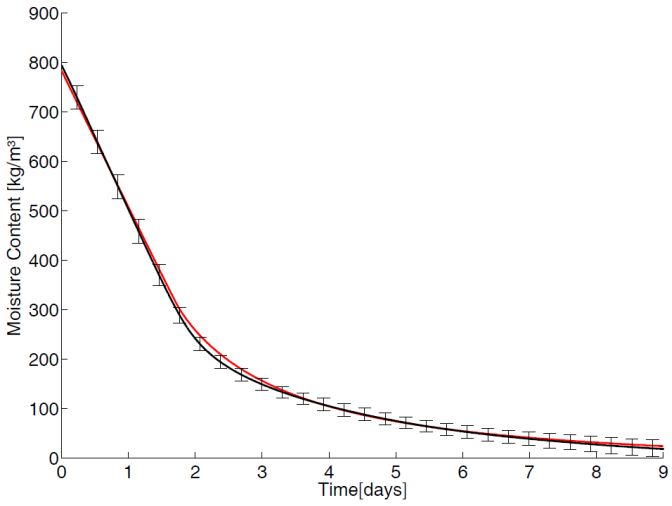

FIG 3. Measured (black) and simulated (grey) moisture content of the sample during the drying experiment

FIG 3 shows, as a result of the continuous weighing of the sample, the evolution of the sample mass during first nine days of the drying experiment. The error bars indicate two times the standard deviation of the successive measurements and are a measure of the uncertainty on the mass loss due to variations in the boundary conditions between the experiments. In FIG 3 two drying phases can be

clearly distinguished. During the first two days of the experiment, the sample mass decreases at a constant rate. This is the constant drying period (CRP). After two days, the mass change slows down and the drying rate decreases accordingly. This period corresponds to the falling period (FRP) or the second drying period.

2.2.2 Temperature

FIG 4 shows the temperature course at 7 mm and 17 mm depth in the calcium silicate during the first nine days of the drying experiment. The temperature evolution clearly shows three drying stages. A constant drying period can be observed during the first two days, as was also seen in the average moisture content measurements (FIG 3). During this period, the temperature in the sample drops near to the wet bulb temperature. After two days, the surface of the sample starts drying out, and the sample enters the second drying period. In this period, the drying rate decreases and temperature in the sample rises.

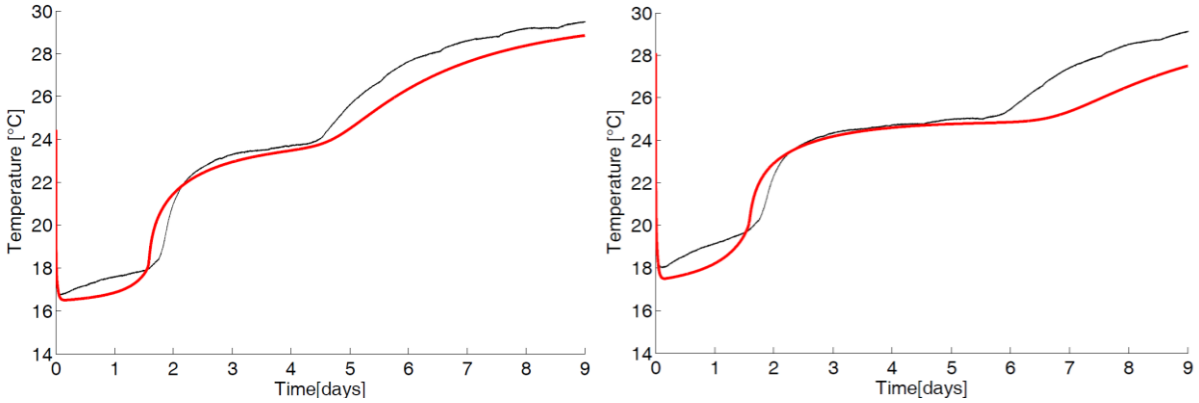

FIG 4. Temperature evolution during the drying experiment (a) at 7mm depth in the sample, and (b) at 17mm depth in the sample : measured (black) and simulated (red)

Furthermore, the temperature rise seems to occur in two phases: first the temperature rises to ± 24°C and a new temperature equilibrium seems to occur. After some time, the temperature rises even further to eventually reach the supply air temperature (± 30°C). At that moment the sample is completely dried. This intermediate temperature platform was also observed by Kowalski (2007) during their experiments in which they have studied the convective drying of a cylindrical kaolin sample.

3. Numerical convective drying model

Next, the convective drying of the calcium silicate sample was modelled using a recently developed heat and mass transfer model that was implemented into a 3D finite element solver (®Fluent). The coupled heat and mass transfer model includes both vapour and liquid moisture transfer. In the model, the driving force for liquid transport was the capillary pressure, the partial vapour pressure was used as the driving force for vapour transport. The model was developed for studying phenomena such as moisture-related damage and drying of building materials more accurately. The model allows for three-dimensional simulations.

For more information about the transport equations for heat and mass that are used in the coupled model the reader is referred to Van Belleghem (2013).

3.1 Simulation model

The convective drying of the calcium silicate sample was modelled using a computational domain representing the actual test section. For symmetry reasons only half of the test sample was modelled. The computational domain is shown in FIG 5. The grid was fine near the top surface of the sample and courser towards the bottom (in total 72390 cells). The polyurethane insulation layer was included in the computational domain. The PUR insulation was assumed impermeable for moisture. At the top surface a constant convective heat transfer coefficient of 25 W/m²K was imposed, at the sides and bottom surface a constant value of 8W/m²K was imposed.

In order to account for potential heat gains by radiation from the environment, an additional radiation heat flux was imposed to the top surface of the sample. The convective drying was simulated for nine days, using a time step of 60s.

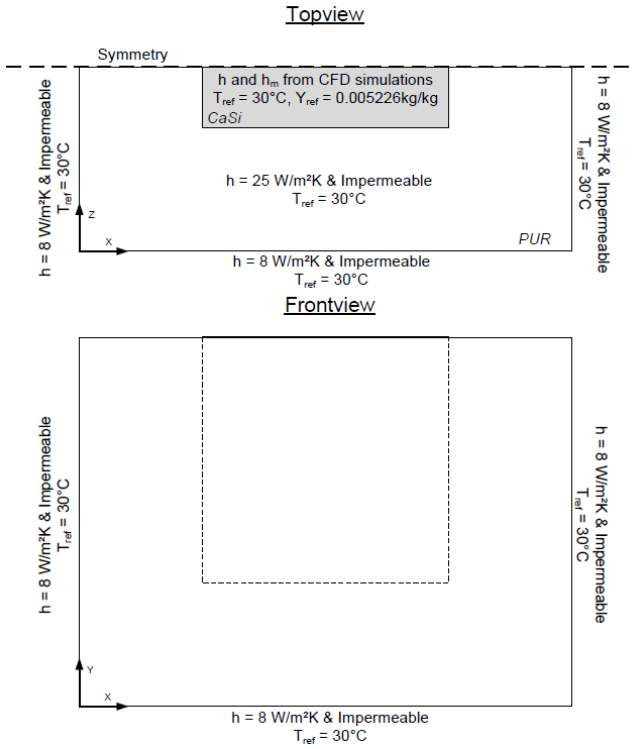

FIG 5 Computational domain with boundary conditions on exterior surfaces

3.1.1 Preliminary simulations

In the current set-up, the boundary condition at the top surface of the calcium silicate material is complicated. Due to the round air inlet in the experiment, the airflow over the calcium silicate sample has a three-dimensional character and the convective heat and mass transfer distribution over the surface is two-dimensional. Therefore, it is not possible to impose a single constant convection coefficient to this surface. Furthermore, previous studies have shown that the convective heat and mass transfer coefficients have a dominant role during the first drying rate period, while during the second drying rate period, the drying rate is mainly determined by the internal transport properties of the porous material.

Preliminary CFD simulations were performed in order to estimate the course and distribution of the convective transfer coefficients at the top surface of the calcium silicate sample. In these simulations only the part near the inlet of the climatic chamber was modelled. These preliminary simulations show that these transfer coefficients have a complex distribution. Near the air inlet where the

boundary layer starts, the convective transfer coefficients are higher. The average heat and mass transfer coefficient are 50.8 W/m²K and 0.0603 s/m respectively. More details on the preliminary simulations and the two-dimensional transfer coefficient distribution can be found in Van Belleghem et.al. 2013.

3.1.2 Material properties

The material properties required in the coupled heat and mass transfer model (TABLE 1) were taken from the HAMSTAD project, where the material properties of calcium silicate were extensively measured (Roels 2003 and Adan 2004). The coupled heat and mass transfer model makes use of the vapour diffusion resistance μ, the liquid permeability K_l and the moisture capacity $\partial w/\partial pc$. The water vapour resistance factor μ and the sorption isotherm are formulated by Eq. (1) and Eq. (2) respectively, where RH is the relative humidity (-), T is the temperature (K) and R_v is the specific gas constant for water vapour (J/kgK). a and n are constants, respectively equal to -2,936 x 10^{-5} and 1,7266. The liquid permeability of calcium silicate is shown in FIG 6.

$$\mu = \left[0.33 + 2.49x10^{-6} \exp\left(6.84RH\right)\right]^{-1} \quad (1)$$

$$w = w_{cap}\left[1 + \left(a\rho_{liq}R_vT\ln\left(RH\right)^n\right)\right]^{\frac{(1-n)}{n}} \quad (2)$$

TABLE 1. Material properties of calcium silicate, based on Roels (2003) and Adan (2004)

Density ρ (kg/m³)	270
Thermal conductivity (W/m.K)	0,06 + 5,6 . 10^{-4} w
Specific heat c_p (J/kg.K)	1000
Vapour resistance μ_{dry} (-)	3
Capillary moisture content w_{cap} (kg/m³)	894
Open porosity ψ_0	0,894

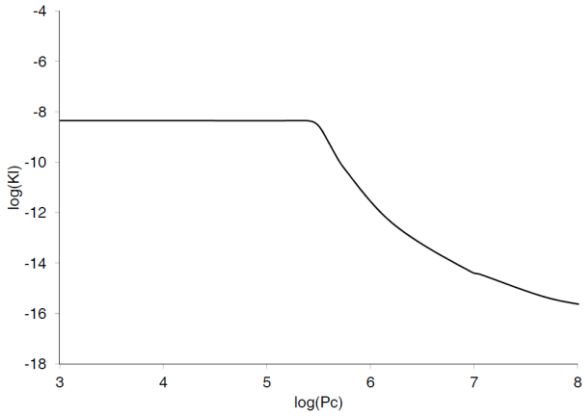

FIG 6 Liquid permeability of calcium silicate, based on Roels (2003) and Adan (2004)

3.2 Simulation results

The drying experiment was modelled using the developed coupled heat and moisture transfer model. The results of the simulated mass loss and the temperatures over time can be found in FIG 3 and FIG 4 and show a good agreement with the measurements. The intermediate temperature platform that was observed in the drying experiment during the second drying period, was also noticed in the numerical simulations. FIG 7 shows the temperature distribution in a longitudinal section of the calcium silicate sample every 24 hours. On the x-axis the length of the sample is shown, on the y-axis the height of the

sample is presented. The PUR insulation layer is also depicted in FIG 7, the calcium silicate sample is indicated with a thin black line. At the start of the simulations, the calcium silicate sample was saturated with water. As the material dries out, a low temperature zone moves into the material. This can be clearly seen in the temperature distribution after the first day of the experiment (FIG 7a). The temperature at the top surface of the calcium silicate sample drops to about 16°C, while the bottom side still has a temperature of about 24°C.

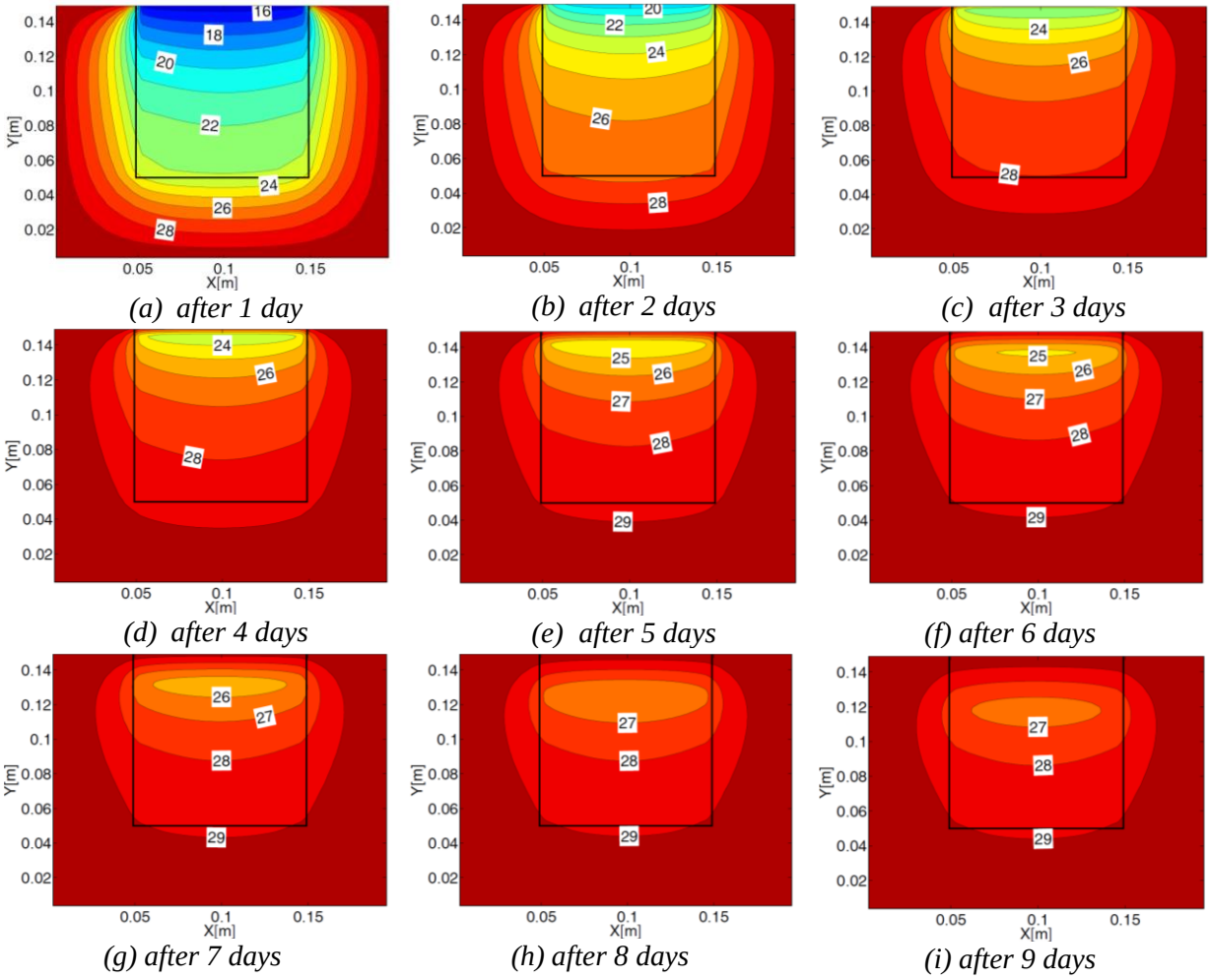

FIG 7 Temperature distribution in a longitudinal section of the calcium silicate sample, shown every 24 hours

The intermediate temperature platform observed in the measurements and the simulations can be explained by the moisture front that is moving in the material, as it dries out. At one side of this moisture front, where the material has already dried out, the relative humidity is low. At the other side of the moisture front, the material is still wet and hence the relative humidity is still close to 100%. At the moisture front, liquid water is evaporating, causing a local drop due to the latent heat accompanied with the evaporation process. For the calcium silicate sample, the intermediate temperature platform is additionally pronounced due to the low heat conductivity of the material when dry. Hence, the dry top layer of the calcium silicate sample acts as an insulation layer on top of the wet material, keeping the temperature in this wet part of the sample low.

The temperature platform that was observed in FIG 4 between the second and the fifth day of the drying experiment can also be noticed in FIG 7: during this time the temperature in the upper layer of

the sample stays more or less stable around 24°C while from the 5th to 7th day on, the temperature increases to about 28°C, which is in accordance with the findings in FIG 4.

4. Conclusions

This paper presents a convective drying experiment conducted with a calcium silicate sample. The experiment showed a very specific drying course of the calcium silicate material: during the second drying period an intermediate temperature platform was observed. By means of simulations this phenomenon could be explained. A recently developed coupled heat and moisture transport model that includes both water vapour diffusion and liquid water transport was used to model the convective drying experiment. The model allows for three-dimensional simulations of the temperature and moisture distribution and is very well-suited to this kind of application. The simulations showed that the intermediate temperature platform could be explained by the low thermal conductivity of calcium silicate when being dry. As the sample dries out, a moisture front moves into the sample. At the top side of the sample the material is already dry, and acts as an insulation layer. By consequence, the heat that is needed for evaporation of liquid water at the moisture front, is taken from the sample, hence lowering locally its temperature. This phenomenon is clearly linked to hygroscopic capillary active insulation materials and cannot be found in non-insulating materials such as ceramic brick.

5. Acknowledgements

The results presented in this paper were obtained within the frame the research project IWT-SB/81322/Van Belleghem funded by the Flemish Institute for the Promotion and Innovation by Science and Technology in Flanders. Their financial support is gratefully acknowledged.

References

Steeman M., Van Belleghem M., De Paepe M. & Janssens A. 2010. Experimental validation and sensitivity analysis of a coupled BES-HAM model. Building and Environment, Volume 45, Issue 10, p. 2202-2217.

Pavlík Z., Mihulka J., Fiala L. & Cerný R. 2012. Application of Time-Domain Reflectometry for Measurement of Moisture Profiles in a Drying Experiment. International Journal of Thermophysics, Volume 33, p. 1661-1673.

Kowalski S.J., Musielak G. & Banaszak J. 2007 Experimental validation of the heat and mass transfer model for convective drying. Drying Technology, Volume 25, p. 107-121.

Adan O., Brocken H., Carmeliet J., Hens H., Roels S. & Hagentoft C.-E. 2004. Determination of liquid water transfer properties of porous building materials and development of numerical assessment methods: Introduction to teh EC HAMSTAD project. Journal of Thermal Envelope and Building Science, Volume 27, Issue 4, p. 253-260.

Roels S., Carmeliet J. & Hens H. HAMSTAD WP 1: Moisture transport properties and material characterisation. Final report. Technical report, KULeuven.

Van Belleghem M., Steeman M., Willockx A., Janssens A. & De Paepe M. 2011. Benchmark experiments for moisture transfer modelling in air and porous materials. Building and Environment, Volume 46, Issue 4, p. 884-898.

Van Belleghem M. 2013. Modelling coupled heat and moisture transfer between air and porous materials for building applications. Ph.D.-thesis. Ghent University, Belgium.

Van Belleghem M., Steeman M., De Geyter W., Stuer G., Janssens A. & De Paepe M. 2013. Drying behaviour of calcium silicate. Submitted to Journal of Construction and Building Materials.

Guidelines on the prevention of built-in moisture

Ernst Jan de Place Hansen, Senior Researcher, Ph.D. [1]
Eva B. Møller, Senior Researcher, Ph.D. [1]

[1] Danish Building Research Institute, Aalborg University, Denmark

KEYWORDS: *Moisture, guideline, building process, humidity risk class, mandatory or voluntary*

SUMMARY:
As a result of built-in-moisture, a number of buildings in Denmark were attacked by moulds even before the users moved in. Therefore, the Danish Building Regulations have since 2008 stipulated that building structures and materials must not, on moving in, have a moisture content that is liable to increase the risk of mould growth. In some cases, authorities can demand that this should be documented by a moisture specialist.

The paper describes a voluntary Danish guideline on how to comply with the requirements and the intentions in the Danish Building Regulations concerning the handling of moisture at each stage of the building process spanning from the proposal phase to delivery of the building and the 1-year and 5-year inspections. This includes categorising a specific building in a humidity risk class as the risk for moisture damages is related both to the expected exposure to moisture during the execution phase and the building's capacity to withstand moisture. It also specifies how moisture should be dealt with in the general quality assurance system of the building industry.

The Danish guideline is compared with similar guidelines and tools in other Nordic countries. The education of moisture specialists is emphasised and it is questioned whether a voluntary guideline will have the desired effect.

1. Introduction

Moisture in buildings often results in an unhealthy indoor climate. This has been known for a long time and many efforts have been made to avoid moisture after moving in. Moisture added to the building during the execution phase has been regarded as unavoidable and it was expected to dry out during the building's first year of use. In a number of cases in Denmark, the completed building was so wet - because of moisture added to the building during the execution phase - that part of the construction was attacked by moulds even before the inhabitants began using the building.

As a result, the Danish Building Regulations (DBR) have since 2008 stipulated that building structures and materials must not, on moving in, have a moisture content that is liable to increase the risk of mould growth (Danish Enterprise and Construction Authority 2008). In 2010, a guideline was introduced to help clients comply with requirements and the intentions outlined in DBR concerning how to deal with moisture at each stage of the building process (Møller 2010). This includes the categorisation of a specific building in a humidity risk class, as the risk of moisture damage is related both to the expected exposure to moisture during the execution phase and the building's susceptibility to moisture. It also specifies how moisture should be handled in the general quality assurance system of the building industry.

2. Moisture requirements in the Danish Building Regulations

A general requirement to construct buildings to prevent water, moisture and damp from causing damage has been part of DBR since 1972 (Ministry of Housing 1972). In 2008, three important requirements concerning control of the moisture content in building structures and materials were added (Danish Enterprise and Construction Authority 2008). The first one states that measures to counter weather conditions that are essential to the proper construction of a building must be taken during planning, design, tendering and execution. The functional requirement may, for example, be complied by:

a. Avoiding materials and constructional solutions that are unduly moisture-sensitive

b. Explicitly allocating time in the client's tendering plan and time schedule for all necessary drying out of building materials and structures

c. The client carrying out a cost-benefit analysis of fully enveloping the building during execution. Further by prescribing total enveloping if it is financially viable, or where the tender documents specify particularly moisture-sensitive materials or constructional solutions

d. The client providing shared facilities for storage of moisture-sensitive materials.

The second requirement states that:

e. Building structures and materials should not, on moving in, have a moisture content that is liable to increase the risk of mould growth.

In both new buildings and renovation projects, this requirement minimises the risk of moving into overly damp buildings and the risk of mould growth.

Finally, in the administrative provisions it is stated that

f. The building permit may impose requirements for the measurement or other types of documentation provided by a moisture specialist in order to verify compliance with requirement e) with respect to the critical moisture content of structures and materials.

This requirement highlights the need of specialists to document moisture conditions at execution.

3. Guideline for dealing with moisture in the execution phase

DBR does not describe how it is documented that these requirements are complied with. To a great extent, the client and the authorities are entrusted with interpreting the requirements in a specific case. Therefore, a guideline for dealing with moisture in the execution phase was prepared for the Danish Enterprise and Construction Authority (Møller 2010). For each step in the building process from the preliminary design phase to the 5-year inspection, the basic decisions are presented and it is suggested, what kind of documentation would be relevant, and how this should be implemented in the quality assurance system of the building industry.

The client defines the kind of competences of the moisture specialist and the amount of documentation that would be relevant in order to comply with requirement f). The moisture specialist does not have to be independent of the contractor. His tasks are described in (Aagaard et al. 2011) and it is emphasised that the requirements in DBR are minimum requirements and that the client may benefit by setting stricter requirements. Therefore the construction client needs guidance to decide

- when it is relevant to consult a moisture specialist
- what kind of competences should be asked for
- how the competences of the specialist should be documented, and
- what kind of requirements can be made to the work of the moisture specialist in the different phases of the construction project.

A number of fundamental decisions on materials and design are taken very early in the building process. Many discontinuities and penetrations will for example increase the risk of moisture entering both during execution and afterwards in the operating phase. From an early stage in the building process, the client must therefore consider if and when a moisture specialist is needed. It is recommended to categorise the building in the relevant humidity risk class (Section 3.2). By doing this, the actors in the building process have from the beginning an idea of whether moisture is expected to demand more than normal attention and can evaluate whether the project would benefit by a involving moisture specialist.

3.1 Documentation

For each stage in the building process, Møller (2010) suggest, what kind of moisture documentation would be relevant as listed in Table 1. The documentation should be part of the quality assurance system of the different companies that at some point or other are involved in the building process.

TABLE 1. List of moisture documentation referring to different stages in the building process.

Stages in the building process	**Documentation of moisture conditions**
Project proposal	A list of conditions subject to risk regarding moisture Description of precautions to respond to the risk
Project design	A moisture strategic plan including • Description of steps that call for special attention in the execution phase • Description of what precautions the project supervisor has taken • A control plan documenting conditions throughout the building process and working as a “warning lamp” • Description of remedies or actions to correct defects
Tender	Tender documents should include • Control plans, describing for each building element when and how to control moisture conditions • Description of how a random check of moisture conditions is to be documented
Execution	Moisture measurements and photos from delivery of the materials and elements to the closing of a construction, according to control plans. Measurement results are evaluated before materials are built-in and again before constructions are closed.
Delivery	Ensure that moisture conditions do not exceed the requirements and if they do, this should be added to the list of deficiencies. Ensure that the documentation report made by the moisture specialist is added to the documents delivered to the authorities if they have requested documentation of the moisture conditions.
1- and 5-year inspection	Control measurements to document whether the moisture conditions are satisfactory. If moisture problems are detected: Documentation of whether the problems are caused by inexpedient operation or defects that can be related to the project design or the execution.

The guideline accentuates the possibility of conducting a preliminary dialogue between the authorities and the client to ensure a higher quality of the completed building, to achieve a better economy during the building process, to reach a better understanding between client and authorities and to improve the quality of the application documents. Finally expectations to the documentation material can be adapted, including an assessment of the need for documentation of the moisture conditions.

3.2 Humidity risk classes

The risk of moisture problems arising during the execution of a building depends primarily on

- how great the moisture exposure is during execution
- how susceptible the building is to moisture.

By combining these two properties, it can be assessed in which humidity risk class a building belongs during execution. Based on this, the actors in the building process can evaluate what measures it would be relevant to take. The Danish guideline (Møller 2010) includes three humidity risk classes labelled 1, 2 and 3, as listed in Table 2.

TABLE 2. Humidity risk classes as a function of exposure to moisture during execution and the susceptibility of the building to moisture.

The susceptibility of the building to moisture	Exposure to moisture during execution		
	Low	Medium	High
Low	class 1	class 2	class 2
Medium	class 1	class 2	class 3
High	class 2	class 3	class 3

Whether the exposure to moisture during execution is low, medium or high depends on

- how wet the construction and assembly processes are, e.g. concrete cast in situ
- to what extent the construction and assembly processes take place without covering.

The susceptibility of a building to moisture is related to

- the ability of materials to absorb moisture
- the mould risk of a specific material
- the time available for drying.

It is highlighted that the combination of materials can be critical, e.g. the combination of moisture-sensitive materials like wood and plaster boards and materials with a high amount of moisture at execution like concrete cast in situ.

TABLE 3. Suggestions of how humidity risk classes can be utilised to determine the need for measures before and during execution. All measures must be documented.

	Risk class 1	Risk class 2	Risk class 3
Before execution	Comply with minimum requirements in DBR	Minimum requirements and: – Setting up a moisture strategy plan	Minimum requirements and: – Setting up a moisture strategy plan – Calculation or simulations if possible – Involve a moisture specialist
During execution	– Moisture measurements at critical times; as minimum before closing the building	– Continuous moisture measurements – Limited measurement programme – Assess specific potential moisture problems	– Continuous moisture measurements – Expanded measurement programme – Involve a moisture specialist

It is not a requirement to categorise a building or a part of a building in a specific humidity risk class before execution or to decide whether the risk class varies during execution. However, by introducing

humidity risk classes, the consulting engineer can make it quite clear to the client that he is taking a risk. The engineer can also demonstrate how the risk can be reduced and where special precautions are necessary, including the use of a moisture specialist, as described in Table 3.

4. Discussion

Moisture related problems in new buildings are well known not only in Denmark but e.g. in Sweden (Samuelsson & Wånggren 2002) and Norway (Mehus et al. 2004). The requirements in the building regulations for airtight buildings to ensure high energy performance as well as the use of moisture sensitive materials highlights the need to control the moisture content of building materials and components during the building process.

4.1 Moisture requirements in building regulations in other Nordic countries

Like in Denmark, the building regulations in Sweden and Norway include a general requirement to prevent moisture from causing damage (Boverket 2011; Ministry of Local Government and Regional Development 2010), e.g. the Norwegian one stating that ground water, surface water, precipitation, construction moisture and vapour must not enter and cause moisture damage, formation of mould or dry rot or hygienic problems.

Additionally, the Norwegian Building Regulations (NBR) states that materials and constructions must be sufficiently dry when they are built in or sealed to avoid problems with mould or dry rot (Ministry of Local Government and Regional Development 2010; Directorate for Building Quality 2011).

The Swedish Building Regulations (SBR) prescribes that the moisture condition of a building element may not exceed the critical moisture conditions (Boverket 2011). SBR even prescribes that the moisture conditions are to be calculated for a worst-case scenario. This is more descriptive than DBR, which does not specify how the critical moisture conditions are to be identified.

In Table 4 requirements in the Danish, Swedish and Norwegian Building Regulations and the existence of guidelines are compared with reference to prevention of built-in moisture.

TABLE 4. Moisture requirements in national building regulations in Denmark, Sweden and Norway and existence of guidelines for a moisture safe building process.

Requirement in national building regulations	Denmark	Sweden	Norway
To prevent moisture from causing damage	General	General	General
That materials and building elements may not exceed a critical moisture content[1]	Yes, at moving in	Yes	Yes, at building in
Documentation by moisture specialist	Yes	No	No
Formal requirements for moisture specialist	No	No	No
Moisture calculation as documentation	No	Yes	No
Guidelines	Voluntary	Voluntary	No
Education for moisture specialist	No[2]	Exists, but not required	No
Critical moisture content	75 %RH	75%RH	20 weight-% [3]

1): Comparable to the Danish requirement presented as e) in Section 2.
2) Post graduate education in building physics established.
3) Critical moisture content for wood.

Since 2008 DBR specifically requires that documentation concerning moisture conditions has to be elaborated by a moisture specialist, presented as requirement f) in Section 2. Neither NBR nor SBR includes a similar requirement. However, since 2009 requirement f) does not apply to detached single-family houses and terraced houses as it was decided to more or less skip the technical aspect of the processing of applications for buildings permits in Denmark for these types of buildings. They are labelled “constructions of limited complexity”. Although this highlights the client's responsibility to

comply with DBR, it can be questioned whether such a simplification is appropriate as no survey has been made to justify that detached single-family houses and terraced houses have less problems with moisture on moving in than other types of buildings. Actually, the most known cases in Denmark with critical moisture content on moving in are in terraced houses.

In Norway a similar transfer of responsibility of the technical contents from the authorities to the client took place in 1997 as the technical aspect of the processing of applications for building permits was radically diminished (Øyen et al. 2008). The volume of defects caused by moisture, and defects in general, related to the execution phase was reduced after the transfer of responsibility (Mehus et al. 2004), but it is not possible to conclude whether this is an effect of the transfer.

4.2 Guidelines and standards for a moisture safe building process

In Sweden, a voluntary building industry standard for a moisture-safe building process (ByggaF) was developed (Mjörnell et al. 2012; Fuktcentrum 2013). The standard describes which actions are to be taken by the different actors in a building process from planning to operation. It includes a number of tools and aids for developers to specify requirements for moisture safety early in the project, and to follow up and document the measures employed by different participants. A moisture specialist is mentioned in ByggaF but not in SBR. Instead the industrial partners behind the standard have developed a voluntary moisture specialist education. In Denmark, postgraduate education in building physics was established with reference to DBR's introduction of moisture specialists. However, the authorities have no plans for setting any formal requirements for moisture specialists.

Tools to help the client and the consulting engineer to evaluate what kind of risk is involved when using different solutions or strategies are included both in the Danish guideline (Møller 2010) and ByggaF. The Danish guideline applies humidity risk classes (Tables 1 and 2) to grade the number of actions to be taken to handle moisture in the building process, while ByggaF includes 20 statements that can affect the moisture safety if they are present or might occur, e.g. that moisture-sensitive materials are expected to be used or that the project lacks a moisture specialist. Each of the statements are rated from 1 (not probable) to 5 (highly probable). The average value of these ratings expresses the complexity of the project, but no specific actions are attached to a certain average rating.

Neither ByggaF nor the Danish guideline is referred to in the national building regulations, but ByggaF is based on cooperation between many partners from the Swedish building industry, universities and authorities thus forming a basis for acceptance of the method, while the Danish guideline was initiated solely by the authorities, although a number of partners from the Danish building industry have contributed to the guideline with rules of thumb. The use of the ByggaF method has led to more focus on the importance of moisture safety and is considered to improve the quality of building projects, although the tools and checklists could be simpler to use (Mjörnell et al. 2012). It might be questioned whether the strategy used in Denmark for developing a guideline is suitable for ensuring implementation in the building industry as documentation of the moisture conditions at moving in is almost never present in the documents sent to the authorities as part of the case (de Place Hansen & Aagaard 2013).

Both the Danish guideline and the Swedish standard place the decisions on the client, concerning what kind of activities to launch to prevent moisture from causing damage, as it is in his interest that the building contains no potential defects. It is also highlighted that moisture safety requirements should be incorporated in the planning and project design by integrating moisture prevention in the quality assurance system of the professionals. As the client is usually the person involved in the building process with the least knowledge of technical aspects both Møller (2010) and Fuktcentrum (2013) highlights the need to involve a moisture specialist – or at least consider to involve such a person helping the client to set up and follow up on the requirements regarding moisture safety.

In Norway the need to focus on the relationship between organising the building process and the prevalence of moisture-related building defects in the completed building, and to develop multidisciplinary organisational guidelines on how to deal with moisture problems during planning, design and execution was addressed as well (Lisø et al. 2005; Øyen et al. 2008). Although such guidelines remain to be developed, NBR refers to a number of building detail sheets, including (SINTEF Byggforsk 1998), which contain control items with special focus on moisture protection during project design and execution.

4.3 Disseminating the measures that prevent built-in moisture

The authorities in Denmark, Sweden and Norway have acknowledged that moisture safety needs to be addressed in their building regulations and that guidelines and tools are necessary to help the client to comply with the requirements as they are function-based. Such guidelines and tools can either be mandatory or voluntary. Often the authorities are reluctant to demand that clients follow a specific guideline as this might be regarded as unnecessary costs by the clients. However, measures introduced to improve the quality and reducing the volume of defects in the Danish construction sector have shown that mandatory systems have the greatest impact (de Place Hansen 2013). Moreover, many non-professional clients only build one house in his or her lifetime and do not have the experience gained from previously completed building projects on how to avoid built-in moisture.

As the initiatives implemented in Denmark and Sweden are relatively new, the effect of these remains to be seen but some kind of campaign to make the guidelines known in the building sector could be beneficial. Only in Denmark are systematic records made of building defects and only for social housing projects (Building Defects Fund 2013). However, these are categorised according to specific building parts and not according to whether they are caused by moisture.

The introduction of guidelines/tools to improve the competences concerning moisture safety, and the introduction of moisture specialist educations highlight the need for persons with such competences.

5. Conclusions

The main findings of this study were:

- Function-based requirements were introduced in Denmark, Sweden and Norway to prevent built-in moisture and highlight the responsibility of the client. In Denmark and Sweden, voluntary guidelines and tools operationalise the requirements and describe how to document that the requirements are complied with.
- The guidelines describe how prevention of built-in moisture should be a part of the quality assurance of all partners in the building process.
- Education of moisture specialists introduced both in Sweden and Denmark is vital to ensure that the guidelines and tools become a success by demonstrating how the risk of built-in moisture can be reduced. Only the Danish Building Regulations refer to a moisture specialist
- The effect of the guidelines and tools remains to be seen, but it is questioned whether voluntary guidelines will have the desired effect and whether it is reasonable to exempt specific types of houses from documentation of moisture conditions like in Denmark.

References

Aagaard N.-J., Høite K. & Møller E.B. 2011. Requirements for moisture documentation and the competences and work of the moisture specialist (author’s translation from Danish). Prepared by the Danish Building Research Institute for the Danish Enterprise and Construction Authority. Copenhagen.

Boverket. 2011. Building Rules – Regulations and General Advice (author's translation from Swedish)]. (BFS 2011:26). BBR 19. The Swedish National Board of Housing, Building and Planning. Karlskrona.

Building Defects Fund. 2013. Annual report 2012 (in Danish). Copenhagen.

Danish Enterprise and Construction Authority. 2008. Building Regulations 2008. Copenhagen.

Danish Enterprise and Construction Authority. 2010. Building Regulations 2010. Copenhagen.

de Place Hansen E.J. & Aagaard N.J. 2013. Constructional documentation in Denmark 2008-2010. Investigation of extent and compliance of requirements for construction of limited complexity (author's translation from Danish). (SBi 2013:05). Danish Building Research Institute, Aalborg University, Copenhagen.

de Place Hansen E.J. 2013. Carrot and stick – how to reduce the amount of defects in Danish construction. Proc. 19th CIB World Building Congress, Brisbane 2013: Construction and Society. (S. Kajewski; K. Manley; K. Hampson; eds). Queensland University of Technology, 2013. 12p.

Directorate for Building Quality. 2011. Guideline on technical requirements for constructions (author's translation from Norwegian). Publication HO-2/2011.Oslo.

Fuktcentrum. 2013. Industrial standard ByggaF. Method for a moisture safe building process (author's translation from Swedish). University of Lund, Lund.

Lisø K.R., Kvande T. & Thue J.V. 2005. Climate 2000 – Building enclosure performance in a more severe climate. Proc. 7th Symposium on Building Physics in the Nordic Countries. The Icelandic Building Research Institute, Reykjavik. Vol. 1, pp. 211-218.

Mehus J., Rolstad A.N., Nordvik V. & Stenstad V. 2004. Change in construction quality. Quantitative registration of volume of building defects. Final report (author's translation from Norwegian). NBI Project Report 379, Norwegian Building Research Institute, Oslo.

Ministry of Housing. 1972. Building Regulations 1972 (in Danish). Copenhagen.

Ministry of Local Government and Regional Development. 2010. Directions on technical requirements for constructions (TEK 10) (FOR 2010-03-26 nr 489) (author's translation from Norwegian). Oslo.

Mjörnell K., Arfvidsson J. & Sikander E. 2012. A method for including moisture safety in the building process. Indoor and Built Environment, Vol. 21, no. 4, pp. 583-594.

Møller E.B. (ed.) (2010): Guideline on handling of moisture in construction (author's translation from Danish). Prepared by the Danish Building Research Institute for the Danish Enterprise and Construction Authority. Copenhagen.

Samuelsson I. & Wånggren B. 2002. Moisture damage. Hammarby Sjöstad, Stockholm (author's translation from Swedish). SP Rapport 2002:15, Technical Research Institute of Sweden, Borås.

SINTEF Byggforsk. 1998. Building details. 474.511. Evaluation of moisture safety. Control items (author's translation from Norwegian). Oslo.

Øyen C.F., Kvande T. & Noreng K. 2008. Insufficient moisture control in the building process – Recommendations for a multi-disciplinary management tool. Proc. 8th Symposium on Building Physics in the Nordic Countries (C. Rode, editor). Report R-189, Dept. of Civil Engineering, Technical University of Denmark, Vol. 3, pp. 1197-1204.

Can painted glass felt or glass fibre cloth be used as vapour barrier?

Amira El-Khattam, M.Sc. [1]
Mie Them Andersen, M.Sc. [2]
Kurt Kielsgaard Hansen, Associate Professor Ph.D. [3]
Eva B. Møller, Senior Researcher Ph.D. [4]

[1] ALECTIA A/S, Denmark
[2] MOE A/S, Denmark
[3] Technical University of Denmark, Denmark
[4] Danish Building Research Institute, Aalborg University Copenhagen, Denmark

KEYWORDS: *Acrylic paint, silicate paint, glass felt, glass fibre cloth, water vapour permeability, water vapour resistance*

SUMMARY:
In most Nordic homes the interior surfaces of walls and ceilings have some kind of surface treatment for aesthetical reasons. The treatments can for example be glass felt or glass fibre cloth which are painted afterwards.

To evaluate the hygrothermal performance of walls and ceilings it is essential to know how much influence a surface treatment has on the water vapour transport. Traditionally, there has been most focus on paints that affect the permeability as little as possible. However, sometimes water vapour resistance is desirable. Especially, this is relevant in existing buildings with a ventilated attic where the ceiling may be air tight but has no vapour barrier; post-insulation of the attic may cause the need for a vapour barrier. Placing a vapour barrier above the ceiling can be tiresome and it is difficult to ensure tightness. A simpler way is to paint a vapour barrier directly on the ceiling e.g. as an ordinary paint.

This paper presents the results of an investigation of the water vapour resistance of surface treatments which are commonly used in-door. The water vapour resistance was measured by the cup method. Aerated concrete was investigated with and without various surface treatments. The surface treatments were glass felt or glass fibre cloth with different types of paints or just paint. The paint types were acrylic paint and silicate paint. The results show that the paint type has high influence on the water vapour resistance while the underlay i.e. glass felt or glass fibre cloth has very little impact.

The measured water vapour resistance for specimens with acrylic paint was the highest, these were measured to be up to approximately $3 \cdot 10^9$ Pa·m^2·s/kg which is considerably less than $50 \cdot 10^9$ Pa·m^2·s/kg as recommended for a vapour barrier. Therefore, two layers of ordinary acrylic paint on glass felt or glass fibre cloth cannot be used instead of a vapour barrier.

1. Introduction

In most Nordic homes the interior walls and ceilings have some kind of surface treatment for aesthetical reasons. Surface treatment will to some extent affect the moisture transport and reduce the moisture transport by diffusion compared to untreated surfaces. How much the diffusion will be reduced depends on the water vapour resistance of the surface treatment. In some cases it is desirable to achieve a high water vapour resistance, e.g. if a vapour barrier is needed but difficult to install. Existing buildings with a ventilated attic where the ceiling may be air tight but has no vapour barrier is

an example of this; post-insulation of the attic may cause the need for a vapour barrier. However, placing a vapour barrier above the ceiling can be tiresome and it is difficult to ensure tightness. A simpler way is to paint a vapour barrier directly on the ceiling e.g. as an ordinary paint.
In the present study aerated concrete was investigated with various surface treatments. The surface treatments were glass felt and glass fibre cloth which were painted with two different types of paints, acrylic paint and silicate paint, respectively. For comparison results without glass felt or glass fibre cloth are also presented.

To investigate the water vapour resistance for the surface treatments the cup method was used.

2. Theory

The vapour resistance is determined by the cup method according to EN ISO 12572 (2001).

It is known that the water vapour resistance is depending on the type of paint, as silicate paint is generally described as an open paint opposed to acrylic paint (Brandt, 2013).

The hypothesis of this paper is, that the water vapour resistance can be increased if the paint layer is supplemented with a layer of glass felt or glass fibre cloth, as these surface treatments are expected to absorb more paint than surfaces without this extra layer. In this way common surface treatments may act as vapour barriers.

3. Materials

Aerated concrete with dry density 535 ± 15 kg/m^3 was used as base material as this material has a high water vapour permeability.

The materials for the surface treatments have been chosen because they are commonly used as surface treatments of walls and ceilings in Denmark, and are expected to have different water vapour permeability.

Seven test specimen series were fabricated:

1. Aerated concrete with no surface treatment (pure aerated concrete)
2. Aerated concrete with two layers of acrylic paint (three series)
    a. Putty and acrylic paint
    b. Putty, glass felt and acrylic paint
    c. Putty, glass fibre cloth and acrylic paint
3. Aerated concrete with two layers of silicate paint (three series)
    a. Putty and silicate paint
    b. Putty, glass felt and silicate paint
    c. Putty, glass fibre cloth silicate paint

For the series with surface treatment a thin layer of putty was applied on one side of the aerated concrete, this was used to level out and fill the coarse pores in the surface. The layer thickness is less than 0.5 mm. On the putty one layer of liquid prime was applied; the liquid prime had a viscosity as water. After this either paint or one of the two kinds of glass fibre and paint was applied. The liquid prime and paint was applied with a roller.

The two kind of glass fibre are called glass felt and glass fibre cloth, which has different structures. They are both made of the same inorganic material; small fibres of glass. However, the differences in the two are the structure; one has a glass fibre mat with a smooth surface where the other is woven glass fibre. The two different structures are shown in FIG 1.

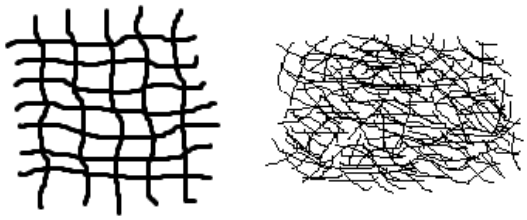

FIG 1 A sketch of the structures of the glass fibre cloth (left) and glass felt (right) which are used in the experiments. It is seen that the structure for glass fibre cloth is rougher compared to glass felt.

The two types of painting were acrylic paint and silicate paint. Acrylic paint consists of i.a. acrylic polymers and water. When the paint dries out the polymers will glue together and establish a layer of polymers.

The silicate paint is a natural mineral product, where the binding agent is silicate.

4. Methods

The experiment was divided into preparation of the specimens and measurements of the water vapour resistance of the seven series.

4.1 Preparation of the specimens with surface treatments

Aerated concrete was used as underlay for the surface treatments. Six different surface treatments were investigated. The constitutions of the specimens are listed in the paragraph of Materials.

When the surface treatments were applied to the aerated concrete slab the surface area of the slab was 600 mm x 400 mm to obtain an evenly distributed surface.

After the surface treatments the specimen were drilled out of the slab. All the specimens had a diameter of 80 mm and a thickness of 24 mm. Four specimens of each surface treatment and eight specimens without surface treatment (pure aerated concrete) were tested. The pure aerated concrete specimens were tested to be used as references.

Afterwards, all the specimens were placed in a ring of plexi glass. The height of the plexi glass ring was 25 mm and had an outer diameter of 100 mm and inner diameter of 93 mm. To achieve that the volume between the plexi glass ring and the specimen was completely sealed epoxy was used.

Furthermore, all the specimens were painted with two layers of epoxy on the vertical perimeter surface to make sure that it was only the surface treated area that would be examined. The specimens which were used for the cup experiment is shown at FIG 2.

FIG 2 Specimens to the cup tests. Left: Specimen, which has just been painted with epoxy on the vertical perimeter surface sides. Middle: Specimen placed in a plexi glass ring with epoxy between the specimen and the plexi glass ring. Right: Specimens ready for the cup test.

4.2 The cup tests

The cup test has been performed according to the European standard EN ISO 12572 (2001) Hygrothermal performance of building materials and products – Determination of water vapour transmission properties. This investigation contained only wet cup tests. The cup equipment that was used is more detailed described in West and Hansen (1988).

The principle for the cup test is that the specimen is sealed to the top of a cup containing a saturated aqueous solution of Potassium Nitrate (KNO_3). The air space between the saturated aqueous solution and the bottom side of the specimen is 6-8 mm, and has a relative humidity of 94 % RH. A net was placed upon the glass cup to avoid the salt solution reached the specimen during handling of the cup. To ensure the sealing between cup and specimen as well as specimen and lid rubber packings were used beneath and above the specimen. A section of the cup used is shown in FIG 3. The cup is placed in a test chamber where the relative humidity and the temperature of the air are controlled to 50 % RH, 23 °C. Between the chamber air and the air inside the cup a water vapour pressure gradient will give a one-dimensional stationary moisture transport through the specimen.

By weighing the cup periodically the weight decrease was determined. The weighing was continued until five successive determinations of change in mass per weighing interval for each specimen were constant within ± 5 % of the mean values for the specimen. The weight change was afterwards used for calculation of the water vapour resistance.

The standard prescribes that the water vapour resistance should be determined as an average of the water vapour resistance of five specimens of this size. However, eight specimens of aerated concrete without surface treatment were used, while four specimens were used for each of the surface treatments.

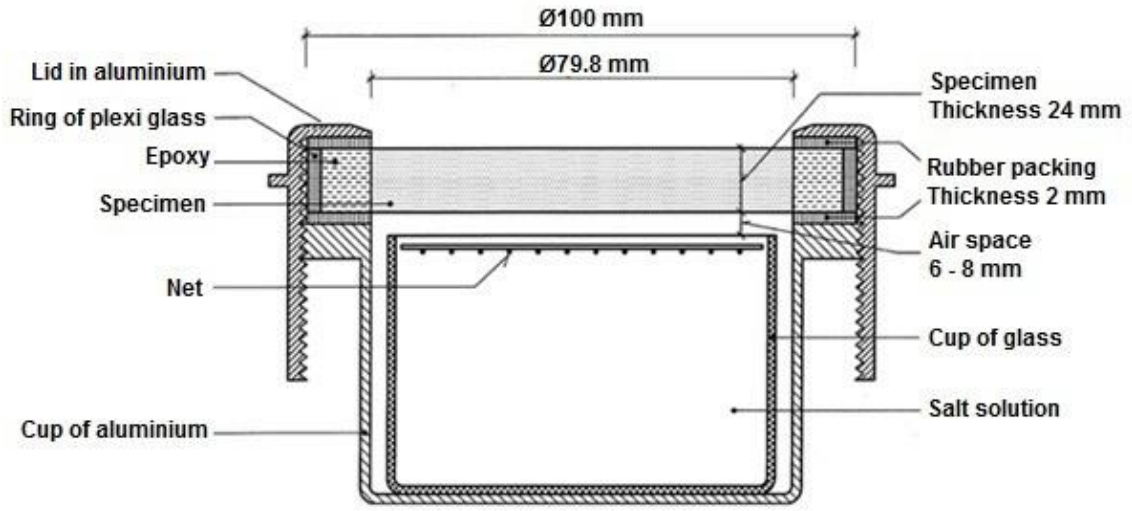

FIG 3 The aluminium cup which was used to the test specimens. Inside the aluminium cup was a glass cup placed were the salt solution (KNO_3) was located. The cup was placed in a climate chamber at 50 % RH and 23 °C.

5. Results

The water vapour permeability δ_p for pure aerated concrete was measured to be $26.6 \cdot 10^{-12}$ kg/(Pa·m·s). The measured water vapour resistance Z_p for the specimens are shown in FIG 4.

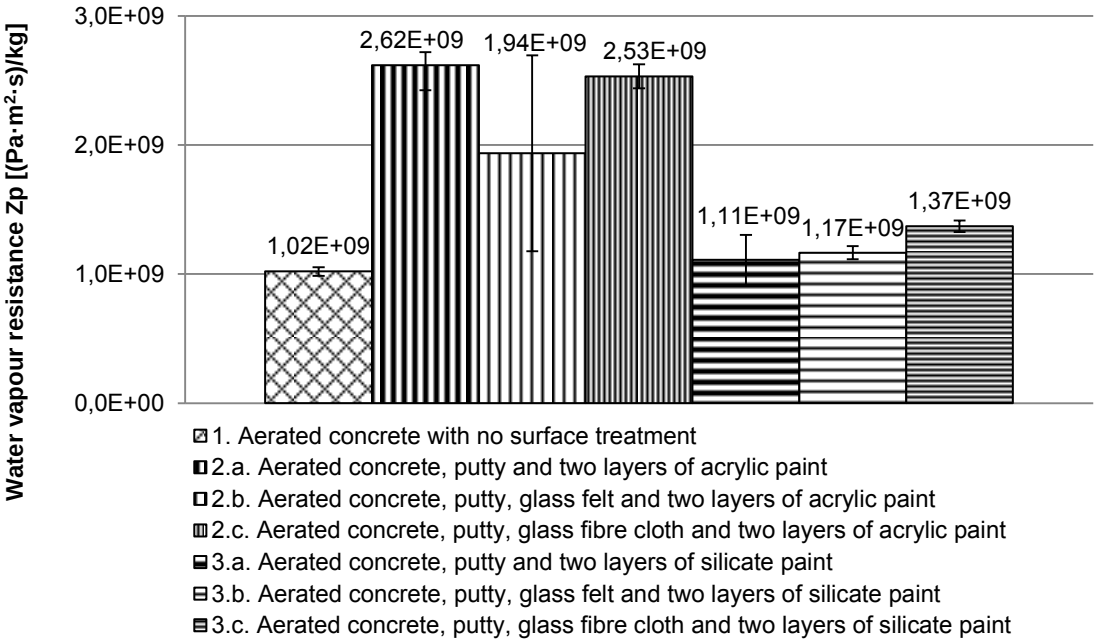

FIG 4 The water vapour resistance, Z_p, with standard deviation for the aerated concrete and the different surface treatment. The vapour resistance and its deviation are calculated from four specimens with same surface treatment and have been tested equally. However, for pure aerated concrete the vapour resistance and its deviation are calculated from eight specimens.

6. Discussion

The water vapour permeability and water vapour resistance factor for the pure aerated concrete were found to be $23.6 \cdot 10^{-12}$ kg/(Pa·m·s) and 8.30, respectively. The water vapour resistance factor is compared with values from IEA – Annex XIV (1991), Gottfredsen and Nielsen (2006) and information from the manufacturer of the aerated concrete slabs. The comparison is shown in FIG 5.

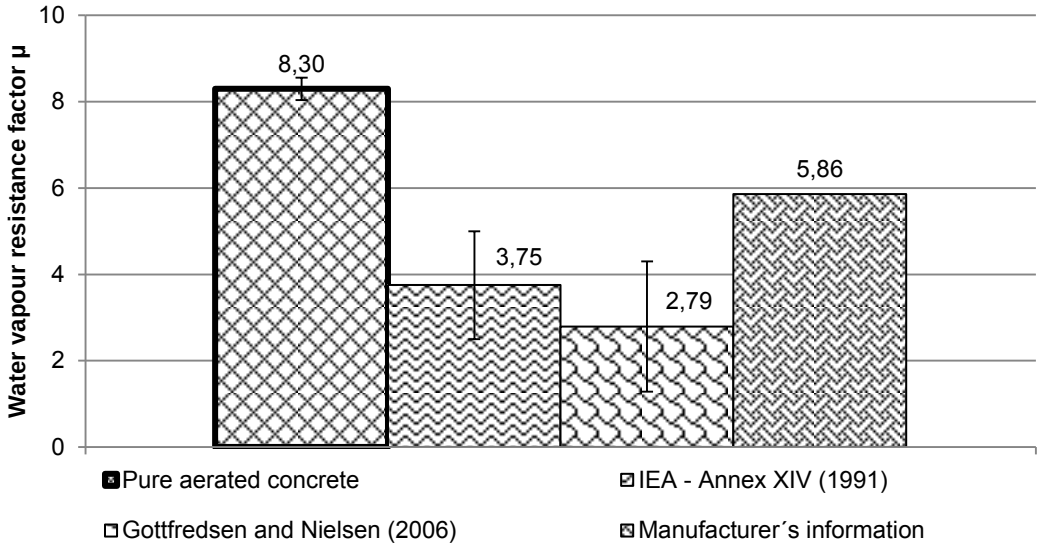

FIG 5 Pure aerated concrete. The water vapour resistance with standard deviation for the cup test compared with Gottfredsen and Nielsen, (2006), IEA – Annex XIV, (1991) and information from the manufacturer of the pure aerated concrete. The manufacturer does not state the standard deviation.

If the measured water vapour resistance factor is compared with information from the manufacturer there is a factor 1.4 in difference which is lower than compared with IEA – Annex XIV (1991) and Gottfredsen and Nielsen (2006). Here is a factor of 2.21 and 2.97 in difference. That means that the recovered water vapour resistance factor is bigger than in the literature. It is important to mention that the water vapour resistance factor is calculated from eight samples, whereas EN ISO 12572 (2001) prescribes that five samples is sufficient. Additionally, the recovered standard deviation is low.

FIG 4 show the water vapour resistance for the different aerated concrete specimens with surface treatment compared to the one without surface treatment. The water vapour resistance is calculated from four specimens that are tested concurrently. It was expected that the surface treatments would have a blocking effect. However, the water vapour resistance in the specimens with silicate paint were not significantly affected; the specimens with only silicate paint have almost the same water vapour resistance as aerated concrete without surface treatment.

It is seen that by using acrylic paint it is possible to get a higher water vapour resistance than when using silicate paint. This was expected as Brandt (2013) characterises silicate paint as more open to water vapour than acrylic paint. Additionally, FIG 4 show paint combined with glass fibre cloth or glass felt has no significant influence on the water vapour resistance, regardless of the paint type. Therefore, glass felt or glass fibre cloths are not able to absorb more paint than surfaces without this extra layer.

Two layers of acrylic paint enhances the water vapour resistance of the aerated concrete by $1\text{-}1.6 \cdot 10^{9}$ Pa·m^2·s/kg. This should be compared to $50 \cdot 10^{9}$ Pa·m^2·s/kg, which by Brandt (2013) is considered to be the lower limit for the water vapour resistance of a vapour barrier. Therefore, two layers of ordinary acrylic paint on glass felt or glass fibre cloth cannot be used instead of a vapour barrier.

The results show that the specimens that were surface treated with glass felt and acrylic paint have a high standard deviation. This could indicate that glass felt makes the distribution of acrylic paint more uneven. A possible explanation could be that the fibres in the glass felt makes it harder for the paint to be evenly distributed so the paint may not cover everywhere even though two layers are applied. As silicate paint has no effect on the water vapour resistance an uneven distribution of silicate paint would not be noticeable.

To test the theory of uneven distribution of paint on glass felt more specimens should have been tested. First of all five specimens should have been used for each surface treatment; this would in general have decreased the standard deviation. Additionally, tests could have been made on specimens with more than two layers of paint. If the theory of uneven distribution is true, more layers of paint would have reduced the unevenness. It would also be interesting to see if e.g. four layers of paint would have doubled the water vapour resistance compared to two layers.

As water vapour resistance of each layer can be added this should theoretically be true. However, the treated surface may not absorb as much paint as the untreated surface. In this test it could have been determined by simply weighing the samples after applying each layer of paint.

7. Conclusions

In the present study it was tested how different surface treatments change the water vapour resistance of aerated concrete. Aerated concrete without surface treatment was compared to aerated concrete with a thin layer of putty and different paint types, silicate paint and acrylic paint, respectively, with and without an underlay of glass felt or glass fibre cloth. The results were:

- The used aerated concrete has lower water vapour permeability than usually reported in the literature and by the manufacturer
- The water vapour resistance is not changed if silicate paint in two layers is used
- Acrylic paint in two layers enhances the water vapour resistance by $1\text{-}1.6 \cdot 10^9$ (Pa·s·m)/kg
- Glass fibre cloth or glass felt as an underlay tissue for the paint has no significant effect on the average water vapour resistance
- Glass felt as an underlay for acrylic paint has higher standard deviation than the other surface treatments. Maybe the glass felt makes the distribution of the paint more uneven.

As a result it must be concluded that glass fibre cloth or glass felt does not absorb more paint than putty without this layer. It might only enhance the unevenness of the distribution of the paint. As two layers of the paint with the highest water vapour resistance (acrylic paint) is about 20 times more open to water vapour than what is recommended for a vapour barrier, two layers of ordinary acrylic paint, with or without glass fibre cloth or glass felt cannot be used as a vapour barrier.

References

Brandt, E. (2013): Moisture in buildings, SBi-guideline 224, 2. edition, Statens Byggeforskningsinstitut, Aalborg Universitet, Copenhagen (in Danish)

EN ISO 12572 (2001): Hygrothermal performance of building materials and products – Determination of water vapour transmission properties.

Gottfredsen, F. R., Nielsen, A. (2006). Construction Materials: Basic Properties. Polyteknisk Forlag (in Danish).

IEA – Annex XIV (1991): International Energy Agency – Energy Conservation in Building and Community Systems. IEA – Annex XIV: Condensation and Energy. Volume 3: Catalogue of Material Proporties.

West, G. P, Hansen, K. K. (1988): Cup equipment for measurement of water vapour transfer, Technical report 179/88. Building Materials Laboratory, Technical University of Denmark (in Danish).

Assessment of the moisture risk in constructions including convection inside air cavities

Michele Bianchi Janetti [1]
Fabian Ochs [1]
Wolfgang Feist [1, 2]

[1] University of Innsbruck, Unit for Energy Efficient Buildings, Austria
[2] Passivhaus Institut, Germany

KEYWORDS: *Moisture risk, hygrothermal analysis, forced convection, internal insulation, timber beam-ends*

SUMMARY:
Mould growth and structural damages can affect timber building components in case critical moisture content is exceeded. Numerical simulation is useful for predicting such a risk, however, in case of constructions including air cavities, realistic modelling becomes very complex. On the one hand, the convective transfer mechanisms which occur in air cavities can significantly influence the moisture distribution; on the other hand, including fluid dynamics in long period hygrothermal simulation leads to high numerical effort and computation time.

In this study the moisture content at the timber beam heads is predicted taking as an example a real building where internal insulation is applied. The effect of streaming air through the gap between timber beams and masonry is taken in to account by means of a simplified approach (line source approach). The employed numerical model has been implemented in Comsol and validated within previous published studies.

In this work different scenarios have been analysed varying the pressure drop over the air gap. It results that, within the realistic range of pressure drop, increasing air flux leads to higher water content inside the construction. The maximal value of the volumetric air flux compatible with a save construction is determined.

1. Introduction

In recent times the use of numerical simulation for predicting heat and moisture transfer inside constructions is increasing.

In external walls with embedded timber beams, the analysis of the moisture risk is of paramount importance, since water condensation can lead to structural damage. If an internal insulation is applied (e.g. in case of historical buildings for which an external insulation is not always possible) the risk of structural damage could arise [1]. Moreover, the presence of air gaps can significantly influence the moisture distribution. In such a situation adequate retrofit design has to be employed, in order to guarantee a long term preservation of the building. More studies on this topic including numerical analysis and in-situ measurements have been published [2],[3].

Numerical simulation can supply important information for a correct design and for the choice of proper materials. At present, specific software for hygrothermal simulation in building-physics application, based on the works of Künzel [4] and Grunewald [5], are available [6], [7]. This software enables HAM (Heat, Air, Moisture) modelling in porous media; however computational fluid dynamic simulation (CFD) is not yet included. In this software convection can be modelled only by means of simplified diffusive models. A study concerning conjugate HAM-CFD modelling and benchmark

experiments has been recently performed by van Belleghem [8], however his model is valid only in the hygroscopic range (RH<98%).

The use of the commercial software Comsol can be profitable for HAM and CFD modelling. Some building-physics applications in this field have been already realized by van Schijndel [9]. Comsol has been tested also in capillary-moisture range (RH>98%), however for moisture values close to the saturation, numerical instability can occur in some cases [10], [11].

Two different approaches of coupling convection in air cavities with heat and mass diffusion in construction materials are possible in Comsol [12]. The first approach includes the calculation of the velocity field inside the air cavities due to computational fluid dynamics. The second approach (line source approach) is based on a simplified model and presents reduced computational effort, hence may be advantageous for long-period simulations. Both these models have been compared with another simulation program [7] and validated against measured data from the literature within another previous work [13].

In this study the line-source approach has been applied to a real construction described in the first part of the paper. Following, a briefly description of the employed mathematical model is reported. In the last part of the paper, results concerning the moisture risk at the beam-ends and considerations about air tightness at the ceiling-wall junction are presented.

2. Problem description

The case presented here refers to a real building which has to be retrofitted within the European project 3ENCULT [14]. *FIG **1*** shows the vertical section through a beam embedded in the external wall.

Air is supposed to stream from the lower to the upper part of the building through the thin air gap between beam-end and masonry (bold line in *FIG 1*. In other cases, which are not investigated here, air can stream from the inside to the outside of the building). Since internal insulation has to be applied, the external wall remains cold during the winter season. Hence significant vapour transfer from the streaming air to the masonry and to the timber beam has to be expected.

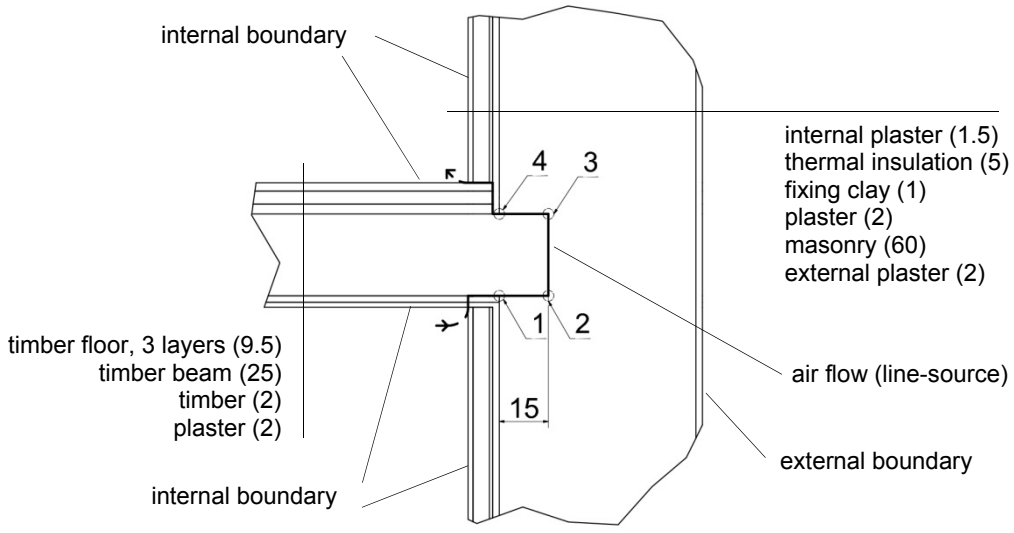

FIG 1. Vertical section of the ceiling-wall junction. The thicknesses of the different layers are reported in centimetres. Positions 1 to 4 refer to the results reported in the following of the paper.

In order to prevent moisture damages, the ceiling-wall junction should be accurately sealed avoiding convection as far as possible. However, a perfect sealing is not practicable in real constructions. The purpose of the simulation presented in the following is to determine the maximal volumetric air flow compatible with a water-damage safe construction.

The simulation is performed in two dimensions, which can be considered an acceptable simplification. A 3D analysis of the same construction, but not including convection inside the gap, has been addressed in [15].

3. Mathematical model

In this paragraph the employed mathematical model is briefly described with focus on the transfer equations and on the volumetric air flow calculation. The detailed derivation of the equations and the models employed for the material functions can be found in the literature cited below.

3.1 Driving equations in porous domains

The heat and moisture transfer in the porous domains (construction materials) is described by a system of two partial differential equations derived by imposing the equilibrium balance of mass and energy within an infinitesimal element of volume:

$$\frac{\partial u}{\partial \varphi}\frac{\partial \varphi}{\partial t} + \nabla \cdot \left(-D_{m,\varphi}\nabla\varphi - D_{m,T}\nabla T\right) = 0 \tag{1}$$

$$\frac{\partial h}{\partial T}\frac{\partial T}{\partial t} + \frac{\partial h}{\partial \varphi}\frac{\partial \varphi}{\partial t} + \nabla \cdot \left(-D_{e,T}\nabla T - D_{e,\varphi}\nabla\varphi\right) = 0 \tag{2}$$

Where temperature *T [K]* and relative humidity *φ [-]* are the dependent variables; *t [s]* and *x [m]* represent time and position; *u [kg/m³]* is the moisture content and h [J/m³] the enthalpy. $D_{m,\varphi}$ *[kg/(m s)]*, $D_{m,T}$*[kg/(m s K)]*, $D_{e,T}$ *[W/(m K)]* and $D_{e,\varphi}$ *[W/m]* are material-specific functions depending from *T* and *φ*. The derivation of these material functions can be found in [4], [5], [16].

3.2 Line-source equations

The convective transfer of moisture and energy along the air gap axis is described by the following one-dimensional balance equations according to [17]:

$$A\left(\frac{\partial \rho_v}{\partial t} + v\frac{\partial \rho_v}{\partial s}\right) = L\beta\left(p_{v,b} - p_{v,a}\right) \tag{3}$$

$$A\left(\frac{\partial h_a}{\partial t} + v\frac{\partial h_a}{\partial s}\right) = L\left[\alpha(T_b - T_a) + \beta\left(p_{v,b} - p_{v,a}\right)h_v\right] \tag{4}$$

where *s [m]* and *t [s]* represent the position along the gap axis and the time respectively. ρ_v *[kg/m³]* and p_v *[Pa]* are the water vapour density and the partial pressure of water vapour in the air. h_a *[J/m³]* and T_a *[K]* are the specific bulk enthalpy of the air and the bulk air temperature. T_b *[K]* and $p_{v,b}$*[Pa]* are the temperature and the partial pressure of the water vapour on the boundary of the air gap; h_v *[J/m³]* represents the enthalpy of water vapour. *β [W/(m² K)]* and *α [W/(m² K)]* are the convective transfer coefficients for moisture and energy at the gap surfaces. *v [m/s]* represents the bulk air velocity, which is supposed to be directed along the gap axis, *A [m²]* is the gap cross-section area and *L [m]* is the length of the cross-section perimeter of the air gap.

The partial pressure of water vapour can be expressed as function of temperature and water vapour density through the ideal gas equation ($p_v=\rho_v R_v T$) and the specific enthalpy of the humid air is described by the following equation:

$$h_a = \rho_{a,d}c_{p,a,d}T_a + \rho_v\left(h_{lv} + c_{p,v}T_a\right) \tag{5}$$

where the term $\rho_{a,d} \cdot c_{p,a,d} \cdot T_a$ represents the enthalpy of dry air, whereas $\rho_v \cdot (h_{lv} + c_{p,v} \cdot T_a)$ represents the enthalpy of water vapour. h_{lv} *[J/Kg]* is the latent heat for condensation of water.

3.3 Volumetric air flow calculation

In the air gap between the beam-ends and the wall, air flows due to the pressure difference between the upper and the lower side of the ceiling as shown in *FIG 1*. The volumetric air flow is determined due to the following empirical power law:

$$\dot{V} = C \cdot \Delta p^n \tag{6}$$

Where C *[m^3/(h Pa^n)]* and n *[n]* are empirical coefficients. Δp *[Pa]* is the pressure drop between upper and lower floor. This pressure drop can be determined by means of in-situ measurements but it is not note in our case. However we know that it is proportional to the difference between internal and external temperature due to the stack effect. For a first approximated assessment of this value equation (7) is employed:

$$\Delta p = \rho g h \frac{T_i - T_e}{2T_i} \quad for \quad T_i > T_e; \qquad \Delta p = 0 \quad for \quad T_i \leq T_e \tag{7}$$

Where ρ is the air density (*1.3 [Kg/m^3]*); g is the gravity acceleration (*9.81 [m/s^2]*); *h[m]* is the height of the ceiling over the ground level; T_e and T_i are the external and internal temperature in [K]

Notice that equation (7) gives the pressure drop between internal and external part of the building, however it is employed here for determining the pressure drop over the ceiling. This approximation is justified, since we are firstly interested in the magnitude order of this value.

4. Boundary conditions, initial conditions and material properties

In TABLE 1 boundary and initial conditions are reported. On the internal/external boundaries and on the line-source third type (Robin) boundary conditions are imposed for both energy and mass transfer. The internal values of temperature and relative humidity are assumed as constant, whereas on the external side periodic functions of the time with an annual period are employed (external temperature range: min 2°C, max 23°C; external RH range: min 65%, max 73%)

The temperature and relative humidity of the air inside the gap are coupled with temperature and relative humidity in the porous medium by means of the line-source model (equations (3) and (4)). The mass and energy transfer coefficients in the air gap have been assumed as constant and calculated under the hypothesis of laminar flow.

The volumetric air flow has been calculated employing equation (6). For the coefficients n and C values measured by PHI (Passivhaus Institut, Darmstadt) are here employed [18]. Different sealing systems have been tested in order to select the most effective one. In TABLE 2 different cases are reported, which refer to different sealing systems (case “a” represents a perfect air-tight construction, case “d” concerns sealing due to adhesive-tape only). Notice that in all the cases the Reynolds number is in laminar range (< 2300). In FIG 2 the pressure drop calculated according to (7) and the volumetric air flow are reported. TABLE 3 reports the employed material properties.

TABLE 1. Boundary and initial conditions

Parameter		Internal	External	Air gap	Initial conditions
ϑ	[°C]	20	$\vartheta_e(t)$	$\vartheta_a(s,t)$	20
φ	[%]	40	$\varphi_e(t)$	$\varphi_a(s,t)$	60
α	[W/(m^2 K)]	6	25	46.2	-
β	[Kg/(m^2 s Pa)]	3e-8	2e-7	3e-7	-

TABLE 2 Simulated cases

Case	n [-]	C [$m^3/(h\ Pa^n)$]	Max. volumetric flow [m^3/h]	Max. air velocity* [m/s]	Re max. * [-]
a (no air flow)	-	-	0	0	-
b	0.6	0.01	0.02	0.0028	0.4
c	0.61	0.034	0.07	0.009	1.3
d	0.59	0.669	1.32	0.183	26.4

*calculated with a gap thickness of 0.002 m

TABLE 3 Material properties

Material	Density [Kg/m^3]	Thermal capacity [J/(Kg K)]	Thermal conductivity [W/(m K)]	Vapour diffusion resistance [-]	Max. water content [Kg/m^3]
Masonry	2453	702	1.7	54	54
Timber	450	2500	0.13	40	600
Fixing clay	2650	1050	2.1	10	427
Th. insulation	49	1400	0.03	27	93
Plaster	1797	850	0.87	12	285
Air	1.2	1006	*	*	-

*value not employed since just convective transfer has been taken in to account in the line-source model

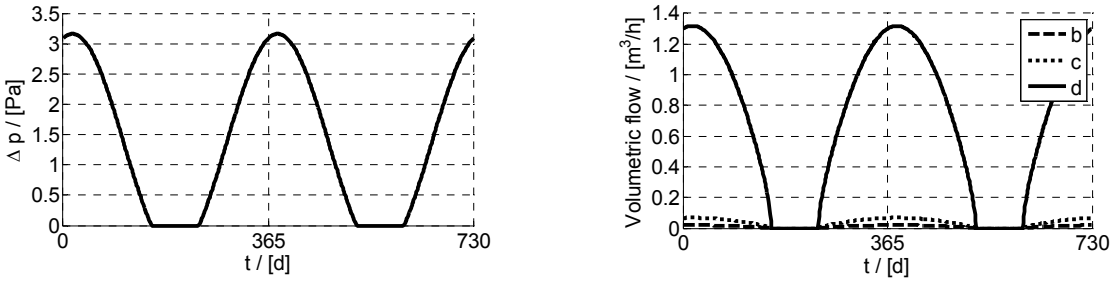

FIG 2. Pressure drop over the gap and volumetric as a function of time air flow calculated according to eq. (6) and (7) for cases b, c and d (TABLE 2)

5. Results

In *FIG 3* the distribution of temperature and relative humidity for case "d" (maximal air flux) are reported after two years. The influence of convective transfer is obvious. Near to the air gap the relative humidity increases up to 95%. Similar behaviour, but less evident, can be observed also in case "b" and "c" which are not reported here.

In *FIG 4* the evolution of the relative humidity at four different positions during the second year is reported. Notice that in the cases "b" and "c" the maximal moisture value is reached at point 1 and 2 respectively (78 and 95%) whereas in case "d" at point 3 (up to 98%).

In *FIG 5* the results concerning the four simulated variants (see TABLE 2) are reported on temperature/relative humidity diagrams. Every point represents the mean values over two weeks. On the same diagrams the wood-damage limit and the mould-germination limit according to [19] and [3] are plotted. As mould germination limit we have assumed the 16-days isopleth for contaminated substrate (after 16 days with values over such limit mould germination can start). Notice that case "a" (air tight construction) and "b" (very good sealing) do not present any kind of risk. In case "c" there is

no wood damage risk, but mould growth can occur. In case “d” (relevant air flow) even wood damage may occur.

Notice that the presence of internal insulation has relevant influence not only on the temperature but also on the humidity distribution. In FIG 6 the results concerning case “c” and case “d” are reported for the same construction without thermal insulation. Notice that neither wood damage nor mould germination would occur in these cases under the given conditions.

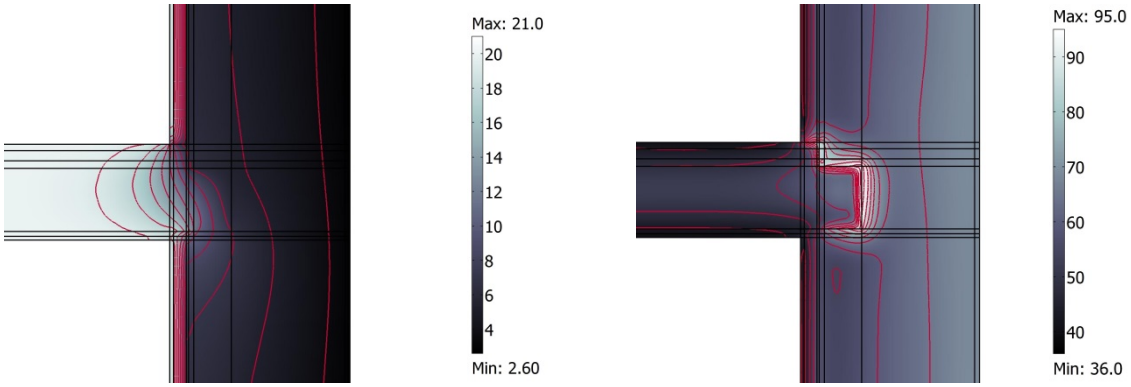

FIG 3. Distributions of temperature [°C] (left) and relative humidity [%] (right) after two years for case d (TABLE 2).

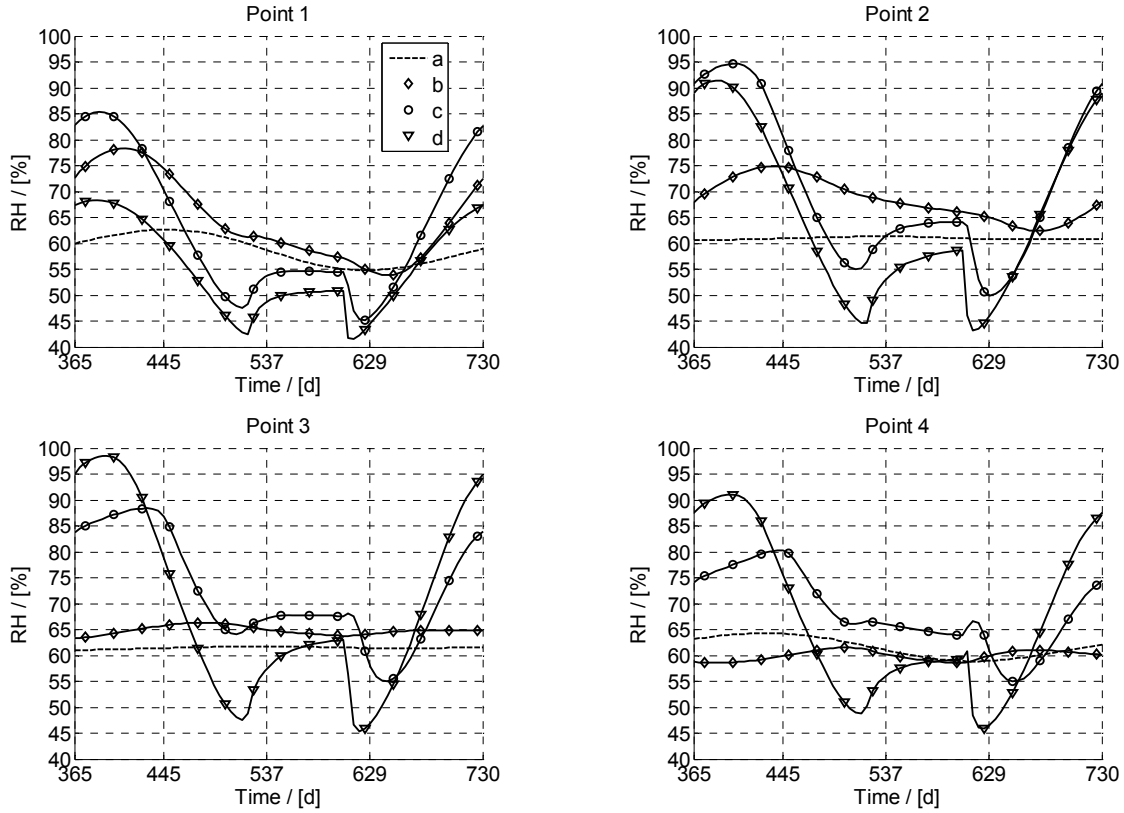

FIG 4. Evolution of relative humidity at four different positions (see FIG 1) during the second year.

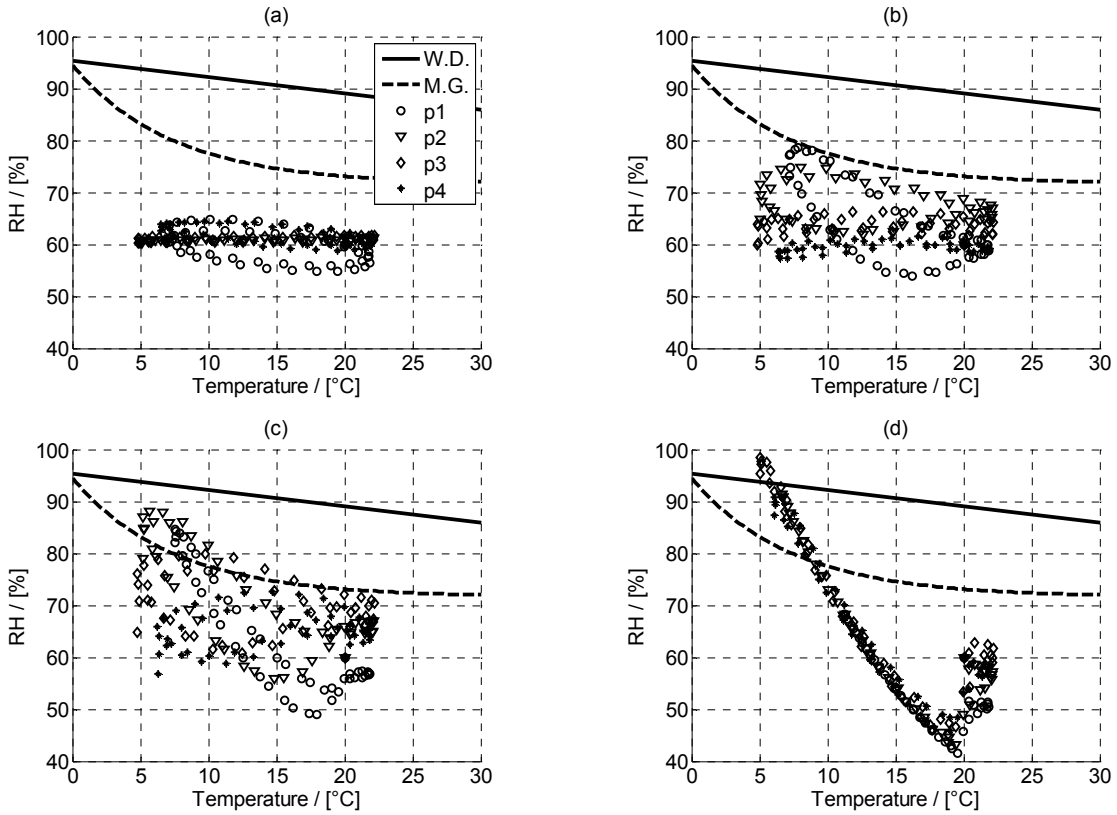

FIG 5. Risk-assessment of wood damage (W.D.) and mould germination (M.G., 16-days isopleth, contaminated substrate) for increasing air velocity in the gap between beam and wall (case (a) to (d)). In the diagrams the values of moisture and temperature at different positions (p1 to p4, FIG 1) are reported. Every point represents mean values over two weeks.

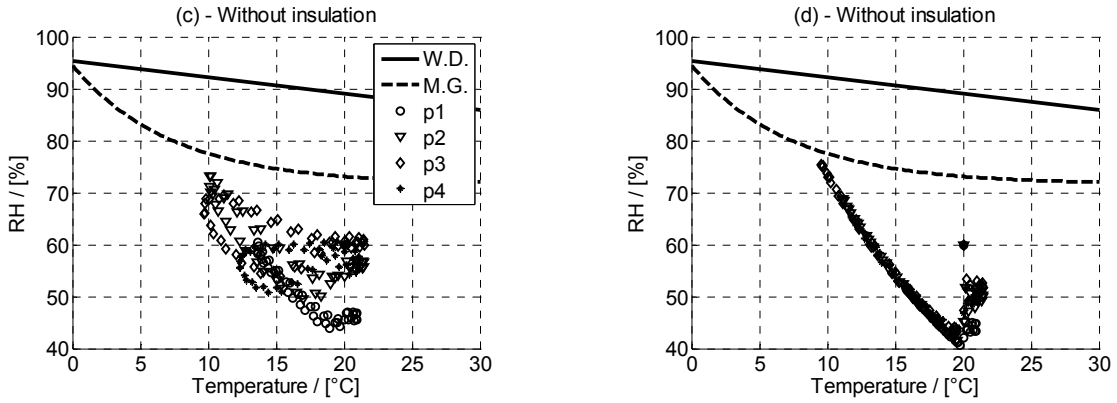

FIG 6. Risk-assessment of wood damage (W.D.) and mould germination (M.G., 16-days isopleth, contaminated substrate) for a construction without internal insulation and for increasing air velocity in the gap between beam and wall (cases (c) and (d), TABLE 2*). In the diagrams the values of moisture and temperature at different positions (p1 to p4, FIG 1) are reported. Every point represents mean values over two weeks.*

6. Conclusions

The moisture risk at timber beam-ends, embedded in a wall with internal insulation, has been assessed. The influence of air convection between beam and masonry has been considered. The maximal value

of volumetric air flow compatible with a water-damage save construction has been determined (case "b", *FIG 5*).

The pressure drop over the air gap has been determined by employing a simple model which may introduce some inaccuracy in the results. This should be verified within further research. Further work will also concern more accurate determination of the volumetric air flow.

7. Acknowledgements

The research presented in this paper is supported by the European project 3ENCULT within the 7th Framework Program (number: 260162, title: Efficient Energy for EU Cultural Heritage, duration: 01.10.2010 – 31.03.2014).

References

[1] R. Pfluger, "Lösungen für den Feuchteschutz. Protokollband Nr.32. Faktor 4 auch bei sensiblen Altbauten: Passivhauskomponeneten + Innendämmung. Darmstadt," 2005.

[2] U. Ruisinger, "Long-term measurements and simulations of five internal insulation systems and their impact on wooden beam heads," *CESBP Vienna*, pp. 313–319, 2013.

[3] D. Kehl, U. Ruisinger, R. Plagge, and J. Grunewald, "Wooden beam ends in masonry with interior insulation - A literature rewiew and simulation on causes and assessment of decay," *CESBP Vienna*, pp. 299–304, 2013.

[4] Künzel, "Simultaneous Heat and Moisture Transport in Building Components," *PhD, Fraunhofer Inst. Build. Phys.*, 1995.

[5] J. Grunewald, "Diffusiver und konvektiver Stoff- und Energietransport in kapillarporösen Baustoffen," *Diss. Tech. Univ. Dresden*, 1997.

[6] "WUFi Software." http://www.wufi.de/, 2011.

[7] "Delphin Software." http://www.bauklimatik-dresden.de/delphin/, 2011.

[8] M. Van Belleghem, M. Steeman, a. Willockx, a. Janssens, and M. De Paepe, "Benchmark experiments for moisture transfer modelling in air and porous materials," *Build. Environ.*, vol. 46, no. 4, pp. 884–898, Apr. 2011.

[9] A. W. M. van Schijndel, "Integrated Heat Air and Moisture Modeling and Simulation," *PhD Diss. Eindhoven, Univ. Technol.*, 2007.

[10] M. Bianchi Janetti, F. Ochs, and W. Feist, "On the conservation of mass and energy in hygrothermal numerical simulation with COMSOL Multiphysics," *Build. Simul. Conf. Chambery*, 2013.

[11] M. Bianchi Janetti, F. Ochs, and W. Feist, "Numerical Quality of a Model for Coupled Heat and Moisture Transport in COMSOL Multiphysics," 2012.

[12] "COMSOL Multiphysics Software." http://www.comsol.com/products/multiphysics/, 2011.

[13] L. Nespoli, M. Bianchi Janetti, and F. Ochs, "Comparing Different Approaches for Moisture Transfer inside Constructions with Air Gaps," *Comsol Conf. Rotterdam*, 2013.

[14] "Efficient Energy for EU Cultural Heritage; http://www.3encult.eu/." .

[15] M. Bianchi Janetti, F. Ochs, R. Pfluger, and W. Feist, "Hygrothermische 3D Simulation von Bauteilen mit COMSOL Multiphysics," *BAUSIM Berlin*, 2012.

[16] M. Bianchi Janetti, F. Ochs, and W. Feist, "3D Simulation of Heat and Moisture Diffusion in Constructions," *Comsol Conf. Stuttgart 2011*, 2011.

[17] M. Bianchi Janetti, F. Ochs, and R. Pfluger, "Coupling Forced Convection in Air Gaps with Heat and Moisture Transfer inside Constructions," *Comsol Conf. Milano 2012*, 2012.

[18] S. Peper, A. Bangert, W. Rupps, and Z. Bastian, "Messungen zur Andichtung von Holzbalkenköpfen und Luftdichtheit von OSB-Platten," *8. Int. BUILDAIR-Symposium, Hann. Ger.*, 2013.

[19] H. Viitanen, T. Toratti, L. Makkonen, R. Peuhkuri, T. Ojanen, L. Ruokolainen, and J. Räisänen, "Towards modelling of decay risk of wooden materials," *Eur. J. Wood Wood Prod.*, vol. 68, no. 3, pp. 303–313, Jun. 2010.

Measurement of water vapour transport through a porous non-hygroscopic material in a temperature gradient

Thor Hansen, M.Sc. [1]
Tim Padfield, MA, Ph.D. [2]
Carsten Rode, Professor [3]
Kurt Kielsgaard Hansen, Associate professor [3]
Ruut Hannele Peuhkuri, Associate professor [3]

[1] Building and construction - Danish Technological Institute, Denmark
[2] Microclimate consultant, United Kingdom
[3] Department of Civil Engineering - Technical University of Denmark, Denmark

KEYWORDS: *diffusion, potential, partial vapour pressure, vapour concentration, temperature gradient, porous, experimental*

SUMMARY:
This was an experiment to identify the driving potential for water vapour diffusion through porous materials in a temperature gradient. The specimen of mineral fibre insulation was placed between a space with controlled temperature and relative humidity and a space with a controlled, higher temperature, and a measured but not controlled relative humidity (RH). This assembly was allowed to reach equilibrium with no vapour movement between the spaces, as tested by a constant RH on each side and by zero flux of water vapour measured in the cold side chamber. The RH and temperature values were converted to partial vapour pressure and to vapour concentration in g/m^3. The concentrations proved to be more equal on either side of the specimen than the partial vapour pressures. This supports an argument that it is concentration difference that drives diffusion of gases. Isothermal diffusion cannot be tested experimentally in this way, but it is reasonable to assume that concentration is the driving potential. The close equality of the concentrations makes it unnecessary to invoke temperature difference as a third possible potential for driving diffusion.

1. Introduction

The experimental work reported in this paper is an attempt to determine whether partial water vapour pressure or concentration of water vapour molecules in kg/m^3 is the driving force for diffusion through a porous material in a temperature gradient.

There has for some years been a discussion about what is the most significant driving potential for moisture transport through porous materials at moderate relative humidity. The story begins with (Fick, 1855). He stated that the driving force for diffusion is concentration difference. However, he studied primarily diffusion in the liquid phase. In the building physics literature and in several numerical models for heat and vapour transport it is assumed that vapour pressure (usually the partial vapour pressure in a mixture of air and water vapour) is the driving potential. In a system at uniform temperature the vapour pressure is proportional to the concentration. However, if there is a temperature gradient the vapour pressure at the higher temperature is higher, for the same vapour concentration in kg/m^3. Around room temperature, the divergence between the two measures is about one part in 300 per degree temperature difference.

This divergence is difficult to measure because there is a practical limit to the temperature difference that can be imposed. At the cool side of the porous material the relative humidity (RH) should be held below around 75%, to avoid capillary liquid flow confusing the process. At the warm side there is no

particular limitation to the RH but it is difficult accurately to obtain a reliable concentration or vapour pressure value from measurement of RH below about 20%.

A number of articles have been published on the effect of temperature on moisture transport through a material. Janssen (2011) has recently published a review which compares eight of the most relevant articles. Five of these articles (Kumaran, 1987), (Dahl, et al., 1996), (Galbraith, et al., 1998), (Stephenson, 2003) and (Peuhkuri, et al., 2008) claim that the temperature has or may have an effect on the moisture transport, while four other papers (Galbraith, et al., 1998), (Thomas, 1999), (Glass, 2007) and (Baker, et al., 2009) state that there is no significant effect of temperature on the moisture transport.

The conclusion of this review was that the papers stating an occurrence of thermal diffusion are flawed, and therefore there is no support for the claim that temperature has an effect on moisture transport.

The purpose of this paper is to test – with a focus on the best possible accuracy of the experimental set-up and method – if either the partial water vapour pressure, or the water vapour content adequately explains the observed diffusion in a temperature gradient, without invoking temperature as a necessary participant in driving the process.

2. Experimental

The principle of the experiment is that a porous specimen is mounted over a cool space with a controlled relative humidity. Above the specimen is a warmed space which is sealed against air flow to the ambient. The RH in this space is measured when the experiment has reached a steady state, when one assumes that there is no net diffusion in either direction. By having the cold climate under the specimen the natural convection within the specimen due to thermal buoyancy is minimised. The specimen is sealed within a cylinder of insulating and an impermeable material to ensure a uniform thermal gradient within the specimen. The temperatures and RH measurements are recalculated to partial vapour pressures in Pascal and to vapour concentrations in kilograms per cubic metre. The parameter which is closest to being identical above and below the specimen is assumed to be the driving potential. If neither parameter seems to be sufficiently similar above and below the specimen, one must accept the possibility of an entirely different transport mechanism being active. The principle of deciding the driving potential by obtaining the same value on both side of the specimen is also described by (Thomas, 1999).

Because of the small difference between these two parameters, the experimental description concentrates on the effort to obtain very accurate RH values.

2.1 The Apparatus

The apparatus is sketched in Figure 1. The specimen is supported over a cylindrical chamber of 791 mm diameter which contains a RH generator. This is basically a water reservoir whose temperature is controlled by a Peltier element. The reservoir is weighed to determine the vapour flux. The chamber air temperature is controlled by an electric heater and a water cooling coil in the annular space around the chamber. The two temperatures, of the water and of the chamber, define the RH but the control system actually uses the signal from a dew point sensor within the chamber and a platinum resistance temperature sensor. The RH on the cool side of the specimen is independently measured by three polymer sensors, which are described in a later section. Above the specimen is a shallow sealed chamber which is heated electrically. This upper chamber also has three RH sensors. The RH sensors incorporate platinum resistance temperature sensors.

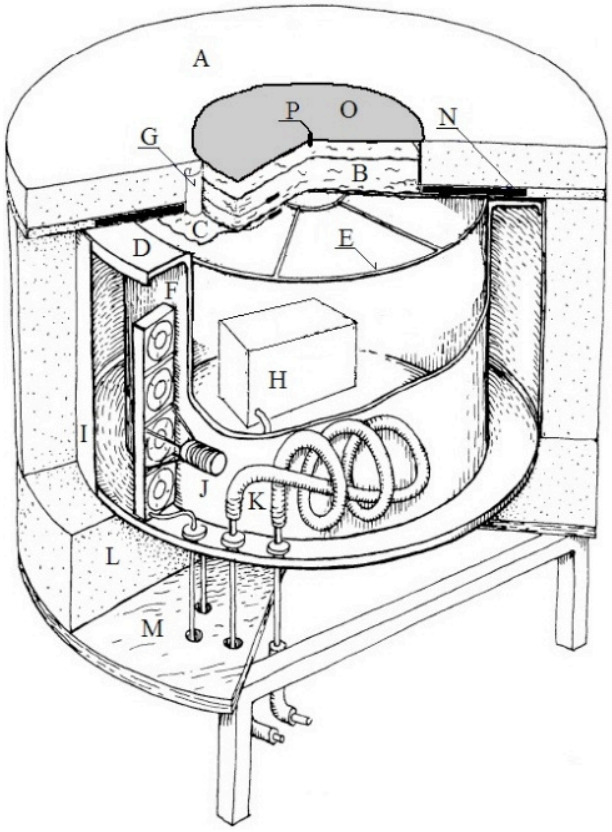

FIG 1. Sketch of the climate chamber. A insulation, B specimen, C Tyvek, D flange over annular space, E open grid, F fans, G polycarbonate foil, H moisture control unit, I stainless steel wall, J heating (electric resistance), K cooling (water circulating in coil), L bottom insulation, M table, N aluminium plate, O Stainless steel plate above sealed airspace, P sensor. [after (Peuhkuri, et al., 2008)].

There is a circular hole 500 mm in diameter in the middle of the aluminium plate, where the specimen is placed, see Figure 2. The specimen is Rockwool, a non-hygroscopic mineral fibre insulation material, with a bulk density of 200 kg/m^3, and a dry thermal conductivity of 0.033 W/(m·K). The underside of the specimen is faced with Tyvek (TM) permeable fabric, to reduce disturbance by the fans which stir the air in the cold space below. The side of the cylindrical specimen is enclosed first by impermeable polycarbonate foil then by foam insulation of equal thickness to the specimen. Above the specimen there is a sealed air space which is heated from above. This space has three RH and temperature sensors.

Each experiment is allowed to run until equilibrium is attained. This is marked by constancy of RH both above and below the specimen. A further check is provided by the weight of water in the reservoir, whose constancy ensured that there was no significant leakage anywhere in the assembly.

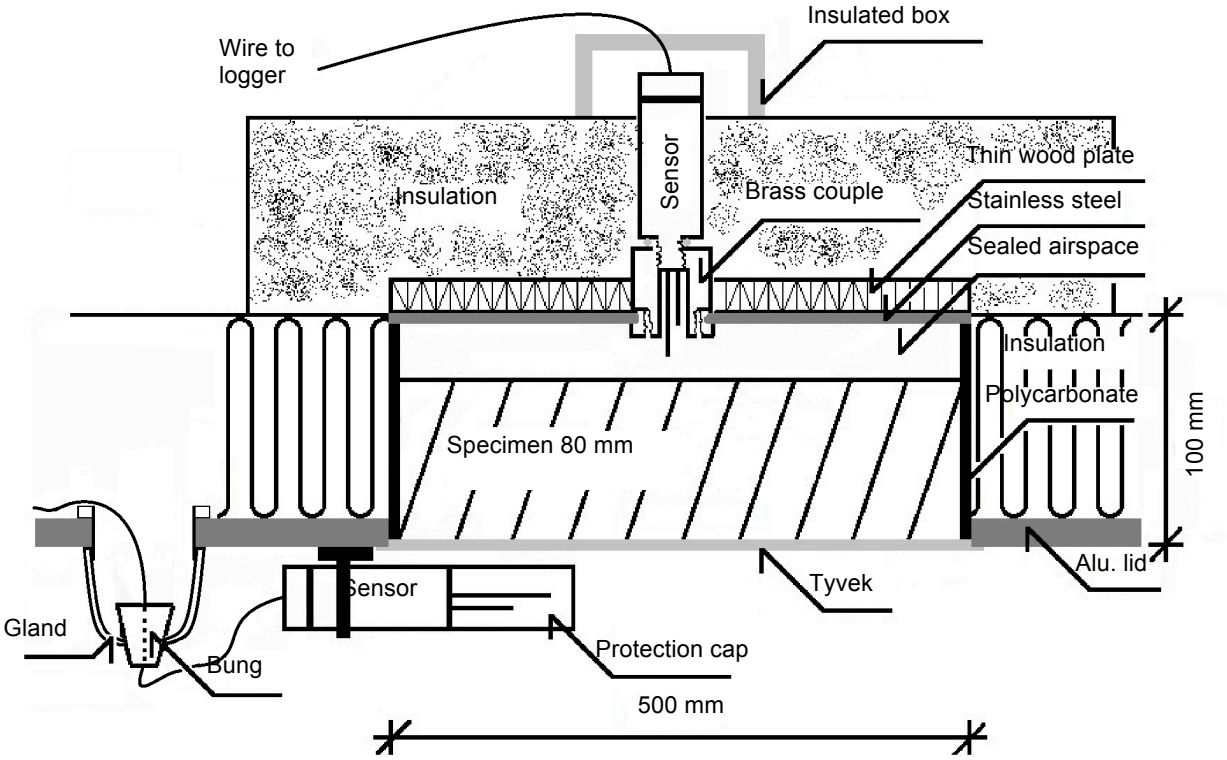

FIG 2. The arrangement of the specimen between the two controlled spaces. A heating plate on top of the sealed airspace creates a temperature of 32°C. Only two of the six temperature and RH sensors are shown.

2.2 Sensor calibration

The temperature and RH sensors were Rotronic HygroClip-S. Three sensors were installed on each side of the specimen. The sensors were calibrated using saturated salt solutions, according to (Greenspan, 1977), and with the manufacturer's ampoules, which are unsaturated salt solutions used just once. The calibration was done by inserting the sensor in a small airtight container containing the saturated salt solution or the ampoule. The calibration temperatures were the same as in the experiment and the same signal processing train was used. Five hours were allowed for equilibration. Calibration was repeated before and after each experimental run. The accuracy of this arrangement was assessed by aggregating the differences between the pairs of calibrations and deriving the standard deviation. For the sensors on the warm side the standard deviation of the RH was 0.9%, and for the cold side it was 0.8%.

The sets of three temperature sensors were tested for accuracy at their operating temperatures against a calibrated mercury thermometer.

These uncertainties convert to an uncertainty in the partial vapour pressure of 44, 24 and 11 Pa for the 32, 22 and 12°C temperatures respectively. The concentration values were derived from the partial vapour pressures, so have proportional uncertainty.

The measurement accuracy was sufficient to ensure that all the measured differences between partial vapour pressures made with a 20K temperature span were significant at the 2σ level, while the experiments with the 10K temperature difference showed significant partial vapour pressure differences at the one standard deviation level.

2.3 Temperature and RH stability

The RH and temperature are shown in Figure 3 for a typical period. The data for relatively stable periods were selected for use. Measurements at one minute intervals were averaged over a 10 hour period.

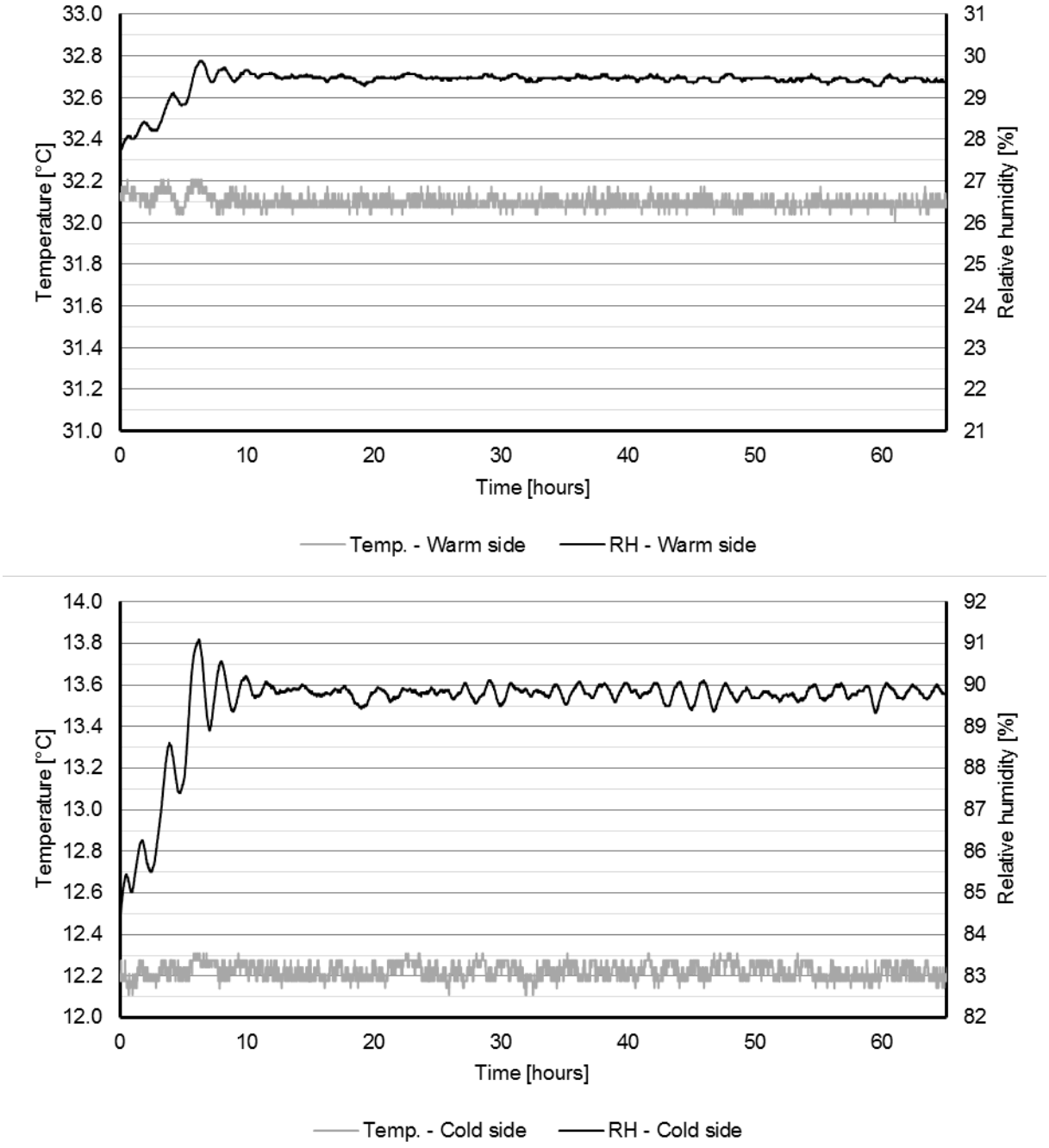

FIG 3. Examples of the measured data above and below the specimen. There was intermittent interference so quiet periods were selected for data processing.

2.4 Calculations

The following equation was used for calculating the saturation partial water vapour pressure and was taken from (Danvak, 1988).

(1)

Where $p_{v,sat}$ saturation partial water vapour pressure (Pa)
T temperature (K)

The concentration in kg/m^3 was derived from the partial vapour pressure using the gas law.

3. Results

3.1 The sequence of experiments

Several combinations of temperature difference and cold side RH were used. The results are summarised in Table 1.

TABLE 1. The experimental results for the seven independent experiments. The per mil differences are calculated from the hot side value minus the cold, divided by the cold side value. Note that runs 5 and 6 are duplicates, but give very different results.

	Warm side				Cold side				Difference	
Run	T °C	RH %	Pressure Pa	Conc. g/m^3	T °C	RH %	Pressure Pa	Conc. g/m^3	Pressure ‰	Conc. ‰
1	31.3	20.2	922	6.56	12.3	60.8	873	6.63	54.2	-9.9
2	32.1	27.7	1325	9.40	12.2	83.8	1191	9.04	106.9	39.6
3	32.1	29.4	1408	9.99	12.2	89.8	1279	9.71	96.0	28.8
4	21.5	36.1	928	6.82	12.3	61.3	876	6.65	58.1	26.1
5	21.6	45.8	1183	8.69	11.9	84.5	1178	8.95	4.3	-29.2
6	21.2	48.5	1225	9.01	12.1	84.0	1189	9.02	30.3	-1.1
7	21.3	51.9	1312	9.65	12.2	90.0	1278	9.70	26.2	-5.2

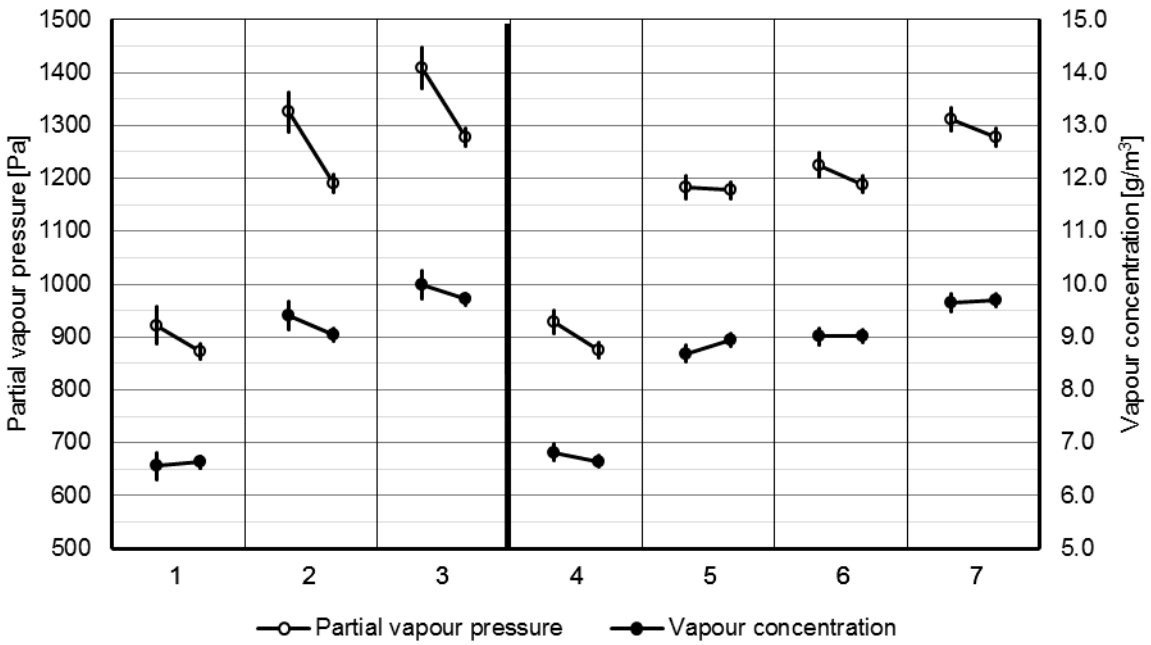

FIG 4. The absolute values of vapour pressures and water vapour concentrations for each experimental run, with σ error bars. The values for hot and cold sides are linked. The flatter links for the pairs of concentration values indicate that this is the potential driving diffusion. The warm side is shown to the left in the illustration of each experimental run.

4. Discussion

All but run 5 show a greater proportional difference in partial vapour pressure across the specimen, and with the higher pressure on the warm side, which would be expected if the concentration were the same on both sides. If one discounts run 5, which was actually the first of the series of experiments, later duplicated as run 6, there is a consistent pattern of vapour pressure excess on the warm side.

The concentration results are more puzzling. Run 1, with relatively low cold side RH and high temperature difference should give the purest result, with little interference from capillary condensation within the porous specimen. It is quite convincing in showing that the concentration above and below is almost equal, while the vapour pressure is higher above, as must then be the case. Runs 2 and 3, with high cold side RH, show the concentration higher at the warm side, and the vapour pressure correspondingly even higher. This sequence of three runs suggests the possibility that at high RH there is condensation at the cold side with liquid flow towards the high temperature side enhancing the concentration above the specimen. However, the experimental runs with the lower temperature difference show an entirely different pattern, with reduced warm side concentration associated with high RH on the cold side.

5. Conclusion

We present strong evidence for concentration rather than vapour pressure being the driving force for vapour diffusion through a porous material. After reaching a steady state with no vapour flow through the specimen, all but one of the seven experiments showed a smaller relative difference in concentration than in vapour pressure across the specimen.

Every experiment showed the vapour pressure higher on the warm side. The concentration differences were more evenly balanced, with three runs showing a higher concentration on the warm side, three runs showing a slightly lower concentration on the warm side and one anomalous run showing considerably lower concentration on the warm side. The experiments performed with the higher temperature gradient, from 12 C to 32 C, and a high cold side RH at 83% showed both vapour pressure and concentration higher on the warm side, hinting at some residual flow process pumping water molecules towards the warm side.

The measurements were at the limit of precision attainable by RH sensors. The temperature difference across the specimen cannot be increased over about 20K without the cold side RH becoming so high that liquid water begins to play a role in the process, or the warm side RH becomes too low to measure with high precision. Absolute certainty is just beyond our grasp but it seems that the unquestioning acceptance of vapour pressure as the driving force for vapour diffusion is not justified. It must also be said that there is no practical significance to this uncertainty because the choice of driving force has scarcely any effect on calculations of the performance of buildings.

References

Baker, P.H., Galbraith, G.H. and McLean, R.C. 2009. Temperature gradient effect on moisture transport in porous building materials. Building Services Engineering Research and Technology. 2009, 30, 37-48.

Dahl, S.D., et al. 1996. Moisture storage and non-isothermal transfer properties of common building materials. HVAC&R Res. 1996, 2, 42-58.

Danvak, Redigeret af Hansen, H. E. et al. 1988. Danvak - Varme- og Klimateknik, Grundbog. s.l. : Danvak, 1988.

Fick, A. 1855. Ann. der. Physik. 94, 59, doi:10.1002/andp.18551700105 (in German). 1855.

Galbraith, G. H., et al. 1998. Nonisothermal moisture diffusion in porous building materials. Build. Res. Inf. 1998, Vols. 26, 330-339.

Glass, S.V. 2007. Measurements of moisture transport in wood-based materials under isothermal and non-isothermal conditions. Clearwater Beach, Florida, United States : Proceedings of Thermal Performance of the Exterior Envelops of Whole Buildings X, 2007.

Greenspan, L.. 1977. Humidity Fixed Points of Binary Saturated Aqueous Solutions. Washington D.C. : JOURNAL OF RESEARCH of the National Bureau of Standards, 1977.

Janssen, H. 2011. Thermal diffusion of water vapour in porous materials: Fact or fiction? International Journal of Heat and Mass Transfer. 2011, Vols. 54, 1548-1562.

Kumaran, M.K. 1987. Moisture transport through glass fiber insulation in the presence of a thermal gradient. J. Therm Insul. 1987, 10, 243-255.

Peuhkuri, R., Rode, C. and Hansen, K. K.. 2008. Non-isothermal moisture transport through insulation materials. Building and Environment. 2008, 43, 811-822.

Stephenson, D.G. 2003. Thermal diffusion of water vapour through glass fiber insulation. J. Therm. Envelope Build. Sci. 2003, 27, 31-48.

Thomas, W.C. 1999. Moisture transfer in porous materials exposed to combined humidity and temperature gradients. s.l. : Final Report ASHRAE 810-RP, 1999.

Hygrothermal assessment of wind-driven rain as a risk for internal insulation retrofit of traditional buildings

Chris Sanders, M.Sc. [1]
Paul Baker, Dr. [1]
Carsten Hermann, Dipl.-Ing. [2]

[1] Glasgow Caledonian University, UK
[2] Historic Scotland, UK

KEYWORDS: *Hygrothermal modelling, hygrothermal monitoring, insulation retrofit, moisture risk assessment, solid stone wall construction, traditional buildings, wind-driven rain*

SUMMARY:

This paper describes a study in which the hygrothermal performance of a traditional Scottish sandstone wall, which is highly exposed to wind-driven rain and had been internally insulated, was monitored and modelled using the simulation software WUFI 2D. Internal and external temperatures and relative humidities and the external solar gain and wind-driven rain load have been recorded from April 2012 to November 2013. Also recorded were temperatures and humidities and the moisture content of timber blocks within the wall. The monitoring results indicate that, despite the concerns that have been expressed about the consequences of applying internal insulation to traditionally constructed masonry walls, no problems have become apparent in this case.

Modelling the wall, using the measured data as boundary conditions, demonstrates the importance of choosing material properties appropriate to the structure under investigation. Three types of sandstone were modelled, with different moisture transport properties, giving very different moisture contents. The modelled temperatures at the interface between the stonework and internal insulation agreed closely with the measured values. The relative humidities measured at the same point followed the same general trend as those calculated using the least porous of the three modelled sandstones, although the values did not agree closely.

1. Introduction

Building regulations in the United Kingdom recommend that the risks of interstitial condensation should be addressed by following the guidance in British Standard BS 5250:2011. This specifies that, when internal insulation is added to a stone wall, a highly air and vapour resistant membrane, an air and vapour control layer (AVCL), should be included on the warm side of the insulation. It is recommended that the risk is assessed with a calculation using the *Glaser method*, specified in EN ISO 13788:2012. However, this 'conventional' assessment method completely ignores liquid moisture transport, for example as a result of wind-driven rain (WDR). Concerns have been raised, especially by heritage professionals, that an AVCL may make conditions within the wall worse by inhibiting evaporation to the inside (Hermann 2013, Little & Ferraro 2014, Rye & May 2012). More advanced methods for hygrothermal assessment, by *numerical simulation*, are now available, taking liquid transport into account. They are based on procedures set out in EN 15026:2007, and software packages for such advanced assessment are available, for example Delphin, MOIST and WUFI.

To provide further information, a sandstone wall in a traditional tenement flat in Glasgow, insulated internally and highly exposed to WDR, has been monitored in detail for 18 months, and hygrothermal conditions have been simulated using the simulation software WUFI 2D 3.3, developed by the Fraunhofer Institute for Building Physics. The simulations were carried out using the measured

internal and external temperatures and relative humidities (RH) and the solar radiation and WDR load measured on the outside wall face. The properties for the materials present were taken from the WUFI database, which contains properties of nine sandstone types: eight from Germany and one from India. As it is not known which of these corresponds most closely to the sandstone used in the Glasgow tenement, the simulations were run with three of these sandstones covering the range of properties in the database.

2. Field measurements

2.1 Location

The monitoring was carried out as part of a retrofit project by Glasgow City Council and Historic Scotland in a top floor corner flat with south and west facing elevations and a fairly open aspect to the west (Figure 1). The building is located near the south bank of the river Clyde in Govan, a suburb of Glasgow. The monitored wall was ca. 600 mm thick and made of sandstone, bedded in mortar. The wall was finished internally with plasterboard which contained a 12.5 mm extruded polystyrene (XPS) insulation backing. This internal finish was presumably installed during the 1980s. The plasterboard was fixed to timber studs, forming a cavity of ca. 90 mm between the stone face and the XPS. This cavity was filled in April 2012 with Knauf Supafil 34, a blown glass fibre mineral wool insulation.

FIG 1. The wall being monitored is the west facing wall of the top floor corner flat with a fairly open aspect and with monitoring equipment installed to the left of the bay window.

The west facing wall was monitored after the retrofit. Climate sensors were installed on the external wall face, primarily to assess the impact of WDR on moisture transport through the wall and its effect (if any) on the risk of moisture problems due to the addition of higher levels of internal insulation. The risk of moisture problems is greatest at the interface between the stonework and the insulation: humidity, temperature and moisture sensors were installed at five locations on the west facing wall. Novel moisture measuring equipment, using the time domain reflectometry (TDR) technique (Philipson 2011), was employed both internally and externally.

This paper covers the monitoring from April 2012 to November 2013. The flat was occupied as of August 2012. The measured TDR data was not yet available at the time of writing of this paper.

Before the retrofit, in situ U-value measurements, carried out during March 2012 at three locations on the west facing elevation, gave an average U-value of 0.77 ±0.03 W/(m^2·K). Measurements on the south elevation after the retrofit gave an improved average U-value of 0.23 ± 0.03 W/(m^2·K). (Measuring on the west elevation was, unfortunately, not possible at the time.)

2.2 Monitoring procedures

Before filling the cavity with insulation, sensors were installed internally in five locations, fixed to the stone surface on the west facing wall (Figure 3). Temperature, relative humidity and wood block moisture content (WBMC) sensors were installed in all five locations, and TDR probes with 75 mm probe length were inserted from the internal stone face at four positions. A combined temperature and relative humidity sensor was also installed to measure the room conditions.

The electrical resistance of the wood blocks was measured and converted into timber moisture contents. The generally recognised safe threshold for timber moisture content is 18%.

FIG 3. Interior sensor locations on west facing wall: temperature, relative humidity and moisture sensors are fixed to the internal stone face in the five locations where plasterboard has been cut away.

The following sensors were mounted on the external west facing elevation (Figure 4):

- combined temperature and relative humidity sensor enclosed in radiation shield
- solarimeter measuring global and diffuse solar radiation incident on the vertical surface
- anemometer (wind speed)
- rain gauge mounted vertically, which senses water hitting its outside surface using infrared light (The gauge can be set up to give a pulse output, emulating a tipping bucket rain gauge.)
- two TDR probes with 75 mm probe length inserted into stonework

Logging commenced on 20th April 2012. Data were logged at 1 minute intervals and stored at 10 minute intervals for all sensors, except for the TDR probes which were recorded hourly.

FIG 4. Instrumentation on external wall from left to right: two TDR moisture probes, vertical rain gauge, solarimeter, anemometer and combined temperature and relative humidity sensor in radiation shield. (Note that the item to the very left, mounted at slightly higher level, is an existing boiler flue.)

2.3 Monitoring results

Figure 5 shows the monthly total solar radiation, measured in the vertical plane, and the total rainfall incident, both on the west facing wall. Figure 6 shows the monthly average relative humidities and WBMCs. Figure 7 shows the temperatures.

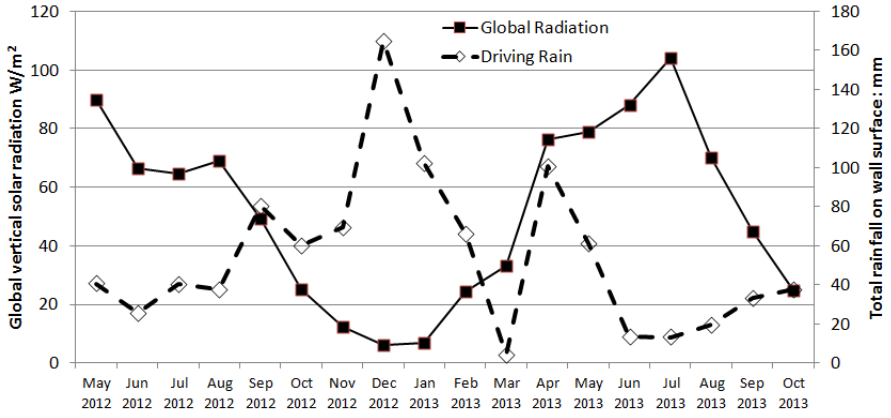

FIG 5. Monthly total solar radiation measured in the vertical plane of the west (facing) wall and total rainfall incident on the same wall

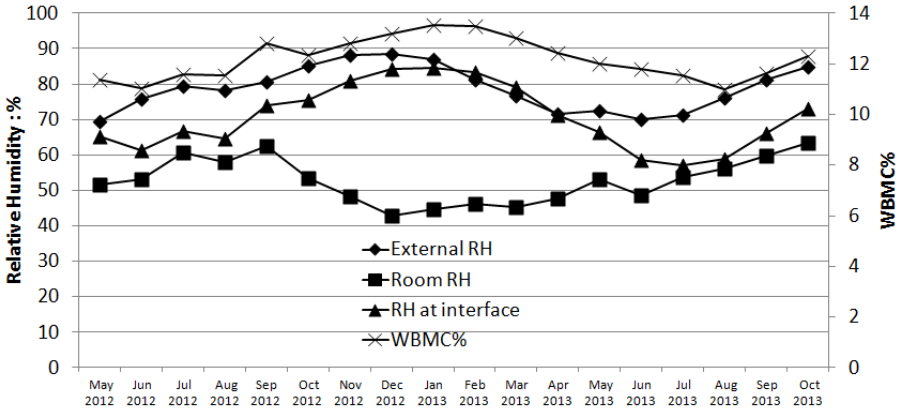

FIG 6. Relative humidities measured externally, within the flat and at interface stonework / insulation (average of 5 measurements); WBMCs measured at the same interface (average of 5 measurements)

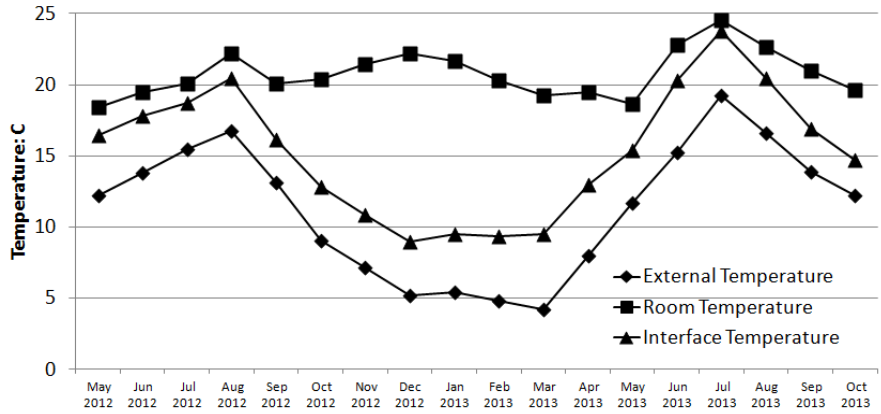

FIG 7. Temperatures measured externally, within the flat and at the interface between the stonework and the insulation (average of 5 measurements)

Figure 6 shows that WBMC follows the change in relative humidity at the interface between the stonework and the insulation. The maximum WBMC is approximately 14%, which indicates low risk of moisture problems so far. Both the WBMC and the relative humidity at the interface generally follow the change in external humidity as well as a seasonal pattern, rising in the winter and falling in the summer.

There is no significant evidence that the amount of rainfall received at the external wall face has an impact on the humidity and WBMC at the interface between the stonework and the insulation. The effect of wind and solar radiation may be sufficient to evaporate moisture from the external wall face and prevent rainwater penetration. Analysis of the TDR data, once available, should clarify the effect of rainfall, wind and solar on the moisture content of the wall.

3. WUFI 2D modelling

3.1 Simulation model

The WUFI software, which complies with EN 15026, was used to develop a model of the wall that had been monitored. Traditionally constructed stone walls in Scotland consist of layers of stones either side, bound together by a mix of smaller stones and mortar, which is likely to contain many air voids. Even if the contents could be defined exactly, it would be impossible to represent them in WUFI. Therefore, a simplified model of homogenous stonework with one horizontal mortar joint was developed using WUFI 2D 3.3, a two dimensional version of the WUFI software family. As no information on the properties of the materials used in the wall was available, the model was run with three German sandstones, representing the range of those available in the material database of WUFI. Table 1 summarises their moisture transport properties.

TABLE 1- Moisture transport properties of the sandstones used in the WUFI model

Sandstone type	Density [kg/m^3]	Porosity	Diffusion resistance factor [-]	Moisture storage at 99% RH [kg/m^3]	Liquid transport coefficient at 50kg/m^3 [m^2/s]
Baumberger	1980	0.23	20.0	115.5	3.9×10^{-9}
Obernkirchner	2150	0.14	32.0	9.4	2×10^{-8}
Zeitzer	2300	0.05	70.0	26	1.0×10^{-8}

The relatively porous Baumberger sandstone has a high moisture storage capacity, but a low liquid transport coefficient, compared to the denser Zeitzer sandstone.

The measured internal and external temperatures and relative humidities and the solar radiation and WDR incident on the external surface were used as the boundary conditions.

3.2 Results

The figures below show the daily means from the hourly data calculated by WUFI. Figure 8 shows the moisture content of the three sandstones modelled, which is very different for the three cases. Figure 9 shows the moisture content of the mineral wool insulation. The high level of liquid transport in Obernkirchner sandstone allows more of the water hitting the outer face of the wall to pass into the mineral wool. It is worth noting, however, that even the highest calculated moisture content (~11 kg/m^3) is well below the level where the thermal conductivity rises (50 – 100 kg/m^3). Figure 10 shows the temperature at the interface between the stonework and the insulation, together with the data measured at this point. There is little difference between the three stone types, and the agreement with measured data is good.

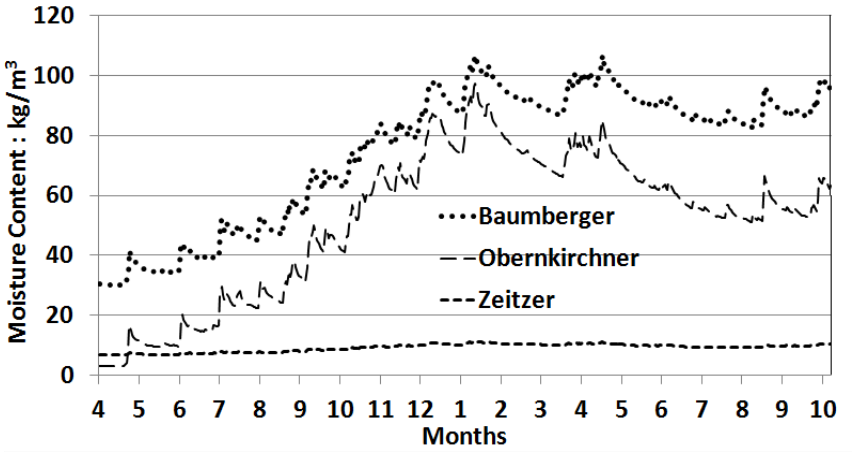

FIG 8. Overall stone moisture content

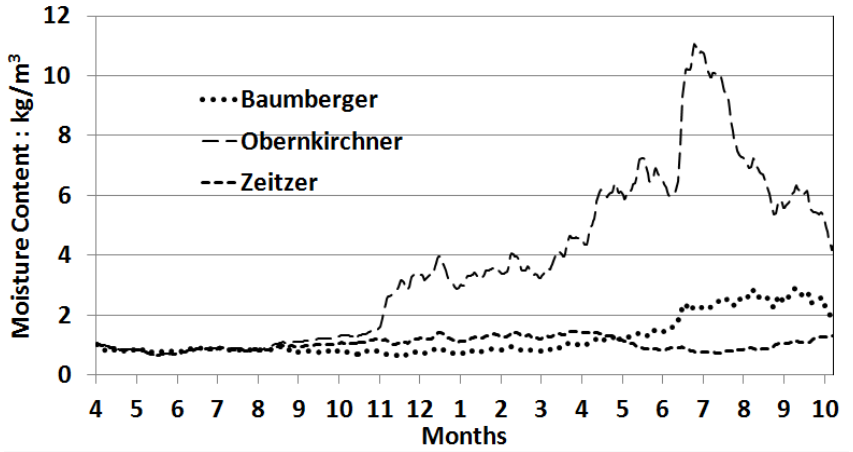

FIG 9. Overall moisture content of the mineral wool insulation

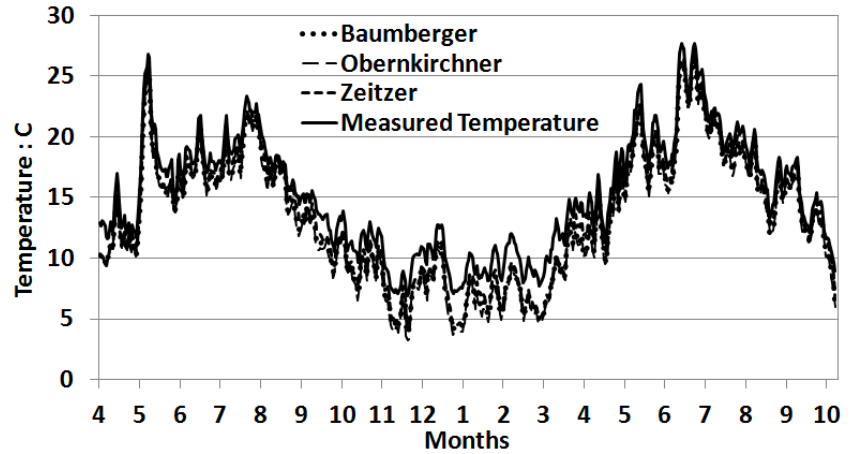

FIG 10. Temperature in the outer 1 mm of the mineral wool insulation (i.e. near interface of stonework and insulation) with the measured data

Figure 11 shows the relative humidity at the same point and measured data. There is considerable variation between the calculated data from the three sandstone types, with that from the Zeitzer sandstone agreeing with the measured data most closely. The simulated RH values for Baumberger and Zeitzer sandstones exceed the measured values continuously as of month 8 of the first

measurement year (i.e. December 2013) and Obernkirchner sandstone as of month 2 of the second year (i.e. February 2013). It is worth noting that the simulated humidity levels of all stone types exceed temporarily RH values of 80%, the generally accepted threshold for mould growth; the values for Baumberger and Zeitzer sandstones remain continuously above this threshold after month 10 of the first measurement year (i.e. February 2013). These simulated results would be cause for concern in situation where the 80% threshold is exceeded for prolonged periods of time. Fortunately, the measured results show that the RH levels only exceed the threshold for suitably short periods of time, followed by period with RH levels substantially below the threshold.

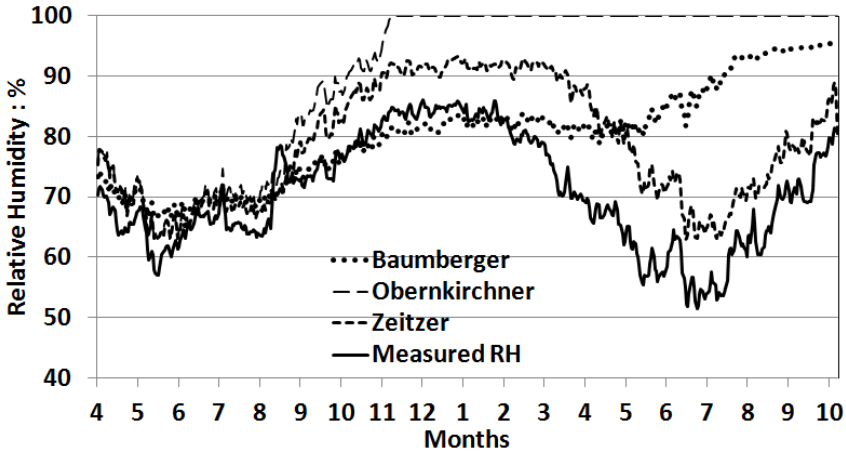

FIG 11. Relative humidities in the outer 1 mm of mineral wool insulation (i.e. near interface of stonework and insulation) with the measured data

4. Discussion

The results from the monitoring and modelling described in this report have indicated that, despite the concerns that have been expressed about the consequences of applying internal insulation to traditional masonry walls, no problems have become apparent in this case. There is no significant evidence that the amount of rainfall received at the external wall face has an impact on the humidity and timber moisture content at the interface between the stonework and the insulation. The effect of wind and solar radiation may be sufficient to evaporate moisture from the external wall face and prevent rainwater penetration. Analysis of the TDR data, once available, should clarify the effect of rainfall, wind and solar radiation on the moisture content of the wall.

Modelling the wall with WUFI 2D, using the measured temperature, humidity, solar and WDR data as boundary conditions, demonstrates the importance of choosing material properties appropriate to the structure under investigation. The three types of sandstone modelled, with different porosities, moisture storage capacities and liquid water transport coefficients, gave very different calculated moisture contents of the sandstone and the mineral wool insulation. It is worth noting, however, that the predicted moisture content of the mineral wool remained well below the levels that have any effect on its thermal conductivity.

The modelled temperatures at the interface between the stonework and the insulation agreed closely with the measured values. Relative humidities measured at the same point followed the same general trend as those calculated using the least porous sandstone, Baumberger sandstone, although the values did not agree closely. This is not surprising, given the great simplification of the model, with one mortar joint in stone, compared to the complex matrix of stone and mortar in reality. Once the TDR data have been analysed, it will be possible to make a more detailed comparison between the measured and calculated moisture contents. It is worth noting that the simulated humidity levels of all stone types exceed, either temporarily or continuously, RH values of 80%, the generally accepted

threshold for mould growth. These simulated results would be cause for concern in situation where the 80% threshold is exceed for prolonged periods of time. Fortunately, the measured results show that the RH levels only exceed the threshold for suitably short periods of time.

It is clear that, if advanced hygrothermal models in accordance with EN 15026:2007, such as WUFI, are to be used to carry out routine assessments of moisture conditions in building structures, considerably more data on the properties of the materials used must be available to achieve realistic simulation results.

5. Acknowledgements

The research was funded by Historic Scotland, an agency of the Scottish Government. The authors thank for their support the occupants of the flat monitored, Govan Housing Association and Glasgow City Council.

References

Baker, P. 2014, forthcoming. Hygrothermal monitoring of energy efficiency retrofits in traditional tenements in Govan, Glasgow. Historic Scotland Technical Paper. [PDF]. Edinburgh, Historic Scotland.

Baker, P. 2013. U-values and traditional buildings. In situ measurements and their comparisons to calculated values. Historic Scotland Technical Paper, 10. [PDF]. Edinburgh, Historic Scotland.

BS 5250. 2011. Code of practice for control of condensation in buildings. British Standards Institution (BSI).

EN 15026. 2007. Hygrothermal performance of building components and building elements. Assessment of moisture transfer by numerical simulation. European Committee for Standardization (CEN).

EN ISO 13788. 2012. Hygrothermal performance of building components and building elements. Internal surface temperature to avoid critical surface humidity and interstitial condensation. Calculation methods. European Committee for Standardization (CEN) and International Organisation for Standardization (ISO).

Hermann, C. 2013. A review of research on the impact of wind-driven rain on Scottish traditional stone wall construction and its internal insulation retrofit. In: Hauser, G. Lützenkopf, T. Eßig, N. (eds.). 2013. SB13 Munich. Implementing sustainability. Barriers and chances. Book of full papers. Stuttgart, Fraunhofer IRB Verlag, 527-42 p.

Little, J. & Ferraro, C. 2014, forthcoming. Assessing insulation retrofits with hygrothermal simulations. Heat and moisture transfer in insulated solid stone walls. Historic Scotland Technical Paper, 15. [PDF]. Edinburgh, Historic Scotland.

Philipson, M. 2011. Application of time domain reflectometry to the measurement of moisture content in porous materials. Ph.D. thesis. Glasgow, Glasgow Caledonian University.

Rye, C. & May, N. 2012. A short paper on the conventions and standards that govern the understanding of moisture risk in traditional buildings. [PDF]. London, Sustainable Traditional Building Alliance.

Sanders, C. 2014, forthcoming. Hygrothermal simulations of internally insulated sandstone walls. A comparison between measured and modelled temperatures and relative humidities using the Glaser method and WUFI simulations. Historic Scotland Technical Paper. [PDF]. Edinburgh, Historic Scotland.

Keeping risks at bay – improving a test method to reliably quantify the capability of capillary active interior insulation

Andrea Binder, M. Eng. [1]
Daniel Zirkelbach, Dipl.-Ing. [1]
Hartwig M. Künzel, Dr.-Ing. [1]

[1]Fraunhofer-Institute for Building Physics, Holzkirchen

KEYWORDS: *Capillary activity, moisture safety, liquid transport, interstitial condensation, material properties, laboratory measurement, measurement method*

SUMMARY:
Conventional laboratory tests for the determination of liquid transport are not fully appropriate for interior insulation purposes, as they tend to overrate the transport ability under non-isothermal conditions in the hygroscopic region, and, in some cases, are not possible at all. A new test method, the Capillary Condensation Redistribution test, has recently been developed by Fraunhofer IBP. This test is specifically designed for the needs of interior insulation and is also appropriate for moisture-sensitive materials. Via hygrothermal simulation, transport characteristics are determined, enabling a close reproduction of CCR-measurement results. The data is cross-checked (where possible) by numerically simulating standard drying tests. While the results of both tests can be simulated with good correlation each, comparisons show that the drying test parameters overestimate the redistribution process of interior insulation. At the same time, the CCR-test parameters partially underestimate the isothermal drying process. To provide a single set of material parameters for hygrothermal simulation, a consolidation of transport characteristics derived from both tests is done. Numerical reproductions of field tests prove the validity and reliability of CCR and combined parameters.

1. Introduction

Interior insulation systems sometimes are met with reservations still by planners and builders (Worch 2010). Due to their complex hygrothermal behaviour, a thorough analysis of all hygrothermal processes is necessary (Worch et al. 2012) in order to keep harm from the construction. For this, transient hygrothermal simulations have proven valuable and are recommended by building physicists (Scheffler & Schoch 2013, Engel 2012, Binder at al. 2012) as well as national and international standards and guidelines (DIN 4108-3:2012, WTA-Guidelines 6-4: 2009 & 6-5:2013, EN ISO 15026:2007). The reliability of the respective simulation results hereby strongly depends on the quality of input parameters such as specific material properties.

In contrast to conventional systems with vapour retarders, capillary active insulation systems utilize the materials ability to store and transport liquid moisture inside their pore system in order to balance the construction moisture content. For this, the specific liquid transport of the insulation material is important; however, the measurement of this characteristic tends to be challenging due to the complex nature of both the materials pore system and the moisture transport processes in general.

For interior insulation, the relevant boundary conditions are non-isothermal, inducing counteracting mass transfer (liquid and vapour). Also, humidification predominantly occurs as a result of water vapour diffusion from the interior air towards the cooler parts of the construction. Here, transport processes are dominated by the rather slow suction velocity inside smaller pores.

This situation cannot be reflected by conventional tests (EN ISO 15148:2003, Holm & Krus 1998). Developed and valid for material in contact with natural weathering, they are not fully appropriate for interior insulation purposes: As the isothermal conditions here produce rectified transport processes, the measured liquid transport may exceed the real one. The high amounts of water applied to the samples additionally lead to an overestimation of the liquid transport, as here, the transport is dominated by the rather high suction velocity inside larger pores. Evidence for this has been found in the context of internal research at IBP and is also supported by external data: Kloseiko et al. (2013) have shown that the results of numerical reproduction of the measured moisture content of interior insulation constructions undercut measurement values. Furthermore, for materials sensitive to liquid moisture, e.g. fibre insulations, the conventional tests sometimes cannot be evaluated at all, as they result in agglutinated or slumped material samples.

Hence, the Fraunhofer-Institute for Building Physics has developed a new laboratory method considering the specific needs and boundary conditions of interior insulation materials. Via numerically simulating the measurement results, liquid transport characteristics for the hygroscopic region are determined. Simulations with respective characteristics have shown good correlation of both measurement and simulation results (Binder et al. 2010) and are valid for these moisture regions and circumstances. Although the respective boundary conditions and transport characteristics clearly are the dominant ones concerning interior insulation and, technically, higher moisture contents should not be reached at all inside interior insulation materials, it cannot be ruled out that sometimes, higher moisture contents or different humidification processes may occur. In order to reliably predict the moisture behaviour of a material, its liquid transport characteristics should therefore also cover the drying behaviour under isothermal conditions as good as possible.

2. Capillary Condensation Redistribution test

2.1 Test concept and procedure

The new method, the Capillary Condensation Redistribution (CCR) test, considers the specific conditions of interior insulation (Binder et al. 2010, Zirkelbach & Binder 2011). In imitation of the real-life boundary conditions of interior insulation, the CCR-test works with non-isothermal conditions and opposing liquid moisture and water vapor flows, with humidification only by vapor diffusion.

In the first phase of testing, the testing device was aligned horizontally, providing for horizontal moisture flows similar to real ones. Experience showed, however, that this may distort the moisture behaviour (Binder et al. 2010), as a runoff of condensation moisture can occur. In continuation of the original idea, the device was modified to vertical orientation. As liquid transport works independent of orientation, unaltered liquid transport characteristics can be expected. Figure 1 shows the set-up of the test.

Under laboratory conditions, a dew-point undercut is applied to one side of a laterally sealed material sample. This produces temperature and partial pressure gradients, and, consequently, vapour diffusion into the material. The adsorbed moisture is condensing at the sealed back side of the material, where it causes an increase of relative humidity. Hence, the moisture content inside the material sample rises. Due to the increasing gradient of relative humidity, a liquid transport back to the front surface of the sample sets in. Eventually, the opposing moisture fluxes will reach dynamic equilibrium. To reveal the hygrothermal behaviour of the material samples during testing, two modes of measuring are taken: Through periodic gravimetrical measurements, the moisture gain is analysed and documented for the entire test period. The moisture distribution in the samples cross-section is measured periodically by using nuclear magnetic resonance spectroscopy. By recomputing both the measured moisture distribution as well as the moisture gain via numerical simulation, highly detailed parameters for the moisture transport in the hygroscopic region are determined.

The tests are executed in a climate chamber with steady-state conditions. The dried and sealed material samples are applied to a carrier plate with heat conductive paste. All boundary conditions are measured and documented for the testing period. Regularly, the samples are removed from the test setup in order to measure their moisture content; the moisture distribution is measured at the beginning and end of the test period, as well as at certain times during test period.

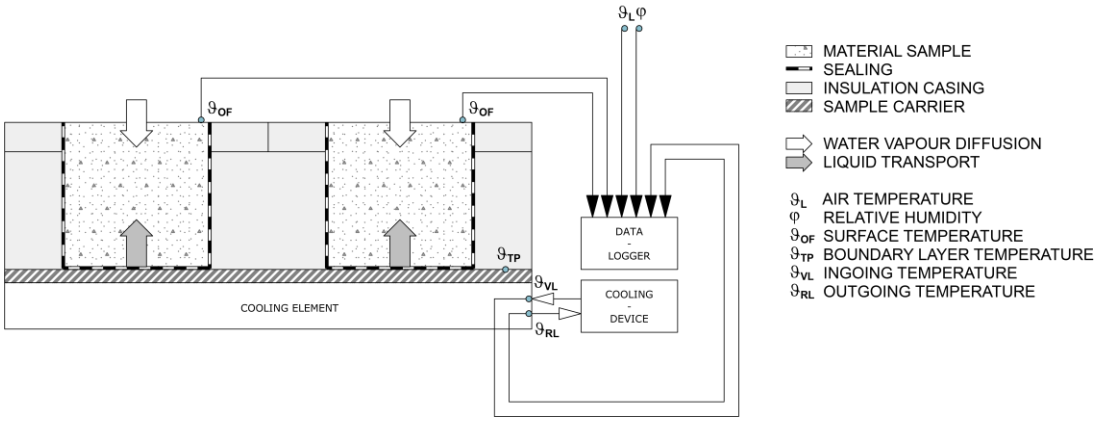

FIG 1. Setup of the new Capillary Condensation Redistribution (CCR) test developed for the measurement of liquid transport inside capillary active insulation material.

2.2 Test results

As an example of conventional capillary active materials, figure 2 shows the moisture development of calcium silicate samples during CCR test. To the right, the moisture content (MC) of three samples is shown for the entire test period of 5 weeks; to the left, the measured moisture distribution (MD) at different points of time (left) is shown for one of the samples. The tests were executed under climate conditions of 72 % RH and 22.7 °C and rear temperatures of 12.0 °C. Starting from sorption moisture content, samples gain weight fast at the beginning of the experiment, with vapour diffusion still taking place to its full extent. With time advancing, the moisture gain is decelerated by an insetting liquid transport (surface diffusion and capillary suction). After 4 weeks, a maximum MC of approximately 50 kg/m³ is reached. Now, there is only little discrepancy to be seen between the results of the different samples. The MD shows steady development: From an even distribution at start of the tests, moisture increases with time advancing, always showing a maximum at the sealed, cool back side of the sample. Towards the open-faced front surface, a comparatively even decrease of moisture is exhibited.

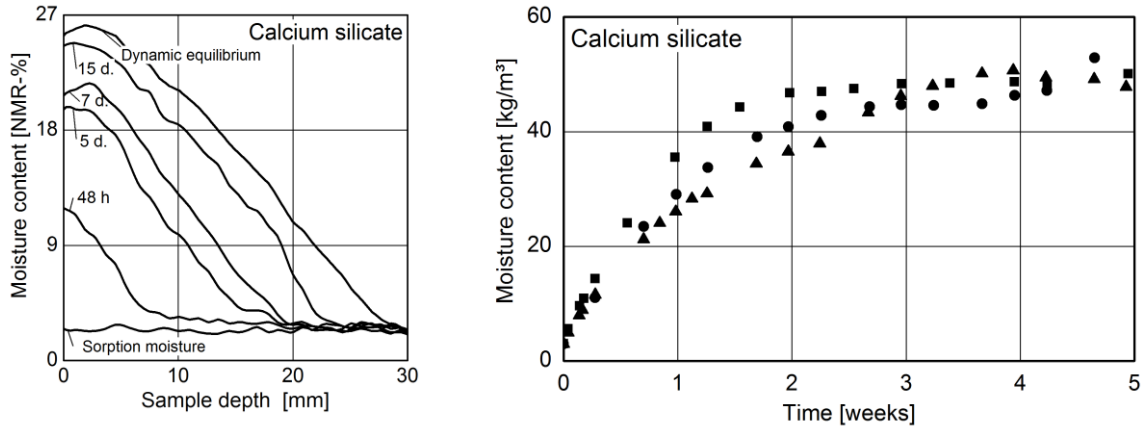

FIG 2. Results of CCR measurements for calcium silicate. Left: moisture distribution at different points of time; right: development of the moisture content for the entire test period

2.3 Determination of transport characteristics

The transport coefficients are determined by numerical simulation with WUFI® (Künzel 1994). For this purpose, the measurement results are processed prior to their implementation into the software, exporting the moisture gain characteristics for the entire test period and the MD at dynamic equilibrium (or at the end of testing). Simple values, based on the A-Value, as described by Holm and Krus (1998), serve as initial values. Step-by-step, these values are adapted in order to gain a good correlation of calculated and measured moisture gain and distribution. Figure 3 shows the measurement results of the CCR test for autoclaved aerated concrete (AAC) compared to simulation results (chain dotted line). When calculated with CCR-test parameters, good correlation can be reached for both moisture distribution (left) and gains (right); only slight deviations can be detected in lower moisture regions. After 12 weeks of testing, still no dynamic equilibrium could be reached; the MC measures up to app. 38 kg/m³. At the rear side of the sample, a maximum MC of app. 110 kg/m³ can be detected, equivalent to a RH level of almost 100 %.

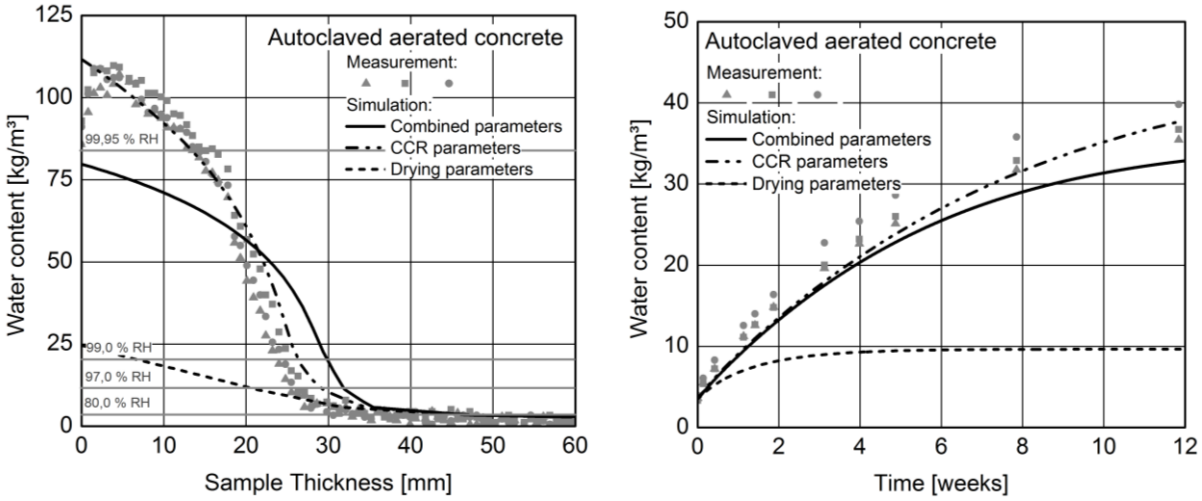

FIG 3. Results of CCR measurements for AAC compared to simulation results with different sets of liquid transport parameters. Left: moisture distribution at different points of time; right: moisture gradient for the entire test period

As mentioned before, the material properties shall enable also a realistic reproduction of the materials drying behaviour. The output of conventional drying tests (where possible/applicable) is reproduced in numerical simulation hence to verify the liquid transport coefficients. Respective results for the AAC material are shown in figure 4. With unaltered CCR parameters (chain dotted line), the drying process is underestimated. After a period of 600 h, the calculated moisture content still outruns the measured values. A cross-check of the drying parameters (dashed line), however, shows that these, on the other hand, do not reflect the measurement results of the CCR test (app. 75 % lower), showing good correlation for the drying test itself, though.

This proves that, while reaching good results in their respective area of implementation, neither of the methods solely is able to reproduce both drying (rectified) and redistribution (counteracting) moisture transport processes. Thus, in an additional step, hence, liquid transport parameters are adapted further, coupling the results of both tests. It showed, however, that it is hardly possible to perfectly reproduce both processes with one single set of combined parameters. This is due on the one hand to the diverging moisture transport processes and boundary conditions, on the other hand to the inevitable simplifications generally needed in simulation tools in order to transform a complex real material into a material data set.

Compromising both tests as good as possible, figures 3 and 4 show the results of simulation (solid line) with combined parameters. Compared to measurements and the “ideal” simulation with separately determined DW_Ws, simulation results still show deviations; however, these deviations are considerably lower than with the respective other parameters (drying and CCR). The selection of the specific parameter set thereby is, to a certain extent, an arbitrary act; however, in consideration of its rather close conformance with real conditions, the reproduction of CCR-test results should be granted priority to that of rectified drying processes.

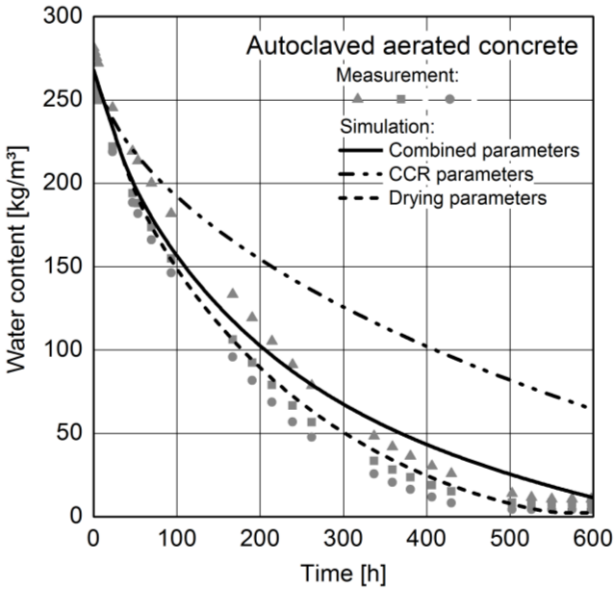

FIG 4. Results of drying tests for AAC compared to simulation results with different sets of liquid transport parameters.

3. Validation & comparison

3.1 Test concept and procedure

To validate both concept and procedures of the CCR test, a field test is done at the facilities in Holzkirchen. In a partitioned test façade (interior climate 25 °C, 50 % RH), an interior insulation assembly is installed into wooden framework with 500 x 500 mm diameter. The basic composition (from the exterior) is 20 mm lime-cement render, 240 mm solid brick and 20 mm plaster (to create an even surface for the insulation layer). The AAC material used for interior insulation is sealed laterally to inhibit any side influences. At the rear side, aluminium foil is applied. Naturally, this is an addition not reflecting the actual situation, but is providing for measurement results that solely reflect the materials hygric behaviour in itself without any manipulation from possible suction processes of backing material. At the interface of insulation and aluminium foil, both temperature and relative humidity are continuously recorded. As traditionally, RH measurement at higher moisture regions is somewhat challenging, additionally, thin wooden plates equipped with wood-moisture probes are embedded. All exterior climate parameters are measured by the IBPs weather station; for interior climate, temperature and relative humidity are measured.

3.2 Test and calculation results

The experiment started in November 2011. As the materials were implemented into the structure without preceding conditioning, their initial moisture contents were not equal. A period of adjustment therefore marks the first weeks of the test period. The following paragraphs only refer to the period

after comparable moisture contents have been reached (1.2.2012 – 31.1.2013). Figure 5 shows the temperature of the exterior air and at the rear side of AAC. Starting at around 5 °C (interface) and -7 °C (exteriorly), temperatures drop in the first days of February and start rising in the 2nd half of February, with maxima showing from late June to August. While larger temperature differences between outside and interface can be detected during winter, towards summer, values are closer.

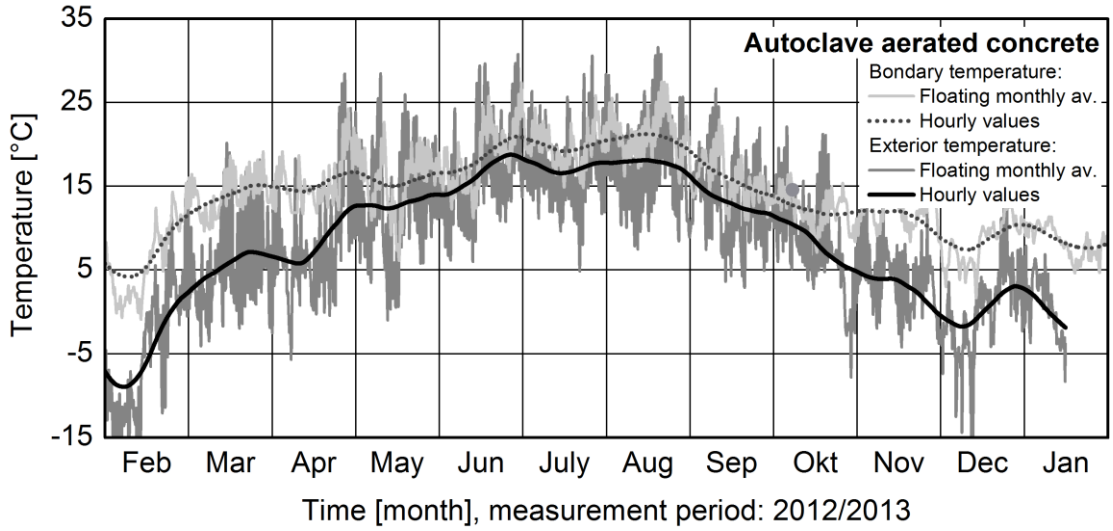

FIG 5. Results of a field test of interior insulation assemblies in Holzkirchen. Temperatures of the exterior air and at the rear side of AAC interior insulation according to measurements.

Figure 6 shows the development of RH at the rear side of AAC. During winter time, approximately 100 % RH are reached, as the moisture settles at the rear side of the insulation. With rising temperatures, redistribution and drying processes (both diffusion and liquid transport) set in; consequently, RH levels fall (starting in April). In autumn, the decrease of temperatures is followed by rising RH levels, reaching 100 % RH again in December.

The graph also shows the results of numerical simulation for the different parameter sets described above. With drying parameters, the rather fast drying process (during spring) can be retraced with good concordance. However, it is not possible to reproduce the high RH levels measured during winter: calculated maxima are approximately 15 % lower than actual ones. Both with CCR as well as with combined parameters, however, 100 % RH are reached during winter time, reflecting the measurements very closely. The rather fast decrease of moisture during spring can be retraced with a setback of approximately one week with combined parameters and two weeks with CCR parameters. With all three parameter sets, RH levels during summer generally can be reproduced with good accordance, levelling out any extremes to a certain extent, however.

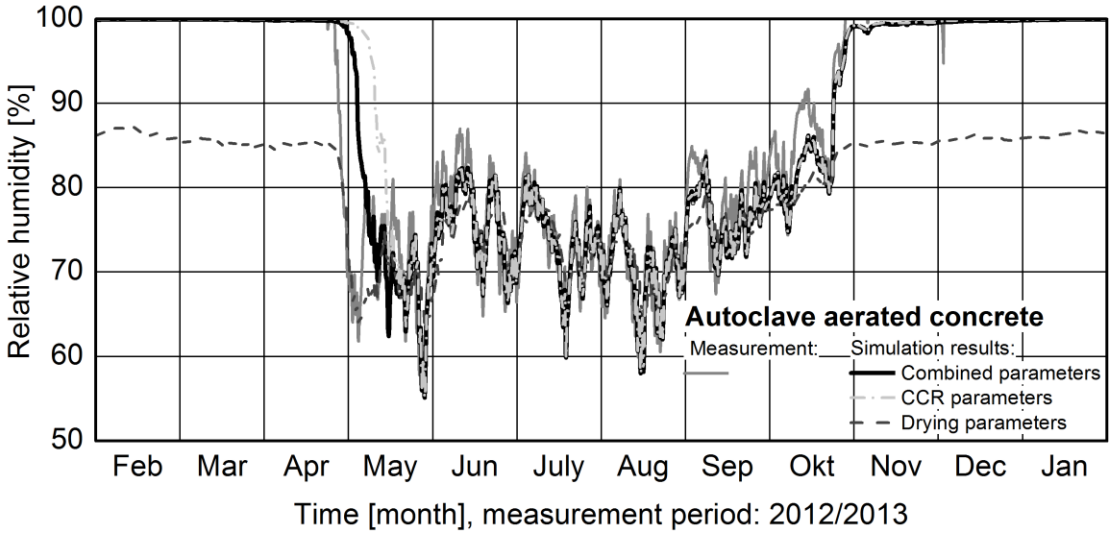

FIG 6. Results of a field test of interior insulation assemblies in Holzkirchen. Level of relative humidity at the rear side of AAC-interior insulation according to measurements and numerical simulation based on different sets of liquid transport parameters.

4. Conclusion

In context with the swiftly developing market of capillary active interior insulation, a reliable data basis of their respective liquid transport ability is important to secure an acceptable performance. Experience has shown that conventional tests, originally developed for materials under influence of natural weathering, are not fully appropriate for interior insulation purposes, tending to overestimate the materials liquid transport abilities and possibly not realizable for moisture sensitive materials. With the development of the CCR-test, the Fraunhofer IBP delivers a test that is especially designed and appropriate for the boundary conditions of interior insulation and also provides a method to determine the liquid transport ability of materials not measureable before.

Showing promising results, the test and its results have been undertaken further cross-checking and validation. The comparison with conventional tests showed that while each test (drying and CCR) delivers good correlation in its respective area of implementation, neither method solely seems to be able to reproduce the respective other test results. Hence, in the desire to cover as best as possible all drying and redistribution processes with just one set of parameters, further processing of the coefficients has been done, compromising the resulting moisture gain and distribution of both tests.

Experience shows that simulations with combined parameters lead to good correlation with results of all tests. The field test done for validation purposes proves the reliability of the respective parameter set, retracing both winterly maxima and summerly minima of RH. The aluminium foil that is used for sealing reasons in the field test adds somewhat to extreme values, as it prohibits any equalizing effects the render or masonry might have on the moisture levels at the interface. Actual MCs may therefore be lower than in this test. However, the large distance between measured results and those of numerical simulation with drying parameters clearly shows the limited adequacy of conventionally determined liquid transport parameters for interior insulation assemblies.

Thus, the new combination method provides reliable and realistic information about the specific liquid transport ability of interior insulation materials both in higher and lower moisture regions under for non-isothermal as well isothermal conditions.

References

Binder, A., Künzel. H. M., Zirkelbach, D. 2012. Ein abschätzender Blick in die Zukunft. Trockenbauakustik, Spezial Innendämmung. Verlagsgesellschaft Rudolf Müller, Köln, Germany. 11 p.

Binder, A., Zirkelbach, D., Künzel, H. M. 2010. Test Method to quantify the wicking properties of insulation materials designed to prevent interstitial condensation. Proceedings of the Buildings XI International Conference. Clearwater Beach, USA. 119 p.

DIN EN 4108-3:2012-01 (draft). Thermal protection and energy economy in buildings – Part 3: Protection against moisture subject to climate conditions – Requirements and directions for design and construction.

DIN EN ISO 15026:2007-07. Hygrothermal performance of building components and building elements – Assessment of moisture transfer by numerical simulation.

DIN EN ISO 15148:2003-03. Wärme- und feuchtetechnisches Verhalten von Baustoffen und Bauprodukten - Bestimmung des Wasseraufnahmekoeffizienten bei teilweisem Eintauchen.

Holm, A., Krus, M. 1998. Bestimmung der Transportkoeffizienten für die Weiterverteilung aus einfachen Trocknungsversuchen und rechnerischer Anpassung. Bauinstandsetzen 4 (1998), Vol. 1. Aedificatio Verlag GmbH, Freiburg, Germany. 33 p.

Kloseiko, P., Arumagi, Endrik & Kalamees, T. 2013. Hygrothermal performance of internally insulated brick wall in a cold climate: field measurement and model calibration. 2nd central European symposium on building physics. Madhavi, A., Martens, B.. Vienna, Austria. 185 p.

Künzel, H. M. 1994 (1995). Simultaneous heat and moisture transport in building components. One- and two-dimensional calculation using simple parameters. Dissertation Lehrstuhl Bauphysik, Fakultät für Bauingenieur- und Vermessungswesen der Universität Stuttgart, Germany.

Scheffler, G., Schoch, T. 2013. Kapillaraktive Innendämmung sicher planen und anwenden. Leitfaden Innendämmung. Bauverlag BV, Gütersloh, Germany. 17 p.

Worch, A. 2010. Innendämmung nach WTA – Das Merkblatt 6-4. Innendämmung im Bestand. Fraunhofer IRB Verlag, Stuttgart, Germany. 9 p.

Worch. A., Hecht C., Ruisinger U. 2012. Und sie funktionieren doch! Trockenbauakustik, Spezial Innendämmung. Verlagsgesellschaft Rudolf Müller, Köln, Germany. 7 p.

WTA-Guideline 6-4:2009-05. Inside insulation according to WTA I: planary guide.

WTA-Guideline E 6-5:2012-11 (draft). Interior insulation according to WTA II. Nachweis von Innendämmsystemen mittels hygrothermischer Berechnungsverfahren.

Zirkelbach, D., Binder, A.. 2011. Mit neuen Kennwerten genauer rechnen. Bauen im Bestand. Vol. 34. Verlagsgesellschaft Rudolf Müller, Köln, Germany. 42. p.

Causes of Condensation in Mechanically Attached Cool Roof Systems

Kehrer Manfred, Senior Researcher [1]
Pallin Simon, Ph.D. [1]

[1] Oak Ridge National Laboratory, TN, USA

KEYWORDS: *Heat, Moisture, Moisture Damage, Hygrothermal Simulation, Durability, Flat Roof, Cool Roof.*

SUMMARY:
A white roof, or cool roof, is constructed to decrease thermal loads from solar radiation, therefore saving energy by decreasing the cooling demand. Unfortunately, cool roofs with a mechanically attached membrane have shown a higher risk of intermediate condensation in the materials below the membrane in certain climates (Ennis and Kehrer 2011) and in comparison with similar constructions with a darker exterior surface (Bludau et al. 2009). As a consequence, questions have been raised regarding the sustainability and reliability of using cool roof membranes in northern U.S. climates. This study focuses on the risk of condensation in cool roof construction with a mechanically attached outer membrane. The risk evaluation is based on 128 simulated scenarios of plausible roof conditions with varying indoor and outdoor climates. Four input parameters are chosen to vary: the outdoor climate, the solar surface properties, the indoor moisture supply, and the indoor air intrusion rate below the surface membrane.

1. Introduction

The hygrothermal performance of a mechanically attached roof system has been investigated with numerical simulations, since such roof constructions have shown a higher risk of intermediate condensation in the materials below the membrane in certain climates (Ennis and Kehrer 2011). The hygrothermal software WUFI is used for the computations of coupled heat and moisture transportation (Künzel 1995) since a tool is required, capable of modelling heat and moisture transport in a transient simulation and with realistic boundary conditions. The simulation tool should be able to include air intrusion and long-wave (infrared) radiation at the exterior surface, since these mechanisms are likely the major causes of risks of condensation.

Roof systems with thermoplastic membranes are prone to be more affected by interior air intrusion into the roof construction, both from wind-induced pressure differences and from the flexibility and elasticity of the membrane (Molleti et al. 2011). Depending on the air permeability of the material underneath the membrane, wind forces increase the risk of fluttering (also referred to as billowing, as seen in FIG. 2) of a flexible single ply thermoplastic membrane. Expectably, the wind-induced pressure differences create a convective air flow into the construction (i.e., air intrusion). If the conditions are right, moisture from the exchanging air may condensate on surfaces with a temperature below the dew-point.

The definite path of convective air flows through the building envelope is usually very difficult to determine, so simplified models (Künzel et al. 2011) help to estimate the additional moisture loads caused by air intrusion. The wind uplifting pressure in combination with wind gusts is an important factor for a fluttering roof. Unfortunately, the effect of fluctuating wind is difficult to estimate as this is a highly dynamic phenomenon and existing standards (ASTM D7586/D7586M-11 2011) take into account only a steady-state approach (i.e., there are no guidelines or regulations on how to estimate the air intrusion rate). Obviously, more detailed knowledge on the hygrothermal performance of

mechanically attached cool roof systems is needed with regard to surface colors, roof airtightness, climate zones, and indoor moisture supply.

FIG. 1 shows the simulated roof assembly, consisting of a traditional metal deck, 3-inch polyisocyanurate insulation boards, and a thermoplastic membrane (representing a flexible single ply membrane). Due to a supposedly air leaky roof construction underneath the thermoplastic membrane, an uplift of the exterior membrane will lead to indoor air intrusion, as seen in FIG. 2. As a consequence of the air intrusion, an air layer is created underneath the membrane. If the surface temperatures in this created volume are lower than the dew point temperature of the indoor air, condensation will occur.

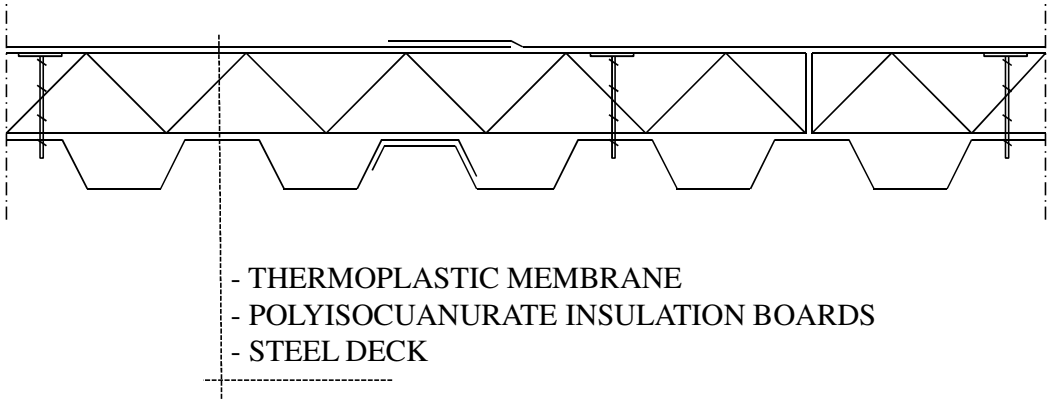

FIG. 1 Model of the investigated mechanically attached roof system. The thermoplastic membrane has either a light or a dark surface that affects the hygrothermal performance of the roof.

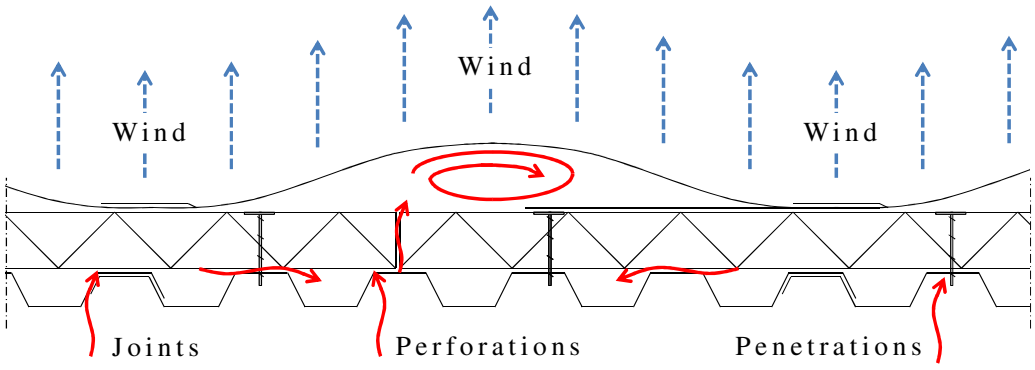

FIG. 2 Wind forces, inducing pressure differences on the outer and inner membrane surfaces, cause the membrane to flutter and balloon. Depending on the condition and workmanship of the construction, air intrusion may arise through overlapping joints of the steel deck, penetrations, or perforations. Plausible locations of air intrusions are indicated with solid arrows. The uplifting forces, due to the wind, are indicated with dashed arrows.

2. Investigations

Air intrusion into a roof construction depends on the wind loads acting on the roof surface and the air permeability of the construction below the thermoplastic membrane. Subsequently, air intrusion is an important parameter to estimate when analyzing the hygrothermal performance of a roof. This section presents an approach to quantify this parameter.

2.1. Wind Forces

The airtightness of a roof construction, together with the existing pressure differences, determines the air leakage rate between the indoor and outdoor environment. In this study, the thermoplastic membrane is assumed to be sealed with satisfactory workmanship, thus minimizing exfiltration or infiltration air exchange; that is, air will not flow between the inner and outer surfaces of the roof. Instead, the exchange of air inside and between the roof materials is a consequence of indoor air intrusion (i.e., an exchange of indoor air in the materials of the building envelope). The air pressure differences influencing the intrusion rate are typically thermally driven (stack effect), with the ventilation system or wind loads acting on the building envelope (Hagentoft 2001). The wind generally creates an uplifting force on the thermoplastic membrane. Due to the flexibility and elasticity of the membrane, it may easily deform in favor of pressure differences, causing the membrane to flutter and balloon (Baskaran and Molleti 2010). This deformation, due to uplifting forces, is also referred to as billowing.

A negative wind-induced air pressure is typically acting on the exterior roof surface and can be estimated by use of ASCE Standard ASCE/SEI 7-10 (ASCE 2010). The wind pressure, P_w, for low-rise buildings is defined in Sections 28.3.2 and 28.4.1. Following the calculation steps of the ASCE Standard and determining the suitable coefficients for the roof construction, exposure and surrounding topography result in an uplift P_w as follows:

$$P_w = 0.273 \cdot V^2 \tag{1}$$

Where P_w Wind uplift pressure (Pa)
V wind speed parallel to the surface (m/s)

The wind speed is typically presented as an average speed for a defined period of time (e.g., 1 hour). Wind speeds that are based on measured averages at shorter time intervals are referred to as gusts (Harper et al. 2010). Gusts have been taken into account by using statistical data derived from minute-based measurements of the wind speed in Holzkirchen, Germany from 2009 to 2010.

2.2. Air Intrusion

The fluttering effect of the roof sheeting causes an exchange of indoor air underneath the membrane. This air intrusion is defined as an air exchange rate per hour, ACH, and can be defined as

$$ACH = \frac{Q}{V} \tag{2}$$

Where ACH Air change rate (1/h)
Q Flow rate (m^3/h)
V Volume of ventilated air space (m^3)

Q, in this study, depends on the pressure difference between the membrane and the indoor environment and also on the airtightness of the roof assembly, as given by

$$Q = A \cdot C \cdot \Delta P^n \tag{3}$$

Where Q Flow rate (m^3/h)
C Air Leakage Coefficient (m^3/(s Pa)
A roof surface area (m^2)
ΔP Pressure difference (Pa)
n Pressure Exponent (-)

A Q_{50}-value refers to air flow rate at a pressure difference of 50 Pa, thus simplifying comparisons between different constructions and measurements.

Consequently, C and n are parameters related to the physical structure of the roof which are typically determined by measurements. Therefore, the roof construction is tested in accordance with the ASTM E2178-11 Standard for testing the air leakage rate (ASTM 2011). The specimen represents the roof construction as defined in Figure 1, except for the exclusion of the outer thermoplastic membrane. The reason for this approach is that the complete roof assembly is assumed to be very airtight and that the air intrusion rate between the indoor environment and underneath the membrane is to be estimated.

TABLE 1. Results from measuring the air leakage coefficient, C, and the pressure exponent, n. Five different assemblies were measured with various repetitions and are presented as average values of the measurements.

Results from airtightness tests	C *(m^3/s,Pa)*	n (-)	Q50 (m^3/s)	Q50 (l/s)
1. Sealed joints and sealed screw penetrations	3.31E-07	0.99	1.74E-05	0.02
2. Steel deck only	6.45E-06	0.95	2.63E-04	0.26
3. Full assembly	6.19E-06	0.96	2.69E-04	0.27
4. Full assembly, 2–4 perforations	6.85E-05	0.54	5.61E-04	0.56
5. Full assembly, 8 perforations	1.25E-04	0.72	2.09E-03	2.09

The results of the measurements are presented in
TABLE 1, in which the different assemblies were measured with various repetitions. The purpose of the first assembly (sealed joints and sealed penetrations) was to ensure a satisfactory seal between the steel deck and the wooden framework, which is confirmed by the results in

TABLE 1. Second, only the steel deck was tested, without the insulation boards mounted on top. This assembly was later compared with the full assembly with both steel deck and insulation boards, though without the thermoplastic membrane. The results from these two assemblies indicate that the airtightness of the steel deck is conclusive (i.e., the airtightness of the insulation boards is much less than that of the steel deck). Further, the steel deck was perforated with varying numbers of 3/16-inch drilled holes. The effects of a perforated steel deck are presented in Table 1, indicating the importance of intact steel sheeting.

The results from measuring the airtightness of the metal roof construction indicate that even small perforations of the steel increase the leakage rate significantly. A well-performed overlap of the steel deck sheets, screwed tight and without further sealing has relatively high airtightness, however.

Further, material properties from the hygrothermal model database are utilized, except for the metal trapezoidal construction where a vapor permeance of 1.0 (perm) is applied. The permeance represents a metal deck including air leakages from penetrations such as screws and is in accordance with earlier investigations done at Oak Ridge National Laboratory (Kyle & Desjarlais, 1994). The initial moisture content of the materials in the simulation model are EMC80 (ASHRAE 160 2011).

3. Parameters

The results of this study are based on multiple iterations of the numerical simulation of the roof construction with varying input parameters. The varying parameters are discussed below.

3.1 Climate

Four different U.S. climates are used, representing climate zones which are:

- Climate Zone 4 – Baltimore, Maryland
- Climate Zone 5 – Chicago, Illinois
- Climate Zone 6 – Minneapolis, Minnesota
- Climate Zone 7 – Fargo, North Dakota

3.2 Surface Solar Reflectance

The solar absorptivity of a surface defines the ratio of solar radiation absorbed by a surface and varies between 0 and 1. The solar absorptivity used in the simulations of this study is set to either 0.3 or 0.85, which is representative of a white or a dark surface.

3.3 Indoor Moisture Supply

Four different variations of indoor relative humidity are used in the simulations. Due to the lack of specific design values for commercial buildings, equivalent rates for residential buildings are applied. The four different variations of indoor moisture supply are presented here:

- EN-15026, normal and high moisture load.
- ASHRAE 160 intermediate method, two bedrooms with ACH = 0.6 and six bedrooms with ACH = 0.2, which supposedly are representative of a low and a high indoor moisture supply.

3.4 Air Intrusion

The air intrusion rates used in the simulations of the roof are as follows.

- Q_{50} = 0.27 (l/s,m^2) A perfectly assembled roof construction
- Q_{50} = 0.56 (l/s,m^2) An assumed satisfactory assembly of roof construction
- Q_{50} = 1.0 (l/s,m^2) Semi-leaky roof construction, arbitrarily chosen.
- Q_{50} = 2.0 (l/s,m^2) Leaky roof construction, based on measurements in (Hens et al. 2003).

4. Results

A total of 128 different scenarios of the mechanically attached roof system are simulated, with varying input parameters as defined in Section 4. Each scenario is numerically simulated for a complete year.

The accumulation of moisture in the air layer between the thermoplastic membrane and the insulation board is evaluated since it is closely related to the amount of condensed water in the roof construction. The moisture content of the air layer is converted into a condensate layer thickness, d_l, in which the moisture content is assumed to be distributed over the complete surface area (FIG. 3).

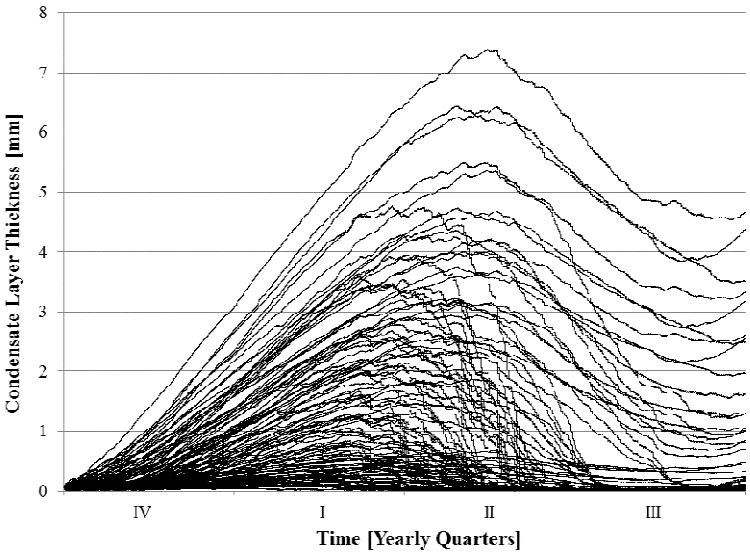

FIG. 3 Condensate layer thickness, d_l, for the 128 simulated roofs with a mechanically attached outer membrane. Typically, the thickness increases during the heating season.

The variations of d_l, illustrated in FIG. 3, give a range of different simulated roofs, without specifying the chosen input parameters of the simulations.

A critical d_l is commonly taken as 0.5 mm to avoid dripping (DIN 4108-3 2001, Hens et al. 2003), hence this value is considered an upper maximum for a safe and reliable roof construction. Additionally, a d_l between 0.5 and 1.0 is considered risky, and values beyond are rated as failures in terms of the risk for condensation. The 1.0 threshold is also recommended in German Standard (DIN 4108-3 2001); it is stated as an upper limit to avoid gravitational flow, but in presence of hygroscopic materials only. However, the standard is mainly used for the surfaces of walls with a sloped roof; consequently, water drips more easily compared to a flat roof. Hence the 1.0 threshold can be assumed conservative and thus applicable for this study.

The results of the risk evaluation for the 128 simulations are given in TABLE 2.

TABLE 2. Results from the 128 simulated scenarios, indicating the reliability of the roof construction at given conditions. Table cells with no background color indicate a safe roof construction, gray indicates risky construction, and black indicates an expected failure with respect to condensation. B stands for a black roof surface, and W stands for white.

Climate Zone 4								
Indoor moisture supply	Q_{50} = 0.27		Q_{50} = 0.56		Q_{50} = 1.0		Q_{50} = 2.0	
ASHRAE - Low	B	W	B	W	B	W	B	W
EN - Normal	B	W	B	W	B	W	B	W
EN - High	B	W	B	W	B	W	B	W
ASHRAE - High	B	W	B	W	B	W	B	W
Climate Zone 5								
Indoor moisture supply	Q_{50} = 0.27		Q_{50} = 0.56		Q_{50} = 1.0		Q_{50} = 2.0	
ASHRAE - Low	B	W	B	W	B	W	B	W
EN - Normal	B	W	B	W	B	W	B	W
EN - High	B	W	B	W	B	W	B	W
ASHRAE - High	B	W	B	W	B	W	B	W
Climate Zone 6								
Indoor moisture supply	Q_{50} = 0.27		Q_{50} = 0.56		Q_{50} = 1.0		Q_{50} = 2.0	
ASHRAE - Low	B	W	B	W	B	W	B	W
EN - Normal	B	W	B	W	B	W	B	W
EN - High	B	W	B	W	B	W	B	W
ASHRAE - High	B	W	B	W	B	W	B	W
Climate Zone 7								
Indoor moisture supply	Q_{50} = 0.27		Q_{50} = 0.56		Q_{50} = 1.0		Q_{50} = 2.0	
ASHRAE - Low	B	W	B	W	B	W	B	W
EN - Normal	B	W	B	W	B	W	B	W
EN - High	B	W	B	W	B	W	B	W
ASHRAE - High	B	W	B	W	B	W	B	W

5. Conclusions

The results emphasize the importance of solar reflectance at the roof surface. The results presented in Table 2, reveals that only about 18% of the simulated roof construction is considered risky when the indoor moisture supply is considered low. (Typically, a low indoor moisture supply is either attained by a low moisture production rate or by a high ventilation air exchange rate.) A comparison between a white and a black surface reveals (for a low moisture supply) that only a white surface can be risky with a high air intrusion rate. The opposite is valid for a white surface with a high indoor moisture supply, where only about 16% of the roof constructions are considered safe. Consequently, a moisture reliable roof construction can only be constructed with a black surface, at a high rate of indoor moisture supply.

The different air intrusion rates applied to the study show similar behavior in comparison with indoor moisture supply. An increased rate increases the maximum condensate layer thickness.

The fourth varying parameter, the climate, was proven to also have an influence on the amount of accumulated moisture. The influence of the climate is proven significant by the comparisons of each climate segments in TABLE 2.

In conclusion, all the varying parameters of this study are highly influential on the hygrothermal cool roof performance. A low indoor moisture supply or a low air intrusion rate ensures a low risk of intermediate condensation. A safe upper limit of air leakage at 50 Pa, Q_{50}, is stated as 0.17 l/s,m^2 for metal roofs (Hens et al. 2003). This limit seems consistent with the low risks of the simulated lower air intrusion rate of 0.27 l/s,m^2, at least for the black roofs of this study.

A cool roof will accumulate approximately twice as much moisture below the surface membrane as a black surface. It is assumed that replacing a black surface with a cool membrane on an existing mechanically attached roof system could result in intermediate condensation.

The mechanical resistance of the roof membrane has not been taken into account in this study. Likely, this means that, at some lower limit of wind-induced pressure, the uplifting force is lower than the weight and flexible resistance of the membrane, thus preventing any air intrusion. Therefore, a complete depressurization analysis of a mechanically attached roof system is needed to fully analyze a cool roof assembly at realistic and fluctuating wind loads.

It is of great concern to emphasize that a single ply roof, including an interior vapor retarder, is not necessarily equivalent with an airtight construction. Either insufficiently sealed overlaps, perforations or penetrations of the vapor retarder, may cause high air intrusion rates.

Finally, the following conclusions can be stated:

- If a very low indoor moisture supply is assumed, no moisture problem is expected, except for white surfaces combined with high air intrusion rates.
- For black roofs, the joints of the steel deck do not necessarily need to be sealed to be considered safe, though penetrations and perforations must.
- The previous statement is valid for white roofs, only with a low or normal indoor moisture supply.
- For all other roof assemblies with varying indoor and outdoor climates, an interior air barrier is recommended.

References

ASCE (2010). *Minimum Design Loads for Buildings and Other Structures*. ASCE/SEI 7-10, American Society of Civil Engineers.

ASHRAE 160 (2011). *ANSI/ASHRAE Addendum a to Standard 160-2009 Criteria for Moisture-Control Design Analysis in Buildings*. Atlanta, GA, American Society of Heating, Refrigerating and Air-conditioning Engineers, Inc.

ASTM (2011). *ASTM E2178-11, Standard Test Method for Air Permeance of Building Materials*, ASTM International.

ASTM D7586/D7586M-11 (2011). *Standard Test Method for Quantification of Air Intrusion in Low-Sloped Mechanically Attached Membrane Roof Aseemblies*, ASTM International.

Baskaran, B. A. and Molleti, S. (2010). *How much air is too much? The National Research Council of Canada studies roof system air intrusion*, NRC Publications Archive.

Bludau, C., Zirkelbach, D. and Kuenzel, H. M. (2009). "*Condensation problems in cool roofs*." Interface, The Journal of RCI XXVII(7): 11-16.

DIN 4108-3 (2001). *Teil 3: Klimabedingter Feuchteschutz, Anforderungen, Berechnungsverfahren und Hinweise für Planung und Ausführung*. Wärmeschutz und Energie-Einsparung in Gebäuden. DIN Deutsches Institut für Normung.

Ennis, M. and Kehrer, M. (2011). *The effects of roof membrane color on moisture accumulation in low-slope commercial roof systems*. Proceedings of NRCA International Roofing Symposium 2011, Washington, MD.

Hagentoft, C.-E. (2001). *Introduction to building physics*. Lund, Sweden, Studentlitteratur.

Harper, B. A., Kepert, J. D. and Ginger, J. D. (2010). *Guidelines for converting between various wind averaging periods in tropical cyclone conditions*, World Meteorological Organization (WMO).

Hens, H., Zheng, R. and Janssens, H. (2003). *Does performance based design impacts traditional solutions? Metal roofs as an example.* Proceedings of the 2nd international conference on building physics, Antwerpen, Belgium.

Künzel, H. M. (1995). *Simultaneous Heat and Moisture Transport in Building Components. - One- and twodimensional calculation using simple parameters*. IRB Verlag, University Stuttgart. Dissertation.

Künzel, H. M., Zirkelbach, D. and Scfafaczek, B. (2011). *Vapour control design in wooden structures including moisture sources due air exfiltration*. 9th Nordic Symposium on Building Physics - NSB 2011, Tampere, Finland.

Molleti, S., Baskaran, B., Kalinger, P. and Beaulieu, P. (2011). *Air Intrusion and Its Effect on Moisture Transport in Mechanically Attached Roof Systems*. Proceedings of the 2011 International Roofing Symposium.

Influence of construction design on moisture damage of wooden buildings

Eva Vahalová[1]
Ruut Peuhkuri, Associate Professor [2]
Carsten Rode, Professor [3]
Karel Šuhajda, Ph.D [4]

[1,4] Brno University of Technology, Department of Civil Engineering, Institute of Building Structures, Czech Republic

[2,3] Technical University of Denmark, Department of Civil Engineering, Section of Building Physic and Services, Denmark

KEYWORDS: *wooden building, wall and floor junction, mould growth, hygrothermal performance*

SUMMARY:
Correct design and use of high quality materials ensure long durability and lifetime of buildings, especially for houses with wooden constructions. The drying potential of a wall construction can be one of the main criteria for durability and healthy indoor environment. Earlier studies have shown that wooden constructions with unventilated, undrained and well-insulated walls can be vulnerable to moisture damage. The damage is often not visible on the surface of the wall, but may be hidden within the wall and at its joints.

This paper presents an analysis of two new wooden experimental buildings with different construction solutions, one from Denmark and the other from the Czech Republic. In order to compare the influence of different construction solutions on the hygrothermal performance and to estimate the durability of the constructions, the details of the joint between wall, floor and foundation was modelled in two dimensions and assessed with respect to risk of mould growth and fungal decay. The vulnerability of the analysed solutions to flaws in moisture design and construction strategy is assessed.

1. Introduction

Wood is a hygroscopic material so its condition depends on its moisture content. From an indoor microclimatic point of view this property of wood is considered an advantage, but with regards to the actual construction of buildings and the dimensional stability of wood-based elements, the sensitivity to the moisture state can often be challenging. The combination of temperature and humidity in the environment in which the timber is located, results in a certain moisture content of the wood, which practically does not depend on the tree species (Havířová 2012).

Since the timber continuously exchanges moisture with the surrounding environment, the moisture content of the timber can increase to a high level when the humidity of the environment is high. If the condition of keeping the wood in a humid environment lasts longer than few weeks in a year, there will be a risk of infection and subsequent degradation of wood components in the construction by wood-destroying micro organisms. Also, in the terms of reliability of the construction the increased moisture content of wood elements will cause the expected increase of deformation of these elements over and/or above the value proved in static calculations.

Several studies mentioned also by Dalehaug (2013) have shown that wooden constructions in unventilated, undrained and well-insulated walls can be susceptible to moisture damage.

Requirements and recommendations for initial moisture conditions of structural wood vary according to the legislation of each country, e.g. in Norway it is allowed to use a wood with 20 weight-% moisture content (MC), in Denmark, Germany, Austria and the Czech Republic it is 18 weight-% MC (Gaare & Løtveit 2012). However, the reality on the construction site is often something else, and it is not unusual to see timber constructions soaking in rain. Although high initial moisture content should never be accepted, but it may still be of interest to see how quickly excessive moisture can be dried from a critical construction element.

The influence of initial moisture content on the performance was based on practical measurements on the site during the construction period of the Danish experimental buildings. The measurements showed that MC of the wood, especially the bottom plate which is in direct contact with concrete screed could reach the value over 35 weight-%.

2. Materials

For this study, two well-insulated timber structures have been chosen for analysis, which are quite different with regards to their possibility to dry out moisture. The two solutions are commonly used in newly built low energy buildings in Czech Republic and Denmark, respectively, and have therefore slightly different thermal properties. Photos of the bottom plate in such walls are shown on Figure 1.

FIG 1. Total view on the wet wall of Czech study case (left), Bottom plate under weather condition in Danish study case (right)

A study of the hygrothermal condition of the two constructions was carried out using numerical simulation. In this study, in order to be able to compare the performance of the two details as well as possible, the insulation thickness was altered in the Czech case to obtain the same U-value of the floor and wall constructions as in the Danish case. The constructions are show on Figure 2.

The insulation layer of the floor construction was in the Czech detail was increased from the normally used 120 mm to 330 mm in order to get the U-value of 0,113W/(m^2K), so the total thickness of the floor construction was for Czech study case 620 mm while it was 380 mm in the Danish case. The main reason for the difference in total thickness is the use of stone as capillary breaking layer in the Czech construction, where the Danish construction uses the EPS insulation as capillary breaking layer. In addition, a thicker concrete slab is used in the Czech construction.

As for wall construction the Czech construction is characterised by having a layer of EPS closed cell foam insulation as the external insulation layer, and mineral wool as insulation between the wooden

posts, while the Danish construction uses cellulose insulation throughout. In order to achieve same U-value, the thickness of the EPS insulation in the Czech case was increased from the typical 100 mm to 155 mm to achieve a U-value of 0,123W/(m^2K). So the total thickness of the wall construction was for the Czech case 376 mm while it was 395 mm in the Danish case. The Danish case was completed on the outside with an air gap and a wooden cladding, which was not included in the numerical simulation model. The dimensions of the Czech bottom plate were 150/120mm (width/height) and Danish 120/45mm (W/H). The compositions of both cases of floor and wall constructions are described in Table 1 and Table 2, respectively.

TABLE 1. U-values for floor constructions for simulated details Czech study case (left), Danish study case (right)

CZE	d[m]	λ[W/mK]	R[m^2K/W]
$R_{internal}$	-	-	0.17
Wooden floor	0.01	0.13	0.078
2x OSB	0.03	0.13	0.23
Mineral wool	0.330	0.04	8.25
Concrete slab	0.150	2.1	0.071
Stone	0.100	2.43	0.041
Σd=	0.620	ΣR=	8.84
		U=1/ΣR=	0.113W/m^2K

DK	d[m]	λ[W/mK]	R[m^2K/W]
$R_{internal}$	-	-	0.17
Wooden floor	0.015	0.13	0.115
Concrete screed	0.100	2.1	0.048
EPS	0.265	0.031	8.549
Σd=	0.380	ΣR=	8.88
		U=1/ΣR=	0.113W/m^2K

TABLE 2. Material layers and calculation of U-values for wall constructions for simulated details Czech study case (left), Danish study case (right)

CZE	d[m]	λ[W/mK]	R[m^2K/W]
$R_{internal}$	-	-	0.13
Gypsum board	0.013	0.2	0.065
Mineral wool	0.04	0.056	0.714
Post, MW	0.15	0.047	3.19
OSB	0.015	0.13	0.115
EPS	0.155	0.04	3.875
Plaster	0.003	0.595	-
$R_{external}$	-	-	0.04
Σd=	0.376	ΣR=	8.13
		U=1/ΣR=	0.123W/m^2K

DK	d[m]	λ[W/mK]	R[m^2K/W]
$R_{internal}$	-	-	0.13
Gypsum board	0.013	0.2	0.065
OSB	0.012	0.13	0.09
Post, cellulose	0.36	0.048	7.5
Wood fireboard	0.01	0.05	0.2
Air gap	0.025	-	-
Cladding	0.025	-	-
$R_{external=internal}$	-	-	0.13
Σd=	0.395	ΣR=	8.12
		U=1/ΣR=	0.123W/m^2K

The corresponding basic material properties used for the heat and moisture simulations are listed in Table 3 and Table 4.

TABLE 3. Material parameters for hygrothermal simulation, part 1 (IBK library version 3.9.1.)

Material parameters	Mineral wool	EPS CZE	Soil, clay	OSB	Climate plaster	Gypsum board
Thickness [mm]	-	155	-	15	3	12.5
Density [kg/m³]	30	34	2650	630	1291	850
Heat capacity [J/kgK]	840	1300	1050	1880	1000	850
Thermal conductivity [W/mK]	0.056	0.04	2.1	0.13	0.595	0.2
Open porosity [m³/m³]	0.92	0.94	0.43	0.4	0.51	0.65
Eff. Water saturation [m³/m³]	0.9	0.935	0.427	0.35	0.32	0.551
Water absorption coefficient [kg/m²$s^{0,5}$]	-	-	0	0.0019	0.0514	0.277
Vapour diffusion resistance [-]	1	30	10	280	17.7	10

TABLE 4. Material parameters for hygrothermal simulation, part 2 (IBK library version 3.9.1.)

Material parameter	Main beam, Spruce	Concrete C20/25	Stone	Light weight concrete	Wood fireboard	Cellulose DK	EPS DK
Thickness [mm]	-	400	100	300	10	365	265
Density [kg/m³]	528	2320	1939	1250	300	55	34
Heat capacity [J/kgK]	2000	850	831	1050	1180	2544	1300
Thermal conductivity [W/mK]	0.13	2.1	2.43	0.18	0.05	0.04	0.031
Open porosity [m³/m³]	0.7	0.14	0.27	0.42	0.42	0.93	0.94
Eff. Water saturation [m³/m³]	0.695	0.143	0.23	0.4	0.4	0.7	0.935
Water absorption coefficient [kg/m²s^{0,5}]	0.0582	0.02	0.07	0.01	0.0674	0.53	-
Vapour diffusion resistance [-]	236.2	110	19.3	10	5	2	30

The vapour barrier behind the wooden post on internal side of the Czech external wall was modelled as a contact resistance between the layers with equivalent air-layer thickness of s_d = 98.3 m. There is no vapour barrier in the Danish construction.

3. Methods

For this investigation, the coupled heat and moisture calculations were performed with the 2D hygrothermal simulation tool Delphin version 5.6.8. The material properties were taken from Delphin material library (IBK library version 3.9.1) and are listed above in Table 3 and Table 4. From the simulation results the temperature and relative humidity at registration points at bottom plate were post-processed.

3.1 Geometry of simulation models

To ensure applicability of an adiabatic boundary for this detail 4.0 m of the floor slab and 1.5 m of the wall was modelled. For the soil 20 m is modelled both in horizontal and vertical direction (EN ISO 10211-1 1997). Figure 2 shows the set up for calculating.

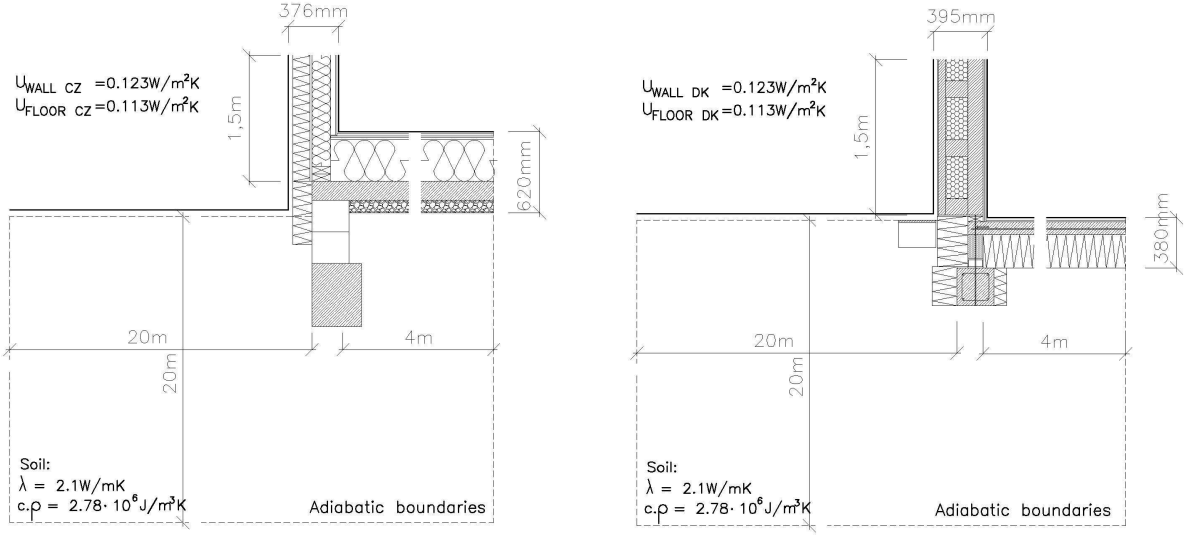

FIG 2. Simulation set up models - Czech study case (left), Danish study case (right)

3.2 Boundary and initial conditions

Simplified interior and exterior climates were described by boundary conditions with a sinusoidally varying air temperature with a sinusoidally varying relative humidity according to WTA (2006) as described in Table 5.

Two sets of calculation were carried out: a “Dry” and a “Wet” set.

The initial conditions for the “Dry” hygrothermal simulations were set to temperature of 20°C and 80% RH. In order to illustrate the possible effect of very wet initial conditions and especially the drying capacity of the different solutions, the bottom plate was assigned to have an initial moisture content equivalent to 35 weight-% MC in the “Wet” set of simulations. Simulations for all cases were performed over 10 years.

TABLE 5. Sinusoidally varying interior and exterior boundary conditions (WTA Merkblatt 6-2-01/D)

Boundary conditions	Interior		Exterior	
	T	RH	T	RH
Mean value [°C], [%]	21	50	9	80
Amplitude [K]	1	10	9	8
Period [year]	1	1	1	1
Phase shift with maximum in	June	August	July	December
Heat exchange coefficient [W/m^{2}K]	8		17	
Vapour diffusion exchange coefficient [kg/m^{2}sPa]	25.10^{-9}		75.10^{-9}	

3.3 Risk of mould growth and decay of the bottom plate

The hygrothermal performance of the studied wooden constructions is assessed by calculating the risk of mould growth around and the risk of decay of the bottom plate. As an input to the risk models, the simulated temperature and relative humidity in given locations were used. As a risk model for mould growth was used the Viitanen model, described e.g. in (Ojanen et al, 2010), and for the decay of wooden construction, a model described in (Viitanen et al. 2010).

3.4 Simulated points

Both study cases were subjected to have the same position of simulating points on the bottom plate. The simulation mesh was settled for dimensions of the registered T and RH in four positions point as shown on Figure 3. Each registration point had dimensions about 16/16 mm (W/H).

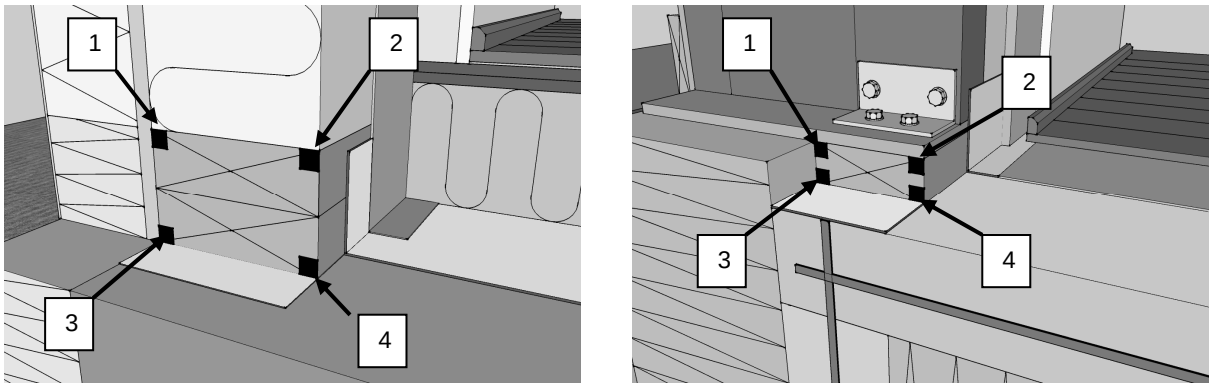

FIG 3. View of simulated details with assigned registration points on bottom plate, Czech study case (left), Danish study case (right)

4. Results

4.1 Relative humidity at registration points

Initial conditions for mould growth index calculation are expressed by graphs in FIG 4 and FIG 5. The graphs are plotted according to the position of the registration points, such as nearby the exterior side (points 01 and 03) and interior side (points 02 and 04).

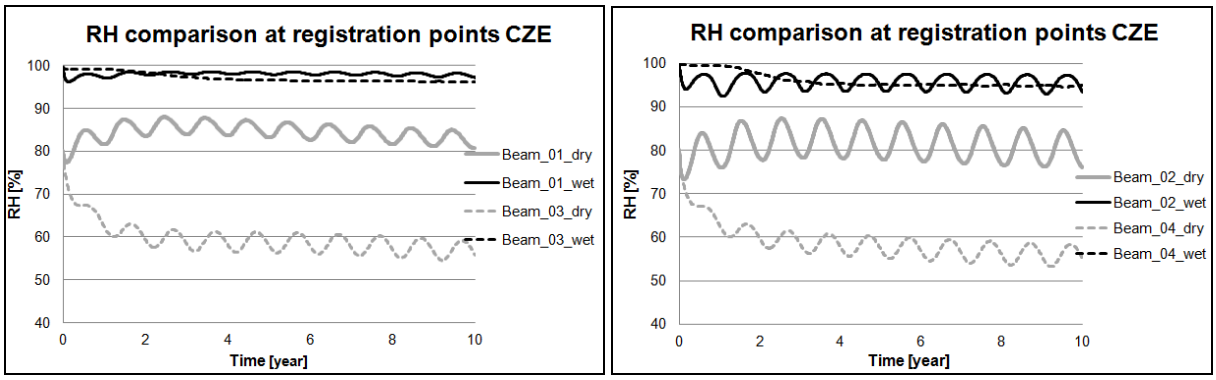

FIG 4. Comparison of RH on CZE bottom plate at registration points 01,03 (left) and 02, 04 (right)

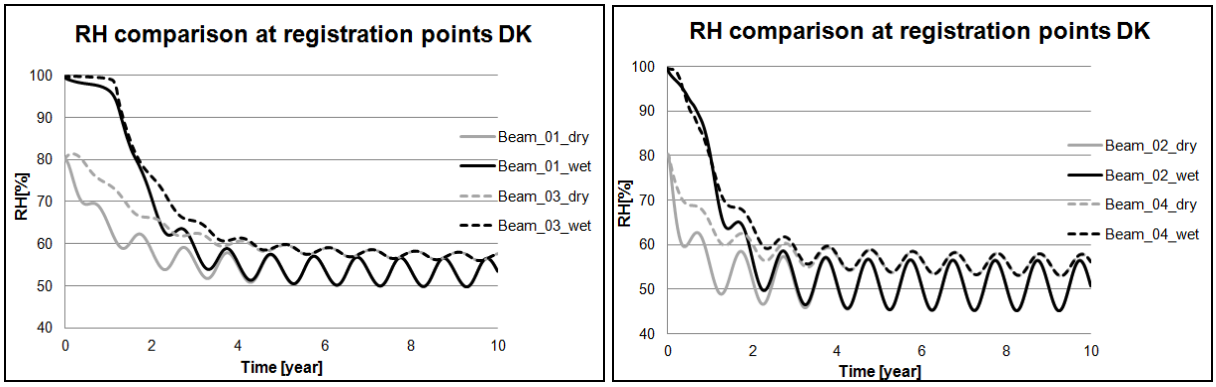

FIG 5. Comparison of RH on DK bottom plate registration points 01,03 (left) and 02,04 (right)

4.2 Calculated mould growth and wood decay risk

Figure 6 shows the calculated mould growth risk for the points given in FIG 3.

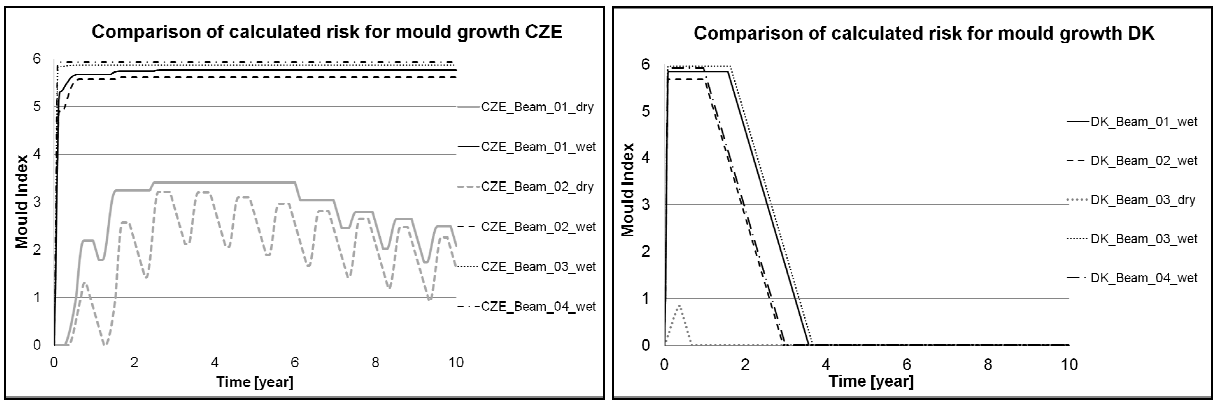

FIG 6. Comparison of the calculated risk of mould growth for registration *points for CZE (left) and DK (right), given in FIG 3. Results showing no risk (Mould index = 0) are omitted*

Figure 7 shows the calculated risk for mass loss of wooden construction as a consequence of decay fungi. Note that the calculated mass loss above 100% makes no physical sense but is an expression of the continuing risk.

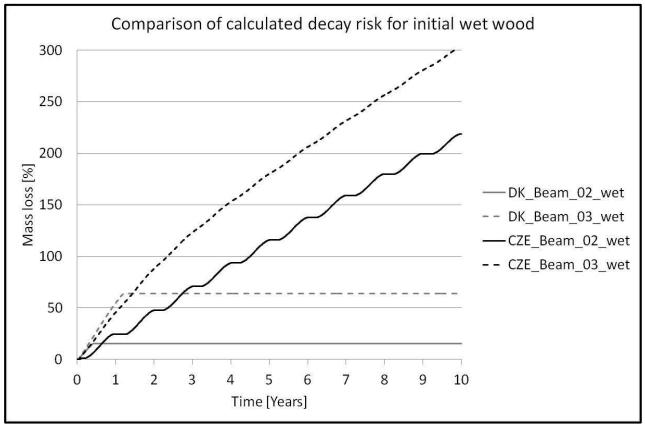

FIG 7. Comparison of Danish and Czech constructions with selected but typical results for the calculated risk of decay fungi (Mass loss). Only cases with initial high moisture content (35 weight-%) showed a risk for decay.

5. Discussion

5.1 Relative humidity at registration points

The relative humidity of all registration points in the study of the Czech case are for the whole simulation period of 10 years in a dangerous range above 90%. Even the relative humidity of initially dry wood near the interior side, respectively in registration points 02 and 03, is oscillating between 75-85%. The usage of relatively vapour diffusion tight material on the exterior side (EPS) is causing minimal drying potential of the wood, conditioned at 35 weight-%. Similar behaviour is visible to be on the bottom of the dry bottom plate, such as registration points 03 and 04, there the relative humidity oscillates between 55-65%.

On the other hand, the relative humidity of all registration points on dry and wet bottom plate of the Danish case will decrease within a few months to two years to less than 60%. Initially wet wood will dry out from all registration points in about 2 years.

5.2 Risk of mould growth and wood decay fungi

The hygrothermal performance of the studied constructions was also assessed with numerical models estimating the risk for both mould and decay fungi. The results in FIG 6 show clearly how the hygrothermal conditions in the initially wet bottom plate are very favourable for initiating biological growth. The better drying potential of the Danish construction is seen as the drop in the mould growth risk over approximately 2 years. The risk of mould growth in the initially dry Czech construction is either not existing or relatively low. A mould growth index below 3 corresponds to growth that is not visible to naked eye.

In FIG 7 some selected but typical cases are presented for the initially wet constructions. The initially dry constructions do not have any risk for decay. While the mass loss of the Danish construction stops at a stage when the construction is dried enough, the mass loss of the Czech construction seems to go on. The initially dry Danish construction does not have any mould growth or risk of decay.

The investigated bottom plate is a part of the load bearing structure and not in a direct contact with interior air. Therefore it can be discussed if calculating mould index makes any sense for the

assessment. However, the mould growth can be seen as the first sign of moisture related failure, even before more severe damage happens with rot and decay.

When using these models for the assessment, it must be kept in mind that the mould growth index and mass loss due to decay fungi only describe how *risky* the hygrothermal conditions are, not the actual mould growth or decay. These methods work best as a *comparison* of different solutions or parameter variations and not as absolute values.

6. Conclusions

The influence of the construction design on the hygrothermal performance of timber constructions was studied with a 2D HAM model of two different construction solution of the wall, floor and foundation junction. In order to see the influence of the different foundation solution the model was adjusted to have the same U-values for the construction of the wall and floor.

Hygrothermal assessment with risk of mould growth and decay fungi highlighted the importance of the correct design of this connection of wooden wall and the foundation that ensures drying potential. Also the necessity of ensuring the usage of construction wood which does not have an excessive initial moisture content was clearly pointed out. This last observation supports also the guidelines that require sheltering of the construction site from rain. The reality on construction sites may be that the constructions are not protected well enough from precipitation and other excessive exposure to moisture, and thus the choice of constructions that are robust to failures during the process should be promoted. The type of insulation and its position in relation to the moisture sensible wood-based construction members may be crucial in this respect.

References

Dalehaug, A. et al. 2013. Laboratory investigation of drying of build-in moisture in wood frame walls at passive house level, page 291-298, Proceedings of 2nd CESBP Building Physics, Austria, 979s.

EN ISO 10211-1.1997. Thermal bridges in building construction – Heat flows and surface temperatures – Part 1: General calculation methods.

Gaare, M. & Løtveit, K. 2012. Kritiske fuktforhold ved lukking av høyisolerte konstruksjoner i bindingsverk av tre, Master Thesis, Norwegian University of Science and Technology, Department of Civil and Transport Engineering

Havířová, Z. 2012. Konstrukční ochrana dřeva zabudovaná ve stavbách. Stavební partner No.1.

Nicolai, A. & Grunewald, J. & Fechner, H. 2010. DELPHIN: Simulation program for coupled heat, air, moisture, salt and VOC transport.

Ojanen, T.; Viitanen, H.; Peuhkuri, R.; Lähdesmäki, K. Vinha, J.; Salminen, K. 2010. Mould growth modeling of building structures using sensitivity classes of materials. Proceedings to Performance of Exterior Envelopes of Whole Buildings XI, Clearwater, Dec 2010. Florida.

Viitanen, H. 1997. Modelling The Time Factor in the Development of Brown Rot Decay in Pine and Spruce Sapwood – The Effect if Critical Humidity and Temperature Conditions, Holzforschung 51, No.2, 99-106.

Viitanen, H; Toratti, T; Makkonen, L; Peuhkuri, R; Ojanen, T.; Ruokolainen, L.; Räisänen, J. (2010) Towards modelling of decay risk of wooden materials. European Journal of Wood and Wood Products. Vol. 68 (2010) No: 3, 303 - 313

WTA 6-2-01/D Simulation wärme- und feuchte technischer Prozesse (Simulation of Heat and Moisture Transfer), Frauhofer IRB Verlag, 2006, ISBN 978-3-8167-6826-5, 20s.

New analysis method for moisture performance of envelope structures

Juha Vinha, Professor

Tampere University of Technology, Finland

KEYWORDS: *Analysis method, moisture performance, envelope structures, moisture reference years, VTT-TUT mould growth model*

SUMMARY:
The new method for analysing the moisture performance of envelope structures has been developed for over ten years at TUT in several research projects. The analysis method allows more reliable research of structural moisture risks in the present and future climates. The main components of this analysis method are: outdoor air conditions, indoor air conditions, material properties, calculation software, performance criteria and analysis principles. An important part of the new analysis method is the new moisture reference years for Finnish climate. These reference years were chosen from current and future climate data. The selected reference years can be used to investigate the critical moisture behaviour of almost all structure types. Another novel part of this method is the use of the improved VTT-TUT mould growth model for mould risk analysis of structures. This improved model can estimate the amount of mould growth on the surfaces of different types of materials.

1. Introduction

Design methods that determine the bearing capacity and durability of structures in extreme conditions have been part of strength calculations of structures already for decades whereas corresponding methods have not been used in building physics.

Main reason is that building physical design analyses are generally much more complicated and difficult to run than strength analyses. Heat and moisture transfer in structures in many different ways which requires considering all key transport modes and their combined effects in analyses. Many more performance criteria also exist for structures than in strength analyses. Materials have several building physical properties that have a significant impact on their hygrothermal behaviour, but often all of them have not even been defined. Different environmental factors effect on structures, but their impact on the moisture behaviour and the formation of critical conditions is not known well enough, especially as concerns the combined effects of various factors. The big challenge in the evaluation of the criticality of outdoor environmental factors is their mutual wide and irregular fluctuation.

A method for analysing the moisture performance of structures, which tries to take into account all of the above factors, has been under development at Tampere University of Technology (TUT) for over ten years. The goal has been to develop a method that is capable of analysing the structures under different conditions and use it in building physical design and dimensioning of structures.

The method has been developed for instance as part of the extensive FRAME project (Future Envelope Assemblies and HVAC solutions) carried out between 2009 and 2012. The central goal of this project was to determine the impacts of climate change and increase of thermal insulation on the moisture behaviour of envelope structures and energy consumption of buildings in Finnish climate. The performance of structures was also examined by this analysis method in the study. Results of the FRAME project have been published in a research report (Vinha et al. 2013), and they will also be published in various scientific publications in the near future.

2. Description of the analysis method

The analysis method developed by TUT examines the moisture behaviour of structures through calculations based on critical indoor and outdoor air conditions. The acceptable moisture behaviour of structures is evaluated on the basis of various performance criteria. Indoor and outdoor air conditions are selected so that they create critical conditions in the structure with regard to the chosen criterion. The criterion must be such that the impact of hygrothermal conditions and changes in them on it can be described by mathematical formulas.

The structure and components of the analysis method are shown in Figure 1.

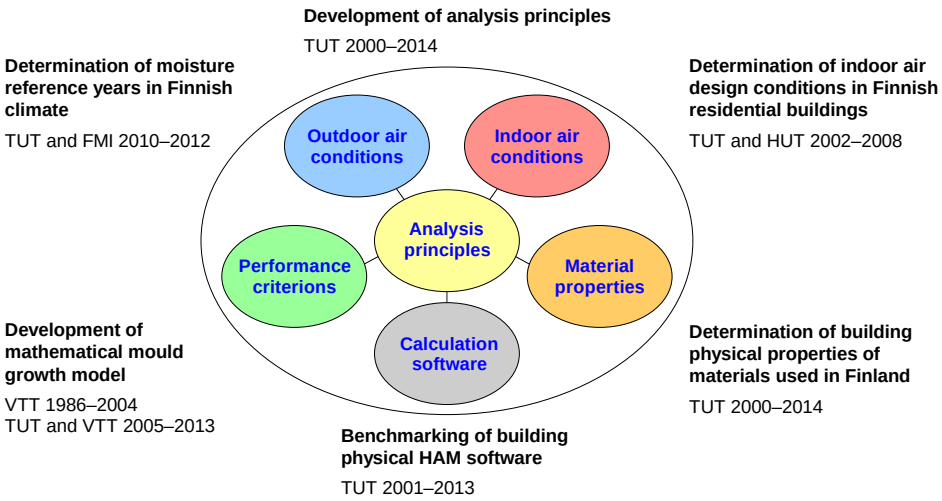

FIG 1. Principle drawing of the TUT analysis method, and research activities regarding to different components of method.

The TUT analysis method consists of the following components: outdoor air conditions, indoor air conditions, material properties, calculation software, performance criteria and analysis principles. The following chapters deal with these components in more detail.

The FRAME study produced the last key component of the analysis method – the moisture reference years (MRYs) for outdoor air. Putting the method into use has, however, also required conducting sufficient research on related components in several earlier studies.

The method still needs development in many areas in order that the accuracy of calculation results can be further improved. Yet, it already provides considerably more accurate research results from the hygrothermal behaviour of structures under changed conditions.

2.1 Outdoor air conditions

The environmental factors, which effect on the moisture behaviour of structures, are temperature, relative humidity, wind, rain (wind-driven rain), solar radiation and long-wave heat radiation to the sky. Moreover, there is always micro-climate around the building, which may differ considerably, for instance, from the conditions measured at a nearby weather station.

Outdoor air conditions, depicted by different reference years, have to be critical with respect to moisture behaviour. Generally, a reference year can be an actual or a synthetic year created by fitting together critical periods of different years. The selected reference year depends on the performance criteria set for the structure in question. In addition, the impacts of different structures must also be considered in the selection of reference years. The same year is not necessarily equally critical with respect to all conditions of all structures, which means that different moisture reference years may have to be selected for different structures.

Earlier the moisture reference year of building physical calculational analyses may have been the year used to determine the energy consumption of buildings, or some other year describing average conditions, or a random year. Thus, the majority of building physical analyses has so far been run under conditions that have not represented critical outdoor air conditions with respect to the moisture behaviour of structures. This is due e.g. the fact that no standard methods for determining such moisture reference years exist. Moreover, the search for the critical reference year for moisture behaviour is very challenging since generally all outdoor environmental factors and their combinations as well as the examined structural solutions affect the criticality level of a year.

One key objective of the FRAME project was to determine critical moisture reference years for envelope structures both in the current climate and those of 2050 and 2100. In this study the reference years were selected so that they correspond to actual years. That ensured that conditions during those years were fully comparable to actual conditions. The reference years were chosen from current and future climate data provided by The Finnish Meteorological Institute FMI. The determination of these years will be described in more detail in upcoming publications.

The research established two moisture reference years in the current climate for structures: Vantaa 2007 (Vantaa is located near Helsinki on the southern coast of Finland) and Jokioinen 2004 (Jokioinen is in southern Finland). Similar years were selected as moisture reference years also for future climate: Vantaa 2050 and 2100 as well as Jokioinen 2050 and 2100. These reference years proved critical for almost all structures when the performance criteria selected for them were those used in this study: mould growth and condensation of moisture within the structure. This was a major advantage since a large number of reference years would make assessment of structures more difficult and take more time.

The moisture reference years for Vantaa are used for those envelope structures whose internal moisture behaviour is remarkably affected by rain/wind-driven rain, and the years for Jokioinen for envelope structures whose moisture behaviour is not affected by rain/wind-driven rain. When using the moisture reference years for Vantaa, the examined orientation of wall structures is south since there wind-driven rain is strongest and solar radiation intensifies migration of the moisture retained in the cladding into the structure by diffusion. With the moisture reference years for Jokioinen, the examined orientation is north where the warming and drying impact of solar radiation is smallest.

Part of the envelope structures are such that rain affects their moisture behaviour to some extent. When examining such structures, it is necessary to study their behaviour with respect to both reference years in order to be able to determine which is more critical for the moisture behaviour of the structure. A good example of this type of structure is a wall assembly with a concrete outer layer. The concrete layer retains some rain water depending on the surfacing, but it migrates into the structure relatively slowly since the water vapour permeability of concrete is generally low and capillary transfer is also quite limited.

2.2 Indoor air conditions

The key indoor climate conditions of building physical analyses are the humidity by volume of indoor air (or moisture excess compared to outdoor air) and indoor air temperature. The moisture stress on wet area structures from washing waters must also be considered in the performance of the structures.

The various activities related to use and occupancy of buildings nearly always add to the moisture of indoor air (moisture excess). Two extensive studies have been conducted in Finland on residential buildings where e.g. indoor air temperature and moisture conditions were examined by long-term monitoring measurements (Vinha et al. 2008). The design indoor air moisture excess and temperature values for different building types in Finland of the current RIL 107 (2012) guideline were determined based on them.

2.3 Material properties

It is important that building physical material properties are known, so that the results of calculations are close enough to the actual behaviour of a structure. The key material properties are thermal conductivity/resistance, specific heat capacity, air permeability/resistance, water vapour permeability/resistance, moisture conductivity/moisture diffusivity, moisture retention curve (sorption and suction curves) and surface emissivity/absorption coefficient.

Material properties always vary to some extent due to changes in the manufacture of products and raw materials. The structure and composition of materials are also often changed as a result of product development. Material properties also vary according to density, temperature and RH. Even properties of materials under the same designation may differ considerably from each other. Therefore, country related material properties should be used in calculations. Moreover, material properties should be defined as a function of temperature and RH.

Building physical properties of materials used in Finland have been determined by TUT for more than 10 years. Part of them has been measured also as a function of temperature and RH. The most extensive related study that defined the key properties of about 40 materials was conducted in 2000–2005 (Valovirta & Vinha 2004; Vinha et al. 2005). Properties have also been defined since in connection with different studies.

Sufficient accuracy of material properties must be ensured by comparing the actual hygrothermal behaviour of structures implemented based on them with calculational modelling of corresponding structures in the same conditions. The key reference material used at TUT has been derived from laboratory tests on timber-framed external wall assemblies (Vinha 2007).

2.4 Calculation software

There are considerable differences between building physical calculation programs, although they are based on quite similar heat and moisture transfer theories. Therefore, one must be very familiar with the properties of these programs to be able to choose the most suitable one for each calculation case and to know how calculations proceed in different situations. This requires a lot of experience from the use of the program. Moreover, calculation results must also be compared to measured test results to determine which factors cause differences between the results of calculations and tests.

In TUT analysis method two calculation programs (WUFI and Delphin) are used in calculational analyses. Their behaviour has also been verified against laboratory test results (Kalamees & Vinha 2003; Laukkarinen & Vinha 2011; Vinha et al. 2013). Calculational comparisons with measurement data from field studies have also been done (Vinha 2007; Vinha et al. 2013).

2.5 Performance criteria

Several building physical performance criteria may be set for the structures. They include e.g.:

- moisture condensation
- mould and microbial growth
- wood rot
- material emissions (VOC)
- colour changes
- weathering and cracking
- flaking of paint
- adhesion failure of glues and paints
- carbonation of concrete
- corrosion of reinforcements and metal parts
- strength of materials or structure
- deformations and settlement
- air tightness of building envelope
- temperatures of interior surfaces

With regard to the above performance criteria, different outdoor environmental factors create critical conditions or phenomena in structures. In the case of almost all performance criteria, there are also several environmental factors and their mutual variation that affect the criticalness of outdoor air conditions. Thus, each performance criterion may require selecting one or more moisture reference years critical particularly in relation to the analysed criterion.

Although several different performance criteria may be set for structures, in practice their number can be limited due the fact that acceptable behaviour of a structure in relation to one criterion often implies acceptable behaviour also in relation to many other criteria. For example, if mould growth is chosen as a criterion of analysis, and the structure performs acceptably in this respect, there is no risk of wood rot or weakening of strength, either. In addition, risks of moisture deformation, material emissions and adhesion failure are also reduced considerably.

The effects of some performance criteria are best analysed under average rather than extreme conditions. In these cases, the phenomenon indicated by the performance criterion develops slowly over several years. Then, the stress caused in a single year is not so essential, but the long-term effects of outdoor air conditions. Such performance criteria include carbonation of concrete, corrosion of metal parts and reinforcement, surface weathering, colour changes and flaking of paint.

Use of performance criteria in calculational modelling requires that the effects of hygrothermal conditions and changes in them on the selected criterion can be depicted by some reference variable and related mathematical formulas. However, there are useful calculation models and reference variables for only very few performance criteria that allow reliable assessment of how indoor and outdoor air conditions and variations in them affect the phenomenon or failure mode of the structure depicted by the criterion. Such a model exists for mould growth developed by VTT and TUT (the VTT-TUT mould growth model) (Viitanen et al. 2010; Ojanen et al. 2010). Therefore, mould growth was also selected as the performance criterion of structures in the FRAME study. Another criterion selected for this study was moisture condensation.

2.6 Analysis principles

The principles of the TUT analysis method describe the procedure with which the hygrothermal performance of envelope assemblies is assessed by calculational analyses in different situations. The procedure involves the subjects, which have been presented in following chapters.

2.6.1 Principles concerning the use of different parts of the analysis method

The moisture reference years determined in the FRAME project are used as outdoor air conditions in the calculations while indoor air conditions are based on the design moisture excess and temperature values presented in RIL 107 (2012). The same values are also used as indoor air conditions when assessing the hygrothermal behaviour and drying of structures during construction.

The building physical properties of building materials are always primarily material properties specified for Finnish materials, which are complemented as necessary with material properties specified in literature and databases of calculation programs.

Used calculation programs are ones whose performance has been verified against test results and whose properties and shortcomings are well known. The programs must also include the necessary heat and moisture transfer modes and they must allow considering the necessary outdoor environmental factors.

The current performance criteria for structures are mould growth and moisture condensation, as they can be assessed fairly reliably by calculations. However, other performance criteria may be added as necessary if reliable calculation models can be developed for them.

Reference variables must be defined for the selected performance criteria which enable assessing the performance of structures. The maximum amount of condensed moisture (or moisture in capillary area) in the structure during a moisture reference year has generally been used as the reference variable for moisture condensation. In the case of mould growth risk, the reference variable is the maximum mould index value during a moisture reference year.

2.6.2 Limit values set for reference variables depicting performance criteria

A key principle of the analysis method is to set limits or other conditions that the reference variables depicting the performance criteria should not exceed/fall short of. These limits depend on the structure under analysis as well as the indoor and outdoor air conditions in which analysis takes place. If the ambient conditions of the structure are highly conducive to, for instance, mould growth or moisture condensation, the selected limit values cannot necessarily be as tight as in less critical climatic conditions. However, the minimum requirement in all cases should be that conditions within structures must not be more critical in relation to the selected performance criteria than those of indoor or outdoor air (Vinha 2007).

Two limit values were selected for the maximum amount of condensed moisture. In structures containing materials highly susceptible to mould growth, the maximum amount of condensed moisture could not exceed 150 g/m^2. This value is based on earlier studies at TUT on timber-framed external walls (Vinha 2007). In the case of materials more resistant to mould growth, the maximum amount of condensed moisture could be 1000 g/m^2 based on standard DIN 4108-3 (1981).

As the maximum mould index value goes very high in outdoor air in the conditions of the reference years, mould growth near the outer surface of the envelope assembly must be accepted. On the other hand, mould growth near the inner surface of structures is not acceptable under any conditions. Therefore, calculational analyses require making a decision about the structural layers where mould growth is no longer permissible. In this analysis method, the limit values are selected so that in the analysis of new buildings, mould growth is not permitted in bearing structures or the thermal insulation layer (including outer surface of insulation material if it is not direct contact with ventilation gap or soil) or material layers on its interior side. In other words, the maximum acceptable mould index value at these points is < 1.0 (in the VTT-TUT mould growth model the mould index value varies between 0 and 6). In renovated structures it may be necessary to exceed this limit in some isolated, highly challenging cases. The objective, however, is to observe the same principle also in renovation.

2.6.3 Principles of modelling moisture leaks and defective structures

The performance of structures has usually been examined in an ideal situation where no moisture leaks into the structure are assumed. However, in practice some leaks always occur during the life cycle of a building, for example, as rain water or water vapour enter the structure through cracks and holes carried by air flows. Earlier calculation programs had no features to allow such analyses, but recent development of programs (e.g. WUFI and Delphin) has made them possible.

Various analyses pertaining to moisture leaks are necessary in the assessment of the fault tolerance of structures, and they are becoming increasingly common as part of building physical calculational analyses. The challenge of these analyses, however, is the need to determine the amount of the moisture leak or the size of the leakage point so that it depicts a typical and probable leak caused by a defect. Some suggestions have already done but this area requires a lot of further research.

The amount of the moisture leak and/or the sizes and locations of the leakage points are selected for moisture leak analyses. The limit values of the performance criteria selected for these analyses may be different than in service state analyses with ideal structures. Typically, various sensitivity analyses as a function of leak amount/size of leakage point are also made as part of these analyses.

If the moisture leak causes a slowly accumulating moisture stress in the structure, the acceptable service life of the building in case the leak remains unchanged must also be assessed. If the analysis is based on a moisture reference year throughout, in calculations spanning several years moisture stress may increase much more rapidly than in reality. On the other hand, the service life estimate of the structure is then on the safe side. If necessary, this fact must be considered for example by changing outdoor air conditions.

2.6.4 Selection of initial conditions and calculation periods

The temperature and moisture content of materials/pore air RH in the initial situation are entered into calculation programs separately for each material layer or alternatively for the entire structure. The values for drying analyses are chosen to represent the situation at the start of drying. For service state analyses, however, the initial conditions of materials must change to correspond to temperature and moisture distributions in the structure before the actual analysis period. In the case of temperature, the change takes place rapidly – typically in a few days, but in the case of moisture the change from initial conditions to service state conditions may take even several years, depending, among other things, on the selected initial conditions.

2.6.5 Selection of examined points

In calculational modelling, the examined points should naturally be located in the structures at points most critical for the studied performance criterion. These points are typically located at interfaces between material layers. In the analysis of mould growth and moisture condensation risk, the points should be located at both sides of the thermal insulation layer and, if necessary, at various cold bridges. Selecting the examined points requires sufficient knowledge of the hygrothermal behaviour of the structure. The number of examined points should be large enough to allow charting the behaviour of the most critical points.

2.6.6 Evaluation of results and sensitivity analyses

The evaluation of results and sensitivity analyses are an important part of assessing the reliability of results. The basic assumptions of calculations must be varied to ensure that the results are logical and change in the right direction. Big sudden or momentary changes in conditions or a large number of convergence errors in calculations may result from various errors related to calculation or input values.

3. Novelty values of the analysis method

The method for analysing the moisture behaviour of structures developed by TUT provides several novelty values, which make it the most sophisticated currently available calculation method for this purpose. These novelty values include:

- Use of outdoor air conditions based on moisture reference years critical for the moisture behaviour of structures (Vantaa 2007 and Jokioinen 2004) which were selected considering all outdoor environmental factors central to the building physical performance of structures, except for the long-wave heat radiation to the sky. The moisture reference years for present climate are actualised years.
- Different types of structures were also considered in the determination of the moisture reference years. The reference year is selected according to the structure to be examined, and the same reference year may be used for the analysis of several different structures.
- Besides the present climate, moisture reference years were also selected from the climates of 2050 and 2100 (Vantaa 2050 and 2100, Jokioinen 2050 and 2100). Future reference years were determined on the basis of the A2 greenhouse gas scenario.
- The design values of indoor air temperature and moisture excess conditions are based on values measured from a large number of Finnish residential buildings.
- The used building physical properties are mainly based on materials used in Finland, and many properties have been determined as a function of temperature and RH.
- The results of calculation software have been compared to test results of several laboratory and field studies, and the assessment and calculation principles of structures have been developed accordingly.

- The mould growth risk of structures is assessed with an improved VTT-TUT mould growth model, which is the most advanced mould growth calculation model in the world. The model allows assessing concrete mould growth amounts in different materials and the interfaces between them. That makes it possible to improve the performance of the assembly by various structural solutions to bring the risk to the desired level or to eliminate it altogether.

Different components of the analysis method were developed for calculational analyses in present and future Finnish indoor and outdoor air conditions, but, based on the same principles; the method can also be used for analyses in other countries. All that is required is to determine the outdoor air moisture reference years and design values for indoor air moisture excess and temperature for the country in question.

4. Acknowledgements

The TUT analysis method has been developed for over ten years at TUT in several research projects. There has also been remarkable collaboration between Aalto University (former Helsinki University of Technology), Technical Research Centre of Finland VTT and the Finnish Meteorological Institute FMI in some of these projects involving a large number of researchers. The main financiers of the projects have been the Finnish Funding Agency for Technology and Innovation TEKES and Finnish construction companies and associations.

References

DIN 4108-3. 1981. Wärmeschutz im Hochbau, Klimabedingter Feuchteschutz, Anforderungen und Hinweise für Planung und Ausführung. Deutches Institut für Normung. 9 p. *(in German)*

Kalamees, T. & Vinha, J. 2003. Hygrothermal calculations and laboratory tests on timber-framed wall structures. Building and Environment, Vol. 38 (5), pp. 689-697.

Laukkarinen, A. & Vinha, J. 2011. Comparison of calculated and measured values of wall assembly tests using Delphin 5. Proceedings of the 9th Nordic Symposium on Building Physics, NSB 2011, Tampere, Finland, May 29–June 2, Vol. 1, pp. 155-162.

Ojanen, T., Viitanen, H., Peuhkuri, R., Lähdesmäki, K., Vinha, J. & Salminen, K. 2010. Mould growth modeling of building structures using sensitivity classes of materials. Proceedings of Thermal Performance of the Exterior Envelopes of Whole Buildings XI International. Conference, Clearwater Beach, Florida, USA, December 5–9. Session II-B, 10 p.

RIL 107-2012. 2012. Buildings' water and damp proofing guidelines. Authors: Laamanen, P., Heimala, A., Heimonen, I., Järvinen, P., Vinha, J. & Åström, G. Finnish Association of Civil Engineers, 219 p. *(in Finnish)*

Valovirta, I. & Vinha, J. 2004. Water vapor permeability and thermal conductivity as a function of temperature and relative humidity. Proceedings of Performance of Exterior Envelopes of Whole Buildings IX International Conference, Clearwater Beach, Florida, USA, December 5–10, Session XIIIA, 16 p.

Viitanen, H., Vinha, J., Salminen, K., Ojanen, T., Peuhkuri R., Paajanen, L. & Lähdesmäki, K. 2010. Moisture and biodeterioration risk of building materials and structures. Journal of Building Physics, Vol. 33 (3), pp. 201-224.

Vinha, J., Valovirta, I., Korpi, M., Mikkilä, A. & Käkelä, P. 2005. Building physical material properties of building materials as a function of temperature and relative humidity. Tampere, Tampere University of Technology, Laboratory of Structural Engineering, Research report 129. 101 p. + 211 p. app. *(in Finnish)*

Vinha, J. 2007. Hygrothermal Performance of Timber-Framed External Walls in Finnish Climatic Conditions: A Method for Determining the Sufficient Water Vapour Resistance of the Interior Lining of a Wall Assembly. Doctoral Thesis. Tampere, Tampere University of Technology, Department of Civil Engineering, Publication 658. 338 p. + 10 p. app.

Vinha, J., Korpi, M., Kalamees, T., Eskola, L., Palonen, J., Kurnitski, J., Valovirta, I., Mikkilä, A. & Jokisalo, J. 2008. A research project on the temperature and humidity conditions, ventilation and air tightness of Finnish detached houses. In: Kumaran, K. & Sanders, C. IEA ECBCS Annex 41 Whole Building Heat, Air, Moisture Response, Subtask 3, Boundary Conditions, Appendix 1. Copenhagen, Denmark, International Energy Agency, pp. 157-174.

Vinha, J., Laukkarinen, A., Mäkitalo, M., Nurmi, S., Huttunen, P., Pakkanen, T., Kero, P., Manelius, E., Lahdensivu, J., Köliö, A., Lähdesmäki, K., Piironen, J., Kuhno, V., Pirinen, M., Aaltonen, A., Suonketo, J., Jokisalo, J., Teriö, O., Koskenvesa, A. & Palolahti, T. 2013. Effects of climate change and increasing of thermal insulation on moisture performance of envelope assemblies and energy consumption of buildings. Tampere, Tampere University of Technology, Department of Civil Engineering, Structural Engineering, Research Report 159. 354 p. + 43 p. app. *(in Finnish)*

Wind-driven rain and runoff on a medium-rise building: experimental and numerical analysis

Thijs Van den Brande, M.Sc. [1]
Bert Blocken, Professor [1,2]
Staf Roels, Professor [1]

[1] Building Physics Section, Department of Civil Engineering, KU Leuven, Belgium
[2] Building Physics and Services, Eindhoven University of Technology, The Netherlands

KEYWORDS: *Driving rain, modelling, full scale experiments, runoff, leaching, surface soiling*

SUMMARY:
As wind-driven rain (WDR) is one of the most important moisture sources for a building envelope, a reliable prediction of the WDR and runoff load is a prerequisite to assess the durability of building facade components. Current state-of-the-art Heat Air and Moisture (HAM) models neglect the influence of runoff.

This study contributes to research efforts to develop models that combine state-of-the-art HAM models with a runoff model. It incorporates excess water that is present at the surface of the material in the form of a runoff layer. Available models for runoff on porous materials are however insufficiently validated. Therefore the experimental part of the present study focuses on collecting a dataset containing WDR intensities and corresponding runoff flow rates on the southwest facade of a medium-rise building.

For this experimental analysis, four modules with known cladding material with incorporated WDR and runoff gauges were mounted on the facade. These gauges are linked to pressure sensors measuring the supplied WDR and runoff every 10 seconds. The dataset is supplemented with detailed meteorological measurements. In this paper, we present the full scale experimental setup and its accuracy, the results of a first measurement campaign and a comparison between measurements and numerical results of a runoff model for a single rain event. From this comparison guidelines for future development of runoff models are deduced.

1. Introduction

Wind-driven rain (WDR) is a significant moisture source for building facades. It affects the hygrothermal behaviour and durability of the building materials and the aesthetic performance of the facade. The interaction of WDR with the building facade is rather complex and is dependent on a large set of urban, building, material and meteorological parameters (Blocken et al. 2013). Distribution of moisture in walls composed of porous building materials has been extensively studied in the past and this aspect can be modelled quite adequately. Splashing, bouncing, spreading and adhesion of raindrops on facades was previously investigated by Abuku et al. (2009). Research on film forming, runoff and film absorption is however limited. Most research on runoff and surface soiling is based on field observations (e.g. Küntz & van Mier 1997; Etyemezian et al. 1998; Etyemezian 2000; Davidson et al. 2000) while numerical work is limited to a few attempts (Blocken & Carmeliet 2012; Van den Brande et al. 2013).

Runoff contributes to surface soiling, both dirty and white washing of facades (Küntz & van Mier 1997; Davidson et al. 2000; Etyemezian 2000), rain infiltration due to preferential runoff paths (Hens 2010) and leaching of nanoparticles into the environment (Kaegi et al. 2008; Kaegi et al. 2010). Kaegi

et al. (2010) clearly related leaching to the runoff that occurred at the walls surface. It is therefore important to get a clear idea of the runoff rate present on the outer facade.

1.1 Experimental measurements of runoff

Previous experimental research towards quantifying runoff rates is, to the authors' knowledge, mainly limited to the work of Beijer & Johansson (1977). They investigated the surface flows on a concrete facade and the ability of these flows to clean the facade. The experiment consisted of combined WDR and runoff measurements at four heights along the facade combined with horizontal rainfall measurements. Due to the limited knowledge of the used building materials and lack of detail in the published measurements it is only possible to estimate the total amount of runoff during a rain event. Beijer & Johansson also pointed out that due to the design of the WDR and especially the runoff gauges, measurement errors were introduced. Blocken & Carmeliet (2006) state that the error on WDR measurements can be very large (up to 100%) and that these errors depend on the type of rain event and on the design of the gauge. They concluded, following Högberg et al. (1999), that a polymethyl-methacrylate (PMMA) finish of the gauge is to be preferred over a polytetra-fluoroethylene (PTFE) finish, a small collection area is preferable to limit adhesion-water-evaporation, the drainage tube from the gauge to the reservoir should be as short as possible, and the height of the rim of the WDR gauge should be limited to reduce wind induced errors.

1.2 Modelling of runoff

The obtained measurements of the runoff flow will be compared with the predicted flow by the lubrification equation (Greenspan 1978; Ruyer-Quil & Manneville 1998). To the authors' knowledge, the only numerical model that has been applied for runoff on facades, is a simplified form of the lubrification equation (Blocken & Carmeliet 2012, Van den Brande et al. 2013). In Van den Brande et al. (2013), a state-of-the-art Heat, Air and Moisture (HAM) model was extended with a module to calculate the runoff of rainwater on the exterior surface of the building envelope. This model takes non-uniform WDR distributions into account as a boundary condition, using catch ratio distributions, and simulates the dynamic distribution of moisture in the wall. The model was then applied to a theoretical example of a low-absorbing building facade under a given WDR load and with constant convective moisture transfer coefficients (CMTC).

In the present paper, the measured WDR and micrometeorological conditions will be used as input and boundary conditions for the model. The thickness of the runoff layer for a non capillary active facade can be described by:

$$\frac{\partial h}{\partial t} + \frac{\rho g}{3\mu}\frac{\partial h^3}{\partial x} = \frac{q_{WDR} - q_{evap}}{\rho} \tag{1}$$

Where
- h the thickness of the runoff layer (m)
- ρ the density of water (kg/m³)
- g the gravitational acceleration, 9.81 m/s²
- μ the dynamic viscosity of water, in function of the temperature (kg/(m s))
- x the vertical coordinate along the wall
- q the supplied (subscript *WDR*) or evaporated (subscript *evap*) moisture flow (kg/(m²s))

the amount of evaporated water in Eq. 1 can be obtained by Eq. 2. If there is no runoff layer present, no evaporation is possible. When a runoff layer is present, a fully saturated surface is assumed.

$$q_{evap} = CMTC \cdot \left(p_{v,surf} - p_{v,air}\right) \tag{2}$$

Where
- CMTC the convective moisture transfer coefficient (s/m)
- $p_{v,surf}$ the vapour pressure at the surface of the wall (Pa)
- $p_{v,air}$ the vapour pressure of the outside air (Pa)

The CMTC used in Eq. 2 is based on empirical relations for the convective heat transfer coefficient (CHTC) and the Lewis analogy (Janssen et al. 2007) between the CHTC and the CMTC. The relation for the CHTC at the sixth floor of a windward facade derived by Sharples (1984) is used for the simulations in this paper:

$$CHTC = 0.5 \cdot W_s + 3.8 \quad (3)$$

Where W_s the reference wind speed at 10 m above the ground (m/s)

More details on the model and its assumptions can be found in (Van den Brande et al. 2013). Runoff however is a complex phenomenon and is dependent on many more parameters as included in this model. For example, surface roughness, near-wall wind speed, adhesion forces of the liquid layer and droplet impact may also influence the behaviour of the runoff layer.

2. Description of the experimental setup

During the late summer – early fall (August 2013 – November 2013) WDR and runoff measurements were conducted on the southwest facade of the medium-rise S.E.G. building, located in Heverlee, Belgium (FIG. 1). An external facade with embedded WDR gauges and runoff gauges was developed, allowing an accurate positioning of the gauges and the possibility to change the finishing material in later experiments. The building has a height of 22 m. Four modules, each consisting of a flat, non capillary active, facade finishing board of 0.6 m by 2.4 m, and each containing a WDR gauge and a runoff gauge were mounted on the top-right corner of the south-west facade, 0.7 m from the side and 0.15 m from the top.

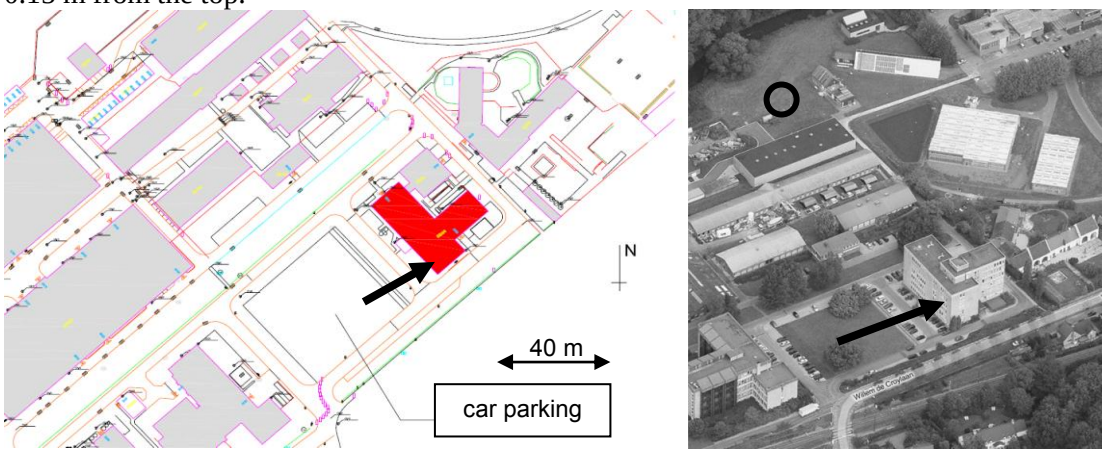

FIG 1. Surroundings of the S.E.G. building, located at the Leuven University Campus in Heverlee, Belgium. The position of the modules is depicted with an arrow, the location of the VLIET weather station is depicted with a circle in the aerial photograph.

In FIG. 2., the positions and dimensions of the WDR gauges and runoff gauges are depicted. The gauges are made of PMMA. The WDR gauges have a collection area of 0.2 by 0.2 m², while the runoff gauges measure runoff along a horizontal line of 0.2 m. The WDR gauge is placed recessed in the plane of the panel. A detailed description of the WDR gauge and its potential measurement errors can be found in (Blocken & Carmeliet 2006; Abuku et al. 2009). The newly developed runoff gauges include a thin slit with rounded edges in the plate material, thus making it possible for the runoff water to flow to the back of the panel where it is collected in a PVC reservoir (FIG. 2., bottom right).

Each of the WDR gauges and runoff gauges is connected to a PVC reservoir with diameter 30 mm by a short PVC tube. The height of the water column in this reservoir is measured every 10 s with a pressure sensor (type PTX 1400). Following the guidelines derived in (Blocken & Carmeliet 2006) by limiting the tubing length, using PMMA and PVC for the gauges, collectors and tubing and limiting evaporation losses, the measurement error of the runoff sensor can be described by the measurement

error on the pressure sensors that monitor the water column, which is equal to 0.15 % of the measured value and a resolution of 2.10^{-4} kg and a small amount of adhesion water in the tubing. For the WDR gauges, an additional absolute error of 0.10 ± 0.02 kg/m² as a result of adhesion water can be considered (Blocken & Carmeliet, 2006).

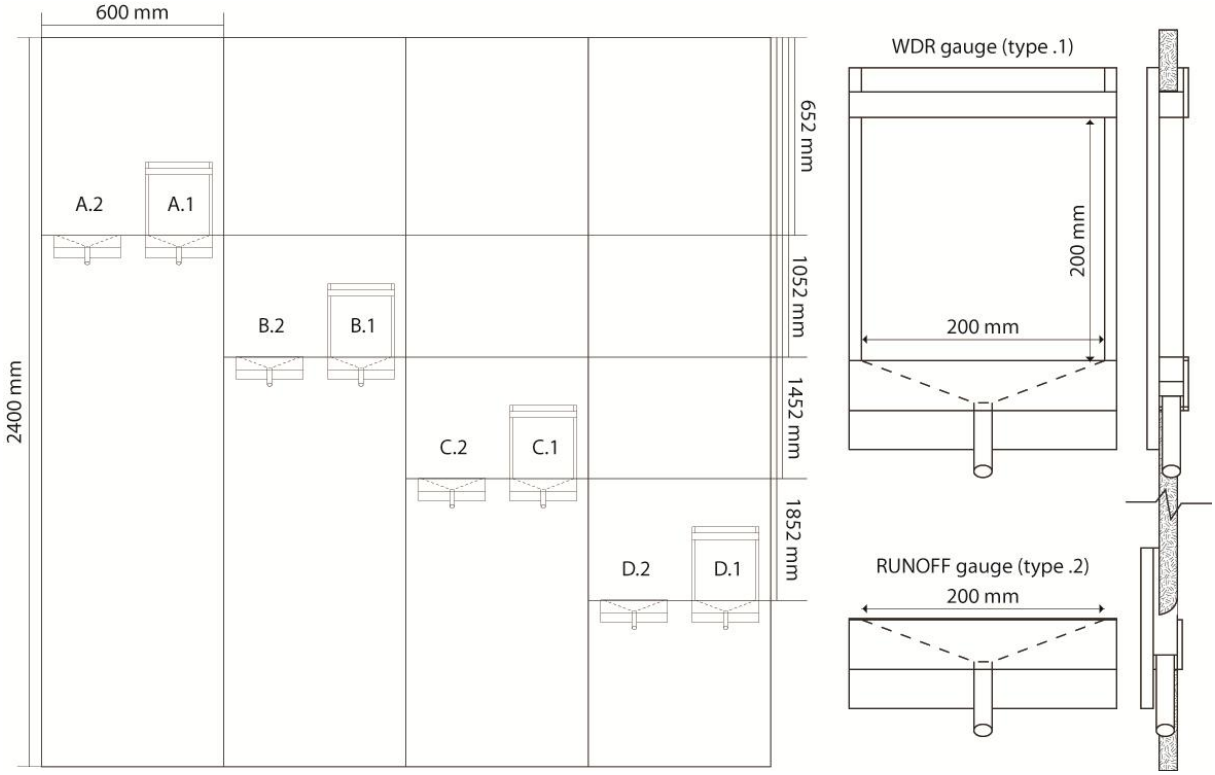

FIG 2. Position, dimensions and numbering of the WDR gauges and runoff gauges. Panels are named A to D, with A the panel the furthest from the top-right corner of the S.E.G. building. WDR gauges are assigned the number .1, runoff gauges the number .2. On the right-hand side of the figure two section views are shown, depicting a side view of the panel with incorporated gauges.

3. Results

A first comparison between measured and simulated runoff rates is made for a particular rain event that occurred on October 23th, 2013 from 16h50 until 17u10 during which a total amount of 2.7 mm horizontal rainfall was measured, which corresponds to a heavy shower. In this paper, only the results of panel C will be discussed. The micrometeorological conditions during this event are summarised in TABLE 1. In the model, the amount of WDR is considered constant over the height of the panel, however a small increase towards the top of the panel is expected.

For the particular shower, the model overestimates the amount of runoff by a factor 2.5 (FIG. 3). Both the flow rate, depicted by the slope of the curve and the total amount of runoff, depicted by the total height, do not correspond to the measured values. In the model, almost all supplied WDR is converted into runoff and the amount of retained water at the surface is limited. In the experiment however, a large amount of WDR does not run off, especially in the second part of the shower when low WDR loads are present.

This difference can be the result of neglecting surface adhesion of water in the runoff model. From experiments, it was found that the total amount of adhesion water on this specific panel can be up to 0.1 kg/m². The difference between measurements and the model can also find its origin in uncertainties on the dynamic viscosity of water, the assumptions made in the runoff model or the simplification of evaporation by the CMTC. Abuku (2009) also attributes the overestimation of the

supplied WDR to the averaging error due to surface averaging the mass of individual droplets and to the error by neglecting splashing and bouncing of the impinging droplets.

In order to determine the origin of the difference between the measured values and the predicted values, a parameter study on a single measurement is performed. The results of this study are summarised in FIG. 4.

TABLE 1. Micrometeorological boundary conditions (wind speed W_s, wind direction W_{dir}, outdoor relative humidity RH an outdoor temperature T) and measured WDR rates Q_{wdr} (sensor C.1) and runoff rates Q_{runoff} (sensor C.2.)

Time from start	Q_{wdr} [kg/(m² s)]	W_s [m/s]	W_{dir} [°N]	RH [%]	T [°C]	Q_{runoff} [kg/(m s)]
0 - 4 min	0	4.31	257	89.9	14.37	0
4 - 8 min	$5.335 .10^{-3}$	3.66	227	89.9	14.37	$4.005 .10^{-3}$
8 - 12 min	$1.035 .10^{-3}$	2.68	235	93.6	14.37	$0.139 .10^{-3}$
12- 16 min	$0.368 .10^{-3}$	3.31	228	93.6	14.37	0
16 - 20 min	$0.138 .10^{-3}$	2.99	223	93.6	14.37	0

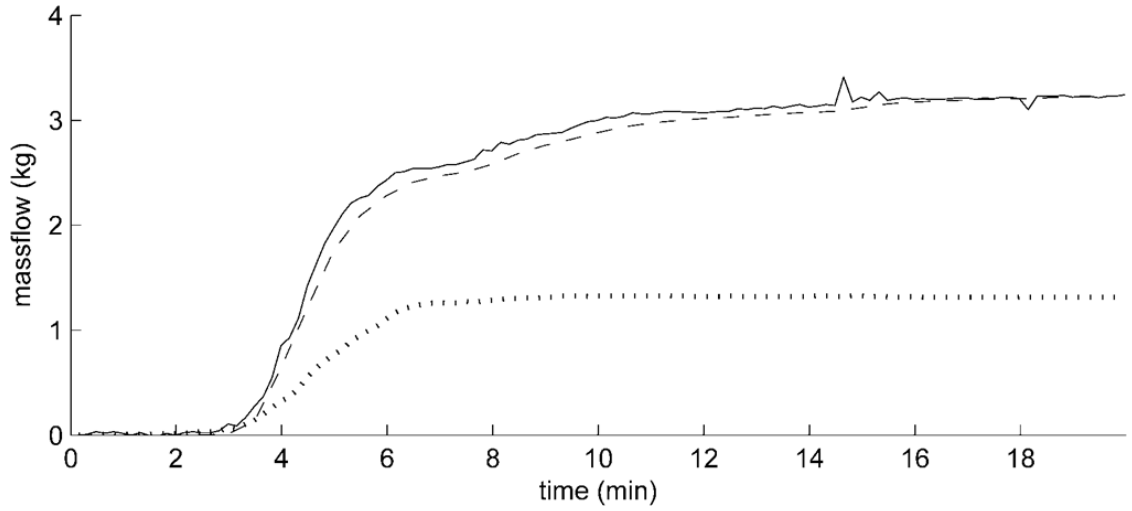

FIG 3. Modelled runoff rate (dashed line) compared to the measured runoff rate (dotted line) for a single shower rain event. The supplied WDR is depicted with a full line.

3.1 Effect of dust particles on the dynamic shear viscosity

The dynamic viscosity determines the flow rate described by the second term in Eq. 1. Higher viscosities result in smaller flows and thus more retained water. In this paper, an empirical relation between viscosity and temperature proposed by Kestin et al. (1978) is used for which is stated that the uncertainty on the absolute viscosity does not exceed 0.1% for a temperature range between -8 °C and 40°C. The uncertainty on the dynamic viscosity can therefore be attributed almost completely to the increase in viscosity as a result of dust particles. Following Einstein (1906) in his definition of the viscosity of slurry, one can say that the uncertainty on the dynamic viscosity is limited to a factor ±1.25, even if the amount of dust particles is high:

$$\mu_s = (1 + 2.5\phi_s)\mu_l \tag{3}$$

Where μ_s the dynamic viscosity of the slurry (kg/(m s))
μ_l the dynamic viscosity of the liquid (kg/(m s))
ϕ_s the volume fraction of the dust particles (-)

As seen in FIG. 4.a the effect of the increased viscosity is limited. At the start of the shower a small extra mass will be held in the runoff layer. Towards the end of the drying period, this mass will also run down the facade, thus barely changing the total amount of runoff. The increased viscosity decreases the runoff rate slightly but cannot account for the difference between the measurements and the model.

3.2 Effect of the uncertainty on the convective moisture transfer coefficients

Moisture transfer from the wall to the outer environment is dominated by forced convection due to wind. Therefore it depends on the local wind speed close to the wall, the pore structure and roughness of the surface, the moisture content at the surface and the local humidity. Determining local wind speeds around the experimental setup is an extensive task and reliable and fast models to determine case specific CMTC are lacking (Janssen et al. 2007). Due to these reasons, a simplified empirical relation between reference wind speed and a case independent CMTC is used (Eq. 3), in which the CMTC does not depend on building geometry, environment topography and surface properties of the material. Given the conclusions of Janssen et al. (2007), one can say that the error on the CMTC can go up to a factor 5.

In FIG. 4b. the results of a simulation with an increased CMTC are depicted with a blue dashed line. Due to the high humidity outdoors during the rain shower (see Table 1.) the evaporation rates are limited. The effect of the increased CMTC is only visible during the drying period, limiting the runoff rate, but cannot account for the difference between the measurements and the model.

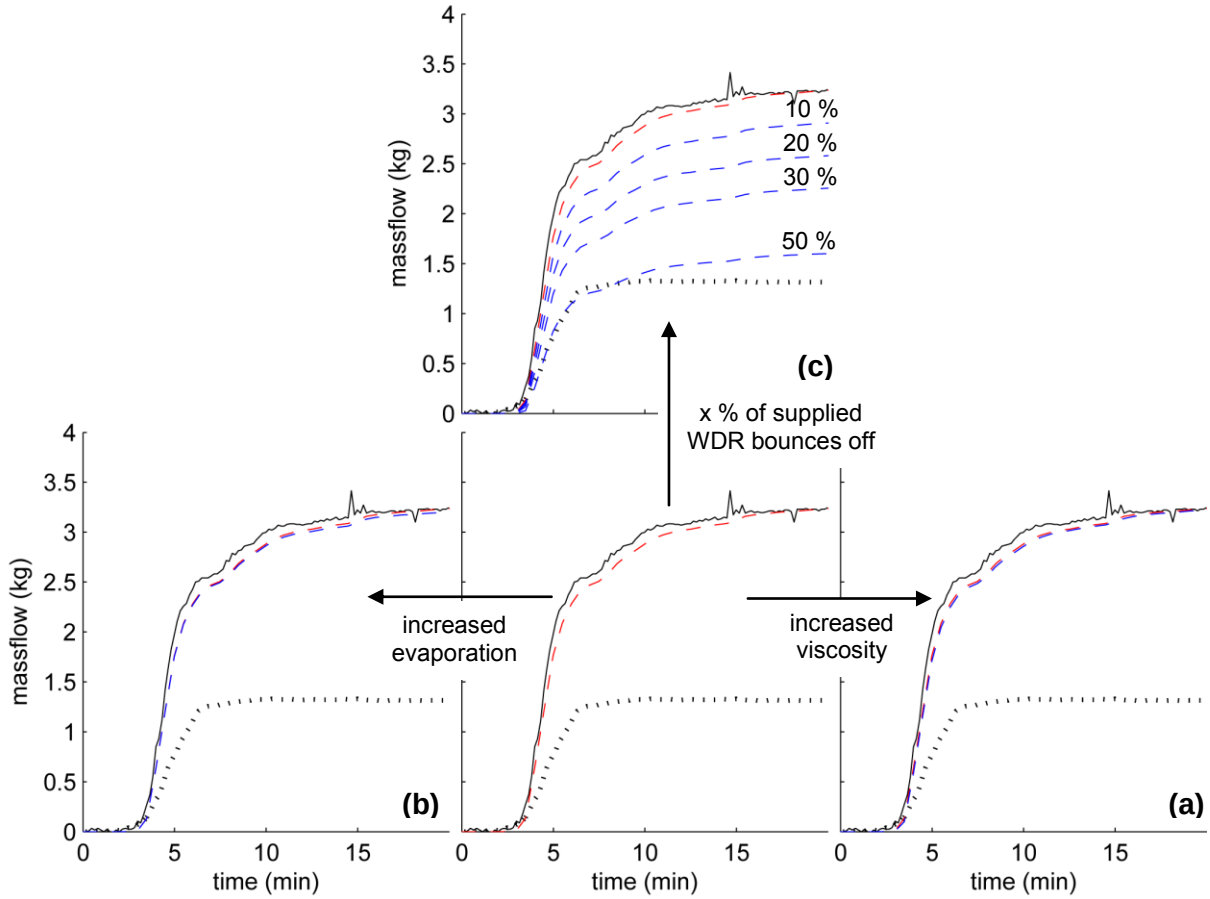

FIG 4. Results of the parameter analysis on the runoff model compared to the measured runoff rate. The measured runoff rate is depicted with a black dotted line, the measured supplied WDR with a full back line. The results of the model described by Van den Brande et al. (2013) are depicted with a red dashed line (equal in all figures), the results of the adjusted models with a blue dashed line.

3.3 Effect of bouncing and splashing of droplets

Due to splashing and bouncing of rain droplets part of the WDR flux is lost and does not contribute to the development of the runoff layer. The impact speed and impact angle of the individual raindrops and surface properties determine if a droplet splashes, bounces or spreads (Abuku et al. 2009). The impact of a droplet on a liquid film is even more unknown. These properties are tedious to measure and it is therefore difficult to correctly quantify the amount of water that actually contributes to runoff. In most WDR simulations, the impact speed and angle of different droplets are not reported making it also difficult to quantify the contribution of bouncing and splashing from simulations.

In FIG. 4c. the effects of the uncertainty on the supplied WDR are depicted. In each simulation a fraction of the supplied WDR is considered to bounce or splash, thus decreasing the supplied WDR. The figure shows that the effect of the uncertainty on the supply determines the result of the model. It is also visible there is also another factor that influences runoff that cannot be described by the model. During the second part of the event no runoff is measured whereas the model predicts a runoff flow due to the small amount of supplied WDR. This difference is in the same order of magnitude as the experimentally determined amount of adhesion water, namely 0.145 kg for the full panel.

4. Conclusions

In this paper the model proposed by Van den Brande et al. (2013) was compared with full scale runoff measurements on a medium-rise building. Measured WDR intensities and detailed micro-meteorological weather measurements were used as boundary conditions for the model. From the first comparison it was found that the model overestimates both the amount of runoff and the actual runoff rate. It was also found that it is necessary to model the adhesion water that is left after the runoff film flows down and to include bouncing and splashing of droplets. The uncertainty on the CMTC and the dynamic shear viscosity are found to be of less importance.

These results points out that future development in the model lies in a more precise experimental and numerical determination of the WDR intensities, including the effects after impact. Reports of WDR simulations should include, next to the moisture fluxes, also impact speed and angles making it possible to estimate splashing and bouncing. The current applied runoff model by Blocken & Carmeliet (2012) and Van den Brande et al. (2013) can also be improved by including surface adhesion of water.

5. Acknowledgements

The results presented in this paper have been obtained in the framework of the research project FWO G.0448.10N, Strategies for moisture modelling of historical buildings in order to reduce damage risks, funded by the FWO-Flanders. The FWO-Flanders (Research Fund-Flanders) supports and stimulates fundamental research in Flanders (Belgium). Their financial contribution is gratefully acknowledged.

References

Abuku, M. et al., 2009. Impact, absorption and evaporation of raindrops on building facades. Building and Environment, 44(1), p.113–124.

Abuku, M., 2009. Moisture Stress of wind-driven rain on building enclosures. Laboratory of Building Physics, KU Leuven.

Abuku, M., Blocken, B. & Roels, S., 2009. Moisture response of building facades to wind-driven rain: Field measurements compared with numerical simulations. Journal of Wind Engineering and Industrial Aerodynamics, 97(5-6), pp.197–207.

Beijer, O. & Johansson, A., 1977. Driving rain against externall walls of concrete [Slagregn mot betongfasader], Stockholm.

Blocken, B. & Carmeliet, J., 2006. On the accuracy of wind-driven rain measurements on buildings. Building and Environment, 41(12), p.1798–1810.

Blocken, B. & Carmeliet, J., 2012. A simplified numerical model for rainwater runoff on building facades: Possibilities and limitations. Building and Environment, 53, p.59–73.

Blocken, B., Derome, D. & Carmeliet, J., 2013. Rainwater runoff from building facades: a review. Building and Environment, 60, p. 339–361.

Davidson, C.I. et al., 2000. Soiling patterns on a tall limestone building: Changes over 60 Years. Environmental Science & Technology, 34(4), p. 560–565.

Einstein, A., 1906. Eine neue Bestimmung der Moleküldimensionen. Annalen der Physik, 324 (2), p. 289-306.

Etyemezian, V. et al., 1998. Vertical gradients of pullutant concentrations and deposition fluxes on a tall limestone building. Journal of the American Institute of Conservation, 37(2), p.187–210.

Etyemezian, V., 2000. Impingement of rain drops on a tall building. Atmospheric Environment, 34(15), p. 2399–2412.

Greenspan, H.P., 1978. On the motion of a small viscous droplet that wets a surface. J. Fluid Mech, 84(1), p. 125–143.

Hens, H., 2010. Wind-driven rain: From Theory to Reality. In Proceedings of Thermal Performance of the Exterior Envelopes of Whole Buildings XI International Conference. Clearwater Beach, Florida, p. paper 15.

Högberg, A., Kragh, M. & van Mook, F., 1999. A comparison of driving rain measurements with different gauges. Proceedings of the 5th Symposium on Building Physics in the Nordic Countries, p. 24–26.

Janssen, H., Blocken, B. & Carmeliet, J., 2007. Conservative modelling of the moisture and heat transfer in building components under atmospheric excitation. International Journal of Heat and Mass Transfer, 50(5-6), p. 1128–1140.

Kaegi, R. et al., 2008. Synthetic TiO2 nanoparticle emission from exterior facades into the aquatic environment. Environmental pollution, 156(2), p. 233–239.

Kaegi, R. et al., 2010. Release of silver nanoparticles from outdoor facades. Environmental pollution, 158(9), p. 2900–2905.

Kestin, J., Sokolov, M. & Wakeham, W., 1978. Viscosity of Liquid Water in the Range -8°C to 150°C. Journal of Chem. Ref. Data, 7(3), p. 941–948.

Küntz, M. & van Mier, J.G.M., 1997. Gravity-driven wetting front instability of water runoffs on concrete structures. HERON, 42(4), p. 231–244.

Ruyer-Quil, C. & Manneville, P., 1998. Modeling film flows down inclined planes. The European Physical Journal B, 6(2), p. 277–292.

Sharples, S., 1984. Full-scale measurements of convective energy losses from exterior building surfaces. Building and Environment, 19(1), p. 31–39.

Van den Brande, T., Blocken, B. & Roels, S., 2013. Rain water runoff from porous building facades: Implementation and application of a first-order runoff model coupled to a HAM model. Building and Environment, 64, p. 177–186.

Method for determination of the critical moisture level for mould growth on building materials

Pernilla Johansson, Lic. Tech. [1]
Annika Ekstrand-Tobin, Ph. D.[1]
Gunilla Bok, Ph. Lic

[1] SP Technical Research Institute of Sweden, Sweden

KEYWORDS: *mould resistance, critical moisture level, mould*

***SUMMARY*:**
Materials that are stored or used in damp climates may be subject to mould growth. However, all materials are not equally susceptible to mould growth. For each specific material, there is a critical moisture level. If this is exceeded, there is a risk that mould growth will develop on the material. In a building, different parts are exposed to different climatic conditions. To minimise the risk of microbial growth, building materials should be choses that are tolerant to the expected climatic conditions.

In this paper we present an innovative test method for determining the critical moisture level for mould growth on a material. It is based on existing test methods for evaluating mould resistance of a material and on a wide range of laboratory tests. The results have been validated by field studies.

1. Introduction

Mould growth on building materials is the consequence of an interaction between environmental factors (temperature and humidity), material properties and the characteristics of the mould fungi. In general, the availability of water in the material is regarded as the crucial element for growth to occur. It is then the surface of the material that is of interest, since the mould fungi are growing at the surface of solid material. At equilibrium, the moisture at the surface is the same as in the surrounding air. Generally, the higher the moisture availability, the higher is the risk for mould growth. However, building materials differ in their mould resistance; some materials can withstand high moisture conditions better than others. Also, while some materials are susceptible to mould growth at low levels of humidity, down to 75% RH, others can tolerate high moisture levels, above 95% RH, without mould growing on them (Ritschkoff et al. 2000) (Nielsen et al. 2004; Hofbauer et al. 2008; Johansson et al. 2012). There is a theoretical level of RH for each material, above which mould growth is possible, the critical moisture level for mould growth. This is dependent on the temperature; the lower the temperature, the higher is the critical moisture level (Johansson et al. 2012).

Traditionally, mould resistance is evaluated by exposing test specimens of the material to spores of mould fungi and then incubating the specimens at a relative humidity and temperature that are favourable to mould growth. The principle behind the test is that most fungi grow well at high RH and if the material is such as to allow mould growth, then it should also grow on the test pieces in the laboratory. Several standardised test methods are available; some are presented in (Adan 1994) and in (Johansson 2012). While being able to discriminate between materials in a general way, these test methods do not provide any information on how a material will perform in a building where the moisture conditions are not that high. It may, therefore, be possible to use materials that have been subject to mould growth in the tests in constructions where the moisture load is lower.

In this paper, we describe and discuss a novel test method (SP Method 4927:2012), the Critical Moisture Level method, for evaluating the critical moisture level of a material. Instead of completely

excluding the use of certain materials that have failed existing mould resistance tests, the CML method can differentiate mould susceptibility at several different moisture levels. With the introduction of this newly developed and validated method, the field for testing materials' susceptibility to mould has widened. It also makes possible a practical application for use in situations with known lower RH. This in turn provides the basis for material choice in designs where moisture and temperature conditions are known.

The CML method is a result of a range of tests conducted in the laboratory over several years (Johansson et al. 2012). These tests have been based on routines from several of the existing testing methods; with some modifications to fit the purpose. The method was validated by field studies in buildings (Johansson et al. 2013b).

The method will be available as a technical specification (SIS/TS 41:2013) and is also presented in (Johansson 2014).

2. Test procedure

The principle underlying the new CLM methodology is the same as in most of the previous test methods of mould resistance: that is, spores from mould fungi are applied to the surface of test pieces of the material, and these are then incubated in conditions of temperature and relative humidity favourable for mould growth. After some weeks of incubation, the surfaces of the test pieces are analysed for mould growth. There are differences among the methods in terms of which species are used, the number of spores and how they are introduced to the test pieces, the incubation environment in which the materials are tested, the assessments of growth of the test pieces, and the evaluation criteria. In (Johansson 2012) some of these parameters are compared between the new CML method and of five selected test methods for determining mould resistance.

In the CML method, a spore solution, containing spores from six mould fungi (*C. sphaerospermum,S. chartarum, E herbariorum, A versicolor, P chrysogenum, A pullulans*) is prepared according to (Johansson et al. 2012) and sprayed onto one surface of the material. Four sets of test specimens are then incubated in four different RH (80%, 85%, 90% and 95%) at 22°C. The test may be performed in parallel in separate moisture chambers with the different RH levels. The specimens are incubated for 12 weeks in each RH and are then visually inspected for fungal growth at x40 magnification. The growth is assessed according to a rating scale where 0=no mould growth, 1=Initial growth, scattered on the surface, 2=clearly established but sparse growth scattered on the surface 3=Patchy, heavy growth, 4=Heavy growth over more or less the entire surface.

To ensure test reproducibility, it is important to control the testing procedure. The CML method provides routines that make this possible. Among these routines are procedures for the preparation and inoculation of spores on test specimens, incubation conditions (including specifications for the test chamber to ensure that the temperature and relative humidity are according to the prescribed values), handling of test specimens and assessment of growth on the test pieces. Also, there are instructions for the action to be taken if deviation occurs. These quality assurance routines are based on our own test results and experiences in research and commissions over more than 15 years.

3. Determining the critical moisture level

The critical moisture is determined by considering the RH at which mould growth is established on the test specimens and the next lower RH where no growth can be detected during analysis. The actual critical moisture level is then expected to be somewhere between these two values or at the RH when the test pieces failed. The actual critical moisture level is therefore reported as a range. The principle is illustrated in FIG 1.

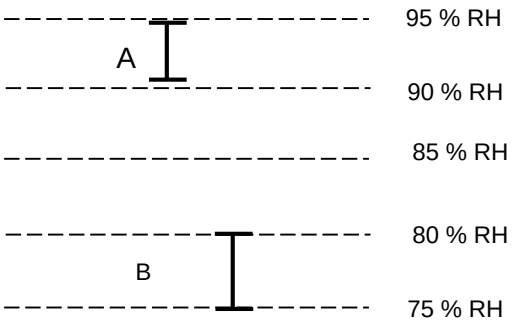

FIG 1. Principle of determination of critical moisture level. The numbers of RH represent the tested RH, except for 75% which is used as the lowest limit for mould growth based on literature. In case A, there is mould growth at 95% RH but not at 90% RH and the critical moisture level is therefore 85%< RH_{crit}, 22°C ≤90%. In case B there is mould growth at 80% RH and the critical moisture level will consequently be established as 75% < RH_{crit}, 22°C ≤ 80%.

As the RH_{crit} is temperature-dependent, the test results are only valid for the temperature tested, that is, 22°C. However, to be able to use the results for applications in buildings, it is important also to assess the critical moisture levels at other temperatures. The results from tests according to the method, the critical moisture level can be calculated for any temperature commonly found in actual buildings (between 0°C and approximately 30°C) according to Eq.1 and Eq. 2. This must be performed for both the upper and lower value of RH_{crit}.

$$RH_{crit\ T2} = 105 + c(T_2^{\ 2} - 54T_2) \qquad (1)$$

Where $RH_{crit\ T2}$ is the critical moisture level (%) at temperature T_2
c is given from Eq.2
T_2 is the chosen temperature (°C) for the extrapolation

$$c = (RH_{crit\ 22} - 105) / (T_1^{\ 2} - 54T_1) \qquad (2)$$

Where c a constant from Eq.2
T_1 is 22°C (the temperature at which the test was performed)
$RH_{crit\ 22}$ is the resulting critical moisture level (%) from the test at temperature T_1

If the calculations are repeated for a series of temperatures, the critical moisture levels can be expressed as growth limit curves, see FIG 2. The equation and procedure for calculating the growth limit curves has been presented by (Johansson et al. 2013a) and is based on both our own (Johansson et al. 2012) and other studies (Sedlbauer 2001; Hofbauer et al. 2008).

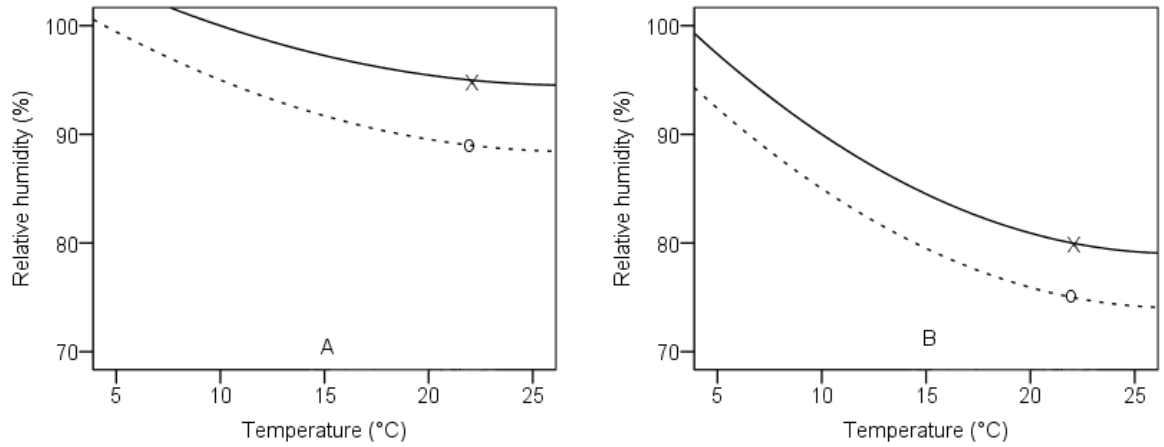

FIG 2. Mould growth limit curves for materials with 90%< $RH_{crit,\ 22°C} \leq$ 5% (A) 75% < $RH_{crit,\ 22°C} \leq$ 80% (B). x is the RH where mould growth was found, o is the next lower RH in the test.

It is essential to have control over the particular values of RH at which the test has been performed. Temperature and RH are logged and recorded every ten minutes with calibrated sensors. The precise mean RH and temperature that the specimens are exposed to will never be exactly the set values. This is because of the expanded measurement uncertainties caused, for example, by variation in each chamber and by measurement error from calibration of the sensors.

In order to distinguish the different incubation RH from each other, there are specified limits, ± 2.5 % of each of the set values for RH and ±2°C for the temperature, within which the mean value together with the measurement uncertainties must fall. The procedure for calculating this is given in the CML method. FIG 3 and TABLE 1 illustrate the principle.

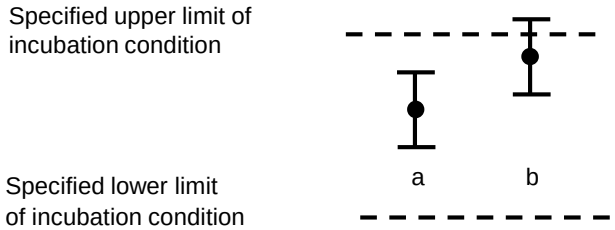

FIG 3. Illustration of the evaluation of incubation criteria. The specified limits of incubation condition are described in TABLE 1. The dots represent mean measured values of RH or temperature and the whiskers represent the calculated expanded uncertainty. In case I the mean value with uncertainties fall into allowed limits. In case II it is not, since the upper limit is exceeded. Therefore, the test is not valid.

TABLE 1 The set points of each incubation condition of the test method

Incubation condition	Set point	Specified lower limit	Specified upper limit
T	22.0°C	20.0°C	24.0°C
RH 1	80.0	77.5%	82.5%
RH 2	85.0	82.5%	87.5%
RH 3	90.0	87.5%	92.5%
RH 4	95.0	92.5%	97.5%

Fewer percentage points between two tested humidity levels would narrow the interval for RH_{crit}. However, measurement uncertainty limits how narrow these intervals may usefully be. Our laboratory study showed that the uncertainty was at most 2.5 percentage points RH, so settings of RH in ranges

smaller than 3 percentage points are not possible with the settings used in the CML method (Johansson 2012).

4. Application of the method

The test is performed in a laboratory at constant conditions of temperature and relative humidity. These environmental factors will vary from the laboratory to in-situ situations. In many parts of a construction, there is a fluctuation in relative humidity and temperature, due to both seasonal and shorter-term variations. This fluctuation causes stress to the fungi growing on materials in the building, which affects not only the rate of growth but also how long the fungi will survive. Also conditions will differ from what the materials encounter in 'real life' including biotic factors, such as spore load, species present and species adaptation.

In spite of all the limitations of and simplifications in the accelerated laboratory method compared to real-life situations, the CML method serves well to predict the mould growth in buildings, as has been shown in (Johansson et al. 2013b). In the present study, the same materials as had been tested in the laboratory test (Johansson et al. 2012) with the CML method was exposed in three crawlspaces and three attics for 2.5 years. If the actual RH and temperature was above the critical moisture level for the material, as had been tested in the laboratory with the routines as prescribed in the CML method, there was growth on the test pieces if the time was long enough. If the RH and temperature did not exceed the critical moisture level, there was no mould growth on the material.

By using the growth limit curves and on the basis of the results from the testing by the CLM method, it can be estimated whether there is risk for mould growth in a building part where the relative humidity and temperature is known, either by measurements or by hygrothermal calculations.

The results from one of the measurements in our field study (Johansson et al. 2013b) serves as an example of how results may be used. FIG 4 shows the measurements of temperature and relative humidity in a crawlspace for 2.5 years. Each value of measured relative humidity is plotted against the temperature, and the growth limit curves for materials are plotted as in FIG 5. If the relative humidity at a specific temperature is below the lowest growth limit curve, no mould growth is expected. If it exceeds the upper limit, mould growth is possible. In between the two curves, there is a zone in which the critical moisture level may fall. To be on the safe side, if the relative humidity is in this zone, mould growth should be regarded as possible.

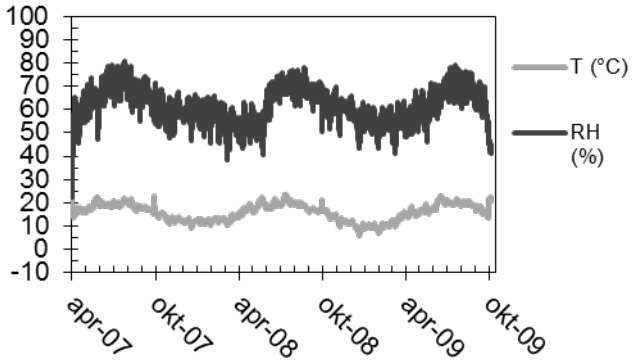

FIG 4. Measured relative humidity and temperature in a crawlspace (Johansson et al. 2013b)

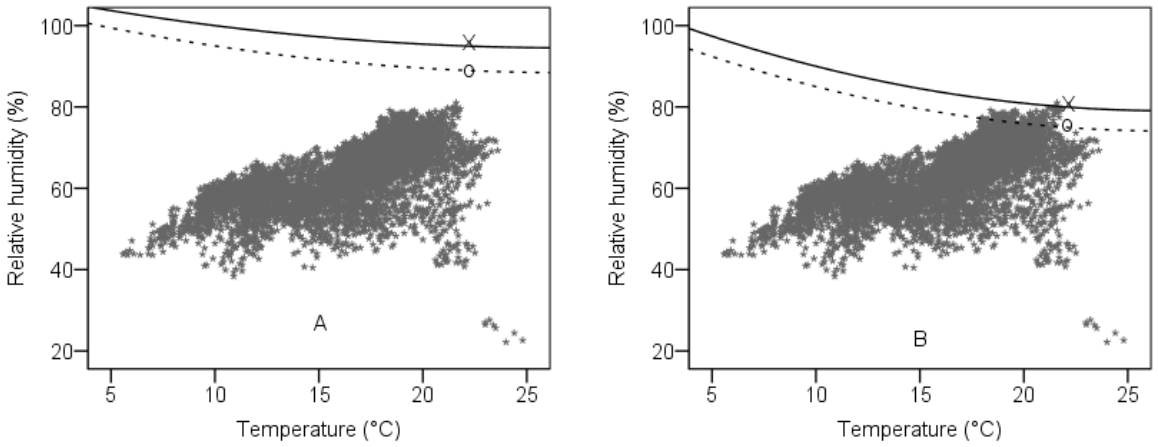

A B

FIG 6. Example of how to use the results from the test. The measured RH conditions in FIG.4 is plotted as a function of measured temperature. The growth limit curves according to FIG. 2 have been introduced to the plots. In case A, no mould growth is expected, since the growth limit curves is well above measured values. In case B, there are values in the critical moisture level interval and hence there is a possible risk for mould growth. If the measured or calculated conditions are expected to be more humid/warm this risk increases since the limit curves then are well exceeded.

One limitation of the method is that the results cannot be used to predict how long the material can withstand the actual conditions in buildings where the temperature and relative humidity fluctuate. The combined RH and temperature conditions must be above the critical moisture level for a sufficient time (Johansson et al. 2013b) for mould growth to develop. If only exceeded occasionally, there is probably no enhanced risk for mould growth. Also, it is the duration of the favourable and unfavourable conditions that is decisive (Johansson et al. 2013a). Based on the field test, we find that when the duration of favourable conditions is not considered, the laboratory test results will not underestimate the risk of mould growth; the results will instead include a certain margin of safety (Johansson et al. 2013b).

Although the simplified approach of considering cumulative time over growth limit curves gave enough information to validate the method, more precise predictions may be needed by more sophisticated models. Several mathematical models for assessing the risk for mould growth have been or are being developed, and some of them are reviewed in (Vereecken and Roels 2012). These methods rely on data from previous published results of mould growth tests. However, two similar materials may have considerably different resistance to mould growth, and so the results from one cannot be applied to the other (Johansson et al. 2012). Therefore, each individual material must be tested separately. In the further development of predictive models, the critical moisture condition should be considered. Results of the test according to the CLM method can then be used as input in the calculations.

5. Conclusions

The CML method for testing the critical moisture level of a material provides a new and enhanced tool to assess the susceptibility of a material for mould growth in buildings in a way that has not been possible earlier. The method contains quality-assured routines and has been validated in real-life conditions.

If the expected temperature and RH in a building part is known, either by measurements or by using heat-and-moisture simulation software, knowledge of the critical moisture levels of a material, as determined by the CML method and the calculated growth limit curves may be used as tools when

choosing materials for construction with minimum risk for mould growth. If the expected exposure of RH and temperature does not exceed the growth limit curves, no mould growth is expected. This is a simplified approach and more precise predictions may be needed by more sophisticated models where consideration is taken to fluctuating conditions of RH and temperature. The results from critical moisture level testing should be included also in those models.

References

Adan OCG. 1994. On the fungal defacement of interior finishes. PhD-Dissertation, University of Eindhoven, Wageningen

Hofbauer W, Kreuger N, Breuer K, Sedlbauer K, Schoch T. 2008. Mould resistance assessment of building materials – Material specific isopleth-systems for practical application. In: Indoor Air 2008, Copenhagen, Denmark. Paper ID: 465

Johansson P. 2012. Critical moisture conditions for mould growth on building materials. Lic Thesis. Report TVBH-3051. Lund University.

Johansson P, Bok G, Ekstrand-Tobin A. 2013a. The effect of cyclic moisture and temperature on mould growth on wood compared to steady state conditions. Building and Environment 65:178-184

Johansson P, Ekstrand-Tobin A, Svensson T, Bok G. 2012. Laboratory study to determine the critical moisture level for mould growth on building materials. International Biodeterioration and Biodegradation 73:23-32.

Johansson P, Svensson T, Ekstrand-Tobin A. 2013b. Validation of critical moisture conditions for mould growth on building materials. Building and Environment 62:201-209.

Johansson P. 2014. Determination of the critical moisture level for mould growth on building materials. Report TVBH-1020. Lund University (in progress)

Nielsen KF, Holm G, Uttrup LP, Nielsen PA. 2004. Mould growth on building materials under low water activities. Influence of humidity and temperature on fungal growth and secondary metabolism. International Biodeterioration and Biodegradation 54 (4):325-336

Ritschkoff A-C, Viitanen HA, Koskela K. 2000. The Response of Building Materials to the Mould Exposure at Different Humidity and Temperature Conditions. In: Healthy Buildings 2000, Espoo, Finland, 2000.

Sedlbauer K. 2001. Vorhersage von Schimmelpilzbildung auf und in Bauteilen.

SIS SIS/TS 41:2013. Laboratory method for determination of critical moisture level for mould growth on building materials. SIS Swedish Standards Insitute.

SP Method 4927. 2012. Laboratory Test Method for Determining Critical Moisture Level for Mould Growth on Building Materials. SP Technical Research Institute of Sweden,

Vereecken E, Roels S. 2012. Review of mould prediction models and their influence on mould risk evaluation. Building and Environment 51:296-310.

Moisture and frost risks for different external walls of test houses under Latvian climate conditions

Ansis Ozolins[1],
Andris Jakovics[1]

[1] University of Latvia, Latvia

KEYWORDS: *multi-layered wall, moisture risks, frost risks*

SUMMARY:
The aim of the current paper is to analyse the moisture and frost risks for different building solutions of external walls. Calculations of heat and moisture transfer through the wall have been done in a long term. It is shown that in case of an external wall consisting only of aerated clay blocks, a significant part is exposed to frost risks. Usage of 5 cm insulation material layer outside does not protect the wall perfectly. Moisture risks for external walls mainly consisting of wooden materials and insulation layer are high even when a vapour barrier is used. Measurements show a good agreement with calculations and any differences can be explained, therefore the results obtained by numerical simulations are reliable.

1. Introduction

The moisture and frost risks in the building components continue to be a highly topical problem. Sedlbauer (2001, pp. 215) gives a generalized isopleths' system for spore germination to predict moisture risks in building constructions. Nowadays these curves are used as a standard according to (German institute for standardisation, 2001). After Sedlbauer (2001) the models for estimating of mould growth risks in different building materials are developed and widely researched. Hazardous classes were defined with the aim to differentiate the mould fungi according to the health dangers in (Sedlbauer & Krus & Breuer, 2003). In (Isaksson & Thelandersson & Extrand-Tobin & Johansson, 2010) the model for predicting onset of mould growth with reasonable reliability is developed. In (Viitanen, 2011) results on mould growth in different materials were shown and existing models on the risk of mould growth development were evaluated. Countless papers about frost damages in different building materials have been published. Comprehensive study about frost damages in concrete is given in (Fagerlund, G. 1995). Relations between the concrete composition, and the frost resistance, are presented and discussed.

Since the critical conditions for mould growth as well as frost risks in different building materials have been widely researched in the laboratory conditions, it is interesting to analyse the moisture risks in real building structures in the real climatic conditions. Although the investigation of moisture risks in building constructions has been implemented recently , e.g. (Mlakar, J. & Strancar, J. 2013), the experiments that compare different building structures with similar conditions (orientation, size, room volume, placement of windows and door, loft, floor, roof, etc) are rarely found. Moreover, this type of analysis for the conditions of Latvian climate has not been available hitherto.

The main aim of this paper is to analyse the moisture and frost risks in case of different building structures of external walls for Latvian climatic conditions.

2. Short description of multi-layered external walls

The current section provides a brief description of external walls of five test stands built in Riga, Latvia.

A detailed description of parameters of some of the external walls is also given in (EEM, 2011; Ozolins, A. & Jakovics, A. 2013; Ozolins, A. & Jakovics, A. & Ratnieks, J. & Gendelis, S. 2012; Ozolins, A. & Jakovics, A. & Ratnieks, J. 2013). The project homepage (EEM, 2011) provides a comprehensive gallery of test stand images.

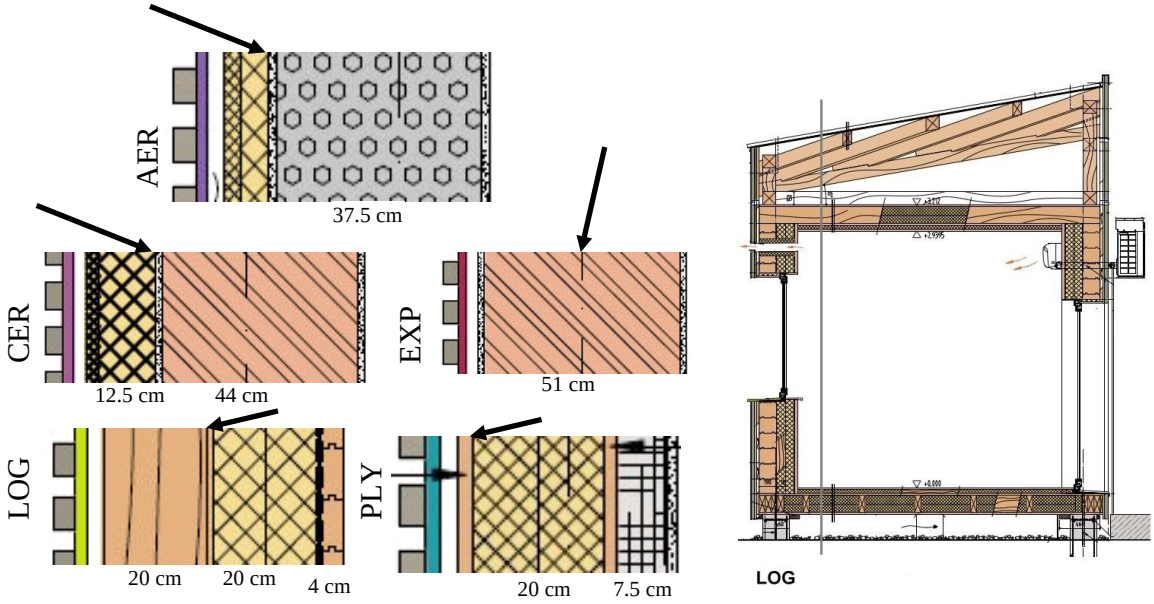

FIG 1. Cross-sections of 5 different external walls. On the right: cross-section of one test house. Arrows indicate temperature and relative humidity sensor placement

TABLE 1. Parameters of building construction walls

AER house	CER house	EXP house	LOG house	PLY house
Material, thermal conductivity λ (W/mK), diffusion resistance factor μ, thickness d (cm)				
Exterior				
Wind protection slab, 0.034, 1, 3	Wind protection slab, 0.034, 1, 3	Lime plaster, 0.7, 7, 1.5	Wooden log, 0.13, 130, 20	Plywood, 0.17, 700, 2
Elasticity stone wool, 0.036, 1, 2	Elasticity stone wool, 0.043, 1, 12.5	Aerated clay bricks with insulation fillings, 0.095, 8, 51	Elasticity stone wool, 0.044, 1, 20	Elasticity stone wool, 0.041, 1, 20
Lime plaster, 0.7, 7, 1.5	Lime plaster, 0.7, 7, 1.5			Plywood, 0.17, 700, 2
Aerated concrete, 0.072, 4, 37.5	Aerated clay bricks, 0.175, 7, 44		Decorative wooden log, 0.13, 130, 4	Fibrolite, 0.068, 2, 7.5
Lime plaster, 0.7, 7, 1.5	Lime plaster, 0.7, 7, 1.5	Lime plaster, 0.7, 7, 1.5		Lime plaster, 0.7, 7, 1.5
Interior				

In Fig. 1 a cross section of each external wall is shown. In Table 1, the multi-layered external walls of each test house are characterized. Ventilated facade is used to protect the walls from the wind and the rain.
Summary, critical conditions for mould growth are on PLY house in the interlayer between the stone wool and the plywood outside and on the LOG house in the interlayer between the outside wooden logs and stone wool. EXP house is the only case where the insulation material is not applied on the external wall. In this case frost risks could be observed because of aerated clay bricks placed outside with no insulation protection. Moisture risks could not be observed on the AER house. However, long drying period of initial moisture at the aerated concrete is expected in this case. It could be predicted that frost and moisture risks may not be observed in case of the CER house. It can be noted that aerated clay bricks consist from the macroscopic cavities.

3. Measurement conditions

Test stands of houses were built in December 2012. The experimental results have been obtained from April, 2013.

3.1 Placement of sensors

Placement of sensors for measurement of relative humidity and temperature are shown in Fig. 1. Arrows indicate the exact placement. For test stands of PLY and LOG, the sensors have been placed in the critical places where the highest moisture risks are predicted. For the test stands of AER and CER the chosen places indicate the highest frost risks on the external wall. For the test stands of EXP, the sensor is placed on the porous domain. One sensor for each of the test stands is also placed by the door jamb. These sensors can also help to estimate the moisture level in each test stand because of their placement near the construction wall.

3.2 Outdoor and indoor climate conditions

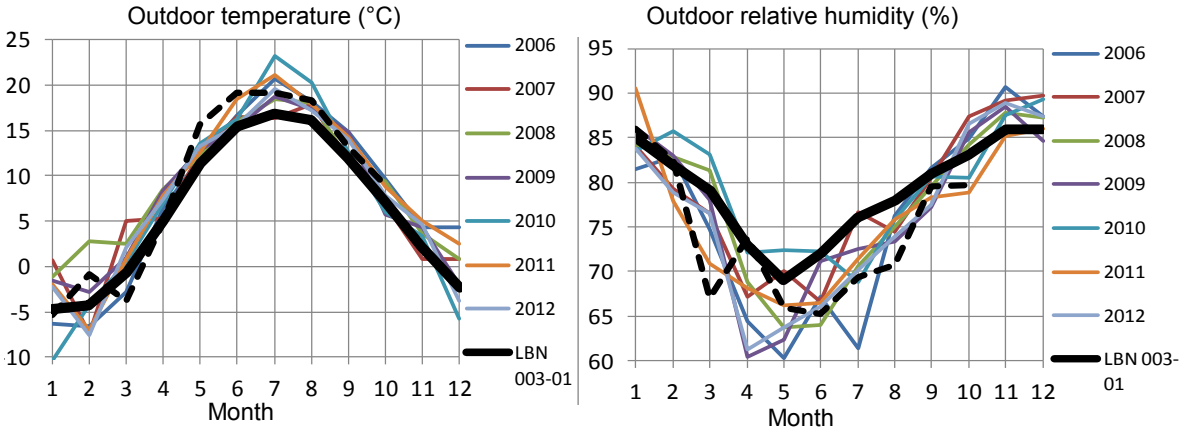

FIG 2. Monthly average outdoor climate conditions in Riga, Latvia. Thicker line denotes the conditions prescribed by the Latvian construction standard

Fig. 2 demonstrates the monthly average outdoor temperature and relative humidity during a period of 7 years. Latvian standard (Latvian Construction Standard, 2001) is also included. According to the illustration, some differences are observed for each year, e.g. colder winters, warmer summers in comparison to those provided for in (Latvian Construction Standard, 2001). Especially significant differences between Latvian construction standard and the real climate conditions are observed in spring and in summer when relative humidity is lower.

4. Results and discussions

In the current section the analysis of results obtained both from measurements and calculations is provided. The software WUFI has been used for the calculations of heat and moisture transfer through building components. In (Kunzel, 1995) the model assumptions are explained in details.

4.1 Moisture risks in a long term

The moisture analysis for external walls of wooden constructions PLY and LOG in a long term will be addressed. A similar analysis was implemented in (Ozolins & Jakovics, 2013). However, the data of outdoor climate is not averaged in the current work. Instead, the calculation has been done throughout a period of 7 years, therefore it is taken into account that some years from this perspective are better (moisture risks are lower) and some years encourage higher moisture risks in a building construction. Indoor climate conditions are defined according to (European Standard, 2007). In (Ozolins & Jakovics & Ratnieks, 2013) it has been shown that measurements are well fitted with the numerical model. It means that the results obtained from simulations in a long term are reliable.

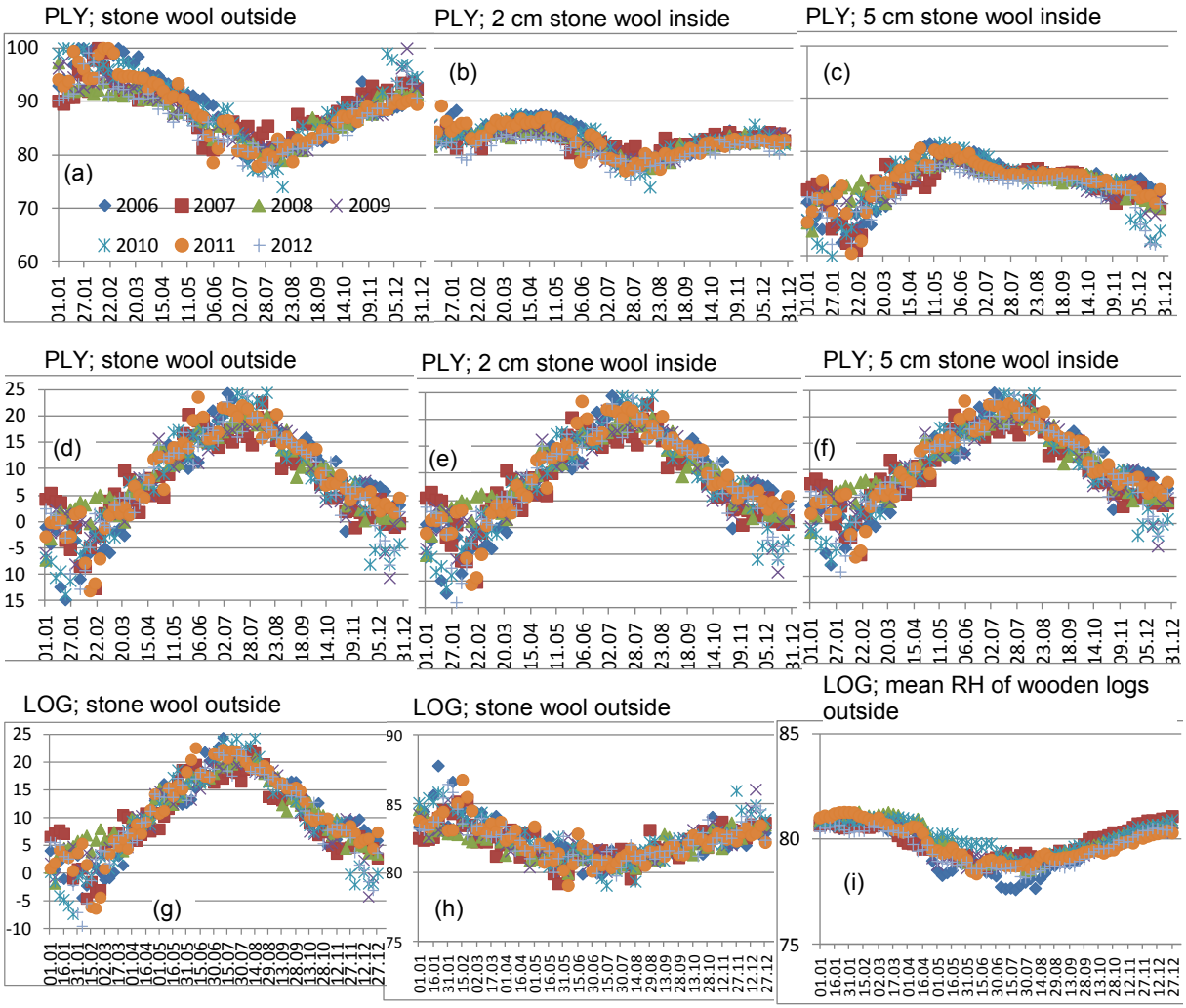

FIG 3. Test stands of LOG and PLY. (a), (b), (c), (h), (i) Relative humidity [%] and (d), (e), (f), (g) temperature [°C] in different places of external walls. Markers describe average 5 day period

Experiments show that even condensation can be observed in case of the external wall of PLY (Fig. 3a). The solution can be to drill small holes on the external plywood plates with the aim to ensure a

better ventilation of the layer consisting of mineral wool. Another alternative could be to replace the external plywood with a low vapour barrier. As it is shown in Fig. 3b, c, the relative humidity is significantly lower just only some centimetres deeper in the stone wool layer in the direction from exterior towards inside. For the test stand of LOG the relative humidity in a critical place is significantly lower and the maximal φ varies between 82-87% in a longer term (Fig. 3h). Mean φ of wooden logs outside is almost identical for each year within the time period of 2006-2012 (Fig. 3i). The relative humidity fluctuates from 77-82% therefore moisture risks are low for outside layer consisting of wooden logs.

Temperature significantly rises in spring (Fig. 3d,e,f,h) therefore mould growth risks are higher in spring because vapour is diffusing significantly slower through the building's construction. Lower limiting humidity level according to (German institute for standardisation, 2001) can be overreached for a longer time period therefore mould growth risks can also be observed for the external wall of LOG despite the usage of vapour barrier. Since the method (German institute for standardisation, 2001) is only applicable for interior surfaces, lower limiting humidity level is not useful for the critical place of the external wall of PLY.

4.2 Frost risks in a long term

In the current subsection the frost risks will be analysed for houses AER, CER and EXP, where aerated concrete and clay bricks are used: material can be damaged due to the low outdoor temperature. Especially high frost risks are for external wall of EXP due to no usage of insulation material on the outside. Since the frost risks are not high for wooden materials, houses LOG and PLY are not inspected in the current subsection.

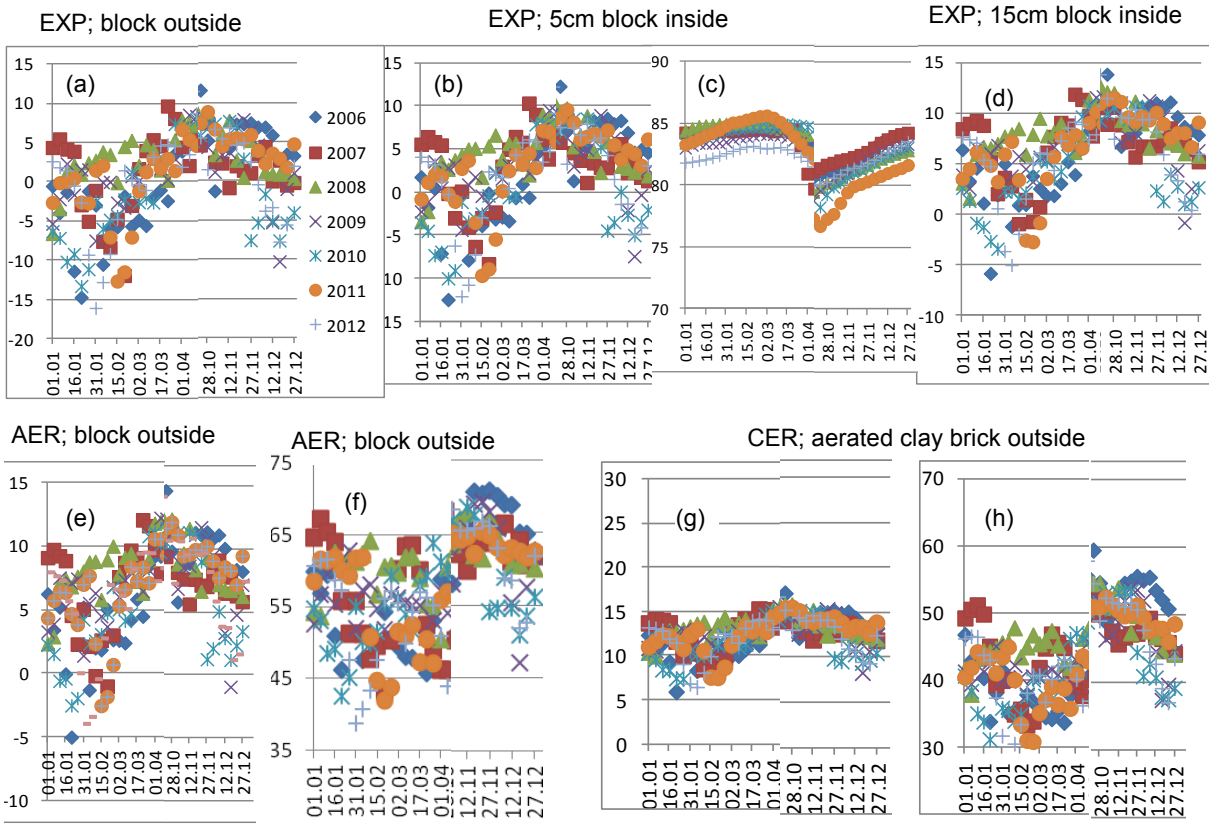

FIG 4. Test stands of AER, CER and EXP. (a), (b), (d), (e), (f), (g) Temperature [°C] and (c), (h) relative humidity [%] in different places of external walls. Markers describe average of 5 day period

As it is shown at the top of Fig. 4, not only the outer side of a block (Fig. 4a) but also the section 5 cm deeper in a block (Fig. 4b) is exposed to the frost risk. The situation can be quite different in each year, e.g. the duration of T_{5cm}<0 is estimated as 3 months (winter 2009-2010) or only a short time period (winter, 2007-2008). However, an overall situation shows that T_{5cm}<0 could often be in case in the winter. φ_{5cm} is estimated approximately between 80 % and 85 % in the winter and the differences between the years are insignificant (Fig. 4c). Since the rain is not taken into account than the water content can forming in the block. Therefore it can be concluded that the total water content can be high enough to encourage moisture damages. During several periods in a winter, the temperature can decrease below 0 °C even in the section up to15 cm deep within the block (Fig. 4d). However, in this case the situation would not be critical because of a low predicted water content in that section.

5 cm and 15 cm thickness of insulation materials have been used for the walls of AER and CER, respectively, therefore frost risks are insignificant in a long term (Fig. 4e, f, g, h). Only a short time period could be critical for the wall of AER (Fig 4e). For CER the situation is safe (Fig. 4g).

4.3 Short overview about measurements at the initial time period

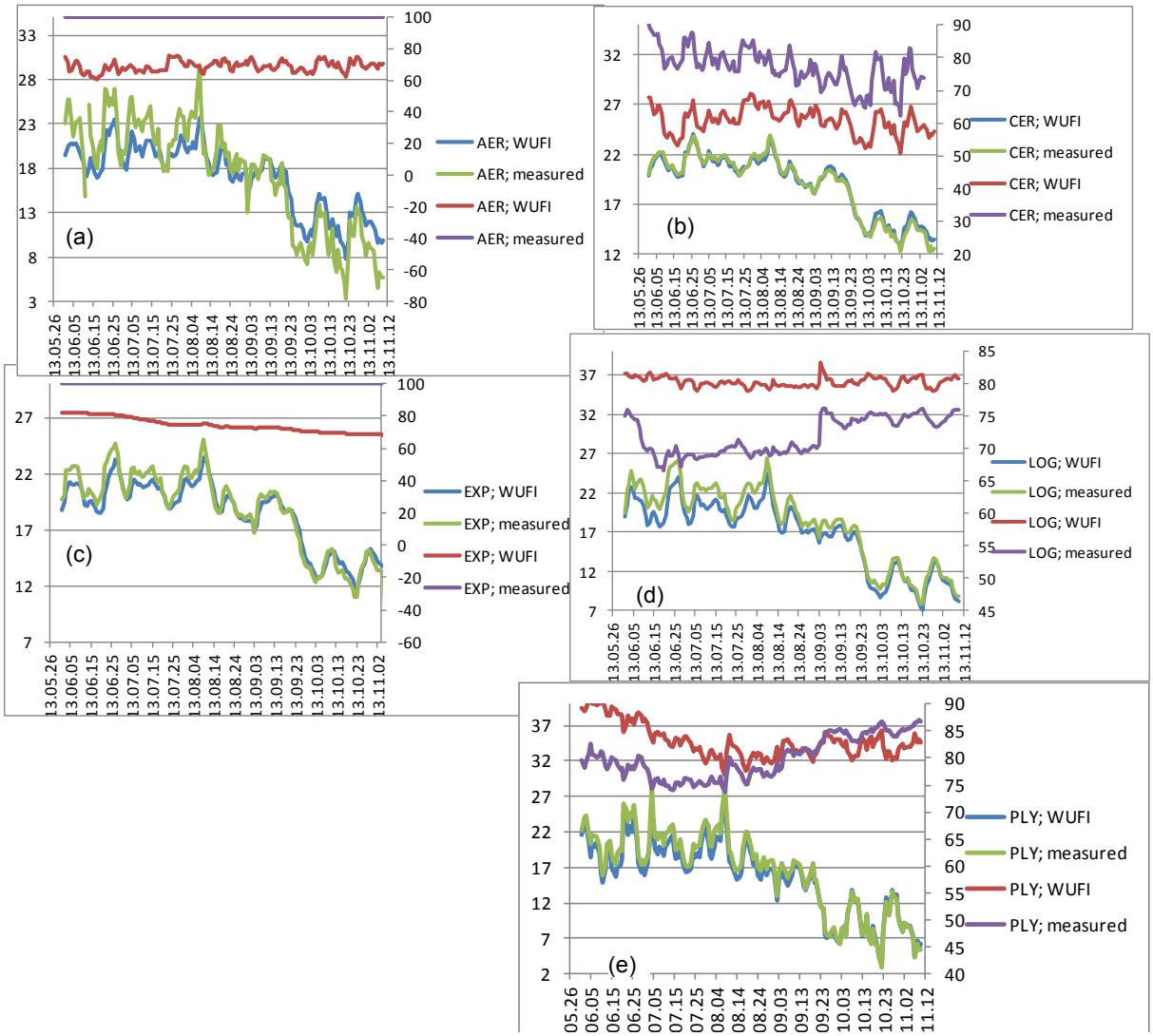

FIG 5. Dynamics of relative humidity and temperature in a specific place of building construction: measurements versus calculations. Specific place for each external wall is shown in Fig. 1, black arrows. Daily average values are used

In the current subsection we will focus on the experimental results at the initial period of test stands' monitoring. These results are compared with the WUFI calculations. The calculation has commenced in December 2012, and it is taken that the initial moisture of external walls equals with 80 % and the time step of 1 hour is chosen. However, initial moisture for each building material can differ significantly.

The real situation shows that high moisture on the wall is observed for external walls of EXP and AER (see Fig. 5a, c). Sensors on the walls show that φ=100 % in the middle of EXP block and on the external side of aerated concrete. Calculated temperatures are almost identical to the real temperatures for test stands of CER, EXP, LOG, PLY (Fig. 5b, c, d, e). Significant differences are observed for the external wall of AER (Fig. 5a). It is explained with a high initial moisture and therefore significantly higher thermal conductivity for the aerated concrete and for insulation materials. From this assumption it follows that the temperature near the external side of aerated concrete is more dependent on T_{out}. However, all temperature curves (see Fig. 5) show that the WUFI model works well for estimating frost risks in a long term, as described in the previous subsection.

The dynamic of measured relative humidity significantly differs from the relative humidity calculated for all test stands. Measurements for AER and EXP (Fig. 5a, c) show 100 % due to the initial moisture. The sensor on the external side of CER block (Fig. 5b) shows a significantly higher relative humidity than the results from calculations. However, fluctuations are similar, therefore with the choice of higher initial moisture in WUFI it will be possible to obtain a good agreement with measurements. The situation is opposite for the LOG (Fig. 5d) and real initial moisture has been lower in this case. Only for the test stand of PLY the differences are not simply explained (Fig. 5e). Currently the only explanation could be different material properties of plywood.

Sensors placed in the door jambs confirm that a high moisture is observed for the AER and EXP at the initial time period despite the same dynamics of a temperature for each case (see Fig. 6).

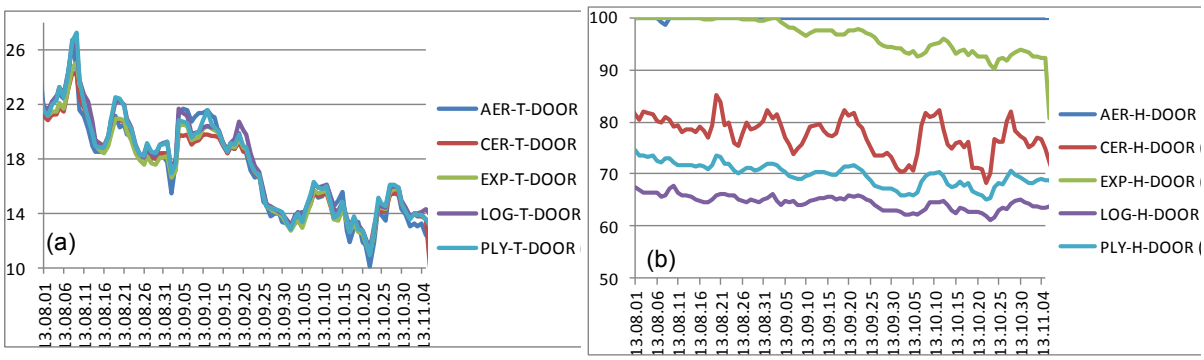

FIG 6. (a) Temperature near the door jamb; (b) Relative humidity near the door jamb

5. Conclusions

Measurements and detailed analysis that have been implemented from several aspects show that the best solution of 5 real external walls inspected in the current work could be the multi-layered wall consisting from aerated clay bricks and insulation materials placed outside of a wall. Moisture and frost risks are not observed in that case either through numerical calculations or measurements. Constructions mainly consisting of wooden materials and insulation materials have been exposed to moisture risks, and further measurements in test houses are recommended to observe, whether the experimental results will confirm the calculations in a long term.

The external wall which consists only of aerated clay bricks with the insulation filling is strongly prone to frost risks. Even in the section 15 cm deep in a block, the temperature below 0 °C could be observed. In case of the test house consisting of aerated concrete and insulation material outside, the frost risks could also be observed. It is planned to implement the analysis to estimate whether real frost damages will be observed for these two test houses.

6. Acknowledgements

The current work was supported by the European Regional Development Fund in Latvia within the project No. 2011/0003/2DP/2.1.1.1.0/10/APIA/VIAA/041.

References

Ozolins, A. & Jakovics, A. 2013. "Risks of condensate formation and mould growth in building under Latvian climate conditions", *Latvian Journal of Physics and Technical Sciences,* Vol. 5, pp.

Ozolins, A. & Jakovics, A. & Ratnieks, J. & Gendelis, S. 2012. "Numerical modelling of thermal comfort conditions in buildings with different boundary structures", *Proceedings of the 11th REHVA World Congress & 8th International Conference on IAQVEC – CLIMA 2013,* Prague.

Ozolins, A. & Jakovics, A. & Ratnieks, J. 2013. "Moisture risks in multi-layered walls – comparison of COMSOL and WUFI@PLUS models with experimental results", *Proceedings of the COMSOL Users Conference 2013,* Rotterdam.

EEM (2011). *Test stand of energy efficiency monitoring project*. [Online] Available from: http:/www.eem.lv.

Mlakar, J. & Strancar, J. 2013. "Temperature and humidity profiles in passive house building blocks", *Building and Environment,* 60. p. 185-193.

German institute for standardisation, 2001. DIN 4108. *Thermal protection and energy economy in buildings*. German: DIN.

Latvian construction standard, 2001. LBN 003-01. *Construction Climatology*. Latvia: LBN.

European standard, 2007. EN 15026. *Hygrothermal performance of building components and building elements - Assessment of moisture transfer by numerical simulation*.

Sedlbauer, K. 2001. "Prediction of mould fungus formation on the surface of and inside building components", PhD thesis, University of Stuttgart, Germany.

Sedlbauer, K. & Krus, M. & Breuer, K. 2003. "Mould Growth Prediction with a New Biohygrothermal Method and its Application in Practice", *Materials Conference*, Lodz.

Isaksson, T., Thelandersson, S., Extrand-Tobin, A., Johansson, P. 2010. "Critical conditions for onset of mould growth under varying climate conditions", *Building and Environment,* Vol. 45. p 1712-1721.

Viitanen, H. 2011. "Moisture and Bio-Deterioration Risk of Building Materials and Structures, Mass Transfer - Advanced Aspects", *InTech,* Finland.

Kunzel, H. M. 1995. "Simultaneous Heat and Moisture Transport in Building Components. One- And two dimensional calculation using simple parameters", PhD thesis, University Stuttgart, Germany.

Fagerlund, G. 1995. *Freeze-thaw resistance of concrete.* Report number: TVBM-3060. Lund.

HAM simulation of the drying out capacity of water ingress in wooden constructions

Glenn De Meersman, M. Sc. [1]
Nathan Van Den Bossche, Assistant Professor[1]
Arnold Janssens, Professor [1]

[1] Ghent University, Belgium

KEYWORDS: *Water penetration, Heat – air – moisture, WUFI, wind driven rain, experimental, water ingress, drying out capacity, static test method, EN 1207*

SUMMARY:
Due to more stringent energy codes, the advantages of wood-frame construction –slender walls in respect to the thermal resistance – have been picked up by the construction market in Belgium. This construction type is not endogenous, and the configuration of building components is often copied from Scandinavian building practice. However, climatic differences may induce additional risks for premature failure due to e.g. water ingress or interstitial condensation. Currently, it remains unclear how much water can be tolerated in wood-frame construction without causing excessive moisture contents. In this paper, the impact of water ingress is evaluated with a 2D hygrothermal model. Static experiments were conducted on the water penetration at window-wall interfaces to relate the water ingress to both wind pressure and the airtightness of the component. A method is proposed to relate these infiltration rates to measured wind pressures to allow for an assessment of the components by means of hygrothermal simulations under a realistic climate. HAM simulation taking into account the expected water ingress loads offers a rapid and realistic method of risk assessment for wooden constructions. Penetrated water was found to be a dominating parameter for the wood moisture content in cases where the initial moisture content and vapour diffusion resistance of the components was altered.

1. Introduction

Compared to masonry buildings, wood frame construction allows for relative slender walls in respect to the thermal resistance. Therefore, despite historical preference for masonry buildings, the share of newly built residential wood frame constructions in Belgium has risen from 5.6% to 11% between 2004 and 2009, and is expected to achieve a market share of 20% by 2020 (WTCB, 2010), mostly driven due to more stringent building codes. Knowledge of the hygrothermal behaviour of wood frame construction remains limited though among building practitioners, and most configurations of wall components are copied from regions with a more prolonged practice of wood-frame construction, such as North-America and Scandinavia. However, climatic differences between these geographic areas are often ignored, increasing the risk of premature building failure. Additionally, Belgian building practice typically consists of SME contractor firms focused on one trade of the building practice, facilitating errors during construction e.g. due to lack of communication or inadequate training. Currently, it remains unclear how robust some construction types are to cope with inadvertent water infiltration, e.g. at window – wall interfaces, and how much water can be tolerated by wood-frame constructions without causing excessive moisture contents leading to deterioration. Therefore, this paper reports on an experimental study on the leak resistance of window-wall interfaces, and a method to relate this risk to climate data is presented. The subsequent drying out capacity of the surrounding wood-frame walls was studied using simulations with a Heat Air Moisture model, allowing for a parametric study of the parameters involved.

2. Experimental results

Depending on the air- and watertightness of the building component water may penetrate into building components due to the co-occurrence of wind and rain. This rainwater can either be drained, buffered or accumulated in the component, potentially leading to deterioration of the building materials, such as due to frost damage, woodrot, … . Although by no means an indication of the long term hygrothermal performance of a building component, laboratory tests of the watertightness of building components allow relating the amount of water ingress to wind pressures. Typically, this is simulated experimentally by submitting building components to forced air pressure differences, either in a cyclic or static fashion, while simultaneously spraying them with water, thereby simulating wind-driven rain. The static test method EN 1027 (NBN, 2000) consists of applying constant pressures, stepwise increasing every 5 minutes. The applied water spray rate is constant at 2 l/min.m². This allows for the determination of water infiltration rates under constant conditions. The dynamic test method EN 12865 (NBN, 2001) subjects the component to pulsating wind pressures by means of 5 second gusts, repeated in cycles of 15 seconds. The water spray rate consists of simulating direct rain impingement, at a constant 1.5 l/min m², and the simulation of water running off the façade, at a constant 1.2 l/min m². By subjecting the building component to both test procedures, the component is subjected to different climate parameters, each with different failure mechanisms.

Experiments on the air- and watertightness of 2 window-wall interfaces were performed following EN 1027 and EN 12865. Two installation concepts were considered: the watertightness of configuration A is guaranteed by a self-expanding sealant tape, configuration B uses self-adhering flashing. The windows in both components are fixed using metal brackets, the airtightness on the interior side is secured using an airtight foil installed with caulking. Mind that the non-operable window itself was sealed meticulously to avoid any air or water leakage that could affect the measurements. Both setups were tested without insulation in place.

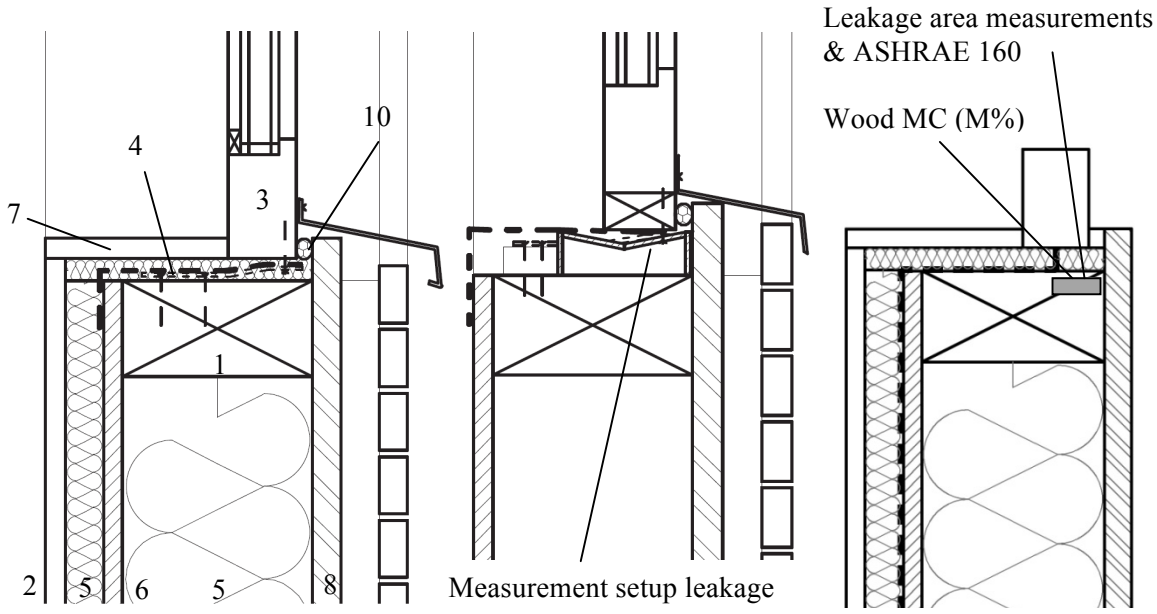

FIG. 1. (l) set up of construction type A, (m) experimental setup of construction type A, (r) input model

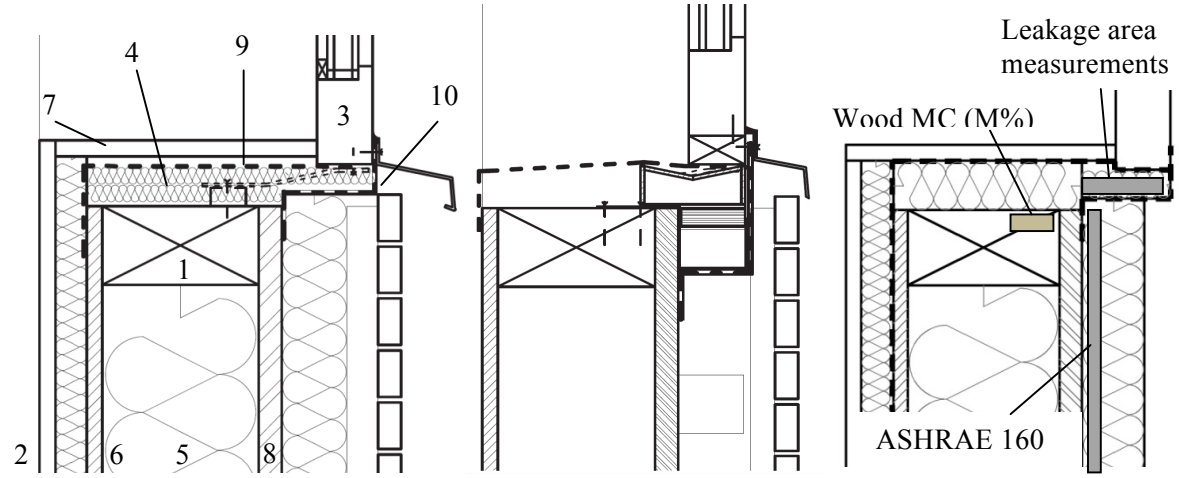

FIG. 2. (l) set up of construction type B, (m) experimental setup of construction type B, (r) input model

TABLE 1. Material properties

	Material	λ (W/mK)	μ (-)	Thickness (mm)
1	Softwood	0.09	200	120
2	Gypsum Board	0.2	8.3	12.5
3	Hardwood	0.13	200	49
4	Polyurethane (PU)	0.03	50	24
5	Mineral wool	0.04	1.3	120
6	Oriented Strand Board	0.13	175	12
7	Plywood	0.13	210	12,5
8	Wood fibre board	0.048	12.5	18
9	Vapour retarder	2.3	20000	1
10	Water resistive barrier	2.3	200	1

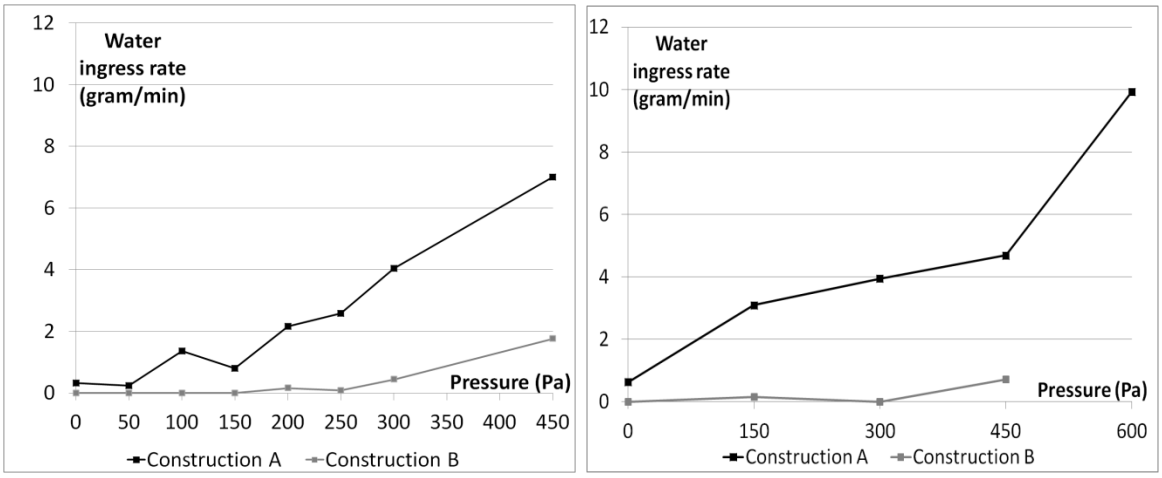

FIG. 3. (l) experimental results of the static method, (r)experimental results of the cyclic method

Results on the static and cyclic test methods are reported in figure FIG. 3. Configuration A is clearly less watertight than configuration B, with 3 – 4 times more water ingress both for the static and cyclic test method. The water ingress rate is not linearly proportional to the applied pressure difference due to the complex reaction of the water tightness membranes and sealant tape due to relaxation phenomena and wind turbulences. In the following only the static test method is considered.

3. Water infiltration

Numerical simulation of the hygrothermal performance of building components is now quite well-established, with several commercial and research packages available. This allows for a quick assessment of the expected performance of a building component over time, for any given climate. One of the remaining difficulties though, is how to take into account the effects of accidental water leaks into the component, and more specifically, how much water can be expected to penetrate. The 2 most important standards for hygrothermal simulations are quite vague on this: the European EN 15026 (NBN, 2007) does not address the subject, whereas the American ASHRAE 160 postulates, as a conservative assumption, that 1 percent of the wind driven rain impinging on the exterior surface will penetrate through that surface if no measured data is available. The specific location where that infiltration is subsequently introduced, is the exterior surface of the water resistant barrier, or equivalent if no water resistant barrier is present. Considering that the tested setups had a total area of 4.5m² the 1% assumption proves to be quite conservative here: for the static test method a penetration rate of 7 g/min at 450 Pa pressure difference is found in component A, as compared to the 90 g/min that would be expected following ASHRAE 160. Additionally, ASHRAE 160 does not consider the locality of leaks, but rather assumes them to be uniformly distributed across the exterior surface of the water barrier. Subsequent accumulation at lower parts of the structure due to gravity are ignored as well. In order to allow for more realistic water penetration rates in the simulations, a relationship between the penetration rates found in the experiments and the actual climatic conditions the component will be subjected to during its service life needs to be developed.

Research on wind speed distributions is rather limited and mainly focuses on extreme wind events, such as hurricanes. Additionally, wind speed data are, at best, only available as sets of 10 minute averaged values, with no information on the peak wind speeds occurring during the 10 minute averaging period. However, research by Davis et al (1968) shows that for higher wind speeds, on a general basis lower gust factors are found, showing an inverse relationship between average wind speed and peak wind speed. Research by Verheij et al (1992) for windspeeds at a height of 20, 40 and 80 meters shows that the distribution of the 10 minute averages can be described using Weibull probability density functions. The distribution of the wind speed fluctuations within these 10 minute periods follows a Gaussian distribution. Nevertheless, virtually no measurements are available on the magnitude of wind peaks for heights under 10 meter. Subsequently, as detailed weather data is scarce, water infiltration rates for building components can only reasonably be based on wind speeds averaged over 10 minute time periods, ignoring temporal variations within the averaging period.

3.1 Static test method

The static test method subjects the building components to static pressure conditions stepwise increasing every 5 minutes. Due to the long duration of every pressure step it seems reasonable that this entails penetration rates at a given pressure difference equivalent to those occurring over averaging periods of at least 5 minutes of the same magnitude under actual wind conditions. Eurocode 1 (2004) allows for calculating the mean velocity pressure based on the mean 10 minute average wind speed using Bernoulli's law:

$$q_{vm} = \frac{1}{2} \cdot c_r(z) \cdot c_0(z) \cdot c_{dir} \cdot c_{season} \cdot v_{b,0} \quad (1)$$

$$c_r(z) = 0.19 \cdot \left(\frac{z_0}{0.05}\right)^{0.07} \cdot ln\left(\frac{z}{z_0}\right) \text{ for } z_{min} \leq z \leq z_{max} \quad (2)$$

$$c_r(z) = c_r(z_{min}) \text{ for } z \leq z_{min} \quad (3)$$

Where q_{vm} mean velocity pressure for 10 minute averaging periods (Pa),
$c_r(z)$ roughness factor (-),
$c_0(z)$ orography factor, taken as 1.0 (-),

c_{dir} directional factor, taken as 1.0 (-),
c_{season} season factor, taken as 1.0 (-),
$v_{b,0}$ fundamental value of the basis wind velocity (m/s),
z_0 roughness length (m),
z height of the wind speed measurement (m),
z_{min} minimum height depending on the terrain category, taken as 5m for category III,
z_{max} taken as 200m.

Wind effects are only assumed to pressurize the building façade if their wind direction is within the range of +-45° to the normal on the building façade.

The peak WDR load at the center of a façade can be determined using (Van Den Bossche, 2013):

$$WDR = 0{,}10 \cdot v(z) \cdot i_h \quad (4)$$

Where WDR wind driven rain load, liter/m²h,
v(z) windspeed at a height z, m/s,
i_h horizontal rain intensity, mm/h.

The rate of water ingress is determined by linearly interpolating the measurements results for the static test method presented in FIG. 3. In the test campaign the water spray rate is held constant and only the applied wind pressure is varied, in the simulations the water ingress rate is corrected for this relative to the actual occurring rain load.

4. Hygrothermal simulations

The transient temperature and moisture distributions in the wood frame wall assemblies are calculated using version 3.3 of the WUFI 2D software package. The modelled geometries are shown in figures 1 and 2. Weather data for the year 2006 measured at the observatory of the KNMI at Cabauw, the Netherlands (Cesar, 2006) was used for the external climatic conditions, the boundary heat transfer coefficient was set to 23 W/m²K. The wall assemblies are oriented to the southwest, as to achieve the highest WDR loading. Solar radiation as measured at the Cabauw observatory is used. The inside of the assembly is subjected to the normal moisture load as described in EN 15026: 2007, the boundary heat transfer coefficient was set to 8 W/m²K. The hygrothermal simulations are run for a period of 2 years, with 10 minute timesteps. Material properties found in the WUFI-database were used in the hygrothermal simulations, shown in table 1.

4.1 General trends

Water leaks in wood frame walls are especially hazardous if the structural members are prone to excessive water contents leading to woodrot. Typically woodrot is assumed to commence at moisture contents of 20 massprocent (M%). FigureFIG. 4 compares hygrothermal simulations of the local wood moisture content of the structural member in configurations A and B for cases with and without accounting for water ingress (location: see figure 1 and 2). The softwood structural member was initially at a moisture content of 15M%.
Typically, hygrothermal calculations only account for moisture loads due to vapour diffusion from the inner climate to the outside and for the absorption of rain water at the exterior surface. However, in the simulations it was found that occasional water ingress has an important effect on the water content of construction A: the general trend found in the simulation without water ingress is followed, yet during rain events significantly higher moisture loads are found in the structural member. Due to the occurrence of wind peaks rainwater is driven into the building components resulting in very localised moisture loads, which depending on the location and used building materials potentially can result in deterioration. In the more watertight construction B the occurrence of water ingress loads as generated by the static test method proves to be of lesser influence on the wood moisture content. The construction is mainly influenced by the vapour diffusion from interior to exterior.

As a comparison the 1% rain penetration guideline in ASHRAE 160 was applied to the structure. One difficulty faced with this was the exact location of the water penetration. ASHRAE 160 explicitly describes the deposit side of the water to be the exterior surface of the water-resistive barrier. If not present, the deposit side shall be described and a technical rationale given. The deposit side in construction A was chosen to be most indicative of the water leaks, figure FIG. 1 shows the deposit site, which is the same as in the experimental setup. In construction B where a clearly defined rainscreen is present due to the self adhering flashing and water resistant wood fibre board the guidelines in ASHRAE 160 were followed. FigureFIG. 4 shows that despite following ASHRAE 160 a nonrealistic moisture content is found in the wooden component. The moisture content of the structural member in construction A tends to follow a somewhat similar trend as compared to the static method, yet because it has no direct connection to the moisture penetration in the component provides an unreliable result.

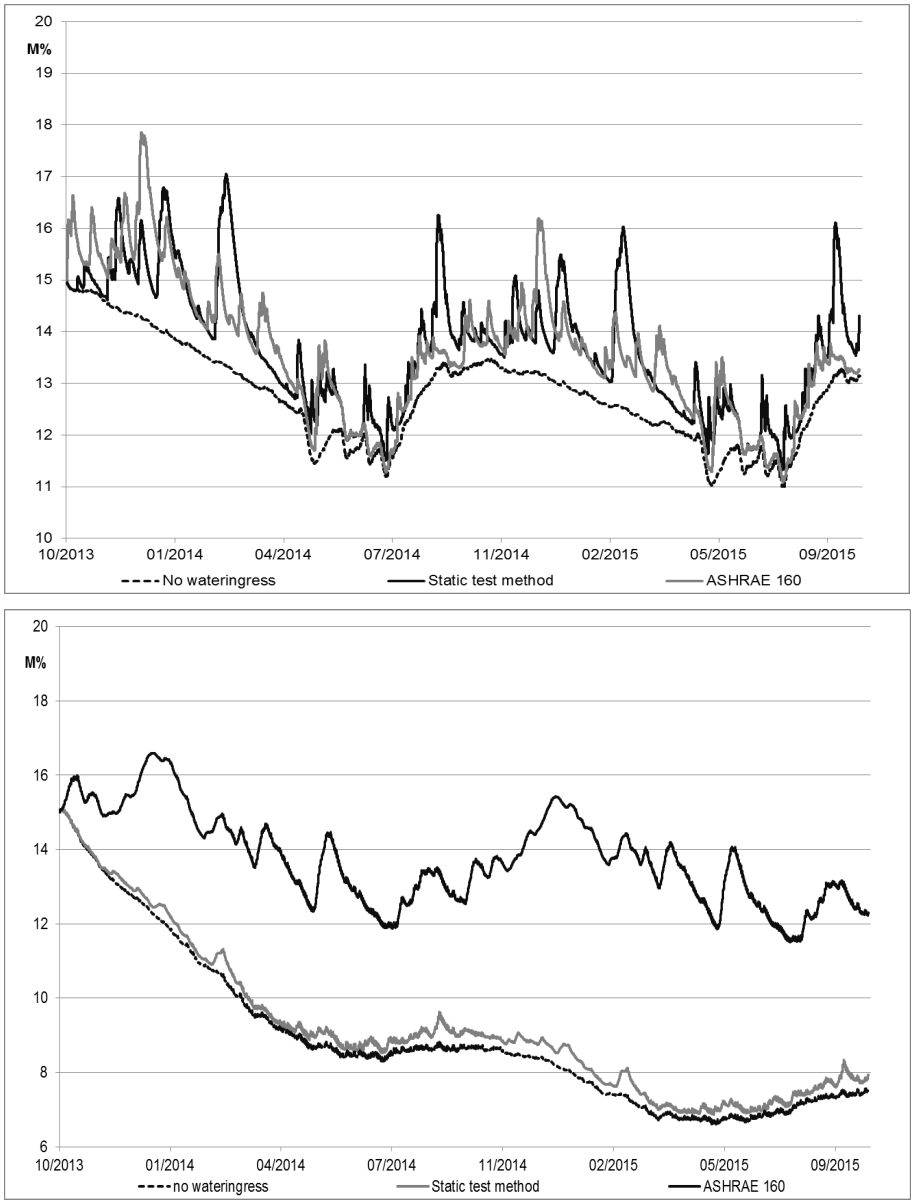

FIG. 4. Hygrothermal simulation results for construction A (above) and B (below)

A parametric study of the material properties influencing the local drying behaviour of the structure was performed for configuration A. Variations were made in the type of insulation material

surrounding the window (polyurethane or mineral wool), the diffusion resistance of the watertight barrier and the initial moisture content. This allows for a qualitative study of their relative importance on the wood moisture content in the case of water ingress. As changing the insulating material from polyurethane to mineral wool equals changing to a more vapour open material with lower thermal performance, the general drying out speed during winter is increased, proving this to be a safer construction type. Similarily, increasing the diffusion resistance of the woodfibre board from 12.5 to 30 slows down the drying of the construction in the case with no water ingress. Though still present, when taking into account water ingress this factor is found to be of lesser importance, as the moisture content of the wooden element is mainly dominated by renewed wetting instead of the vapour diffusion from the interior to exterior. Construction elements initially at a moisture content of 20M% will take significantly longer to dry out when taking into account water ingress, potentially leading to deterioration.

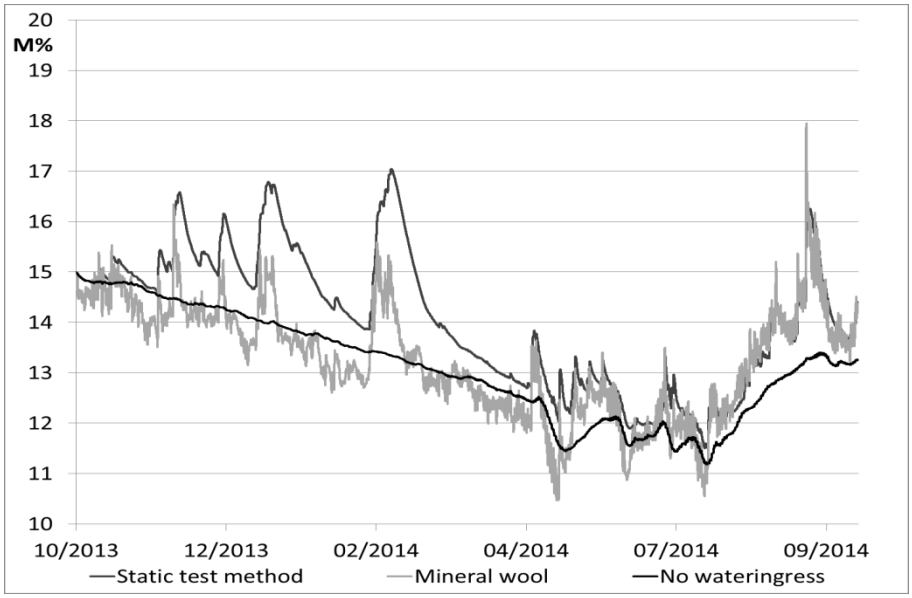

FIG. 5. Simulation result for construction A with polyurethane and mineral wool insulation.

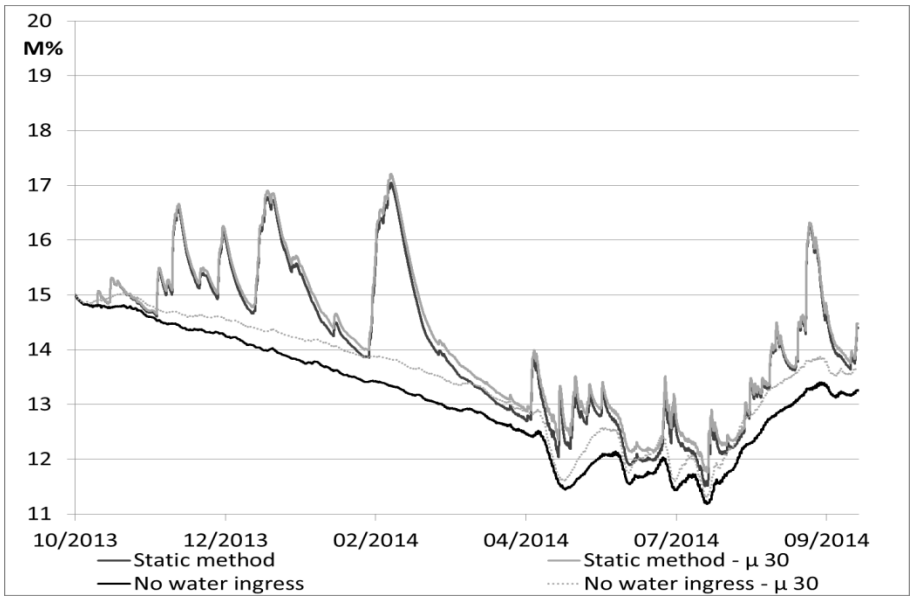

FIG. 6. Simulation result for construction A with $\mu_{wood\ fibre\ board}$ 12.5 and 30.

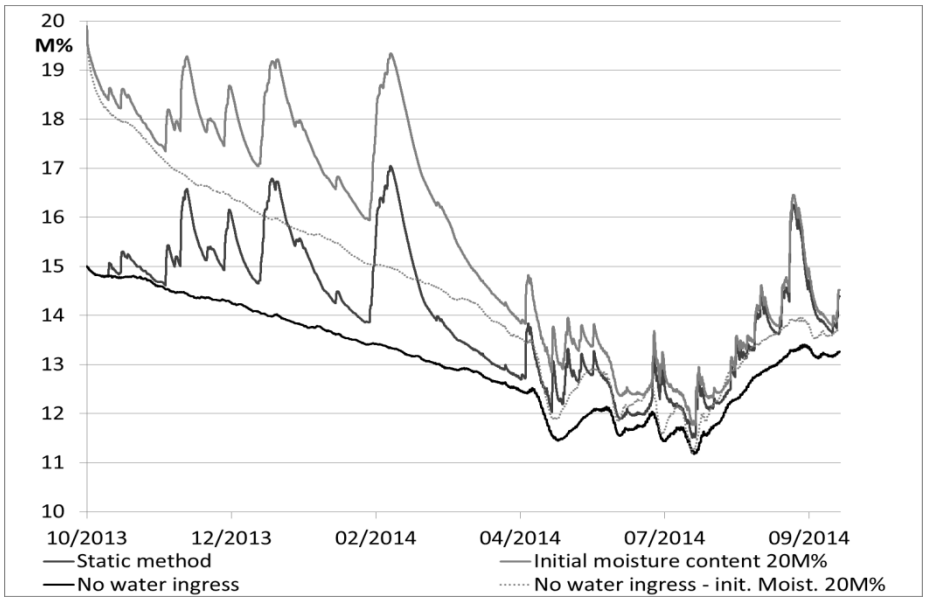

FIG. 7. Simulation result for construction A with initial moisture content at 15 and 20 M%

5. Conclusions

In this paper, a method to relate experimental data on water penetration rates to actual weather conditions is presented. Based on water ingress rates found using the static method EN 1207, a realistic source term is defined correlated to the occurring wind driven rain load for use in hygrothermal simulations. Comparison with ASHRAE 160 shows significant differences in the moisture content of the wooden elements, especially for more watertight components. This is mainly due to the conservative approach in ASHRAE 160 where a fixed penetration rate of 1 % of the impinging water is said to penetrate, with no connection to the actual watertightness of the system. In the parametric study it is found that the water leakage significantly influences the performance of the components.

6. Acknowledgements

Special thanks goes to Silke Maertens and Lynn Devos for the experiments used in this paper.

References

ASHRAE, 2009, ASHRAE 160: Criteria for moisture-control design analysis in buildings, Atlanta
DAVIS, F.K et al; 1968, The variation of gust factors with mean wind speed and with height, Journal of applied meteorology, vol 7.
CEN, 2000, EN 1027: Windows and doors. Watertightness. Test method, Brussel
CEN, 2001, EN 12865: Determination of the resistance of external wall systems to driving rain under pulsating air pressure, Brussel
CEN, 2007, EN 15026: Hygrothermal performance of building components and building elements. Assessment of moisture transfer by numerical simulation, Brussel
Cesar, 2006, meteorological surface data, KNMI, Cesar Observatory: Cabauw
VAN DEN BOSSCHE, N., 2013; Watertightness of Building components: principles, testing and design guidelines, PhD Thesis, Universiteit Gent: Gent
VERHEIJ, F.J. et al.; 1992, Gust modelling for wind loading, Journal of wind engineering and industrial aerodynamics, 41-44, p. 947-958
WTCB, 2010, Onderzoek naar mogelijke nieuwe bouwconcepten en het effect ervan op het gebruik van oppervlaktedelfstoffen. WTCB, VITO, K.U.Leuven: Vlaanderen. p.166-180.

Moisture assessment by fast and non-destructive in- situ measurements

Eva B. Møller, Ph.D. [1]
Ernst Jan de Place Hansen, Ph.D. [1]
Erik Brandt, M.Sc. [1]
Kurt Kielsgaard Hansen, Associate Professor, Ph.D. [2]

[1] Danish Building Research Institute/Aalborg University Copenhagen, Denmark
[2] Technical University of Denmark, Denmark

KEYWORDS: Moisture measurements, inorganic building materials, non-destructive, absolute moisture, vapour tight surface treatment.

SUMMARY:
A building inspection report is made in connection with the resale of 90% of all single-family houses in Denmark. The building inspection is visual with the option of using simple hand-held instruments but with no destructive measures allowed. However, many construction components have a high moisture content, which is not revealed by this inspection. The moisture content may become a problem for the buyers. This problem might have been avoided if the moisture content of the building materials was measured on inspection. This is easily done in wood-based materials but for example in concrete and brick the moisture content is difficult to determine within a short period time. There is political pressure to include moisture measurements in the report if it does not increase the cost of the inspection significantly.

Therefore, a moisture-measuring method is needed that is non-destructive, fast to use, easily applicable and suitable for most porous building materials. Furthermore, the measurements must be reliable at the high end of the hygroscopic area and describe absolute moisture content or corresponding relative humidity. The existing methods for moisture measuring cannot meet these requirements, and those who come close are very expensive. This paper describes a method under development; with simple means and within a few hours, the method can measure the absolute moisture content or the corresponding relative humidity in constructions in a non-destructive way. The method is based on measurements of the relative humidity of the air in a small hood placed tightly and sealed to the surface of the construction. Results with aerated concrete covered with acrylic paint are presented.

1. Introduction

In Denmark a building inspection report is made by a certified building inspector at more than 90% of all resales of single-family houses. The report points out building components that are in worse condition than is to be expected in a well-maintained house of the same age and style. The building inspection report has two purposes:

- To point out weaknesses of the house to potential byers (consumer guidance)
- Form the basis for an insurance that exempts the seller from his 10-year period of liability for hidden building damages and defects. The buyer will have insurance against hidden building damages and defects. The cost of the insurance is split evenly between seller and buyer.

The insurance companies may exclude building components mentioned in the inspection report.

It is only possible to take out this insurance if there is a building inspection report made by a certified building inspector and reported to a central secretariat. The arrangement is administered by the Danish Ministry of Housing, Urban and Rural Affairs.

The building inspection is visual with the option of using simple hand-held instruments but no destructive measures are allowed. The inspection includes all kinds of damages and defects; however, the experience is that one of the major problems is that some construction components have a high moisture content, which is not revealed by this inspection. The moisture may become a problem for the buyers. The problem could have been avoided if the moisture content of the building materials was measured on inspection. This is easily done in wood-based materials but e.g. in concrete and brick the moisture content is difficult to determine within a short period of time. There is political pressure to include moisture measurements in the report if it does not increase the cost of the inspection significantly.

Measuring relative humidity in indoor air would only provide information on the hygrothermal conditions in that specific moment. By extra airing and heating of the house before the inspection takes place, the result can easily be manipulated to give the impression of less humidity than would have been the case under normal conditions. However, materials act relatively slowly within a short period of airing and heating, and they therefore represent the memory of the house; if materials in general are moist, it would take a long time to reduce the moisture content simply by airing and heating. Depending on the reasons for moist materials, it is not possible in this way to reduce the moisture content in materials significantly.

Therefore, a moisture-measuring method is needed that should be non-destructive, fast to use, easily applicable and suitable for most porous building materials. Furthermore, the measurements must be reliable at the high end of the hygroscopic area and describe absolute moisture content or the corresponding relative humidity (RH). The existing methods for moisture measuring cannot meet this requirement, and those that come close are very expensive.

This paper describes a method under development that meets the above criteria. The method is based on measurements of the relative humidity of the air under a small hood placed tightly and sealed to the surface of the construction. The first experiments were conducted and described in Andersen & El-Khattam (2012). The experiments described in this article concentrated on how the method could be used in inorganic porous building materials covered by acrylic paint, a common surface treatment with a relatively high vapour resistance.

2. Methods for measuring moisture in materials and air

2.1 Existing methods

There are several instruments available for moisture measurements; some are destructive some are not, some measure relative humidity, some measure the moisture content in materials. The accuracy of the measurements varies considerably and so does the use of different methods and instruments. The methods described in the following are all used in practice, mainly for non-destructive in-situ measurements. Other methods are available but these are either expensive and therefore not commonly used or mostly used in laboratories.

2.1.1 Accurate measurements

The most accurate way to determine moisture content in materials is, in brief, to collect a sample of the material, weigh it, dry it at 103-105 ºC until the weight is stable and determine the weight of the dry material. The water content can then be determined as the difference of the weight before and after the drying divided by the dry weight.

This method is accurate but destructive, takes time and is not suitable for in-situ measurements.

2.1.2 Absolute measurements in materials

An effective way to determine the absolute moisture content of timber is by measuring the electrical resistance between two pins pressed into the timber. This method is almost non-destructive; it only leaves two pinholes which may disappear after some time. Most timber is made of pine or spruce and therefore many instruments with two pins directly convert the resistance to moisture content in weigh-% for pine or spruce, but ideally the instrument or the scale must be calibrated to the actual wood species.

The moisture content in other materials could theoretically be measured in the same way if properly calibrated. However, in most other materials, e.g. gypsum, it is difficult to ensure that there is no slip between the material and each pin; slips influence the measurement.

Most other moisture measurements are relative; the absolute moisture content can only be determined if an absolute scale is established by a destructive measuring of the absolute moisture content in a few points and by correlating this to the scale.

2.1.3 Relative measurements in materials

There is a variety of methods for determining how the moisture content in a material varies relatively. This is practical when the moistest areas are to be identified. However, it does not determine the absolute moisture level. The methods are used on porous materials, where different properties depend on the moisture content. The techniques used in practice include measuring impedance, capacitance, dielectricity, hydrogen content and temperature (Phillipson et al. 2007).

Most of these methods are non-destructive and measures conditions on or near the surface.

2.1.4 Relative humidity

Moisture in air can be measured in different ways ranging from traditional mechanical hygrometers where humidity determines the expansion and contraction of a specific material, over methods using the dew point temperature (chilled mirror hygrometer) or wet and dry temperature (wet and dry bulb psychrometer) to different optical methods and methods of measuring dielectric changes in a thin hygroscopic film. More thorough descriptions are for example given in Yeo et al. (2008).

2.2 Relative humidity or moisture content in materials

Sorption curves connect moisture content in materials with relative humidity, however, there are many sorption curves within the same material type. Hansen (1986) compiled sorption curves for the most common building materials and the collection contains five sorption curves for aerated concrete alone, illustrating that it is not enough to know the material type, as the sorption curve for the specific material must be known to determine the absolute moisture content from the relative humidity and vice versa.

The main concern about moisture is the risk of deterioration of materials and mould growth. For wood-based materials the moisture limits are normally given as weigh-% of wood (e.g. 20 weigh-% for deterioration and 16 weigh-% for mould growth) as well as humidity (85% RH and 75% RH respectively), but for other materials the limits are less clear. Deterioration is mainly a concern in wood-based materials and metals. This paper does not deal with corrosion and metals are therefore not treated. Mould growth can appear at a lower moisture level than deterioration, and on all surfaces, so therefore limits for mould growth should be used to determine whether the moisture levels in a building element are too high.

Mould grow on surfaces and limits for mould growth depend on the material and the degree of contamination, as mould live on organic material including what might be available in dust and dirt. The simplest way to describe the risk of mould growth is to describe the relative humidity on the

surface of a building element without discriminating between different materials. The method might be too simple with a risk of overestimating the risk of mould growth on inorganic, relatively clean surfaces or underestimating the risk on diffusion-open organic surfaces e.g. wallpaper with sawdust. However, it may be sufficient for fast determination of whether the moisture level is elevated or not.

2.3 New near-surface measurement

Sometimes practitioners make a simple assessment of moisture transport through a building component by covering e.g. 0.5-1.0 m^2 of a surface with plastic foil for a few days; if there is condensation in the area coved by plastic, moisture is transported to the surface. A more standardised method is described in ASTM (2013), where moisture content in concrete floors is determined by placing a hood on the clean floor, sealing it to the surface and after 72 hours the relative humidity under the hood describes how moist the concrete is. Most flooring and surface treatments cannot be applied if the concrete is too moist and most manufacturers describe this upper limit for moisture in floors by the relative humidity.

This project was inspired by these simple methods; the hypothesis was:

It is possible to measure the near-surface moisture in the material by placing and sealing a hood tightly to the surface. After 1-2 hours the relative humidity under the hood is similar to the relative humidity in the surface-near pores in the material.

If this hypothesis is true, the method could be used as a non-destructive way to determine the moisture content in the materials in existing houses. The result would be given as the relative humidity close to the surface, which would be sufficient, as the reasons for making these measurements is to determine whether the moisture content is acceptable in terms of risk of mould growth.

3. Previous findings

Initial experiments were conducted by Andersen and El-Khattam (2012); their research was mostly conducted on aerated concrete. They developed a “moisture hood” to be placed on the surface of the material of which the moisture content was to be measured. A sensor, measuring temperature and relative humidity was placed inside the box. In brief, their findings were:

- *Design of the hood.* Experiments were initially conducted with an aluminium hood (80 mm diameter, 50 mm high), later smaller hoods were used; the smallest and simplest was fastening the temperature and humidity sensor to the surface with aluminium tape. The different hoods were tested with and without thermal insulation. The conclusion was that the results of the measurements were not affected by the volume of the hood. Furthermore, thermal insulation had no effect.
- *Sealing to the surface.* To avoid the influence of the relative humidity in the surrounding air, the hood itself must be vapour tight. The sealing between edge of the hood and the surface of the material must also be tight and at the same time removable to ensure that the method is non-destructive. The aluminium tape was not easy to remove, however, reusable adhesive gum, which is normally used for pasting e.g. drawings on painted walls, was found to be easy to place and remove, the gum itself had a vapour resistance (Z-value) of 233 $\cdot 10^9$ $Pa \cdot m^2 \cdot s/kg$ at a thickness of 3.5 mm. This was considered to be sufficiently vapour tight.
- *Tightness of the surface, depth of measurement and time to equilibrium.* The hood was tested on aerated concrete with different surface treatments. The Z-value of the treatments varied from $0.09 \cdot 10^9$ and 1.58 $\cdot 10^9$ $Pa \cdot m^2 \cdot s/kg$ (two layers of silicate and acrylic paint, respectively). The specimens were conditioned at 85% RH and sealed at all sides except the painted side. The specimens were left to dry and had dried from one side for 9-14 days at 65% RH. Sensors were placed in drilled holes in different depths to determine a moisture profile. Apparently the surface treatment had an influence on the drying of the specimens and on the relative humidity under the hood. The relative humidity under the hood placed on silicate paint (low vapour

resistance) became constant after approximately 10 hours; the relative humidity corresponded to the relative humidity at a depth of 15 mm. When placed on acrylic paint, the relative humidity under the hood was also constant after 10 hours but at a lower level than 15 mm inside the material, probably corresponding to the moisture level on the surface.

4. Materials and methods

Based on the findings of Andersen and El-Khattam (2012) it was decided to investigate whether the "moisture hood" could be modified making it possible to determine the relative humidity of an inorganic building material immediately behind a layer of acrylic paint. As neither the thermal insulation nor the volume of the hood seemed to have any influence, the experiments were conducted without thermal insulation and with a hood size that fitted the size of a wireless sensor.

4.1 Building materials and equipment

Emphasis was put on using materials and surface treatments that are commonly used in the Danish building stock and equipment that is commercially available and suitable for measurements in the field.

4.1.1 Building materials and surface treatments

Typical inorganic building materials were used as materials, the moisture content of which was to be determined. The specific materials are listed in Table 1.

Table 1. Building materials used in most experiments. Values are average values determined by simple weighing and distance measurements.

	Concrete	Aerated concrete	Brick
Density	2200 kg/m^3	535 kg/m^3	1830 kg/m^3
Size	400 x 400 x 50 mm	600 x 400 x 50 mm	230 x 110 x 55 mm

One side of all specimens was given a surface treatment of one layer of putty (less than 0.5 mm thick) and one layer of liquid primer with a viscosity like water as well as two layers of acrylic paint. It was the same type of paint as used by Andersen and El-Khattam (2012), e.g. the Z-value of the surface treatment was 1.58 $\cdot 10^9$ Pa$\cdot$m$^2\cdot$s/kg.

4.1.2 Materials for moisture measuring device

The hood consisted of an aluminium hood (diameter 85 mm, height 15 mm), sealed to the surface with reusable adhesive gum (Z-value = 233 $\cdot 10^9$ Pa$\cdot$m$^2\cdot$s/kg at a thickness of 3.5 mm). A wireless sensor (ClimaSpot) was placed under the hood. All sensors were new and therefore calibrated.

4.2 Methods

Modification of the method involved one small destructive measure; the surface was penetrated by a nail (3 mm in diameter). The idea was that air and thereby moisture from the pores in the aerated concrete behind the acrylic paint would be transported into the hood much faster than if it could be transported only through the relatively tight acrylic paint. As the number of holes could be important, the theory was tested with different numbers of penetrations of the surface treatment under the hood. Furthermore, the effect of a small negative pressure under the hood was investigated. Consequently, the following parameters were investigated:

- Number of penetrations: 1, 2 and 3
- Pressure difference under the hood: 0 and -0.5 atm
- Three different building materials
- Conditioning of the building material prior to testing: 90% ± 5% RH and 65% ± 3% RH

Each experiment was repeated twice reaching a total of 108 experiments.

The procedure was always the same:

- After applying the surface treatment, the specimens were conditioned in a climate chamber with the prescribed relative humidity at 22 ± 2 °C until the weight was constant.
- Each specimen was wrapped in 0.2 mm PE-foil. Only the painted side was left unsealed
- The penetrations were made by a nail
- The specimen was placed in a climate chamber at 50% ± 3% RH and 22°C ± 2 °C.
- The hood including sensor and possibly suction device was sealed to the treated surface.
- Temperature and relative humidity under the hood were registered every 4 minutes for more than 50 hours.

The set-up is shown in Figure 1.

Figure 1. Experimental set-up showing moisture hoods sealed at the edge to the surface of bricks wrapped in PE-foil. Two experiments are conducted at the same time; one with under pressure (with suction device) and one without pressure difference.

5. Results and discussion

The project included many experiments and only selected data representative of the experiments are shown in this paper. Figure 2 shows the results for aerated concrete for the first 12 hours of the experiments. After this time, changes were very small. Concrete and brick show similar results.

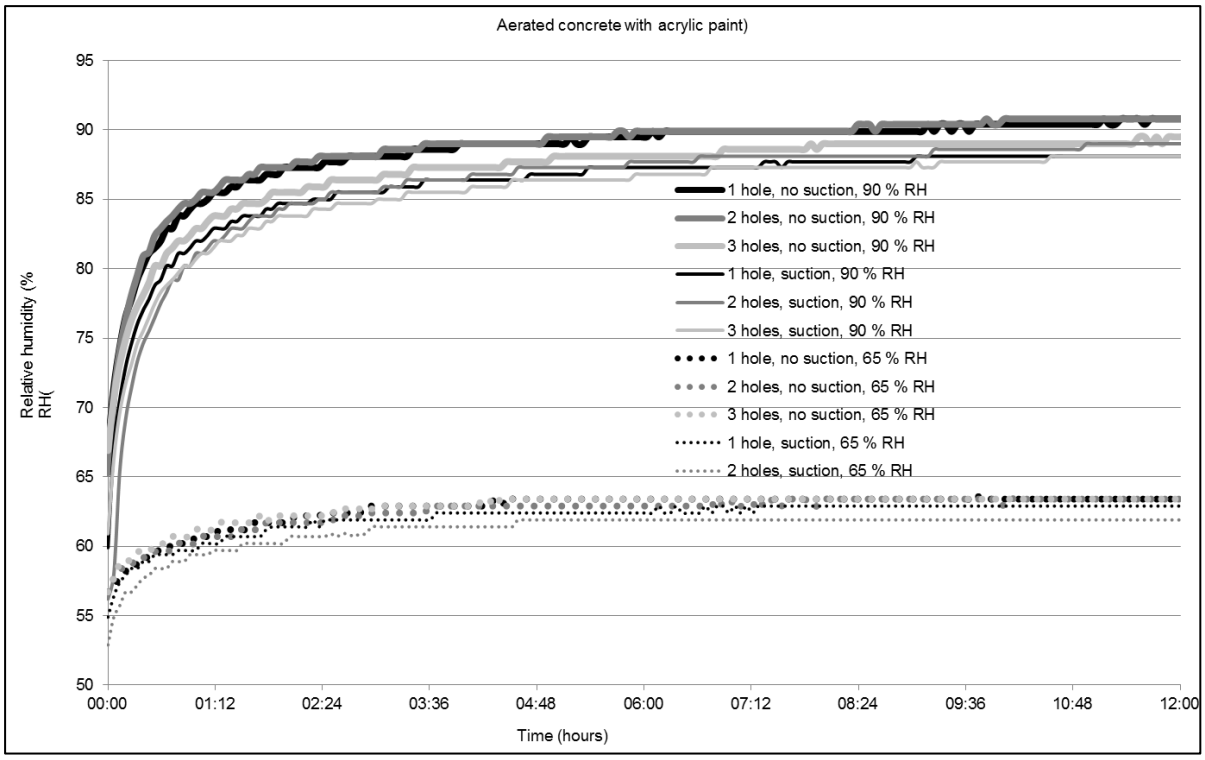

Figure 2. Results for aerated concrete, time (hours vs. RH). Measurements with 3 holes and suction at 65 % RH are missing. Concrete and brick show similar results.

The relative humidity under the hood in some of the experiments with suction (not shown here) stayed at a level similar to the relative humidity in the room. Apparently the leakage was too significant to measure the moisture from the building material. In one case, the relative humidity started at a low level but after approximately one day it went up to the expected level. Maybe the suction had tightened the sealing after some time.

Experiments without suction did not show these unexpected results but were more stable. Consequently, suction did not seem to improve the method. On contrary; measurements without suction reacted faster and were more close to the expected value than when suction was used. Moreover, establishing controlled suction might be difficult in the field. Therefore, suction should be omitted.

5.1 Penetrations

Apparently the number of penetrations did not affect the readings; there was no difference whether there was one or three holes. The number of penetrations should therefore be kept to a minimum, as this modification of the method was destructive, although the holes were very small.

5.2 Time to equilibrium

There is a clear difference in the readings in Figure 2 between the specimens conditioned at 90% ± 5% RH and at 65% ± 3% RH. The difference showed almost instantly. Therefore, the method would be fast for relative measurements. However, the aim is to find the absolute moisture content or the corresponding relative humidity. Apparently the measurements became stable after approximately 5 hours. For the purpose of this method, this was too long.

However, after 1 hour 30 minutes the measurements showed a clear tendency of what to expect; in Figure 2, the specimens conditioned at 90% RH and 65% RH had reached 90% and 80%, respectively, of the total rise in relative humidity. If the method should be used as planned, it must be evaluated

whether it is possible to create a tendency line and from this estimate the final rise. This should be evaluated together with results from measurements on surfaces covered by silicate paint or with no paint, to see whether it is possible to use the method independently of the surface treatment.

5.3 Surface or in-depth measurements

For silicate paint it was possible to measure the relative humidity 15 mm inside aerated concrete after leaving the hood on the surface for 10 hours. With a single penetration of an acrylic paint, the relative humidity immediately behind the paint, could be directly determined after 5 hours. The main concern of the buyer of a house is whether there is a risk of mould growth or not; as mould growth occurs at the surface it might be sufficient to determine the moisture level immediately behind the paint or at the surface itself.

As surface measurements are very uncertain, measurements immediately behind the paint may be more reliable; if the moisture level is high, it is a reasonable assumption that the risk of mould growth is high. It is therefore sufficient to determine the relative humidity immediately behind the paint.

6. Conclusion

The experiments showed that it is possible to measure the near-surface moisture in the material by placing a tightly sealed hood on the surface and measure the relative humidity in the box. However, if the material had a surface treatment of acrylic paint, it took approximately 5 hours until equilibrium was reached if the surface had a small penetration under the hood. For the purpose of doing non-destructive in-situ measurements within 1-2 hours, the results must be extrapolated by creating a tendency line based on early measurements as this will increase the uncertainty of the final result.

There is no need for establishing suction under the hood; the risk of sucking air from the room instead of air from the pores in the material is too high, as the sealing between hood and surface becomes very critical. At the same time, only one small penetration of the paint is needed, as more penetrations will neither enhance the precision of the measurement nor shorten the time to equilibrium.

7. Acknowledgements

The authors wish to thank M. Them Andersen an A. El-Khattam for their thorough work as master students to develop a suitable hood for the measurements.

References

ASTM. 2013 Standard Test Method for Determining Relative Humidity on the Surface of Concrete Floor Slabs Using Humidity Probe and Insulated Hood Measurements. F2420 – (draft 2013) WK40341

Andersen M.T & El-Khattam A. 2012. Ikke-destruktiv måling af fugt i uorganiske byggematerialer Hovedrapport. (Authors translation: Non-destructive moisture measurements in inorganic construction materials. Main rapport). Department of Civil Engineering, Danish Technical University, Denmark

Hansen K. K. 1986. Sorption isotherms A catalogue. Technical Report 162. The Technical University of Denmark, Department of Civil Engineering, Building Materials Laboratory. Lyngby, Denmark.

Phillipson M.C., Baker P.H., Davies M., Ye Z., McNaughtan A., Galbraith G.H. & McLean R.C. 2007. Moisture measurement in building materials: an overview of current methods and new approaches. Building Services Engineering Research and Technology, 28:303-316

Yeo T.L., Sun T. & Grattan K.T.V. 2008. Fibre-optic sensor technologies for humidity and moisture measurement. Sensors and Actuators A 144: 280-295

Smart vapour barriers in passive house wall – a way to make the structure more moisture robust?

Arvid Dalehaug, Assosiate Professor
[1] Magne Agnalt, M.Sc. [1]
Stig Geving, Professor [1]

[1] Norwegian University of Science and Technology, Norway

KEYWORDS: *smart vapour barriers, drying capability, built in moisture*

SUMMARY

Highly insulated envelope constructions, such as passive house walls, are claimed to be less moisture robust than more traditionally insulated constructions. This is due to several reasons, one of them is that built-in moisture or moisture from accidental leakages may use more time to dry for these structure compared to the traditional ones. In Norway this has led to stricter recommendations in regard to moisture safety during construction of passive houses.

It could be advantageous if we were able to improve the moisture robustness of passive house walls. One way to improve the moisture robustness could be by using so-called smart vapour barriers. Smart vapour barriers are products with adaptable vapour resistance, giving the possibility for moisture to dry to the indoor air during summer – while maintaining a high vapour resistance during winter to reduce the risk for condensation.

In this study, the use of smart vapour barriers in highly insulated wood frame walls were investigated by the use of a hygrothermal simulation tool, both in regard to possibly improved drying of built-in moisture and possible problems by using such products. Simulations were performed for Scandinavian climates and typical wood frame walls and for various types of commercial available smart vapour barriers. Recommendations for when and under what conditions smart vapour barriers are useful for highly insulated wood frame walls are given.

1. Introduction

Highly insulated envelope constructions, such as passive house walls, are claimed to be less moisture robust than more traditionally insulated constructions. This is due to several reasons; one of them is that it may take more time to dry out built-in moisture or moisture from accidental leakages from these structures compared to the traditional ones.

In Norway this has led to stricter recommendations in regard to moisture safety during construction of passive houses. Such recommendations could be to protect the constructions and house from rain, another could be to dry the wooden materials down to lower levels of moisture content before allowing the closure of the wall cavity.

Even if these recommendations may be considered reasonable in any way, it could be advantageous if we were able to improve the moisture robustness of passive house walls, and possibly use less strict requirements on some projects. One way to improve the moisture robustness could be by using so-called smart vapour barriers. Smart vapour barriers are products with adaptable vapour resistance, giving the possibility for moisture to dry to the indoor air during summer – while maintaining a high vapour resistance during winter to reduce the risk for condensation.

2. Methods

To find out about the performance of the available smart vapour barriers in well insulated wood frame constructions we have done computer simulations of a variety of material combinations. Wufi 2D and 3D from Frauenhofer Institut für Bauphysik were selected for the simulation

2.1 The purpose of the simulations

The moisture simulations were carried out to document the effect of using Smart Vapour Barriers (SVB) in wood frame walls and to find out about how other parameters also influence the results. Several calculations have been done before with SVB (Tariku et al., 2009) and vapour retarders (Geving et al., 2010) in wood frame walls. The specific goal for these simulations were to investigate the usefulness, possibilities and limitations for SVB in very well insulated wood frame walls under Norwegian climate conditions.

2.2 Description of the simulated construction for 1D calculations

Two thicknesses of insulation were used in the simulation programme. The wall was built up as displayed in figure 1.

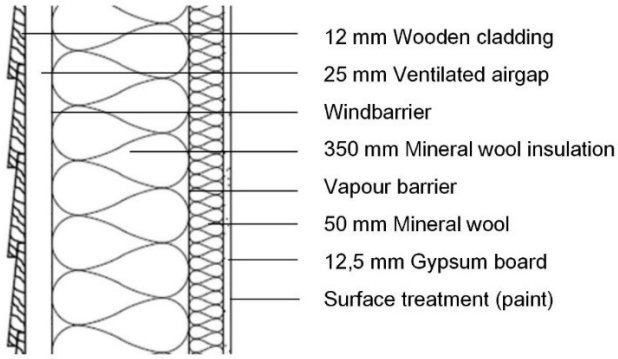

FIG 1. The standard simulated wall

For the simulation we selected two commercial available Smart Vapour Barriers (SVB) to be compared to a vapour barrier (PE foil).

2.3 Material properties of PE-foil and smart vapour barriers

The diffusion resistance depending on relative humidity is shown in figure 1.

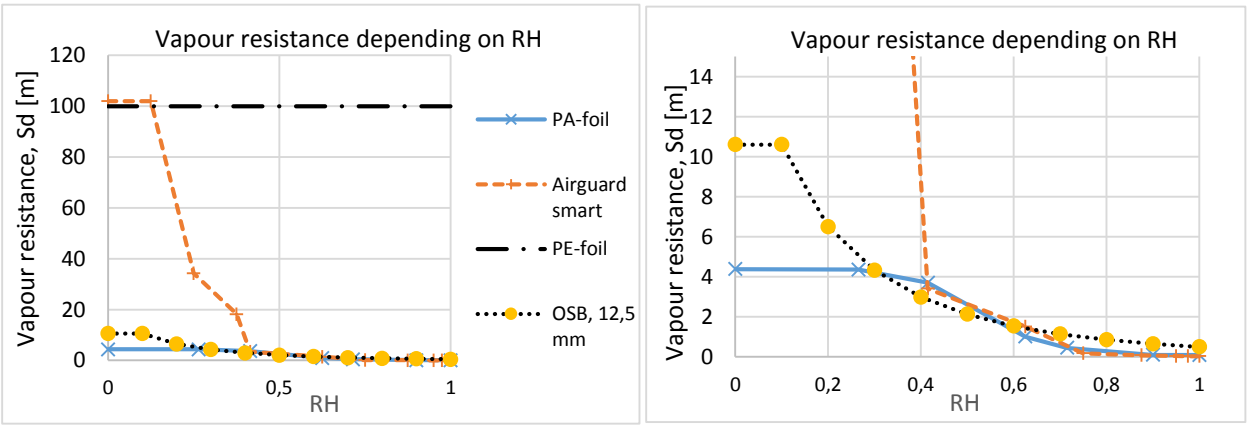

FIG 2. Diffusion resistance depending on relative humidity, Graph to the right is the enlarged lower part of the diagram.

Stellander (2011) made a list of available SVBs on the market and we selected two of them. Novaflexx is made from polyamide and is produced by the German company Dörken. It has not been possible to find test results from how the S_d-value varies with RH, but according to Stellander (2012) the importer confirmed that Novaflexx' properties were according to the PA-foil listed in the material database defined by Frauenhofer Institut für Bauphysik in WUFI. The given range of variation of S_d-value is between 0,08 – 4,38 m. Novaflexx is more vapour open and does not have a variation range for the S_d-value as vide as the other product used in the simulations.

AirGuard Smart is produced by Dupont Tyvek and has a S_d-value that vary from 0,02 – 102,5 m (DuPont, 2013). The great variation in water vapour diffusion resistance should provide good drying performance at high water contents in the surrounding materials, and should at the same time be tight enough when the construction is dry. AirGuard Smart was not define in the Wufi database and data was entered manually. The properties of PA-foil was used as a starting point, that had to be changed according to the product declaration for AirGuard Smart and extra S_d-data produced by DuPont. In practise, the high S_d value for the driest conditions is not of interest because the moisture level at the vapour barrier even in very cold climate seldom go below 20-25% RH.

2.4 Parameter variation in the construction and climate for the simulations

For the other materials data from the Wufi database were used with some modifications.

TABLE 1. Variation of parameters for the simulation

Type of vapour barrier	The data for the materials except from SVB are given in table 1. One simulation was performed with an OSB board as vapour barrier.
Thickness of insulation	Two thicknesses are tried. 400 mm for passive house standard and 250 mm for comparison.
Wind barrier	Standard wind barrier is rather vapour open. For comparison an OSB board is also tested.
Orientation of the facade	Standard orientation is north. For comparison south is also tested.
The position of the SVB in the wall	Standard position is 50 mm into the insulation of wall from the inside. For comparison calculations are also done for 0 and 100 mm from the inside.
Internal moisture supply for the indoor climate.	Medium moisture supply is chosen from figure 3. Because of the dependency of outdoor humidity and temperature the indoor climate will be varying from place to place. See point 2.4.1.
Internal surface material and treatment.	Standard inside is painted (2 layers of acryl based paint) gypsum board with a total Sd-value of 0,15 m.

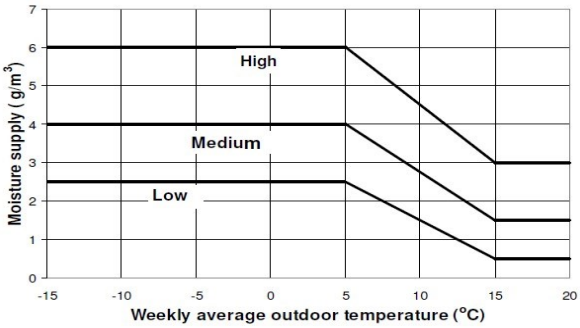

FIG 3. Suggestion of design values for «low», «medium» and «high» moisture supply in buildings (Geving et al., 2008)

2.4.1 Outdoor moisture load, external climate.

Outdoor climate is one of the factors that has the greatest influence on moisture conditions in walls to the external (Geving and Thue, 2002). To see what happens in a rough year and to check for possible moisture problems "Moisture Design Reference Year" (MDRY) has been made and is available for 12 different places in Norway. By using series of MDRY for the simulation the moisture load will be more severe than in a normal year (Thue et al., 2007).

The Oslo climate is chosen as standard climate for the simulations. Calculations have also been done for Bergen, Trondheim, Røros and Tromsø. To compare with climate in other parts of Europe calculations are also done with climate from Gothenburg in Sweden and Holzkirchen in Germany.

2.4.2 External cladding.

All simulations were done with a ventilated wooden cladding. In the simulation the air exchange rate of the cavity was 20 h^{-1}. In practise, the cladding is a rain screen and it also protects the wind barrier from direct radiation from the sun. The temperature on the wind barrier does not become as high as it would have been without a cladding during daytime. It also reduces the effect from clear sky radiation during nights. The wetting of the cladding during rain is obvious and not of interest for the testing of well insulated framework. Therefore the calculated water content in the cladding is subtracted from the total water content of the wall to find the resulting water content in the rest of the wall structure.

2.4.3 Initial moisture content in the construction for the simulation.

To simulate initial moisture content of a serious magnitude in mineral wool it is necessary to check the moisture storage function of mineral wool in the Wufi-library. We chose to distribute the extra moisture in all mineral wool between wind- and vapour barrier. By using the material properties of ISOVER GW Integra ZSF – 032 the moisture storage function is ok.

2.5 Parameter variation in the construction and climate for all the simulations

2.5.1 Starting conditions, initial moisture content

The moisture content at the start of the simulation was set to 80% RH for the whole construction except from the insulation between wind and vapour barrier that must contain the extra water from built in moisture. 80 % is the normal moisture content in materials that has been stored in outdoor climate protected from rain (Geving og Thue, 2002). The start temperature in the construction has little influence on the results, because the temperature will adapt to the surroundings after a short time. In the calculations the start temperature is set to 20°C.

TABLE 2. Material and climate combinations for the simulation

		Simulated combinations of wood frame wall																
Parameters	**Variables**	1	2	3	4	5	6	7	8	9	10	11	12	13	14	15	16	17
Vapour barrier	**Novaflexx**	**x**	**x**	**x**	**x**	**x**	**x**	**x**	**x**	**x**	**x**	**x**	**x**	**x**	**x**	**x**	**x**	
	AirGuard Smart	**x**	**x**	**x**	**x**	**x**	**x**	**x**	**x**	**x**	**x**	**x**	**x**	**x**	**x**	**x**	**x**	
	PE-foil	**x**	**x**	**x**	**x**	**x**	**x**	**x**	**x**	**x**	**x**	**x**	**x**	**x**	**x**	**x**	**x**	
Insulation thickness	**400 mm**	**x**		**x**	**x**	**x**	**x**	**x**	**x**	**x**	**x**	**x**	**x**	**x**	**x**	**x**	**x**	**x**
	250 mm		x															
Wind barrier	**Roll product S_d=0,1m**	**x**	**x**		**x**	**x**	**x**	**x**	**x**	**x**	**x**	**x**	**x**	**x**	**x**	**x**	**x**	**x**
	OSB-board,S_d=2-13m			x														
Facade orientation	**North**	**x**	**x**	**x**		**x**	**x**	**x**	**x**	**x**	**x**	**x**	**x**	**x**	**x**	**x**	**x**	**x**
	South				x													
Location of SVB (from the inside)	0 mm					x												
	50 mm	**x**	**x**	**x**	**x**			**x**	**x**	**x**	**x**	**x**	**x**	**x**	**x**	**x**	**x**	**x**
	100 mm						x											

		Simulated combinations of wood frame wall																
Indoor moisture supply	2,5 – 0,5 g/m^3							x										
	4,0 – 1,5 g/m^3	**x**	**x**	**x**	**x**	**x**	**x**			**x**	**x**	**x**	**x**	**x**	**x**	**x**	**x**	**x**
	6,0 – 3,0 g/m^3								x									
Built in moisture	**8,57 kg/m^3**	**x**	**x**	**x**	**x**	**x**	**x**	**x**	**x**		**x**	**x**	**x**	**x**	**x**	**x**	**x**	**x**
	80 % RH in the whole layer									x								
Inside surface treatment	**S_{dTOT} = 0,15 m**	**x**	**x**	**x**	**x**	**x**	**x**	**x**	**x**	**x**		**x**	**x**	**x**	**x**	**x**	**x**	**x**
	S_{dTOT}= 0,5 m										x							
Outdoor climate	**Oslo**	**x**	**x**	**x**	**x**	**x**	**x**	**x**	**x**	**x**	**x**							**x**
	Bergen											x						
	Trondheim												x					
	Røros													x				
	Tromsø														x			
	Gøteborg															x		
	Holzkirchen																x	
OSB-board as SVB																		**x**

The part of the insulation with the extra water content is given a moisture content of 8,57 kg/m^3. That represents a 3 mm water film evenly distributed in the insulation layer of 350 mm.

2.5.2 Calculation period

The calculation period is one year from midsummer to midsummer to see the effect of using SVPs.

3. Results

In this paper only some few of the results can be presented. For more information see: (Agnalt 2013). In all the graphs the curves have been smoothed by presenting only day values. Hourly plots become very difficult to read.

3.1.1 Standard wall and Oslo climate

The total moisture content is displayed in figure 4. The flows through wind- and vapour-barrier are shown in figure 5.

In table 3 the sum of the moisture flows is calculated. The flows outwards through the wind barrier are equal as long there is enough moisture in the construction. The flow inwards is about half of the flow outwards in the wet period with SVBs. Later on, the flow through the vapour barriers turns and becomes more normal with almost continuous flows through the walls.

TABLE 3. Distribution of moisture flow in kg/m2 from the wall during one year

Vapour barrier Wind barrier	AirGuard Roll product		NovaFlexx Roll product		PE-foil Roll product	
	Through inside	Through outside	Through inside	Through outside	Through inside	Through outside
First 3 months	1.088	1.870	1.002	1.955	0.083	2.791
Last 9 months	-0.520	0.485	-0.330	0.637	-0.034	0.088
Sum out of wall	0.568	2.355	0.672	2.592	0.049	2.879
Sum of both sides out of wall	2.923		3.264		2.928	

Negative numbers in table 3 are transport into the wall construction, positive out of the wall

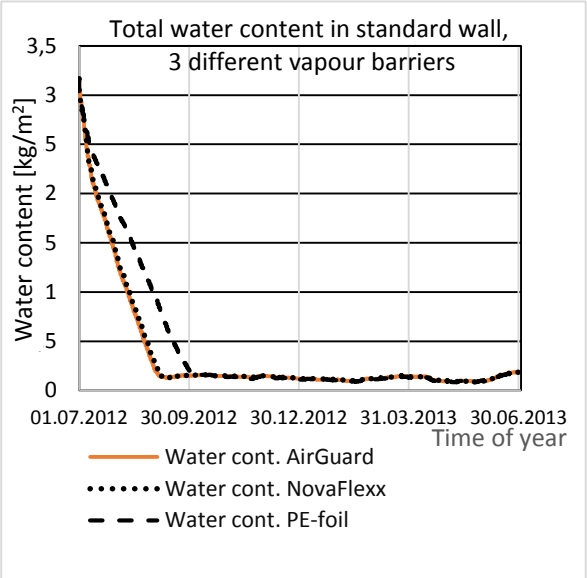

FIG 4. Total water content in external standard wall (400 mm insulation) dependent of type of vapour barrier

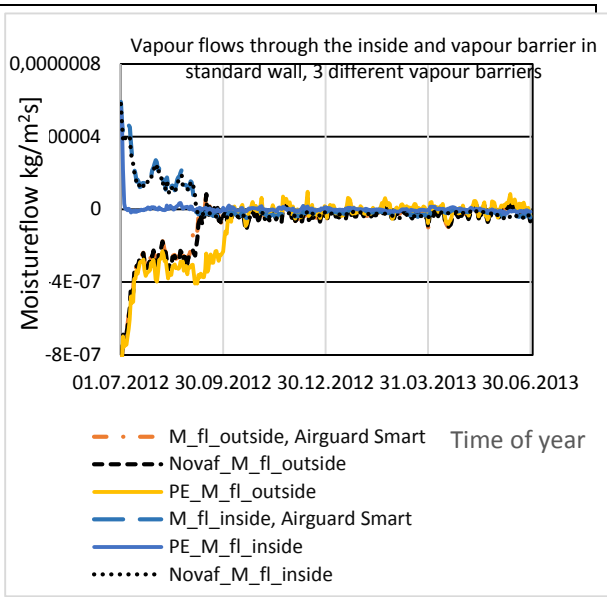

FIG 5. Vapour flows through inside and vapour barrier in standard wall, 3 different vapour barriers (negative numbers are transport form inside to outside)

To fig 6: The RH right inside the wind barrier is varying from about 80% up to 90% for the first 10,5 months. The wall with PE-foil are wetter than the two others in September because the water in the wall did not escape as fast (see figure 4). It took about 2 weeks more to get the water out with PE-foil. After about 4 months, the moisture level becomes more equal. The risk of developing mould growth in the outer part of the wall is therefore higher with PE-foil than with SVBs due to higher RH in the warmer period. In the wall with PE-foil it is about 4% dryer during winter.

To fig 7: The RH behind the vapour barrier goes down from near 100% to less than 80% within two months with smart vapour barriers. It takes 3 weeks more with PE-foil. After about 3 months, the moisture level becomes equal. The risk of developing mould growth in the inner part of the wall is therefore higher with PE-foil than with SVBs.

3.1.2 Standard wall, Oslo climate, OSB as wind barrier

To see the influence from using a more vapour tight wind barrier with a large moisture capacity the wind barrier is replaced with a 12,5 mm OSB. The Sd-value for the board is displayed on figure 2. The ratio of Sd for vapour barrier to Sd vind barrier then becomes about 1 for the smart vapour barriers when the RH at the wind barrier is above 25%. In most climates this is the normal condition.

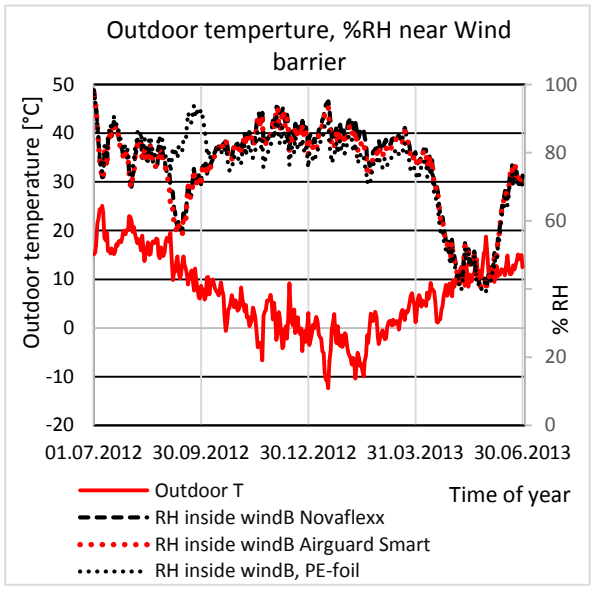

FIG 6. Relative humidity (RH) on inside of wind barrier

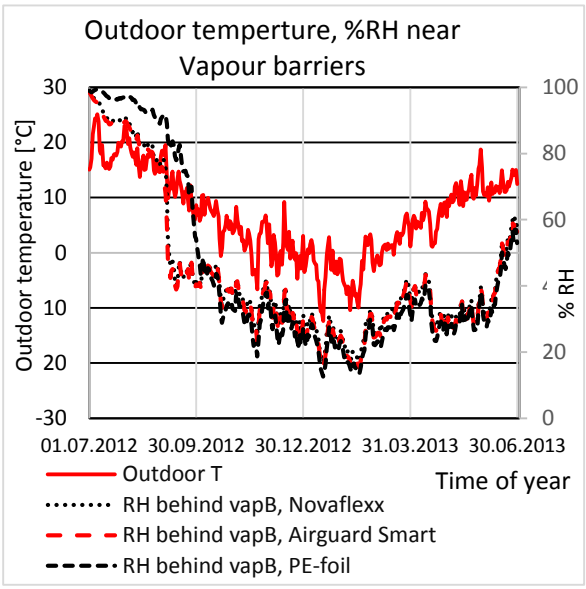

FIG 7. Relative humidity (RH) behind vapour barrier

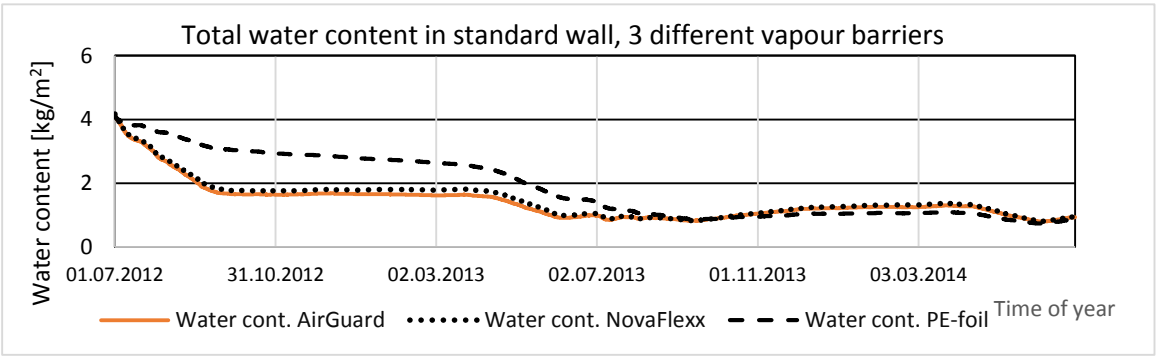

FIG 8. Total moisture content during 2 years in standard wall with 3 different vapour barriers and OSB-wind barrier

As can be seen by comparing to figure 4, the water content is much higher and does not reach normal level before after one year with smart vapour barriers. About 1 kg/m^2 of the water content is in the OSB-board (0,75 kg//m^2 in summer and 1,1 kg/m^2 in winter). After 14 months the water content for the construction with PE-foil also reaches 1 kg/m^2. Due to the more vapour open inside, the moisture flow outwards in winter is higher and therefor the OSB becomes wetter and RH near the OSB stays higher as shown in figure 8.

The moisture at the inside of OSB wind barrier stays high much longer than in walls with a vapour open wind barrier. When running the calculation for two years, it appears that the RH on the inside the wind barrier is reduced to 70% after one year for walls with SVB and after 14 months with PE-foil. Next winter the situation is opposite, the wall with PE-foil is driest (at about 75% RH) while the others rise to 90%.

3.1.3 Influence from changing insulation thickness from 400 to 250mm

The moisture from the start is as in the standard situation. I.e. the concentration of extra water is in the insulation between the barriers is the same. The total water content is therefore lower as it would be in a real wall with less wood and less insulation that can contain moisture.

By comparing RH on inside of wind barrier to figure 5, the first month is the same. Then, when most of the extra water is evacuated from the 250 mm wall, the RF go down to 50% for all walls before rising again during winter. For the PE-foil the increase, shown in figure 5, in RH is finished after 1,5 months.

3.1.4 Influence from changing climates

To see the influence from different climates simulations were done for Trondheim, Oslo and Gothenburg climate. The result is shown in figure 9.

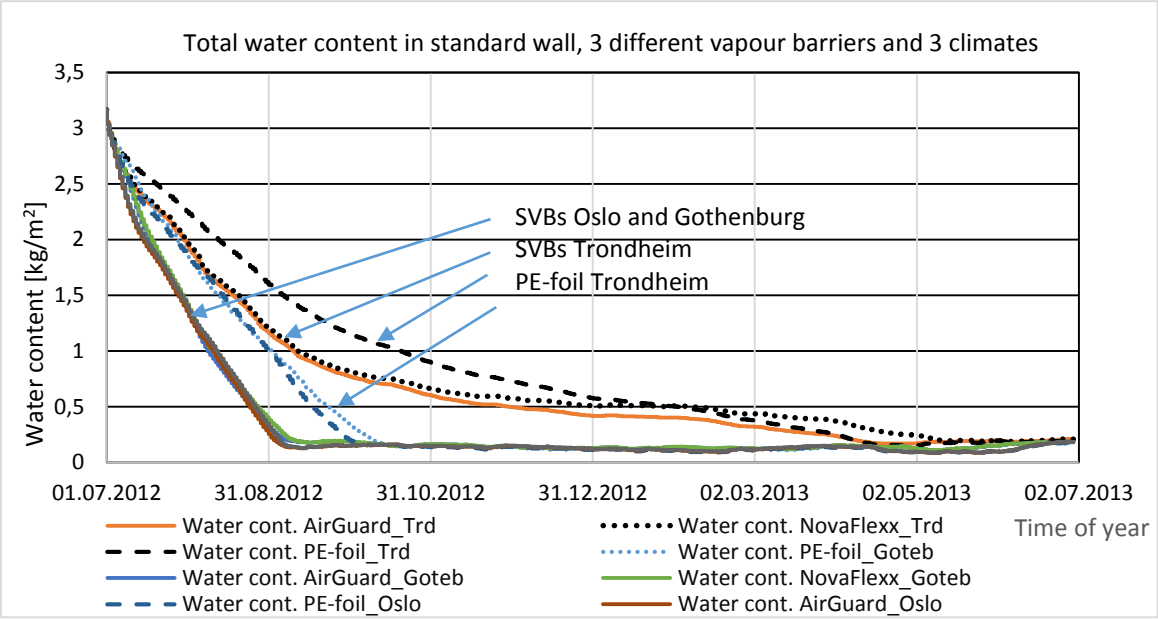

FIG 9. Water content at 3 different climates and vapour barriers

3.1.5 Influence from other parameters

On facades facing south, the drying is faster and results in lower moisture level. The results from the total simulation series are reported in (Agnalt, Magne. 2013)

4. Conclusions

Using smart vapour barriers is effective to reduce the moisture content in well insulated wall structures. The ratio of vapour resistance, vapour barrier/wind barrier is important or the long time performance of the construction.

To keep the robustness of the structure the initial level of moisture must be under control even while using smart vapour barriers.

References

Agnalt, Magne. 2013. Smarte dampsperrer i bindingsverksvegger. Master thesis from Norwegian University of Science and Technology. Department of civil and transport engineering.

GEVING, S., HOLME, J. and UVSLØKK, S. 2010. Prosjektrapport 65 - Alternative dampsperrer med uttørkingsmulighet mot innelufta, Oslo, SINTEF akademisk forlag.

GEVING, S., HOLME, J. and JENSSEN, J. A. 2008. Indoor air humidity in Norwegian houses. Proceedings of the 8th Symposium on Building Physics in the Nordic Countries vol. 2.

GEVING, S. and THUE, J. V. 2002. Håndbok 50 - Fukt i bygninger. Oslo, Norges byggforskningsinstitutt.

DUPONT. 2013. *Dupont AirGuard Smart - AVCL with variable vapour resistance* [Online]. http://www.siginsulation.co.uk/Literature/Airguard%20Smart%20flyer%20final.pdf: Dupont. [Accessed 18.05.2013].

STELLANDER, M. 2011. Litteraturundersøkelse vedrørende smarte dampsjikt med uttørkingsmulighet mot innelufta. Trondheim: NTNU.

THUE, J. V., OUSTAD, M. and GUSTAVSEN, A. 2007. WUFI 1D Pro 4.1 Brukermanual.

TARIKU, F., MAREF, W., LENARDO, B. D. og GATLAND, S. 2009. Hygrothermal performance of RH-dependent vapour retarder in a Canadian coastal climate.

Hygrothermal simulations of internally insulated massive masonry walls exposed to driving rain in cold climate

Jon Ivar Belghaug Knarud, M.Sc. [1]
Stig Geving, Professor [1]
Tore Kvande, Professor [1]

[1] Norwegian University of Science and Technology, Norway

KEYWORDS: *Masonry walls, interior insulation, relative humidity, parameter sensitivity, insulation materials, WUFI*

SUMMARY:
In order to lower energy consumption and improve indoor climate conditions interior insulation retrofitting of massive masonry buildings with protected exterior facades has become needed. As a way to investigate the hygrothermal performance of such walls, a range of simulations have been conducted using software for heat and moisture transport. The impact of driving rain in cold climate lacks much attention in previous studies described in the literature, and therefore this has been given extra concern in the present work. By varying parameters such as, location, wall orientation, short wave radiation, insulation material, vapor barrier solution and indoor moisture load, the effect on the relative humidity in the interior insulation has been investigated. Results show that the amount of driving rain accessing the wall plays an imperative role, making the performance of the wall especially sensitive to location and orientation.

1. Introduction

Energy consumption has during the past few decades become a larger and larger focus as the human society has become aware of the serious challenges we face, in the time forward, with regard to CO_2 greenhouse gas emissions and the possible scarceness of cheap energy. In order to reduce the energy consumption, retrofitting old buildings with more insulation has become a topic. However, a lot of the old masonry buildings have a protected external facade due to their cultural and historical heritage value. Applying insulation on the interior side of the walls seem to be the only option for these buildings, but from a building physics point of view, interior insulation is unfortunately often associated with moisture related problems, including frost damage in the brickworks. Great care must therefore be taken when choosing if and how a wall should be insulated on the inside.

Several studies have looked into the challenge of applying insulation to the inside of massive masonry brick walls, but most of these studies have been based on an external environment corresponding to a continental climate or a costal, relatively warm climate. A few studies have looked at colder climates (climates experiencing cold winters and having many days with temperatures below freezing), like Saïd et al. (2003), Straube and Schumacher (2003), Kloseiko et al. (2013), but in these cases the exposure from wind driven rain was either limited or not described.

Since many parameters may influence the hygrothermal performance of an internally insulated masonry wall, it's of interest to analyze how sensitive the wall is to variations in the influencing parameters. Nielsen et al. (2012) performed a sensitivity analysis focusing on a limited set of parameters including insulation thickness, insulation conductivity, air exchange rate, wall orientation, driving rain exposure and vapor barrier performance. The analysis was done on a solid brick wall, insulated internally with mineral wool, in an external environment corresponding to the Danish design

reference year. The driving rain exposure coefficient and wall orientation were without doubt the most influential parameters on moisture content in the innermost part of the masonry. The vapor barrier and the insulation thickness had only minor influence. Nielsen concludes that the overall effort should be on preventing driving rain. Similarly, Zhao et al. (2011) also conducted a numerical sensitivity analysis of hygrothermal performance. Although this was on a wood-framed wall with an external layer of cement based plaster, different boundary conditions and material properties were analyzed for whether having a positive or negative effect on the total moisture content in the wall. In addition to the hygroscopic properties of the materials the external boundary conditions; short wave absorption, long wave emissivity and rain exposure, were the most influential parameters. The importance of solar radiation (short wave radiation) is supported by Straube and Schumacher (2003).

2. Hygrothermal simulations

A span of different interior insulation solutions was simulated with WUFI PRO 5.2. 1D (Fraunhofer, 2014), which is a numerical software for solving heat and moisture transport in building materials. A description of the capabilities and weaknesses of the software can be found in WUFI online help (Fraunhofer, 2012).

2.1 Materials and variations in wall assembly

The insulation solutions investigated includes the use of mineral wool, expanded polystyrene (EPS) boards, closed and open cell polyurethane spray-on foam, calcium silicate boards, vacuum insulation panels (VIP) and wood fiber boards.

In the numerical model a default 1D wall assembly was designed with an external 20 mm thick layer of render protecting the masonry brick layer behind it. The brick layer was chosen to be 360 mm thick corresponding to $1^1/_2$ stone walls. On the interior side of the brick layer there is an insulation layer with thickness of 50, 100 or 200 mm, depending on the solution in question (with the exception of VIP; thickness 20 mm). On the interior side of the wall assembly there is a gypsum board, 13.5 mm thick. For some of the wall assemblies a vapor barrier (PE-foil) or a smart vapor retarder is present between the insulation layer and the interior gypsum board. The default wall assembly is shown in FIG 1, while the hygrothermal properties of all the materials used can be found in TABLE 1. The liquid transport coefficient for suction and redistribution has been chosen for the render and brick by using the generate function in WUFI after supplying values for the water absorption coefficient (A-value) appropriate for use in Norway. Resulting coefficients and their referred source is listed in TABLE 1.

2.2 Boundary conditions

The simulations have been conducted for three different Norwegian climate exposures, corresponding to the “Moisture Design Reference Year” (MDRY) of Oslo, Trondheim (measure location at Vaernes) and Bergen. The MDRY is the 10th percentile year of the climatic distribution measured over a range of years. Mainly related to the severity of temperature and relative humidity, the MDRY corresponds to a return-period of 10 years. Oslo has been chosen as a default location for the simulations.

The exterior facade has been chosen as default to be oriented normal to the most severe driving rain direction in order to get a dimensioning rain exposure. For Trondheim the resulting facade orientation is towards west, while for Oslo and Bergen its south, corresponding to an annual free driving rain exposure of approximately 500 mm, 200 mm and above 1500 mm respectively. As a comparison the driving rain exposure described by Straube and Schumacher (2003) for Prince Albert was only 50 mm/annum for the maximum driving rain direction. However, a set of simulations have been done using other orientations for Oslo, getting a range of driving rain from approximately 50-200 mm/annum.

TABLE 1 Material properties

Material	Density [kg/m^3]	Heat cap. [J/kgK]	Heat cond. [W/mK]	Sorption at RH = 80%, (100) [kg/m^3]	Diffusion resistance μ [-] at RH = 0%, (100)	Liquid suction at normalized water content 0 (1) [m^2/s]
Render[1,5]	1900	850	0.8	45 (210)	15 (const.)	1.9E-9* (4.2E-7)
Brick open[1,6]	1800	850	0.6	4.5 (230)	10 (const.)	2.9E-9 (2.6E-6)
Brick tight[4]	1800	850	0.6	4.5 (230)	15 (const.)	2.9E-10 (2.6E-7)
Mineral wool[4]	30	840	0.035	0.12 (8.5)	1.3 (const.)	non
EPS[1]	20	1500	0.04	0.18 (0.6)	21.7 (const.)	non
PUR open cell[1]	7.5	1470	0.037	0.21 (5.27)	2.38 (const.)	non
PUR closed cell[1]	39	1470	0.025	1.12 (28)	88.93 (62.1)	non
Calcium Silicate[3,1]	222	1303	0.07	3.0 (899)	6.0 (const.)	3.4E-10 (2.9E-7)
VIP[2]	200	850	0.008	non	inf. (const.)	non
Wood fiber[1]	53	2100	0.039	7.0 (180)	1.35 (1.58)	2E-14 (2.1E-7)
PE-foil, 0.1 mm[1]	130	2200	2.2	0.2	70000 (const.)	non
Smart vapor retarder 0.4mm[4]	347.5	1925	0.05	0	75000 (125)	-
Gypsum plasterboard[1]	625	850	0.2	5.0 (25)	8.33 (2.63)	-

[1] WUFI PRO 5.2 Material database
[2] Johansson (2011)
[3] (Binder et al. (2013))
[4] Custom defined based on an evaluation of realistic values
[5] (Time et al. (2004))
[6] New measurements from the building physics laboratory at the department of Civil and Transport Engineering, NTNU.
[*] at normalized water content of 0.2

In WUFI the driving rain coefficient was set as 0.1 s/m, corresponding to mid wall surfaces of buildings up to 10-20m according to WUFI. The amount of wind driven rain hitting the facade is not necessarily the most important parameter since the exterior material often has limited ability to absorb all the water. For such cases, the duration of facade wetting is a more important parameter. The latter parameter is governed by the location and orientation of the facade in question. However, in the present case, initial simulations showed that the render had the capacity to transport large amounts of water from the surface, making both the driving rain coefficient and the “adhering fraction of rain” coefficient very important for simulation results. The latter being 0.7 as default in WUFI. Since both of these factors are difficult to assess without detailed knowledge of the specific building facade and its micro environment, the proposed values in WUFI was used.

For an exterior wall often wetted by driving rain, the drying potential, which is depending much on the temperature in the wall, is important. When applying internal insulation the drying potential of the brick layer is seriously decreased due to the resulting low temperature across the layer most of the year. Still, effective drying of the layer can occur when the external environmental exposure conditions are favorable, as for instance when sunshine heat up the wall. Unfortunately, there is an uncertainty related to whether the exterior facade is subjected to sunshine or not, since it also could be shaded someway. In the present simulations a favorable situation, without any shading, has been

chosen as default, making the exterior facade subjected to both long and shortwave radiation. The shortwave absorptivity and the long-wave emissivity are chosen to 0.6 and 0.9 respectively, corresponding to aged dark stucco.

It is assumed that the interior side of the gypsum board is painted, thereby adding extra moisture diffusion resistance. An interior S_d-value of 0.5m is chosen for the cases with or without vapor barrier, while a S_d-value of 0.05m is chosen for the cases with smart vapor retarder to give more effect to the retarder.

The interior climate has been chosen according to EN 13788 using humidity classes 1 (low), 2 (medium) and 3 (high) for the different cases, class 2 chosen as default. The interior temperature has been set to 23 ^{o}C, making it a non-conservative parameter. Values and options in WUFI not mentioned in this sub chapter have not been altered from their inherent default.

2.3 Initial conditions

As a simplification, a temperature of 20 ^{o}C and a RH level of 90 % have been chosen throughout the wall assembly. All the simulations were run over 5 years in order to achieve stable yearly variations, i.e. equal variations over each year. Only the last simulated year is presented in the results.

3. Results

A total of 42 simulations were conducted by varying the parameters as mentioned earlier. Since that many simulations give a lot of data only the assumed most interesting results are presented here. The results are taken as the RH 0.6 mm into the insulation layer from the interior brick surface. As also mentioned earlier some input parameters were given a chosen default. This encompassing the location being Oslo, orientation being what gives maximum driving rain, insulation material being mineral wool, insulation thickness being d=100 mm, masonry consisting of open old brick + render and indoor moisture load being medium. The result presentation will mainly mention the parameters which differ from the default, indicating the default is used for parameters not mentioned.

3.1 Location

For both mineral wool and EPS three simulations were run for the locations Oslo, Trondheim and Bergen, keeping all other parameters as default. As can be seen in FIG 2 both Trondheim and Bergen suffer a high RH of approximately 100 % in the mineral wool cases. Oslo mainly experiences a RH in the interval 92 - 96.5 %. The EPS cases (not shown) experience approximately the same situation.

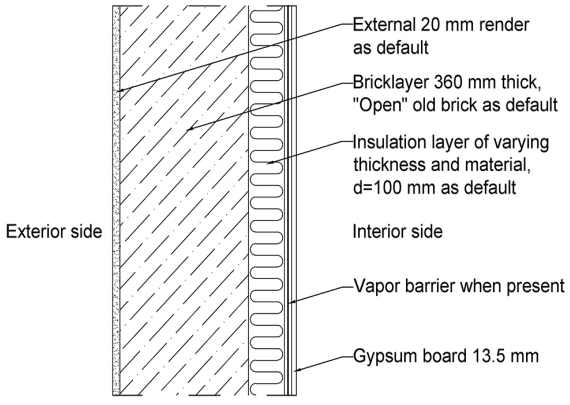

FIG 1. Default wall assembly

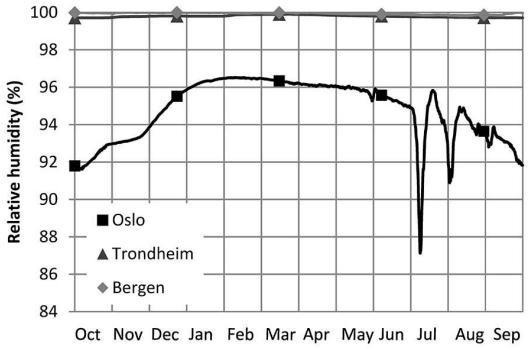

FIG 2. Mineral wool d=100mm and PE vapor barrier for three locations with widely different driven rain exposure.

3.2 Masonry, and retrofitting impact

Four cases were simulated varying the brick and external render between the default open old brick + render and the tight old brick without external render. These are shown in FIG 3. Although the tight old brick has no protecting render it has a lower RH level (average RH of 47 %) compared to the open old brick with external render (average RH of 53 %) when both solutions are without insulation. When insulated and given an PE-vapor barrier the situation becomes reversed giving the tight old brick case a considerably higher RH of about 100 % (average RH of 99 %) compared to the open old brick + render which reach a maximum RH of 97 % (average RH of 95 %).

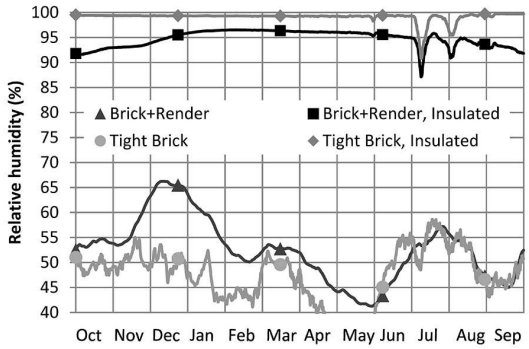

FIG 3. Non-retrofitted walls and walls retrofitted with d=100mm mineral wool and PE vapor barrier, for open brick + render and tight brick masonry.

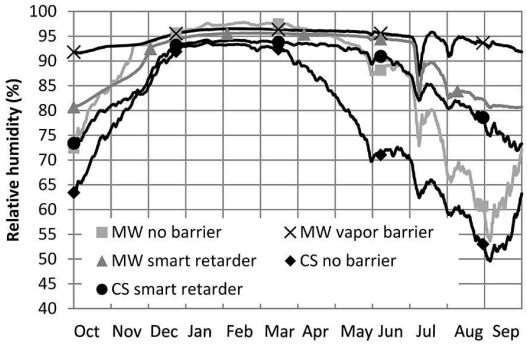

FIG 4. Effect of vapor barrier, no barrier and smart vapor retarder for d=100 mm of mineral wool (MW) insulation and for d=50mm of calcium silicate (CS) insulation.

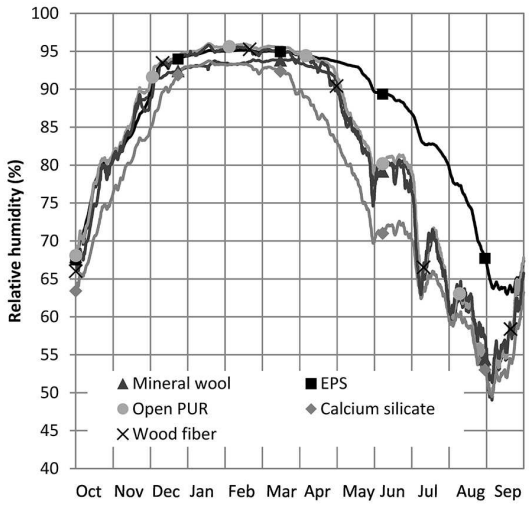

FIG 5. Wall with different insulation materials of thickness d=50mm. No vapor barrier.

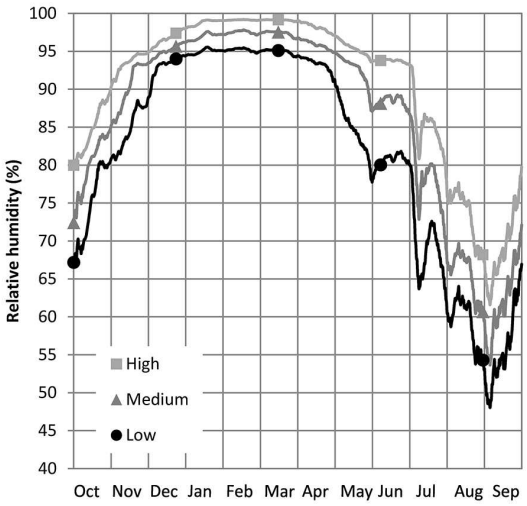

FIG 6. Mineral wool d=100mm for different indoor moisture levels. No vapor barrier.

3.3 Smart vapor retarder

Mineral wool and calcium silicate was simulated without vapor barrier as well as with smart vapor retarder. In FIG 4 and TABLE 2 these results can be seen compared to the result of mineral wool with vapor barrier. Mineral wool without vapor barrier experience a higher RH in the winter compared to mineral wool with smart vapor retarder. The latter does not occur for calcium silicate. Mineral wool with vapor barrier has the overall highest RH level, although the mineral wool case without vapor barrier experiences the highest RH during the year.

3.4 Insulation materials

Seven insulation materials where tried and, with the exception of closed cell PUR and VIP, the results when they were applied with thickness of 50 mm and no vapor barrier is shown in FIG 5. It can be seen that mineral wool, open cell PUR and wood fiber exhibit the same trend in RH. Calcium silicate has a lower RH development over the whole year and start drying out earlier in the spring compared to the others. EPS experience a considerably higher RH level during the summertime than the other materials. Although not shown in any figure, both closed cell PUR and VIP where simulated without a vapor barrier since their vapor diffusivity resistance is so high that a vapor barrier becomes more or less redundant. Modeled thicknesses of closed cell PUR and VIP was 100 mm and 20 mm respectively. With VIP the RH level never falls below 90 % in the autumn. The RH level stays a little bit above 96 % from end of December to June. The closed cell PUR experience quite similar conditions to that of VIP although the RH level falls down to 89 % in the autumn.

3.5 Indoor moisture level

Two cases for 100 mm of mineral wool without vapor barrier were simulated changing only the indoor moisture load from the default medium to high and low. The results are shown in FIG 6. For the high and low moisture load, the RH change in similar magnitude (5-6 % change in average RH level, TABLE 2) to a higher and lower level respectively compared to the default medium moisture load.

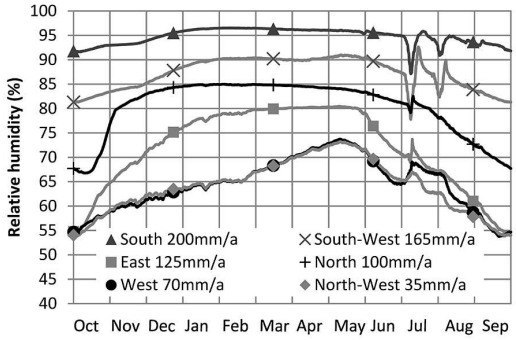

FIG 7. Results for varying orientations. Wall with vapor barrier.

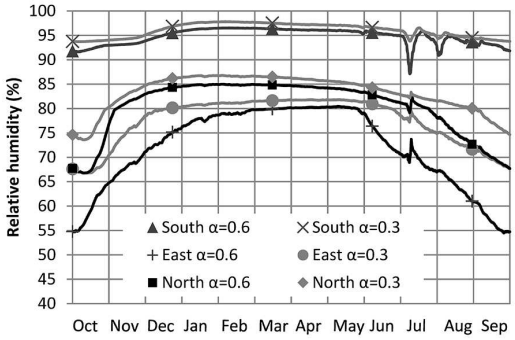

FIG 8. Results for varying short wave radiation exposure where α=0.6 is the normal absorptivity of the wall and α=0.3.

3.6 Orientation

As the orientation changes the amount of driving rain also changes due to the fact that the wind are more likely to follow some directions compared to others. In FIG 7 the effect of changing the orientation is shown with the corresponding wind driven rain levels. As can be seen from the figure, the RH level widely differs for the different orientations, from a low 55 % RH in the autumn for the least exposed orientations to a high of above 90 % RH for the most exposed orientation. It should be noted that the trend is broken when comparing east and north orientation, where north has a higher RH level even though it experience less driving rain exposure.

3.7 Short wave radiation

Since the drying potential of the wall is very dependent on the temperature, it is interesting to see how the short wave radiation from the sun can help with drying out the moisture. The amount of short wave radiation hitting the facade is closely linked to the wall orientation. Located in Oslo the radiation amount is almost half at north oriented walls and about 80 % at east and west oriented walls

compared to south oriented ones. The influence of the absorptivity of short wave radiation is shown in FIG 8 for three orientations trying to investigate why the east orientation had lower RH than the north orientation when east actually experience more driving rain (FIG 7). As can be seen in FIG 8 the RH level increase more for the east orientation than for the north orientation when a reduced absorptivity is used, but still it does not nearly account for the whole discrepancy seen in FIG 7. The halved absorptivity used is assumed to correspond to approximately 50 % shading of the wall.

TABLE 2 RH data from some chosen simulated cases. Parameters not mentioned kept as default.

Simulation case	Yearly mean RH [%]	% of year with RH ≥ 85 % [1]	% of year with RH ≥ 95 % [1]
Vapor barrier	95	100	55
No vapor barrier	87	67	37
50 mm, no vapor barrier	81	49	0
Smart vapor retarder	91	74	37
No vapor barrier, low moisture load	82	49	17
No vapor barrier, high moisture load	93	90	45
Vapor barrier, east oriented, α=0.6	72	0	0
Vapor barrier, north-west	64	0	0
Vapor barrier, east oriented, α=0.3	77	0	0
CS, 50 mm, no vapor barrier	78	40	0
CS, 50 mm, smart vapor barrier	87	60	0
EPS, 50 mm, no vapor barrier	86	63	12

[1] In literature, critical RH for mold growth is usually 75-85% and 95 % for wood and mineral wool respectively

4. Discussion

The simulations done in the present work have in a way been kind of a “brute force” sensitivity analysis meaning a broad range of cases has manually been simulated with parameter variations. Compared to the more automated and fully post processed sensitivity analyzes done by Zhao et al. and Nielsen et al., it has here been focused on presenting the actual impact parameters have on specific cases in form of RH levels in the insulation. What seems clear from the current simulations is the high impact from the driving rain exposure. By varying the location from Oslo to Trondheim and Bergen a RH level of about 100 % was reached, making it difficult to analyze Trondheim and Bergen any further due to the limited possibility of getting a result impact (sending the RH below 100 %). Focus therefore had to be on Oslo. By varying the orientation it could easily be seen how large impact direct driving rain exposure has on the wetting of the wall. It seems this is the most influential parameter if the location is locked, capable to reduce the average RH level from 95 down to 64 % (TABLE 2). Closely related to orientation is the short wave radiation access, varying with a factor of 2 from lowest access to highest. From FIG 8 the impact of reduced access to short wave radiation, assumed due to shading of the wall, clearly gave an increase in RH. For east orientation a 50 % reduction to short wave radiation led to an increase in average RH of 5 %. However, the correlation between wetting and drying due to orientation and short wave radiation was not investigated enough to establish any conclusion. The reason for why the east and north orientation had a discrepancy related to the RH level when the short wave radiation and driving rain exposure were considered has not been identified. A hypothesis may be that it is also affected by the long wave radiation and air temperature in some way. A more thorough investigation in the climate data of the MDRY file of Oslo, and possibly also comparison to other locations could perhaps identify whether this is the case. In the cases where there is no vapor barrier, the insulation material has a certain effect especially if categorized out from low and high vapor diffusion resistance, as well as capillary capability. When looking at the effect of smart vapor retarder in connection with mineral wool and calcium silicate the

drying potential in the autumn was effectively reduced from the no vapor barrier cases (4 % and 9 % for mineral wool and calcium silicate respectively), but for mineral wool there were also a small improvement in form of lower RH level during the winter and spring.

5. Conclusions

It is a clear challenge related to locations having a high driving rain exposure, when looking at retrofitting of masonry walls with interior insulation. Although no focus was given the damage potential due to moisture in the present work, it still became evident that the retrofitting solutions investigated here have a certain limit to how large driving rain exposure they can endure.

Keeping the location locked the parameters making the greatest impact on hygrothermal performance were in descending order, with overall potential change in yearly mean RH, derived from TABLE 2, in parenthesis; orientation (31 %), indoor moisture load (11 %), vapor barrier solution (8-9 %), insulation material (8 % or 3-4 % excl. EPS). The effect of short wave radiation was inconclusive due to insufficient investigation into this parameter, although it seems to have a significant impact. More investigation into the correlation effects on hygrothermal performance between driving rain, short and long wave radiation and possibly external air temperature should be conducted, due to influence on the drying potential of the wall.

References

Binder A, Künzel H and Zirkelbach D. (2013) A new approach to measure liquid transport in capillary active interior insulation. *2nd Central European Symposium on Building Physics.* Vienna, Austria: Vienna University of Technology, 393-400.

Fraunhofer. (2012) WUFI Pro 5.2 online help.

Fraunhofer. (2014) *WUFI PRO, 2D, Plus*. Available at: http://www.wufi-pro.com/.

Johansson P. (2011) Assessment of the Risk for Mold Growth in a Wall Retrofitted with Vacuum Insulation Panels. *9th Nordic Symposium on Building Physics - NSB 2011*. Tampere, Findland: Tampere University of Technology.

Kloseiko P, Arumägi E and Kalamees T. (2013) Hygrothermal performance of internally insulated brick wall in a cold climate: field measurement and model calibration. *2nd Central European Symposium on Building Physics.* Vienna, Austria: Vienna University of Technology, 185-192.

Nielsen A, Møller EB, Rasmussen TV, et al. (2012) Use of sensitivity analysis to evaluate hygrothermal conditions in solid brick walls with interior insulation. *5th International Building Physics Conferance.* Kyoto, JApan: 5th IBPC Organizing Committee, 377-384.

Saïd MNA, Demers RG and McSheffrey LL. (2003) Hygrothermal performance of a masonry wall retrofitted with interior insulation. *Proceedings of the 2nd International Conference on Building Physics.* Leuven, Belgium: Balkema Publishers.

Straube J and Schumacher C. (2003) Comparison of Modeled and Monitored Performance of a Wall Insulation Retrofit in a Solid Masonry Building. In: Duncan Hill HTG, Policy and Research Division (ed). Canada: Canada Mortgage and Housing Corporation, 56.

Time B, Kvande T, Terjesen T, et al. (2004) *Moisture tranport in mineral building materials - material properties (in Norwegian)*, Blindern, Oslo: Norges byggforskningsinstitutt.

Zhao J, Plagge R, Nicolai A, et al. (2011) Stochastic study of hygrothermal performance of a wall assembly—The influence of material properties and boundary coefficients. *HVAC&R Research* 17: 591-601.

A method for status determination of historical buildings

Jesper Arfvidsson, professor[1]
Björn Bjelke-Holtermann, conservation consultant [2]
Johan Mattsson, M.Sc.[3]

[1] Lund University, Sweden
[2] Tyréns AB, Sweden
[3] Mycoteam AS, Norway

KEYWORDS: *Building Physics, Building Biology, Building Antiquarian, Historical Buildings*

SUMMARY:
Today there is a need for energy-efficiency measures in historic buildings. To ensure that such measures will provide the planned result without damage to the building or poor indoor climate, a skilled holistic approach is required. To be able to propose accurate measures requires a thorough understanding of the individual cultural heritage, the existing building's function and how the measures will affect the building. This requires a multidisciplinary knowledge, for example building antiquarian, building biological and building physical expertise.

This paper presents a method for determining the status of the existing building and a method for risk assessment of energy saving measures. The goal is to develop safe concepts for energy saving measures in different types of buildings.

1. Introduction

1.1 Background

There is currently a major focus on how climate and climate influence on the service life of materials in historic buildings. Less known is the problem how other changes significant can influence in the building physics and any consequential damages due to this (Haugen et al. 2012). Most of Scandinavia's historic buildings have at various times undergone changes in design and usage. Older structures have been renovated with new construction solutions and materials. Changed requirements for indoor climate and energy use has led to new heating and ventilation systems have been installed. The results of these changes have not always been satisfactory, and sometimes resulted in building damages of various kinds or a non-acceptable indoor climate (Mattsson 1995, 2014). These mistakes have led to extensive costs in damage remediation. In addition, in many cases are important historical values lost during the restoration work.

Building a new energy efficient house requires considerable expertise in a number of areas. To implement energy-saving measures in existing buildings often require even more. Changes into thicker insulation, intermittent heating, new types of building materials and reduced or modified ventilation affects buildings thermal and hygroscopic properties. These changes increase the risk for moisture and mould damages (Mundt-Petersen 2013, Mattsson 2004). Unfortunately, it is usually the case that the sensitivity and thus the risk of for example moisture damage have increased by these measures. A number of structures, which we know is critical to moisture, will become even more sensitive, and new parts of the building, which previously functioned well, will be in the risk zone. We have many examples of this in buildings with crawl space or cold attics that was remedied after the energy crisis in 1970's. When additional insulation is used in the building envelope of poorly insulated buildings, the temperature in the crawl space, attic and parts of the outer wall will be lower than before during the cold period. If warm moist air can be transported from the heated space in the building up of the attic it cools down and the relative humidity increases. Also during cold clear winter nights sometimes the inside of the outer roof will be so cold that the outside air, through ventilation, may condense on the inside of the attic. The inside of the roof becomes damaged, but also attic

floor because of the condensation that forms on the inside of the outer roof drops down into structure and cause moisture and mould (Nunez et al 2013). Thermal insulated basement walls were up to the 1994-95 thermal insulated on the inside, normally in combination with a windbreaker against the foundation wall and a damp barrier on the warm side of the insulation. Such construction is a high risk construction with respect to moisture problem, and in old buildings where it might be some intrusion of water through the wall, the risk of both mould fungi and decay fungi is extreme high (Alfredsen et al, Gobakken et al 2014). If we look at the crawl space it is another season that becomes dangerous moisture. In winter, the crawlspace cools down and then when spring and summer arrive, warm and humid outdoor air gets into the crawlspace through ventilation openings. The crawl space is still cold and when hot humid outdoor air enters the crawl space it cools down and the relative humidity of the air increases. When humid air comes into contact with sufficiently cold surfaces, condensation and free water occurs. This increases both the risk of moisture and mould damages (Viitanen 1995) and decay problems (Austigaard et al. 2014). Use of modern building materials, such as gypsum boards and fibre boards instead of traditional wooden materials does also increase the risk of mould damages due to a poor mould resistance capacity in the modern materials (Nunez et al 2013, Nore et al. 2014).

A number of measures to reduce the risk of moisture damages are found in modern construction. These should however be adapted to be used in historical buildings. Often change is heating systems is made, for example from a local system to district heating. A chimney that previously was hot and warmed up the cold attic gets cold. The negative pressure created through the "chimney effect ", and contributed to the ventilation, is gone. The result can be a building, which is indeed energy efficient but has a very high risk of damp and mould, poor ventilation and therefore a bad environment for both the building and humans. A critical side effect in access to moisture problems is also often elevated radon values in these poorly ventilated buildings, especially in basements and ground floor. Change of windows and more efficient air-tightening reduce the natural ventilation in old buildings. In concrete building this can be critical and change from a ventilation rate about 0,5 to less than 0,15 air change/hour has been documented after replacement of windows (Mycoteam 2013).

To be able to improve energy efficiency of an existing building in a proper way demands considerable expertise and holistic thinking of those involved. To handle the hygrothermal function of modern energy efficient buildings requires different types of computational tools and knowledge of the material properties. Energy update existing buildings required additional understanding of how the existing building works in the present situation. A status determination in a sufficient level of detail is of crucial importance in order to consider what measures should be considered.

1.2 Aim

The goal is to develop a methodology and to produce different types of tools required to ensure proper status determination and risk assessment of energy update measures in historical buildings.

1.3 Limitations

Effects due to actions in connection with the accessibility and fire safety have so far been neglected.

2. Method

Performing a risk assessment of existing and future problems and damages is complicated. No complete method of dealing with this is used today. In order to make an accurate assessment of risk requires knowledge of a number of factors.

The work to develop a methodology for status determination and risk assessment of energy conservation in historic buildings evolves different experts working together. In our case it is limited to Building physicists, building biologists and building antiquarians. However, other relevant disciplines can easily be supplemented as needed. Through frequent meetings and discussions, with a goal to understand more of each other's specific areas and way of thinking, a first common method has been developed. The input has been already developed methods or guidelines in the different specialisations.

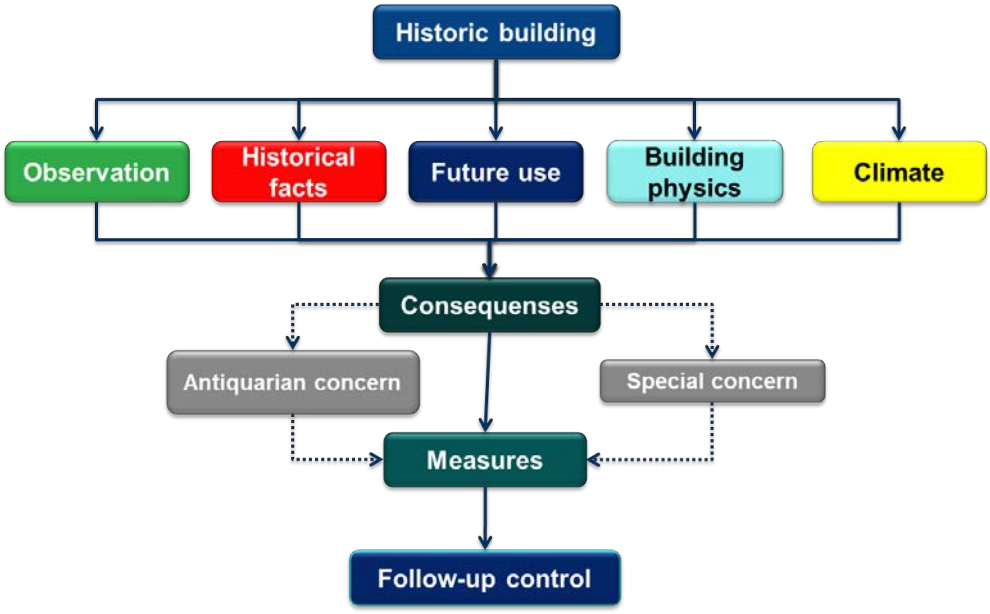

FIG 1. At survey of historical buildings, several aspects has to be taken into account in order to be able to perform an optimal understanding and evaluation of the situation.

3. Result

The work has resulted in a method (3B-method) to address the **B**uilding Physical, **B**uilding Biological and **B**uilding Antiquarian aspects of a building at present and after certain measures.

Each of the three areas has been treated in a similar way that makes it possible to handle them all within the same system. The systematics in the method is inspired from the ByggaF-method (Mjörnell et al. 2012), which is developed to assess the moisture safety in buildings though out the whole building process.

The Building physics part deals with energy efficiency, moisture safety, ventilation and indoor climate, but also building technology. A number of checklists will be used to cover and assess the different building physical aspects.

The Building biological part deals with the presence of different kinds of fungi and insects. Examples of checklists have been designed to facilitate the possibility to assess the degree of attack and how dangerous it is but also the reason behind and the way to minimize the future effects (Mattsson 2010).

It is important to distinguish between old, inactive and ongoing active attacks of various biodeterioration. One must also be able to assess the occurring organisms and the current building physics that cause the suitable conditions for biodeterioration. In addition, it is important to distinguish between species that can easily be developed further by even low humidity values and those that die out if it is not very wet. This knowledge and understanding is in fact the foundation in order to be able to assess the consequences of various energy efficiency measures in the building in question.

The Building antiquarian (conservation consultant) deals with building technology, traditional building materials and heritage values. The care of the historically valuable buildings is governed by certain general principles and of special requirements and legislations, based on each building's individual cultural and technical characteristics. Some general guidelines are; preserving the character, using minimally invasive procedures, preventing damages, using traditional materials and traditional techniques. This does not necessarily exclude modern technology as long as it preserves both the character and the life of the house, both in whole and detail.

The method is divided in different modules:

1. The building (building envelope)
2. The interior (lose and solid)
3. Building services installations
4. Climate (outdoor, indoor)
5. Current laws and regulations (informative part)

The information is build up by the different experts from “bottom to top”. All details are dealt with and successively put together in bigger and bigger units and modules that are either approved or not. In Figure 2 a schematic picture of the process is showed.

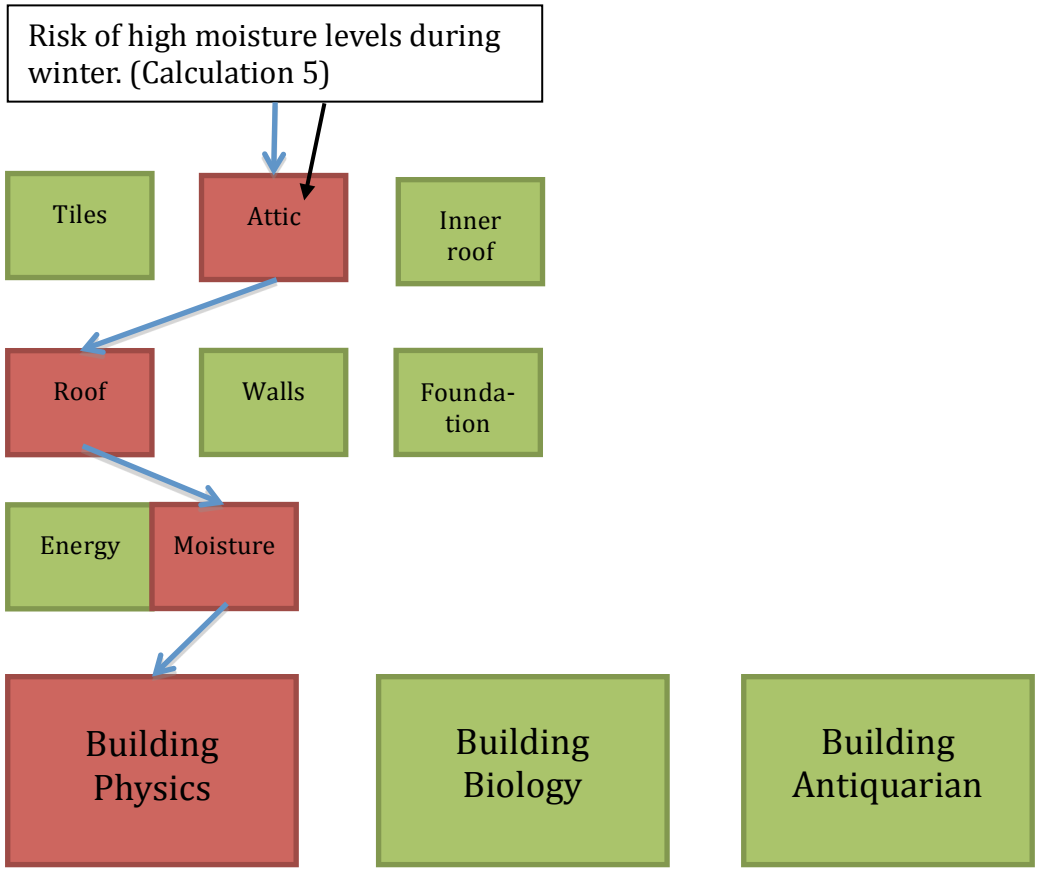

FIG 2. The “bottom to top” process. All details are successively put together in bigger and bigger units. The objective is to give an, easy to understand, overview as a base for decision makers.

When the status determination is made, it is much easier to see what has to be done and what is the most urgent to take care of. Different measures and how they may influence other parts in the system have to be assessed. A kind of risk assessment has to be made; in this stage a simple one is introduced.

All together the result of the method gives an overview of the present status of the building and also the possibilities for different measures. It forms a more holistic base for decision makers to be able to decide what to do and at what risk.

Now the method is used the other way, “top to bottom”. If a module is not approved, it is possible to step down in the hierarchy and in detail find the reason why a special part has failed to pass. The reason could be found in any of the main three different parts; Building physical, Building biological or Building antiquarian aspects. .

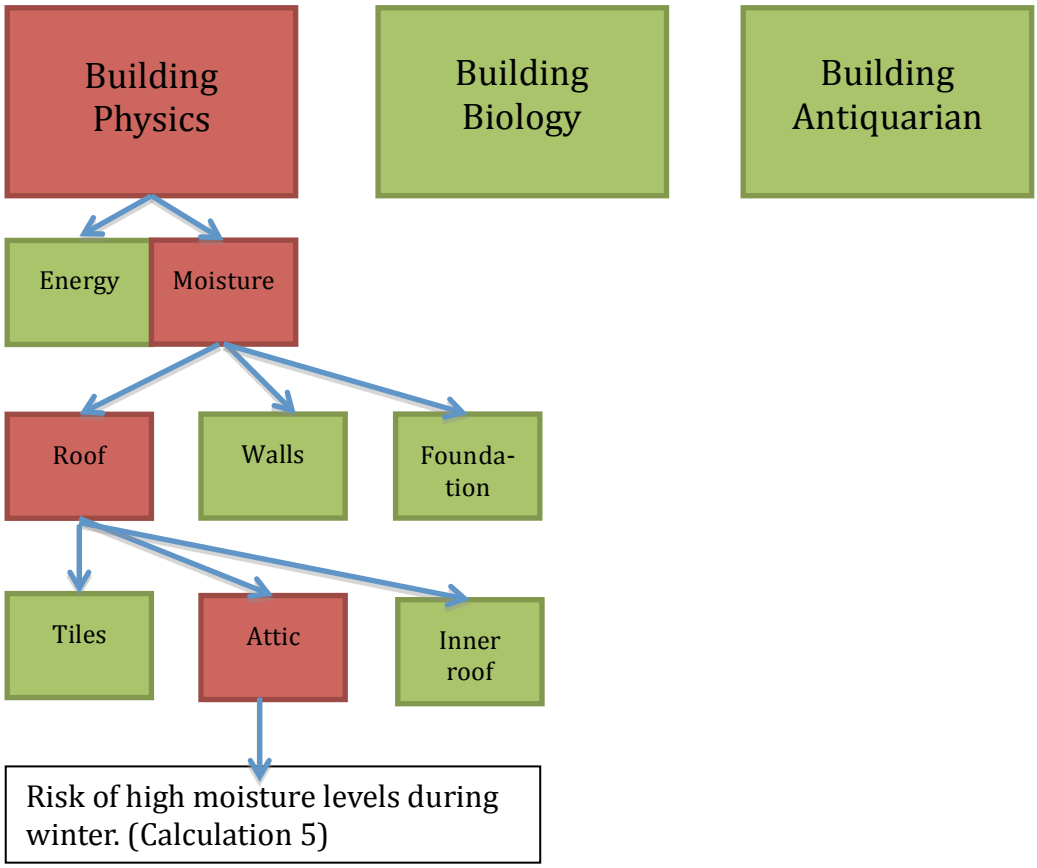

FIG 3. The overview of the status of the building is shown with coloured boxes. For more detailed information it is possible to get more and more information about the background to different problems or damages.

One challenge in the “Building Antiquarian aspects” is to find levels and adequate information and guidelines within the method so that cultural and historical values can be identified and preserved. As a user of the method one must also be aware of, and accept, that conservation aspects will not always lead to optimal improvements and vice versa. Another challenge is to make the whole method user-friendly.

For historic buildings and those of traditional construction an appropriate balance needs to be achieved between building conservation and measures to improve energy efficiency if lasting damage is to be avoided both to the building’s character and significance and its fabric, (English Heritage. 2012).

An understanding of what constitutes the special interest or significance of a historic building requires experience. Very often technical, philosophical and aesthetic conflicts will need to be resolved and on occasion highly creative solutions to problems will be necessary. In such circumstances there is no substitute for the knowledge, skill and judgment of qualified and experienced professional advisor such as an architect or surveyor experienced with historic buildings. Such people have both the technical ability and wide working knowledge of historic buildings essential to properly informed

maintenance and adaptation. Their advice can thus prevent damage and unnecessary expense and heartache, (English Heritage. 2012).

4. Discussion

In order to propose measures in an existing building, it is important to know the status of the building in the starting position. One must get a clear picture of how the existing building works building physically today (and maybe even how it was intended to work from the beginning), considering heat-, air- and moisture transfer in materials and structures and what influence various changes might have

The condition of the materials and structures must be determined with respect to moisture exposure, mould, wood decaying fungi and wood-destroying insects. This has importance both on the potential need for repair or replacement, and in evaluation of the risk for a possible further development of the occurring damages, such as in cases with dry rot damages.

Due to the fact that damages caused by biodeterioration in old buildings are the result of an accumulated damage development through the buildings service life, it is important to clarify when and why the damages have been established and what the yearly development has been (Mattsson 2010). Such knowledge of the damages does often give a detailed understanding in both what the general risk for biodeterioration in the actual building is and the consequences of a possible further development.

Also the lack of expected attack provides information that must be considered and analysed.

An accurate description of the initial state facilitates the selection of measures and reduces the risk of undesirable effects such as dampness and poor indoor climate. In cases with a risk for critical reduction of air exchange rate, proper actions can be planned and performed before damages and complaints occur.

5. Conclusion

Energy efficiency measures in old buildings are a challenging task. By using a multi-disciplinary approach, it is possible to interpret how the building has functioned so far and what consequences various changes in use and construction may have. This provides an opportunity to optimize measures regarding energy efficiency while maintain the cultural heritage values and reduce the risk of the occurrence of fungal and insect damage and a poor indoor-air climate.

References

Brischke, C., Bayerbach, R., Rapp, A., 2006. Decay-influencing factors: A basis for service life prediction of wood and wood-based products. Wood Material Science and Engineering (1):91-107.

Coggins, C.R., 1980. Decay of timber in buildings. Dry rot, wet rot and other fungi. The Rentokil library, East Grinstead.

Gobakken, L., Mattsson, J. and Alfredsen, G., 2008. In service performance of wood depends upon the critical in-situ conditions. Case-studies. International Research Group on Wood Protection, IRG/WP 08-20382.

Gravesen, S., Frisvald, J. and Samson, R. A., 1994. Microfungi. Munksgaard, Copenhagen.

Grøntoft, T., 2008. Effekten av klima og klimaendringer på den bygde kulturarven. Online at http://www.klimakommune.no/kulturarv/Effekter_av_klima_og_klimaendringer_p_den_bygde_kulturarven_Nedbrytningsmekanismer_og_s_rbarhet.shtml .

English Heritage. Energy Efficiency and Historic Buildings. Application of Part L of the Building Regulations to historic and traditionally constructed buildings. 2012.

Mattsson, J., 1995. Råte- og insektskader. Tilstandsanalyse og utbedringstiltak. FOK-programmets skriftserie nr 23. Norges Forskningsråd

Mattsson, J., 2010. Råtesopp i bygninger. Mycoteam, Oslo

Mattsson, J. and Flyen, A.C., 2011. Preventive methods against biodeterioration of protected building materials in Svalbard. Polar Settlements – Location, Techniques and Conservation. ICOMOS. ISBN 978-82-996891-3-7. Pp. 44 – 50

Mattsson, J. and Flyen, A.C., 2008. Biodeterioration in buildings in Svalbard (Spitsbergen). Historical Polar Bases – Preservation and Management. ICOMOS. ISBN 978-82-996891-2-0. Pp 23 – 29.

Mattsson, J., Flyen, A.-C., Nunez, M., 2010. Wood- decaying fungi in listed buildings and structures at Svalbard. Agarica. Vol. 29, p. 5 – 14.

Mjörnell, K., Arfvidsson, J., and Sikander, E., 2012: A method for including moisture safety in the building process. Indoor and build Environment 21(4), pp 583-594.

Nunez, M., Sivertsen, M.S., Mattsson, J., 2012. Indoor mould ecology: Substrate and construction preferences for Actinomycetes and 13 mould genera. Healthy Buildings 2012. Brisbane (Proceedings).

Rayner, A.D.M., Boddy, L., 1988. Fungal decomposition of wood. Its biology and ecology. John Wiley & sons, Chichester.

Scheffer, T.C., 1971. A climate index for estimating potensial for decay in wood structures above ground. Forest products Journal, 21(10): 25-30.

Stokland, J.N., Siitonen, J., Jonsson, B.G., 2012. Biodiversity in dead wood. Cambridge University press.

Viitanen, H., 1995. Models of the critical time of humidity and temperature conditions for the development of mould fungi in pine and spruce sapwood. IRG/WP 95 – 20066. International Research Group of Wood Protection. Stockholm.

Infrared thermography in the diagnosis of moisture in building components

Eva Barreira, Assistant Professor [1]
João M. P. Q. Delgado, PhD [1]

[1] University of Porto, Faculty of Engineering, Civil Engineering Department, Building Physics Laboratory, Portugal

KEYWORDS: *Infrared thermography, moisture, building diagnosis*

SUMMARY:
Moisture is one of the most deteriorating factors of building components. Moisture may have different sources: it can result from wind-driven rain infiltrations through cracks in the building envelope, it can be due to rising damp from the ground, it may be caused by surface condensations, etc. To avoid severe degradation it is very important to detect moisture in an earlier stage, i.e., before significant visible signs occur, and to trace the leak through the building elements. Using non-destructive technics is very important, especially when the building is occupied, as further work is avoid during the assessment.

In this work it was analysed the applicability of infrared thermography, a non-destructive technique (NDT), to assess moisture in building components. Thermograms were obtained from moist areas, caused by different sources (infiltrations and rising damp), existing in occupied buildings. Simultaneously, a moisture detector was also used in the same areas to evaluate, qualitatively, the moisture content of the components under study. The comparison between the two methods showed a good accordance of the results and proved that infrared thermography it is a very useful NDT to detect moisture in an earlier stage. However, some cautions must be taken into account when analysing the results, as thermography also detects other kind of defects that cause temperature differences in the surface of the component.

1. Introduction

The problem of moisture in buildings has always aroused great interest, since moisture is one of the main causes of buildings pathology. Moisture may cause degradation of building materials and components, compromising their performance concerning durability, mechanical resistance, waterproofness and appearance. It can also cause unhealthy conditions for users, resulting from biological growth and degradation of materials and building components. Moisture may have different causes that can be divided into 6 groups: built-in moisture; rising damp; infiltrations due to wind-driven rain; surface condensations; moisture due to hygroscopic phenomena; and moisture due to accidental causes, etc.

Infrared thermography is a non-contact and non-destructive testing technology that can be applied to determine the surface temperature of an object. The detectors collect infrared radiation emitted by the surface and convert it into a thermal image with the distribution of the body superficial temperature, the thermograms. In this process, each colour expresses a certain range of temperatures (see Figure 1).

Two approaches can be used to obtain the surface temperature distributions using infrared cameras: the passive and the active approach. In the passive thermography the surface temperature under study is naturally different than ambient temperature and defects are detected without the use of any

equipment to heat or cool the surface. In active thermography, however, an external energy source is used to induce and emphasise relevant thermal contrast between the damaged and not damaged areas (Maldague 1993).

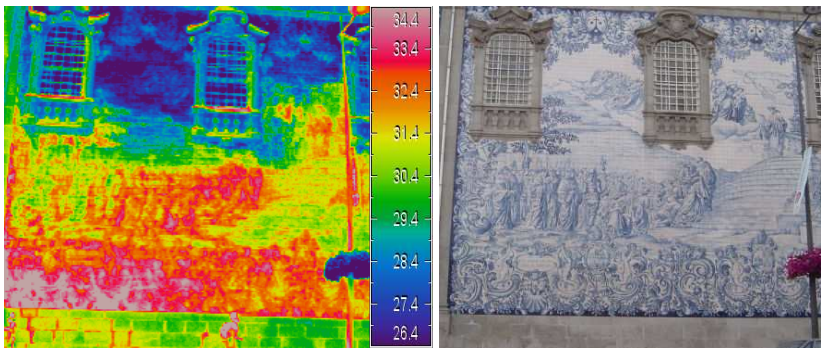

FIG 1. Thermogram and visible image of the Carmo Church's façade covered with "azulejos" (ceramic tile) in Porto, Portugal

The thermal images can be analysed qualitatively or quantitatively. The qualitative analysis only considers the relative differences in the surface temperature distribution given by the thermal image. It is faster and easier to interpret but it can be used, only, for a more superficial approach of the problem. In the quantitative analysis real surface temperatures are calculated based on the thermal image and the necessary analytical parameters. This approach requires more rigorous test conditions, it is more time consuming and requires that the equipment used is strictly calibrated (Hart 2001).

This technology has been applied to buildings for a couple of decades, to evaluate the building performance (Hart 2001). It has been used to detect insulation defects, air leakages and heat losses. Inspection procedures are well defined in standards such as ASTM C 1060-90 (2003), ISO 6781 (1983) and CEN-EN 13187 (1998).

However, procedures to detect moisture in building components using infrared thermography are still under development. It is still not clear if infrared thermography can be used to detect moisture before any visible marks occur, such as efflorescence, biological growth, detachments or degradation of the material, avoiding severe degradation, and to trace a water leak through the building elements.

Changes in moisture content can be related with changes in surface temperature and can be detected by infrared thermography, due to three physical phenomena:

- Evaporative cooling at the moist area: The evaporation at the surface is an endothermic reaction, which induces a decrease on the surface temperature (Rosina & Ludwig 1999, Moropolou et al. 2002, Barreira & Freitas 2007, Grinzato et al. 2010).
- Reduced thermal resistance (Rajewski & Devine 1996, ASTM C 1060-90 2003): The heat flow through wet materials is higher than through dry materials, which creates a thermal pattern as the surface temperature over the wet material is higher, if the inspection is made from the outside during the colder season. This effect is pushed to extremes when the wetting occurs in thermal insulation materials.
- Increased heat storage capacity of the moist material (Balaras & Argiriou 2002, ASTM C 1060-90 2003, Lerma et al. 2011): The surface temperature over a wet area responds more slowly to a change in the air temperature than the surface temperature over a dry area. Thus, when the whole surface is cooling, wet areas will cool more slowly. During the course of a sunlit day, wet areas will store more solar energy than dry areas, thus, they will cool more slowly during the evening.

In this work, the qualitative and passive approaches were used. Moist areas in building components were assessed considering the effect of evaporative cooling. Simultaneously, a moisture detector was

also used in the same areas to evaluate, qualitatively, the moisture content of the components under study. The comparison between the two methods is presented.

2. Equipment and procedures used in the measurements

2.1 Infrared camera

The thermography equipment used was Thermo Tracer TH7800 made by NEC Avio Infrared Techonologies Co., Ltd (Figure 2a). The main specifications are described in Table 1.

TABLE 1. Specifications of Thermo Tracer TH7800 (NEC nd)

Measuring range	-20º C to 100º C
Resolution	0,1º C
Accuracy	± 2º C or ± 2% of the reading
Detector	Uncooled focal plane array (microbolometer)
Spectral range	8 to 14 μm
Thermal image pixels	320 (H) x 240 (V) pixels
Focusing range	50 cm to infinite
IFOV	1.5 mrad

2.2 Moisture detector

The moisture detector used was TRAMEX LS made by Tramex, Ltd (Figure 2b). This non-destructive equipment operates on the principle that the electrical impedance of a material varies in proportion to its moisture content. The instrument measures the electrical impedance of a material by creating a low frequency alternating electric field between the electrodes. The reading displayed by the equipment is a relative scale in percentage, which indicates the greater or lesser signal (lower values indicates lesser signal that corresponds to lower moisture content). To obtain precise moisture content the equipment must be calibrated (TRAMEX nd). During this work, only the qualitative approach was used as the moisture detector was not calibrated.

a)

b)

FIG 2. Equipment used in the measurements: a) Thermo Tracer TH7800; b) TRAMEX LS

2.3 Test procedures and treatment of results

The main objective of the tests carried out was to assess whether thermography can be used to detect moisture in building elements. To this end, thermograms of the damaged areas due to moisture were taken and were compared with the results of the moisture detector. Different building elements with moist areas caused by different sources (infiltrations and rising damp), were analysed:

- Infiltrations: (a) classroom wall of the University of Porto – Engineering Faculty; (b) cafeteria ceiling and walls of the University of Porto – Engineering Faculty.
- Rising damp: exterior wall of a basement with the inner surface damaged.

Thermograms were taken considering emissivity 0.9. This value may not correspond to the real emissivity value of the surfaces under study, however, as the qualitative approach was used, an estimated value of emissivity was considered acceptable.

To compare the results obtained by thermography with the ones given by the moisture detector, a correlation between the relative scale of the detector results and the thermograms colour scale was established. As lower temperatures correspond to moister areas, because evaporation is more intense, the colder colour was related with higher values of the detector relative scale and the warmer colour with the lower values (Figure 3).

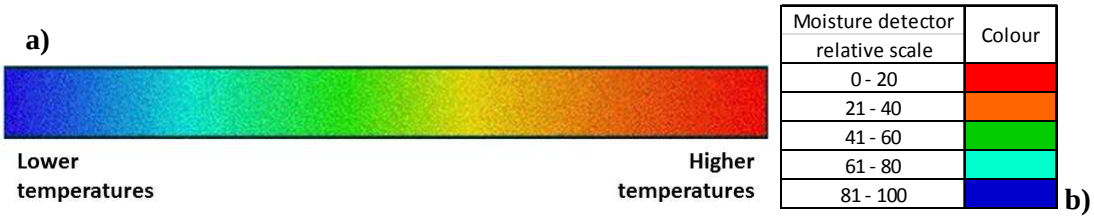

FIG 3. a) Thermograms colour scale; b) Correlation between the relative scale of the detector results and the thermograms colour scale

Before using the moisture detector it was defined a grid dividing the entire area to be analysed. The grid span was assigned depending on the size of the area under study (Figure 4a). Using the measured values in each point of the grid a graph was created (Figure 4b).

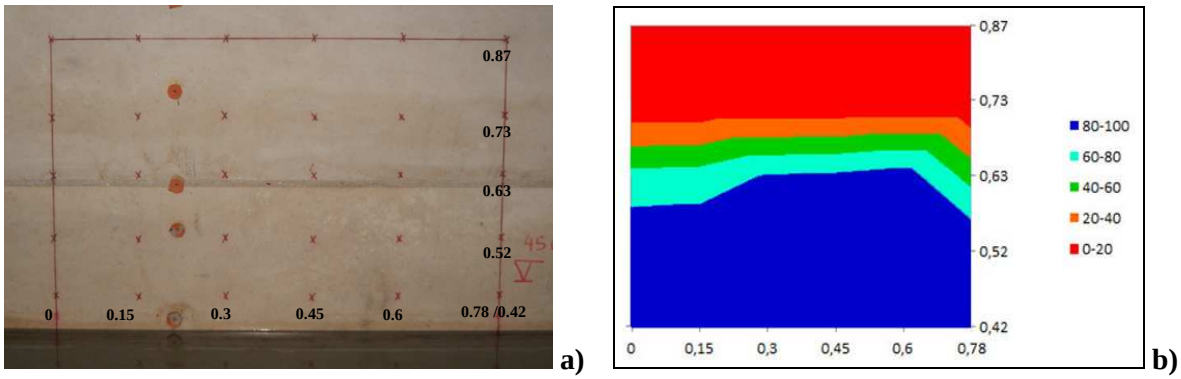

FIG 4. a) Grid dividing the area under study; b) Moisture detector results

3. Measurements results

3.1 Infiltrations

3.1.1 Classroom wall of the University of Porto – Faculty of Engineering

This study was carried out in a classroom of University of Porto – Faculty of Engineering where it was visible the degradation of the coating caused by the presence of water. The moisture source in the wall was an infiltration through the roof. This problem had already been repaired some months before the test was performed. Figure 5 shows, respectively, the visible and the thermal image. Figure 6 shows the results obtained using the moisture detector.

The results of the moisture detector show that the wall is not moist, as it was expected (Figure 6). These results are in accordance with the thermal image, because the colder area is not located were the coating is damaged but aligned with the ventilation grille located in the ceiling.

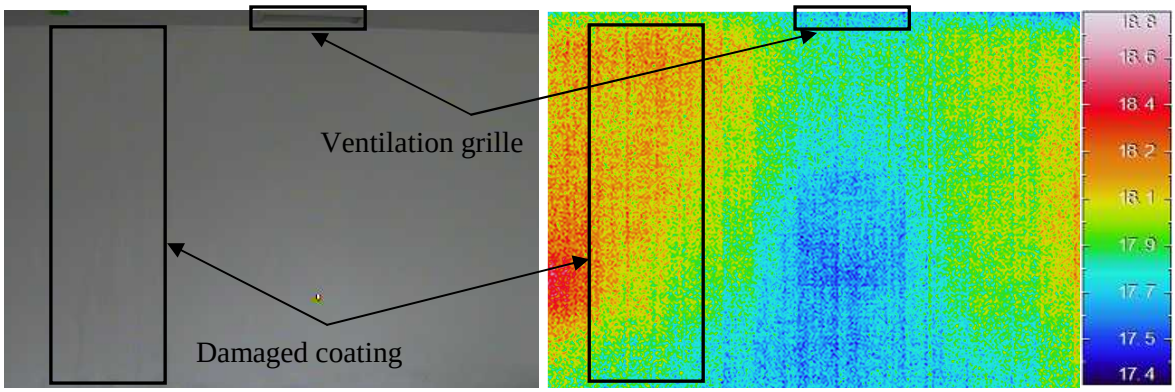

FIG 5. Visible and thermal image of the classroom wall

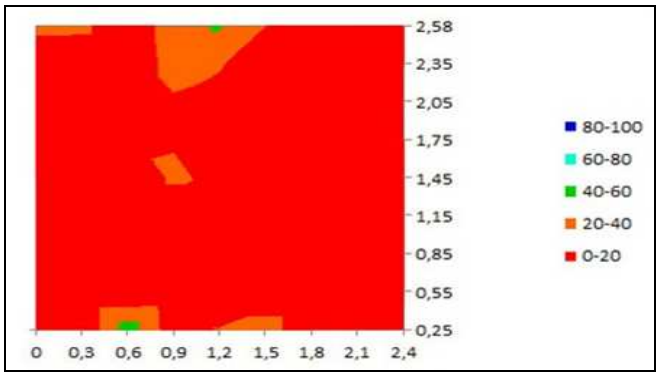

FIG 6. Moisture detector results of the classroom wall

3.1.2 Cafeteria ceiling and walls of the University of Porto – Faculty of Engineering

This study was carried out in the cafeteria of University of Porto – Faculty of Engineering, where it was visible the degradation of the coating caused by water infiltration through the roof. As three walls were damaged, the area under study was divided into 3 sections (Figure 7). This infiltration was detected a few days before the test was performed and was not repaired by that time. Figure 8 shows the thermal images of the area under study. Figure 9 shows the results obtained using the moisture detector, for sections A, B and C.

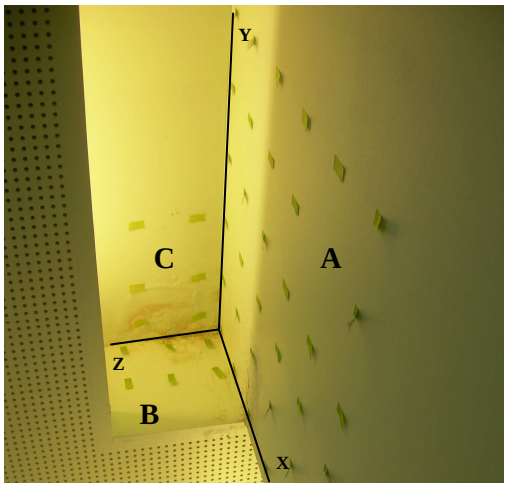

FIG 7. Cafeteria ceiling and walls – Area under study

The thermal images (Figure 8) clearly show a colder area near the corner, resulting from the evaporation of water infiltration. The colder area in the thermal image covers more area than the visible degradation of the surface, which means that thermography allows “see” further than the human eye. The results of the moisture detector (Figure 9) are in accordance with the thermal images, pointing the moister area near the corner.

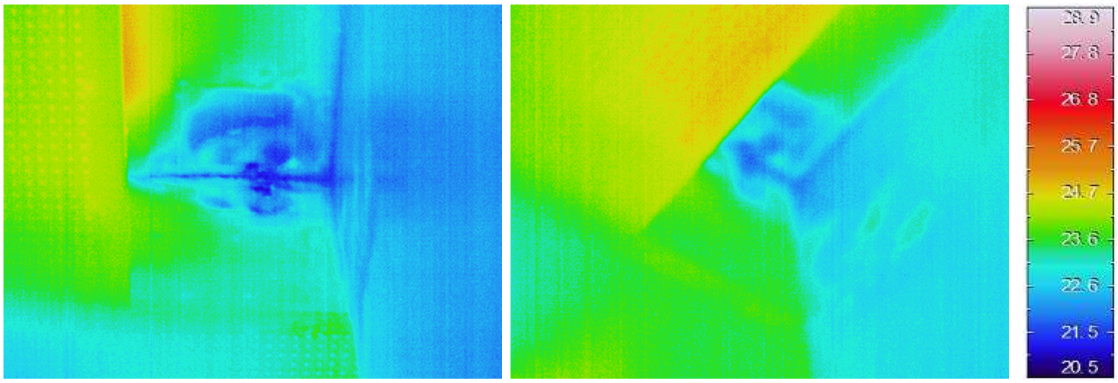

FIG 8. Thermal images of the ceiling and walls of the cafeteria

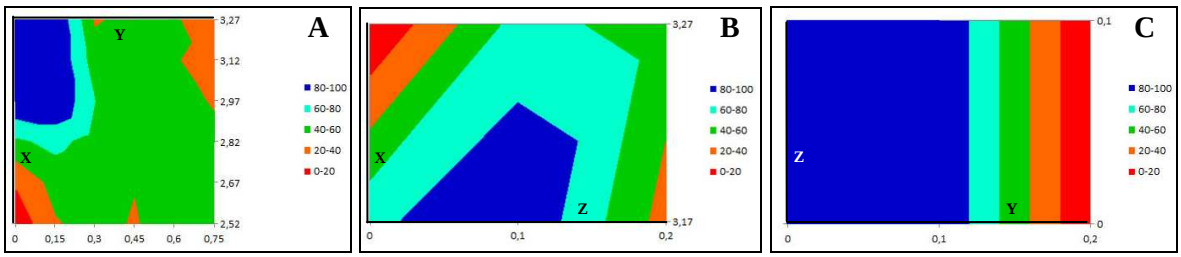

FIG 9. Moisture detector results of the ceiling and walls of the cafeteria (sections A, B and C)

3.2 Rising damp: exterior wall of a basement with the inner surface damaged

The wall under study is located in the basement of a building, used as a garage. It is next to the ground and it has clear signs of rising damp (Figure 10a shows degradation of the inner coating near the ground). Figures 11 and 10b show, respectively, the thermal image (as background is the visible image) and the results obtained using the moisture detector.

The thermal image (Figure 11) clearly shows a colder area near the ground, resulting from the rising damp evaporation. The upper lever of the colder area in the thermal image is above the visible degradation of the surface, which means that thermography allows “see” further than the human eye. The moisture detector (Figure 10b) shows that the wall is moister until 1.7 m from the ground, corresponding to the change in the superficial coating. That may related with the characteristics of the coat, as the lower coating seems to be less vapour-permeable than the upper one. Comparing the thermal image with the results of the moisture detector, they are not completely in accordance. Than may be related with the fact that thermography only detects surface evaporation and the moisture detector assesses inner moist.

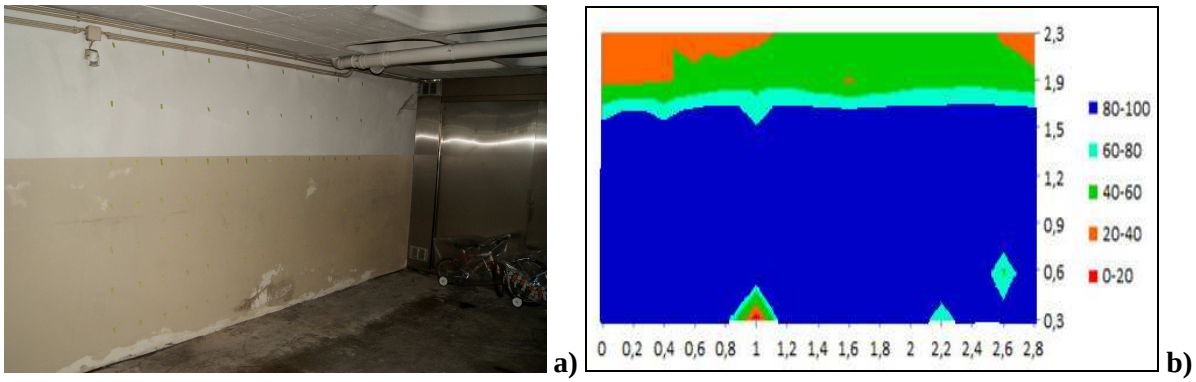

FIG 10. a) Basement wall under study; b) Moisture detector results for the basement wall

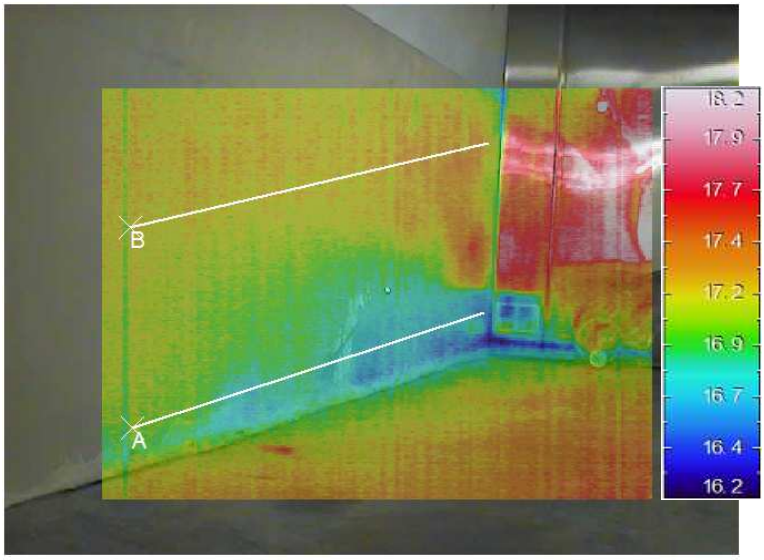

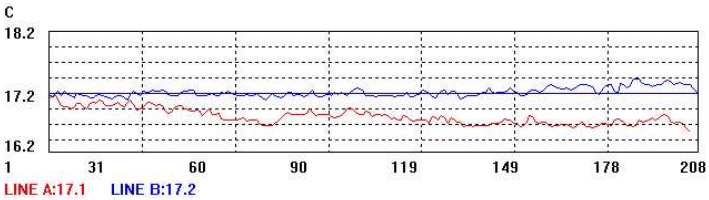

FIG 11. Thermal image of the basement wall (as background is the visible image)

4. Conclusions

Experimental tests showed that there is an agreement between the thermal images and the results obtained with the moisture detector. Besides, it was also possible to assess that thermography detects moisture beyond the visible signs of moist (stained or damaged areas). In conclusion, the results of this work indicate that thermography ought to be considered as a nondestructive assessment tool for the detection of moisture in porous materials, even when there are no visible signs on the surface.

However, further test must be carried out, namely, it is necessary to evaluate the potential of thermography using specimens in which the infiltration of water and the test conditions are well controlled and compare the experimental results with numerical simulation results. One the other hand, it is also necessary to establish test procedures and evaluation criteria, as the effect of other kind

of defects that cause temperature differences in the surface of the component can induce misinterpretation.

5. Acknowledgements

The research work presented herein was supported by FEDER funds through the Operational Programme for Competitiveness Factors – COMPETE and by national funds through the Portuguese Foundation for Science and Technology – FCT, under research project PTDC/ECM/114189/2009. J.M.P.Q. Delgado would like to thank FCT for financial support through the grant SFRH / BPD / 84377 / 2012.

References

ASTM-C 1060-90. 2003. Standard practice for thermographic inspection of insulation installations in envelope cavities of frame buildings. American Society for Testing and Materials ASTM.

Balaras C. A. & Argiriou A. A. 2002. Infrared thermography for building diagnostics. Energy and Building, 34(2), 171–183.

Barreira E. & Freitas V. P. 2007. Evaluation of building materials using infrared thermography. Construction and Building Materials, 21(1), 218–224.

CEN-EN 13187. 1998. Thermal performance of buildings – Qualitative detection of thermal irregularities in building envelops - Infrared method. European Committee for Standardization CEN.

Grinzato B., Cadelano G. & Bison P. 2010. Moisture map by IR thermography. J. Modern Optics, 57(18), 1770–1778.

Hart J. 2001. A practical guide for infra-red thermography for building surveys. BRE.

ISO 6781. 1983. Thermal Insulation – Qualitative detection of thermal irregularities in building envelopes – Infrared method. International Organization for Standardization ISO.

Lerma J. L., Cabrelles M. & Portalés C. 2011. Multitemporal thermal analysis to detect moisture on a building façade. Construction and Building Materials, 25(5), 2190–2197.

Maldague X. P. V. 1993. Nondestructive Evaluation of Materials by Infrared Thermography.Springer-Verlag.

Moropoulou, A., Avdelidis, N.P., Haralampopoulos, G., and Anagnostopoulou, S. 2002. Detection of Moisture in Porous Materials by Infrared Thermography, Proceedings of Thermosense XXIV, 4710:324-332, The International Society for Optical Engineering (SPIE), Bellingham, WA.

NEC nd. Thermo Tracer TH7800/TH7800N Operation Manual. NEC Avio Infrared Technologies Co.

Rajewski G. & Devine G. 1996. Building Envelope – Infrared thermography. Preventative roof maintenance workshop, Building operator association.

Rosina E., & Ludwig N. 1999. Optimal thermographic procedures for moisture analysis in building materials. Proceedings of society of photographic instrumentation engineers (SPIE), 3827, 22–33.

TRAMEX nd. Tramex LS Operation Manual.

Industry Standard ByggaF

Method for Including Moisture Safety in the Construction Process

Kristina Mjörnell, PhD, Business Area Manager for The Built Environment[1], Adjunct professor[2]

[1] SP Technical Research Institute of Sweden
[2] Building Physics, Lund University

KEYWORDS: *Moisture safety, moisture requirements, industry standard, construction process*

SUMMARY:
Bygga F – A methodology for including moisture safety in the construction process was presented in 2007. Since then, the methodology has been developed into a Swedish industry standard for the construction sector. ByggaF includes a method that secure, documents and communicates moisture safety throughout the construction process, from planning to management. The method involves a standardized way of working designed to meet the demands of society and the client's requirements for moisture safety. The purpose of ByggaF is to highlight moisture issues at an early stage in new construction, renovation and refurbishment projects and to document the activities and actions that are required and performed in a structured way to ensure a moisture-proof building. By formulating and setting moisture requirements and requirements for the activities, these can be incorporated into the program documents, system documents, construction documents and control plans, etc. This means that the important selection of system, materials and production methods that will impact the moisture safety of the building can be made from the beginning. The aim is to make it clear and easy for the building owner to work according to the methodology and support him or her in the formulation and following up of moisture requirements during the different phases in the construction process. The industry standard includes terms and definitions, a general description of the method and one section for each phase in the construction process. Under each heading there is text that contains "must-have" requirements that must be met. In addition, there is a guidance text to clarify, explain or give examples of what the "must-have" requirements mean.

1. Introduction

Moisture damage that affects our buildings is a major problem. Despite today's modern construction methods, the trend is not declining in terms of this type of damage. Moisture damage often causes a deterioration of the indoor environment, which in turn can have an adverse effect on human health. For home-owners, moisture problems often cause major unexpected expenses. The reason for moisture-damage arising in buildings is due to a number of different factors. This could be an ambiguous allocation of responsibilities, unclear requirements, lack of monitoring, unrealistic schedules, unclear communication between the stages, a lack of skills and inadequate procedures for moisture safety, but it could just as well be due to many different and often new types of structures, materials and components that are used where the materials are liable to degrade in the presence of moisture, with emissions, microbial growth and stability problems as a result. It is therefore extremely important to design moisture-proof structures composed of materials that can withstand the moisture load that the structure is expected to be exposed to during its service life, and to ensure a suitable environment for the building both during the construction stage and the operational stage. Requirements for moisture safety may often conflict with other requirements such as accessibility,

architectural and design requirements as well as energy requirements. These conflicts need to be addressed and resolved throughout the entire construction process.

In order to put more focus on the moisture issues and to work with them in a structures way in the construction process, Bygga F – A methodology for including moisture safety in the construction process was developed and presented in 2007. The methodology was then introduced to the Swedish construction sector and is today widely used by building owners (here referred to as clients), designers and contractors. The purpose of ByggaF is to highlight moisture issues at an early stage in new construction, renovation and refurbishment projects and to document the activities and actions that are required and performed in a structured way to ensure a moisture-proof building. By formulating and setting moisture requirements and requirements for the activities, these can be incorporated into the program documents, system documents, construction documents and control plans, etc. This means that the important systems as well as choice of material and production methods that will impact the moisture safety of the building can be made from the beginning. There have though been doubts about what parts of the ByggaF methodology are compulsory and what parts are optional. Therefore, the methodology was developed into a Swedish industry standard for the construction sector. The aim with this paper is to disseminate awareness and knowledge about the Swedish industry standard and make it available for other countries to apply in their quality management work.

2. Description of the method

2.1 Overall description

Industry standard ByggaF includes a method that secure, documents and communicates moisture safety throughout the construction process, from planning to management. The method involves a way of working designed to meet the demands of society and the client's requirements for moisture safety.

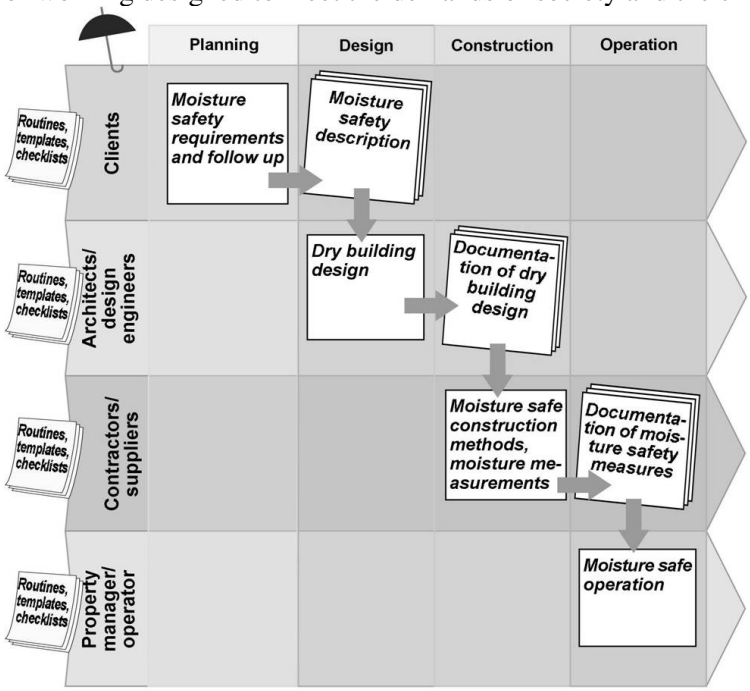

FIG 1 Overall picture of the ByggaF method.

Under each heading in the standard there is text that contains “must-have requirements” that must be met. In addition, there is a guidance text that can clarify, explain or give examples of what the “must-have requirement” means. The guidance may also contain advice.

2.2 The client is responsible

The client is the one who performs or fails to perform the planning, construction, alteration, renovation, demolition or excavation work. In Sweden the client must ensure that this is carried out in accordance with the requirements applicable to the measures in the Swedish Planning and Building Act (PBL), or regulations or decisions communicated with support of the Act. If the measures are subject to permits or notification, the client must ensure that they are checked according to the inspection plan that the local building committee determines in the start-up statement. (Chap 10, Section 5). Regulations are given in The Swedish National Board of Housing, Building and Planning’s building regulations that set society’s minimum requirements for the building.

In order for the building to be planned and designed correctly, the client should engage the appropriate skills for the different work tasks. In many cases, the client hires a project manager as an extended arm in the construction process. However, the client is still responsible for compliance with the laws and regulations.

The client does not always possess enough knowledge or time to pursue and monitor the moisture safety work in the project. It can be very helpful for the client to hire a person who is an expert in moisture safety, a moisture expert. The moisture expert can help the client to set requirements for moisture safety and to monitor compliance of the requirements.

2.3 Organization for moisture safety work

However, the practical moisture safety work is performed by all participants, planners, designers, contractors and suppliers.

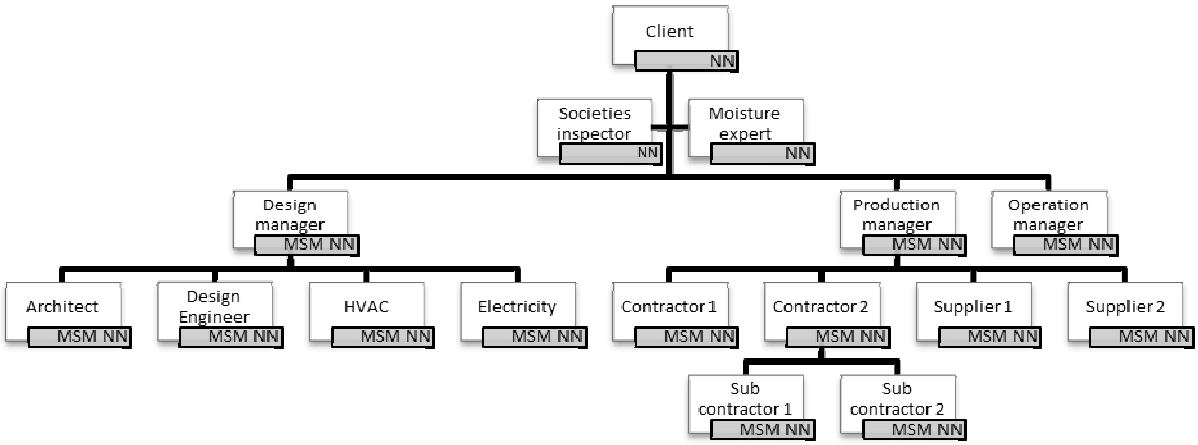

FIG 2 Example of the organization of the responsibility for the moisture safety work. Each participant designates a moisture safety manager (MSM) whose name (NN) is listed in the organizational chart.

The allocation of responsibility for different activities at different stages may vary with different forms of construction contract. Depending on the contract form, the responsibility boundaries are moved between systems planning, detailed planning and production. In the forms of contracts where the contractor also has the role of the planner, the contractor must also take responsibility for what in this document are called planners’ activities and responsibilities. In design and construct contracts, the responsibility for continually monitoring the moisture safety work lies with a coordinating moisture

safety manager for production. The client usually establishes the moisture safety specification, but for a design and construct contract the client may want to transfer all responsibility to the contractor. In these cases, the design and construct contractor can formulate the moisture safety specification on behalf of the client. The information in the moisture safety specification can also be found in other documents. In the following sections the compulsory activities are as shown.

2.4 Moisture safety in the program stage

2.4.1 Moisture expert

The first thing the client should do is to appoint a moisture expert. Our experience is that involving a moisture expert following up the moisture safety work in the project is of crucial importance for the result. The moisture expert will support the building owner in decision making, information, following up on design, reviewing of construction documents, following up on production, handling non-confirmations and compilation and handing over of final moisture safety documentation etc.

2.4.2 Early risk assessment

To start with the moisture expert will support the client making the early moisture risk analysis which he or she is responsible for. By making an early risk analyses before the mayor decisions about the buildings location, foundation practices, principles for handling rainwater, drainage systems, supporting framework, construction methods etc. are made, moisture critical constructions and designs could be avoided, which will save time and money in the long run.

2.4.3 The clients' requirements

The moisture expert may also help the client to decide on the moisture safety requirements to be set in the project. It must be possible to verify and monitor the moisture safety requirements. The requirements must include both technical requirements and requirements for activities and skills. It is of crucial importance that the moisture safety requirements are documented in a moisture safety program, in the moisture safety specification or in other contract documents, in order to be in force in agreements between the client and consultants and contractors. It is also required that the client describes the methods to be used in the project to monitor compliance with these requirements as well as actions to take in case of non-conformance.

2.5 Moisture safety in the systems planning and design stage

Depending on the contract form, the responsibility boundaries are moved between systems planning and detailed planning as mentioned in section 2.3. In many construction projects there are two different groups of people engaged in planning and design of the building, one team working with the early stages and one team responsible for detailed design. The following procedures must be carried out by all teams, however on a completely different level of detail.

2.5.1 Information to planners and designers

Already in the procurement and contracting of planners and designers it is important to inform them about the moisture safety requirements and the methods that will be used to monitor compliance of the requirements. This is appropriately done by the moisture expert.

2.5.2 Moisture safety design

Each participant in the design phase who selects, designs, draws and constructs materials, building elements or installations that affect the moisture safety of the building must designate a person as responsible for performing a moisture risk analysis and inspection ensuring the systems and material

selections meet moisture safety requirements and that this is documented and reported to the moisture expert and client. They must also present a procedure for how they plan to carry out a moisture risk analysis and inspection showing that the chosen systems meet the moisture safety requirements and how this is to be documented. In the subsequent design they should follow the procedure for moisture safety design. To start with, all structures and materials sensitive to moisture and moisture critical work operations must be identified. The next step is to estimate the moisture condition that the various building elements and materials as well as combination of materials will be exposed to and describe how they vary in time. Then the estimated moisture conditions are to be compared with the permitted moisture conditions in order to evaluate the probability of damage to occur.

2.5.3 Moisture risk analyses

In the end of the planning or design process, the team must jointly conduct and document moisture risk analysis, even though it is the design manager who is responsible for the coordination of the risk analysis. A new moisture risk analysis should be performed if conditions change, for example if materials or designs are changed. In the risk analyses the probability of any damage caused by moisture to occur is evaluated as well as the consequence of the damage. If the risk value is high the design of the construction has to be altered in order to fulfil the requirements.

2.6 Moisture safety in the production stage

2.6.1 Ahead of production

When contractors, sub-contractors and suppliers are contracted it is important that the moisture expert informs about the moisture safety requirements and the methods that will be used to monitor compliance of the requirements.

Ahead of production, the moisture expert supported by project planners and designers must notify the main contractor of the result of the moisture safety planning. This could be arranged as a joint meeting with all actors participating in planning and design process as well as the contractor assigned for the production stage. At this meeting the planners and designers have the opportunity to motivate their choice of construction and designs and can also answer questions regarding the drawings and technical descriptions. This is also an opportunity for feedback on the planning and design process.

Each planner and designer must also forward any written documentation to the moisture safety manager for production regarding identified critical elements, structures and installations resulting from the moisture safety planning and design. The documentation must specify the type of measures along with the documentation required by the moisture safety manager for production in order to reduce the risk of moisture damage and other inconveniences caused by moisture arising in production.

Before production starts, all participant who produces, assembles materials, building elements or installations that affect the moisture safety of the building must designate a person responsible for ensuring moisture safety work is performed, documented and reported in the production stage to the client.

2.6.2 Moisture safety plan for production

The first thing to start with for the moisture safety manager is to identify moisture-sensitive elements, structures and installations that are important in production and to prepare a moisture safety plan. A moisture safety plan describes the moisture safety measures to be undertaken in order to protect the building and construction materials from damaging moisture during production and must also include the control points identified during the planning stage. The moisture safety manager for production

must ensure the implementation of the activities in the moisture safety plan as well as implementation and documentation the measurement and inspection according to the moisture safety plan.

2.6.3 Measurement and inspections

The moisture safety manager for production is responsible for executing and documenting the measurements and controls according to the moisture safety plan. The measurements have to be performed using standardized measuring methods.

2.6.4 Following up meetings

It is the client's moisture expert who is responsible for convening, conducting and documenting regular monitoring meetings with contractors and suppliers.

2.6.5 Moisture inspection rounds

The moisture safety manager for production is responsible for conducting and documenting moisture inspection rounds at the construction site at a rate agreed between the contractor and the client depending upon what activities are on-going. However, the moisture expert is also to conduct moisture inspection rounds by himself or together with the moisture safety manager for production. In case any non-conformance in relation to the moisture safety plan occurs, it is the moisture safety manager who is responsible for documentation and reporting on the proposed measures to the client's moisture expert.

2.6.6 Documentation of the work

The moisture safety manager for production is responsible for collecting data for operation and maintenance instructions for moisture safety from subcontractors and suppliers as well as data from the moisture safety work carried out by subcontractors and suppliers, and submit this to the moisture expert, who in turn compiles the moisture safety documentation from planning and production and submits it to the client.

2.7 Moisture safety in the operation stage

In the commissioning stage when the building is handed over to the building owner, the client's moisture expert and the moisture safety manager for production are to hold a review with the responsible administrator and operations manager about the moisture critical structures of the building and the measures to be carried out to ensure that moisture safety is maintained. During subsequent management of the building, it is the operation manager, on behalf of the building owner, who is responsible for carrying out recurrent operational inspection rounds, in which moisture safety is one of many aspects to be considered.

3. Conclusions

The industry standard ByggaF includes a method that guarantees, documents and communicates moisture safety throughout the construction process, from planning to management. The industry standard involves a standardized way of working designed to meet the demands of society and the client's requirements for moisture safety. The purpose of the industry standard ByggaF is to highlight moisture issues at an early stage in new construction, renovation and refurbishment projects and to document the activities and actions that are required and performed in a structured way to ensure a moisture-proof building. By formulating and setting moisture requirements and requirements for the activities, these can be incorporated into the program documents, system documents, construction documents and control plans, etc. This means that the important systems and material selection and production methods that will impact the moisture safety of the building can be made from the

beginning. The aim is to make it clear and easy for the building owner to work according to the methodology and support him or her in the formulation and following up of moisture requirements during the different phases in the construction process. The industry standard includes terms and definitions, a general description of the method and one section for each phase in the construction process. Under each heading there is text that contains “must-have requirements” that must be met. In addition, there is a guidance text that can clarify, explain or give examples of what the “must-have requirement” means. The guidance may also contain advice. One part of the standard describes the methodology for moisture design and moisture risk assessment. There are also templates for estimation of probability, consequence and risk assessment for each construction detail. The industry standard has been developed in collaboration between researchers, building owners, contractors, design engineers and authorities. It is an open access standard available to down load at www.fuktcentrum.se. The English version makes it possible to use the industry standard not only in Sweden but also in other countries and in international construction projects. It is however necessary to adapt the requirements in the standard according to existing conditions and regulations in other countries.

4. Acknowledgements

The development of the industry standard ByggaF has been founded by SBUF, the Development Fund of the Swedish Construction Industry, participating organisations and companies. A number of persons from different organisations and companies have participated in the work developing the industry standard: PEAB, NCC, Skanska, JM, SydArk Konstruera AB, Akademiska Hus, Polygon Sverige AB, FuktCom, SP, IVL, LTH, CTH, Sveriges Byggindustrier, FoU-Väst, Säker Vatten AB, Boverket och Byggherrarna. The industry standard is administered by Fuktcentrum (Swedish Moisture Research Center).

References

ByggaF metod för fuktsäker byggprocess. *ByggaF method for moisture safe building process*. FoU Väst Reprt 2007/02. In Swedish.

Branschstandard – ByggaF, *Industry Standard ByggaF*. Version 2013-05-08. Available at www.fuktcentrum.se. Access date 6/12/2013, Swedish and English versions are available.

Mjörnell, K, Arfvidsson, J, Sikander, E, A Method for Including Moisture Safety in the Building Process, Indoor and Built Environment, 2012;21;4:583-594.

Swedish Building Regulations, BBR

The Planning and Building Act, PBL

WUFI®, PC-Program for calculating the coupled heat and moisture transfer in building components, Fraunhofer Institute for Building Physics.

TorkaS 3.0, PC program for estimation of drying times for concrete slabs. Available at http://www.fuktcentrum.se. Access date: 02/07/2013.

BIDry, PC program for estimation of drying times for concrete slabs. Available at http://www.bidry.se. Access date 02/07/2013.

RäknaF, Instructions and recommendations for moisture calculations. Available at http://www.fuktcentrum.se. Access date: 02/07/2013.

TOPIC
Retrofitting of Buildings

Page.....1172-1356

Holistic retrofit and follow-up through monitoring: Case Virkakatu, Oulu, Finland

Yrsa Cronhjort, M.Sc. Architecture [1]
Simon le Roux, M.Sc. Architecture [1]

[1] Aalto University School of Arts, Design and Architecture, Finland

KEYWORDS: *E2ReBuild, monitoring, retrofit, residential, TES-system, user interface*

SUMMARY:
Case Virkakatu, Oulu, exemplifies an extensive retrofit of an apartment building representing the prefabricated concrete element BES system. The original house was built according to Finnish building standards of the early 1980´s. Building works included a complete refurbishment of the interiors, a renewal of the building envelope including floor slabs, facades, windows, doors and the roof. New building service systems were installed. The apartments were equipped with separate air ventilation units with efficient heat recovery, and the target was for passive house level according to the local suggestion by VTT. This site is the second building in Finland in which the facades have been retrofitted using timber based elements, the TES-system. The demonstration is one of seven pilots realized within the EU Fp7 funded project E2ReBuild. The project has developed a monitoring plan that was adopted and extended in case Virkakatu. The building envelope is monitored for moisture and temperature, the indoor air quality is surveyed through following ventilation operation, carbon dioxide levels, and room temperature. Energy usage including heating, hot water and electricity is measured. The monitoring is completed with an own weather station on site. The user is involved with apartment wise user interfaces. The monitoring scheme has proved a useful means to prove retrofit results, follow energy use, and secure the functionality of building service systems.

1. Introduction

Case Virkakatu, Oulu exemplifies an extensive energy retrofit of an apartment building representing the concrete element BES-system developed in the 1960´s and typical Finnish housing production. The system is based on the use of standardized prefabricated elements and joint details. The load bearing structure of the demonstration building is a bookshelf frame with a precast concrete sandwich facade.

The building in Oulu is two storeys high, and contains 8 student apartments. The original gross floor area was 744 m^2 and the heating was based on district heating. The building was constructed according to Finnish building standards of the early 1980´s.

Before building works the condition of the building and its structures was analysed: The original floor slab consisted of a 70 mm reinforced concrete slab isolated with 50 mm expanded polystyrene and the original facades of an 80-85 mm thick external layer of brickwork, 130-140 mm of thermal wool insulation and an inner layer of concrete. The facade structure was additionally analysed using GPR survey, as an experiment, as to verify the surface profile of the inner concrete layer.

The building is part of a housing cooperative with five apartment buildings and a service building with communal facilities. As part of the EU FP7 funded project E2ReBuild one of the buildings was refurbished. The other buildings will be renovated at a later stage in a conventional manner with less demanding targets for energy efficiency. These will be monitored for comparison.

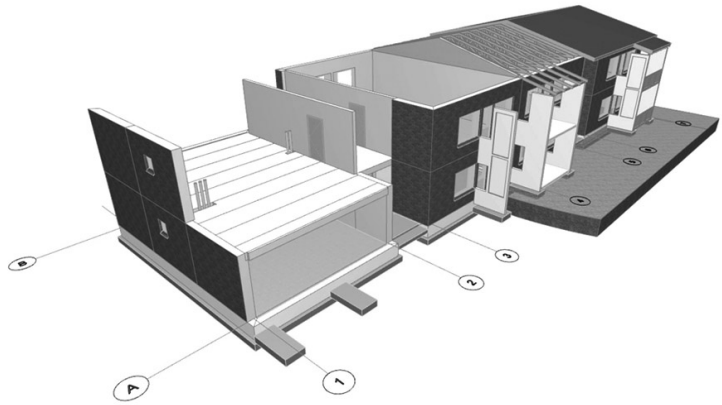

FIG 1. The structural core of the case building in Finland represents the BES system with a load bearing concrete frame and precast concrete sandwich façade elements. Image Simon le Roux.

2. Refurbishment Case Virkakatu

Case Virkakatu is one of seven demonstrations within the EU FP7 funded project E2ReBuild. The project applies, demonstrates, evaluates and follows up the results of various cost effective and advanced strategies for industrialized retrofitting of residential buildings. The common targets for the demonstrations are to improve the overall energy efficiency as to fulfil at least national limit values for the energy use in new buildings and to reduce the space heating demand by at least 75%. (E2ReBuild 2013)

The objective for the refurbishment in Oulu was to reach passive house level of energy efficiency according to the local suggestion by VTT (Nieminen Lylykangas 2009), a level above current demands for new building. The chosen strategy was a holistic retrofit including the application of TES Energy Facade for improving the thermal insulation and air tightness of the building envelope.

Building works included a complete refurbishment of the interiors and the building envelope including floor slabs, facades, windows, doors and the roof. New building service systems were installed. The aim was to create student family apartments responding to modern living requirements.

Building works on site started with the removal of the original in-situ ground floor slabs and the external layer of concrete and brickwork from the precast facade elements. The old thermal insulation layer was stripped away. New facades were manufactured from prefabricated, timber based elements (TES, FIG 2-4). The facade elements consisted of a load bearing timber frame and glass mineral wool thermal insulation, gypsum wind barrier boarding on the outside and plywood on the inside. A thin thermal insulation layer was added to the elements on site as an adjustment layer between the elements and the uneven existing concrete surface. External cladding and windows were assembled on site. The total thickness of new thermal insulation in the completed facade is 300 mm with a U-value of 0.11 W/m^2K (FIG 5). A 200 mm thick layer of graphite-enhanced EPS thermal insulation was installed beneath the new ground floor slab and 550 mm of blown loose fill mineral wool was installed in the roof, with U-values of 0.11 W/m^2K and 0.08 W/m^2K respectively (FIG 6). Inward opening wood aluminium passive house casement windows were installed, with an average U-value of 0,8 W/m2K. Special attention was paid to improving the airtightness of the building envelope, with an original measured n50 value of 3.3 l/h and 0.8 l/h after renovation works (Puotiniemi 2012, Puotiniemi 2013). Corresponding measured q50 values were 3.1 m3/h*m2 and 1.2 m3/h*m2 (Puotiniemi 2012, Puotiniemi 2013).

This site is the second building in Finland in which the facades have been retrofitted using timber based elements, the TES system, and the most northern demonstration in project E2ReBuild. The EnerPhiT Passive House Certificate for old buildings in accordance with EnerPhiT criteria for Residential-Use Refurbished Buildings (Feist 2010) is to be considered.

FIG 2-4. The façade retrofit started with the removal of redundant structures and an uneven inner concrete surface was revealed. A thin layer of thermal insulation was added as an adjustment layer to the prefabricated timber based façade elements prior to assembly. TES-elements were finally assembled directly onto the existing building, thus forming a new façade. The cladding was installed on site. Image to the left: Simon le Roux. Images 3 and 4: Jaakko Kallio-Koski M3 Architects.

The old roof of the building was also demolished and replaced by a new roof and thermal insulation. The roof structure was prefabricated in four sections on site and lifted onto the building as elements.

Air-tightness of the building was improved by several measures. The original concrete frame was repaired before adding the new facades and ground floor slab as it had significant air leaks which were filled with cement grout. The TES-elements were encapsulated with plywood and a wind barrier. The air-tightness of window and door fittings, ceilings and duct penetrations was ensured on site during installation works. Windows were sealed to the inner concrete frame with a polyurethane based elastomeric joint sealant. The remaining air leaks after refurbishment were determined to derive from shrinkage of the new in-situ concrete floor slab during the drying of the concrete (Puotiniemi 2013).

The internal works included a remodelling of the student flats into family apartments with renewed floor plans, new kitchens and bathrooms including saunas and new surfaces. The lighting was replaced with energy efficient LED fixtures. The apartments were additionally upgraded with separate air ventilation units with rotary heat exchangers of an annual heat recovery efficiency rated 75.7%.

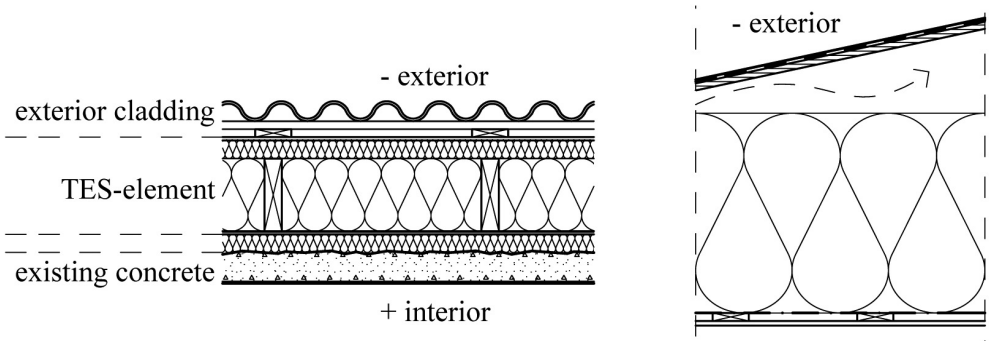

FIG 5-6. Façade and roof structure after refurbishment. Outer façade layers were removed leaving the inner concrete layer in place. A new façade was retrofitted with prefabricated timber based elements. The U-value of the finished wall is 0.11 W/m2K. The old roof was completely replaced, adding 550 mm thermal insulation, resulting in a U-value of 0.08 W/m2K. The external wall structure from the outside: cladding, 22+22 mm air gap, 9mm wind barrier GU 9, 50 mm thermal insulation layer, 200 mm thermal insulation layer, 9 mm plywood board, 50 mm thermal insulation (adjustment layer), old inner concrete layer. The thermal insulation is glass mineral wool. Images: Simon le Roux.

3. Monitoring Scheme

Project E2ReBuild includes one Work Package devoted to the monitoring and follow up of the implemented retrofit strategies; WP5 Innovation in Operation and Use. Within this Work Package a monitoring scheme was designed to be applied in all demonstrations of the project. This monitoring scheme was implemented and extended in case Virkakatu to also include monitoring the building physics performance in addition to measuring the attributes directly related to energy use.

The building facades, ground floor slab and roof are monitored for moisture and temperature. Indoor air quality is surveyed by following the ventilation operation, carbon dioxide levels, and room temperatures in selected apartments. Energy usage including space heating, domestic hot water and electricity is separately measured for the building as a whole and for individual apartments. The monitoring is completed with an onsite weather station. The user is provided with a digital display of real-time information on private electricity and water usage in each apartment. In this paper our focus is on the follow-up of the energy use in the building and the effects of the monitoring scheme. See Table 1 below.

TABLE 1. Oulu demonstration monitoring scheme

Main parameters for comparison	Comments	User interface
Purchased energy	Shared by 5 houses	
Space heating	District heating	
Domestic hot water	Flow and temperature	x (volume)
Building electricity		
Household/tenant electricity		x (kWh)
Additional parameters		
Indoor dwelling temperatures and RH	2 apartments	
Indoor CO_2	1 apartment	
Outdoor temperature, RH and irradiation		x (temperature)
Airtightness and thermal imaging		
Ventilation rates, electricity	Operation	
Building envelope performance		

The monitoring is followed up through an online interface with access to all data. The interface includes an alarm function, allowing for early intervention in case of malfunction of i.e. an air ventilation unit.

Airtightness was measured before and after refurbishment using a blower door test and thermal imaging (Puotiniemi 2012, Puotiniemi 2013). Reference data on purchased energy, space heating and building electricity was collected also prior to building works.

The monitoring is realized using a digital building automation system, which collects measurement input to a programmable substation (FIDELIX FX-2025a Digital Controller), from which data is transferred via virtual private network to outside monitoring. The controller interface has input/output modules to directly connect the network of different monitoring points around the building (36 channel combination module, 16 channel digital input and 8 channel analogue input modules). The substation communicates with the input modules using Modbus communication protocol (Modbus RTU RS-485), and also collects monitoring input from all eight apartment ventilation units (ENERVENT PINGVIN eco ECE ventilation unit Multi Web-ModBus). Each apartment has a FIDELIX Multi-LCD room panel with 3,5” colour LCD touch screen, programmed to display hot and cold water volume, electricity meter and outdoor temperature, daily, weekly and monthly use.

The building automation controls the supply of heating water from the district heating heat exchanger according to the current outdoor temperature using a valve actuator (HRYD24-SR). Outdoor

conditions are monitored with a weather station (DAVIS Vantage Pro2 Plus) and outdoor illumination and temperature sensors (PRODUAL LUX 11 + NTC 10).

An ultrasonic compact energy meter (SHARKY 775) is installed to measure and calculate the total energy demand in district heating for space heating and domestic hot water. Immersion temperature sensors (PRODUAL TEAT NTC10) and the flow meter together measure the overall space heating delivered to the radiators and the domestic hot water supplied to each apartment.

Two apartments are monitored for indoor temperature/humidity with transmitters in 4 rooms (PRODUAL KLH100), and with $C0_2$ transmitters in air intake and exhaust ducts (PRODUAL HDK).

Structure humidity and temperature sensors are installed in four TES elements which face north, south, east and west, and in the ground floor slab (HONEYWELL HIH-4010 moisture sensors and PRODUAL TE NTC10 temperature sensors). The roof insulation is monitored with PRODUAL KLU-100 outdoor humidity and temperature transmitters. (Palosaari 2013)

4. Experiences and Results

The building works on site were finished in February 2013 with the first tenants moving in 1st of March. Hence the monitoring is in its early phases covering a period of 9 months and excluding the winter period, but nevertheless, shows the effects of the refurbishment.

As to illustrate the results of the energy retrofit the energy demand for space heating and domestic hot water before, as simulated and after were compared (FIG 7). The energy demand before is the monthly average based on the last eight year purchased district heating for the whole building complex. The simulation prior to renovation was done using the IDA Indoor Climate and Energy dynamic simulation tool for studying thermal indoor climate and energy consumption of the building (Equa). Assumptions were made in the simulation of the average domestic hot water demand based on Finnish regulations. As seen in the graph, the simulated heating demand after refurbishment is higher in summer than the previous average purchased energy for the same months of June to August, which suggests that the simulation has a large safety margin for worst cases, or that students use less water in summer than expected. Estimates were made in the simulation to include the influence of additional heating coming from tenants' use of under floor electrical comfort heating. A calculation was also made of the average heat losses in the transfer of space heating and hot water in underground heating pipes from the centralised district heating heat exchanger of the building complex. The actual monitored heating use excludes the heat losses in underground pipes, which are outside the case study building. However the heat losses are estimated to be at worst 10 – 15%, and even so the current monitored energy use is less that the simulated energy demand.

The energy demand in the graph (FIG 7) is calculated according to the Finnish standard calculation methodology for the total gross floor area of the building. The comparison of energy performance is complicated by the variety of definitions for floor and volume. Care had to be taken to check for inconsistencies in figures used by different designers, energy calculations, planners and authorities. The size of the building grew slightly after refurbishment, since the volume was filled in places, which increased the net floor area. The thickness of the external walls, ground slab and roof insulation was increased, but the leasable floor area remained approximately the same. The volume calculation of the building was particularly complex, since the external surface is multi-layered and irregular. (TABLE 2)

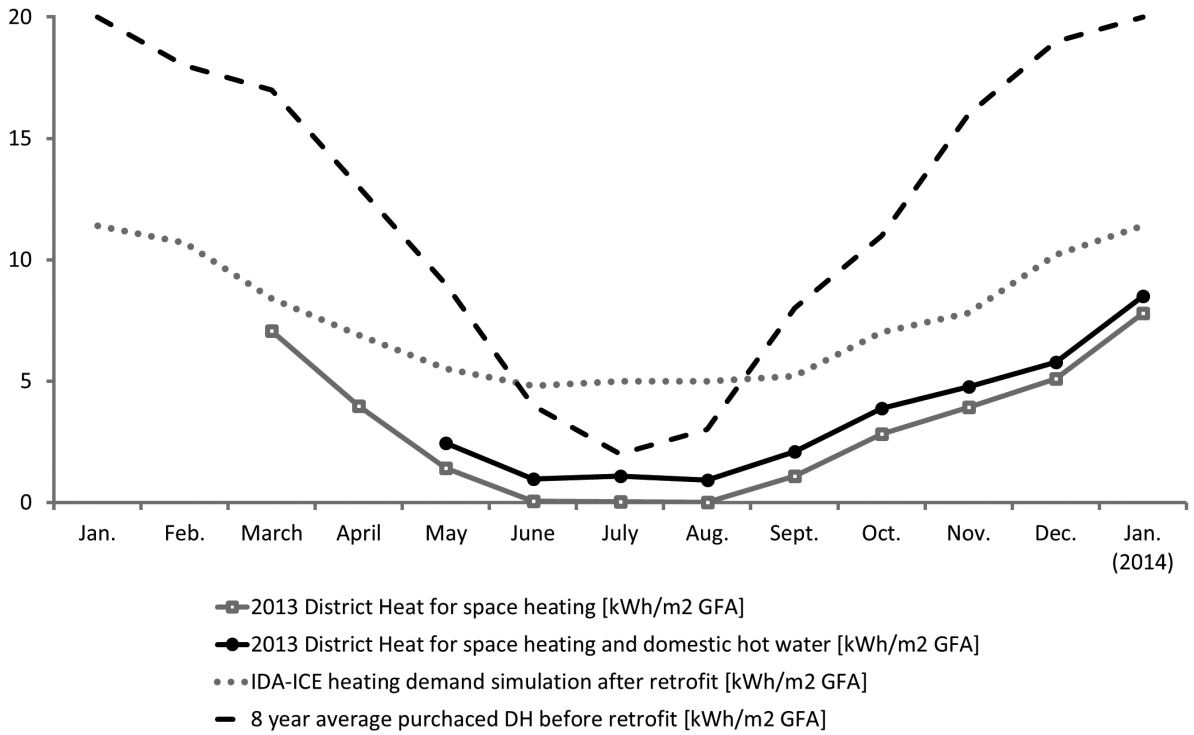

FIG 7. First 9 months monitoring results of energy use for space heating and hot water case Virkakatu, Oulu, Finland. Graphs from the top: Average purchased district heating energy for space heating and hot water before, IDA-ICE simulated energy demand for space heating and hot water after, Monitored energy demand for space heating and hot water after, Monitored energy demand for space heating only after refurbishment. Numbers are net energy without normalization. The demand is calculated for the gross floor area of the building. The image shows a dramatic drop in energy demand, averaging a 60% decrease in energy consumption for space heating and hot water after refurbishment. Image Simon le Roux.

TABLE 2. Case Virkakatu, Oulu, Finland details of the building

Parameters	Before	After
Total gross building volume	2196 m3	2439 m3
Total heated/cooled net volume	1802 m3	1875 m3
Air volume	1732 m3	1798 m3
Total gross area	744 m2	791 m2
Leasable area	572 m2	578 m2
Apartments and stairwells	633 m2	661 m2
Total heated/cooled net floor area (internal)	652 m2	680 m2

The savings in energy demand for space heating and hot water benefits in this case the building owner, PSOAS. In Finland, the rent for an apartment includes space heating and hot water, sometimes paid for separately as a lump sum based on the number of dwellers in the apartment.

In addition to the rent, the tenant pays separately for his own electricity directly to the electricity distributor. As to allow for user control of their own, personal energy consumption for electricity, the apartments were equipped with user interfaces monitoring the apartment´s use of hot water and electricity. Over the period of the first 8 months the results show a great variety in usage with less consumption during the summer months, typical vacation time in Finland. However, the tenants of one

apartment reported on following their electricity use from the interface and having saved 25% in electricity by changing their own behaviour accordingly. (FIG 8)

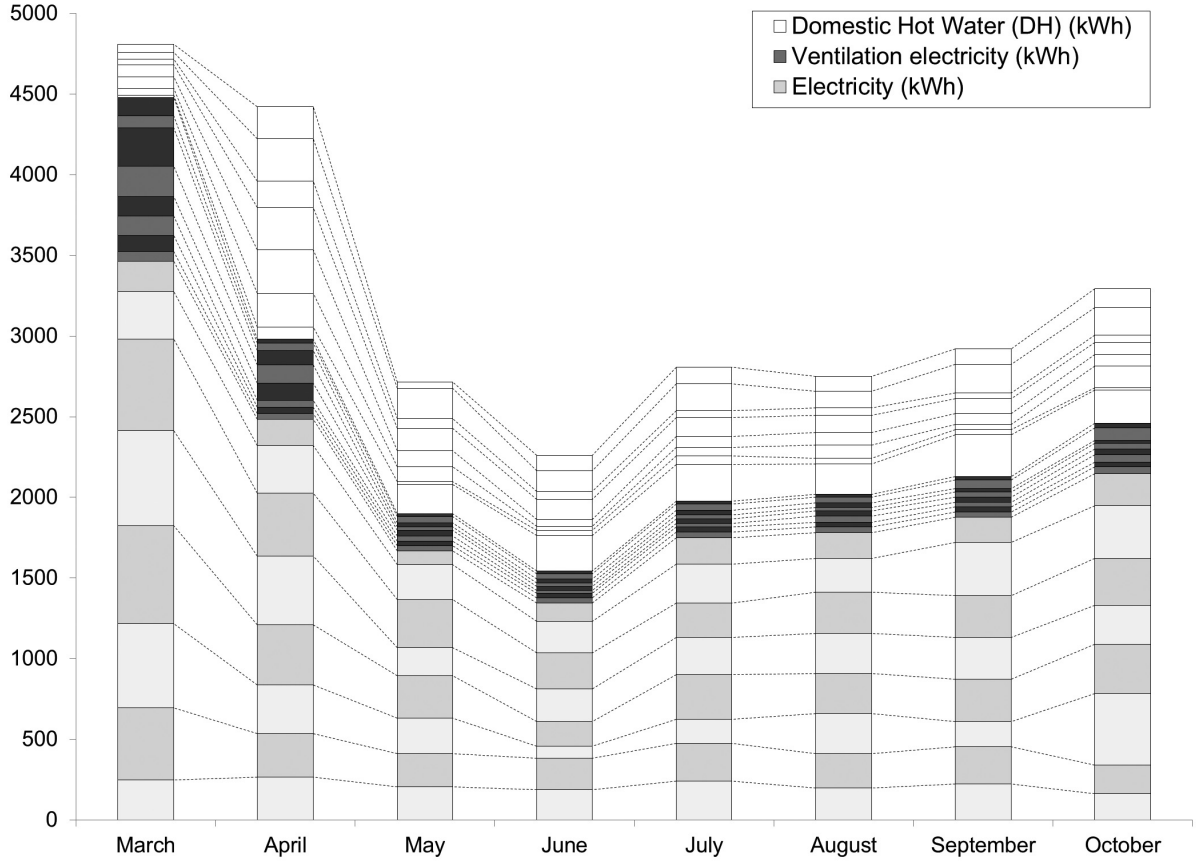

FIG 8. First 8 months monitoring results of energy use for hot water, ventilation and electricity in single apartments case Virkakatu, Oulu, Finland. Graphs from the top: Hot water use 8 apartments, ventilation 8 apartments, and electricity use 8 apartments. Measurement units in kWh. After the first months the energy demand for ventilation units has stabilized as well as the average demand for hot water. The user electricity shows the biggest fluctuation. This fluctuation may be caused by vacations in summer time and the increased need for artificial interior light towards the dark winter months. Only one apartment shows a fairly constant level of electricity use after the first two months. The graph shows full measures for the months from March through October 2013. Image Simon le Roux.

The monitoring scheme has proved a useful means to prove retrofit results, follow energy use and secure the functionality of building service systems. The first two months showed unreliable measures for the use of hot water, but since then the monitoring results have stabilized at average levels of 30,2 kWh energy used for ventilation and 98,5 kWh energy used for hot water per apartment and month. With an average leasable floor area of 71,5 m2/apartment this equals, on average, 0,42 kWh/m2 leasable area of net energy used for ventilation per month or 5 kWh/m2/annum, with 1,38 kWh/m2 leasable area of net energy used for hot water per month or 16,5 kWh/m2/annum. These results indicate that by using water saving showerheads and dual flush toilets in the apartments, the average water usage after refurbishment is 55% less than assumed in building regulations. The building owner had already installed water saving showerheads in the apartments in 2009. The user interface has proven useful for affecting user behaviour in one of the eight case apartments.

5. Conclusions

The paper presents a comparison of energy use before an extensive building refurbishment, simulated energy use and monitored energy use after refurbishment. The case building is a two storey high apartment building situated in Oulu, Finland. Coordinates of the location are 65° 01' N, 25° 28' E (Oulu). The aim for the refurbishment was passive house level of energy efficiency according to local suggestion by VTT. A comprehensive monitoring scheme was applied to the project as to verify and follow up achieved results for energy efficiency, functionality of applied timber structures and achieved interior air quality. The results for the first eight months indicate a high level of energy efficiency including 55% savings in the use of hot water as compared to simulation. Additionally, the results indicate a positive effect on tenant´s use of electricity and hot water as a result of their access to real-time data through apartment wise user interfaces. Overall the monitoring scheme has proven an efficient and easy approach to verifying the results of an ambitious refurbishment project.

6. Acknowledgements

The paper is based on research and academic support for the passive house demonstration in Oulu, Finland, realized within the EU FP7 funded project E2ReBuild Industrialised energy efficient retrofitting of resident buildings in cold climates. The project is coordinated by Christina Claeson-Jonsson, NCC AB. The project started in January 2011 and ends in June 2014. Partners from Finland include the Aalto University, NCC Rakennus Oy and Pohjois-Suomen Opiskelija-Asuntosäätiö PSOAS. The monitoring scheme for the Oulu demonstration project was developed in collaboration with Carl Magnus-Capener, SP Sveriges Tekniska Forskningsinstitut AB, leader of Work Package 5 Innovation in Operation and Use.

The research leading to these results has received funding from the European Union's Seventh Framework Programme (FP7/2007-2013) under grant agreement n° 260058.

References

Feist W. 2010. EnerPHit Certification as “Quality-Approved Energy Retrofit with Passive House Components” Criteria for Residential-Use Refurbished Buildings. 16 p.

Nieminen J. & Lylykangas K. 2009. Passiivitalon määritelmä. www.passiivi.info – ohjeita passiivitalon arkkitehtisuunnitteluun. p 9.

Palosaari M. 2013. Rakennemittausten liittäminen Fidelix-automaatiojärjestelmään. Opinnäytetyö. Automaatiotekniikan koulutusohjelma. Oulun seudun ammattikorkeakoulu. Oulu, Finland. 42 p.

Puotiniemi J. 2012. Ilmatiiveysmittausraportti Psoas Virkakatu 8 90570 Oulu 15.07.2012. CRAMO. Oulu, Finland. p 4.

Puotiniemi J. 2013. Tiiviysmittausraportti Psoas Virkakatu 8 90570 Oulu. CRAMO. Oulu, Finland. p 1.

IDA ICE software, Equa Solutions: www.equa-solutions.co.uk/en/software/idaice accessed 12.11.2013

Fenestra FW-Passive window U-values: www.fenestra.fi/~/media/Files/Tuotetiedot/ikkunoiden_energiatekniset_ominaisuudet.ashx accessed 13.11.2013

Project E2ReBuild www.e2rebuild.eu/ accessed 30.10.2013

The City of Oulu www.ouka.fi/oulu/english/information-about-oulu accessed 14.11.2013

Energy retrofitting of an old multi-storey building with heritage value. A case study in Copenhagen with full-scale measurements

Maria Harrestrup, M.Sc. [1]
Svend Svendsen, Professor [1]
Agis M. Papadopoulos, Professor [2]

[1] Technical University of Denmark, Denmark
[2] Aristotle University of Thessaloniki, Greece

KEYWORDS: *Energy renovation, Energy savings, Heritage Building, Internal Insulation.*

SUMMARY:
Europe has a vision of reducing energy consumption significantly and Denmark has set up an even more ambitious goal aiming at being completely fossil-free by 2050. But already in 2035 the energy-supply mix for buildings are aimed to be free of fossil fuels. Energy retrofitting of buildings is an important solution of securing energy reductions. But challenges occur when it comes to retrofitting of heritage buildings. A case study on a typical multi-storey building with heritage value in Copenhagen has been carried out. Theoretical investigations are validated with full-scale measurements on energy consumptions before and after the renovation. Energy-saving measures that pay regard to the heritage values of the building are in focus. This implies solutions such as internal insulation. When insulating the facade from the inside, the facade will become cold and condensation in the interface can occur. Furthermore the beam construction will not be insulated, which create a large thermal bridge and the moisture and temperature conditions in the wooden beams will change and attention needs to be given to risk of degradation of the wood. The investigation showed that the actual energy consumption was reduced by 42% whereas the calculated was reduced by 58%. The deviation might be due to altered occupant behaviour. Furthermore relative humidity and temperature measurements in the beam-ends showed no risk of wood decay.

1. Introduction

Europe has a vision of reducing greenhouse gas emissions and energy consumptions by 20 % by 2020 and 80% in 2050 compared to 1990-levels (European Commission 2010) and Denmark has set an even more ambitious goal, aiming at being completely fossil-fuel-free by 2050. Even more, the energy-supply mix for buildings is aimed to be free of fossil fuels as soon as 2035 (Danish Minister of Climate 2011; Danish Energy Agency 2010). Since the building sector is responsible for approximately 40% of the total energy consumption in EU today (Lechtenböhmer and Schüring, 2011) and less than 1% is replaced with new low-energy buildings (Hartless 2003), focus needs to be given to the old inefficient building stock. Different legislative frameworks have been introduced within the area of energy efficiency and buildings with the main legislative instrument in Europe to be the Energy Performance in Buildings Directive (EPBD) implemented in 2002 (EU 2002). In 2010 a recast of the directive was introduced stating that new and retrofitted buildings should consume 'nearly zero' energy (EU, 2010). Energy retrofitting of buildings is an important solution of securing energy reductions, but challenges occur when it comes to retrofitting of heritage buildings where the facade cannot be modified due to the architectural value of the building. The study (Morelli et al. 2011) investigated an energy retrofit of a multi-storey building with heritage value from 1930 constructed with brick facades and found that it was possible to save 70% of the energy consumption. In such cases internal insulation is the only solution for insulating the facade. When insulating the facade from the inside, the facade will become cold and the drying potential of the wall will be reduced. Condensation in the interface between the insulation and the brick wall can occur, which can lead to mould growth (Christensen and Bunch-Nielsen 2009; Munch-Andersen 2008). Furthermore the

horizontal division separating the floors will not be insulated, which will lead to the occurrence of a thermal bridge, where the load bearing beam construction is placed. Many buildings with heritage value are constructed with wooden beams as load bearing structural elements (Engelmark 1983). The moisture and temperature conditions in the wood will change and attention needs to be given to the risk of the wood's degradation, which can, in extremis, lead to a risk of fatal structural damage. Multiple studies have investigated the effect on the wooden beam constructions when applying internal insulation, including Krebs and Collet (1981), Chistensen and Bunch-Nielsen (2009), Munch-Andersen (2008) and Rasmussen (2010). These studies, however, do not include detailed investigation of the impact of Wind Driven Rain (WDR). Morelli & Svendsen (2012) investigated different intensities of WDR on the facade and concluded that the WRD has a great impact on the performance and durability of the wooden beam ends. Kehl et al. (2013a) provides a literature review that also concludes that WDR has an important influence on the behaviour of moisture content and the risk of decay of the beam ends. Other studies that investigate the impact of internal insulation are Ruisinger (2013) and Kehl et al (2013b).

This paper presents results from an energy retrofit of a typical multi-storey building in Copenhagen with heritage value. The aim of the project was to demonstrate a method of how to energy renovate a heritage building focusing on energy savings and to demonstrate the efficiency of different technologies and products. Theoretical investigations are validated with full-scale measurements of energy consumption before and after the renovation. Since the building is protected, energy-saving measures complying with its heritage value have been considered. Economic aspects are not discussed in this paper, since they had already been evaluated before the renovation took place in order to determine the most feasible energy saving measures. The results from that phase (the planning phase of this study) are described by Morelli et al (2012).

2. Methodological approach

2.1 Approach

Step 1: The existing energy consumption is calculated with the building simulations software IDA ICE 4.5 and validated with the measured energy consumption. The measured energy consumption consists of space heating and domestic hot water consumption and is an average consumption from the period 2007-2009. *Step 2:* The energy consumption of the renovated building is calculated with the retrofit measures implemented in the IDA ICE model and the reduction in energy consumption is evaluated based on the results. *Step 3:* The actual energy consumption of the renovated building is measured including heating consumption, domestic hot water consumption and electricity consumption for mechanical ventilation. The heating consumption was measured for the entire building including space heating and domestic hot water provided by HOFOR A/S. Three different mechanical ventilation systems were implemented in the building. A comparison between the electricity usages for each system was carried out. *Step 4*: Since the building is of heritage value, the use of internal insulation was used. The relative humidity and temperature conditions are measured in the wooden beam end embedded in the masonry wall. The measurements are carried out in the apartment that is more exposed to wind, rain, and sun. The measurements are used to evaluate the risk of moisture and degradation problems in the beam that may occur when implementing internal insulation.

2.2 Description of the existing building

The building is located in Copenhagen, Denmark, and was built in 1896. It is a multi-storey building with 6 floors with a heated area of 2717 m^2 and an unheated basement. The building consists of 30 apartments located in three apartment blocks (Block A, B and C). The plan view of the building together with a 3D-view of the model build in IDA ICE 4.5 can be seen in Figure 1. The load-bearing construction is made of wooden beams and brick walls. The thickness of the brick wall varies from 320-645mm. There is no insulation in the building envelope and the windows are old 1-layer inefficient windows. The building has a heritage value corresponding to Class 4 from the SAVE

classification system in Denmark (SAVE 2011), which imply that the building envelope cannot be changed. The U-values for the existing building can be seen in Table 1. The building is heated with district heating and fresh air is provided by natural ventilation from opening windows and leaks. In the toilet/bathrooms and kitchens an exhaust ventilation system was installed but in most apartments the ducts were blocked and did not work. Many of the apartments did not have a shower.

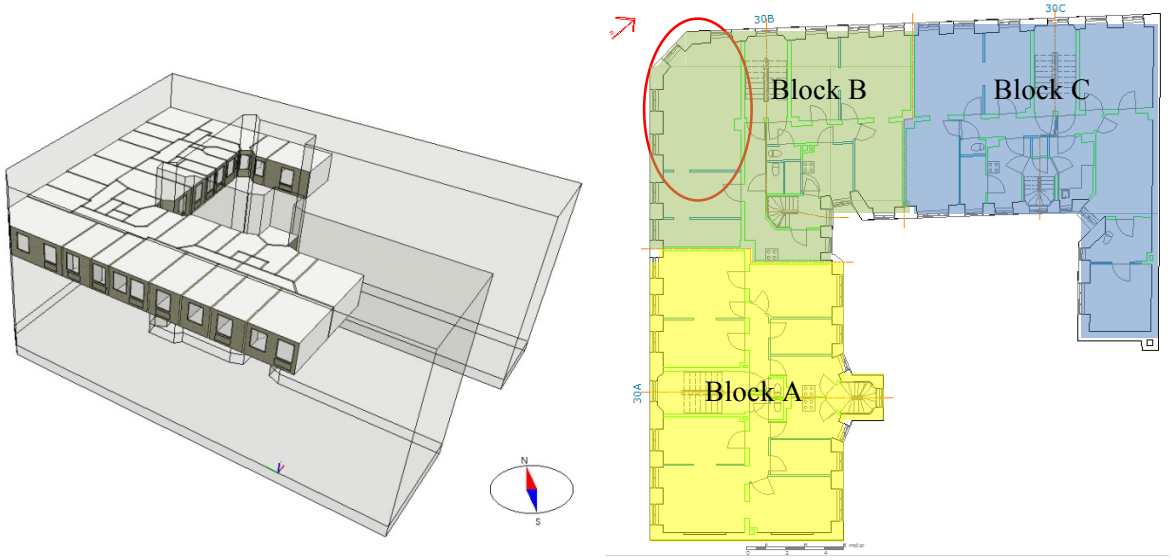

FIG 1. Left: 3D-view of IDA ICE model. Right: Plan drawing of the apartments. The red circle indicates the apartment for moisture and temperature measurements for evaluating the use of internal insulation.

TABLE 1. U-values for the existing building.

	U- values $W/(m^2 \cdot K)$
Average brick wall	1.40
Roof	0.52
Floor to basement	1.50
Windows 1 pane	4.20

2.3 Retrofitting approach

2.3.1 General improvements

The building went through a deep retrofitting where energy saving measures were in focus, but also the interior comfort was improved by installing bathrooms in all the apartments, which were lacking previously. Furthermore permission was given from the municipality to install penthouse flats with roof terraces and solar cells, increasing the total value of the building.

2.3.2 Building envelope

Before choosing which energy saving measures that should be used for the renovation, different energy saving measures were tested in a test apartment on the first floor in Block C. Different window-solutions and different internal insulation products were installed and tested with regards to costs, energy performance, and moisture and temperature conditions. The different solutions are described in Morelli et al. (2012). Since the building has heritage value, the facade cannot be changed. However, the municipality accepted that the windows were changed to new windows since it was proven from the test apartment that they are the most cost- and energy-optimal choice. The windows for the deep retrofitting were from Frovin Windows and Doors A/S and reconstructed as the old

windows. The frame is made of wood and the U-value for the window is U = 0.89 W/m^{2}K. Due to the heritage value of the building internal insulation was used except from the north-east facade (Block C). This facade is facing a narrow passage and 250mm external mineral wool from Rockwool was applied (U-value = 0.39 W/m^{2}K). The remaining facades were insulated with internal insulation. The apartments in Block A and B were insulated with Aerorock (a mix of Rockwool and Aerogel) with a U-value of 0.19 W/m^{2}K and in the apartments in Block C Kingspan (PUR) were applied with a U-value of 0.20 W/m^{2}K.

The installation of internal insulation can create a risk of mould growth at the interface between the insulation material and the brick-wall since the temperature at the interface will decrease when applying internal insulation. Experience from the test apartment showed that it is crucial to clean the brick wall from organic material before applying the internal insulation in order to minimise the risk.

2.3.3 Moisture and temperature measurements

In order to evaluate the implementation of internal insulation and the effect on the beam ends, temperature and relative humidity measurements are carried out in the beam ends. In the test apartment a similar investigation was done and showed no risk. However, the test apartment was orientated north-east facing a small passage and was located on the 1st floor, which implies a minimised amount of wind-driving rain. The measurements for this study are therefore implemented in the apartment that is exposed to the most extreme weather conditions (wind driven rain, sun, wind etc.). The apartment is facing south-west and is on the 5th floor where no shadow or shelter is present. The measuring points and a drawing of how the internal insulation was installed are seen in Figure 2. Due to wall socket and the cables for electricity the insulation was stopped 200 mm above the floor (see Figure 2). This solution is supported by investigations carried out by Morelli and Svendsen (2012) who concluded that if the insulation is stopped 200 mm above the floor, the risk of wood decay is decreased significantly.

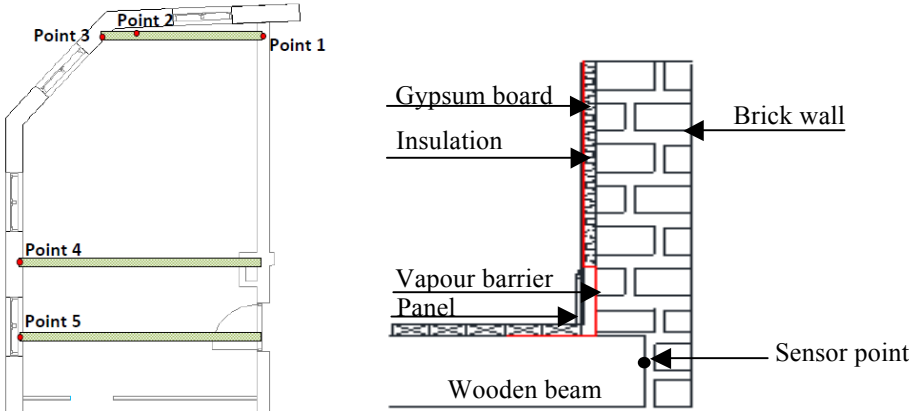

FIG 2. Left: Measurement points for temperature and relative humidity in the beam-ends. Right: Drawing of how the internal insulation was mounted.

2.3.4 Mechanical ventilation

Three different mechanical ventilation systems with heat recovery were installed in the three apartment blocks respectively. *Block A:* A traditional central mechanical ventilation system is installed. The air handling unit (AHU) is placed in the basement and the existing chimneys are used for the exhaust from the bathrooms and kitchens. The supply air to the living rooms is at a constant rate of 140 m^3/h. The exhaust air from the bathrooms is constant at 20 m^3/h when the relative humidity is below 55% and 54 m^3/h when it exceeds 55%. In the kitchen the exhaust rate is 72 m^3/h, but increases to 144 m^3/h when the cooker hood is activated. *Block B:* The ventilation system in Block B is a central ventilation system with the AHU placed in the basement. The ventilation system is

operated as demand controlled based on CO_2, relative humidity and temperature. Furthermore there is a user panel to regulate specific needs. During unoccupied hours a dispensation was given from the municipality to ventilate only with an air exchange rate of 22 m^3/h. *Block C*: The ventilation systems in Block C are decentralized systems on apartment level. This implies that each apartment has an AHU. The control for the ventilation system is demand controlled as for the system in Block B.

3. Results

3.1 Energy consumption

The annual energy consumption calculated and measured is shown in Table 2. The measured energy consumption for the existing building is an average from 2007-2009 and includes space heating and domestic hot water. The deviation between the measured and calculated annual heating and hot water consumption for the existing building is 2.5 % which is considered acceptable. The calculated energy consumption for the renovated building is 63.0 kWh/m^2/yr, which corresponds to a reduction in the energy use of 58% compared to the calculated energy use before the renovation. The biggest reduction is found in Block C (65 %) since the north/east facades with no sunlight were insulated with 250 mm external insulation reducing the heat loss dramatically. Morelli et al. (2012) calculated the energy consumption to be reduced by 68% with the building energy simulation software BE10 that is based on Danish standards. The software BE10 is however a simplified software and is working as a one-zone-model whereas IDA ICE software is a multi-zonal software providing more details. The calculated electricity consumption for ventilation is seen to be less for the demand controlled systems followed by the traditional central ventilation with constant airflow, but the calculated energy consumptions are very similar in all three cases.

TABLE 2. Calculated and measured energy consumption for existing building. Calculated energy consumption for the renovated building.

	Existing building		**Renovated building**		
[kWh/m^2/yr]	**Measured**	**Calculated**	**Calculated**		
	Space heating and hot water	Space heating and hot water	Space heating and hot water	Mechanical ventilation	Total
Block A	-	127.5	78.4	7.0	85.4
Block B	-	134.6	37.1	6.9	57.0
Block C	-	191.1	60.4	6.8	67.2
Total weighted	**155.5**	**151.6**			**63.0**

3.2 Measured energy consumption in the renovated building

3.2.1 Heating consumption

The energy consumption was measured after the renovation was carried out. The total heating consumption for the entire building including space heating and domestic hot water was measured and is shown in Figure 3. Since the measured values include space heating and domestic hot water, the monthly hot water consumption is estimated based on an average value of the heat consumption from June, July and August. It is expected that there is no space heating consumption during these month and even though variations in the hot water consumption occurs over the year, it gives a reasonable estimate. The month November and December are estimated values in order to calculate the annual heating consumption per meter square. The total heated floor area after the renovation is 2892 m^2. This gives a total annual heat consumption of 88.8 kWh/m^2 (see Table 3). Considering weather data it was found that the monthly average temperature in 2013 was 1.5°C higher than that of the design reference year used in the simulation model.

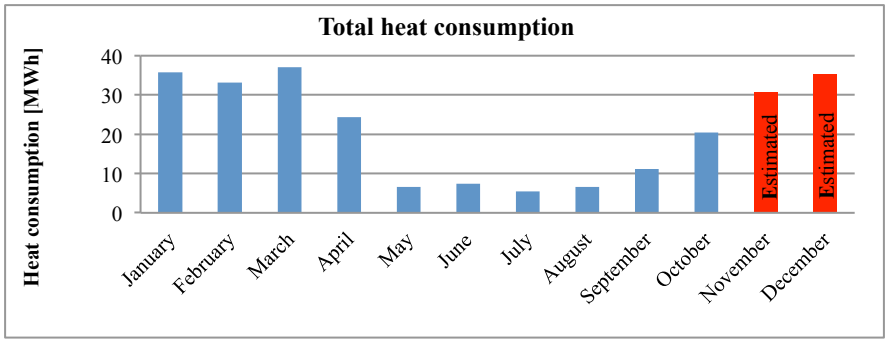

FIG 3. Total heat consumption for the entire building.

3.2.2 Electricity consumption for ventilation

The electricity consumption from the three different ventilation systems was measured and presented in Figure 4. Based on the measurements in Figure 4 the annual consumption per meter square was estimated for each system in order to compare them. As seen from Table 3 the ventilation system in Block B (Centralised demand controlled ventilation) is using the most electricity followed by Block C (Decentralised demand controlled ventilation) and A (Centralised constant ventilation). Table 3 shows that the measured annual energy consumption is 90.7 kWh/m^2, which is 28 % more than the calculated energy consumption.

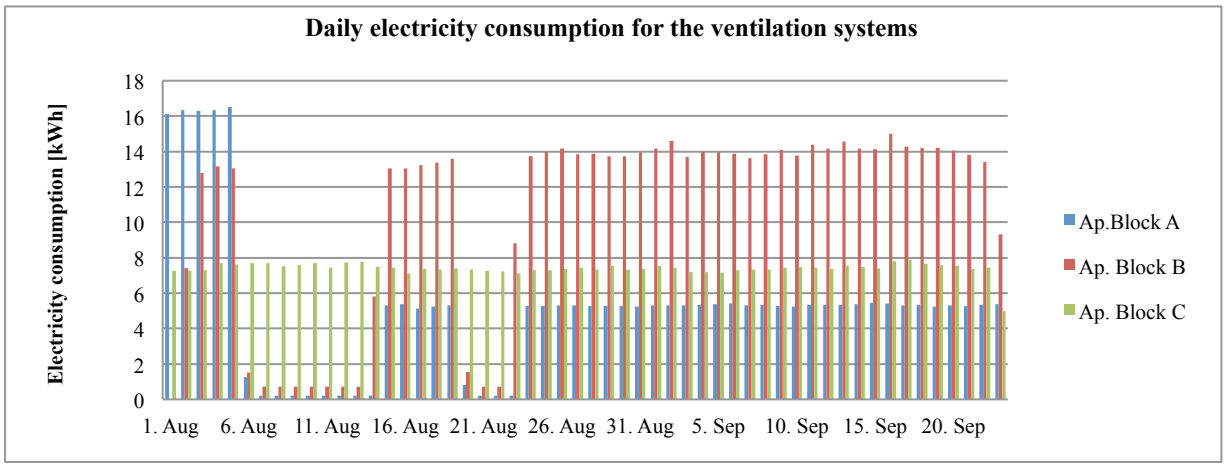

FIG 4. Daily measure electricity consumption for the ventilation systems

TABLE 3. Estimated annual energy consumption per meter square based on measurements

[kWh/m^2/year]	Energy consumption	Total
Heating		87.8
Hot water	27.0	
Space heating	60.8	
Ventilation (weighted)		2.9
Block A	1.9	
Block B	3.9	
Block C	2.9	
Total energy consumption		**90.7**

3.3 Moisture and temperature measurements

Figure 5 shows the measured temperature and relative humidity in the beam ends. According to Viitanen (1997) there is no risk of degradation of the beam when the RH is less than 75%. As seen

from Figure 5 the RH is less than 75% except from point 3 that has RH>75% during the first month. Point 3 has generally higher RH than the other points. The reason for that may be due to the orientation of this beam end, which is facing straight west and therefore exposed to less sun compared to point 4 and 5. Point 1 and 2 are not mounted in the facade and therefore these points are not as critical with regards to high relative humidity. This is also indicated in Figure 5 where the temperature in point 1 and 2 is higher in October/November.

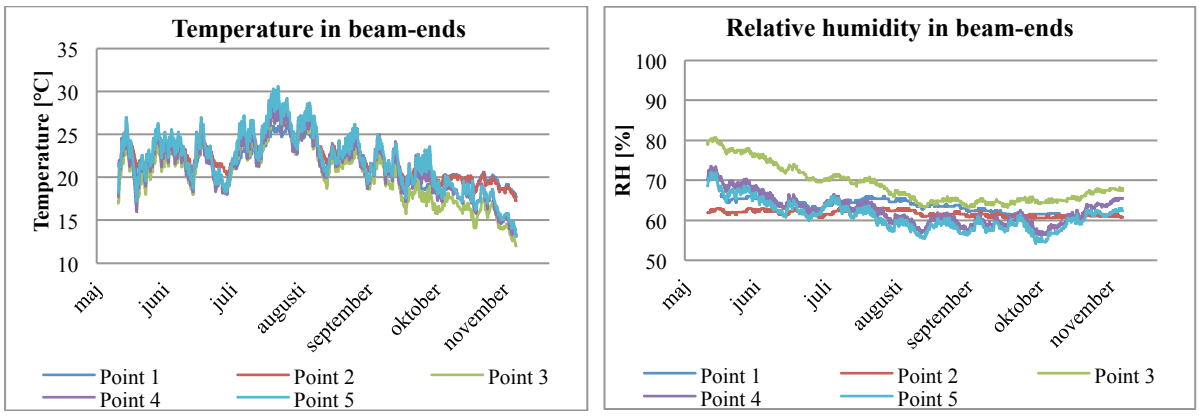

FIG 5. Left: Temperature in the beam ends. Right: Relative humidity in the beam ends.

4. Discussion

While the measured and calculated energy consumption before the renovation deviated with only 2.5%, the measured energy consumption of the renovated building was 28% higher than the calculated energy consumption for the renovated building. One reason for this can be the occupant behaviour. It is often seen that when a building undergo a renovation, the occupant feels an increased comfort and a tendency of an increased room temperature is often seen (Harrestrup and Svendsen 2013). Therefore the actual energy consumption is often higher than what has been calculated. The study showed that when the room set point temperature is increased with 2 °C, the space heating consumption increases by approximately 30 %. Since the monthly average temperature in 2013 in average is 1.5°C higher than the average temperature from the DRY used in the simulation, the increased consumption cannot be explained based on colder weather conditions in 2013 and therefore increased energy consumption. Another reason could be that when insulating from the inside the thermal capacity of the building is decreased, and therefore less heat might be stored during the day and released during night, which might increase the heating consumption. These reasons are to be investigated but are not within the scope of this paper. The measured and calculated electricity consumption for ventilation is seen to deviate with the actual consumptions being approximately 40-70% less than the calculated consumption. Furthermore the calculated results show that the demand controlled systems are more energy efficient than the traditional central system with constant airflow, whereas the actual consumptions show that the traditional central ventilation system with constant air flow is the most energy efficient system.

5. Conclusions

This paper presents a method on how to energy-renovate an old heritage multi-storey building in Copenhagen and document the energy use before and after the renovation. The calculated energy consumption was found to be reduced by 58% but the actual energy consumption was estimated to be reduced by 42% compared to the measured energy consumption before the renovation. A reason for this deviation can be due to altered occupant behaviour. Three different ventilation systems were installed in the building, one in each apartment block. The results from the simulations showed that

the decentralised systems were slightly more energy efficient compared to the traditional centralised system with constant airflow, whereas the measurements on the actual energy consumption showed the opposite. When applying internal insulation, as was done in the studied building, the risk of moisture problems and wood decay can be present. The temperature and relative humidity measurements carried out in the wooden beam ends showed no risk even in the facade of the apartment exposed to more wind driven rain. In this case study the internal insulation was stopped 200mm above the floor, which can be the reason that no risk of moisture problems seems to be present. This solution can therefore be a durable solution for insulating from the inside and still save a considerable amount of energy.

6. Acknowledgements

The results provided in this paper were financed by the Danish Energy Agency under the project: "Development and 1:1 –demonstration of concepts for renovation of older multi-storey building to low energy class 1". The project team consist of DTU Civil Engineering, COWI, Rönby.dk, and Ecolab.

References

Danish Energy Agency. 2010. Grøn Energi – vejen mod et dansk energisystem uden fossile brændsler. Copenhagen: Danish Energy Agency (in Danish).

Danish Ministry of Climate, Energy and Buildings. 2011.Vores Energi. Copenhagen: Danish Energy Agency (in Danish).

Christensen G. & Bunch-Nielsen T. 2009. Indvendig Efterisolering Af Ældre Ydermure (BYG-ERFA erfaringsblad (31) 09 10 29). Ballerup: BYG-ERFA.

European Commission, 2010. Roadmap for a low carbon economy by 2050. Directorate-General Climate Action, European Commission, Bruxelles

EU 2002. Directive 2002/91/EC of the European Parliament and of the Council of 16 December 2002 on the energy performance in buildings, Official Journal of the European Communities, 4/1/2003.

EU 2010. Directive 2010/31/EU of the European Parliament and of the Council of 19 May 2010 on the energy performance in buildings (recast), Official Journal of the European Union, 18/06/2010.

Engelmark J. 1983. Københavns Etageboligbyggeri 1850-1900. En Byggeteknisk Undersøgelse. Hørsholm: Danish Building Research Institute (in Danish).

Harrestrup M., Svendsen S., 2013. Changes in heat load profile of typical Danish multi-storey buildings when energy-renovated and supplied with low-temperature district heating. International Journal of Sustainable Energy, DOI: 10.1080/14786451.2013.848863

Hartless R. 2003. Application of Energy Performance Regulations to Existing Buildings, Final Report of the Task B4, ENPER TEBUC, SAVE 4.1031/C/00-018/2000."Watford, UK: Building Research Establishment.

Kehl D., Ruisinger U., Plagge R., Grunewald J. 2013a. Wooden Beam Ends in Masonry with Interior Insulation – A Literature Review and Simulation on Causes and Assessment of Decay, 2nd Central European Symposium on Building Physics, Vienna.

Kehl D., Ruisinger U., Plagge R., Grunewald J. 2013b. Holzbalkenköpfe bei innengedämmten Mauerwerk – Ursachen der Holzzerstörung und Beurteilung von Holz zerstörenden Pilzen, 2nd International Congress on interior Insulation, Dresden (in German)"

Krebs HJ and Collet PF (1981) Indvendig Efterisolering: Indmurede Bjælkeenders Fugt 2 Og Temperaturforhold i Etagekryds. 1st ed. Tåstrup: Danish Technological Institute.

Lechtenböhmer S. & Schüring A. 2011. The Potential for Large-Scale Savings from Insulating Residential Buildings in the EU. Energy Efficiency 4 (2): 257–270

Morelli M., Rönby L., Mikkelsen S.E., Christensen M.G., Kildemoes T. & Tommerup H. 2012. Energy retrofitting of a typical old Danish multi-family building to a "nearly-zero" energy building based on experiences from a test apartment. Energy and Buildings 54: 395–406.

Morelli M. & Svendsen S. 2012. Investigation of interior post-insulated masonry walls with wooden beam ends. Journal of Building Physics 36(3): 265–293

Morelli M., Tommerup H., Tafdrup M.K. & Svendsen S. 2011. Holistic energy retrofitting of multi-storey building to low energy level. Proceedings of the 9th Nordic Symposium on Building physics, Tampere, Finland: Tampere University of Technology, Vol. 3, Session C10, 1323-1330

Munch-Andersen J. 2008. SBi-Anvisning 221. Efterisolering Af Etageboliger. Hørsholm: Danish Building Research Institute, Aalborg University (in Danish).

Rasmussen T.V. 2010. Post-insulation of existing buildings constructed between 1850 and1920. In: Thermal performance of the exterior envelopes of whole buildings XI, Clearwater Beach, FL, 5–9 December. Atlanta, GA: ASHRAE.

Ruisinger U.2013. Long-term measurements and simulations of five internal insulation systems and their impact on wooden beam heads, 2nd Central European Symposium on Building Physics, Vienna.

SAVE. 2011. SAVE Kortlægning og registrering af bymiljøers og bygningers bevaringsværdi. Copenhagen: Ministry of Culture, Cultural heritage board.

Viitanen H.A. 1997. Modelling the time factor in the development of mould fungi-The effect of critical humidity and temperature conditions on pine and spruce sapwood, Holzforschung-International Journal of the Biology, Chemistry, Physics and Technology of Wood. 51 (1997) 6-14.

Low Energy Retrofitting in Sweden – Thirty-one feasibility studies

Katarina Högdal, M.Sc. [1]
Emma Karlsson, B.Sc. [1]

[1] WSP Environmental, Sweden

KEYWORDS: *Energy efficiency, Retrofitting, Feasibility studies*

SUMMARY:

To accelerate the energy efficiency rate in the residential sector, the Swedish Energy Agencies network for energy efficient apartment buildings has implemented the campaign Halvera Mera (Halve More). The campaign aimed to produce feasibility studies that would identify the measures needed to halve the energy consumption in apartment buildings. A total of 31 studies where completed within Halvera Mera. The studies show that there are significant differences among property owners regarding which measures they are interested in, how they carry out their energy and profitability calculations and which measures they plan to invest in.

An analysis of the reports show that municipal property owners, property owners who have their building in a larger city and property owners with buildings that have a high energy usage seem to be more likely to invest in energy efficiency measures.

The analysis also shows that the calculated energy savings in the feasibility studies are widely spread. The estimated energy savings range from 30 percent up to 82 percent and the new estimated energy performance range from 20 kWh/m^2 and year to100 kWh/m^2 and year. The estimations, assumptions and results presented in the reports indicate that the property owners knowledge lever differ greatly, as well as the knowledge level of the consultants. To ensure that energy measures are being adequately implemented, and that the targets for energy efficiency will be reached, a general knowledge lift is required.

1. Introduction

1.1 Background

In 2007, the European Council decided on energy and climate goals for 2020, the so-called '20-20-20 targets'. These state that by year 2020 greenhouse gas emissions shall be reduced by 20 percent, the share of renewable energy shall increase by 20 percent and energy efficiency must improve by 20 percent, relative to 1990. In 2011, a new energy strategy was adopted where energy efficiency was highlighted as a key factor for the long-term energy and climate goals. (SEK(2010)1349)

Sweden has set their own climate targets, based on the same foundations as the 20-20-20 targets. The Swedish environmental goals for built environment set specific targets for energy efficiency in the housing stock. These targets are that the energy consumption in the residential sector shall decrease by 20 percent by 2020, and by 50 percent by 2050, relative to 1995. (2008/09:NU25)

The Swedish Energy Agency has a mission to accelerate the energy efficiency rate in the residential sector, and a method that has proven to be effective in Sweden is demonstration projects. The Energy Agencies network for energy efficient apartment buildings, BeBo, has developed the concept

Rekorderlig Renovering (Smart Renovation). The purpose of Rekorderlig Renovering is to ensure that demonstration projects for low energy retrofitting, which will improve the energy performance by at least 50 percent, is carried out. The concept involves a combination of energy efficiency measures, customized to each individual project, which in addition to halve the energy usage also shall result in an increased living comfort, reduced environmental impact and economic benefits for the property owner. To increase the number of demonstration projects in accordance with Rekorderlig Renovering the campaign Halvera Mera was implemented.

1.2 Goal

The goal of the campaign Halvera Mera was to produce feasibility studies, in accordance with Rekorderlig Renovering, which identifies the measures and actions needed to halve the energy consumption in apartment buildings while retrofitting.

2. Project Description – Halvera Mera

2.1 Scope

The goal of Halvera Mera was to produce 25 feasibility studies in accordance with the concept Rekorderlig Renovering. The campaigns target group was property owners in the private and community sectors, as well as housing associations. As the interest for the campaign turned out to be larger than expected, it was decided to expand the number of studies to 35. Despite this, there were still property owners on the waiting list. To encourage these owners to implement energy-saving measures, they were offered an energy inspection.

The feasibility study reports were written according to a given template, containing information such as the condition of the building, descriptions of the investigated energy measures, reports of calculated energy savings and LCC analysis for selected measures. A grant of 17 000 EUR was paid to the property owners who presented a preliminary report to the specified criteria.

A total of 31 studies and 17 energy inspections were carried out. After the reports from the feasibility studies were compiled the results were summarized and analysed.

2.2 Implementation

Halvera Mera was coordinated by WSP Environmental and led by a project team consisting of:

- Fred Nordstrom, NENET, NENET
- Maria Malmkvist (project manager), WSP Environmental (later replaced by Saga Ekelin, WSP Environmental)
- Bengt Linné, Bengt Dahlgren AB
- Christina Andersson, WSP Environmental (later replaced by Emma Karlsson, WSP Environmental)
- Katarina Högdal, WSP Environmental

The project group also included Göran Werner, coordinator of BeBo, and Mats Björs, the then president of Byggherrarna AB.

2.2.1 Feasibility Studies

The feasibility studies were conducted by the property owners, with the support from the project team. Some property owners conducted the feasibility study within the company, but many took help of external consultants. BeBo offered support for designing a survey of inhabitants, information about moist problems and in some cases financing for additional measurements.

3. Results

3.1 Feasibility Studies

A total of 36 property owners entered the campaign Halvera Mera. During the project some property owners left the project, due to various reasons. At the end of the project 31 reports were submitted and approved by BeBo board.

The goal for the property owners was to identify measures that would halve their energy consumption. The average calculated energy saving in the reports is 78 kWh/m^2 and year, corresponding to 54 percent. However, the results are widely spread. The estimated energy saving ranges from 30 kWh/ m^2 and year to 150 kWh/ m^2 and year, equivalent to a reduction of energy use ranging between 30 percent and 82 percent.

The new, calculated energy performances are also widely spread. In the reports values between 20 kWh/ m^2 and year and 100 kWh/ m^2 and year are presented, with a mean of 63 kWh/m^2 and year.

Figure 1 show which energy measures that have been investigated. The most common measures to examine are the exhaust air heat pump, façade insulation, attic insulation, energy-efficient windows and commissioning of the heating system.

Installing energy-efficient windows was the most popular measure. This was examined in 75 percent of the feasibility studies, and 55 percent plan to implement it. About 10 percent opted out the action, usually because it was too costly in relation to the energy saving, and 10 percent had not yet made a decision. When replacing or upgrading with an energy-efficient window a U-value between 0.7 and 1.8 were chosen in this project. The average U-value was 1.1.

Commissioning the heating system was not investigated as often as the energy-efficient windows was, but almost as many property owners planned to carry out the action. The implementation of these two measures should reasonably be linked to each other, since an adjustment of the heating system is recommended for greater measures in the building envelope.

Facade insulation, both external and internal, was examined in about 70 percent of the feasibility studies, but only 20 percent planned to implement the measure and nearly 30 percent opted it out. This was mainly due to the fact that façade insulation often requires large and expensive actions that can only be motivated if the façade also needs to be renovated. Some property owners chose to go ahead with facade insulation, even though it was unprofitable as an energy measure, to achieve other positive effects such as improved indoor climate.

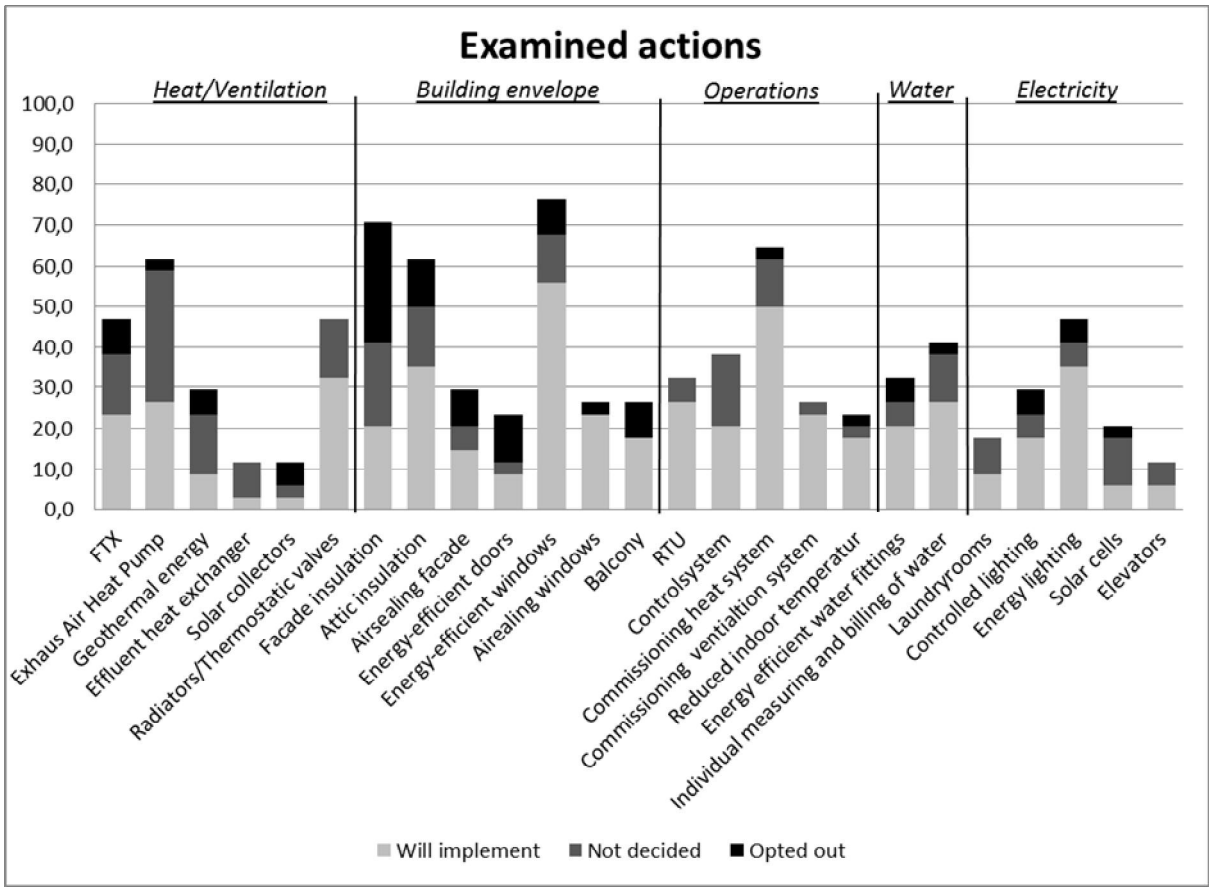

FIG 1. Energy measures examined in the feasibility studies. The bars show the percentage of the property owners who have studied each measure. The lighter portion of the bars show the fraction that plan to carry out the action and the black portion of the bars shows the proportion that has opted out the action. The grey areas represent the property owner who have investigated the action but has not yet made a decision about implementation.

4. Analysis

4.1 Energy Calculations

In Halvera Mera, there were no requirements on how the energy calculations should be performed, or which method or tool that was to be used. This resulted in a differentiation in the calculated energy savings.

Table 1 shows the span of the estimated energy savings for some measures. Low estimated energy savings can in some reports be explained by the fact that the energy measure was already implemented, and only needed to be updated or replaced. High estimated energy savings can in some reports be due to that additional measures are implemented at the same time, but are not fully described in the report. However, in most cases it has been difficult to find a good explanation for the large variations. This indicates that there are significant differences in how property owners and consultants perform their energy calculations, and that these differences will affect the result of the energy calculation.

TABLE 1. Calculated energy savings for chosen action. Figures presented in kWh/m^2 and year

Water supply system	Heating system	Exhaust Air Heat Pump	FTX
2	2	7	17
3	3	8	19
3	3	21	20
3	4	27	21
4	4	29	22
4	7	30	24
4	8	32	24
4	9	36	24
5	9	36	26
5	11	36	34
6	12	43	38
6	12	44	38
7	12	45	46
8	14	47	51
8	14	53	56
9	19	53	
12	23	55	
19	31		
35			

When the potential energy savings have been calculated, assumptions have been made, as to e.g. the efficiency of heat pumps and the potential of individual measure and billing of water. The large differences in energy reduction suggest that these assumptions also differ. An examination of the energy calculations suggests that the assumptions are often too optimistic, which leads to results that presents unrealistically high energy savings.

4.2 Investment cost

Investment costs for the different measurements have been estimated from experiences from other projects or theoretically calculated costs. How the investment costs have been presented differ in the reports. In some reports only the total cost is presented, but in other reports the marginal cost is

described as well. In some reports, it has been difficult to determine whether the given cost intends the total cost or the marginal cost.

Figure 2 shows the investment cost for various measures against their potential energy saving. The cost is presented as EUR per square meter A_{temp} (floorarea heated to above 10°C). The energy saving for the various measures is presented in kWh per square meter during the actions presumed lifetime. For installation measures a lifetime of 15 years has been assumed and for construction measures measures a lifetime of 40 years, according to BeBo guidelines.

The points represent averages, calculated from the reports. The average investment cost has been calculated from the marginal cost, when presented. The measures found in the lower left corner has a relatively low investment cost, but also gives a rather small energy saving. The measures that are found in the upper right corner provide a greater energy saving, but also have a higher investment cost. In the lower right corner are the measures that could be considered the most cost-effective, that give a fairly large energy saving but still has a low investment cost.

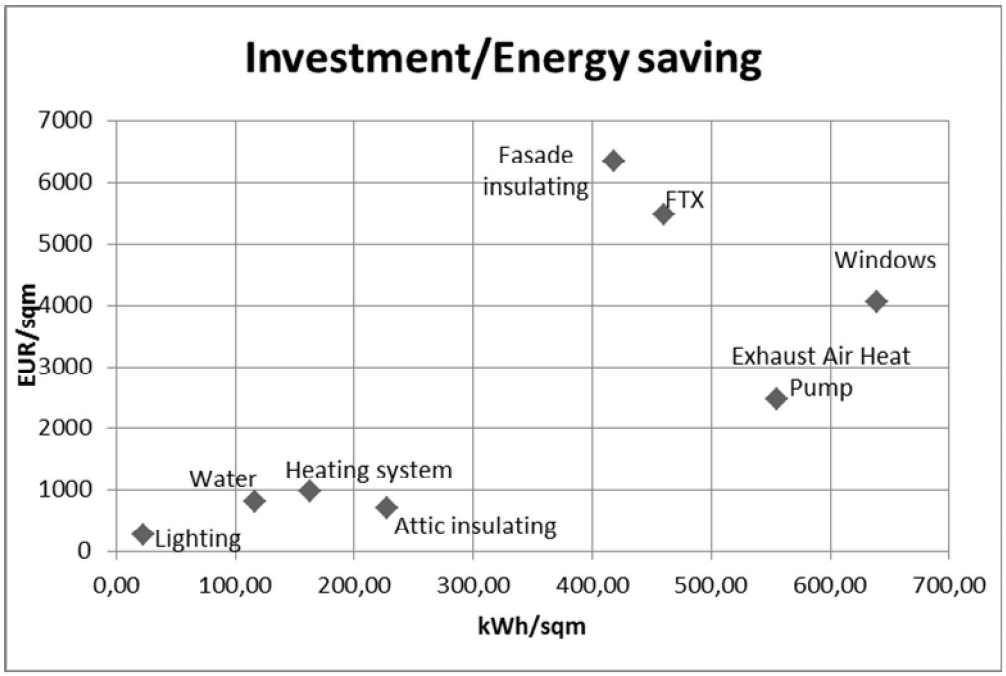

FIG 2. Investment vs. potential energy saving. The y-axis presents the cost as EUR per square meter A_{temp}. The x-axis present the energy savings for the various measures is presented in kWh per square meter based on the actions presumed lifetime. For installations a lifetime of 15 years has been assumed and for construction measures a lifetime of 40 years.

4.3 Profitability

A requirement in the feasibility studies was to perform both an LCC analysis for each measure as well as a profitability analysis. A summary of the property owners calculations show that the cost of capital rate is set to 5.2 percent at average, while the rate of return is generally a bit lower with an average of 4.8 percent.

Profitability requirements and calculations have not always been presented in a similar way, why it has been difficult to get a general picture of the economic circumstances. Since so few property owners have indicated their profitability requirements, it has not been possible to make a deeper analysis on the subject.

In the profitability calculations it has not always been clear whether the measures have been considered as energy measures or as maintenance. Nor has it always been clarified whether the costs that are presented include both maintenance and investment, or only investment cost. However, there seems to be a difference in how property owners carry out their profitability calculations, and if they consider their measures to be investments or as maintenance.

When investing in energy-saving measures, and when performing profitability calculations for energy measures, it is important to first determine the buildings need for maintenance, in order to make a correct profitability analysis. For example, if the windows need to be replaced, it is not correct to start from a zero-cost position in your profitability calculations for energy efficient windows. Instead, you should estimate the cost for a conventional window replacement, and use the margin cost for investing in energy efficient window in the profitability calculation. This way, the energy savings that the energy efficient windows gives only have to cover the cost of the actual investment, to be consider profitable.

A measure that is performed with the sole purpose to reduce energy usage should be considered as an energy measure, and its cost should be counted as an investment. If a measure is necessary due to needs of restoration, it should instead be considered as maintenance or a raise of standards, even if it results in a reduction in energy use as well. However, this distinction is sometimes difficult to make, since some renovations could include both maintenance and energy reducing measures. In this project some property owners have performed their profitability calculations using the total cost for a measure, even if the measure also met a maintenance need. This made it difficult to find energy investments that were profitable.

5. Conclusions

The feasibility studies in Halvera Mera show that there are large differences among property owners in what measures they are interested in, how they carry out their energy calculations and how they implement their profitability calculations.

A summary of the results of the feasibility studies show that measures on the heating and ventilation systems and measures in the building envelope are the keys to significant energy savings. The analysis indicates that housing associations, property owners with buildings in small towns and property owners whose buildings have a low energy usage seems to have difficulties to make decisions about these measures.

The analysis of the feasibility studies shows three circumstances that make property owners more likely to invest in energy measures.

1. Municipal ownership. Municipal property owners often plan for more and larger investments in energy measures than private owners and housing associations do.
2. Larger cities. Property owners who have their building in a city with more than 140,000 residents have greater ambitions for implementing energy measures than property owners in smaller cities. This is probably linked to better market conditions.
3. High energy usage. Property owners with buildings that have an energy usage greater than 150 kWh/m^2 and year more frequently plans to implement their action than the property owners whose buildings have a lower energy usage. This is probably due to the greater incentive to implement energy measures that comes with a high energy usage.

The reports also show that the calculated energy savings in the feasibility studies are widely spread. The estimated energy savings range from 30 percent up to 82 percent and the new estimated energy performance range from 20 kWh/m^2 and year to100 kWh/m^2 and year. The estimations, assumptions and results presented in the reports indicate that the property owners knowledge lever differ greatly, as

well as the knowledge level of the consultants. To ensure that energy measures are being adequately implemented, and that the national targets for energy efficiency will be reached, a general knowledge lift is necessary.

6. Acknowledgements

We wish to acknowledge Arne Elmroth, Prof Em at Lund University, for his valuable audit of the calculations in the reports and his advice on how to best carry out the analysis.

We would also like to acknowledge Göran Werner and Saga Ekelin at WSP Environmental for their feedback and inputs on the project summary and the analysis.

References

SEK(2010)1349. Energi 2020 – En strategi för hållbar och trygg energiförsörjning på en konkurrenssatt marknad. The European Commission KOM (2010) 639

2008/09:NU25T. Riktlinjer för energipolitiken. The Swedish Commission for Industry and Trade

Methodology to ensure good indoor environment in energy efficient retrofitting

Tuomo Ojanen, M.Sc. [1]
Riikka Holopainen, Ph.D. [1]
Hannu Viitanen, Ph.D. [1]
Jorma Lehtovaara, M.Sc. [2]
Paavo Kero, M.Sc.[3]
Juha Vinha, Professor [3]

[1] *VTT Technical Research Centre of Finland*
[2] *Aalto University, Finland*
[3] *Tampere University of Technology, Finland*

KEYWORDS: *Building renovation, methodology, indoor environment, moisture, energy efficiency,*

SUMMARY:
The main challenge in renovation is how to focus typically limited resources in the right renovation actions. The target of the renovation is a building with healthy and comfortable indoor conditions, safe moisture performance of structures and improved energy efficiency. Prioritization is needed and it should be based on reliable information and a concept of the performance of the whole building.

This paper presents a methodology developed to assist the decision-makers in the renovation process. The objective was to form a practical and simple methodology that is aimed especially for the assessment of the present state of the building and to set priorities for different needs in a renovation project. A three level risk and condition classification is used to form a survey of the indoor environment, structure and system performance and the energy efficiency aspects. The user is guided through the survey using the depth suitable for the building, ranging from check-list to finer analysis. Depending on the performance classification and risk analysis of the building, suitable tools and check-lists are presented to help in the analysis of the different elements.

The technical present value of the building before and after renovation can be used to study the cost-effectiveness of the renovation actions. A school building renovation project will be presented as a practical application of the methodology.

1. Introduction

The motivation for building renovation is typically in problems with the perceived indoor environment, deterioration or aging of structures or other building components or moisture damages. Energy efficient renovation of old building stock is in major role when trying to meet with the regulations aimed to reduce the emission of green-house gases.

The challenge in renovation is how to choose the right action to reach the required level of performance: Improved energy efficiency allowing healthy and comfortable indoor conditions with safe moisture performance of structures. There is typically lots of information of the maintenance processes, moisture problems and accidents, possible conditions surveys, energy consumption and earlier renovations through the history of the building. Proper analysis of the present state condition of the building is the requirement for proper design of the renovation so that the typically limited resources can be used in an efficient way.

A methodology and tool has been developed to help in the decision making and design of a renovation. The objective was to develop user-friendly, practical, simple and clear methodology to help the stakeholders in the planning, design and implementation phases of a building renovation process. The aim was to create a concept that could guide the user to through the process. The focus of the methodology is in the present state analysis revealing the renovation needs and in the evaluation of the risk levels of different building systems. The risks are studied from different perspectives: indoor safety and comfort (thermal comfort, air quality, illumination), building physical performance and energy efficiency aspects for different structures and systems. Also a cost study is integrated in the tool.

2. Objectives for renovation methodology

The objective of the ENERSIS concept is to form a clear survey of the present state of the building to be renovated. The decisions made in the planning phase of the project are the most important for the success of the renovation. Right renovation action has to be chosen to ensure good results.

2.1 Aims of the methodology

The aim was to form a simple and user friendly methodology that could be used to clarify and illustratively present the present state analysis of the building. The methodology is meant only to help and guide in the design phase of the renovation process. The user of the methodology makes decisions and sets the priorities using the results of the methodology when found suitable. The methodology only clarifies and justifies the actions according to the information given by the user (Ojanen & al. 2013).

2.2 Evaluation principles

The ENERSIS concept was developed to guide the user of the methodology to take into account not only the primary reason for renovation, but also the indoor environment performance and the overall energy efficiency of the building. This approach includes the building physical performance, thermal comfort, perceived indoor air quality and lighting conditions

The methodology advises which aspects should be considered to achieve the set performance goals and how to evaluate the interactions, possible risks and energy saving potentials of different building components. Suitable tools and check-lists are presented to help in the analysis of the different elements. The methodology reveals the risks linked to a straight -forward renovation which does not consider the overall performance of the building or the risks and potentials that are included. The cost-effectiveness of the renovation can be evaluated by solving the apparent technical value of the building before and after different renovation actions.

3. Structure of the methodology tool

The methodology was formed in an Excel format tool. The structure of the methodology and the development principles of the tool are presented in the following. Figure 1 presents the decision making process of a building renovation and Figure 2 the structure of the tool to help in the methodology application.

4. Renovation tool application in a case study

The use of the renovation tool was studied in a renovation case study. The case study was carried out for the renovation process of a school building built in 1966. This school building had reported to have poor indoor air (IAQ) and environment (IEQ) quality and modest energy efficiency.

The renovation process was followed during the research project and the methodology could be applied in this case study by using the information from the site. The conditions and results of the application of the methodology are presented in the following.

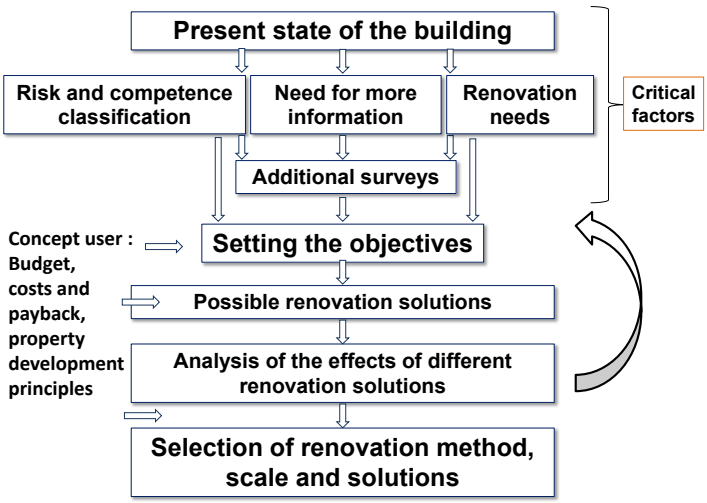

FIG 1.Decision making process of a building renovation.

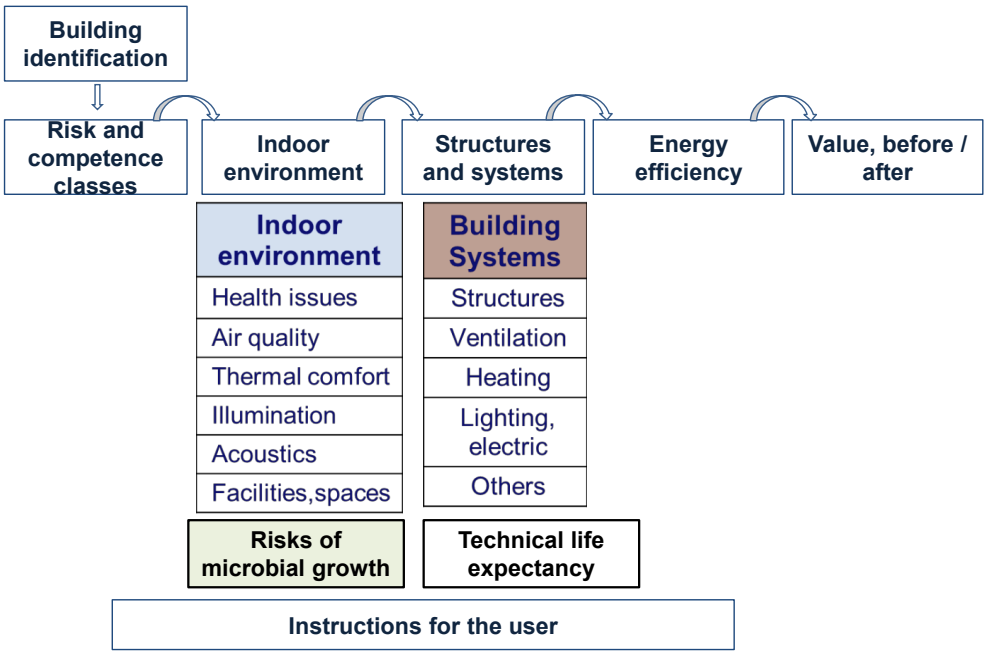

FIG 2. Structure of the Enersis-tool for the evaluation of renovation needs.

4.1 Indoor environment

The symptoms on bad IAQ and thermal comfort were evaluated based on the building user inquiries. The feedback from the users of the buildings is the first step when evaluating the present state of the building and possibly needed additional surveys and focused conditions studies.

Indoor air quality in many times related to insufficient ventilation and or also moisture damages causing bio-deterioration of structures. Several different organisms can be involved in the moisture

problems and damage of buildings, but their effect on IAQ are often indirect: particles, smell and Microbial Volatile Organic Compounds (MVOC:s). Other aspect of indoor climate is the thermal comfort. This more technical orientated performance depends on the temperature, air flow velocity and partly also humidity conditions that can be studied by measurements.

In the site case the indoor conditions evaluation was based on user questionnaires and further micro-biological studies and the evaluation results are presented in FIG 3.

Class	Definitions
2,5 - 3	Essential need for renovation, severe risks included
1,5 – 2,5	Renovation needed, increased risks
1 – 1,5	Performance lower than required, low risks
1 < 1	Fulfills current requirements Better than required

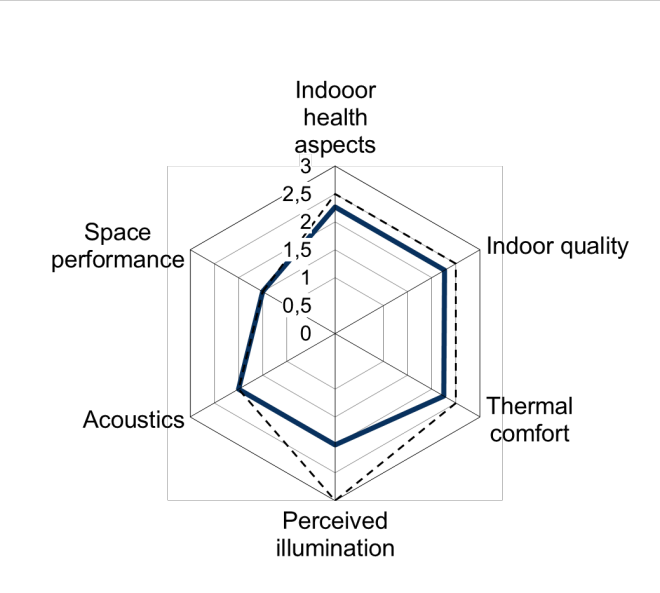

FIG 3. *Classification categories for risks and renovation needs (left) and the presentation of the evaluation results. Continuous line for average levels, dashed for maximum values of each sub area.*

4.2 Structures and systems

The critical structures and systems for heat and moisture performance were evaluated. The design and implementation requirements vary by structures and the analysis was done for different parts of the building envelope and ground supported structures.

The moisture performance of the building envelope parts can be evaluated. One of the most suitable criterias for the moisture performance analysis is the risk of bio-deterioration that can be studied numerically using mould and decay models incorporated with the hygroscopic simulations (Viitanen 1997a, 1997 b, Viitanen et al 2000, 2010, Ojanen et al 2010). Mould development depends on factors like ambient temperature, exposure time and the type and surface conditions of building material. Mould typically affects the quality of the adjacent air space with volatile compounds and spores.

Degradation in one structure or system increases the risk for damage to other structures. Therefore it is important to pay attention also to the starting degradation. Other evaluation criterion in this section is the performance of design solutions, their functionality and fault tolerance. For example wood-frame walls can be more sensitive to the excess of moisture than massive brick walls, and generally ventilated structures are more tolerant against additional moisture than unventilated structures.

In addition to structures, also the present state of the building systems (ventilation, heating, plumbing) were evaluated. The evaluation results for the school building are presented in Figure 4 (left).

4.3 Microbial condition of building and materials

The role of microbes is important for the performance of buildings and for indoor air quality (IAQ). Visual inspection of structure and analysis of the eventual damage of the building are the first step to

evaluate the condition of the materials and structure. Especially the details where moisture can be accumulated during the service live of the building are important to notice. In the next step, more detailed analysis of the critical parts of the structures should to be performed, when also samples from materials will be taken.

Based on the analysis, an evaluation of the condition of the building will be performed using a systematic process. Different methods can be used. The direct microscope analyses are also very useful especially for damage analytic. Figure 4 (right) presents the results of the evaluation of the school building. The evaluation is based on different microbial analysis of the structures of the school building. Three different levels of classification were used: 1) no microbial problems, 2) local problems or microbial growth, 3) severe or large microbial problems or damage. The most attacked structures were the inside parts of outdoor walls caused by water penetration through the brick façade. Also the outer part of constructions in ground were wet and attacked by micro-organisms. A part of the floor structure (crawl base) was partially attacked by decay.

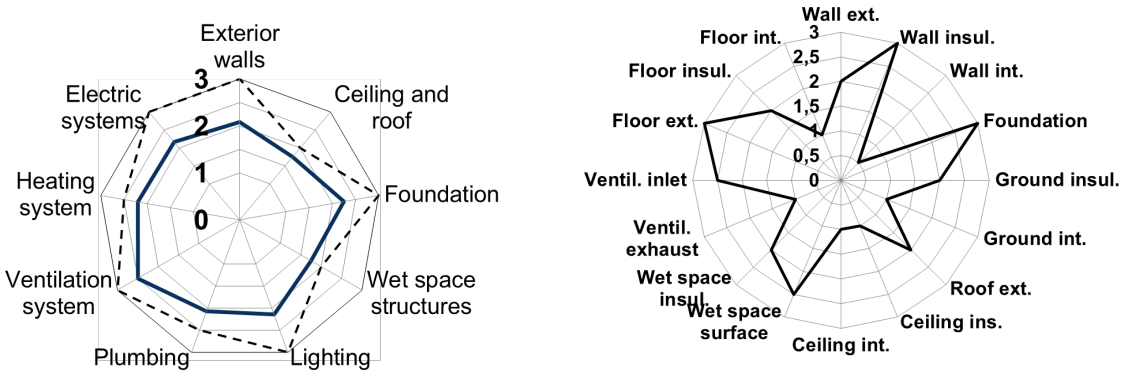

FIG 4. *Evaluation results of the structures and building systems (left) and microbial condition of a school building (right). Continuous line for average levels and dashed line for maximum values of each sub area.*

4.4 Lighting

The main goal of the lighting renovation process is to improve lighting quality and energy efficiency and to achieve light levels mentioned in latest recommendations. User acceptance and visual comfort is improved with advanced daylight use, modern controls and attractive luminaire outlook.

Renovation of lighting system is normally a part of large building renovation process of the building. The lighting evaluation part of the tool helps the experts to find the biggest risks of the old lighting systems and to make decisions for the future lighting plans. The “check list” of lighting tool concern age of installation, quality and quantity of lighting, types of light source and luminaires, lacks and faults of luminaires and parts, controls and sensors, use of daylight and overall energy efficiency. Again, the three level risk classification is used to present the current and future risks of the lighting system. The lighting evaluation is presented in Figure 5 (left).

The first and even sufficient reason to renew the old lighting installation is the high age of fixtures. Expected life period of the lighting installation is typically 25 years. During this period all the components, especially plastic lamp holders and light diffusing materials, electrical parts like ballasts are normally aged. Energy efficiency of old luminaires may be poor due to missing or darkened reflectors and diffusers or glare shields. Lamp types may be out of date even, in some cases like incandescent and mercury lamps, already denied by the European directives.

With LED technology it is already possible to gain better energy efficiency than with the present T5 tubular fluorescent technology. The main disadvantages of led general lights are higher luminaire price, so far limited selection of systems for general indoor lighting, and only moderate glare reduction due to the lacks in intensity distributions.

4.5 Energy efficiency

The normalized specific heating energy use of the school building was 48 kWh/m^3 and the specific electricity use 8.3 kWh/m3 (year 2009). The original energy class of the school building was class D (Finnish energy classification of buildings) representing a quite average energy use. This reasonable high energy class is due to the insufficient ventilation rate. Besides being under-dimensioned, the existing mechanical outlet ventilation system also had no heat recovery. The renovation will increase the energy-efficiency of the school building by means of ventilation heat recovery, increased insulation levels of wall and roof structures and a new energy-efficient lighting system.

The evaluation of the energy efficiency of the original school building is presented in Figure 5 (right).

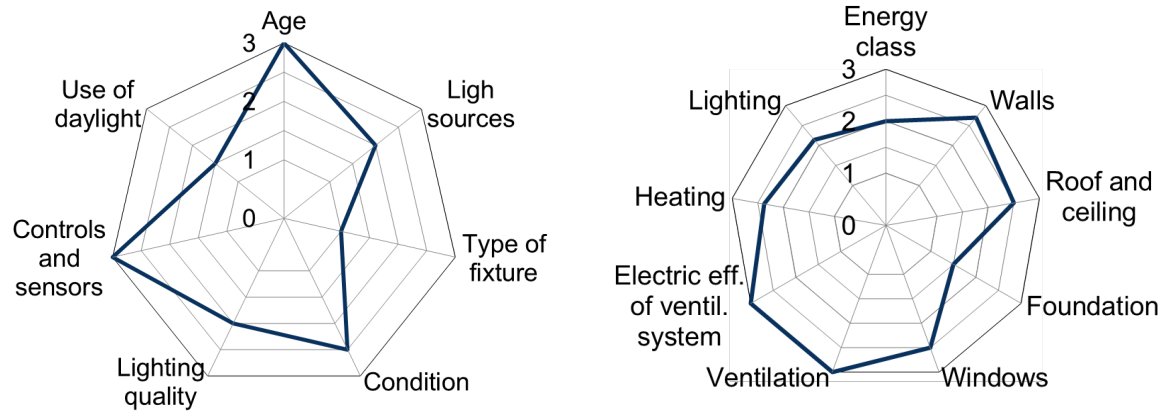

FIG 5. Evaluation results for lighting quality (left) and energy efficiency (right) of the school building.

The new mechanical inlet and outlet ventilation system with heat recovery will increase the electricity use of the building. Some of this increase can be compensated using on-demand ventilation, which was estimated to reduce the average ventilation airflow by 50-60 %. Also the more efficient fans will reduce the electricity use of the ventilation system: the specific fan power (SPF) of the original outlet air fans was estimated to be 2.5 kW/(m3/s), whereas that of the new inlet and outlet ventilation fans was estimated to be 1.9 kW/(m3/s). With these assumptions the annual electricity use of the ventilation system would increase 9 MWh.

Including lighting improvements the total effect of the renovation on the annual electricity use is -10 MWh. The estimated decrease of the annual heating energy use of the building is 400 MWh, which represents the annual saving of 21 700 € with the average heating energy price of 54 €/MWh. The renovation will increase the energy class of the school building from class D to class A and the total annual energy saving due to the renovation is 22 550 €. Besides energy savings the new ventilation system will also improve the thermal comfort of the occupants and improve the indoor air quality, which have been linked to better learning results of the pupils.

4.6 Renovation cost evaluation

Renovation actions affect both book value and technical value of a real estate. Book value is usually calculated subtracting the annual depreciation from the value of the new building and adding the cost of repairs.

Renovation actions are not always properly aligned, damaged structures may remain unrepaired and undamaged structures may be repaired. Such renovation does not raise directly the book value as calculation model assumes. Therefore, book value and technical value may differ significantly.

New calculation model to estimate technical value of real estate was developed in research project. In the model building is divided in seven parts: Roof, external wall, ground-supported and bathroom constructions, and plumbing, heating and ventilation systems.

Firstly, each part is defined as the percentage of its share in the total value of the building by its current condition. Secondly, each part is evaluated by the risk for moisture problems by its design solution. A combination of condition and risk evaluation gives a comprehensive approximation of the value of building. Model can be used to evaluate technical value before and after renovation. This gives valuable information when deciding the extent of renovation or prioritizing renovations. The technical value of case building before and after renovation is shown in Table 1.

TABLE 1. *The technical value of case building before and after renovation*.

Area 4 485 brm^2 Price of new building 2400 €/brm^2								
	Before renovation				**After renovation**			
Structure	Cond.	%	Risk	%	Cond.	%	Risk	%
Roof constructions	2	9 %	2	5 %	1	13 %	1	1 %
External wall constructions	3	5 %	3	6 %	1	14 %	2	4 %
Ground-supported constructions	2	7 %	2	5 %	2	7 %	2	5 %
Bathroom constructions	2	6 %	3	7 %	1	9 %	1	1 %
Plumbing systems	2	7 %	3	9 %	1	12 %	2	7 %
Heating systems	2	5 %	2	6 %	1	10 %	1	2 %
Ventilation systems	3	6 %	2	4 %	1	16 %	1	1 %
Total		45 %		42 %		81 %		21 %
	26 %				**64 %**			
	Price		**2 809 404 €**		**Price**		**6 887 884 €**	

5. Discussion and conclusions

The renovation methodology and tool developed in a project are described in a concise way. The methodology guides the user through the renovation process, emphasizing the present state analysis and the evaluation of the renovation needs. Different levels of analysis depths can be applied varying from a check-list approach to detailed performance analysis. The concept methodology tool only guides the user to take into account the needed actions and gives information about the performance requirements. The final decisions remain always to the user who is responsible for the aims and allowed costs of the renovation actions.

A case study was carried out using the information of a school building. The case study showed that using this approach the risks related to different parts and systems of the building can be better taken into account than without a systematic tool. The simple three-level presentation of the risks and

renovation needs of building structures and systems reveals the actual problem areas and helps to prioritize the renovation actions. Also the interactions and reciprocal risks of different renovation solutions are easier to comprehend. The improvement of the indoor conditions were evaluated by numerical thermal comfort analysis of different renovation solutions. Survey after the renovation is ready will show the effects on indoor air conditions and energy efficiency.

The renovation cost evaluation shows the best ways to increase the value of the building. This approach takes into account the present and renovated conditions and risk evaluations of different parts of the building and gives a comprehensive approximation of the value before and after selected renovation actions.

Using this methodology the renovation process will lead to solutions where the existing problems of the old building will be sorted and mended and the renovation will be directed to good energy efficient solutions with healthy and comfortable indoor environment. Due to the simple structure of the tool it is easy to use and update according the new requirements, research results and user needs.

6. Acknowledgements

Project ENERSIS (A Concept Ensuring High Indoor Environment Quality and Structure Moisture Performance in Energy Efficiency Renovations) was financed by TEKES (The Finnish Funding Agency for Technology and Innovation), VTT (Technical Research Centre of Finland), City of Helsinki and industry, and it was carried out at VTT Technical Research Centre of Finland, Aalto University and Tampere University of Technology during 2010 – 2013.

References

Viitanen, H. 1997a. Modelling the time factor in the development of brown rot decay in pine and spruce sapwood - the effect of critical humidity and temperature conditions. Holzforschung, vol. 51, 1, pp. 6 - 14

Viitanen, H. 1997b. Critical time of different humidity and temperature conditions for the development of brown rot decay in pine and spruce. Holzforschung, vol. 51, 2, pp. 99 – 106

Viitanen, H; Hanhijärvi, A; Hukka, A; Koskela, K. Modelling mould growth and decay damages. Healthy Buildings 2000: Design and Operation of HVAC Proceedings. Espoo, 6 - 10 August 2000. Vol. 3. SIY Indoor Air Information, pp. 341 - 346

Viitanen, H; Vinha,J.; Salminen, K.; Ojanen, T.; Peuhkuri, R; Paajanen, L.; Lähdesmäki, K.. 2010. Moisture and bio-deterioration risk of building materials and structures. Journal of Building Physics, vol. 33, 3, pp. 201-224

Ojanen, T., Viitanen, H., Peuhkuri,R., Lähdesmäki, K., VinhaJ., Salminen K. Mould growth modeling of building structures using sensitivity classes of materials. Thermal Performance of the Exterior Envelopes of Whole Buildings XI. Clearwater Beach, 5.-9. Dec.2010. CD. ASHRAE, DOE, ORNL. Atlanta, USA (2010).

Ojanen, Tuomo; Holopainen, Riikka; Viitanen, Hannu; Lehtovaara, J.; Vinha, J.; Kero, P. Methodology to integrate energy efficiency, safe moisture performance and indoor environment quality in building renovation projects. 2nd Central European Symposium on Building Physics, CESBP 2013, 9 - 11 September 2013, Vienna, Austria. Proceedings. WienUniversity of Technology (2013), pp. 937 – 942

Individual energy savings for individual flats in blocks of flats

Anker Nielsen, Professor [1]
Jørgen Rose, Ph.D.[1]

[1] Danish Building Research Institute, Aalborg University, Denmark

KEYWORDS: *Energy savings, individual flats, lower temperature, variation*

SUMMARY:
It is well known that similar flats in a block do not have the same energy demand. Part of the explanation for this is the location of the flat in the building, e.g. on the top floor, at the house end or in the middle of the building. It is possible to take this into account when the heating bill is distributed on the individual flats. Today, most blocks of flats have individual heat meters to save energy and to ensure a fair distribution of the cost. If all flats have the same indoor temperature, the distribution is correct.

In practice, the inhabitants of the different flats maintain different indoor temperatures. The result is that heat flows between individual flats. This decreases the energy consumption in the flat where the owner maintains a lower temperature. The neighbouring flats will have higher energy consumption. Calculations were performed for Danish blocks of flats from 1920, 1940, 1960 and 1980. Normally, we expect the reduction in energy consumption to be around 20% for a 2 °C lower temperature, but for an inner flat the reduction can be up to 71%. The owners of the adjoining flats get an increase in energy demand of 10 to 20% each. They will not be able to figure out whether this is because the neighbour maintains a low temperature or the fact that they maintain a higher temperature. The best solution is to keep your own indoor temperature low. We can also turn the problem around: if you maintain a higher temperature than your neighbours, then you will pay part of their heating bill.

1. Introduction

It is a well-known fact that energy consumption in dwellings varies significantly depending on the number of inhabitants and their individual behaviour. This has been documented in several previous publications, e.g. (Hiller 2003) showing measurements of variations in energy consumption for 38 individual single-family houses over a period of 10 years, (Pettersen 1997) presenting the mean value and standard deviation of energy consumption in more than 900 flats spread over 9 different blocks and (Mørck 2011) showing the variations in heating energy consumption for 64 individual housing units.

For blocks of flats, it is interesting to know not only the energy demand of the entire building, but also the energy demand of each flat. It is typical that flats immediately below the roof, above an unheated basement and at the building ends have a higher energy demand. This is the effect of different heat losses, but another factor also has an impact. That is the indoor temperature. A lower indoor temperature results in energy savings that are very economic as it does not cost any money. If we calculate with Danish climate conditions, a lowering of the temperature by 2 °C will result in a 20% energy saving or 10% per °C. That is the case if you live in a single-family house, where you can control the temperature yourself.

If we lower the temperature by 2 °C in all flats in the block, we get the 20% energy saving. But that is not the case when we consider lowering the temperature in a individual flat. Here, a lowering of the temperature gives a much higher energy saving as you receive heat from your neighbours if they do not lower their temperature. It is important to be aware of this effect if you make individual

measurements of the heating demand and perform calculations of the expected heating bill. It is normal in Denmark to have a central heating system and each flat pays part of the total heating bill of the building. Typically this is based on measuring the indoor temperature or the heating consumption of each flat.

2. Energy calculation

The calculations of the energy demand presented in this paper is done with the model described in Nielsen 1980 based on a monthly energy balance. The model can calculate multi-zones, where each flat is a zone and staircases, basement etc. are other zones. The zones can be heated to a fixed constant temperature or the temperature in each zone can be dependent on the heat balance with other zones. In each zone, the heat loss and ventilation loss to the outdoor air and the heat gain from solar radiation, persons and equipment is taken into account. The heat flow between individual flats, i.e. transmission heat flow, is also taken into account in the model. The outdoor climate is the Danish standard climate data. The outdoor temperature is given as a monthly mean value. Solar radiation through a typical pane is given as a monthly sum depending on the orientation of the window. The calculation method also takes into account that the heat gain cannot always be fully utilized and could instead give rise to overheating. This is determined by the energy balance calculated month by month. For each heated zone (as flats), a heating demand is calculated for a constant indoor temperature of 21 °C. The heat flows between zones can be positive or negative depending on the temperature difference.

This method is similar to that of Be10 (Aggerholm and Grau 2005), which is used for most small buildings in Denmark today. But Be10 only considers the building as a single zone. For multi-zone models, it is normal to use much more complex models that calculate the energy balances hour by hour, but the effect of lowering the temperature in individual flats the model by (Nielsen 1980) should be sufficient.

3. Selected buildings

In a thesis work Rasmussen 1980 calculated energy savings and energy economy in blocks of flats from different time periods. The buildings were selected as typical for the period, but it was important to have drawings and descriptions as a basis. All U-values and areas were calculated and the method by Nielsen 1980 was used in the energy calculations. The thesis work presented different calculated energy savings for individual energy-saving measures such as new windows or extra wall insulation and their economy.

The selected buildings were:

Struenseegade, Nørrebro, København, 1920, built from bricks, with wooden floors and single glazing.

Bispeparken, Bispebjerg, København, 1940, built from bricks, with floors of concrete and single glazing.

Hedeparken, Ballerup, 1960, industrialised construction built from concrete, with wooden façade elements and double glazing.

Tinggården, Herfølge, 1980, low-dense buildings with good insulation.

Eremitageparken, Lyngby, 1972, modern industrialised buildings.

This paper concentrates on “Struenseegade” from 1920 and “Hedeparken” from 1960, but the effect of later changes in the building methods, insulation levels etc. are discussed.

4. The case: Struenseegade

The buildings in Struenseegade were built in 1920. They are 5 storeys high and consist of two- and three-room flats. Calculations were done based on drawings and descriptions of the flats, and in order

to represent all types and locations in the buildings, 40 flats were included in the analysis. The overall insulation level of the buildings was extremely poor with a solid brick wall thickness of 36-60 cm with a U-value ranging from 1.0 to 1.5 W/m^{2}K.

Heat flows between individual flats depend on the nature of the partition walls and floors. In 1920, Denmark did not have any particular requirements concerning thermal insulation of buildings, and there were no requirements concerning sound insulation either. In this particular building, the partition walls consisted of brick and the floors were wooden joists with clay deposits. The U-value of the partition walls were 2.2 W/m^{2}K and the U-value of the floors were 0.7 W/m^{2}K and therefore differences in indoor temperature in individual flats have had a huge impact on the energy consumption in the surrounding flats.

The block of flats was grouped with other buildings meaning that it did not have gable flats.

Figure 1 shows the individual energy demand of flats around 4 staircases in MWh per year calculated at an indoor temperature of 21 °C.

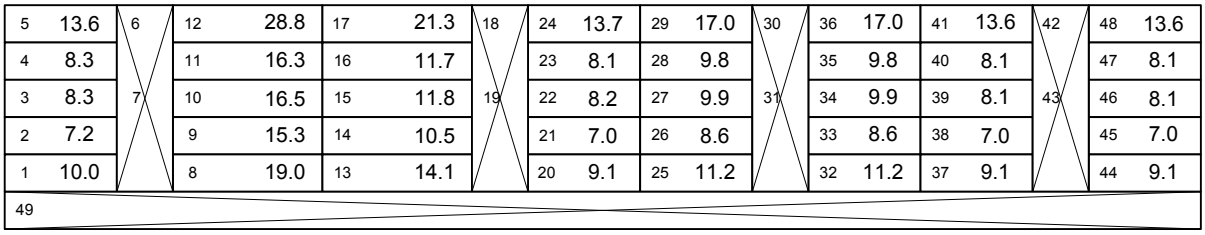

FIG 1. Energy demand of flats around 4 staircases in MWh per year

Figure 1 shows the energy demand of the flats around four staircases, if the indoor temperature was 21 °C in all flats. Flats nos. 1 to 5 were located at the building end but since the building was grouped with other buildings, they had no extra heat loss. The four staircases, nos. 6+7, 18+19, 30+31 and 42+43 as well as the basement 49 were unheated. Flats nos. 8-17 were three-room flats while the rest were two-room flats. The result was that the flats on the ground floor like nos. 1, 8, 13, 20, 25, 32, 37 and 44 had a higher energy demand than more centrally located flats. A similar effect was seen on the top floor with flats nos. 5, 12, 17, 24, 29, 36, 41 and 48 which had an even higher heat demand due to the extra heat loss through the roof.

The calculated energy demand of the flats varied from 7.0 MWh/year for a two-room flat placed in the centre of the building to 28.8 MWh/year for a three-room flat at the top of the building.

Temperature lowered by 2 °C		Flat Above	Flat Right	Flat Left	Flat Below
Entryway 6 and 7 Left	5 -25		12 +1		4 +6
	4 -34	5 +4	11 +1		3 +6
	3 -34	4 +6	10 +1		2 +7
	2 -36	3 +6	9 +1		1 +5
	1 -29	2 +7	8 +1		
Entryway 6 and 7 Right	12 -25		17 +4	5 +2	11 +6
	11 -35	12 +3	16 +7	4 +3	10 +5
	10 -35	11 +6	15 +6	3 +3	9 +6
	9 -36	10 +5	14 +7	2 +3	8 +5
	8 -30	9 +6	13 +6	1 +2	
Lowering everywhere		-20			

FIG 2. Energy demand of flats nos. 1-5 and 8-17 if the temperature is lowered by 2 °C in one flat. Small numbers are flat numbers, large numbers are changes in energy demand in % compared with normal. Negative numbers are energy savings and positive numbers increased energy consumption

Temperature lowered by 2 °C		Flat Above	Flat Right	Flat Left	Flat Below
Entryway 18 and 19 Left	17 -28		24 +2	12 +3	16 +8
	16 -40	17 +4	23 +3	11 +5	15 +7
	15 -40	16 +8	22 +3	10 +4	14 +8
	14 -42	15 +7	21 +3	9 +5	13 +6
	13 -35	14 +8	20 +3	8 +4	
Entryway 18 and 19 Right	24 -32		29 +6	17 +1	23 +7
	23 -45	24 +4	28 +10	16 +2	22 +7
	22 -45	23 +7	27 +10	15 +2	21 +8
	21 -48	22 +6	26 +11	14 +2	20 +6
	20 -41	21 +8	25 +9	13 +2	
Lowering everywhere		-20			

FIG 3. Energy demand of flats nos. 8-17 and 20-29 if temperature is lowered by 2 °C in one flat. Small numbers are flat numbers, large numbers are changes in energy demand in % compared with normal. Negative numbers are energy savings and positive numbers increased energy consumption

Figures 2 and 3, had the same layout as the flats located in the building. For example, if we look at flat (3) in Figure 2; if the temperature in this flat is lowered by 2 °C, the savings will be 34 %. In turn, this increased the energy consumption of the neighbouring flat (10) by 1% for the upstairs neighbour (4) 6% and the downstairs neighbour (2) 7%. Results for the other flats can be read in a similar manner.

For a single-family house you would expect savings corresponding to approximately 20% if the temperature was lowered by 2 °C, but here the results showed significantly higher savings. This was due to the transmission of heat to the flat from adjacent flats.

The savings of two-room flats were:

- Top floor (on the roof) approx. 30%
- Between floors approx. 45%
- Lower floor (against basement) approx. 30%

As a result of these savings, the energy consumption of the adjoining flats increases by up to 11%. The exact figures are shown in Figs. 2 and 3. The building's total energy consumption is almost unaffected by individual flats lowering temperature.

5. The case: Hedeparken

The buildings in ”Hedeparken” were built in 1960 as one of the large industrialised buildings consisting of four-storey blocks of flats. All flats in this block are of the same size – three-roomed. The calculation was performed based on the drawings and descriptions of the flats. The calculation was performed for three staircases in a block of flats. The thermal insulation of 75 mm mineral wool was typical for the period around 1960. The windows had double glazing with a U-value of 2.50 W/m^{2}K. The walls were a light wooden prefabricated solution with a U-value of 0.44 W/m^{2}K. The floor between the cellar and the flats had a U-value of 0.60 W/m^{2}K. The roof had a U-value of 0.48 W/m^{2}K.

The heat flows between the individual flats depend on the constructions in the building. The Danish Building Regulations from 1960 specify rules for the sound insulation between the flats but there are no regulations concerning heat flow. To achieve good sound insulation, it is important to use heavy constructions, e.g. concrete. This, however, results in a high U-value. The partition walls between flats were 150 mm concrete with a U-value of 2.8 W/m^{2}K. For floors between flats the U-value was 1.35 W/m^{2}K.

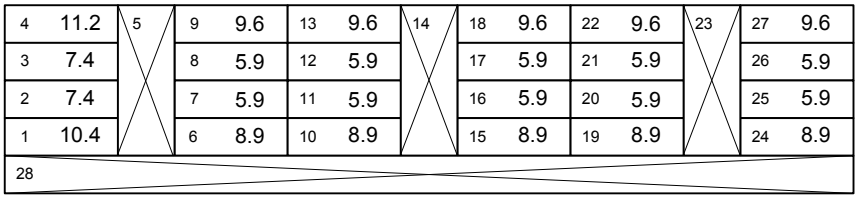

FIG 4. Energy demand of flats around three staircases in MWh per year

The drawing in Figure 4 shows the energy demand for the flats around three staircases, if the indoor temperature was 21 °C in all flats. Flats nos. 1 to 4 are located at the gable with extra heat loss. The three staircases nos. 5, 14 and 23 were calculated as unheated. The only heat comes from the adjoining flats and solar radiation. Below the block of flats was a basement – no. 28, which was also unheated. The result was that the flats nos. 1, 6, 10, 15, 19 and 24 on the ground floor had a higher energy demand than most inner flats. The calculated energy demand of the flats varied from 5.9 MWh per year in an inner flat to 11.2 MWh per year for the flats at the top floor at the gable. The average

temperature in the staircases had a variation from 17.0 °C in December to 21.2 °C in July. The variation in energy demand gives a variation on the energy bill of the flats, also if we had the same indoor temperature and free heat from solar radiation, electricity and persons. In real life, the energy bill depends on the inhabitants' use of the flats, i.e. some have a higher temperature and some could have more ventilation and also an effect of the variation in the number of inhabitants in each flat.

Temperature lowered by 2 °C		Flat Above	Flat Right	Flat Left	Flat Below
Entryway 5 Left	4 -35		9 +5		3 +17
	3 -54	4 +11	8 +8		2 +16
	2 -54	3 +16	7 +8		1 +12
	1 -38	2 +17	6 +6		
Entryway 5 Right	9 -47		13 +11	4	8 +5
	8 -71	9 +11	12 +16	3 +7	7 +18
	7 -71	8 +18	11 +16	2 +7	6 +13
	6 -51	7 +20	10 +13	1 +6	
Lowering everywhere		-20			

FIG 5. Energy demand of flats nos. 1-9 if temperature is lowered by 2 °C. Small numbers are flat numbers, large numbers are changes in energy demand in % compared with normal. Negative numbers are energy savings and positive numbers increased energy consumption

Figure 5 shows the result of a calculation on the energy demand of flats nos. 1-9 if the temperature was lowered by 2 °C – from 21 °C to 19 °C. This is not unrealistic if you want to save energy and reduce your energy bill. For flats in the middle of the building, like nos. 7 and 8 the energy demand for heating and ventilation would be reduced by 71%. The result was of course that flats above, below and next door to the left and right had a higher energy demand and a higher bill. The increase of these flats was 7-18%.

If we take an example flat no. 8, the saving were 71%. For the flat above no. 9, the increase was 11%. For the flat below no. 7 the increase was 18%. For the neighbours to the right, no. 12, the increase was 16%. For the neighbour to the left, no. 3, the increase was 7%.

For the top floor, the saving was 47% and for the first floor above the basement 38%.

The energy saving was less if you lived in a flat at the gable. The savings were:

Top floor at the end and under the roof:	35%
Floors 2 and 3 at the end:	54%
First floor at the end and above basement:	38%

All the savings and extra heat demand of the neighbours are given in Figure 5.

These savings correspond to the obtained 20% saving if all flats reduced the indoor temperature by 2 °C.

All calculation were performed with a lower temperature but we can reverse it so a 2 °C higher temperature for a flat in the inner part of the building gets a 71% higher energy demand. If you have a

higher temperature than your neighbours, then you get a high energy bill as you also pay for your neighbours' heating. They would save 7-18% on their individual energy bills.

6. Discussion

Calculations for the other buildings show similar effects of variations in energy demand between the flats and that lowering the temperature in an individual flat gives much more saving than the 20% for 2 °C. The numerical values can be less but the effect of the heat flow between the flats is very important for the savings. Is this still relevant today – many years after the calculation? The answer is yes. Many of the buildings have been extra insulated or had new windows so the energy demand of the flats has been reduced. But you cannot do anything with the heat flow between flats. So there is still a heat flow between the flats if we lower the temperature and the saving from a lower temperature is the same or slightly higher.

New buildings are typically built with constructions as described in Rasmussen 2011 in order to obtain the necessary sound insulation. There are no rules regarding thermal insulation between flats. Looking at the cases in the report, we can find the best insulated constructions. For the floor, this is 25 mm insulation and for the wall it is 50 mm insulation material, if the construction is made as cavity wall with a 60 mm space with 50 mm mineral wool. In reality, this wall construction is seldom used as it is quite complicated to build.

We can now look at Hedegården and look at the changes that will occur if extra insulation is added. For walls between flats, the extra 50 mm insulation decreases the U-value from 2.80 W/m^{2}K to 0.62 W/m^{2}K. For floors between flats, the extra 25 mm insulation decreased the U-value from 1.35 W/m^{2}K to 0.73 W/m^{2}K.

If we again look at flat no. 7, Table 1 shows the effect of a change in the constructions.

TABLE 1. Savings with original wall/floor or better insulated wall/floor between flats

	Original	New constructions	Realistic
Flat 7	-71%	-40%	-58%
Flat 8 above	18%	10%	14%
Flat 6 below	13%	7%	10%
Flat 2 left	7%	2%	5%
Flat 11 right	16%	4%	13%

The new constructions reduces the heat flow between the flats as flat 8 goes from 18% to 10% increase of energy demand. The savings in flat 8 is now reduced to 40%, but still a very large effect. The new constructions are a theoretical case as there are some practical problems. If we look at the solution with 25 mm insulation; this is only possible under a wooden floor and not under inner walls in the flat and probably not under bathrooms and toilets. So there will be thermal bridges and some areas that do not have 25 mm insulation. We must also remember that some of the sound insulation solutions do not have thermal insulation. A best estimate is given in the last column. For the wall between flats it is, as mentioned, more complicated to build the wall as two separate walls with thermal insulation between, so only few houses will have this solution. A more realistic estimate is therefore shown in the right column of Table 1.

7. Conclusions

The calculations presented in this paper show that it is much easier to achieve energy savings by lowering the temperature in a flat in the central part of a block than for flats closer to the top, bottom

or end of the building since it will receive heat from the flats around it. This effect is still relevant even in new blocks of flats as the floors and walls between individual flats typically do not have specific thermal insulation. The most efficient way of saving energy is that all inhabitants know that you increase savings if the neighbours do not lower the temperature. If all flats lower the temperature, we will achieve the highest total energy savings.

Is it possible to determine whether your neighbours are "stealing" your heat? This is probably not possible as there will always be variations in the behaviour and number of people in the flats. So you have to take the risk, but we could also look at it, so that if your neighbour maintain a high temperature you will achieve an energy saving.

References

Aggerholm, S. and Grau, K. 2005; Bygningers energibehov - Pc-program og beregningsvejledning. (Building energy demand – PC program and user guide) SBi-Anvisning 213. Statens Byggeforskningsinstitut (SBi), Hørsholm, Denmark

Hiller, C. 2003; Sustainable energy use in 40 houses – A study of changes over a ten-year period, Report TVBH-3044, Department of Building Physics, Lund Institute of Technology, Lund University, Sweden.

Mørck, O., Thomsen, K. E. and Rose, J. 2012; The EU CONCERTO project Class 1 - Demonstrating cost-effective low-energy buildings - Recent results with special focus on comparison of calculated and measured energy performance of Danish buildings, Applied Energy, Vol. 97, 09.2012, pp 319-326.

Nielsen, A 1980: Beregning af ruminddelte bygningers energiforbrug. Metoderne EFB2 og EFB3 (Calculation of energy demand for building divided in rooms), meddelelse nr. 103, Thermal Insulation Laboratory, Technical University of Denmark

Pettersen, T. D. 1997; Uncertainty analysis of energy consumption in dwellings, NTNU, Trondheim, Doktor ingeniøravhandling 1997:122, Høgskolen i Narvik, Norway.

Rasmussen, N.H. 1980: Energibesparelser og energiøkonomi i etageboliger, (Energy savings and energy economy for blocks of flats), Thesis work, Thermal Insulation Laboratory, Technical University of Denmark

Rasmussen, B. 2011. Lydisolering mellem boliger – nybyggeri (sound insulation between flats) SBi-anvisning 237, Statens Byggeforskningsinstitut (SBi), Hørsholm, Denmark

Renovation vs. demolition of an old apartment building: energy use, economic and environmental analysis

Kalle Kuusk, M.Sc.
Simo Ilomets, M.Sc.
Targo Kalamees, Professor
Sten Tuudak, M.Sc.
Andre Luman, M.Sc.

Tallinn University of Technology, Estonia

KEYWORDS: *renovation scenarios; energy performance; cost effectiveness; embodied energy; apartment buildings.*

SUMMARY:
The paper analyses four renovation scenarios for one concrete element building type. These scenarios were: major renovation, low-energy renovation, low-energy renovation with extensions, demolition of the original building and construction of a new building. Results reveal that in the current case an existing building can be renovated to meet the same energy-efficiency levels as a new building. Demolition of an existing building and construction of a new one raises the global cost at least four-fold. Analyses of embodied energy via CO_2 emissions from the materials and energy production for a building during 20 years show that a new building has at least three times higher environmental impact than low-energy renovation. Therefore, the condition and low energy efficiency of an old concrete element apartment building are not the reasons to consider its demolition.

1. Introduction

Increasing energy prices and energy saving policies have shifted attention to the energy performance of dwellings. EU has made a commitment to reduce the emission of greenhouse gases by 20% by the year 2020 compared to the level of 1990. Estonia has set the goal of maintaining the final energy consumption at the same level as in 2010. However, this will require a decrease in energy use and an increase in energy efficiency. Energy economy and heat retention were included as basic requirements for construction works (Construction Production Regulation 2011) earlier but sustainable use of natural resources is a recent addition. This means that focus should also be on the durability and low long-term environmental impact of the construction process and exploitation (often expressed via carbon dioxide CO_2 emission).

The design of renovation raises the question of the extent and economic viability of renovation. Frequent discussions also address the demolition of an existing building and the construction of a new building. The agenda of Tallinn Vision Council contains a target to demolish 103 of the oldest prefabricated concrete large panel element apartment buildings (hereinafter: concrete element buildings) in Tallinn (Sarv 2013). The concept targeted to demolishing existing buildings introduces new economic and environmental challenges. Previous studies have pointed out that such areas as exact embodied energy values, the costs and applicability of refurbishment, direct energy impact of demolition and its wider environmental impact still remain unclear. However, both broad arguments and concrete evidence support maintaining a focus on renovation rather than on large-scale demolition (Power 2008).

Results of research covering the current technical condition of Estonian old concrete element housing stock refer to satisfactory condition in terms of load-bearing but to insufficient energy performance, indoor climate and hygrothermal performance of the building envelope (Kalamees 2011). Also, durability of concrete façades has been found to be problematic regarding to corrosion and frost damage (Ilomets 2011).

This study analyses different renovation scenarios for one concrete element building type. The aim was to find out how renovation, renovation with extensions, and construction of a new building affect the energy efficiency, economic viability, and embodied energy.

2. Methods

2.1 Studied building

The study object was a five-storey apartment building with prefabricated concrete large panel elements (TABLE 1, FIG 1) constructed in 1966. That type of construction was typical in Estonia and in other countries in Eastern Europe during the period 1961-90. In total, there are almost 3500 old concrete element buildings in Estonia (National Register of Construction Works).

During renovation works in 2011, additional insulation was placed to the building envelope, old windows were replaced, a new two-pipe heating system and a ventilation system with heat recovery were installed.

TABLE 1. Characterisation of the studied building

Net area, m^2	3519
Heated area, m^2	2968
Number of apartments	60
Compactness: Building envelope, m^2 / volume, m^3	0.35

FIG 1. Picture of the studied building before (left) and after major renovation (right).

2.2 Simulations and calculations

Indoor climate and energy simulations were made for different stages of the building:

- original building without any renovation measures
- major renovation
- renovation on a low-energy building level
- renovation on a low-energy building with extensions of the building
- demolition of the original building and construction of a new building

As occupant behaviour related to energy usage is variable and unrelated to the building type, the energy calculations were made at standard indoor climate and by a unified calculation methodology. The methodology is specified in local regulations (Estonian Government's Ordinance No. 68 and Ministry of Economic Affairs and Communications' Ordinance No. 63. 2012). Energy performance of buildings was calculated with dynamic simulations using the IDA Indoor Climate and Energy 4.5 simulation program.

During the first phase of our calculations, simulation models for the pre- and the post-renovation stage were validated using the measured indoor climate and energy consumption data from the building. In the second step, validated models were calculated at standard usage and energy efficiency packages for a low-energy building, for a low-energy building with extensions, and for a new building were composed (TABLE 2).

TABLE 2. Variables of the simulation model

Variables	Without renovation	Major renovation	Low-energy	Low-energy (extensions)	New building
Thermal transmittance, W/(m^2·K) :					
walls $U_{wall,}$	0.90	0.17	0.14	0.14	0.12
roof U_{roof}	0.80	0.11	0.11	0.11	0.08
basement ceiling $U_{basement}$	0.60	0.60	0.23	0.23	0.23
windows U_{window}	1.90	1.40	0.80	0.80	0.80
doors U_{door}	1.10	1.10	1.10	1.10	1.10
Additional insulation, mm:					
external wall	-	+150	+200	+200	+250
roof	-	+300	+300	+300	+400
basement ceiling	-	-	+100	+100	+100
Air leakage rate q_{50}, m^3/(h·m^2)	5.0	5.0	3.0	3.0	1.0
HVAC systems:					
heating	1-pipe	2-pipe, thermostats	2-pipe, thermostats	2-pipe, thermostats	2-pipe, thermostats
ventilation	natural ventilation	exhaust air heat pump	apartment based AHU	apartment based AHU	apartment based AHU
renewable energy				solar collectors	

Extensions were attached to kitchens and staircases in the simulations of low-energy buildings with extensions. Additional space was used to accommodate the ventilation air handling units and increase the small floor area of the existing kitchen. Solar collectors were installed for heating domestic hot water (DHW) to compensate the increased heat loss caused by the additional constructions.

The construction of the new building scenario followed the principle that its energy efficiency would be higher than minimum requirements and would comply with the low-energy requirements for energy efficiency.

Estonian Test Reference Year (Kalamees and Kurnitski 2006) was used to simulate outdoor climate conditions.

Primary energy (PE) was used as the indicator for the energy efficiency. The requirements for the apartment buildings were as follows:

- major renovation: PE ≤ 180 kWh/(m^2·a)
- new buildings: PE ≤ 150 kWh/(m^2·a)
- low-energy buildings: PE≤ 120 kWh/(m^2·a)

According to the energy source, the use of the primary energy and the environmental impact were taken into account with the weighting factors:

- district heating 0.9
- electricity 2.0

2.3 Economic analysis

The global cost (EN 15459, Eq. (1)) calculation was used to assess the cost effectiveness of different renovation strategies.

$$C_g(\tau) = \frac{C_i + \sum_{i=1}^{20}(C_{ai}(j) \times R_d(i))}{A_{floor}} \quad (1)$$

where:
- $C_g(\tau)$ global incremental cost (€/m^2)
- C_i initial investment cost (€)
- $C_{a,i}(j)$ annual cost year i for component j (energy cost) (€)
- $R_d(i)$ discount factor for year i
- A_{floor} net floor area (m^2)

A period of 20 years was selected because the maximum period for renovation loans for apartment owners' associations in Estonia is 20 years. Global cost was calculated at the interest rate 4%. To show sensitivity to the escalation rate, five escalation rate scenarios were considered: 1% escalation, 3% escalation, 5% escalation, 7% escalation, and 9% escalation. Construction costs (TABLE 3) were taken from a database of apartment owners' associations containing reports of their real renovation costs and from the estimations of construction companies. The energy price levels used were 0.14 €/kWh for electricity and 0.075 €/kWh for district heating (mainly based on gas).

TABLE 3. Construction costs

Scenario	Cost, €	Cost, €/net m^2
Major renovation	450 000	128
Low-energy	773 000	220
Low-energy + extensions	1 051 000	278
New building	4 742 000	1348

2.4 Environmental analysis

Environmental impact of the five scenarios was analysed via the emission of CO_2 during the renovation/construction and 20 years of exploitation. An existing building before the renovation was chosen as the reference point, which means that CO_2 emissions of the construction materials used in 1966 and CO_2 emissions of energy carriers until the major renovation in 2011 were excluded from the analysis. Embodied energy of the renovation scenario was calculated for the quantity of each material from CO_2 emissions of the construction materials based on the literature. Also, thermal energy and electricity consumption were calculated and multiplied with CO_2 emissions to produce that energy.

To simplify the analysis, the following aspects were not taken into account:

- transportation
- energy and water demand at the building site
- workmanship
- HVAC systems installed into the building and the solar collector at low-energy with an extensions scenario
- small details and fixing (glue mortar, fastening, sealing foam and tapes etc.)
- thin layers (floor covering, rendering, filler, colour)
- transmission loss of district heating and electricity from the plant to the building site

It was also assumed that the impact of recycling the materials from a demolished building is negligible when replacing the existing building with a new one. The reason was that no dangerous waste (asbestos etc.) originates from the existing building and the majority of the remaining materials can be reused to a landfill construction site nearby. A minority of materials unsuitable for reuse can be sorted and handed over to the licenced company of construction waste management.

CO_2 emissions of the construction materials and the energy carriers used in the analysis are presented in TABLE 4.

TABLE 4. CO_2 emissions of the construction materials and the energy carriers (Kurnitski 2011 and Hegger 2008)

Material	CO_2 emission, kg/CO_2 eq/kg	Energy carrier	CO_2 emission, t/MWh
Expanded polystyrene	3.4	District heating	0.278
Stone wool	0.99	(mainly based on gas)	
Bitumen polymer sheeting	1.21	Electricity	1.01
Glass	0.66	(mainly based on oil shale)	
Precast concrete element	0.182		
Steel	0.73		
PVC	2.28		
Gypsum board	0.39		

3. Results

3.1 Energy usage

Delivered energy calculation results showed that the use of the delivered space heating energy can be decreased from 153 kWh/(m^2·a) to 15 kWh/(m^2·a) (FIG 2 left). The low-energy renovation scenario with extensions has a higher space heating energy need (32 kWh/(m^2·a)) than the low-energy scenario with the current building body shape (19 kWh/(m^2·a)) due to decreased compactness and additional linear thermal bridges. Solar collectors are used for heating DHW to compensate the increased heat loss through the building envelope. Use of the primary energy in the standard usage is shown in FIG 2 right. Electricity accounts for the largest share of the primary energy consumption in different renovation scenarios. For further reduction of the primary energy, it is necessary to reduce the electricity demand. Comparison of the energy use for low-energy renovation and for a new building shows no substantial differences. Thus, existing buildings can be renovated to meet the same energy-efficiency levels as new buildings.

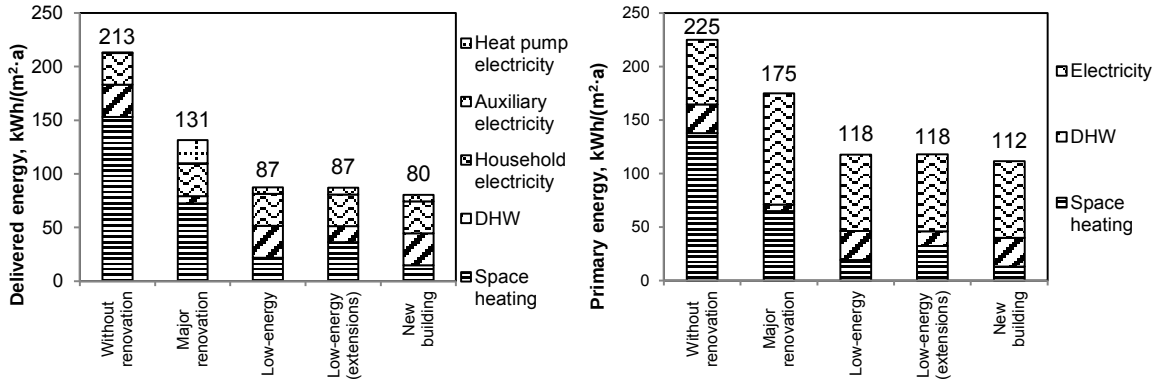

FIG 2. Delivered energy usage (left) and primary energy usage (right) of different renovation strategies.

3.2 Economic analysis

The global cost was selected to assess the cost effectiveness of renovation strategies (TABLE 5). Before the renovation stage, the global cost is lower than in other scenarios because the calculations do not take into account the maintenance costs. If the pre-renovation stage is taken as the reference point, the escalation should be 9% for the global cost to decrease in the renovation scenarios. The implemented low-budget major renovation has the lowest global cost values in the renovation strategies. Low-energy renovation with extensions has ca 15% higher global cost than the low-energy renovation without additional extensions. Demolishing of an existing building and building a new one has ca four times higher global cost than the low-energy renovation and the low-energy renovation with extensions.

TABLE 5. Global incremental cost values

Renovation Scenario	Global cost, €/net m^2				
	Escalation 1%	Escalation 3%	Escalation 5%	Escalation 7%	Escalation 9%
Without renovation	218	264	326	410	524
Major renovation	290	325	370	432	517
Low-energy	330	353	383	425	481
Low-energy (extensions)	388	412	443	485	543
New building	1463	1484	1513	1552	1605

3.3 Environmental analysis

Embodied energy of a renovation scenario can be expressed as a sum of CO_2 emitted from the production of the construction materials and CO_2 emitted from the energy production that a building consumes during the period of 20 years. Results presented in TABLE 6 indicate that the smallest embodied energy (3901 tons) is achieved by renovating an existing building to the low-energy level, being also lower than the reference case before renovation. In that case only 1029 tons of embodied energy originate from the materials (26% of total); that is close to major renovation but the impact from energy consumption has decreased notably, especially from electricity. Extensions in the case of low-energy lead to a higher need for materials and end up with a higher total value because of deteriorated compactness. Construction of a new building with the same volume has about nine times

higher need of resources for materials; that leads to more than three times higher total embodied energy compared to low-energy renovation, despite low energy consumption during exploitation.

TABLE 6. Emission of CO_2 from the production of construction materials and from energy production

Scenario	CO_2 emissions, t			
	Materials	District heating	Electricity	Total
Without renovation	0	2891	1717	4608
Major renovation	774	1251	2990	5015
Low-energy	1029	812	2060	3901
Low-energy (extensions)	2089	895	2283	5267
New building	9576	701	2060	12337

4. Discussion

Our results showed that in terms of energy efficiency, economic viability, and embodied energy, no direct reasons exist to demolish old concrete element buildings and build new apartment buildings.

Energy performance of existing low-energy and low-energy buildings with extensions is close to that of a new building; however, the construction cost of a new building is about four times higher. Also, the environmental impact of a new building is the highest because most (78%) of embodied energy comes from the materials and the improvement of energy performance during the exploitation will have no further impact. The result of approximately three times higher environmental impact of a new building refers to similar conclusions found in previous studies (Ireland 2008 and Yates 2006). They report that new homes use four to eight times more resources than an equivalent refurbishment. It should be noticed that some of the additional factors related to a new building (transportation, HVAC systems, construction waste management) were excluded, in the opposite case, the difference between renovation vs new building would even have been larger.

Load bearing structures are not a critical issue as the condition of the main load bearing structures was found to be sufficient, allowing planning of renovation works instead of demolition (Kalamees 2011). Therefore, the condition and low energy efficiency of old concrete element buildings are not the reasons to consider their demolition. Tallinn Vision Council has pointed out that floor planning of these old dwellings is unsuitable for families (Sarv 2013) because of small-sized bathrooms and kitchens. In addition, in the five-storey buildings, narrow staircases and absence of elevators restrict movement of families with small children and older people on higher floors. Demolition is a plausible solution when some region is intended to be thoroughly renewed. At higher volumes, the construction costs would be lower and a larger macro-economic impact would be also an important factor, but here further detailed analysis is required. On a single building level, renovation is substantially cheaper than building a new dwelling. The number of old concrete element buildings reveals a potential solution in favour of renovation due to enormous construction capacity. Power (2008) has stated that even with the highest feasible level of demolition, the existing stock would remain the dominant energy challenge in the built environment far into the future. From here on, focus should be on sustainable design from the materials that contain a low amount of energy, on the use of local and nearby materials and the durability of buildings during both renovation and new construction.

5. Conclusions

Main findings of this study reveal that in the current case an existing building can be renovated to meet the same energy-efficiency levels as a new building and demolition of an existing building and construction of a new one raises the global cost at least four-fold as compared to renovation. Analyses of embodied energy via CO_2 emissions from the materials and the energy production used in a

building during 20 years demonstrate that a new building has at least three times higher environmental impact than low-energy renovation. Therefore, energy efficiency, economic and environmental issues show no support to the idea of demolition instead of renovation.

6. Acknowledgements

This work was supported by institutional research funding IUT1−15 "Nearly-zero energy solutions and their implementation on deep renovation of buildings" of the Estonian Ministry of Education and Research, "Reducing the environmental impact of buildings through improvements of energy performance, AR12059" (financed by SA Archimedes) and Research European with Social Foundation financing task 1.2.4 Cooperation of Universities and Innovation Development, Doctoral School project "Civil Engineering and Environmental Engineering" code 1.2.0401.09-0080.

References

Construction Production Regulation 2011 - Regulation (EU) No 305/2011 of the European Parliament and of the Council of 9 March 2011

EN 15459, Energy performance of buildings – economic evaluation procedure for energy systems in buildings, November 2007.

Estonian Government's Ordinance No. 68. Minimum requirements for energy performance of buildings. RT I, 05.09.2012, 4, 2012.

Hegger, M.; Fuchs, M.; Stark, T.; Zeumer, M. Energy Manual. Birkhäuser Verlag AG 2008.

Ilomets, S.; Kalamees, T.; Agasild, T.; Õiger, K.; Raado, L.-M. (2011). Durability of concrete and brick facades of apartment buildings built between 1960-90 in Estonia. International Conference on Durability of Building Materials and Components. Porto, Portugal:, 1171 - 1178.

Ireland, D. 2008. New Tricks with Old Bricks. The Empty Homes Agency, London.

Kalamees, T.; Kurnitski, J. 2006. "Estonian Test Reference Year for Energy Calculations," Proceedings of the Estonian Academy of Science, Engineering 12 pp. 40-58.

Kalamees, T.; Õiger, K.; Kõiv, T-A.; Liias, R.; Kallavus, U.; Mikli, L.; Lehtla, A.; Kodi, G.; Arumägi, E. 2011. Technical condition of Prefabricated Concrete Large Panel Apartment Buildings in Estonia. International Conference on Durability of Building Materials and Components. Porto, Portugal:, 973 - 981.

Kurnitski, J. 2011. Lessons learnt from Viikki Synergy building sustainable development design competitions: proposed criteria for sustainability. http://www.senaatti.fi/document.asp?siteID=1&docID=852

Ministry of Economic Affairs and Communications' Ordinance No. 63. Methodology for calculating the energy performance of buildings; RT I, 18.10.2012, 1, 2012.

National Register of Construction Works, www.ehr.ee

Power, A. 2008. Does demolition or refurbishment of old and inefficient homes help to increase our environmental, social and economic viability? Energy Policy 36 pp. 4487–4501.

Sarv, M. 2013. Mustamäe maha, püsti uus Mustamäe! Eesti Päevaleht, 19 January, http://epl.delfi.ee/news/lp/mustamae-maha-pusti-uus-mustamae.d?id=65551478 (in Estonian).

Yates, T. 2006. Sustainable Refurbishment of Victorian Housing. BRE Press, Bracknell.

Building Performance Simulation software for planning of energy efficiency retrofits

Thomas Fænø Mondrup, Ph.D.
Jan Karlshøj, Associate Professor
Flemming Vestergaard, Associate Professor

Department of Civil Engineering, Technical University of Denmark, Denmark

KEYWORDS: *Retrofitting, energy efficiency, building performance simulation, information flow*

SUMMARY:
Designing energy efficiency retrofits for existing buildings will bring environmental, economic, social, and health benefits. However, selecting specific retrofit strategies is complex and requires careful planning. In this study, we describe a methodology for adopting Building Performance Simulation (BPS) software as an energy conscious decision-making tool. The methodology has been developed to screen buildings for potential improvements and to support the development of retrofit strategies. We present a case study of a Danish renovation project, implementing simulation-based approaches to energy efficiency retrofits in social housing. To generate energy savings, we focus on optimizing the building envelope. We evaluate alternative building envelope actions using procedural solar radiation and daylight simulations. In addition, we identify the digital information flow and the exchange requirements for each simulation.

1. Introduction

1.1 Background to study

The impetus to energy efficiency comes from a variety of sources. In the European Union (EU), the Commission has adopted an action plan aimed at achieving 20% reduction in primary energy consumption by 2020, the *20-20-20 goal*. This reduction will require major improvements in the energy efficiency of buildings, which represent around 40% of the EU's total consumption (European Union 2009). Recently, the EU's drive to reduce consumption mainly focused on new buildings. However, considering that the average lifetime of a building is over 50 years, and a complete renewal of the existing European building stock would take more than 100 years (Kaderják et al. 2012), a substantial reduction in total consumption will not occur if no energy is saved through retrofitting existing buildings (Verbeeck et al. 2005).

Selecting specific retrofit strategies is a complex endeavor with many actions to be considered. A decision support approach is therefore needed (Kolokotsa et al. 2009). Here, Building Performance Simulation (BPS) software has an important role to play (Peltormäki 2009). With the evolution of information technology (IT), virtual models have been developed to simulate the performance of buildings (Doukas et al. 2009). Consequently, today's simulation software allows any aspect of a retrofit strategy to be simulated and assessed before it is built, helping project team members to understand the implications of their choices and to make informed decisions (Beaven 2011).

1.2 Multifaceted study

Based on the above, this study has two goals. The first is to explore the current approaches to energy efficiency retrofits in the Architecture, Engineering, and Construction (AEC) industry. The second is

to describe a methodology to facilitate software as an energy conscious decision-making tool. The methodology has been developed to screen buildings for potential improvements and to support sustainable retrofit strategies.

Using an integrated and experience-based approach (Towns 2001), the study goals are addressed by: (1) a review of trends in the field of energy efficiency retrofits to establish a knowledge base, and (2) a case study of a Danish renovation project to explore the effect of BPS software as an informative decision-making aid.

2. Methodology

2.1 Review of current approaches

A review of current approaches to energy efficiency retrofits has been conducted and included articles and research conducted by academic institutes; industry work practice; and guidelines generated by government institutions. The review was carried out to understand and identify current trends in energy efficiency retrofits, and specifically focused on the uptake of integrating BPS software as a tool for design decision-making.

2.2 Qualitative case study research

A qualitative case study of energy efficiency retrofits in Danish social housing has been conducted. The case study approach facilitates "in-depth, multi-faceted explorations of complex issues in their real-life settings" (Crowe et al. 2011). In the present case study, multiple context-specific retrofit actions were compared to identify and evaluate trade-offs and post-retrofit benefits, which were defined as reduced energy consumption and improved indoor environmental quality. To achieve improvements, the case study retrofit actions focused on optimizing the building envelope.

A key feature of this case study was that BPS software was used to predict the influence of the investigated retrofits. In particular, the researchers used a comprehensive suite of solar radiation and daylight simulations to show how building performance is affected by specific retrofit choices. Solar radiation simulations were performed using Autodesk Ecotect Analysis (Autodesk 2011); daylight simulations were performed using IES Virtual Environment (IES 2012). Both Ecotect and IESVE use data interpolation from the EPW weather file. As part of the simulation process, the case study identified the task/tool-specific exchange requirements for each simulation, that is the required data input for each solar radiation [Ecotect] and daylight simulation [IESVE]. Based on these simulations, knowledge was provided prior to the decision-making/retrofit planning, thereby facilitating an informative decision approach (Attia 2012).

Notably, the primary purpose of this case study was to demonstrate the benefits of adopting BPS software as an informative decision-making tool for pre-retrofit investigations, not to present specific building performance figures.

Based on a *Triple Helix* of university-industry-government interactions, an interdisciplinary project team of clients, project managers, contractors, architects, engineers, and manufacturers collaborated in the case study (Etzkowitz 2003). Here, representing the university and engineering link, the corresponding author of this article was involved in simulation and design activities.

3. Review

3.1 Energy efficiency retrofits

Retrofitting is "the process of modifying something after it has been manufactured" (City of Melbourne 2013). For buildings, energy efficiency retrofits are defined as actions that allow an

upgrade of the building's energy and environmental performance to a higher standard than was originally planned (Jaggs et al. 1999). An overview of potential retrofit strategies, and retrofit actions which may improve performance figures, is illustrated in FIG 1 below.

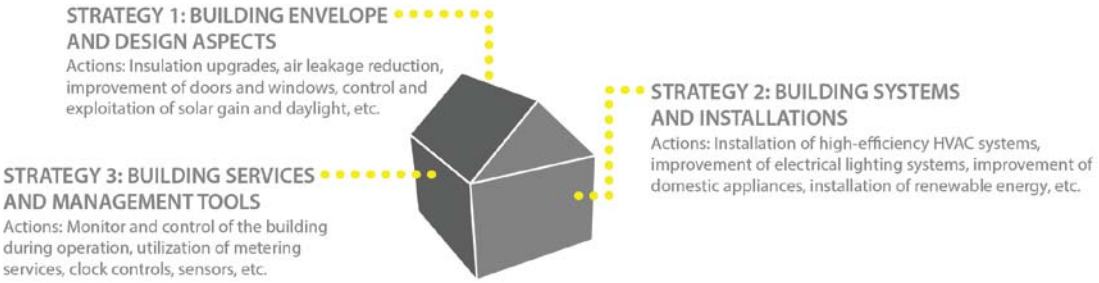

FIG 1. Retrofit strategies/actions [Inspired by (Kolokotsa et al. 2009)]

An example of a retrofitting action is the upgrading of insulation levels. Here, re-insulation of the building envelope – external walls, roofs, and floors – will improve the energy consumption of the building by reducing thermal losses through the fabric. Another example is the replacement of traditional single/double glazed windows with energy efficient triple glazed windows. As with the insulation upgrade, triple glazed windows will improve the building's thermal performance. Replacing or changing the position, size, and shape of the windows may also result in improved solar gains, and better daylight exploitation, thereby reducing heat consumption and electrical lighting consumption respectively (Bokel 2007).

Furthermore, a key feature of retrofit is the objective of improved indoor environmental quality, usually measured by occupant comfort. Indoor environmental quality (IEQ) is determined by several factors, including air quality, acoustics, temperature, and lighting conditions. Consequently, some retrofit strategies integrate natural ventilation for better air quality, thermo-active building systems for thermal stability, and natural lighting for a better quality of illumination (Osso et al. 1996) (Paul et al. 2008).

The green agenda is generally a powerful tool in a retrofit argument. However, retrofits also allow an upgrade of functionality, architectural quality, and aesthetic value of the building (Kalc 2012).

3.2 Retrofit performance criteria

The planning and evaluation of energy efficiency retrofits depend on well-defined project goals and carefully constructed criteria (Jaggs et al. 1999). Accordingly, the main criteria for efficiency and sustainable performance in a retrofit include: (1) improvement of energy consumption, (2) limited impact on global environment, (3) improvement of indoor environmental quality (IEQ), and (4) upgrading of functionality, architectural quality, and aesthetic value. Furthermore, the expected cost of a specific retrofit is key to its effective value. In this study, however, cost-effectiveness is not included as a criterion for retrofit evaluations.

Several of these criteria often appear to be in conflict, for example, energy consumption improvements versus architectural quality. Therefore, finding the optimum retrofit strategy is an optimization procedure. Here, the optimization involves iterative evaluations of proposed retrofit strategies/actions against selected criteria. Therefore, because optimization is complex, efforts for energy efficiency retrofits often focus on specific strategies/actions without the adoption of a holistic approach (Kolokotsa et al. 2009).

3.3 Simulation-based decision-making methodology

Generally, decisions taken during the early phases of the design process, where the impact of design decisions on building performance is more significant than decisions made in later design phases, can

determine the success or failure of a retrofit. For this reason, ensuring informed decision-making in the early design phases of both new builds and retrofitting is important (Shaviv et al. 1996).

Here, intelligent models and simulation-based approaches can be supportive. In the simulation-based process, a virtual model is developed to identify the most beneficial retrofit strategies/actions through performance simulations. More specifically, BPS software is used to simulate the performance of a virtual model representing a specific retrofit strategy/action. Then, simulation results are evaluated against predefined performance criteria. If the results are not satisfactory, the retrofit strategy/action is modified and the simulation process is repeated (Attia 2012). This iterative procedure is illustrated in FIG 2 below.

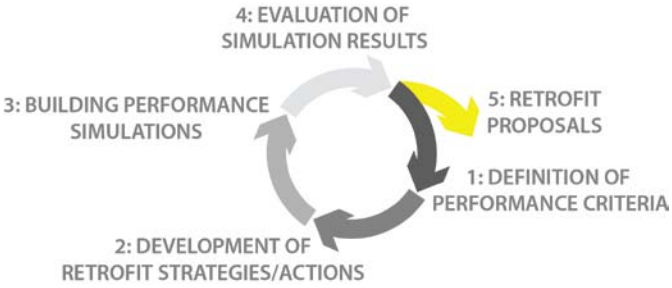

FIG 2. Iterative decision methodology [Inspired by (Kolokotsa et al. 2009)]

3.4 Simulation-based retrofit design process

In contrast to design processes aimed at new-build, the retrofit design process is strongly influenced by the conditions of an existing building. The simulation-based retrofit design process is illustrated in FIG 3 below, here integrating the above mentioned simulation-based decision methodology. As illustrated, the simulation-based retrofit design process consists of three phases: (1) analysis of existing conditions, (2) development of retrofit strategies/actions, including evaluation against performance criteria, and (3) implementation of retrofit strategies/actions.

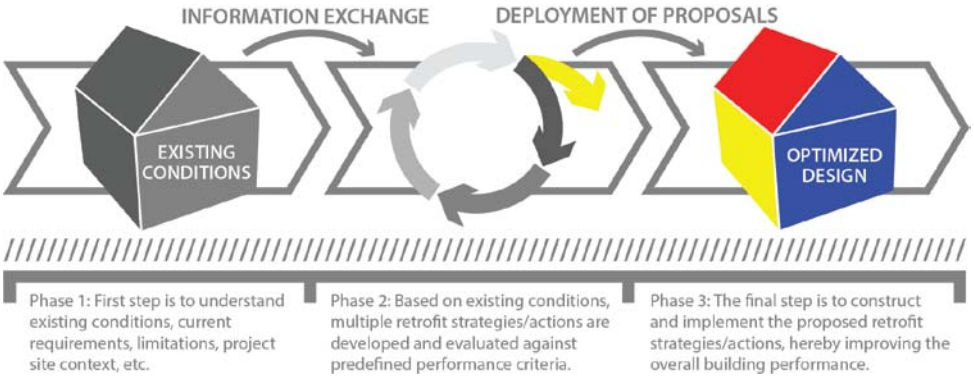

FIG 3. Retrofit design process

A key challenge to simulation-based retrofit design processes is the digital information flow between functional phases. In most cases, this information flow is defined by task/tool-specific exchange requirements, that is the required data input for specific BPS software applications.

4. Case study

4.1 Analysis of existing conditions

The framework of this case study was directed toward the *Gate 21* pilot project *Building Envelope Retrofits* (GATE 21 2013). The aim of this project was to investigate the benefits of energy efficiency

building envelope retrofits in Danish social housing, referring to *Strategy 1*, implementing retrofit actions related to the building envelope and design aspects. In particular, Gate 21 was looking for creativity in developing multiple *exemplar* building envelope designs, with the aim of identifying successful actions that could be adopted into future building envelope retrofit projects. Another issue that was highlighted was that of developing building envelope designs optimized for solar radiation and daylight exploitation.

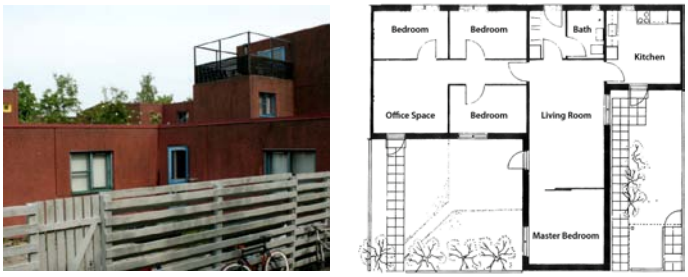

FIG 4. Pre-retrofit conditions of case study house

The dwelling used for the retrofit case study was a precast concrete construction, 1970s single storey house in Albertslund, Denmark (55.39°N 12.21°E). Pre-retrofit buildings typically have aging window units, poor insulation, air leakage, and mould growth due to surface condensation. These factors result in increased energy bills and poor indoor environmental quality. FIG 4 shows the house exterior and plan.

4.2 Development of building envelope retrofit actions

Based upon review findings, the practice procedure for the development and evaluation of optimized building envelope retrofit actions followed five steps: (1) definition of performance criteria, (2) development of retrofit strategies/actions, (3) building performance simulations, (4) evaluation of simulation results, and (5) retrofit proposals.

4.2.1 Definition of performance criteria

Case study performance criteria were defined to establish a basis for evaluation. Performance criteria were generated with two main purposes: (1) to improve energy consumption by optimizing the exploitation of solar radiation and (2) to improve indoor environmental quality by optimizing the exploitation of daylight. In many cases, such performance criteria will be some combination of potential improvements. For example, optimizing the exploitation of solar radiation may not only improve energy consumption figures, but also indoor environmental quality levels by supporting occupants' thermal comfort. Equally, optimizing the exploitation of daylight may not only improve indoor environmental quality levels, but also energy consumption figures.

4.2.2 Development of retrofit strategies/actions

In collaboration with the case study project team, a list of retrofit actions was developed. Since the aim of this case study was to investigate the effects of multiple building envelope designs, basic retrofit actions included re-insulation of external walls and upgrading of existing windows. Specifically for this case study, the influence of selected building envelope design variables was investigated, particularly that of alternative window positions, sizes, and shapes to investigate the resulting effects on solar gains and daylight conditions. The retrofit options consisted of nine building envelope designs/retrofit actions:

- Action 1: Energy efficient windows.
- Action 2: Energy efficient windows + increased window width.
- Action 3: Energy efficient windows + increased window height.

- Action 4: Energy efficient windows + extra window section at patio doors.
- Action 5: Energy efficient windows + double patio doors.
- Action 6: Energy efficient windows + small skylight in living room.
- Action 7: Energy efficient windows + large skylight in living room.
- Action 8: Energy efficient windows + extra window section in living room.
- Action 9: Energy efficient windows + extra window section in master bedroom.

4.2.3 Building performance simulations

BPS software was used to investigate the retrofit actions. Simulations were performed on two levels: (1) simulation of solar radiation striking exterior surfaces [Ecotect] and (2) simulation of interior solar gains and daylight distribution [IESVE]. Before simulating, specific exchange requirements for each simulation were identified:

- Site: Global coordinates, weather data, elevation, 3D geometry, context [Ecotect + IESVE].
- Building: Global coordinates, orientation, elevation, 3D geometry [Ecotect + IESVE].
- Spaces: Elevation, 3D geometry, space boundaries, [IESVE].
- External constructions: 3D geometry, U-values, [IESVE].
- Internal constructions: 3D geometry, U-values, surface reflectance values [IESVE].
- Windows: Orientation, 3D geometry, U-values, g-values, VT-values, shadings [IESVE].

In FIG 5 below, selected solar radiation simulations are illustrated. Here, average hourly solar radiation is mapped over existing conditions, hours in question 06-18, all year, summer, and winter, contour range 0-200 Wh/m^2. The Ecotect case study models were kept simple, representing outer volumes/exterior surfaces only. As illustrated, surrounding vegetation was not included.

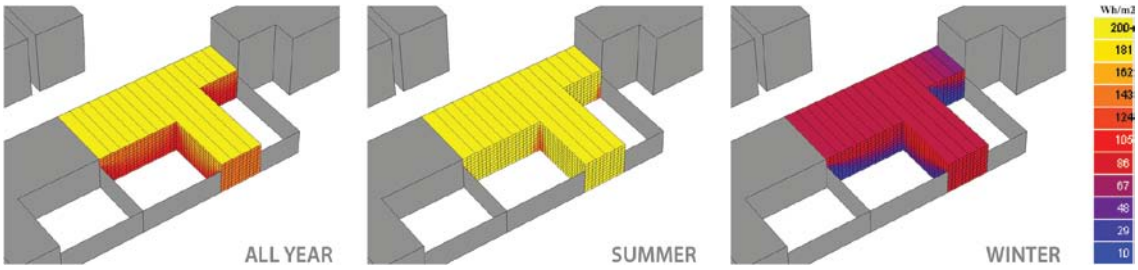

FIG 5. Incident solar radiation on exterior surfaces (south view)

In FIG 6 below, selected daylight simulations are illustrated. Here, average annual solar gains and daylight distribution are mapped over existing conditions, retrofit *Action 1* with energy efficient windows, and retrofit *Action 7* with energy efficient windows and a large skylight in the living room, contour range 40-760 LUX. The base-case model was created to understand the existing conditions of the case study building. This model was used as a reference to estimate improvements from retrofit actions 1 to 9.

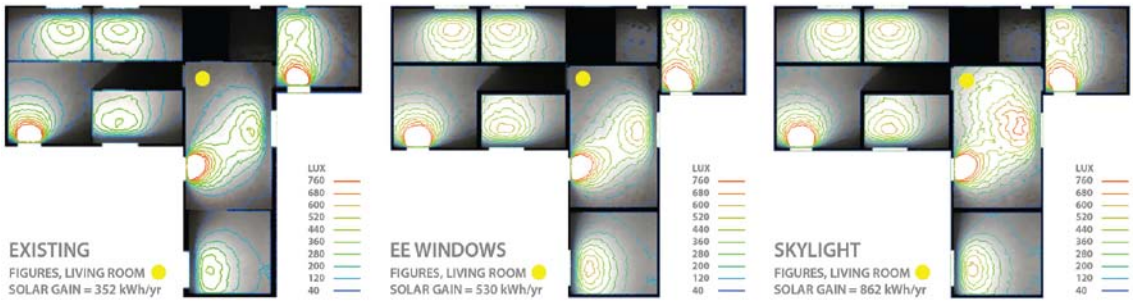

FIG 6. Correlation of interior solar gains and daylight distribution (top view)

4.2.4 Evaluation of simulation results

Based upon the BPSs, several kinds of correlations were demonstrated. For example, FIG 5 shows that an obstructed context greatly influences radiation values. As illustrated, the surrounding wooden fence causes overshadowing, particularly during winter when the sun is low. Therefore, upper parts of the façades and freely exposed roofs should be prioritized when optimizing the exploitation of solar radiation.

FIG 6 shows that the replacement of existing windows with energy efficient windows brings significant improvements. Energy efficient windows have smaller frames, allowing more sunlight and daylight to penetrate. In addition, the installation of the large skylight further improves the solar gains and daylight distribution and is particularly effective at bringing solar radiation and daylight into deep spaces/darker areas of the case study building.

4.2.5 Retrofit proposals

The evaluation of simulation results forms a solution space for potential building envelope retrofit actions. This solution space does not define any specific optimum retrofit, rather a wide range of applicable retrofit actions. Nevertheless, installing large window openings will improve solar radiation and daylight exploitation. Note, however, that high intensity solar radiation is the commonest cause of overheating in buildings and should therefore be controlled, for example with adjustable external solar shading.

4.3 Implementation of retrofit strategies/actions

The final step is to implement specific building envelope retrofit actions into the case study building. For implementation, the case study project team members should select specific retrofit actions within the developed solution space. This selection process is currently being conducted.

5. Conclusions

In the decision-making process of selecting specific retrofit strategies, multiple actions are available. The decision maker has to take into consideration energy, environmental, functional, architectural, and financial aspects to develop a sustainable retrofit strategy. For this purpose, a decision support approach is needed.

In this study, the critical role of Building Performance Simulation (BPS) software as an energy conscious decision-making tool was emphasized. In the case study, this was particularly illustrated by solar radiation and daylight simulations results. Based upon this tendency, BPS software is generally evaluated as a useful methodology for planning of energy efficiency retrofits.

6. Acknowledgements

The authors would like to thank all of the people and organizations involved in this study, particularly the case study project team members. The work presented in this study was performed in the scope of the pilot project *Building Envelope Retrofits*, funded by *Gate 21*.

References

Attia S. 2012. A Tool for Design Decision Making – Zero Energy Residential Buildings in Hot Humid Climates Université catholique de Louvain, UCL, Department for Architecture and Climate. 298 p.

Autodesk. 2011. http://usa.autodesk.com/ecotect-analysis/

Beaven M. 2011. Building Information Modelling – Across Arup, digital collaboration is redefining the possible in performance and design. ARUP. http://www.arup.com/Services/Building_Modelling.aspx

Bokel R.M.J. 2007. The Effect of Window Position and Window Size on the Energy Demand for Heating, Cooling and Electrical Lighting. Proceedings of Building Simulation. 117-121.

City of Melbourne. 2013. What is a Building Retrofit? City Of Melbourne, 1200 Buildings. http://www.melbourne.vic.gov.au/1200buildings/what/Pages/WhatIsRetrofit.aspx

Crowe S., Cresswell K, Robertson A., Huby G. & Avery A., Sheikh A. 2011. The Case Study Approach. BMC Medical Research Methodology. 11:100-108.

Doukas H., Nychtis C. & Psarras J. 2009. Assessing Energy-Saving Measures in Buildings Through an Intelligent Decision Support Model. Building and Environment. 44:290-298.

Etzkowitz H. 2003. Innovation in Innovation: The Triple Helix of University-Industry-Government Relations. Social Science Information. 42:293-337.

European Union. 2009. Summaries of EU legislation. http://europa.eu/legislation_summaries/energy/energy_efficiency/en0002_en.htm

GATE 21. 2013. About GATE 21. http://www.gate21.dk/UK/

IES. 2012. VE-Pro. http://www.iesve.com/software/ve-pro

Jaggs M. & Palmer J. 1999. Energy Performance Indoor Environmental Quality Retrofit – a European Diagnosis and Decision Making Method for Building Refurbishment. Energy and Buildings. 31:97-101.

Kaderják P., Meeus L., Azevedo I., Kotek P., Pató Z., Szabó L. & Glachant J. 2012. How to Refurbish All Buildings by 2050 – Final Report June 2012. THINK. 72 p.

Kalc I. 2012. Energy Retrofits of Residential Buildings – Impact on Architectural Quality and Occupant's Comfort. Norwegian University of Science and Technology, NTNU. 83 p.

Kolokotsa D., Diakaki C., Grigoroudis E., Stavrakakis G. & Kalaitzakis K. 2009. Decision Support Methodologies on the Energy Efficiency and Energy Management in Buildings. Advances in Building Energy Research. 3:121-146.

Osso A., Walsh, T., Gottfried, D. & Simon, L. 1996. Sustainable Building Technical Manual: Green Building Design, Construction, and Operations. Public Technology, Inc, USA. 292 p.

Paul W. & Taylor P. 2008. A Comparison of Occupant Comfort and Satisfaction between a Green Building and a Conventional Building. Building and Environment. 43:1858-1870.

Peltormäki A. 2009. ICT for a Low Carbon Economy – Smart Buildings. European Commission. Brussels. 48 p.

Shaviv E., Yezioro A., Capeluto I.G., Peleg U.J. & Kalay Y.E. 1996. Simulations and Knowledge-based Computer-aided Architectural Design (CAAD) Systems for Passive and Low Energy Architecture. Energy and Buildings. 23:257-269.

Towns M.H. 2001. Kolb for Chemists: David A. Kolb and Experimental Learning Theory. Journal of Chemical Education. 78:1107-1117.

Verbeeck G. & Hens H. 2005. Energy Savings in Retrofitted Dwellings: Economically Viable? Energy and Buildings. 37:747-754.

Uncertainty of indoor boundary conditions at calculation of energy consumption for heating of residential buildings determined by inhabitants´ behaviour

Peter Matiasovsky, Dr. Ing [1]
Pavol Hrebik, PhD [2]
Peter Mihalka, PhD [1]

[1] Institute of Construction and Architecture, Slovak Academy of Sciences, Slovakia
[2] Slovak University of Technology in Bratislava, Bratislava

KEYWORDS: *Inhabitants´ behaviour, indoor temperature, air change rate, internal heat gains, uncertainty*

SUMMARY:
The paper is focused on an analysis of the indoor boundary conditions uncertainty influencing the reliability of energy assessment of the buildings for housing. The distribution of input parameters that enter into a calculation of the heat demand for heating, indoor temperature, air change rate and internal heat gains given by the inhabitants´ behaviour were analysed. From available literature data and from the results of measurements it was proved that the uncertainty of the input energy simulation parameters can be modelled with suitable distribution functions.

1. Introduction

The sensitivity analysis carried out for residential buildings energy rating by Corrado and Mechri (2009) highlights that only a few factors are responsible of most energy rating uncertainties given by the inhabitants´ behaviour: in decreasing order of importance, indoor temperature, air change rate, number of occupants, metabolism rate, and equipment heat gains. Thus, in this study a further investigation was performed on the factors. The indoor temperature, air change rate and internal heat gains were analysed for the best assessment of the energy needs calculation uncertainty. These three factors were supposed to be determined by the behaviour and habits of a household. Each of the factors was specified by the parametric probability distribution.

2. Indoor temperature

Thermal comfort is defined as that state of mind in which satisfaction is expressed with the thermal environment (Olesen, 1982). At creating the satisfactory thermal environment the homoiotermia of human organism (keeping the body temperature at certain level of 37°C) is required. The environment is evaluated by the psychophysical scale in which *PMV* (Predicted Mean Vote) index expresses supposed mean value of thermal feeling of larger group of persons. Fanger (1970) developed the dependence of *PMV* index on certain combination of activity and clothing and four factors of thermal comfort: air temperature, mean effective temperature of ambient surfaces, relative humidity and air velocity.

When all factors of thermal comfort except the temperature are supposed to be constant it is possible to express *PMV* as a linear function of temperature. At the modelling of indoor temperature uncertainty in various dwellings we considered that each household tries to maintain the constant indoor temperature satisfying its particular thermal comfort requirements. These requirements are

TABLE 1. Values of PMV index for indoor temperature values at activity 1 met, clothing 1 clo and air velocity < 0.1 m/s

PMV	-0.85	-0.57	-0.3	-0.02	0.26	0.53	0.81	1.08
Temperature (°C)	20	21	22	23	24	25	26	27

expressed by thermal index *PMV*. Considering the activity 1 met, clothing 1 clo and air velocity < 0.1 m/s according to the Fanger's thermal comfort equation (Kaclík 1984) *PMV* = 0 at temperature of 23°C. In Table 1 there are *PMV* values corresponding the temperatures interval 20 - 27°C.

The *PPD* index (Predicted Percentage of Dissatisfied) expresses supposed percentage of dissatisfied, which in given environment will feel thermal discomfort. *PPD* index (%) is determined from *PMV* according to standard (ISO 7730:2005):

$$PPD = 100 - 95.\exp(-0{,}03353.PMV^4 - 0.2179.PMV^2) \quad (1)$$

With use of Equation (1) from values in Tab. 1 we get the distribution of predicted percentage of dissatisfied with temperature (Tab. 2), which we transformed to the "predicted percentage of satisfied" with temperature *PPS* = 1 – *PPD*, in order to express the accepted temperature probability.

In Figure 1 the satisfaction of inhabitants with indoor temperature, *PPS* is approximated as the normal distribution with standard deviation 4°C.

A comparison of this distribution with distributions of indoor temperature measured in real dwellings shows that real distributions are significantly narrower. The data determined by Piršel (1989) have the means of 22.71 and 22.14°C and standard deviations of 1.82 and 2.18°C for living rooms and bedrooms respectively. The model indoor temperature distribution proposed by Corrado and Mechri (2009) is the normal distribution with the mean of 22°C and standard deviation of 2°C for Sweden. The results of survey presented by Haldi (2010) give the values of 23.5°C and 1.5°C for the mean and standard deviation respectively.

The standard (ISO 7730:2005) recommends the following limits for acceptable thermal environment:

$$-0.5 < PMV < 0.5 \quad (2)$$

or *PPD* < 10 %, which corresponds the temperature interval from 21.5 to 24.5°C. That recommendation represents a reduction of the interval of acceptable temperatures given by the standard deviation 4°C, to the interval of recommended values with standard deviation 0.5°C (Fig. 1). This, 0.5°C value is supposed by (Jaraminienea & Juodis 2006).

The comparison of relative distributions of acceptable, recommended and real indoor temperatures results in a conclusion that real temperatures in dwellings lie in the interval determined by acceptable and recommended values. A real uncertainty of indoor temperature can be modelled by normal distribution with standard deviation 1.5°C. The distribution with standard deviation 0.5°C represents an ideal situation with reliable control system.

TABLE 2. Probability of temperature unacceptability PPD or acceptability PPS

Temperature (°C)	17	18	19	20	21	22	23	24	25	26	27	28	29
PPD (%)	61	45	32	20	12	7	5	6	11	19	30	43	58
PPS (%)	39	55	68	80	88	93	95	94	89	81	70	57	42

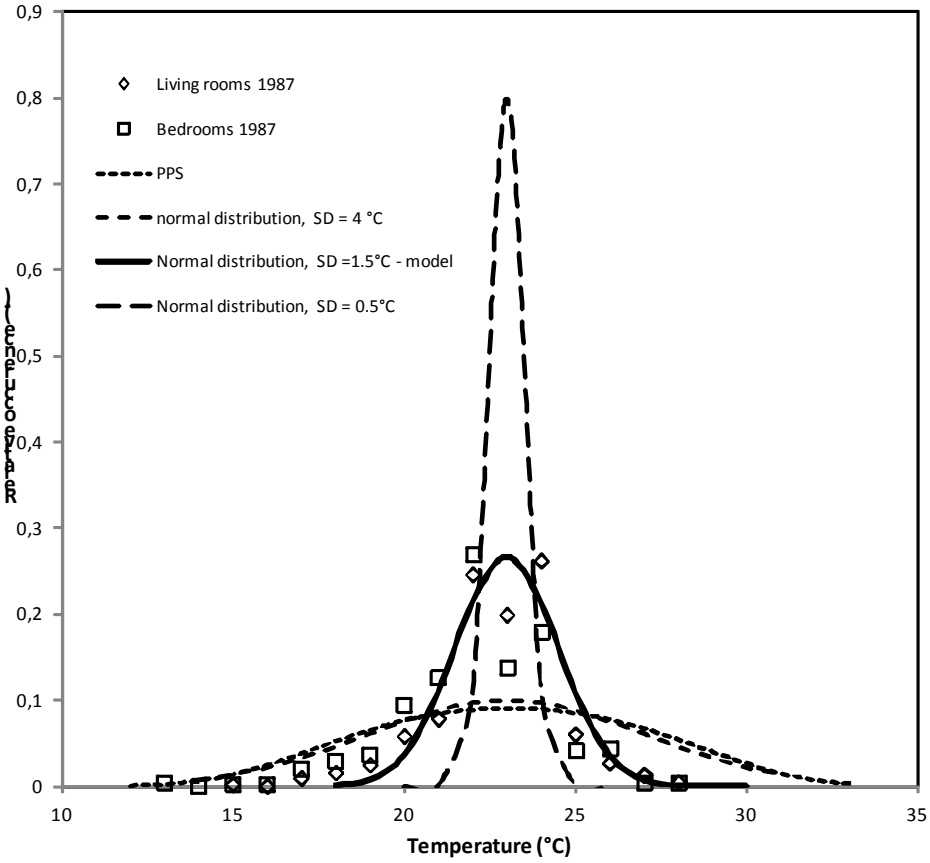

FIG 1. Normal distributions of acceptable (SD = 4°C), recommended (SD = 0.5°C) and real - model (SD = 1.5°C) indoor temperature compared with data from (Piršel 1989)

3. Air change rate

The air change in a household depends on weather conditions, air permeability of envelope structures, operating of technical equipment and activity of occupants. The air change in buildings consists of two components: the basic air change provided by infiltration and the air change due to occupants behaviour. The windows opening is characterised by the number of windows open during monitored period per dwelling (IEA-Annex VIII 1987) defined as:

$$N_o = \frac{\sum_{i=1}^{N} N_i \cdot t_i}{t_m} \tag{3}$$

Where N total number of windows (-)
t_i opening duration of particular window (h)
t_m monitored period (h)

The air change rates can be calculated according to universal empirical relationship (De Gids & Phaff 1982) adopted in standard EN 15242 (2007) for case of single-sided ventilation. The hourly values of total air change rate in a dwelling n (1/h) represent the sum of minimum required air change rate n_0 due to infiltration and air change rate Δn due to open windows:

$$n = n_0 + \Delta n = 0.5 + \frac{3600}{V} \cdot S_w \cdot \mu \cdot 0.5 \cdot N_o \cdot \left(0.001 \cdot v^2 + 0.0035 \cdot (\theta_i - \theta_a) \cdot H + 0.01\right)^{0.5} \quad (4)$$

Where S_w window area (m^2)
μ coefficient reducing window area to equivalent open window area (-)
H window height (m)
V volume of a dwelling (m^3)
$\theta_i \theta_a$ indoor, outdoor temperature respectively (°C)
V wind velocity (m/s).

The ventilation heat loss (kWh) is then calculated as:

$$Q_v = 0.361.n.V.(\theta_i - \theta_a) \quad (5)$$

Equation (4) was verified in the case study (Matiašovský P. & Koronthályová O. 2003) where a relationship between real duration of the windows opening and the air change rate in identical dwellings characteristic in Slovakia was estimated. In Fig. 2 there is a linear dependence between the number of open windows and the air change rate, for the average weekly values. The found regression corresponds to Equation (4) and gives the actual minimum air change rate n_0 = 0.57 with the regression coefficient a = 0.57.After inserting the actual parameters of dwellings and the actual mean values of wind velocity and air temperature during a heating season into Equation (4) the resulting regression coefficient a = 0.58 which confirms an universality of Equation (4).
In Annex VIII (1987) the distribution of average air change rates in dwellings due to windows opening during a heating season was determined. The distribution has an asymmetric character, with minimum 0.1 h^{-1}, median 0.14 h^{-1} and maximum 0.8 h^{-1}. For arbitrary household, the average air change rate in dwelling during heating season is determined by dwelling inhabitants´ behaviour and can be expressed as the value of random distribution, introducing the relative average air change rate in a dwelling K:

$$n = n_0 + a \cdot N_o = n_0 + a \cdot m_{N_o} \cdot K \quad (6)$$

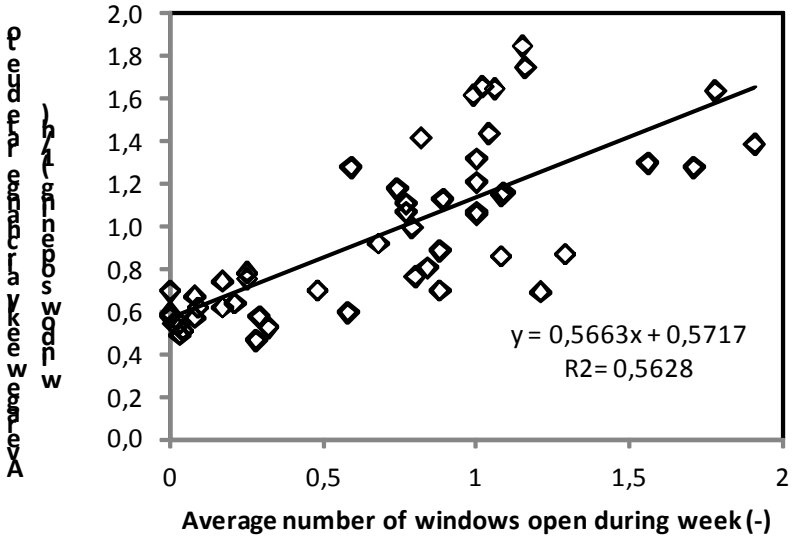

FIG 2. Dependence of average weekly air change rate on average weekly number of windows during week (Mihálka & Matiašovský 2007)

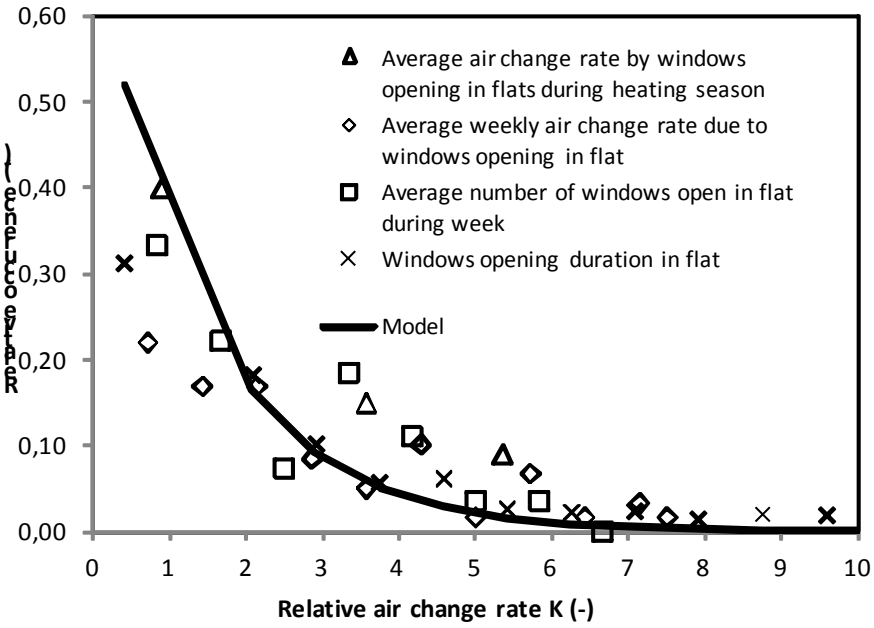

FIG 3. Distribution and uncertainty model of relative average air change rate due to windows opening - exponential distribution (λ = 0.69)

The relative air change rate by windows opening in a dwelling K is defined as the ratio of air change rate to median air change rate, or the ratio of number of open windows in a dwelling to median number of open windows:

$$K = \frac{\Delta n}{m_{\Delta \bar{n}}} = \frac{N_o}{m_{\bar{N}_o}} \tag{7}$$

The introduction of relative air change rate K enables to compare the distributions of relative air change rate in dwellings due to windows opening during a heating season with the distributions of relative air change rate and weekly values of number of open windows and windows opening duration in dwellings, presented in (Mihálka & Matiašovský 2007). The compared distributions are similar and compatible mutually, which indicates that the distribution of all windows opening activities lies in one general interval, independently on its time interval scale. In Fig. 3 there is a comparison of the analysed distributions of relative air change rates due to windows opening, as well as relative numbers of open windows and durations of windows opening in the heating season K. As the uncertainty model, the exponential distribution $f(K,\lambda) = \lambda \cdot e^{-\lambda \cdot K}$, with $\lambda = 0.69$, was identified. The model proposed by Corrado and Mechri (2009) allows the air change rates smaller than minimum required air change rate 0.5 h^{-1}.

4. Internal heat gains

Modelling the internal heat gains is based on an assumption that households use the electric energy solely. The analysis issues from the data on yearly consumption of electric energy in households (kWh/year) and on their electrical appliances equipment (Stanek kps.fsv.cvut.cz/file_ download.php?fid=2413), based on the results of detailed analysis of statistical survey of ČSÚ (2003, 2005 and 2011), the outputs of project REMODECE (2008) and the values received from the report JRC-IES (2007). Considering the data presented in Tables 3 and 4 the heat gains from electrical equipment were expressed as a function of the number of household members. The internal heat gains were then calculated as a sum of the heat gains from electrical appliances and constant metabolic heat

gains. The hourly courses of heat gains from electrical appliances represent 90 W per person in an average household and they were developed on the basis of type household electricity load profiles of class 4 (http://support.okte.sk) - the consumption without the use of electricity for heating per year in Slovakia, defining the load expressed by the values of relative hurly loads in the year within the range from 0 to 1. The heat produced by household members was considered as 1 met per person and it was reduced by coefficient 0.8 expressing the percentage of assumed presence in dwelling. The resulting relation for hourly data (kWh) has the form:

$$Q_i = TDO4 \cdot 90 \cdot (1.272 + 0.0159 \cdot P - 0{,}032 \cdot P^2) + 104 \cdot 0.8 \cdot P \qquad (8)$$

Where *TDO4* type household electricity load profiles of class 4 (-)
P number of persons in household (-)

The polynomial of second order expresses the dependence of consumption on number of household members in Fig. 4. It is developed from the data in Table 4 where is the energy consumption per household member in relation to the energy consumption of member of average household (Tab. 3) for dwellings with various numbers of persons in household.

The distribution of household members has developed during last decades. In Fig. 5 there is the comparison of household size distribution in Slovakia in years: 1961 (Keilman 1987), 1981 and 2004 (Dol & Haffner 2010), 1991 and 2001 (Dzianová 2001), 2010 (Senaj & Zavadil, 2012).

The model of household size distribution was chosen from the results of last survey from 2010 (Senaj & Zavadil, 2012). It is gamma distribution $f(P,\alpha,\beta) = \frac{\beta^{\alpha} P^{\alpha-1} e^{-\beta P}}{\Gamma(\alpha)}$, with parameters $\alpha = 2.85$, $\beta = 1$.

The model proposed by Corrado and Mechri (2009) supposes the one person households as the most probable ones.

TABLE 3. Parameters of average household

Period	Electricity consumption (kWh/year)	Number of persons (-)	Electricity consumption per person (kWh/person.year)
2006 - 2008	2125	2.7	787

TABLE 4. Yearly consumption of electric energy in household in dependence on number of inhabitants

Number of persons in household	Consumption (kWh/year)	Consumption per person (kWh/persons.year)	Consumption per person/Consumption per member of average household (-)
1	1010	1010	1.28
2	1783	891	1.13
3	2398	799	1.02
4	2758	689	0.88
5	2056	411	0.52

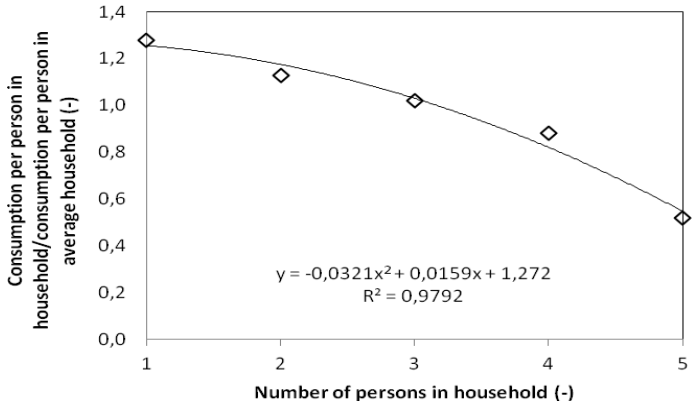

FIG 4. Energy consumption per person in relation to energy consumption per person in average household in dependence on number of persons

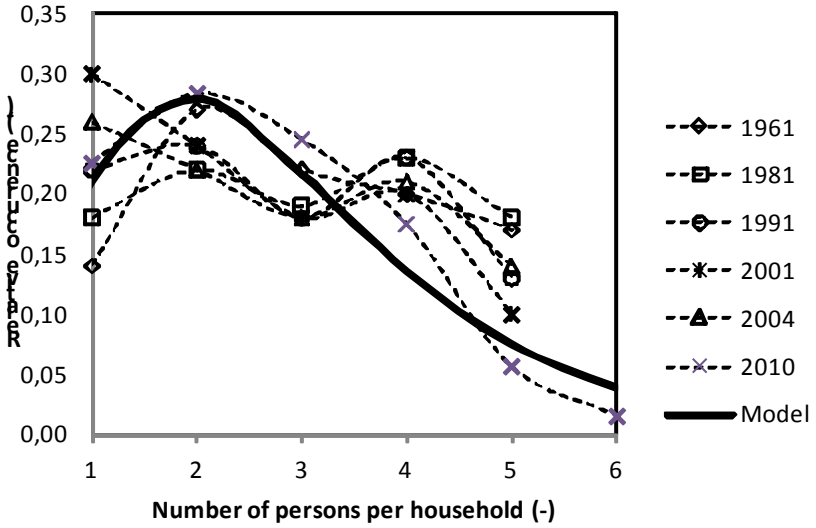

FIG 5. Distribution of household size in Slovakia Uncertainty model of number of persons in household - gamma distribution ($\alpha = 2.85$, $\beta = 1$)

Conclusions

The consumption of energy for heating of residential buildings is significantly determined by the behaviour of their inhabitants, determining the indoor boundary conditions. The uncertainty of indoor boundary conditions in households: indoor temperature, air change rate and internal heat gains was analysed with the following results.

The household temperature uncertainty can be characterised by a normal distribution with the mean value determined by a combination of activity, clothing, relative humidity, air velocity and by the standard deviation determined by an acceptability of the deviation from mean value by household inhabitants.

An analysis of the uncertainty of ventilation habits in households showed the correlation of the windows opening activities and air change rates, independently on the analysed time interval. The normalisation of their distributions, dividing by their medians enables to use the exponential distribution of the relative air change rate by opening windows as a universal model.

The internal heat gains have two components. The first of them are the gains from appliances, which can be modelled under the assumption of electricity use only. The appliances amount in a dwelling is a function of the household members. The distribution of household members is developing and changing during longer periods. The contemporary distribution for Slovakia can be modelled by gamma distribution with one resident household as the mode.

5. Acknowledgements

The authors wish to thank the Slovak Research and Development Agency APVV, project No. 0031-10 for the financial support of this work.

References

Corrado V. & Mechri H. E. 2009. Uncertainty and Sensitivity Analysis for Building Energy Rating. Journal of Building Physics 33, 125-156.

De Gids W. & Phaff H. 1982. Ventilation rates and energy consumption due to open windows: A brief overview of research in the Netherlands. Air infiltration review 4, 4-5.

Dol K. & Haffner M. 2010. Housing Statistics in the European Union. OTB Reasearch Institute for the Built Environment, Delft University of Technology.

Dziranová O. 2001. Households and families according to Census of population and housing in 2001. Statistical Office of the Slovak Republic. www.statistics.sk/files/Sekcie/.../Domacnosti.doc. (in Slovak)

EN 15242. 2007. Ventilation for buildings - Calculation method for the determination of air flow rates in buildings including infiltration. Brussels: CEN.

Fanger P. O. 1970. Thermal Comfort: Analysis and applications in environmental engineering. McGraw-Hill.

Haldi F. 2010. Towards a Unified Model of Occupants' Behaviour and Comfort for Building Energy Simulation, École Polytechnique Fédérale de Lausanne (Thesis).

Hrebik P. 2013. Impact of uncertainty of selected parameters for calculation of heat demand for heating, Slovak University of Technology in Bratislava, PhD thesis (in Slovak).

http://support.okte.sk/isom/sk/index.html?typove_diagramy.htm

IEA- Annex VIII 1987. Inhabitants´ Behaviour with Respect to Ventilation, Summary.

ISO 7730:2005 Ergonomics of the thermal environment - Analytical determination and interpretation of thermal comfort using calculation of the PMV and PPD indices and local thermal comfort criteria.

Jaraminienea E. & Juodis E. 2006. Heat demand uncertainty evaluation of typical multi-flat panel building Journal of Civil Engineering and Management 12, 69-75

Kaclík J. 1984 Economical heating of buildings, ALFA Bratislava.

Keilman N. 1878. Recent trends in family houshold composition. European Journal of Population 3, 297-325.

Matiašovský P. & Koronthályová O. 2003. Passive solar gains versus ventilation by openning windows. Proceedings of 2nd International Conference on Building Physics. Balkema. Lisse, 765 – 770.

Mihálka P. & Matiašovský P. 2007. Water vapour production and ventilation regimes in large panel building flats. Building Research Journal 55, 209-226.

Olesen B. W. 1982. Technical Review No. 2: Thermal Comfort.

Piršel L. et al. 1989. Determinants of thermal comfort in buildings. Final Report II-8-4/02,1,1. STU in Bratislava, Faculty of Civil Engineering, Bratislava. (in Slovak).

Senaj M. & Zavadil T. 2012. Results of survey of financial situation of Slovakian households. Casual study of National Bank of Slovakia. Bratislava. (in Slovak)

Stanek K. Perspectives of further research kps.fsv.cvut.cz/file_download.php?fid=2413. (in Czech)

Richardson, I., Thomson, M. and Infield, D. (2008) A high-resolution domestic building occupancy model for energy demand simulations. Energy and Buildings 40, 1560-1566.

Effect of orientation on the hygrothermal behaviour of a capillary active internal wall insulation system

Valentina Marincioni, M.Sc. [1]

Hector Altamirano-Medina, Ph.D. [1]

[1]University College London, UK

KEYWORDS: *internal insulation, capillary active, relative humidity, orientation, solar radiation*

SUMMARY: *UK authorities are promoting energy efficiency schemes to improve the performance of buildings as a result of the high levels of energy consumption and consequent CO2 emissions. A quarter of these emissions are due to requirements for space heating. Installation of insulation is one of the most common alternatives to thermally improve buildings, especially on buildings built of solid masonry (~20 percent of the housing stock). However, the thermal improvement of buildings located in conservation areas, listed buildings, decorative façades, or traditional buildings could be only achieved through the use of internal wall insulation. Solid masonry walls with high surface water absorption coefficients have a higher dependence on external climate conditions (e.g. rain, solar radiation), which are likely to affect the performance of internal wall insulation. This paper examines the effect of walls orientation on the hygrothermal behaviour of an internally insulated 16th century building. External walls have been insulated with a capillary active system that allows moisture movement towards indoor environments. Sensors to monitor relative humidity and temperature between the existing brick wall and the insulation were installed in the north-facing and south-facing walls of the building. Both walls are exposed to the same internal environmental conditions (teaching area). The study showed that drying of the south-facing wall occurred faster than drying of the north-facing wall and that drying of the south-facing wall was enhanced by the effect of direct solar radiation.*

1 Introduction

Improving the energy efficiency performance of the building stock is a priority if the UK is to meet at least 80% carbon reduction by 2050. Wall insulation is one of the measures considered for buildings built of solid masonry (~20 percent of the housing stock) (DECC, 2011).

Due to planning requirements, traditional buildings built before 1920 (generally buildings located in conservation areas, listed or with decorative façades) and characterised by solid walls are likely to be thermally improved through the installation of internal wall insulation. However, internal wall insulation can undermine the durability of a building, increasing the risk of mould growth and timber decay. Solid walls would be exposed to lower temperatures and, depending on the insulation system applied, there may be an increase in the vapour resistance of the building envelope.

This paper presents the results of a case study where the effect of orientation on the heat and moisture transfer within internally insulated solid walls was assessed. The building analysed is a grade II listed barn, with 330 mm solid brick walls and internally insulated with a capillary active insulation system made out of dense woodfibre.

2 Methodology

2.1 The building

The building studied is a grade II listed 16th century barn located in Maidenhead, west of London. The building was refurbished in 2011 and converted into an education centre, featuring a large teaching area, open-plan offices and one exhibition area.

The external walls (solid brick) were insulated internally with 100 mm of Pavadentro, a composite board formed by woodfibre and a mineral layer that creates a light vapour diffusion resistance; the total equivalent air layer thickness of the dry composite board is s_d = 1.6 m.

The existing wall was levelled with a lime-based coat before the insulation was applied and then a bonding coat was used to provide full contact between the insulation and the existing wall. External façades were left exposed, without any impregnation treatment or installation of damp proof courses; therefore not limiting moisture penetration into the building. The building durability could be maintained if potential moisture accumulation were counterbalanced by subsequent moisture drying (a process formed by evaporation and vapour transfer).

a) b)

FIG 1. Building and external walls insulated a) north facing wall; b) south facing wall (access to teaching area)

TABLE 1. Wall assembly

Wall construction (outside to inside)		Thickness (mm)
Brick		330
Levelling coat (3:1 NHL and sand)		0 to 6
Bonding coat (Lime plaster)		5
Pavadentro (composite insulation)	woodfibre board	20
	mineral layer	1
	woodfibre board	80
Internal finish (Lime plaster)		8

2.2 Monitoring method

The aim of the study was to estimate the effect of orientation on the hygrothermal behaviour of internally insulated walls. Four thermocouples and resistive probes (sensors) to measure temperature (T) and relative humidity (ϕ) respectively were installed at the interface between the existing wall and the insulation; sensors (NH, NL) were installed at 30 cm (low – L) and at 200 cm from the ground (high – H) on the north-facing wall and on the south façade (SH, SL) respectively, as shown in figure 1. Sensors were set with a sampling interval of Δt = 30 min and an accuracy of T = ± 0.7 °C and ϕ = ± 5 % at 21 °C. Data were collected for 22 months starting on 01/11/2011 and ending on 11/09/2013.

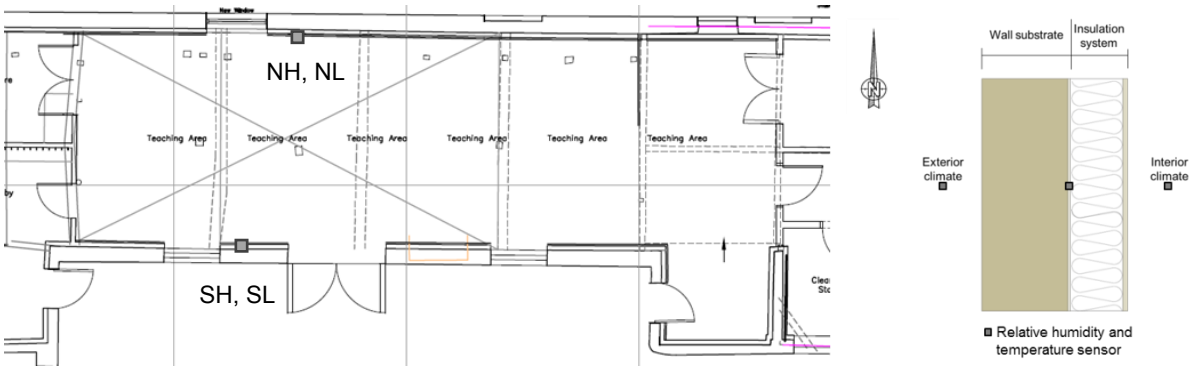

FIG 2. Building plan with focus on the teaching area and locations of sensors

2.3 Climate

The building is located within the Wind Driven Rain zone 2 (where 33 l/m^2 < WDR < 56.5 l/m^2 per spell) in an area where the prevalent wind direction is WSW. Minimum and maximum mean daily temperatures (data from the period 1971-2000) vary from 1 °C to 9 °C and from 7 °C to 23 °C respectively. Monthly average sunshine fluctuates from 50 to 200 hours. (Met Office, 2013a)

The main source of internal moisture comes from the people occupying the teaching room, generally large groups for short periods of time; occupation patterns depend on the frequency of school visits. The room is naturally ventilated (all windows are openable).

3 Results and discussion

Temperature and relative humidity at the interface between the existing wall and the insulation were collected and the profiles related to the north and south orientations compared. The reduction and increase of relative humidity (drying and wetting period respectively) at the interface were analysed and the causes of such events identified.

Profiles of relative humidity at the four interstitial locations studied are shown in Figure 3. The initial relative humidity varied from 82 % to 94.6 % as sensors were applied on the surface of the insulation board and surrounded by the bonding coat (wet when applied). The initial moisture of the construction system started drying out after 2 months on the south elevation and 4 months on the north elevation.

As shown in Figure 3, there was a reduction of the interstitial relative humidity in both insulated walls, however with a higher reduction observed in the south-facing wall. In both walls, the relative humidity was lower at the end of the study at high level (NH and SH). Drying occurred approximately from January to September, whereas wetting occurred from September to January.

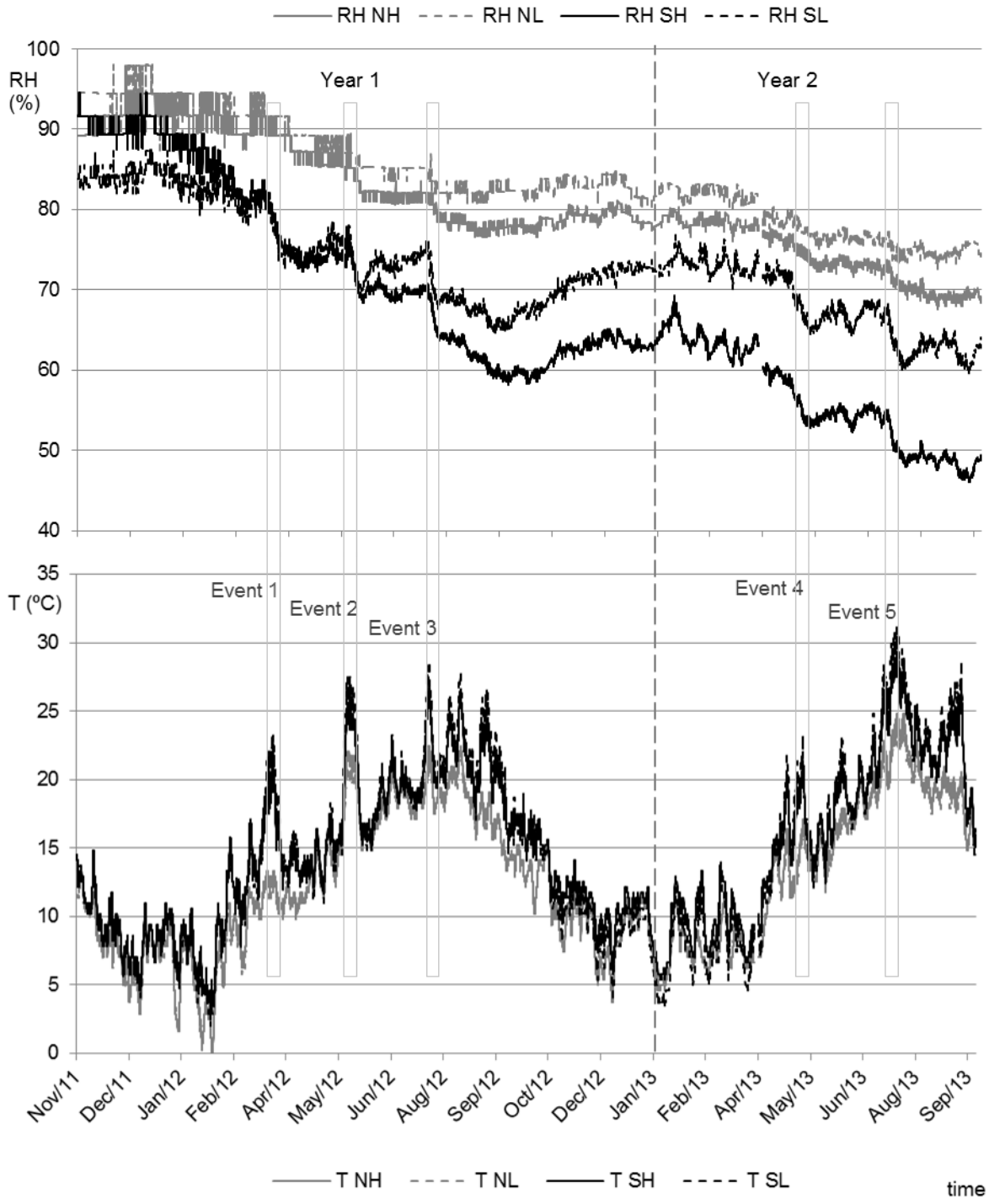

FIG 3. Relative humidity and temperature measured at four location of the existing wall-insulation interface.

Drying periods in 2012 and 2013 were characterised by events of sudden relative humidity reduction; sudden reductions were defined as events when at least one sensor shows a decrease of relative humidity ϕ (%), in function of time t (d), for minimum 7 days and with an average rate of 0.5 % per day or above:

$$\frac{\Delta\phi}{\Delta t} \geq 0.5\ \%/d \qquad (1)$$

According to these criteria, three major events occurred on year 1, followed by two on year 2.

TABLE 2. *Events of sudden decrease in relative humidity (Δϕ/Δt) and difference in the temperature averages*

Event	Start date	End date	Duration (days)	Δϕ/Δt south wall (%/d)		Δϕ/Δt north wall (%/d)		$T_{south\ wall}$ - $T_{north\ wall}$ (ºC)
				High	Low	High	Low	
1	24/3/12	6/4/12	13	0.62	0.77	0.15	0.15	6.1
2	23/5/12	3/6/12	11	0.64	0.82	0.37	0.37	3.6
3	23/7/12	1/8/12	9	0.67	0.78	0.22	0.33	3.6
4	25/4/13	9/5/13	14	0.43	0.5	0.22	0.14	4.3
5	6/7/13	20/7/13	14	0.43	0.57	0.29	0.14	4.8

The events of sudden relative humidity reduction lasted from 9 to 14 days, with a rate of decrease from 0.43 to 0.82 % per day in the south-facing wall and from 0.14 to 0.37 % per day in the north-facing wall.

A difference in temperature at the interface of the existing wall and insulation was noted during the events of sudden relative humidity reduction (Figure 3, below), which was not observed during the wetting period. Temperatures at the four locations were comparable; however in the drying period, and in particular during the relative humidity reduction events, the temperature at the interface of the existing wall and the insulation on the south-facing wall was higher than the temperature within the north-facing wall. Table 2 shows the average difference of interstitial temperature between the sensors located in the south wall and the ones in the north wall.

The difference in temperature seems to be related to orientation and more specifically to solar radiation. Direct radiation would allow an increase in surface temperature in the south-facing wall and a higher rate of evaporation compared to the north-facing wall, which is only affected by diffuse radiation. The observed sudden reductions in the internal humidity of the south-facing wall coincided with events reported by the Met Office (2013b) as "remarkably sunny" periods: from the 23rd to 30th March 2012 and from the 21st to the 28th May 2012. The same happened in July 2012, a cold and wet month until the 21st, when the weather became warmer and sunnier. In Figure 4, the monitored relative humidity for the period November 2011 – August 2012 was plotted along with daily averaged solar radiation intensity (W/m^2); events of sudden relative humidity reduction match periods of consistently high solar radiation intensity.

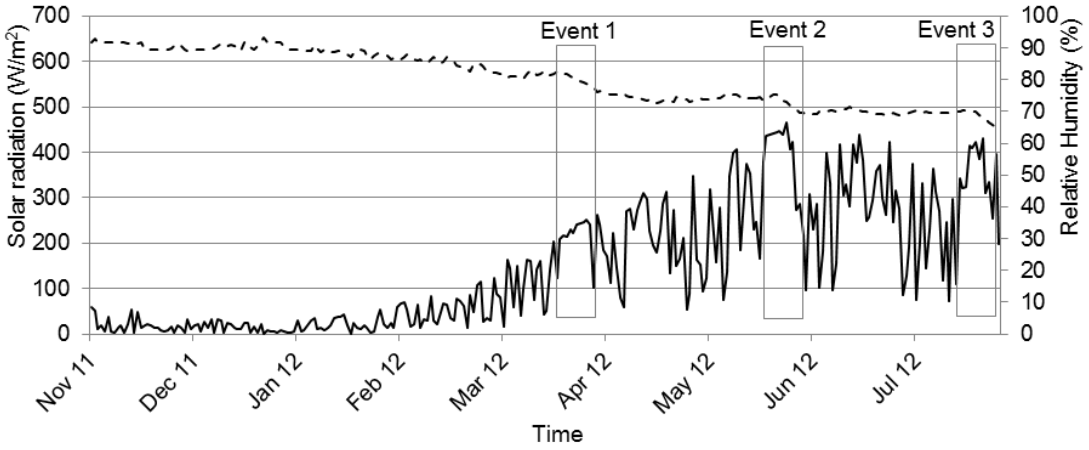

FIG 4. Events of sudden relative humidity (dashed line) reduction and solar radiation (solid line)

4 Conclusion

This paper examines the effect of walls orientation on the hygrothermal behaviour of internally insulated walls of a traditional building.

Temperature and relative humidity at the interface between the existing wall and the insulation were monitored for a period of two years. It was observed that the walls have a different hygrothermal performance. The south-facing wall presented a faster reduction in relative humidity compared to the north-facing wall. Discrepancy in the performance was found to be associated to wall orientation; in particular solar radiation.

The hygrothermal performance of a capillary active internal wall insulation system was found to allow dry-out of moisture within the building envelope enhanced by changes of temperature in the external wall due to longer and constant periods of solar radiation. Other studies have shown that capillary active insulation is beneficial to the building structure helping to reduce the risk of mould growth (Häupl, Fechner et al. 2006, Wegerer and Bednar, 2011).

The effect of solar radiation and wind driven rain on the performance of various conventional and capillary active insulation systems is being further investigated.

Acknowledgments

The authors would like to thank Natural Building Technologies and Technology Strategy Board who funded the research project and to Oxley Conservation for providing the case study building.

References

DECC. 2011. Extra help where it is needed : a new Energy Company Obligation. © Crown copyright.

Häupl P., Fechner H. et al. 2006. Moisture atlas for building envelopes. 3rd International Conference on Building Physics, Montreal, QC.

Wegerer P. & Bednar T. 2011. Long-term Measurement and Hygrothermal Simulation of an Interior Insulation Consisting of Reed Panels and Clay Plaster. 9th Nordic Symposium on Building Physics, Tampere, Finland.

Met Office. 2013 a. South England: climate. [http://www.metoffice.gov.uk/climate/uk/so/ accessed on 22/11/2013]

Met Office. 2013 b. UK climate summaries. [http://www.metoffice.gov.uk/climate/uk/2012/ accessed on 28/11/2013]

Hygrothermal Performance of TES Energy Façade at two European residential building demonstrations – Comparison between Field Measurements and Simulations

Carl-Magnus Capener, Ph.D. [1]
Stephen Burke, Ph.D. [2]
Simon Le Roux, Architect [3]
Stephan Ott, Architect [4]

[1] SP Technical Research institute of Sweden, Energy Technology, Sweden
[2] NCC Construction Sverige AB, NCC Teknik, Sweden
[3] Aalto University, Department of Architecture, Finland
[4] TU Munich, Chair of Timber Structures and Building Construction, Germany

KEYWORDS: *E2ReBuild, monitoring, hygrothermal simulations, TES-system*

SUMMARY:
In this study, the retrofitted facades of two European multi-unit residential buildings built in the 1950's and 1980's are investigated. The demonstration buildings, situated in Munich, Germany and Oulu, Finland, are part of the EU FP7 project E2ReBuild, a European collaboration project, researching and demonstrating industrialised energy efficient retrofitting of residential buildings in cold climates. The demonstration project in Munich, Germany, consisted of two blocks of residential multi-storey buildings in the suburb of Sendling, built in 1954. The buildings were typical examples of the concrete brick constructions, built throughout Germany in the post-war era. The pilot building in Oulu, northern Finland is one of five student apartment buildings in a housing corporation. The building was completed in 1985 according to a Finnish industrialized building system developed in the late 1960's using prefabricated concrete elements for residential buildings, called the "BES system". To improve their energy performance, the retrofit included a façade refurbishment with the TES method utilizing timber based, prefabricated façade elements for the renewal of the building envelope and improved thermal insulation. As part of an advanced monitoring programme, hygrothermal gauges were installed in the walls and they have been monitored for more than one year after the retrofitting. This paper presents the results from the in-situ measurements of the two demonstrations and compares the findings to calculated transient hygrothermal 2D-simulations of the facades utilising the monitored data from the sites in Finland and Germany.

1. Introduction

According to European standards and the EU's energy roadmap, the energy performance of multi-unit residential buildings from the 1950's and later in Europe is poor. External thermal insulation systems are commonly used to improve the thermal performance of such buildings, and for the two selected buildings of the E2ReBuild project the TES-method was chosen for improving the building envelope performance. The TES-system and method utilises timber based and insulated prefabricated façade elements for the renewal of the building envelope and to improve its thermal performance (Lattke 2011, Cronhjort 2014). In this study, the hygrothermal effects caused by the refurbishment are investigated and the TES-system is monitored.

This paper presents the findings from two investigated European multi-unit residential demonstration buildings. The demonstration buildings, situated in Munich, Germany and Oulu, Finland, are part of

the EU FP7 project E2ReBuild, a European collaboration project, researching and demonstrating industrialised energy efficient retrofitting of residential buildings in cold climates.

The demonstration project in Munich, Germany, consisted of two blocks of residential multi-storey buildings in the suburb of Sendling, built in 1954. The buildings were typical examples of the concrete brick constructions, built throughout Germany in the post-war era.

The pilot building in Oulu, northern Finland is one of five student apartment buildings in a housing corporation. The building was completed in 1985 according to a Finnish industrialized building system developed in the late 1960's using prefabricated concrete elements for residential buildings, called the "BES system" (Cronhjort 2014).

To improve the buildings' energy performance, the retrofit included a façade refurbishment with the TES method utilizing timber based, prefabricated façade elements for the renewal of the building envelope and improved thermal insulation. As part of an advanced monitoring programme, hygrothermal gauges were installed in the walls and they have been monitored after the completion of the retrofitting.

This paper presents the results from the in-situ measurements of the two demonstrations and compares the findings to calculated transient hygrothermal 2D-simulations (Künzel 1995, Holm 2000) of the facades utilising the monitored data from the sites in Finland and Germany.

2. Description of the demonstration buildings and field measurements

The FP7 project E2ReBuild includes seven demonstration buildings throughout northern and central Europe and this paper investigates the hygrothermal performance of timber element system (TES) (Lattke 2011) as external thermal insulation method and compares measured hygrothermal performance with simulation results from WUFI 2D models.

In this paper two of these demonstration buildings are presented and monitoring results from their retrofitted north-facing walls are shown.

2.1 Demonstration buildings

2.1.1 Background on Munich demo

The Munich demonstration was built in 1954 and is located in the suburb of Sendling. It consists of two blocks of residential buildings. They are examples of typical concrete block constructions built throughout Germany after World War 2.
(http://www.e2rebuild.eu/en/demos/munich/Sidor/default.aspx)

The heating demand of the building after the retrofit is calculated to be about 21 kWh/m²a. This is about 38 % lower, than the national requirement, EnEV2009. The overall energy demand after the retrofit is equivalent to a primary energy use of 23.5 kWh/m²a. This number is low because it includes a bonus for regenerative energy sources like solar thermal collectors, and a primary energy factor of fp = 0.7 for district heating.

The refurbishment concept includes a significant dismantling of the existing dwellings, built from light weight concrete block walls and concrete ceilings. The building was stripped down to the primary structure and the roof was taken off, see Figure 1, left. Additional changes in floor plan layout and new circulation cause interventions on the interior walls as well as on the window openings. A new attic floor and a roof were added together with an entire new building envelope made from TES Energy Façade elements.

Figure 1: Left: Dismantled structure of Munich demonstration with new elevator shaft (Picture: Lichtblau Architects). Right: Oulu demonstration during assembly of prefabricated TES elements (Picture: Simon Le Roux).

The highly insulated exterior wall with triple glazed windows is the backbone of the building envelope, see Table 1. The heating system is supplied from the district heating grid. On sunny days it is supported by solar thermal panels on the roof with a large accumulator tank containing 20000 litres of water as buffer. Room heating is done by radiators. The apartments have decentralised ventilation units with plate heat exchangers. The highly insulated building envelope, together with a modern and efficient ventilation system with heat recovery, means that the tenants enjoy an energy-efficient apartment with a high level of thermal comfort.

Table 1 Facts about thermal performance of envelope and building services, Munich demonstration.

	before	after
Exterior walls and roof	1.8 W/m²K	0.15 W/m²K
Windows	2.5 W/m²K	0.9 W/m²K
Basement ceiling	1.55 W/m²a	0.45 W/m²K
Heating energy (calculated)	280 kWh/m²a	21.2 kWh/m²a
Primary energy (calculated)	343 kWh/m²a	23.5 kWh/m²a

2.1.2 Background on Oulu demo

The E2ReBuild demo building in Oulu, northern Finland is one of five student apartment buildings in a housing corporation.

(http://www.e2rebuild.eu/en/demos/oulu/Sidor/default.aspx)

The Finnish demonstration building underwent a complete retrofitting of the envelope, see Table 12. The old façade layers of the previous BES-systems were removed leaving only the inner concrete layer in place. A new façade was retrofitted using prefabricated timber based elements, see Figure 1, right. The old roof was replaced completely by a new timber truss roof and a new thermal insulation layer of 550 mm resulting in a U-value of 0.08 W/m2K. ISOVER blown loose fill mineral wool, λ=0.041 W/mK. The existing ground floor slab was replaced, with a new in-situ concrete ground floor slab with 200 mm BASF Neopor EPS insulation.

Table 2 Facts about thermal performance of building envelope, Oulu demonstration.

	before	After
Exterior walls and roof	0.28 W/m²K	0.11 W/m²K
Windows	2.1 W/m²K	0.8 W/m²K
Ground slab	0.24/0.36 W/m²a	0.11/0.15 W/m²K
Roof	0.22 W/m²a	0.08 W/m²a

2.2 On-site hygrothermal monitoring of the facades

Part of this project includes an analysis of the TES Energy Façade elements with regards to hygrothermal performance, or the temperatures and moisture performance of the exterior wall. Figure 2 shows where each of the GE HygroTrac sensors was placed in the north façade of the Munich demonstration.

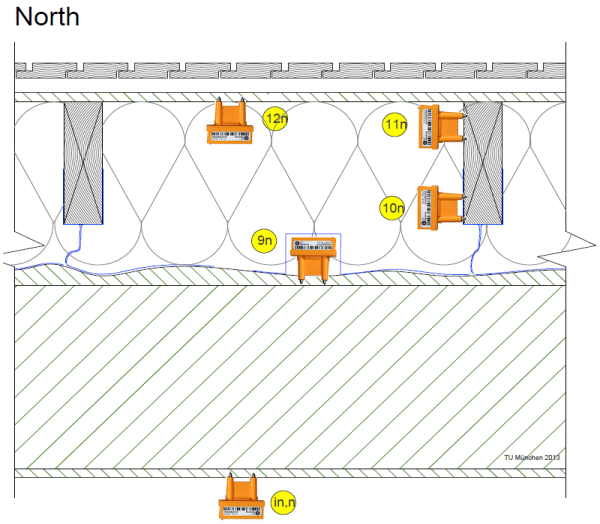

- wood shuttering formwork 24 mm
- air layer / lathing horizontal 24 mm
- gypsum fibre board 15 mm
- construction wood / cellulose 200 mm
- adaption layer – cellulose 60 mm
- membrane, Sd-value = 5 m
- exist. plaster, lime-cement plaster 25 mm
- existing exterior wall, light-weight concrete building blocks 300 mm
- exist. plaster, lime-cement plaster 15 mm

Figure 2: Monitoring positions of the presented Munich TES Façade element.

For the Oulu demonstration in Finland there was a similar set up of monitoring positions of the facades, as shown in Figure 3. Also facing north, the retrofitted wall construction consisted of:

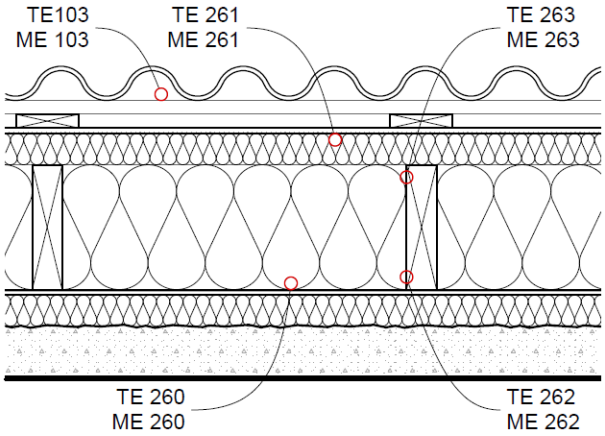

TES façade element description: US10YK
Declared U-value of the finished wall is 0.11 W/m^{2}K

- 7mm corrugated fibre cement cladding
- 44 mm air gap
- 22 + 22x100mm timber battens
- 9mm gypsum wind barrier
- 50 + 200mm glass mineral wool slab (Lambda 0,033 W/mK)
- 42x48mm c600mm horizontal timber battens
- 42x198mm c600mm timber load bearing frame
- 9 mm plywood board
- 50 mm soft thermal insulation
- 80mm existing precast concrete

Figure 3: Monitoring positions of the presented Oulu TES Façade element.

2.2.1 Measured data

For the Munich demo temperature, RH, and moisture content were measured at the measurement points shown in Figure 3 between 2012 and 2013. This data was measured every hour and was uploaded to GE's homepage where it could be monitored and downloaded. The sensors are wireless and had difficulties in sending their data every hour during the measurement period so a number of data points are missing. The sensors have also stopped recording data between February and April, 2013.

The data has been downloaded and sorted to match the times from the WUFI calculations for comparison purposes.

Similarly, for the Oulu demo, temperature and relative humidity is monitored at the measurement points shown in Figure 3 since February 2013.

3. Hygrothermal modelling and simulation

The hygrothermal behaviour of the demonstration buildings facades has been modelled by the two-dimensional hygrothermal building envelope tool WUFI 2D 3.3. The software has been experimentally verified for many types of building component assemblies (Künzel 1995, Karagiozis 2001) and similar set-ups (Holm 2000, Tariku 2006).

Material data and initial moisture conditions were supplied from material databases such as MASEA Datenbank (Materialdatensammlung für die energetische Altbausanierung) and the IBP Fraunhofer Material Database. As the buildings are between 30 to 60 years old, the German demonstration originates from the early 1950-ies, there is some lack of precise historic material data and appropriate assumptions had to be made.

3.1 Munich demonstration

WUFI 2D simulations were done using the drawing shown in Figure 2 together with measured climate data during the period of January 1, 2012 to October 28, 2013. Material properties were mostly taken from the Default materials database in WUFI.

The specific material in the existing wall is unknown with unknown thermal and moisture properties. It is known that the material is a type of Leca block with aerated aggregate. The real lambda value of the old wall was calculated using the measured indoor temperatures, temperatures in the adaption layer and temperatures in the exterior part of the mineral wool. These calculations showed that the lambda value of the old wall in reality is between 0.09 and 0.12 W/mK, which is similar to the thermal properties of the default materials Light Expanded Clay Aggregate and Aerated concrete. The default material's lambda value in WUFI 2D was modified to the measured value for the actual wall. Other thermal and moisture properties were obtained based on a report from an on-line database U-wert (www.u-wert.net). The default moisture properties for Light Expanded Clay Aggregate were used in the calculation since the actual moisture properties of the existing wall are unknown. At the beginning of the calculation, the initial moisture levels of all materials were set to about 80 % RH, based on measured values.

3.2 Oulu demonstration

For the Finnish demonstration the WUFI 2D simulations were set-up according to the drawing shown in Figure 3 together with measured climate data for the period of March 2013 to March 2014. An initial relative humidity throughout the existing construction of 60 % was assumed since this was an old construction and should not contain any excess moisture and a modest ventilation rate in the air gap behind the cladding of 5 air changes per hour (5 ACH) was selected.

4. Results

Both the Munich and Oulu simulated results agree quite well with the measured results in the new wall. The temperatures correlate very well with the measured results. The moisture levels also correlate very well, however the measured data shows much more variation in moisture levels than the simulated data.

4.1 Munich

The measured data indicates that the moisture measurement points are in a mineral wool layer. The simulated results are also taken from mineral wool. It is interesting to see that even though they are the same points, the calculations show a much more stable moisture level in the wall than in reality.

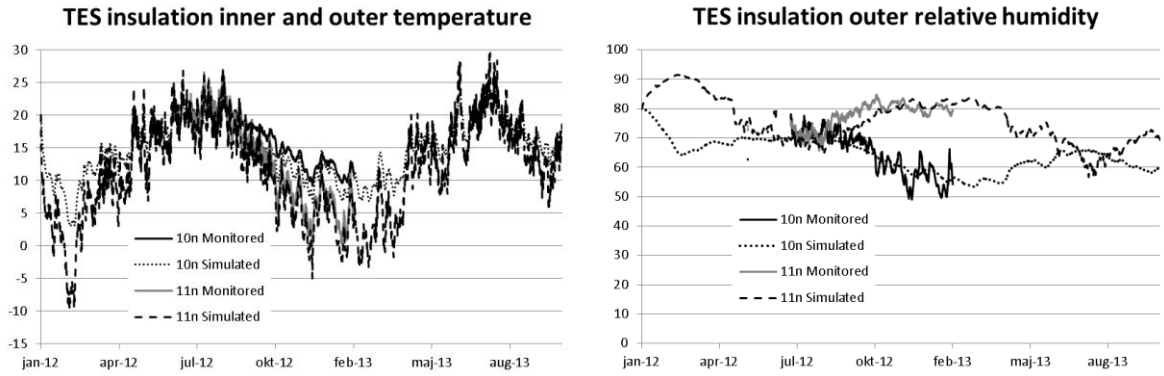

Figure 4: Temperature and relative humidity for the Munich TES Façade elements insulation, inner (10n) and outer (11n) locations.

The moisture levels in the exterior of the wall correlate well however, the calculated moisture level in the middle of the wall (point 9n in Figure 2) does not match the measured values. Further calculations seem to indicate that the plastic may be punctured at the sensor. If we calculate the moisture levels of the wall with the vapour barrier (SD 5m), the moisture level at the interior of the vapour barrier is both more stable and much higher than calculated, while the remaining moisture levels show very good correlation between measured and calculated values. If we lower the SD value of the vapour barrier to that of a weather barrier (SD = 0,1m) the simulated moisture values at point 9n agree with the measured data, however all the other measurement points have more error than simulations with the vapour barrier. This seems to indicate that measurement point 9n is affected by the exterior climate more than it should be if the vapour barrier was complete.

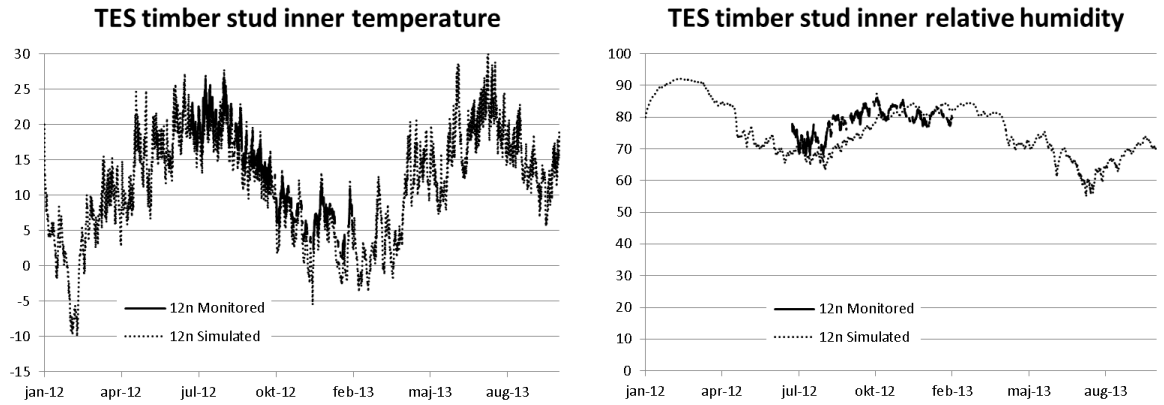

Figure 5: Temperature and relative humidity for the Munich TES Façade elements timber stud (12n).

In both the calculated and measured results, there does not appear to be a significant moisture risk associated with TES Energy Façade in Munich over the long term. The trend that can be seen in the WUFI calculation is that the construction dries out over time.

4.2 Oulu

The measured results correlate well with the simulated figures. It is clear that the initial moisture level has a great influence on the simulated values, the relative humidity is too low for the outer part of the wooden studs but for the inner part the simulation is well in accordance with the monitored result. After some months however, the levels are very close to the measured values, as the monitored wall gets drier. Also, the ventilation rates seem to have an influence, at least for the outer parts of the simulated wall. The low, 5 ACH, ventilation rate give accurate readings during many periods, but often seem to be underestimated as larger fluctuations can be seen in the relative humidity on the inside of the outdoor gypsum board. Another possible reason for the fluctuations can indicate insufficient air tightness over the wind barrier, causing larger fluctuations in the monitored results of the insulation compared to the simulated results.

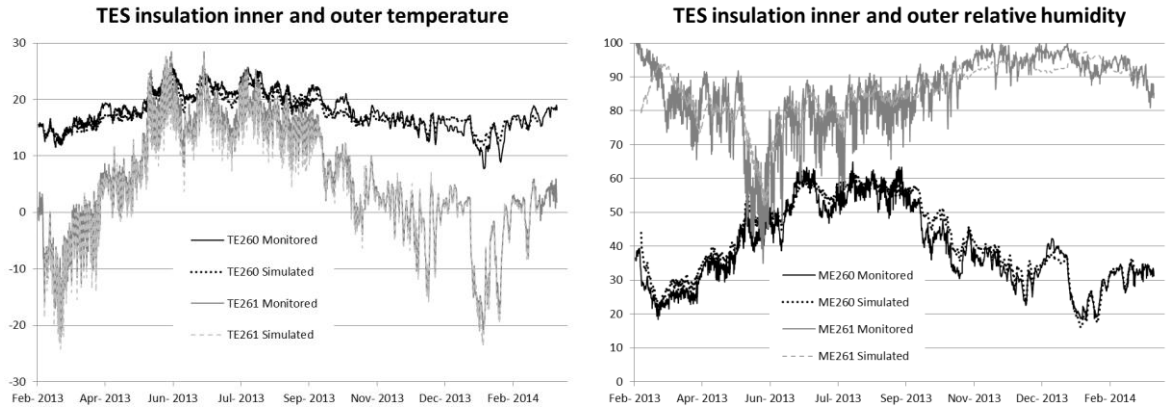

Figure 6: Temperature and relative humidity for the Oulu TES Façade elements insulation, inner (TE/ME260) and outer (TE/ME261) locations.

It is clear that the extra insulation placed outside the wooden studs has a beneficial influence on the temperature and relative humidity of the studs. Comparing the relative humidity for the monitoring position of the TES outer insulation (ME261) to the relative humidity at the TES outer part of the timber studs (ME263), clearly shows the reduction in relative humidity. Not only does the insulation break the thermal bridge, it also raises the temperature of the studs outer parts compared to a case without extra insulation, and this gives lower relative humidity and risk of moisture damage.

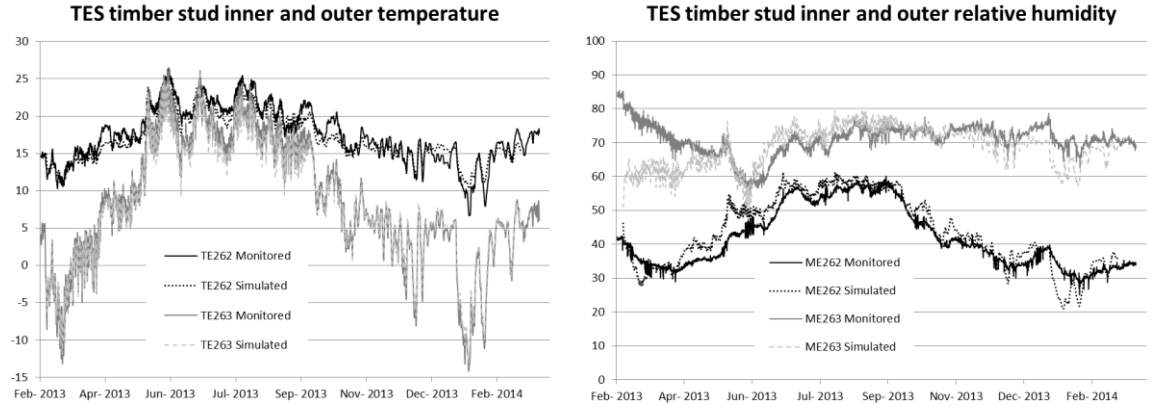

Figure 7: Temperature and relative humidity for the Oulu TES Façade elements timber studs, inner (TE/ME262) and outer (TE/ME263) locations.

5. Conclusions

In conclusion, the two cases from Munich and Oulu show that WUFI 2D is a good tool to determine the moisture performance of the TES Energy Façade after a renovation however, the results are very sensitive to the input data such as the existing wall, climate data, the new building materials and if there is any problem with the quality of the work. The demo cases also show that the risks for moisture damage in the form of mould growth in the TES Energy Façade are quite low in both cases for the measured climate. This gives an excellent possibility to evaluate TES Energy Façade with different modifications and in new locations using WUFI 2D before actually starting the retrofit of a building. Initial moisture can pose a risk for wooden construction, both elevated moisture contents in the TES wooden studs themselves, but also in the interior and existing wall material where the TES will be placed can be a source of excess moisture, especially for materials such as concrete and lightweight concrete.

For future work it would be interesting to see the effect of built-in moisture in the existing wall on the hygrothermal performance of the external TES timber studs and the risk of moisture damage this would impose. Also, the robustness and sensitivity of the system to moisture from envelope leakage or from transport to construction site is a topic that needs further investigation, as well as the effect of the extra layer of insulation on the timber studs in the Finnish demo compared to the German TES build-up without extra insulation.

6. Acknowledgements

This paper is based on research and results from the EU FP7 funded project E2ReBuild Industrialised energy efficient retrofitting of resident buildings in cold climates. The project started in January 2011 and ends in June 2014. The project is coordinated by Christina Claeson-Jonsson, NCC AB.

The research leading to these results has received funding from the European Union's Seventh Framework Programme (FP7/2007-2013) under grant agreement n° 260058.

References

Cronhjort, Y., Le Roux, S. 2014. Holistic retrofit and follow-up through monitoring: Case Virkakatu, Oulu, Finland, Submitted to the Nordic Symposium on Building Physics 2014, Lund, Sweden

Holm, A., Künzel, H.M. 2000. Two-Dimensional Transient Heat and Moisture Simulations of Rising Damp with WUFI 2d, 12th Int. Brick/Block Masonry Conf. Proc. Vol. 2, Madrid, Spain

Karagiozis, A., Künzel, H.M., Holm, A. 2001. WUFI ORNL/IBP – A North American Hygrothermal Model: Proceedings of the Thermal Performance of the Exterior Envelopes of Whole Buildings VIII (Buildings VIII), Clearwater Beach, Florida, USA, December 2-7, 2001

Künzel, H.M. 1995. Simultaneous Heat and Moisture Transport in Building Components – One- and two-dimensional calculation using simple parameters, IRB Verlag, Germany

Lattke, F., Larsen, K., Ott, S., Cronhjort, Y. 2011. TES Energy Façade – prefabricated timber based building system for improving the energy efficiency of the building envelope, funded by: Woodwisdom Net, Research project from 2008-2009

Tariku, F., Kumaran, M.K. 2006. Hygrothermal modelling of aerated concrete wall and comparison with field experiment, Proceedings of the 3rd International Building Physics Conference, Montreal, Canada, August 27, 2006, pp 321-328

New sustainable and insulating building material made of cattail

Martin Krus [1]
Werner Theuerkorn [2]
Theo Großkinsky [1]
Hartwig Künzel [1]

[1] Fraunhofer Institute for Building Physics IBP, Holzkirchen, Germany
[2] typha technik, Naturbaustoffe, Schönau, Germany

KEYWORDS: Insulation, sustainability, cattail, half timbered framework, heritage

SUMMARY:
Due to the special structural properties of cattail (typha) building materials can be produced offering a combination of insulation and strength, which is unique on the market. The leaf mass of typha is especially suited due the structure of the plant. The leaves have a fiber-reinforced supporting tissue filled with soft open-cell spongy tissue providing for amazing statics and an excellent insulating effect. In the past few years, the Fraunhofer Institute for Building Physics investigated various product developments in cooperation with the inventor Dipl.-Ing. Werner Theuerkorn. The newly developed magnesite-bound typha board has an extremely high strength and dynamic stability despite a low thermal conductivity of about 0.055 W/mK and can solve energetic as well as static problems. This innovative building material possesses a lot of positive properties. With the typha board as infill of the timber frames and as an additional inside insulation layer an extremely slender exterior wall construction with wall heating is realized. Due to the simple processability and inherent stiffness the material could be adjusted to the irregular inclined walls. The suitability of the wall structure has been investigated over a measuring period of 1.5 years. The U-value of the whole building (infill and timber construction) is about 0.35 W/m²K. The low level of moisture applied by the mortar and plaster dried out fast to a constant moisture contents in the wooden supports of below 20 M.-%.

1. Introduction

Cattails are, due to their enormous growth rate and yield, optimally suited as raw material for industrial use. Typha stock (Fig. 1, left) comprises resilient, natural monocultures with an annual production rate of 15 to 20 tonnes of dry matter per hectare. This corresponds to four to five times the amount that local evergreen forests produce. Cattail crops create ecologically precious wetlands, which fulfill other important functions besides the absorption of nutrients and CO_2 (Faulstich 2012). Cultivation in lowland moors and valley plains in Germany would offer a sufficient basis to cover the total demand for insulation and wall construction materials. The special structural characteristics of cattails support the production of construction materials that offer a unique combination of load bearing capacity and insulation. The plant's structure (Fig. 1, right) entails the particular suitability of the typha leaf mass for creating innovative building materials (Pfadenhauer 2001, Theuerkorn 1998). Due to the combination of tensile strength of stem fibre and elastic sponge-like tissue, leaves are tear and break resistant, flexible and maintain their shape even in dried condition. These characteristics provide remarkable load-bearing capacity and excellent insulation properties. Behaviour of leaf mass under tensile and compressive stress is completely different along the leaf axis from base to tip than perpendicular to it: along the axis, the leaf material resists high compression loads of approximately 1 N/ mm and even higher tensile stress. Perpendicular to this axis, elastic deformation sets in already at very low stress of 0.01 N/mm and predominantly remains within reversible ranges.

Fig. 1. Typha sprout with leaf fan, left picture by TU Munich and section of a typha leaf, right picture by Chr. Gruber BLfD

The special qualities of typha insulation panels originate in these diverse characteristics. Their production is based on laying out typha-leaf particles randomly, yet parallel to the panel plane and binding them with magnesite. The result is a material that can be created within a relatively simple procedure. This product contains only plant ingredients, purely mineral-based adhesive and no further additives. Thus, it is completely compostable. At the same time, it features a beneficial ratio of compressive strength along the panel plane, thermal conductivity, vapour diffusion properties, as well as storage mass for summertime heat protection. Variations in strength values and insulation capacities depend on bulk density and the percentage of magnesite (Table 1).

Table 1:Measured heat conductivities and bearing loads for different bulk densities and parts of mangesite bond, from Theuerkorn (2013).

Type	Density [kg/m³]	Magnesite part [%]	Bearing load [N/mm²]	Heat conductivity* [W/Km]
1a	257	50	0,54	0,055
1b	283	60	0,46	0,058
1c	233	40	0,34	0,053
2a	237	50	0,36	-
2b	243	60	0,36	-
2c	217	40	0,29	0,048
3a	318	50	1,01	-
3b	346	60	0,76	0,061

* orientative, not normative measurement

The complete range of hygrothermal key values was registered for a material sample with a particularly effective combination of stability and thermal conductivity. The material, despite relatively high bulk mass and high solidity, features a comparably low thermal conductivity of 0.055 W/mK and displays capillary action at a medium vapour diffusion rate (Table 2). By using it, vapour barriers could be avoided completely in many applications. Moreover, this innovative building material possesses a lot of other positive properties:

- renewable building materials with a very high resistance to mould growth
- good protection against fire, noise control and thermal insulation in summer
- simple processability with all common tools
- relatively diffusion open and capillary active
- low energy consumption in production
- recyclability.

Table 2: Hygrothermal material properties of type 1a.

Material property	Unit	Result
Bulk density	kg/m³	270
Porosity	Vol.-%	75
Diffusion resistance dry-cup (23 0/50)	-	28
Wet-cup (23 50/93)	-	20
Water absorption coefficient	Kg/m²√h	1.1
Sorption moisture content 23 °C 65 % r. H:	Vol.-%	0.65
23 °C 80 % r. H:	Vol.-%	1.2
23 °C 93 % r. H:	Vol.-%	2.9
23 °C 97 % r. H:	Vol.-%	6.9
Capillary saturation	Vol.-%	59
Heat conductivity	W/mK	0.055

2. Insulation of half timbered framework

Due to the immanent energy transition, new requirements are also placed on historic buildings. In general, they can hardly be met. This is why it is necessary to develop new materials and concepts for energy optimization meeting historic preservation needs specifically for such objects. The newly developed building material made of cattails seems appropriate for the task. In the case of a timbered building in Nuremberg with asymmetrical design and inadequate bracing of the structural frame (see Fig. 2, left) the timbers were supposed to be made visible again - while maintaining EnEV 2009 regulations as well as historic preservation requirements (Theuerkorn 2013; Fritsch 2013), and at the same time, providing stability to the building. These requirements were met by employing typha-panels. The model project made use of the material and was supported by the Federal German Foundation for the Environment and the Bavarian State Office for the Preservation of Historical Monuments. After comprehensive research on the existing construction, the details for the wall composition were designed and realized in close cooperation with construction management and craftsmen. A model frame served to develop a slender exterior wall construction of only 20 cm depth featuring integrated wall heater (Fig. 2, right).

Fig. 2. Condition of the wooden framework before restoration (left) and sheme of the insulation (right), pictures by Alexandra Fritsch.

The framework timbers were covered with slats according to carpentry standards for renovating such structures. The typha panels were cut to provide a continuous 10 mm wide groove. First, external panels with a thickness of 60 mm were fixed on the outside to the slats with drywall screws and

washers. A second panel with 60 mm thickness was fit internally and connected to the external panels with screws, while leaving a gap between the edge of the interior panels and the timbers. To enable wind proofing and force-fit connections, the gaps between timbers and typha panels are infilled with a typha-based joint compound. The seams are covered and smoothed with a taping knife. By including ground typha material, the joint compound can expand if water is introduced later on. After creating a uniform plane wall surface by use of compensating panels, additional 40 mm thick typha panels were attached to the interior wall. Due to panels being screw-tight and easy to render, their surface served to directly mount wall heat pipes with screw connectors. Voids were infilled with a lime-gypsum based mortar. The finishing coat is a loam render enriched with cattail seed parachutes. This render reinforcement is an effective means to ensure crack resistance without a fabric lining. Fig. 3 shows the layout of the construction.

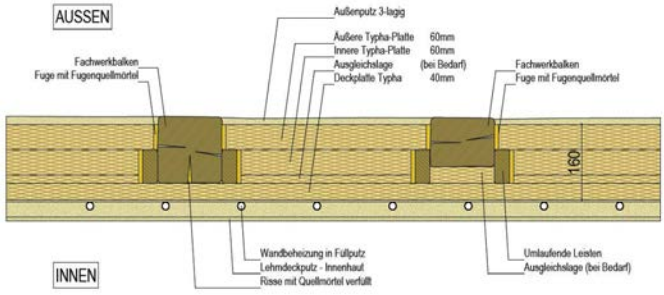

Fig. 3. Layout wall structure planning guide, picture by Fritsch+Knodt&Klug.

The functional capability of the wall construction was tested by monitoring during a one and a half years testing period. For this purpose, sensors were distributed along the cross section of a selected infill area to determine temperature, relative humidity, wood moisture, and heat flow (Fig.4).

Fig. 4. Outer sensors at layer 1 beneath the outside rendering (left) as well as Temperature sensor, heat flow wafer and humidity sensor on barrier layer 3, beneath internal insulation on the second insulation board layer (right).

The course of boundary layer temperatures as hourly average values from January 2011 to September 2012 is displayed in Fig 5, left. The typical thermal stratification from the interior (room air temperature RLLT / interior surface temperature IOFT) to the exterior along boundary layer 4 (GS4T) is evident. Prior to operating the wall heater, the space was heated via an open door to the heated neighbouring room. The initial adjustment attempts of the renter after begin of operation clearly display excessive use (marked by a blue circle). Fig 5, right side, shows the measured heat flow behind the interior insulation (boundary layer 3) and the temperature distribution along this area, as well as the exterior along boundary layer 1.

The thermal insulation characteristics of the wall construction can be calculated based on this heat flow in relation to the temperature difference. Two selected measuring periods (indicated in orange)

result in a heat transfer coefficient (U-value) of 0.26 W/m²K, taking the additional interior insulation into account. For the entire construction including frame timbers the result is a value of 0.31 W/m²K. Since measurements also include thermal gains due to solar intake (including diffuse irradiance), this heat transfer resistance is called “relational” U-value.

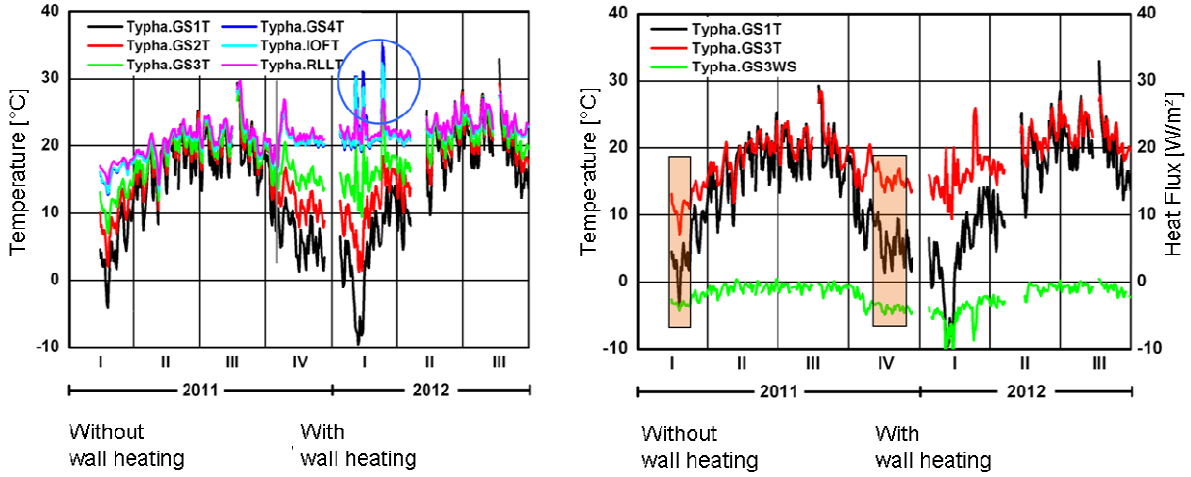

Fig. 5. Measured course of the temperature as daily mean values for the period from January 2011 to September 2012 (left) and heat flow measured behind the internal insulation (layer 3) with course of the temperature at layer 1 and 3. The bars show time periods suited for assessing the thermal resistance (right).

When calculating the “real” U-value based on the material properties, the outcomes are slightly higher values of 0.29 W/m²K for the infill and 0.35 W/m²K for the entire construction. Due to the building moisture that is introduced via the exterior render and the relatively good absorption capacity of wood, the results show a very high initial wood moisture content of more than 100 %. However, drying occurs quickly, and the wood moisture content of all four measurement areas along the wood surface located immediately behind the exterior render layer decreased to 20 % (Fig. 6).

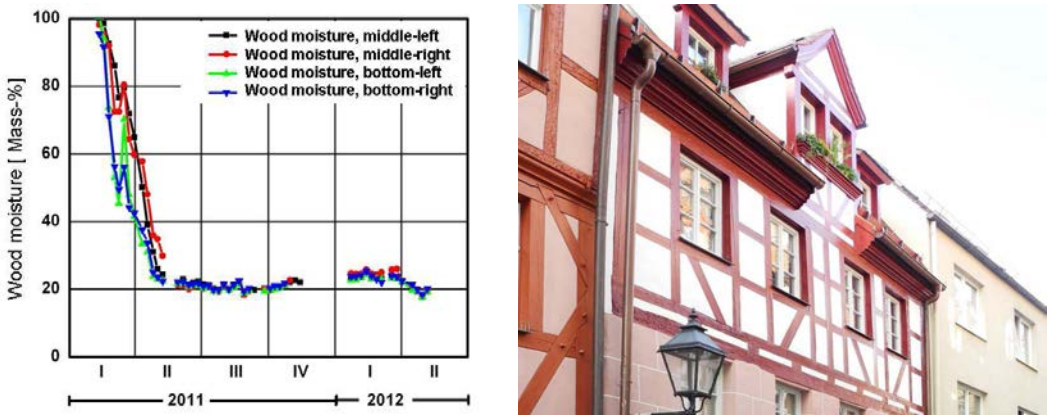

Fig. 6. Course of the wood moisture (left) and view of the building after restoration (right).

By adding the typha panels as a combination of infill insulation and interior insulation, a heat transfer coefficient of approximately 0.35 W/ m²K was achieved for this wall construction - at an overall wall thickness not exceeding 20 cm, including wall heater. For a timbered building, this is an extraordinarily good result. The measurements of temperatures and air humidity undertaken across two heating periods prove the suitability of the construction in regard to building physics. Altogether, the entire insulation procedure based on applying magnesite bonded typha panels comprises an extremely effective solution in terms of building physics and historic preservation.

3. Calculational investigations for the magnesite-bound typha board as internal insulation on masonry

The half-timbered building in Pfeiffergasse in Nuremberg has a ground floor of massive masonry as many other buildings of the same kind. For the energetic restoration of this building it was planned to install an internal insulation by magnesite-bound typha boards of a material thickness of 4 cm furnished with fiber-reinforced clay plaster. The boards were installed edge to edge and fixed by dowels on the internal surface of the external wall. Since an accompanying measurement was not planned due to financial reasons hygrothermal calculations were carried out to assess whether this measure will be free of damage. The IBP developed a proved and frequently validated one-dimensional and two-dimensional computer program WUFI®-Pro (Künzel 1994) for the calculation of coupled heat and moisture transfer processes. Previous descriptions of the moisture transfer behavior of building materials by means of this method have achieved good compliance of calculation and practical investigations of the test specimen (Krus 1996; Künzel 1999).

Climate data of Holzkirchen are used as climate boundary conditions allowing assessments on more unfavorable weather conditions than those in Nuremberg. Living conditions with normal moisture load (meaning normal use of living areas) serve as indoor climate. The heat transmission coefficients are 8 W/m²K on the inside and 17 W/m²K on the outside. Material parameters of the masonry and clay plaster are taken from the WUFI® material database. Calculations of the typha board are based on the hygrothermal material parameters determined before. If necessary, it is possible to assess by means of the prognosis tool WUFI®-Bio (Sedlbauer 2001; Sedlbauer 2003), whether mould growth may occur. Since an all-over contact of the typha board with the brick work cannot be secured a thin air layer was suggested between insulation and masonry.

If the most critical point of the wall between external wall and internal insulation is considered, the characteristic seasonal fluctuations of temperature and humidity can be observed. Maximum relative humidity of approx. 65 %, however, is achieved in this point (Fig. 7, left). Therefore, mould growth can be excluded. The calculation results show that no moisture damage will occur in case of careful implementation with good permanent convection tightness.

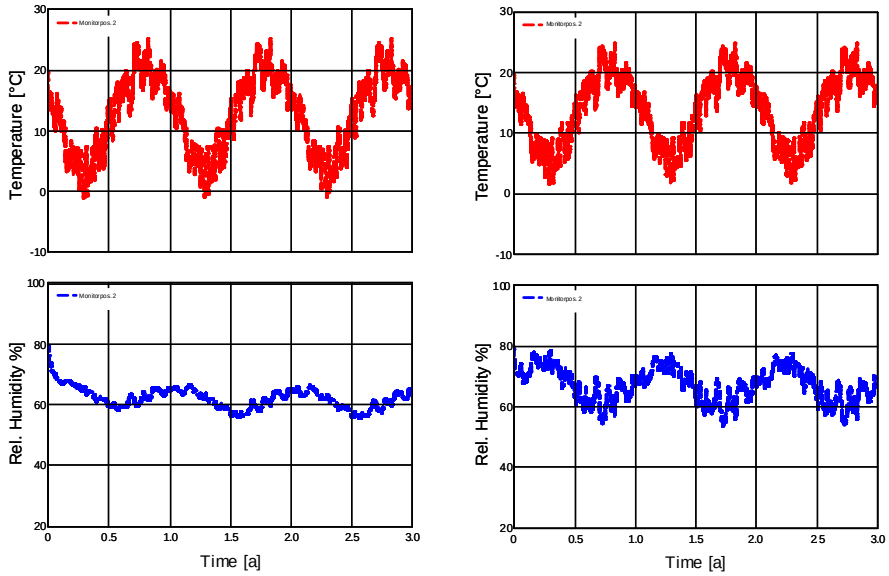

Fig. 7. Course of temperature (top) and relative humidity (bottom) between external wall and internal insulation with careful implementation (left) and without perfect tightness with back flow of 1 l/mh (right).

Since it cannot be suggested that this is always the case, the tolerance of the construction must be investigated. To find an answer to the question the following investigations were based on a defined leakage with a back flow of the insulation board by warm and humid air from the interior. The following calculations were based on a back flow of 1 liter per hour and running meter wall length. Fig. 7, right side, shows the situation behind the insulation. Due to the inflowing warm air minimum temperatures of barely below 0 °C are raised to scarcely above freezing temperature. The rel. humidity doesn`t exceed 80 % despite the back-flow.

Fig. 8, left side, shows the result of a further increase of the back flow up to one cubic meter per day and running meter wall length. In winter, however, 80 % r. h. is temporarily exceeded so that mold growth could no longer be excluded. For verification the calculated course of temperature and relative humidity at this point is used for the mould growth prognosis program WUFI®-Bio. As the results in Fig. 8, right side, show the spore water content never exceeds the limit water content. Despite back flow no mould growth must be expected under these conditions. Therefore, the wall structure with this kind of internal insulation shows a considerable tolerance of untightness, one reason may be the relatively low thickness of the insulation material.

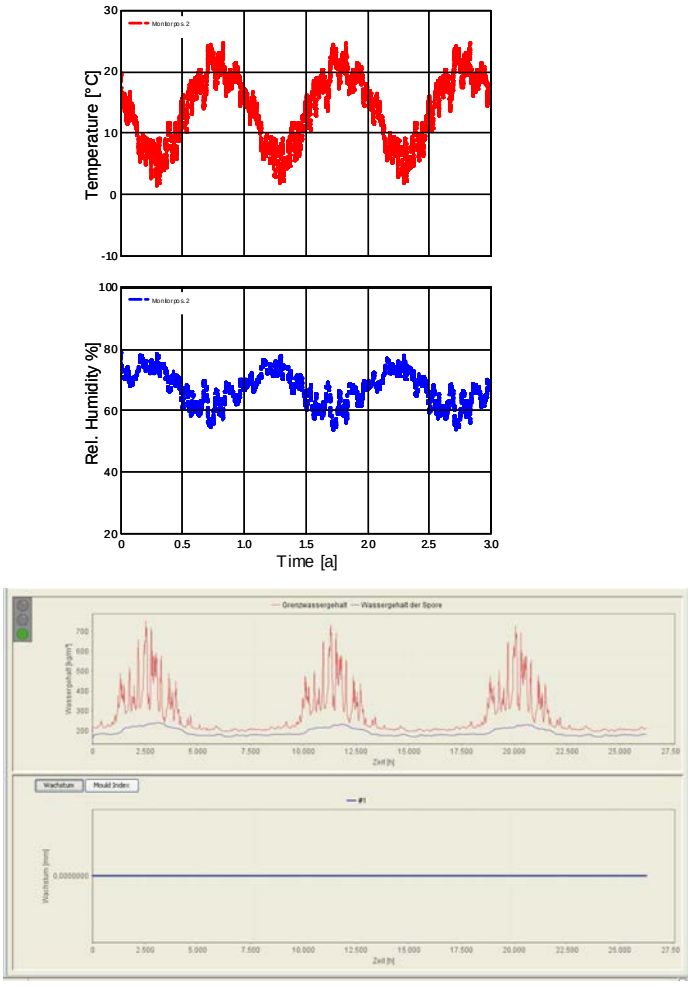

Fig. 8. Course of temperature (top) and relative humidity (bottom) between external wall and internal insulation at a back flow of 1 m³/md (left) and calculated results by WUFI®-Bio for the area behind the internal insulation.

4. Conclusions

A product has been developed by means of optimizations concerning the structure of the board and the material properties showing numerous positive characteristics. For the first time ever, a material is available showing a relatively high bearing capacity and simultaneously good insulation properties, which is manufactured from renewable material at low energy consumption and entails great advantages for the environment. Moreover, susceptibility to mould growth in practical application is relatively low, what is frequently a problem in case of renewable insulation materials. The material is sufficiently diffusion-open to support drying-out processes but diffusion-tight enough to work without any vapor barrier in many applications. Calculations of the internal insulation showed that at least in case of moderate thickness the typha boards can be directly doweled to the wall and coated by an internal plaster, and thus can function free of damage from the building physical point of view and have a considerable tolerance for errors in installation. The installation of the typha boards in the framework building in Nuremberg allowed the achievement of a thermal transmittance coefficient of approx. 0.35 W/m²K with a total thickness of the wall structure of only 20 cm including wall panel heating by a combination infilling with the typha board and internal wall surface area insulation. This result is extremely good for a framework building.

The measurements of temperatures and humidity in various depths of the structure carried out at the object during two heating periods prove the building physical suitability. In the beginning, slightly higher initial humidity occurred due to the built-in moisture added by internal and external plasters, and then the framework dried out rapidly and humidity remained low and uncritical. The measurements of the heat flow confirmed the positive results of the calculations. The measurements of the moisture contents of the timber also showed that due to the rapid drying-out only relatively low and uncritical moisture occurred in the timber. All in all, an extremely positive result is achieved from the building physical point of view and as concerns the preservation of historical monuments by the installation of magnesite-bound typha boards as insulation measure.

5. Acknowledgements

Thanks to Altstadtfreunde Nürnberg e.V. and to Deutsche Bundesstiftung Umwelt who have not only financially supported these investigations.

References

Faulstich, M. 2012. SRU-Umweltgutachten 2012, Verantwortung in einer begrenzten Welt, Berlin.

Fritsch, A. & Theuerkorn, W. 2013 Fachwerksanierung und Energieeffizienz. In Denkmalpflege Informationen.

Krus, M. & Künzel, H.M. 1996. Vergleich experimenteller und rechnerischer Ergebnisse anhand des Austrocknungsverhaltens von Ziegelwänden. Internationales Symposium of CIB W67 Energy and Mass Flow in the Life Cycle of Buildings. Wien, 4.-10. August 1996, S. 493-498.

Künzel, H.M. 1994. Verfahren zur ein- und zweidimensionalen Berechnung des gekoppelten Wärme- und Feuchtetransports in Bauteilen mit einfachen Kennwerten. Dissertation Universität Stuttgart 1994.

Künzel, H.M. (1999): Praktische Beurteilung des Feuchteverhaltens von Bauteilen durch moderne Rechenverfahren. WTA-Schriftenreihe, Heft 18, Aedificatio Verlag.

Pfadenhauer, J.& Heinz, S. 2001. Multitalent Rohrkolben -Ökologie, Forschung, Verwertung Broschüre zum Abschlussbericht des DBU-Projektes „Rohrkolbenanbau in Nierdermooren - Integration von Rohstoffgewinnung, Wasserreinigung zu einem nachthaltigen Nutzungskonzept“ im Donaumoos 1998-2001, TU München, Lehrstuhl für Vegetationsökologie.

Sedlbauer, K. 2001. Vorhersage von Schimmelpilzbildung auf und in Bauteilen. Dissertation Universität Stuttgart (2001).

Sedlbauer, K. & Krus, M. 2003. Schimmelpilze in Gebäuden – Biohygrothermische Berechnungen und Gegenmaßnahmen. Berlin : Ernst und Sohn Verlag S. 435-531, Bauphysik-Kalender 2003.

Theuerkorn, W. , Reizky, Lenz, Kleyn. 1998. Rohrkolben, ein nachwachsender Rohstoff.

Theuerkorn, W.; Fritsch, A.; Mach, M.; Krus, M; Großkinsky, Th.; Fitz,C. Theuerkorn, D. Knodt, H. Walter, U. 2013. Neuer Baustoff für umweltfreundliche und bautechnische Sanierung in der Denkmalpflege. DBU-Bericht (Förderkennzeichen AZ 27918).

Cross Laminated Timber vs. timber frame walls in water damage – comparing drying and mould growth

Kristine Nore, Ph.D. [1]
Johan Mattsson, Cand.Scient [2]
Mari Sand Austigard, Ph.D. [2]

[1] Norwegian Institute of Wood Technology, Norway
[2] Mycoteam AS, Norway

KEYWORDS: *Water damage, CLT, Cross Laminated Timber, wood, mould growth, drying.*

SUMMARY:
In Norway 83 000 water damages were reported to insurance companies in 2013. Risk management and renovation procedures are needed in order to reduce the costs generated by these incidents. In the presented experiment one square meter dwelling partition walls were submerged for 48 hours prior to full assembly and drying in a dry environment. Dwelling partition walls are between two separate residential apartments, and have to fulfil requirements regarding fire safety, sound insulation, moisture control and more. The edges of the wall samples were sealed in order to obtain drying mainly through the wall surfaces. The results show different drying patterns in standard light weight timber frame walls and Cross Laminated Timber (CLT) walls. The CLT walls were not fully wetted after 48 hours, and could still absorb water from the soaked mineral wool between the CLT elements. The CLT partition walls therefore gave lower risk of mould growth, and lower actual mould growth. However, the drying period was longer compared to the timber frame wall.

1. Introduction

Water damages are common in Norway, reaching 83 000 water damages reported to insurance companies in 2013 (Finance Norway, 2014). There is always a risk of mould growth following water damage. Mould is unacceptable in dwellings, and avoiding mould damage is a major aspect in handling water damages. The crucial factor in order to avoid mould growth is to obtain quick drying of the wetted materials. It has been shown that log walls and massive timber walls are damaged by mould fungi after 3-4 weeks, while light timber frame walls are damaged after about one week of wet conditions due to more accessible cellulose in the gypsum boards (Mattsson & Stensrød 2009). Mould growth depends on available water at the surface of the substrate (Rayner and Boddy, 1988, Samson et al. 2004). It is therefore of great importance to establish dry surfaces as fast as possible, at least within one week, in order to avoid mould damages after water damages.

The main question is how to handle water damages in such a way that mould growth can be avoided in every single case, regardless of construction type. Despite the large number of water damages every year, there is a general lack of understanding regarding how to perform a satisfactory handling of water damages. Mattsson & Stensrød (2009) reported that about 50% of investigated water damages where inadequately managed by the contracted professional companies.

Given the general lack of knowledge about how to handle well-known structures, there is great uncertainty regarding how to handle water damages in new and more unknown materials and structures, e.g. in CLT assemblies. It is therefore important to clarify how wet these constructions might get during leakage incidents, how fast they dry out, and how extensively they may be attacked by mould.

CLT elements are still emerging as a construction concept, and experience is limited. The first erected CLT buildings are now ten-fifteen years old. Risk handling in the event of water damage is not developed for CLT buildings, neither in terms of survey methods, adequate instruments for moisture measurements or suitable drying equipment. Knowing the hygrothermal performance after water damage will allow better procedures for risk handling actions.

Hygrothermal performance for external walls, including common CLT build ups, is tested and calculated in McClung (2013). She concludes that built in moisture alone is not likely to cause building failure. One limit found is the ability to calculate actual performance for different climates. Available simulation tools are not sufficiently accurate for this purpose, and experimental data are needed.

Two experiments were performed: One large scale drying test on square meter dwelling partition wall elements and one smaller scale test of mould growth on smaller wall elements. Dwelling partition walls used in multistory wooden buildings often consist of separate load bearing walls, most often with additional insulation in between for sound insulation.

2. Measurement set-up

The CLT provided was 120 mm thick. This is usually more than needed for loadbearing inner walls, but was considered an advantage concerning moisture uptake and drying out period. The light weight timber frame was built using standard 48×98 mm wood, assembled as shown in BDS 524.305 (2002). In each test element two wall elements were combined, with insulation in between. All elements used in both tests were insulated with mineral wool, which mainly provides sound insulation in such partition walls.

The drying test was performed using large-scale elements measuring B×H = 0.8 × 1.2 m. Three CLT partition wall elements and one timber framed reference element were used. The mould growth test was performed on smaller elements measuring 0.6 x 0.37 m. Four CLT elements and four timber frame elements were used.

2.1 Large scale laboratory drying test

The large scale buildup is shown in Figure 2. The elements were submerged for 48 hours. After wetting the pieces were assembled to dwelling partition walls. In order to ensure the correct distance between the separate wall elements in each test element, chipboards were attached to all four edge surfaces. PE foil was inserted between the chipboards and the elements in order to seal the edges. For additional sealing, an acrylic sealing compound was applied along the edges of the chipboards.

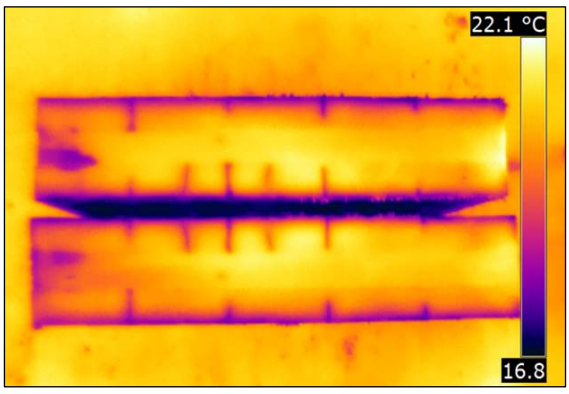

FIG 1. A thermal photograph of two of the CLT elements after wetting. Colder areas (blue) have higher water content in the wood than warmer (yellow) areas. The elements have mainly absorbed water along their outer edges, leaving the middle of each element relatively dry.

a b

FIG 2. Construction principle for the large-scale drying test. a: Two wall elements combined to form a dwelling partition wall, with mineral wool in between for sound insulation. b: the elements suspended in the weighing rig. The reference timber frame test element is seen in front.

The elements were instrumented with weight cells and Hygrotrac sensors (Omnisense, 2014). Each element was suspended from a weight cell, so that their weight could be monitored continuously. Unfortunately the weight cells did not operate prior to January 8th. The Hygrotrac sensors measure air temperature, relative humidity and wood moisture content. In each CLT element three Hygrotrac sensors were mounted, on the inside (wet part of partition wall), in the middle of the element (holes drilled from outside) and on the outside (also measuring laboratory climate), as shown in Figure 2a.

After 80 days in the drying rig, air sampling for total count of mould spores was performed in all four test elements. The method used was the Air-O-Cell air sampling cassette in which 75 litres of air was sucked from inside each element using a calibrated wall pump (BioAire), see Figure 3. The air is passed through a sticky surface where the mould spores and other airborne particles are captured, and the filter is subsequently analysed under a microscope.

FIG 3. Sampling of air from inside a CLT element, via a hole drilled in the particleboard on the edge surface of the element.

2.2 Mycotest

The elements used in the mould growth test were contaminated by soaking the elements in a mould spore suspension. The suspension was a mixture of commonly occurring mould fungi, e.g. *Cladosporium* spp., *Penicillium* spp., *Aspergillus versicolor* and *Chaetomium globosum* of about 500 000 spores/ml water. After contamination, Hygrotrac instruments were installed and the elements were assembled and the edges sealed using PE-foil and moisture tight sealing tape (Figure 4a).

The elements were placed in climate chambers with 20 °C and 70% relative humidity. Temperature, relative humidity and wood moisture in each test element was measured every 30 minutes. Each week one CLT and one timber frame element were dissembled for assessment of mould growth (Figure 2b). The amount of mould growth was assessed using microscopic analysis of tape lifts.

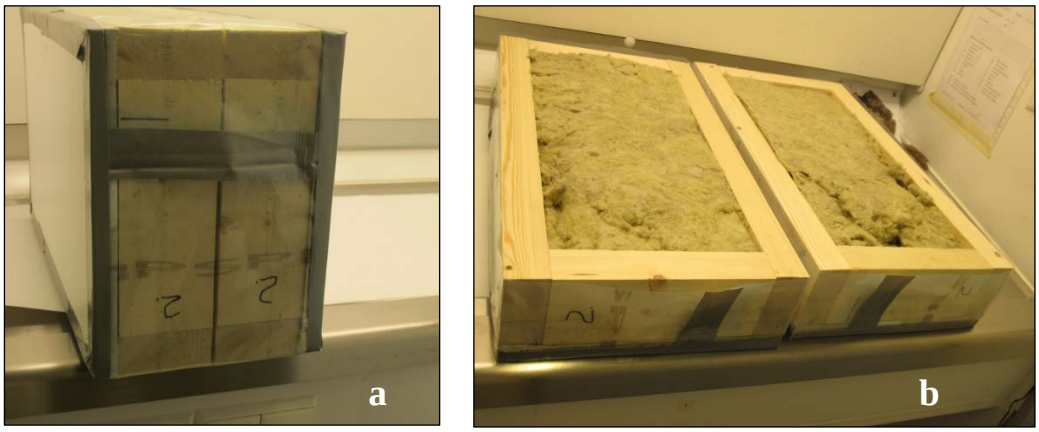

FIG 4a. Timber frame test element for mould growth after contamination and assembly. b. Timber frame test element after dissemble for mould growth assessment.

3. Results

3.1 Drying test

The climate in the room where the drying test was performed is not controlled. The temperature and relative humidity varied throughout the test as shown in Figure 5. The temperature was [19-24] °C and the relative humidity [25-60] %. The standard deviation is included in the graph to show the variation of the six sensors. The test elements were placed only 10 cm apart in the drying rig. This caused higher air humidity in the in-between spaces, especially in the beginning of the test. This is seen in the standard deviation of the relative humidity in Figure 5. The drying process, which is most rapid in the beginning of the test, is responsible for the lower air temperature shown in the start of the drying. This is due to the fact that the transfer of bound water moleculesto free water molecules in the air reduces the moisture enthalpy, which again requires energy. This energy is taken from heat in the air and in the wood, reducing temperature of both in the process.

The temperature and relative humidity inside the partition walls are shown in Figure 6. The temperature follows the room temperature, only with smaller amplitudes. A time lag is clearly evident in the CLT elements, as well as even smaller amplitudes than in the timber frame element. This is due to the larger hygrothermal capacity of the CLT elements. The fact that the relative humidity reaches values above 100 % is obviously a measurement failure. Anyhow, the moisture inside the timber frame element levels out at a level that is probably close to saturation. The relative humidity in the timber frame element probably falls to a level slightly below saturation on February 6th, but no further drying seems to take place during the test period. The air inside the CLT elements increases in humidity during the first few days, and then dries steadily throughout the test period. The CLT elements clearly had more moisture capacity to remove the moisture from the locked void of the walls.

The moisture content of the wood in the CLT elements is shown in Figure 7. The wood moisture content was decreasing from the inside towards the outside of the element throughout the test period. The moisture content at the outer surface very quickly decreased below 10 weight percent. In the middle of the element the moisture remained relatively stable at 15 weight percent, while the inner surface dried from around fiber saturation point to 20 weight percent during the 12 weeks of drying.

Figure 8 shows the development in weight for all elements. The CLT weighed around 130 kg , while the timber frame element weighed around 70 kg. The timber frame element lost 5 litres from Jan 8th to Feb 24th. The CLT elements lost inaverage 1.5 litres in the same period.

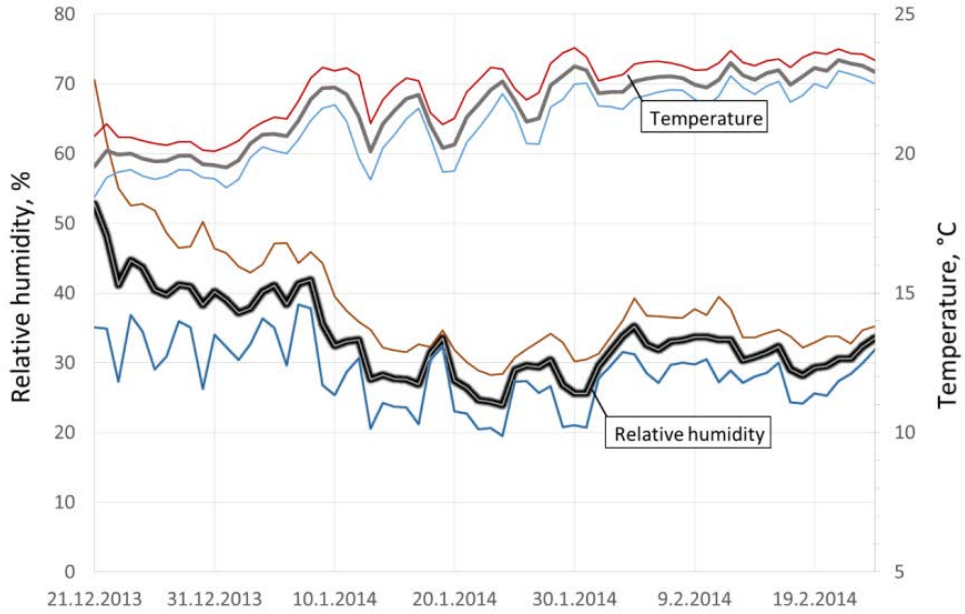

FIG 5. Climate around the test walls given by six temperature and relative humidity sensors and presented as average values with standard deviations.

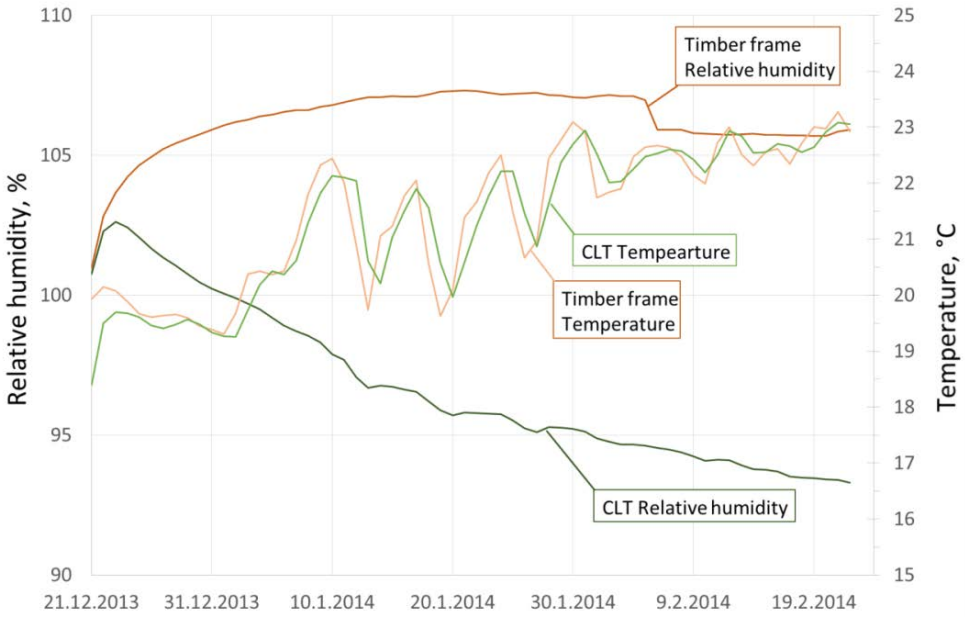

FIG 6. Temperature and relative humidity inside the test elements. The values for the CLT elements are average data from the three elements. The temperature delay for the CLT walls is due to their larger hygrothermal inertia.

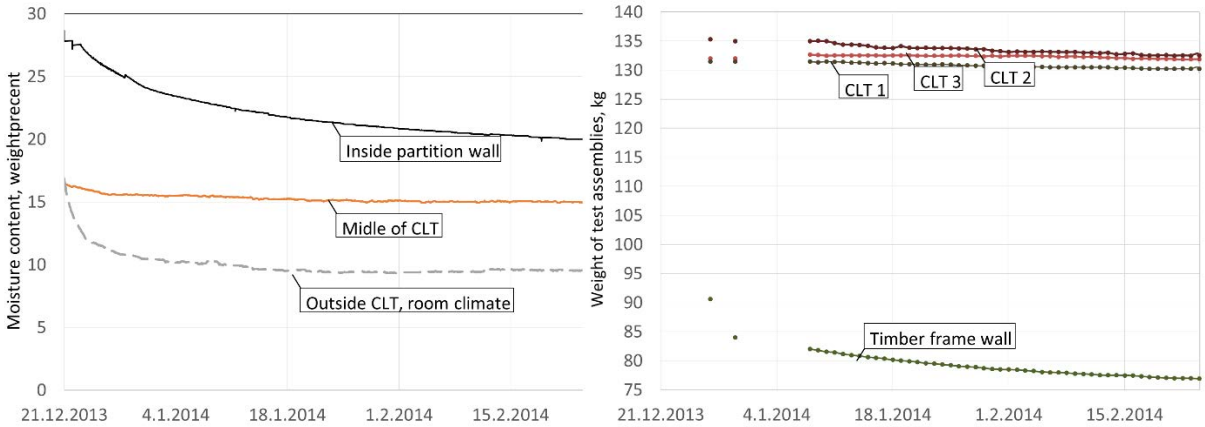

FIG 7a: Wood moisture content in weight percent on the inner surface, in the middle of the CLT elements and on the outer surface. The moisture gradient shows that the elements are drying from the inside towards the outside. b. Development of the weight in all four elements in the drying test. The timber frame wall element had a lower initial weight than the CLT elements, and lost weight at a higher rate.

3.2 Mould growth test

Logging of relative humidity in the test elements showed clearly lower relative humidity inside the CLT elements compared to the timber framed elements. The relative humidity in the timber frame elements was around 100% throughout the test period, while the relative humidity in the CLT elements was 70-80%. The analyses of the test elements dissembled after 1, 2, 3 and 4 weeks of exposure show large differences in mould growth between the timber framed and the CLT elements (Table 1).

The growth of mould fungi was well established in the timber framed elements during the first week of the mould growth test and increased to extensive growth during the second week. The mould growth was mainly found on the gypsum boards, and on the wood surfaces directly attached to the gypsum boards. In the CLT elements mould growth was slow to establish and only reached sparse growth in the fourth and final week of the test period.

Results from air sampling in the test elements in the drying test show after 80 days a large amount of mould spores was found in the timber frame element, 230904 mould spores/m^3. In the CLT elements the number of mould spores was similar to that in the ambient air, counting 108 mould spores/m^3 air.

TABLE 1. Mould growth in the test elements after one, two, three and four weeks.

Element	Mould growth
One week	
Timber framed element	Moderate growth
CLT element	No growth
Two weeks	
Timber framed element	Extensive growth
CLT element	No growth
Three weeks	
Timber framed element	Extensive growth
CLT element	No growth
Four weeks	
Timber framed element	Extensive growth
CLT element	Sparse growth

4. Discussion

Water damages occur in all type of buildings and constructions. The main questions are how to handle such damages and which risk there is for mould growth in various situations. Mattsson & Stensrød (2009) reported that about 50% of controlled water damages were inadequately managed. Greater knowledge of the development of mould growth in different damage situations should make proper damage management easier to obtain.

The results display the influence of hygrothermal inertia. Even after 48 hours of submersion the water did not reach more than centimeters into the CLT as shown in Figure 1. This proves slow water uptake, and the corresponding slow drying is also shown in Figure 6 and 7 a and b. This corresponds to former research like given in Hameury (2006). Regarding water leakages this effect is beneficial. The water is slowly absorbed and dried, not providing free surface moisture. This gives time for renovation. However, it is of great importance never to hinder diffusion drying in wet biological material, including CLT elements. Thus, a risk management procedure in case of water leakage in such structures should be developed.

Our results in this project show that CLT wall constructions dry out more slowly than timber frame walls. Nevertheless, the results regarding mould growth after deliberate contamination show that the risk for mould damages is significantly lower in the CLT construction compared to the more commonly used timber frame wall structure which had established mould damage within one week as expected.

There was no active contamination of the large elements that were soaked for monitoring of the drying process. The air sampling for mould spores showed that a natural contamination occurred in the test elements, even though the test was started in December when there are very few mould spores in the air (Mattsson et al 2014) and only new materials without any previous moisture problems or mould growth were used. This shows that that the mould spores available in the ambient air and tap water are sufficient to cause extensive mould damage, even in winter when spore counts are low. This is also what is found in normal water damages; given a little time, mould growth almost always occurs. The evident occurrence of mould damages in the timber frame wall construction and evident absence of similar damages in the CLT elements also confirms the same pattern as the controlled test with active contamination of mould fungi.

The positive result from the CLT elements regarding mould growth despite a very long exposure time can be explained by the large amount of wood in the CLT. Wood is a highly hygroscopic material with a vast number of available sorption sites, efficiently transporting water molecules from the air into the wooden structure. Thus the water activity at the surface is kept at a low level, and mould spores are unable to germinate (Samson et al 2004). The extensive mould growth in the timber frame elements is probably caused by a combination of two factors: lasting high relative humidity and the presence of gypsum boards. Gypsum boards are extremely susceptible to mould growth, due to a combination of accessible cellulose in the paper and good water retaining properties of the gypsum (Mattsson & Stensrød 2009).

4.1 CLT elements as construction material

We have only tested standard CLT elements. In this type of element water slowly if not at all penetrate between the lamellae in the element, and water uptake takes place mainly at the outer surfaces of the element. Timber elements fastened by wooden plugs, screws or other methods might allow water to penetrate into the element, and water uptake can take place in each lamella. This could give more hospitable conditions for mould fungi. Different insulation materials can be expected to affect the relative humidity inside the partition walls. Further studies should be performed using different massive timber elements and different insulation materials as well as different modes of wetting,

simulating leakages, wetting in the construction process and/or other common sources of water damage.

5. Concluding remarks

The testing of CLT elements compared with standard timber framed wall shows promising results regarding the risk of mould growth after water leakages. Despite a clearly slower drying process in the CLT elements, there was significantly less mould growth. This shows that CLT elements do not increase the risk of mould damages after possible water damages, and even indicates that the risk may be smaller where CLT elements are used. This is important, as mould growth has a negative impact on indoor air quality. However, there is still need to develop proper risk management procedures in case of water damage in CLT constructions. The authors foresee a development of pre-applied drying out slots available for mounting drying equipment in case of water leakage.

6. Acknowledgements

The authors highly acknowledge Innovation Norway who party funded this project and Massiv Lust who provided the CLT.

References

BDS 524.305 2002. Partition walls between row house dwellings. Building Design Sheet. SINTEF Building and infrastructure, Trondheim, Norway *(in Norwegian).*

Finance Norway (FNO). Water damages statistics 2013. http://www.fno.no/Hoved/Statistikk/skadeforsikring/VASK/ Cited January 20th 2014.

Hameury S., 2006. The hygrothermal Inertia of Massive Timber Constructions. Doctoral Thesis. Royal Institute of Technology, Architecture and the Built Enviroment. Stockholm, Sweden.

McClung, V. R. (2013). Field study of Hygrothermal Performance of Cross-Laminated Timber Wall Assemblies with Built-In Moisture. Thesis and dissertation Paper 1059. Ryerson University, USA.

Mattsson J, 2004. Muggsopp i bygninger. Forekomst, påvisning, vurdering og utbedring. Mycoteam, Oslo *(in Norwegian).*

Mattsson J, Grønli I, Whist CM, Ødegaard AT, 2014.Muggsoppsporer i luftprøver. Agarica 2014, vol. 34, 69-76 *(in Norwegian).*

Mattsson J, Magnusen K, 2005. NBI-blad 701.401 Muggsopp i bygninger. SINTEF Byggforsk, Oslo *(in Norwegian).*

Mattsson J, Stensrød O, 2009. Håndbok om vannskader. Årsak, undersøkelser, tiltak og gjenoppbygging. Mycoteam, Oslo *(in Norwegian).*

Nunez M, Sivertsen MS, Mattsson J, 2012. Substrate and construction preferences for Actinomycetes and 20 mould genera. Proceedings in Healthy Buildings 2012, Brisbane. International society of indoor air.

Rayner ADM, Boddy L, 1988. Fungal decomposition of wood: Its biology and ecology. John Wiley & sons, Chichester.

Samson RA, Hoekstra E, Frisvad J, Filtenborg O, 2004. Introduction to food- and airborne fungi. Centraalbuerau voor schimmelcultures, Utrecht.

Retrofitting a brick wall using vacuum insulation panels: measured hygrothermal effect on the existing structure

Pär Johansson, Lic.Tech. [1]
Stig Geving, Professor [2]
Carl-Eric Hagentoft, Professor [1]
Bjørn Petter Jelle, Professor [2, 3]
Egil Rognvik [3]
Angela Sasic Kalagasidis, Assistant Professor [1]
Berit Time, Ph.D. [3]

[1] Chalmers University of Technology, Sweden
[2] Norwegian University of Science and Technology (NTNU), Norway
[3] SINTEF Building and Infrastructure, Norway

KEYWORDS: *listed building, brick wall, interior insulation, vacuum insulation panel, measurement, laboratory, driving rain*

SUMMARY:
Old listed buildings need to be retrofitted to reduce the energy use for heating. Vacuum insulation panels (VIPs) require less thickness than conventional insulation materials to reach the same thermal resistance. The aim of this paper is to investigate the hygrothermal performance of a brick wall with wooden beam ends after it was insulated on the interior with VIPs. The paper presents the first part of a laboratory study where a brick wall was built in the laboratory and exposed to simulated driving rain. Different measurement techniques of the relative humidity in the construction have been used. The relative humidity in the wall increased substantially when exposed to driving rain. The moisture content in the wooden beams also increased. However, it has not been possible to fully determine the influence by the added insulation layer. It is clear that the drying capacity to the interior side is substantially reduced. These investigations are ongoing and will be reported in future publications.

1. Introduction

In Europe, the majority of the future building stock has already been built. The increasing energy prices and the pressure to reduce the energy use in society urge for energy retrofitting measures in the existing building stock (IEA 2013). External walls of old buildings in Sweden and Norway often have a low thermal resistance in comparison to current standards. In Swedish buildings built before 1960, the average U-value of the walls is 0.58 W/(m^2·K) (Boverket 2009) while it is 0.9 W/(m^2·K) for at least 100 000 Norwegian buildings from before 1945 (Thyholt *et al.* 2009). For retrofitted walls the general target U-value is 0.18 W/(m^2·K) in Sweden (Boverket 2011) and 0.22 W/(m^2·K) in Norway (KRD 2010). Many old buildings are considered to be of great historical value and are protected for their external appearance which limits the possible retrofitting measures. Retrofitting on the exterior side of the wall is, in many cases, not allowed so the only possible solution is to add interior insulation. The available additional thickness of the wall is limited by the allowed reduction in rentable internal floor area. Novel highly efficient thermal insulation materials such as vacuum insulation panels (VIPs) increases the thermal resistance of the wall compared to conventional insulation materials with the same thickness. The thermal resistance of a VIP is 5-10 times higher than for conventional insulation materials (Baetens *et al.* 2010), reducing the required thickness to reach a targeted thermal resistance.

VIPs are rigid panels which, unlike most insulation materials, cannot be adapted on the construction site and have to be preordered in the correct dimensions. They are sensitive to damages which could lead to puncturing and a fivefold increase in thermal conductivity. Therefore special care has to be taken in all stages of the construction process to avoid damaged VIPs. Also, thorough hygrothermal investigations are needed to ensure that the relative humidity in the wall is below the critical levels for mold growth and dry rot fungi in wood and freeze thaw damages in brick and mortar.

When retrofitting old buildings, the prerequisites are given by the existing construction. The intermediate floors in old brick buildings are often carried by wooden beams which are embedded in the brick. Mold and dry rot can damage the wooden beams and the risk for that is higher when interior insulation is added because of the higher relative humidity in the wall. Driving rain raises the moisture content in the wall and wooden beam ends, increasing the risk for damages. Also air leakages from the interior into the area around the wooden beam ends can transport moist air from the interior which will raise the moisture content even higher (Kehl *et al.* 2013). Unprotected brick walls may also have freeze-thaw damages. The movement of water through brick masonry has many important consequences in building constructions and it has therefore been studied by a number of authors, e.g. Hall (1977) and Brocken (1998). While the majority of these studies involved water suction experiments from a free water surface, large scale experiments where water suction in brick walls is studied during a real or artificial rain load, such as presented by Abuku *et al.* (2009) and Piaia *et al.* (2013), are rare. To the knowledge of the authors, similar studies for brick masonry are not available.

The aim of this paper is to investigate the hygrothermal performance of a brick wall with wooden beam ends after the wall was insulated on the interior side with VIPs. The brick wall was built in laboratory according to the methods used in the late 19th century to the early 20th century in Sweden and Norway. Wooden beam ends were studied since these are a known risk area when insulating brick walls (Kehl *et al.* 2013; Rasmussen 2010; Ueno 2012). The wall was tested in a large-scale building envelope climate simulator where it was exposed to a temperature gradient and cycling climate with driving rain. In the first sequence, the wall without interior insulation was tested. Before the second sequence VIPs were added to the interior of the wall. A pre-study using the hygrothermal simulation tool WUFI 2D was presented by Johansson *et al.* (2013) where suitable materials, wall layout and testing climate were proposed. The study is part of a research project which is run in cooperation between Chalmers University of Technology in Gothenburg, Sweden, the Norwegian University of Science and Technology (NTNU) and SINTEF Building and Infrastructure, in Trondheim, Norway.

2. Wall layout and material selection

A common wall thickness in brick buildings from the late 19th century is 380 mm which is equal to 1.5 bricks thick walls. The brick walls of multiple floors often have wooden beams inserted around 200 mm into the brickwork to carry the intermediate floors (Kvande & Edvardsen 2013). In the pre-study, Johansson *et al.* (2013) studied three wall thicknesses, 120 mm, 250 mm and 380 mm, to investigate the possibility to decrease the (expensive) testing time by using a thinner wall in the laboratory study. It was found that the moisture accumulation rate was not decreasing linearly with increasing thickness, but had a more exponential relationship. However, the same water flow was found during wetting for the different wall thicknesses. Therefore, the same conclusions could be drawn by using a 250 mm thick brick wall as for using a 380 mm thickness. The schematics of the brick wall built in the laboratory and investigated in this paper are presented in FIG 1.

Two VIP sizes, 20 mm thick, were used in the study, larger 600x1 000 mm and smaller 500x600 mm, as shown in FIG 1. Three types of sensors were installed in the wall to monitor the wetting and drying; 10 relative humidity sensors (E+E Elektronik EE060), 8 Sahlén sensors (wood moisture sensors) and 12 resistance moisture meters (pin-type). The relative humidity sensors measure the relative humidity and temperature in the range of 0-100% and -40-60°C. They were located in the mortar between the bricks, see FIG 2b, together with the Sahlén sensors. These measure the mass percentage moisture in

birch wood inside the sensor which gives a measurement range of 60-100% relative humidity. The size of the relative humidity sensor is 116x12 mm (length, diameter) and the Sahlén sensor is 40x13 mm. The resistance moisture meters were made of two insulated metal pins located 25 mm apart, installed on three different locations in the wooden beams as shown in FIG 1. One sensor was drilled into the center of the beam at the interior surface of the wall (a). Two other sensors were installed 10 mm from the end of the beam, one with insulated pins in the center of the beam (b) and one on the wooden surface (c). The relative humidity sensors were monitored hourly in the first sequence and every 6 minutes in the second sequence by a computerized system. The Sahlén sensors and resistance moisture meters were monitored daily at the start of the climate sequence, and later every 2 days.

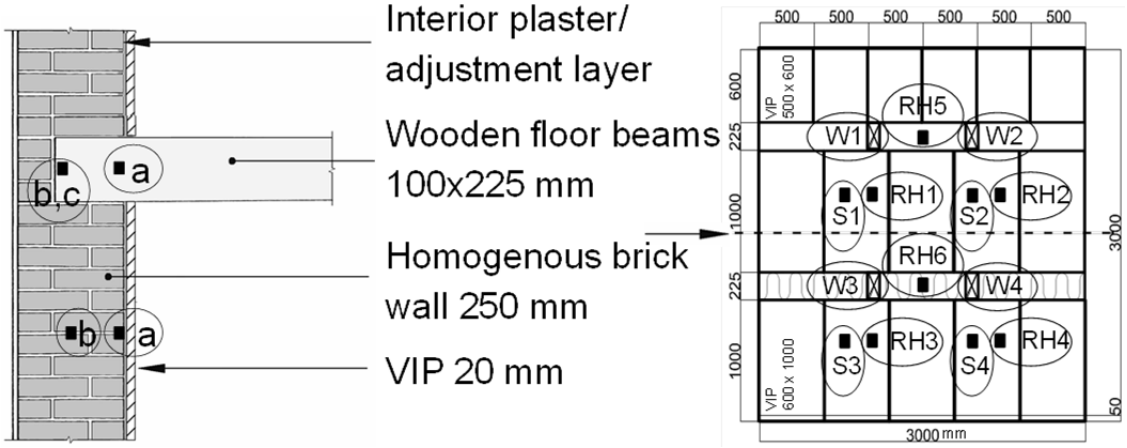

FIG 1. Left: schematics of the brick wall tested in the laboratory. The sensor locations at different depths of the wall are indicated by a, b and c. Right: measurements of the wall with the locations and sizes of the VIPs and sensor positions. RH = RH sensors, S = Sahlén sensors and W = resistance moisture meters. A layer of mineral wool was located around the two lower wooden beams. The horizontal dashed black line, indicated by an arrow, shows the symmetry line of the wall where a rubber strip was installed on the exterior side of the wall to break the water run-off.

The brick wall was built inside a 3x3 m steel frame to allow it to be moved from the laboratory to the climate simulator. The lower part of the frame was filled with 200 mm cellular glass insulation to insulate the lower boundary from the steel frame. The size of the bricks was 226x104x60 mm (length x width x height) and the thickness of the mortar joints between the bricks were 10-12 mm, see FIG 2a. The water accumulation in the upper part of the wall could interfere with the measurement results for the lower part of the wall. Therefore a rubber strip was installed on the exterior side of the wall to stop liquid water from being transported along the wall. Mortar was applied on the entire interior brick surface to make an even surface for attaching the VIPs. Four voids of each 100x225 mm, see FIG 2c, were created where the wooden beams were installed after the wall had dried. The gaps between the brick and wooden beams were sealed with a mix of modelling clay and beeswax. Around the two lower wooden beams, a layer of mineral wool was added to simulate the thermal resistance of the intermediate floor while the space around the two upper beams was left as it was, see FIG 1. A polyethylene foil was wrapped around the beams and over the space between them to simulate the vapor resistance of an intermediate floor, see FIG 2d. In the second sequence of the laboratory study, the interior side of the brick, between the intermediate floors, was covered by VIPs, see FIG 2e.

To resemble the properties of an old brick wall in the laboratory study it was essential to use a brick and mortar similar to what was used in Sweden and Norway in the late 19th century to the early 20th century. The modern brick types are formed by dry-pressing, molding or extruding the clay to form the wanted size and shape (Brick Industry Association 2006), giving other properties to the bricks than what manual production methods does. The liquid water transport coefficient is lower for modern bricks than for the historical bricks which are targeted in this study. The bricks and mortar used in the laboratory study were chosen based on the conclusions from the pre-study by Johansson *et al.* (2013).

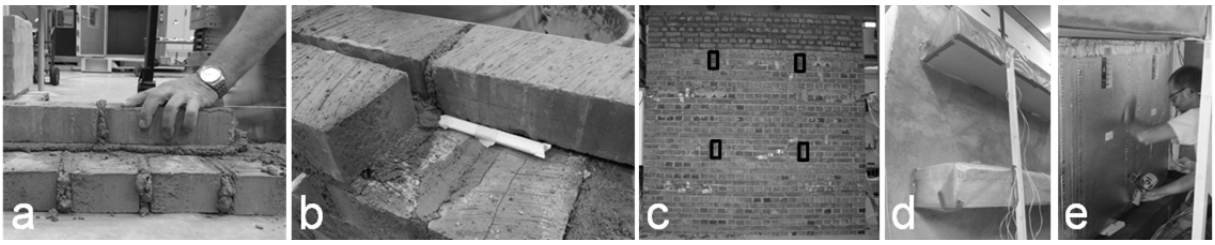

FIG 2. Photos from the construction of the wall in the laboratory. a: brick and mortar laid out, b: relative humidity sensor installed in the mortar in the middle of the wall, c: finished brick wall with the four voids for the wooden beams marked with black rectangles, d: wooden beams installed and wrapped in polyethylene foil, e: installation of the VIPs which were glued to the wall with taped edges.

The mortar type used to bind the bricks together has varied over time. Hydraulic lime mortar was used in the early days but later replaced by cement mortar and finally by mixtures of lime and cement mortar (Kvande & Edvardsen 2013). The liquid water transport coefficient is substantially larger for lime and cement mortars and hydraulic lime mortars than for pure cement mortar. Hydraulic lime mortar requires a longer curing time than a mixture of lime and cement mortar would. It was also expected to be more difficult to fully control the adhesion of the hydraulic lime mortar. Therefore, a lime and cement mortar was chosen which resembles the hygrothermal properties of the historic hydraulic lime mortar and minimizes the curing and adhesion times, allowing for faster construction.

3. Measurements of hygric properties of the brick and mortar

The hygric properties of the brick and mortar were tested in the laboratory of NTNU and SINTEF Building and Infrastructure in Trondheim, Norway. The procedures in the standards NS-EN ISO 15148 and NS-EN 1015-18 were followed using 6 samples each of the brick and mortar. The average values and standard deviations for the brick and mortar are presented in TABLE 1

TABLE 1. Measured hygric properties of the brick and mortar used in the laboratory study. The uncertainties are given as the standard deviation of the mean with a confidence interval of 68.3%.

Material	Density (kg/m^3)	A_w-value ($kg/(m^2 \cdot s^{0.5})$)	Moisture content at 75% RH (wt-%)	Moisture content at saturation (wt-%)
Brick	1 810 ± 30	0.19 ± 0.03	0.046 ± 0.004	13.1 ± 0.6
Mortar	1 670 ± 40	0.0655 ± 0.0004	2.04 ± 0.08	11.7 ± 0.2

The A_w-value is defined in NS-EN ISO 15148 as the short term liquid water absorption coefficient which is a measure of the rate of water absorption by e.g. driving rain on a material. To assess the liquid water transport coefficient, D_{ws} (m^2/s) dependent on the moisture content, w (kg/m^3), there is an approximate relationship between A_w and D_{ws} which is used in WUFI 2D (Fraunhofer IBP 2010):

$$D_{ws}(w) = 3.8 \cdot \left(\frac{A_w}{w_f} \right)^2 \cdot 1000^{\left(\frac{w}{w_f} - 1 \right)} \qquad (1)$$

where A_w short term liquid water absorption coefficient ($kg/(m^2 \cdot s^{0.5})$)
w moisture content (kg/m^3)
w_f moisture content at saturation (kg/m^3)

In order to use Equation (1), the moisture sorption isotherm for the material has to be defined. The approximate equation for the sorption isotherm based on measured data is (Fraunhofer IBP 2010):

$$w(\varphi) = w_f \cdot \frac{(b-1) \cdot \varphi}{b - \varphi} \qquad (2)$$

where w_f moisture content at saturation (kg/m^3)
b fitting parameter (-)
φ relative humidity (-)

The liquid water transport coefficient was calculated using Equation (1), based on the measurement results. The liquid water transport coefficients for the brick used in the laboratory study compared to the data from WUFI 2D (Fraunhofer IBP 2010) at 80% relative humidity (assuming D_{ws} = 0 m^2/s at 0% RH with a linear relation to 80% RH) and at saturation are presented in TABLE 2.

TABLE 2. Liquid water transport coefficient at 80% relative humidity and at saturation for the brick used in this study compared to data from WUFI 2D (Fraunhofer IBP 2010).

	Material	D_{ws} at 80% RH 10^{-9} (m^2/s)	D_{ws} at saturation 10^{-6} (m^2/s)
	Measured brick	2.5	2.4
WUFI 2D	Masonry	1 600	1.7
	Extruded	7.5	70
	Historical	14	300
	Hand-formed	9.5	200
	Vienna 1900s	0.44	17

The liquid water transport coefficient increases with a factor of 1 000 when the moisture content in the brick used here becomes saturated. The relation is similar for the other brick types. “Historical” has the highest liquid water transport coefficient. The brick used in this study has a 100 times lower liquid water transport coefficient which is more in line with the properties of “Masonry” at saturation. The moisture diffusion resistance factor, μ (-), was not measured here but it is around 10-15 for most bricks (Fraunhofer IBP 2010).

The measured properties of the lime and cement mortar was similar to what is found in the WUFI 2D database for mortars of this type. The sorption isotherm was very similar to the sorption isotherm of the brick, but with a maximum moisture content of 195 kg/m^3 compared to 237 kg/m^3 in the brick. The liquid water transport coefficient was $1.5 \cdot 10^{-9}$ at 80% relative humidity and $0.4 \cdot 10^{-6}$ at saturation which is 60% and 18% of the brick. A parametric study of these different properties was performed by Johansson *et al.* (2013) which showed that the capillary active bricks gave a faster wetting of the wall.

4. Climate simulator and climate sequence

To make the results of the laboratory study applicable to the conditions in Gothenburg (Sweden) and Bergen (Norway), the climate sequence was based on the climate in these cities. They are both located close by the sea which means a large portion of driving rain will hit the façades of the buildings. Measurements of the amount of rain during a rain event were used as input. The climate simulator is designed to generate a controlled dynamic climate condition on both sides of the brick wall. On the interior side a constant temperature of 25°C and relative humidity of 40% was chosen.

The temperature and relative humidity was 5°C and 70% on the exterior side in the first sequence. In the second sequence it had to be changed to 10°C and 90% relative humidity because the equipment was overloaded and broke down during the first sequence. The rain period in the first sequence was supposed to be four hours long, but due to equipment malfunction the rain was not turned off in time but first after 14 hours. In the second sequence the rain period was reduced to 30 minutes since the rain intensity and the rate of the capillary suction were much higher than anticipated. The rain amount hitting the wall was 5 mm/hour, i.e. 5 l/(m$^2 \cdot$h). After the wetting sequence, the drying climate was 10°C and 60% on the exterior side and kept at 25°C and 40% on the interior side. After 1 month drying with VIPs on the interior side of the wall, the panels were removed to allow for drying out from both sides of the wall. The climate was then changed to 40°C and 10% relative humidity on both sides.

5. Results of the hygrothermal measurements in the climate simulator

The plans for the measurements in the climate simulator had to be changed during the course of running the experiment. The malfunction during the first climate sequence meant that the wall was saturated after a very short time and also the interior side of the wall was wet. All the relative humidity sensors in the wall showed a relative humidity of 100% within less than 36 hours. The temperature could not be kept constant during this sequence so the temperature in the wall varied between 8.2°C and 21.2°C which makes an evaluation of the moisture measurement results complicated.

During the second sequence, the equipment worked more in line with the expectations. The temperature was kept constantly around 10°C on the exterior side of the wall which gave a temperature between 9.4°C and 11.2°C in the middle of the wall. The measurements of the relative humidity in the wall during the second climate sequence are presented in FIG 3.

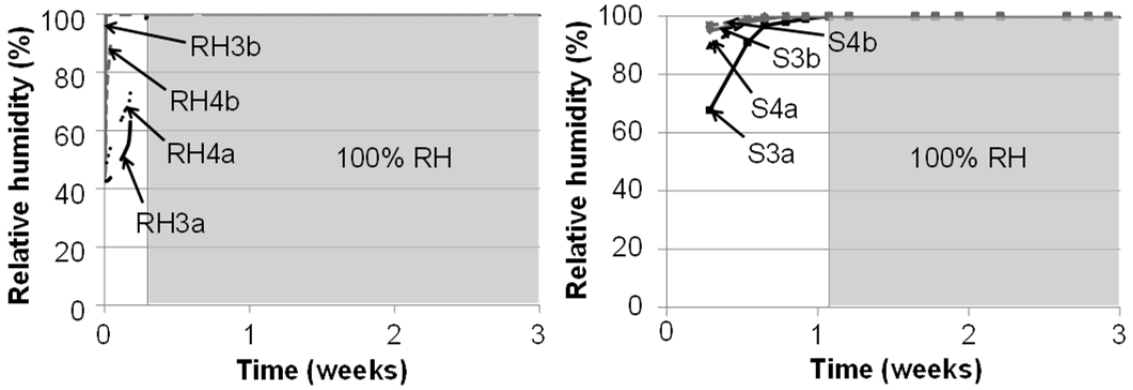

FIG 3. Relative humidity in the wall. Left: relative humidity measured with the relative humidity sensors. Right: relative humidity measured with the Sahlén sensors translated from the wood moisture content by using the sorption isotherm for birch wood. The sensors are located in the mortar in the middle of the wall (RH3b, RH4b, S3b, S4b) and in the mortar in the inner part of the brick wall (RH3a, RH4a, S3a, S4a). The Sahlén sensor only measures relative humidity above 60%.

It is clear that the moisture sensors in the middle of the wall are reached by the moisture faster than the sensors in the inner part of the brick wall. The Sahlén sensors show a significantly slower increase in relative humidity in the wall since the sensors uses a wooden material that has to absorb the moisture before the sensor can register the increasing moisture content. Also here, the relative humidity increases slower in the inner part of the brick wall in the first few days, but is then equal as in the middle of the wall. The relative humidity in the four wooden beams is shown in FIG 4.

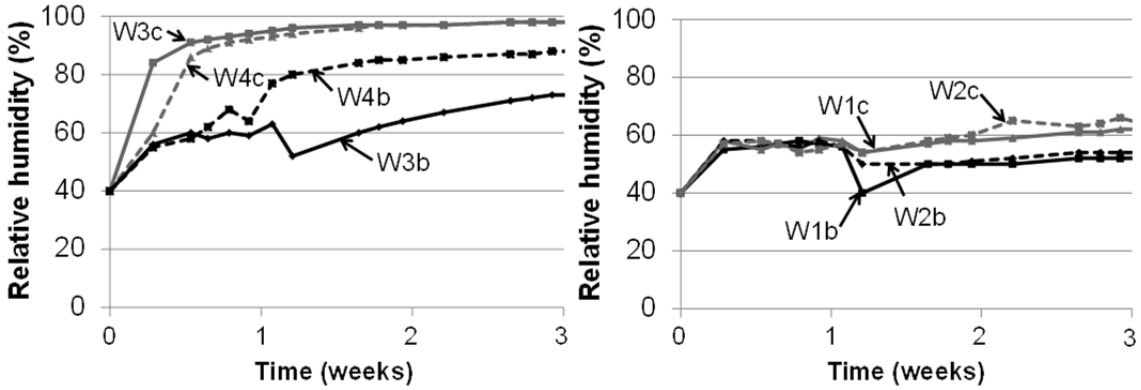

FIG 4. Relative humidity in the beams translated from the wood moisture content by using the sorption isotherm for spruce, in the middle of the beam end (b) and at the surface of the beam end (c). Left: lower beams (with mineral wool). Right: upper beams (without mineral wool).

There is a large difference between the relative humidity in the beams in the upper and lower part of the wall. This difference may partly be caused by the mineral wool insulation which is placed around the two lower beams, but not around the upper ones. The higher temperature in the wall results in a lower relative humidity, but this effect cannot explain the large difference on its own. The relative humidity sensors and Sahlén sensors in the upper part of the wall also showed a significantly lower relative humidity than what is shown for the lower part in FIG 3. The reason for this behavior is not clear. Part of it might be caused by the force of gravity on the liquid water flow.

6. Conclusions

A laboratory study with a brick wall built in the laboratory and exposed to simulated driving rain in a large-scale building envelope climate simulator was conducted. The relative humidity in the wall increased substantially when exposed to driving rain. As expected from the simulations in the pre-study, the moisture increased faster in the mortar in the middle of the wall compared to in the inner part. The brick and mortar was more capillary active than expected. The lower part of the wall had a higher relative humidity which could be caused by the force of gravity, acting on the liquid water flow. The different sensors gave consistent results, although the Sahlén sensor is more appropriate to be used in measurements where the relative humidity is expected to change slower than what was the case in this study. In the wooden beams, the moisture content increased more in the end of the beam than close to the interior brick surface. Due to equipment malfunction, data from important measurement periods are missing, making it difficult to draw conclusions from the first sequence of the laboratory investigations. In the next phase of this project, a wall without VIPs will again be tested and compared to the wall with VIPs. The simulations will be compared to hygrothermal simulations.

7. Acknowledgements

The work is supported by The Swedish Research Council Formas, the Lars Hierta Memorial Foundation, and finally the Research Council of Norway and several partners through The Research Centre on Zero Emission Buildings (www.ZEB.no). Porextherm Dämmstoffe GmbH is acknowledged for supplying the vacuum insulation panels and Wienerberger and St-Gobain Weber are acknowledged for supplying the brick and mortar.

References

Abuku, M., Blocken, B., & Roels, S. 2009. Moisture response of building facades to wind-driven rain: field measurements compared with numerical simulations. Journal of Wind Engineering and Industrial Aerodynamics, 97(5-6), 197-207.

Baetens, R., Jelle, B. P., Thue, J. V., Tenpierik, M. J., Grynning, S., Uvsløkk, S., & Gustavsen, A. 2010. Vacuum insulation panels for building applications: A review and beyond. Energy and Buildings, 42(2), 147-172.

Boverket. 2009. Så mår våra hus - redovisning av regeringsuppdrag beträffande byggnaders tekniska utformning m.m. (The state of our buildings - report of governmental mission on the technical design of buildings etc.). [In Swedish]. Karlskrona, Sweden: Boverket.

Boverket. 2011. Regelsamling för byggande, BBR 2012 (Regulations for construction, BBR 2012). [In Swedish]. Karlskrona, Sweden: Boverket.

Brick Industry Association. 2006. Manufactoring of Brick. Reston, Virginia, USA: The Brick Industry Association.

Brocken, H. J. P. 1998. Moisture Transport in Brick Masonry: The Grey Area Between Bricks (Dissertation). Eindhoven, The Netherlands: Eindhoven University of Technology, Faculty of Architecture, Building and Planning, and Faculty of Applied Physics.

Fraunhofer IBP. (2010). WUFI 2D Transient Heat and Moisture Transport (Version 3.3.2) [Computer Program]. Holzkirchen, Germany: Fraunhofer IBP.

Hall, C. 1977. Water movement in porous building materials - I. Unsaturated flow theory and its applications. Building and Environment, 12(2), 117-125.

IEA. 2013. Policy Pathway: Modernising Building Energy Codes. Paris, France: OECD/IEA and New York, NY, USA: United Nations Development Programme (UNDP).

Johansson, P., Time, B., Geving, S., Jelle, B. P., Sasic Kalagasidis, A., Hagentoft, C.-E., & Rognvik, E. 2013. Interior insulation retrofit of a brick wall using vacuum insulation panels: design of a laboratory study to determine the hygrothermal effect on existing structure and wooden beam ends. Proceedings of the 12th International Conference on Thermal Performance of the Exterior Envelopes of Whole Buildings, Clearwater Beach, Florida, USA, December 1-5, 2013.

Kehl, D., Ruisinger, U., Plagge, R., & Grunewald, J. 2013. Wooden beam ends in masonry with interior insulation - A literature review and simulation on causes and assessment of decay. Proceedings of the 2nd Central European Symposium on Building Physics, Vienna, Austria, September 9-11, 2013.

KRD. 2010. Byggteknisk forskrift (TEK 10). FOR-2010-03-26-489 Forskrift om tekniske krav til byggverk (Building Code. Regulations on technical requirements for construction). [In Norwegian]. Oslo, Norway: Kommunal- og regionaldepartementet, Bolig- og bygningsavd.

Kvande, T., & Edvardsen, K. I. 2013. Eldre yttervegger av mur og betong. Metoder og materialer (Older exterior brick and concrete walls. Methods and materials). [In Norwegian]. Oslo, Norway: SINTEF Building and Infrastructure.

Piaia, J. C. Z., Cheriaf, M., Rocha, J. C., & Mustelier, N. L. 2013. Measurements of water penetration and leakage in masonry wall: Experimental results and numerical simulation. Building and Environment, 61, 18-26.

Rasmussen, T. V. 2010. Post-Insulation of Existing Buildings Constructed Between 1850 and 1920. Proceedings of the 11th International Conference on Thermal Performance of the Exterior Envelopes of Whole Buildings, Clearwater Beach, Florida, USA, December 5-9, 2010.

NS-EN 1015-18:2002. Methods of test for mortar for masonry - Part 18: Determination of water absorption coefficient due to capillary action of hardened mortar. Brussels, Belgium: European Committee for Standardization (CEN).

NS-EN ISO 15148:2002. Hygrothermal performance of building materials and products - Determination of water absorption coefficient by partial immersion. Geneva, Switzerland: International Organization for Standardization (ISO).

Thyholt, M., Pettersen, T. D., Haavik, T., & Wachenfeldt, B. J. 2009. Energy Analysis of the Norwegian Dwelling Stock. Subtask A - Internal working document. IEA SHC Task 37 Advanced Housing Renovation by Solar and Conservation: International Energy Agency, Solar Heating and Cooling Programme.

Ueno, K. 2012. Masonry Wall Interior Insulation Retrofit Embedded Beam Simulations. Proceedings of the Building Enclosure Science & Technology Conference, BEST 3: High Performance Buildings - Combining Field Experience with Innovation, Atlanta, GA, USA, April 2-4, 2012.

Energy savings in the Danish building stock until 2050

Kim B. Wittchen, Senior scientist, M.Sc., Civ. Eng. [1]
Jesper Kragh, Senior scientist, M.Sc., Civ. Eng. [1]

[1] Danish Building Research Institute, Aalborg University, Denmark

KEYWORDS: *Renovation, Existing buildings, Energy savings, Regulation compliance, Energy projection*

SUMMARY: (Style: Summary Heading)
A study has been conducted analysing the energy savings for space heating and domestic hot water in the Danish building stock due to renovation of building components at the end of their service life. The purpose of the study was to estimate the energy savings until 2050 as building components are energy upgraded according to the requirements stipulated in the Danish Building Regulations 2010. Furthermore, scenario analyses was made for the potential impact on the energy consumption of introducing different levels of tightening of the energy requirements for existing buildings in the Danish Building Regulations.

Compliance with the requirements in the Danish Building Regulations will potentially result in energy savings for space heating and domestic hot water around 30 % until 2050. Further tightening of the component insulation level requirements will only result in marginally higher savings, due to the level of the current requirements. Higher energy savings can, though, be achieved e.g. by setting requirements for balanced mechanical ventilation with heat recovery and use of solar heating for domestic hot water.

1. Introduction

As something relatively new, requirements for the minimum insulation level of building components have been introduced in the Danish Building Regulations 2010 (BR10) to be applied when the building components are being renovated, e.g. replacement of roof covering. However, it is a question how much these requirements will influence the energy consumption in the existing Danish building stock in 2050. Furthermore, the impact of further tightening of the requirements needs to be investigated.

A calculation model for the net heating consumption in the entire existing Danish building stock until 2050 have been established in order to investigate the consequences of continuing with the current requirements and the effect of introducing stricter rules.

The purpose of the analyses was to clarify the energy savings until 2050 if the building components are being upgraded according to the requirements stipulated in the Danish Building Regulation 2010. Upgrading is assumed to be introduced when the building components need renovation anyway due to the building materials used having reached the end of their service life. Additionally, the analyses were targeted at an investigation of the effect of introducing stricter requirements for the energy upgrading of building components in combination with planned refurbishment.

Assumptions of when building components are going to be replaced originate from the Danish building and dwelling stock register (BBR) which holds information about the building materials used in facades and roofs. This information combined with knowledge about the age of the building and estimates for the probable service life of different building materials gives an

estimate of the replacement rate and hence the rate of energy upgrading of the existing building stock.

2. Background

In the Danish Building Regulations 2010 there are ultimate minimum energy requirements that must be followed when replacing windows. For roofs, external walls etc. there are requirements that must be met if it is economically, architecturally and technically feasible to meet them as part of a retrofitting process. The examples in Table 1 are specifically listed in BR10 as normally being economically feasible.

Table 1. Examples, mentioned in the Danish Building Regulation 2010, BR10, as "often being economically feasible".

Building component	Insulation thickness that is economically feasible to upgrade [mm]	Total insulation thickness after upgrading [mm]
Accessible attic	< 175	300
Sloping walls and ceiling to ridge	< 200	300
Space under the roof slope	< 175	300
Flat roof	< 200	250
Lightweight external wall	< 150	250
Cavity masonry wall	Uninsulated	Cavity wall insulation
Massive external wall in brickwork	-	200
External wall in lightweight concrete	< 50	150
Floor structure above unheated basement	-	Insulation between beams
Floor above unheated basement	< 50	100
Floor above accessible crawl space	< 150	250
Floor above free space	< 175	300
Slab on ground	Uninsulated	250

In the analyses, the above values imply that an accessible attic is insulated if the total U-value of the roof construction is above 0.20 W/m²K, and that it will have a U-value of 0.15 W/m²K after upgrading.

BR10 also set rules for the replacement of windows, and here new windows must have an annual average energy balance of no less than -33 kWh/m² per year calculated for a standard window regarding size, configuration and average orientation. This requirement will become stricter in 2015 when the energy balance should be at least -17 kWh/m² per year, and even stricter in 2020 where the energy balance should be at least 0 kWh/m² per year. The table below shows an overview of the energy requirements for building components that should be complied with in combination with renovation and extensions of existing buildings. Compliance is mandatory unless it is not economically, architecturally or technically feasible to comply with the level of the requirements. In these cases, the building components should be insulated up to the feasible level.

Table 2. Requirements to building components in combination with renovation and extensions of existing buildings as stated in the Danish Building Regulations 2010.

Building component	W/m²K
External walls and basement walls towards the ground	0.2
Internal walls and floors towards unheated rooms or rooms heated to a temperature more than 5 K lower than the current room	0.4
Slab on ground, basement floors towards ground and floors above outdoor spaces or ventilated crawl spaces	0.12
Ceiling and roof constructions, including walls towards spaces under the roof, flat roofs and sloping walls directly towards the roof	0.15
External doors, gateways, hatches, removable windows and dome lights[1)]	1.65
Windows	**kWh/m² per year**
In facades[2)]	-33
In roofs[2)]	-10

1) When replacing windows after 1 January 2015, the U-value (incl. frame) should not exceed 1.40 W/m²K.
2) When replacing windows after 1 January 2015, the energy balance over the heating season should not be lower than -17 kWh/m² per year and for roof windows not lower than 0 kWh/ m² per year. When replacing windows after 1 January 2020, the energy balance for facade windows should not be lower than 0 kWh/m² per year.

3. Method and assumptions

The purpose of the analyses was to estimate the energy savings to be expected until 2050 if buildings and building components are being upgraded according to the requirements laid down the in the Danish Building Regulations 2010, when they have to be replaced or renovated for other reasons.

A model of the energy consumption in the existing Danish building stock was set up, based on information extracted from the database of the Danish energy performance certification scheme (EMO) and extrapolated to cover all Danish buildings using data from the Danish building and dwelling stock register (BBR). The model compares the calculated energy consumption of the building stock according to registrations made by energy certification experts with the theoretical energy consumption in the same buildings after energy upgrading. Energy flows included in the model are: space heating energy, ventilation, and domestic hot water. The calculated energy consumption for the building stock "as-is" was compared with the 2011 energy statistics by the Danish Energy Agency (Energy statistics, 2011) and showed a discrepancy of 6 % in comparable building categories.

Potential energy savings from improvements of the technical installations in the buildings are thus not part of the analyses.

Often, there will be architectural considerations in combination with external insulation of external walls made of masonry, which is the predominant building material for external walls in Denmark. This, in combination with the long service life of this kind of external walls, sets limits for the share of masonry external walls that are expected to have external insulation. For older blocks of flats in major cities constructed before 1950, there is a potential for external insulation of the walls on the back of the buildings without violating the architectural impression of the street view. The amount of this area is difficult to estimate from the available information. For other types of materials used in external walls, e.g. concrete and lightweight facades, there will normally not be the same architectural constraints against adding external insulation. It is thus assumed that 0.5 % of the masonry walls are being energy upgraded every year until 2050.

The share of energy upgrades of slabs on ground is evaluated to be modest and normally related to establishing floor heating, e.g. in bathrooms. In contrast to this, floors above basements and

accessible crawl spaces are expected to be subject to energy upgrading. It is not possible to identify a certain point in the lifetime of a building when these floors will be upgraded. Therefore, it was estimated that 15 % of the floors above basements and accessible crawl spaces will be upgraded up to 2050.

3.1 Energy upgrading

The material used as roof covering is registered in the BBR. From knowledge about the year of construction and average service life of different building materials (GI, 2013), the future replacement rate of roofs are estimated and used to calculate the upgraded energy performance of the existing building stock. Roof covering of older buildings is expected already to have been replaced, but not necessarily energy upgraded, one or more times since the building was constructed. The share of these roofs that are being replaced every year is estimated to be 1 divided by the average service life of the roofing material. Similar assumptions are made for the other building components.

The insulation level for the existing building stock is based on registrations made by building experts in the building energy certification scheme. The average insulation levels were calculated for different typical construction periods and building types as area-weighted U-values.

3.1.1 Ventilation systems and solar thermal systems

Establishing balanced mechanical ventilation systems with heat recovery will have a growing relative impact as the insulation level of the buildings increases. It is therefore expected that these systems will increase in numbers over time. The effect of heat recovery was calculated by introducing an average efficiency in combination with an estimated airchange rate. It is further assumed that airtightness of the renovated buildings are being dealt with in combination with replacement of windows and external doors.

As a starting point, mechanical ventilation is not anticipated in combination with ordinary renovation works as it is not mandatory according to BR10. The effect of this measure was evaluated in a special scenario where mechanical ventilation with heat recovery was assumed to be installed in combination with replacement of roof covering of buildings with sloping roofs. The same consideration is valid for the installation of solar thermal systems for covering of a share of the energy consumption for domestic hot water.

3.2 Energy model for the existing building stock

The Danish building stock is divided into different types of buildings and furthermore into different typical age classes. Within each type and age class, the original buildings' energy performance is assumed to be more or less uniform. Based on statistical data from the EMO scheme regarding the current insulation levels and areas per unit for each of the buildings components (facades, roofs, floors, windows and doors), it is possible to create a model for each type and period, e.g. single family houses constructed between 1961 and 1972. From the calculated average energy consumption in each type and age class, it is possible to extrapolate to the consumption of the entire Danish building stock. The results of these calculations were then compared with and tuned according to the energy consumption in the same groups in the Danish Energy Agency's energy statistics (Energy statistics, 2011).

The model for the energy consumption in each class includes heat losses through the thermal envelope, ventilation losses and energy used for domestic hot water. On the gains side, loads from persons, appliances and sun through windows are included. A degree-day method was used to calculate the energy consumption in the existing building stock and for calculation of energy savings in combination with planned building refurbishment.

3.3 Service life for building materials

The service life for building components is base for the expected life time for the various building materials used for external constructions. The expected life times for building materials is extracted from GI (2013) and Larsen (1992). The life time for a material depends on many factors like roof covering, roof boarding and exposure. The average material life times are shown in the table below.

Table 3. Estimated average life times for external building materials used in the analyses.

Roof covering	Life time [years
Flat roofs	35
Asphalt board (sloping roofs)	35
Fibre concrete, incl. asbestos tiles and slates	40
Cement tiles	60
Roof tiles	60
External wall covering	
Bricks (clay, lime-sand stone, cement stone)	75
Lightweight concrete (light blocks, porous concrete)	60
Sheets of fibre cement, incl. asbestos	45
Wooden boards	40
Concrete components	40
Windows	25

For new windows, especially those made of plastic or combined wood/metal, the life time of the frame can be longer, but in this analysis it is not of major importance for the energy savings by 2050.

The figure below indicates the works associated with energy upgrading of roof insulation by 2050. The drop in activity after 2044 is due to the fact that some roof coverings are changed twice during the period and only the first replacement results in energy upgrading. Under this assumption, 81 % of the total roof area will be thermally upgraded by 2050.

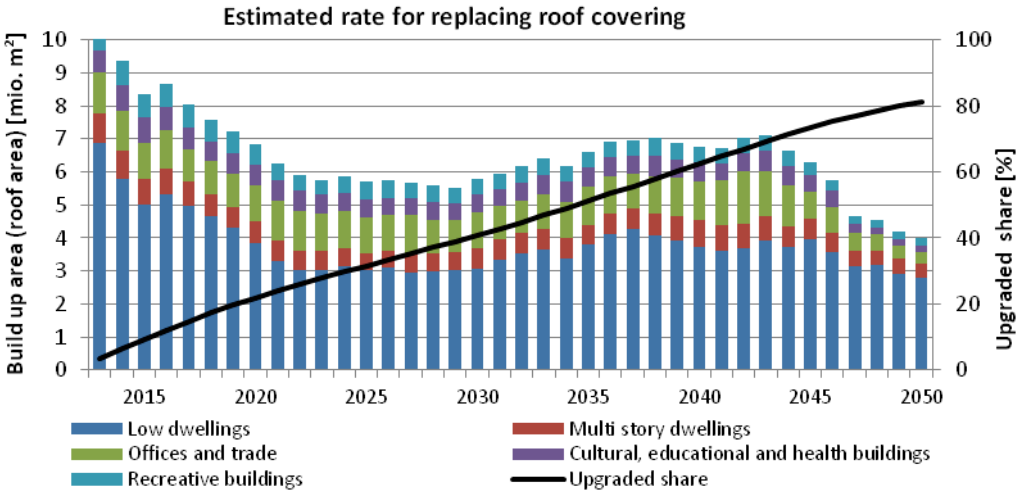

FIG 1. Estimated development in roof covering replacements that lead to energy upgrading of the roofs on the existing buildings. Over the period 82 % of the roofs are estimated to be replaced and consequently energy upgraded.

Over the period leading up to 2050, all windows are estimated to be replaced and 18 % of the external walls to be thermally upgraded. The low ratio of upgraded external walls is due to the long lifetime of the dominant masonry wall and because of architectural constraints for changing the appearance of these kinds of walls. A fixed share of 0.5 % of the available area of external masonry walls is assumed to be upgraded every year, and this dominates the total refurbishment works on external walls.

4. Calculation results

The table below shows results from 11 different scenarios. The scenarios set out to investigate the effects of different suggestions for more strict requirements to building components and other initiatives to increase energy savings in the existing building stock by 2050 and compare this with what happens if rules will remain at the same level as the current requirements. Furthermore, one scenario analysed the consequence of a prolonged service life of the roofing materials.

In the business-as-usual scenario A0, only 80 % of the potential area is assumed to be upgraded due to architectural or technical constraints. The A scenarios analyses different levels of implementing building energy upgrading by 2050. The B scenarios analyse different tightening of the component requirements in the Danish Building Regulations.

Table 4. Calculated net heating energy consumption by 2050 in each of the different scenarios.

Scenario		Energy consumption in 2050 TJ/year	Energy savings compared with today %	Energy savings compared with scenario A0 %-point
	Status 2011	206 178	-	-
A0	Business-as-usual	148 978	27.7 %	-
A1	Full BR compliance	141 446	31.4 %	3.7 %
A2	90 % BR compliance	145 212	29.6 %	1.8 %
A3	Longer life of roofs [1)]	156 072	24.3 %	-3.4 %
A4	All roofs insulated before 2050	145 943	29.2%	1.5%
A5	Fast implementation of A windows [2)]	148 978	27.7 %	0.0 %
B1	More tight requirements for roofs + A2	144 075	30.1 %	2.4 %
B2	More tight requirements for external walls + A2	143 445	30.4 %	2.7 %
B3	More tight component requirements + A2	142 308	31.0 %	3.2 %
B4	Extra tight requirements for roofs + A2	143 318	30.5 %	2.7 %
B5	Extra tight requirements for external walls + A2	141 839	31.2 %	3.5 %
B6	Requirements for A+ windows + A2	140 067	32.1 %	4.3 %
B7	Automation and effectiveness + A2	141 683	31.3 %	3.5 %
B8	Extra tight component requirements = B4+B5+B6	134 799	34.6 %	6.9 %
B9	More tight component requirements and A+ windows = B1+B2+B6	137 163	33.5 %	5.7 %
B10	Automation and effectiveness + B9	133 695	35.2 %	7.4 %
C1	BMV with VGV + B10	109 342	47.0 %	19.2 %

Faster implementation of stricter requirements when replacing windows (Scenario A5) will not result in lower energy consumption by 2050, unless new window types are invented. The reason

for this is the short lifetime of windows that ensures that all windows have been upgraded to comply with the 2020 requirements before 2050 even for windows replaced in 2019.

The general insulation level of existing Danish buldings is rather high, and only a limited number of the traditional energy-saving measuers are thus economically feasible. To be able to meet the government's target that Denmark is to become free of fossil fuels by 2050 while for heating of buildings by 2035, more rigid requirements need to be considered. Among those are requirements for implementing balanced mechanical ventilation with heat recovery in residential buildings with a sloping roof (enough free space in the attic to install the ventilation system) in combination with roof retrofit (Scenario C1).

The estimated service life of roof covering materials can be questioned and a special scenario have thus been made to analyse the effects of a longer service life of these materials. A 25 % extension of the service life for roofs (Scenario A3) only results in a decrease of the retrofitted area of about 5 %, which only has a marginal influence on energy savings by 2050. Furthermore, there is a hump of roofs on buildings constructed in the 1970s, which even with a 25 % prolonged service life will need to be replaced before 2050.

The next figure shows the development of energy use for space heating, ventilation and domestic hot water in each scenario. It is clear that installation of balanced mechanical ventilation with heat recovery in combination with renovation of sloping roofs will have a significant effect on the energy consumption by 2050. This is not surprising as only a marginal share of the existing building stock has been equipped with this kind of systems yet. To be able to save this amount of energy, it is however a pre-condition that airtightness of the buildings have been improved at the same time, e.g. in combination with replacement of windows.

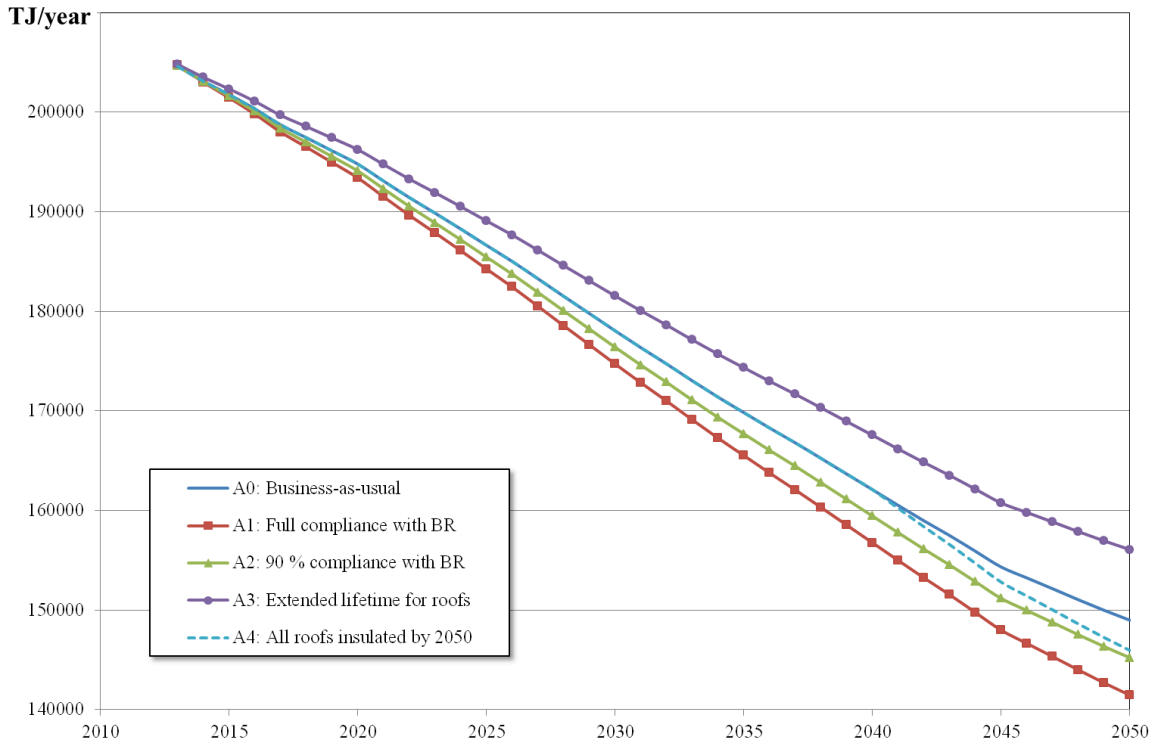

FIG 2. Development in net energy consumption for space heating, ventilation and domestic hot water in the existing Danish building stock as analysed in the A Scenarios. Energy saving measures are assumed to be implemented at the same rate as the building components are being retrofitted due to the end of their service life.

Generally, all curves bend around 2037 and that is the time when all windows have been upgraded at least once during the period, and no further energy savings can be expected from window upgrading – except if further technical improvements of window technology are implemented and requirements in the Danish Building Regulations are being tightened further.

5. Conclusions

It is the aim of the Danish government that Denmark should be free of fossil fuels by 2050 while for heating buildings this should happen in 2035. To be able to reach that goal, it is estimated that the energy consumption in the existing building stock should be reduced by about 60-70 %. Following the current path, with energy upgrading of building components in compliance with the requirements in the Danish Building Regulations 2010 (BR10) when retrofitting the buildings due to termination of service life for the building components, will not result in enough energy savings (about 30 % of the 2011 national energy use in buildings) to reach that goal.

To be able to come closer to that goal there is a need for more strict requirements in combination with refurbishment works and also improvements of the energy performance of windows. It is possible to get more energy efficient windows with an annual energy balance value of +15 kWh/m² per year for facade windows. Introduction of mechanical ventilation with heat recovery can also contribute to fulfilment of the goal.

The analyses have not taken into account demolishing of existing buildings and replacement with new buildings by 2050. Historically, about 1 % of the Danish building stock is replaced every year. If this trend continues over the next 30 years, about one third of the buildings will be newly built by 2050 and have a significant lower energy need.

6. Acknowledgements

The work has been funded as part of the Danish Energy Agency's activities for establishing a national strategy for energy upgrading of the existing building stock.

7. References

Energy statistics 2011, Danish Energy Agency, 2011. Available at: www.ens.dk.

Larsen, E. S. 1992. Service life of concrete constructions (In Danish: Betonkonstruktioners levetid). SBi report 225. Danish Building Research Institute, Hørsholm, Denmark.

GI: Danish Building Owners Investment Fund (GI: Grundejernes Investeringsfond), 2013. www.levetider.dk

Danish Building Regulations 2010 (December 2010). The Danish Ministry of Economic and Business Affairs, Copenhagen, 2010. Available at: http://bygningsreglementet.dk/link/42549/link

Wittchen K.B., Kragh J. and Aggerholm S. (March, 2014). Potential heating energy savings in the Danish building stock until 2050. (In Danish: Potentielle varmebesparelser ved løbende bygningsrenovering frem til 2050). SBi-2014-01. Danish Buildings Research Institute, Aalborg University, Copenhagen, Denmark.

User behaviour impact on energy savings potential

Jørgen Rose, MSc. Civ. Eng., Ph.D[1]

[1] Danish Building Research Institute, Aalborg University, Denmark

KEYWORDS: *User behaviour, energy upgrading, energy savings potential, indoor temperature, internal heat gain, domestic hot water consumption, air change rate*

SUMMARY: (Style: Summary Heading)
When buildings are to undergo energy upgrading in Denmark, the national compliance checker, Be10, is often used to calculate expected energy savings for different energy-saving measures. The Be10 calculation is, however, very dependent on a variety of standard assumptions concerning the building and the residents' behaviour and if these defaults do not reflect actual circumstances, it can result in non-realisation of expected energy savings. Furthermore, a risk also exists that residents' behaviour change after the energy upgrading, e.g. to obtain improved comfort than what was possible before the upgrading and this could lead to further discrepancies between the calculated and the actual energy savings. This paper presents an analysis on how residents' behaviour and the use of standard assumptions may influence expected energy savings. The analysis is performed on two typical single-family houses corresponding to different levels of energy consumption. The purpose of the analysis is to identify the importance of each of the four primary user-related parameters in terms of their relative and combined impact on the overall energy needs before/after upgrading; 1) Indoor temperature, 2) Internal heat gain, 3) Domestic hot water consumption and 4) Air change rate. Based on the analysis, a methodology is established that can be used to make more realistic and accurate predictions of expected energy savings associated with energy upgrading taking into account user behaviour.

1. Introduction

User behaviour plays an important role for a building's energy consumption and in connection with energy upgrading of existing buildings, user behaviour may lead to non-realisation of expected energy savings. Most often failure to achieve energy savings occur because users gain the possibility and focuses on increased comfort instead, e.g. through a slight increase in temperature or air change rate.

User behaviour influence on energy consumption in buildings has been dealt with in numerous articles and reports and is not a new topic, e.g. (Lundström, 1986). A state-of-the-art review on occupants influence on the energy consumption in buildings was performed by Larsen et al (2010).

This analysis was performed as part of the Danish Energy Agency "Network for Energy Renovation" aiming to support the establishing of future energy-policies in Denmark.

The purpose of the analysis is to identify the importance of four primary user-related parameters in terms of their relative and combined impact on the overall energy consumption before/after the energy upgrading:

1. Indoor temperature
2. Internal heat gain
3. Domestic hot water consumption
4. Air change rate

Based on the analysis, a methodology is established that can be used to make more realistic and accurate predictions of expected energy savings associated with energy renovation taking into account

user behaviour. The purpose is to develop a method which provides an energy calculation, based on a specific combination of parameters corresponding to a specific family in a specific building.

Furthermore, the purpose of the analysis is to provide an overview of how user behaviour affects the expected energy savings in buildings, and thus try to establish a method for determining the expected energy savings, taking into account user behaviour.

2. Method

The analysis is performed using 2 buildings representing typical single-family houses from 2 different periods; the 1930s and the 1960s. The following gives a brief description of the 2 buildings.

2.1 1930s

The house is a typical bungalow from 1932 with a gross heated area of 103 m^2. The building has a full, unheated basement less than half below ground level with a gross area of 103 m^2. The total window area on the ground floor is 16% of the floor area. The total glass area on the ground floor is 12.0 m^2.

FIG 1. Typical single-family house from 1930s.

2.1.1 U-values for building constructions

The U-values are summarised in Table 1. Note that windows are assumed to have been changed during the 1960s, and now correspond to traditional double-glazed windows.

TABLE 1. U-values for building constructions

Building construction	U-value [W/m^2K]
Floor separation	1.02
Exterior wall, mean	1.45
Ceiling	0.55
Windows	2.70
Basement wall	1.24
Basement floor	0.40

2.1.2 Heating and ventilation

The house has an old oil boiler in the basement connected to a 2-pipe heating system. All pipes are insulated with 10 mm insulation. The hot water tank holds 200 l with 30 mm insulation.

The building has natural ventilation and can be categorised as leaky, which means that the total air change rate in the house is set at 0.45 l/s per m^2.

2.1.3 Calculated energy consumption

Calculation of energy consumption is based on the Danish compliance checker, Be10 (Aggerholm and Grau, 2012). The calculation covers energy consumption for heating, cooling, ventilation and domestic hot water. The 1930s house has a calculated energy consumption of 417 kWh/m^2 per year.

2.2 1960s

The house is a typical single-family house from the 1960s with a gross heated area of 108 m^2. The house consists of lounge, kitchen/dining area, utility room/bathroom, hall, toilet and 3 bedrooms. The total window area is 22% of the floor area. The total glass area is 19.9 m^2.

FIG 2. Typical single-family house from 1960s.

2.2.1 U-values for building constructions

The U-values are summarised in Table 1.

TABLE 2. U-values for building constructions

Building construction	U-value [W/m^2K]
Exterior wall, heavy	0.46
Exterior wall, light	0.49
Ceiling	0.39
Windows	2.70
Slab on ground	0.30

2.2.2 Heating and ventilation

The heating distribution system is a 2-pipe heating system with a flow temperature of 80 °C and return temperature of 60 °C. The heating system is an old oil boiler unit located in the utility room. All pipes are insulated with 30 mm insulation. Domestic hot water is produced in a 200 l hot water tank with 30 mm insulation.

The building has natural ventilation and can be categorised as leaky, which means that the total air change rate in the house is set at 0.45 l/s per m^2.

2.2.3 Calculated energy consumption

The single-family house has a calculated energy consumption of 240 kWh/m^2 per year.

2.3 Energy-saving measures

For each building, 2 packages of energy-saving measures are suggested.

2.3.1 1930s, energy-saving measures, Package 1

The following measures are carried out:

1. Floor separation: 70 mm clay replaced by 75 mm insulation
2. Ceiling: New 300 mm insulation
3. Exterior wall: 150 mm exterior insulation
4. Windows: Replaced by Class A windows (U = 0.9 W/m^2K and g = 0.62)
5. Heating supply: Connection to district heating instead of old oil boiler

The total energy consumption is reduced from 417.3 kWh/m^2 per year to 143.8 kWh/m^2 per year.

2.3.2 1930s, energy-saving measures, Package 2

The following measures are carried out:

1. Floor separation: 70 mm clay replaced by 75 mm insulation
2. Ceiling: New 300 mm insulation
3. Exterior wall: 150 mm exterior insulation
4. Windows: Replaced by Class C windows (U = 1.3 W/m^2K and g = 0.62)
5. Air tightness: Improved (from 0.45 to 0.30 l/s per m^2)
6. Mechanical ventilation: 90% heat recovery
7. Heating supply: District heating instead of old oil boiler

The total energy consumption is reduced from 417.3 kWh/m^2 per year to 126.6 kWh/m^2 per year.

2.3.3 1960s, energy-saving measures, Package 1

The following measures are carried out:

1. Exterior wall: 160 mm insulation for the heavy wall and 125 mm insulation for the light wall
2. Ceiling: New 200 mm insulation added to existing 100 mm
3. Windows: Replaced by Class A windows (U = 0.9 W/m^2K and g = 0.62)
5. Air tightness: Improved (from 0.45 to 0.30 l/s per m^2)
6. Mechanical ventilation: 90% heat recovery
7. Heating supply: Ground source heat pump instead of old oil boiler

The total energy consumption is reduced from 239.9 kWh/m^2 per year to 78.5 kWh/m^2 per year.

2.3.4 1960s, energy-saving measures, Package 2

The following measures are carried out:

1. Exterior wall: 160 mm insulation for the heavy wall and 125 mm insulation for the light wall
2. Ceiling: New 200 mm insulation added to existing 100 mm
3. Windows: Replaced by Class A windows (U = 0.9 W/m^{2}K and g = 0.62)
5. Air tightness: Improved (from 0.45 to 0.30 l/s per m^2)
6. Heating supply: District heating instead of old oil boiler

The total energy consumption is reduced from 239.9 kWh/m^2 per year to 97.7 kWh/m^2 per year.

3. Energy savings as a function of user behaviour

Chapter 2.3 has shown expected energy savings for two different buildings and for different energy saving measure packages. These calculations are based on standard assumptions concerning user behaviour, e.g. 20 °C indoor temperature etc. To evaluate influence of user behaviour, new sets of calculations are performed where four primary user-related parameters vary. Table 5 shows variations.

TABLE 5. Variation of parameters in calculations

Parameter	Variation	Unit
Indoor temperature	18 – 23	°C
Internal heat gain	2.0 – 7.0	W/m^2
Domestic hot water consumption	150 – 400	l/m^2
Air change rate (natural ventilation)	0.30 – 0.45	l/s per m^2
Air change rate (infiltration)	0.13 – 0.31	l/s per m^2

Calculations are performed for each individual package for the parametric variations shown in Table 5. Calculation results for the 1930s single-family house are shown in Tables 6 – 9.

TABLE 6. 1930s, Package 1. Relative energy savings in % as a function of indoor temperature before/after energy upgrading.

		Indoor temperature after [°C]					
		18	19	20	21	22	23
Indoor temperature before [°C]	18	**100.0**	96.7	93.1	89.3	85.7	81.9
	19	103.0	**100.0**	96.6	93.1	89.8	86.3
	20	106.0	103.1	**100.0**	96.7	93.6	90.4
	21	108.6	106.0	103.1	**100.0**	97.1	94.0
	22	110.9	108.4	105.6	102.8	**100.0**	97.2
	23	112.9	110.6	108.0	105.3	102.7	**100.0**

TABLE 7. 1930s, Package 1. Relative energy savings in % as a function of internal heat gain before/after energy upgrading.

		Internal heat gain after [W/m^2]					
		2	3	4	5	6	7
Internal heat gain before [W/m^2]	2	**100.0**	102.3	104.5	106.8	109.0	111.0
	3	97.7	**100.0**	102.2	104.5	106.7	108.8
	4	95.4	97.7	**100.0**	102.3	104.5	106.6
	5	93.1	95.4	97.7	**100.0**	102.2	104.3
	6	90.9	93.2	95.4	97.8	**100.0**	102.1
	7	88.7	91.1	93.4	95.7	97.9	**100.0**

TABLE 8. 1930s, Package 1. Relative energy savings in % as a function of domestic hot water use before/after energy upgrading.

		Domestic hot water use after [l/m^2]					
		150	200	250	300	350	400
Domestic hot water use before [l/m^2]	150	**100.0**	99.1	98.1	97.2	96.2	95.2
	200	100.9	**100.0**	99.1	98.1	97.1	96.1
	250	101.9	101.0	**100.0**	99.0	98.1	97.1
	300	102.9	101.9	101.0	**100.0**	99.0	98.0
	350	103.8	102.9	101.9	101.0	**100.0**	99.0
	400	104.8	103.9	102.9	102.0	101.0	**100.0**

TABLE 9. 1930s, Package 1. Relative energy savings in % as a function of air change rate before/after energy upgrading.

		Air change rate [l/s per m^2]			
		0.30	0.35	0.40	0.45
Air change rate [l/s per m^2]	0.30	**100.0**	98.0	96.0	94.0
	0.35	102.0	**100.0**	97.9	95.9
	0.40	104.2	102.1	**100.0**	97.9
	0.45	106.4	104.3	102.2	**100.0**

The tables show the relative energy savings, e.g. if the indoor temperature is 20 °C before the energy upgrading and 22 °C after, then the relative energy savings are 93.6% of the expected energy savings. The "before" situation could also correspond to a situation where no data is available and therefore a standard value is assumed.

Similar calculations are performed for the remaining packages, i.e. Package 2 for 1930s and Packages 1 and 2 for 1960s.

A cross comparison shows that the lower the total energy consumption is, the more the relative savings are influenced, i.e. the expected energy savings for the 1960s building are more sensitive to discrepancies between parameters in the "before" and "after" situations.

4. Discussion

4.1 Indoor temperature

The indoor temperature greatly affects the energy consumption of the building, and the analysis shows that for every degree the inside temperature deviates from standard assumptions, the energy consumption is increased/decreased by 6 – 8%. This applies regardless of the level of the total energy consumption.

The analysis also shows that the higher the indoor temperature, the greater energy savings will be achieved in connection with an energy upgrading. If the indoor temperature changes in connection with an energy upgrading, e.g. 2 °C, then the relative savings are reduced by 4 – 7% in a house from the 1930s and 8 – 12% in a house from the 1960s.

4.2 Internal heat gain

The internal heat gain greatly affects the energy consumption of the building and the lower the energy consumption of the building, the greater the relative importance of variations in the internal heat gain. In the non-upgraded buildings, 1 W/m^2 deviation in the internal heat gains influences the energy

consumption by 2 – 3%, for the upgraded buildings from the 1930s about 4 – 5% and the upgraded buildings from the 1960s about 5 – 6%.

The analysis also shows that the energy savings achieved are largely independent of the level of the internal heat gain if it is the same after as before. The energy-saving potential is thus largely independent of the internal heat gain. If the internal heat gain changes in connection with energy upgrading, then the relative savings are reduced by 2 – 3% in a house from the 1930s and 3 – 4% in a house from the 1960s for each 1 W/m^2 change.

4.3 Domestic hot water consumption

Consumption of domestic hot water affects the total energy consumption of the building with the same level, regardless of the building's overall energy state, and therefore the deviations in hot water consumption is most important in buildings that have undergone extensive energy upgrading. The analysis shows that for every 50 litres/m^2 per year, the consumption of hot water differs from the standard assumption of 250 litres/m^2 per year, the total energy consumption is increased/decreased by approximately 1% for the non-upgraded buildings and approximately 2 – 3% for the energy-upgraded buildings.

The analysis also shows that the energy savings achieved are largely independent of the consumption of domestic hot water, if the level of consumption is the same after as before. The energy-saving potential is thus largely independent of the consumption of domestic hot water. If the consumption of domestic hot water changes in the course of an energy upgrading e.g. increases by 50 litres/m^2 per year, then the relative savings are reduced by approximately 1% in a house from the 1930s and 1-2% in a house from the 1960s.

4.4 Air change rate

The air change rate affects the energy consumption of the building to some extent and the lower the energy consumption the greater the significance of the air change rate. In the 1930s house an increase in air change of 0.05 l/s per m^2 results in an increase in energy demand of approximately 4%. In the 1960s house, an increase in air change results in an increase in energy demand of approximately 6%.

The analysis also shows that the lower the air change rate, the greater the savings that are achieved in the context of an energy upgrading. The energy-saving potential is thus dependent on air change rate. If the air change rate increases, e.g. 0.05 l/s per m^2 in the context of an energy upgrading, then the relative savings are reduced by approximately 2% for the 1930s house and approximately 4% for the 1960s house.

4.5 Combined effects

Domestic hot water consumption does not influence the energy balance of the building and effects can be calculated independently of other parameters. The other three parameters are, however, interdependent, and the overall impact on the building's energy needs cannot be determined by a simple summation of individual effects. However, the effect of combining parameters is still quite limited and the only case where it is actually necessary to adjust the total energy savings is for the combination of “indoor temperature” and “ventilation rate”. This can be achieved by a simple calculation of the extra ventilation heat loss that occurs based on the change in temperature (compared to 20 °C) and the change in air change rate (compared to 0,13 l/s pr. m^2), i.e.:

$$\Phi_v = 1005 kg/m^3 \cdot 1{,}205 J/kgK \cdot (v_a - 0{,}13) l/s\ pr.m^2 \cdot (T_a - 20) K$$

Where v_a is the actual ventilation rate in l/s pr. m^2 and T_a is the actual temperature in °C.

The error introduced by simply adding the individual effects but taking into account the above-mentioned correction for combinations of “indoor temperature” and “ventilation rate” will be in the

order a few percent maximum. This way a method for predicting the energy saving potential can be based on similar analysis for different types of buildings and building use.

5. Conclusions

This analysis has shown that the levels of the internal heat gain and the consumption of domestic hot water only has a modest impact on the energy-saving potential of buildings, as long as the value of the parameters does not change in the course of an energy upgrading. None of these parameters are directly related to comfort, and therefore they will typically not be changed in the process.

The indoor temperature and air change rate in the building both affect the energy-saving potential. Both parameters are directly related to the comfort in the buildings and are therefore parameters that could potentially be changed in connection with an energy upgrading.

The indoor temperature is clearly the more important of the two parameters, and the results of the analysis shows that for every degree the indoor temperature is raised after an energy upgrading, the expected savings are reduced by approximately 6 – 8%, i.e. the lower the total energy demand of the building the more significant the influence of the indoor temperature.

The air change rate is less important, but it is clear that if there are large differences between the assumption of level and actual level it can affect energy savings significantly. The significance of the air change rate is highly dependent on the building's total energy consumption and the lower the energy consumption, the greater the significance of the air change rate. The results of the analysis show that for every 0.01 l/s per m^2 difference between the air change rate before and after the energy upgrading, the expected energy savings are reduced by approximately 0.4 to 0.8%, depending on the overall energy consumption. This may not sound of much, but if the air change rate changes from the minimum requirement for new buildings (0.30 l/s per m^2) to a level where it can be categorised as a leaky building (0.45 l/s per m^2), the expected energy savings are reduced by up to 12%.

Based on the analysis a relatively simple method for determining of energy savings for energy upgrading measures can be developed. The aim would be to develop a method that can predict energy savings for specific energy saving measures in a specific building, taking into account user behaviour.

6. Acknowledgements

This work was financed by the Danish Energy Agency (Energistyrelsen).

References (Times New Roman 14 pt bold, Style: References Heading)

Lundström, E. 1986; Occupant influence on energy consumption in single-family dwellings. Swedish Council for Building Research, Document D5:1986, Sweden.

Larsen, T. S., Knudsen, H. N., Kanstrup, A. M., Christiansen, E., Gram-Hanssen, K., Mosgaard, M., Brohus, H., Heiselberg, P. and Rose, J. 2010; Occupants influence on the energy consumption of Danish domestic buildings - State of the art. DCE Technical Report No. 110. Aalborg University, Denmark.

Aggerholm, S. and Grau, K. 2005; Bygningers energibehov - Pc-program og beregningsvejledning. (Building energy demand – PC program and user guide) SBi-Anvisning 213. Statens Byggeforskningsinstitut (SBi), Hørsholm, Denmark.

Façade integrated active components in timber-constructions for renovation - a case study

Fabian Ochs, Dr.-Ing.[1]
Georgios Dermentzis, Dipl.-Ing. [1]
Dietmar Siegele, Dipl.-Ing. [1]
Alexandra Konz, Dipl.-Ing. [1]
Wolfgang Feist, Prof. Dr. [2]

[1] University of Innsbruck, Unit for Energy Efficient Buildings, Austria
[2] Passive House Institute, Darmstadt, Germany

KEYWORDS: *Façade integrated active components Deep Renovation*

SUMMARY:
Deep renovation to high energy efficiency plays a key role in saving energy and in reducing CO_2-emissions. In the framework of the EU project iNSPiRe (fp7), renovation kits are developed and energy efficient renovation packages are investigated with the aim to achieve a primary energy demand of maximum 50 kWh/(m2 a) for heating, domestic hot water, auxiliary energies and lighting).

As one approach a façade integrated micro-heat pump (mechanical ventilation with heat recovery and exhaust-air heat pump) is being developed. A prototype is measured in PASSYS test cells and will later monitored in a demo building in Ludwigsburg, Germany. In the paper the approach of the micro-heat pump is discussed considering building physics and energy performance. The potential of the system is investigated by means of building and system simulation.

The façade integrated micro-heat pump is a promising concept for renovated and new buildings with a very low heating demand. With the prefabricated elements a minimum invasive renovation is enabled. The concept has the potential to deliver heat with reasonable efficiency at very low cost.

1. Introduction

The majority of existing building stock in Europe and worldwide consists of poor energy performance buildings. Deep renovation to a high energy efficiency standard e.g. according to the EnerPHit standard (heating demand of 25 kWh/(m^2 a)) plays a key role in saving energy and in reducing CO2-emissions (Feist 2012). In order to meet the target of a primary energy demand of maximum 50 kWh/(m^2 a) the aim of the EU project iNSPiRe (fp7) is:

- Deep renovation of the existing buildings through a systemic approach which includes integrated concepts consisting of building and system technologies.
- Development of energy efficient renovation packages (integrated solutions) and of energy efficient 'kits' such as multifunctional systems, including energy production, distribution and storage technologies, integrated into the envelope system

2. Concept of Micro-heat Pump

The micro-heat pump (µHP) is a concept for very efficient buildings - renovated and new buildings with a very low heating demand of 25 kWh/(m² a) or below such as e.g. EnerPHit standard (see www.passipadia.org), corresponding to a specific heat load in the range of 10 W/m². For such high performance buildings reasonable energy efficient and cost effective heating systems are required. A façade integrated µHP (mechanical ventilation with heat recovery and exhaust-air heat pump) is

developed as one renovation kit in the framework of the project iNSPiRe for very efficient residential buildings. The µHP has a heating capacity of approx. 1 kW (300 W_{el} speed controlled compressor).

Basically, the µHP concept would work for water (radiator, floor heating, radiant ceiling) and air based systems (supply air and principally also recirculated air). As source ambient air and/or exhaust air or brine are possible. The exhaust air-to-supply air has the highest potential to be really micro and thus compact, see FIG. 1.

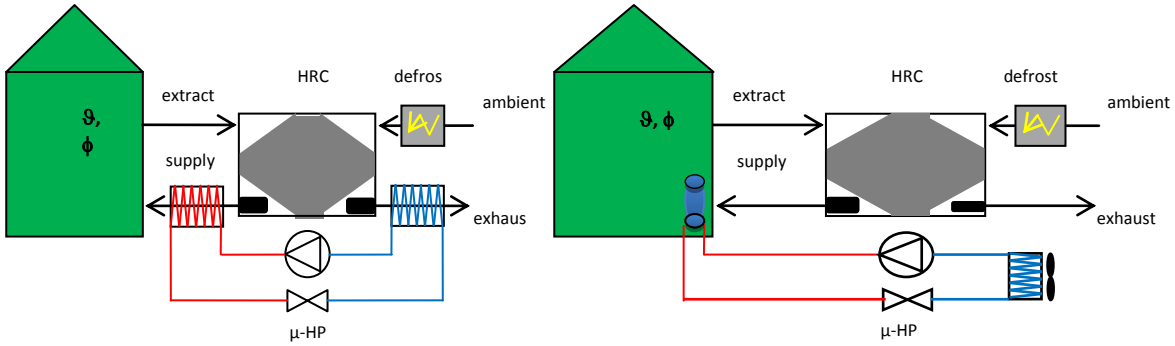

FIG 1. Scheme µHP with mechanical ventilation with heat recovery (MVHR); extract air-to-air (left) and ambient air-to-water (right)

The µHP is a system for decentralized heating. With a reversible heat pump the system could be used also for cooling. Domestic hot water (DHW) preparation has to be solved separately. For multi-family houses domestic hot water can be prepared by a central system using e.g. heat pump and/or solar thermal collectors. In Ochs et al. 2014 heating of very efficient SFH such as a passive house (heating demand of 15 kWh/(m² a)) with a heat pump in combination with a simple solar DHW preparation with direct electric backup is investigated (see FIG. 2). Reasonable to good performance (PE < 50 kWh/(m² a)) can be obtained if a high solar fraction of about 70 % is obtained (equal to about 10 m² of SC) and the heat pump is operated with a SPF of about 2.5.

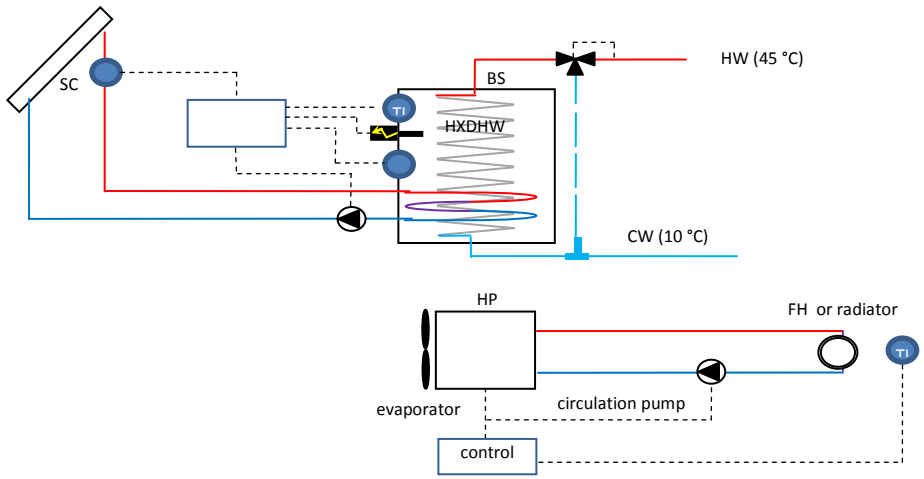

CW: cold water
HW: hot water
FH: floor heating
BH: backup heater
SC: Solar collector
HP: Heat pump
BS: Buffer storage

FIG 2. Scheme of a ambient air-to-water µHP for heating and independent solar DHW preparation

Façade integration offers several advantages (see the floor plan of the demo building in Ludwigsburg in FIG 3 as an example, the demo building is discussed below in detail):

1. No additional space for MVHR and heating system is required.
2. Cold ducts (i.e. ambient air and exhaust air) are short and outside the thermal envelope.
3. Extract air ducts are completely placed inside the façade. The inlet of the extract air is placed in the reveal of the window; all ducts are prefabricated and part of the façade.
4. Minimum installation inside the flat (i.e. minimum disturbance of tenants)

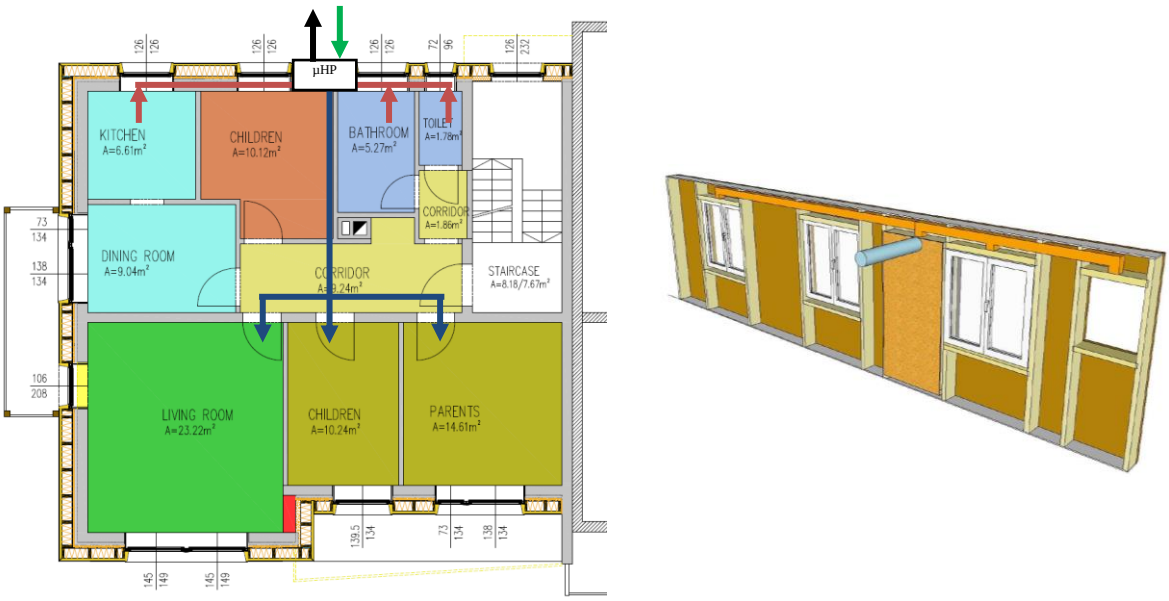

FIG 3. (left) Floor plan of GF of demo building in Ludwigsburg (D) with position of the façade integrated MVHR with µHP; (right) integration of extract air ducts in the timber frame façade

Filter accessibility from inside is possible via the reveal, however one important issue has to be solved: maintenance of the MVHR and heat pump from outside in case of high rise buildings.

3. Lab Measurements and Prototype

A prototype of a timber frame façade with an integrated MVHR is produced and measured in the lab at UIBK, see FIG 4. A second prototype with MVHR and µHP is under construction.

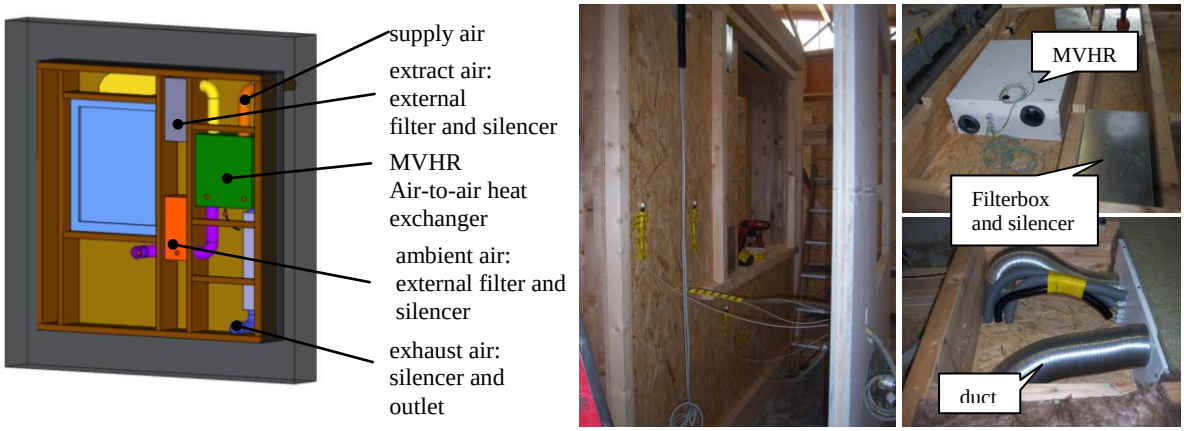

FIG 4. *(left) 3D Sketchup model and (right) photos of the production of the prototype (façade integrated MVHR), photos: Gumpp & Maier GmbH*

During lab measurements aspects of building physics and the energy performance of the MVHR and the µHP will be measured. Two so-called PASSYS test cells and an acoustic test cell are available. The following parameters will be measured:

- building physics (U-Value, g-Value, avoidance of moisture accumulation inside the construction and of mould growth, sound emission and sound insulation)
- energy performance of the active component (ηhr efficiency of mechanical ventilation with heat recovery, COP (coefficient of performance of heat pump)

For the façade integrated MVHR thermal and hygrothermal simulations have been conducted on component level (2D) and the system has been optimized to allow a secure operation. By means of lab measurements of a prototype these aspects are investigated in detail and simulation results will be proven. First measurement results are expected to be available in spring 2014.

4. Demo Building Ludwigsburg

The "Lubu demo building" is a multi-family house is located in a town area in Ludwigsburg. The 1971 residential building consists of four flats: Basement floor with living area approx. 40 m²; Ground floor and first floor: each 1 flat, living area approx. 90 m² (with south loggia); Attic storey: 1 flat, living area approx. 60 m² (with west balcony); (see Ochs et al. 2013 for details)

The east wall is adjacent to another multi-family house, see Figure 1. Some refurbishment measures have been implemented so far. In the 80's the façade (including the outside basement wall) was insulated with 5 cm external insulation. The timber roof, the ceiling of the attic storey and the basement floor are not insulated. The heating demand of the building is calculated with the PHPP with approx. 125 kWh/(m² a) assuming heated staircase and cellar (A_T = 366.6 m²) or 180 kWh/(m² a) assuming unheated staircase and cellar, see also section *Simulation results*, below).

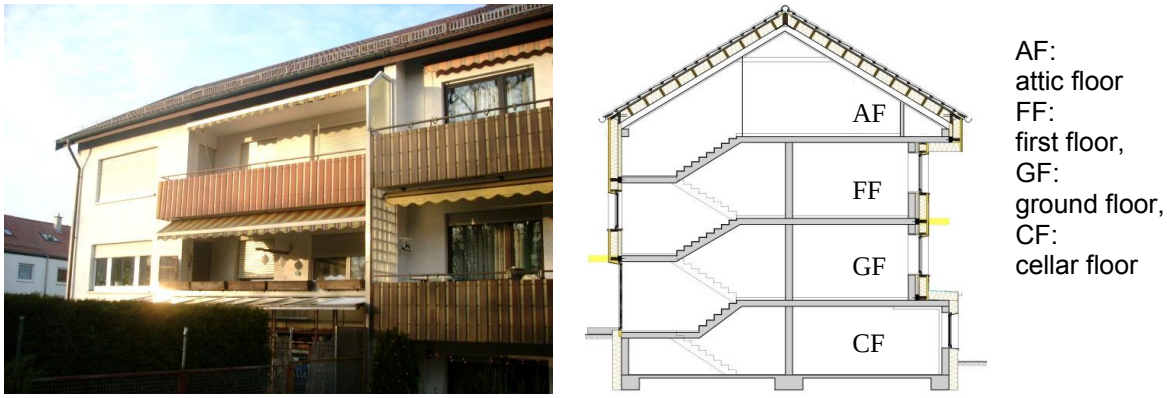

FIG 5. (left) South façade of the multi-family house, which adjacent neighbouring building, (right) section with prefabricated timber frame façade;

5. Feasibility of the Concept - Simulation Study

5.1 Simulation Model

TRNSYS is used to simulate the performance of the building and the heat pump. Since TRNSYS 17 a new plug-in is available that allows importing data from a 3D drawing, see FIG 6 for the Sketchup-model of the Lubu demo building with five zones.

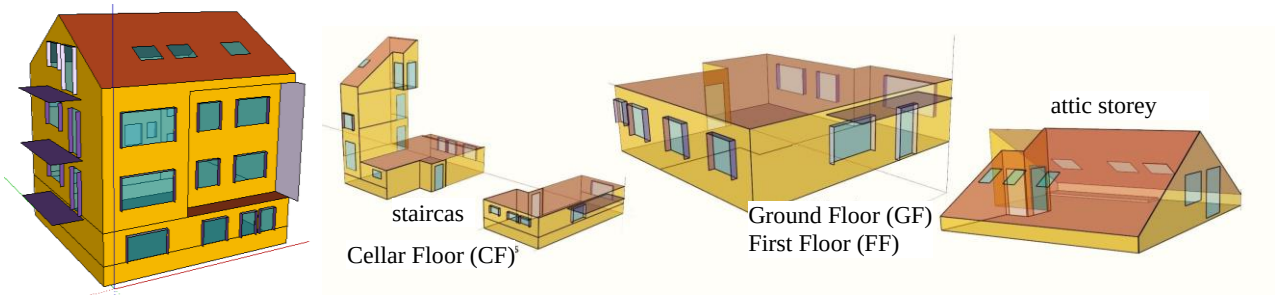

FIG 6. 3D Sketchup-Model of the Lubu demo building with the five zones (CF, GF, FF, AF and staircase)

5.2 Simulation Results

The heating demand can be reduced from 125 kWh/(m² a) (related to the treated area incl. staircase and cellar) to about 22 kWh/(m² a) using a prefabricated timber frame façade element, perimeter insulation, 3 pane windows in PH quality and a MVHR, see TABLE 1. Renovation to 15 kWh/(m² a) is also possible from the technical point of view if enhanced components are used and ground insulation is applied but is (here) not recommended from the economic point of view. For the detailed renovation solution (parametric study of different envelope solutions) incl. details of the timber frame façade and U-values of walls and windows, etc. see Ochs et al. 2013.

REMARK: Here, the staircase is assumed to be heated to the same temperature as the four flats, i.e. to 20 °C. The specific heating demand of the existing building is 180 kWh/(m² a) if the staircase and cellar are considered to be unheated. (There is also an absolute difference as a result of differences in geometry (treated area and external surface: cellar, staircase external wall, basement and roof) and boundary conditions (staircase and neighbour temperature, i.e. $\Delta\vartheta = 4$ K).

TABLE 1. Specific heating demand (HD) of the demo building before and after the renovation simulated with the five zone TRNSYS model for the four flats and heated staircase and in comparison with the PHPP results (total heating demand); reference area is treated area

	Zone	Total	CF	GF	FF	AT	ST
	Area / [m²]	366.6	47.3	92	92	58.1	77.2
existing building	TRNSYS	124.5	161.1	77.6	73.5	160.1	192.6
366.6 m²	PHPP	124.6					
renovated building	TRNSYS	20.3	43.8	2.4	2.2	20.9	48.1
366.6 m²	PHPP	20.6					

In the renovated case, if the staircase is assumed to be heated the heating demand is about 1500 kWh/a higher than in the case of unheated staircase. The heat load is 500 W higher (maximum of daily average) as can be seen in TABLE 2. With additional controlled shading and night ventilation (for overheating protection) and summer-bypass of the MVHR the heating demand and the heat load increases slightly.

TABLE 2. Absolut and specific heating demand (HD) and heat load (HL) simulated with the TRNSYS 5 zone model for different boundary conditions; reference area is treated area

	Area / [m²]	HD / [kWh/a]	spec. HD / [kWh/(m² a)]	HL / [W]	spec. HL / [W/m²]
TRNSYS 1Z	366.6	7515.3	20.5	4032.6	11.0
TRNSYS 5Z [*)]	366.6	7439.5	20.3	4086.0	11.1
TRNSYS 5Z fl. adia.[#)]	289.4	5997.8	20.7	3473.4	12.0
TRNSYS 5Z fl. perio.[+)]	289.4	6176.9	21.3	3557.9	12.3
TRNSYS 5Z fl. perio. summer[$)]	289.4	6468.0	22.3	3648.0	12.6

[*)] heated staircase, [#)] floating staircase temperature, adiabatic neighbour [+)] floating staircase temperature and floating periodic temperature of neighbour staircase; [$)] summer over-heating with protection by means of controlled shading, night ventilation and summer-bypass

5.3 Sensitivity Analysis

For the design of the µHP with a heating capacity of 1 kW the heat load of the flats is the important design criterion. To investigate the robustness of such as system a sensitivity analysis is performed. Following aspects are investigated:

1. Boundary conditions – staircase and neighbour
2. Non-heated neighbour flat

3. Additional window ventilation
4. Different set point temperatures (single flat and all flats)
5. Occupation profile (internal gains and design air change rate)
6. Heat pump system concept (with/without storage)

5.3.1 Building and User Behaviour

For the reference case the following heating demands (HD) and heat loads (HL) of the flats have been obtained by means of simulation. The boundary conditions have strong influence.
The µHP with air heating is suitable for the GF and FF with the HD below 10 kWh/(m² a) (GF has slightly higher heating demand due to the colder cellar). For the CF a µHP concept with a hydronic heat distribution system would be possible. In the AF with a heat load of about 2 kW the µHP concept is hardly feasible.
If one of both neighbouring flats is not heated (the entire winter, e.g. due to long term absence of a tenant) the heat load increases from 880 W to 1120 W. With an additional backup heater the comfort level can be maintained. The increase of the HL with increasing set point temperatures is shown in FIG. 7. If all flats have higher set point, the increase of the HL is less significant. Additional window ventilation (every night! not occasional window ventilation) in the sleeping room would increase the heat load by a factor of 3.

TABLE 3. spec. heating demand HD in kWh/(m² a) and heat load HL in W/m² in brackets (TRNSYS 5Z floating staircase, periodic neighbour, summer overheating protection)

	Area / [m²]	TRNSYS 5Z	TRNSYS 5Z fl. adia.[#)]	TRNSYS 5Z fl. perio.[+)]	TRNSYS 5 Z (TABLE 1, PHPP)	PHPP
CF	47.3	43.8 (15.8)	54.8 (17.9)	54.8 (18.1)	44.02	59.7 (18.4)
GF	92.0	2.4 (5.4)	8.3 (8.4)	9.0 (8.8)	4.70	1.4 (8.8)
FF	92.0	2.3 (5.2)	5.1 (6.7)	5.4 (6.8)	4.43	1.4 (8.8)
AT	58.1	20.9 (15.3)	37.4 (21.3)	38.9 (21.8)	38.07	34.6 (22.2)

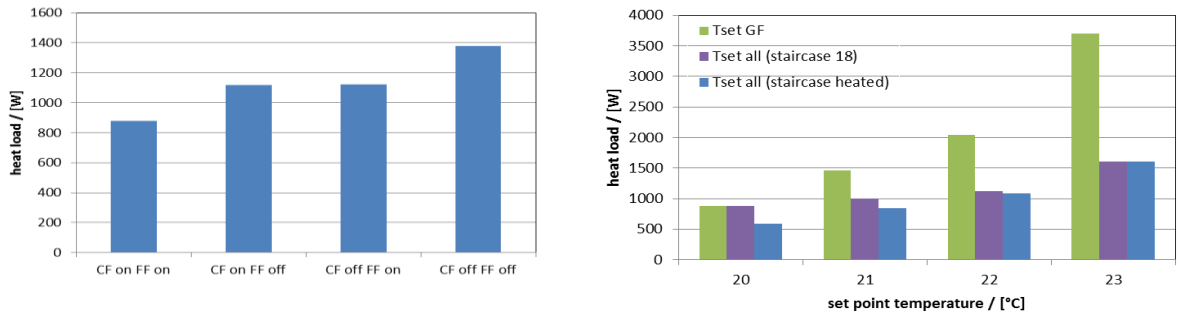

FIG 7. (left) heat load of GF for heated (“CF on FF on”) and unheated neighbour flats (heating off either in CF or FF or in both) and (right) heat load for different set point temperatures

5.3.2 System Concept and Sizing

In the previous section simulation results for heating demand and heat load apply for the case of ideal heating. In a further step a simulation study using ambient air to water µHP is performed. Different heating systems concepts (with and without storage) and different sizing of heat pump and buffer storage are investigated. Radiators are used with different flow temperatures in case of the system with storage. The heat pump used for the simulation is scaled to match the required power (with constant performance map, COP(35/2) = 3.9, see Konz 2013 for further details). The system with storage is shown in FIG 8 and the one without in FIG 2.

REMARK: As experience shows, small heat pumps are less efficient than large heat pumps for several reasons (e.g. thermal losses, efficiency of compressor, dead volume, parasitic energies). Hence, the performance of larger (i.e. up-scaled) heat pumps is supposed to be slightly higher than calculated and that of the down-scaled heat pumps slightly lower.

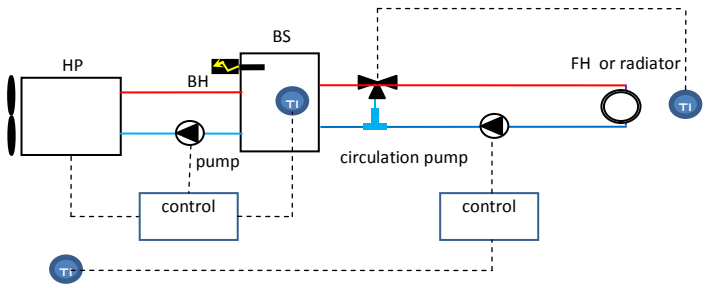

FH: floor heating

BH: backup heater

HP: Heat Pump

BS: Buffer Storage

FIG 8. Heating system with µHP with buffer storage

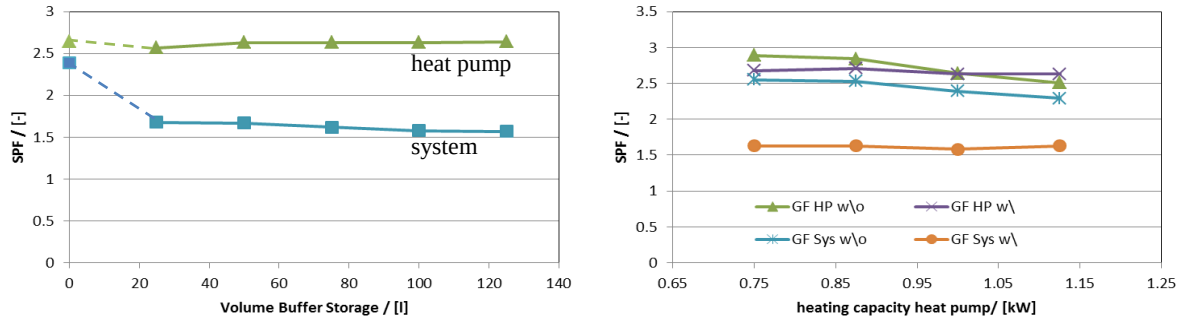

FIG 9. (left) SPF as a function of the storage size and (right) SPF as a function of the heat pump size

With sufficient storage (> 50 l) the SPF of the heat pump can be slightly increased, however the SPF of the system is significantly reduced due to storage losses and parasitic energies. The SPF without storage is significantly higher. A System SPF of about 2.4 can be obtained. The size of the heat pump (here for the case of a constant speed compressor) is important for a good performance. If the heat pump is over-dimensioned the SPF decreases significantly.

The heat load of the building is influenced by the occupation profile – on the one hand via the internal gains and on the other hand via the ventilation rate (here, 30 m³/h/person). In addition the ventilation rate limits the maximum heating capacity according to equation 1 in case of air heating.

$$\dot{Q} = n \cdot \rho \cdot c \cdot V \cdot (\vartheta_{max} - \vartheta_{room}) \qquad (1)$$

With $\dot{Q}$ heat flow (W),
n air change rate (1/h),
ρ density, 1.24 (kg/m³),
c specific heat capacity, 1004 J/(kg K),
V Volume (m³),
ϑ temperature (°C)

With a maximum temperature of 55 °C and a room temperature of 20 °C the maximum heating capacities shown in TABLE 4 are obtained and compared to the simulated heat load of the GF flat. For a normal occupation of 2 adults and 2 children (2A2C) or 2 adults and 1 child (2A1C) the maximum heating capacity is sufficient. In case of lower occupation level there is a mismatch between heat load and heating capacity which has to be considered during the design. An additional backup heater (e.g. in the bathroom and/or corridor) should be considered for comfort reasons anyway.

TABLE 4. simulated spec. heat load HL and max. heating capacity in case of air heating (acc. equ. 1)

Occupation	Ventilation rate / [m³/h]	HL / [W]	max. heating capacity / [W]
2A2C	120	881	1453
2A1C	90	908	879
2A	60	1203	586

REMARK: in a very efficient house a slightly under-dimensioned heating system does not lead to a significant temperature drop due to the high inertia (time constant) of the building. Temperatures will hardly drop below 19 °C (Bisanz 1998).

6. Conclusions and Outlook

It is shown by means of an extensive simulation study that the system concept of a façade integrated µHP is feasible for renovated buildings (EnerPHit standard or better). Reasonable performance with high economic efficiency can be obtained. A more detailed physical heat pump model is under development considering air heating and speed controlled compressor. A multi-zone model of the GF flat has been established and will be used for future investigations and optimization.

A prototype with façade integrated MVHR has been developed and will be measured in the lab at UIBK. A second prototype with an exhaust air-to-air heat pump in combination with MVHR will be developed in the near future and optimized for the demo building in Ludwigsburg, where two of the four flats will be renovated with the proposed system in late 2014. Monitoring of the performance will be conducted for a period of at least one year.

7. Acknowledgements

These results are part of the research and simulation work of the European project iNSPiRe funded under the 7th Framework Program (Proposal number: 314461, title: Development of Systematic Packages for Deep Energy Renovation of Residential and Tertiary Buildings including Envelope and Systems, duration: 01.10.2012 – 30.09.2016).

References

Bisanz, C., Heizlastauslegung im Niedrigenergie- und Passivhaus, 1. Auflage, Darmstadt, Januar 1999

Feist, W. (editor), EnerPHit Planerhandbuch - Altbauten mit Passivhaus Komponenten fit für die Zukunft machen. Autoren: Zeno Bastian, Wolfgang Feist

Konz A., Thermische Simulation von Sanierungsvarianten eines Mehrfamilienhauses mit Fokus auf den Einsatz von Wärmepumpen in zentraler und dezentraler Gebäudetechnik, Master Thesis, TUM, UIBK, 2013

Ochs F., Dermentzis G., Siegele D., Konz. A., Feist W. 2013 Use of Building Simulation Tools for Renovation Strategies - a renovation case study, EnergyForum 2013, Bressanone

Ochs F., Dermentzis G., Siegele D., Konz. A., Loose A., Drück H., Feist W. 2014, Thermodynamic analysis of ground coupled heat pumps with solar thermal regeneration, IEA Heat Pump Conference, Montreal 2014 (abstract accepted).

Siegele D., Modellierung und Simulation Fassadenintegrierter Aktiver Komponenten, Master Thesis, UIBK, 2013

PASSYS, The *PASSYS Test Cells*: A Common European Outdoor Test Facility for Thermal and Solar Building Research, Commission of the European Communities, Directorate-General XII for Science, Research and Development, Edited by BBRI - Brussels 1990

The influence from input data provided by the user on calculated energy savings.

Jimmy Vesterberg, M.Sc[1,2], Staffan Andersson, Ph.D [1], Thomas Olofsson, Ph.D [1]

[1] Applied Physics and Electronics, Umeå University, Sweden
[2] Industrial Doctoral School, Umeå University, Sweden

KEYWORDS: *Simulation, energy savings, retrofit, model calibration, regression*

SUMMARY:
It is generally accepted that the most correct decisions are made when the used support system provides the most accurate description of the starting point as possible. That is, in this case, a detailed initial description of a building, planned to be refurbished and evaluated with the building energy simulation software IDA ICE (v 4.5).

In order to assess this statement, we have used two different models to predict energy savings due to different planned energy conservation measures (ECMs):

- A basic model based on inputs from currently available standards and as-built drawings.

- A calibrated model based on an analysis of measurements from two months, together with measured air handling unit parameters, hourly electricity usage and indoor temperatures.

The relative prediction differences between the models are investigated as well as compared with the actual outcome in a neighboring building where the analyzed ECMs have been implemented.

The result indicates that a calibrated model should be used, in order to accurately determine the post-retrofit energy demand. However, if only investigation of ECMs which aims to decrease a buildings transmission loss is of interest, the findings suggest that BES calibration is of minor importance.

1. Introduction

To stimulate investments in different energy conservation measures (ECMs) in existing buildings it is important that these measures meet the expected or by the supplier promised performance. This implies an increasing demand for reliable evaluation methods and accurate input parameters to simulation models, since the question of liability is expected to become more frequent.

Typically, implementation of ECMs in existing buildings is preceded by calculations with whole Building Energy Simulation (BES) models to predict the expected savings. Often these BES models are based on standardized building and user templates, even though it is generally accepted that the most reliable analysis of retrofit options are made with calibrated BES models (Reddy, 2006; Zhen, 2013; Heo, Choudhary and Augenbroe 2012; Raftery, Keane and O'Donnell, 2011). A hindering factor for the widespread use of calibrated simulations is that it typically demands considerable more resources than a typical design stage simulation.

This study was designed to investigate discrepancies between outputs from uncalibrated (standardized) and calibrated BES models, when they are used to calculate energy savings. For this purpose, we have used two different models: The first is based on inputs from currently available standards and as-built drawings (basic model). The second, calibrated model is based on extracted thermal performance parameters from an analysis of measurements from two months as well as measured air handling unit performance parameters, hourly electricity usage and indoor temperatures.

The calibrated model comfortably passes the calibration acceptance criteria's for total energy demand for space heating suggested in ASHRAE guideline 14 (ASHRAE, 2002).

In addition to investigating prediction differences between the models, the plausibility of the models predicted post-retrofit energy demand are analyzed through a comparison with the actual outcome in a neighboring building in which the modeled ECMs already have been implemented (with the only difference of a slightly larger addition of an attic room). A verification, possible due to identical building designs as well as very similar energy characteristics, pre-retrofit.

The used BES tool in this study is IDA Indoor Climate and Energy (IDA ICE) (EQUA, 2013) which has been used in numerous previous studies e.g. (Pavlovas, 2004; Molin, Rohdin and Moshfegh 2011; Salvalai, 2012; Hesaraki and Holmberg, 2013; Loutzenhiser et al, 2009)

1.1 Buildings and considered ECMs

The studied building is a ten apartment multifamily building, constructed during the years 1970/71 for the municipal housing company, AB Bostaden. The building is at the time of writing, part of a large refurbishment project, that includes 21 multifamily buildings located in the city district Ålidhem, Umeå, Sweden. Due to a relative high demand of District Heating (DH) for space heating, a number of ECMs were considered to reduce this energy demand: (ranked in a most likely implementation order)

1. New attic room for placement of a new air handling unit and retrofitting of roof
2. Ventilation system with heat recovery on the exhaust air
3. Improved roof insulation
4. Window upgrade (from two to three glazed)
5. Adjustment of domestic hot water circulation losses
6. Additional interior insulation of exterior walls

2. Modeling

The basic model was defined in IDA ICE based on inputs from current available standards and as-built drawings including floor plan, dimensions of different parts of the building envelope and heating and ventilation system (one serving all of the thermal zones). The calibrated model was obtained by changing different input data in the basic model to coincide with a performed analysis of measurements.

2.1 Weather file

The used weather file contained, an onsite measured outdoor dry-bulb temperature and relative humidity. The global solar radiation was measured at Umeå University weather station (Applied Physics and Electronics, 2013) approximately 1 km from the studied buildings. However no wind measurements were available, instead typical mean year data for wind speed and direction was synthetically generated with the climate software (Meteonorm, 2013).

2.2 Basic model

The basic model was heavily based on standardized building and user templates to mimic the situation when detailed measured data does not exists or given time constraints do not allow a typical labor intensive calibration process. Input, regarding: household electricity usage, indoor temperature, window airing, internal shading, heat gain from the occupants and electric heat gain factor were estimated with a widely used guideline in Sweden (SVEBY, 2012).

This source was further used to distribute the household electricity usage in the kitchens, living rooms, bathrooms, bedrooms and halls to 51%, 27% and 3 × 7% of the total household electricity

load, similar to the assumed distribution in a previous study in Sweden (Molin, 2011). The air rates to and from the air handling unit as well as the air leakage were estimated based on the Swedish building regulations (SBN 1975) and (SBN 1980).

The most common method in praxis to account for thermal bridges in Sweden has been found to utilize standardized values in the literature (Berggren, 2013). Thus, in this study, the heat loss due to thermal bridges was estimated with standard linear thermal transmittance values, tabulated in the ISO standard (ISO 14683, 2007). This approach applied on the investigated building resulted in a ratio of thermal bridges to total transmission losses of 25%.The definition of U-values were thereafter completely defined with program defaults complemented by design values in literature (Petterson, 2009).

In contrast to the above standardized values, the annual measured building electricity was used as input, due to the wide accessibility of this information in Sweden, since it is regulated (SFS 2006:985) to be measured for new buildings. For older buildings as in this study, it was gathered from utility bills. Based on performed site surveys, 85% of the total measured building electricity usage was assigned to the ventilation room (where the majority of the equipment was installed). The remaining 15% was evenly distributed between the stairwells in the model to cover the power need of a few remaining lights.

The internal heat gain due to occupancy was estimated from public records and guidelines given in (SVEBY, 2012). This heat gain was modeled as constant heat contributions and evenly distributed over the living areas. An occupancy schedule could have been used but as these heat contributions are small relative to the total heat demand, the increase in model accuracy was assessed to be negligible.

A zone strategy that follows the guidelines given in (ASHRAE, 2007) was used to agglomerate actual zones in the building of the same zone type into a single zone, if the actual thermal zones in the building varied less than 45 degrees in orientation from each other. This zone approach led to 21 zones in the final model of which a 3D façade view is shown in fig 1.

FIG 1. 3D façade view of the analysed building defined in IDA ICE software, where the location and geometrical model correspond to the real situation before the planned refurbishment.

Further model preparation concerned the buildings mechanical supply and exhaust ventilation system with constant air change rate. It was simulated accordingly, as a constant air volume system and with a heating coil in the air handling unit. The heating coil was activated when the supply air was below the set, constant supply temperature.

In addition, the radiators were modeled as ideal heaters in the IDA ICE environment, placed in respective zones with a sufficient capacity to sustain the set indoor temperature, during all conditions.

The interior walls were treated as adiabatic, the inside air was allowed to move between the zones in each floor through interior door openings and external infiltration was distributed over the zones according to external surface area.

Finally, the heat transfer to the ground was simulated according the standard (EN ISO 13370, 2007) and as the building lacks a air conditioning system, no cooling energy was considered in the simulations. However, when the indoor temperature was above 25°C, the occupants were assumed to increase the ventilation by airing.

The use of the above input values resulted in a simulated energy demand (electricity and DH for space heating) of 172.7 MWh/yr, this is an overestimation by approximately 19.1% compared to the measured data of 145.0 MWh/yr. Discrepancies of this magnitude have been reported in other studies (Pedrini, Westphal and Lamberts 2002; Ahmad and Culp, 2006; Danielski, 2012) and are not unusual for BES models heavily based on standardized input values.

2.3 Calibrated model

The calibrated model was developed from the basic model by adjusting the previous assumed thermal performance parameters to coincide with a regression analysis of measured data from two months, when the solar gain was the smallest, i.e. a thorough analysis based on the energy signature principles was conducted (pre-retrofit) with a method developed in (Andersson et al, 2011). In addition, the basic model was complemented with hourly measured building and household electricity usage as well as air handling unit performance parameters and temperature data. To summarize, the revised input parameters were:

- The actual electricity use was loaded into the program at an hourly time step as recommended in (Raftery, Keane and O'Donnell, 2011) for the complete year of simulation.
- The dynamic influence of the indoor temperature was considered.
- IDA ICE calculation of ground heat loss was adjusted to coincide with the results from a regression analysis of measured data.
- The buildings loss factor (transmission + leakage) was adjusted to coincide with the results from the regression analysis.
- Measured air handling unit performance parameters (air rate, supply temperature, efficiency) was loaded into the program as average values during the heating season (Oct-Mar).

The use of the above building unique input values resulted in a simulated energy demand (electricity and DH for space heating) of 139.6 MWh/yr. This corresponds to a modest underestimation (MBE) of -3.7% and a Coefficient of Variation of the root mean squared error (CV) of 5.7% calculated with monthly data. The suggested calibration tolerance limits suggested in (ASHRAE, 2002) is a MBE within ± 5% and CV less than 15% relative to monthly data. Thus the model passes these thresholds comfortably.

2.4 Model predictions

The predictions from the basic and the calibrated models were investigated using the six previous mentioned individual ECMs as well as three different sets of ECMs:

- Set1, Composed of ECM 1 and 2
- Set2, Composed of ECM 3, 4 and 6
- Set3, All individual measures implemented.

The individual and sets of ECMs were evaluated separately so that a decision could be made for each category. This enables the building manager to choose to implement only one ECM at a time or select a group of measures. The energy savings were estimated by adding each individual ECM to the models and the predicted energy demand ($\hat{E}_{ECM,i}$) was compared with the forecast of the previous

prediction ($\hat{E}_{ECM,i-1}$). This adding of measures continued until all measures were included and thus represented the post-retrofit situation. The predicted percentage savings for both models was calculated, according to:

$$\%E_{save,i} = 100 \times \frac{\hat{E}_{ECM,i-1} - \hat{E}_{ECM,i}}{E_{measured,DH}} \quad (1)$$

Where $E_{measured\ DH}$ is the measured DH demand for space heating (radiators and air handling unit), during the analyzed year, pre-retrofit. Eq. 1 was further used to analyze model differences for the sets of ECMs, then with $\hat{E}_{ECM,i-1}$ substituted against the predicted model energy demand in the present situation (i.e. held fixed) and $\hat{E}_{ECM,i}$ then corresponded to the model forecast for the ith set of ECMs.

The implementation of an attic room (ECM 1) is necessary for installment of a new air handling unit and would result in increased energy demand. However, the focus in this study is to investigate prediction differences of simulation models when subject to input parameter changes. In that analysis the direction of the energy change is of minor importance.

In table 1, the shared baseline values for both models (basic and calibrated) and the adjusted values in the post-retrofitted models are shown. For consistency, ECM 1 been excluded in table 1 due to the fact that the basic and calibrated models have different overall UA-values.

The overall UA-values increased in the basic model from 920.1 WK^{-1} to 946.0 WK^{-1} and from 799.3 WK^{-1} to 817.4 WK^{-1} in the calibrated model respectively due to the addition of ECM 1 in the models. The reason for the different changes in the two models overall UA-values originates from that the models assumes different settings of thermal bridges which is also assumed to hold for the installation of ECM 1.

TABLE 1. Shared baseline values in the used simulation models and the new (modified) values to simulate the ECMs considered.

Design alternative	Affected building components	Pre-retrofit value	Post-retrofit value
ECM 2	Air handling unit efficiency	0%	85%
ECM 3	U-value roof	0.29 $WK^{-1}m^{-2}$	0.07 $WK^{-1}m^{-2}$
ECM 4	U-value window/SHGC*	2.2 $WK^{-1}m^{-2}$/73%	1.1 $WK^{-1}m^{-2}$/55%
ECM 5	Heat losses from dhwc**	31 kWh/m^2	5.0 kWh/m^2
ECM 6	Heated area/U-value walls	880 m^2/0.32 $WK^{-1}m^{-2}$	868 m^2/0.24 $WK^{-1}m^{-2}$

*Solar Heat Gain Coefficient. **Constant domestic hot water circulation (dhwc) losses modified to standardized level according to (SVEBY, 2012).

3. Results

The predicted savings for both models are shown in fig 2 for all individual as well as for the different sets of ECMs. The smallest discrepancies between the models are seen for the ECMs which affects the buildings transmission losses i.e. individual ECMs (1,3,4,6 max deviation 1.8%) as well as for the combined measure Set2, with a 2.6% difference between the two model predictions.

The difference is significant, 14.2% regarding the saving potential for the implementation of heat recovery in the ventilation system (ECM 2). This is mainly due to that different air rates are assumed in the models. In the basic model a higher standardized air rate is assumed compared to the calibrated model, which uses the measured air rate, hence a larger saving potential exists in the basic model for this ECM. This creates subsequent errors by the basic model in the combined measure sets, Set1and Set3 with a 12.4% and 12.2% deviation in comparison with the calibrated model.

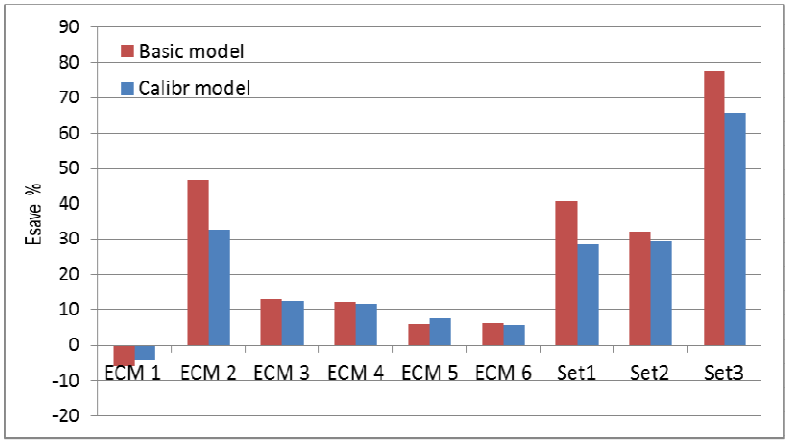

Fig 2.Annual predicted percentage savings with the two BES models due to individual as well as sets of ECMs.

Minor discrepancies are also seen between the models in the predicted change in energy use associated with the adjustment of the buildings dhwc losses, (ECM 5) of 1.6%. This energy saving potential depends on the length of the heating season in the models. The basic model has a longer heating season and can therefore utilize a larger part of the constant dhwc losses compared to the calibrated model. A reduction of the dhwc loss in the basic model must then be replaced by a larger part of the temperature dependent heat load, which results in a smaller predicted overall heat saving, compared to the calibrated model.

3.1 Analyze of predicted post-retrofit energy demand.

Measured post-retrofit energy use, for an entire year, does not yet exist for the studied building. However, the reasonableness of some forecasts can be estimated by comparing the predicted post-retrofit energy demand with the actual outcome in a neighboring building, in which the simulated ECMs already have been implemented, with the only difference of a slightly larger attic room. The comparison is possible due to identical building designs as well as heating and ventilation systems, before the refurbishment. The similarities were also confirmed through a comparison of the buildings measured heat demand, during a couple of months prior to the refurbishment.

Before the model outputs were compared with the neighboring building, the measured input parameters previously used in the calibrated model were changed to the measured operating conditions in the retrofitted neighboring building. (No modifying was done in the basic model as it assumes standardized operating conditions). This resulted in deviations of the magnitude of +17% for the basic model and less than -1% for the calibrated model in predicted post-retrofit demand of total energy demand for space heating (electricity and DH demand).

An additional test was done for the implementation of ECM 2, by comparing the measured supplied DH to the air handling unit in the neighboring building with the same in the studied building, pre-retrofit, the difference was measured to 26.8 MWh/yr. Thus this magnitude of energy savings is what is reasonable to be expected due to installment of ECM2.

The basic model predicted an energy saving of 40.5 MWh/yr, that is +51% more than the comparative value of 26.8 MWh/yr, whereas the calibrated model estimated 28.2 MWh/yr which corresponds to a much more moderate discrepancy of +5%.

4. Conclusions

This study was designed to investigate the necessity of using calibrated simulation models in order to get reliable energy saving predictions. We focused on a few selected ECMs implemented in one studied building.

Based on the observed agreement between the predicted post-retrofit energy demand with the calibrated model and the actual outcome in the neighboring building, it is indicated that a calibrated model should be used in order to accurately predict the post-retrofit energy demand. In addition, the calibrated model yielded accurate forecast of the energy saving due to heat recovery of the exhaust air.

However, in the calculations of the ECMs which affected the transmission losses, small differences were found between the basic and calibrated model. This indicates that BES models based on standardized input parameters can be used to predict energy savings for that purpose.

The main conclusion is that, accurate predictions of energy savings can be obtained with standardized BES models, complemented by measured air handling unit performance parameters. However, in order to accurately predict the post-retrofit energy demand, the starting point of the used BES model is crucial, i.e. in such situations the input parameters needs to be thoroughly calibrated.

5. Acknowledgements

The project is funded by The Industrial Doctoral School at Umeå University and AB Bostaden, Umeå, Sweden. The authors also thank Umeå Energi for their assistance with data collection.

References

Ahmad M. & Culp C.H. 2006. Uncalibrated building energy simulation modeling. HVAC & R Research, 12, 1141-1155.

Andersson S. et al, 2011. Building performance based on measured data. World Renewable Energy Congress – Sweden, 8-13 May, 2011, Linköping, 899-906

ASHRAE. 2002. ASHRAE Guideline 14-2002. Measurement of Energy and Demand Savings. Atlanta: American Society of Heating, Refrigerating and Air-Conditioning Engineers, Inc.

ASHRAE. 2007. ANSI/ ASHRAE Standard 90.1. Energy Standard for Buildings Except Low-Rise Residential Buildings. Atlanta: American Society of Heating, Refrigerating and Air-Conditioning Engineers, Inc.

Applied Physics and Electronics. http://www8.tfe.umu.se/weather/1024/1080/10/sv-SE/station.htm [2013-12-03]

Berggren B. & Wall M. 2013. Calculation of thermal bridges in (Nordic) building envelopes – Risk of performance failure due to inconsistent use of methodology. Energy and Buildings, 65. 331-339.

Danielski, I. 2012. Large variations in specific final energy use in Swedish apartment buildings: Causes and solutions. Energy and Buildings. 49, 276-285.

EN ISO 13370. 2007. Thermal performance of buildings-Heat transfer via the ground-Calculation methods.

EQUA. http://www.equa-solutions.co.uk [2013-12-03]

Meteonorm. http://meteonorm.com/ [2013-12-03]

Heo Y, Choudhary R. & Augenbroe G.A. (2012). Calibration of building energy models for retrofit analysis under uncertainty. Energy and Buildings. 47, 550-560.

Hesaraki A. & Holmberg S. (2013). Energy performance of low temperature heating systems in five new-built Swedish dwellings: A case study using simulations and on-site measurements. Building and Environment. 64, 85-93.

ISO 14683. 2007. Thermal bridges in building construction - Linearthermal transmittance - Simplified methods and default values.

Molin A., Rohdin P. & Moshfegh B. 2011. Investigation of energy performance of newly built low-energy buildings in Sweden. Energy and Buildings. 43(10), 2822-2831.

Loutzenhiser P. et al, 2009. An empirical validation of window solar gain models and the associated interactions. International Journal of Thermal Sciences. 48(1), 85-95.

Pavlovas V. 2004. Demand controlled ventilation: A case study for existing Swedish multifamily buildings. Energy and Buildings. 36(10), 1029-1034.

Pedrini A., Westphal F.S & Lamberts R. 2002. A methodology for building energy modelling and calibration in warm climates, Building and Environment. 37(8–9), 903-912.

Petterson, B.Å. 2009. TILLÄMPAD BYGGNADSFYSIK. Lund, Studentlitteratur

Raftery P., Keane M & O'Donnell J. 2011. Calibrating whole building energy models: An evidence-based methodology. Energy and Buildings. 43(9), 2356-2364.

Reddy, T. A. 2006. Literature review on calibration of building energy simulation programs: uses, problems, procedures, uncertainty and tools. ASHRAE Transactions, 226–240.

Salvalai, G. 2012. Implementation and validation of simplified heat pump model in IDA-ICE energy simulation environment. Energy and Buildings. 49, 132-141.

SBN. 1975. Statens Planverk. Svensk Byggnorm, Supplement No 1.

SBN. 1980. Statens Planverk. Svensk Byggnorm, Utgåva 2.

SFS 2006:985. Lag om energideklaration för byggnader, Näringsdepartementet, Stockholm

SVEBY. 2012. Brukarindata för energiberäkningar i bostäder.

The Swedish National Board of Housing Building and Planning.2009. Så mår våra hus-Redovisning av regeringsuppdrag beträffande byggnaders tekniska utformning m.m.

Tian, Z. & Love J.A 2013. Energy performance optimization of radiant slab cooling using building simulation and field measurements. Energy and Buildings. 41(3), 320-330.

An approach for holistic energy retrofitting based on assessment of economic viability and durability of energy saving measures

Martin Morelli, Ph.D.

Department of Construction and Health, Danish Building Research Institute, Aalborg University Copenhagen, Denmark

KEYWORDS: *Cost of conserved energy, risk assessment, FMEA, wooden beam, windows, full-scale experiment, measurement*

SUMMARY

The majority of renovation projects are driven by the possibility of reducing energy consumption of buildings. This, however, might result in retrofitting projects that neglects the longevity of the building. Furthermore, many evaluation techniques only consider the profitability of the energy saving measures and forget to consider, whether it is more prudent to demolished the building and erect a new building.

An evaluation approach is presented to assess whether to retrofit an existing building or to demolish and replace it. The primary concept of the method is to develop a retrofitting proposal with a profitably combination of energy saving measures. The cost of the combination of energy saving measures is evaluated against the cost of demolishing the existing building and erecting a new building including consideration of maintenance costs and operational costs. The energy price is used as constraint to determine the amount of building retrofitting for implementation. The approach includes also durability assessments of the energy saving measures.

An example is carried out to illustrate the application of the approach. The example highlights the importance of including risk assessment and durability evaluation of the energy saving measures when performing holistic energy retrofitting of buildings.

1. Introduction

In recent years, major focus is addressed to building renovation given that new buildings add at most 1% a year to the existing building stock. The stimulus for carry out building renovation is reducing the energy consumption of buildings. In Denmark the government has adopted a long-term policy, implying that Denmark should be independent of fossil fuels by 2050, and by 2035 energy supply to buildings should be from renewable energy sources (Danish Government, 2011). To meet this objective, it is of significance to improve the energy efficiency of the existing building stock, but also to invest in and convert the supply network to renewable energy sources. Ideally, a balance must be found between the costs for improving energy efficiency of the existing building stock and the costs of buying energy from heating and power plants based on renewable energy sources.

Several approaches exist for optimisation of building renovation, where the commonly used economic techniques are simple payback time and net present value (NPV) (Verbeeck and Hens, 2005; Tommerup and Svendsen, 2006). Both techniques, as well as their limitations, are described by Martinaitis et al. (2004). A method derived from NPV is cost of conserved energy (CCE), which gives the cost to save 1 kWh of energy and is directly comparable to the cost of supplied energy. This makes the CCE technique more transparent and practicable for understanding the profitability of the measures as compared to the monetary result obtained using e.g. the NPV method. The CCE method was applied in building renovation by Martinaitis et al. (2004; 2007) and for design of new buildings by (Petersen and Svendsen, 2012). In common, the methods focus on energy consumption and not the

durability of the energy saving measures (ESMs). The stimulus for saving energy neglects the fact that the longevity of the building could be challenged due to changed hygro-thermal conditions. Therefore, it is important to include both an assessment of the whole building as well as ESMs in the retrofitting approach.

The presented approach determines the viability of various ESMs including an assessment whether to renovate the existing building or to replace it with a new building. Furthermore, the approach evaluates the durability of the ESMs. The first part of the method is adapted to building retrofitting from the method presented by Petersen and Svendsen (2012), and the energy price is used as constraint to determine the amount of building retrofitting for implementation. The durability of the measures is evaluated based on hygro-thermal measurements and experiences in a test apartment of a multi-family building.

2. Approach for holistic energy retrofitting

The approach for holistic energy retrofitting is shown in Figure 1, which consider both the profitability of the retrofitting project and the durability of the ESMs. First step was to determine the needed retrofitting and whether the retrofitting should be executed or the building should be demolished and rebuild. Second step was to investigate the ESMs regarding their durability.

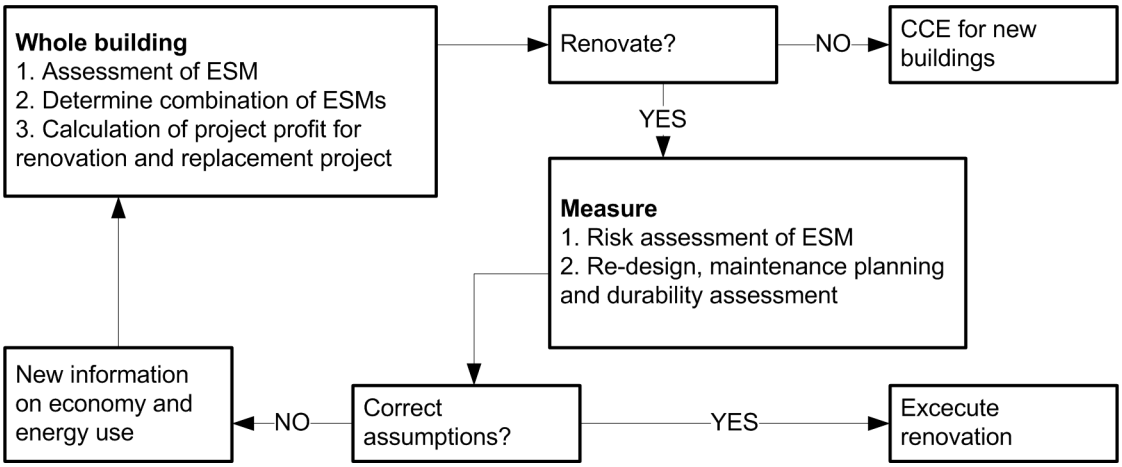

FIG. 1. Holistic energy retrofitting from whole building to energy saving measure (ESM)

2.1 Whole building

The profitability of the whole building retrofitting is based on the cost of conserved energy (CCE) concept described by Morelli et al. (2014) and in the following bullets 1-3. This concept allows for a decision-making on whether to invest in ESMs or buying energy, as the CCE results are directly comparable with the energy price.

1. Assessment of ESM and determining the inter-relationship between the CCE_R (€/kWh), which is the marginal CCE for the different measures. From Eq. (1) the energy use can be expressed as a function of the CCE_R which enable a direct comparison of the ESMs.

$$CCE_R = \frac{t \cdot a(n_r, d) \cdot I_{measure} + \Delta M_{year} + \Delta E_{operation,\,year} \cdot P_{energy\ type}}{\Delta E_{year}} \quad (1)$$

where, t is a reference period that enables a comparison of measures with different service life and is defined as the ratio between the reference period, n_r (years), and the useful lifetime, n_u (years); $a(n_r, d)$ is the capital recovery rate, for which d is the real interest rate (absolute number); $I_{measure}$ is the marginal investment cost (€), where $a(n_r, d)$ I is the marginal*

annualised investment cost(€); ΔM_{year} is the change in annual maintenance cost (€); $\Delta E_{operation,year}$ is the annual change in energy consumption during operation of the measure (kWh); $P_{energy\ type}$ is the energy price for the energy type used for operational energy (€/kWh); ΔE_{year} is the annual change in annual energy conserved by the measure (kWh).

This, however, is easily applicable for continuous ESMs e.g. insulation materials, but not for discrete measures e.g. windows and ventilation. Therefore, a five step algorithm was formulated to rank the discrete ESMs (Morelli et al., 2014).

A. A first reference is determined among a number of components based on their investment cost and annual energy use. The components are ranked according to investment cost, and the component with lowest cost is chosen as reference. If the investment cost is identical for two or more components, the component with lowest energy use should be chosen as reference, and the other components should be omitted due to the higher energy use. For existing components the investment cost will be the refurbishment cost, thus the component performs as when it was newly installed.
B. The marginal CCE_R for each component is calculated applying Eq. (1) using the reference component determined in step A. Components with negative values of CCE_R are omitted because they use more energy combined with a higher investment than the reference component determined in step A.
C. A new reference is determined based on the marginal CCE_R derived in step B. The component with the smallest positive marginal CCE_R is chosen as a new reference to form a curve. From the remaining components, those with an energy use equal or higher than the new reference are omitted as they are not ESMs compared to the new reference
D. The marginal CCE_R for each component is calculated applying Eq. (1) using the reference component determined in step C and its respective investment cost and energy savings. Step C and D are repeated until there are no more components to consider.
E. The reference component found in step A and those determined in step C are listed in the order they are determined. These discrete components are thereby transformed in to a continuous CCE_R function by calculating the marginal CCE_R according to Eq. (1).

2. The method suggest that the determination of a combination of ESMs is defined as the energy weighted average marginal CCE_R of the measures ($CCE_{R,average}$ [€/kWh]) equal to the energy price, Eq. (2). First the discrete measures must be chosen as close to the energy price as possible, and thereafter adjusting the $CCE_{R,average}$ by choosing the continuous measures, thus the $CCE_{R,average}$ equals the energy price.

$$CCE_{R,average} = \frac{\Delta E_1 \cdot CCE_{R,1} + \Delta E_2 \cdot CCE_{R,2} + \ldots + \Delta E_n \cdot CCE_{R,n}}{\sum_1^n \Delta E_i} \leq P_{energy\ type} \qquad (2)$$

where, E_n is the energy consumption for the ESM n (kWh); $CCE_{R,n}$ is the cost of conserved energy for the ESM n (€/kWh);and, $\sum_1^n \Delta E_i$ is the sum of the individual energy consumptions of all ESMs (kWh).

3. Calculation of the economic project profit considering whether to renovate the building or replace it with a new building. The profit of any given project is determined on the basis of the market value (MV) for the retrofitted building, or a newly erected building, minus the investment cost (I),which can also including the transaction costs, and the discounted (1/capital recovery rate) maintenance and operational (M&O) costs, as given in Eq. (3). If a new building is erected at the exact same location as the existing building, the cost for demolishing (D) the existing building must also be included. The building project that should be undertaken in economic terms will be the one having the highest profit.

$$Profit = MV - \left(I + D + \frac{M\,\&\,O}{a(n_r, d)} \right) \quad (3)$$

2.2 Measures

Two types of ESMs were investigated, i.e. 1) two types of interior insulation and 2) four different measures to improve the windows. These measures were investigated in full scale in the test apartment.

The risk of failures was identified for an interior insulated masonry-wooden beam assembly applying Failure Mode and Effect Analysis (FMEA) (Stamatis, 2003). The critical points, found in the FMEA, were investigated by full scale measurements of temperature and relative humidity behind the interior insulation and in the wooden beam embedded in the masonry.

The four window measures were installed in the test apartment and their energy performance was calculated based on the energy balance (Morelli et al., 2012).

3. Multi-family building – a case study

A typical building in Copenhagen, Denmark, dated from the period 1850-1930 was used as case. The building with 30 apartments had six storeys with a floor to floor height of 2.6 m and a gross floor area at each storey of 453 m^2. The solid masonry facades were deemed worthy of preservation and the windows constituted 27% of the overall façade area. The windows were with a single pane; however, the windows on the street façade had a secondary glazing installed. The un-insulated floor divisions were constructed with wooden beams and clay pugging. The building was natural ventilated by opening windows, infiltration and ventilation ducts located in the kitchens and bathrooms. Furthermore, the building employed central heating produced from district heating. A detailed description of the building is given in (Morelli et al., 2012) where the pre-renovation energy consumption for the building was determined to approx. 160 kWh/(m^2 year).

3.1 Description of energy saving measures

Two interior insulation materials were tested. i) A combination of aerogel and stone wool fibres with a gypsum board mounted on the surface, hereafter referred to as MiWo-Aero, which has a thermal conductivity of 0.019 W/(m2 K). ii) Vacuum insulation panel (VIP) having a thermal conductivity of 0.005 W/(m^2 K) for a thickness of 20 mm under 1 mbar pressure. The four window measures are briefly described in Table 1 where the numbers of panes refer to the total amount of panes in the window (Morelli et al., 2012).

TABLE 1. Energy data for window measures

#	Window type and retrofit measure	U_W [W/(m^2K)]	g_w [-]	E_{ref} [kWh/(m^2 year)]
	Ref. with 1 layer normal pane	4.05	0.51	-266
	Ref. with secondary pane (2 panes)	2.20	0.45	-109
1	Refit with secondary pane (3 panes)	1.09	0.38	-24
2	Refit with secondary pane (2 panes)	1.62	0.44	-59
3	Refit with sash on casement (2 panes)	1.76	0.44	-72
4	New with coupled frames (3 panes)	0.96	0.33	-21

3.2 Whole building assessment

For the economical assessment of the whole building retrofitting, a reference period of 30 years was considered, which corresponds to a typical loan period for building investments but also the

approximated service life of many building components. The real interest rate was set to 2.5% and expresses the amount that the nominal interest rate is larger than the rate of inflation. The energy price in 2040 for heat based on renewable energy sources was determined to 0.15 €/kWh by Morelli et al. (2014), whereas todays energy price was 0.09 €/kWh. The graphs in Figure 2 for interior insulation and window measures are based on Eq. (1). Similar figures were developed for each ESM. Applying Eq. (2) and choosing discrete ESMs before continuous ESMs the amount of ESMs in Table 2 were obtained, which correspond to an energy consumption for the building of about 45-50 kWh/(m^2 year) depending on the energy price (Morelli et al., 2014). The measures implemented were: demand controlled ventilation, new windows, insulation towards basement and attic as well insulation on the inside and outside of the walls.

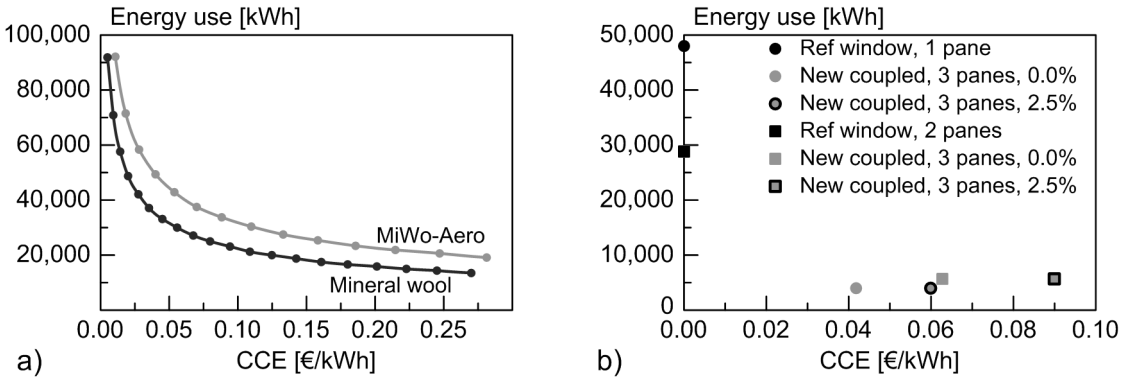

FIG 2. Energy use as a function of CCE_R for a) 2 types of interior insulation and b) windows with single pane and single pane with secondary pane (Morelli et al., 2014)

TABLE 2. Amount of energy saving measures in relation to energy price and interest rate of 2.5%

Energy price	0.09 €/kWh		0.15 €/kWh	
Measure #	CCE [€/kWh]	Type [-]	CCE [€/kWh]	Type [-]
Mechanical ventilation	0.22	Central DCV	0.22	Central DCV
Windows – yard	0.06	New 3 panes	0.06	New 3 panes
Windows – street	0.09	New 3 panes	0.09	New 3 panes
Floor to basement	0.06	50 mm	0.14	105 mm
Floor to attic	0.06	260 mm	0.14	435 mm
Wall- interior insul.	0.06	80 mm	0.14	140 mm
End wall – exterior insul.	0.06	50 mm	0.14	90 mm

The evaluation of whether to renovate the building or build a new, according to Eq. (3), was based on presumptions of market values, renovation cost of the building and theoretically energy consumption (Morelli et al., 2014).

In connection with the building renovation new bathrooms and kitchens would be installed, which was included in the investment cost of the renovation given in Table 3. The retrofitted building was compared to a new building fulfilling the Danish Building Regulations in 2015 corresponding to a total energy consumption of approx. 30 kWh/(m^2 year).

TABLE 3. Economic evaluation of retrofitted and new building

Energy price	0.09 €/kWh		0.15 €/kWh	
	Refit [€/m^2]	New [€/m^2]	Refit [€/m^2]	New [€/m^2]
Market value	3100	4000	3100	4000

Expenses:				
Investment	695	2200	745	2200
Demolish		90		90
Heat	11	6	18	11
Electricity	3	3	3	3
Profit ±	**2391**	**1701**	**2334**	**1696**

3.3 Experiences with interior insulation from a test apartment

The FMEA conducted on the interior insulated masonry and wooden beam assembly focused on the three main structural parts; masonry, wooden beam, and insulation including vapour barrier. The results were as given below in prioritised order (Morelli & Svendsen, 2013).

1. Collapse of the wooden beam due to moisture penetration into the structure.
2. Loss of adherence between the brick and mortar.
3. Mould growth behind the interior insulation.

The first and last failures were investigated by measurements of temperature and relative humidity in the beam and behind the insulation. Figure 3 shows the results for insulation installed to a northeast facing wall and placed between the ground and first floor. After dismantling the MiWo-Aero product on first floor no visible signs of mould growth were present, which was documented through Mycrometer surface tests (measurements on bio-mass from a swap).

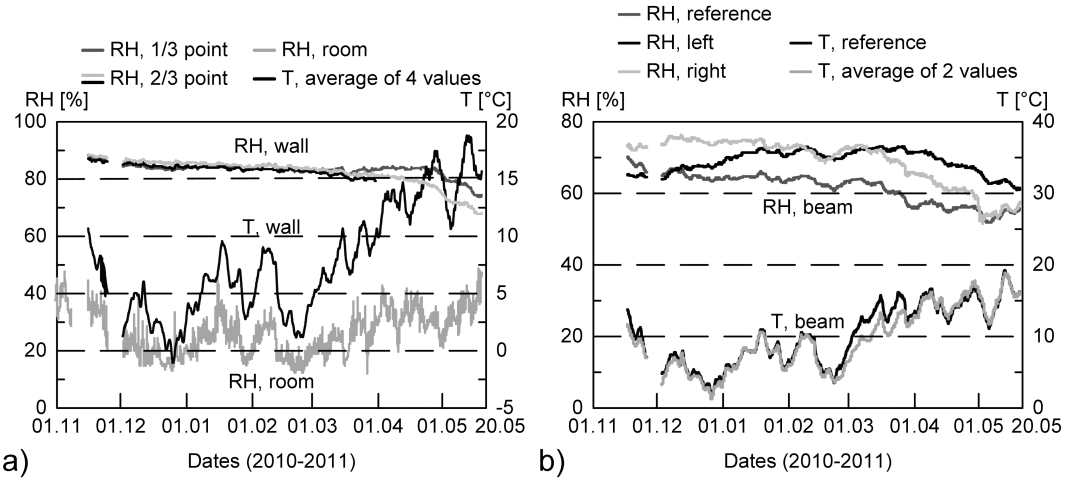

FIG 3. Temperature and relative humidity a) behind inside insulation and indoor relative humidity; and b) in the wooden beam and temperature in the exterior climate (Morelli et al., 2012)

The MiWo-Aero product was reasonably easy to work with, but the product could not take up any deviations on the surface of the wall. Consequently, the preparation of the wall ensuring a relatively smooth surface was very important, thus the applied insulation likewise provided an even, flat surface. However, the mineral fibers in the MiWo-Aero product did not have enough adhesion to keep the gypsum board fixed to the surface of the insulation resulting in a gap between insulation and gypsum board. In comparison to the MiWo-Aero product, the VIP product was a challenge to work with. Specifically, the VIP product needed to be ordered in specific sizes, given that no on site changes could be made, if incorrect sizes were delivered. Furthermore, the VIP product needed special care as the VIP panels were easily punctured; thereby increasing their thermal transmittance from 0.005 W/(m^2 K) to 0.019 W/(m^2 K).

4. Discussion

The economical assessment can be used by decision-makers to determine whether to renovate their building or demolish it and thereafter erect a new building. The approach can be applied at different stages of projects, and for a comparison of different ESMs. The method is easily adjustable to different energy prices, what on the one hand is an advantage of the method, because the energy price is difficult to forecast. On the other hand, this implies that care must be taken using the method, because the energy price strongly influences the optimised combination of ESMs. However, the study showed that doubling the energy price did not change the buildings energy usage significant. This could indicate that an upper limit for implementing ESMs is reached regarding insulation measures. Nevertheless, other measures might further reduce the building's energy consumption, e.g. technical installations excluding mechanical ventilation, as technical installations were not considered in this study. A reduction of approx. 70% in energy consumption is achieved after retrofitting, which is close to the expected requirement for nearly zero energy buildings.

The economical assessment, in the twofold holistic energy retrofitting approach, relies on two main assumptions, i.e. maintenance cost and operational costs. A verification of these assumptions is needed for the holistic energy retrofitting method before making the final decision whether to retrofit or replace the building. Installing interior insulation on solid masonry walls with embedded wooden beams, the wooden structure becomes critical parts, due to the outer wall's changed moisture balance. This could cause premature deterioration of the beam. However, the measurements are about 5-10% RH higher as compared to the reference measurement. A RH below 75% does not pose a risk for the durability of the beam end. These measurements were performed in a northeast facing wall that received, given its orientation and location on the building (between ground and first floor), a limited amount of wind driven rain and direct exposure to sunlight. Based on Isopleths information provided in (Sedlbauer, 2002) a risk for mould growth could be present when interpreting the measurements. The temperature is around 10 °C and the RH is 85%; in such instances under these conditions the germination time is about 2 days. However, there were no visible signs of mould growth on the wall after dismantling the MiWo-Aero product. In case, the measurements indicated risk for wood rot or mould growth, new retrofit measure should have been suggested, installation of monitoring devices or planning maintenance including economically considerations. These new assumptions should then be included in a second round of calculation according to Figure 1 determining an optimised retrofitting.

The two critical points related to mould growth and wood rot reveal, in this study, no expected increase in maintenance or operational cost for the ESM. However, the durability of the MiWo-Aero product itself did not show the expected service life, as the gypsum board and insulation material could not stay fixed. This would increase the maintenance cost, if this insulation material was to be used. Relying on the VIP product a significant cost for planning had to be included, thus the needed sizes of VIP panels are ordered and installed in the building. In worst case, this could lead to many poor assemblies and together with a potential increased thermal transmittance by punctured VIP panels this would result in overestimations of the energy savings or increases in operational cost.

Through these two simple examples of insulation materials the significant of the durability is shown when approaching a holistic energy retrofitting in an early project stage. Especially, when considering new materials such as the MiWo-Aero and VIP products. In instances, where either the MiWo-Aero or VIP products are the only materials considered as interior insulation, one could have entailed a significant increase in cost for maintenance, operation or even installation. A more difficult parameter to appraise is the loss of living space due to installed interior insulation, which also should be accounted for in the holistic energy retrofitting approach.

5. Conclusion

An approach for holistic energy retrofitting is developed that consider both the economical profitability of the energy saving measures (ESMs), whether to retrofit the building or demolish it and

build a new building, and the durability of the ESMs. The economic assessment integrates methods of component-based optimisation and evaluation of the project economy for building renovation measures. A trade-off between investing in ESMs and buying energy is established entirely on the predicted future renewable energy price. The method uses the marginal cost of conserved energy (CCE) to identify an optimised combination of ESMs having the energy weighted average marginal CCE_R equal to the energy price. The profit of the project is determined as the market value deducting the cost for renovation/new building (including demolishing), maintenance and operation. The building with highest profit must be chosen. In cases where replacement of buildings is not an option because of preservation value on facades, not heritage buildings, the method can be used to evaluate, whether it is reasonably to preserve these buildings. Furthermore, the holistic method includes and risk assessment and durability evaluation of the ESMs, thus the energy savings are not the only stimulus for executing the building renovation.

The holistic energy retrofitting approach for building renovation developed is highly relevant to and useful for the many future retrofitting projects.

References

Danish Government. 2011. Our Future Energy. Danish Ministry of Climate, Energy and Buildings. Available from ⟨http://www.ens.dk⟩. (accessed 06.02.13).

Martinaitis, V., Kazakevičius, E. & Vitkauskas, A. 2007. A two-factor method for appraising building renovation and energy efficiency improvement projects. Energy Policy 35, 192–201.

Martinaitis, V., Rogoža, A. & Bikmaniene, I. 2004. Criterion to evaluate the "twofold benefit" of the renovation of buildings and their elements. Energy & Buildings 36, 3–8.

Morelli, M., Harrestrup, M. & Svendsen, S. 2014. Method for a component-based economic optimisation in design of whole building renovation versus demolishing and rebuilding. Energy Policy 65, 305-314.

Morelli, M., Rønby, L., Mikkelsen, S.E., Minzari, M.G., Kildemoes, T. & Tommerup, H.M. 2012. Energy retrofitting of a typical old Danish multi-family building to a "nearly-zero" energy building based on experiences from a test apartment. Energy & Buildings 54, 395–406.

Morelli, M. & Svendsen, S. 2013. Investigation of interior post-insulated masonry walls with wooden beam ends. Journal of Building Physics 36(3), 265-293.

Petersen, S. & Svendsen, S. 2012. Method for component-based economical optimisation for use in design of new low-energy buildings. Renewable Energy 38, 173–180.

Sedlbauer, K. 2002. Prediction of mould growth by hygrothermal calculation. Journal of Building Physics 25, 321-336.

Stamatis, D.H. 2003. Failure Mode and Effect Analysis: FMEA From Theory to Execution. 2nd ed. Milwaukee, WI: ASQ Press.

Tommerup, H. & Svendsen, S. 2006. Energy savings in Danish residential building stock. Energy & Buildings 38, 618–626.

Verbeeck, G. & Hens, H. 2005. Energy savings in retrofitted dwellings: economically viable? Energy & Buildings 37, 747–754.

Destructive testing in buildings – building performance investigation and comparisons with non-destructive testing

Dennis Johansson, Ph.D. [1]
Jesper Arfvidsson, Professor [2]
Hans Bagge, Ph.D. [2]
Lars-Erik Harderup, Ph.D. [2]
Johan Stein, Ph.D. student [2]
Petter Wallentén, Ph.D. [2]

[1] Building Services, Lund University, Sweden
[2] Building Physics, Lund University, Sweden

KEYWORDS: *Destructive, measurements, investigation, inspection, health, status, renovation*

SUMMARY:
It is important to investigate building performance and relate it to health and satisfaction of the occupants in order to enable sustainable and healthy buildings. Studies have been made on performance of buildings and relationships between indoor environment and occupants´ health and satisfaction. However, to really obtain the building performance and construction conditions, such as moisture conditions or material degeneration, it is necessary to look into the construction behind the surface layers, which means that the building must be taken apart. This is usually not possible because it is not allowed or economically reasonable in inhabited dwellings. This paper presents a pilot study of a project that owns the unique possibility of investigating building performance where the buildings will be taken apart to reach behind the surface layers. In this pilot study, the aim was to provide an image of the normal state of normal detached houses after normal aging to assist in the design of energy-saving measures, and to compare with non-destructive testing. Non-destructive and destructive tests were carried out in 14 houses in Malmberget in Sweden. Examples of results are damages found in attics and in wet rooms, but also working houses and good correlation between non-destructive and destructive test results. The pilot study also resulted in a number of useful methods for destructive testing behind the surface layers to enable efficient destructive testing in the main project where 148 apartments will be investigated in Kiruna starting 2013.

1. Introduction

Much of the housing stock built since the late 1940s, not to forget the Swedish ‘Miljonprogram’, where one million apartments were built, is currently in need of major energy improvements and renovations. The design of such actions is today often based on assumptions and estimates from the original drawings and descriptions. The materials and properties of the design is assumed to be as new in absence of better information. In practice, the building does not even need to match the drawings geometrically and materially. Beside possible changes between drawings and actual construction, aging, movements and normal use adds to influence on design thermal performance, airtightness, moisture protection and other building technical performance. The uncertainties are thus embedded in the structure and become even more pronounced over time. Normally it is not considered to be an option to study the current status of renovation projects in detail, which leads to unsafe conditions and hence uncertain results. A good knowledge of the condition of a building is necessary to assure the quality of the final result with redevelopment. At design of the redevelopment, and if there are no

reported or presumed damages, the condition of an assumed "standard building" is highly relevant for the controlled construction process and subsequent operation and maintenance.

The condition of the building and its components are essential starting points for energy and moisture design and also for the assessment of estimated remaining life time. Early in the planning phase of renovation it must be analysed and identified whether it is reasonable and profitable to replace certain parts of structures or not. The existing components often have unknown properties due to aging, unknown material data, large variations from manufacturing, unknown version, etc. These factors are very important for calculations of moisture levels and energy use. Interaction of these factors will in turn also affect the renovated building's energy use, indoor environment and life time.

Today cases of damaged buildings are inspected and documented. Typical damages are connections between exterior walls and foundation, and exterior walls and windows. Unfortunately, these reports are not easily accessible and also describe damage houses and not the normality of the building stock. Purchase inspections could provide an overall picture of a building's normal state, but they include only inspection of the visible surfaces and are not normally at the hand of the actors of the building process. The Swedish National Board of Housing, Building and Planning has recently presented preliminary results from the 'BETSI' study containing surveys and some measurements, but due to type of the study - no destroying testings. Previous studies of non-damaged buildings have been made on a few detached houses (Örtengren, 1988) but otherwise there is very little available material. There are also studies comparing occupants with building conditions but not with the option to get behind the surface materials (Folkhälsoguiden, 2010; Hägerhed, 2006).

1.1 Prerequisites

Ore mining, once founding the cities of Kiruna and Malmberget, is now undermining part of these cities which means that new built areas must be created. A large amounts of buildings will be affected and need to be evacuated and then demolished. Access to some of these buildings has been provided prior to demolition to provide an opportunity to develop methods for studies using destructive testing. In the future, a larger amount of buildings will be studied based on the methods found in this study. The focus is on areas that affect energy efficiency, moisture control and indoor environment and the users of the buildings. The projects was carried out in collaboration with the real estate owner LKAB Fastigheter and Kirunabostäder, which own and run a large number of the buildings to be demolished.

1.2 Aim

The overall aim of developing methods that use destructive testing is to reduce uncertainty in the implementation of energy improvement measures in existing buildings with regard to energy, indoor environment and sustainability. Objectives are to

- reduce uncertainty in the implementation of measures in existing buildings
- develop better models and input data for efficient and optimized new construction
- develop methods for efficient and optimized renovation
- describe relationships between residents' health and experience of their indoor environment and the physical conditions of the building
- develop methods for non-destructive testing

The part of the study reported in this paper aims to develop methods and efficiency for destructive testing and to connect the results to indoor environmental questionnaires in a few, still habited, houses in Malmberget. This will result in

- a picture of the condition of a number of cross sectional buildings after normal aging

- methods for combining destructive testing of buildings with epidemiological surveys of the buildings' occupants as a basis for studies on a larger scale in Kiruna
- condition of selected structural elements beyond what normal inspections provide
- a comparison between destructive and non-destructive testing methods
- an overview of the experienced indoor environment in the houses

Only a few houses were investigated which means that the result will not be statistically founded and conclusions must be drawn with caution.

2. Method

Suitable buildings to study was provided in the city of Malmberget, lat N67.2°, lon E20.6°, 69 km north from the Arctic circle. The area is called 'Elevhemsområdet' and was be completely erased during 2012. These buildings were from the 1960s. Methods of destructive testing were developed in this area by Arfidsson et al (2011) (Johansson et al (2012). On previous visits an overview of the area was made together with the mining company LKAB who has the responsibility to find new homes for people in the area. The selection was also made in cooperation with GMG Bygg och Maskintjänst who carried out the demolitions in the area. The remaining houses were remaining due to different aspects such as to demolish entire neighbourhoods at a time. In total the study contained 19 houses in Elevhemsområdet, see Figure 1, noted house 1-19, of which 7 were also investigated by non-destructive methods, houses 1-7. Questionnaires based on the Swedish BETSI study with some additional questions concerning the life span of the house were distributed to the 13 houses that were supposed to be demolished last during the summer of 2011. Heating season would have been preferred but since the demolition was not scheduled, that would be a risk of losing the data.

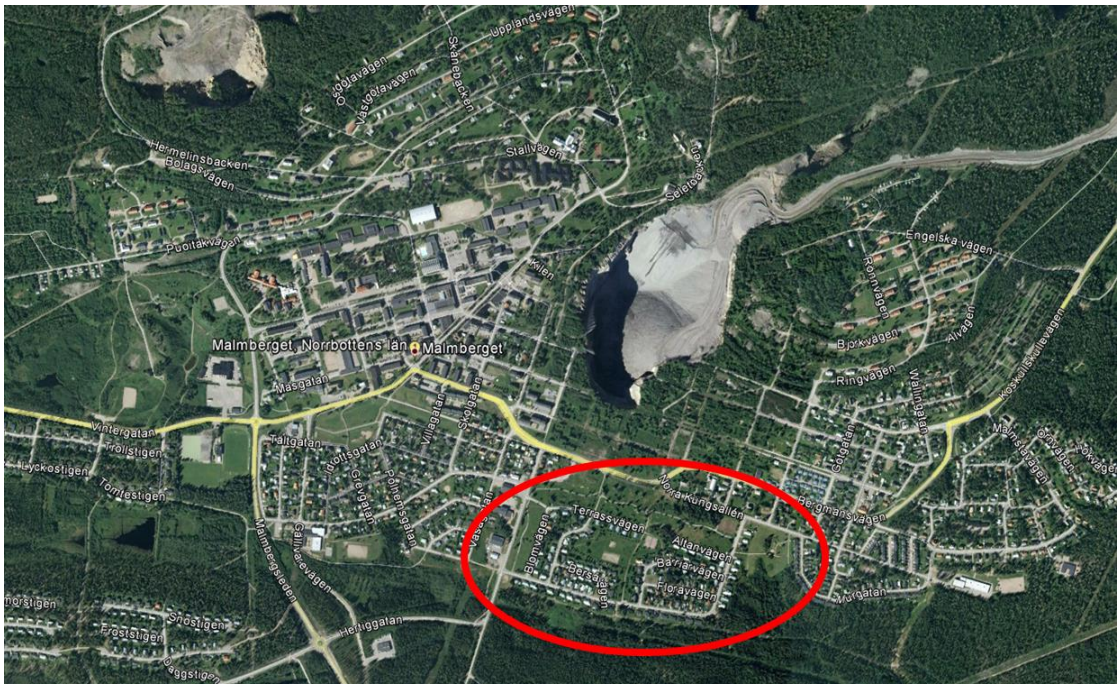

FIG 1. Elevhemsområdet in Malmberget that was the base for selecting the tested 19 houses and is now erased.

The implementation followed the following steps

- Selection of questionnaire for the investigation of the indoor environment and distribution together with loggers for temperature and relative humidity in some of the houses
- Non-destructive testing, which means normal sales inspection
- Planning of specific sampling in the houses.
- Sampling of the houses in place in Malmberget
- Analysis of samples in the laboratory and compilation of results.

2.1 Mould index analyses

Mould is quantified by the method of Johansson (2012) described in Figure 2.

Rating		Description of extent of growth
0		No mould growth.
1		Initial growth, one or a few hyphae and no conidiophores.
2		Sparse but clearly established growth; often conidiophores are beginning to develop.
3		Patchy, heavy growth with many well-developed conidiophores.
4		Heavy growth over more or less the entire surface.

FIG 2. Mould quantification by Johansson (2012).

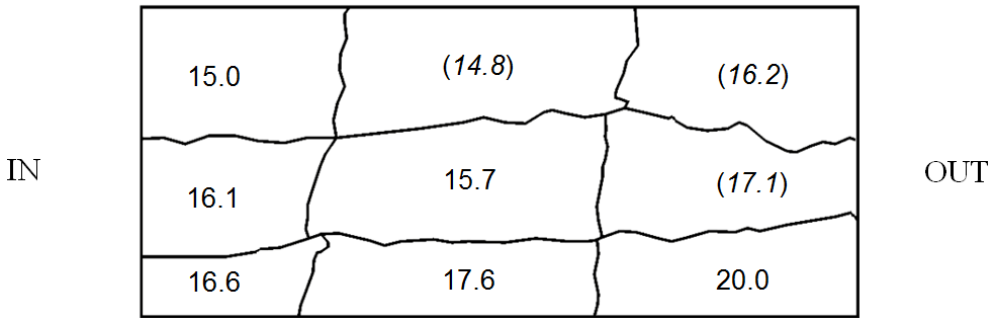

FIG 3. Moisture content in % for house 1.Paragraphed values mean that there was resin indicating a too high value in the measurements.

3. Results

Houses 1-7 were examined by non-destructive inspections and destructive testing including a hole between two studs in a systematically chosen outer wall. Houses 8-14 were examined by smaller holes in the walls, and in all, 1-14, samples were taken from the attic. Houses 15-19 were having answers on the questionnaires together with three of the houses 1-14. Arfvidsson et al (2013) give a comprehensive presentation of findings from each house. Physical examinations were made in May 2012.

FIG 4. The wall investigation of house 1. It is dirty in the outer parts from the outside asphalt impregnated board but without apparent moisture damages.

3.1 Sill tests

A part of the sill at the ground level was taken out from houses 1-7. Figure 3 shows the moisture content in % from house 1. The methods of measurements are specified by Arfvidsson et al (2013). This sample had a clear mould odour and there was a moisture damage. All the other samples showed lower values. It is not clear if the normally lower values depend on houses not habited for a while, dry outdoor climate, high quality wood or something else.

3.2 Walls

All 7 examined outer walls between studs except 1 had brick facade. These brick facades are all lacking ventilation in the intended air gap and in some cases air gap is missing. Most commonly, an intended air gap behind the bricks was followed by asphalt impregnated soft fibre board. The supporting structure varies between standing studs with mineral wool between to standing boards with outside insulation. If there are standing studs, generally there is an inner surface of boards. The inner surface material is in all cases a soft porous wooden fibre sheet with wallpaper. Asphalt impregnated paper is usually used as air and vapour barrier on the inside. In many cases the insulation material is mineral wool, and in some cases paper or saw dust. Figure 4 gives examples from the wall investigation between the studs in house 1.

3.3 Attics

All houses, 1-14, had cold attics which is a known risk construction. Boverket showed that 18% of houses built before 1976 with cold attics had mould odour or mould. Viitanen (1996) described mould growth. Table 1 gives the mould index for all houses, 1-14. All attics were affected by mould to very varying extents. Figure 5 shows the most extreme example where the occupant had installed a ventilation duct between the washroom and the attic. The joist between living volume and attic was most problematic, insulation was not apparently correlated to moisture, and there was some cases of mould even if visual inspections did not show it.

TABLE 1.Mould index in the attics of house 1-14. 'Paral roof' means parallel roof. If there is no metal roof, there is brick roof. 'Insul' and 'Saw dust' means number of cm of insulation material. Then there is mould indexes for the different construction elements of the attic.

Nr	Metal roof	Paral roof	Poor vent	Leak	Insul	Saw dust	Tot	Board index	Upp beam index	Truss index	Joist index	Other index
1	yes	yes			15		15			4		4
2	yes			yes	10	20	30			2	4	
3	yes				10	20	30		1	2	3	
4	yes					14	14			3	3	
5	yes		yes			20	20		4	3	4	
6	yes		yes		10	15	25	4		2	1	
7	yes					15	15			1	4	
8					20	25	45	2		2	2	
9	yes		yes		10	25	35	1		3	2	
10	yes					20	20		3	2	2	
11	yes	yes			22		22	2		3		3
12					20		20	1		2	4	
13	yes					15	15	4		2		4
14		yes			10		10	4		4		

FIG 5. Mould growth in the cold attic of house 13.

3.4 Questionnaires

In 4 of the 8 houses with responses of the 13 questionnaires distributed, the occupants had lived in the house for more than 10 years, in 1 house between 6 and 10 years, and in 3 houses in between 3 and 5 years. In 3 of the houses they were very happy with the dwelling, while in the other houses they were quite happy with the dwelling. In the houses there are different types of window opening patterns from not at all to several hours a day. There were complaints about high indoor temperatures during summers and low during winters and that it was difficult to control indoor temperature. .In 6 houses there was complaint on food smell spread, and in 5 there was sometimes bad odour. Symptoms from eyes or nose are reported in 6 houses but not believed by the occupant to be caused by the indoor environment.

4. Discussion and conclusions

The opportunities with destructive testing in buildings have been shown and methods have been developed to enable future research to deepen understanding of how buildings act as systems over their life cycle. This provides an opportunity to knowledge feedback to the building industry and ultimately it will lead to both better and more optimal buildings and better competitiveness in the construction industry. The study has also given results from some houses that have been normally aged.

Comparisons between non-destructive and destructive tests can be done at two different levels. Firstly, one can compare if damages are consistent, secondly, the construction can be compared. Inspections, which are normally non-destructive, should give fewer and more uncertain results of a building performance because the destructive testing enables access to more of the construction. On the other hand, the time that has elapsed since the occupants have moved out affect moisture damages and conditions. In this and related studies, there has usually elapsed some time between move out and investigation.

What was seen in this study was that a lot coincide between inspections and destructive investigations, but there are differences both regarding construction details and actual damages. Looking at the exterior of the building should imply almost similar constructions, but the destructive testing shows discrepancies in for example air and vapour barriers and air gaps. The clear damage that was found in house 1 was shown in both inspection and investigation. On the other hand, the destructive testing in this study is also based on random checks and not total. There can be damages everywhere even if it is reasonable to believe that the construction details are the same within the same house. In the study, the choice of check points has been systematic in a random way and not based on suspected risk of damage.

Moisture measurements that reflect the habited conditions are a problem when there is the time elapsed between move out and investigations. An alternative could be to keep the dwelling heated and with a synthetic moisture production to that preferable should have been measured in the same dwelling. Arfvidsson et al (2011) showed that out of 3 outdoor wash room walls 2 were mouldy. In the present study there was no systematic way to test outdoor washroom walls.

The demolition schedule together with the relatively low number of houses in the study unfortunately resulted on only a few investigated houses with questionnaire response. Therefore it is difficult to compare questionnaire outcome with physical findings. An example of an indicative correlation is house 5 where a leaky window frame connection coincided with complaints on cold draught. A more extensive project is funded and will start during 2013 dealing with 148 apartments in Kiruna where hopefully there will be more options to find significance.

Mould in cold attics is a non-solved problem and the study points at a need of better constructions for new buildings, renovation projects and existing buildings in operation. This problem is also referring to attics with low amount of insulation, and inspections did not show all the actual problems.

5. Acknowledgements

Thanks to SBUF, NCC, LKAB and GMG Bygg och Maskintjänst for funding and helping out with the study.

References

Arfvidsson, J, Bagge, H, Harderup, LE, Johansson, D, Stein, J, Wallentén, P, 2011, Tillståndsbedömning av naturligt åldrade byggnadskomponenter inför energieffektiviserande åtgärder – en förstudie med fält och laboratorieundersökningar, Department of Building Physics, Lund University, Sweden, TVBH-7234, in Swedish

Arfvidsson, J, Bagge, H, Harderup, LE, Johansson, D, Stein, J, Wallentén, P, 2013, Tillståndsbedömning av byggnader med hjälp av förstörande provning av byggnads-komponenter – kopplingar till brukarnas hälsa och upplevd innemiljö, Department of Building Physics, Lund University, Sweden, TVBH-7236, in Swedish

Folkhälsoguiden, 2010, Bamse – en studie om barn och allergi, Institutet för miljömedicin, Stockholm, http://www.folkhalsoguiden.se/Projekt.aspx?id=1005, in Swedish

Hägerhed Engman, L. 2006, Indoor Environmental Factors and its Association with Asthma and Allergy Among Swedish Pre-School Children, doctoral thesis, Department of Building Physics, Lund University, Sweden, TVBH-1015, http://www.byfy.lth.se

Johansson, D, 2012, Building Performance Investigation in the Arctic by Help of Destructive Testing in Buildings – a Pilot Study, proceedings of Cold Climate HVAC conference, Calgary, Canada

Johansson, P, 2012, Critical Moisture Conditions for Mould Growth on Building Materials, Rapport TVBH-3051 Lund, Department of Building Physics, Lund University, Sweden

Viitanen, H, Vinha, J, Salminen, K, Ojanen, T, Peuhkuri, R, Paajanen, L, Lähdesnäki, K, 2010, Moisture and biodeterioration risk of building materials and structures, Journal of Building Physics, Vol. 33, No 3, pp. 201-224

Örtengren (Sikander), E, 1988, Mögelpåväxt i friska hus, ISBN: 91-7848-148-1, in Swedish

Measurement of heat loss from hot water supply system in a hotel and insulation retrofit

Shuichi Hokoi, Professor[1], Yoshinori Masuda, M. Eng.[1], Tsutomu Goi, Engineer[2]

[1] Kyoto University, Japan [2], Kansai Electric Power Co. Inc. Japan

KEYWORDS: *Hot water supply, Hotel, Heat loss, Storage tank, Heat bridge, Insulation retrofit*

SUMMARY:
In Japanese hotels, 30% or more of the total energy is consumed by the hot water supply. Significant heat loss from such a supply system can be expected because the hot water is continuously circulated throughout the building. In this study, the heat loss was measured from one such hot water supply system for a hotel in the Kansai area. This hotel is 11 stories high with a floor area of 4708 m^2. It is aimed towards businessmen and has a shower in each guest room. The supply water is heated in a gas boiler, stored in a hot water tank, and then circulated via a piping system throughout the building. The temperature and flow rate of the hot water in the piping system were measured in order to calculate the heat loss from both the piping system and storage tank. More than 40% of the heat of the water was lost during circulation via the piping system. Additional thermal insulation was applied to the pipes and storage tank to examine the effect; the heat loss was significantly reduced.

1. Introduction

As of 2012, carbon dioxide emissions in Japan have increased by 6.3% over 1990 levels (National Institute for Environmental Studies 2013). Thus, enormous efforts are required to reduce these emissions, even though the rate of increase in carbon dioxide emissions is decreasing. In the five sectors of industry, housing, commerce, transportation, and power generation, the growth rate of carbon dioxide emissions has remained high in the housing and commerce sectors. A breakdown of energy consumption by hotels shows that 31% is for domestic hot water use (Institute for Building Environment and Energy Conservation. 2001). Thus, reducing the energy consumption of the hot water supply is very important.

In order to reduce the energy consumption of a hot water supply, the whole hot water supply system (HWSS) needs to be optimized. Different types of high-efficiency hot water boilers and heat pumps have been introduced to optimize HWSS operation and reduce heat loss. Since the insulation method and the characteristics of the hot water supply and demand have a great influence on the heat loss, the actual situation should be surveyed. With respect to heat loss through hot water pipes, a wide range of studies have been carried out: from fundamental studies such as investigating the thermal properties of pipes (Iwamoto et al. 2003) and modeling the temperature change in water plugs (Mizuno et al. 1995) to practical examinations of actual systems (Wang et al. 2004, Mae et al. 2004). While there have also been many studies on HWSS and heat loss in houses (Kondo et al. 2011), few studies have considered the heat loss through piping in actual use and minimization of the heat loss of HWSS to reduce the overall energy consumption with regard to hotels.

This study measured the heat loss of the HWSS for a hotel where each guest room is equipped with a shower.

2. Outline of measurement

2.1 Measured hotel and system

2.1.1 Measured hotel

The hotel under study is a business hotel in the Kansai area of Japan with a floor area of 4708 m^2. It has 11 stories with one underground floor for 168 guest rooms. It is made of reinforced concrete with a partial steel structure. The hotel has a restaurant and store with two large baths for common use that are partly exposed to the outside on the top floor. The check-in and check-out times are 15:00 and 11:00, respectively.

2.1.2 Hot water system

Figure 1 shows the schematics of the hotel's hot water supply system (HWSS). The hot water is produced by six gas furnaces on the roof (heating capacity: 551.4 kW, gas consumption: 45.0 m^3/h (13 A)), stored in one storage tank (volume: 4454 L, dimensions: 1400 mm diameter × 2500 mm length), and then sent to the large common-use baths and guest rooms, as well as a cooking room and staff rooms. The unused water returns to the storage tank. Running water is supplied to the tank. When the water temperature drops below 65 °C, the water is sent from the lower part of the tank to the gas furnace and heated before returning to the upper part of the tank.

This HWSS supplies the following facilities with hot water: a washbasin and shower in each guest room, the showers in the large common-use baths, the hot water tap in the cooking room, and the staff rooms. The guest rooms have no bathtub. Since the common-use baths are supplied with hot water from a separate hot water supply system, it was not measured in the present study.

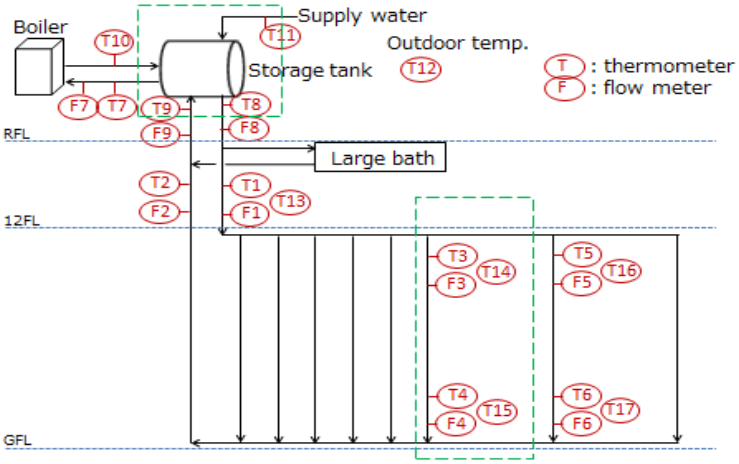

FIG 1. Schematics of measured hot water supply system

2.2 Measurement of temperature and water flow rate

The temperature and flow rate of the hot water in the pipes and the air temperatures at several points in the pipe shafts were measured. Table 1 lists the details of the measured items, and Figure 1 shows the measured points. The letters "T" and "F" denote the temperature and flow rate, respectively. The flow rate of the hot water and running water were measured by the flow meter set in the pipe in units of 0.1 L every 10 s. The hot water temperatures were measured by thermocouples set in the pipes every 10 s. The measurement was started in May 2011.

TABLE 1. Measured items and locations

Location	Measured item
T1/F1	water temperature and flow rate at branch to guest rooms
T2/F2	return water temperature and flow rate at branch from guest rooms
T3/F3, T5/F5	water temperature and flow rate to guest rooms
T4/F4, T6/F6	return water temperature and flow rate from guest rooms
T7/F7	water temperature and flow rate at inlet of gas boiler
T8/F8	water temperature and flow rate to guest rooms,
T9/F9	return water temperature and flow rate from guest rooms
T10	return water temperature from gas boiler
T11	temperature of supplied running water
T12	outdoor temperature
T13	air temperature in pipe shaft at branch to guest rooms
T14/T16, T15, T17	air temperature in pipe shaft on 11th , 3rd, and 2nd floors

3. Measured results

3.1 Water temperature and flow rate between gas boiler and storage tank

As an example, Figures 2 and 3 shows temperature T7 and flow rate F7 of the hot water flowing from the storage tank to the boiler and hot water temperature T10 from the boiler to the tank on October 1. When the water temperature dropped below 65 °C, the water in the lower part of the storage tank was sent to the boiler and returned to the tank after being heated. On this day, the boiler was turned on 13 times. The water was sent from the tank to the boiler at a flow rate of 26 L/10s when the boiler was in operation (Fig. 3).

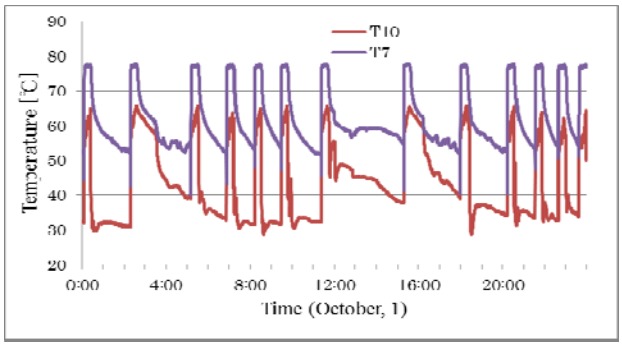

FIG. 2 Hot water temperatures (T7 and T10): October 1

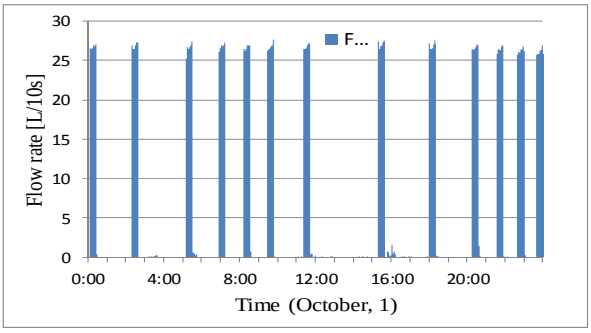

FIG. 3 Hot water flow rate (F7): October 1

3.2 Water temperature and flow rate at exit of storage tank

Figures 4 and 5 show temperature T8 and flow rate F8 of the hot water flowing from the tank to the guest rooms and T9 and F9 of the water returning from the guest rooms to the tank on October 1. The temperature peaks in Fig. 4 occurred at almost the same times as those in Fig. 2. Since return water flow rate F9 was nearly constant (Fig. 5), the difference between the flow rates from the tank to the guest rooms (F9 and F8) can be regarded as the amount of used water (showers at common-use baths, water basin and shower in each guest room, and cooking room and staff rooms) at that time. The water consumption was 0–5 L/10 s.

3.3 Guest rooms

Figures 6 and 7 shows temperatures T3 and T4 and flow rates F3 and F4, respectively, for one vertical

pipeline from the eleventh floor to the second floor. Fig. 6 shows that the difference between inlet temperature T3 (eleventh floor) and exit temperature T4 (second floor) was 2–3 °C. Since such a large temperature drop occurred during the flow from the eleventh floor to the second floor, the heat loss was not negligible.

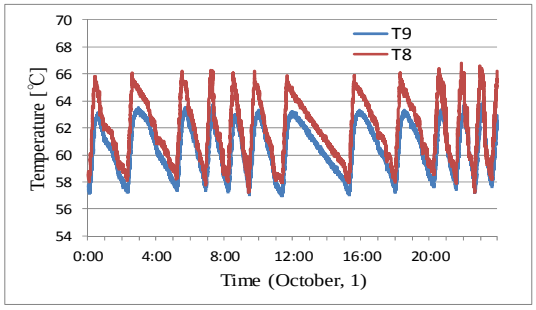

FIG. 4 Hot water temperatures (T8 and T9): October 1

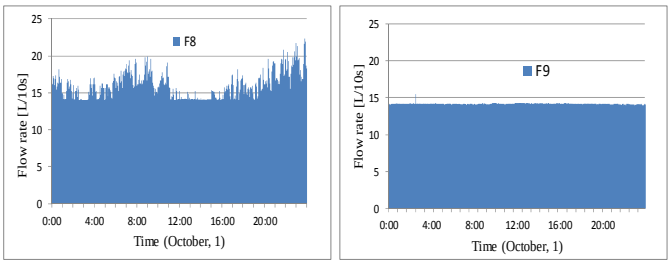

FIG. 5 Hot water flow rates (F8 and F9): October 1

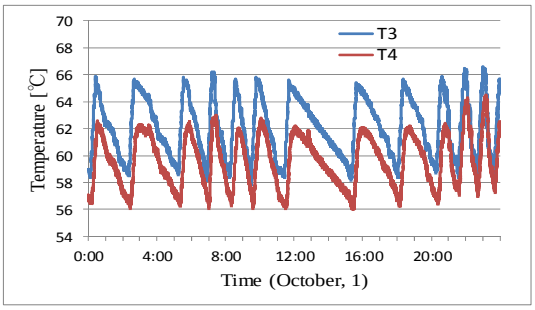

FIG. 6 Hot water temperatures (T 3 and T4): October 1

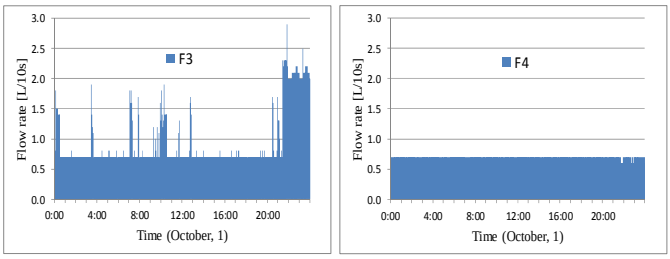

FIG. 7 Hot water flow rate (F3 and F4): October 1

4. Heat loss through hot water system

4.1 Measurement of surface temperatures of HWSS

The infrared radiation temperature was measured around the boiler and storage tank on the roof and at several points in the pipe shafts.

The hot water pipes are insulated by glass wool insulation with aluminum craft and steel mesh, while the storage tank is insulated by a glass wool insulating mold, polyethylene film, and Galvalume plate. Since the reflectivity of the pipe surface was so high that measuring the surface temperature was very difficult, the surface temperature was approximated by attaching tape to the pipes, which lowered the surface reflectivity.

Figure 9 shows the surface temperatures of the hot water pipe in the pipe shaft on the eleventh floor. Since the air temperature in the pipe shaft was about 25 °C, the pipe surface temperature was more than 10 °C higher than the air temperature despite the insulation. Figure 10 shows the temperature of the metal plate supporting the pipe: contact point A was at 45.1 °C. Figure 11 shows the bulb and flange connecting the upper and lower pipes, which had surface temperatures of 56.7 °C. The bulb temperature was also high at 36.9 °C.

Fig. 12 shows the storage tank and supporting leg on the roof floor. All (four) legs showed an area with high temperature. As the outdoor temperature decreased, the amount of outgoing heat became significant despite the surface area not being very large.

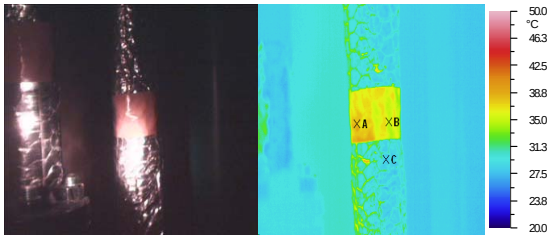

FIG. 9 Pipe surface temperature (T3-T4 pipeline)

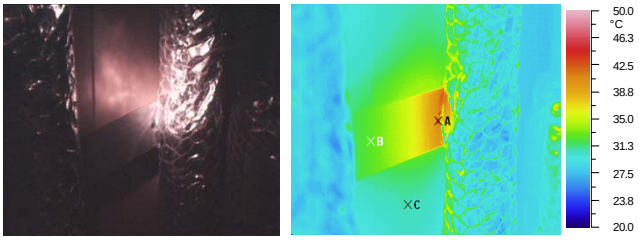

FIG. 10 Temperature of metal support

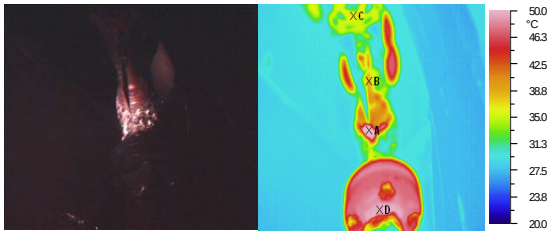

FIG. 11 Temperatures of valve and flange

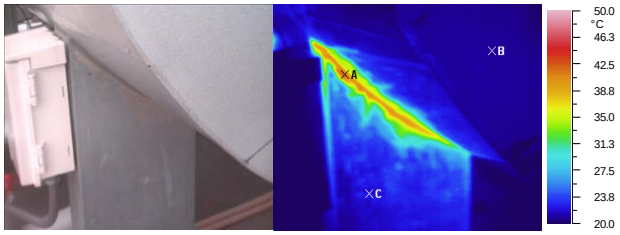

FIG. 12 Temperature of hot water storage tank

4.2 Estimate of heat loss

4.2.1 Method of calculation

The heat losses in the guest rooms and storage tank were evaluated.

Heat loss in guest rooms

Heat loss Q1 [MJ/day] in the guest rooms was determined by the following equation:

$$Q_1 = \sum_t [T_8(t) - T_9(t)] F_9(t) \rho \, c \Delta t \qquad (1)$$

Where ρ [kg/L]: density of water, c [MJ/℃kg]: specific heat of water.

Here, the heat dissipated by cooling of the water remaining in the branch pipes from the main piping to the guest room is neglected and regarded as used heat Q2.

Heat loss from storage tank (Fig. 13)

Used heat in the guest rooms Q2 [MJ/day], heat supplied to storage tank Q3 [MJ/day], and heat lost from storage tank Q4 [MJ/day] were determined by the following equations:

$$Q_2 = \sum_t [T_8(t) - T_{11}(t)][F_8(t) - F_9(t)] \rho \, c \Delta t \qquad Q_3 = \sum_t [T_7(t) - T_{10}(t)] F_7(t) \rho \, c \Delta t \qquad (2)\ (3)$$

$$Q_4 = Q_3 - Q_1 - Q_2 \qquad (4)$$

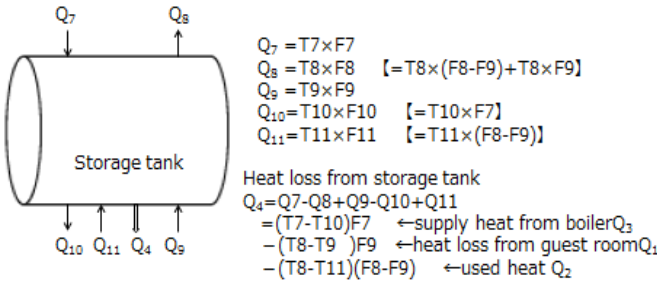

FIG. 13 Thermal calculation of storage tank

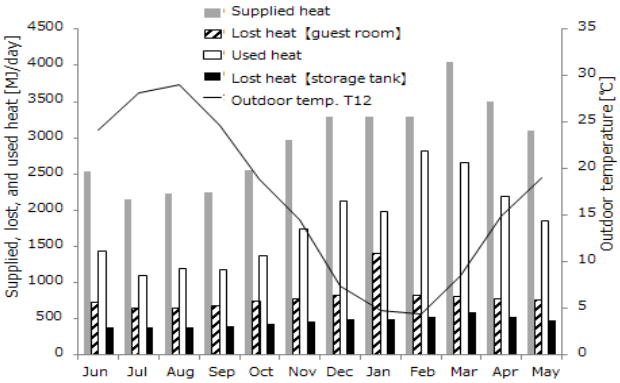

FIG. 14 Supplied, lost, and used heat [June 2011–May 2012]

4.2.2 Calculated results

Figure 14 shows the calculated results from June 2011 to May 2012. The daily values of Q1–Q4 [MJ/day] are shown along with the monthly average outdoor temperature. The supplied heat to the storage tank (Q3) and used heat at the guest rooms (Q2) were low in the summer season while high in the winter season. They were negatively correlated with the outdoor temperature. The heat lost from the guest rooms (Q1) showed a similar seasonal change ranging from 650 MJ (August) to 830 MJ (February). The heat lost from the storage tank Q4 had the same seasonal trend ranging from 380 MJ (August) to 590 MJ (March). This seems to have been influenced by the temperature difference between the outdoor air and storage tank.

5. Insulation retrofit for reducing heat loss

5.1 Outline of insulation retrofit

Based on the measured surface temperatures by the infrared thermo-camera (section 4.1), a significant amount of heat loss occurred. Therefore, the insulation of the hot water pipes and storage tank was retrofitted.

The insulation retrofit area is shown by broken lines in Figure 1, and the outline of the retrofit is shown in Figures 15 and 16. The retrofit to the hot water pipes took place over October 1–3, 2012 and replaced 25 mm glass wool insulation with pipe covers made of 20 mm thick expanded insulation. The retrofit was done for only one pipeline from the eleventh floor to the second floor. The glass wool insulation was replaced with a pipe cover because it seemed to be too tight. Additional insulating cover was attached to exposed parts such as the bulbs and flanges (25th and 26th October 2012). Glass wool insulation with aluminum craft was added to the exposed parts of the connecting flanges and bulbs for the same insulated vertical pipeline.

Figure 16 shows the schematics of insulation retrofit for the legs of the storage tank; this was carried out on October 18–20, 2012. The entire leg was covered by 50 mm thick glass wool insulation and finished by Galvalume plates.

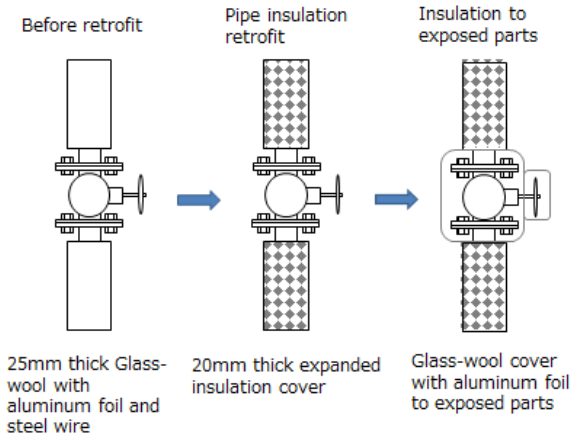

FIG. 15 Insulation on pipe, bulb, and flange

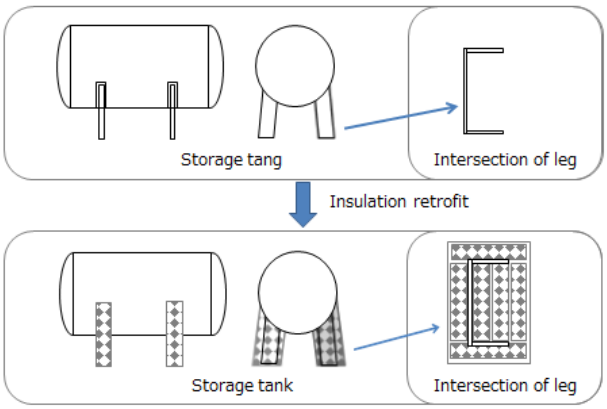

FIG. 16 Thermal insulation to storage tank

5.2 Effect of insulation retrofit

The heat losses before and after the insulation retrofit were compared; heat loss Q3-4 of the retrofitted vertical line (second to eleventh floors) and heat loss Q5-6 of the non-retrofitted line (third to eleventh

floors) were evaluated. Figures 17 and 18 show the results. Heat losses Q3-4 and Q5-6 were calculated from the following equations.

$$Q_{3-4} = \sum_t [T_3(t) - T_4(t)]F_3(t)\rho\, c\Delta t \quad Q_{5-6} = \sum_t [T_5(t) - T_6(t)]F_6(t)\rho\, c\Delta t \quad (5)\ (6)$$

5.2.1 Replaced insulation around hot water pipe (October 1–3, 2012)

The heat loss temporarily increased on October 1 and 2 due to the replacement work. The heat loss of the retrofitted line decreased from 60 MJ/day before the retrofit to 50 MJ/day afterward. Since the heat loss of the non-retrofitted line did not change from 50 MJ/day, the retrofit can be concluded to have reduced the heat loss by 10 MJ/day.

5.2.2 Addition of insulation cover to exposed parts (October 25–26, 2012)

After the insulation was added, the heat loss of the retrofitted line decreased from 50 MJ/day to 40 MJ/day. Since the heat loss of the non-retrofitted line did not change from 50 MJ/day, the retrofit can be concluded to have reduced the heat loss by about 10 MJ/day.

5.2.3 Addition of insulation to storage tank (October 18–20, 2012)

Figure 19 compares heat losses Q4 in March 2012 to those in January 2013 when the mean outdoor temperature was almost the same as that in the previous year (8.6 and 7.7 °C, respectively). The heat loss was 590 MJ/day before the retrofit and 340 MJ/day afterward; thus, the reduction was more than 250 MJ/day.

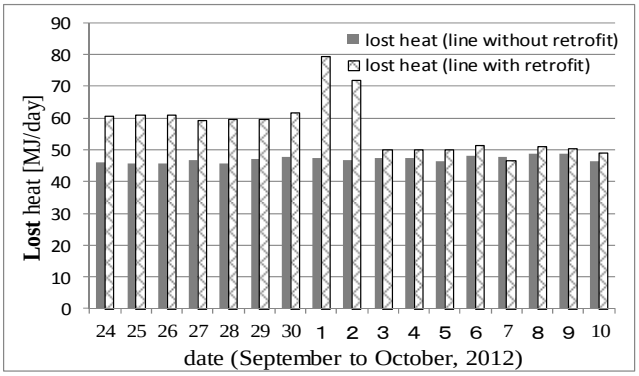

FIG. 17 Heat loss from hot water piping [September 24–October 10, 2012]

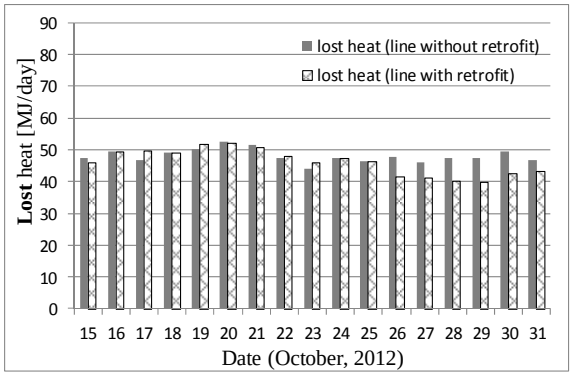

FIG. 18 Heat loss from hot water piping [October 15–31, 2012]

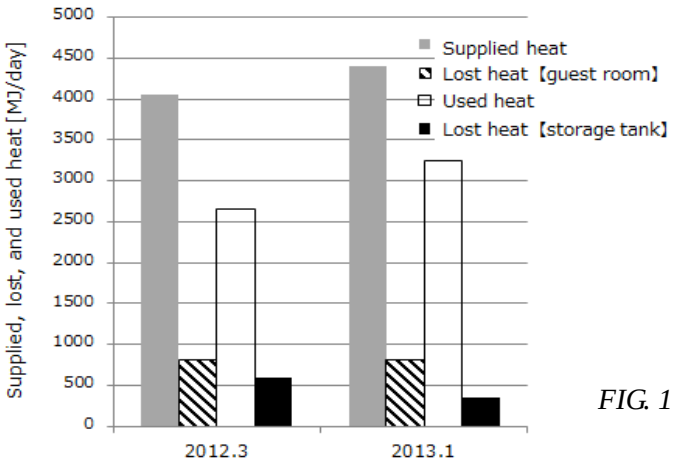

FIG. 19 Heat loss from hot water storage tank

6. Conclusions

In this study, the heat loss was measured from a hot water supply system of a hotel aimed at businessmen in the Kansai area of Japan. The insulation was retrofitted in order to reduce the heat loss. The main results are as follows.

1. During the flow process in a vertical pipeline from the eleventh floor to second floor, the hot water temperature decreased by 2–3 °C, which is a significant heat loss.
2. Thermal bridges were identified at several areas, such as flanges connecting upper and lower pipes, bulbs, and the concrete slab in contact with the pipe. Since the surface temperature of the insulated pipes was rather high, improving the insulation seemed necessary.
3. The heat loss due to hot water circulation throughout the building was more than 600 MJ/day.
4. The supplied heat to the storage tank and guest rooms had a strong negative correlation with the outdoor temperature.
5. Replacing the usual 25 mm thick glass wool insulation with a 20 mm expanded insulation pipe cover reduced the heat loss of one vertical pipeline by about 10 MJ/day (20%).
6. Adding an insulation cover on exposed parts such as the connecting flanges and bulbs of the hot water pipe reduced the heat loss of one vertical pipeline by about 10 MJ/day (20%).
7. Retrofitting the insulation of the storage tank reduced the heat loss by more than 250 MJ/day (42%).

References

Institute for Building Environment and Energy Conservation. 2001. Handbook for Energy Conservation of Residential and Non-residential Buildings.

Iwamoto S., et al. 2003. Study on Evaluation and Design Method of Hot Water Supply System for Dwelling Part 11 A Study on Heat Loss from Hot Water Pipe and Tap, Summaries of Technical Papers of Annual Meeting. The Society of Heating, Air-conditioning Sanitary Engineers of Japan.HASE. PP.1601-1604.

Kondo S. & Hokoi S. 2011. Heat Loss from Hot Water Supply Line in a Residential Building. J. of Environmental Engineering (Transactions of AIJ). No. 669. PP.981-989.

Mae M., et al. 2004. Experimental Study on Low Energy and Resource Saving Technologies for Autonomous Housing. Part 9 Experiment on energy efficiency of hot water boiler. Summaries of Technical Papers of Annual Meeting Architectural Institute Japan. PP.165-166.

Mizuno M. et al. 1995. Heat Loss from Hot Water Drain Pipe. Part 2 Heat Loss from Vertical Drainage Stack. The Society of Heating, Air-conditioning Sanitary Engineers of Japan. No.58. PP.13-21.

National Institute for Environmental Studies 2013. http://www.nies.go.jp/whatsnew/2012/

Wang X., Mae M., Iwamoto S., & Kamata M. Examination on a Thermal Efficiency and Heat Loss of Hot Water Supply System in Dwellings Part 1. J. of Environmental Engineering (Transactions of AIJ). No. 580. PP.61-68.

The role of thermal investigations and user involvement in energy renovation

Marlene Hagen Eriksen, PhD Student [1]
Anne Sofie Lorentzen, M.Sc. Civil Engineering[1]
Carsten Rode, Professor[1]
Søren Peter Bjarløv, Associate Professor[1]

[1] Technical Univeristy of Denmark, Civil Engineering, Denmark

KEYWORDS: *Energy renovation, holistic approach, thermal indoor climate, user involvement, multi-story residential buildings.*

SUMMARY:
Around 75 % of the Danish building stock is built before the early 1970s where the national building regulations started addressing energy. Most of the buildings have not undergone thorough renovation, however the buildings have not exhausted their lifetime either and therefore the potential for energy renovation of the buildings is large. A wide range of technical solutions already exists for energy renovation of buildings, but full benefit of their potential can only be achieved by a holistic approach and by including the users of the buildings.

This paper presents results of technical investigations performed as part of a case study of a holistic energy renovation of a typical pre-war multi-storey residential building in Copenhagen, Denmark. Findings from measurements of the thermal indoor climate are supported by indications from a questionnaire survey among the users of the building. By involving the users early in the renovation process, it is possible to create ownership of the suggested solutions, and thus to enhance the realised performance of the implemented technical solutions. The presented results have been part of a thorough investigation that forms basis for a new concept for holistic energy renovation.

1. Introduction

In the municipality of Copenhagen 90 % of housing stock are multi-storey residential buildings and 85 % of these buildings are built before 1970 (Danmarks Statistik, 2013), where new regulations regarding energy was implemented in the building code. Today 43 % of the Danish energy consumption is for electricity and heating of buildings (Havelund, 2011). Since the regulations concerning energy before 1972 were much less demanding than today there is a huge energy saving potential by renovating old and highly energy consuming buildings. And since quite similar multi-storey buildings represent a large part of the building stock, there is a potential to find generic solutions which can be duplicated, adjusted and applied.

This paper presents the role of pre-renovation investigations of the thermal indoor climate for a multi-storey residential building, covering user perception based on workshops, user surveys and thermal measurements. Based on the results of the survey, it was chosen to do the thermal measurements to investigate if the tendencies seen would be confirmed or disconfirmed by a traditional measure.

The main idea is to involve the residents in the renovation process so the knowledge of the inhabitants, which can be difficult to obtain otherwise, will be taken into account early in process. It is believed that a thorough involvement of users in the building renovation process can increase the value of the project and lead to more holistic projects. This can be obtained through ongoing communication, understanding of the proposed solutions and the sense of being part of the project and being heard. By

giving the end users a share in the early stages of a renovation the chance of them feeling ownership of solutions adopted in the building will increase.

2. Method

As part of the Danish development project "Holistic Energy Renovation of Buildings", different investigations were conducted on a typical pre-war multi-storey building in Copenhagen.
The case building is a 5 storey building from 1935 and it consists of massive brick walls, wooden decks, older windows and an unused attic. The building is naturally ventilated and the flats are heated by radiators in the bedroom and in the living room. The flats are in the size 39 m^2 – 123 m^2 with the main part of the flats about 50 m^2 (OIS, 2013). No thorough renovation of the building has been performed.

The investigations presented in this paper are based on a questionnaire survey conducted on the residents, followed by a workshop including owner, caretaker and residents and finally followed by measurements conducted in different flats. The purpose of combining the activities is to get as much information as possible about both the experienced and the actual thermal indoor climate and to find possible correlations between the different investigations.

The questionnaire consisted of 36 questions concerning general information about the participants, economy, architecture and quality of the building, the building conditions and the perceived indoor climate. The response rate of the 136 possible replies was approximately 18 %. The questionnaire was sent out in May 2012.

The workshop was facilitated by an industrial psychologist from a larger Danish consultant company, focusing on wishes of the participants and the need of the building. Around 15 people participated in the workshop and the output was a sketch of what according to the participants would be "the perfect solution" for the renovation of the building.

The thermal measurements were used to determine the thermal indoor climate in the building. The measurements conducted took place in the last week of February 2013 in four flats. The flats were found representative for the building, being located different places in the building and containing bedroom, living room, hallway, bathroom and kitchen. In all the flats temperature, relative humidity and CO_2 measurements were done, in order to determine the thermal indoor climate. Temperatures and relative humidity was measured in the bedroom, kitchen and bathroom and living room. Additionally the CO_2 concentration was measured in the living room. The loggers were in the living rooms placed in a height 45-100 cm and in the rest of the rooms in heights in the range 90-190 cm.

Flat 1 and 2 have kitchen and bedroom oriented NNE and living room oriented SSE. Flat 2 and 4 have kitchen and bedroom oriented WSW and living room oriented ENE. There were two permanent residents in flat 2 and one permanent resident in the rest of the flats.

3. Results

The results presented in this paper are based mainly on the questionnaire survey and the thermal measurements. The results of the questionnaire survey have influenced the type of measurements chosen to be performed in the flats.

3.1 Temperatures

A part of the questionnaire referred to the residents' perception of the economy also related to energy use. In *FIG. 1* it is seen that more than 50 % of the residents perceive their energy use on heating as

above average or high. This indicates that there perhaps is an issue regarding the use of heating in the building, however it does not imply the reasons for the problems.

According to the replies only 48 % respond positively that they use heating in the bedroom whereas 92 % respond positively on the question regarding the living room.

Furthermore, the residents were then asked if they experienced problems with adjusting the heating in the apartment. The result that can be seen in *FIG. 2* indicates that approximately 50% or more experience problems adjusting the heat sometimes or weekly, most often in the living room.

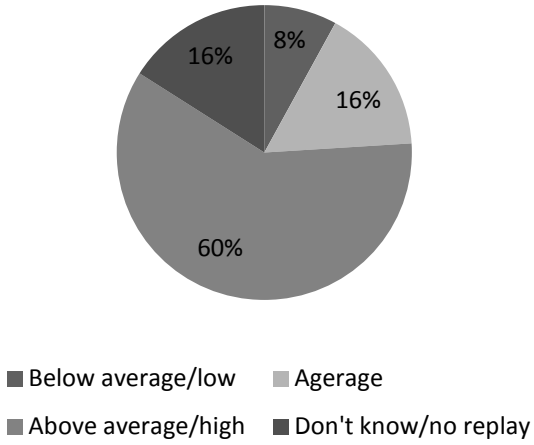

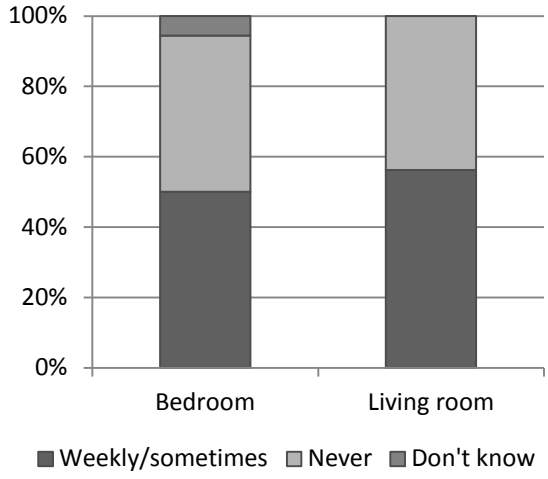

FIG. 1 Perception of energy use for heating

FIG. 2 Problems by regulating the heating

As the last question regarding heating, the residents were asked if it was typically too cold in their apartment during the winter time. The result is to be found in *FIG. 3* and shows that around 50 % or more of the resident's experience that it is often or sometimes too cold in the main part of the apartment during wither time.

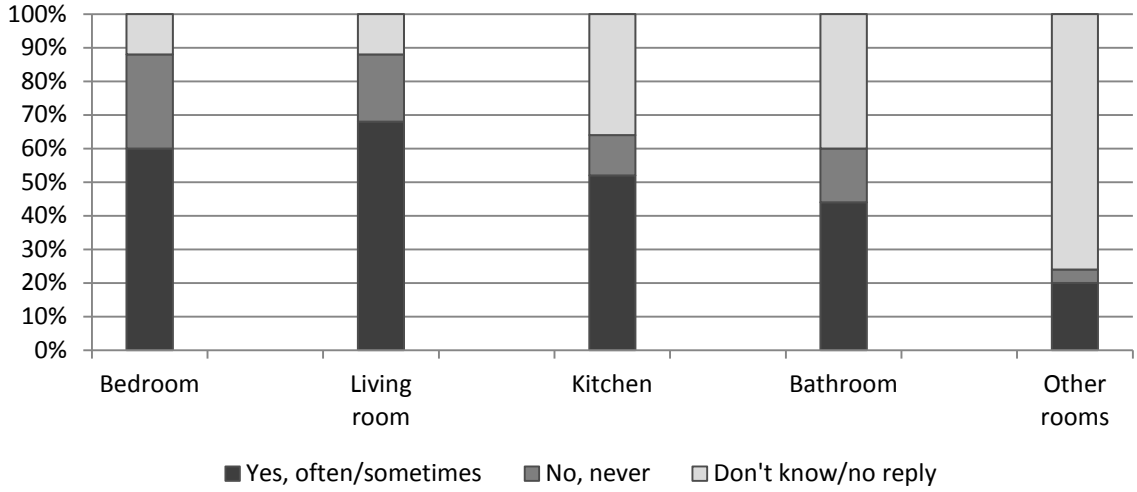

FIG. 3 Perception of too cold in the winter period

The indications found in the questionnaire points towards problems with the heating systems, leaving the flats too cold during wintertime, without the residents being able to influence.

Furthermore, the workshop indicated that a new heating system was a priority for the residents, when asked what they wanted from a renovation.

Therefore temperatures were measured in 4 flats, distributed across most of the building investigated. The results of the measurements in the kitchen can be seen in *FIG. 4*. This graph shows that the measured temperatures in general are in the lower end or outside the comfort zone (20°C-24°C) (Dansk Standard, 1993) in the kitchens, where there is no heating, with an average temperature in three of the kitchens is about 18°C.

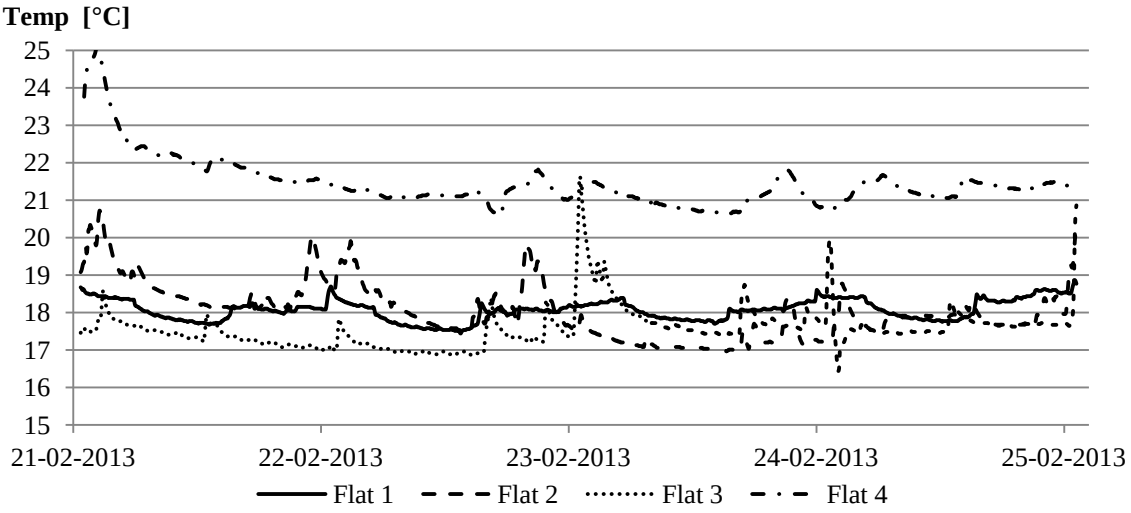

FIG. 4 Measured temperatures in kitchens

Both in the living rooms and the bedrooms, where the radiators are placed, the temperature is most often 18°C – 20°C as seen in *FIG. 5* and *FIG. 6*. In one bedroom the temperature is very low between 10-16°C.

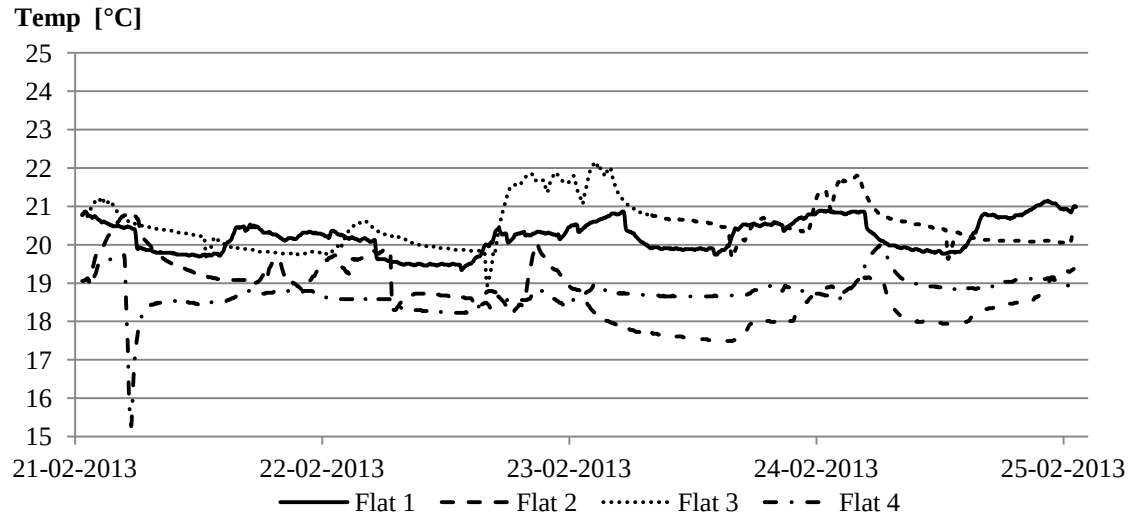

FIG. 5 Measured temperatures in living rooms

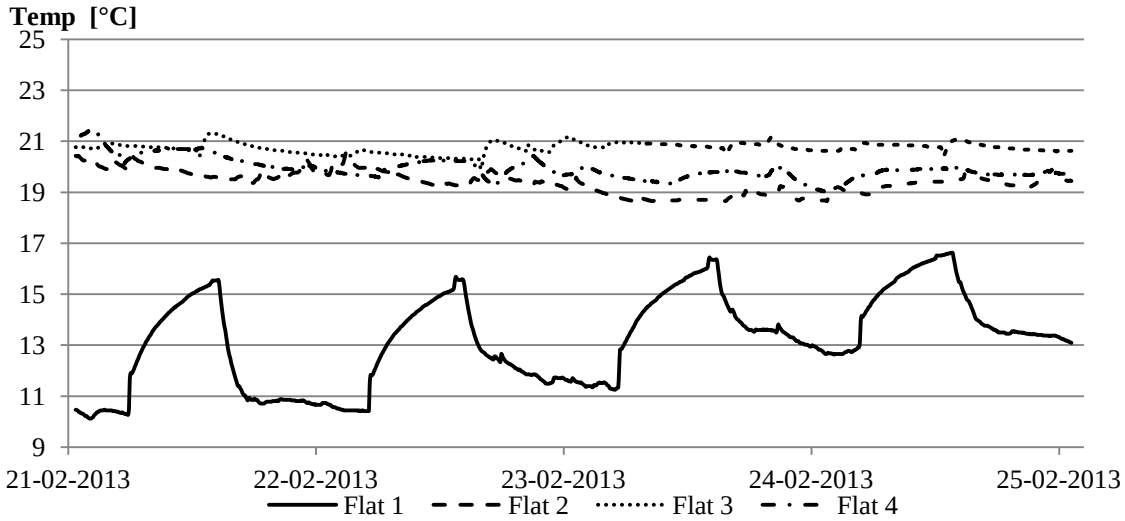

FIG. 6 Measured temperatures in bedrooms

The results of the questionair are supported by the temperature measurements performed, indicating that the heating of the building should be a focus area in renovation of the building.

3.2 Relative humidity

As part of the questionnaire the residents were asked questions regarding the indoor climate, among others about their perception of moisture spots and mould growth. 12 % of the residents responded that they have experienced moisture spots in the living room or the kitchen or in the bathroom and 20 % have according to the questionnaire experienced mould growth on floor, wall or ceiling in the bathroom.

The measurements afterwards performed of the relative humidity in the bathroom underpin the problems with high moisture content and possible problems with mould growth. In peak periods with assumed longer use of hot water, the humidity increases from the normal level between 30-45 % RH up to 95 %, *FIG. 7*. This is a wet though, but for one of the flats the relative humidity first drops to a level under 45 % RH after almost three hours after the peak. This gives longer periods with humidity above 75 % and an increased risk of mould growth on organic materials. Furthermore, this is much higher than the recommended humidity for living rooms below 40-45 % (SBi, 2009).

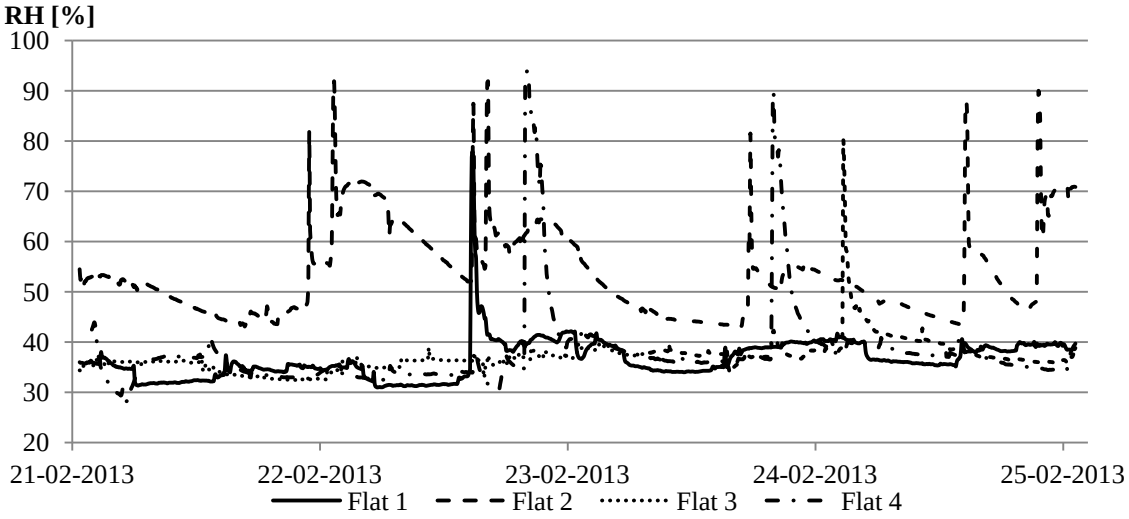

FIG. 7 Measured relative humidity in bathrooms

Also in the kitchen the relative humidity was measured and even without mechanical ventilation, the relative humidity only increased to a level above 45 % RH in one of the flats in peak periods, as seen in *FIG. 8*.

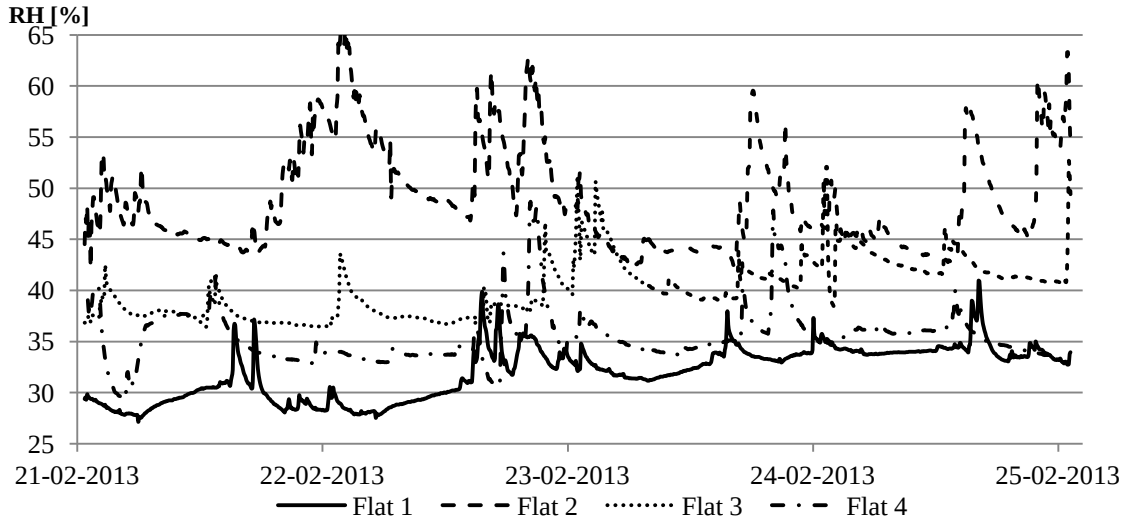

FIG. 8 Measured relative humidity in kitchens

3.3 Carbon dioxide – air exchange with outdoor air

As a measure of the indoor climate, also the CO_2 concentration in the living room was measured. The measurements show that the normal level of CO_2 does not rise much above the assumed outdoor CO_2-concentration on 380 ppm (Indeklimaportalen, 2013), *FIG. 9*. For flat 2 with two permanent residents, the CO_2-concentration in peak load periods does not exceed the level on 1000 ppm recommended for workspaces and for the rest of the flats, the CO_2-concentration in peak load periods is between 450 and 600 ppm.

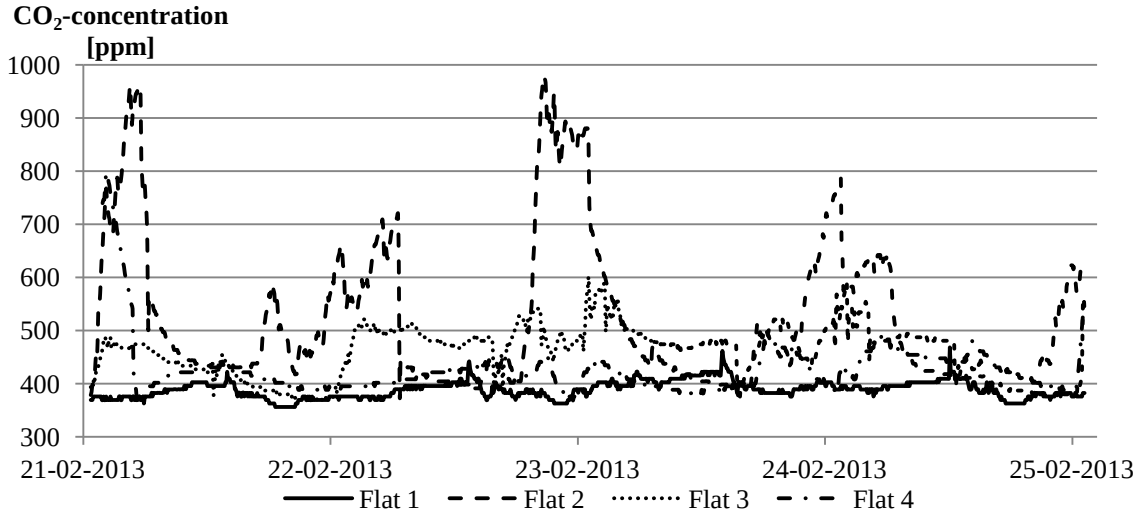

FIG. 9 Measured CO2-consentration in living rooms

These values indicate that there is a large uncontrolled exchange of air with the outside.
As the last part of the questionnaire the residents were asked to evaluate if they would be willing to pay more in rent if the indoor climate would be improved. The result can be seen in *FIG. 10* below, showing that 52 % are not willing to pay a higher rent for an improvement of the indoor climate and another 32 % have not made up their mind.

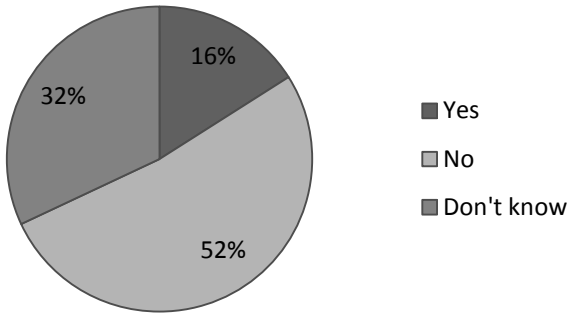

FIG. 10 Willingness to pay a higher rent if the indoor climate is improved

This indicates that most of the residents can point out areas where the indoor climate can be improved, but the willingness to pay for it is low. This is a challenge for the building owner and underpins a problem in the Danish legalisation often referred to as the owner-tenant paradox.

4. Discussion

The temperature levels, the level of relative humidity and the leakiness in the flats are problem areas that are all applicable for improvements in a renovation project of the building. This is indicated in the questionnaire and is in general supported by the measurements performed in four of the respondents' flats. This underlines the problem areas of the case building and it is reasonable to believe that the problem areas and solutions could be the same in buildings of the same type and therefore the results are useable in similar buildings.

It is clear that the building needs thorough renovation to improve the thermal indoor climate, however economical challenges such as who has to pay for the increased comfort is still present.

4.1 Data basis

By comparing user survey and measurements it is possible to show a connection between perceived and actual thermal indoor climate. The reliability of both the user survey and the thermal measurements are questionable regarding the low response rate in the questionnaire and the very few flats used for thermal investigations. With the relative low response rate of 18 % for the questionnaire, the quality of the composition of the replies can be questioned compared to the actual composition of residents in the building. Furthermore, also the choice of flats for the thermal measurements could be questioned as representative for the average resident. Nevertheless, the findings in the survey along with the workshop for the residents are supported by the measurements.

Another uncertainty is the difference in time between the user survey and thermal measurements. However no improvements were done to the building in the period in-between, but the year-to-year difference in the winter may have influenced the replies. Furthermore, the measurements took place only in the winter period and data from the other seasons are thus not available for comparison.

4.2 Further investigations

It is evident that more investigations would be preferable in order to give a more precise picture of the thermal conditions of the building. For example it would be relevant to measure the inside wall temperatures of the cold un-insulated exterior walls and compare these with the relative humidity in order to examine the probability of moisture and mould growth on the walls.

The infiltration level and hence the draught problems should also be further investigated. This could be done by a Blower Door test that could be used for both investigation of leakiness of doors and windows.

As the building has not yet been renovated, it is difficult to evaluate the influence of the user involvement, however it can already now be seen that the early involvement has given a broader and more holistic perspective of the renovation and caused more detailed investigations of the building. The challenge will be through the renovation process to keep up the user involvement and thereby creating ownership of the solutions proposed and implemented in the renovation.

5. Conclusions

Based on the user survey and the technical investigations it is clear that there is a potential for renovation of the building. Especially the heating system seems insufficient and the ventilation that is uncontrolled and comes in places where it is not desired.

The measurements underline the thermal problems identified in the user survey and the conclusions are more reliable when there is a match between measured and perceived conditions. Even though further investigations would have clarified the problem areas even more, the performed measurements gives technical evidence of the main problems perceived by the residents.

These investigations and their results once again indicates the importance of early user involvement, as picking up on some of the areas proposed by the users have broadened the perspective of the renovation and added knowledge to a more holistic approach.

It is likely that the found problem areas can be used generally for buildings in the same category since the results were consistent and in agreement with the expected. It will be preferable to do more investigations for similar buildings to document the findings.

References

Danmarks Statistik. (2013). Statistikbanken. Retrieved November 11, 2013, from http://statistikbanken.dk/bol101

Dansk Standard. (1993). DS 474 Norm for specifikation af termisk indeklima, *1. udgave*.

Havelund, M. (2011). *Hvidbog om bygningsrenovering - Et overblik over den eksisterende viden og de væsentligste studier af renoveringseffekter*. Bygherreforeningen og Grundejernes Investeringsfond.

Indeklimaportalen. (2013). Indeklimaportalen - Alt om indeklima - Indendørs CO2. Retrieved November 11, 2013, from http://indeklimaportalen.dk/indeklima/luftkvalitet/maaling/indendors_co2/

OIS. (2013). Ejendomsdata for Kretahus. Ministeriet for By, Bolig og Landdistrikter.

SBi. (2009). Skimmelblog - Relativ fugtighed. Retrieved November 11, 2013, from http://blog.sbi.dk/skimmel/2009/12/relativ-fugtighed-og-absolut-fugtighed-dugpunkt.html

Predicting energy savings at district level: representative vs. individual dwelling approach

Mieke Deurinck, Ph.D. [1]
Dirk Saelens, Professor [1]
Staf Roels, Professor [1]

[1] KU Leuven, Department of Civil Engineering, Building Physics Section

KEYWORDS: *residential buildings, energy savings, aggregated level, Monte-Carlo analysis*

SUMMARY:
When predicting energy savings at aggregated level, a common simplification is the representation of a large group of similar houses by one single representative dwelling, occupied by one specific inhabitant. The calculated energy savings for this representative dwelling are then multiplied with the number of houses to obtain the expected aggregated energy savings. In this paper, this representative dwelling approach is compared with the individual dwelling approach where multiple different dwellings are modelled separately and their energy savings are added. When combined with probabilistic user behaviour, it is found that the representative dwelling approach predicts similar mean aggregated savings, but underestimates the actual spread due to the lack of variety in building characteristics.

1. Introduction

Policy makers often rely on aggregated building stock models to estimate the energy saving potential of future policy measures. Due to the aggregated scale, assumptions and simplifications have to be made to keep the building stock models manageable. A simplification often used is the representation of similar housing groups by a single dwelling model with most probable characteristics like size, orientation, insulation level, equipment etc. This is called the 'representative dwelling' approach (Cyx 2011). A single user behaviour profile which best reflects the 'average' user is then chosen and the calculated energy savings for this single dwelling are multiplied with the number of houses to obtain the expected aggregated energy savings. The main advantage of this approach is the limited modelling work and reduced calculation time. However, there are some important disadvantages. The existing variability in building use and characteristics, even for houses belonging to the same district, cannot be reflected by one single building model and a single user, which limits its applicability for policy makers. Also, the specific choice and combination of both the representative dwelling and average inhabitant have an important impact on the predicted energy savings. If one would select another dwelling and /or user, the aggregated outcome could be heavily influenced.

In this paper, two different approaches in modelling energy savings at district level will be compared: (i) the *representative dwelling* approach where a fictitious dwelling is modelled, based on average characteristics from the district, and where its energy savings are scaled up to district level and (ii) the *individual dwelling* approach where 10 individual dwellings, sampled from the district, are modelled in detail and where their individual energy savings are added up to compose the district savings. In both approaches, the user behaviour will be implemented in a probabilistic way, meaning that heating patterns and temperature setpoints are given by probability distributions instead of fixed values. A Monte Carlo analysis based on the maximin Latin-hypercube sampling is performed to obtain the overall spread on the energy savings due to this user behaviour.

In the next section, the case district and the generic building model are described and the composition of the representative dwelling is discussed. The third section shows how the probabilistic user

behaviour is modelled and how the Monte Carlo analysis is performed. The final section discusses the results of the simulations.

2. Case study

2.1 Description

The case study in this paper is a small district in Leuven, Belgium, consisting of 52 identical dwellings built by the same building company around 1970. They are relatively large 2-storey dwellings with uninhabited attic, both in detached and in semi-detached typology. Some pictures and the original floor plan of the dwellings are given in Figure 1. The total volume V is 432 m³ and gross floor area (including garage) is 162 m². Due to the limited floor area of the ground floor, many owners have enlarged the dwellings by adding a ground floor extension at the backside. Outer walls are cavity walls in brick. Both slab-on-ground and internal floors are concrete structures, while the pitched and flat roofs are wooden structures.

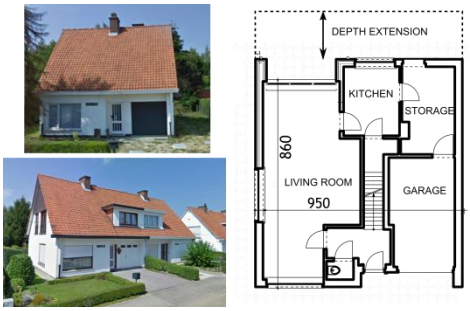

FIG 1. Casestudy dwelling (open and semi-terraced) and floor plan of ground floor (dimensions in mm).

The detailed survey information of 10 randomly sampled dwellings can be found in Table 1. Although all dwellings were originally uninsulated, roof insulation (mineral wool) and cavity wall insulation (blown-in foam) is recently installed in most of them and original windows sometimes have been replaced by better performing ones. The overall mean U-value, U_m [W/(m²K)], varies between 0.76 and 1.34.

TABLE 1. Survey data of 10 individual dwellings

Dwelling		1	2	3	4	5	6	7	8	9	10
Typology	(Semi)-Detached	D	D	D	D	D	S-D	S-D	S-D	S-D	S-D
orientation front facade		NW	SE	SE	SE	NE	SE	SE	SE	SE	SW
$depth_{extension}$	[m]	3.3	0	3.6	2.8	1.8	2. 6	2.7	0	0	3.9
$d_{wall,PUR}$	[m]	0.06	0	0	0.06	0	0	0	0.06	0	0
$d_{roof,MW}$	[m]	0	0	0.05	0	0	0.13	0	0.08	0	0.12
$d_{floor,PUR}$	[m]	0	0	0.03	0.06	0	0	0.10	0	0	0.10
U_{window}	[W/(m²K)]	1.1	1.1	2.83	2.83	2.83	1.4	1.1	2.83	1.4	1.4
v_{50}	[m³/(h.m²)]	7.3	7.0	17.5	4.6	12.3	4.8	3.8	7.0	15.9	13.2
Condensing boiler?	[Yes/No]	Y	Y	Y	N	Y	Y	Y	N	N	N
U_m	[W/(m²K)]	0.85	1.26	0.89	0.76	1.34	1.13	1.04	1.04	1.31	1.03

2.2 BES-model

A generic building model, easy adaptable to simulate the different building variants, is developed in TRNSYS, a dynamic building energy simulation (BES) software package. The dwelling is divided in 2 zones: a dayzone at the ground floor (V_{day} = 243 m³, $A_{fl,day}$ = 80 m²) and a nightzone at the second

floor (V_{night} = 189 m³, $A_{fl,night}$ = 82 m²). The depth of the extension (if present - see Figure 1 and Table 1) is treated as a parameter in the BES-model, leading to an enlarged volume and heat loss area of the dayzone. Different temperature settings are applied in both zones. Each zone is considered as one node for which heat balances are solved every time step. The time step is set at 30 minutes. Heat transfer between the different zones is assumed to occur only by heat conduction through the internal walls and floors, thereby neglecting possible heat transfer via interzonal air flows. Hourly outside conditions are taken from the Meteonorm weather data file of Ukkel, Belgium.

Air infiltration rates are expressed as a function of the heat loss surface area A_i and the measured air permeability at 50 Pa, v_{50} [m³/(h.m²)], given in Table 1: $\dot{V}_{inf} = 0.04\ v_{50}\ A_i$ [m³/h]. Since none of the dwellings are equipped with a ventilation system, no additional ventilation rates are incorporated in the BES-model. Hence, the heat loss due to the occasional air flows from opening windows and doors is not included in the calculated heat loss, leading to a slight underestimation of total energy use. Internal gains are assumed only function of the heated volume and set constant throughout the year ($\Phi_{int} = (220 + 0.67/V)*V\ [W]$), which is consistent with the Flemish implementation of the EPBD. 70% of this value is attributed to the dayzone, the remaining part to the nightzone.

To reduce the calculation time, the heating system is not explicitly modelled in TRNSYS. Instead, a monthly overall efficiency of the heating system $\eta_{TOT,m}$ [-] is used to obtain the monthly total energy use $E_{use,m}$ [kWh] = $E_{net,m}$ / $\eta_{TOT,m}$ with $E_{net,m}$ [kWh] the monthly net energy demand. $E_{net,m}$ is obtained by using an ideal heater (no production, distribution or emission losses and no thermal inertia) in the TRNSYS model and is defined as the energy the ideal heater would need to deliver to reach the zone set point temperatures at any time. 30% of the heat is emitted by radiation and the remaining part by convection, which corresponds with convecto-radiators, an emission system commonly used in Flanders. The heating power for each zone is limited by the maximum heating power as determined by the European standard EN 12831. The monthly overall heating efficiency $\eta_{TOT,m}$ for different systems and control parameters is obtained from Peeters et al. (2008) in function of the monthly heat balance ratio, being the ratio of the occurring heat gains (internal and solar gains) and the occurring heat losses (ventilation, infiltration and transmissions losses). Here, two systems are chosen: (i) an on/off non-condensing high efficiency boiler and (ii) a modulating condensing boiler, both with central room thermostat and no thermostatic valves on the convecto-radiators.

2.3 Composition of the representative dwelling

Given the survey information in Table 1, a representative dwelling could be composed in different ways. One could choose to search for a dwelling likely to occur in reality and as close to the average values as possible, or one could choose to compose a fictive dwelling that equals the average values, even if these values do not occur in reality.
In this paper, the last approach is chosen: a fictive dwelling is made by averaging all dwelling parameters (see Table 2). This is also done for the typology and geometry, resulting in a semi-terraced typology with a common wall area half the common wall area of the semi-terraced typology and an extra outer wall area equal to half the outer wall area of the open typology. For the 'averaged' heating system, the weighted average efficiency of both monthly system efficiencies is applied. Yet, the modelling software imposes an important limitation in averaging the U-value of the window, since a predefined window has to be chosen in the simulation software. The mean U-value of the representative dwelling should equal 1.88 W/(m²K), a U-value which is not commercially available and thus, not readily available in the software. Therefore, the representative dwelling model is duplicated: once with a window type with U=1.4 W/(m²K) and once with a window type with U=2.83 W/(m²K). The energy uses of both dwelling models are then weighted averaged with weighing factor $f_{2.83}$ = (1.88-1.4)/(2.83-1.4) and $f_{1.4}$=1-$f_{2.83}$ to obtain the final energy use of the representative dwelling. Yet, one has to be aware of the limitations of the latter procedure. The window type does not only influence the transmission losses by its U-value, but also influences the amount of solar gains by its solar transmission factor (*g*-value). Or thus, the representative dwelling should in fact also have the

average *g*-value of all 10 dwellings. Since the predefined window types come with a fixed combination of U-value and *g*-value, a choice has to be made which of both values will be averaged in the representative dwelling. For moderately insulated dwellings as in this paper, the heating season energy use is proven to be more sensitive to the exact U-value than to the solar gains (see Brohus et al. 2009, Firth et al. 2010), so the U-value is chosen here.

TABLE 2. Composition of the representative dwelling

		Representative dwelling
Typology	Free/Semi-Terraced	S-T
orientation front facade		216° (S=0°/W =90°)
$depth_{extension}$	[m]	2.1
$d_{wall,PUR}$	[m]	0.018
$d_{roof,MW}$	[m]	0.038
$d_{floor,PUR}$	[m]	0.029
U_{window}	[W/(m²K)]	(1.88) →(1-*f*)*1.4 + *f**2.83
v_{50}	[m³/(h.m²)]	9.33
Heating system		60% eff condensing + 40 % eff non-cond

3. Incorporating probabilistic user behaviour

Instead of using a fixed heating schedule and/or temperature setpoints, all dwelling models are subjected to different possible combinations of heating schedules and setpoints. As such, the expected energy consumption of every dwelling will be formulated as a probability distribution rather than a fixed deterministic value. The possible heating patterns and temperature setpoints and their respective probability distributions are defined in 3.1. The procedure to compose stochastic user behaviour from these distributions is explained in 3.2.

3.1 Heating patterns and setpoints

By lack of reliable and extended datasets, realistic user behaviour is defined based on the approach of Deurinck et al. (2012). Based on mainstream employment status (full-time out to work, halftime out to work, continuously home), the different time schedules from Table 3 are imposed in both day- and nightzone.

TABLE 3 - Overview of the different deterministic time schedules in the dayzone and nightzone. All 7 days of the week are identical, except for the dayzone where during the weekend dayzone pattern 4 is always used. 'X' = set temperature presence, '--' = set temperature absence, ' ' = no heating.

	dayzone				nightzone		
	1	2	3	4	1	2	3
00:00 – 06:00	--	--	--	--	X	X	X
06:00 – 09:00	X	X	X	X			X
09:00 – 12:30	--	X	--	X			
12:30 – 17:00	--	--	X	X			
17:00 – 22:00	X	X	X	X		X	
22:00 – 00:00	--	--	--	--	X	X	X
PROBABILITY	0.5	0.125	0.125	0.25	0.33	0.33	0.33

Table 4 summarizes the probability distributions used. In total, 11 parameters are to be altered per simulation run. The set temperature in the dayzone during presence is picked from a uniform distribution between [19-21] °C. During absence and during night, the set temperature in the dayzone is picked from [15-18] °C. The nightzone is never heated during the day. During the night, a probability of 0.3 is attributed to the chance that the nightzone is heated to a temperature of

[13-18] °C; the remaining 0.7 probability is attributed to the nightzone being unheated. Probabilities of occurrence are arbitrary attributed to each of the time schedules. After a time schedule is chosen, each of the start and end times of every heating period is altered with a random value picked from a uniform distribution between [+0.5h,-0.5h]. Finally, the internal gains are uniformly changed by [-20%; +20%] of their initial value of section 2.2. Remark how all parameters are assumed to be uncorrelated, which is unlike reality. For example, elderly persons are likely to be at home all day (see schedule 4) and tend to choose higher temperature settings. However, for the pragmatic modelling of user behaviour in this paper, correlations are not considered.

TABLE 4 – Probability distributions for the 11 user behaviour parameters (p = probability; U(a,b) = uniform continuous distribution between a and b; Bern(p) = Bernoulli distribution with p = chance at success)

nr	parameter	distribution
1	$T_{day,presence}$	U(19 °C , 22 °C)
2	$T_{day,absence}$	U (15 °C , 18 °C)
3 – 4	$T_{night,presence}$	U(13 °C , 18 °C) * Bern(0.3)
5 – 8	start and end times (max #4)	initial start/end time + U(-0.5 h,+0.5 h)
9	Heating pattern dayzone	p(1)=0.5 ; p(2) = p(3) = 0.125 ; p(4) = 0.25
10	Heating pattern nightzone	p(1) = p(2) = p(3) = 1/3
11	Internal Gains	initial value * U(0.8,1.2)

3.2 Monte-Carlo analysis using maximin Latin-Hypercube sampling scheme

The Monte Carlo technique is used to vary all 11 user behaviour parameters simultaneously in multiple simulation runs, leading to a large range of possible output values per dwelling. The parameter sampling is done with a distance-based space-filling maximin sampling scheme that maximizes the minimal distance between Latin Hypercube sampling points and that proves to be more efficient than a random or Latin Hypercube sampling (Janssen 2013). Due to this efficient sampling scheme the number of simulation runs per dwelling can be limited to 100 runs. Note that only one single sampling scheme (with 100 user profiles) is generated and re-used for all dwellings, since this is the only way one can be assured that the observed differences in output are to be attributed to the different user characteristics and not to different sampling schemes. Or, this means that the same set of 100 stochastically defined inhabitants is used for all dwelling simulations.
For the calculated energy savings in this paper, this also implies that the user and its heating habits remain the same before and after retrofit. However, it is generally known that inhabitants tend to take back part of the potential energy savings in enhanced indoor comfort by increasing the set temperature, heating more rooms more often etc. This effect, known as the *rebound* or *temperature takeback* effect, is not incorporated here.

4. Predicting energy savings

To illustrate the methodology, only one retrofit measure is discussed here: all pitched (MW) and flat roofs (PUR) and the ceiling (MW) between nightzone and unheated attic are insulated to reach a total insulation thickness of 0.2 m. Note that this might not be an economically viable retrofit measure for every single dwelling, since some cases already have (partly) insulated roofs. However, for this study the economical viability of a retrofit measure is not assessed, but the applicability of aggregated models evaluated. To calculate the energy savings, the BES-model of every dwelling with every sampled user profile thus needs to be simulated twice, both for the original and retrofitted situation. Per dwelling, this leads to 100 calculated energy use values before and after retrofit and thus, to 100 values of net energy savings.

4.1 At dwelling level

In this section, the simulation results of the 11 separate dwelling models (10 individual dwellings and 1 representative dwelling) are discussed. Figure 2 shows the empirical cumulative distributions of the total heating season energy use, both before and after retrofit. These cumulative curves show both the influence of the insulation levels on the energy use (compare the lateral position along the x-axis between left and right curves) and the impact of user behaviour on the calculated energy use (the steeper the cumulative curves, the lower the impact of the user behaviour on the energy use). The mean energy use can differ by a factor two, with the representative dwelling situated in the middle of all curves. The curves before retrofit are slightly flatter than the ones after retrofits. This indicates that the energy use in pre-retrofit dwellings is more sensitive to inhabitants than post-retrofit dwellings.

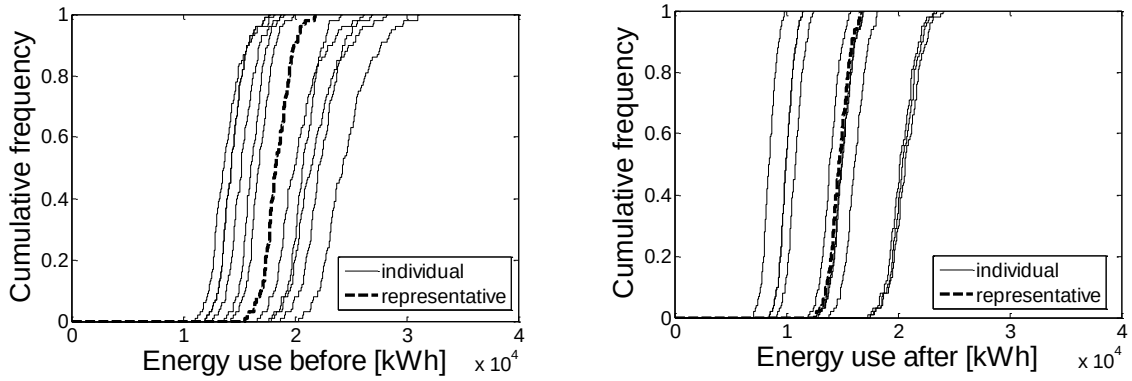

FIG 2. Cumulative plots of total heating season energy use for every individual and the representative dwelling model, both before (left) and after (right) retrofit.

Figure 3 shows the empirical cumulative distributions of the resulting energy savings at dwelling level. Here, user behaviour heavily impacts the distributions. Around the cumulative frequency of 0.7, a clear shift in distribution is seen. This shift divides the users who do not heat the nightzone (70% of them, see Table 4) and those who do heat the nightzone. Although it is an artificial division due to the rigid application of the proposed user behaviour in section 3.1 and thus, unlikely to occur in reality in this extent, it does show how heating patterns can have a great impact on calculated energy savings. If only part of the dwelling is heated, the energy savings will be lower and less influenced by temperature setpoints and time schedules (see first steep part of curves). If one chooses to heat the nightzone during the night, the energy savings will be higher and a larger spread is found around the mean value (see flatter second part of curves). Since the representative dwelling already has some roof insulation before renovation, as is the case for the 4 dwellings at the left of it, the impact on the energy savings of heating the nightzone is less pronounced.

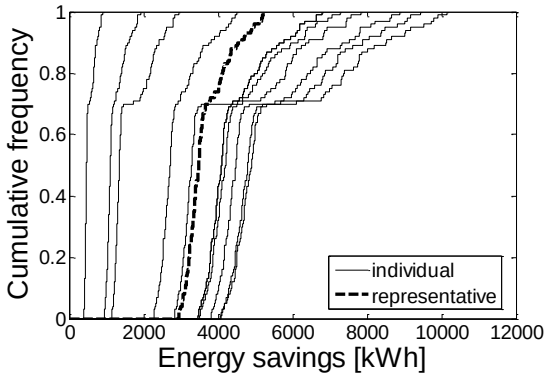

FIG 3. Cumulative plot of total heating season energy savings of every dwelling model.

4.2 At district level

4.2.1 Composing the district data

The district level is defined here on a small scale, the sum of 10 dwellings. To compose the data at this level, single datapoints are randomly picked from every dwelling and added up. Due to the small calculation time of this procedure, this can easily be repeated 10000 times, resulting in 10000 aggregated values for each approach. For the representative dwelling approach, 10 values are picked only from the representative dwelling values. For the individual dwelling approach, one value is picked from each of the 10 dwellings, so every dwelling is always represented once in the aggregated sample.
Note that the composition of the district data by (randomly) sampling 10 values, adding them and repeating this multiple times, is the appropriate procedure to obtain a reliable distribution of the aggregated outcome. Another procedure would be to obtain 100 aggregated energy values by multiplying the 100 representative dwelling values by 10 (representative dwelling approach) or by adding all 10 energy uses under the first user to obtain a first aggregated energy use value, adding all energy uses under the second user for a second value etc. (individual dwelling approach). However, a housing group is then composed in which all 10 dwellings are each time inhabited by the same type of user, which is very unlikely in reality and which leads to an overestimation of the actual spread in aggregated energy use.

4.2.2 Results

Figure 4 (left) shows the empirical probability distributions of the total heating season energy use at the district level. All are best fitted with normal distributions (see Table 5). The mean values of the fitted distributions before retrofit differ by about 1%, while after retrofit, the mean values differ by only 2%. Or, both approaches predict almost equal mean aggregated energy use, both before and after retrofit. The spread for the individual dwelling approach is slightly higher before retrofit (due to the variation in building characteristics), but the difference with the representative dwelling approach remains quite small. This means almost all variation is defined by the user behaviour. This is an important finding in favour of the representative dwelling approach: if the user behaviour is indeed as variable as assumed in section 3, the spread in aggregated energy use might be predicted equally well by a single dwelling model and stochastic user behaviour than by 10 separate dwelling models with the same stochastic user behaviour.

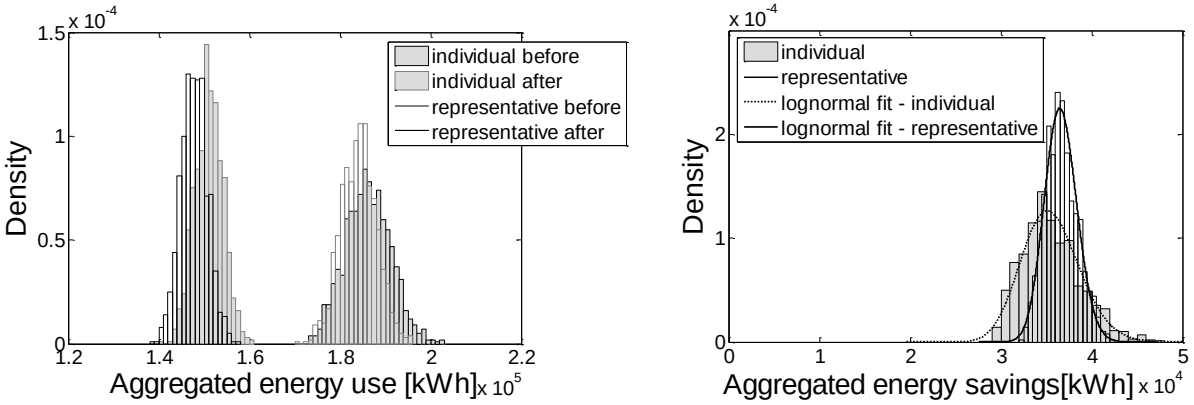

FIG 4. Probability distribution of total heating season aggregated energy use (left) and aggregated energy savings (right).

The district energy savings are also shown in Figure 4 (right). Both proved to be best fitted by lognormal distributions. The mean energy savings values practically equal the difference between the before and after values of Table 5 and also, the difference in mean value between the 2 approaches is

very small. Due to the probabilistic approach however, additional information is available about the possible spread in energy savings, given the user behaviour from section 3. Now, the two approaches do differ from each other. The standard deviation of the individual approach is almost twice as large as the standard deviation from the representative approach. Based on the fitted distributions in Table 5, the probability that the predicted aggregated energy savings are lower than 33 MWh, is only 5% for the representative dwelling approach but still more than 25% for the individual dwelling approach. So, the representative approach could easily overpredict the amount of district energy savings. This might be important when also costs are to be involved in the analysis, because lower energy savings than expected lead to larger payback times and lower return on investment rates.

TABLE 5. Fitted probability distributions: normal ~N(μ ; σ) and lognormal ln(μ ; σ) with μ = mean and σ = standard deviation – in kWh.

	individual dwelling approach	representative dwelling approach
before	~N($1.86 \cdot 10^5$; 5055)	~N($1.84 \cdot 10^5$; 3906)
after	~N($1.51 \cdot 10^5$; 2974)	~N($1.47 \cdot 10^5$; 2960)
savings	~ln (35320 ; 3186)	~ln (36536 ; 1834)

5. Conclusion

Using a representative dwelling to represent a larger group of similar houses does not automatically lead to bad energy saving predictions. If rigorously composed to match the average building characteristics and when combined with probabilistic user behaviour, the mean predicted energy savings of the representative dwelling approach are almost equal to the mean energy savings predicted by the individual dwelling approach. However, if one is also interested in the calculated spread on the energy savings, the representative dwelling approach performs less, since no spread due to differences in building characteristics can be taken into account. For districts with a uniform housing population, e.g. low renovation rates in the past, the representative dwelling approach thus could be an option. For districts where a considerable part of the houses already has been renovated to a small or large extent, it could be important to gain more information about the spread on building characteristics and to include more dwelling types as is done in the individual dwelling approach.

References

Brohus, H., Heiselberg, P., Hesselholt, A., & Rasmussen, H. (2009). Application of partial safety factors in building energy performance assessment. *Eleventh International IBPSA Conference*, July 27-30 2009, Glasgow, Schotland.

Cyx, W., Renders, N., Van Holm, M., & Verbeke, S. (2011). *Report "IEE TABULA - Typology Approach for Building Stock Energy Assessment."*

Deurinck, M., Saelens, D., & Roels, S. (2012). Assessment of the physical part of the temperature takeback for residential retrofits. *Energy and Buildings*, 52, 112–121.

Firth, S. K., Lomas, K. J., & Wright, A. J. (2010). Targeting household energy-efficiency measures using sensitivity analysis. *Building Research & Information*, 38(1), 25–41.

Janssen, H. (2013). Monte-Carlo based uncertainty analysis: Sampling efficiency and sampling convergence. *Reliability Engineering & System Safety*, *109*, 123–132.

Peeters, L., Van der Veken, J., Hens, H., Helsen, L., & D'haeseleer, W. (2008). Control of heating systems in residential buildings: Current practice. *Energy and Buildings*, *40*(8), 1446–1455.

Testing a new method for VIP interior insulation for heritage buildings

Stefan Bichlmair[1]
Martin Krus[1]
Ralf Kilian[1]

[1]Fraunhofer Institute for Building Physics IBP Holzkirchen

KEYWORDS: *VIP interior insulation, reversible mounting, retrofitting historic buildings, listed buildings*

SUMMARY:
In old traditional buildings and even more in listed, historic buildings energetic refurbishment has to be planned thoroughly. For small rooms it may be of advantage to use thin and high efficient internal wall insulation systems like vacuum insulation panels (VIP). These systems have the best ratio of thickness to insulation, but they are also absolutely diffusion tight. This tightness makes a VIP system sensible to air leakage and air flows behind the panels. Also the mounting of interior insulation mostly affects disadvantageously the original surfaces and plasters. In case of valuable buildings this can lead to restrictions in retrofitting energy saving measures such as interior insulation.

A special focus is therefore put on reversible application in historic buildings. Refurbishments in old and valuable buildings should be carried out without or at least minimal damage to original surfaces and plasters compared to typical mounting systems. The presented mounting system reduces possible damage to original surfaces and plasters if a removal is necessary. The new system uses an additional layer between interior insulation and original surfaces to protect the surface and enable a save fixing.

The interior insulation system also has been tested experimentally to assess the influence to the original surface and possible damages to the plaster. Therefore the original surface was evaluated before mounting and after removal of the VIP interior insulation. The performance of the interior insulation was measured for one heating period.

This paper highlights the concepts of reversible application of the system. Also the measured data of the interior insulation and comparison of the simulation results with the measured data are shown.

1. Introduction

The use of internal wall insulation with vacuum insulation panels (VIP) provides a way for energetic building stock refurbishments, where special consideration to the external appearance of a building has to be taken into account and thin insulation thicknesses are required. The installation of VIP internal wall insulation in building stock often faces design problems and issues of removal and reversibility. Conventionally, fully adhered assemblies could not be dismantled without damage to the original surface.

1.1 Mounting of VIP

One problem of vapor-proof systems such as VIPs is a possible backside air flows between VIP-Panels and wall if there are cracks in the surface layer and cavities behind the Panels. These backside air flows can transport moisture and mould spores from the indoor air to the cold wall surface

underneath the interior insulation and may lead to mould growth. To avoid backside air flows is full bonding of the panels to the wall, but this cannot always be guaranteed under the conditions of typical construction sites. The best method is to put the adhesive on both sides. But unevenness of old wall constructions, stiffness of panels and a thin use of adhesive makes failures possible. Not durable tight joints to adjacent building components in conjunction with cavities may lead to back side air flows.

Existing wall surfaces with loose plaster or painting could make an addition doweling of the panels necessary. Doweling of VIP panels is mostly only in additional edge zones made of e.g. polystyrene possible. This edge zones or dowel zones are additional thermal bridges.

1.2 Conservation of original surfaces and plaster in cultural heritage preservation

In the view of cultural heritage preservation a mostly comprehensive tradition of the historical building substance is aspired (Charta of Venice 1964). Also plasters or paint layers are informative about the ancient way of live and therefore worth to conserve. The use of typical adhesives based on cement with additional plastic additives may damage or destroy these near surface layers. Furthermore substances of the adhesive may migrate into deeper material layer. With this procedure an irreversible damage may occur to these layers. A good adhering system may destroy additionally the plaster if removed. One example of near surface layers in a historic building shows FIG 1. The exposed layers are documents of the historic of the building and give an impression of the taste of the epochs.

FIG 1: Exposed historic paint layers of a rectory oft he 16th century in Haimhausen in greater Munich (Picture: Klaus Klarner, conservator, Munich)

2. Experimental setup and measurements

The general aim of the project is the innovative application of an exemplary wall construction with vacuum insulation panels (VIPs) in combination with adhesive mats in the field of internal wall insulation of the building stock. New solutions and approaches should be developed, tested and demonstrated by the investigations. In conjunction with an adhesive mat as a separating layer, it is possible to design the internal wall insulation removable, as an important aspect of the reversibility for renovation and repair work in old buildings and historic preservation areas. The mats are pinned with only a few dowels to the wall. The adhesive mats are made of thin mesh with single-lined fleece. The fleece protects the original surface from the adhesive mortar used for fixing the VIPs to the wall, and thus enables an almost completely reversible attachment. Similarly, these mats enable a better adaptation of the dowel position given on the ground, which offers the possibility of placement in voids and thus help to protect valuable wall areas, e.g. with decorative historic paintings, and therefore can be beneficial for conservation reasons.

In this project, a combination of measurements in a case building object and computational simulation is performed, which serve to check a prototype wall construction for the economic and safe use of VIPs for existing buildings. In addition, a possible change of condition of the masonry surface will be examined and the measured data will be processed.

In a first step different adhesive matt systems that are available on the market, have been looked for and one of them is selected for use. Prior to installation, the construction was checked by calculation with the hygrothermal building simulation software WUFI® (Bichlmair et al 2012) developed by Fraunhofer IBP (Künzel 1994). The experiments took place in a building at the test site of the Fraunhofer IBP Holzkirchen. Here suitable test buildings, laboratories and workshops for the implementation of the project exist and also the required climate data for the site are known. FIG 2 shows the interior of the test building with test setup during mounting.

FIG 2. Interior view of the experimental building with the east and south walls with color swatches and some already mounted adhesive mat.

FIG 3. Component opening with layer indication of the interior insulation at the east wall.

If the interior insulation is not fixed accurate backside air flows with infiltrated indoor air may occur and then mold growth is possible. For specific measurements of backside air flow, the application of adhesive mat is suitable, since a defined layer of air of approximately 1 cm is present in the mesh (FIG 2 and 3). To achieve a higher level of security against backside air flow in the adhesive mat special horizontal seal joint was formed dividing the masonry in three sectors. To implement this sealing without thermal bridging a double layer VIP system with ca. 10 cm thickness were used for this purpose, originally developed for exterior insulation (Kolbe 2012). To assess the impact of the seal joint on the original wall surface different sealing methods were developed. Four different systems were selected therefrom and applied (Bichlmair et al 2012). In addition, some specific open joints as a gap with ca. 1 mm width were produced to the adjacent bottom and ceiling as a reference for not tight seals to adjacent building parts. The test setup for measuring backside air flows was planned and carried out (Bichlmair et al 2012) with the homogenous tracer gas emission method (NTVVS 118, 1997) due to good experiences with this method in historic buildings (Kilian et al

2011). The measuring period were too long, therefore the results cannot be used for interpretation. The further investigations on backside air flow were made computationally, based on the measured data for temperature and used test set up for the experiment.

The surface of the wall was painted with defined colors with different historical binders (FIG 2 and 4) to assess changes in consequence of the insulation (Bichlmair et al 2012). The color values were measured prior to mounting, using the standard method of CIELAB (EN ISO 11664, 2012). After removing the interior insulation, a further check on the original wall was made in order to assess the surface concerning degree of damage-freeness and change of the color values. The measured color lightness and color space are shown in FIG 4 in the right graph. There are only small deviations of the two measurements before mounting of the internal insulation and after removing almost 6 month later.

The left picture in FIG 4 shows the removed internal insulation with some leavings of the adhesive mat and adhesive. The first image shows almost complete conservation of the original surface. Only a small strip (rectangle 1) has high losses of substances. This strip was made as a reference sealing with adhesive directly mounted on the surface. Removing this directly applied adhesive led to the typical loss of the upper layers of the original wall, i.e. in this case the newly applied test colors.

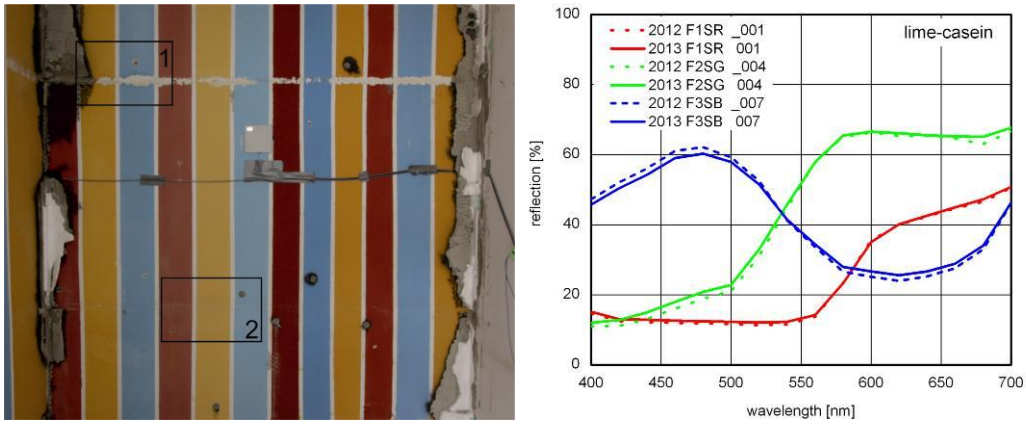

FIG 4. Left picture: South wall after removal of the interior insulation. For the areas of the numbered rectangles visual macro photos exist. Right graph: Color reflection on the binder system lime-casein on the south wall with the colors red, yellow and blue before and after application of interior insulation.

With examination of the surface visually mold growth could be observed on several areas. Within the different colors and binder systems no obvious pattern was recognizable. As mentioned several cracks were built for some test fields. The bottom fields with cracks had only a few and small mold spots, the fields at the ceiling had the most intense mold growth. The least mold growth but still visually recognizable has been observed in fields with no deliberately installed gaps in the middle of the wall.

To assess the effect of the internal insulation monitoring measurements were made with temperature sensors, relative humidity sensors and heat flow meters at the boundary layer and additionally with an infrared camera In addition, a combination of measurement and calculation is used for checking the developed component structure. In FIG 5 the north façade of the test building is shown with visual image and infrared (IR) image. The different thermal behavior is made visible with the IR image. In the center of the IR Image the insulated wall partition is shown with blue colors. The right wall partition remained with its original wall brick structure and is shown yellow-red colored. Two rectangular arranged measurement fields refer to the measured IR temperature within the insulated and untouched wall partition. The PT 100 temperature measurement is also located within the rectangular IR measurement field. One part is insulated with the internal insulation. The IR camera has an absolute accuracy of ± 1.5 °C and a thermal sensitivity of 0.07 K at 23 °C.

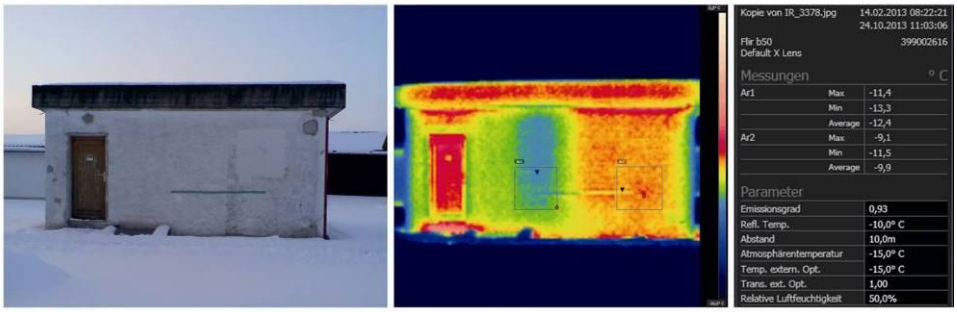

FIG 5. Exterior view of the north side of the test building with IR image, before sunrise, 14th Feb 2013.The temperature measured with IR correspond to the measurement with calibrated PT 100 temperature sensor within the accuracy of the measurements.

The left graph in FIG 6 shows the course of temperature of the insulated and not insulated wall partition from 01. 02. 2013 to 01.03. Comparing the both wall partitions the former original surface behind the interior insulation is cooling down almost to the level of the outside wall surface temperature. The temperature drops below 0 °C on the former original surface. The right graph in FIG 6 shows the temperature course of the insulated wall partition with additionally measured relative humidity on the former original wall surface. During the complete measuring period of almost 6 month the relative humidity was at 100 % RH, measured with a capacitive sensor with an accuracy of ± 2% RH and ±0.3 °C. The PT 100 temperature sensor was calibrated to ± 0.1 K. The temperature sensor of the humidity sensor was checked with an additional PT 100 sensor at the same interstitial layer whereas the PT 100 was fixed on the original wall surface. The humidity sensor measured the air in the small air cavity within the adhesive mat.

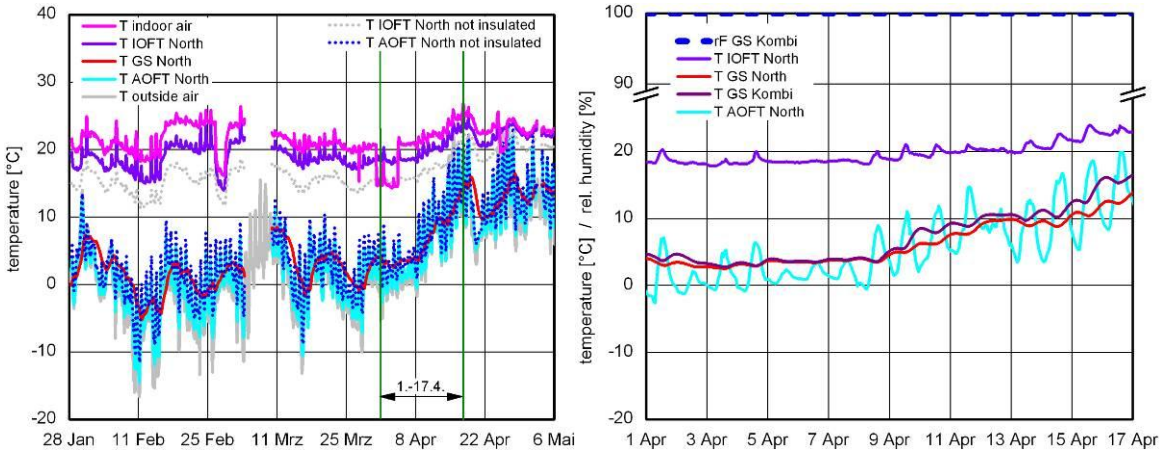

FIG 6. The left graph shows the temperature course of the north wall from 28th Jan to 6th May 2013. T AOFT names the outer surface temperature, T GS the temperature of the original surface behind the internal insulation, T IOFT the inuslated wall surface temperature inside. The right graph shows the period form 1st April to 17th April 2013 with relative Humidity and temperatur courses, whereas TGS Kombi and RH GS Kombi names the temperature and relative Humidity on the orgininal surface unterneath interal insulation.The level of RH is constant at 100 % RH.

3. Simulation

Further computational studies were carried out on the basis of the first simulation which were calculated with the measured data as boundary condition and compared to measured data in the

interstitial layer. The influence of the assumed backside air flow was taken into account and the results of the simulation were also compared to the measured data. With this calibrated simulation long term calculations were performed with and without backside air flow and their impact calculated on the moisture balance. For the boundary conditions for the long term calculation a typical indoor moister load of residential housing between 40 % RH at 20 °C in winter and 60 % RH at 22 °C in summer were used. For the outdoor climate the Holzkirchen climate of 1991 were implemented and repeated for 10 years. The heat transmission coefficient was assumed outside with 0.0588 [m²*K/W] and indoors with 0.125 [m²*K/W]. The results on the water content of the plaster and brick wall are shown in (FIG 7) on the left side and the temperature and relative humidity course on the surface of the original plaster underneath the adhesive mat on the right side in (FIG 7). The leaky construction with backside air flow shows for the plaster with the red line a certain increase in the water content within the annual cycle and also a long term increase over ten years. The water content of the brick wall with backflow air current is only increasing slightly compared to the tight construction. The relative humidity shows a similar behavior to the plaster with an annual cycle and a continuous small long term increase.

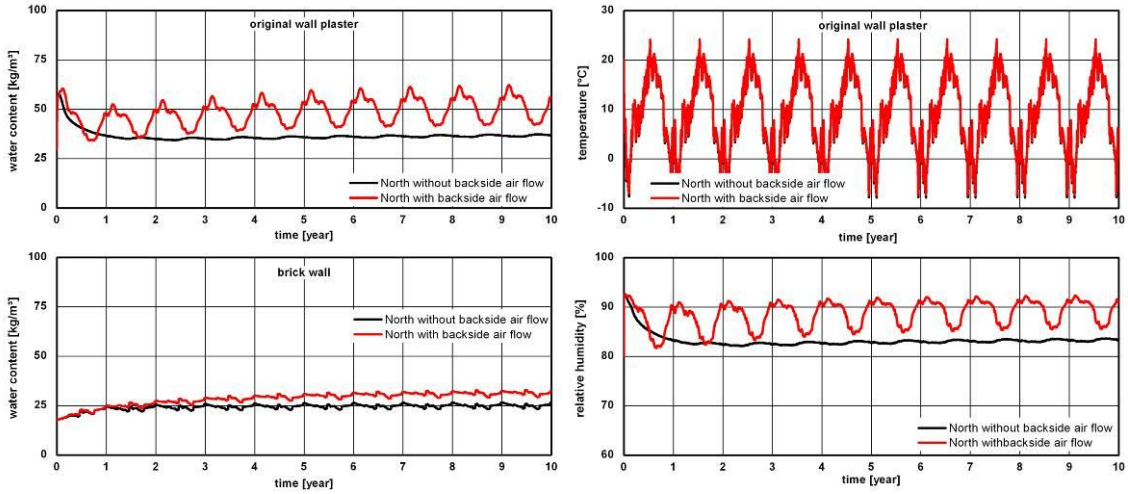

FIG 7: Sequence of water content in the existing original wall plaster and brick wall of the north side with and without backside air flow of the VIP interior insultion over a time span of ten years. The right graphs shows the temperature and humidity on the surface of the original plaster underneath the interstitial layer between original plaster and new applied adhesive mat calculated with tight (black line) and leaky (red line) construction on a north oriented facade over a time span of ten years.

To assess the influence of the increase of moister in the construction an additional simulation with WUFI® Bio (Sedlbauer 2001) was performed on the results of the previous simulation. With this tool a predicted mould growth can be calculated based on relative humidity, temperature and substrate with transient boundary conditions. With combining the results of the bio hygrothermal model with the mould index of the Viitanen model (Viitanen H. & Ritschkoff A.1991) it is possible to use an accepted and demonstrative measure for WUFI® Bio (Krus et al 2011). The mould index reaches from 0 (no mould growth) to 6 (100 % mould coverage of the surface).

With a mould index of 3 a mould growth is clearly visible. For Mould Index below 1 only low risk of mould growth exists. In (FIG 8) the Mould-Index is calculated for the shown data in (FIG 7) of the 10th year with and without backside air flow. The simulation with backside air flow shows a visible mould growth. If the construction is tight only a very low risk of mould growth can be calculated at that position of the wall construction.

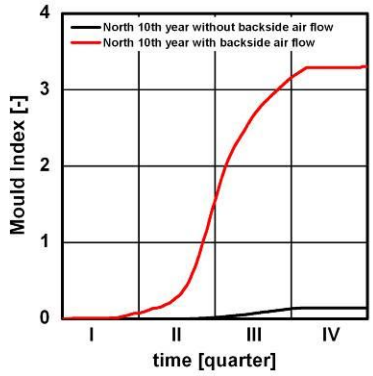

FIG 8. Sequence of the mould-indexes in the interstitial layer between original plaster and new applied adhesive mat calculated with tight and leaky construction on a north oriented facade of the last calculated year.

4. Conclusions

The investigations for removable assembly contribute to a significant development of reversible internal wall insulation. It was possible to dismantle the VIP largely non-destructive to the orginal surface. The results in terms of the conservation status of the colored surfaces and changes of the colors are encouraging. The mold growth by backside air flow could not be resolved despite the effort for sealing. With simulation the effect of the background current was reproduced and the long-term performance was calculated. From the perspective of conservation of historic surfaces the separation with lamination of the original surface from the cement adhesive is a promising option for internal insulation.

5. Acknowledgements

These examinations were funded by the national public funding body BBSR, Aktenzeichen SF-10.08.18.7-11.29 / II 3-F20-10-1-087, and conducted in cooperation with St. Gobain Weber GmbH.

References

Bichlmair S. Krus M. & Kilian R.2012. Eine neue Mehtode zur VIP-Innendämmung im Bereich der Denkmalpflege. Konzepte – Aufbau – Erste Ergebnisse. In: Tagungsunterlage. 2. Internationale Innendämmkongress. TU Dresden. Dresden.

Charta of Venice. 1964. download of the homepage of ICOMOS, 2013 http://www.icomos.org/charters/venice_e.pdf

EN ISO 11664 – 4. 2012. Farbmetrik - Teil 4: CIE 1976 L*a*b* Farbenraum. Beuth-Verlag.Berlin.

Kilian R. Bichlmair S. Wehle B. & Holm A. 2011. Passive sampling as a method for air exchange measurements for whole building simulation of historic buildings. 9th Nordic Symposium on. Building Physics. Proceedings V3, p. 1135- 1142. Tampere University of Technology, Tampere, Finland.

Kolbe G. 2012. Fit mit Vakuumdämmung. Ausbau+Fassade 02/2012, p. 21-24. Geislingen.

Künzel H.M.1994. Verfahren zur ein- und zweidimensionalen Berechnung des gekoppelten Wärme- und Feuchtetransports in Bauteilen mit einfachen Kennwerten. Dissertatiton. Universität Stuttgart.

Krus M. Seidler C.M. & Sedlbauer, K.: Übertragung des Mould-Indexes auf das biohygrothermisches Modell zur Schimmelpilzvorhersage. IBP-Mitteilung 38, Valley 2011.

NTVVS 118.1997. Ventilation: Local Mean Age of Air-Homogeneous Emission Technique; Nordtest Method, Finland.

Sedlbauer K.2001. Vorhersage von Schimmelpilzbildung auf Bauteilen. Dissertation, Stuttgart.

Viitanen H. & Ritschkoff A.1991. Mould growth in pine and spruce sapewood in relation to air humidity and temmperature. Uppsala: Swedish University of Agriculture Sciences, Department of Forest Products.

TOPIC
RAP-RETRO

Page.....1358-1406

Hygrothermal Risk Assessment - Retrofit of External Wall by the Application of Interior Insulation

Simon Pallin, PhD [1]
Angela Sasic Kalagasidis, Associate Professor [2]

[1] Oak Ridge National Laboratory in Tennessee, U.S.A.
[2] Chalmers University of Technology, Sweden

KEYWORDS: *Hygrothermal, probabilistic, simulation, risk, retrofit, sensitivity analysis, mould growth.*

SUMMARY:

Inside insulation of external walls of timber-framed construction is an adequate retrofitting measure in cases where there is an interest of preserving the existing façade. According to certain recommendations, and for the purpose of minimizing the work efforts, the additional insulation is placed directly on an existing wall, leaving the existing vapour retarder in the area that is substantially colder than before the retrofitting and thus increasing the risk of mould growth in the wall. The hygrothermal conditions inside the retrofitted wall are investigated for various indoor and outdoor conditions, and with and without indoor air intrusion in the wall. According to the results, 32% of 500 simulated scenarios obtained an annual average of relative humidity larger than the critical value for mould growth at the most critical spot inside the wall. The corresponding ratio was 43% in the wall assembly with an assumed air intrusion. Suggestions for the improvements of the moisture performance of the wall are also suggested. The used methodology of risk assessment is fully presented in the paper; it is of a general character and can be used in other retrofitting studies.

1. Introduction

Hygrothermal design of building envelopes is associated with standards, procedures, data and tools that help engineers in finding solutions in accordance with performance goals and applicable regulations. These ordinances are consistent with a proven knowledge in this engineering field and they are essentially developed as means for minimizing failures in the design. Nevertheless, undesirable deviations between a predicted and actual performance of building envelopes do happen. One reason for this can be found in a lack of design practice to evaluate the performance of building envelopes under different operational scenarios. Another reason is the lack of expert knowledge in situations when a design contains details that are not covered by design references.

This paper applies a hygrothermal risk assessment approach for the evaluation of a building retrofit design for which there is a lack of design guidelines. The assessment approach is based on existing algorithms (Ljungquist 2005, Vose 2008, Sasic Kalagasidis and Rode 2011, Pallin 2013) and involves testing of a large number of operation scenarios. The risk assessment algorithm is designed for residential retrofitting but may also be used in the energy and moisture safety design of new building constructions.

2. Method

The risk assessment algorithm is based on a step-by-step approach and presented in FIG. 1. It is a set of guidelines on how to perceive conditions for possible variations and to systematically test, evaluate and document the effects of these deviations on the performance of a building envelope in question. The first step of the risk assessment is to define the **Scope**, which consists of *System Formulation*,

Targets and Concerns, *Existing Conditions* and *Strategy Identification*. This section intends to describe the purpose of the retrofitting project, gather knowledge and experience from similar projects and to formulate the performance criteria of the risk assessment (such as energy efficiency, moisture durability, occupants' expected level of comfort, etc.). The purpose is also to describe valuable and available information of the building status, properties of technical equipment, occupants' comfort issues and other information needed for a suitable retrofit design. The final outcome of this section is to present the retrofitting strategies.

The section of **Qualitative Risk Analysis** (QlRA) in FIG. 1 consists of two analysis segments; the *Risks Identification*, which serves to identify possible unwanted events or consequences on the hygrothermal performance; and the definition of *Influential Parameters, Uncertainties and Correlations,* which purpose is to gather an in-depth understanding of the interaction between the influencing parameters and the performance criteria of the risk assessment. The QlRA is followed by a first evaluation of the analysis, in which the result of the first analysis is presented together with decisions on the necessity for further analyses. This step is referred to as a *Qualitative Risk Evaluation.*

The section of the **Quantitative Risk Analysis** (QRA) consists of defining *Method and Performance Indicators*; *Input Values and Probability Distributions;* determine the *Design and Run Simulation Model;* and making *Result, Sensitivity and Uncertainty Analyses* of the results. In *Method and Performance Indicators,* the type of simulation method for the analysis is determined and the availability of existing models is investigated. Performance indicators are defined to enable the result and sensitivity analyses of the risk assessment. The values of the input parameters must be established and their variability, uncertainty and correlations; to ensure realistic and reliable simulation results.

Once all the information needed is implemented into the model, the simulations can get started. The number of simulations depends on the prescribed convergence criteria for the simulations, the nature of the input parameter variability and uncertainty and also on the defined performance criteria. The simulation results enable a sensitivity and uncertainty analysis, which may be conducted for several reasons; to determine which of the input parameters require additional research in order to reduce the output uncertainty; which input parameters are insignificant and can be neglected in the risk assessment model; which of the varying parameters contribute the most and how are they correlated (Hamby 1994).

However, a QRA is not necessarily required. The risk assessment can come to a halt depending on the outcome of the evaluation of the QlRA. If the proposed retrofitting measure, thus the studied object of the risk assessment, is considered as safe and reliable in the qualitative risk evaluation, a QRA is not needed. In addition, the risk assessment can come to a halt if crucial information is missing or if the credibility of the QlRA is low; as a result, the risk assessment is redirected back to the start of the QlRA; or if necessary, back to the section of the Scope. Such interrupting measures are also taken if the studied retrofit is considered to fail based on the defined targets and concerns.

A second evaluation determines whether the results obtained from the QRA is sufficient for risk tolerability decisions. If essential information is missing or if further analyses are required, the risk assessment is redirect back to the start of the QRA or, if necessary, redirected back to the QlRA.

In **Documentation**, the products of the risk analysis are presented in a *Risk Analysis Report* and *Options and Recommendations* for further analyses are presented together with suggestions on possible alternatives for improvement of the studying object. The documentation of the risk assessment serves as the foundation on which the decision makers should base their *Risk Tolerability Decisions*. While the above presented analysis is normally done by design engineer, this final step should be taken by a risk management team.

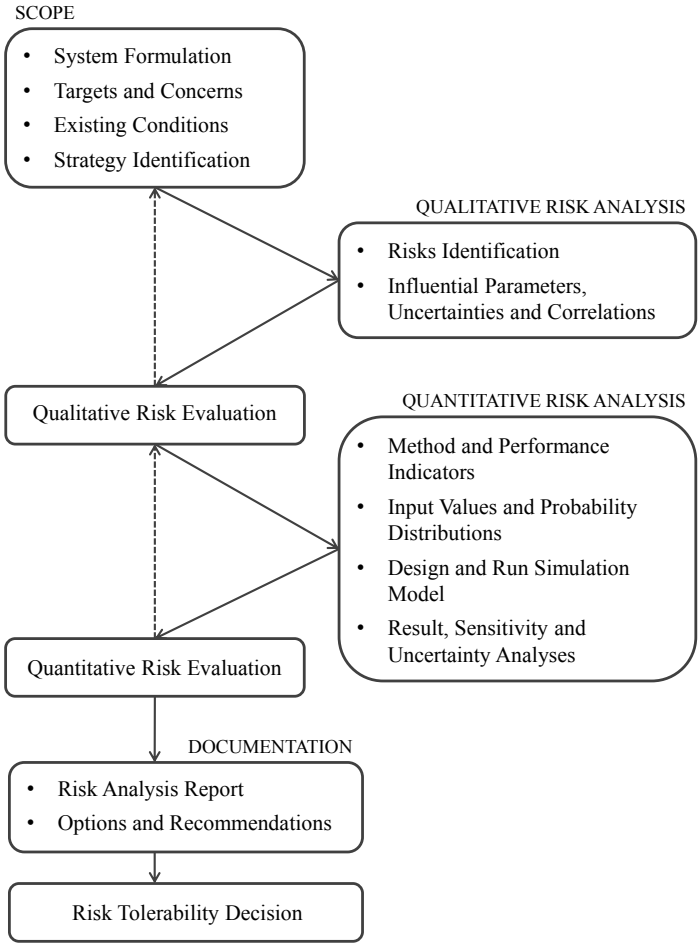

FIG. 1 A flowchart for hygrothermal risk assessment (adapted from Ljungquist 2005, Vose 2008, Sasic Kalagasidis and Rode 2011). *The dashed lines with arrows indicate possible redirections, based on the decisions made during the risk assessment procedure.*

3. Case study

A case study has been defined to evaluate the risk assessment algorithm presented in FIG. 1. The object of the case study is a recommended design of an exterior wall retrofit. The proposed retrofit involves addition of an insulation layer on the inside of the existing wall, thus not affecting the exterior cladding of the wall. Necessary conditions of the studied object are presumed to make the analysis credible and will be presented shortly. The procedure of analysing the hygrothermal performance of the wall after the retrofitting follows each step of the proposed risk assessment algorithm.

3.1 Scope

Energy efficiency improvements are planned for an existing exterior wall. Due to the preserving interest of the exterior cladding, a supplement of insulation must be constructed on the inner side of the wall. The proposed design of the retrofitting measure is presented in FIG. 2, and consists of a new timber-framed wall, directly constructed onto the inner surface of the existing wall (also timber framed). The insulation material in the new construction is glass wool, which is mounted between the wooden studs. An additional gypsum board is mounted on the interior side of the new timber frame.

The intention of the retrofitting measure is to improve the thermal performance while maintaining a durable and moisture resistant wall assembly. However, the suggested solution is also motivated by

minimum changes on the existing wall which, naturally, will minimize the costs from additional building material and optimize the construction time. Apparently, the conditions and functions of the existing building materials are considered acceptable. It is of great concern to create a design which enables a satisfying interaction between the existing and supplementary building materials. A possible unwanted consequence of interest for the risk assessment is the risk of mould.

The studied retrofitting measure is assumed to be constructed in Gothenburg, Sweden, which is considered as an oceanic climate. The retrofit is assumed to be constructed with satisfying workmanship. It is worth noting that the suggested retrofitting measure is not widely practiced.

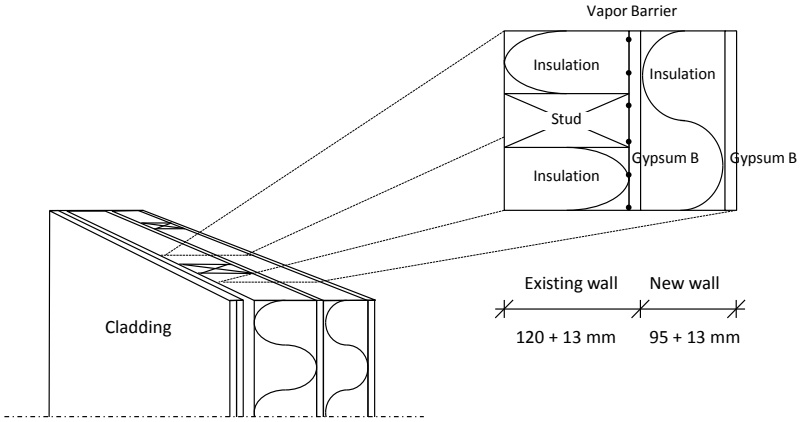

FIG. 2 An illustration of the design of the exterior wall retrofit, together with thicknesses of the applied materials, in both the new and existing wall assemblies.

3.2 Qualitative risk analysis

The major risks of concern in this risk assessment are mould growth, or other damages related to critical levels of moisture. The development of mould depends on the nutrients in the building material, the temperature, the relative humidity, φ, and the fluctuation and exposure time (Viitanen 2001, Johansson et al. 2005). Therefore, this case study aims at investigating the hygrothermal performance of the retrofitted wall and resistance to such moisture related damages.

A *Fault Tree Analysis* (FTA) can be a useful method to determine the mechanisms and influential parameters that will have an effect on the hygrothermal performance. FIG. 3 illustrates a FTA of the investigated retrofit and in concerns of the risk of mould in the wall assembly. FIG. 3 also includes a legend, describing the Boolean operators and the descending events of a FTA.

In concerns of FIG. 3; capillary suction, water leakages and built-in moisture (moisture damp) are assumed to be checked upon due to inspections of the wall prior the construction of the retrofit. Therefore, these mechanisms can be excluded from being decisive on the risk of mould. Neither is moisture infiltration by convection important, if the conditions and functions of the exisiting building materials are considered acceptable. However, two mechanisms probably possess a higher impact on the moisture performance. These are the indoor air exfiltration and the moisture transport by diffusion and shall be investigated further.

3.3 Qualitative Risk evaluation

The area around the existing studs, as seen in FIG. 2 and FIG. 4, will have a decreased temperature during the heating season in comparison with prior the retrofit. As a consequence, the existing gypsum board will have a lower moisture acceptance. Unfortunately, this critical position will commonly exist due to a shift in the placement of the existing and new studs, with the intention of avoiding thermal bridges.

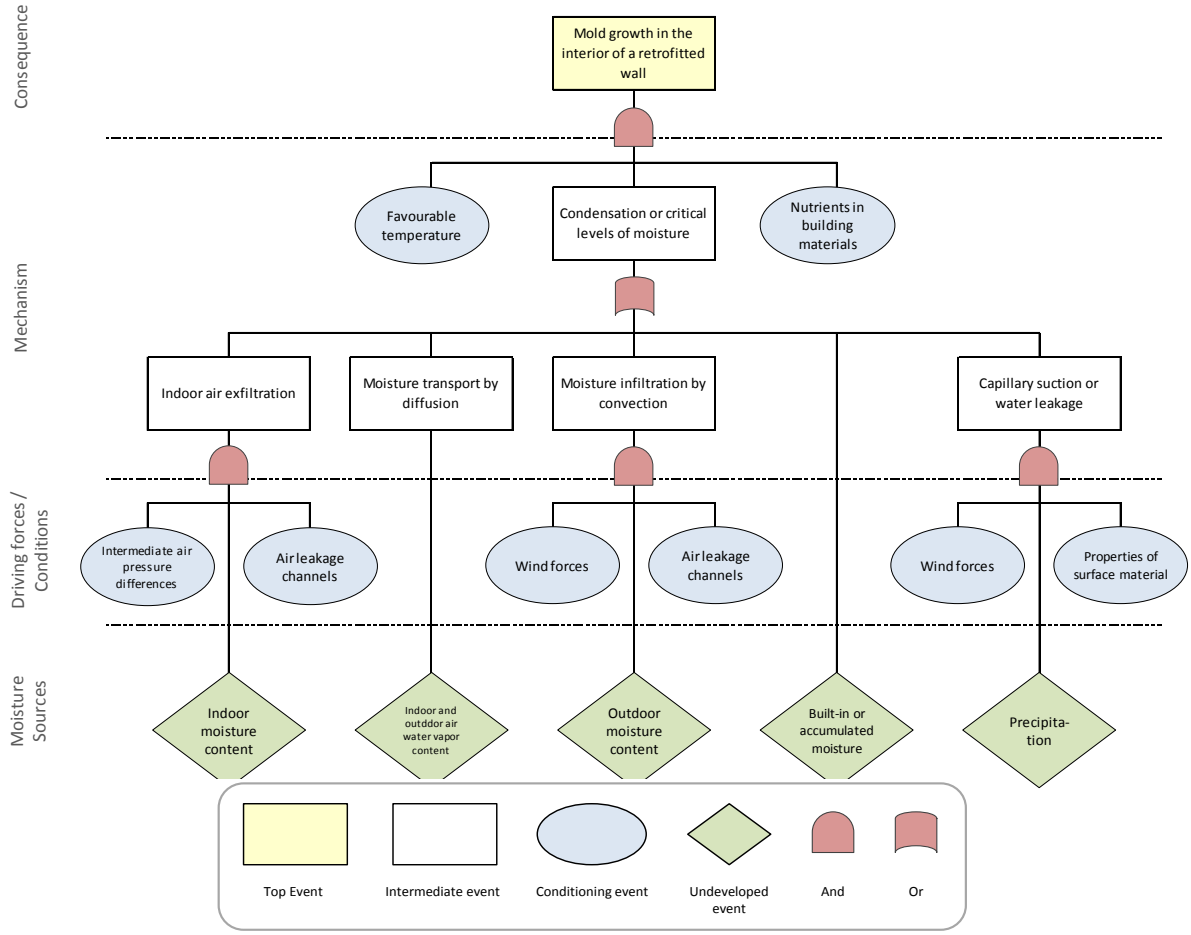

FIG. 3 A Fault Tree Analysis (FTA) depicts the most important mechanisms, driving potentials and sources of potential mould growth in the wall assembly. A legend illustrates the operators of the FTA.

A vapour retarder of the original wall remains in the same place, between the existing studs and the intermediate gypsum board, which is a substantially colder region than before the retrofitting. As a consequence, there will be moisture diffusion from the indoor environment during the cold periods and moisture accumulation in all materials on the inner side of the vapour retarder. All this will increase the risk of mould growth in the wall. An additional aspect that will affect the function and future performance of the retrofit is possible indoor air intrusion in the wall since the wall bearing is made of timber which will shrink, bend and crack depending on moisture content, temperature, quality of the material and the applied load (Breyer et al. 1998). A plausible scenario is that minor air gaps are created between the existing and new wall structures due to these structural movements.

In conclusion of the first risk evaluation, the studied retrofitting measure possesses a higher risk of mould growth in the wall assembly in comparison with prior the retrofit. However, the variability of the performance is difficult to estimate based on solely a QlRA. Therefore a QRA is recommended in order to evaluate influential parameters, likeliness of failure and possible actions of improvement.

3.4 Quantitative risk analysis

A model of the presented retrofit design in FIG. 2 was created in HAM-tools, which is a library of models developed in Simulink® and especially constructed to simulate heat and mass transport in building and building components (Sasic Kalagasidis 2004). The simulation model consists of a one-dimensional wall model and an air gap. The path of heat and mass transport through the wall, crossing the assumed critical position of the retrofit, can be seen in the left-hand illustration of FIG. 4.

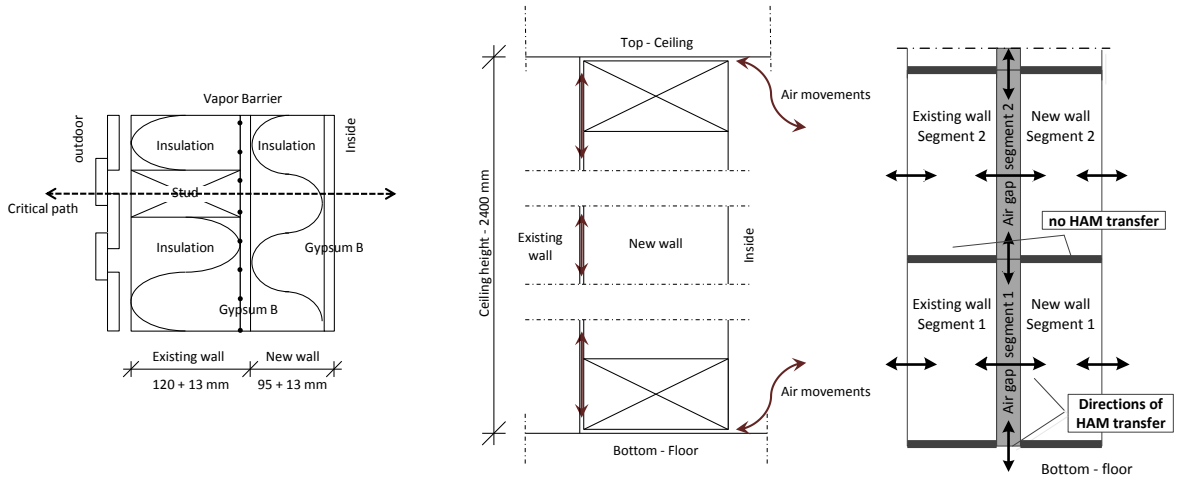

FIG. 4 The left-hand plan drawing illustrates the assumed critical path of the retrofitted wall. The middle picture illustrates a section drawing of the simulated wall, in which the two-headed arrows demonstrate possible positions and directions of air intrusion. The right-hand scheme illustrates numerical coupling between the wall elements and the air gaps.

An additional simulation model was made with an assumed 3 mm air gap between the new timber frame and the existing gypsum board, in accordance with the middle illustration of FIG. 4. The assumed width of the air gap is based on plausible deformations. The air movement inside the gap is driven by air pressure differences due to the variations in temperature along the air gap and in the inner environment. The air gap is discretized in five equally long segments, which are serially coupled along the wall height as shown in the right-hand picture in Figure 4. The temperature and moisture content of the air in each segment are found from the heat and mass balance between the air in the gap, adjacent wall elements as well as with the preceding and following air gaps. A well-mixed air is modelled in each segment. The resulting model of the wall is combination of one-dimensional wall segments and quasi two-dimensional air gaps.

The Monte Carlo method is applied for the sampling of the varying input parameters in the simulation model. The variability of three input parameters are implemented; the outdoor climate, the indoor moisture production and the ventilation rate. The weather data consists of 44 simulated years of the climate in Gothenburg, Sweden between 1960-2004 (Nik 2010). The applied ventilation rates are based on measurements made in 417 apartments in Sweden from 2008 to 2009 (Boverket 2009), while the variability of the indoor moisture production are based on simulations of 10 000 plausible scenarios of residential multi-family households (Pallin et al. 2011). Altogether, 500 consecutive years was simulated with hourly varying climate data, indoor moisture production rates area and with an annually constant ventilation rate.

As discussed, the area around the existing studs is assumed to be the most critical position of the wall in concerns of the risk of mould. FIG. 5 presents the probability distribution of the annual average of relative humidity in this critical position, both with and without an assumed air intrusion. Apparently, 32% of the simulated scenarios has an average above 80% relative humidity, which can be associated with a risk of mould (Hukka and Viitanen 1999). In the case of an assumed air intrusion, the corresponding number of the simulated scenarios with a critical average is 43%.

A sensitivity analysis was performed, using three different methods. The three analyses methods indicate that the ventilation rate has the highest influence on the annual average relative humidity in the intermediate gypsum board. Also the indoor moisture production proves to be influential, though slightly less. According the result of the sensitivity analysis in FIG. 6, the outdoor climate has the lowest influence. This means that the same risk may exist in other climates.

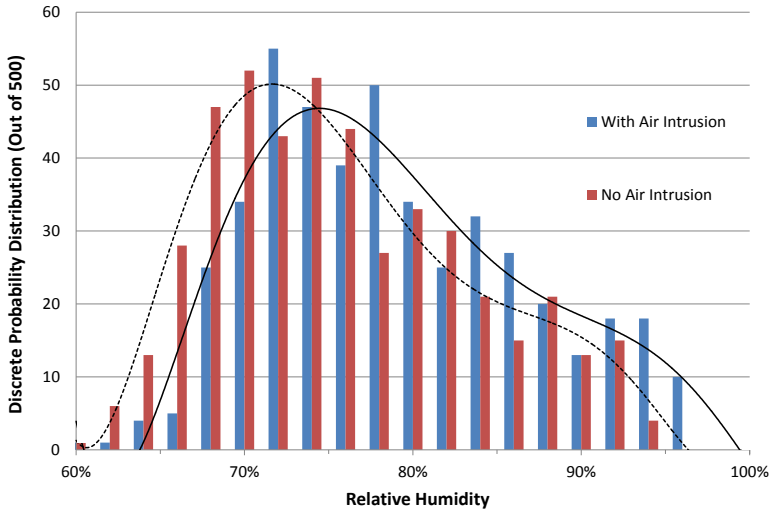

FIG. 5 Two discrete probability distributions illustrate the variability of the annual average of relative humidity in the assumed critical position (i.e. the intermediate gypsum board) post-retrofit. The disparity between the plots is whether an air intrusion is assumed or not. In addition, trend lines are added for both plots, hence representing two probability density functions.

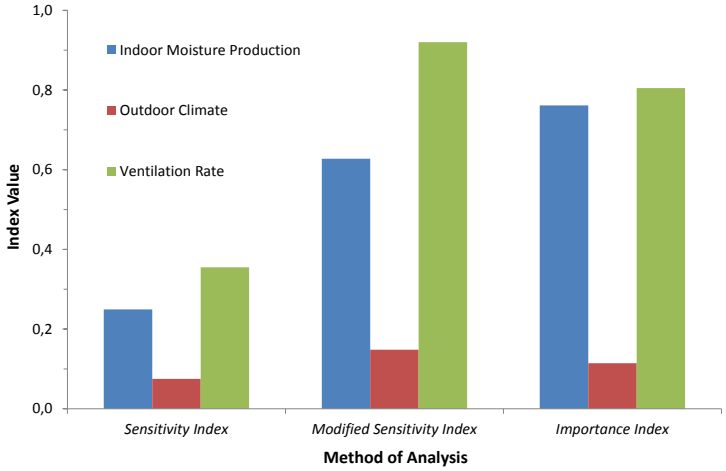

FIG. 6 present the results from the sensitivity analyses from three sensitivity analyses methods. The ventilation rate has the highest influence on the variability of the moisture content in the intermediate gypsum board close to the existing timber studs. The moisture production also has a high influence, though the outdoor climate has not. A high index value indicates a high influence.

4. Conclusion

The conclusion of this paper also serves as the *Risk evaluation, Options and Recommendations* of the case study, as seen in FIG. 1.

A recommended design for an external wall retrofit with interior additional insulation has been evaluated with a hygrothermal risk assessment procedure. The most decisive parameters in concerns of the moisture performance were identified; the outdoor climate, the indoor moisture production and the ventilation rate. Further, a critical position was identified in the wall assembly, which was assumed to have a higher risk of developing mould post-retrofit. Finally, the retrofit design was simulated using stochastic variations of the three most decisive parameters in a hygrothermal calculation tool.

According to the results, 32% of the simulated scenarios obtained an annual average of relative humidity larger than the critical value for mould growth. The corresponding ratio was 43% in the wall assembly with an assumed air intrusion of indoor air into to the wall assembly. The sensitivity analyses indicated that the air flow rate of the ventilation system has the highest influence on the moisture content in the intermediate gypsum board. The indoor moisture production is also influential, though the impact from the outdoor climate is low. This means that the same risk may exist in other climates.

However, the moisture performance of the studied retrofit can be improved if any of the following actions is taken; decrease the indoor moisture production or increase the ventilation rate; assemble a new vapour retarder behind the new gypsum board; ecrease the thickness of the additional insulation.

References

Boverket (2009). Så mår våra hus - redovisning av regeringsuppdrag beträffande byggnaders tekniska utformning m.m. Karlskrona, Sweden, Boverket.

Breyer D. E., Fridley K. J. & Cobeen K. E. (1998). Design of wood structures ASD. New York, McGraw Hill.

Hamby D. M. (1994). A review of techniques for parameter sensitivity analysis of environmental models. Environmental Monitoring and Assessment 32(2): 135-154.

Hukka A. & Viitanen H. A. (1999). A mathematical model of mould growth on wooden material. Wood Science and Technology 33.

Johansson P., Samuelson I., Ekstrand-Tobin A., Mjörnell K., Sandberg P. I. & Sikander E. (2005). Microbiological growth on building materials – critical moisture levels. Borås, SWEDEN, SP Swedish National Testing and Research Institute.

Ljungquist K. (2005). A probabilistic approach to Risk Analysis - A comparison between undesirable indoor events and human sensitivity. Luleå University of Technology. Luleå. Doctoral thesis.

Nik V. M. (2010). Climate Simulation of an Attic Using Future Weather Data Sets - Statistical Methods for Data Processing and Analysis. Building Technology, Building physics division. Gothenburg, Chalmers university of Technology, Sweden. Licentiate thesis.

Pallin S. (2013). Risk Assessment of Hygrothermal Performance - Building Envelope Retrofit. Department of Civil and Environmental Engineering. Gothenburg, Sweden, Chalmers University of Technology. Doctoral thesis.

Pallin S., Johansson P. & Hagentoft C.-E. (2011). Stochastic modeling of moisture supply in dwellings based on moisture production and moisture buffering capacity. IBPSA - Building simulation 2011. Sydney, Australia.

Sasic Kalagasidis A. (2004). HAM-Tools. Building Technology, Building physics division. Gothenburg, Chalmers University of Technology.

Sasic Kalagasidis A. & Rode C. (2011). Framework for Probabilistic assessment of performance of Retrofitted Buildings. IEA-ANNEX 55, Reliability of Energy Efficient Building Retrofitting - Probability Assessment of Performance and Cost, . San Antonio, TX.

Viitanen H. (2001). Factors affecting mould growth on kiln dried wood, VTT Building and Transport.

Vose D. (2008). Risk analysis: A quantitative guide. Chichester, England; Hoboken, NJ, Wiley.

Moisture safe cold attics - Assessment based on risk analyses of performance and cost

Carl-Eric Hagentoft, Professor
Angela Sasic Kalagasidis, Associate Professor

Department of Civil and Environmental Engineering, Chalmers University of Technology, Sweden

KEYWORDS: *Mould growth, probabilistic, risk, weather, attics, life cycle cost, drying potential*

SUMMARY
Problems with high humidity levels and mould growth in cold attics have been increasing over the last few years. A recent Swedish study showed that as many as up to 60 – 80 % of the single-family houses in Västra Götaland (largely, the Gothenburg region) are showing significant mould growth and thereby risk developing serious moisture problems. The high humidity levels are to a large extent a consequence of the increasing demand on energy efficiency. Houses are frequently retrofitted with additional attic insulation, which leads to a colder attic space and hence a higher humidity. Furthermore, furnace heating is often replaced in favour of heat pumps or district heat. This may alter the air-pressure balance of the house, resulting in an increased thermal pressure on the ceiling with subsequent air-leakage up to the attic. Also newly built attics have problems. A risk assessment of the risk for mould growth is performed for different design of the attic. Also a simplified life cycle cost is estimated for the different design alternatives. The alternative with controlled ventilation is estimated to be risk free with lowest life cycle cost. Roof insulation gives low risk for mould growth in northern part of Sweden.

1. Introduction

Problems with high humidity levels in cold attics have been remarkably increasing in Sweden over the last decade. Beside clear evidence – the significant mould growth on the wooden parts of cold attics, which is recently confirmed in about 60-80 % single-family houses in Västra Götaland region (largely, the Gothenburg region; (Ahrnens C., Borglund E., 2007), mould odours in indoor air seem to be one of the most frequent side effects. Thus, cold attics are together with crawl spaces singled out as the two worst constructions in existing Swedish buildings with large existing and future mould problems.

The high humidity levels are to a large extent a consequence of the increasing demand on energy efficiency. Houses are frequently retrofitted with additional attic insulation, which leads to a colder attic space and hence a higher humidity (Hagentoft et.al. 2008). Leaks of indoor air up to the attic through the attic floor, and the under cooling of the roof due to sky radiation, increase the problem (Holm and Lengsfeld 2006, Sanders et. al 2006, Essah et. al 2009). The moist air might condensate at the underlay and small droplets of liquid water can build up. The water will then be absorbed and accumulated in the surface area. High moisture content can even lead to rot.

Another important moisture source influencing the attic hygrothermal condition is the water vapour in the surrounding outdoor air. The advice given to the building sector in Sweden today is to have a not too high or not too low ventilation rate, by outdoor air, of the attic. A too high ventilation rate, in combination with under cooling, results in high relative humidity (Sasic 2004). Too low ventilation is also risky in case of construction damp or leaky attic floor (Arfvidsson and Harderup 2005, Sanders 2006, Essah 2009). The optimal air exchange rate varies with the outdoor climate, and fixed ventilation through open eaves and/or gable and ridge vents are not always the best choice (Hagentoft et. al 2008,2011, 2012).

The results from a recently finished SBUF-financed Swedish research project *Risk assessment for Cold Attics* is presented in this paper (Hagentoft, Sasic, 2103).

2. Probabilistic Analysis – Type of attics

The probabilistic model of attic performance presented in this paper uses validated deterministic models for the heat and moisture transfer (see section 4). The Monte Carlo method will be used to calculate the maximum mould growth index for multiple randomly chosen and simulated whole year. One of 30 weather data years (1961- 1990) with hourly values will be selected randomly for each simulation. The attic is assumed to be damaged by mould growth if the Mould Growth Index (MGI) according to Hukka and Viitanen (1999) exceeds 1.

The reference case is represented by the conventional design of a cold attic today. It has a -sloped roof (between 10 to 30 degrees), which is built from the inside starting with 22 mm wooden T&G board, moisture tight board, litter and batten and counter batten and roof tiles. The cold attic floor is insulated with 400 mm loose fill insulation. The reference house is ventilated by 20 mm wide open slots along the eaves. The building is five storeys high (a multi-family house), has an attic floor area of 220 m^2. There is an exhaust ventilation system in the building resulting in a ventilation rate of 0.5 h^{-1}. The leakage of the building envelope at 50 Pa is 0.6 litre/m^2/s. Two alternative attic floor constructions are considered; a 200 mm thick concrete floor with a vapour barrier on top or a wooden frame construction with gypsum board and a vapour barrier. In the simulations, three alternative airtightness's of the attic floor are considered; Totally tight, tight (0.06 air exchanges of the indoor air at 50 Pa alternatively expressed as a specific leakage area of $6.4 \cdot 10^{-6}$ m^2/m^2) or leaky (0.3 air exchanges of the indoor air at 50 Pa/$3.8 \cdot 10^{-5}$ m^2/m^2). Different Swedish locations are considered and the orientation of the building (North, East, West and South) is varied. The indoor moisture supply is either low (1± 0.5 g/m^3) or medium (3± 0.5 g/m^3), and normally distributed.

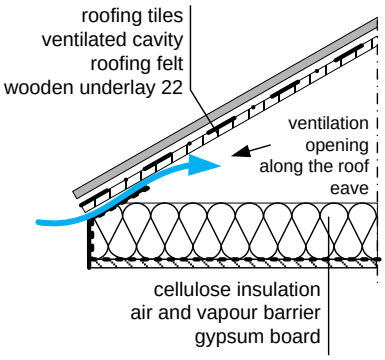

FIG 1. The conventional cold attic - the traditional reference construction.

The following alternative designs are used (see also Figure 2):

- Conventional
- Thermally insulated roof
- Controlled ventilation
- Diffusion open membrane
- Moisture buffering insulation material

3. Risk indicators for alternative design – Results in a nutshell

In the next chapter, some results for the hygrothermal performances of the attic are presented for some cases. Here, we present the findings in terms of a risk levels for the different construction designs. The color used are then representing:

- Risk free (Green)
- Low risk (Yellow)

- Semi high risk (Orange)
- High risk (red)

In Figure 2 the risk levels of the various designs are presented together with some requirements for the risk evaluation. One important finding is that it is very important to dry out the building damp immediately after construction for all cases.

	Cold attic construction	Requirements and sensitivity
Risk free	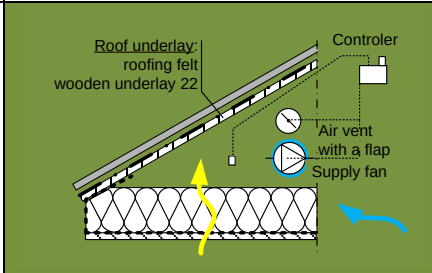 Controlled mechanical ventilation	• The airtightness of the attic should be at least 10 1/h@50Pa • Ventilation should start directly after completeness of attic construction • Requires alarm function for failure of mechanical devices • Lowest total life cycle cost
Low risk	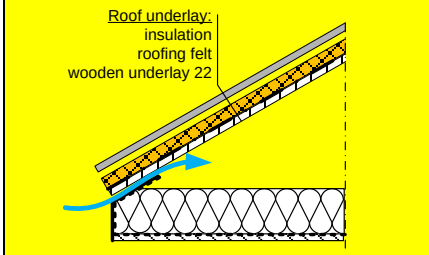 Insulated roof, good air tightness of the attic floor	• Requires durable solution for the airtightness of the attic floor. • Works better at low moisture excess in the building (well ventilated housing - preferably exhaust only mechanical ventilation system). • Sensitive to the building orientation. • Some sensitivity to the local and future climate. • Should be supplemented with dehumidifiers in the construction phase to eliminate built-in moisture.
Semi-high risk	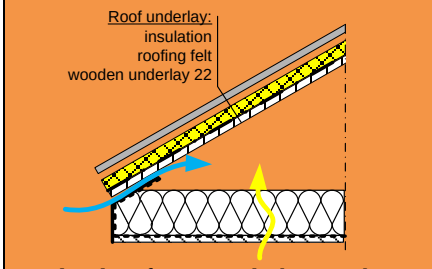 Insulated roof, some air leakage in the attic floor	• Works better at low moisture excess in the building (well ventilated housing - preferably exhaust only mechanical ventilation system). • Sensitive to the local and future climate. • Should be supplemented with dehumidifiers in the construction phase to eliminate built-in moisture.
High risk	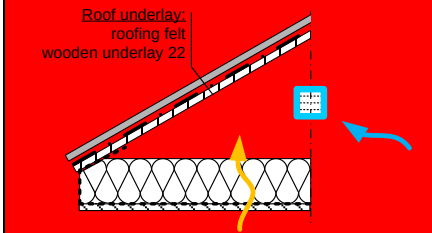 Reduced ventilation – only through gable vents; air tight roof eaves.	• Extra sensitive to the lack of air-tightness in the attic floor and high moisture excess in the home. • Should be supplemented with dehumidifiers in the construction phase to eliminate built-in moisture. • Sensitive to future climate.
High risk	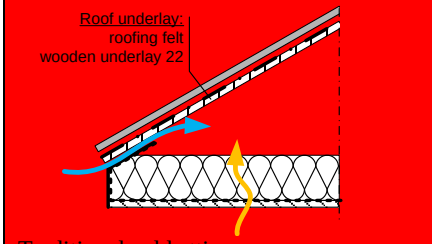 Traditional cold attic	• Extra sensitive to the lack of air-tightness in the attic floor and high moisture excess in the home. • Sensitive to future climate. • The most expensive technical solution when lifecycle cost is assessed. • Should be supplemented with dehumidifiers in the construction phase to eliminate built-in moisture.

FIG 2. Summarized risk levels of the various designs presented together with some requirements.

4. Hygrothermal performance

Only some samples of results from total findings in the project will be given in this chapter. The complete report (In Swedish) can be found in the reference list (Hagentoft, Sasic, 2013), with a direct link.

Figure 3 shows a number of simulations based on randomly chosen years. In the simulations the cold attic starts from dry conditions, in the middle of the summer. The risk assessment is based on the fraction of simulations that results in a mould growth index exceeding one. In this example 17 of total of 128 simulations results in a failure, i.e. the risk for mould growth is 13% (17/128=0.13).

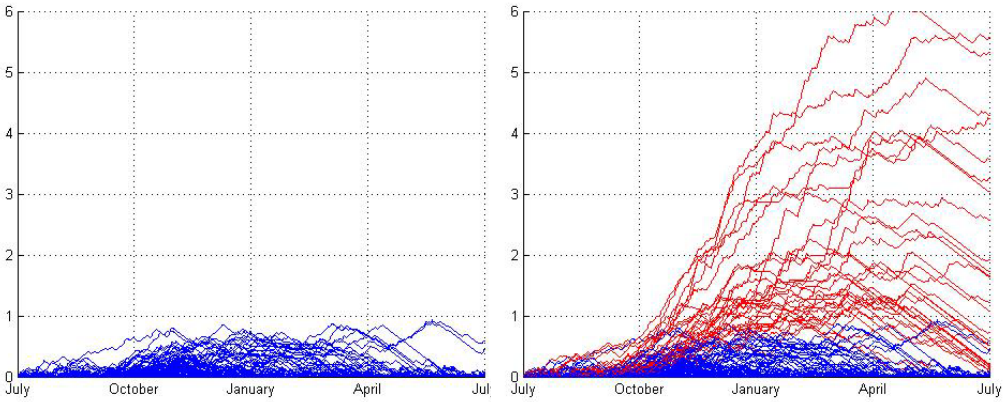

FIG 3. Example of simulation results for randomly chosen years and input parameters. The figure to the left represent the damaged free simulations and the additional ones in the right hand figure represent additional cases with mould growth.

The cases with controlled ventilation do not result in any mould growth exceeding 1. The second best alternative is represented by the case with insulation on the roof. Table 1 shows the results for some of these cases.

TABLE 1. Results from the probabilistical simulations. The table presents the maximum mould growth rates for two different slope angles of the roof (10 and 20 degrees). The roof structure is covered with 0,1 m cellular plastic insulation. The location is Gothenburg or Stockholm and the orientation of the building is varied. For the Stockholm case with a tight attic floor no mould growth is registered.

	Leaky attic floor				Tight attic floor			
Gothenburg, roof slope 10°	N	S	E	W	N	S	E	W
Average of max MGI*	1.40	1.09	0.81	0.83	0.28	0.23	0.08	0.10
Risk that max MGI* >1, (%)	41	33	24	25	8	5	0	0
Gothenburg, roof slope 20°								
Average of max MGI*	1.74	1.07	0.95	1.09	0.34	0.25	0.11	0.08
Risk that max MGI* >1, (%)	50	33	30	29	9	5	0	0
Stockholm, roof slope 10°								
Average of max MGI*	0.55	0.38	0.70	0.50				
Risk that max MGI* >1, (%)	17	12	17	13				
Stockholm, roof slope 20°								
Average of max MGI*	0.68	0.38	0.54	0.57				
Risk that max MGI* >1, (%)	20	9	12	14				

* max MGI means the maximum MGI during one year of simulations.

5. Simulation tool

SimpleColdAttic is a stand-alone software for HAM-simulations of cold attic temperature, relative humidity as well as mould growth index. The program can simulate both in deterministic as well as in probabilistic (random) mode. With the program similar cases as presented here in this paper can be analysed. The program is based on a simplified HAM-model for an attic, theory can be found in (Hagentoft, 2011) and (Hagentoft and Sasic, 2011).

The free software can be down loaded from: http://www.byggnadsteknologi.se/downloads.html.

6. Life cycle cost

Table 2 shows the final results for the total cost (life-cycle cost) for alternative construction designs of the attic. Location, airtightness of the attic floor and moisture supply is varied as random parameters in the calculations.

TABLE 2. Total cost (in SEK) for attic floor and roof (104 m^2) for the case with a one-family residential building. In the case with roof insulation, the insulation thickness of 0.1m is considered. The roof slope angle is fixed to 20 degrees and the orientation is North-South.

Alternative Design	Base Investment	Operational Cost	City	Airtightness Moisture supply	Risk MGI>1	Damage Investm.	Yearly Cost
Conventional	76380	0	Gothenburg	Any	100%	38400	5739
Ins. roof	94135	0	Gothenburg	Good Low	10%	3840	4889
Ins. roof	94135	0	Stockholm	Not good High	50%	19200	5657
Ins. roof	94135	0	Stockholm	Good Low	0%	0	4697
Ins. roof	94135	0	Stockholm	Not Good High	20%	7680	5081
Controlled ventilation	88427 (80927)	600	Anywhere	Any	0%	0	4639

The yearly cost is based on a 5% interest rate on investments. The damage investment represents a simplification representing the cost for the fraction of the buildings damaged that has to be cleaned and added a controlled ventilation system. For the controlled ventilation the fan is assumed to be replaced after 15 years which gives a yearly operational cost of 500 SEK. The use of electricity for the fan ads further 100 SEK to the yearly cost. The investment cost for the controlled ventilation, in brackets, is the value after reduction of cost for exchange of the fan (7500 SEK) which is given as a yearly cost instead. Ill-will (bad-will) is not included. Initial cost for drying of building damp is included with 5000 SEK (for the cases with conventional solutions or insulated roof). No inflation is considered, the numbers represent the real value.

7. New findings on drying potential for cold attics and ventilated structures

Although one could expect a close correlation between the mould growth risk in cold attics and outdoor climate, specifically outdoor temperature and solar radiation intensity, previous investigations (Nik et al., 2012) and also the results presented in Table 1 show that such correlation is not straightforward. The results suggest that the risk is also correlated to the ventilation flow rate through the attic, which is determined by the wind and the orientation of the attic. This is further investigated by the means of a *drying potential*, DΠ, a new performance criterion which can be seen as an upgraded Π-factor (Hagentoft, 1993,; Hagentoft and Harderup, 1996). For the period between the times t_a and t_b, DΠ is found as

$$D\Pi = \frac{1}{t_b - t_a}\int_{t_a}^{t_b} \tilde{R}(w,\theta)\cdot\left(v_{sat}(T_{eq}) - v_{out}\right)dt, \quad 1/\tilde{R}(w,\theta) = 1/R_a(w,\theta) + \frac{1}{A/Z(R_a)} \tag{1}$$

Where T_{eq} equivalent outdoor temperature, (^{o}C)
v_{out}, v_{sat} water vapour content in outdoor air and at saturation, (g/m^3)
R_a air flow rate through the ventilation opening in the attic, (m^3/s)
w wind speed, (m/s)
θ angle between the wind direction and the azimuth of the ventilation opening, (deg)
A area of the roof slope (only shed roofs), (m^2)
Z resistance to convective moisture transfer between the air and the roof slope, (s/m)

While Π-factor is basically calculated from the weather parameters and radiation surface conditions, DΠ accounts in addition for the attic geometry and ventilation flow rate through the attic. Figure 4 shows DΠ for a conventional cold attic, which can be located in Gothenburg or in Stockholm, and over the period of 1975-2100. The climate data are obtained from the climate scenarios RCA3-ERA40 (1975-2004) and RCA3-ECHAM5-A1B-1 (2010-2100), (Nik et al., 2012). The geometry and roof slope (20 deg) of the attic are same in every case, while the orientation of the roof varies. The values included in the figures refer to annual mean DΠ, g/(m^2·h). Based on the results, the lowest DΠ is found for the attic in Gothenburg with north roof orientation. At the same location, DΠ for the attics with west and east roofs is approximately the same, and twice the value for the north roof. Finally, DΠ for the south roof is close albeit somewhat lower in the later period than of the west and east roof. By comparing these findings with the mould risks from Table 1, we can conclude that the lower DΠ, the higher risk for mould growth and vice versa.

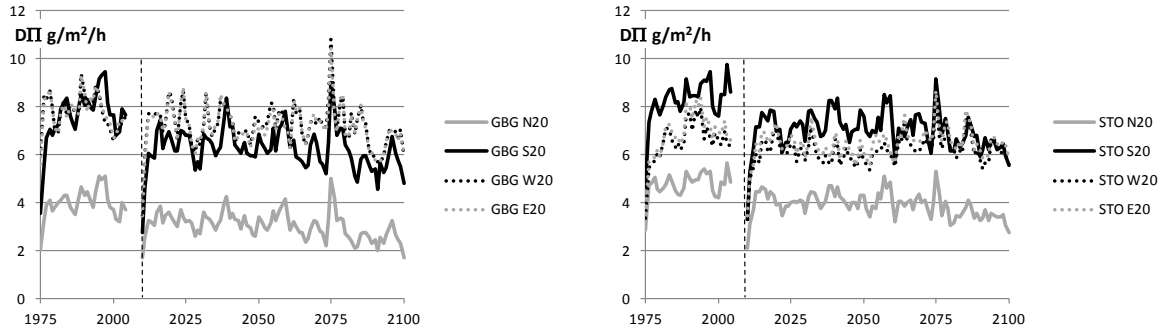

FIG 4. Drying potentials for a cold attic with different roof orientation and geographical location. The results up to 2004 are obtained with the climate data from RCA3-ERA40. From the vertical dashed lines, the results are obtained with the climate data from RCA3-ECHAM5-A1B-1.

The results for the cold attic in Stockholm are similar, with one exception that the DΠ for the south roof is somewhat higher than for the west and east roofs. Even these results are well correlated with the mould risks from Table 1, i.e. the largest DΠ (for the south roof) corresponds to the lowest risk (also the south roof).

We can also observe a declining trend of DΠ over time that can be interpreted as the predicted climate changes will increase the risk of mould growth in the attic.

For comparisons of drying potentials between different locations, a normalized drying potential is used:

$$n D\Pi_j^{City,period} = \frac{30^{-1}\cdot\sum_{i=year}^{year+30} D\Pi_j^{City,i}}{\overline{D\Pi}_W^{LUND,1975-2004}} \tag{2}$$

Where

City, period Location and 30-year period for which nDΠ accounts for
j roof orientation, N, S, E, W

year start year, for example 2010, 2014, 2070

$D\overline{\Pi}_W^{LUND,1975-2004}$ 30-year averaged DΠ at a location with the highest drying potential in the country (*LUND*), in the past, 1975-2004, and for the roof orientation with the highest average drying potential at the same location (*W*=west)

The normalized drying potential is a relative measure that takes values between 0-1, where 0 means no drying potential and 1 the maximum potential for the climate in Sweden. Figure 5 shows the normalized drying potential for four representative cities in the country and for the past and predicted future climate conditions. Based on the past climate data (1975-2004), the maximum drying potential for a cold attic is found in Lund, for the west or east roof orientation, and the minimum in Östersund for the north roof orientation. The south roof direction in Lund has the next largest normalized drying potential (0.9). South, west and east roof orientations in Gothenburg and Stockholm show moderately high nDΠ (0.6-0.7), while the north roof direction has a low potential (0.5 or lower) at all locations. As the latitude increases, nDΠ decreases, reaching the lowest values in Östersund for all roof directions.

Although the predicted future climate changes indicated a noteworthy increment of outdoor air temperature (see Figure 5), the normalized drying potential at all locations and directions decreases. The main reason for this is increasing outdoor air humidity, which is about 2 g/m^3 larger in 2070-2100 than in the past period.

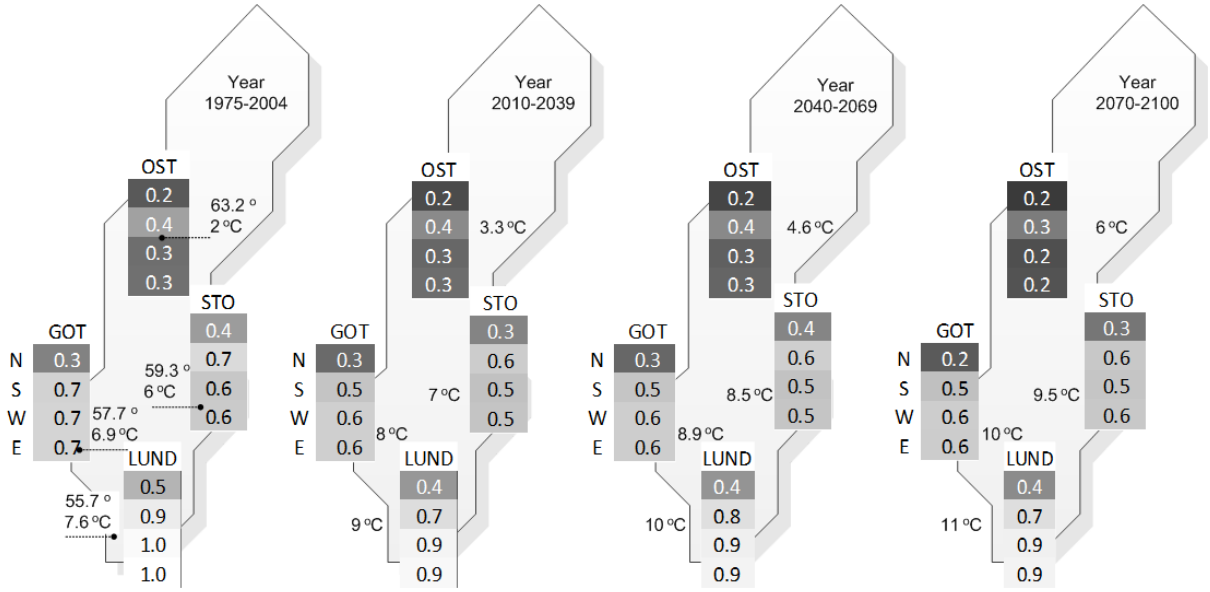

FIG 5. Normalized drying potentials for a cold attic with different roof orientations and geographical locations in Sweden (GOT=Gothenburg;STO=Stockholm;OST=Östersund and LUND). For each location, the latitudes and 30-year average of annual outdoor temperatures are shown.

8. Conclusions

The results from the research project gives:

- The moisture safety of a cold attic is improved if: the attic floor is airtight, building damp is removed directly after the building has been erected, the indoor environment is well ventilated and the attic has a positive pressure in relation to the dwelling.
- Conventionally designed attics with ventilations at the eaves are not moisture safe, neither are the ones with reduced ventilation with gable ventilation openings. However, the risk becomes lower further north in Sweden.
- Insulation of the roof improves the moisture conditions of the attic. However, the risk levels are determined by the location in the country and the orientation of the building.
- Controlled ventilation represents a robust technical solution, which can withstand the spread in workmanship (airtightness) and moisture supply as well as future climate.
- Controlled ventilation represents the most cost effective alternative.

- A revised drying potential represents a promising new indicator for the moisture safety of ventilated structures such as attics for evaluation and comparison of alternative designs, locations and orientation, including estimates for future climates.

Acknowledgements

The work is supported by the Swedish Research Council for Environment, Agricultural Sciences and Spatial Planning (FORMAS-BIC) and SBUF (The construction industry's organisation for research and development).

References

Ahrenens, C., Borglund E. 2007. Fukt på kallvindar. Master thesis 2007:11. Chalmers, Building Physics.

Arfvidsson, J. and Harderup, L-E. 2005. Moisture Safety in Attics Ventilated by Outdoor Air. 7th Symposium in Building Physics, Reykjavik, Island.

Essah, E.A. 2009. Modelling and measurements of airflow and ventilation within domestic pitched roofs. Doctoral thesis. Glasgow Caledonian University, Scotland, UK.

Hagentoft, C-E. 1993. Indoor Climate Classes. The Use of the & Pi;-Factor, Report T2-S-93/03. IEA-Annex 24 HAMTIE, and (1994) Lund University Department of Building Physics. Report TVBH-7170.

C. E. Hagentoft, E. Harderup, 1996, Moisture Conditions in a North Facing Wall with Cellulose Loose Fill Insulation: Constructions with and without Vapor Retarder and Air Leakage. Journal of Thermal Insulation and Building Envelopes, vol. 19.

Hagentoft C-E, Sasic Kalagasidis A. Ahrnens C., Borglund E. 2007. Effekter på funktion och kostnad av styrd ventilation av kallvindar. Bygg&Teknik, No 4, 2007.

Hagentoft CE, Sasic Kalagasidis A., Thorin M., Nilsson S.,2008. Mould growth control in cold attics through adaptive ventilation. 8th Nordic Symposium on Building Physics, Copenhagen, June 16-19, 2008.

Hagentoft CE, Sasic Kalagasidis A. 2011. Probabilistic analysis of hygrothermal conditions and mould growth potential in cold attics. Nordic Symposium in Building Physics. Tampere, Finland

Hagentoft CE, Probabilistic analysis of hygrothermal conditions and mould growth potential in cold attics. Impact of weather, building system and construction design characteristics. XII DBMC, April 2011, Porto, Portugal.

Hagentoft CE, Sasic Kalagasidis A. 2012. Chapter: Hygrothermal Conditions and Mould Growth Potential in Cold Attics: Impact of Weather, Building System and Construction Design Characteristics in Building Pathology and Rehabilitation. Editors: Freitas, V. Peixoto de, Costa, Anibal, Delgado, João M.P.Q. Springer.

Hagentoft CE, Sasic Kalagasidis A. 2013. Riskanalyser för ventilerade kallvindskonstruktioner. http://www.sbuf.se/ProjectArea/Documents/ProjectDocuments/213A85DA-36F8-438A-8053-E7A5E2740AF7/FinalReport/SBUF%2012438%20Slutrapport%20Riskanalyser%20för%20kallvindskonstruktioner.pdf

Holm, A., Lengsfeld, K. 2006. Hygrothermal performance of unfinished attics (ventilated roofs) – an experimental study. Research in Building Physics and Building Engineering. Proceedings from the third International Building Physics Conference, Montreal, Canada.

Hukka E., Viitanen H.A., 1999. A mathematical model of mould growth on wooden material. Wood Science and Technology 33, Springer-Verlag.

Nik M.V., Sasic Kalagasidis A., Kjellström, E. 2012. Assessment of hygrothermal performance and mould growth risk in ventilated attics in respect to possible climate changes in Sweden. pp. 96-109(55),.Building and Environment.

Sanders, C.H. 2006. Modelling condensation and airflow in pitched roofs – Building Research and Establishment (BRE) information paper, IP 05/06. BRE Press, Garston, Watford – UK. ISBN 1-86081-912-5, pp. 1-7

Sasic Kalagasidis A. 2004. HAM-Tools. An Integrated Simulation Tool for Heat, Air and Moisture Transfer Analyses in Building Physics. Doctoral thesis. Chalmers University of Technology, Sweden.

Prediction of indoor climate based on questionnaires

Christoph Harreither, M.Sc.[1]
Naomi Morishita, M.Sc.[1]
Thomas Bednar, Professor, Ph.D.[1]

[1] Vienna University of Technology, Institute of Building Construction and Technology, Austria

KEYWORDS: *indoor climate, relative humidity, indoor temperature, air tightness, questionnaire*

SUMMARY:
The main goal of our study was the validation of a formerly presented model to calculate the indoor humidity. Indoor humidity is the most important boundary condition for the hygrothermal behaviour of building components. With the presented model, the durability and life-cycle costs of building components can be predicted. The presented work forms the basis for decision making during the design process.

In this study, questionnaires from 38 households were collected regarding indoor moisture production and ventilation behaviour. The questionnaire answers and values from literature were used as inputs in the formerly presented model. Temperature, relative humidity, and air tightness measurements were performed in parallel. The outcome was compared to the calculation results and used to validate and refine the model.

The calculated results fit well to the measured values, if the humidity is in the low to average range. When absolute indoor humidity is very high, the calculation shows variance from the measured values. The calculated maximum is 15 g/m³, which exceeds the measured maximum of 11 g/m³. Theories for the variance have been postulated; however, specific questions for airtight buildings should be included in future questionnaires to determine the reasons for the variance.

The work forms part of the Austrian contribution to IEA Annex 55.

1. Introduction

Different aspects must be considered during the building design process. Cost minimization, durability (over the building's lifespan) and high energy efficiency are three typical performance goals, which can result in different design solutions. The most important aspects for durability are indoor and outdoor climate and the fault tolerance of the construction.

This study focuses on the prediction of indoor climate, which is the first step in the formerly presented probabilistic model to calculate life-cycle costs (Harreither et al. 2012). Values for moisture production in residential buildings were published by Kalamees et al. (2006), Hartmann et al. (2009) and Geving & Holme (2011). Even standardized values can be found (DIN Fachbericht 2010). In this study, daily production rates in homes were calculated based on the above literature values and applied to the data from the questionnaires. Values to quantify the ventilation rates by window opening were taken from Reiß & Erhorn (2009). The ventilation rates by infiltration or a mechanical ventilation system were taken from standards. Monthly mean values were calculated in this study, which will form the basis to calculate the building components lifespans.

2. Investigation

Two housing projects were investigated during winter 2012/2013 in Vienna and summarized in this study.

PSG is a low-rise high-density housing project on the east side of Vienna and is the first project in our study. Questionnaires were distributed to all 91 households in November 2012. By the end of January, we received 39 completed questionnaires, performed 34 Blower-Door tests and measured temperature and relative humidity in 28 houses.

The second project is KW, a multi-storey residential apartment building on the north side of Vienna. Ten flats took part in our study by completing questionnaires and joining the temperature and relative humidity measurements during January 2013.

2.1 Investigated houses in PSG-project

The PSG housing project is described in detail in Zingerle (2013). 91 nearly identical detached houses were built within a social housing project in 2009. All houses have two floors with 52 m² gross floor area (GFA). Each house has dimensions of 4.75 m x 11.00 m. The net floor area is 84 m². Most of the houses have cellars too. Half of the houses are orientated east-west and the other half are orientated north-south.

The houses consist of timber frame walls and a timber frame roof. The ground floor slab and the cellars are composed of reinforced concrete. The exterior wall assembly on the ground floor is gypsum board, OSB, vapour barrier, timber platform framing with thermal insulation and an ETICS on the exterior. The exterior walls on the upper floor have wooden cross-battens and a ventilated curtain-wall facing instead of the ETICS. The timber frame roof is composed of gypsum board, battening, a vapour barrier, wooden beams with thermal insulation, wooden planking, a ventilation layer, wooden planking, and an EPDM foil on the exterior.

None of the houses in PSG have a balanced mechanical ventilation system, but all the houses have fans in the toilet on the ground floor and in the upper floor bathroom. The toilets on the ground floor are windowless but the bathrooms on the upper floor have two windows on opposite walls with dimensions 2 m x 1 m.

We equipped 28 houses in PSG in January 2013 with two data loggers each. One logger was mounted on the ground floor in the middle of the open plan kitchen/dining/living rooms at head height. On the upper floor, the loggers were placed in the bedrooms. When it was not possible to place the data logger in the bedroom, the loggers were placed in another upper floor room (nursery or study). Most inhabitants state that the internal doors are always open, so it was assumed that the upstairs was also hygrothermally coupled.

Blower-door-tests were also conducted in these 28 houses and six other houses.

2.2 Investigated flats in KW-project

An apartment building with 45 flats was built in 2009 as a social housing project. The GFA of the five-storey building is 5300 m² and the investigated flats have 55 - 110 m² net floor area. There are one storey flats and two storey maisonettes. Four of the investigated flats have bathrooms with a window; the other bathrooms have no window. A centralized balanced mechanical ventilation system is provided for all flats.

The external walls are made of reinforced concrete with ETICS on the exterior and plaster finish on the interior. The flat concrete roof has external thermal insulation. The external covering is either gravel or green roof. The interior partitions are either made of concrete or insulated stud walls with gypsum board.

Temperature and relative humidity loggers were placed in the living room and bedrooms of each investigated flat.

2.3 Questionnaires

Each participating household received a questionnaire regarding moisture production and ventilation behaviour.

The moisture production related questions were (a) How many persons live in the house/flat? (b) How many persons use the house/flat as a home office? (c) How often do you shower/bath per week? (d) Do you have a tumble dryer? (e) How often is the tumble dryer in use? (f) Where do you dry your clothes (if the tumble dryer is not in use)? (g) How many indoor plants do you have? (h) How often do you cook during one week? (i) Which pets do you have? (j) Do you use a humidifier/dehumidifier?

The ventilation related questions were (a) Do you have a mechanical ventilation system? (b) On which level does it operate? (c) How often do you open the windows per day? (d) How many windows are open the whole day/night? (e) Do you have an additional fan in the bathroom or the toilet? (f) At what levels do you use it?

2.4 Measurement equipment

The temperature and relative humidity was measured using T&D RTR 53 and HOBO U12 data logger. Loggers collected instantaneous values at 15 minutes (PSG) or hourly intervals (KW) for this study. The n_{50}-values were measured with a Minneapolis Blower Door™.

3. Questionnaire results

3.1 Questionnaire results in PSG

3.1.1 Moisture production

One to four persons live in the houses. All households use this house as their principal residence. Some of the families have small children and the house is occupied more often during the day. In other houses, the people work all day and the house is only occupied during the evening and night. Ten households have a tumble dryer. Most of the others hang the laundry in the living area (living room, bedroom, study, …). Some of the houses do not have any indoor plants. One household has 39 plants. The families cook lunch or dinner between one and twelve times per week. The number of pets varies between zero and three. No household has an aquarium. The household that produces the most moisture due to pets is a family with two dogs. One family has a humidifier.

3.1.2 Ventilation behaviour

None of the houses have a mechanical ventilation system. Seven families open some windows in the morning for a short time. Fifteen families open windows for short periods in the morning and in the evening. Only six families open several windows more than twice a day. Two families have a window open for half a day. In four houses, there is one window open the whole night. All households use the fans in the bathroom and in the toilet. The fans switch on at a relative humidity between 50 % and 100 %.

3.2 Questionnaire results in KW

All moisture production-related answers are in the same range as in the PSG-project. Two families have a tumble dryer.

The largest difference to the PSG-project is the mechanical ventilation system in the KW project. One family uses the ventilation system on high; all others set it on low. The families open their windows less often than in the PSG-project. No additional fans are installed in the bathrooms and toilets as the mechanical system constantly extracts air from the bathrooms and toilets.

4. Measurement results

4.1 Measurement results in PSG

Monthly average temperatures vary between 19 and 24 °C on the ground floor and between 18 and 24 °C upstairs (FIG 1). The mean temperature of all measured houses in the basement (20.9 °C) is 0.5 K higher than the mean value of all measured upper floors (20.4 °C). The monthly mean relative humidity varies from 40 % to 70 %.

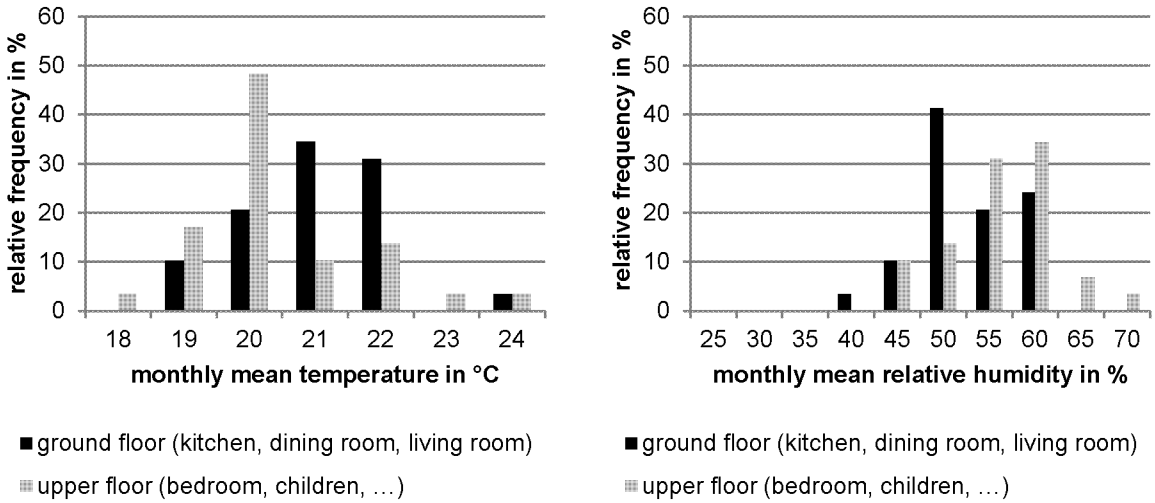

FIG 1. Histograms of measured monthly mean temperature (left) and monthly mean relative humidity (right) in January 2013 in the PSG-project.

The mean of all measured n_{50}-values is 0.68/h. The lowest n_{50}-value is 0.45/h, the second highest is 0.87/h. All houses are very airtight probably as the houses are prefabricated.

4.2 Measurement results in KW

Histograms of measured temperature and relative humidity can be seen in FIG 2.

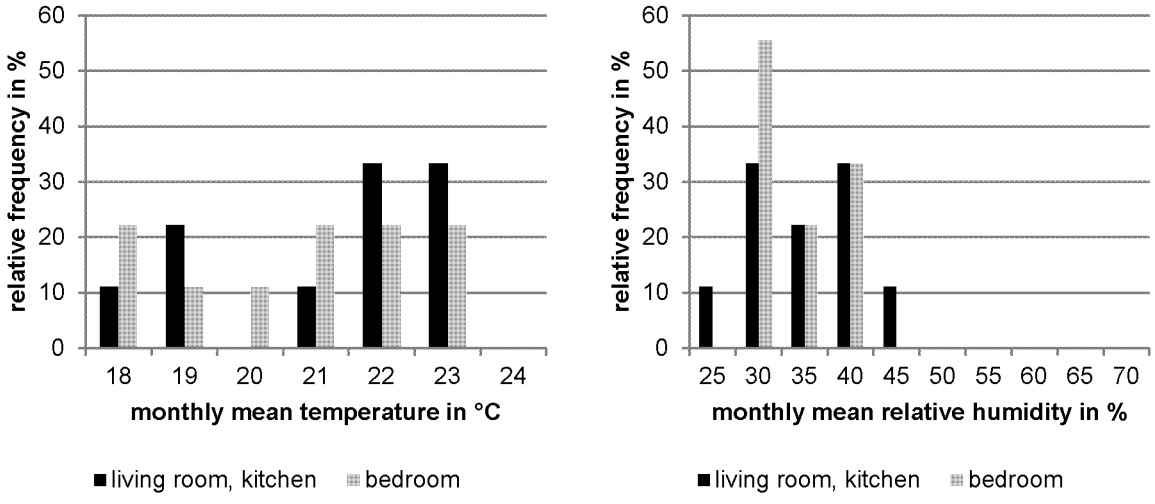

FIG 2. Histograms of measured monthly mean temperature (left) and monthly mean relative humidity (right) in January 2013 in the KW-project.

4.3 External climate

The external temperature and relative humidity were measured at the PSG-project, at the KW-project and at our institute. All three positions are within 6 km distance of each other.

The monthly mean values in January 2013, measured by the two loggers in PSG, were 0.35 °C and 77 % relative humidity which results in an absolute humidity of 0.0039 kg/m³. At the KW-project 1.80 °C and 69 % were measured with two loggers similar to PSG. The weather station at our institute measured monthly mean values of 1.30 °C and 74 % relative humidity. Both result in the same absolute humidity of 0.0039 kg/m³.

5. Prediction of indoor humidity using questionnaire-results

For the prediction of indoor humidity from the questionnaires a formerly presented model was used (Harreither et al. 2012), improved and described in detail. The absolute humidity in the flats was calculated from the measured external temperature and literature values for moisture production and ventilation, applied to the data from the questionnaires. The internal volume of the flats was taken from the architectural plans. Internal moisture excess, Δν, is than calculated by using EN ISO 13788 (2012).

$$\Delta\nu = \nu_i - \nu_e = \frac{G}{n \cdot V} \quad (1)$$

Where ν_i humidity of indoor air by volume (kg/m³)
ν_e humidity of outdoor air by volume (kg/m³)
G internal moisture production rate (kg/h)
n air change rate (1/h)
V internal volume of building (m³)

5.1 Moisture production

According to Kalamees et al. (2006), a person who is at home all the time produces 0.9 kg water vapour per day caused by respiration, transpiration, etc. Furthermore, it was assumed that a full-time employee is at home half a day (12 hours) and produces 0.45 kg/day. A part-time employee is at home 18 hours a day and produces 0.68 kg/day. Small children are assumed to be at home 18 hours a day and produce only 50 % the moisture an adult does (0.34 kg/day). Children in high school are assumed to be at home 14 hours a day and produce 75 % the moisture of an adult (0.39 kg/day). Someone who works from a “home-office” is considered to always be at home.

Literature values for moisture production due to personal hygiene are around 0.16 kg/shower, 0.33 kg/bathing and 0.08 kg/towel-drying (Kalamees et al. 2006, Hartmann et al. 2009, DIN Fachbericht 4108-8 2010). If the bathroom has a window or a fan, half of the value (for showering and bathing) is taken. If there are two windows, a quarter of the literature values is taken for the calculation. It is assumed that most of the moisture goes directly to the outside by windows or the fan and does not affect the measurement in the bedroom.

We identified out of the questionnaires that people in KW do their laundry approximately every fourth day. Assuming that one load evaporates 2.25 kg water (Hartmann et al. 2009), one person produces 0.55 kg water vapour per day by hanging laundry to dry. Some households are assumed to produce only 0.1 kg moisture per day due to drying the laundry with a tumble dryer or hanging the laundry outside the flat such as in a cellar or on a balcony.

For plants, moisture production of 0.05 kg/day/plant (Hartmann et al. 2009) was adopted. The mean number of plants per household is 6.6.

Cooking was assumed to produce 0.2 kg water vapour per event and per person (Kalamees et al. 2006, Hartmann et al. 2009).

15 households have pets. Dogs were assumed to produce 0.4 kg moisture/day; cats produce 0.1 kg/day. There were no other animals relevant for internal moisture production.

An additional production rate of 1.6 kg/day was calculated in one flat because of a humidifier. Nevertheless the absolute humidity is still low in this flat because of a tumble dryer, their inhabitants being at work all the time and open a window at night.

FIG 3 shows box plots of the moisture production rates per event and the overall internal moisture load per person.

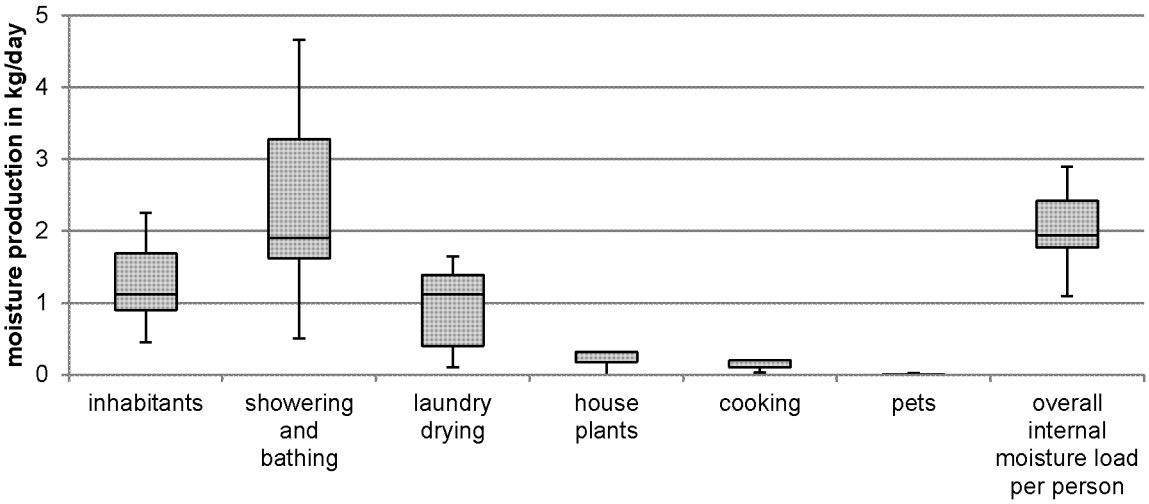

FIG 3. Box plots of moisture production per household caused by different events and overall per person

5.2 Ventilation

The air change rates by a mechanical ventilation system, window opening and infiltration were summed to get the total air change rate (FIG 4).

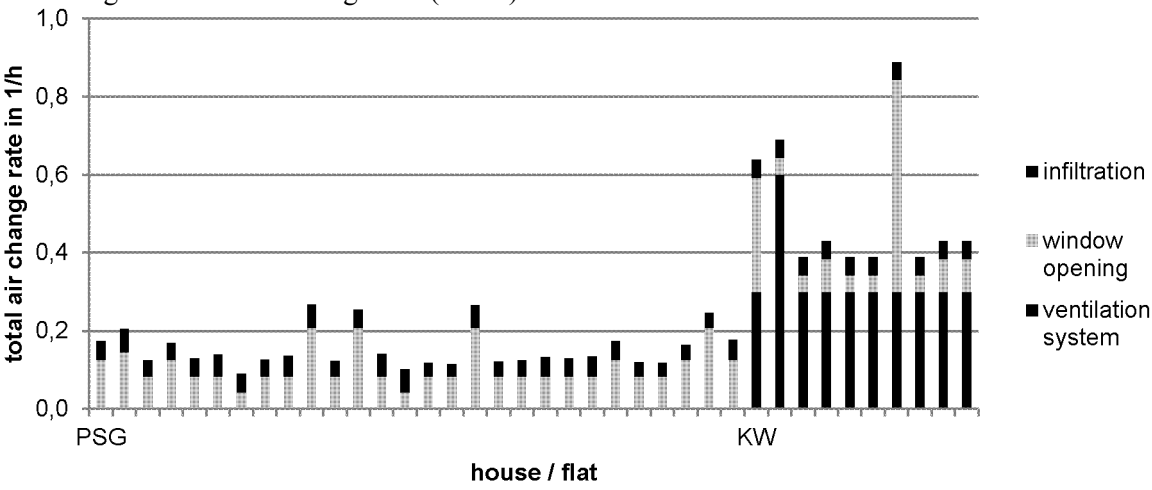

FIG 4. Total air change rates in the flats/households due to different ventilation measures

The high air change rate due to the ventilation system was assumed to be 0.6/h and low 0.3/h.

The air change by window opening was calculated according to Reiß et al. (2009). An air change rate of 1/h for the whole flat was assumed for short airing periods by window opening in the morning or in the evening. For long periods of open windows during night or day (12 hours either during the day or night) an air change rate of 1/h is calculated for the room with the open window.

The fans in the bathroom are already taken into account when calculating the moisture production by showering or bathing.

The air change rate due to infiltration is calculated using Annex C in EN ISO 13789 (2007). The air change rate due to infiltration is 7 % of the n_{50}-value. In the KW-project, no n_{50}-values were measured. Therefore the mean n_{50}-value of the PSG-project was used to calculate the air change rate due to infiltration.

An additional air change rate of 0.05/h was assumed in one flat because of a dehumidifier.

5.3 Comparison of calculations and measurements

FIG 5 shows the calculated absolute humidity on the horizontal axis and the measured absolute humidity on the vertical axis.

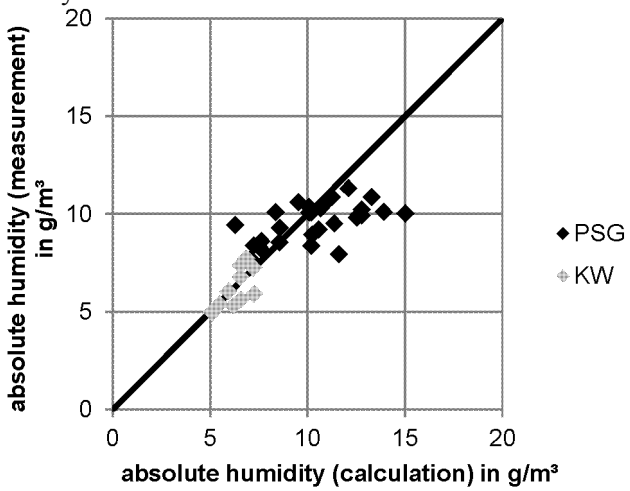

FIG 5. Comparison of calculated and measured absolute humidity

The calculated results match the measured values if the humidity is low to average. When absolute indoor humidity is very high, the calculation shows variance from the measured values. The calculation with a maximum of 15 g/m³ exceeds the measured maximum of 11.9 g/m³. There seems to be a maximum moisture content, which is not exceeded.

The seven houses with the highest calculated indoor humidity were occupied during January 2013. In the measured data it can be seen that none of the families were on holiday. One theory for the deviation is condensation on the windows or other "condensate-catchers". Some families told us during the survey that they sometimes wipe condensation from the windows in PSG. Moisture production rates as well as ventilation rates are not constant values, but vary (Johansson et al. 2011). The calculation could more accurately reproduce the measurements by using the upper boundary production value and the lower ventilation boundary value.

6. Conclusions and future work

An improved model for the prediction of indoor humidity was presented in this work. The correlation is very good for low to medium indoor humidity. Further research is needed for airtight residences with high indoor humidity.

The number of questionnaires returned was high in both projects. The period of time to complete the questionnaires seems to be acceptable due to the high return rate. Perhaps an even more accurate questionnaire can be used during the planning process for individual homeowners when designing their own homes.

Future work should be done to determine why an already high indoor humidity is still overestimated using this model. A more probability-based approach can also be implemented in the model if the literature provides distributions for moisture production and ventilation rates instead of single values.

7. Acknowledgements

The authors acknowledge the participants of our study, the Austrian Research Promotion Agency (FFG) and the Federal Ministry for Transport, Innovation and Technology (BMVIT), who founded this work within the IEA-Project Annex 55 (www.nachhaltigwirtschaften.at/results.html/id6578). Thanks to Harald Hofbauer, Martin Zingerle and Astrid Lederer for assisting in data collection.

References

DIN Fachbericht 4108-8. 2010. Wärmeschutz und Energie-Einsparung in Gebäuden – Teil 8: Vermeidung von Schimmelwachstum in Wohngebäuden. DIN Deutsches Institut für Normung e.V. Beuth Verlag. Berlin.

EN ISO 13788. 2012. Hygrothermal performance of building components and building elements – Internal surface temperature to avoid critical surface humidity and interstitial condensation – Calculation methods (ISO 13788:2012). European Committee for Standardization.

EN ISO 13789. 2007. Thermal performance of buildings – Transmission and ventilation heat transfer coefficiants – Calculation method (ISO 13789:2007). European Committee for Standardization.

Geving S. & Holme J. 2011. Mean and diurnal indoor air humidity loads in residential buildings. Journal of Building Physics 35. 392-421.

Harreither C., Nusser B. & Bednar T. 2012. Decision Support Method for Flat Roofs using Probabilistic Tools to calculate Life Cycle Costs and Energy Efficiency. 5th International Building Physics Conference (IBPC), Kyoto, Japan; 28.05.2012 - 31.05.2012; in: "The Role of Building Physics in Resolving Carbon Reduction Challenge and Promoting Human Health in Buildings", Paper-Nr. P 481-488, 8 S.

Hartmann T., Reichel D. & Richter W. 2009. Feuchteabgabe in Wohnungen. in Wohnungslüftung und Raumklima. Helmut Künzel (Hrsg.). 2., überarbeitete und erweiterte Auflage. Stuttgart, Fraunhofer IRB Verlag. 109 pp.

Johansson P., Pallin S. & Shahriari M. 2011. Development of a Risk Assessment Procedure Applied on Building Physics: Part One, Model Development. XIIth International Conference on Durability of Building Materials and Components (DBMC), Porto, Portugal; 12.4.2011-15.4.2011.

Kalamees T, Vinha J, Kurnitski J. 2006. Indoor Humidity Loads and Moisture Production in Lightweight Timber-frame Detached Houses. Journal of Building Physics 29. 219-246.

Reiß J. & Erhorn H. 2009. Klassifizierung des Nutzerverhaltens bei der Fensterlüftung – Querauswertung der Fensteröffnungszeiten von 67 messtechnisch erfassten Wohnungen. In Wohnungslüftung und Raumklima. Helmut Künzel (Hrsg.). 2., überarbeitete und erweiterte Auflage. Stuttgart, Fraunhofer IRB Verlag. 125 pp.

Zingerle M. 2013. Entwicklung einer statistischen Methode für die Ermittlung der erforderlichen Stichprobengröße zur Qualitätssicherung der Luftdichtheit von Gebäuden. Master's Thesis. Vienna University of Technology.

Uncertainty of climate related parameters of a building envelope – case of leakage characteristics

Krystyna Pietrzyk, Associate Professor

Chalmers University of Technology, Department of Architecture, Sweden

KEYWORDS: *building envelope, blower door tests, leakage characteristics, discharge coefficient, uncertainty, reliability*

SUMMARY:

Airflow through the building envelope depends on the airtightness of the structure specified by the type of construction and the quality of the workmanship. If we neglect the latter reason, the actual airtightness performance of the building depends on the regime of the airflow through the openings which is a combination of laminar and turbulent ones. The leakage characteristics of a building vary according to the changes of the regime of the flow with the pressure difference across the building envelope. The leakage characteristics are presented by a dimensionless discharge coefficient that relates the flow rate through the openings to the area of building components and the corresponding pressure difference across the openings. It is proposed to treat the discharge coefficient as a variable, which could be estimated from the blower door tests. The results of pressurization and depressurization tests carried out on the single-family house using reductive sealing method related to the different parts of the structure are presented. The uncertainties coupled to the regime of the airflow are reflected by the variation of dimensionless discharge coefficient which in terms of probability density function could be applied in the reliability models of, for example, air exchange performance of buildings.

1. Introduction

This study is in line with the research area being developed during 2010 to 2013, under the custody of Annex 55 within IEA-EXCO "Reliability of Energy Efficient Building Retrofitting – Probability Assessment of Performance and Cost (RAP-RETRO)". The paper relates to the concept and program of measurements described in (Pietrzyk 2000).

Reliability of a design considers the stochastic variability of different sort of data that could be divided in to 3 groups (Pietrzyk 2005a). The first group consists of the load data treated as random variables, which can be described by the typical, for the site or the living style, family of distributions. The second group consists of the parameters, which variations oscillate around the mean value. The example of such parameter can be a material property randomly varying in space due to uneven quality of the product. This group contains also the coefficients, which values are uncertain or inaccurate stated, and as a consequence, a certain interval of that value has to be taken into account. The third group of random variables is formed by load related data describing the properties of a construction, which are load dependent, like for example thermal transmittance (especially dynamic U-value), or leakage characteristic. The important research task is to find the probabilistic regularities typical for the climate-construction interaction (Pietrzyk & Hagentoft 2004).

Leakage characteristics of the building envelope are treated as climate related parameters of construction and presented in this study in terms of dimensionless discharge coefficient.

2. Airflow through a building envelope

Airflow through a building envelope is a combination of laminar and turbulent flows.
It depends on the type of construction and conforms to a relationship expressed by the Power Law Equation (Etheridge & Sandberg 1996):

$$Q = k(\Delta p)^{n_k} \quad (1)$$

Where

Q - airflow rate (m^3/h)
k - flow coefficient depending on the total size of all the leakage passages ($m^3/h/Pa^{n_k}$)
Δp - pressure difference across building envelope (Pa)
n_k - flow exponent varying between 0.5 for turbulent flow and 1.0 for laminar flow

The flow coefficient and flow exponent are usually assumed to be constant and can be estimated from the results of blower door tests.

Air leakage through the building envelope depends on the applied pressure difference. It is important to know the relationship between airflow and pressure difference since it is unique for every house. It can be estimated from the leakage values assumed for adventitious and purpose provided openings. This relationship can also be measured by means of blower door tests. Sometimes, instead of Equation 1, it is more convenient to use a different form for the relationship between the flow and pressure difference which is based on the fixed power $n_k = 0.5$ (as for orifice flow). A flow coefficient varies with Δp depending on the changes of real regime of the flow and the leakage characteristics of the openings. Assuming a mostly turbulent regime of the flow through the openings we arrive at the following equation describing the flow Q (Wirén 1985):

$$Q = IA\sqrt{\frac{2|\Delta p|}{\rho}} \quad (2)$$

Where

Q - airflow (m^3/s),
Δp - pressure difference across a building envelope (Pa),
A - area of building envelope (m^2),
ρ - density of air (kg/m^3)
I - dimensionless discharge coefficient characterising leakage properties of the building, relating the flow rate through the openings to the area of building component and the corresponding pressure drop across openings (-).

$$I = f(Re)\,\alpha \quad (3)$$

$$\alpha = \frac{A_1}{A} \quad (4)$$

α - relative leakage area (-)
A_1 - area of leakage openings (m^2)
f(Re)- coefficient dependent on Reynolds number and including the effect of frictional characteristic of the openings, cracks and leaks (-)

The coefficient I can be presented as a linear function of "frictionless flow velocity" through the openings v_q, which in turn depends on the pressure difference.

$$I = a\,v_q + b \quad (5)$$

Where

a - parameter of linear regression $I(v_q)$ (s/m)
b - parameter of linear regression $I(v_q)$ (-)

$$v_q = \sqrt{\frac{2|\Delta p|}{\rho}} \quad (6)$$

In the case of big openings, the flow is turbulent and the leakage parameter can be considered to be constant (the minor losses are independent of the Reynolds number). For the other openings, where a boundary flow occurs, leakage properties can vary significantly with the magnitude of pressure difference (Wirén 1985). The changes of Reynolds number with an increase of flow velocity induced by larger pressure differences make the parameters I and K dependent on Δp.

Evaluation of the parameters of the regression $I(v_q)$ is possible using the results of blower door test. Examples of the function $I(v_q)$, evaluated for the experimental house, for a turbulent flow through the opening and boundary flow through the walls are presented in the following section.

3. Experiment

The experimental building is a two-storey timber-framed single family detached house with a concrete basement. A garage with doors facing south is located in the extended south part of the cellar. Figure 1 shows photographic view of the Southern side of the building together with the drawing of the façade. The external walls as well as the roof are insulated with a 0.265 m layer of mineral wool. A plastic sheet is mounted inside the insulation to provide good air-tightness. The external face of the wall is timber clad with an air cavity behind it.

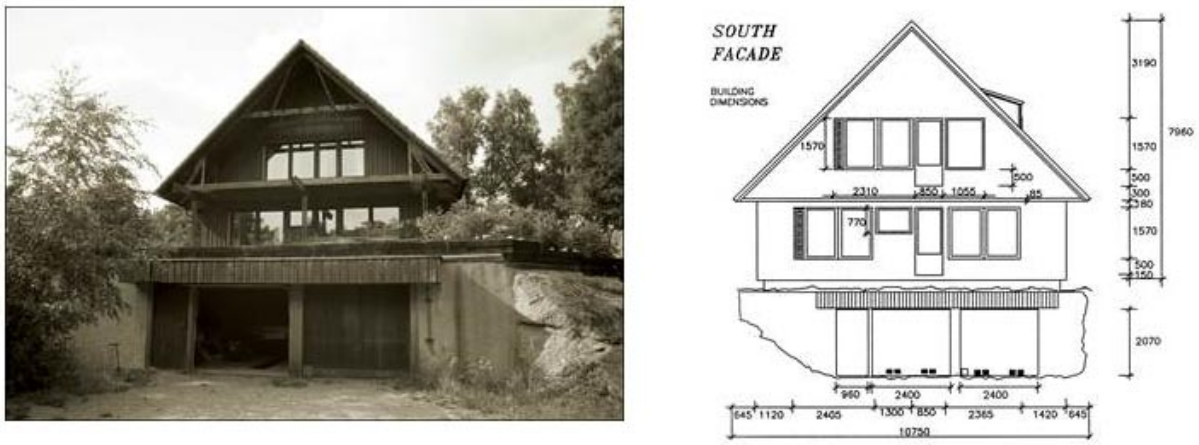

Figure 1. The Southern façade of the experimental building

The leakage characteristics of the building were evaluated using blower door tests. In the case when discharge coefficient I is evaluated for the whole building, big openings should be treated separately in the model with own leakage characteristics. Location of the leakage associated with the opening can be identify by means of thermograph and measured by reductive sealing method.

3.1 Air-tightness of the building

According to the Code of Practice (Boverkets Byggregler 1994) air tightness of a building is characterised by the average air leakage through the part of the building forming the boundary with outdoor air or an unheated space, and measured at a pressure difference of 50 Pa. An estimation of the total leakage at a pressure difference of 50 Pa Q(50) was done by means of pressurisation and depressurisation tests according to the Swedish Standard (SS 021551, 1987). The measurements were carried out in 1991 and the instrumentation used is described in (Schechinger & Handa 1993).

Investigations of the air tightness of the building have been made in different conditions according to the different area of intentional openings existing in the envelope: the outlet of ventilation system, the passage to the attic, the ventilation windows, the door for the cat and the opening under the garage door situated in the cellar.

The configurations of the openings measured by blower door tests that were eventually used to estimate discharge coefficients for the whole building and for the big opening under the garage door are listed in Table 1.

Table 1. Configuration of the openings during the blower door tests

	Case no.	Ventilation duct	Attic	Ventilation window	Cat door	Opening under the garage door
Whole build.	2	Not sealed	closed	closed	sealed	Not sealed
	6	Not sealed	closed	closed	sealed	sealed
Cellar	11	The floor between the cellar and the living part of the house is sealed			sealed	Not sealed
	12				Not sealed	Not sealed
	13				Not sealed	sealed

The results are presented in terms of parameters of the power law equation (Equation 1) in Table 2. The table contains the flow coefficients and the flow exponents estimated for different cases from the results of pressurisation and depressurisation tests. The root-mean-square error, evaluated for each set of parameters fitted, is found to be proportional to the magnitude of airflow through the building envelope.

Table 2. Parameters of the leakage curves fitted to pressurisation and depressurisation data for different cases.

Case no.	Pressurisation test $Q = k\Delta p^n$			Depressurisation test $Q = k\Delta p^n$		
	k	n	rms error	k	n	rms error
2	214.2	0.67	25.4	190.2	0.67	15.4
6	95.7	0.69	6.7	80.3	0.72	7.3
11	225.8	0.64	27.5	219.9	0.62	25.2
12	229.7	0.66	22.3	240.2	0.62	35.6
13	94.2	0.73	12.2	106.0	0.69	14.3

The example of fitting of leakage curves for pressurisation and depressurisation data for cases 11, 12 and 13 described above are presented in Figure 2.

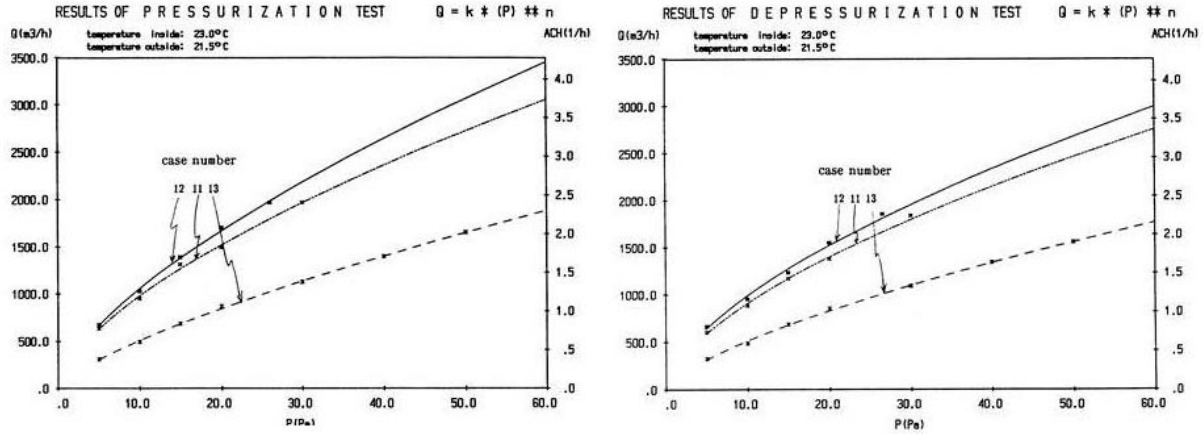

Figure 2. Results of the blower door tests for the cases: 11, 12, 13 (Table 1)

The analysis of the results from Table 2 exemplified by Figure 2 gives an idea of the possible influence of the above-mentioned openings on the air tightness of the building. Generally, from the all cases measured (Pietrzyk 2000) (1-14 that are not listed here) it was realised that: the outlet of the ventilation duct in the range of 0 to 30 Pa, which is particularly interesting for our study, seems to be less important; the passage to the attic hardly has any influence on the exchanged air due to the fact that the insulation is not put in the attic floor but directly under the roof; the ventilation windows could have a significant influence on the air tightness of the building but they were usually closed.

The opening under the garage door has the greatest influence (compare cases no. 11 and 13). At a pressure difference of 10 Pa it causes approximately 0.5/hour ACH whereas the pressure difference of 30 Pa increases this value to 1./hour. At 50 Pa ACH caused by this opening reaches a value of 1.2/hour which is about 40% of the air change rate caused by all of the openings existing in the building envelope. The cat door situated in the garage door at the ground level contributed significantly less to the amount of air being exchanged. It was more important at pressure differences less than -15 Pa (see cases no.11 and no.12 for pressurisation tests). The cat door and the big opening under the garage door could be treated as one opening in the model for air change rate.

The results of the measurements for cases no. 11, no. 12 and no. 13 show that investigated openings in the cellar work more efficiently to transport air into the house than out of the house (the flow exponent estimated for the pressurisation test is greater than the flow exponent from the depressurisation test).

Cases no. 12 and no. 13 have been measured with a fan situated in the cellar, with the floor between the cellar and the upper part of the building sealed. In that way the influence of cracks in the living area was limited. A subtraction of the results of case no. 13 from the results of case no. 12 also cancels the effect of openings in the garage room. The configuration of the openings in the case no. 2 is close to ordinary serviceability conditions during the measurement period. Case no. 6 characterises the air tightness of the building under the same conditions but with the influence of the near-to-ground opening under the garage door and the cat door excluded. Cases no. 6 and case no. 12 minus no. 13 are complementary and together fully describe the air tightness of the house during the measurement period.

3.2 Discharge coefficient – deterministic evaluation

The airflow through the envelope (Equation 2) can be presented in the following form (Wirén 1985):

$$Q = K\ A\ \sqrt{|\Delta p|} \tag{7}$$

Where $$K = I\sqrt{\frac{2}{\rho}} \tag{8}$$

K - leakage function [$\sqrt{m^3/kg}$]

Similarly to discharge coefficient I (Equation 5), a leakage function K is also presented as a linear function of v_q:

$$K = a_K v_q + b_K \tag{9}$$

Cases no. 2 and no. 6 describe the air tightness of the whole building with a certain configuration of openings while case no.12 minus no.13 is characteristic only for the opening under the garage door together with the cat door.

The example of detailed results of the evaluation of the parameters like flow through the openings, air change rate, I and k coefficients for different pressure differences and estimation of the functions of $K(v_q)$ is shown in Table 3 for the pressurisation test for case 6. The definitions of the symbols are:

p - pressure difference applied in the building during the test (Pa)
fl - pressure difference measured as a result of test (Pa)
q - flow through the openings (m^3/h)
Q - flow through the openings corrected due to the difference of temperature of the air outside T_{ext} and inside T_{int} the building (m^3/h) or (m^3/s)
rms - rms error of approximation
I - dimensionless discharge coefficient (-)
K - leakage function [$\sqrt{m^3/kg}$]
k - flow coefficient depending on the total size of all the leakage passages $(m^3/h/Pa^{n_k})$

Table 3. Detailed results of pressurisation test - case no. 6.

The results of p r e s s u r i s a t i o n test case 6
for a house with A= 413.0 m2 and V= 819.0 m3
Tint = 23.5 Text = 21.0

p(Pa)	fl(Pa)	q(m3/h)	Q(m3/h)	k	ACH(1/h)
5.0000	3.0000	285.2710	287.6955	128.6613	.3513
10.0000	8.0000	462.2045	466.1328	147.4041	.5691
15.0000	14.0000	608.7079	613.8813	158.5035	.7495
20.0000	21.0000	743.0975	749.4131	167.5739	.9150
30.0000	36.0000	968.7568	976.9902	178.3732	1.1929
40.0000	56.0000	1203.9890	1214.2220	191.9853	1.4826
50.0000	74.0000	1380.9440	1392.6800	196.9547	1.7005
	k = 180.73370		n = .50000		rms = 87.77390
	Q(50.)=1278.0 m3/h				

p(Pa)	fl(Pa)	v_q(m/s)	Q(m3/s)	K	I
5.0000	3.0000	2.8859	.0799	.00008654	.00006705
10.0000	8.0000	4.0813	.1295	.00009914	.00007682
15.0000	14.000	4.9986	.1705	.00010661	.00008260
20.0000	21.000	5.7718	.2082	.00011271	.00008733
30.0000	36.000	7.0690	.2714	.00011997	.00009296
40.0000	56.000	8.1626	.3373	.00012913	.00010005
50.0000	74.000	9.1261	.3869	.00013247	.00010264
	K = .00012156		n = .50000		rms = .0243816

$K = .00000728 * v_q + .00006856$

The estimated function $I(v_q)$ for these cases are presented in Figure 3. The parameters of these relationships are shown in Table 4, together with the flow exponents evaluated from Equation 1.

Table 4. Parameters of relationship $I = a_I v_q + b_I$ and the flow exponent related to the case.

case no.	parameter a_I * 10^{-4}	parameter b_I * 10^{-4}	flow exponent
2	0.1247	1.0247	0.668
6	0.0570	0.5300	0.686
12-13	0.0095	0.7354	0.530

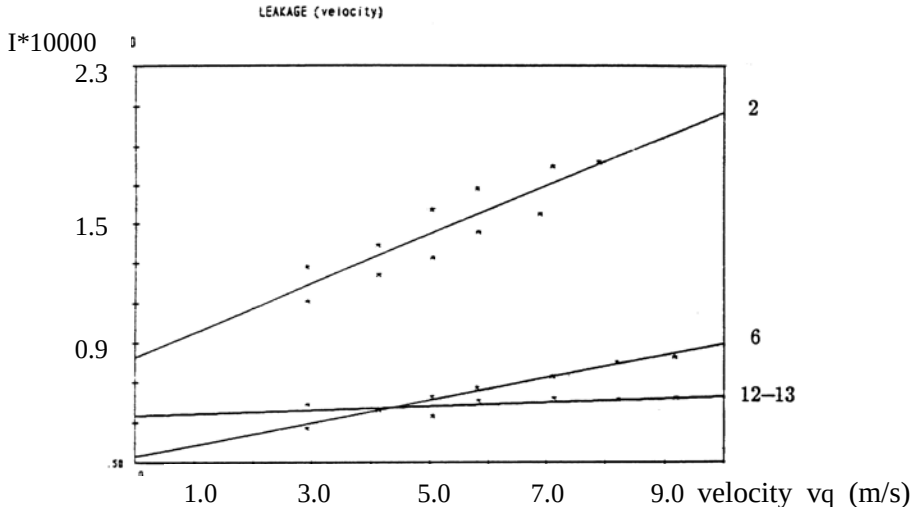

Figure 3. The function $I(v_q)$ estimated for different cases: 12-13 - when turbulent flow occurs 2, 6 - when boundary flow occurs

The flow through the opening under the garage door (see case no. 12 minus case no. 13) seems to be turbulent according to the value of the flow exponent (see Table 4). The line describing the relationship $I(v_q)$ related to this case presented in Figure 3 is almost horizontal because for fully turbulent flow minor losses are constant and do not depend on Reynolds number.

3.3 Discharge coefficient – stochastic representation

Discharge coefficient can be evaluated for specified periods of time using design parameters of the house together with climatic characteristics of the site: local wind speed for specified wind directions and outdoor temperature. Probability density function of I has been approximated using FORM (First-Order Reliability Method) where the wind and buoyancy driven pressure drop was a function of two random variables: the wind speed given wind direction sector and the temperature difference across the building envelope. Both variables have been represented by statistical parameters of probability density functions for one-hour mean data. The procedure is described in (Pietrzyk 2000, Pietrzyk & Hagentoft 2008a,b). The probabilistic description of discharge coefficient I described by Equations 5 and 6 is illustrated in Figure 4. It relates to the case 6 (see Tables 3 and 4).

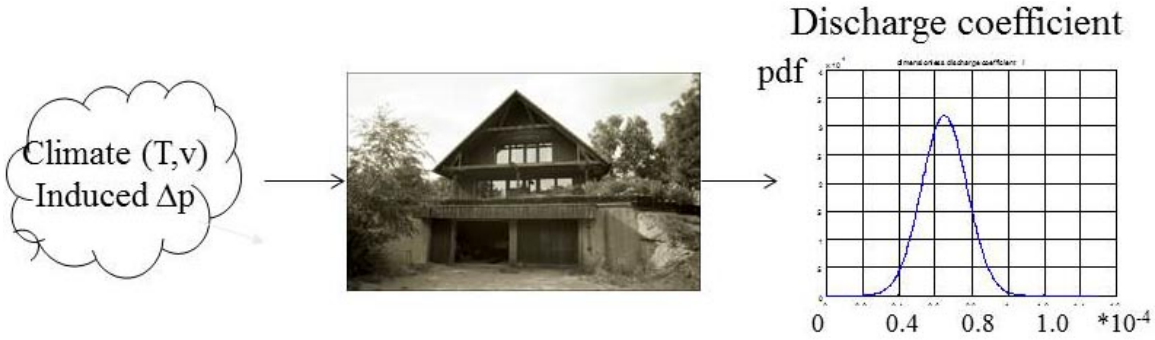

Figure 4. Probabilistic model of discharge coefficient of a building envelope.

The flow through the opening under the garage door (together with cat door) is close to turbulent. Coefficient *I* does not seem to be dependent on the pressure drop (see case 12-13 in Figure 3), and neither does the leakage parameter *K*. Due to this fact, a fully turbulent flow through that opening has been assumed in the model. A flow exponent of 0.5 and a constant value of the discharge coefficient *I* have been assigned to describe flow through this opening.

4. Conclusions

Dimensionless discharge coefficient is represented by a unique function for the building component or for the whole building envelope. Its variation reflects the microclimatic impact of the environment on air-tightness performance.

Dimensionless discharge coefficient could be treated as a climate dependent parameter of the building defined by the probability density function. The leakage characteristics of a building vary with the pressure difference across the building envelope according to the changes of real regime of the flow (laminar, turbulent) through the openings. Dimensionless discharge coefficient relates the flow rate through the openings to the area of building components and the corresponding pressure difference across the openings.

The dimensionless discharge coefficient *I* in the form of regression coefficients *a* and *b* could be used as the input data to the reliability model: Parameters *a* and *b* of Equation 5 can be evaluated from the results of blower door tests carried out on the standard components or they can be assumed according to design values of the leakage area. In the case when leakage characteristics are evaluated only for the whole house the dimensionless discharge coefficient should be estimated also for a dominant opening, if it exists.

The application of the dimensionless discharge coefficient in the probabilistic model of air infiltration in a building is described in (Pietrzyk 2000, 2005b and Pietrzyk & Hagentoft 2008b).

5. Acknowledgments

The measurements were carried out by Bernt Schechinger.
The financial support provided by Swedish Council for Building Research is gratefully acknowledged.

References

Boverkets Byggregler (Swedish Building Code) BBR 94:1, (1994). Stockholm, Sweden.

Etheridge D., Sandberg M. (1996). *Building Ventilation: Theory and Measurements*, John Wiley& Sons.

Pietrzyk K. (2000). Probabilistic modelling of air infiltration and heat loss in low-rise buildings. *Ph.D. thesis*, ISSN 0346-718X, School of Architecture, Chalmers University of Technology, Gothenburg, Sweden.

Pietrzyk K., Hagentoft C.-E. (2004). Probabilistic modelling of dynamic U-value. Performance of Exterior Envelopes of Whole Buildings IX, Florida, USA.

Pietrzyk K. (2005a). Reliability analysis in interior climate and building envelope design. The 7th *Nordic Symposium on Building Physics*, ISBN 9979-9174-6-6, vol.2, pp 1049-1056, Reykjavik, Iceland, June 2005.

Pietrzyk K. (2005b). Probability-based design in ventilation. *The International Journal of Ventilation*. Vol. 4 Number 2, pp 143-156.

Pietrzyk K., Hagentoft C-E. (2008a). Reliability analysis in building physics design. *Building and Environment*. Vol. 43/4, pp 558-568.

Pietrzyk K., Hagentoft C-E. (2008b). Probabilistic analysis of air infiltration in low-rise buildings. *Building and Environment*. Vol 43/4 pp 537-549.

Schechinger B., Handa K. (1993). Risk analysis of air infiltration in building structures – description of test house and instrumentation. Building Aerodynamics Research Group. School of Architecture, Chalmers University of Technology. Publ. 1993:BA11.

Swedish Standard SS 02 15 51 Buildings – Determination of airtightness, (1987) Standariseringskomissionen i Sverige.

Wirén, B.G. (1985). *Effects of surrounding buildings on wind pressure distributions and ventilation losses for single-family houses*, The National Swedish Institute for Building Research, bulletin M85:19. Gävle, Sweden.

Relevance of site location on heat stress in a naturally ventilated residential building

Zoltán Sadovský, D.Sc. [1]
Oľga Koronthályová, Ph.D. [1]
Peter Mihálka, Ph.D. [1]
Peter Matiašovský, Ph.D. [1]
Katarína Mikulová, Ph.D. [2]

[1] Institute of Construction and Architecture of the Slovak Academy of Sciences, Slovakia
[2] Slovak Hydrometeorological Institute, Slovakia

KEYWORDS: *Residential building, natural ventilation, indoor environment, heat wave, heat stress period, probabilistic model, mean return period.*

SUMMARY:
The indoor environment performance of a naturally ventilated residential building during heat waves is studied focusing on the relevance of site location. Recently developed probabilistic model of the heat stress induced by heat waves is employed. For the assessment of extremely hot indoor environment a heat stress period (HSP) related to high PPD or operative temperature thresholds is defined. The annual probabilities of exceeding considered HSP durations are estimated. The annual exceedance probability is interpreted by the mean return period. A typical section of a naturally ventilated residential building represented by two opposite rooms connected by a corridor is studied. The indoor environment is simulated by the ESP-r software tool. Hourly time series of meteorological data recorded during 14 years at two lowland stations and one mountainous station in Slovakia represent site (and climate) variability.

1. Introduction

For moderate thermal indoor environments the current standards ISO 7730: 2005, ASHRAE 55: 2004 and EN 15251: 2007 specify several levels of thermal comfort in buildings. For air conditioned buildings the corresponding limits are based on the PMV/PPD index, while for naturally ventilated buildings the concept of adaptation expressed in terms of the operative temperature limits is applied. As an overheating discomfort the up-crossing of the established limits is considered. For buildings and spaces where the design of mechanical cooling or natural ventilation is not adequate to meet the required categories the design documents shall state how often the indoor conditions are outside the required range, see EN 15251: 2007. This is carried out by one of the given methods evaluating general thermal comfort conditions, assessed by measurements in real buildings or by dynamic computer simulations, over season or year. A review of indices for such long term evaluation is presented in Carlucci & Pagliano (2012).

An extreme overheating heat stress may cause heat exhaustion and heat stroke, particularly within vulnerable populations as are e.g. the elderly, children, socially isolated and the ill. However, also a wide range of medical conditions can be exacerbated by heat exposure, Kravchenko et al. 2013. Heat stress indications are often based on thresholds of air temperature or a combination of air temperature and relative humidity. The indices are being checked for their ability of predicting heat induced mortality (Barnett et al. 2010). Increased attention is paid to relationship between outdoor and indoor temperatures in homes occupied by the elderly (White-Newsome et al. 2012) and hospital wards (Lomas & Giridharan 2012). Complex heat stress indicators derive from Fanger's (1970) predicted mean vote, which includes all important meteorological and physiological parameters in a complete

heat budget (energy balance) model of the human body. As an important factor of heat stress effects duration of heat exposure and lack of overnight relief is accepted, cf. McGeehin and Mirabelli (2001), Montero et al. (2010).

Heat waves causing extreme heat exposures are rare events in moderate climate zones. Their temporal structure can not be revealed by the long term criteria, which essentially provide overall – integral indices. For the study of indoor environment performance of a naturally ventilated residential building during heat waves a probabilistic model of the heat stress has been recently developed Sadovský et al. (2014). The extremely hot indoor environment is characterised by a heat stress period (HSP). HSP is related to a high value of PPD index, alternatively an operative temperature threshold can be considered.

The heat stress period was defined by continuous intervals of hours at which a high PPD threshold was exceeded. However, two continuous intervals may be separated by an interval of PPD values below the threshold, the short duration of which does not provide sufficiently long relief for occupants. Therefore a working rule allowing consideration of the sum of two continuous intervals “A” an “B” separated by a short period “d” as one continuous interval was suggested. For application of the rule two necessary conditions have to be satisfied: 1) $d < 8$ hours considered as expected normal sleeping time 2) $d < \min \{A / 2; B / 2\}$. Note that sometimes a concatenation of intervals may occur, e.g. HSP may be obtained as the sum $A + B + C$ of three intervals. Thereby, the HSP concept captures also prolonged durations of heat waves.

The previous study (Sadovský et al. 2014) aimed at probabilistic description of HSP, particularly at estimating the probability of annual exceedance of considered durations. For interpretation of the annual exceedance probability the mean return period was used. The approach was illustrated on example of a typical section of a naturally ventilated residential building represented by two opposite rooms connected by a corridor in original and retrofitted state, see Figure 1. A temperate continental climate variability represented by the 14 years hourly time series of the external temperature, air relative humidity, solar radiation, wind velocity and direction recorded at meteorological station in Bratislava Koliba (BA Koliba) was considered. The hourly PPD values were calculated by a dynamic simulation employing the code ESP-r within the summer season from the 1st May to the 30th September. These ESP-r calculations are carried out in accordance with the standard ISO 7730: 2005. The PPD calculation was done for the occupant’s CLO = 0.14, MET = 1.0 (ISO 7730. 2005) and the maximum air velocity near the occupant up to 0.1 m/s. On that account the applied PPD threshold PPD > 60 % corresponds to the operative temperature above 31°C.

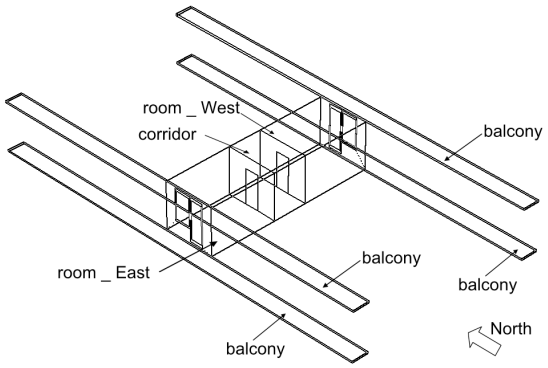

FIG 1. View on the considered section of residential building

The present paper extends the previous study focusing on the relevance of site. The same example of building structure in original state is adopted in another two locations (Milhostov and Ganovce in Slovakia). According to the Kőppen-Geiger climate classification Bratislava in the western lowland

part and Milhostov in the eastern lowland part of Slovakia are in class Dfb, while Ganovce in the mountainous region are in Dfc. The ESP-r input data characterising the section and occupants' behaviour are the same at each site; for details see the paper Sadovský et al. (2014). Thus only the affects of site conditioned climate on indoor environment performance of the section in a naturally ventilated residential building are studied.

2. Probabilistic analysis

The probability of annual exceedance of a given HSP duration at high PPD index is studied by the theory of extreme values employing the block maxima method. Considering the annual (seasonal) maxima of HSP as statistically independent the corresponding sample distribution function can be fitted by the general extreme value distribution (GEV):

$$\mathrm{GEV}(x) = \exp\left\{-\left[1+\xi\left(\frac{x-\mu}{\sigma}\right)\right]^{-1/\xi}\right\} \qquad (1)$$

Where μ, σ, ξ are the location, scale and shape parameters
x is defined on $\{x: 1+\xi(x-\mu)/\sigma > 0\}$

Alternatively, the family of general Pareto distributions (GP) possessing the same shape parameter and the additional advantage that the location parameter is the left end point of the distribution can be applied:

$$\mathrm{GP}(x) = 1-\left[1+\xi\left(\frac{x-\mu}{\sigma}\right)\right]^{-1/\xi} \qquad (2)$$

see Coles (2001), Reiss and Thomas (2007).

The sample (empirical) distribution function is given by

$$F(s_i) = \frac{i}{N_S+1}, \qquad i = 1,\ldots,N_S \qquad (3)$$

Where N_S = 14 is the number of summer seasons (years)
s_i is the seasonal HSP maximum ordered into ascending sequence

Figures 2 and 3 show calculated annual maxima of the heat stress period HSP at PPD > 60 % for Bratislava and Milhostov site distinguishing eastern and western room. Since for the Ganovce site only few hours satisfying the condition of overheating set on PPD-s have been obtained, there was no reason for the probabilistic study at this site.

The sample distribution functions are approximated by the theoretical probability distribution (2) or (3) applying non-linear regression. By the fitted theoretical cdf the annual probability of exceeding the HSP durations denoted by x are obtained as 1 – GEV(x) or 1 – GP(x). Figures 4 and 5 show the resulting annual exceedance probabilities of the heat stress period HSP related to PPD > 60 %. Again eastern and western room are distinguished plotting together Bratislava and Milhostov site results.

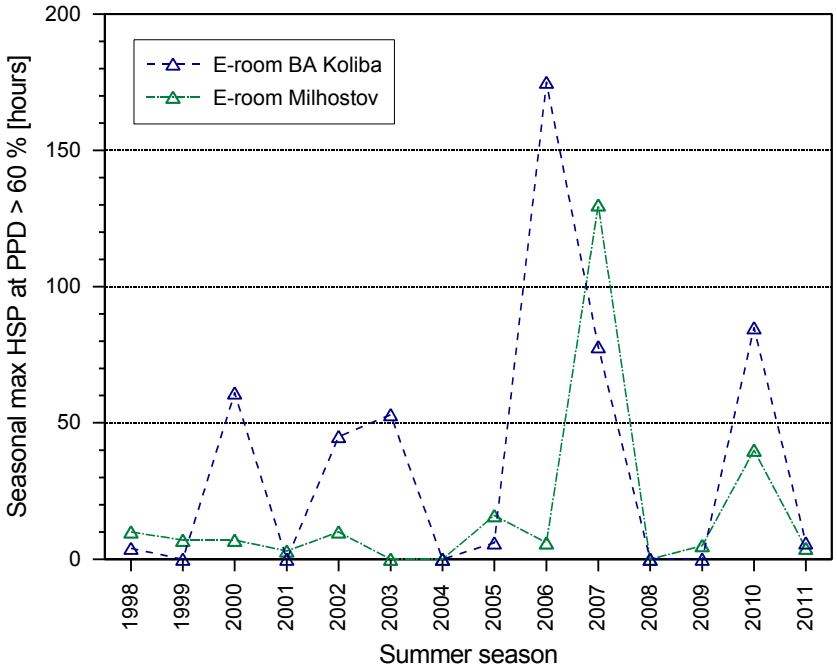

FIG 2. Annual – seasonal maxima of the heat stress period HSP at PPD > 60; eastern room

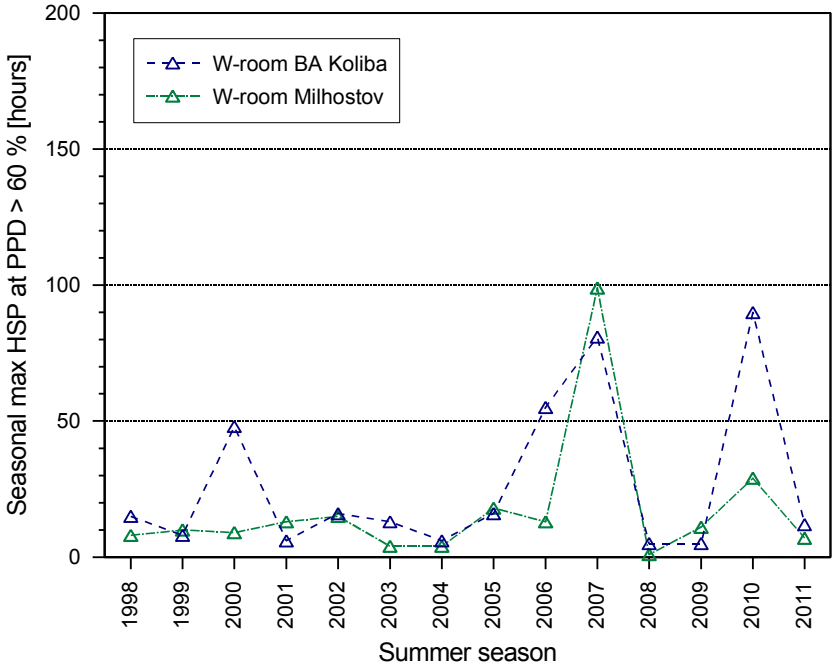

FIG 3. Annual – seasonal maxima of the heat stress period HSP at PPD > 60; western room

The inverse of the annual probability of exceedance represents the mean return period (in years). By the mean return periods a better perceivable presentation of the annual exceedance probabilities is obtained. Figures 6 and 7 show the mean return periods corresponding to the probabilities visualised in Figures 4 and 5.

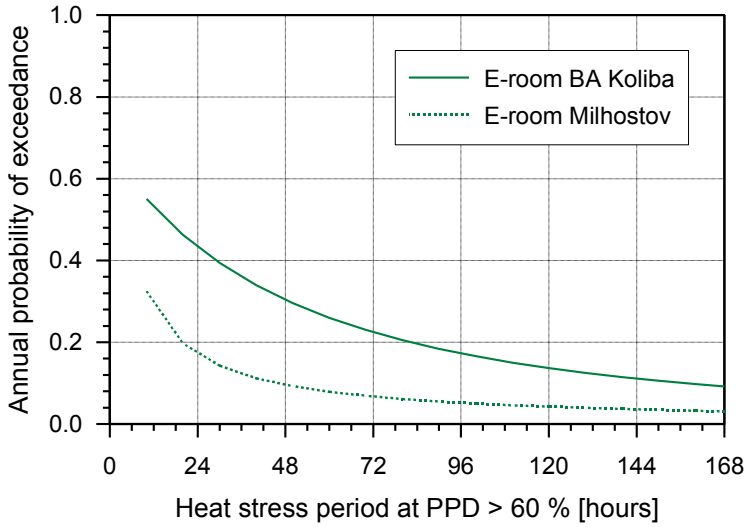

FIG 4. Annual probability of exceedance of HSP at PPD > 60 %; eastern room

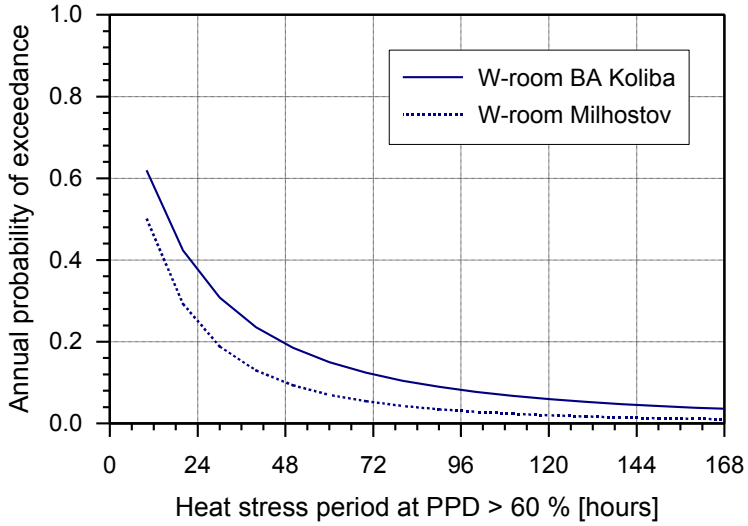

FIG 5. Annual probability of exceedance of HSP at PPD > 60 %; western room

3. Discussion and conclusions

A common definition of heat wave is still missing. The statistical-meteorological criteria are particularly useful in introducing systems of warning alerts triggering preventive measures. However, they may not adequately describe thermal performance of indoor environment like PMV/PPD model. Another approach defines heat wave by the relationship between temperature and mortality Montero et al. (2010) or by a sum of days with average of night time bedroom temperature above a given threshold Patidar et al. (2014).

The present paper adopts the working definition of the heat stress period HSP (Sadovský et al. 2014) based on the PMV/PPD index. The idea was to introduce a simple criterion on duration of the exposure of occupants to an extreme thermal indoor environment, which may adversely impact their health. Further improvements of the criterion are foreseen. The applied dynamic computer simulation allows analysis of correlations of the obtained HSP and of the outdoor temperature and humidity with supposed outcome of providing indication of heat wave alert dates.

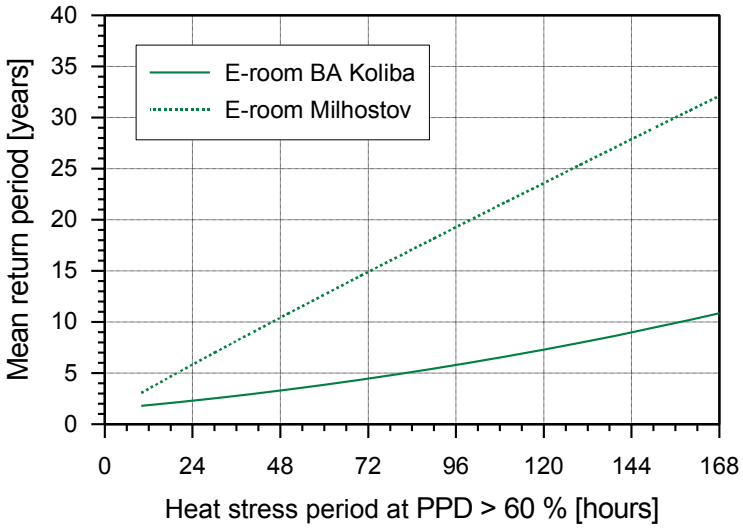

FIG 6. Mean return periods of HSP at PPD > 60 %; eastern room

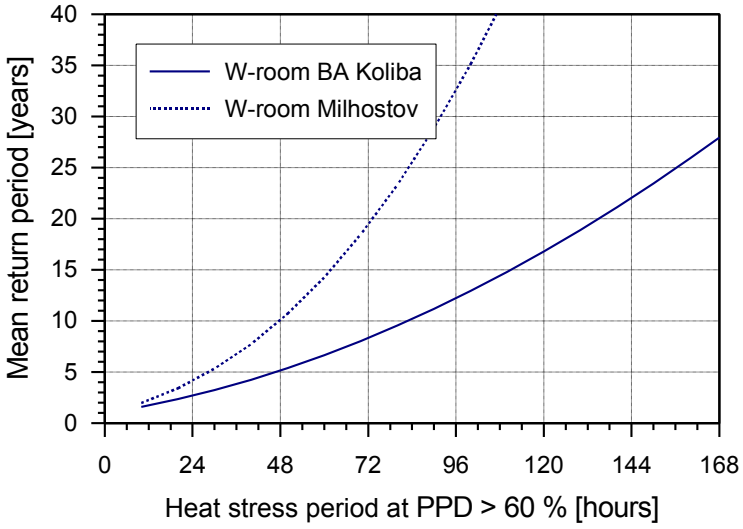

FIG 7. *M*ean return periods *of HSP at PPD > 60 %; western room*

The estimated probabilities of annual exceedances of HSP (or any other relevant period) are of special interest offering essential information for a health cost-benefit analysis. The corresponding mean return period provides tangible interpretation of the probabilities with a potential of being used for regulatory purposes.

The obtained annual exceedance probabilities and particularly the corresponding mean return periods show the importance of climate variation related to the site location in the same Dfb class. Moreover, it supports the view that for probabilistic approaches the climate variability can not be covered by Test Reference Year or Design Summer Year (for definitions see Lomas & Giridharan 2012).

4. Acknowledgements

This work was supported by the Slovak Research and Development Agency under the contract No. APVV-0031-10.

References

ASHRAE, ASHRAE 55. 2004. Thermal Environmental Conditions for Human Occupancy, American Society of Heating Refrigerating Air-Conditioning Engineers, Atlanta, USA.

Barnett A.G., Tong S., Clements A.C.A. 2010. What measure of temperature is the best predictor of mortality. Environmental Research 110:604-611.

Carlucci S. & Pagliano L. 2012. A review of indices for the long-term evaluation of the general thermal comfort conditions in buildings. Energy and Buildings 53: 194–205.

CEN, EN 15251. 2007. Indoor environmental input parameters for design and assessment of energy performance of buildings addressing indoor air quality, thermal environment, lighting and acoustics, European Committee for Standardization, Brussels, Belgium.

Coles S., 2001. An Introduction to Statistical Modeling of Extreme Values. Springer Verlag, London.

Fanger P.O. 1970. Thermal Comfort. Copenhagen, Danish Technical Press.

ISO, ISO 7730. 2005. Ergonomics of the thermal environment – Analytical determination and interpretation of thermal comfort using calculation of the PMV and PPD indices and local thermal comfort criteria, International Organization for Standardization, Switzerland.

Kravchenko J., Abernethy A.P., Fawzy M., Lyerly H.K. 2013. Minimization of Heatwave Morbidity and Mortality. American Journal of Preventive Medicine 44(3):274-282.

Lomas K.J. & Giridharan R. 2012. Thermal comfort standards, measured internal temperatures and thermal resilience to climate change of free-running buildings: A case-study of hospital wards. Building and Environment 55:57-72.

McGeehin M.A., Mirabelli M. 2001. The Potential Impacts of Climate Variability and Change on Temperature-Related Morbidity and Mortality in the United States. Environmental Health Perspectives 109(2):185-189.

Montero J.C., Mirón I.J., Criado J.J., Linares C. & Díaz J. 2010. Comparison between two methods of defining heat waves: A retrospective study in Castile-La Mancha (Spain). Science of the Total Environment 408:1554-1550.

Patidar S., Jenkins D., Banfill P. & Gibson D. 2014. Simple statistical model for complex probabilistic climate projections: Overheating risk and extreme events. Renewable Energy 61:23-28.

Reiss R-D. & Thomas M. 2007. Statistical Analysis of Extreme values. 3rd Edition. Basel: Birkhäuser Verlag AG.

Sadovský Z., Koronthályová O., Mihálka P., Matiašovský P. & Mikulová K. 2014. Probabilistic study of overheating discomfort in residential building. ESREL 2013: Safety, Reliability and Risk Analysis: Beyond the Horizon – Steenbergen et al. (Eds). Taylor & Francis Group, London, 1629-1635.

White-Newsome J.L., Sánchez B.N., Jolliet O., Zhang Z., Parker E.A., Dvonch J.T., O'Neill M.S. 2012. Climate change and health: Indoor heat exposure in vulnerable populations. Environmental Research 112:20-27.

Variability of building airtightness and ventilation due to user actions on envelope and systems

Nuno M. M. Ramos, Assistant Professor [1]
António Curado, Assistant Professor [2]
Pedro F. Pereira, M.Sc. [1]

[1] University of Porto - Faculty of Engineering, Portugal
[2] Instituto Politécnico de Viana do Castelo - Escola Superior de Tecnologia e Gestão, Portugal

KEYWORDS: *airtightness, blower-door, ventilation, user*

SUMMARY:
A large social housing renovation program was recently implemented in Porto, Portugal. One of the projects renovated 179 dwellings with focus on the upgrade of windows and ventilation systems. An increased airtightness was expected and mechanical extraction on kitchens and bathrooms was implemented. Two years after the renovation process was concluded, a sample of 25 of those dwellings was tested with a blower-door and all the visible actions of the users were recorded. Additionally, temperature and, relative humidity were measured in most of the dwellings.

This paper is focused on analysing the patterns of user actions on envelope and systems and the effect they have on airtightness and ventilation. The first part of the study correlates the observed user actions with factors that could have triggered them. The second part of the study analyses the consequences of the user actions on the ventilation of the dwellings during the heating season. The consequences are evaluated with the measurements of the dwellings indoor environment.

1. Introduction

1.1 Motivation

Dwellings should be designed for user's well-being but frequently user actions seem to contradict the logic adopted in the design, resulting in a high variability of hygrothermal performance. An enhanced knowledge of the users is critical for an effective design. Studies on user behaviour and its influence on dwellings performance can be found in literature. (Santin, 2011) tried to find a correlation of the energy spent on heating with household profiles and building characteristics in more than 300 different types of dwellings located in The Netherlands. Some relationships between user behaviour and household characteristics were found. As this study didn't take into account the differentiation of the energy use (heating or other), the relationship between the energy consumption for heating and the household profiles or behavioural patterns could not be found. A study in Seattle, USA (Emery and Kippenhan, 2006) compared the energy demand during 15 years of four similar single houses built in the same period, based on the same standards. The results showed that the energy demand is strongly affected by user behaviour. During the 15 years of monitoring the houses were occupied by different tenants. The results showed that the space heating energy consumption remained constant, even though it should have been strongly influenced by the different ventilation strategies of the several families. (Kalamees et al., 2009) measured the indoor climate of 170 detached houses in terms of temperature and relative humidity over 1 year. A direct correlation between the interior temperature and RH with the exterior conditions was found. The ventilation rate and its influence in the indoor climate were also studied. The authors found that if the ventilation rate is high, variations in the outdoor climate have a greater influence and if the ventilation rate is low, the variation of moisture

production has a higher influence. In the present paper, a social housing refurbishment project is used as case study to evaluate how user actions affect actual ventilation rates and how that reflects in the building performance.

1.2 Studied buildings

A large social housing retrofitting program was implemented in Porto, Portugal. The interventions included the upgrade of windows and ventilation systems. One of the renovated neighborhoods was chosen as a case study for this work. The neighbourhood has 4 detached buildings with similar typologies (FIG. 1). The renovation work was performed in 2009 and 2010 by two different companies, based on the same design project for all buildings (Freitas, 2007-2009). The neighbourhood has a total of 179 dwellings, including the following typologies: 19 T1(1 bedroom) dwellings, 31 T2, 72 T3, 56 T4 and 1 T5.

In the retrofit solution, the original natural ventilation system was improved by introducing continuous mechanical extraction in the kitchens, including a fan of variable flow. A mechanical fan was installed in the bathrooms, to be turned on when the facility is used. In the main rooms self-regulating air inlets were installed. The laundry had a fixed air inlet of 1x30 cm^2. It must be stressed that the retrofitting process had several constraints, including a low budget and a very small allocation period of each dwelling tenants.

FIG. 1. Location and image of the retrofitted buildings (Freitas, 2007-2009)

1.3 Methodology

A sample of the retrofitted dwellings was selected for an in-depth analysis, including air permeability tests and continuous measurement of indoor climate, temperature (T) and relative humidity (RH).

The air permeability measurements were carried out using the Retrotec 1000 blower door model. The standard (EN-13829, 2001) was applied in the tests, following method A described in the standard. According to that, air terminal devices of mechanical ventilation were sealed while openings for natural ventilation were closed but not sealed. In each dwelling, both pressurization and depressurization tests were performed. The in situ measurements were done in four days of two consecutive weeks during spring, with average temperature ranging from 13.5 ºC to 21.0 ºC during that period, as recorded by LFC weather station (Freitas, 2001). The wind velocity during tests varied between 1.2 m/s and 2.4 m/s.

Additionally, a questionnaire was submitted to the users, collecting information for each of the days that measurements took place. That information included: window opening, heating, cooking and bathing.

2. User actions

The sample dwellings are presented in TABLE 1, including the typology of each dwelling, the number of users, the age range and the potential skills of the users. The last field of the table presents the modifications with a possible impact on airtightness that were observed in each dwelling.

The collected information reveals that the number of users per dwelling is low which would not be expected in social housing. The explanation for this is that the houses were occupied decades ago, and meanwhile children grew and moved out. This is confirmed by the age of the users, sometimes quite high. It was possible to see that the modified dwellings include users that are active workers.

All the actions on the envelope intended an increase in airtightness.

TABLE 1. Sample dwellings

Dwelling	Typology	Users	Age	Skills	Modifications
1	T1	3	60-85	Retired	No modification observed
2	T1	2	50-80	Unskilled worker	No modification observed
3	T3	3	40-65	HVAC technician	Laundry opening sealed
4	T3	5	15-80	Unskilled worker	Laundry opening sealed
5	T4-B	5	15-60	Unskilled worker	No modification observed
6	T3	3	30-60	School teacher	No modification observed
7	T3	4	20-80	Unskilled worker	No modification observed
8	T3	3	50-65	Unskilled worker	Self-regulating devices and laundry openings sealed
9	T3	3	15-65	Unskilled worker	Self-regulating devices sealed
10	T3	4	10-60	Unskilled worker	No modification observed
11	T3	1	80	Retired	No modification observed
12	T3	2	35-65	Unskilled worker	No modification observed
13	T3	3	15-90	Unemployed	No modification observed
14	T1	2	50-90	Retired	No modification observed
15	T1	1	90	Retired	No modification observed
16	T4-A	2	65-70	Retired	No modification observed
17	T3	2	50-60	Unskilled worker	Self-regulating devices sealed
18	T4-A	2	70-80	Retired	No modification observed
19	T3	4	10-50	Unskilled worker	No modification observed
20	T4-B	4	20-60	Gym Teacher	Self-regulating devices and laundry openings sealed
21	T3	3	40-70	Unskilled worker	Laundry opening sealed
22	T4-B	5	10-50	Unskilled worker	No modification observed
23	T3	2	50-80	Retired	No modification observed
24	T4-B	6	15-60	Unskilled worker	No modification observed
25	T3	2	60-70	Retired	No modification observed

3. Airtightness and ventilation

The values obtained in the tests of pressurization and depressurization were averaged and are presented in FIG. 2. The dwellings without modifications are shaded in the graph.

The sample was divided in modified and non-modified apartments, and the average ACH50 for each group was calculated, resulting in ACH_{50} = 4.2 h^{-1} for the first group and ACH_{50} = 8.0 h^{-1} for the latter.

In addition to the users modifications performed in specific dwellings, the mechanical extract systems were shut down in all buildings during most of the day, by the tenants administration, and only turned on during meal preparation time. Some tenants installed, in addition, an exhaust hood in the cooktop of the kitchen. Hence, the buildings ended up without an actual ventilation system, as no mechanical exhaust operates continuously and a purpose provided natural ventilation system is not really there since fully functional vertical ducts that would facilitate stack effect do not exist. This means that adventitious ventilation is the only strategy that can be considered. According to (Liddament, 1996) the ACH_{50} should than be greater than 8 h^{-1}. The users that made modifications, without technical knowledge, tried to lower the ventilation rate by acting on airtightness, resulting in values that are inadequately low for the ventilation conditions.

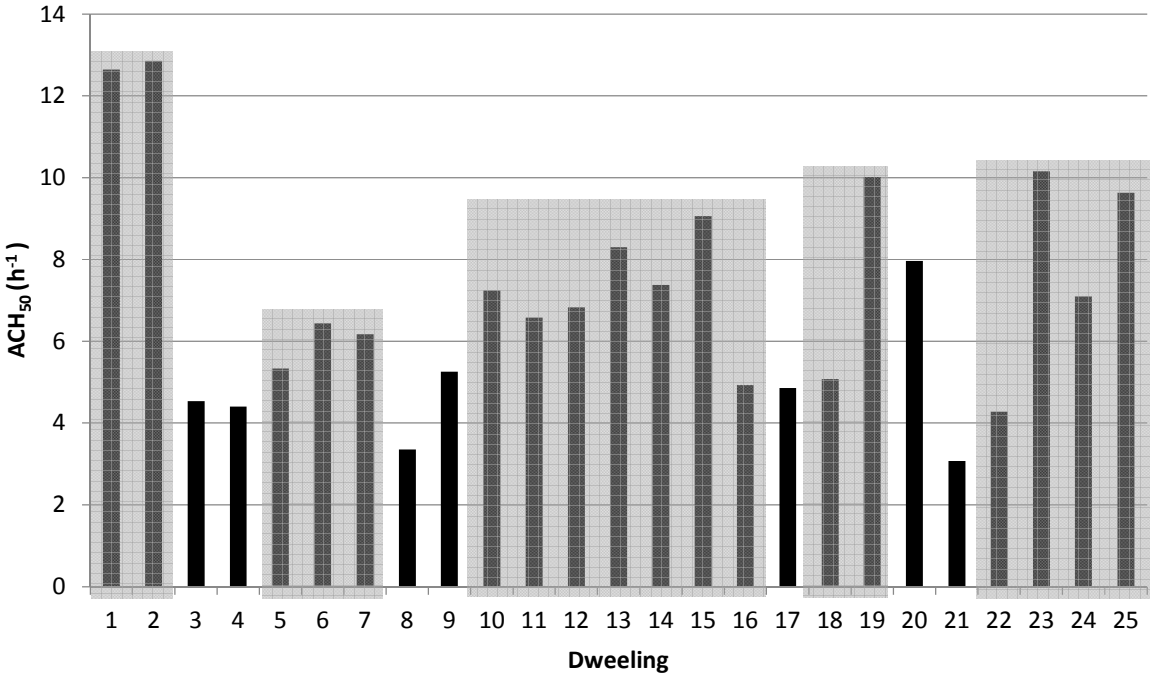

FIG. 2. Measured ACH50 values (shaded results correspond to non-modified dwellings).

The evaluation of window opening action relied on questionnaires that were supposed to be filled every day of the surveying period. The outdoor temperature effect was therefore considered to be the same for all the dwellings. With that information, the total number of hours users said the windows were opened was divided by the number of days the survey took place in each dwelling resulting in the NWO parameter, expressed in hours/day. The correlation between that parameter and airtightness is presented in FIG. 3. It shows a tendency of decreasing hours of opened windows with the increase of ACH_{50} especially if the number of users per dwelling is included in the analysis. This observation confirms that, turning the dwellings more airtight without a working ventilation system compels the users to increase ventilation by opening windows. Of course that this is more a trend than an actual correlation as user behaviour is complex and cannot be assessed in a too simplified way.

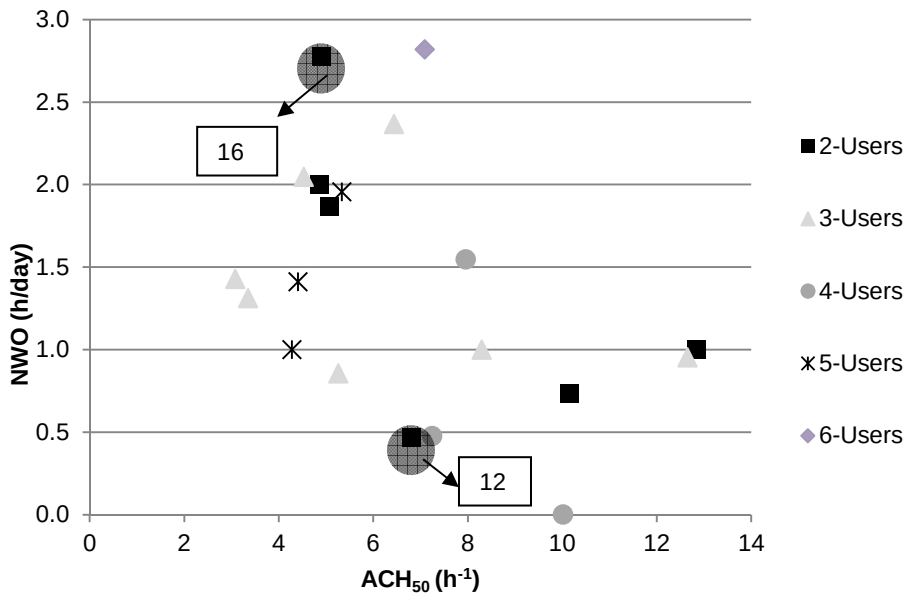

FIG. 3. ACH50 vs. NWO.

Two apartments, 12 and 16, were chosen as examples, as they presented very different window opening activity, although airtightness was in the same range and number of users was identical. The dwellings are highlighted in FIG. 3 and are analysed in detail in the next section.

4. Activity profiles and Indoor climate

Using the information from the questionnaires, the operation profiles were generated for each of the dwellings (12 and 16). TABLE 2 presents average activity indicators for each of the dwellings and FIG. 4 presents the activity profiles in each dwelling, regarding cooking, taking showers and opening windows. The profiles were created by defining the probability that a certain activity could take place during the studied period. In the case of window opening, for instance, in dwelling 12 windows were only opened from 11 to 12. Note that it doesn't mean they are opened everyday but rather that, if opened, the activity occurs only at that hour of the day. In dwelling 16 they could be opened during a significant part of the day. In addition, using TABLE 2 information it can be confirmed that window opening activity was quite more intense in dwelling 16. It must also be stressed that, according to the questionnaires, no heating was used during the survey period.

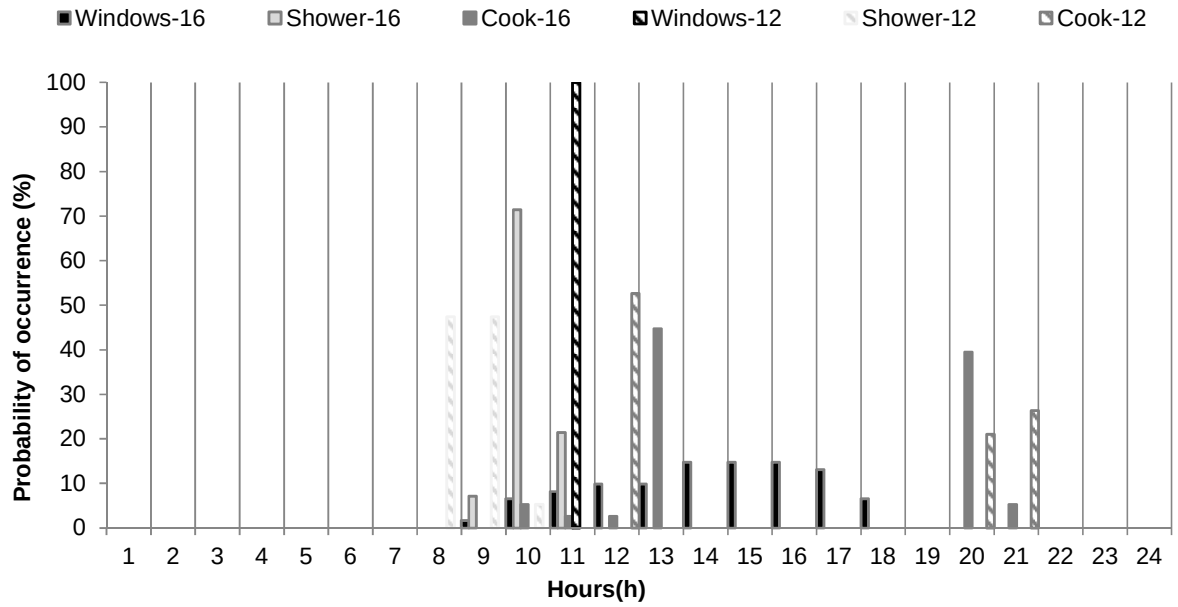

FIG. 4. Activity profiles for dwellings 12 and 16.

TABLE 2. Activity and indoor environment in dwellings 12 and 16

Dwelling	Shower h/ day	Cooking h/day	NWO h/day	ACH_{50} h^{-1}	Ti-Te ºC	(Pi-Pe)/users Pa/user
12	*1.27*	1.27	0.47	6.82	4.91	53.13
16	*0.64*	1.73	2.77	4.92	3.21	53.33

From the information in TABLE 2 it's clear that the window opening activity was decisive for a better performance of dwelling 12 as it was almost 2 ºC warmer for identical moisture excess. It can also be

Correlations between user actions, including airtightness modification and window opening, and indoor climate, including Temperature (T) and relative humidity (RH), were pursued for the whole sample.

T and RH were continuously measured, during each specific survey period, in at least one bedroom in each of the 25 dwellings. The mean hourly difference between exterior and interior temperature (Ti-Te) and Mean hourly vapour excess (Pi-Pe) divided by number of users were tested for correlation with ACH_{50} resulting in FIG. 5 and FIG. 6. No correlation was found there which proves the importance of the additional ventilation introduced by window opening activity and how it can actually result in colder dwellings. The windows opening activity has a high variability related with various factors such as routines and schedules of the users. The results presented in Figure 5 highlight the importance of the human action regarding window operation, and hence on the thermal performance of dwellings as more airtight buildings aren't necessarily warmer.

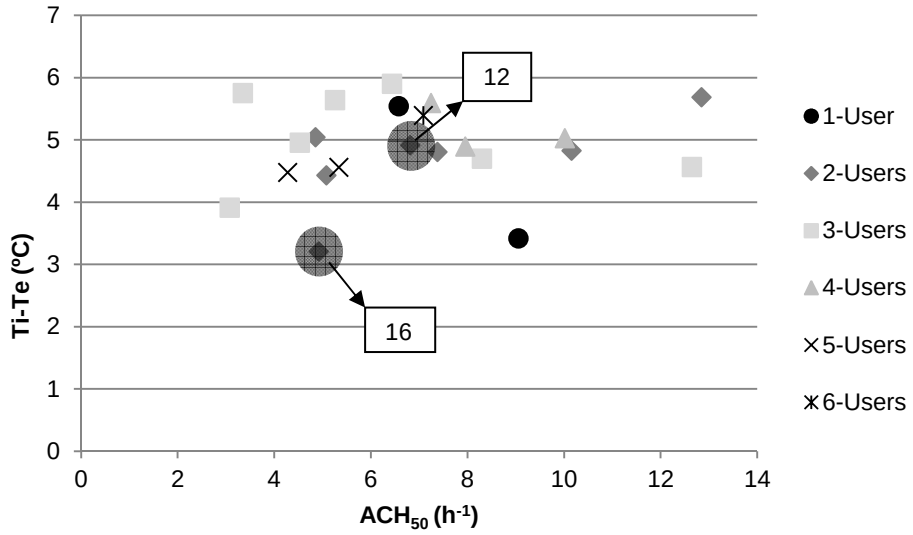

FIG. 5. ACH50 vs.Ti-Te.

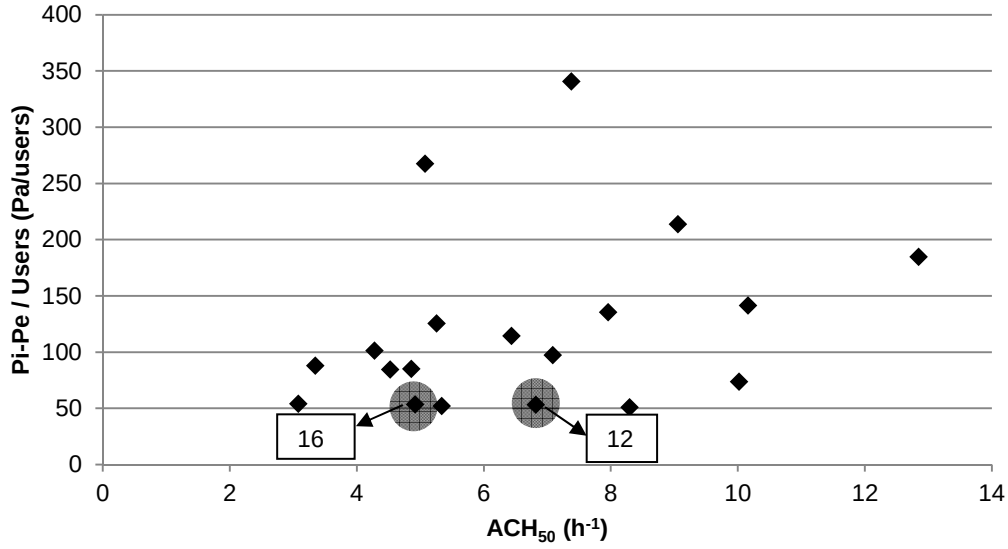

FIG. 6. ACH50 vs. (Pi-Pe)/users.

5. Conclusions

The main conclusions of this work are the following:

- The airtightness of a sample of what should be identical buildings was found to have a high variability, with user actions being one of the causes;
- User action can have an important effect on building airtightness. In this case of social housing where heating is reduced to an absolute minimum, the users acted on air inlets in several apartments, reducing ACH_{50} mean values to almost 50% of the initial values. Actions to increase airtightness were linked to active workers among the dwelling users;
- The window opening action presented different patterns in each dwelling. The number of hours per day windows were opened was used as a rough indicator of those patterns, and differences between 0 and 3, were found;

- Correlating ACH_{50} and window opening activity showed a tendency of decreasing hours of opened windows with the increase of ACH_{50} which results in more airtight dwellings not being necessarily the warmer;
- The robustness of the ventilation systems regarding user action must be explored as the data shows that those actions will not necessarily produce a better indoor environment;
- The complexity of human behaviour is a challenge for designers but the authors believe that increasing the knowledge of user actions is decisive for building better homes.

6. Acknowledgements

This work is funded by FEDER funds through the Programa Operacional Factores de Competitividade – COMPETE and by National Funds through the FCT – Fundação para a Ciência e a Tecnologia on the frame of the project FCOMP-01-0124-FEDER-041748 and EXPL/ECM-COM/1999/2013.

References

EMERY, A. F. & KIPPENHAN, C. J. 2006. A long term study of residential home heating consumption and the effect of occupant behavior on homes in the Pacific Northwest constructed according to improved thermal standards. *Energy,* 31**,** 677-693.

EN-13829 2001. Thermal performance of buildings - Determination of air permeability of buildings - Fan pressurization method

FREITAS, V. P. D. 2001. *Building Phisics Laboratory - METEOROLOGICAL STATION* [Online]. Available: http://experimenta.fe.up.pt/estacaometeorologica/index.php?lang=en.

FREITAS, V. P. D. 2007-2009. Projeto de Reabilitação do Bairro de Lordelo do Ouro.

KALAMEES, T., KORPI, M., VINHA, J. & KURNITSKI, J. 2009. The effects of ventilation systems and building fabric on the stability of indoor temperature and humidity in Finnish detached houses. *Building and Environment,* 44**,** 1643-1650.

LIDDAMENT, M. 1996. A Guide to Energy Efficient Ventilation. *AIVC,254*.

SANTIN, O. G. 2011. Behavioural patterns and user profiles related to energy consumption for heating. *Energy and Buildings,* 43**,** 2662-2672.

Concepts for development of stochastic data bases for building performance simulation - a material database pilot project

Jianhua Zhao, Dr.[1]
Rudolf Plagge, Dr.-Ing[1]
Nuno M.M. Ramos, Professor [2]
M. Lurdes Simões, Professor [2]
John Grunewald, Professor, Dr.-Ing[1]

[1] Institute of Building Climatology, Dresden University of Technology, Germany
[2] Laboratório de Física das Construções, Universidade do Porto, Portugal

KEYWORDS: *Stochastic database, uncertainty analysis, specific material, generic material, probability density function*

SUMMARY: Probabilistic assessment of hygrothermal performance of building components has received an increasing attention. Comparing to deterministic simulation, probabilistic simulation provides a wide range of the possibilities that could cover the unexpected scenarios. However, the lack of knowledge of inputs variability becomes one of the obstacles in probabilistic simulation.

In this paper, the concept to build a stochastic material database was illustrated. The sources of uncertainty in different data levels were analyzed. Uncertainty in basic parameters will also lead to the variation of functionalized data depending on the modeling approach. In addition to specific material, generic material which owns the common material characteristics of one type of specific materials can be also included in stochastic database for probabilistic simulation. The range and distribution of the inputs determine the corresponding range of simulation outputs. Therefore, probability density functions of material properties in building brick category were investigated by statistical tests as one example.

1. Introduction

Current hygrothermal tools mainly execute deterministic simulations due to the fact that each parameter uses a desired value. Thus, the corresponding outputs will be a predictably determined value or function. However, the simulation inputs in the real world, e.g., user behavior, material properties, and weather condition, will not always follow the way defined in the simulation. For instance, material properties obtained from reference laboratory condition may differ from those at environmental conditions when the material was incorporated in the building envelope, due to the change of the surrounding environment. Weather condition used in the simulation is either the measured data of past years or the synthetic data, e.g., test reference year. The stochastic nature of the inputs leads to the variations in the simulation outputs.

Material data is one of the most important inputs in the hygrothermal building simulation. In the heat, air, and moisture models the material is usually assumed as a homogenous and isotropic entity composed of the matrix and pore. On the macroscopic level, if the studied portion is larger than the representative element volume (REV), material property is assumed to be independent of the size, shape, and the orientation of the volume (Bear and Bechmat 1991). Thus, material property is postulated as a deterministic value in the hygrothermal model. Those simplifications and assumptions make the simulation of complex physical phenomena possible. However, the physical phenomena indicate there exists a considerable variation in material property in reality.

The knowledge of material properties is achieved by experimental measurements. The experiment shows that the non-homogeneity of porous building material could introduce substantial uncertainty (Kumaran *et al.* 2004). There are many factors interactively influencing the measurement of material properties. Total uncertainty is the cumulative uncertainty of those factors. A simulation using deterministic inputs cannot adequately take into account the variable conditions and unexpected scenarios occurring during building construction and operation. Therefore, uncertainty analysis of the input data should be conducted before a probabilistic performance evaluation. This paper conducts material property uncertainty analysis and builds a concept of a stochastic material database for probabilistic simulations.

2. Uncertainty in material properties

Uncertainty in material properties may result from three sources: material's natural inhomogeneity, the production and measurement, and modeling methodology concerning the functionalization of discrete measured data.

- Natural errors arise from the natural variability of physical properties of a specific material. It is an intrinsic property of the material. Even for the same batch of the material, their behaviors may also exhibit distinction.
- Production and measurement errors are caused by producing technique, experimental setup, evaluation and interpretation of experiments. For a specified R-value, the thicknesses, densities, and thermal conductivities of the studied insulations may vary over considerable ranges due to the differences in manufacturing processes (ASHRAE 2009). To the same parameter, the inconsistent standards may also have different interpretations. In addition, although some of the measurement procedures have been outlined by the standards, the measurements are susceptible to uncertainty. For example, in water absorption measurement, initial moisture content and environmental relative humidity will influence the water absorption coefficient.
- Modeling error comes from the difference between mathematical model and real material property. Different models can result in the discrepancy in explanation of physical phenomenon. For instance, moisture transport in porous material can be modeled by diffusivity method and conductivity method, depending on the adopted driving forces (water vapor, moisture content, capillary pressure, etc.), with different parameters in the model. Thus, the applied methods lead to the different transport functions approximating the reality of moisture transport.

In this paper, uncertainties in specific material and generic material are discussed, respectively. First, the definitions of specific material, generic material, and material category are given:

- A specific material is an individual material, usually associated with a specific producer. It has its particular name to differentiate from others. Its material properties are obtained by measuring representative samples of the production line.
- A generic material is a "derived" or "artificial" material from one material cluster. First, material cluster is identified from a collection of specific materials, according to the similarity between specific materials by comparing their differences in material properties. Then, synthetic process is applied to derive a generic material from each identified cluster. Generic material represents one type of specific materials which have similar characteristics (Zhao 2012).
- A material category defines a group of specific and generic materials with common natural characteristics and overall designation.

The definitions of these three terms can be exemplified as follows: historical "brick a" and "brick b" are two specific materials. These two bricks have similar material properties and can be aggregated

into a brick cluster called “historical brick fabricated by the classic loam and clay”, represented by one generic material named “historical building brick”, which belongs to the category “brick”.

2.1 Uncertainty in specific material

Generally, material properties include basic parameters and functionalized data. A set of international standards have been developed to measure those properties. In addition to these well described standards, the HAM modeling tools may require extra tests to acquire additional material information, e.g., drying test, tension infiltrometer or head permeameter to measure liquid water conductivity (Plagge *et al.* 2007).

Uncertainty in material property of specific material depends on its porous structure and the conducted experiments. The measurements of water absorption, drying test, moisture retention, desorption, adsorption and water vapor diffusion resistance factor of one specific brick are shown in Figure 1. In the graph, each colored mark represents one specimen. The blue curve is the connection of mean values of the measurements from several specimens. The graphs show there is no consistent result among the measured specimens. Each property has more or less variation. Brick exhibits a large variation in water absorption coefficient and capillary saturation moisture content. Its water vapor diffusion resistance factor also has a great discrepancy.

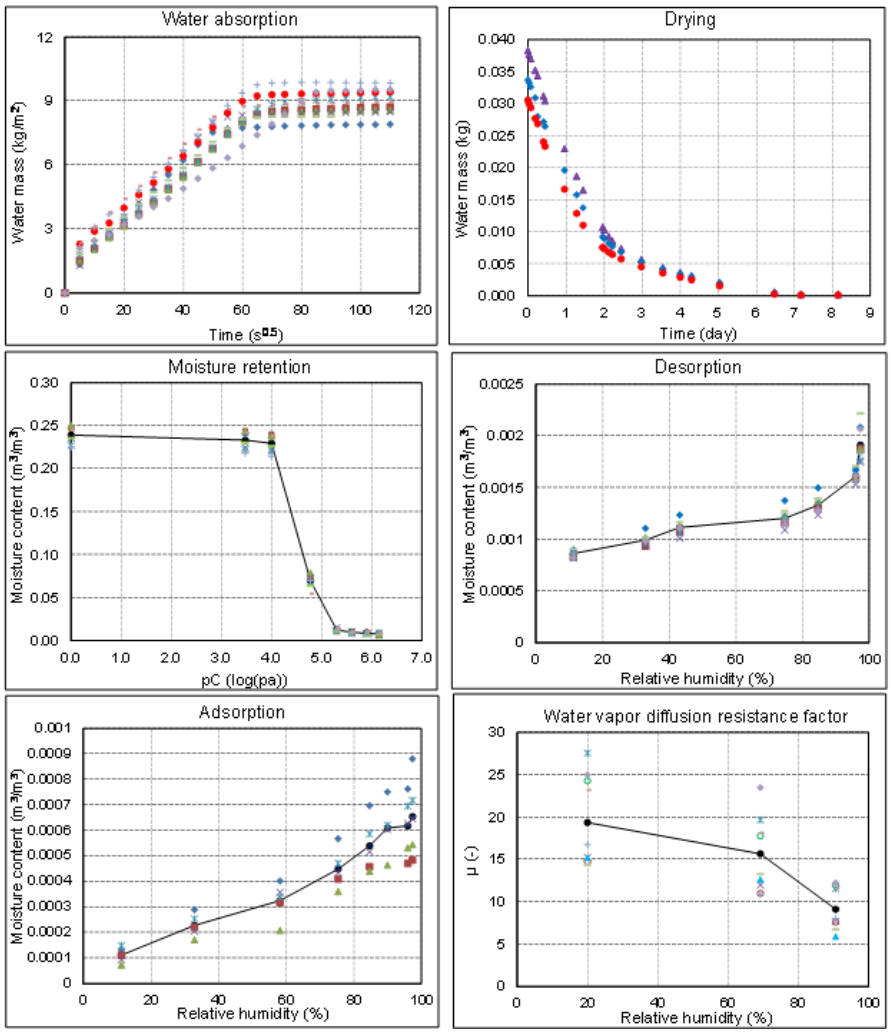

FIG 1.Water absorption, drying test, moisture retention, desorption, adsorption and water vapor diffusion resistance factor of brick

Uncertainty in material properties of a specific material is usually obtained from statistical data of experimental measurements: mean value, standard deviation, maximum, and minimum values calculated from measured representative specimens. This knowledge is straightforward and considers the possible range of each property of a specific material. The limitation is that adequate specimens are required to get reliable statistical information, especially for the inhomogeneous materials.

The functionalized data, also called material function, corresponds to properties that are dependent on state variables, such as moisture retention curve is moisture content as a function of capillary pressure. Functionalized data suffers from the uncertainty in the relevant basic material parameters, depending on the adopted mathematical model. For instance, open porosity and water vapor diffusion resistance factor are related to water vapor permeability function; effective saturation moisture content is the upper limit of moisture content in moisture retention function and liquid water conductivity function. When those basic parameters vary, the corresponding material functions will also shift in a certain range. For the engineering model (Grunewald *et al.* 2003), material functions and related basic material parameters are listed in Table 1.

TABLE 1. Material functions and their related material parameters

Material function	Unit	Symbol	Parameters that affect material function
Moisture retention function	m^3/m^3	$\theta(pC)$	θ_{eff}
Water vapor permeability	s	$K_v(\theta)$	θ_{por} *and* μ_{dry}
Liquid water conductivity	s	$K_l(\theta)$	θ_{eff} *and* K_l
Thermal conductivity	$W/m{\cdot}K$	$\lambda(\theta)$	θ_{eff}

Moisture retention curve, thermal conductivity, water vapor permeability and liquid water conductivity of the brick, with account of the uncertainty measured from experiment, are shown in Figure 2. In each graph, the red curve presents the design material function for the deterministic simulation. The grey shadow region is the possible variation range of material functions obtained from total 400 randomly generated samples.

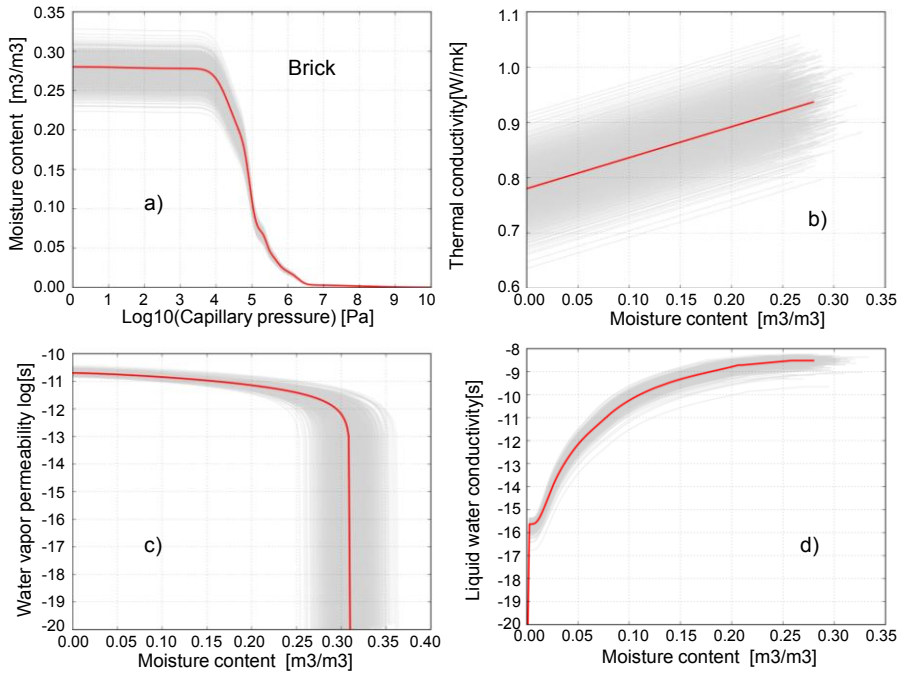

FIG 2. Material functions of brick a) moisture retention curve b) thermal conductivity c) water vapor permeability d) liquid water conductivity

2.2 Uncertainty in generic material

Generic material is a derived material that represents one type of specific materials (Zhao 2012). To obtain generic material, cluster analysis which can detect natural groups in data is first applied to identify material clusters from a bunch of specific materials in a material category. The clustering is a process that successively fuses specific materials into groups until a single group containing all the specific materials, as shown in Figure 3.

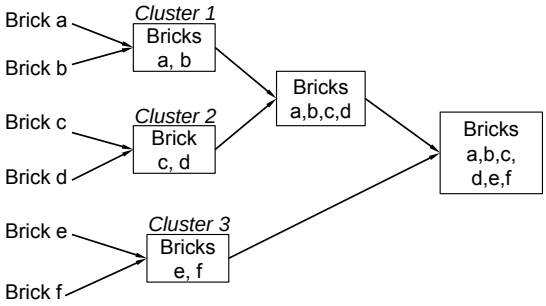

FIG 3. The process of clustering individuals to a single group

Cluster analysis relies on criterion variables based on which the distance is measured between two individuals or groups. In Zhao (2012), the selected criterion variables include basic material parameters and characteristic moisture contents, in consideration of correlations between material parameters. The similarity between two specific materials is determined by their distance. The smaller the distance, the more similar two specific materials. The most similar specific materials are then aggregated into one cluster. In each cluster, specific materials own the common material characteristics. Once the material cluster is identified, generic synthesis process is conducted to derive one generic material from each material cluster by arithmetically averaging material property of specific materials in this cluster.

Descriptive statistics of material properties of all collected bricks from IBK laboratory measurement and literature data (ASHRAE 2009, Kumaran 1996, and Kumaran *et al*. 2004), and descriptive statistics of specific bricks in one identified brick cluster (Zhao 2012), are presented in Table 2 and 3. COVs of material properties of specific bricks in one cluster are less than those of all bricks in brick category since the properties are more similar each other in one cluster compared to those of other bricks.

TABLE 2. Descriptive statistics of material properties of all bricks in brick category

All Bricks	N	Mean	StdDev	Min.	Max.	Median	COV(%)
ρ [kg/m^3]	70	1791.0	218.3	1100.0	2400.0	1794.0	12.19
c [J/kgK]	41	867.32	65.07	772.22	1092.18	860.88	7.5
λ [W/mK]	56	0.684	0.220	0.373	1.340	0.667	32.19
θ_{por} [m^3/m^3]	47	0.313	0.063	0.110	0.446	0.314	20.10
θ_{cap} [m^3/m^3]	42	0.207	0.071	0.071	0.350	0.204	34.35
μ [-]	53	33.5	40.1	6.8	212.0	19.4	119.50
A_w [kg/m^{2}s$^{0.5}$]	51	0.177	0.141	0.001	0.500	0.142	79.74
θ_{eff} [m^3/m^3]	33	0.285	0.071	0.156	0.419	0.292	24.84
k_l [s]	26	1.53E-08	3.02E-08	2.91E-11	1.16E-07	3.16E-09	197.04

TABLE 3. Descriptive statistics of material properties of bricks in one cluster

Clustered Bricks	N	Mean	StdDev	Min.	Max.	Median	COV(%)
ρ [kg/m^3]	8	1741.0	44.0	1657.2	1787.5	1746.5	2.53
c [J/kgK]	8	939.09	72.70	867.97	1092.18	918.35	7.74
λ [W/mK]	8	0.656	0.117	0.543	0.871	0.633	17.84
θ_{por} [m^3/m^3]	8	0.352	0.011	0.336	0.375	0.352	3.07
θ_{cap} [m^3/m^3]	8	0.253	0.012	0.231	0.266	0.256	4.82
μ [-]	8	18.0	5.8	8.6	24.5	18.6	32.13
A_w [kg/m^{2}s$^{0.5}$]	8	0.167	0.046	0.107	0.227	0.167	27.25
θ_{eff} [m^3/m^3]	8	0.332	0.016	0.313	0.357	0.329	4.79
k_l [s]	7	3.37E-09	3.54E-09	8.64E-10	1.07E-08	1.77E-09	105.06

Comparing to the deviation in material property of a specific material which only accounts for the uncertainty among the specimens, the deviation in material properties of a generic material provides the knowledge of the possible variation range of material property of this type of specific materials in the stochastic simulations. Thus, generic materials, together with specific materials, comprise of a stochastic material database.

2.3 Probability distribution of material properties

Uncertainty can be quantified from a probability distribution, which approximates the possible range and distribution of the variable. Probability distribution of the inputs will influence the range and distribution of the outputs, thus, they should be carefully selected. Three statistical tests were carried out in the analysis of the distribution of material property: Chi-squared test, Kolmogorov-Smirnov (K-S) test, and Shapiro-Wilk (S-W) test. Chi-squared test and Kolmogorov-Smirnov test can evaluate if the data follows the specified distribution. Shapiro-Wilk test is used to examine if the sample is drawn from a normally distributed population. The null hypothesis is that the data comes from a particular theoretical distribution. The null hypothesis is accepted, if the calculated *p*-value is larger than the predefined significance level α.

Probability density functions of material properties in building brick category, with collected data from IBK laboratory, ASHRAE (2009), Kumaran (1996), and Kumaran *et al*. (2004), were evaluated. Histogram plots of bulk density, specific heat capacity, thermal conductivity, capillary saturation moisture content, effective saturation moisture content, water absorption coefficient, liquid water conductivity at saturation moisture content, and water vapor diffusion resistance factor were illustrated in Figure 4. The number of materials analyzed for each property was also indicated. Chi-squared test, Kolmogorov-Smirnov test and Shapiro-Wilk test were conducted for each material category. The significance level α is set to 0.05.

From statistical analysis, bulk density, specific heat capacity, thermal conductivity, capillary saturation moisture content, effective saturation moisture content, and liquid water conductivity at saturation moisture content in common logarithm (log10) scale mainly follow normal distribution. Water absorption coefficient and water vapor diffusion resistance factor can be postulated to come from a lognormal distribution.

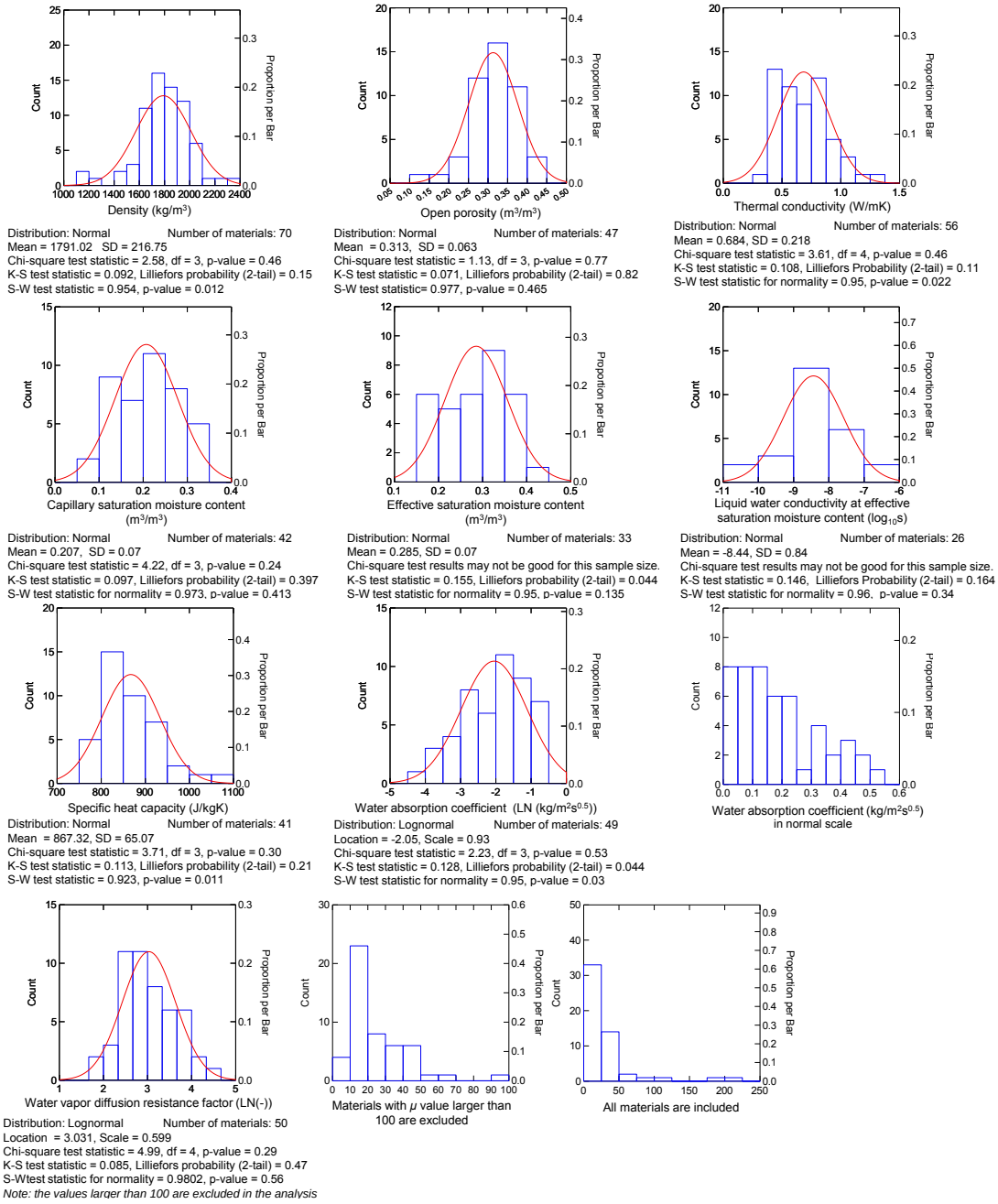

FIG 4. Histogram plots and statistical analyses of material properties of bricks

3. Conclusions

A probabilistic simulation needs a stochastic database which contains the information of the possible range and distribution of input data. This paper presents the concept for establishing a stochastic material database.

Uncertainty in material property comes from its natural inherence, production and measurement, and modelling errors. The variance in the measured data is the sum of those uncertainties. Uncertainty can be considered in different data levels, i.e., specific material, generic material, and material category. Uncertainty in properties becomes larger as more materials are included in the analysis.

The range and distribution of input data determine corresponding simulation outputs. Therefore, probability density function of material property of building bricks collected from different sources

were analyzed. Bulk density, specific heat capacity, thermal conductivity, capillary saturation moisture content, effective saturation moisture content, liquid water conductivity at effective saturation moisture content in common logarithm (log10), basically follow normal distribution. Water vapor diffusion resistance factor and water absorption coefficient can be postulated to be from lognormal distribution.

The concept of stochastic material database can be widely applied to build other inputs database, e,g., indoor load, weather data, and air tightness and ventilation.

Acknowledgement

This paper is accomplished under the framework of IEA Annex 55 RAP-RETRO and authors thank for all the advice from the collaborators.

Nomenclature

ρ	Bulk density
c	Specific heat capacity
λ	Thermal conductivity
μ	Water vapor diffusion resistance factor
A_w	Water absorption coefficient
θ_{por}	Open porosity
θ_{cap}	Capillary saturation moisture content
θ_{eff}	Effective saturation moisture content
K_l	Liquid water conductivity at saturation
N	Number of specific materials
IBK	Institute of Building climatology, Dresden University of Technology, Germany
ASHRAE	American Society of Heating, Refrigerating and Air-Conditioning Engineers

References

ASHRAE. 2009. ASHRAE Handbook of Fundamentals. Atlanta, GA: American Society of Heating, Refrigerating and Air-Conditioning Engineers

Bear, J. and Bechmat, Y.1992 Introduction to modeling of transport phenomena in porous media. Kluwe Academic Publishers.

Grunewald, J., Häupl, P., and Bomberg, M. 2003. Towards an Engineering Model of Material Characteristics for Input to Ham Transport Simulations - Part 1: An Approach. Journal of Building Physics 26 (4):343-366.

Kumaran, M.K. 1996. Final Report, IEA-Annex 24, Task 3: Material Properties, IRC/NRC, Canada.

Kumaran, M.K., Lackey, J.C., Normandin, N., Tariku, F., and Van Reenen, D. 2004. Heat, air and moisture transport properties of several North American bricks and mortar mixes. Journal of Testing and Evaluation,Vol 32, no 5, pp. 383–389

Plagge, R., Scheffler, G., and Nicolai, A. 2007. Experimental Methods to Derive Hygrothermal Material Functions for Numerical Simulation Tools. Paper read at Buildings X Proceedings, at Clearwater Beach, Florida.

Roels, S., Carmeliet, J., Hens, H., Adan, O., Brocken, H., Cernym, R., Pavlik, Z., Ellis, A. T., Hall, C., Kumaran, K., Pel, L., and Plagge, R.. 2004. A Comparison of Different Techniques to Quantify Moisture Content Profiles in Porous Building Materials. Journal of Thermal Envelope and Building Science 27 (4):261-276.

Zhao, J. 2012. Development of a Novel Statistical Method and Procedure for Material Characterization and a Probabilistic Approach to Assessing the Hygrothermal Performance of Building Enclosure Assemblies. Ph.D. Dissertation. Syracuse University, USA, pp.298

Influence of Ice Formation on Thermal Conductivity and Liquid Water Conductivity in Hygrothermal Transport Models

Luisa Sontag, Dipl.-Ing. [1]
Andreas Nicolai, Dr. [1]
John Grunewald, Prof. Dr.-Ing. [1]

[1] Institut of Building Climatology, Germany

KEYWORDS: *ice formation, thermal conductivity, liquid water conductivity, material model, porous media, simulation, Delphin*

SUMMARY:
This article investigates the influence of ice formation on transport processes in porous media. Previously, an ice model was implemented in the hygrothermal simulation program Delphin, with the focus on thermodynamic effects. The physical model includes a moisture content specific freezing point depression and considers the phase transition enthalpy of the ice crystallization. The model is now extended to consider the effect of ice in the porous medium on thermal and liquid moisture transport through adaptation of liquid water conductivity and thermal conductivity. We present the relevant equations and investigate their influence in comparative simulation cases. The adaptation of transport coefficients has a significant impact on simulation results.

1. Introduction

Ice formation in porous materials has already been investigated by several authors before (e.g. Hens 1996). But the development of these models was mostly discontinued or was not sufficient to been integrated in current hygrothermal simulation programs (Nicolai 2007; Künzel 1994; Janssen et al. 2007). This is the reason we developed a new ice formation model based on theoretical approaches which shall afterwards be compared with experimental data.

The ice model is implemented in the hygrothermal simulation program Delphin (Sontag 2012). With this extension it is possible to simulate ice formation and freeze-thaw-cycles in porous media. The focus was on the thermodynamic effects at first. This means the physical model includes a moisture specific freezing point depression and considers the phase transition enthalpy of the ice crystallization. Simulation results obtained with this implementation showed that the temperature decreases slower when the freezing point temperature is reached, than without the ice model. The approximation with the simulation is now significantly better than before.

But the ice mass has also an influence on the transport processes which take place in the pore system of the material. Especially the influence of the ice mass on the liquid water transport is very important. The more ice will be formed the less liquid water for the transport exists. Consequently, less pore space is available for liquid transport and part of the pore space is blocking liquid transport. But also the fact that the ice mass has a higher thermal conductivity than liquid water mass should be taken into account. These effects are considered in our extension to the existing hygrothermal transport model Delphin. We introduced ice-dependent models for liquid water conductivity and thermal conductivity.

To quantify the importance of these model extensions before conducting own experiments or using literature data, we analyzed the influence of the transport model adaptation in comparative simulation cases. We chose a simple drying test of a single material layer which is nearly saturated. First, however, we will briefly discuss the current state of art in the hygrothermal transport model including ice formation.

2. Ice Formation Model

If ice crystallization is neglected in hygrothermal simulation programs, simulation results for cases with material temperatures below 0 °C may significantly deviate from practical observations. The primary source of error is the ice crystallization enthalpy. Thus, we incorporated an ice formation model into the current Delphin version 5.8.1 (Nicolai & Sontag 2013) with particular focus on said crystallization enthalpy. A second component of the model is the consideration of freezing point depression.

2.1 Modeling of Porous Material

The capillary porous material can be described on the macroscopic level as mixture of pores of different radii. Assuming cylindrical pores the pore size can be associated with a capillary pressure using the Kelvin equation. With decreasing pore radius capillary pressures will increase. Capillary pressures inside the material are responsible for liquid capillary moisture transport and moisture update. We assume that the porous medium will always be filled from the smallest to the biggest pores with liquid water (Grunewald 1997).

The relation between the capillary pressure, defined negatively, and the moisture content can be experimentally determined. The resulting moisture retention curve is material specific. With increasing moisture content the capillary pressure gets smaller in magnitude, until the material is saturated. Then the capillary pressure is zero and no more water can be absorbed from the material.

2.2 Ice Crystallization

When temperatures drop below 0 °C ice crystallization in the material is possible. Liquid water has the property to freeze at a free water surface with normal pressure at 0 °C. Inside the pore system the capillary pressure and related surface tension requires lower temperatures for crystallization to begin. This effect is called freezing point depression. This relation can be expressed with a thermodynamic model that gives the capillary pressure of the largest pore not yet frozen (Xu 1998). All smaller pores will still have liquid water.

This means, the temperature in small pores must decrease more than in bigger pores to allow ice formation. Because of this fact we assume that the capillary porous material always freezes from the biggest to the smallest pores. The larger in magnitude the capillary pressure (the less moisture in the material) the more the temperature must decrease so that ice can be formed. This also means that ice crystallization near 0 °C is only possible when the material is saturated. To summarize, the freezing point inside the porous medium depends on temperature and moisture content.

A very important effect of the ice formation is the consideration of the phase transition enthalpy. The ice crystallization is an exothermic reaction, that means during the phase transition heat is released. The result is that the temperature during the ice crystallization decreases more slowly while phase transitions occur. The phase transition enthalpy of ice crystallization has a huge impact on the hygrothermal simulation results and was therefore in the focus of the modeling.

2.3 Simplifications

Other effects of the ice formation were initially neglected. This includes for example the volume expansion. Ice has a smaller density than liquid water. The result is that liquid water is displaced from the ice or, if not enough space exist, the solid matrix can be damaged. This effect is currently neglected and in the model we assume that ice mass has the same density than liquid water mass.

Also kinetic processes during the ice crystallization were neglected. A thermodynamic equilibrium between liquid water and ice is used instead. That means that at any time of the simulation it is possible to separate liquid and ice masses depending on given temperatures and the freezing point depression. When the freezing point is reached the ice will be formed immediately and without time

delay. At the same time the liquid water is reduced by the same amount. The total moisture content in the material is composed of liquid water, ice and water vapor, whereby the mass density of water vapor is very small compared to the other. With respect to volumetric moisture contents, we use the sum of liquid and ice contents θ_{l+ice} (Eq. 1).

$$\theta_{l+ice} = \theta_l + \theta_{ice} \tag{1}$$

Where θ_{l+ice} Total volumetric moisture content (without vapour) in [m³/m³]

θ_l Liquid water content in [m³/m³]

θ_{ice} Ice content in [m³/m³]

With respect to liquid transport we assume that ice formation will not influence the driving potential for liquid flow, the gradient of capillary pressure.

In the reality the freezing point and the thaw point are not the same, so that the freezing and thawing have different temporal progress. This effect is called hysteresis and also omitted in this ice model. We assume that the freezing point is equal to the thaw point.

Crystallization may cause cracks in the material matrix which may have an impact on all material specific properties. Property modifications like this are very complex and require much experimental data. Currently, we are interested in most important influencing factors of ice formation and such secondary effects are currently outside of the scope of this article. Also the modifications of the transport properties were unconsidered at first (Sontag 2012).

3. Ice-Dependent Transport Parameter Models

The ice model is now extended to consider the effect of ice crystallization on thermal and liquid moisture transport in porous medium. This shall be done by adaptation of the liquid water conductivity and the thermal conductivity. It can be expected that models with ambition to capture experimental observations very accurately will be, at the same time very complex and include many parameters. We choose to use simple models with few fitting parameters first, in order to analyse principle effects and gain an understanding of important model sensitivities.

3.1 Thermal Conductivity

The thermal conductivity of a material depends on the water content. With increasing moisture content in the material the thermal resistance decreases. Previously we assumed that ice has the same thermal conductivity as liquid water. However, the thermal conductivity of ice is about four times higher than that of water. This results in further reduction of thermal resistance whenever ice is formed.

In our porous media model we assume that the different pore components and phases contribute area- or volume-weighted to the thermal conductivity (parallel model). In this simple linear model the thermal conductivity depends on the properties of the dry material and volumetric contents of the liquid water and ice multiplied with their respective thermal conductivities, Eqn. (2).

The consideration of ice mass in the calculation of the thermal conductivity increases the thermal conductivity compared to the original model, where the total moisture content was multiplied with the specific thermal conductivity of liquid water. We can expect temperature profiles and heat fluxes to change accordingly.

$$\lambda = \lambda_{dry} + \lambda_{liquid} \cdot \theta_l + \lambda_{ice} \cdot \theta_{ice} \tag{2}$$

Where λ_{dry} Thermal conductivity of the dry material in [W/m·K]

λ_{liquid} Thermal conductivity of liquid water, 0.56 W/(m·K)

λ_{ice} Thermal conductivity of ice, 2.2 W/(m·K)

3.2 Liquid Water Conductivity

The liquid water conductivity in the porous medium depends on the pore volume und the pore distribution. In bigger pores the liquid water can flow faster than in smaller pores, based on comparison to Hagen-Poiseuille pipe flow. In combination with a bundle-of-tubes modeling approach we obtain a moisture-dependent liquid conductivity for a capillary-pressure driven Darcy flow model. Materials with many big pores have a higher liquid water transport than materials with same porosity but mostly small pores. The liquid water conductivity is typically described through a model and subsequently calibrated in experiments (Scheffler 2010).

If the material begins to dry, the capillary transport decreases significantly. Then only small pores can transport water resulting in slow capillary transport. Therefore, it is very important to consider the ice crystallization in the liquid water transport. We assume in the ice model, that the ice will be formed from the biggest to the smallest pores. This means these bigger pores are no longer available for the liquid water transport. But, we disregards that in reality also areas with bigger pores may still contain liquid water while smaller pores are already frozen. In this situation also bigger pores which still contain liquid water can be also take part in the liquid water transport.
To investigate the influence of the ice formation on the liquid water transport, we determine the liquid water conductivity now in dependency only of the liquid water fraction and no longer on the total volumetric moisture content θ_{l+ice} (Eq. 3). Because of this modification we expect the capillary transport to get smaller with beginning of the ice formation.

$$K_l = K_l\left(\theta_l\right) \tag{3}$$

Where K_l Liquid water conductivity in [s]

4. Simulation Case

4.1 Test Case Setup

To analyze the influence of ice formation on the heat and moisture transport processes, comparative simulations were performed. We use a simple drying test of a 36.5 cm thick brick wall construction (Wienerberger Normal Brick ID #264, Delphin 5.8 material database), with constant climate conditions on the inside and outside (see TABLE 1). To enforce ice formation the temperature on the outside is set to -10 °C.

TABLE 1. Climate conditions

Inside (right surface)	Temperature	20 °C
	Relative Humidity	50 %
Outside (left surface)	Temperature	-10 °C
	Relative Humidity	80 %

To perform a drying test, the material must be wet in the beginning. Therefore the initial moisture content is set to 90 % of the effective saturation. The drying process is possible to both sides of the construction. The initial temperature is set uniformly to 20 °C.

The numerical model used initially a non-uniform spaced discretization grid with boundary element sizes of 1 mm increasing up to a maximum of 10 mm in the material center. Further grid refinement showed that equidistant grids (0.5 mm cell size) are better suited since step gradients appear also

inside the construction. The time integration was controlled to be accurate to 4 digits of the monitored quantities. The project files with detailed simulation input data are available for further reference from the authors. The simulations were done using the Delphin 5.8.1 version (Nicolai et al. 2013).

4.2 Description of Principle Effects Observed in the Test Case

When materials starts to dry out, the liquid water from the inside of the construction is transported with capillary transport to the surface and evaporates there. During the first stage of the drying the capillary transport is much larger than evaporation rate at the surface. Therefore, moisture content decreases nearly uniformly in the material. But the capillary transport gets smaller with decreasing moisture content. Is the evaporation rate at the surface bigger than the capillary transport in the inside of the construction, that means not enough liquid water can be transported to the surface, the moisture content near the evaporation surface drops quickly. This marks the end of the first drying period with near constant moisture removal rate. Afterwards, a moisture profile characteristic for drying processes forms. As soon as the material surface gets dry, the water transport from the inside to the surface is dominated by vapour diffusion processes now, which are significantly slower than capillary transport. Hence, the remainder of the drying process takes very long.

In our test case we have set different temperatures on either side of the material. Vapour pressure difference is the driving force for evaporation from the material surface. On the cold side of the material the difference between saturation vapour pressure and ambient vapour pressure is much smaller than on the inside of the material, resulting in higher drying rate at the warm side. Since the outside temperature is -10 °C and the material is in the beginning nearly saturated, the ice formation starts immediately with simulation start. Because of that the amount of unfrozen liquid water reduces. The phase transition enthalpy involved in this process slows down the cooling of the initially warm material.

4.3 Without Influence of Ice on Transport Coefficients

First we simulate the drying test without modification of the transport coefficients. This simulation can serve later as comparative case. FIG. 1 shows the moisture and temperature profile after five days.

The left diagram shows computed liquid, ice and total moisture mass densities of the simulation case with ice formation and phase transition enthalpy included. From the moisture profile we see that the drying process is still in the first drying stage and the total moisture mass density is nearly uniformly distributed in the construction. This means the capillary transport is large enough to transport the water to the surfaces where it evaporates. Only after 25 days the drying process reaches the second stage. The ambient temperature of -10 °C results in ice formation in the first 15 cm.

In the right diagram is shown the temperature profile of the previously model without ice calculation and the new ice model. Because of the consideration of the phase transition enthalpy temperatures decrease slower with beginning of ice formation. The results are slightly higher temperatures in the construction visible even after 5 days. Note, the thermal conductivities are computed exactly the same in both cases based on the total moisture content and the temperature difference do not stem from different heat flux calculations.

The effect of freezing point depression is also visible in the left diagram. Since the total moisture content across the simulation domain is nearly the same, the computed ice content follows the temperature dependent freezing point depression model. Even at the cold surface about 10% of the total moisture content are still liquid.

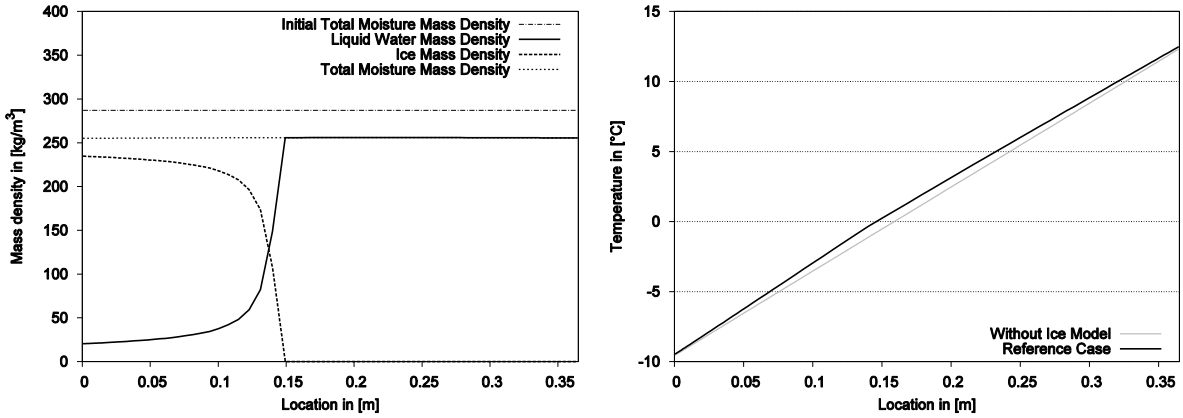

FIG 1. Initial model version without modification of transport coefficients, profiles after 5 days

Now we want to analyze the influence of the ice formation on the transport coefficients through adaptation the thermal conductivity and the liquid water conductivity. To analyze the influence of each adaptation of the transport coefficients, we investigate each modification separately at first, and combined afterwards.

4.4 Influence of Ice on Thermal Conductivity

Because of the ice crystallization in the outer layer, the thermal conductivity in this area increases significantly with our extended thermal conductivity model. The surface temperature at the outside increases marginally, which appears to have no significant influence on the evaporation rate. But, a shift of the temperature in the middle of the constructions can be observed. Because of the higher thermal conductivity are the temperatures lower (see FIG. 2, right). The ice formation now reaches up to the middle of the construction (see FIG. 2, left). The left diagram also shows the ice mass profile of the reference case for comparison.

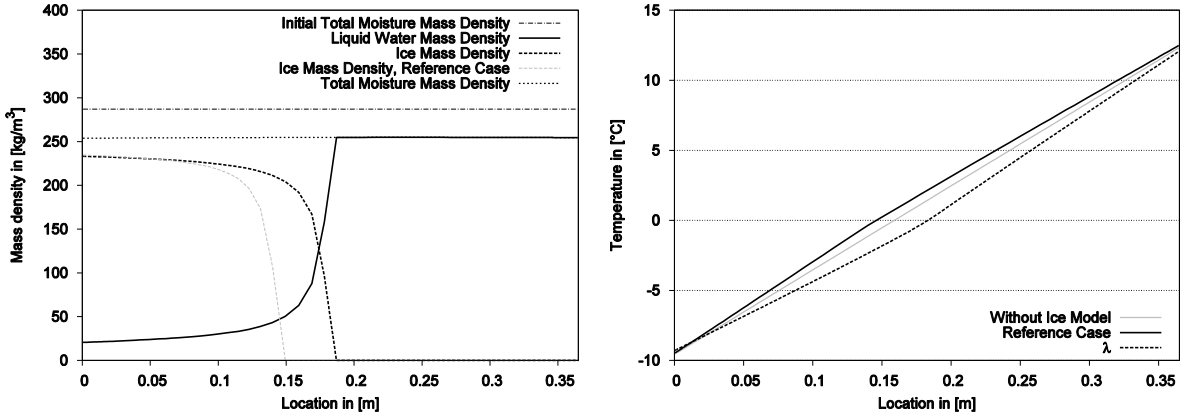

FIG 2. Simulation with improved thermal conductivity model, profiles after 5 days

Because of the reason that the ice formation has no influence of the liquid water transport, the drying potential does not change. The moisture mass density and also the moisture distribution are the same as the reference simulation. Consequently, the adaptation of the thermal conductivity has no significant influence on the drying process in the first stage.

4.5 Influence of Ice on Liquid Water Conductivity

Because ice formation at the outside of the construction occurs immediately, the related pores are no longer available for the capillary transport. The liquid water conductivity in our modified model decreases extremely in this area and the moisture transport is very quickly dominated by diffusion.

This transport process is now significantly slower, so that the drying process occurs now mainly over the inside of the construction. Consequently, the overall moisture content in the construction is higher than in the reference simulation (see FIG. 3, left). Also, the reduction of liquid conductivity in the ice formation zone hinders liquid capillary transport to the inside, resulting in non-uniform moisture distribution.

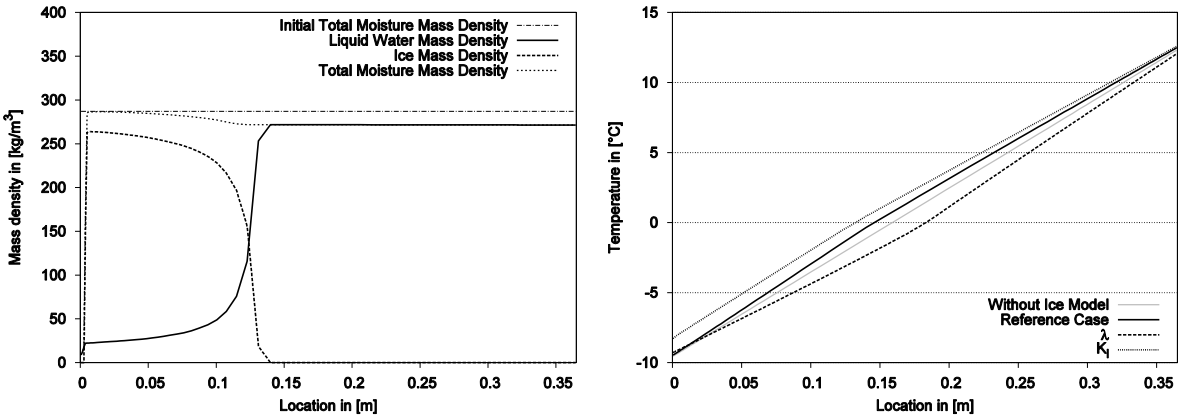

FIG 3. Simulation with improved liquid water conductivity model, profiles after 5 days

Because of the higher ice content in the leftmost 13 cm of the material more phase transition enthalpy is released during the freezing process. However, this is not the reason for the higher temperatures in the construction. Indeed, at the left surface evaporation and corresponding evaporation cooling effects are much smaller than before, resulting in higher temperatures.

4.6 Combined Model

In the last simulation case we investigate the combined influence of ice formation on the thermal conductivity and the liquid water conductivity. Because of the higher thermal conductivity, the temperature in the middle of the construction is lower compared to the reference simulation, while being higher at the cold surface (see FIG. 4, right). Ice crystallization now extends deeper into the construction, to about 17 cm (see FIG. 4, left). The influence of the ice-dependent liquid water conductivity dominates the process. Because of the ice formation the liquid water conductivity decreases and drying takes significantly longer, as in the previous variant.

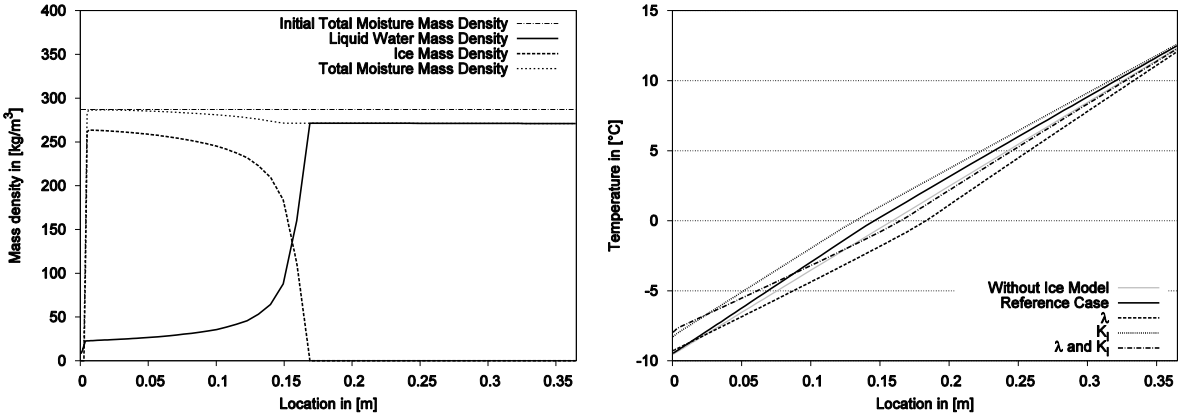

FIG 4. Simulation with full model, profiles after 5 days

5. Conclusions

In the article we showed the influence of ice formation on the hygrothermal transport. We adapted the thermal conductivity and the liquid water conductivity models and presented the relevant equations. The influence on the hygrothermal transport was shown in comparative simulation cases.

It was found that both, the thermal conductivity and the liquid water conductivity, have a large impact on the results. The assumption of ice crystallizing in large pores which leaves only small pores available for capillary transport leads to an extreme reduction of the liquid transport coefficient. Application of this model will give another extreme case compared to ice-free modelling approaches, which likely underestimates liquid capillary transport in the presence of ice.

In our ice model particularly the low moisture content range of the liquid conductivity is used. This sets high demands on material modelling and material function calibration. Next research steps will be comparison of simulations with simple experiments, for example the drying-freezing test presented here. Other model features currently simplified or ignored in the model may then be gradually included to gain better approximation of measured results.

References

Grunewald, J. 1997. Diffusiver und konvektiver Stoff- und Energietransport. PhD Thesis. TU Dresden. Germany.

Hens, H. 1996. Final Report. Volume 1. Task 1: Modelling. International Energy Agency. IEA ANNEX 24 – Heat, Air and Moisture Transfer Through New and Retrofitted Insulated Envelope Parts. 25 ff.

Janssen, J. & Blocken, B. & Carmeliet, J. 2007. Conservative modelling of the moisture and heat transfer in building components under atmospheric excitation, International Journal of Heat and Mass Transfer 50 (2007): 1128-1140.

Künzel, H. M. 1994. Simultaneous Heat and Moisture Transport in Building Components. PhD Thesis. Fraunhofer Institute of Building Physics. Germany.

Nicolai, A. 2007. Modeling and Numerical Simulation of Salt Transport and Phase Transitions in Unsaturated Porous Building Materials. PhD Thesis. Syracuse University. NY. USA

Nicolai, A. & Fechner, H. & Vogelsang, St. & Sontag, L. & Paepcke, A. & Grunewald, J. 2013. DELPHIN 5.8 Model Reference. TU Dresden. Germany.

Nicolai A. & Sontag L. 2013. Implementation of an Efficient Numerical Solution Method to Simulate Freezing Processes in Porous Media. 2nd Central European Symposium on Building Physics. Vienna. Austria. 599-603.

Scheffler, G. A. & Plagge, R. 2010. A Whole Range Hygric Material Model: Modelling Liquid and Vapour Transport Properties in Porous Media. International Journal of Heat and Mass Transfer 53 (2010): 286-296.

Sontag L. 2012. Numerische Simulation von Gefrierprozessen in porösen Medien. Master Thesis. TU Dresden. Germany.

Xu, Y. 1998. Numerische Simulation der Eisbildung in kapillarporösen Baustoffen unter Berücksichtigung der gekoppelten Wärme- und Feuchtetransportprozesse. PhD Thesis. TU Dresden. Germany.

AUTHOR INDEX

Adl-Zarrabi, Bijan 317, 467
Agnalt, Magne 1132
Alev, Üllar 55
Allard, Ingrid 7
Almeida, Ricardo 370
Alonso Álvarez, María 734
Altamirano-Medina, Hector 119, 1238
Andersen, Claus Wessel 718
Andersen, Mie Them 1030
Andersson, Staffan 1301
Andreas, Nicolai 231
Antretter, Florian 483, 854, 879
Arfvidsson, Jesper 1149, 1317
Arumägi, Endrik 616
Bacher, Peder 255
Bagel, Lubomir 443
Bagge, Hans 63, 1317
Baker, Paul 1053
Barreira, Eva 1156
bauwens, geert 199, 255
Bednar, Thomas 39, 47, 102, 1374
Bejat, Timea 191
Belleudy, Clément 79
Berger, Julien 582
Bertelsen, Niels H. 271
Bianchi Janetti, Michele 1037
Bichlmair, Stefan 1349
Binder, Andrea 1061
Bishara, Nadja 892
Bjarløv, Søren Peter 1333
Bjelke-Holterman Björn 1149
Björk, Folke 924
Blocken, Bert 1093
Blomsterberg, Åke 87
Bok, Gunilla 500, 1101
Bonath, Victoria 863
Brandt, Erik 1124
Brinks, Pascal 726
Broström, Tor 608, 648
Burke, Stephen 87, 1244
Bustamante, Waldo 303
Cai, Hong 991
Capener, Carl-Magnus 1244
Carbonez, Kim 313
Carlsson, Peter 330
Cerny, Robert 223, 354
Chhay, Marx 79, 582
Claesson, Johan 338
Claesson, Leif 656
Colinart, Thibaut 475
Collet, Florence 378
Craven, Colin 710
Cronhjort, Yrsa 1172
Curado, António 1397
Dahlblom, Mats 814, 830
Dalehaug, Arvid 1132
De Backer, Lien 71
De Meersman, Glenn 127, 1116
De Paepe, Michel 71, 1014
de Place Hansen, Ernst Jan 1124
Deconinck, An-Heleen 525
Delgado, João 1156
Delghust, Marc 678, 998
Dermentzis, Georgios 1293
Deurinck, Mieke 1341
Devos, Lynn 127
Eder, Katharina 39, 47
Ekstrand-Tobin, Annika 460, 1101
El-Khattam, Amira 1030
Englund, Finn 900
Eriksson, Petra 608
Fænø Mondrup, Thomas 1221

Fauchoux, Melanie 386, 774
Fazio, Paul 79
Feist, Wolfgang 1037, 1293
Feng, Chi 394, 435
Feng, Ya 394, 435
Ferreira, Cláudia 600
Fink, Marcus 879
flamant, gilles 255, 263
Flyen, Anne Cathrine 632
Fontanini, Anthony 135
Fort, Jan 354
Frade, Dina 183
Fransson, Victor 846, 908
Freitas, Vasco P. de 183
Gawin, Dariusz 411
Ge, Hua 79, 144, 838
Gendelis, Staņislavs 871
Georgiev, Georgi 1252
Geving, Stig 207, 1132, 1141, 1269
Glouannec, Patrick 475
Gohardani, Navid 924
Goi, Tsutomu 1325
Gorgolewski, Mark 533
Goto, Yutaka 932
Großkinsky, Theo 1252
Grunewald, John 1399, 1405
Grynning, Steinar 279
Gudmundsson, Kjartan 508
Guernouti, Sihem 582
Gullbrekken, Lars 419
Gustavsen, Arild 279, 419
Gustavsson, Thorbjörn 608
Hagen Eriksen, Marlene 1333
Hagentoft, Carl-Eric 1269, 1366
Hallik, Jaanus 694, 758
Hannu, Viitanen 1197
Hansen, Ernst Jan de Place 1022
Hansen, Kurt Kielsgaard 1030, 1124
Hansen, Kurt 1045
Hansen, Thor 1045
Harderup, Lars-Erik 1317
Harreither, Christoph 1374
Harrestrup, Maria 1180
Hermann, Carsten 1053
Hokoi, Shuichi 1325
Holubek, Matus 451
Hrebik, Peter 1229
Huizing, Ryan 774
Hutchinson, Thomas 167
Huttunen, Petteri 295
Hviid, Christian Anker 718, 734, 822, 916
Högdal, Katarina 1189
Ifka, Tomas 443
Ilomets, Simo 1213
Jakovics, Andris 782, 871, 1108
Janssen, Hans 394, 435, 750
Janssens, A. 71, 127, 313, 678, 998, 1014, 1116
Jansson, Anders 960
Jansson, Helén 467
Jelle, Bjørn Petter 322, 1269
Jensen, Lars 814, 830
Jerman, Milos 223
Jiménéz, Maria José 255
Johansson, Dennis 63, 1317
Johansson, Ingrid 330, 991
Johansson, Pernilla 460, 500, 1101
Johansson, Pär 338, 1269
Jorma, Lehtovaara 1197
Juha, Vinha 1197
Järnström, Helena 983
Jönsson, Dan 63
Jørn, Toftum 790
Kadylak, David 774
Kalamees, Targo 55, 758, 1213
Kalbe, Kristo 694, 758
Kallert, Anna 766

Karami, Peyman 508
Karlshøj, Jan 1221
Karlsson, Emma 1189
Kayello, Ahmad 79
Kedowide, Yannick 191
Kehrer, Manfred 1069
Kettunen, Ari-Veikko 346
Kiesel, Kristina 566
Kilian, Ralf 664, 1349
Kjellsson, Elisabeth 702
Klenz Larsen, Poul 648
Kläth, Mikael 95
Knarud, Jon Ivar Belghaug 1141
Koci, Vaclav 223
Kok, Reinier 798
Konder, Hannes 39
Koniorczyk, Marcin 411
Konz, Alexandra 1293
Kopecky, Pavel 742
Kornadt, Oliver 31, 726
Koronthalyova, Olga 443, 1390
Korsnes, Silje 419, 492
Kosny, Jan 135
Kotol, Martin 710
Koulani, Chrysanthi Sofia 790, 822
Krag, Jesper 1277
Kramer, Rick 558, 624
Krause, Michael 159
Kronvall, Johnny 247
Krus, Martin 664, 1252, 1349
Kuliffayova, Marta 443
Kumlin, Anders 330, 991
Kurkinen, Eva-Lotta 863
Kurkinen, Kimmo 975
Kurnitski, Jarek 806
Kuusk, Kalle 758, 1213
Kvande, Tore 1141
Künzel, Hartwig M. 947, 967, 1061
Laamanen, Jarmo 983
Langmans, Jelle 215
Lappalainen, Vuokko 983
Larsen, Poul Klenz 640
Laukkarinen, Anssi 295
Laverge, Jelle 71, 998
Le Pierres, Nolwenn 191
le Roux, Simon 1172, 1244
Leenknegt, Sarah 15, 23
Leimer, Ing H.-P 152
Lelièvre, Dylan 475
Lethé, Guillaume 263
Liao, Zaiyi 838
Lidholm, Anders 671
Lindberg, Ola 846, 908
Liu, Linn 608
Lorentzen, Anne Sofie 1333
Luman, Andre 1213
Lysholt Hansen, Mathias Young Bok 790
M. M. Ramos, Nuno 600
Maas, Marco 624
Madera, Jiri 223
Madsen, Henrik 255
Maertens, Silke 127
Mahdavi, Ardeshir 550, 566
Marciniak, Alicja 411
Mari Sand, Austigard 1261
Marincioni, Valentina 119, 1238
Martens, Marco 624
Masuda, Yoshinori 1325
Matiasovsky, Peter 402, 451, 1229, 1390
Mattsson, Johan 632, 1149, 1261
Mauring, Tõnu 694, 758
Meng, Qinglin 394, 435
Mihalka, Peter 402, 451, 1229, 1390
Mikulova, Katarina 1390
Miljan, Martti-Jaan 55
Mjörnell, Kristina 1164

Morelli, Martin 1309
Morishita, Naomi 1374
Mosfegh, Bahram 608
Månsson, Tommie 940
Møller, Eva B. 1030
Møller, Eva Birgit 1022
Møller, Eva 1124
Neusser, Maximilian 47
Nicolai, Andreas 287, 1399
Nielsen, Anker 175, 271, 1205
Nik, Vahid 317, 574
Nilsson, Lars-Olof 427
Norbäck, Dan 991
Nordquist, Birgitta 830, 846, 908
Nore, Kristine 483, 900, 1261
Nunes, Ângela 183
Ochs, Fabian 1037, 1293
Ohlsson, Ulf 863
Ojanen, Tuomo 591, 1197
Olofsson, Thomas 7, 1301
Olsson, Lars 954
Oly, René 726
Ostermeyer, York 932, 940
Ott, Stephan 1244
Ozolins, Ansis 782, 1108
Paap, Leena 758
Paavo, Kero 1197
Padfield, Tim 1045
Paepcke, Anne 231
Pallin, PhD, Simon 1358
Pallin, Simon 1069
Papadopoulos, Agis 1180
Pasanen, Pertti 983
Pavlik, Zbysek 354
Pazold, Matthias 854
Peixoto de Freitas, Vasco 600
Pereira, Pedro F. 183, 1397
Petersen, Steffen 239, 916
Petzold, Hans 686
Peuhkuri, Ruut 790, 1045, 1077
Pietrzyk, Krystyna 1382
Pinto Seppä, Isabel 591
Piot, Amandine 191
Plagge, Rudolf 892, 1405
Pretot, Sylvie 378
Prieto, Alejandro 303
Q. Nyrud, Anders 900
Quenard, Daniel 79
Radon, Jan 854
Rafati Nasr, Mohammad 774
Ramos, Nuno M. M. 183, 1397
Ramos, Nuno 370, 1405
Ratnieks, Jānis 871
Ravanfar, Afrooz 838
Ridley, Ian 119
Riikka, Holopainen 1197
Rode, Carsten 710, 1045, 1077, 1333
Roelens, Wina 678
Roels, S. 199, 215, 255, 525, 750, 1093, 1341
Rognvik, Egil 279, 419, 1269
Rohdin, Patrik 608
Rose, Jørgen 1205, 1285
Rosenlund, Hans 247
Sadovsky, Zoltan 1390
Saelens, Dirk 15, 23, 1341
Sandberg, Mats 656
Sandberg, Mikael 330
Sanders, Chris 1053
Sasic K., A. 467, 574, 1269, 1358, 1366
Schellen, Henk 624
Schiøtt Sørensen, Lars 175
Schmidt, Dietrich 766
Schmidt, Jens 31
Schuß, Matthias 550
Sedlbauer, Klaus 664
Seng, Billy 467

Shukla, Nitin 135
Siegele, Dietmar 1293
Simões, Lurdes 1405
Simonson, Carey 386, 774
Sohlberg, Elina 983
Sontag, Luisa 1399
Sousa, Hipólito 183
Sousa, Rui 183
Stanek, Kamil 742, 1006
Steeman, Marijke 313, 1014
Stein, Johan 1317
Steskens, Paul 263
Ståhl, Fredrik 608
Stöckl, Beate 967
Šuhajda, Karel 1077
Sunvisson, Peter 95
Svendsen, Svend 1180
Tahmasebi, Farhang 550
Tanghe, Tine 678
Teder, Marko 55
Terkildsen, Søren 822
Thalfeldt, Martin 806
Theuerkorn, Werner 1252
Thorsrud, Erik 207
Time, Berit 279, 419, 1269
Tkaczyk, Alan Henry 758
Torvi, David 386
Tuudak, Sten 1213
Urban, Bryan 135
Uus, Andres 55
Uvsløkk, Sivert 207, 419, 492
Vahalová, Eva 1077
Wahlgren, Paula 110
Walbaum, Holger 932
Valge, Margus 758
Wallentén, Petter 1317
Van Belleghem, Marnix 1014
Van De Vijver, Sven 313
Van Den Bossche, Nathan 127, 313, 1116
Van den Brande, Thijs 1093
Van Gelder, Liesje 750
van Schijndel, Jos 542, 558, 624
Wang, Lin 144
Wegerer, Paul 102
Weiss, Dirk 686
Weitzmann, Peter 734
Vera, Sergio 303
Wessberg, Magnus 648
Vesterberg, Jimmy 1301
Vestergaard, Flemming 1221
Vickers, Andrea 533
Widström, Torun 656
Viitanen, Hannu 983
Viljanen, Klaus 346
Vinha, Juha 295, 1085
Winkler, Matthias 483
Wittchen, Kim B. 271, 1277
Vogelsang, Stefan 287
Woloszyn, Monika 79, 191, 582
Vuckovic, Milena 566
Vågen, Magnus 492
Zhao, Jianhua 1405
Ziegler, Matthias 159
Zirkelbach, Daniel 967, 1061
Åhs, Magnus 362

We thank our sponsors!